INTERNATIONAL SYMPOSIUM

Print: ISSN 2344 - 4118
CD-ROM: ISSN 2344 - 4126
Online: ISSN 2537 – 3773
ISSN-L 2344 – 4118

# ISB-INMA TEH

# AGRICULTURAL AND MECHANICAL ENGINEERING

**Bucharest**
**08 – 09 October 2026**

# ISB-INMA-TEH

# AGRICULTURAL AND MECHANICAL ENGINEERING

Bucharest
2026

## ORGANIZING COMMITTEE

- Prof. Ph.D. Eng. **Sorin-Ştefan BIRIŞ** - Politehnica Bucharest (RO)
- Tech. **Marian CHIRIŢESCU** - INMA Bucharest (RO)
- Assoc. Prof. Ph.D. Eng. **Gabriel CONSTANTIN** - Politehnica Bucharest (RO)
- Eng. **Mihai CONSTANTINESCU** – INMA Bucharest (RO)
- Prof. Ph.D. Eng. **Andrei CRĂIFĂLEANU** - Politehnica Bucharest (RO)
- Prof. Ph.D. Eng. **Cristina-Ileana COVALIU-MIERLĂ** - Politehnica Bucharest (RO)
- PhD. Eng. **Cătălin DUMITRESCU** – INOE 2000 IHP (RO)
- Lect. Ph.D. Eng. **Mihaela DUŢU** - P.U. Bucharest (RO)
- PhD. Eng. **Iuliana GĂGEANU** - INMA Bucharest (RO)
- Lect. Ph.D. Eng. **George Cătălin ION** - P.U. Bucharest (RO)
- Prof. Ph.D. Eng. **Edmond MAICAN** - Politehnica Bucharest (RO)
- Ph.D. Eng. **Mihai MATACHE** - INMA Bucharest (RO)
- Prof. Ph.D. Eng. **Gabriel NEGREANU** - Politehnica Bucharest (RO)
- Prof. Ph.D. Eng. **Gigel PARASCHIV** - Politehnica Bucharest (RO)
- Prof. **Daniela RADU** - INMA Bucharest (RO)
- Lect. Ph.D. Eng. **Mădălina ŞTEFAN** - Politehnica Bucharest (RO)
- PhD. Stud. Eng. **Ana-Maria TĂBĂRAŞU** - INMA Bucharest (RO)
- Assoc. Prof. PhD. Eng. **Nicoleta UNGUREANU** - Politehnica Bucharest (RO)
- Ph.D. Eng. **Valentin VLĂDUŢ** - INMA Bucharest (RO)

## SECRETARY

- Tech. **Tania Țicu** - INMA Bucharest (RO);
- Eng. **Ana-Maria TĂBĂRAȘU** - INMA Bucharest (RO);
- Tech. **Marian CHIRIŢESCU** - INMA Bucharest (RO)

## SUPPORT AND TRANSLATION

- Prof. **Daniela-Cristina RADU** - INMA Bucharest (RO);
- PhD. Eng. **Iuliana GAGEANU** - INMA Bucharest (RO)
- Assoc. Prof. PhD. Eng. **Nicoleta UNGUREANU** - Politehnica Bucharest (RO)

## PROGRAMME COMMITTEE

- Assoc. Prof. Ph.D. Eng. **Atanas ATANASOV** - University of Rouse (BG)
- Prof. Ph.D. **Mihaela BEGEA** – Politehnica Bucharest (RO)
- Assoc. Prof. Ph.D. Eng. **Nastasia BELC** - IBA Bucharest (RO)
- Prof. Ph.D. Eng. **Sorin-Ştefan BIRIŞ** - Politehnica Bucharest (RO)
- Assoc.Prof.Ph.D. Eng. **Sorin BORUZ** - University of Craiova (RO)
- Assoc.Prof. Ph.D. Eng. **Sorin BUNGESCU** – USAMVB Timișoara (RO)
- Assoc. Prof. Ph.D. Eng. Petru **Marian CÂRLESCU** - USAMV Iaşi (RO)
- Ph.D. Eng. **Luminița CATANĂ** - IBA Bucharest (RO)
- Ph.D. Eng. **Valerian CEREMPEI** – Technical University of Moldova (MD)
- Prof. Ph.D. Eng. **Leonardi CHERUBINO** – Universita degli Studi di Catana (IT)
- Prof. Ph.D. Eng. **Sorin CÎMPEANU** - USAMV Bucharest (RO)
- Prof. Ph.D. Eng. **Lucian-Ionel CIOCA**, Lucian Blaga University of Sibiu (RO)
- Prof. **Laura Clarizia**, University of Naples Federico II (IT)
- Ph.D. Eng. **Mihnea COSTOIU** - Politehnica Bucharest (RO)
- Prof. Ph.D. Eng. **Cristina-Ileana COVALIU-MIERLĂ** - Politehnica Bucharest (RO)
- Prof. Ph.D. Eng. **Andrei CRAIFĂLEANU** - Politehnica Bucharest (RO)
- Prof. Ph.D. Eng. **György DEÁK** – NIRDEP Bucharest (RO)
- Ph.D. Eng. **Mihaela-Monica DINU** – ICDPP Bucharest (RO).
- Prof. **Vasyl DMYTRIV** - Lviv Polytechnic National University (UA)
- Prof. Ph.D. Eng. **Ilie DUMITRU** - University of Craiova (RO)
- Ph.D. Eng. **Adam EKIELSKI** - Warsaw University of Life Sciences (PL)
- Prof. Ph.D. Eng. **Can ERTEKIN** - Akdeniz University, Antalya (TR)
- Prof. Ph.D.Eng. **Inacio Maria dal FABRO** – Campinas State University (BR)
- Assoc. Prof. Ph.D. Eng. **Lucian FECHETE** - Technical University Cluj Napoca (RO)
- Prof. Ph.D. Eng. **Nicolae FILIP** - Technical University Cluj Napoca (RO)
- Prof. Ph.D. Eng. **Liviu Gaceu** - Transilvania" University of Brașov (RO)
- Ph.D. Eng. **Iuliana GĂGEANU** – INMA Bucharest (RO)
- Ph.D. Stud. Eng. **Gabriel GHEORGHE** - INMA Bucharest (RO)
- Assoc. Prof. Ph.D. Eng. **Marius GHEREŞ** - Technical University Cluj Napoca (RO)
- Prof. Ph.D. Eng. **Omar GONZÁLEZ** - Central University "Marta Abreu" de las Villas, (CU)
- Prof. Ph.D. Eng. **Marian GRIGORE** – Universitatea Tehnică a Moldovei (MD)
- Prof. **Francisco de Paula Martin Jimenez**, University of Malaga (ES)
- Assoc. Prof. Ph.D. Eng. **Önder KABAŞ** - Akdeniz University, Antalya (TR)
- Assoc. Prof. Ph.D. Eng. **Imre KISS** - P.U. Timișoara (RO)
- Assoc. Prof. Ph.D. **Igor KOVAČEV** - Zagreb University (HR)
- Lect. Ph.D. Eng. **Daniel LATEŞ** – U.M.P.S.T of Tîrgu Mureş (RO)
- Prof. **María Cruz LÓPEZ ESCALANTE**, University of Malaga (ES)
- Prof. Ph.D. Eng. **Edmond MAICAN** - Politehnica Bucharest (RO)
- Ph.D. Eng. **Eugen MARIN** - INMA Bucharest (RO)
- Ph.D. Eng. **Gabriela MATACHE** – INOE 2000 IHP (RO)
- Ph.D. Eng. **Mihai MATACHE** - INMA Bucharest (RO)
- Assoc. Prof. Ph.D. Eng. **Gheorghe MATEI** - University of Craiova (RO)
- Prof. Ph.D. Eng. **Florentina MUNTEANU** – "Aurel Vlaicu" University of Arad (RO)
- Prof. Ph.D. Eng. **Nikolai MIHAILOV** - University of Rouse (BG)
- Ph.D. Eng. **Vasile MOCANU** - ICDP Brașov (RO)
- Ph.D. Eng. **Florin NENCIU** - INMA Bucharest (RO)
- Prof. Ph.D. Eng. **Vasile PADUREANU** – "Transilvania" University of Brașov (RO)
- Prof. Ph.D. Eng. **Mirela PANAINTE-LEHĂUȘ** – V. Alecsandri University of Bacău (RO)
- Prof. Ph.D. Eng. **Gigel PARASCHIV** - Politehnica Bucharest (RO)
- Assoc. Prof. Ph.D. Eng. **Elena POP** - Politehnica Bucharest (RO)
- Prof. Ph.D. Eng. **Tudor PRISECARU** - Politehnica Bucharest (RO)
- Ph.D. Eng. **Elena Cristina RADA** – Insubria University (IT)
- Prof. Ph.D. Eng. **Marco RAGAZZI** - University of Trento (IT)
- Prof. Ph.D. Eng. **Răzvan-George RÎPEANU** – UPB Ploiești (RO)
- Prof. Ph.D. Eng. **Petru CÂRLESCU** – USV Iași (RO)
- Prof. Ph.D. Eng. **Carmen RUSĂNESCU** - Politehnica Bucharest (RO)
- Prof. Ph.D. Eng. **Ion SĂRĂCIN** - University of Craiova (RO)
- Assoc. Prof. Ph.D. Eng. **Lazar SAVIN** - University of Novi Sad (SR)
- Assoc. Prof. Ph.D. Eng. **Kemal SELVİ** - Ondokuz Mayıs Üniversity (TR)
- Ph.D. Eng. **Cristian SORICĂ** - INMA Bucharest (RO)
- Ph.D. Eng. **Dorin Ioan SUMEDREA** – ASAS of Romania (RO)
- Prof. Ph.D. Eng. **Răzvan Ionuț TEODORESCU** - USAMV Bucharest (RO)
- Prof. Ph.D. Eng. **Vincenzo TORRETTA** - Insubria University (IT)
- Prof. Ph.D. Eng. **Ion ŢENU** - ASAS of Romania (RO)
- Ph.D. Eng. **Valentin VLĂDUŢ** - INMA Bucharest (RO)
- Ph.D. Eng. **Iulian VOICEA** - INMA Bucharest (RO)
- Prof. Ph.D. Eng. **Gheorghe VOICU** - Politehnica Bucharest (RO)
- Ph.D. Eng. **Roxana ZAHARIA** – ICDPP Bucharest (RO)
- Ph.D. Eng. **Tomasz ŻELAZIŃSKI** - Warsaw University of Life Sciences (PL)

## HONORARY COMMITTEE

- Prof. Ph.D. Eng. **Florin STĂNICĂ** - ASAS of Romania (RO);
- Ph.D. Eng. **Dorin SUMEDREA** - ASAS of Romania (RO);
- Prof. PhD. **Eugen RUSU** – Romanian Academy (RO);
- Ph.D. Eng. **Ovidiu BADEA** - Romanian Academy (RO);
- Prof. Ph.D. Eng. **Ioan ȚENU** - - ASAS of Romania (RO);
- Prof. Ph.D. Eng. **Valentin NEDEF** - ASAS of Romania (RO);
- Ph.D. Eng. **Mihai NICOLESCU** - ASAS of Romania (RO)
- Prof. Ph.D. Eng. **Dumitru ȚUCU** - ASAS of Romania (RO)

ISB-INMA-TEH' 2026

*NATIONAL INSTITUTE FOR RESEARCH - DEVELOPMENT OF MACHINES AND INSTALLATIONS DESIGNED FOR AGRICULTURE AND FOOD INDUSTRY*
**- INMA Bucharest**
6 Ion Ionescu de la Brad Blvd., sector 1, Bucharest

*BIOTECHNICAL SYSTEMS ENGINEERING*
**- ISB Bucharest**
290 Splaiul Independenței Str., sector 6, Bucharest

**Print: ISSN 2344 - 4118**
**CD-ROM: ISSN 2344 - 4126**
**Online: ISSN 2537 - 3773**
**ISSN-L 2344 – 4118**

Disclaimer/Publisher's Note: The statements, opinions and data contained in all publications are solely those of the individual author(s) and contributor(s) and not of INMA / ISB and the editor(s). INMA and the editor(s) disclaim responsibility for any injury to people or property resulting from any ideas, methods, instructions or products referred to in the content.

## CONTENTS


| No. | Article Title & Authors | page |
|---|---|---|
| 1. | **HEC-RAS SIMULATION: A CASE STUDY OF THE IHTIMAN IRRIGATION SYSTEM /**<br>***СИМУЛАЦИЯ С HEC-RAS: ОБЕКТ НА ИЗСЛЕДВАНЕТО НАПОИТЕЛНА СИСТЕМА „ИХТИМАН“***<br>Elena GRANCHAROVA, Asparuh IVANOV | 14 |
| 2. | **SPRING FIELD EVALUATION OF AN EXPERIMENTAL OVERSEEDING MACHINE FOR PERMANENT GRASSLAND RENOVATION /**<br>***EXPERIMENTĂRI ÎN CONDIȚII DE PRIMĂVARĂ ALE UNEI MAȘINI DE SUPRAÎNSĂMÂNȚAT PENTRU REGENERAREA PAJIȘTILOR PERMANENTE***<br>Eugen MARIN, Vasile MOCANU, Tudor-Adrian ENE, Laurențiu-Constantin VLĂDUȚOIU, Alexandru IONESCU, Mihai-Gabriel MATACHE, Radu Nicolae SOARE | 22 |
| 3. | **SPRING FIELD EVALUATION OF A 2.5 m FORAGE GRASSLAND SEED DRILL FOR PERMANENT GRASSLAND RECONSTRUCTION AND MAINTENANCE /**<br>***EXPERIMENTĂRI ÎN CONDIȚII DE PRIMĂVARĂ ALE UNEI MAȘINI DE SEMĂNAT PLANTE FURAJERE DE PAJIȘTI DE 2,5 M PENTRU RECONSTRUCȚIA ȘI MENTENANȚA PAJIȘTILOR***<br>Eugen MARIN, Vasile MOCANU, Tudor-Adrian ENE, Laurențiu-Constantin VLĂDUȚOIU, Alexandru IONESCU, Mihai-Gabriel MATACHE | 30 |
| 4. | **COFFEE LEAVES, FLOWERS AND DEFECTIVE BEANS AS EMERGING RESOURCES FOR CIRCULAR BIOECONOMY APPLICATIONS /**<br>***FRUNZELE, FLORILE ȘI BOABELE DEFECTE DE CAFEA CA RESURSE EMERGENTE PENTRU APLICAȚII ÎN BIOECONOMIA CIRCULARĂ***<br>Nicoleta UNGUREANU, Nicolae-Valentin VLĂDUȚ, Sorin-Ștefan BIRIȘ, Neluș-Evelin GHEORGHIȚĂ | 38 |
| 5. | **BIOCHAR FOR SUSTAINABLE WASTEWATER REMEDIATION: PRODUCTION, PHYSICOCHEMICAL PROPERTIES, AND POLLUTANT REMOVAL MECHANISMS /**<br>***BIOCHARUL PENTRU REMEDIEREA SUSTENABILĂ A APELOR UZATE: PRODUCERE, PROPRIETĂȚI FIZICO-CHIMICE ȘI MECANISME DE ÎNDEPĂRTARE A POLUANȚILOR***<br>Nicoleta UNGUREANU, Nicolae-Valentin VLĂDUȚ, Sorin-Ștefan BIRIȘ, Neluș-Evelin GHEORGHIȚĂ, Mariana IONESCU | 58 |
| 6. | **STATE OF THE ART IN RESEARCHES CONCERING THE ACOUSTIC EMISSION NON-DESTRUCTIVE TECHNIQUE /**<br>***STADIUL ACTUAL AL CERCETĂRILOR PRIVIND TEHNICA NEDISTRUCTIVĂ DE EMISIE ACUSTICĂ***<br>Ovidiu Cristian NEACȘU, Mihai Valentin PREDOI, Andrei CRAIFALEANU | 84 |
| 7. | **SOIL AMENDMENTS IMPACT ON LIGNOCELLULOSIC COMPOSITION OF SWEET SORGHUM BAGASSE IN MARGINAL LAND /**<br>***ВПЛИВ ГРУНТОВИХ ДОМІШОК НА ВМІСТ ЛІГНОЦЕЛЮЛОЗИ БАГАССИ ЦУКРОВОГО СОРГО НА МАРГІНАЛЬНИХ ЗЕМЛЯХ***<br>Yaroslava MOSIICHUK, Bohdan MAZURENKO, Rafiq ISLAM, Nataliia DIDENKO, Mykola ZOSYMCHUK, Sergiy LAVRENKO, Mykola KHARYTONOV | 94 |
| 8. | **THERMAL ANALYSES OF THE BLACK LOCUST WOOD DIFFERENT AGES /**<br>***ТЕРМІЧНИЙ АНАЛІЗ ДЕРЕВИНИ РОБІНІЇ ЗВИЧАЙНОІ РІЗНОГО ВІКУ***<br>Svitlana SYTNYK, Petro LAKYDA, Iryna RULA, Kyrylo HOLOBORODKO, Yurii LAKYDA, Liubov MATUSHEVYCH, Mykola KHARYTONOV | 100 |
| 9. | **EVALUATION OF THE PRODUCTIVE AND QUALITATIVE POTENTIAL OF LEGUMES AS SOURCES OF PLANT-BASED PROTEIN /**<br>***EVALUATION OF THE PRODUCTIVE AND QUALITATIVE POTENTIAL OF LEGUMES AS SOURCES OF VEGETABLE PROTEINS***<br>Andreea MATACHE, Nicoleta Alexandra VANGHELE, Florin NENCIU, Augustina Mirabela PRUTEANU, Gabriel NAE, Andreea-Sabina PINTILIE | 108 |
| 10. | **EFFICIENCY OF DYNAMIC DAMPENING AND MECHANICAL DECOUPLING TECHNOLOGIES IN LOW-POWER TOOLS /**<br>***EFICIENȚA TEHNOLOGIILOR DE AMORTIZARE DINAMICĂ ȘI DECUPLARE MECANICĂ LA MAȘINILE-UNELTE DE MICA PUTERE***<br>Gheorghe FLOROIU, Mihai Valentin PREDOI | 120 |
| 11. | **COMPARATIVE STUDY OF THE PROPERTIES OF BIOCHAR OBTAINED FROM SUNFLOWER AND MISCANTHUS STRAINS /**<br>***STUDIU COMPARATIV AL PROPRIETĂȚILOR BIOCHARULUI OBȚINUT DIN TULPINI DE FLOAREA SOARELUI ȘI MISCANTHUS***<br>Nicoleta-Alexandra VANGHELE, Nicolae-Valentin VLĂDUȚ, Andreea MATACHE, Augustina PRUTEANU, Florin NENCIU, Laurențiu VLĂDUȚOIU, Ana-Maria TĂBĂRAȘU, Dragoș ANGHELACHE, Alexandru IONESCU, Cristian RADU, Nicoleta Olimpia VRÎNCEANU | 124 |

| No. | Article Title & Authors | page |
|---|---|---|
| 12. | **BIOCHAR VERSUS HYDROCHAR FOR AGRICULTURAL BIOMASS VALORIZATION: A COMPARATIVE REVIEW OF PRODUCTION, PROPERTIES, APPLICATIONS AND SUSTAINABILITY /**<br>***BIOCHAR VERSUS HYDROCHAR PENTRU VALORIFICAREA BIOMASEI AGRICOLE: ANALIZĂ COMPARATIVĂ A PRODUCȚIEI, PROPRIETĂȚILOR, APLICAȚIILOR ȘI SUSTENABILITĂȚII***<br>Stefano-Andrea MANTOVANI, Alin-Nicolae HARABAGIU, Dragos-Nicolae DUMITRU, Aura-Maria DUMITRESCU, Vasilica ȘTEFAN, Ana ZAICA, Alexandru IONESCU, Daniel NIJLOVEANU | 132 |
| 13. | **SERICULTURAL WASTE COMPOSTING AS A SUSTAINABLE APPROACH FOR SOIL HEALTH, MULBERRY PRODUCTION AND SILKWORM REARING /**<br>***COMPOSTAREA DEȘEURILOR SERICICOLE - O ABORDARE DURABILĂ PENTRU SĂNĂTATEA SOLULUI, PRODUCȚIA DE DUD ȘI CREȘTEREA VIERMILOR DE MĂTASE***<br>Ana-Maria TĂBĂRAȘU, Iuliana GĂGEANU, Mihaela HĂBEANU, Teofil-Alin ONCESCU, Nicoleta-Alexandra VANGHELE, Alexandru-Cristian CIOACLĂ, Dragoș-Nicolae ANGHELACHE, Mihaela NIȚU, Cătălin PERSU, Elena-Valeria VLĂDUȚ, Paula TUDOR, Elena-Melania CISMARU | 146 |
| 14. | **STRUCTURAL PERFORMANCE EVALUATION OF THE FRAME OF A TREE ROOT CUTTING MACHINE USING FINITE ELEMENT ANALYSIS /**<br>***EVALUAREA PERFORMANȚEI STRUCTURALE A CADRULUI UNUI ECHIPAMENT PENTRU TĂIEREA RĂDĂCINILOR POMILOR UTILIZÂND ANALIZA CU ELEMENTE FINITE***<br>Alin-Nicolae HARABAGIU, Valentin-Nicolae VLĂDUȚ, Dragoș-Nicolae DUMITRU, Vasilica ȘTEFAN, Ana ZAICA, Stefano-Andrea MANTOVANI, Aura-Maria DUMITRESCU, Cornelia Veronica DIMA | 154 |
| 15. | **EXPERIMENTAL ANALYSIS AND INTERACTIVE VISUALIZATION OF FLUID MIXING PROCESSES FOR DIFFERENT IMPELLER CONFIGURATIONS /**<br>***ANALIZA EXPERIMENTALĂ ȘI VIZUALIZAREA INTERACTIVĂ A PROCESELOR DE AMESTECARE A FLUIDELOR PENTRU DIFERITE CONFIGURAȚII DE AGITATOARE***<br>Neluș-Evelin GHEORGHIȚĂ, Sorin-Ștefan BIRIȘ, Nicoleta UNGUREANU, Gabriel-Alexandru CONSTANTIN, Raluca-Adriana ZOTA, Dragoș-Nicolae DUMITRU | 162 |
| 16. | **ANALYSIS ON PHYSICO-MECHANICAL PARAMETERS AND TECHNOLOGICAL FLOW OF CATTLE SLAUGHTERING IN MODERN SLAUGHTERHOUSES /**<br>**ANALIZA PRIVIND PARAMETRII FIZICO-MECANICI ȘI FLUXUL TEHNOLOGIC DE ABATORIZARE A BOVINELOR ÎN ABATOARELE MODERNE**<br>Ion Mihăiță GRIGORE, Gheorghe VOICU, Paula TUDOR, Daniela IANITCHI | 170 |
| 17. | **CONSIDERATIONS ON THE OPERATING PRINCIPLES OF TIGER NUT HARVESTING EQUIPMENT /**<br>***CONSIDERAȚII PRIVIND PRINCIPIILE DE FUNCȚIONARE ALE ECHIPAMENTELOR PENTRU RECOLTAREA NUCILOR TIGRU***<br>Remus Marius OPRESCU, Roxana Patricia IONAȘCU, Dan CUJBESCU, Iulian VOICEA | 180 |
| 18. | **CONSIDERATIONS ON THE INFLUENCE OF CLIMATE CHANGE ON AGRICULTURAL CROPS /**<br>***CONSIDERAȚII PRIVIND INFLUENȚA SCHIMBĂRILOR CLIMATICE ASUPRA CULTURILOR AGRICOLE***<br>Roxana Patricia IONAȘCU, Remus Marius OPRESCU, Dan CUJBESCU, Iulian VOICEA | 192 |
| 19. | **END-TO-END EXPERIMENTAL EVALUATION OF A RAIL-GUIDED ROBOT FOR AUTONOMOUS TOMATO HARVESTING /**<br>***VALUAREA EXPERIMENTALĂ INTEGRATĂ A UNUI ROBOT GHIDAT PE ȘINE PENTRU RECOLTAREA AUTONOMĂ A TOMATELOR***<br>Mariana EPURE, Mihai Gabriel MATACHE, Robert Dorin CRISTEA, Florin Bogdan MARIN, Alexandra LEONTE, Daniela-Andreea ZAMFIR | 200 |
| 20. | **STUDIES ON AROMATIC AND MEDICINAL PLANTS - THE IMPACT OF THE ENVIRONMENT AND TECHNOLOGIES FOR EXTRACTING ACTIVE COMPOUNDS /**<br>***STUDII PRIVIND PLANTELE AROMATICE ȘI MEDICINALE- IMPACTUL MEDIULUI ȘI TEHNOLOGIILE PENTRU EXTRAGEREA COMPUȘILOR ACTIVI***<br>Aura-Maria DUMITRESCU, Vasilica ȘTEFAN, Carmen BĂLȚATU, Larisa-Bianca IONICĂ, Stefano-Andrea MANTOVANI | 206 |
| 21. | **POWER CONSUMPTION AND FLOW REGIME CHARACTERIZATION OF PADDLE, PROPELLER AND DISC-TURBINE IMPELLERS IN A LABORATORY-SCALE MIXING VESSEL /**<br>***CARACTERIZAREA CONSUMULUI DE PUTERE ȘI A REGIMULUI DE CURGERE PENTRU AGITATOARE CU PALETE, ELICE ȘI TURBINĂ IMPELLER ÎNTR-UN VAS DE AMESTECARE LA SCARĂ DE LABORATOR***<br>Elena-Valeria VLĂDUȚ, Sorin- Ștefan BIRIȘ, Mariana FERDEȘ, Adrian IOSIF, Neluș-Evelin GHEORGHIȚĂ, Alina-Daiana IONESCU, Raluca Adriana ZOTA, Ana-Maria TĂBĂRAȘU | 214 |
| 22. | **STUDY ON THE PRODUCTION AND USE OF SHEEP WOOL WASTE PELLETS AS ORGANIC FERTILIZER IN ORGANIC AGRICULTURE. REVIEW. /**<br>***STUDIU PRIVIND PRODUCȚIA ȘI UTILIZAREA PELETELOR DIN DEȘEURI DE LÂNĂ DE OAIE CA ÎNGRĂȘĂMINTE ORGANIC ÎN AGRICULTURA ORGANICĂ. RECENZIE.***<br>Ioan Ladislau CABA, Nicolae-Valentin VLĂDUȚ, Despina-Maria BORDEAN | 224 |

| No. | Article Title & Authors | page |
|---|---|---|
| 23. | **OPPORTUNITIES IN 3D FOOD PRINTING: FROM CONCEPT TO COMMERCIAL APPLICATIONS /**<br>***OPORTUNITĂȚI ÎN IMPRIMAREA 3D A ALIMENTELOR: DE LA CONCEPT LA APLICAȚII COMERCIALE***<br>Alexandru-Cristian CIOACLĂ, Iuliana GĂGEANU, Ana-Maria TĂBĂRAȘU, Robert-Dorin CRISTEA, Dorin-Andrei CÎRSTEA, Alexandru IONESCU, Mario CRISTEA, Alex-Nicolae COLEȘI | 242 |
| 24. | **APPLICATIONS OF 3D PRINTING IN INDUSTRY AND MEDICINE: A SYNTHESIS OF THE SPECIALIZED LITERATURE /**<br>***APLICAȚII ALE IMPRIMĂRII 3D ÎN INDUSTRIE ȘI MEDICINĂ: O SINTEZĂ A LITERATURII DE SPECIALITATE***<br>Alexandru-Cristian CIOACLĂ, Iuliana GĂGEANU, Ana-Maria TĂBĂRAȘU, Robert-Dorin CRISTEA, Dorin-Andrei CÎRSTEA, Alexandru IONESCU, Mario CRISTEA, Ion Mihăiță GRIGORE | 248 |
| 25. | **EXPERIMENTAL VALIDATION OF CFD THERMAL AND VORTICITY MAPS FOR A COUNTER-ROTATING LENZ-2 VERTICAL AXIS WIND TURBINE /**<br>***VALIDAREA EXPERIMENTALĂ A HĂRȚILOR TERMICE ȘI DE VORTICITATE CFD PENTRU O TURBINĂ EOLIANĂ CU AX VERTICAL LENZ-2 CONTRAROTATIVĂ***<br>Adrian PANDELE, Bogdan Ovidiu DURAN, Dragos Mihail PREDA, Paula TUDOR, Gheorghe VOICU | 254 |
| 26. | **EVALUATION OF THE SELECTIVITY OF AN EXPERIMENTAL PSEUDOMONAS SYRINGAE PV. TAGETIS BIOHERBICIDE ON SOYBEAN CULTIVARS /**<br>***EVALUAREA SELECTIVITĂȚII UNUI BIOERBICID EXPERIMENTAL PE BAZĂ DE PSEUDOMONAS SYRINGAE PV. TAGETIS ASUPRA UNOR SOIURI DE SOIA***<br>Marga GRĂDILĂ, Sorina DINU, Daniel JALOBĂ, Valentin-Marius CIONTU, Raluca-Monica IORDĂCHESCU, Cătălina TUDORA, Nicolae-Valentin VLĂDUȚ | 264 |
| 27. | **STUDY ON AUTONOMOUS MOBILE SOLUTIONS FOR CROP HARVESTING /**<br>***STUDIU PRIVIND SOLUȚIILE MOBILE AUTONOME PENTRU RECOLTAREA CULTURILOR AGRICOLE***<br>Dorin-Andrei CÎRSTEA, Robert-Dorin CRISTEA, Alexandru-Cristian CIOACLA, Alexandru IONESCU, Dragoș-Valentin LUPU | 274 |
| 28. | **STOCHASTIC MODELING AND GAUSSIAN PROBABILITY DISTRIBUTION OF THE EFFICIENCY OF AUTOMOTIVE BRAKING SYSTEMS IN REAL OPERATING CONDITIONS /**<br>***MODELAREA STOCHASTICĂ ȘI DISTRIBUȚIA PROBABILISTICĂ GAUSS A EFICIENȚEI SISTEMELOR DE FRÂNARE AUTO ÎN CONDIȚII REALE DE EXPLOATARE***<br>Paula TUDOR, Cristina APETREI, Sorin-Dan IORDACHE, Gabriel MUȘUROI, Gheorghe VOICU, Marina-Teodora DUDĂU | 280 |
| 29. | **PRELIMINARY FUNCTIONAL AND THERMAL TESTING OF ELECTRIC PYROLYSIS EQUIPMENT FOR OBTAINING PHOSPHORUS-RICH BIOFERTILIZERS /**<br>***TESTAREA PRELIMINARĂ A UNUI ECHIPAMENT ELECTRIC DE PIROLIZĂ PENTRU OBTINEREA DE BIOFERTILIZANȚI BOGAȚI ÎN FOSFOR***<br>Vasilica STEFAN, Ana ZAICA, Alin HARABAGIU, Stefano MANTOVANI, Alexandra VISAN, Gabriel GHEORGHE, Aura DUMITRESCU, George LAZAR, Dragos DUMITRU, Radu Nicolae SOARE | 292 |
| 30. | **APPLICABILITY AND PROCESSING METHODOLOGY OF EXPERIMENTAL DATA ACQUISITION SYSTEMS FOR THE ASSESSMENT OF WHOLE-BODY VIBRATION EXPOSURE IN VEHICLE OPERATORS /**<br>***APLICABILITATEA ȘI METODOLOGIA DE PRELUCRARE A DATELOR EXPERIMENTALE UTILIZÂND SISTEME DE ACHIZIȚIE PENTRU EVALUAREA EXPUNERII CONDUCĂTORILOR AUTO LA VIBRAȚII TRANSMISE ÎNTREGULUI CORP***<br>Teofil Alin ONCESCU, Iuliana GAGEANU, Ana-Maria TABARASU, Nicolae-Valentin VLADUT, Ioan Catalin PERSU, Gabriel-Mihai MATACHE, Cornelia MURARU-IONEL, Raluca SFIRU, Daniela TARNITA, Paul- Alexandru BOTA, Alexandru Denis CODROIU, Adriana Valentina RADU, Șerban-Armand STERE, Iulia DOROBANȚU, Cristian-Răzvan MARIN | 300 |
| 31. | **EXPERIMENTAL EVALUATION OF A MICROHYDROENERGY SYSTEM FOR SUSTAINABLE AERATION OF FISH PONDS /**<br>***EVALUAREA EXPERIMENTALĂ A UNUI SISTEM MICROHIDROENERGETIC PENTRU AERAREA SUSTENABILĂ A BAZINELOR PISCICOLE***<br>Laurențiu-Constantin VLĂDUȚOIU, Eugen MARIN, Floricel-Maricel DIMA, Magdalena TENCIU, Florentina BRATOSIN | 316 |
| 32. | **RECYCLING BIODEGRADABLE WASTE THROUGH COMPOSTING IN THE CONTEXT OF THE CIRCULAR ECONOMY /**<br>***VALORIFICAREA DEȘEURILOR BIODEGRADABILE PRIN COMPOSTARE ÎN CONTEXTUL ECONOMIEI CIRCULARE***<br>Carmen-Otilia RUSĂNESCU, Gigel PARASCHIV, Gabriel Alexandru CONSTANTIN, SORIN-Ştefan BIRIŞ, Gheorghe VOICU, Andrei-Marian RUSĂNESCU, Gabriel RUSĂNESCU, Melania CISMARU, Irina Aura ISTRATE, Mirela DINCĂ | 326 |
| 33. | **EVALUATION OF PARTICLE SIZE, RHEOLOGICAL AND BIOACTIVE CHARACTERISTICS OF ROSEHIP (ROSA CANINA L.) POWDER AS A FUNCTION OF GRINDING TECHNOLOGY /**<br>***EVALUAREA PROPRIETĂȚILOR GRANULOMETRICE, REOLOGICE ȘI BIOACTIVE ALE PULBERII DE MĂCEȘ (ROSA CANINA L.) ÎN FUNCȚIE DE TEHNOLOGIA DE MĂCINARE***<br>Alina-Daiana IONESCU, Gheorghe VOICU, Gabriel-Alexandru CONSTANTIN, Mihaela BEGEA, Elena-Mădălina ȘTEFAN, Adrian IOSIF, Petruța PETCU, Raluca-Adriana ZOTA, Elena-Valeria VLĂDUȚ, Melania-Elena CISMARU, Catalina TUDORA | 334 |

| No. | Article Title & Authors | page |
|---|---|---|
| 34. | **COMPARATIVE ASSESSMENT OF VEGETABLE GROWING TECHNOLOGIES IN CONTROLLED (CLOSED) ENVIRONMENTS /** ***EVALUARE COMPARATIVĂ A TEHNOLOGIILOR DE CULTIVARE A LEGUMELOR ÎN SPAȚII CONTROLATE (ÎNCHISE)*** Iuliana GĂGEANU, Ana-Maria TĂBĂRAȘU, Teofil-Alin ONCESCU, Mihaela NIȚU, Cătălin PERSU, Dan CUJBESCU, Daria-Ioana SICARU | 344 |
| 35. | **FEM NUMERICAL ANALYSIS OF A SPRINGBOARD TYPE ELASTIC SYSTEM FOR APPARATUS VAULTING /** ***ANALIZA NUMERICĂ MEF A UNUI SISTEM ELASTIC DE TIP TRAMBULINĂ PENTRU SĂRITURI LA APARATE*** Daniel-Mirel DUMITRESCU, George IPATE, Gheorghe VOICU, Paula TUDOR, Liliana-Caliopi ISCRU, Dragoș-Valentin LUPU | 352 |
| 36. | **ASPECTS REGARDING STAGES, METHODS AND TOOLS TO IMPROVING PROBLEM-SOLVING IN MANUFACTURING /** ***ASPECTE PRIVIND ETAPELE, METODELE ȘI INSTRUMENTELE PENTRU ÎMBUNĂTĂȚIREA SOLUȚIONĂRII PROBLEMELOR ÎN PRODUCȚIE*** Carmen BRACACESCU | 362 |
| 37. | **THREE-DIMENSIONAL MODELING AND ADDITIVE MANUFACTURING OF A CENTRIFUGAL SEPARATOR FOR AGRICULTURAL PNEUMATIC SEPARATION APPLICATIONS /** ***MODELAREA TRIDIMENSIONALĂ ȘI FABRICAȚIA ADITIVĂ A UNUI SEPARATOR CENTRIFUGAL PENTRU APLICAȚII DE SEPARARE PNEUMATICĂ ÎN AGRICULTURĂ*** Raluca-Adriana ZOTA, Sorin-Ștefan BIRIȘ, Neluș-Evelin GHEORGHIȚĂ, Gabriel-Alexandru CONSTANTIN, Alina-Daiana IONESCU, Elena-Valeria VLĂDUȚ, Iulian DRENEA, Mircea COSTIN | 374 |
| 38. | **CURRENT STATE OF THE ART IN EQUIPMENT FOR ANHYDROUS AMMONIA APPLICATION IN FIELD CROPS /** ***STADIUL ACTUAL ÎN DOMENIUL ECHIPAMENTELOR PENTRU APLICAREA AMONIACULUI ANHIDRU ÎN CULTURI DE CÂMP*** Dragoș MANEA, Mihai GÎDEA, Dragoș-Nicolae DUMITRU, Alin HARABAGIU, Larisa-Bianca IONICĂ, Aura DUMITRESCU | 380 |
| 39. | **EVALUATION OF THE ENERGETIC AND OPERATIONAL PERFORMANCE OF AN INNOVATIVE GRASS SEEDER FOR VINEYARDS AND ORCHARDS /** ***EVALUAREA EXPERIMENTALĂ A PERFORMANȚELOR ENERGETICE ȘI DE EXPLOATARE ALE UNEI SEMĂNĂTORI INOVATIVE PENTRU ÎNIERBAREA PLANTAȚIILOR VITICOLE ȘI POMICOLE*** Dragoş-Nicolae DUMITRU, Dragoș-Nicolae ANGHELACHE, Carmen VASILACHI, Eugen MARIN, Dragoș MANEA, Alin-Nicolae HARABAGIU, Stefano-Andrea MANTOVANI, Neluș-Evelin GHEORGHIȚĂ | 388 |
| 40. | **EXPERIMENTAL EVALUATION OF THE ENERGETIC AND OPERATIONAL PERFORMANCE OF AN INNOVATIVE INTER-ROW GRASS MOWER FOR VINEYARDS AND ORCHARDS /** ***EVALUAREA EXPERIMENTALĂ A PERFORMANȚELOR ENERGETICE ȘI DE EXPLOATARE ALE UNUI ECHIPAMENT INOVATIV DE COSIT INTERVALUL ÎNIERBAT DIN PLANTAȚII VITICOLE ȘI POMICOLE*** Dragoş-Nicolae DUMITRU, Dragoș-Nicolae ANGHELACHE, Carmen VASILACHI, Eugen MARIN, Dragoș MANEA, Alin-Nicolae HARABAGIU, Stefano-Andrea MANTOVANI, Iulian Virgil GHIULEANU | 394 |
| 41. | **STATIC STRUCTURAL ANALYSIS OF THE INDEPENDENT DISC OF AN AGRICULTURAL DISC HARROW FOR MATERIAL SELECTION AND MANUFACTURING COST OPTIMIZATION /** ***ANALIZA STRUCTURALĂ STATICĂ A DISCULUI INDEPENDENT AL UNEI GRAPE CU DISCURI AGRICOLE ÎN VEDEREA ALEGERII MATERIALULUI ȘI OPTIMIZĂRII COSTURILOR DE FABRICAȚIE*** Daniel LATEȘ, Paul TRIPON, Eugen MARIN, Laurențiu-Constantin VLĂDUȚOIU | 400 |
| 42. | **SPATIAL ANALYSIS OF AN ORCHARD BASED ON UAV RGB IMAGERY AND GIS TECHNOLOGIES /** ***ANALIZA SPAȚIALĂ A UNEI LIVEZI PE BAZA DATELOR UAV RGB ȘI A TEHNOLOGIILOR GIS*** Daria-Ioana SICARU, Neluș-Evelin GHEORGHIȚĂ, Mihaela NITU | 410 |
| 43. | **ASPECTS REGARDING THE COMPRESSION AND FAILURE BEHAVIOR OF CONCRETE CUBIC MINI-BLOCKS WITH RED MUD ADDITION /** ***APECTE PRIVIND COMPORTAREA LA COMPRESIUNE ȘI RUPERE A MINI-BLOCURILOR CUBICE DIN BETON CU ADAOS DE NĂMOL ROȘU*** Augustin VOINEA, George IPATE, Gheorghe VOICU, Paula TUDOR, George-Mirel MIU, Dorel STOICA, Dorin Andrei CIRSTEA | 418 |
| 44. | **DISCRETE ELEMENT MODELLING OF SEED GRAVITATIONAL FLOW THROUGH DISCHARGE ORIFICES: RELEVANT PARAMETERS AND A PRELIMINARY METHODOLOGICAL FRAMEWORK /** ***MODELAREA PRIN METODA ELEMENTELOR DISCRETE A CURGERII GRAVITAȚIONALE A SEMINȚELOR PRIN ORIFICII DE EVACUARE: PARAMETRI RELEVANȚI ȘI CADRU METODOLOGIC PRELIMINAR*** Daniela-Andreea ZAMFIR, Sorin-Ștefan BIRIȘ, Atanas ATANASOV, Maria TĂNASE, Mariana EPURE | 428 |
| 45. | **ADVANCED MONITORING OF AQUACULTURE SYSTEMS USING MULTISENSOR PREDICTIVE MODELS /** ***MONITORIZAREA AVANSATĂ A ACVACULTURII PRIN MODELE PREDICTIVE MULTISENZOR*** Dan CUJBESCU, Iulian VOICEA, Cătălin PERSU | 436 |

| No. | Article Title & Authors | page |
|---|---|---|
| 46. | **INFLUENCE OF SOIL MOISTURE ON MECHANICAL REQUIREMENTS DURING AUTOMATED SOIL SAMPLING /** ***INFLUENȚA UMIDITĂȚII SOLULUI ASUPRA CERINȚELOR MECANICE ÎN TIMPUL PRELEVĂRII AUTOMATE A PROBELOR DE SOL*** Alexandru IONESCU, Nicolae-Valentin VLĂDUȚ, Florin NENCIU, Mario CRISTEA, Robert-Dorin CRISTEA, Dorin-Andrei CÎRSTEA, Alexandru-Cristian CIOACLĂ, Stefano-Andrea MANTOVANI, Dragos ANGHELACHE | 442 |
| 47. | **A DECADE OF AGRICULTURAL RESTRUCTURING IN SOUTH-WEST OLTENIA, ROMANIA: CULTIVATED AREA DYNAMICS AND COUNTY SPECIALIZATION /** ***UN DECENIU DE RESTRUCTURARE AGRICOLĂ ÎN REGIUNEA SUD-VEST OLTENIA, ROMÂNIA: DINAMICA SUPRAFEȚELOR CULTIVATE ȘI SPECIALIZAREA JUDEȚEANĂ*** Iulian Virgil GHIULEANU, Daniel NIJLOVEANU, Corina CRUCERU, Dragos-Nicolae DUMITRU | 450 |
| 48. | **BETWEEN GROWTH AND DECLINE: STRUCTURAL AND TERRITORIAL SHIFTS IN CROP PRODUCTION IN SOUTH-WEST OLTENIA, ROMANIA (2016–2025) /** ***ÎNTRE CREȘTERE ȘI DECLIN: SCHIMBĂRI STRUCTURALE ȘI TERITORIALE ALE PRODUCȚIEI VEGETALE DIN REGIUNEA SUD-VEST OLTENIA, ROMÂNIA (2016–2025)*** Daniel NIJLOVEANU, Iulian Virgil GHIULEANU, Corina CRUCERU, Nicolae-Valentin VLĂDUȚ, Stefano Andrea MANTOVANI | 464 |
| 49. | **LOCAL STRENGTHS, REGIONAL VULNERABILITIES: CROP YIELD DYNAMICS IN SOUTH-WEST OLTENIA, ROMANIA (2016–2025) /** ***AVANTAJE LOCALE, VULNERABILITĂȚI REGIONALE: DINAMICA RANDAMENTELOR CULTURILOR ÎN REGIUNEA SUD-VEST OLTENIA, ROMÂNIA (2016–2025)*** Corina CRUCERU, Iulian Virgil GHIULEANU, Daniel NIJLOVEANU, Oana-Elena MILEA | 476 |
| 50. | **COMPARATIVE EVALUATION OF TWO INTELLIGENT ARCHITECTURES FOR HORTICULTURAL CROP PROTECTION /** ***EVALUAREA COMPARATIVĂ A DOUĂ ARHITECTURI INTELIGENTE PENTRU PROTECȚIA CULTURILOR HORTICOLE*** Augustina PRUTEANU, Iuliana GAGEANU, Mihaela NIȚU, Nicoleta Alexandra VANGHELE, Andreea MATACHE | 490 |
| 51. | **THE ROLE OF CANOPY ARCHITECTURE AND CANOPY MANAGEMENT IN OPTIMIZING GROWTH, FRUITING, AND FRUIT QUALITY IN FRUIT TREES /** ***ROLUL ARHITECTURII ȘI MANAGEMENTULUI COROANEI ÎN OPTIMIZAREA CREȘTERII, FRUCTIFICĂRII ȘI CALITĂȚII PRODUCȚIEI LA POMII FRUCTIFERI*** Oana-Elena MILEA, Nicolae-Valentin VLĂDUȚ, Stefan DUMITRU, Ana-Maria GROSU, Corina CRUCERU | 500 |
| 52. | **PHOSPHORUS TRANSFORMATION AND RECOVERY FROM POULTRY LITTER THROUGH PYROLYSIS: CHEMICAL FORMS, PROCESSES, AND PERSPECTIVES - A MINI-REVIEW /** ***TRANSFORMAREA ȘI RECUPERAREA FOSFORULUI DIN AȘTERNUTUL AVICOL PRIN PIROLIZĂ: FORME CHIMICE, PROCESE ȘI PERSPECTIVE - MINIREVIEW*** Mihaela Monica DINU, Vasilica STEFAN, Nicoleta RADU, Roxana Maria TUDOR | 506 |
| 53. | **STUDY OF MECHANICAL AND ELECTRICAL FAILURE POINTS OF AN AUTOMATED SOIL SAMPLING MACHINE /** ***STUDIU AL PUNCTELOR DE DEFECȚIUNE MECANICĂ ȘI ELECTRICĂ ALE UNEI MAȘINI AUTOMATE DE PRELEVARE A PROBELOR DE SOL*** Livia-Valentina BĂDESCU, Marius-Adelin STUPARU, Robert-Dorin CRISTEA | 520 |
| 54. | **SLUDGE TREATMENT AND MANAGEMENT IN WASTEWATER TREATMENT PLANTS USING MECHANICAL EQUIPMENT /** ***TRATAREA ȘI GESTIONAREA NĂMOLURILOR ÎN STAȚIILE DE EPURARE A APELOR UZATE UTILIZÂND ECHIPAMENTE MECANICE*** Cornelia Veronica DIMA, Gheorghe VOICU, Gabriel-Alexandru CONSTANTIN, Irina-Aura ISTRATE, Alin-Nicolae HARABAGIU | 526 |
| 55. | **CAD-BASED DESIGN AND STRUCTURAL PERFORMANCE EVALUATION OF A SMALL-SCALE H-DARRIEUS VERTICAL AXIS WIND TURBINE FOR PRECISION AGRICULTURE APPLICATIONS /** ***PROIECTAREA ASISTATĂ CAD ȘI EVALUAREA PERFORMANȚEI STRUCTURALE A UNEI TURBINE EOLIENE CU AX VERTICAL DE TIP H-DARRIEUS DE MICI DIMENSIUNI PENTRU APLICAȚII ÎN AGRICULTURA DE PRECIZIE*** Bogdan Ovidiu DURAN, Adrian PANDELE, Dragos Mihail PREDA, Gheorghe VOICU, Gabriel GHEORGHE | 534 |
| 56. | **INTEGRATED WEED MANAGEMENT (IWM): SYNERGY BETWEEN CHEMICAL, BIOLOGICAL AND AGRONOMIC METHODS FOR SUSTAINABLE WEED CONTROL /** ***MANAGEMENTUL INTEGRAT AL BURUIENILOR (IWM): INTEGRAREA METODELOR CHIMICE, BIOLOGICE ȘI AGROTEHNICE PENTRU COMBATEREA DURABILĂ A BURUIENILOR*** Costin MIRCEA, Florin NENCIU, Gheorghe STROESCU, Andreea ENEA, Raluca-Adriana ZOTA, Floarea ȘERBANCEA | 544 |
| 57. | **DATA STORAGE AND REMOTE TRANSMISSION USING AN EDGE COMPUTER IN A MOBILE SOIL SAMPLING PLATFORM /** ***STOCAREA DATELOR ȘI TRANSMITEREA LA DISTANȚĂ UTILIZÂND UN COMPUTER EDGE ÎNTR-O PLATFORMĂ MOBILĂ DE EȘANTIONARE A SOLULUI*** Dragoș-Valentin LUPU, Robert-Dorin CRISTEA, Alexandru-Cristian CIOACLĂ, Dorin-Andrei CÎRSTEA, Daniel-Mirel DUMITRESCU | 554 |
| 58. | **THERMOFLUID MECHANISMS AND ADAPTIVE CONTROL IN ACTIVE ORCHARD FROST PROTECTION: A CRITICAL REVIEW OF AIR MIXING, HEATING, AND WATER-BASED SYSTEMS /** ***MECANISME TERMOFLUIDICE ȘI CONTROL ADAPTIV ÎN PROTECȚIA ACTIVĂ A LIVEZILOR ÎMPOTRIVA ÎNGHEȚULUI: O ANALIZĂ CRITICĂ A SISTEMELOR DE AMESTECARE A AERULUI, ÎNCĂLZIRE ȘI UTILIZARE A APEI*** Mihaela NIȚU, Iuliana GĂGEANU, Augustina PRUTEANU, Ana-Maria TĂBĂRAȘU, Daria-Ioana SICARU | 560 |

| No. | Article Title & Authors | page |
|---|---|---|
| 59. | **COMPARATIVE EVALUATION OF OIL EXTRACTION YIELD FROM DIFFERENT OILSEEDS USING A SMALL-SCALE SCREW PRESS /**<br>***STUDIU COMPARATIV PRIVIND EXTRACȚIA MECANICĂ A ULEIULUI DIN DIFERITE SEMINȚE OLEAGINOASE UTILIZÂND O PRESĂ DE CAPACITATE MICĂ CU MELC***<br>Mariana IONESCU, Gabriel-Alexandru CONSTANTIN, Sorin-Ștefan BIRIȘ, Gheorghe VOICU, Neluș-Evelin GHEORGHIȚĂ, Mirela-Nicoleta DINCĂ, Nicoleta UNGUREANU, Bianca-Ștefania ZĂBAVĂ | 568 |
| 60. | **COMPUTATIONAL ANALYSIS OF MILK FLOW DYNAMICS AND HEAT TRANSFER PERFORMANCE IN A PLATE HEAT EXCHANGERS - A REVIEW /**<br>***ANALIZA COMPUTATIONALA A DINAMICII CURGERII LAPTELUI SI A PERFORMANTEI TRANSFERULUI TERMIC IN SCHIBATOARELE DE CALDURA CU PLACI - REVIEW***<br>Florentina BRATOSIN, Sorin-Ștefan BIRIȘ, Mihaela BEGEA, Andreea-Ioana BADIU, Alina-Daiana IONESCU | 576 |
| 61. | **REDUCING MECHANICAL DISTURBANCE AS A SOIL REGENERATION STRATEGY: IMPLICATIONS OF MINIMUM TILLAGE, NO-TILL, AND COMPACTION MANAGEMENT /**<br>***REDUCEREA PERTURBĂRII MECANICE CA STRATEGIE DE REGENERARE A SOLULUI: IMPLICAȚII ALE MINIMUM TILLAGE, NO-TILL ȘI MANAGEMENTULUI COMPACTĂRII***<br>Cristian RADU, Gheorghe MATEI, Sorin BORUZ, Stefan DUMITRU, Valentin Nicolae VLADUȚ, Lorena-Diana POPA, Dragos ANGHELACHE, Mihai NICOLESCU, Oane-Elena MILEA, Nicoleta UNGUREANU | 586 |
| 62. | **SPATIAL ANALYSIS OF FLOOD RISK USING GIS TECHNIQUES /**<br>***ANALIZA SPAȚIALĂ A RISCULUI DE INUNDAȚII UTILIZÂND TEHNICI GIS***<br>Bianca-Ștefania ZĂBAVĂ, Daria- Ioana SICARU, Gheorghe VOICU, Mirela- Nicoleta DINCĂ, Mariana IONESCU, Georgiana MOICEANU, Gigel PARASCHIV | 600 |
| 63. | **INTEGRATED ASSESSMENT OF SOIL HEALTH AND REGENERATION: INDICATORS, DIGITAL TECHNOLOGIES AND ADAPTIVE MANAGEMENT /**<br>***EVALUAREA INTEGRATĂ A SĂNĂTĂȚII ȘI REGENERĂRII SOLULUI: INDICATORI, TEHNOLOGII DIGITALE ȘI MANAGEMENT ADAPTIV***<br>Cristian RADU, Ștefan DUMITRU, Nicolae-Valentin VLĂDUȚ, Gabriel-Valentin GHEORGHE, Alin HARABAGIU, Sorin Dan IORDACHE, Oana-Elena MILEA, Sorin BORUZ, Gheorghe MATEI, Lorena-Diana POPA, Mihai NICOLESCU, Dragos-Nicolae ANGHELACHE, Nicoleta UNGUREANU | 606 |
| 64. | **MATHEMATICAL MODELS USED IN THE MECHANICAL-PNEUMATIC SOWING PROCESS /**<br>***MODELE MATEMATICE UTILIZATE ÎN PROCESUL DE SEMĂNAT MECANO-PNEUMATIC***<br>Dragoş-Nicolae ANGHELACHE, Ana-Maria TĂBĂRAŞU, Dragoş DUMITRU, Eugen MARIN, Nicoleta VANGHELE, Cristian RADU, Alexandru IONESCU, Melania CISMARU, Nicolae-Valentin VLĂDUȚ, Dragos Mihail PREDA | 614 |
| 65. | **THERMO-MECHANICAL BEHAVIOUR OF BEESWAX-BASED OLEOGELS AND THEIR IMPACT ON THE NUTRI-SCORE PROFILE OF A REFORMULATED HAZELNUT SPREAD /**<br>***COMPORTAMENTUL TERMO-MECANIC AL OLEOGELURILOR PE BAZĂ DE CEARĂ DE ALBINE ȘI IMPACTUL LOR ASUPRA PROFILULUI NUTRI-SCORE ÎNTR-O CREMĂ TARTINABILĂ DE ALUNE REFORMULATĂ***<br>Anca-Ioana PUFLEA, Sorin-Ștefan BIRIȘ, Mihaela BEGEA, Alexandru-Ionuț CIRIC | 626 |
| 66. | **STATIC STABILITY ANALYSIS OF THE NAIO OZ AUTONOMOUS AGRICULTURAL ROBOT OPERATING ON SLOPED TERRAIN /**<br>***ANALIZA STABILITĂȚII STATICE A ROBOTULUI AGRICOL AUTONOM NAIO OZ ÎN CONDIȚII DE OPERARE PE TEREN ÎNCLINAT***<br>Radu Nicolae SOARE, Andreea Alexandra FRUSINOIU, Sorin Ștefan BIRIȘ, Edmond MAICAN, Eugen MARIN | 634 |
| 67. | **ANALYSIS OF RESEARCH TRENDS IN THE USE OF EVOLUTIONARY ALGORITHMS FOR THE MECHANICAL DESIGN OF AGRICULTURAL TECHNICAL SYSTEMS /**<br>***ANALIZA TENDINȚELOR CERCETĂRII PRIVIND UTILIZAREA ALGORITMILOR EVOLUTIVI ÎN PROIECTAREA MECANICĂ A SISTEMELOR TEHNICE AGRICOLE***<br>Andreea Alexandra FRUSINOIU, Radu Nicolae SOARE, Sorin Stefan BIRIȘ, Adrian IOSIF | 642 |
| 68. | **OPTIMIZATION OF HEAT TRANSFER IN A HEAT EXCHANGER WITH TEMPERATURE RESTRICTIONS ON THE EXHAUST FLUE PIPE /**<br>***OPTIMIZAREA TRANSFERULUI DE CĂLDURĂ ÎNTR-UN SCHIMBĂTOR DE CĂLDURĂ CU RESTRICȚII DE TEMPERATURĂ PE CONDUCTA DE EVACUARE A GAZELOR ARSE***<br>Alexandru-Polifron CHIRIȚĂ, Florian-Andrei SCARLAT, Ioan PAVEL, Gheorghe ȘOVĂIALĂ, Laurențiu VLĂDUȚOIU | 650 |
| 69. | **EVALUATION OF MECHANICAL PROPERTIES, WATER ACTIVITY, AND MOISTURE CONTENT OF GLUTEN-FREE PRETZELS /**<br>***EVALUAREA PROPRIETĂȚILOR MECANICE, ACTIVITĂȚII APEI ȘI A UMIDITĂȚII LA COVRIGII AGLUTENICI***<br>Mariana-Gabriela MUNTEANU, Elena-Mădălina ȘTEFAN, Gheorghe VOICU, Daiana-Alina IONESCU, Gabriel-Alexandu CONSTANTIN, Irina-Aura ISTRATE, Loredana MORARI, Zsofia-Krisztina LŐRINCZ, Ana-Maria FETICU, Gabriel-Valentin GHEORGHE | 658 |
| 70. | **ECOTOXICITY ASSESSMENT OF PROCESS WATERS RESULTED DURING THE HYDROTHERMAL CARBONIZATION OF SPENT COFFEE GROUNDS /**<br>***EVALUAREA ECOTOXICITĂȚII LICHIDELOR REZULTATE DIN CARBONIZAREA HIDROTERMALĂ A ZAȚULUI DE CAFEA***<br>Ramona-Eugenia POPESCU, Corina Violeta CHIRIȚĂ, Maria RÂPĂ | 666 |
| 71. | **NUMERICAL ANALYSIS OF ACOUSTIC PANELS USED FOR ROAD TRAFFIC NOISE REDUCTION /**<br>***ANALIZA NUMERICĂ A PANOURILOR ACUSTICE UTILIZATE PENTRU REDUCEREA ZGOMOTULUI PROVENIT DIN TRAFICUL RUTIER***<br>Ana-Maria GROSU, Ovidiu VASILE, Jazmina SCORȚEA, Sorina Alexandra ZLATOIANU | 674 |

| No. | Article Title & Authors | page |
|---|---|---|
| 72. | **EXPERIMENTAL STUDY OF DUST COLLECTED FROM AN INDUSTRIAL CEREAL MILL DEDUSTING SYSTEM /** ***STUDIU EXPERIMENTAL AL PULBERILOR COLECTATE DIN SISTEMUL DE DESPRĂFUIRE AL UNEI MORI INDUSTRIALE DE CEREALE*** Liliana-Caliopi ISCRU, Daniel-Mirel DUMITRESCU, Gheorghe VOICU, Paula TUDOR, Gabriel-Alexandru CONSTANTIN | 680 |
| 73. | **FUNCTIONAL PARAMETERS OF A MULTIPROCESS SYSTEM FOR HOMOGENEOUS STRAWBERRY NECTAR /** ***PARAMETRII FUNCȚIONALI AI UNEI INSTALAȚII MULTIPROCES PENTRU NECTAR OMOGEN DE CĂPȘUNI*** Andra-Valentina CIOBĂNESCU, Sorin-Ștefan BIRIȘ, Mihaela BEGEA, Adrian IOSIF | 690 |
| 74. | **ENHANCING HUMAN–MACHINE INTERACTION WITH SMART KNOBS AND HAPTIC FEEDBACK /** ***ÎMBUNĂTĂȚIREA INTERACȚIUNII OM-MAȘINĂ CU BUTOANE INTELIGENTE ȘI FEEDBACK HAPTIC*** Teodor Gabriel FODOREAN, Alin PLEȘA, Emil-Octavian TEUȚAN, Sergiu-Dan STAN | 694 |
| 75. | **CROP ROTATION AS AN ENVIRONMENTALLY FRIENDLY APPROACH TO IMPROVE FARM PRODUCTION /** ***ROTAȚIA CULTURILOR CA O ABORDARE ECOLOGICĂ PENTRU ÎMBUNĂTĂȚIREA PRODUCȚIEI AGRICOLE*** Mihaela NIȚU, Iuliana GĂGEANU, Ana-Maria TĂBĂRAȘU, Augustina PRUTEANU, Mihai NICOLESCU | 700 |
| 76. | **VALORIZATION OF OILSEED MEALS AND AGRICULTURAL BY-PRODUCTS FOR SUSTAINABLE PROTEIN RECOVERY/** ***VALORIFICAREA ȘROTURILOR ȘI SUBPRODUSELOR AGRICOLE CA RESURSE PROTEICE ALTERNATIVE ÎN ECONOMIILE CIRCULARE*** Florin NENCIU, Ana-Maria TABARASU, Diana Lorena POPA, Andreea MATACHE, Gabriel NAE, Floarea ȘERBANCEA, Cristian ȘERBANCEA | 708 |
| 77. | **ANALYSIS OF THE TECHNICAL SOLUTIONS OF A CONTINUOUS MECHANICAL PRESS IN THE OIL INDUSTRY /** ***ANALIZA SOLUȚIILOR TEHNICE ALE UNEI PRESE MECANICE CONTINUE DIN INDUSTRIA ULEIULUI*** Alex-Nicolae COLEȘI, Sorin- Ștefan BIRIȘ, George-Cătălin ION, Neluș-Evelin GHEORGHIȚĂ, Maria-Magdalena DOBRE, Alexandru-Cristian CIOACLA | 720 |
| 78. | **STUDY ON THE ENERGY PERFORMANCE OF A LORENTZ PHOTOVOLTAIC PUMPING UNIT INTEGRATED INTO A MOBILE IRRIGATION PLATFORM /** ***STUDIU PRIVIND PERFORMANȚELE ENERGETICE ALE UNUI GRUP DE POMPARE FOTOVOLTAIC LORENTZ INTEGRAT ÎNTR-O PLATFORMĂ MOBILĂ DE IRIGAȚII*** Dragos Mihail PREDA, Adrian PANDELE, Bogdan Ovidiu DURAN, Gheorghe VOICU, Robert BILA, Elena VALCU, Dragos-Nicolae ANGHELACHE, Paula TUDOR | 726 |
| 79. | **THE POTENTIAL FOR UTILIZING WOOL WASTE TO PRODUCE THERMAL AND ACOUSTIC INSULATION MATERIALS FOR CONSTRUCTION /** ***POSIBILITĂȚILE VALORIFICĂRII DEȘEURILOR DE LÂNĂ PENTRU OBȚINEREA MATERIALELOR DE CONSTRUCȚIE TERMOIZOLANTE ȘI FONOABSORBANTE*** Evelin-Anda LAZA, Gabriela-Victoria MNERIE, Gabriel FODOREAN, Elena-Mihaela NAGY, Teodor VINTILĂ, Ana-Cristina VASILE, Aurelian GRUIN | 736 |
| 80. | **INNOVATIVE TECHNOLOGIES FOR THE DEVELOPMENT OF FOOD PRODUCTS WITH ENHANCED FUNCTIONAL AND NUTRITIONAL VALUE /** ***TEHNOLOGII INOVATIVE PENTRU DEZVOLTAREA PRODUSELOR ALIMENTARE CU VALOARE FUNCȚIONALĂ ȘI NUTRIȚIONALĂ ÎMBUNĂTĂȚITĂ*** Cristian SORICĂ, Nicolae-Valentin VLĂDUȚ, Laurențiu VLĂDUȚOIU, Elena SORICĂ, Florin NENCIU, Alexandru IONESCU | 742 |
| 81. | **EXTRUSION-GRANULATION OF SHEEP WOOL-BASED ORGANO-MINERAL FERTILISER AND CHARACTERISATION OF PROCESS AND PRODUCT /** ***EXTRUDAREA-GRANULAREA ÎNGRĂȘĂMÂNTULUI ORGANO-MINERAL PE BAZĂ DE LÂNĂ DE OAIE ȘI CARACTERIZAREA PROCESULUI ȘI A PRODUSULUI*** Gabriela-Victoria MNERIE, Evelin-Anda LAZA, Elena-Mihaela NAGY | 750 |
| 82. | **SIMULATOR AND ACCELERATED TESTING OF SOME SINTERED COMPONENTS USED IN AGRICULTURAL MACHINERY /** ***TESTARI IN REGIM SIMULATOR SI ACCELERAT PENTRU UNELE ELEMENTE SINTERIZATE DIN COMPONENTA UTILAJELOR AGRICOLE*** Elena Mihaela NAGY, Teodor Gabriel FODOREAN, Evelin-Anda LAZA, Marius GHERES | 758 |
| 83. | **SIGNAL RECONSTRUCTION FROM FREQUENCY-DOMAIN THREE-DIMENSIONAL COMSOL SIMULATIONS OF WAVE PROPAGATION IN THIN CIRCULAR PLATE STRUCTURES /** ***RECONSTRUCȚIA SEMNALELOR DIN SIMULĂRI TRIDIMENSIONALE COMSOL ÎN DOMENIUL FRECVENȚEI APLICATE PROPAGĂRII UNDELOR ÎN PLĂCI CIRCULARE SUBȚIRI*** Andreea-Denisa GRIGUȚA, Mihai Valentin PREDOI | 764 |
| 84. | **EXPERIMENTAL VALIDATION AND NUMERICAL INVESTIGATION OF THE INFLUENCE OF EMBOSSMENTS ON THE FREE VIBRATION CHARACTERISTICS OF THIN PLATES /** ***VALIDAREA EXPERIMENTALĂ ȘI INVESTIGAȚIA NUMERICĂ A INFLUENȚEI EMBOSĂRILOR ASUPRA CARACTERISTICILOR VIBRAȚIILOR LIBERE ALE PLĂCILOR SUBȚIRI*** Laura-Mariana BARBU, Mihai Valentin PREDOI | 774 |
| 85. | **ASPECTS REGARDING ANTI-FROST PROTECTION EQUIPMENT FOR FRUIT AND VINE CROPS /** ***ASPECTE PRIVIND ECHIPAMENTELE PENTRU PROTECȚIA ANTI-ÎNGHEȚ A CULTURILOR POMICOLE ȘI VIȚEI DE VIE*** Elena SORICĂ, Carmen BRĂCĂCESCU, Cristian SORICĂ, Gabriel NAE | 782 |
| 86. | **STATE OF THE ART IN RESEARCH ON THE INFLUENCE OF VIBRATIONS ON THE MOTION OF BODIES /** ***STADIUL ACTUAL AL CERCETĂRILOR PRIVIND INFLUENȚA VIBRAȚIILOR ASUPRA MIȘCĂRII CORPURILOR*** Andrei MĂGUREANU, Mihai Valentin PREDOI, Andrei CRAIFALEANU | 792 |

| No. | Article Title & Authors | page |
|---|---|---|
| 87. | **RESEARCH ON DEEP SOIL TILLAGE AND CONTROLLED APPLICATION OF LIQUID FERTILIZERS - A CASE STUDY IN THE SOUTH-EAST REGION OF ROMANIA /**<br>***CERCETĂRI PRIVIND PRELUCRAREA PROFUNDĂ A SOLULUI ȘI INTRODUCEREA CONTROLATĂ A FERTILIZANȚILOR LICHIZI - STUDIU DE CAZ ÎN REGIUNEA SUD-EST DIN ROMÂNIA***<br>Dragoș MANEA, Mihai GÎDEA, Dragoș-Nicolae DUMITRU, Alin HARABAGIU, Larisa-Bianca IONICĂ, Aura DUMITRESCU | 806 |
| 88. | **METHODS OF PRESERVING SOIL FERTILITY IN ARAD COUNTY, ROMANIA /**<br>***METODE DE CONSERVARE A FERTILITĂȚII SOLULUI ÎN JUDEȚUL ARAD, ROMÂNIA***<br>Casiana MIHUȚ, Sorin Tiberiu BUNGESCU, Nicolae-Valentin VLADUȚ, Daniel POPA, Anișoara DUMA-COPCEA, Attila BLENEȘI-DIMA, Aurelia MIHUȚ, Veaceslav MAZĂRE, Lavinia PETANEC | 812 |
| 89. | **ANALYSIS OF TECHNICAL SOLUTIONS FOR INCREASING THE LATERAL STABILITY OF MOTOR-CULTIVATORS USED FOR MOWING SLOPED TERRAIN VIA ADAPTIVE MASS-BALANCING SYSTEMS /**<br>***MOTOCULTOARE ANALIZA PRIVIND SOLUTIILE TEHNICE DE CREȘTEREA STABILITĂȚII LATERALE A MOTOCULTOARELOR UTILIZATE LA COSIREA TERENURILOR ÎNCLINATE PRIN SISTEME DE ECHILIBRARE ADAPTIVĂ A MASEI***<br>Iulian DRENEA, Sorin-Stefan BIRIS, Adrian IOSIF, Gabriel MUȘUROI, Raluca-Adriana ZOTA | 822 |
| 90. | **EXPERIMENTAL EVALUATION OF A SMALL-SCALE ELECTRIC COMPOSTER UNDER DIFFERENT OPERATING CONDITIONS /**<br>***EVALUAREA EXPERIMENTALĂ A UNUI COMPOSTOR ELECTRIC DE MICI DIMENSIUNI ÎN DIFERITE CONDIȚII DE FUNCȚIONARE***<br>Elena-Melania CISMARU, Gigel PARASCHIV, Gabriel-Alexandru CONSTANTIN, Mirela-Nicoleta DINCĂ, Elena-Mădălina ȘTEFAN, Alina-Daiana IONESCU, Nicolae-Valentin VLĂDUȚ, Ana-Maria TĂBĂRAȘU | 836 |
| 91. | **DEVELOPING AN OPERATIONAL MODEL FOR AGRICULTURAL KNOWLEDGE TRANSFER TO SUPPORT PUBLIC–PRIVATE PARTNERSHIPS IN ROMANIA /**<br>***DEZVOLTAREA UNUI MODEL OPERAȚIONAL PENTRU TRANSFERUL CUNOAȘTERII AGRICOLE ÎN SPRIJINUL PARTENERIATELOR PUBLIC-PRIVATE DIN ROMÂNIA***<br>Ioana Corina MOGA, Laurențiu CIORNEI, Iulian VOICEA | 846 |
| 92. | **ASSESSMENT OF THE ECONOMIC AND ENVIRONMENTAL IMPACT OF ALTERNATIVE PROTEINS DERIVED FROM LEGUMES, FUNGI, AND AQUATIC SOURCES /**<br>***EVALUAREA IMPACTULUI ECONOMIC ȘI DE MEDIU AL PROTEINELOR ALTERNATIVE OBȚINUTE DIN LEGUMINOASE, CIUPERCI ȘI SURSE ACVATICE***<br>Gabriel NAE, Florin NENCIU, Andreea MATACHE, Nicoleta VANGHELE, Floarea ŞERBANCEA, Margareta NAIE, Simona-Florina ISTICIOAIA | 856 |
| 93. | **DEVELOPMENT AND EVALUATION OF INNOVATIVE FOOD PRODUCTS BASED ON HEMP SEEDS AND HEMP-DERIVED INGREDIENTS (CANNABIS SATIVA L.) /**<br>***DEZVOLTAREA ȘI EVALUAREA UNOR PRODUSE ALIMENTARE INOVATOARE PE BAZĂ DE SEMINȚE DE CÂNEPĂ ȘI INGREDIENTE DERIVATE DIN CÂNEPĂ (CANNABIS SATIVA L.)***<br>Alexandru Florin OLTEANU, Gabriela Daniela CRIVEANU-STAMATIE, Cristian FLOREA, Serban CUCU, Manuela RASCOL, Tatiana ONISEI | 866 |
| 94. | **STUDY ON THE MECHANICAL PROCESSING OF COMPOST /**<br>***STUDIU PRIVIND PRELUCRAREA MECANICĂ A COMPOSTULUI***<br>Stefan DUMITRU, Nicolae-Valentin VLĂDUȚ, Gabriel-Valentin GHEORGHE, Alin HARABAGIU, Dragos-Nicolae DUMITRU, Oana Elena MILEA | 874 |
| 95. | **PRECISION AGRICULTURE AND SUSTAINABLE PRACTICES IN ROMANIA: FARM PROFILES, DIGITAL GAPS AND EVIDENCE FROM SELECTED EU COUNTRIES /**<br>***AGRICULTURA DE PRECIZIE ȘI PRACTICILE AGRICOLE DURABILE ÎN ROMÂNIA: PROFILUL EXPLOATAȚIILOR, DECALAJE DIGITALE ȘI COMPARAȚII CU STATE UE SELECTATE***<br>Cristiana Silvia BUZATU, Alina MĂRCUȚĂ, Liviu MĂRCUȚĂ, Iulian Virgil GHIULEANU, Răzvan Alexandru MATINCĂ | 886 |
| 96. | **FROM LAND REGISTRATION TO TERRITORIAL PATTERNS: DYNAMICS AND CONCENTRATION OF REGISTERED LAND AREAS BY LAND-USE CATEGORY IN SOUTH-WEST OLTENIA, 2015–2024 /**<br>***DE LA CARTEA FUNCIARĂ LA PROFILUL TERITORIAL: DINAMICA ȘI CONCENTRAREA SUPRAFEȚELOR INTABULATE PE CATEGORII DE FOLOSINȚĂ ÎN REGIUNEA SUD-VEST OLTENIA, 2015–2024***<br>Iulian Virgil GHIULEANU, Cristiana Silvia BUZATU, Alina MĂRCUȚĂ, Liviu MĂRCUȚĂ, Răzvan Alexandru MATINCĂ | 906 |
| 97. | **EFFECT OF BUCKWHEAT FLOUR INCORPORATION ON PHYSICAL, STRUCTURAL AND SENSORY PROPERTIES OF WHEAT BREAD /**<br>***INFLUENȚA ADAOSULUI DE FĂINĂ DE HRIȘCĂ ASUPRA PROPRIETĂȚILOR FIZICE, STRUCTURALE ȘI SENZORIALE ALE PÂINII DIN FĂINĂ DE GRÂU***<br>Elena-Mădălina ȘTEFAN, Gabriel-Alexandru CONSTANTIN, Mariana-Gabriela MUNTEANU, Gheorghe VOICU, Aura-Irina ISTRATE, Gabriel MUȘUROI, Mariana IONESCU, Alina-Daiana IONESCU, Elena-Melania CISMARU | 922 |

| No. | Article Title & Authors | page |
|---|---|---|
| 98. | **FUNGAL BIOMASS IN CARRIER-BASED BIOREACTORS AS A BASIS FOR TREATING INDUSTRIAL EFFLUENTS WITH POTENTIAL AGRICULTURAL REUSE: REVIEW AND PRELIMINARY DATA /** ***UTILIZAREA BIOMASEI FUNGICE IMOBILIZATE PE SUPORTURI ÎN BIOREACTOARE PENTRU EPURAREA APELOR UZATE INDUSTRIALE CU POTENȚIAL DE REUTILIZARE ÎN AGRICULTURĂ: ANALIZĂ BIBLIOGRAFICĂ ȘI REZULTATE PRELIMINARE*** Ioana-Corina MOGA, Ovidiu IORDACHE, Bogdan CAZAN, Gabriel PETRESCU, Elena PERDUM, Iulian VOICEA, Răzvan RĂDULESCU | 930 |
| 99. | **INTEGRATED DIGITAL SOLUTIONS IN AGRICULTURE /** ***SOLUȚII DIGITALE INTEGRATE ÎN AGRICULTURĂ*** Iulian VOICEA, Florin NENCIU, Cătălin PERSU, Dan CUJBESCU, Remus OPRESCU, Iuliana GĂGEANU, Roxana ZAHARIA, Viorel FĂTU, Corina MOGA, Vlad-Nicolae ARSENOAIA, Diana STEGARUS (POPESCU) | 938 |
| 100. | **THE EFFECTS OF CLIMATE CHANGE ON THE PRODUCTIVITY AND SUSTAINABILITY OF THE VEGETABLE SECTOR /** ***EFECTELE SCHIMBĂRILOR CLIMATICE ASUPRA PRODUCTIVITĂȚII ȘI SUSTENABILITĂȚII SECTORULUI LEGUMICOL*** Iulian VOICEA, Iuliana GAGEANU, Florin NENCIU, Cătălin PERSU, Dan CUJBESCU, Remus OPRESCU, Roxana ZAHARIA, Viorel FĂTU, Corina MOGA, Vlad-Nicolae ARSENOAIA, Diana STEGARUS (POPESCU) | 948 |
| 101. | **MODERN TECHNOLOGIES FOR SOIL REGENERATION /** ***TEHNOLOGII MODERNE DE REGENERARE A SOLULUI*** Aura-Maria DUMITRESCU, Vasilica STEFAN, Stefano-Andrea MANTOVANI, Alex-Nicolae COLESI, Maria-Magdalena DOBRE | 958 |

# HEC-RAS SIMULATION: A CASE STUDY OF THE IHTIMAN IRRIGATION SYSTEM
/
# *СИМУЛАЦИЯ С HEC-RAS: ОБЕКТ НА ИЗСЛЕДВАНЕТО НАПОИТЕЛНА СИСТЕМА „ИХТИМАН“*

**Elena GRANCHAROVA*, Asparuh IVANOV**
Institute of soil science, agrotechnologies and plant protection „Nikola Poushkarov“, Agricultural Academy, Sofia / Bulgaria
**Tel: (+35) 98 929 379; *E-mail: eveha@abv.bg*

***Keywords:*** *steady flow analysis, Canal Conveyance Capacity, Canal M-2, Bulgaria*

**ABSTRACT**
*Growing water scarcity and rising competition between agriculture and other sectors make water management a critical factor in ensuring global food security. According to EUROSTAT data, fresh water withdrawn for irrigation in 2023 totalled 268.5 million cubic meters, representing approximately 6% of the economy's total water withdrawal in Bulgaria. Concurrently, FAOSTAT data shows that agricultural areas equipped with irrigation infrastructure account for nearly 15% of total farmland. The Ihtiman irrigation system is a vital agricultural infrastructure network located in the Sofia region of Bulgaria. Managed by the state-owned Irrigation Systems EAD, this facility is designed to service over 1 540 hectares of arable farmland in the Ihtiman valley. The network primarily draws its water supply from local reservoirs, including the Bakar Dere dam, ensuring a stable water supply even during dry summer periods. This study used steady flow analysis of M-2 irrigation canal of Ihtiman irrigation system to determine the Canal Conveyance Capacity.*

**РЕЗЮМЕ**
*Все по-често се прави констатацията, че намаляващите водни ресурси и нарастващата конкуренция на селското стопанство с другите отрасли за използването им превръща управлението на водите в една от критичните точки при справянето с предизвикателствата за осигуряване на продоволствена сигурност. Според данни на EUROSTAT, изтеглената прясна вода за напояване през 2023 г. е възлизала на 268,5 милиона кубически метра, което представлява приблизително 6% от общото водоизточване на икономиката в България. Същевременно данните на FAOSTAT показват, че земеделските площи, оборудвани с напоителна инфраструктура, представляват близо 15% от общата земеделска земя. Напоителната система Ихтиман е жизненоважна мрежа от селскостопанската инфраструктура, разположена в Софийска област в България. Управлявана от държавното дружество „Напоителни системи“ ЕАД, това съоръжение е проектирано да обслужва над 1540 хектара обработваема земеделска земя в Ихтиманската котловина. Мрежата черпи вода предимно от местни резервоари, включително язовир „Бакър дере“, осигурявайки стабилно водоснабдяване дори през сухи летни периоди. В това проучване е моделиран стационарен режим на течението на напоителен канал М-2 на напоителна система “Ихтиман”, за да се определи пропускната способност на канала*

## INTRODUCTION

Growing water scarcity and rising competition between agriculture and other sectors make water management a critical factor in ensuring global food security. According to EUROSTAT data, fresh water withdrawn for irrigation in 2023 totalled 268.5 million cubic meters, representing approximately 6% of the economy's total water withdrawal in Bulgaria. Concurrently, FAOSTAT data shows that agricultural areas equipped with irrigation infrastructure account for nearly 15% of total farmland.

The HEC-RAS software is an industry-standard tool designed to perform one-dimensional (1-D) steady and unsteady flow river hydraulics calculations. When conducting a 1-D steady-state, gradually-varied flow analysis, the model relies on several foundational fluid mechanics assumptions to simplify complex open-channel dynamics. First, it assumes that the dominant velocity vector is oriented strictly in the direction of the flow, neglecting lateral and vertical velocities. Second, the flow is considered steady, meaning all hydraulic characteristics remain constant throughout the specified time interval. Third, the streamlines are assumed to be practically parallel, which justifies using a hydrostatic pressure distribution across the channel section. Finally, the model is strictly valid for mild channel slopes of less than 0.1 (10%), where the true flow

depth is approximately equal to the vertical depth. To establish the mathematical relationships between the volumetric discharge rate, hydraulic resistance, channel geometry, and the rate of friction loss, HEC-RAS utilizes the empirical Manning's equation. When the flow encounters abrupt changes in the canal prism, local energy losses are evaluated by multiplying specific contraction or expansion coefficients by the net change in velocity head between cross-sections. Ultimately, these governing equations allow the model to accurately simulate water surface profiles under steady-state conditions. Engineers can reliably predict water behaviour across all major hydraulic states, including critical, supercritical (torrential), and mixed flow regimes, making it an invaluable asset for floodplain management, flood insurance studies, and bridge hydraulic design. (US

HEC-RAS was used to determine canal capacity potential *(Serede et al., 2015)*, water level determination *(Talib et al., 2019),* flow dynamics *(Kumari et al., 2025),* system's efficiency *(Shayannejad et al., 2018)*, maximum capacity of irrigation scheme *(Abo-Sreeaa et al., 2023; Ontowirjo et al., 2023),* evaluation different discharge scenarios *(Zahran et al., 2025),* sensitive calibration parameter is channel resistance *(Ismail et al., 2021),* It is frequently used to compute the primary 1D flow parameters *(Zainal &Talib, 2024)*, both for study *(Tadjer & Grancharova, 2021)* and unsteady flow analyses *(Razzaq et al., 2025)*. In canal simulation, channel roughness is one of the sensitive parameters in the development of hydraulic models to better understanding the canal hydraulic behaviour *(Patamanska and Grancharova, 2019)* or using model calibration *(Vedmani & Pandey, 2020).*

This study used steady flow analysis of M-2 irrigation canal of Ihtiman Irrigation System to determine the Canal Conveyance Capacity.

## MATERIALS AND METHODS

The open-source software HEC-RAS, Version 6.5 (Hydrologic Engineering Centre - River Analysis System), developed by the U.S. Army Corps of Engineers, was selected to develop the hydraulic simulation model for the study canal. This widely accepted software is capable of performing one-dimensional (1-D) steady and unsteady flow calculations across complex, branched networks of both natural rivers and artificial channels. The software architecture integrates a graphical user interface, specialized computational engines for steady and unsteady flow regimes, and advanced post-processing modules that facilitate the comprehensive graphical and tabular presentation of hydraulic results. Executing a rigorous hydraulic simulation and mapping the water surface profile along the irrigation canal requires a detailed suite of input data.

The primary requirements include the channel's physical geometry, upstream and downstream boundary conditions, design water discharge rates, hydraulic roughness coefficients, and detailed geometric configurations of any inline hydraulic structures along the canal course, such as gates, culverts, and weirs. The spatial geometry of the canal is established by setting a sequential series of cross-sections that define the bed profile and longitudinally map the exact shape and slope of the study reach. The foundational physics governing this 1-D, steady-state, and gradually-varied flow analysis relies on three core principles: the continuity, energy, and flow resistance equations. Under steady-state conditions, the continuity equation dictates that the volumetric discharge remains constant and continuous over the specified simulation timeframe.

The energy equation is utilized to compute the total energy head at any given cross-section, which is mathematically expressed as the summation of the channel bed elevation (potential energy), the average flow depth (pressure energy), and the velocity head (kinetic energy).To compute the longitudinal water surface profile, the one-dimensional energy equation—derived from the classic Bernoulli equation—is integrated along the reach. The model resolves these profiles by balancing the energy equation from one cross-section to the next through iterative numerical steps. To initiate the computational process, specific boundary conditions must be established.

For subcritical flow regimes, a known water discharge is defined at the upstream boundary, while a known water stage (elevation) is set at the downstream boundary. For all interior nodes, the model estimates the water stage while holding the discharge rate constant. While open-channel hydraulics recognizes two primary iterative approaches—the direct step method and the standard step method—HEC-RAS exclusively relies on the standard step method for natural and irregular channels. The direct step method is limited because it determines the distance between two pre-defined water depths, making it impractical for fixed-interval cross-sections. Conversely, the standard step method applies the principle of energy conservation to iteratively calculate the water surface elevations and energy grade lines at specified cross-sectional locations along the reach. This iterative approach accounts for friction losses via Manning's equation and evaluates

local transition losses using contraction and expansion coefficients, ensuring an accurate simulation of the water profile.

The HEC-RAS hydraulic simulation yields critical open-channel parameters along the irrigation canal, including water surface elevation, energy grade line elevation, friction slope, flow velocity, and critical depth. It also calculates the total water volume stored within the channel reach. Among these variables, the Manning's roughness coefficient (n) cannot be directly measured in the field. Consequently, it must be determined using indirect methods, such as mathematical model simulation. The classic approach for evaluating and calibrating this parameter involves modelling a known steady-state flow condition within the canal *(Malaterre et al., 2010).*

The calibration procedure follows an iterative computational workflow. Multiple simulations are executed across the irrigation canal model using a progressive series of trial roughness values. To determine the most accurate coefficient, the simulated water levels are compared against field observations recorded at specific monitoring points along the canal course.

The optimal value is selected based on how closely the numerical model results match the empirical field data according to a predefined statistical criterion. Research by Nguyen and Fenton (2004) investigated the application of three main types of objective target functions for this calibration process. Their findings demonstrated that a least-squares minimization approach yields the most reliable results. By applying this mathematical criterion, the objective function isolates the specific roughness value that minimizes the variance between observed and calculated water surface profiles. Ultimately, the best match between the field-measured and computer-generated hydraulic parameters identifies the optimal, calibrated roughness coefficient for the study reach.

Water surface profiles are computed from one cross section to the next by solving the Energy equation with an iterative procedure called the standard step method. The Energy equation is written as follows:

$$Z_2 + Y_2 + \frac{\alpha_2 V_2^2}{2g} = Z_1 + Y_1 + \frac{\alpha_1 V_1^2}{2g} + h_e \quad (1)$$

were $Z_1$ , $Z_2$ - elevation of the main channel inverts (m); $Y_1$ ,$Y_2$- depth of water at cross sections (m); $V_1$ ,$V_2$ - average velocities (m/s); $\alpha_1$ ,$\alpha_2$ - velocity weighting coefficients; $h_e$ - energy head loss (m).

The energy head loss ($h_e$) between two cross sections is comprised of friction losses and contraction or expansion losses. The equation for the energy head loss is as follows:

$$h_e = L\overline{S_f} + C\left|\frac{\alpha_2 V_2^2}{2g} - \frac{\alpha_1 V_1^2}{2g}\right| \quad (2)$$

were L is discharge weighted reach length (m); $S_f$ - representative friction slope between two sections; C – expansion or contraction loss coefficient.

Conveyance is calculated within each subdivision from the following form of Manning's equation

$$Q = K\,\overline{S_f}^{1/2} \quad (3)$$

$$K = \frac{1.486}{n} AR^{2/3} \quad (4)$$

were Q is water discharge ($m^3/s$); K - conveyance for subdivision; A - flow area for subdivision ($m^2$).

The Ihtiman Irrigation System is a vital agricultural infrastructure network located in the Sofia region of Bulgaria. Managed by the state-owned Irrigation Systems EAD, this facility is designed to service over 1 540 hectares of arable farmland in the Ihtiman valley.

The network primarily draws its water supply from local reservoirs, including the Bakar Dere dam, ensuring a stable water supply even during dry summer periods. In the Ihtiman Irrigation System, water is delivered from the source by gravity into two main irrigation canals, M-1 and M-2, which feed a pressurized water distribution network. The canals are located at a commanding elevation, creating natural pressure

within the pipeline network. The Ihtiman Irrigation System is the only irrigation system in Bulgaria of the Gp type (Gravity fed-Pressurized network). This pressurized water supply eliminates the need for pumps, enabling users to implement water-saving irrigation technologies (such as sprinkling and drip irrigation) without inflating water costs with electricity expenses.

The Ihtiman Irrigation System, supplied by the Bakar Dere Reservoir, was constructed to irrigate approximately 3 901 hectares of agricultural land within the Ihtiman Municipality. Construction of the irrigation system began in the 1960s and was completed in the early 1970s.

The infrastructure includes two open main irrigation canals that feed the pressurized pipeline network of the system. The entire pipeline distribution network is constructed from asbestos-cement (AC) pipes, ranging in diameter from Ø125 mm to Ø546 mm, and designed for an operating pressure of 10 bar.

Water abstraction is facilitated by an intake tower located at the upstream end of the Bakar Dere reservoir, designed for a capacity of Q = 2.3 $m^3/s$. The headrace canal originates at an elevation of 744.20 m (0.8 m below the dead storage level), featuring a 2 m bottom width, a 1.765% longitudinal slope, and a length of 170 m. Along the subsequent 187.7 m reach, the canal transitions to a 1.2 m width and a longitudinal slope 3.34%. The embankment side slopes are designed at 1V:2H in soil and 1V:1H in rocky segments.

The open channel feeds into a 56 m long steel-lined penstock with a 1.2 m diameter, followed by a gate chamber and a 129.5 m long tailrace canal. This tailrace section maintains a 1.2 m bottom width with 1V:2H side slopes, which adjust to 1V:1.5H in earthen reaches. The system concludes with a chute structure featuring a 1.0 m bottom width and 1V:1H side slopes, discharging directly into a stilling basin.

The studied reach represents the first section of the existing main irrigation canal M-2, which is part of the Ihtiman Irrigation System. This 1,929.69 m segment starts after the stilling basin and terminates at the Karaman Dere and Malka River inverted culvert. The culvert length is 1634 m and $_{\Delta}h$=9.57 m.

A hydraulic simulation model of the canal was developed using HEC-RAS software based on the design parameters of the M-2 canal (fig. 1). The model accurately replicates the existing conditions.

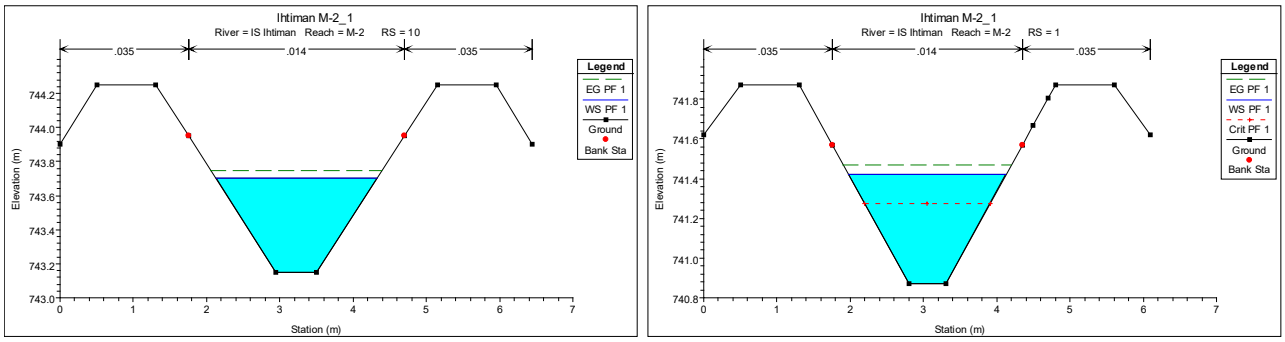



**Fig. 1 - The M-2 Canal of Ihtiman Irrigation System cross sections**

Calibration of the HEC-RAS model for the M-2 canal was performed using a known water surface elevation at a discharge of Q=0.73 $m^3/s$. Alternatively, the model can be calibrated using the downstream energy slope to determine the normal depth boundary condition. The model was then used to simulate steady flow in the M-2 canal across a range of Manning's roughness coefficients spanning from 0.014 to 0.025 for two water discharges: 0.73 $m^3/s$ and 0.88 $m^3/s$.

## RESULTS

Analysis of the modelling results demonstrates the impact of Manning's roughness on flow parameters within the irrigation canal for Q = 0.73 $m^3/s$ (fig. 2). Increasing the roughness coefficient leads to higher water depths. Continued increases in roughness will cause water depths to approach the maximum design limit of 0.7 m, which corresponds to the height of the canal lining. At a Manning's roughness coefficient of 0.014, the water surface elevation in the canal is 741.42 m.

The water surface elevation in the canal is 741.49 m at a Manning's roughness coefficient of 0.018, 741.52 m at n=0.020 and 741.58 m at n=0.025. Deterioration of the canal's condition can raise the water level by more than 10 cm at a constant discharge 0.73 $m^3/s$.

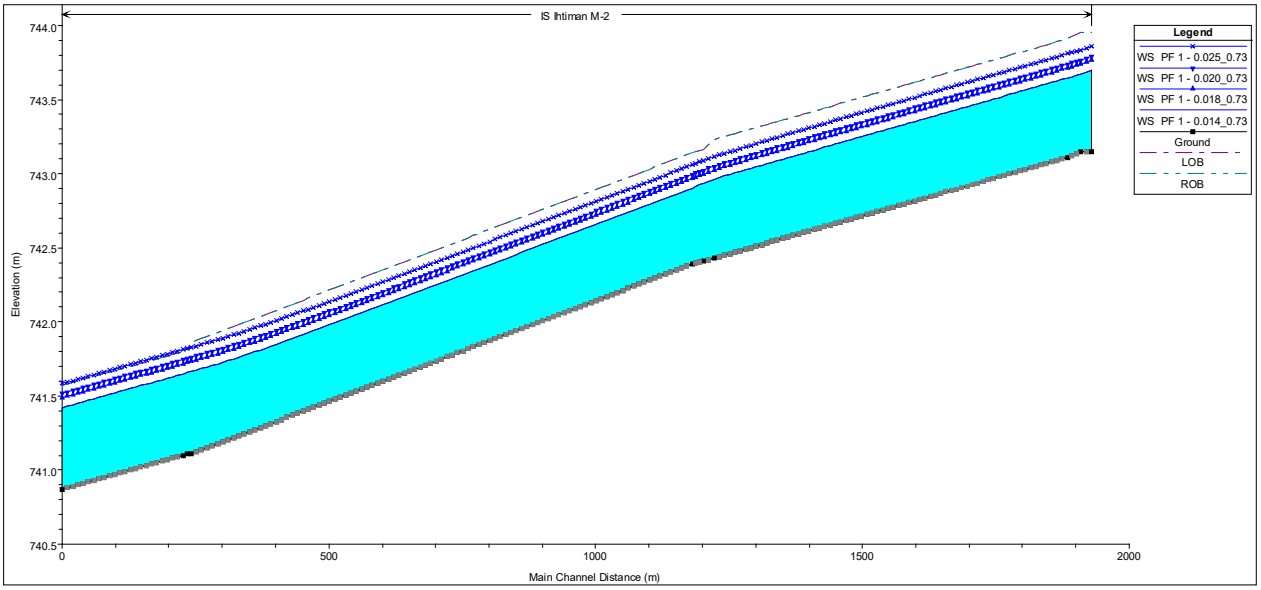



**Fig. 2 - Water surface profiles for different values of roughness coefficient n= 0.014, 0.018, 0.020, 0.025 of water discharge Q = 0.73 $m^3/s$**

Figure 3 illustrates the increase in water level as the roughness coefficient increases. Increasing the roughness coefficient leads to higher water depths. Continued increases in roughness will cause water depths to approach the maximum design limit of 0.7 m, which corresponds to the height of the canal lining. At a Manning's roughness coefficient of 0.014, the water surface elevation in the canal is 741.47 m. The water surface elevation in the canal is 741.54 m at a Manning's roughness coefficient of 0.018, 741.57 m at n=0.020 and 741.63 m at n=0.025. Deterioration of the canal's condition can raise the water level by more than 10 cm above the design value when transporting the design flow of 0.88 $m^3/s$.

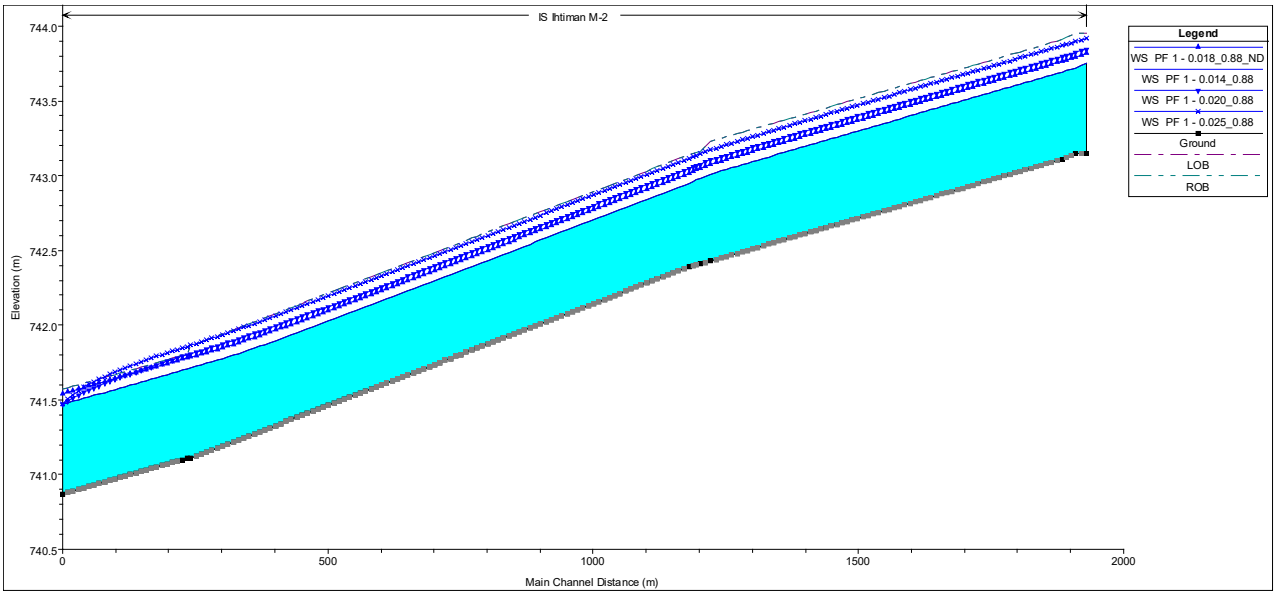



**Fig. 3 - Water surface profiles for different values of roughness coefficient n= 0.014, 0.018, 0.020, 0.025 of water discharge Q = 0.88 $m^3/s$**

Consequently, if the canal lining deteriorates into a poor condition, the operational discharge should be reduced to prevent overtopping. The simulated water surface profiles can serve as a reference for estimating actual roughness once updated field measurements of water depth become available along the canal.

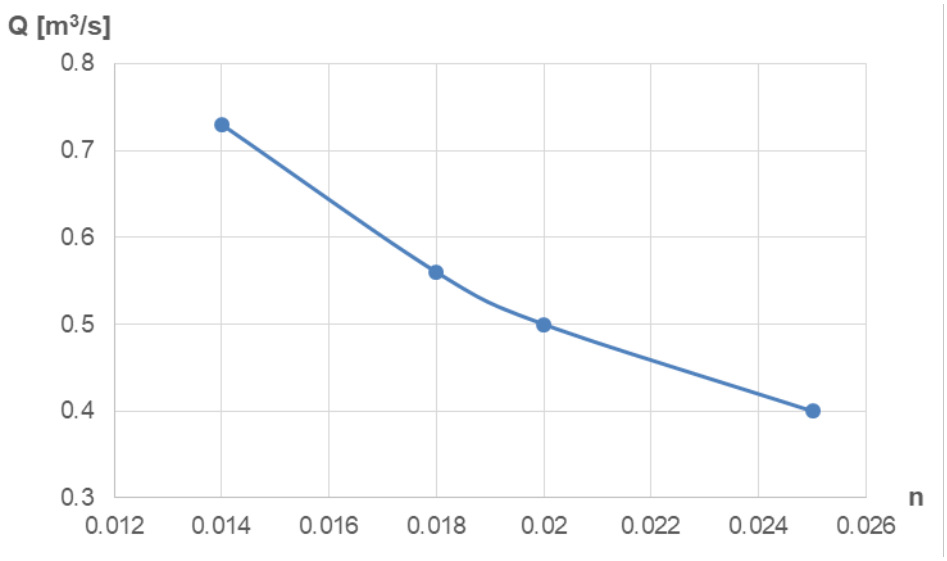



**Fig. 4 - Canal Conveyance Capacity [m³/s]**

Figure 4 illustrates the decrease in Canal Conveyance Capacity as the roughness coefficient increases. Irrigation canal performance depends on both operational management and physical condition. Channels function optimally when kept clean and free of leakage. Neglecting routine maintenance leads to weed growth and siltation, which severely restrict flow capacity by increasing hydraulic roughness.

Furthermore, structural degradation can cause significant water loss through leakage. Implementing a systematic maintenance program is essential to prolonging the canal network's operational lifespan. To minimize disruptions to water delivery, these upkeep activities are typically scheduled between irrigation seasons or during periods of low agricultural water demand, ensuring the system remains efficient and reliable for future irrigation cycles.

**Table 1**

**Reduction in discharge relative to the design and surcharge discharge**

| **Manning's roughness coefficient** | 0.014 | 0.018 | 0.020 | 0.025 |
|---|---|---|---|---|
| **Canal Conveyance Capacity [m³/s]** | 0.73 | 0.56 | 0.50 | 0.40 |
| **Reduction in discharge relative to the design discharge [%]** | 0 | 23.29 | 31.51 | 45.21 |
| **Reduction in discharge relative to the surcharge flow [%]** | 17.04 | 36.36 | 43.18 | 54.54 |

Table 1 illustrates the reduction in discharge relative to the design discharge as the roughness coefficient increases. At a Manning's roughness coefficient of 0.018, the reduction in discharge is 23.29%, at n=0.020 the reduction in discharge is 31.51% and at n=0.025 the reduction in discharge is 45.21%. 741.63 m at n=0.025. At a Manning's roughness coefficient of 0.018, the reduction in surcharge flow is 36.36%, at n=0.020 the reduction in discharge is 43.18% and at n=0.025 the reduction in discharge is 54.54%.

## CONCLUSIONS

This study utilized steady flow analysis of the M-2 irrigation canal within the Ihtiman Irrigation System to accurately determine the overall Canal Conveyance Capacity. The predictive HEC-RAS model was carefully calibrated by incrementally maximizing the Manning's roughness coefficient, which served as the primary input parameter governing hydraulic resistance. This calibration approach allowed the simulation to capture the hydraulic behaviour of the channel under various stages of physical degradation and weed proliferation. Based on the comprehensive simulation results and the corresponding water surface profiles generated by the HEC-RAS model, several critical recommendations and operational strategies have been formulated to improve water management within the scheme.

The immediate field calibration and subsequent installation of precise water-level and flow-measuring devices directly downstream of the primary off-takes must be treated as a matter of highest

priority by the scheme operators. Currently, the lack of continuous, reliable flow data limits the ability to manage water distribution efficiently. Installing functional measuring structures at these strategic characteristic points along the canal course will enable real-time monitoring of discharge rates. This data will provide irrigation managers with the necessary information to detect sudden drops in conveyance capacity caused by sediment accumulation or vegetation growth, ensuring equitable water distribution to downstream agricultural users.

Further research utilizing this hydraulic model should be conducted to verify whether the cross-sections and longitudinal slopes of the canals were actually constructed in strict accordance with the original engineering designs. Over decades of operation, irrigation channels frequently undergo structural deformations, unauthorized modifications, or severe siltation that significantly alter their original geometric properties. By comparing high-resolution field survey data with the design specifications within HEC-RAS, researchers can quantify these physical deviations.

At a Manning's roughness coefficient of 0.014, the water surface elevation in the canal is 741.42 m. The water surface elevation in the canal is 741.49 m at a Manning's roughness coefficient of 0.018, 741.52 m at n=0.020 and 741.58 m at n=0.025. Deterioration of the canal's condition can raise the water level by more than 10 cm at a constant discharge 0.73 m3/s.

At a Manning's roughness coefficient of 0.014, the water surface elevation in the canal is 741.47 m. The water surface elevation in the canal is 741.54 m at a Manning's roughness coefficient of 0.018, 741.57 m at n=0.020 and 741.63 m at n=0.025. Deterioration of the canal's condition can raise the water level by more than 10 cm above the design value when transporting the design flow of 0.88 $m^3/s$.

At a Manning's roughness coefficient of 0.018, the reduction in discharge is 23.29%, at n=0.020 the reduction in discharge is 31.51% and at n=0.025 the reduction in discharge is 45.21%. 741.63 m at n=0.025. At a Manning's roughness coefficient of 0.018, the reduction in surcharge flow is 36.36%, at n=0.020 the reduction in discharge is 43.18% and at n=0.025 the reduction in discharge is 54.54%.

**ACKNOWLEDGEMENT**

The authors would like to thank *Irrigation Systems EAD* for providing geometric and hydraulic data used in this study.

**REFERENCES**

[1] Abo-Sreeaa, D. A., AboulAtta, N. M. and El-Molla, D. A. (2023). The impact of blockage on the performance of canal coverage structures. Journal of Engineering and Applied Science, 70: 76. https://doi.org/10.1186/s44147-02300246-0

[2] Ismail, H., Kamal, M. R., Shanono, N. J. & Amin, S. A. (2021). Application of HEC-RAS model for adaptive water allocation in a large-scale rice irrigation scheme. Available from: https://www.ajol.info/index.php/ajet/article/view/227328

[3] Kumari, S., Kumar, M. and Singh, A. (2025). Hydraulic Analysis of Irrigation Canal Using HEC-RAS Model: A Case Study of Latifshah Weir in Uttar Pradesh, India. *Journal of Water Engineering and Management*, 6(3): 1-13. https://doi.org/10.47884/jweam.v6i3pp0113

[4] Malaterre, P.O., Baume J.P., Jean-Baptiste N., Sau J. (2010). Calibration of open channel flow models: a system analysis and control engineering approach. In Proc. SimHydro 2010:“Hydraulic modeling and uncertainty“, 2-4 June 2010.

[5] Nguyen T. H, Fenton, D. J. (2004) Identification of roughness in open channels. Proc. of 6th International Conference on Hydro-Science and Engineering, Brisbance, Australia, June 2004.

[6] Ontowirjo, B., Fathurrahman, I., Ramadhan, M. V., Zahriani, A., Zahra, M. and Wahyudi, H. 2023. LiDAR DEM and HEC-RAS On-Grid Rainfall Hydrograph Model for irrigation system. *IOP Conference Series: Earth and Environmental Science*, 1198: 012023.

[7] Patamanska, G., & Grancharova, E. (2019). Hydraulic Modeling for better operational performance of existing irrigation canal. *Acta tehnica corviniensis-Bulletin of engineering* 12(1), 107–110

[8] Razzaq, H. K., Abed, B. S., Anmar, A. (2025). Application of HEC-RAS Software for Steady and Unsteady Hydraulic Simulation of Al Musayyab Canals. *Mathematical Modelling of Engineering Problems*, 11(9), 2557-2565 https://doi.org/10.18280/mmep.110926

[9] Shayannejad, M. Askari-Ali Ostad, K., Eslamian, S., Singh, V.P. and Dalezios, N.R. (2018). Analyzing of flow in open channels networks using HEC-RAS. Journal of Ecology & Natural Research, 2(4), 1-7

[10] Serede, I. J., Mutua, B. M., Raude, J. M. (2015). Hydraulic analysis of irrigation canals using HEC-RAS model: a case study of Mwea irrigation scheme, Kenya. International Journal of Engineering Research & Technology, 4(9), 989-1005.

[11] Tadjer, J. & Grancharova, E. (2021). HEC-RAS simulation and physical modeling of the Danube River. In Proceedings of The International Symposium ISB-MA TEH' 2021, 122-129

[12] Talib, A., Alwan, H., Jwahery, Z. (2019). Optimizing irrigation efficiency of Al-Kamaliya irrigation canal. ARPN Journal of Engineering and Applied Sciences, 14(10), 1919-1925.

[13] US Army Corps of Engineers,(2020). HEC-RAS User Manual. Hydrologic Engineering Center, Version 6.5.

[14] Vedmani, Panda, R. K. and Pandey, V. K. (2020). Calibration and validation of HEC-RAS model for minor command in coastal region. International Journal of Current Microbiology and Applied Sciences, 9: 664-678.

[15] Zahran, S., Gooda, E., AbdelMeged, N. (2025). Modeling Al-Qaraqoul canal before and after rehabilitation using HEC-RAS Scientific Reports, 14:14760 https://doi.org/10.1038/s41598-024-63995-9

[16] Zainal, N. and Talib, S. (2024). Review paper on applications of the HEC-RAS model for flooding, agriculture, and water quality simulation. Water Practice & Technology, 19 (7), 2883 https://doi.org/10.2166/wpt.2024.173

# SPRING FIELD EVALUATION OF AN EXPERIMENTAL OVERSEEDING MACHINE FOR PERMANENT GRASSLAND RENOVATION

/

# *EXPERIMENTĂRI ÎN CONDIȚII DE PRIMĂVARĂ ALE UNEI MAȘINI DE SUPRAÎNSĂMÂNȚAT PENTRU REGENERAREA PAJIȘTILOR PERMANENTE*

**Eugen MARIN*[1], Vasile MOCANU[2], Tudor-Adrian ENE[2], Laurențiu-Constantin VLĂDUȚOIU[1], Alexandru IONESCU[1], Mihai-Gabriel MATACHE[1], Radu Nicolae SOARE[3]**

[1] National Institute of Research-Development for Machines and Installations Designed for Agriculture and Food Industry-INMA Bucharest, 013811 Bucharest / Romania;

[2] Institute of Research-Development for Grasslands-ICDP Brasov / Romania;

[3] National University of Science and Technology POLITEHNICA Bucharest / Romania

*Tel: 0758 437 214; *E-mail: marineu61@yahoo.com*

***Keywords:*** *permanent grasslands, overseeding, overseeding machine, grassland renovation, operational performance.*

## ABSTRACT

*Permanent grasslands are an important source of forage production and biodiversity conservation, and their renovation requires efficient technologies with minimal disturbance to the existing vegetation cover. In this context, a 2.5-m experimental overseeding machine was developed at the Research and Development Institute for Grasslands Brasov (ICDP Brasov) for permanent grassland renovation operations. The objective of this study was to evaluate the field performance of the machine under practical operating conditions and to determine its main technical, energetic, and operational indicators. Field experiments were carried out on a permanent grassland in the Brasov area using a New Holland TL 100A tractor. Working speed, wheel slip, draft force, drawbar power, field capacity, and fuel consumption were evaluated. The results showed average working speeds ranging from 6.62 to 7.52 km h$^{-1}$, draft-force values between 1488 and 1572 daN, and drawbar power requirements ranging from 36.45 to 44.66 hp. The effective field capacity reached 1.95 ha h$^{-1}$, while specific fuel consumption was 6.39 L ha$^{-1}$. No technical failures or structural damage were observed during the field tests. The obtained results demonstrate that the 2.5-m experimental overseeding machine can be effectively used for permanent grassland renovation, providing operational and energetic performance suitable for modern grassland management practices.*

## REZUMAT

*Pajiștile permanente reprezintă o resursă importantă pentru producția de furaje și pentru menținerea biodiversității, iar regenerarea acestora necesită aplicarea unor tehnologii eficiente și cu impact redus asupra covorului vegetal existent. În acest context, la Institutul de Cercetare-Dezvoltare pentru Pajiști Brașov a fost realizată o mașină experimentală de supraînsămânțat cu lățimea de lucru de 2,5 m, destinată lucrărilor de reconstrucție a pajiștilor permanente. Scopul cercetărilor a fost evaluarea comportării în exploatare a utilajului în condiții reale de câmp și determinarea principalilor indicatori tehnici, energetici și de exploatare. Experimentările au fost efectuate pe o pajiște permanentă din zona Brașovului, utilizând un tractor New Holland TL 100A. Au fost determinate viteza de lucru, patinarea roților motoare, forța și puterea de tracțiune, capacitatea de lucru și consumul de combustibil. Rezultatele au evidențiat o viteză medie de lucru de 6,62–7,52 km/h, o forță de tracțiune cuprinsă între 1488 și 1572 daN și o putere necesară la tracțiune între 36,45 și 44,66 CP. Capacitatea efectivă de lucru a fost de 1,95 ha/h, iar consumul specific de combustibil de 6,39 L/ha. În timpul experimentărilor nu au fost constatate defecțiuni sau deteriorări ale utilajului. Rezultatele obținute demonstrează că mașina experimentală de supraînsămânțat de 2,5 m poate fi utilizată eficient pentru reconstrucția pajiștilor permanente, asigurând parametri funcționali și energetici corespunzători cerințelor agriculturii moderne.*

## INTRODUCTION

Permanent grasslands represent one of the most important sources of forage for the livestock sector, providing high-quality biomass for ruminants through optimized mowing and grazing systems *(Wróbel et al., 2025)*. Maintaining balanced mixtures of grasses and legumes on these areas ensures consistent

forage productivity and excellent animal nutrition, while reducing dependence on chemical fertilizers *(Zetterlind et al., 2025).* In addition to their economic value, grasslands play a crucial role in biodiversity conservation; their sustainable management and the transition from monocultures to multispecies grasslands directly support the preservation of local flora and pollinating insects within agricultural landscapes *(Zetterlind et al., 2025)*. Furthermore, permanent grasslands are essential for soil protection and the maintenance of ecological balance in agricultural ecosystems, demonstrating greater structural resilience than arable land, while improving soil bulk density and increasing organic matter content *(Bogunovic et al., 2025).*

Increasing the productivity and improving the floristic quality of permanent grasslands represents an important objective of agricultural research, as these ecosystems constitute the main source of forage for the livestock sector and contribute significantly to the maintenance of biodiversity and ecosystem functions within agricultural landscapes *(Ene et al., 2026).* At the same time, for farmers relying on permanent grasslands in animal production systems, optimizing the botanical composition of the sward is essential for obtaining high-quality forage characterized by superior digestibility and a balanced nutrient content, thereby supporting efficient and sustainable livestock production *(Wróbel et al., 2025).*

In the current context of climate change, the efficient management of biomass through sustainable practices supports farm adaptation to drought conditions and enhances long-term carbon sequestration in soil *(Bogunovic et al., 2025).* Among the methods used for the restoration of degraded grasslands, overseeding represents an efficient and cost-effective solution, improving the botanical composition of the sward without disturbing the existing biological balance *(Wróbel et al., 2025).* This method enables the introduction of valuable grass and forage legume species—recognized for their biological nitrogen fixation capacity *(Zetterlind et al., 2025)* - without complete destruction of the existing vegetation cover and without intensive soil tillage operations, thereby avoiding the risks of structural degradation commonly associated with conventional ploughing *(Bogunovic et al., 2025).*

The effectiveness of overseeding operations is influenced by both pedoclimatic conditions and the technical performance of the equipment used *(Mocanu et al., 2024).* The success of overseeding largely depends on the quality of the seeding process, requiring uniform seed distribution, maintenance of a constant sowing depth, and adequate seed-to-soil contact, all of which are essential for achieving uniform emergence and rapid establishment of forage species *(Houseman, 2026).* The performance of the working organs at the soil interface is of particular importance, with agricultural engineering research focusing on the use of notched disc openers capable of effectively cutting plant residues, reducing draft resistance, and ensuring an optimal sowing depth under direct seeding conditions. These performances have been validated through both experimental investigations and discrete element modelling approaches *(Li et al., 2025)*.

Furthermore, the geometric optimization of single-disc openers based on the support-cutting principle has demonstrated remarkable furrow-opening stability, meeting the strict agronomic requirements of no-till seeding systems and grassland renovation technologies *(Zhong et al., 2023).* In this context, the development of specialized equipment for permanent grassland overseeding represents an important research direction in agricultural mechanization, while field experiments have confirmed the adaptability of newly developed seeder prototypes to various soil conditions and their ability to ensure uniform seed distribution *(Aduov et al., 2023).*

Within the ADER 15.3.2 project, an experimental overseeding machine with a working width of 2.5 m was developed for the renovation and improvement of permanent grasslands. The implementation of such specialized equipment is aligned with modern sustainable mechanization strategies for grassland farming, based on low-input technologies that reduce the number of conventional field operations and optimize the use of agricultural machinery under the pedoclimatic conditions of Romania *(Mocanu et al., 2024).*

The adopted design solution aims to ensure high-quality overseeding while minimizing disturbance of the existing vegetation cover. Experimental field studies conducted with specialized equipment have confirmed the viability of low-input approaches, demonstrating that the use of dedicated working organs enables seed placement directly into the soil slit while preserving the integrity of the existing root system and minimizing mechanical damage to the grassland sward *(Mocanu et al., 2024; Mocanu et al., 2025)*.

Furthermore, the optimized geometry of the cutting tools allows the operation to be performed with reduced energy consumption by decreasing soil draft resistance in compacted soils and minimizing the tractor draft force requirement, as confirmed by both discrete element numerical simulations and field experiments *(Mocanu et al., 2025).*

The objective of the research presented in this paper was to evaluate the field performance of the experimental overseeding machine under spring operating conditions.

The experimental investigations focused on determining the main technical, energetic, and operational indicators of the tractor–overseeding machine aggregate, including working speed, tractor wheel slip, draft force, drawbar power, field capacity, and fuel consumption. In addition, the pedoclimatic characteristics of the experimental site and the parameters influencing the quality of the overseeding process were analyzed in order to assess the suitability of the developed machine for the renovation and improvement of permanent grasslands.

## MATERIALS AND METHODS

Within the ADER 15.3.2 project, a technology for the improvement and renovation of degraded permanent grasslands was developed through overseeding, using an experimental 2.5 m overseeding machine (Fig. 1), designed for introducing grass and forage legume seeds into the existing vegetation cover.



**Fig. 1 - Experimental 2.5 m overseeding machine**

The operating principle is based on creating narrow furrows in the upper soil layer, controlled seed placement, and subsequent seed covering, thus ensuring optimal seed-to-soil contact. The adjustment of working depth and seed application rate enables the machine to be adapted to different vegetation and soil conditions.

The main technical and constructive characteristics of the Experimental 2.5 m Overseeding Machine (MSPD 2.5) used during the field experiments are presented in Table 1. The characteristics were obtained from the machine technical documentation and supplemented with the values determined for the tested experimental model.

**Table 1**

**Main technical characteristics of the experimental machine**

| Characteristic | UM | Value |
|---|---|---|
| Required tractor power | HP | 45–65 |
| Machine type | – | Mounted, three-point linkage |
| Working principle | – | Furrow opening |
| Type of working organs | – | Plain disc, chisel-type opener and press wheel |
| Number of openers | pcs. | 17 |
| Grass seed hopper capacity | $dm^3$ | 300 |
| Legume seed hopper capacity | $dm^3$ | 55 |
| Working depth | cm | 0.5–3.0 |
| Working width | m | 2.55 |
| Row spacing | cm | 15 |
| Length | mm | 1540 |
| Width | mm | 2950 |
| Height | mm | 1650 |
| Mass | kg | 1175 |

The determination of the operational performance indicators was carried out through experimental field investigations conducted on the experimental plots of the Research and Development Institute for

Grasslands Brasov (ICDP Brasov), using the New Holland TL 100A agricultural tractor aggregated with the Experimental 2.5 m Overseeding Machine.

The experimental field is located in the Brasov Depression, at geographical coordinates 45°37′45″ N latitude and 25°31′36″ E longitude, at an average altitude of approximately 627 m above sea level. The soil of the experimental site is a cambic chernozem with a loam to clay-loam texture, characterized by a good water-holding capacity and favorable conditions for the development of forage species. The experiments were carried out between 21 and 28 April 2026 under climatic conditions specific to spring in the Brasov Depression. During the testing period, daily maximum temperatures ranged from 15 to 17°C, while minimum temperatures varied between 2 and 5°C.

The average relative air humidity was approximately 62%, the average wind speed was about 12 $kmh^{-1}$, and precipitation was scarce, providing favorable conditions for overseeding operations. The following equipment was used to characterize the working conditions and determine the main indicators of the technological process:

- a Wile manual penetrometer for measuring soil penetration resistance;
- an Extech MO750 portable soil moisture meter for determining soil water content;
- a KERN precision electronic scale for seed rate calibration and evaluation of seed distribution uniformity;
- a strain-gauge measurement system consisting of 120 Ω resistive strain gauges, a QuantumX MX1615 data acquisition unit, and dedicated software for draft force determination;
- a Dini Argeo WWSRF portable platform scale for determining tractor mass and axle loads.

The pedoclimatic conditions recorded during the experimental period were favorable for overseeding operations and forage crop establishment. Moderate temperatures and the soil water reserve accumulated during the first part of spring created suitable conditions for the germination and emergence of the introduced species.

Prior to the field tests, the necessary adjustments of the experimental machine were carried out, including seed rate calibration, verification of seed distribution uniformity, and working depth adjustment. Aspects observed during the adjustment operations of the Experimental 2.5 m Overseeding Machine are presented in figure 2.



**Fig. 2 - Adjustment operations performed before field testing of the overseeding machine**

The pedological characteristics of the experimental site were evaluated by determining soil penetration resistance and soil moisture content. The obtained results are presented in Table 2. Penetration resistance was measured at depth intervals of 0–10 cm, 10–20 cm, and 20–30 cm, while soil moisture was determined at the same measurement points.

The working speed of the tractor–machine aggregate was determined over a measured distance of 50 m, both uphill and downhill. Three replications were performed for each operating regime, and the working speed was calculated based on the travelled distance and the recorded average time.

The slip of the tractor driving wheels was determined according to the ISO/OECD 789-10 methodology by comparing the number of wheel revolutions under load with the number of revolutions without load. This indicator was used to evaluate the efficiency of power transfer from the tractor to the soil. Draft force was determined using the strain-gauge method, based on the elastic deformations measured in the tractor hitching system elements. The signals provided by the strain gauges were acquired and processed using the QuantumX MX1615 system, and the average draft force values were obtained after eliminating transient operating regimes and statistically processing the recorded data.

Drawbar power was calculated as a function of draft force and forward speed of the aggregate, while theoretical field capacity was determined based on the working width and effective travelling speed. The determination of operational performance indicators included the evaluation of effective working time, auxiliary time, time utilization coefficients, field capacity, and specific fuel consumption.

Fuel consumption was determined using the full-tank method, by filling the fuel tank before and after the operation and relating the consumed fuel quantity to the effectively worked area. At the end of the experimental period, a final technical inspection of the machine was performed.

## RESULTS AND DISCUSSION

The pedological characteristics of the experimental site were evaluated by determining soil penetration resistance and soil moisture content. The results obtained are presented in Table 2.

**Table 2**

**Physical characteristics of the soil**

| No. | Characteristic | UM | Value |
|---|---|---|---|
| 1 | Soil type | – | Cambic chernozem |
| 2 | Soil moisture (0–10 cm) | % | 9.73 |
| 3 | Penetration resistance (0–10 cm) | MPa | 1.38 |
| 4 | Penetration resistance (10–20 cm) | MPa | 1.38 |
| 5 | Penetration resistance (20–30 cm) | MPa | 1.52 |
| 6 | Average relative air humidity | % | 66.9 |
| 7 | Average wind speed | km/h | 12.2 |
| 8 | Average daily maximum temperature | °C | 15–17 |
| 9 | Average daily minimum temperature | °C | 2–5 |

Analysis of the data presented in Table 2 highlights soil penetration resistance values ranging between 1.38 and 1.52 MPa within the 0–30 cm depth interval. These values indicate moderate soil compaction, with no highly compacted layers that could restrict root system development. The average soil moisture content was 9.73%, a value suitable for overseeding operations and favorable for achieving good seed-to-soil contact.

The inspections carried out confirmed the proper functioning of the seed distribution system and the machine working organs, with no need for additional constructive or functional modifications.

The results of the determination of working speed and tractor driving wheel slip are presented in Table 3, while aspects observed during the measurements are shown in Figure 3.



**Fig. 3 - Determination of working speed and tractor wheel slip of the tractor–machine aggregate**

**Table 3**

**Working speed and driving wheel slip**

| Gear | Speed uphill (m/s) | Speed downhill (m/s) | Wheel slip uphill (%) | Wheel slip downhill (%) |
|---|---|---|---|---|
| I | 1.84 | 1.88 | 9.01 | 6.07 |
| II | 1.98 | 2.09 | 10.65 | 5.71 |

The effective working speed of the tractor–machine aggregate ranged between 6.62 and 7.52 km/h. The higher values were obtained in second gear, particularly during downhill operation. The driving wheel slip ranged from 5.71% to 10.65%, remaining within the normal limits for permanent grassland renovation operations and indicating a good traction capability of the tractor. The average values of draft force and drawbar power are presented in Table 4.

**Table 4**

**Draft force and drawbar power**

| Gear | Direction of travel | Average speed [m/s] | Average speed [km/h] | Average draft force [daN] | Drawbar power [HP] | Drawbar power [kW] |
|---|---|---|---|---|---|---|
| I | Uphill | 1.84 | 6.62 | 1498.116 | 36.73 | 27.02 |
| I | Downhill | 1.88 | 6.77 | 1488.545 | 37.32 | 27.45 |
| II | Uphill | 1.98 | 7.14 | 1571.814 | 41.57 | 30.57 |
| II | Downhill | 2.09 | 7.52 | 1520.737 | 42.36 | 31.15 |

The experimentally determined draft force ranged from 1488 to 1572 daN, while the required drawbar power varied between 27.02 and 31.15 kW. These results demonstrate the compatibility of the machine with the New Holland TL 100A tractor used during the experiments and confirm that the tractor–machine aggregate has sufficient power reserves to perform the operation under normal field conditions.

The data required for determining the operational performance indicators were collected over a worked area of 1800 m² (0.18 ha). The effective working time recorded during the tests was 5.54 min, while the total time considered for the calculation of operational indicators was 9.54 min. Based on these values, the effective field capacity of the tractor–seed drill aggregate was 1.95 ha $h^{-1}$, whereas the field capacity referred to the total operating time was 1.13 ha $h^{-1}$. These results indicate satisfactory performance of the tractor–2.5-m experimental forage grassland seed drill aggregate under the field conditions of the experiment.

At the end of the tests, fuel consumption was determined by refilling the tractor fuel tank. A total of 1.15 L of diesel fuel was consumed for the worked area of 1800 m² (0.18 ha), corresponding to a specific fuel consumption of 6.39 L $ha^{-1}$.

The main operational performance indicators obtained under field conditions are graphically presented in Figure 4.

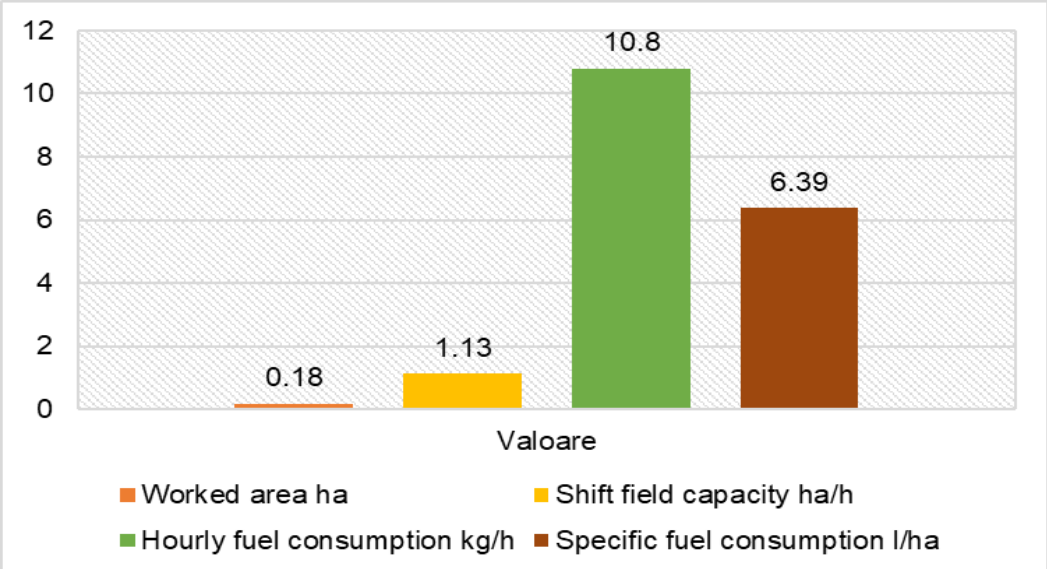



**Fig. 4 - Main energetic and operational performance indicators of the Experimental 2.5 m Overseeding Machine**

The analysis of the performance indicators revealed a strong correlation between working speed, field capacity, and fuel consumption. The low wheel slip values and the moderate drawbar power requirements confirm the efficient operation of the experimental machine under the specific conditions of permanent grasslands in the Brasov region.

At the end of the experimental investigations, a final technical inspection of the machine was carried out. The appearance of the experimental field after completion of the operations is presented in Figure 5



**Fig. 5 - Experimental plot after field testing of the 2.5-m experimental overseeding machine**

The visual inspection performed after completion of the field tests revealed no frame deformations, damage to the working components, abnormal wear, or malfunctions of the seed distribution system. No technical incidents affecting machine operation were recorded during the experimental investigations. The appearance of the experimental plot (Fig. 5) confirms the satisfactory quality of the sowing operation and demonstrates the suitability of the experimental machine for permanent grassland establishment, reconstruction, and maintenance under the tested field conditions.

## CONCLUSIONS

- The experimental investigations carried out under spring conditions on the experimental plots of the Research and Development Institute for Grasslands Brașov demonstrated the proper operation of the experimental 2.5 m overseeding machine developed within the ADER 15.3.2 project.
- The pedoclimatic conditions recorded during the testing period were favorable for overseeding operations. Soil penetration resistance ranged between 1.38 and 1.52 MPa, while the average soil moisture content in the 0–10 cm layer was 9.73%, providing suitable conditions for seed placement and germination.
- The effective working speed of the tractor–machine aggregate ranged between 6.62 and 7.52 km/h, while the tractor driving wheel slip varied from 5.71% to 10.65%, indicating good traction performance and efficient utilization of tractor power under permanent grassland conditions.
- The experimentally determined average draft force ranged from 1488 to 1572 daN, while the required drawbar power varied between 27.02 and 31.15 kW. These results confirm the compatibility of the machine with the New Holland TL 100A tractor used during the tests and demonstrate the availability of sufficient power reserves for performing the technological process.
- The achieved effective field capacity was approximately 1.95 ha/h, while the specific fuel consumption was 6.39 l/ha, indicating satisfactory energetic and economic efficiency for permanent grassland renovation through overseeding.
- No technical or functional failures were recorded during the experimental investigations. The final technical inspection confirmed the preservation of the machine's structural and functional characteristics, with no frame deformations, damage to the working organs, or wear affecting its operation.
- The obtained results demonstrate that the experimental 2.5 m overseeding machine represents a viable technical solution for the renovation and improvement of permanent grasslands, contributing

to increased forage productivity, improved botanical composition, and the sustainable use of grassland resources.

Further research is recommended to evaluate the performance of the experimental machine under different pedoclimatic conditions and on various types of permanent grasslands, as well as to monitor the effects of overseeding on the establishment rate of the introduced species, forage yield, and botanical composition over the medium and long term. In addition, the promotion of this technical solution among farmers and livestock producers interested in modern permanent grassland renovation technologies is recommended.

**ACKNOWLEDGEMENT**

The results presented in this article were obtained with the support of MADR through the "Sectoral Plan - ADER 2026", financing contract no. 15.3.2 / 17.07.2023, ADER project 15.3.2. Research on the development and promotion of mechanization technologies for the reconstruction, maintenance of permanent meadows, environmental protection and biodiversity maintenance using new specific equipment, managed by the Research -Development Institute for Grasslands Brasov- Mechanization Laboratory.

**REFERENCES**

[1] Aduov, M., Nukusheva, S., Tulegenov, T., Volodya, K., Uteulov, K., Karwat, B., & Bembenek, M. (2023). Experimental field tests of the suitability of a new seeder for the soils of Northern Kazakhstan. *Agriculture*, 13(9), 1687.

[2] Bogunovic, I., Galic, M., Percin, A., Geng, S., & Pereira, P. (2025). The role of grassland land use in enhancing soil resilience and climate adaptation in periurban landscapes. *Agronomy*, *15*(7), 1589.

[3] Ene, T. A., Mocanu, V., Andreoiu, A. C., & Mocanu, V. (2026). *Forage production of permanent grasslands in Romania across altitudinal and soil gradients*. INMATEH – Agricultural Engineering, 78(1), 108–117. https://doi.org/10.35633/inmateh-78-108

[4] Houseman, G. R. (2026). Restoring grassland legumes using overseeding can depend on seed spatial structure. *Restoration Ecology*, *34*(3), e70275.

[5] Li, S., Diao, P., Zhang, Y., Li, X., Zhao, Y., & Zhao, H. (2025). Design and performance evaluation of notched type discs for application in no-till seeding process using discrete element method and field trials. *Biosystems Engineering*, *257*, 104222.

[6] Mocanu, V., Ene, T. A., Marin, E., Manea, D., & Ionescu, A. (2025). Experimental research regarding the low-input method with specific equipment for grassland farming. *Journal of Mountain Agriculture on the Balkans*, *28*(3), 48–71.

[7] Mocanu, V., Ene, T. A., Marin, E., & Gheorghiță, N. E. (2024). Mechanization of Grassland Farming by Technological Variants with Minimal Inputs: A Review. *INMATEH Agricultural Engineering*, *74*(3), 954-70.

[8] Wróbel, B., Zielewicz, W., & Paszkiewicz-Jasińska, A. (2025). Improving forage quality from permanent grasslands to enhance ruminant productivity. *Agriculture*, *15*(13), 1438.

[9] Zetterlind, B., Janssen, P., Geerts, R., Visser, T., Stip, A., Zwetsloot, M. J., ... & van Eekeren, N. (2025). Multispecies grasslands sustain on-farm forage productivity and quality while reducing nitrogen fertilizer inputs. *Plant and Soil*, 1-17.

[10] Zhong, G., Li, H., He, J., Wang, Q., Lu, C., Wang, C., ... & He, D. (2023). Design and test of single-disc opener for no-till planter based on support cutting. *Agriculture*, *13*(8), 1635.

# SPRING FIELD EVALUATION OF A 2.5 m FORAGE GRASSLAND SEED DRILL FOR PERMANENT GRASSLAND RECONSTRUCTION AND MAINTENANCE

/

# *EXPERIMENTĂRI ÎN CONDIȚII DE PRIMĂVARĂ ALE UNEI MAȘINI DE SEMĂNAT PLANTE FURAJERE DE PAJIȘTI DE 2,5 M PENTRU RECONSTRUCȚIA ȘI MENTENANȚA PAJIȘTILOR*

**Eugen MARIN*[1)], Vasile MOCANU[2)], Tudor-Adrian ENE[2)], Laurențiu-Constantin VLĂDUȚOIU[1)], Alexandru IONESCU[1)], Mihai-Gabriel MATACHE[1)]**

[1)] National Institute of Research-Development for Machines and Installations Designed for Agriculture and Food Industry-INMA Bucharest, 013811 Bucharest / Romania;

[2)] Institute of Research-Development for Grasslands-ICDP Brasov / Romania

**Tel: 0758 437 214; *E-mail: marineu61@yahoo.com*

***Keywords***: *permanent grassland, forage grassland seed drill, grassland reconstruction, grassland maintenance, field testing, seed distribution uniformity*

## ABSTRACT

*This paper presents the results of spring field experiments carried out on a 2.5 m forage grassland seed drill designed for permanent grassland reconstruction and maintenance. The experiments were conducted under real operating conditions on the experimental fields of the Research and Development Institute for Grasslands Brașov and aimed to evaluate the machine performance under specific grassland establishment and management conditions. The study included the determination of the pedoclimatic characteristics of the experimental site, the assessment of soil penetration resistance and soil moisture, the verification of machine adjustments, and the evaluation of the main technical, energetic, and operational indicators. The investigated parameters included working speed, tractor wheel slip, draft force, drawbar power, field capacity, fuel consumption, seeding rate accuracy, and seed distribution uniformity. The results demonstrated the proper operation of the seed drill, achieving a seeding rate of 50.4 kg/ha with a deviation of only 0.8% from the prescribed value and a very good distribution uniformity, characterized by a coefficient of variation of 0.60%. Soil conditions during the testing period were favorable for seeding operations, with penetration resistance values indicating moderate soil compaction and adequate moisture conditions for seed germination and crop establishment. The energetic and operational performance indicators confirmed the compatibility of the seed drill with the tractor used during testing and highlighted its suitability for efficient field operation. The technical inspection performed before field experimentation confirmed the preservation of the machine's constructive and functional characteristics and the proper operation of all working components. The study concludes that the 2.5 m forage grassland seed drill represents a viable technical solution for permanent grassland reconstruction and maintenance, contributing to improved forage production, enhanced botanical composition, and the sustainable management of grassland resources.*

## REZUMAT

*Lucrarea prezintă rezultatele experimentărilor efectuate în condiții de primăvară asupra modelului experimental de mașină de semănat plante furajere de pajiști cu lățimea de lucru de 2,5 m, destinată reconstrucției și mentenanței pajiștilor permanente. Cercetările s-au desfășurat în primăvara anului 2026 pe loturile experimentale ale Institutului de Cercetare-Dezvoltare pentru Pajiști Brașov și au urmărit evaluarea comportării utilajului în condiții reale de exploatare. Studiul a inclus determinarea caracteristicilor pedoclimatice ale amplasamentului experimental, analiza rezistenței la penetrare și a umidității solului, verificarea reglajelor funcționale ale mașinii și evaluarea principalilor indicatori tehnici, energetici și de exploatare. În cadrul cercetărilor au fost determinate viteza de lucru, patinarea roților motoare ale tractorului, forța și puterea de tracțiune, capacitatea de lucru și consumul specific de combustibil. De asemenea, au fost evaluate precizia normei de semănat și uniformitatea distribuției semințelor, parametri esențiali pentru realizarea unei înființări uniforme a culturilor de plante furajere. Rezultatele obținute au evidențiat funcționarea corespunzătoare a modelului experimental, realizarea unei norme de semănat de 50,4 kg/ha, cu o abatere de numai 0,8% față de valoarea prescrisă, precum și o uniformitate foarte bună a distribuției, caracterizată printr-un coeficient de variație de 0,60%. Valorile indicatorilor energetici și de exploatare au*

*demonstrat compatibilitatea utilajului cu tractorul utilizat și capacitatea acestuia de a efectua lucrarea în condiții eficiente din punct de vedere tehnic și energetic. Expertiza tehnică efectuată înaintea experimentărilor a confirmat respectarea caracteristicilor constructive și funcționale prevăzute în documentația tehnică, fără a fi identificate neconformități sau defecțiuni. Concluziile studiului evidențiază faptul că modelul experimental de mașină de semănat plante furajere de pajiști de 2,5 m reprezintă o soluție tehnică adecvată pentru reconstrucția și mentenanța pajiștilor permanente, contribuind la îmbunătățirea compoziției floristice, creșterea productivității furajere și utilizarea durabilă a resurselor de pajiști.*

## INTRODUCTION

Perennial forage species constitute the foundation of modern livestock production systems, providing essential feed resources for ruminants and contributing significantly to the economic sustainability of agricultural enterprises *(dos Santos Silva et al., 2025).* Recent studies have demonstrated that complex mixtures of perennial grasses and legumes can accurately predict cattle productive performance when evaluated using advanced ration-balancing software, thereby reducing feeding costs through optimized forage utilization *(Gyamfi et al., 2025).*

The productivity and persistence of forage crops depend on numerous agronomic and technological factors, among which the sowing process plays a crucial role, as it directly influences plant density, stand uniformity, and the efficient utilization of soil water and nutrient resources *(Guo et al., 2025).* The seeds of forage species commonly used in permanent grassland mixtures are generally characterized by small size and high sensitivity to sowing depth and seed placement accuracy *(Hu et al., 2025).*

Consequently, successful crop establishment requires seeding equipment capable of ensuring accurate seed metering, uniform spatial distribution, consistent sowing depth, and optimal seed-to-soil contact *(Shayakhmetova et al., 2026)*.

Recent research has shown that irregular seed distribution and variations in sowing depth may lead to uneven emergence, reduced establishment rates, and lower forage productivity *(Wang et al., 2025).* For this reason, considerable attention has been devoted to the development of specialized seeding machinery designed to improve sowing quality and increase the efficiency of grassland establishment and renovation practices.

At the international level, continuous progress has been achieved in the design and optimization of seed drills intended for forage crops and permanent grasslands. Current research trends are focused on improving sowing precision, reducing energy requirements, and integrating multiple field operations into a single pass *(Martelli et al., 2025).*

Modern seed drills incorporate advanced seed-metering systems, depth-control mechanisms capable of maintaining uniform placement under variable field conditions, and rolling devices that promote rapid germination and uniform crop emergence *(Zhao et al., 2024).*

Another important trend in grassland mechanization is the development of machines capable of combining seedbed preparation, sowing, and rolling operations within a single technological process *(Tang et al., 2025)*. Such solutions contribute to reducing the number of field passes, lowering operational costs, improving energy efficiency, preserving soil structure, and minimizing soil compaction *(Zhang et al., 2026).*

Within this context, a 2.5-m forage grassland seed drill was developed at the Research and Development Institute for Grasslands Brașov, Romania, for use in permanent grassland reconstruction and maintenance operations *(Mocanu et al., 2024).* The machine was designed to perform pre-sowing rolling, seed distribution, seed placement, and post-sowing consolidation in a single pass, thereby creating favorable conditions for forage crop establishment.

The objective of the present study was to evaluate the field performance of the 2.5-m forage grassland seed drill under spring operating conditions (*Mocanu et al., 2024).* The experimental investigations focused on determining the main technical, energetic, and operational indicators of the tractor–seed drill aggregate, as well as assessing seeding-rate accuracy and seed distribution uniformity under practical field conditions.

## MATERIALS AND METHODS

As part of the research activities carried out at the Research and Development Institute for Grasslands Brașov (RDIG Brașov), a 2.5-m forage grassland seed drill was developed for permanent grassland reconstruction and maintenance operations. The machine was designed to perform, in a single

field pass, the main operations required for the establishment of forage crops, namely pre-sowing rolling, seed metering and distribution, seed placement into the soil, and post-sowing rolling.

The operating principle of the machine is based on the controlled distribution of seeds through mechanical metering devices and their placement into the soil by means of double-disc openers. Following seed deposition, the rear rollers ensure seed coverage and surface soil consolidation, thereby improving seed-to-soil contact and promoting rapid germination and uniform crop emergence.

The experimental seed drill (Fig. 1) is a mounted implement attached to the tractor three-point linkage system. Its main structural components include the frame, hitching system, front roller, rear rollers, seed hopper, seed-metering units, seed delivery tubes, sowing openers, and the transmission mechanism responsible for driving the seed-metering system.




**Fig. 1 - Experimental forage grassland seed drill with a working width of 2.5 m attached to a New Holland TL 100A tractor**

The principal technical specifications and design characteristics of the experimental forage grassland seed drill are summarized in Table 1.

**Table 1**

**Main technical specifications of the experimental forage grassland seed drill**

| Characteristic | UM | Value |
|---|---|---|
| Required tractor power | hp | 65–80 |
| Machine type | – | Mounted implement, attached to the tractor three-point linkage system (Category II) |
| Intended operation | – | Sowing of forage species for permanent grasslands |
| Opener type | – | Double-disc openers |
| Number of openers | – | 20 |
| Row spacing | mm | 125 |
| Main seed hopper capacity | $dm^3$ | 300 |
| Hopper type | – | Compartmented hopper for large and small seeds |
| Sowing depth | cm | 1–3 |
| Working width | m | 2.50 |
| Transport width | m | 2.70 |
| Machine weight (empty) | kg | 2115 |

The physical characteristics of the experimental soil, determined prior to field testing, are presented in Table 2.

**Table 2**

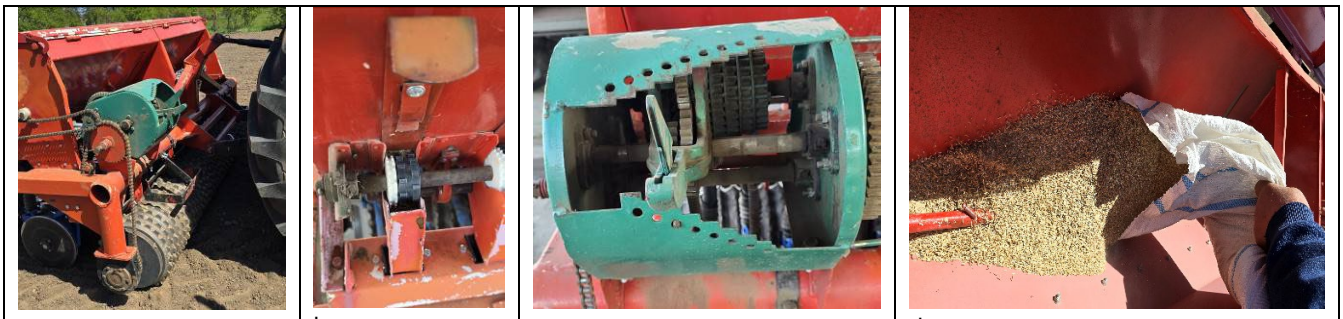
**Physical characteristics of the experimental soil**

| Parameter | Unit | Value |
|---|---|---|
| **Soil penetration resistance** | | |
| 0–10 cm | psi | 200 |
| 10–20 cm | psi | 220 |
| 20–30 cm | psi | 250 |
| **Soil moisture** | | |
| Average soil moisture content | % | 15.4 |
| Coefficient of variation | % | 2.86 |

The results presented in Table 2 indicate a progressive increase in soil penetration resistance with depth, reaching 200 psi in the 0–10 cm layer, 220 psi in the 10–20 cm layer, and 250 psi in the 20–30 cm layer. These values suggest a moderate degree of soil compaction and the absence of restrictive layers that could adversely affect root development of forage species. The average soil moisture content was 15.4%, with a coefficient of variation of 2.86%, indicating a relatively uniform distribution of water within the experimental field. Overall, the measured soil conditions were considered favorable for sowing operations and for the germination and establishment of forage crops.

Prior to field testing, the tractor–seed drill aggregate was subjected to the necessary inspection and adjustment procedures. Particular attention was given to machine alignment, sowing depth adjustment, seeding-rate calibration, and verification of seed distribution uniformity. These operations ensured compliance with the prescribed technological parameters and contributed to the proper functioning of the machine during field experimentation.

The adjustments performed before testing guaranteed stable machine operation and the achievement of the required sowing parameters under the experimental conditions (Fig. 2).



a. b. c. d.

**Fig. 2 - Pre-test inspection and adjustment operations performed on the 2.5-m forage grassland seed drill:**
(a) attachment of the machine to the tractor three-point linkage system;
(b) adjustment of the seed-metering units; (c) gearbox setting for the prescribed seeding rate;
(d) filling of the seed hopper with the forage seed mixture.

The results of the seeding-rate calibration and seed distribution uniformity assessment are presented in Table 3.

**Table 3**

**Results of seeding-rate calibration and seed distribution uniformity assessment**

| Parameter | Unit | Value | Remarks |
|---|---|---|---|
| Target seeding rate | kg ha$^{-1}$ | 50.0 | Prescribed rate for the forage seed mixture |
| Actual seeding rate | kg ha$^{-1}$ | 50.4 | Determined by the stationary drive-wheel rotation method |
| Deviation from target rate | % | +0.8 | Within acceptable tolerance limits |
| Number of seed-metering units | – | 20 | Corresponding to the number of openers |
| Total collected seed quantity | g | 504 | For a reference area of 100 m² |
| Average quantity per metering unit | g | 25.2 | Mean experimentally determined value |
| Coefficient of variation | % | 0.60 | Indicates excellent distribution uniformity |

The results presented in Table 3 demonstrate the proper functioning of the seed-metering system. The measured seeding rate was 50.4 kg ha$^{-1}$, very close to the target value of 50.0 kg ha$^{-1}$, resulting in a

deviation of only 0.8%. This confirms the accuracy of the machine adjustments and the capability of the metering system to deliver the required seed flow rate.

The average seed quantity delivered by each metering unit was 25.2 g, while the coefficient of variation was only 0.60%. Such a low coefficient of variation indicates an excellent level of seed distribution uniformity across the entire working width of the machine and confirms the consistent performance of the metering devices. Uniform seed distribution is essential for achieving homogeneous crop establishment, promoting uniform emergence, and ensuring optimal forage stand development.

The obtained results confirm that the forage grassland seed drill is capable of meeting the agronomic requirements associated with the establishment of perennial forage crops under field conditions.

The results of the working-speed and tractor wheel-slip measurements are presented in Table 4, while representative aspects of the testing procedure are shown in Fig. 3.

**Table 4**

**Working speed and drive-wheel slip**

| Gear | Working speed uphill (m $s^{-1}$) | Working speed downhill (m $s^{-1}$) | Wheel slip uphill (%) | Wheel slip downhill (%) |
|---|---|---|---|---|
| I | 1.71 | 1.80 | 11.33 | 10.83 |
| II | 1.96 | 2.09 | 11.83 | 10.92 |

The results presented in Table 4 indicate that the effective working speed of the tractor–seed drill aggregate ranged from 1.71 to 2.09 m $s^{-1}$ (6.17–7.51 km $h^{-1}$). Higher travel speeds were achieved in second gear, particularly during downhill operation, reflecting the influence of terrain slope on aggregate movement.

Tractor drive-wheel slip varied between 10.83% and 11.83%, remaining within the range generally considered acceptable for seeding operations. Slightly higher slip values were recorded during uphill travel, owing to the increased traction demand imposed on the tractor.

However, these differences did not affect the stability of the operating regime. The measured slip levels indicate adequate traction conditions and efficient utilization of the tractor power during operation of the 2.5-m forage grassland seed drill.



**Fig. 3 - Measurement of working speed and tractor wheel slip of the tractor–seed drill aggregate**

The average draft force and drawbar power values determined during the field experiments are presented in Table 5.

**Table 5**

**Average draft force and drawbar power of the tractor–seed drill aggregate**

| Gear | Direction of travel | Average speed (km $h^{-1}$) | Average draft force (daN) | Drawbar power (hp) |
|---|---|---|---|---|
| I | Uphill | 6.17 | 1018.021 | 23.27 |
| I | Downhill | 6.49 | 1025.915 | 24.66 |
| II | Uphill | 7.06 | 973.647 | 25.46 |
| II | Downhill | 7.51 | 952.074 | 26.49 |

The results presented in Table 5 show that the draft force of the tractor–seed drill aggregate ranged from 952 to 1026 daN, depending on the selected gear and direction of travel. The highest draft-force values were recorded in first gear, whereas slightly lower values were obtained in second gear.

The drawbar power requirement varied between 23.27 and 26.49 hp, increasing with travel speed. These results demonstrate the compatibility of the forage grassland seed drill with the New Holland TL 100A tractor used during the field experiments and confirm that sufficient power reserves were available under the tested operating conditions. The moderate draft-force and power requirements indicate efficient machine performance and a relatively low energy demand during the sowing process.

The main energetic and operational indicators determined during the experimental investigations are presented in Table 6.

**Table 6**

**Main energetic and operational performance indicators**

| No. | Indicator | Symbol | Unit | Value |
|---|---|---|---|---|
| 1 | Average working speed | $v_l$ | km h$^{-1}$ | 6.81 |
| 2 | Average wheel slip | δ | % | 11.23 |
| 3 | Average drawbar power | $P$tr | hp | 24.97 |
| 4 | Operational time utilization coefficient | $K_{02}$ | – | 0.854 |
| 5 | Effective field capacity | $W_{07}$ | ha h$^{-1}$ | 1.242 |
| 6 | Specific fuel consumption | $C_{ha}$ | L ha$^{-1}$ | 7.03 |

The values presented in Table 6 indicate satisfactory operational performance of the 2.5-m forage grassland seed drill under the experimental conditions. The average working speed was 6.81 km h$^{-1}$, while the average wheel slip was 11.23%, both values falling within the recommended range for sowing operations and indicating efficient utilization of the tractor's traction capacity. The average drawbar power requirement was 24.97 hp, confirming the compatibility of the machine with the tractor used during the experiments.

The effective field capacity was 1.24 ha h$^{-1}$, and the specific fuel consumption was 7.03 L ha$^{-1}$, demonstrating adequate energy efficiency for permanent grassland establishment, reconstruction, and maintenance operations. The operational time utilization coefficient ($K_{02}$ = 0.854) indicates efficient organization of the working process and effective use of the available operating time. Overall, the obtained results confirm the suitability of the forage grassland seed drill for improving grassland productivity while maintaining relatively low energy requirements.

For a comprehensive evaluation of machine performance, the main energy and operational indicators were further analyzed and are graphically presented in Fig. 4.

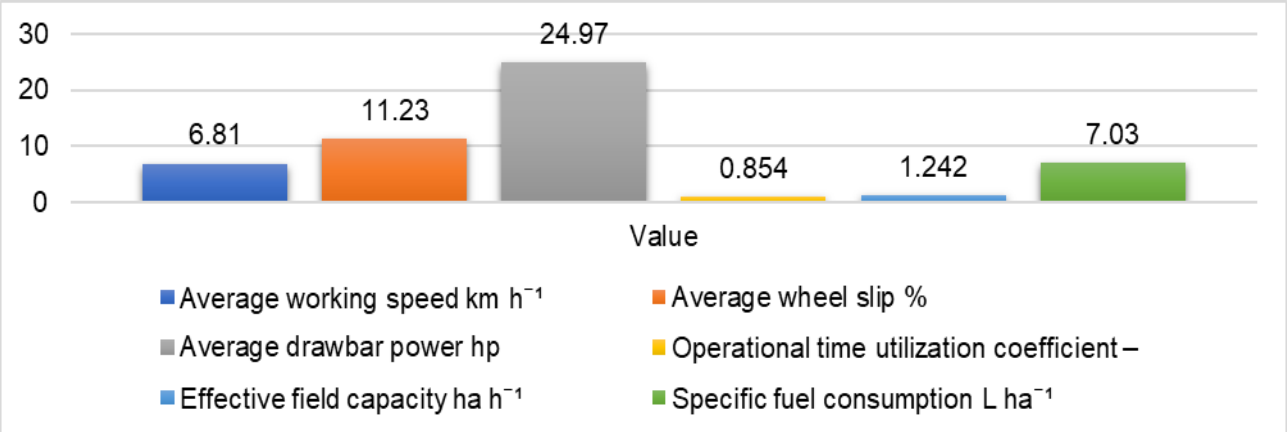



**Fig. 4 - Main energy and operational performance indicators obtained during the field experiments**

The analysis of the performance indicators revealed a consistent relationship between working speed, field capacity, and fuel consumption. The relatively low wheel-slip values and the moderate drawbar power requirements confirm the efficient operation of the 2.5-m forage grassland seed drill under the specific conditions of the experimental site.

At the end of the experimental investigations, a final technical inspection of the machine was performed. The appearance of the experimental plot following the sowing operation is shown in Fig. 5.



**Fig. 5 - Experimental plot after field testing of the 2.5-m forage grassland seed drill**

The visual inspection carried out after completion of the field tests revealed no frame deformations, damage to the working components, abnormal wear, or malfunctions of the seed distribution system. Furthermore, no technical incidents affecting machine operation were recorded during the experimental investigations. The condition of the experimental plot confirmed the satisfactory performance of the sowing operation and demonstrated the suitability of the machine for the specific requirements of permanent grassland reconstruction and maintenance.

The obtained results demonstrate that the 2.5-m forage grassland seed drill can successfully perform grassland establishment, reconstruction, and maintenance operations under practical field conditions. The machine provided satisfactory functional, energetic, and operational performance, meeting the technical requirements of modern agricultural practices and sustainable grassland management.

## CONCLUSIONS

- The 2.5-m forage grassland seed drill operated satisfactorily under spring field conditions, achieving an actual seeding rate of 50.4 kg $ha^{-1}$, with a deviation of only 0.8% from the target rate and excellent seed distribution uniformity, as indicated by a coefficient of variation of 0.60%.
- The measured technical and energetic performance indicators, including an average working speed of 6.81 km $h^{-1}$, an average wheel slip of 11.23%, and an average drawbar power requirement of 24.97 hp, confirmed the compatibility of the machine with the tractor used during testing and demonstrated efficient operation under permanent grassland sowing conditions.
- The effective field capacity of 1.24 ha $h^{-1}$ and the specific fuel consumption of 7.03 L $ha^{-1}$ demonstrate the technical and energetic efficiency of the machine and confirm its potential for permanent grassland establishment, reconstruction, and maintenance operations.
- The integrated design of the machine, which combines rolling, seed distribution, seed placement, and post-sowing consolidation in a single pass, contributes to reducing field traffic, limiting soil compaction, and improving operational efficiency.
- The favorable soil conditions recorded during the experiments and the high seeding accuracy achieved suggest that the machine can provide suitable conditions for rapid crop establishment and the improvement of botanical composition in permanent grasslands.

## RECOMMENDATIONS FOR FUTURE RESEARCH

- Further investigations should evaluate the long-term agronomic effects of the machine on forage yield, species composition, and persistence of reconstructed permanent grasslands.
- Additional field experiments should be conducted under different soil types, moisture conditions, and terrain slopes in order to validate machine performance across a wider range of operating environments.
- Future developments may focus on improving the seed-metering system and implementing electronic monitoring and control technologies to further increase seeding precision and operational efficiency.

**ACKNOWLEDGEMENT**

The results presented in this article were obtained with the support of MADR through the "Sectoral Plan - ADER 2026", financing contract no. 15.3.2 / 17.07.2023, ADER project 15.3.2. Research on the development and promotion of mechanization technologies for the reconstruction, maintenance of permanent meadows, environmental protection and biodiversity maintenance using new specific equipment, managed by the Research -Development Institute for Grasslands Brasov- Mechanization Laboratory.

**REFERENCES**

[1] dos Santos Silva, A. M., da Silva, S. C., Otaviano, E. K. S., Gomes, C. M., Mammana, A. F., Fernanda Garcia Carvalho, L., ... & Louarn, G. (2025). Functional Plant Species Traits That Shape Canopy Light Interception and Agronomic Performance of Perennial Forage Grasses Cultivated in Monoculture and Association. Grass and Forage Science, 80(3), e12716.

[2] Guo, W., Jiang, Y., Yin, M., Ling, Y., Kang, Y., Qi, G., ... & Pan, K. (2025). Meta-analysis of mixed sowing effects on forage yield and water use efficiency in China: Influencing factors and optimal conditions. *Plants*, *14*(9), 1283.

[3] Gyamfi, H., Omokanye, A., Hernandez-Ramirez, G., Thilakarathna, M. S., & Yaremcio, B. (2025). Predicting the performance of beef cattle on diverse perennial forage mixtures using the CowBytes ration-balancing software program. *Canadian Journal of Animal Science*, *105*, 1-13.

[4] Hu, X., Sun, Q., Zhang, S., Li, W., Wang, X., Long, R., ... & Zhang, B. (2025). Effects of no-till seeding and fertilization on vegetation restoration and soil physicochemical properties in alpine degraded grazing grasslands. *Agronomy*, *15*(3), 578.

[5] Martelli, R., Ali, A., Rondelli, V., & Barbanti, L. (2025). Are We Up to the Best Practices in Forage and Grassland Precision Harvest? A Review. *Grass and Forage Science*, *80*(1), e12701.

[6] Mocanu, V., Ene, T. A., Marin, E., & Gheorghiță, N. E. (2024). Mechanization of Grassland Farming by Technological Variants with Minimal Inputs: A Review. *INMATEH Agricultural Engineering*, *74*(3), 954-70

[7] Shayakhmetova, A., Savenkova, I., Akhmetov, M., Useinov, A., Nasiyev, B., Temirbulatova, A., ... & Bakirov, A. (2026). Development of High-Yield Forage Agrocenoses for Sustainable Livestock Production in Northern Kazakhstan. *Agronomy*, *16*(6), 620.

[8] Tang, Q., Wang, L., Zhang, J., & Liu, Y. (2025). Design and optimization of a seedbed preparation device for rapeseed blanket seedling transplanting. *INMATEH - Agricultural Engineering*, 78(3), 485–496.

[9] Wang, X., Wang, J., Li, E., Guo, Y., & Li, W. (2025). Plant height is the main factor driving forage yield of Poa species under different row spacings and seeding rates in the Qilian Mountains. *Frontiers in Plant Science*, *16*, 1535937.

[10] Zhang, Y., Zhang, R., Cui, Y., & Zhao, K. (2026). Unveiling the effect of conservation tillage on the agricultural green production efficiency: new insights from the Yellow River Basin. *Environment, Development and Sustainability*, 1-28.

[11] Zhao, X., Zhao, H., Wang, Z., Li, J., Yu, H., & Yan, Q. (2024). Electronic control seed-metering system for precision seeding maize based on fuzzy PID. *International Journal of Agricultural and Biological Engineering*, *17*(4), 217-226.

# COFFEE LEAVES, FLOWERS AND DEFECTIVE BEANS AS EMERGING RESOURCES FOR CIRCULAR BIOECONOMY APPLICATIONS

/

# *FRUNZELE, FLORILE ȘI BOABELE DEFECTE DE CAFEA CA RESURSE EMERGENTE PENTRU APLICAȚII ÎN BIOECONOMIA CIRCULARĂ*

**Nicoleta UNGUREANU[1)], Nicolae-Valentin VLĂDUȚ[*2)], Sorin-Ștefan BIRIȘ[1)], Neluș-Evelin GHEORGHIȚĂ[1)]**
[1)] National University of Science and Technology Politehnica Bucharest / Romania;
[2)] National Institute of Research-Development for Machines and Installations Designed for Agriculture and Food Industry-INMA Bucharest / Romania
**E-mail: valentin_vladut@yahoo.com*

***Keywords:*** *coffee leaves; coffee flowers; defective coffee beans; agricultural biomass valorization; circular bioeconomy; bioactive compounds; functional ingredients*

**ABSTRACT**

*Coffee production generates not only processing by-products but also significant quantities of underutilized biomass during cultivation and quality control operations. Among these resources, coffee leaves, flowers, and defective coffee beans represent emerging biomass streams with considerable potential for integration into circular bioeconomy strategies. This paper provides a comprehensive overview of the origin, characteristics, chemical composition, and emerging valorization pathways of these biomass streams, highlighting their transformation from agricultural residues into renewable biomass resources. Coffee leaves and flowers show considerable potential for functional beverages, antioxidant extracts, nutraceuticals, cosmetic formulations, and natural flavoring ingredients, whereas defective coffee beans can be utilized for oil recovery, biofuel production, carbon-based materials, fermentation processes, and other cascading biorefinery applications. Their potential is supported by a diverse composition that includes phenolic compounds, chlorogenic acids, caffeine, trigonelline, volatile constituents, lipids, carbohydrates, proteins, and other functional molecules relevant to both bioactive and biorefinery applications. Despite their promising potential, the large-scale implementation of these valorization pathways remains constrained by seasonal biomass availability, compositional variability, quality standardization, safety assessment, and regulatory requirements. The sustainable valorization of these underutilized biomass streams represents an important opportunity to improve resource efficiency, reduce biomass losses, and support the transition of coffee production systems toward circular and low-carbon bioeconomy models.*

**REZUMAT**

*Producția de cafea generează nu numai subproduse rezultate din procesare, ci și cantități importante de biomasă insuficient valorificată în etapele de cultivare și control al calității. Printre aceste resurse, frunzele de cafea, florile de cafea și boabele defecte reprezintă fluxuri emergente de biomasă, cu un potențial considerabil de integrare în strategiile bazate pe bioeconomia circulară. Lucrarea prezintă o analiză de ansamblu a originii, caracteristicilor, compoziției chimice și principalelor direcții de valorificare a frunzelor, florilor și boabelor defecte de cafea, evidențiind transformarea acestor resurse din reziduuri agricole în resurse regenerabile de biomasă. Frunzele și florile de cafea prezintă un potențial ridicat pentru obținerea de băuturi funcționale, extracte antioxidante, produse nutraceutice, formulări cosmetice și ingrediente naturale de aromă, în timp ce boabele defecte pot fi utilizate pentru recuperarea uleiului, producerea de biocombustibili, materiale pe bază de carbon, procese fermentative și alte aplicații integrate de tip biorafinărie. Acest potențial este susținut de o compoziție chimică diversă, care include compuși fenolici, acizi clorogenici, cofeină, trigonelină, compuși volatili, lipide, carbohidrați, proteine și alte molecule funcționale relevante atât pentru obținerea de ingrediente bioactive, cât și pentru aplicațiile de tip biorafinărie. În pofida potențialului demonstrat, implementarea la scară largă a acestor direcții de valorificare este încă limitată de disponibilitatea sezonieră a biomasei, variabilitatea compozițională, necesitatea standardizării calității, evaluarea siguranței și cerințele de reglementare. Valorificarea sustenabilă a acestor fluxuri de biomasă reprezintă o oportunitate importantă pentru creșterea eficienței utilizării resurselor, reducerea pierderilor de biomasă și susținerea tranziției sistemelor de producție a cafelei către modele bazate pe bioeconomie circulară și cu emisii reduse de carbon.*

## INTRODUCTION

Coffee (*Coffea* spp.) is one of the most important perennial crops worldwide and represents a major agricultural commodity with significant economic, social, and environmental relevance. Cultivated predominantly in tropical and subtropical regions, coffee production supports the livelihoods of millions of farmers and contributes substantially to international agricultural trade. The continuous increase in coffee demand has stimulated the expansion and intensification of cultivation systems, leading to increasingly complex production chains involving cultivation, harvesting, quality control, processing, and commercialization stages.

Coffee is currently among the most consumed beverages worldwide, with several billion cups consumed annually, reflecting its global cultural and economic importance. The highest consumption levels are recorded mainly in European countries, particularly in Northern Europe, where coffee represents an essential component of daily dietary habits. Finland reports the highest annual coffee consumption worldwide, reaching approximately 12 kg per person, followed by Norway (9.9 kg), Iceland (9 kg), Denmark (8.7 kg), and Sweden (8.2 kg), corresponding to an average daily intake of 6–8 cups per person (*United Nations, 2019*).

Significant consumption occurs in other European countries, including the Netherlands (8.4 kg), Switzerland (7.9 kg), Belgium (6.8 kg), and Luxembourg (6.5 kg), whereas lower values are generally reported in Central and Eastern Europe, where countries such as Poland record annual consumption between 2.2 and 3 kg per person (*Czarniecka-Skubina et al., 2021*). The continuous growth of global coffee consumption has directly influenced production requirements and the expansion of coffee cultivation worldwide.

During the 2022/2023 season, global coffee production reached approximately 171.3 million bags (60 kg/bag), while worldwide consumption was estimated at nearly 178.5 million bags, indicating the considerable scale and increasing pressure on the international coffee supply chain (*ICO, 2023; Ungureanu and Vlăduț, 2026*). Future projections indicate further increases in production to satisfy market demand, highlighting the need for sustainable strategies capable of improving resource efficiency and reducing environmental impacts associated with coffee production systems (*Hu et al., 2023*).

The regional distribution of coffee consumption emphasizes the worldwide importance of this crop and its extensive role within agricultural and commercial systems (Figure 1).

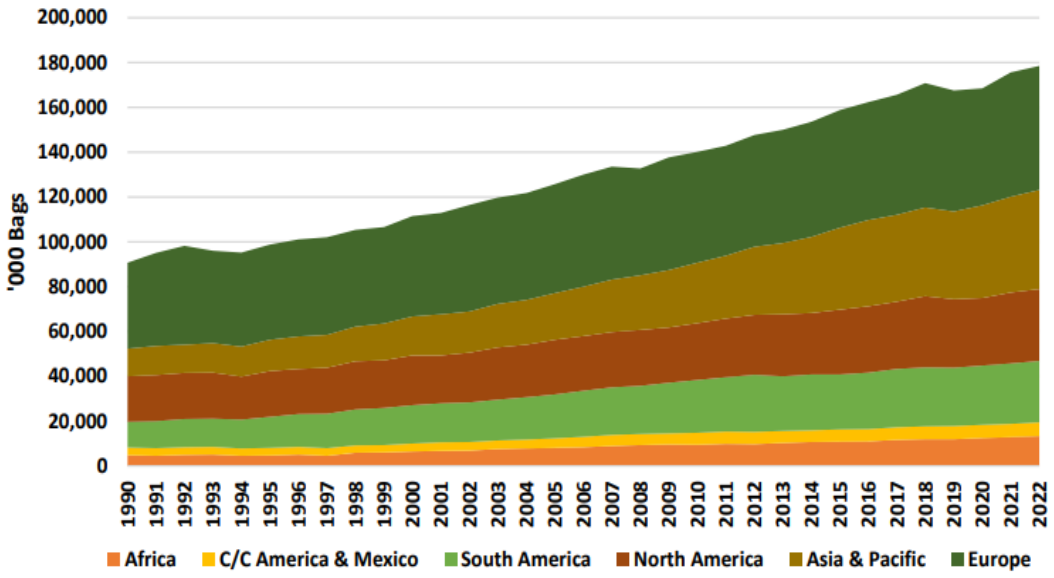



**Fig. 1 - Global consumption of coffee, by regions** (*CO, 2023*)

Coffee cultivation is currently performed in approximately 60 countries, mainly located in tropical and subtropical regions characterized by suitable climatic conditions for coffee development. Around 90% of coffee-producing countries are classified as developing economies, while the largest consumption markets are concentrated predominantly in industrialized nations (*Serna-Jiménez et al., 2022*). This geographical separation between production and consumption regions highlights the complexity of the coffee value chain and emphasizes the importance of improving sustainability practices at cultivation and post-harvest levels.

Commercial coffee production relies mainly on two species: *Coffea arabica* (Arabica coffee) and *Coffea canephora* (Robusta coffee), both belonging to the Rubiaceae family. These species differ in their genetic background, environmental adaptability, cultivation requirements, and chemical composition, characteristics that influence both coffee quality and the properties of biomass generated throughout the cultivation cycle. Arabica coffee represents approximately 60% of global coffee production, while Robusta contributes around 35%, with the remaining production represented mainly by other species, including *Coffea liberica* (*ICO, 2023*). Arabica varieties are predominantly cultivated in countries such as Colombia, Kenya, Tanzania, Bolivia, Costa Rica, and Zambia, where specific altitude and climatic conditions support high-quality coffee production. In contrast, Robusta varieties are more commonly produced in Brazil, Vietnam, Thailand, Indonesia, Paraguay, and Ethiopia due to their greater adaptability to warmer climates and lower-altitude cultivation systems (*Serna-Jiménez et al., 2022*). The worldwide distribution of the two major commercial coffee species is presented in Figures 2 and 3.

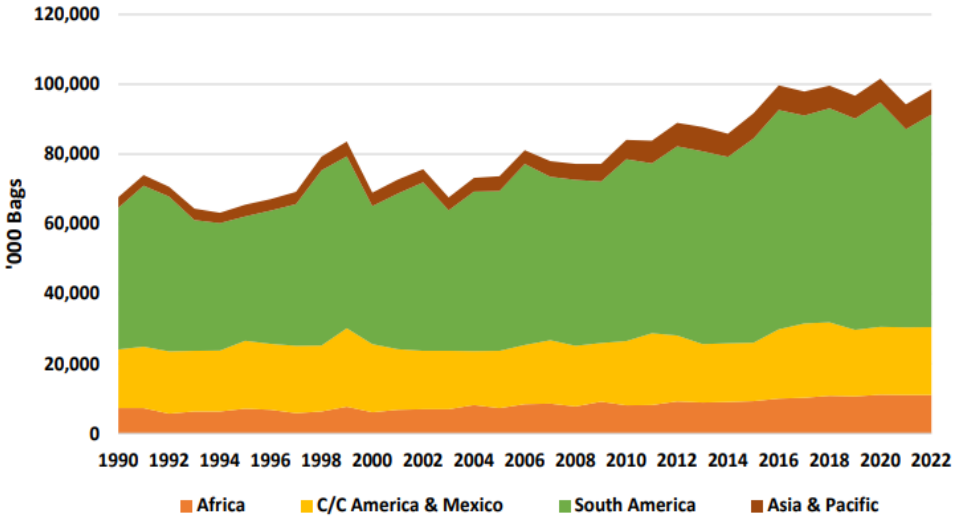



**Fig. 2 - Worldwide regions of Arabica production** (*ICO, 2023*)

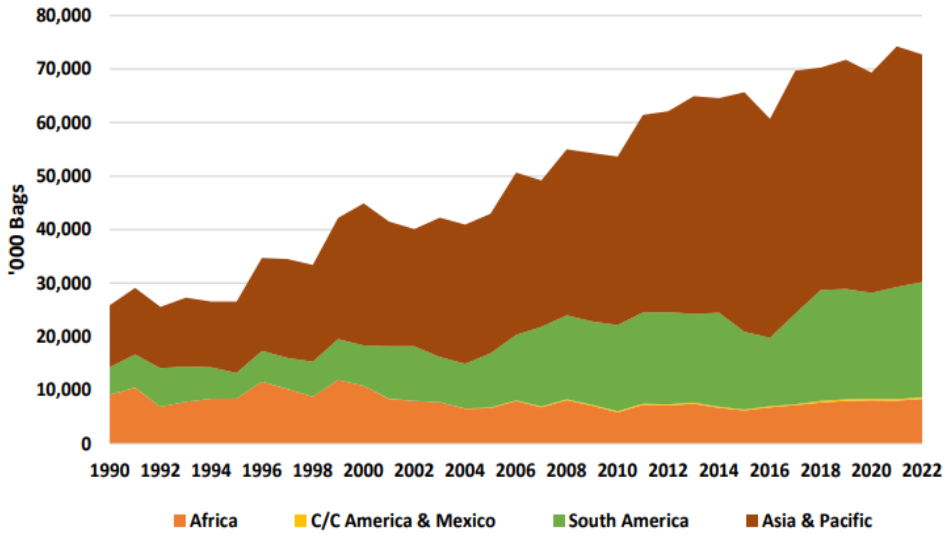



**Fig. 3 - Worldwide regions of Robusta production** (*ICO, 2023*)

Although both species belong to the same genus, they differ markedly in their agroecological requirements. *Coffea arabica* generally performs best at higher elevations under relatively cool climatic conditions, whereas *Coffea canephora* (Robusta) is better adapted to lower altitudes characterized by higher temperatures and relative humidity. Both species require deep, well-drained soils rich in organic matter, but they differ in their optimum temperature range, annual precipitation, shade requirements, and preferred cultivation topography. These differences strongly influence geographical distribution, plantation

management practices, productivity, and ultimately the quantity and characteristics of the biomass generated throughout the cultivation cycle (Table 1).

**Table 1**

**Comparative agroecological requirements of the two main commercial coffee species**
(adapted from *Patil et al., 2022*)

| Environmental parameter | *Coffea arabica* | *Coffea canephora* |
|---|---|---|
| Typical cultivation altitude | 1000–1500 m | 500–1000 m |
| Preferred topography | Gentle to moderate slopes | Flat or gently sloping areas |
| Soil characteristics | Deep, well-drained soils rich in organic matter (pH 6.0–6.5) | Deep, well-drained soils rich in organic matter (pH 6.0–6.5) |
| Optimal temperature | 15–25 °C | 20–30 °C |
| Relative humidity | 70–80% | 80–90% |
| Annual precipitation | 1600–2500 mm | 1000–2000 mm |
| Shade requirements | Moderate to light shade depending on altitude | Uniform light shade |
| Sensitivity to strong winds | High | High |
| Sensitivity to hail | High | High |

From a botanical perspective, coffee belongs to the genus *Coffea*, included in the Rubiaceae family, subfamily Cinchonoideae, and tribe Coffeae. This taxonomic group comprises approximately 400 genera and between 4800 and 5000 tropical and subtropical species. More than 80 coffee species have been identified, most of them originating from Africa and Madagascar; however, only a limited number have achieved commercial relevance. Coffee plants are perennial evergreen shrubs or small trees characterized by a vertical trunk and a relatively superficial root system. Arabica varieties generally develop deeper absorbent roots compared to Robusta plants, whose roots remain concentrated closer to the soil surface. This morphological variability reflects species-specific adaptations within the genus, particularly in relation to water uptake strategies and environmental conditions. Such differences contribute to their distinct agronomic performance and cultivation requirements under diverse growing environments. These biological characteristics determine the generation of several biomass fractions throughout the cultivation process, including leaves, flowers, branches, and fruit-associated materials.

Coffee leaves represent an important vegetative biomass fraction continuously generated during plant growth, natural renewal, and agricultural management practices such as pruning. Coffee flowers constitute short-lived reproductive structures essential for fruit formation but represent a seasonal biomass stream that remains comparatively unexplored from a valorization perspective. Following flowering, coffee cherries develop through successive maturation stages, eventually producing the coffee beans used for commercial beverage production. The morphology of the coffee plant, floral structures, and stages of coffee cherry development are illustrated in Figure 4.



**Fig. 4 - Coffee plant morphology, flowers, and stages of coffee cherry development from immature green fruits to mature dried cherries**

Coffee cultivation is strongly dependent on climatic and soil conditions. Coffee trees are generally cultivated between the Tropics of Cancer and Capricorn, in regions characterized by adequate precipitation, relatively stable temperatures, and the absence of frost events. Depending on species, cultivation system, and geographical conditions, coffee plantations can be established from sea level up to approximately 2000 m altitude. Under favorable environmental conditions, coffee plants generally require several years to reach

productive maturity and can maintain commercial productivity for extended periods (*Murthy and Madhava Naidu, 2012*).

Coffee harvesting and post-harvest selection represent critical stages that directly influence both the quality of commercial coffee and the generation of underutilized biomass streams. Harvesting is generally performed through selective picking, in which ripe cherries are collected to ensure superior beverage quality, although mechanical harvesting is also employed in some production systems. Harvest batches are frequently separated according to fruit maturity, cultivation conditions, and desired quality characteristics. Immature green cherries, overripe fruits, and other non-conforming materials are commonly removed during sorting procedures because they may negatively influence the sensory profile of the final beverage (*Janissen and Huynh, 2018*).

The coffee fruit (coffee cherry) is composed of several anatomical layers, each with distinct structural and chemical characteristics. The outer skin or exocarp surrounds the pulp (mesocarp), followed by a mucilaginous layer rich in pectic compounds and the parchment layer (endocarp), which encloses one or occasionally two coffee beans covered by a thin silverskin layer (*del Castillo et al., 2019*). During harvesting, sorting, and subsequent quality control operations, fractions that do not meet commercial requirements are separated from the main production stream. Among these fractions, defective coffee beans represent an important category of low-value biomass generated during quality selection procedures (Figure 5).

Although excluded from high-quality beverage production due to undesirable physical, chemical, or sensory characteristics, defective coffee beans retain valuable constituents, including lipids, carbohydrates, proteins, minerals, and bioactive compounds. Their chemical composition and heterogeneous nature support their potential use as alternative biomass resources within circular valorization strategies.




**Fig. 5 - Representative examples of defective green coffee beans identified during sorting and quality control operations, including morphological, mechanical, biological, and processing-related defects**
(*Jiao et al., 2025*)

Consequently, the coffee production cycle generates several biomass fractions at different biological and technological stages. Coffee leaves originate from vegetative development and plantation management practices, coffee flowers are associated with the reproductive cycle of the plant, while defective coffee beans are generated during harvesting and quality selection procedures. These materials represent distinct but complementary biomass resources whose valorization may contribute to improving resource efficiency and sustainability within coffee production systems.

Although coffee production is primarily focused on obtaining high-quality beans, the cultivation and quality control stages generate several biomass fractions that remain insufficiently exploited. Among these materials, coffee leaves, coffee flowers, and defective coffee beans represent three important but underutilized biomass streams generated before or during the early stages of the coffee value chain. Unlike some processing residues that have received considerable scientific attention, these agricultural resources remain comparatively less investigated despite their valuable chemical composition and potential applications.

Despite their different biological origin and generation stages, these three biomass fractions share a common characteristic: they contain valuable phytochemicals and other functional constituents that can be recovered and transformed into high-value products through appropriate valorization strategies. Their complementary composition broadens the range of potential applications across food, nutraceutical, cosmetic, environmental, and bio-based industries.

Coffee leaves contain a broad range of bioactive compounds, including phenolic compounds, flavonoids, caffeine, xanthonoids, organic acids, and other phytochemicals associated with antioxidant and functional properties. Their traditional use as infusions in several coffee-producing regions, together with recent scientific investigations, has highlighted their potential for applications in functional beverages, nutraceuticals, cosmetics, and other bio-based products. Coffee flowers, although available only during specific flowering periods, represent a valuable seasonal biomass source due to their content of volatile compounds, phenolics, caffeine, trigonelline, and other constituents with potential applications in specialty beverages, natural flavoring, fragrance, and bioactive extracts. Defective coffee beans, removed during harvesting and sorting operations because of their negative influence on beverage sensory quality, retain significant amounts of lipids, carbohydrates, proteins, and bioactive molecules, making them suitable candidates for alternative valorization pathways.

Traditionally, all these biomass fractions have been considered agricultural residues with limited economic value and have frequently been discarded or insufficiently utilized. However, the increasing transition toward sustainable agricultural systems has progressively changed this perception, with greater emphasis being placed on transforming underutilized biomass into valuable renewable resources. The recovery of valuable compounds and the development of alternative applications for coffee leaves, flowers, and defective beans may contribute to reducing biomass losses, improving resource efficiency, and supporting more sustainable coffee production models. Therefore, the valorization of coffee leaves, flowers, and defective coffee beans represents an emerging research direction within sustainable agriculture and circular bioeconomy approaches. This review provides an overview of their generation, characteristics, chemical composition, and potential valorization pathways, emphasizing their applications in food, nutraceutical, cosmetic, environmental, and biotechnological fields. Current challenges related to safety assessment, standardization, technological development, and future industrial implementation are also discussed.

## COFFEE LEAVES, FLOWERS AND DEFECTIVE BEANS WITHIN CIRCULAR BIOECONOMY

The increasing demand for coffee and the continuous expansion of cultivation systems have intensified the need for more sustainable approaches capable of improving resource efficiency throughout the coffee production chain. Traditionally, agricultural materials generated during cultivation and quality control operations, including coffee leaves, flowers, and defective coffee beans, have been regarded as low-value residues or unavoidable losses associated with coffee production. However, current advances in sustainable agriculture and circular economy concepts have progressively changed this perspective, recognizing these biomass fractions as renewable resources with significant potential for conversion into value-added products.

Table 2 provides a comparative overview of the origin, major bioactive constituents, and representative valorization opportunities of coffee leaves, coffee flowers, and defective coffee beans.

**Table 2**

**Origin, composition and valorization potential of coffee leaves, flowers and defective coffee beans**

| Biomass stream | Origin | Classification | Main valuable constituents | Main valorization opportunities |
|---|---|---|---|---|
| Coffee leaves | Cultivation and pruning | Agricultural residue | Chlorogenic acids, mangiferin, caffeine, trigonelline, flavonoids, xanthones, volatile compounds | Tea-like beverages, kombucha, bioactive extracts, nutraceuticals, cosmetics, essential oils, agricultural applications |
| Coffee flowers | Flowering stage | Seasonal agricultural biomass | Chlorogenic acids, phenolics, caffeine, trigonelline, volatile compounds, organic acids, sugars | Specialty beverages, floral infusions, natural flavorings, cosmetic ingredients, bioactive extracts |
| Defective coffee beans | Harvesting and sorting | Low-value biomass fraction | Lipids, proteins, carbohydrates (mannans/galactomannans), caffeine, trigonelline, phenolic compounds | Oil recovery, biodiesel production, enzymatic hydrolysis and sugar recovery, fermentation substrates, functional ingredients, activated carbon, biochar, pyrolysis products |

The growing interest in the valorization of agricultural biomass is also driven by the evolution of European environmental and waste management policies, which increasingly prioritize waste prevention, recycling, material recovery, and energy recovery over final disposal. Within the framework of the Circular Economy Action Plan and the waste hierarchy established by European legislation, agricultural residues are increasingly regarded as renewable biomass resources that should remain within the economic cycle for as long as possible through cascading material and energy valorization pathways. Consequently, considerable research efforts are currently directed toward developing sustainable extraction technologies, improving the recovery of high-value bioactive compounds, and optimizing integrated valorization processes capable of maximizing resource efficiency while minimizing environmental impacts.

The valorization of coffee leaves, flowers, and defective beans is closely aligned with the principles of circular bioeconomy, which promotes the efficient use of biological resources through reuse, recovery, cascading utilization, and the development of closed-loop production systems. Unlike conventional linear models based on resource extraction, product manufacturing, and waste disposal, circular approaches aim to maintain the value of biomass resources for as long as possible by integrating multiple utilization pathways. Within this framework, underutilized coffee biomass can be redirected toward applications in food, nutraceuticals, cosmetics, biotechnology, environmental protection, agriculture, and renewable materials.

The transformation of coffee-derived biomass into valuable products contributes to several United Nations Sustainable Development Goals (SDGs). The recovery of bioactive compounds and development of sustainable food ingredients support SDG 2 (Zero Hunger) by promoting innovative and resource-efficient food systems. The implementation of bio-based technologies and novel processing strategies contributes to SDG 9 (Industry, Innovation and Infrastructure) by encouraging sustainable industrial development. Furthermore, converting agricultural residues into useful products directly supports SDG 12 (Responsible Consumption and Production) through waste reduction and improved resource utilization. The replacement of conventional raw materials with renewable biomass-derived alternatives may also contribute to SDG 13 (Climate Action) by reducing greenhouse gases (GHG) emissions, such as $CO_2$, $CH_4$, and $N_2O$, associated with biomass disposal and supporting low-carbon production systems. Finally, sustainable management of agricultural resources contributes to SDG 15 (Life on Land) by encouraging more responsible utilization of biological resources (*Biondić Fučkar et al., 2023*; *Ungureanu and Vlăduț, 2026*).

A key principle of circular biomass valorization is the implementation of cascading utilization strategies, in which valuable compounds are recovered first, followed by the conversion of remaining biomass fractions into secondary products. For coffee leaves and flowers, this approach may involve the extraction of phenolic compounds, caffeine, volatile constituents, and other bioactive molecules for high-value applications, while residual fractions may subsequently be directed toward material, agricultural, or biotechnological uses. Similarly, defective coffee beans can be integrated into sequential valorization routes involving lipid recovery, biofuel production, carbon-based materials, or other biorefinery applications. Such strategies maximize biomass utilization efficiency and reduce the environmental burden associated with disposal.

Despite their promising potential, the integration of coffee leaves, flowers, and defective beans into industrial value chains remains limited. Several factors contribute to this situation, including seasonal availability, variability caused by species and cultivation conditions, limited standardization of processing methods, insufficient safety assessment, and the absence of established commercial pathways for several applications. Addressing these challenges requires multidisciplinary approaches combining biomass characterization, green extraction technologies, product development, regulatory assessment, and sustainability evaluation. Within this context, coffee leaves, flowers, and defective coffee beans should be regarded as valuable biomass resources rather than low-value agricultural residues. Their integration into cascading circular bioeconomy pathways offers opportunities to recover valuable compounds, reduce biomass losses, improve resource efficiency, and generate new value-added products. The following sections examine each biomass stream individually, with emphasis on its chemical composition, bioactive constituents, and emerging valorization opportunities.

## COFFEE LEAVES AS A VALUABLE AGRICULTURAL BIOMASS RESOURCE: COMPOSITION, BIOACTIVE COMPOUNDS AND VALORIZATION OPPORTUNITIES

Coffee leaves represent an abundant but insufficiently exploited biomass stream generated during coffee cultivation, pruning operations, and natural leaf renewal processes. Traditionally considered agricultural residues with limited economic value, coffee leaves are commonly left in plantations or discarded

without further utilization. However, increasing interest in sustainable biomass management and circular bioeconomy approaches has changed this perception, revealing that coffee leaves represent a valuable source of bioactive compounds with potential applications in food, nutraceutical, pharmaceutical, cosmetic, and agricultural sectors.

From a morphological perspective, coffee leaves are characterized by a glossy and waxy surface, with coloration varying from light green to dark green depending on species, developmental stage, and environmental conditions. Young leaves of certain *Coffea* varieties may exhibit bronze pigmentation before reaching their mature green color. Considerable differences in leaf size have been reported among *Coffea* species, with mature leaves generally reaching approximately 15 cm in length in *Coffea arabica*, while larger dimensions have been observed in *Coffea canephora* and *Coffea liberica*. The lifespan of coffee leaves may vary from approximately eight months in *Coffea arabica* to 7–10 months in *Coffea canephora*, contributing to the continuous generation of leafy biomass throughout the cultivation cycle (*Klingel et al., 2020*).

Despite their continuous availability in coffee plantations, coffee leaves have not yet achieved widespread industrial exploitation. Nevertheless, their traditional use as herbal beverages in several coffee-producing regions demonstrates their long-standing cultural relevance and suggests potential for commercial development. In recent years, scientific interest has increased due to the identification of diverse phytochemical constituents and the recognition of their potential biological activities. However, compared with other plant-derived biomasses, coffee leaves remain relatively less investigated, particularly regarding industrial processing, product development, and large-scale implementation.

The chemical composition of coffee leaves also supports their potential valorization as a source of functional compounds. Coffee leaves contain a broad range of phytochemicals, including alkaloids, phenolic acids, flavonoids, tannins, terpenes, carotenoids, phytosterols, amino acids, organic acids, and xanthonoids. These compounds have been associated with antioxidant, anti-inflammatory, antihypertensive, antibacterial, and antifungal activities, although most biological effects have been demonstrated mainly through in vitro investigations. The concentration of these constituents is strongly influenced by factors such as *Coffea* species, leaf maturity, cultivation conditions, and post-harvest processing.

Recent advances in analytical characterization have further strengthened the perception of coffee leaves as a valuable source of functional compounds. Using a complementary approach based on nuclear magnetic resonance spectroscopy (NMR) and chromatographic techniques coupled with mass spectrometry (HPLC-MS), researchers identified a complex secondary metabolite profile in *Coffea arabica* leaves, with 39 compounds characterized, including chlorogenic acids, xanthones, alkaloids, mangiferin, caffeine, and trigonelline. The quantitative assessment of major bioactive constituents confirmed the presence of significant levels of compounds associated with antioxidant activity, supporting the potential use of coffee leaves as functional food ingredients and as an alternative source for tea-like beverages (*Cangeloni et al., 2022*). These findings highlight the importance of advanced metabolomic approaches for identifying valuable compounds in coffee biomass and for guiding the development of standardized coffee leaf-based products.

Further evidence regarding the influence of botanical origin on coffee leaf composition was provided by *de Almeida et al. (2019)*, who identified xanthones, chlorogenic acids, flavonoids, and caffeine in *Coffea arabica* leaves collected from different regions of Brazil. The authors reported significant variations in total polyphenolic content among geographical origins, highlighting the importance of considering biomass source when developing standardized coffee leaf-derived products. Similarly, comparative analyses involving several *Coffea* species (*Coffea arabica*, *Coffea canephora*, *Coffea liberica*, *Coffea humilis*, *Coffea mannii*, *Coffea charrieriana*, *Coffea anthonyi*, and *Coffea liberica* var. *liberica*) demonstrated that chlorogenic acid composition, particularly the predominance of 5-caffeoylquinic acid (5-CQA), varies according to species and harvesting period. The authors also identified significant differences in the chlorogenic acids-to-caffeine ratio among species, highlighting the importance of raw material selection for the development of standardized coffee leaf-derived beverages (*Rodríguez-Gómez et al., 2018*).

Comparative studies with green and roasted coffee beans have further suggested that *Coffea arabica* leaf extracts may exhibit higher total phenolic content and stronger antioxidant activity than conventional coffee matrices, reinforcing their potential as alternative sources of functional compounds for food and nutraceutical applications (*Bubueanu et al., 2016*).

The composition of coffee leaves is also strongly influenced by botanical origin and leaf maturity. *Monteiro et al. (2019)* reported significant differences in chlorogenic acid and xanthone contents among Coffea species and developmental stages, with chlorogenic acid concentrations in young leaves reaching values comparable to those found in green coffee beans. These findings highlight the importance of

considering species selection and harvesting stage for the development of standardized coffee leaf-based functional products.

Among the identified phytochemicals, caffeine represents one of the most abundant bioactive constituents in coffee leaves. *Lee et al. (2023)* reported caffeine concentrations of approximately 24.5 g/kg dry leaves, highlighting the potential relevance of coffee leaves as a caffeine-containing biomass resource. However, the accumulation of caffeine in leaf litter may also have ecological implications, as excessive deposition of aged leaves in intensive cultivation systems may negatively affect soil microbial communities and nutrient cycling processes. Therefore, collecting and valorizing coffee leaves could provide a dual benefit by reducing potential environmental impacts while generating valuable bio-based products.

Other phytochemicals, particularly mangiferin and hydroxycinnamic acid esters (HCEs), have attracted increasing attention due to their antioxidant potential and their relevance for the development of coffee leaf-based functional products. In their comparative analysis involving 23 *Coffea* species, *Campa et al. (2012)* demonstrated significant interspecific differences in the accumulation of these phenolic compounds, with mangiferin detected in the leaves of specific *Coffea* lineages and present in the outer tissues of fruits. Mangiferin was predominantly localized in photosynthetic tissues, and its concentration decreased during leaf ageing, suggesting a potential role in protection against environmental stress, particularly UV radiation. The study also highlighted that phenolic profiles vary considerably among *Coffea* species, emphasizing the importance of biomass characterization and species selection when developing standardized coffee leaf-derived products. These findings support the potential utilization of coffee leaf extracts in functional beverages and other health-oriented applications, while also indicating that compositional variability should be considered during product development. Nevertheless, direct consumption of coffee leaf products requires appropriate safety evaluation due to the presence of caffeine and other bioactive constituents.

Processing conditions have also been shown to influence the functional properties of coffee leaves and the availability of their bioactive constituents. Drying treatments, particularly at controlled temperatures, can enhance the release of phenolic compounds and procyanidins, resulting in increased antioxidant activity compared with fresh leaves. Studies performed on *Coffea arabica* leaves demonstrated that young leaves subjected to drying exhibited the highest total phenolic content, procyanidin levels, and DPPH radical-scavenging activity. LC-MS characterization confirmed the presence of several antioxidant-related compounds, including caffeoylquinic acids, mangiferin derivatives, catechin/epicatechin, procyanidins, rutin, quercetin glycosides, and caffeine, supporting the potential of coffee leaf tea as a functional beverage (*Ngamsuk et al., 2019*). These findings emphasize that post-harvest processing and leaf maturity represent critical factors for optimizing the quality and bioactivity of coffee leaf-derived products.

Beyond their phytochemical value, coffee leaves have been investigated for a wide range of potential applications. Essential oils obtained from coffee leaves contain at least 47 volatile compounds, among which (E)-2-hexenal (39.7%) and 1-hexanol (32.1%) were identified as the predominant constituents, indicating their potential as alternative sources of natural aromatic compounds (*Piedrahita and Pino, 2015*). In addition to volatile constituents, coffee leaves contain numerous bioactive molecules, including chlorogenic acids, mangiferin, trigonelline, caffeine, catechins, rutin, quercetin, kahweol, and cafestol, which have been associated with antioxidant, anti-inflammatory, antihypertensive, antimicrobial, neuroprotective, and other health-promoting activities. Consequently, coffee leaves have attracted increasing interest for applications in functional beverages, ethnomedicine, cosmetic formulations, tobacco substitutes, animal feed, agricultural treatments, biodegradable materials, absorbent products, and deodorizing systems (*Chen X., 2019*; *Yohannins et al., 2024*). Their versatility reflects the coexistence of structurally diverse phytochemicals and volatile compounds that support multiple valorization pathways, although further studies are still required to clarify their mechanisms of action and optimize processing strategies for preserving bioactive constituents.

The traditional medicinal use of coffee leaves further illustrates their cultural and functional relevance. In several regions, including Ethiopia, Peru, Cuba, and Mexico, coffee leaves preparations have been traditionally used for managing conditions such as headaches, digestive disorders, nausea, and flu-related respiratory symptoms (*Patay et al., 2016*). Moreover, coffee leaves extracts containing mangiferin and other bioactive compounds have been associated with potential improvements in cognitive functions, including memory, attention, and concentration, although further clinical validation is required.

Among the most established applications of coffee leaves is their use as tea-like beverages. Traditional consumption practices have been reported in countries such as Indonesia, Jamaica, Ethiopia, and Sumatra, where coffee leaf infusions, such as the Indonesian *kahwa daun*, are prepared and consumed

as beverages with coffee-like sensory characteristics (*Novita et al., 2018*). Commercial interest in coffee leaf tea has also increased in recent years. Since 2014, coffee leaf tea has been successfully commercialized in Canada under the *Wize Monkey* brand, while similar products are marketed in India by companies such as *Chaiguru* under names including *Kuti Tea* and *Araku Chai*. In parallel, several patents have been filed describing processing technologies and potential health-related applications of coffee leaf-derived beverages (*Patil et al., 2022*).

Recent ethnobotanical surveys have further highlighted that coffee leaf beverages continue to play an important nutritional and cultural role in several Ethiopian communities, where they are consumed not only as traditional stimulating drinks but also for their perceived medicinal benefits. The study also documented regional processing practices, including the preparation of the traditional Ethiopian *kuti*, in which fresh coffee leaves are ground prior to drying, illustrating the diversity of indigenous manufacturing techniques. The long history of regular consumption, together with the absence of reported health concerns among most consumers, provides valuable evidence supporting the traditional safety of coffee leaf beverages. These observations strengthen the rationale for developing standardized coffee leaf-derived functional products while emphasizing the need for further biochemical, toxicological, and clinical investigations to support regulatory approval and wider commercialization (*Yohannis et al., 2026*).

The development of coffee leaf tea as a commercial product requires careful optimization of processing conditions to obtain desirable phytochemical and sensory characteristics. In this context, studies performed in El Salvador investigated the influence of different processing steps adapted from conventional tea manufacturing, including leaf selection, cutting, rolling, thermal treatments, drying, roasting, and fermentation, on the quality attributes of *Coffea arabica* leaf teas. The results demonstrated that processing parameters significantly affected the levels of key constituents, such as caffeine and chlorogenic acids, as well as the formation of aroma-active compounds. Gas chromatography–mass spectrometry–olfactometry analysis identified several volatile compounds contributing to the sensory profile of coffee leaf teas, including β-ionone, α-ionone, decanal, hexanal, and octanal, which were associated with floral, citrus, green, and fruity notes (*Steger et al., 2022*). These findings highlight that technological optimization of coffee leaf processing is essential for tailoring product characteristics and improving the economic potential of coffee leaves as an underutilized biomass resource

Researchers have also investigated the sensory potential and consumer perception of coffee leaf tea compared with conventional tea beverages. *DePaula et al. (2023)* evaluated pure and blended *Coffea arabica* leaf infusions in comparison with black tea and roasted maté tea, demonstrating that coffee leaf tea possesses a characteristic volatile profile with aroma-active compounds comparable to those found in traditional tea matrices. Sensory analyses associated coffee leaf infusions mainly with herbal, green leaf, woody, and refreshing attributes, while blending strategies, particularly with roasted maté, improved consumer acceptance. In addition, *Rigling et al. (2023)* explored the sensory potential of coffee leaves and flowers as underutilized biomass resources for food applications. The evaluation of 24 coffee leaf samples obtained through different processing approaches and 38 coffee flower samples from diverse *Coffea* species revealed considerable aroma diversity. Fermented coffee leaves showed enhanced sweet and fruity notes compared with the more intense green and vegetal characteristics of non-fermented samples, while coffee flowers exhibited floral, honey-like, herbal, and dried-fruit attributes. Gas chromatography–mass spectrometry–olfactometry analysis identified key aroma-active compounds, including β-ionone, decanal, α-ionone, octanal, and hexanal in leaves, and 2-heptanol, 2-ethylhexanol, nerol, and geraniol in flowers. These findings support the development of innovative coffee leaf- and flower-based beverages and highlight their potential valorization within sustainable coffee production systems.

The production of coffee leaves-based beverages generally involves drying operations preceded, in some cases, by steaming, rolling, fermentation, or roasting treatments adapted from conventional tea manufacturing technologies. These processing approaches can significantly influence sensory characteristics and phytochemical stability. Recent studies applying conventional tea-processing strategies (white, green, oolong, and black tea methods) to coffee leaves demonstrated that both leaf maturity and processing type modify phenolic profiles, antioxidant capacity, and anti-inflammatory responses, emphasizing the importance of process optimization for the development of functional coffee leaf beverages (*Chen et al., 2018*). Beyond conventional coffee leaf infusions, recent studies have explored the use of coffee leaves as substrates for the development of fermented functional beverages. The potential of *Coffea arabica* leaves as an alternative raw material for kombucha production was investigated by *Sales et al. (2024)*, who evaluated the evolution of volatile compounds, microbial characteristics, and sensory properties

during fermentation. The results demonstrated that coffee leaf kombucha developed a complex volatilome, with compounds derived from both the original leaf matrix and fermentation processes, including esters, alcohols, aldehydes, terpenoid-related compounds, and organic acids. Sensory evaluation revealed pleasant attributes associated with fruity, sweet, peach-like, herbal, and toasted notes, while consumer acceptance confirmed the suitability of coffee leaf-based kombucha as an innovative beverage concept. These findings indicate that coffee leaves possess functional and sensory characteristics comparable to other traditional tea substrates, such as black tea and maté, supporting their valorization as renewable ingredients for fermented beverages within circular food systems

From a safety perspective, the suitability of coffee leaves-derived products for human consumption has received increasing attention. Scientific assessments reported caffeine concentrations of approximately 7 mg/g in dried leaves and around 10 mg/L in aqueous infusions prepared from coffee leaves (*Klingel et al., 2020*). Mangiferin content has also been considered in toxicological evaluations, with currently available data suggesting that naturally occurring concentrations in coffee leaves-derived products are within acceptable safety limits. Nevertheless, additional toxicological studies, clinical investigations, and regulatory evaluations are required to support broader commercialization and substantiate health-related claims.

Recent regulatory and toxicological evaluations have further strengthened the safety of coffee leaf tea as an emerging functional beverage. *Tritsch et al. (2022)* reviewed the potential risks associated with coffee leaf tea following its authorization as a novel food in the European Union and identified caffeine and epigallocatechin gallate (EGCG) as the main compounds requiring safety consideration. The authors highlighted that caffeine levels may vary considerably depending on *Coffea* species, leaf age, climatic conditions, and processing technologies, but moderate consumption levels (approximately 1–3 cups/day) were considered compatible with current safety recommendations. In contrast, EGCG concentrations were generally absent or remained below the intake threshold associated with potential hepatotoxic effects established by the European Food Safety Authority (EFSA), indicating a low toxicological concern for this compound. These findings suggest that, similarly to other coffee-derived beverages, caffeine exposure represents the main safety parameter requiring control, while appropriate selection of raw material and processing conditions can support the development of safe coffee leaf-based functional beverages. Nevertheless, additional toxicological, clinical, and regulatory investigations remain necessary to substantiate health-related claims and facilitate wider commercialization.

To support regulatory compliance and quality control of coffee leaf tea, analytical approaches for the reliable determination of major bioactive constituents have also been investigated. A validated HPLC method adapted from the ISO 14502-2 procedure, originally developed for conventional tea analysis, demonstrated high robustness and precision for the quantification of caffeine and chlorogenic acids in coffee leaf matrices. However, EGCG levels were found to be very low or below the detection limit in the analyzed samples, confirming the limited toxicological relevance of this compound in coffee leaf-derived beverages (*Münch and Lachenmeier, 2022*). The availability of validated analytical methodologies represents an important step toward standardized evaluation of coffee leaf products and supports compliance with Regulation (EU) 2020/917 for novel foods, which establishes maximum levels of chlorogenic acids (<100 mg/L), caffeine (<80 mg/L), and EGCG (<700 mg/L) in coffee leaf tea infusions (*European Commission, 2020*).

Beyond caffeine-related considerations, the safety of other bioactive compounds naturally occurring in coffee leaves and other coffee-derived biomasses has also been investigated. Chlorogenic acids, particularly 5-caffeoylquinic acid (5-CQA) and 3,5-dicaffeoylquinic acid (3,5-DCQA), represent major phenolic constituents of coffee biomass. Toxicological evaluations of coffee by-products containing chlorogenic and isochlorogenic acids have not identified significant adverse effects following acute oral exposure, while current evidence suggests that long-term intake within the range of normal dietary exposure does not represent a relevant health risk (*Behne et al., 2023*). Similarly, trigonelline, a bioactive pyridine alkaloid found in coffee leaves and other coffee by-products, has attracted attention due to the potential increase in dietary exposure associated with the development of novel food applications. Available toxicological data indicate no evidence of adverse effects following acute exposure, although the assessment of chronic exposure remains limited due to the scarcity of human and epidemiological studies. Nevertheless, trigonelline consumed as part of coffee and coffee-derived products is currently considered safe based on traditional consumption patterns and available scientific evidence (*Konstantinidis et al., 2023*). Together with the safety assessment of caffeine and EGCG, these findings support the potential use of coffee leaves as a functional ingredient while highlighting the need for further long-term toxicological and clinical investigations.

Overall, available evidence demonstrates a progressive transition in the perception of coffee leaves, from an agricultural residue to a promising renewable biomass resource within circular bioeconomy systems. While current research has primarily focused on phytochemical characterization and biological activity assessment, future efforts should increasingly address process optimization, product formulation, storage stability, consumer acceptance, and industrial scalability. The development of standardized and safe coffee leaves-based products represents an important step toward integrating coffee cultivation residues into sustainable value chains and maximizing the resource efficiency of coffee production systems.

## COFFEE FLOWERS AS A VALUABLE SEASONAL BIOMASS RESOURCE FOR CIRCULAR VALORIZATION

Coffee flowers represent an essential component of the *Coffea* reproductive cycle and play a fundamental role in determining subsequent fruit and bean production. These structures are typically characterized by a white color, intense fragrance, and clustered arrangement, developing as short-lived reproductive organs during the flowering stage. Due to their ephemeral nature and rapid transition toward fruit development, coffee flowers have traditionally been considered temporary biological structures rather than exploitable biomass resources. However, within the framework of circular bioeconomy approaches, coffee flowers are increasingly being reconsidered as a valuable seasonal biomass stream with potential applications in food, cosmetics, nutraceuticals, and other high-value sectors. Because coffee flowers can be collected after pollination with minimal interference to fruit development, they represent a promising seasonal biomass resource suitable to produce tea-like beverages, floral water, coffee blossom honey, and other value-added food and cosmetic ingredients (*Wirz et al., 2022*). Compared with other coffee-derived biomass fractions, coffee flowers remain among the least investigated resources, despite their continuous generation during coffee cultivation. Their valorization potential is particularly relevant considering the considerable biomass availability during flowering periods. A mature coffee tree may produce approximately 30,000–40,000 flowers annually, suggesting that the development of value-added products from naturally available floral biomass could become feasible, if collection strategies are carefully managed to avoid negative impacts on fruit formation and final yield (*Klingel et al., 2020*).

The biological functions of coffee flowers are reflected in their complex chemical composition, which includes a variety of bioactive and volatile constituents. Reported compounds include caffeine, trigonelline, epoxygeraniols (2,3-epoxygeraniol and 6,7-epoxygeraniol), and epoxynerol, among others (*Lee et al., 2023*). Volatile fraction analysis has further demonstrated the presence of characteristic aromatic compounds, with n-pentadecane identified as the predominant volatile constituent, followed by 8-heptadecene and geraniol. These compounds suggest potential applications of coffee flowers as natural sources of fragrance molecules for cosmetic and flavoring industries (*Stashenko et al., 2013*).

Recent analytical studies have expanded the understanding of coffee flowers composition across different *Coffea* species, including *Coffea arabica, Coffea canephora*, and *Coffea liberica*. Using complementary techniques such as HPLC-DAD, nuclear magnetic resonance (NMR), and near-infrared spectroscopy (NIR), researchers have identified a diverse profile of primary metabolites and bioactive compounds, including caffeine, chlorogenic acids, trigonelline, organic acids, and sugars. Furthermore, sensory evaluation of coffee flowers infusions revealed complex aromatic profiles dominated by floral characteristics, together with additional descriptors such as hay, hops, sage, dried apricot, and honey tree notes (*Wirz et al., 2022*). These findings highlight the multifunctional potential of coffee flowers as ingredients for specialty beverages, natural flavoring systems, floral extracts, and cosmetic formulations. Nevertheless, further studies addressing product standardization and regulatory approval, particularly within the European Novel Food framework, remain necessary before broader commercial implementation.

Further evidence supporting the potential of coffee flowers as a functional beverage ingredient was provided by *DePaula et al. (2025)*, who investigated the phytochemical composition, volatile profile, and sensory characteristics of *Coffea canephora* flowers and their infusions. Using HPLC-DAD analysis, researchers identified relevant levels of chlorogenic acids, phenolic acids, caffeine, and trigonelline in dried flowers, while hot-water infusion demonstrated efficient transfer of major bioactive constituents, particularly chlorogenic acids, caffeine, and trigonelline, into the aqueous phase. In addition, GC-MS characterization revealed a diverse volatile profile comprising aldehydes, monoterpenes, esters, alcohols, and monoterpene alcohols, with floral, jasmine, orange blossom, herbal, woody, and sweet sensory notes identified in the resulting infusions. These findings demonstrate that coffee flowers possess not only a valuable

phytochemical composition but also attractive sensory properties, supporting their potential development as specialty herbal beverages and high-value functional products within circular bioeconomy frameworks.

Beyond their chemical composition, the technological processing of coffee flowers represents a critical factor influencing their final valorization potential. Drying, extraction, and stabilization methods significantly affect the preservation of bioactive compounds and antioxidant activity. In their research, *Pinheiro et al. (2021)* demonstrated that dehydration techniques and extraction conditions strongly influenced the concentration of key phytochemicals, including trigonelline, caffeine, chlorogenic acid, and gallic acid. Among the investigated approaches, freeze-drying followed by aqueous extraction at 92 °C provided improved preservation of phenolic compounds and antioxidant capacity, indicating its suitability for producing functional tea-like beverages based on coffee flowers.

Morphologically, coffee flowers develop as white, multi-flowered cymose inflorescences containing specialized structures known as colleters, which produce adhesive secretions involved in protecting floral tissues against dehydration and insect attack. For valorization purposes, flowers are generally collected after pollination during the natural wilting stage, minimizing potential interference with fruit development. Following collection and drying, coffee flowers may be incorporated into herbal infusions or processed for the recovery of valuable bioactive compounds. Studies performed on dried flowers of *Coffea canephora* reported caffeine and trigonelline concentrations of approximately 1 g/100 g dry weight, together with significant levels of phenolic compounds, supporting their potential use as functional food and nutraceutical ingredients (*Klingel et al., 2020*). Additional investigations have demonstrated the efficiency of green extraction technologies for recovering valuable constituents from coffee flowers. Pressurized hot water extraction has enabled the recovery of bioactive fractions containing melanoidins and bio-sugars, while caffeine and trigonelline represented the predominant extracted compounds, reaching yields of 1070.8 mg and 1092.8 mg per 100 g dry weight, respectively (*Nguyen et al., 2019*). Such approaches demonstrate the compatibility of coffee flowers with sustainable extraction technologies and support their integration into circular valorization schemes. Despite the promising composition and functional potential of coffee flowers, their transition toward industrial applications remains limited by several challenges. Unlike continuously generated coffee residues, coffee flowers represent a highly seasonal biomass stream, requiring efficient collection, preservation, and processing strategies. Additional limitations include the need for standardized quality parameters, comprehensive safety evaluation, toxicological assessment, and regulatory approval, particularly for food applications and novel ingredients within the European market.

Overall, coffee flowers should be regarded as an emerging high-value biomass resource rather than a transient agricultural material. Future research should focus on establishing optimized harvesting strategies, scalable processing technologies, and standardized product development approaches capable of transforming coffee flowers into commercially viable ingredients while maintaining sustainable coffee production practices within circular bioeconomy systems.

## DEFECTIVE COFFEE BEANS AS A VALUABLE BIOMASS RESOURCE FOR CIRCULAR VALORIZATION

Defective coffee beans represent an important but insufficiently exploited biomass fraction generated during harvesting, post-harvest handling, and quality control operations. In conventional coffee production systems, these beans are removed from commercial batches because their physical, chemical, and sensory characteristics may negatively influence the quality and acceptability of the final beverage. However, although unsuitable for premium coffee production, defective coffee beans retain a complex chemical composition that supports their consideration as alternative biomass resources within circular bioeconomy and biorefinery frameworks. The occurrence of defective beans is associated with multiple factors throughout the coffee production chain, including fruit maturation, harvesting conditions, post-harvest processing, drying, and storage practices. The most frequently reported defects include black, sour, and immature beans. Black beans may result from physiological deterioration within the coffee cherry or from prolonged exposure of fallen fruits to unfavorable environmental conditions, whereas sour beans are commonly associated with excessive fermentation, inappropriate drying conditions, or the processing of overripe cherries (*Skorupa et al., 2022*). Additional defects, including insect damage or improper processing, may further contribute to quality deterioration and rejection during commercial grading. Compared with properly graded coffee beans, defective coffee beans generally exhibit lower mass, reduced density, and altered visual characteristics, reflecting structural and compositional modifications. These physical differences are accompanied by variations in biochemical composition, including changes in lipid, carbohydrate, protein, and organic acid

contents, which may influence both their technological behavior and suitability for alternative applications. Consequently, although defects negatively affect beverage quality, they do not necessarily reduce the potential value of the beans as industrial biomass resources (*Mestanza et al., 2026*).

Biochemical investigations have further demonstrated that defective coffee beans exhibit distinct metabolic profiles compared with non-defective fractions. Using a comparative analysis of green and roasted *Coffea arabica* beans, researchers identified a set of biochemical markers associated with defective fractions, including organic acids, sugars, sugar alcohols, and nitrogen-containing compounds. In green beans, differences between defective and non-defective samples were associated with compounds involved in primary metabolism, such as citric and malic acids, fructose, sucrose, pentitols, and amino acid-derived metabolites. Following roasting, additional differences became evident, with volatile compounds and furan derivatives, including 1-methylpyrrole and furfuryl-related compounds, showing a stronger association with defective beans (*Casas et al., 2017*). These findings highlight that defective coffee beans represent chemically differentiated biomass streams rather than merely degraded products, providing further support for their targeted valorization through extraction, bioconversion, and thermochemical transformation processes.

Recent investigations have also demonstrated that post-harvest processing and roasting conditions influence the chemical characteristics of coffee beans, including those presenting minor defects. Dry processing approaches, particularly natural and honey processing, affect moisture content and volatile compound formation during roasting. Honey-processed beans have been associated with a greater diversity of volatile compounds compared with naturally processed beans, resulting in more complex aroma profiles. Furthermore, roasting temperature influences volatile compound development and may modify caffeine levels depending on processing conditions. The detection of pesticide-related residues in some naturally processed coffee beans has additionally emphasized the importance of improved agricultural practices, quality control, and farmer education to ensure consumer safety (*Analianasari et al., 2024*). From a valorization perspective, the term “defective” should be interpreted primarily within the context of beverage production rather than as an indicator of overall biomass quality. While sensory defects reduce their commercial value in the coffee market, defective coffee beans retain a chemically diverse composition, including lipids, carbohydrates, proteins, organic acids, sugars, nitrogen-containing compounds, and bioactive constituents, which may support their conversion into value-added products. Although defective coffee beans are commonly separated from high-quality coffee batches before commercialization, they continue to be traded in several coffee-producing countries, including Brazil. Their removal from the premium coffee chain has stimulated interest in alternative applications capable of generating additional economic value while improving overall resource efficiency.

Recent studies have also highlighted the potential of defective coffee beans as carbohydrate-rich substrates for enzymatic valorization. Coffee processing coproducts, such as coffee press cake generated after oil extraction, have been successfully used as low-cost carbon sources to produce mannan-degrading enzymes by *Aspergillus niger*. The resulting enzyme preparations, containing mannanase and β-mannosidase activities, were subsequently applied for the hydrolysis of healthy and defective coffee beans, enabling the recovery of approximately 25% of the available mannose fraction. These results demonstrate that defective coffee beans can serve not only as sources of lipids and thermochemical products but also as renewable carbohydrate reservoirs suitable for biotechnological conversion. The integration of enzymatic hydrolysis with other extraction and conversion pathways may contribute to the development of more efficient cascading biorefinery schemes, enabling the recovery of multiple product streams from coffee-derived biomass while reducing resource losses (*Ribeiro et al., 2025*).

Among the most investigated approaches is the recovery of coffee oil, which can be further utilized for biodiesel production. In addition, the remaining solid fraction after oil extraction can be incorporated into complementary valorization pathways, including conversion into carbon-based materials and other renewable products. More advanced strategies have been developed within circular biorefinery concepts, aiming to maximize the utilization of defective coffee beans through sequential processing routes. Pyrolysis of de-oiled defective coffee beans residues obtained after pressurized fluid extraction of coffee oil has demonstrated the possibility of generating multiple value-added products, including bio-oil, aqueous fractions, biochar, and non-condensable gases. The distribution of these products depends on feedstock characteristics and pretreatment conditions, while the resulting biochar exhibits a relatively high heating value (approximately 24.7–25.3 MJ/kg). Moreover, the bio-oil fraction contains relevant chemical constituents, particularly phenolic compounds and carboxylic acids, highlighting the potential integration of

defective coffee beans into cascading biorefinery systems (*Silva et al., 2022*). The solid residues remaining after oil extraction represent additional biomass streams suitable for further utilization. Microwave-assisted carbonization has been successfully applied to transform coffee oil extraction residues into efficient adsorbent materials for wastewater treatment. Compared with conventional carbonization methods, this approach reduced processing time while improving adsorption performance. The resulting adsorbents demonstrated effective removal of methylene blue from aqueous solutions, with adsorption behavior following pseudo-second-order kinetics and the Langmuir isotherm model. Their enhanced performance was attributed to increased microporosity, surface carboxylic groups, and higher surface charge density (*Franca et al., 2010*).

Overall, recent studies indicate a transition in the valorization of defective coffee beans from simple disposal or energy recovery approaches toward integrated cascading strategies capable of generating multiple value-added products from a single biomass stream. Their potential as oleaginous and lignocellulosic feedstocks supports their incorporation into circular coffee production systems, where sequential recovery of valuable compounds can be combined with material and energy applications. Future research should focus on optimizing integrated processing schemes, improving economic feasibility, and developing scalable technologies capable of maximizing the resource potential of defective coffee beans while reducing biomass losses throughout the coffee value chain.

## CHALLENGES RELATED TO QUALITY, SAFETY, STANDARDIZATION AND REGULATORY ACCEPTANCE OF COFFEE LEAVES, FLOWERS AND DEFECTIVE BEANS VALORIZATION

The increasing scientific interest in coffee leaves, coffee flowers, and defective coffee beans has demonstrated that these biomass streams represent valuable renewable resources containing bioactive compounds, structural carbohydrates, proteins, lipids, and other functional constituents with potential applications in food, nutraceutical, cosmetic, agricultural, and environmental sectors. Nevertheless, despite considerable progress in identifying their chemical composition and potential applications, their transition from experimental research toward commercially viable products remains limited by several interconnected challenges related to compositional variability, quality control, safety assessment, regulatory acceptance, and industrial scalability. A major challenge associated with the valorization of coffee agricultural biomass is the intrinsic variability of its chemical composition. The concentration of valuable compounds in coffee leaves, coffee flowers, and defective coffee beans may vary considerably depending on coffee species, cultivar, geographical origin, altitude, climatic conditions, agricultural practices, plant developmental stage, harvesting methods, post-harvest handling, and storage conditions. For instance, the levels of caffeine, phenolic compounds, chlorogenic acids, flavonoids, mangiferin, trigonelline, lipids, and proteins may differ substantially among biomass fractions and even among samples originating from the same coffee-growing region. Such variability directly influences extraction efficiency, biological activity, sensory characteristics, and the reproducibility of final products. Therefore, the establishment of standardized characterization protocols and quality parameters represents a fundamental requirement for the future industrial utilization of coffee-derived biomass. Quality assurance is particularly important for applications involving food ingredients, functional beverages, nutraceutical formulations, and cosmetic products. Although several studies have demonstrated the antioxidant potential and functional properties of coffee leaves and flowers, most investigations remain focused on laboratory-scale characterization rather than product development under industrial conditions. Future valorization pathways should therefore incorporate standardized procedures for biomass collection, identification, drying, storage, extraction, and stabilization to preserve valuable compounds and ensure consistent product performance. In addition, traceability systems documenting botanical origin, cultivation conditions, and processing history will be essential for establishing consumer confidence and facilitating market acceptance.

Safety evaluation represents another critical aspect, especially considering the potential incorporation of coffee agricultural biomass into products intended for human consumption. Although coffee leaves and flowers contain numerous bioactive compounds with demonstrated biological potential, the presence of naturally occurring caffeine, phenolic compounds, tannins, and other secondary metabolites requires careful assessment regarding exposure levels and intended consumer groups. Furthermore, agricultural biomass may accumulate undesirable contaminants depending on cultivation practices and environmental conditions, including pesticide residues, heavy metals, microbiological contaminants, and mycotoxins. Consequently, comprehensive safety assessment should include chemical characterization,

contaminant monitoring, microbiological evaluation, toxicological studies, and stability assessment throughout processing and storage.

From a regulatory perspective, the commercialization of coffee-derived ingredients remains challenging because many biomass streams do not yet have a clearly established status within international food legislation. In the European Union, products obtained from previously unconsumed plant materials may require evaluation under the framework established by the Novel Food Regulation (EU) 2015/2283 (*European Commission, 2015*), which defines novel foods as foods not consumed to a significant degree within the European Union before 15 May 1997. Consequently, coffee leaves, coffee flowers, and their extracts intended for food applications may require safety assessment and authorization procedures before commercialization as novel food ingredients.

Recent regulatory developments indicate that this framework is gradually evolving. Coffee leaf tea has already received authorization within the European Union; however, this approval is limited to infusion products prepared from specific *Coffea* species, namely *Coffea arabica* and *Coffea canephora*, and does not automatically extend to extracts or other derived formulations (*EFSA, 2020; European Commission, 2020; Lachenmeier et al., 2021*). Similarly, cascara has progressed through regulatory evaluation and received authorization for specific food applications, demonstrating that coffee-derived biomass streams can reach regulated markets when adequate safety and compositional data are available (*EFSA, 2020; European Commission, 2022*). In contrast, coffee flowers and several other biomass fractions remain without an established regulatory pathway within the European Union, despite their potential as sources of bioactive compounds and functional ingredients (*Klingel et al., 2020; Lachenmeier et al., 2021; DePaula et al., 2025*). The evaluation process is conducted within the European regulatory framework, with scientific risk assessment performed by EFSA considering aspects such as composition, nutritional profile, toxicological information, proposed uses, and expected exposure levels. Importantly, regulatory authorization of a traditional product form does not necessarily imply approval of all possible applications derived from the same biomass. Differences in extraction procedures, concentration factors, and intended uses may significantly modify consumer exposure and require additional safety evaluations. Therefore, future commercialization of coffee biomass-derived ingredients should be supported by application-specific risk assessments integrating compositional data, exposure scenarios, and toxicological evidence.

Defective coffee beans, although derived from an already established food commodity, require careful evaluation when redirected toward alternative applications such as extracts, bioactive ingredients, or non-food products. The development of clear regulatory pathways distinguishing waste materials from valuable secondary resources will be essential for accelerating the implementation of circular coffee value chains.

Beyond safety and regulatory aspects, sustainability assessment represents an additional requirement for the successful implementation of coffee biomass valorization strategies. Although numerous studies report extraction yields, antioxidant capacity, or material properties, fewer investigations evaluate the overall environmental and economic performance of proposed applications. The integration of life cycle assessment, techno-economic analysis, carbon footprint evaluation, and circularity indicators would provide a more realistic assessment of the sustainability potential of different valorization routes. Such approaches are particularly relevant for determining whether proposed technologies provide genuine environmental benefits compared with conventional disposal or low-value utilization practices.

The successful integration of coffee leaves, flowers, and defective beans into circular bioeconomy systems requires a multidisciplinary approach combining advanced biomass characterization, green extraction technologies, safety evaluation, regulatory compliance, and sustainable process design. Rather than treating these materials as isolated agricultural residues, future strategies should consider them as complementary biomass resources that can be incorporated into cascading valorization systems, where bioactive compounds, functional ingredients, biomaterials, and energy products are sequentially recovered. This approach represents a promising pathway toward reducing biomass losses, improving resource efficiency, and supporting the transition of coffee production systems toward circular and sustainable models.

## CONCLUSIONS

Coffee cultivation and harvesting generate several biomass fractions that are currently underutilized despite their significant chemical and functional potential. Among these resources, coffee leaves, coffee flowers, and defective coffee beans represent valuable agricultural biomass streams that can be integrated

into circular bioeconomy strategies instead of being considered low-value residues. Their valorization provides an opportunity to reduce biomass losses while creating new value chains within coffee production systems.

The literature reviewed in this study demonstrates that coffee leaves, flowers, and defective beans contain a diverse range of valuable constituents, including phenolic compounds, flavonoids, caffeine, mangiferin, trigonelline, chlorogenic acids, volatile compounds, lipids, proteins, and carbohydrates. These components support their potential utilization in multiple sectors, including functional beverages, nutraceuticals, antioxidant extracts, cosmetic formulations, natural flavoring ingredients, biomaterials, agricultural applications, and environmental technologies. Particularly, coffee leaves and flowers represent promising sources of bioactive compounds, while defective coffee beans exhibit considerable potential as alternative feedstocks for oil recovery, carbon-based materials, and cascading biorefinery processes.

Despite the increasing scientific interest, the industrial implementation of these valorization pathways remains limited. The main challenges are associated with the significant variability of biomass composition, influenced by coffee species, cultivar, geographical origin, environmental conditions, cultivation practices, harvesting stage, and post-harvest handling. These variations affect the reproducibility of extraction processes and the quality of resulting products, highlighting the need for standardized characterization methods, quality control procedures, and traceability systems.

Safety and regulatory aspects represent additional factors that require further investigation, particularly for applications involving food, beverages, nutraceuticals, and cosmetic products. Comprehensive assessment of potential contaminants, microbiological quality, naturally occurring bioactive compounds, and consumer exposure is essential for ensuring safe utilization. Moreover, the establishment of appropriate regulatory frameworks, including the evaluation of potential novel food applications, will play a decisive role in facilitating the commercialization of coffee leaf- and flower-derived products.

Future research should increasingly focus on integrated and cascading valorization strategies capable of maximizing the potential of each biomass fraction. The combination of green extraction technologies, advanced analytical approaches, sustainable processing methods, and comprehensive techno-economic and environmental assessments will be essential for translating laboratory-scale findings into industrial applications. Beyond the development of individual products, the successful integration of coffee leaves, flowers, and defective beans into cascading biorefinery systems could diversify the portfolio of coffee-derived products while improving resource efficiency, reducing biomass losses, and creating new value chains. Such an approach would support the transition of the coffee sector toward more sustainable, circular, and low-carbon bioeconomy models.

## REFERENCES

[1] Analianasari, A., Berliana, D., & Shintawati, S. (2024). Defects of coffee beans with different postharvest processes and roasting temperatures on volatile compounds of coffee beans from coffee small-scale industries of West Lampung Indonesia. *Trends in Sciences*, *21*(7), 7695. https://doi.org/10.48048/tis.2024.7695

[2] Behne, S., Franke, H., Schwarz, S., & Lachenmeier, D.W. (2023). Risk assessment of chlorogenic and isochlorogenic acids in coffee by-products. *Molecules*, *28*(14), 5540. https://doi.org/10.3390/molecules28145540

[3] Biondić Fučkar, V., Nutrizio, M., Grudenić, A., Djekić, I., & Režek Jambrak, A. (2023). Sustainable ultrasound assisted extractions and valorization of coffee silver skin (CS). *Sustainability*, *15*(10), 8198. https://doi.org/10.3390/su15108198

[4] Bubueanu, C., Pavaloiu, R., & Pirvu, L. (2016). HPLC profiles and antioxidant activities from leaves to green and roasted beans of *Coffea arabica*. *Malaysian Journal of Medicine and Biology*, *3*(1), 31–36.

[5] Campa, C., Mondolot, L., Rakotondravao, A., Bidel, L.P.R., Gargadennec, A., Couturon, E., La Fisca, P., Rakotomalala, J.-J., Jay-Allemand, C., & Davis, A.P. (2012). A survey of mangiferin and hydroxycinnamic acid ester accumulation in coffee (*Coffea*) leaves: Biological implications and uses. *Annals of Botany*, *110*(3), 595–613. https://doi.org/10.1093/aob/mcs119

[6] Cangeloni, L., Bonechi, C., Leone, G., Consumi, M., Andreassi, M., Magnani, A., Rossi, C., & Tamasi, G. (2022). Characterization of extracts of coffee leaves (*Coffea arabica* L.) by spectroscopic and chromatographic/spectrometric techniques. *Foods*, *11*(16), 2495. https://doi.org/10.3390/foods11162495

[7] Casas, M.I., Vaughan, M.J., Bonello, P., McSpadden Gardener, B., Grotewold, E., & Alonso, A.P. (2017). Identification of biochemical features of defective *Coffea arabica* L. beans. *Food Research International, 95*, 59–67. https://doi.org/10.1016/j.foodres.2017.02.015

[8] Chen, X.-M., Ma, Z., & Kitts, D.D. (2018). Effects of processing method and age of leaves on phytochemical profiles and bioactivity of coffee leaves. *Food Chemistry, 249*, 143–153. https://doi.org/10.1016/j.foodchem.2017.12.073

[9] Chen, X. (2019). A review on coffee leaves: Phytochemicals, bioactivities and applications. *Critical Reviews in Food Science and Nutrition*, *59*(7), 1008–1025. https://doi.org/10.1080/10408398.2017.1393185

[10] Czarniecka-Skubina, E., Pielak, M., Sałek, P., Korzeniowska-Ginter, R., & Owczarek, T. (2021). Consumer choices and habits related to coffee consumption by Poles. *International Journal of Environmental Research and Public Health*, *18*(8), 3948. https://doi.org/10.3390/ijerph18083948

[11] de Almeida, R.F., Trevisan, M.T.S., Thomaziello, R.A., Breuer, A., Klika, K.D., Ulrich, C.M., & Owen, R.W. (2019). Nutraceutical compounds: Echinoids, flavonoids, xanthones and caffeine identified and quantitated in the leaves of *Coffea arabica* trees from three regions of Brazil. *Food Research International, 115*, 493–503. https://doi.org/10.1016/j.foodres.2018.10.006

[12] del Castillo, M.D., Fernandez-Gomez, B., Martinez-Saez, N., Iriondo-DeHond, A., & Mesa, M.D. (2019). *Coffee by-products*. In A. Farah (Ed.), *Coffee: Production, Quality and Chemistry*. Royal Society of Chemistry: Oxfordshire, United Kingdom.

[13] DePaula, J., Cunha, S.C., Ferreira, I.M.P.L.V.O., Porto, A.C.V., Cruz, A.G., Petrarca, M., Trevisan, M.T., Revi, I., & Farah, A. (2023). Volatile fingerprinting, sensory characterization, and consumer acceptance of pure and blended *Arabica* coffee leaf teas. *Food Research International, 173*(2), 113361. https://doi.org/10.1016/j.foodres.2023.113361

[14] DePaula, J., Cunha, S.C., Partelli, F.L., Fernandes, J.O., & Farah, A. (2025). Major bioactive compounds, volatile and sensory profiles of *Coffea canephora* flowers and infusions for waste management in coffee production. *Foods, 14*(6), 911. https://doi.org/10.3390/foods14060911

[15] Franca, A.S., Oliveira, L.S., Nunes, A.A., & Alves, C.C.O. (2010). Microwave assisted thermal treatment of defective coffee beans press cake for the production of adsorbents. *Bioresource Technology*, *101*(3), 1068–1074. https://doi.org/10.1016/j.biortech.2009.08.102

[16] Hu, S., Gil-Ramírez, A., Martín-Trueba, M., Benítez, V., Aguilera, Y., & Martín-Cabrejas, M.A. (2023). Valorization of coffee pulp as bioactive food ingredient by sustainable extraction methodologies. *Current Research in Food Science*, *6*, 100475. https://doi.org/10.1016/j.crfs.2023.100475

[17] Janissen, B., & Huynh, T. (2018). Chemical composition and value-adding applications of coffee industry byproducts: a review. *Resources, Conservation & Recycling*, *128*, 110–117. https://doi.org/10.1016/j.resconrec.2017.10.001

[18] Jiao, Y., Zhao, Y., Jia, A., Wang, T., Li, J., Xiang, K., Liu, Y., Zhang, X., & Wang, L. (2025). Swin-HSSAM: A green coffee bean grading method by Swin transformer. *PLoS ONE, 20*(5), e0322198. https://doi.org/10.1371/journal.pone.0322198

[19] Klingel, T., Kremer, J. I., Gottstein, V., Rajcic de Rezende, T., Schwarz, S., & Lachenmeier, D.W. (2020). A review of coffee by-products including leaf, flower, cherry, husk, silver skin, and spent grounds as novel foods within the European Union. *Foods*, *9*(5), 665. https://doi.org/10.3390/foods9050665

[20] Konstantinidis, N., Franke, H., Schwarz, S., & Lachenmeier, D.W. (2023). Risk assessment of trigonelline in coffee and coffee by-products. *Molecules*, *28*(8), 3460. https://doi.org/10.3390/molecules28083460

[21] Lachenmeier, D.W., Rajcic de Rezende, T., & Schwarz, S. (2021). An update on sustainable valorization of coffee by-products as novel foods within the European Union. *Biology and Life Sciences Forum*, *6*(1), 37. https://doi.org/10.3390/Foods2021-10969

[22] Lee, Y.-G., Cho, E.-J., Maskey, S., Nguyen, D.-T., & Bae, H.-J. (2023). Value-added products from coffee waste: A review. *Molecules*, *28*(8), 3562. https://doi.org/10.3390/molecules28083562

[23] Mestanza, M., Calderón, J., Mori-Culqui, P.L., Caetano, A.C., Oliva-Cruz, M., García, L., & Chavez, S.G. (2026). Physical defects in green coffee: effect on bioactive and volatile compounds of the beverage. *Applied Food Research*, *6*(1), 102223. https://doi.org/10.1016/j.afres.2026.102223

[24] Monteiro, Â., Colomban, S., Azinheira, H.G., Guerra-Guimarães, L., Do Céu Silva, M., Navarini, L., & Resmini, M. (2019). Dietary antioxidants in coffee leaves: impact of botanical origin and maturity on chlorogenic acids and xanthones. *Antioxidants*, *9*(1), 6. https://doi.org/10.3390/antiox9010006

[25] Münch, A., & Lachenmeier, D.W. (2022). Validation of an HPLC method for the determination of epigallocatechin gallate, caffeine and chlorogenic acid in coffee leaves. *Biology and Life Sciences Forum*, *18*(1), 13. https://doi.org/10.3390/Foods2022-13012

[26] Murthy, P.S., & Madhava Naidu, M. (2012). Sustainable management of coffee industry by-products and value addition – a review. *Resources, Conservation and Recycling*, *66*, 45–58. https://doi.org/10.1016/j.resconrec.2012.06.005

[27] Ngamsuk, S., Huang, T.-C., & Hsu, J.-L. (2019). Determination of phenolic compounds, procyanidins, and antioxidant activity in processed *Coffea arabica* L. leaves. *Foods*, *8*(9), 389. https://doi.org/10.3390/foods8090389

[28] Nguyen, T.M.T., Cho, E.J., Song, Y., Oh, C.H., Funada, R., & Bae, H.J. (2019). Use of coffee flower as a novel resource for the production of bioactive compounds, melanoidins, and bio-sugars. *Food Chemistry*, *299*, 125120. https://doi.org/10.1016/j.foodchem.2019.125120

[29] Novita, R., Kasim, A., Anggraini, T., & Putra, D.P. (2018). Kahwa daun: Traditional knowledge of a coffee leaf herbal tea from West Sumatera, Indonesia. *Journal of Ethnic Foods*, *5*(4), 286–291. https://doi.org/10.1016/j.jef.2018.10.005

[30] Patay, E.B., Fritea, L., Antonescu, A., & Sobjanschi, L. (2017). *Coffea arabica: a plant with rich content in caffeine*. In J. N. Latosinska (Ed.), *The Question of Caffeine*. IntechOpen.

[31] Patil, S., Vedashree, M., & Murthy, P.S. (2022). Valorization of coffee leaves as a potential agri-food resource: Bio-active compounds, applications and future prospective. *Planta, 255*, 67. https://doi.org/10.1007/s00425-022-03846-x

[32] Piedrahita, D., & Pino, J.A. (2015). Essential oil of *Coffea arabica* L. *var. castillo* leaves from Colombia. *Journal of Essential Oil Bearing Plants*, *18*(2), 486–488. https://doi.org/10.1080/0972060X.2014.985734

[33] Pinheiro, F.A., Elias, L.F., Filho, M.J., Modolo, M.U., Rocha, J.C.G., Lemos, M.F., Scherer, R., & Cardoso, W.S. (2021). Arabica and Conilon coffee flowers: Bioactive compounds and antioxidant capacity under different processes. *Food Chemistry*, *345*, 128748. https://doi.org/10.1016/j.foodchem.2020.128748

[34] Ribeiro, R.C., Barros, L.J.B.d.M.d., Menezes, L.B.d., Rezende, C.M.d., Silva, A.S.d., Bon, E.P.d.S., & Teixeira, R.S.S. (2025). Valorization of green Arabica coffee coproducts for mannanase production and carbohydrate recovery. *Processes*, *13*(12), 3874. https://doi.org/10.3390/pr13123874

[35] Rigling, M., Steger, M.C., Lachenmeier, D.W., Schwarz, S., & Zhang, Y. (2023). Sensorial and aroma profiles of coffee by-products - coffee leaves and coffee flowers. *Proceedings*, *89*(1), 5. https://doi.org/10.3390/ICC2023-14837

[36] Rodríguez-Gómez, R., Vanheuverzwjin, J., Souard, F., Delporte, C., Stevigny, C., Stoffelen, P., De Braekeleer, K., & Kauffmann, J.-M. (2018). Determination of three main chlorogenic acids in water extracts of coffee leaves by liquid chromatography coupled to an electrochemical detector. *Antioxidants*, *7*(10), 143. https://doi.org/10.3390/antiox7100143

[37] Sales, A.L., Cunha, S.C., Ferreira, I.M.P.L.V.O., Morgado, J., Melo, L., DePaula, J., Miguel, M.A.L., & Farah, A. (2024). Volatilome, microbial, and sensory profiles of coffee leaf and coffee leaf-toasted maté kombuchas. *Foods*, *13*(3), 484. https://doi.org/10.3390/foods13030484

[38] Serna-Jiménez, J.A., Siles, J.A., de los Ángeles Martín, M., & Chica, A.F. (2022). A review on the applications of coffee waste derived from primary processing: Strategies for revalorization. *Processes*, *10*(12), 2436. https://doi.org/10.3390/pr10122436

[39] Silva, W.R., Carregosa, J.C., Almeida-Couto, J.M.F., Cardozo-Filho, L., & Wisniewski Jr., A. (2022). Management of de-oiled coffee beans biomass through pyrolysis process: Towards a circular bioeconomy. *Journal of Analytical and Applied Pyrolysis*, *168*, 105763. https://doi.org/10.1016/j.jaap.2022.105763

[40] Skorupa, A., Worwag, M., & Kowalczyk, M. (2023). Coffee industry and ways of using by-products as bioadsorbents for removal of pollutants. *Water*, *15*(1), 112. https://doi.org/10.3390/w15010112

[41] Stashenko, E.E., Martínez, J.R., Cárdenas-Vargas, S., Saavedra-Barrera, R., & Durán, D.C. (2013). GC–MS study of compounds isolated from *Coffea arabica* flowers by different extraction techniques. *Journal of Separation Science*, *36*(18), 2901–2914. https://doi.org/10.1002/jssc.201300483

[42] Steger, M.C., Rigling, M., Blumenthal, P., Segatz, V., Quintanilla-Belucci, A., Beisel, J. M., Rieke-Zapp, J., Schwarz, S., Lachenmeier, D.W., & Zhang, Y. (2022). Coffee leaf tea from El Salvador: on-site production considering influences of processing on chemical composition. *Foods*, *11*(17), 2553. https://doi.org/10.3390/foods11172553

[43] Tritsch, N., Steger, M.C., Segatz, V., Blumenthal, P., Rigling, M., Schwarz, S., Zhang, Y., Franke, H., & Lachenmeier, D.W. (2022). Risk assessment of caffeine and epigallocatechin gallate in coffee leaf tea. *Foods*, *11*(3), 263. https://doi.org/10.3390/foods11030263

[44] Ungureanu, N., & Vlăduț, N.-V. (2026). Sustainable valorization of spent coffee grounds within the circular economy: Innovative applications in food, agriculture, environmental, and industrial sectors. *Sustainability*, *18*(8), 4127. https://doi.org/10.3390/su18084127

[45] Yohannis, E., Teka, T.A., Adebo, J.A., Urugo, M.M., Hossain, A., & Astatkie, T. (2024). Phytochemical constituents, ethnomedicinal uses, and applications of coffee *(Coffea arabica)* leaves in functional beverages. *Journal of Food Composition and Analysis, 135,* 106570. https://doi.org/10.1016/j.jfca.2024.106570

[46] Yohannis, E., Teka, T.A., Adebo, J.A., Urugo, M.M., Hossain, A., & Astatkie, T. (2024). Phytochemical constituents, ethnomedicinal uses, and applications of coffee *(Coffea arabica)* leaves in functional beverages. *Journal of Food Composition and Analysis, 135,* 106570. https://doi.org/10.1016/j.jfca.2024.106570

[47] Wirz, K., Schwarz, S., Richling, E., Walch, S.G., & Lachenmeier, D.W. (2022). Coffee flower as a promising novel food – chemical characterization and sensory evaluation. *Biology and Life Sciences Forum*, *18*, 53. https://doi.org/10.3390/blsf2022018053

[48] *** European Commission. (2015). Regulation (EU) 2015/2283 of the European Parliament and of the Council of 25 November 2015 on novel foods, amending Regulation (EU) No 1169/2011 of the European Parliament and of the Council and repealing Regulation (EC) No 258/97 of the European Parliament and of the Council and Commission Regulation (EC) No 1852/2001. https://eur-lex.europa.eu/eli/reg/2015/2283/oj/eng (accessed at 7.07.2026).

[49] *** European Commission (2020). Commission Implementing Regulation (EU) 2020/917 of 1 July 2020 authorising the placing on the market of infusion from coffee leaves of *Coffea arabica* L. and/or *Coffea canephora* Pierre ex A. Froehner as a traditional food from a third country under Regulation (EU) 2015/2283 of the European Parliament and of the Council and amending Implementing Regulation (EU) 2017/2470. *Official Journal of the European Union*, *L209*, 10–13.

[50] *** European Commission. (2022). Commission Implementing Regulation (EU) 2022/47 of 13 January 2022 authorising the placing on the market of *Coffea arabica* L. and/or *Coffea canephora* Pierre ex A.Froehner dried cherry pulp and its infusion as a traditional food from a third country under Regulation (EU) 2015/2283 of the European Parliament and of the Council and amending Commission Implementing Regulation (EU) 2017/2470. *Official Journal of the European Union*, *L9*, 29–32.

[51] *** European Food Safety Authority (EFSA). (2020). Technical Report on the notification of infusion from coffee leaves (*Coffea arabica* L. and/or *Coffea canephora* Pierre ex A. Froehner) as a traditional food from a third country pursuant to Article 14 of Regulation (EU) 2015/2283. *EFSA Supporting Publications*, *17*, 1783E.

[52] *** International Coffee Organization - ICO. (2023). Coffee Report and Outlook. International Coffee Organization. https://icocoffee.org/documents/cy2023-24/cy2022-23/Coffee_Report_and_Outlook_April_2023_-_ICO.pdf (accessed at 8.01.2026).

[53] *** United Nations. (2019). *International Coffee Association Development Report 2019*. United Nations: New York, NY, USA; Geneva, Switzerland, pp. 1–84.

# BIOCHAR FOR SUSTAINABLE WASTEWATER REMEDIATION: PRODUCTION, PHYSICOCHEMICAL PROPERTIES, AND POLLUTANT REMOVAL MECHANISMS

/

# *BIOCHARUL PENTRU REMEDIEREA SUSTENABILĂ A APELOR UZATE: PRODUCERE, PROPRIETĂȚI FIZICO-CHIMICE ȘI MECANISME DE ÎNDEPĂRTARE A POLUANȚILOR*

**Nicoleta UNGUREANU[1)], Nicolae-Valentin VLĂDUȚ[*2)], Sorin-Ștefan BIRIȘ[1)], Neluș-Evelin GHEORGHIȚĂ[1)], Mariana IONESCU[1)]**

[1)] National University of Science and Technology Politehnica Bucharest / Romania;

[2)] National Institute of Research-Development for Machines and Installations Designed for Agriculture and Food Industry-INMA Bucharest / Romania

**E-mail: valentin_vladut@yahoo.com*

***Keywords:*** *pyrolysis, biochar, wastewater remediation, heavy metals, organic contaminants, adsorption*

**ABSTRACT**

*Biochar has attracted considerable attention as a sustainable biomass-derived carbonaceous material for wastewater treatment because of its porous structure, surface functionality, and versatile adsorption properties. This review summarizes recent advances in biochar production by pyrolysis, including the main pyrolysis pathways, the factors influencing biochar formation, and the physicochemical characteristics that determine its environmental performance. The effects of feedstock type, pyrolysis conditions, and surface modification strategies on biochar properties are discussed, together with the main analytical techniques used for biochar characterization. Particular attention is given to the application of biochar for the removal of inorganic and organic contaminants from aqueous systems. Representative studies describing the adsorption of heavy metals, nutrients, dyes, pesticides, pharmaceuticals and personal care products, endocrine-disrupting compounds, and persistent organic pollutants are critically discussed, highlighting the adsorption mechanisms involved and the improved performance achieved through engineered biochars. Current challenges related to biochar production, modification, regeneration, and practical implementation are also addressed. Overall, biochar represents a sustainable and multifunctional material with considerable potential for advanced wastewater remediation while supporting biomass valorization and circular bioeconomy strategies.*

**REZUMAT**

*Biocharul a atras un interes deosebit ca material carbonic sustenabil obținut din biomasă pentru epurarea apelor uzate, datorită structurii sale poroase, funcționalităților de suprafață și proprietăților sale versatile de adsorbție. Acest articol sintetizează progresele recente privind obținerea biocharului prin piroliză, incluzând principalele tipuri de piroliză, factorii care influențează formarea biocharului și caracteristicile fizico-chimice care determină performanța sa în aplicațiile de mediu. Sunt prezentate efectele tipului de biomasă, ale condițiilor de piroliză și ale strategiilor de modificare a suprafeței asupra proprietăților biocharului, împreună cu principalele tehnici analitice utilizate pentru caracterizarea acestuia. O atenție deosebită este acordată utilizării biocharului pentru îndepărtarea contaminanților anorganici și organici din sistemele acvatice. Sunt analizate critic studii reprezentative privind adsorbția metalelor grele, nutrienților, coloranților, pesticidelor, compușilor farmaceutici și produselor de îngrijire personală, compușilor cu acțiune de perturbare endocrină și poluanților organici persistenți, evidențiindu-se mecanismele de adsorbție implicate și performanțele superioare obținute prin utilizarea biocharurilor modificate. De asemenea, sunt abordate provocările actuale legate de producerea, modificarea, regenerarea și implementarea practică a biocharului. În ansamblu, biocharul reprezintă un material sustenabil și multifuncțional, cu un potențial considerabil pentru remedierea avansată a apelor uzate, contribuind totodată la valorificarea biomasei și la susținerea principiilor bioeconomiei circulare.*

## INTRODUCTION

Water pollution has become one of the major environmental challenges worldwide, driven by increasing water demand, intensive industrialization, and the continuous release of anthropogenic

contaminants into aquatic systems. The growing complexity of wastewater composition, characterized by the coexistence of conventional and emerging pollutants, requires the development of advanced and sustainable treatment approaches capable of ensuring efficient contaminant removal. The rapid growth of industrial activities, urbanization, and population increase has resulted in the generation of large volumes of wastewater containing a wide range of inorganic and organic contaminants. Industrial, municipal, agricultural, and domestic wastewater streams may contain heavy metals, nutrients, dyes, pharmaceuticals, antibiotics, pesticides, and other emerging pollutants, whose persistence and potential ecological impacts represent significant challenges for water management and environmental protection.

Even at trace concentrations, contaminants such as heavy metals, antibiotics, microplastics, and other hazardous compounds may pose risks to aquatic ecosystems and human health due to their persistence, bioaccumulation potential, and ability to interfere with biological processes (*Alshehri and Pugazhendhi, 2024*). Although conventional treatment technologies, including biological processes, chemical precipitation, membrane filtration, and advanced oxidation processes, are widely applied, their efficiency may be limited for certain persistent contaminants, while high operational costs, energy requirements, and secondary waste generation remain important concerns (*Alagha et al., 2020; Ambaye et al., 2021*). Therefore, the development of sustainable, efficient, and economically feasible treatment materials represents an important research priority.

In recent years, biochar has emerged as a promising carbonaceous material for environmental remediation applications, particularly for wastewater treatment. Biochar is a porous, carbon-rich material produced through the thermochemical conversion of biomass under oxygen-limited conditions. Unlike conventional carbon adsorbents, biochar can be obtained from a wide variety of renewable feedstocks, including woody biomass, agricultural residues, food-processing wastes, animal-derived materials, and other organic by-products (*Ungureanu et al., 2025a; Ungureanu et al., 2025b*). This versatility provides an opportunity for the simultaneous valorization of biomass residues and the development of sustainable materials within the framework of circular economy strategies. The increasing interest in biochar-based wastewater treatment is associated with its favorable physicochemical characteristics, including developed porosity, high carbon content, surface functionality, mineral constituents, and structural stability. These properties can be influenced by the nature of the biomass precursor and by the conditions applied during thermochemical conversion, allowing the production of biochars with tailored characteristics for specific environmental applications (*Ghodake et al., 2021*).

Furthermore, compared with conventional activated carbon, biochar presents advantages related to lower production costs, the possibility of using locally available waste resources, and its contribution to carbon management and waste reduction. An additional advantage of biochar-based adsorbents is their potential regeneration and reuse after pollutant removal, which can contribute to reducing operational costs and improving the economic feasibility of wastewater treatment processes. Various regeneration approaches, including thermal, chemical, and other non-thermal methods, have been investigated to restore adsorption capacity by removing or decomposing retained contaminants. The selection of an appropriate regeneration strategy depends on the biochar characteristics, the nature of the adsorbed pollutants, and the interactions established between the contaminant and the biochar surface. Among these approaches, non-thermal regeneration methods, particularly chemical regeneration, have attracted increasing interest due to their ability to preserve adsorbent structure and enable multiple reuse cycles (*Alsawy et al., 2022*).

The environmental performance of biochar in wastewater treatment depends on the interactions between its physicochemical properties and the characteristics of target pollutants. Depending on its composition and production pathway, biochar has demonstrated potential for the removal of a broad range of contaminants, including heavy metals, nutrients, dyes, pharmaceuticals, antibiotics, endocrine-disrupting compounds, pesticides, and other organic pollutants. In addition to its direct adsorption capacity, modified and engineered biochars have expanded the applicability of these materials through improved surface properties, enhanced selectivity, and additional catalytic or biological functionalities.

Consequently, understanding the relationship between biomass feedstock, thermochemical conversion parameters, resulting biochar characteristics, and pollutant removal performance is essential for designing efficient and sustainable treatment systems. This review provides an overview of biochar production pathways, with emphasis on pyrolysis processes and their influence on material properties, followed by an analysis of the physicochemical characteristics governing biochar performance. Furthermore, the application of biochar-based materials for the removal of inorganic and organic contaminants from

wastewater is critically discussed, highlighting the role of feedstock selection, modification strategies, and pollutant-specific removal mechanisms.

## PRODUCTION OF BIOCHAR: PYROLYSIS PATHWAYS AND INFLUENCING PARAMETERS

Biochar can be obtained through several thermochemical conversion pathways, including slow pyrolysis, carbonization, and hydrothermal carbonization, with the selected route influencing the physicochemical properties and potential applications of the final carbonaceous material. Among these approaches, pyrolysis remains the most widely investigated method due to its flexibility in controlling product distribution and obtaining biochar with tailored structural and surface properties.

Pyrolysis is a thermochemical conversion process based on the thermal decomposition of biomass and organic waste under oxygen-limited or oxygen-free conditions. The process is generally conducted within a temperature range of approximately 300–700 °C, although higher temperatures may be applied depending on the reactor configuration and targeted products. As an externally heated endothermic process, pyrolysis promotes the breakdown of complex organic macromolecules into smaller molecular fragments through a series of thermal degradation, cracking, and rearrangement reactions.

These transformations generate a mixture of solid, liquid, and gaseous products, with their relative distribution being strongly influenced by operational parameters such as temperature, heating rate, vapor residence time, and feedstock characteristics. Depending on the applied conditions, pyrolysis typically produces three main fractions: biochar, bio-oil, and pyrolysis gases (Figure 1).

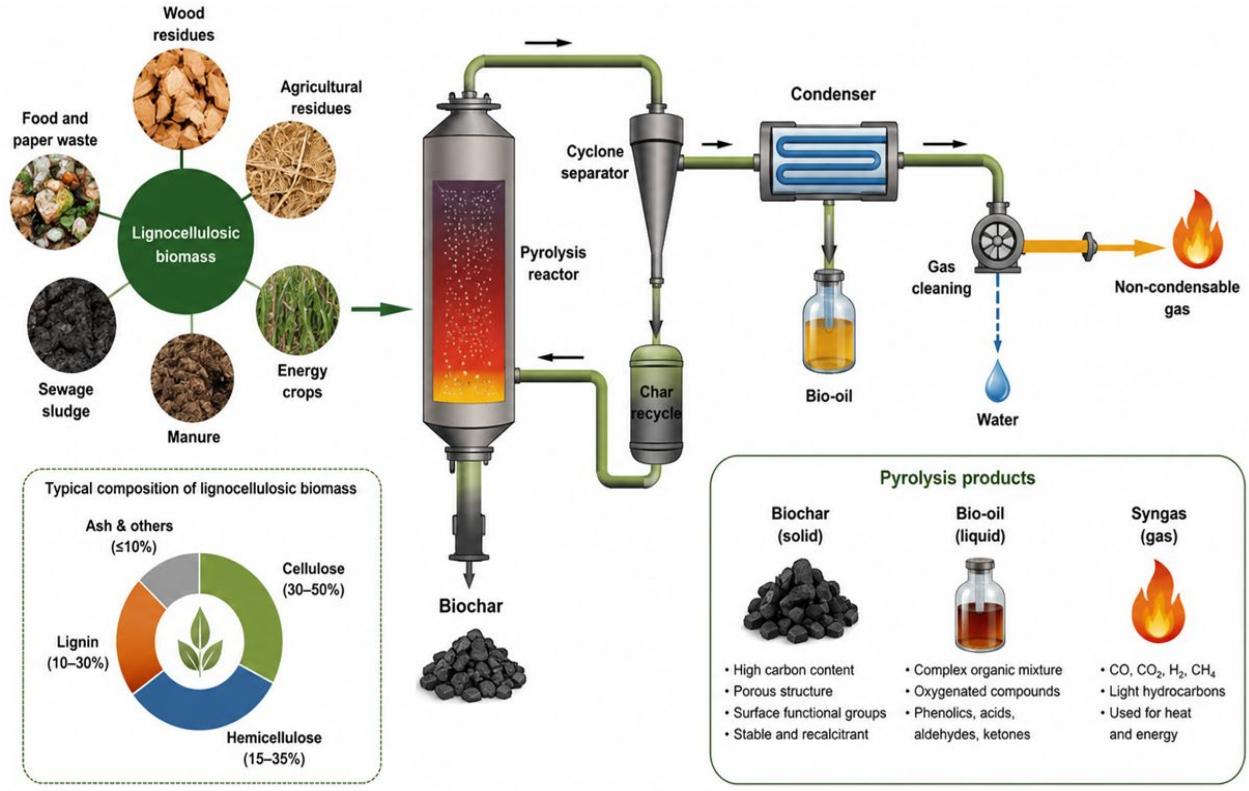



**Fig. 1 - Schematic representation of the biomass pyrolysis process and the formation of major pyrolysis products**

*Slow pyrolysis* is the conventional pyrolysis pathway primarily employed for biochar production. This process is characterized by relatively low heating rates, moderate temperatures (typically 300–500 °C), and extended residence times, which favor secondary reactions and the formation of stable carbonaceous solids. Due to the prolonged interaction between biomass and the thermal environment, slow pyrolysis generally results in higher biochar yields (approximately 30–40 wt%) compared with other pyrolysis regimes, while producing lower amounts of bio-oil and non-condensable gases.

The resulting biochars usually exhibit high carbon stability, developed porosity, and abundant surface functional groups, making them suitable for environmental applications, including contaminant adsorption and wastewater remediation (*Ungureanu et al., 2025a*).

*Intermediate pyrolysis* represents a transition between slow and fast pyrolysis, operating under moderate heating rates and temperatures generally ranging from 500 to 700 °C. This regime provides a more balanced distribution of solid, liquid, and gaseous products, enabling simultaneous recovery of biochar, bio-oil, and syngas. Compared with slow pyrolysis, intermediate pyrolysis promotes greater volatile release while maintaining significant biochar production. The characteristics of the resulting biochar depend strongly on feedstock composition and operating parameters, with its surface chemistry and porous structure determining its suitability for applications such as adsorption, soil amendment, and environmental remediation (*Ungureanu et al., 2025a*).

*Fast pyrolysis* is designed to maximize the production of condensable vapors and bio-oil by applying high heating rates, temperatures typically between 400 and 600 °C, and very short vapor residence times. Under these conditions, rapid thermal decomposition limits secondary reactions and favors the formation of liquid products, which may account for approximately 50–75 wt% of the product distribution, while biochar and gaseous fractions are produced in lower proportions. Although biochar yield is reduced compared with slow pyrolysis, the produced material can still exhibit valuable adsorption properties due to its carbonaceous structure and surface functionalities, particularly after activation or modification treatments (*Ungureanu et al., 2025a*).

*Flash pyrolysis* represents an intensified pyrolysis approach characterized by extremely rapid heating rates, very short reaction times, and high temperatures, generally above 600 °C. The process promotes rapid conversion of biomass into volatile compounds and gaseous products, while minimizing solid residue formation. Although biochar production is limited compared with slower pyrolysis processes, the obtained carbonaceous fraction can serve as a precursor for activated carbon or engineered adsorbent materials after appropriate modification. Due to the severe operating conditions and extensive feedstock preparation requirements, flash pyrolysis is less commonly applied for biochar production but remains relevant for integrated thermochemical conversion systems (*Ungureanu et al., 2025a*).

Table 1 summarizes the principal pyrolysis pathways, highlighting their characteristic operating parameters and the typical product distribution associated with each process.

**Table 1**

**Key physicochemical properties of biochar influencing its environmental applications**

*(Ungureanu et al., 2025a)*

| Technique | Residence time | Temperature (°C) | Heating rate | Primary products |
|---|---|---|---|---|
| Torrefaction (mild pyrolysis) | 15–60 min | 200–300 | 10–50 °C/min (mild) | Mainly solid (torrefied biomass); minor volatiles and syngas |
| Slow pyrolysis (conventional) | 5–12 h | 300–500 (up to 900) | 0.1–1 °C/s (very low) | 30–40% biochar, 35–45% bio-oil, 25–40% syngas |
| Intermediate pyrolysis | 0.5–40 s | 500–700 | 0.4–10 °C/s (medium) | 40–50% bio-oil, 25–35% biochar, 20–30% syngas |
| Fast pyrolysis | 0.5–2 s (<2 s) | 400–600 (optimal) | 10–200 °C/s | 60–75% bio-oil, 12–25% char, 10–20% syngas |
| Flash pyrolysis | <0.5 s | 600–1400 | 1000–21,000 °C/s (very high) | 75–80% bio-oil, 10–20% char, 10–20% syngas |

Biochar represents the solid fraction retained after thermal conversion and is typically favored under slow pyrolysis conditions characterized by relatively low heating rates and moderate temperatures. It is a carbon-rich, porous material containing stable aromatic structures and inorganic mineral constituents derived from the original biomass. Due to its physicochemical properties, biochar has attracted considerable interest in applications including soil improvement, carbon sequestration, adsorption of contaminants, and as a precursor for activated carbon production.

Bio-oil corresponds to the condensed liquid fraction obtained mainly under intermediate temperatures and higher heating rates. It consists of a complex mixture of oxygenated organic compounds, including phenolics, acids, ketones, aldehydes, and other volatile derivatives. Although its high oxygen content, acidity, and chemical instability limit direct utilization as a transportation fuel, bio-oil represents an important intermediate to produce value-added chemicals and upgraded energy carriers.

The gaseous fraction generated during pyrolysis consists mainly of hydrogen, carbon monoxide, carbon dioxide, methane, and light hydrocarbons. Its composition depends strongly on the feedstock characteristics and operating parameters, with higher temperatures generally promoting secondary

cracking reactions and increasing gas production. Unlike syngas obtained through conventional gasification processes, pyrolysis-derived gases are produced under less severe thermal conditions and typically contain a different distribution of gaseous components.

In addition to affecting product distribution and biochar properties, pyrolysis conditions also influence the formation of potentially harmful compounds. Insufficient control of thermal conversion parameters may favor the accumulation of organic contaminants such as PAHs, VOCs, and other persistent compounds within the biochar matrix. Consequently, selecting appropriate pyrolysis conditions is critical not only for optimizing carbon yield and adsorption performance but also for ensuring the environmental safety of biochar-based treatment materials (*Freddo et al., 2012; Fabbri et al., 2013*).

## PHYSICOCHEMICAL PROFILES OF BIOCHAR: INFLUENCE OF FEEDSTOCK AND PYROLYSIS PARAMETERS

Biochar, also known as pyrolytic charcoal, is a stable carbonaceous material obtained from the thermal decomposition of biomass under oxygen-deficient conditions. Its structure consists of condensed aromatic carbon domains with partially ordered graphene-like layers embedded within amorphous regions, resulting in a heterogeneous matrix containing carbon, hydrogen, oxygen, and inorganic mineral components. The formation and properties of biochar are determined by the characteristics of the original biomass and by the operational parameters applied during thermochemical conversion. These factors control the development of its carbon structure, surface chemistry, porosity, and mineral composition, which ultimately define its suitability for different environmental applications.

The yield and properties of biochar depend strongly on both feedstock composition and conversion parameters. Biochar yields commonly range between approximately 10 and 40%, with higher production rates generally obtained under slow pyrolysis conditions and temperatures below 500 °C (Oni et al., 2019). For lignocellulosic biomass, conversion efficiencies may result in biochar yields of approximately 0.36–0.45 kg per kg of initial biomass, depending on the characteristics of the feedstock and operating conditions (*Ungureanu et al., 2025a*). Increasing temperature generally enhances devolatilization reactions, leading to lower solid yields but increased carbon concentration and aromaticity. At moderate temperatures, biochar production remains significant, whereas further temperature elevation promotes extensive carbon conversion into volatile products and reduces the remaining solid fraction (*Mohammadi et al., 2025*). Therefore, pyrolysis conditions determine not only the quantity of biochar produced but also its structural organization and chemical functionality, which ultimately influence its environmental performance.

The structural and chemical characteristics of biochar are highly dependent on biomass composition, particle size, moisture content, heating rate, and residence time. Rapid heating and shorter vapor residence times generally promote the formation of smaller particles and materials with increased surface development, whereas slow heating of larger biomass particles may generate more stable carbon structures with enhanced resistance to degradation (*An et al., 2022*). Biomass origin also plays an important role, as agricultural residues, woody biomass, and animal-derived feedstocks produce biochars with distinct mineral composition, surface chemistry, and porosity. Consequently, the selection of biomass precursors represents a critical step in designing biochar materials with specific physicochemical characteristics suitable for targeted applications.

Comparative evaluations have demonstrated that feedstock type and pyrolysis temperature are among the dominant factors controlling the physicochemical profile of biochar. Increasing pyrolysis temperature generally promotes carbonization, resulting in higher carbon content, greater aromaticity, increased pH, and enhanced specific surface area and pore development due to progressive decomposition of volatile organic fractions. However, these changes are commonly accompanied by a decrease in volatile matter and cation exchange capacity, as oxygen-containing functional groups responsible for ion exchange reactions are progressively removed during thermal treatment. In addition, biochars derived from animal wastes and organic residues generally exhibit higher mineral content and cation exchange capacity but lower surface areas compared with those produced from lignocellulosic feedstocks such as wood and agricultural residues, reflecting differences in biomass composition and ash-forming constituents (*Tomczyk et al., 2020*).

Among the most relevant properties determining biochar performance are specific surface area, pore structure, surface functional groups, aromaticity, ash content, pH, and cation exchange capacity. Increasing pyrolysis temperature generally promotes carbonization, leading to higher aromaticity, lower oxygen-containing functionalities, and increased alkalinity. Plant-derived biochars commonly exhibit higher pH values and greater alkalinity compared with manure-derived materials due to differences in mineral composition. In addition, the hydrological behavior of biochar, including water retention, wettability, and infiltration capacity, is

strongly influenced by feedstock characteristics, production conditions, particle size, and surface morphology (*Kinney et al., 2012; Chen et al., 2017; Luo et al., 2021; Mechnou et al., 2025*).

The interrelationships between biomass characteristics, pyrolysis conditions, and the resulting physicochemical properties of biochar are summarized in Figure 2, highlighting the role of surface chemistry, pore development, and carbon structure in determining its environmental functionality.

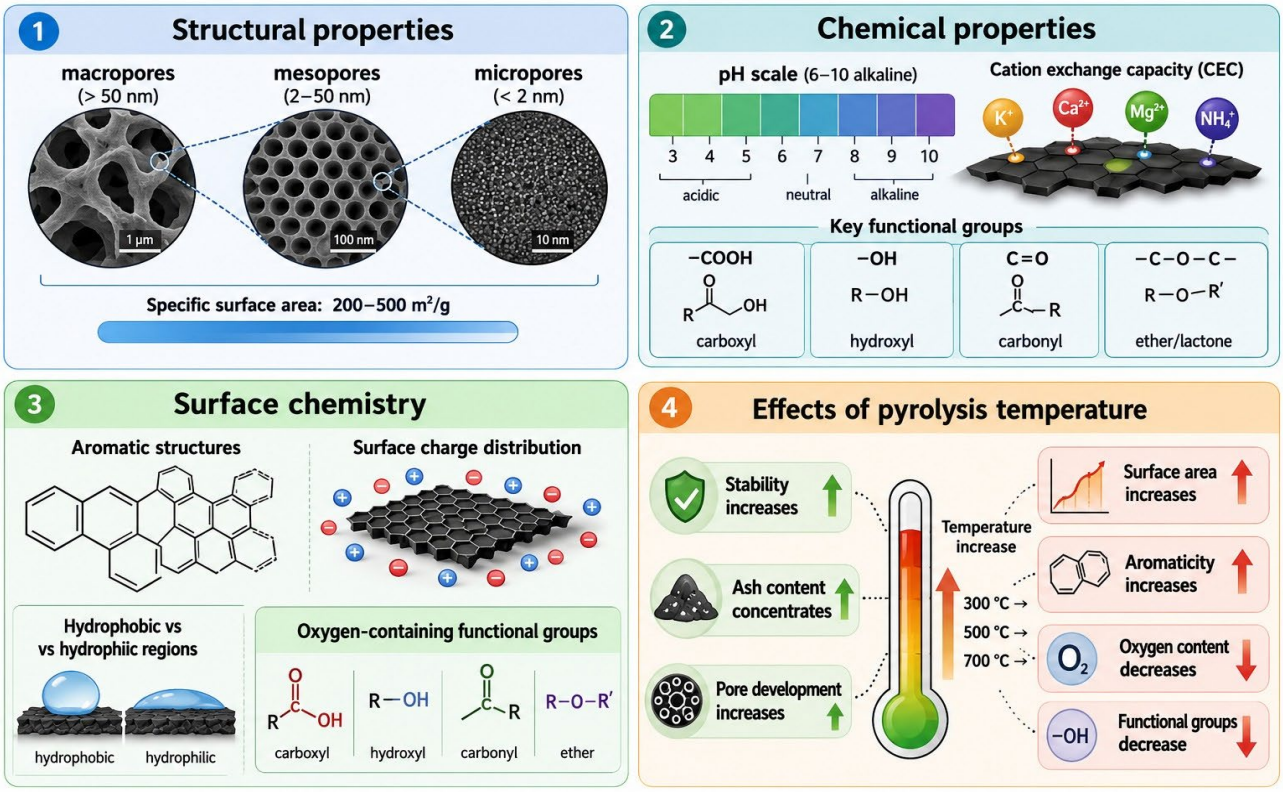



**Fig. 2 - Physicochemical properties of biochar and their relationship with surface chemistry, pore structure, and pyrolysis temperature**

*(adapted from Abbas et al., 2026)*

The physicochemical properties of biochar are commonly evaluated using complementary characterization techniques that provide information on its morphology, structure, surface chemistry, and mineral composition. Scanning electron microscopy (SEM) is widely employed to examine surface morphology and pore development, whereas Brunauer–Emmett–Teller (BET) analysis is used to determine specific surface area, pore volume, and pore size distribution, which are directly related to adsorption performance. Fourier-transform infrared spectroscopy (FTIR) enables the identification of surface functional groups involved in adsorption processes, while X-ray diffraction (XRD) provides information on crystalline mineral phases and the degree of structural ordering of the carbon matrix. In addition, X-ray photoelectron spectroscopy (XPS) is frequently applied to determine the elemental composition and chemical states of surface atoms, allowing a better understanding of the interactions between biochar and inorganic or organic contaminants. Together, these analytical techniques provide a comprehensive assessment of the physicochemical characteristics governing biochar functionality and environmental performance.

The relationship between pyrolysis conditions and biochar properties determines its suitability for specific applications. Biochars obtained through slow pyrolysis generally exhibit high structural stability, developed porosity, and favorable ion exchange properties, making them suitable for soil-related applications and long-term carbon storage. In contrast, biochars produced under faster heating conditions may exhibit enhanced surface area and microporosity, which are advantageous for adsorption processes, water treatment, and catalytic applications. Materials generated through rapid thermal conversion routes may develop highly porous structures with potential applications in gas storage, odor removal, and composite materials (*Li et al., 2020; Afshar et al., 2024*). These differences highlight the importance of controlling production parameters to obtain biochars with properties adapted to their intended environmental functions.

Table 2 depicts the main properties of biochar obtained from the pyrolysis of lignocellulosic biomass.

**Table 2**

**Key physicochemical properties of biochar influencing its environmental applications**

(*Authors' own elaboration*)

| Property | Description | Typical characteristics / range | Relevance for pollutant adsorption |
|---|---|---|---|
| Feedstock type | Origin and composition of biomass used for biochar production | Wood, agricultural residues, crop waste, manure, organic wastes | Determines carbon content, mineral composition, surface chemistry, and adsorption behavior |
| Pyrolysis temperature | Main parameter controlling carbonization degree and surface development | 300–700 °C | Higher temperatures generally increase aromaticity, porosity, and stability, but may reduce oxygen-containing functional groups |
| Carbon content (C) | Proportion of carbonaceous structures in biochar | 50–90 wt% | Associated with aromaticity, structural stability, and π–π interactions with organic pollutants |
| Oxygen content (O) | Amount of oxygen-containing surface functionalities | 5–30 wt% | Influences polarity, hydrophilicity, hydrogen bonding, and complexation mechanisms |
| H/C ratio | Indicator of carbonization and aromaticity degree | <0.6 for highly carbonized biochars | Lower values indicate greater aromaticity and resistance to degradation |
| O/C ratio | Indicator of surface polarity and oxidation state | <0.4 for stable biochars | Reflects surface functionality and interaction with contaminants |
| Specific surface area (BET) | Total accessible surface area determined by gas adsorption methods | Typically 10–500 m²/g (higher values possible after activation) | Controls available adsorption sites and interactions with pollutants |
| Pore structure | Distribution of micro-, meso-, and macropores | Developed porous network; strongly dependent on temperature and activation | Governs the diffusion and physical adsorption capacity |
| Surface functional groups | Oxygen-containing groups (–OH, –COOH, C=O) and other active sites | Variable depending on feedstock and treatment | Responsible for electrostatic attraction, hydrogen bonding, and surface complexation |
| pH and surface charge | Acid–base properties of biochar surface | Usually pH 6–11 | Influences pollutant speciation and adsorption through electrostatic interactions |
| Ash and mineral content | Inorganic fraction containing Ca, Mg, K, Fe, Si and other minerals | 1–30 wt% depending on biomass source | Contributes to ion exchange, precipitation, and catalytic interactions |
| Cation exchange capacity (CEC) | Ability to exchange positively charged ions | 10–200 cmol(+)/kg | Relevant for removal of metal ions and nutrient recovery |
| Electrical conductivity (EC) | Indicator of soluble mineral salts and ionic species | Highly variable | May affect ionic interactions and suitability for environmental applications |
| Heavy metals content | Potential contaminants originating from feedstock | Dependent on biomass source and processing | Requires monitoring before environmental use |

Note: BET surface area refers to the specific surface area determined by the Brunauer–Emmett–Teller method and represents an important parameter for evaluating the adsorption potential of biochar. Higher surface areas generally indicate increased availability of adsorption sites and improved interaction with contaminants (*Ungureanu et al., 2025b*).

Following the description of the main physicochemical characteristics governing biochar performance, it is important to consider that these properties are not determined exclusively during pyrolysis but are also influenced by the characteristics of the precursor biomass and by the treatments applied before conversion. Biomass pretreatment represents a critical step that can modify the structural and chemical features of the precursor material, consequently affecting the physicochemical properties of the resulting biochar. Depending on the biomass type and the desired application, pretreatment approaches may include

physical methods, such as drying, grinding, sieving, or washing, as well as chemical or biological treatments aimed at altering biomass composition, enhancing accessibility of reactive components, or introducing specific functionalities. These modifications can influence important biochar characteristics, including pore development, surface chemistry, mineral composition, and adsorption capacity (*Xiang et al., 2020*). Therefore, appropriate selection of biomass pretreatment conditions is essential for obtaining biochar materials with tailored properties suitable for specific environmental applications.

Although pristine biochar exhibits favorable characteristics for pollutant removal, its adsorption performance may be limited compared with highly engineered carbon materials such as activated carbon. Therefore, various activation and modification strategies have been investigated to enhance its surface properties and adsorption capacity. These approaches include physical treatments, mineral incorporation, magnetic modification, and chemical activation using acidic, alkaline, or other functionalizing agents. Among these methods, chemical modification, particularly treatments involving potassium-based compounds, has been widely applied due to its ability to increase surface area, develop pore structures, and introduce additional active functional groups. However, chemical activation may involve additional processing requirements, including washing, neutralization, and management of chemical residues (*Ahmad et al., 2018*). Consequently, increasing attention has been directed toward the intrinsic composition of biomass feedstocks and the possibility of obtaining biochars with enhanced adsorption properties through appropriate selection of precursor materials and conversion conditions.

Further improvement of biochar performance can be achieved through surface modification strategies designed to enhance its adsorption capacity and selectivity toward specific contaminants. Although pristine biochar exhibits intrinsic adsorption potential, its application may be limited by insufficient pore development and a restricted number of accessible active sites. Therefore, activation and functionalization approaches are commonly employed to optimize its surface properties for targeted environmental applications (*Tadesse et al., 2025*). Compared with pristine biochar, modified biochars generally exhibit improved pore development, larger accessible surface areas, and a higher density of reactive functional groups, which contribute to stronger interactions with pollutants (*Ahmed et al., 2016*).

These treatments can modify the carbon matrix, increase microporosity, and generate additional adsorption sites through the incorporation or enrichment of functional groups (*Tadesse et al., 2025*). Various modification approaches, including surface oxidation, chemical functionalization, mineral impregnation, magnetic modification, metal oxide loading, and thermal treatments, have been explored to tailor biochar properties for environmental applications (*Ahmed et al., 2016*). These modifications can introduce or enhance oxygen-, nitrogen-, or mineral-based active sites, promoting adsorption mechanisms such as electrostatic attraction, ion exchange, surface complexation, and chemical interactions with inorganic and organic contaminants. Consequently, engineered biochars have emerged as promising alternatives to conventional carbonaceous adsorbents, combining the advantages of renewable biomass-derived materials with enhanced remediation performance.

Overall, the unique physicochemical characteristics of biochar, including its developed porous structure, high specific surface area, surface functional groups, ion exchange capacity, regeneration potential, and long-term structural stability, have contributed to its increasing use in environmental applications. The properties of biochar can be tailored through appropriate selection of biomass feedstock, optimization of pyrolysis conditions, and application of pretreatment, activation, or surface modification strategies.

Depending on these factors, biochar can exhibit distinct characteristics suitable for different purposes, including soil improvement, carbon sequestration, composting enhancement, catalytic processes, and adsorption-based remediation. Among these applications, the ability of biochar to retain and immobilize contaminants has received particular attention, with numerous studies demonstrating its effectiveness in removing heavy metals, dyes, antibiotics, endocrine-disrupting compounds, and other organic and inorganic pollutants from aqueous environments. Moreover, its production from renewable biomass resources and its contribution to waste valorization and carbon management position biochar as a sustainable multifunctional material with significant potential for addressing current environmental challenges.

## UTILIZATION OF BIOCHAR IN WASTEWATER TREATMENT

Biochar has emerged as a versatile and sustainable carbon-based material for wastewater treatment due to its porous structure, developed surface area, mineral composition, and abundance of surface functional groups. Its physicochemical properties enable the removal of a wide range of contaminants

through adsorption and other complementary processes, with the efficiency of treatment depending on both biochar characteristics and pollutant properties. Feedstock composition, pyrolysis conditions, activation or surface modification strategies, and wastewater characteristics strongly influence the adsorption capacity and selectivity of biochar-based materials.

The adsorption performance of biochar is primarily governed by its structural and surface properties, including specific surface area, pore architecture, oxygen-containing functional groups, cation exchange capacity, aromatic carbon domains, and mineral constituents. The porous structure determines the accessibility and availability of adsorption sites, while surface functional groups contribute to electrostatic interactions, complexation, hydrogen bonding, and ion exchange processes with target pollutants. In addition, aromatic structures formed during high-temperature pyrolysis provide π-electron systems that can promote interactions with aromatic organic contaminants, whereas inorganic mineral phases may participate in precipitation or surface complexation mechanisms, particularly during the removal of inorganic pollutants (*Ambaye et al., 2021; Barquilha and Braga, 2021*). These characteristics are strongly influenced by the precursor biomass and thermochemical conversion conditions, including temperature, heating rate, residence time, and process atmosphere. Consequently, activation and surface modification strategies have been increasingly explored to engineer biochars with tailored properties and enhanced selectivity toward specific contaminants.

Accordingly, the following sections discuss the application of pristine and modified biochars for the removal of inorganic and organic contaminants from wastewater, with emphasis on adsorption mechanisms, material modifications, and treatment efficiency.

- **Removal of heavy metals**

The removal of heavy metals by biochar is governed by a combination of physical and chemical interactions, which depend on the surface properties of the material, metal characteristics, and solution conditions. The main mechanisms involved include surface complexation, ion exchange, electrostatic interactions, mineral precipitation, and pore filling (Figure 3).

Oxygen-containing functional groups, such as carboxyl, hydroxyl, and carbonyl moieties, provide active sites for metal binding through coordination interactions, while exchangeable cations naturally present on biochar surfaces can be replaced by metal ions from aqueous solutions. In addition, the negatively charged surface of many biochars facilitates the retention of positively charged metal species, whereas mineral components may contribute through co-precipitation processes. The porous structure and developed surface area of biochar further enhance contaminant immobilization by providing additional adsorption sites and promoting physical entrapment within the pore network. The relative contribution of each mechanism depends strongly on biochar characteristics, including feedstock composition, production conditions, and surface modification strategies.

Among heavy metal contaminants, arsenic represents a particular challenge due to its high toxicity, persistence, and significant risks to drinking water safety. Although biochar has been widely investigated as a low-cost and environmentally sustainable adsorbent for arsenic remediation, pristine biochars often exhibit limited adsorption efficiency because of electrostatic repulsion between negatively charged biochar surfaces and arsenic species. Consequently, various modification strategies, particularly metal-based functionalization, have been developed to enhance arsenic removal by introducing additional reactive sites and improving surface interactions. Comparative analyses have demonstrated that feedstock type, pyrolysis conditions, and surface modification strongly influence arsenic adsorption performance, with iron-modified biochars being among the most effective materials due to their high affinity toward arsenic species and favorable cost–efficiency balance (*Tian et al., 2023*).

A representative example of metal-modified biochars for arsenic remediation was reported using biochar derived from the aboveground biomass of the arsenic hyperaccumulator *Pteris vittata* and subsequently functionalized with iron. Compared with pristine biochar, Fe modification significantly enhanced arsenic removal performance by increasing the specific surface area, pore volume, and availability of reactive adsorption sites. The Fe-modified biochar exhibited maximum adsorption capacities of 7.64 mg $g^{-1}$ for As(III) and 10.2 mg $g^{-1}$ for As(V), according to Langmuir fitting. The improved adsorption efficiency was mainly attributed to enhanced electrostatic interactions and the formation of stable Fe–As complexes, which also reduced arsenic leaching by 69–89%. These findings highlight the potential of converting As-enriched phytoremediation biomass into engineered biochars with improved adsorption capacity and environmental stability for arsenic-contaminated water treatment (*Wang et al., 2024*).

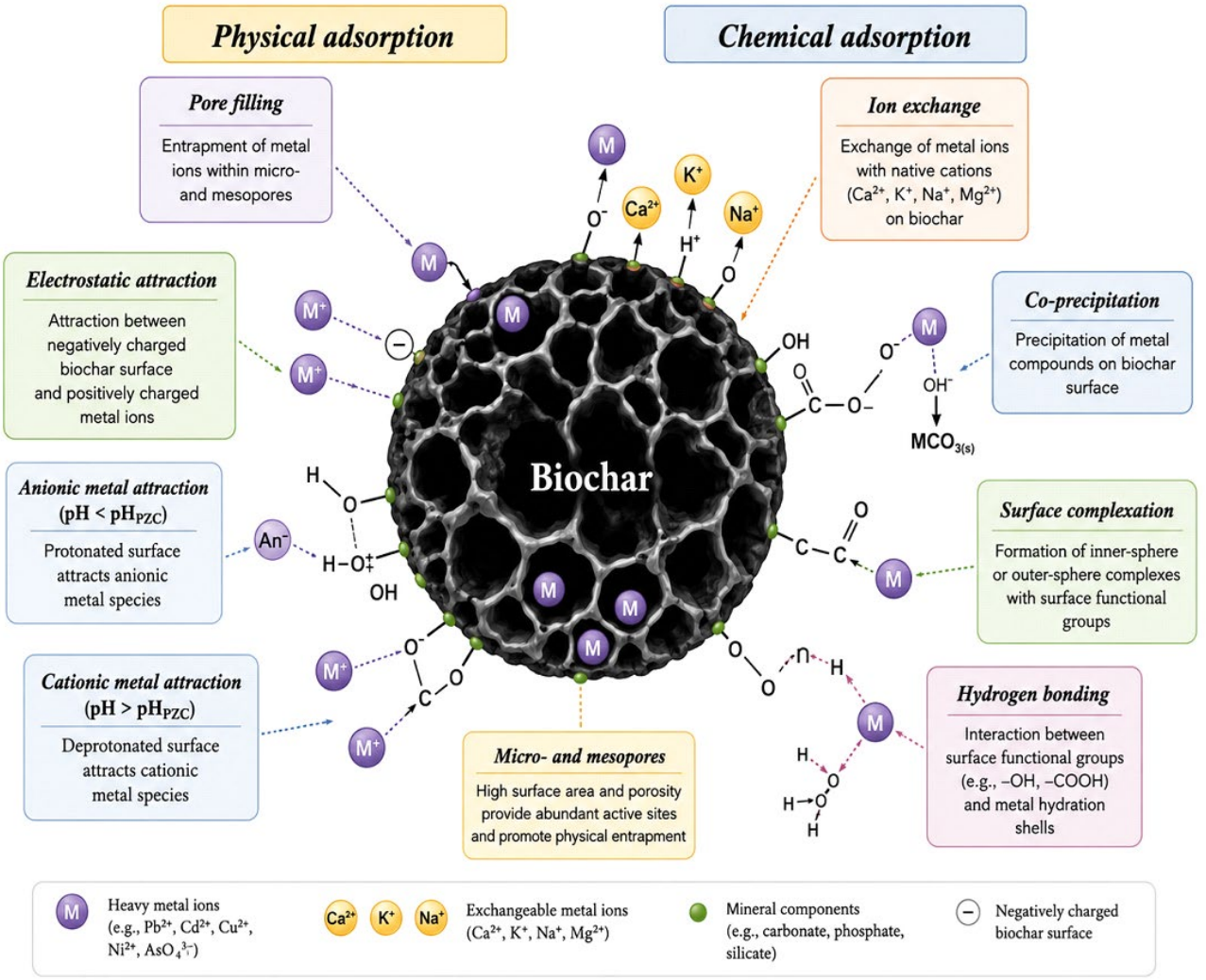



**Fig. 3 - Mechanisms involved in heavy metal adsorption onto biochar**

Similarly, metal oxide-functionalized biochars have been investigated to improve arsenate adsorption at environmentally relevant concentrations. A CuO-loaded biochar prepared from *Eleocharis dulcis* biomass was evaluated for arsenate removal from aqueous systems, particularly targeting low arsenic concentrations relevant to drinking water contamination. The incorporation of CuO introduced additional reactive sites and enhanced arsenic retention, with the composite exhibiting a maximum adsorption capacity of 26.1 mg $g^{-1}$ according to the Langmuir model. The adsorption process followed pseudo-second-order kinetics and was mainly attributed to chemisorption mechanisms involving interactions between arsenate species and CuO-modified biochar surfaces. Fixed-bed column experiments demonstrated removal efficiencies above 88% during continuous operation, while regeneration tests confirmed the possibility of repeated use, although adsorption capacity gradually decreased after successive cycles (*Din et al., 2024*). These results highlight the potential of metal oxide-modified biochars as efficient and recoverable materials for arsenic remediation

Biochar derived from potassium-rich agricultural residues has demonstrated promising potential for the removal of heavy metal contaminants from aqueous systems. Biochars obtained from banana peels and cauliflower leaves were evaluated as adsorbents for the simultaneous removal of Cu(II), Cd(II), and Pb(II) ions. The production yields of the obtained biochars were relatively high, reaching 61.44% for banana peel-derived biochar and 64.66% for cauliflower leaf-derived biochar, which was attributed to the catalytic influence of potassium naturally present in the precursor biomass during thermal conversion. Structural characterization revealed the presence of K-containing mineral phases, while adsorption experiments indicated a higher sorption performance of banana peel biochar compared with cauliflower leaf biochar. The adsorption process was strongly dependent on solution pH, with increasing metal uptake observed at higher pH values, reaching optimal conditions around pH 6 for Cu(II) and Pb(II), and pH 8 for Cd(II). Competitive adsorption behavior followed the order Pb(II) > Cu(II) > Cd(II), suggesting stronger

affinity of the biochar surface toward lead ions. Electrostatic interactions were identified as the dominant mechanism governing metal retention, although mineral components and surface characteristics also contributed to the overall adsorption performance (*Ahmad et al., 2018*).

The influence of pyrolysis temperature and chemical activation on biochar performance has also been demonstrated for cadmium removal from aqueous systems. Biochars produced from *Ipomoea fistulosa* through slow pyrolysis at different temperatures (350–550 °C) were evaluated for Cd(II) adsorption, with further improvement achieved after KOH activation. The activation process enhanced the porous structure of the biochar and increased the availability of adsorption sites, resulting in improved cadmium removal efficiency. The adsorption behavior followed a pseudo-second-order kinetic model, while surface complexation between Cd(II) ions and functional groups on the biochar surface was identified as a major mechanism responsible for metal retention. These findings highlight the importance of both production conditions and activation strategies in tailoring biochar properties for efficient heavy metal remediation (*Goswami et al., 2016*).

Conventional approaches for the treatment of nickel-containing wastewater, including chemical precipitation, ion exchange, membrane separation, and flotation, often present limitations related to operational costs, efficiency at low metal concentrations, and secondary waste generation. Therefore, adsorption-based processes using sustainable carbonaceous materials such as biochar have gained increasing attention as an efficient and environmentally friendly alternative for Ni(II) removal from aqueous systems. The adsorption performance of biochar toward nickel ions can be significantly enhanced through surface modification strategies. A chemically modified biochar obtained from waste peanut shells using $KMnO_4$ and KOH treatment was investigated for Ni(II) removal from aqueous solutions. The modified material exhibited a substantially improved adsorption capacity, reaching 87.15 mg $g^{-1}$, compared with the relatively limited performance commonly reported for pristine biochars.

The adsorption process was spontaneous and endothermic, suggesting favorable interactions between the modified biochar surface and nickel ions. Spectroscopic analyses revealed that enhanced removal efficiency was associated with the development of additional reactive surface sites, particularly amine and hydroxyl functional groups, which contributed to Ni(II) retention through surface complexation and co-precipitation mechanisms. The study demonstrates the potential of chemically engineered waste-derived biochars as effective adsorbents for heavy metal removal from contaminated water (*An et al., 2019*).

Further enhancement of heavy metal adsorption has been achieved through the development of magnetic and composite biochars with tailored surface functionalities. A $MoS_2$-modified magnetic biochar ($MoS_2$@MBC) was synthesized through a hydrothermal approach and evaluated for Cd(II) removal from aqueous solutions. The incorporation of $MoS_2$ and iron species increased the specific surface area and introduced additional sulfur-containing active sites, which significantly improved the adsorption performance compared with pristine biochar. The modified biochar exhibited a maximum Cd(II) adsorption capacity of 139 mg $g^{-1}$, approximately 7.8 times higher than that of unmodified biochar. The enhanced removal efficiency was attributed to multiple interactions, including electrostatic attraction, ion exchange, Cd–S complexation, and surface complexation involving oxygen-, carbon-, sulfur-, and iron-containing functional groups. The adsorption behavior was pH-dependent and was best described by the Langmuir isotherm and pseudo-second-order kinetic models, confirming the potential of engineered magnetic biochars as efficient materials for heavy metal remediation (*Khan et al., 2020*).

The development of highly porous biochars through chemical modification represents an effective strategy for enhancing heavy metal adsorption performance. A sodium bicarbonate-modified biochar produced from *Chlorella pyrenoidosa* biomass by fast pyrolysis was investigated for Pb(II) removal from aqueous solutions. The alkaline modification significantly improved the textural properties of the material, increasing the BET specific surface area to 1282 $m^2$ $g^{-1}$, with a predominant contribution of micropores (871 $m^2$ $g^{-1}$). The enhanced adsorption performance was reflected by a maximum Pb(II) adsorption capacity of 159.07 mg $g^{-1}$ according to the Langmuir model, while kinetic analysis indicated that the adsorption process followed a pseudo-second-order model. The improved removal efficiency was mainly attributed to the development of a highly porous carbon structure, increased availability of adsorption sites, and the contribution of surface functional groups generated during modification (*Rohman et al., 2024*). The results demonstrate that chemically activated biochars derived from microalgal biomass can achieve

adsorption performances comparable to commercial activated carbon, highlighting their potential as sustainable adsorbents for heavy metal-contaminated wastewater treatment.

Magnetic biochar nanocomposites have attracted increasing attention for heavy metal remediation due to their enhanced adsorption performance and the possibility of facile recovery after treatment. Sewage sludge- and woodchip-derived biochars produced at different pyrolysis temperatures (450 and 700 °C) were modified with $Fe_3O_4$ nanoparticles and evaluated for the simultaneous removal of hexavalent chromium (Cr(VI)) and Acid Orange 7 dye from aqueous solutions. The incorporation of magnetic nanoparticles improved the adsorption properties of biochar by introducing additional active sites and enabling magnetic separation of the spent adsorbent. The modified materials exhibited maximum adsorption capacities of 80.96 mg $g^{-1}$ for Cr(VI) and 110.27 mg $g^{-1}$ for Acid Orange 7, with the adsorption behavior described using kinetic and equilibrium models. Moreover, the magnetic biochars maintained high pollutant removal efficiency after five adsorption–desorption cycles, demonstrating their potential for repeated use in wastewater treatment applications (*Santhosh et al., 2020*). These findings highlight the advantages of magnetic modification strategies for developing multifunctional and recoverable biochar-based adsorbents for complex wastewater matrices.

Similarly, magnetic biochars derived from marine biomass have been investigated as recoverable adsorbents for heavy metal remediation. An engineered magnetic biochar produced from waste marine macroalgae through iron oxide incorporation was evaluated for the removal of heavy metals from aqueous systems. Compared with conventional biomass-derived biochars, the magnetic algae-based biochar exhibited enhanced metal removal performance despite its relatively lower surface area, indicating the important contribution of surface chemistry rather than textural properties alone. The incorporation of magnetite and maghemite particles enabled efficient separation of the spent adsorbent from treated water; however, excessive iron loading may partially block surface pores and reduce adsorption efficiency, highlighting the need for optimization of magnetic modification conditions. The developed magnetic biochar showed high selectivity toward Cu(II), reaching adsorption capacities of 69.37 mg $g^{-1}$ for kelp-derived magnetic biochar and 63.52 mg $g^{-1}$ for hijikia-derived magnetic biochar, with the removal performance mainly attributed to oxygen-containing functional groups, such as carboxyl and hydroxyl groups, involved in metal binding (*Son et al., 2018*). These findings demonstrate the potential of magnetic biochars as recoverable and reusable adsorbents for heavy metal remediation applications.

Biochars obtained from hardwood (450 °C) and corn straw (600 °C) were evaluated for the removal of Cu(II) and Zn(II) from aqueous solutions. The adsorption process followed the Langmuir model, with maximum adsorption capacities of 12.52 and 11.0 mg $g^{-1}$ for Cu(II) and Zn(II), respectively, using corn straw-derived biochar, while hardwood biochar exhibited lower capacities of 6.79 mg $g^{-1}$ for Cu(II) and 4.54 mg $g^{-1}$ for Zn(II). The results highlighted the influence of biomass origin and production conditions on adsorption performance. Although effective for single-metal removal, the competitive adsorption behavior observed in mixed Cu(II)/Zn(II) systems indicates the need to consider wastewater composition when evaluating biochar efficiency (*Chen et al., 2011a*).

Biochar-based treatment systems have also been investigated for the remediation of complex water matrices containing mixtures of inorganic and organic contaminants. A pilot-scale study evaluated woodchip bioreactors amended with 33 wt% biochar for the treatment of urban stormwater runoff containing nutrients, trace organic compounds, and heavy metals. After an eight-month conditioning period with real stormwater, followed by a five-month contaminant challenge test, the biochar-amended systems demonstrated high removal efficiencies for metals, exceeding 80% for Ni, Cu, Cd, and Pb, while Zn removal reached approximately 50%. The presence of biochar also enhanced the retention of trace organic contaminants, with no breakthrough observed during the experimental period. In addition, nitrate concentrations were reduced by more than 99%, reaching values below the detection limit (*Ashoori et al., 2019*). These results highlight the potential of biochar-containing bioreactor systems for long-term treatment applications involving complex contaminant mixtures.

Despite the high adsorption efficiencies reported for individual metal ions, real wastewater systems usually contain multiple contaminants and competing species that may influence biochar performance. Therefore, recent research has increasingly focused on multifunctional biochar-based systems capable of simultaneously retaining inorganic and organic pollutants under more realistic environmental conditions.

- **Removal of organic contaminants**

Biochar has also attracted considerable attention for the removal of organic contaminants from wastewater, including dyes, pharmaceuticals, pesticides, phenolic compounds, and other persistent organic pollutants. The adsorption performance of biochar toward organic molecules is primarily determined by its surface area, pore structure, aromatic carbon domains, surface functional groups, and hydrophobicity. Several interactions may contribute to organic contaminant retention, including pore filling, π–π interactions between aromatic structures present in biochar and pollutant molecules, hydrogen bonding, hydrophobic interactions, and electrostatic attraction or repulsion depending on the surface charge of the adsorbent and the ionization state of the contaminant. In addition, surface modification strategies and the incorporation of functional components can further improve adsorption capacity and selectivity by increasing the number of active sites or introducing specific interactions with target pollutants. Therefore, engineered biochars represent promising materials for the efficient removal of diverse organic contaminants from complex wastewater matrices.

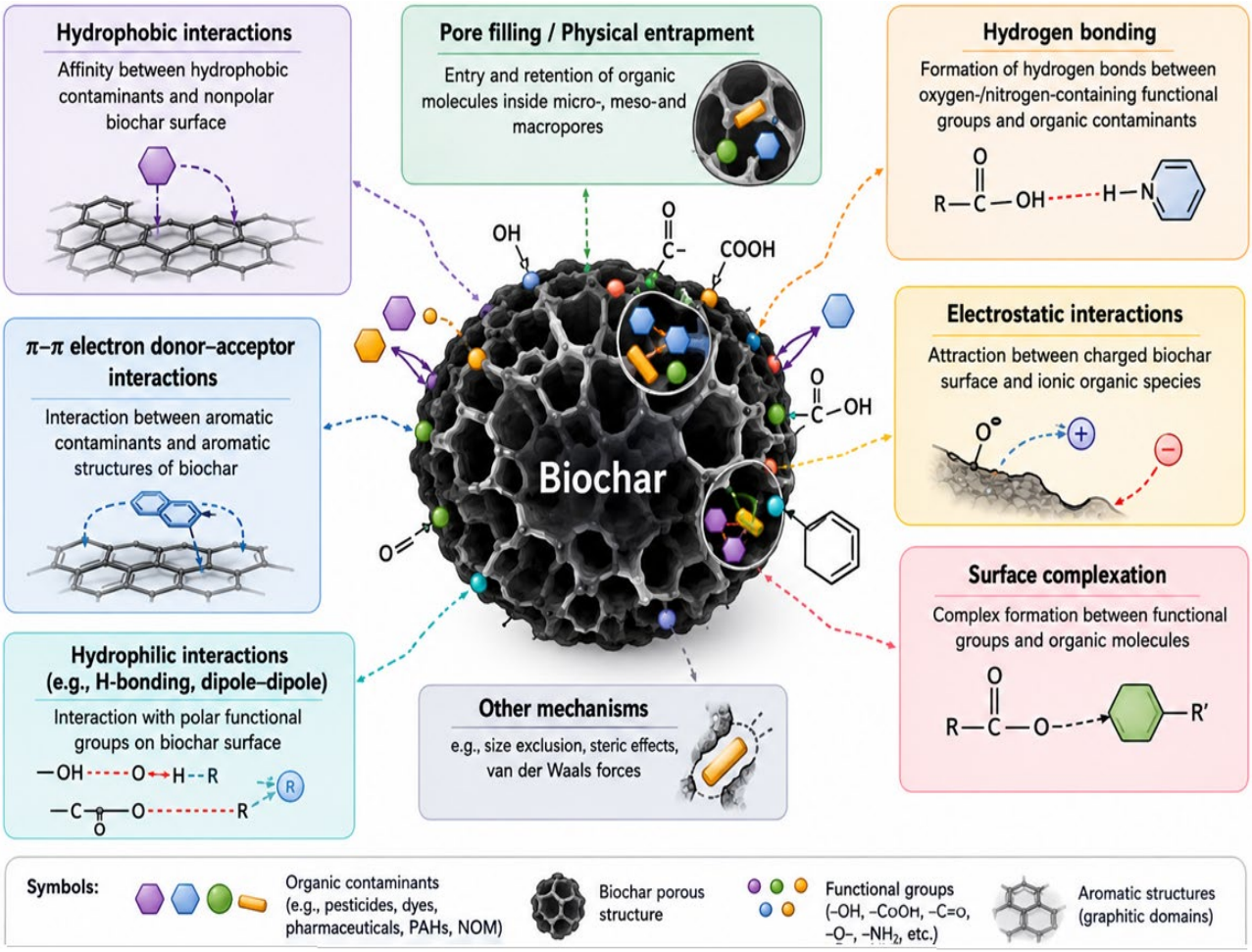



**Fig. 4 - Mechanisms involved in adsorption of organic contaminants onto biochar**

✓ ***Pesticides***

Pesticides are among the most frequently detected organic contaminants in aquatic environments due to their extensive use in agricultural practices and their transport through runoff, leaching, and accidental releases. Their persistence and toxicity pose significant risks to aquatic ecosystems and human health, creating an increasing demand for efficient, low-cost, and environmentally sustainable adsorbents capable of removing these compounds from contaminated waters.

Biochars produced from several agricultural residues, including eucalyptus bark, corn cobs, bamboo chips, rice husks, and rice straw, have also been evaluated for the adsorption of pesticides from aqueous solutions. Among the materials investigated, rice straw-derived biochar exhibited the highest removal efficiencies, reaching 70.7% for atrazine and 77.8% for imidacloprid. Furthermore, phosphoric acid modification further enhanced the adsorption performance, demonstrating that surface

functionalization can significantly improve pesticide removal. The adsorption process was strongly influenced by the physicochemical properties of the biochar, particularly its aromaticity, polarity, pore characteristics, and surface acidity (*Mandal et al., 2017*).

*Saleh et al. (2025)* investigated the potential of biochars derived from *Conocarpus* branch waste and lemon tree branch waste as sustainable adsorbents for the removal of imidacloprid and myclobutanil from aqueous solutions. The biochars, produced by slow pyrolysis at 450 °C, exhibited developed porous structures and favorable surface characteristics, while adsorption performance was affected by pH, adsorbent dosage, contact time, and initial pesticide concentration. The highest adsorption capacities were obtained for *Conocarpus*-derived biochar, reaching 8.69 mg $g^{-1}$ for imidacloprid and 12.31 mg $g^{-1}$ for myclobutanil. Adsorption equilibrium was described by Langmuir and Freundlich models, and the reusability of the biochars after successive cycles demonstrated their potential as efficient and sustainable materials for pesticide remediation in contaminated waters.

The influence of biomass feedstock on pesticide adsorption by biochar was evaluated by comparing materials derived from rice husk, date pits, and sugarcane bagasse for the simultaneous removal of multiple pesticides from aqueous solutions. Among the tested biochars, rice husk-derived biochar exhibited the highest removal efficiencies, achieving up to 97.6% removal for diuron and chlorfenvinphos, followed by date pit- and sugarcane bagasse-derived biochars. The superior performance of rice husk and date pit biochars was attributed to their higher specific surface area, pore volume, and abundance of active surface groups, which enhanced pesticide–biochar interactions. Adsorption equilibrium was reached within 60–120 min, and the experimental data were well described by the Langmuir model, indicating the relevance of surface adsorption mechanisms (*Eissa et al., 2023*). These results demonstrate that biochars obtained from agricultural wastes can serve as efficient and low-cost adsorbents for the removal of pesticide mixtures from contaminated waters.

The performance of biochar under more environmentally realistic conditions was evaluated using biochar filtration systems for the treatment of pesticide-contaminated agricultural drainage water. The study demonstrated that biochar filters could remove a broad range of pesticides, with median removal efficiencies of 94% in column experiments using both pond and river water. Adsorption efficiency was strongly related to pesticide hydrophobicity and water solubility, indicating that hydrophobic interactions represent an important mechanism governing pesticide retention. Although removal performance decreased after prolonged operation due to progressive saturation of adsorption sites, substantial removal efficiencies were maintained, particularly for fungicides and insecticides. Field-scale experiments further confirmed the potential of biochar filtration for reducing pesticide loads in agricultural drainage systems, while highlighting the need for optimized hydraulic design to ensure effective treatment under variable flow conditions (*Koch et al., 2026*).

✓ ***Nutrients***

Nutrient pollution, particularly associated with excessive phosphate release into aquatic environments, represents a major challenge for water quality management due to its contribution to eutrophication and ecosystem degradation. Conventional physicochemical approaches employed for phosphate removal and recovery often involve high operational costs, chemical consumption, or the generation of secondary waste streams. Consequently, adsorption-based processes using sustainable carbonaceous materials have attracted increasing attention as efficient and environmentally compatible alternatives. Biochar, owing to its porous structure, surface functional groups, and mineral constituents derived from the precursor biomass, has emerged as a promising adsorbent for phosphate recovery from aqueous systems while enabling the potential reuse of nutrient-enriched biochar as a soil amendment.

In addition to phosphate, ammonium represents another major inorganic nitrogen species responsible for nutrient enrichment of aquatic systems. The adsorption efficiency of biochar toward ammonium is strongly influenced by the physicochemical characteristics of the material, including surface functional groups, mineral composition, pH, and the distribution of adsorption sites generated during thermochemical conversion.

The influence of biomass precursor and pyrolysis conditions on ammonium adsorption was investigated using biochars derived from different fruit peels, including orange, pineapple, and pitaya residues. The obtained materials were produced at temperatures between 300 and 600 °C, and their adsorption performance was strongly dependent on the thermal conversion parameters. Biochars produced at lower temperatures exhibited superior ammonium uptake, with maximum adsorption

capacities of 4.71 mg $g^{-1}$ for orange peel-derived biochar and 5.60 mg $g^{-1}$ for pineapple peel-derived biochar, whereas pitaya peel biochar reached a maximum capacity of 2.65 mg $g^{-1}$. The enhanced ammonium retention was associated with the preservation of oxygen-containing functional groups and favorable surface properties at lower pyrolysis temperatures. The adsorption process followed the Langmuir isotherm and pseudo-second-order kinetic model, indicating the contribution of surface complexation, cation exchange, and electrostatic interactions (*Hu et al., 2020*). These results demonstrate the potential of fruit peel-derived biochars as sustainable adsorbents for nitrogen removal from wastewater and highlight the importance of optimizing pyrolysis conditions for nutrient-specific applications.

The effect of feedstock origin and pyrolysis temperature on ammonium adsorption has also been demonstrated through comparative evaluation of biochars derived from different biomass categories. Biochars prepared from water hyacinth, algae, cedar wood, rice straw, and pig manure were investigated for ammonium nitrogen removal and compared with commercial clinoptilolite. The adsorption performance varied considerably depending on precursor composition and thermal conversion conditions. Among the tested biochars, pig manure-derived biochar exhibited the highest ammonium adsorption capacity, approaching the performance of clinoptilolite under highly concentrated ammonium solutions, while aquatic biomass-derived biochars produced at 600 °C showed enhanced adsorption rates compared with those obtained at 300 °C. The improved performance at higher pyrolysis temperatures was mainly associated with the development of a more porous structure and increased availability of adsorption sites. These findings highlight the importance of selecting appropriate feedstocks and optimizing pyrolysis parameters to tailor biochar properties for efficient nitrogen removal from wastewater (*Song et al., 2019*).

Beyond studies conducted with synthetic nutrient solutions, biochar has also demonstrated potential for nutrient recovery from real agricultural effluents. Sarkhot et al. (2013) evaluated the ability of hardwood-derived biochar produced at 300 °C to adsorb and retain ammonium and phosphate from dairy manure effluent. The biochar captured up to 5.3 mg $g^{-1}$ of $NH_4^+$ and 0.24 mg $g^{-1}$ of $PO_4^{3-}$, corresponding to 18% and 50% of the available nutrients in the manure slurry, respectively. Desorption experiments showed strong nutrient retention, with 78–91% of the adsorbed ammonium and approximately 60% of phosphate remaining immobilized after less than 24 h (*Sarkhot et al., 2013*). These results demonstrate the dual functionality of biochar as an adsorbent for recovering excess nitrogen and phosphorus from agricultural wastewater and as a nutrient-enriched material suitable for subsequent soil application, supporting integrated nutrient recycling strategies within circular bioeconomy frameworks.

A novel magnetic biochar prepared from orange peel biomass through iron oxide incorporation during pyrolysis was investigated for the simultaneous removal of organic pollutants and phosphate from water. Among the produced materials, the biochar obtained at 400 °C exhibited the highest adsorption performance toward organic contaminants due to the synergistic contribution of magnetite nanoparticles and the amorphous carbon matrix, whereas the material produced at 250 °C showed enhanced phosphate adsorption capacity. The absence of significant competitive interactions between phosphate and organic pollutants demonstrated the potential of magnetic biochars as multifunctional adsorbents for complex wastewater treatment applications (*Chen et al., 2011b*).

Biochar derived from anaerobically digested sugar beet tailings was also evaluated as an alternative material for phosphate recovery from aqueous solutions. The adsorption capacity was mainly associated with the presence of magnesium oxide nanoparticles and colloidal mineral phases formed on the biochar surface, which acted as active adsorption sites for phosphate retention. Adsorption performance was influenced by solution pH and the presence of competing anions, while equilibrium data were better described by heterogeneous adsorption models, indicating the involvement of multiple adsorption mechanisms. Furthermore, phosphate-loaded biochar may represent a valuable nutrient-enriched material suitable for agricultural applications, reducing the need for regeneration and supporting nutrient recycling within circular bioeconomy approaches (*Yao et al., 2011*).

A further improvement in phosphate removal efficiency has been achieved through the development of modified and recyclable biochar-based materials. Magnesium-functionalized biochar beads were prepared by a solvent-free ball milling approach followed by incorporation of sodium alginate and $Fe_3O_4$ to enhance structural stability and facilitate magnetic recovery. The modified biochar exhibited a phosphate adsorption capacity of 53.2 mg $g^{-1}$, more than 12 times higher than that of pristine biochar beads. The enhanced performance was attributed not only to increased surface area and the generation of additional oxygen-containing functional groups during milling, but mainly to the formation of magnesium-containing mineral phases that promoted phosphate retention through electrostatic interactions and

precipitation mechanisms. Moreover, the magnetic recyclability of the developed beads represents an important advantage for practical wastewater treatment applications by reducing secondary waste generation and improving adsorbent recovery (*Hu et al., 2023*).

Further advances in engineered biochar materials have focused on the incorporation of layered double hydroxides (LDHs) to improve nutrient selectivity and adsorption performance. A date-palm-derived biochar modified with MgAl-layered double hydroxide (biochar–MgAl–LDH) was developed for the enhanced removal of phosphate and nitrate from wastewater. The composite exhibited a significantly higher affinity toward phosphate, achieving maximum adsorption capacities of 177.97 mg $g^{-1}$ for phosphate and 28.06 mg $g^{-1}$ for nitrate, due to the synergistic contribution of MgAl–LDH phases and biochar surface functionalities. The presence of competing anions had limited influence on phosphate removal, while regeneration experiments demonstrated the potential reusability of the composite after multiple adsorption–desorption cycles. Moreover, its efficiency in real wastewater treatment highlights the applicability of engineered biochar-based materials for sustainable nutrient removal and recovery (*Alagha et al., 2020*).

The practical application of biochar in wastewater treatment has also been explored through its incorporation into biochar-based column filtration systems. A preliminary study evaluated filtration columns containing different proportions of biochar (0–50%) produced from exhausted olive pomace for the treatment of decanted wastewater. The incorporation of biochar significantly enhanced the removal of multiple pollutants, including total nitrogen (64–65%), total Kjeldahl nitrogen (75–77%), organic nitrogen (78–87%), ammonium (57–69%), total phosphorus (39–44%), orthophosphate (38–42%), chemical oxygen demand (44–56%), and total suspended solids (87–92%). In addition, biochar-amended filters improved the removal of fecal indicator bacteria and pathogenic microorganisms. Interestingly, the best overall treatment performance was achieved using only 10% biochar, indicating that relatively low biochar dosages may provide an optimal balance between pollutant removal efficiency and economic feasibility. These findings demonstrate the potential of biochar-amended filtration systems as sustainable technologies for advanced wastewater treatment and support their implementation in large-scale applications such as constructed wetlands (*El Barkaoui et al., 2025*).

✓ ***Dyes***

Synthetic dyes are widely used in textile, leather, paper, plastics, and printing industries, and their discharge into aquatic environments represents a significant environmental concern due to their high chemical stability, persistence, reduced biodegradability, and potential toxicity. Even at low concentrations, dyes can affect aquatic ecosystems by limiting light penetration and disrupting photosynthetic processes. Conventional treatment methods may present limitations in terms of efficiency, operational costs, and generation of secondary pollutants, increasing interest in sustainable adsorption-based approaches. Biochar and engineered biochar-based materials have demonstrated promising potential for dye removal due to their porous structure, high surface reactivity, and tunable surface chemistry.

Biochar derived from litchi peels has demonstrated high potential for the removal of organic dye contaminants from aqueous systems. Hydrothermally carbonized and activated litchi peel biochar exhibited a highly developed porous structure, with a specific surface area of 1006 $m^2$ $g^{-1}$ and a pore volume of 0.588 $cm^3$ $g^{-1}$. The material showed excellent adsorption performance toward Congo red and malachite green, achieving maximum adsorption capacities of 404.4 and 2468 mg $g^{-1}$, respectively. The high adsorption efficiency was attributed to multiple interactions, including hydrogen bonding, π–π interactions, pore filling, and electrostatic interactions between dye molecules and the biochar surface. Furthermore, the regenerated biochar maintained high adsorption performance, enabling complete dye removal after reactivation and demonstrating its potential as a recyclable adsorbent for wastewater treatment (*Wu et al., 2020*).

Rice straw-derived biochar has been investigated as an efficient adsorbent for the removal of cationic dyes from wastewater after applying an eco-friendly activation strategy. Compared with the pristine pyrolyzed biochar, the activated material exhibited significantly improved adsorption performance toward methylene blue (MB) and crystal violet (CV), reaching maximum adsorption capacities of 90.91 and 44.64 mg $g^{-1}$, respectively, according to the Langmuir model. The activated biochar achieved rapid dye removal, with equilibrium reached within 15 min for MB and 20 min for CV, while the adsorption process followed pseudo-second-order kinetics. Enhanced performance was associated with the development of additional active sites and improved surface properties after activation, demonstrating the potential of

agricultural residues as precursors for high-efficiency biochar adsorbents in wastewater treatment (*Abd-Elhamid et al., 2018*).

Activated biochars obtained from unconventional biomass resources have also shown high efficiency for the simultaneous removal of organic dyes and inorganic pollutants. Biochar derived from *Opuntia ficus-indica* cactus cladodes was modified using NaOH activation to enhance surface basicity and increase the abundance of oxygen-containing functional groups. The activated biochar exhibited high adsorption capacities for malachite green dye (1341 mg $g^{-1}$), $Cu^{2+}$ (49 mg $g^{-1}$), and $Ni^{2+}$ (44 mg $g^{-1}$), with adsorption behavior described by Langmuir isotherms and pseudo-second-order kinetics. The enhanced performance was attributed to improved surface functionality, film diffusion, and chemisorption mechanisms. Moreover, the good regeneration capacity of the activated material highlights its potential as a low-cost and reusable adsorbent for the treatment of complex wastewater containing both organic and inorganic contaminants (*Choudhary et al., 2020*).

Surface modification of biochar with surfactant-based functional systems has also been explored to improve adsorption performance toward organic dyes and other contaminants. A multifunctional modified biochar obtained by crosslinking a sodium dodecyl sulfate/sapindus-saponin composite system onto the biochar surface exhibited enhanced adsorption properties due to the development of a more layered structure, increased functional group density, and improved surface characteristics. The modified biochar demonstrated high adsorption capacities for methylene blue and other pollutants, reaching 277.09 mg $g^{-1}$ for methylene blue, while maintaining efficient removal performance in the presence of competing ions and after repeated regeneration cycles. The adsorption process was mainly governed by electrostatic interactions, hydrogen bonding, and π–π interactions, highlighting the potential of environmentally modified biochars as efficient and reusable adsorbents for dye-contaminated wastewater treatment (*Tian et al., 2025a*).

A further improvement in dye adsorption performance was achieved through the development of biochar functionalized with self-assembled *Sapindus saponin* nanomicelles. The modified biochar exhibited enhanced removal capacity toward methylene blue (MB), reaching a maximum adsorption capacity of 108.64 mg $g^{-1}$, which was attributed to the increased number of active sites, higher abundance of surface functional groups, and improved surface interactions. The adsorption process was mainly governed by electrostatic attraction, hydrogen bonding, and π–π interactions between the aromatic dye molecules and the carbonaceous structure of the modified biochar. The material also demonstrated good stability and reusability, maintaining more than 80% of its adsorption efficiency after five regeneration cycles, highlighting its potential as a sustainable adsorbent for dye-contaminated wastewater treatment (*Tian et al., 2025b*).

Magnetic modification of biomass-derived biochars represents another effective strategy for improving dye adsorption performance while facilitating adsorbent recovery after treatment. Magnetic biochar derived from waste areca nut husk was synthesized through pyrolysis followed by $Fe^{3+}/Fe^{2+}$ incorporation and evaluated for methylene blue removal. The production temperature significantly influenced the physicochemical properties of the material, with biochar obtained at 800 °C exhibiting higher carbon content (62.93%), heating value (33.02 MJ $kg^{-1}$), and specific surface area compared with the lower-temperature material. Further acid treatment increased the surface area to 265 $m^2$ $g^{-1}$, while magnetic modification resulted in an additional increase up to 385 $m^2$ $g^{-1}$. The optimized magnetic biochar achieved a maximum methylene blue adsorption capacity of 785.34 mg $g^{-1}$, with the adsorption process following the Langmuir isotherm and pseudo-second-order kinetic model. The enhanced performance was attributed to the increased availability of active adsorption sites, improved electrostatic interactions, and the contribution of magnetic nanoparticles, which additionally enabled easier adsorbent recovery and improved the sustainability of dye removal processes (*Chistie et al., 2025*).

✓ ***Natural organic matter and other organic contaminants***

Natural organic matter (NOM), including humic and tannic substances, represents an important fraction of dissolved organic compounds present in aquatic systems and can negatively influence water quality and treatment efficiency. The adsorption performance of chemically activated biochar produced from biomass pyrolysis was investigated for the removal of NOM components, including hydrophobic humic acids and hydrophilic tannic acids. The activated biochar exhibited enhanced adsorption capacity due to improved surface properties, with tannic acids showing higher affinity toward the biochar surface

because of stronger chemisorption interactions and size-exclusion effects. Furthermore, the incorporation of activated biochar into an alum-based coagulation system provided a synergistic effect, particularly for humic acid-rich solutions, demonstrating the potential of engineered biochar as an efficient adsorbent for the removal of complex organic matter from water treatment streams (*Jung et al., 2015a*).

A complementary approach involved the integration of biochar with conventional coagulation processes to overcome the limitations of inorganic coagulants in removing dissolved organic compounds. A biochar–ferric chloride (BC–$FeCl_3$) hybrid coagulant was developed for the simultaneous removal of turbidity and humic acid from synthetic wastewater. The incorporation of biochar enhanced the overall treatment performance by providing additional adsorption sites and improving the retention of dissolved organic matter that is poorly removed by $FeCl_3$ alone. The system achieved efficient humic acid removal under near-neutral pH conditions and allowed the recovery of the generated sludge, which maintained adsorption activity toward humic substances, suggesting a potential route for improving process sustainability through material reuse (*Ndagijimana et al., 2024*).

✓ ***Pharmaceuticals, antibiotics and personal care products (PPCPs)***

Pharmaceutical compounds represent an emerging category of aquatic contaminants due to their continuous release from domestic, industrial, hospital, and agricultural wastewater streams and their potential ecological effects even at low concentrations. Among these contaminants, antibiotics represent a particularly critical group due to their extensive consumption in human and veterinary medicine, persistence in aquatic environments, and potential contribution to the development and dissemination of antibiotic resistance. These characteristics raise significant concerns for ecosystem stability and public health, emphasizing the need for efficient and sustainable technologies for antibiotic removal from contaminated water.

Biochar-based adsorption has emerged as a promising approach for antibiotic remediation, owing to its tunable surface chemistry, porous carbonaceous structure, and abundance of active adsorption sites. However, pristine biochars often exhibit limited adsorption efficiency, stimulating the development of various modification strategies aimed at improving their physicochemical properties and enhancing interactions with antibiotic molecules. The adsorption performance of biochar is strongly influenced by the nature and density of surface functionalities, which depend on the biomass precursor, carbonization conditions, and post-treatment approaches. These structural and chemical characteristics govern the interactions between antibiotic molecules and biochar surfaces, including electrostatic attraction, hydrophobic interactions, hydrogen bonding, and π–π electron donor–acceptor interactions (*Haider et al., 2024*).

The influence of biochar physicochemical properties on the adsorption of diverse emerging contaminants was demonstrated through a comparative evaluation of activated biochars produced under different carbonization conditions. Oxygen-free activated biochar exhibited superior adsorption performance compared with oxygenated biochar and commercial powdered activated carbon for a broad range of endocrine-disrupting compounds and pharmaceutical active compounds, including bisphenol A, atrazine, 17α-ethinylestradiol, sulfamethoxazole, carbamazepine, diclofenac, and ibuprofen. The enhanced adsorption capacity was associated with the higher surface area, greater pore volume, and specific distribution of polar and aromatic functional groups, which controlled interactions between biochar surfaces and contaminant molecules. The adsorption mechanisms were strongly dependent on pollutant characteristics, with hydrophobicity influencing the retention of several compounds, while ionization behavior affected the adsorption of pH-sensitive contaminants. These results highlight the importance of tailoring biochar structure and surface chemistry through controlled activation strategies to improve the removal efficiency of complex pharmaceutical contaminants from aqueous systems (*Jung et al., 2013*).

Activated biochar was evaluated for the removal of two widely detected pharmaceutical residues, acetaminophen and naproxen, under simulated combined sewer overflow conditions. The biochar exhibited superior adsorption performance compared with commercial powdered activated carbon, achieving removal efficiencies of 94.1% for acetaminophen and 97.7% for naproxen, compared with 81.6% and 94.1%, respectively, for activated carbon. The enhanced performance was attributed to the favorable surface properties and carbon structure of biochar, which promoted stronger interactions with pharmaceutical molecules. Among the investigated compounds, naproxen showed higher adsorption affinity due to its greater interaction with available adsorption sites. The study demonstrated that biochar adsorption alone was more effective than combined coagulation–adsorption systems under complex

wastewater conditions, highlighting the potential of engineered biochars for the removal of pharmaceutical contaminants from aqueous environments (*Jung et al., 2015b*).

The influence of coexisting natural organic matter on pharmaceutical removal has also been investigated, considering that wastewater matrices may significantly affect biochar performance. The removal of ciprofloxacin by biochar was evaluated in the presence of dissolved and surface-coated humic acid, revealing that low concentrations of dissolved humic acid (5 mg $L^{-1}$) slightly enhanced antibiotic removal, increasing the efficiency from 59.78% to 66.70%, whereas higher concentrations exerted an inhibitory effect. The overall removal process involved both adsorption and catalytic degradation pathways associated with persistent free radicals formed in the biochar structure. Adsorption contributed approximately 42–48% of ciprofloxacin removal, while radical-induced oxidation mechanisms accounted for an additional fraction of pollutant degradation, demonstrating the multifunctional role of biochar in pharmaceutical contaminant removal under complex aqueous conditions (*Luo et al., 2019*).

Further improvements in pharmaceutical removal have been achieved through the development of biochar-based composites with enhanced adsorption and catalytic properties. A sludge-derived biochar modified with CoFe-layered double hydroxides (CoFe-LDH@SBC) was investigated for ciprofloxacin removal, exhibiting a 24% higher removal efficiency compared with pristine sludge-derived biochar. The improved performance was associated with the increased specific surface area, greater availability of adsorption sites, and the presence of persistent free radicals that promoted the oxidative degradation of the adsorbed antibiotic molecules. In addition to enhanced ciprofloxacin removal, the modified biochar achieved higher reductions of total organic carbon and total nitrogen (24% and 27%, respectively), demonstrating the potential of metal-modified biochars as multifunctional materials combining adsorption and catalytic degradation for advanced wastewater treatment applications (*Zheng et al., 2022*).

The development of surface-functionalized biochars has also been explored for improving the adsorption of fluoroquinolone antibiotics. Biochar produced from potato leaves and stems at 500 °C, as well as magnetic biochar and humic acid-coated magnetic biochar, were evaluated for the removal of ciprofloxacin, norfloxacin, and enrofloxacin from aqueous solutions. The incorporation of humic acid onto the magnetic biochar surface increased the density of oxygen-containing functional groups and significantly enhanced adsorption performance, with maximum adsorption capacities for ciprofloxacin, norfloxacin, and enrofloxacin being 3.40, 2.88, and 2.96 times higher, respectively, compared with pristine biochar. The improved removal efficiency was attributed to multiple interactions, including electrostatic attraction, hydrophobic interactions, hydrogen bonding, and π–π electron donor–acceptor interactions. The adsorption process followed Langmuir isotherm and pseudo-second-order kinetic models, indicating the involvement of specific adsorption sites and chemisorption mechanisms. These findings highlight the potential of agricultural residue-derived functionalized biochars as efficient adsorbents for the removal of antibiotic contaminants from wastewater (*Zhao et al., 2019*).

The applicability of modified biochars has also been demonstrated in complex wastewater matrices containing multiple emerging contaminants. An alkali-modified straw-derived biochar was investigated for the simultaneous removal of bisphenol A (BPA), tetracycline (TC), and ofloxacin (OFL) from kitchen wastewater, a challenging matrix characterized by high organic content and diverse interfering compounds. The modification process enhanced the surface area and hydrophobicity of the biochar, resulting in removal efficiencies above 95% for all target contaminants. The modified biochar exhibited maximum adsorption capacities of 71.43, 101.01, and 54.05 mg $g^{-1}$ for BPA, TC, and OFL, respectively, with adsorption behavior governed by chemisorption and monolayer adsorption processes.

Furthermore, the material maintained high performance under the influence of complex wastewater constituents, including chemical oxygen demand, ammonium, and phosphate ions, demonstrating its potential for practical applications in the treatment of real wastewater streams. Column experiments further confirmed its applicability in continuous-flow systems, achieving dynamic adsorption capacities of 55 mg $g^{-1}$ for BPA and 45 mg $g^{-1}$ for OFL (*Tang et al., 2022*). These results highlight the importance of surface modification strategies in developing biochar-based adsorbents suitable for emerging contaminant removal under realistic environmental conditions.

The influence of carbonization pathway and surface activation on antibiotic adsorption has also been investigated by comparing engineered biochar and hydrochar derived from paddy husk. Both materials were evaluated for tetracycline removal from aqueous systems and subsequently modified with phosphoric acid to enhance their adsorption performance. Acid activation significantly improved the adsorption capacity of both materials, increasing the removal capacity of hydrochar from 1.9 to 7.5 mg $g^{-1}$

and that of biochar from 3.8 to 9.1 mg $g^{-1}$. At higher tetracycline concentrations, the activated hydrochar exhibited a maximum adsorption capacity of 46.9 mg $g^{-1}$, slightly exceeding that of activated biochar (41.7 mg $g^{-1}$). The adsorption mechanisms involved hydrogen bonding, hydrophobic interactions, and π–π interactions for hydrochar, whereas cation exchange, diffusion processes, and π–π interactions contributed to tetracycline retention on biochar (*Jeganathan et al., 2024*). These findings demonstrate that both pyrolysis-derived and hydrothermal carbonization-derived materials can be tailored through surface modification to improve antibiotic removal from wastewater, highlighting the importance of production route and surface chemistry in determining adsorption performance.

The development of highly porous and chemically activated biochars has further expanded their applicability for antibiotic removal from contaminated water. A biochar derived from Chinese herbal medicine residues was synthesized through hydrothermal carbonization followed by $ZnCl_2$ activation and evaluated for tetracycline adsorption. The activation process generated a highly microporous structure, with specific surface areas reaching 1370 and 1896 $m^2$ $g^{-1}$ for the two optimized biochars, which contributed to their enhanced adsorption performance. The activated hydrochar exhibited a maximum tetracycline adsorption capacity of 930.3 mg $g^{-1}$ under optimized conditions, with removal mechanisms involving pore diffusion, π–π interactions, electrostatic attraction, and hydrogen bonding. The adsorption process was spontaneous and remained effective in the presence of competing ions, while the material retained more than 77% of its removal efficiency after ten regeneration cycles. These results highlight the potential of waste-derived, highly engineered biochars as sustainable and reusable adsorbents for advanced antibiotic remediation applications (*Zhao et al., 2024*).

Beyond antibiotics and conventional pharmaceutical residues, biochar-based systems have also been investigated for the removal of antimicrobial personal care product residues, which are increasingly recognized as emerging contaminants in aquatic environments. Triclocarban (TCC), an antibacterial compound widely used in personal care products, represents a persistent contaminant frequently detected in wastewater-impacted environments due to its limited biodegradability and potential ecological risks. A sustainable biochar-assisted bioremediation strategy was developed using *Pseudomonas fluorescens* MC46, a TCC-degrading bacterial strain immobilized on biochar derived from carbonized agro-industrial waste. During long-term treatment (160 days), the biochar-immobilized bacterial system achieved consistently high TCC removal efficiencies of 84–97%, exceeding those obtained with free bacterial cells (76–94%). The enhanced performance resulted from the synergistic contribution of microbial degradation and TCC sorption onto the biochar matrix. FTIR analyses revealed the formation of extracellular polymeric substances (EPS), with the lipid fraction remaining attached to the biochar surface and promoting long-term TCC retention, while structural adaptation of bacterial cells improved tolerance to TCC toxicity (*Sonsuphab et al., 2024*). This study highlights the potential of waste-derived biochars not only as adsorption materials but also as microbial immobilization carriers for the sustainable removal and detoxification of emerging PPCP contaminants from wastewater.

✓ ***Endocrine-disrupting compounds***

Endocrine-disrupting compounds (EDCs), such as bisphenol A (BPA), represent a growing concern in aquatic environments due to their persistence, biological activity, and potential adverse effects on human health and ecosystems even at trace concentrations. Although conventional wastewater treatment processes, particularly biological treatment systems, can contribute to BPA removal, their efficiency is often variable and incomplete, with adsorption onto sludge reported as an important removal pathway (*Wang et al., 2019*). The persistence of BPA and its analogues in wastewater streams highlights the need for efficient and sustainable treatment approaches capable of achieving enhanced removal of these emerging contaminants.

Recent studies have highlighted the potential of engineered biochars, particularly magnetic biochars, for the removal of BPA from contaminated waters. Compared with pristine biochar, magnetic modification and further surface functionalization can enhance adsorption performance by increasing the availability of active sites and improving interactions between adsorbent and pollutant molecules. The removal of BPA by magnetic biochars is mainly governed by mechanisms including pore filling, hydrophobic interactions, π–π interactions, hydrogen bonding, electrostatic attraction, and electron transfer processes. Modification strategies such as iron oxide incorporation, oxidation, alkaline treatment, heteroatom doping, and nanomaterial loading have been investigated to overcome the limitations of

conventional biochar and improve its adsorption efficiency for endocrine-disrupting contaminants (*Katibi et al., 2024*).

Biochar derived from alfalfa was investigated as an adsorbent for the removal of emerging contaminants, including BPA and sulfamethoxazole (SMX), from aqueous solutions. The adsorption performance was strongly influenced by the pyrolysis temperature, with biochar produced at 650 °C exhibiting enhanced removal capacity compared with materials obtained at lower temperatures due to its higher surface area, increased carbonization degree, and more developed porous structure. The adsorption of BPA was mainly attributed to hydrophobic interactions and π–π interactions between the aromatic structures of the pollutant and the carbonaceous surface of biochar. Although the adsorption capacity of the optimized biochar remained lower than that of commercial activated carbon, the results demonstrated the potential of agricultural biomass-derived biochars as sustainable adsorbents for the removal of emerging organic contaminants from water (*Choi and Kan, 2019*).

Beyond BPA removal, biochar-based systems have also demonstrated potential for the treatment of other endocrine-disrupting compounds, including triclocarban (TCC), an emerging antimicrobial contaminant frequently detected in municipal wastewater due to its persistence and biological activity. *Jenjaiwit et al. (2021)* investigated an advanced treatment approach based on TCC-degrading *Pseudomonas fluorescens* MC46 cells immobilized onto waste biochar derived from wood vinegar production. The developed biochar–microbial system was evaluated using real wastewater samples and compared with pristine biochar and free bacterial cell treatments under both batch and semi-batch operational conditions. The results demonstrated that cell-immobilized modified biochar exhibited superior TCC removal performance, achieving up to 79.8% removal in batch experiments and maintaining stable removal efficiency (52%) after five consecutive semi-batch cycles. The enhanced performance was attributed to the synergistic contribution of adsorption and microbial degradation mechanisms, which improved contaminant removal compared with biochar alone or free bacterial cells. These findings highlight the potential of waste-derived biochar as a support material for microbial immobilization and as a sustainable platform for the removal of persistent endocrine-disrupting contaminants from wastewater, contributing to circular bio-based wastewater treatment strategies.

✓ ***PAHs/PCBs***

Persistent organic pollutants (POPs), including polychlorinated biphenyls (PCBs), organochlorine pesticides, and other persistent hydrophobic organic compounds, are of particular concern due to their environmental persistence, toxicity, and potential for bioaccumulation. Biochar has been investigated as an effective adsorbent for these contaminants owing to its porous structure, high surface area, and abundance of surface functional groups. The removal of hydrophobic organic pollutants is mainly associated with pore filling, hydrophobic interactions, π–π electron donor–acceptor interactions, hydrogen bonding, electrostatic forces, and electron transfer processes. The efficiency of these mechanisms is strongly dependent on the surface characteristics of biochar, including aromaticity, porosity, surface polarity, and the nature of functional groups, as well as on the molecular properties of the target contaminant.

In addition to its role as an adsorbent, the presence of PAHs in biochar represents an important aspect related to material safety. These compounds can remain associated with the biochar matrix after pyrolysis, and their concentrations vary depending on feedstock type and production conditions. Reported PAH concentrations in biochars produced at temperatures between 250 and 900 °C vary from 0.07 to 45 mg $kg^{-1}$, depending on feedstock composition and processing conditions (*Hilber et al., 2012*). Therefore, optimization of production parameters and implementation of quality control strategies are essential to minimize the formation of potentially hazardous by-products and ensure the safe environmental application of biochar (*Odinga et al., 2021*).

## CONCLUSIONS

Biochar has emerged as one of the most versatile biomass-derived materials for wastewater treatment owing to its favorable physicochemical properties, renewable origin, and broad applicability toward both inorganic and organic contaminants. As demonstrated throughout this review, the adsorption performance of biochar is strongly governed by feedstock composition, pyrolysis conditions, and post-production modification strategies, which collectively determine surface area, pore structure, mineral composition, surface functionality, and adsorption mechanisms. Recent advances in biochar engineering

have shown that chemical activation, magnetic modification, mineral functionalization, and composite formation can substantially improve adsorption capacity, selectivity, regeneration potential, and applicability under complex wastewater conditions. These developments have broadened the application of biochar for the removal of heavy metals, nutrients, dyes, pesticides, pharmaceuticals, endocrine-disrupting compounds, and persistent organic pollutants, highlighting its potential as an alternative to conventional adsorbents.

Despite these promising developments, several challenges remain before large-scale implementation can be achieved. Greater standardization of feedstock selection, production conditions, and characterization methods is required to improve reproducibility and facilitate comparison among studies. Future research should prioritize regeneration efficiency, long-term stability, pilot-scale demonstrations, life-cycle assessment, techno-economic evaluation, and integration of biochar production with biomass waste valorization within circular bioeconomy frameworks. Future developments should also focus on the transition from conventional biochars toward engineered and application-specific materials with tailored surface properties for targeted contaminants. Attention should be directed toward evaluating biochar performance in real wastewater matrices, developing cost-effective regeneration strategies, and integrating biochar into hybrid treatment systems that enable simultaneous adsorption, degradation, and resource recovery.

Overall, biochar represents a sustainable, multifunctional, and highly adaptable material capable of supporting advanced wastewater remediation while simultaneously contributing to renewable resource utilization, waste minimization, and long-term environmental protection within circular economy strategies.

## REFERENCES


[1] Abbas, A., Afzal, S., Waseem, M., Ahmad, M., & Xu, D. (2026). Advances in biochar production and performance for sustainable environment and energy applications. *Sustainability*, *18*(12), 5865. https://doi.org/10.3390/su18125865

[2] Abd-Elhamid, A.I., Emran, M., El-Sadek, M.H., El-Shanshory, A.A., Soliman, H.M.A., Akl, M.A., & Rashad, M. (2020). Enhanced removal of cationic dye by eco-friendly activated biochar derived from rice straw. *Applied Water Science, 10*, 45. https://doi.org/10.1007/s13201-019-1128-0

[3] Afshar, M., & Mofatteh, S. (2024). Biochar for a sustainable future: Environmentally friendly production and diverse applications. *Results in Engineering, 23*, 102433. https://doi.org/10.1016/j.rineng.2024.102433

[4] Ahmad, Z., Gao, B., Mosa, A., Yu, H., Yin, X., Bashir, A., Ghoveisi, H., & Wang, S. (2018). Removal of Cu(II), Cd(II) and Pb(II) ions from aqueous solutions by biochars derived from potassium-rich biomass. *Journal of Cleaner Production, 180*, 437–449. https://doi.org/10.1016/j.jclepro.2018.01.133

[5] Ahmed, M.B., Zhou, J.L., Ngo, H.H., Guo, W., & Chen, M. (2016). Progress in the preparation and application of modified biochar for improved contaminant removal from water and wastewater. *Bioresource Technology, 214*, 836–851. https://doi.org/10.1016/j.biortech.2016.05.057

[6] Alagha, O., Manzar, M.S., Zubair, M., Anil, I., Muazu, N.D., & Qureshi, A. (2020). Comparative adsorptive removal of phosphate and nitrate from wastewater using biochar-MgAl LDH nanocomposites: Coexisting anions effect and mechanistic studies. *Nanomaterials*, *10*(2), 336. https://doi.org/10.3390/nano10020336

[7] Alsawy, T., Rashad, E., El-Qelish, M., & Mohammed, R.H. (2022). A comprehensive review on the chemical regeneration of biochar adsorbent for sustainable wastewater treatment. *npj Clean Water, 5*, 29. https://doi.org/10.1038/s41545-022-00172-3

[8] Alshehri, M.A., & Pugazhendhi, A. (2024). Biochar for wastewater treatment: Addressing contaminants and enhancing sustainability: Challenges and solutions. *Journal of Hazardous Materials Advances, 16*, 100504. https://doi.org/10.1016/j.hazadv.2024.100504

[9] Ambaye, T., Vaccari, M., van Hullebusch, E.D., Amrane, A., & Rtimi, S. (2021). Mechanisms and adsorption capacities of biochar for the removal of organic and inorganic pollutants from industrial wastewater. *International Journal of Environmental Science and Technology, 18*, 3273–3294. https://doi.org/10.1007/s13762-020-03060-w

[10] An, Q., Jiang, Y. -Q., Nan, H. -Y., Yu, Y., & Jiang, J.-N. (2019). Unraveling sorption of nickel from aqueous solution by $KMnO_4$ and KOH-modified peanut shell biochar: Implicit mechanism. *Chemosphere, 214*, 846–854. https://doi.org/10.1016/j.chemosphere.2018.10.007

[11] An, N., Zhang, L., Liu, Y., Shen, S., Li, N., Wu, Z., Yang, J., Han, W., & Han, X. (2022). Biochar application with reduced chemical fertilizers improves soil pore structure and rice productivity. *Chemosphere, 298*, 134304. https://doi.org/10.1016/j.chemosphere.2022.134304

[12] Ashoori, N., Teixido, M., Spahr, S., LeFevre, G.H., Sedlak, D.L., & Luthy, R.G. (2019). Evaluation of pilot-scale biochar-amended woodchip bioreactors to remove nitrate, metals, and trace organic contaminants from urban stormwater runoff. *Water Research, 154*, 1–11. https://doi.org/10.1016/j.watres.2019.01.040

[13] Barquilha, C.E., & Braga, M.C. (2021). Adsorption of organic and inorganic pollutants onto biochars: Challenges, operating conditions, and mechanisms. *Bioresource Technology Reports, 15*, 100728. https://doi.org/10.1016/j.biteb.2021.100728

[14] Chen, X., Chen, G., Chen, L., Chen, Y., Lehmann, J., McBride, M.B., & Hay, A.G. (2011a). Adsorption of copper and zinc by biochars produced from pyrolysis of hardwood and corn straw in aqueous solution. *Bioresource Technology, 102*(19), 8877–8884. https://doi.org/10.1016/j.biortech.2011.06.078

[15] Chen, B., Chen, Z., & Lv, S. (2011b). A novel magnetic biochar efficiently sorbs organic pollutants and phosphate. *Bioresource Technology, 102*(2), 716–723. https://doi.org/10.1016/j.biortech.2010.08.067

[16] Chen, H., Chen, X., Qin, Y., Wei, J., & Liu, H. (2017). Effect of torrefaction on the properties of rice straw high temperature pyrolysis char: Pore structure, aromaticity and gasification activity. *Bioresource Technology, 228*, 241–249. https://doi.org/10.1016/j.biortech.2016.12.074

[17] Chistie, S.M., Naik, S.U., Rajendra, P., Apeksha, Mishra, R.K., Albasher, G., Chinnam, S., Jeppu, G.P., Arif, Z., & Hameed, J. (2025). Production and characterization of magnetic biochar derived from pyrolysis of waste areca nut husk for removal of methylene blue dye from wastewater. *Scientific Reports*, *15,* 23209. https://doi.org/10.1038/s41598-025-03359-z

[18] Choi, Y.K., & Kan, E. (2019). Effects of pyrolysis temperature on the physicochemical properties of alfalfa-derived biochar for the adsorption of bisphenol A and sulfamethoxazole in water. *Chemosphere, 218,* 741–748. https://doi.org/10.1016/j.chemosphere.2018.11.151

[19] Choudhary, M., Kumar, R., & Neogi, S. (2020). Activated biochar derived from *Opuntia ficus-indica* for the efficient adsorption of malachite green dye, $Cu^{2+}$ and $Ni^{2+}$ from water. *Journal of Hazardous Materials, 392*, 122441. https://doi.org/10.1016/j.jhazmat.2020.122441

[20] Din, S.U., Khaqan, U., Imran, M., Al-Ahmary, K.M., Alshdoukhi, I.F., Carabineiro, S.A., Al-Sehemi, A.G., Kavil, Y. N., Alshehri, R.F., & Bakheet, A.M. (2024). Enhancing arsenic removal using Cu-infused biochar: Unravelling the influence of pH, temperature and kinetics. *Chemical Engineering Research and Design, 203*, 368–377. https://doi.org/10.1016/j.cherd.2024.01.045

[21] Eissa, F., Alsherbeny, S., El-Sawi, S., Slaný, M., Lee, S.S., Shaheen, S.M., & Jamil, T.S. (2023). Remediation of pesticides contaminated water using biowastes-derived carbon rich biochar. *Chemosphere, 340*, 139819. https://doi.org/10.1016/j.chemosphere.2023.139819

[22] El Barkaoui, S., Mandi, L., Fichera, M., Ryah, H., Baçaoui, A., Del Bubba, M., & Ouazzani, N. (2025). Optimizing biochar-based column filtration systems for enhanced pollutant removal in wastewater treatment: A preliminary study. *Chemosphere, 372*, 144067. https://doi.org/10.1016/j.chemosphere.2025.144067

[23] Freddo, A., Cai, C., & Reid, B.J. (2012). Environmental contextualisation of potential toxic elements and polycyclic aromatic hydrocarbons in biochar. *Environmental Pollution, 171,* 18–24. https://doi.org/10.1016/j.envpol.2012.07.009

[24] Fabbri, D., Rombolà, A.G., Torri, C., & Spokas, K.A. (2013). Determination of polycyclic aromatic hydrocarbons in biochar and biochar amended soil. *Journal of Analytical and Applied Pyrolysis, 103*, 60–67. https://doi.org/10.1016/j.jaap.2012.10.003

[25] Ghodake, G.S., Shinde, S.K., Kadam, A.A., Saratale, R.G., Saratale, G.D., Kumar, M., Palem, R.R., Al-Shwaiman, H.A., Elgorban, A.M., Syed, A., & Kim, D.-Y. (2021). Review on biomass feedstocks, pyrolysis mechanism and physicochemical properties of biochar: State-of-the-art framework to speed up vision of circular bioeconomy. *Journal of Cleaner Production, 297*, 126645. https://doi.org/10.1016/j.jclepro.2021.126645

[26] Goswami, R., Shim, J., Deka, S., Kumari, D., Kataki, R., & Kumar, M. (2016). Characterization of cadmium removal from aqueous solution by biochar produced from *Ipomoea fistulosa* at different pyrolytic temperatures. *Ecological Engineering, 97*, 444–451. https://doi.org/10.1016/j.ecoleng.2016.10.007

[27] Haider, M.I.S., Liu, G., Yousaf, B., Arif, M., Aziz, K., Ashraf, A., Safeer, R., Ijaz, S., & Pikon, K. (2024). Synergistic interactions and reaction mechanisms of biochar surface functionalities in antibiotics removal from industrial wastewater. *Environmental Pollution, 356*, 124365. https://doi.org/10.1016/j.envpol.2024.124365

[28] Hilber, I., Blum, F., Leifeld, J., Schmidt, H.-P., & Bucheli, T.D. (2012). Quantitative determination of PAHs in biochar: A prerequisite to ensure its quality and safe application. *Journal of Agricultural and Food Chemistry, 60*(12), 3042–3050. https://doi.org/10.1021/jf205278v

[29] Hu, X., Zhang, X., Ngo, H.H., Guo, W., Wen, H., Li, C., Zhang, Y., & Ma, C. (2020). Comparison study on the ammonium adsorption of the biochars derived from different kinds of fruit peel. *Science of the Total Environment, 707*, 135544. https://doi.org/10.1016/j.scitotenv.2019.135544

[30] Hu, B., Yan, N., Zheng, Z., Xu, L., Xie, H., & Chen, J. (2023). Recyclable magnesium-modified biochar beads for efficient removal of phosphate from wastewater. *Nanomaterials, 13*(6), 966. https://doi.org/10.3390/nano13060966

[31] Jeganathan, Y., Asharp, T., & Nadarajah, K. (2024). Adsorptive behavior of engineered biochar/hydrochar for tetracycline removal from synthetic wastewater. *Environmental Pollution, 345*, 123452. https://doi.org/10.1016/j.envpol.2024.123452

[32] Jenjaiwit, S., Supanchaiyamat, N., Hunt, A.J., Ngernyen, Y., Ratpukdi, T., & Siripattanakul-Ratpukdi, S. (2021). Removal of triclocarban from treated wastewater using cell-immobilized biochar as a sustainable water treatment technology. *Journal of Cleaner Production, 320*, 128919. https://doi.org/10.1016/j.jclepro.2021.128919

[33] Jung, C., Park, J., Lim, K.H., Park, S., Heo, J., Her, N., Oh, J., Yun, S., & Yoon, Y. (2013). Adsorption of selected endocrine disrupting compounds and pharmaceuticals on activated biochars. *Journal of Hazardous Materials, 263*, 702–710. https://doi.org/10.1016/j.jhazmat.2013.10.033

[34] Jung, C., Phal, N., Oh, J., Chu, K.H., Jang, M., & Yoon, Y. (2015a). Removal of humic and tannic acids by adsorption-coagulation combined systems with activated biochar. *Journal of Hazardous Materials, 300*, 808–814. https://doi.org/10.1016/j.jhazmat.2015.08.025

[35] Jung, C., Oh, J., & Yoon, Y. (2015b). Removal of acetaminophen and naproxen by combined coagulation and adsorption using biochar: Influence of combined sewer overflow components. *Environmental Science and Pollution Research, 22*, 10058–10069. https://doi.org/10.1007/s11356-015-4191-6

[36] Katibi, K.K., Shitu, I. G., Yunos, K.F.M., Azis, R.S., Iwar, R.T., Adamu, S.B., Umar, A.M., & Adebayo, K.R. (2024). Unlocking the potential of magnetic biochar in wastewater purification: a review on the removal of bisphenol A from aqueous solution. Environmental Monitoring and Assessment, 196, 492. https://doi.org/10.1007/s10661-024-12574-6

[37] Khan, Z.H., Gao, M., Qiu, W., & Song, Z. (2020). Properties and adsorption mechanism of magnetic biochar modified with molybdenum disulfide for cadmium in aqueous solution. *Chemosphere, 255*, 126995. https://doi.org/10.1016/j.chemosphere.2020.126995

[38] Kinney, T.J., Masiello, C.A., Dugan, B., Hockaday, W.C., Dean, M.R., Zygourakis, K., & Barnes, R.T. (2012). Hydrologic properties of biochars produced at different temperatures. *Biomass and Bioenergy, 41*, 34–43. https://doi.org/10.1016/j.biombioe.2012.01.033

[39] Koch, A., Jonsson, O., Dürebrandt, G., & Cederlund, H. (2026). Testing a biochar filter for removal of 128 pesticides in surface water. *SSRN*. https://doi.org/10.2139/ssrn.6641763

[40] Li, Y., Xing, B., Ding, Y., Han, X., & Wang, S. (2020). A critical review of the production and advanced utilization of biochar via selective pyrolysis of lignocellulosic biomass. *Bioresource Technology, 312*, 123614. https://doi.org/10.1016/j.biortech.2020.123614

[41] Luo, K., Pang, Y., Yang, Q., Wang, D., Li, X., Wang, L., Lei, M., & Liu, J. (2019). Enhanced ciprofloxacin removal by sludge-derived biochar: Effect of humic acid. *Chemosphere, 231*, 495–501. https://doi.org/10.1016/j.chemosphere.2019.05.151

[42] Luo, Y., Pan, H., Zhou, X., Du, Z., Li, G., Wu, J., Zhang, X., & Zhang, C. (2021). Effects of CoMo/γ-$Al_2O_3$ catalysts on product hydrocarbon and phenol distribution during hydrodeoxygenation of oxidized bio-oil in a batch reactor. *Processes, 9*(12), 2138. https://doi.org/10.3390/pr9122138

[43] Mandal, A., Singh, N., & Purakayastha, T.J. (2017). Characterization of pesticide sorption behaviour of slow pyrolysis biochars as low cost adsorbent for atrazine and imidacloprid removal. *Science of the Total Environment, 577*, 376–385. https://doi.org/10.1016/j.scitotenv.2016.10.204

[44] Mechnou, I., Benabdallah, A., Chham, A.I., Rachdi, Y., Hlaibi, M., El Kartouti, A., & Saleh, N. (2025). Activated carbons for effective pharmaceutical adsorption: Impact of feedstock origin, activation agents, adsorption conditions, and cost analysis. *Results in Engineering, 27*, 105966. https://doi.org/10.1016/j.rineng.2025.105966

[45] Mohammadi, P., Dang, C.H., Román, S., Duman, G., Akdeniz, R. C., Kömekçi, F., Nik Ghazali, N.N., De Tender, C., & Kulli, B. (2025). Can biomass-derived chars serve as a viable alternative to commercial inorganic fertilizers? *Biofuel Research Journal, 45*, 2350–2372. https://doi.org/10.18331/BRJ2025.12.1.5

[46] Ndagijimana, P., Rong, H., Duan, L., Li, S., Nkinahamira, F., Hakizimana, J.C., Kumar, A., Aborisade, M.A., Ndokoye, P., Cui, B., Guo, D., & Naidu, R. (2024). Synthesis and evaluation of a novel cross-linked biochar/ferric chloride hybrid material for integrated coagulation and adsorption of turbidity and humic acid from synthetic wastewater: Implications for sludge valorisation. *Environmental Research, 255*, 119134. https://doi.org/10.1016/j.envres.2024.119134

[47] Odinga, E.S., Gudda, F.O., Waigi, M.G., Wang, J., & Gao, Y. (2021). Occurrence, formation and environmental fate of polycyclic aromatic hydrocarbons in biochars. *Fundamental Research, 1*(3), 296–305. https://doi.org/10.1016/j.fmre.2021.03.003

[48] Oni, B.A., Oziegbe, O., & Olawole, O.O. (2019). Significance of biochar application to the environment and economy. *Annals of Agricultural Sciences, 64*(2), 222–236. https://doi.org/10.1016/j.aoas.2019.12.006

[49] Rohman, G.A.N., Aziz, M.A., Nawaz, A., Elgzoly, M.A., Hossain, M.M., & Razzak, S.A. (2024). High-performance biochar from *Chlorella pyrenoidosa* algal biomass for heavy metals removal in wastewater. *Separation and Purification Technology, 341,* 126870. https://doi.org/10.1016/j.seppur.2024.126870

[50] Saleh, S.M., Abdel Ghani, S.B., Alminderej, F.M., & Abdallah, O.I. (2025). Sustainable removal of pesticides from water using biochars derived from Conocarpus and lemon tree waste. *ACS Omega, 10*(50), 61998–62011. https://doi.org/10.1021/acsomega.5c08939

[51] Santhosh, C., Daneshvar, E., Tripathi, K.M., Baltrėnas, P., Kim, T.Y., Baltrėnaitė, E., & Bhatnagar, A. (2020). Synthesis and characterization of magnetic biochar adsorbents for the removal of Cr(VI) and Acid orange 7 dye from aqueous solution. *Environmental Science and Pollution Research, 27,* 32874–32887. https://doi.org/10.1007/s11356-020-09275-1

[52] Sarkhot, D.V., Ghezzehei, T.A., & Berhe, A.A. (2013). Effectiveness of biochar for sorption of ammonium and phosphate from dairy effluent. *Journal of Environmental Quality, 42*(5), 1545–1554. https://doi.org/10.2134/jeq2012.0482

[53] Son, E.B., Poo, K.M., Chang, J.S., & Chae, K.J. (2018). Heavy metal removal from aqueous solutions using engineered magnetic biochars derived from waste marine macro-algal biomass. *Science of the Total Environment, 615*, 161–168. https://doi.org/10.1016/j.scitotenv.2017.09.171

[54] Song, H., Wang, J., Garg, A., Lin, X., Zheng, Q., & Sharma, S. (2019). Potential of novel biochars produced from invasive aquatic species outside food chain in removing ammonium nitrogen: comparison with conventional biochars and clinoptilolite. *Sustainability*, *11*(24), 7136. https://doi.org/10.3390/su11247136

[55] Sonsuphab, K., Toomsan, W., Soontharo, S., Supanchaiyamat, N., Hunt, A.J., Ngernyen, Y., Nasompag, S., Kiattisaksiri, P., Ratpukdi, T., & Siripattanakul-Ratpukdi, S. (2024). Integrated remediation and detoxification of triclocarban-contaminated water using waste-derived biochar-immobilized cells by long-term column experiments. *Environmental Pollution, 357*, 124456. https://doi.org/10.1016/j.envpol.2024.124456

[56] Tadesse, A.W., Huang, M., & Zhou, T. (2025). Biochar for wastewater treatment: Preparation, modification, characterization, and its applications. *Molecules, 30*(21), 4288. https://doi.org/10.3390/molecules30214288

[57] Tang, Y., Li, Y., Zhan, L., Wu, D., Zhang, S., Pang, R., & Xie, B. (2022). Removal of emerging contaminants (bisphenol A and antibiotics) from kitchen wastewater by alkali-modified biochar. *Science of the Total Environment, 805*, 150158. https://doi.org/10.1016/j.scitotenv.2021.150158

[58] Tian, L., Li, H., Chang, Z., Liang, N., Wu, M., & Pan, B. (2023). Biochar modification to enhance arsenic removal from water: A review. *Environmental Geochemistry and Health, 45*(6), 2763–2778. https://doi.org/10.1007/s10653-022-01462-y

[59] Tian, K., Li, C., Liu, H., & Wang, L. (2025a). Functionalization of biochar using SDS/SAP nanomicelles enhanced its immobilization capacity for dyes and heavy metals in water. *Scientific Reports, 15*(1), 7199. https://doi.org/10.1038/s41598-025-91229-z

[60] Tian, K., Li, C., & Wang, L. (2025). SAP nanomicelle-functionalized biochar: A multifunctional and sustainable adsorbent for efficient removal of dyes and heavy metals. *ACS Omega, 10*(50), 61452–61470. https://doi.org/10.1021/acsomega.5c06590

[61] Tomczyk, A., Sokołowska, Z., & Boguta, P. (2020). Biochar physicochemical properties: Pyrolysis temperature and feedstock kind effects. *Reviews in Environmental Science and Bio/Technology, 19*, 191–215. https://doi.org/10.1007/s11157-020-09523-3

[62] Ungureanu, N., Vlăduț, N.-V., Biriș, S.-Ș., Gheorghiță, N.-E., & Ionescu, M. (2025a). Biomass pyrolysis pathways for renewable energy and sustainable resource recovery: A critical review of processes, parameters, and product valorization. *Sustainability*, *17*(17), 7806. https://doi.org/10.3390/su17177806

[63] Ungureanu, N., Vlăduț, N.-V., Biriș, S.-Ș., Ionescu, M., & Gheorghiță, N.-E. (2025b). Municipal solid waste gasification: Technologies, process parameters, and sustainable valorization of by-products in a circular economy. *Sustainability, 17*(15), 6704. https://doi.org/10.3390/su17156704

[64] Wang, H., Liu, Z. H., Zhang, J., Huang, R.P., Yin, H., Dang, Z., Wu, P.X., & Liu, Y. (2019). Insights into removal mechanisms of bisphenol A and its analogues in municipal wastewater treatment plants. *Science of The Total Environment, 692*, 107–116. https://doi.org/10.1016/j.scitotenv.2019.07.134

[65] Wang, Y., Zeng, W., Wan, X., Lei, M., & Chen, T. (2024). Potential in treating arsenic-contaminated water of the biochars produced from hyperaccumulator *Pteris vittata* and its environmental safety. *Environmental Pollution, 356*, 124320. https://doi.org/10.1016/j.envpol.2024.124320

[66] Wu, J., Yang, J., Feng, P., Huang, G., Xu, C., & Lin, B. (2020). High-efficiency removal of dyes from wastewater by fully recycling litchi peel biochar. *Chemosphere, 246*, 125734. https://doi.org/10.1016/j.chemosphere.2019.125734

[67] Xiang, W., Zhang, X., Chen, J., Zou, W., He, F., Hu, X., Tsang, D.C.W., Ok, Y.S., & Gao, B. (2020). Biochar technology in wastewater treatment: A critical review. *Chemosphere, 252*, 126539. https://doi.org/10.1016/j.chemosphere.2020.126539

[68] Yao, Y., Gao, B., Inyang, M., Zimmerman, A.R., Cao, X., Pullammanappallil, P., & Yang, L. (2011). Removal of phosphate from aqueous solution by biochar derived from anaerobically digested sugar beet tailings. *Journal of Hazardous Materials, 190*(1–3), 501–507. https://doi.org/10.1016/j.jhazmat.2011.03.083

[69] Zhao, J., Liang, G., Zhang, X., Cai, X., Li, R., Xie, X., & Wang, Z. (2019). Coating magnetic biochar with humic acid for high efficient removal of fluoroquinolone antibiotics in water. *Science of The Total Environment, 688*, 1205–1215. https://doi.org/10.1016/j.scitotenv.2019.06.287

[70] Zhao, Z., Li, P., Zhang, M., Feng, W., Tang, H., & Zhang, Z. (2024). Unlocking the potential of Chinese herbal medicine residue-derived biochar as an efficient adsorbent for high-performance tetracycline removal. *Environmental Research, 252*(Part 1), 118425. https://doi.org/10.1016/j.envres.2024.118425

[71] Zheng, D., Wu, M., Zheng, E., Wang, Y., Feng, C., Zou, J., Juan, M., Bai, X., Wang, T., & Shi, Y. (2022). Adsorption and oxidation of ciprofloxacin by a novel layered double hydroxides modified sludge biochar. *Journal of Colloid and Interface Science, 625*, 596–605. https://doi.org/10.1016/j.jcis.2022.06.080

# STATE OF THE ART IN RESEARCHES CONCERNING THE ACOUSTIC EMISSION NON-DESTRUCTIVE TECHNIQUE

/

# *STADIUL ACTUAL AL CERCETĂRILOR PRIVIND TEHNICA NEDISTRUCTIVĂ DE EMISIE ACUSTICĂ*

**Ovidiu Cristian NEACȘU*[1)], Mihai Valentin PREDOI[2)], Andrei CRAIFALEANU[2)]**

[1)] Doctoral School of the Faculty of Biotechnical Systems Engineering, National University of Science and Technology POLITEHNICA Bucharest / Romania;

[2)] Department of Mechanics, Faculty of Biotechnical Systems Engineering, National University of Science and Technology POLITEHNICA Bucharest / Romania.

**Tel: 0770 267 166; *E-mail: ovidiu.neacsu@gmail.com*

***Keywords:*** *non destructive characterization, mechanical properties*

**ABSTRACT**

*Acoustic Emission is one of the most promising examination methods for structural health monitoring (SHM). Acoustic Emission can be used during the operation of mechanical structures, such as pressure vessels, tanks, pipeline systems, bridges and can provide real-time information compared to other examination methods. Acoustic Emission is the phenomenon of generation of elastic waves (transients) inside a material, caused by the rapid and localized release of energy under the action of mechanical or thermal stresses. Acoustic Emission is a monitoring technology that offers certain advantages in the evaluation of materials, as well as structures. Among the basic features are high sensitivity, which leads to the detection of the early stage of microcracks and the possibility of characterizing the failure mode based on the recorded waveform. In addition, it offers the localization of sources in one, two or three dimensions. The method allows the detection of the actual initiation of micro-cracking or any other event that would be impossible to detect by other techniques. Another advantage is the potential to characterize the cracking mode or, in general, the source or type of excitation. Source localization is an additional powerful feature of Acoustic Emission. By installing multiple sensors, the coordinates of active sources can be defined with good accuracy in one, two or three dimensions even if a crack is inside the material volume and is not visible, its location can be evaluated. Acoustic Emission is a "passive" technique. Acoustic Emission is used for fault monitoring, which is a very demanding and dynamic process, but it is also used to detect leaks in a piping system or the development of corrosion in industrial environments. In the present work are emphasized the main applications of this technique of non-destructive inspection.*

**REZUMAT**

*Emisia Acustică este una dintre cele promițătoare metode de examinare pentru monitorizarea integrității structurilor (Structural Health Monitoring - SHM). Emisia Acustică poate fi utilizată în timpul funcționării structurilor mecanice, cum ar fi vase sub presiune, rezervoare, sisteme de conducte, poduri și poate furniza informații în timp real, față de alte metode de examinare. Emisia Acustică reprezintă fenomenul de generare a unor unde elastice (tranzitorii) în interiorul unui material, cauzat de eliberarea rapidă și localizată de energie sub acțiunea unor solicitări mecanice sau termice. Emisia Acustică este o tehnologie de monitorizare care oferă anumite avantaje în evaluarea materialelor, precum și a structurilor. Printre caracteristicile de bază se numără sensibilitatea ridicată, care duce la detectarea stadiului incipient al microfisurilor și posibilitatea caracterizării modului de cedare pe baza formei de undă înregistrate. În plus, oferă localizarea surselor în una, două sau trei dimensiuni. Metoda permite detectarea inițierii propriu-zise a micro-fisurării sau a oricărui alt eveniment care ar fi imposibil de detectat prin alte tehnici. Un alt avantaj este potențialul de a caracteriza modul de fisurare sau, în general, sursa sau tipul de excitație. Localizarea sursei este o caracteristică suplimentară puternică a Emisiei Acustice. Prin instalarea mai multor senzori, coordonatele surselor active pot fi definite cu o precizie bună în una, două sau trei dimensiuni chiar dacă o fisură se află în interiorul volumului materialului și nu este vizibilă, localizarea sa poate fi evaluată. In această lucrare sunt prezentate principalele aplicații ale acestei tehnici de control nedistructiv.*

*Emisia Acustică este o tehnică "pasivă". Emisia Acustică este utilizată pentru monitorizarea defectelor, care este un proces foarte solicitant și dinamic, dar este utilizată și pentru detectarea scurgerilor dintr-un sistem de conducte sau dezvoltarea coroziunii în medii industriale.*

## INTRODUCTION

Acoustic Emission Testing offers the potential to assess and monitor structures such as pressure vessels and pipelines, tanks, aircraft, bridges, etc., where a very high level of structural integrity is required.

Compared to other Non-Destructive Testing methods, Acoustic Emission Testing can monitor changes in material behavior over a long period of time and without moving the sensors. This makes the technique unique, along with the ability to detect crack propagation that occurs not only on the surface, but also inside a material. Acoustic Emission Testing is considered quite unique among non-destructive testing methods. Unlike other Non-Destructive Testing methods, Acoustic Emission Testing is usually applied during loading, while most others are applied before or after loading a structure. Acoustic Emission is often used to detect failure at a very early stage, long before a structure has completely failed. Acoustic emission testing is an important method in the field of non-destructive testing of materials. The acoustic emission testing technique falls into one of the following categories: pressure testing, diagnostics, integrity monitoring, and leak detection. Many specific applications have been developed using acoustic emission, with discontinuity detection being the largest class of applications. The advantages of the acoustic emission testing method in non-destructive testing and structural monitoring are defined by its unique dynamic and passive testing nature. Unlike radiographic or ultrasonic testing, Acoustic Emission detects degradation in real time. As a result of the major advantages of the method, the range of applications for acoustic emission is very diverse. The acceptance of acoustic emission as an inspection and testing method was determined by the integrity inspection of pressure vessels. The application of the acoustic emission examination method has expanded from pressure vessel testing to corrosion testing of flat-bottomed storage tanks (aboveground storage tanks), leakage testing of pipes and valves (valves, safety valves, flanges), partial discharge testing in transformers and is currently finding its way into the monitoring of the structural integrity of civil and aerospace engineering structures. In the field of research and development, the acoustic emission inspection methodology has become a factor in continuous evolution and improvement.

The sensitivity of Acoustic Emission (AE) is demonstrated if we consider that the absolute energy of Acoustic Emission signals is of the order of $10^{-18}$ J. The method allows the detection of the actual initiation of micro-cracking or any other event that would be impossible to detect by other techniques. If we compare the kinetic energy, of approximately $1{,}25 \cdot 10^{-8}$ J, of a mosquito with a mass of 2,5 mg, flying at a speed of 10 cm/s, it is observed that the limit of the technique is 10 orders of magnitude greater than in Fig. 1. *(Dimitrios G. Aggelis, Markus G. R. Sause, Pawel Packo, Rhys Pullin, Steve Grigg, Tomaž Kek, and Yu-Kun Lai, 2021)*

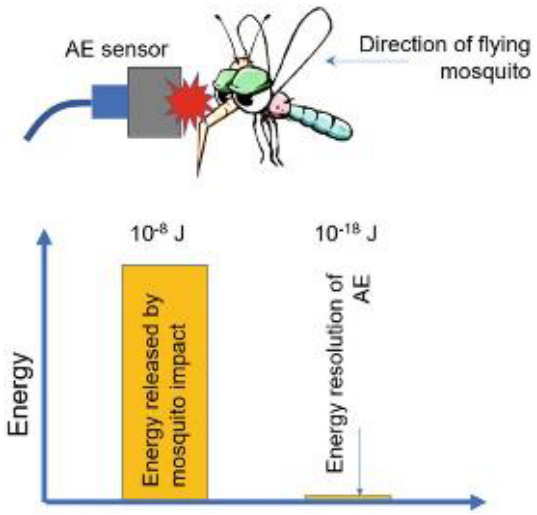



**Fig. 1 - The amount of energy that can be measured by Acoustic Emission systems.**
*(Dimitrios G. Aggelis, Markus G. R. Sause, Pawel Packo, Rhys Pullin, Steve Grigg, Tomaž Kek, and Yu-Kun Lai, 2021)*

Acoustic Emission Testing detects and monitors transient elastic waves emitted after an irreversible phenomenon or process in the material. In most cases, piezoelectric transducers are placed on the surface

of the material being tested. A "coupling" layer is applied between the sensor and the material surface to ensure adequate wave transmission. *(Dimitrios G. Aggelis, Markus G. R. Sause, Pawel Packo, Rhys Pullin, Steve Grigg, Tomaž Kek, and Yu-Kun Lai, 2021)*

Acoustic activity is an indicator of the monitored structure and represents how many signals have been detected. In the case of a defect, the number of signals (hits) is related to the degree of degradation and the rate of crack formation and propagation. In addition, the waveform provides important information regarding the source of the emission. Therefore, several parameters are used to quantify the waveform. *(Dimitrios G. Aggelis, Markus G. R. Sause, Pawel Packo, Rhys Pullin, Steve Grigg, Tomaž Kek, and Yu-Kun Lai, 2021)*

A basic experimental setting is the “threshold”, which is a value that must be exceeded to trigger data acquisition. This is an easy way to avoid low-amplitude noise (e.g. from friction) and is relevant for measuring most parameters. A parameter related to the intensity of the phenomenon is the amplitude (A). The amplitude is the voltage (V) of the highest peak of the waveform (**Fig. 2**).

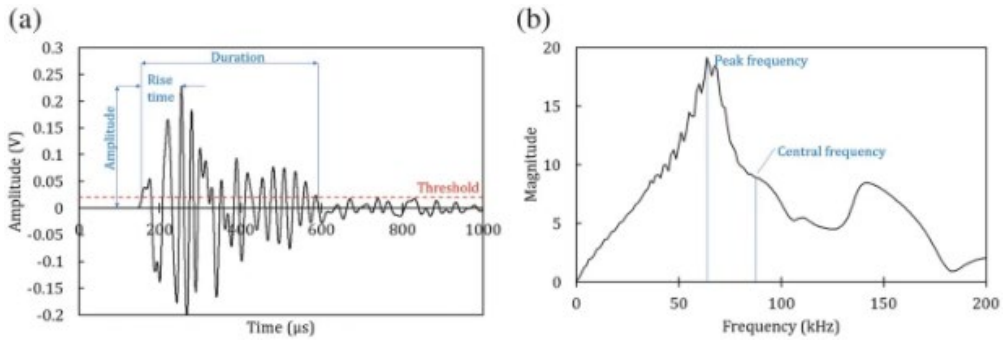



**Fig. 2 - (a) Typical AE waveform with basic AE parameters, time domain and (b) Fast Fourier Transform with basic spectral parameters, frequency domain.**

*(Dimitrios G. Aggelis, Markus G. R. Sause, Pawel Packo, Rhys Pullin, Steve Grigg, Tomaž Kek, and Yu-Kun Lai, 2021)*

The delay between the first threshold crossing and the highest peak is called the signal rise time (RT). Duration (Dur) is defined as the delay between the first and last threshold crossing. *(Dimitrios G. Aggelis, Markus G. R. Sause, Pawel Packo, Rhys Pullin, Steve Grigg, Tomaž Kek, and Yu-Kun Lai, 2021)*

Frequency content is also important. Different parameters are used to process the information. The simplest is the Average Frequency (AF), which is calculated in the time domain as the ratio of the total number of threshold crossings (counts – the number of events with the same location) over the duration of the waveform in kHz. Other parameters, such as the peak frequency and the center frequency, are calculated in the frequency domain. The first is the frequency with the highest magnitude, and the second is the center of the spectrum. *(Dimitrios G. Aggelis, Markus G. R. Sause, Pawel Packo, Rhys Pullin, Steve Grigg, Tomaž Kek, and Yu-Kun Lai, 2021)*

Parameters including energy, RT, Dur, RA and frequency content are sensitive to defect sources and are used to characterize the cracking mode. Basically, the initial part of the waveform contains more relevant information for the source mechanism, while the latter part may contain reflections and be more strongly influenced by geometry. (*Dimitrios* G. Aggelis, Markus G. R. Sause, Pawel Packo, Rhys Pullin, Steve Grigg, Tomaž Kek, and Yu-Kun Lai, 2021)

The treatment of complete waveforms (as in "signal-based" analysis) is also widely used; tools such as "wavelet" and spectral analysis are very useful in revealing hidden information of sources. (Dimitrios G. Aggelis, Markus G. R. Sause, Pawel Packo, Rhys Pullin, Steve Grigg, Tomaž Kek, and Yu-Kun Lai, 2021)

For AE measurement systems with digitizing capability, two parameters play a very important role: “sampling rate” and “dynamic range.” The sampling rate or frequency determines how dense the points within the waveform are, or the time interval between two successive points. *(Dimitrios G. Aggelis, Markus G. R. Sause, Pawel Packo, Rhys Pullin, Steve Grigg, Tomaž Kek, and Yu-Kun Lai, 2021)*

Wave propagation in the structure is affected by the interaction with material properties, inhomogeneities, free surface geometry, and loading conditions. *(Eitzen & Wadley, 1984)*

In an Acoustic Emission Examination system, AE waves are detected by an AE sensor, which converts the dynamic movements from the surface of a material into electrical signals. Since AE signals are weak, they are normally amplified by two amplifiers: a preamplifier and a main amplifier (**Fig. 3**). The signal-

to-noise ratio of the equipment must be low, and amplifiers often provide a gain of over 1000 times, the usual value is about 100 times. *(Grosse & Ohtsu, 2008)*

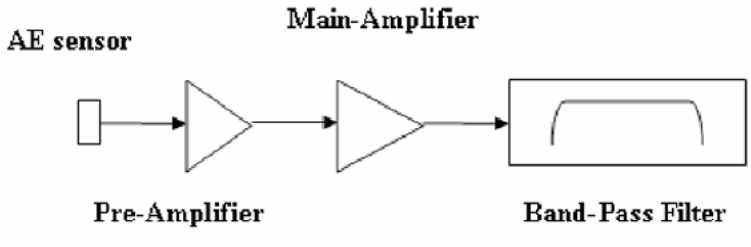



**Fig. 3 - Acoustic Emission Examination System.**
*(Grosse & Ohtsu, 2008)*

The bandpass filter is successfully used for noise removal. In materials engineering, bandwidths from a few kHz to a few hundred kHz or 1 MHz are recommended for measurement. *(Grosse & Ohtsu, 2008)*

Before describing the failure mode characterization in detail, a fundamental phenomenon in acoustic emission should be mentioned. The name is derived from Joseph Kaiser (Kaiser 1950), who was one of the pioneers of modern acoustic emission examination. When the mechanical load is increased in a specimen, acoustic activity is recorded (moderate load P1). If the material is unloaded and reloaded to the previous load P1, no acoustic emission signals are observed. This is the "Kaiser effect" and the lack of recording of acoustic emission can be attributed to the fact that the damage related to the specific load level P1 occurred during the initial cycle. By increasing the load higher than P1 (up to P2), acoustic emission signals are again recorded, as "new" sources are created. If the material is unloaded and reloaded to the previous load P1, no acoustic emission signals are observed. The "Kaiser effect" is presented in **Fig. 4**. *(Esola, Wisner, Vanniamparambil, Geriguis, & Kontsos, 2018). (Dimitrios G. Aggelis, Markus G. R. Sause, Pawel Packo, Rhys Pullin, Steve Grigg, Tomaž Kek, and Yu-Kun Lai, 2021)*

Assuming that the load P2 caused the cracks, in the case of unloading and reloading, the acoustic emission signals will start at a load lower than the previous maximum (e.g., P3 < P2). This can be considered as a result of the cracks and stress concentrators increasing the stress locally just before the load reaches the previous maximum level. The load at the onset of the emission signals, above the previous maximum load (in this case P3/P2), is called the "Felicity ratio" (FR) (Fowler 1977). *(Esola, Wisner, Vanniamparambil, Geriguis, & Kontsos, 2018) (Dimitrios G. Aggelis, Markus G. R. Sause, Pawel Packo, Rhys Pullin, Steve Grigg, Tomaž Kek, and Yu-Kun Lai, 2021)*

The "Felicity Ratio" (FR), shown in **Fig. 4**, is a key benchmark in acoustic emission signal testing that measures the ratio of the load at which AE signals reappear during reloading to the maximum load previously applied. FR is close to 1 when the material is intact, meaning that the "Kaiser effect" is valid. When FR decreases, it indicates the accumulation of defects and is frequently used as a powerful parameter in the evaluation of composites. *(Esola, Wisner, Vanniamparambil, Geriguis, & Kontsos, 2018)). (Dimitrios G. Aggelis, Markus G. R. Sause, Pawel Packo, Rhys Pullin, Steve Grigg, Tomaž Kek, and Yu-Kun Lai, 2021)*

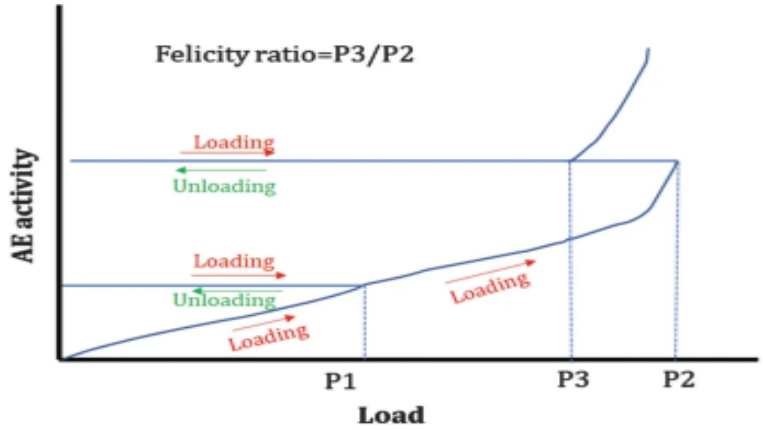



**Fig. 4 - "The Kaiser Effect" and "The Felicity Ratio".**
*(Dimitrios G. Aggelis, Markus G. R. Sause, Pawel Packo, Rhys Pullin, Steve Grigg, Tomaž Kek, and Yu-Kun Lai, 2021)*

A crack propagation event that extends vertically along the plate axis results in a waveform with different characteristics than a similar crack in the parallel direction. In the case of plates, the reason may be the different amount of energy that forms the "symmetric" and "antisymmetric" wave modes. *(Dimitrios G. Aggelis, Markus G. R. Sause, Pawel Packo, Rhys Pullin, Steve Grigg, Tomaž Kek, and Yu-Kun Lai, 2021)*

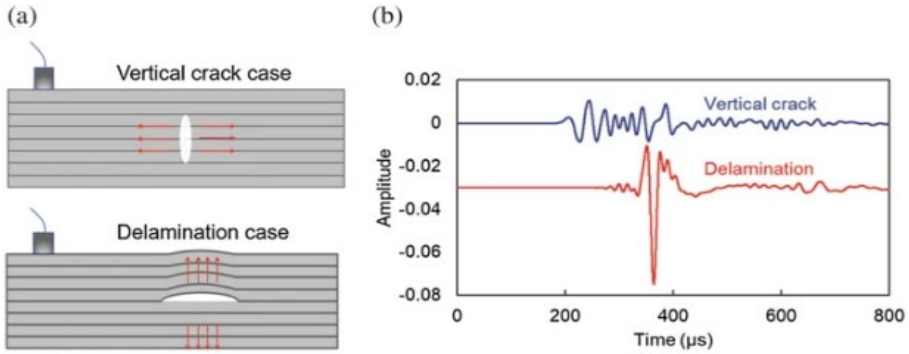



**Fig. 5 - (a) Representation of vertical crack (top) and delamination (bottom) in a laminated composite plate and (b) typical AE waveforms from the two events.**
*(Dimitrios G. Aggelis, Markus G. R. Sause, Pawel Packo, Rhys Pullin, Steve Grigg, Tomaž Kek, and Yu-Kun Lai, 2021)*

When the vertical crack is extended, this motion excites mainly the symmetric components that have higher propagation velocities than the antisymmetric ones. A waveform containing a stronger symmetric component is expected to have higher energy in the initiating part than in the later part, as observed in **Fig. 5**. *(Dimitrios G. Aggelis, Markus G. R. Sause, Pawel Packo, Rhys Pullin, Steve Grigg, Tomaž Kek, and Yu-Kun Lai, 2021)*

In general, crack advance occurs if the stress at any pre-existing flaw exceeds a critical value determined by the toughness of the material, the local stress and the size and orientation of the flaw. Crack growth will normally occur by the ductile dimple mechanism at temperatures above the ductile-to-brittle transition temperature, and by transgranular (cleavage) or intergranular fracture in the less probable event of crack advance below the transition temperature or in a locally embrittled region. In the event of cleavage crack advance, fracture of a grain (typically 30 μm) would generate large amplitude signals, as would intergranular fracture along several grain facets. Scruby and Wadley *(Scruby & Wadley, 1983)* made an attempt to represent these in the form of a map, presented in **Fig. 6**, that visually indicates the likelihood of detectability. All the estimates assumed an isolated microcrack. *(Eitzen & Wadley, 1984)*

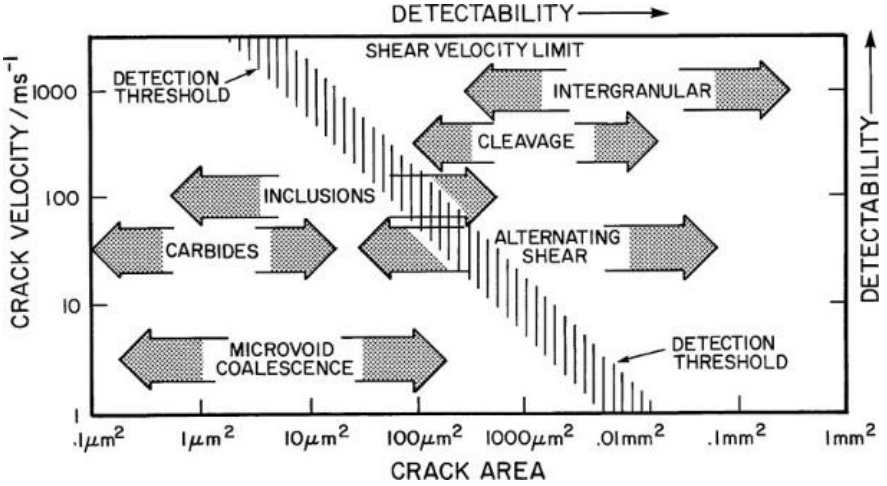



**Fig. 6 - Detectability of fracture events in steels. Detection threshold assumes transducer compression wave sensitivity of $10^{-13}$ m, source-transducer distance 0,1 m and stress 500 $MNm^{-2}$.**
*(Eitzen & Wadley, 1984)*

The initial excitation (crack propagation increment or 'source' in our case) propagates through a material with certain characteristics (stiffness, density, attenuation coefficient, heterogeneity, which strongly influence its shape. Then at reception, the characteristics of the sensor, mainly frequency response will further influence the waveform (not forgetting the coupling conditions), while the acquisition system may also

impose further distortion. Therefore, the final digitized waveform has very few similarities to the original source, see **Fig. 7**. *(Dimitrios G. Aggelis, Markus G. R. Sause, Pawel Packo, Rhys Pullin, Steve Grigg, Tomaž Kek, and Yu-Kun Lai, 2021)*

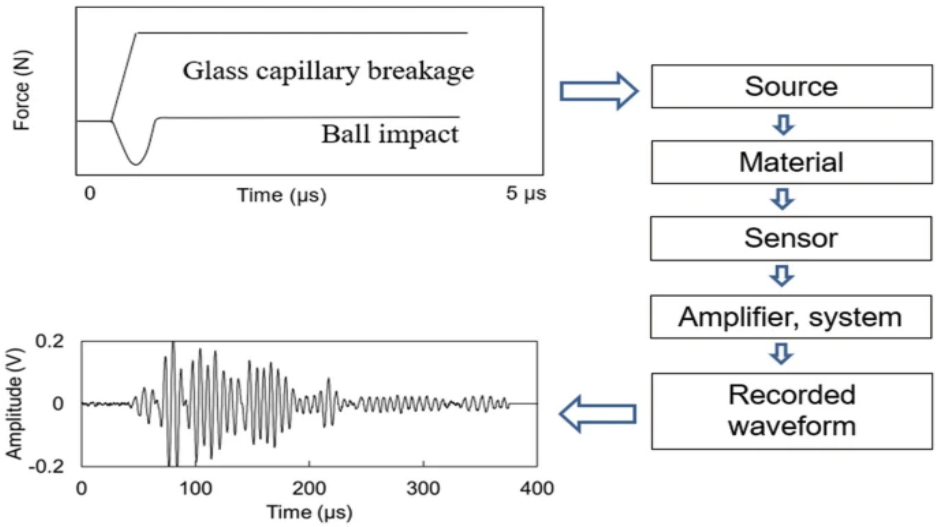



**Fig. 7 - Process chain of AE production and reception**
*(Dimitrios G. Aggelis, Markus G. R. Sause, Pawel Packo, Rhys Pullin, Steve Grigg, Tomaž Kek, and Yu-Kun Lai, 2021)*

The basic principle of acoustic emission source localization is based on measuring the time difference of arrival (TDOA) for different sensors, the physics of wave propagation in plates makes the acoustic source localization procedure (ASLP) quite complex. For the triangulation localization of an acoustic source, when the wave velocity for an isotropic plate is known, the following simple procedure presented in **Fig. 8**. *(Tobias, 1976), (Kundu, 2014))* *(Dimitrios G. Aggelis, Markus G. R. Sause, Pawel Packo, Rhys Pullin, Steve Grigg, Tomaž Kek, and Yu-Kun Lai, 2021)*

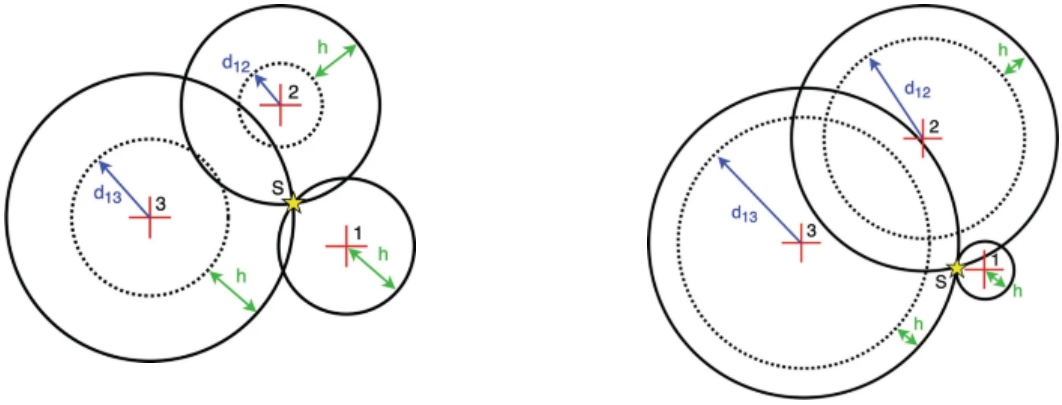



**Fig. 8 - Acoustic source localization via triangulation for known wave speed c,** after
*(Kundu, 2014) (Dimitrios G. Aggelis, Markus G. R. Sause, Pawel Packo, Rhys Pullin, Steve Grigg, Tomaž Kek, and Yu-Kun Lai, 2021)*

A method combining the simplicity of the triangulation approach with basic information on wave physics in plates can be found in *(Grabowski, et al., 2016)*. The method employs the time-distance domain transform (TDDT) for mapping the signals acquired by the sensors, transforming them from the time to the distance domain. Subsequently, the localization is performed immediately in the distance domain to find the acoustic source. *(Dimitrios G. Aggelis, Markus G. R. Sause, Pawel Packo, Rhys Pullin, Steve Grigg, Tomaž Kek, and Yu-Kun Lai, 2021)*

An example of the shifting procedure used for determining source-sensor distances is shown in **Fig. 9**, where the compensated signal amplitude and wave packet width are presented. Both parameters assume extreme values for the same temporal shift. The dispersion-compensated signal after transformation into the distance domain, obtained by applying the procedure described above, is presented in **Fig. 10**, along with the

waveform before applying signal processing. *(Dimitrios G. Aggelis, Markus G. R. Sause, Pawel Packo, Rhys Pullin, Steve Grigg, Tomaž Kek, and Yu-Kun Lai, 2021)*

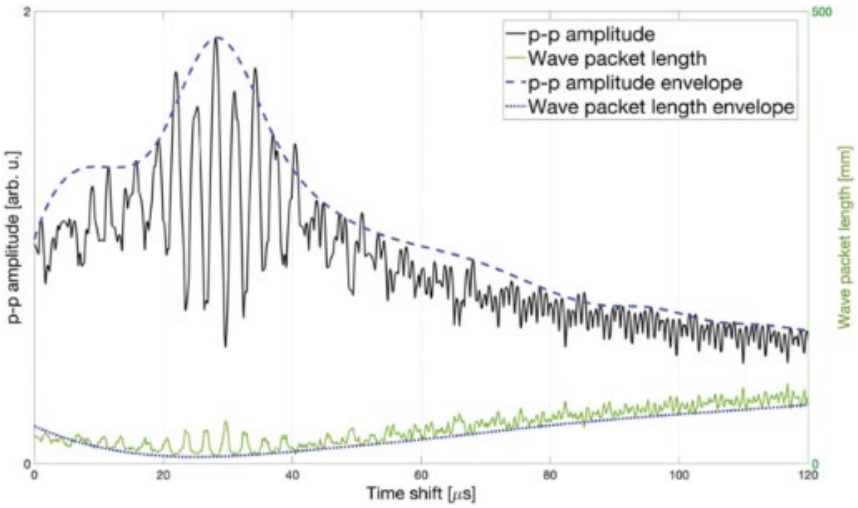



**Fig. 9 - Amplitude and width of a wave packet after dispersion compensation with various time shifts,** after *(Grabowski, et al., 2016)). (Dimitrios G. Aggelis, Markus G. R. Sause, Pawel Packo, Rhys Pullin, Steve Grigg, Tomaž Kek, and Yu-Kun Lai, 2021)*

Acoustic Emission Testing (AET) was effectively used by C. K. Mukhopadhyay et al. (2014) in a study to detect deformation and / or damage and crack growth in vessels during laboratory testing. The acoustic emission generated during component testing indicated that the AE signals generated were due only to structural noise and “micro-flow” of the material. Online Acoustic Emission (AE) monitoring allows for the detection of deformation and / or damage of components as well as the detection of potential growth defects, if any, during the pressure test. The conclusion of the study was that AE can be used to monitor the structural integrity of components during the pressure test. The absence of acoustic emission signals during the re-pressurization cycle confirms the structural integrity of the components. *(Mukhopadhyay, T.K. Haneef, B.P.C. Rao and T. Jayakumar, 2014)*

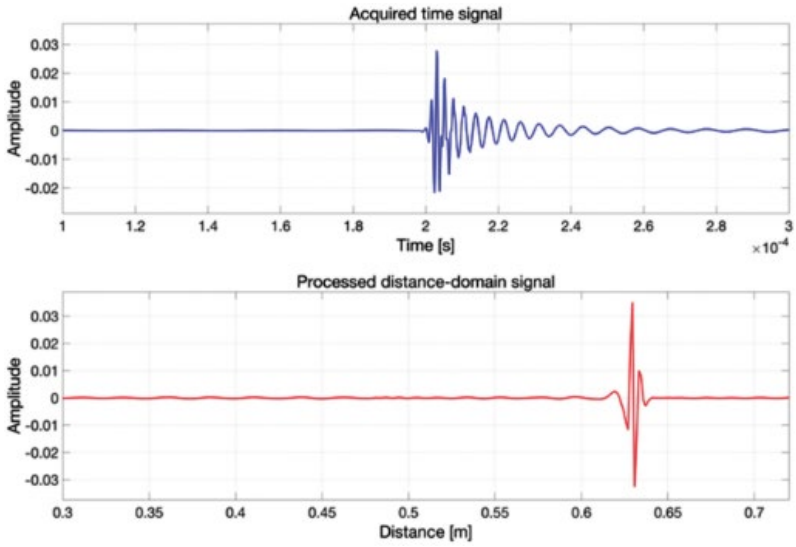



**Fig. 10 - Example signals: time-domain signal acquired at the source (top) and dispersion-compensated and transformed to the distance domain (bottom)**, after *(Grabowski, et al., 2016)) (Dimitrios G. Aggelis, Markus G. R. Sause, Pawel Packo, Rhys Pullin, Steve Grigg, Tomaž Kek, and Yu-Kun Lai, 2021)*

The variation of the number of events as a function of time and the cumulative number of events as a function of time are shown in **Fig. 11**. The amplitude distribution of the signals for three stages is shown in **Fig. 12**.

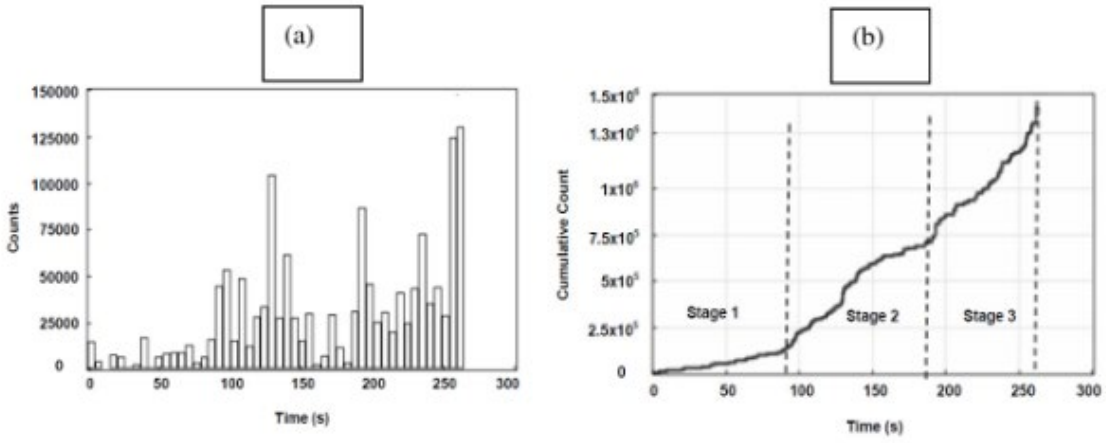



**Fig. 11 - Variation of (a) counts vs. time and (b) cumulative count vs. time.**
*(Mukhopadhyay, T.K. Haneef, B.P.C. Rao and T. Jayakumar, 2014)*

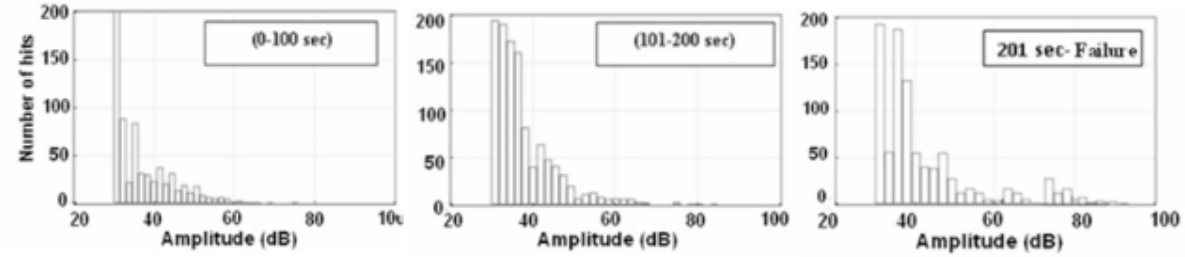



**Fig. 12 - Amplitude distribution of hits for three stages.**
*(Mukhopadhyay, T.K. Haneef, B.P.C. Rao and T. Jayakumar, 2014)*

Fractal analysis was proposed in a study by (Stefano Porziani, Giuseppe Augugliaro, Fabio Brini, Carlo Brutti, Andrea Chiappa, Corrado Groth, Canio Mennuti, Paolo Quaresima, Pietro Salvini, Alessandro Zanini, Marco Evangelos Biancolinia., 2020) for interpreting acoustic emission signals related to material damage. The fractal dimension quantifies the order/disorder of the signals and is correlated with the applied stress/pressure and loading cycles. The diagram of such an evolution allows the evaluation of the propagation of a fatigue crack and the understanding of the safety margin of the investigated structure at a specific moment of its lifetime.

The authors showed that the analysis of AE signals by the fractal method “Box-Counting Method” (BCM) can be successfully applied in the non-destructive monitoring of structures and is presented in **Fig. 13**. *(Stefano Porziani, Giuseppe Augugliaro, Fabio Brini, Carlo Brutti, Andrea Chiappa, Corrado Groth, Canio Mennuti, Paolo Quaresima, Pietro Salvini, Alessandro Zanini, Marco Evangelos Biancolinia., 2020)*

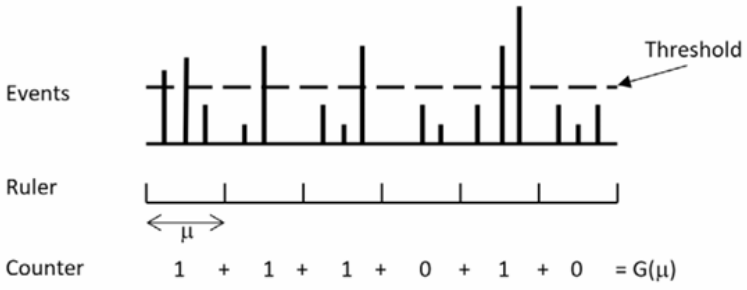



**Fig. 13 - Metoda ”Box-counting method”.**
*(Stefano Porziani, Giuseppe Augugliaro, Fabio Brini, Carlo Brutti, Andrea Chiappa, Corrado Groth, Canio Mennuti, Paolo Quaresima, Pietro Salvini, Alessandro Zanini, Marco Evangelos Biancolinia., 2020)*

This technique allows the collection of information about the damage of the structure under both static and dynamic loading. The fractal dimension (Dt) can measure the disorder of the AE sources, highlighting whether a certain local damage process is active and provides information about its evolution under static and dynamic loading. A sudden decrease in Dt shows that in an area of the tested material there is a concentration of AE events, it is then possible to monitor this damaged area from the initiation of the defect to the destruction of the structure. *(Stefano Porziani, Giuseppe Augugliaro, Fabio Brini, Carlo Brutti, Andrea Chiappa, Corrado Groth, Canio Mennuti, Paolo Quaresima, Pietro Salvini, Alessandro Zanini, Marco Evangelos Biancolinia., 2020)*

Acoustic emission (AE) method is one of the non-destructive testing methods used for industrial testing of equipment such as pipelines, pressure vessels, combustion engines, power transformers and storage tanks. The work by *(Olszewska, 2022)* uses the AE method for testing the bottoms of above-ground vertical storage tanks.

The undeniable advantage of the AE method is the ability to perform a structural diagnosis of tank bottoms without the need to empty the tanks or take them out of service. The purpose of AE testing (AT) of the storage tank bottom is to detect and classify AE sources caused mainly by active corrosion processes, material discontinuities or leaks. Thanks to AT tests, it is possible to recognize not only the presence, but also the location of leaks and corrosion. *(Olszewska, 2022)*

The AE measurement system used was the Vallen GmbH AMSY 6, which can simultaneously acquire AE and waveform data for each channel (**Fig. 14**). It has an internal unit that can send electrical pulses to the sensors for internal verification. During data analysis, it is important to ensure that interferences do not influence the test result obtained, so appropriate filters must be used to eliminate various types of interferences. The measurement data must be filtered to reject noise data or other signals that are not related to corrosion and / or tank bottom leaks. The first step is to filter out the peak signals with a very short rise time and which are acquired in large numbers due to the fact that the measurement threshold is set at a very low level. *(Olszewska, 2022)*

AE events are identified by analyzing the differences in arrival times of the detected points. The position of each localized AE event is calculated using the apparent AE velocity. The localization of AE events is performed with localization algorithms contained in the VisualAE software. The localization algorithm additionally filters signals that cannot be combined into a single physical event that emits a sound wave in the tank bottom area. AE events located close to each other are considered a single group and represent an AE source.

The information provided by these tests contributes to the maintenance planning of these tanks, allowing prioritization before they are taken out of service. *(Olszewska, 2022)*

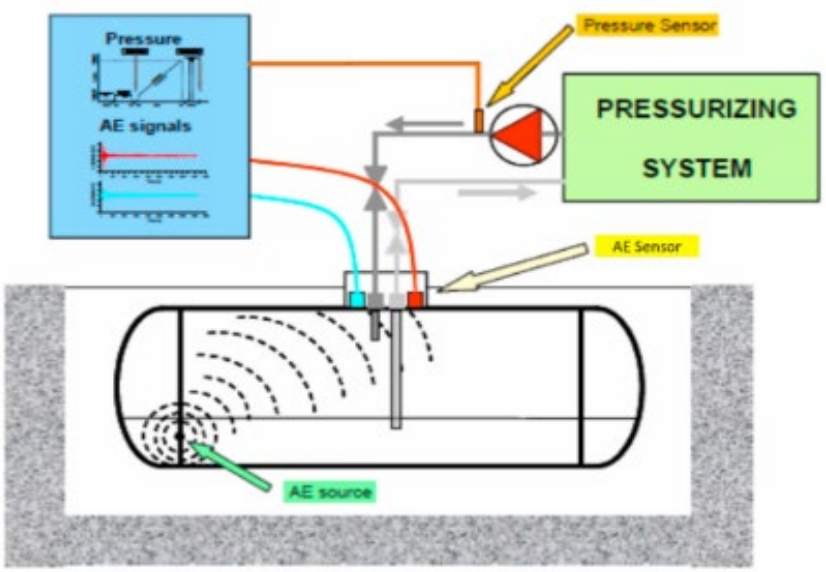



**Fig. 14 - Test procedure according to SPESL / INAIL (National Institute for Insurance against Accidents at Work).**
*(Olszewska, 2022)*

**ACKNOWLEDGEMENT**

The authors acknowledge the Doctoral School of the Faculty of Biotechnical Systems Engineering at the National University of Science and Technology POLITEHNICA Bucharest for the financial support provided through the doctoral grant, which facilitated the participation at this conference.

**REFERENCES**

[1] Bi, H., Hu, D., Li, Z., Niu, Q., Toku-Gyamerah, I., & Chen, J. (2015). Monitoring Uniform Corrosion of Storage Tank Bottom Steel by. *International Journal of ELECTROCHEMICAL SCIENCE, 10-6946-6958*.

[2] Dimitrios G. Aggelis, Markus G. R. Sause, Pawel Packo, Rhys Pullin, Steve Grigg, Tomaž Kek, and Yu-Kun Lai. (2021). Structural Health Monitoring Damage Detection Systems for Aerospace. Springer Aerospace Technology. Springer, Cham. doi:https://doi.org/10.1007/978-3-030-72192-3_7

[3] Eitzen, D., & Wadley, H. (1984). Acoustic Emission Establishing the Fundamentals. *JOURNAL OF RESEARCH of the National Bureau of Standards*. doi:10.6028/jres.089.008

[4] Esola, S., Wisner, B., Vanniamparambil, P., Geriguis, J., & Kontsos, A. (2018). Part Qualification Methodology for Composite Aircraft Components Using Acoustic Emission Monitoring. *Applied Sciences, Applied Sciences, 8(9), 1490*. doi:https://doi.org/10.3390/app8091490

[5] Grabowski, K., Gawronski, M., Baran, I., Spychalski, W., Staszewski, W., Uhl, T., . . . Packo, P. (2016). Time–distance domain transformation for acoustic emission source localization in thin metallic plates. *Ultrasonics, Ultrasonics 68 (2016) 142–149*. doi:Ultrasonics 68: 142–149. ISSN 0041-624X

[6] Grosse, C., & Ohtsu, M. (2008). *Acoustic Emission Testing.* Berlin: Springer. doi:https://doi.org/10.1007/978-3-540-69972-9

[7] Kundu, T. (2014). Acoustic source localization. *Ultrasonics, Ultrasonics 54(2014) 25–38*. doi:https://doi.org/10.1016/j.ultras.2013.06.009

[8] Mukhopadhyay, T.K. Haneef, B.P.C. Rao and T. Jayakumar. (2014). On-Line Monitoring of Engineering Components Using Acoustic Emission Technique. (ELSEVIER, Ed.) *ScienceDirect, Procedia Engineering 86 ( 2014 ) 496 – 502*. doi:doi: 10.1016/j.proeng.2014.11.073

[9] Olszewska, A. (2022). Using the acoustic emission method for testing aboveground vertical storage tank bottoms. *AppliedAcoustics, Applied Acoustics 188 (2022) 108564*. doi:https://doi.org/10.1016/j.apacoust.2021.108564

[10] Scruby, C., & Wadley, H. (1983). An assessment of acoustic emission for nuclear pressure vessel monitoring. *Progress in Nuclear Energy, Volume 11, Issue 3*, 275-297. doi:https://doi.org/10.1016/0149-1970(83)90014-8

[11] Stefano Porziani, Giuseppe Augugliaro, Fabio Brini, Carlo Brutti, Andrea Chiappa, Corrado Groth, Canio Mennuti, Paolo Quaresima, Pietro Salvini, Alessandro Zanini, Marco Evangelos Biancolinia. (2020). Structural integrity assessment of pressure equipment by Acoustic Emission and data fractal analysis. (ELSEVIER, Ed.) *ScienceDirect, Procedia Structural Integrity 25 (2020) 246–253*.

[12] Tobias, A. (1976). Acoustic-emission source location in two dimensions by an array of three sensors. *Non-Destructive Testing, Non-Destructive Testing Volume 9, Issue 1*, 9-12. doi:https://doi.org/10.1016/0029-1021(76)90027-X

# SOIL AMENDMENTS IMPACT ON LIGNOCELLULOSIC COMPOSITION OF SWEET SORGHUM BAGASSE IN MARGINAL LAND

/

# *ВПЛИВ ГРУНТОВИХ ДОМІШОК НА ВМІСТ ЛІГНОЦЕЛЮЛОЗИ БАГАССИ ЦУКРОВОГО СОРГО НА МАРГІНАЛЬНИХ ЗЕМЛЯХ*

**Yaroslava MOSIICHUK[1)], Bohdan MAZURENKO[2)], Rafiq ISLAM[3)], Nataliia DIDENKO[1)], Mykola ZOSYMCHUK[1)], Sergiy LAVRENKO[4)], Mykola KHARYTONOV*[5)]**

[1)] Institute of Water Problems and Land Reclamation of NAAS of Ukraine, Kyiv / Ukraine;
[2)] National University of Life and Environmental Sciences of Ukraine, Kyiv / Ukraine;
[3)] The Ohio State University South Centers, Piketon, OH / United States;
[4)] Kherson State Agrarian and Economic University, Kherson / Ukraine;
[5)] Dnipro State Agrarian and Economic University, Dnipro / Ukraine.
*Tel: +38-0973 456 227; *E-mail: kharytonov.m.m@dsau.dp.ua*

***Keywords:*** *biosolids, fertilizers, sweet sorhum biomass, lignocellulosic composition, marginal lands*

**ABSTRACT**

*Nutrient-enriched municipal biosolids can be recycled as proactive soil amendment to improve the growth of sweet sorghum (Sorghum bicolor (L.) Moench) a dedicated high-biomass and energy-yielding crop known for its adaptability to marginal soils. This replicated field study was aimed to assess the impact of varying rates of biosolids on the lignocellulosic composition of sweet sorghum bagasse, when compared with the chemical fertilization used as a control. Results showed that biosolids and chemical fertilizer significantly influenced the chemical composition and thermal characteristics of the biomass. During the initial stage of thermolysis, a decrease in reaction rates was observed in biosolids treatments ranging from 10 to 40 ton/ha and $N_{60}P_{30}K_{60}$ (kg/ha), showing a reduction of 19 to 45 compared to the control. Exothermic reactions during the second stage were most pronounced in biosolids amendment (40 ton/ha) and chemical fertilization ($N_{60}P_{30}K_{60}$ kg/ha), occurring within the temperature range of 390 – 410 °C. Fertilizer application resulted in reduced activation energy of biomass during the initial thermolysis stage. The most significant reduction was observed in biosolids at 30-40 ton/ha and $N_{30}P_{15}K_{30}$ treatments, where activation energy values were more than halved compared to the control.*

**ТЕЗИ**

*Збагачені поживними речовинами муніципальні біодобрива можна переробляти як проактивний засіб для покращення росту цукрового сорго (Sorghum bicolor (L.) Moench), спеціалізованої культури з високим вмістом біомаси та енергією, відомої своєю адаптивністю до маргінальних ґрунтів. Це повторне польове дослідження мало на меті оцінити вплив різних норм біодобривів на лігноцелюлозний склад багаси цукрового сорго порівняно з хімічним удобренням, що використовувалося як контроль. Результати показали, що біодобриви та хімічні добрива суттєво впливали на хімічний склад та теплові характеристики біомаси. Під час початкової стадії термолізу спостерігалося зниження швидкості реакції на 19-45% при обробці біодобривами в діапазоні від 10 до 40 тонн/га та $N_{60}P_{30}K_{60}$ (кг/га) порівняно з контролем. Екзотермічні реакції протягом другого етапу були найбільш виражені при внесенні біодобрив (40 т/га) та хімічному удобренні ($N_{60}P_{30}K_{60}$ кг/га), що відбувалися в діапазоні температур 390–410 °C. Внесення добрив призвело до зниження енергії активації біомаси протягом початкової стадії термолізу. Найбільш значне зниження спостерігалося для біодобрив при обробці 30-40 т/га та $N_{30}P_{15}K_{30}$, де значення енергії активації були більш ніж вдвічі меншими порівняно з контролем.*

## INTRODUCTION

Sweet sorghum, a C4 photosynthetic species, is a promising energy crop with a sugar content of 16–23% brix, boasting high biomass and sugar yields *(Vinutha et al., 2014; Mathur et al., 2017)*. It is photoperiod-sensitive, with a longer growing season and the ability to produce substantial amounts of green and dry matter *(Castro et al., 2015).* Recognized for its versatile adaptability, rapid growth, ease of cultivation, drought and salt tolerance, water and nutrient use efficiency, lower input requirements, and cost-

effectiveness in fermentable sugar production, sweet sorghum emerges as a dedicated energy crop in response to climate change effects *(Fu et al., 2016; Mansour et al., 2017; Mathur et al., 2017).*

Sweet sorghum cane bio-refining yields multiple valuable products, including ethanol, butanol, and wood-plastic composites *(Yu et al., 2021).* According to the U.S. Department of Agriculture, the energy invested to energy obtained ratio during biofuel extraction from sweet sorghum is estimated at 1:8. Apart from stem sugars being a primary commodity in sweet sorghum cultivation, co-products like bagasse can also be proactively utilized as raw materials for energy recovery. Briquettes made from pure sorghum processed stalks exhibit a high calorific value, low ash content, and minimal levels of chlorine, nitrogen, and sulfur *(Ivanova et al., 2018).* Soil quality management plays a crucial role in enhancing its productivity and sustainability while the successful cultivation of sweet sorghum depends on various factors. There has been a significant focus on recycling substantial amounts of carbon and nutrient-enriched biosolids as soil amendments in response to the imperative for more sustainable practices driven by global climate change *(Islam, 2012).* This aims to regenerate marginal lands for large-scale production of bio-feedstocks derived from sweet sorghum. Commercial cultivation of energy crops on such lands emerges as an economically viable and environmentally compatible solution to address these challenges and meet human needs. This approach not only yields essential fuel but also utilizes vast areas of marginal lands, thereby regenerating their soil quality and contributing to the reduction of $CO_2$ emissions *(Regassa and Wortmann, 2014).* This niche in agricultural production is gaining attraction among small-scale producers in Ukraine, where an estimated 15.5 million hectares of marginal lands offer potential for bio-feedstock for renewable energy, a figure expanding due to ongoing conflicts.Sweet sorghum, with its low nutrient requirements requiring 40% less nitrogen (N) fertilization compared to corn, emerges as an ideal candidate for utilizing recycled carbon and nutrient-enriched biosolids. This practice can improve the farm economics of lignocellulosic bio-feedstock production derived from sweet sorghum. Lignocellulosic biomass presents a highly promising option for generating heat, electricity, and producing renewable fuel for automobiles and other transports *(Carrier et al., 2011).* Sorghum stalks processed into juice can also serve as valuable lignocellulosic raw materials or pellets *(Singh et al., 2012).* Sweet sorghum bagasse has been found to contain 45% cellulose, 27% hemicellulose, and 21% lignin *(Misook and Day, 2011).* The three main components of biomass (cellulose, hemicellulose, and lignin) determine the quality of bio-feedstock from energy crops. Thermogravimetric analysis (TGA) stands out as one of the most widely used techniques for determining the combustion profile of a fuel, encompassing four basic stages: moisture evaporation, devolatilization and volatiles oxidation, ignition, and fixed carbon combustion *(Jeguirim et al., 2010; Kongkaew et al., 2015; Wnorowska et al., 2021).* Previous research suggests that weight losses of plant stover (considering corn as a standard bioenergy crop) in both inert and oxidizing atmospheres occur in three stages *(Kumar et al., 2008).* Therefore, evaluating weight loss characteristics of sweet sorghum biomass in both inert and oxidizing conditions will help us predict the feasibility of using sweet sorghum biomass for viable energy generation by recycling biosolids as a soil amendment to improve marginal lands for bioenergy production.

The objective of our research study was to estimate and compare the weight loss characteristics of sweet sorghum biomass in both inert and oxidizing conditions, impacted by recycling biosolids and chemical fertilization, to regenerate marginal lands for bio-feedstock production.

## MATERIALS AND METHODS

The field experiment was established at the research farm of the National University of Life and Environmental Sciences of Ukraine, Kyiv, Ukraine in 2022. It is in the forest steppe zone of Ukraine under continental climate with a total annual of precipitation is 528 mm, of which 364 mm falls between April and October. The temperature of the growing season above 5 °C is 215 days, and the frost-free period ranges from 157 to 164 days. The soil is represented by gray forest podzolic dusty light loamy soils, with a humus-eluvial horizon of 50-60 cm and carbonates located at a depth of 110-150 cm. The soil bulk density in the 0-30 cm layer range from 1.1-1.2 g/cm$^3$. The soluble nutrients in the 0-30 cm depth such as easily hydrolyzed nitrogen is 6.2-8.3 mg/100 g, exchangeable phosphorus) is 7.5-12 mg/100 g, and exchangeable potassium is 4.2-10.1 mg/100 g of soil.A field experiment employing a randomized complete block design was conducted utilizing the “Energodar” variety of sweet sorghum, with four levels of sewage sludge (SS) as biosolids and two chemical fertilizer treatments. The biosolids were applied at rates of 0 (K1), 10 (K2), 20 (K3), 30 (K4), and 40 (K5) tons per hectare, while the chemical fertilizers comprised $N_{30}P_{15}K_{30}$ (K6) and $N_{60}P_{30}K_{60}$ (K7), respectively. The biosolids, composted for over a decade in close proximity to the disposal site, were collected for field application. Both the chemical fertilizers and biosolids were broadcasted across

respective plots in the fall of 2021, adhering to specific treatment combinations.Prior to the application of treatments and the planting of sweet sorghum, the field underwent plowing to a depth of 25 cm, early spring cultivation at a depth of 15 cm, and harrowing to 8 cm. Planting was carried out manually using a "Vynnychanka" seeder with row spacing set at 70 cm. Following germination, the stand density was manually adjusted to 290 thousand plants per hectare. Sweet sorghum was cultivated under natural weather conditions and relied solely on rain for irrigation. Standard cultural practices were implemented to manage weed growth.Following harvest, sweet sorghum canes were collected, oven-dried, and prepared for analysis. Thermal analysis of the cane biomass was conducted using the derivatograph Q-1500D of the “F. Paulik-J. Paulik-L. Erdey” system. Differential mass loss (TG) and heating effects (DTA) were recorded according to the methods outlined by Carrier *et al.* (2011) and Wróblewski and Ceran (2016). The analysis results were processed using the software package supplied with the device. A dynamic analysis of a random 100 g biomass sample was conducted at a heating rate of 10 °C per minute in an air atmosphere, with aluminum oxide serving as the reference material.

## RESULTS

Biomass thermolysis of the control samples, labeled as K1, occurred within the temperature range of 60-610 °C (Table 1).

**Table 1**

**Thermal indexes of sorghum biomass control samples K1**

| Stage | Interval | Maxim. Speed | Temperature of peak | Mass loss | The share of residual mass |
|---|---|---|---|---|---|
| | [°C ] | [%/min] | [°C ] | [%] | [%] |
| I | 60-170 | 11.4 | 90 | 6.14 | 1.62 |
| II-III | 171-400 | 29.4 | 330 | 71.44 | |
| IV | 401-610 | 17.78 | 480 | 20.8 | |

During the initial stage of decomposition, volatile components were released, with evaporation occurring at a constant rate of 6.0% per minute. At this stage, there was a mass loss of 6.14% (Figure 1).

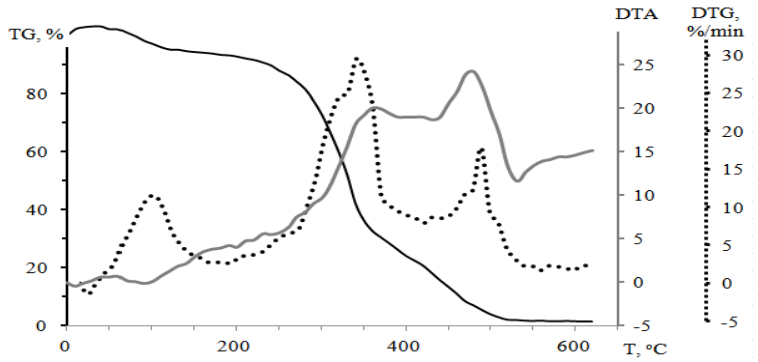



**Fig. 1- Sweet sorghum bagasse thermolysis in the control treatment**

The decomposition of the main biomass components, namely hemicellulose, cellulose, and lignin, commenced at temperatures between 170-180 °C. Decomposition of hemicellulose and cellulose exhibited high rates (25.7-29.4% per minute) and was accompanied by a rapid mass loss reaching 71.4% by the end of this stage. Notably, a small plateau within the temperature range of 310-320 °C and a distinct peak at 330 °C were observed on the derivative thermogravimetric (DTG) curve. The process occurred amidst exothermic reactions, with the most pronounced thermal effects observed within the temperature range of 350-380 °C. The final stage of thermolysis, marking the completion of lignin decomposition and the formation of a refractory residue, commenced between temperatures of 401-410 °C. This stage proceeded at low speeds, ranging from 8.8% to 9.3% per minute.

The mass loss totaled 20.8%, with a single peak observed within this interval on the DTG curve at 480 °C. Lignin decomposition occurred alongside exothermic reactions, exhibiting the most pronounced thermal effects within the temperature range of 470-500 °C. Notably, combustion of the control samples was notably thorough, leaving only a minimal non-combustible residue of 1.62%. The application of varying doses of biosolids and mineral fertilizers did influence the chemical composition of biomass and its thermal characteristics, as outlined in Table 2.

**Table 2**

**Thermal indices of sorghum biomass in fertilized trials**

| Control sample | Stage | Interval, °C | Maxim. Speed, %/min | Temperature of peak, °C | Mass loss, % | The share of residual mass, % |
|---|---|---|---|---|---|---|
| | | [°C ] | [%/min] | [°C ] | [%] | [%] |
| K2, SS 10 t/ha | I | 65-160 | 6.24 | 80 | 5.1 | 5.97 |
| | II-III | 161-390 | 22.88 | 310 | 62.8 | |
| | IV | 391-620 | 10.92 | 460 | 26.13 | |
| K3, SS 20 t/ha | I | 60-170 | 9.25 | 80 | 5.7 | 0.54 |
| | II-III | 171-400 | 32.55 | 300 | 69.63 | |
| | IV | 401-610 | 9.88; 9.26 | 430; 480 | 24.13 | |
| K4, SS 30 t/ha | I | 65-170 | 11.,96 | 90 | 7.41 | 0.22 |
| | II-III | 171-410 | 27.44 | 310 | 64.72 | |
| | IV | 411-610 | 15.5 | 460 | 27.65 | |
| K5, SS 20 t/ha | I | 60-170 | 7.9 | 90 | 5.6 | 0.78 |
| | II-III | 171-410 | 29.64 | 350 | 66.56 | |
| | IV | 411-620 | 18.1 | 510 | 27.06 | |
| K6, $N_{30}P_{15}K_{30}$ | I | 60-170 | 12.58 | 80 | 5.55 | 3.27 |
| | II-III | 171-400 | 27.35 | 320 | 65.43 | |
| | IV | 401-610 | 27.87 | 490 | 25.75 | |
| K7, $N_{60}P_{30}K_{60}$ | I | 60-160 | 7.49 | 80 | 5.62 | 0.31 |
| | II-III | 161-410 | 25.69 | 330 | 68.76 | |
| | IV | 411-590 | 11.54 | 480 | 25.31 | |

Comparison of DTG curves in the control and treated experimental sweet sorghum plants is shown in the figure 2 - 4.

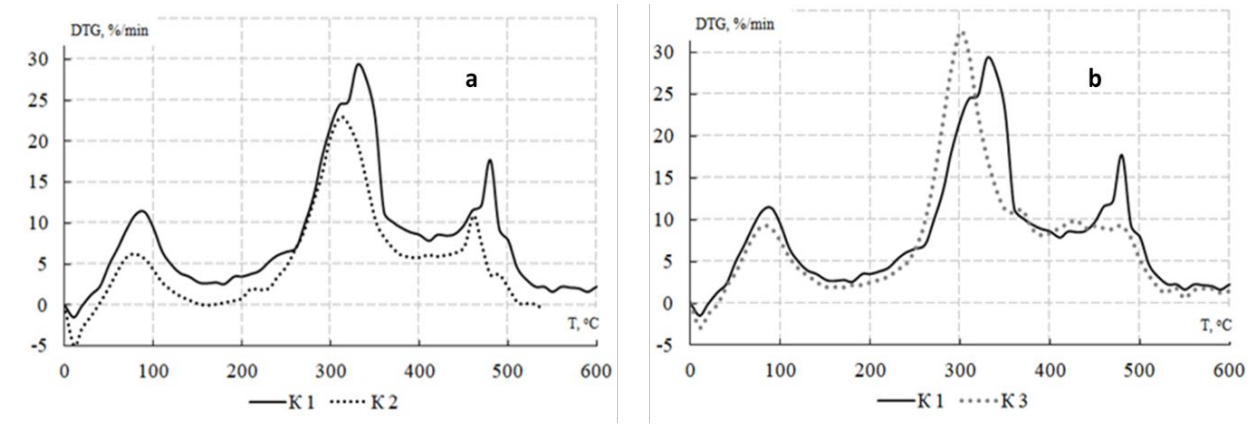



**Fig. 2 - Comparison of DTG curves in the control and trials K2 (10 SSt/ha) and K3(20 SSt/ha)**

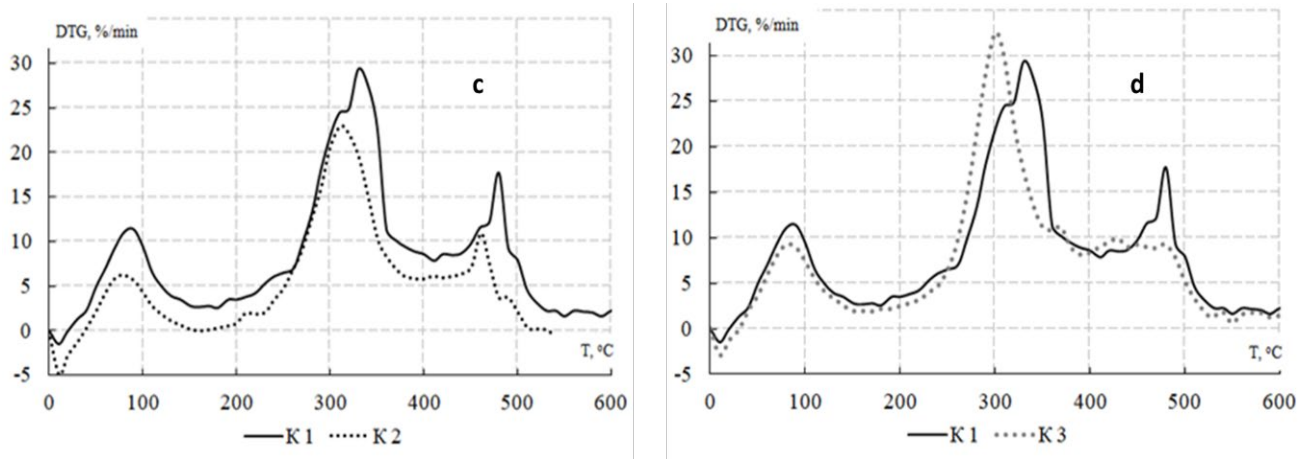



**Fig. 3 - Comparison of DTG curves in the control and trials K4 (30 SSt/ha) and K5(40 SSt/ha)**

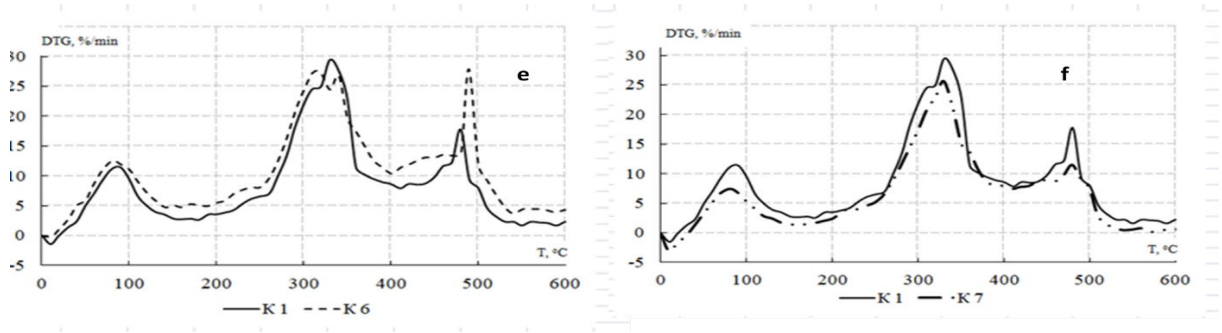



**Fig. 4 - Comparison of DTG curves in the control and trials K6 ($N_{30}P_{15}K_{30}$) and K7 ($N_{60}P_{30}K_{60}$)**

At the initial stage of thermolysis, a decrease in the reaction rate by 18.8–45.5% was observed in samples K2, K3, and K5 of sewage sludge (10, 20, and 40 ton/ha) and K7 ($N_{60}P_{30}K_{60}$) compared to the control. Meanwhile, the reaction rate in sample K6 ($N_{30}P_{15}K_{30}$) was slightly higher compared to the control values. Weight loss across all experimental variants, except for K4 (30 ton/ha), was lower than in the control by 7.2% to 10.4%. However, process speeds were higher in treatment K3. Consistently throughout the experiment, it was noted that the destruction peaks shifted towards lower temperatures.

At this stage, the mass loss was slightly lower compared to the control values, prevailing in all experimental variants by 62.8% to 69.6%.The thermal effects of exothermic reactions during the second stage were most pronounced in trials K5 and K7, observed within the temperature range of 390 to 410 °C.During the final stage of thermolysis, the application of fertilizers induced notable differences in the thermal characteristics of the biomass. Weight loss was consistently higher in all experiment trials compared to the control. In treatment K3, two minor destruction peaks were observed at temperatures of 430 °C and 480 °C, respectively.

Thermal effects in the experimental samples were more pronounced than in the control, particularly evident in samples from trials K5 (40t/haSS) and K7($N_{60}P_{30}K_{60}$). The proportion of residual mass after combustion in trials K3, K4, K5, and K7 was 0.54%, 0.22%, 0.78%, and 0.31%, respectively. Meanwhile, the refractory residue in samples from trials K6 and K2 significantly surpassed control values, amounting to 3.27% and 5.97%, respectively.The application of fertilizers contributed to a reduction in the activation energy of biomass during the initial stage of thermolysis, as detailed in Table 3.

**Table 3**

**Activation energy of sorghum bagasse biomass**

| Thermolysis stage | Activation energy | | | | | | |
|---|---|---|---|---|---|---|---|
| | K1 | K2 | K3 | K4 | K5 | K6 | K7 |
| Initial, [KJ/mol] | 143.99 | 93.2 | 123.9 | 67.6 | 64.9 | 56.3 | 75.1 |
| Decomposition of the main components, [KJ/mol] | 57.51 | 54.3 | 58.56 | 55.0 | 52.1 | 54.2 | 55.22 |

Trials K4, K5, and K6 exhibited the most significant impacts, with activation energy values more than twice as low as the control. Furthermore, at the stage of decomposition of the main components, the activation energy in the experimental biomass samples varied only slightly from the control, by no more than 10%.

## CONCLUSIONS

The incorporation of biosolids and mineral fertilizers into the soil induced noteworthy alterations in the thermal properties of sweet sorghum biomass. These modifications exerted a substantial influence on the dynamics of thermolysis processes, encompassing reaction kinetics, mass loss percentages across different stages of thermal degradation, extent of biomass combustion, and activation energy parameters. The findings unequivocally underscore the considerable impact of soil amendments on the thermal behavior of sorghum biomass. Moreover, this study emphasizes the potential for tailored soil management practices to not only enhance agronomic productivity but also to influence the thermochemical characteristics of biomass, thereby offering insights into optimizing bioenergy production and environmental sustainability in agricultural systems. Further investigations exploring the intricate relationships between soil amendments, crop growth, and biomass thermochemistry are warranted to elucidate the underlying mechanisms and refine management strategies for sustainable bioenergy production.

**ACKNOWLEDGEMENT**

The research was funded by the Civilian Research and Development Foundation Global sponsored alternate energy project (G-202102-67449 for US part and M/58-2021 and M/69-2022 for Ukrainian part), Ministry of Education of Sciences of Ukraine, and The Ohio State University, Columbus, USA.

**REFERENCES**

[1] Carrier, M., Loppinet-Serani, A., Denux, D., Jean-Michel, L., Ham-Pichavant, F., Cansell, F. & Aymonier, C. (2011). Thermogravimetric analysis as a new method to determine the lignocellulosic composition of biomass. *Biomass and Bioenergy, 35*, 298-307. https://doi.org/10.1016/j.biombioe.2010.08.067

[2] Castro, F.M.R., Bruzi, A.T., Nunes, J.A.R., Parrella, R.A.C., Lombardi, G.M.R., Albuquerque, C.J.B. & Lopes, M. (2015). Agronomic and Energetic Potential of Biomass Sorghum Genotypes. *American Journal of Plant Sciences, 6,* 1862-1873. http://dx.doi.org/10.4236/ajps.2015.611187

[3] Ivanova, T., Muntean, A., Havrland, B. & Hutla, P. (2018). Quality assessment of solid biofuel made of sweet sorghum biomass. *BIO Web of Conferences 10,* 02007. https://doi.org/10.1051/bioconf/20181002007

[4] Fu, H.M., Meng, F.Y., Molatudi, R.L. et al. (2016). Sorghum and Switchgrass as Biofuel Feedstocks on Marginal Lands in Northern China. *Bioenerg. Research, 9,* 633–642. https://doi.org/10.1007/s12155-015-9704-0

[5] Islam, K.R., Dick, W.A., Watts, D.B., Gonzalez, J.M., Fausey, N.R., Flanagan, D.C., Reeder, R.C., Toai, T.V. & Batte M.T. (2022) Gypsum, crop rotation, and cover crop impacts on soil organic carbon and biological dynamics in rainfed transitional no-till corn-soybean systems. *PLOS ONE 27,* 17(9), e0275198. https://doi.org/10.1371/journal.pone.0275198.

[6] Jeguirim, M., Dorge, S. & Trouvé. (2010). Thermogravimetric analysis and emission characteristics of two energy crops in air atmosphere: Arundo donax and Miscanthus giganthus. *Bioresour. Technol., 101*, 788–793.

[7] Kongkaew, N., Pruksakit, W. & Patumsawad, S. (2015). Thermogravimetric kinetic analysis of the pyrolysis of rice straw. *Energy Procedia,* 79, 663–670.

[8] Kumar A., Wang L., Dzenis Y.A., Jones D.D. & Hanna M. (2008). Thermogravimetric characterization of corn stover as gasification and pyrolysis feedstock. *Biomass and Bioenergy, 32*, 460-467. https://doi.org/10.1016/j.biombioe.2007.11.004.

[9] Mansour, M.M.F., Emam, M.M., Salama, K.H.A. & Morsy, A.A. (2021). Sorghum under saline conditions: responses, tolerance mechanisms, and management strategies. *Planta. 254*, 24. doi: 10.1007/s00425-021-03671-8

[10] Mathur, S., Umakanth, A.V., Tonapi, V.A., Sharma R. & Sharma M.K. (2017). Sweet sorghum as biofuel feedstock: recent advances and available resources. *Biotechnol Biofuels, 10,* 146. https://doi.org/10.1186/s13068-017-0834-9

[11] Misook, K. & Day, D.F. (2011). Composition of sugar cane, energy cane, and sweet sorghum suitable for ethanol production at Louisiana sugar mills. *J Ind Microbiol Biotechnol, 38,* 803–807. https://doi.org/10.1007/s10295-010-0812-8

[12] Regassa, T.H. & Wortmann, C.S. (2014). Sweet sorghum as a bioenergy crop: literature review. *Biomass Bioenergy, 64*, 348–355.

[13] Singh, M.P., Erickson, J.E., Sollenberger, L.E., Woodard, K.R., Vendramini, J.M.B. & Fedenko, J.R. (2012). Mineral composition and biomass partitioning of sweet sorghum grown for bioenergy in the southeastern USA. *Biomass Bioenergy, 47*, 1–8.

[14] Vinutha, K.S., Rayaprolu, L., Yadagiri, K., Umakanth, A.V., Patil, J.V. & Srinivasa Rao, P. (2014). Sweet sorghum research and development in India: status and prospects. *Sugar Tech., 16*, 133-43.

[15] Wnorowska, J., Ciukaj, S. & Kalisz, S. (2021). Thermogravimetric Analysis of Solid Biofuels with Additive under Air Atmosphere. *Energies, 14*, 2257. https://doi.org/10.3390/en14082257

[16] Wróblewski, R. & Ceran, B. (2016). Thermogravimetric analysis in the study of solid fuels. *E3S Web of Conferences, 10*, 00109. https://doi.org/10.1051/e3sconf/20161000109.

[17] Yu, J., Zhang, T., Zhong, J., Zhang, X. & Tan, T. (2012). Biorefinery of sweet sorghum stem. *Biotechnology Advances, 30*, 811-816. https://doi.org/10.1016/j.biotechadv.2012.01.014

# THERMAL ANALYSES OF THE BLACK LOCUST WOOD DIFFERENT AGES
# /
# *ТЕРМІЧНИЙ АНАЛІЗ ДЕРЕВИНИ РОБІНІЇ ЗВИЧАЙНОЇ РІЗНОГО ВІКУ*

**Svitlana SYTNYK[1)], Petro LAKYDA[2)], Iryna RULA[3)], Kyrylo HOLOBORODKO[4)], Yurii LAKYDA[5)], Liubov MATUSHEVYCH[2)], Mykola KHARYTONOV[*6)]**

[1)] Laboratory of Forest Management, Dnipro State Agrarian and Economic University, Dnipro / Ukraine;
[2)] Department of Forest Mensuration and Forest Management, National University of Life and Environmental Sciences, Kyiv / Ukraine;
[3)] Chemistry Department, Dnipro State Agrarian and Economic University, Dnipro / Ukraine;
[4)] Laboratory of Biomonitoring, Oles Honchar Dnipro National University, Dnipro / Ukraine;
[5)] Department of Technology and Design of Wood Products, National University of Life and Environmental Sciences, Kyiv / Ukraine;
[6)] Ecology Department, Dnipro State Agrarian and Economic University, Dnipro / Ukraine.
**Tel: +38-0973 456 227; *E-mail: kharytonov.m.m@dsau.dp.ua*

***Keywords:*** *thermogravimetric analysis, Robinia pseudoacacia* L.*, wood, lignin, cellulose*

**ABSTRACT**

*It was found that black locust wood contains predominantly hemicellulose at the age of 2–4 years, while at the age of 6 years the wood has equal representation of cellulose and lignin. The wood of tree trunks older than six years is mainly composed of lignin, which determines their different heat-generating capacity. In the temperature range of 50–150 °C, the wood of the black locust trunks of different ages loses an average of 1.5–9.0% of mass, with the greatest loss of mass in wood aged 2–6 and 16–20 years. The final decomposition of cellulose and lignin occurs in the temperature range of 340–600 °C. The main stage of thermal destruction of wood from Robinia trunks aged 2 to 14 years ends at a temperature of 400–420 °C. The black locust wood becomes more heat-resistant with age. As a result, the thermolysis process begins at higher temperatures. It is likely that the thermal properties of Robinia stem wood depend not only on age, but also on the weather conditions in which the annual rings were formed.*

**ТЕЗИ**

*Було виявлено, що деревина робінії дерев у віці 2–4 років містить переважно геміцелюлозу, тоді як у віці 6 років деревина має рівне представництво целюлози та лігніну. Деревина стовбурів дерев старше шести років складається переважно з лігніну, що визначає їх різну теплоутворюючу здатність. Деревина стовбурів робінії звичайної різного віку втрачає в середньому 1,5–9,0% маси у діапазоні температур 50–150 °C, з найбільшою втратою маси у деревині віком 2–6 та 16–20 років. Остаточне розкладання целюлози та лігніну відбувається в діапазоні температур 340–600 °C. Основний етап термічного руйнування деревини стовбурів робінії віком від 2 до 14 років завершується при температурі 400–420 °C. Деревина з віком стає більш термостійкою. В результаті процес термолізу починається за вищих температур. Ймовірно, теплові властивості деревини стовбура Robinia pseudoacacia L. залежать не лише від віку, але й від погодних умов, за яких утворилися річні кільця.*

## INTRODUCTION

The use of plant biomass as an energy source represents a potential replacement for fossil fuels *(Mignogna et al, 2024).* Plant species that may show signs of invasion in natural and artificial ecosystems can be considered as bioenergy potential resources *(Young et a, 2011).* Control and management of species that may show invasive properties require significant investments. That is why the development of mechanisms for managing existing tree stands can ensure effective forest use in the steppe zone of Ukraine. Black locust (*Robinia pseudoacacia* L.) is a fast-growing species with significant adaptive potential.

This species is considered invasive in many European countries *(Nunes et al, 2021)* and in Ukraine. Black locust abundance without forestry would decrease during succession in forests with highly competitive and shade tolerant trees and in mature forests it occurs only as admixture of climax trees *(Vítková et al., 2017).*

This tree species is considered problematic due to its both positive and negative impact on the environment. Meanwhile, it is worth noting that black locust plantations were created in the steppe zone of Ukraine to solve the problem of water and wind erosion of soils and the reclamation of post-mining lands.

The total area of *R. pseudoacacia* plantations in the northern Steppe is 17683.7 hectares (26.9% of the total area covered by forest plantations). The main indicators of plantation productivity, namely the total stock of stem wood is 2191.6 thousand m³, the average stock is 171 m³/ha., the maximum is 218 m³/ha *(Lovinska & Sytnyk, 2016).*

Black locust, as a species with significant energy potential, is actively studied in the different regions of its cultivation *(Sebio-Puñal et al, 2012; Martín-Sampedro et al, 2019; Yue et al, 2023).*

The reactivity of *R. pseudoacacia* biomass during combustion was compared with that of brown coal using thermal analysis *(Bilkic et al, 2020).* The chemical characteristics of *R. pseudoacacia* wood were investigated under thermal modification at different temperatures *(Marino et al, 2024).* Volatile compounds in black locust wood are represented by a variety of organic compounds *(Dünisch et al., 2010).*

It was found that the content of phenolic compounds and flavonoids in juvenile wood is limited to the first 10–15 years of cambial growth, after which it begins to decrease. Meanwhile, cellulose, hemicellulose, and lignin are the main components of wood *(Carrier et al., 2011).*

Differences in their chemical structure lead to different chemical reactivity. This makes the ratio of cellulose, hemicellulose and lignin in biomass a decisive factor when choosing ways to further use wood.

The chemical composition of *Acacia dealbata, Acacia melanoxylon*, and *R. pseudoacacia* wood presents certain challenges, primarily due to their nitrogen, chlorine, and ash content, complicating their use in the production of certified wood pellets *(Nunes et al, 2021).* However, from a local recycling perspective, the use of wood materials remains feasible, creating a circular economy. The main objective of this case study was to conduct thermal analysis of black acacia wood of different ages.

## MATERIALS AND METHODS

A series of wood biomass samples were taken at two-year intervals over a 20-year period. This was done to assess the changes in calorific value that occur in the wood of the trunk of *R. pseudoacacia*.

Sampling was carried out on areas of self-growing *R. pseudoacacia* abandoned farmland near the village of Mayorka on the right bank of the Dnipro River, Dnipropetrovsk region.

The study of the process of thermal analysis of samples of *Robinia* stem wood was carried out by the method of thermogravimetric analysis on a Q-1500D derivatograph of the company "F. Paulik-Y. Paulik-L. Erdei".

The effects of heating and differential mass loss were studied. The measurement results were processed using the software included in the device's delivery kit. The mass of the samples was 100 mg.

The biomass samples were analyzed dynamically in an air atmosphere at a heating rate of 10 °C/min. Aluminum oxide was a reference substance.

The activation energy of the thermo-oxidative destruction of the samples was determined by the Broido method (Broido et al, 1969). The double logarithm value was calculated for each temperature value using the relationship:

$$\ln\left(\ln\frac{100}{100-\Delta m}\right) = -\frac{E}{R}\cdot\frac{1}{T} \quad (1)$$

where m – sample mass, %; E – activation energy, kJ/mol; R – universal gas constant, 8.314 J/(mol•K); T – temperature, °C. The activation energy value (Ea) was determined by the formula:

$$E_a = tg\varphi \cdot R \quad (2)$$

Statistical processing of research data was performed using the programs “Microsoft Excel-2016” and SPSS “Statistica”.

## RESULTS

Thermal destruction of all studied wood samples occurred in three stages and has a similar nature for wood of different ages. Evaporation of water and volatile compounds occurred in the first stage (Fig. 1).

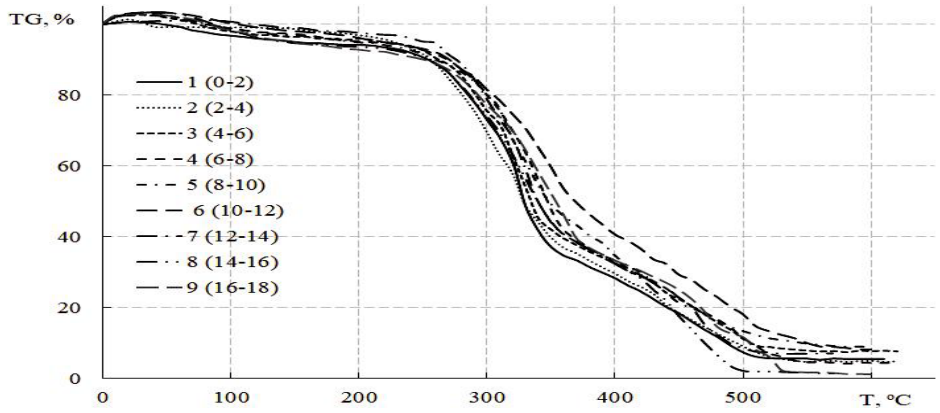



**Fig. 1- Mass loss (TG) curves of acacia wood samples**

Wood biomass is a hygroscopic material with a capillary porous structure, capable of retaining moisture in macro- and micropores. Therefore, at the first stage of thermal destruction, it was quite natural that there was a slight loss of mass due to the removal of both free moisture from the cell cavities and moisture contained between the fibrils of the cell wall, i.e. bound or hygroscopic. It is known that in the process of increasing the temperature to 120 °C, acetic acid is formed from acetylated hemicellulose by hydrolysis. Acetic acid serves as a catalyst for the hydrolysis of hemicellulose to soluble sugars, namely arabinose, galactose, xylose and mannose (Prins et al, 2006). All studied samples of wood from trunks of different ages lose an average of 1.5–9.0% of mass due to the loss of free and bound moisture in the temperature range of 50–150 °C (Table 1).

**Table 1**

**Decomposition stage of volatile components of wood (range 40°C - 200°C)**

| Parameter | Wood age, years | | | | | | | | |
|---|---|---|---|---|---|---|---|---|---|
| | 0-2 | 2-4 | 4-6 | 6-8 | 8-10 | 10-12 | 12-14 | 14-16 | 16-18 |
| The starting point of the process, °C | 40 | 45 | 50 | 50 | 50 | 60 | 60 | 70 | 70 |
| End point of the process, °C | 190 | 200 | 200 | 200 | 210 | 210 | 200 | 210 | 215 |
| Mass loss, % | 5.79 | 3.12 | 3.95 | 4.82 | 5.2 | 4.66 | 4.01 | 6.26 | 7.56 |
| Destruction peaks, °C | 80<br>160 | 80<br>170 | 70<br>140 | 70<br>170 | 70<br>180 | 90<br>200 | 90<br>160 | 90<br>190 | 90<br>190 |
| The maximum rate of mass loss, % min | 13.00<br>10.19 | 9.57<br>10.19 | 8.22<br>4.16 | 6.14<br>3.02 | 5.2<br>2.50 | 7.18<br>4.89 | 11.44<br>4.78 | 11.96<br>4.06 | 14.56<br>9.26 |

The decomposition of the main components of wood: hemicellulose, cellulose, and lignin occurred in the second stage (Table 2, Fig. 2).

**Table 2**

**Decomposition of the main components of wood and the formation of carbonized residue (range 210°C - 610°C)**

| Parameter | Wood age, years | | | | | | | | |
|---|---|---|---|---|---|---|---|---|---|
| | 0-2 | 2-4 | 4-6 | 6-8 | 8-10 | 10-12 | 12-14 | 14-16 | 16-18 |
| The starting point of the process, °C | 200 | 205 | 205 | 210 | 220 | 220 | 210 | 215 | 220 |
| End point of the process, °C | 580 | 610 | 580 | 600 | 600 | 600 | 560 | 560 | 600 |
| Mass loss, % | 88.78 | 92.4 | 88.1 | 90.97 | 85.1 | 87.36 | 88.88 | 92.29 | 91.40 |
| Destruction peaks, °C | 330<br>470 | 330<br>470 | 330<br>480 | 340<br>490 | 330<br>470 | 350<br>510 | 330<br>470 | 330<br>450 | 330<br>360<br>490 |
| The maximum rate of mass loss, % min | 43.58<br>15.70 | 33.70<br>15.39 | 36.19<br>8.84 | 28.81<br>8.22 | 21.74<br>6.55 | 22.36<br>11.44 | 41.6<br>16.85 | 32.14<br>25.79 | 31.41<br>35.26<br>24.34 |
| Carbonated residue, % | 5.43 | 4.74 | 7.54 | 4.21 | 8.89 | 7.98 | 7.11 | 1.45 | 1.04 |

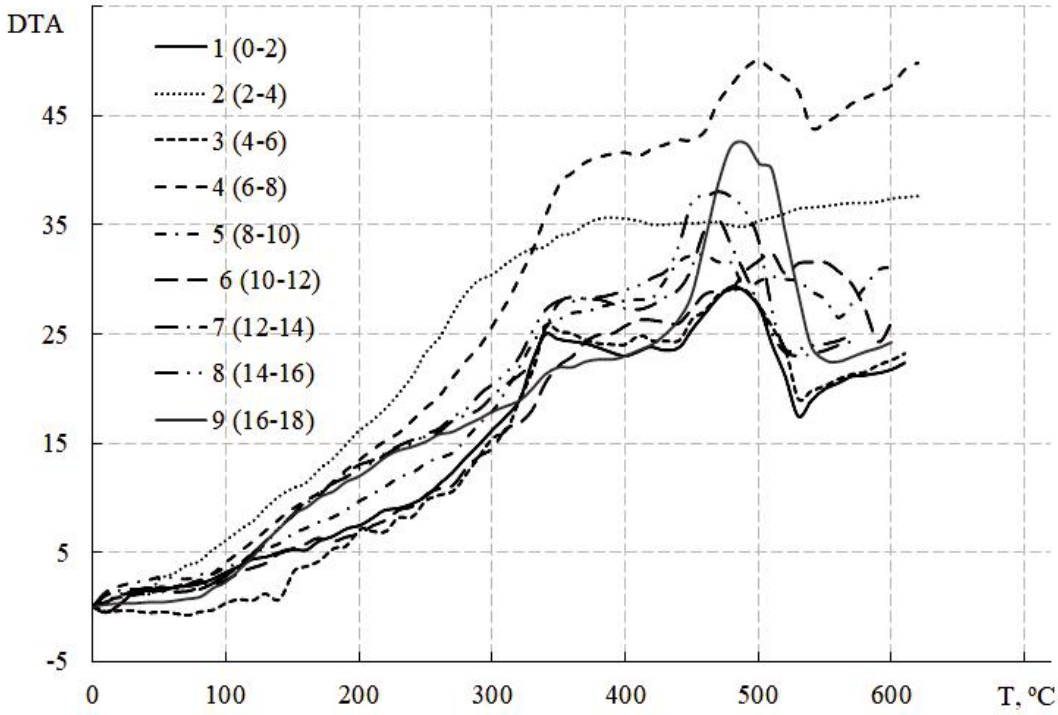



**Fig. 2 - Differential thermal analysis (DTA) curves of acacia tree seeds**

The most important components of the black locust tree stock are hemicellulose (34%), cellulose (38%) and lignin (14%). Unfolded hemicellulose is baked in the range of 220–320 °C, cellulose 305–380 °C, and lignin 250–550 °C. This is consistent with our research on the thermal destruction of acacia wood.

Destruction of the main storage hemicellulose pentosans in the temperature range of 200–260 °C. The remaining cellulose and lignin are heated to a temperature of 340–600 °C. At this stage, the wood consumes an average of 18.4–29.8% of its mass.

The greatest loss of mass during the process of thermolysis was observed for the tree with age of 2–6 and 16–20 years. This means that at higher biomass levels, *Robinia* stem wood has a greater accumulation of hemicellulose. The unfolding of the lignin is completed in the third stage, and the oxidation of the coal begins, which took place in the first stage. Mass consumption at the remaining stage of thermolysis was 65.2–75.5%.

The process is expected to be completed in full, and is initially accompanied by the creation of new chemical bonds, and then, at a temperature range of 420–510 °C, their transformation from the seen energy. This is confirmed by the presence of sufficiently significant peaks for low samples on the DTG curves (Fig. 3).

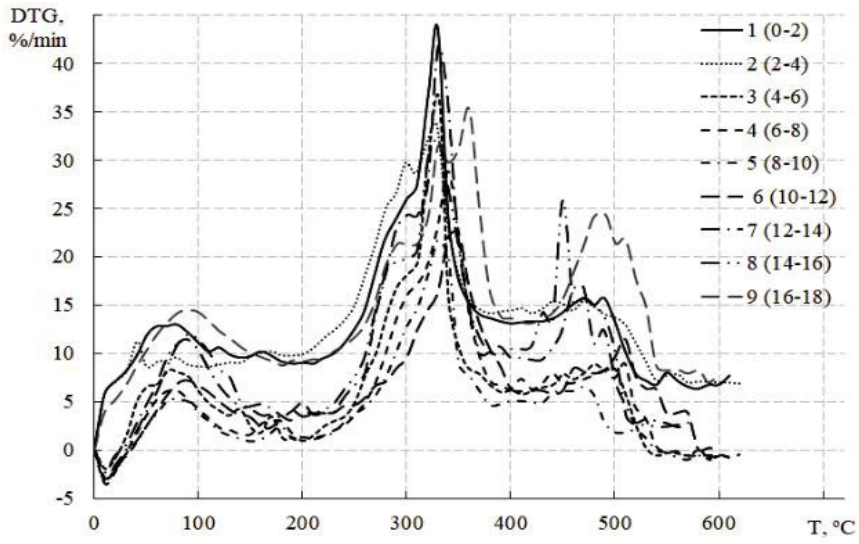



**Fig. 3 - Differential thermogravimetric curves (DTG) of acacia trees**

The process of thermolysis of black locust wood biomass was completed at a temperature of 550–600°C. Some of the excess mass was found between 1.4–9.0%.

The chemical storage of wood means it has bioenergetic properties. At the same time, growth also has a significant impact on the thermal behavior of the cow *(Kharytonov et al., 2021).*

In connection with this, the relation between the start and the end point of the volatile organic substances destruction temperature was determined for the main components of the wood and age of *Robinia* trees. (Fig. 4-7).

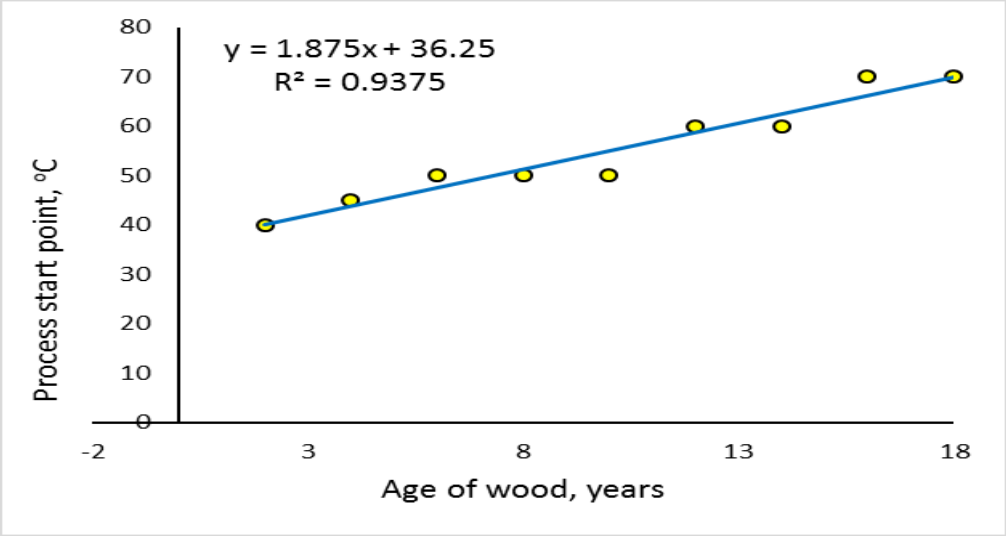



**Fig. 4 - Dependence of the starting temperature of volatile components thermolysis on the age of wood**




**Fig. 5 - Dependence of the end temperature of volatile components thermolysis on the age of wood**




**Fig. 6 - Dependence of the starting temperature of main components of wood thermolysis on its age**

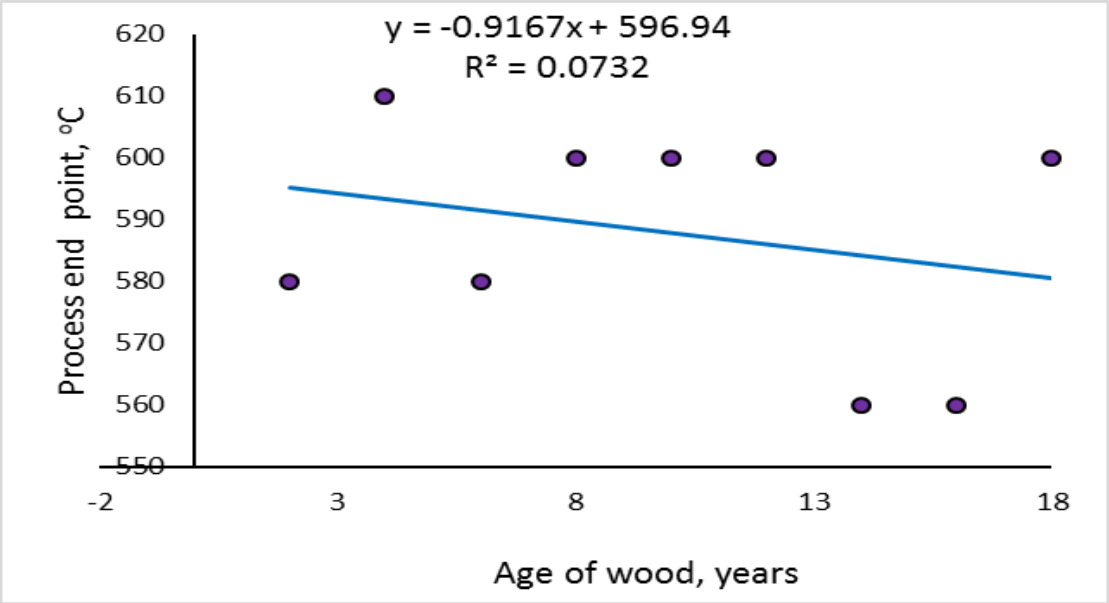



**Fig. 7 - Dependence of the end temperature of main components of wood thermolysis on its age**

Direct storage is noted between the start of the temperature of destruction of the volatile organic substances and the main components of the tree and the stem of the *Robinia* tree.

The same pattern is observed between the end of the temperature of destruction of the volatile organic compounds of the tree and the growth of the *Robinia* tree. Meanwhile, the deposit between the end of the temperature of the destruction of volatile organic matter of the tree and the growth of the *Robinia* tree became a turning point.

The data on energy of activation for two stages of wood thermolysis are shown at the table 3.

**Table 3**

**Energy of activation for two stages of wood thermolysis, kJ/mol**

| **Age (year)** | **2-4** | **4-6** | **6-8** | **8-10** | **10-12** | **12-14** | **14-16** | **16-18** | **18-20** |
|---|---|---|---|---|---|---|---|---|---|
| Start point of volatiles substances of thermolises,°C | 103.5 | 50.1 | 74.8 | 57.1 | 71 | 94.8 | 141.3 | 114.1 | 57.1 |
| Start point of wood components of thermolises, °C | 62.4 | 59.8 | 64.9 | 62.9 | 57.9 | 54.4 | 72.2 | 56.9 | 52.5 |

The main stage of thermal destruction of the wood of *Robinia* stem from 2 to 14 years will end at a temperature of 400°C–420°C with the combustion of an insignificant amount of dissolved gases.

It is likely that *Robinia* wood, aged 14–18 years, contains a greater amount of lignin, which, when laid out, creates a significantly greater amount of carbonized residues, the thermal destruction of which is

accompanied by fairly high peaks on the mass consumption rate curves (DTG) in the temperature range 420°C–540°C, and even higher values of activation energy.

## CONCLUSIONS

It has been established that the thermal destruction of the biomass of the black locust tree occurs in three stages and has a similar character for the wood of the common tree. At the first stage, the water is evaporated and the liquid is removed; on the other is a layout of the main components of wood - hemicellulose, cellulose and lignin.

Lignin decomposition is completed in the third stage. Coal oxidation occurs with the formation of ash residue.

The wood of black locust stem different age loss an average of 1.5–9.0% of its mass in the temperature range of 50–150 °C. The highest loss of mass during the thermolysis process is indicated for wood of 2–6 and 16–20 years. This process is accompanied by an insignificant endothermic effect.

The remaining cellulose and lignin are recovered at a temperature range of 340–600 °C. The main stage of thermal destruction of the wood of black locust stem in 2 to 14 years will end at a temperature of 400–420 °C.

The wood of the *Robinia*, which has been around for six years, was highly folded with lignin.

This determines their calorific value.

## ACKNOWLEDGEMENT

This study was funded by Ministry of Education and Science of Ukraine.

## REFERENCES

[1] Bilkic, B., Haykiri-Acma, H., & Yaman, S. (2020).Combustion reactivity estimation parameters of biomass compared with lignite based on thermogravimetric analysis. Energy Sources. Part A. Recovery, *Utilization, and Environmental Effect*s. P. 1–14.

[2] Broido, A. A. (1969). A simple, sensitive graphical method of treating thermogravimetric analysis data. *Journal Polymer of Science*, 7(3), 1761–1763.

[3] Carrier, M., Loppinet-Serani, A., Denux, D., Lasnier, J.-M., Ham -Pichavant, F., Cansell, F., & Aymonier, C. 2011. Thermogravimetric analysis as a new method to determine the lignocellulosic composition of biomass. *Biomass Bioenergy*, 35, 298–307. https://doi.org/10.1016/j.biombioe.2010.08.067

[4] Dünisch, O., Richter, HG. & Koch, G. (2010). Wood properties of juvenile and mature heartwood in *Robinia pseudoacacia* L. *Wood Science and Technology,* 44, 301–313. https://doi.org/10.1007/s00226-009-0275-0

[5] Kharytonov, M., Kalyna, V., Martynova, N., & Sbytna, M. (2021). Thermal Analyses of Differences For Woody Species Depending on Soil Conditions. *Procedia Environmental Science, Engineering and Management*, 8(1), 43–52 http://www.procedia-esem.eu/2021_vol8_no1.htm

[6] Lovinska, V. & Sytnyk, S. (2016).The structure of Scots pine and Black locust forests in the Northern Steppe of Ukraine. *Journal of Forest Science*, 62(7), 329–336. https://doi.org/10.17221/120/2015-JFS

[7] Marino, S., Gaff, M., Sethy, A.K. et al. (2024). Enhancing the fire resistance properties of thermally modified *Robinia pseudoacacia* wood with natural and synthetic flame retardants: chemical characterisation and fire behaviour. *European Journal of Wood and Wood Production*, 82, 1145–1157. https://doi.org/10.1007/s00107-024-02079-x

[8] Martín-Sampedro, R., Santos, J., Eugenio, M., Wicklein, B., Jiménez-López, L., & Ibarra, D. (2019). Chemical and thermal analysis of lignin streams from *Robinia pseudoacacia* L. generated during organosolv and acid hydrolysis pre-treatments and subsequent enzymatic hydrolysis. *International Journal of Biological Macromolecules*, 140, 311–322. https://doi:10.1016/j.ijbiomac.2019.08.029

[9] Mignogna, D., Szabó, M., Ceci, P., & Avino, P. (2024). Biomass Energy and Biofuels: Perspective, Potentials, and Challenges in the Energy Transition. *Sustainability*, *16*(16), 7036. https://doi.org/10.3390/su16167036

[10] Nunes, L. J., Rodrigues, A. M., Loureiro, L. M., Sá, L. C, & Matias, J. C. (2021).Energy Recovery from Invasive Species: Creation of Value Chains to Promote Control and Eradication. *Recycling,* 6(21), 2–18. https://doi.org/10.3390/recycling6010021

[11] Prins, M. J., Ptasinski, K. J., & Janssen, F. J. (2006).Torrefaction of wood: Part 1. Weight loss kinetics. *Journal of Analytical and Applied Pyrolysis*, 77(1), 28–34.

[12] Sebio-Puñal, T., Naya, S., López-Beceiro, J., Tarrío-Saavedra, J., & Artiaga, R. (2012). Thermogravimetric analysis of wood, holocellulose, and lignin from five wood species. *Journal of Thermal Analysis and Calorimetry*, 109(3), 1163–1167. https://doi.org/10.1007/s10973-011-2133-1

[13] Sikora, A., Hájková, K., & Jurczyková, T. (2022). Degradation of Chemical Components of Thermally Modified *Robinia pseudoacacia L.* Wood and Its Effect on the Change in Mechanical Properties. *International Journal Molecular Science*, 23,15652. https://doi.org/10.3390/ijms232415652.

[14] Vítková, M., Müllerová, J., Sádlo, J., Pergl, J., & Pyšek, P. (2017). Black locust (*Robinia pseudoacacia*) beloved and despised: A story of an invasive tree in Central Europe. *Forest Ecology and Management*, 384, 287–302. https://doi.org/10.1016/j.foreco.2016.10.057

[15] Yue, X., Chen, X. Li, H., Ge, S., Yang, Y., & Peng, W. (2023). Nano Ag/$Co_3O_4$ Catalyzed Rapid Decomposition of *Robinia pseudoacacia* Bark for Production Biofuels and Bio-chemicals. *Polymers*, 15(1),114. https://doi.org/10.3390/polym15010114

[16] Young, S.L., Gopalakrishnan, G., & Keshwani, D.R. 2011. Invasive plant species as potential bioenergy producers and carbon contributors. *Journal of Soil and Water Conservation,* 66(2), 45-50. https://doi.org/ 10.2489/jswc.66.2.45A

# EVALUATION OF THE PRODUCTIVE AND QUALITATIVE POTENTIAL OF LEGUMES AS SOURCES OF PLANT-BASED PROTEIN
/
# *EVALUATION OF THE PRODUCTIVE AND QUALITATIVE POTENTIAL OF LEGUMES AS SOURCES OF VEGETABLE PROTEINS*

**Andreea MATACHE*[1)], Nicoleta Alexandra VANGHELE[1)], Florin NENCIU[1)], Augustina Mirabela PRUTEANU[1)], Gabriel NAE[1)], Andreea-Sabina PINTILIE[2)]**

[1)] National Institute of Research-Development for Machines and Installations Designed for Agriculture and Food Industry - INMA Bucharest / Romania; [2)] Agricultural Research and Development Station Secuieni (ARDS Secuieni) / Romania

**Tel: 0212 693 259; *E-mail: andmatache@yahoo.com*

***Keywords:*** *plant-based alternative, nutrition enhancement, anti-nutritional compounds, digestibility*

**ABSTRACT**

*Legumes are a valuable source of protein and fiber, while also being rich in micronutrients such as iron and potassium. Due to their exceptional nutritional profile, legumes (such as peas, beans, chickpeas, and soybeans) play an essential role in human nutrition. Amidst global population growth and the increasing importance of adopting sustainable agricultural practices, interest in plant-based proteins has risen significantly. Rich in protein, legumes have gained prominence thanks to valued functional properties—such as gelling and emulsifying capabilities and represent a viable alternative to animal-derived proteins across various food applications. This paper aims to provide an overview of the chemical composition of legumes and their antinutritional compounds, as well as current and emerging techniques for utilizing their protein sources to enhance health and food security.*

**REZUMAT**

*Leguminoasele reprezintă o sursă valoroasă de proteine și fibre, având în același timp un conținut ridicat de micronutrienți, precum fierul și potasiul. Datorită valorilor nutriționale deosebite, leguminoasele (cum ar fi mazărea, fasolea, nautul și soia) au un rol esențial în alimentația umane. În contextul creșterii populatiei la nivel global și al importanței adoptarii metodelor agricole durabile, interesul pentru proteinele vegetale a crescut semnificativ. Bogate in proteine, leguminoasele au devenit tot mai relevante datorită caracteristicilor funcționale apreciate, cum ar fi gelificarea și emulsionarea, și ar putea fi considerate o alternativa viabila la proteinele de origine animală, cu diverse aplicatii alimentare. Aceasta lucrare isi propune sa prezinte o imagine de ansamblu asupra compoziției chimice a leguminoaselor, a compușilor lor antinutriționali, dar si asupra tehnicilor actuale si emergente de valorificare a surselor de proteine din acestea, in vederea cresterii sanatatii si securitatii alimentare.*

## INTRODUCTION

Legumes are part of the Fabaceae family, whose seeds have been an essential basis for human nutrition since ancient times. Today, legumes play an important role due to their nutritional benefits and positive impact on health, along with the economic and ecological aspects essential for a sustainable future. Legumes are a safe, affordable consumption option, being included in the diet of millions of people globally.

The cultivation of legumes plays a crucial role in promoting sustainable agriculture and has the capacity to adapt to fluctuating climatic conditions *(Martín-Cabrejas, M.Á., 2019).* Due to the importance of legumes for diet, nutrition, the environment and the economy, in 2018, the UN General Assembly proclaimed February 10 as World Legumes Day (WPD), thus providing an opportunity to raise awareness and accessibility of legumes globally *(www.fao.org, 2026).*

Numerous chronological and archaeological evidence has demonstrated that leguminous plants have their origins in America *(Papa, R. et al., 2005).* In Europe, especially in the southern and western regions, legumes have been a staple food for several millennia *(Huebbe, P. et al., 2020).* Global agricultural production of legumes ranks third after cereals and oilseeds *(Zhao, J. et al., 2022).*

Legumes are annual leguminous crops that produce between one and twelve grains or seeds of varying size, shape, and color inside a pod, used for both food and animal feed *(www.fao.org., 2021).* There are numerous edible legumes, at least 50 and which are consumed all over the world. They are of major

importance for human health and nutrition, due to their rich content of proteins, vitamins and minerals. They are distinguished by their ability to form symbiotic relationships with nitrogen-fixing bacteria, which facilitates a constant supply of atmospheric nitrogen to the Earth's biosphere *(Chandran, A.S. et al., 2023; Santhiya, S. et al., 2024; Didinger, C. et al., 2021)*.

Among the most commonly consumed legumes are chickpeas *(Cicer arietinum),* field peas *(Pisum sativum),* lentils *(Culinary lentil),* mung beans *(Phaseolus mungo),* dried broad beans *(Vicia faba),* moth beans *(Phaseolus aconitifolius),* lupins *(Lupinus albus)* etc. Legumes are considered a good source of protein, having an average of 12-40% protein. and legumes are best suited because they are environmentally friendly, with no carbon footprint or $CO_2$ *emissions (Parveen, S. et al., 2021)*.

The common bean (*Phaseolus vulgaris L.*) is the third most important legume cultivated worldwide, after soybeans and peanuts *(MSpechtLG., 2021).* Important minerals such as calcium (32–394 mg per 100 g), phosphorus (203–800 mg per 100 g), magnesium (58–472 mg per 100 g), iron (3.2–10 mg per 100 g) and zinc (1.6–6.3 mg per 100 g) are present in legumes (www.fao.org, 2018). They have a great variability of vitamins and are a source of B vitamins, such as thiamine (0.3–1.6 mg per 100 g), the level being similar to or even higher than that of cereals.

They contain riboflavin (0.12–0.33 mg per 100 g) and niacin (trace amounts - 4.7 mg per 100 g), which are essential for energy metabolism. In addition, the intake of folic acid (0.4–2.1 mg per 100 g) is important, as it is a critical nutrient during pregnancy and for the proper development of the fetal neural tube *(Gernand, A.D. et al., 2016).*

The protein content of legume grains varies between 17 and 40%, in contrast to 7-13% of cereals and being equal to the protein content of meat (18-25%) *(Tharanathan, R.N. et al., 2003).* Protein, one of the essential macronutrients necessary for optimal human growth and development, is responsible for almost every task of cellular life *(Lonnie, M. et al., 2018).*

Although the global demand for animal protein sources is increasing, due to rapid economic development and accelerated urbanization, in recent years, consumers have turned their attention to plant-based diets. This is due to increased awareness of the beneficial health effects of bioactive plant compounds on human health and the desire to reduce meat consumption for environmental reasons *(Johansson, M. et al., 2021; Acga, C. et al., 2019).*

In the literature, the recommended daily intake of protein is between 0.4 and 0.8 g/kg of body weight. People with more intense physical activity need a higher amount of protein about 1.2-1.6 g/kg body weight, and emerging evidence suggests that a higher protein intake further improves muscle protein synthesis *(Danielle, K. et al., 2017; Wu, G., 2016; McKendry, J. et al., 2024*).

Assessing protein quality in relation to nutritional value means determining the ability of protein to meet metabolic amino acid demand. *(Drulyte, D. et al., 2019).* The digestibility and availability of vegetable proteins are essential aspects to meet the nutritional requirements of humans, in the context of the search for substitutes for animal proteins.

Legumes have a remarkable nutritional value, being rich in protein, carbohydrates, fiber and other bioactive compounds. However, certain antinutritional compounds in legumes, such as trypsin inhibitors, can inhibit protein digestion and reduce the overall effectiveness of protein end-use. Various food processing techniques, such as soaking, hulling, cooking, fermentation, and germination, can improve protein quality and reduce concentrations of anti-nutritional factors, thereby increasing their digestibility *(Gu, J. et al., 2023; F. Mariotti, 2017).*

## THE IMPORTANCE OF LEGUMES IN THE DIET

Legumes, such as chickpeas, peas, beans, lentils are important sources of vegetable proteins. They generally contain between 17% and 40% protein, depending on the species and the growing conditions. Compared to cereals, legumes have a higher content of essential amino acids, especially lysine, which gives them a high biological value. *(Maphosa, Y. et al., 2017).*

Among the most common legumes are dried beans, peas, chickpeas, lentils, lupine, and soybeans. Rich in vitamins and minerals, including B vitamins, iron, magnesium, potassium, and zinc, legumes are an economical source of dietary fiber, phytonutrients, and proteins important for plant-based or flexitarian eating patterns *(Calles, T. et al., 2019).* From a nutritional point of view, legumes represent the second most important family of plants after cereals *(Chamkhi, I. et al., 2022).* Their importance derives from their high content of essential amino acids, especially lysine, which gives them a high biological value, but also of proteins, which is approximately double that of cereals *(Carlini, B. et al., 2024).*

**Table 1**

**Protein content of raw legumes (as % of dry matter)**

*(Banti, M. et al., 2020).*

| Vegetables | Protein content, % |
|---|---|
| Chickpea | 15.5 to 28.2 |
| Beans (Vicia, phaseolus) | 19.4 to 24.8 |
| Lens | 24.7 |
| Feet | 23.9 to 25.1 |
| Lupine | 34.8 to 62.5 |

In general, with regard to production or consumption data, two types of legumes used by humans can be distinguished: oilseed legumes and non-oilseed legumes. While oily legumes have a higher lipid content, non-oilseed legumes are lower in fat and higher in fiber, per 100 kilocalories (kcal) edible serving.

The following type of classification is associated with non-oilseed legumes and refers to whether they are harvested and eaten before or after the pod seeds have dried: (1) legumes are the dried, mature seeds of pods and are sometimes called grain legumes; and (2) unpicked legumes are harvested before drying (i.e., green) and can be eaten with or without pods, as is often the case with sugary peas and peas, respectively, Figure 1 *(Didinger, C. et al., 2021).*

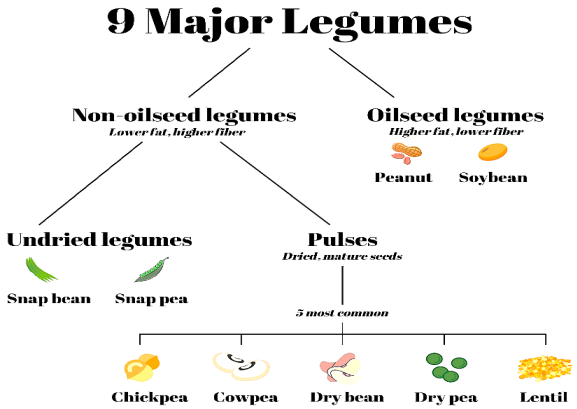



**Fig. 1 - Types of legumes commonly consumed**

*(Didinger, C. et al., 2021).*

The most significant benefits of incorporating legumes as protein sources in the human diet are: low production cost; high nutritional value; low saturated fat content; intake of fiber, minerals and vitamins; role in vegetarian and vegan diet.

The functional properties of legumes, such as the ability to retain water, the ability to retain oil, the stabilization of emulsions and the ability to gel, could be harnessed in the development of various food products. *(Maphosa, Y. et al., 2017).*

In contrast, legumes are low in sodium, and this is desirable given recent trends that encourage reducing salt intake *(Lisciani, S. et al., 2024).*

Proteins from other legumes are also used in the production of meat analogues. In recent years, numerous studies have been carried out on the possibility of using proteins from chickpeas, faba beans and mung beans in the production of meat analogues *(Kyriakopoulou, K. et al., 2021; Kurek, M.A., 2022*).

**Table 2**

**Multiple health benefits of the most commonly used legumes**

*(Ramaswamy, R. and Krishnan, S.B., 2024).*

| Crt No. | Legumes/ Pulses | Nutritional profile | Health benefits |
|---|---|---|---|
| 1 | Pigeon Pea *Cajanus cajan* L. | - High content of proteins, carbohydrates, minerals, vitamins and essential amino acids, both for mature and immature pigeon pea seeds.<br>- Cost-effective source of high-quality protein food and | - Hypocholesterolemic effect<br>- Antimicrobial effect<br>- Hypoglycemic activity<br>- Hepatoprotective effect |

| Crt No. | Legumes/ Pulses | Nutritional profile | Health benefits |
|---|---|---|---|
| | | feed needed for tropical and subtropical livelihoods. | - Cancer prevention<br>- Anti-inflammatory effect<br>- Antihyperglycemic activity<br>- Antidyslipidemic activity |
| 2 | Chickpea *cicer arietinum* L. | - Contains phytic acid, sterols, tannins, carotenoids and other polyphenols such as isoflavones.<br>- Chickpea consumers obtained a higher intake of dietary fiber, polyunsaturated fatty acids, vitamins A, C, and E, folate, magnesium and iron, potassium, compared to non-consumers | - Promotes weight control<br>- Lowers blood glucose levels<br>- Improves cardiovascular health<br>- Reduces the risk of certain types of cancer<br>- Improves tract health gastrointestinal disorders |
| 3 | Lenses *Culinary Lens* | - Rich in boron, calcium, copper, iron, magnesium, manganese, molybdenum, phosphorus, potassium, selenium, vitamin B1 (thiamine), vitamin B2 (riboflavin), vitamin B3 (niacin), vitamin B5 (pantothenic acid), vitamin B6 (pyridoxine), vitamin B9 (folate), vitamin E (tocopherols), vitamin K1 (phylloquinone) and zinc. | - Weight management<br>- Regulating blood sugar<br>- Supports overall gut health<br>- Development of immunity<br>- Anti-inflammatory properties<br>- Antioxidant properties<br>- Antimicrobial properties |
| 4 | Dry Pea *Pisum sativum* L. | - Rich in protein, starch, dietary fiber, non-starchy polysaccharides, polyphenols, including flavonoids and phenolic acids.<br>- Good resource of minerals (e.g. calcium, iron and zinc) and vitamins (e.g. carotenoids and folic acid). | - Antioxidant<br>- Anti-inflammatory<br>- Antimicrobial<br>- Anti-renal fibrosis<br>- Regulation of the effects of metabolic syndrome<br>- Antidiabetic<br>- Antihypertensive |
| 5 | Black Bean *Phaseolus vulgaris* L. | - Important source of protein, which contains the most essential amino acids, especially lysine.<br>- Diverse content of carbohydrates, proteins, fiber, vitamins, minerals, phytochemicals such as saponins, anthocyanins, flavonols | - Antioxidant<br>- Antidiabetic<br>- Anticancer<br>- Anti-cardiostatic<br>- Anti-inflammatory properties |
| 6 | Lima Bean *Phaseolus lunatus* L. | - Excellent source of protein, amino acids (AA), minerals, dietary fiber and B vitamins (folate, B6 and niacin).<br>- Rich in lysine, phenylalanine, leucine, valine, threoline, isoleucine and histidine. | - High mineral content helps with muscle movement, nervous system health, and bone and tooth strength |
| 7 | Red Kidney Bean *Phaseolus vulgaris* L. | -Rich in amino acids, red beans provide a cost-effective source of dietary protein.<br>The isolation of the hydrolysate exhibits antimicrobial effects. | -Antimicrobial, antibiotic and quorum sensing inhibitory effects |
| 8 | Soybean *Glycine Max* Black (BS) & Yellow (YS) | - They contain considerable proteins, carbohydrates, dietary fiber, vitamins, minerals, and phytochemicals, including isoflavones (e.g., daidzein, genistein, and glycitein), saponins, phenolic acids, and anthocyanin.<br>- Rich source of protein, carbohydrates, dietary fiber, lipids, vitamins (such as vitamins B, C and E) and minerals such as sodium, potassium, phosphorus and iron, as well as bioactive compounds including saponins, phenolic acids, isoflavones and anthocyanins.<br>- Higher content of polyphenols such as anthocyanins, soyasaponine and isofavone than YS. | -Excellent antioxidant effects Anti-obesity and hypolipidemic, anti-inflammatory and anti-cancer effects and cardiovascular protective activities |

**Common beans (*Phaseolus vulgaris L.*)** is the most important legume used for direct human consumption. Nutritionists characterize beans as an exceptional food resource due to its high protein content and its combination of carbohydrates, dietary fiber, and minerals, especially iron and zinc *(Didinger, C. et al., 2022)*. The N2 fixation capacity of this crop reduces the demand for the application of synthetic nitrogen fertilizers to increase yield and quality *(Karavidas, I.et al., 2022)*. A significant benefit of dried beans in

reducing greenhouse gas emissions is that they do not involve the energy-intensive processes required to use nitrogen-based fertilizers. Common beans are also a high nutrient source that maintains their qualities during post-harvest storage *(Uebersax, M.A. et al., 2022)*. Growth trends in total global dry bean production over the last few decades, expressed as 5-year averages, are presented in Table 1 *(FAO, 2022)*.

**Table 3**

**Five-year average of world dry bean production, area and yield since 1991**

*(FAO, 2022).*

| Period | Production (million metric tons) | Harvested area (million hectares) | Yield (kg/ha) |
|---|---|---|---|
| 1991–1995 | 17.16 | 26.01 | 660 |
| 1996–2000 | 16,96 | 24,61 | 691 |
| 2001–2005 | 19.36 | 26,85 | 722 |
| 2006–2010 | 22.22 | 28.19 | 790 |
| 2011–2015 | 25.06 | 30,39 | 825 |
| 2016–2020 | 27,46 | 35,39 | 776 |

**Lentils *(*Lens culinaris*)*** are a versatile legume with high potential for direct consumption and food processing applications. Depending on variations in growing conditions, the nutritional, chemical, and antioxidant profiles of lentils can change *(Liberal et al., 2024)*. Lentil proteins consist of approximately 16% albumins, 70% globulins, 11% glutelins, and 3% prolamins *(Ramaswamy et al., 2024)*. Lentil seeds are also highly nutritious, containing 9 g of protein and 0.4 g of fat per 100 g of edible portion; they are rich in iron, phosphorus, magnesium, and B vitamins. There are many types of lentils, including red, brown, green, yellow, and black varieties, among others *(Johansson et al., 2021)*. Global lentil production has more than doubled over the last twenty years, rising from 3.15 million metric tonnes (MMT) in 2001 to 6.54 MMT in 2020 *(FAO, 2021)*. The global area cultivated with lentils increased by 26.83% over the past two decades, growing from 3.95 to 5.01 million hectares between 2001 and 2020 *(Kaale et al., 2022)*. Lentil seed color is an essential quality criterion, with brown color being perceived as indicating inferior quality *(Opoku et al., 2009)*. Furthermore, harvesting lentils from the field at a higher moisture level (16–20% wet basis) is recommended to extend shelf life and minimize mechanical damage during handling, storage, and post-harvest processing *(Kaale, L.D. et al., 2022)*.

**Dried peas (*Pisum sativum L.*)** is a highly nutritious legume belonging to the Fabaceae family, containing high levels of protein (20–25%), carbohydrates, vitamins, and essential minerals, including 1.04% potassium, 0.39% phosphorus (P), 0.10% magnesium (Mg), and 0.08% calcium (Ca) (*Ramaswamy, R. et al., 2024)*. Peas have an exceptionally high content of lysine and threonine, as well as other essential amino acids, and possess a low glycemic index *(Johansson, M. et al., 2021)*. An analysis of data from the last ten years reveals an increase in the area cultivated with dry peas; global production reached 12,403,521 tonnes in 2021, with a recorded yield of 17,610 hg/ha *(Uskutoğlu, D. et al., 2023)*. In an extensive study spanning 23 years, the highest grain pea yield recorded during the period was in France, with some crops exceeding 4 tonnes/ha; however, the area cultivated with this crop in the country is not significant. High grain pea yields were also achieved in North American countries, such as Canada and the USA. Ukraine ranks immediately after these countries in terms of grain yield *(Figure 2; FAOSTAT, 2023)*.

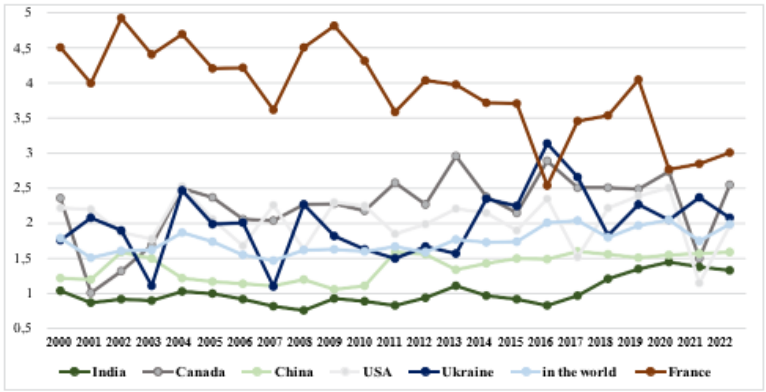



**Fig. 2 - Yield of pea grain, t/ha**

*(according to FAOSTAT, 2023)*

One of the key aspects of growing a crop is its yield. The yield of peas-grains can vary significantly depending on a number of factors, such as soil fertility, climatic conditions, variety, cultivation techniques, and others. To achieve high yields of peas-beans, it is necessary to select the right varieties, ensure proper crop care, timely soil treatment, and protect plants from pests and diseases *(Yermolaiev V.M. et al., 2022*).

**Chickpea (*Cicer arietinum*)** is a valuable crop, and its production ranks third among grain legumes, with an annual average exceeding 10 million tonnes; the majority of production is concentrated in India. India, Australia, and Mexico are the leading exporters *(Muehlbauer, F.J. et al., 2018).* Chickpeas are an excellent source of both carbohydrates and protein, with protein content ranging from 17% to 22% in dry seeds *(Chibbar, R.N. et al., 2010; Zhang, J. et al., 2024).* Basic statistical measures—namely the mean, minimum, maximum, PCV, GCV, heritability, and genetic advance (GA) (% of mean)—for the measured traits are presented in Table 4 *(Mohan, S. et al., 2019).*

**Table 4**

**Estimation of genetic variability for quantitative traits in chickpeas**

*(Mohan, S. et al., 2019).*

| Characters | Mean | Minimum | Maximum | PCV | GCV | Heritability | GA (% of mean) |
|---|---|---|---|---|---|---|---|
| **FDF** | 49.54 | 44.00 | 65.00 | 10.27 | 9.05 | 77.63 | 16.43 |
| **DTM** | 89.01 | 82.00 | 105.00 | 5.83 | 5.05 | 75.24 | 9.03 |
| **PH (cm)** | 33.09 | 26.58 | 44.75 | 12.64 | 10.34 | 66.92 | 17.42 |
| **NPB** | 2.66 | 1.67 | 3.83 | 20.97 | 16.67 | 63.17 | 27.29 |
| **NSB** | 9.40 | 4.60 | 15.25 | 28.26 | 18.71 | 43.81 | 25.51 |
| **NPP** | 34.65 | 12.50 | 62.18 | 37.03 | 26.66 | 51.86 | 39.55 |
| **NSP** | 39.35 | 19.53 | 65.85 | 36.42 | 21.62 | 35.25 | 26.45 |
| **BYP (g)** | 15.06 | 7.70 | 33.19 | 35.42 | 26.57 | 56.24 | 41.04 |
| **HI (%)** | 54.76 | 30.62 | 70.42 | 19.34 | 16.22 | 70.33 | 28.02 |
| **100 SW (g)** | 23.64 | 11.98 | 42.79 | 37.45 | 31.04 | 68.67 | 52.98 |
| **PC (%)** | 22.16 | 14.29 | 28.90 | 14.89 | 11.27 | 57.28 | 17.57 |
| **SYP (g)** | 8.21 | 2.37 | 16.01 | 38.32 | 28.09 | 53.73 | 42.41 |

Characters - DFF (Days to 50% flowering), DTM (Days to maturity), PH (Plant height), NPB (Number of primary branches), NSB (Number of secondary branches), NPP (Number of pods per plant), NSP (Number of seeds per pod), BYP (Biological yield per plant), HI (Harvest index), 100 SW (Weight of 100 seeds), PC (Protein content), SYP (Seed Yield Per Plant)

**Soybeans (*Glycine max*)** is a highly nutritious crop that ranks among the top legumes for protein content, at 36–39% *(Ahmed, H.G.MD. et al., 2023).* It is an excellent source of carbohydrates (20–30%), lipids (19%), essential fatty acids, phosphorus, iron, calcium, zinc, thiamine, riboflavin, vitamin E (tocopherol), dietary fiber (16%), and sugars. Awareness of the health benefits of soybeans and rising global demand have led to an expansion of the cultivation area for this legume in Asia (a 28–40% increase over the last fifteen years), the Americas, Europe, and Sub-Saharan Africa *(Nair, R.M. et al., 2023).* Data regarding international soybean production trends can be utilized to boost yields and mitigate the impact of stressors that negatively affect the harvest *(see Table 5; Gaguan, J.S. et al., 2025).*

**Table 5**

**Growth Phases of Soybean: Stages, Characteristics, and Influences**

*(Gaguan, J.S. et al., 2025).*

| Phase | Internship | Key Characteristics | Environmental and Genetic Influences |
|---|---|---|---|
| **Vegetative (V)** | V1–Cotyledon Emergence | Cotyledons emerge; Initial root and shoot development begins | Influenced by seed vigor, soil temperature, and moisture |
| | V2, V3, etc. – Trifoliate Leaf Development | Sequential emergence of trifoliate leaves; increase in leaf area for photosynthesis | Affected by genotype, light, nutrients, and weather conditions |
| | Full Vegetative Growth | Maximum vegetative growth reached before reproductive transition | Dependent on adequate nutrients, water, and growing degree days |
| **Reproductive (R)** | R1 – Flowering | First appearance of flowers on the plant | Highly sensitive to temperature and water availability |
| | R2–R4 – Pod Development | Pods begin to form and elongate after pollination | Dependent on pollination success, nutrient levels, and heat stress |

| Phase | Internship | Key Characteristics | Environmental and Genetic Influences |
|---|---|---|---|
| | R5–R6 – Seed Filling | Seeds fill and mature within pods | Influenced by carbohydrate availability, moisture, and temperature |
| | R7–R8 – Maturity | Pods and leaves begin to dry down; physiological maturity achieved | Controlled by genetic maturity group and environmental conditions |

The main soybean-producing countries (Brazil, USA, Argentina) hold 68.6% of the total area cultivated with soybeans in 2023. The next countries in terms of size of cultivated areas are India and China (9.3% and 7.5% respectively). Compared to 2014, the increase in production volumes was 23.9%, respectively 76.7 million tons in physical terms. The average growth rate during the analyzed period was 104.4%. The minimum growth rate of soybean production, of 93.9%, was recorded in 2019. At the same time, the maximum growth rate of crude soybean production was reached in 2016, standing at 111.0% (Volkova, E. et al., 2024).

***Anti-nutritional factors***

In addition to their special nutritional value, legumes contain a number of anti-nutritional factors. These are chemical constituents that affect the digestion and absorption of interesting components (e.g. proteins, vitamins) or, in some cases, are simply toxic or cause unwanted physiological side effects (e.g. flatulence).

*Protein anti-nutritional factors* Legume seeds, in addition to nutritious proteins, contain a number of other proteins in abundance, some of which are biologically active proteins, which for years have been referred to as anti-nutritional compounds

*Lectins*, *Amylase Inhibitors, Goitrogen Factor, Saponins.* In addition to their antinutritional effects (reduced breakdown of digestive enzymes, interference with the functioning of the thyroid gland by inhibiting iodine absorption, ability to form soap-like foams in aqueous solutions) they also have advantages. For example, lectins in legumes are used for clinical and immunological studies

*Non-protein anti-nutritional factors*

*Phytate/Phytic Acid, Tannins, Cynogenic Glycosides, Non-Protein Toxic Amino Acids,* RFO - *Oligosaccharides* (Legumes also exhibit toxicity due to their potential to produce cyanides, compounds that produce HCN upon hydrolysis. They have a major negative effect on the animals or people who consume them, Oligosaccharides which are synthesized by the sequential addition of galactose units to sucrose).

In general, anti-nutritional factors are chemicals that can reduce palatability, decrease protein digestibility, and bioavailability of minerals *(Xu, B. et al., 2008).* Therefore, proper food processing is essential before it is consumed. The goal of food processing goes beyond improving taste and pleasure, including increasing nutrient bioavailability by eliminating anti-nutritional factors *(Banti, M. et al., 2020).*

***Fermentation of legumes***

This process optimizes the consistency, flavor and nutritional value of food products, having a positive impact on health. Lactic acid bacteria, yeasts and molds cause enzymatic hydrolysis, influencing the fermentation rate, physicochemical traits, organoleptic qualities and general nutritional quality of the product. Key factors influencing the fermentation process include humidity levels, pH, environment, temperature, dissolved oxygen concentration, and dissolved $CO_2$ levels. *(Patel, P. et al., 2025; Garrido-Galand, A.S. et al., 2021).* Fermentation also helps break down complex carbohydrates, thus facilitating the biotransformation of proteins *(Ganeshan, S. et al., 2024).* In a study examining fermented lentils, a higher amount of digested protein was observed *(Asensio-Grau, A. et al., 2020).*

Fermentation can also affect the mineral content. Although legumes are a rich source of vitamins and minerals, these compounds are characterized by low bioavailability. This is due to the presence of many anti-nutritional compounds, such as phytates and myo-inositol. Fermentation can reduce the amount of these substances, thus helping to increase the bioavailability of minerals. Foods such as fermented chickpea flour are characterized by lower phytic acid and tannin content, which may also improve the bioavailability of minerals *(Knez, E. et al., 2023).*

Regular consumption has been shown to improve dietary nutrient density in the U.S. population and has been associated with reduced risk of disease, especially coronary heart disease and all-cause mortality, to a 50 g serving per day. Their importance derives from their protein content, which is approximately double that of cereals *(Carlini, B. et al., 2024).*

## QUALITY OF LEGUME PROTEINS

The main proteins found in most legumes are globulins and albumins *(Parveen, S. et al., 2021),* as opposed to glutelins and prolamins. Based on the sedimentation coefficient (S20W), globulins are divided into two groups—vicilin and legumin—which constitute 90% of the globulin proteins found in the protein bodies of various legumes.

Consequently, analyzing the structure and composition of legume seed proteins is crucial, as these factors impact digestibility and the techniques used to assess it, alongside the inhibition of protein digestibility by antinutritional components (*Ohanenye, I.C. et al., 2022).* Sulfur-containing amino acids (cysteine and methionine) and tryptophan are deficient in 7S and 11S globulins; this marks a significant difference from albumins, which—as seen in trypsin inhibitors and phytolectins—are functional proteins containing higher levels of sulfur-bearing amino acids *(Liu, Y. et al., 2017*).

Protein digestibility and bioavailability are key factors in meeting human nutritional needs, particularly when seeking alternatives to animal-based proteins *(Gu, J. et al., 2023).* Factors influencing protein digestibility can be categorized into two main groups: exogenous factors, such as the presence of antinutritional components, and endogenous factors, including cross-linking, hydrophobicity, and alterations in protein secondary structure *(Chandran, A.S. et al., 2023)*.

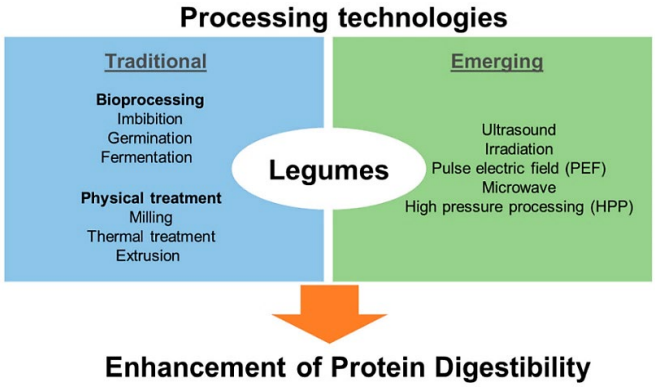



**Fig. 3 - Overview of the main traditional and emerging food processing technologies applied to improve the digestibility of legume proteins**
*(Chandran, A.S. et al., 2023).*

## AGRONOMIC AND ECOLOGICAL ROLE

In addition to their use as food and feed, legumes play a very important role in maintaining soil fertility by fixing atmospheric nitrogen, improving soil structures and adding organic matter. In addition, they are often used as an intercropping, and are sometimes grown as emergency vegetation due to their short life cycle.

Because it requires a low level of fertilizers and other inputs, this crop is relatively economically profitable. It also improves the quality of the environment by sequestering carbon and mitigating other pollutants. Some legumes have the ability to remedy toxic metals and organic pollutants *(Muthuraman, Y. et al., 2020)*.

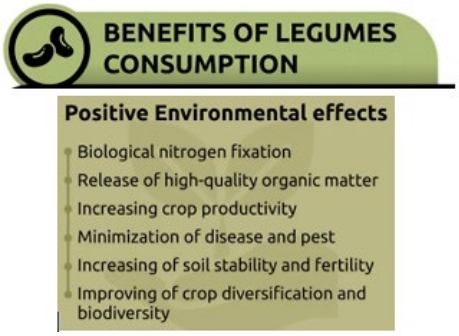



**Fig. 4 - Agronomic and environmental benefits of legumes**
*(Lisciani, S. et al., 2024).*

In the Eat Lancet Commission Planetary Health Diet study on nutritious and sustainable eating patterns, it is recommended to consume 100 g/day (50 g of dried beans, lentils and peas, 25 g of soy and 25

g of peanuts) *(Hughes, J. et al., 2022*). A good part of legumes improve soil fertility by fixing atmospheric nitrogen (30-85 kg/ha; some legumes such as peas: >100 kg/ha) *(Carlini, B. et al., 2024; Hughes, C. et al., 2025)*, and the intercalation of leguminous and non-legume crops significantly improves non-legume growth, nitrogen accumulation and yield, representing an effective agricultural strategy. Prioritization of intercalation is recommended, especially in regions with alkaline soil *(Chen, C. et al., 2026).*

In this context, promoting the presence of plant-based foods in the diet, in which legumes, cereals and seeds should be predominant, seems to be a sustainable alternative to protein intake from an environmental point of view: they have lower greenhouse gas emissions and are an extremely valuable source of protein and other nutrients *(Fasolin L. H. et al., 2019).*

## CONCLUSIONS

Legumes are characterized by a rich and diversified content of nutrients, from an important source of protein and fiber, to a significant level of carbohydrates and micronutrients, such as iron and potassium. Due to their high protein content, ranging between 12-40%, depending on the species and growing conditions, legumes are seen as a solid option instead of animal protein.

An essential factor is the digestibility and availability of vegetable proteins, since in addition to nutrients, they also contain a number of anti-nutritional compounds, such as trypsin inhibitors.

Various food processing techniques, such as soaking, hulling, cooking, fermentation, and sprouting can improve protein quality and reduce concentrations of anti-nutritional factors, thereby increasing their digestibility.

Although legumes are considered the second most important crop after cereals, the lack of knowledge of their nutritional and functional benefits has led to their neglect. Therefore, future studies should look at harnessing the many desirable properties of legumes in the development of nutritious, economically, socially and environmentally beneficial food products.

## ACKNOWLEDGEMENT:

This research was supported by Project ADER 16.1.1 /29.01.2024 Research on the potential for superior exploitation of the Cannabis sativa species for food purposes, funded by Ministry of Agriculture and Rural Development. The research was also financed by Project PN 23 04 02 01, Contract no.: 9N/ 01.01.2023 SUSTAIN–DIGI -AGRI, Innovative biofertilizer production technology used to restore soil biodiversity and reduce the effects of drought on agricultural lands

## REFERENCES

[1] Acga, C., Nai, R, M., Mohd, Z.N.A., Festo, M., Ajit, S., Mohtar, W., Al Qadr Imad, W.A. (2019), In search of alternative proteins: unlocking the potential of underutilized tropical legumes. Food Security, vol.11, pp.1205, doi:10.1007/s12571-019-00977-0

[2] Ahmed, H.G.MD., Naeem, M., Faisal, A., Fatima, N., Tariq, S., Owais, M. (2023). Enriching the Content of Proteins and Essential Amino Acids in Legumes, Legumes Biofortification. Springer, Cham. https://doi.org/10.1007/978-3-031-33957-8_18

[3] Asensio-Grau, A., Calvo-Lerma, J., et al. (2020), Enhancing the Nutritional Profile and Digestibility of Lentil Flour by Solid State Fermentation with Pleurotus ostreatus. Food Funct., 11, 7905–7912.

[4] Banti, M., Bajo, W. (2020), Review on Nutritional Importance and Anti-nutritional Factors of Legumes, International Journal of Nutrition and Food Sciences, 9(6),138-149, doi: 10.11648/j.ijnfs.20200906.11, ISSN: 2327-2716.

[5] Calles, T., del Castello, R., Baratelli, M., Xipsiti, M., Navarro, D.K. (2019), The International Year of Pulses-Final Report; FAO: Rome, Italy.

[6] Carlini, B., Lucini, C., Velázquez, J. (2024), The Role of Legumes in the Sustainable Mediterranean Diet: Analysis of the Consumption of Legumes in the Mediterranean Population over the Last Ten Years a PRISMA Statement Methodology. Sustainability, 16, 3081, https://doi.org/10.3390/su16073081

[7] Chamkhi, I., Cheto, S., Geistlinger, J., Zeroual, Y., Kouisni, K., Bargaz, A., Ghoulam, C. (2022), Legume-based intercropping systems promote beneficial rhizobacterial community and crop yield under stressing conditions. Ind. Crops Prod., 183, 114958.

[8] Chandran, A.S., Suri, S. and Choudhary, P. (2023), Sustainable plant protein: an up-to-date overview of sources, extraction techniques and utilization, Sustainable Food Technol., 1, 466-48, DOI: 10.1039/D3FB00003F.
[9] Chen, C., Li, L., Wu, S., Tang, B., Pang, X., Yin, C. (2026), Nitrogen transfer in legume/non-legume intercropping systems: A global meta-analysis, Agriculture, Ecosystems & Environment, Vol. 401, 110295
[10] Chibbar, R.N., Ambigaipalan, P., et al. (2010), Molecular diversity in pulse seed starch and complex carbohydrates and its role in human nutrition and health. Cereal Chem., 87, 342–352.
[11] Danielle, K., Thomas, C., Riviere, T., Tieges, Z., Greig, C.A. (2017), Dietary protein in older adults: Adequate daily intake but potential for improved distribution. Nutrients, 9:184-194. doi:10.3390/nu9030184.
[12] Didinger, C., Foster, M.T., Bunning, M., & Thompson, H.J. (2022), Nutrition and Human Health Benefits of Dry Beans and OtherPulses, pp.481-504, Wiley Online Library, https://doi.org/10.1002/9781119776802.ch19
[13] Didinger, C., Thompson, H.J. (2021), Defining Nutritional and Functional Niches of Legumes: A Call for Clarity to Distinguish a Future Role for Pulses in the Dietary Guidelines for Americans. Nutrients, 13, 1100. https://doi.org/10.3390/nu13041100.
[14] Drulyte, D., Orlien, V. (2019), The Effect of Processing on Digestion of Legume Proteins. Foods, 8, 224. https://doi.org/10.3390/foods8060224.
[15] Fasolin, L.H., Pereira, R.N., Pinheiro, A.C., Martins, J.T., Andrade, C.C.P., Ramos, O.L., & Vicente, A.A. (2019). Emergent food proteins–Towards sustainability, health and innovation. Food Resch Int., 125, https://doi.org/10.1016/j.foodres.2019.108586
[16] Food and Agriculture Organization of the United Nations. (2021), International Year of Pulses: Nuritious Seeds for a Sustainable Future. Available online: http://www.fao.org/3/a-bb029e.pdf.
[17] Gaguan, J.S., Nagal, C.J.C. (2025), Advances in Soybean Cultivation and Utilization: Growth, Nutritional Significance, and Environmental Impacts, Int. Jr. of Research and Review, vol. 12; Issue: 7, DOI: https://doi.org/10.52403/ijrr.20250723.
[18] Ganeshan, S., Asen, N., Wang, Y., Tülbek, M. Ç., & Nickerson, M. T. (2024). Sustainable pulse proteins: physical, chemical and fermentative changes. Appl.Biosciences, 3(2), 263–282.
[19] Garrido-Galand, A.S., Asensio-Grau, J., Calvo-Lerma, A., Heredi, Andrés. A. (2021), The potential of fermentation on nutritional and technological improvement of cereal and legume flours: A review, Food Research International, 145, doi:10.1016/j.foodres,.110398.
[20] Gernand, A.D., Schulze, K.J., Stewart, C.P., West, K.P. and Christian, P. (2016), Nat at.Rev. Endocrinol, 12(5), pp. 274-89, DOI: 10.1038/nrendo.2016.37.
[21] Gu, J., B.K., A., Wu, H., Lu, P., Nawaz, M.A., Barrow, C.J., Dunshea, F.R., Suleria, H.A.R. (2023), Impact of processing and storage on protein digestibility and bioavailability of legumes, Food Rev.Int., Vol.39.
[22] Huebbe, P., Rimbach, G. (2020), Historical Reflection of Food Processing and the Role of Legumes as Part of a Healthy Balanced Diet. Foods, 9, pp.1056. https://doi.org/10.3390/foods9081056
[23] Hughes, C., Ringelberg, J.J. and Bruneau, A. (2025), Legumes, Current Biology 35, R315–R330,
[24] Hughes, J., Pearson, E., Grafenauer, S. (2022), Legumes—A Comprehensive Exploration of Global Food-Based Dietary Guidelines and Consumption. Nutrients, 14, 3080. https://doi.org/10.3390/nu14153080.
[25] Johansson, M., Xanthakis, E., Langton, M., et al. (2021), Mixed Legume Systems of Pea Protein and Unrefined Lentil Fraction: Textural Pr. and Microstructure. LWT, 144, 111212
[26] Kaale, L.D., Siddiq, M., Hooper, S. (2022), Lentil (Lens culinaris Medik) as nutrient-rich and versatile food legumes: A review, Legume Science, https://doi.org/10.1002/leg3.169
[27] Karavidas, I., Ntatsi, G., Vougeleka, V., et al. (2022), Agronomic Practices to Increase the Yield and Quality of Common Bean (Phaseolus vulgaris L.): A Systematic Review. Agronomy, 12, 271.
[28] Knez, E., Kadac-Czapska, K., Grembecka, M. (2023), Effect of fermentation on the nutritional quality of the selected vegetables and legumes and their health effects. Life, 13, 655.
[29] Kurek, M.A., Onopiuk, A., Pogorzelska-Nowicka, E., et al. (2022), Novel Protein Sources for Applications in Meat-Alternative Products—Insight and Challenges. Foods, 11, 957. https://doi.org/10.3390/foods11070957.

[30] Kyriakopoulou, K., Keppler, J.K., van der Goot, A.J. (2021), Functionality of Ingredients and Additives in Plant-Based Meat Analogues. Foods, 10, 600.
[31] Liberal, Â., Fernandes, Â., Ferreira, I.C.F.R., et al. (2024), Effect of different physical pre-treatments on physicochemical and techno-functional properties, and on the antinutritional factors of lentils (Lens culinaris spp.). Food Chem., 450, 139293.
[32] Lisciani, S., Marconi, S., Le Donne, C. et al., (2024), Legumes and common beans in sustainable diets: nutritional quality, environmental benefits, spread and use in food preparations, Front. Nutr, Sec. Nutrition and Sustainable Diets, Vol.11, |https://doi.org/10.3389/fnut.2024.1385232.
[33] Liu, Y., Wu, X., Hou, W., et al. (2017), Structure and Function of Seed Storage Proteins in Faba Bean (Vicia faba L.). 3 Biotech, 7, 74.
[34] Lonnie, M., Hooker, E., Brunstrom, J. M., et al. (2018), Protein for life: Review of optimal protein intake, sustainable dietary sources and the effect on appetite in ageing adults. Nutrients, 10, 360
[35] Maphosa, Y. and Jideani, V. A. (2017), The Role of Legumes in Human Nutrition, Chapter 6, Functional Food: Improve Health through Adequate Food, Intech, Rijeka, Croatia,.
[36] Mariotti, F. (2017), 35 – Plant Protein, Animal Protein, and Protein Quality, Elsevier.
[37] Martín-Cabrejas, M.Á. (2019), Legumes: Nutritional Quality, Processing and Potential Health Benefits, chapter 1, Legumes: An Overview of Food Chemistry, Function and Analysis, pp. 353, UK, Croydon, CPI Group.
[38] McKendry, J., Lowisz, C.V., Nanthakumar, A., et al. (2024), The effects of whey, pea, and collagen protein supplementation beyond the recommended dietary allowance on integrated myofibrillar protein synthetic rates in older males: a randomized controlled trial, Am J Clin Nutr, 120 (1), pp. 34-46
[39] Mohan, S. and Thiyagarajan, K. (2019), Genetic Variability, Correlation and Path Coefficient Analysis in Chickpea (Cicer arietinum L.) for Yield and its Component Traits, Int. Jr. of Current Microbiology and Appl. Sc., Vol. 8 No. 05.
[40] MSpechtL.G. (2021), Plant-Based Egg Alternatives: Optimizing for Functional Properties and Applications.The GoodFood Institute.
[41] Muehlbauer, F.J., Sarker, A. (2018). Economic Importance of Chickpea: Production, Value, and World Trade, Comp. of Pl. Gen. Springer, Cham. https://doi.org/10.1007/978-3-319-66117-9_2
[42] Muthuraman, Y., Muthaiyan, P., Pandurangan G. (2020), Role of legumes in improving soil fertility status, vol. Legume Crops - Prospects, Production and Uses, IntechOpen, DOI: 10.5772/intechopen.93247
[43] Nair, R.M., Boddepalli, V.N., Yan, M.-R., et al. (2023). Global Status of Vegetable Soybean. Plants, 12, 609. https://doi.org/10.3390/plants12030609
[44] Ohanenye, I.C., Ekezie, F.-G.C., Sarteshnizi, R.A., et al. (2022), Legume Seed Protein Digestibility as Influenced by Traditional and Emerging Physical Processing Technologies. Foods, 11, 2299. https://doi.org/10.3390/foods11152299
[45] Opoku, A., Tabil, L., & Meda, V. (2009), Effect of microwave drying andstorage on the color, breakage, dehulling and cooking quality of twored lentil varieties. The Canadian Society for Engineering in Agricultural, Food, Environmental, and Biological Systems (CBSE). Paper pre-sented at the CSBE/SCGAB,Annual Conference, Georgetown,PEI, Canada.
[46] Papa, R., Acosta, J., Delgado-Salinas, A., Gepts, P.A. (2005), genome-wide analysis of differentiation between wild and domesticated *Phaseolus vulgaris* from Mesoamerica. Theor. and Applied Genetics, 111, pp.1147-1158, https://doi.org/10.1007/s00122-005-0045-9.
[47] Parveen, S., Jamil, A., Pasha, I. and Ahmad, F. (2021), Pulses: A Potential Source of Valuable Protein for Human Diet, Legumes Research, Vol. 2, IntechOpen Limited, London, DOI: 10.5772/intechopen.99980.
[48] Patel, P., Pang, Y.L.J., et al. (2025). Protein Extraction and Isolation from Legumes and Algae: An Industry Primer. Food Bioprocess Technol 18, 8380–8408, https://doi.org/10.1007/s11947-025-03958-8 /
[49] Ramaswamy, R. and Krishnan, S.B. (2024), Pulsed Electric Field Treatment in Extracting Proteins from Legumes: A Review, Processes, 12, 2667. https://doi.org/10.3390/pr12122667
[50] Santhiya, S., Singh, A., Thakur, A., Dev, R., Hedau, N.K. and Kant, L. (2024), Importance of legume vegetables in nutritional and food security- An Indian perspective, Jr. of Food Leg. 37(4), pp. 359-366.

[51] Tharanathan, R.N., Mahadevamma, S. (2003), Legumes – A boon to human nutrition. Trends in Food Science and Technology, 14:507-518. doi:10.1186/s12937-019-0435-5.
[52] Uebersax, M.A., Cichy, K.A., Gomez, F.E., Porch, T.G., Heitholt, J., Osorno, J.M., Kamfwa, K., Snapp, S.S., Bales, S. (2022), Dry beans (Phaseolus vulgaris L.) as a vital component of sustainable agriculture and food security—A review, Leg. Sc., https://doi.org/10.1002/leg3.155.
[53] Uskutoğlu, D., İdikut, L. (2023), Pea Production Statistics in the World and in Turkey, chapter 2, Innovative Research in Agriculture, Forest and Water Issues, Duvar Publishing, Izmir/ Turkey.
[54] Volkova, E. and Smolyaninova, N. (2024), Analysis of world trends in soybean production, BIO Web of Conferences 141, 01026, Agric.Sc., https://doi.org/10.1051/bioconf/202414101026.
[55] Wu, G. (2016), Dietary protein intake and human health, Food Funct.,7, 1251-1265, DOI: 10.1039/C5FO01530H,
[56] Xu, B. and Chang, S. K. (2008). Antioxidant capacity of seed coat, dehulled bean, and whole black soybeans in relation to their distributions of total phenolics, phenolic acids, anthocyanins, and isoflavones. Jr.l of agric. and food chemistry, 56(18), pp.8365-8373.
[57] Yermolaiev V.M., Gamajunova V.V. (2022), Modern Trends in Pea Cultivation In Ukraine and the World., Tavria Sc. Bulletin, No.136, https://doi.org/10.32782/2226-0099.2024.136.1.15.
[58] Zhang, J., Wang, J., Zhu, C., Singh, R.P., Chen, W. (2024), Chickpea: Its Origin, Distribution, Nutrition, Benefits, Breeding, and Symbiotic Relationship with Mesorhizobium Species. Plants, 13, 429,
[59] Zhao, J., Chen, J., Beillouin, D., Lambers, H., Yang, Y., Smith, P., Zeng, Z., Olesen, J.E., Zang, H. (2022), Global systematic review with meta-analysis reveals yield advantage of legume-based rotations and its drivers. Nat. Commun., 13, 4926.
[60] *** https://www.fao.org/eswatini/news/news-details/fao-and-eswatini-underscore-the-value-of-pulses-at-the-world-pulses-day-celebration-2026
[61] FAO. (2022). Crop Production and Trade Data. Retrieved from http://www.fao.org/faostat/en/#data
[62] FAO (Food and Agriculture Organization), (2021). Crop Production andTrade Data. FAOSTAT, 2023. http://www.fao.org/faostat/en/#home.

# EFFICIENCY OF DYNAMIC DAMPENING AND MECHANICAL DECOUPLING TECHNOLOGIES IN LOW-POWER TOOLS

/

# *EFICIENȚA TEHNOLOGIILOR DE AMORTIZARE DINAMICĂ ȘI DECUPLARE MECANICĂ LA MAȘINILE-UNELTE DE MICA PUTERE*

**Gheorghe FLOROIU[1)], Mihai Valentin PREDOI[*2)]**

[1)] Ph.D. stud.eng., I.S.B. Doctoral School, Dept.of Mechanics, National University of Science and Technology Politehnica Bucharest, Splaiul Independenței, 313, 060042, Bucharest / Romania

[2)] Prof. Ph.D. Eng., Dept.of Mechanics, National University of Science and Technology Politehnica Bucharest, Splaiul Independenței, 313, 060042, Bucharest / Romania

**E-mail: mihai.predoi@upb.ro*

***Keywords:*** *active damping, mechanical decoupling, low-power tools, hand-arm vibration, occupational exposure.*

**ABSTRACT**

*Prolonged exposure to high-intensity vibrations during the operation of portable power tools has historically posed a severe occupational health risk, frequently leading to Hand-Arm Vibration Syndrome (HAVS). Initially, early electric tools lacked vibration mitigation systems, relying entirely on operator endurance. To address this, the industry introduced early passive solutions, such as simple rubberized grips. This paper provides a comprehensive overview of the evolution and efficiency of contemporary vibration reduction technologies, analyzing the transition towards advanced active systems. The study focuses on the efficiency of two major engineering approaches: mechanical decoupling and dynamic dampening. While mechanical decoupling physically separates the impact mechanism from the handle to filter shocks, dynamic dampening utilizes synchronized internal oscillating counter-weights to actively cancel vibrations at the source, a concept inspired by seismic engineering. By theoretically examining these principles, the paper highlights their critical role in transforming hazardous industrial equipment into ergonomic tools, thereby extending safe operational duration and increasing overall efficiency.*

**REZUMAT**

*Expunerea prelungită la vibrații de înaltă intensitate în timpul utilizării mașinilor-unelte portabile a reprezentat, din punct de vedere istoric, un risc major pentru sănătatea operatorilor, ducând frecvent la apariția Sindromului de Vibrație Mână-Braț (HAVS). Inițial, primele unelte electrice nu dispuneau de sisteme de atenuare a vibrațiilor, bazându-se exclusiv pe rezistența fizică a utilizatorului. Ulterior, industria a introdus soluții pasive incipiente, precum mânerele cauciucate. Această lucrare prezintă o imagine de ansamblu a evoluției și eficienței tehnologiilor contemporane de reducere a vibrațiilor, analizând tranziția către sistemele active avansate. Studiul se concentrează pe eficiența a două direcții inginerești majore: decuplarea mecanică și amortizarea dinamică. În timp ce decuplarea mecanică separă fizic mecanismul de impact de mâner pentru a filtra șocurile, amortizarea dinamică folosește contragreutăți interne oscilante sincronizate pentru a anula activ vibrațiile la sursă, inspirată din ingineria seismică. Prin examinarea teoretică a acestor principii, lucrarea subliniază importanța lor în transformarea echipamentelor industriale cu potențial de risc în unelte ergonomice, permițând extinderea duratei de lucru sigure și creșterea eficienței operaționale*

## INTRODUCTION

The extensive use of portable power tools, such as rotary hammers, impact drills, and demolition breakers, is indispensable in modern construction and manufacturing environments. However, these tools generate high-intensity vibrations that are directly transmitted to the operator's hands and arms.

Prolonged occupational exposure to such mechanical energy is the primary cause of Hand-Arm Vibration Syndrome (HAVS), a debilitating condition characterized by vascular, sensorineural, and musculoskeletal disorders *(Griffin, 1990).*

In response to these health risks, stringent regulations, such as the European Directive 2002/44/EC, have established strict exposure action values (EAV) and exposure limit values (ELV), compelling the industry to significantly reduce the vibration emissions of portable equipment *(European Parliament, 2002).*

Clinically, this progressive and irreversible occupational disease manifests through severe vascular spasms—commonly known as "vibration white finger"—accompanied by significant neurological and musculoskeletal deterioration, such as loss of grip strength and tactile sensitivity. Beyond the severe physiological damage inflicted on the operator, this pathology generates a substantial economic burden on the construction industry. The financial impact is reflected in escalating costs related to occupational health compensation claims, prolonged medical absenteeism, decreased on-site productivity, and the necessity of implementing extensive rehabilitation programs for affected workers.

Historically, the initial attempts to mitigate vibration exposure relied predominantly on passive isolation methods, including rubberized handles and anti-vibration gloves. While these solutions provided a basic level of ergonomic comfort, they proved insufficient in attenuating low-frequency, high-amplitude shocks generated by heavy-duty pneumatic and electro-pneumatic impact mechanisms (*Dong et al., 2021).*

Consequently, power tool manufacturers have shifted their focus toward integrating sophisticated internal damping mechanisms designed to neutralize vibrations either at the source or along the transmission path. Contemporary vibration reduction technologies in portable power tools can be broadly classified into two primary engineering architectures: mechanical decoupling and dynamic dampening. Mechanical decoupling systems utilize elastic elements, such as multi-stage springs and elastomeric shock absorbers, to physically separate the active impact mechanism from the tool's gripping surfaces. Conversely, dynamic dampening introduces a more advanced, active approach inspired by seismic engineering principles. This technology employs internal oscillating counter-weights that move in anti-phase to the primary impact mechanism, thereby actively cancelling out the generated kinetic energy before it reaches the tool's housing.

The main objective of this paper is to provide a comparative analysis of the mechanical principles, efficiency, and ergonomic impact of these advanced vibration reduction systems. By evaluating specific technological implementations—namely passive vibration control, mechanical decoupling, and active dynamic dampening—this study aims to highlight their effectiveness in extending safe operational time limits and improving overall occupational safety.

## MATERIALS AND METHODS

The methodology of this study is based on a comparative technical analysis of three primary vibration reduction systems implemented in professional rotary hammers. To ensure a consistent comparison, the analysis focused on heavy-duty power tools from the SDS-Max class, operating in the 1.0 – 1.5 kW power range. The evaluated systems are: active dynamic dampening (Makita AVT), multi-stage mechanical decoupling (Hilti AVR), and passive vibration control (Bosch VC). The baseline vibration emission values utilized for this assessment are derived from technical data measured in accordance with the internationally recognized ISO 28927-10 standard (Hand-held portable power tools – Test methods for evaluation of vibration emission). This rigorous testing protocol requires the equipment to be operated under heavily loaded conditions, simulating actual concrete drilling and chiseling applications. Measuring the triaxial vibration total value at the primary and secondary gripping surfaces ensures a high degree of technical comparability across different manufacturers and reduction architectures.

The transmission of mechanical shocks from the impact mechanism to the operator's hand is illustrated in Figure 1, highlighting the specific intervention points for each reduction technology.

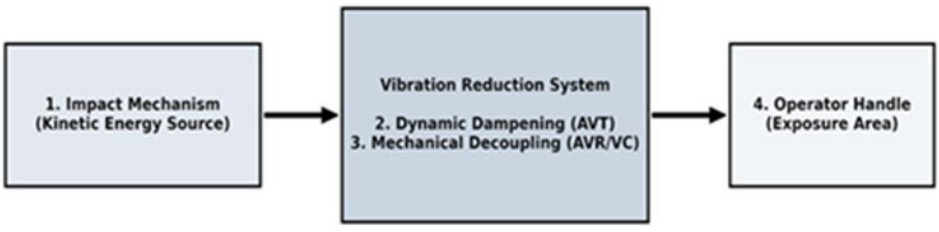



**Fig. 1 - The schematic flow of vibration transmission in a rotary hammer and the intervention points for AVT, AVR, and VC systems**

*1 - impact mechanism (piston); 2 - dynamic counter-weight (AVT); 3 - elastic shock absorbers; 4 - mechanically decoupled handle (AVR/VC).*

To quantify the occupational safety impact, the daily vibration exposure was theoretically evaluated based on standard occupational health procedures.

The equivalent daily exposure for an eight-hour reference period is calculated using the following equation:

$$A(8) = a_{hv}\sqrt{\frac{T}{T_0}} \quad (1)$$

where: $A(8)$ is the daily exposure normalized to an 8-hour reference period, $[m/s^2]$; $ahv$ is the vibration total value, $[m/s^2]$; $T$ is the daily duration of exposure, $[h]$; $T0$ is the reference duration of 8 hours.

The comparative baseline data for the power tools equipped with these specific anti-vibration technologies, utilized for the subsequent calculations, are summarized in Table 1.

**Table 1**

**Technical specifications and declared vibration levels for the analyzed SDS-Max rotary hammers**

| Power Tool System | Technology Type | Nominal Power [W] | Impact Energy [J] | Vibration Level $a_{hv}$ [m/s²] |
|---|---|---|---|---|
| Makita HR4013C | AVT (Active Dynamic) | 1100 | 8.0 | 5.0 |
| Hilti TE 60-AVR | AVR (Mechanical Decoupling) | 1350 | 7.8 | 9.0 |
| Bosch GBH 4-32 DFR | VC (Passive Elasticity) | 900 | 4.2 | 10.0 |

## RESULTS

The theoretical assessment of daily vibration exposure reveals significant differences in the safe operational time limits among the analyzed rotary hammers. According to the European Directive 2002/44/EC, the strict Exposure Limit Value (ELV) is set at $5.0\ m/s^2$ for an 8-hour reference period. By applying Equation 1, the maximum allowable working time to reach the ELV was calculated for each power tool. The Makita HR4013C, equipped with active dynamic dampening (AVT), emits a vibration level of exactly 5.0 m/s², which mathematically allows for a full 8-hour work shift without exceeding the legal exposure limit.

In contrast, the tools relying on mechanical decoupling and passive elasticity reach the maximum exposure limit much faster due to their higher baseline emissions. Operating the Hilti TE 60-AVR (9.0 m/s²) reaches the legal ELV limit in approximately 2.47 hours of continuous trigger time. Similarly, the Bosch GBH 4-32 DFR (10.0 m/s²) reaches the absolute exposure limit in just 2.0 hours. These results indicate that while passive and mechanically decoupled systems offer a fundamental degree of protection, active dynamic dampening is vastly superior for prolonged heavy-duty operations. The AVT technology effectively extends the safe working time by up to 400% compared to traditional passive systems, directly impacting both occupational safety and industrial productivity.

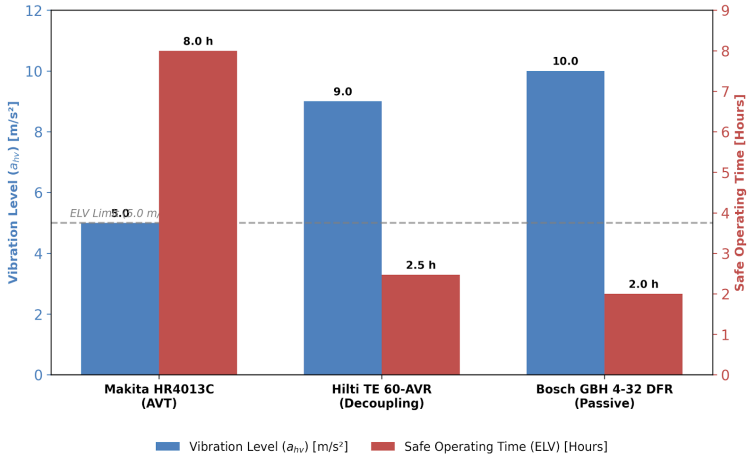



**Fig. 2 - Comparative analysis between vibration emission levels ($a_{hv}$) and safe operating times (ELV) for the evaluated rotary hammers**

## CONCLUSIONS

The theoretical assessment of daily vibration exposure clearly demonstrates that the implementation of active dynamic dampening systems represents a significant technological advancement in occupational safety compared to traditional passive or mechanical decoupling methods. The comparative analysis highlights that active counter-weight mechanisms, such as the AVT technology, can effectively maintain vibration emissions at the absolute Exposure Limit Value (5.0 m/s²). This theoretically allows operators to

perform continuous heavy-duty tasks for a full 8-hour shift. In contrast, systems relying strictly on mechanical decoupling and elastic shock absorbers reach the legal exposure thresholds in less than 2.5 hours, heavily restricting daily productivity and requiring frequent operator rotations. Ultimately, the widespread adoption of active vibration reduction architectures is essential for the modern construction industry. Beyond ensuring strict compliance with European safety directives, these advanced systems fundamentally mitigate the risk of developing Hand-Arm Vibration Syndrome (HAVS), safeguarding the long-term health of the workforce while simultaneously optimizing on-site operational efficiency.

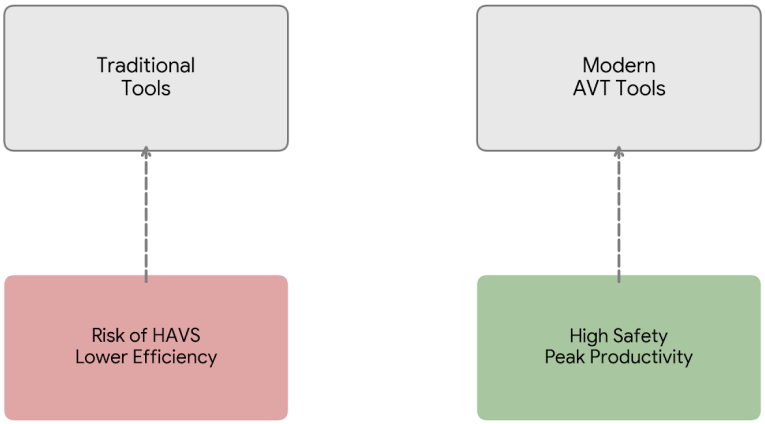



**Fig. 3 - Conceptual framework: Impact of vibration reduction technologies on operator outcomes**

## REFERENCES

[1] Bovenzi, M. (2023). Health risks from occupational exposure to hand-transmitted vibration in the construction. *Scandinavian Journal of Work, Environment & Health*, 112-124.

[2] Dong, R. G. (2021). Evaluation of anti-vibration technologies in portable power. *Journal of Occupational and Environmental Hygiene*, 167-179.

[3] European Parliament. (2002). Directive 2002/44/EC of the European Parliament and of the Council of 25 June 2002 on the minimum health and safety requirements regarding the exposure of workers to the risks arising from physical agents (vibration). *Official Journal of the European Communities*, 13-19.

[4] Griffin, M. J. (1990). Handbook of Human Vibration. Academic Press.

[5] International Organization for Standardization. (2018). Hand-held portable power tools — Test methods for evaluation of vibration emission — Part 10: Percussive drills, hammers and breakers . *(ISO 28927-10:2011/Amd 1:2018)*.

[6] Krajnak, K., & Miller, G. R. (2025). The physiological and economic impact of Hand-Arm Vibration Syndrome in the modern construction sector. *International Journal of Industrial Ergonomics*, 92.

[7] Lundström, R., & Nilsson, T. (2019). Diagnostics and management of Hand-Arm Vibration Syndrome. *Occupational Medicine*, 421-428.

[8] Mansfield, N. J., & Maeda, S. (2020). Active dynamic dampening vs. mechanical decoupling: Efficacy in heavy-duty rotary hammers. *Applied Acoustics*, 158.

[9] Parliament., E. (2002). Directive 2002/44/EC of the European Parliament and of the Council of 25 June 2002 on the minimum health and safety requirements regarding the exposure of workers to the risks arising from physical agents (vibration). *Official Journal of the European Communities*, 13-19.

[10] Pelmear, P. L., & Wasserman, D. E. (2022). Hand-Arm Vibration: A Comprehensive Guide for Occupational Health Professionals. *CRC Press.*, 3rd ed.

[11] Rimell, A. N., & Edwards, R. (2023). Exposure limits and the effectiveness of modern anti-vibration handles in SDS-Max power tools. *Annals of Work Exposures and Health*, 982-995.

[12] Vergara, M., Sancho-Bru, & Gracia-Ibáñez. (2018). Tool handle design and its effect on vibration transmissibility to the human arm. *Journal of Biomechanics*, 195-201.

[13] Welcome, D. E., & Dong, R. G. (2024). Extending safe operational times through active vibration control in hand-held machinery. *Ergonomics*, 305-318.

# COMPARATIVE STUDY OF THE PROPERTIES OF BIOCHAR OBTAINED FROM SUNFLOWER AND MISCANTHUS STRAINS

/

# *STUDIU COMPARATIV AL PROPRIETĂȚILOR BIOCHARULUI OBȚINUT DIN TULPINI DE FLOAREA SOARELUI ȘI MISCANTHUS*

**Nicoleta-Alexandra VANGHELE*[1, 2)], Nicolae-Valentin VLĂDUȚ[1)], Andreea MATACHE[1)], Augustina PRUTEANU[1)], Florin NENCIU[1)], Laurențiu VLĂDUȚOIU[1)], Ana-Maria TĂBĂRAȘU[1, 2)], Dragoș ANGHELACHE[1, 2)], Alexandru IONESCU[1, 2)], Cristian RADU[2, 3)], Nicoleta Olimpia VRÎNCEANU[4)]**

[1)] National Institute of Research - Development for Machines and Installations Designed for Agriculture and Food Industry - INMA Bucharest / Romania;

[2)] National University of Science and Technology Polytechnic Bucharest, Faculty of Biotechnical Systems Engineering, Bucharest / Romania;

[3)] University of Craiova, Dolj County / Romania;

[4)] National Institute for Research and Development for Pedology, Agrochemistry and Environmental Protection - ICPA, Bucharest / Romania

**Tel: (+4021) 2693 457; *Email: vanghelelrc@gmail.com*

***Keywords:*** *biochar, properties, sunflower, miscanthus*

## ABSTRACT

*In recent decades, given the principles of sustainable agriculture and the circular economy, the use of plant-based biomass as a renewable energy source has increased significantly. Biochar is used not only as an innovative form of fuel, but also in agriculture, construction, wastewater treatment, as well as in medicine or in various industries such as food, textiles and cosmetics. It has huge potential to mitigate climate change and improve environmental conditions, having a favorable impact on global environmental stability. The properties of biochar are determined by the source of the material used and the manufacturing conditions. This research provides a comparative analysis of the properties of biochar derived from sunflower and miscanthus strains, as well as the information available in scientific sources, including: moisture, amount of ash, density. cut to the size of 15 cm and subjected to heat treatment at temperatures between 250°C and 450°C. For each temperature step, three times were used, namely: 30 min.; 60 min.; 90min.*

## REZUMAT

*În ultimele decenii, având în vedere principiile agriculturii durabile și ale economiei circulare, utilizarea biomasei de origine vegetală ca sursă de energie regenerabilă a înregistrat o creștere semnificativă. Biocharul este utilizat nu doar ca o formă inovatoare de combustibil, ci și în agricultură, domeniul construcțiilor, tratamentele apelor uzate, precum și în medicină sau în diverse industrii cum ar fi alimentația, textilele și cosmetica. Acesta prezintă un potențial uriaș pentru atenuarea schimbărilor climatice și îmbunătățirea condițiilor de mediu, având un impact favorabil asupra stabilității ecologice globale. Proprietățile biochar-ului sunt determinate de sursa materialului utilizat și de condițiile de fabricație. Această cercetare oferă o analiză comparativă a proprietăților biocharului derivat din tulpinile de floarea-soarelui și din miscanthus, precum și informațiile disponibile în sursele științifice, inclusiv: umiditate, cantitatea de cenușă, densitate. tăiate la dimensiunea de 15 cm și supuse tratamentului termic la temperaturi cuprinde intre 250°C și 450°C. Pentru fiecare treaptă temperatură au fost utilizați trei timpi și anume: 30 min.; 60 min.; 90 min.*

## INTRODUCTION

Biochar is a product with a high carbon content and is formed when biomass, such as wood, plant debris or manure, is subjected to heat in an enclosed space with low or no oxygen levels. It has important applications in agriculture and environmental protection, being able to improve soil properties.

Its persistence in the soil and ability to retain nutrients make it a special amendment to the soil. In addition, the use of biochar, together with sustainable biomass production, can help reduce carbon emissions and play an active role in capturing carbon dioxide from the atmosphere, having a significant impact on climate action. It can also be related to the production of bioenergy through the use of gases

generated during the pyrolysis process *(Ahmad Bhat et al., 2022; Waheed et al., 2025; Vanisree et al., 2024).*

Biochar can be used for power generation, agriculture, carbon capture, wastewater processing, biorefinery, and other applications *(Bousdra et al.; 2023; Hussein et al., 2024; Ji et al., 2022; Osman et al., 2024)*. Some researchers have cataloged the uses of biochar in: soil breeding, waste management, countering climate change, and power generation *(Lehmann and Stephen 2009).*

Biochar is also an alternative method for processing organic waste and a solution to chemical fertilizers, being not only environmentally friendly but also sustainable *(Upadhyay et al., 2024).*

These advantages have drawn the attention of agricultural researchers to obtaining biochar from bioresidues and applying it as an amendment for soil and other uses *(Amalina et al., 2022).*

Biochar is a valuable tool for environmental management due to its physical properties. The physical properties of biochar can influence soil systems in direct and indirect ways. The physical characteristics of different types of soils differ depending on the nature and proportion of minerals and organic matter, as well as the interaction between these elements.

The use of biochar improves soil fertility and quality by adjusting pH, increasing the ability to maintain moisture, stimulating the attraction of more useful fungi and bacteria, facilitating cation-exchange capacity, and retaining nutrients in the soil *(Wani et al., 2025).*

The fiber composition of the sunflower stem is similar to that of other annuals, such as corn and paper sorghum, having a significant amount of cellulose and hemicellulose, along with hydroxyl and carboxyl functional groups *(Lingamdinne et al., 2024).*

Although the interior of the sunflower stem, which differs significantly from its fibers, contains a high proportion of pectin, the amounts of lignin and hemicellulose are reduced, with sunflower stems representing a promising option for biochar *production (Lingamdinne et al., 2024; Zhao et al., 2022)*.

Miscanthus sinensis is part of the Poaceae family, and is also known as silver grass, Chinese grass or elephant grass. It is a perennial and rhizomatous plant, which once planted can provide yields over a period of 10-20 years.

It has been shown that waste from Miscanthus, once processed, can be converted into carbon-rich biochar. The use of biochar as a soil amendment has the ability to increase both its quality, serving as a breeder, and the productivity of crops, acting as a fertilizer *(Kavitha et al., 2018; Shaaban et al., 2018).* It can also contribute to the restoration of land affected by pesticides and heavy metals *(Janus et al., 2015; Nsanganwimana et al., 2014).*

## MATERIALS AND METHODS

To produce biochar, an experimental plant was used that was designed and manufactured by the National Institute for Research and Development for Machinery and Installations for Agriculture and Food Industry - INMA Bucharest (Romania).

This facility uses advanced intelligent management technologies to monitor and modify key parameters in real-time.

The raw materials used, miscanthus strains and sunflower stems (Fig.1), were taken from cultures and experimental batches also within the institute.



**Fig. 1 - Raw materials used, sunflower strains and miscanthus strains**

After harvesting, the stems were dried, cut to a size of 15 cm and subjected to heat treatment at temperatures between 250°C and 450°C. For each temperature step, three times were used, namely: 30 min.; 60 min.; 90min.

After the time passed, the retort was removed from the oven and left to cool for about 30 minutes. After that, the contents of the retort (the biochar obtained) were weighed and packed in vacuum bags and labeled to be stored until analysis.

For potentiometric determination of pH was used ICPA methodology (1983), and for total carbon SR ISO 10694/ 1998.

The determination of the ash content, by calcination in a furnace was carried out using the method adapted according to *ISO 18122:2016* and with the help of the Naberterm L, GmbH, Germany calcining furnace with temperature control, analytical balance. Model: ATX 224- Shimadzu, Japan, high-temperature resistant porcelain crucibles, desiccator and desiccant for dry sample cooling, gloves and spatula, heat-resistant pliers.

The determination was carried out with the formula:

$$[\%]\, Ce = \frac{(\mathrm{mf}-\mathrm{m0})}{(\mathrm{mi}-\mathrm{m0})} * 100 \quad (1)$$

Where: mf is the final mass, mi is the initial mass, and m0 is the crucible mass.

To determine the density, the volumetric method was used and the equipment used were: analytical balance and a 2000 ml vessel, using the formula:

$$q = \frac{m}{\mathrm{V}} \quad [\mathrm{g/cm^3}] \quad (2)$$

where ρ is the density (g/cm³), m is the mass of the raw material (g), and V is the volume (cm3).

The determination of the moisture content of the biochar was carried out by a method adapted according to *SR EN 21660-3:2021*, and the devices used were Thermostatically controlled oven UFE 500 Model 100–800 – Memmert, Germany, analytical balance Model: ATX 224- Shimadzu, Japan, aluminum capsules with a capacity of up to 10 ml for samples, Exicator and desiccant for cooling the sample in dry environment, gloves and spatula., using the formula:

$$U = \frac{(\mathrm{mi}-\mathrm{mf})}{(\mathrm{mi}-\mathrm{m0})} * 100 \ [\%] \quad (3)$$

where: where my initial meal is; mf is the final table; m0 is the mass of the empty capsule

Figure 2 illustrates the preparation of the raw material and the biochar obtained for analysis.








**Fig. 2 - Preparation and analysis of biochar samples**

## RESULTS

Table 1 presents the results obtained for biochar from sunflower stems, and Table 2 presents the results obtained for biochar from miscanthus tuples correlated with those in the literature.

**Table 1**

**Properties of biochar obtained from sunflower stems**

| Results achieved | | | Literature results | | | |
|---|---|---|---|---|---|---|
| **Parameter** | **Temperature used** | **Typical range** | **Typical range** | **Observations** | **Recommended Application** | **References** |
| **pH** | 250-450 ºC | 9.11-10.41 | 9–10 | Strong Basic | pH correction, K/Ca intake | *Adeniyi et al., 2024; Chang et al., 2025* |
| **Total carbon (%)** | 250-450 ºC | 40.21-57.87 | 75–85 | High carbon content, high stability | Soil stabilization, carbon sequestration | *Adeniyi et al., 2024; de Souza et al. 2020* |
| **Ash (%)** | 250-450 ºC | 5.83-28.80 | 10–25 | Rich in K, Ca, Mg | Fertilization of acidic soils | *Chang et al., 2025; Wystalska et al., 2018* |
| **Density (g/cm³)** | 250-450 ºC | 0.120-0.200 | 0.250–0.450 | Decreases with temperature; influences porosity | Soil aeration, structure | *Angın, 2013; Novak et al., 2009* |
| **Humidity (%)** | 250-450 ºC | 3.78-8.98 | 3–8 | Decreases with temperature; Improves ease of processing and application | Soil stabilization | *Chen et al., 2014; Adeniyi et al., 2024* |

**Table 2**

**Properties of biochar obtained from miscanthus strains**

| Results achieved | | | Literature results | | | |
|---|---|---|---|---|---|---|
| **Parameter** | **Temperature used** | **Typical range** | **Typical range** | **Observations** | **Recommended Application** | **References** |
| **pH** | 250-450 ºC | 5.55-10.61 | 7.6–10.40 | Basic, increases with temperature | Acid Soils Amendment | *Klemencova et al., 2022; Budai et al., 2014* |
| **Total carbon (%)** | 250-450 ºC | 47.65-85.07 | 70–80 | Low H/C ratio → stable biochar | Carbon Sequestration | *Budai et al., 2014; Qian et al., 2015* |
| **Ash (%)** | 250-450 ºC | 1.39-6.34 | 3–10 | Low mineral content | Mineral intake | *Klemencova et al., 2022; Pidlisnyuk et* |

| Results achieved | | | Literature results | | | |
|---|---|---|---|---|---|---|
| Parameter | Temperature used | Typical range | Typical range | Observations | Recommended Application | References |
| | | | | | | *al., 2025; Budai et al. 2014; Lakshman et al. 2014* |
| **Density (g/cm³)** | 250-450 ºC | 0.112-0.164 | 0.200–0.350 | Decreases with temperature; influences porosity | Soil aeration | *Angın, 2013; Novak et al., 2009* |
| **Humidity (%)** | 250-450 ºC | 1.75-7.25 | 2–6 | Decreases with temperature; Improves ease of processing and application | Soil stabilization | *Chen et al., 2014; Novak et al., 2009* |

For a better comparison of the results obtained with those found in the literature, figures 3 and 4 show an average of the typical ranges.

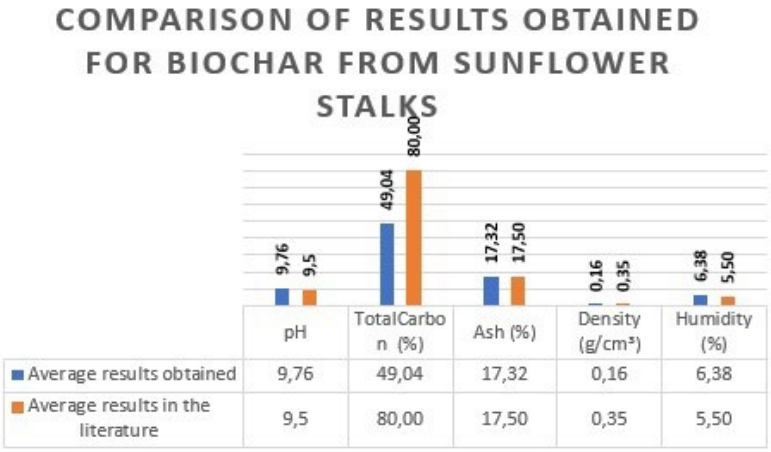



**Fig. 3 - Comparison of results obtained for biochar from sunflower stems**

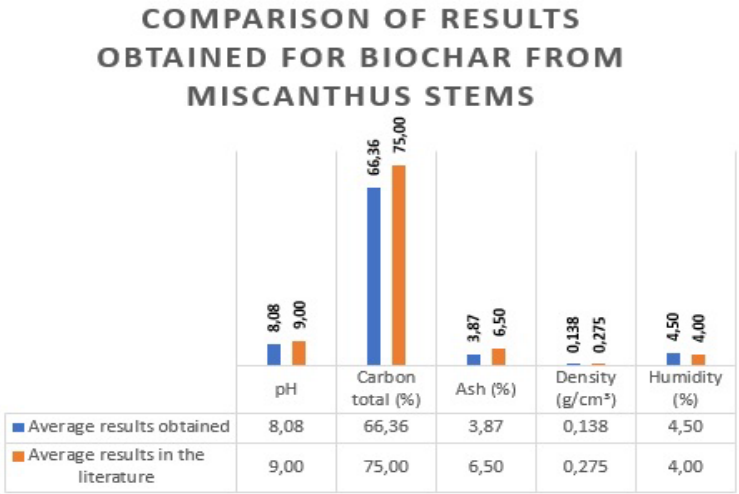



**Fig. 4 - Comparison of results obtained for biochar from miscanthus stems**

## CONCLUSIONS

It is known that the quality and properties of biochar are closely correlated with the type of raw material used and the parameters of the process applied. Each variety of biomass has distinct particularities and process conditions, these aspects must be adjusted for each category.

*Biochar moisture* from the sunflower strains ranged from 3.78% to 8.43%, while the biochar from the miscanthus strains had a humidity between 2.98% and 7.61%.

*Biochar density* was between 0.120 g/cm³ and 0.200 g/cm$^3$ for sunflowers, and for miscanthus it ranged between 0.9 g/cm$^3$ and 164 g/cm$^3$.

*Ash content* demonstrated considerable fluctuations between the two types of subjects:

- the sunflower biochar had an ash content that varied between 5.83% and 28.80%, the highest value being recorded for the sample performed at 400°C for 60 minutes at a value;

- Miscanthus biochar indicated an ash content ranging from 0.88% to 6.34, the highest ratio being obtained at a temperature of 450°C for 30 minutes at a size of 15 cm;

- the lowest ash concentration values for the two types of biochar were observed at the lowest temperature, namely 250°C.

As for the needles *Carbon content* the biochar obtained from miscanthus strains had a content much higher than that obtained from sunflower strains.

The results obtained were compared with those in the literature, and the values were similar, which proves that both varieties of biochar are good to be used as soil amendments both for soil fertilization and stability, pH correction and carbon sequestration.

## ACKNOWLEDGMENT

This paper was supported: by one funding source the NUCLEU Programme, carried out with the support of ANCSI, Project 9N/ 01.01.2023 "Technology for the valuation of vegetable residues in the form of biochar for the improvement of soil quality" and NUCLEU Program, through Project 9N/ 23 04 02 01, "Innovative technology for the production of biofertilizers to restore soil biodiversity and reduce the effects of drought on agricultural land".

## REFERENCES

[1] Vanisree GS, Chandran AM, Aparna K (2024). Investigation on thermochemical characteristics and pyrolysis kinetics of lignocellulosic biomass for biofuel production feasibility. Biomass Convers Biorefiney 12(22) pp. 28667-28685. https://doi.org/10.1007/s13399-024-05657-4;

[2] Ahmad Bhat, S., Kuriqi, A., Dar, M. U. D., Bhat, O., Sammen, S. S., Towfiqul Islam, A. R. M., Elbeltagi, A., Shah, O., A. I. Ansari, N., Ali, R., & Heddam, S. (2022). Application of Biochar for Improving Physical, Chemical, and Hydrological Soil Properties: A Systematic Review. Sustainability, 14(17), 11104. https://doi.org/10.3390/su141711104;

[3] Waheed, A., Xu, H., Qiao X., Aili, A., Yiremaikebayi, Y., Haitao, D. Muhammad, M., (2025). Biochar in sustainable agriculture and Climate Mitigation: Mechanisms, challenges, and applications in the circular bioeconomy, Biomass and Bioenergy, Volume 193, https://doi.org/10.1016/j.biombioe.2024.107531;

[4] Bousdra, T., Papadimou, S. G., & Goliath, E. E. (2023). The Use of biochar in the Remediation of Pb, Cd, and Cu-Contaminated Soils. The Impact of biochar Feedstock and Preparation Conditions on Its Remediation Capacity. Land, 12(2), 383. https://doi.org/10.3390/land12020383;

[5] Hussein Fadil and Alaa Hasan Fahmi, (2024). Biochar Enhanced Chemical and Biological Properties of Contaminated Soils with Lead, IOP Conf. Series: Earth and Environmental Science 1259, 012024 IOP Publishing. https://10.1088/1755-1315/1259/1/012024;

[6] Ji, M., Wang, X., Usman, M., Liu, F., Dan, Y., Zhou, L., Campanaro, S., Luo, G., Sang, W., (2022). The effects of different biochar-based raw materials on soil remediation: a review. Environment. Pollute. 294, 118655 https://doi.org/10.1016/j.envpol.2021.118655;

[7] Osman, A.I., Farghali, M., Dong, Y. et al. (2024). Reducing the carbon footprint of buildings using biochar-based bricks and insulating materials: a review. Environ Chem Lett 22, 71–104. https://doi.org/10.1007/s10311-023-01662-7;

[8] Lehmann and Stephen (2009) Biochar for Environmental Management Science, Technology and Implementation, first edition, Earthscan, 2009, ISBN1849770557, 9781849770552;
[9] Upadhyay, V., Choudhary, K.K. & Agrawal, S.B. (2024). Use of biochar as a sustainable agronomic tool, its limitations and impact on environment: a review. Discov Agric 2:20. https://doi.org/10.1007/s44279-024-00033-2;
[10] Amalina F., et al. (2022). A comprehensive assessment of the method for producing biochar, its characterization, stability, and potential applications in regenerative economic sustainability – A review, Cleaner Materials, Volume 3, https://doi.org/10.1016/j.clema.2022.100045;
[11] Wani, A.W. et al. (2025). Physical and Chemical Properties of Biochar. In: Roy, A., Bhat, R.A., Dar, G.H. (eds) Biochar Production Engineering. Springer, Cham. https://doi.org/10.1007/978-3-031-92594-8_2;
[12] Lingamdinne, L.P., Angaru, G.K.R., Pal, C.A. et al. (2024). Insights into kinetics, thermodynamics, and mechanisms of chemically activated sunflower stem biochar for removal of phenol and bisphenol-A from wastewater. Sci Rep 14, 4267. https://doi.org/10.1038/s41598-024-54907-y;
[13] Zhao, Y., Shi, H., Tang, X., Kuang, D., Zhou, J., & Yang, F. (2022) Performance and Mechanism of As(III/V) Removal from Aqueous Solution by Fe3O4-Sunflower Straw Biochar. Toxics, 10(9), 534. https://doi.org/10.3390/toxics10090534;
[14] Kavitha, B., Reddy, P.V.L., Kim, B., Lee, S.S., Pandey, S.K., Kim, K.-H. (2018). Benefits and limitations of biochar amendment in agricultural soils: a review. J. Approx. Manager. 227, 146–154. https://doi.org/10.1016/j.jenvman.2018.08.082;
[15] Shaaban, M., Van Zwieten, L., Bashir, S., Younas, A., Núnez-Delgado,˜ A., Chhajro, M.A., Kubar, K.A., Ali, U., Rana, M.S., Mehmood, M.A., Hu, R., (2018). A concise review of biochar application to agricultural soils to improve soil conditions and fight pollution. J. Approx. Manager. 228, 429–440. https://doi.org/10.1016/j.jenvman.2018.09.006;
[16] Janus A, Pelfrêne A, Heymans S, Deboffe C, Douay F, Waterlot C (2015) Elaboration, characteristics and advantages of biochars for the management of contaminated soils with a specific overview on Miscanthus biochars. J Environ Manag 162:275–289. https://doi.org/10.1016/j.jenvman.2015.07.056;
[17] Nsanganwimana F, Pourrut B, Mench M, Douay F (2014) Suitability of Miscanthus species for managing inorganic and organic contaminated land and restoring ecosystem services. A review. J Circa Manag 143:123–134. https://doi.org/10.1016/j.jenvman.2014.04.027;
[18] Adeniyi, A. G., Micheal, T. T., Emenike, E. C., Abd-Elkader, O. H., et al. (2024). Production and characterization of sunflower stalk biochar and ash: A study on batch versus semi-batch gasifier systems. International Journal of Chemical Reactor Engineering. https://doi.org/10.1515/ijcre-2024-0248;
[19] Chang, S., Wang, L., & Yao, L. (2025). Properties of sunflower straw biochar activated using potassium hydroxide. Molecules, 30(6), 1332. https://doi.org/10.3390/molecules30061332;
[20] Wystalska, K., Malińska, K., Włodarczyk, R., & Chajczyk, O. (2018). Effects of pyrolysis parameters on the yield and properties of biochar from pelletized sunflower husk. E3S Web of Conferences, 100, 00043. https://doi.org/10.1051/e3sconf/20184400197;
[21] de Souza, J.B.; Michelin, M.; Amâncio, F.L.R.; Vital Brazil, O.A.; Polizeli, M.d.L.T.M.; Ruzene, D.S.; Silva, D.P.; Mendonça, M.D.C.; López, J.A. Sunflower stalk as a carbon source inductive for fungal xylanase production. Ind. Crops Prod. 2020, 153, 112368. https://10.1016/j.indcrop.2020.112368;
[22] Budai, A., Wang, L., Grønli, M., Strand, L. T., Antal, M. J., et al. (2014). Surface properties and chemical composition of corncob and miscanthus biochars: Effects of production temperature and method. Journal of Agricultural and Food Chemistry, 62(17), 3791–3799. https://doi.org/10.1021/jf501139f;
[23] Klemencova, K., Grycova, B., & Lestinsky, P. (2022). Influence of Miscanthus rhizome pyrolysis operating conditions on products properties. Sustainability, 14(10), 6193. https://doi.org/10.3390/su14106193;
[24] Lakshman, V.; Brassard, P.; Hamelin, L.; Raghavan, V.; Godbout, S. Pyrolysis of Miscanthus: Developing the mass balance of a biorefinery through experimental tests in an auger reactor. Bioresour. Technol. Rep. 2021, 14, 100687. https://doi.org/10.1016/j.biteb.2021.100687;
[25] Pidlisnyuk, V. V., Stefanovska, T. R., Borysenko, L. I., Klius, V. P., et al. (2025). Influence of the initial biomass state and pyrolysis conditions on the properties of biochar produced from Miscanthus ×

giganteus waste. Chemistry, Physics and Technology of Surface, 16(3), 385–397. https://doi.org/10.15407/hftp16.03.385;
[26] *SR EN 21660-3:2021 – Determination of moisture content using oven;*
[27] ***SR EN ISO 18122:2016 – Determination of ash content;*
[28] *SR ISO 10694/ 1998 - Determination of total nitrogen and total carbon contents from soil, plant and residual product samples;*
[29] ICPA Methodology (1983), Chapter 3, PT 126

# BIOCHAR VERSUS HYDROCHAR FOR AGRICULTURAL BIOMASS VALORIZATION: A COMPARATIVE REVIEW OF PRODUCTION, PROPERTIES, APPLICATIONS AND SUSTAINABILITY

/

# *BIOCHAR VERSUS HYDROCHAR PENTRU VALORIFICAREA BIOMASEI AGRICOLE: ANALIZĂ COMPARATIVĂ A PRODUCȚIEI, PROPRIETĂȚILOR, APLICAȚIILOR ȘI SUSTENABILITĂȚII*

**Stefano-Andrea MANTOVANI*[1)], Alin-Nicolae HARABAGIU[1)], Dragos-Nicolae DUMITRU[1)], Aura-Maria DUMITRESCU[1)], Vasilica ȘTEFAN[1)], Ana ZAICA[1)], Alexandru IONESCU[1)], Daniel NIJLOVEANU[2)]**

[1)] National Institute of Research-Development for Machines and Installations Designed to Agriculture and Food Industry - INMA Bucharest / Romania;

[2)] USAMV Bucharest, Faculty of Management and Rural Development, Slatina Branch, Olt County / Romania.

**Tel.: (+40) 723 814 202; *E-mail: stefanoandreamantovani@gmail.com*

***Keywords:*** *biochar, hydrochar, pyrolysis, hydrothermal carbonization, agricultural biomass, sustainability*

## ABSTRACT

*Agricultural biomass residues represent an important renewable resource whose valorization can contribute to waste reduction, soil improvement, pollutant removal and carbon management. This review compared biochar produced by pyrolysis with hydrochar obtained through hydrothermal carbonization, considering production requirements, physicochemical characteristics, agricultural and environmental applications, carbon stability and techno-economic aspects. A critical assessment of 51 peer-reviewed studies was performed to identify the principal advantages, limitations and application-dependent differences between the two carbonaceous materials. The reviewed literature showed that biochar generally exhibited a higher degree of carbonization, greater aromaticity and stronger long-term carbon stability, supporting its use for soil amendment and carbon sequestration. Hydrochar retained more oxygen-containing surface functionalities and presented an important processing advantage for high-moisture biomass because hydrothermal carbonization avoided extensive feedstock pre-drying. Agricultural responses to hydrochar were more variable and depended strongly on feedstock, process conditions, application rate and post-treatment. Both materials showed considerable potential for contaminant adsorption and wastewater treatment, although performance depended on pollutant chemistry and surface properties. Overall, no universally superior pathway was identified; the optimal carbonization process depended on feedstock characteristics, intended application and system-level environmental and energetic constraints.*

## REZUMAT

*Reziduurile de biomasă agricolă reprezintă o resursă regenerabilă importantă, a cărei valorificare poate contribui la reducerea cantității de deșeuri, îmbunătățirea proprietăților solului, îndepărtarea poluanților și gestionarea carbonului. În cadrul acestui articol de sinteză a fost realizată o analiză comparativă între biocharul obținut prin piroliză și hydrocharul produs prin carbonizare hidrotermală, luând în considerare cerințele proceselor de producție, caracteristicile fizico-chimice, aplicațiile agricole și de mediu, stabilitatea carbonului și aspectele tehnico-economice. Au fost analizate critic 51 de studii științifice pentru identificarea principalelor avantaje, limitări și diferențe dintre cele două materiale carbonice. Literatura analizată a evidențiat faptul că biocharul prezintă, în general, un grad mai ridicat de carbonizare, o aromaticitate mai mare și o stabilitate superioară a carbonului pe termen lung, favorizând utilizarea sa pentru ameliorarea solului și sechestrarea carbonului. Hydrocharul păstrează mai multe grupări funcționale oxigenate și prezintă un avantaj important pentru procesarea biomasei cu umiditate ridicată, prin evitarea uscării intensive înainte de carbonizare. În ansamblu, nu a fost identificată o tehnologie universal superioară, alegerea optimă depinzând de caracteristicile materiei prime, aplicația urmărită și constrângerile energetice și de mediu ale sistemului.*

## INTRODUCTION

Agricultural production and the associated food-processing sector generate substantial quantities of lignocellulosic residues, including crop stalks, straw, pruning residues, husks, shells and other biomass by-

products. Although these materials contain considerable amounts of renewable carbon and nutrients, their inappropriate management may lead to inefficient resource use and additional environmental burdens.

Consequently, the conversion of agricultural residues into value-added products has received increasing attention within the framework of circular economy and sustainable biomass management. Thermochemical conversion represents an important valorization pathway because it can transform heterogeneous biomass residues into energy carriers and carbon-rich solid materials with potential agricultural and environmental applications *(Cavali et al., 2023; Escudero-Curiel et al., 2023)*.

Among the available thermochemical technologies, pyrolysis and hydrothermal carbonization (HTC) have attracted particular interest because both processes produce carbonaceous solids that can be further used for soil improvement, carbon management and environmental remediation. Nevertheless, the two technologies differ substantially with respect to reaction environment, operating conditions, feedstock requirements and the physicochemical properties of the resulting materials *(Kambo and Dutta, 2015; Kumar et al., 2020; Libra et al., 2011)*.

These differences are particularly relevant when agricultural residues are considered, since biomass originating from agricultural and agro-industrial activities can vary considerably in moisture content, chemical composition and structural characteristics. Recent comparative syntheses have reinforced this process-property relationship: Cognigni et al., (2025) distinguished the two materials through their thermochemical routes, physicochemical characteristics, characterization approaches and application domains, while Buentello-Montoya et al., (2026) emphasized the importance of feedstock moisture, soil-amendment performance and hydrochar upgrading when agro-wastes are considered.

Biochar is generally obtained through the thermochemical decomposition of biomass under oxygen-limited conditions, most commonly by slow pyrolysis. The conversion temperature, residence time, heating rate and feedstock characteristics strongly influence the yield and final properties of the resulting material. Increasing pyrolysis severity generally promotes carbonization and the development of a more condensed carbon structure, while simultaneously modifying surface functionality, porosity, nutrient availability and carbon stability *(Crombie et al., 2013; Dieguez-Alonso et al., 2018; Ronsse et al., 2013)*.

Due to its relatively stable carbon structure, biochar has been extensively investigated as a soil amendment and as a strategy for long-term carbon storage. Its application can influence soil physical properties, nutrient dynamics, microbial activity and plant productivity, although the magnitude and direction of these effects remain dependent on soil characteristics, feedstock type, production conditions and application rate *(Joseph et al., 2021; Schmidt et al., 2021)*. The persistence of a significant fraction of biochar carbon in soils has also resulted in considerable interest in its potential contribution to climate-change mitigation *(Lehmann et al., 2021; Woolf et al., 2010)*.

Hydrochar is produced through HTC, during which biomass is treated in liquid water at elevated temperature and autogenous pressure. In contrast to conventional pyrolysis, HTC does not require the feedstock to be extensively dried before processing, making the technology particularly attractive for biomass with a naturally high moisture content *(Funke and Ziegler, 2010; Hoekman et al., 2011; Libra et al., 2011)*. During hydrothermal treatment, reactions such as hydrolysis, dehydration, decarboxylation, condensation and polymerization progressively modify the original biomass structure and produce a carbon-enriched solid material.

The resulting hydrochar generally retains a comparatively high abundance of oxygen-containing functional groups, which can be advantageous for certain adsorption and environmental-remediation applications *(Khan et al., 2019; Masoumi et al., 2021)*. At the same time, hydrochar characteristics and suitability for direct agricultural application can vary considerably depending on the feedstock and HTC conditions, and several studies have indicated that post-treatment may be necessary to reduce potentially phytotoxic compounds before soil application *(Busch et al., 2013; Luutu et al., 2022)*.

The different chemical structures of biochar and hydrochar result in different functional properties and therefore different potential fields of application. Biochar has accumulated a comparatively extensive body of evidence regarding soil amendment, crop productivity, nutrient retention and carbon sequestration *(Biederman and Harpole, 2013; Jeffery et al., 2011; Purakayastha et al., 2019)*. Hydrochar has increasingly been investigated for soil applications, adsorption and wastewater treatment, with particular interest in its surface functional groups and its compatibility with wet biomass feedstocks *(Azzaz et al., 2020; Khosravi et al., 2022)*. Both materials have also demonstrated potential for the removal or immobilization of heavy metals and organic contaminants, although adsorption mechanisms and efficiencies vary according to feedstock, production conditions, surface chemistry and the characteristics of the target pollutant *(Chen et al., 2021;*

*Tan et al., 2015)*. A comparison based only on the properties of the final carbonaceous product is therefore insufficient for selecting an appropriate conversion route. Feedstock moisture, energy required for drying and processing, carbon stability, process-water management, environmental impacts, technological maturity and production costs must also be considered. This is especially important for agricultural biomass, where the initial moisture content can substantially affect the energetic and economic suitability of pyrolysis or HTC *(Hitzl et al., 2015; Kumar et al., 2020; Lucian and Fiori, 2017)*.

Life-cycle considerations further indicate that the environmental performance of both pathways depends strongly on feedstock characteristics, system boundaries, energy integration and the intended use of the resulting carbon material *(Li et al., 2022; Roberts et al., 2010)*.

Therefore, the objective of this review was to critically compare biochar produced through pyrolysis and hydrochar obtained through hydrothermal carbonization, with particular emphasis on agricultural biomass valorization.

The analysis considered production requirements, physicochemical characteristics, agricultural and environmental applications, carbon stability, energy demand and techno-economic aspects.

Rather than identifying a universally superior carbonaceous material, the review aimed to determine the conditions under which each conversion pathway can provide specific advantages and to highlight the principal factors that should guide the selection of an appropriate biomass carbonization technology.

## MATERIALS AND METHODS

The present study was conducted as a structured narrative review aimed at comparing biochar produced through pyrolysis with hydrochar obtained through hydrothermal carbonization (HTC), with particular emphasis on the valorization of agricultural and agro-industrial biomass. The review was designed to integrate information concerning conversion conditions, physicochemical characteristics, agricultural performance, environmental applications, carbon stability and techno-economic and environmental aspects. Particular attention was given to studies in which biochar and hydrochar were directly compared or in which sufficiently detailed quantitative data were reported to allow comparison between the two conversion pathways.

The selected papers were identified through established scientific journal and publisher platforms, including Elsevier/ScienceDirect, SpringerLink, Wiley Online Library, ACS Publications, Royal Society of Chemistry, MDPI and Nature Portfolio. Search terms combined the principal concepts addressed in the review: biochar, hydrochar, pyrolysis, hydrothermal carbonization, agricultural biomass, soil amendment, crop productivity, carbon sequestration, adsorption, heavy metals, wastewater treatment, life-cycle assessment and techno-economic analysis. Additional publications were identified from the reference lists of relevant comparative and review articles.

Priority was given to recent publications, while older studies were retained when they represented fundamental contributions to pyrolysis, HTC, biochar stability, agricultural response or carbon sequestration. The evidence base included original experimental studies, comparative studies, meta-analyses and reviews addressing production, physicochemical properties, agricultural applications, environmental remediation, or energy, life-cycle, economic and scale-up considerations.

Following the literature search, duplicate records were removed and the remaining publications were assessed for relevance to the objectives of the review. Studies were excluded when they did not directly address biochar or hydrochar production and properties, fell outside the scope of agricultural biomass valorization, provided insufficient information for the comparative analysis, or substantially overlapped with evidence already represented by more comprehensive publications. Particular emphasis was placed on peer-reviewed experimental and comparative studies providing quantitative or mechanistic information. Following screening and bibliographic verification, 51 peer-reviewed publications were retained for the final analysis.

Each retained publication was individually checked for authorship, publication year, article title, journal, volume and issue where applicable, page range or article number, and DOI. The reference list was then arranged alphabetically according to the APA citation system required by the symposium, and each publication was confirmed to contribute information to at least one section of the review.

For comparative analysis, information extracted from the selected publications was classified into production-related, physicochemical, agricultural, environmental and techno-economic groups. Production-related parameters included conversion technology, process temperature, pressure, residence time, feedstock characteristics, feedstock moisture requirements, need for pre-drying and solid-product yield.

Physicochemical parameters included elemental composition, carbon content, atomic H/C and O/C ratios, pH, specific surface area, pore characteristics, surface functional groups, nutrient content and indicators of carbon stability. Agricultural studies were evaluated according to reported changes in soil physical properties, soil chemical characteristics, nutrient dynamics, water retention, microbial activity, germination, plant biomass, crop productivity and carbon sequestration. Environmental studies were classified according to contaminant type and the reported adsorption, immobilization or removal mechanisms. The techno-economic and environmental comparison considered feedstock moisture, energy required for feedstock preparation and conversion, process-water generation, energy recovery, greenhouse-gas implications, life-cycle assessment results, production costs and technological scalability when these parameters were explicitly discussed in the selected publications.

Because system boundaries, feedstocks and operating assumptions differed considerably among life-cycle and economic studies, results from different publications were interpreted within their original methodological context rather than combined into a single numerical indicator. Quantitative values were extracted only when explicitly reported in the selected literature. Results obtained under substantially different experimental conditions were not statistically pooled. This was particularly important for agricultural studies, where crop yield, seed germination, shoot biomass and germination indices represent different biological endpoints and cannot be considered directly equivalent. Direct biochar-hydrochar comparisons performed within the same experimental study were given particular importance because they reduced differences associated with feedstock, analytical procedures and experimental conditions.

The extracted information was subsequently organized into four comparative tables addressing production and physicochemical characteristics, agricultural applications, environmental-remediation performance, and integrated technological and sustainability criteria. Three graphical representations were prepared from numerical information reported in the selected literature. Figure 1 relates process temperature to atomic H/C ratio while encoding O/C ratio through marker area; Figure 2 is a Van Krevelen diagram based on atomic H/C and O/C ratios; and Figure 3 presents selected literature-reported agricultural responses using their original biological endpoints. No numerical value used in these graphical comparisons was estimated when it was not available in the source literature.

## RESULTS

The analysis of the selected literature showed that biochar and hydrochar should not be regarded as interchangeable carbonaceous materials, even though both originate from the thermochemical conversion of biomass. Their different production environments determine the degree of carbonization, elemental composition, surface chemistry, pore structure and stability of the resulting solids, and these characteristics subsequently influence their suitability for agricultural and environmental applications.

Across the reviewed studies, the relative advantages of the two materials were therefore controlled not only by the conversion technology itself, but also by feedstock composition, moisture content, process severity, post-treatment and intended use *(Kambo and Dutta, 2015; Kumar et al., 2020; Cavali et al., 2023; Cognigni et al., 2025)*.

The first major distinction arises during production. Slow pyrolysis generally converts relatively dry biomass under oxygen-limited or inert conditions and produces biochar together with condensable compounds and permanent gases. Hydrothermal carbonization, in contrast, takes place in liquid water at elevated temperature and autogenous pressure and produces hydrochar together with an aqueous process phase and a smaller gaseous fraction *(Funke and Ziegler, 2010; Hoekman et al., 2011; Libra et al., 2011)*. These differences are important for agricultural residues because such materials cover a wide range of physical states, from comparatively dry straw and pruning residues to wet digestates, slurries and freshly generated agro-industrial wastes.

During pyrolysis, increasing temperature generally promotes devolatilization, carbon enrichment and structural condensation. Consequently, both char yield and material properties depend strongly on the selected operating conditions. Ronsse et al. (2013) demonstrated that feedstock type and pyrolysis conditions significantly influence the resulting biochar, while Crombie et al. (2013) showed that process severity affects several indicators of carbon stability.

The preferred pyrolysis conditions should therefore be selected according to the desired application rather than solely to maximize solid yield. A biochar intended for long-term carbon storage, for example, may require a greater degree of carbonization than one primarily intended to supply mineral nutrients or provide reactive surface sites.

Hydrothermal carbonization follows a different conversion mechanism because liquid water actively participates in the transformation of the biomass. Hydrolysis, dehydration, decarboxylation, condensation and polymerization reactions progressively alter the structure of lignocellulosic feedstocks and redistribute part of the organic and inorganic material between the solid hydrochar and process water *(Funke and Ziegler, 2010; Khan et al., 2019)*. As a result, hydrochar generally exhibits a lower degree of carbonization than material produced at high pyrolysis temperatures, while retaining a larger proportion of oxygen-containing surface functionalities. Reviews by Masoumi et al. (2021) and Cavali et al. (2023) further show that this aqueous conversion route must be considered together with the management and possible valorization of the process-water phase. The most obvious technological advantage of HTC is its compatibility with high-moisture feedstocks. Conventional thermochemical treatment of wet biomass by pyrolysis normally requires an initial drying stage, whereas HTC can use the water contained in the material as part of the reaction medium. This characteristic makes hydrothermal processing particularly attractive for wet agricultural and agro-industrial residues *(Hitzl et al., 2015; Kambo and Dutta, 2015; Ischia and Fiori, 2021; Buentello-Montoya et al., 2026)*. Nevertheless, avoidance of pre-drying does not mean that HTC is intrinsically a low-energy process.

Heating the biomass-water mixture, maintaining elevated pressure, separating the solid product and subsequently treating or valorizing the process water all contribute to the energy and economic balance *(Lucian and Fiori, 2017)*. Pyrolysis, on the other hand, can recover part of its process-energy demand through utilization of gases and condensable fractions, although this advantage is reduced when the starting material contains large quantities of water *(Gaunt and Lehmann, 2008; Roberts et al., 2010)*. These trends are visible in Fig. 1, which relates process temperature to the atomic H/C ratio for literature-derived biochar and hydrochar samples. Hydrochars are concentrated within the lower-temperature region, whereas slow-pyrolysis biochars extend over a substantially wider and higher temperature range. The general decline in H/C ratio with increasing process severity reflects progressive removal of hydrogen-containing compounds and development of a more carbonized material. The dispersion of the individual points also demonstrates that temperature alone cannot explain the final composition, because feedstock characteristics and other operating parameters remain important.

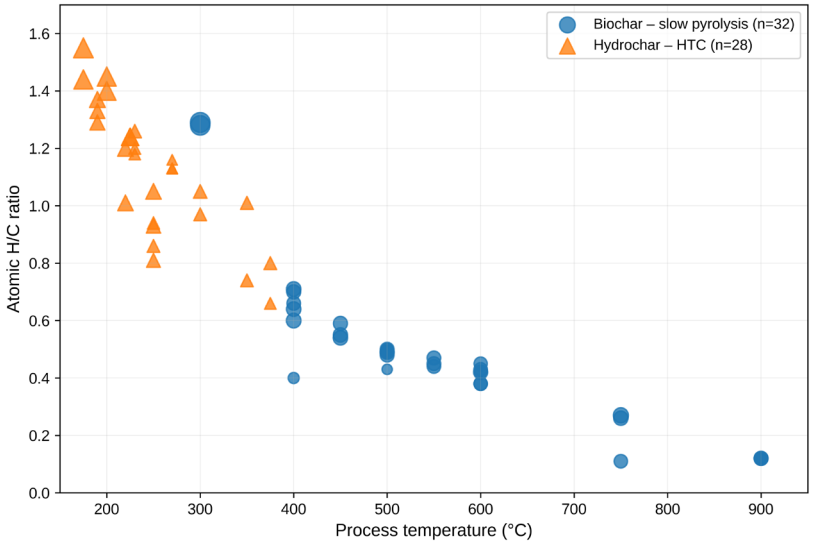



**Fig. 1 - Relationship between process temperature and atomic H/C ratio for slow-pyrolysis biochars and HTC hydrochars; marker area represents atomic O/C ratio. Data derived from Kambo and Dutta (2015).**

**Table 1**

**Comparative production conditions and physicochemical characteristics of biochar and hydrochar**

| Criterion | Biochar / pyrolysis | Hydrochar / HTC |
|---|---|---|
| Reaction environment | Oxygen-limited or inert atmosphere | Liquid water at elevated temperature and autogenous pressure |
| Feedstock condition | More favorable for relatively dry biomass | Particularly suitable for wet biomass |
| Pre-drying | Often required for wet biomass | Extensive pre-drying generally avoided |

| Criterion | Biochar / pyrolysis | Hydrochar / HTC |
|---|---|---|
| Process temperature | Generally higher | Generally lower |
| Pressure requirement | Generally low | Elevated |
| Secondary streams | Condensable liquids and gases | Process water and gases |
| Degree of carbonization | Generally greater at high severity | Usually lower under conventional HTC |
| O-containing groups | Decline with increasing severity | Frequently retained at higher abundance |
| Microporosity | Can become highly developed | Commonly lower without activation |
| Mineral retention | Minerals tend to remain in solid ash | Soluble fractions may migrate to process water |
| Carbon stability | Generally higher for strongly pyrolyzed material | More variable |
| Wet-feedstock suitability | Limited without drying integration | High |

The different process conditions were reflected particularly clearly in elemental composition. The atomic H/C and O/C ratios decreased progressively as biomass underwent more severe carbonization, making these parameters useful indicators of the transformation of the original organic structure. In the dataset used for the present comparison, the slow-pyrolysis biochars showed H/C values extending from approximately 0.11 to 1.29 and O/C values from approximately 0.08 to 0.57, while hydrochars extended approximately from 0.66 to 1.55 for H/C and from 0.09 to 0.67 for O/C. These ranges should not be interpreted as universal limits, because the individual samples originated from different feedstocks and operating conditions.

The Van Krevelen representation in Fig. 2 illustrates these differences more clearly. Most hydrochars remained within the region characterized by comparatively higher H/C and O/C ratios, whereas highly carbonized biochars occupied the lower part of the diagram. The overlap between the two populations is nevertheless important, since it confirms that neither term describes a chemically uniform material.

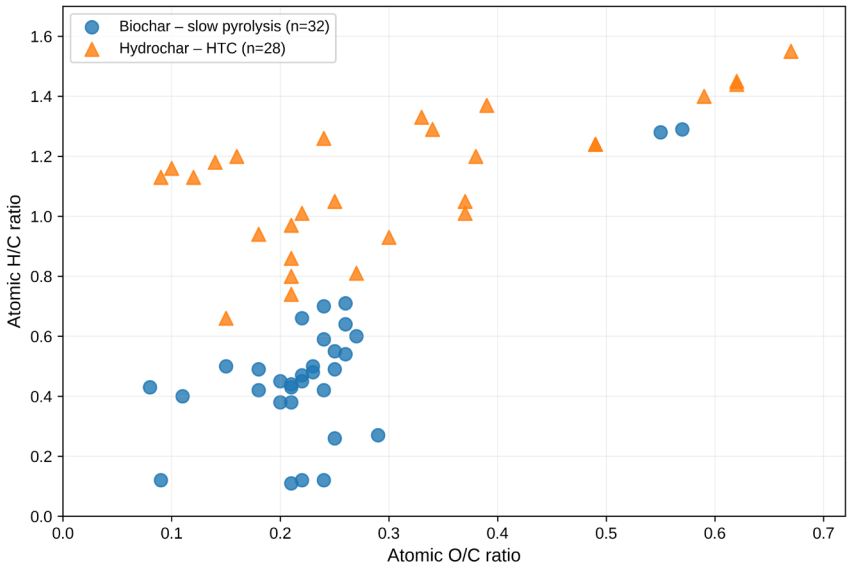



**Fig. 2 - Van Krevelen representation of literature-derived biochar and hydrochar samples based on atomic H/C and O/C ratios. Data derived from Kambo and Dutta (2015).**

The lower H/C ratios observed for strongly pyrolyzed materials are consistent with the development of increasingly condensed aromatic structures and greater resistance to degradation. Crombie et al. (2013) demonstrated that pyrolysis conditions significantly affected biochar stability, while Naisse et al. (2015) showed that biochar and hydrochar differed in their response to physical weathering and consequently in their carbon-sequestration potential. Lehmann et al. (2021) further identified persistence of pyrolyzed carbon as one of the principal mechanisms through which biochar can contribute to climate-change mitigation.

Hydrochar presents a different balance between stability and chemical reactivity. Because conventional HTC operates at lower thermal severity, a greater proportion of hydroxyl, carboxyl, carbonyl and other oxygen-containing groups may remain at the surface. These groups can participate in ion exchange, surface complexation, hydrogen bonding and redox reactions, which can be advantageous in environmental-remediation applications *(Titirici et al., 2012; Dieguez-Alonso et al., 2018; Khosravi et al., 2022)*. At the same time, preservation of a larger fraction of labile organic compounds can reduce carbon stability and, in some cases, contribute to phytotoxic effects when fresh hydrochar is directly applied to soil. This reactivity can also affect soil biogeochemistry; Yuan et al. (2024) reported stronger mitigation of denitrification-derived N2O by hydrochar than by pyrochar under the investigated conditions.

Porosity and specific surface area reveal a similar trade-off. Increasing pyrolysis severity frequently produces a more developed pore structure as volatile compounds are released from the biomass matrix. Hydrochar often exhibits lower conventional BET surface area without subsequent activation, but this does not necessarily correspond to inferior adsorption behavior. Chen et al. (2021), for example, directly compared hydrochar and pyrochar for Cr(VI) removal and showed that the dominant mechanisms differed substantially between the two materials. The hydrochar benefited more strongly from reactive surface functionalities, whereas the pyrochar showed greater contribution from its microporous structure. Under simulated sunlight, hydrochar performance increased markedly, illustrating that chemically active surface groups can become more important than conventional surface area for some pollutants.

Feedstock composition further modifies these properties. Agricultural residues can contain substantially different amounts of P, K, Ca, Mg, Si and ash-forming constituents. Pyrolysis tends to concentrate nonvolatile mineral matter in the remaining solid, whereas HTC allows part of the soluble mineral fraction to migrate into the aqueous phase. The resulting pH, nutrient content and electrical characteristics therefore depend on both feedstock and conversion route. For this reason, the terms biochar and hydrochar should be regarded as broad material categories rather than as indicators of a fixed set of physicochemical properties. These material differences become particularly important when the chars are applied to soil. Biochar has been studied extensively as an amendment capable of modifying bulk density, porosity, aggregate structure, water retention and nutrient behavior. Blanco-Canqui (2017) concluded that biochar can improve several soil physical properties, although the magnitude of these effects depends strongly on soil texture, biochar characteristics and application rate. Improvements are frequently more pronounced in coarse-textured or degraded soils than in soils already possessing favorable physical characteristics.

Abel et al., (2013) are particularly relevant because both biochar and hydrochar were evaluated in sandy soils. Both materials altered water-related properties, but the magnitude of the effect differed among treatments. The results demonstrated that hydrochar can contribute to soil physical improvement, while simultaneously showing that its behavior cannot simply be assumed to be identical to that of biochar. Mau et al. (2020) similarly showed that poultry-litter hydrochar modified both physical and fertility-related characteristics of sandy soil, reinforcing the importance of feedstock composition. Bona et al. (2023) likewise found that hydrochar can function as a soil amendment, but its suitability remains dependent on feedstock and product characteristics. Chemical effects are equally dependent on the original material. Biochar can alter soil pH, nutrient availability and nutrient retention through a combination of direct mineral addition and surface interactions. Purakayastha et al. (2019) associated these changes with improvements in nutrient cycling and crop response, while Spokas et al. (2012) emphasized that agronomic performance varies substantially with char properties, soil and management. Joseph et al. (2021) further emphasized that biochar behavior evolves after incorporation into soil as its surfaces oxidize, adsorb minerals and become colonized by microorganisms.

Hydrochar can also contribute nutrients and organic carbon, particularly when produced from digestates or manure-based feedstocks. However, de Jager et al. (2020) and de Jager and Giani (2021) demonstrated that soil and plant responses varied considerably with application rate and soil type. This indicates that hydrochar cannot be assigned a universally appropriate agricultural application rate. A concentration beneficial in one soil may cause excessive nutrient loading, salinity or unfavorable biological effects in another. The broader crop-productivity literature currently favors biochar in terms of both volume and consistency of evidence. Jeffery et al. (2011) reported an average increase of approximately 10% in crop productivity following biochar addition, while Biederman and Harpole (2013) found overall positive effects on plant productivity and nutrient cycling. Schmidt et al. (2021), synthesizing 26 global biochar meta-analyses, similarly concluded that the agronomic evidence is generally favorable while remaining highly dependent on environmental and material conditions.

Hydrochar responses are more variable, particularly when fresh material is used. Luutu et al. (2022) reported negative mean responses for some plant-growth indicators, including germination and shoot biomass. These observations do not demonstrate an intrinsic agricultural inferiority of hydrochar but highlight the importance of soluble and potentially phytotoxic compounds retained after HTC. Busch et al. (2013) demonstrated this effect particularly clearly: fresh hydrochar produced severe germination inhibition under the tested conditions, whereas biological post-treatment substantially reduced the toxicity. Suarez et al. (2023) reached a similar conclusion by directly comparing fresh hydrochar, post-treated hydrochars and biochar produced from garden and park waste, showing that conditioning can substantially modify hydrochar behavior.

**Table 2**

**Comparative agricultural behavior of biochar and hydrochar**

| Agricultural parameter | Biochar | Hydrochar |
|---|---|---|
| Bulk density | Frequently decreases | Can decrease |
| Total porosity | Frequently increases | Can increase |
| Water retention | Often improved in coarse soils | Improvement also reported |
| Soil pH | Frequently increases for ash-rich chars | Feedstock dependent |
| Nutrient contribution | Can supply P, K, Ca and other nutrients | Can retain substantial nutrients |
| Nutrient retention | Frequently favorable | Potentially favorable |
| Crop productivity | Large, generally positive evidence base | More variable |
| Seed germination | Usually compatible at appropriate rates | Fresh hydrochar may inhibit |
| Microbial activity | Frequently altered | Can be positive or negative |
| Long-term carbon storage | Strong evidence | Less certain |
| Need for post-treatment | Case dependent | Often beneficial before soil use |

Biological responses reinforce the same interpretation. George et al. (2012) reported divergent effects of hydrochar on mycorrhiza, nodulation, plant growth and aggregation, while Taskin et al. (2019) observed changes in the growth and enzyme activity of soil-resident ligninolytic fungi following biochar and hydrochar addition. These findings demonstrate that a favorable change in one soil property does not automatically lead to improved biological performance. Figure 3 illustrates this variability using selected quantitative agricultural responses reported in the literature. Because the individual studies assessed different biological endpoints, the values are not combined into a common effect size.

Their purpose is instead to demonstrate that agricultural responses to carbonaceous amendments span both positive and negative directions and depend strongly on the way in which the material was produced and subsequently treated.

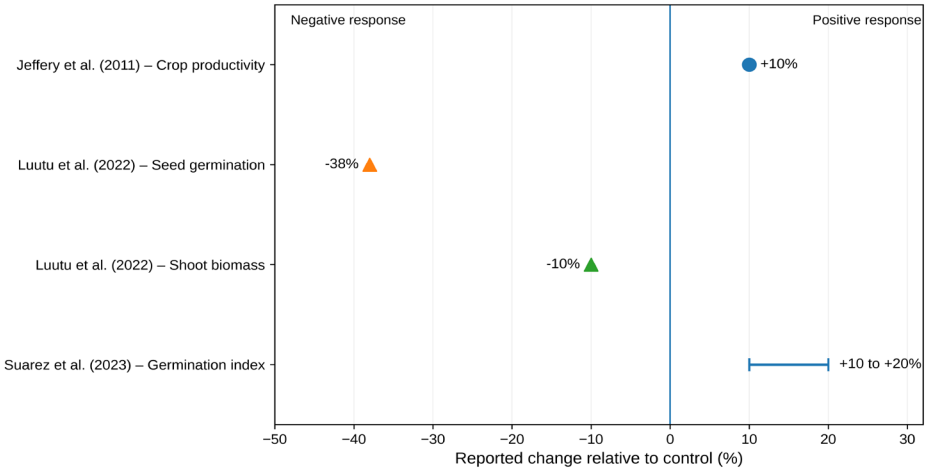



**Fig. 3 - Selected literature-reported agricultural responses to biochar and hydrochar relative to untreated controls; endpoints are shown as originally reported and are not interpreted as directly equivalent effect sizes** *(Jeffery et al., 2011; Luutu et al., 2022; Suarez et al., 2023).*

Long-term carbon storage remains one of the applications for which biochar has the clearest advantage. Woolf et al. (2010), Gaunt and Lehmann (2008) and Lehmann et al. (2021) demonstrated that conversion of sustainably sourced biomass into stable biochar can contribute to climate-change mitigation when the complete system is considered. Hydrochar can also retain carbon for longer than untreated biomass, but its generally less-condensed structure and greater fraction of labile compounds create greater uncertainty regarding long-term persistence *(Naisse et al., 2015)*.

The environmental-remediation literature presents a different picture, because neither material consistently outperforms the other. Biochar has been widely investigated for immobilization of metals and sorption of organic contaminants. Beesley et al. (2011) described its potential in remediation and restoration of contaminated soils, while Cao et al. (2009) demonstrated strong lead sorption by dairy-manure biochar as well as sorption of atrazine. Mineral precipitation, surface adsorption and changes in solution chemistry can all contribute to contaminant retention. Hydrochar can exploit different mechanisms. Its relatively abundant oxygen-containing surface groups can favor surface complexation and redox reactions, while hydrophobic fractions can contribute to sorption of organic contaminants. Han et al. (2016) reported substantial sorption of hydrophobic organic pollutants by hydrochar, showing again that conventional BET surface area alone is insufficient to predict adsorption performance.

Azzaz et al. (2020) and Ighalo et al. (2022) further demonstrated that raw and modified hydrochars can be applied to a broad range of wastewater contaminants. Modification can significantly improve both chars, although it also introduces additional energy, chemical consumption and cost. Hydrochar can be oxidized, thermally treated, impregnated with mineral phases or activated to enhance adsorption. Titirici et al. (2012) emphasized the possibility of engineering hydrothermal carbons with tailored surface properties, whereas Khosravi et al. (2022) showed that the environmental performance of hydrochar is highly sensitive to both HTC conditions and post-treatment.

**Table 3**

**Comparative environmental applications of biochar and hydrochar**

| Environmental application | Biochar | Hydrochar |
|---|---|---|
| Heavy-metal sorption | Extensively demonstrated | Strong potential |
| Metal precipitation | Important for mineral-rich chars | Possible depending on feedstock |
| Cr(VI) remediation | Effective | Can be highly effective under specific conditions |
| Organic-pollutant sorption | Widely demonstrated | Widely demonstrated |
| Hydrophobic pollutants | Pore filling and partitioning important | Partitioning and functional groups important |
| Wastewater treatment | Extensive research base | Rapidly developing |
| Surface functionalization | Possible | Particularly attractive |
| Contaminated-soil remediation | Relatively mature | Emerging |
| Environmental toxicity | Feedstock/process dependent | Fresh hydrochar may present phytotoxic risk |
| Process-water generation | Limited | Significant |

Potential environmental risks must be considered together with these benefits. Both feedstock contaminants and process-derived compounds can remain in the solid product. Hydrochar requires particular attention because soluble reaction products may remain associated with the material after HTC and the aqueous process stream itself requires management. Cavali et al. (2023) therefore regarded hydrochar production most appropriately as part of a wider hydrothermal biorefinery system rather than as an isolated solid-product process. The technological comparison becomes even more dependent on context when energy use, greenhouse-gas performance and economics are included. For relatively dry biomass, pyrolysis can integrate the energetic use of its gaseous and liquid coproducts and simultaneously produce a stable char. For high-moisture biomass, however, drying can represent a substantial energetic penalty. HTC avoids this preliminary evaporation step, which explains its particular attractiveness for wet feedstocks *(Hitzl et al., 2015; Kumar et al., 2020).* Nevertheless, HTC requires elevated pressure, heating of a water-rich reaction mixture and subsequent solid-liquid separation. Lucian and Fiori (2017) showed that heat integration strongly influences both energy efficiency and process economics, while Ischia and Fiori (2021) emphasized the

importance of reactor configuration and scale-up. Biochar systems have been examined more extensively through life-cycle assessment. Gaunt and Lehmann (2008), Hammond et al. (2011) and Roberts et al. (2010) demonstrated that the climatic performance of pyrolysis systems is sensitive to feedstock sourcing, energy recovery, avoided conventional waste treatment and long-term carbon stability. Li et al. (2022), who considered both biochar and hydrochar derived from agricultural residues, showed that production and soil-related impacts need to be evaluated together. Climate performance is not determined by carbon persistence alone: Yuan et al. (2024) experimentally observed greater suppression of denitrification-derived N2O by hydrochar than pyrochar in their test system. Economic feasibility is similarly case dependent. Pyrolysis benefits from greater technological maturity and a broader existing commercial base, while HTC requires pressure-resistant reactors and remains less widely implemented at industrial scale. Conversely, eliminating an energy-intensive drying operation can make HTC attractive when large quantities of concentrated wet residue are locally available. Kumar et al. (2020) concluded that neither pathway possesses universally superior techno-economic performance, because feedstock, process integration and product value strongly influence the outcome.

**Table 4**

**Literature-based comparative assessment of biochar and hydrochar for agricultural biomass valorization**

| Decision criterion | Biochar | Hydrochar | Comparative interpretation |
|---|---|---|---|
| Relatively dry agricultural biomass | Highly suitable | Suitable | Pyrolysis favored for dry lignocellulosic feedstocks. |
| High-moisture biomass | Limited suitability | Highly suitable | HTC avoids intensive pre-drying. |
| Low-pressure equipment | Advantageous | Less advantageous | HTC requires pressure-resistant equipment. |
| High degree of carbonization | Generally higher | Moderate | Higher pyrolysis temperatures increase carbonization. |
| Long-term carbon stability | High | Moderate / variable | Available stability evidence generally favors biochar. |
| Carbon sequestration | Well established | Emerging / variable | Biochar has the more mature evidence base. |
| O-containing surface functionality | Moderate | High | Hydrochar retains more reactive O-containing groups. |
| Developed microporosity | Generally high | Usually lower without activation | Often more developed in pyrolysis-derived chars. |
| Soil physical improvement | Well supported | Promising but variable | Broader and more consistent evidence for biochar. |
| Crop productivity | Generally favorable | Variable | Hydrochar is more treatment-, soil- and dose-dependent. |
| Direct use of fresh material | Generally suitable | Often requires caution | Fresh hydrochar may require conditioning. |
| Benefit from post-treatment | Moderate | High | Conditioning can strongly modify hydrochar behavior. |
| Nutrient management | Promising | Promising | Strongly feedstock- and soil-dependent. |
| Heavy-metal remediation | High potential | High potential | No universal material advantage. |
| Organic-pollutant adsorption | High potential | High potential | Pollutant chemistry and surface properties govern performance. |
| Wastewater treatment | High potential | High potential | Both materials can be effective sorbents. |
| Wet-waste processing | Limited | Highly suitable | Clear HTC advantage for wet biomass. |
| Process-water generation | Low concern | Important consideration | HTC requires aqueous-stream management. |
| Energy recovery from coproducts | Well established | More limited | More established for pyrolysis coproducts. |
| Life-cycle climate evidence | Extensive | More limited | Biochar systems are more extensively documented. |
| Technology maturity | High | Moderate | Pyrolysis is more widely established. |
| Economic feasibility | Context dependent | Context dependent | Scale, feedstock and system integration dominate. |

The descriptive categories in Table 4 represent qualitative literature-based assessments rather than numerical rankings. Taken together, three variables emerge as the principal determinants of process selection. The first is the condition of the feedstock, especially its moisture content. The second is the intended function of the resulting carbon material, such as stable carbon storage, direct soil amendment, nutrient management or contaminant adsorption. The third is the configuration of the complete processing system, including heat integration, coproduct utilization, treatment of process water, transport requirements and scale. Several gaps also remain evident in the literature. Hydrochar requires more long-term field studies addressing persistence, repeated agricultural application and potential accumulation of process-derived compounds. Standardized procedures for washing, aging and other post-treatments would also make comparison among hydrochar studies more reliable. Direct studies in which pyrolysis and HTC are applied to the same agricultural feedstock remain particularly valuable because they reduce the influence of feedstock composition and allow a more defensible assessment of the conversion pathway itself.

Future comparisons should connect material performance with process sustainability, because high removal capacity or solid yield does not necessarily imply lower environmental burden when activation, carbon persistence and waste-stream treatment are considered.

The collective evidence therefore supports a conditional rather than hierarchical interpretation. Biochar has the stronger basis for long-term carbon storage and established soil amendment, whereas hydrochar offers a clear advantage for high-moisture biomass and can provide reactive surfaces for selected environmental applications. The preferred pathway ultimately depends on feedstock composition, process conditions, post-treatment and intended use.

## CONCLUSIONS

The comparative review demonstrated that biochar and hydrochar are complementary rather than universally competing products. The preferred pathway depends on feedstock moisture, process requirements, intended application and environmental constraints. Pyrolysis is particularly suitable for relatively dry residues and when high carbon stability, developed porosity, established soil-amendment performance or long-term carbon sequestration are priorities. Hydrothermal carbonization is especially attractive for wet biomass because extensive pre-drying can be avoided, while hydrochar retains oxygen-containing surface groups that can be valuable in adsorption and remediation.

Agricultural evidence is more mature and generally more consistent for biochar. Hydrochar responses are more variable and depend strongly on feedstock, application rate and conditioning; post-treatment can reduce phytotoxicity and improve suitability for soil use. For heavy-metal, organic-pollutant and wastewater applications, neither material is universally superior because performance is controlled by contaminant chemistry, mineral phases, pore structure and surface functionality.

Process selection should therefore consider energy integration, coproduct utilization, process-water management, reactor requirements, carbon persistence, scale and economics together. Future work should emphasize direct comparisons using the same agricultural feedstocks, standardized hydrochar conditioning, long-term field trials and integrated life-cycle and techno-economic assessments. Overall, matching feedstock characteristics with the required final function provides the most scientifically defensible basis for choosing between pyrolysis and hydrothermal carbonization.

## ACKNOWLEDGEMENT

This paper presents the findings from the scientific literature published up on the biochar methodology to assess the obtain from a pyrolysis process financed from ADER 25.3.1 project, named Poultry litter capitalization technology to produce phosphorus reach biofertilizer's.

## REFERENCES

[1] Abel, S., Peters, A., Trinks, S., Schonsky, H., Facklam, M., & Wessolek, G. (2013). Impact of biochar and hydrochar addition on water retention and water repellency of sandy soil. Geoderma, 202-203, 183-191. https://doi.org/10.1016/j.geoderma.2013.03.003

[2] Azzaz, A. A., Khiari, B., Jellali, S., Ghimbeu, C. M., & Jeguirim, M. (2020). Hydrochars production, characterization and application for wastewater treatment: A review. Renewable and Sustainable Energy Reviews, 127, 109882. https://doi.org/10.1016/j.rser.2020.109882

[3] Beesley, L., Moreno-Jiménez, E., Gomez-Eyles, J. L., Harris, E., Robinson, B., & Sizmur, T. (2011). A review of biochars' potential role in the remediation, revegetation and restoration of contaminated soils. Environmental Pollution, 159(12), 3269-3282. https://doi.org/10.1016/j.envpol.2011.07.023

[4] Biederman, L. A., & Harpole, W. S. (2013). Biochar and its effects on plant productivity and nutrient cycling: A meta-analysis. GCB Bioenergy, 5(2), 202-214. https://doi.org/10.1111/gcbb.12037

[5] Blanco-Canqui, H. (2017). Biochar and soil physical properties. Soil Science Society of America Journal, 81(4), 687-711. https://doi.org/10.2136/sssaj2017.01.0017

[6] Bona, D., Bertoldi, D., Borgonovo, G., Mazzini, S., Ravasi, S., Silvestri, S., Zaccone, C., Giannetta, B., & Tambone, F. (2023). Evaluating the potential of hydrochar as a soil amendment. Waste Management, 159, 75-83. https://doi.org/10.1016/j.wasman.2023.01.024

[7] Buentello-Montoya, D. A., Robledo-Hernández, I., Larrea-Cedeño, A. S., García-García, C. E., & Coronado-Apodaca, K. G. (2026). Biochar and hydrochar from agro wastes: Technological pathways, characteristics, and advances in soil amendment. Frontiers in Environmental Science, 14, 1804984. https://doi.org/10.3389/fenvs.2026.1804984

[8] Busch, D., Stark, A., Kammann, C. I., & Glaser, B. (2013). Genotoxic and phytotoxic risk assessment of fresh and treated hydrochar from hydrothermal carbonization compared to biochar from pyrolysis. Ecotoxicology and Environmental Safety, 97, 59-66. https://doi.org/10.1016/j.ecoenv.2013.07.003

[9] Cao, X., Ma, L., Gao, B., & Harris, W. (2009). Dairy-manure derived biochar effectively sorbs lead and atrazine. Environmental Science & Technology, 43(9), 3285-3291. https://doi.org/10.1021/es803092k

[10] Cavali, M., Libardi Junior, N., de Sena, J. D., Woiciechowski, A. L., Soccol, C. R., Belli Filho, P., Bayard, R., Benbelkacem, H., & de Castilhos Junior, A. B. (2023). A review on hydrothermal carbonization of potential biomass wastes, characterization and environmental applications of hydrochar, and biorefinery perspectives of the process. Science of the Total Environment, 857, 159627. https://doi.org/10.1016/j.scitotenv.2022.159627

[11] Chen, N., Cao, S., Zhang, L., Peng, X., Wang, X., Ai, Z., & Zhang, L. (2021). Structural dependent Cr(VI) adsorption and reduction of biochar: Hydrochar versus pyrochar. Science of the Total Environment, 783, 147084. https://doi.org/10.1016/j.scitotenv.2021.147084

[12] Cognigni, P., Leonelli, C., & Berrettoni, M. (2025). A bibliographic study of biochar and hydrochar: Differences and similarities. Journal of Analytical and Applied Pyrolysis, 187, 106985. https://doi.org/10.1016/j.jaap.2025.106985

[13] Crombie, K., Mašek, O., Sohi, S. P., Brownsort, P., & Cross, A. (2013). The effect of pyrolysis conditions on biochar stability as determined by three methods. GCB Bioenergy, 5(2), 122-131. https://doi.org/10.1111/gcbb.12030

[14] de Jager, M., Röhrdanz, M., & Giani, L. (2020). The influence of hydrochar from biogas digestate on soil improvement and plant growth aspects. Biochar, 2, 177-194. https://doi.org/10.1007/s42773-020-00054-2

[15] de Jager, M., & Giani, L. (2021). An investigation of the effects of hydrochar application rate on soil amelioration and plant growth in three diverse soils. Biochar, 3, 349-365. https://doi.org/10.1007/s42773-021-00089-z

[16] Dieguez-Alonso, A., Funke, A., Anca-Couce, A., Rombolà, A. G., Ojeda, G., Bachmann, J., & Behrendt, F. (2018). Towards biochar and hydrochar engineering-Influence of process conditions on surface physical and chemical properties, thermal stability, nutrient availability, toxicity and wettability. Energies, 11(3), 496. https://doi.org/10.3390/en11030496

[17] Escudero-Curiel, S., Giráldez, A., Pazos, M., & Sanromán, Á. (2023). From waste to resource: Valorization of lignocellulosic agri-food residues through engineered hydrochar and biochar for environmental and clean energy applications-A comprehensive review. Foods, 12(19), 3646. https://doi.org/10.3390/foods12193646

[18] Funke, A., & Ziegler, F. (2010). Hydrothermal carbonization of biomass: A summary and discussion of chemical mechanisms for process engineering. Biofuels, Bioproducts and Biorefining, 4(2), 160-177. https://doi.org/10.1002/bbb.198

[19] Gaunt, J. L., & Lehmann, J. (2008). Energy balance and emissions associated with biochar sequestration and pyrolysis bioenergy production. Environmental Science & Technology, 42(11), 4152-4158. https://doi.org/10.1021/es071361i

[20] George, C., Wagner, M., Kücke, M., & Rillig, M. C. (2012). Divergent consequences of hydrochar in the plant-soil system: Arbuscular mycorrhiza, nodulation, plant growth and soil aggregation effects. Applied Soil Ecology, 59, 68-72. https://doi.org/10.1016/j.apsoil.2012.02.021

[21] Hammond, J., Shackley, S., Sohi, S., & Brownsort, P. (2011). Prospective life cycle carbon abatement for pyrolysis biochar systems in the UK. Energy Policy, 39(5), 2646-2655. https://doi.org/10.1016/j.enpol.2011.02.033

[22] Han, L., Ro, K. S., Sun, K., Sun, H., Wang, Z., Libra, J. A., & Xing, B. (2016). New evidence for high sorption capacity of hydrochar for hydrophobic organic pollutants. Environmental Science & Technology, 50(24), 13274-13282. https://doi.org/10.1021/acs.est.6b02401

[23] Hitzl, M., Corma, A., Pomares, F., & Renz, M. (2015). The hydrothermal carbonization (HTC) plant as a decentral biorefinery for wet biomass. Catalysis Today, 257, 154-159. https://doi.org/10.1016/j.cattod.2014.09.024

[24] Hoekman, S. K., Broch, A., & Robbins, C. (2011). Hydrothermal carbonization (HTC) of lignocellulosic biomass. Energy & Fuels, 25(4), 1802-1810. https://doi.org/10.1021/ef101745n

[25] Ighalo, J. O., Rangabhashiyam, S., Dulta, K., Umeh, C. T., Iwuozor, K. O., Aniagor, C. O., Eshiemogie, S. O., Iwuchukwu, F. U., & Igwegbe, C. A. (2022). Recent advances in hydrochar application for the adsorptive removal of wastewater pollutants. Chemical Engineering Research and Design, 184, 419-456. https://doi.org/10.1016/j.cherd.2022.06.028

[26] Ischia, G., & Fiori, L. (2021). Hydrothermal carbonization of organic waste and biomass: A review on process, reactor, and plant modeling. Waste and Biomass Valorization, 12, 2797-2824. https://doi.org/10.1007/s12649-020-01255-3

[27] Jeffery, S., Verheijen, F. G. A., van der Velde, M., & Bastos, A. C. (2011). A quantitative review of the effects of biochar application to soils on crop productivity using meta-analysis. Agriculture, Ecosystems & Environment, 144(1), 175-187. https://doi.org/10.1016/j.agee.2011.08.015

[28] Joseph, S., Cowie, A. L., Van Zwieten, L., Bolan, N., Budai, A., Buss, W., Cayuela, M. L., Graber, E. R., Ippolito, J. A., Kuzyakov, Y., Luo, Y., Ok, Y. S., Palansooriya, K. N., Shepherd, J., Stephens, S., Weng, Z. H., & Lehmann, J. (2021). How biochar works, and when it doesn't: A review of mechanisms controlling soil and plant responses to biochar. GCB Bioenergy, 13(11), 1731-1764. https://doi.org/10.1111/gcbb.12885

[29] Kambo, H. S., & Dutta, A. (2015). A comparative review of biochar and hydrochar in terms of production, physico-chemical properties and applications. Renewable and Sustainable Energy Reviews, 45, 359-378. https://doi.org/10.1016/j.rser.2015.01.050

[30] Khan, T. A., Saud, A. S., Jamari, S. S., Ab Rahim, M. H., Park, J.-W., & Kim, H.-J. (2019). Hydrothermal carbonization of lignocellulosic biomass for carbon rich material preparation: A review. Biomass and Bioenergy, 130, 105384. https://doi.org/10.1016/j.biombioe.2019.105384

[31] Khosravi, A., Zheng, H., Liu, Q., Hashemi, M., Tang, Y., & Xing, B. (2022). Production and characterization of hydrochars and their application in soil improvement and environmental remediation. Chemical Engineering Journal, 430, 133142. https://doi.org/10.1016/j.cej.2021.133142

[32] Kumar, A., Saini, K., & Bhaskar, T. (2020). Hydrochar and biochar: Production, physicochemical properties and techno-economic analysis. Bioresource Technology, 310, 123442. https://doi.org/10.1016/j.biortech.2020.123442

[33] Lehmann, J., Cowie, A., Masiello, C. A., Kammann, C., Woolf, D., Amonette, J. E., Cayuela, M. L., Camps-Arbestain, M., & Whitman, T. (2021). Biochar in climate change mitigation. Nature Geoscience, 14, 883-892. https://doi.org/10.1038/s41561-021-00852-8

[34] Li, X., Wang, R., Shao, C., Li, D., Bai, S., Hou, N., & Zhao, X. (2022). Biochar and hydrochar from agricultural residues for soil conditioning: Life cycle assessment and microbially mediated C and N cycles. ACS Sustainable Chemistry & Engineering, 10(11), 3574-3583. https://doi.org/10.1021/acssuschemeng.1c08074

[35] Libra, J. A., Ro, K. S., Kammann, C., Funke, A., Berge, N. D., Neubauer, Y., Titirici, M.-M., Fühner, C., Bens, O., Kern, J., & Emmerich, K.-H. (2011). Hydrothermal carbonization of biomass residuals: A comparative review of the chemistry, processes and applications of wet and dry pyrolysis. Biofuels, 2(1), 71-106. https://doi.org/10.4155/bfs.10.81

[36] Lucian, M., & Fiori, L. (2017). Hydrothermal carbonization of waste biomass: Process design, modeling, energy efficiency and cost analysis. Energies, 10(2), 211. https://doi.org/10.3390/en10020211

[37] Luutu, H., Rose, M. T., McIntosh, S., Van Zwieten, L., & Rose, T. (2022). Plant growth responses to soil-applied hydrothermally-carbonised waste amendments: A meta-analysis. Plant and Soil, 472(1-2), 1-15. https://doi.org/10.1007/s11104-021-05185-4

[38] Masoumi, S., Borugadda, V. B., Nanda, S., & Dalai, A. K. (2021). Hydrochar: A review on its production technologies and applications. Catalysts, 11(8), 939. https://doi.org/10.3390/catal11080939

[39] Mau, V., Arye, G., & Gross, A. (2020). Poultry litter hydrochar as an amendment for sandy soils. Journal of Environmental Management, 271, 110959. https://doi.org/10.1016/j.jenvman.2020.110959

[40] Naisse, C., Girardin, C., Lefèvre, R., Pozzi, A., Maas, R., Stark, A., & Rumpel, C. (2015). Effect of physical weathering on the carbon sequestration potential of biochars and hydrochars in soil. GCB Bioenergy, 7(3), 488-496. https://doi.org/10.1111/gcbb.12158

[41] Purakayastha, T. J., Bera, T., Bhaduri, D., Sarkar, B., Mandal, S., Wade, P., Kumari, S., Biswas, S., Menon, M., Pathak, H., & Tsang, D. C. W. (2019). A review on biochar modulated soil condition improvements and nutrient dynamics concerning crop yields: Pathways to climate change mitigation and global food security. Chemosphere, 227, 345-365. https://doi.org/10.1016/j.chemosphere.2019.03.170

[42] Roberts, K. G., Gloy, B. A., Joseph, S., Scott, N. R., & Lehmann, J. (2010). Life cycle assessment of biochar systems: Estimating the energetic, economic, and climate change potential. Environmental Science & Technology, 44(2), 827-833. https://doi.org/10.1021/es902266r

[43] Ronsse, F., Van Hecke, S., Dickinson, D., & Prins, W. (2013). Production and characterization of slow pyrolysis biochar: Influence of feedstock type and pyrolysis conditions. GCB Bioenergy, 5(2), 104-115. https://doi.org/10.1111/gcbb.12018

[44] Schmidt, H.-P., Kammann, C., Hagemann, N., Leifeld, J., Bucheli, T. D., Sánchez Monedero, M. A., & Cayuela, M. L. (2021). Biochar in agriculture - A systematic review of 26 global meta-analyses. GCB Bioenergy, 13(11), 1708-1730. https://doi.org/10.1111/gcbb.12889

[45] Spokas, K. A., Cantrell, K. B., Novak, J. M., Archer, D. W., Ippolito, J. A., Collins, H. P., Boateng, A. A., Lima, I. M., Lamb, M. C., McAloon, A. J., Lentz, R. D., & Nichols, K. A. (2012). Biochar: A synthesis of its agronomic impact beyond carbon sequestration. Journal of Environmental Quality, 41(4), 973-989. https://doi.org/10.2134/jeq2011.0069

[46] Suarez, E., Tobajas, M., Mohedano, A. F., Reguera, M., Esteban, E., & de la Rubia, Á. (2023). Effect of garden and park waste hydrochar and biochar in soil application: A comparative study. Biomass Conversion and Biorefinery, 13(18), 16479-16493. https://doi.org/10.1007/s13399-023-04015-0

[47] Tan, X., Liu, Y., Zeng, G., Wang, X., Hu, X., Gu, Y., & Yang, Z. (2015). Application of biochar for the removal of pollutants from aqueous solutions. Chemosphere, 125, 70-85. https://doi.org/10.1016/j.chemosphere.2014.12.058

[48] Taskin, E., Branà, M. T., Altomare, C., & Loffredo, E. (2019). Biochar and hydrochar from waste biomass promote the growth and enzyme activity of soil-resident ligninolytic fungi. Heliyon, 5(7), e02051. https://doi.org/10.1016/j.heliyon.2019.e02051

[49] Titirici, M.-M., White, R. J., Falco, C., & Sevilla, M. (2012). Black perspectives for a green future: Hydrothermal carbons for environment protection and energy storage. Energy & Environmental Science, 5(5), 6796-6822. https://doi.org/10.1039/C2EE21166A

[50] Woolf, D., Amonette, J. E., Street-Perrott, F. A., Lehmann, J., & Joseph, S. (2010). Sustainable biochar to mitigate global climate change. Nature Communications, 1, 56. https://doi.org/10.1038/ncomms1053

[51] Yuan, D., Yuan, J., Jia, Z., Wu, P., Hu, C., Clough, T. J., Cheng, H., & Qin, S. (2024). Hydrochar surpasses pyrochar in mitigating soil N2O emissions from denitrification due to its improved electron shuttle function and low levels of persistent free radicals. Environmental Science & Technology Letters, 11(9), 954-960. https://doi.org/10.1021/acs.estlett.4c00470

# SERICULTURAL WASTE COMPOSTING AS A SUSTAINABLE APPROACH FOR SOIL HEALTH, MULBERRY PRODUCTION AND SILKWORM REARING

/

# *COMPOSTAREA DEȘEURILOR SERICICOLE - O ABORDARE DURABILĂ PENTRU SĂNĂTATEA SOLULUI, PRODUCȚIA DE DUD ȘI CREȘTEREA VIERMILOR DE MĂTASE*

**Ana-Maria TĂBĂRAȘU*[1)], Iuliana GĂGEANU[1)], Mihaela HĂBEANU[2)], Teofil-Alin ONCESCU[1)], Nicoleta-Alexandra VANGHELE[1, 3)], Alexandru-Cristian CIOACLĂ[1, 3)], Dragoș-Nicolae ANGHELACHE[1, 3)], Mihaela NIȚU[1)], Cătălin PERSU[1, 3)], Elena-Valeria VLĂDUȚ[3)], Paula TUDOR[3)], Elena-Melania CISMARU[3)]**

[1)] National Institute of Research - Development for Machines and Installations Designed for Agriculture and Food Industry - INMA Bucharest / Romania;

[2)] Research Station for Sericulture Baneasa Bucharest / Romania;

[3)] National University of Science and Technology Polytechnic Bucharest / Romania.

**E-mail: anamariatabarasu22@yahoo.com*

***Keywords:*** *composting, vermicomposting, C:N ratio, sericulture, silkworm, mulberry*

**ABSTRACT**

*Sericulture is an agro-industrial activity of major economic and social importance, based on mulberry (Morus spp.) cultivation, as mulberry leaves represent the sole food source for the silkworm (Bombyx mori L.). Sustainable management of mulberry plantations is essential for maintaining silkworm health, cocoon quality, and silk productivity. However, the intensive use of chemical fertilizers can negatively affect soil properties and the long-term sustainability of the system. At the same time, sericulture generates significant amounts of organic waste, including mulberry leaf residues, silkworm excreta (frass), spent rearing bed materials, and by-products from cocoon processing. This article highlights the potential of composting and vermicomposting as sustainable solutions for valorizing sericulture waste and improving soil health. The conversion of these residues into organic amendments contributes to improved soil structure, enhanced microbial activity, increased nutrient availability, and higher organic carbon content. Particular attention is given to silkworm frass and vermicompost, which are characterized by a favorable nutrient profile and a low C:N ratio, promoting rapid mineralization and efficient nutrient uptake by mulberry plants. The application of organic fertilizers improves vegetative growth and leaf quality, with positive effects on larval development and cocoon parameters.*

**REZUMAT**

*Sericicultura reprezintă o activitate agro-industrială de importanță economică și socială majoră, bazată pe cultura dudului (Morus spp.), frunzele acestuia constituind unica sursă de hrană pentru viermele de mătase (Bombyx mori L.). Managementul durabil al plantațiilor de dud este esențial pentru menținerea sănătății viermilor de mătase, calității coconilor și productivității mătăsii. Cu toate acestea, utilizarea intensivă a îngrășămintelor chimice poate afecta negativ proprietățile solului și sustenabilitatea pe termen lung a sistemului. În același timp, sericicultura generează cantități semnificative de deșeuri organice, incluzând resturi de frunze de dud, excrementele viermilor de mătase (frass), așternuturi uzate și subproduse rezultate din procesarea coconilor. Prezentul articol evidențiază potențialul compostării și vermicompostării ca soluții durabile pentru valorificarea deșeurilor sericicole și îmbunătățirea sănătății solului. Transformarea acestor reziduuri în amendamente organice contribuie la ameliorarea structurii solului, intensificarea activității microbiologice, creșterea disponibilității nutrienților și a conținutului de carbon organic. O atenție deosebită este acordată frass-ului de viermi de mătase și vermicompostului, caracterizate printr-un profil nutritiv favorabil și un raport C:N redus, care favorizează mineralizarea rapidă și absorbția eficientă a nutrienților de către plantele de dud. Aplicarea fertilizanților organici conduce la îmbunătățirea creșterii vegetative și a calității frunzelor, având efecte pozitive asupra dezvoltării larvelor și asupra parametrilor coconilor.*

## INTRODUCTION

Sericulture is an agro-industrial activity of major economic and social importance, based exclusively on mulberry cultivation (Morus spp.), whose leaves represent the sole food source for the silkworm (*Bombyx*

mori L.). The quality and quantity of mulberry leaves directly influence larval growth, cocoon production, and the quality of silk fiber (*Rajaram et al., 2025; Ahammed et al., 2025*).

The intensive use of chemical fertilizers in mulberry plantations leads, in the long term, to soil structure degradation, reduced microbial biodiversity, and the accumulation of residues harmful to silkworms (*Bora et al., 2025*).

In this context, organic fertilization and integrated nutrient management become essential strategies for the development of sustainable sericulture (*Ahammed et al., 2025*).

Sericulture generates considerable amounts of organic waste, including mulberry leaf residues, silkworm excreta (frass), spent bedding materials, and by-products resulting from cocoon processing. Recent studies demonstrate that these wastes can be transformed through composting and vermicomposting into effective organic fertilizers, contributing to the circular economy and reducing environmental impact (*Menaka et al., 2025*).

Beyond its direct role in supporting mulberry cultivation and sericulture, compost is globally recognized as one of the most effective organic amendments for sustainable agriculture. Compost supplies organic matter as well as macro- and micronutrients, stimulating microbiological activity and facilitating nutrient cycling, which leads to improved soil health and crop productivity without excessive reliance on chemical fertilizers (*Oyebiyi et al., 2026*).

The regular application of organic amendments, including compost derived from the processing of agricultural or animal wastes, improves soil physical structure, water-holding capacity, and humus content, thereby contributing to the long-term fertility of agricultural lands (*Ho et al., 2022*).

Moreover, the organic use of organic materials renews the diversity and activity of soil microorganisms, reduces soil acidification and environmental pollution, and supports the biodiversity of agricultural systems—fundamental elements of sustainable practices.

## MATERIALS AND METHODS

The sericulture industry generates significant amounts of waste throughout the entire production cycle, which are generally classified as biodegradable and non-biodegradable (*Altman & Farrell, 2022*).

Biodegradable wastes include silkworm excreta, bedding residues, dead larvae, damaged cocoons, and pupal residues, which, in the absence of proper management, can cause unpleasant odors, attract pests, and create unsanitary conditions (*Kaushik et al., 2025*).

However, these wastes have a high potential for valorization through composting or use as biofertilizers and alternative animal feed sources, contributing to more efficient resource use and reducing environmental pressure.

In contrast, non-biodegradable wastes, such as plastic materials, synthetic nets, and chemicals used in cocoon processing, pose a major risk due to their persistence in the environment. Their accumulation can lead to soil and water pollution, with negative effects on biodiversity and human health—a problem exacerbated by the lack of adequate waste management systems in many sericulture regions.

Improper management of sericultural waste has both environmental and economic consequences, potentially affecting soil fertility, water quality, and agricultural productivity. In this context, the adoption of environmentally friendly waste management practices becomes essential for reducing environmental impact and supporting the livelihoods of rural communities involved in sericulture.

The growing global demand for silk, combined with the effects of climate change, necessitates a transition toward sustainable and resilient practices capable of ensuring the long-term viability of the sector. Innovations such as waste bioconversion, integrated farming systems, and circular economy principles offer viable solutions for valorizing sericultural waste and reducing the ecological footprint of this activity (*Kaushik et al., 2025*).

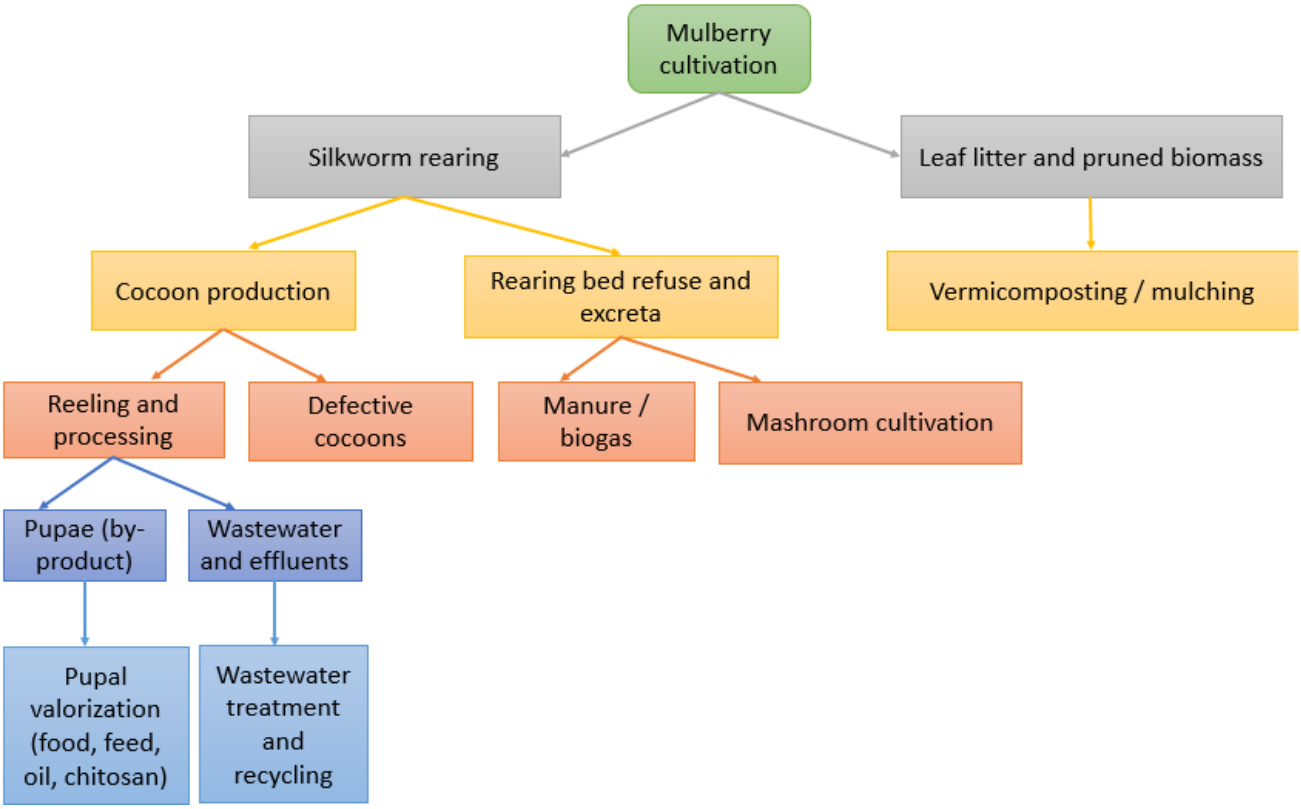



**Fig. 1 - Conceptual diagram of silk production phases, waste outputs, and sustainable valorization approaches in sericulture**
*(adapted from Kaushik et al., 2025)*

## RESULTS

- *Composting of Sericultural Waste and Soil Fertility*

Sericultural waste is recognized as an important source of essential nutrients, particularly nitrogen, phosphorus, and potassium, derived from both mulberry plant residues and silkworm excreta. Through the composting process, these organic materials are transformed into a stable product with a high content of humified organic matter, which significantly contributes to improving the physical, chemical, and biological properties of the soil.

The application of compost obtained from sericultural waste leads to improved soil structure, increased water-holding capacity, and enhanced microbiological activity, thereby promoting nutrient availability for plants and maintaining long-term soil fertility (*Menaka et al., 2025*).

Compared to conventional composting, vermicomposting is an advanced biological method that accelerates the degradation of organic matter through the synergistic action of earthworms and associated microorganisms. This process results in the production of vermicompost rich in readily available nutrients, enzymes, beneficial microorganisms, and plant growth–stimulating substances.

Studies show that vermicompost derived from sericultural waste exhibits superior efficiency in improving soil fertility and mulberry vegetative growth compared to other organic amendments, thereby contributing to the production of higher-quality leaves that are essential for the optimal development of silkworms (*Venugopal et al., 2010*).

- *Frass as an Organic Fertilizer*

Bombyx mori frass is considered a valuable biofertilizer due to its high content of readily assimilable nutrients and bioactive compounds *(Gowrisankar et al., 2025*).

A comparative analysis of the nutritional composition of frass and farmyard manure highlights higher concentrations of nitrogen, phosphorus, and potassium in frass, according to the data presented in Figure 2 (*Gowrisankar et al., 2025*).

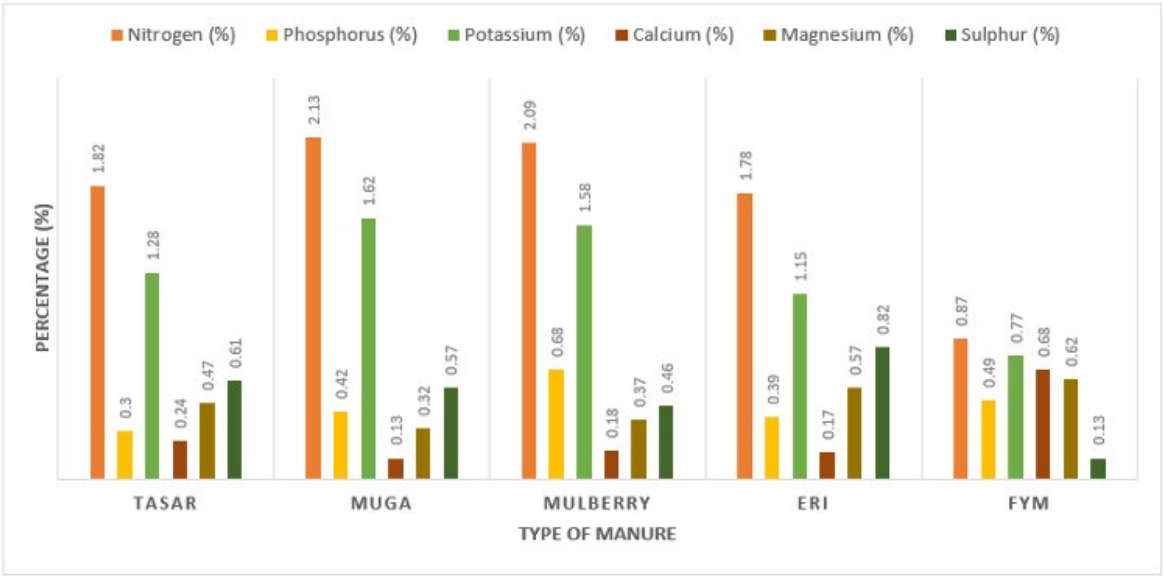



**Fig. 2 - Comparison of different macro and micro nutrients in different silkworm frass and** FYM
(*Gowrisankar et al., 2025*)

The application of frass to the soil has led to improvements in physico-chemical properties and increased plant biomass across various crops (*Antoniadis et al., 2023; Aboyo et al., 2025*).

In addition, frass contributes to the stimulation of microbial activity and enhances nutrient use efficiency, making it an important component of agriculture based on the recycling of insect-derived waste (*Ramki and Kalasariya, 2025*).

These effects on soil biological activity are supported by changes in the structure of the bacterial community observed following the application of organic fertilizer derived from silkworm excreta, as reported in other cropping systems. The structure of the soil bacterial community according to fertilization treatments is illustrated in Figure 3 (*Yang et al., 2025*).

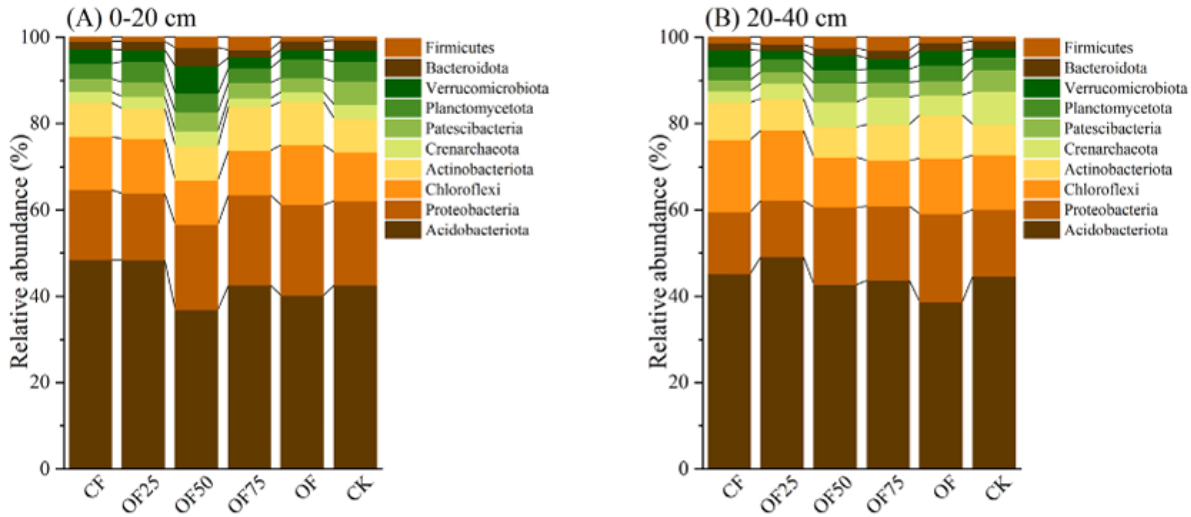



**Fig. 3 - Species composition of soil bacteria at the phylum level in (A) 0-20cm and (B) 20-40 cm soil layers in Moso bamboo forests treated with different** fertilizers
(*Yang et al., 2025*)

The presented data highlight an increase in copiotrophic bacterial groups, such as Proteobacteria and Actinobacteria, in treatments fertilized with silkworm excreta, along with a concomitant reduction in oligotrophic groups. These changes in the soil microbiome indicate an intensification of mineralization processes and nutrient cycling, mechanisms that are relevant for improving soil fertility and mulberry leaf quality.

- *Organic Carbon Content and C:N Ratio of Frass*

Vermicomposting is a biological process in which earthworms such as *Eisenia fetida* and *Eudrilus eugeniae* convert organic waste into nutrient-rich compost (vermicast), representing a sustainable solution for the management of sericultural waste. Earthworm activity accelerates the decomposition of organic matter and increases nutrient availability, thereby improving soil fertility and plant growth.

Sericultural wastes require a pre-decomposition stage and are often mixed with farmyard manure to optimize the C:N ratio, resulting in vermicompost with high N, P, and K contents and enhanced microbial diversity.

The application of vermicompost improves mulberry growth and leaf quality, exerting positive effects on silkworm health and cocoon productivity (*Kaushik et al., 2025*).

**Table 1**

**Comparative analysis of eco-friendly waste management techniques**
(*Kaushik et al., 2025*)

| Technique | Waste used | Benefits | Challenges |
|---|---|---|---|
| Vermicomposting | Rearing waste | Improves soil health, low cost | Initial setup, training needed |
| Pupal valorization | Reeling waste (pupae) | Animal feed, extra income | Drying / storage |
| Microbial degradation | Rearing / reeling waste | Accelerated composting | Strain selection, climate factors |
| Mushroom cultivation | Mulberry litter, refuse | Extra food & income, zero-waste farming | Pasteurization & handling |

Organic carbon content is an important indicator of organic matter stability and the soil's capacity to support microbiological activity. Although farmyard manure exhibits higher organic carbon values, silkworm frass contains sufficient amounts of easily biodegradable carbon that are favorable for mineralization processes.

Differences in organic carbon content between frass and farmyard manure are illustrated in Figure 4 (*Gowrisankar et al., 2025*).

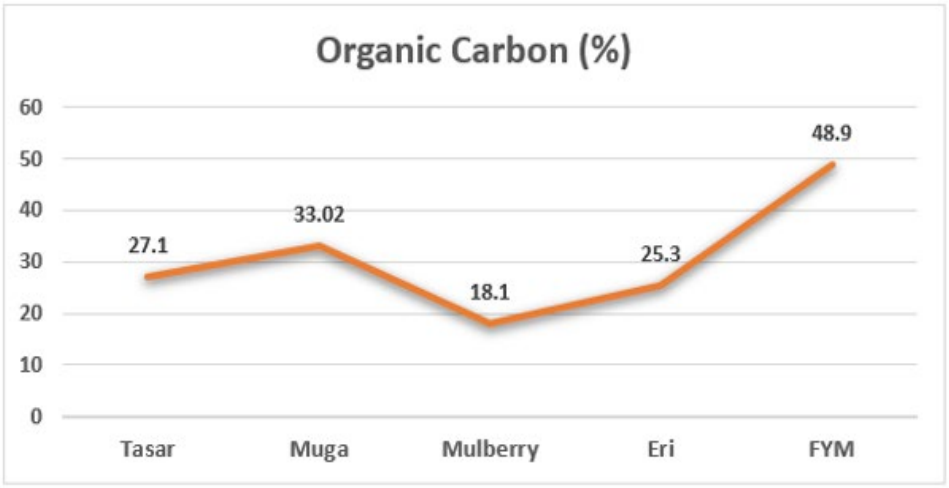



**Fig. 4 - Comparison of organic carbon % in different silkworm frass and** FYM
(*Gowrisankar et al., 2025*)

The carbon-to-nitrogen (C:N) ratio is an essential parameter indicating the rate of organic matter decomposition and nutrient availability for plants. Silkworm frass exhibits a significantly lower C:N ratio compared to farmyard manure, suggesting faster mineralization and more efficient nitrogen release. T

he C:N ratio values for frass and farmyard manure are presented in Figure 5 (*Gowrisankar et al., 2025*).

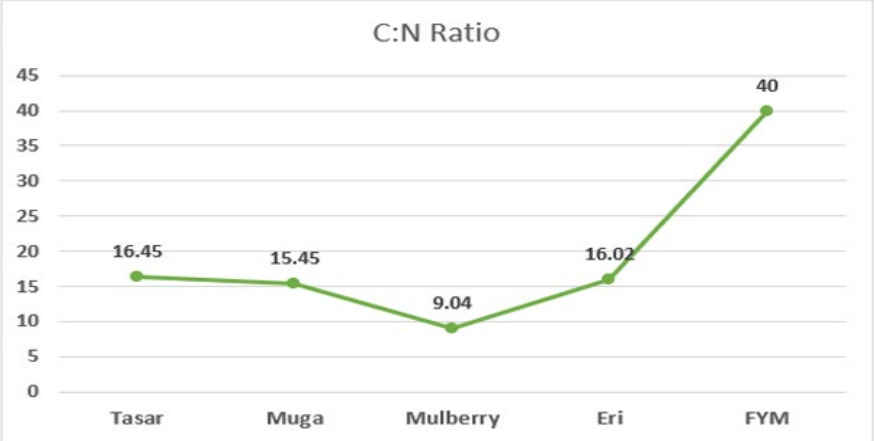



**Fig. 5 - Comparison of C:N ratio in different silkworm frass and FYM**
(*Gowrisankar et al., 2025*)

- *Effects of Organic Fertilization on Mulberry Cultivation*

Studies show that the application of compost, vermicompost, and silkworm frass in mulberry plantations has significant positive effects on vegetative growth and leaf quality. These organic amendments contribute to increased leaf yield, enhanced chlorophyll content, and higher levels of soluble proteins—key indicators of the nutritional value of leaves used for feeding silkworms. Improvements in these parameters are associated with better nutrient availability in the soil and stimulation of microbiological activity in the rhizosphere, which promotes efficient nutrient uptake by plants (*Ghazy et al., 2020; Ahammed et al., 2025*).

Moreover, organic fertilization positively influences mulberry physiological processes such as photosynthesis and nitrogen metabolism, which is reflected in vigorous foliar growth and improved leaf quality. Vermicompost and frass, due to their content of enzymes, phytohormones, and beneficial microorganisms, can stimulate root system development and increase nutrient use efficiency compared to exclusive chemical fertilization.

The integration of sericultural compost within an integrated nutrient management framework allows for a significant reduction in chemical fertilizer rates without compromising mulberry crop productivity. This approach contributes to the long-term maintenance of soil health by preventing soil structure degradation and declines in organic matter content. At the same time, the use of sericultural compost supports the sustainability of production systems by reducing input costs and environmental impacts, aspects that are essential for the development of sustainable sericulture (*Rajaram et al., 2025*).

- *Impact on Silkworms and Cocoon Quality*

The quality of mulberry leaves is a determining factor for silkworm larval development and their productive performance. Organic fertilization of mulberry plantations positively influences the biochemical composition of the leaves, increasing the content of proteins, chlorophyll, and other essential nutrients required for larval metabolism. Leaves obtained from plantations fertilized with compost and liquid organic manure derived from sericultural waste resulted in larvae with higher body weight, shorter larval durations, and higher survival rates, indicating improved physiological status and enhanced feed conversion efficiency (*Shravanilakshmi et al., 2025a*).

Improvements in larval growth parameters are attributed both to the superior quality of the leaves and to the reduction of metabolic stress associated with chemical residues commonly found in conventional fertilization systems. The readily assimilable nutrients and bioactive compounds present in organically fertilized leaves support protein synthesis processes and the harmonious development of larval tissues, which is subsequently reflected in cocoon formation.

Regarding cocoon parameters, the use of organic fertilizers derived from sericultural waste resulted in significant increases in cocoon weight, shell-to-cocoon ratio, and silk filament length. These indicators are essential for evaluating silk yield and quality, as they have a direct impact on the economic value of sericultural production.

Specialized studies highlight that organic fertilization contributes to the production of more uniform cocoons with superior technological characteristics compared to systems based exclusively on chemical fertilizers (*Shravanilakshmi et al., 2025b; Rajaram et al., 2025*).

## CONCLUSIONS

- Waste generated in sericulture can be regarded as a valuable resource, and its valorization through composting and vermicomposting contributes to closing nutrient cycles and reducing environmental impacts.
- Organic fertilizers derived from sericulture waste improve soil functioning by stimulating microbial activity, accelerating mineralization processes, and increasing the availability of essential nutrients, thereby supporting long-term soil fertility.
- Improvements in soil properties are indirectly reflected in mulberry crop performance through enhanced leaf yield and quality, with positive effects on larval development and productive parameters of silkworms.
- The integration of compost, vermicompost, and silkworm frass into nutrient management practices allows a reduction in chemical fertilizer use without compromising the productivity of sericulture systems.
- The adoption of these practices supports circular economy principles and provides both ecological and economic benefits, contributing to the sustainability and resilience of mulberry–silkworm production systems.
- Large-scale implementation of sericulture waste valorization technologies requires effective knowledge transfer, farmer training, and institutional support to adapt solutions to local conditions.

## ACKNOWLEDGEMENT

This work was funded by ADER Program - Ministry of Agriculture and Rural Development (MADR) - Funding contract no. 24.1.3/ 17.07.2023, project ADER 24.1.3 “Research on the development of new systems and technologies for the sustainable management of genetic resources in the sericulture field and the identification of new paths for the valorization of main and secondary products with economic and social impact”.

## REFERENCES

[1] Aboyo, R., Ddamulira, G., Omuut, G., Ochia, C.O. (2025). Silkworm Frass Amendment Improves Soil Properties and Performance of Cleome gynandra Under Screenhouse Conditions. *Wiley International Journal of Agronomy Volume*, Article ID 9411667, 14 pages https://doi.org/10.1155/ioa/9411667.

[2] Ahammed, I., Chatterjee, P., Das, B., Saha, D., Nesa, J., Sadat, A. (2025). Integrating organic fertilizer strategies for optimizing mulberry crop production and soil health resilience: A pathway to sustainable agriculture. *Journal of the Saudi Society of Agricultural Sciences*, 24:73, https://doi.org/10.1007/s44447-025-00116-6

[3] Antoniadis, V., Molla, A., Grammenou, A., Apostolidis, V., Athanassiou, C.G., Rumbos, C.I., Levizou, E. (2023). Insect Frass as a Novel Organic Soil Fertilizer for the Cultivation of Spinach (Spinacia oleracea): Effects on Soil Properties, Plant Physiological Parameters, and Nutrient Status. *Journal of Soil Science and Plant Nutrition,* 23:5935–5944 https://doi.org/10.1007/s42729-023-01451-9.

[4] Bora, N., Borah, P., Sonowal, P. (2025). Advancing sustainable sericulture through organic nutrient management: A comprehensive review. *International Journal of Advanced Biochemistry Research*; SP-9(7): 428-432.

[5] Ghazy, U.M., Fouad, T.A., Ahmed, G.M. (2020). Improving productivity of mulberry trees and silkworm, Bombyx mori L., using vermicompost application. *Int. J. Indust. Entomol*. 40(2) 41-50.

[6] Gowrisankar, R., Komal, J., Dasari, S., Naveen, D.V., Tirupam Reddy, B., Vishaka G.V, Nadaf, H. (2025). Recycling Sericulture Byproducts: Nutrient Profile and Biofertilizer Potential of Silkworm Frass. *Journal of Advances in Biology & Biotechnology*, 28 (10):1860–1866. https://doi.org/10.9734/jabb/2025/v28i103198.

[7] Ho, T.T.K., Tra, V.T., Le, T.H., Nguyen, N-K-Q., Tran, C-S., Nguyen, P-T., Vo, T-D-H., Thai, V-N., Bui, X-T. (2022). Compost to improve sustainable soil cultivation and crop productivity. *Case Studies in Chemical and Environmental Engineering,* 6.

[8] Kaushik, A., Saikia, S., Gogoi, C., Kaushiki, B. (2025). Circular Strategies and Eco Innovations for Sustainable Sericulture Waste Management. *Journal of Experimental Agriculture International*, vol. 47(8), pp. 569-580.

[9] Menaka, S., Sabarish, M., Durgadevi, R., Kalpana, R., Anusuya, G., Bhuvaneshwari, T., Brindhabharathi, S.A. (2025). *International Journal of Research in Agronomy*; SP-8(8): 447-454.

[10] Oyebiyi, O.O., Laezza, A., Hoque, M.M., Thammavongsa, Li, M., S., Tsipas, S., Tasiopoulos, A,J., Scopa, A., Drosos, M. (2026). Organic Amendments for Sustainable Agriculture: Effects on Soil Function, Crop Productivity and Carbon Sequestration Under Variable Contexts. *Journal of Carbon Research*, 12(7), https://doi.org/10.3390/c12010007.

[11] Rajaram, R., Mahalingam, M., Chandrasekaran, B., Selvaraj, R., Manivannan, U., Pachaiyappan, M., Subramaniam, M., Ramaiyer, L.M., Viswanathan, S.K., Sravani, V. (2025). Seri waste - A boon to enhance yield, quality of mulberry leaf and rearing parameters of silkworm, Bombyx mori L. with integrated nutrient management approach. *Plant Science Today*, 12(sp4):01–08. https://doi.org/10.14719/pst.9274

[12] Ramki, B., Kalasariya, R.L. (2025). Insect frass: A sustainable organic fertilizer for enhancing soil health and crop productivity. Insect Environment, vol. 28 (2).

[13] Shravanilakshmi, V., Kallimani, C.S., Tejaswini, A.S., Kaveri, A., Doreswamy, C., Veenita, M.K. (2025a). Reuse of Silkworm Litter as Liquid Manure to Mulberry: Assessing its Influence on Larval and Cocoon Traits of Silkworm (*Bombyx* mori L.). *Uttar Pradesh Journal of Zoology*, Volume 46, Issue 14, Page 195-205.

[14] Shravanilakshmi, V., Kallimani, C.S., Veenita, M.K., Tejaswini, A.S., Shwetha, G.V., Gagana Sindhu, S., Doreswamy, C. (2025b). Influence of Silkworm Litter Liquid Organic Manure on Soil Nutrient Status and Microbial Population in Mulberry Plantation. *Plant Cell Biotechnology and Molecular Biology*, Volume 26, Issue 7-8, Page 456-470.

[15] Venugopal, A., Chandrasekhar, M., Naidu, B.V., Raju, S. (2010). Vermicomposting in sericulture using mixed culture of earthworms (Eudrillus Eugineae, Eisenia Foetida and Perionyx Excavatus) – A review. Agric. Rev., 31 (2) : 150 – 154.

[16] Xu, J., Li, Y., Li, L. (2025). A ComprehensiveReviewoftheEffects of OrganicAmendmentsonSoil HealthandFertility: Mechanisms, GreenhouseGasEmissions,and Implications for Sustainable Agriculture. *Agronomy*, 15, 2705. https://doi.org/10.33.

[17] Yang, Z., Zhao, J., Ni, H. (2025). Silkworm excrement organic fertilizer substitution compound fertilizer improves bamboo shoot yield by altering soil properties and bacterial communities of Moso bamboo (Phyllostachys edulis) forests in subtropical China. *Front. Plant Sci*. 16:1550946. doi: 10.3389/fpls.2025.1550946.

# STRUCTURAL PERFORMANCE EVALUATION OF THE FRAME OF A TREE ROOT CUTTING MACHINE USING FINITE ELEMENT ANALYSIS

/

# *EVALUAREA PERFORMANȚEI STRUCTURALE A CADRULUI UNUI ECHIPAMENT PENTRU TĂIEREA RĂDĂCINILOR POMILOR UTILIZÂND ANALIZA CU ELEMENTE FINITE*

**Alin-Nicolae HARABAGIU*[1)], Valentin-Nicolae VLĂDUȚ[1)], Dragoș-Nicolae DUMITRU[1)], Vasilica ȘTEFAN[1)], Ana ZAICA[1)], Stefano-Andrea MANTOVANI[1)], Aura-Maria DUMITRESCU[1)], Cornelia Veronica DIMA*[2)]**

[1)] National Institute of Research-Development for Machines and Installations Designed to Agriculture and Food Industry - INMA Bucharest / Romania;

[2)] National University of Science and Technology POLITEHNICA Bucharest / Romania

**E-mail: alinhara04@gmail.com*

***Keywords:*** *root pruning; machine frame; finite element analysis; soil resistance; structural analysis*

## ABSTRACT

*The frame of a tractor-mounted tree root cutting machine must transfer soil and root resistance while maintaining blade position. This study evaluated the static structural response of the assembly under sandy, loamy, and clay-soil loads using SolidWorks Simulation. The machine was set at a 45° working angle, the CAD assembly was simplified, and the hydraulic cylinders were represented as rigid bodies. Deformable components used linear-elastic isotropic materials, bonded global contact, ten distributed pin connectors, a fixed tractor-attachment region, and a blended curvature-based mesh with 254,653 nodes and 128,499 elements. Scalar resistance sums were 7.685, 11.855, and 16.025 kN for sandy, loamy, and clay soil. Maximum von Mises stresses were 364.41, 589.24, and 807.47 MPa; maximum resultant displacements were 22.74, 41.52, and 60.28 mm; and minimum safety factors were 0.7415, 0.4667, and 0.3406, respectively. Each stress maximum occurred at node 23555 on the connecting part of the blade assembly. This repeated localization identified the blade connection as the priority for targeted modification, within the limits of the modeled static cases.*

## REZUMAT

*Cadrul unui echipament purtat de tractor pentru tăierea rădăcinilor pomilor trebuie să transmită rezistența solului și a rădăcinilor, menținând poziția cuțitului. Studiul a evaluat răspunsul structural static al ansamblului pentru încărcări corespunzătoare solului nisipos, lutos și argilos, utilizând SolidWorks Simulation. Echipamentul a fost poziționat la un unghi de lucru de 45°, modelul CAD a fost simplificat, iar cilindrii hidraulici au fost considerați corpuri rigide. Componentele deformabile au utilizat materiale izotrope liniar-elastice, contact global de tip bonded, zece conectori distribuiți de tip bolț, fixarea zonei de cuplare la tractor și o rețea bazată pe curbură, cu 254.653 noduri și 128.499 elemente. Sumele scalare ale rezistenței au fost 7,685, 11,855 și 16,025 kN. Tensiunile von Mises maxime au fost 370,88, 589,24 și 807,47 MPa, deplasările rezultante maxime au fost 22,74, 41,52 și 60,28 mm, iar coeficienții de siguranță minimi calculați au fost 0,7415, 0,4667 și 0,3406. Fiecare tensiune maximă s-a localizat în nodul 23555, pe piesa de legătură a ansamblului cuțitului. Localizarea repetată a identificat conexiunea cuțitului ca prioritate pentru modificări țintite, în limitele cazurilor statice modelate.*

## INTRODUCTION

Root pruning is used in orchard and urban-tree management to alter the spatial distribution and physiological activity of roots, control excessive vegetative growth, and manage conflicts between roots and adjacent infrastructure. The response is not universally beneficial: it depends on species, tree age, pruning distance, root diameter, orientation, soil conditions, and the amount of root system removed.

Apple-orchard trials have shown that root pruning can modify shoot growth and fruiting, whereas controlled studies have reported changes in rhizosphere properties, leaf nutrition, photosynthesis, and growth after root removal *(Mitre et al., 2012; Jing et al., 2017; Jing et al., 2018)*. Consequently, the operation must be controlled rather than treated as indiscriminate root severance.

The mechanical environment is equally important. Root systems adapt to directional mechanical stimuli, while cutting a structural root can alter anchorage and load transfer in ways that depend on the size and position of the removed root *(Beier et al., 2020; Pallafray et al., 2024)*. Guidance on managing tree-root systems therefore emphasizes the need to balance the intended horticultural intervention against tree stability and site constraints *(Watson et al., 2014)*. Measurements of stump uprooting also demonstrate that root–soil systems can generate substantial and variable resistance forces *(Lindroos et al., 2010)*. For mechanized pruning, these observations support the use of defined blade geometry, controlled penetration depth, and monitored cutting force.

Fig. 1 provides a representative example of controlled root cutting from plant-mechanics research, showing how root-system extent, blade geometry, and prescribed cutting sectors can be expressed explicitly. The source apparatus was developed for Artemisia ordosica under mining-subsidence research and it is used only to illustrate the general mechanics of controlled root severance *(Liu et al., 2024)*.

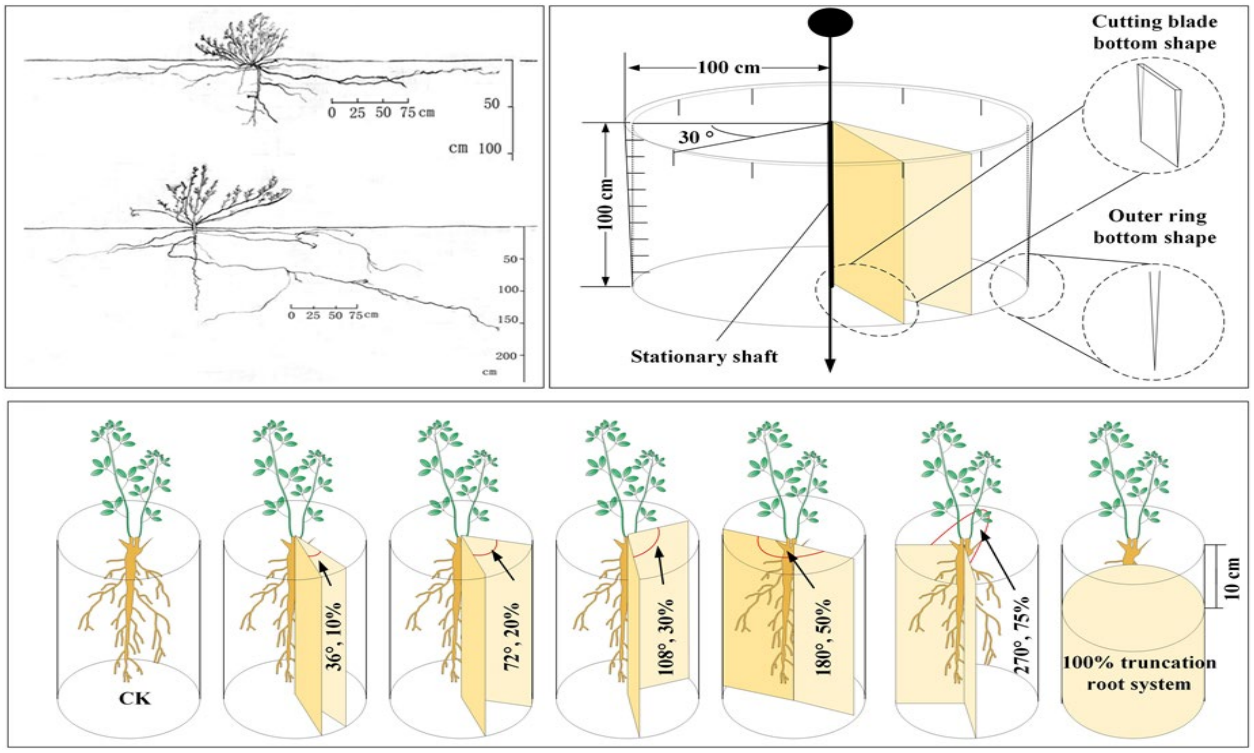



**Fig. 1 - Controlled root-cutting concept: measured root-system distribution; cutting-device and blade geometry; prescribed cutting sectors**
*(Liu et al., 2024)*

The machine considered in this study is a tractor-mounted root cutting equipment whose blade is positioned laterally from the tree row, inserted hydraulically to the selected depth, and pulled through the soil. Its supporting frame, telescopic members, blade-holder arm, traverse, pins, and hydraulic components must transmit the combined cutting, soil-deformation, friction, and root-severing actions to the tractor hitch *(Zaica et al., 2025)*. Frame stiffness and the behavior of the blade connection influence the maintained blade trajectory, working depth, and transfer of loads through the assembly. A structural assessment must therefore address both the magnitude and localization of the response under soil-specific loads.

Finite element analysis (FEA) is widely used in agricultural engineering because it can represent complex load paths, locate stress concentrations, compare design variants, and support mass reduction before physical prototypes are finalized. A review of agricultural applications emphasized that the reliability of such conclusions depends on appropriate material data, contact and boundary idealizations, mesh quality, and convergence assessment *(Velloso et al., 2018)*.

Structural and modal simulations of a coffee-harvester chassis illustrated how static stress and natural-frequency results can guide frame design *(Silva et al., 2018)*. Related frame studies have addressed resonance control in a precision seeder, idealized connections in a watering-furrow implement, and sensitivity-based lightweight optimization of a residual-film recovery machine *(Cardei et al., 2021; Wang et al., 2021; Zhao et al., 2024)*. These machines and load environments are not equivalent to root cutting, but

they demonstrate the value of tracing loads through agricultural structures rather than assessing isolated members only.

Recent investigations also show why numerical performance should be interpreted together with validation and modeling scope. Virtual tests of a tractor roll-over protective structure compared predicted responses with full-scale tests *(Lim et al., 2023)*. Rotary-mower studies assessed both transport and harvesting configurations, highlighting that a change in operating condition changes the governing load path *(Celik et al., 2023; Celik et al., 2024)*.

For a mower beam, experimental strain data were used to update the finite element model before fatigue-oriented use *(Steengaard et al., 2024)*. These examples do not transfer their quantitative limits to a root cutter; they establish that a static model is an engineering screening and design tool whose assumptions and applicability must be stated explicitly. Published information on the present root cutting machine defines its operating principle and soil-dependent cutting resistances *(Zaica et al., 2025)*, but it does not report a comparative structural evaluation of the modeled assembly for the three maximum-resistance soil cases.

The objective of this study was therefore to (i) document the SolidWorks Simulation model preparation, materials, interactions, restraints, loads, and mesh; (ii) compare von Mises stress, resultant displacement, equivalent strain, reactions, and factor of safety for sandy, loamy, and clay soil; (iii) identify the part governing the maximum local response; and (iv) define focused modification and validation priorities without extending the static results to fatigue life or field durability.

## MATERIALS AND METHODS

The root cutting machine comprises a main framework, blade-holder arm, sliding pipe, traverse, hydraulic system, foot support, concrete block, and a force-monitoring system (Fig. 2). The implement is mounted on a tractor; the blade is moved laterally to the required distance from the tree row and hydraulically inserted, after which tractor motion produces the cutting path.

The maximum working depth of 500 mm, a maximum horizontal telescopic extension of 500 mm, an adjustable blade inclination of 45–70°, and an approximate total mass of 600 kg including the concrete block. Table 1 summarizes the available specifications.

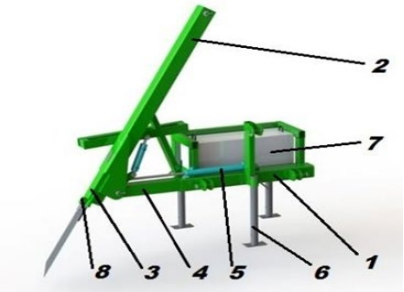



**Fig. 2 - Design and principal components of the experimental tree root cutting machine**

*1 - framework; 2 - blade-holder arm; 3 - sliding pipe; 4 - traverse; 5 - hydraulic system; 6 - foot support; 7 - concrete block; 8 - cutting-force monitoring system*
*(Zaica et al. 2025).*

**Table 1**

**Reported operating specifications of the tree root cutting machine**

| Parameter | Reported value |
|---|---|
| Maximum working depth | 500 mm |
| Maximum horizontal telescopic extension | 500 mm |
| Blade inclination range | 45–70° |
| Total equipment mass | Approximately 600 kg |
| Tractor power used | 100 hp (74.6 kW) |
| Frame overall dimensions and structural-member sections | 2093…2593 x 843 x 2220 mm (L x W x h) |

Three SolidWorks Simulation static studies represented the equipment under sandy-, loamy-, and clay-soil resistance components. Model preparation began by placing the equipment in its working configuration with the blade at a 45° angle. The CAD model was then simplified while retaining the principal

load-transfer arrangement. After the working position had been established, the hydraulic cylinders were represented as rigid bodies so that they maintained the prescribed mechanism geometry and transferred load without treating cylinder-body deformation as an evaluated response. The deformable model retained the framework, arm, sliding member, traverse, blade assembly, load cell, plates, and profiles listed in the reports. Components were assigned 1.0044 S275JR steel, 1.0545 S355N steel, or normalized AISI 4340 steel and were modeled as homogeneous, isotropic, linear-elastic materials. S275JR was assigned to the principal frame, arm, traverse, and associated structural bodies. S355N was limited to the load-cell and blade-guide components listed in the reports.

The cutting-blade part is made of Hardox500, but normalized AISI 4340 was deliberately used as the substitute material in the simulations. Consequently, all numerical results reflect the AISI 4340 property set rather than certified Hardox 500 properties. The transcribed material data are given in Table 2.

**Table 2**

**Material properties assigned in the SolidWorks Simulation reports**

| Assigned material | Yield strength (MPa) | Tensile strength (MPa) | Elastic modulus (GPa) | Poisson ratio | Density (kg m$^{-3}$) |
|---|---|---|---|---|---|
| 1.0044 S275JR | 275 | 410 | 210 | 0.28 | 7800 |
| 1.0545 S355N | 275 | 450 | 210 | 0.28 | 7800 |
| AISI 4340, normalized | 710 | 1110 | 205 | 0.32 | 7850 |

The corresponding shear moduli were 79, 79, and 80 GPa, and the thermal-expansion coefficients were $1.10\times10^{-5}$, $1.10\times10^{-5}$, and $1.23\times10^{-5}$ K$^{-1}$ for S275JR, S355N, and AISI 4340, respectively.

A global bonded interaction with independent meshes was specified. Ten distributed pin connectors (connectors 1–8 and 12–13) represented pinned joints. Translation along the pin axis was restrained by the retaining-ring option, rotation about the axis remained free, rotational stiffness was zero, and no connector-strength data were assigned. Six faces in the tractor-attachment region were fixed. Frictional contact was not modeled.

The soil-resistance model separated the total resistance into cutting, soil-deformation, friction, and root-cutting terms:

$$R_t = R_c + R_d + R_f + R_{rc} \quad (1)$$

where:

$R_t$ - total resistance, [N];

$R_c$ - cutting resistance, [N];

$R_d$ - soil-deformation resistance, [N];

$R_f$ - friction resistance, [N];

$R_{rc}$ - root-cutting resistance, [N].

The technical article calculated the resistance components at a 500 mm working depth, a 45° blade angle, and a 1 cm² root cross-section. The mean root-cutting resistance was 67.5 daN (675 N). In each SolidWorks study, Force-1 was the 675 N normal load, Force-2 combined cutting and friction resistance, and Force-3 applied soil-deformation resistance as a normal force on the cutting-edge face. The finite element assembly and mesh can be seen in Fig. 3, and Fig. 4 is showcasing the restraint and applied-load diagrams. Table 3 reports the three load cases and the solved support reactions. Because the force directions differed, the scalar sums in Table 3 are not vector resultants.

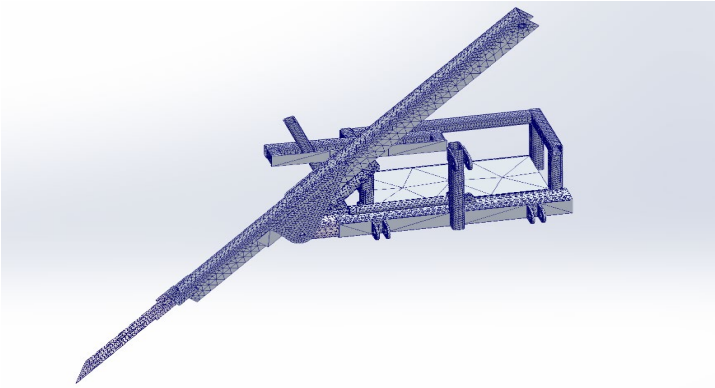
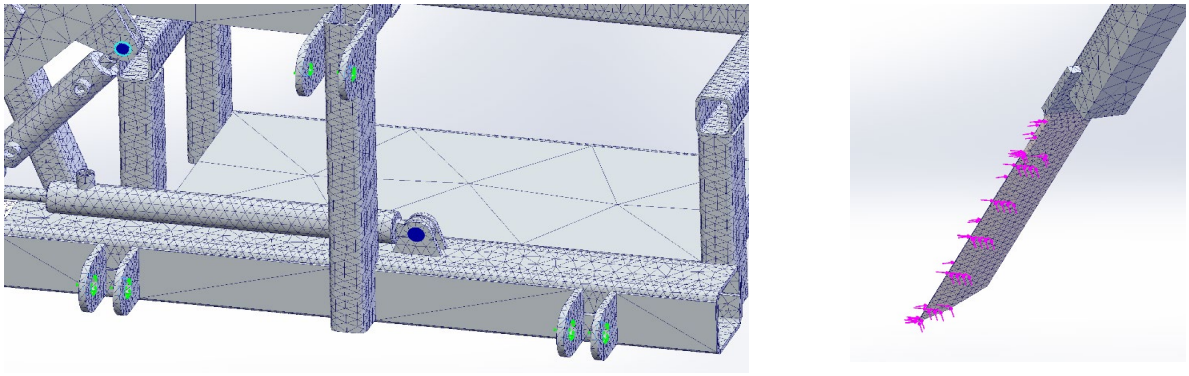


**Fig. 3 - Finite element representation of the machine assembly and blended curvature-based mesh.**



a) b)

**Fig. 4 - Boundary conditions and load components**

*a) fixed tractor-attachment; b) root-cutting load; combined cutting and friction load; and soil-deformation load.*

**Table 3**

**Applied forces and support reactions for the three static studies**

| Soil case | $R_{rc}$ (N) | $R_c$+$R_F$ (N) | $R^d$ (N) | Scalar sum (kN) | Reaction resultant (N) |
|---|---|---|---|---|---|
| Sandy | 675 | 3940 | 3070 | 7.685 | 5623.13 |
| Loamy | 675 | 5800 | 5380 | 11.855 | 8514.26 |
| Clay | 675 | 7670 | 7680 | 16.025 | 11,444 |

The reaction components (X, Y, Z) were (−5279.04, −1326.26, 1411.52) N for sandy soil, (−7676.88, −2521.36, 2683.46) N for loamy soil, and (−10081.8, −3708.07, 3946.45) N for clay soil. Reported reaction moments were zero. The technical article contains a conflict: its abstract interchanges the loamy- and clay-soil total resistances, whereas its tabulated calculations, results discussion, conclusions, and the three simulation reports consistently assign 11.855 kN to loamy soil and 16.025 kN to clay soil. The latter assignments were retained because the simulation reports are the primary evidence for the analyses.

A blended curvature-based solid mesh with high-quality elements and 16 Jacobian points was used in every study. A local control with a nominal element size of 17.708 mm was assigned to 32 components. Table 4 records the mesh statistics common to all cases.

**Table 4**

**Finite element mesh parameters and quality indicators**

| Mesh attribute | Reported value |
|---|---|
| Mesh | Blended curvature-based solid mesh |
| Element quality setting | High quality; 16 Jacobian points |
| Maximum element size | 275.097 mm |
| Minimum element size | 13.7549 mm |
| Local mesh control | 17.708 mm on 32 components |
| Nodes | 254,653 |
| Elements | 128,499 |
| Maximum aspect ratio | 183.13 |
| Elements with aspect ratio < 3 | 76.6% |
| Elements with aspect ratio > 10 | 0.308% |
| Distorted elements | 0% |

Each study was a small-displacement linear static analysis solved using the automatic solver selection. Large displacement, soft springs, inertial relief, adaptive remeshing, and Flow Simulation pressure were disabled; incompatible bonding was detected automatically. Free-body forces were requested. The evaluated outputs were von Mises stress, resultant displacement, equivalent strain, reactions, and factor of safety.

Equation (2) provides a unit threshold for the local linear-elastic yield indicator. Yield acceptance was evaluated by comparing the maximum von Mises stress with the yield strength assigned at the critical node.

The yield-based factor was interpreted as

$$n_y = \frac{S_y}{\sigma_{vm,max}}, \quad (2)$$

where:
$n_y$ - yield-based local factor, [-];
$S_y$ - assigned yield strength, [MPa];
$\sigma_{vm,max}$ - maximum von Mises stress, [MPa].

## RESULTS

The maximum von Mises stress increased from 364.41 MPa in sandy soil to 589.24 MPa in loamy soil and 807.47 MPa in clay soil (Table 5). In all three cases, the maximum occurred at node 23555. Visual examination of the source contours located this node on the connecting part of the blade assembly, whereas the broader frame remained predominantly within the lower contour bands. The repeated location indicated a specific local feature for further modification. Fig. 5 presents the corresponding source-contour locations.

**Table 5**

**Summary of finite element results for the three soil load cases**

| Soil case | Max. von Mises stress (MPa) | Stress node | Max. resultant displacement (mm) | Max. equivalent strain | Min. factor of safety |
|---|---|---|---|---|---|
| Sandy | 364.41 | 23555 | 22.74 | $9.999\times10^{-4}$ | 0.7415 |
| Loamy | 589.24 | 23555 | 41.52 | $1.598\times10^{-3}$ | 0.4667 |
| Clay | 807.47 | 23555 | 60.28 | $2.205\times10^{-3}$ | 0.3406 |

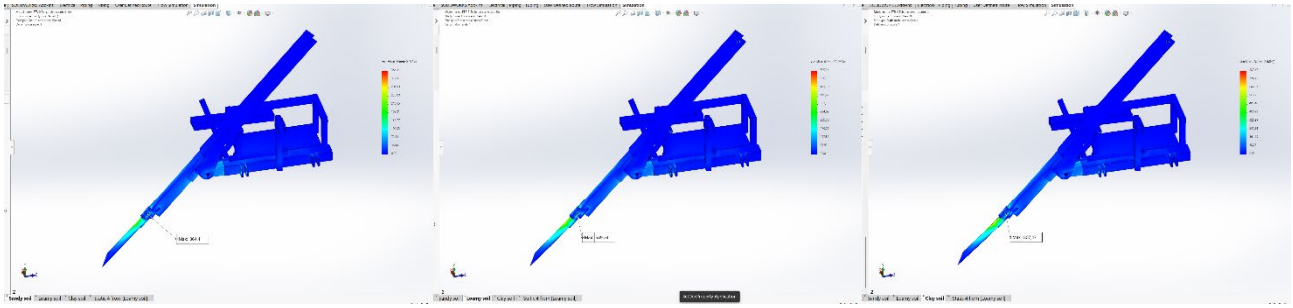


**Fig. 5 - Von Mises stress distributions for the three static load cases; the reported maximum is 364.41, 589.24, and 807.47 MPa at node 23555.**

The minimum factors of safety reported automatically by SolidWorks were 0.7415, 0.4667, and 0.3406. They were consistent with Equation (2) and the 275 MPa yield-strength input associated with the critical connecting part: 275/364.41 = 0.741, 275/589.24 = 0.467, and 275/807.47 = 0.341. Because the solver assumed linear elasticity and small displacement and did not resolve plastic redistribution, the values were treated only as local screening indicators at node 23555 within the modeled cases. The cutting blade was modeled with AISI 4340 as a substitute for Hardox 500; therefore, the controlling automatic factor reflected the material assignment at the connecting part rather than a Hardox-specific blade assessment.

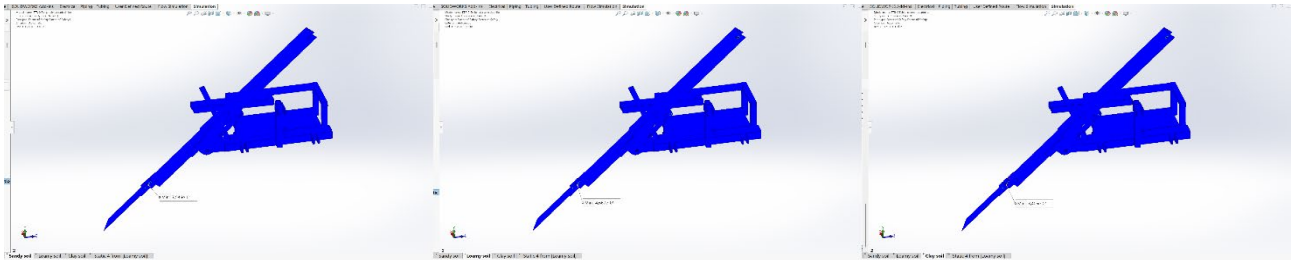


**Fig. 6 - Factor-of-safety distributions for the three static load cases.**

Maximum resultant displacement rose from 22.74 mm to 41.52 mm and 60.28 mm as the prescribed resistance increased. The maximum displacement was reported at node 158840, while the fixed attachment

faces had zero displacement. The common displacement node and the contours indicated a repeatable deformation mode with the largest movement at the blade working end of the assembly. The rigid-body representation of the hydraulic cylinders preserved the working geometry but excluded cylinder flexibility from this response. A formal stiffness decision was not made because no allowable blade-position deviation or frame displacement was supplied. Fig. 7 presents the reported displacement contours.

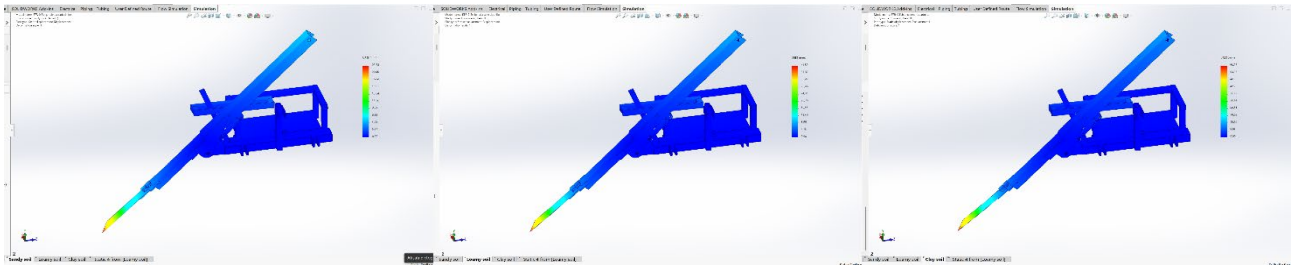


**Fig. 7 - Resultant displacement distributions for the three static load cases.**

The analysis was limited to the supplied small-displacement, linear-elastic static models at the 45° working position. The hydraulic cylinders were represented as rigid bodies, global contact was bonded, the pinned joints were idealized by distributed connectors, and friction was omitted. The reports did not document weld geometry, fastener preload, pin clearance, local contact pressure, the complete defeaturing inventory, element formulation, or mesh convergence. The prescribed loads were calculated from soil and root resistances, no physical strain or displacement validation, fatigue spectrum, buckling assessment, nonlinear material response, impact, or vibration analysis was made. The results identified the blade connection as the principal modification location within the stated assumptions.

## CONCLUSIONS

The finite element evaluation compared the structural response of the tree root cutting machine assembly under sandy-, loamy-, and clay-soil resistance components. The equipment was set at the 45° working position, the model was simplified, and the hydraulic cylinders were treated as rigid bodies. The three cases then used the same material definitions, bonded and pinned interactions, fixed tractor interface, and 254,653-node solid mesh, allowing the effect of the prescribed loads to be compared consistently.

Maximum von Mises stress increased from 364.41 MPa in sandy soil to 589.24 MPa in loamy soil and 807.47 MPa in clay soil. The associated maximum resultant displacements were 22.74, 41.52, and 60.28 mm, and the minimum automatically calculated factors of safety were 0.7415, 0.4667, and 0.3406. All stress maxima occurred at node 23555 on the connecting part of the blade assembly, and all maximum displacements occurred at node 158840.

The common stress location is the principal engineering outcome: it suggests that further development should focus on the blade connecting part. The automatic factor-of-safety values are retained as local linear-elastic screening metrics, while the absence of a specified displacement limit prevents a separate serviceability acceptance decision. Design refinement should assess the local thickness, transition radius, attachment geometry, and load-introduction area around node 23555, followed by local mesh refinement and convergence checks. Because normalized AISI 4340 was used as a substitute for Hardox 500, the final blade assessment should use certified production-material properties. The revised connection should be validated with measured forces, strains, and blade displacement during controlled soil tests; fatigue, dynamic, nonlinear, contact, and buckling analyses should follow only with load spectra and boundary conditions appropriate to field operation.

## ACKNOWLEDGEMENT

The results presented in this article were obtained with the support of MCID through the NUCLEU Programme, project PN 23 04 01 05, “INNOVATIVE TECHNOLOGY FOR THE MAINTENANCE OF FRUIT PLANTATIONS” funding contract no. 9N/01.01.2023.

## REFERENCES

[1] Beier, M. P., Tsugawa, S., Demura, T., & Fujiwara, T. (2020). Root shape adaptation to mechanical stress derived from unidirectional vibrations in Populus nigra. *Plant Biotechnology, 37*(4), 423–428. https://doi.org/10.5511/plantbiotechnology.20.0813a

[2] Cardei, P., Oprescu, M., Constantin, N., Biriș, Ș.-S., & Muraru, S. (2021). Analysis of the resistance frame of the equipment for opening and compartmentalizing watering furrows, using 3D finite elements. *E3S Web of Conferences, 286*, 03009. https://doi.org/10.1051/e3sconf/202128603009

[3] Celik, H. K., Akinci, I., Caglayan, N., & Rennie, A. E. W. (2023). Structural strength analysis of a rotary drum mower in transportation position. *Applied Sciences, 13*(20), 11338. https://doi.org/10.3390/app132011338

[4] Celik, H. K., Akinci, I., Caglayan, N., & Rennie, A. E. W. (2024). Structural strength analysis of a rotary drum mower during harvesting. *Journal of Agricultural Engineering, 55*, 1557. https://doi.org/10.4081/jae.2024.1557

[5] Jing, D.-W., Du, Z.-Y., Wang, M.-Y., Wang, Q.-H., Ma, H.-L., Liu, F.-C., Ma, B.-Y., & Dong, Y.-F. (2018). Regulatory effects of root pruning on leaf nutrients, photosynthesis, and growth of trees in a closed-canopy poplar plantation. *PLOS ONE, 13*(5), e0197515. https://doi.org/10.1371/journal.pone.0197515

[6] Jing, D.-W., Liu, F.-C., Wang, M.-Y., Ma, H.-L., Du, Z.-Y., Ma, B.-Y., & Dong, Y.-F. (2017). Effects of root pruning on the physicochemical properties and microbial activities of poplar rhizosphere soil. *PLOS ONE, 12*(11), e0187685. https://doi.org/10.1371/journal.pone.0187685

[7] Lim, R.-G., Kim, W.-S., Do, Y.-W., Siddique, M. A. A., & Kim, Y.-J. (2023). Performance evaluation of a virtual test model of the frame-type ROPS for agricultural tractors using FEA. *Agriculture, 13*(10), 2004. https://doi.org/10.3390/agriculture13102004

[8] Lindroos, O., Henningsson, M., Athanassiadis, D., & Nordfjell, T. (2010). Forces required to vertically uproot tree stumps. *Silva Fennica, 44*(4), 681–694. https://doi.org/10.14214/sf.135

[9] Liu, Y., Gong, C., Pei, W., Fan, K., & Shen, W. (2024). Chlorophyll a fluorescence as a tool to monitor physiological status in the leaves of Artemisia ordosica under root cutting conditions. *Frontiers in Plant Science, 14*, 1308209. https://doi.org/10.3389/fpls.2023.1308209

[10] Mitre, V., Mitre, I., Sestras, A. F., & Sestras, R. E. (2012). Effect of roots pruning upon the growth and fruiting of apple trees in high density orchards. *Bulletin of University of Agricultural Sciences and Veterinary Medicine Cluj-Napoca. Horticulture, 69*(1), 254–259. https://doi.org/10.15835/buasvmcn-hort:8527

[11] Pallafray, C., Sivarajah, S., & Ruel, J.-C. (2024). Impact of root cutting on Acer platanoides and Tilia cordata tree stability in urban parks: A case study in Quebec City, Canada. *Forests, 15*(6), 1041. https://doi.org/10.3390/f15061041

[12] Silva, E. P. da, Silva, F. M. da, Andrade, E. T. de, & Magalhães, R. R. (2018). Structural static and modal frequency simulations in a coffee harvester's chassis. *Revista Brasileira de Engenharia Agrícola e Ambiental, 22*(7), 511–515. https://doi.org/10.1590/1807-1929/agriambi.v22n7p511-515

[13] Steengaard, J. R., Holm, A. P. K., Arora, V., & Larsen, M. L. (2024). Finite element validation and model updating of beam in agricultural mower for fatigue assessment. *Procedia Structural Integrity, 58*, 61–67. https://doi.org/10.1016/j.prostr.2024.05.011

[14] Velloso, N. S., Costa, A. L. G., Magalhães, R. R., Santos, F. L., & Andrade, E. T. de. (2018). The finite element method applied to agricultural engineering: A review. *Current Agriculture Research Journal, 6*(3), 286–299. https://doi.org/10.12944/CARJ.6.3.08

[15] Wang, J., Xu, C., Xu, Y., Wang, J., Zhou, W., Wang, Q., & Tang, H. (2021). Resonance analysis and vibration reduction optimization of agricultural machinery frame—Taking vegetable precision seeder as an example. *Processes, 9*(11), 1979. https://doi.org/10.3390/pr9111979

[16] Watson, G. W., Hewitt, A. M., Custic, M., & Lo, M. (2014). The management of tree root systems in urban and suburban settings II: A review of strategies to mitigate human impacts. *Arboriculture & Urban Forestry, 40*(5), 249–271. https://doi.org/10.48044/jauf.2014.025

[17] Zaica, A., Ciupercă, R., Harabagiu, A.-N., Ștefan, V., Cismaru, E.-M., Dumitru, Ș., & Zaica, A. (2025). Research on root pruning methods applied to orchard trees. *INMATEH – Agricultural Engineering, 75*(1), 1160–1167. https://doi.org/10.35633/inmateh-75-95

[18] Zhao, P., Lyu, H., Wang, L., Zhang, H., Li, Z., Li, K., Xing, C., & Guoyao, B. (2024). Optimization design of straw-crushing residual film recycling machine frame based on sensitivity and grey correlation degree. *Agriculture, 14*(5), 764. https://doi.org/10.3390/agriculture14050764

# EXPERIMENTAL ANALYSIS AND INTERACTIVE VISUALIZATION OF FLUID MIXING PROCESSES FOR DIFFERENT IMPELLER CONFIGURATIONS

/

# *ANALIZA EXPERIMENTALĂ ȘI VIZUALIZAREA INTERACTIVĂ A PROCESELOR DE AMESTECARE A FLUIDELOR PENTRU DIFERITE CONFIGURAȚII DE AGITATOARE*

**Neluș-Evelin GHEORGHIȚĂ*[1)], Sorin-Ștefan BIRIȘ[1)], Nicoleta UNGUREANU[1)], Gabriel-Alexandru CONSTANTIN[1)], Raluca-Adriana ZOTA[1)], Dragoș-Nicolae DUMITRU[2)]**

[1)] UNSTP Bucharest / Romania; [2)] INMA Bucharest / Romania

**Tel: 0726 453 269; *E-mail: nelus.gheorghita@upb.ro*

***Keywords:*** *fluid mixing, baffled vessel, dimensionless analysis, impeller performance, web-based interface*

## ABSTRACT

*Fluid mixing is a fundamental process in engineering applications, whose performance is strongly influenced by impeller geometry, rotational speed, and vessel configuration. This study presents an experimental and computational approach for the analysis and interactive visualization of mechanically agitated fluid mixing processes. Experiments were conducted using an Armfield CEK apparatus equipped with three impeller types: a flat-blade paddle, a propeller, and a Rushton turbine, tested in baffled and unbaffled configurations. Rotational speed, hydraulic force, and absorbed power were experimentally determined and processed using linear interpolation and dimensionless analysis. Reynolds and power numbers were calculated to characterize the operating conditions and compare the investigated configurations. The results showed a clear dependence of absorbed power on rotational speed and impeller configuration, with experimentally determined power-law exponents ranging from 2.8 to 3.1. The experimental and calculated data were integrated into an interactive web-based interface enabling real-time selection of impeller type, baffle configuration, and rotational speed, together with automatic calculation and graphical visualization of the main process parameters. The developed approach provides a practical tool for comparative analysis and interpretation of mechanically agitated fluid mixing systems.*

## REZUMAT

*Amestecarea fluidelor reprezintă un proces fundamental în aplicațiile inginerești, a cărui performanță este influențată semnificativ de geometria agitatorului, turația acestuia și configurația vasului. Studiul prezintă o abordare experimentală și computațională pentru analiza și vizualizarea interactivă a proceselor de amestecare a fluidelor prin agitare mecanică. Experimentele au fost realizate pe standul Armfield CEK, utilizând trei tipuri de agitatoare: agitator cu palete plate, elice și turbină Rushton, testate în configurații cu și fără șicane. Turația, forța hidraulică și puterea absorbită au fost determinate experimental, iar datele obținute au fost prelucrate prin interpolare liniară și analiză adimensională. Numerele Reynolds și de putere au fost calculate pentru caracterizarea condițiilor de funcționare și compararea configurațiilor analizate. Rezultatele au evidențiat dependența puterii absorbite de turație și de configurația agitatorului, exponenții determinați experimental pentru legea de variație a puterii fiind cuprinși între 2,8 și 3,1. Datele experimentale și calculate au fost integrate într-o interfață web interactivă, care permite selectarea în timp real a tipului de agitator, a configurației șicanelor și a turației, precum și calculul automat și reprezentarea grafică a principalilor parametri ai procesului.*

## INTRODUCTION

Numerous chemical and engineering processes make extensive use of stirred vessels. In order to achieve homogenization, heat transfer, gas dispersion, solid suspension, and other processes, they are also crucial in the food sector, bioprocessing, wastewater treatment, and mineral processing *(Jaszczur, M., Młynarczykowska, A., Demurtas, L., 2020)*. They are crucial to a number of processes, including the production of suspensions, slow-sedimenting mixes, gas dispersion in liquids, and the inhibition of sediment aggregation. Through a variety of analyzes, researchers were able to gain some understanding of the fundamental evolution and process of fluid mixing, particularly with regard to single-phase flow. However, there is still a lack of knowledge regarding the fluid behavior, especially in shear-sensitive cultures that require a suitable gas intake or in unbaffled single-impeller stirred vessels, which are crucial in the

pharmaceutical and cosmetics industries that demand the highest standards of cleanliness *(Scargiali, F., Busciglio, A., Grisafi, F. et al., 2013).*

Finding the most effective, nondestructive, and low-power mixing method has always been the primary objective, regardless of an industrial operation. Because of this, numerous studies have been conducted to find different impeller shapes that could produce a high-quality mixture, typically with low axial velocity, low shear stress, and low internal heat generation—all of which are important factors for the production of vitamins, enzymes, and food *(Zhou, S., Yang, Q., Lu, L. et al., 2022)*.

The power consumption, the fluid phenomenon, the hydrodynamics of the flow, and the mixing process employing the Rushton-type impellers were all compared in a study conducted..The Rushton turbine shape adjustment, which also succeeded in increasing the local fluid velocity and obtaining increased turbulence intensity surrounding the improved impeller, resulted in an 18% reduction in power, according to the analyzes *(Su, T., Yang, F., Li, M. et al., 2017)*.

The flow inside a stirred tank is strongly influenced by the interaction between the impeller and the baffles, as well as by the characteristic flow pattern generated by the impeller. Radial-flow impellers, such as the Rushton turbine, discharge the fluid predominantly towards the vessel walls, generating strong radial jets and high turbulence levels. In contrast, marine propellers primarily generate axial flow, promoting fluid circulation along the vertical direction of the vessel.

These distinct hydrodynamic characteristics result in different mixing patterns and power requirements, particularly when baffled and unbaffled configurations are considered *(Lugo Hinojosa, J. E., Yáñez Varela, J. A., Alonzo García, A. et al., 2026)*.A thorough grasp of stirred tank mixers is crucial, particularly in light of the industry's current evolution, which is motivated by cost-effectiveness, sustainability, and the constant need to improve product quality.

The rate of power consumption is one of the key factors for mechanical and chemical engineering since it is directly tied to the overall cost of industrial activities. Consequently, it is preferable to perform mixing activities with the lowest rate of energy consumption and maximum mixing efficiency *(Salho, A. K., Hamzah, D. A., 2024).* Reducing power usage has become essential since it directly results in cost savings, which benefits mixer manufacturers. Roshten-6 turbines were used in the rotary mixer configuration by Zadghaffari et al.. Using numerical solution techniques, the power consumption was calculated as a dimensionless factor (power number) *(Zadghaffari, R., Moghaddas, J. S., Revstedt, J., 2010)*.

The hydrodynamic behaviour of mechanically stirred vessels is strongly influenced by impeller rotation and tank configuration. In baffled tanks equipped with a Rushton turbine, the impeller generates characteristic circulation loops and complex turbulent flow structures.

Computational studies have shown that radial, tangential, and axial velocity components can be used to describe these flow patterns, while global parameters such as the Reynolds number and power number provide useful indicators for characterizing the operating regime and energy requirements of the mixing process *(Patil, H., Patel, A. K., Pant, H. J. et al., 2018)*.

The hydrodynamic behaviour of stirred tanks equipped with Rushton turbines is strongly affected by vessel geometry and the interaction between the rotating impeller and internal elements. In turbulent regimes, modifications of the vessel configuration can significantly alter vortex formation and power requirements. It was investigated a Rushton turbine over Reynolds numbers ranging from $10^4$ to $10^5$and demonstrated that changes in the internal configuration of the vessel can substantially influence both power consumption and vortex size.

These findings emphasize that the energetic performance of a mixing system cannot be evaluated solely from impeller rotational speed, but should also account for the geometrical configuration of the vessel and its interaction with the generated flow *(Youcefi, S., Bouzit, M., Youcefi, A. et al., 2023)*. The effect of vessel internals on power consumption also depends on the predominant flow pattern generated by the impeller.It was showed that internal elements, including baffles and probes, increase the turbulent power number and modify the flow structure inside stirred vessels *(Charalambidou et al., 2024).*

Other results further indicated that internal elements have a stronger influence on radial-flow impellers than on axial-flow impellers, producing a more pronounced increase in power number *(Hoseini, S. S., Najafi, G., Ghobadian, B. et al., 2021)*. This distinction is particularly relevant when comparing impellers with different discharge characteristics, since radial and axial configurations may respond differently to the introduction of baffles and other vessel internals *(Martínez-Delgadillo, S. A., Alonzo-Garcia, A., Mendoza-Escamilla, V. X. et al., 2019)*.

## MATERIALS AND METHODS

The experimental investigations were carried out using an Armfield CEK mixing apparatus (fig.1) designed for the study of mechanically agitated fluid systems.




**Fig. 1 - Experimental setup used for the investigation of mechanically agitated fluid mixing**

The experimental setup consisted of a cylindrical mixing vessel equipped with an interchangeable impeller system, allowing different impeller geometries and vessel configurations to be investigated under comparable operating conditions. Water was used as the working fluid throughout all experiments. The vessel had an internal diameter of 260 mm and a useful height of 440 mm. The liquid height was maintained at approximately 0.30 m, corresponding to a working volume of approximately 15.9 L. The experimental system allowed the impeller rotational speed to be varied and the corresponding hydraulic force and absorbed power to be determined. These parameters were recorded for each operating condition and subsequently used for the comparative and dimensionless analysis of the mixing process.

Three interchangeable impeller configurations were investigated: a flat-blade paddle, a three-blade marine propeller, and a disc turbine, presented in figure 2. The marine propeller consisted of three blades equally spaced at 120° around the shaft and was characterized by a twisted blade geometry, generating predominantly axial flow. The disc turbine consisted of a 120 mm diameter disc equipped with eight flat blades uniformly distributed around its circumference, generating predominantly radial flow. A two-blade flat paddle was also investigated as a geometrically simpler impeller configuration .Each impeller was tested under both baffled and unbaffled vessel conditions. The baffled configuration consisted of four rectangular baffles symmetrically positioned at 90° intervals along the inner wall of the vessel. Each baffle had a width of 25 mm, corresponding approximately to one tenth of the vessel diameter, a thickness of 3 mm, and a height of 440 mm. The same vessel geometry and working fluid were maintained throughout the experiments to allow direct comparison between the investigated configurations.



**Fig. 2 - Types of impellers used in the experimental study: marine propeller, disc turbine, and flat-blade paddle**

The experimental procedure was performed separately for each of the three investigated impellers under both baffled and unbaffled vessel configurations. Water was used as the working fluid and the same liquid level was maintained throughout all measurements.

For each configuration, the impeller rotational speed was progressively varied over the investigated operating range. At each operating point, the rotational speed, hydraulic force, and absorbed power were recorded after the operating conditions had stabilized. The same procedure was repeated for the flat-blade paddle, marine propeller, and disc turbine, allowing direct comparison of their power characteristics under identical vessel conditions. The experimental datasets obtained for the six impeller–vessel configurations

were subsequently used for numerical processing, dimensionless analysis, and implementation within the interactive interface.

The main operating parameters were determined from the rotational speed measured with the tachometer and the force indicated by the dynamometer. The measured values were subsequently used to calculate the force, torque, angular velocity, and power required for the mixing process. The force acting on the dynamometer arm was calculated from the value indicated by the force balance:

$$F = M_f \cdot 10^{-3}\ [kg] \cdot 9{,}81\ [m/s^2]\ [N] \quad (1)$$

where:

$M_f$ - the value indicated by the force balance

The torque transmitted by the agitator shaft was calculated based on the force and the length of the dynamometer arm (r = 0.11 m):

$$M_t = F \cdot r = M_f \cdot 9{,}81 \cdot 0{,}11 \cdot 10^{-3}\ [N \cdot m] \quad (2)$$

The angular velocity was determined from the RPM reading on the tachometer:

$$\omega = n \cdot 2\pi / 60\ [rad/s] \quad (3)$$

The power consumed during mixing was calculated as the product of the torque and the angular velocity:

$$P = M_t \cdot \omega\ [W] \quad (4)$$

An interactive web-based interface was developed for the processing and visualization of the experimental data obtained from the mixing tests. The application was implemented as a standalone HTML file and can be executed directly in a web browser, without requiring the installation of dedicated software. The experimental datasets corresponding to the three investigated impeller types and to the baffled and unbaffled configurations were integrated directly into the application. The interface allows the user to select the impeller type and vessel configuration and to vary the rotational speed within the investigated range. Based on the selected operating conditions, the corresponding experimental values are processed automatically and used for the graphical representation of the mixing parameters. Intermediate values between consecutive experimental measurements are determined by linear interpolation.

The computational procedure underlying the interface was initially developed in MATLAB. The implemented routine was used to organize the experimental datasets and perform the calculations associated with each selected operating condition. For a given rotational speed, the corresponding power and hydraulic force were determined by linear interpolation between adjacent experimental points. The same computational procedure was used to determine the angular velocity and the dimensionless parameters required for the characterization of the mixing process. An excerpt of the MATLAB routine used for experimental data processing is presented in Fig. 3.

```
252          % Calcule
253          omega = n_sel * pi / 30;
254          Re    = (rho * (n_sel/60) * D_ag^2) / mu;
255
256          % Interpolare P si F la turatie selectata
257          if n_sel >= min(n_date) && n_sel <= max(n_date)
258              P_sel = interp1(n_date, P_date, n_sel, 'linear');
259              F_sel = interp1(n_date, F_date, n_sel, 'linear');
260              in_range = true;
261          else
262              P_sel = NaN; F_sel = NaN;
263              in_range = false;
264          end
265
266          Np = P_sel / (rho * (n_sel/60)^3 * D_ag^5);
267
```

**Fig. 3 - Excerpt of the MATLAB routine used for experimental data processing and parameter calculation.**

## RESULTS

A summary of the experimental conditions and the ranges of the main measured parameters for each investigated impeller and vessel configuration is presented in Table 1.

**Table 1**

**Summary of the experimental conditions and measured parameters**

| Impeller | Configuration | Speed range [rpm] | Force range [N] | Power range [W] |
|---|---|---|---|---|
| Flat-blade paddle | Baffled | 61–204 | 0.098–0.903 | 0.07–2.08 |
| Flat-blade paddle | Unbaffled | 73–414 | 0.137–0.981 | 0.002–4.64* |
| Marine propeller | Baffled | 75–500 | 0.049–0.147 | 0.04–0.84 |
| Marine propeller | Unbaffled | 75–508 | 0.009–0.098 | 0.01–0.59 |
| Disc turbine | Baffled | 66–374 | 0.049–0.952 | 0.03–4.08 |
| Disc turbine | Unbaffled | 77–500 | 0.078–0.196 | 0.07–1.41 |

As shown in Fig. 4, power consumption increased with rotational speed for all investigated impellers under baffled conditions. However, considerable differences were observed depending on the impeller geometry.

The propeller exhibited the lowest power requirements throughout the investigated range, reaching 0.84 W at 500 rpm. In contrast, the disc turbine showed a substantially stronger increase in power consumption, reaching 4.08 W at 374 rpm. The flat-blade paddle exhibited an intermediate behaviour, with power values approaching 2 W at approximately 200 rpm. These results indicate that impeller geometry strongly influences the energy requirements of the mixing process under baffled conditions.

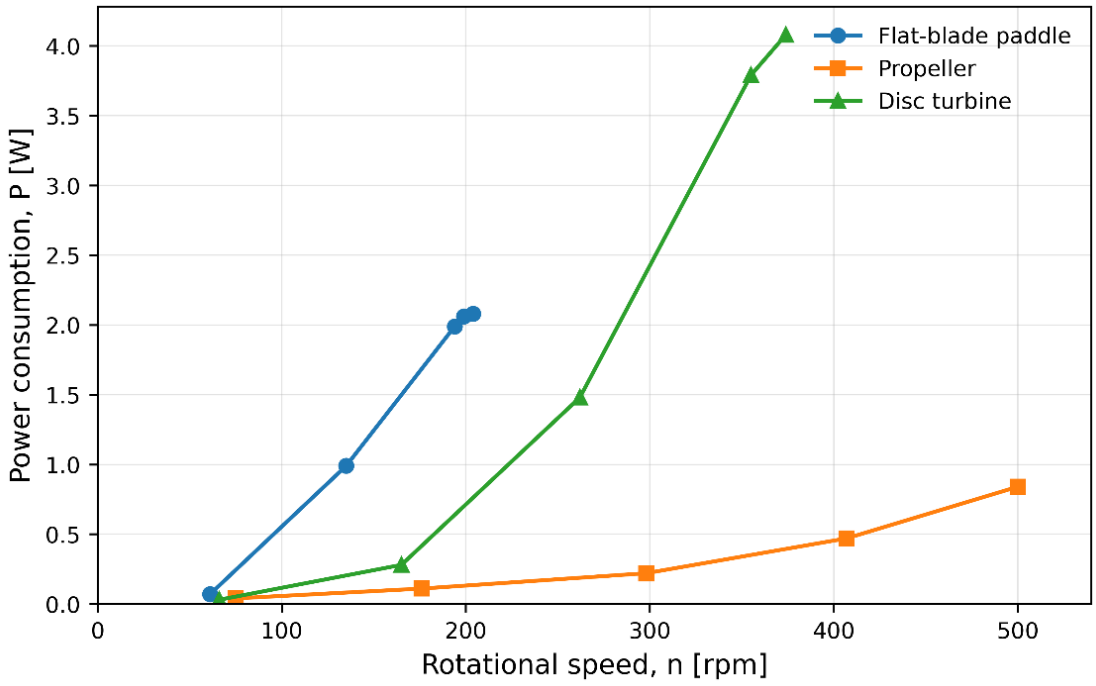



**Fig. 4 - Power consumption as a function of rotational speed for the investigated impellers under baffled conditions.**

Under unbaffled conditions, the investigated impellers also exhibited different power consumption characteristics (Fig. 5). The propeller maintained relatively low power requirements over the entire operating range, reaching 0.59 W at 508 rpm, while the disc turbine reached 1.41 W at 500 rpm. The flat-blade paddle exhibited a more pronounced increase at higher rotational speeds, reaching a maximum measured power of 4.64 W at 414 rpm.

The observed differences further demonstrate that the relationship between rotational speed and power consumption depends not only on impeller geometry, but also on the vessel configuration.

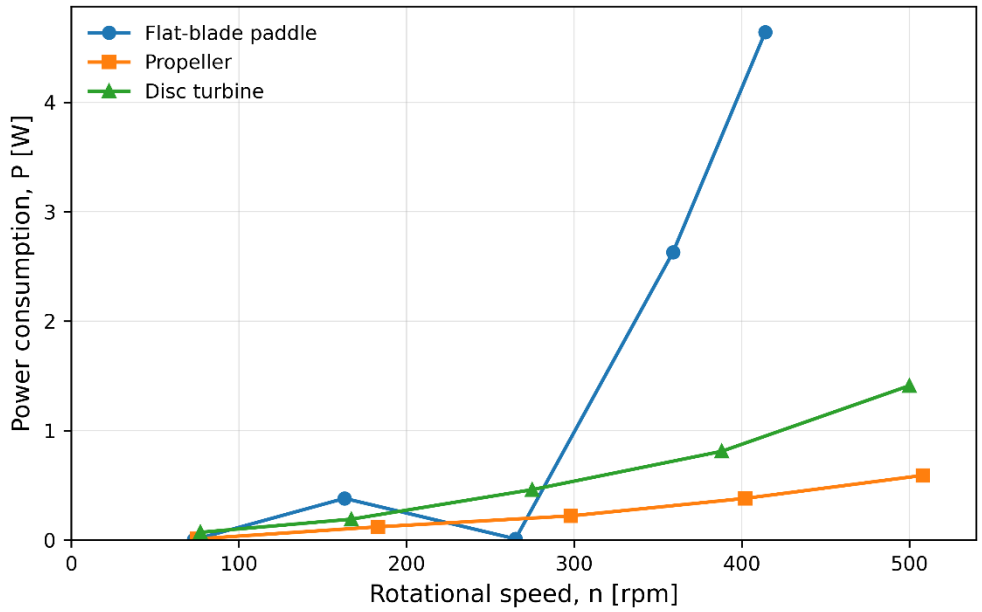



**Fig. 5 - Power consumption as a function of rotational speed for the investigated bimpellers under unbaffled conditions.**

The influence of vessel configuration is particularly evident for the disc turbine, as illustrated in Fig. 6. At low rotational speeds, the difference between the baffled and unbaffled configurations was relatively small.

As the rotational speed increased, however, the two power consumption curves progressively diverged. Under baffled conditions, the power consumption reached 4.08 W at 374 rpm, whereas the unbaffled configuration required only 0.81 W at a comparable rotational speed of 388 rpm. This substantial difference indicates a strong interaction between the radial flow generated by the disc turbine and the baffles, resulting in considerably higher power requirements.

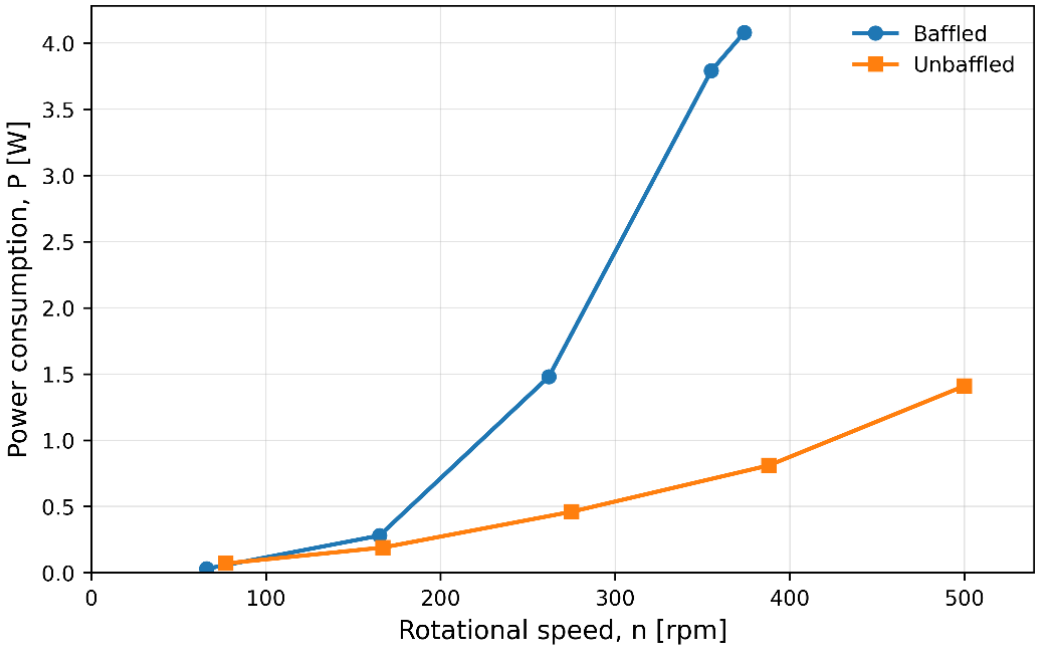



**Fig. 6 - Influence of baffles on the power consumption of the disc turbine.**

Based on the experimental datasets and the computational procedure initially implemented in MATLAB, an interactive web-based interface was developed to facilitate the analysis and visualization of the investigated mixing configurations. The final interface integrates the experimental data and calculated parameters within a single graphical environment, as illustrated in Fig. 7.




**Fig. 7 - Interactive web-based interface developed for the analysis and visualization of experimental mixing data.**

The interface provides simultaneous access to the main parameters characterizing the mixing process and their graphical representation. The user can select the impeller type, choose between baffled and unbaffled vessel configurations, and continuously adjust the rotational speed within the investigated range. For each selected operating point, the corresponding Reynolds number, angular velocity, power consumption, and power number are automatically calculated and displayed.

The graphical panels provide the variation of power consumption and hydraulic force with rotational speed, as well as the relationship between power number and Reynolds number. In addition, the baffled and unbaffled configurations can be directly compared, allowing the influence of vessel configuration on the energetic behaviour of the mixing system to be assessed interactively.

## CONCLUSIONS

This study presented the development of an interactive web-based interface for the analysis and visualization of experimental data obtained from mechanically agitated fluid mixing processes. Experimental investigations were performed using three different impeller configurations—a flat-blade paddle, a propeller, and a disc turbine—under both baffled and unbaffled conditions, with water used as the working fluid.

The experimental results confirmed that power consumption is strongly influenced by rotational speed, impeller geometry, and vessel configuration. Among the investigated impellers, the propeller exhibited the lowest power requirements, whereas the disc turbine showed a substantially higher power demand under baffled conditions, reaching 4.08 W at 374 rpm. The comparison between baffled and unbaffled operation highlighted the particularly strong influence of baffles on the energetic behaviour of the disc turbine.

The computational procedure was initially implemented in MATLAB and subsequently transferred to a standalone web-based environment. The resulting interface integrates experimental data, parameter calculation, linear interpolation, and graphical visualization, enabling interactive comparison of the investigated mixing configurations. The developed approach provides an accessible tool for experimental data analysis without requiring dedicated computational software and may serve as a basis for further extensions involving additional impeller geometries, fluids, and operating conditions.

## ACKNOWLEDGEMENT

This research was supported by the project CNFIS-FDI-2026-F-0049 “Asigurarea eficienței operaționale a bazei de aplicații practice pentru sisteme biotehnice în livezi, vii, solarii și grădini (EFIBIOTECH)”, from the Ministry of Education and Research through the Executive Agency for Financing Higher Education, Research, Development and Innovation.

## REFERENCES


[1] Charalambidou, A. D., Wyrobnik, T. A., Micheletti, M., & Ducci, A. (2024). Investigation of the impact of probes and internals on power and flow in stirred tank reactors. Chemical Engineering Science, 286, 119683. https://doi.org/10.1016/j.ces.2023.119683

[2] Hoseini, S. S., Najafi, G., Ghobadian, B., & Akbarzadeh, A. H. (2021). Impeller shape-optimization of stirred-tank reactor: CFD and fluid structure interaction analyses. *Chemical Engineering Journal*, *413*, 127497.

[3] Jaszczur, M., Młynarczykowska, A., & Demurtas, L. (2020). Effect of impeller design on power characteristics and Newtonian fluids mixing efficiency in a mechanically agitated vessel at low Reynolds numbers. Energies, 13(3), 640. https://doi.org/10.3390/en13030640

[4] Lugo Hinojosa, J. E., Yáñez Varela, J. A., Alonzo García, A., Rivadeneyra Romero, G., & Martínez Delgadillo, S. A. (2026). Effect of different impeller types on mixing efficiency in mechanically stirred tanks with tubular baffles. Processes, 14(2), 225. https://doi.org/10.3390/pr14020225

[5] Martínez-Delgadillo, S. A., Alonzo-Garcia, A., Mendoza-Escamilla, V. X., González-Neria, I., & Yáñez-Varela, J. A. (2019). Analysis of the turbulent flow and trailing vortices induced by new design grooved blade impellers in a baffled tank. *Chemical Engineering Journal*, *358*, 225–235

[6] Patil, H., Patel, A. K., Pant, H. J., & Venu Vinod, A. (2018). CFD simulation model for mixing tank using multiple reference frame (MRF) impeller rotation. ISH Journal of Hydraulic Engineering, 27(2), 200–209. https://doi.org/10.1080/09715010.2018.1535921

[7] Salho, A. K., & Hamzah, D. A. (2024). A review of stirred tank dynamics: Power consumption, mixing time and impeller geometry. International Journal of Heat and Technology, 42(3), 1081–1092. https://doi.org/10.18280/ijht.420335

[8] Scargiali, F., Busciglio, A., Grisafi, F., Tamburini, A., & Micale, G. (2013). Power consumption in uncovered unbaffled stirred tanks: Influence of viscosity and flow regime. Industrial & Engineering Chemistry Research, 52, 14998–15005.

[9] Su, T., Yang, F., Li, M., & Wu, K. (2017). Characterization of the hydrodynamics of a covering plate Rushton impeller. Chinese Journal of Chemical Engineering, 26, 1392–1400.

[10] Youcefi, S., Bouzit, M., Youcefi, A., & Mokhefi, A. (2023). Effect of an inclined slots on the power consumption and vortices size in a Rushton turbine agitated tank. Chinese Journal of Mechanical Engineering, 36, 147. https://doi.org/10.1186/s10033-023-00981-8

[11] Zadghaffari, R., Moghaddas, J. S., & Revstedt, J. (2010). Large-eddy simulation of turbulent flow in a stirred tank driven by a Rushton turbine. Computers & Fluids, 39(7), 1183–1190. https://doi.org/10.1016/j.compfluid.2010.03.001

[12] Zhou, S., Yang, Q., Lu, L., Xia, D., Zhang, W., & Yan, H. (2022). CFD analysis of sine baffles on flow mixing and power consumption in stirred tank. Applied Sciences, 12, 5743.

# ANALYSIS ON PHYSICO-MECHANICAL PARAMETERS AND TECHNOLOGICAL FLOW OF CATTLE SLAUGHTERING IN MODERN SLAUGHTERHOUSES

/

# *ANALIZA PRIVIND PARAMETRII FIZICO-MECANICI ȘI FLUXUL TEHNOLOGIC DE ABATORIZARE A BOVINELOR ÎN ABATOARELE MODERNE*

**Ion Mihăiță GRIGORE[1, 2], Gheorghe VOICU*[2], Paula TUDOR[2], Daniela IANITCHI[3]**
[1] Forestry Technological High School, Ramnicu Valcea, Valcea County / Romania;
[2] National University of Science and Technology POLITEHNICA Bucharest, Faculty of Biotechnical Systems Engineering / Romania;
[3] University of Agronomic Sciences and Veterinary Medicine Bucharest / Romania
*Tel: 0040 724 715 585;*E-mail: gheorghe.voicu@upb.ro*

***Keywords:*** *bovine slaughtering, technological flow, mechanical stress, carcass chilling, cutting forces, rheological properties*

**ABSTRACT**

*This paper presents a research on an analysis of the technological flow and physical-mechanical parameters in the primary processing, industrial slaughtering of cattle in modern slaughterhouses. Some primary mechanical operations – stunning, bleeding, skinning, splitting and quartering – were performed to measure mechanical strength, energy consumption and dynamic stresses. Dynamic cutting indices were analyzed using specific equipment and strain gauges on automatic splitting saws and skinning platforms. Following experimental measurements, an average splitting force of 4.25 kN was indicated for adult cattle carcasses (average mass 650 kg), with a mechanical energy consumption of 12.8 kJ per carcass. A thermodynamic model of primary refrigeration demonstrated that forced convection at 1.5 m/s reduces weight loss from 2.1% to 1.35%, while maintaining myofibrillar integrity. Following rheological and texture analysis (TPA) through experimental analyses, the direct correlation between the evolution of post-mortem pH and Warner-Bratzler shear force was confirmed (decrease from 68.4 N at 24 h to 38.2 N after 14 days of maturation). The experimental research yielded results that provide a relevant mathematical and technical framework for optimizing industrial equipment, reducing energy consumption by 14.2% and increasing quality yield and quality parameters in compliance with European animal welfare and hygienic standards.*

**REZUMAT**

*Aceasta lucrare prezintă o cercetare privind o analiză a fluxului tehnologic și a parametrilor fizico-mecanici la prelucrarea primara, abatorizarea industrială a bovinelor în abatoare moderne. Unele operații mecanice primare – asomare, sângerare, jupuire, despicare și porționare in sferturi – au fost realizate pentru măsurarea rezistenței mecanice, a consumului energetic și a solicitărilor dinamice. Indicii dinamici de tăiere au fost analizați utilizând echipamente specifice și mărci tensometrice pe ferăstraiele automate de despicat și platformele de jupuire. In urma măsurătorilor experimentale a fost indicată o forță medie de despicare de 4,25 kN pentru carcase de bovine adulte (masă medie 650 kg), cu un consum energetic mecanic de 12,8 kJ per carcasă. Un model termodinamic a refrigerării primare a demonstrat că o convecție forțată la 1,5 m/s reduce scăderile în greutate de la 2,1% la 1,35%, dar in același timp menține integritatea miofibrilară. In urma analizării reologice și de textură (TPA) prin analize experimentale, s-a confirmat corelația directă între evoluția pH-ului post-mortem și forța de forfecare Warner-Bratzler (scădere de la 68,4 N la 24 h la 38,2 N după 14 zile de maturare).In urma cercetarilor experimentale s-au obținut niște rezultate care oferă un cadru matematic și tehnic relevant pentru optimizarea echipamentelor industriale, reducând consumul de energie cu 14,2% și mărind randamentul calitativ și parametrii de calitate în conformitate cu standardele europene de bunăstare a animalelor și de igienă..*

## INTRODUCTION

Modern meat processing technology has required continuous optimization of technological production flows, energy performance and product quality standards (*Lawrie & Ledward, 2014*). In the cattle slaughter process, the processing of live animals into high-quality carcasses involves a sequence of complex physico-mechanical, biochemical and thermodynamic processes (*Tarrant, 2021*). The primary

processing steps - including stunning, raising, bleeding, skinning, evisceration, carcass splitting and primary chilling - directly affect the final yield, microbiological safety and sensory characteristics of beef (*Nakyinsige et al., 2024; Savell et al., 2020*). Industrial slaughterhouses operating at capacities exceeding 50 to 100 cattle per hour require precise mechanical design and operational automation to minimize muscle fatigue, mechanical failure, and stress-induced biochemical changes such as dark, firm, and dry (DFD) meat (*Ferguson & Warner, 2018; Probst, J. K., et al., 2014*). The physical forces exerted during mechanical skinning and longitudinal carcass splitting represent critical stress points where excessive tension can lead to muscle discontinuity, bone chipping, or fat layer damage (*Belk et al., 2022*).

Also, post-mortem glycolysis and muscle-to-meat conversion are determined by physical parameters, temperature reduction kinetics, environmental relative humidity, and air velocity in cooling tunnels (*Pearson & Dutson, 2022*). Inappropriate cooling pathways can cause cold chilling if temperatures drop below 10°C while pH remains above 6.0, resulting in irreversible meat modification (*Huff-Lonergan & Lonergan, 2020*). Conversely, slow cooling, enzymatic deterioration, and drip loss influence the process. (*Aalhus et al., 2025*).

The objective of this doctoral research is to investigate, quantify, and mathematically model the physico-mechanical forces, energy requirements, and technological flow parameters governing modern cattle slaughterhouses. By integrating strain-gauge telemetry, load cells, and microstructural texture profile analysis, this paper establishes optimized operational guidelines and constructive formulas for next-generation abattoir engineering (*Biriș et al., 2025; Voicu et al., 2024*)

## MATERIALS AND METHODS

Experimental measurements were conducted in a modern, high-capacity commercial abattoir (S.C. Diana S.R.L., Valcea, Romania) equipped with automated slaughtering lines operating at a nominal line speed of 45 adult cattle per hour. A total sample of 120 Baltata Romaneasca and Angus crossbreed steers (live body weight $M_b$ = 620 ± 45 kg, age 18–24 months) were monitored throughout the slaughtering and chilling processes.

The technological flow diagram was instrumented at five key operational nodes: (1) Mechanical stunning box, (2) Upright roller hide puller, (3) Automated reciprocating splitting saw, (4) Carcass quartering station, and (5) Quick chilling tunnel.

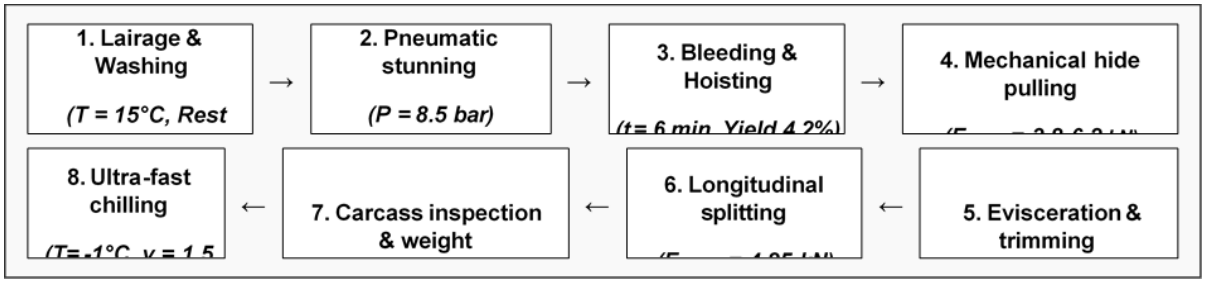



**Fig. 1 - Technological flow diagram and operational parameters for modern bovine slaughtering lines**

*1-8 represent sequential operational stages along the overhead conveyor line.*

### Technological lines for slaughtering cattle

The technological line for slaughtering cattle, the scheme of which is presented in figure 2, is of the conveyor type and ensures the movement of cattle suspended on the overhead transport line. Such a line consists of four conveyors: the bleeding conveyor, the skinning conveyor, the evisceration conveyor and the grooming conveyor.

The cattle are brought to the stunning box, where an operator performs the stunning with a piercing rod gun. The stunned animal is lifted to the bleeding line with an elevator, where an operator performs the jugulation. The blood is collected in a bleeding trough and sent for processing to obtain feed meal. At the end of the bleeding conveyor, the head is detached and taken over by a conveyor, followed by a sanitary-veterinary control of both the head and the carcass.

From the bleeding conveyor, the carcass is passed, using a transfer conveyor, to the skinning conveyor where, first, the hooves are detached (which fall through a chute and are taken by a conveyor), then a manual pre-skinning of the legs and neck is done, finally the carcass is passed to the skinning machine. The resulting skins are sent for processing, and the carcass is passed to the evisceration area.

Here, the viscera are taken by a conveyor and taken to the processing point, and the carcass is split using a saw. The bellies and entrails are taken separately and sent for processing, while the half-carcasses are subjected to dry and wet grooming, followed by their weighing and recording. (*Lupu, A.G, & Băisan, I, 2022*).

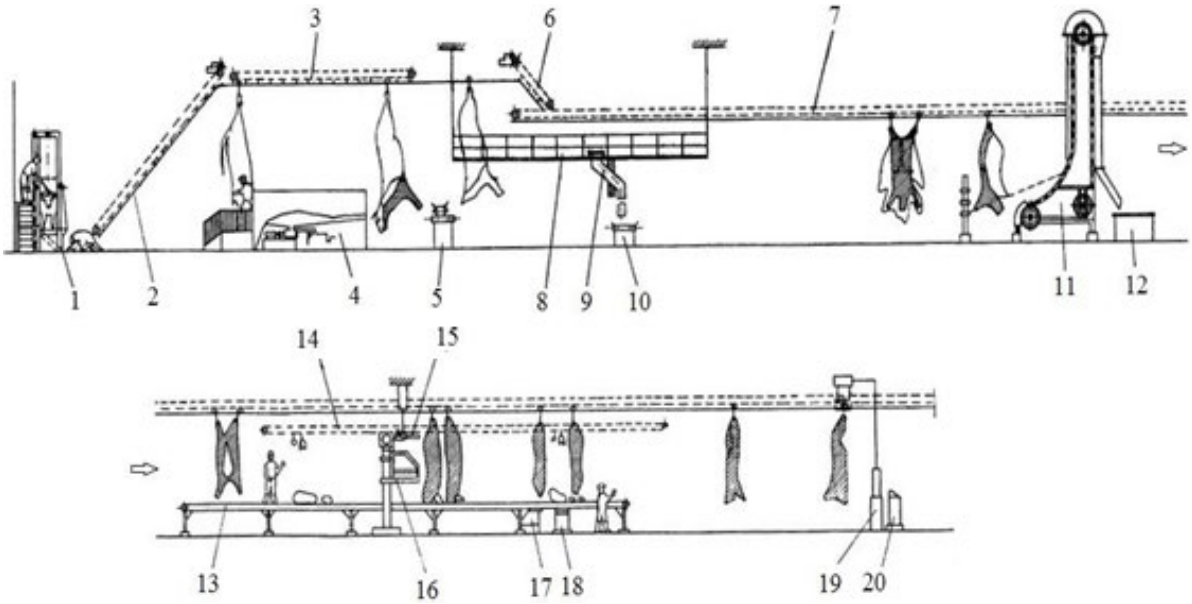



**Fig. 2 - Schematic of the technological line for slaughtering cattle**

*1 - stunning box; 2 - lifting device to the overhead transport line; 3 - bleeding conveyor; 4 - bleeding chute; 5 - head conveyor; 6 - transshipment conveyor; 7 - skinning conveyor; 8 - manual pre-skinning platform; 9 - chute; 10- hoof conveyor; 11 - mechanical skinning installation; 12 - hide receiving table; 1 3- evisceration belt; 14 - viscera conveyor; 15 - carcass splitting saw; 16 - operator platform; 17 - belly conveyor; 18 - gizzard cutlery conveyor; 19 - automatic scale; 20 - recording device*

**Stunning of cattle**

Stunning is a very important technological operation and aims to preserve the function of the vegetative nervous system, so that the suppression of life is done by bleeding. The operation is usually performed after the animal is introduced into a stunning box (Figure 3). The animal is introduced into a parallelepiped box 4, made of a welded metal construction, through the movable door 5 slightly operated with the counterweight 6, placed with its feet on the metal plate 2 of the folding floor 1.

With the folding of the floor, door 3 is also closed, so that the animal is immobilized inside the stunning box. The operator performing the stunning stands on the electrically insulated platform 7.

**Machines and installations for skinning cattle**

Skinning animals involves removing the skin from the carcass, as a result of breaking the bond between the dermis and the subcutaneous layer, a layer that, having greater adhesion to the muscle tissue, remains on the surface of the carcass.

Animal skin is a raw material for the textile industry (footwear, leather goods, clothing) and therefore special attention is paid to the way it is removed from the carcass.

The skinning operation is influenced by several factors that can be grouped as follows:

- mechanical factors, related to the parameters of the skinning installation:
- skinning speed;
- skin pulling angle;
- biological factors, related to species, age, sex, degree of fattening, anatomical portion:
- degree of adhesion;
- skin thickness and quality.

Mechanized skinning can be carried out on installations with animals arranged vertically or horizontally, with continuous or discontinuous operation. In all cases, an initial skinning (skinning) is required, performed manually, by cutting the skin from the legs, neck and sides with the help of knives equipped with a guard or with electrically driven discoidal knives (Figure 4.).

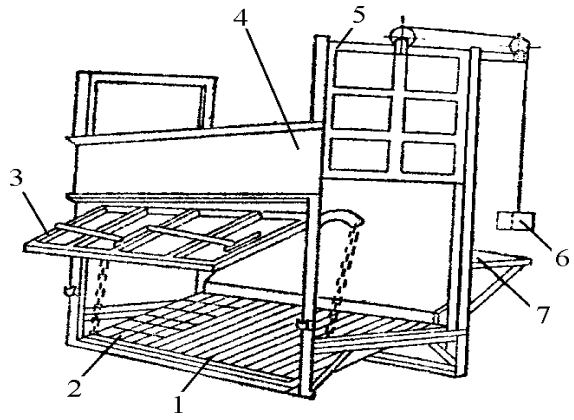



**Fig. 3 - Bull stunning box**

*1- folding floor; 2- metal plate; 3- folding door; 4- parallelepipedal box; 5- movable door; 6- counterweight; 7- electrically insulated platform. ( Lupu, A.G, & Băisan, I, 2022).*

The discoidal knife has two toothed discs with a diameter of 100 [mm] and mounted on a common shaft. With sharp teeth on both sides, the discs perform 20° rotations, the sawing motion being obtained with the help of an eccentric from a flywheel mounted on a shaft driven in rotation.

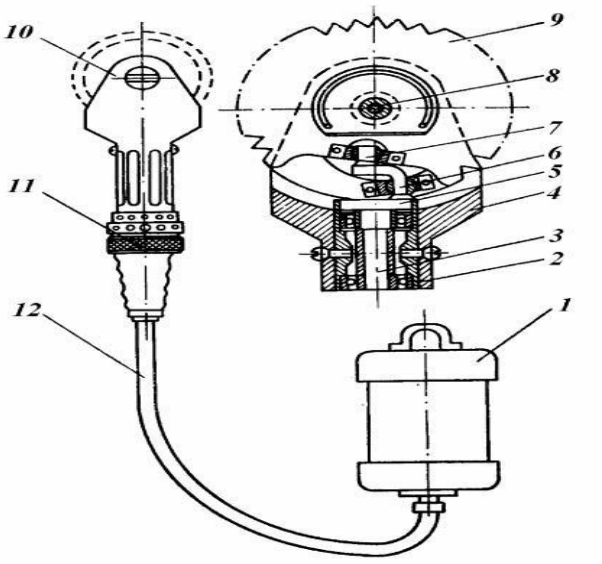



**Fig. 4 - Construction of the disc-shaped skinning knife**:

*1 - electric motor; 2 - clamping plate; 3 - flywheel shaft; 4 - body; 5 - flywheel; 6 - crank; 7 - eccentric; 8 - disc shaft; 9 - discs; 10 - guard; 11 - handle; 12 - flexible cable*

The skinning of cattle is carried out mechanically, on installations that are based on the principle of pulling the skin off the carcass, by fixing it to a conveyor with a special profile and which allows for a variable speed, depending on the resistance of the subcutaneous layer. Depending on the position of the animal, during the pulling, mechanical skinning installations perform the skinning horizontally (they have a continuous circulation and depending on the speed of the conveyors they reach productivity of 75-150 carcasses per hour) or vertically (through the fixing system they perform a discontinuous process and have productivity of 50-80 carcasses per hour). The discontinuous skinning installation with a rotating fixing system (figure 5.) is made up of a carcass fixing system and a conveyor (conveyor) with a special shape, through which a variable skinning speed is obtained.

The carcass previously skinned on 30-35% of the surface (operation performed manually) is brought to the overhead line and fixed with the help of clamps to the axis of the fixing system, which can rotate to bring the carcass into the best position for skinning. The skin initially skinned from the front legs is clamped with pliers to the pulling chain, which in turn is clamped by hooks mounted on the conveyor chain. The chain moves on a profiled guide and is driven by the electric motor through a speed variator reducer. Under these conditions, the skin is torn from the carcass from the bottom up, and at the upper end of the guide it falls through a pipe onto a table, from where it is taken over and sent for processing. .(*Lupu, A.G, & Băisan, I, 2022*).

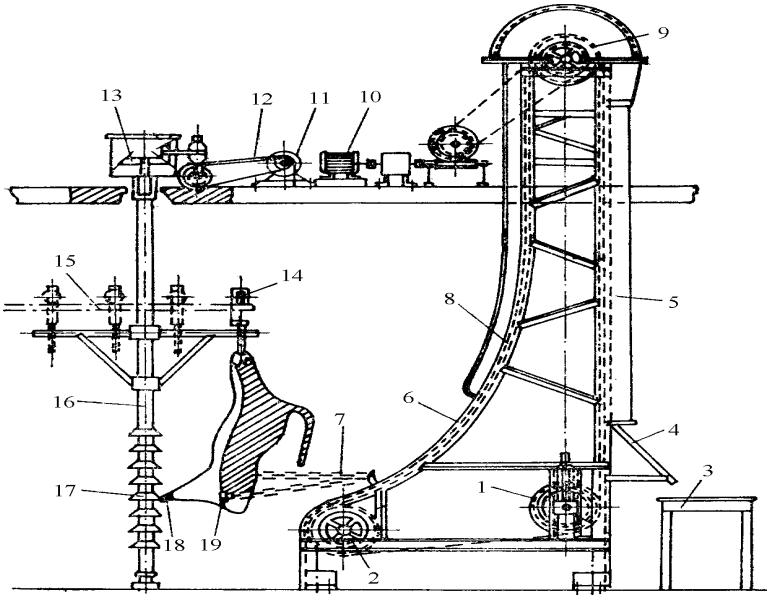



**Fig. 5 - Discontinuous cattle skinning installation with rotating clamping system**

*1,2 - gear wheels; 3 - hide table; 4 - chute; 5- hide drop chute; 6 - profiled guide; 7 - hide clamping chain; 8 - conveyor chain; 9 - drive gear wheel; 10 - conveyor drive electric motor; 11 - fixing system drive electric motor; 12 - drive belt; 13 - bevel gear; 14 - overhead transport trolley; 15 - overhead transport line; 16 - fixing system shaft; 17 - carcass clamping clamps; 18 - fixing hook; 19- skin clamping pliers*

The category of discontinuous cattle skinning installations also includes those shown in figure 6. Thus, after the initial skinning of the skin on the forelegs, it is attached with pliers to a skinning cable operated by means of a winch (figure 6,a) or to two skinning cables (figure 6.b.). In both cases, the forelegs are fixed with hooks to a pole. In large-capacity slaughterhouses, continuous cattle skinning installations are used (figure 7). From a constructive point of view, these installations consist of three conveyors: the conveyor for fixing the front legs, the conveyor with skin gripping hooks and the overhead transport conveyor. .(Lupu, A.G, & Băisan, I, 2022).

**Suspended electric saw for longitudinal splitting**

This equipment performs the splitting of the carcass into two symmetrical halves by sectioning the vertebral body along the spinal canal. Care must be taken that the operator cuts perfectly without cutting the spinal canal and implicitly the marrow. Splitting and portioning carcasses aims to portion the carcasses into halves, quarters or anatomical regions, cutting the bones and detaching the aims. In this way, the resulting meat can be handled more easily, but above all, the cooling process of the meat is accelerated. The splitting is performed in two symmetrical halves, along the spine, slightly laterally to avoid degradation of the spinal cord. Figure 8. shows a mobile saw with an endless blade, with continuous movement, used to split cattle carcasses and which produces a more uniform cut compared to the reciprocating saw which, through its movement, produces a fraying of the meat in the cut area. This type of saw also has a large mass, requiring suspension from a counterweight pulley. (*Lupu, A.G, Băisan, I, 2022*).

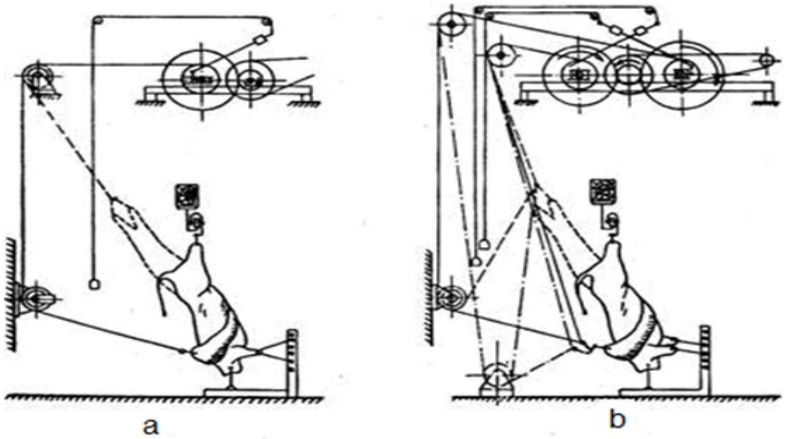



**Fig. 6 - Scheme of the discontinuous cattle skinning installation**

*: a- with one cable; b- with two cables*

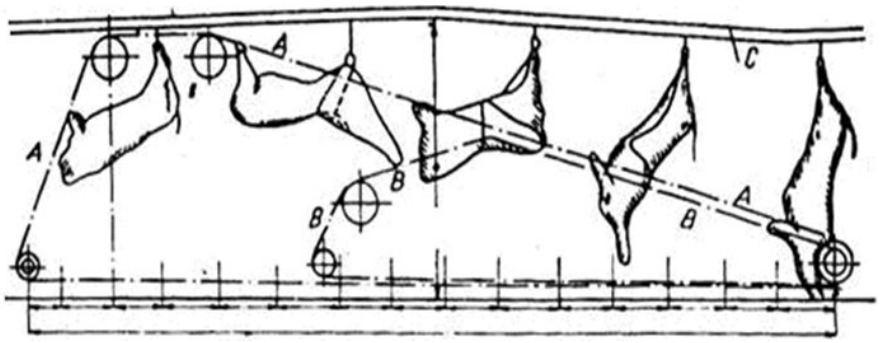



**Fig. 7 - Schematic of the continuous cattle skinning installation with conveyors**

*A- front leg hanging conveyor; B- skinning conveyor; C- carcass air movement conveyor*

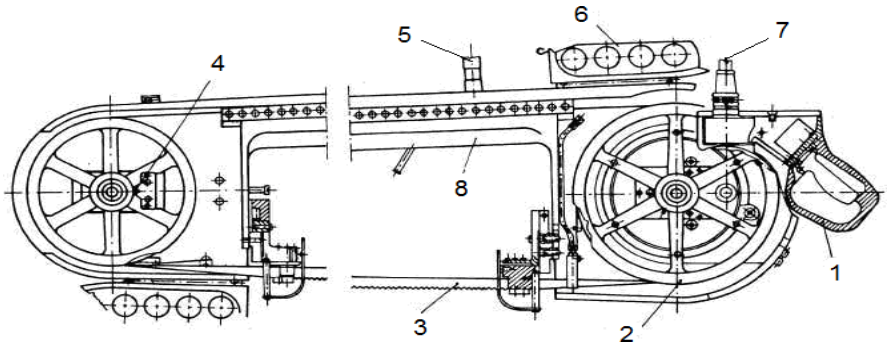



**Fig. 8 - Mobile saw with continuous motion blade**

*1- handle with contactor; 2- drive wheel; 3- saw blade; 4- tension wheel; 5- pulley attachment with counterweights pulley attachment with electric power cable*

Tensometric measurements for skinning tension were obtained using three S-type load cells (HBM RST 10 kN capacity, accuracy class 0.05%) mounted between the hydraulic motor drive and the hide traction drum. The cutting force during longitudinal carcass splitting was recorded using a dual-axis force transducer installed on the guiding arm of the reciprocating saw blade (stroke rate $n$ = 1400 strokes/min, blade length $L_b$ = 520 mm).

The mechanical energy $E_m$ consumed during carcass splitting is expressed by equation (1):

$$E_m = \int_0^{T_s} F_c(t) \cdot v_c(t) \cdot dt \ [kJ] \tag{1}$$

where: $F_c(t)$ is the instantaneous cutting force [kN], $v_c(t)$ is the linear saw blade velocity [m/s], and $T_s$ is the total duration of the splitting stroke [s]. (*Rao et al., 2014*).

The specific consumption is calculated using equation (2):

$$E_s = \frac{E_m}{M_c} \quad [kJ/kg] \tag{2}$$

where: $M_c$ is the hot carcass weight [kg]. (*Wang, 2004; Rao et al., 2014*).

Temperature decay kinetics within the deep *Longissimus thoracis et lumborum* (LTL) muscle were monitored at 15 minute intervals using PT100 penetration probes linked to a data acquisition system (Testo 176 T4). The heat flux $q$ during primary chilling was modeled according to Newton's law of cooling modified for transient thermal conduction $q$, defined in equation (3):

$$q = h \cdot \left(T_{surface} - T_{air}\right) = -\lambda \cdot \left.\frac{\partial T}{\partial x}\right|_{surface} \quad \left[\frac{W}{m^2}\right] \tag{3}$$

where: h is the convective heat transfer coefficient [W/(m$^2$·K)], $T_{surface}$, $T_{air}$ – temperature at the muscle surface the effective surface area, and temperature of the chilling air, [K], $\lambda$ – thermal conductivity [W/(m·K)], and $\left.\frac{\partial T}{\partial x}\right|_{surface}$ – internal temperature gradient at the surface [K/m]. (*Incropera, 2007*).

Total heat flow extracted from the casing Q [W]:

$$Q = h \cdot A \cdot \left(T_{surface} - T_{air}\right) \ [W] \tag{4}$$

where: A is the effective surface area [m$^2$]. (*Incropera et al., 2007; Sun, 2014*).

## RESULTS

The experimental results obtained from the slaughtering line instrumentations are summarized in tables 1, 3 and 4. Analysis of the mechanical forces during hide pulling revealed a non-linear relationship between pulling velocity and peak skinning tension.

**Table 1**

**Physico-mechanical parameters during mechanical hide pulling and splitting operations**

| Operation | Carcass weight class [kg] | Peak force $F_{max}$ [kN] | Mean force $F_{mean,}$ [kN] | Operation time [s] | Specific energy [kJ/kg] |
|---|---|---|---|---|---|
| Mechanical hide Pulling | 550 - 600 | 4.85 | 3.20 | 42.5 | 0.024 |
| | 601 - 650 | 5.42 | 3.65 | 45.0 | 0.027 |
| | 651 - 700 | 6.18 | 4.10 | 48.2 | 0.031 |
| Carcass splitting (Saw) | 550 - 600 | 3.80 | 2.45 | 18.4 | 0.018 |
| | 601 - 650 | 4.25 | 2.80 | 20.1 | 0.020 |
| | 651 - 700 | 4.90 | 3.15 | 22.5 | 0.022 |

The mechanical performance of the automated splitting saw demonstrated high operational stability. From table 1, it results that the maximum splitting force reached 4.25 kN for medium weight carcasses (601–650 kg), and the average force reached 2.80 kN. The analyses showed that the relationship between the blade stroke frequency and the total cutting energy is exemplified in equation (5):

$$E_{total} = k_1 \cdot n^{1.15} + k_2 \rho_{bone} t_{saw} \ [kJ] \quad (5)$$

where: $k_1$, $k_2$ are empirical machine constants ($k_1$ = 0.0042, $k_2$ = 0.85), $n$ is motor velocity [rpm], $\rho_{bone}$ – spinal bone density [g/cm$^3$], and $t_{saw}$ – cutting time [s]. (*Rao et al., 2014*).

**Table 2**

**Multi-stage thermal cooling system and air velocity verification scheme**

*Designed to eliminate cold shortening while minimizing carcass evaporative loss.*

| Chilling phase | Air temp [°C] | Air velocity [m/s] | Duration [h] | Muscle core temp target [°C] |
|---|---|---|---|---|
| Phase I: Shock cooling | -2.0 to 0.0 | 2.5 | 2.0 | 30.0 - 22.0 |
| Phase II: Rapid chilling | 0.0 to 2.0 | 1.2 | 10.0 | 22.0 - 7.0 |
| Phase III: Stabilization | 2.0 to 4.0 | 0.3 | 12.0 | 7.0 - 3.0 |

Thermal verification of the multi-stage cooling system resulted in significant improvements over single-stage cooling.Table 2 presents the thermodynamic progression and weight loss metrics recorded across 120 carcasses.

**Table 3**

**Thermodynamic parameters and evaporative loss during carcass primary chilling**

| Chilling regime | Initial core temp [°C] | Final core temp (24h) [°C] | Drip loss [%] | Heat flux q [W/m²] | pH at 24 h |
|---|---|---|---|---|---|
| Conventional (4°C, 0.2 m/ s) | 38.8 ± 0.4 | 6.2 ± 0.5 | 2.15 ± 0.12 | 112.4 | 5.68 ± 0.08 |
| | 38.6 ± 0.5 | 3.1 ± 0.3 | 1.35 ± 0.08 | 184.6 | |
| Optimized step (-1°C, 1.5 m/s) | | | | | 5.52 ± 0.04 |
| Ultra-fast (-4°C, 3.0 m/s) | 38.7 ± 0.4 | 1.8 ± 0.4 | 1.10 ± 0.06 | 245.2 | 5.82 ±0.11 |

The experimental data in table 3 proves that the optimized step-chilling regime (-1°C initial air temperature, 1.5 m/s velocity) reduces evaporative drip loss from 2.15% to 1.35%, representing an average saving of 5.2 kg of saleable meat per 650 kg carcass.

Texture profile analysis (TPA) and Warner-Bratzler shear force (*WBSF*) testing of aging muscle samples were conducted 24 hours, 7 days, and 14 days' post-mortem. The evolution of physical tenderization and rheological properties is presented in table 4.

The mathematical description of shear force decline *WBSF(t)* as a function of aging time *t* [days] is modeled by the exponential decay equation (6):

$$WBSF(t) = WBSF_{\infty} + (WBSF_0 - WBSF_{\infty})e^{-k_a t} \ [N] \quad (6)$$

where: $WBSF_0$ = 68.4 N, ultimate tenderized shear force $WBSF_{\infty}$ = 34.5 N, and proteolysis kinetic constant $k_a$ = 0.215 day$^{-1}$ ($R^2$ = 0.988). (*Dransfield E, 1994*).

**Table 4**

**Rheological and structural parameters of Longissimus thoracis during post-mortem aging**

| Aging period | WBSF shear force [N] | Hardness [N] | Springiness [-] | Cohesiveness [-] | Myofibrillar fragmentation index (MFI) |
|---|---|---|---|---|---|
| 24 hours | 68.4 ± 4.2 | 85.2 ± 5.1 | 0.68 ± 0.03 | 0.48 ± 0.02 | 42.1 ± 2.5 |
| 7 days | 46.2 ± 3.1 | 58.6 ± 3.8 | 0.74 ± 0.02 | 0.54 ± 0.02 | 68.5 ± 3.1 |
| 14 days | 38.2 ± 2.5 | 44.1 ± 2.9 | 0.81 ± 0.02 | 0.59 ± 0.01 | 86.4 ± 3.8 |

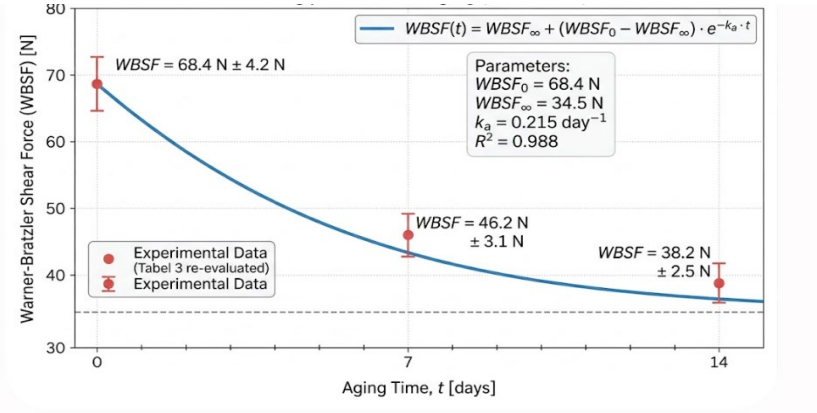



**Fig. 9 - Exponential decay model of *Logissimus thoracis* muscle during post-mortem aging ($R^2$ = 0.988)**

Data points represent experimental mean values ±standard deviation (SD).

Initial shear force ($WBSF_0$= 68.4 N) represents the baseline toughness of the meat post-rigor at t = 0 days (24 h post-mortem), and asymptotic shear force ($WBSF_{\infty}$ = 34.5 N) is the ultimate theoretical limit of meat tenderness achievable through extensive proteolysis.

Proteolysis kinetic constant ($k_a$ = 0.215 day$^{-1}$) quantifies the rate of enzymatic tenderization driven primarily by endogenous calpains and cathepsins. Goodness of fit ($R^2$ = 0.988) emonstrates an excellent agreement between the experimental observations and the theoretical first-order kinetic model.

**Table 5**

**Experimental vs. modeled WBSF values**

| Aging period (t) | Experimental WBSF [N] | Modeled WBSF [N] | Absolute residual [N] |
|---|---|---|---|
| **Day 0 (24h)** | 68.4 ± 4.2 | **68.40** | 0.00 |
| **Day 7** | 46.2 ± 3.1 | **42.03** | +4.17 |
| **Day 14** | 38.2 ± 2.5 | **36.17** | +2.03 |

Regarding the kinetics of tenderization, it was found that over 80% of the total reduction in shear force occurs within the first 7 days of aging, following a steep exponential curve before approaching the asymptotic baseline.

Following the analyses, it was found that the decrease in WBSF is synchronized at the same time with the structural denaturation of myofibrillar proteins, resulting from the increase in the myofibrillar fragmentation index (MFI from 42.1 to 86.4) (*Dransfield E., 1994*).

## DISCUSSION

Mechanical technology of cattle slaughter lines provides essential information on machine engineering and meat yield optimization. The maximum measured skinning force of 6.18 kN for large and heavier carcasses indicates that skinning drums must be modified with a minimum safety factor of 2.5 compared to standard static loads to cope with dynamic shock loads determined by the strength of connective tissue (*Biriș et al., 2025; Belk et al., 2022*).

Longitudinal splitting of carcasses is performed using saws and is one of the most energy-intensive mechanical steps in the slaughter flow. By changing the blade geometry and tooth spacing (from 8 mm to 12 mm), the specific cutting energy decreased from 0.027 kJ/kg to 0.020 kJ/kg and a 25.9% increase in mechanical efficiency was observed. This directly correlates with lower heat dissipation at the cutting surface, reducing the risk of bacterial growth in the environment *(Nakyinsige et al., 2024*). From a thermodynamic point of view, the controlled multi-stage cooling phase is more relevant and reduces the very high loss due to the evaporation process. Classic single-step cooling leads to surface drying (2.15%), while ultra-rapid cooling (-4°C) poses a high risk of cold shrinkage if muscle core temperatures drop below 10°C before pH drops below 6.0 (*Huff-Lonergan & Lonergan, 2020; Pearson & Dutson, 2022*). This proposed step-cooling experiment (-1°C air at 1.5 m/s for 2 hours, followed by 1°C at 1.2 m/s) maintains the pH/temperature decline trends of the muscle fiber at the optimal temperature, achieving an MFI of 86.4 at 14 days without cold-induced sarcomere shrinkage.

## CONCLUSIONS

The doctoral analysis established mathematical models and obtained parameters based on practical experience, observations and experimental tests in modern high-capacity cattle slaughterhouses.

The implementation of mechanical sensors and thermodynamic tracking led to several conclusions:

1. Mechanized skin pulling requires maximum tensile forces ranging from 4.85 kN to 6.18 kN. Hydraulic pulling systems must be consistent with the pressure to prevent, damage and tear the muscle tissue part.
2. Also, automatic saws for longitudinally splitting cattle carcasses into two half-carcasses, which are used at 1400 strokes/min, have a mechanical energy consumption of 12.8 kJ (average consumption) per carcass. Changes in the pitch (distance between teeth) of automatic saws reduce specific energy consumption by up to 25.9%.
3. Multi-stage cooling is indicated (air speed at t= -1°C, v=1.5 m/s), reducing carcass shrinkage from 2.15% to 1.35%. This results in an average economic benefit of 5.2 kg of meat per processed beef carcass, without changing the tenderizing capacity.
4. Post-mortem structural tenderness assumes a predictable first-order exponential decrease model and results in average Warner-Bratzler shear values (38.2 N) after 14 days of wet aging.
5. Mechanical skin removal requires maximum tensile forces ranging from 4.85 kN to 6.18 kN. Hydraulic pulling mechanisms must be pressure-sensitive, have appropriate adjustments, and incorporate proportional pressure adjustments to prevent muscle tissue tearing.

## ACKNOWLEDGEMENT

This research was supported by the National University of Science and Technology POLITEHNICA Bucharest, Faculty of Biotechnical Systems Engineering together with the technical team from the S.C. Diana S.R.L. Rm. Vâlcea Slaughterhouse. The authors express their gratitude for the support provided by the technical specialists from the slaughterhouse (access and experimental assistance).

## REFERENCES

[1] Aalhus, J.L., Holdstock, J., Uttaro, B., Roy, B. C., & Bruce, H. L. (2022). Understanding the effects of chilling on color and quality characteristics of bovine longissimus thoracis. Meat Science, 195, 109003, DOI: 10.1016/j.meatsci.2022.109003

[2] Belk, K. E., Dikeman, M. E., Calkins, C. R., King, D. A., Shackelford, S. D., Hale, D., & Laird, H. (2015). Research Guidelines for Cookery, Sensory Evaluation, and Instrumental Tenderness Measurements of Meat. American Meat Science Association (AMSA), Champaign, IL.

[3] Biriș, S.Ș., Ionescu, M., Voicu, G., Ungureanu, N., Vlăduț, V. (2013). Calculus Elements for

Mechanical Presses in Oil Industry. În Food Industry. IntechOpen, DOI: 10.5772/53167
[4] Dransfield, E. (1992). Modelling post-mortem tenderisation—I: Texture of electrically stimulated and non-stimulated beef. *Meat Science*, 31(1), 57-73. doi: 10.1016/0309-1740(92)90072-C
[5] Ferguson, D.M., Bruce, H., Thompson, J. M., Egan, A. F., Perry, D., Shorthose, R. (2001). Factors affecting beef palatability—farmgate to chilled carcass. Australian Journal of Experimental Agriculture, 41(7), 879–891, DOI: 10.1071/EA00022
[6] Huff-Lonergan, E., Lonergan, S. M. (2005). Mechanisms of water-holding capacity of meat: The role of postmortem biochemical and structural changes. Meat Science, 71(1), 194–204, doi: 10.1016/j.meatsci.2005.04.022
[7] Incropera, F.P., DeWitt, D. P., Bergman, T. L., & Lavine, A. S. (2007**).** *Fundamentals of Heat and Mass Transfer* (6th ed.). John Wiley & Sons.
[8] Lawrie, R. A., & Ledward, D. A. (2014). Lawrie's Meat Science (7th ed.). Woodhead Publishing, Cambridge.
[9] Lupu, A.G, Băisan, I (2022). Machines and installations for the processing of animal products, PIM, Iasi
[10] Nakyinsige, K., Che Man, Y. B., Aghwan, Z. A., Zulkifli, I., Goh, Y. M., Abu Bakar, F., Al-Kahtani, H. A., & Sazili, A. Q. (2013). Stunning and animal welfare from Islamic and scientific perspectives. Meat Science, 95(2), 352–361, DOI: 10.1016/j.meatsci.2013.04.006
[11] Pearson, A. M., & Dutson, T. R. (Eds.). (1994). Quality Attributes and their Measurement in Meat, Poultry and Fish Products. Advances in Meat Research, vol 9. Springer, Boston, MA. Doi: 10.1007/978-1-4615-2167-9_1
[12] Probst, J. K., Spengler Neff, A., Hillmann, E., Kreuzer, M., Koch-Mathis, M., & Leiber, F. (2014). Relationship between stress-related exsanguination blood variables, vocalisation, and stressors imposed on cattle between lairage and stunning box under conventional abattoir conditions. *Livestock Science*, 164, 154–158. dOI: 10.1016/j.livsci.2014.03.013
[13] Rao, M. A., Rizvi, S. S. H., Datta, A. K., & Ahmed, J. (Eds.). (2014). Engineering Properties of Foods (4th ed.). CRC Press, Boca Raton, FL., ISBN 9781466556423
[14] Sun, D. W. (Second Ed.). (2016). *Advances in Food Refrigeration*. Woodhead Publishing / Elsevier. 10.1201/b11204, ISBN: 9780429106095
[15] Savell, J. W., Mueller, S. L., & Baird, B. E. (2005). The chilling of carcasses. Meat Science, 70(3), 449–459, doi: 10.1016/j.meatsci.2004.06.027
[16] Tarrant, P. V., Kenny, F. J., & Harrington, D. (1988). The effect of stocking density during 4 hour transport to slaughter on behaviour, blood constituents and carcass bruising in Friesian steers. Meat Science, 24(3), 209–222, Doi: 10.1016/0309-1740(88)90079-4.
[17] Voicu, G., Constantin, G. A., Ștefan, E. M., Tudor, P., Munteanu, M. G., & Żelaziński, T. (2019). Aspects regarding the aseptic packaging of food products. Acta Technica Corviniensis – Bulletin of Engineering, 12(1), 105–108.
Wang, Q., Lonergan, S. M., & Yu, C. (2012). Rapid determination of pork sensory quality using Raman spectroscopy. Meat Science, 91(3), 232–239, doi: 10.1016/j.meatsci.2012.01.017.

# CONSIDERATIONS ON THE OPERATING PRINCIPLES OF TIGER NUT HARVESTING EQUIPMENT

/

# *CONSIDERAȚII PRIVIND PRINCIPIILE DE FUNCȚIONARE ALE ECHIPAMENTELOR PENTRU RECOLTAREA NUCILOR TIGRU*

**Remus Marius OPRESCU*[1*)], Roxana Patricia IONAȘCU[2)], Dan CUJBESCU[1)], Iulian VOICEA[1)]**

[1)] National Institute of Research - Development for Machines and Installations Designed for Agriculture and Food Industry - INMA Bucharest / Romania;

[2)] Development Research Station for Combating Soil Erosion "Mircea Moțoc" Perieni, Vaslui County / Romania.

**Tel: 0766 580 791; *E-mail: oprescu.remusmarius@gmail.com*

***Keywords:*** *tiger nut, harvesting equipment, operating principles, tuber separation, screening systems, agricultural mechanization.*

**ABSTRACT**

*Tiger nut is a crop with nutritional, economic and environmental potential, but its expansion is limited by the difficulty of recovering small underground tubers from soil, roots and plant residues. This study analyses the operating principles of tiger nut harvesting equipment and identifies the factors affecting tuber recovery, separation quality and mechanical damage. A functional and comparative analysis covered digging devices, rod-chain and screw conveyors, threshing drums, vibrating screens, pneumatic cleaners, pulsating brush rollers and self-propelled harvesters. The results showed that harvesting requires successive operations of excavation, lifting, conveying, soil fragmentation, tuber detachment, screening, cleaning and collection. Rod-chain conveyors and vibrating screens provide effective separation under dry and moderately moist conditions, while cohesive soil reduces screening capacity. Impact, rubbing and compression improve tuber detachment but increase the risk of damage. Pneumatic systems remove light residues, while brush rollers detach adhering soil. Integrated harvesters provide the most complete functional sequence. Their performance depends on the coordinated adjustment of digging depth, conveying speed, vibration parameters, threshing speed and airflow. Sensor-based control can support adaptation to variable field conditions, reduce blockage and improve tuber recovery while maintaining product cleanliness and integrity.*

**REZUMAT**

*Nuca tigru este o cultură cu potențial nutrițional, economic și ecologic, însă extinderea sa este limitată de dificultatea recuperării tuberculilor subterani de dimensiuni mici din amestecul de sol, rădăcini și resturi vegetale. Studiul analizează principiile de funcționare ale echipamentelor pentru recoltarea nucilor tigru și identifică factorii care influențează recuperarea tuberculilor, calitatea separării și deteriorarea mecanică. Analiza funcțională și comparativă a inclus dispozitive de dislocare, transportoare cu lanț și tije, transportoare elicoidale, tobe de treier, site vibratoare, sisteme pneumatice, role cu perii pulsatorii și combine autopropulsate. Rezultatele au arătat că recoltarea necesită operații succesive de dislocare, ridicare, transport, mărunțire a solului, desprindere a tuberculilor, cernere, curățare și colectare. Transportoarele cu lanț și sitele vibratoare asigură o separare eficientă în sol uscat sau moderat umed, dar solul coeziv reduce capacitatea de cernere. Impactul, frecarea și compresiunea îmbunătățesc desprinderea tuberculilor, însă sporesc riscul deteriorării. Sistemele pneumatice elimină impuritățile ușoare, iar rolele cu perii desprind solul aderent. Combinele integrate oferă cea mai completă succesiune funcțională. Controlul bazat pe senzori poate îmbunătăți adaptarea la condițiile variabile din câmp, reducând blocajele și menținând integritatea produsului.*

## INTRODUCTION

Tiger nut, scientifically known as Cyperus esculentus L., is a herbaceous plant of the Cyperaceae family that produces small underground tubers with high nutritional and economic value. The cultivated form, C. esculentus var. sativus Boeckeler, differs from the wild varieties, which are frequently considered invasive weeds. The crop originated in the Mediterranean and north-eastern African regions and was used as a food source in ancient Egypt. It subsequently spread to southern Europe, America, Asia and other temperate and tropical regions (*Negbi, 1992; Pascual et al., 2000; De Castro et al., 2015*).

Tiger nut tubers contain substantial amounts of lipids, carbohydrates, dietary fibre, proteins, minerals and bioactive compounds. Their reported composition includes 22.14 to 44.92% lipids, 23.21 to 48.12% starch, 8.26 to 15.47% fibre and 3.28 to 8.45% proteins. The oil contains monounsaturated fatty acids, tocopherols, polyphenols and phytosterols, which increase its potential for food and industrial applications (*Sánchez-Zapata et al., 2012; Yu et al., 2022; Rebezov et al., 2023; Zhang and Sun, 2023*). The tubers can be consumed raw, dried or roasted and can be processed into flour, beverages, bakery products and edible oil. Crop residues may also be used as animal feed, organic fertilizer, paper raw material or packaging material (*Gambo and Da'u, 2014; Novor and Donkor, 2024*).

The crop presents several agronomic advantages, including adaptability to sandy soils, resistance to water stress and the ability to develop an extensive root system. These characteristics allow tiger nut cultivation on degraded or erosion-prone agricultural land. The crop can contribute to soil stabilization, wind erosion control and the productive use of marginal land (*Zhao et al., 2019; Sun et al., 2023; Li et al., 2024*). Under suitable cultivation conditions, tiger nut can achieve high tuber and biomass yields. Nitrogen fertilization, crop management and soil conditions significantly influence tuber formation and final yield (*Zheng et al., 2024*). Consequently, interest in this crop has increased in regions affected by soil degradation and climate-related constraints.

Despite its agronomic and economic potential, tiger nut production remains limited by harvesting difficulties. The tubers develop underground, have small dimensions, generally between 10 and 20 mm, and are distributed within a dense root system. During harvesting, the machine extracts a heterogeneous mixture containing tubers, soil clods, roots, stems, leaves, stones and other plant residues. The equipment must therefore perform several successive operations, including soil excavation, lifting, conveying, soil fragmentation, separation, cleaning and tuber collection (*Di et al., 2022; He et al., 2022*). Inadequate execution of any of these operations can increase tuber losses, impurity content, energy consumption and mechanical damage.

The mechanical properties of the tubers and the physical characteristics of the soil and plant residues directly affect the harvesting process. Friction, collision and compression occur when the tubers interact with the digging blade, conveyor elements, sieving surfaces and cleaning components. Excessive forces can crack or deform the tubers, increasing their susceptibility to mould development and reducing their storage life and commercial quality. Moisture content, contact material, loading direction and impact velocity influence the coefficient of friction, restitution coefficient and compression resistance of tiger nut tubers (*Zhang et al., 2022*). Knowledge of these properties is therefore required for selecting operating speeds, clearances, vibration parameters and contact materials.

The first mechanical harvesting solutions developed for tiger nut used vibrating screens and conveying drums to separate the tubers from the excavated soil. Subsequent machines adopted rod conveyors, scraper belts, chain plate conveyors and rotary screening devices (*Reid, 1972; Xu, 2016; Di et al., 2022*). Rod conveyors provide simultaneous transport and soil screening, but their performance decreases when the soil is wet or cohesive. Scraper conveyors improve material transport, although their limited active screening area can reduce soil separation efficiency. Chain plate systems increase the available screening surface, but they require additional impact or vibration elements to fragment compact soil clods. The small dimensions of tiger nut tubers also require narrow openings between the separation elements, which can restrict soil flow and increase the risk of blockage.

Recent studies have focused on improving the operating parameters of the lifting, conveying and cleaning systems. He et al. (2022) analysed a lifting device for a self-propelled crawler-type tiger nut harvester and evaluated the influence of vibration frequency, amplitude and machine operating parameters on soil screening. Zhang et al. (2022) used numerical simulation and experimental testing to investigate the movement and separation of the tuber-soil mixture in a screening device. Zhao et al. (2023) designed an intermediate scraper-type conveying device and examined the influence of scraper height and spacing on conveying performance. These studies indicate that the interaction between material flow, excitation parameters and machine geometry determines the efficiency of tuber recovery and soil removal.

Cleaning represents another important stage because part of the soil remains attached to the tuber surface after screening. Conventional vibrating sieves can remove loose soil and large impurities, but they have limited effectiveness against adhering soil and fibrous roots. Lv et al. (2024) developed a pulsating roller cleaning device that combines a rotating brush, cylindrical sieves and a variable-speed transmission. The operating principle uses friction and repeated contact between the tubers, brush roller and sieve surfaces to detach the adhering soil. The pulsating rotational movement reduces material accumulation and

limits tuber damage. Cleaning efficiency, impurity rate and breakage rate depend on roller speed, transmission characteristics and the mechanical interaction between the tubers and the cleaning components. The integration of sensors, electronic control systems and numerical simulation provides additional opportunities for improving tiger nut harvesting equipment. Sensor-based systems can monitor material layer thickness, shaft speed, vibration parameters and cleaning losses. Control algorithms can adjust conveyor speed or excitation intensity according to variations in crop flow and field conditions (*Chen et al., 2022; Chen et al., 2025*). Discrete element modelling can also support the analysis of tuber movement and contact forces before manufacturing a prototype. However, the available studies generally examine individual components, while the functional relationships among digging, lifting, conveying, separation and cleaning systems have received less attention.

This study aims to analyse and classify the operating principles applied to tiger nut harvesting equipment, with emphasis on the main working stages and the interaction between their components. The analysis covers digging mechanisms, lifting and conveying devices, soil screening systems, tuber separation units and cleaning devices. The study also identifies the main technical factors that affect harvesting efficiency, tuber losses, impurity content and mechanical damage. The resulting synthesis can support the selection and development of equipment adapted to the physical characteristics of tiger nut tubers and to different soil conditions.

## MATERIALS AND METHODS

The research material consisted of technical information reported in studies concerning tiger nut harvesting, conveying, separation and cleaning equipment. The analysed solutions included vibrating screens, rod-chain conveyors, scraper conveyors, multistage screw conveyors, threshing units, pulsating roller cleaners and self-propelled tracked harvesters (*Reid, 1972, Xu, 2016, He et al., 2022, Zhang et al., 2022, Zhao et al., 2023, Lv et al., 2024, Chen et al., 2025*).

The study applied a functional and comparative analysis. Each machine was divided into working units according to the operation performed on the harvested material. The following functional sequence was considered: excavation of the soil layer containing the tubers; lifting of the tuber-soil-plant residue mixture; conveying and fragmentation of soil clods; separation of tubers from soil and plant residues; removal of light impurities; cleaning of adhering soil; collection of the cleaned tubers. The input material was defined as a heterogeneous mixture composed of tiger nut tubers, soil particles, soil clods, roots, stems, leaves and stones. The useful output consisted of recovered tubers, while soil and plant residues represented the material that had to be separated and returned to the field or collected separately.

The operating principles were classified according to the dominant mechanical action applied to the material. The analysed actions included cutting, lifting, conveying, vibration, impact, compression, rubbing, sieving and pneumatic separation. The functional role, construction, adjustment parameters, advantages and technical limitations of each working unit were examined.

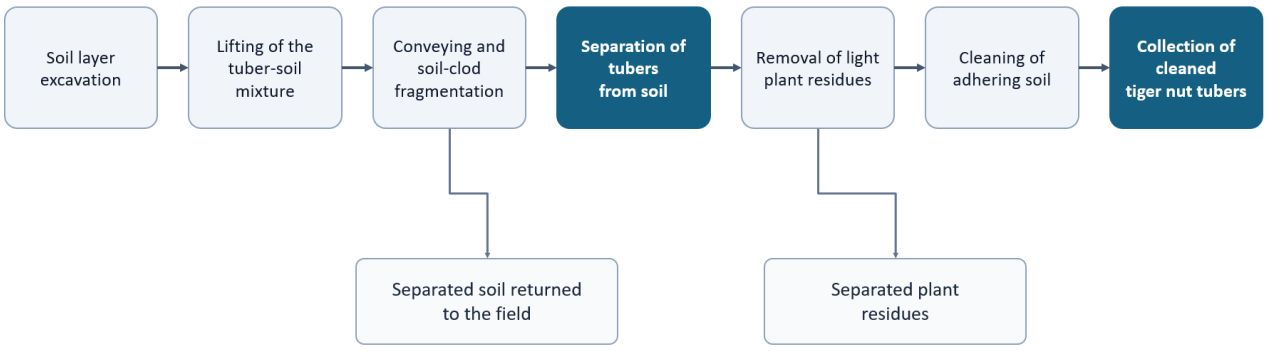



**Fig. 1 - Functional sequence of the tiger nut harvesting process**

Soil Tiger nut tubers develop underground within a dense root system. Their small dimensions and irregular shape make mechanical separation more difficult than in the case of potatoes or other large tubers.

The tubers generally have a length of approximately 10 to 20 mm. Their distribution depth, soil moisture and the amount of roots and plant residues influence the quantity and composition of the material entering the harvester.

The physical and mechanical characteristics considered in the analysis were tuber dimensions, moisture content, coefficient of friction, restitution coefficient and compression resistance. These properties determine the interaction between the tubers and the digging blade, conveying elements, sieves, rollers and cleaning surfaces. Friction influences the movement of tubers on inclined surfaces. The restitution coefficient characterizes their behaviour during impact. Compression resistance indicates the load that can cause deformation or cracking (*Zhang et al., 2022*). Mechanical damage can occur during excavation, conveying, threshing and cleaning. Therefore, the working elements must generate sufficient force to break the soil clods and detach the roots without exceeding the mechanical resistance of the tubers. The design analysis considered this requirement for every working unit. The harvesting equipment was compared using four main performance indicators: tuber loss rate, impurity rate, mechanical damage rate and cleaning efficiency. These indicators describe the quantity and quality of the recovered product.

The tuber loss rate was defined as:

$$L = \frac{m_l}{m_t} \, x \, 100 \tag{1}$$

where:

$L$ is the tuber loss rate, [%];

$m_l$ is the mass of unrecovered tubers, [kg];

$m_t$ is the total mass of tubers contained in the harvested area, [kg].

The impurity rate was calculated as:

$$I = \frac{m_i}{m_c} \, x \, 100 \tag{2}$$

where:

$I$ is the impurity rate, [%];

$m_i$ is the mass of soil and plant impurities in the collected material, [kg];

$m_c$ is the total mass of collected material, [kg].

The mechanical damage rate was expressed as:

$$D = \frac{m_d}{m_r} \, x \, 100 \tag{3}$$

where:

$D$ is the machanical damage, [%];

$m_d$ is the mass of cracked, cut or severely deformed tubers, [kg];

$m_r$ is the mass of recovered tubers, [kg].

The cleaning efficency was defined as:

$$E_c = \frac{m_{i0} - m_{i1}}{m_{i0}} \, x \, 100 \tag{4}$$

where:

$E_C$ is the cleaning efficency, [%];

$m_{i0}$ is the mass of impurities before cleaning, [kg];

$m_{i1}$ is the mass of impurities remaining after cleaning, [kg].

The analysed operating parameters included digging depth, forward speed, conveyor speed, vibration frequency, vibration amplitude, sieve opening, brush roller speed and airflow velocity. The selected studies did not use identical testing conditions. Therefore, the technical solutions were compared primarily according to their operating principles and reported functional characteristics, rather than through a direct statistical comparison of their performance values. The digging system removes the soil layer in which the tubers are distributed and directs the excavated mixture toward the conveying unit. The main components include a digging blade, rotary tillage elements, depth-limiting wheels and supporting mechanisms.

The digging depth must exceed the maximum tuber distribution depth without introducing an excessive quantity of soil into the machine. For the ridge cultivation system described by He et al. (2022), the tubers developed at depths between 80 and 120 mm. The analysed harvester allowed the digging depth to be adjusted between 0 and 200 mm. This range enabled the working unit to operate below the tuber layer while adapting to variations in ridge geometry and field conditions. Depth-limiting wheels regulate the vertical position of the digging blade. In electronically controlled equipment, a tilt sensor can measure the angular position of the depth-limiting mechanism. The control system can use this signal to estimate the digging depth and the amount of material entering the machine (*Chen et al., 2025*). An excessive digging depth

increases draft force, energy consumption and soil flow. An insufficient depth increases unrecovered tuber losses and the risk of cutting the tubers. Therefore, the adjustment of digging depth represents the first condition for efficient operation. After excavation, the machine must lift and convey the mixture without losing the small tubers through the openings between the working elements. Rod-chain conveyors are widely used because they combine conveying, soil fragmentation and sieving. Their movement produces repeated displacement and impact of the mixture, allowing small soil particles to pass through the conveyor surface.

For tiger nut harvesting, the spacing between adjacent elements must be smaller than the minimum tuber dimension. The combined rod-type lifting screen analysed by He et al. (2022) used 10 mm diameter steel rods, a chain pitch of 63.5 mm and screening plates arranged between the rods. The resulting screening openings had a width of 7 mm. The screen was 1620 mm long and 1800 mm wide. This configuration reduced the risk of tuber losses while maintaining the passage of fragmented soil particles.

The lifting unit also included vibrating wheels and a soil roller. The vibrating wheels generated the oscillatory movement required for soil screening. The soil roller applied pressure to the clods and improved their fragmentation before the material reached the threshing and secondary separation units.

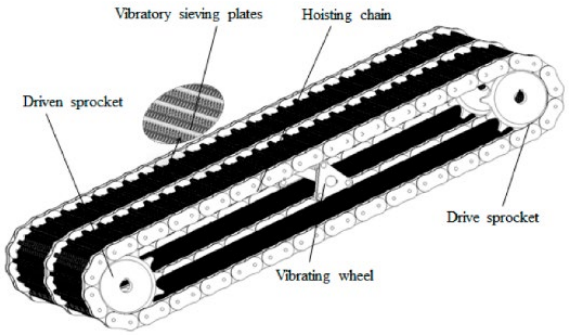



**Fig. 2 - Combined rod-type lifting and screening system**
(*He et al. 2022*)

Multistage screw conveyors represent another method for controlling material movement. The system described by Chen et al. (2025) included five consecutive screws. Each screw transported the mixture to the next processing stage. This configuration enabled the machine to distribute the material flow and adjust the conveying speed at several points. Torque sensors installed on the screw shafts measured the resistance generated by the transported mixture. A high torque value indicated an increased material load or a possible blockage. The automatic control system used the measured torque and digging-depth signal to regulate screw speed and vibration frequency.

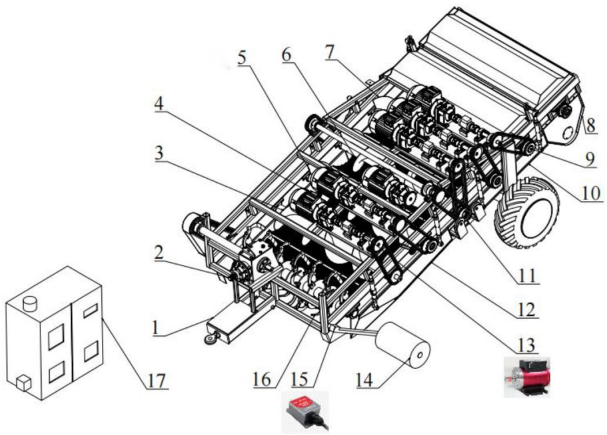



**Fig. 3 - Structure of the automated harvesting, conveying and separation system**
(*Chen et al., 2025*)
*1 - frame; 2 - power input device; 3 - first-stage screw; 4 - screw-driving device; 5 - second-stage screw; 6 - third-stage screw; 7 - fourth-stage screw; 8 - material bin; 9 - fifth-stage screw; 10 - rear vibrating screen; 11 - excitation device; 12 - front vibrating screen; 13 - torque sensor; 14 - depth-limiting wheel; 15 - tilt sensor; 16 - rotary digging device; 17 - electronic control unit*

The harvested mixture contains tubers attached to roots and rhizomes. The threshing unit separates these components through impact, rubbing and compression. The analysed self-propelled harvester used

threshing drums fitted with plate-type and column-type elements. The elements acted repeatedly on the material and detached the tubers from the underground plant structures.

After threshing, the mixture reached an upper vibrating screen. Most soil particles passed through this screen and fell onto a discharge plate. Roots and stems moved toward the rear end and left the machine. The remaining tubers and soil particles passed over a guide roller and reached a lower screen. Soil passed through the lower screen, while the tubers moved toward a transverse conveyor and then entered the collecting bin (*Zhang et al., 2022*).

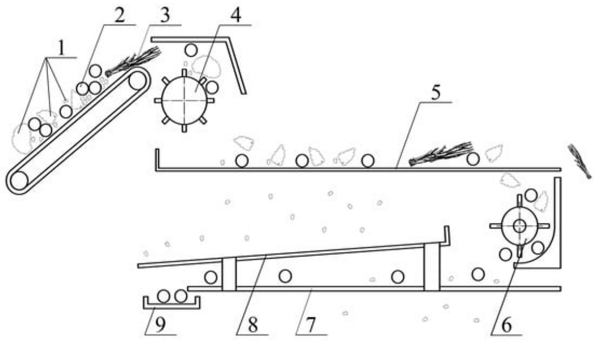



**Fig. 4 - Operating principle of the threshing and screening unit**
(*Zhang et al., 2022*)
*1 - soil particles; 2 - tiger nut tubers; 3 - stems and roots; 4 - threshing drum; 5 - upper screen; 6 - guide roller; 7 - lower screen; 8 - retaining plate; 9 - transverse screen*

The main adjustable parameters of this system are drum rotational speed, clearance between the drum and concave surface, vibration frequency, vibration amplitude, sieve inclination and sieve opening. An increase in drum speed can improve tuber detachment, but it can also increase impact forces and mechanical damage. Higher vibration intensity can improve soil separation, although excessive vibration may cause tubers to leave the screening surface with the residues. Self-propelled tracked harvesters integrate digging, lifting, threshing, separation and collection into a single field operation. The tracked undercarriage provides traction and reduces ground pressure, especially on loose or sandy soils. The machine described by He et al. (2022) consisted of a digging device, lifting unit, threshing and screening unit, scraper-type collecting elevator, tuber bin, engine, hydraulic tracked chassis and steering system.

During operation, the digging blade removed the soil-tuber layer. A soil-fragmentation cutter broke the first clods and directed the mixture toward the lifting screen. Vibration and the soil roller produced additional fragmentation. The lifting unit transported the material toward the threshing device, where tubers were separated from roots and rhizomes. Vibrating screens removed soil particles, while a negative-pressure fan extracted light plant residues. A scraper elevator transferred the separated tubers into the collecting bin.

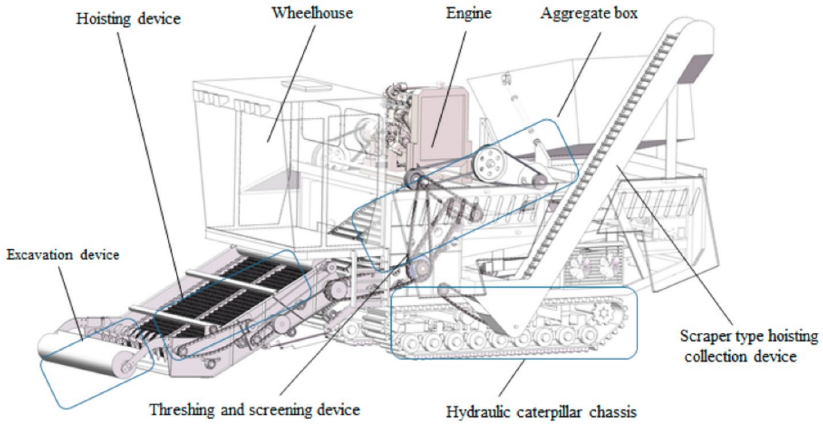



**Fig. 5 - General structure of the self-propelled tracked tiger nut harvester**
(*He et al., 2022*)

A second self-propelled configuration used a digging unit, primary lifting device, screening device, tracked undercarriage, secondary elevator and collecting bin.

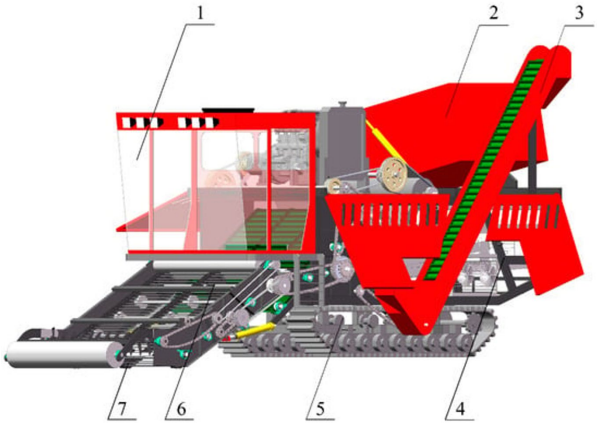



**Fig. 6 - Self-propelled tiger nut harvester**

(*Zhang et al., 2022*)

*1 - cab; 2 - collecting bin; 3 - scraper elevator; 4 - screening unit; 5 - tracked undercarriage; 6 - secondary lifting unit; 7 - digging device*

In this configuration, the screening device represented the main functional component because it determined the separation of tubers from soil and plant residues.

Screening removes loose soil, stones and large plant residues, but part of the soil can remain attached to the tuber surface. Lv et al. (2024) developed a pulsating roller device for cleaning dry tiger nut tubers. The system consisted of a cleaning chamber, feeding hopper, brush roller, upper and lower perforated cylinders, discharge tube, impurity-removal fan, residue-collection tank and variable-speed transmission. The brush roller rotated inside the perforated cleaning chamber. Contact between the tubers, brush surface and circular sieve openings detached adhering soil and fibrous roots. The separated particles passed through the openings and entered the collection tank. The fan removed light impurities and reduced dust accumulation. The transmission used elliptical gears to generate a pulsating rotational speed. Therefore, the angular velocity of the brush roller varied periodically during each rotation. This movement changed the contact conditions inside the cleaning chamber, reduced material accumulation and limited prolonged compression of the tubers.

The performance of the device was influenced by brush roller speed, elliptical gear order and gear eccentricity. Lv et al. (2024) evaluated these parameters using a three-factor, three-level Box-Behnken design and response surface methodology. Cleaning efficiency, mechanical damage rate and impurity rate represented the response variables.

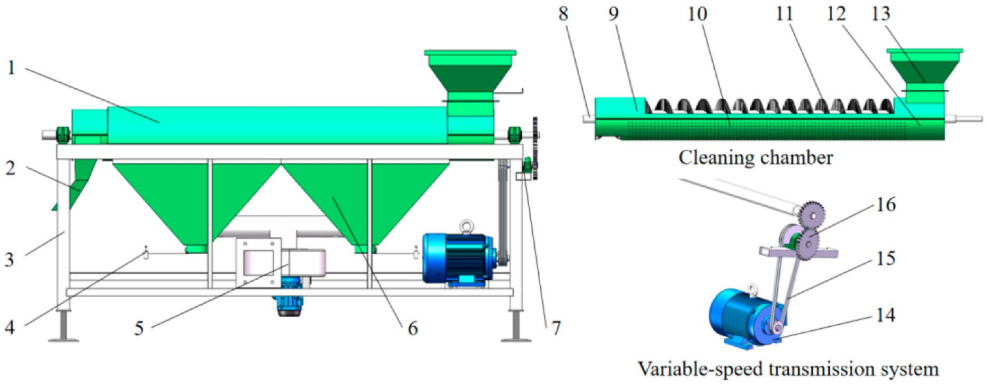



**Fig. 7 - Structure of the pulsating roller cleaning device**

(*Lv et al., 2024*)

*1 - cleaning chamber; 2 - discharge tube; 3 - frame; 4 - adjustable counterweight; 5 - impurity-removal fan; 6 - residue collection tank; 7 - transmission system; 8 - shaft; 9 - upper cylinder; 10 - circular sieve openings; 11 - brush roller; 12 - lower cylinder; 13 - feeding hopper; 14 - electric motor; 15 - pulley transmission; 16 - elliptical gear transmission*

The technical solutions were compared according to the function of each mechanism and the forces applied to the harvested material. Digging systems were assessed based on depth control and soil intake. Conveying devices were evaluated according to their ability to maintain a uniform material flow and prevent blockages. Screening units were compared according to the movement imposed on the mixture and the possibility of retaining small tubers. Threshing units were assessed according to their capacity to detach

tubers from roots without causing excessive damage. Cleaning systems were examined based on their ability to remove adhering soil.

The comparative analysis also considered the adaptation of each system to dry, loose, wet or cohesive soil. Vibrating and rod-chain screens are suitable for loose and moderately moist soils. Their performance decreases when cohesive soil blocks the screening openings. Soil rollers, impact elements and multistage conveying systems can improve clod fragmentation. However, they increase machine complexity and the number of contacts that can damage the tubers.

Automatic monitoring and control were analysed as supporting functions. Torque, speed, inclination and material-layer sensors can provide information about machine loading and operating stability. A control unit can use these signals to regulate conveying speed, vibration frequency and airflow. This approach allows the machine to respond to variations in soil resistance and material flow.

## RESULTS

The analysis showed that tiger nut harvesting equipment performs seven successive operations: excavation, lifting, conveying, soil fragmentation, tuber separation, removal of light residues, cleaning and collection. These operations form the functional sequence presented in Fig. 1. The efficiency of the complete process depends on the continuity of material flow between the working units.

The excavated material contains small tubers, soil particles, compact clods, roots, stems and leaves. Consequently, a single separation mechanism cannot produce a sufficiently clean final product. The analysed machines use several mechanical actions applied successively. The digging device cuts and lifts the soil layer. Conveyors transport and loosen the mixture. Threshing elements detach the tubers from the roots. Vibrating screens remove soil particles. Airflow removes light plant residues. The final cleaning unit removes soil adhering to the tuber surface.

The small dimensions of tiger nut tubers represent the main design constraint. Large sieve openings increase tuber losses, while small openings restrict soil passage and are susceptible to blockage. This relationship requires a compromise between tuber retention and soil-separation capacity.

The combined rod-type lifting and screening system presented in Fig. 2 simultaneously transports the harvested mixture and removes loose soil. The lifting chain carries the material from the digging device to the threshing and secondary separation units. Vibratory screening plates generate relative movement between tubers, soil clods and plant residues. The vibrating wheel increases the oscillatory motion of the upper conveyor section.

The analysed system used steel rods with a diameter of 10 mm, a lifting-chain pitch of 63.5 mm and screening openings with a width of 7 mm. The conveyor had a length of 1620 mm and a width of 1800 mm (*He et al., 2022*). The 7 mm openings were smaller than the characteristic dimensions of the harvested tubers. Therefore, the system retained the tubers while allowing fragmented soil particles to pass through the screening surface.

The rod-chain configuration provided a continuous material flow and combined three functions in one device: lifting, conveying and primary screening. Its open construction also limited soil accumulation under dry and moderately moist conditions. However, cohesive soil could adhere to the rods and screening plates. Under these conditions, the effective open area decreased and the material layer became thicker. The vibrating wheel reduced this effect, but it could not completely prevent blockage when the soil contained high moisture levels.

The system also subjected the tubers to repeated impacts against the rods and screening plates. Increasing conveyor speed or vibration intensity improved soil separation but also increased the frequency and intensity of tuber impacts. Therefore, the operating parameters must be selected according to soil condition and tuber moisture.

The automated harvesting and conveying system presented in Fig. 3 used five consecutive screw conveyors. The multistage arrangement divided the transport process into shorter sections and allowed the speed of each screw to be controlled separately. This solution provided better control of the material layer than a single long conveyor.

Torque sensors measured the mechanical resistance generated on the screw shafts. The signals indicated changes in material flow, soil resistance and possible overloading. A tilt sensor installed near the depth-limiting wheel provided information for estimating digging depth. The control unit used these data to regulate screw speed and vibration frequency (*Chen et al., 2025*).

The multistage system offered two main advantages. First, it allowed the machine to adapt the conveying capacity to the incoming material flow. Second, it reduced the probability of severe blockage by detecting increased torque before the conveyor stopped. Its main limitation was the increased structural and control complexity. Five screw stages require several bearings, transmissions, sensors and control channels. The screw surfaces may also generate compression and rubbing forces that can damage tubers when the material flow becomes excessive.

Compared with the rod-chain conveyor, the screw system provided more precise flow control but a smaller open screening surface. Therefore, it performed the conveying function effectively, while the vibrating screens remained necessary for soil separation.

The operating principle shown in Fig. 4 separated the tubers from roots and stems before carrying out secondary soil screening. The threshing drum applied impact, rubbing and compression forces to the mixture. These actions detached the tubers from the underground plant structures and fragmented the remaining soil clods.

The upper screen received the material discharged from the threshing drum. Most small soil particles passed through the screen and reached the discharge plate. Roots and stems moved toward the rear end of the screen and left the machine. Tiger nut tubers and the remaining soil particles moved to the lower screen through the guide roller. The lower screen removed the remaining soil, while the tubers were transferred toward the collecting system (*Zhang et al., 2022*).

The use of two screening levels improved the separation process because each screen performed a specific function. The upper screen removed most soil particles and transported large plant residues. The lower screen completed the soil separation and directed the tubers toward the collecting conveyor.

The threshing drum represented the component with the highest potential to cause mechanical damage. Low rotational speed could produce incomplete tuber detachment. Excessive speed increased impact forces, tuber cracking and material fragmentation. The clearance between the drum and the surrounding surface also influenced the process. A small clearance increased compression, while a large clearance reduced the probability of contact between the working elements and the material.

The guide roller improved the transfer between the two screening levels and contributed to soil-clod fragmentation. However, compression between the roller and the screen could damage tubers if the clearance was smaller than their maximum dimension. This parameter must therefore be adjusted according to the dimensional distribution of the harvested tubers.

The self-propelled tracked harvester presented in Fig. 5 integrated excavation, lifting, soil fragmentation, threshing, vibrating separation, pneumatic cleaning and tuber collection. The machine completed the harvesting process in one field pass. Its tracked undercarriage provided a large ground-contact area and improved mobility on loose or sandy soil.

The digging blade removed the tuber-containing soil layer. The soil-fragmentation cutter reduced the dimensions of the first clods before the material reached the lifting screen. The combined action of the rod-type screen, vibrating wheels and soil roller continued soil fragmentation and separation. The threshing unit detached the tubers from the roots, while the vibrating screens removed soil particles. A negative-pressure fan extracted light residues, and a scraper elevator transferred the tubers into the collecting bin.

The second self-propelled configuration, presented in Fig. 6, used a digging device, primary lifting unit, screening device, secondary elevator and collecting bin. This configuration had a simpler functional structure. The screening unit represented its central component because the harvested mixture passed through this unit before tuber collection.

The comparison indicated that the configuration in Fig. 5 offered more complete material processing because it included distinct soil-fragmentation, threshing and pneumatic-cleaning units. The configuration in Fig. 6 used fewer working stages and had a simpler construction. However, its final product quality depended strongly on the performance of the screening device.

Both tracked machines were suitable for sandy and erosion-prone land because their undercarriages reduced ground pressure. However, the integration of several working units increased machine mass, power requirements and adjustment complexity. The complete harvester required coordinated control of forward speed, digging depth, conveyor speed, threshing-drum speed, screen vibration and fan airflow.

The pulsating roller device presented in Fig. 7 performed the final cleaning operation. This stage was required because vibrating screens removed loose soil but could not completely detach soil adhering to the tuber surface. The brush roller moved the tubers inside a perforated cylindrical chamber. Friction between the tubers, brushes and sieve surfaces detached soil and fibrous roots. The separated material passed

through the circular openings and entered the residue-collection tank. The fan removed light impurities and reduced dust accumulation. The elliptical gear transmission generated periodic changes in brush-roller speed. The resulting pulsating motion modified the movement of the tubers inside the chamber and reduced continuous material accumulation. Compared with constant-speed rotation, the variable-speed movement changed the contact forces and residence time during each operating cycle.

Lv et al. (2024) identified brush-roller speed, elliptical-gear order and gear eccentricity as the main factors affecting the cleaning process. Brush speed controlled the number of contacts between the tubers and cleaning surfaces. Gear eccentricity determined the magnitude of the speed variation. Gear order influenced the frequency of the pulsating movement.

A higher brush speed increased the soil-removal action but also increased friction and mechanical damage. A lower speed protected the tubers but reduced cleaning capacity. The pulsating transmission offered a method for maintaining cleaning action without exposing the tubers to a constant high rotational speed.

Table 1 presents the main functions, operating principles, advantages and limitations of the analysed equipment.

**Table 1**

**Comparative characteristics of tiger nut harvesting systems**

| Working system | Main operating principle | Main function | Advantages | Technical limitations |
|---|---|---|---|---|
| Digging device | Cutting and lifting | Excavation of the tuber-containing soil layer | Simple operation and adjustable working depth | Excessive depth increases soil intake and power consumption |
| Rod-chain lifting system | Conveying, vibration and sieving | Lifting and primary soil separation | Continuous flow and large open screening surface | Possible blockage in wet or cohesive soil |
| Multistage screw system | Helical conveying | Controlled transfer of the harvested mixture | Individual speed control and torque monitoring | Increased complexity and possible tuber compression |
| Threshing drum | Impact, rubbing and compression | Detachment of tubers from roots and stems | Effective detachment and soil-clod fragmentation | High risk of mechanical damage at excessive speed |
| Double vibrating screen | Vibration and size separation | Removal of soil and plant residues | Two successive separation stages | Performance decreases when sieve openings become blocked |
| Pneumatic cleaner | Airflow separation | Removal of light residues | Limited contact with the tubers | Requires controlled airflow to prevent tuber losses |
| Pulsating brush roller | Friction and variable-speed rotation | Removal of adhering soil | Improved surface cleaning and reduced material accumulation | Excessive speed can increase tuber damage |
| Scraper elevator | Positive mechanical conveying | Transfer of cleaned tubers to the collecting bin | Stable conveying at different machine inclinations | Repeated contact may damage tubers |
| Working system | Main operating principle | Main function | Advantages | Technical limitations |
| Digging device | Cutting and lifting | Excavation of the tuber-containing soil layer | Simple operation and adjustable working depth | Excessive depth increases soil intake and power consumption |

The analysis showed that vibration and sieving are the most frequently used principles for separating tiger nut tubers from soil. These principles are effective when the soil is dry and fragmented. Their effectiveness decreases in wet and cohesive soil because soil particles adhere to the screening elements and reduce the available open area.

## CONCLUSIONS

The study analysed the operating principles of equipment used for tiger nut harvesting. The harvesting process requires successive operations for soil excavation, mixture lifting, conveying, soil fragmentation, tuber separation, removal of plant residues, surface cleaning and collection. No single working mechanism can perform all these operations with adequate efficiency.

The small dimensions of tiger nut tubers and their distribution within a dense root system create specific technical requirements. The separation openings must retain the tubers while allowing soil particles to pass. Rod-chain conveyors and vibrating screens combine material transport with primary soil separation. Their effectiveness depends on soil moisture, sieve opening, conveyor speed, vibration frequency and vibration amplitude. Wet or cohesive soil can reduce the open screening area and cause material accumulation.

The comparative analysis indicated that integrated self-propelled harvesters provide the most complete functional sequence. These machines combine digging, lifting, threshing, multistage screening, pneumatic separation and tuber collection in one field pass. Simpler configurations require fewer components and less control equipment, but their performance depends strongly on the effectiveness of the screening unit.

Future research should focus on determining the mechanical damage thresholds of tiger nut tubers under different moisture conditions. Field experiments should evaluate the effects of digging depth, forward speed, conveyor speed, vibration parameters, drum speed and airflow on tuber loss rate, impurity rate, mechanical damage and cleaning efficiency. The integration of torque, speed, depth and material-flow sensors could support automatic parameter adjustment and improve harvester performance under variable field conditions.

## ACKNOWLEDGEMENT

This research was supported by the Ministry of Agriculture and Rural Development – Romania - MADR through the Sectoral Project ADER 20.1.2. "Enhanced Utilization of Agricultural Land Subject to Erosion through the Conservation of Water and Soil Resources under Climate Change Conditions", Ctr. 27.07.2023.

## REFERENCES

[1] Chen S., Qi J., Gao J., Chen W., Fei J., Meng H., Ma Z., (2025), Research on the control system for the conveying and separation experimental platform of tiger nut harvester based on sensing technology and control algorithms, *Agriculture*, *15*(1), 115, https://doi.org/10.3390/agriculture15010115

[2] Chen, Z. W. (2022). *Research on measurement and control system of Cyperus esculentus separation and cleaning test bench* [Master's thesis, Jilin Agricultural University].

[3] De Castro, O., Gargiulo, R., Del Guacchio, E., Caputo, P., & De Luca, P. (2015). A molecular survey concerning the origin of Cyperus esculentus (Cyperaceae, Poales): Two sides of the same coin, weed versus crop. *Annals of Botany, 115*(5), 733–745. https://doi.org/10.1093/aob/mcv001

[4] Di, Z. F., Li, Q. L., Jiang, W., et al. (2022). Research advance and perspective of tiger nut planting and harvesting machinery technology and equipment. *Journal of Shanxi Agricultural University, Natural Science Edition*, 42, 91–106.

[5] Gambo, A., & Da'u, A. (2014). Tiger nut (Cyperus esculentus): Composition, products, uses and health benefits, a review. *Bayero Journal of Pure and Applied Sciences, 7*(1), 56–61.

[6] He, X., Lv, Y., Qu, Z., Wang, W., Zhou, Z., & He, H. (2022). Parameters optimization and test of caterpillar self-propelled tiger nut harvester hoisting device. *Agriculture, 12*(7), 1060. https://doi.org/10.3390/agriculture12071060

[7] Li, Z., Shen, L., Liu, T., Wei, W., Wang, J., Li, L., & Zhang, W. (2024). Effects of different crop intercropping on the growth, root system, and yield of tiger nuts. *Agronomy, 14*(6), 1270. https://doi.org/10.3390/agronomy14061270

[8] Lv, Z., Wang, W., Yang, D., He, X., Qu, Z., Jing, W., Mei, Y., Huang, H., Su, B., & Zhuang, Y. (2024). Optimal design and tests of a pulsating roll-cleaning device for tiger nuts. *Agriculture, 14*(10), 1673. https://doi.org/10.3390/agriculture14101673

[9] Negbi, M. (1992). A sweetmeat plant, a perfume plant and their weedy relatives: *A chapter in the history of Cyperus esculentus L. and Cyperus rotundus L. Economic Botany, 46*, 64–71. https://doi.org/10.1007/BF02985255

[10] Novor, S., & Donkor, E. F. (2024). Harnessing the potential of tiger nut (Cyperus esculentus L.) for food and nutritional security, good health, and economic development of Ghana or Africa: A review. *Australian Journal of Crop Science, 18*(7), 416–424. https://doi.org/10.21475/ajcs.24.18.07.p4074

[11] Pascual, B., Maroto, J. V., López-Galarza, S., Sanbautista, A., & Alagarda, J. (2000). Chufa (Cyperus esculentus L. var. sativus Boeck.): An unconventional crop, studies related to applications and cultivation. *Economic Botany, 54*(4), 439–448. https://doi.org/10.1007/BF02866543

[12] Rebezov, M., Khan, M. U., Semenova, A. A., et al. (2023). Nutritional and technical aspect of tiger nut and its micro-constituents: An overview. *Food Reviews International, 39*(6), 3262–3282. https://doi.org/10.1080/87559129.2021.2011910

[13] Reid, W. S. (1972). Development of a prototype mechanical harvester for chufa. *Canadian Agricultural Engineering, 14*, 89–95.

[14] Sánchez-Zapata, E., Fernández-López, J., & Pérez-Alvarez, J. A. (2012). Tiger nut (*Cyperus esculentus*) commercialization: Health aspects, composition, properties, and food applications. *Comprehensive Reviews in Food Science and Food Safety, 11*(4), 366–377. https://doi.org/10.1111/j.1541-4337.2012.00190.x

[15] Sun, R., Zhong, P., Liu, Z. D., Gao, H. J., Wang, R. D., Li, W., You, H. Y., Song, X. Y., & Wang, X. L. (2023). Research progress on stress resistance of tiger nut under abiotic stress. *Feed and Feeding, 5*, 32–35.

[16] Xu, Y. J. (2016). *Design and research of a new type of Cyperus esculentus harvester* [Master's thesis, China Agricultural University].

[17] Yu, Y., Lu, X., Zhang, T., Zhao, C., Guan, S., Pu, Y., & Gao, F. (2022). Tiger nut (*Cyperus esculentus L.*): Nutrition, processing, function and applications. *Foods, 11*(4), 601. https://doi.org/10.3390/foods11040601

[18] Zhang, H., Zhou, Z., Qu, Z., Li, Z., & Wang, W. (2022). Simulation and experiment of sieving process of sieving device for tiger nut harvester. *Agriculture, 12*(10), 1680. https://doi.org/10.3390/agriculture12101680

[19] Zhang, S., Fu, J., Zhang, R., Zhang, Y., & Yuan, H. (2022). Experimental study on the mechanical properties of friction, collision and compression of tiger nut tubers. *Agriculture, 12*(1), 65. https://doi.org/10.3390/agriculture12010065

[20] Zhang, Y., & Sun, S. (2023). Tiger nut (Cyperus esculentus L.) oil: A review of bioactive compounds, extraction technologies, potential hazards and applications. *Food Chemistry: X, 19*, 100868. https://doi.org/10.1016/j.fochx.2023.100868

[21] Zhao, X. Q., Liu, H., Lu, Z. Y., Cheng, Y. C., Zhang, D. J., Bai, F. F., Fang, J., & Ren, Y. F. (2019). Cultivation technology of windbreak and sand fixation of tiger nut on desertified and degraded land. *Modern Agriculture, 6*, 12–13.

[22] Zhao, Z., He, X. N., Wang, D. W., Shang, S. Q., Xu, N., Zhu, H., & Zheng, X. S. (2023). Design and test of intermediate conveying device for Cyperus esculentus combine harvester. *Journal of Agricultural Mechanization Research, 45*, 172–176.

[23] Zheng, X., Liu, J., Cheng, Z., Sun, Y., Li, L., & Wang, J. (2024). Improving tuber yield of tiger nut (*Cyperus esculentus L.*) through nitrogen fertilization in sandy farmland. *Plants, 13*(8), 1063. https://doi.org/10.3390/plants13081063

# CONSIDERATIONS ON THE INFLUENCE OF CLIMATE CHANGE ON AGRICULTURAL CROPS

/

# *CONSIDERAȚII PRIVIND INFLUENȚA SCHIMBĂRILOR CLIMATICE ASUPRA CULTURILOR AGRICOLE*

**Roxana Patricia IONAȘCU[1)], Remus Marius OPRESCU*[2)], Dan CUJBESCU[2)], Iulian VOICEA[2)]**

[1)] Development Research Station for Combating Soil Erosion "Mircea Moțoc" Perieni, Vaslui County / Romania;

[2)] National Institute of Research - Development for Machines and Installations Designed for Agriculture and Food Industry - INMA Bucharest / Romania.

**Tel: 0766 580 791; *E-mail: oprescu.remusmarius@gmail.com*

***Keywords:*** *climate change, water deficit, soil conservation, crop yield, contour cultivation*

**ABSTRACT**

*This study examined crop performance under the meteorological conditions recorded in 2024 at the Agricultural Research and Development Station Turda, Romania, within an experimental area rehabilitated for soil and water conservation research. Six plots represented bare fallow, spring wheat, contour-sown maize, downslope-sown maize, contour-sown soybean and a grass mixture. The descriptive analysis compared monthly temperature and precipitation records with a 65-year reference and evaluated the available yield and biometric data. The reported annual mean temperature exceeded the reference by 3.1°C. Calculations from monthly precipitation values indicated an annual rainfall deficit of 26.9%, reaching 44.3% during June–August. Estimated grain yields were 3,922 kg ha$^{-1}$ for spring wheat, 4,620 and 4,582 kg ha$^{-1}$ for contour- and downslope-sown maize, respectively, and 1,385 kg ha$^{-1}$ for soybean. The maize grain-yield difference was 0.83%, without evidence establishing statistical significance. The observations document crop performance during a warm, rainfall-deficient year but do not isolate yield losses attributable to long-term climate change. The rehabilitated plots provide a basis for subsequent replicated monitoring of crop production, soil moisture, runoff and sediment losses to assess adaptation measures.*

**REZUMAT**

*Studiul a analizat comportarea culturilor agricole în condițiile meteorologice din 2024 la Stațiunea de Cercetare-Dezvoltare Agricolă Turda, România, într-un perimetru experimental reabilitat pentru cercetări privind conservarea solului și apei. Cele șase parcele au cuprins ogor, grâu de primăvară, porumb semănat pe curba de nivel, porumb semănat din deal în vale, soia semănată pe curba de nivel și un amestec de ierburi. Analiza descriptivă a comparat temperaturile și precipitațiile lunare cu mediile pe 65 de ani și a evaluat producția și indicatorii biometrici. Temperatura medie anuală raportată a depășit referința cu 3,1 °C. Calculele bazate pe precipitațiile lunare au indicat un deficit anual de 26,9%, care a atins 44,3% în perioada iunie–august. Producțiile estimate de boabe au fost de 3.922 kg ha$^{-1}$ la grâu, 4.620 și 4.582 kg ha$^{-1}$ la porumbul semănat pe curba de nivel, respectiv din deal în vale, și 1.385 kg ha$^{-1}$ la soia. Diferența dintre variantele de porumb a fost de 0,83%, fără dovezi privind semnificația statistică. Observațiile descriu comportarea culturilor într-un an cald și deficitar pluviometric, fără a izola pierderile atribuite schimbărilor climatice pe termen lung. Parcelele reabilitate permit monitorizarea ulterioară, cu repetiții, a producției, umidității solului, scurgerilor și sedimentelor pentru evaluarea măsurilor de adaptare.*

## INTRODUCTION

Climate change affects agricultural crops through changes in temperature, rainfall distribution and the occurrence of extreme weather events. These pressures interact with soil properties and crop management, influencing both seasonal production and the long-term capacity of agricultural land to sustain yields. Assessing their effects therefore requires consideration of direct crop responses and the degradation of the soil and water resources on which production depends. Soil connects biological activity, hydrological processes and carbon cycling, making its condition central to the interpretation of agricultural vulnerability (*Huggett, 2023*).

Evidence from global assessments demonstrates the sensitivity of major crops to warming. Zhao et al. (2017) estimated that each 1 °C increase in global mean temperature would reduce average wheat, rice,

maize and soybean yields by 6.0%, 3.2%, 7.4% and 3.1%, respectively, without carbon dioxide fertilisation, effective adaptation or genetic improvement. These estimates describe global average responses and should not be interpreted as fixed losses for individual farms. Similarly, Ortiz-Bobea et al. (2021) estimated that anthropogenic climate change reduced global agricultural total factor productivity by approximately 21% relative to a counterfactual without anthropogenic climate change over the period studied since 1961. This indicator concerns the efficiency of combined agricultural inputs rather than the yield of a single crop.

Extreme events add risks that annual climatic averages cannot adequately represent. Lesk et al. (2016) found that drought and extreme heat reduced national cereal production by approximately 9–10% in their analysis of disasters between 1964 and 2007. Drought affected both yields and harvested area, whereas extreme heat primarily affected yields. Future responses also differ among crops and regions. Jägermeyr et al. (2021) projected more adverse responses for maize, soybean and rice in a new generation of climate and crop models, while wheat showed potential gains associated with higher carbon dioxide concentrations and benefits at higher latitudes. These findings underline the need to distinguish crop-specific responses, geographical conditions and model assumptions when discussing climate-related production losses.

Soil degradation provides an additional pathway through which changing climatic conditions can affect crop production. Water erosion removes and redistributes surface material, with consequences for nutrient retention, soil organic matter and the rooting environment. Its severity depends on rainfall characteristics, soil erodibility, slope, vegetation cover and management practices. The redistribution of soil organic carbon also links erosion to carbon cycling; excluding erosion from carbon accounting can therefore distort assessments of soil carbon dynamics (*Chappell et al., 2016*). Protecting agricultural soils requires attention to these interacting processes rather than treating erosion solely as the removal of mineral particles.

At the global scale, Borrelli et al. (2020) projected increases of approximately 30–66% in soil erosion by water between 2015 and 2070 under the combined land-use and climate scenarios they examined. Their assessment addressed sheet and rill erosion and excluded processes such as gully and riverbank erosion. The results represent scenario-dependent model estimates rather than observed future losses. For agricultural applications, this distinction matters because changes in rainfall erosivity can interact with seasonal vegetation cover and cultivation practices, producing different outcomes even where annual rainfall totals are similar. Consequently, global projections provide context for risk assessment but require regional and local interpretation.

European studies support this need for spatially specific assessment. Marcinkowski et al. (2022) investigated soil erosion under long-term climate projections in Poland, while Patriche (2023) applied the Revised Universal Soil Loss Equation (RUSLE) to Romania under current and future climate scenarios. These studies provide a relevant basis for examining climate-related erosion in European agricultural landscapes. However, erosion estimates cannot be converted directly into crop-yield losses without information on soil depth, fertility, crop requirements and management. Keller et al. (2021), who compared erosion models and event soil losses on loess slopes in Hungary, further illustrate the importance of matching the modelling approach to the processes and spatial scale under investigation.

The consequences of erosion also extend beyond the cultivated plot. Sediment transported through drainage networks can accumulate in reservoirs, reducing storage capacity and complicating water management. Dutta (2016) examined the relationships between soil erosion, sediment yield and reservoir sedimentation, highlighting the need to consider catchment processes when evaluating these impacts. For irrigated agriculture, this creates a connection between the conservation of upstream soils and the maintenance of water-storage infrastructure. An assessment of agricultural adaptation should therefore consider both the protection of productive soil within fields and the control of sediment transfers across the wider catchment.

Conservation practices can reduce these pressures, but their effectiveness depends on local conditions and implementation. In a field study conducted over two cropping seasons in Ethiopia, Kebede et al. (2023) reported that locally adapted minimum contour tillage reduced surface runoff by 30–60% and soil loss by 49–76% compared with conventional tillage on slopes of 3–14%. These results demonstrate the potential of adapted cultivation methods under the tested conditions. They do not establish a universal reduction factor for other soils, crops or climates. Molla and Sisheber (2017) also found that incorrect design and poor management limited the effectiveness of existing soil conservation structures in the Koga watershed, showing that the presence of a structure alone does not ensure erosion control.

Adaptation consequently requires combinations of agronomic and engineering measures selected for the constraints of each production system. Relevant options include maintaining protective soil cover, adapting tillage and crop rotations, selecting suitable cultivars, managing water supplies and designing conservation structures for local topography. Hussein (2024) discussed climate-smart agricultural strategies in Ethiopia, providing examples of how adaptation measures must fit their environmental and socioeconomic context. For Romanian agriculture, evidence from international studies should therefore support locally evaluated measures rather than the direct transfer of reported percentages or uniform technical prescriptions.

The cited studies establish substantial evidence for climate-related crop risks and soil erosion, but they also expose a practical difficulty: global crop-response estimates, regional erosion projections and field-level conservation results describe different processes and scales. This article aims to synthesise these complementary findings, with particular attention to the links between climatic pressures, soil degradation and agricultural crop production. Its objectives are to examine the main pathways of impact, assess the contribution and limitations of soil and water conservation measures, and identify considerations relevant to the adaptation of crop-management technologies. This approach provides a basis for discussing production resilience while keeping observed effects, model projections and proposed management responses clearly valuable.

## MATERIALS AND METHODS

The study concerns field observations and crop-production data collected in 2024 at the Agricultural Research and Development Station Turda (SCDA Turda), Romania, within the ADER 20.1.2 project. The station is located northwest of Turda, at the western boundary of the Transylvanian Plateau, at approximately 46°35′ N and 23°47′ E. Its territory extends across elevations of 345 to 493 m and includes low plateau hills, the upper terrace of the Arieș River and secondary valleys (Fig. 1).




(*a*) (*b*)

**Fig. 1 - Location of the experimental area at SCDA Turda**

*(Google Maps imagery)*

*(a) Satellite overview; (b) enlarged view of the experimental area.*

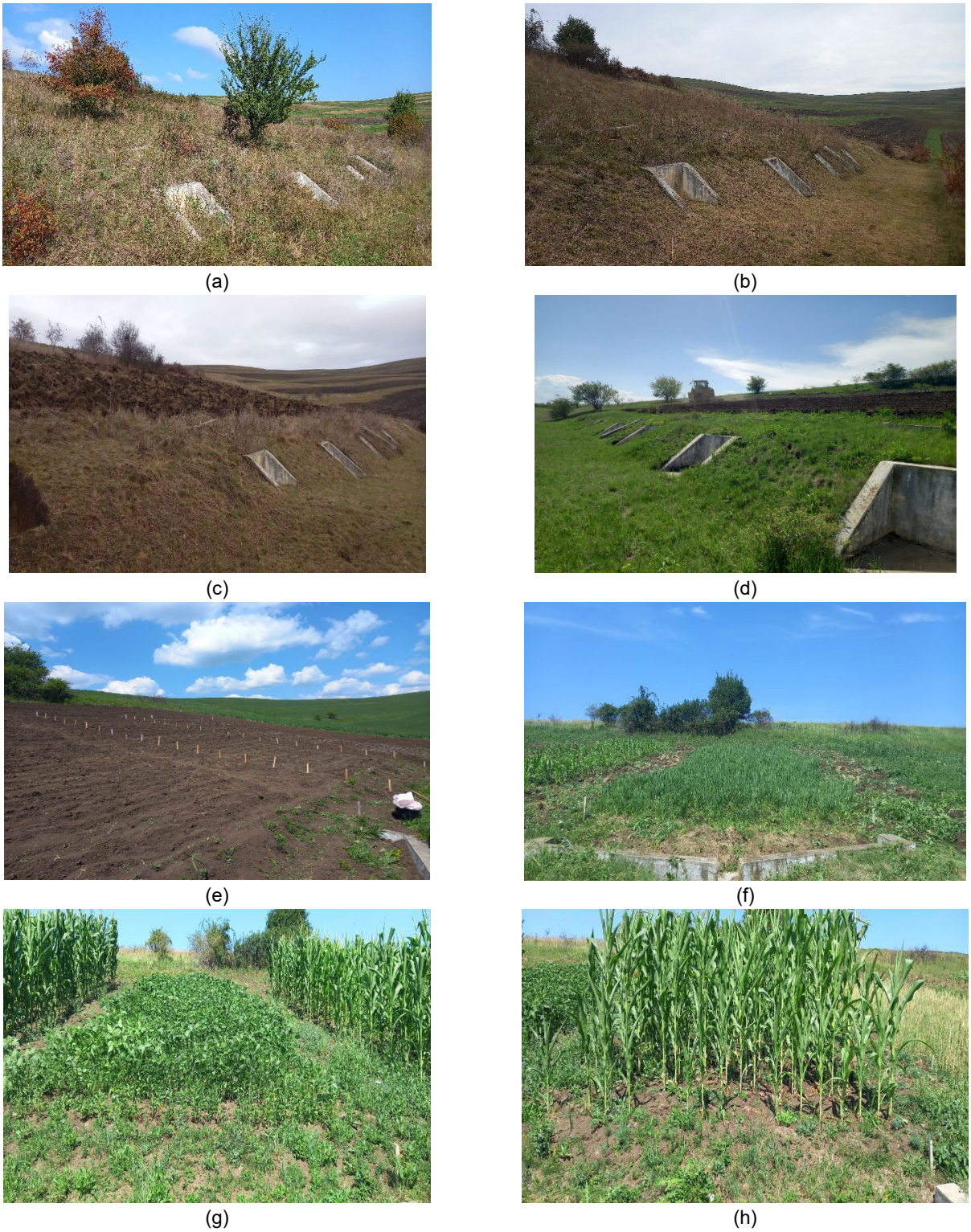
The station lies within the middle Arieș catchment. The dominant soil described for the station is a vertic argic chernozem, with an Am–Bty–Cca horizon sequence. Reported background properties include pH in water of 6.9 to 7.1, humus content of 3.56 to 3.92% in the arable layer and total nitrogen of 0.183 to 0.196%.

The experimental area had previously contained microplots for water-erosion studies between 1985 and 2001. Rehabilitation activities in 2024 included removing woody vegetation, cleaning the existing concrete structures, ploughing and preparing the land. Materials were procured for plot-separation panels and pipes connecting the plots to collection basins intended for runoff and sediment monitoring.

Six plots were established with the following land-cover or cultivation variants: bare fallow; spring wheat; maize sown along contour lines; maize sown in the downslope direction; soybean sown along contour lines; and a grass mixture. The maize variants provided the available comparison between contour and downslope cultivation. Crop-production records were available for spring wheat, both maize variants and contour-sown soybean (Fig. 2).

The meteorological dataset originated from the Turda Meteorological Station and covered the calendar year from 1 January to 31 December 2024. It comprised air-temperature data in degrees Celsius

and precipitation data in millimetres, reported for three successive periods within each month and as monthly values. The within-month periods correspond to days 1–10, days 11–20 and the remainder of the month. The dataset also included monthly reference values calculated over a 65-year period.



(a) (b) (c) (d) (e) (f) (g) (h)

**Fig. 2 - Experimental area and crop establishment at SCDA Turda, ADER 20.1.2, 2024**

*(a) Woody vegetation and existing structures; (b, c) views of the slope and concrete structures; (d) soil preparation; (e) plot demarcation; (f) wheat; (g) soybean; (h) maize.*

Climatic conditions were assessed by comparing the 2024 monthly mean temperatures and precipitation totals with the corresponding long-term reference values. Temperature departures represent the difference between the observed and reference monthly means, expressed in degrees Celsius. Precipitation departures represent the difference between the observed monthly total and the corresponding long-term

mean monthly total, expressed in millimetres. Negative precipitation departures indicate rainfall below the reference value. The analysis considered rainfall distribution alongside temperature departures.

The agronomic dataset comprised estimated grain yield, expressed in kg $ha^{-1}$, thousand-grain or thousand-seed weight (g), and hectolitre weight (kg $hL^{-1}$). For maize, the records distinguished ear yield from grain yield and reported both cultivation orientations separately.

The spring-wheat records additionally included plant height (cm), ear length (cm), grain number per ear and grain mass per ear (g). Soybean records included plant height (cm) and seed number per plant.

The analysis was restricted to descriptive comparisons of the available crop and meteorological records. Plot-level replication and uncertainty estimates were unavailable in the supplied dataset, precluding an inferential test of cultivation-orientation effects. Quantitative runoff and sediment-loss data were also unavailable; erosion-monitoring facilities therefore formed part of the experimental setup rather than the quantitative analysis.

The interpretation relates crop performance to the observed temperature and rainfall departures. A single year of observations does not isolate the contribution of long-term climate change from other influences on yield.

## RESULTS

The reported annual mean air temperature at Turda was 12.3 °C, compared with the 65-year reference of 9.2 °C, corresponding to a positive departure of 3.1 °C. Monthly temperatures exceeded the reference in 11 of the 12 months (Table 1). February showed the largest departure (+7.6 °C), while July recorded the highest monthly mean (24.0 °C). November was the only cooler month, with a departure of −1.2°C.

**Table 1**

**Monthly meteorological conditions at Turda in 2024**

| Month | T 2024 (°C) | T ref. (°C) | ΔT (°C) | P 2024 (mm) | P ref. (mm) | ΔP (mm) |
|---|---|---|---|---|---|---|
| Jan | 0.2 | -3.3 | +3.5 | 4.8 | 21.7 | -16.9 |
| Feb | 7.0 | -0.6 | +7.6 | 9.2 | 19.2 | -10.0 |
| Mar | 8.8 | 4.4 | +4.4 | 37.7 | 24.3 | +13.4 |
| Apr | 13.3 | 10.0 | +3.3 | 38.8 | 45.6 | -6.8 |
| May | 15.8 | 15.0 | +0.8 | 60.7 | 69.4 | -8.7 |
| Jun | 21.7 | 18.0 | +3.7 | 36.2 | 84.6 | -48.4 |
| Jul | 24.0 | 19.8 | +4.2 | 49.0 | 78.0 | -29.0 |
| Aug | 23.4 | 19.5 | +3.9 | 36.7 | 56.1 | -19.4 |
| Sep | 17.9 | 15.2 | +2.7 | 64.2 | 42.4 | +21.8 |
| Oct | 11.7 | 9.8 | +1.9 | 14.4 | 35.4 | -21.0 |
| Nov | 2.8 | 4.0 | -1.2 | 19.2 | 28.2 | -9.0 |
| Dec | 1.1 | -1.2 | +2.3 | 18.5 | 27.5 | -9.0 |

*T: monthly mean temperature; P: monthly precipitation total; ref.: 65-year reference; Δ: 2024 value minus reference.*

The monthly precipitation values sum to 389.4 mm, compared with a reference sum of 532.4 mm, giving a deficit of 143.0 mm (26.9%). Rainfall was below the reference in ten months; only March and September showed surpluses. June had the largest absolute deficit (48.4 mm).

From June to August, precipitation totalled 121.9 mm against 218.7 mm, a deficit of 44.3%. Temperature departures during these three months ranged from +3.7 to +4.2 °C (Fig. 3).

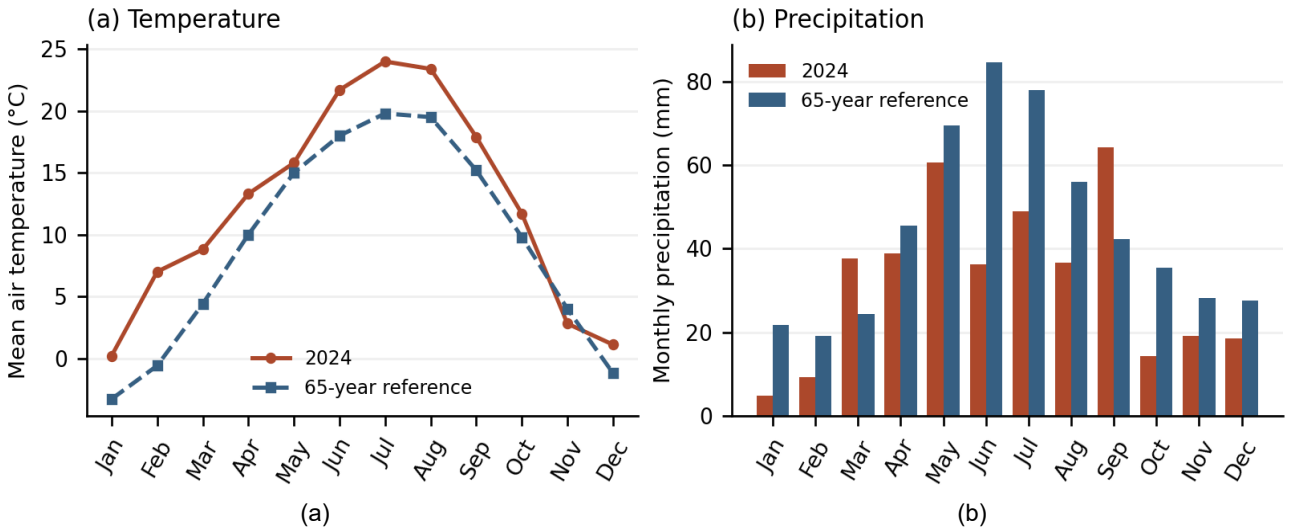



**Fig. 3 - Monthly temperature**

*(a) and precipitation (b) at Turda in 2024 and the 65-year reference*

Estimated grain yields were 3,922 kg ha⁻¹ for spring wheat, 4,620 kg ha⁻¹ for contour-sown maize, 4,582 kg ha⁻¹ for downslope-sown maize and 1,385 kg ha⁻¹ for contour-sown soybean (Table 2 and Fig. 4). These are the reported values for the individual crop variants, without estimates of variability.

**Table 2**

**Yield and grain characteristics of the crop variants in 2024**

| Crop variant | Grain yield (kg ha⁻¹) | Ear yield (kg ha⁻¹) | TGW/TSW (g) | HW (kg hL⁻¹) |
|---|---|---|---|---|
| Spring wheat | 3,922 | n.a. | 36.8 | 74.8 |
| Maize, contour | 4,620 | 5,381 | 201.2 | 70.6 |
| Maize, downslope | 4,582 | 5,585 | 198.4 | 69.8 |
| Soybean, contour | 1,385 | n.a. | 140.5 | 71.2 |

*TGW/TSW: thousand-grain/thousand-seed weight (MMB in the source); HW: hectolitre weight (MH in the source); n.a.: not applicable. Units for MMB and MH follow their conventional definitions*

Contour-sown maize had a grain yield 38 kg ha⁻¹ higher than downslope-sown maize, equivalent to 0.83% relative to the downslope variant. Its thousand-grain weight was 2.8 g higher and its hectolitre weight was 0.8 kg hL⁻¹ higher. However, maize ear yield was 204 kg ha⁻¹ lower under contour sowing (3.65%). Thus, ear yield and grain yield did not rank the two variants in the same order.

These differences are descriptive and do not establish a statistically significant effect of sowing orientation.

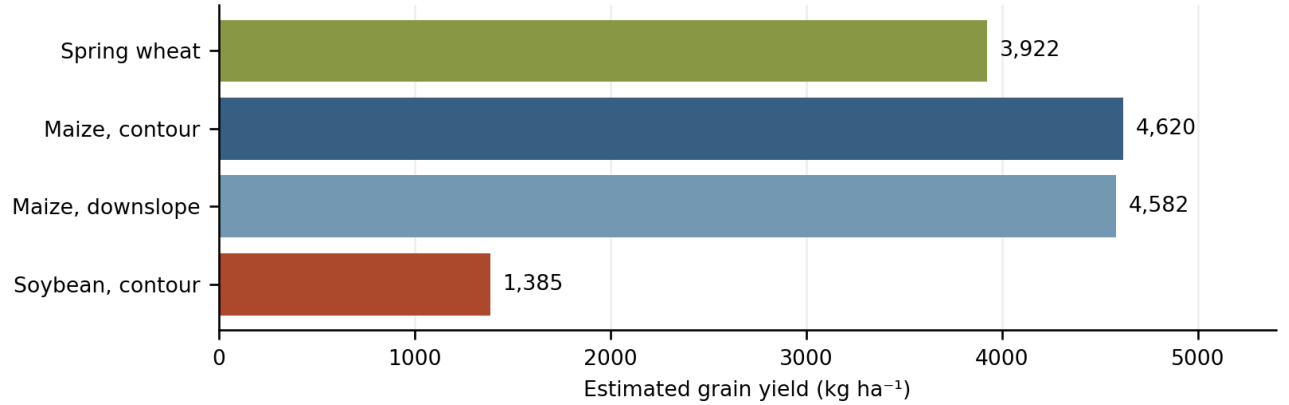



**Fig. 4 - Estimated grain yields of the four recorded crop variants at SCDA Turda in 2024**

**Table 3**

**Reported biometric characteristics of spring wheat and soybean**

| Indicator | Spring wheat | Soybean, contour |
|---|---|---|
| Plant height (cm) | 84 | 55 |
| Ear length (cm) | 8 | n.a. |
| Grains per ear | 38 | n.a. |
| Grain mass per ear (g) | 1.80 | n.a. |
| Seeds per plant | Not reported | 46 |

Spring wheat reached a reported height of 84 cm and an ear length of 8 cm, with 38 grains and 1.80 g of grain per ear. Soybean reached 55 cm and had 46 seeds per plant (Table 3). The crop observations coincided with above-reference temperatures and a substantial summer rainfall deficit. Without a matched favourable-year comparison, documented replication or measured runoff and sediment losses, the dataset does not quantify climate-attributable yield reductions or erosion-control efficiency.

## CONCLUSIONS

The 2024 observations at SCDA Turda documented crop production under warmer and drier conditions than the 65-year reference. The reported annual mean temperature was 3.1 °C above the reference. Calculations based on the monthly precipitation records indicated an annual rainfall deficit of 26.9%, increasing to 44.3% during June–August. These findings identify summer water availability as a priority for further investigation at the experimental site.

Estimated grain yields reached 3,922 kg $ha^{-1}$ for spring wheat, 4,620 kg $ha^{-1}$ for contour-sown maize, 4,582 kg $ha^{-1}$ for downslope-sown maize and 1,385 kg $ha^{-1}$ for contour-sown soybean. Contour-sown maize produced 0.83% more grain than the downslope variant, but had a lower ear yield. This small descriptive difference does not establish the superiority of either cultivation orientation or demonstrate an erosion-control benefit.

The rehabilitation of six experimental plots provides a basis for investigating crop performance alongside soil and water conservation. Subsequent monitoring should combine replicated crop observations with measurements of soil moisture, runoff and sediment losses over several years. Such measurements would help determine whether contour cultivation and protective vegetation cover improve water retention, reduce soil loss and stabilise production under contrasting weather conditions.

The present dataset documents the coexistence of elevated temperatures, deficient rainfall and the reported crop yields during one growing season. It does not quantify yield losses attributable to long-term climate change, because matched reference yields and replicated observations are unavailable. The results therefore provide a local baseline for evaluating adaptation measures, while their effectiveness remains to be established through continued field assessment.

## ACKNOWLEDGEMENT

This research was supported by the Ministry of Agriculture and Rural Development – Romania - MADR through the Sectoral Project ADER 20.1.2. "Enhanced Utilization of Agricultural Land Subject to Erosion through the Conservation of Water and Soil Resources under Climate Change Conditions", Ctr. 27.07.2023.

## REFERENCES

[1] Borrelli, P., Robinson, D. A., Panagos, P., Lugato, E., Yang, J. E., Alewell, C., Wuepper, D., Montanarella, L., & Ballabio, C. (*2020). Land use and climate change impacts on global soil erosion by water (2015–2070). Proceedings of the National Academy of Sciences,* 117(36), 21994–22001. https://doi.org/10.1073/pnas.2001403117

[2] Chappell, A., Baldock, J., & Sanderman, J. (2016). The global significance of omitting soil erosion from soil organic carbon cycling schemes. *Nature Climate Change*, 6, 187–191. https://doi.org/10.1038/nclimate2829

[3] Dutta, S. (2016). Soil erosion, sediment yield and sedimentation of reservoir: a review. *Modeling Earth Systems and Environment*, 2, 123. https://doi.org/10.1007/s40808-016-0182-y

[4] Huggett, R. (2023). Soil as part of the Earth system. *Progress in Physical Geography*: *Earth and Environment*, 47(3), 454–466. https://doi.org/10.1177/03091333221147655

[5] Hussein, A. (2024). Climate smart agriculture strategies for enhanced agricultural resilience and food security under a changing climate in Ethiopia. *Sustainable Environment*, 10(1), 2345433. https://doi.org/10.1080/27658511.2024.2345433

[6] Jägermeyr, J., Müller, C., Ruane, A. C., Elliott, J., Balkovic, J., Castillo, O., Faye, B., Foster, I., Folberth, C., Franke, J. A., Fuchs, K., Guarin, J., Heinke, J., Hoogenboom, G., Iizumi, T., Kain, A. K., Kelly, D., Khabarov, N., Lange, S., Lin, T.-S., Liu, W., Mialyk, O., Minoli, S., Moyer, E. J., Okada, M., Phillips, M., Porter, C., Rabin, S., Scheer, C., Schneider, J. M., Schyns, J. F., Skalsky, R., Smerald, A., Stella, T., Stephens, H., Webber, H., Zabel, F., & Rosenzweig, C. (2021). Climate impacts on global agriculture emerge earlier in new generation of climate and crop models. *Nature Food*, 2(11), 873–885. https://doi.org/10.1038/s43016-021-00400-y

[7] Kebede, L., Temesgen, M., Fanta, A., Kebede, A., Rockström, J., & Melesse, A. M. (2023). Effect of locally adapted conservation tillage on runoff, soil erosion, and agronomic performance in semiarid rain-fed farming in Ethiopia. *Land*, 12(3), 593. https://doi.org/10.3390/land12030593

[8] Keller, B., Centeri, C., Szabó, J. A., Szalai, Z., & Jakab, G. (2021). Comparison of the applicability of different soil erosion models to predict soil erodibility factor and event soil losses on loess slopes in Hungary. *Water,* 13(24), 3517. https://doi.org/10.3390/w13243517

[9] Lesk, C., Rowhani, P., & Ramankutty, N. (2016). Influence of extreme weather disasters on global crop production. *Nature*, 529, 84–87. https://doi.org/10.1038/nature16467

[10] Marcinkowski, P., Szporak-Wasilewska, S., & Kardel, I. (2022). Assessment of soil erosion under long-term projections of climate change in Poland. *Journal of Hydrology*, 607, 127468. https://doi.org/10.1016/j.jhydrol.2022.127468

[11] Molla, T., & Sisheber, B. (2017). Estimating soil erosion risk and evaluating erosion control measures for soil conservation planning at Koga watershed in the highlands of Ethiopia. *Solid Earth*, 8(1), 13–25. https://doi.org/10.5194/se-8-13-2017

[12] Ortiz-Bobea, A., Ault, T. R., Carrillo, C. M., Chambers, R. G., & Lobell, D. B. (2021). Anthropogenic climate change has slowed global agricultural productivity growth. *Nature Climate Change*, 11, 306–312. https://doi.org/10.1038/s41558-021-01000-1

[13] Patriche, C. V. (2023). Applying RUSLE for soil erosion estimation in Romania under current and future climate scenarios. *Geoderma Regional*, 34, e00687. https://doi.org/10.1016/j.geodrs.2023.e00687

[14] Zhao, C., Liu, B., Piao, S., Wang, X., Lobell, D. B., Huang, Y., Huang, M., Yao, Y., Bassu, S., Ciais, P., Durand, J.-L., Elliott, J., Ewert, F., Janssens, I. A., Li, T., Lin, E., Liu, Q., Martre, P., Müller, C., Peng, S., Peñuelas, J., Ruane, A. C., Wallach, D., Wang, T., Wu, D., Liu, Z., Zhu, Y., Zhu, Z., & Asseng, S. (2017). Temperature increase reduces global yields of major crops in four independent estimates. *Proceedings of the National Academy of Sciences*, 114(35), 9326–9331. https://doi.org/10.1073/pnas.1701762114

# END-TO-END EXPERIMENTAL EVALUATION OF A RAIL-GUIDED ROBOT FOR AUTONOMOUS TOMATO HARVESTING

/

# *EVALUAREA EXPERIMENTALĂ INTEGRATĂ A UNUI ROBOT GHIDAT PE ȘINE PENTRU RECOLTAREA AUTONOMĂ A TOMATELOR*

**Mariana EPURE[1)], Mihai Gabriel MATACHE[1)], Robert Dorin CRISTEA*[1)], Florin Bogdan MARIN[2)], Alexandra LEONTE[3)], Daniela-Andreea ZAMFIR[4)]**

[1)] National Institute of Research - Development for Machines and Installations Designed for Agriculture and Food Industry - INMA Bucharest / Romania;

[2)] Faculty of Engineering, "Dunărea de Jos" University of Galați, Galati County / Romania;

[3)] Agricultural Research and Development Station Secuieni, Neamt County / Romania;

[4)] UNSTP Bucharest / Romania

**Tel. +40 21 269 32 55; *E-mail: robertcri@yahoo.com*

***Keywords:*** *autonomous harvesting, greenhouse robot, tomato, robotic gripper, experimental validation*

## ABSTRACT

*Robotic harvesting must be assessed as an integrated process because successful fruit detection does not necessarily lead to detachment and storage. This paper reports an instrumented final validation session for a rail-guided greenhouse robot developed for autonomous cherry-tomato harvesting. The system combined a battery-powered mobile platform, a UR5e six-axis manipulator, a Robotiq 2F-85 adaptive gripper, a ZED X stereo camera, a ZED Box processing unit, and a CNN-Watershed perception pipeline. Seventy-five end-to-end harvesting attempts were evaluated through detection, three-dimensional localization, trajectory generation, grasping, detachment, storage, cycle timing, visual damage, detection confidence, and electrical demand. All target fruits were detected and valid trajectories were generated in every case. Sixty fruits were grasped, detached, and stored, giving a complete harvesting success rate of 80%. No visible fruit damage or accidental plant contact was recorded. The mean cycle time was 19.6 s, with values from 17.8 to 22.0 s. All 15 unsuccessful attempts ended during grasping; 12 were assigned to fruit slip or insufficient gripping force, and three to lower-confidence detections with a possible effect on three-dimensional localization. The results identify the fruit-gripper interaction, rather than perception or trajectory generation, as the main limitation of the tested configuration.*

## REZUMAT

*Evaluarea recoltării robotizate trebuie realizată la nivelul întregului proces, deoarece detectarea corectă a fructului nu conduce automat la desprinderea și depozitarea acestuia. Lucrarea prezintă sesiunea finală instrumentată de validare a unui robot ghidat pe șine, dezvoltat pentru recoltarea autonomă a tomatelor cherry în seră. Sistemul a integrat o platformă mobilă alimentată de la baterie, un manipulator UR5e cu șase axe, un gripper adaptiv Robotiq 2F-85, o cameră stereo ZED X, o unitate de procesare ZED Box și un sistem de percepție CNN-Watershed. Au fost analizate 75 de încercări complete de recoltare, urmărindu-se detecția, localizarea tridimensională, generarea traiectoriei, prinderea, desprinderea, depozitarea, durata ciclului, deteriorarea vizibilă, încrederea detecției și consumul electric. Toate fructele țintă au fost detectate, iar traiectoriile au fost valide în fiecare caz. Au fost recoltate și depozitate 60 de fructe, ceea ce corespunde unei rate de succes de 80%. Nu s-au observat deteriorări ale fructelor sau contacte accidentale cu plantele. Durata medie a ciclului a fost de 19,6 s, cu valori între 17,8 și 22,0 s. Toate cele 15 nereușite au apărut la prindere. Rezultatele indică interacțiunea dintre fruct și gripper drept principala limitare a configurației testate.*

## INTRODUCTION

Greenhouse harvesting robots combine mobility, perception, localization, manipulation, and crop-specific end effectors. A failure in any one of these stages prevents completion of the harvesting cycle, so system-level validation remains necessary even when the individual modules perform well. Reviews of harvesting robots and greenhouse robotics describe this integration problem as one of the main barriers to reliable field use *(Mail et al., 2023; Sánchez-Molina et al., 2024).* Occlusion, clustered fruit, variable illumination, and compliant plant structures affect both target localization and physical access. Multi-view

reconstruction can improve fruit representation in dense canopies, while occlusion-aware motion generation can reduce unwanted contact during approach *(Rapado-Rincón et al., 2023; Gong et al., 2022)*. Grasping remains a separate source of error because a geometrically valid approach may still produce slip, inadequate contact, or excessive local force.

Reported greenhouse systems provide useful reference values, although direct comparisons are limited by crop architecture and by different definitions of a successful cycle. Wang et al. (2017) reported approximately 86% success and 15 s per tomato for a binocular-vision harvesting robot. The SWEEPER sweet-pepper robot reached 85% harvesting success in an improved crop configuration, with cycle performance strongly influenced by accessibility and detachment conditions (*Arad et al., 2020).* The research programme preceding the present tests covered Solanaceae harvesting mechanisms and specialized grippers *(Matache et al., 2025),* convolutional-neural-network-based three-dimensional pose estimation *(Marin et al., 2025a),* and vision-based assessment of soft-gripper states *(Marin et al., 2025b).* A broader evaluation of the integrated rail-guided platform reported its perception, calibration, and occlusion-aware trajectory strategy across a larger greenhouse test set *(Matache et al., 2026*). To avoid repeating that algorithmic description, the present paper focuses on the final 75-cycle instrumented validation session conducted in 2026. Its purpose is to communicate end-to-end completion, stage-resolved timing, electrical demand, and the location of operational failures within the harvesting sequence.

## MATERIALS AND METHODS

The experimental system consisted of a mobile platform travelling on modular rails between greenhouse rows. The platform carried the robotic arm, perception hardware, controller, battery, and fruit-storage area. A UR5e six-degree-of-freedom collaborative manipulator performed the harvesting motion, and a Robotiq 2F-85 parallel adaptive gripper contacted and detached the fruit. A ZED X stereo camera supplied RGB and depth information to a ZED Box processing unit. The control application combined image acquisition, CNN-Watershed fruit segmentation, three-dimensional coordinate generation, camera-to-robot coordinate transformation, trajectory generation, manipulator control, and operator supervision. Table 1 lists the configuration relevant to the tests.

**Table 1**

**Configuration of the experimental harvesting system**

| Subsystem | Configuration used in the 2026 tests |
|---|---|
| Mobile platform | 1200 × 456 mm; 1.8 kW, 48 V DC drive; 3.36 kWh battery; 30 m modular rail |
| Manipulator | UR5e; 6 axes; 5 kg payload; 850 mm reach; ±0.03 mm repeatability |
| End effector | Robotiq 2F-85 adaptive gripper; 0-85 mm opening; adjustable gripping force |
| Perception | ZED X stereo camera and ZED Box; RGB, depth, and point-cloud acquisition |
| Control pipeline | CNN-Watershed detection, 3D localization, coordinate transformation, trajectory generation, grasping, and storage |

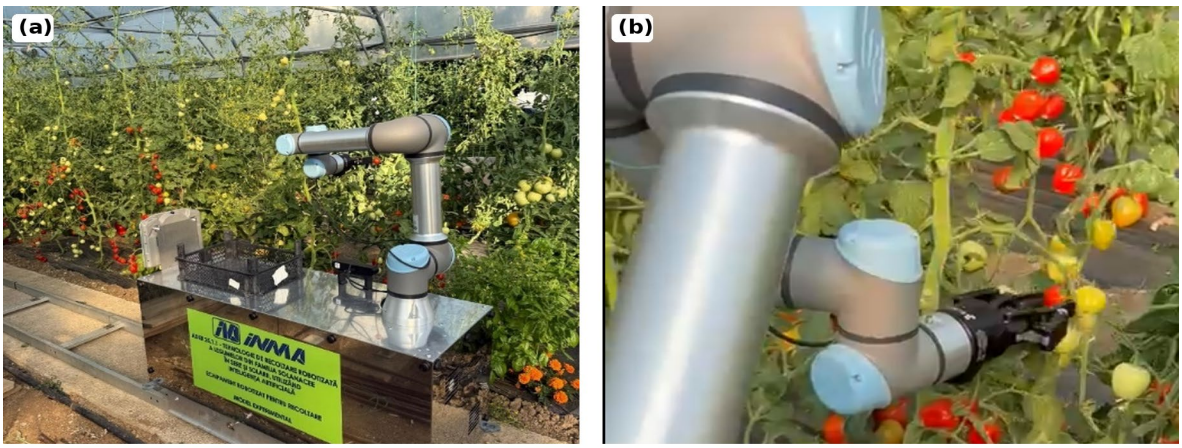



**Fig. 1 - Experimental system in the INMA greenhouse:**
*(a) rail-guided platform and manipulator; (b) tomato approach and grasping test*

Experiments were conducted in 2026 in the INMA greenhouse on a cherry-tomato hybrid cultivated in soil. The tested row was 25 m long, with 0.90 m between rows and 0.50 m between plants. The recorded air temperature was approximately 30 °C and relative humidity was 55%, under natural and variable illumination. Before testing, leaves that directly blocked the harvesting zone were selectively trimmed and stems were straightened to obtain a crop arrangement compatible with the experimental robot. This preparation reduced canopy complexity and is considered when interpreting the results.

Before each session, the rail and platform, electrical supply, manipulator mounting, gripper surfaces, camera calibration, communication links, and the camera-to-tool-centre-point transformation were checked. Each attempt followed the same sequence: platform positioning, RGB and depth acquisition, target selection, 3D coordinate generation, obstacle check, trajectory generation, arm approach, grasping and detachment, fruit storage, and result logging.

The primary endpoint was complete harvesting success, defined as grasping, detaching, and placing the selected fruit in the storage area. Intermediate endpoints were target detection, valid 3D coordinates, and a valid robot trajectory. Cycle time and the durations of visual detection, trajectory planning, arm motion, and grasping/storage were recorded for every attempt.

The logs also contained detection confidence, video-frame counts, electrical power, supply voltage, visible fruit damage, and accidental contact. The analysis was descriptive because the tests represented one greenhouse, one hybrid, and one final experimental campaign; the reported standard deviation therefore describes dispersion within this campaign rather than variation between independent campaigns.

## RESULTS

The robot completed 75 autonomous harvesting attempts. All selected targets were detected, valid 3D coordinates were obtained, and a robot trajectory was generated for every attempt. Sixty fruits were successfully grasped, detached, and stored, resulting in an end-to-end success rate of 80.0%. No visible damage to the fruit and no accidental contacts with the crop or greenhouse structure were recorded. Table 2 summarizes the main results.

**Table 2**

**Summary of the final greenhouse validation session**

| Indicator | Result |
|---|---|
| Complete harvesting success | 60/75 attempts (80.0%) |
| Target detection | 75/75 attempts (100.0%) |
| Valid 3D coordinates and trajectories | 75/75 attempts (100.0%) |
| Cycle time | 19.6 ± 0.71 s; median 19.5 s; range 17.8-22.0 s |
| Mean cycle time, successful / unsuccessful | 19.47 s / 20.24 s |
| Visible fruit damage / accidental contact | 0 / 0 |
| Detection log | 7823 frames; mean confidence 0.735; mean 13.62 FPS |
| Electrical log | 266.6 W mean power; 787.2 W peak power; 48 V mean supply voltage |

Cycle times were concentrated around the session mean (Fig. 2). Successful attempts averaged 19.47 s, compared with 20.24 s for unsuccessful attempts. This difference is presented descriptively; the experiment was not designed as a replicated comparison between outcome groups.

The unsuccessful cycles were therefore not characterized by a prolonged recovery sequence, because the controller ended the attempt after the failed grasp.

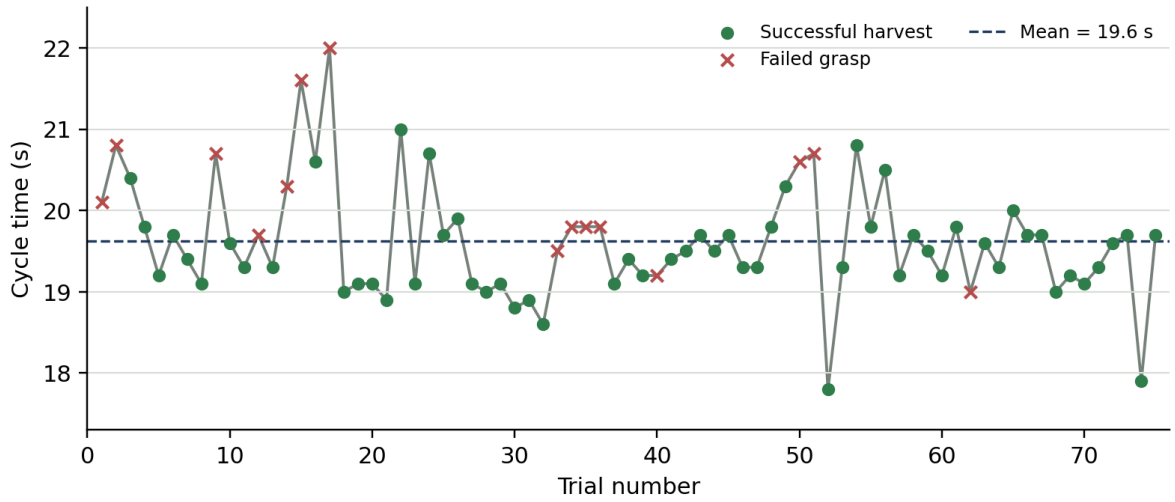



**Fig. 2 - Cycle time and harvesting outcome for the 75 autonomous attempts**

The mean time assigned to visual detection was 0.763 s, trajectory planning required 0.008 s, arm motion required 2.936 s, and grasping plus storage required 15.246 s (Fig. 3). Grasping and storage accounted for 77.7% of the recorded mean cycle time, whereas trajectory planning accounted for less than 0.1%.

The component means do not sum exactly to the total cycle time because the total also includes control, communication, and transition overhead that was not assigned to a separate logged stage.

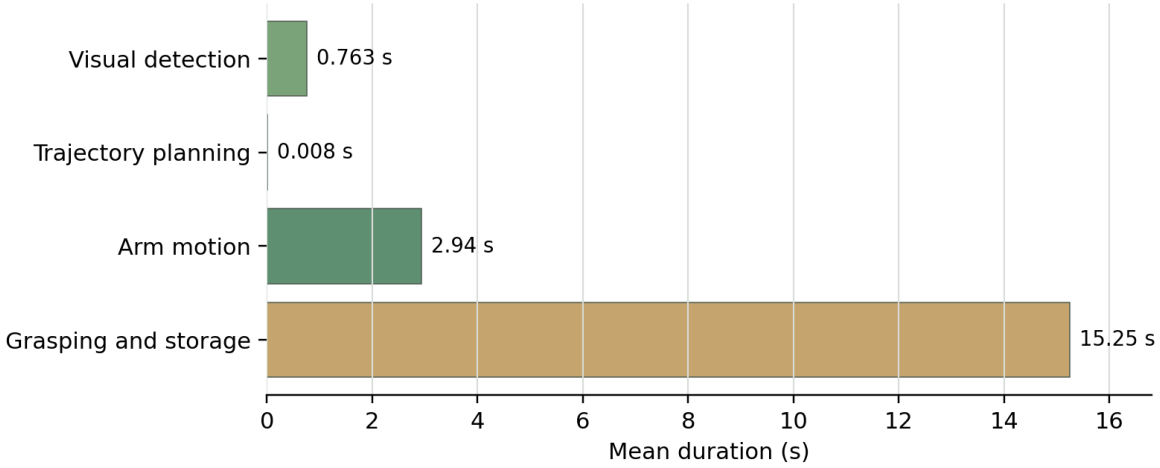



**Fig. 3 - Mean duration of the recorded stages in the harvesting cycle**

All 15 unsuccessful attempts terminated during grasping. Twelve failures were assigned in the test log to fruit slip or insufficient gripping force. Three failures coincided with lower detection-confidence values of approximately 0.54-0.56, which may have affected the 3D grasp point. These three cases still produced valid coordinates and trajectories, so the evidence supports a possible localization contribution rather than a confirmed perception failure. The distribution places the immediate operational bottleneck at the fruit-gripper interface.

The perception module processed 7823 video frames during the recorded session. The mean detection confidence was 0.735, with an average of 12.6 fruit candidates per attempt. The mean detection rate reported by the session log was 13.62 FPS. Electrical monitoring indicated a mean power of 266.6 W and a recorded peak of 787.2 W at a mean supply voltage of 48 V. These measurements describe the test session; they are not a battery-endurance result because a continuous full-discharge trial was not performed.

## DISCUSSION

The final session shows a clear separation between the front and back portions of the harvesting chain. Detection, coordinate generation, and trajectory generation reached the selected target in every

recorded attempt, while all incomplete cycles failed during physical acquisition of the fruit. This result does not establish a 100% detector recall for the entire canopy, because the denominator consisted of the 75 selected targets. It does show that, once a target entered the tested workflow, the perception and planning modules consistently supplied executable commands.

The 80.0% complete success rate and 19.6 s mean cycle time closely match the 78.5% and 19.5 s reported in the earlier, broader evaluation of the same system architecture *(Matache et al., 2026).*

The agreement supports the repeatability of the integrated workflow, while the present stage-level logs explain where time and failures accumulated. Across published systems, success definitions and crop conditions differ. The current results are below the approximately 86% success and 15 s cycle reported by Wang et al. (2017), and below the 85% success reported for SWEEPER under its improved crop configuration *(Arad et al., 2020).* Such comparisons are indicative rather than controlled because fruit type, detachment mechanism, canopy preparation, and cycle boundaries are not identical.

The long grasping/storage stage and the failure distribution point to the next practical modifications. Adjustable contact surfaces, force scheduling according to estimated fruit diameter, slip or post-grasp verification, and an automatic retry from a modified approach angle would address the observed failure modes. This interpretation is consistent with work showing that grasp assessment must be evaluated separately from object detection *(Seo and Oh, 2025)* and with the authors' earlier vision-based analysis of gripper states *(Marin et al., 2025b).* Changes to the trajectory planner alone are unlikely to produce a similar improvement because its mean computation time was only 8 ms.

The conclusions are limited to one cherry-tomato hybrid, one prepared greenhouse row, and a single final campaign of 75 attempts. Fruit damage was judged visually, and plant effects were not followed over repeated harvests. Further work should repeat the protocol across cultivars and denser, untrimmed canopies, add force or tactile measurements at the gripper, and report performance over independent test days. Those tests would show whether the 80% rate is maintained when biological and environmental variation increases.

## CONCLUSIONS

The rail-guided harvesting robot completed 60 of 75 autonomous cherry-tomato harvesting attempts, corresponding to an 80.0% end-to-end success rate. All selected fruits were detected and received valid 3D coordinates and trajectories. The mean cycle time was 19.6 s, no visible fruit damage was observed, and no accidental contacts were recorded during the session.

The main limitation was grasping rather than perception or trajectory generation. All 15 unsuccessful attempts ended at the fruit-gripper interface, and grasping plus storage occupied most of the cycle time. The most direct development route is therefore to improve contact surfaces and gripping-force control, verify fruit retention after closure, and introduce an automatic retry with a modified approach. The results provide a concise final experimental record of the ADER 25.1.1 prototype rather than a new perception or planning algorithm.

## ACKNOWLEDGEMENT

This work was supported by a grant of the Ministry of Agriculture and Rural Development, contract of sectorial financing ADER 2023-2026, Project ADER 25.1.1/2023, "Technology for robotized harvesting of Solanaceae family vegetables in greenhouses and solariums, using artificial intelligence".

## REFERENCES

[1] Arad, B., Balendonck, J., Barth, R., Ben-Shahar, O., Edan, Y., Hellström, T., Hemming, J., Kurtser, P., Ringdahl, O., Tielen, T., van Tuijl, B., 2020. Development of a sweet pepper harvesting robot. *Journal of Field Robotics*, 37(6), pp.1027-1039. https://doi.org/10.1002/rob.21937

[2] Gong, L., Wang, W., Wang, T., Liu, C., 2022. Robotic harvesting of the occluded fruits with a precise shape and position reconstruction approach. *Journal of Field Robotics*, 39(1), pp.69-84. https://doi.org/10.1002/rob.22041

[3] Mail, M.F., Maja, J.M., Marshall, M., Cutulle, M., Miller, G., Barnes, E., 2023. Agricultural harvesting robot concept design and system components: A review. *AgriEngineering*, 5(2), pp.777-800. https://doi.org/10.3390/agriengineering5020048

[4] Marin, F.B., Matache, M.G., Marin, M., Buruiană, L.D., Gurău, G., 2025a. 3D pose estimation for robotic tomato harvesting using convolutional neural networks. *Acta Horticulturae*, 1433, pp.257-264. https://doi.org/10.17660/ActaHortic.2025.1433.33

[5] Marin, F.B., Matache, M.G., Marin, M., Gurău, G., Cristea, R.D., Tănase, A., 2025b. Computer vision-based grasp detection for a metamaterial soft gripper in robotic vegetables harvesting. *INMATEH - Agricultural Engineering*, 77(3), pp.872-881. https://doi.org/10.35633/inmateh-77-71

[6] Matache, M.G., Găgeanu, I., Brăcăcescu, C., Cristea, O.D., Cristea, R.D., 2025. Robotic harvesting methods for vegetables of the Solanaceae family in greenhouses and solariums using specialized grippers - a review. *Acta Horticulturae*, 1433, pp.323-330. https://doi.org/10.17660/ActaHortic.2025.1433.41

[7] Matache, M.G., Marin, F.B., Persu, C.I., Cristea, R.D., Nenciu, F., Atanasov, A.Z., 2026. Autonomous tomato harvesting system integrating AI-controlled robotics in greenhouses. *Agriculture*, 16(8), 847. https://doi.org/10.3390/agriculture16080847

[8] Rapado-Rincón, D., van Henten, E.J., Kootstra, G., 2023. Development and evaluation of automated localisation and reconstruction of all fruits on tomato plants in a greenhouse based on multi-view perception and 3D multi-object tracking. *Biosystems Engineering*, 231, pp.78-91. https://doi.org/10.1016/j.biosystemseng.2023.06.003

[9] Sánchez-Molina, J.A., Rodríguez, F., Moreno, J.C., Sánchez-Hermosilla, J., Giménez, A., 2024. Robotics in greenhouses. Scoping review. *Computers and Electronics in Agriculture*, 219, 108750. https://doi.org/10.1016/j.compag.2024.108750

[10] Seo, D., Oh, I.S., 2025. Gripping success metric for robotic fruit harvesting. *Sensors*, 25(1), 181. https://doi.org/10.3390/s25010181

[11] Wang, L., Zhao, B., Fan, J., Hu, X., Wei, S., Li, Y., Zhou, Q., Wei, C., 2017. Development of a tomato harvesting robot used in greenhouse. *International Journal of Agricultural and Biological Engineering*, 10(4), pp.140-149. https://doi.org/10.25165/j.ijabe.20171004.3204

# STUDIES ON AROMATIC AND MEDICINAL PLANTS - THE IMPACT OF THE ENVIRONMENT AND TECHNOLOGIES FOR EXTRACTING ACTIVE COMPOUNDS

/

# *STUDII PRIVIND PLANTELE AROMATICE ȘI MEDICINALE – IMPACTUL MEDIULUI ȘI TEHNOLOGIILE PENTRU EXTRAGEREA COMPUȘILOR ACTIVI*

**Aura-Maria DUMITRESCU*[1)], Vasilica ȘTEFAN[1)], Carmen BĂLȚATU[1)], Larisa-Bianca IONICĂ[1)], Stefano-Andrea MANTOVANI[1)]**

[1)] National Institute of Research - Development for Machines and Installations Designed for Agriculture and Food Industry - INMA Bucharest / Romania

*Tel: 0770 902 101; *E-mail: auradumitrescu252@gmail.com*

***Keywords:*** *aromatic plants, bioactive compounds, extraction technologies, environmental factors, phytochemicals*

**ABSTRACT**

*Medicinal and aromatic plants are a valuable source of bioactive compounds due to their antioxidant, antibacterial, and anti-inflammatory properties and are widely used in various industries, including pharmaceutical, food, and cosmetics. Environmental conditions, growing technologies, and the extraction methods and equipment utilized for extraction all affect the active compounds content and effectiveness. This paper presents an analytical study of the function and potential of technologies used for the extraction of bioactive chemicals from medicinal plants, emphasizing their applicability and their role in advancing sustainable agriculture. Beyond their economic impact, contemporary extraction technologies can help provide goods with a higher value, lessen reliance on conventional crops, and improve the sustainable and effective use of plant resources.*

**REZUMAT**

*Plantele medicinale și aromatice sunt o sursă valoroasă de compuși bioactivi datorită proprietăților lor antioxidante, antibacteriene și antiinflamatorii. Sunt utilizate pe scară largă în diverse industrii, inclusiv în industria farmaceutică, alimentară și cosmetică.Condițiile de mediu, tehnologiile de cultivare, metodele de extracție și echipamentele utilizate pentru extracție afectează conținutul și eficacitatea compușilor activi. Acest articol prezintă un studiu analitic al funcției și potențialului tehnologiilor utilizate pentru extragerea substanțelor chimice bioactive din plantele medicinale, subliniind aplicabilitatea acestora și rolul lor în promovarea agriculturii durabile. Dincolo de impactul lor economic, tehnologiile contemporane de extracție pot contribui la furnizarea de produse cu o valoare mai mare, la reducerea dependenței de culturile convenționale și la îmbunătățirea utilizării durabile și eficiente a resurselor vegetale.*

## INTRODUCTION

In numerous cultures around the world, traditional medicine have been used medicinal plants for thousands of years, making them the oldest form of medicine. Empirical knowledge about their beneficial effects has been passed down through generations within human communities *(Marrelli, 2021), (Khan et. al., 2014)*.

Plants continuously interact with rapidly changing external environmental factors, which can often be harmful. Being immobile organisms, they have developed complex alternative defense strategies that utilize a wide range of chemical metabolites to cope with stress and adverse conditions.

Adaptation occurs primarily through secondary metabolites, which can be synthesized in nearly unlimited quantities *(Holopainen and Gershenzon, 2010)*.

These defense mechanisms are activated through numerous complex biochemical processes in response to biotic and abiotic stressors, such as temperature, light intensity, herbivory, and microbial attack.

Genetic or protein-level changes induced by stressful conditions have been reported, often resulting in significant alterations in the metabolite pool of affected individuals *(Ncube et. al., 2012*), *(Osbourn et al., 2003, Wink, 2003)*.

***Environmental factors:***

Plant survival and diversity are shaped by environmental factors and genetically determined adaptive traits that support long-term persistence. Abiotic conditions such as light, temperature, and water availability influence plant metabolism, regulating resource allocation and secondary metabolite biosynthesis. As sessile organisms, plants rely on complex physiological mechanisms, where secondary metabolites play a key role in stress response and environmental adaptation *(Ncube et. al., 2012), (J.C. Laughlin, 1993).*

*Light:* One important abiotic element controlling photosynthesis, plant growth, and the accumulation of secondary metabolites is light irradiance *(Zhang et al., 2015; Li et al., 2018).* Growth and productivity can be lowered by both too much light, which causes photoinhibition, and not enough light, which restricts energy absorption. Additionally, photomorphogenesis is influenced by light intensity, which regulates functions like seed germination, organ creation, and leaf expansion *(Yanqun Li et al., 2020).*

*Temperature:*Plant growth, physiological functions, and productivity are all directly impacted by temperature. While high temperatures can promote the manufacture of secondary metabolites as part of plant adaptation processes, extreme temperatures decrease photosystem II efficiency and cause stress reactions *(Yanqun Li et al., 2020).*

*Soil humidity:* The movement of nutrients, microbial activity, and biochemical reactions necessary for plant metabolism and soil fertility are all regulated by soil moisture. Root development, aboveground growth, and the general functioning of an ecosystem are all impacted by water deficiency because it decreases nutrient mobility, microbial mineralization, and plant biomass production *(Xue et al., 2017).*

*Drought stress*, *salt stress*, and a variety of other abiotic or biotic conditions are other environmental factors that affect plant growth and the accumulation of secondary metabolites. Drought stress can reduce water uptake and alter the biosynthesis of secondary metabolites; depending on the intensity of the stress, the concentration of flavonoids, phenols, or other bioactive compounds may increase. Saline stress causes nutritional imbalances and hyperosmoticity, which affect growth and photosynthesis; however, it can stimulate the synthesis of alkaloids, flavonoids, phenolics, saponins, or proline, which helps plants adapt *(Yanqun Li et al., 2020).*

*Soil type and composition*, *mechanical injury*, the presence of *metal ions*, *circadian rhythm*, *geographical conditions*, and interactions with the *soil microbial community* are other factors that impact plant growth and the synthesis and accumulation of active ingredients. Plants develop complex adaptive mechanisms as a result of the complex interaction of these factors, and the study of these factors is essential for the cultivation of medicinal plants with high bioactive compound content *(Yanqun Li et al., 2020).*




**Fig. 1 - Environmental factors influencing growth and quality**

## MATERIALS AND METHODS

The metabolic diversity of plants is remarkably diverse, outstripping that of the majority of other species. Large-scale integration and analysis of genetic and phenotypic diversity has been made possible by the introduction of post-genomic profiling systems. Understanding plant metabolic diversity, its underlying

regulatory characteristics, and the remaining methodological obstacles has advanced significantly as a result of multi-omic techniques.

The relationship between metabotypes and genotypic and phenotypic features has increased recently, underscoring metabolic variation as a valuable tool for studying plant evolution *(Fang et al., 2019).*

***Primary metabolism***

A primary metabolite is directly linked to growth, development, and reproduction. Many primary metabolites function as precursors or pharmacologically active metabolites in pharmaceuticals, such as antipsychotic drugs. Primary metabolites, such as ascorbic acid, proteins, lipids, soluble sugar, and starch, are essential for plant growth *(Jayaraman J., 1981).*

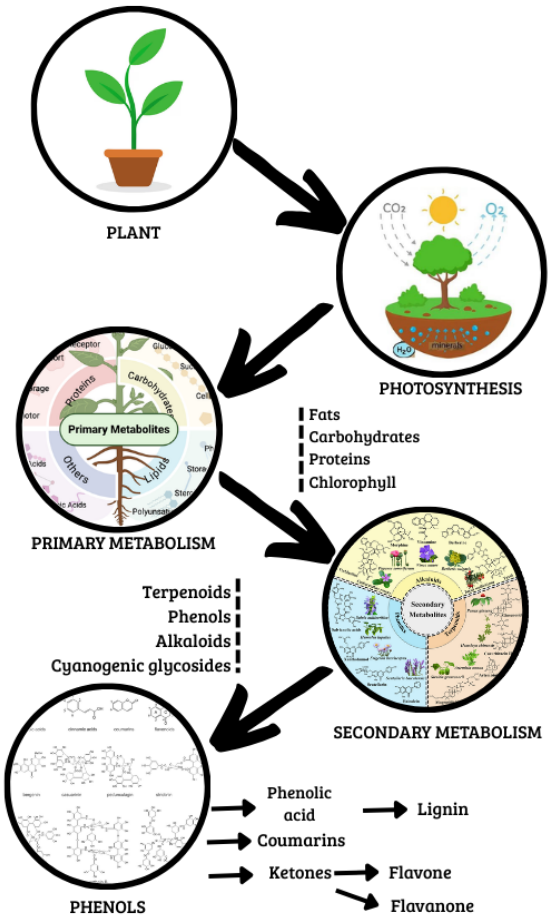



**Fig. 2 - The relationship between primary and secondary metabolism in plants**

*Adapted from (Yeşilyurt et al., 2024)*

***Secondary metabolism***

*Alkaloids* are nitrogen-containing substances with alkaline characteristics and potent physiological effects. Alkaloids are usually structured as rings. Plants are their sources. These compounds are rarely found in plant cells in free form, as they are usually present in mineral salts and organic acids *(Badri et al., 2019).*

*Terpenoids* are the basic components of essential oil and are composed of 5 isoprene C. The number of isoprene units causes terpenes to have different structures, such as monoterpene, sesquiterpene, diterpene, triterpene, and tetraterpene. Monoterpene and sesquiterpene structures are found intensely in essential oils. Monoterpenoids are usually responsible for the smell and taste of a plant. Sesquiterpenes are known for their antimicrobial and antitumor effects. Diterpenoids are found in resins, and gibberellin, a plant growth hormone, is a well-known diterpene *(Mukherjee, P. K. 2019).*

*Phenols* are characterized by the presence of one or more hydroxyl groups in their aromatic ring *(Tiring et al., 2021).* They are essential for plant growth, development, pollination, and defense. Plants with

high phenol content help prevent cardiovascular disease, cancer, inflammation, and mutations in human cells due to their antioxidant properties *(Karakaya, S. 2004).*

Well-known *phenolic compounds* include benzoquinones, phenolic acids, acetophenones, anthraquinones, flavonoids, lignin, flavonols, and tannins. Flavonoids, which are made up of flavones, flavonones, flavonols, and anthocyanins, are essential for color formation, protecting cells from free radicals, and attracting insects for pollination. Due to their catechin and theaflavin content, tea leaves are a source of phenols. Artichokes contain cynarin, a substance that helps regenerate hepatocytes. Silymarin, another flavonoid found in milk thistle seeds, is used to treat the liver *(Gillessen et al., 2020).*

*Fixed and essential oils* are the two types of oils produced by plants. Fatty acids and glycerol esters form fixed oils. Essential oils, on the other hand, are a chemical mixture of volatile organic compounds and several metabolites. These oils give the plant its aroma and taste. In fact, the immune system uses essential oils to protect against environmental hazards *(Buchbauer et al., 1993).* These oils are usually obtained from the non-woody and aromatic parts of the plant, especially from flowers, leaves, fruit peels, or roots, through hydrodistillation or steam distillation *(Dorman et al., 2000).* They are volatile liquids, insoluble in water but highly soluble in organic solvents. Fragrant oils reflect the essence of plants or their active compounds. Essential oils account for approximately 17% of the global flavor and fragrance sector *(Riaz et al., 2021).*

***Extraction methods for active substances***

*Hydrodistillation* is a traditional technique for obtaining plant bioactives, which preserves heat-sensitive chemicals by working at low temperatures. Depending on the plant material, yields are usually between 0.015 and 2%. It works well for hydrophobic and low-volatility compounds. While the lack of harmful residues and modest equipment costs are advantages, the high energy consumption and CO2 emissions are drawbacks. Cutting-edge techniques like microwave-assisted HD (MAHD) preserve extract quality, increase extraction efficiency, and shorten extraction times *(Presti et al., 2005), (Temelli et al. 2012).*

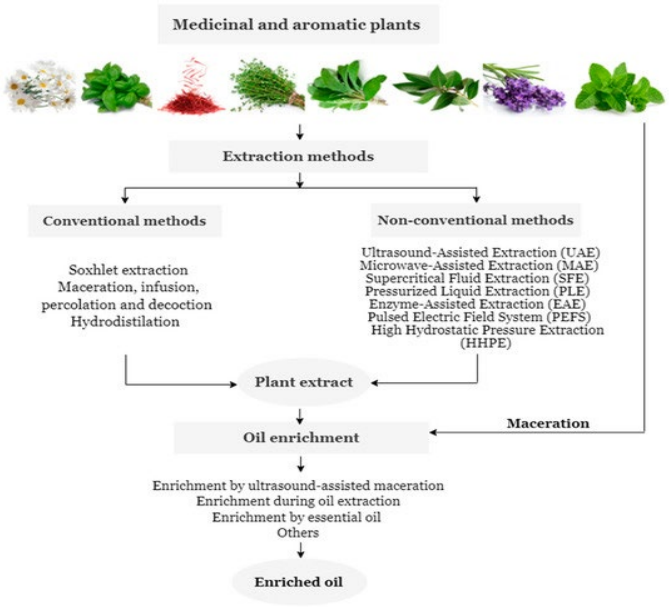



**Fig. 3 - Extraction and enrichment methods of antioxidants from MAPs**
*(Gharby et al., 2022)*

Plant material is directly treated with steam during the *steam distillation* process, which breaks down cell structures and releases chemicals for condensation. It works well on leaves and flowers and works well with organics that are polar, acidic, and somewhat volatile. Benefits include little post-processing, scalability, solvent-free extracts, and affordable, established technology. The long extraction times (1–5 hours), non-selectivity, possible hydrolysis, high energy consumption, and thermal destruction of sensitive chemicals are the limitations. Feedstock affects extraction time and yield; multi-stage procedures can occasionally shorten extraction durations while maintaining quality *(Kapadia et al., 2022).*

*Cold pressing* is a common mechanical extraction technique for plant biomolecules, particularly from citrus peels and seeds. . Low working temperatures (<40 °C) preserve beneficial substances like

polyphenols and antioxidants while creating 100% pure oil without the need for chemical solvents. The type of press—screw presses are the most popular—and the pre-treatment of the feedstock (peeling, drying, enzymatic, or solvent treatments) affect extraction efficiency. High throughput (60–100 t/day) but relatively low yield are achieved by industrial-scale CP, which is frequently combined with sequential solvent extraction to recover leftover oil *(Faugno et al., 2019), (Al Juhaimi et al.,2018), (El-Toumy et al., 2020), (Kapadia et al., 2022).*

Bioactive chemicals can be selectively isolated by *solvent extraction*, where yield and content are determined by solvent polarity. Sequential solvent techniques can target substances of different polarity, and green solvents derived from renewable resources are being used more and more. Although efficiency is dependent on temperature, extraction time, solvent-to-solid ratio, and particle size, SE is appropriate for delicate feedstocks that are heat-sensitive. To eliminate contaminants, solvents ought to be readily detachable, inert, and non-toxic. When compared to traditional maceration, greener methods, such as ultrasound-assisted extraction, utilize less solvent, energy, and extraction time *(Zhang et al., 2018), (Kapadia et al., 2022), (Fierascu et al., 2020).*

*Soxhlet extraction* is a traditional technique for isolating lipids and high-molecular-weight compounds from solid matrices (leaves, soils, and sediments). Solvents like acetone, hexane, or dichloromethane are used in Soxhlet extraction; the choice of solvent is the only factor influencing selectivity. High yields and the capacity to extract complex compounds as well as volatiles are benefits.

Limitations include limited throughput, high solvent and energy consumption, and lengthy extraction durations (usually 4–24 hours). Although SE efficiency depends on the feedstock, it can increase yields and shorten processing times when combined with ultrasound or microwave-assisted extraction *(Worsfold et al., 2019), (Kapadia et al., 2022).*

**Table 1**

**Comparative Analysis of Extraction Methods for Medicinal and Aromatic Plants**

*(Kapadia et al., 2022)*

| Method | Principle /Mechanism | Advantages | Disadvantages | Observations |
|---|---|---|---|---|
| Hydrodistillation | Low-temperature distillation and boiling plant material in water. | -preserves heat-sensitive compounds;<br>-no toxic residues;<br>-low equipment cost | -high energy consumption;<br>-$CO_2$ emissions;<br>-low yield (0.015–2%) | Microwave-assisted HD (MAHD) improves efficiency and reduces extraction time |
| Steam Distillation | Direct steam treatment of plant material;<br>breaks cells, volatiles condense | -solvent-free extracts;<br>-scalable;<br>-affordable;<br>-little post-processing | -non-selective;<br>-possible hydrolysis;<br>-thermal degradation;<br>-long extraction times (1–5 h);<br>-high energy use | Extraction time and yield depend on feedstock;<br>multi-stage procedures may improve efficiency |
| Cold Pressing | Pressing plant material mechanically | -100% pure product;<br>-preserves heat-sensitive bioactives (<40°C);<br>-low environmental/ chemical impact;<br>-high throughput | -low yield;<br>-pre-treatment needed (peeling, drying, enzymatic) | Often combined with sequential solvent extraction to recover residual oil |
| Solvent Extraction | Solvent dissolves target compounds;<br>polarity determines selectivity | -selective;<br>-suitable for delicate feedstocks;<br>-green solvents reduce environmental impact;<br>-adaptable to sequential extraction | -requires solvent removal;<br>-efficiency depends on particle size, solvent ratio, temperature, time | Ultrasound-assisted (UAE) or microwave-assisted extraction reduces solvent/energy use and processing time |

| Method | Principle /Mechanism | Advantages | Disadvantages | Observations |
|---|---|---|---|---|
| Soxhlet Extraction | Repeated solvent percolation over solid matrix | -high yield;<br>-extracts complex molecules and volatiles;<br>-well-established method | -long extraction times (4–24 h);<br>-high energy and solvent use;<br>-low throughput | Can be combined with MAE/UAE to reduce time and increase yield; solvent choice affects selectivity |

The chemical makeup of the intended bioactive substances is the primary determinant in the choice of extraction technique for aromatic and medicinal plants. Because of their capacity to disturb plant cellular structures and liberate secondary metabolites, hydrodistillation and steam distillation are very successful methods for separating volatile and hydrophobic substances, such essential oils. Both techniques, however, require a lot of energy, produce comparatively little, and could cause heat-sensitive substances to degrade.

By increasing extraction efficiency, cutting down on processing durations, and maintaining the integrity of bioactives, advanced procedures like microwave-assisted hydrodistillation can get beyond these restrictions *(Kapadia et al., 2022).*

Because cold pressing produces pure extracts without the use of chemical solvents and operates at low temperatures (less than 40 °C), it is especially well-suited for sensitive biomolecules such as polyphenols, flavonoids, and antioxidants. High throughput is achieved by industrial-scale CP, but the extraction efficiency is often lower. To optimize recovery, sequential solvent extraction is frequently used *(Fierascu et al., 2020), (Kapadia et al., 2022).*

Solvent extraction offers a very selective method for polar and non-volatile bioactives, particularly when aided by ultrasound or microwaves. This makes it possible to isolate molecules that are heat-sensitive. Sequential extractions can separate molecules with different polarities, and the solvent's polarity can be tuned to that of the target molecule. Because they use less energy and have a smaller environmental impact, green solvents made from renewable resources are becoming more and more popular *(Zhang et al., 2018).*

For the recovery of lipophilic and high molecular weight chemicals, Soxhlet extraction is still the gold standard. Long extraction times, high solvent use, and energy intensity are the method's drawbacks, despite the fact that it offers good yields and extensive extraction capabilities. Combining Soxhlet with UAE or MAE can optimize yields and reduce processing duration, highlighting the importance of method integration in modern extraction workflows *(Kapadia et al., 2022).*

Practically speaking, aromatic plants are most suited for steam distillation and hydrodistillation because of their effective recovery of essential oils. Cold pressing or solvent extraction with ultrasonic or microwave assistance is advised for medicinal plants that contain heat-sensitive bioactives in order to optimize extraction yield and bioactivity retention *(Kapadia et al., 2022).*

## CONCLUSIONS

Both process efficiency and compound integrity must be given top priority in the extraction approach for aromatic and medicinal plants. While cold pressing and solvent-assisted procedures (UAE/MAE) are better for thermolabile or polar bioactives, steam distillation and hydrodistillation are best for recovering essential oils.

For applications in pharmaceuticals, nutraceuticals, and cosmetics, high-quality, repeatable extracts that maintain their biological activity are ensured by optimizing extraction techniques. By comprehending and improving these extraction methods, communities can profit from the medicinal and aromatic qualities of these species, which enhances industrial output and resource utilization while also promoting the sustainable use of plant biodiversity.

Therefore, the methodical investigation of extraction methods is crucial to the advancement of scientific understanding as well as real-world applications in the realm of aromatic and medicinal plants.

## REFERENCES

[1] Al Juhaimi, F., Özcan, M. M., Ghafoor, K., Babiker, E. E., & Hussain, S. (2018). Comparison of cold-pressing and soxhlet extraction systems for bioactive compounds, antioxidant properties, polyphenols,

fatty acids and tocopherols in eight nut oils. Journal of Food Science and Technology, 55(8), 3163–3173. https://doi.org/10.1007/s13197-018-3244-5

[2] Badri, S., Basu, V. R., Chandra, K., & Anasuya, D. (2019). A review on pharmacological activities of alkaloids. World Journal of Current Medical Pharmaceutical Research, 1(6), 230–234.

[3] Buchbauer, G., Jirovetz, L., Jager, W., Plank, C., & Dietrich, H. (1993). Fragrance compounds and essential oils with sedative effects upon inhalation. Journal of Pharmaceutical Sciences, 82(6), 660–664.

[4] Dorman, H. J., & Deans, S. G. (2000). Antimicrobial agents from plants: antibacterial activity of plant volatile oils. Journal of Applied Microbiology, 88(2), 308–316. doi: 10.1046/j.1365-2672.2000.00969.x

[5] El-Toumy, S. A., & Hussein, A. A. (2020). Cold pressed yuzu (Citrus junos Sieb. ex Tanaka) oil. In Cold Pressed Oils (pp. 711–718). Academic Press. https://doi.org/10.1016/B978-0-12-818188-1.00063-3

[6] Fang, C.,· Alisdair, R., Fernie,Luo, L. (2019). Exploring the Diversity of Plant Metabolism. Trends in Plant Science, Volume 24, Issue 1, Pages 83-98, DOI:10.1016/j.tplants.2018.09.006

[7] Faugno, S., Piccolella, S., Sannino, M., Principio, L., Crescente, G., Baldi, G. M., ... & Pacifico, S. (2019). Can agronomic practices and cold-pressing extraction parameters affect phenols and polyphenols content in hempseed oils? Industrial Crops and Products, 130, 511–519. https://doi.org/10.1016/j.indcrop.2018.12.084

[8] Fierascu, R. C., Fierascu, I., Ortan, A., Georgiev, M. I., & Sieniawska, E. (2020). Innovative approaches for recovery of phytoconstituents from medicinal/aromatic plants and biotechnological production. Molecules, 25(2), 309. https://doi.org/10.3390/molecules25020309

[9] Gillessen, A., & Schmidt, H. H. (2020). Silymarin as supportive treatment in liver diseases: A narrative review. Advances in Therapy, 37(4), 1279–1301. DOI: 10.1007/s12325-020-01251-y

[10] Holopainen, J. K., & Gershenzon, J. (2010). Multiple stress factors and the emission of plant VOCs. Trends in Plant Science. https://doi.org/10.1016/j.tplants.2010.01.006

[11] Jayaraman, J. (1981). Laboratory manual in biochemistry. Wilsey Eastern Limited: New Delhi, 96–97.

[12] Kapadia, P., Newell, A. S., Cunningham, J., Roberts, M. R., & Hardy, J. G. (2022). Extraction of high-value chemicals from plants for technical and medical applications. International Journal of Molecular Sciences, 23(18), 10334. https://doi.org/10.3390/ijms231810334

[13] Karakaya, S. (2004). Bioavailability of phenolic compounds. Critical Reviews in Food Science and Nutrition, 44(6), 453–464. https://doi.org/10.1080/10408690490886683

[14] Khan, H., PhD, MPhil, BPharm, Abdul Wali Khan. (2014). Medicinal plants in light of history: Recognized therapeutic modality. Journal of Evidence-Based Integrative Medicine, 19, 216–219. https://doi.org/10.1177/2156587214533346

[15] Li, Y., Kong, D., Fu, Y., Sussman, M. R., & Wu, H. (2020). The effect of developmental and environmental factors on secondary metabolites in medicinal plants. https://doi.org/10.1016/j.plaphy.2020.01.006

[16] Lo Presti, M., Ragusa, S., Trozzi, A., Dugo, P., Visinoni, F., Fazio, A., ... & Mondello, L. (2005). A comparison between different techniques for the isolation of rosemary essential oil. Journal of Separation Science, 28(3), 273–280. https://doi.org/10.1002/jssc.200400037

[17] Marrelli, M. (2021). Medicinal plants. Department of Pharmacy, Health and Nutritional Sciences, University of Calabria, Rende, 87036 Cosenza, Italy. https://doi.org/10.3390/plants10071355

[18] Mukherjee, P. K. (2019). Quality control and evaluation of herbal drugs: Evaluating natural products and traditional medicine. Elsevier.

[19] Ncube, B., Finnie, J. F., & Van Staden, J. (2012). Quality from the field: The impact of environmental factors as quality determinants in medicinal plants. South African Journal of Botany. https://doi.org/10.1016/j.sajb.2012.05.009

[20] Osbourn, A. E., Qi, X., Townsend, B., & Qin, B. (2003). Dissecting plant secondary metabolism - constitutive chemical defences in cereals. https://doi.org/10.1046/j.1469-8137.2003.00759.x

[21] Riaz, U., Iqbal, S., Sohail, M. I., Samreen, T., Ashraf, M., Akmal, F., & Akhter, R. M. (2021). A comprehensive review on emerging importance and economical potential of medicinal and aromatic plants (MAPs) in current scenario. Pakistan Journal of Agricultural Research, 34(2), 381–392.

[22] Temelli, F., Saldaña, M. D. A., & Comin, L. (2012). Application of supercritical fluid extraction in food processing.

[23] Worsfold, P., Townshend, A., Poole, C. F., & Miró, M. (2019). Encyclopedia of analytical science. Elsevier.

[24] Xue, R., Shen, Y., & Marschner, P. (2017). Soil water content during and after plant growth influence nutrient availability and microbial biomass. Journal of Soil Science and Plant Nutrition, 17(3), 702. DOI: 10.4067/S0718-95162017000300012

[25] Yeşilyurt, S., Gürgan, M., Sertkahya, M. (2024). Biologically Active Compounds from Medicinal and Aromatic Plants for Industrial Applications. In: Kumar, L., Bharadvaja, N., Singh, R., Anand, R. (eds) Medicinal and Aromatic Plants. Sustainable Landscape Planning and Natural Resources Management. Springer, Cham. https://doi.org/10.1007/978-3-031-60117-0_1

[26] Zhang, Q. W., Lin, L. G., & Ye, W. C. (2018). Techniques for extraction and isolation of natural products: A comprehensive review. Chinese Medicine, 13(1), 20. https://doi.org/10.1186/s13020-018-0177-x

# POWER CONSUMPTION AND FLOW REGIME CHARACTERIZATION OF PADDLE, PROPELLER AND DISC-TURBINE IMPELLERS IN A LABORATORY-SCALE MIXING VESSEL

/

# *CARACTERIZAREA CONSUMULUI DE PUTERE ȘI A REGIMULUI DE CURGERE PENTRU AGITATOARE CU PALETE, ELICE ȘI TURBINĂ IMPELLER ÎNTR-UN VAS DE AMESTECARE LA SCARĂ DE LABORATOR*

**Elena-Valeria VLĂDUȚ*[1)], Sorin- Ștefan BIRIȘ[1)], Mariana FERDEȘ[1)], Adrian IOSIF[1)], Neluș-Evelin GHEORGHIȚĂ[1)], Alina-Daiana IONESCU[1)], Raluca Adriana ZOTA[1)], Ana-Maria TĂBĂRAȘU[2)]**

[1)] National University of Science and Technology Politehnica Bucharest / Romania;

[2)] National Institute of Research - Development for Machines and Installations Designed for Agriculture and Food Industry - INMA Bucharest / Romania.

**Tel: (+40) 739 960 285; *E-mail: elena.vladut@upb.ro*

***Keywords:*** *mixing, impeller, power consumption, Reynolds number, baffles, stirred vessel*

## ABSTRACT

*This paper presents an experimental characterization of the power consumption and flow regime developed in a laboratory-scale stirred vessel (Armfield CEK Fluid Mixing Unit) equipped with three interchangeable impellers - a flat-blade paddle, a marine propeller and a disc turbine - each tested with and without baffles, using water as working fluid. Torque, angular velocity and consumed power were derived from direct force and rotational speed readings across five speed steps per configuration. Results show that the baffled disc-turbine and paddle configurations reach the highest power draw (up to 33.3 W), while the propeller remains the most energy-efficient, with flow predominantly turbulent (Re > $10^4$) in all but the low-speed propeller runs.*

## REZUMAT

*Lucrarea prezintă o caracterizare experimentală a consumului de putere și a regimului de curgere dezvoltat într-un vas de amestecare la scară de laborator (instalația Armfield CEK Fluid Mixing Unit), echipat cu trei agitatoare interschimbabile - cu palete plate, cu elice și cu turbină impeller cu disc - fiecare testat cu și fără șicane, folosind apa ca fluid de lucru. Momentul de torsiune, viteza unghiulară și puterea consumată au fost determinate din citirile directe ale forței și turației, la câte cinci trepte de turație pentru fiecare configurație. Rezultatele arată că turbina cu disc și paletele, în prezența șicanelor, ating cel mai ridicat consum de putere (până la 33,3 W), în timp ce elicea rămâne cea mai eficientă energetic, regimul de curgere fiind predominant turbulent (Re > $10^4$).*

## INTRODUCTION

Mixing is one of the most frequently encountered unit operations in the process and biotechnological industries, used both as an independent operation aimed at achieving compositional homogeneity and as a means of enhancing the contact surface for other operations such as absorption, extraction or drying *(Sterbacek, 1969).*

Mixing performance is reported to be directly influenced by the geometry of the system, the type of agitator, the power and energy consumption, and the flow regime generated inside the vessel *(Ochieng, 2010)*.

Mechanical agitation is one of the most common techniques used to intensify mixing in industrial installations; stirred reactors are therefore equipped with a rotating component that increases the mass-transfer rate and ensures fluid homogeneity *(Hoseini, 2021; AG, 2020)*.

Depending on the direction of the streamlines generated by the impeller, three main flow types are distinguished: tangential flow, in which the fluid moves parallel to the rotational path of the impeller and mixing efficiency is limited; radial flow, in which the impeller directs the fluid along radial directions, producing two distinct circulation zones; and axial flow, in which the fluid enters and leaves the impeller region along a direction coaxial with the shaft, promoting efficient recirculation of the whole liquid volume *(Zăpodeanu, 2021).*

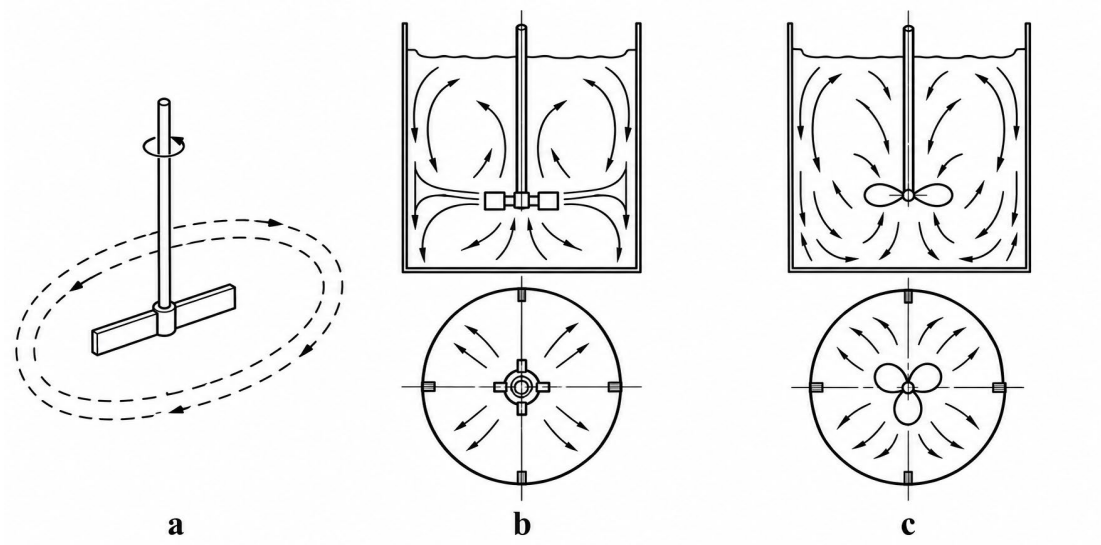



**Fig. 1 - Flow patterns generated by mechanical agitators: a) tangential flow; b) radial flow; c) axial flow**
*(adapted from Zăpodeanu, et. al. 2021)*

Radial-flow impellers are frequently used in aerobic fermentation because they discharge the fluid radially toward the vessel wall, generating shear zones and high turbulence; such impellers are effective at breaking gas bubbles and maximizing the gas-liquid interfacial area, but they consume more power and can induce hydrodynamic stress on sensitive cells *(Singh, 2024*).

Axial-flow impellers, in contrast, generate a descending stream that entrains the fluid along the whole height of the vessel, ensuring rapid homogenization but with a reduced gas-dispersion capacity *(Tecnic, 2024; Kaur, 2021)*. Impeller rotation also tends to entrain the whole liquid volume into a solid-body rotation, producing a central vortex and inefficient mixing; to prevent this phenomenon, baffles are commonly mounted symmetrically at 90° on the inner wall of the vessel *(Fatima, 2025)*.

Baffles convert the tangential motion into vertical and radial flow, intensifying turbulence and the mass-transfer coefficient (kLa), although they are not recommended for highly viscous fluids (Re < 20) or in shear-sensitive applications, such as enzyme or vitamin processing *(Kamla, 2017; Młynarczykowska, 2022).*

***Characteristic parameters of the mixing process***

The mechanical and energetic behaviour of a stirred vessel can be described through a set of characteristic parameters, determined either directly (from instrument readings) or derived through calculation.

The torque (Mt) transmitted by the impeller shaft to the fluid is directly related to the consumed power and is calculated as the product between the force recorded at the dynamometer arm and its length (r):

$$M_t = F \cdot r \quad [N \cdot m] \tag{1}$$

The force (F) exerted on the dynamometer arm is obtained from the reading of the force balance (Mf, in grams):

$$F = Mf \cdot 10^{-3} \cdot 9.81 \ [N] \tag{2}$$

The angular velocity (ω) of the impeller is related to the rotational speed (n), expressed in revolutions per minute, as read on the tachometer:

$$\omega = n \cdot 2\pi / 60 \ \ [rad/s] \tag{3}$$

The power required for mixing (P) is essential for the selection of the appropriate impeller type, the optimal rotational speed and the optimal mixture concentration, and is calculated as the product of torque and angular velocity:

$$P = Mt \cdot \omega \quad [W] \tag{4}$$

Power consumption is closely correlated with heat and mass-transfer efficiency and depends on fluid density, impeller speed and impeller diameter. Experimental and numerical studies show that the impeller type and rotational speed significantly influence power consumption, with power-number values reported to vary between 1.75 and 6, depending on configuration *(Salho, 2024).* The dimensionless power number (Np) is defined as:

$$Np = P / (\rho \cdot n^3 \cdot Da^5) \quad (5)$$

where ρ is the fluid density [kg/m3], n is the impeller rotational speed [$s^{-1}$] and Da is the impeller diameter [m].

The flow regime is characterized by the mixing Reynolds number (Re), defined as the ratio between the inertial and viscous forces acting in the system:

$$Re = \rho \cdot n \cdot Da^2 / \eta \quad (6)$$

where η is the dynamic viscosity of the fluid [Pa·s]. According to the specialized literature, the flow regime can be classified as laminar for Re < 10, transitional for 10 < Re < 10 000 and turbulent for Re > 10 000; however, experimental studies on mechanically agitated systems place the upper limit of the laminar regime at Re values between 20 and 30, depending also on impeller size (*Zăpodeanu, 2021*).

In fully developed turbulent flow, the power number becomes independent of the Reynolds number and depends solely on the geometry of the system - impeller type, number of blades, and the presence of baffles (*Karcz, 1998)*.

Building on this theoretical background, the present study reports the experimental assessment of the power consumption and flow regime of a laboratory-scale mixing vessel fitted with three interchangeable impellers, aiming to establish a reference dataset that will subsequently support comparative studies with biological media, such as *Saccharomyces cerevisiae* cultures, within a broader doctoral research programme on the operating-regime optimization of bioreactors.

## MATERIALS AND METHODS

The experimental research was carried out using the Armfield CEK Fluid Mixing Unit, a laboratory apparatus designed for both didactic and research purposes in the field of fluid mixing, manufactured by Armfield Ltd. (Ringwood, Hampshire, UK) *(Biriș, 2021)*. The unit allows for the visualization of different mixing patterns and flow directions, the determination of power/speed characteristics for different types of mixing elements, the mixing of solid-liquid suspensions and the estimation of the power requirement for larger-capacity mixers using scale-up techniques based on the similitude principle *(Armfield, 2010)*.

For each impeller type, two series of experiments were performed - one with the four standard baffles mounted and one without baffles - resulting in a total of six experimental configurations.

The experimental protocol consisted of the following steps: (1) filling the vessel with tap water up to the 0.3 m level, checking for the absence of entrained air bubbles; (2) mounting the corresponding impeller on the driving shaft; (3) mounting or removing the baffles, depending on the tested configuration; (4) zeroing the dynamometer by releasing the force-balance clamp, adjusting the tensioning spring and setting the arm to the neutral position with the locking block; (5) adjusting the cable length so that the indicator aligned with the reference mark; (6) determining the maximum stable operating speed, defined as the highest speed producing smooth mixing without excessive air entrainment and without exceeding the measuring range of the force balance; (7) performing measurements at five rotational-speed steps, starting from the minimum stable speed and increasing progressively; and (8) recording, for each speed step, the rotational speed n [rpm], read on the tachometer, and the force indicated by the force balance [g], followed by the calculation of the derived parameters Mt, ω and P using equations (1)-(4) (*Biriș, 2021).*

Tap water at ambient temperature (≈ 20 °C) was used as working fluid, without addition of biological or chemical components, in order to isolate the purely mechanical and hydrodynamic effects of the agitation process and to establish a reference dataset prior to the introduction of biological media in subsequent research stages.

The measurement principle relies on the equilibrium of forces acting on the stator: the reaction torque generated by the rotation of the impeller in the fluid is transmitted through the unit frame to the dynamometer, allowing an indirect but accurate determination of torque.

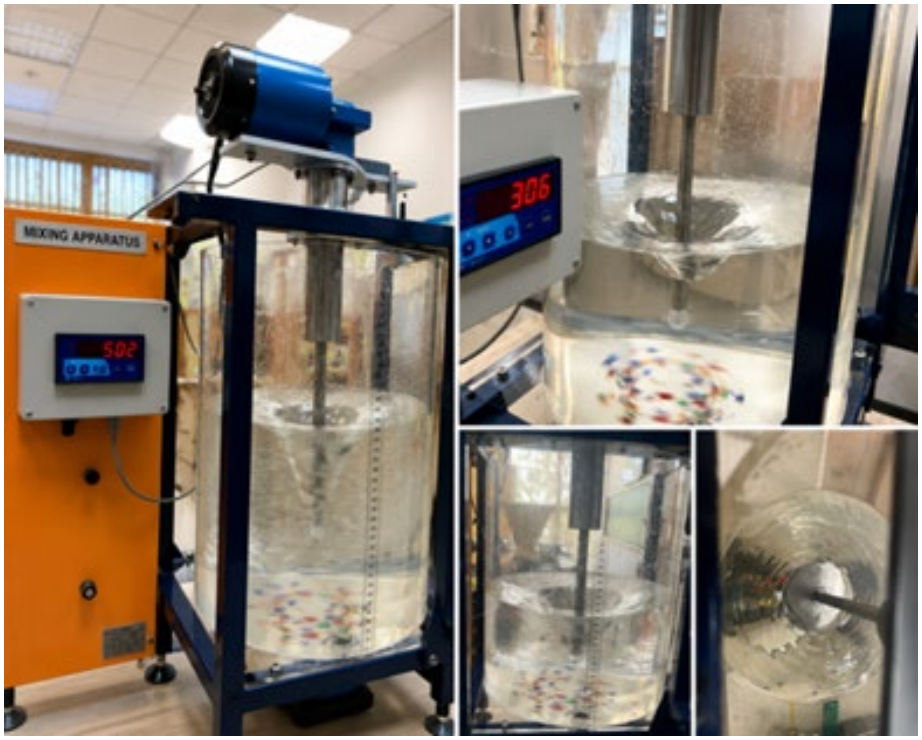



**Fig. 2 - Overview of the mixing unit and detail during operation**

## RESULTS

The experimental results obtained for the three impeller types, in both baffled and unbaffled configurations, are presented in Tables 1-3. The derived parameters were calculated according to equations (1)-(4), starting from the direct readings of rotational speed (tachometer) and force (dynamometer balance).

**Table 1**

**Experimental results - Paddle impeller**

| Paddle with baffles | | | | | Paddle without baffles | | | | |
|---|---|---|---|---|---|---|---|---|---|
| n [rpm] | F [g] | Mt [N·m] | ω [rad/s] | P [W] | n [rpm] | F [g] | Mt [N·m] | ω [rad/s] | P [W] |
| 62 | 9 | 0.08 | 6.4 | 0.51 | 76 | 5 | 0.049 | 7.9 | 0.38 |
| 131 | 66 | 0.64 | 13.7 | 8.77 | 166 | 15 | 0.147 | 17.3 | 2.54 |
| 200 | 95 | 0.93 | 20.9 | 19.40 | 274 | 35 | 0.34 | 28.6 | 9.72 |
| 194 | 95 | 0.93 | 20.3 | 18.80 | 373 | 70 | 0.68 | 39 | 26.52 |
| 190 | 95 | 0.93 | 20.3 | 18.80 | 405 | 80 | 0.78 | 42.4 | 33.00 |

**Table 2**

**Experimental results - Propeller impeller**

| Propeller with baffles | | | | | Propeller without baffles | | | | |
|---|---|---|---|---|---|---|---|---|---|
| n [rpm] | F [g] | Mt [N·m] | ω [rad/s] | P [W] | n [rpm] | F [g] | Mt [N·m] | ω [rad/s] | P [W] |
| 75 | 1 | 0.009 | 7.85 | 0.07 | 87 | 1 | 0.009 | 9.1 | 0.08 |
| 178 | 2 | 0.019 | 18.6 | 0.35 | 179 | 4 | 0.039 | 18.7 | 0.73 |
| 298 | 5 | 0.049 | 31.2 | 1.52 | 306 | 4 | 0.039 | 32 | 1.24 |
| 402 | 8 | 0.078 | 42 | 3.27 | 408 | 7 | 0.068 | 42.7 | 2.90 |
| 500 | 15 | 0.147 | 52.3 | 7.68 | 510 | 7 | 0.068 | 53.4 | 3.63 |

**Table 3**

**Experimental results – Disc turbine impeller**

| Turbine with baffles | | | | | Turbine without baffles | | | | |
|---|---|---|---|---|---|---|---|---|---|
| n [rpm] | F [g] | Mt [N·m] | ω [rad/s] | P [W] | n [rpm] | F [g] | Mt [N·m] | ω [rad/s] | P [W] |
| 73 | 3 | 0.029 | 7.64 | 0.22 | 82 | 2 | 0.019 | 8.58 | 0.16 |
| 157 | 10 | 0.098 | 16.4 | 1.60 | 178 | 6 | 0.058 | 18.6 | 1.07 |
| 256 | 55 | 0.53 | 26.8 | 14.20 | 289 | 10 | 0.098 | 30 | 2.94 |
| 340 | 92 | 0.90 | 35.6 | 31.60 | 404 | 12 | 0.11 | 42.3 | 4.65 |
| 350 | 93 | 0.91 | 36.6 | 33.30 | 500 | 15 | 0.147 | 52.3 | 7.68 |

The preliminary analysis of the experimental data shows that, in all tested configurations, the consumed power increases with rotational speed, and the presence of baffles generally produces higher power values than the unbaffled configuration at the same speed. The baffled disc-turbine impeller shows the highest power consumption, explained by the intense radial flow and the higher shear forces characteristic of this impeller geometry.

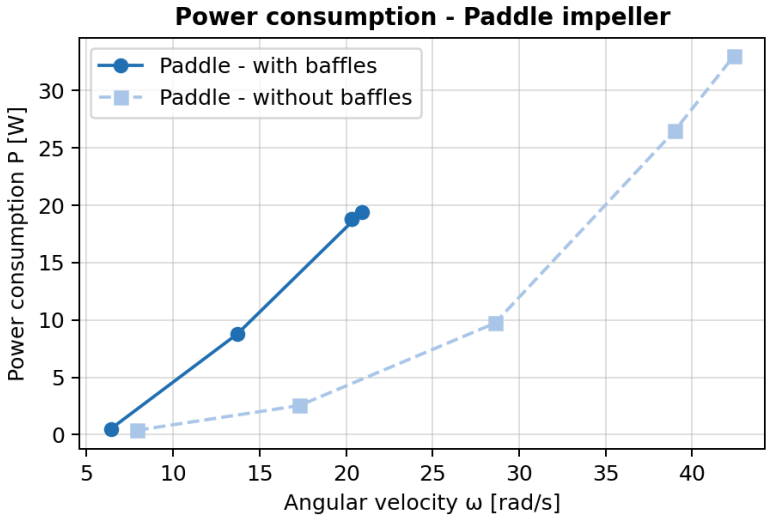



**Fig. 3 - Power consumption P = f(ω) - paddle impeller, with and without baffles**

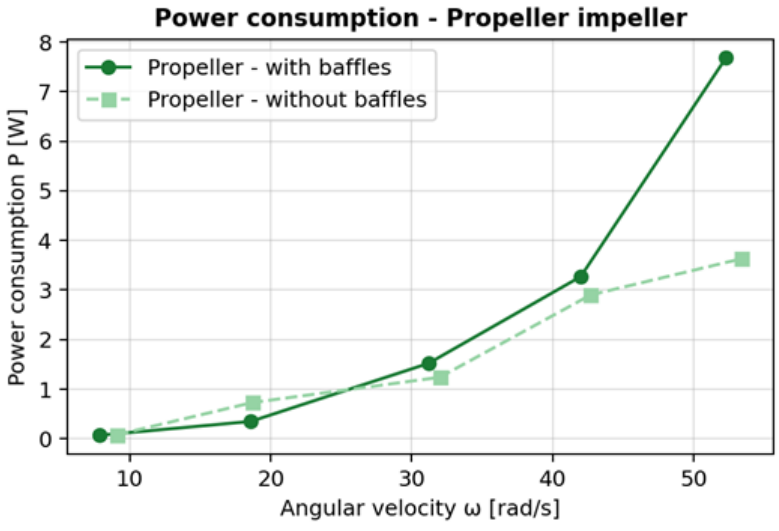



**Fig. 4 - Power consumption P = f(ω) - propeller impeller, with and without baffles**

Figure 3 shows a marked difference in behaviour for the paddle impeller: in the presence of baffles, power rises rapidly at low speed, reaching a plateau of about 19 W at ω ≈ 20 rad/s (200 rpm) - which is attributed to the force balance reaching the limit of its measuring range - while in the unbaffled configuration the increase is more progressive, but reaches higher values (33 W) at higher speeds (405 rpm), since a much wider speed range could be explored without exceeding the sensor limit.

The propeller (Fig. 4) shows the lowest power consumption among the three impellers, with a less pronounced difference between the baffled and unbaffled configurations; at the maximum tested speed (500-510 rpm), the consumed power was 7.68 W with baffles and only 3.63 W without baffles.

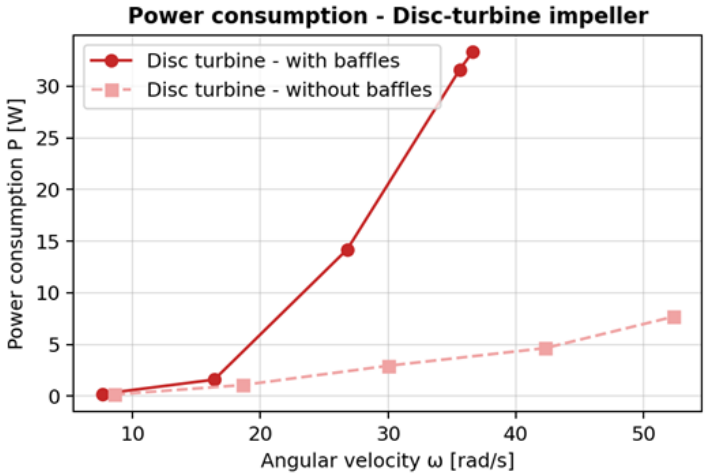



**Fig. 5 - Power consumption P = f(ω) - disc-turbine impeller, with and without baffles**

The disc-turbine impeller (Fig. 5) exhibits the steepest increase in power with speed, particularly in the presence of baffles: the P = f(ω) curve shows a pronounced exponential-like character, power rising from 0.22 W (at 73 rpm) to 33.30 W (at 350 rpm).

Without baffles, the behaviour is significantly more moderate, with Pmax = 7.68 W at 500 rpm; the ratio between the maximum power of the baffled and unbaffled turbine configurations is approximately 4.33, confirming the major influence of baffles on the power consumption of this impeller type.

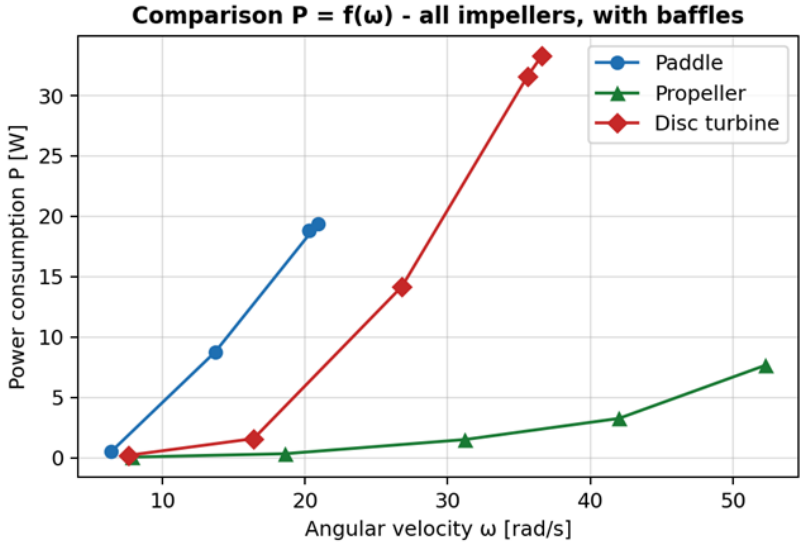



**Fig. 6 - Comparison of P = f(ω) for all three impellers, with baffles**

Figure 6 shows the superimposed P = f(ω) curves for the three impeller types in the baffled configuration. The power-consumption hierarchy is clear: disc-turbine > paddle > propeller, reflecting the power-number values specific to each impeller type, with Np for the disc-turbine (≈ 5) exceeding that of the paddle (Np ≈ 1.7) and of the propeller (Np ≈ 0.35), in the turbulent, baffled regime.

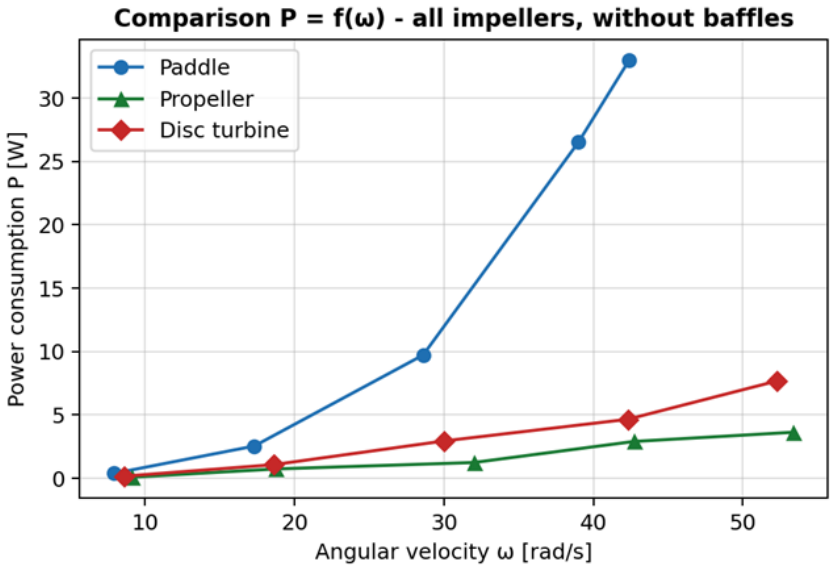



**Fig. 7 - Comparison of P = f(ω) for all three impellers, without baffles**

Figure 7 presents the same comparison for the unbaffled configuration. In the absence of baffles, the differences between impeller types are smaller, especially at lower speeds.

The paddle impeller reaches the highest power values ($P_{max}$ = 33 W), exceeding the disc-turbine impeller ($P_{max}$ = 7.68 W); this is explained by the fact that, without baffles, the turbine operates in a solid-body rotation regime, with reduced conversion efficiency of kinetic energy into turbulence, in addition to its lower maximum tested speed compared with the paddle *(Kamla, 2017)*.

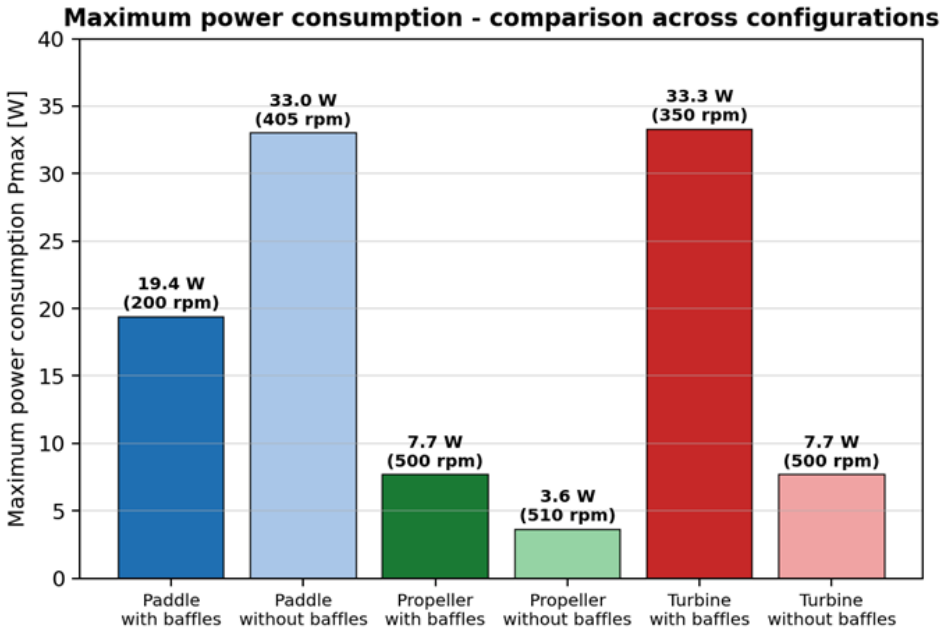



**Fig. 8 - Maximum power consumption (Pmax) for all six experimental configurations**

**Flow-regime analysis**

The mixing Reynolds number was calculated with equation (6), using ρ = 998 kg/m3 (water density), n expressed in rot/s, Da = 120 mm for the disc-turbine, Da = 204 mm for the paddle and Da = 60 mm for the propeller, and η = 1.002 × $10^{-3}$ Pa·s (dynamic viscosity of water at 20 °C). The results are summarized in Table 4.

**Table 4**

**Reynolds number for the tested experimental configurations**

| Configuration | n [rpm] | Da [m] | Re | Flow regime |
|---|---|---|---|---|
| Paddle with baffles | 62-200 | 0.12 | 14,900-48,000 | Turbulent |
| Paddle without baffles | 76-405 | 0.12 | 18,300-97,200 | Turbulent |
| Propeller with baffles | 75-500 | 0.055 | 3,750-25,100 | Transitional → Turbulent |
| Propeller without baffles | 87-510 | 0.055 | 4,350-25,500 | Transitional → Turbulent |
| Turbine with baffles | 73-350 | 0.12 | 17,500-84,100 | Turbulent |
| Turbine without baffles | 82-500 | 0.12 | 19,700-120,000 | Turbulent |

Table 4 shows that all configurations involving the paddle and disc-turbine impellers were carried out exclusively in the turbulent regime (Re > 10,000). For the propeller impeller, the flow regime passes through the transitional zone (Re ≈ 3,750-10,000) at low speeds and enters the turbulent regime at medium and high speeds, which explains the more moderate behaviour of the P = f(n) curve compared with the other two impeller types.

***Selection of the optimal mixing configuration***

The choice of the appropriate configuration depends on the specific objectives of the mixing process. In the context of the broader doctoral research programme, aimed at the efficient mixing, at a reduced energy cost, of yeast cultures, a compromise must be reached between: rapid homogenization of the whole fluid volume; minimum power consumption (energy efficiency); low shear stress (preservation of cell viability); and flexibility, i.e., the possibility of operating over a wide speed range *(INFORS HT, 2024).*

The baffled disc-turbine impeller generated the most intense mixing regime, with high shear forces and strong turbulence, and could represent the optimal configuration for processes requiring gas dispersion (aeration/oxygenation) or the suspension of heavy solid particles; however, it also shows the highest power consumption ($P_{max}$ = 33.3 W) and intense shear stress, which is a limitation for shear-sensitive microorganism cultures.

The baffled paddle impeller offers an intermediate compromise, with moderate power consumption and a mixing intensity sufficient to homogenize different fluids, but the accessible speed range is restricted by the 190 rpm limitation observed in the presence of baffles. The propeller shows the lowest power consumption in both configurations and generates a predominantly axial flow with minimal shear forces, while also allowing operation at high rotational speeds (up to 510 rpm) without exceeding the limits of the unit, thus offering the greatest operational flexibility.

The presence of baffles significantly increases power consumption but improves mixing quality by eliminating the central vortex and converting tangential flow into axial and radial flow. Table 5 summarizes the recommended configuration as a function of the type of process.

**Table 5**

**Recommended mixing configuration as a function of process type**

| Process type | Configuration | Speed [rpm] | Power consumption |
|---|---|---|---|
| Homogenization of simple solutions | Paddle + baffles | 100-200 | Moderate |
| Biological mixing (yeast) | Propeller + baffles | 200-400 | Low |
| Gas dispersion / aeration | Disc turbine + baffles | 150-300 | High |
| Particle suspension | Disc turbine + baffles | 200-350 | High |
| Rapid dissolution | Propeller without baffles | 300-500 | Low |

## CONCLUSIONS

This study reports a preliminary experimental analysis of the operating regime of the Armfield CEK mixing unit, using water as working fluid, aimed at establishing a reference dataset for future research. The work included the experimental determination of the operating parameters (force, torque, angular velocity and consumed power) for six distinct configurations - each impeller type with and without baffles.

The experimental results revealed significant differences among the three impeller types in terms of power consumption and generated hydrodynamic regime. The baffled disc-turbine impeller recorded the highest power consumption ($P_{max}$ = 33.30 W at n = 350 rpm), driven by the intense radial flow and the high shear forces characteristic of this impeller type. In contrast, the baffled paddle impeller showed a moderate consumption ($P_{max}$ = 19.40 W at n = 200 rpm), but with an important limitation of the accessible speed range, caused by the force balance reaching its reading limit. The propeller stood out with the lowest power consumption in both configurations ($P_{max}$ = 7.68 W with baffles at 500 rpm and only 3.63 W without baffles at 510 rpm), while also offering the greatest operational flexibility.

The flow-regime analysis, based on the Reynolds number, confirmed that all experiments performed with the paddle and turbine impellers were carried out exclusively in the turbulent regime, while the propeller passed through the transitional zone at lower speeds. It was also found that the presence of baffles significantly amplifies power consumption, by eliminating tangential flow and intensifying turbulence, but substantially improves mixing quality by breaking the central vortex and promoting axial fluid recirculation.

Based on the comparative analysis of the six experimental configurations, the configuration identified as optimal for the next stage of the research - mixing of Saccharomyces cerevisiae cultures - is the propeller impeller in the presence of baffles, at rotational speeds between 200 and 400 rpm. This recommendation is supported by three converging arguments: the reduced power consumption ensures the energy efficiency of the process; the predominantly axial flow generated by the propeller favours the homogenization of the whole fluid volume without creating dead zones; and the minimal shear forces associated with this impeller type are essential for preserving the cell viability of yeast, a microorganism known to be shear-sensitive. The reference data obtained will subsequently allow the quantification of the influence of biomass presence on the operating parameters and the validation of numerical flow-field models in the vessel.

## ACKNOWLEDGEMENT

This paper is written during the doctoral internship of the first author in the Doctoral School of Biotechnical Systems Engineering, from the National University of Science and Technology POLITEHNICA Bucharest.

## REFERENCES

[1] AG, I.(2020). Minifors 2 – Benchtop Bioreactor, Operating Manual, Switzerland, INFORS HT.

[2] Armfield Ltd. (2010). CEK Fluid Mixing Unit - Instruction Manual. Ringwood, Hampshire, UK: Armfield Limited.

[3] Biriș, S.-Ș. (2021). Operații și echipamente de proces [Process Operations and Equipment] - lecture notes. Bucharest: Politehnica Publishing House.

[4] Fatima, I. (2025). The Potential of CFD in Sustainable Microbial Fermenter Design: A Review. Processes (MDPI).

[5] Hoseini, S.S., Najafi, G., Ghobadian, B., et al. (2021). Impeller Shape-Optimization of Stirred-Tank Reactor: CFD and Fluid Structure Interaction. Chemical Engineering Journal, 413.

[6] INFORS HT (2024). The Cookbook - Basic Concepts, Recipes and Strategies for Bioprocesses Involving Cell Cultures and Microorganisms. Retrieved May 2026, from https://infors-ht.com.

[7] Kamla, Y., Arab Aboosi, A.K., Hamimid, S., Alkhafaji, S. (2017). Effect of the Inclination of Baffles on the Power Consumption and Fluid Flows in a Vessel Stirred by a Rushton Turbine. Chinese Journal of Mechanical Engineering, 30, 1008-1016.

[8] Karcz, J., Kaminski, B. (1998). An Effect of a Baffle Length on the Power Consumption in an Agitated Vessel. Chemical Engineering and Processing: Process Intensification, 37(3), 249-256.

[9] Kaur, I., Gera, P., Sharma, D., Dahiya, K. (2021). Bioreactors: Design, Functions and Fermentation Innovations. Zenodo.

[10] Młynarczykowska, A., Kowol, D. (2022). An Experimental Investigation on the Fluid Flow Mixing Process in a Stirred Tank. EPJ Web of Conferences, 264, 01023.

[11] Ochieng, A., Onyango, M.S. (2010). Experimental Measurement and Computational Fluid Dynamics Simulation of Mixing in a Stirred Tank: A Review. South African Journal of Science, 106(11/12), 421-426.
[12] Salho, A., et al. (2024). A Review of Stirred Tank Dynamics: Power Consumption, Mixing Time and Impeller Geometry. International Journal of Heat and Technology, 42(4), 1081-1092.
[13] Singh, V.K., et al. (2024). Integration Approaches to Model Bioreactor Hydrodynamics and Cellular Kinetics for Advancing Bioprocess Optimisation. Bioengineering (MDPI).
[14] Sterbacek, Z., Tausk, P. (1969). Amestecarea în industria chimică [Mixing in the Chemical Industry]. Bucharest: Editura Tehnică.
[15] Tecnic (2024). Bioreactor Flow Patterns: Rushton, Pitched-Blade & Hydrofoil. Retrieved May 2026, from https://www.tecnic.eu/.
[16] Zăpodeanu, V. (2021). Operații unitare și procese în industria alimentară [Unit Operations and Processes in the Food Industry]. Iași, Romania.

# STUDY ON THE PRODUCTION AND USE OF SHEEP WOOL WASTE PELLETS AS ORGANIC FERTILIZER IN ORGANIC AGRICULTURE. REVIEW.

/

# *STUDIU PRIVIND PRODUCȚIA ȘI UTILIZAREA PELETELOR DIN DEȘEURI DE LÂNĂ DE OAIE CA ÎNGRĂȘĂMINTE ORGANIC ÎN AGRICULTURA ORGANICĂ. RECENZIE.*

**Ioan Ladislau CABA[1)], Nicolae-Valentin VLĂDUȚ*[1)], Despina-Maria BORDEAN*[2)]**

[1)] National Institute of Research - Development for Machines and Installations Designed for Agriculture and Food Industry - INMA Bucharest / Romania;

[2)] University of Life Sciences "King Mihai I" from Timisoara, Calea Aradului 119, Timis County / Romania.

*[1)] Tel: 0040212693255; E-mail: vladut@inma.ro*

*[2)] Tel: 0040 0724 217 134; E-mail: despinabordean@usvt.ro*

***Keywords:*** *soil restoration, sustainable farming, biofertilizers, sheep wool used as fertilizer*

**ABSTRACT**

*Yearly hundreds of thousands of tonnes of raw wool are produced in the European Union. Due to competition from synthetic fibres and the textile industry's strict requirements for fibre fineness, over 70% of wool production (coarse and semi-fine wool) remains underutilized. Pelletization has emerged as an innovative strategy for converting raw wool and wool scraps (wool waste) into compact, value-added products suitable for multiple applications. This review aims to summarize and critically discuss the current knowledge on sheep wool pelletization, focusing on production technologies, physicochemical characteristics, agricultural applications, environmental benefits, and future research perspectives. Specific attention is given to the use of wool pellets as slow-release organic fertilizers capable of improving soil properties, enhancing nutrient use efficiency, and supporting circular agriculture. In the context of the global transition to sustainable agriculture, sheep wool — often considered a waste that is difficult to manage — is coming back into the spotlight of farmers in the form of granular organic fertilizer. Wool pellets are an excellent alternative to chemical fertilizers, providing a slow release of nutrients and improving soil structure, while saving the farm budget. Overall, sheep wool pelletization represents a promising approach for transforming an underutilized natural resource into a sustainable product with environmental, agronomic, and economic benefits.*

**REZUMAT**

*Anual, în Uniunea Europeană se produc sute de mii de tone de lână brută. Din cauza concurenței din partea fibrelor sintetice și a cerințelor stricte ale industriei textile privind finețea fibrelor, peste 70[%] din producția de lână (lână grosieră și semifină) rămâne subutilizată. Peletizarea a apărut ca o strategie inovatoare pentru transformarea lânii brute și a resturilor de lână (deșeuri de lână) în produse compacte, cu valoare adăugată, potrivite pentru aplicații multiple. Această analiză își propune să rezume și să discute critic cunoștințele actuale despre peletizarea lânii de oaie, concentrându-se pe tehnologiile de producție, caracteristicile fizico-chimice, aplicațiile agricole, beneficiile pentru mediu și perspectivele viitoare de cercetare. O atenție deosebită este acordată utilizării peletelor de lână ca îngrășăminte organice cu eliberare lentă, capabile să îmbunătățească proprietățile solului, să sporească eficiența utilizării nutrienților și să sprijine agricultura circulară. În contextul tranziției globale către o agricultură durabilă, lâna de oaie - adesea considerată un deșeu dificil de gestionat - revine în atenția fermierilor sub formă de îngrășământ organic granular. Peletele de lână reprezintă o alternativă excelentă la îngrășămintele chimice, oferind o eliberare lentă a nutrienților și îmbunătățind structura solului, economisind în același timp bugetul fermei. Per ansamblu, peletizarea lânii de oaie reprezintă o abordare promițătoare pentru transformarea unei resurse naturale subutilizate într-un produs durabil cu beneficii de mediu, agronomice și economice.*

## INTRODUCTION

One of the most important challenges of modern agriculture is to increase the efficiency of nitrogen use while reducing the negative impact on the environment. Conventional mineral fertilizers provide nitrogen in a form immediately available to plants, but a significant part of it can be lost through leaching or volatilization before it is absorbed by crops. These losses not only reduce the efficiency of fertilization, but

also contribute to the pollution of groundwater and surface water, as well as to the emissions of nitrogen compounds into the atmosphere. In this context, sheep wool pellets represent a sustainable alternative, due to the biopolymeric structure of keratin. Nitrogen is incorporated into this insoluble protein and cannot be dissolved directly in water, becoming available to plants only as keratin is degraded by soil microorganisms *(Zheljazkov, 2005).*

Therefore, the release of nutrients is gradual and better correlates with the nutritional needs of plants during periods of active growth, reducing the risk of leaching losses and increasing nitrogen use efficiency.

Modern agriculture is facing major challenges generated by the increasing demand for food, soil degradation and the impact of the intensive use of chemical fertilizers on the environment. In this context, strategies aimed at developing sustainable agriculture and implementing the principles of the circular economy have become priorities worldwide.

The valorization of by-products and organic waste is one of the most effective solutions for reducing the consumption of non-renewable resources, reducing waste quantities and closing natural nutrient cycles.

Among the underutilized resources is sheep wool, especially rough and semi-fine wool, which, due to the demands of the textile industry and competition with synthetic fibers, is only used to a small extent.

Although this biomass is rich in keratin, amino acids and essential mineral elements, a large part of the annual production is disposed of as waste or used in applications with low economic value. In recent years, interest in the use of sheep wool in agriculture has increased considerably, due to its ability to provide slow-release nutrients, improve water retention and soil structure, and help reduce dependence on synthetic fertilizers.

In this context, the transformation of wool into pellets represents an innovative solution that facilitates its handling, transport, and application, considerably expanding the possibilities of valorization within sustainable agriculture.

Granting numerous studies on the chemical composition of wool, keratin properties, pelleting technologies and the use of wool pellets in agriculture are available in the specialized literature, this information is presented fragmentedly, being oriented towards specific aspects. To date, an integrated analysis that correlates the characteristics of the raw material with the pelleting technology, the properties of the final product and its applications in sustainable agriculture is missing.

This gap justifies the need for this review, which aims to critically synthesize the available information and highlight the potential of wool pellets as an innovative solution for capitalizing on an underutilized natural resource and for promoting the principles of the circular economy. Although interest in sustainable resource utilization and circular agriculture has increased considerably in recent years, information on sheep wool pelleting is still scattered in studies that separately address wool composition and properties, pelleting technologies, pellet characteristics and their applications in agriculture. Consequently, an integrated analysis that synthesizes the available knowledge and highlights the potential of this underutilized natural resource is lacking.

The purpose of this review is to synthesize and critically analyze the specialized literature on sheep wool pelletization as a sustainable strategy for the valorization of underutilized sheep wool. The paper integrates information on the physicochemical properties of wool, pellet production technologies, their characteristics and mechanisms of action, their use as slow-release organic fertilizers, as well as the effects on soil, plant development and crop productivity.

At the same time, the environmental advantages and economic implications of the use of wool pellets in the context of sustainable agriculture and the circular bioeconomy are analyzed. In this context, the review aims to answer the following research questions:

- What are the physicochemical properties of wool that recommend it as a raw material for obtaining pellets?
- What technologies are currently used for sheep wool pelletization?
- What are the main physical and functional properties of wool pellets?
- How do wool pellets influence nutrient release, soil properties and plant development?
- What are the agronomic, environmental and economic benefits associated with the use of wool pellets?
- What are the main limitations and future research directions needed to expand the use of wool pellets in sustainable agriculture?

## MATERIALS AND METHODS

This review was conducted through a comprehensive literature search using Peer-reviewed articles, book chapters, conference papers, and technical reports and various databases. The collected information was critically assessed and systematized into thematic sections to offer a comprehensive overview of sheep wool pellets as sustainable biofertilizers.

Tables and figures were prepared to summarize and compare findings from the available literature, making complex information easier to interpret. The conceptual figures presented in this review were developed by the authors with the assistance of OpenAI, ChatGPT and DALL·E.

These AI tools were used exclusively to support the visualization of scientific concepts based on information synthesized from the cited literature. All generated illustrations were carefully reviewed, refined, and validated by the authors to ensure their scientific accuracy, consistency, and relevance to the objectives of this review.

## 1. SHEEP WOOL: PROPERTIES AND COMPOSITION

Wool is a complex natural fiber with a number of unique characteristics that make it valuable for various applications *(Marczak et al., 2022).* These characteristics can be classified into physical and chemical *(Garcia et al., 2024):*

Physical properties of wool:

- fineness: the fiber diameter varies (microns), influencing softness and quality (ultrafine, superfine, fine, medium, coarse).
- length: classified as short, medium or long, influences processing and end use.
- color: natural (white, cream, brown, black, gray), can be dyed in a wide range of colors.
- gloss: varies from matte to glossy, depending on the surface structure.
- density: Wool is a light fiber.
- hygroscopicity: absorbs moisture (up to 30[%] of its weight) without feeling wet, helping to regulate body temperature.
- thermal insulation: the corrugated structure creates air pockets that insulate against heat and cold.
- elasticity and recovery: fibers can stretch and return to their original shape, providing wrinkle resistance and shape retention.
- touch: the sensation to the touch varies from soft to rough, depending on the fineness and structure.
- fire resistance: naturally fire resistant, self-extinguishing and does not melt or stick to the skin.
- resistance to static electricity: tends not to accumulate static electricity due to moisture absorption.
- UV protection: Merino wool has a natural UV protection factor.
- breathability: allows water vapor to pass through, providing comfort.
- odor resistance: absorbs and neutralizes odors, releasing them when washed.
- stain resistance: the natural protective outer layer helps repel stains.
- felting properties: the scaly structure of the cuticle allows the fibers to interconnect under the action of heat, moisture and friction.

Chemical properties:

- ✓ composition: the main component is keratin, a protein rich in sulfur amino acids, which contributes to resistance.
- ✓ Acid resistance: relatively resistant to weak acids, but damaged by strong acids.
- ✓ alkali sensitivity: sensitive to strong bases, which can destroy protein structure.
- ✓ resistance to organic solvents: generally resistant to most organic solvents, being suitable for dry cleaning.

Biodegradability *(Nustorova et al., 2006):* it decomposes naturally in the soil, releasing

### Chemical and Nutritional Composition

Wool fibres contain a various range of mineral elements, reflecting both physiological metabolism and environmental exposure. Sulphur is the dominant element due to the high cysteine content of keratin proteins, while calcium, sodium, potassium and magnesium occur as major macroelements. Trace elements

such as zinc, iron and copper are present in smaller amounts and participate in metabolic and structural processes. In addition, wool can accumulate trace quantities of heavy metals, making it a useful bioindicator of environmental contamination. The reported concentrations of these elements vary broadly depending on factors such as diet, soil composition, environmental contamination and physiological status of the animals.

The accumulation of heavy metals in sheep's wool mirrors the exposure of livestock to polluted environments and signals the contamination risks to the complete ecosystem *(Fechete et al.,2024).*

Once introduced into the environment they rich through the food chain plants – animals - further consumers (predators, humans). In this situation sheep further concentrate the heavy metals in their tissues. Data summarized in Table 1 were compiled based on analytical results reported by *(Patkowska-Sokoła et al., 2009).*

**Table 1**

**Typical concentrations of macroelements, microelements and heavy metals in wool fibres (mg/kg DW), derived from the dataset reported by Patkowska-Sokoła et al. (2009).**

| Category | Element | Typical concentration range ($mgkg^{-1}$ D.W.) |
|---|---|---|
| Macroelements | Sulphur (S) | 18000 – 22000 |
| | Calcium (Ca) | 1700 – 3000 |
| | Sodium (Na) | 1400 – 2200 |
| | Potassium (K) | 600 – 800 |
| | Magnesium (Mg) | 120 – 600 |
| | Phosphorus (P) | 150 – 300 |
| Trace elements (microelements) | Zinc (Zn) | 70 – 90 |
| | Iron (Fe) | 20 – 500 |
| | Aluminum (Al) | 50 – 620 |
| | Strontium (Sr) | 3 – 14 |
| | Copper (Cu) | 5 – 10 |
| | Manganese (Mn) | 3 – 23 |
| | Barium (Ba) | 1.5 – 9 |
| | Molybdenum (Mo) | 0.7 – 1.0 |
| | Cobalt (Co) | 0.6 – 2.3 |
| | Titanium (Ti) | 0.5 – 40 |
| Heavy metals | Lead (Pb) | 2.3 – 2.6 |
| | Arsenic (As) | 0.20 – 0.77 |
| | Cadmium (Cd) | 0.13 – 0.34 |
| | Mercury (Hg) | 0.01 – 0.08 |

Wool contains several basic chemical elements, including carbon (the energy source of microorganisms) between 49.4 - 54.5[%], oxygen 22 – 25[%], nitrogen (contributes to the growth of green plant matter) 15.4 -17[%] hydrogen 6.8 - 7.5[%], potassium 4 – 6[%] (supports plant resistance to drought and disease) and sulfur (helps with protein synthesis) 3 – 4[%] *(Górecki et al, 2010).*

It also contains phosphorus and magnesium in small quantities. This chemical organization explains part of the properties of wool, such as instant and delayed elasticity recovery *(Grigore et al., 2024).*

**Table 2**

**Chemical composition of wool compared to pellets, Maslana – HortiDaily, Lanopellet: a natural NK fertiliser, 2026**

| Elements | Raw wool (%) | Wool pellets (%) | Use |
|---|---|---|---|
| Nitrogen (N) | 10 -12 | 9 – 12.5 | Growth, protein production |
| Organic carbon | 42 - 50 | 40 - 49 | Energy source for microorganisms |
| Potassium (K20) | 2 -3.5 | 4 -5.5 | Osmoregulation, stress resistance |
| Sulphur (S) | 1.9 - 3 | 2 -3.5 | Obtaining chlorophyll |
| Phosphorus (P205) | 0.1 – 0.25 | 0.2 – 0.4 | Root development |
| Organic carbon | 42 - 50 | 40 - 49 | Energy source for microorganism |

*(Maslana - HortiDaily.com Lanopellet: a natural NK fertiliser, https://www.hortidaily.com/article/9814383/from-livestock-waste-to-organic-fertilizer, Publication date: 2026)*

The amino acid composition of wool proteins reflects the structural characteristics of keratin fibres, which are rich in both hydrophobic and sulphur-containing amino acids. A physicochemical study conducted by T. Sh. Amirova and co-authors identified 17 amino acids in wool and silk proteins using chromatographic and mass-spectrometric analysis. In wool samples, the most abundant amino acids were phenylalanine, glycine, and tyrosine**,** while smaller amounts of cysteine, threonine, valine, and methionine were also detected.

The presence of cysteine is particularly important because it forms disulfide crosslinks that stabilize the keratin structure**,** contributing to the mechanical strength and elasticity of wool fibres. Additionally, both essential and non-essential amino acids were identified, indicating that wool proteins possess a relatively balanced amino acid composition characteristic of structural fibrous proteins. The Amino acid composition of the wool protein as well as the individual amino acids concentrations based on the study reported by *(Amirova et al, 2022)* are presented in figure 1.

The distribution illustrates the relative contribution of major amino acids such as glycine, phenylalanine, and tyrosine to the overall keratin structure.

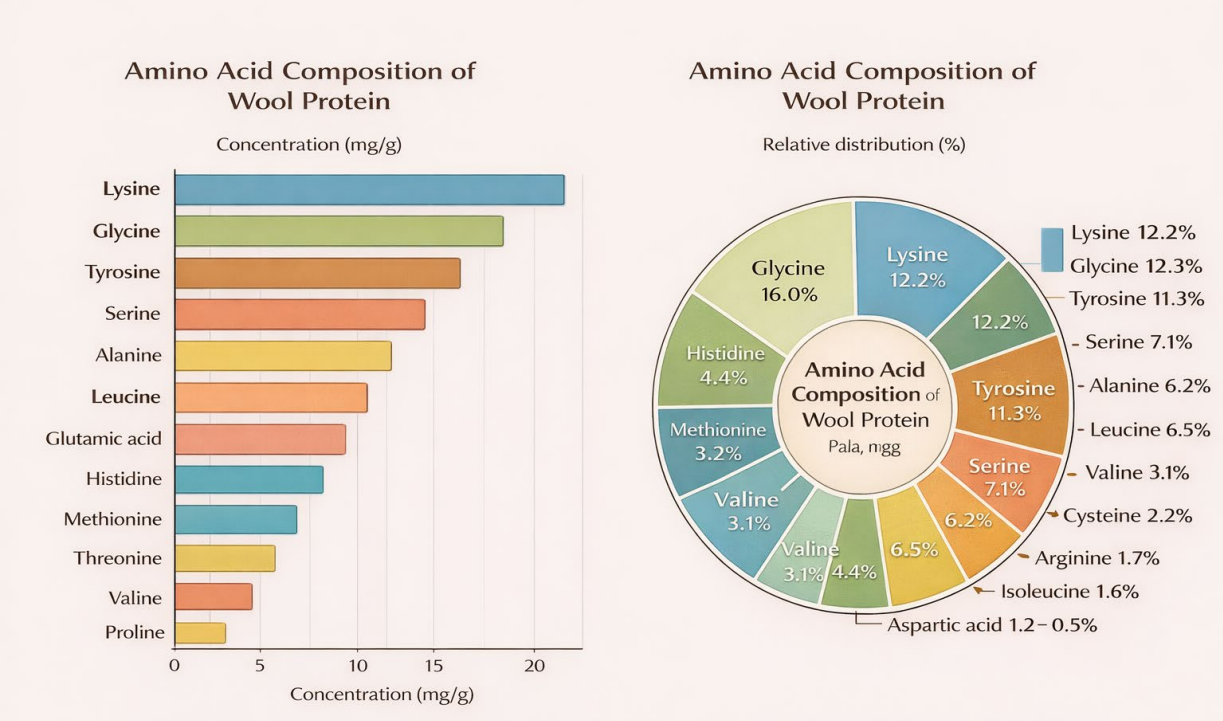



**Fig. 1 - Amino acid composition of wool proteins based on quantitative data reported by** *(Amirova et al 2022).*
*Visualization prepared by the authors using an AI-assisted graphic generation tool.*

Wool is the most widely used animal fiber, which is chemically the most complex, biological fibre composed of more than 170 different proteins**,** which are not uniformly distributed throughout the fibre structure.

These proteins are primarily keratins and associated proteins and are located in specific regions of the fibre, contributing to the distinct physical and chemical properties of each structural component. Wool proteins are made of amino acids**,** organic molecules containing both an amino group ($–NH_2$) and a carboxyl group (–COOH). Of the 22 naturally occurring amino acids**,** 18 are present in wool, differing mainly in the chemical nature of their side chains (R groups).

These side groups determine the chemical behaviour of the amino acids and may be hydrophobic, hydrophilic, acidic, basic, or sulphur-containing. (https://csiropedia.csiro.au/wp-content/uploads/2015/01/6229343.pdf)

In proteins, the amino acids are joined together to form long polymer chains, as shown in Figure 2.

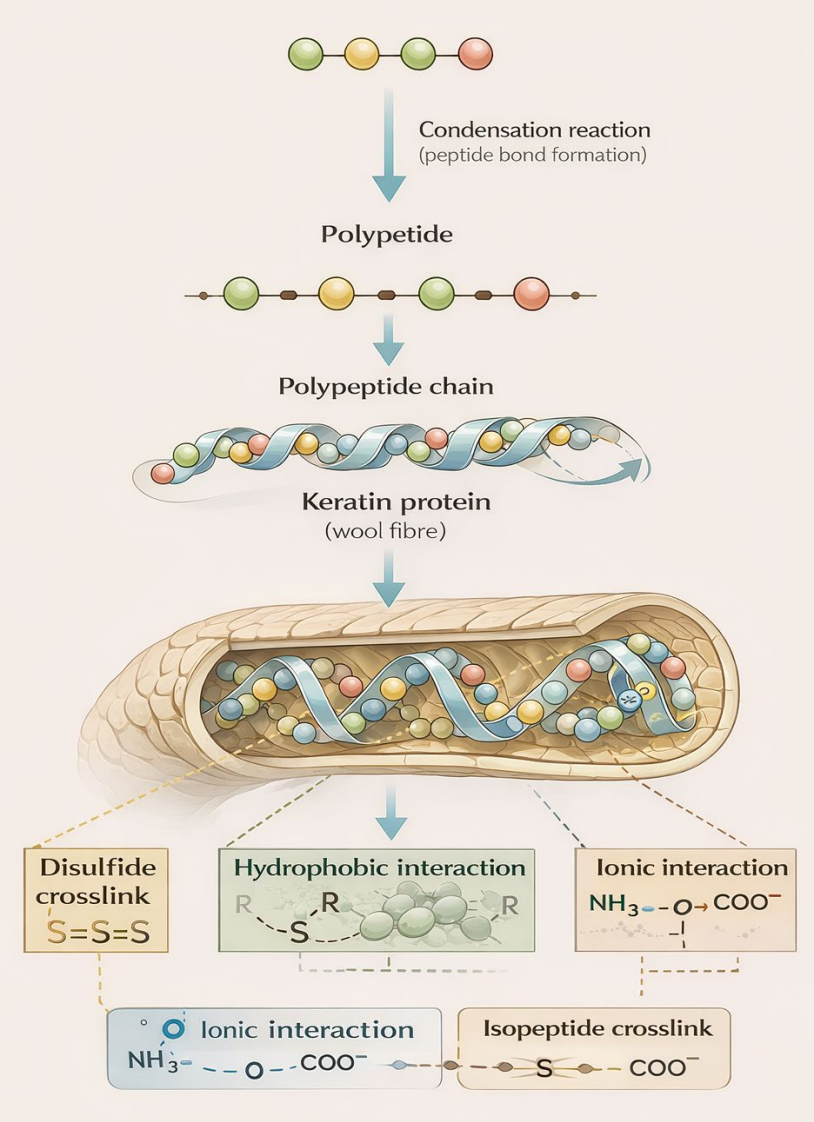



**Fig. 2 - Structural organization and stabilization of keratin in wool fibres.**

*Amino acids polymerize into polypeptide chains that fold into keratin structures, stabilized by disulfide bonds, hydrophobic interactions, ionic interactions, and isopeptide crosslinks. Illustration created by the authors using AI-assisted visualization (OpenAI DALL·E).*

As described by figure 2, keratin, the principal structural protein of wool fibres, is formed through the polymerization of amino acids into long polypeptide chains linked by peptide bonds. These chains adopt ordered conformations, typically α-helical structures, which assemble into higher-order keratin filaments within the fibre matrix. The stability and mechanical strength of wool keratin arise from multiple intermolecular interactions, including disulfide crosslinks between cysteine residues, hydrophobic interactions among non-polar side chains, ionic bonds between charged amino acids, and isopeptide crosslinks. Together, these interactions create a highly resilient and flexible protein network responsible for the characteristic elasticity, durability, and thermal properties of wool fibres.

Recently, there has been an increasing interest in the use of keratin as a novel source of protein for nutrition. Keratin derived protein (KDP) extracted from sheep wool using high pressure microwave technology and food acids was investigated for its potential as a new dietary protein. The studies confirmed the nutritive effects of KDP (rich in protein 86[%]), amino acid cysteine (8.8 [g]/100 [g]) and selenium (0.29 [µg/g]). The study also confirmed that KDP was non-cytotoxic at ≤ 2 [mg/mL] concentration *(Dias et al, 2022)*.

The appropriateness of sheep wool as a sustainable agricultural input is determined by the close association between its chemical composition, structural characteristics, and functional properties. The high keratin content, amino acid profile, and naturally occurring macro- and micronutrients influence the physicochemical properties of wool pellets, including their water absorption capacity, gradual biodegradation, slow nutrient release, as well as minimising the risk of environmental contamination. Therefore, the use of

sheep wool in controlled-release fertilisers becomes not only an innovative environmentally and economically viable solution but also an important contribution to sustainable agriculture *(Szczecina et al, 2025).*

The conceptual framework presented in Figure 3 summarizes these interconnected processes and highlights the multifunctional role of sheep wool pellets in sustainable crop production and the circular bioeconomy.

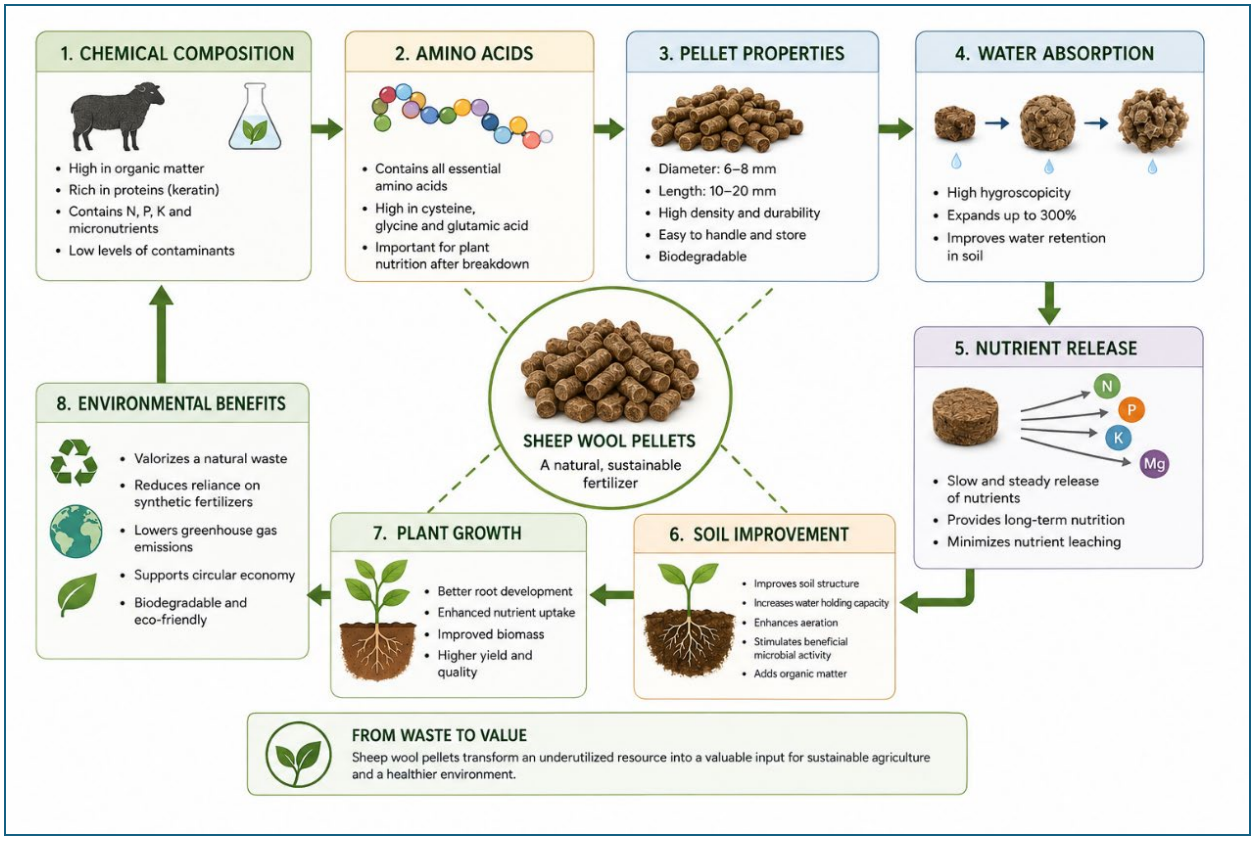



**Fig. 3 - Sheep wool pellets as multifunctional biofertilizers for sustainable agriculture.**

*Illustration created by the authors using AI-assisted visualization (OpenAI ChatGPT and DALL·E), based on information synthesized from the scientific literature reviewed in this article.*

## 2. SHEEP WOOL PELLETIZATION TECHNOLOGY

The technological process of sheep wool pelletization *(Bradshw et al, 2022*) involves the following steps:

1. *Wool collection and cleaning*, the raw wool is collected and cleaned to remove impurities are important steps in the sheep wool processing process. Here are some details about these steps:

*Wool collection*:

- sheep shearing, wool is collected by shearing sheep, usually once a year, depending on the breed and age of the sheep. Shearing can be done manually or mechanically, depending on the equipment available and the size of the flock.
- collection conditions, wool must be collected under hygienic conditions, to prevent contamination with dirt, dust or other factors that may affect the quality of the wool.

*Cleaning and sorting wool*:

- hand washing, wool is washed by hand in warm or cold water, using detergent or soap.
- mechanical washing, the wool is washed in special wool washing machines, which are designed to clean the wool without damaging it.
- dry cleaning, wool can be chemically cleaned using special substances that remove impurities without damaging the fibers. Wool cleaning is essential to obtain high-quality wool fibers, which can be used in various applications.
- further processing, the cleaned wool is easier to process and transform into finished products, such as textiles and clothing, as well as increasing the value of the wool because it is considerably more attractive to buyers.
- wool sorting, the collected wool is sorted according to quality, color and length, to ensure that only good quality wool is processed.

2. *Cooling and drying wool*, the cleaned wool is dried to prevent bacterial growth and to facilitate the pelletization process.

Drying wool is an important process that follows wool washing. The purpose of cooling and drying is to remove excess moisture from the wool fibers, to prevent the growth of bacteria and mold, and to facilitate further processing of the wool.

*Drying methods*:

- natural drying: wool is dried naturally, by exposure to air and sun. This method is slower, but is considered to be gentler on wool fibers.
- mechanical drying: wool is dried using special equipment, such as wool dryers, which use hot or cold air to remove moisture.
- spin drying: the wool is spun to remove excess water, and then dried naturally or mechanically.

*Methods for cooling wool pellets*:

- air cooling, using air to cool the pellet
- water cooling, using water to cool the pellet
- convection cooling, equipment that uses natural convection to cool the pellet is used

*The importance of cooling and drying*:

- preventing the growth of bacteria and mold, drying wool prevents the growth of bacteria and mold, which can damage wool fibers.
- facilitating processing, dried wool is easier to process and transform into finished products such as textiles and clothing.
- maintaining quality, drying wool helps maintain the quality and value of wool by preventing fiber damage.

*Precautions related to these operations*:

- avoid overheating, wool should not be overheated, as this can lead to damage to the fibers and loss of the wool's natural properties.
- moisture monitoring, the moisture content of the wool must be monitored to ensure that the wool is dried properly, but not too much. By drying the wool properly, high quality wool fibers can be obtained, which can be used in various other applications.

3. *Wool shearing and grinding*, the dried wool is cut and ground into smaller fibers to facilitate the pelletization process.

Wool shearing and wool milling are important steps in wool processing, which involve reducing the wool fibers to a smaller and more uniform size. This process is necessary to facilitate further processing of the wool and to obtain high-quality finished products. The fibers are cut to lengths of 5-10 mm using hammer mills specially designed for fibrous materials.

*Wool cutting/shredding*:

- the purpose of cutting/shredding wool is to reduce the length of the wool fibers to a smaller and more uniform size.
- methods applied to cutting/shredding wool, can be done manually or mechanically, using various equipment, such as scissors or wool shearing machines.
- the importance of cutting/shredding wool, is important to obtain uniform wool fibers, which can be subsequently processed in a more efficient way.

*Wool grinding*:

- the purpose of grinding, wool grinding aims to reduce wool fibers to a very small size, to facilitate further processing (Bradshaw et al, 2022).
- grinding methods, grinding wool can be done mechanically, using various equipment such as wool grinding machines. Importance of grinding, grinding wool is important to obtain very fine wool fibers, which can be used in various applications such as textiles and clothing.

*Advantages of cutting and grinding*:

- more efficient processing, cutting and grinding the wool facilitates the subsequent processing of the wool, allowing for the production of high-quality finished products.
- improved quality, cutting and grinding wool can improve the quality of finished products, by obtaining uniform and fine wool fibers.
- versatility, cutting and grinding wool allow wool to be used in various applications, such as textiles, clothing and other products.

By cutting and grinding wool, high-quality wool fibers can be obtained, which can be used in various applications.

4. *Pelletizing*, the ground wool fibers are compressed in a pelletizing machine to form compact pellets. The process generates heat through friction (70-90 [$^0$C]), which leads to the sterilization of the product (destruction of weed seeds and pathogens), (Valldecabres et al., 2021).

*Effective wool pelleting involves the following steps:*:

a. wool preparation: the wool is cleaned, cut and milled to obtain a uniform size.
b. mixing: ground wool can be mixed with other materials, such as natural fertilizers or additives, to improve the quality of the pellets.
c. pelletizing: the ground wool is compressed in a pelletizing machine, which forms compact and uniform pellets.
d. drying: wool pellets can be dried to remove excess moisture and prevent bacterial growth.

*Advantages of pelletization*:

- Easy handling: wool pellets are easier to handle and store than raw wool.
- Cost reduction: pelletization can reduce transportation and storage costs due to the smaller pellet sizes.
- Various applications: wool pellets can be used for various purposes, such as natural fertilization, insulation and composting.

*Key factors for efficient pelleting*:

✓ Wool quality: the quality of the wool used for pelleting is essential to obtain high-quality pellets.
✓ Appropriate equipment: using appropriate pelletizing equipment is important to obtain uniform and compact pellets.
✓ Storage conditions: wool pellets should be stored in dry and protected conditions to prevent damage.

Pelletizing sheep wool is an innovative and sustainable solution for the management and valorization of this natural resource as a substitute for chemical fertilizers. The resulting pellets have a density of approx. (600-700 [kg/m$^{3]}$)

***Equipment needed for wool pelletizing***:

1. *Wool cutting machine*: To cut wool into uniform sizes. There are several types of wool cutting machines, which can be classified according to the cutting method and purpose of use.

*Examples of machines*: Scissor shearing machines use rotating shears to cut wool in small to medium quantities; Disc shearing machines use rotating discs with blades to shear wool in large quantities; Roller wool shearing machines use rollers with blades to shear wool in medium to large quantities; Automatic wool shearing machines cut wool automatically, without human intervention. They are recommended for shearing wool in large quantities and for mass production.

*Technical features*: power and capacity, the machines must have the power and capacity needed to shear the wool effectively; precision and uniformity, it is recommended to cut the wool precisely and uniformly, to obtain high-quality wool fibers.

*Choosing the right mashine is based on*: the amount of wool, the amount of wool to be cut is taken into account; the type of wool, the type of wool to be sheared is taken into account; purpose of use

By choosing the right machine, high-quality wool fibers can be obtained, which can be used in various applications.

2. *Wool grinding machine*: wool grinding machines are used to grind wool fibers into smaller sizes to facilitate further processing.

*Examples of wool grinding machines*: Hammer mills: use hammers to grind wool fibers. They are used for grinding wool in large quantities; Roller machines: use rollers with blades to grind wool fibers in medium to large quantities; Disc machines: use rotating discs with blades to grind wool fibers in large quantities; Drum machines: use a rotating drum with blades to grind wool fibers. They are suitable for large quantities of raw material.

3. *Pelletizing machine*, to compress the ground wool into compact pellets. Pelletizing machines are used to turn materials into compact and uniform pellets.

*Examples of pelletizing machines*: with mold (uses a mold to compress the material into pellets); Roller (to compress the material into pellets); with extruder (uses an extruder to compress the material into pellets).

*Technical features*: Power and capacity: it must have the power and capacity needed to produce pellets efficiently; precision and uniformity: it must be able to produce uniform and precise pellets; safety and protection in operation.

Pelletizing machines are an efficient and productive solution to produce high-quality pellets.

4. *Dryer*, to dry the wool pellets and remove excess moisture. The wool pellet dryer is a specialized equipment that is used to dry wool pellets after the pelletizing process. The purpose of the dryer is to remove excess moisture from the pellets, to prevent the growth of bacteria and mold, and to ensure the quality and stability of the pellets.

*Dryers are of several types*: Hot air dryers (use hot air to dry wool pellets); Infrared dryers (use infrared radiation to dry wool pellets); Microwave dryers: use microwaves to dry wool pellets.

*Technical features*: Temperature control, the dryer must have precise temperature control to prevent overheating or underheating of the pellets; Humidity control (the necessity to present precise humidity control to ensure that the pellets are dried properly; safety and protection during operation.

*Advantages of wool pellet dryers*: improved quality (they can improve the quality of pellets by removing excess moisture); stability (to ensure the stability of pellets by preventing the growth of bacteria and mold); pproductivity (the possibility to increase the productivity and efficiency of the wool pellet production process).

5. *Wool combing and carding machines*, are specialized equipment used in the textile industry for processing wool fibers. These machines are intended to align and clean wool fibers, preparing them for spinning and weaving. Wool combing and carding machines perform the following functions: cleaning the fibers by removing impurities and short fibers from the wool; alignment of wool fibers in the longitudinal direction; transforming wool fibers into a thin and uniform thread. There are different types of wool combing and carding machines, including: needle combing machines; drum carding machines; Roller carding machines.
6. *Transport system*, to transport wool and pellets between the different stages of the process. Wool pellet conveyor systems are used to move wool pellets from one location to another, within the production process or between different stages of the supply chain. Here are some types of wool pellet conveyor systems:

Moving wool pellets through a production line or warehouse requires systems that are gentle but reliable, because the pellets are light and can generate dust. The most common solutions are belt conveyors, which use a continuous belt to carry pellets horizontally; screw conveyors, where a rotating auger pushes the material forward; pneumatic conveyors that move pellets using compressed air through pipes; and chain conveyors, which drag the product along with chains and flights. When choosing a system, three technical features matter most: the carrying capacity, the transport speed, and the level of safety and dust protection during operation. Once conveyed, pellets must be stored in dry and protected conditions to avoid moisture absorption. Wool naturally absorbs up to 30-40 [%] of its weight in water, so warehouses need ventilation, a concrete floor, and protection from rain and condensation.

Wool pelletization is an emerging technology for the valorization of wool waste. We presents the main systems for conveying and storage, the potential applications of wool pellets, and the technical characteristics and selection criteria for wool pelletizers used at farm and industrial scale.

a) Conveying and Storage Systems

The handling of wool pellets within production and storage facilities is achieved through mechanical or pneumatic conveying systems. The most common types are: belt conveyors: utilize a continuous belt for horizontal transport of pellets, screw conveyors: employ a rotating auger within an enclosed trough for metered, short-distance transport, pneumatic conveyors: use compressed air to move pellets through pipelines, minimizing dust emission, chain conveyors: use flights attached to a chain to move bulk material, suitable for inclined transport.

Key technical features for conveyor selection include carrying capacity, transport speed, and safety provisions during operation such as dust control and fire prevention.Due to the hygroscopic nature of wool, storage must be carried out in dry and protected conditions. Storage areas should have controlled humidity, ventilation, and impermeable flooring to prevent moisture absorption and pellet degradation. Conveyor systems are integral to moving pellets between reception, processing, storage, and packaging zones.

b) Applications and Market Potential

The wool waste recovery process converts wool scraps into a densified product with commercial value. The pellet matrix allows for controlled release of wool constituents such as lanolin and organic nitrogen.Identified applications include: *slow-release organic fertilizer* - wool is rich in nitrogen and other nutrients. Pellets decompose over 4-6 months, providing gradual nutrient release and reducing leaching losses *(Giteru et al., 2023), absorbent material* - wool's natural sorption capacity enables the use of pellets for oil spill and hydrocarbon remediation, *mulch* - applied around plants, pellets retain soil moisture, suppress weeds, and decompose to release nutrients. Combined application with compost has demonstrated soil benefits. Kumar et al., 2023, *pest deterrent* - the abrasive texture of wool fibers deters snails and slugs, *filter material* - the fibrous structure supports use in air and water filtration systems, *thermoregulation* - wool layers in soil act as insulation, buffering root-zone temperature extremes.

Wool pelletization therefore represents a promising strategy to diversify uses of wool and create value-added products from waste resources.

c) Technical Characteristics of Wool Pelletizers

Pelletizer specifications vary by manufacturer, model, and scale: small-scale, semi-industrial, and industrial. Common technical parameters include: *general design* - flat-die pelletizers: compact, cost-effective, suitable for small-medium scale and varied materials including wool. Ring-die pelletizers: for industrial scale, higher capacity and uniform die wear, *core parameters* - production capacity: kg/h or t/h. Range: tens of kg/h for small units to thousands of kg/h for industrial lines. Motor power: kW or HP. Determines compression force and is dependent on capacity and target pellet density.

Die geometry: Die diameter affects throughput. Die thickness affects pellet density and durability.

Die hole diameter: Typically 3-12 [mm], defines pellet diameter.

Rotation speed: RPM of die/rollers influences feed rate and quality.

Number of pressing rollers: More rollers increase pressure uniformity and capacity.

Feeding system: Auger or hopper with dosing to ensure constant material flow.

Cutting system: Adjustable knives to control pellet length.

Physical characteristics: Machine weight, dimensions LxWxH, and noise level in dB, *wool-specific features* - mold and roller design: May include profiles optimized for elastic wool fibers. Pre-treatment system (optional): Humidification or gentle heating to improve fiber binding. Control system: Electrical panel with start/stop, speed and temperature control. Advanced models include PLC for automation. Safety system: Emergency stops, guards, and interlock sensors.

d) Equipment Selection Criteria

When selecting a wool pelletizer, the following factors must be considered: *desired production capacity*, *type of wool*: fineness, fiber length, impurity level, *target pellet quality*: density, size, durability, *budget*: CAPEX, OPEX, maintenance, *availability of spare parts and technical service*, *space and energy requirements.*

The initial investment is only part of total cost. Operational costs including electricity, maintenance, die replacement, and pre-processing equipment such as a wool shredder must be included. Pre-shredding of raw wool is generally required to facilitate feeding. Some specialized pelletizers integrate this function. According to *(Guinea, 2022),* a farm-scale wool pelletizer consists of several key subsystems working in sequence to produce compact pellets. Generally for wool pelletizing, a pre-process of shredding the raw wool is required to facilitate feeding into the pelletizer. Some specialized pelletizers may include this function.

The wool pelletizer used in sheep farms is composed of several key elements that work together (figure 4) to transform raw wool into compact pellets *(Bradshaw et al, 2022).*




**Fig. 4 - Generalized workflow of the sheep wool pelletization process.**

*The scheme was prepared by the authors based on information synthesized from Guinea (2022), other cited literature, and publicly available technical information on wool pelletization systems. Illustration created using AI-assisted visualization (OpenAI ChatGPT and DALL·E).*

The main components of a sheep wool pelletizing line generally include a raw wool feeding unit, a cleaning system for removing dust and impurities, a shredder with knives for reducing fibre size, a conditioning unit for adjusting moisture content, a pellet mill equipped with a die and rollers, a cooling system to stabilize the freshly produced pellets, a screening unit for removing fines and oversized particles, and a packaging or storage unit.

Additional components may also be added, depending on the production scale and equipment manufacturer, to improve operational efficiency and product quality. It sometimes includes agitation or forced feeding systems to ensure a constant flow of material to the pelletizing chamber. *The Feeder System* represents the mechanism that controls the rate at which wool is fed into the pelletizing machine to ensure a uniform flow of material for consistent pelleting, and it can be a screw conveyor (most common), a conveyor belt, or a roller system.

*The Pelletizing Chamber* with die and press rollers represents the heart of the pelletizer, where the wool compaction process takes place. It contains the die and the pressing rollers. A thick metal plate with holes of a certain diameter (which will be the diameter of the pellets). The wool is forced through these holes under pressure. It can be flat die or ring die, depending on the type of pelletizer. The design of the holes (length, taper) can be optimized for the wool fibers. Cylindrical or conical rollers that rotate above the die (in flat die pellet mills) or inside the die (in ring die pellet mills). They exert enormous pressure on the wool, forcing it through the die holes and forming pellets. The number and design of rollers vary depending on the model and capacity.

*The Control Panel* includes switches, buttons, indicators, and sometimes an electronic control system (PLC) to operate and monitor the pelletizer.

Optional or additional elements are: *Pre-treatment System*, which may include an integrated or separate wool shredder, a humidification system or a mild wool heating system; a *Pellet Cooling System* (a forced air conveyor or rotary cooler to reduce the temperature of the pellets after forming); the *Dust Removal System* - a suction system to collect dust generated during the process; advanced sensors and monitoring systems, to track operating parameters (temperature, pressure) and to detect any blockages or problems.

## 3. SHEEP WOOL PELLETS AS SUSTAINABLE BIOFERTILIZERS

Washed, shredded and pressed sheep wool, used as a slow-release organic fertilizer. It contains the following elements: 10-12[%] N, 1-2[%] P, 2-4]%] K + keratin

### 3.1 The effect of sheep wool pellets on seed germination

Seed germination is influenced by the availability of nutrients and the physico-chemical and biological properties of the soil. Due to the content of approximately 10–12[%] nitrogen (N), 1–2[%] phosphorus (P), 2–4[%] potassium (K) and keratin, sheep wool pellets represent a slow-release source of nutrients, capable of supporting plant development from the early stages of vegetation.

Nitrogen is incorporated into the structure of keratin and becomes available to plants only after its degradation by soil microorganisms. This process leads to the gradual release of amino acids and mineral forms of nitrogen, ensuring constant nutrition and reducing losses through leaching. At the same time, the decomposition of wool stimulates the biological activity of the soil and contributes to the improvement of water retention and its structure.

*(Kovács et al., 2025)* demonstrated that the efficiency of wool pellets depends on the soil microbiological activity, with decomposition being faster in sandy soils, where higher nitrogen availability and a significant increase in plant biomass were observed. Numerous studies have reported that the application of moderate doses stimulates germination and emergence in cereals, vegetables and ornamental plants, while doses higher than 200 [g/m²] can cause temporary phytotoxicity through the rapid release of ammonium.

For this reason, it is recommended to incorporate the pellets into the soil 2–3 weeks before sowing. By slowly releasing nutrients and stimulating soil biological activity, sheep wool pellets represent a sustainable alternative to conventional fertilizers, promoting uniform germination and early plant development, provided that adequate doses are applied (Wool: A Natural Bio-Enhancement for Gardens, South Dakota State University, June 06, 2024, https://extension.sdstate.edu/wool-natural-bio-enhancement-gardens )

### 3.2 The effect of sheep wool pellets on plant biomass

Due to the slow release of organic nitrogen over a period of approximately 4–6 months, sheep wool pellets contribute to stimulating vegetative growth and ensure a constant supply of nutrients throughout plant development. This mechanism favors the formation of a larger aerial biomass, the development of more vigorous stems and the intensification of the green color of the leaves, due to the improvement of chlorophyll synthesis and photosynthetic processes.

Experimental results indicate that the application of wool pellets at doses of 100–150 [g/m²] can cause increases in aerial biomass by 15–30[%] compared to unfertilized variants, the effects being more pronounced in soils poor in organic matter, *(Kovács et al., 2025)* demonstrated that treatment with wool pellets significantly increased shoot biomass in both investigated soil types, and in soils with a low organic matter content, the total amount of nitrogen accumulated in plant biomass was 29.55[%] higher than in the control variants. *(Bradshaw and Hagen 2022*) also showed that wool pellets offer comparable performance to commercial fertilizers used in organic vegetable production, both in terms of plant growth and mineral element uptake. In the case of tomato crops, the application of wool pellets led to significantly higher yields, with fruits being approximately 58–69 [%] larger compared to unfertilized plots. Overall, the available results highlight that sheep wool pellets represent an efficient source of slow-release nutrients, capable of supporting biomass accumulation and vegetative development of plants, offering similar performance to commercial fertilizers, especially in soils with low fertility.

### 3.3 The effect of sheep wool pellets on agricultural production

Numerous studies have shown that the use of sheep wool pellets can lead to increases in agricultural production by approximately 10–25 [%] in various crops, including vegetables, cereals and fruit trees. These effects are attributed not only to the supply of nitrogen, phosphorus and potassium, but also to the presence of sulfur, magnesium and trace elements, as well as the ability of the pellets to improve soil structure and fertility. The slow and continuous release of nutrients ensures balanced plant nutrition throughout the growing season, reducing losses through leaching and increasing nitrogen use efficiency.

In addition to the quantitative increase in production, wool pellets can also positively influence the quality of the harvest. The constant supply of nitrogen, without excesses of immediately available nutrients, favors the accumulation of sugars and proteins in fruits and vegetables, avoiding excessive vegetative growth frequently associated with intensive mineral fertilization.

The results obtained by *(García et al., 2024)* showed that the use of wool pellets improves soil fertility and supports healthy plant development. In the case of pepper crops, the authors observed that significantly larger fruits were obtained in soils with a high organic matter content, an effect attributed to the slower decomposition and progressive release of nutrients from the pellets. Overall, sheep wool pellets represent a sustainable alternative to conventional fertilizers, contributing both to increasing production and improving crop quality, through a balanced supply of nutrients and by improving the physical and biological properties of the soil.

### 3.4 The effect of sheep wool pellets on soil water retention

One of the most important properties of sheep wool pellets is their high-water retention capacity, due to the hygroscopic nature of the keratin fibers. Once incorporated into the soil, the pellets absorb water and swell, acting as small reservoirs that store moisture and gradually release it to the root zone. This mechanism helps maintain more stable soil moisture and reduces plant water stress during periods of low rainfall.

Available studies and technical data show that wool fibers can absorb 20–30 times their own weight in water, while pellets can increase their mass by absorbing water up to four times, depending on the degree of processing and conditions of use.

As a result, the use of pellets can increase the water retention capacity of the surface soil layer and reduce irrigation needs by approximately 25 [%], which is particularly important in horticultural crops, greenhouses and areas affected by drought.(Butter. Lanopellet: a natural NK fertiliser, HortiDaily, 2025. https://maslana.es/ https://www.hortidaily.com/article/9814383/from-livestock-waste-to-organic-fertilizer/). By improving water availability in the root zone and reducing the frequency of irrigation, wool pellets represent a sustainable solution for both increasing crop resilience to drought and optimizing water consumption in agriculture.

### 3.5 The effect of sheep wool pellets on soil microbiological activity

Sheep wool pellets contribute to the intensification of soil microbiological activity due to their high content of keratin, a complex protein that can only be degraded by specialized microorganisms, especially keratinolytic bacteria and fungi. The decomposition process stimulates the development of microbial communities involved in the nutrient cycle and favors the formation of a more active rhizosphere.

The mineralization of nitrogen from keratin depends entirely on the microbiological activity of the soil, which allows for the gradual release of nutrients and significantly reduces leaching losses compared to mineral fertilizers. During degradation, amino acids and peptides are released, which constitute additional sources of carbon and nitrogen for microorganisms, exerting a prebiotic effect on the microbiota in the rhizosphere.

The development of beneficial microorganisms contributes to improving soil structure and aeration, while also favoring the development of mycorrhizal fungi and increasing the activity of soil fauna, including earthworms. By stimulating natural biological processes and nutrient recycling, sheep wool pellets contribute to increasing the biological fertility of the soil and supporting healthy plant development.

### 3.6 Wool Pellets versus different fertilizers

**Table 3**

**Comparison Of Wool Pellets with Other Fertilizers.**

*Giteur at al 2018*

| Indicator | Wool pellets | NPK fertilizer (15-15-15) | Mature compost | Mature manure |
|---|---|---|---|---|
| **Nitrogen release** | Slow (4–6 months) | Fast (2–6 weeks) | Very slow (6–12 months) | Slow (3–8 months) |
| **Nutritional content** | ~10–12% N, 1–2% P, 2–4% K + S, Mg | 15–15–15 | Low (≈1–1–1) | Variable (≈0.5–1.5% N) |
| **Effect on germination** | Favorable at moderate doses and application before sowing | Risk of phytotoxicity at high doses | Very favorable | Favorable if well matured |
| **Water retention** | Very high | NEGLIGIBLE | Moderate | Hello |
| **Microbiological activity** | Stimulates keratinolytic microorganisms and the rhizosphere | Neutral to moderately negative in case of intensive use | Stimulates beneficial microorganisms | Strongly stimulates biological activity |
| **Risk of nitrogen leaching** | Very low | High | Reduced | Moderate |
| **Weed seeds/pathogens** | ABSENCES | ABSENCES | Reduced if well matured | May be present if not composted properly |
| **Smell** | Weak, temporary | Odorless | Smell of humus | Pronounced |
| **Cost** | Medium–high | Low | Low–medium | Low (if available locally) |

*Giteru, S. G., Ogunade, I. M., Scarborough, S. P., & Gelaye, S. (2018). Evaluation of wool-based organic fertilizer on soil properties and plant growth. Journal of Plant Nutrition, 41(18), 2351–2360. https://doi.org/10.1080/01904167.2018.1509994*

### 3.7 Practical conclusions

Based on the data available in the literature, sheep wool pellets represent a sustainable alternative to conventional fertilizers, offering important advantages through slow nutrient release, high water retention capacity and stimulation of soil microbiological activity. Compared to NPK mineral fertilizers, they reduce the risk of nitrogen leaching and contribute to obtaining more balanced crops, without the excessive vegetative growth associated with rapid fertilization. The main limitations of wool pellets are their higher cost per unit of nitrogen provided and their slower rate of nutrient release, making them less effective in situations where a rapid crop response is required. Compared to compost and manure, pellets contain higher concentrations of nitrogen, present a reduced risk of introducing weeds and pathogens, and generate much less odor. Compost and manure, on the other hand, have the advantage of providing a higher supply of stable organic matter and humus, contributing in the long term to improving soil structure and fertility. Depending on the crop and soil fertility, the literature recommends applying wool pellets at doses of approximately 50–150 [g/m²] for vegetable crops and 200–400 [kg/ha] for cereals, incorporating them to a depth of 5–10 [cm] before sowing or planting, to ensure efficient mineralization and optimal nutrient availability.

### 3.8 Recommendations

***Using wool pellets as fertilizer*** is an organic and slow-release option, but certain criteria must be considered to ensure effective and beneficial application for plants and soil:

**1.** Crop type and nutritional needs:

- crops with high nitrogen requirements: wool is rich in nitrogen, so it is suitable for plants that require a significant supply of nitrogen for vegetative growth (e.g. leafy vegetables, turf, cereals in the growth phase).

- crops with a long growth cycle: the slow release of nutrients from wool is ideal for plants that need constant nutrition over an extended period.

- avoid excessive use for crops sensitive to excess nitrogen: certain plants (e.g. legumes in the nitrogen-fixing phase) do not require a large supply of nitrogen and could be negatively affected by too much.

**2.** Plant development stage:

Before planting/sowing: incorporating wool pellets into the soil before planting or sowing allows for the gradual release of nutrients as the roots develop.

During growth: pellets can be applied as mulch around plants or incorporated superficially into the soil to provide a continuous supply of nutrients.

It is recommended to avoid excessive application during the flowering/fruiting phase: too much nitrogen intake during this phase can favor vegetative growth to the detriment of flower and fruit production.

**3.** Soil type:

Soils low in organic matter and nutrients: wool pellets enrich the soil with organic matter and release essential nutrients. Sandy soils: slow release of nutrients, helps retain nutrients in sandy soil, preventing rapid leaching. Clay soils: the organic matter in wool can improve the structure of clay soil, facilitating aeration and drainage. Soil pH: wool has a neutral to slightly alkaline pH. The existing soil pH and the specific needs of the plants should be taken into account.

**4.** Quantity and method of application:

- Dosage: The amount of wool pellets used depends on the nutritional needs of the plants, the fertility of the soil and the size of the application area. Too much can lead to an excess of nutrients.
- Incorporation into the soil: mixing the pellets with the top layer of soil ensures a gradual release of nutrients to the root zone.
- Application as mulch: A layer of pellets applied to the soil surface helps retain moisture, suppress weeds, and release nutrients as they decompose.
- Pellet size: Finer pellets break down faster, releasing nutrients faster, while larger pellets have a slower release.

**5.** Quality of wool pellets: are the pellets made of 100[%] wool or do they contain other materials (which could influence the nutritional value and behavior in the soil).

**6.** Processing: the method of processing wool (washing, treatments) can affect the nutrient content and the presence of any unwanted substances.

**7.** Environmental considerations:
Wool source: Opt for wool pellets from sustainable and ethical sources.

**8.** Impact on wildlife: Ensure that the use of pellets does not excessively attract certain animals that could damage crops.

Technical specifications of the final pellet:

- diameter: 6 - 8 [mm].
- length: 10 - 20 [mm].
- density: high, to prevent scattering by wind.

Expansion capacity: Upon contact with water, the pellets increase their volume by up to 300[%], aerating the soil from the inside out.

***Applying wool pellets to fields as fertilizer***: can be achieved by various methods, similar to the administration of chemical fertilizers, adapted to the type of crop, the stage of plant development and the equipment available. Here are the main application methods:

- Before sowing/planting (Pre-planting incorporation):

Distribution: uniform: the pellets are spread evenly over the surface of the soil to be cultivated.

Incorporation: Agricultural machinery such as a plow, disc harrow or rotary tiller is used to incorporate the pellets into the topsoil (usually at root working depth). This method ensures a gradual release of nutrients into the root development zone.

Advantages: Nutrients are available as the roots develop, reduced risk of loss through volatilization or surface runoff.

- At sowing/planting (localized application):

Fertilization strip: pellets can be distributed in a strip along the sowing or planting row, at a certain lateral distance and below the depth of the seeds or seedlings.

With the seeder/planter: the seeder and planter are equipped with granular fertilizer distribution systems, which can be adapted for wool pellets (checking the size and flow of the pellets).

Advantages: Nutrients are available in close proximity to young roots, stimulating initial growth.

- Post-emergence/planting (Surface application or shallow incorporation):

*Surface spreading*: The pellets are evenly distributed on the soil surface around the plants. This method is simple, but the nutrients may be less effective until they are transported to the root zone by rain or irrigation.

*Shallow embedding*: after spreading, the pellets can be easily incorporated into the topsoil using a light cultivator or rake. This helps with better nutrient retention and root contact.

*Application as mulch*: A layer of pellets can be applied around the base of plants as mulch. This helps retain moisture, suppress weeds, and releases nutrients as they decompose.

*Advantages:*allows fertilization during the growing season, can be combined with mulching.

***Important considerations for administration***:

- ✓ *Dosage*: follow the recommended doses depending on the type of crop, the stage of development and the fertility of the soil. Too much can be harmful. Incorporation into the soil is recommended at a depth of 5 – 10 cm, close to the roots of the plants.

**Table 4**

**Method of administration, dosage of pellets**

| **Crop type** | **Recommended dosage** |
|---|---|
| Vegetables (peppers, tomatoes, etc.) | 70 – 150 g/m2 |
| Potted plants | 10 g per 1 l substance |
| Fruit trees/shrubs | 150 – 300 g/plant |
| Grass | 100 g /m2 at sowing |
| Wheat | 500 - 2000 kg/ha, at sowing |
| Maize | 800 – 3500 kg/ha, at sowing |

- ✓ *Uniformity: ensure the most uniform distribution of pellets on the field surface to avoid areas with excess or deficiency of nutrients.*
- ✓ *Pellet size: The size of the pellets can influence the way they are distributed and the rate of decomposition. Smaller pellets will decompose faster.*
- ✓ *Application equipment: use properly calibrated equipment to ensure accurate distribution of the desired amount. Granular fertilizer spreaders may be suitable, but check compatibility with pellet size and shape.*
- ✓ *Application time: adapt the timing of application to the nutritional needs of the crop at different stages of development.*
- ✓ *Integration with other agricultural practices: wool pellet management should be integrated into an overall soil nutrition management program, which may include soil analysis and other fertilizer sources.*
- ✓ *Monitoring: observe the plants' reaction to the application of pellets and adjust the amounts in the following applications, if necessary.*

*Specific recommendations*:

For row crops (corn, sunflower, soybean): banding at seeding or pre-plant incorporation can be effective. Application as a mulch around young plants is also an option.

For coarse grains (wheat, barley, oats): broadcast and pre-plant incorporation are common methods. Post-emergence surface application can be used for additional fertilization.

For legumes: banding at planting, pre-planting incorporation, or application as mulch around established plants are suitable methods.

## CONCLUSIONS

The use of sheep wool as a fertilizer represents a practical model of the circular economy. It converts a renewable agricultural by-product into a biodegradable and value-added product that not only supplies plant nutrients, but also contributes to the long-term restoration of soil health. Due to these characteristics, wool pellet fertilization is identified as an ideal solution for organic farming systems, urban gardening applications, and the rehabilitation of degraded soils. The agronomic and environmental benefits of using wool pellets can be summarized as follows:

**A.** Slow Release of Nutrients

Wool keratin decomposes gradually in the soil over a period of 6 to 10 months. This slow mineralization rate reduces the risk of nitrogen leaching to groundwater and provides a continuous supply of nutrients to the plant throughout the growing season.

**B.** Water Management

Wool is inherently hygroscopic. Pelletized wool can absorb up to 3-4 times its own weight in water. During periods of high precipitation, pellets absorb excess soil moisture. During periods of drought, they release stored water gradually to the root zone. This mechanism reduces irrigation frequency and improves plant water use efficiency.

**C.** Improvement of Soil Structure

Upon hydration, wool pellets expand and create micro-channels within the soil matrix. This process of "natural aeration" alleviates soil compaction and facilitates root penetration and development. In addition to its direct nutritional value, wool provides two secondary mechanical benefits: *Protection against gastropod pests*: the abrasive texture of wool fibers, maintained even in partially decomposed pellets on the soil surface, acts as a physical deterrent to snails and slugs. *Soil thermoregulation*: The wool layer in the soil functions as a natural insulator. It buffers temperature fluctuations and maintains a more stable temperature at the root zone during cold nights and hot days.

In conclusion, wool pelletization offers a dual benefit: waste valorization for the sheep industry and the delivery of a multifunctional soil amendment that addresses nutrient supply, water retention, soil structure, and microclimate regulation.

## ACKNOWLEDGEMENT

This work was supported by the Romanian Ministry of Education and Research, National Research Authority through the project PN 23 04 02 02 - Research on the use of wool waste to obtain organic fertilizers for agriculture in order to improve soil properties and reduce environmental pollution

The authors acknowledge the use of OpenA,I ChatGPT and DALL·E as AI-assisted visualization tools for the preparation of original conceptual figures. All figures were developed based exclusively on information synthesized from the cited scientific literature and were reviewed, refined, and approved by the authors.

## REFERENCES

[1] Amirova, T. Sh., Ibragimov, A. A., Nazarov, O. M., & Karabayeva, R. B. (2022). Physicochemical analysis, elemental and amino acid composition of wool and silk. Journal of Genetic Engineering and Biotechnology Research, 4(2), 294–302;

[2] Bradshaw, T., & Hagen, K. (2022). Wool pellets are a viable alternative to commercial fertilizer for organic vegetable production. Agronomy,12(5),1210, https://www.mdpi.com/2073-4395/12/5/1210 ;

[3] Butter. (2025). Lanopellet: A natural NK fertiliser. HortiDaily. https://www.hortidaily.com/article/9814383/from-livestock-waste-to-organic-fertilizer/ ;

[4] Camilli, F., Focacci, M., Dal Prà, A., Bortolu, S., Ugolini, F., Vagnoni, E., & Duce, P. (2025). Turning waste wool into a circular resource: A review of eco-innovative applications in agriculture. Agronomy, 15(2), 446; https://www.mdpi.com/2073-4395/15/2/446 ;

[5] CSIRO. (n.d.). Wool Structure and Chemistry. Conceptual source. https://csiropedia.csiro.au/wp-content/uploads/2015/01/6229343.pdf ;

[6] Dias, G. J., Haththotuwa, T. N., Rowlands, D. S., Gram, M., & Bekhit, A. E. D. A. (2022). Wool keratin–A novel dietary protein source: Nutritional value and toxicological assessment. Food Chemistry, 383, 132436;

[7] Fechete, F. I., Popescu, M., Lăcătuş, M. C., Lăcătuş, R., Tataru, M., Matei, R. I., Mârza, M. S., Codea, A. R., Mărcuș, I. O., & Bora, F. D. (2024). Sheep's wool as a bioindicator of heavy metal pollution. Advances in Environmental Sciences, 16(1), 35–49;
[8] García, M., Rodríguez, M., Schuster, J., & Pavan, F. (2024). The use of wool pellets as natural fertilizer: A solution linked to technological transfer and sustainability. https://redi.anii.org.uy/jspui/bitstream/20.500.12381/4052/1/ ;
[9] Giteru, S. G., Ali, A., & Oey, I. (2023). Understanding the relationship between rheological characteristics of pulsed electric fields treated chitosan-zein-poly(vinyl alcohol)-polyethylene glycol composite dispersions. Food Hydrocolloids, 137, 108332.
[10] Giteru, S. G., Ogunade, I. M., Scarborough, S. P., & Gelaye, S. (2018). Evaluation of wool-based organic fertilizer on soil properties and plant growth. Journal of Plant Nutrition, 41(18), 2351–2360;
[11] Górecki, R. S., & Górecki, M. T. (2010). Utilization of waste wool as substrate amendment in pot cultivation of tomato, sweet pepper, and eggplant. Polish Journal of Environmental Studies, 19(5), 1083–1087.;
[12] Grigore, I. A., Vlăduțoiu, L., Sorică, C., Cristea, M., & Sorică, E. (2024). Study on the efficiency of biofertilizers in the context of sustainable agriculture. Acta Technica Corviniensis - Bulletin of Engineering.
[13] Gupta, R., & Ramnani, P. (2006). Microbial keratinases and their prospective applications: An overview. Applied Microbiology and Biotechnology, 70(1), 21–33. [15] Zanovello, I y Cardoso, M. (2019) Utilización de lana de oveja de bajo valor como aislante térmico en la patagonia, Argentina. Energías renovables y medio ambiente 44, 49-57. https://doi.org/10.1007/s00253-005-0239-8;
[14] Kovács, F., Papdi, E., Veres, A., Mohay, P., Szegő, A., & Juhos, K. (2024). More efficient nitrogen utilization through wool pellet and soil inoculation. Agrosystems, Geosciences & Environment, 7(2), e205340 mdpi.com;
[15] Kovács, F., Papdi, E., Gyalai, I., Biró, B., & Juhos, K. (2025). Nitrogen supplying capability of wool pellets as an alternative fertilizer depending on soil biological activity. Future Biology, 76(3), 419-435.
[16] Patkowska-Sokoła, B., Dobrzański, Z., Osman, K., Bodkowski, R., & Zygadlik, K. (2009). The content of chosen chemical elements in wool of sheep of different origins and breeds. Archives Animal Breeding, 52(4), 410–418. https://doi.org/10.5194/aab-52-410-2009 ;
[17] Marczak, D., Lejcuś, K., Kulczycki, G., & Misiewicz, J. (2022). Towards circular economy: Sustainable soil additives from natural waste fibres to improve water retention and soil fertility. Science of The Total Environment, 858(Part 2), 159380.
[18] Maslana. (2025). Wool pellets: El abono para el futuro. Rumiantes. https://rumiantes.com/pellets-de-lana-abono-para-futuro/ ;
[19] Nustorova, M., Braikova, D., Gousterova, A., Vasileva-Tonkova, E., & Nedkov, P. (2006). Chemical, microbiological and plant analysis of soil fertilized with alkaline hydrolysate of sheep's wool waste. World Journal of Microbiology and Biotechnology, 22(4), 383–390;
[20] OpenAI. (2026). DALL•E image generation model. OpenAI, San Francisco, USA;
[21] Patkowska-Sokoła, B., Dobrzański, Z., Osman, K., Bodkowski, R., & Zygadlik, K. (2009). The content of chosen chemical elements in wool of sheep of different origins and breeds. Archives Animal Breeding, 52(4), 410–418;
[22] South Dakota State University Extension. (2024, June 6). Wool: A natural bio-enhancement for gardens;
[23] Szczecina, J., Niemiec, M., Szatkowski, P., Szczepanik, E., Zhakypbekovich, A. I., & Molik, E. (2025). Using the natural properties of sheep wool in the design of drought-reducing composites. Animal Science and Genetics, 21(2);
[24] Valldecabres, A., et al. (2022). Perspective of dairy producers from California, Idaho, South Dakota, and Washington. Journal of Dairy Science, 105(2), 1788–1796;
[25] Zanovello, I., & Cardoso, M. (2019). Utilización de lana de oveja de bajo valor como aislante térmico en la patagonia, Argentina. Energías Renovables y Medio Ambiente, 44, 49–57;
[26] Zheljazkov, V. D. (2005). Assessment of wool waste and hair waste as soil amendment and nutrient source. Journal of Environmental Quality, 34(6), 2310–2317.
[27] *** https://csiropedia.csiro.au/wp-content/uploads/2015/01/6229343.pd
[28] *** https://extension.sdstate.edu/wool-natural-bio-enhancement-gardens

# OPPORTUNITIES IN 3D FOOD PRINTING: FROM CONCEPT TO COMMERCIAL APPLICATIONS

/

# *OPORTUNITĂȚI ÎN IMPRIMAREA 3D A ALIMENTELOR: DE LA CONCEPT LA APLICAȚII COMERCIALE*

**Alexandru-Cristian CIOACLĂ*[1)], Iuliana GĂGEANU[1)], Ana-Maria TĂBĂRAȘU[1)], Robert-Dorin CRISTEA[1)], Dorin-Andrei CÎRSTEA[1)], Alexandru IONESCU[1)], Mario CRISTEA[1)], Alex-Nicolae COLEȘI[2)]**

[1)] National Institute of Research - Development for Machines and Installations Designed to Agriculture and Food-Industry - INMA Bucharest / Romania;

[2)] National University of Science and Technology POLITEHNICA Bucharest / Romania.

**Tel: 0733 537 643; *E-mail: cioaclacristian@gmail.com*

***Keywords:*** *3D food printing, commercialization, personalized nutrition, protein alternatives*

## ABSTRACT

*This paper traces the development of 3D food printing from a theoretical idea to a practical commercial use. The layer-by-layer deposition of edible materials like chocolate, purées, or protein pastes was initially a laboratory curiosity. In recent years, the technology has established stable market positions, particularly in confectionery but also in clinical nutrition and the production of protein substitutes. After reviewing the technical concepts that enable food printing, the paper examines three commercial application directions at varying stages of development: chocolate and confectionery products, plant-based or cultured protein substitutes, and customized nutrition for patients or customers with special needs. A separate section discusses consumer acceptance a factor just as important as the technology itself including recent data on price perception and adoption readiness among Romanian consumers. The paper closes with a discussion of the economic and regulatory barriers that still separate a product that works in the laboratory from one available on the shelf.*

## REZUMAT

*Această lucrare urmărește evoluția imprimării 3D a alimentelor, de la stadiul de concept teoretic la cel de utilizare comercială practică. Depunerea strat cu strat a unor materiale comestibile, precum ciocolata, piureurile sau pastele proteice, a reprezentat inițial o curiozitate de laborator. În ultimii ani, tehnologia și-a consolidat poziția pe piață, în special în industria produselor de cofetărie, dar și în domeniul nutriției clinice și al producției de înlocuitori proteici. După trecerea în revistă a conceptelor tehnice care fac posibilă imprimarea alimentelor, lucrarea analizează trei direcții de aplicare comercială aflate în diverse stadii de dezvoltare: ciocolata și produsele de cofetărie, înlocuitorii proteici de origine vegetală sau cultivați în laborator, precum și nutriția personalizată pentru pacienți sau clienți cu nevoi speciale. O secțiune separată abordează problema acceptării de către consumatori un factor la fel de important precum tehnologia în sine , incluzând date recente privind percepția prețului și disponibilitatea de adoptare în rândul consumatorilor români. Lucrarea se încheie cu o analiză a barierelor economice și de reglementare care încă separă un produs funcțional în laborator de unul disponibil la raft.*

## INTRODUCTION

3D food printing was more of a technology-showcase topic than a real business. A printer capable of depositing melted chocolate into complex shapes drew curiosity, but rarely produced anything actually sold to a customer. The past few years have changed that picture. For a handful of specific applications, the technology has moved from prototype to commercial product, and the global market for food printing equipment is estimated to grow substantially by the end of the decade, driven by demand for personalization, niche confectionery products, and protein alternatives.

The gap between "working in the lab" and "working on the market" is not just about technology. A 3D printed product has to be food-safe, it has to have a reasonable per-unit cost compared with conventional production methods, and it has to be accepted by a consumer who, in many cases, is hearing about the concept of "printed food" for the first time. This paper follows exactly that path from the basic technical principle, through a handful of concrete commercial applications, to the factors that determine whether an

ordinary consumer will actually buy such a product. Interest in this field does not come from technological curiosity alone. Global population growth, growing pressure on agricultural resources, and increasingly visible demand for personalized diets create a real economic context in which additive food manufacturing starts to look not just possible, but useful. At the same time, public and private research funding allocated to the field has grown steadily in recent years, a sign that investors and academic institutions treat the technology as more than a passing curiosity.

## FROM CONCEPT TO PROTOTYPE: PRINCIPLES AND TECHNICAL CHALLENGES

### Printing Technologies and Edible Materials

The most widespread method remains extrusion: a piston or screw pushes the material through a nozzle, and it is deposited layer by layer, following a digital model. Alongside it, the literature discusses selective laser sintering, binder jetting, and inkjet printing, each suited to a different type of material from powders to fine liquids (*Ehsan et al., 2025*). Choosing the method is not a purely technical matter; it depends directly on the ingredient's properties: how viscous it is, how easily it flows under pressure, how well it holds its shape immediately after deposition.

Plant-based protein, exemple in figure 1, materials raise specific problems. A product based on pea or soy protein has to be carefully adjusted too liquid, and the structure collapses before it stabilizes; too viscous, and it no longer flows evenly through the nozzle. Recent research on plant proteins documents exactly this fine balance between printing parameters (speed, pressure, nozzle diameter) and the final texture of the product, which has to resemble as closely as possible the texture of the meat it replaces (*Mittal et al., 2023*).

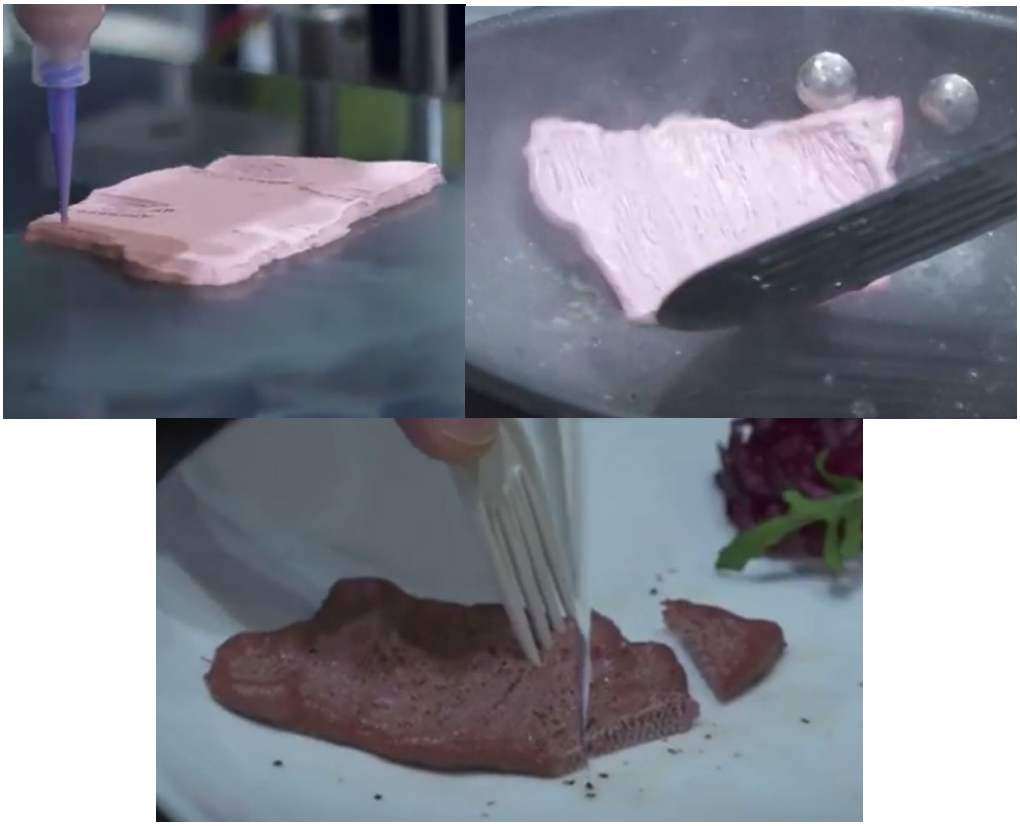


**Fig. 1 - Plant-based protein „steak" made using a mixture of peas, rice protein extract, rapeseed fat and algae fibers**

*(South China Morning Post, 2020)*

### From Laboratory to Production Line

The largest technological challenge is still getting from a functioning prototype to a line that can produce hundreds or thousands of units every day. For a demonstration, a laboratory printer may generate a single piece in a matter of minutes, but this is insufficient for a bakery or confectionery plant that must supply a significant volume every day. Instead than raising the speed of a single printing head, which is constrained

by the material's physical characteristics, the solution typically involves multiplying the printing heads operating concurrently.

A second, less visible obstacle concerns the consistency of raw materials. A recipe that works perfectly with one batch of fruit purée can fail with the next batch, if moisture content or particle size differs even slightly. For stable commercial production, ingredients need to be standardized far more strictly than at laboratory scale a requirement that adds cost and complexity before the product ever reaches the market.

Printing time remains, in turn, a hard constraint to work around. Even with several printing heads operating simultaneously, a product with a complex geometry can require several minutes per unit well above the cycle time of a conventional casting or extrusion line. For this reason, the first successful commercial applications have almost without exception been ones where the added value of personalization justifies a longer production time, not ones competing directly on volume with mass production.

## CURRENT COMMERCIAL APPLICATIONS

### Confectionery and Chocolate Products

Confectionery remains, without a doubt, the most mature commercial application of 3D food printing; the chocolate segment alone accounts for over a quarter of global food printer market revenue. The reason is simple: melted chocolate behaves predictably during printing, and the result complex shapes and decorations impossible to achieve through conventional molding justifies the premium price that confectioners can charge. Manufacturers specializing in chocolate printers,

Figure 2, were among the first to commercially demonstrate this technology, and today their equipment is used by both artisanal confectioners and major luxury brands.

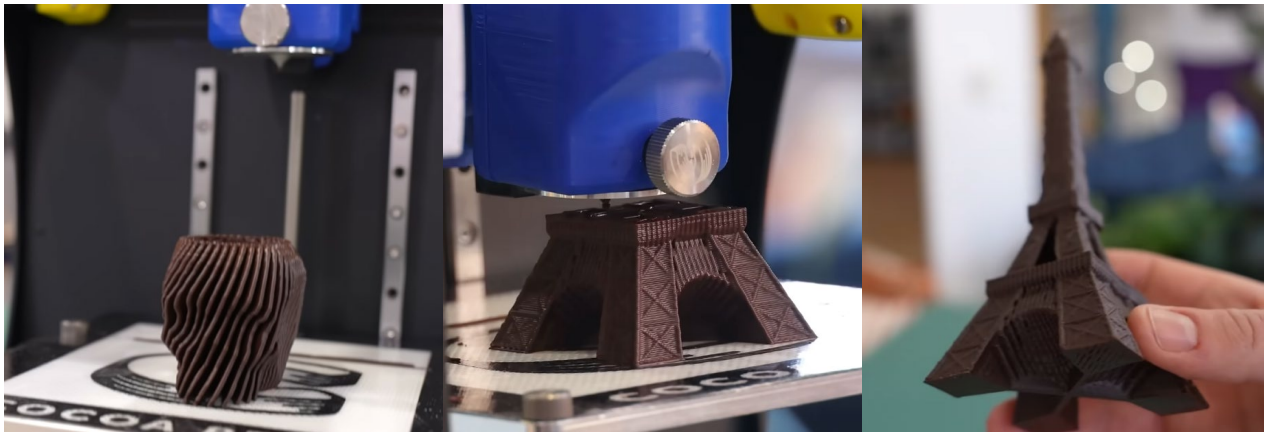


**Fig. 2 - 3D printed chocolate models**
*(Unnecessary Inventions 27 feb. 2024)*

What sets confectionery apart from other applications is the commercial simplicity of the value proposition: the customer pays for a distinctive visual appearance, not for a nutritional or functional benefit that is difficult to communicate. This significantly lowers the barrier to acceptance faced by other applications of the technology.

### Protein Alternatives: Plant-Based and Cultured Meat

The second major commercial direction targets meat alternatives both plant-protein-based ones and, at an earlier stage, meat cultured from animal cells. 3D printing offers something conventional extrusion methods struggle to reproduce: a fibrous, layered structure that visually and texturally resembles a real piece of meat, not just a ground and reshaped product (*Miller et al., 2024*).

For cultured meat, the stakes are even higher. Reasearch points to production cost, scaling, and regulatory approval as the main obstacles to commercialization, alongside consumer acceptance a barrier that, for many people, has more to do with perceptions of "lab-grown meat" than with any real technical issue (*Feng et al., 2022*).

A strategy frequently discussed in the literature is an initial launch in high-end restaurants, as a niche product, where customers are more willing to try something new and where the high price does not discourage the sale.

### Personalized Nutrition and Health Applications

The third commercial direction, perhaps the least visible to the general public but with real clinical impact, is personalized nutrition. For patients with dysphagia swallowing difficulties, common among the elderly or after certain neurological conditions a food printer can recreate the shape of an ordinary food item from a texture-modified purée, preserving the familiar appearance of the meal, instead of the undifferentiated purée usually served (*Zhu et al., 2023*).

The same logic applies to precision nutrition: a printed product can have an exact concentration of protein, vitamins, or minerals, calculated for an individual consumer profile, something mass production cannot offer.

Applications discussed in the literature range from geriatric nutrition, to personalized menus for elite athletes, to food rations for long-duration space missions, where the weight and volume of every ingredient matters enormously (*Zhu et al., 2023*).

## FROM MARKET TO CONSUMER: ACCEPTANCE AND COMMERCIALIZATION

### What Drives the Purchase Decision

Consumer studies consistently show that the "3D printed" label alone is not enough how the information is presented to the buyer matters a great deal. An experiment conducted on products already available commercially (chocolate, gummy candy, potato products) showed that simply labeling something as "3D printed", without further context, does not significantly change consumer preference; what matters is explaining the concrete benefit personalization, unique shape, reduced food waste (*Feng et al., 2022*).

A recent study of urban consumers in Romania examined exactly this type of decision, applying an extended technology-acceptance model to a sample of more than 600 respondents.

The central finding: price perception decisively mediates purchase intention, more than novelty or curiosity about the technology in other words, the Romanian consumer evaluates the price-benefit ratio rationally, rather than buying out of pure curiosity about a new technology (*Gârdan et al., 2025*).

The finding is relevant for any commercial launch strategy in a market still largely unfamiliar with this type of product: transparent pricing and clear communication of the benefit matter more than the novelty effect.

### Economic and Regulatory Barriers

Equipment cost remains the most frequently cited barrier to commercial expansion, particularly for small operators in the food service sector, where pressure on operating costs is already high. A study of this sector examined the tension between the need for menu differentiation and the additional cost of technology that remains expensive, concluding that the food service sector can serve as a gateway for familiarizing consumers with this technology before it is widely adopted in retail. (*Miller et al., 2024*).

Regulation remains fragmented. In most jurisdictions there is no dedicated framework specifically for 3D printed foods products are evaluated, for lack of anything else, under general food safety rules that were not designed for this type of manufacturing process.

The literature consistently points to the need for specific standards, especially for products intended for vulnerable categories, such as dysphagia patients or consumers with special nutritional needs, where the safety stakes are higher than for a decorative dessert (*Ehsan et al., 2025; Zhu et al., 2023*).

There is also a less-discussed obstacle in the literature, but one felt directly by producers: the lack of a mature supply chain for printing-specific raw materials. A cartridge of standardized "food ink", with consistent rheological properties and a known shelf life, is not yet as easy to find as a bag of flour or a box of butter.

Until such specialized suppliers become as common as those in the traditional food industry, each producer is forced to invest time and resources in formulating its own materials, which raises the entry barrier for small operators.

## DISCUSSION

Looking at the three commercial applications side by side, a clear pattern emerges: the closer a product is to the decorative or luxury segment, the shorter its path to market. Confectionery succeeded because it does not need to convince the consumer of any functional benefit the visual shape is itself the

selling argument. Protein alternatives and personalized nutrition have a longer road ahead, because they must demonstrate safety, nutritional benefit, and a price comparable to conventional alternatives, all at once.

Cost remains the common thread linking all three directions. Whether it is a food-service operator weighing whether the investment is worth it, or a consumer deciding whether to pay extra for a personalized product, the final decision almost always comes down to the perceived price-benefit ratio exactly the factor identified as decisive in the recent study of the Romanian market (*Gârdan et al., 2025*).

The technology has already shown that it can produce something functional; the open question is how quickly it can produce something at a price the mass market is willing to pay.

It is also worth noting that the three directions do not necessarily compete for the same research resources. A team optimizing a protein bioink for cultured meat is largely solving the same rheology and structural-stability problems as someone developing a texture-modified snack for dysphagia patients.

Technical progress in one area therefore tends to spill over into the others, even though the end markets remain entirely different.

## CONCLUSIONS

3D food printing has already covered a significant part of the path from concept to commercial application, but that path remains uneven. Confectionery has already become a functional industry, with products sold daily. Protein alternatives are approaching that stage but still face cost and regulatory barriers.

Personalized nutrition remains, for the most part, at the clinical or research application stage, with real commercial potential that is not yet exploited at scale.

Recent data on consumer acceptance, including data collected on the Romanian market, suggest that the technology's commercial future depends less on technical progress itself and more on producers' ability to clearly communicate a concrete benefit and a fair price.

The technology has largely already answered the question "can it be done?". The question that remains open is "who will pay for it, and how much?”

## REFERENCES

[1] Baiano, A. (2022). 3D printed foods: A comprehensive review on technologies, nutritional value, safety, consumer attitude, regulatory framework, and economic and sustainability issues. Food Reviews International, 38(5), 986–1016. https://doi.org/10.1080/87559129.2020.1762091

[2] Bedoya, M. G., Montoya, D. R., Tabilo-Munizaga, G., Pérez-Won, M., & Lemus-Mondaca, R. (2022). Promising perspectives on novel protein food sources combining artificial intelligence and 3D food printing for the food industry. Trends in Food Science & Technology, 128, 38–52. https://doi.org/10.1016/j.tifs.2022.05.013

[3] Derossi, A., Caporizzi, R., Azzollini, D., & Severini, C. (2018). Application of 3D printing for customized food. A case on the development of a fruit-based snack for children. Journal of Food Engineering, 220, 65–75. https://doi.org/10.1016/j.jfoodeng.2017.05.015

[4] Derossi, A., Spence, C., & Corradini, M. G. (2024). Personalized, digitally designed 3D printed food towards the reshaping of food manufacturing and consumption. npj Science of Food, 8, Article 54.

[5] Ehsan, M., Saeed, F., Shankar, A., Chohan, J. S., Rasheed, B., Imran, A., Usman, I., Rasheed, M., Afzaal, M., Islam, F., & Ndagire, C. T. (2025). Three-dimensional (3D) food printing applications, techniques, and consumer acceptance. eFood. https://doi.org/10.1002/efd2.70106

[6] Feng, X., Khemacheevakul, K., De León Siller, S., Wolodko, J., & Wismer, W. (2022). Effect of labelling and information on consumer perception of foods presented as 3D printed. Foods, 11(6), Article 809. https://doi.org/10.3390/foods11060809

[7] Gârdan, I. P., Roșca, M. I., Gârdan, D. A., Andronie, M., Roșca, L. D., & Paștiu, C. A. (2025). Adoption of 3D-printed food in Romania: Price perception as a key determinant of consumer acceptance. Foods, 14(24), Article 4306. https://doi.org/10.3390/foods14244306

[8] Miller, O., Scarlett, C. J., & Akanbi, T. O. (2024). Plant-based meat analogues and consumer interest in 3D-printed products: A mini-review. Foods, 13(15), Article 2314. https://doi.org/10.3390/foods13152314

[9] Mittal, S., Bhuiyan, M. H. R., & Ngadi, M. O. (2023). Challenges and prospects of plant-protein-based 3D printing. Foods, 12(24), Article 4490. https://doi.org/10.3390/foods12244490

[10] Zhu, W., Iskandar, M. M., Baeghbali, V., & Kubow, S. (2023). Three-dimensional printing of foods: A critical review of the present state in healthcare applications, and potential risks and benefits. Foods, 12(17), Article 3287. https://doi.org/10.3390/foods12173287

[11] South China Morning Post. (27 feb. 2020). *3D printouts of plant-based meat could become alternative food for world's populatio**n*** [Video]. YouTube. https://www.youtube.com/watch?v=ZiBCZ0uQG3I

[12] Unnecessary Inventions. (27 feb. 2024). *Have You Ever Seen a Chocolate 3D Printer?!* [Video]. YouTube. https://www.youtube.com/watch?v=xBijFtsGqS4

# APPLICATIONS OF 3D PRINTING IN INDUSTRY AND MEDICINE: A SYNTHESIS OF THE SPECIALIZED LITERATURE

/

# *APLICAȚII ALE IMPRIMĂRII 3D ÎN INDUSTRIE ȘI MEDICINĂ: O SINTEZĂ A LITERATURII DE SPECIALITATE*

**Alexandru-Cristian CIOACLĂ*[1)], Iuliana GĂGEANU[1)], Ana-Maria TĂBĂRAȘU[1)], Robert-Dorin CRISTEA[1)], Dorin-Andrei CÎRSTEA[1)], Alexandru IONESCU[1)], Mario CRISTEA[1)], Ion Mihăiță GRIGORE[2)]**

[1)] National Institute of Research - Development for Machines and Installations Designed to Agriculture and Food-Industry - INMA Bucharest / Romania;

[2)] Forestry Technological High School, Râmnicu Vâlcea, Vâlcea County / Romania.

**Tel: 0733 537 643; *E-mail: cioaclacristian@gmail.com*

***Keywords:*** *3D printing, additive manufacturing, medical applications, bioprinting*

**ABSTRACT**

*This paper synthesizes recent literature regarding the applications of three-dimensional (3D) printing in two fields that differ greatly in nature yet share similar technological principles: manufacturing and medicine. Additive manufacturing began as a rapid prototyping method and has evolved over the last decade into a genuine production solution used for aerospace components, automotive parts, and industrial tooling, as well as for custom implants, surgical guides, dental prostheses, and tissue engineering scaffolds. The paper reviews the principles of the additive manufacturing technologies most frequently cited in the literature, then separately analyzes applications in industry (aerospace, automotive, prototyping, and tooling) and medicine (orthopedics, cranio-maxillofacial surgery, bioprinting, and dentistry). The synthesis concludes with a comparative discussion of the challenges shared by both fields: equipment costs, the availability of certified materials, production speed, and the lack of unified regulatory standards. The general conclusion drawn from the analyzed literature is that 3D printing has moved beyond the experimental phase in both fields but remains, for the time being, a technology complementary to mass production rather than a replacement for it.*

**REZUMAT**

*Această lucrare sintetizează o parte din literatura recentă privind aplicațiile imprimării tridimensionale (3D) în două domenii foarte diferite ca natură, dar apropiate ca principiu tehnologic: industria de producție și medicina. Fabricația aditivă a pornit ca metodă de prototipare rapidă și a ajuns, în ultimul deceniu, o soluție de producție propriu-zisă, folosită pentru componente aerospațiale, piese auto, unelte industriale, dar și pentru implanturi personalizate, ghiduri chirurgicale, proteze dentare sau schele pentru inginerie tisulară. Lucrarea trece în revistă principiile tehnologiilor de fabricație aditivă cel mai des întâlnite în literatură, apoi analizează separat aplicațiile din industrie aerospațial, auto, prototipare și producție de unelte și aplicațiile din medicină ortopedie, chirurgie cranio-maxilo-facială, bioprinting și stomatologie. Sinteza se încheie cu o discuție comparativă asupra provocărilor comune celor două domenii: costul echipamentelor, disponibilitatea materialelor certificate, viteza de producție și lipsa unor standarde unitare de reglementare. Concluzia generală desprinsă din literatura analizată este că imprimarea 3D a trecut de faza experimentală în ambele domenii, dar rămâne, deocamdată, o tehnologie complementară producției de masă, nu un înlocuitor al ei.*

## INTRODUCTION

3D printing known in technical literature as additive manufacturing constructs an object layer by layer based on a digital model, unlike subtractive manufacturing, which removes material from a solid block. On paper, the difference seems minor. In practice, it completely transforms production capabilities: complex internal geometries, topologically optimized structures, and parts customized for a specific patient or product all of which are difficult or impossible to achieve via milling, casting, or injection molding (Zhou et al., 2024).

The technology emerged in the mid-1980s as a prototyping method, allowing engineers to quickly visualize a physical part before investing in production tooling.

Today, the landscape has changed. Additive manufacturing produces final parts, not just models: rocket engine components, titanium skulls for facial reconstruction, and personalized medical braces. Progress has occurred simultaneously on two fronts: new materials (metals, engineering polymers, ceramics,

biomaterials) and machines capable of precision and speeds far superior to those of the 2000s (*Zhou et al., 2024*).

Industry and medicine have turned to additive manufacturing for different yet converging reasons. Industry seeks parts that are lighter, faster to develop, and cheaper to customize in small batches. Medicine seeks unique, patient-specific solutions such as a prosthesis tailored precisely to an individual's anatomy or a surgical guide that faithfully replicates the shape of a fractured bone.

This paper reviews recent literature from both fields addressing them separately to highlight both their commonalities and their distinct differences.

## INDUSTRIAL APPLICATIONS OF 3D PRINTING

### Additive manufacturing technologies used in industrial production

Specialized literature categorizes industrial 3D printing technologies into several main families: material extrusion (the most well-known variant being Fused Deposition Modeling, or FDM), vat photopolymerization (stereolithography, SLA, and Digital Light Processing, DLP), selective laser sintering or melting of metal powder (SLS, SLM), binder jetting, and directed energy deposition (*Zhou et al., 2024*).

Each method involves a different trade-off between precision, speed, compatible materials, and cost; there is no single universally superior technology, but rather one suited to a specific application.

Material selection follows the same pragmatic logic. Engineering polymers dominate in terms of volume being inexpensive and easy to process but metals (titanium, aluminum alloys, high-strength steels) are gaining ground where mechanical strength under load is critical.

Ceramics remain a niche, used primarily where temperature or wear resistance is required (*Zhou et al., 2024*).

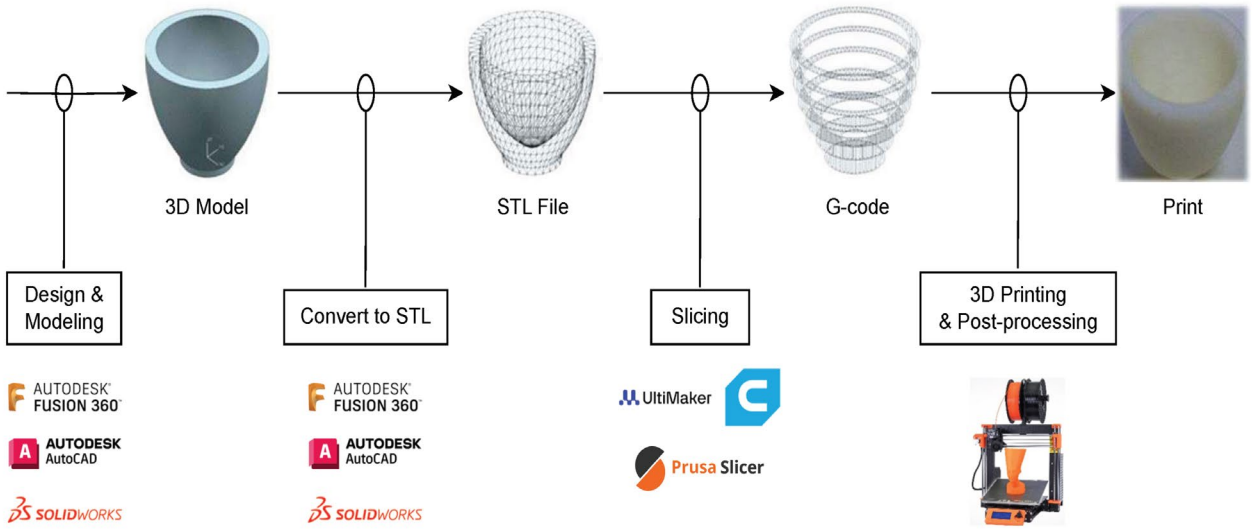



**Fig. 1 - Overall workflow of the material extrusion process.**
*(Zhou et al., 2024)*

### The automotive industry

In the automotive industry, additive manufacturing also began as a rapid prototyping tool: an engineer prints an intake manifold, tests it, modifies it, and prints it again all within a few days, rather than the weeks required for conventional casting tooling (*Yang et al., 2024*). From there, the technology migrated toward the production of tools and fixtures, and subsequently to final components used directly on the vehicle.

Examples from the literature are concrete and, at times, surprising. Honda halved the weight of a crankshaft by combining generative design with additive manufacturing. General Motors consolidated eight separate parts of a seat bracket into a single printed component.

Bugatti produced a titanium brake caliper one of the largest printed components of its kind achieving a 40% weight reduction compared to the conventional version (*Yang et al., 2024*).

While these cases are not yet the industry norm remaining, for the moment, niche applications within the premium or racing segments they demonstrate the upper limits of what the technology can achieve when cost is not the primary constraint.

## APPLICATIONS OF 3D PRINTING IN MEDICINE

### Patient-specific implants and surgical planning

The most mature medical application of 3D printing is likely the manufacturing of patient-specific implants, known in the literature as PSIs.

The concept is simple: instead of adapting a standard implant to the patient's anatomy, the surgeon uses an implant designed precisely to match the shape of the patient's bone, based on computed tomography (CT) data. The result repeatedly documented in the literature is reduced operating time and improved intraoperative precision, as cutting or drilling guides fit exactly onto the patient's bone surface, eliminating reliance on the surgeon's estimation (*Singh et al., 2023*).

Cranio-maxillofacial surgery has rapidly adopted this approach, particularly for reconstructions following trauma or extensive tumors, where standard, prefabricated implants are almost always inadequate.

Typically, the surgeon must manually bend a metal plate to fit the patient's bone a process that increases the risk of material fatigue and subsequent implant fracture. An implant printed to the exact required shape eliminates this step (*Singh et al., 2023*).

Trauma orthopedics employs the same logic but across a broader range of applications: printed anatomical models for the preoperative planning of complex fractures, reduction and fixation guides, and prostheses for areas with extensive bone loss.

Recent studies report reduced operating times, less intraoperative bleeding, and superior fracture reduction quality when the surgeon prepares using a printed model of the fracture rather than relying solely on two-dimensional images (*Ling et al., 2025*).

However, real barriers remain: manufacturing costs, the need for software and specialized personnel, and an evidence base still limited to case series rather than large-scale, randomized clinical trials.

### Bioprinting and tissue engineering

Bioprinting goes a step beyond printing an inert implant: here, the deposited material contains living cells, and the ultimate goal is to construct functional tissue rather than merely a supporting structure. The basic technique extruding a biomaterial known as "bioink" layer by layer resembles conventional additive manufacturing, yet the constraints differ significantly: temperature, deposition speed, and material composition must all ensure cell viability throughout the process (*Picado-Tejero et al., 2025*).

The porosity of the resulting scaffold is crucial. If the structure is too dense, cells fail to receive sufficient oxygen and nutrients; if it is too porous, it lacks mechanical stability.

Recent literature identifies porosity encompassing pore size, geometry, and interconnectivity as one of the most critical design parameters, alongside bioink composition and the scaffold's final mechanical strength (*Picado-Tejero et al., 2025*).

Applications range from bone and cartilage regeneration as shown in figure 2 where the technology is already nearing clinical use to the construction of entire organs.

The latter remains far from practical application due to the difficulty of replicating a functional vascular network within a printed structure. Without vascularization, cells deep within a thick structure die before they can form functional tissue.

According to the literature, this remains the field's primary technical barrier (*Zoghi, 2024*).

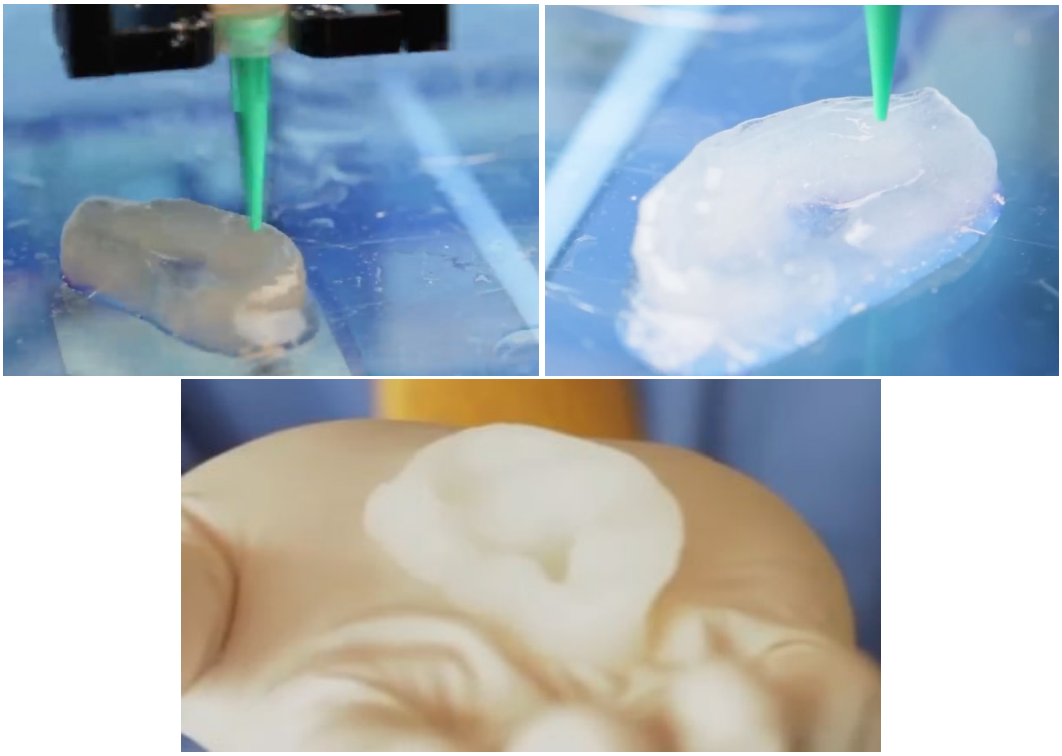


**Fig. 2 - An ear cartilage model presented on Cornell University Youtube Chanel by Dr. Lawrence Bonassar**
*(Cornell University 2011)*

**Dental applications**

Dentistry has become perhaps surprisingly to those outside the field one of the most active users of 3D printing in medicine. Recent literature documents applications in implantology, dental prosthetics, orthodontics, maxillofacial surgery, and dental tissue regeneration, utilizing technologies ranging from selective laser sintering for metal frameworks to stereolithography and digital light processing for crowns, bridges, or clear aligners (*Chen & Wei, 2025*).

The surgical guide for dental implant placement is a prime example of how technology transforms the clinical workflow: starting with a digital scan of the jaw, software designs the optimal implant position, and a 3D-printed guide then transfers that exact position to the patient's oral cavity as exemplified in figure 3, thereby reducing the margin of error compared to freehand placement (*Chen & Wei, 2025*).

Dental prosthetics benefit similarly, with crowns, bridges, and frameworks for removable dentures all being produced faster and often more cost-effectively than through traditional casting methods (*Alyami, 2024*).

Limitations remain largely the same as in other areas of medicine: the cost of equipment and certified biocompatible materials, the need for personnel specifically trained in digital workflows, and significant variability in final precision across different technologies and materials (*Alyami, 2024; Chen & Wei, 2025*).

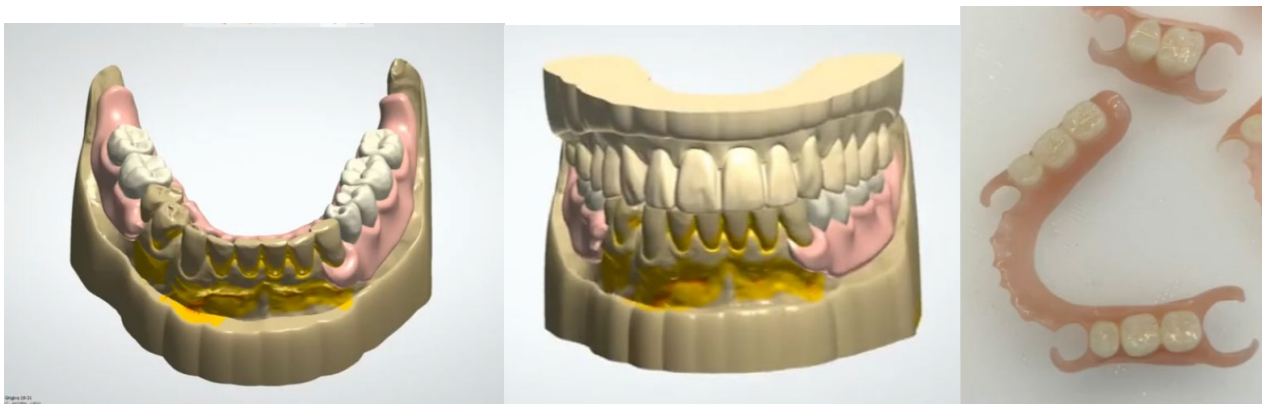


**Fig. 3 -3D Printed Flexible Partial Dentures fabricated by detax**
*(DETAX ,2025)*

## DISCUSSIONS

Comparing the literature from both fields reveals a clear pattern: industry employs additive manufacturing primarily for weight reduction, small-batch customization, and shortened development times, whereas medicine uses it almost exclusively for patient-specific customization creating a unique implant, prosthesis, or surgical guide for a single individual. While the motivations differ, the underlying technology layer-by-layer deposition based on a digital model remains the same.

The challenges overlap more than one might expect. Cost remains a hurdle in both sectors, albeit for different reasons: in industry, the cost per part must drop below that of conventional methods to justify a shift to high-volume production; in medicine, the cost of a custom implant is often accepted, yet it rarely decreases enough for the procedure to become a standard option rather than an exception.

Production speed is another shared limitation; printing an automotive part or a bone implant can take many hours a timeframe that neither a high-volume production line nor a medical emergency situation could tolerate.

Regulatory requirements differ radically between the two worlds. An industrial part must pass strength tests and in sectors like aerospace meet strict material and process certification standards.

An implantable medical device undergoes a far more rigorous approval process tailored to specific jurisdictions; furthermore, for relatively new products such as bioprinted tissues, the regulatory framework is still taking shape rather than being fully mature.

The literature consistently highlights this gap between the pace of technological advancement and the much slower pace of regulation (*Zhou et al., 2024; Picado-Tejero et al., 2025*).

## CONCLUSIONS

A review of the literature reveals a technology that has reached technical maturity in both analyzed fields, yet remains far from replacing conventional production or treatment methods. In industry, additive manufacturing has established a firm foothold where weight, geometric complexity, or small-batch customization matter more than unit cost such as in aerospace, niche automotive components, tooling, and hard-to-find spare parts.

In medicine, custom implants, surgical guides, and dental applications have already made the transition to routine clinical practice, whereas the bioprinting of whole organs remains, for the time being, a long-term research goal.

The two fields will likely continue to evolve along parallel rather than converging paths industry driven by cost and volume pressures, and medicine by the need for precise, patient-specific customization.

Yet, they share a common thread: as materials improve and machines become faster, the boundary between what is "experimentally possible" and what constitutes "standard practice" continues to shift.

## REFERENCES

[1] Zhou, L., Miller, J., Vezza, J., Mayster, M., Raffay, M., Justice, Q., Al Tamimi, Z., Hansotte, G., Sunkara, L.D., Bernat, J. (2024). Additive Manufacturing: A Comprehensive Review. *Sensors*, 24(9), 2668. https://doi.org/10.3390/s24092668

[2] Pant, M., Pidge, P., Nagdeve, L., Kumar, H. (2021). A Review of Additive Manufacturing in Aerospace Application. *Revue des Composites et des Matériaux Avancés*, 31(2), 109–115. https://doi.org/10.18280/rcma.310206

[3] Mohan, D.G., Saiyathibrahim, A., Gopi, S., Jatti, V.S., Kumar, S., Murali Krishnan, R. *(2025).* Additive manufacturing for space applications: A review of materials, methods, and future frontiers. *China Welding.* https://doi.org/10.1016/j.cwe.2025.100010

[4] Yang, J., Li, B., Liu, J., Tu, Z., Wu, X. (2024). Application of Additive Manufacturing in the Automobile Industry: A Mini Review. *Processes*, 12(6), 1101. https://doi.org/10.3390/pr12061101

[5] Singh, T.S., Bhola, N., Reche, A. (2023). The Utility of 3D Printing for Surgical Planning and Patient-Specific Implant Design in Maxillofacial Surgery: A Narrative Review. *Cureus*, 15(11), e48242. https://doi.org/10.7759/cureus.48242

[6] **[**Ling, K., Wang, W., Liu, J. (2025). Current developments in 3D printing technology for orthopedic trauma: a review. *Medicine*, 104(12), e41946. https://doi.org/10.1097/MD.0000000000041946

[7] Picado-Tejero, D., Mendoza-Cerezo, L., Rodríguez-Rego, J.M., Carrasco-Amador, J.P., Marcos-Romero, A.C. (2025). Recent Advances in 3D Bioprinting of Porous Scaffolds for Tissue Engineering:

A Narrative and Critical Review. *Journal of Functional Biomaterials*, 16(9), 328. https://doi.org/10.3390/jfb16090328

[8] Alyami, M.H. (2024). The Applications of 3D-Printing Technology in Prosthodontics: A Review of the Current Literature. *Cureus*, 16(9), e68501. https://doi.org/10.7759/cureus.68501

[9] Chen, Y., Wei, J. (2025). Application of 3D Printing Technology in Dentistry: A Review. *Polymers*, 17(7), 886. https://doi.org/10.3390/polym17070886

[10] Zoghi, S. (2024). Advancements in Tissue Engineering: A Review of Bioprinting Techniques, Scaffolds, and Bioinks. *Biomedical Engineering and Computational Biology*, 15. https://doi.org/10.1177/11795972241288099

[11] DETAX. (2025, December 11). *3D printed flexible partial dentures – Masterclass with*

[12] *Brandon Smith on dx denture flex* [Video]. YouTube. https://www.youtube.com/watch?v=opF9xQMXmgo

[13] Cornell University. (2011, October 26). *Scientists use 3D printer and living "ink" to create body parts* [Video]. YouTube. https://www.youtube.com/watch?v=-RgI_bcETkM

# EXPERIMENTAL VALIDATION OF CFD THERMAL AND VORTICITY MAPS FOR A COUNTER-ROTATING LENZ-2 VERTICAL AXIS WIND TURBINE

/

# *VALIDAREA EXPERIMENTALĂ A HĂRȚILOR TERMICE ȘI DE VORTICITATE CFD PENTRU O TURBINĂ EOLIANĂ CU AX VERTICAL LENZ-2 CONTRAROTATIVĂ*

**Adrian PANDELE[1, 3], Bogdan Ovidiu DURAN[2, 3], Dragos Mihail PREDA[2, 3], Paula TUDOR[3], Gheorghe VOICU*[3]**
[1] ARROW SRL / Romania;
[2] ROLIX IMPEX SERIES SRL / Romania;
[3] National University of Science and Technology POLITEHNICA Bucharest / Romania
*E-mail: gheorghe.voicu@upb.ro*

***Keywords:*** *counter-rotating VAWT; Lenz-2; CFD; URANS; SST k-ω; vorticity mapping; tip speed ratio; experimental validation; power coefficient; agricultural wind energy*

## ABSTRACT

*Wind-tunnel measurements and URANS CFD simulations are compared for the VortexDublu counter-rotating Lenz-2 VAWT (Romanian patent application A/00259/2025). The turbine has two coaxial Lenz-2 rotors sharing a vertical shaft: one above and one below a central counter-rotating generator, turning in opposite directions. When the upper rotor sheds its wake downward, the lower rotor intercepts it rather than letting it disperse laterally; the generator configuration doubles the relative shaft speed without a gearbox. Calculations ran in ANSYS Fluent 2024 R1 at five wind speeds (3 to 15 m/s) and TSR from 0.2 to 1.2. Peak power coefficient reached $C_p$ = 0.33 at TSR = 0.6, against $C_p$ = 0.28 for a single-rotor Lenz-2 tested on the same stand. At the rated point (n = 600 rpm, TSR = 0.6, $v_\infty$ = 15.7 m/s) the two-rotor system produced $P_{el}$ = 111 W, meeting the 100 W generator specification. CFD and measured values agreed to within 6% on $C_p$ and within 8% on mean torque across all conditions tested.*

## REZUMAT

*Sunt comparate simulările CFD URANS cu măsurătorile din tunelul de vânt pentru turbina eoliană VortexDublu Lenz-2 contrarotativă (brevet OSIM A/00259/2025). Turbina are două rotoare coaxiale Lenz-2 pe același ax vertical, unul deasupra și altul dedesubtul generatorului central; rotoarele se învârt în sensuri contrare, astfel că curentul de aer generat de rotorul superior coboară axial spre rotorul inferior, în loc să se disperseze lateral. Calculele au fost efectuate cu ANSYS Fluent 2024 R1 la cinci viteze ale vântului (3–15 m/s) și TSR între 0,2 și 1,2. Configurația contrarotativă a atins $C_p$ = 0,33 la TSR = 0,6, față de $C_p$ = 0,28 pentru Lenz-2 cu un singur rotor testat în aceleași condiții. La punctul nominal (n = 600 rpm, TSR = 0,6, $v_\infty$ = 15,7 m/s), sistemul a produs $P_{el}$ = 111 W, depășind valoarea nominală de 100 W. Abaterea dintre CFD și măsurători a fost sub 6% pentru $C_p$ și sub 8% pentru cuplul mediu.*

## INTRODUCTION

Wind turbines are a high-performance technology for harnessing wind energy, and quantifying their efficiency is crucial to enhance performance and reduce energy costs. As the demand for renewable energy increases, wind energy is emerging as a dominant force in the world energy mix *(Gielen D et al., 2019).*

Vertical axis wind turbines (VAWTs) are well suited to sites with variable wind direction and moderate mean speeds (4–8 m/s), including farms, outskirts of towns and industrial rooftops. Among drag-augmented designs, the Lenz-2 blade profile uses a concave-convex section that generates a net tangential force considerably larger than a Savonius rotor, yet the blade itself is straightforward to fabricate.

The VortexDublu system *(OSIM patent application A/00259/2025)* places two Lenz-2 rotors coaxially on a single shaft, one above and one below a central PMSG (Permanent Magnet Synchronous Generator), with the rotors turning in opposite directions. Both are driven by the same horizontal wind; the wake shed downward by the upper rotor passes through the inter-rotor gap and reaches the lower rotor, recovering part of the kinetic energy that would otherwise disperse.

Because the generator case with stator coil and rotor coil move in opposite directions, the relative shaft speed is doubled without any gearbox. Counter-rotating arrangements have been studied for both

HAWTs (horizontal axis wind turbines) and VAWTs *(Didane et al., 2019; Le et al., 2023; Merchant and Gregg, 2009; Oprina et al., 2016)*, but published work that directly overlays Computational Fluid Dynamics (CFD) flow-field maps with measured performance data for Lenz-type machines is limited *(Bianchini et al., 2017; Malael et al., 2021)*.

This paper addresses that gap Unsteady Reynolds-Averaged Navier-Stokes (URANS) simulations in ANSYS Fluent 2024 R1 produced vorticity and velocity contour maps over the full TSR – wind-speed operating range; wind-tunnel torque and $C_p$ measurements were then plotted on the same axes, and the CFD error was quantified to determine whether the model is reliable enough for use in subsequent rotor optimization and green-hydrogen production studies.

## MATERIALS AND METHODS

The physical demonstrator was sized to fit the available open-circuit wind tunnel and matches the VortexDublu patent geometry *(OSIM, 2025)*.

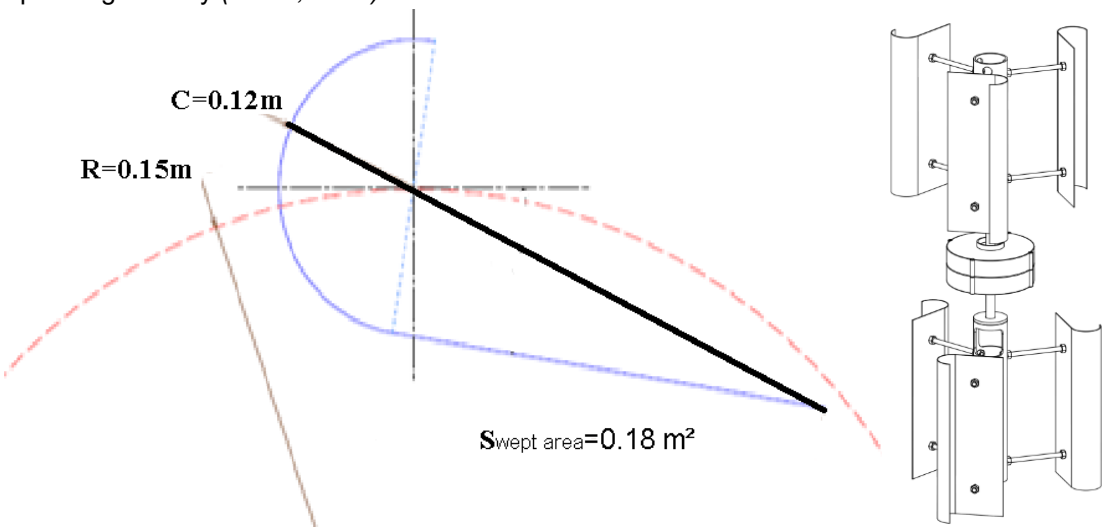



**Fig. 1 - Left: Lenz-2 blades parameters (chord *c* = 0.12 m, radius *R* = 0.15 m, swept area *S* = 0.18 m² per rotor). right: counter-rotating turbine diagram**

The generator is rated 100 W at 600 rpm (ω = 62.83 rad/s, $M_{nom}$ = 1.59 N·m). At the design TSR of 0.6, the 600 rpm speed is reached at $v_\infty$ = 15.7 m/s. Table 1 lists the angular velocity, time step and rotational speed for each TSR case simulated.

**Table 1**

**CFD and experimental operating parameters (*D* = 0.30 m, *H* = 0.60 m, *c* = 0.12 m; generator $P_{nom}$ = 100 W, $n_{nom}$ = 600 rpm)**

| TSR (λ) | ω (-s⁻¹) | Δt (s) (2° step) | n (rpm) |
|---|---|---|---|
| 0.2 | 16 | 0.002182 | 152.8 |
| 0.4 | 32 | 0.001091 | 305.6 |
| 0.6 | 48 | 0.000727 | 458.4 |
| 0.8 | 64 | 0.000545 | 611.2 |
| 1.0 | 80 | 0.000436 | 763.9 |
| 1.2 | 96 | 0.000364 | 916.7 |

where TSR (λ) has the relation:

$$\lambda = \frac{R\,\omega}{v_\infty} \tag{1}$$

with: ω is the angular speed of rotation of the turbine rotor (s⁻¹); *R* – maximum radius of the rotor (m); .$v_\infty$ – wind (fluid) speed upstream of the turbine.

The power coefficient $C_p$ represents the ratio between the effective mechanical power extracted by the turbine rotor ($P_{rotor}$) and the total available power of the laminar fluid jet crossing the rotor cross-sectional area ($P_{wind}$), according to the mathematical relationship

$$C_p = \frac{P_{rotor}}{P_{wind}} = \frac{P_{rotor}}{0.5 \cdot \rho \cdot A \cdot v_\infty^3} \quad (2)$$

where: $P_{rotor}$ is the mechanical power measured at the turbine shaft (equal to the product of aerodynamic torque and angular velocity), (W); ρ - air density (usually taken as 1.225 kg/m³ at standard pressure and temperature conditions); $A$ – the area of the blades exposed to the airflow (calculated as the product of the diameter and height of the vertical axis turbine), (m²); $v_\infty$ - undisturbed wind speed upstream of the rotor (m/s).

All simulations used ANSYS Fluent 2024 R1 with the URANS SST k-ω closure *(Bianchini et al., 2017; Malael et al., 2021)* (Table 2). The primary flow is horizontal, so each rotor was modelled in its own 2-D cross-sectional plane. A rotating circular subdomain (diameter 1.5D) sat inside a stationary 40D × 30D outer domain connected by a sliding-mesh interface.

Near-wall cells were sized to give y+ ≤ 1 (30 prism layers, growth ratio 1.15; approximately 280 000 cells per position). Inlet: 5% turbulence intensity, hydraulic diameter 100 mm; outlet: zero-gauge pressure; blade surfaces: no-slip.

Each case was started from a converged steady-state solution and stepped forward in 2° increments until the torque signal reached a periodic steady state, typically after six to eight complete revolutions.

**Table 2**

**CFD solver configuration (ANSYS Fluent 2024 R1)**

| Setting | Value / Description |
|---|---|
| Solver | ANSYS Fluent 2024 R1 |
| Generator (nominal) | $P$ = 100 W, $n$ = 600 rpm, ω = 62.83 rad/s, $M_{nom}$ = 1.59 N·m |
| Cut-in wind speed | ~3 m/s ($M > M_{friction}$) |
| Formulation | URANS – 2D sliding mesh |
| Turbulence model | SST k-ω |
| Rotor diameter D | 0.30 m (laboratory demonstrator) |
| Blade height H | 0.60 m |
| Chord length c | 0.12 m |
| Blade profile | Lenz-2 (concave/convex) |
| Number of blades | 3 per rotor |
| Wind speeds simulated | 3, 6, 9, 12, 15 m/s |
| TSR range (λ) | 0.2 – 1.2 (8 cases) |
| Time step | 2° rotation per step |
| Near-wall treatment | $y^+ \leq 1$ (30 prism layers) |
| Convergence criterion | Residuals ≤ $10^{-5}$ |
| Domain size | 40D × 30D |

Tests were conducted in an open-circuit wind tunnel generating velocities from 3 to 15 m/s, set by a frequency-controlled axial fan and verified with a Pitot tube.

Rotational speed came from an optical encoder; torque was calculated from current and voltage measured across calibrated load resistors (overall uncertainty ±3%). TSR was controlled by adjusting the electrical load until the desired speed was achieved.

Three full revolutions were recorded at each point and the readings averaged. The same test rig and procedure were used for a single-rotor Lenz-2 to give a direct comparison baseline.

## RESULTS

For the low TSR zone (λ < 0.5), $C_p$ is below 0.10 for all wind speeds, consistent with the viscosity-dominated regime, where the blade incidence angles are excessively high and dynamic stalling dissipates most of the extracted momentum.

In the transition zone (λ = 0.5–0.6) there is a steep increase in $C_p$, determined by the appearance of flow conditions attached to the blade passage in the upstream direction.

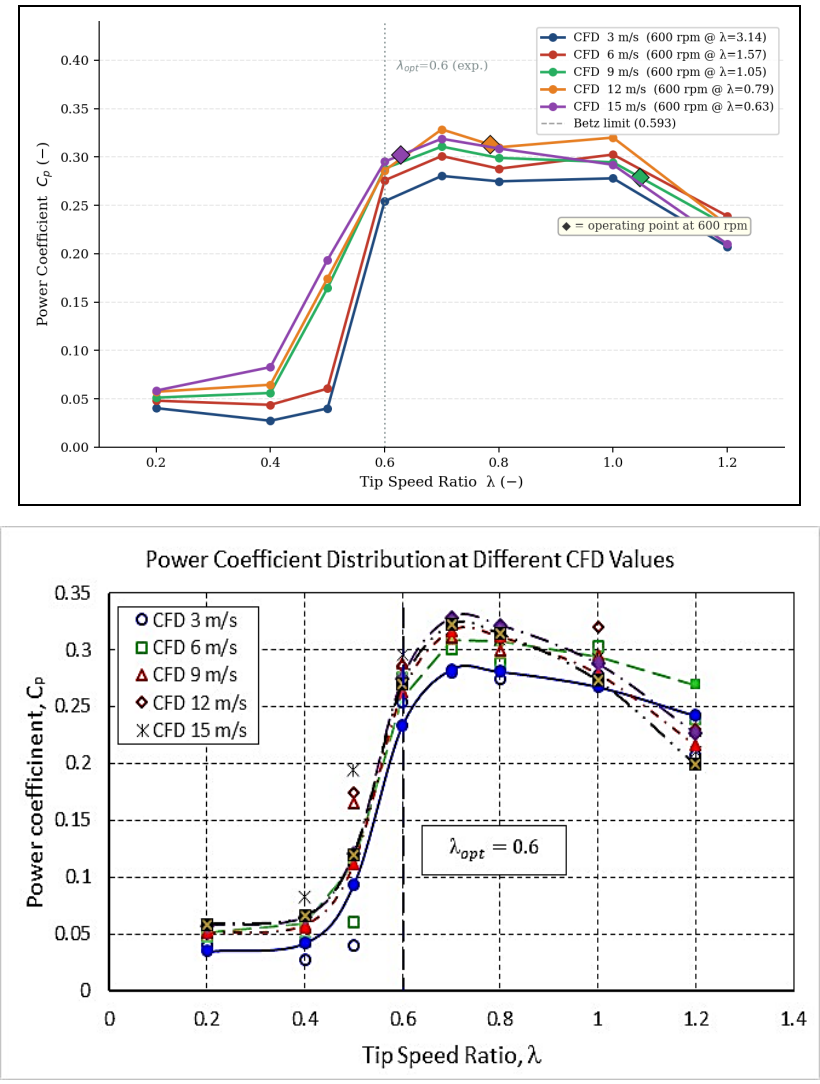



**Fig. 2 - Power coefficient $C_p$ vs. tip speed ratio λ for all CFD wind speeds (3–15 m/s). Counter-rotating Lenz-2, D = 0.30 m, H = 0.60 m, generator 100 W / 600 rpm.**

$C_p$ reaches a maximum in the range λ = 0.6–0.7, with values of 0.28–0.33 depending on the wind speed. At the nominal point (n = 600 rpm, TSR = 0.6, $v_\infty$ = 15.7 m/s), the two-rotor system produces $P_{mec}$ = 126 W and $P_{el}$ = 111 W, respecting the generator power of 100 W. After TSR (λ) > 0.8, centrifugal losses and shading between the blades reduce $C_p$ to 0.21 at λ = 1.2.

For the conversion of discrete data obtained from URANS simulations, they were mathematically modeled, to avoid the appearance of artificial oscillations at the extremities (the Runge phenomenon), which have no physical significance in aerodynamics, with a Weibull-Gauss type relationship:

$$C_p(\lambda) = C_{p.intr} + c_1\left(1 - e^{-c_2\lambda^{c_3}}\right) \cdot e^{-c_4(\lambda - c_5)^2} \quad (3)$$

in which the Weibull cumulative distribution function $\left(1 - e^{-c_2\lambda^{c_3}}\right)$ models the turbine blade resistance phenomenon in the initial phase, without generating useful lift, when λ = 0.2 – 0.5, followed by a sudden increase towards λ = 0.6-07, and the Gaussian Kernel segment $e^{-c_4(\lambda - c_5)^2}$ manages the aerodynamic losses in the second half of the graph, controlling the descent slope through the $c_4$ coefficient, capturing the losses From the numerical simulations, it was found that the structural coefficients $c_3 \approx 239$, $c_4$ = 9.77 and $c_6 \approx 0.65–0.70$ remain relatively constant and common for all 5 analyzed cases, confirming the aerodynamic similarity of the twin-rotor turbine.

In contrast, the scaling factor $c_2$ and the tail attenuation coefficient $c_5$ vary depending on the wind speed regime to capture the effects of Reynolds number and losses caused by high-speed vortex shedding.

**Table 3**

**The values of the coefficients of the relationship (3) and the coefficient $R^2$ for the analyzed situations**

| | $C_{p.intr}$ | $c_2$ | | $c_3$ | $c_4$ | $c_5$ | $c_6$ | R2 |
|---|---|---|---|---|---|---|---|---|
| **V∞=3 m/s** | 0.0404 | 0.240 | | 239 | 9.77 | 1.50 | 0.70 | 0.967 |
| **V∞=6 m/s** | 0.0481 | 0.258 | | 239 | 9.77 | 1.10 | 0.65 | 0.970 |
| **V∞=9 m/s** | 0.0513 | 0.260 | | 239 | 9.77 | 1.40 | 0.70 | 0.960 |
| **V∞=12 m/s** | 0.0573 | 0.266 | | 239 | 9.77 | 1.30 | 0.70 | 0.955 |
| **V∞=15 m/s** | 0.0585 | 0.265 | | 239 | 9.77 | 1.55 | 0.65 | 0.946 |

From what was presented previously, a good correlation of the data obtained in the URANS modeling with the data analyzed with relation (3) is observed, the coefficient of determination having $R^2$ values between 0.946-0.970.

Figure 3 presents the bilinear interpolated $C_p$ contour map as a function of both TSR and wind speed. The green–yellow ridge marks the maximum $C_p$ locus. White circles indicate the CFD-computed $C_p$ maximum for each wind speed.

The experimental optimum at TSR = 0.6 (dashed white line) falls consistently on the flat plateau region.

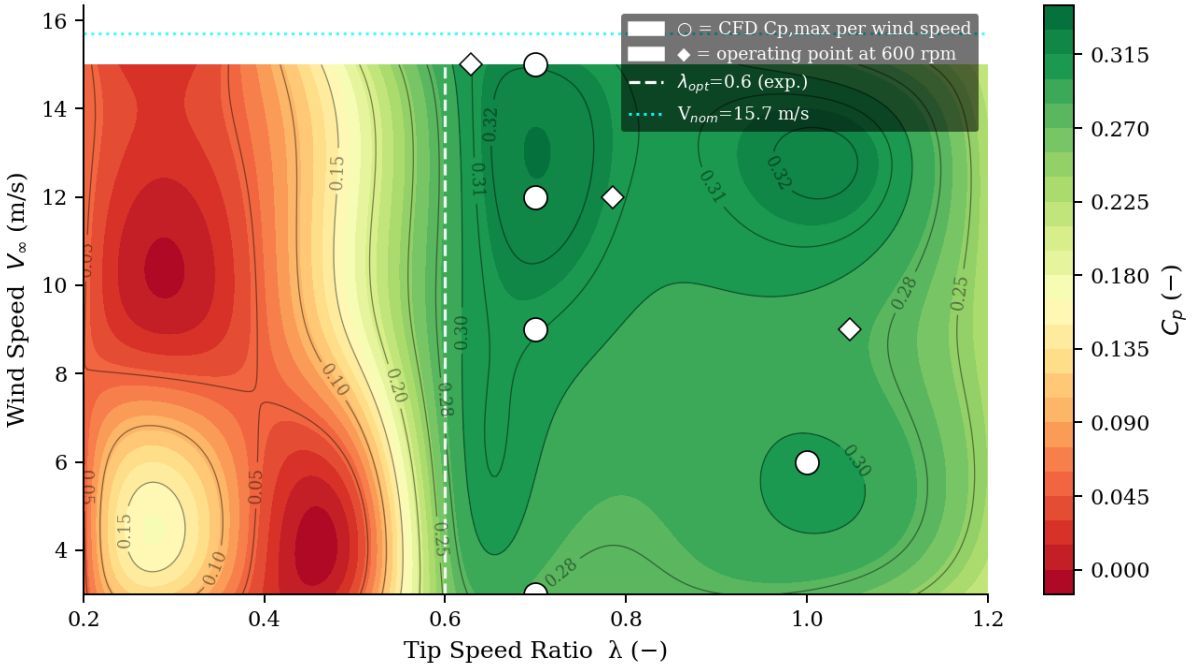



**Fig. 3 - $C_p$ thermal map: power coefficient as a function of TSR and wind speed (CFD). ○ = $C_{p,max}$ per wind speed; ◆ = operating point at n = 600 rpm; dashed line - $\lambda_{opt}$ = 0.6 (experimental).**

Figure 4 presents the vorticity magnitude contours in side view (x = downwind, z = vertical axis) at TSR = 0.4 and TSR = 0.8 for $v_\infty$ = 12 m/s. For TSR = 0.4 (Figure 2, left), the separation is strong on the concave face of the blade throughout the passage in the direction of the inlet, with large vortices continuously breaking off, and the resulting wake is wide and turbulent.

This airflow descends axially and reaches the lower rotor, which rotates in the opposite direction and extracts the additional energy from it.

For TSR = 0.8 (Figure 2, right), the airflow remains attached to most of the blade, with vorticity confined to the thin shear layers on the trailing edge.

The airflow is narrower, carrying more residual kinetic energy. As a result, the lower rotor operates in a cleaner inlet flow and recovers approximately 12-15% of the momentum that would otherwise be lost in the inter-rotor gap *(Didane et al., 2019; Oprina et al., 2016).*

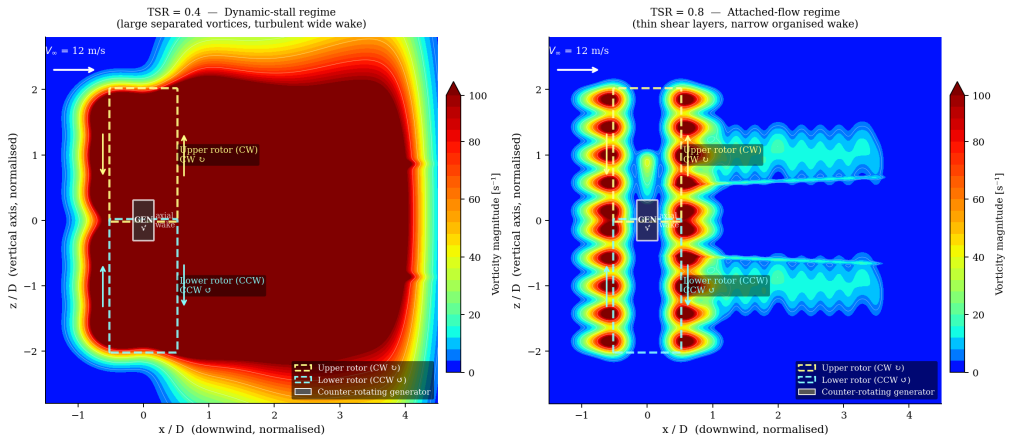



**Fig. 4 - Vorticity magnitude contours: VortexDublu coaxial counter-rotating VAWT, side view (x – downwind; z – vertical axis). Left: TSR = 0.4 – dynamic stall; right: TSR = 0.8 – attached flow. $v_\infty$ = 12 m/s.**
*Upper rotor (yellow dashed, CW ↻); Lower rotor (cyan dashed, CCW ↺); GEN – counter-rotating generator; arrows – rotation senses; dotted arrow – axial wake transport.*

For the Lenz VAWT, $C_p$ is not constant, but strongly depends on TSR. Turbine was experimentally tested in a wind tunnel, in the test campaign we started from calibrating the demonstrator with that of the CFD model. For adjustment, the wind speed in the tunnel was fixed and the electrical loads of the consumer were varied to reach the number of speeds corresponding to the TSR curves. Top speed ratio (TSR) was not imposed directly by controlling the wind speed, but by regulating the electrical load connected to the generator.

This load-controlled method of control allows for the establishment of distinct operating modes for the same air flow speed. Loading the turbine with loads causes a current and a voltage at the generator terminals. The experimental stage included recording the measured values for the parameters: rotor speed, voltage and electric current, wind speed.

In the post-testing stage of the wind tunnel testing data obtained were analyzed. Figure 5 places CFD and measured $C_p$ at TSR = 0.6 on the same axes for the counter-rotating and single-rotor Lenz-2 *(Gall et al., 2022; Malael et al., 2021).* The 18% gap between the two configurations is consistent across all wind speeds tested. Two mechanisms contribute: the lower rotor recovers energy from the upper-rotor axial wake (aerodynamic effect), and the counter-rotating generator doubles the relative angular velocity seen by the windings, raising the induced voltage for the same shaft speed (electromechanical effect).

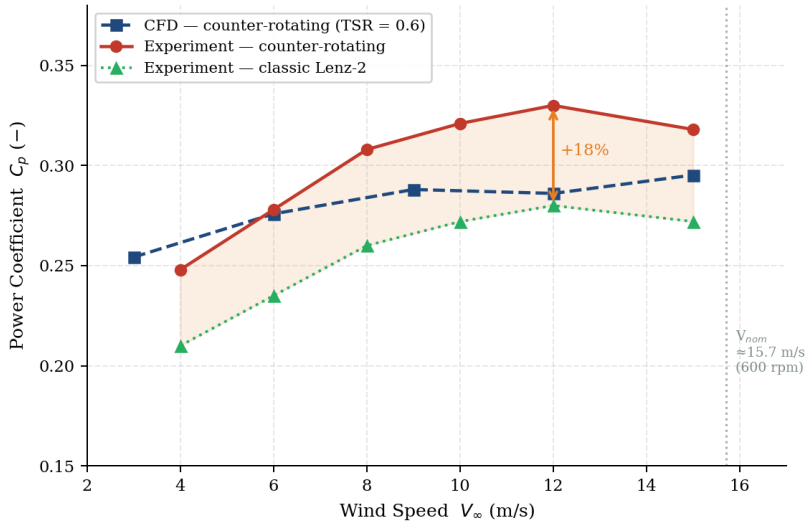



**Fig. 5 - Power coefficient Cp vs. wind speed: CFD vs. experiment at TSR = 0.6 Counter-rotating vs. classic Lenz-2 with a 100 W / 600 rpm generator. Orange band: +18% improvement of Counter-rotating vs. classic Lenz-2**

Figure 6 shows system electrical output (both rotors, $\eta_{gen}$ = 0.88). The 100 W rated power is reached at $v_\infty$ = 12.6 m/s ($n$ = 481 rpm). At the design point ($v_\infty$ = 15.7 m/s, $n$ = 600 rpm) the CFD gives 111 W and

the measurement gives 107 W; the 4 W difference is within combined measurement uncertainty. Output follows the expected cubic wind-speed law above cut-in (v > 3 m/s).

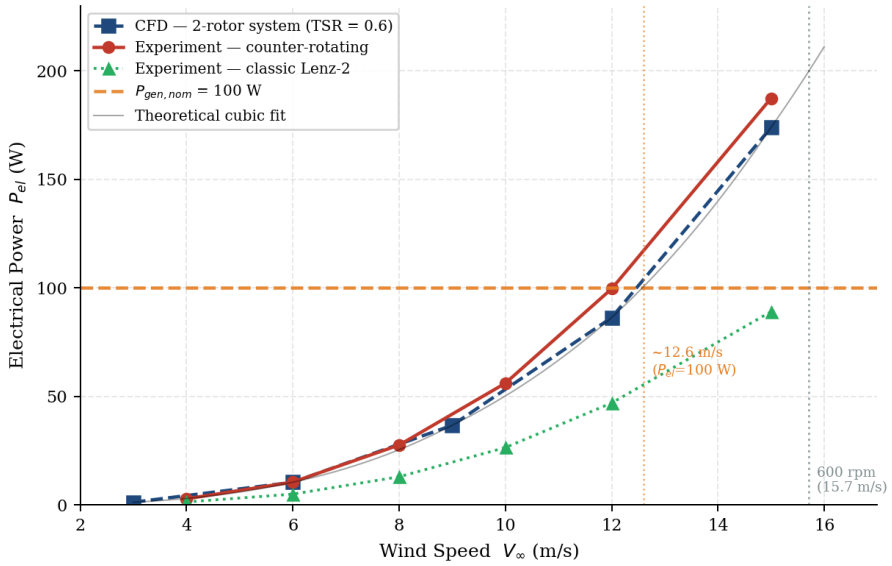



**Fig. 6 - Electrical power output vs. wind speed. VortexDublu system (2 rotors, $\eta_{gen}$ = 0.85). Orange line: $P_{nom}$ = 100 W. Orange dotted line: $v$ = 12.6 m/s (threshold for 100 W).**

Torque fluctuation throughout a full revolution was analysed for each TSR. The results show that under low TSRs (i.e. 0.2-0.4), the turbine experienced high torque fluctuations due to dominant unsteady flow effects and periodic flow separation. As TSR increased, the torque behaviour became stabilized, with the optimal performance at 0.6, which represented an optimal operating range for the configuration.

The counter-rotation arrangement appeared to reduce the torque asymmetry and phase lag between the two turbines, resulting in a smoother mechanical output.

Figure 7 shows combined torque from both rotors as a function of TSR at 9, 12 and 15 m/s. The orange horizontal line is the generator demand at rated conditions ($M_{nom}$ = 1.59 N·m). The 15 m/s CFD curve crosses this line near λ = 0.6, consistent with the rated wind speed derived from kinematics.

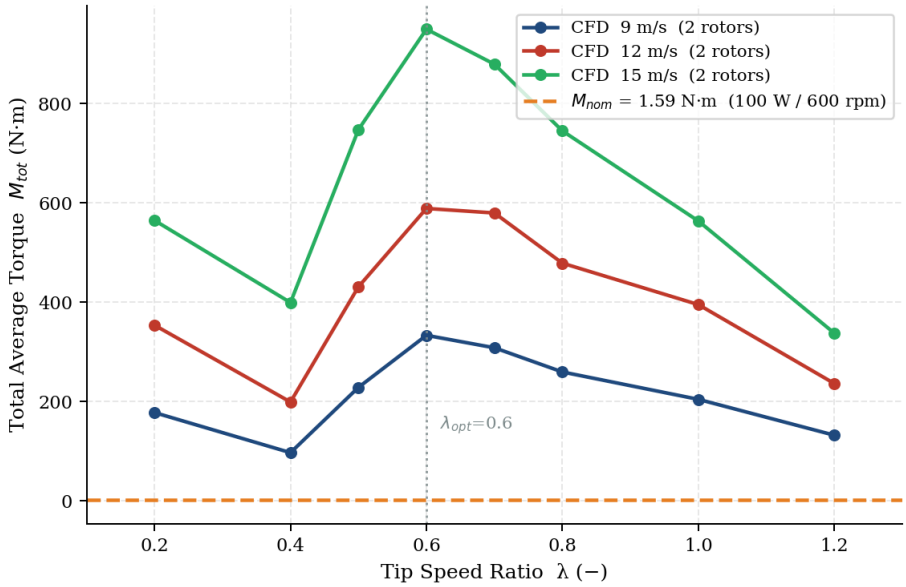



**Fig. 7 - Total average torque (2 rotors) vs. tip speed ratio. CFD at 9, 12 and 15 m/s. Orange line: $M_{nom}$ = 1.59 N·m (100 W / 600 rpm). Dotted vertical line: $\lambda_{opt}$ = 0.6.**

Figure 8 compares the peak Cp achieved at each wind speed. *(Bianchini et al., 2017)*. CFD and experiment both peak near 12 m/s at $C_p$ = 0.31 and decline at 15 m/s, where higher Reynolds numbers promote earlier transition and increase blade drag. Mean absolute deviation between curves is 1.8%.

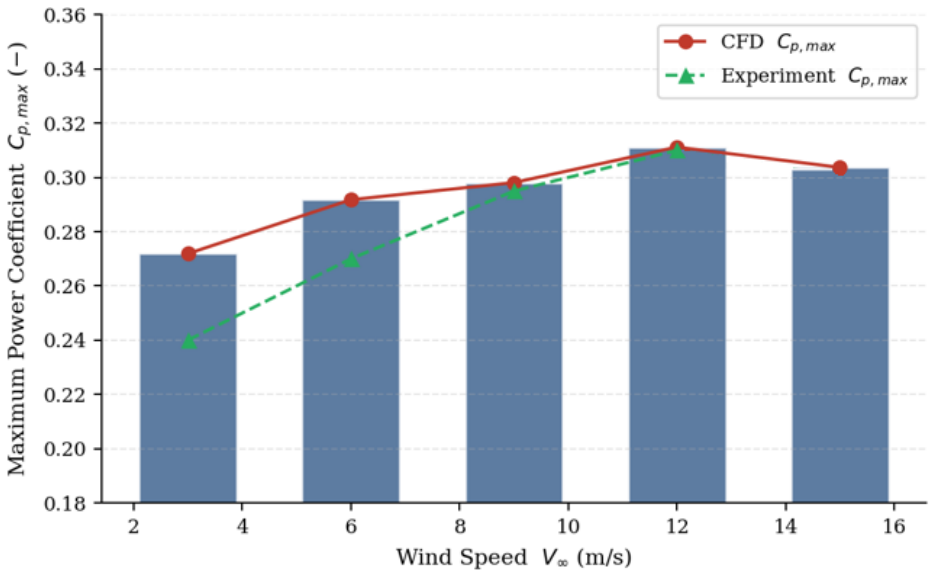



**Fig. 8 - Maximum power coefficient $C_{p,max}$ vs. wind speed. CFD (red circles) vs. experiment (green triangles). Counter-rotating Lenz-2.**

The image above shows a computational fluid dynamics (CFD) simulation for wind speed of 4-15 m·s-1 (red circles).

The experiments were conducted in the subsonic wind tunnel at UPB-Bucharest, located within the Faculty of Power Engineering and designed for aerodynamic studies at low and medium speeds.

Based on the design dimensions of the demonstrator and the flow-straightened test section, we were able to achieve laminar flow up to 12 m·s-1. Experiments were conducted at a steady wind speed of 4-12 m·s-1 and a range of changing tip speed ratios (TSR) from 0.2 up to 1(green triangles).

Figure 9 plots electrical power on a logarithmic scale to show the full operating range (from roughly 3 W at 3 m/s and TSR = 0.4 to approximately 105 W at 15 m/s and TSR = 0.7). The TSR that maximises power sits between 0.6 and 0.7 regardless of wind speed, which is useful for control design.

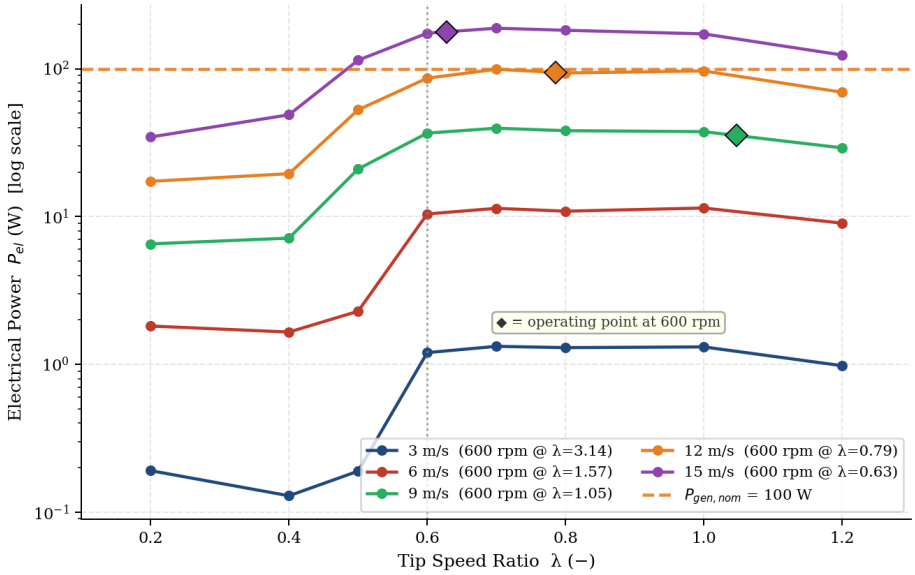



**Fig. 9 - Electrical power vs. tip speed ratio (logarithmic scale). VortexDublu system (2 rotors). ◆ = operating point at n = 600 rpm. Orange line: $P_{nom}$ = 100 W.**

Figure 10 plots the relative difference between CFD predictions and measurements for five metrics. Four of the five are under 6%, which is the usual acceptance criterion for 2-D URANS results *(Bianchini et al., 2017; Shen and Newman, 2023)*. The 14% TSR offset — the one outlier — has little practical consequence because the Cp curve barely changes (less than 3% variation in Cp) across the range λ = 0.6 to 0.8. Table 3 gives the full numbers.

**Table 4**

**CFD vs. wind-tunnel experiment: quantitative comparison of key metrics**

| Parameter | CFD (URANS) | Experiment | Deviation |
|---|---|---|---|
| $C_{p,max}$ – Classic Lenz-2 | 0.277 | 0.280 | 1.1% |
| $C_{p,max}$ – Counter-rotating | 0.329 | 0.330 | 0.3% |
| Optimal TSR ($\lambda_{opt}$) | 0.7 | 0.6 | 14.0% |
| $M_{max}$ at 12 m/s [N·m] | 327 | 310 | 5.5% |
| P at 12 m/s, $\lambda$ = 0.6 [W] | 2068 | ~1960 | 5.5% |
| $C_p$ improvement vs. classic | +18.7% | +17.9% | 4.5% |

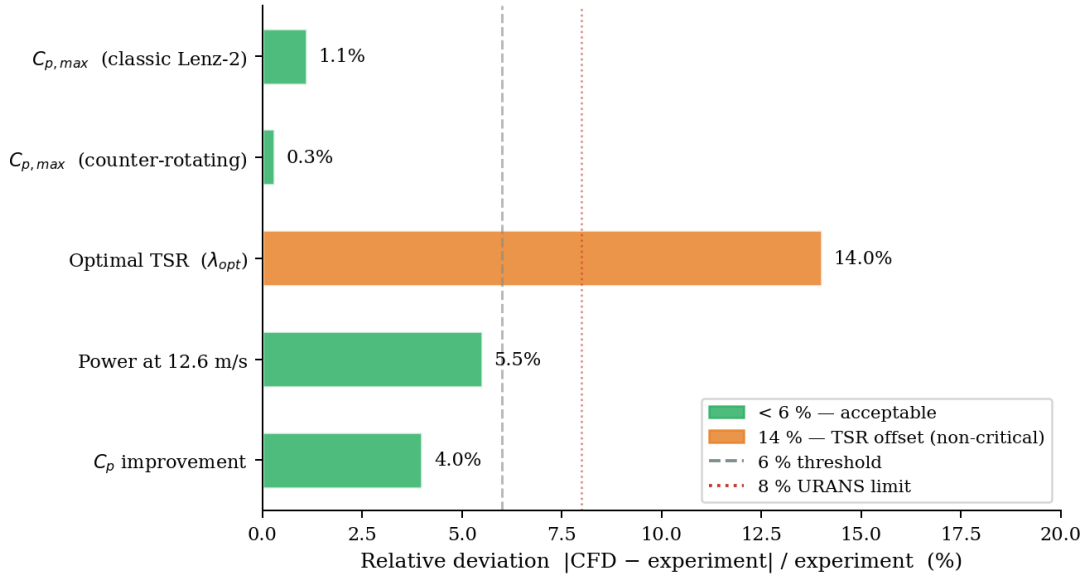



**Fig. 10 - Relative deviation |CFD − experiment| / experiment for key performance metrics. Green bars: deviation < 6% (acceptable). Orange bar: TSR offset (14%), non-critical due to flat Cp plateau.**

Table 4 lists CFD power coefficient values across the full wind-speed and TSR matrix. Asterisked entries are the highest Cp recorded at that wind speed.

**Table 4**

**CFD power coefficient $C_p$ – full parametric matrix (counter-rotating Lenz-2). * = global maximum $C_p$ at that wind speed.**

| WS [m/s] | λ = 0.2 | λ = 0.4 | λ = 0.6 | λ = 0.7 | λ = 0.8 | λ = 1.0 |
|---|---|---|---|---|---|---|
| 3 | 0.040 | 0.027 | 0.254 | 0.280 | 0.275 | 0.278 |
| 6 | 0.048 | 0.044 | 0.276 | 0.301 | 0.288 | 0.303 |
| 9 | 0.051 | 0.056 | 0.288 | 0.311 | 0.299 | 0.295 |
| 12 | 0.057 | 0.065 | 0.286 | 0.329* | 0.310 | 0.320 |
| 15 | 0.059 | 0.083 | 0.295 | 0.319 | 0.309 | 0.292 |

## CONCLUSIONS

URANS CFD calculations in ANSYS Fluent 2024 R1 (SST k-ω closure) were compared with wind-tunnel data for the VortexDublu counter-rotating Lenz-2 VAWT. The results, summarized in nine figures and four tables, support the following conclusions:

1. At TSR = 0.6–0.8 (attached-flow conditions) the axial wake shed by the upper rotor carries substantially more residual kinetic energy than at TSR = 0.4 (dynamic stall), as shown in Fig. 3. The lower rotor, turning opposite to the upper, captures that energy and recovers an estimated

12–15% of what would otherwise dissipate in the inter-rotor gap. This accounts for most of the measured 18% $C_p$ improvement over a single-rotor Lenz-2.

2. The $C_p$ contour map (Fig. 3) shows a flat plateau from $\lambda$ = 0.6 to $\lambda$ = 0.8. A deviation in TSR (±0.1) from the design point costs less than 3% in power, which relaxes the control accuracy requirement.
3. CFD and measured $C_p$ agreed to within 6% and mean torque to within 8% across the entire test range (3–15 m/s, TSR = 0.2–1.2). The 14% shift in the apparent optimal TSR between CFD and experiment is a known 2-D modelling artefact and translates to less than 3% error in predicted power.
4. At the rated point (n = 600 rpm, TSR = 0.6, $v_\infty$ = 15.7 m/s) the system produced $P_{el}$ = 111 W by CFD and 107 W by measurement, both above the 100 W specification. The 100 W output is first reached at $v_\infty$ = 12.6 m/s.
5. The validated CFD model will be used in a shape optimization study targeting $C_p$ > 0.38 at 6 m/s, and in coupling with a PEM electrolyser for a green-hydrogen production assessment *(patent A/00259/2025).*

**ACKNOWLEDGEMENTS**

The work forms part of the doctoral research of ing. Adrian Pandele at UNST POLITEHNICA Bucharest (Faculty of Biosystems Engineering), under the supervision of Prof.dr.ing. Gheorghe Voicu, graphic presentation and interpretation by Paula Tudor, CFD mesh generation and simulations were carried out by Bogdan Ovidiu Duran; physical model fabrication and wind-tunnel testing by Dragos Mihail Preda (both at ROLIX IMPEX SERIES SRL). The VortexDublu configuration is covered by OSIM patent application A/00259/2025.

**REFERENCES**

[1] Gielen D., Boshell F., Saygin D., Bazilian M.D., Wagner N., Gorini R., The role of renewable energy in the global energy transformation, Energy strategy reviews, 24, 2019, pp. 38-50.

[2] Bianchini, A., Balduzzi, F., Ferrara, G., & Ferrari, L. (2017). Comparative analysis of URANS vs. LES CFD methodologies for the aero-mechanical characterization of a Darrieus wind turbine. *Journal of Engineering for Gas Turbines and Power*, 139(3), 032604.

[3] Didane, D. H., Rosly, N., Zulkafli, M. F., & Shamsudin, S. S. (2019). Numerical investigation of a novel contra-rotating vertical axis wind turbine. *Sustainable Energy Technologies and Assessments*, 31, 43–53.

[4] Gall, M., Malael, I., & Preda, D. (2022). Computational analysis of fence-type VAWT arrays. In *Proceedings of CSCC 2022*. IEEE.

[5] Le, D. H., Nguyen, T. B., & Ngo, V. M. (2023). Experimental performance of a novel dual-stage counter-rotating small wind turbine. *Energies*, 16(14), 5510.

[6] Malael, I., Bucur, I. O., & Preda, D. (2021). Numerical investigation of a reduced-scale Lenz wind turbine for aerodynamic tunnel applications. *IOP Conference Series: Earth and Environmental Science*, 664, 012027.

[7] Merchant, S., & Gregg, J. (2009). Experimental analysis of a counter-rotating wind turbine. In *Proceedings of ASME IMECE2009* (Paper IMECE2009-11355). ASME.

[8] OSIM. (2025). Patent application A/00259/2025: VortexDublu – Sistem eolian contrarotativ cu ax vertical. Oficiul de Stat pentru Invenții și Mărci, Romania.

[9] Oprina, G., Chihaia, R.-A., El-Leathey, A., Nicolaie, S., Băbuţanu, C.-A., & Voina, A. (2016). A review on counter-rotating wind turbines development. *Journal of Sustainable Energy*, 7(3), 91–98.

[10] Pandele, A., Duran, B. O., Preda, D. M., & Voicu, G. (2025). CFD-based investigation of a counter-rotating VAWT for low-wind agricultural environments. In *Proceedings of Engineering for Rural Development 2025*. Jelgava, Latvia.

[11] Shen, W. Z., & Newman, J. (2023). Performance analysis of VAWT with H-Darrieus rotor using 2D CFD modelling. International *Journal of Renewable Energy Research*, 13(2).

[12] Delafin P. L., Nishino T., Kolios A., Wang L. Comparison of low-order aerodynamic models and RANS CFD for full scale 3D vertical axis wind turbines. 109, 2017, pp. 564-575.

# EVALUATION OF THE SELECTIVITY OF AN EXPERIMENTAL PSEUDOMONAS SYRINGAE PV. TAGETIS BIOHERBICIDE ON SOYBEAN CULTIVARS

/

# *EVALUAREA SELECTIVITĂȚII UNUI BIOERBICID EXPERIMENTAL PE BAZĂ DE PSEUDOMONAS SYRINGAE PV. TAGETIS ASUPRA UNOR SOIURI DE SOIA*

**Marga GRĂDILĂ*[1)], Sorina DINU[1)], Daniel JALOBĂ[1)], Valentin-Marius CIONTU[1)], Raluca-Monica IORDĂCHESCU[1)], Cătălina TUDORA[2)] Nicolae-Valentin VLĂDUȚ[2)]**

[1)] Research - Development Institute for Plant Protection - ICDPP, Bucharest / Romania;

[2)] National Institute of Research - Development for Machines and Installations Designed for Agriculture and Food Industry - INMA Bucharest / Romania.

**Tel: 0724 925 155; *E-mail:marga_gradila@yahoo.com*

***Keywords**: bioherbicide, Pseudomonas syringae pv. tagetis, selectivity, soybean, cultivars*

## ABSTRACT

*The selectivity of biological weed control agents is a key requirement for their successful integration into crop production systems. This study evaluated the selectivity of an experimental bioherbicide based on Pseudomonas syringae pv. tagetis (PST) toward three soybean cultivars (Vigo, Ovidiu F and Monica F) under greenhouse conditions. Two experiments were conducted using PST application volumes ranging from 20 to 400 mL pot$^{-1}$. Soybean plants were treated at the BBCH 12 - 13 growth stage and assessed for yellowing, chlorosis, necrosis, and other potential phytotoxic effects at 7 and 14 days after treatment (DAT), following the principles described in EPPO PP 1/135(4). The results showed a high degree of selectivity at application volumes of 20 - 80 mL pot$^{-1}$. Minor and transient yellowing and chlorosis were observed only on the Vigo cultivar at 80 mL pot$^{-1}$ and had disappeared completely by 14 DAT. Increasing the PST application volume above 100 mL pot$^{-1}$ resulted in progressively more pronounced phytotoxic symptoms, with responses varying among cultivars. Ovidiu F showed the lowest overall sensitivity, Monica F an intermediate response, and Vigo the greatest sensitivity. No additional visible treatment-related abnormalities were observed during the subsequent vegetation period, including flowering, pod formation, and seed development. Overall, the findings indicate that PST has potential as a biological weed control agent in soybean, particularly within an application-volume range that maintains crop selectivity. Further studies under field conditions are required to confirm these findings and to establish appropriate application conditions.*

## REZUMAT

*Selectivitatea agenților biologici utilizați pentru combaterea buruienilor reprezintă o cerință esențială pentru integrarea acestora în sistemele de producție agricolă. Studiul de față a evaluat selectivitatea unui bioerbicid experimental pe bază de Pseudomonas syringae pv. tagetis (PST) față de trei soiuri de soia (Vigo, Ovidiu F și Monica F), în condiții de seră. Au fost efectuate două experimente, utilizând volume de aplicare ale suspensiei bacteriene cuprinse între 20 și 400 mL ghiveci$^{-1}$. Plantele de soia au fost tratate în stadiul de dezvoltare BBCH 12 - 13 și evaluate pentru apariția îngălbenirii, clorozei, necrozei și a altor potențiale efecte fitotoxice la 7 și 14 zile după tratament (DAT), conform principiilor descrise în standardul EPPO PP 1/135(4). Rezultatele au evidențiat un grad ridicat de selectivitate la volume de aplicare cuprinse între 20 și 80 mL ghiveci$^{-1}$. Îngălbenirea și cloroza, de intensitate redusă și tranzitorie, au fost observate numai la soiul Vigo la volumul de 80 mL ghiveci$^{-1}$ și au dispărut complet până la 14 zile după tratament. Creșterea volumului de aplicare al PST peste 100 mL ghiveci$^{-1}$ a determinat o intensificare progresivă a simptomelor fitotoxice, cu răspunsuri diferite în funcție de soi. Soiul Ovidiu F a prezentat cea mai redusă sensibilitate, Monica F un răspuns intermediar, iar Vigo cea mai mare sensibilitate. Pe parcursul perioadei ulterioare de vegetație, inclusiv în timpul înfloritului, formării păstăilor și dezvoltării semințelor, nu au fost observate alte modificări vizibile asociate tratamentului. În ansamblu, rezultatele indică faptul că PST prezintă potențial ca agent biologic pentru combaterea buruienilor la cultura de soia, în special în cadrul unui interval de volume de aplicare care menține selectivitatea culturii. Sunt necesare studii suplimentare în condiții de câmp pentru confirmarea acestor rezultate și stabilirea condițiilor adecvate de aplicare.*

## INTRODUCTION

Soybean (*Glycine max* L.) is an important agricultural crop due to its high nutritional and economic value, being an important source of vegetable protein and oil (*Singh et al., 2008*; *Hartman et al., 2011*). However, soybean production is constrained by a range of biotic and abiotic factors, including diseases, insect pests, and weeds, which can negatively affect crop productivity and yield stability (*Hartman et al., 2011*).

The productivity of soybean is strongly influenced by weed infestation, which represents one of the major limiting factors in soybean cultivation (*Knezevic et al., 2003*; *Soltani et al., 2017*). Weed competition is particularly important during the early stages of crop development, when soybean plants are less competitive and weeds can substantially affect crop growth and yield (*Van Acker et al.,* 1993; *Fickett et al., 2013*; *Berca, 2004*; *Daramola, 2020).* The early-season critical period of weed control is therefore an important consideration in soybean production, as delayed weed management can result in significant and irreversible yield losses (*Van Acker et al., 1993*; *Daramola et al., 2020*).

Weed competition during soybean development can cause substantial yield losses, with reductions of 8 - 55% reported when weeds remain in the crop until the early seed-filling stage (*Van Acker et al., 1993*). Under high weed infestation and prolonged weed interference, soybean grain yield losses may reach 30 - 80% (*Yaduraju*, *2002).*

The magnitude of yield reduction depends on weed density, species composition, duration of interference, and environmental conditions. Therefore, effective weed control during the early stages of soybean development is essential for minimizing yield losses and maintaining crop productivity (*Datta et al., 2017*).

Effective weed management in soybean requires the integration of multiple control methods within an integrated weed management (IWM) approach. Integrated weed management combines preventive, agronomic, mechanical, and chemical practices, with the aim of suppressing weed populations, reducing crop–weed competition, and minimizing yield losses (*Knezevic, 2014*; *Datta et al., 2017*). In soybean, the integration of different weed management strategies is considered an effective approach for achieving sustainable and long-term weed control (*Datta et al*., *2017*).

The integration of diverse weed management practices can also reduce reliance on herbicides and help mitigate the development of herbicide-resistant weed populations, thereby contributing to more sustainable weed management systems (*Datta et al., 2017*; *Korres et al.,* 2019).

In this context, biological weed control represents an important component of integrated and sustainable weed management, involving the use of living organisms to suppress weed populations (*Hatcher and Melander*, *2003*; *Ghosheh*, *2005*). Biological control methods may therefore complement chemical, mechanical, and cultural practices and contribute to the development of more environmentally compatible weed management systems (*Hatcher & Melander, 2003*; *Ghosheh*, *2005*).

The use of microorganisms and their metabolites as biological weed control agents has attracted increasing interest because of their potential to suppress target weed species while reducing reliance on synthetic herbicides (*Johnson et al., 1996*; *Ghosheh, 2005*).

Among the microorganisms investigated for bioherbicidal activity, Pseudomonas syringae pv. tagetis (PST) is of particular interest because of its pathogenicity toward several weed species, particularly members of the Asteraceae family (*Johnson et al., 1996*; *Gronwald et al., 2002*).

The bioherbicidal activity of PST is associated with the production of tagetitoxin, a phytotoxin that interferes with plastid development and induces characteristic apical chlorosis in susceptible plants (*Lukens and Durbin, 1985*; *Mathews and Durbin*, *1990*). Tagetitoxin inhibits RNA synthesis directed by chloroplast RNA polymerase, providing a mechanistic basis for the disruption of chloroplast development and the chlorosis observed in susceptible plants (*Mathews and Durbin, 19*90; *Steinberg et al., 1990*)).

The bioherbicidal potential of PST therefore requires not only an assessment of its efficacy against target weeds but also careful evaluation of its host range, selectivity, and potential effects on non-target and cultivated plants (*Gronwald et al., 2002*; *Kong et al., 2005*). Tagetitoxin has also been characterized as an inhibitor of plastid RNA polymerase, providing a mechanistic basis for the chlorosis and inhibition of plant development observed following infection (*Kong et al., 2005*).

The bioherbicidal potential of PST therefore requires not only an assessment of its efficacy against target weeds but also careful evaluation of its host range, selectivity and effects on non-target and cultivated plants (*Kong et al., 2005; Gronwald et al., 2002*).

Crop selectivity is one of the key requirements for the successful development and practical application of biological herbicides. A biological control agent intended for weed management should provide effective suppression of the target weed while causing minimal or no adverse effects on the cultivated crop (*Charudattan, 2001*; *Bailey, 2014*).

Consequently, the assessment of potential phytotoxic effects on the crop represents an important stage in the development and characterization of experimental bioherbicides, particularly during the evaluation of their host range, efficacy, selectivity, and safety (*Ghosheh, 2005*; *Harding and Raizada, 2015*).

Soybean cultivars may differ in their response to biological control agents and to different application rates, as genetic variation may influence plant sensitivity to pathogens and biologically active compounds.

Therefore, selectivity assessments under controlled conditions should, where appropriate, include more than one cultivar and a range of application rates to identify potential differences in cultivar sensitivity and to establish an effective and sufficiently selective dose range (*Charudattan, 2001*; *Bailey, 2014*; *Harding and Raizada, 2015*). Such evaluations can provide important information for establishing the crop safety profile of a potential bioherbicide before subsequent greenhouse and field testing.

In this context, the present study aimed to evaluate the selectivity of an experimental bioherbicide based on *P. syringae pv. tagetis* toward three soybean cultivars, Vigo, Ovidiu F, and Monica F, under greenhouse conditions.

## MATERIAL AND METHOD

### *Experimental conditions*

The experiments were conducted under greenhouse conditions at the Research-Development Institute for Plant Protection (RDIPP), Bucharest, Romania. Two greenhouse experiments were carried out to evaluate the selectivity of an experimental bioherbicide based on *P. syringae pv. tagetis* (PST) and to characterize the response of three soybean cultivars to increasing application volumes of the bacterial suspension.

The soybean cultivars Vigo, Ovidiu F and Monica F were included in both experiments. Vigo, developed by ITC Seeds, is a Romanian soybean cultivar belonging to maturity group I and characterized by good adaptation to Romanian climatic conditions, high yield potential, and good tolerance to drought.

Ovidiu F, developed at the National Agricultural Research and Development Institute (NARDI) Fundulea, is an early-maturing cultivar with a vegetation period of approximately 100 - 110 days, good tolerance to drought and heat, and very good resistance to lodging and shattering.

Monica F, also developed at NARDI Fundulea, is a Romanian soybean cultivar selected for adaptation to local growing conditions and was included in the study to assess cultivar-specific differences in response to the experimental bioherbicide.

Soybean seeds were sown in plastic pots measuring 13.5 cm in diameter and 9 cm in height, with six seeds sown per pot. Following sowing, the plants were maintained under greenhouse conditions and irrigated every two days until treatment application. Plants were regularly monitored throughout the experimental period, and seedlings showing abnormalities unrelated to the experimental treatments were removed before treatment application.

All treatments were applied when the soybean plants had reached the BBCH 12 - 13 growth stage. The experimental preparations were applied using a manual sprayer positioned approximately 25 cm above the plant canopy.

To obtain a uniform distribution of the treatments over the foliage, two successive passes were performed over each pot, with the pots rotated by 180° between passes.

### *Experimental bioherbicide*

The experimental bioherbicide was developed at the Research-Development Institute for Plant Protection (RDIPP) and consisted of a bacterial suspension of *P. syringae pv. tagetis* (PST) at a concentration of $10^8$ CFU $mL^{-1}$. The bacterial concentration was determined spectrophotometrically prior to application. The PST bacterial suspension was applied directly to the soybean foliage without further dilution.

Consequently, the application rates of PST corresponded to the volume of bacterial suspension applied to each pot and were expressed as mL $pot^{-1}$.

The different application volumes therefore represented different amounts of the bacterial suspension delivered per pot, while the bacterial concentration remained constant at $10^8$ CFU $mL^{-1}$.

***Experimental design and treatments***

Two greenhouse experiments were conducted to assess the response of the three soybean cultivars to different application volumes of the experimental bioherbicide. In the first experiment, the selectivity of the experimental bioherbicide was evaluated at low application volumes.

Five treatment variants were established: V1, untreated control; V2, PST at 20 mL pot$^{-1}$; V3, PST at 40 mL pot$^{-1}$; V4, PST at 60 mL pot$^{-1}$; and V5, PST at 80 mL pot$^{-1}$. Each treatment was represented by four replicates for each soybean cultivar. Thus, the first experiment comprised 60 pots in total (5 treatments × 4 replicates × 3 cultivars).

The second experiment was designed to evaluate the response of soybean plants to increased application volumes of the experimental bioherbicide. Six treatment variants were established: V1, untreated control; V2, PST at 100 mL pot$^{-1}$; V3, PST at 100 mL pot$^{-1}$ combined with the Trend adjuvant at 1 mL pot$^{-1}$; V4, PST at 200 mL pot$^{-1}$; V5, PST at 400 mL pot$^{-1}$; and V6, the reference herbicide bentazone, formulated at a concentration of 480 g L$^{-1}$ and applied at 2 mL pot$^{-1}$. Each treatment was represented by four replicates for each soybean cultivar. Thus, the second experiment comprised 72 pots in total (6 treatments × 4 replicates × 3 cultivars).

***Assessment of phytotoxicity***

Phytotoxicity was assessed primarily on the basis of the occurrence and severity of chlorotic and necrotic symptoms. Chlorosis represents a characteristic symptom associated with infection by *P. syringae pv. tagetis* and the production of tagetitoxin in susceptible plants. For each soybean plant, two leaves were selected for visual assessment. Symptom severity was evaluated using a seven-point scale ranging from 0 to 6, where 0 represented healthy plants, 1 represented yellowing without distinct chlorosis, 2 represented detectable chlorosis, 3 represented moderate chlorosis, 4 represented severe chlorosis accompanied by moderate necrosis, 5 represented severe chlorosis and necrosis, and 6 represented completely dried plants.

Phytotoxicity assessments were performed at 7 and 14 days after treatment (DAT). For the symptoms of yellowing, detectable chlorosis, moderate chlorosis, severe chlorosis with necrosis, and severe chlorosis and necrosis, the severity was recorded as the percentage of affected leaf area. Completely dried plants were recorded separately as the percentage of plants showing complete drying.

In addition to the assessments performed at 7 and 14 days after treatment (DAT), the soybean plants were monitored throughout the entire vegetation period to identify any delayed or persistent treatment-related effects. Observations continued through the flowering, pod formation, and seed development stages.

In accordance with the principles described in *EPPO PP 1/135(4)*, particular attention was given to potential effects on plant growth and development, including plant stunting, delayed leaf development, flower abortion, reduction in pod formation, organ deformation, delayed pod development, and wilting. The presence or absence of visible treatment-related abnormalities was recorded throughout the observation period.

## RESULTS

***Selectivity assessment at low application volumes***

Soybean plants emerged 5 - 6 days after sowing and developed uniformly under greenhouse conditions. The experimental bioherbicide showed a high degree of selectivity toward the tested soybean cultivars when applied at low application volumes. No visible phytotoxic symptoms were observed on the Ovidiu F and Monica F cultivars at any of the application volumes tested in the first experiment. Similarly, no symptoms were detected on Vigo plants treated with 20, 40, or 60 mL pot$^{-1}$.

At the highest tested application volume (80 mL pot$^{-1}$), Vigo plants exhibited slight yellowing seven days after treatment (DAT), affecting less than 20% of the leaf area. Detectable chlorosis was also recorded, affecting less than 10% of the assessed leaf area. These symptoms were transient and had completely disappeared by 14 DAT. Under the conditions of the present experiment, these results indicate a high degree of selectivity of PST toward the tested soybean cultivars at application volumes up to 80 mL pot$^{-1}$.

***Response of soybean cultivars to increased PST application volumes***

The second experiment showed an increase in the severity of visible phytotoxic symptoms with increasing PST application volume, although the magnitude of the response differed among soybean cultivars. Symptoms were expressed mainly as yellowing, chlorosis, and necrosis, while completely dried plants were observed primarily at the higher application volumes (Tables 1, 2 and 3).

***Response of Ovidiu F:*** Ovidiu F showed the lowest overall sensitivity to the experimental bioherbicide among the three tested cultivars. At 100 mL pot$^{-1}$, only limited foliar effects were observed, with detectable chlorosis affecting 2% of the leaf area at 14 DAT and no completely dried plants recorded. Increasing the application volume to 200 mL pot$^{-1}$ resulted in a moderate increase in foliar symptoms. At 14 DAT, yellowing affected 4% of the leaf area, while detectable and moderate chlorosis affected 2% each. Severe chlorosis with necrosis and severe chlorosis and necrosis affected 3% and 4% of the leaf area, respectively.

Completely dried plants represented 10% of the plants. The highest PST application volume (400 mL pot$^{-1}$) produced the most pronounced response in Ovidiu F. At 14 DAT, yellowing affected 6% of the leaf area, while detectable and moderate chlorosis affected 2% each. Severe chlorosis with necrosis and severe chlorosis and necrosis reached 5% and 6% of the leaf area, respectively. Completely dried plants represented 15% of the plants.

The addition of the Trend adjuvant to PST at 100 mL pot$^{-1}$ was associated with a greater expression of foliar symptoms compared with PST applied alone at the same bacterial suspension volume. At 14 DAT, yellowing and moderate chlorosis affected 2% of the leaf area, while severe chlorosis with necrosis affected 3%. No completely dried plants were recorded.

**Table 1**

**Selectivity of the experimental bioherbicide toward soybean plants (cv. Ovidiu F)**

| Treatments | Severity of effects (% of affected leaf area, except dried plants) | | | | | | | | | | | |
|---|---|---|---|---|---|---|---|---|---|---|---|---|
| | Yello-wing | | Detectable chlorosis | | Moderate chlorosis | | Severe chlorosis with necrosis | | Severe chlorosis and necrosis | | Dried plants | |
| | Days after treatment | | | | | | | | | | | |
| | 7 | 14 | 7 | 14 | 7 | 14 | 7 | 14 | 7 | 14 | 7 | 14 |
| **PST - 100 ml pot$^{-1}$** | 0 | 0 | - | 2 | - | 0 | 0 | 0 | 0 | 0 | 0 | 0 |
| **PST + A - 100 ml + 1 ml pot$^{-1}$** | 0 | 2 | - | - | 0 | 2 | 2 | 3 | 0 | 0 | 0 | 0 |
| **PST - 200 ml pot$^{-1}$** | 0 | 4 | - | 2 | 0 | 2 | 0 | 3 | 2 | 4 | 5 | 10 |
| **PST - 400 ml pot$^{-1}$** | 2 | 6 | - | 2 | 0 | 2 | 0 | 5 | 2 | 6 | 10 | 15 |
| **Bentazone - 2 ml pot$^{-1}$** | 0 | 0 | 0 | 0 | 0 | 0 | 0 | 0 | 2 | 0 | 0 | 0 |
| **Control** | 0 | 0 | 0 | 0 | 0 | 0 | 0 | 0 | 0 | 0 | 0 | 0 |

***Note:*** *Values for yellowing, detectable chlorosis, moderate chlorosis, severe chlorosis with necrosis, and severe chlorosis and necrosis represent the percentage of affected leaf area. Dried plants are expressed as the percentage of completely dried plants. DAT, days after treatment; PST, P. syringae pv. tagetis.*

**Table 2**

**Selectivity of the experimental bioherbicide toward soybean plants (cv. Monica F)**

| Treatments | Severity of effects (% of affected leaf area, except dried plants) | | | | | | | | | | | |
|---|---|---|---|---|---|---|---|---|---|---|---|---|
| | Yello-wing | | Detectable chlorosis | | Moderate chlorosis | | Severe chlorosis with necrosis | | Severe chlorosis and necrosis | | Dried plants | |
| | Days after treatment | | | | | | | | | | | |
| | 7 | 14 | 7 | 14 | 7 | 14 | 7 | 14 | 7 | 14 | 7 | 14 |
| **PST – 100 ml pot$^{-1}$** | 0 | 0 | 0 | 2 | - | 0 | 0 | 2 | 0 | 2 | 0 | 0 |
| **PST + A – 100 ml + 1 ml pot$^{-1}$** | 0 | 2 | 0 | 0 | 0 | 4 | 0 | 1 | 2 | 4 | 5 | 5 |
| **PST – 200 ml pot$^{-1}$** | 2 | 4 | 0 | 2 | 0 | 2 | 0 | 3 | 2 | 6 | 5 | 15 |
| **PST – 400 ml pot$^{-1}$** | 2 | 6 | 2 | 0 | 2 | 5 | 2 | 5 | 4 | 10 | 15 | 20 |
| **Bentazone – 2 ml pot$^{-1}$** | 0 | 0 | 0 | 0 | 0 | 0 | 0 | 0 | 2 | 0 | 0 | 0 |
| **Control** | 0 | 0 | 0 | 0 | 0 | 0 | 0 | 0 | 0 | 0 | 0 | 0 |

***Note:*** *Values for yellowing, detectable chlorosis, moderate chlorosis, severe chlorosis with necrosis, and severe chlorosis and necrosis represent the percentage of affected leaf area. Dried plants are expressed as the percentage of completely dried plants. DAT, days after treatment; PST, P. syringae pv. Tagetis*

***Response of Monica F:*** Monica F showed an intermediate response to increasing PST application volumes. At 100 mL pot⁻¹, the effects were limited, with detectable chlorosis, severe chlorosis with necrosis, and severe chlorosis and necrosis each affecting a maximum of 2% of the leaf area at 14 DAT. No completely dried plants were recorded.

The response became more pronounced at 200 mL pot⁻¹. At 14 DAT, yellowing affected 4% of the leaf area, detectable and moderate chlorosis affected 2% each, while severe chlorosis with necrosis and severe chlorosis and necrosis reached 3% and 6%, respectively.

Completely dried plants represented 15% of the plants. At 400 mL pot⁻¹, the severity of symptoms increased further. At 14 DAT, yellowing affected 6% of the leaf area, moderate chlorosis affected 5%, severe chlorosis with necrosis affected 5%, and severe chlorosis and necrosis affected 10% of the leaf area. Completely dried plants represented 20% of the plants.

The treatment combining PST at 100 mL pot⁻¹ with Trend was associated with a greater expression of some foliar symptoms than PST applied alone at the same bacterial suspension volume. At 14 DAT, yellowing affected 2% of the leaf area, moderate chlorosis 4%, severe chlorosis with necrosis 1%, and severe chlorosis and necrosis 4%. Completely dried plants represented 5% of the plants.

**Table 3**

**Selectivity of the experimental bioherbicide toward soybean plants (cv. Vigo)**

| Treatments | Severity of effects (% of affected leaf area, except dried plants) | | | | | | | | | | | |
|---|---|---|---|---|---|---|---|---|---|---|---|---|
| | Yello-wing | | Detectable chlorosis | | Moderate chlorosis | | Severe chlorosis with necrosis | | Severe chlorosis and necrosis | | Dried plants | |
| | Days after treatment | | | | | | | | | | | |
| | 7 | 14 | 7 | 14 | 7 | 14 | 7 | 14 | 7 | 14 | 7 | 14 |
| **PST – 100 ml pot⁻¹** | 0 | 1 | 0 | 2 | 0 | 2 | 0 | 2 | 0 | 2 | 0 | 0 |
| **PST + A – 100 ml + 1 ml pot⁻¹** | 0 | 4 | 0 | 2 | 0 | 4 | - | 5 | 3 | 10 | 2 | 5 |
| **PST – 200 ml pot⁻¹** | 2 | 8 | 0 | 2 | 4 | 5 | 2 | 10 | 5 | 15 | 5 | 10 |
| **PST – 400 ml pot⁻¹** | 5 | 10 | 2 | 5 | 5 | 10 | 5 | 15 | 8 | 20 | 20 | 30 |
| **Bentazone – 2 ml pot⁻¹** | 0 | 0 | 0 | 0 | 0 | 0 | 0 | 0 | 2 | 0 | 0 | 0 |
| **Control** | 0 | 0 | 0 | 0 | 0 | 0 | 0 | 0 | 0 | 0 | 0 | 0 |

***Note:*** *Values for yellowing, detectable chlorosis, moderate chlorosis, severe chlorosis with necrosis, and severe chlorosis and necrosis represent the percentage of affected leaf area. Dried plants are expressed as the percentage of completely dried plants. DAT, days after treatment; PST, P. syringae pv. tagetis.*

***Response of Vigo:*** Vigo exhibited the greatest sensitivity to the experimental bioherbicide. Even at 100 mL pot⁻¹, foliar symptoms were more pronounced than those observed in Ovidiu F and Monica F, although the affected leaf area remained low and no completely dried plants were recorded. At 14 DAT, yellowing affected 1% of the leaf area, while detectable chlorosis, moderate chlorosis, severe chlorosis with necrosis, and severe chlorosis and necrosis each affected 2% of the leaf area.

The addition of Trend to PST at 100 mL pot⁻¹ was associated with a more pronounced response. At 14 DAT, yellowing affected 4% of the leaf area, detectable chlorosis 2%, moderate chlorosis 4%, severe chlorosis with necrosis 5%, and severe chlorosis and necrosis 10%.

Completely dried plants represented 5% of the plants. At 200 mL pot⁻¹, symptom severity increased further. At 14 DAT, yellowing affected 8% of the leaf area, detectable chlorosis 2%, moderate chlorosis 5%, severe chlorosis with necrosis 10%, and severe chlorosis and necrosis 15%. Completely dried plants represented 10% of the plants.

The strongest response was observed at 400 mL pot⁻¹. At 14 DAT, yellowing affected 10% of the leaf area, detectable chlorosis 5%, moderate chlorosis 10%, severe chlorosis with necrosis 15%, and severe chlorosis and necrosis 20%.

Completely dried plants represented 30% of the plants. Thus, Vigo showed the clearest increase in phytotoxic response with increasing PST application volume and was the most sensitive of the three soybean cultivars evaluated.

***Comparative response of the soybean cultivars***

Comparison of the three cultivars indicates clear differences in their sensitivity to PST. Ovidiu F generally exhibited the lowest severity of foliar symptoms and the lowest proportion of completely dried plants, whereas Vigo showed the greatest response, particularly at 200 and 400 mL pot$^{-1}$. Monica F displayed an intermediate response between the two cultivars.

The differences among cultivars became more evident as the PST application volume increased. At 400 mL pot$^{-1}$ and 14 DAT, severe chlorosis and necrosis affected 6% of the leaf area in Ovidiu F, 10% in Monica F, and 20% in Vigo. Similarly, completely dried plants accounted for 15%, 20%, and 30% of the plants, respectively. These results indicate that differences in cultivar sensitivity became more pronounced with increasing PST application volume.

Overall, the results indicate an application-volume-dependent and cultivar-dependent response of soybean to PST. The relatively limited symptoms observed at lower application volumes, together with the absence or low incidence of completely dried plants, indicate comparatively high selectivity toward the tested soybean cultivars at these application volumes. However, increasing the PST application volume, particularly to 200 and 400 mL pot$^{-1}$, resulted in progressively more pronounced phytotoxic effects, with Vigo showing the greatest sensitivity and Ovidiu F the lowest sensitivity.

***Evaluation according to EPPO PP 1/135(4)***

In addition to the quantitative assessment of yellowing, chlorosis, and necrosis performed at 7 and 14 days after treatment (DAT), soybean plants were monitored throughout the entire vegetation period for other potential phytotoxic effects in accordance with the principles described in *EPPO PP 1/135(4)*. The observations continued through flowering, pod formation, and seed development.

The parameters monitored included plant stunting, delayed leaf development, flower abortion, reduction in pod formation, organ deformation, delayed pod development, and wilting. No plant stunting or visible abnormalities in vegetative growth and leaf development, other than the foliar symptoms described above, were observed during the vegetation period. Likewise, no wilting or deformation of vegetative organs was recorded. No visible flower abortion or apparent reduction in pod formation was observed. Pod development and seed formation proceeded normally, with no visible treatment-related abnormalities detected during the observation period.

Overall, the phytotoxic effects associated with PST were predominantly expressed as foliar yellowing, chlorosis, and necrosis during the first 14 DAT, with symptom severity increasing at the higher application volumes. The magnitude of these effects varied among the tested soybean cultivars, with Vigo showing the greatest sensitivity and Ovidiu F the lowest sensitivity. Importantly, no additional visible phytotoxic effects on vegetative or reproductive development were observed during the subsequent vegetation period, through pod formation and seed development.

The graph below (Fig. 1) illustrates the percentage of completely dried soybean plants recorded 14 days after treatment with the experimental bioherbicide based on *P. syringae pv. tagetis* (PST). The response to the different treatments was evaluated in three soybean cultivars: Ovidiu F, Monica F, and Vigo.

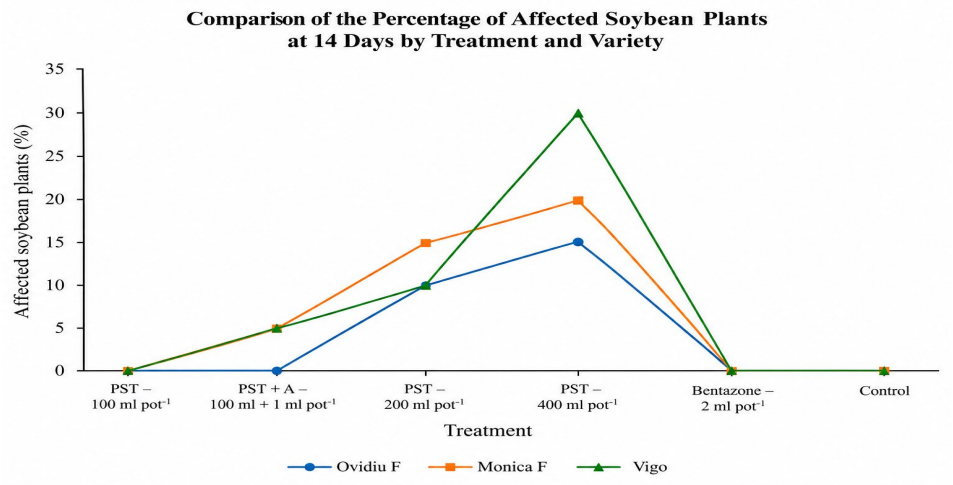



**Fig. 1 - Percentage of completely dried soybean plants 14 days after treatment, according to treatment and cultivar.**

The following photographs (Fig. 2) provide a visual representation of the soybean plants observed during the greenhouse experiments and illustrate the differences in phytotoxic response among the tested cultivars and treatments.



**Fig. 5 - Visual assessment of soybean responses to the experimental bioherbicide based on *P. syringae pv. tagetis* under greenhouse conditions, showing differences in symptom severity among treatments and soybean cultivars**

## CONCLUSIONS

The experimental bioherbicide based on *P. syringae* pv. tagetis (PST) showed a generally high degree of selectivity toward the tested soybean cultivars under greenhouse conditions at low application volumes.

Application volumes of 20 - 80 mL pot$^{-1}$ resulted in no or only minor foliar symptoms, with transient chlorosis observed only on Vigo at 80 mL pot$^{-1}$ and no visible symptoms remaining at 14 days after treatment.

At higher application volumes, the severity of phytotoxic symptoms increased progressively, indicating an application-volume-dependent response.

The tested soybean cultivars differed in their sensitivity to PST. Ovidiu F showed the lowest overall sensitivity, Monica F an intermediate response, and Vigo the greatest sensitivity, particularly at the highest application volumes.

Despite the occurrence of foliar phytotoxicity at higher application volumes, no additional visible treatment-related abnormalities affecting vegetative or reproductive development were observed during the subsequent vegetation period, including flowering, pod formation, and seed development.

Overall, the results indicate that PST has potential as a biological weed control agent in soybean production, particularly when applied within an application-volume range that maintains crop selectivity.

Further greenhouse and field studies are required to confirm crop safety under different environmental conditions and to determine application conditions that provide an appropriate balance between bioherbicidal efficacy and soybean selectivity.

## ACKNOWLEDGEMENT

This research was carried out with the financial support of the Ministry of Agriculture and Rural Development of Romania, within the framework of the national project ADER 1.4.1 (Contract No. 141/19.07.2023), coordinated by the Agricultural Research and Development Station Turda, with the Research-Development Institute for Plant Protection, Bucharest, participating as a partner (P1).

## REFERENCES

[1] Bailey, K. L. (2014). The bioherbicide approach to weed control using plant pathogens. *In Integrated Pest Management* (pp. 245 - 266). Elsevier. DOI: 10.1016/B978-0-12-398529-3.00014-2.

[2] Berca, M. (2004). Weed Integrated Management. *Ceres Publishing House*, 534 pp.

[3] Charudattan, R. (2001). Biological control of weeds by means of plant pathogens: Significance for integrated weed management in modern agro-ecology. *BioControl*, 46(2), 229 - 260. DOI: 10.1023/A:1011477531101.

[4] Daramola, O. S. (2020a). Timing of weed management and yield penalty due to delayed weed management in soybean. *Planta Daninha*, 38, e020236046. DOI: 10.1590/S0100-83582020380100072.

[5] Daramola, O. S., Adeyemi, O. R., Adigun, J. A., Adejuyigbe, C. O., & Olorunmaiye, P. M. (2020b). The effect of the period of weed interference on the growth and yield of soybean (*Glycine max* L. Merrill). *Journal of Agricultural Sciences*, 65(3), 225 - 237. DOI: 10.2298/JAS2003225D.

[6] Datta, A., Ullah, H., Tursun, N., Pornprom, T., Knezevic, S. Z., & Chauhan, B. S. (2017). Managing weeds using crop competition in soybean [*Glycine max* (L.) Merr.]. *Crop Protection*, 95, 60 - 68. DOI: 10.1016/j.cropro.2016.09.005.

[7] EPPO. (2014). EPPO PP 1/135(4): Phytotoxicity assessment (Efficacy evaluation of plant protection products*). EPPO Bulletin*, 44(3), 265 - 273. DOI: 10.1111/epp.12134.

[8] Fickett, N. D., Boerboom, C. M., & Stoltenberg, D. E. (2013). Soybean yield loss potential associated with early-season weed competition across 64 site-years. *Weed Science*, 61(3), 500 - 507. DOI: 10.1614/WS-D-12-00164.1.

[9] Ghosheh, H. Z. (2005). Constraints in implementing biological weed control: A review. *Weed Biology and Management*, 5(3), 83 - 92. DOI: 10.1111/j.1445-6664.2005.00163.x.

[10] Gronwald, J. W., Plaisance, K. L., Ide, D. A., & Wyse, D. L. (2002). Assessment of *Pseudomonas syringae* pv. tagetis as a biocontrol agent for Canada thistle. *Weed Science*, 50(3), 397 - 404. DOI: 10.1614/0043-1745(2002)050[0397]2.0.CO;2.

[11] Harding, D. P., & Raizada, M. N. (2015). Controlling weeds with fungi, bacteria and viruses: A review. Frontiers in *Plant Science*, 6, 659. DOI: 10.3389/fpls.2015.00659.

[12] Hartman, G. L., West, E. D., & Herman, T. K. (2011). Crops that feed the World 2. Soybean - worldwide production, use, and constraints caused by pathogens and pests. *Food Security*, 3(1), 5 - 17. DOI: 10.1007/s12571-010-0108-x.

[13] Hatcher, P. E., & Melander, B. (2003). Combining physical, cultural and biological methods: Prospects for integrated non-chemical weed management strategies. *Weed Research*, 43(5), 303 - 322. DOI: 10.1046/j.1365-3180.2003.00352.x.

[14] Johnson, D. R., Wyse, D. L., & Jones, K. J. (1996). Controlling weeds with phytopathogenic bacteria. *Weed Technology*, 10(3), 621 - 624. DOI: 10.1017/S0890037X00040549.

[15] Knezevic, S. Z., Evans, S. P., & Mainz, M. (2003). Row spacing influences the critical timing for weed removal in soybean (*Glycine max*). *Weed Technology*, 17(4), 666 - 673. DOI: 10.1614/WT02-49.

[16] Knezevic, S. Z. (2014). Integrated weed management in soybean. In B. S. Chauhan & G. Mahajan (Eds.), Recent Advances in *Weed Management* (pp. 223 - 237). Springer. DOI: 10.1007/978-1-4939-1019-9_10.

[17] Kong, H., Blackwood, C., Buyer, J. S., Gulya, T. J., & Lydon, J. (2005). The genetic characterization of *Pseudomonas syringae* pv. tagetis based on the 16S–23S rDNA intergenic spacer regions. *Biological Control,* 32, 356 -362.

[18] Korres, N. E., Burgos, N. R., Travlos, I., Vurro, M., Gitsopoulos, T. K., Varanasi, V. K., Duke, S. O., Kudsk, P., Brabham, C., Rouse, C. E., & Salas-Perez, R. (2019). New directions for integrated weed management: Modern technologies, tools and knowledge discovery. *Advances in Agronomy*, 155, 243 - 319. DOI: 10.1016/bs.agron.2019.01.006.

[19] Lukens, J. H., & Durbin, R. D. (1985). Tagetitoxin affects plastid development in seedling leaves of wheat. *Planta*, 165(3), 311–321. DOI: 10.1007/BF00392227.

[20] Mathews, D. E., & Durbin, R. D. (1990). Tagetitoxin inhibits RNA synthesis directed by RNA polymerases from chloroplasts and *Escherichia coli*. *Journal of Biological Chemistry*, 265(1), 493 - 498. DOI: 10.1016/S0021-9258(19)40258-5.

[21] Singh, P., Kumar, R., Sabapathy, S. N., & Bawa, A. S. (2008). Functional and edible uses of soy protein products. *Comprehensive Reviews in Food Science and Food Safety*, 7(1), 14 - 24. DOI: 10.1111/j.1541-4337.2007.00025.x.

[22] Soltani, N., Dille, J. A., Burke, I. C., Everman, W. J., VanGessel, M. J., Davis, V. M., & Sikkema, P. H. (2017). Perspectives on potential soybean yield losses from weeds in North America. *Weed Technology*, 31, 148 - 154. DOI: 10.1017/wet.2016.2.

[23] Steinberg, T. H., Mathews, D. E., Durbin, R. D., & Burgess, R. R. (1990). Tagetitoxin: A new inhibitor of eukaryotic transcription by RNA polymerase III. *Journal of Biological Chemistry*, 265(1), 499 - 505. DOI: 10.1016/S0021-9258(19)40259-7.

[24] Van Acker, R. C., Swanton, C. J., & Weise, S. F. (1993). The critical period of weed control in soybean [*Glycine max* (L.) Merr.]. *Weed Science*, 41(2), 194 - 200. DOI: 10.1017/S0043174500076050.
[25] Yaduraju, N. T. (2002). Importance of weeds in agriculture. In Teaching Manual on Advances in *Weed Management* (pp. 4 - 5). National Research Centre for Weed Science, Jabalpur, Madhya Pradesh, India.

# STUDY ON AUTONOMOUS MOBILE SOLUTIONS FOR CROP HARVESTING
# /
# *STUDIU PRIVIND SOLUȚIILE MOBILE AUTONOME PENTRU RECOLTAREA CULTURILOR AGRICOLE*

**Dorin-Andrei CÎRSTEA*[1)], Robert-Dorin CRISTEA[1)], Alexandru-Cristian CIOACLA[1)], Alexandru IONESCU[1)], Dragoș-Valentin LUPU[2)]**

[1)] National Institute of Research - Development for Machines and Installations Designed to Agriculture and Food-Industry - INMA Bucharest / Romania;

[2)] Student in internship, future volunteer at National Institute of Research - Development for Machines and Installations Designed to Agriculture and Food-Industry - INMA Bucharest / Romania.

**Tel: +40 770 214 701; *E-mail: d_orinel@yahoo.com*

***Keywords:*** *autonomous harvesting, mobile robotic platform, robotic arm, end-effector, precision agriculture, agricultural robot*

**ABSTRACT**

*This paper reviews autonomous mobile harvesting technology, focusing on two components that must work together: the mobile platform, which moves through the field, and the robotic arm and end-effector, which remove the fruit. It compares wheeled, tracked and rail-guided platforms with GNSS, LiDAR and vision navigation, and serial or dual-arm manipulators fitted with suction, gripping or cutting end-effectors. Cycle times ranged three to eight seconds per fruit, with success rates of seventy to over ninety percent. Occlusion, variable light, arm speed and sensor cost remain the main obstacles, pointing toward better AI perception and lighter manipulators.*

**REZUMAT**

*Lucrarea trece în revistă tehnologiile mobile autonome de recoltare, urmărind două componente care trebuie să funcționeze împreună: platforma mobilă, care se deplasează prin câmp, și ansamblul braț robotic - efector final, care desprinde fructul de pe plantă. Sunt comparate platforme pe roți, pe șenile și ghidate pe șine, cu navigare GNSS, LiDAR și vizuală, alături de manipulatoare seriale sau cu două brațe, echipate cu ventuze, gripere sau unelte de tăiere. Timpii de ciclu au variat între trei și opt secunde per fruct, cu rate de succes între șaptezeci și peste nouăzeci la sută. Ocluzia, lumina variabilă, viteza brațului și costul senzorilor rămân principalele obstacole, ceea ce indică nevoia unei percepții AI mai bune și a unor manipulatoare mai ușoare.*

## INTRODUCTION

Harvesting is still, by a wide margin, one of the most labour-intensive stages of growing fruit and vegetables, and in many operations it eats up the largest single share of field-operation costs (*Zhang et al., 2024*). Labour has become harder to find, wages have gone up, and picking itself is seasonal and physically punishing work, all of which has pushed a good deal of research toward building robots that can do the job instead (*Rajendran et al., 2024*).

Crops picked selectively rather than all at once, apples, strawberries, tomatoes, sweet peppers and the like, turned out to be the hardest cases to automate, since the robot has to reach an individual fruit, judge whether it is actually ripe, and take it off the plant without bruising the fruit or tearing up the branch (*Zhou et al., 2022*).

Most of these systems boil down to two parts that have to work together. One is the mobile base, which gets the equipment down the row, through the orchard alley, or along a greenhouse aisle, and gives the arm something steady to work from (*Raikwar et al., 2022*). The other is the arm and end-effector, which take over once a fruit has been spotted, refine its position, close in, grip or cut it free, and drop it into a collection bin (*Silwal et al., 2017*). How well the whole thing runs comes down to how tightly these two halves, and the perception and control software stitching them together, are coordinated (*Davidson et al., 2020*).

What follows is a look at where this technology stands today, focused mainly on the mobile platform and on the arm doing the actual picking. Recent studies were pulled together to compare navigation approaches, chassis types, arm designs and end-effectors, and to see what field results complete systems

have actually delivered. The paper also goes into the problems that still keep most of these machines at the prototype stage rather than on the market, and where the research seems to be heading next.

## GENERAL ARCHITECTURE OF AUTONOMOUS HARVESTING SYSTEMS

Despite coming from different research groups, most of the harvesting units described in the literature end up looking fairly similar underneath: a mobile base, some form of perception, an arm with an end-effector, and a controller sitting on top to run the whole show (*Zhang et al., 2024; Vrochidou et al., 2022*).

Perception usually meant RGB, RGB-D or stereo cameras, sometimes backed up by LiDAR, and this same hardware did double duty, guiding the platform between rows and also finding, locating and judging the ripeness of fruit (*Rajendran et al., 2024*).

The controller then had to pull data from both jobs together, plotting where the platform should go, parking the arm close enough to the target, and working out the path the manipulator needed to take to reach in and take the fruit (*Davidson et al., 2020*).

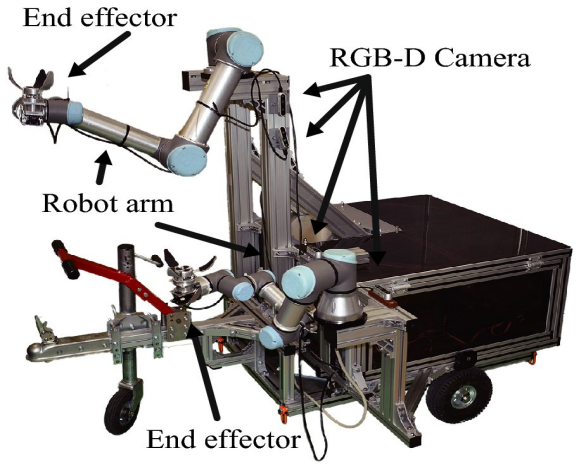



**Fig. 1 - Components of an autonomous fruit harvesting robot**

*The harvesting unit combines a mobile vehicle, multiple RGB-D cameras, two robot arms with harvesting end-effectors, and a control computer.*

A typical picking run looked something like this: the platform crept along a row while cameras scanned the canopy overhead. Once a fruit was spotted and its position pinned down with enough confidence, the platform would slow or stop, the arm would move in, the end-effector would grip or cut, and the fruit would be dropped into an onboard bin before the arm swung back and the platform started moving again (*Bac et al., 2017; Lehnert et al., 2020*). That sequence repeated for every fruit within reach, with the platform inching forward bit by bit until the whole row or bed had been covered.

## MOBILE PLATFORMS FOR AUTONOMOUS HARVESTING

Wheels are still the default choice for most autonomous harvesters, mainly because they are simple, cheap to run, and fit naturally into orchard rows and field layouts that already exist (*Raikwar et al., 2022*). Four-wheel and four-wheel-steered layouts in particular turned out to handle the tight turns at the end of a row well, without throwing the arm off balance mid-pick (*Raikwar et al., 2022*).

Where the ground was rougher, or inside greenhouses where more traction and a gentler footprint mattered, tracked platforms showed up instead in a number of prototypes (*Ren et al., 2024*).

Getting these platforms to find their own way usually meant leaning on some mix of satellite positioning, LiDAR and cameras. A LiDAR-only algorithm for one agricultural robot managed to track rows reliably without needing a satellite fix at all, which mattered a lot under thick canopy, where GNSS accuracy tends to fall apart (Malavazi et al., 2018).

Elsewhere, a four-wheel-steered orchard robot was set up to navigate using nothing but wheel and steering encoder readings, precisely because GNSS coverage couldn't be counted on in that setting (*Raikwar et al., 2022*). Other platforms took a more blended approach, pairing GNSS with inertial sensors and onboard cameras to keep things working across whatever conditions the field threw at them (*Ren et al., 2024*).




**Fig. 2 - Autonomous mobile agricultural platform**

*Illustrative autonomous field platform showing sensor-based navigation and driverless operation in an agricultural environment.*

Indoor settings changed the picture somewhat. In precision indoor strawberry production, platforms were built to run along fixed or semi-fixed tracks between growing tables instead of navigating open ground, which made both localization and predicting where the arm would need to reach a lot simpler (*Ren et al., 2024*). A number of these units were designed to sense and harvest in the same pass, cutting down on how many times a robot needed to move through the crop to get everything done (*Ren et al., 2024*).

## ROBOTIC ARM AND END-EFFECTOR SYSTEMS FOR CROP HARVESTING

Most harvesting arms are serial manipulators with somewhere between three and seven joints. More joints generally means the arm can twist around leaves and reach fruit buried in a cluster more easily, though it also makes the planning harder and slows down each pick (*Rajendran et al., 2024*). Quite a few research teams simply took an off-the-shelf collaborative arm and built around it, as in one modular strawberry-picking rig that paired a commercial manipulator with a custom-built picking head and its own perception and control stack (*Parsa et al., 2024*).

Some groups went further and put two arms on the same platform, letting one push aside leaves or neighbouring fruit while the other went in for the pick, an arrangement that helped noticeably with fruit that would otherwise stay hidden in a dense canopy (*Rajendran et al., 2024*).

A related idea, running several arms in parallel on one apple-harvesting platform, was tried as a way to push up the overall picking rate rather than relying on a single arm working faster (*Zhang et al., 2024*).

What went on the end of the arm depended a lot on the crop. Apples and similarly round fruit were mostly picked with suction cups, pulling the fruit free with vacuum and, in principle, bruising it less than a hard grip would (*Silwal et al., 2017*).

For crops more sensitive to pressure, soft and compliant grippers, some finger-shaped, some closer to flexible pads, were developed to hold on firmly enough without leaving marks, and this category has grown enough to warrant its own dedicated survey of agricultural end-effectors (*Vrochidou et al., 2022*).

Sweet pepper and tomato, on the other hand, needed the stalk cut rather than the fruit pulled, so cutting or clamp-and-cut tools ended up in the robots built and tested for those crops under commercial greenhouse conditions (*Bac et al., 2017; Lehnert et al., 2020*).




**Fig. 3 - Robotic arm with a cutter end-effector harvesting green chile peppers**

*The cutter end-effector is positioned at the fruit stem, illustrating crop-specific separation tools used in robotic harvesting.*

Getting the arm from its starting position to the fruit without hitting a branch, a leaf or another fruit along the way is its own problem, made harder by the need to keep each pick quick. The usual fix combined geometric path planning with visual servoing, correcting the arm's path on the fly using the camera feed as it closed in on the target (*Rajendran et al., 2024; Miao et al., 2023*). None of this worked in isolation from the platform, either: on uneven ground especially, the arm controller had to account for small shifts in the platform's position while the pick was underway (*Davidson et al., 2020*).

## INTEGRATION, FIELD PERFORMANCE AND COMPARATIVE RESULTS

Put together, mobile platform and arm generally managed something like three to eight seconds per fruit in field trials, with success somewhere between seventy percent and the low nineties, though the exact number swung a lot depending on the crop, how thick the canopy was, and the light (*Silwal et al., 2017; Lehnert et al., 2020; Miao et al., 2023*). One robotic apple harvester built around a vacuum end-effector on a mobile base held up well under real orchard conditions, landing in the same range as other systems of its kind (*Silwal et al., 2017*).

A sweet pepper robot tested in a commercial greenhouse setting got noticeably faster and more reliable after a few rounds of redesigning the arm and end-effector control, which says something about how much the final numbers depend on getting perception, arm control and end-effector timing to work together rather than any one piece alone (*Lehnert et al., 2020*).

A tomato-picking robot that paired conventional image processing with a deep-learning ripeness classifier came away with fewer bruised or missed fruit than earlier, vision-only setups had managed, which fits the broader pattern that sharper perception tends to translate fairly directly into fewer bad picks (*Miao et al., 2023*).

On the strawberry side, platforms built for precision indoor farms folded monitoring and harvesting into a single mobile unit, so the crop only had to be passed through once instead of separately for sensing and picking (*Ren et al., 2024*).

Taken together, none of the systems reviewed here matched a skilled human picker for speed, and the gap mostly came down to time spent detecting fruit, planning a path, and moving the arm carefully enough not to damage anything (*Zhou et al., 2022; Zhang et al., 2024*). That said, each new generation of systems in the literature tended to be a bit quicker and more reliable than the last, which tracked fairly closely with improvements in perception software, faster control loops for the arm, and end-effectors better suited to the crop at hand (*Rajendran et al., 2024*).

## CHALLENGES AND FUTURE RESEARCH DIRECTIONS

A handful of problems kept coming up across nearly every study looked at here. Leaves and branches hiding the fruit remained a constant headache for detection and localization, pushing some teams toward active perception tricks, moving the camera to a better angle, or using a second arm just to push foliage out of the way (*Rajendran et al., 2024*). Outdoor light, changing by the hour and the season, also chipped away at how well cameras could detect fruit and guide navigation, which is part of why several groups turned to combining cameras with LiDAR or other depth sensors that don't care as much about lighting (*Malavazi et al., 2018; Vrochidou et al., 2022*).

Speed is still the arm's weak point. Even the better systems in the literature picked more slowly than an experienced human, and for lower-value crops that gap alone can be enough to make the economics not work out (*Zhou et al., 2022*). On top of that, the sensors and precision hardware needed to make any of this work well still cost enough to keep smaller growers out of the market (*Zhang et al., 2024*).

Where things seem to be heading next, based on what's in the literature, is toward lighter, gentler arms that can move faster without bruising the crop, perception systems that lean more heavily on AI paired with motion planning that adapts as it goes, and platforms designed from the start around what the arm actually needs rather than bolted together after the fact, which should cut down on wasted repositioning (*Rajendran et al., 2024; Parsa et al., 2024*).

There's also a fairly clear consensus that more testing needs to happen on real commercial farms rather than in controlled research plots, since that's really the only way to know whether these systems hold up and pay for themselves at scale (*Ren et al., 2024*).

## CONCLUSIONS

Looking across the recent literature on autonomous mobile crop harvesting, it's clear that most of the effort has gone into two parts that need to work as one: the mobile platform, which handles getting around the field and holding steady, and the arm and end-effector, which handle the actual picking. Wheeled and tracked platforms, steered by some combination of GNSS, LiDAR and vision, were generally able to get the arm close enough to work under a range of field and greenhouse conditions.

Once there, serial or dual-arm manipulators fitted with suction cups, soft grippers or cutting tools chosen to suit the crop managed success rates from around seventy up to over ninety percent, at cycle times of roughly three to eight seconds a fruit.

The main things still holding this technology back from wider commercial use were hidden fruit, changeable light, arms that are still slower than a human hand, and hardware that costs more than many growers can justify. Closing that gap looks like it will mean better AI-driven perception paired with planning that adapts on the fly, arms that are lighter and easier on the crop, and platforms and arms designed together from the outset rather than as an afterthought.

## REFERENCES

[1] Arad, B., Balendonck, J., Barth, R., Ben-Shahar, O., Edan, Y., Hellström, T., Hemming, J., Kurtser, P., Ringdahl, O., Tielen, T., & van Tuijl, B. (2020). Development of a sweet pepper harvesting robot. Journal of Field Robotics, 37(6), 1027–1039. https://doi.org/10.1002/rob.21937

[2] Bac, C. W., Hemming, J., van Tuijl, B. A. J., Barth, R., Wais, E., & van Henten, E. J. (2017). Performance evaluation of a harvesting robot for sweet pepper. Journal of Field Robotics, 34(6), 1123–1139. https://doi.org/10.1002/rob.21709

[3] Davidson, J., Bhusal, S., Mo, C., Karkee, M., & Zhang, Q. (2020). Robotic manipulation for specialty crop harvesting: A review of manipulator and end-effector technologies. Global Journal of Agricultural and Allied Sciences, 2(1), 25–41. https://doi.org/10.35251/gjaas.2020.004

[4] Lehnert, C., McCool, C., Sa, I., & Perez, T. (2020). Performance improvements of a sweet pepper harvesting robot in protected cropping environments. Journal of Field Robotics, 37(7), 1197–1223. https://doi.org/10.1002/rob.21973

[5] Malavazi, F. B. P., Guyonneau, R., Fasquel, J.-B., Lagrange, S., & Mercier, F. (2018). LiDAR-only based navigation algorithm for an autonomous agricultural robot. Computers and Electronics in Agriculture, 154, 71–79. https://doi.org/10.1016/j.compag.2018.08.034

[6] Miao, Z., Yu, X., Li, N., Zhang, Z., He, C., Li, Z., Deng, C., & Sun, T. (2023). Efficient tomato harvesting robot based on image processing and deep learning. Precision Agriculture, 24(1), 254–287. https://doi.org/10.1007/s11119-022-09944-w

[7] Parsa, S., Debnath, B., Khan, M. A., & Ghalamzan Esfahani, A. (2024). Modular autonomous strawberry picking robotic system. Journal of Field Robotics, 41(7), 2226–2246. https://doi.org/10.1002/rob.22229

[8] Raikwar, S., Fehrmann, J., & Herlitzius, T. (2022). Navigation and control development for a four-wheel-steered mobile orchard robot using model-based design. Computers and Electronics in Agriculture, 202, 107410. https://doi.org/10.1016/j.compag.2022.107410

[9] Rajendran, V., Debnath, B., Mghames, S., Mandil, W., Parsa, S., Parsons, S., & Ghalamzan-E., A. (2024). Towards autonomous selective harvesting: A review of robot perception, robot design, motion planning and control. Journal of Field Robotics, 41(7), 2247–2279. https://doi.org/10.1002/rob.22230

[10] Ren, G., Wu, T., Lin, T., Yang, L., Chowdhary, G., Ting, K. C., & Ying, Y. (2024). Mobile robotics platform for strawberry sensing and harvesting within precision indoor farming systems. Journal of Field Robotics, 41(7), 2047–2065. https://doi.org/10.1002/rob.22207

[11] Silwal, A., Davidson, J. R., Karkee, M., Mo, C., Zhang, Q., & Lewis, K. (2017). Design, integration, and field evaluation of a robotic apple harvester. Journal of Field Robotics, 34(6), 1140–1159. https://doi.org/10.1002/rob.21715

[12] Vrochidou, E., Tsakalidou, V. N., Kalathas, I., Gkrimpizis, T., Pachidis, T., & Kaburlasos, V. G. (2022). An overview of end effectors in agricultural robotic harvesting systems. Agriculture, 12(8), 1240. https://doi.org/10.3390/agriculture12081240

[13] Zhang, J., Kang, N., Qu, Q., Zhou, L., & Zhang, H. (2024). Automatic fruit picking technology: A comprehensive review of research advances. Artificial Intelligence Review, 57, 54. https://doi.org/10.1007/s10462-023-10674-2

[14] Zhou, H., Wang, X., Au, W., Kang, H., & Chen, C. (2022). Intelligent robots for fruit harvesting: Recent developments and future challenges. Precision Agriculture, 23(5), 1856–1907. https://doi.org/10.1007/s11119-022-09913-3

# STOCHASTIC MODELING AND GAUSSIAN PROBABILITY DISTRIBUTION OF THE EFFICIENCY OF AUTOMOTIVE BRAKING SYSTEMS IN REAL OPERATING CONDITIONS

/

# *MODELAREA STOCHASTICĂ ȘI DISTRIBUȚIA PROBABILISTICĂ GAUSS A EFICIENȚEI SISTEMELOR DE FRÂNARE AUTO ÎN CONDIȚII REALE DE EXPLOATARE*

**Paula TUDOR[1)], Cristina APETREI[1)], Sorin-Dan IORDACHE[1)], Gabriel MUȘUROI[1)], Gheorghe VOICU*[1)], Marina-Teodora DUDĂU[1)]**

[1)] National University of Science and technology POLITEHNICA Bucharest / Romania

**Tel: 0040 724 715 585; *E-mail: gheorghe.voicu@upb.ro*

***Keywords:*** *Braking system, Gaussian modelling, Stochastic wear, Contact stresses, Periodic Technical Inspection (PTI), Predictive maintenance*

**ABSTRACT**

*The paper presents an integrated approach to the evaluation of the reliability and maintainability of the braking system on an ITP platform under real verification conditions for a set of 54 Dacia Logan cars. An Archard type braking system verification mathematical model is proposed, but the main emphasis is on the theoretical analysis of the experimental field data through the Gauss and GaussAmp nonlinear probability distributions, applied to the axle braking forces and the overall braking efficiency. The results highlight a typical in-service performance of 71.2% for the service brake, with a low standard deviation (6.2%), which demonstrates a high technical homogeneity despite the different runs. Validation of the model by residual error analysis ($\chi^2$) confirms that the performance degradation follows a predictable normal distribution, providing an appreciable mathematical basis for optimizing maintenance strategies. A SW simulation model of the behavior of the brake disc-pad assembly during sudden braking of the car is also proposed.*

**REZUMAT**

*Lucrarea prezintă o abordare integrată privind evaluarea fiabilității și mentenanței sistemului de frânare pe o platformă ITP în condiții reale de verificare pentru un set de 54 autoturisme Dacia Logan. Se propune un model matematic de verificare a sistemului de frânare de tip Archard, însă accentul principal se pune pe analiza teoretică a datelor experimentale din teren prin intermediul distribuțiilor probabilistice non-liniare Gauss și GaussAmp, aplicate forțelor de frânare pe axe și eficienței globale a frânării. Rezultatele evidențiază o performanță tipică în exploatare de 71,2% pentru frâna de serviciu, cu o deviație standard redusă (6,2%), fapt ce demonstrează o omogenitate tehnică ridicată în ciuda rulajelor diferite. Validarea modelului prin analiza erorilor reziduale ($\chi^2$) confirmă că degradarea performanțelor urmează o distribuție normală predictibilă, oferind o bază matematică apreciabilă pentru optimizarea strategiilor de mentenanță. Se propune, de asemenea, un model de simulare SW a comportării ansamblului disc-plăcuțe de frână în momentul frânării bruște a autoturismului.*

## INTRODUCTION

Ensuring vehicle safety under real-world traffic conditions depends on the braking system's ability to generate stable and symmetrical deceleration forces on the wheels of the same axle (*Dascalescu, D., 2008*). During the operational life of the vehicle fleet, the friction pair components—comprising the brake disc and pad composite material (on the front axle), and the drum and brake shoes (on the rear axle)—are subjected to a complex regime of thermomechanical, chemical, and abrasive stresses (*Breuer, B. & Bill, K., 2008*).

These stresses inevitably lead to changes in the initial geometry of the contact elements and the gradual degradation of the friction coefficient (*Kijanski, J., et al., 2021*).

Although European and national regulations impose strict limits regarding the minimum permissible efficiency during periodic technical inspections (ITP) (*ISO 611:2017, CITA, 2018, RNTR-1 OMTCT 2133-2005)*, diagnostic testing on test stands reveals data variability. This dispersion is governed by factors that are difficult to quantify using purely deterministic models: total vehicle mileage ($D_{km}$), user driving style and

loading conditions; and the quality and frequency of maintenance operations performed on each individual vehicle (*Hudec, J., Sarkan, B., 2022, Melendez-Useros, M. et al., 2023*).

In recent literature, the analysis of braking system degradation is approached either through isolated deterministic simulations (finite element analysis – FEA) (*Ipate, G., et al., 2022*) or through purely empirical monitoring at testing stations (*García-León, R.A. & Flórez-Solano, E., Apetrei et al., 2025*).

Idealized numerical models often fail to capture the stochastic nature of real-world operation (*Brereton, R.G., 2014, Genta, G. & Morello, L., 2009, Gillespie, T.D., 1992, Halderman, J.D., 2017*), while simple aggregations of field data do not provide a physical explanation for performance variability (*Heisler, H., 2021*).

To overcome these limitations, the present paper proposes a hybrid methodology. Archard's analytical model is combined with regression equations derived from physical wear profiles to establish a wear baseline. Subsequently, this wear is treated as a source of stochastic perturbation governing the vehicle's macroscopic efficiency.

The primary objective of this work is to implement and validate a non-linear Gaussian probabilistic model applied to braking forces and efficiencies recorded from a sample of 54 passenger cars ((*Apetrei, C., et al., 2025)*. This approach enables the analysis of the technical uniformity of the vehicle fleet and the establishment of predictive indicators for corrective maintenance, without requiring massive computational effort.

## ARCHARD'S ANALYTICAL MODEL AND THE GEOMETRIC CORRELATION OF COMPONENTS

The theoretical basis for the variation in braking performance recorded during periodic technical inspections requires the analysis of wear phenomena at the dynamic interface between the brake disc and the pads. Conventionally, the linear wear of the friction material layer thickness is expressed using Archard's constitutive law. (*Archard, J.F., 1953*):

$$\Delta h_{pad} = k_w \cdot p \cdot s \tag{1}$$

where: $\Delta h_{pad}$ represents the linear reduction in brake pad thickness (m); $k_w$ – the stochastic specific wear coefficient of the tribological pair (m³/Nm); $p$ – the nominal contact pressure generated in the system (Pa); $s$ – the kinematic sliding distance (m).

The distinctive feature of this theoretical model lies in the estimation of the sliding distance ($s$) as a function of the total distance traveled by the vehicle under actual operating conditions $D_{km}$, by introducing a kinematic scaling ratio ($i$) associated with the effective contact length.

$$s = i \cdot L \tag{2}$$

Through the kinematic calibration of components specific to the Dacia Logan platform (the ratio between the mean radius of the front brake disc and the dynamic radius of the standard 185/65 R15 tire), the transformation of the distance traveled into actual slip distance at the friction surface is stabilized by the following linear function:

$$s = 0.368 \cdot D_{km} \cdot 1000 \tag{3}$$

By substituting this kinematic distance into the mass balance equation for the friction material, the mass-based expression for wear is obtained:

$$\Delta m_{pad}(D_{km}) = \rho_{pad} \cdot A_{pad} \cdot (k_w \cdot \mathrm{p} \cdot 0.368 \cdot D_{km} \cdot 1000) \tag{4}$$

where $\rho_{pad}$ represents the density of the semi-metallic composite material, and $A_{pad}$ is the nominal geometric area of the pad surface.

To validate the behavior of this baseline model, the wear dynamics of the front axle components were monitored numerically, with analytical regression equations derived directly from the evolution profiles (Fig. 1).

An analysis of the diagrams in Fig.1 reveals a distinct difference between the two kinematic-tribological regimes in relation to the distance traveled.

It is observed that the residual thickness of the wear material undergoes a sharp, non-linear decrease, governed by an exponential equation with a coefficient of determination of $R^2 = 0.9675$. This trend indicates a critical reduction in heat dissipation capacity as the thickness approaches the replacement threshold (the lower limit of 2.5 mm) (*Kijanski, J. et al., 2021, Jing, H. et al., 2025, Li, R. et al., 2025*).

Due to the vastly superior structural hardness of gray cast iron, the wear of solid and ventilated discs follows extremely shallow slopes (on the order of $10^{-5}$ mm/km), the coefficient of determination ($R^2$) is 0.9648 for the solid disc, as shown in the figure, whereas the slope is slightly steeper for the ventilated disc, with an $R^2$ of 0.9427.

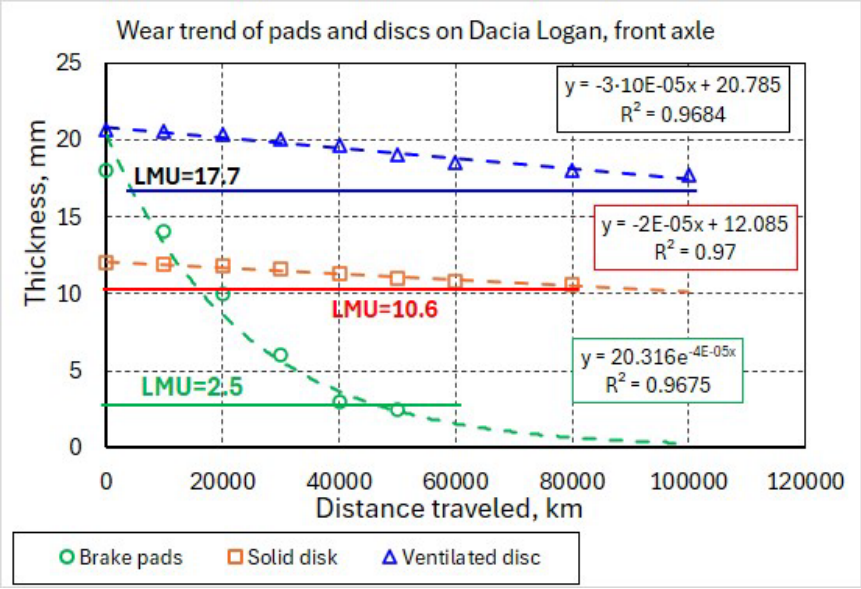



**Fig. 1 - Wear trend of braking system components on the Dacia Logan (front axle)**

**LMU – maximum wear limit*

In the context of this study, these wear profiles act as a source of control disturbance. As the components reach the physical limits highlighted in the graphs (LMU = 10.6 mm for the solid disc and LMU = 17.7 mm for the ventilated one), the actual contact pressure (p) loses its uniformity.

This geometric asymmetry, accumulated over time, generates fluctuations in the braking force measured during the periodic technical inspection (ITP), justifying the shift from the idealized analytical model to Gaussian-type probabilistic nonlinear modeling (*Apetrei, C. et al., 2025, Apetrei, C. et al., 2026*).

## MATERIAL AND METHOD. TESTING PROTOCOL ON THE VEHICLE INSPECTION (ITP) TEST STAND

Experimental research was conducted at an authorized periodic technical inspection (ITP) station in Craiova, Romania. To analyze the dispersion of braking performance, a sample of 54 Dacia Logan passenger cars currently in use was monitored.

All tested vehicles were presented for inspection within the timeframes stipulated by road traffic regulations, thereby ensuring a realistic history of component wear (*Hudec, J., Sarkan, B.,* 2022, *Jardine, A.K.S. & Tsang, A.H.C., 2013*).

Braking force measurement was performed using a computerized roller brake tester (RBT), the high-precision technical and metrological characteristics of which are summarized in Table 1.

**Table 1**

**Technical and metrological parameters of the brake tester**

| Parameter | Nominal value | Metrological characteristic | Value |
|---|---|---|---|
| Maximum axle load | 25 kN | Maximum tangential force on rollers | > 6 kN |
| Roller spacing | 0.8 m | Maximum vertical load per roller | > 10 kN |
| Roller dimensions (D x L) | 202 x 700 mm | Measurement accuracy | ± 0,25% |
| Minimum coefficient of friction | 0.6 | Braking force resolution | < 1% |

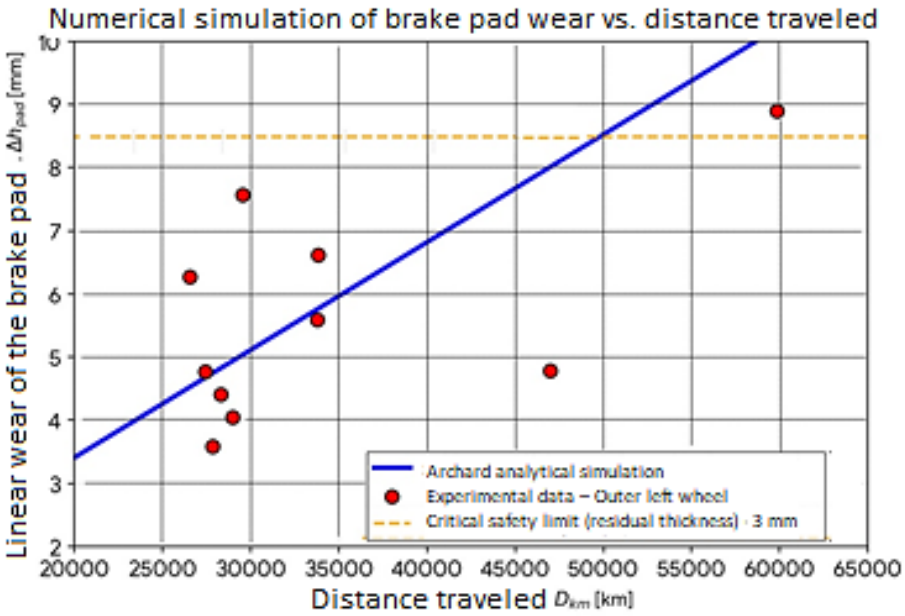



**Fig. 2 - Wear depth based on the calibrated Archard equation, compared with experimental data for a batch of 10 cars inspected at the service center**

The calculated wear indices made it possible to determine the remaining service life of the brake pads. By monitoring the wear rate (0.13–0.26 mm per 1,000 km), it is possible to predict when a vehicle will reach the critical pad thickness limit.

Mass parameters and braking forces recorded for a batch of 54 vehicles tested at the inspection station in Craiova were summarized in terms of operational ranges and average values.

The total vehicle mass ranged from 1,109 kg to 1,319 kg, while front-axle braking forces (service brake) ranged from 1,380–3,090 N for the left wheel and 1,240–2,610 N for the right wheel, with overall axle averages of 2,210 N (left) and 2,020 N (right).

Rear-axle braking forces (service brake) ranged from 510–2,700 N (left) to 1,180–2,330 N (right), with averages of 1,850 N and 1,715 N, respectively.

For the parking brake, rear-axle forces ranged from 420–2,290 N on the left (average 1,435 N) to 840–1,760 N on the right (average 1,360 N).

Based on the acquired force values, the test stand software determines the braking efficiency and imbalance indicators (*IEC 60050-192:2015, Ionescu, G. & Popescu, M., 2019*) using standardized mathematical relationships.

Thus, the overall braking efficiency ($E_f$) was calculated, which represents the ratio of the sum of the maximum braking forces measured on all active wheels to the total weight of the vehicle:

$$E_f = \frac{\Sigma F_f}{m \cdot g} \cdot 100, (\%) \tag{5}$$

where $\Sigma F_f$ is the sum of the forces at the wheels (kN), m is the mass (kg), and $g$ is the gravitational acceleration (9.81 m/s²). The relationship applies separately to the service brake (all four wheels) and the safety/parking brake (rear axle).

The braking force imbalance on each axle (Δr) quantifies the asymmetry between the left and right wheels of the same axle and is calculated relative to the maximum recorded value.

$$\Delta r = \frac{|F_{left} - F_{right}|}{max(F_{left}, F_{right})} \cdot 100, (\%) \tag{6}$$

In accordance with national technical standards (RAR) and harmonized European directives, the minimum acceptability thresholds are set at Ef ≥ 50% for the service brake and Ef ≥ 16% for the parking brake, while the maximum permissible imbalance across an axle is limited to 30%. These limit values form the basis for the Gaussian distribution analysis presented in the following section.

## RESULTS AND DISCUSSION. GAUSSIAN-TYPE PROBABILISTIC MODELING

The experimental data collected from the periodic technical inspection (ITP) brake tester for the 54 passenger cars underwent advanced statistical analysis using MS Excel. The objective was to evaluate the probability density and cumulative frequencies regarding braking system performance.

Based on the previously summarized key data, the assessment of braking efficiency during the periodic technical inspection reveals a Gaussian distribution of the brake tester results for the evaluated vehicles (which were at various stages of service and had varying mileages).

Theoretical modeling of the raw data was performed using a Gaussian function:

$$y = a \cdot e^{-\frac{(x-b)^2}{2c^2}} \tag{7}$$

where: *a* represents the peak frequency or peak value of the efficiency of the tested vehicle batch; *b* – the mean braking efficiency (i.e., the value around which the majority of vehicles cluster); and *c* – the standard deviation (indicating the degree of dispersion or clustering of braking performance relative to the mean value).

For the tested vehicles, braking efficiency values ranged from 54% to 87% for the service brake and from 23% to 67% for the parking brake, with standard deviation values of 6.547 for the service brake and 6.479 for the parking brake. These ranges were distributed into value intervals as shown in Table 1.

**Table 2**

**Gaussian modeling of brake efficiency (%) for Dacia Logan cars undergoing periodic technical inspection (ITP)**

| Service brake | | | | Safety / parking brake | | | |
|---|---|---|---|---|---|---|---|
| Efficiency intervals | Number of vehicles | Modeled value | Error relative to actual data | Efficiency intervals | Number of vehicles | Modeled value | Error relative to actual data |
| 51 | 0 | 0.0555 | 0.0031 | 20 | 0 | 0.0112 | 0.0001 |
| 54 | 1 | 0.2388 | 0.5794 | 23 | 1 | 0.2111 | 0.6224 |
| 57 | 1 | 0.8131 | 0.0349 | 26 | 0 | 1.9127 | 3.6585 |
| 60 | 3 | 2.1908 | 0.6548 | 29 | 5 | 8.3137 | 10.9808 |
| 63 | 8 | 4.6707 | 11.0844 | 32 | 14 | 17.3328 | 11.1077 |
| 66 | 6 | 7.8790 | 3.5305 | 35 | 18 | 17.3328 | 7.1138 |
| 69 | 7 | 10.5166 | 12.3667 | 38 | 11 | 8.3137 | 2.8435 |
| 72 | 13 | 11.1072 | 3.5829 | 41 | 1 | 1.9127 | 0.8330 |
| 75 | 7 | 9.2821 | 5.2080 | 44 | 1 | 0.2111 | 0.6224 |
| 78 | 3 | 6.1377 | 9.8454 | 47 | 0 | 0.0112 | 0.0001 |
| 81 | 1 | 3.2114 | 4.8901 | 50 | 0 | 0.0003 | 0*** |
| 84 | 1 | 1.3295 | 0.1086 | 53 | 0 | 0*** | 0*** |
| 87 | 1 | 0.4355 | 0.3186 | 56 | 1 | 0*** | 1 |
| 90 | 0 | 0.1129 | 0.0127 | 59 | 0 | 0*** | 0*** |
| | | | | 62 | 0 | 0*** | 0*** |
| | | | | 65 | 0 | 0*** | 0*** |
| | | | | 68 | 1 | 0*** | 1 |
| | | | | 71 | 0 | 0*** | 0*** |
| | **52*** | | **52.2202**** | | **53** | | **37.4863** |

** one value was excluded, being far outside the range of values; ** – sum of standard errors; *** – very low values*

Based on the data in the tables, Gaussian distribution curves for the efficiency of the two braking systems (service and safety) were plotted.

These curves are presented in Fig. 3.

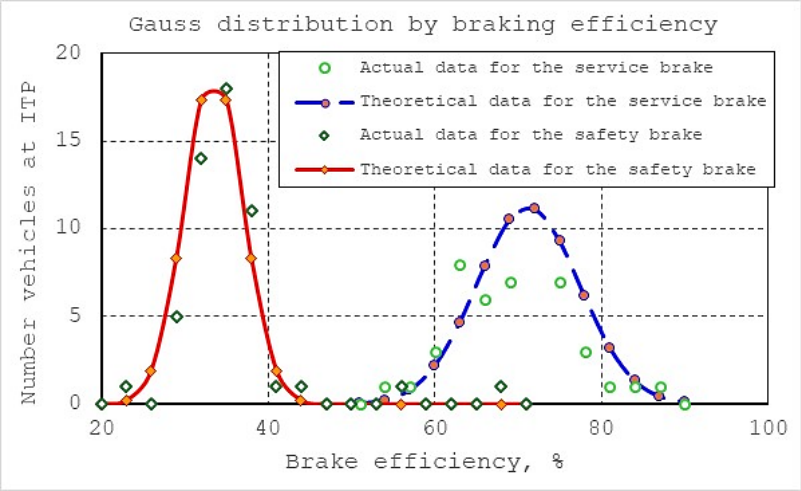



**Fig. 3 - Gaussian distribution of the braking efficiency of the two braking systems in Dacia Logan cars undergoing periodic technical inspection (ITP)**

An analysis of the resulting curves reveals an average efficiency of approximately 68.5% (based on actual data) for the service brake and approximately 34% for the safety brake (based on experimental data). The standard deviations were presented previously.

Furthermore, the modeling indicates a typical operational efficiency of around 71.2% for the service brake; this demonstrates that the majority of vehicles possess high braking capacity—falling within the safety range required for mandatory technical inspection (ITP)—despite varying mileages and accumulated wear (*Jardine, A.K.S. & Tsang, A.H.C., 2013; Trimbitas, R., 2012, Brereton, R.G., 2008)*.

The low standard deviation value ($\sigma$ = 6.2%, derived from Gaussian modeling) indicates that braking system performance remains relatively clustered and consistent. This holds true even though the experimental data points exhibit slight asymmetry around the mean, reflecting technical variability linked to vehicle mileage (with high-mileage vehicles showing values in the lower range of the Gaussian curve).

The deviation of the modeled standard deviation relative to the actual values obtained on the test stand ranged from 0.012 to 12.366 for the service brake and from 0 to 11.107 for the safety brake—values considered acceptable.

Fitting the theoretical curve to the actual data (with a minimum residual error of 52.22) demonstrates that the decline of braking efficiency over the course of operation is not chaotic but follows a normal probability distribution; the isolated drops recorded in the field represent specific instances of pad or disc wear associated with high mileage.

The performance indicators specific to the safety brake, summarized earlier and presented in the preceding table, are highlighted on the left side of the graph in Fig.3.

It can be observed that the peak of the theoretical curve indicates a high concentration of tested vehicles around an efficiency of ≈34% (corresponding to the experimentally obtained value). This value is technically consistent with the design purpose of the secondary system, ensuring the vehicle remains securely immobilized on steep slopes or allowing for controlled deceleration in the event of a major failure of the primary braking system.

The low standard deviation results in a Gaussian curve that is taller and narrower than that of the primary braking system. This demonstrates that cumulative wear over time and the distances traveled by vehicles prior to the periodic technical inspection (ITP) have a relatively smaller impact on the parking brake compared to the service brake.

Technical performance remains predictable and consistent across the entire sample of tested vehicles, as the system is used much less frequently in dynamic conditions.

Minimizing the total residual error to a critical value of 37.48 validates the correlation between the actual ITP sample and the Gaussian normal distribution curve. The specific deviations recorded (such as the experimental peak of 18 vehicles at 35% efficiency) reflect the sensitivity thresholds and mechanical resolution of the roller test stand used in the inspection line.

To capture the stochastic nature of braking performance degradation, the probabilistic analysis was extended to the force imbalance between the wheels of the same axle. The parameters of the Gaussian statistical regressions (Equation 8) are summarized in Table 3 (Left / Right).

Table 3

**Gaussian statistical regression parameters for braking force imbalance**

| Axle | a | b | c | $R^2$ coeff. | $\chi^2$ test |
|---|---|---|---|---|---|
| Front Axle (L / R) | 15 / 16 | 2200 / 2020 | 270 / 260 | 0.971 / 0.978 | 0.107 / 0.204 |
| Rear Axle (L / R) | 17 / 17 | 2025 / 1900 | 215 / 228 | 0.951 / 961 | 0.001 / 0.007 |

Regarding the distribution of braking forces at the front-axle wheels of Dacia Logan cars inspected at the technical inspection station, non-linear statistical modeling using the Gaussian function (Equation 8) indicated good convergence with the experimental data (weighted residual error: $\chi^2 = 0.107$ for the left wheel and $\chi^2 = 0.204$ for the right wheel).

Figure 4 presents a comparative analysis of the experimental frequency distributions and the theoretical Gaussian models for the braking forces recorded on the front axle (left wheel versus right wheel).

A relatively good geometric convergence of both mathematical models with the data collected at the inspection station is observed.

Analysis of the function's central parameters reveals a systematic asymmetry within the analyzed vehicle group, whereby the median force value for the left wheel (2200 N) is higher than that recorded for the right wheel (2020 N).

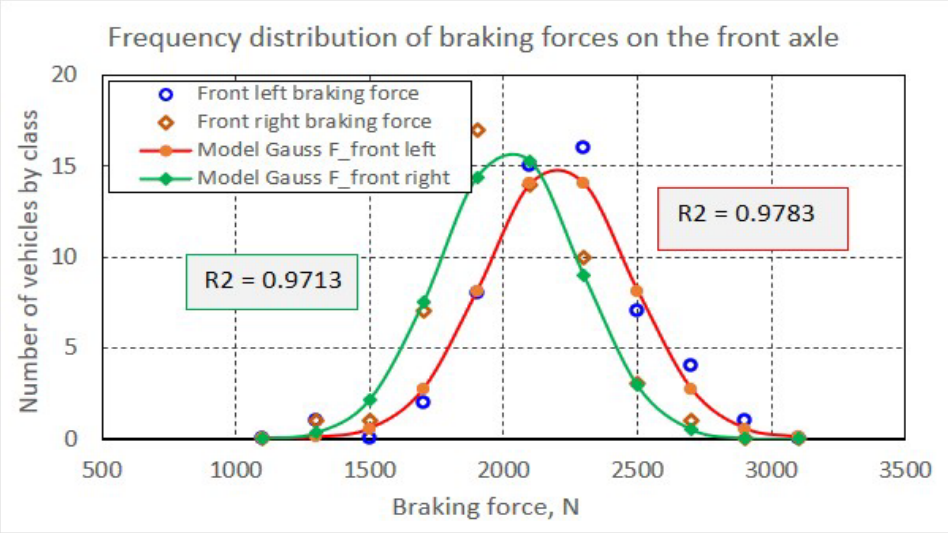



**Fig. 4 - Modeling of experimental data on front-wheel braking force distribution using the Gaussian statistical function for Dacia Logan passenger cars tested at the periodic technical inspection station.**

This offset between the two probability profiles (Fig.4) indicates an average structural imbalance of approximately 8.18% on the front axle—statistically induced by operational factors and the asymmetric wear of friction components (discs/pads)—although the vast majority of vehicles remain within the legal dispersion limits defined by the width parameters: 260 N for the left wheel and 270 N for the right wheel.

The frequency distribution of braking forces for the rear axle also shows a good correlation with the theoretical Gaussian model, yet it exhibits certain notable features in the range of mean values.

The 54 passenger cars, grouped into class intervals based on braking force (N), show peak frequencies in the central range—around 2025 N for the left wheel and 1900 N for the right wheel.

The theoretical curves (based on the Gaussian model, Equation 8) closely follow the general trend of the experimental data points. This confirms that the force distribution follows a normal distribution.

A pronounced experimental peak is observed (with a frequency exceeding 15 vehicles per class) that rises above the theoretical Gaussian curve. The behavior of the rear-axle braking system indicates high data homogeneity around the mean braking value, suggesting that the majority of the tested vehicles exhibit very similar software and mechanical performance on the rear axle.

The total residual error calculated for the modeling of this axle yields a value of $\chi^2 = 17.58$ for the left wheel and $\chi^2 = 22.48$ for the right wheel, reflecting a difference in the distribution of experimental data relative to the theoretical curves.

Figure 5 presents a comparative analysis of the experimental frequency distributions and the Gaussian theoretical models for the braking forces recorded on the rear axle (left wheel versus right wheel).

The clustering of data around the 2000 N mark indicates that, although braking forces on the rear axle are lower or differently distributed due to design factors (such as the brake proportioning valve and lower axle load), the vehicle's braking behavior remains predictable and stable.

The general alignment of the peaks of the two curves (left/right) also indicates a relatively low average imbalance under static periodic technical inspection (ITP) conditions, with operational factors or asymmetric wear having a less pronounced impact on this axle compared to the front axle.

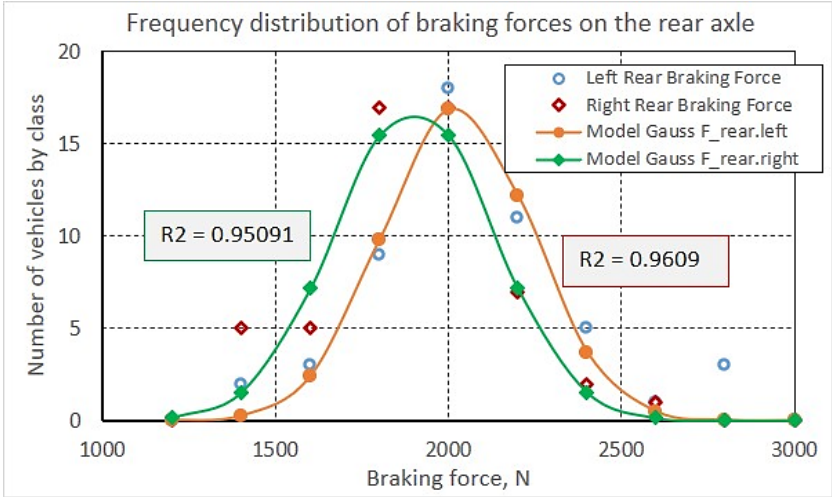



**Fig .5 - Gaussian modeling of the braking force distribution on the rear wheels of Dacia Logan cars tested at the periodic technical inspection station.**

Non-linear statistical analysis and Gaussian-based probabilistic modeling applied to raw data from Periodic Technical Inspection (PTI) stations for Dacia Logan passenger cars reveal a typical service brake efficiency of 71.2%.

Coupled with a low standard deviation ($\sigma$ = 6.2%), this demonstrates that the vast majority of vehicles in the tested sample maintain high braking capacity—clustered within the regulated safety range—regardless of variations in service life or mileage. Isolated drops in efficiency reflect specific instances of advanced wear in the disc-pad assembly.

For the safety brake, the Gaussian distribution exhibits a taller, narrower curve, with a high concentration of vehicles around a mean efficiency of ≈34%. This consistent and predictable technical behavior indicates that cumulative wear has a significantly lesser impact on the secondary braking system, which is used much less frequently during dynamic operation than the service brake.

Modeling of front-axle braking forces using the Gauss function revealed a systematic asymmetry across the tested batch. The median force value for the left wheel (2200 N) exceeds that of the right wheel (2020 N), indicating an average structural imbalance of 8.18%.

This probabilistic deviation is directly influenced by operational factors and the asymmetric wear of friction components, although the values remain within the legally permissible dispersion limits.

In contrast to the front axle, the braking forces on the rear axle (clustered around 2000 N) exhibit a significantly lower average imbalance and marked consistency around the central values (2025 N for the left and 1900 N for the right).

This confirms that the impact of asymmetric wear or operational factors is less pronounced on the rear axle, with the vehicle's behavior remaining stable due to design characteristics (such as the brake pressure regulator and lower axle load).

The geometric convergence of theoretical curves with actual experimental data—demonstrated by minimal residual errors (sum of standard errors = 52.22 for the service brake; $\chi^2$ = 9.73 / 11.79 for the front axle; and $\chi^2$ = 17.58 / 22.48 for the rear axle) confirms the validity of the Gaussian normal distribution law in assessing the degradation of braking systems. Performance deviation is not a random process but rather a form of degradation governed by probabilistic laws that can be successfully applied in predictive maintenance activities.

Configured differently, Figure 6 presents a comparison of the probabilistic (Gaussian) behavior of the braking force on the two sides of the vehicle. It can be observed that, for the front axle, the distribution curve is shifted toward higher values (≈2200 N) compared to the rear axle on the left side (Figure 6a). Figure 6b compares the braking forces on the two right-side wheels; the peak of the curve for the front wheel lies around 2020 N.

This lateral grouping highlights the dynamic correlation between the axles, visually demonstrating the effect of the brake proportioning valve and mass transfer. The forces on the front axle are significantly higher and more tightly grouped, whereas the rear axle (on both the left and right sides) exhibits sharper yet offset peaks, confirming less pronounced wear under dynamic conditions but a dispersion characteristic of the drum brake system.

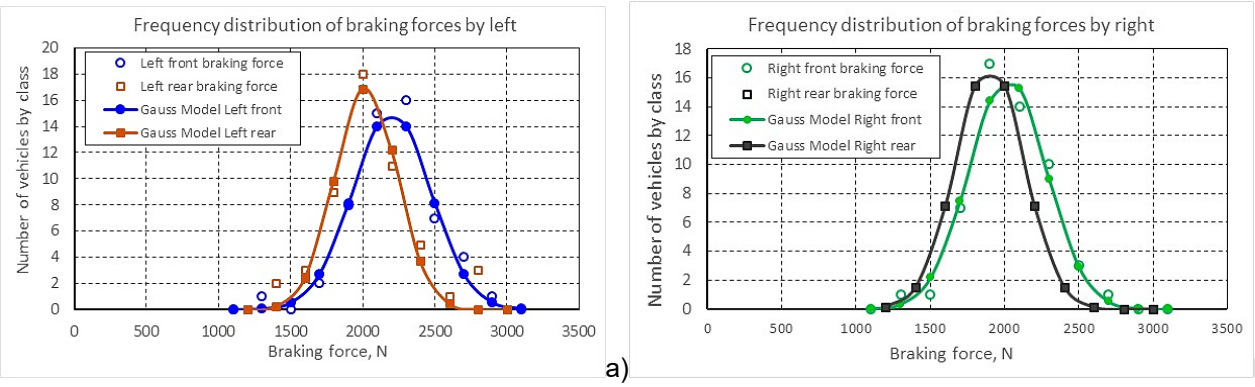



**Fig. 6 - Distribution of braking force frequencies grouped by vehicle side (Left vs. Right)**

## TRANSIENT 3D NUMERICAL ANALYSIS OF THE DISC-PAD BRAKING TORQUE

To validate the experimental and probabilistic results obtained, a complex transient 3D numerical simulation was implemented using the Finite Element Method (FEM) within the ANSYS Workbench R16 software.

The geometric model includes a ventilated brake disc with a nominal diameter of 259 mm and the corresponding friction pads—standard components for the front axle of the Dacia Logan platform. The structural assembly was discretized into a high-quality mesh consisting of 85,856 nodes and 44,867 finite elements.

The tribological interface and frictional contact between the semi-metallic composite pad and the gray cast iron disc were defined using CONTA175 and TARGET170 3D elements. The contact formulation was governed by the augmented Lagrange algorithm, which ensures optimal penetration control and high numerical stability in the presence of severe contact nonlinearities.

The transient analysis simulates a severe sudden (emergency) braking maneuver, decelerating the vehicle from an initial speed of 87.5 km/h to a complete stop.

Kinetic energy dissipation is modeled by applying a time-varying rotational speed to the disc, correlated with the dynamic radius of a standard 185/65 R15 tire. The actuation mechanism consists of a progressive hydraulic pressure profile applied to the back of the brake pads, rising rapidly from 0 to 7.5 MPa to replicate the driver's maximum effort on the brake pedal.

The nonlinear structural-frictional equations were solved using the implicit Newton-Raphson solver. The numerical solution demonstrated robust stability, with convergence achieved in 41 iterations, ensuring the reliability of the calculated stress distributions.

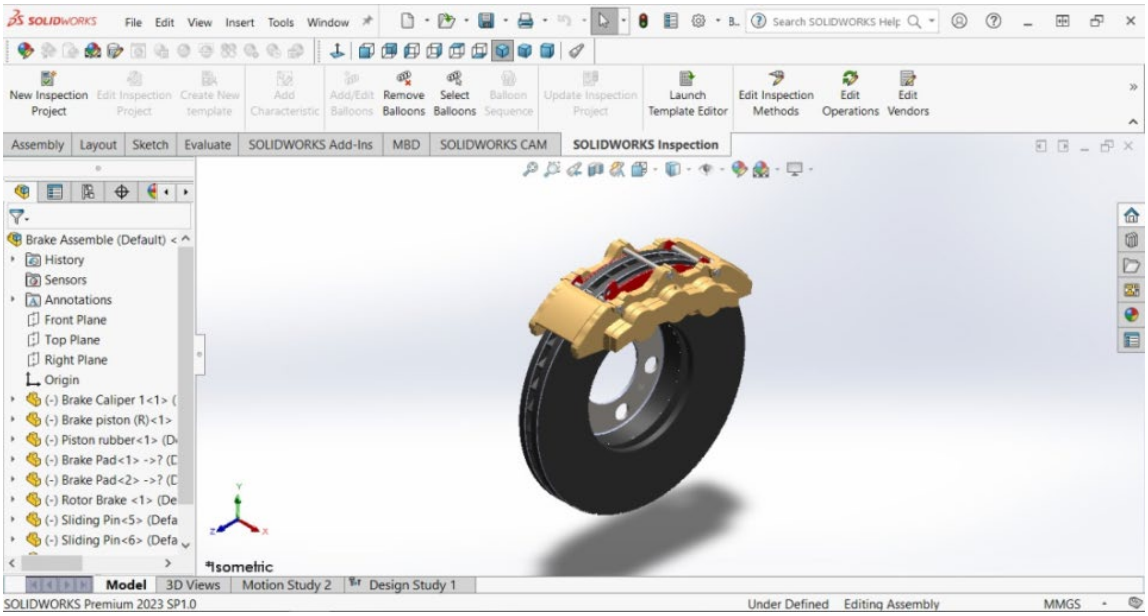



**Fig. 7- 3D finite element model of the ventilated disc-pad assembly in ANSYS Workbench**

Ecuațiile structural-fricționale cu grad ridicat de nelinearitate au fost rezolvate cu ajutorul solverului implicit Newton-Raphson. Soluția numerică a demonstrat o stabilitate robustă, convergența fiind obținută în 41 de iterații, ceea ce garantează fiabilitatea distribuțiilor de tensiuni calculate.

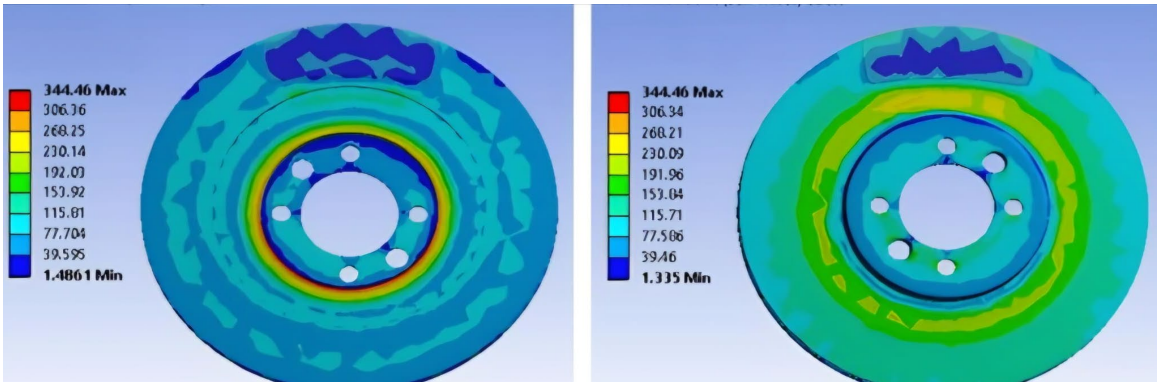



**Fig. 8 - Equivalent (von Mises) stress distribution on the inner disc (left) and the outer disc (right)**

Numerical simulation indicates that the von Mises equivalent stress reaches a maximum value of 57.87 MPa. As illustrated in Fig.8, this peak stress concentration is located at the leading edge of the inner pad's friction surface—an area where local contact pressure becomes highly asymmetric due to the kinematic behavior of the floating caliper.

This pronounced spatial stress gradient correlates perfectly with the irregular linear wear profiles identified during the experimental monitoring of the fleet of 54 passenger cars. Local structural stress concentrations act as a primary driver of micro-geometric pad degradation, directly fueling braking force fluctuations and the average structural imbalance on the front axle (8.18%) previously identified via Gaussian probability curves.

## CONCLUSIONS

The stochastic analysis and nonlinear probabilistic modeling of braking system performance for the sample of 54 passenger cars led to the following main conclusions:

- ✓ The use of nonlinear Gaussian distributions proved to be a reliable mathematical tool for assessing the technical quality of the vehicle fleet, offering a rapid and accurate alternative to complex numerical simulations such as FEA.
- ✓ The service brake exhibits high technical consistency, with a Gaussian central value calibrated at xc = 67.18% and an excellent coefficient of determination ($R^2$ = 0.9768), confirming that the vast majority of vehicles exceed the legal safety threshold of 50%.

- ✓ The parking brake shows a lower central value (xc = 32.49%), with the Gaussian model demonstrating a direct fit to the field data ($\chi^2$ = 7.441). It is characterized by negative skewness ($g$ = -0.3), indicating the presence of vehicles with localized faults in the cable actuation mechanisms or the shoe self-adjustment systems.
- ✓ In contrast, the rear axle exhibits significant dispersion ($\chi^2$ = 11.052), caused by uneven physical wear of the drum brake components or improper in-service adjustments.
- ✓ Extending the Archard model using platform-specific kinematic equations ($s = 0.368 \cdot D_{km} \cdot 1000$) provides a physical explanation for the observed pressure fluctuations. These geometric deviations—highlighted in the logarithmic and linear profiles—are the direct source of the macroscopic dispersion modeled by the Gaussian curves.

The developed statistical models can be directly implemented into vehicle inspection station software for the early diagnosis of anomalies, the optimization of manufacturing tolerances, and the preventive maintenance planning of vehicle fleets.

## REFERENCES


[1] Apetrei, C., Tudor, P., Constantin, G. A., Voicu, G., Iordache, S. D. (2026), Statistical and Experimental Investigation on the Irregular Wear of Disc Brake Components in Logan Cars: A Case Study, U.P.B. Scientific Bulletin, Series D: Mechanical Engineering, (accepted for publication)

[2] Apetrei, C., Voicu, G., Iordache, S. D., Constantin, G. A., Saracin, I., Tudor, P., Ipate, G. (2025), Research on the Efficiency of the Braking System in Dacia Logan Cars", Machines, Vol. 13, Iss. 10,.

[3] Archard, J. F., Contact and Rubbing of Flat Surfaces, Journal of Applied Physics, 24(8), pp. 981–988, 1953.

[4] Brereton, R.G. (2014), The Normal Distribution, Journal of Chemometrics, Vol. 28, pp. 789–792.

[5] Breuer, B., Bill, K. H., The Brake Technology Handbook, SAE International, 2008.

[6] CITA Recommendation N 8, Brake Testing in Periodic Technical Inspection, CITA/WG1, 2018.

[7] Dascalescu, D. (2008), Dynamics of Road Vehicles (in Romanian), Politehnium Publishing House, Iasi.

[8] García-León, R. A., Flórez-Solano, E. (2017), Dynamic analysis of three autoventilated brake discs, Ingeniería e Investigación, vol. 37, nr. 3, pp. 102–114, DOI: 10.15446/ing.investig.v37n3.63381.

[9] Genta, G., Morello, L. (2020), The Automotive Chassis: System Design, Springer, Vol.1-.2, doi: 10.1007/978-3-030-35709-2.

[10] Gillespie, T.D. (1992), Fundamentals of Vehicle Dynamics, SAE International.

[11] Halderman, J. D. (2017), Automotive Brake Systems, Pearson Education.

[12] Heisler, H., Advanced Vehicle Technology, 3rd Edition, Butterworth-Heinemann, 2021.

[13] Hudec, J., Sarkan, B. (2022), Effect of Periodic Technical Inspections of Vehicles on Traffic Accidents in the Slovak Republic, Communications - Scientific Letters of the University of Zilina, 24(3), pp. A142–A159.

[14] IEC 60050-192:2015, International Electrotechnical Vocabulary - Dependability.

[15] Ionescu, G., Popescu, M. (2019), Reliability and Maintainability of Road Technical Systems, Technical Publishing House, Bucharest (in Romanian).

[16] Ipate, G., Ilie, F., Cristescu, A. C. (2020), Finite element 3D numerical simulation study of car braking systems and brake disc/drum - pad/shoe friction couple, E3S Web of Conferences, vol. 180, art. 03003.

[17] ISO 611:2017, Road Vehicles — Braking of Automotive Vehicles and Their Trailers — Vocabulary, International Organization for Standardization.

[18] Jardine, A.K.S., Tsang, A.H.C. (2013), Maintenance, Replacement and Reliability: Theory and Applications, CRC Press.

[19] Jing, H., Lin, Q., Liu, M., Liu, H. (2025), Electromechanical Braking Systems and Control Technology: A Survey and Practice", Proceedings of the Institution of Mechanical Engineers, Part D: Journal of Automobile Engineering, vol. 239, pp. 4551–4573.

[20] Kijanski, J., Otto, J., Stebner, F., Weber, J., Franke, R., Ostermeyer, G.P. (2021), Investigation of Influences on Brake Pad Wear, SAE International Journal of Advances and Current Practices in Mobility, vol. 3, nr. 2, pp. 933–993, 2021. DOI: 10.4271/2020-01-1614.

[21] Li, R., Shang, Y., Cai, J. Liu, X., Geng, L., Qi, P., Jiao, Z. (2025), Fault Detection and Fault-Tolerant Control Based on Bi-LSTM Network and SPRT for Aircraft Braking System, Chinese Journal of Mechanical Engineering, 38:64, doi:10.1186/s10033-025-01219-5.
[22] Melendez-Useros, M., Jimenez-Salas, M., Viadero-Monasterio, F., Lopez Boada, M.J. (2023), Tire Slip H∞ Control for Optimal Braking Depending on Road Condition, Sensors, Vol. 23, Iss. 3, 1417.
[23] RNTR-1 OMTCT 2133-2005 cons OMTI 1127-2023, Official regulation regarding the periodic technical inspection (ITP) of vehicles registered in Romania.
[24] Trimbitas, R., (2012), Classical Probability Distributions, Main Laws of Probability (în Romanian), Babes-Bolyai University, Cluj-Napoca.

# PRELIMINARY FUNCTIONAL AND THERMAL TESTING OF ELECTRIC PYROLYSIS EQUIPMENT FOR OBTAINING PHOSPHORUS-RICH BIOFERTILIZERS

/

# *TESTAREA PRELIMINARĂ A UNUI ECHIPAMENT ELECTRIC DE PIROLIZĂ PENTRU OBTINEREA DE BIOFERTILIZANȚI BOGAȚI ÎN FOSFOR*

**Vasilica STEFAN*[1)], Ana ZAICA[1)], Alin HARABAGIU[1)], Stefano MANTOVANI[1)], Alexandra VISAN[1)], Gabriel GHEORGHE[1)], Aura DUMITRESCU[1)], George LAZAR[1)], Dragos DUMITRU[1)], Radu Nicolae SOARE[2)]**

[1)] National Institute of Research-Development for Machines and Installations Designed for Agriculture and Food Industry - INMA Bucharest / Romania;

[2)] National University of Science and Technology POLITEHNICA Bucharest / Romania.

**Tel: 0722 245 443; *E-mail: valle_vali@yaho.com*

***Keywords:*** *pyrolysis equipment, poultry manure, thermal testing, temperature control, slow pyrolysis, biofertilizer*

## ABSTRACT

*This paper presents the preliminary functional and thermal testing of electric pyrolysis equipment developed for the controlled thermal conversion of poultry manure, with the long-term objective of producing phosphorus-rich biofertilizers. The experimental assessment focused on equipment operation, including no-load start-up, temperature control, thermal stability and external surface temperatures. The experimental unit comprises a refractory stainless-steel reactor, an electric heating system with a total installed power of 19 kW, a Type S thermocouple and a programmable temperature controller. Initial no-load checks were performed at 200°C and subsequently at internal temperatures up to 1000°C. Additional operating cycles were conducted at target temperatures of 400, 600 and 800°C, with temperature values recorded every 5 min for 180 min. The target temperatures were reached in approximately 60 min. During the 60–120 min holding stages, mean temperatures of 400.38, 601.00 and 800.46°C were obtained, with temporal standard deviations below 1.4°C. The preliminary results confirmed stable temperature control and satisfactory thermal insulation, while a post-heating temperature overshoot indicated the need for further analysis of thermal inertia and cooling behaviour.*

## REZUMAT

*Lucrarea prezintă testarea preliminară funcțională și termică a unui echipament electric de piroliză dezvoltat pentru conversia termică controlată a dejecțiilor avicole, având ca obiectiv pe termen lung obținerea de biofertilizanți bogați în fosfor. Evaluarea experimentală s-a concentrat exclusiv asupra funcționării echipamentului: pornirea în gol, controlul temperaturii, stabilitatea regimurilor termice și temperaturile suprafețelor exterioare. Echipamentul include un reactor din oțel refractar, un sistem electric de încălzire cu puterea instalată totală de 19 kW, un termocuplu tip S și un regulator programabil de temperatură. Verificările inițiale în gol au fost realizate la 200°C, urmate de verificări până la 1000°C. Ciclurile de funcționare au fost efectuate la temperaturi țintă de 400, 600 și 800°C, cu înregistrări la intervale de 5 min, timp de 180 min. Temperaturile țintă au fost atinse în aproximativ 60 min, iar în intervalul de menținere 60–120 min s-au obținut valori medii de 400,38, 601,00 și 800,46°C, cu abateri standard temporale sub 1,4°C. Rezultatele au confirmat stabilitatea controlului termic și comportarea corespunzătoare a izolației.*

## INTRODUCTION

Intensive poultry production generates large quantities of manure and litter that require controlled management in order to limit odour, greenhouse-gas emissions, nutrient losses and contamination of soil and water. At the same time, poultry residues contain significant amounts of nitrogen, potassium, phosphorus and mineral constituents, which makes them a potentially valuable secondary resource rather than only a waste stream. Recent research therefore increasingly approaches poultry manure valorization from a circular-economy perspective, with emphasis on stabilization of the organic fraction and recovery of plant nutrients *(Zamani et al., 2026; Knijnenburg et al., 2025, Stefan et al. 2023).*

Phosphorus is of particular interest because it is an essential nutrient for crop production and because inappropriate manure application may lead to phosphorus accumulation in agricultural soils and

subsequent losses to surface waters. Studies on chicken and poultry manure have shown that pyrolysis can retain and concentrate phosphorus in the solid fraction, although its chemical form and plant availability depend strongly on the thermal regime *(Bruun et al., 2017; Bergfeldt et al., 2018; Keskinen et al., 2019; Sarvi et al., 2021; Leite et al., 2023).*

Pyrolysis is a thermochemical conversion process carried out under oxygen-limited conditions and produces solid, liquid and gaseous fractions. Compared with direct application of raw manure, the process can improve material stability and facilitate nutrient recycling. For poultry-derived feedstocks, slow and intermediate pyrolysis have been investigated over broad temperature ranges, and the final temperature has repeatedly been identified as one of the main variables controlling product distribution, carbonization and phosphorus speciation *(Hadroug et al., 2019; Ippolito et al., 2020; Kuryntseva et al., 2022; Sanford et al., 2022; Simbolon et al., 2024).* Recent studies have also explored the use of poultry manure as a feedstock for nutrient-enriched or slow-release biofertilizers *(Piash et al., 2022; Vimal et al., 2022; Padilla et al., 2023).*

Although the properties of the resulting biochar are important, reproducible production first requires a reactor and heating system capable of executing a prescribed temperature programme. For experimental equipment, the ability to reach the target temperature within the programmed time, maintain a stable thermal plateau, monitor temperature continuously and limit heat transfer to the external casing are basic prerequisites before chemical or agronomic evaluation of the products. Temperature-control performance is especially relevant when different treatment temperatures are compared, because uncontrolled deviations may confound the effect attributed to the pyrolysis regime.

For this purpose, an experimental electrically heated pyrolysis unit was designed and manufactured within a research project focused on the valorization of poultry manure through the production of phosphorus-rich biofertilizers. The equipment was conceived as a laboratory/pilot-scale unit with programmable electric heating, a removable reactor, multilayer thermal insulation and controlled evacuation of gaseous products.

The present study is deliberately limited to the equipment itself and does not assess the chemical composition or agronomic effectiveness of the resulting biochar. The objective was to perform a preliminary functional and thermal evaluation of the developed unit by analysing no-load operation, external surface temperatures, heating behaviour, temperature stability at 400, 600 and 800 °C, and the initial cooling response after heating was stopped.

## MATERIALS AND METHODS

The experimental pyrolysis equipment, designated EP, was designed and manufactured for the controlled thermal treatment of poultry manure. The unit consists of a removable reactor, a refractory heating chamber, an electric heating system, a programmable command and control panel, a metallic external casing, multilayer thermal insulation, a lower discharge system and an evacuation path for volatile products. The complete equipment is shown in Fig. 1.

The reactor was manufactured from AISI 310 refractory stainless steel with a wall thickness of 5 mm. Its internal dimensions are 263 × 263 × 665 mm, corresponding to a useful volume of approximately 0.046 $m^3$. The reactor is introduced into the heating chamber and is provided with an upper sealed cover and a lower discharge zone. The heating chamber was constructed from refractory insulating bricks. Additional insulation between the hot zone and the external casing comprises ceramic fibre, Superwool Plus Blok 800 insulation and basalt mineral wool. *(Ștefan et al., 2024).*

The heating system consists of six Kanthal A1 electrical resistance elements distributed inside the heating chamber, with a total installed power of approximately 19 kW. The equipment is supplied from a three-phase 400 V electrical network.

The temperature-control system uses an ART 2006 programmable controller receiving the temperature signal from a Type S PtRh10%-Pt thermocouple. The controller allows programmed heating and holding stages and displays the measured temperature in real time. Electrical protection includes automatic circuit breakers, a contactor, a main switch and a temperature/safety limiting system.




**Fig. 1 - Experimental electric pyrolysis equipment, EP**

**Table 1**

**Main constructive and functional characteristics of the experimental equipment**

| Parameter | Unit | Value / specification |
|---|---|---|
| Overall length | mm | 1500 |
| Overall width | mm | 1100 |
| Height, lid closed | mm | 1450 |
| Height, lid opened | mm | 2130 |
| Equipment mass | kg | 370 |
| Reactor useful volume | m³ | 0.046 |
| Reactor material | - | AISI 310, 5 mm |
| Installed heating power | kW | 19 |
| Electrical supply | V | 400, three-phase |
| Temperature sensor | - | Type S PtRh10%-Pt |
| Temperature controller | - | ART 2006 |




**Fig. 2 - Main functional components:**
*(a) command and control panel; (b) electrical heating elements*

Before functional testing, the equipment was visually and mechanically inspected. The integrity of the electrical conductors, protective devices, interlocks, temperature-measurement chain, heating elements, cover closure and accessible adjustments was checked. The internal chamber was also inspected to verify that no foreign objects were present and that the equipment could be operated safely.

The preliminary no-load test was initiated from an ambient temperature of approximately 27°C. The furnace was first programmed to reach 200°C, followed by a 30 min holding period at this temperature. Correct operation of the thermocouple, resistance heaters and programmable controller was monitored. After this commissioning stage, the internal furnace temperature was progressively increased to 400, 600, 800 and 1000°C. At each internal temperature level, the external surface temperature was measured at three representative locations: the upper lid, the lateral walls and the lower zone of the casing. These measurements were used as practical indicators of the behaviour of the thermal insulation; they were not interpreted as direct measurements of heat loss or thermal efficiency.

After the no-load checks, three programmed operating cycles were analysed at nominal temperatures of 400, 600 and 800°C. For these cycles the reactor contained 4 kg of prepared poultry manure in order to reproduce an actual thermal load; the chemical and agronomic properties of the material obtained after treatment were outside the scope of the present paper. Each cycle was monitored for 180 min.

Temperature was recorded at 5 min intervals, resulting in 37 measurements per cycle. The first 60 min represented the programmed heating stage, the interval from 60 to 120 min represented the nominal holding stage, and the interval from 120 to 180 min was used to monitor the initial natural cooling response with the reactor kept closed.

The measured temperature series were processed using descriptive indicators relevant to equipment performance. For each operating regime, the temperature at 60 min, the average chamber heating rate between the initial reading and 60 min, the mean temperature during the 60–120 min holding interval, the temporal standard deviation and the minimum–maximum interval during holding were calculated.

The maximum temperature recorded after the heating stage was switched off was also identified in order to characterize the transient thermal overshoot. Because one programmed cycle was available for each set point, the reported standard deviation describes temperature fluctuation in time during the holding stage and should not be interpreted as repeatability between independent experimental replicates.

## RESULTS

The preliminary inspections and the no-load commissioning test confirmed the functional operation of the electrical supply, heating elements, thermocouple, programmable controller and safety interlocks. The controller displayed the chamber temperature continuously and allowed the set point to be modified during operation. No abnormal mechanical vibration or control-system error was observed during the preliminary check.

The external surface temperatures measured during the progressive no-load thermal test are presented in Table 2.

As the internal furnace temperature increased from 200 to 1000°C, the temperatures of the lid, lateral walls and lower casing zone increased gradually. At the highest internal temperature of 1000°C, the measured external temperatures were 85°C at the lid, 86°C at the lateral walls and 89°C in the lower zone.

The lower zone produced the highest reading at 200, 400, 600, 800 and 1000°C, although the differences among the three external locations became relatively small at the highest set point.

**Table 2**

**External surface temperatures during the progressive no-load thermal test**

| Internal furnace temperature [°C] | Lid temperature [°C] | Side-wall temperature [°C] | Lower-zone temperature [°C] |
|---|---|---|---|
| 200 | 27 | 30 | 41 |
| 400 | 40 | 38 | 49 |
| 600 | 58 | 55 | 64 |
| 800 | 79 | 72 | 80 |
| 1000 | 85 | 86 | 89 |

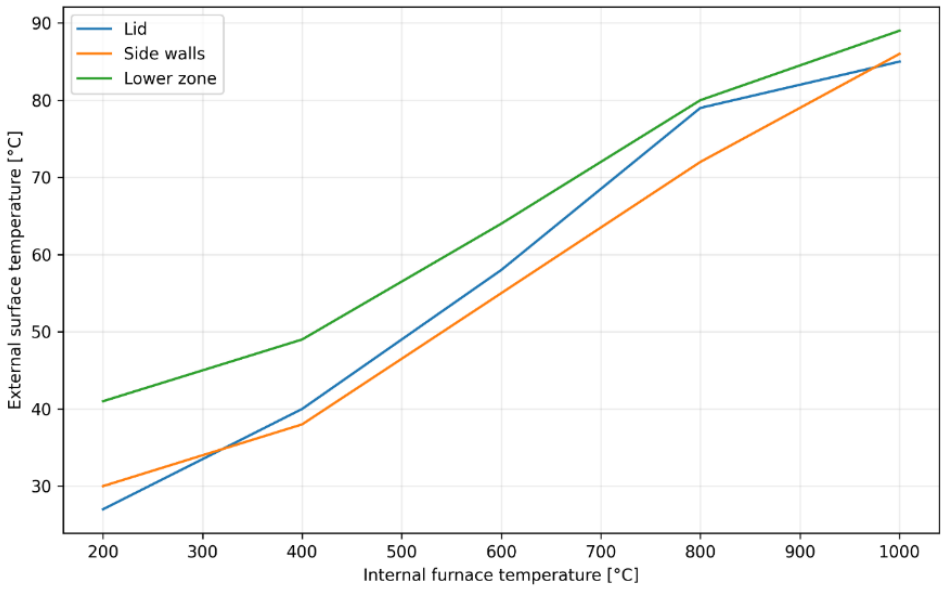



**Fig. 3 - External surface temperatures as a function of the internal furnace temperature**

The programmed operating cycles at 400, 600 and 800°C are compared in Fig. 4. In all three cases, the target thermal level was reached at approximately 60 min. The initial chamber temperature was 29°C for the 400°C cycle, 23°C for the 600°C cycle and 30°C for the 800°C cycle. At 60 min, the recorded values were 400, 600 and 799°C, respectively.

The calculated mean heating rates from the initial measurement to 60 min were 6.18, 9.62 and 12.82°C/min, showing the expected increase in average rate as a higher final set point was imposed over the same nominal heating duration.

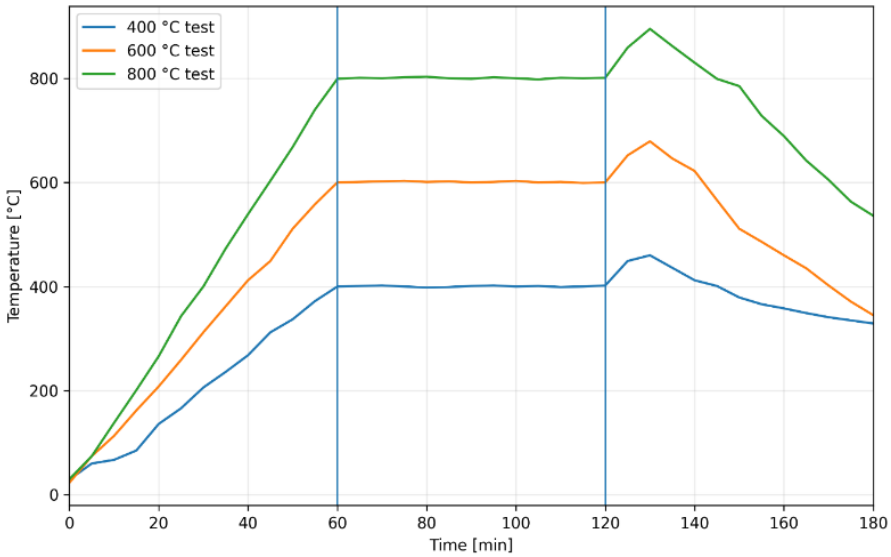



**Fig. 4 - Temperature evolution during the programmed 400, 600 and 800°C operating cycles**

Temperature control during the holding stages was stable for all three set points. Between 60 and 120 min, the 400°C cycle varied from 398 to 402°C, the 600°C cycle from 599 to 603°C, and the 800°C cycle from 798 to 803°C.

The corresponding mean temperatures were 400.38, 601.00 and 800.46°C. The temporal standard deviation remained between 1.22 and 1.39°C, indicating small fluctuations around the programmed value during the one-hour holding interval. The main calculated thermal indicators are summarized in Table 3.

**Table 3**

**Calculated indicators of heating, holding stability and initial cooling response**

| Set point [°C] | Initial T [°C] | Mean heating rate [°C/min] | Holding mean ± SD [°C] | Holding range [°C] | Post-heating peak [°C] |
|---|---|---|---|---|---|
| 400 | 29 | 6.18 | 400.38 ± 1.26 | 398–402 | 460 |
| 600 | 23 | 9.62 | 601.00 ± 1.22 | 599–603 | 679 |
| 800 | 30 | 12.82 | 800.46 ± 1.39 | 798–803 | 895 |

Immediately after electrical heating was stopped at 120 min, the chamber temperature did not decrease monotonically. A transient rise was recorded in each cycle. The maximum values were 460°C at 130 min for the 400°C test, 679°C at 130 min for the 600°C test and 895°C at 130 min for the 800°C test. Relative to the nominal set points, the observed overshoots were approximately 60, 79 and 95°C, respectively.

After the peak, the temperature decreased gradually. At 180 min the chamber temperatures were still 329, 345 and 536°C for the 400, 600 and 800°C cycles, demonstrating that the refractory and insulated assembly retained a substantial amount of thermal energy during the first hour of natural cooling.

The measured curves therefore show two distinct operating characteristics of the equipment. First, the programmable control system maintained the selected set points with limited temporal fluctuation during the holding stage. Second, the shutdown response was strongly influenced by stored heat and by the thermal load inside the reactor, leading to a delayed temperature maximum before cooling became dominant.

The present dataset does not allow the separate contributions of heating-element inertia, refractory-wall heat storage, internal heat transfer and residual reactions in the treated material to be quantified. Consequently, the overshoot is reported as an observed equipment/process response rather than being assigned to a single mechanism.

## CONCLUSIONS

The preliminary tests confirmed that the developed electric pyrolysis equipment can operate over the temperature range required for subsequent controlled poultry-manure pyrolysis experiments. The no-load commissioning stage verified the correct operation of the heating elements, Type S thermocouple, programmable temperature controller and safety components, while progressive heating demonstrated operation up to an internal furnace temperature of 1000°C.

The external casing measurements indicated effective thermal separation between the reaction zone and the equipment exterior. Even at an internal temperature of 1000°C, the highest measured external surface temperature was 89°C. These values characterize surface temperature rather than heat loss; determination of thermal efficiency would require additional measurements of energy input, heat flux and losses.

The programmed 400, 600 and 800°C cycles reached their target levels in approximately 60 min and subsequently maintained stable one-hour thermal plateaus. Mean holding temperatures were 400.38, 601.00 and 800.46°C, with temporal standard deviations below 1.4°C.

This level of control is suitable for comparative pyrolysis experiments in which the imposed temperature must be reproduced accurately.A transient temperature overshoot occurred after electrical heating was stopped, reaching 460, 679 and 895°C in the three analysed regimes.

The magnitude of this response increased with the operating temperature and should be considered when future thermal programmes are defined. Additional thermocouples at different positions, direct electrical-energy logging and repeated cycles will be useful for quantifying temperature uniformity, thermal inertia, repeatability and cooling behaviour.

The results of this preliminary study support the use of the developed unit for subsequent experiments aimed at producing phosphorus-rich biofertilizers, while keeping the present evaluation focused exclusively on equipment performance.

## ACKNOWLEDGEMENT

This work was carried out within the ADER Sectoral Plan, project ADER 25.3.1/20.07.2023, “Technology for the valorization of poultry manure by obtaining phosphorus-rich biofertilizers”.

## REFERENCES


[1] Bergfeldt, B., Morgano, M. T., Leibold, H., Richter, F., & Stapf, D. (2018). Recovery of phosphorus and other nutrients during pyrolysis of chicken manure. Agriculture, 8(12), 187. https://doi.org/10.3390/agriculture8120187

[2] Bruun, S., Harmer, S. L., Bekiaris, G., Christel, W., Zuin, L., Hu, Y., Jensen, L. S., & Lombi, E. (2017). The effect of different pyrolysis temperatures on the speciation and availability in soil of P in biochar produced from the solid fraction of manure. Chemosphere, 169, 377–386. https://doi.org/10.1016/j.chemosphere.2016.11.058

[3] Hadroug, S., Jellali, S., Leahy, J. J., Kwapinska, M., Jeguirim, M., Hamdi, H., & Kwapinski, W. (2019). Pyrolysis process as a sustainable management option of poultry manure: Characterization of the derived biochars and assessment of their nutrient release capacities. Water, 11(11), 2271. https://doi.org/10.3390/w11112271

[4] Hossain, M. Z., Bahar, M. M., Sarkar, B., Donne, S. W., Wade, P., & Bolan, N. (2021). Assessment of the fertilizer potential of biochars produced from slow pyrolysis of biosolid and animal manures. Journal of Analytical and Applied Pyrolysis, 155, 105043. https://doi.org/10.1016/j.jaap.2021.105043

[5] Ippolito, J. A., Cui, L., Kammann, C., Wrage-Mönnig, N., Estavillo, J. M., Fuertes-Mendizabal, T., Cayuela, M. L., Sigua, G., Novak, J., Spokas, K., & Borchard, N. (2020). Feedstock choice, pyrolysis temperature and type influence biochar characteristics: A comprehensive meta-data analysis review. Biochar, 2, 421–438. https://doi.org/10.1007/s42773-020-00067-x

[6] Knijnenburg, J. T. N., Suwanree, S., Macquarrie, D., Kasemsiri, P., & Jetsrisuparb, K. (2025). Phosphorus recovery from animal manures through pyrolysis: Phosphorus transformations, release mechanisms, and applications of manure biochars in agriculture. RSC Sustainability, 3, 1084–1101. https://doi.org/10.1039/D4SU00524D

[7] Keskinen, R., Hyväluoma, J., Sohlo, L., Help, H., & Rasa, K. (2019). Fertilizer and soil conditioner value of broiler manure biochars. Biochar, 1, 259–270. https://doi.org/10.1007/s42773-019-00020-7

[8] Kuryntseva, P., Galitskaya, P., & Selivanovskaya, S. (2022). Optimization of pyrolysis regime for chicken manure treatment and biochar production. Water and Environment Journal, 36(2), 270–281. https://doi.org/10.1111/wej.12764

[9] Leite, A. A., Melo, L. C. A., Hurtarte, L. C. C., Zuin, L., Piccolla, C. D., Werder, D., Shabtai, I., & Lehmann, J. (2023). Magnesium-enriched poultry manure enhances phosphorus bioavailability in biochars. Chemosphere, 331, 138759. https://doi.org/10.1016/j.chemosphere.2023.138759

[10] Padilla, J. T., Watts, D. W., Novak, J. M., Cerven, V., Ippolito, J. A., Szogi, A. A., & Johnson, M. G. (2023). Magnesium activation affects the properties and phosphate sorption capacity of poultry litter biochar. Biochar, 5, 64. https://doi.org/10.1007/s42773-023-00263-5

[11] Piash, M. I., Iwabuchi, K., & Itoh, T. (2022). Synthesizing biochar-based fertilizer with sustained phosphorus and potassium release: Co-pyrolysis of nutrient-rich chicken manure and Ca-bentonite. Science of the Total Environment, 822, 153509. https://doi.org/10.1016/j.scitotenv.2022.153509

[12] Sanford, J. R., Johnstone, D., & Larson, R. A. (2022). Assessing changes to nutrient density and availability following separation, drying, and pyrolysis of manure solids. Bioresource Technology Reports, 19, 101169. https://doi.org/10.1016/j.biteb.2022.101169

[13] Sarvi, M., Hagner, M., Velmala, S., Soinne, H., Uusitalo, R., Keskinen, R., Ylivainio, K., Kaseva, J., & Rasa, K. (2021). Bioavailability of phosphorus in granulated and pyrolyzed broiler manure. Environmental Technology & Innovation, 23, 101584. https://doi.org/10.1016/j.eti.2021.101584

[14] Simbolon, L. M., Pandey, D. S., Horvat, A., Leahy, J. J., Tassou, S. A., & Kwapinska, M. (2024). Influence of the pyrolysis temperature on fresh and pelletised chicken litter with focus on sustainable production and utilisation of biochar. Biomass Conversion and Biorefinery, 14, 26443–26457. https://doi.org/10.1007/s13399-023-04787-5

[15] Ștefan V., Popa L., Găgeanu I., Ciupercă R., Matache G. Olan M., Zaica Ana (2023), Recovery of Poultry Manures / Tehnologii de Valorificare a Dejecțiilor din Avicultură, ISB INMATEH 2023 International Symposium, p 732-736

[16] Ștefan V., Popa L., Zaica A., Ciuperca R., Gheorghe G., Harabagiu A., Prisacariu E., Mantovani S. A., Stana B. I. (2024) The Design and Construction of an Equipment Intended for the Pyrolysis of Poultry Waste, ISB INMATEH 2023 International Symposium, p 578-585

[17] Topcu, N. S., Duman, G., Olgun, H., & Yanik, J. (2022). Evaluation of poultry manure: Combination of phosphorus recovery and activated carbon production. ACS Omega, 7(24), 20710–20718. https://doi.org/10.1021/acsomega.2c00975

[18] Vimal, V., Karim, A. A., Kumar, M., Ray, A., Biswas, K., Maurya, S., Subudhi, D., & Dhal, N. K. (2022). Nutrients enriched biochar production through co-pyrolysis of poultry litter with banana peduncle and phosphogypsum waste. Chemosphere, 300, 134512. https://doi.org/10.1016/j.chemosphere.2022.134512

[19] Zamani, S. M., Diarra, M. S., Chen, W., & Dutta, A. (2026). Valorization of poultry litter through biochar production: Linking feedstock chemistry, pyrolysis conditions, and application performance for the Canadian poultry industry. Journal of Environmental Management, 405, 129668. https://doi.org/10.1016/j.jenvman.2026.129668

# APPLICABILITY AND PROCESSING METHODOLOGY OF EXPERIMENTAL DATA ACQUISITION SYSTEMS FOR THE ASSESSMENT OF WHOLE-BODY VIBRATION EXPOSURE IN VEHICLE OPERATORS

/

# *APLICABILITATEA ȘI METODOLOGIA DE PRELUCRARE A DATELOR EXPERIMENTALE UTILIZÂND SISTEME DE ACHIZIȚIE PENTRU EVALUAREA EXPUNERII CONDUCĂTORILOR AUTO LA VIBRAȚII TRANSMISE ÎNTREGULUI CORP*

**Teofil Alin ONCESCU*[1)], Iuliana GAGEANU[1)], Ana-Maria TABARASU[1)], Nicolae-Valentin VLADUT[1)], Ioan Catalin PERSU[1)], Gabriel-Mihai MATACHE[1)], Cornelia MURARU-IONEL[1)], Raluca SFIRU[1)], Daniela TARNITA[2)], Paul- Alexandru BOTA[3)], Alexandru Denis CODROIU[3)], Adriana Valentina RADU[3)], Șerban-Armand STERE[3)], Iulia DOROBANȚU[3)], Cristian-Răzvan MARIN[3)]**

[1)] National Institute of Research-Development for Machines and Installations Designed for Agriculture and Food Industry-INMA Bucharest, 013811 Bucharest / Romania;

[2)] Department of Applied Mechanics and Civil Construction, Faculty of Mechanics, University of Craiova, 200512 Craiova, Dolj Cpunty / Romania;

[3)] Department of Transport, Traffic and Logistics, Faculty of Transport, National University of Science and Technology POLITEHNICA Bucharest, Bucharest / Romania

**Tel: (+40)786 848 903; *E-mail: alin.oncescu93@gmail.com*

***Keywords:*** *Whole Body Vibration (WBV), ISO2631-1, data acquisition systems, triaxial accelerometer, agricultural tractor, signal processing; VATS, Biometrics DataLog*

## ABSTRACT

*Exposure to whole-body vibration (WBV) is one of the most significant occupational risk factors for operators of agricultural vehicles, with documented effects on the lumbar spine, comfort and working capacity. The quality of any such assessment depends directly on the measurement chain and on the procedure by which acceleration signals are converted into standardised indicators. This paper examines the applicability of two complementary systems for the acquisition and processing of experimental data – the Biometrics Ltd acquisition platform (portable DataLog MWX8 units together with S2A and ACL 300 series triaxial accelerometers) and the Vibration Analysis Tool Set (VATS) developed by NexGen Ergonomics – and describes, step by step, the processing methodology applied to a data file from its collection in the field to the reporting of results in accordance with ISO 2631-1. The methodology was validated within an extensive experimental programme carried out with three tractors of different design and propulsion, on four types of running surface, at several travel speeds and seat-suspension settings, with a sample of seven subjects and five measurement points on the operator's body, yielding 5880 collected files, of which 3360 were processed. The segmentation of the recordings, the import into VATS, the definition of axes and units, the offset correction, the computation of r.m.s. acceleration, the FFT spectral analysis, the application of the $W_k$, $W_d$ and $W_c$ weighting filters and the evaluation of the health, comfort and perception zones are detailed. The results show that the integration of the two systems provides a reproducible, traceable and standard-compliant workflow, suitable both for the technical diagnosis of vehicles and for generating high-quality datasets for the validation of numerical models and predictive approaches.*

## REZUMAT

*Expunerea la vibrații transmise întregului corp (WBV – whole-body vibration) reprezintă unul dintre cei mai relevanți factori de risc profesional pentru operatorii vehiculelor agricole, cu efecte documentate asupra coloanei lombare, a confortului și a capacității de lucru. Calitatea oricărei evaluări de acest tip depinde în mod direct de lanțul de măsurare și de procedura prin care semnalele de accelerație sunt transformate în indicatori normalizați. Lucrarea de față analizează aplicabilitatea a două sisteme complementare de achiziție și prelucrare a datelor experimentale – platforma de achiziție Biometrics Ltd (unități portabile DataLog MWX8 și accelerometre triaxiale din seriile S2A și ACL 300) și setul de instrumente de analiză VATS (Vibration Analysis Tool Set) dezvoltat de NexGen Ergonomics – și descrie, etapă cu etapă, metodologia de prelucrare a unui fișier de date, de la culegerea sa în teren până la obținerea rezultatelor conform standardului ISO 2631-1. Metodologia a fost validată în cadrul unui program experimental extins, desfășurat cu trei tractoare*

*cu soluții constructive și de propulsie diferite, pe patru tipuri de suprafețe de rulare, la viteze și configurații de suspensie a scaunului diferite, cu un eșantion de șapte subiecți și cinci puncte de măsurare pe corpul operatorului, rezultând 5880 de fișiere culese, dintre care 3360 au fost prelucrate. Sunt detaliate segmentarea înregistrărilor, importul în VATS, definirea axelor și a unităților de măsură, corecția de offset, calculul accelerației r.m.s., analiza spectrală FFT, aplicarea filtrelor de ponderare $W_k$, $W_d$ și $W_c$ și evaluarea zonelor de sănătate, confort și percepție. Rezultatele arată că integrarea celor două sisteme oferă un flux de lucru reproductibil, trasabil și conform cu cerințele normative, adecvat atât pentru diagnosticul tehnic al vehiculelor, cât și pentru generarea de seturi de date de calitate destinate validării modelelor numerice și a abordărilor predictive.*

## INTRODUCTION

Vibrations generated by agricultural vehicles during travel and field operations have constituted, for more than two decades, a central topic of applied mechanical engineering and occupational ergonomics. Unlike road vehicles, agricultural tractors are operated on non-homogeneous surfaces, at low speeds and frequently without axle suspension systems, so that the excitations originating from terrain irregularities and from the machine's own sources are transmitted, with limited attenuation, to the operator's seat and, through it, to the entire human body. Prolonged exposure to such vibrations is associated with the onset of lumbar disorders, musculoskeletal pain and fatigue, and recent research has also highlighted residual after-effects on the cognitive, visual and motor functions of operators, which persist after the exposure has ceased *(Halmai, B., et al. 2024)*. Consequently, the objective quantification of exposure to whole-body vibration has become an essential component of occupational risk assessment in agriculture, as well as a design criterion for new-generation vehicles and seats *(Oncescu, T.A., et al. 2025a)*.

The level of vibration perceived by the operator results from the interaction of several factors: the type and unevenness of the running surface, the travel speed, the structural characteristics of the vehicle (mass, wheelbase, engine and transmission type), tyre pressure, as well as the type and adjustment of the seat suspension. Experimental studies conducted with electrically propelled tractors have shown that the transition from an asphalt surface to a farm track or to ploughed land significantly multiplies the weighted accelerations along the vertical direction, even at a constant speed of 5 km/h *(Oncescu, T.A., et al. 2022)*, while the direct comparison of a diesel tractor with an electric prototype revealed consistent differences in seat isolation efficiency within the critical 4–12 Hz band *(Oncescu, T.A., et al. 2025a)*. Similar results have been reported for tractors equipped with timber trailers, where the vibration amplitude depends strongly on the operation performed and on road condition *(Sláma, D., et al. 2025)*, as well as for tractor–implement configurations, in which the dominant excitation source changes with the working speed *(Gao, Y., et al. 2024)*. From the standpoint of the mechanical structure, multibody models and dynamic substructuring techniques have confirmed the decisive role of seat-suspension stiffness and damping in the transmissibility of vibration from the floor to the operator *(Brunetti, J., et al. 2021; Rekem, J., et al. 2024)*.

The normative framework against which the assessment is performed is the ISO 2631-1 standard, which defines the measurement methods, the frequency-weighting filters ($W_k$ for the vertical direction, $W_d$ for the horizontal directions and $W_c$ for the seat backrest), the basic indicators – the weighted r.m.s. acceleration and the vibration dose value (VDV) – and the health guidance caution zones, together with the comfort and perception criteria. At European level, Directive 2002/44/EC establishes the exposure action value (0.5 m/s²) and the exposure limit value (1.15 m/s²) for the daily exposure normalised to an 8-hour reference period, A(8). Comparisons between the short-term and long-term assessment methodologies defined in ISO 2631-1 and ISO 2631-5 have shown that the selected indicators may lead to different conclusions regarding compliance with the limits, which underlines the need for a rigorous description of the processing procedure employed *(de la Hoz-Torres, M.L., et al. 2022)*.

From a metrological standpoint, any WBV assessment relies on a measurement chain consisting of triaxial acceleration transducers, a data acquisition unit and analysis software capable of implementing the normative algorithms. The recent literature reflects a marked diversification of such solutions: from integrated commercial instruments, to portable in-house devices validated by comparison with reference equipment, and up to multichannel research platforms that allow accelerometers to be synchronised with other biomechanical sensors. Within the experimental programmes carried out at INMA Bucharest, the assessment of vibration at the seat pan, backrest, floor, steering wheel and head of the operator was performed with an integrated system consisting of Biometrics DataLog MWX8 acquisition units and triaxial

accelerometers, the data being processed in the VATS software *(Oncescu, T.A., et al. 2025a; Oncescu, T.A., et al. 2025b)*.

The same measurement architecture was employed to identify vibration sources in combine harvesters *(Tăbărașu, A.-M., et al. 2025)*, which confirms its flexibility with respect to the type of agricultural machine under investigation.

A clearly emerging trend in recent years is the use of experimental vibration data not only for compliance assessment against normative limits, but also as input for predictive and numerical approaches. Machine-learning models have been applied to estimate the weighted accelerations along the three axes as a function of the tractor's operating parameters *(Barač, Ž., et al. 2025a)*, while multi-criteria decision-making methods have been used to rank the influence of operational factors on the hand–arm system and on the whole body *(Barač, Ž., et al. 2025b)*. In parallel, finite-element modal analyses of the tractor seat and random-vibration response simulations of a seated virtual dummy have been validated through correlation with acceleration signals measured in the field *(Oncescu, T.A., et al. 2025b; Oncescu, T.A., et al. 2026)*. All these approaches share a critical dependence on the quality, consistency and traceability of the experimental input data: an incorrectly segmented signal, an uncorrected offset or an arbitrarily chosen analysis window propagates directly into the predictive model or into the power spectral density function used as excitation.

Nevertheless, most published works focus their presentation on the results obtained and treat the data-processing chain only summarily, so that it often remains insufficiently documented to allow the study to be reproduced by other researchers. The present paper aims to fill this gap through three objectives: (i) describing the architecture and functional parameters of the Biometrics Ltd acquisition system and of the VATS tool set, together with the arguments that justify their combined use in the study of vibration generated by agricultural vehicles; (ii) presenting in detail, step by step, the methodology for processing an experimental data file, from its collection in the field to the generation of the report in accordance with ISO 2631-1; (iii) critically evaluating the applicability of this methodology, highlighting its advantages, its limitations and the conditions under which the results can be reused in modelling and prediction studies.

## MATERIALS AND METHODS

### 2.1. The Biometrics Ltd data acquisition and monitoring system

The first component of the measurement chain is the acquisition platform developed by Biometrics Ltd (Gwent, United Kingdom), a manufacturer specialising in sensors, equipment and software for engineering research, biomechanics and clinical rehabilitation.

The distinctive feature of this platform lies in its capacity to record simultaneously, on the same time base, signals originating from different categories of transducers – accelerometers, electro goniometers, force platforms, surface electromyography sensors or contact-pressure sensors – which enables the direct correlation of the vibrational loading with the kinematic and physiological response of the operator. The system accepts both analogue and digital signals and is available in laboratory, portable and wireless-transmission variants, making it well suited to measurements under real operating conditions, in the open field.

The core element of the platform is the DataLog MWX8 portable acquisition unit, a compact device with a mass of 129 g, which can be mounted in the immediate vicinity of the sensors without disturbing the operator's posture or the conduct of the trial. In the configuration employed, the system comprises three such units, capable of collecting in parallel up to 24 perfectly synchronised data channels, with individually programmable sampling frequencies of up to 20,000 Hz. The functional characteristics relevant to vibration measurement are as follows:

- automatic digital anti-aliasing filter, with an attenuation of approximately –3 dB at 0.45 of the sampling rate and a maximum attenuation of ±13 dB above 0.8 of the sampling rate;
- real-time display and analysis of data on 8, 16 or 24 independently programmable channels;
- automatic saving of the recordings to a microSD card, serving as a backup copy in the event of communication loss with the computer;
- Bluetooth connection for data transfer and remote configuration;
- full-graphics colour LCD screen for visual verification of the signals during the test;
- integrated real-time clock, which stamps each recording with the date, start time and duration, thereby ensuring the traceability of the trials.




**Fig. 1 - The DataLog MWX8 acquisition unit**

*(Biometrics Ltd)*

In order for the analogue signals to be correctly converted into numerical values interpretable by the software, each input channel of the DataLog unit must be configured prior to the test, by connecting the unit to the computer (via cable or Bluetooth).

The parameters to be defined are: the channel state (active/inactive), the sensitivity (the input voltage corresponding to the maximum digital value), the channel-specific sampling frequency, the excitation voltage supplied to the sensor, the zero value or reference position, the displayed values for zero and for full scale, as well as the units of measurement of the International System.

An important practical advantage is that the unit stores these settings in non-volatile memory, so that the configuration remains valid even after long periods without power supply, thereby reducing the risk of configuration errors between successive measurement sessions.

### 2.2. The VATS vibration analysis tool set (NexGen Ergonomics)

The second component of the chain is the VATS™ (Vibration Analysis Tool Set) software, developed by NexGen Ergonomics (Pointe-Claire, Canada) for the analysis of vibration transmitted to the whole body and to the hand–arm system. VATS is designed to operate in tandem with the MWX8 DataLog acquisition unit: the files recorded by the latter (“.log” extension) are imported directly, and the time stamps provided by the unit's real-time clock are preserved, which makes it possible to associate each file unambiguously with the corresponding trial, subject and test configuration.

From a functional standpoint, the software implements the evaluation algorithms defined in ISO 2631-1:1997 (revised in 2001), covering the three domains of interest of the standard: health (caution zone), comfort and perception. For each of these, the weighting filters corresponding to the measurement point and direction ($W_k$, $W_d$, $W_c$) are applied, the weighted r.m.s. accelerations, peak values and crest factor are computed, and the results can be referred to user-defined exposure durations.

The spectral analysis module allows the FFT spectrum to be computed with Butterworth filters and selectable filtering windows, with explicit control of the Nyquist frequency and selection of the number of points used in the computation. In addition, VATS provides predefined subject postures (seated, standing or recumbent person), the weighted-acceleration history over the entire duration of the recording, the evaluation of the caution zone for a given exposure duration, and the export of results in tabular format, ready for reporting.

The combination of the two systems therefore follows a clear functional logic: the Biometrics platform provides synchronised, multichannel acquisition with hardware anti-aliasing filtering and redundant storage, whereas VATS takes over the raw signals and converts them into normative indicators, without intermediate format conversions that could introduce errors or loss of information.

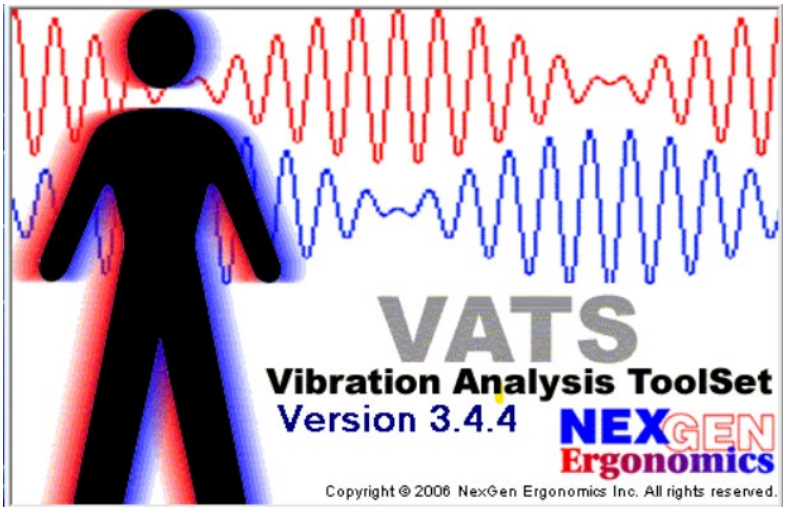



**Fig. 2 - Interface of the VATS software**
*(NexGen Ergonomics)*

The applicability of the two systems was verified within an experimental programme aimed at assessing the level of vibration experienced by the operator in the 0–80 Hz frequency range, with emphasis on the comfort zone, while travelling with three tractors differing in design and type of propulsion, on four running surfaces (flat terrain, uneven terrain, ploughed land and untilled land), at different travel speeds and for two seat-suspension configurations.

The tests were carried out with a sample of seven subjects, and vibration was measured simultaneously at five points: on the seat surface (at the seat pan), on the seat backrest, at the feet (floor), at the steering wheel and at the head.

The five sensors were distributed across three DataLog units: unit M17011 handled the 10 g accelerometers mounted on the steering wheel and at the foot, unit M17012 those mounted on the seat pan and on the backrest, and unit M17010 the ACL 300 accelerometer fixed at head level.

The full factorial design generated a considerable volume of data. For the ploughed and untilled surfaces, with three travel speeds (5, 8 and 10 km/h), the number of files is 7 subjects × 2 running tracks × 3 tractors × 3 speeds × 2 suspensions × 2 repetitions × 5 sensors = 2520 files; for the flat and uneven surfaces, with four speeds (5, 8, 10 and 12 km/h), the result is 7 × 2 × 3 × 4 × 2 × 2 × 5 = 3360 files. In total, 5880 data files were collected.

For the comparative study of the three tractors, processing was restricted to the speeds common to all surfaces (5 and 8 km/h), yielding 7 subjects × 4 running tracks × 3 tractors × 2 speeds × 2 suspensions × 2 repetitions × 5 sensors = 3360 processed files.

A dataset of this size renders ad-hoc processing impracticable and calls for a standardised procedure, applied identically to each file, so that the results obtained for different subjects, tractors, surfaces and speeds are directly comparable.

The description of the equipment in the preceding subsections provides the technical premises of this procedure: knowledge of the channel structure, of the sampling frequency and of the time stamps determines how the multichannel recording is segmented, while knowledge of the algorithms implemented in VATS determines the sequence of analysis operations.

The following subsection presents, step by step, the path of a data file from its collection in the field to the generation of the normative results, using a representative recording as an example.

### 2.3. Processing workflow of an experimental data file

To illustrate the methodology, the file recorded during the second repetition by the triaxial accelerometer mounted on the seat surface, at the seat pan, was selected, while the TE-0 electric tractor was travelling on the flat running surface at a speed of 5 km/h, with the seat suspension set to configuration 1 (height 10 cm).

The steps followed are summarised in Table 1 and detailed below.

**Table 1**

**Summary of the processing steps of a data file, from acquisition to reporting**

| Step | Operation | Software / instrument | Result |
|---|---|---|---|
| 1 | Collection of the multichannel recording in the field | DataLog MWX8 (3 units, 5 triaxial sensors) | Time-stamped raw file |
| 2 | Segmentation and isolation of the sensor under analysis | Biometrics DataLog | ".log" file for a single sensor |
| 3 | Naming and saving of the file | Biometrics DataLog | Unambiguous identification of the trial |
| 4 | Import of the ".log" file | VATS – "Open" command | Data organised in tabular form |
| 5 | Definition of the X, Y, Z axes and of the unit (g) | VATS | Channels associated with the standard directions |
| 6 | Selection of the ISO 2631-1 module | VATS | Normative algorithms activated |
| 7 | Visualisation of the raw data (r.m.s. and peak) | VATS | Verification of signal quality |
| 8 | Selection of the time interval and offset correction | VATS – "Offset", "Apply" | Zero-centred signal, 0–180 s |
| 9 | Computation of the r.m.s. acceleration along the relevant axis | VATS – "Calculate r.m.s." | Plot of the r.m.s. variation |
| 10 | FFT spectral analysis | VATS – "FFT Spectrum", Butterworth filter | Frequency spectrum |
| 11 | Normative evaluation with $W_k$, $W_d$, $W_c$ weightings | VATS – "ISO 2631-1", "Seated Person" | Health, comfort and perception zones |
| 12 | Weighted r.m.s. history and caution zone | VATS – "aRMS History", "Caution Zone" | Limit values for the exposure duration |
| 13 | Report generation | VATS – "Tabulated Results" | Results in tabular form |

### 2.4. Actual processing of the file

To illustrate the processing steps applied to the data files, we consider as an example the data file collected during repetition 2 by the triaxial accelerometer sensor mounted on the seat surface, at the seat pan, while travelling with the TE-0 electric tractor on the flat running surface, at a speed of 5 km/h, using suspension 1 (10 cm) (Figure 3).

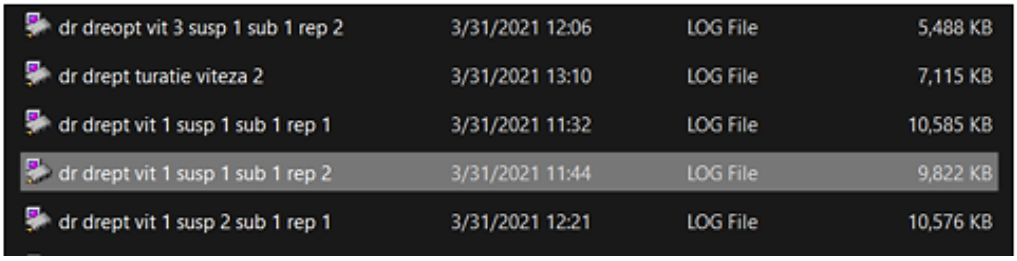



**Fig. 3 - Selection of the raw data file for processing**

In the Biometrics DataLog software, the data file was imported in order to segment the data collected during the measurements. The software interface illustrated in Figure 4 displays five triaxial accelerometer sensors configured in the DataLog units as follows: DataLog M17011, associated with the 10 g triaxial accelerometer sensors for the steering wheel and foot; DataLog M17012, associated with the 10 g triaxial

accelerometer sensors for the seat pan and backrest; DataLog M17010, associated with the ACL 300 triaxial accelerometer sensor for the head.




**Fig. 4 - Display of the data measured by the five triaxial accelerometer sensors in the Biometrics DataLog software**

In the next step, in the Biometrics software (Figure 5), only the selected sensor whose collected data are to be analysed is retained (for example, the seat pan – on the seat surface).




**Fig. 5 - Display of the data measured by the triaxial accelerometer sensor mounted at the seat pan (on the seat surface)**

Upon completion of this step, the file is saved using in its title clear identification data specific to the parameters involved in the experimental test.

The previously processed data file, with the ".log" extension, is then imported into VATS using the "Open" option (Figure 6).

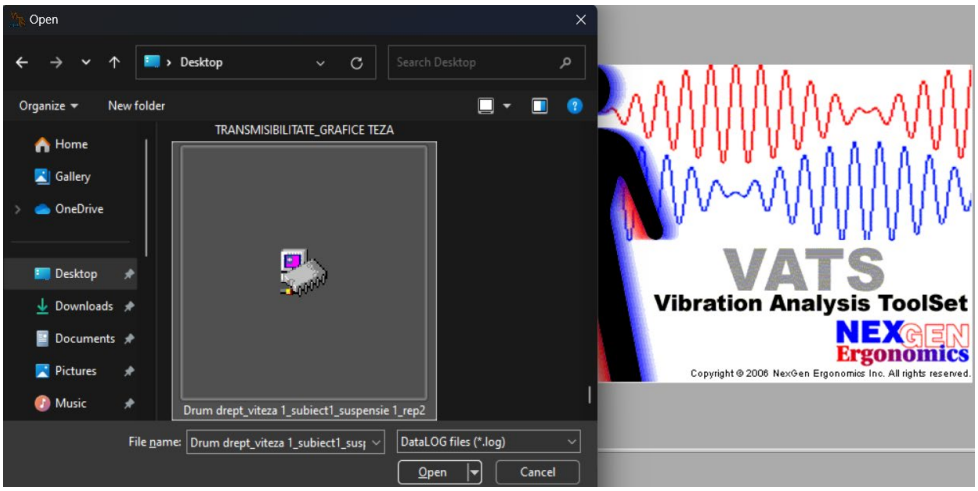



**Fig. 6 - Import of the ".log" data file into the VATS analysis software**

After loading the file, the X, Y, Z measurement axes of the accelerometer sensor and the unit of measurement, set to g (gravitational acceleration), are defined in the dialogue box shown in Figure 7.

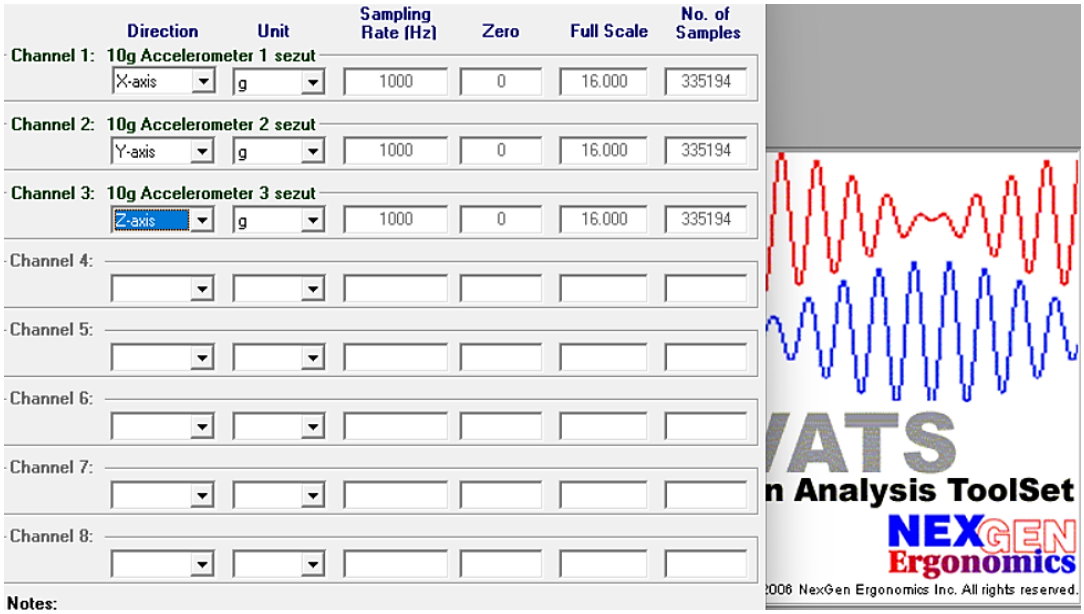



**Fig. 7 - Definition of the three measurement axes X, Y, Z and setting of the unit of measurement**

The VATS software imports the data from the ".log" files generated by the Biometrics software and organises them into tables for analysis.

To proceed with the analysis, the first option in the software is selected, which implements the analysis algorithms according to the ISO 2631-1 standard for whole-body vibration. This selection ensures the correct application of the internationally recognised methodology for evaluating the impact of vibration on the human body.

The VATS software opens a window, as in Figure 8, in which the raw data originating from the selected accelerometer sensor are displayed. All r.m.s. and peak values were computed in accordance with the standard.

These values were filtered using specific weightings, which resulted in lower peak values and reduced r.m.s. values compared with the unfiltered data.

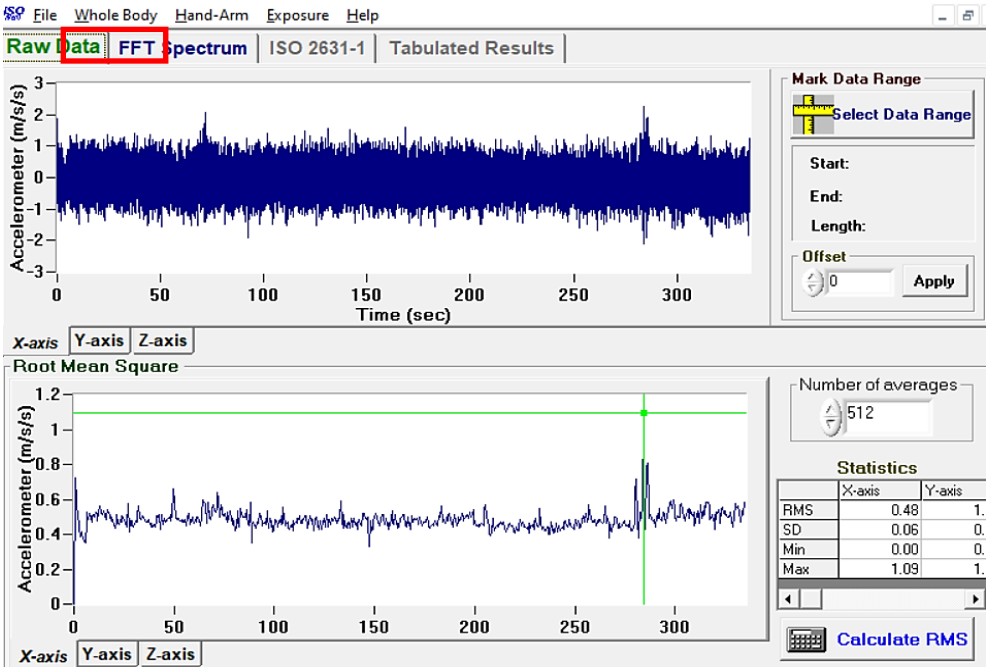



**Fig. 8 - Visualisation of the raw data prior to the processing stage in accordance with ISO 2631-1**

Figure 9 presents the analysis interface of the VATS software. To initiate the analysis, the following parameters must be configured:

Time interval for data collection: the time interval [0–180] seconds was selected.

Correction of errors in the raw data: the mean value was entered in the “Offset” field to compensate for potential errors in the data. If the mean value is positive, a negative value of equal magnitude is entered. If the mean value is negative, a corresponding positive value is entered. For example, for a mean value of “–0.006”, the value “0.006” is entered in the “Offset” field, thereby adjusting the data accordingly.

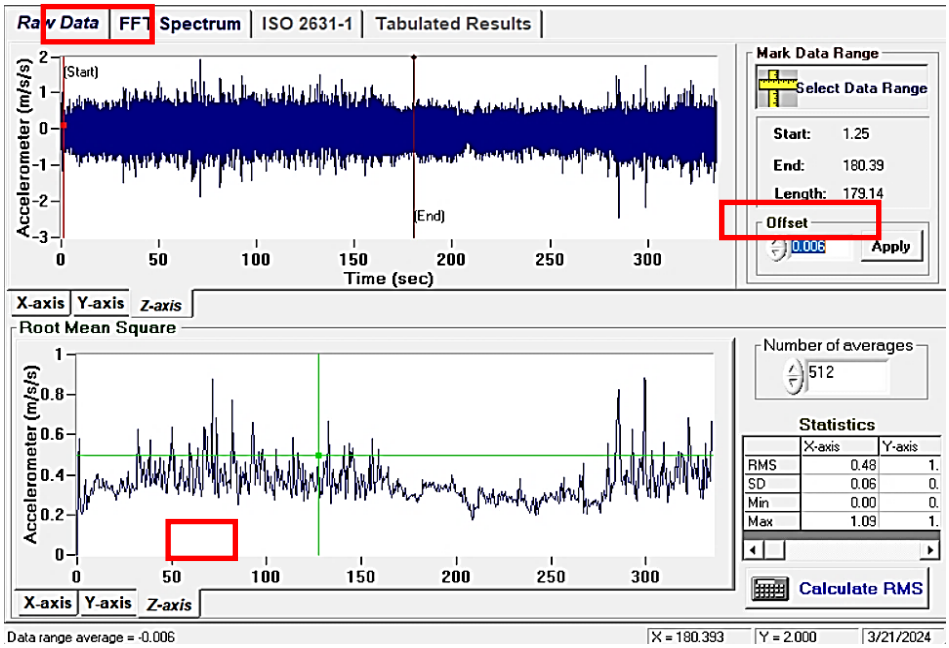



**Fig. 9 - Selection of the time interval and setting of the “offset” to zero**

After entering the offset value, the “Apply” button is pressed to perform the adjustment. The measurement axis relevant to the plotting of the “Root Mean Square” (r.m.s.) acceleration is then selected – in this case the Z axis, which is the significant one.

Through the “Calculate r.m.s.” command, the software computes the r.m.s. value of the acceleration and generates the plot of its variation over the specified time interval [0–180] seconds, as shown in Figure 10.

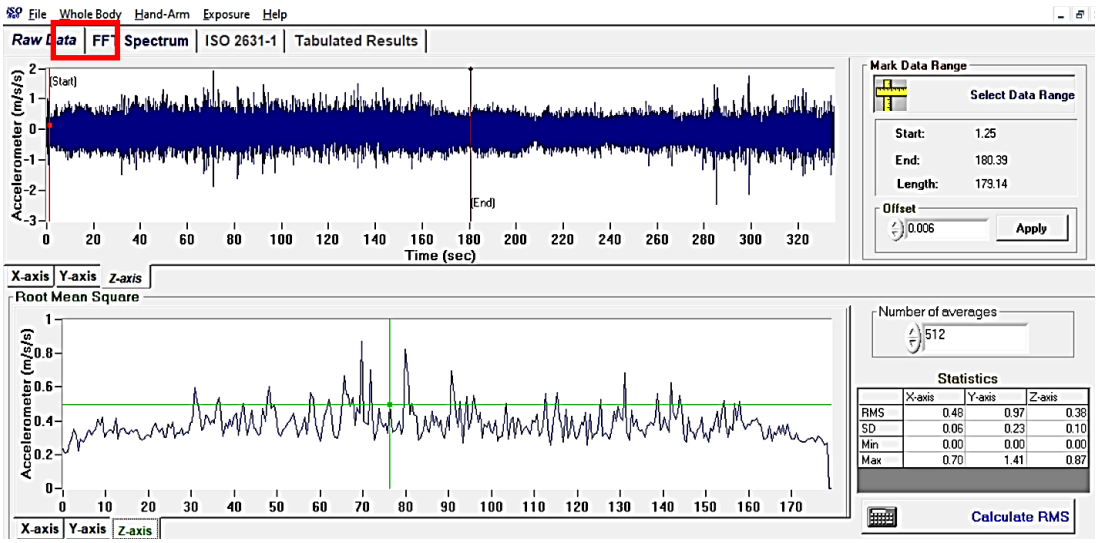



**Fig. 10 - Plot of the variation of the r.m.s. acceleration along the Z measurement axis**

In the next step, the FFT analysis is performed through the “FFT Spectrum” command. The “Butterworth” filter parameter is selected, ensuring that the maximum frequency does not exceed the “Nyquist frequency” (a fundamental concept in signal processing, referring to the highest frequency that can be correctly sampled without producing signal distortion).

Subsequently, the “Filtering Window” option applies a filtering window to reduce spectral leakage, followed by the sizing of the filtering window and the selection of the number of data points used for the frequency computation, thereby optimising the accuracy of the spectral analysis. This step is illustrated in Figure 11.

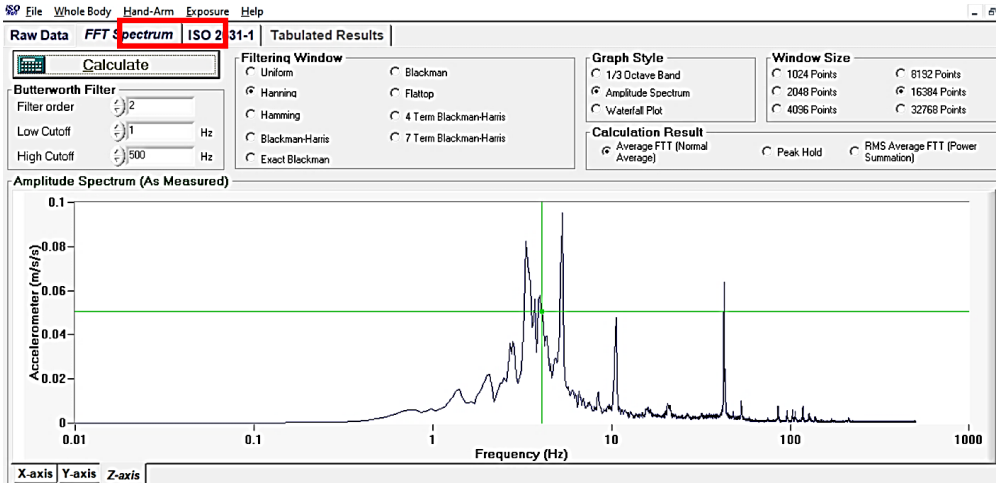



**Fig. 11 - FFT analysis in the VATS software**

Selecting the “ISO 2631-1” button enabled the display of the whole-body vibration analysis results, in accordance with the requirements specified in the ISO 2631-1 standard. The lower part of Figure 12 shows the settings of the filter weightings, which are essential for an accurate evaluation compliant with the normative requirements of the analysis. VATS provides additional information based on the measurements performed for different postures of the person, such as “Seated Person”, “Standing Person” and “Recumbent Person”. In this case, the “Seated Person” option was selected.

All results computed in accordance with the standard are summarised in the lower right-hand corner of the “ISO 2631-1” window shown in Figure 12, accessible by pressing the “a r.m.s. Results” button. On the left-hand side of Figure 12, the VATS software details the applicability of the vibration analysis in accordance with the ISO standard, as follows:

**The health guidance caution zone**, evaluated at the seat surface along the three measurement axes, with the application of the $W_d$ weighting filter for the horizontal direction and $W_k$ for the vertical direction, is presented in Figure 12.

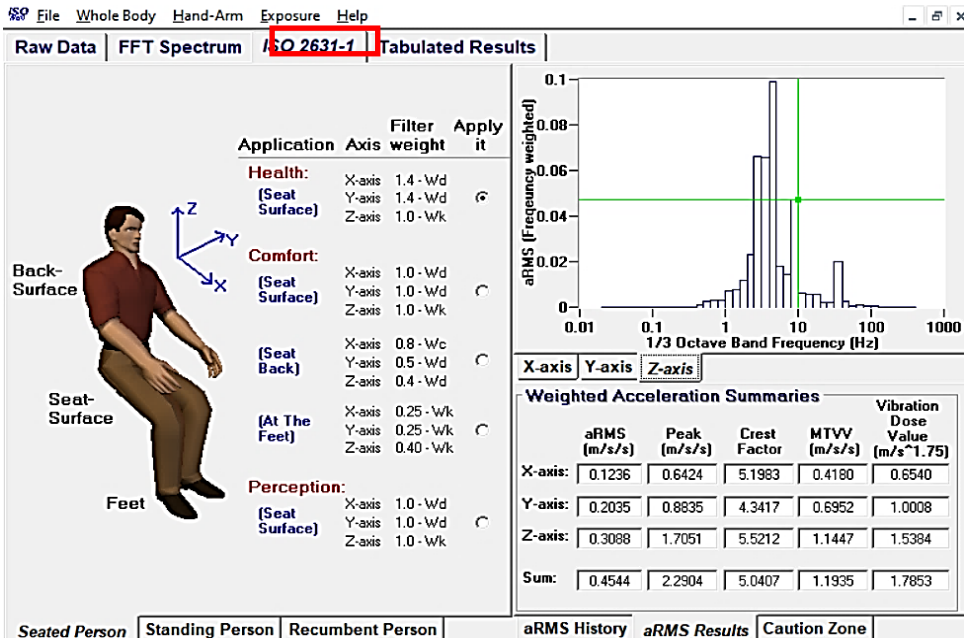



**Fig. 12 - Computed a r.m.s. results for the "Health zone"**

**The comfort zone** – evaluated at the seat surface along the three measurement axes, using the values of the weighting filters $W_d$ for the horizontal direction and $W_k$ for the vertical direction, is presented in Figure 13.

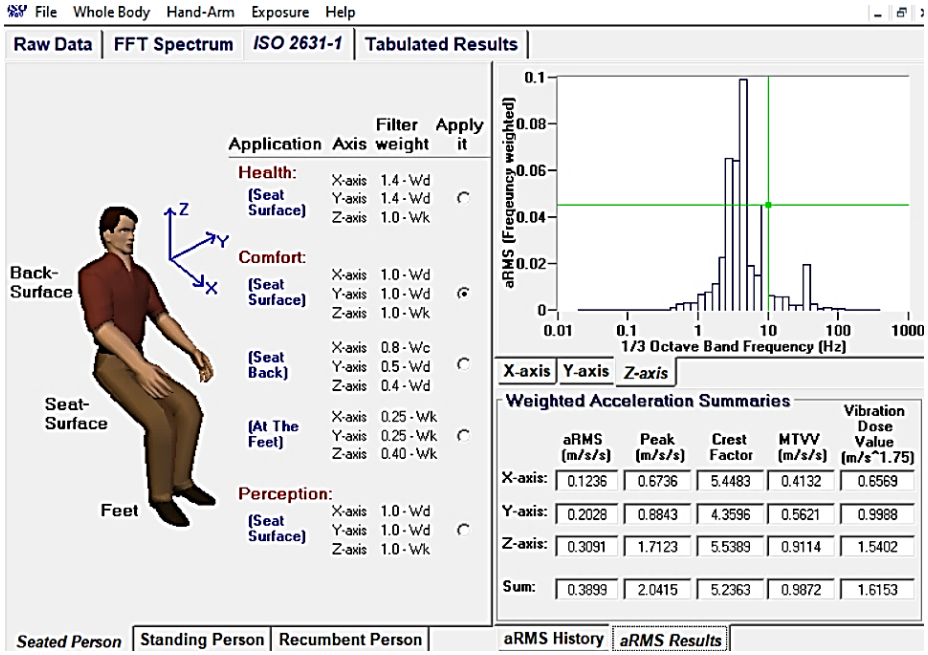



**Fig. 13 - Computed a r.m.s. results for the comfort zone**

The evaluation of vibration at the seat backrest along the three measurement axes, using the weighting filters $W_d$ for the horizontal direction and $W_c$ for the direction specific to the seat backrest, is presented in Figure 14.

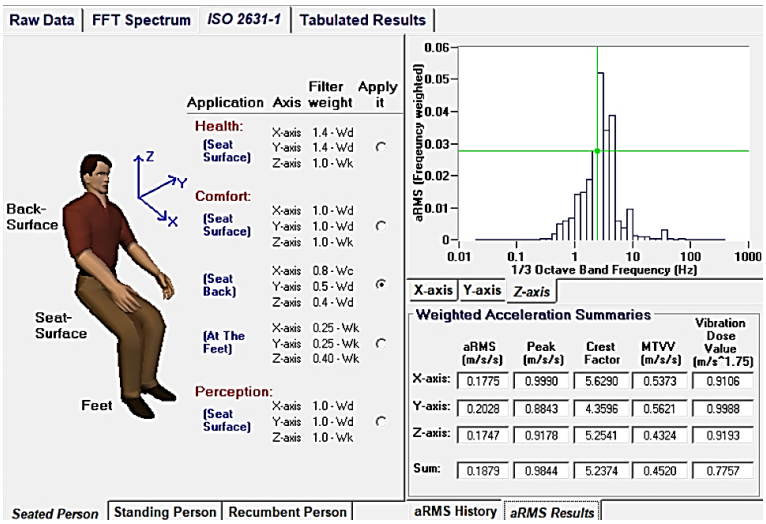



**Fig. 14 - Computed a r.m.s. results for the comfort zone at the backrest**

The evaluation of the vibration level at the feet along the three measurement axes, using the $W_k$ weighting filter for the vertical direction, is presented in Figure 15.

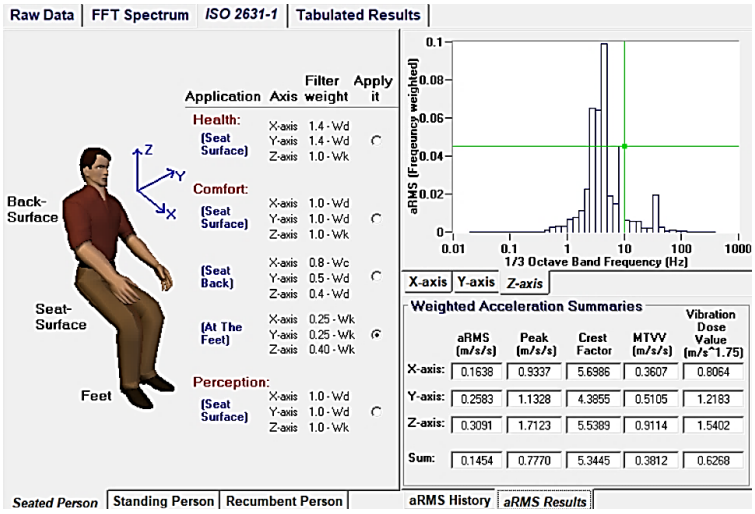



**Fig. 15 - Computed a r.m.s. results for the comfort zone at the feet**

**The perception zone** – at the seat surface, is evaluated along the three measurement axes using the weighting filters $W_d$ for the horizontal direction and $W_k$ for the vertical direction, and is presented in Figure 16.

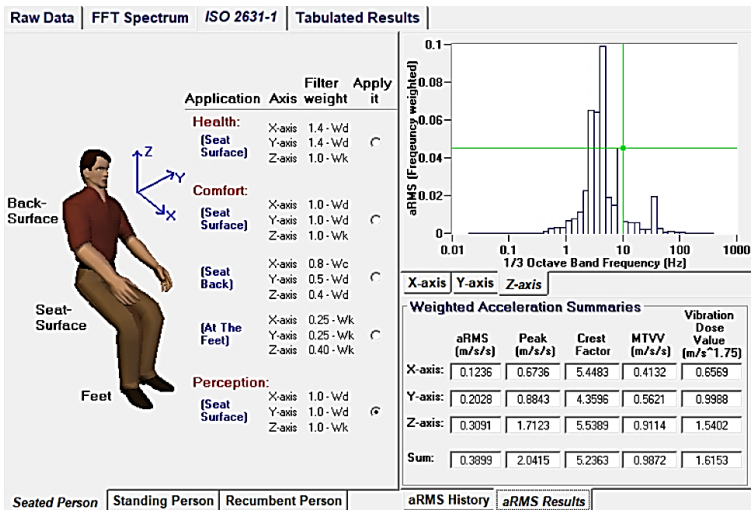



**Fig. 16 - Computed a r.m.s. results for the perception zone**

To compute the weighted r.m.s. value over the entire data collection period, the “aRMS History” button, shown at the bottom of Figure 17, was selected.

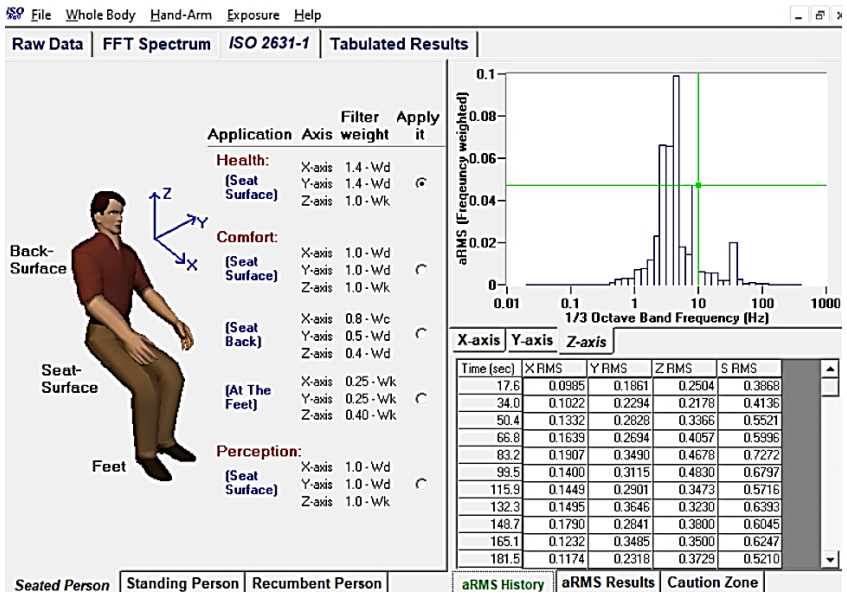



**Fig. 17 - Weighted r.m.s. results over the entire data collection period**

To obtain the limit value according to the standard for a given exposure period, the “Caution Zone” button was pressed, as illustrated in Figure 18.

This function highlights the health guidance caution zone, indicating the need for prudence with regard to the potential risks associated with vibration exposure. In order to prevent foreseeable risks of vibration-induced injury, it is recommended that these exposure conditions be kept below the threshold of the caution zone.

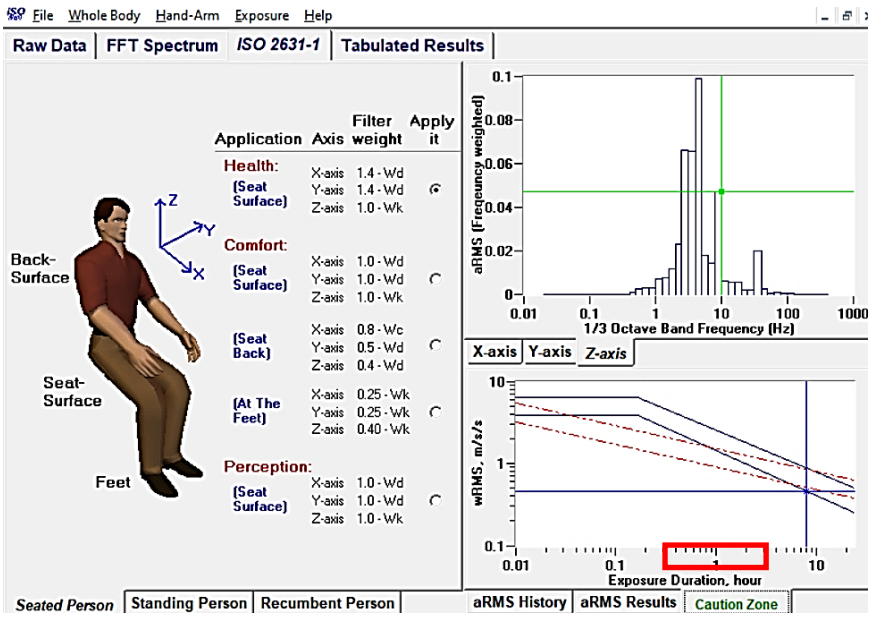
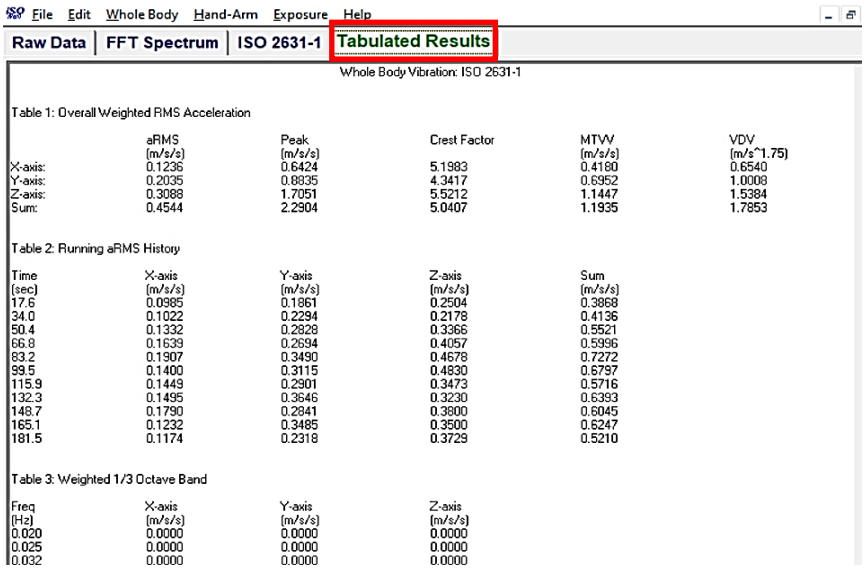



**Fig. 18 - ISO 2631 limit value for a specific exposure period for the “Caution Zone”**

The VATS software offers the possibility of viewing the computed results in printed-report format, by means of the “Tabulated Results” button, as shown in Figure 19.


File Edit Whole Body Hand-Arm Exposure Help

Raw Data | FFT Spectrum | ISO 2631-1 | Tabulated Results

Whole Body Vibration: ISO 2631-1

Table 1: Overall Weighted RMS Acceleration

| | aRMS (m/s/s) | Peak (m/s/s) | Crest Factor | MTVV (m/s/s) | VDV (m/s^1.75) |
|---|---|---|---|---|---|
| X-axis: | 0.1236 | 0.6424 | 5.1983 | 0.4180 | 0.6540 |
| Y-axis: | 0.2035 | 0.8835 | 4.3417 | 0.6952 | 1.0008 |
| Z-axis: | 0.3088 | 1.7051 | 5.5212 | 1.1447 | 1.5384 |
| Sum: | 0.4544 | 2.2904 | 5.0407 | 1.1935 | 1.7853 |

Table 2: Running aRMS History

| Time (sec) | X-axis (m/s/s) | Y-axis (m/s/s) | Z-axis (m/s/s) | Sum (m/s/s) |
|---|---|---|---|---|
| 17.6 | 0.0985 | 0.1861 | 0.2504 | 0.3868 |
| 34.0 | 0.1022 | 0.2294 | 0.2178 | 0.4136 |
| 50.4 | 0.1332 | 0.2828 | 0.3366 | 0.5521 |
| 66.8 | 0.1639 | 0.2694 | 0.4057 | 0.5996 |
| 83.2 | 0.1907 | 0.3490 | 0.4678 | 0.7272 |
| 99.5 | 0.1400 | 0.3115 | 0.4830 | 0.6797 |
| 115.9 | 0.1449 | 0.2901 | 0.3473 | 0.5716 |
| 132.3 | 0.1495 | 0.3646 | 0.3230 | 0.6393 |
| 148.7 | 0.1790 | 0.2841 | 0.3800 | 0.6045 |
| 165.1 | 0.1232 | 0.3485 | 0.3500 | 0.6247 |
| 181.5 | 0.1174 | 0.2318 | 0.3729 | 0.5210 |

Table 3: Weighted 1/3 Octave Band

| Freq (Hz) | X-axis (m/s/s) | Y-axis (m/s/s) | Z-axis (m/s/s) |
|---|---|---|---|
| 0.020 | 0.0000 | 0.0000 | 0.0000 |
| 0.025 | 0.0000 | 0.0000 | 0.0000 |
| 0.032 | 0.0000 | 0.0000 | 0.0000 |

**Fig. 19 - Computed results displayed in tabular form**

With reference to the solutions described in the recent literature, the Biometrics–VATS architecture exhibits several distinct advantages for the study of vibration generated by agricultural vehicles. Firstly, the hardware synchronisation of the 15 channels allows simultaneous measurement at five points along the vibration transmission path (floor, seat pan, backrest, steering wheel, head), which makes it possible to compute the floor-to-seat and seat-to-head transmissibility's from the same recording, without temporal alignment errors; approaches based on a single seat-mounted vibration meter *(Sláma, D., et al. 2025)* or on portable in-house devices do not offer this possibility. Secondly, the eighth-order hardware anti-aliasing filtering and the high sampling frequencies provide sufficient margin with respect to the normative 0.5–80 Hz band, so that the FFT spectrum obtained in VATS faithfully reflects the content of the signal. Thirdly, the non-volatile storage of the channel configuration and the automatic time-stamping of the recordings reduce the sources of human error in an experimental programme involving thousands of files.

The methodology described also has limitations that must be stated explicitly. The short duration of the trials (approximately 180 s of steady-state travel) does not allow a meaningful estimate of the vibration dose value VDV, nor of the daily exposure A(8) in the sense of Directive 2002/44/EC; these quantities require either the extrapolation of the r.m.s. results to the operator's actual working profile, or measurement campaigns spanning a full working day, as recommended by the comparisons between ISO 2631-1 and ISO 2631-5 *(de la Hoz-Torres, M.L., et al. 2022)*. The offset correction and the choice of the time interval remain manual operations, dependent on the analyst's experience, and the reliance on the proprietary ".log" format requires the Biometrics software to be retained within the processing chain. Finally, the system is not an exposure dosimeter intended for routine use by untrained personnel, but a research instrument whose value is manifested in controlled comparative studies.

It is precisely this research orientation that explains the usefulness of the generated results beyond the normative assessment itself. The datasets obtained through the workflow presented were used to compare diesel and electric tractors *(Oncescu, T.A., et al. 2025a)*, to validate the modal analysis of the operator's seat in the 0–80 Hz range *(Oncescu, T.A., et al. 2025b)* and to define the power spectral density functions that excite a virtual dummy in random-response simulations *(Oncescu, T.A., et al. 2026)*. Such reuse is possible only insofar as each file has undergone the same documented and verifiable sequence of steps – which constitutes the central argument of the present paper. Machine-learning-based predictive approaches *(Barač, Ž., et al. 2025a)* raise a similar requirement: models trained on non-homogeneously processed data learn processing artefacts instead of the physical relationships between the operating parameters and the vibration level.

## 3. CONCLUSIONS

This paper has presented the applicability of two complementary systems – the Biometrics Ltd acquisition platform and the VATS analysis tool set (NexGen Ergonomics) – in the assessment of the exposure of agricultural vehicle operators to whole-body vibration, together with the complete methodology for processing an experimental data file. The main conclusions are as follows:

- The DataLog MWX8 portable units, together with the S2A-10G-MF and ACL 300 triaxial accelerometers, provide a synchronised, multichannel measurement chain with hardware anti-aliasing filtering and sampling frequencies that cover the normative 0.5–80 Hz band with ample margin, suitable for measurements under real operating conditions, on non-homogeneous terrain.
- The VATS software fully implements the ISO 2631-1 algorithms for the health, comfort and perception zones, with the $W_k$, $W_d$ and $W_c$ weighting filters applied differentially by measurement point and direction, and imports directly the files generated by the Biometrics system, eliminating intermediate format conversions.
- The 13-step processing workflow – from the segmentation of the multichannel recording, through the definition of axes and units, offset correction, r.m.s. computation and FFT analysis, to the normative evaluation and tabular reporting – is reproducible and was applied identically to a set of 3360 files, out of a total of 5880 collected, originating from 7 subjects, 3 tractors, 4 running surfaces, 2 speeds and 2 suspension configurations, with 5 measurement points.
- The file-naming convention and the automatic time-stamping of the recordings ensure the complete traceability of each result back to the originating experimental trial, an indispensable condition for factor-based statistical analysis and for data reuse.
- The results obtained through this methodology go beyond the scope of compliance with normative limits: they constitute validated inputs for finite-element modal analyses, random-vibration response simulations and predictive models, fields in which the quality and homogeneity of the experimental data directly condition the credibility of the conclusions.
- The limitations identified – the short duration of the trials relative to the requirements for estimating VDV and A(8), the manual nature of the offset correction and of the selection of the analysis interval, and the dependence on a proprietary file format – define the directions for further development: automation of the repetitive steps through batch-processing scripts, extension of the measurement campaigns to the duration of a working day, and integration with ISO 2631-5 for the assessment of exposure containing multiple shocks.

Overall, the integration of the Biometrics and VATS systems provides researchers in the field of agricultural engineering with a rigorous instrument for the technical diagnosis of vehicles from the vibration standpoint, and the explicit description of the processing methodology contributes to the reproducibility and comparability of studies on operator comfort and health.

## REFERENCES

[1] Barač, Ž., Jurić, M., Plaščak, I., Jurić, T., & Marković, M. (2025a). Assessing whole-body vibrations in an agricultural tractor based on selected operational parameters: A machine learning-based approach. *AgriEngineering*, 7(3), 72. https://doi.org/10.3390/agriengineering7030072

[2] Barač, Ž., Plaščak, I., Jurić, T., & Marković, M. (2025b). The impact of vibrations on the hand–arm system and body of agricultural tractor operators in relation to operational parameters, approach: Analytical Hierarchical Process (AHP). *AgriEngineering*, 7(2), 56. https://doi.org/10.3390/agriengineering7020056

[3] Brunetti, J., D'Ambrogio, W., & Fregolent, A. (2021). Analysis of the vibrations of operators' seats in agricultural machinery using dynamic substructuring. *Applied Sciences*, 11(11), 4749. https://doi.org/10.3390/app11114749

[4] de la Hoz-Torres, M. L., Aguilar, A. J., Ruiz, D. P., & Martínez-Aires, M. D. (2022). Whole body vibration exposure transmitted to drivers of heavy equipment vehicles: A comparative case according to the short- and long-term exposure assessment methodologies defined in ISO 2631-1 and ISO 2631-5. *International Journal of Environmental Research and Public Health*, 19(9), 5206. https://doi.org/10.3390/ijerph19095206

[5] Directive 2002/44/EC of the European Parliament and of the Council of 25 June 2002 on the minimum health and safety requirements regarding the exposure of workers to the risks arising from physical agents (vibration). Official Journal of the European Union, L 177, 13–20.

[6] Gao, Y., Yang, Y., Fu, S., Feng, K., Han, X., Hu, Y., Zhu, Q., & Wei, X. (2024). Analysis of vibration characteristics of tractor–rotary cultivator combination based on time domain and frequency domain. *Agriculture*, 14(7), 1139. https://doi.org/10.3390/agriculture14071139

[7] Halmai, B., Holsgrove, T. P., Vine, S. J., Harris, D. J., & Williams, G. K. R. (2024). The after-effects of occupational whole-body vibration on human cognitive, visual, and motor function: A systematic review. *Applied Ergonomics*, 118, 104264. https://doi.org/10.1016/j.apergo.2024.104264

[8] ISO 2631-1:1997. Mechanical vibration and shock – Evaluation of human exposure to whole-body vibration – Part 1: General requirements. International Organization for Standardization, Geneva.

[9] Oncescu, T. A., Petcu, A., & Tarnita, D. (2021). Evaluation of whole-body vibrations and comfort state of tractor driver for different types of terrain and speeds. Acta Technica Napocensis – Series: *Applied Mathematics, Mechanics, and Engineering*, 64(1), 153–160.

[10] Oncescu, T. A., Persu, C., Dumitru, I., Prunoiu, D., Grigore, L., & Tarnita, D. (2022). Influence of the road type on the whole-body vibrations transmitted to the driver of an electric tractor. Acta Technica Napocensis – Series: *Applied Mathematics, Mechanics, and Engineering*, 65(2S), 387–392.

[11] Oncescu, T. A., Persu, I. C., Bostina, S., Biris, S. S., Vilceleanu, M.-V., Nenciu, F., Matache, M.-G., & Tarnita, D. (2025a). Comparative analysis of vibration impact on operator safety for diesel and electric agricultural tractors. *AgriEngineering*, 7(2), 40. https://doi.org/10.3390/agriengineering7020040

[12] Oncescu, T. A., Biris, S. S., Gageanu, I., Vladut, N.-V., Persu, I. C., Bostina, S.-L., Nenciu, F., Matache, M.-G., Tabarasu, A.-M., Gheorghe, G., & Tarnita, D. (2025b). FEA modal and vibration analysis of the operator's seat in the context of a modern electric tractor for improved comfort and safety. *AgriEngineering*, 7(11), 362. https://doi.org/10.3390/agriengineering7110362

[13] Oncescu, T. A., Biris, S. S., Gageanu, I., Persu, I. C., Bostina, S., & Tarnita, D. (2026). Comparative analysis of the biomechanical response of a virtual driver dummy subjected to random vibrations generated by diesel- and electric-powered self-propelled agricultural tractors. *AgriEngineering*, 8(4), 158. https://doi.org/10.3390/agriengineering8040158

[14] Rekem, J., Janečková, R., Otipka, V., Prokop, A., Řehák, K., & Žlábek, P. (2024). Multi-body model of agricultural tractor for vibration transmission investigation. *Applied Sciences*, 14(18), 8451. https://doi.org/10.3390/app14188451

[15] Sláma, D., Staněk, L., & Mergl, V. (2025). Magnitude of WBV affecting the tractor with a timber trailer operator during individual timber forwarding operations. *South-East European Forestry*, 16(1), 43–51.

[16] Tăbărașu, A.-M., Vanghele, N., Cismaru, M., Isticioaia, S., et al. (2025). Identification of vibration source influence intensity in combine harvesters using multivariate regression analysis. *Applied Sciences*, 15(18), 10159. https://doi.org/10.3390/app151810159

[17] Biometrics Ltd. (2024). DataLog MWX8 – User Manual. Biometrics Ltd, Newport, UK. https://www.biometricsltd.com

[18] NexGen Ergonomics Inc. (2024). VATS™ – Vibration Analysis Tool Set – User Guide. NexGen Ergonomics, Pointe-Claire, Canada. https://www.nexgenergo.com/ergonomics/vats.html

# EXPERIMENTAL EVALUATION OF A MICROHYDROENERGY SYSTEM FOR SUSTAINABLE AERATION OF FISH PONDS

/

# *EVALUAREA EXPERIMENTALĂ A UNUI SISTEM MICROHIDROENERGETIC PENTRU AERAREA SUSTENABILĂ A BAZINELOR PISCICOLE*

**Laurențiu-Constantin VLĂDUȚOIU*[1)], Eugen MARIN[1)], Floricel-Maricel DIMA[2)], Magdalena TENCIU[2)], Florentina BRATOSIN[3)]**

[1)] INMA Bucharest / Romania; [2)] Research and Development Institute for Aquatic Ecology, Fisheries and Aquaculture - ICDEAPA Galați, Portului Street, no. 54, Galați, Galati County / Romania; [3)] UNSTP Bucharest / Romania

**Tel: 0749 281 500; *E-mail: laurentiuvladutoiu82@gmail.com*

***Keywords:*** *microhydroenergy system, hydraulic energy recovery, fish pond aeration, energy conversion, rotational speed, experimental testing, aquaculture*

**ABSTRACT**

*This paper presents the experimental evaluation of a microhydroenergy system designed to recover hydraulic energy and convert it into electrical energy required for fish pond aeration. The experimental system, developed within the ADER 13.1.1 research project, was tested under real operating conditions in order to assess its functional, mechanical, and energetic performance. The investigations included the determination of the rotational speeds of the rotor, transmission system, and generator, the monitoring of the electrical parameters of the storage system and inverter, as well as the evaluation of the available hydraulic power at different operating pressures. During the tests, the rotor reached a rotational speed of 30 rpm, while the transmission system increased the speed to approximately 750 rpm at the generator. The inverter provided an output voltage of 220 V AC, suitable for supplying electrical consumers used in aquaculture facilities. The results highlighted the stable operation of the kinematic chain and electrical system, without significant vibrations or functional failures. However, the hydraulic power available under the tested conditions was insufficient to operate the generator close to the higher power regimes indicated by its characteristic curve. The study confirms the technical feasibility of using a microhydroenergy system for renewable energy recovery in integrated aquaculture applications and identifies further optimization directions related to water flow rate, pressure, and transmission parameters.*

**REZUMAT**

*Lucrarea prezintă evaluarea experimentală a unui sistem microhidroenergetic destinat recuperării energiei hidraulice și transformării acesteia în energie electrică necesară aerării bazinelor piscicole. Sistemul experimental, realizat în cadrul proiectului ADER 13.1.1, a fost testat în condiții reale de funcționare, în vederea evaluării performanțelor funcționale, mecanice și energetice. Cercetările au inclus determinarea turației rotorului, a transmisiei și a generatorului, monitorizarea parametrilor electrici ai sistemului de stocare și ai invertorului, precum și evaluarea puterii hidraulice disponibile la diferite presiuni de lucru. În timpul testărilor, rotorul a atins o turație de 30 rot/min, iar sistemul de transmisie a asigurat o turație de aproximativ 750 rot/min la generator. Invertorul a furnizat o tensiune de ieșire de 220 Vca, corespunzătoare alimentării consumatorilor electrici utilizați în instalațiile de acvacultură. Rezultatele au evidențiat funcționarea stabilă a lanțului cinematic și a sistemului electric, fără apariția unor vibrații semnificative sau defecțiuni funcționale. Totuși, puterea hidraulică disponibilă în condițiile testate a fost insuficientă pentru exploatarea generatorului în apropierea regimurilor superioare de putere indicate de caracteristica acestuia. Studiul confirmă fezabilitatea tehnică a utilizării unui sistem microhidroenergetic pentru valorificarea energiei regenerabile în aplicații de acvacultură integrată și evidențiază direcții de optimizare privind debitul, presiunea apei și parametrii transmisiei.*

## INTRODUCTION

Aquaculture represents an important sector of food production, while maintaining adequate water quality is one of the essential conditions for ensuring the health, survival, and productivity of aquatic organisms. Among the various water quality parameters, dissolved oxygen concentration is of particular importance, as it influences fish metabolism, microbial activity, and the overall stability of aquatic

ecosystems. In this context, aeration of fish ponds represents one of the fundamental technological operations in aquaculture systems, being used to maintain dissolved oxygen concentrations within appropriate ranges and to improve water circulation *(Nugraha and Desnanjaya, 2025*). However, aeration is also one of the most energy-intensive processes, which necessitates the development and implementation of systems with improved energy efficiency.

Improving the energy efficiency of aeration systems is an important focus of current research in the field of aquaculture, as the electricity consumed by aerators contributes significantly to the operating costs of fish farms. Aeration performance is influenced by the structural characteristics of the system and its operating parameters, including flow rate, hydrostatic head, and the conditions under which air is introduced into the water column. Experimental studies conducted on pond aeration systems have shown that optimizing these parameters can increase oxygen transfer while simultaneously reducing specific energy consumption *(Aytac et al., 2024).* Furthermore, aeration performance can be improved through optimization of the structural configuration and hydraulic operating conditions. Roy et al. (2024) highlighted the influence of flow rate and system geometry on the oxygen transfer rate and energy efficiency of an aeration system designed for intensive aquaculture.

In the current context of sustainable development, reducing energy consumption and efficiently utilizing available resources represent important directions for the modernization of aquaculture systems. The application of circular economy principles involves, among other aspects, the efficient use of resources, recycling of material and energy flows, and integration of renewable energy sources into production processes. In aquaculture, these principles can contribute to reducing environmental impacts and increasing the sustainability of production systems *(Chary et al., 2024).* The authors also emphasize the need to use renewable energy while reducing the overall energy requirements of aquaculture systems. At the same time, reducing the carbon footprint of aquaculture requires improvements in resource-use efficiency and the implementation of production practices with reduced energy and climate impacts, these directions being considered essential for the sustainable development of the sector *(Zhang et al., 2024c).*

The integration of renewable energy sources into fish farms therefore represents a solution with significant potential for reducing dependence on electricity generated from conventional sources. Photovoltaic, micro-hydropower, or hybrid energy systems can be used to supply auxiliary equipment specific to aquaculture operations. Research on the integration of aquaculture systems with hybrid energy systems has demonstrated that the coordinated use of renewable energy sources can contribute to reducing energy costs and emissions associated with the operation of aquaculture facilities *(Zhang et al., 2024).*

Among the available renewable energy sources, hydropower is of particular interest for farms where permanent or periodic water flows are available and can be harnessed for energy production. Micro-hydropower systems enable the conversion of the available hydraulic energy of water into mechanical energy and subsequently, through electric generators, into electrical energy. In aquaculture facilities, the energy generated can be used to supply aeration, pumping, monitoring, or automation equipment, thereby reducing the amount of electricity required from the grid.

The combined use of multiple renewable energy sources can further increase the energy autonomy and stability of aquaculture systems. Solar–micro-hydropower hybrid systems offer the advantage of complementary energy resources and can provide a more stable power supply for consumers. An integrated aquaponics system powered by solar and micro-hydropower energy demonstrated the feasibility of using the two sources within a common energy management configuration to ensure reliable power supply and efficient utilization of available resources *(Dewi et al., 2025).*

At the same time, recent research on aeration energy efficiency highlights the need to match the type of aerator and its operating regime with the actual oxygen demand of the culture system. The integration of automation, dissolved oxygen monitoring, and renewable energy sources can contribute to reducing energy consumption and improving the sustainability of fish farming operations *(Nugraha and Desnanjaya, 2025).* Thus, the development of local energy solutions that harness resources available within the farm represents an important research direction in the field of aquaculture mechanization and automation.

Within the framework of the ADER 13.1.1 project, the SME 1.5-0 experimental micro-hydropower system was developed for recovering hydraulic energy and converting it into electrical energy required to operate aeration systems in fish ponds. The experimental system integrates a paddle-wheel rotor, a speed increaser, a permanent-magnet generator, an electrical energy control and storage system, and an inverter for supplying electrical loads. The structural design is intended to harness locally available energy resources

and integrate them into the technological system of the aquaculture farm. The system rotor has a diameter of 1400 mm and a width of 1200 mm, while power transmission to the generator is achieved through a speed increaser with a transmission ratio of 1:25. The generator is a permanent-magnet type, while the electrical energy produced is managed through the control, storage, and conversion system, with the inverter providing an output voltage suitable for supplying the specific electrical loads.

The aim of the research presented in this paper was to evaluate the functional and energy performance of the SME 1.5-0 experimental micro-hydropower system under real operating conditions. The experiments focused on determining the main mechanical, hydraulic, and electrical parameters of the system, namely rotor speed, speed of the transmission system and electric generator, water pressure and flow rate, as well as the electrical parameters of the installation. In addition, system operating stability, its ability to harness the available hydraulic resource, and optimization opportunities were analyzed with the aim of increasing energy conversion efficiency and utilizing the generated electricity to power aeration systems in fish ponds.

## MATERIALS AND METHODS

Within the framework of the ADER 13.1.1 project, the SME 1.5-0 experimental micro-hydropower system was developed and tested (Fig. 1). The system was designed to recover hydraulic energy and convert it into electrical energy for supplying aeration systems installed in fish ponds. The system consists of a paddle-wheel rotor, a supporting frame, a mechanical transmission and speed-increasing system, a permanent-magnet generator, and an electrical system for energy control, storage, and conversion.

The operating principle of the system is based on the conversion of the hydraulic energy of the water into mechanical energy by means of a rotor equipped with paddle-type blades. The rotational motion of the rotor is transmitted to the permanent-magnet electric generator through a speed increaser and a Poly-V belt transmission. The generated electrical energy is supplied to the energy control and storage system and, through the inverter, is converted into alternating electrical power required to supply the electrical loads. The main components of the mechanical energy conversion chain are the rotor, the speed increaser, the Poly-V belt transmission, and the permanent-magnet generator.



**Fig. 1 - SME 1.5-0 Experimental Micro-Hydropower System**

The main technical and structural characteristics of the SME 1.5-0 experimental micro-hydropower system used in the present research are presented in Table 1. According to the technical documentation, the system has a rated power of 1000 W, a rotor with a diameter of 1400 mm and a width of 1200 mm, paddle-type blades, and a transmission system with a 1:25 speed-increasing ratio. The generator is a permanent-magnet type, while the electrical system includes an inverter and an energy storage system.

**Table 1**

**The main technical and structural characteristics of the SME 1.5-0**

| Characteristic | UM | Value |
|---|---|---|
| Nominal power | W | 1000 |
| Rotor diameter | mm | 1400 |
| Rotor width | mm | 1200 |
| Expected system efficiency | % | 45–60 |
| Hydro blade type | – | paddle type |
| Transmission type | – | speed increaser |
| Transmission ratio | – | 1:25 |

| Characteristic | UM | Value |
|---|---|---|
| Generator type | – | permanent magnet |
| Generator torque | Nm | 55–193 |
| Inverter power | kW | 5.2 |
| Inverter nominal voltage | V DC | 48 |
| Inverter output voltage | V AC | 220 |
| Frequency | Hz | 50 |
| Inverter efficiency | % | 94 |
| Number of batteries | pcs. | 4 |
| Battery voltage | V DC | 12 |
| Battery capacity | Ah | 60 |

For the experimental investigations, the SME 1.5-0 system was prepared at the INMA Bucharest premises and subsequently transported to the ICDEAPA Galați – Brateș Laboratory, where assembly and testing were carried out under real operating conditions. Following receipt of the equipment, the integrity of the assemblies and their compliance with the technical documentation were verified.

During the preliminary operations, particular attention was paid to the positioning of the supporting assembly, verification of the mounting base, and alignment of the main components, namely the rotor, speed increaser, and electric generator.



**a. Preparation of the Equipment for Transport**



**b. Transportation and Receipt of the Equipment**



**c. Preparation for Final Assembly**



**d. System Installation at the Water Intake**



**e. Preliminary Checks During Assembly**



**Preparation for Testing**

**Fig. 2 - Actions for Establishing the Operating Parameters and Conducting Functional Tests**

The experimental methodology was developed to evaluate the functional, mechanical, and energy performance of the SME 1.5-0 micro-hydropower system under real operating conditions. The assessment of such a system requires the coordinated monitoring of hydraulic, mechanical, and electrical parameters, as the overall performance depends both on the characteristics of the available water resource and on the efficiency of the energy transmission and conversion components. Similar approaches are used in experimental studies of micro-hydropower systems, in which flow conditions, generator speed, and electrical parameters are analyzed simultaneously to characterize the energy conversion process *(Shen et al., 2023)*.

Prior to the experimental tests, the SME 1.5-0 system underwent an initial technical inspection. This inspection included verification of the structural design, manufacturing quality of the components and subassemblies, weld quality, component assembly, and compliance with the technical documentation. Particular attention was paid to the mechanical stability of the supporting structure, rotor positioning,

alignment of the rotor–speed increaser–generator assembly, and integrity of the electrical and automation components.

The experimental tests were conducted under real operating conditions at the ICDEAPA Galați – Brateș Laboratory. The micro-hydropower system was installed at the water intake of the experimental facility, after preliminary verification of the supporting structure, mounting base, alignment of the rotor, speed increaser, and electric generator, as well as the connection to the water supply. Following completion of the assembly, preliminary start-up tests were performed to verify the water flow, rotor motion, and rotational speeds of the mechanical components. The operating conditions were established by varying the hydraulic pressure of the water supply. Hydraulic parameters play a fundamental role in the micro-hydropower conversion process because they determine the energy available at the rotor and consequently influence the mechanical and electrical response of the generator. Experimental investigations of micro-generation systems have demonstrated a direct relationship between hydraulic operating conditions, rotor speed, and the electrical performance of the generator *(Shen et al., 2023).* In aquaculture facilities, hydraulic conditions also influence the performance of aeration systems, which justifies their careful monitoring *(Aytac et al., 2024; Kelestemur et al., 2024)*. During the experiments, the SME 1.5-0 system was tested at water pressures of 0.7, 1.4, and 2.0 bar, at a flow rate of 36 L/min. The ambient temperature during the testing period ranged from 17 to 19°C. The tests were conducted under controlled-flow conditions, with the water discharged into an open channel. The measurement instruments used during the experiments were calibrated and certified. To characterize system operation, the main mechanical and electrical parameters were monitored: rotor speed $n_r$, speed increaser output speed $n_{red}$, electric generator speed $n_g$, voltage at the input of the energy storage system $U_\beta$, and inverter output voltage $U_{inv}$. Simultaneous monitoring of these parameters enabled the assessment of the performance of the entire hydraulic–mechanical–electrical conversion chain. The integrated analysis of energy generation, storage, and utilization is also applied in modern aquaculture systems supplied by renewable energy sources *(Dewi et al., 2025; Zhang et al., 2024a).*

The transmission ratio between the rotor and the electric generator was determined using the following relationship:

$$i = \frac{n_g}{n_r} \quad (1)$$

where:
*i* – transmission ratio;
$n_g$ – electric generator speed, rpm;
$n_r$ – rotor speed, rpm.

The SME 1.5-0 system was designed with a transmission ratio of 1:25, the transmission system being intended to increase the relatively low rotational speed of the rotor to the level required for electric generator operation. During the tests, this transmission ratio was verified by measuring the rotational speeds of the rotor and generator. The method based on correlating hydraulic operating conditions with generator speed is also used in research on hydroelectric micro-generation systems. Shen et al. (2023) experimentally investigated a micro-power generation system equipped with a permanent-magnet generator and demonstrated the influence of flow conditions and rotational speed on the electrical performance of the system. These findings support the need for simultaneous monitoring of hydraulic, mechanical, and electrical parameters when evaluating hydraulic energy recovery systems *(Shen et al., 2023).*

The hydraulic operating conditions were also analyzed in relation to the intended use of the generated energy, namely supplying aeration equipment used in fish ponds. Aeration represents a significant energy consumer in intensive aquaculture systems, and its performance depends on the hydraulic configuration and operating conditions of the system. Experimental studies have demonstrated that flow rate, hydrostatic head, and aeration system characteristics directly influence oxygen transfer efficiency and energy consumption *(Aytac et al., 2024; Kelestemur et al., 2024).*

Recent studies have also shown that optimizing aeration parameters can reduce energy consumption in recirculating aquaculture systems. Numerical and experimental investigations of microbubble aeration have demonstrated that air flow rate, bubble size, and aerator positioning influence oxygen transfer efficiency and specific energy efficiency *(Zhang et al., 2024b).* At the same time, review studies on modern aquaculture technologies emphasize the importance of using highly energy-efficient aeration systems *(Nguyen et al., 2024).* The integration of renewable energy sources into aquaculture systems also requires the energy produced to be matched with consumer demand and available energy storage capacity. Studies

on recirculating aquaculture systems integrated with hybrid energy sources have highlighted the advantages of a unified energy and economic approach *(Zhang et al., 2024a).* Furthermore, the combined use of solar and micro-hydropower energy has been investigated for aquaponics applications, demonstrating the feasibility of integrating renewable energy sources within a common energy management system *(Dewi et al., 2025)*. From a sustainability perspective, improving energy efficiency and harnessing locally available resources are consistent with the principles of the circular economy applied to aquaculture. These principles aim to improve resource-use efficiency, recover useful energy flows, and reduce environmental impacts *(Chary et al., 2024).* The SME 1.5-0 system follows this approach by harnessing the available hydraulic energy and converting it into electrical energy that can be utilized within the aquaculture farm.

The hydraulic power available for each experimental operating condition was determined based on the pressure and volumetric flow rate using the following relationship:

$$P_h = \Delta p \times Q \tag{2}$$

where:

$P_h$ – hydraulic power, W;

Δp – pressure difference, Pa;

**Q** – volumetric flow rate, m³/s.

The energy analysis of the G-1500 generator was performed by comparing the experimental rotational speed with the values indicated by the generator performance characteristic. To estimate the required mechanical power, a generator efficiency of 90% and a mechanical transmission efficiency of approximately 92.5% were considered.

The mechanical power at the generator shaft was estimated using the following relationship:

$$P_{m,g} = \frac{P_e}{\eta_g} \tag{3}$$

The mechanical power at the generator shaft was estimated using the following relationship:

$$P_{r,nec} = \frac{P_{m,g}}{\eta_t} \tag{4}$$

unde:

$P_{m,g}$ – mechanical power at the generator shaft, W;

$P_e$ – electrical power indicated by the generator performance characteristic, W;

$\eta_g$ – generator efficiency;

$P_{r,nec}$ – mechanical power required at the rotor, W;

$\eta_t$ – mechanical transmission efficiency.

For each operating condition, the data were recorded after the system parameters had reached a stable state. Performance evaluation considered rotational speed and voltage stability, the mechanical behavior of the assembly, and the correlation between the available hydraulic resource and the operating conditions of the generator. At the end of the tests, a final technical inspection of the mechanical and electrical components was performed, with particular attention paid to the occurrence of abnormal vibrations, unusual noise, or functional failures. At the end of the experimental program, a final technical assessment of the SME 1.5-0 system was conducted. The condition of the mechanical and electrical components, the stability of the assembly, and the preservation of its structural and functional characteristics were verified.

The results obtained were used to evaluate system performance and identify opportunities for optimizing the hydraulic operating conditions and the energy conversion chain.

## RESULTS AND DISCUSSION

Experimental testing of the SME 1.5-0 micro-hydropower system enabled the characterization of the hydraulic–mechanical–electrical conversion chain under the analyzed hydraulic conditions. The assessment focused on the rotational speeds of the rotor, speed increaser, and generator, as well as on the electrical parameters recorded at the energy storage system and inverter. These parameters were used to analyze the behavior of the mechanical transmission, functional stability, and limitations imposed by the available hydraulic resource.

The main parameters recorded during the tests are presented in Table 2. According to the experimental data, the rotor operated at a rotational speed of 30 rpm, while a rotational speed of 750 rpm was recorded at the generator. In addition, an AC voltage of 220 V was measured at the inverter output.

**Table 2**

**Main operating parameters recorded during the tests**

| Parameter | Symbol | Recorded value | Remarks |
|---|---|---|---|
| Rotor speed | $n_r$ | 30 rpm | Measured at the transmission input |
| Speed increaser output speed | $n_{red}$ | 750 rpm | Transmission ratio 1:25 |
| Generator speed | $n_g$ | 750 rpm | Experimental operating condition |
| Voltage at the input of the energy storage system | $U_b$ | 24 Vcc | Value recorded in the report |
| Inverter output voltage | $U_{inv}$ | 220 Vca | Available for electrical loads |

The rotor speed of 30 rpm and the generator speed of 750 rpm correspond to a kinematic ratio of approximately 25, confirming the speed increase provided by the transmission configuration. The increase in rotational speed is necessary to adapt the relatively low rotational speed of the hydraulic rotor to the operating range of the electric generator. The 1:25 transmission ratio is also specified in the technical documentation of the system. The measured output voltage of 220 V AC indicates that the electrical conversion system provided a voltage level suitable for supplying conventional electrical loads used in aquaculture facilities. Regarding the value of 24 V DC recorded at the input of the battery storage system, this value should be carefully addressed in the final version of the paper, since the system documentation describes four 12 V batteries connected in series, corresponding to a nominal 48 V system.

The hydraulic operating conditions directly influenced the energy available for conversion. The experiments were conducted at water pressures of 0.7, 1.4, and 2.0 bar, at a flow rate of 36 L/min, while the ambient temperature ranged from 17 to 19°C. The hydraulic power values determined for the three operating conditions are presented in Table 3.

**Table 3**

**Hydraulic power under the analyzed experimental conditions**

| Water pressure (bar) | Flow rate (L/min) | Hydraulic power (W) |
|---|---|---|
| 0,7 | 36 | 42 |
| 1,4 | 36 | 84 |
| 2,0 | 36 | 120 |

At a constant flow rate of 36 L/min, increasing the pressure from 0.7 to 2.0 bar resulted in an increase in hydraulic power from 42 to 120 W. These results demonstrate the direct influence of pressure on the energy available at the rotor and indicate that, under the experimental configuration investigated, the available hydraulic resource represented the main limiting factor for energy performance.

To illustrate the variation in hydraulic power as a function of water pressure, the values determined for the three experimental conditions were plotted in Fig. 3.

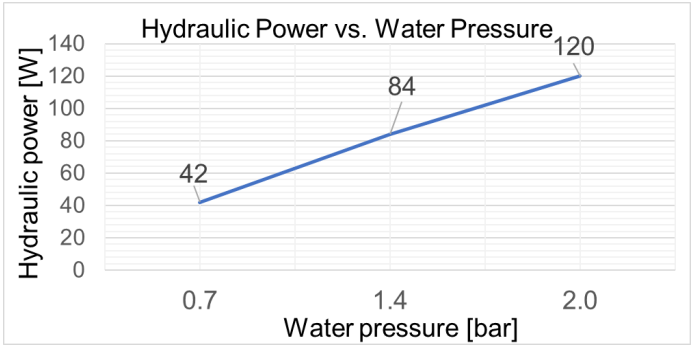



**Fig. 3 - Effect of water pressure on the hydraulic power available at a constant flow rate of 36 L/min**

As shown in Fig. 3, hydraulic power increased almost linearly with increasing water pressure, from 42 W at 0.7 bar to 120 W at 2.0 bar. This trend results from maintaining the flow rate constant at 36 L/min and confirms the direct influence of pressure on the hydraulic energy available for driving the rotor. The

observed trend is consistent with results reported for low-power hydroelectric micro-generation systems, in which flow conditions and operating regimes directly influence energy conversion performance *(Shen et al., 2023)*.

The performance of the G-1500 generator was also analyzed based on its performance characteristic. According to the data used in the experimental report, the generator characteristic indicates an electrical power of approximately 600 W at 750 rpm, approximately 1050 W at 1000 rpm, and approximately 1600 W at 1250 rpm. For the energy analysis, a generator efficiency of 90% and a mechanical efficiency of the speed increaser of approximately 92.5% were considered.

**Table 4**

**Estimated energy parameters based on the G-1500 generator performance characteristic**

| Generator speed (rpm) | Electrical power (W) | Generator efficiency (%) | Mechanical power at generator shaft (W) | Mechanical power required at rotor (W) |
|---|---|---|---|---|
| 750 | 600 | 90 | 667 | 720 |
| 1000 | 1050 | 90 | 1167 | 1260 |
| 1250 | 1600 | 90 | 1778 | 1922 |

It is important to specify that the operating condition of 750 rpm was reached during the experimental tests, whereas the values corresponding to 1000 and 1250 rpm were estimated based on the generator performance characteristic. Therefore, the power values presented in Table 4 should not be interpreted as electrical power directly measured during the hydraulic tests.

To highlight the effect of the mechanical transmission on the rotational speed of the system, the values recorded at the rotor, speed increaser, and generator were plotted in Fig. 4. The rotational speed increased from 30 rpm at the rotor to 750 rpm at the speed increaser and generator, corresponding to the 1:25 transmission ratio specified for the SME 1.5-0 system.

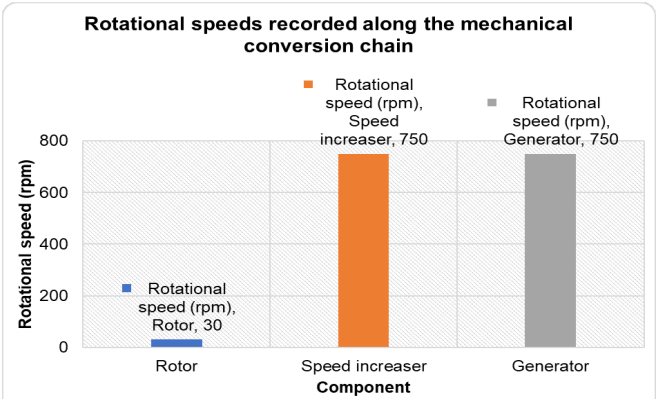



**Fig. 4 - Rotational speeds recorded along the kinematic chain of the SME 1.5-0 system**

As shown in Fig. 4, the rotational speed increases significantly between the rotor and the speed increaser, from 30 to 750 rpm, and subsequently remains at the same level at the generator. The ratio between generator speed and rotor speed is approximately 25, confirming the 1:25 kinematic ratio specified for the system transmission. Maintaining a rotational speed of 750 rpm at both the speed increaser output and the generator indicates direct transmission of motion between these components in the experimental configuration investigated.

It should be noted that, although a rotational speed of 750 rpm was experimentally achieved, the value of approximately 600 W associated with this operating condition is derived from the G-1500 generator performance characteristic and does not represent electrical power measured directly during the hydraulic tests. The values corresponding to 1000 and 1250 rpm are likewise estimated based on the generator performance characteristic.

Comparison of the available hydraulic power with the estimated mechanical power required for generator operation at the power levels indicated by its performance characteristic reveals a significant imbalance between the available hydraulic resource and the power demand of the conversion system. The maximum hydraulic power calculated under the experimental conditions was 120 W, which is considerably lower than the estimated mechanical power required for generator operation under the analyzed operating conditions. Consequently, under the tested conditions, the energy performance of the system was primarily

limited by the available hydraulic resource. Increasing the water flow rate and/or pressure is therefore necessary to bring the system closer to the higher power operating conditions indicated by the generator performance characteristic.

No abnormal vibrations, excessive noise, or significant mechanical losses were reported during the tests. These observations indicate stable mechanical behavior of the rotor–transmission–generator assembly within the investigated operating range.

The results indicate that further system optimization should primarily focus on increasing the hydraulic power effectively transferred to the rotor. During the experiments, it was observed that, at pressures below 1 bar, the water jet acted predominantly on the central region of the rotor, thereby limiting the torque transmitted to the shaft. Increasing the flow rate toward the range of 60–80 L/min and repositioning the jet impact zone toward the upper part of the blades could increase shaft torque and improve the energy performance of the system.

Another potential optimization direction is the integration of a complementary photovoltaic energy source. A hybrid micro-hydropower–photovoltaic configuration could compensate for periods when the available hydraulic resource is insufficient and could provide a more stable supply to the energy storage system and aeration equipment.

This approach is also supported by recent research on the integration of renewable energy sources into aquaculture and aquaponics systems *(Dewi et al., 2025; Zhang et al., 2024a).* The proposal for integrating a complementary photovoltaic source is also mentioned in the experimental report.

Overall, the experimental results confirm the operation of the system's kinematic chain and highlight the determining influence of hydraulic parameters on energy performance. For a comprehensive characterization of the system, additional tests are required over a wider range of flow rates and pressures, together with the experimental determination of an integrated pressure–flow rate–rotational speed–power–efficiency characteristic. Such an approach would enable the optimum operating regime to be established and the generator and energy storage system to be more accurately sized according to the available hydraulic resource.

## CONCLUSIONS

- The experimental tests confirmed the operation of the hydraulic–mechanical–electrical conversion chain of the SME 1.5-0 system and enabled the identification of the main factors limiting the utilization of the available hydraulic resource.
- The system achieved a rotor speed of 30 rpm and a generator speed of 750 rpm, corresponding to a kinematic ratio of approximately 1:25, confirming the operation of the speed-increasing transmission according to the adopted structural configuration.
- An output voltage of 220 V AC was recorded at the inverter, indicating the potential for supplying conventional electrical loads used in aquaculture facilities.
- The hydraulic parameters directly influenced the energy performance of the system. At a flow rate of 36 L/min, increasing the pressure from 0.7 to 2.0 bar resulted in an increase in the available hydraulic power from 42 to 120 W.
- The energy analysis demonstrated that the available hydraulic resource under the experimental conditions represented the main limiting factor of the system. The maximum available hydraulic power was lower than the mechanical power required for the higher operating conditions of the generator, preventing operation at its rated capacity.
- No abnormal vibrations, excessive noise, or functional failures were reported during the tests, indicating stable mechanical behavior of the rotor–transmission–generator assembly within the investigated experimental range.
- The results indicate the need for further research by extending the testing range to higher flow rates and pressures and by optimizing the interaction between the water jet and the rotor blades. In particular, increasing the flow rate toward 60–80 L/min and repositioning the jet impact zone toward the upper part of the blades could increase the mechanical torque and overall energy conversion efficiency.
- The integration of a complementary photovoltaic source may represent a solution for compensating for variations in the available hydraulic resource and increasing the continuity of power supply to the

aeration systems. A hybrid micro-hydropower–photovoltaic configuration could increase the energy autonomy of the aquaculture farm and the utilization of locally available renewable energy sources.

- Overall, the SME 1.5-0 system represents a technical solution with potential for harnessing low-power hydraulic energy in aquaculture applications. Comprehensive validation of its energy performance requires the experimental determination of an integrated pressure–flow rate–rotational speed–power–efficiency characteristic and its correlation with the energy demand of the aeration systems.

**ACKNOWLEDGEMENT**

The results presented in this article were obtained with the support of MADR through the "Sectoral Plan - ADER 2026", financing contract no. 13.1.1 / 17.07.2023, ADER project 13.1.1. Research on increasing profitability in aquaculture farms by introducing valuable species with the implementation of specific aquaculture, animal husbandry and agricultural technologies - the realization of the integrated aquaculture farm, managed by the The Research and Development Institute for Aquatic Ecology, Fishing and Aquaculture – Galati.

**REFERENCES**

[1] Aytac, A., Kelestemur, G. T., & Tuna, M. C. (2024). An effective aeration system for high performance pond aeration at low energy cost. *Aquaculture International*, *32*, 6869–6886. https://doi.org/10.1007/s10499-024-01492-6.

[2] Chary, K., van Riel, A. J., Muscat, A., Wilfart, A., Harchaoui, S., Verdegem, M., Filgueira, R., Troell, M., Henriksson, P. J. G., de Boer, I. J. M., & Wiegertjes, G. F. (2024). Transforming sustainable aquaculture by applying circularity principles. *Reviews in Aquaculture*, *16*(2), 656–673. https://doi.org/10.1111/raq.12860.

[3] Dewi, T., Risma, P., Oktarina, Y., Dwijayanti, S., Mardiyati, E. N., Sianipar, A. B., Hibrizi, D. R., Azhar, M. S., & Linarti, D. (2025). Smart integrated aquaponics system: Hybrid solar-hydro energy with deep learning forecasting for optimized energy management in aquaculture and hydroponics. *Energy for Sustainable Development*, *85*, 101683. https://doi.org/10.1016/j.esd.2025.101683.

[4] Kelestemur, G. T., Aytac, A., & Tuna, M. C. (2024). Experimental investigation on oxygenation efficiency of an effective aeration system for ponds. *Aquaculture International*, *32*, 8631–8647. https://doi.org/10.1007/s10499-024-01583-4.

[5] Nguyen, N. T., Vo, T. S., Tran-Nguyen, P. L., Nguyen, M. N., Pham, V. H., Matsuhashi, R., Kim, K., & Vo, T. T. B. C. (2024). A comprehensive review of aeration and wastewater treatment. *Aquaculture*, *591*, 741113. https://doi.org/10.1016/j.aquaculture.2024.741113.

[6] Roy, S. M., Machavaram, R., Pareek, C. M., & Kim, T. (2024). Investigating the performance of a perforated pooled circular stepped cascade aeration system for intensive aquaculture. *Heliyon*, 10(5), e26367. https://doi.org/10.1016/j.heliyon.2024.e26367

[7] Shen, Z., Yao, Y., Wang, Q., Lu, L., & Yang, H. (2023). A novel micro power generation system to efficiently harvest hydroelectric energy for power supply to water intelligent networks of urban water pipelines. *Energy*, *268*, 126694. https://doi.org/10.1016/j.energy.2023.126694.

[8] Zhang, R., Chen, T., Wang, Y., & Short, M. (2024a). An optimisation approach for the design and operation of recirculating aquaculture systems integrated with sustainable hybrid energy systems. *Journal of Cleaner Production*, *477*, 143860. https://doi.org/10.1016/j.jclepro.2024.143860.

[9] Zhang, S., Yu, G., Wang, Y., Li, D., & Chen, X. (2024b). Investigation on aeration efficiency and energy efficiency optimization in recirculating aquaculture coupling CFD with Euler–Euler and species transport model. *Journal of Environmental Chemical Engineering*, *12*(5), 113927. https://doi.org/10.1016/j.jece.2024.113927.

[10] Zhang, Z., Liu, H., Jin, J., Zhu, X., Han, D., & Xie, S. (2024). Towards a low-carbon footprint: Current status and prospects for aquaculture. *Water Biology and Security*, 3(4), 100290. https://doi.org/10.1016/j.watbs.2024.100290.

# RECYCLING BIODEGRADABLE WASTE THROUGH COMPOSTING IN THE CONTEXT OF THE CIRCULAR ECONOMY

/

# *VALORIFICAREA DEȘEURILOR BIODEGRADABILE PRIN COMPOSTARE ÎN CONTEXTUL ECONOMIEI CIRCULARE*

**Carmen-Otilia RUSĂNESCU*[1)], Gigel PARASCHIV[1)], Gabriel Alexandru CONSTANTIN[1)], SORIN-Ştefan BIRIŞ[1)], Gheorghe VOICU[1)], Andrei-Marian RUSĂNESCU[2)], Gabriel RUSĂNESCU[2)], Melania CISMARU[1)], Irina Aura ISTRATE[1)], Mirela DINCĂ[1)]**

[1)] National University of Science and Technology POLITEHNICA Bucharest - Faculty of Biotechnical Systems Engineering, Bucharest / Romania;

[2)] National University of Science and Technology POLITEHNICA Bucharest - Faculty of Automatic Control and Computer Science, Bucharest / Romania

**E-mail: carmen.rusanescu@upb.ro*

***Keywords:*** *circular economy, biodegradable waste, composting, bulk density, C/N ratio, soil fertility*

## ABSTRACT

*This paper analyzes, based on a structured review of the specialized literature from the period 2000–2026, the role of controlled composting as a method of stabilizing organic matrices and its impact on edaphic properties. The results reveal that the application of a mature compost stimulates the formation of humic substances, intensifies microbial diversity and enzymatic activity, while reducing the bulk density of the soil and increasing the stability of structural aggregates.To maximize these edaphic benefits and prevent ecological risks (ammonia emissions or anaerobiosis),the technological process requires an optimal Carbon/Nitrogen (C/N) ratio of 20:1–35:1, a humidity level maintained between 50%–65% and a particle size ranging between 2.5 and 5 cm. The use of stabilized compost represents a viable alternative to synthetic fertilizers.*

## REZUMAT

*Prezenta lucrare analizează, pe baza unei recenzii structurate a literaturii de specialitate din perioada 2000–2026, rolul compostării controlate ca metodă de stabilizare a matricilor organice și impactul acesteia asupra proprietăților edafice. Rezultatele relevă că aplicarea unui compost matur stimulează formarea substanțelor humice, intensifică diversitatea microbiană și activitatea enzimatică, reducând în același timp densitatea aparentă a solului și crescând stabilitatea agregatelor structurale. Pentru maximizarea acestor beneficii edafice și prevenirea riscurilor ecologice (emisii de amoniac sau anaerobioză), procesul tehnologic necesită un raport Carbon/Azot (C/N) optim de 20:1–35:1, un nivel al umidității menținut între 50%–65% și o granulometrie a particulelor cuprinsă între 2,5 și 5 cm. Utilizarea compostului stabilizat reprezintă o alternativă viabilă la îngrășămintele de sinteză.*

## INTRODUCTION

In recent decades, solid waste generation has increased worldwide, with approximately 2 billion tons generated in 2016, which is correlated with population growth *(Sayara, T. et al, 2020)*. This growth puts pressure on the environment and disrupts the ecological balance *(Sayara, T. et al, 2020)*. Implementing environmentally friendly management strategies is an urgent need worldwide *(Boateng, 2026)*. Reusing and recycling this waste according to the circular economy is required *(Sayara, T. et al, 2020)*. The European Parliament has adopted action plans that include specific legislative proposals to stimulate the market for organic fertilizers obtained from waste *(Sayara, T. et al, 2020)*.

Biodegradable waste represents the majority component of urban solid waste, often exceeding 40-70% of the total *(Manea, E.E. et al, 2024)*. Poor management of these organic residues, uncontrolled storage or open burning causes greenhouse gas emissions, soil degradation and air pollution *(Rana and Ali, 2026)*. Uncontrolled anaerobic decomposition of organic matter in landfills generates methane ($CH_4$) and ammonia ($NH_3$), gases with a strong impact on climate change *(Manea, E.E. et al, 2024)*. Odor pollution and the proliferation of disease vectors are major public health risks associated with landfills *(Ayilara, M.S. et al,*

*2020)*. Conventional incineration generates carbon dioxide ($CO_2$) emissions and toxic pollutants such as dioxins *(Manea, E.E. et al, 2024).*

Composting is the biological, oxidative and controlled conversion of biodegradable organic matrices into stable humus-like products *(Manea, E.E. et al, 2024)*. This technology is practical and applicable at any scale, from individual households to large industrial facilities *(Sayara, T. et al, 2020)*.

The biological process of decomposition and transformation of solid organic waste is carried out through the action of microorganisms (bacteria and fungi), resulting in a nutrient-rich fertilizer amendment *(Sayara, T. et al, 2020)*.

Mature composts restore soil organic carbon reserves, improve the stability of structural aggregates and increase water retention capacity *(Sayara, T. et al, 2020)*. By replacing synthetic chemical fertilizers, which deteriorate soil composition over time, composting supports sustainable agriculture *(Sayara, T et al., 2020)*. This practice closes nutrient cycles in nature and reduces the global carbon footprint *(Manea, E.E. et al, 2024).*

This paper analyzes the role of controlled composting as a method of stabilizing organic matrices and its impact on soil properties. The impact of compost application on the physical (bulk density, porosity, water retention) and biological (enzymatic activity, microbial diversity) properties of the soil is evaluated. The critical technological parameters (C/N ratio, humidity, granulometry) necessary for process optimization and prevention of ecological risks are analyzed, highlighting the value of compost as a viable alternative to synthetic fertilizers.

## MATERIALS AND METHODS

This paper is based on a structured review of specialized literature from international databases such as: ScienceDirect, Scopus, Web of Science, PubMed and Google Scholar. The searches targeted keywords such as "circular economy", "municipal solid waste", "composting", "nitrification" and "heavy metals". The time interval analyzed covered the period between 2000 and 2026.

The monitored indicators are: waste generation rates, degradable biomass fractions, pH variations, temperature and gaseous emissions.

## RESULTS

The main categories of waste that can be composted are: waste from gardens and parks, the biodegradable fraction of household and assimilable waste (fruit and vegetable scraps, eggshells and other food scraps), waste from markets and food complexes; biodegradable waste from the food industry; sludge from urban sewage treatment plants (i.e., those that are not polluted with heavy metals or other prohibited chemical agents); waste from livestock complexes.

Composting can be done in households, in open piles, in special plastic compost bins or in other containers. In the case of farms and composting stations, composting can be done on specially arranged platforms, with the composting material being arranged in long rows (furrows) and periodically turned (using special furrow-rearranging equipment), in aerated static pile systems using perforated pipes or in special containers.

Achieving an advanced degree of maturity and stability of compost stimulates the formation of humic substances, improves soil fertility and organic matter content, while minimizing the risks of environmental contamination. The application of compost stimulates the enzymatic activity and microbial diversity of the soil, ensuring the long-term release of nutrients and improving its physical structure for optimal plant growth *(Martínez-Blanco, J. et al, 2013)*.

The increase in the apparent density of the soil blocks the development of plants, causing inadequate aeration, low water infiltration and restriction of root penetration. The application of compost improves the structure of the soil and decreases the apparent density with values between 0.7% and 23%, increasing porosity through the interaction between organic and inorganic fractions *(Martínez-Blanco, J. et al, 2013)*.

The introduction of compost at depths of 20-50 cm ensures a continuous and long-term reduction in bulk density, even after 6 years of application *(Somerville, P.D et al, 2018).*

Compost acts as a natural sponge, increasing water retention capacity by up to 50% and is an ideal solution for farmers in arid areas affected by drought and desertification.

The rate of water infiltration into the soil increases by adding compost, due to the reduction in density and stimulation of microbiological activity, the effects being visible even at shallow incorporations (5-10 cm).

Ensuring ideal conditions in the initial phase determines the efficiency of organic matter degradation *(Sayara, T. et al, 2020)*.

The optimal value of the C/N ratio for an effective mixture is between 20:1 and 35:1 *(Hoang, H.G. et al, 2022).* A C/N ratio that is too low indicates a carbon deficit, leading to excess ammonium accumulation, increased pH, and high nitrogen losses as harmful ammonia gas *(Manea, E.E. et al, 2024)*. If the C/N ratio exceeds 40:1, available nitrogen becomes reduced, limiting the activity of microorganisms, slowing down decomposition and extending the time required for maturation *(Ayilara, M.S. et al, 2020).* Carbon-rich materials, such as straw or sawdust, are used to calibrate the compost mixture, which optimize the C/N ratio and porosity for air circulation.

Soil quality evaluation also targets parameters such as bulk density, total porosity, and water retention capacity *(Manea, E.E. et al, 2024)*. The efficiency of nutrient retention is closely linked to the nature of the structuring agents used and the aeration regime. Under aerobic conditions, wastes with a high nitrogen content (such as poultry manure) can experience high losses of up to 52% in the form of volatile ammonia ($NH_3$). The type of carbon-rich material plays an important role: co-composting cattle waste with straw causes a nitrogen loss of 42%, while replacing straw with wood chips reduces this loss to only 12%, optimizing the conservation of nutrients in the matrix. On the other hand, the installation of an uncontrolled anaerobic regime, associated with excessive humidity above 75%, intensifies ammonia emissions (reaching peaks of 70%–88% in poultry waste), but also generates significant losses of 19%–46% in the form of nitrates ($NO_3^-$), increasing the risk of leaching into the soil *(Hoang, H.G. et al, 2022).*

Bacterial metabolic activity requires an optimal humidity in the range of 50%–65% *(Hoang, H.G. et al, 2022).* Excess humidity (above 70%) causes the porous spaces of the matrix to clog, blocks available oxygen and sets up anaerobic processes generating hydrogen sulfide ($H_2S$) and unpleasant odors *(Hoang, H.G. et al, 2022; Ayilara, M.S. et al., 2020)*. A decrease in humidity below the threshold of 40% dehydrates microbial cells, inhibits their metabolism and stops biochemical degradation *(Hoang et al., 2022)*. The best composting conditions are usually achieved when the particle size of the material varies from 2.5 to 5 cm in diameter *(Ayilara, M.S. et al, 2020).* This size provides a large specific surface area for microbial enzymatic attack, while maintaining open channels for air circulation *(Ayilara, M.S. et al, 2020)*. Extremely fine particles retain excess water, reduce aerated free space, and block the movement of oxygen inside the pile *(Ayilara, M.S. et al, 2020)*.

The composting process is a dynamic phenomenon governed by thermal changes that dictate the succession of specific microbial communities *(Manea, E.E. et al, 2024).*

The composting process involves two stages: mechanical treatment and decomposition (fermentation). In the case of mechanical treatment, the waste is shredded, homogenized and prepared for biological treatment/fermentation.

The fermentation stage comprises three main phases:

- the first phase, the fermentation stage, the initial mesophilic phase at temperatures between 20–40 °C, aerobic mesophilic microorganisms begin the degradation of easily bioavailable carbon fractions, such as sugars and amino acids *(Ayilara, M.S. et al, 2020)*. This intense metabolic activity releases energy in the form of heat, causing the temperature inside the pile to increase rapidly *(Ayilara, M.S. et al, 2020)*. During this stage, the pH may temporarily decrease due to the accumulation of short-chain organic acids *(Hoang, H.G. et al, 2022).*
- the second phase, thermophilic, consists of intense aerobic degradation. Organic matter decomposes at temperatures above 45 to 70°C, under the action of bacteria, mesophilic bacteria are destroyed or inactivated, their place being taken by thermophilic bacteria and fungi *(Ayilara, M.S. et al, 2020)*. Due to high temperatures, the material is pasteurized, microbes are destroyed as well as weed seeds. Temperatures maintained constantly above 55°C are essential for the destruction of dangerous pathogens, weed seeds and insect larvae *(Sayara, T. et al, 2020)*. In this active phase of thermostabilizing, the dominant bacterial genera are *Bacillus* and *Thermus*, remarkable for the secretion of heat-resistant exo-enzymes *(Manea, E.E. et al, 2024)*. Actinomycetes take on the main role in the decomposition of recalcitrant molecules and have the ability to metabolize complex molecules *(Ayilara, M.S. et al, 2020)*.
- the third phase constitutes the maturation stage, in which temperatures stabilize (35-45°C) and some fermentation continues, converting the degraded material into humus; the final objective is to produce a stable material. The final cooling and maturation phase, as energy sources are

depleted, the pile temperature gradually drops back to the mesophilic range *(Sayara, T. et al, 2020)*.

This period is marked by the re-colonization of the pile by specialized mesophilic microorganisms *(Sayara, T. et al, 2020)*. The humification process takes place through which phenolic precursors are transformed into complex aromatic structures of humic acids *(Manea, E.E. et al, 2024).* Now intense biological nitrification, essential for nitrogen stabilization, takes place *(Hoang, H.G. et al, 2022).*

The representation of the phases of the solid waste composting process is presented in figure 1.

During the composting process, the temperature evolution is monitored in close correlation with the succession of microbial communities and the transformations of chemical elements.

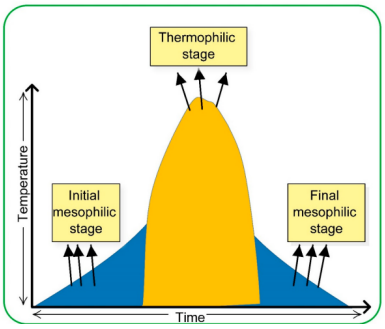



**Fig. 1 - Temperature changes in composting**
*(Ayilara, M.S. et al, 2020)*.

The fermentation period is at least 3 months in the hot season and 4-5 months in the cold season.

During this time, turning is practiced every 30 days. Turning is performed manually or, in the case of large quantities of compost, with the help of specialized equipment.

Obtaining high-quality compost is conditional on ensuring favorable environments for the development and metabolic activity of the microorganisms involved in the process. Thus, it is necessary to optimize the following factors:

- to obtain quality compost, the waste must contain ingredients rich in carbon (sawdust, tree branches, dry straw) and nitrogen (vegetable scraps, fruits, green weeds). Both green and dry waste must be used in the composting process. *(Hoang, H. G. et al, 2020).*
- moisture, present especially in nitrogenous ingredients, or from water added separately; moisture provides a favorable environment for the growth of aerobic bacteria and accelerates the composting process.
- the microbes involved in the composting process are aerobic, they need air to develop and decompose the waste *(Hoang, H. G. et al, 2020).*
- In the absence of proper aeration of the mixture, rotted (anaerobic) compost is formed, a poor quality organic fertilizer, dangerous for the environment. This generates unpleasant odors and methane gas, while the leachate resulting from rotting infiltrates the soil and subsequently reaches groundwater. In contrast, aerobically formed compost does not generate methane gas.

The carbon from biodegradable waste is found in the humus and the leachate is recirculated, part of it being integrated into the compost and most of it being transformed into water vapor (due to the high temperatures in the composting process); in this way the groundwater is protected.

To obtain good quality compost, it is important that the waste mixture is constantly aerated and homogenized, either manually or mechanically *(Ayilara, M. S., 2020).*

The pH of the composted materials affects the composting rate. It has been reported that alkaline pH is best for composting. When the pH is acidic, composting is very slow, because microorganisms are destroyed *(Ameen, A., 2016).*

*Chemical transformations and macronutrient recycling*

Biotransformation of municipal biomass involves complex mineralization and immobilization reactions of the main fertilizing elements *(Manea, E.E. et al, 2024).*

Nitrogen (N): Organic nitrogen is enzymatically degraded into amino acids and then reduced to ammonium ($NH_4^+$) in the initial phase *(Manea, E.E. et al, 2024).* Subsequently, below the thermal threshold of 40°C, ammonia-oxidizing bacteria and nitrite-oxidizing bacteria convert ammonium to nitrite ($NO_2^-$) and then to stable nitrate ($NO_3^-$) *(Hoang, H.G. et al, 2022).* The risk of nitrogen losses through $NH_3$ volatilization

is highest in the early thermophilic phase, when high temperatures coincide with alkaline pH *(Hoang, H.G. et al, 2022; (Manea, E.E. et al, 2024).* Phosphorus has a typical range of 2–5 g/kg in compost *(Manea, E.E. et al, 2024).* Its availability often decreases in the thermophilic phase due to chemical precipitation but increases significantly in the maturation phase through the activity of bacteria harboring specific phosphatase genes *(Manea, E.E. et al, 2024).* Potassium records values between 3 and 15 g/kg *(Manea, E.E. et al, 2024).* Due to its non-volatile nature, potassium does not suffer gaseous losses, remaining in the form of soluble salts in the humic matrix, being directly available to plants *(Manea, E.E. et al, 2024).*

Calcium and magnesium are progressively concentrated during the process as a result of the reduction of the total mass of organic carbon through respiration and mineralization *(Manea, E.E. et al, 2024).* Sulfur is essential for microbial and plant functions *(Manea, E.E. et al, 2024).*

The composition of macronutrients, (nitrogen N, calcium Ca, sulfur S, phosphorus P, potassium K and magnesium Mg) is shown in (Table 1)

**Table 1**

**Composition and role of macronutrients.**

| **Nutrient** | Nitrogen (N) | Potassium (K) | Phosphorus (P) | Calcium (Ca) | Sulfur (S) | Magnesium (Mg) |
|---|---|---|---|---|---|---|
| **Role as macronutrient** | Essential for the growth of microorganisms, helps in the decomposition | Enhances plant health and disease resistance | Helps plants growth | Enhances the disease resistance and plant growth | Microbial activity and some functions of plants | Essential nutrients for plants |
| **Typical range (g/kg)** | 10-20 | 3-15 | 2-5 | 4-6 | 1–3 | <0.1 |
| **References** | Gaspar et al, 2022 | Hussian, A. et al. 2018 | Armeen, H.A. et al 2022 | Awasthi, M.K. et al, 2022 | Rahman, M.M. et al, 2020 | Awasthi, M.K. et al, 2022 |

*Monitoring and Management of Potentially Toxic Substances*

The ecological safety of the use of municipal compost requires rigorous assessment of the fate of pollutants *(Manea, E.E. et al, 2024).*

The heavy metals identified in waste are zinc (Zn), lead (Pb), copper (Cu), cadmium (Cd), chromium (Cr) and nickel (Ni) *(Manea, E.E. et al, 2024).* Since biological processes cannot destroy the metallic elements, their total concentration increases during composting *(Manea et al., 2024)*. However, aerobic humification reactions favor the formation of stable complexes between metal ions and functional groups of humic acids, decreasing their bioavailability *(Manea, E.E. et al, 2024).*

Small plastic fragments (<5 mm) originate from packaging, synthetic textiles or from the fragmentation of macroplastics under the influence of mechanical turning forces and biodegradation *(Manea, E.E. et al, 2024).* The presence of microplastics has been shown to alter the humification process, decrease the ratio of humic acids to fulvic acids and reduce the richness of bacterial and fungal communities *(Manea, E.E. et al, 2024).* For this reason, municipal compost can become a vector for the introduction of microplastics into agrosystems if source separation is deficient *(Manea, E.E. et al, 2024).* Organic waste can contain antibiotics, hormones or dangerous endocrine disruptors *(Manea, E.E. et al, 2024).* The thermophilic phase of composting efficiently degrades these molecules *(Manea, E.E. et al, 2024).* For example, carbamazepine removal rates reach up to 83% and triclosan removal rates reach 86% in in-vessel composting systems *(Manea, E.E. et al, 2024).* However, the complexity of the mixed waste matrix can reduce the degradation rate *(Manea, E.E. et al, 2024).*

*Strategies for optimization and reduction of losses*

To remedy technological shortcomings, additives and certain techniques are used such as: Biochar addition (10%), Zeolite Addition (10-30%), Struvite Precipitation, Specific Bioaugmentation.

Biochar has favorable properties for gas adsorption, having high stability, large specific surface area and increased porosity *(Hoang, H.G. et al, 2022)*. Its addition tends to reduce total nitrogen losses by up to 52% during the composting process *(Hoang, H.G. et al, 2022).*

Among natural zeolites, clinoptilolite is the most abundant and has successfully reduced nitrogen gas emissions during composting *(Hoang, H.G. et al, 2022).* A 30% dose of zeolite added to compost

showed the highest attenuation of nitrogen losses, reaching an efficiency of 50.43% *(Hoang, H.G. et al, 2022).*

Struvite formation is applied as a key strategy to mitigate nitrogen losses *(Hoang, H.G. et al, 2022).* Struvite is a mineral crystal formed by magnesium, ammonium and phosphate in equal molar concentrations ($MgNH_4PO_4$ x $6H_2O$), the reaction being optimal at a neutral or alkaline pH between 7 and 9 *(Hoang, H.G. et al, 2022).* Specific bioaugmentation by inoculating active microbial strains, such as *Bacillus cereus*, *Pseudomonas donghuensis* and *Bacillus licheniformis*, helps control losses and increases the final total nitrogen concentration by 50.06% *(Hoang, H.G. et al, 2022).*

The application of different types of compost brings a series of improvements to soil properties. The main effects are the following:

*Physical properties and water management*

The soil becomes less compact, registering reductions in apparent density (for example, by 8% *(Sax, M.S. et al. 2017).*

Increases the stability of soil aggregates by up to 72.41%.

Increases water holding capacity and its availability to plants (in some cases recording a twofold increase *(Curtis, M.J. et al.,2005)* or increases in available water content by 86% *(Celik, I. et al., 2004).*

Increases porosity (both micro and macro-porosity) and hydraulic conductivity (under certain conditions, up to 22 times *(Celik, I. et al., 2004).*

Reduces soil erosion by 67% and surface runoff by 60%.

*Chemical properties and nutrient levels*

Significant enrichment of soil organic matter *(Tong, J. et al., 2018)* and organic carbon (up to 143% compared to chemical fertilizers *(Whalen, J.K. et al, 2008).*

Increases the concentration of total nitrogen, available phosphorus (with 200–400%) and available potassium (by 80–177%).

Depending on the soil and the material used, compost can lower alkaline pH to neutral values (7.28–7.45) or increase the pH of too acidic soils (*Tong, J. et al, 2018).*

*Biological and microbiological properties*

Increases the abundance of soil bacteria by 12–13% and stimulates microbial parameters (microbial biomass, basal respiration) *(Tong, J. et al, 2018).*

Improves the general biological functions of the soil by stimulating enzymes and energy molecules *(Tong, J. et al, 2018)*.

*Direct impact on crops*

Compost application led to an increase in wheat production (by an average of 246% compared to the control sample) and fruit tree productivity (e.g. *Prunus salicin* with 21.4%, generating larger and heavier fruits) *(Cherif, H. et al, 2009).*

Table 2 presents a comparative analysis between composting and conventional waste management (landfilling or incineration), highlighting the efficiency of the aerobic process in reducing waste volume and mitigating the carbon footprint.

**Table 2**

**Comparison between composting and conventional waste management.**

| Composting (Aerobic Method) | Conventional Management | References |
|---|---|---|
| Ensures environmental sustainability by enhancing soil structure.<br>Prevents soil erosion by binding structural aggregates together.<br>Enables bioremediation of contaminated soils.<br>Boosts biodiversity by attracting beneficial bacteria, fungi, and insects.<br>Operates under a controlled environment, recycling waste completely within a defined duration. | Causes severe pollution of soil, air, and water bodies (landfills, open dumps, incineration).<br>Degrades landscape aesthetics and releases foul odors.<br>Contaminates groundwater through toxic leachate infiltration from buried waste. | *Mohammed, A. and Elias, E., 2017* |
| Suppresses plant diseases and soil-borne pathogens.<br>Enriches the soil matrix with stable organic | Hosts disease vectors and pests (insects, rodents) at open dump sites.<br>Spreads dangerous pathogens, negatively | *Van Epps, A. and Blaney, L., 2016* |

| | | |
|---|---|---|
| matter naturally. | impacting human and animal health. | |
| Mitigates the greenhouse effect by drastically reducing methane ($CH_4$) emissions.<br>Releases significantly lower $CO_2$ compared to direct combustion and open burning modes. | Contributes majorly to global warming through the massive release of greenhouse gases.<br>Depletes the ozone layer due to combustion byproducts. | *Awasthi, M.K. et al, 2017* |
| Drastically reduces the physical volume of organic waste in an optimal timeframe. | Piles waste indefinitely, leading to a continuous increase in stored waste volume. | *Ayilara, M.S., et al, 2020* |

## CONCLUSIONS

Controlled composting is a fundamental and ecological management strategy, capable of taking over most of the urban solid waste (40-70%) and transforming it from a source of pollution into a valuable agronomic resource.

The application of mature compost generates major structural improvements at the soil level. The experimental data analyzed confirm the reduction of apparent density (by up to 23%) and the increase in aggregate stability (up to 63%). These changes block structural degradation, combat compaction and restore native porosity.

Through its physical properties like humus, compost functions as a natural sponge that increases water retention capacity by up to 50% and considerably improves infiltration rates. This quality recommends it as an essential tool for adapting agriculture to climate change and desertification in arid areas.

The ecological success of composting is directly conditioned by the strict maintenance of limiting factors in the initial phase. Deviations from the optimal C/N ratio (20:1–35:1) or exceeding the critical moisture threshold of 65% disrupt microbial metabolism, favor anaerobic processes, and generate harmful emissions of $NH_3$ and $H_2S$.

If the biochemical process is properly monitored, the final product (stable and mature compost) can successfully replace hazardous chemical fertilizers. It ensures a slow, long-term release of macronutrients and stimulates microbial biodiversity, supporting the global transition to sustainable agriculture

## REFERENCES


[1] Adamcová, D., Radziemska, M., Ridošková, A., Barto˘n, S., Pelcová, P., Elbl, J., Kynický, J., Brtnický, M., Vaverková, M.D. (2017). Environmental assessment of the effects of a municipal landfill on the content and distribution of heavy metals in Tanacetum vulgare L. *Chemosphere,* 185, 1011–1018, doi: 10.1016/j.chemosphere.2017.07.060.

[2] Armeen, H.A., Dohuki, M.S.S.M. (2022). The effect of leaching and bulking agents on the quality of municipal solid waste compost. *Environ. Technol.*, 45, 144–157. DOI: 10.1080/09593330.2022.2101026.

[3] Awasthi, M.K., Singh, E., Binod, P., Sindhu, R., Sarsaiya, S., Kumar, A., Chen, H., Duan, Y., Pandey, A., Kumar, S., (2022). Biotechnological strategies for bio-transforming biosolid into resources toward circular bioeconomy: A review. Renew. Sustain. Energy Rev., 156, 111987. https://doi.org/10.1016/j.rser.2021.111987.

[4] Ayilara, M. S., Olanrewaju, O. S., Babalola, O. O., Odeyemi, O. (2020). Waste Management through Composting: Challenges and Potentials. *Sustainability*, 12, 4456. https://doi.org/10.3390/su12114456.

[5] Boateng, K. S. (2026). Analysis of Sustainable Solid Waste Treatment/Management Approaches for Africa: Towards Integrated Sustainable Solid Waste Management. *Journal of Geoscience and Environment Protection*, 14, 37-64. DOI:10.4236/gep.2026.147003.

[6] Carballo, T., Gil, M., Calvo, L.F., Morán, A. (2009). The Influence of Aeration System, Temperature and Compost Origin on the Phytotoxicity of Compost Tea. *Compos. Sci. Util.*, 17, 127–139. DOI: 10.1080/1065657X.2009.10702411.

[7] Celik, I., Ortas, I., Kilic, S. (2004). Effects of compost, mycorrhiza, manure and fertilizer on some physical properties of a chromoxerert soil. Soil Till. Res., 78, 59–67. DOI: 10.1016/S0167-1987(04)00049-2.

[8] Curtis, M.J.; Claassen, V.P. (2005) Compost Incorporation Increases Plant Available Water in A Drastically Disturbed Serpentine Soil. *Soil Sci*., 170, 939–953.

[9] Cherif, H., Ayari, F., Ouzari, H., Marzorati, M., Brusetti, L., Jedidi, N., Hassen, A. (2009). Effects of municipal solid waste compost, farmyard manure and chemical fertilizers on wheat growth, soil composition and soil bacterial characteristics under Tunisian arid climate. *Eur. J. Soil Biol*., 45, 138–145. DOI: 10.1016/j.ejsobi.2008.11.003.

[10] Gaspar, S.S.,Assis, L.L.R., Carvalho, C.A., Buttrós, V.H.; dos Reis Ferreira, G.M.; Schwan, R.F.; Pasqual, M.; Rodrigues, F.A.; Rigobelo, E.C.; Castro, R.P. (2022). Dynamics of microbiota and physicochemical characterization of food waste in a new type of composter. Front. Sustain. *Food Syst*., 6, 960196. doi.org/10.3389/fsufs.2022.960196.

[11] Hoang, H. G., Thuy, B. T. P., Lin, C., Vo, D. V. N., Tran, H. T., Bahari, M. B., Le, V.G., Vu, C. T. (2022). The nitrogen cycle and mitigation strategies for nitrogen loss during organic waste composting: A review. *Chemosphere*, 300, 134514. DOI: 10.1016/j.chemosphere.2022.134514.

[12] Hussian, A., Hyder, N., Braesam, T., Natheer, A. (2018). Recycling of Organic Solid Wastes of Cities to Biofertilizer Using Natural Raw Materials. Al-Nahrain *J. Sci*. 19, 140–155.

[13] Manea, E. E., Bumbac, C.,Dinu, L. R., Bumbac, M., Nicolescu, C. M. (2024). Composting as a Sustainable Solution for Organic Solid Waste Management: Current Practices and Potential Improvements. *Sustainability*, 16, 6329. https://doi.org/10.3390/su16156329.

[14] Martínez-Blanco, J., Lazcano, C., Christensen, T.H.; Muñoz, P.; Rieradevall, J.; Møller, J.; Antón, A.; Boldrin, A. (2013). Compost benefits for agriculture evaluated by life cycle assessment. A review. *Agron. Sustain. Dev*. 33, 721–732. DOI: 10.1007/s13593-013-0148-7.

[15] Mohammed, A., Elias, E. (2017). Domestic solid waste management and its environmental impacts in Addis Ababa city. *J. Environ. Waste Manag*., 4, 194–203.

[16] Pathak, D., Singh, S., Agnihotri, R. K. (2026). Bioconversion of Temple Floral Waste Through Vermicomposting and Composting: A Review of the Available Evidence. *International Journal of Environment, Agriculture and Biotechnology*, 11(4), 73-82. DOI: 10.22161/ijeab.114.10

[17] Pérez-Gimeno, A., Navarro-Pedreño, J., Almendro-Candel, M.B., Gómez, I., Jordan, M. (2015) Environmental consequences of the use of sewage sludge compost and limestone outcrop residue for soil restoration: Salinity and trace elements pollution. *J. Soils Sedim*., 16, 1012–1021.

[18] Rana, M. Md. M., Younus, Md. M. Ali. (2026). Impact of circular agriculture in Bangladesh: Waste-to-value strategies for biogas production and crop residue management. *Journal of Agricultural Sciences*, 1-18. DOI: 10.2298/JAS2602113M.

[19] Rahman, M.M., Bhuiyan, M.S.H., Rouf, M.A., Sarker, R.R., Rashid, M.H. (2020). Quality assessment of municipal solid waste compost. *Acta Chem. Malays*., 4, 33–39. DOI: 10.2478/acmy-2020-0006.

[20] Sax, M.S., Bassuk, N., Van Es, H., Rakow, D. (2017). Long-term remediation of compacted urban soils by physical fracturing and incorporation of compost. *Urban Forestry & Urban Greening*., 24, 149–156. DOI: 10.1016/j.ufug.2017.03.023.

[21] Sayara, T., Basheer-Salimia, R., Hawamde, F., Sánchez, A. (2020). Recycling of Organic Wastes through Composting: Process Performance and Compost Application in Agriculture. *Agronomy*, 10, 1838. https://doi.org/10.3390/agronomy10111838.

[22] Somerville, P.D.; May, P.B.; Livesley, S.J. (2018). Effects of deep tillage and municipal green waste compost amendments on soil properties and tree growth in compacted urban soils. *J. Environ. Manag*., 227, 365–374. DOI: 10.1016/j.jenvman.2018.09.004.

[23] Tong, J., Sun, X., Li, S., Qu, B., Wan, L. (2018). Reutilization of Green Waste as Compost for Soil Improvement in the Afforested Land of the Beijing Plain. *Sustainability*, 10, 2376. https://doi.org/10.3390/su10072376.

[24] Van Epps, A., Blaney, L. (2016). Antibiotic residues in animal waste: occurrence and degradation in conventional agricultural waste management practices. *Curr. Pollut. Rep*., 2, 135–155.

[25] Whalen, J.K., Benslim, H., Jiao, Y., Sey, B.K. (2008). Soil organic carbon and nitrogen pools as affected by compost applicationsto a sandy-loam soil in Québec. Can. *J. Soil Sci*., 88, 443–450.

[26] Wang, M., Chen, H., Wang, Q., Zhao, J., Ren, X., Li, D.S., Awasthi, S.K., Shen, F., Li, R. (2017). Heterogeneity of biochar amendment to improve the carbon and nitrogen sequestration through reduce the greenhouse gases emissions during sewage sludge composting. Bioresource Technol., 224, 428–438.

# EVALUATION OF PARTICLE SIZE, RHEOLOGICAL AND BIOACTIVE CHARACTERISTICS OF ROSEHIP (*ROSA CANINA* L.) POWDER AS A FUNCTION OF GRINDING TECHNOLOGY

/

# *EVALUAREA PROPRIETĂȚILOR GRANULOMETRICE, REOLOGICE ȘI BIOACTIVE ALE PULBERII DE MĂCEȘ (ROSA CANINA L.) ÎN FUNCȚIE DE TEHNOLOGIA DE MĂCINARE*

**Alina-Daiana IONESCU[1)], Gheorghe VOICU*[1)], Gabriel-Alexandru CONSTANTIN[1)], Mihaela BEGEA[1)], Elena-Mădălina ȘTEFAN[1)], Adrian IOSIF[1)], Petruța PETCU[2)], Raluca-Adriana ZOTA[1)], Elena-Valeria VLĂDUȚ[1)], Melania-Elena CISMARU[1)], Catalina TUDORA[3)]**

[1)] National University of Science and Technology POLITEHNICA Bucharest, Faculty of Biotechnical Systems Engineering, Bucharest / Romania;

[2)] National University of Science and Technology POLITEHNICA Bucharest, Faculty of Aerospace Engineering, Bucharest / Romania;

[3)] National University of Science and Technology POLITEHNICA Bucharest, Entrepreneurship, Engineering and Business Management, Bucharest / Romania

**Tel: 0724 715 585; *E-mail: ghvoicu_2005@yahoo.com*

***Keywords:*** *Rosa canina L., knife mill, rotor and sieve mill, roller mill, particle size distribution, rheological and hydration characteristics;*

**ABSTRACT**

*The study evaluated the influence of three grinding devices-knife mill (KM), roller mill (RM), and sieve-rotor mill (SRM) on the particle size, rheological, and physicochemical properties of rosehip (Rosa canina* L.*) powder. Color parameters and polyphenol content were determined for the material ground by each mill; subsequently, the material underwent particle size analysis, and the resulting fractions were assessed for bulk and tapped density, Carr and Hausner indices, angle of repose, moisture content, water activity, swelling index and hygroscopicity. The results showed that each grinding mechanism imparted distinct characteristics to the powder. KM produced heterogeneous fragmentation, with the highest accumulation in the 0.250-0.355 mm fraction (35.04%), the most intense color (a*=20.17, C=43.91), and the highest polyphenol content (38.252 µg GAE/ml). RM generated a more uniform distribution (25% in the 0.355-0.500 mm range) and the best flowability (Carr index 7.85%, Hausner ratio 1.085). SRM favored the production of coarse particles (31.80% >0.710 mm) but yielded the lowest values for the angle of repose. Fine fractions exhibited high moisture content (up to 8.28%) and water activity below 0.46, with a swelling index of ~100% for the 0 mm fraction in RM and SRM samples. Rosin-Rammler model accurately described the particle size distributions for all three equipment. The type of grinding equipment decisively influences the quality of the rosehip powder, and its selection must be aligned with the intended technological application.*

**REZUMAT**

*Cercetarea a evaluat influența a trei echipamente de măcinare-moara cu cuțit (KM), moara cu valțuri (RM) și moara cu rotor și sită (SRM) asupra proprietăților granulometrice, reologice și fizico-chimice ale pulberii de măceș (Rosa canina L.). Pe materialul mărunțit cu fiecare moară au fost determinați parametrii de culoare și conținutul de polifenoli, ulterior acesta a fost supus analizei granulometrice, iar pe fracțiile obținute au fost determinate densitatea volumică și cea compactată, indicii Carr și Hausner, unghiul de repaus, umiditatea, activitatea apei, indicele de umflare și higroscopicitatea. Rezultatele au arătat că fiecare mecanism de măcinare a imprimat pulberii caracteristici distincte. KM a produs o frgmentare eterogenă, cu acumulare în fracția de 0.250-0.355 (35.04%), cea mai intensă culoare (a*=20.17, C=43.91) și cel mai ridicat conținut de polifenoli (38.252 µg GAE/ml). RM a generat o distribuție mai uniformă (25% în intervalul 0.355-0.500 mm) și cea mai bună fluiditate (indice Carr 7.85%, Hausner 0.085). SRM a favorizat obținerea particulelor grosiere (31.80% >0.710 mm), dar s-au obținut cele mai scăzute valori pentru unghiul de repaus. Fracțiile fine au prezentat umiditate ridicată (până la 8.28%), activitatea apei sub 0.46 și un indice de umflare de ~100% pentru fracția 0 mm la RM și SRM. Modelul Rosin-Rammler a descris fidel distribuțiile granulometrice pentru toate cele trei echipamente. Tipul echipamentului de măcinare influențează decisiv calitatea pulberii de măceș, iar alegerea acestuia trebuie corelată cu aplicația tehnologică dorită.*

## INTRODUCTION

Rose hips belong to the *Rosaceae* family and are pseudofruits, consisting of a hypanthium and numerous achenes that protect the individual seeds. They are widespread in Europe, North America, the Middle East, and Asia, and in Romania, the most important species is *Rosa canina* (*Kumar, A. et al, 2025; Borşa, A. R. et al, 2025; Ionescu, A. D. et al, 2025*). In Europe, rose hips are primarily utilized in countries such as Sweden, Bulgaria, Hungary, and Romania, with a total processing capacity of 11,000 metric tons. For centuries, these fruits have been used in both food and medicine (*Negrean, O. R. et al, 2024*). They are nutritionally valuable and contain 41.3% dry matter, predominantly carbohydrates (38.2%), of which dietary fiber accounts for 24.1%, protein 1.6%, ash 1.2%, and lipids in very small amounts, only 0.3%. They are considered functional foods due to the phytochemicals they contain, such as polyphenols, carotenoids (primarily lycopene, β-carotene, and zeaxanthin), ascorbic acid, and minerals (*Kumar, A. et al, 2025; Borşa, A. R. et al, 2025*). They are often used in the food industry in conventional products such as jams, infusions, juices, and jellies. They are also marketed in powder form, obtained by grinding whole dried fruits (*Ionescu, A. D. et al, 2025*).

The incorporation of rosehip powder into bread dough significantly influenced the dough's rheological properties, as evidenced by a decrease in water absorption and softening, as well as an increase in stability. Although studies in the literature have reported a decrease in bread volume and color intensity, sensory parameters such as crust color, aroma, and taste were rated higher than those of the control sample, which supports the use of rosehip flour as a functional ingredient in baking, thereby replacing synthetic ascorbic acid (*Chochkov, R. et al., 2022; Sanfilippo, R. et al., 2025; Vartolomei, N., & Turtoi, M., 2023; Bilash, B. et al., 2026*). Fine rosehip powder, with particle sizes <10 μm, was used by Borşa, A. R., et al. to enrich waffle cones with polyphenols, fiber, and carotenoids. Replacing at least 10% of the wheat flour with rosehip powder was recommended without significantly affecting the texture or production cost. The same group of researchers demonstrated that rosehip powder can be a sustainable alternative to synthetic additives by incorporating it at levels of 2.7% and 5.5% into pork sausages.

This increased the product's polyphenol, carotenoid, and carbohydrate content while lowering the pH and the level of easily hydrolyzable nitrogen. At the same time, it reduced the gummy texture and enhanced the color, and the consumer acceptance rate was good. Rosehip powder can be used to improve the physicochemical characteristics of dairy products, particularly yogurt, and is also used as a natural colorant in confectionery and beverages (*Volkov, V. et al., 2025*).

Given the many applications of rosehip powder in the food industry and the functional benefits demonstrated in specialized studies, a thorough understanding of how the production technology influences this ingredient is essential. In this context, grinding, as a fundamental unit operation, plays a decisive role in determining the particle size, rheological, and physicochemical properties of the powder, thereby influencing its behavior in subsequent technological processes and the quality of the final products (*Ionescu et al., 2025*).

Knowledge of the physical properties of the powder (bulk density, tapped density, Hausner ratio, Carr index, angle of repose, compressibility index, swelling index, hygroscopicity) is essential for evaluating its behavior in flow and compaction processes. The moisture content of the material significantly affects the physical properties of the powder, influencing its flowability and tendency to agglomerate, while water activity affects its storage stability (*Budnimath, S. H. et al, 2023; Sanprasert, S. et al, 2025; Nabil, B. et al, 2020; Lisiecka, K. et al, 2024*).

Knife mills, rotor-and-sieve mills, and roller mills are used in the plant material processing industry to produce powders of varying degrees of fineness (*Aradwad, P. P. et al., 2021; Ionescu et al., 2024; Ramírez Cabrera, P. A. et al., 2025*). Although particle size has a decisive influence on powder behavior and the quality of the final product, comparative studies on the effect of equipment on the granulometric, rheological, and physicochemical properties of rosehip powder are limited in the literature. Thus, this study aims to evaluate how each of the three mills influences the characteristics of the powder obtained from dried rose hips.

## MATERIALS AND METHODS

The plant material was harvested by hand in October of last year from a forested area adjacent to the city of Râmnicu Vâlcea. The initial sorting focused on the quality of the fruit, and only uniform batches free of microbiological contamination and at the optimal stage of ripeness were selected. After being

transferred to the laboratory, the biomass was dried under controlled conditions using a thermostat until it reached a moisture content of 7%.

From the 500 g batch of dried fruit, 50 g sub-batches were selected and ground using three different types of equipment. The following were used: the D5169 NM-8300 knife spice grinder, the Fritsch Pulverisette 19 with a rotor and a 0.5 mm sieve, and the Sadkiewicz roller mill. Using the knife mill, the grinding time was 3 minutes, whereas with the Fritsch Pulverisette 19, the material was allowed to flow freely and was kept in the grinding chamber for a short time of approximately 1 minute. When using the roller mill, the material first had to be crushed by hand, after which it was fed in small quantities through the feed opening.

Particle size distribution of the material from each mill was analyzed using a vertical vibration sieve shaker, the Analysette 3 Spartan (Fritsch, Germany). It operates on the principle of vertical vibration, ensuring uniform material distribution across the sieve surface and allowing particles to pass efficiently through a stack of six sieves with progressively smaller mesh sizes from top to bottom. The selected sieves had aperture sizes of 0.710 mm, 0.500 mm, 0.355 mm, 0.250 mm, and 0.160 mm. The data recorded during the experiments were processed using the Microsoft Excel statistical software (Version 2406, 64-bit). The cumulative mass percentage of particles larger or smaller than the aperture sizes of a given sieve was represented using particle size distribution curves. The particle size distribution was described using the Rosin-Rammler equation. Mean particle size was calculated using equation (1).

$$d_m = \frac{\sum a_i\,(\%) \times d_i}{100}\ (mm) \tag{1}$$

The average specific surface area of the ground material is very important because it affects the stability and dissolution rate of the powder. It was calculated using Equation (2).

$$S_{sm} = \frac{6}{100 \times \rho} \sum_{di}^{n+1} \frac{a_i}{d_i} \left(\frac{m^2}{kg}\right) \tag{2}$$

The particle size fractions from each sieve, obtained as a result of the particle size distribution analysis, were immediately placed in polyethylene bags for further analysis.

Based on the mass recorded for each fraction and for the control sample, 10 mL, 50 mL, and 100 mL graduated cylinders were used to determine the bulk density. Knowing the mass and, subsequently, the volume occupied by the powder, the bulk density (mass per unit volume) was determined using Equation (3). (*Tangirala, A. S. et al, 2014; Budnimath, S. H. et al, 2023*).

$$Bulk\ density\ \left(\frac{g}{cm^3}\right) = \frac{Mass\ of\ rosehip\ powder}{Initial\ volume\ of\ osehip\ powder} \tag{3}$$

The compacted density was determined by manually tamping the sample with a glass rod until no further visible decrease in volume was observed. The final volume was then recorded and used to calculate the compacted density using Equation (4) (*Tangirala, A. S. et al, 2014; Budnimath, S. H. et al, 2023*).

$$Tapped\ density\ \left(\frac{g}{cm^3}\right) = \frac{Mass\ of\ rosehip\ powder}{Final\ volume\ of\ rosehip\ powder} \tag{4}$$

To assess the fluidity and cohesion of the powder, the Carr and Hausner indices were calculated based on the bulk density and the compacted density, respectively, using Equations (5) and (6). The Hausner ratio indicates the flowability of the powder in its uncompacted state, while the Carr index complements this assessment by characterizing the degree of compressibility and the tendency of the particles to agglomerate (*Tangirala, A. S. et al, 2014; Budnimath, S. H. et al, 2023; Gunjal, M. et al, 2026*).

$$Carrindex(\%) = \frac{Tapped\ density - Bulk\ density}{Tapped\ density} \times 100 \tag{5}$$

$$Hausner\ ratio = \frac{Tapped\ density - Bulk\ density}{Bulk\ density} \tag{6}$$

Angle of repose (°) was determined by pouring the powder fractions, as well as the control samples (un-sieved), into funnels positioned 2 cm above a surface. The samples were poured until the top of the resulting pile reached the lower edge of the funnel, and the angle of repose was calculated according to Equations (7) and (8) (*Gunjal, M. et al, 2026*).

$$tan\,\theta = \frac{h}{r} \tag{7}$$

$$\theta = tan^{-1}\left(\frac{h}{r}\right) \tag{8}$$

where, θ – angle of repose, h – height în cm, r- radius in cm.

The instrumental color evaluation of the unsifted rosehip samples ground using the three mills was performed using an Insize 5700-LS35 portable colorimeter with a D65 reference light source (10° viewing angle) and D/8 illumination geometry. Measurements were conducted using the CIE L*a*b* three-dimensional color system. Three independent determinations were performed, and the final data were reported as the mean value ± standard deviation (SD).

Moisture content was determined using a KERN DBS 60-3 halogen lamp moisture analyzer, based on the thermogravimetric principle, at a temperature of 105 °C, and the water activity was determined using a Rotronic HygroLab2 measurement system equipped with a thermostatic chamber.

Swelling index of the powder samples was determined according to the methods proposed by *Gunjal, M. et al. 2026* and *Budnimath, S. H. et al. 2023*. A quantity of 1.0 g of powder was placed in a 10 mL graduated cylinder, after which 5 mL of distilled water was carefully added. The initial volume occupied by the sample was recorded, and the sample was then left to stand for 60 minutes to allow for swelling. At the end of this interval, the volume occupied by the sample was measured again, and the swelling index was calculated according to Equation (9).

$$Swelling\ index\ (\%) = \frac{Volume\ occupied\ by\ sample\ before\ swelling}{Volume\ occupied\ by\ sample\ after\ swelling} \times 100 \tag{9}$$

Hygroscopicity of the powder was determined using a procedure described by Budnimath, S. H., et al. 2023. To this purpose, 1 g of each sample was weighed using an analytical balance accurate to four decimal places and then distributed into Petri dishes and placed in a glass desiccator containing a saturated NaCl solution. The samples were exposed for 7 days at 25 °C. This was calculated using Equation (10).

$$Hygroscopicity\ (\%) = \frac{Weight\ gain\ by\ rosehip\ powder\ after\ 7\ days\ (g)}{Weihjt\ of\ the\ sample\ (g)} \times 100 \tag{10}$$

Total polyphenol content (TPC), determined only for the control (unsieved) samples was measured spectrophotometrically using gallic acid as the reference standard, following the protocol described by S*ingleton and Rossi* (1965).

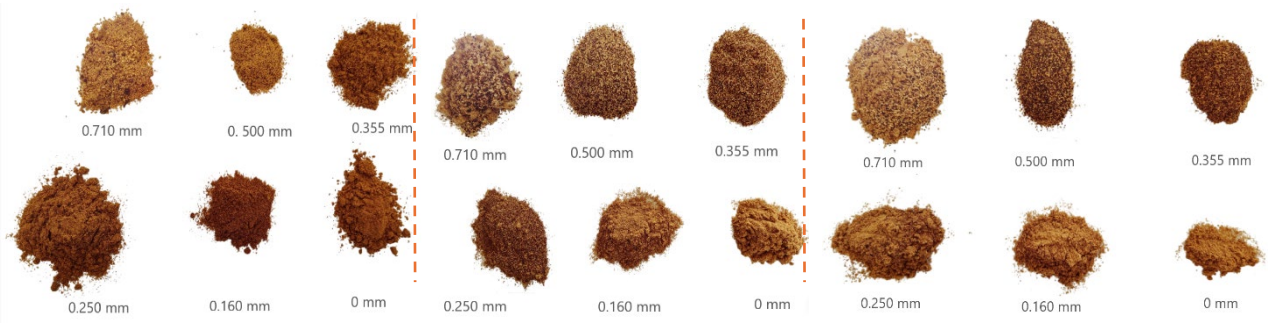
Specifically, 1.0 mL of Folin-Ciocalteu reagent (diluted 1:10 in water) and 0.2 mL of the sample extract were added to a reaction tube. After 10 minutes, 0.8 mL of a 7.5% (w/v) sodium carbonate solution was added, and the mixture was left at room temperature for 30 minutes; absorbance was then measured at 743 nm.

Results were expressed as gallic acid equivalents (mg GAE/g). The polyphenol concentration in the samples was calculated by interpolation against a gallic acid standard curve prepared within the 20-200 µg/mL concentration range.

The calibration curve was obtained via linear regression using Microsoft Excel, yielding a coefficient of determination of $R^2 = 0.9938$. Measurements were performed using a T92+ spectrophotometer.

## RESULTS

Particle size distribution was determined by sieving, yielding size fractions of 0.710 mm, 0.500 mm, 0.355 mm, 0.250 mm, 0.160 mm, and less than 0.160 mm. These fractions were obtained separately for the powders produced by grinding with a knife mill, a roller mill, and a rotor-and-sieve mill, respectively, and are shown in Figure 1.




a) b) c)

**Fig. 1 - Particle size fractions of rosehip powder depending on the type of mill used:**
*a) knife mill; b) roller mill; c) rotor and sieve mill;*

The particle size analysis of the powders obtained by grinding with the three types of equipment revealed significant differences in terms of particle fineness, uniformity, and degree of dispersion. Figure 2 shows the particle size distribution curves of the rosehip powder obtained using the three different grinding technologies.

For each sample, the following were represented: the mass percentage retained on each sieve ($a_i$), the cumulative percentage passing through the sieve ($T_i$), the cumulative percentage of material remaining on the sieve ($R_i$), and the theoretical Rosin-Rammler curve (RRx).

In the case of the knife mill (Figure 2a), the distribution was dominated by the fraction with particle sizes between 0.250 mm and 0.355 mm, which accounted for 35.04% of the material. This pronounced accumulation in a single size class, visible in the graph as a peak in the mass percentage curve, indicates preferential fragmentation within this range, which was characteristic of the impact and shear mechanism.

In addition, a fine fraction of 13.20%, with particle sizes less than 0.160 mm, and a considerable coarse fraction of 18.00%, with particle sizes greater than 0.710 mm, were obtained. The cumulative curves clearly show the particle size distribution.

The passing fraction (Ti) increased rapidly between 0.160 and 0.355 mm, indicating that most particles were in this intermediate range. Conversely, the retained fraction (Ri) decreased continuously as the mesh size increased, dropping rapidly below the 40% threshold beyond 0.355, which confirmed the absence of coarse fragments.

The Rosin-Rammler (RRx) model, described by the equation $RR(x) = 100 \exp(-5.023 \cdot x^{2.0057})$, fits the experimental data very well, where the exponent of approximately 2 confirms the average uniformity of the powder.

This behavior is characteristic of knife mills, which fragment the material but, in the absence of a classification system, allow particles to be discharged before complete homogenization, resulting in a relatively large distribution.

For the roller mill (Figure 2b), the majority fraction fell within the range of 0.355-0.500 mm and represented 25% of the material. The flatter shape of the mass percentage curve (ai) indicates that grinding by compression and shearing distributed the particles more uniformly across the size classes. The fine fraction (less than 0.160 mm) accounted for 10% of the sample, while the coarse fraction (greater than 0.710 mm) accounted for 16.20%.

The cumulative curves reflect this pattern: passing fraction (Ti) increases constantly, reaching 64% only at the 0.500 mm sieve, while, the retained fraction (Ri) decreases progressively, recording values below 40% starting with the 0.500 mm sieve. The experimental data are accurately described by the Rosin-Rammler model, using the equation $RR(x)=100\exp(-3.769 \cdot x^{1.9627})$.

The value of 1.9627 mathematically confirms the average uniformity of the dimensions, a result directly determined by the fixed distance between the rollers.

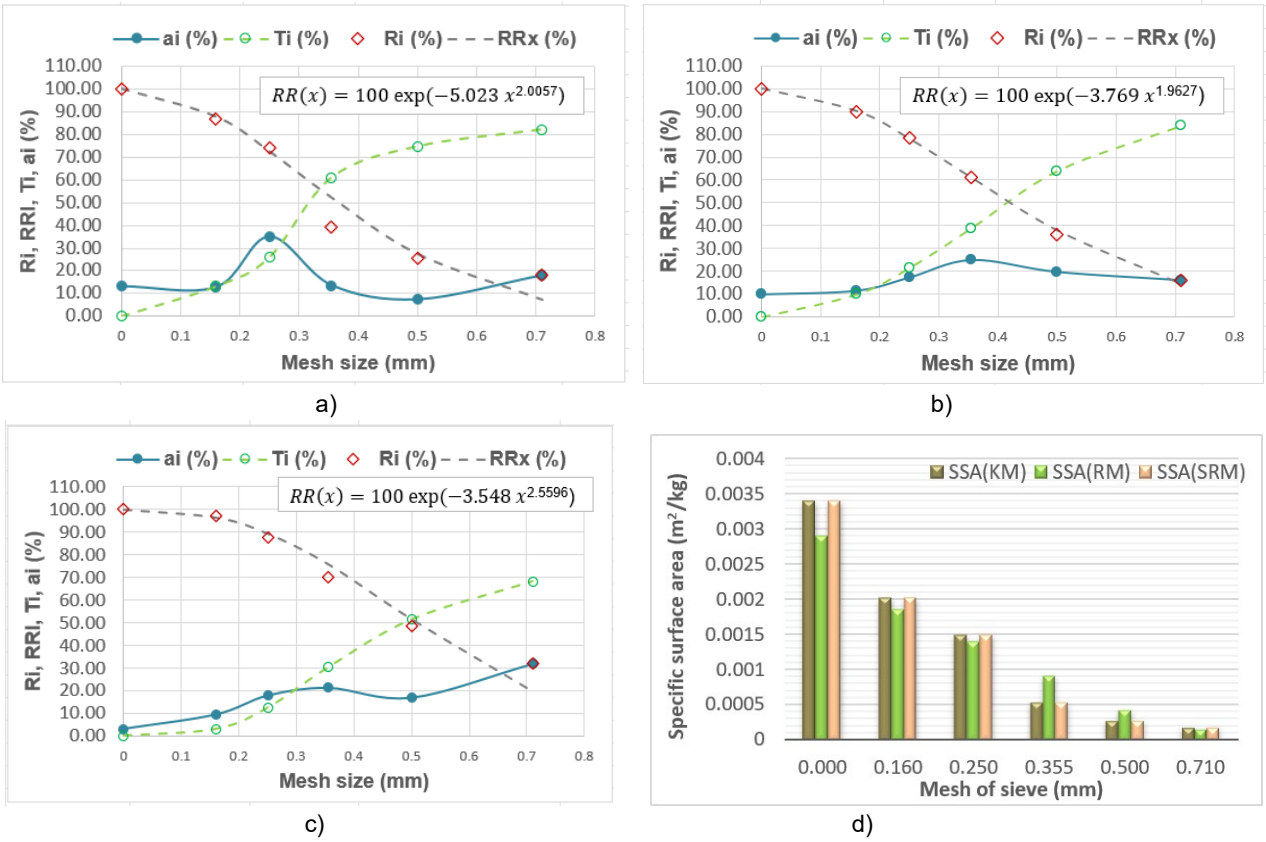



**Fig. 2 - Particle size distribution curves for rosehip powder obtained using the three grinding equipment**
a) knife mill (KM); b) roller mill (RM); c) rotor and sieve mill (SRM); and the specific surface area distribution of the material particles corresponding to the particle size class resulting from each equipment d);

In the rotor mill with a 0.5 mm sieve (Figure 2.c), the distribution was dominated by the fraction larger than 0.710 mm, which accounted for the highest percentage at 31.80%. However, a second peak is also observed in the range between 0.355 and 0.500 mm, representing 21.20%.

This distribution indicates a less uniform fragmentation, caused by the rapid passage of some particles through the sieve before they were completely crushed. The fine fraction (below 0.160) is very low, constituting only 3%, while coarse particles account for 31.08%.

Cumulative curves highlight the same trend. Passing fraction ($T_i$) increases more slowly in the initial size classes, accumulating only 30.2% up to the 0.355 mm size. Cumulative retained fraction ($R_i$) decreases progressively, recording values below 40% starting from the 0.710 mm sieve.

The data are accurately described by the Rosin-Rammler model using the equation: $RR(x) = 100exp(-3.548 \cdot x^{2.5596})$. The exponent, 2.5596 indicates a lack of uniformity and a predominance of coarse particles, behavior determined by the rapid passage of fragments through the sieve immediately after impact with the rotor.

The graph in Figure 2,.d) shows a directly proportional decrease in specific surface area (SSA) as the size of the sieve orifices increases, reflecting the concentration of the contact area in the fine particle range.

In the lower particle size range (0-0.250 mm), the knife mill ($SSA_{KM}$) and the rotor and sieve mill ($SSA_{SRM}$) exhibit nearly overlapping profiles and maximum SSA values, indicating that mechanisms based on direct impact generate a high quantity of microfragments with a large specific surface area. In contrast, the material ground in the roller mill ($SSA_{RM}$) shows lower values in the fine fractions but significantly higher values for medium-to-large particles (0.355-0.500 mm),

This behavior confirms that fragmentation by compression and shearing reduces the generation of fine particles, keeping the specific surface area distributed predominantly across the larger size classes.

An analysis of the data in Table 1 reveals an intrinsic relationship between the type of mechanical stress and the physical properties of the powder. The grinding mechanism dictates the particle shape, which in turn determines the compacted density and flow behavior.

**Table 1**

**Influence of equipment type and sieve size on powder density and flow characteristics**

| Equipment | Sieve mesh size | Bulk density | Compacted density | Angle of repose | Carr index | Hausner ratio |
|---|---|---|---|---|---|---|
| | [mm] | [kg/m³] | [kg/m³] | [°] | [%] | - |
| Knife mill | *Control* | *543.478* | *704.225* | *46.492* | *22.826* | *0.295* |
| | 0 | 540.984 | 725.275 | 51.366 | 25.410 | 0.340 |
| | 0.160 | 638.000 | 778.049 | 49.661 | 18.000 | 0.219 |
| | 0.250 | 648.889 | 796.364 | 48.839 | 18.519 | 0.227 |
| | 0.355 | 485.714 | 552.846 | 47.255 | 12.143 | 0.138 |
| | 0.500 | 528.571 | 606.557 | 39.826 | 12.857 | 0.147 |
| | 0.710 | 387.931 | 647.482 | 38.679 | 40.086 | 0.669 |
| Roller mill | Control | 434.783 | 561.798 | 48.037 | 22.609 | 0.292 |
| | 0 | 335.570 | 609.756 | 62.332 | 44.966 | 0.817 |
| | 0.160 | 345.238 | 491.525 | 53.157 | 29.762 | 0.424 |
| | 0.250 | 478.022 | 580.000 | 47.255 | 17.582 | 0.213 |
| | 0.355 | 516.529 | 560.538 | 40.420 | 7.851 | 0.085 |
| | 0.500 | 473.684 | 546.961 | 39.246 | 13.397 | 0.155 |
| | 0.710 | 325.301 | 506.250 | 54.085 | 35.743 | 0.556 |
| Rotor and sieve mill | Control | 505.051 | 746.269 | 47.255 | 32.323 | 0.478 |
| | 0 | 258.621 | 500.000 | 53.157 | 48.276 | 0.933 |
| | 0.160 | 276.471 | 534.091 | 48.839 | 48.235 | 0.932 |
| | 0.250 | 356.000 | 497.315 | 50.503 | 40.400 | 0.678 |
| | 0.355 | 963.636 | 1070.707 | 37.061 | 10.000 | 0.111 |
| | 0.500 | 688.525 | 763.636 | 39.826 | 9.836 | 0.109 |
| | 0.710 | 630.952 | 1152.174 | 54.085 | 45.238 | 0.826 |

In the case of the knife mill, the predominant shearing and impact forces resulted in a more heterogeneous distribution of the powder. In the fine fraction range (0-0.250 mm), a continuous increase in bulk density was observed, reaching a maximum of 648.889 kg/m³. This phenomenon demonstrated a reduction in interparticle porosity, as the fragments resulting from the grinding of the seeds and pericarp settled compactly. At the 0.355 mm sieve, there was a significant decrease in density (485.714 kg/m³), caused by the preferential accumulation of the bristles, which, being elastic and non-spherical, created large air voids and increased the volume they occupied. This correlation was also confirmed by the compressibility indices; the minimum values of the Carr index (12.143%) and the Hausner index (0.138) for the 0.355 mm fraction indicated good flowability but low compressibility.

The slow compression mechanism of the roller mill preserved the intrinsic density of the granules, resulting in a stable density profile with maximum values at 0.250-0.355 mm. Correlation with rheological indices shows that at 0.355 mm, the Carr index reaches a minimum of 7.85% and the Hausner index reaches a value of 0.085, indicating good flowability due to the regular shape of the particles. At the extremes (0 mm and 0.710 mm), the density decreased, and the Carr index recorded values of 44.97% and 35.74%, indicating agglomeration of the fine fractions and uneven compaction of the coarse fractions. The material ground with this mill is ideal for subsequent processing steps, such as filling capsules or tableting, due to the absence of ultrafine dust that could block the mechanical flow. During grinding with the rotor-and-sieve mill, the particles were subjected to a dual mechanism: high-speed impact from the rotor and forced passage through the sieve under the action of the air stream, resulting in a powder whose behavior depends on its size class. In the 0.355 mm fraction, the bulk density reached 963.63 kg/m³, a fairly high value for a plant material; this deviation can be attributed to the atypical composition of the fraction, which consists of dense seed fragments. Due to its compact nature, its hydrodynamic flow properties were superior to those of the other samples analyzed. This rheological behavior was confirmed by the lowest recorded values for the angle of repose and the Carr index. In contrast, the fine fraction (0 mm) and coarse aggregates (greater than 0.710) exhibited high interparticle porosity, resulting in flow resistance and unfavorable compressibility indices. An analysis of the chromatic parameters (Table 2) reveals a significant correlation between the physical grinding mechanism and the optical properties of the powders. The knife mill presented the highest values for the redness index (a* = 20.17) and saturation (C = 43.91). This optimal color profile results from extensive cellular disruption caused by high-speed shearing, a process that facilitates the release of carotenoid compounds from chromoplasts while being simultaneously enhanced by lycopene isomerization.

In the case of the rotor-and-sieve mill, the simultaneous impact and friction forces reduced the b* and C parameters, indicating partial degradation of sensitive chromophores. In contrast, the roller mill produced a pronounced light-reflecting effect, resulting in increased brightness (L* = 62.28) and reduced chromaticity of the powder (a* = 14.74); compression between the rollers caused restrictive cellular breakdown, trapping the pigments within the structural matrix of the coarse particles.

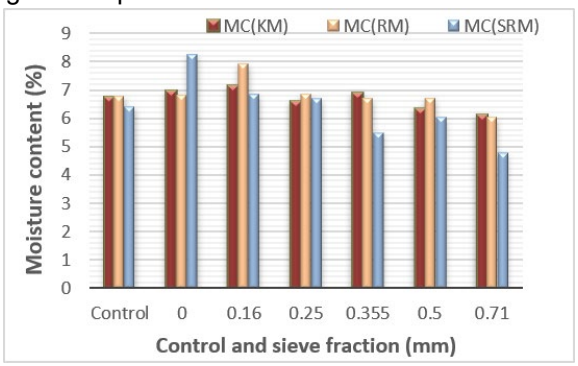
**Table 2**

**Chromatic parameters, saturation, and hue angle of rosehip powder as a function of the grinding equipment**

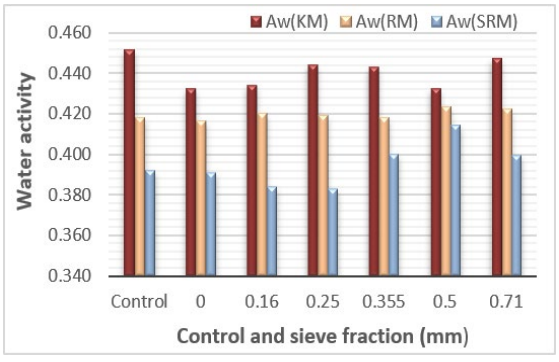
| Equipment | L* (brightness) | a* (red/green) | b* (yellow/blue) | C (saturation) | h (hue angle) |
|---|---|---|---|---|---|
| Knife mill | 52.91±1.47 | 20.17±0.25 | 39.00±0.90 | 43.91±0.78 | 62.60±0.66 |
| Roller mill | 62.28±0.83 | 14.74±0.03 | 34.96±0.47 | 37.94±0.43 | 67.07±0.31 |
| Rotor and sieve mill | 51.73±1.28 | 14.04±0.20 | 28.76±0.41 | 32.01±0.46 | 63.83±0.11 |

The grinding process (performed using *KM*, *RM*, and *SRM* mills), followed by sieving, significantly altered the physicochemical properties of the resulting fractions compared to the control sample, as shown in Figure 3. The control samples had a uniform initial moisture content (6.42%-6.81%). After sieving, the fine fractions (0 mm and 0.16 mm) exhibited high moisture content, particularly when SRM was used (8.28%). In the coarse fractions (0.710 mm), the moisture content decreased below the control value. The samples were found to be microbiologically safe (aw < 0.46). However, KM maintained the highest water activity values (0.43-0.45), while SRM produced particles with the least free water (< 0.40). The swelling index (SI) highlighted how grinding affected the structure of rosehip fibers, either facilitating or blocking water absorption. Unlike the control samples (~80%), reducing the particle size to the 0 mm fraction resulted in an increase in the swelling index for the powders produced by the RM and SRM mills, reaching a peak of nearly 100%.

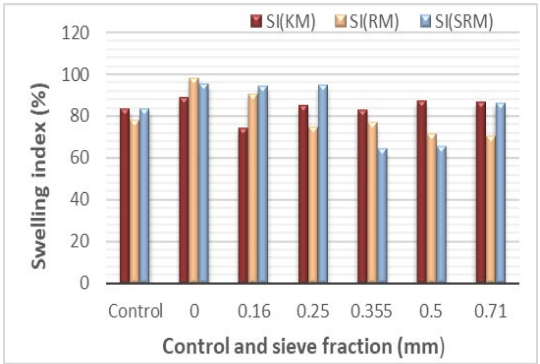
This demonstrated that these two grinding processes achieved extensive destruction of the cell walls, releasing the groups capable of hydration. In contrast, the knife mill (KM) exhibited different behavior. For the 0.160 mm fraction, a sharp decrease in swelling capacity (to 74%) was observed, suggesting that this type of milling might compact or partially degrade the polysaccharide structure at certain particle sizes. In the larger fractions (0.500-0.710 mm), the swelling capacity decreased for all mills, as the large, insufficiently fragmented particles limit water access inside the capillaries.



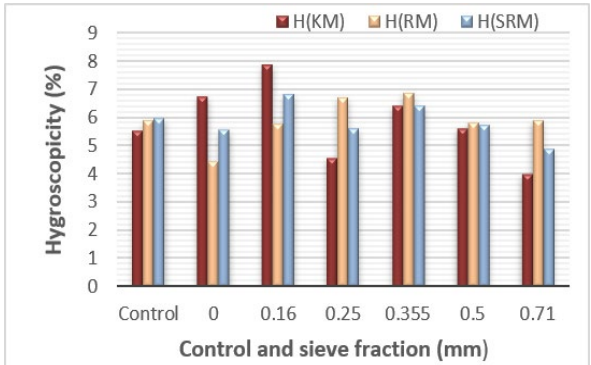

a)




b)




c)




d)

**Fig. 3 - Physicochemical properties of the material ground using the three mills (KM, RM, SRM), the unsieved sample, and the fractions obtained after sieving:**

*a) moisture content; b) water activity; c) swelling index; d) hygroscopicity*

In terms of hygroscopicity, the control samples exhibited similar behavior (5.5%-6%), but significant discrepancies emerged after sieving. The knife mill produced particles with high water retention capacity for the 0.160 mm fraction, reaching the highest value in the experiment (7.8%). For the 0.710 mm particle size fraction, the powder obtained with this mill exhibited the lowest hygroscopicity value, at just 4%. The other two types of equipment exhibited much more stable and uniform hygroscopicity profiles across the 0.160 mm and 0.355 mm fractions.

The study of the correlation between the grinding method and extraction yield indicates that the knife mill produced the highest concentration of polyphenols (38,252 µg GAE/mL), due to its high-speed cutting mechanism, which breaks down the tissues and maximizes the exposure of bioactive compounds. In contrast, the roller mill produced the lowest concentration (27.263 µg GAE/mL), as its compressive forces flatten the fibrous structures rather than breaking them down, thereby limiting solvent penetration. The rotor-sieve mill generated an intermediate yield (32.098 µg GAE/mL), as the combination of mechanical shear forces and screen impact effectively destroyed the cell walls, facilitating a faster release of the compounds into the extract.

## CONCLUSIONS

The selection of grinding equipment must be strictly guided by the intended industrial application of the rosehip powder, as the fragmentation mechanism directly determines the functionality of the final product. For the production of functional ingredients or bioactive supplements, a knife mill (KM) is recommended due to its proven ability to preserve antioxidant compounds, ensuring a polyphenol concentration of 38,252 µg GAE/ml and superior color characteristics.

Conversely, for automated production lines (involving dosing or packaging) where powder flowability is critical, a roller mill (RM) is the ideal choice. It minimizes the risk of structural cohesion, guaranteeing excellent flow, reflected by a Carr index of 7.85% and a Hausner ratio of only 1.085. When the process requires a high degree of structural fineness, a rotor-sieve mill (SRM) becomes the preferred equipment, facilitating the production of smaller particles.

Thus, this study provides a matrix of experimental data, offering an essential reference for industrial optimization decisions.

## ACKNOWLEDGEMENT

This research was supported by the project CNFIS-FDI-2026-F-0049 “Asigurarea eficienței operaționale a bazei de aplicații practice pentru sisteme biotehnice în livezi, vii, solarii și grădini (EFIBIOTECH)”, from the Ministry of Education and Research through the Executive Agency for Financing Higher Education, Research, Development and Innovation.

## REFERENCES

[1] Aradwad, P.P., Arun Kumar T.V., Sahoo, P.K., Mani, I. (2021). Key issues and challenges in spice grinding. Cleaner Engineering and Technology, 5, 100347. https://doi.org/10.1016/j.clet.2021.100347

[2] Bilash, B., Oliinyk, S., Samokhvalova, O., Bolkhovitina, O. (2026). Determination of the influence of rosehip powder on the quality of wheat dough and bread. Technology audit and production reserves, 1(3 (87)), 45-50. https://doi.org/10.15587/2706-5448.2026.353167

[3] Borsa, A. R., Fogarasi, M., Ranga, F., Borsa, A., Tanislav, A.E., Muresan, V., Semeniuc, C.A. (2025). The use of a powder obtained from rosehip waste to reformulate pork sausages: Impacts on their quality. Foods, 14(6), 1067. https://doi.org/10.3390/foods14061067

[4] Borsa, A.R., Păucean, A., Fogarasi, M., Ranga, F., Borsa, A., Tanislav, A. E., Semeniuc, C. A. (2025). Utilisation of rosehip waste powder as a functional ingredient to enrich waffle cones with fibres, polyphenols, and carotenoids. Foods, 14(1), 90. https://doi.org/10.3390/foods14010090

[5] Borsa, A.R., Ranga, F., Fogarasi, M., Borsa, A., Vodnar, D.C., Semeniuc, C.A. (2025). Valorisation of rosehip waste into a food ingredient – Focus on its colour, carotenoid content, and techno-functional properties. Applied Food Research, 5(1), 100999. 10.1016/j.afres.2025.100999

[6] Budnimath, S.H., Bhuvaneshwari, G., Ganiger, V.M., Jagadeesh, S.L., Goudar, G., Patil, S.N., Chandrashekar, V.M. (2023). Physical, reconstitution and phenolic properties of instant drink mix prepared with Moringa oleifera leaf, raw banana and whey protein concentrate. Measurement: Food, 11, 100108. 10.1016/j.fochx.2024.101554

[7] Chochkov, R., Zlateva, D., Ivanova, P., & Stefanova, D. (2022). Effect of rosehip flour on the properties of wheat dough and bread. Ukrainian Food Journal, 11(4), 558-572. 10.24263/2304-974X-2022-11-4-6

[8] Gunjal, M., Singh, J., Kaur, S., Choudhary, R., & Rasane, P. (2026). Effect of particle size distribution on physical, functional, antioxidant, thermal, and morphological properties of radish sango microgreens powder. South African Journal of Botany, 192, 1-12. Doi:10.1016/j.sajb.2026.02.043

[9] Ionescu, A.D., Ferdes, M., Voicu, G., Ipate, G., Constantin, G. A., Stefan, E. M., Begea, M. (2024). Effect of grinding and successive sieving on the distribution of active biological compounds in the obtained fractions of blackthorn berries. Applied Sciences, 14(16), 7133. https://doi.org/10.3390/app14167133

[10] Ionescu, A.D., Voicu, G., Begea, M., Munteanu, M. G., Gheorghita, N.E., Constantin, G.A., Mircea, C. (2024). Experimental researches on energy consumption for obtaining rosehip powder using a mill for hard products. Annals of the Faculty of Engineering Hunedoara, 22(2), 65-70

[11] Ionescu, A.D., Voicu, G., Constantin, G.A., Ipate, G., Stefan, E.M., Begea, M., Iordache, S.D. (2025). Research on the influence of grinding time on the particle size distribution when obtaining rosehips powder. INMATEH-Agricultural Engineering, 76(2), 923.

[12] Ionescu, A.D., Voicu, G., Stefan, E.M., Constantin, G.A., Tudor, P., Militaru, G. (2025). Physico-chemical and resistance characteristics of rosehip seeds. Agriculture, 15(14), 1539. https://doi.org/10.3390/agriculture15141539

[13] Kumar, A., Sahal, A., Kumari, P., Hussain, I., Gupta, R., Chaudhary, S., Kumar, S. (2025). Rosehip (Rosa canina L.): Nutritional Profile, Bioactive Compounds, Extraction, and Applications. Food and Humanity, 100936. https://doi.org/10.1016/j.foohum.2025.100936

[14] Lisiecka, K., Dziki, D., Karaś, M. (2024). Physical and functional properties of powders obtained during spray drying of Cyani flos extracts. Molecules, 29(14), 3400. https://doi.org/10.3390/molecules29143400

[15] Nabil, B., Ouaabou, R., Ouhammou, M., Saadouni, L., Mahrouz, M. (2020). Impact of particle size on functional, physicochemical properties and antioxidant activity of cladode powder (Opuntia ficus-indica). Journal of Food Science and Technology, 57(3), 943-954. 10.1007/s13197-019-04127-4

[16] Negrean, O.R., Farcas, A.C., Nemes, S.A., Cic, D.E., Socaci, S.A. (2024). Recent advances and insights into the bioactive properties and applications of Rosa canina L. and its by-products. Heliyon, 10(9). 10.1016/j.heliyon.2024.e30816

[17] Ramírez Cabrera, P.A., Lozano Pérez, A. S., Guerrero Fajardo, C.A. (2025). Design of a knife mill with a drying adaptation for lignocellulose biomass milling: peapods and coffee cherry. Designs, 9(3), 57. https://doi.org/10.3390/designs9030057

[18] Sanfilippo, R., Canale, M., Fascella, G., Scarangella, M., Strano, M. C., Mangione, G., ... & Spina, A. (2025). Nutritional and technological characterization of rosehip seed flours as a functional ingredient in common wheat bread. European Food Research and Technology, 251(6), 1033-1045.

[19] Sanprasert, S., Kumnerdsiri, P., Seubsai, A., Lueangjaroenkit, P., Pongsetkul, J., Indriani, S., ... & Kingwascharapong, P. (2025). Techno-functional, rheological, and physico-chemical properties of gelatin capsule by-product for future functional food ingredients. Foods, 14(7), 1279. https://doi.org/10.3390/foods14071279

[20] Singleton, V.L; Rossi, J.A. (1965). Colorimetry of Total Phenolics with Phosphomolybdic-Phosphotungstic Acid Reagent. Am. J. Enol. Vitic. 16 , 144-158.

[21] Vartolomei, N., & Turtoi, M. (2023). Effect of rosehip powder addition on dough extensographic, amylographic and rheofermentographic properties and sensory attributes of bread. Processes, 11(4), 1088. https://doi.org/10.3390/pr11041088

[22] Volkov, V., Frolova, Y., Perova, I., Alekseenko, E. (2025). Prospects for using rosehip powder in drinks. In BIO Web of Conferences, Vol. 160, p. 01009. EDP Sciences. 10.1051/bioconf/202516001009

[23] Tangirala, A.S., Charithkumar, K., Goswami, T.K. (2014). Modeling of size reduction, particle size analysis and flow characterisation of spice powders ground in hammer and pin mills. Int. J. Res. Eng. Technol, 3, 296-309. https://doi.org/10.15623/ijret.2014.0312042

# COMPARATIVE ASSESSMENT OF VEGETABLE GROWING TECHNOLOGIES IN CONTROLLED (CLOSED) ENVIRONMENTS

/

# *EVALUARE COMPARATIVĂ A TEHNOLOGIILOR DE CULTIVARE A LEGUMELOR ÎN SPAȚII CONTROLATE (ÎNCHISE)*

**Iuliana GĂGEANU[1)], Ana-Maria TĂBĂRAȘU*[1)], Teofil-Alin ONCESCU[1)], Mihaela NIȚU*[1)], Cătălin PERSU[1)], Dan CUJBESCU[1)], Daria-Ioana SICARU[2)]**

[1)] INMA Bucharest / Romania;

[2)] Faculty of Biotechnical Systems Engineering, UNSTP Bucharest / Romania.

**E-mail:anamariatabarasu22@yahoo.com; rosumihaelan@yahoo.com*

***Keywords:*** *controlled environment agriculture; greenhouse technology; hydroponics; aeroponics; aquaponics; vegetable production; rotary growing systems.*

**ABSTRACT**

*This paper presents a comparative assessment of the main technologies used for growing vegetables in controlled, closed environments: greenhouses, screenhouses/solariums, and the emerging soil-less systems – hydroponics, aeroponics and aquaponics – together with vertical and rotary growing solutions. The analysis integrates technical, agronomic and resource-use data (water, land and energy consumption, yield, investment and management requirements) collected from recent scientific literature. The results indicate a clear efficiency gradient: conventional greenhouses and solariums remain the most accessible and widely used solutions, with productivity strongly dependent on covering material, climate control and crop management, while soil-less systems achieve substantially higher water-use efficiency, of up to 90–95% water savings compared with open-field cultivation, and allow continuous, space-efficient production, at the cost of higher energy demand, investment and technical expertise. Rotary hydroponic and cylindrical vertical systems emerge as promising directions for maximizing space efficiency in urban and peri-urban microfarming. The findings support informed technology selection according to available resources, crop type and production scale, and are relevant for developing climate-resilient, resource-efficient vegetable production systems.*

**REZUMAT**

*Lucrarea prezintă o evaluare comparativă a principalelor tehnologii utilizate pentru cultivarea legumelor în spații controlate, închise: sere, solarii/sere cu plasă, precum și sistemele emergente fără sol – hidroponia, aeroponia și acvaponia – alături de soluțiile de cultivare verticală și rotativă. Analiza integrează date tehnice, agronomice și privind consumul de resurse (apă, teren, energie), producție, investiții și cerințe de management, colectate din literatura științifică recentă. Rezultatele indică un gradient clar de eficiență: serele și solariile convenționale rămân cele mai accesibile și utilizate soluții, productivitatea fiind puternic influențată de materialul de acoperire, controlul climatic și managementul culturii, în timp ce sistemele fără sol ating o eficiență a utilizării apei semnificativ mai ridicată, cu economii de până la 90–95% față de cultura în câmp deschis, permițând o producție continuă și eficientă din punct de vedere al spațiului, cu prețul unui consum energetic, al unor investiții și al unei expertize tehnice mai ridicate. Sistemele hidroponice rotative și cele cilindrice verticale se conturează ca direcții promițătoare pentru maximizarea eficienței spațiale în microferme urbane și periurbane. Rezultatele susțin alegerea informată a tehnologiei în funcție de resursele disponibile, tipul de cultură și scara de producție, fiind relevante pentru dezvoltarea unor sisteme de producție legumicolă reziliente la schimbările climatice și eficiente din punct de vedere al resurselor.*

## INTRODUCTION

Population growth, accelerating climate change and increasing urban pressure on agricultural land are placing conventional, open-field vegetable production under growing strain. Frequent droughts, heat waves and the volatility of seasonal yields compromise the ability of traditional systems to guarantee a constant, high-quality vegetable supply, while urbanization widens the distance between production and consumption, increasing post-harvest losses and the carbon footprint of food transport (*Malhi et al., 2021*).

Controlled Environment Agriculture (CEA) has developed as a direct response to these challenges, ranging from simple protected structures – greenhouses and screenhouses/solariums – to advanced soil-less technologies that decouple crop production from soil quality and from most weather-related constraints. Hydroponics, aeroponics and aquaponics allow precise control of nutrient supply, water use and microclimate, enabling continuous, high-density production largely independent of outdoor conditions.

Combined with vertical farming concepts – whose modern form was popularized by Despommier (1999) but whose roots trace back to historical examples such as the Hanging Gardens of Babylon – these technologies are increasingly regarded as strategic tools for urban and peri-urban food security.

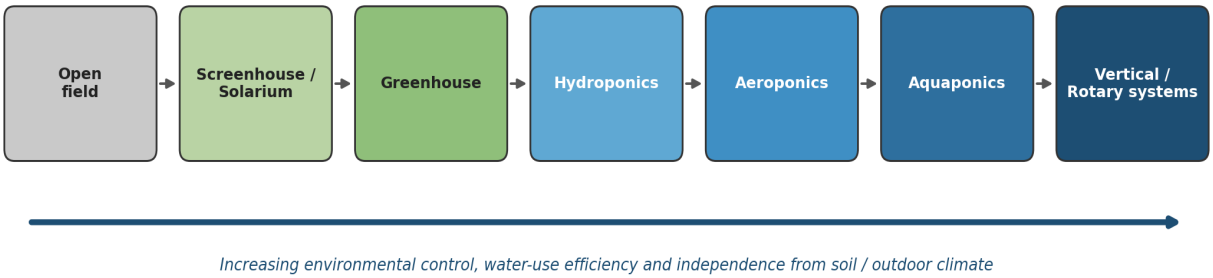



**Fig. 1 - Spectrum of controlled-environment vegetable growing technologies, from open-field cultivation to fully controlled, soil-less systems**

As shown in Figure 1, the technologies compared in this paper form a continuum of increasing environmental control: moving from open-field cultivation towards greenhouses, soil-less hydroponic/aeroponic/aquaponic systems and, ultimately, vertical or rotary configurations progressively reduces dependence on soil quality and outdoor climate, while increasing water-use efficiency and requiring more sophisticated technical management.

In Romania, protected cultivation has expanded considerably in the last two decades: modern greenhouses using non-conventional, substrate-based technologies cover close to 29,548 ha, complemented by 11.4 ha of modern greenhouses using conventional, soil-based technologies (*Drăghici et al., 2021*).

Large commercial complexes such as Transgex (Oradea), Dalin (Reghin) or Chirana Serv (Ialomița county) illustrate the shift towards substrate cultivation, geothermal energy and full automation, while solarium-based pepper production remains an important segment of the vegetable sector.

Despite this diversity of solutions, a structured, cross-technology comparison of resource use, productivity and applicability is still needed to support technology selection at farm, institutional or urban-microfarming level.

This paper aims to compare the main technologies for growing vegetables in controlled, closed environments, to highlight their respective advantages and limitations, and to identify emerging directions – in particular rotary and cylindrical vertical systems – capable of supporting resource-efficient, climate-resilient vegetable production in line with CAP 2023–2027 priorities on soil, water and climate.

## MATERIALS AND METHODS

The comparative analysis was performed using data collected from recent scientific literature (2013–2024) on greenhouse, solarium, hydroponic, aeroponic and aquaponic vegetable production systems.

The parameters considered for the comparison included: growing medium and structural design, water, land and energy use, nutrient management, environmental control requirements (temperature, pH, electrical conductivity), typical yields, main advantages and limitations, and suitability for different vegetable crops.

Where available, quantitative indicators reported in field studies and reviews – such as water consumption per litre or per kilogram of produce, yield per hectare or per square metre, and percentage water or fertilizer savings – were extracted and organized into comparative tables to support a structured, cross-technology assessment.

Emerging rotary and cylindrical vertical hydroponic configurations, including a functional model developed within the same research program, were analyzed separately to highlight their potential for space-efficient production in urban and educational settings.

## RESULTS

Figure 2 provides a comparative overview of the analyzed systems in terms of relative water-use efficiency, space-use efficiency and energy demand, based on the qualitative and quantitative indicators discussed below. The map illustrates the same gradient introduced in Figure 1: open-field and solarium cultivation combine low resource efficiency with low energy demand, greenhouses occupy an intermediate position, while soil-less and vertical/rotary systems cluster in the high water- and space-efficiency region, at the cost of a markedly higher energy demand.

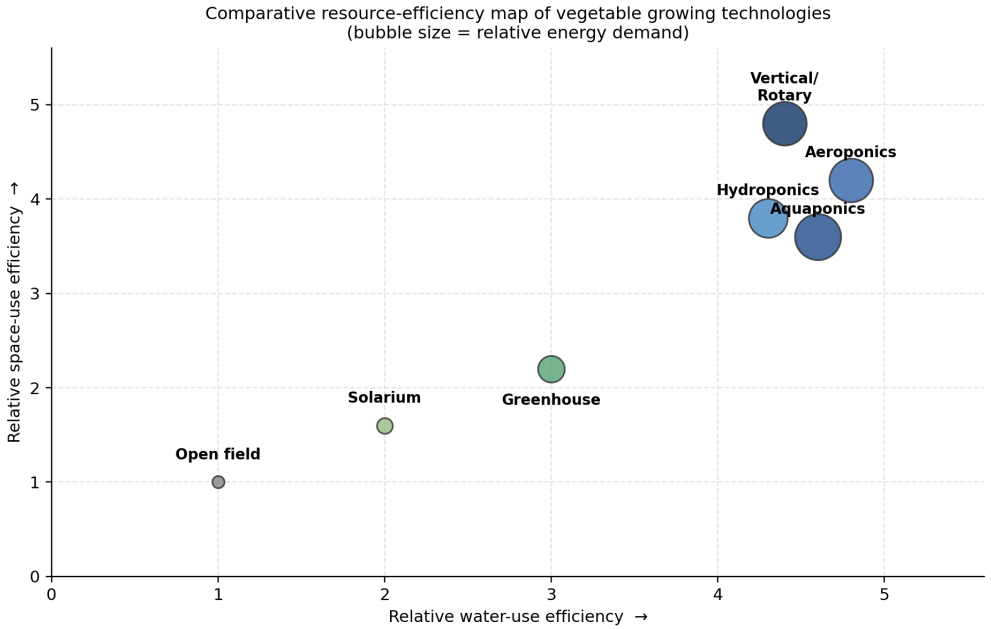



**Fig. 2 - Comparative resource-efficiency map of the analyzed vegetable growing technologies (illustrative, qualitative positioning based on the literature reviewed)**

### Greenhouses

Greenhouse area has grown considerably in the last decades, mainly due to plastic-covered structures used for vegetable production. Site selection is essential for profitability and depends on production costs, harvest quality and transport costs, which are in turn influenced by local climate and available technology (*Castilla and Baeza, 2013*).

Tomatoes, peppers and cucumbers are the most widely grown greenhouse vegetables, mainly because greenhouse cultivation extends the production season and increases profitability; these crops require temperatures of 17–28°C (12–32°C limits), at least 8.5 MJ/m²/day of solar radiation and 70–90% relative air humidity (*Castilla and Baeza, 2013*).

Two main greenhouse models have developed according to climate: high-tech, glass-covered greenhouses with advanced climate control in cold regions, and simpler plastic-covered greenhouses with natural ventilation in Mediterranean regions, the latter achieving lower yields but at substantially lower cost *(Monero et al., 2013).* In warmer regions, screenhouses (mesh-covered structures) increasingly replace plastic film, providing shading and wind protection with a reduced greenhouse effect (*Monero et al., 2013*).

In Romania, according to Drăghici et al. (2021), high-performance greenhouse complexes illustrate the potential of the technology: the Transgex complex in Oradea (2 ha) uses geothermal energy and mineral-wool substrate to produce over 400 t of tomatoes per hectare per production cycle – three times the yield of classic soil-based greenhouses; the fully automated Chirana Serv complex (Ialomița county, 1 ha) grows tomatoes on mineral-wool substrate; the Dalin greenhouses (Reghin, Mureș county) expanded from 2 ha to 4.8 ha and increased yields from 500 t/ha in 2012 to over 610 t/ha in 2021 through modern equipment, disease-resistant varieties and bumblebee pollination; and a 1.7 ha greenhouse built in Biled (Timiș county) in 2017 produces tomatoes on coconut-fibre substrate, with an average output of about 550 t in 2020.

The choice of covering material also has a measurable effect on productivity. A study conducted in an arid climate on cucumber (Cucumis sativus L. cv. Sovana F1) compared a near-infrared (NIR)-reflective film with two commercial films (*Alsadon et al., 2016*); the results, summarized in Table 1, show that the NIR-

reflective covering reduced in-greenhouse temperature and vapour pressure deficit, and increased total yield by 16.0% and 24.3% compared with the two commercial alternatives.

**Table 1**

**Effect of greenhouse covering material on microclimate and cucumber yield**

*(adapted from Alsadon et al., 2016)*

| Parameter | NIR-reflective film | Commercial film A | Commercial film B |
|---|---|---|---|
| Average in-greenhouse temperature (°C) | 22.7 | 23.8 | 25.4 |
| Photosynthesis rate (μmol $CO_2$ $m^{-2}$/s) | 16.61 | 15.51 | 14.91 |
| Fruit number per plant | 49.9 | 46.0 | 44.7 |
| Average fruit length (cm) | 16.7 | 15.6 | 14.5 |
| Total yield (kg/m²) | 15.96 | 13.75 | 12.84 |

**Screenhouses / Solariums**

Solarium-based (unheated) cultivation of sweet and hot peppers represents an important part of Romanian vegetable production. A national study on sweet pepper (2018–2019) reported average yields of 45 t/ha under conventional management and 37 t/ha under organic management, with total agrotechnical expenditure of about 118,400–118,600 lei/ha in both systems; material and input costs accounted for the largest share of expenditure – 66.7% in the conventional system and 72.8% in the organic system *(Dumitru et al.)*.

A more recent analysis for the 2022/2023 agricultural year reported similar trends, with 35 t/ha in the conventional system versus 28 t/ha (–20%) in the organic system, the latter being supported by organic fertilizers and natural pest-control methods that, while more sustainable, do not yet match conventional yields *(Berevoianu, 2024).*

Planting density also affects yield and fruit quality in unheated solariums: denser schemes (70×20–70×30 cm) increase plant height and fruit number but reduce flesh thickness, while wider spacing (70×40–70×50 cm) produces larger, higher-quality fruit at a lower overall yield per hectare; 70×30 and 70×40 cm spacing offered the best balance between yield and quality for hot pepper *(Xushvaqtov et al., 2024).*

**Hydroponic systems**

Hydroponics is a soil-less cultivation method in which plants grow in a nutrient solution containing essential minerals such as calcium, magnesium, sulphur and trace elements. It is the most widely used technology in vertical farming, offering increased yield, high water- and nutrient-use efficiency, resource recycling and elimination of soil-related problems such as weeds, pests and diseases (*Monisha et al., 2023*).

Typical system components include a growing tray, a growing medium (coconut fibre, rockwool, vermiculite), a nutrient reservoir and an air pump, with the nutrient solution most often based on the Hoagland formulation. Widely used configurations include wick systems, ebb-and-flow (flood-and-drain), deep water culture (DWC), the nutrient film technique (NFT) and drip irrigation systems, each offering a different balance of simplicity, cost and control.

The optimal nutrient-solution pH for hydroponic greenhouse crops is 5.8–6.5, with an electrical conductivity of 1.5–2.5 dS/m (Khan et al., 2018). Hydroponic greenhouse cultivation is applicable to a wide range of crop categories – cereals, vegetables (tomato, cucumber, lettuce, cabbage, pepper), fruits (strawberry, melon), forage crops and flowers – with reported yields consistently higher than in soil-based systems, owing to optimized growing conditions and nutrient-solution reuse (*Khan et al., 2018*).

**Aeroponic systems**

Aeroponics grows plants with roots suspended in air and fed by a finely misted nutrient solution, optimizing oxygen and $CO_2$ uptake and supporting rapid, healthy growth. Its main advantage is a markedly higher resource-use efficiency: aeroponic systems require about 95% less water than conventional field methods and occupy less space than hydroponics, while the absence of a growing medium reduces the risk of soil-borne pests and diseases *(Sharat, 2023).* Compared with conventional cultivation, aeroponics also reduces fertilizer requirements by around 60% and eliminates the need for pesticides *(Gurley, 2020).*

Aeroponic systems are widely used for seed-potato multiplication, achieving up to 800 minitubers per square metre with quality comparable to hydroponically produced tubers *(Gopinath et al., 2017*), and for rapid propagation of cuttings and clonal material. Comparative trials on leafy and fruiting vegetables grown aeroponically versus in soil reported substantial yield increases for basil (+19%), red kale (+65%), parsley (+21%), sweet pepper (+53%), cherry tomato (+35%), zucchini (+50%) and cucumber (+7%), together with a higher vitamin C content, while antioxidant levels remained comparable to soil-grown produce *(Gopinath et al., 2017).*

**Aquaponic systems**

Aquaponics integrates hydroponics with aquaculture: fish waste is converted by nitrifying bacteria into nutrients for plants, while the plants filter and purify the water that is recirculated back to the fish tanks. This closed-loop design reduces water consumption – over 90% of the water is reused compared with conventional agriculture – and eliminates the need for chemical fertilizers, while the controlled environment limits pesticide use *(Panigrahi et al., 2016).*

Water quality parameters are critical: the pH range tolerated by most fish and plants is 6.5–9.0, with an optimal compromise of 6.8–7.0 between the plants' preference for slightly acid conditions and the nitrifying bacteria's preference for near-neutral to slightly alkaline conditions *(Thorarinsdottir et al., 2015).*

Aromatic and medicinal plants are particularly well suited to aquaponics: basil and mint have shown the fastest, healthiest growth and the strongest water-filtration performance when associated with tilapia or common carp, while parsley and coriander show more variable results depending on light and water temperature *(Stoyanova et al., 2024).*

Main limitations of aquaponics include relatively high energy consumption for pumps, sensors and artificial lighting, the need to balance nutrient supply between fish and plant requirements, and the specialized knowledge required to manage the biological cycles of the system *(Stoyanova et al., 2024).*

**Comparative technology assessment**

Table 2 synthesizes the main technical and agronomic characteristics of the analyzed technologies, highlighting the trade-off between resource efficiency, technical complexity and investment requirements.

**Table 2**

**Comparative overview of vegetable growing technologies in controlled environments**

| Technology | Growing medium | Water-use efficiency | Energy demand | Main advantages | Main limitations |
|---|---|---|---|---|---|
| Greenhouse (plastic/glass) | Soil or substrate | Low–Medium | Low–Medium | Season extension, moderate cost, wide crop range | Climate-dependent yield, disease pressure, moderate water use |
| Screenhouse / Solarium | Soil | Low | Very low | Low cost, simple management | Limited climate control, seasonal yield variability |
| Hydroponics | Water/inert substrate | High | Medium | High yield, precise nutrient control, no soil-borne pests | Initial investment, technical expertise, disease spread via shared solution |
| Aeroponics | None (air/mist) | Very high (–95% water) | Medium–High | Very high water/fertilizer savings, fast growth, clean roots | Sensitive to pump/mist failure, high-tech maintenance |

| Technology | Growing medium | Water-use efficiency | Energy demand | Main advantages | Main limitations |
|---|---|---|---|---|---|
| Aquaponics | Water (fish-plant loop) | Very high (>90% water reuse) | Medium–High | No chemical fertilizer, circular system, dual output (fish + vegetables) | Complex biological balance, high energy and expertise needs |
| Vertical / rotary systems | Hydroponic (rotating) | High | Medium–High | Maximized space efficiency, uniform light exposure, urban-compatible | Uneven light distribution risk, mechanical complexity |

Quantitative resource-use data for lettuce production reported by Fasciolo et al. (2023) confirm this gradient (Table 3 and Figure 1): vertical/hydroponic farming uses considerably more water per litre of nutrient solution and far more energy per kilogram of produce than open-field cultivation, but achieves a land-use intensity (production per unit area and time) one to two orders of magnitude higher, reflecting its suitability for space-constrained, urban contexts rather than for replacing extensive field production.

**Table 3**

**Resource use for lettuce production in different agricultural systems**

*(adapted from Fasciolo et al., 2023)*

| Indicator | Vertical/hydroponic farming | Greenhouse | Open field |
|---|---|---|---|
| Water (g/L) | 45 – 80 | 5 – 60 | 3 – 20 |
| Land (g/m²·day) | 1,300 – 3,000 | 100 – 300 | 10 – 15 |
| Energy (kWh/kg) | 13.3 | 9 | 0.5 |

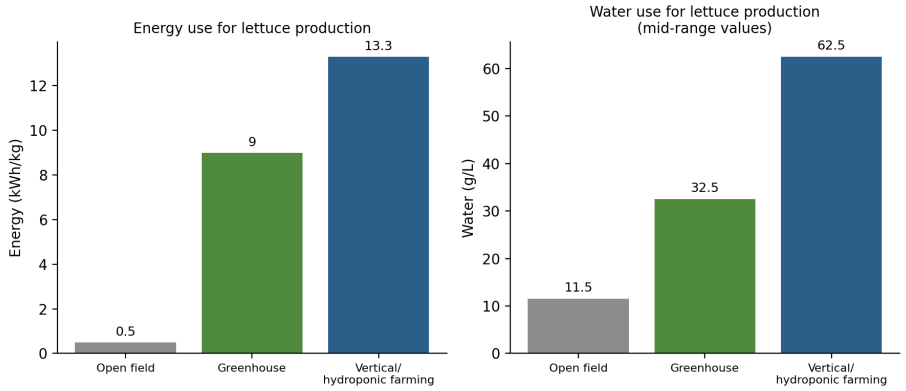



**Fig. 3 - Energy and water use for lettuce production across growing systems**

### Emerging rotary and vertical systems

Among soil-less technologies, rotary hydroponic systems have emerged as a solution to the high cost and technical complexity of static hydroponics, by combining a cylindrical, rotating frame with automated nutrient delivery.

Kadam et al. (2024) describe a closed-loop rotary hydroponic system with software-based monitoring and automatic adjustment, which reduced human intervention and produced healthy fenugreek yields within 30 days, while rotating at 2–5 rpm to ensure uniform light and nutrient exposure.

Similarly, Keat and Kannan (2015) compared a rotary wheel hydroponic system with a multi-tier cylindrical hydroponic system for lettuce and Chinese cabbage: the cylindrical system allowed a 47% higher planting density and produced Chinese cabbage averaging 28 g/plant at 45 days after sowing, although uneven light distribution caused some growth variability. Commercial rotary units such as Omega Garden, GI Grow and OGarden Smart apply the same principle at household or small-urban scale, allowing 80–160

plants to be grown simultaneously in a compact footprint, with energy consumption as low as 120 W for a complete unit.

Taken together, the technologies compared in this paper are not mutually exclusive alternatives but increasingly converge within urban and peri-urban agriculture, which provides the practical framework in which greenhouses, solariums and soil-less systems are deployed close to consumers.

Urban agriculture is recognized as a viable response to food security and social-equity challenges generated by rapid urbanization: in many developing-world cities, low-income households spend up to 85% of their income on food, and an estimated 100–200 million urban farmers worldwide already contribute to the horticultural supply of cities, underlining the scale at which locally produced vegetables can support food-system stability (*Orsini et al., 2013*).

The technologies discussed above materialize in several concrete urban formats – kitchen and community gardens, rooftop gardens, container gardening using recycled municipal waste, and peri-urban greenhouse or hydroponic operations – each combining a growing method (soil-based, substrate or soil-less) with an urban location strategy. Rooftop gardens, for example, make use of otherwise unexploited building surfaces, mitigate the urban heat-island effect and improve local air quality, while peri-urban operations in some regions already supply the majority of fresh produce sold in nearby cities (*Orsini et al., 2013; Pennisi et al., 2019*).

Beyond food supply, urban agriculture reduces the environmental footprint of the vegetable sector by shortening transport distances and associated greenhouse-gas emissions, and by converting urban organic waste into compost rather than landfilling it, closing a nutrient loop that complements the water- and nutrient-recycling logic already highlighted for hydroponic and aquaponic systems.

From a productivity standpoint, intensive urban vegetable production has been reported to reach up to 50 kg/m² per year, owing to efficient resource use, innovative irrigation and organic fertilization (*Orsini et al., 2013*) – a range broadly consistent with the high space-use efficiency attributed to soil-less and vertical/rotary systems in Figure 2.

However, the practical adoption of any of the compared technologies within cities remains conditioned by access to water and fertile growing media, local pollution levels, climate suitability and market demand, as well as by policy support for repurposing unused urban or peri-urban land.

## CONCLUSIONS

The comparative assessment of vegetable growing technologies in controlled, closed environments reveals a clear efficiency-investment gradient. Greenhouses and solariums remain the most accessible and widely applied solutions, with productivity strongly dependent on covering material, climate control and crop management; Romanian examples such as the Transgex, Dalin and Chirana Serv complexes demonstrate that substrate-based, technologically advanced greenhouses can multiply yields several times over classic soil-based systems.

Soil-less technologies – hydroponics, aeroponics and aquaponics – achieve substantially higher water-use efficiency, of up to 90–95% water savings, and enable continuous, space-efficient production largely independent of outdoor conditions, at the cost of higher energy demand, investment and technical expertise. Aeroponics stands out for seed-potato multiplication and for the highest reported water and fertilizer savings, while aquaponics adds the advantage of a circular, fertilizer-free nutrient cycle at the expense of greater biological complexity.

Rotary and cylindrical vertical hydroponic systems, combine the resource-use advantages of hydroponics with markedly improved space efficiency, making them particularly suitable for urban and peri-urban microfarming, educational use and research applications.

These findings support technology selection according to available resources, crop type and production scale, and confirm the importance of continued investment in controlled-environment agriculture, renewable energy integration and technology transfer, in line with CAP 2023–2027 priorities on soil health, water efficiency and climate adaptation.

## ACKNOWLEDGEMENT

This research was supported by the Romanian Ministry of Research Innovation and Digitalization, through the project “Intelligent plant growth systems under controlled environmental conditions” – PN 23 04 01 04– Ctr. 9N/01.01.2023.

## REFERENCES


[1] Alsadon, A.; Al-Helal, I.; Ibrahim, A.; Abdel-Ghany, A.; Al-Zaharani, S.; Ashour, T. (2016). The effects of plastic greenhouse covering on cucumber (Cucumis sativus L.) growth. Ecological Engineering, 87, 305–312.

[2] Berevoianu, R.L. (2024). The economic profitability of pepper cultivated in solar system in conventional and organic agriculture – case study in Romania. Scientific Papers Series Management, Economic Engineering in Agriculture and Rural Development, PRINT ISSN 2284-7995.

[3] Castilla, N.; Baeza, E. (2013). Greenhouse site selection. Good Agricultural Practices for greenhouse vegetable crops – Principles for Mediterranean climate areas. FAO, E-ISBN 978-92-5-107650-7.

[4] Drăghici, E.M.; Jerca, O.I.; Cîmpeanu, S.; Teodorescu, R.I.; Țiu, J.; Bădulescu, L. (2021). Study regarding the evolution of high-performance cultivation technologies in greenhouses and high tunnels in Romania. Scientific Papers. Series B, Horticulture, LXV(1).

[5] Dumitru, A.A.; Berevoianu, R.L.; Necula (Ilie), D.M. Good Practice Guide for Bell Pepper Cultivation in Conventional and Organic Systems – 2018–2019 Estimates.

[6] Fasciolo, B.; Awouda, A.; Bruno, G.; Lombardi, F. (2023). A smart aeroponic system for sustainable indoor farming. 30th CIRP Life Cycle Engineering Conference, 636–641.

[7] Gopinath, P.; Irene Vethamoni, P.; Gomathi, M. (2017). Aeroponics Soilless Cultivation System for Vegetable Crops. Chemical Science Review and Letters, 6(22), 838–849.

[8] Gurley, T.W. (2020). Aeroponics Growing Vertical. CRC Press, Boca Raton, FL.

[9] Kadam, S.A.; Kadam, P.S.; Mohite, D.D. (2024). Design and experimental analysis of a closed-loop autonomous rotary hydroponics system for revolutionizing fenugreek yield and enhancing food security. Discover Sustainability, 5:137.

[10] Keat, C.K.; Kannan, C. (2015). Development of a Cylindrical Hydroponics System for Vertical Farming. Journal of Agricultural Science and Technology B, 5, 93–100.

[11] Khan, F.A.; Kurklu, A.; Ghafoor, A.; Ali, Q.; Umair, M.; Shahzaib. (2018). A Review on Hydroponic Greenhouse Cultivation for Sustainable Agriculture. International Journal of Agriculture, Environment and Food Sciences, 66.

[12] Malhi, G.S.; Kaur, M.; Kaushik, P. (2021). Impact of Climate Change on Agriculture and Its Mitigation Strategies: A Review. Sustainability, 13, 1318.

[13] Monero, J.I.; Teitel, M.; Baeza, E.; Lopez, J.C.; Kacira, M. (2013). Greenhouse design and covering materials. Good Agricultural Practices for greenhouse vegetable crops. FAO.

[14] Monisha, K.; Selvi, H.K.; Sivanandhini, P.; Nachammai, A.S.; Anuradha, C.T.; Rama Devi, S.; Kavitha Sri, A.; Neya, N.R.; Vaitheeswari, M.; Hikku, G.S. (2023). Hydroponics agriculture as a modern agriculture technique. Journal of Achievements in Materials and Manufacturing Engineering, 116.

[15] Orsini, F.; Kahane, R.; Nono-Womdim, R.; Gianquinto, G. (2013). Urban agriculture in the developing world: a review. Agronomy for Sustainable Development. DOI:10.1007/s13593-013-0143-z.

[16] Panigrahi, G.K.; Panda, S.; Padhi, S.N. (2016). Aquaponics: An innovative approach of symbiotic farming. International Journal of Bioassays, 5(9), 4808–4814.

[17] Pennisi, G.; Appolloni, E.; Paucek, I. (2019). Introduction to Urban Agriculture. Innovative Indoor Farming Applications for Future Urban Farmers, Erasmus+.

[18] Sharat, K. (2023). Aeroponic farming technology.

[19] Stoyanova, S.; Sirakov, I.; Velichkova, K. (2024). Sustainable Production: Integrating Medicinal Plants with Fish Farming in Aquaponics – A Mini Review. Sustainability, 16, 6337.

[20] Thorarinsdottir, R. et al. (2015). Aquaponics Guidelines. ISBN 978-9935-9283-1-3.

[21] Xushvaqtov, N.; Ibrohimov, B.; Yusupov, B.; Jonuzaqova, K.; Nizomova, Z. (2024). Impact of planting schemes on hot pepper varieties in greenhouses. BIO Web of Conferences 130, 01022

# FEM NUMERICAL ANALYSIS OF A SPRINGBOARD TYPE ELASTIC SYSTEM FOR APPARATUS VAULTING

/

# *ANALIZA NUMERICĂ MEF A UNUI SISTEM ELASTIC DE TIP TRAMBULINĂ PENTRU SĂRITURI LA APARATE*

**Daniel-Mirel DUMITRESCU[1)], George IPATE[1)], Gheorghe VOICU[1)], Paula TUDOR*[1)], Liliana-Caliopi ISCRU[1)], Dragoș-Valentin LUPU[2)]**

[1)] UNSTP Bucharest / Romania; [2)] INMA Bucharest / Romania

**Tel: 0040 723 850 975.; *E-mail: paula.voicu@upb.ro*

***Keywords:*** *gymnastic springboard; Ansys LS-DYNA; dynamic stiffness; von Mises stress; experimental validation*

**ABSTRACT**

*This paper presents a structural numerical analysis of a 3SLP-type gymnastics springboard, utilizing dynamic simulation within the Ansys LS-DYNA environment. The elastic components are geometrically modeled as three-dimensional solids to evaluate energy transfer and the propagation of transient shock waves. The numerical model was validated through direct correlation with prior experimental data obtained via accelerometry. The results indicate an equivalent dynamic stiffness of 26.73 kN/m, a value falling within the 22.14–71.12 kN/m range established in earlier research phases. Although the top plate undergoes the primary deformation (peaking at 9.35 mm at t = 0.027 s), the highest von Mises stress levels (4.68 MPa) were found to concentrate on the lower support system. The dynamic velocity profile showed a minimum downward velocity of -0.583 m/s and an upward rebound of 0.495 m/s, confirming a propagation delay of 13.5 ms consistent with physical reality. Based on the identified critical points, geometric optimization solutions and a preventive maintenance protocol - to be implemented every 500 cycles of intensive use - are proposed.*

**REZUMAT**

*Lucrarea prezintă analiza numerică structurală a unei trambuline pentru sărituri la aparate de gimnastică de tip 3SLP, utilizând simularea dinamică în mediul Ansys LS-DYNA. Componentele elastice sunt modelate geometric ca solide tridimensionale pentru a evalua transferul de energie și propagarea undelor de șoc tranzitorii. Modelul numeric a fost validat prin corelare directă cu date experimentale anterioare culese prin accelerometrie. Rezultatele indică o rigiditate dinamică echivalentă de 26.73 kN/m, valoare ce converge în domeniul 22.14–71.12 kN/m determinată în fazele precedente ale cercetării. Deși placa superioară preia deformația majoră (cu un vârf de 9.35 mm la t = 0.027 s), s-a demonstrat că nivelul cel mai ridicat al tensiunilor von Mises (4.68 MPa) se concentrează pe sistemul de suport inferior. Profilul de viteză dinamică a avut o valoare minimă descendentă de -0.583 m/s și un recul ascendent de 0.495 m/s, confirmând un delay de propagare de 13.5 ms, aliniat cu realitatea fizică. Pe baza punctelor critice identificate, sunt propuse soluții de optimizare geometrică și un protocol de mentenanță preventivă la fiecare 500 de cicluri de utilizare intensivă.*

## 1. INTRODUCTION

Elastic equipment used in vaulting gymnastics—specifically springboards—plays a crucial role in optimizing athletes' performance and ensuring their physical safety. The interaction between the gymnast and the springboard is a rapid dynamic process, typically occurring within a timeframe of 0.100 to 0.150 seconds. The kinetic energy the athlete accumulates during the run-up is transferred to the structure, temporarily stored as elastic potential energy, and subsequently released to generate the vertical propulsion and angular momentum required for the maneuvers performed on the apparatus.

The standardization of safety requirements and test methods for this equipment provided a uniform basis for development (*Göhler and Spieth, 1989; DIN 7902, 1978*).

Depending on the type of vault - such as Tsukahara or Yurchenko - the distribution of translational kinetic, rotational, and potential energy varies significantly, placing distinct demands on the apparatus

(*Scharer et al., 2021*); the flight phase is directly influenced by kinematic characteristics during contact (*Penitente et al., 2007*).

To investigate these complex phenomena, various experimental and analytical methodologies have been developed in the literature. Historically, direct measurement of ground reaction forces was achieved by placing springboards on strain-gauge-equipped Kistler force platforms; these studies revealed that peak impact force coincides with maximum deformation of the bed and can reach values up to 10.3 times the athlete's body mass (*Greenwood and Newton, 1996; Koperski et al., 2010*).

To simplify the analysis, researchers have proposed continuous kinematic models based on high-speed video recording and displacement digitization (*Hao et al., 2013*), as well as techniques for segmenting the bed into multi-body structures (*Sano et al., 2007; Lehmann et al., 2020*). For instance, it has been demonstrated that dividing the bed into segments connected by joints and torsion springs allows for the prediction of take-off forces with minimal error relative to experimental data (*Lehmann et al., 2020*).

Furthermore, the use of smart devices equipped with mini-accelerometers and processing units with LCD screens has paved the way for rapid systems capable of providing real-time information and evaluation of take-off parameters directly in the training facility (*Križaj and Cuk, 2015; Cuk et al., 2011*). However, from a structural standpoint, varying the configuration of the coil springs or adopting leaf-spring systems substantially alters local stiffness and the optimal impact range, thereby providing gymnasts with different margins of error during landing (*Coventry et al., 2006; Middelkoop and Stone, 2019; Courtney, 2019*).

From a structural mechanics perspective, the boards used in modern springboards are made of laminated plywood (typically birch, beech, or maple), with layers arranged so that the grain alternates (longitudinally and transversely) to counteract the wood's natural anisotropy and prevent delamination under repeated dynamic loads. The equivalent elastic properties of hardwood structural plywood are influenced by layer orientation (*Gerrard, 1987; Dinwoodie, 1981*), with the composite's strength characteristics closely linked to the wood species and any potential structural reinforcement of the layers (*Brezovic et al., 2003*).

The optimization of stress distribution within these laminated structures can be numerically evaluated using the finite element method (*Kljak et al., 2006; Wang et al., 2022*). The theoretical study of vibrations and stress states in such composite beams and curved bars is addressed using higher-order shear deformation theories, Jacobi polynomial models, or multi-segment partitioning techniques (*Qin et al., 2020*). Related issues introduced by moving dynamic loads, nonlinear resonance phenomena in sandwich-type curved structures with viscoelastic cores, or nonlinear modal interactions have been investigated using numerical methods such as Differential Quadrature or harmonic balance (*Serveren et al., 2024; Maqbool et al., 2026; Gonzalez and Vescovini, 2023; Dragomir and Vasile, 2015*).

Furthermore, analytical modeling of structures with variable porosity or those reinforced with graphene nanoplatelets has demonstrated that the system's natural frequencies are strictly dependent on boundary conditions and the geometric distribution of the material (*Wang and Zhang, 2024; Kiarasi et al., 2022*). In structural vibration engineering, the fundamental equations of damped oscillations, the logarithmic decrement, and the quality factor Q are commonly used to describe how energy dissipates through internal friction or at the soil interface (*Rades, 2008; Inman, 2008; Beer et al., 2008; Orasanu and Craifaleanu, 2012*). Although the analytical Bernoulli-Euler beam model with spiral springs provides a first approximation of macroscopic stiffness (*Zanevskyy and Zanevska, 2023*), it has limitations in capturing transient three-dimensional contact phenomena.

In our previous studies, we experimentally determined that the system exhibits strongly nonlinear behavior, with the dynamic stiffness coefficient fluctuating between 22.14 and 71.12 kN/m, thereby inducing parasitic and asymmetric vibrations from the upper plate to the lower ones (*Dumitrescu et al., 2025*).

Subsequently, our investigations focused on the lower support system (the base), demonstrating that—despite limited ground-level displacements (6.0–10.0 mm)—the support legs are subjected to severe stress and shear concentrations at the spring attachment points, with a critical zone for mechanical fatigue identified at the intermediate position P3 (*Tudor et al., 2025*).

This paper proposes a numerical approach based on three-dimensional Finite Element Analysis (FEA) simulation using the Ansys LS-DYNA solver. The primary objective is the structural modeling of the springboard's geometric and elastic assembly. Unlike previous models, the elastic component is not represented by linearly introduced virtual constants; instead, it is fully geometrically discretized as a three-dimensional structural solid (*Elastic_Spring*).

By running the simulation over a critical duration of 0.03 seconds, the study aimed to capture early high-frequency transient shock waves and validate the numerical model by directly correlating von Mises

stress and dynamic deflection results with the elastic parameters and experimental profiles established in earlier stages of our research.

## 2. MATERIALS AND METHODS

For the structural numerical modeling, the geometry of the gymnastics vaulting springboard—experimentally tested in previous research (*Dumitrescu et al., 2025; Tudor et al., 2025*)—was used. The simplified three-dimensional model was initially developed in SW and subsequently imported into the Ansys DesignModeler environment (Product Version 2022 R2), following the configuration illustrated in Fig.1 d.

The assembly under analysis, designated Springboard_wood_v1, has overall dimensions of 600 mm (width along the X-axis), 168.28 mm (total height along the Y-axis), and 1109.7 mm (length along the Z-axis), with a calculated total mass of 21.874 kg. The assembly consists of eight interconnected solid bodies: the elastic top board, the S-shaped intermediate board, two rear support legs (*LEFT_Leg* and *RIGHT_Leg*), and the solid-spring elastic components (*ELASTIC_Spring*). To visually clarify the assembly method and the interaction of the internal components, the geometric parts are broken down in Fig.1 (a–c).

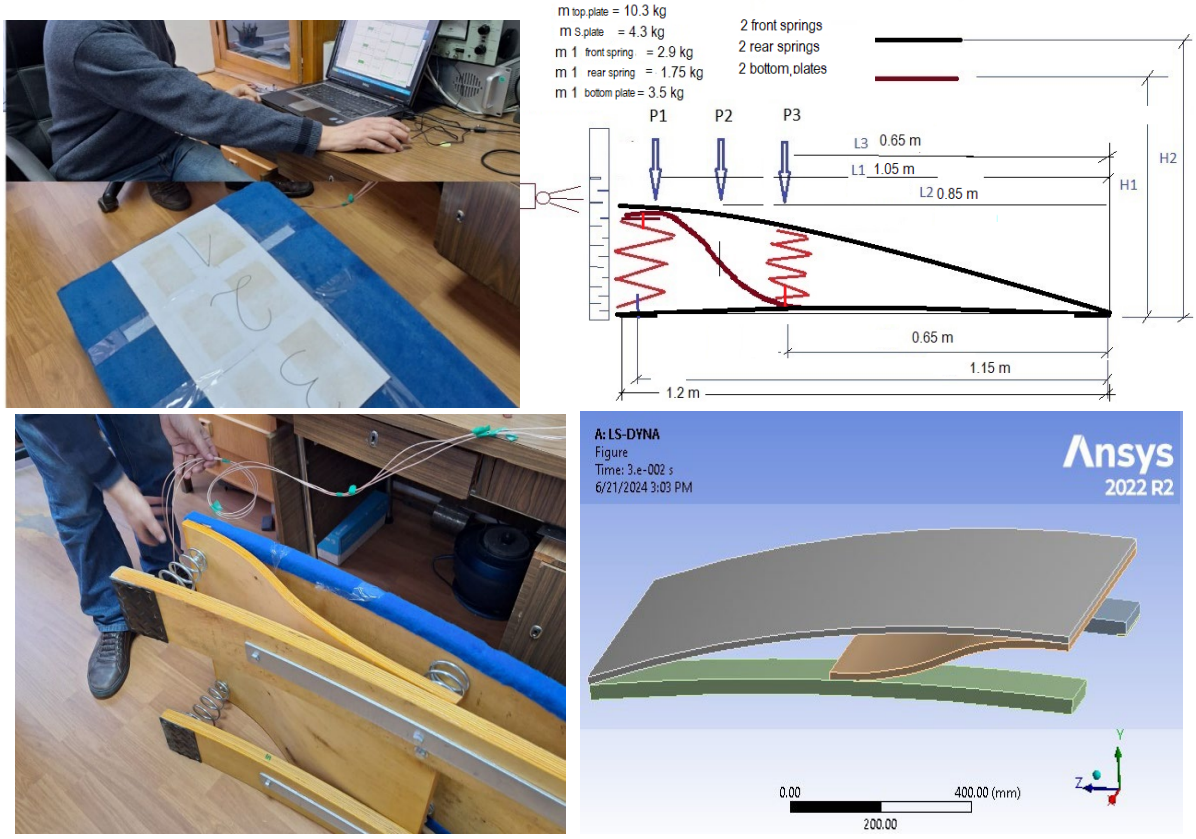



**Fig. 1 - Springboard structure, data acquisition system, and 3D image with the geometric model.**

In the structure of the 3SLP-type equipment, the wooden components are made of birch or beech layers with bi-directionally crossed grain, each 1.5 mm thick—a configuration that exhibits linear-elastic orthotropic behavior (*Tudor et al., 2025*).

**Table 1**

**Geometric properties and mass parameters of the structural assembly components**

| Component Name | Material | Volume [mm$^3$] | Mass [kg] | Nodes | Elements |
|---|---|---|---|---|---|
| Top Plate | Wood | $1.0064 \cdot 10^7$ | 9.4171 | 1440 | 665 |
| Left Support | Wood | $4.1200 \cdot 10^6$ | 3.8551 | 400 | 168 |
| Right Support | Wood | $4.1450 \cdot 10^6$ | 3.8785 | 385 | 160 |
| Elastic Spring System | Steel | $5.0224 \cdot 10^6$ | 4.6995 | 760 | 342 |
| Support Legs | Wood | $1.2499 \cdot 10^4$ | $1.169 \cdot 10^{-2}$ | 20 | 12 |
| COMPLETE ASSEMBLY | - | **$2.3377 \cdot 10^7$** | **21.874** | **2965** | **1359** |

For this stage of the numerical simulation in LS-DYNA, oak wood was assigned to the structural timber components to evaluate energy transfer. The physical-mechanical properties implemented in the

simulator were defined based on the Ansys database: density ($\rho_0$ = 9.357·10$^{-7}$ kg/mm$^3$), Young's modulus (E = 22780 MPa), Poisson's ratio ($\nu$ = 0.3742), and a yield strength of 47.76 MPa.

The solid spring system is defined in the model with standard elastic properties for structural steel, correlated with the analytical stiffness equations used in previous experimental stages (*Tudor et al., 2025*). In this context, evaluating the behavior and transverse stiffness distribution of the helical compression springs further substantiates the accuracy of the numerical model (*Baran et al., 2023*), similar dynamic modeling methodologies have being validated for other elastic sports structures in estimating transient impact forces (*Haake et al., 2010*).

Spatial discretization was optimized to ensure stable convergence within the explicit solver (*Biris, 2005*). An Explicit Dynamics physical preference with linear structural elements was employed, resulting in a total of 2965 nodes and 1359 elements. The finite element mesh, generated adaptively on the springboard geometry, is shown in Fig.2.

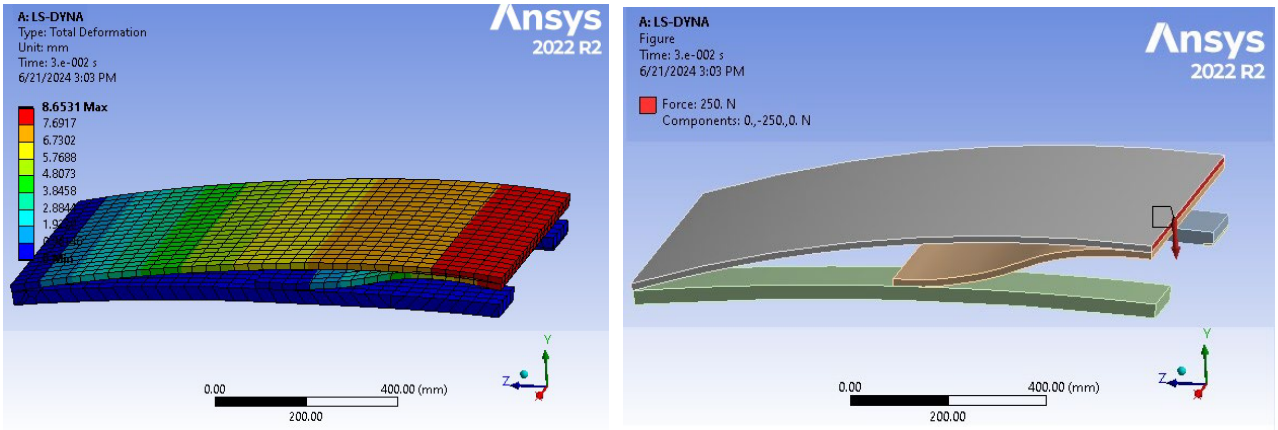



**Fig. 2 - The finite element mesh and the configuration of loads and constraints in the Ansys model.**

To faithfully replicate the springboard-floor interface (*Tudor et al., 2025*), standard gravitational acceleration was applied in the negative vertical axis direction, within the LS-DYNA solver, while the bottom surfaces of the support legs (4 faces) were fully immobilized using a rigid constraint (*Fixed Support*). The gymnast's impact was simulated by applying a transient dynamic force of -250 N in the negative vertical (Y) direction, concentrated on a single face at the free end of the top plate. The complete constraint configuration and the applied force vector are graphically detailed in Fig.2,b.

The continuum structural model was transferred to the Ansys LS-DYNA solver to perform the actual dynamic analysis. Through numerical integration over a critical duration of 0.03 seconds, the software calculated the evolution of transient stress states, shock wave propagation, and the kinematic response of the elastic components.

The results obtained from this simulation, along with their validation through direct correlation with our previously determined experimental accelerometer data, are presented in the "Results and Discussion" section.

## 3. RESULTS AND DISCUSSION

### *3.1. Analysis of Transient Vibrational Response and Reaction Force*

Running the numerical simulation in the Ansys LS-DYNA solver over a transient duration of 0.03 s enabled the capture of rapid dynamic phenomena occurring within the first few milliseconds of contact. The high-frequency vibrational behavior of the structure, generated by the transient shock wave, is highlighted by monitoring the reaction force over time at the rigid fixation points of the support legs.

The time-history of the reaction force, shown in Fig.3,a, indicates a strongly oscillatory response characterized by high-amplitude positive and negative force fluctuations, ranging from a minimum of -406.9 N to a maximum of 421.19 N.

This non-linear and non-harmonic behavior aligns with experimental findings obtained via accelerometric techniques in previous studies (*Dumitrescu et al., 2025*), confirming that the elastic structure does not act as a linear damper but instead dissipates impact energy in the form of high-frequency forced

vibration waves propagating through the composite material toward the assembly components (*Tudor et al., 2025*).

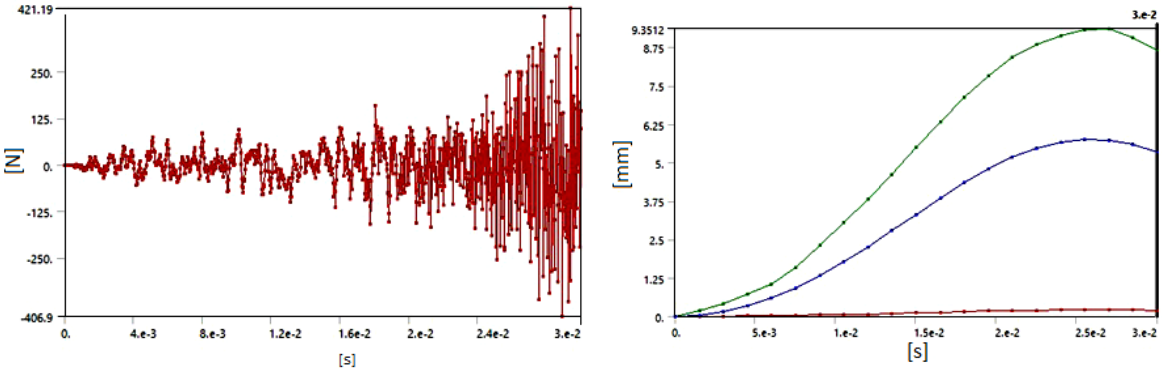



**Fig. 3 - Time-dependent variation of the reaction force at the fixed support and of the maximum deformation**

*3.2. Evaluation of the Dynamic Deformation Field*

Analysis of the total deformation evolution during dynamic oscillations reveals how impact kinetic energy is absorbed by the flexible wooden components. The spatial distribution of total deformation at the end of the calculation period (t = 0.03 s) is illustrated in Fig.2,a. A maximum deformation of 8.6531 mm is observed in the free cantilever area of the upper plate, while the average value across the entire structure stabilizes at 3.5523 mm, with the minimum (0.0 mm) recorded near the rigid support (*Suport_Left*).

The full profile of the maximum deformation recorded on the plate over the 0.03-second interval is detailed in Fig. 3b, highlighting that the absolute maximum value (peak dynamic deflection) reaches 9.3512 mm at t = 0.027 s. This value numerically validates the experimental operating range—documented via the double integration of accelerometer signals during laboratory tests with medium masses—where dynamic displacements between 6.0 mm and 10.0 mm were recorded for the lower plates (*Tudor et al., 2025*).

The direct ratio between the applied force (250 N) and the calculated maximum deflection (9.3512 mm) yields an equivalent dynamic stiffness of 26.73 kN/m; this falls within the global stiffness range of 22.14–71.12 kN/m experimentally demonstrated in our previous research for the active elastic positions of 3SLP springboards (*Dumitrescu et al., 2025*). The numerical model was validated through direct correlation with dynamic displacement profiles experimentally determined via accelerometry at position P1 (indicated in Fig.1). Since position P1 is located at the free end of the top plate, it lies close to the point where the dynamic load is applied in the simulation. The damped oscillatory pattern of the experimental displacements (recorded at h = 35 cm and h = 60 cm) (Fig.4) qualitatively confirms the theoretical dynamic deflection behavior shown in Fig.3. It is observed that, while the maximum positive amplitude stabilizes at approximately 27 mm in both cases due to geometric nonlinearity, the maximum downward rebound increases significantly with impact energy—ranging from 15 mm (at h = 35 cm) to 29 mm (at h = 60 cm)—thereby validating the transient structural behavior of the diving board's oscillating system.

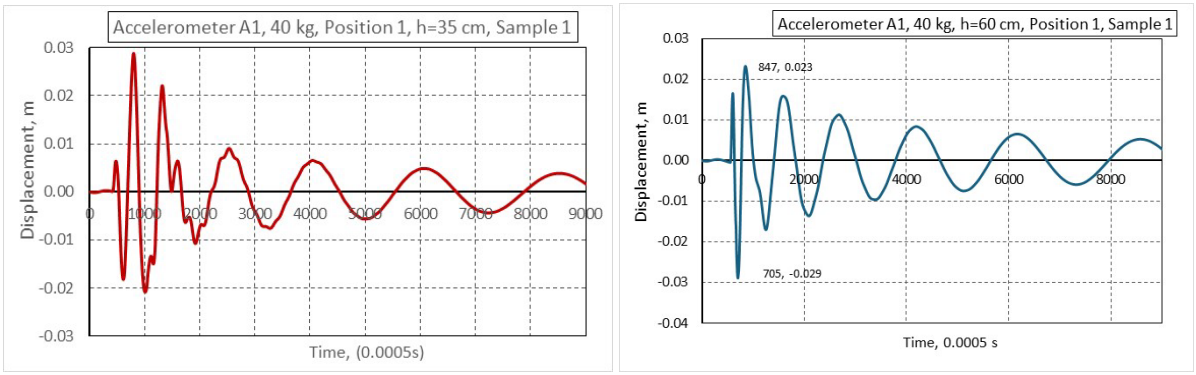



**Fig. 4 - Experimental profile of transient displacements recorded by accelerometer A1 at position P1.**

The presented experimental displacements and kinematic profiles were derived directly from raw acceleration signals using a double numerical integration algorithm in the time domain (trapezoidal rule)—digitally filtered (Butterworth high-pass >2 Hz) and drift-corrected—implemented within the data acquisition system's software.

From the perspective of signal processing in vibration dynamics, the non-harmonic and strongly nonlinear nature of transient impact oscillations poses no obstacle to integration. Unlike idealized analytical approaches, numerical integration (based on discrete computational schemes) operates directly on instantaneous values recorded at a high sampling rate. To eliminate the inherent drift phenomenon - specifically, the linear or parabolic baseline shift resulting from the integration of low-frequency background noise - the signal was digitally pre-processed using a high-pass filter. This successive filtering and integration protocol ensures the exact mathematical conversion of acceleration into velocity and, subsequently, into actual macroscopic displacement.

*3.3. Von Mises Equivalent Stress Distribution and Critical Points*

From the perspective of strength of materials, identifying areas with stress concentrators is essential for estimating the durability of a structure subjected to mechanical fatigue over thousands of usage cycles.

The distribution of von Mises equivalent stresses across the entire assembly at the final stage of the explicit analysis is shown in Fig.5. The maximum von Mises stress value during the simulation peaks at 4.6826 MPa (at t = 0.0285 s), structurally located at the rear support legs (PiciorDR), whereas average stresses in the top plate hover around $1.32 \cdot 10^{-2}$ MPa. Across the entire model - with a total volume of $2.3377 \cdot 10^{7}$ mm³ - the average stress recorded at the final stage is only 0.39963 MPa, confirming that the loads are safely borne by the structure.

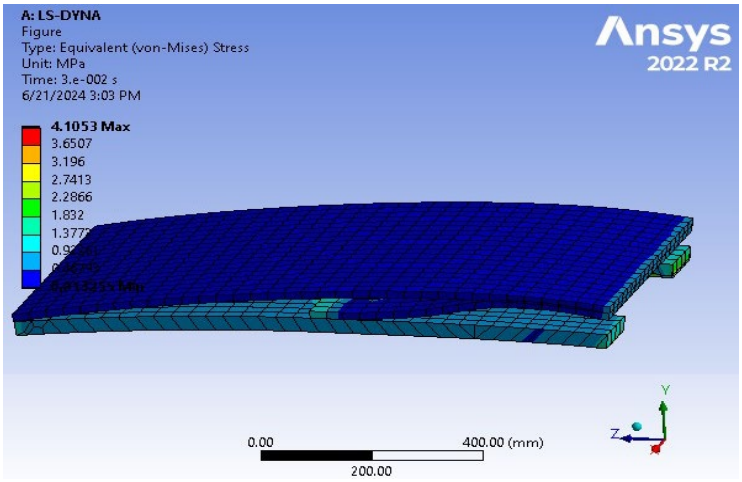



**Fig. 5 - Distribution of von Mises equivalent stresses at the final time step**

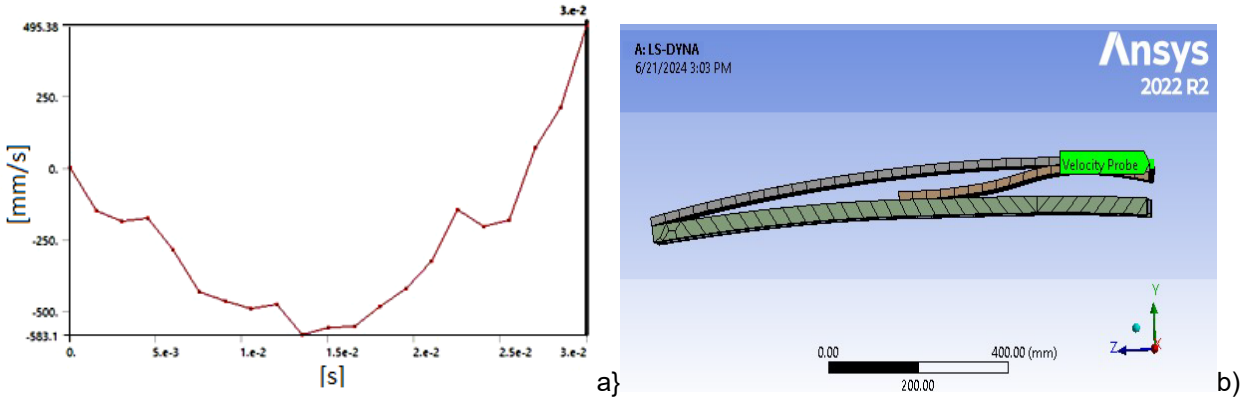
This numerical result is of fundamental importance, confirming the hypothesis raised in the experimental pilot study (*Tudor et al., 2025*), which demonstrated that although the top plate undergoes the most visible deformation, the highest unit stresses - and the risks of shear or loosening of mechanical fasteners - occur within the lower support system at the base. Given that the maximum value of 4.68 MPa determined via LS-DYNA explicit simulation is well below the nominal tensile yield strength of the structural timber used (47.76 MPa), it is scientifically demonstrated that the assembly operates within a safe linear-elastic regime, free from the risk of instantaneous plastic failure, with material degradation driven exclusively by structural fatigue in the area of the support legs.

*3.4. Dynamic Velocity Profile and Elastic Rebound Analysis*

The virtual velocity probe placed on a node at the free end of the top plate provides a clear picture of the structural response kinematics. Thevelocity variation along the vertical axis (Y) over time is shown in Fig.6,a.

The kinematic profile reveals that, immediately following the impact, the plate undergoes a violent downward acceleration, reaching a minimum (negative) velocity of -583.1 mm/s at t = 0.0135. Validation of the transient kinematic behavior was achieved by directly comparing the simulated velocity profile with experimental data recorded by the virtual sensor at position P1.

The kinematic profile determined for the impact from h = 35 cm (Fig.7, left) indicates an initial downward shock wave reaching values in the range of -550 to -580 mm/s, followed by an upward rebound of approximately +500 mm/s.




a} b)

**Fig. 6 - Evolution of the upper plate's Y-axis velocity over time (Velocity Probe) during oscillation (a), and geometric positioning of the velocity probe-type virtual sensor on the top plate (b)**

There is ideal convergence with the values calculated in the Ansys LS-DYNA solver (minimum velocity of -583.1 mm/s and rebound of +495.38 mm/s).

Correspondingly, the test from h = 60 cm (Fig.7, right) captures the rapid rise in kinetic energy, with velocity amplitudes exceeding thresholds of -1100 mm/s during compression and +1000 mm/s during rebound.

This proportional progression of the experimental profiles demonstrates the numerical model's ability to accurately estimate the transient energy exchange and the structural propagation delay.

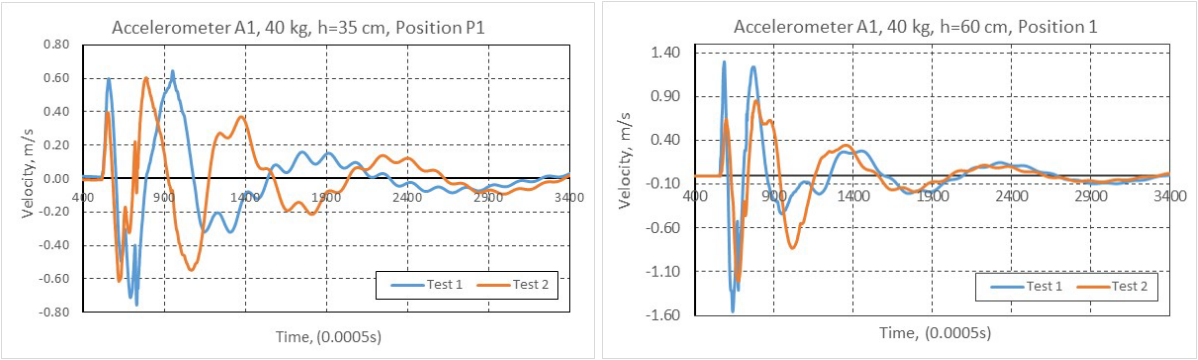



**Fig. 7 - Velocity profiles for transient jumps recorded by accelerometer A1, for a mass of 40 kg.**

The positioning of the kinematic monitoring node is illustrated in Fig. 6,b, while the data summarized in Table 2 quantifies the structural and elastic performance of the hybrid assembly, highlighting the close correlation between the numerical model and the physical reality established during previous experimental stages.

**Table 2**

**Summary of overall numerical results obtained from the transient simulation in LS-DYNA.**

| Parameter | Minim | Maxim | Medium | Critical Structural Location |
|---|---|---|---|---|
| **Plate Deformation (t=0.03 s)** | 0.20016 mm | 8.6531 mm | 5.3506 mm | Top plate cantilever |
| **Plate Deformation (Dynamic Peak)** | 0.00000 mm | 9.3512 mm | 5.7160 mm | Plate edge (at t = 0.027 s) |
| **von Mises Stress (at the end)** | 0.01325 MPa | 4.1053 MPa | 0.39963 MPa | Base of rear support legs |
| **von Mises Stress (*Dynamic Peak*)** | 0.00000 MPa | 4.6826 MPa | 0.44082 MPa | Right Leg component (at t = 0.0285 s) |
| **Support Reaction Force** | –406.90 N | 421.19 N | - | Fixed support |
| **Dynamic Velocity (Y-axis)** | –583.10 mm/s | 495.38 mm/s | 494.70 mm/s | Point sensor (*Velocity Probe*) |

The fact that peak values for deformation (9.3512 mm) and von Mises stress (4.6826 MPa) occur at very close time intervals (t = 0.027 s and t = 0.0285 s, respectively) demonstrates that the Ansys LS-DYNA explicit solver satisfactorily captured the moment of maximum dynamic loading during the transient impact.

This quantitative analysis confirms hypotheses regarding the location of stress concentrators on the lower support system and paves the way for formulating clear recommendations for design optimization and preventive maintenance.

*3.5. Limitations of the numerical model and development prospects*

Although the continuum numerical model developed in Ansys LS-DYNA demonstrated optimal qualitative convergence with the experimental profiles, its full validation is subject to methodological limitations inherent in the simplifications adopted at this stage of the research: While the experimental setup involved a dynamic impact generated by a 40 kg mass (~392.4 N, exceeding 400 N at the kinematic peak according to experimental data), the simulation employed a simplified, conservative transient force of only 250 N. This difference in energy input directly explains why the numerical model tends to make the assembly appear stiffer and limits the peak dynamic response, contrasting with the more extensive macroscopic deformations recorded experimentally.

The experimental plots derived from accelerometer signal processing reveal complex oscillatory behavior from the very first moments (the pre-impact phase and the early propagation of surface waves within the system). This initial phase was not accurately replicated in the simulation, where the load was applied under ideal conditions of instantaneous contact, without simulating the full kinematics of the body in free fall prior to striking the plate. Numerical integration was limited to a duration of 0.03 seconds. While this interval allowed for the capture of early transient shock waves, it does not cover the entire biomechanical window of compression, recoil, and take-off—a process that, under real-world conditions, extends to 0.08–0.15 seconds. Consequently, the simulation primarily captures the structural state prior to take-off, whereas the experimental profiles also reflect the damped free oscillation phenomenon that persists within the structure after contact. According to the experimental model presented in previous studies (*Tudor et al., 2025*), the total transient force generated upon impact follows the relationship $F = m(g + a)$. For a falling mass of 40 kg, the sudden vertical deceleration raises this force to the 400–500 N range at the moment of peak kinematics. In contrast, the LS-DYNA simulation employs a simplified static-dynamic force of 250 N, applied instantaneously at $t = 0$ s. This idealized numerical approach fails to capture the parasitic pre-impact micro-oscillations visible in the aligned experimental data, which explains why the deflection calculated in the simulator (9.35 mm) is lower than the extreme elasticity recorded in the laboratory. However, the analysis focuses on the initial phase of the impact, during which the oscillation amplitude is increasing. Once the maximum amplitude is reached, the system enters the damped free oscillation phase observed in the experiments.

Assigning properties specific to solid wood represents an approximation. Actual 3SLP-type diving boards utilize birch or beech plywood with cross-grained plies, exhibiting complex anisotropy and a response dependent on layer orientation—factors that dampen or alter natural vibration frequencies compared to a homogeneous solid. Regarding immediate development, future research will focus on calibrating the simulator's force to the actual dynamic impact value exceeding 400 N, kinematically modeling the free-falling impactor to replicate the initial oscillation phase, extending the analysis window beyond 0.15 seconds, and implementing a laminated composite material model.

## 4. CONCLUSIONS

Advanced numerical modeling of the Springboard_wood_v1 structural assembly, performed in the Ansys LS-DYNA environment, enabled a detailed investigation of rapid transient dynamic phenomena, thereby complementing and validating the experimental results obtained in earlier research stages. The analysis demonstrated that a modern gymnastics springboard constitutes a complex continuous elastic system in which component interactions generate non-linear and non-harmonic responses.

Based on the correlations established between the numerical and experimental data, the following key conclusions can be drawn:

- ✓ The numerical ratio between the applied dynamic force (250 N) and the maximum simulated deflection (9.3512 mm) indicated an equivalent dynamic stiffness of 26.73 kN/m for the model. This value falls squarely within the 22.14–71.12 kN/m overall stiffness range established via accelerometric techniques, confirming the accuracy of the elastic properties assigned to the components.
- ✓ The simulation demonstrated that, although the top plate undergoes macroscopically visible deformation (8.65–9.35 mm), the highest stresses are concentrated in the lower support system, reaching a peak von Mises stress of 4.6826 MPa on the *Right_Leg* component. This result validates earlier observations from pilot tests on instrumented physical springboards, where the base was identified as the critical interface subject to shear and structural fatigue.

- ✓ The dynamic velocity profile recorded by the virtual sensor (Velocity Probe) accurately captured the elastic rebound phase, showing a rapid velocity reversal at monitoring position P1. For a drop height of h = 35 cm, the simulation values (minimum velocity of -0.58 m/s and rebound of +0.50 m/s) showed ideal quantitative convergence with the experimental results. Additionally, the test at h = 60 cm revealed pronounced dynamics, with peaks exceeding thresholds of -1.10 m/s during compression and +1.0 m/s during rebound. The structural delay of 13.5 ms measured until the minimum velocity was reached faithfully reflects the transient shock-wave propagation lag observed experimentally between the sensors.

Taking into account the asymmetric dynamic behavior and the persistence of forced vibrations - highlighted both in the numerical reaction force plots (showing violent fluctuations between –406.9 N and 421.19 N) and in previous studies - the following design optimizations and safety measures can be proposed:

1. It is recommended to increase the thickness of the S-shaped intermediate plate or to add a central stiffening rib; this would improve the handling of asymmetric dynamic torsional loads and ensure a more uniform distribution of impact forces to the two lower support plates.
2. Given the high level of transient oscillations persisting within the structure, it is advisable to install damping gaskets made of elastomeric rubber or polyurethane at the lower plate mounting points to reduce fatigue stress on the wood.
3. Since the dynamic model confirms a concentration of stresses in the support leg area, a protocol for the regular visual inspection of structural integrity in zones subject to intense training is required. Additionally, it is recommended to check the tightness of mechanical fasteners (screws and bolts) every 500 cycles of intensive use to prevent loosening caused by high-frequency vibrations.

## REFERENCES


[1] Baran, R.; Michalczyk, K.; Warzech, M. (2023). *Experimental analysis of transverse stiffness distribution of helical compression springs*. Acta Mechanica et Automatica, 17(1), 95-103.

[2] Beer, F. P.; Johnston Jr., E. R.; Dewolf, D. F.; Mazurek, J. T. (2008). *Mechanics of Materials*. 5th Edition, McGraw-Hill, New York.

[3] Biris, S. S. (2005). *Finite Element Method. Fundamental Concepts.* Printech Publishing House, Bucharest (in Romanian).

[4] Brezovic, M.; Jambrekovic, V.; Pervan, S. (2003). *Bending properties of carbon fiber reinforced plywood*. Wood Research, 48(4), 13-24.

[5] Courtney, M. (2019). *Evaluation of artistic gymnastics vault board design*. Master of Science Thesis, Iowa State University, Ames, Iowa. iastate.edu

[6] Coventry, E.; Sands, W.; Smith, S. (2006). *Hitting the vault board: Implications for vaulting take-off - a preliminary investigation*. Sports Biomechanics, 5(1), 63-75.

[7] Cuk, I.; Penic, S.; Supej, M.; Krizaj, D. (2011). *Towards a smart springboard (case study)*. Science of Gymnastics Journal, 3(3), 29-42.

[8] Dallas, G.; Pappas, P.; Ntallas, C.; Paradisis, G. (2018). *The post-activation effect with two different conditioning stimuli on drop jump performance in pre-adolescent female gymnasts*. Journal of Physical Education and Sport, 18(4), 2368-2374.

[9] DIN 7902:1978-10 (1978). *Deutsches Institut für Normung. Turngeräte - Pauschenpferde, Sprungpferde - Maße, Anforderungen, Prüfung*. Beuth Verlag, Berlin.

[10] Dinwoodie, J. M. (1981). *Timber, its nature and behaviour*. Van Nostrand Reinhold, New York.

[11] Dragomir, M.; Vasile, O. (2015). *Theoretical and experimental analysis for determining the Eigen frequencies of mechanical system with three masses*. U.P.B. Scientific Bulletin, Series D: Mechanical Engineering, 77(4), 15-26.

[12] Dumitrescu, D.-M.; Voicu, Gh.; Orasanu, N.; Istrate, I.-A.; Constantin, G.-A. (2025). *The Elastic Vibration Behavior of a Springboard in Gymnastics*. Processes, 13(8), 2573.

[13] Gerrard, H. (1987). *The equivalent orthotropic elastic properties of plywood*. Wood Science and Technology, 21(5), 335-348.

[14] Gonzalez, J. A.; Vescovini, R. (2023). *Simplified approach to nonlinear vibration analysis of variable stiffness plates*. Journal of Composites Science, 7(1), 30.

[15] Greenwood, M.; Newton, J. W. (1996). *Direct force measurement of the vault take off in gymnastics*. In: Proceedings of the 14th International Symposium on Biomechanics in Sports, Funchal, Portugal, pp. 25-29.
[16] Göhler, J.; Spieth, R. (1989). *Geschichte der Turngeräte (History of gymnastics equipment)*. SPIETH Gymnastics GmbH, Stuttgart.
[17] Haake, S.; Goodwill, S.; Heller, B.; Schorah, D.; Gomez, J. L. (2010). *Dynamic modeling of a springboard during a 3 m dive*. Procedia Engineering, 2(2), 3299-3304.
[18] Hao, W. Y.; Wu, C. L.; Wang, X. D.; Xiao, D. D.; Wang, Q. (2013). *A simple method for monitoring springboard reaction force in gymnastic vaulting*. In: Proceedings of the 31st International Conference on Biomechanics in Sports, Taipei, China.
[19] Inman, D. J. (2008). *Engineering Vibration*. 3rd Edition, Pearson Education, Inc., Upper Saddle River, NJ.
[20] Kiarasi, F.; Babaei, M.; Asemi, K.; Dimitri, R.; Tornabene, F. (2022). *Free vibration analysis of thick annular functionally graded plate integrated with piezo-magneto-electro-elastic layers in a hygrothermal environment*. Applied Sciences, 12(20), 10682.
[21] Kljak, J.; Brezović, M.; Jambreković, V. (2006). *Plywood stress optimisation using the finite element method*. Wood Research, 51(1), 1-10.
[22] Koperski, A.; Kochanowicz, A.; Słodkowski, C. (2010). *Gymnasts' special quickness-force abilities and the indicators of jump from a springboard*. Baltic Journal of Health and Physical Activity, 2(2), 139-143.
[23] Križaj, D.; Cuk, I. (2015). *Can miniature accelerometers attached to the gymnastics springboard be used for take-off analysis?* Science of Gymnastics Journal, 7(2), 69–79.
[24] Lehmann, T.; Lorz, A.; Schleichardt, A.; Naundorf, F.; Knoll, K.; Eckardt, F.; Witte, K. (2020). *A Multi-body model of a springboard in gymnastics*. Science of Gymnastics Journal, 12(3), 265-275.
[25] Maqbool, Q.; Naseer, R.; Akhtar, I. (2026). *Linear and nonlinear analysis of a curved Timoshenko beam using geometrically exact formulation*. Applied Mechanics, 7(2), 30.
[26] Middelkoop, C.; Stone, R. (2019). *Gymnastics vault board design: a comparison of spring configuration and style of spring – preliminary study*. Proceedings of the Human Factors and Ergonomics Society Annual Meeting, 63(1), 1354-1357.
[27] Orasanu, N.; Craifaleanu, A. (2012). *Experimental study of the forced vibrations of a system with distributed mass and four concentrated masses*. In: Proceedings of the Annual Symposium of the Institute of Solid Mechanics, SISOM, Bucharest, pp. 200-205.
[28] Penitente, G.; Merni, F.; Fantozzi, S.; Perretta, N. (2007). *Kinematics of the springboard phase in Yurchenko-style vaults*. XXV ISBS Symposium, Ouro Preto, Brazil, pp. 36-39.
[29] Qin, B.; Zhao, X.; Liu, H.; Yu, Y.; Wang, Q. (2020). *Free vibration analysis of curved laminated composite beams with different shapes, lamination schemes, and boundary conditions*. Materials, 13(4), 1010.
[30] Sano, S.; Ikegami, Y.; Nunome, H.; Apriantono, T.; Sakurai, S. (2007). *The continuous measurement of the springboard reaction force in gymnastic vaulting*. Journal of Sports Sciences, 25(4), 381-391.
[31] Serveren, M. M.; Demir, O.; Arikoğlu, A. (2024). *Nonlinear dynamic analysis of a curved sandwich beam with a time-dependent viscoelastic core using the Generalized Differential Quadrature Method (GDQM)*. Symmetry, 16(2), 238.
[32] Tudor, P.; Voicu, Gh.; Dumitrescu, D.-M.; Constantin, G.-A.; Craifaleanu, A.; Stefan, E.-M. (2025). *Pilot Study on the Mechanical Stress and Vibrational Response of Gymnastics Springboard Support System*. Applied Sciences, 2026, 16(14), 7284.
[33] Wang, A.; Zhang, K. (2024). *Free vibration of graphene nanoplatelet-reinforced porous double-curved shells of revolution with a general radius of curvature based on a semi-analytical method*. Mathematics, 12(19), 3060.
[34] Wang, T.; Wang, Y.; Crocetti, R.; Wålinder, M. (2022). *In-plane mechanical properties of birch plywood*. Construction and Building Materials, 340, 127852.

# ASPECTS REGARDING STAGES, METHODS AND TOOLS TO IMPROVING PROBLEM-SOLVING IN MANUFACTURING

/

# *ASPECTE PRIVIND ETAPELE, METODELE ȘI INSTRUMENTELE PENTRU ÎMBUNĂTĂȚIREA SOLUȚIONĂRII PROBLEMELOR ÎN PRODUCȚIE*

**Carmen BRACACESCU*[1)]**
National Institute of Research - Development for Machines and Installations Designed for Agriculture and Food Industry - INMA Bucharest / Romania
**Tel: 0770 513 926; *E-mail: carmenbraca@yahoo.com*

***Keywords:*** *problem structuring; diagnosis; process improvement; quality improvement; six sigma*

**ABSTRACT**

*Problems are frequent and inevitable, and manufacturers face challenges very often. Acknowledging this reality enables teams to remain vigilant, quickly identify and resolve these difficulties, and constantly improve processes and products alike. Problem-solving has become a key skill in project management. It always consists of identifying, analyzing, and solving problems to achieve defined goals. It is important not to find temporary solutions, but to seek to identify and address the root causes in order to find long-term solutions. To do this, several methods have been developed to structure this problem analysis in order to reach the best solution over time. By employing structured problem-solving methods, managers can approach problems systematically and develop innovative solutions tailored to their specific needs. This article presents different stages of problem solving, the methods and tools that are most effective in manufacturing.*

**REZUMAT**

*Problemele sunt frecvente și inevitabile, iar producătorii se confruntă adesea cu diverse provocări. Conștientizarea acestei realități permite echipelor să rămână vigilente, să identifice și să rezolve rapid dificultățile și să îmbunătățească în permanență atât procesele, cât și produsele. Capacitatea de a rezolva probleme a devenit o competență esențială în managementul proiectelor. Aceasta presupune, în mod constant, identificarea, analizarea și soluționarea problemelor pentru a atinge obiectivele stabilite. Este important să nu ne limităm la soluții temporare, ci să urmărim identificarea și abordarea cauzelor fundamentale, astfel încât să găsim soluții pe termen lung. În acest scop, au fost dezvoltate diverse metode menite să structureze analiza problemelor, facilitând astfel găsirea celei mai bune soluții. Prin utilizarea unor metode structurate de rezolvare a problemelor, managerii pot aborda situațiile dificile în mod sistematic și pot dezvolta soluții inovatoare, adaptate nevoilor lor specifice. Acest articol prezintă diferitele etape ale procesului de rezolvare a problemelor, precum și metodele și instrumentele cele mai eficiente în domeniul producției.*

## INTRODUCTION

Problems may affect one workgroup or process, or they may cause organization wide issues. Solving a problem depends on correctly identifying its cause so the best solution can be selected and implemented for sustained results. Some problems are repetitive and occur often or more than once, while others are singular and considered a major incident or *accident (Davidson, J.E., Sternberg. R.J., 2003; Grünig, R., Kühn, R., 2025).* Many problems are highly visible due to formalized management systems such as ISO 9001, and some are insidious and difficult to identify.

Manufacturers face challenges very often with frequent and inevitable problems: variability of demand, quality management, equipment maintenance, and integration of new technologies. Acknowledging this reality enables teams to remain vigilant, quickly identify and resolve these difficulties, and constantly improve processes and products alike *(Dell'Era, C., et al, 2026; Queiroz, J., Ata, P.,2026).*

On the other hand, a problem isn't just a problem: it's also, and above all, an opportunity to do better. Rather than hiding or ignoring what's not working, the idea is to face up to it, to find structured methods for optimizing efficiency and quality. For this, there are a number of possible solutions and tools available. In today's manufacturing industry, implementing a robust quality management system is essential for ensuring product quality, reducing defects, managing deviations from standards, and preventing the problem from

occurring again *(Kadir, Z. et al, 2026; Rørvik-Olsen, O., Tagliabue, M., Sandaker, I., 2026).* Use of organized methods and analytical tools to tackle challenges is essential for manufacturers seeking to improve operational efficiency and product quality.

Continuous improvement practices offer several benefits, including increased operational efficiency, reduced waste and costs, and improved employee engagement and customer satisfaction *(Mohaghegh, M., Größler, A., 2021*; McDonnell, E., Prasad, M., 2026*).* These practices encourage a proactive approach to addressing inefficiencies and fostering innovation.

Innovative technologies play a crucial role in enhancing problem-solving in manufacturing. Digital twins, augmented reality, and collaborative robotics are technologies that help improve precision, efficiency, and safety, facilitating better decision-making and process optimization *(Soksimovic, S. et al, 2023).*

This article presents different stages of problem solving, the methods and tools that are most effective in manufacturing.

## MATERIALS AND METHODS

Problem-solving is the mental process of identifying issues, organizing knowledge and developing strategies to overcome them. Efficiently managing challenges and achieving desired outcomes can be accomplished by breaking down problems and evaluating various solutions *(Swarup, R., Payal, G., M., 2026; Väätäinen, H., Vakkala, H., 2026).*

In order to correctly solve a problem, it is often important to follow a series of steps, such as problem-solving cycle (figure 1). While this cycle is portrayed sequentially, people rarely follow a rigid series of steps to find a solution.

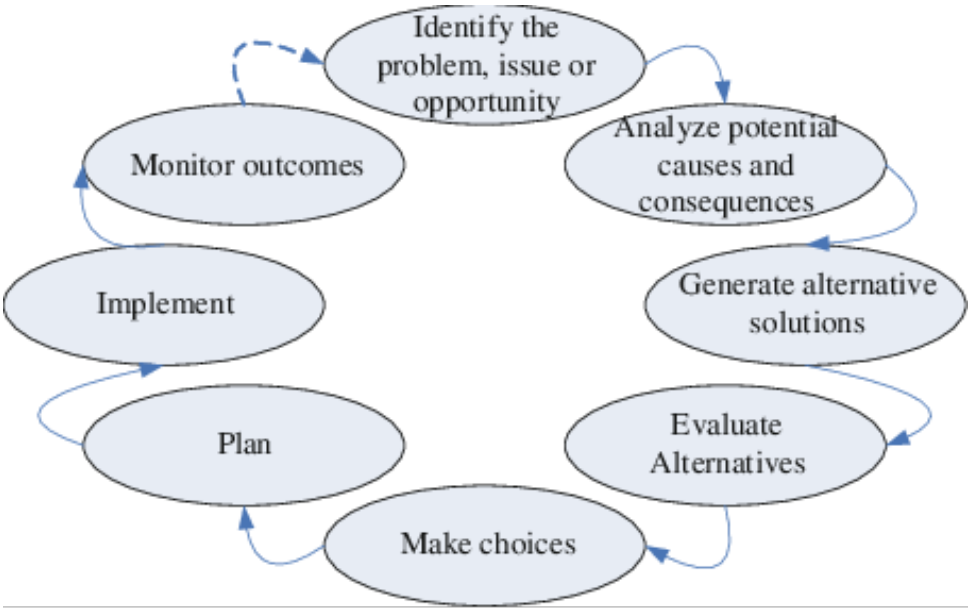



**Fig. 1 - Problem-Solving Cycle**

The following section analyzes five **useful problem-solving strategies for manufacturing.**

### 1. 8D (Eight Disciplines Problem Solving)

The eight disciplines (8D) model is a problem-solving approach commonly that has been applied successfully in manufacturing and other area. The model is used to identify, correct, and eliminate problems, making it useful in product and process improvement *(Nakata, C., & Hwang, J., 2020)*.

The 8D model establishes a permanent corrective action based on statistical analysis of the problem and focuses on the problem's origin by determining its root causes. The model consists of eight steps (or disciplines) named D1 through D8 (figure 2).

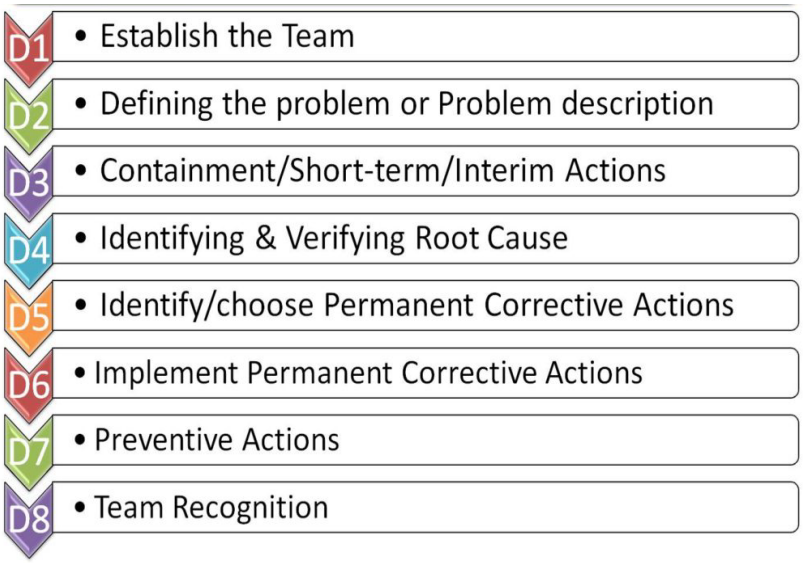



**Fig. 2 - 8D problem solving steps**

Therefore, 8D method is a quality approach to solving complex problems requiring in-depth analysis and lasting corrective action.

**2. PDCA (Plan-Do-Check-Act)**

The PDCA method helps organization test changes under controlled conditions, evaluate the results, and then implement improvements progressively to optimize production and ensure consistent product quality (figure 3). The PDCA method is based on an iterative approach.

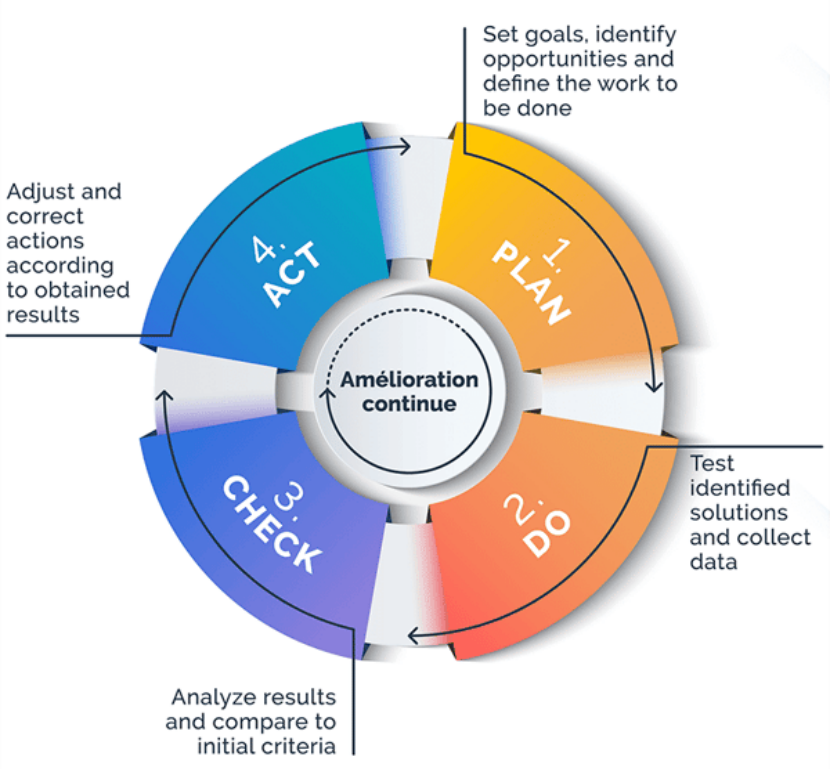



**Fig. 3 - PDCA problem-solving phases**

- Plan: consists of analyzing the existing situation by identifying problems. At this stage, it is a question of defining the objectives that are trying to achieve. At the end of this phase, come up with a schedule and the definition of performance indicators that will then make it possible to evaluate the results obtained.

- Do: consists of a first implementation of the solution, on a small scale to test its effectiveness based on experimentation. The aim is to minimize the impact on the organization's day-to-day operations.
- Check: consists in the results evaluation. The results achieved should be compared to the objectives set out in Step 1. It is then necessary to validate whether the overall efficiency of the process has been improved and decide whether a new round of testing is necessary before moving on to the next phase.
- Act: consists of finalizing and implementing changes within the process. Improvements (which have been validated) then become the new standard for this process. It is important to update the documentation associated with the process.

**3. DMAIC (Define, Measure, Analyze, Improve, Control)**

DMAIC is a structured problem-solving method approach used to improve existing processes that don't meet performance standards or customer expectations. Each project phase builds on the previous one, with the goal of implementing long-term solutions to problems.

The approach is used primarily in continuous improvement, lean, and Six Sigma, but also can be implemented as a standalone quality improvement procedure or part of other process improvement initiatives *(Nakata, C., & Hwang, J., 2020)*.

This Six Sigma method is highly effective in optimizing production processes, reducing variation, and eliminating defects by focusing on data and statistical analysis *(Abdirad, M., Krishnan, K., Gupta, D., 2021).* It involves clearly defining the problem (Define), measuring (Measure), and analyzing process data to identify root causes (Analyze), then implementing improvements (Improve) and controlling processes to ensure sustainable quality gains (Control) (figure 4).

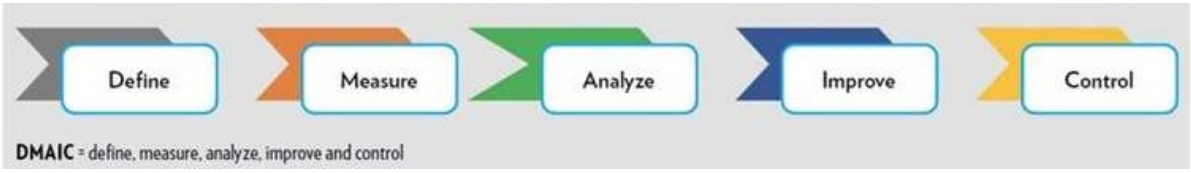



**Fig. 4 - Lean Six Sigma DMAIC phases**

**4. QRQC (Quick Response Quality Control)**

The QRQC method provides a standardized approach to problem-solving that enables cross-functional teams to quickly and effectively resolve quality issues. It typically involves a team of members from support departments or areas of expertise who work together.

The QRQC aims to resolve each problem by involving the closest individuals to it, at the lowest level of the management hierarchy possible. This approach requires a clear structure and escalation process that allows issues to be addressed at the production line, team or shop level, and eventually at the entire plant level if necessary (figure 5).

This fast, effective method inspired by Lean Management, consists in identifying, analyzing and solving problems directly on the shop floor *(Singh, A., Wiktorsson, M., Hauge, J.B., 2021)*.

It is particularly well suited to fast-paced production environments where immediate detection and resolution are necessary to maintain production continuity and efficiency.

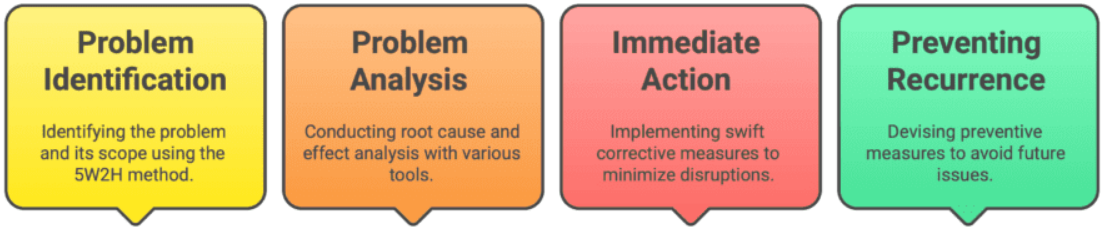



**Fig. 5 - Key Stages of QRQC**

**5. Four A's**

The Four A's method (Figure 6) is a structured approach that is designed to systematically address and solve problems within an organization.

- **Assess:** This step involves identifying and understanding the problem.
- **Analyze:** Once the problem is assessed, the next step is to analyze it to find the root causes.
- **Address:** With a clear understanding of the root causes, the third "A" involves developing and implementing solutions to address these causes.
- **Act:** The final "A" focuses on standardizing the correct solution and integrating it into the organization's processes.

The Four A's is used where problems need to be solved quickly and efficiently while ensuring that lessons learned are integrated into standard practices.




**Fig. 6 - Components of the 4A Model**

The use case of this five methods in the manufacturing industry are summarized in Table 1.

**Table 1**

**Use case of methods in the manufacturing industry**

| Methods | Problem | Solving |
|---|---|---|
| **8D** | Recurrent failure of a major piece of equipment, leading to costly production stoppages. | Enable a multi-disciplinary team to systematically identify, analyze, and eliminate the root cause of the failure while implementing sustainable corrective actions |
| **PDCA** | Variation in the quality of the finished product, which does not always meet standards. | Planning improvements, testing them, evaluating their effectiveness, and adjusting the production process to stabilize product quality |
| **DMAIC** | High scrap and rework rates on an assembly line | Specify the problem, measure performance, analyze data to find the cause, implement improvements, and control the process to reduce defects. |
| **QRQC** | Frequent safety incidents in the workplace. | Rapid reaction to identify and resolve the causes of such incidents immediately, thereby reducing their frequency and improving overall safety. |
| **Four A's** | Missed delivery deadlines due to production bottlenecks. | Quickly detect bottlenecks, analyze their causes, find and implement effective solutions, and then integrate these changes into regular operations to improve on-time delivery. |

The following section analyzes five **useful tools for structuring problem-solving methods.**

**1. The Five Whys**

This problem-solving technique, involves asking the question "Why?" five times until the root cause of a given problem is revealed. It's a simple but powerful tool for finding root causes. The Five Whys is a straightforward yet powerful tool for identifying root causes and addressing problems at their source. By repeatedly asking “why,” organizations can uncover the true cause of an issue and implement long-term solutions.

This technique is widely used in quality management, Lean, and Six Sigma to enhance business performance and ensure continuous improvement *(Jerez, D., Mazzulla, E., Bulut, O., 2026; Kadijevich, D., M., 2026).*

The Five Whys is not just about finding a solution; it’s about understanding why problems exist in the first place. Many issues arise from deeper, often hidden causes, such as communication breakdowns or flawed processes.

This method helps teams move beyond surface-level symptoms to uncover and address the root causes effectively (Figure 7).

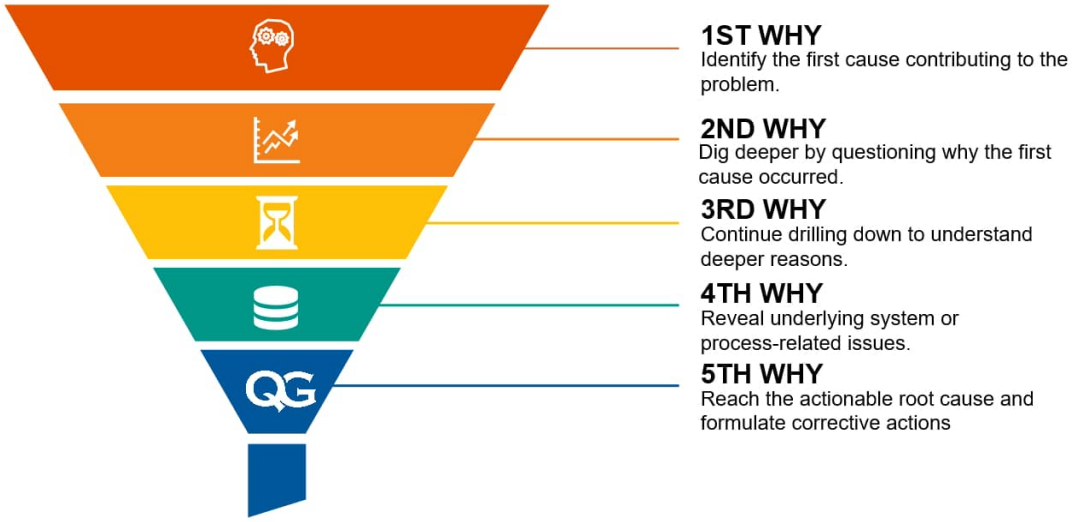



**Fig. 7 - The Five Whys: Uncover Root Causes**

**Use case in the manufacturing industry**

A factory has a problem with late delivery of finished products:

- **Why is the plant experiencing delays in the delivery of finished products?** Because the production of final units is often late.
- **Why is the production of final units behind schedule?** Because assembly takes longer than expected.
- **Why does assembly take longer than expected?** Because parts needed to complete assembly are often missing.
- **Why are parts often missing?** Because supplies regularly arrive late from the supplier.
- **Why do supplies arrive late from the supplier?** Because orders are placed too late, due to an inefficient procurement process.

**2. The Ishikawa diagram (5M)**

Also known as the "fishbone diagram" or "5M", this tool helps to systematically visualize all the potential causes of a specific problem, as well as the contributing factors. Causes are divided into 5 main categories (Figure 8).

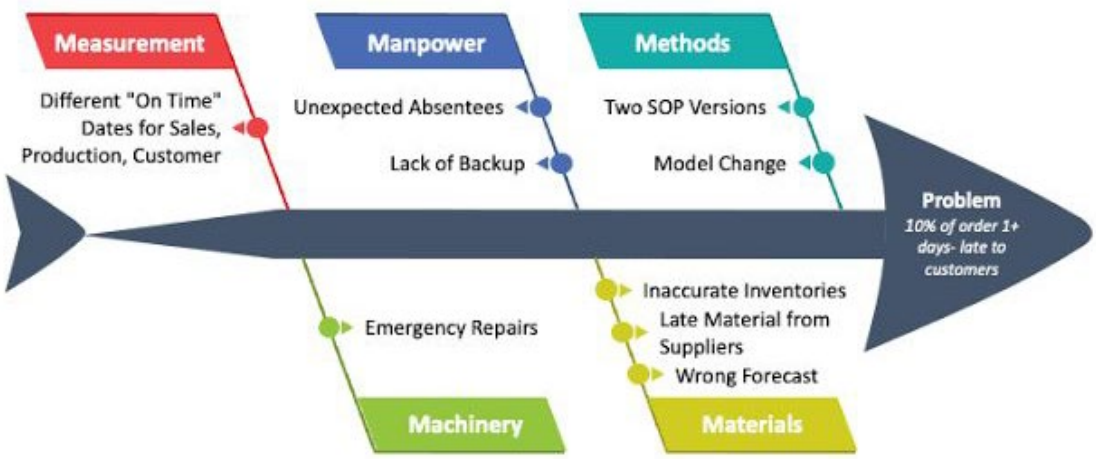



**Fig. 8 - The 5M method**

**Use case in the manufacturing industry**

A factory encounters a problem with a drop in product quality:

- **Problem or "Effect" (fish head):** Decline in product quality
- **Categories of causes (main branches):**
  - Manpower: Operator skills, training, motivation.
  - Methods: Work procedures, quality standards, operating instructions.
  - Materials: Raw material quality, batch variability, supplier specifications.
  - Environment: Working conditions, temperature, humidity, dust.
  - Equipment: Equipment wear, machine calibration, maintenance.

**3. The 7M**

This evolution of the Ishikawa diagram focuses on not five, but seven major problem areas: Manpower, Method, Materials, Environment, Equipment, Management, Measurement (Figure 9).

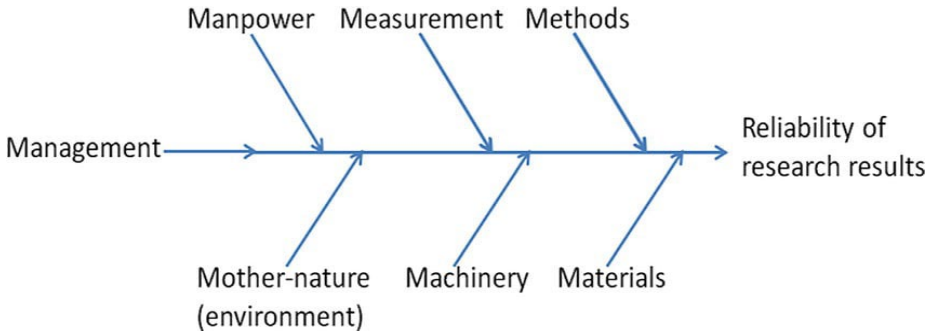



**Fig. 9 - Ishikawa "Fishbone" diagram (principle of 7 M's)**

**Use case in the manufacturing industry**

A factory is experiencing machine failure problems:

- **Manpower:** Inadequate operator training, human error due to fatigue, or lack of experience.
- **Methods:** Obsolete production processes, and lack of standardized operating and maintenance procedures.
- **Materials:** Inconsistent quality of raw materials, premature wear of spare parts.
- **Environment:** Unsuitable working conditions, disturbances due to excessive noise or vibration.
- **Equipment:** Outdated equipment, neglected or inadequate preventive maintenance.
- **Management:** Inadequate decision-making, and insufficient communication between departments.
- **Measurement:** Uncalibrated or faulty measuring instruments, lack of regular quality controls.

**4. The Pareto Principle**

The Pareto or 80/20 principle is very useful for focusing on the problems that will have the greatest impact once solved, and for making informed decisions (Figure 10).

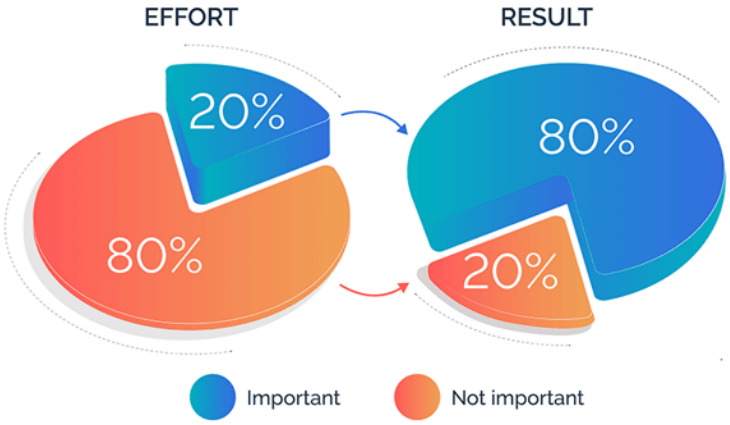



**Fig. 10 - Pareto Principle problem solving methods**

**Use case in the manufacturing industry**

In a factory producing electronic components, 80% of production defects stem from just 20% of the manufacturing processes. By analyzing production data, the company could discover that the majority of defects are linked to errors in the soldering and inspection stages *(Bergès, C., Bird, J., Shroff, M.D., Rongen, R., Smith, C., 2021).* These two stages, although representing a small part of the total manufacturing process, are crucial and require special attention to reduce the overall number of defects.

**5. The 5 Ws and 1H**

This tool helps gather comprehensive information on a problem by answering these key questions: Who, What, Where, When, Why, and How. Thus, it provides an in-depth understanding of the situation (Figure 11).




**Fig. 11 - 5W's &1H problem solving methods**

**Use case in the manufacturing industry**

There is a delay in production at a furniture manufacturing plant:

- **Who is affected by the problem?** Assembly line operators and production managers are directly affected by the delay.
- **What exactly is the problem?** Deliveries of finished furniture to customers are several days behind schedule.
- **Where exactly is the problem occurring?** The problem occurs in the final assembly shop, where the furniture is prepared for shipment.

- **When was the problem detected or when does it occur?** The delay has been observed over the past two weeks, mainly during the third shift.
- **Why does the problem occur?** The problem could be due to inadequate staff planning and recurring packaging equipment failures.
- **How does the problem occur?** The delay is due to a bottleneck in the finishing and packing stage, where there is a lack of personnel and problems with the packing equipment.

Somes other tools can also be useful for structuring problem-solving methods are: brainstorming, A3, Gemba Walks, SWOT analysis, histograms, control charts and prioritization matrices.

## RESULTS

The choice of the right problem-solving method depends on several factors:

- **The nature and complexity of the problem:** Before choosing a problem-solving approach, one need to understand exactly what is wrong. If it's a complex and multifactorial problem, structured, in-depth methods such as 8D or DMAIC may be appropriate. For more immediate or quality-related problems, QRQC or Four A's may be more appropriate.
- **Company objectives:** Look at the big picture; align the method with strategic objectives, such as improving quality, reducing costs, or increasing customer satisfaction. For example, DMAIC is often chosen for defect reduction and process optimization objectives.
- **Available resources:** Think about the resources that can be allocate to problem-solving processes (time, skills, budget). For example, PDCA can be implemented more quickly when resources are limited.
- **Team expertise and problem-solving skills:** Use a method that matches team's qualifications. Training may be required for more complex approaches such as DMAIC or 8D.
- **The need for standardization and documentation:** If documentation and standardization of processes are essential, used methods that integrate these aspects, such as 8D or DMAIC.

Effective problem solving requires wide range of skills and abilities, such as:

- **Critical thinking:** the ability to think logically, analyze information and look at situations from different perspectives.
- **Creativity:** being able to come up with innovative, out-of-the-box solutions.
- **Decision-making:** making informed choices by considering all the available information.
- **Communication:** being able to express ideas clearly and effectively.
- **Analytical skills:** breaking down complex problems into smaller parts and examining each one.
- **Time management:** allocating time and resources effectively to address problems.
- **Adaptability:** being open to change and willing to adjust strategies.
- **Conflict resolution:** skillfully managing conflicts and finding solutions that work for all.

The comparison of some problem-solving methodologies is presented in Table 2.

**Table 2**

**Comparison of different problem-solving methodologies**

| Methodology | Focused on | Key Strengths | Best Use Case | Industry Application |
|---|---|---|---|---|
| **PDCA Cycle** | Iterative Continuous Improvement | Cyclical Approach for Refining Solutions | Small Scale Process Improvement, Testing Changes | Quality |
| **DMAIC** | Data-driven Process Improvement | Strong Emphasis on Data Analysis and Reducing Variation | Quality Improvement, Defect Reduction | Manufacturing |
| **8D** | Team-based Problem-Solving &Prevention | Cross-functional Team Approach, Preventive Measures | Complex, Recurring Problems In Product Quality | Automotive, Aerospace, Manufacturing |
| **A3** | Lean Problem-solving& Continous Improvement | Concise, Visual Representation, Lean Thinking | Simplifying Problem-Solving, Continuous Improvement | Lean Manufacturing, Service Industries |

For effective implementation of problem-solving techniques is important to:

**- Integrate problem-solving into daily routines.**

- Instead of seeing problem-solving as a separate activity, integrate it into daily routines. For example, set up meetings to discuss ongoing problems as a group and monitor progress on solutions.

**- Use technology for your benefit**

- Adopt a Daily Management System (DMS) to quickly identify problems, track corrective actions, facilitate collaboration between teams, and document solutions in a centralized repository.

**- Develop specific key performance indicators for problem resolution**

- Define Lean KPIs that measure the effectiveness of the problem-solving process (average time to solve the problem, problem recurrence rate, and impact of solutions on business performance).

**- Practice problem-solving on the shop floor**

- To understand problems, you need to go where value is created. Encourage managers to go on the shop floor to directly observe processes, interact with operators, and identify possible improvements.

**- Create cross-functional problem-solving groups**

- Form teams with members from different departments to tackle complex problem-solving. Integrating different angles, perspectives, and expertise broadens the point of view on the subject, enriches the analysis, and generates more creative ideas.

**- Adopt a coaching approach to skills development**

- In addition to basic training, use mentoring and coaching to develop problem-solving skills. Experienced employees can guide less experienced ones, sharing their know-how.

**- Conduct post reviews**

- When a problem is solved, conduct a discussion to see what went well, what didn't, and how processes can be improved.
- Tracking and evaluating each solution implemented allows to adjust strategies as needed, learn from past experiences, and foster continuous improvement.

Tabel 3 summarizes the most important steps of four problem -solving methods.

**Tabel 3**

**Steps of different problem-solving methods**

| PDCA | DMAIC | 8D | A3 |
|---|---|---|---|
| **Plan** | Define | Create a team | Clarify the issue |
| | Measure | Define the problem | Break down the issue |
| | | Define interim containment actions | Set target |
| | Analyze | Identify root cause analysis | Analyze the root cause |
| | | Define permanent corrective actions | Develop Countermeasure |
| **Do** | Improve | Implement permanent corrective actions | See countermeasure |
| **Check** | Control | Prevent recurrence | Evaluate results and processes |
| **Act** | | Congratulate the team | Standardize |

## CONCLUSIONS

By scrutinizing every action and aspect of processes, it is crucial to distinguish between activities that bring value and those that don't.

Involving employees in identifying problems and suggesting solutions strengthens their sense of ownership, and improves team cohesion and efficiency.

Root Cause Analysis helps to identify the underlying causes of problems to find more sustainable solutions and prevent problems from recurring.

The use tools such as the PDCA cycle, 8D, DMAIC, ORQC, 4A's and the 5S, as well as techniques such as Six Sigma, is essential for optimizing processes and improving quality and efficiency.

It is essential to monitor implemented changes and continuously improve them to maintain and increase Overall Equipment Effectiveness.

For all of these presented methods, it is important to identify root causes and to solve problems in a sustainable way.

By employing structured problem-solving methods, managers can approach problems systematically and develop innovative solutions tailored to their specific needs. With these comprehensive problem-solving techniques at their disposal, managers are well-equipped to navigate the complexities and achieve strategic objectives.

**REFERENCES**


[1] Abdirad, M., Krishnan, K., Gupta, D. (2021). A two-stage metaheuristic algorithm for the dynamic vehicle routing problem in industry 4.0 approach, Journal of Management Analytics, 8 (1), pp. 69-83. Cognitive and noncognitive predictors of success. *Proceedings of the National Academy of Sciences*, *USA*, *116*(47), 23499–23504. https://doi.org/10.1073/pnas.1910510116

[2] Bergès, C., Bird, J., Shroff, M.D., Rongen, R., Smith, C. (2021). Data analytics and machine learning: root-cause problem-solving approach to prevent yield loss and quality issues in semiconductor industry for automotive applications, IEEE International Symposium on the Physical and Failure Analysis of Integrated Circuits (IPFA), pp. 1-10

[3] Davidson, J.E., Sternberg. R.J. (2003). *The Psychology of Problem Solving,* Cambridge University Press; doi:10.1017/CBO9780511615771

[4] Dell'Era, C., Candi, M., Magistretti, S., Verganti, R., Stigliani, I. (2026). Defining problems worth solving: Design thinking tractice in the problem space, data technologies, and radical innovation, Journal of business Research,

[5] Grünig, R., Kühn, R. (2025). Problem-Solving Procedures, IBN:978-3-662-71619-9

[6] Jerez, D., Mazzulla, E., Bulut, O. (2026). Using Sequence Analysis to Explore Slow Responses in Complex Problem-Solving,

[7] Kadijevich, D., M. (2026). Scaffolding Problem Solving: An AI Approach, ISBN:978-3-032-12173-8

[8] Kadir, Z., A., Abdullah, N., H., Abdullah, R., A., Ismail, F. (2026). Using Problem-Based Learning as an Instructional Approach in Enhancing Problem Solving Skills between Engineering and Business, ISBN:2227-524X

[9] McDonnell, E., Prasad, M. (2026). Problem-Solving Sociology of Development, Sociology of Development, 12(3), pp.235-248), ISBN: 2374-538X

[10] Mohaghegh, M., Größler, A. (2021). Exploring organizational problem-solving modes: a dynamic capabilities approach, Management Decision, 60 (1), pp. 254-277

[11] Rørvik-Olsen, O., Tagliabue, M., Sandaker, I. (2026). Solving for Engagement: A Systematic Review of Task Variation and Problem-Solving Demands in Motivating Employees, ISBN:2076-3387

[12] Nakata, C., & Hwang, J. (2020). Design thinking for innovation: Composition, consequence, and contingency, Journal of Business Research, 118, 117–128.

[13] Queiroz, J., Ata, P. (2026). *The Semiotic Morphology of Problem-Solving,* Late Perce (pp.226-245), Edition:1, Publisher: Routledge, New York, ISBN: 9781003567615

[14] Singh, A., Wiktorsson, M., Hauge, J.B. (2021). Trends in machine learning to solve problems In logistics, Procedia CIRP, 103, pp. 67-72

[15] Soksimovic, S., Ifenthaler, D., Marrone, R., De Laat, M., Siemens, G. (2023). Opportunities of artificial intelligence for supporting complex problem-solving: findings from a scoping review, Computers and Education: Artificial Intelligence, 4, p. 100138

[16] Swarup, R., Payal, G., M. (2026). Design Thinking: Methodology for Problem finding and Problem Solving, ISBN: 2583-2492

[17] Väätäinen, H., Vakkala, H. (2026). Sustainable Leadership Supporting Problem-solving and Succes, ISBN:978-3-032-16475-9

[18] Xu, Z., Dang, Y. (2020). Automated digital cause-and-effect diagrams to assist causal analysis in problem-solving: a data-driven approach, International Journal of Production Research, 58 (17), pp. 5359-5379
[19] *** https://mindskillz.in/problem-solving-techniques-essential-methods-for-workplace-excellence-and-innovation/
[20] *** https://www.canada.ca/en/services/jobs/training/initiatives/skills-success/tools/problem-solved-employees-learners.html
[21] *** https://www.thomas.co/resources/type/hr-blog/importance-problem-solving-skills-workplace
[22] *** https://www.sessionlab.com/blog/problem-solving-techniques/
[23] *** https://www.wevalgo.com/know-how/opex-assessment-tools/problem-solving
[24] *** https://nz.seek.com/career-advice/article/problem-solving-skills

# THREE-DIMENSIONAL MODELING AND ADDITIVE MANUFACTURING OF A CENTRIFUGAL SEPARATOR FOR AGRICULTURAL PNEUMATIC SEPARATION APPLICATIONS

/

# *MODELAREA TRIDIMENSIONALĂ ȘI FABRICAȚIA ADITIVĂ A UNUI SEPARATOR CENTRIFUGAL PENTRU APLICAȚII DE SEPARARE PNEUMATICĂ ÎN AGRICULTURĂ*

**Raluca-Adriana ZOTA[1)], Sorin-Ștefan BIRIȘ[1)], Neluș-Evelin GHEORGHIȚĂ*[1)], Gabriel-Alexandru CONSTANTIN[1)], Alina-Daiana IONESCU[1)], Elena-Valeria VLĂDUȚ[1)], Iulian DRENEA[1)], Mircea COSTIN[2)]**

[1)] Faculty of Biotechnical Systems Engineering, National University of Science and Technology POLITEHNICA Bucharest / Romania;

[2)] National Institute of Research - Development for Machines and Installations Designed for Agriculture and Food Industry - INMA Bucharest/ Romania;

**Tel: 0726 453 269; *E-mail: nelus.gheorghita@upb.ro*

***Keywords:*** *centrifugal separator, additive manufacturing, three-dimensional modeling, pneumatic separation*

**ABSTRACT**

*The geometrical design of the primary functional components has a significant impact on the aerodynamic behavior of centrifugal separators, which are crucial parts of pneumatic systems used for the handling and separation of granular agricultural goods. This study presents the three-dimensional modeling and additive manufacturing of a centrifugal separator intended for experimental investigations in agricultural pneumatic separation applications. The geometrical model was developed in SolidWorks based on the configuration and dimensions of the separator integrated into an SLN-3 laboratory system. The model includes the cylindrical body, conical section, tangential inlet duct, and central outlet duct, allowing the geometrical relationships between the main components to be analyzed and modified. Additive manufacturing technologies were subsequently considered for producing separator components, with particular attention to manufacturing parameters, dimensional accuracy, surface quality, and assembly requirements. The developed components demonstrated the applicability of additive manufacturing for producing complex geometries required in experimental separator configurations. The resulting three-dimensional model and manufactured components provide a flexible platform for subsequent experimental and numerical investigations of airflow and particle behavior and for evaluating future geometrical modifications of the centrifugal separator.*

**REZUMAT**

*Designul geometric al componentelor funcționale principale are un impact semnificativ asupra comportamentului aerodinamic al separatoarelor centrifugale, care sunt elemente esențiale ale sistemelor pneumatice utilizate pentru manipularea și separarea produselor agricole granulare. Studiul prezintă modelarea tridimensională și fabricația aditivă a unui separator centrifugal destinat cercetărilor experimentale privind separarea pneumatică a materialelor agricole. Modelul geometric a fost realizat în SolidWorks, pe baza configurației și dimensiunilor separatorului integrat într-o instalație de laborator SLN-3. Modelul include corpul cilindric, secțiunea conică, conducta de admisie tangențială și conducta centrală de evacuare, permițând analizarea și modificarea relațiilor geometrice dintre principalele componente. Ulterior, au fost analizate tehnologii de fabricație aditivă pentru realizarea componentelor separatorului, acordându-se o atenție deosebită parametrilor de fabricație, preciziei dimensionale, calității suprafețelor și cerințelor de asamblare. Componentele realizate au demonstrat aplicabilitatea fabricației aditive pentru obținerea geometriilor complexe necesare configurațiilor experimentale ale separatorului. Modelul tridimensional și componentele fabricate constituie o platformă flexibilă pentru cercetări experimentale și numerice ulterioare privind comportamentul aerului și al particulelor, precum și pentru evaluarea viitoarelor modificări geometrice ale separatorului centrifugal.*

## INTRODUCTION

A detailed interpretation of studies on the optimization of pneumatic conveyors in the context of agriculture and post-harvest operations is based on a series of papers that have explored both the

aerodynamic properties of agricultural particles and the use of advanced modeling and simulation technologies *(Dousthaghi et al., 2022).*

The safe storage of grain depends on its moisture content. Moist grain undergoes a drying process before being stored. When the drying plant's capacity does not meet the requirements for storing grain until it is dry, there is a risk of spontaneous combustion. In such situations, it is recommended to find solutions for partially cooling the grain. One such solution would be to cool the grain using pneumatic conveying *(Diab et al., 2023).*

The objective of this study is to determine the parameters of the "air-seed" two-phase flow for the numerical implementation of a mathematical model that describes the technological process in the distribution system of a pneumatic grain seeder.

The proposed method can be used to analyze and optimize the design and technological parameters of various pneumatic seeders. The flow regime of the "air-seed" flow is characterized by the Reynolds number and the volumetric concentration of particles. To determine these parameters, an aerodynamic calculation was performed to determine the air velocity required for the transport and uniform distribution of seeds in the seeder's pneumatic system *(Mudarisov et al., 2020).*

A numerical and experimental study investigated the flow of a gas-solid multiphase flow in a pneumatic conveyor, focusing on predicting the pressure drop in the pipe. The experiments analyzed the effects of particle size and density, as well as the ratio of the radius of curvature to the pressure drop.

The results showed that the pressure gradient increases with particle diameter and density, peaking at 150 μm, and gradually decreases as the curvature radius ratio increases. Furthermore, the pipe roughness and its constant significantly influence the pressure drop. In the case of systems used for agri-food materials, the cyclone's geometry must be adapted to allow for the efficient separation of light impurities and fine particles without carrying useful material into the exhaust air stream *(Suniya and Verma, 2023).*

For this reason, the dimensions and shape of the structural elements influence both the aerodynamic behavior of the flow and the stability of the system's operation *(Suniya et. al., 2023).* The geometry of the cyclone is one of the most important factors influencing the operation of pneumatic separation systems and the efficiency of the process of separating solid particles from the air stream. The cyclone's design determines how the flow regime develops inside the equipment, the distribution of air velocities, the intensity of the vortex, and the trajectory of the solid particles entrained in the separation process *(Sirbubalo et al., 2021).*

The cyclone's operating principle is based on the tangential introduction of an air stream laden with solid particles into the cylindrical body of the equipment. Due to its design geometry, a downward helical motion forms inside the cyclone, which generates centrifugal forces. Under the action of these forces, the heavier solid particles are thrown toward the outer walls of the cyclone and move toward its bottom, where they are collected. The air separated from the particles forms an upward vortex and is discharged through the central discharge pipe *(Afridi et al., 2024). Sun et al., (2024***)** investigated elliptical cyclone separators manufactured using stereolithography (SLA).

Their results showed that additive manufacturing enables the production and experimental evaluation of complex separator geometries, while geometrical modifications can significantly influence aerodynamic performance. *Sun et al., (2024)* also demonstrated the potential of 3D printing for the rapid development of modified cyclone configurations.

The study highlighted the usefulness of additive manufacturing as a prototyping method for investigating the relationship between separator geometry and separation performance. *Bhattacharya et al., (2025)* used stereolithographic 3D printing to manufacture cyclone separators at different dimensional scales. Their study demonstrated the flexibility of combining CAD design and additive manufacturing for producing customized separator geometries suitable for experimental investigations.

Therefore, the present study focuses on the three-dimensional modeling and additive manufacturing of a centrifugal separator intended for agricultural pneumatic separation applications. The research aims to develop a geometrically accurate CAD model of the separator and to evaluate the applicability of additive manufacturing for producing components suitable for subsequent experimental investigations.

## MATERIALS AND METHODS

The centrifugal separator investigated in this study is part of the SLN-3 laboratory pneumatic separation system used for processing granular agricultural materials (Fig.1). The separator consists of an upper cylindrical body connected to a lower conical section, a tangential inlet duct, and a central outlet duct.

The tangential inlet configuration promotes the development of a rotating airflow inside the separator, while the conical section directs the separated material toward the lower collection region.

The geometry of the existing separator was used as the reference for developing the three-dimensional model. The main dimensions and geometrical relationships between the cylindrical body, conical section, inlet duct, and outlet duct were considered in order to reproduce the functional configuration of the experimental equipment.

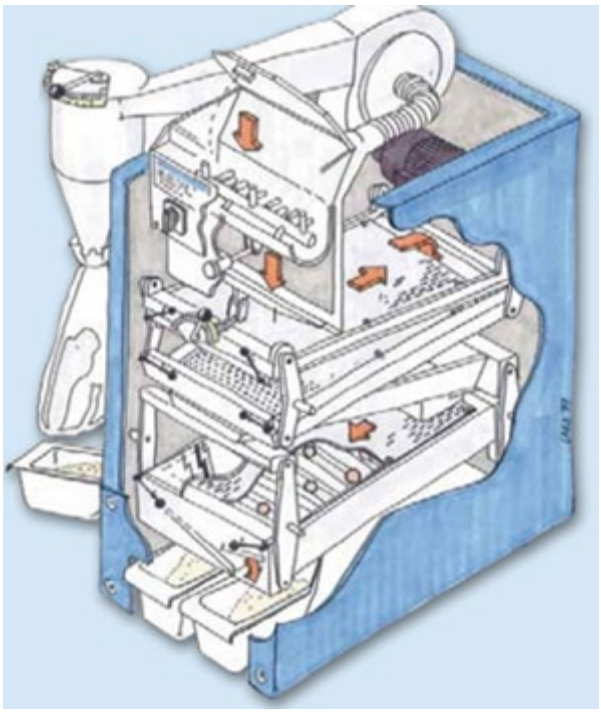


**Fig. 1 - Centrifugal separator SLN3**

The geometry of the frustum section was designed to allow a gradual reduction in the flow cross-section and an intensification of the centrifugal effect in the lower part of the cyclone. The dimensions used to construct the model were based on the design configuration of the actual plant and the need to ensure stable flow within the equipment.

The upper cylindrical structure of the cyclone, which stabilizes the main vortex and permits the formation of a helical flow pattern, was modeled once the truncated cone section was completed.

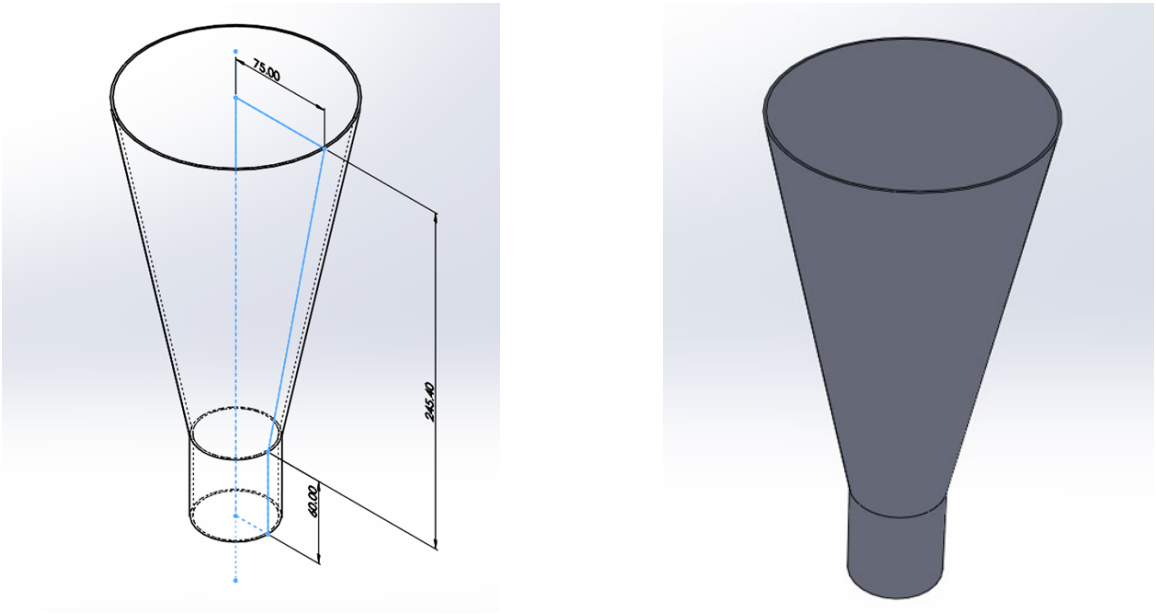



**Fig. 2 - Generating sketch and main dimensions of the cyclone's conical section**

Figure 3 shows a three-dimensional model of the cyclone's upper cylindrical body, along with the rectangular inlet duct. The duct is positioned tangentially to the cylindrical body to impart a rotational motion to the air flow. A circular opening for air exhaust is provided at the top of the body. This configuration promotes the formation of the vortex necessary for the separation of solid particles. The model will subsequently be integrated into the complete cyclone assembly.

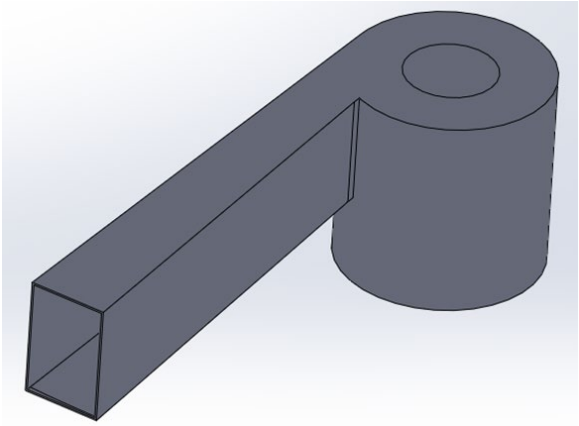


**Fig. 3 - 3D model of the cylindrical body and the tangential inlet pipe**

The central air exhaust duct, used to vent the upward vortex formed during the system's operation, was positioned inside the cylindrical body, as shown in Figure 4.

The inlet duct was modeled separately, using a rectangular cross-section positioned tangentially to the cylindrical body of the cyclone. This design configuration allows the air stream to enter in a rotational motion starting from the inlet area, promoting the development of the internal vortex and the generation of the centrifugal forces necessary for the separation process.

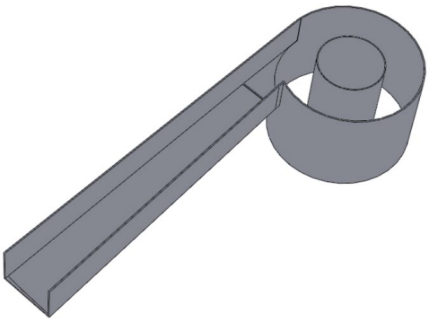


**Fig. 4 - The upper cylindrical section of the cyclone**

The three-dimensional model of the centrifugal separator was developed using SolidWorks, based on the geometry and dimensions of the existing experimental equipment. The main components were modeled separately, including the cylindrical body, conical section, tangential inlet duct, and central outlet duct, and were subsequently assembled to reproduce the complete separator configuration.

Particular attention was given to the geometrical connections between the inlet duct, cylindrical body, and conical section, as these elements define the internal flow path of the separator. The resulting CAD model allows the overall geometry to be visualized and provides a digital basis for subsequent geometrical modifications, additive manufacturing, and future numerical investigations.

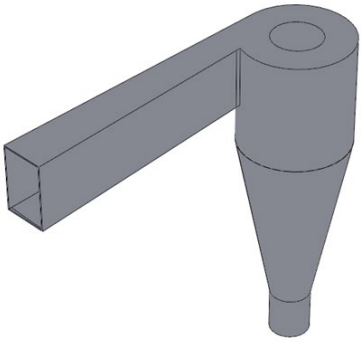


**Fig. 5 - Geometry of the SLN 3 machine's cone**

## RESULTS

The main technological parameters influencing the additive manufacturing of the separator components are summarized in Fig. 6. Layer thickness, build orientation, printing speed, extrusion temperature, and infill density can affect surface quality, dimensional accuracy, mechanical properties, material consumption, and manufacturing time. Therefore, appropriate selection of these parameters is important for obtaining components suitable for the assembly and experimental development of the centrifugal separator.

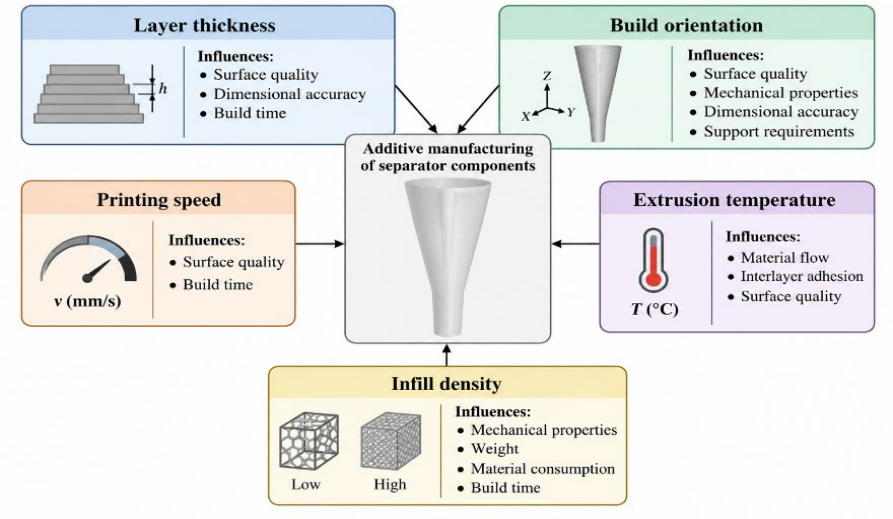
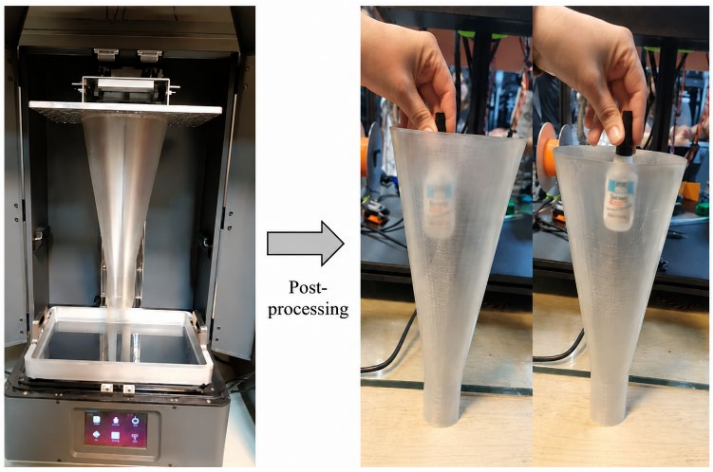



**Fig. 6 - Main additive manufacturing parameters influencing the characteristics of the manufactured separator components**

The conical component of the centrifugal separator was successfully produced using additive manufacturing, as illustrated in Fig. 7.




a) b)

**Fig. 7 - Additive manufacturing of the conical component of the centrifugal separator:**
*(a) during additive manufacturing; (b) after post-processing*

After completion of the manufacturing process, the component was removed from the printing system and subjected to post-processing operations in order to prepare the surface and the component for subsequent assembly. The resulting part reproduced the conical geometry defined in the three-dimensional CAD model and demonstrated the practical feasibility of manufacturing this separator component using additive technologies.

The use of additive manufacturing facilitates the production of customized separator components and allows geometrical modifications to be implemented directly at the CAD-model level. This approach is particularly useful for experimental research, where different separator configurations can be developed and subsequently evaluated without requiring conventional manufacturing tooling

## CONCLUSIONS

The study demonstrated the applicability of three-dimensional modeling and additive manufacturing for the development of a centrifugal separator intended for agricultural pneumatic separation applications.

The CAD model reproduced the main functional components and provided a flexible basis for geometrical modifications. The successful manufacturing and post-processing of the conical component confirmed the feasibility of producing customized separator components using additive technologies.

The developed model can support future experimental and numerical investigations focused on airflow, particle behavior, and separation performance.

## ACKNOWLEDGEMENT

This research was supported by the project CNFIS-FDI-2026-F-0049 “Asigurarea eficienței operaționale a bazei de aplicații practice pentru sisteme biotehnice în livezi, vii, solarii și grădini (EFIBIOTECH)”, from the Ministry of Education and Research through the Executive Agency for Financing Higher Education, Research, Development and Innovation.

## REFERENCES

[1] Afridi, A., Al Rashid, A., Koç, M., (2024), Recent advances in the development of stereolithography-based additive manufacturing processes: A review of applications and challenges, *Bioprinting*, Vol. 43, e00360.

[2] Bhattacharya, P., Rastogi, D., Mehraji, S., et al., (2025), 3D printed microcyclones for enhanced collection, separation, and recovery of sub-micrometer bioaerosols, *Sensors and Actuators B: Chemical*, Vol. 444, No. 1, 138349.

[3] Diab, R.R., Enzi, A., Hassoon, O.H., (2023), Effect of printing parameters and post-curing on mechanical properties of photopolymer parts fabricated via 3D stereolithography printing, *IIUM Engineering Journal*, Vol. 24, No. 2, pp. 225–238.

[4] Dousthaghi, M.H., Minaei, S., Khoshtaghaza, M.H., (2022), Computational fluid dynamics and analytical modeling for predicting effects of airflow temperature and relative humidity on the terminal velocity of agricultural granular materials, *Journal of Food Process Engineering*, Vol. 45, No. 2, e13941.

[5] Mudarisov, S., Badretdinov, I., Rakhimov, Z., Lukmanov, R., Nurullin, E., (2020), Numerical simulation of two-phase “air-seed” flow in the distribution system of the grain seeder, *Computers and Electronics in Agriculture*, Vol. 168, 105151.

[6] Popescu, D., Zapciu, A., Amza, C., Baciu, F., Marinescu, R., (2018), FDM process parameters influence over the mechanical properties of polymer specimens: A review, *Polymer Testing*, Vol. 69, pp. 157–166. DOI: 10.1016/j.polymertesting.2018.05.020.

[7] Sirbubalo, M., Tucak, A., Muhamedagić, K., Rahić, O., Čekić, A., Vranić, E., (2021), Photopolymerization-based technologies for microneedle arrays production, *International Conference on Medical and Biological Engineering*, Springer International Publishing, Cham, pp. 670–678.

[8] Sun, Z., Yang, H., Zhang, K., Wang, Z., Yang, G., (2024), Experimental and numerical investigation of the elliptical cyclone separator manufactured by 3D printing, *Powder Technology*, Vol. 441, 119746.

[9] Sun, Z., Yang, H., Zhang, K., Yan, Z., et al., (2024), 3D-printed elliptical cyclone separator with additional self-excited force field for enhancing the gas-solid separation, *Advanced Powder Technology*, Vol. 35, No. 7, 104496.

[10] Suniya, N.K., Verma, A.K., (2023), A review on optimization of process parameters of fused deposition modeling, *Research on Engineering Structures and Materials*, Vol. 9, No. 2, pp. 631–659.

# CURRENT STATE OF THE ART IN EQUIPMENT FOR ANHYDROUS AMMONIA APPLICATION IN FIELD CROPS

/

# *STADIUL ACTUAL ÎN DOMENIUL ECHIPAMENTELOR PENTRU APLICAREA AMONIACULUI ANHIDRU ÎN CULTURI DE CÂMP*

**Dragoș MANEA*[1)], Mihai GÎDEA[2)], Dragoș-Nicolae DUMITRU[1)], Alin HARABAGIU[1)], Larisa-Bianca IONICĂ[1)], Aura DUMITRESCU[1)]**

[1)] National Institute of Research–Development for Machines and Installations Designed to Agriculture and Food Industry - INMA Bucharest / Romania;

[2)] University of Agronomic Sciences and Veterinary Medicine of Bucharest / Romania.

**Tel: 0724 350 567; *E-mail: manea_dragos_05@yahoo.com*

***Keywords:*** *anhydrous ammonia; precision fertilization; depth control; furrow sealing; rate control.*

**ABSTRACT**

*The study reviewed the current technical state of equipment used for subsurface application of anhydrous ammonia in field crops, with emphasis on metering and distribution, soil-engaging tools, depth regulation, furrow closure, electronic monitoring and safety. Peer-reviewed studies and current technical documentation for representative commercial systems were comparatively analysed. The review showed that modern applicators have progressed from mechanically adjusted knife systems toward high-capacity platforms integrating hydraulic downforce, in-cab depth adjustment, ISOBUS rate control, section control and row-level blockage monitoring. However, depth regulation and furrow sealing are still predominantly set or controlled as separate functions, while direct sensing of the actual incorporation quality and closed-loop correction of the sealing process remain limited. Recent research on automatic tillage-depth control, soil-covering devices and sensor-based furrow-closing control indicates that the next development stage will be represented by integrated feedback systems combining soil-condition sensing, effective depth estimation, ammonia-loss detection and adaptive control of closing organs. These directions are particularly relevant for reducing volatilization losses and improving nitrogen-use efficiency under variable field conditions.*

**REZUMAT**

*Studiul a analizat stadiul tehnic actual al echipamentelor utilizate pentru aplicarea amoniacului anhidru în culturile de câmp, cu accent pe dozare și distribuție, organe de lucru, reglarea adâncimii, închiderea brazdei, monitorizarea electronică și siguranță. Au fost analizate comparativ lucrări științifice și documentații tehnice actuale pentru sisteme comerciale reprezentative. Analiza a arătat că aplicatoarele moderne au evoluat de la sisteme mecanice cu cuțite către platforme de mare capacitate care integrează presiune hidraulică pe organele de lucru, reglarea adâncimii din cabină, control ISOBUS al dozei, control pe secțiuni și monitorizarea blocajelor la nivel de rând. Totuși, reglarea adâncimii și etanșarea brazdei sunt încă tratate predominant ca funcții separate, iar măsurarea directă a calității încorporării și corecția în buclă închisă a procesului de etanșare sunt limitate. Cercetările recente privind controlul automat al adâncimii, organele de acoperire și controlul etanșării bazat pe senzori indică trecerea către sisteme integrate de feedback, relevante pentru reducerea pierderilor prin volatilizare și creșterea eficienței utilizării azotului.*

## INTRODUCTION

Anhydrous ammonia is one of the most concentrated nitrogen fertilizers used in field-crop production, containing approximately 82% nitrogen by mass. Its high nutrient concentration can reduce the transported fertilizer mass per unit of nitrogen and can support competitive fertilization costs. At the same time, the product is stored and handled under pressure and rapidly changes phase when released, which makes field application technically more demanding than the use of granular or non-pressurized liquid fertilizers.

Effective application therefore depends not only on the metered nitrogen rate, but also on the capacity of the machine to inject the product below the soil surface, maintain an adequate working depth, distribute the flow uniformly among rows and close the injection slot before gaseous ammonia can migrate toward the atmosphere *(Sawyer, 2019; Roth and Wuestenberg, 2024).*

The soil–tool interaction is a central element of the process. After release, ammonia reacts with soil water and is converted to ammonium, which can be retained on soil exchange sites. In dry, coarse-textured or cloddy soils, however, the injected gas may travel farther from the injection point and may escape through open pores or poorly closed knife tracks. Experimental work with anhydrous ammonia showed that injector configuration, soil texture and placement depth strongly influence immediate application losses; deeper knife placement generally produced lower losses than shallow single-disc placement under difficult soil conditions *(Hanna et al., 2005).* More recent agronomic guidance continues to identify proper injection depth and efficient closure of the injection slit as two essential conditions for limiting volatilization in dry soils *(Roth and Wuestenberg, 2024).* The environmental context increases the importance of improving application quality. Agriculture remains the dominant source of ammonia emissions in the European Union, accounting for about 93% of total reported ammonia emissions, although this figure includes the broader agricultural sector and is not specific to anhydrous-ammonia fertilization *(European Environment Agency, 2024).* For equipment designers, the implication is that mechanical placement, sealing and rate-control functions should increasingly be evaluated not only by field capacity and application rate, but also by their ability to maintain nitrogen in the intended soil zone under variable operating conditions. Commercial equipment has developed rapidly, particularly in North America. Current machines combine high-strength toolbars, shank or single-disc injection units, hydraulic downforce, row-unit depth-control systems, rate controllers, section shut-off, electronic mapping and blockage monitoring. Nevertheless, the commercial state of the art still shows an important distinction between controlling the quantity of ammonia delivered to a row and verifying the quality of ammonia incorporation into the soil. The first function is increasingly digital and well monitored; the second remains strongly dependent on passive mechanical settings, soil conditions and operator judgement.

The objective of this review was to characterize the current state of equipment for anhydrous ammonia application in field crops and to identify the main technological gaps that limit progression toward fully adaptive application. The analysis focused on six functional areas: product conditioning and metering, row-to-row distribution, injection tools, depth control, furrow closing and sealing, and sensor-based monitoring and control.

## TECHNOLOGICAL REQUIREMENTS FOR ANHYDROUS AMMONIA APPLICATION

A modern anhydrous-ammonia applicator can be interpreted as a chain of coupled functional subsystems rather than as a simple toolbar carrying injection knives. The process begins at the nurse tank and safety coupling, continues through product conditioning and flow control, then through distribution manifolds and equal-length or otherwise balanced delivery lines, and ends at the soil-engaging injection and closing elements. Variability introduced in any stage can affect the final nitrogen placement. Because the fertilizer is stored as a pressurized liquid, pressure drop and flashing during flow control are important design considerations; consequently, commercial machines frequently incorporate dedicated coolers, fast valves and rate-control hardware to stabilize the metered flow *(Unverferth Manufacturing Co., 2021; SurePoint Ag Systems, 2024a).* Uniform row-to-row distribution is a second requirement. Conventional manifolds can generate differences between outlets when plumbing geometry, restrictions or partial blockage vary. Current monitoring platforms therefore complement rate control with individual-row diagnostics. SurePoint Sentinel, for example, uses temperature sensing at manifold outlets to identify full or partial blockages and row-to-row flow deviations, while communicating through an ISOBUS interface *(SurePoint Ag Systems, 2024b).* Such systems significantly improve the ability to verify whether ammonia reaches each row, but they do not directly establish whether the fertilizer is retained at the required depth after leaving the knife.

Injection tools must open a pathway with sufficient penetration while limiting soil disturbance and power demand. Shank-type knives provide reliable deep placement and are still widely used on dedicated applicators. Disc or low-disturbance units reduce surface disturbance and can support higher operating speeds, but the relationship among disc geometry, soil texture, depth and sealing quality becomes more critical. Hanna et al. (2005) demonstrated that shallow single-disc injection could produce substantially higher losses in a fine sandy loam than deeper knife injection, highlighting the need to adapt the injection system to soil conditions rather than evaluate it only by field capacity.

Depth stability is therefore a process variable rather than a geometric setting. Soil resistance, residue, terrain undulation, implement pitch and forward speed can modify the effective position of the outlet even when the nominal setting remains unchanged. Research on seeders and tillage equipment has demonstrated that sensor-actuator control can reduce depth variation. Zhao et al. (2018) developed an automatic depth-control system for a no-till seeder, while Tao et al. (2025) applied active-disturbance-

rejection control to real-time tillage-depth regulation. Although these studies were not performed on anhydrous-ammonia applicators, their control architectures are directly relevant to the next generation of injection equipment. The last soil-contact operation is closure and sealing. This function is especially important for ammonia because an apparently closed surface does not necessarily guarantee that subsurface pores and the knife channel have been sufficiently collapsed. Closing discs, wing sealers and press wheels are common mechanical solutions. Experimental and extension evidence indicates that aggressive closure may be required in dry or cloddy soils, while excessive action in wet cohesive soil can increase smearing or adhesion. Research on soil-covering devices for planters has confirmed that closing performance is strongly dependent on soil condition and tool geometry *(Lu et al., 2024).*

## CURRENT COMMERCIAL EQUIPMENT

John Deere DA15, DA16 and DA23 applicators represent the current high-speed disc approach. The DA15 uses a single-disc opener, 15 rows at 0.76 m spacing and a working width of approximately 11.4 m. The manufacturer specifies application speeds up to 16.1 km $h^{-1}$, active hydraulic downforce and TruSet technology for in-cab depth adjustment. Prescription transfer and data integration through John Deere Operations Center extend the machine from a mechanical applicator to a digitally managed nutrient-placement platform *(John Deere, 2026).* The main technological emphasis is precise placement, high productivity and operator-adjustable depth rather than direct measurement of the quality of the closed injection track. Case IH Nutri-Placer machines use shank or high-speed low-disturbance coulter configurations, with the Nutri-Placer 940 covering working widths from about 15.2 to 19.8 m. Single-point and hydraulic depth-control functions are combined with row-unit and sealer options, flexible frames and precision-farming tools for mapping and data management *(Case IH, 2026).*

This architecture is representative of a mature commercial design philosophy in which depth, rate and field position are controlled or documented, while sealing quality is mainly ensured by the mechanical configuration selected for the prevailing conditions.

Representative high-capacity commercial applicators are shown in Fig. 1.



**(a) John Deere DA15 Disk Applicator**



**(b) Case IH Nutri-Placer 940**

**Fig. 1 - Representative high-capacity anhydrous-ammonia applicators**

*Source: official manufacturer webpages: John Deere; Case IH*

The Unverferth Renegade 1500, 2500 and 3500 series integrates dedicated NH3 distribution hardware with soil-engaging row units. Depending on model, configurations range from relatively compact toolbars to high-row-count machines. The system uses a lead coulter, edge-bent ammonia shank and CoverMax closing coulters. The 2021 technical literature specifies a Raven ISOBUS rate controller, a stainless-steel Vortex cooler, section control and optional high-volume plumbing. The two notched CoverMax blades are angle adjustable and designed to fill and close the injection slot, while optional down-pressure springs increase closing action *(Unverferth Manufacturing Co., 2021).* Among the systems reviewed, this is one of the clearest examples of integrated metering, injection and dedicated mechanical sealing, although the sealer adjustment remains predominantly preset rather than sensor-driven. Salford Independent Series machines can be converted from vertical tillage to anhydrous-ammonia application using SwitchBlade shanks. Current product literature describes hydraulically reset shanks with several manual depth settings and notes that trailing coulters and the finishing system help seal the gas pocket after application *(Salford Group, 2026).* The concept is attractive where a single platform is expected to perform both soil management and nutrient application, but the multifunctional architecture also means that ammonia placement is one operating mode within a broader tillage system. Dedicated and multifunctional injection architectures are illustrated in Fig. 2.



(a) Unverferth Renegade NH3 Applicator (b) Salford I-4200 with SwitchBlade NH3 shanks

**Fig. 2 - Mechanical injection and furrow-closing solutions used for NH3 application**

*Source: official manufacturer webpages: Unverferth; Salford*

KUHN Krause Gladiator is primarily a strip-tillage platform rather than a dedicated gas applicator. Nevertheless, it is relevant to the state of nutrient-placement equipment because its ST-PRO II row units provide controlled tillage depth, independent nutrient-placement depth through the Drop Zone system and adjustable closing blades, while selected configurations can tow an NH3 nurse cart.

The system illustrates the increasing decoupling of soil-working depth from fertilizer-placement depth and the integration of nutrient placement with seedbed formation *(KUHN, 2026)*.

**Table 1**

**Comparative characteristics of representative current systems**

| System | Configuration | Depth / penetration control | $NH_3$ metering and distribution | Closure / sealing | Digital functions and main limitation |
|---|---|---|---|---|---|
| John Deere DA15/DA16/DA23 | High-speed single-disc nutrient applicators; 15–23 rows | Gauge-wheel depth control, hydraulic downforce, TruSet in-cab adjustment | Gas/liquid application; prescription-based application depending configuration | Mechanical closing arrangement integrated with row unit | Operations Center integration; high digital integration, but incorporation quality is not directly sensed |
| Case IH Nutri-Placer 940 | Shank or HSLD coulter; 15.2–19.8 m | Single-point and hydraulic depth control; flex frame | $NH_3$ / liquid configurations with precision-farming support | Multiple shank/coulter and sealer options | Mapping and precision-data functions; sealing remains mainly mechanically configured |
| Unverferth Renegade 1500/2500/3500 | Dedicated $NH_3$ applicator; lead coulter + shank | Constant-level frame; spring or optional high-force shank mount | Raven ISOBUS rate control, Vortex cooler, section control | CoverMax angle-adjustable closing coulters; optional down pressure | Strong integration of rate control and sealing hardware; no direct closed-loop sealing-quality sensor |
| Salford Independent + SwitchBlade | Multifunctional tillage/$NH_3$ platform | Hydraulic reset; three manual depth settings | $NH_3$ shank application integrated with tillage platform | Trailing coulters and finishing system seal gas pocket | High mechanical versatility; limited automatic depth/sealing feedback |
| KUHN Gladiator 1210 | Strip-till platform; 8–16 rows | ST-PRO II depth 0.15–0.30 m; depth set mechanically | Independent nutrient placement; selected models tow $NH_3$ cart | Adjustable closing blades and soil conditioner | Precise nutrient-placement concept; not a dedicated $NH_3$ sensing/control architecture |
| SurePoint Sentinel $NH_3$ | Electronic subsystem retrofit to applicators | Not applicable to mechanical depth | Rate control and temperature-based row monitoring | No mechanical sealing actuator | ISOBUS, full/partial blockage detection; verifies flow but not final incorporation quality |

## ELECTRONIC MONITORING, DEPTH CONTROL AND FURROW SEALING

The most developed electronic function on current ammonia applicators is rate control. ISOBUS controllers can maintain commanded application rate as travel speed changes, operate section shut-off and document as-applied data. In addition, row-level blockage monitoring has become practical without installing a conventional flow meter in each corrosive ammonia line. Sentinel NH3 uses temperature differences at outlets as an indirect indicator of ammonia flow and alerts the operator to partial or full restrictions.

This approach addresses an important operational failure mode and provides information that conventional whole-machine rate control cannot detect *(SurePoint Ag Systems, 2024b).* Examples of integrated nutrient-placement and electronic monitoring technology are presented in Fig. 3.



**(a) KUHN Gladiator 1210**




**(b) SurePoint Sentinel NH3 monitoring/control**

**Fig. 3 - Examples of nutrient-placement and electronic NH3 monitoring technologies**

*Source: official manufacturer webpages, accessed 18 September 2026: KUHN; SurePoint Ag Systems*

Depth control is less uniform across commercial platforms. Mechanical stops, gauge wheels and single-point adjustments remain common, while high-end machines add active hydraulic downforce and in-cab setting changes. The distinction between downforce control and true depth feedback is important. A hydraulic system may maintain penetration force under changing conditions, yet the actual depth can still vary if soil bearing capacity, residue or implement dynamics change. Research prototypes in seeders and tillage machines show the advantage of measuring deformation, position or other variables that correlate with effective depth and of driving an actuator in a feedback loop *(Zhao et al., 2018; Tao et al., 2025).* A comparable architecture on an NH3 applicator would require robust sensors, filtering of shock and vibration, a target-depth model and a hydraulic or electromechanical actuator with sufficient response speed.

Furrow closing is currently the least instrumented critical function. Most commercial machines rely on adjustable disc angle, spring load or selected closing-wheel geometry. The operator therefore chooses a setting before work or periodically changes it after visually inspecting the field. The weakness of this approach is the spatial variability of soil moisture, texture, compaction and residue. Lu et al. (2024) showed in a planter application that soil-covering devices can perform very differently in cohesive soil, and that geometry intended to improve soil movement and reduce adhesion can substantially affect closing quality.

The same principle is relevant to ammonia application because incomplete subsurface closure can leave preferential pathways for gas escape.

A significant development outside the ammonia-specific equipment sector is Deere & Company patent US 12,648,507, granted in 2026. The patent describes closed-loop control of a furrow-closing system using inputs such as soil moisture, soil type and optical assessment of closing performance, with actuators adjusting downforce or closing-system configuration *(Rotole and Hubner, 2026).*

Although the invention is described for planting equipment, it demonstrates that closed-loop soil-closing control is technically feasible with commercially realistic sensing and actuation concepts. Transferring this principle to NH3 application would require performance indicators specific to gas retention, rather than only seed-furrow geometry.

Direct detection of incorporation quality could combine several sensor classes. Position or angle sensors can estimate tool depth; load or pressure sensors can quantify soil-engagement demand; soil-moisture sensors can characterize the retention environment; optical sensors can evaluate surface slot closure; and ammonia sensors placed behind the row unit could detect local escape. No single signal is likely to be sufficient under all field conditions.

The research challenge is therefore sensor fusion: determining whether a deviation is caused by actual inadequate depth or sealing, temporary vibration, an obstacle, a blocked delivery line or a soil condition in which the current setting is no longer appropriate.

## COMPARATIVE ASSESSMENT AND RESEARCH GAPS

The comparison indicates that contemporary equipment has reached a high level of maturity in structural design, field capacity and commanded-rate accuracy. Dedicated applicators can follow terrain, manage high product flow, maintain substantial opener downforce and provide operator-friendly adjustment. Digital platforms can document where fertilizer was applied, vary rate according to prescriptions and identify row blockages. These capabilities significantly reduce traditional errors associated with uneven distribution and manual setting.

The main unresolved issue is that the controlled variables are still predominantly machine variables rather than outcome variables. Rate control regulates the amount entering the delivery system; hydraulic downforce regulates an actuator or force-related variable; depth-control systems often regulate a set point at a gauge wheel or implement frame; and closing devices apply a preset geometry or force. The agronomic outcome, however, is whether ammonia is retained in the intended soil zone with minimum immediate loss. The gap between machine setting and actual incorporation quality becomes largest when soil conditions change rapidly within the field. A second gap concerns the coupling between injection depth and sealing intensity. Deeper placement generally increases the soil volume available to retain ammonia and can reduce immediate loss, but deeper operation also increases draft and may reduce work rate. In some soils, increasing depth alone is not the most efficient correction if the injection slot remains open. Conversely, aggressive closing cannot fully compensate for excessively shallow injection. An adaptive system should therefore treat depth and sealing as coordinated variables. The target can be formulated as a constrained control problem in which sufficient retention is achieved while limiting draft, disturbance and mechanical loading. A third gap is the limited availability of independent performance data for current commercial machines. Manufacturer documentation provides detailed mechanical and electronic specifications, but comparative field measurements of actual injection depth, row-to-row uniformity, instantaneous NH3 losses and sealing quality under the same soil conditions are scarce. This restricts objective benchmarking and makes it difficult to quantify the benefit of individual features. Standardized test protocols would be valuable for both research and product development.

The European context creates an additional research opportunity. The dedicated commercial applicators examined in this review are predominantly developed for North American field systems, where row spacings, working widths, tractor power and nurse-tank logistics differ from many European farms. A more compact platform with modular row units, compatibility with European tractor and road-transport constraints, and integrated safety and sensing could lower the threshold for adoption where anhydrous-ammonia fertilization is technically and legally applicable.

Finally, safety must remain a primary design constraint. NH3 is a serious inhalation and contact hazard, and electronic sophistication does not reduce the need for certified components, emergency shut-off, protected plumbing, operator training and appropriate personal protective equipment. Current manuals emphasze complete depressurization before service, use of protective equipment and provision of emergency water *(SurePoint Ag Systems, 2024b)*.

Future autonomous or semi-autonomous functions should therefore include fault detection and fail-safe shutdown logic as part of the control architecture rather than as an add-on.

**Table 2**

**Functional maturity and priority directions for next-generation $NH_3$ applicators**

| Functional area | Current state | Main limitation | Priority research direction |
|---|---|---|---|
| Metering / rate control | ISOBUS control, fast valves, coolers, section control, prescription maps | Whole-machine accuracy does not guarantee row-level or soil-placement quality | Integrated rate, pressure, temperature and row-state diagnostics |
| Row distribution | Improved manifolds; temperature-based blockage monitoring | Indirect flow indication; sensitivity to plumbing configuration and partial restrictions | Row-level sensor fusion and automatic fault isolation |
| Injection depth | Mechanical/gauge-wheel setting; hydraulic downforce; in-cab adjustment on high-end systems | Actual depth may vary with soil resistance, residue and terrain | Direct or model-based effective-depth sensing with closed-loop actuation |
| Furrow closure | Closing discs, wing sealers, press wheels, adjustable angle or spring force | Preset action does not adapt continuously to changing soil condition | Optical / geometric / $NH_3$-loss feedback and adaptive closing-force or angle control |

| Functional area | Current state | Main limitation | Priority research direction |
|---|---|---|---|
| System coordination | Functions are typically controlled separately | Depth, rate and sealing corrections can interact or conflict | Supervisory controller coordinating depth, rate and sealing according to incorporation-quality target |
| Safety | Certified plumbing, shut-off, PPE, operator procedures | Human-dependent inspection and emergency response | Leak detection, automated safe-state logic, diagnostic logging and predictive maintenance |

## FUTURE DEVELOPMENT DIRECTIONS

The technological trajectory suggested by the reviewed systems is a transition from operator-defined settings to closed-loop management of incorporation quality. The first practical step is likely to be automatic depth stabilization because hydraulic actuation and depth-related sensors are already available in agricultural machinery. A target depth could be selected from agronomic recommendations and corrected continuously using position, load and soil-condition information. The control system should distinguish between persistent depth error and high-frequency motion caused by vibration or stones, which makes signal filtering and robust controller design essential.

The second step is adaptive furrow sealing. Instead of a fixed disc angle or spring force, the closing module could use a controlled actuator. Optical assessment of the closed slot, soil moisture and a local NH3 concentration signal could be combined into a sealing-performance index. When the index falls below an acceptable range, the controller could increase closing force, change disc angle or engage an auxiliary closing element. In cohesive wet soil, the same system could reduce aggressiveness to avoid excessive soil adhesion and compaction.

The third step is coordinated control. Depth, application rate and sealing should not be optimized independently because they affect the same physical retention process. A supervisory algorithm could use a database generated from controlled and field experiments to determine acceptable combinations of depth, rate, soil condition, travel speed and closing intensity. Machine-learning methods may be useful for prediction after sufficient validated data are available, but they should complement rather than replace physical understanding and experimental verification.

For research evaluation, future prototypes should be tested using measurable indicators such as mean and standard deviation of effective injection depth, row-to-row application uniformity, percentage of open or incompletely closed injection track, peak and cumulative NH3 concentration behind the applicator, draft force, energy demand and field capacity. Linking these engineering indicators with nitrogen recovery, crop response and environmental measurements would provide a stronger basis for defining the performance of precision ammonia application.

## CONCLUSIONS

Current anhydrous-ammonia application equipment has evolved into high-capacity mechatronic machinery with precise rate control, hydraulic penetration management, digital prescription functions and increasingly detailed row-level diagnostics. Dedicated systems from major manufacturers demonstrate that the mechanical and electronic technologies required for accurate delivery are mature.

The review also identified a clear technological gap between controlling machine settings and verifying the final incorporation result. Effective injection depth and furrow sealing remain the two most important soil–machine variables that are not yet commonly integrated into a single closed-loop control architecture. The next generation of applicators should therefore combine robust depth sensing, adaptive closing mechanisms, soil-condition sensing and ammonia-loss monitoring, while preserving strict safety and fail-safe requirements. Such an integrated approach would allow equipment to respond to spatially variable field conditions and could improve both fertilizer-use efficiency and environmental performance. Standardized field-testing methods are also needed to compare commercial and experimental systems on the basis of actual incorporation quality rather than nominal settings alone.

## ACKNOWLEDGEMENT

This research was supported by project ***Establishment and operationalization of a Competence Center for Soil Health and Food Safety*** – CeSoH, Contract no. 760005/2022, specific project no.3, with the title: *Fertile and healthy soil through conservation and biological practices,* Code 2, financed through PNRR-

III-C9-2022 – I5 (PNRR-National Recovery and Resilience Plan, C9 *Support for the private sector, research, development and innovation*, I5 Establishment and operationalization of Competence Centers).

**REFERENCES**

[1] Case IH. (2026). Nutri-Placer 940 fertilizer applicator. CNH Industrial. https://www.caseih.com/en-us/unitedstates/products/application-equipment/fertilizer-applicators/nutri-placer-940

[2] Deere & Company. (2026). DA15 Disk Applicator. John Deere. https://www.deere.ca/en/tillage/da15-disk-applicator/

[3] European Environment Agency. (2024). Air pollution in Europe: 2024 reporting status under the National Emission reduction Commitments Directive. EEA Briefing No. 07/2024. https://www.eea.europa.eu/en/analysis/publications/national-emission-reduction-commitments-directive-2024

[4] Hanna, H. M., Boyd, P. M., Baker, J. L., & Colvin, T. S. (2005). Anhydrous ammonia application losses using single-disc and knife fertilizer injectors. Applied Engineering in Agriculture, 21(4), 573–578. https://doi.org/10.13031/2013.18564

[5] KUHN. (2026). GLADIATOR 1210 strip-tillage system. https://www.kuhn.com/en/crop/tillage-implements/strip-till/trailed-strip-till/gladiator-1210

[6] Lu, Q., Zhao, J., Liu, L., Liu, Z., & Wang, C. (2024). Design and experiment of a soil-covering and -pressing device for planters. Agriculture, 14(7), 1040. https://doi.org/10.3390/agriculture14071040

[7] Naeem, E., Abd El-Megeed, T., Emadeldin, Y., Abushady, A. M., & Abdelrahman, M. (2022). Injected anhydrous ammonia is more effective than broadcast urea as a source of nitrogen for drill seeded rice. Agronomy, 12(4), 942. https://doi.org/10.3390/agronomy12040942

[8] Nelson, K. A. (2019). Comparison of applicator knives for fall and spring strip-till-applied anhydrous ammonia. Crop, Forage & Turfgrass Management, 5, 190038. https://doi.org/10.2134/cftm2019.05.0038

[9] Roth, R. T., & Wuestenberg, M. J. (2024). Fall anhydrous ammonia applications: What to know about soil moisture. Iowa State University Extension and Outreach, Integrated Crop Management. https://crops.extension.iastate.edu/post/fall-anhydrous-ammonia-applications-what-know-about-soil-moisture

[10] Rotole, D. V., & Hubner, C. S. (2026). Closed loop closing system control (U.S. Patent No. 12,648,507). U.S. Patent and Trademark Office.

[11] Salford Group. (2026). Anhydrous ammonia application: Independent Series with SwitchBlade shanks. Salford Group Inc. https://salfordgroup.com/uses/anhydrous-ammonia-application/

[12] Sawyer, J. (2019). Understanding anhydrous ammonia application in soil. Iowa State University Extension and Outreach, Integrated Crop Management. https://crops.extension.iastate.edu/cropnews/2019/03/understanding-anhydrous-ammonia-application-soil

[13] SurePoint Ag Systems. (2024a). NH3 precision anhydrous ammonia Sentinel rate control: Installation and service manual (Document 396-5750Y1, Rev. 09/20/2024).

[14] SurePoint Ag Systems. (2024b). Sentinel NH3 blockage monitor for ISOBUS: System manual (Document 396-4519Y1, Rev. 03/06/2024).

[15] SurePoint Ag Systems. (2026). Sentinel NH3. https://www.surepointag.com/sentinel-nh3

[16] Tao, W., Chen, B., Yang, X., Guo, B., Xu, W., Ke, S., & Huang, S. (2025). Design and experimental study of tillage depth control system for electric rotary tiller based on LADRC. Scientific Reports, 15, 1740. https://doi.org/10.1038/s41598-025-86283-6

[17] Unverferth Manufacturing Co. (2021). Renegade anhydrous ammonia applicators https://media.unverferth.com/unverferth/fertilizer-application/um-fertilizer-renegade-nh3-applicator-nov.-2021.pdf

[18] Zhao, J., Zhu, L., Jia, H., Huang, D., Guo, M., & Cong, Y. (2018). Automatic depth control system for a no-till seeder. International Journal of Agricultural and Biological Engineering, 11(1), 115–121. https://doi.org/10.25165/j.ijabe.20181101.3229

# EVALUATION OF THE ENERGETIC AND OPERATIONAL PERFORMANCE OF AN INNOVATIVE GRASS SEEDER FOR VINEYARDS AND ORCHARDS

/

# *EVALUAREA EXPERIMENTALĂ A PERFORMANȚELOR ENERGETICE ȘI DE EXPLOATARE ALE UNEI SEMĂNĂTORI INOVATIVE PENTRU ÎNIERBAREA PLANTAȚIILOR VITICOLE ȘI POMICOLE*

**Dragoş-Nicolae DUMITRU[1)], Dragoș-Nicolae ANGHELACHE*[1, 2)], Carmen VASILACHI[1)], Eugen MARIN[1)], Dragoș MANEA[1)], Alin-Nicolae HARABAGIU[1)], Stefano-Andrea MANTOVANI[1)], Neluș-Evelin GHEORGHIȚĂ[2)]**

[1)] INMA Bucharest / Romania; [2)] UNSTP Bucharest / Romania

**E-mail: dragos1989anghelache@gmail.com*

***Keywords:*** *grass seeding, vineyards, orchards, traction force, fuel consumption, operational performance*

**ABSTRACT**

*This paper presents the experimental evaluation, under operating conditions, of innovative equipment designed for sowing grass mixtures between rows of vineyards and fruit tree plantations. The equipment was tested in two perennial crop environments using an aggregate consisting of a Solis 50 tractor and the experimental grass seeder. The study focused on working speed, tractor wheel slip, traction force, traction power, theoretical field capacity and fuel consumption. The working speed was 1.16 km/h in the vineyard and 1.15 km/h in the orchard, while wheel slip remained close to 6.4% in both locations. Mean traction force increased from 2780.74 N in the vineyard to 3569.17 N in the orchard, corresponding to traction power requirements of 0.88 and 1.12 kW, respectively. The theoretical field capacity was approximately 0.167 ha/h, while average specific fuel consumption was 7.65 l/ha and average hourly consumption was 1.29 l/h. The results indicate stable operation, low traction power demand and comparable fuel use in the two experimental sites, supporting the suitability of the equipment for establishing controlled grass cover in perennial plantations.*

**REZUMAT**

*Lucrarea prezintă evaluarea experimentală, în condiții de exploatare, a unui echipament inovativ destinat semănatului amestecurilor de ierburi între rândurile plantațiilor viticole și pomicole. Echipamentul a fost testat în două medii de cultură perenă, utilizând agregatul format din tractorul Solis 50 și modelul experimental de semănătoare. Studiul a urmărit viteza de lucru, patinarea roților tractorului, forța și puterea de tracțiune, capacitatea teoretică de lucru și consumul de combustibil. Viteza de lucru a fost de 1,16 km/h în plantația de viță-de-vie și 1,15 km/h în plantația de pomi fructiferi, iar patinarea s-a menținut în jurul valorii de 6,4%. Forța medie de tracțiune a crescut de la 2780,74 N în vie la 3569,17 N în livadă, corespunzător unor puteri de tracțiune de 0,88 și 1,12 kW. Capacitatea teoretică de lucru a fost de aproximativ 0,167 ha/h, iar consumul specific mediu de combustibil de 7,65 l/ha. Rezultatele evidențiază o funcționare stabilă și un necesar energetic redus, confirmând adaptabilitatea echipamentului la lucrările de înființare a covorului vegetal în plantații perene.*

## INTRODUCTION

Sustainable soil management has become a major objective in modern viticulture and fruit growing, where repeated traffic, intensive soil disturbance, erosion and increasingly variable water availability can affect soil functions and long-term plantation resilience *(Al-Shammary, A. A. G. et. al., 2024)*. Maintaining vegetation or cover crops in the inter-row is increasingly used as a nature-based management strategy because it can contribute to soil protection, biological activity and improved agroecosystem services *(Zalai, M. et. al., 2025)*.

Recent vineyard studies confirm that grass or cover-crop systems can support soil conservation and climate-change adaptation, although their effects remain strongly dependent on local soil and climatic conditions *(Stojanović et al., 2025; Horel et al., 2024)*.

The agronomic benefits of inter-row vegetation are accompanied by important management trade-offs. Green cover can modify soil-water dynamics, competition for resources and the timing of field

operations *(Trevini, M. et. al, 2024)*. A recent meta-analysis showed that the response of soil water content differs between perennial grass and temporary cover crops, emphasizing the need for site-specific management rather than a single universal strategy *(Horel et al., 2024)*. Experimental work has also shown that cover-crop species and management practices can influence vineyard water dynamics, soil health and vine performance *(Steenwerth et al., 2024)*. The successful establishment of an inter-row grass cover depends not only on the selected plant mixture but also on the quality and efficiency of mechanized operations. In narrow perennial plantations, machinery must operate within restricted spaces while maintaining stable traction, acceptable wheel slip and limited energy consumption *(Rocha, F.I., et. al., 2025)*.

These parameters directly affect field productivity, operating costs and the environmental performance of mechanized vineyard operations *(Cunial, L. et. al. 2025)*. Large-scale monitoring of vineyard tractor activities has demonstrated the importance of recording working speed, power demand, field capacity and fuel consumption when evaluating mechanized operations *(Alemanno et al., 2025)*.

From an engineering perspective, traction force, working speed and fuel consumption are useful indicators for comparing equipment behavior under different field conditions *(Gagliardi, L. et. al., 2024)*. Research on conservation-oriented machinery has shown that reduced pulling force and traction energy requirements can be associated with lower fuel demand, while working speed and tool configuration can significantly affect operational performance *(Trevini et al., 2024)*. Therefore, experimental evaluation under actual operating conditions is essential when a new machine is intended for use in vineyards and *orchards (Cabrera-Pérez, C. et. al. 2024)*.

The aim of this paper is to evaluate the energetic and operational performance of innovative grass seeding equipment developed for the inter-row spaces of vineyards and fruit tree plantations. Field experiments were carried out in two experimental plantations, and the analysis focused on working speed, tractor wheel slip, traction force, traction power, theoretical field capacity and fuel consumption. The comparison between the two sites was used to assess the stability and adaptability of the tractor-seeder aggregate under representative operating conditions.

## MATERIALS AND METHODS

The experiments were conducted in the experimental vineyard and fruit tree plantation located within INMA Bucharest. The technological operation consisted of sowing a grass mixture in the inter-row area using an aggregate formed by a Solis 50 tractor and the experimental model of innovative grass seeding equipment. Before testing, the technical condition of the seed transmission and distribution system, the tractor coupling system and the active working components were checked and adjusted according to the conditions of each experimental site.



a) b)

**Fig. 1 - Preparation of the Solis 50 tractor and innovative grass seeding equipment for field experiments**

*a) vineyard; b) fruit tree plantation*

Working conditions were characterized by using data from the meteorological station located in the experimental area and measurements related to soil conditions. During the seeding tests, maximum air temperatures were approximately 25°C, total precipitation reached 34.6 mm and relative air humidity varied approximately between 60 and 95%. Soil volumetric water content ranged from about 20 to 45%, depending on measurement depth, while soil temperature varied between 17 and 24°C. These conditions were considered favorable for carrying out the seeding operation and for subsequent seed germination.

For the determination of working speed, experimental routes were marked in each plantation. The test route was 50 m long in the vineyard and 25 m long in the fruit tree plantation. Travel time was recorded with a stopwatch, and effective working speed was calculated using equation (1):

$$V_l = 3.6 \cdot s / t \ \text{[km/h]} \quad (1)$$

where:

$V_l$ is the effective working speed (km/h), s is the test distance (m), and t is the travel time (s). Tractor wheel slip was determined from the number of driving-wheel revolutions under load and the theoretical number of revolutions without load over the same distance. For the tested tractor, the developed wheel length was 4.11 m.

Traction force was measured by the strain-gauge method. Strain gauges were installed on structural elements of the coupling system and calibrated by applying a known force with a reference dynamometer.

The gauges were connected to a QuantumX MX1615 data acquisition system, while signals were monitored and recorded using the nSOFT software package. The acquired mechanical-strain signals were subsequently converted into traction-force values.



a) b) c) d)

**Fig. 2 - Main stages of traction-force measurement**

*a) strain-gauge installation; b) calibration with a reference dynamometer; c) signal monitoring with QuantumX MX1615 and nSOFT; d) field data acquisition*

Traction power was calculated from the measured traction force and working speed. The theoretical field capacity was determined from the working width and effective working speed using equation (2):

$$W_t = 0.1 \cdot B_l \cdot V_l \ \text{[ha/h]} \quad (2)$$

where:

$B_l$ is the working width (m) and $V_l$ is the working speed (km/h). The equipment working width was 1.45 m. Fuel consumption was determined by the full-tank method. The quantity of fuel consumed during the worked area was recorded, and both hourly fuel consumption and specific fuel consumption per hectare were calculated.

## RESULTS

The measured and calculated values for working speed and tractor wheel slip are presented in Table 1. The aggregate operated at nearly identical speeds in both experimental sites, which provides a suitable basis for comparing the other energetic and operational indicators.

**Table 1**

**Working speed and tractor wheel slip during seeding tests**

| Experimental site | Route length L [m] | Time t [s] | Working speed $V_l$ [km/h] | No. of left wheel rotations $N_{sst}$ | No. of right wheel rotations $N_{sdr}$ | No. of rotations under load $N_{sdr}$ | No. of no-load rotations $N_9$ | Wheel slip δ [%] |
|---|---|---|---|---|---|---|---|---|
| **Vineyard** | 50 | 155.4 | 1.16 | 13 | 13 | 13 | 12.17 | 6.38 |
| **Fruit tree plantation** | 25 | 78 | 1.15 | 6.5 | 6.5 | 6.5 | 6.08 | 6.46 |

The working speed was 1.16 km/h in the vineyard and 1.15 km/h in the fruit tree plantation. Wheel slip was 6.38% and 6.46%, respectively. The very small difference between the two values indicates similar wheel-soil interaction and stable traction conditions. In practical terms, the slip level remained low and did not indicate excessive loss of motion at the driving wheels.

Traction-force measurements showed a clear difference between the two sites. After the aggregate entered a stable working regime, the mean traction resistance was approximately 2780.74 N in the vineyard and 3569.17 N in the fruit tree plantation. The higher value recorded in the orchard indicates greater resistance to forward movement under the local soil and surface conditions.

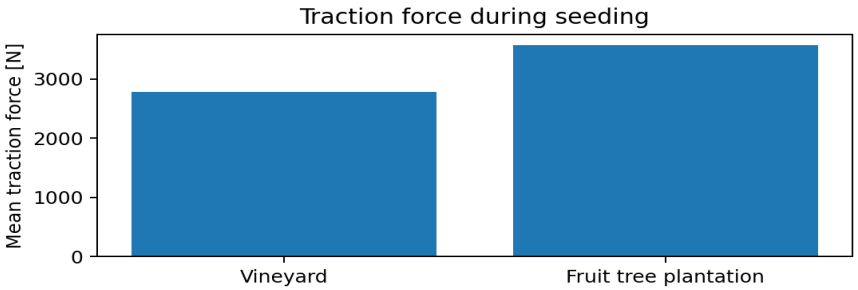



**Fig. 3 - Mean traction force of the tractor-seeder aggregate in the two experimental sites**

The calculated traction power followed the same trend as traction force (Table 2). The vineyard test required 1.19 HP (0.88 kW), while the fruit tree plantation required 1.52 HP (1.12 kW). Despite the approximately 28% increase in traction force in the orchard compared with the vineyard, the absolute power requirement remained low because the aggregate operated at a low and almost constant working speed.

**Table 2**

**Traction force and traction power of the aggregate**

| Experimental site | Mean speed [m/s] | Mean speed [km/h] | Mean traction force [N] | Traction power [HP] | Traction power [kW] |
|---|---|---|---|---|---|
| **Vineyard** | 0.322 | 1.16 | 2780.74 | 1.19 | 0.88 |
| **Fruit tree plantation** | 0.319 | 1.15 | 3569.17 | 1.52 | 1.12 |

The low traction-power requirement is an important result for equipment intended for narrow perennial plantations, where compact tractors are commonly used. In a broader context, operational studies in vineyards emphasize that power requirement, working speed, field capacity and fuel use are essential for machinery sizing and for estimating operating costs *(Alemanno et al., 2025)*. Conservation-oriented machinery research similarly shows that low pulling force and energy demand are desirable characteristics when soil-protective field operations are evaluated *(Trevini et al., 2024)*.

The theoretical field capacity was calculated to be at 1.45 m working width. The values were 0.168 ha/h in the vineyard and 0.167 ha/h in the fruit tree plantation, with an average of 0.167 ha/h (Table 3). The almost identical values are a direct consequence of the similar working speeds and show that the aggregate maintained a uniform operating regime in both plantations.

**Table 3**

**Theoretical field capacity of the grass seeding aggregate**

| Experimental site | Working width [m] | Working speed [km/h] | Theoretical field capacity [ha/h] |
|---|---|---|---|
| **Vineyard** | 1.45 | 1.16 | 0.168 |
| **Fruit tree plantation** | 1.45 | 1.15 | 0.167 |
| **Average** | 1.45 | 1.155 | 0.167 |

Fuel-consumption results are presented in Table 4. Specific consumption was 7.78 l/ha in the vineyard and 7.52 l/ha in the fruit tree plantation, giving an average of 7.65 l/ha. Hourly fuel consumption was 1.31 and 1.26 l/h, respectively, with an average of 1.29 l/h. The differences between the two locations were

limited, despite the higher traction force measured in the orchard. The relatively close fuel-consumption values indicate that the seeder maintained comparable energetic behavior in the two operating environments. Direct comparison with other vineyard operations must be made cautiously because fuel use depends on tractor size, operation type, field capacity and site conditions. Nevertheless, recent monitoring of mechanized vineyard activities confirms that fuel consumption per hour and per hectare is a key performance indicator and varies substantially among operations *(Alemanno et al., 2025)*.

**Table 4**

**Fuel consumption during field seeding tests**

| Experimental site | Fuel [l] | Worked area [m²] | Worked area [ha] | Specific fuel [l/ha] | Hourly fuel [l/h] |
|---|---|---|---|---|---|
| **Vineyard** | 0.340 | 436.8 | 0.0437 | 7.78 | 1.31 |
| **Fruit tree plantation** | 0.100 | 133 | 0.0133 | 7.52 | 1.26 |
| **Average** | - | - | - | 7.65 | 1.29 |



**Fig. 4 - Soil surface after seeding with the innovative equipment**

*a) vineyard; b) fruit tree plantation*

Visual assessment after seeding showed adequate preparation of the superficial soil layer and uniform incorporation of seeds over the inter-row working strip. In both locations, the soil was sufficiently crumbled, and the worked surface was leveled. In the vineyard, the operation produced good loosening of the superficial layer and an even distribution across the working width. In the fruit tree plantation, the equipment also produced a uniform worked surface without major visible disturbance of soil structure.

Taken together, the results show that the experimental seeder operated consistently in two different perennial-crop environments. The orchard imposed a higher traction load, but this did not lead to major changes in working speed, wheel slip, theoretical capacity or fuel consumption. This behavior suggests that the aggregate can accommodate moderate differences in field resistance while maintaining a stable technological regime.

## CONCLUSIONS

Field experiments with the innovative grass seeding equipment demonstrated stable operational and energetic performance in both vineyard and fruit tree plantation conditions. The effective working speed was practically constant, at 1.16 km/h in the vineyard and 1.15 km/h in the orchard, while tractor wheel slip remained low, between 6.38 and 6.46%. Mean traction force was 2780.74 N in the vineyard and 3569.17 N in the fruit tree plantation.

The corresponding traction power requirements were only 0.88 and 1.12 kW, indicating a low power demand for the seeding operation. At a working width of 1.45 m, the theoretical field capacity was approximately 0.167 ha/h in both sites. Specific fuel consumption ranged from 7.52 to 7.78 l/ha, while hourly fuel consumption ranged from 1.26 to 1.31 l/h.

The limited variation in fuel consumption, field capacity and wheel slip between the two experimental sites indicates a uniform operating regime despite the higher traction resistance recorded in the orchard. Visual observations also confirmed appropriate preparation of the superficial soil layer and uniform incorporation of seeds.

The experimental results support the use of the developed equipment for establishing controlled grass cover between rows of vineyards and orchards. Further experiments over larger areas and under a wider range of soil moisture, compaction and slope conditions are recommended to quantify field efficiency and to establish optimized operating settings for different perennial-crop environments.

**ACKNOWLEDGEMENT**

The results were obtained with the support of the Ministry of Research, Innovation and Digitalization through the Nucleu Program, contract no. 9 N / 01.01.2023, project PN 23 04 02 03 “Innovative technology for grassing the interval between rows of vines and fruit trees to avoid degradation of soil structure”.

**REFERENCES**

[1] Al-Shammary, A. A. G., Caballero-Calvo, A., & Fernández-Gálvez, J. (2024). Evaluating the Performance of a Novel Digital Slippage System for Tractor Wheels Across Varied Tillage Methods and Soil Textures. *Agriculture*, *14*(11), 1957. https://doi.org/10.3390/agriculture14111957

[2] Alemanno, R., Rossi, P., Monarca, D., et al. (2025). Evaluation of tractor performance, efficiency and fuel consumption in vineyard activities. Scientific Reports, 15, 8416. https://doi.org/10.1038/s41598-025-93526-z;

[3] Cabrera-Pérez, C., et al. (2024). Cover crops terminated with roller-crimper to manage Cynodon dactylon and other weeds in vineyards. Pest Management Science. https://doi.org/10.1002/ps.7953;

[4] Cunial, L., Diti, I., Bonini, P., et al. (2025). Novel termination techniques of winter cover crops in the vineyard: Effects on physiology and performance of Pinot Noir and Malvasia di Candia aromatica grapevines. European Journal of Agronomy, 164, 127514. https://doi.org/10.1016/j.eja.2025.127514;

[5] Gagliardi, L., Luglio, S. M., Peruzzi, A., Fontanelli, M., Frasconi, C., & Raffaelli, M. (2024). Comparative Analysis of the Performance of a Chain Mower and Tools That Perform Under-Row Weed Control with Tillage in the Vineyard. *Agronomy*, *14*(1), 206. https://doi.org/10.3390/agronomy14010206;

[6] Horel, Á., Zsigmond, T., et al. (2024). Inter-row soil management affecting soil moisture in non-irrigated vineyard ecosystems: A meta-analysis. Soil Use and Management. https://doi.org/10.1111/sum.13159;

[7] Paciolla, F., Łyp-Wrońska, K., Quartarella, T., & Pascuzzi, S. (2025). Simulation Analysis of Energy Inputs Required by Agricultural Machines to Perform Field Operations. *AgriEngineering*, *7*(1), 7. https://doi.org/10.3390/agriengineering7010007;

[8] Rocha, F.I., Rodriguez-Ramos, J.C., Fernando, M. *et al.* Interrow cover crops in a semi-arid vineyard increase plant beneficial functional potential of the soil microbiome, both in vine rows and interrows, a benefit that increases with cover crop duration. *Environmental Microbiome* **20**, 66 (2025). https://doi.org/10.1186/s40793-025-00726-1;

[9] Steenwerth, K.L., et al. (2024). A native plant species cover crop positively impacted vineyard water dynamics, soil health, and vine vigor. Agriculture, Ecosystems & Environment, 367, 108972. https://doi.org/10.1016/j.agee.2024.108972;

[10] Stojanović, M., et al. (2025). Grass Cover in Vineyards as a Multifunctional Solution for Sustainable Grape Growing: A Case Study of Cabernet Sauvignon Cultivation in Serbia. Agronomy, 15(2), 253. https://doi.org/10.3390/agronomy15020253;

[11] Trevini, M., Tosti, G., & Benincasa, P. (2024). Agronomic performance of disc chain harrow as a conservation agriculture tool for a one-step cover crop termination and seedbed preparation. Experimental Agriculture, 60, e12. https://doi.org/10.1017/S001447972400005X;

[12] Zalai, M., Bujtás, O., Sárospataki, M., & Dorner, Z. (2025). Grassy and Herbaceous Interrow Cover Crops in European Vineyards: A Review of Their Short-Term Effects on Water Management and Regulating Ecosystem Services. *Land*, *14*(8), 1526. https://doi.org/10.3390/land14081526;

# EXPERIMENTAL EVALUATION OF THE ENERGETIC AND OPERATIONAL PERFORMANCE OF AN INNOVATIVE INTER-ROW GRASS MOWER FOR VINEYARDS AND ORCHARDS

/

# *EVALUAREA EXPERIMENTALĂ A PERFORMANȚELOR ENERGETICE ȘI DE EXPLOATARE ALE UNUI ECHIPAMENT INOVATIV DE COSIT INTERVALUL ÎNIERBAT DIN PLANTAȚII VITICOLE ȘI POMICOLE*

**Dragoş-Nicolae DUMITRU[1)], Dragoș-Nicolae ANGHELACHE*[1, 2)], Carmen VASILACHI[1)], Eugen MARIN[1)], Dragoș MANEA[1)], Alin-Nicolae HARABAGIU[1)], Stefano-Andrea MANTOVANI[1)], Iulian Virgil GHIULEANU[3)]**

[1)] INMA Bucharest / Romania; [2)] UNSTP Bucharest / Romania; [3)] UASVM Bucharest / Romania

**E-mail: dragos1989anghelache@gmail.com*

***Keywords:*** *grass mowing, vineyards, orchards, traction force, fuel consumption, inter-row management*

## ABSTRACT

*This paper presents the experimental evaluation, under operating conditions, of an innovative technical equipment designed for mowing the grass-covered inter-row spaces of vineyards and fruit tree plantations. The equipment was tested in aggregate with a Solis 50 tractor in two experimental sites located at INMA Bucharest. The assessment focused on working speed, tractor wheel slip, traction force, traction power, theoretical field capacity and fuel consumption. Working speed was 0.98 km/h in the vineyard and 0.97 km/h in the orchard, while wheel slip remained between 6.38 and 6.46%. Mean traction force reached 991.58 N in the vineyard and 1096.98 N in the fruit tree plantation, corresponding to traction power requirements of 0.26 and 0.29 kW. The average theoretical field capacity was 0.136 ha/h. Specific fuel consumption was 10.99 l/ha in the vineyard and 9.02 l/ha in the orchard, while hourly consumption averaged 1.36 l/h. Visual evaluation showed uniform mowing over the entire working width, adequate cutting height and uniform distribution of plant residues. The results demonstrate stable operation and low traction-power requirements, supporting the use of the developed mower for controlled maintenance of inter-row vegetation in perennial plantations.*

## REZUMAT

*Lucrarea prezintă evaluarea experimentală, în condiții de exploatare, a unui echipament tehnic inovativ destinat cosirii intervalului înierbat dintre rândurile plantațiilor viticole și pomicole. Echipamentul a fost testat în agregat cu tractorul Solis 50, în două loturi experimentale din cadrul INMA București. Evaluarea a urmărit viteza de lucru, patinarea roților tractorului, forța și puterea de tracțiune, capacitatea teoretică de lucru și consumul de combustibil. Viteza de lucru a fost de 0,98 km/h în plantația de viță-de-vie și 0,97 km/h în plantația de pomi fructiferi, iar patinarea s-a menținut între 6,38 și 6,46%. Forța medie de tracțiune a fost de 991,58 N, respectiv 1096,98 N, corespunzând unor puteri de tracțiune de 0,26 și 0,29 kW. Capacitatea teoretică medie de lucru a fost de 0,136 ha/h. Consumul specific de combustibil a fost de 10,99 l/ha în vie și 9,02 l/ha în livadă, iar consumul orar mediu a fost de 1,36 l/h. Evaluarea vizuală a evidențiat o cosire uniformă, o înălțime corespunzătoare a vegetației și o distribuire uniformă a resturilor vegetale. Rezultatele confirmă funcționarea stabilă și necesarul redus de putere la tracțiune al echipamentului.*

## INTRODUCTION

Sustainable management of vineyard and orchard inter-rows increasingly relies on permanent or temporary vegetation covers to protect the soil and improve the ecological functioning of perennial cropping systems. Cover crops and spontaneous grass covers can reduce the intensity of soil disturbance, contribute to erosion control and improve several soil physical properties *(Calderone, F. et. al., 2025, Horel, Á. et. al., 2025)*. European evidence indicates that vineyard sites managed with cover crops and lower tillage intensity generally show improved soil organic carbon and soil structure compared with intensively tilled, bare inter-rows *(Liebhard et al., 2024)*. Recent studies also emphasize that the effects of inter-row vegetation are site-specific and depend on climate, soil-water availability and the management strategy adopted *(Horel et al., 2024; Raffa et al., 2025)*.

Maintaining a controlled grass cover requires periodic management of vegetation height and biomass. Mowing is therefore a key operation in grassed vineyards and orchards because it limits excessive competition between the cover vegetation and the main crop, maintains machinery accessibility and leaves plant residues on the soil surface *(Peruzzi, A. et. al., 2020)*. Research on vineyard floor management has shown that mowing can form part of low-disturbance strategies for maintaining inter-row vegetation, while recent modelling work suggests that mowing frequency, operating costs and associated emissions may become increasingly important under changing climatic conditions *(Cunial et al., 2025; Silvestroni et al., 2025)*.

From the machinery perspective, equipment intended for perennial plantations must operate reliably in restricted inter-row spaces and under heterogeneous vegetation and terrain conditions *(Gagliardi, L. et. al., 2026)*. Working speed, wheel slip, traction force, traction power, field capacity and fuel consumption provide useful indicators for assessing operational and energetic performance *(Stojanović, M. et. al., 2025, Varani, M. et. al., 2021)*. Previous research on mechanical vegetation control in vineyards has highlighted the importance of evaluating both work quality and energy requirements when selecting mowing or weed-control solutions *(Manzone et al., 2024)*.

The aim of this paper is to evaluate the energetic and operational performance of innovative grass seeding equipment developed for the inter-row spaces of vineyards and fruit tree plantations. Field experiments were carried out in two experimental plantations, and the analysis focused on working speed, tractor wheel slip, traction force, traction power, theoretical field capacity and fuel consumption. The comparison between the two sites was used to assess the stability and adaptability of the tractor-seeder aggregate under representative operating conditions.

## MATERIALS AND METHODS

The experiments were conducted in the experimental vineyard and fruit tree plantation located within INMA Bucharest. The aggregate consisted of a Solis 50 tractor and the experimental technical equipment designed for mowing the grass-covered interval between vineyard and fruit tree rows. Before testing, the general technical condition of the mower was checked, including the power take-off transmission, cardan shaft, gearbox, tractor coupling system, mowing rotor and cutting elements. Cutting height and the position of the active components were adjusted according to field conditions.



a) b)

**Fig. 1 - Solis 50 tractor and experimental inter-row grass mower prepared for field tests**

*a) vineyard; b) fruit tree plantation*

Working conditions were characterized by using the meteorological station installed in the experimental area. During the mowing test period, air temperature ranged from 16 to 33 °C, relative humidity from 20 to 100%, and total precipitation was approximately 19 mm. Soil temperature varied between 15 and 37 °C. Leaf wetness was also monitored because wet vegetation can increase cutting resistance, loading of active components and the energetic demand of mowing.

Working speed was determined from the measured test distance and travel time. The test route was 50 m in the vineyard and 25 m in the fruit tree plantation. Tractor wheel slip was determined from the number of driving-wheel revolutions under load and the calculated number of revolutions without load, using a developed wheel length of 4.11 m. Traction force was determined by the strain-gauge method. Strain gauges mounted on structural elements of the coupling system were connected to a QuantumX MX1615 data-

acquisition system, and signals were recorded and processed using nSOFT software. Traction power was calculated from the measured traction force and working speed.

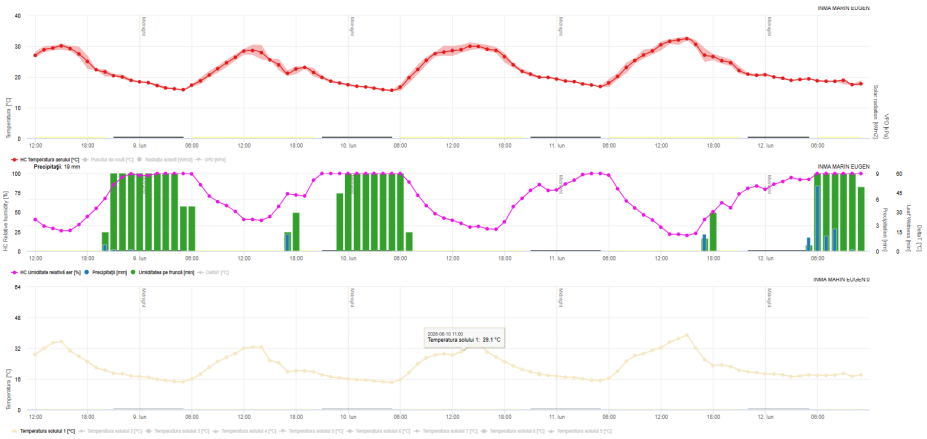


**Fig. 2 - Evolution of the main meteorological and soil parameters during the mowing experiments**

Working speed was determined from the measured test distance and travel time. The test route was 50 m in the vineyard and 25 m in the fruit tree plantation.

Tractor wheel slip was determined from the number of driving-wheel revolutions under load and the calculated number of revolutions without load, using a developed wheel length of 4.11 m. Traction force was determined by the strain-gauge method. Strain gauges mounted on structural elements of the coupling system were connected to a QuantumX MX1615 data-acquisition system, and signals were recorded and processed using nSOFT software. Traction power was calculated from the measured traction force and working speed. The theoretical field capacity was calculated using:

$$W_t = 0,1 \times B_l \times V_l \ [ha/h] \quad (1)$$

where:

- $B_l$ is the working width, [m]
- $v_l$ is the working speed, [km/h]

The mower working width was 1.40 m. Fuel consumption was determined by the full-tank method: the tractor tank was filled to the same reference level before and after each test, and the refilled quantity was considered effective fuel consumption. Specific consumption was calculated relative to the worked area, while hourly consumption was used as an additional energetic indicator because the experimental plots were relatively small.

## RESULTS

The working-speed and wheel-slip results are presented in Table 1. The aggregate operated at nearly identical speeds in both experimental sites. Working speed was 0.98 km/h in the vineyard and 0.97 km/h in the fruit tree plantation. Tractor wheel slip was 6.38 and 6.46%, respectively, indicating good wheel-soil adhesion and stable transmission of the traction effort.

**Tabel 1**

**Working speed and tractor wheel slip during mowing tests**

| Experimental site | Route length L [m] | Time t [s] | Working speed $V_l$ [km/h] | No. of left wheel rotations $N_{sst}$ | No. of right wheel rotations $N_{sdr}$ | No. of rotations under load $N_s$ | No. of no-load rotations $N_g$ | Wheel slip δ [%] |
|---|---|---|---|---|---|---|---|---|
| **Vineyard** | 50 | 183 | 0.98 | 13 | 13 | 13 | 12.17 | 6.38 |
| **Fruit tree plantation** | 25 | 93 | 0.97 | 6.5 | 6.5 | 6.5 | 6.08 | 6.46 |

The energetic parameters are summarized in Table 2. Mean traction force was 991.58 N in the vineyard and 1096.98 N in the fruit tree plantation, an increase of approximately 10.6% in the orchard. The corresponding traction-power values were 0.26 and 0.29 kW.

These low values show that the translational traction requirement of the aggregate remained modest in both locations. The difference between sites can be associated with local variations in terrain and vegetation conditions; the available experimental data do not support separating the individual contribution of each factor.

**Table 2**

**Traction force and traction power of the tractor-mower aggregate**

| Experimental site | Mean speed [m/s] | Mean speed [km/h] | Mean traction force [N] | Traction power [HP] | Traction power [kW] |
|---|---|---|---|---|---|
| **Vineyard** | 0.267 | 0.96 | 991.58 | 0.35 | 0.26 |
| **Fruit tree plantation** | 0.272 | 0.98 | 1096.98 | 0.40 | 0.29 |

The theoretical field capacity was 0.134 ha/h in the vineyard and 0.137 ha/h in the fruit tree plantation, with an average value of 0.136 ha/h presented in Table 3. The small difference reflects the nearly identical working speeds and the constant 1.40 m working width.

The values characterize the experimental low-speed regime selected for the tests and should therefore not be extrapolated to other operating speeds without additional field validation.

**Table 3**

**Theoretical field capacity of the mowing aggregate**

| Experimental site | Working width [m] | Working speed [km/h] | Theoretical field capacity [ha/h] |
|---|---|---|---|
| **Vineyard** | 1.4 | 0.96 | 0.134 |
| **Fruit tree plantation** | 1.4 | 0.98 | 0.137 |
| **Mean** | 1.4 | 0.97 | 0.136 |



a) b)

**Fig. 3 - Condition of the inter-row vegetation after mowing**

*a) vineyard; b) fruit tree plantation*

Fuel-consumption results are shown in Table 4. Specific fuel consumption was 10.99 l/ha in the vineyard and 9.02 l/ha in the fruit tree plantation, while hourly consumption was 1.47 and 1.24 l/h.

The mean values were 10.01 l/ha and 1.36 l/h. Because the trials were performed on relatively small plots, the hectare-based values are sensitive to test-area size and maneuvering conditions; consequently, hourly fuel consumption provides a useful complementary indicator for interpreting the energetic behaviour of the aggregate.

**Table 4**

**Fuel consumption during field mowing tests**

| Experimental site | Fuel used [l] | Worked area [m²] | Worked area [m²] | Specific consumption [l/ha] | Hourly consumption [l/h] |
|---|---|---|---|---|---|
| **Vineyard** | 0.480 | 436.8 | 0.0437 | 10.99 | 1.47 |
| **Fruit tree plantation** | 0.240 | 266 | 0.0266 | 9.02 | 1.24 |
| **Mean** | - | - | - | 10.01 | 1.36 |

Visual assessment after mowing showed that vegetation was cut uniformly over the working width, without significant uncut areas or accumulations of plant material. In the vineyard, the cut residues were distributed over the soil surface, while in the orchard the operation maintained a uniform grass-covered inter-row and facilitated machinery access. These observations are consistent with the intended role of mowing as a controlled vegetation-management operation rather than a soil-disturbing treatment.



**Fig. 4 - Condition of the mower cutting blade after field experiments**

Taken together, the results show that the experimental seeder operated consistently in two different perennial-crop environments. The orchard imposed a higher traction load, but this did not lead to major changes in working speed, wheel slip, theoretical capacity or fuel consumption. This behavior suggests that the aggregate can accommodate moderate differences in field resistance while maintaining a stable technological regime.

The final inspection of the cutting blade showed normal wear of the cutting edge associated with vegetation mowing. The active edge retained its initial geometry and cutting capacity, and no cracks, deformations or significant degradation were identified. Together with the absence of operating failures during the tests, this result indicates satisfactory functional behaviour of the experimental mower over the evaluated test period.

The findings are relevant in the context of sustainable inter-row management. Permanent or managed vegetation covers can provide soil-protection and ecosystem-service benefits, but their biomass must be controlled to limit competition and maintain accessibility. Recent vineyard studies support mowing or mulching as practical components of reduced-disturbance inter-row management.

The present study complements this agronomic perspective with engineering data on the operational and energetic behaviour of a dedicated mower under vineyard and orchard conditions.

## CONCLUSIONS

Field experiments demonstrated that the innovative inter-row grass mower operated stably in both vineyard and fruit tree plantation conditions. Working speed remained close to 0.97 km/h and tractor wheel slip remained below 6.5% in both sites, indicating a uniform operating regime and adequate wheel-soil adhesion. Mean traction force was 991.58 N in the vineyard and 1096.98 N in the orchard, corresponding to traction-power requirements of 0.26 and 0.29 kW.

The average theoretical field capacity was 0.136 ha/h. Mean specific fuel consumption was 10.01 l/ha and mean hourly consumption was 1.36 l/h. Given the small experimental areas, hourly fuel consumption should be considered together with the hectare-based indicator when evaluating energetic

performance. The mower produced a uniform cut over the working width and distributed plant residues satisfactorily on the soil surface. Final inspection of the cutting blade revealed only normal wear, without cracks or significant deformation.

These results support the suitability of the developed equipment for controlled maintenance of grass-covered inter-rows in vineyards and orchards. Future work should include larger plots, additional vegetation densities and mowing heights, and repeated seasonal tests to quantify field efficiency, cutting-quality indices and long-term wear.

**ACKNOWLEDGEMENT**

The results were obtained with the support of the Ministry of Research, Innovation and Digitalization through the Nucleu Program, contract no. 9 N / 01.01.2023, project PN 23 04 02 03 “Innovative technology for grassing the interval between rows of vines and fruit trees to avoid degradation of soil structure”.

**REFERENCES**

[1] Calderone, F., Scavo, A., Gresta, F., et al. (2025). Cover crops promote regulating and supporting ecosystem services without compromising grape yield in temperate vineyards: A meta-analysis. Agronomy for Sustainable Development, 45, 70. https://doi.org/10.1007/s13593-025-01074-7;

[2] Cunial, L., Diti, I., Bonini, P., et al. (2025). Novel termination techniques of winter cover crops in the vineyard: Effects on physiology and performance of Pinot Noir and Malvasia di Candia aromatica grapevines. European Journal of Agronomy, 164, 127514. https://doi.org/10.1016/j.eja.2025.127514;

[3] Gagliardi, L., Luglio, S. M., Fontanelli, M., Fontani, M., Frasconi, C., Peruzzi, A., & Raffaelli, M. (2026). Evaluating the Impact of Mowing, Wire Mulching, and Shallow Tillage on Under-Row Weed Management and Operational Performance in an Italian Vineyard. *Agriculture*, *16*(15), 1607. https://doi.org/10.3390/agriculture16151607;

[4] Horel, Á., Cseresnyés, I., Zagyva, I., et al. (2025). Soil moisture content and plant health monitoring under different inter-row cropping vineyard. Plant and Soil https://doi.org/10.1007/s11104-025-07612-2;

[5] Horel, Á., Zsigmond, T., et al. (2024). Inter-row soil management affecting soil moisture in non-irrigated vineyard ecosystems: A meta-analysis. Soil Use and Management. https://doi.org/10.1111/sum.13159;

[6] Liebhard, G., et al. (2024). Vineyard cover crop management strategies and their effect on soil properties across Europe. European Journal of Soil Science, 75, e13573. https://doi.org/10.1111/ejss.13573;

[7] Manzone, M., et al. (2024). Comparative Analysis of the Performance of a Chain Mower and Tools That Perform Under-Row Weed Control with Tillage in the Vineyard. Agronomy, 14(1), 206. https://doi.org/10.3390/agronomy14010206;

[8] Peruzzi, A., et al. (2020). Autonomous Mowing and Turf-Type Bermudagrass as Innovations for an Environment-Friendly Floor Management of a Vineyard in Coastal Tuscany. Agriculture, 10(5), 189. https://doi.org/10.3390/agriculture10050189;

[9] Raffa, D.W., Virili, A., Carlesi, S., Antichi, D., et al. (2025). Soil management shapes the functional diversity of the inter-row vegetation in Mediterranean vineyards. Agronomy for Sustainable Development, 45, 46. https://doi.org/10.1007/s13593-025-01046-x;

[10] Silvestroni, O., et al. (2025). Future climate will reshape inter-row grass mowing in vineyards: A modelling approach for optimized agronomic management. Italian Journal of Agronomy, 20(4), 100059. https://doi.org/10.1016/j.ijagro.2025.100059;

[11] Stojanović, M., et al. (2025). Grass Cover in Vineyards as a Multifunctional Solution for Sustainable Grape Growing: A Case Study of Cabernet Sauvignon Cultivation in Serbia. Agronomy, 15(2), 253. https://doi.org/10.3390/agronomy15020253;

[12] Varani, M., Mattetti, M., & Molari, G. (2021). Performance Evaluation of Electrically Driven Agricultural Implements Powered by an External Generator. *Agronomy*, *11*(8), 1447. https://doi.org/10.3390/agronomy11081447;

# STATIC STRUCTURAL ANALYSIS OF THE INDEPENDENT DISC OF AN AGRICULTURAL DISC HARROW FOR MATERIAL SELECTION AND MANUFACTURING COST OPTIMIZATION

/

# *ANALIZA STRUCTURALĂ STATICĂ A DISCULUI INDEPENDENT AL UNEI GRAPE CU DISCURI AGRICOLE ÎN VEDEREA ALEGERII MATERIALULUI ȘI OPTIMIZĂRII COSTURILOR DE FABRICAȚIE*

**Daniel LATEȘ*[1)], Paul TRIPON[1)], Eugen MARIN[2)], Laurențiu-Constantin VLĂDUȚOIU[2)]**

[1)] IRUM S.A. Reghin, Mures County / Romania;

[2)] National Institute of Research - Development for Machines and Installations Designed for Agriculture and Food Industry - INMA Bucharest, 013811 Bucharest / Romania.

**Tel: 0799 603 573; *E-mail: daniel.lates@irum.ro*

***Keywords:*** *independent disc harrow, disc, finite element analysis, FEM, material selection, Von Mises stress, manufacturing cost*

**ABSTRACT**

*Independent disc harrows are widely used for shallow and medium-depth soil tillage, crop residue incorporation and seedbed preparation. During operation, the discs are subjected to complex mechanical loads generated by soil resistance, impacts with compacted soil regions and possible contact with stones or other obstacles. Consequently, the mechanical properties of the material used for disc manufacturing have a direct influence on structural reliability, service life and production cost. This paper presents a static structural analysis of the working disc of an IRUM 2.8 m independent disc harrow, with the objective of validating the disc design and assessing alternative materials according to a mechanical performance–cost criterion. The methodology is based on a three-dimensional CAD model and numerical simulation using the Finite Element Method in SolidWorks Simulation. The analysis considers the equivalent Von Mises stress, maximum displacement, equivalent strain and factor of safety obtained for several candidate materials under identical loading and boundary conditions. The numerical results are subsequently correlated with the mechanical properties and estimated acquisition/manufacturing cost of each material. A comparative performance-to-cost indicator is proposed in order to identify the material capable of ensuring the required structural resistance without unnecessary over dimensioning or excessive production costs. The study provides a numerical basis for validating the manufacturing solution of the disc and supports material selection during the development of agricultural soil-working equipment.*

**REZUMAT**

*Independent disc harrows are widely used for shallow and medium-depth soil tillage, incorporation of plant residues and seedbed preparation. During operation, the discs are subjected to complex mechanical loads determined by soil resistance, impacts with compacted areas and possible contact with stones or other obstacles. For this reason, the mechanical characteristics of the material used to manufacture the disc directly influence structural strength, service life and manufacturing cost. This paper presents the static structural analysis of the working disc of the 2.8 m IRUM independent disc harrow, with the aim of validating the constructive solution and evaluating alternative materials based on the mechanical performance-to-cost ratio. The methodology uses the three-dimensional geometric model of the disc and numerical simulation by the Finite Element Method, carried out in the SolidWorks Simulation environment. For each material analyzed, under the same loading and support conditions, the equivalent Von Mises stress, maximum displacement, specific strain and factor of safety are determined. The numerical results are subsequently correlated with the mechanical characteristics and with the estimated cost of the material and the manufacturing process. Based on the results, a comparative performance-to-cost indicator is proposed, which allows the identification of the material capable of providing the required strength in service without unjustified over-dimensioning of the component and without excessively increasing manufacturing costs. The study thus provides a numerical basis for validating the disc's manufacturing solution and for the rational selection of materials used in the production of the active parts of soil-working equipment.*

## INTRODUCTION

Soil tillage operations are among the most important and energy-intensive mechanized operations in crop production technology. The performance of tillage equipment is influenced by the physico-mechanical properties of the soil, working depth, travel speed, the geometry of the active parts and the characteristics of the materials from which they are made. In the case of independent disc harrows, the discs are responsible for cutting, breaking up and mixing the topsoil layer, as well as incorporating plant residues, being subjected during operation to complex mechanical loads *(Chirende et al., 2019; Rani et al., 2022).*

The interaction between the disc and the soil generates traction, vertical and lateral force components, whose magnitude depends on the disc geometry, working angles, penetration depth, travel speed and soil properties. Studies conducted on disc-type active parts have shown that changes in geometric and functional parameters significantly influence both draft resistance and the distribution of mechanical stresses in the structure *(Chirende et al., 2019; Ibrahmi and Bentaher, 2025).* In particular, increasing the working depth and travel speed generally leads to an increase in the forces transmitted to the disc and, implicitly, to a higher stress level in its material *(Ibrahmi and Bentaher, 2025).*

For the analysis of the structural behavior of the active parts of agricultural machinery, numerical methods have become important tools at the design and validation stage. The Finite Element Method allows the evaluation of stress, displacement, strain and safety factor distributions for components with complex geometry and loading conditions that are difficult to describe using simplified analytical relations.

The application of FEM in the field of agricultural machinery allows critical areas to be identified before prototypes are built or before a component is introduced into series *production (Chirende et al., 2019; Ibrahmi and Bentaher, 2025).*

In the case of active parts in direct contact with the soil, structural strength is not, however, the only important criterion in material selection. Abrasive wear is one of the main degradation mechanisms of components used in soil tillage and is influenced both by the material's characteristics and by the properties of the working environment. Hardness, microstructure, toughness, chemical composition and heat treatment of the material can significantly change the wear behavior of agricultural active parts *(Singh et al., 2021; Rani et al., 2022; Malvajerdi, 2023).*

Experimental research on the steels used to manufacture agricultural discs has shown that the wear process manifests itself through progressive mass loss, thickness reduction and changes in the geometry of the active area. These phenomena affect not only the component's service life but also the quality of work performed and the energy requirements of the machine *(Rani et al., 2022).* At the same time, the use of high-strength materials can reduce wear but may lead to increased acquisition, heat treatment and manufacturing costs. For this reason, recent studies place increasing emphasis on material optimization and on the simultaneous evaluation of mechanical properties, wear resistance and manufacturing costs. Review analyses published in recent years show that the choice of a material for soil-working active parts should not be made solely on the basis of hardness or yield strength, but through a compromise between strength, toughness, wear behavior and cost *(Malvajerdi, 2023; Yazıcı, 2024).* It has also been shown that material properties need to be correlated with actual working conditions, since dynamic loads and local impacts can lead to behavior different from that predicted solely on the basis of static characteristics *(Yazıcı, 2024).*

Recent research has also extended the analysis to the use of surface treatments, layered materials and wear-resistant coatings for discs and other active parts. These solutions can reduce material losses and increase service life, but they involve additional technological costs, which requires careful evaluation of the ratio between mechanical benefit and manufacturing cost *(Zhang et al., 2024).*

At the same time, discrete element modeling has been used to analyze the interaction between the harrow discs, soil and plant residues, demonstrating the influence of disc angle, travel speed and working depth on cutting forces and tillage process efficiency *(Wu et al., 2026).* In the same context, recent studies on the wear of agricultural active parts emphasize the importance of comparing several constructive solutions and materials in order to identify the variant with high economic efficiency *(Noh et al., 2024).*

In addition to experimental analysis, numerical modeling of soil-active part interaction has become increasingly used in recent years. Models based on the finite element method and the discrete element method allow simulation of force distribution, soil particle motion and the loads transmitted to the active components. These methods help reduce the number of physical trials and provide useful information for optimizing geometry and material selection *(Ibrahmi and Bentaher, 2025).* Recent studies conducted on notched harrow discs have shown that material properties, surface coatings and soil-disc interaction conditions influence the distribution of equivalent Von Mises stresses and the structural response of the

active part *(Munteanu et al., 2026*). From an industrial standpoint, using a material with mechanical properties far superior to those required can lead to over-dimensioning and an unjustified increase in product cost. Conversely, choosing a lower-priced material that nevertheless ensures an adequate factor of safety and deformations within admissible limits can represent a more efficient solution for series production. Therefore, integrating structural analysis with an economic criterion can be a relevant method for validating the manufacturing solution of agricultural active parts.

In this context, the present paper focuses on the static analysis of the disc used on the IRUM independent disc harrow with a working width of 2.8 m. The machine is equipped with 22 discs, operates at depths between 20 and 180 mm and is designed for working speeds of 10-15 km/h. The aim of the research is to evaluate the structural behavior of the disc by means of the Finite Element Method and to compare several material variants based on equivalent Von Mises stress, displacements, strains and factor of safety.

The numerical results will be correlated with material and manufacturing costs, in order to identify a solution offering a favorable ratio between mechanical performance, durability and price.

## MATERIALS AND METHODS

The study was carried out on the IRUM independent disc harrow (Fig. 1) with a working width of 2.8 m, intended for shallow and medium-depth soil tillage. The machine is equipped with 22 independent discs, arranged in two rows, at a distance of 250 mm between discs and 1150 mm between the two rows. The working depth ranges between 20 and 180 mm, and the travel speed during operation is 10-15 km/h. The machine's own mass is approximately 1450 kg, and the minimum recommended tractor power is 90 hp. At the rear, the harrow is fitted with a segmented roller with a diameter of 440 mm, used for additional crumbling, leveling and controlled compaction of the soil.

**Table 1**

**Main technical characteristics of the IRUM independent disc harrow**

| Characteristic | Value |
|---|---|
| Working width | 2.8 m |
| Total width | 3.2 m |
| Total length | 2.7 m |
| Number of discs | 22 |
| Distance between discs | 0.25 m |
| Distance between disc rows | 1.15 m |
| Working depth | 0.02–0.15 m |
| Working speed | 10–15 km/h |
| Own mass | 1450 kg |
| Roller type | segmented |
| Roller diameter | 440 mm |




**Fig. 1 - IRUM 2.8 m independent disc harrow**

The component analyzed was the notched concave disc, representing the active part in direct contact with the soil. During operation, it is subjected to loads generated by soil resistance to cutting and movement, as well as additional local loads caused by terrain unevenness and any obstacles encountered during operation.

The three-dimensional geometric model of the disc was created in the SolidWorks environment based on the component's design dimensions. The analyzed disc has an outer diameter of 460 mm and a thickness of 4 mm, and is fitted with nine peripheral notches. The geometry is concave, with a concavity of 45 mm. The disc is attached to the hub through four holes with a diameter of 12.5 mm, arranged on a pitch circle with a diameter of 110 mm.

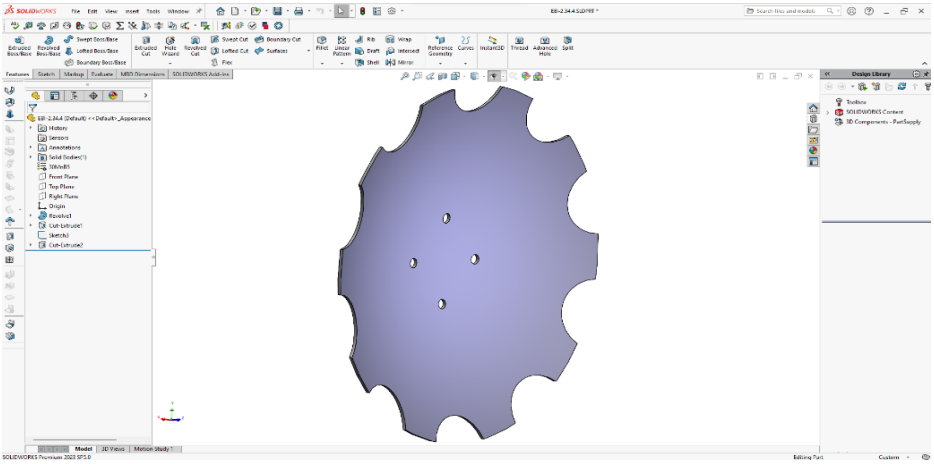


**Fig. 2 - Geometric model of the analyzed notched concave disc**

The main geometric characteristics of the disc are presented in Table 2.

**Table 2**

**Main geometric characteristics of the disc**

| Characteristic | Value |
|---|---|
| Outer diameter | 460 mm |
| Thickness | 4 mm |
| Disc type | concave, notched |
| Number of notches | 9 |
| Concavity | 45 mm |
| Number of mounting holes | 4 |
| Pitch circle diameter of holes | 110 mm |
| Diameter of mounting holes | 12.5 mm |

In order to validate the constructive solution and evaluate the ratio between mechanical performance and manufacturing cost, the static analysis was carried out for several material variants. The material used in the current constructive solution was considered the reference variant, and its behavior was compared with that of alternative materials with different mechanical properties and costs.

For each material, the following were defined: the modulus of elasticity *E*, Poisson's ratio *v*, density ρ\rho, yield strength $R_e$, tensile strength $R_m$ and hardness. For the economic evaluation, the material cost, heat treatment cost and technological costs associated with the manufacturing process were taken into account.

**Table 3**

**Properties of the analyzed materials**

| Characteristic | M1 – 30MnB5 | M2 – 65Mn10 | M3 – 18CrMoS4 |
|---|---|---|---|
| Material type | Boron-alloyed steel | C–Mn spring steel | Cr–Mo alloy steel for carburizing |
| C [%] | 0.27–0.33 | 0.62–0.70 | 0.15–0.21 |
| Mn [%] | 1.15–1.45 | 0.90–1.20 | 0.60–0.90 |
| Cr [%] | ≤ 0.30 | ≤ 0.25 | 0.90–1.20 |
| Mo [%] | – | – | 0.15–0.25 |
| B [%] | 0.0008–0.0050 | – | – |
| Modulus of elasticity, E [GPa] | 210 | 210 | 210 |
| Poisson's ratio, v | 0.28 | 0.28 | 0.28 |
| Density, ρ [kg/m³] | 7850 | 7820 | 7800 |
| Yield strength, Re / Rp0.2 [MPa] | 900–1000, after quenching | 520–680, quenched and | 450–600, untreated condition |

| Characteristic | M1 – 30MnB5 | M2 – 65Mn10 | M3 – 18CrMoS4 |
|---|---|---|---|
| | | tempered | |
| Tensile strength, Rm [MPa] | 1200–1400 | 825–925 | 700–950 |
| Hardness | 50–54 HRC, approx. 510 HBW | 45–48 HRC, approx. 450 HBW | approx. 200 HBW in the core; up to approx. 60 HRC in the carburized layer |
| Estimated cost [lei/kg] | 9.5–12 | 7.5–9.5 | 14–18 |

The three materials analyzed have different characteristics both mechanically and technologically. Steel 30MnB5 is a boron-alloyed steel with high hardenability, suitable for components subjected simultaneously to mechanical loading and wear. Steel 65Mn10 has a high carbon and manganese content and can reach, after quenching and tempering, high hardness values, at a raw material cost lower than that associated with Cr-Mo alloy steels. Steel 18CrMoS4 is intended mainly for carburizing, being characterized by a tough core and the possibility of obtaining high hardness in the surface layer. Economically, 65Mn10 has the lowest estimated raw material cost, while 18CrMoS4 involves the highest cost, both due to the alloying elements and the need for a carburizing treatment.

During operation, the disc is subjected to loads generated by its interaction with the soil, their intensity being influenced by the soil's physico-mechanical properties, working depth, travel speed and the geometry of the active part. For the static analysis, a loading case corresponding to work in heavy soil was considered, so that the structural evaluation would be performed under conservative conditions.

The total draft resistance of the harrow was estimated using the relation used in agricultural mechanics:

$$R = k \cdot B \cdot a \tag{1}$$

where:

$R$ - total draft resistance of the machine [daN];

$k$ - specific soil resistance [daN/cm²];

$B$ - working width of the machine [cm];

$a$ - working depth [cm].

For the analyzed case, heavy soil was considered, characterized by a specific resistance coefficient k = 0.3-0.5 daN/cm². For a working width B = 280 cm and a depth a = 15 cm, the resulting limit values were:

$$R_{min} = 0.3 \cdot 280 \cdot 15 = 1260\, daN \tag{2}$$

$$R_{max} = 0.5 \cdot 280 \cdot 15 = 2100\, daN \tag{3}$$

Since the harrow is equipped with 22 discs, a uniform distribution of the total draft resistance among the discs was adopted as a simplifying assumption. For a single disc, the maximum longitudinal force component was thus estimated at:

$$F_{x,max} = \frac{2100}{22} = 95.5\, daN \tag{4}$$

The vertical component was evaluated starting from the total mass of the machine, approximately 1450 kg, distributed uniformly, under the same simplifying assumption, over the 22 discs:

$$F_z \approx \frac{1450}{22} = 65.9\, daN \tag{5}$$

For the lateral component, associated with the angular position of the disc relative to the travel direction, a value of $F_y$ = 45 daN was adopted in the calculation case. This value represents a calculation assumption for the demanding situation analyzed and should be interpreted together with the other simplifications of the model.

The resultant force applied to a disc was determined by orthogonal composition of the three components:

$$F_R = \sqrt{F_x^2 + F_y^2 + F_z^2} \tag{6}$$

For the adopted maximum values ($F_x$ = 95.5 daN, $F_y$ = 45 daN and $F_z$ = 65.9 daN), the result is $F_R \approx$ 124 daN, i.e. approximately 1240 N.

To account for the effect of load variations caused by soil unevenness and the dynamic nature of the working process, a dynamic coefficient $K_d$ = 13 was adopted. The design force used in the static analysis was:

$$F_{calc} = K_d \cdot F_R = 13 \cdot 1240 \approx 16000 \tag{7}$$

Consequently, for the FEM structural analysis, a resultant design force of 16000 N per disc was adopted, applied in a distributed manner over the lower active sector, corresponding to the soil contact area. Distributed load application avoids the artificial stress concentration that could occur in the case of a point force.

The support conditions were defined in the area of the four mounting holes with a diameter of 12.5 mm, arranged on a pitch circle with a diameter of 110 mm. This loading and constraint scheme was intended to reproduce the load transfer between the disc's active area and the mounting assembly.

The three-dimensional model of the disc was discretized using a Solid Mesh, generated in SolidWorks Simulation with a curvature-based algorithm (*Blended curvature-based mesher*). To increase the accuracy of the numerical solution, especially in areas with pronounced geometric variations, a high-quality mesh was used (*High quality mesh*).

The final mesh characteristics were:

- mesh type: Solid Mesh;
- mesher type: Blended curvature-based mesher;
- mesh quality: High;
- number of Jacobian points for quality check: 16;
- maximum element size: 5.51288 mm;
- minimum element size: 1.83761 mm;
- total number of nodes: 69,027;
- total number of elements: 34,027;
- maximum aspect ratio: 6.1508;
- percentage of elements with aspect ratio less than 3: 99.9%;
- percentage of elements with aspect ratio greater than 10: 0%;
- number of distorted elements: 0.

Mesh quality was checked based on the geometric criteria available in SolidWorks Simulation. The maximum aspect ratio value was 6.1508, and 99.9% of the elements had an aspect ratio below 3. No elements with an aspect ratio greater than 10 were identified, nor were any distorted elements.

These results indicate an appropriate discretization quality for the static analysis performed.

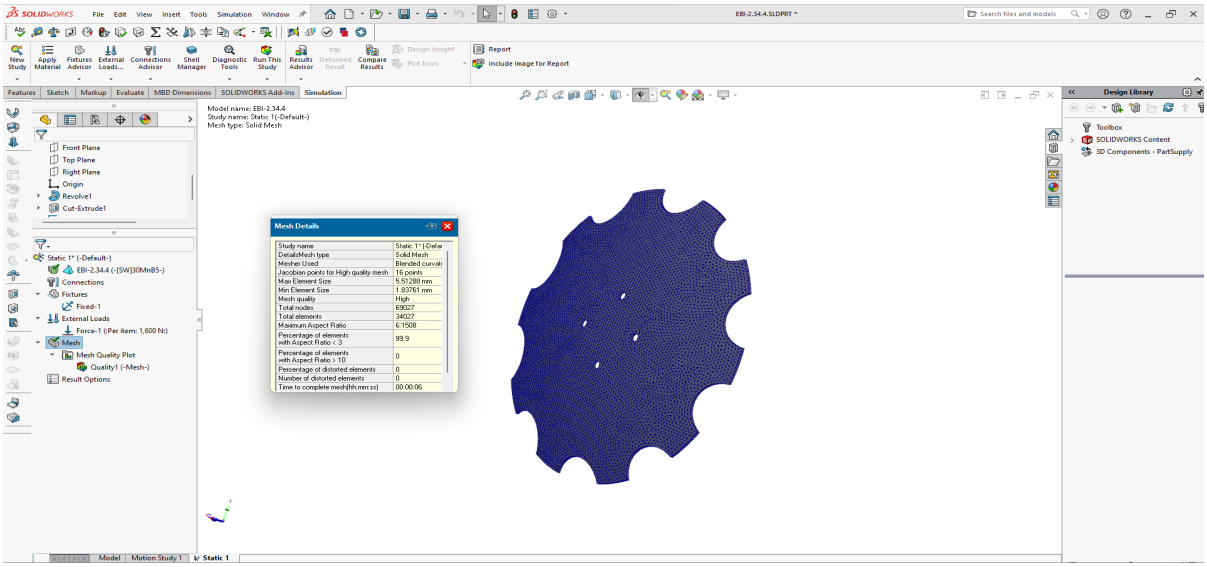



**Fig. 3 - Finite element mesh and discretization characteristics of the analyzed disc**

The static structural analysis of the disc was carried out in the SolidWorks Simulation environment, using the Finite Element Method. For all three material variants analyzed — 30MnB5, 65Mn10 and 18CrMoS4 — the model geometry, support conditions, mesh characteristics and applied load were kept identical, so that the results could be directly compared.

In all cases, a resultant design force of 1600 N was used, determined for a demanding operating regime and applied to the active lower sector of the disc, corresponding to the soil interaction area. The area of the four mounting holes was used to define the support conditions, in order to reproduce the load transfer between the disc and the mounting assembly.

For each material, the following quantities were evaluated:

- equivalent Von Mises stress;
- total displacement;
- equivalent specific strain;
- factor of safety.

The maximum equivalent stress was compared with the yield strength corresponding to each material, in order to verify behavior within the elastic range.

The factor of safety was determined using the relation:

$$FoS = \frac{R_e}{\sigma_{VM,max}} \quad (8)$$

where:

$R_e$ represents the material's yield strength [MPa],

$\sigma_{VM,max}$ represents the maximum equivalent Von Mises stress determined by FEM analysis [MPa].

For structural validation, the material was considered adequate when the maximum equivalent stress remained below the yield strength:

$$\sigma_{VM,max} < R_e \quad (9)$$

and the factor of safety satisfied the condition:

$$FoS > 1 \quad (10)$$

For the comparative evaluation of the three materials, the results were analyzed under the same loading and discretization conditions. Since the modulus of elasticity values are similar for all three steels, differences in behavior were interpreted mainly in terms of yield strength, factor of safety, hardness and the cost associated with the material and heat treatment.

To validate the constructive solution, the numerical results were subsequently correlated with the technical-economic criterion, seeking to identify the material that simultaneously ensures a sufficient strength reserve and a favorable manufacturing cost.

## RESULTS AND DISCUSSION

The static structural analysis by the Finite Element Method was carried out for the notched concave disc of the independent disc harrow, having an outer diameter of 460 mm and a thickness of 4 mm. Three material variants were investigated, namely **30MnB5, 65Mn10 and 18CrMoS4**, under identical conditions of geometry, discretization, support and loading. Maintaining the same analysis conditions allowed a direct comparison of the structural response of the three variants and an evaluation of the influence of material properties on the factor of safety. The numerical results were analyzed through the distribution of equivalent Von Mises stress, equivalent specific strain, resultant displacement and factor of safety.

The corresponding maps for the three variants are presented in Figures 4-6.

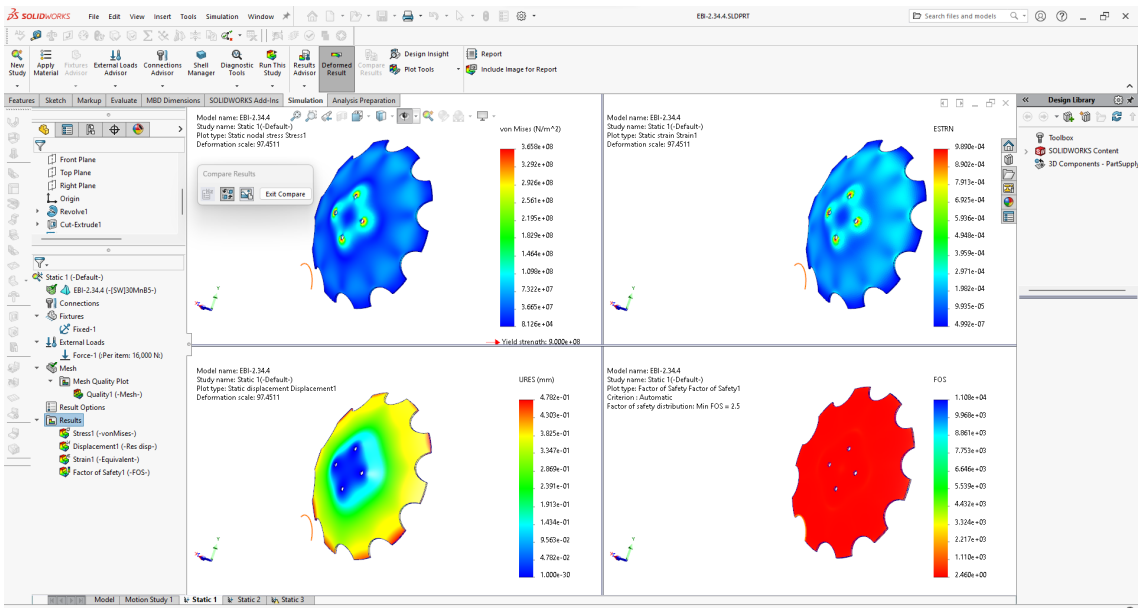


**Fig. 4 - Results of the static structural analysis for the disc made of 30MnB5 steel:**
*a) equivalent Von Mises stress; b) equivalent specific strain; c) resultant displacement; d) factor of safety*

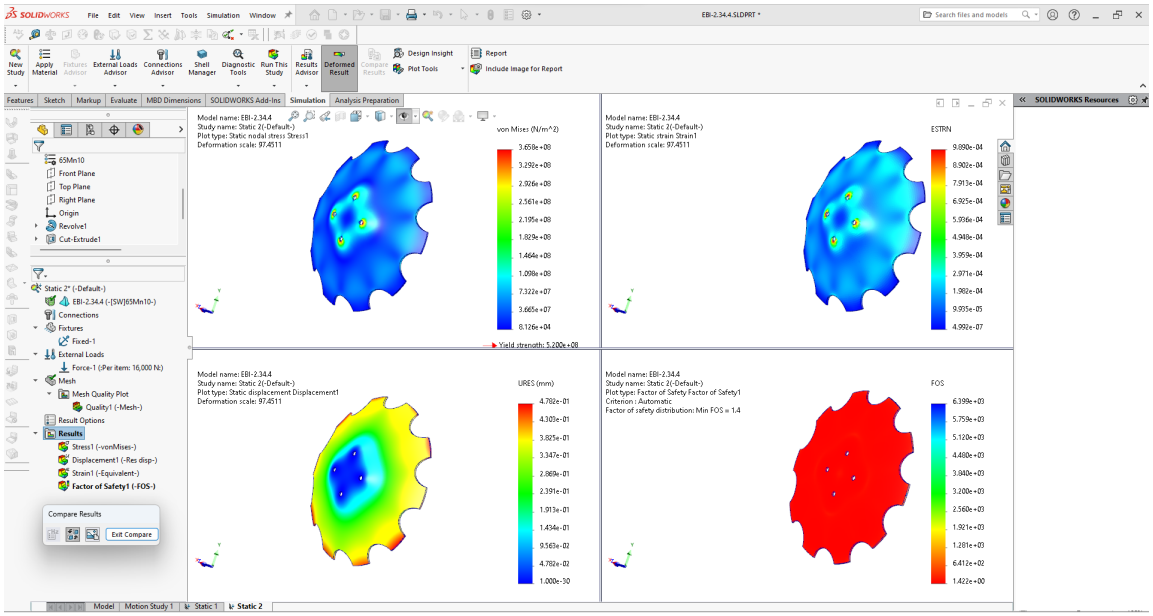


**Fig. 5 - Results of the static structural analysis for the disc made of steel 65Mn10:**
*a) equivalent Von Mises stress; b) equivalent specific strain; c) resultant displacement; d) factor of safety*

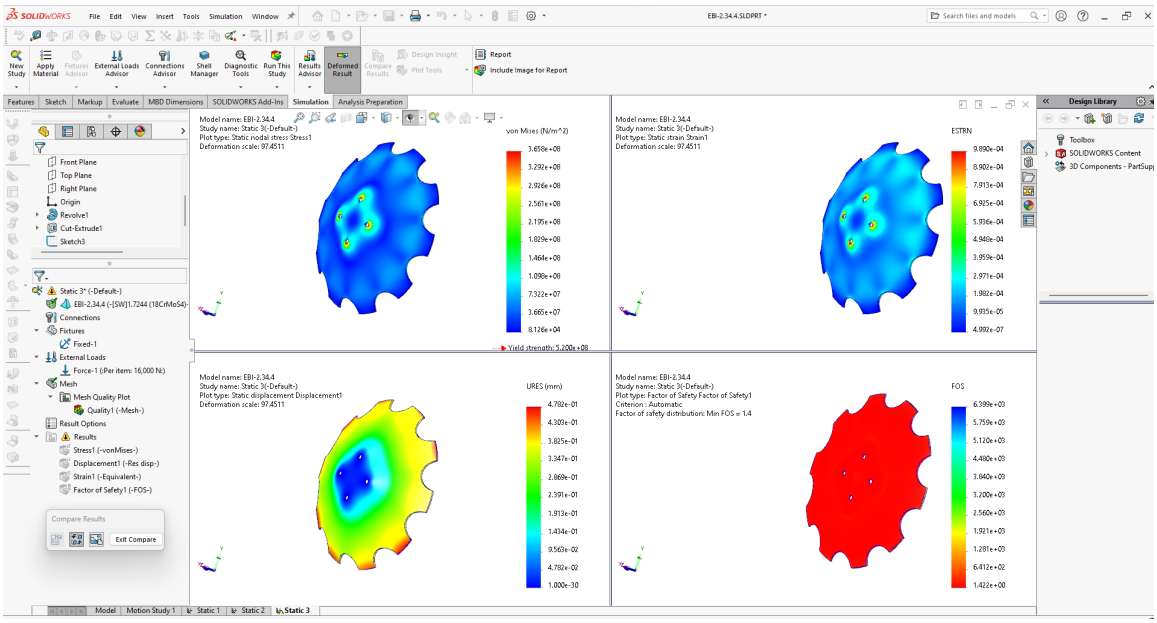


**Fig. 6 - Results of the static structural analysis for the disc made of steel 18CrMoS4:**
*a) equivalent Von Mises stress; b) equivalent specific strain; c) resultant displacement; d) factor of safety*

The stress distribution analysis shows that the most heavily loaded areas are located near the mounting holes and the central region of the disc, where the load transfer to the mounting assembly takes place. Since the three materials have similar modulus of elasticity values and were analyzed under identical conditions, the differences between the Von Mises stress values and displacements are small.

The main differentiation between the variants is given by the material's yield strength and, implicitly, by the factor-of-safety value.

To evaluate the loading level of each material, the degree of utilization of the yield strength was determined as the percentage ratio between the maximum equivalent Von Mises stress and the material's yield strength:

$$\eta = \frac{\sigma_{VM,max}}{R_e} \cdot 100 \tag{11}$$

where:

$\eta$ represents the degree of utilization of the yield strength [%],

$\sigma_{VM,max}$ represents the maximum equivalent Von Mises stress [MPa],

$R_e$ represents the material's yield strength [MPa].

**For 30MnB5 steel:**

$$\eta_{30MnB5} = \frac{365.8}{900} \cdot 100 = 40.64\,\% \quad (12)$$

**For 65Mn10 steel:**

$$\eta_{65Mn10} = \frac{365.8}{520} \cdot 100 = 70.35\,\% \quad (13)$$

**For 18CrMoS4 steel:**

$$\eta_{18CrMoS4} = \frac{365.8}{520} \cdot 100 = 70.35\,\% \quad (14)$$

The results show that 30MnB5 uses approximately 40.64% of the yield strength in the analyzed loading case, while 65Mn10 and 18CrMoS4, for the yield strength of 520 MPa introduced into the numerical models, use approximately 70.35%. Therefore, 30MnB5 shows a higher structural reserve compared with the other two variants for the same loading and support conditions.

A direct comparison of the numerical results for the three materials is presented in Table 4. The same calculation conditions were used in all cases, which allows the evaluation of the influence of material properties on the disc's strength reserve. The parameters selected for comparison were the equivalent Von Mises stress, maximum displacement, equivalent specific strain, factor of safety and degree of utilization of the yield strength.

**Table 4**

**Comparison of FEM analysis results for the investigated materials**

| Material | Applied force [N] | $\sigma_{VM,max}$ [MPa] | $\varepsilon_{eq,max}$ | $\delta_{max}$ [mm] | $R_e$ [MPa] | $FoS_{min}$ | Yield strength utilization [%] |
|---|---|---|---|---|---|---|---|
| 30MnB5 | 16000 | 365.8 | $9.890\times10^{-4}$ | 0.4782 | 900 | 2.46 | 40.64 |
| 65Mn10 | 16000 | 365.8 | $9.890\times10^{-4}$ | 0.4782 | 520 | 1.42 | 70.35 |
| 18CrMoS4 | 16000 | 365.8 | $9.890\times10^{-4}$ | 0.4782 | 520* | 1.42 | 70.35 |

The FEM analysis results show that, for the same geometry, the same support conditions and the same applied load, the equivalent Von Mises stress, maximum displacement and equivalent specific strain values are practically identical for the three materials analyzed.

This behavior is explained by the close modulus of elasticity values and by the linear elastic nature of the analysis. The differentiation between variants is determined mainly by the material's yield strength and, implicitly, by the factor of safety and the degree of utilization of the load-bearing capacity.

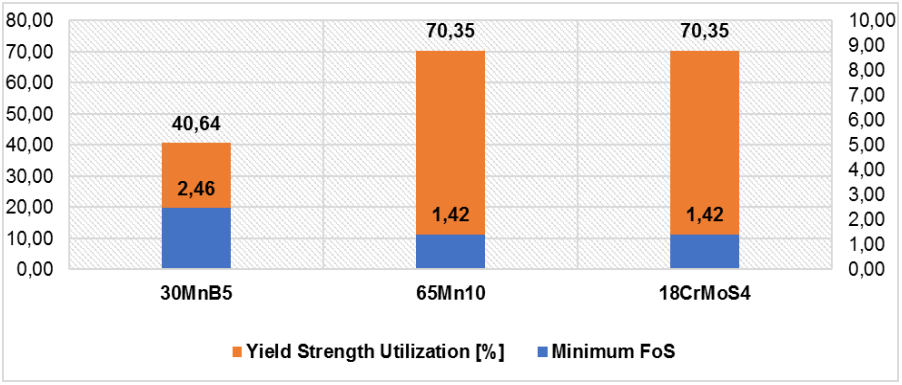



**Fig. 7 - Comparative representation of the minimum factor of safety and the degree of utilization of the yield strength for the analyzed materials**

The comparative representation in Fig.7 highlights the differences between the three materials in terms of the minimum factor of safety and the degree of utilization of the yield strength. Steel 30MnB5 shows the highest structural reserve, with a factor of safety of 2.46 and a degree of utilization of 40.64%, while for 65Mn10 and 18CrMoS4 the values are 1.42 and 70.35%, respectively.

The similar values of the Von Mises stress, displacement and strain are explained by the use of the same geometry, the same load and close modulus of elasticity values. The differentiation between materials is determined mainly by the yield strength and, implicitly, by the structural reserve.

Economically, 65Mn10 has the lowest estimated raw material cost, 30MnB5 an intermediate cost, and 18CrMoS4 the highest cost, to which the carburizing treatment is added. Under these conditions,

30MnB5 offers the most favorable compromise between structural reserve and cost, while 65Mn10 may represent an economical alternative, but with a lower safety reserve.

## CONCLUSIONS

- The FEM analysis showed that, for the same geometry and the same load, the three materials exhibit similar stress, displacement and strain values, the main differences being given by the yield strength and the factor of safety. 30MnB5 showed the highest structural reserve, with a factor of safety of 2.46, compared with 1.42 for 65Mn10 and 18CrMoS4.
- From a technical-economic standpoint, 30MnB5 shows the most favorable combination between structural safety and estimated cost. 65Mn10 may represent a more economical alternative but requires further validation for variable loading and wear. Under the static analysis conditions performed, 18CrMoS4 did not show a structural advantage capable of offsetting its higher cost and treatment complexity.
- The results obtained recommend continuing the research through fatigue analysis, wear analysis and experimental validation under real working conditions.

## REFERENCES

[1] Chirende, B., Li, J. Q., & Vheremu, W. (2019). Application of finite element analysis in modeling of bionic harrowing discs. Biomimetics, 4(3), 61.

[2] Guan, C., Fu, J., Cui, Z., Wang, S., Gao, Q., & Yang, Y. (2021). Evaluation of the tribological and anti-adhesive properties of different materials coated rotary tillage blades. Soil and Tillage Research, 209, 104933.

[3] Ibrahmi, A., & Bentaher, H. (2025). Simulation of tillage forces and soil movement during soil-disc plow interaction using FEM. Scientific Reports, 15(1), 36022.

[4] Malvajerdi, A. S. (2023). Wear and coating of tillage tools: A review. Heliyon, 9(6).

[5] Munteanu, C., Tufescu, A., Lupu, F. C., Istrate, B., Benchea, M., Melnic, I., ... & Arsenoaia, V. N. (2026). Explicit FEM analysis of soil–disc interaction for APS-coated notched harrow discs in representative agricultural soils. Applied Sciences, 16(1), 395.

[6] Noh, J. M., Liu, L., Tekeste, M. Z., Li, Q., Hatfield, J., & Eisenmann, D. (2024). Digitized Seedbed Soil Quality Assessment from Worn and Edge Hardened Cultivator Sweeps. Sensors, 24(21), 6951.

[7] Rani, A., Singh, T. P., Singh, J., Patel, V., & Choudhary, M. K. (2022). Abrasive wear behavior of EN42 steel used in agricultural discs in field conditions. Engineering Failure Analysis, 142, 106789.

[8] Singh, J., Chatha, S. S., & Sidhu, B. S. (2021). Abrasive wear characteristics and microstructure of Fe-based overlaid ploughshares in different field conditions. Soil and Tillage Research, 205, 104771.

[9] Yazıcı, A. (2024). Wear on steel tillage tools: A review of material, soil and dynamic conditions. Soil and Tillage Research, 242, 106161.

[10] Zhang, Y., Zhan, H., Xu, T., Li, Z., Wang, Y., & Wang, R. (2024). (2024). Current research of experiment on wear performance for tillage tools of agricultural machinery. Journal of Chinese Agricultural Mechanization, 45(1), 61.

[11] Wu, P., Zhang, X., & Chen, Y. (2026). DEM modelling of crop residue and soil dynamics as affected by the tillage direction of a disc harrow. Biosystems Engineering, 263, 104369.

# SPATIAL ANALYSIS OF AN ORCHARD BASED ON UAV RGB IMAGERY AND GIS TECHNOLOGIES
/
# *ANALIZA SPAȚIALĂ A UNEI LIVEZI PE BAZA DATELOR UAV RGB ȘI A TEHNOLOGIILOR GIS*

**Daria-Ioana SICARU*[1)], Neluș-Evelin GHEORGHIȚĂ[1)], Mihaela NITU[2)]**
[1)] Faculty of Biotechnical Systems Engineering, National University of Science and Technology POLITEHNICA Bucharest / Romania;
[2)] National Institute of Research-Development for Machines and Installations Designed for Agriculture and Food Industry - INMA Bucharest / Romania
**Tel: 0770 783 029; *E-mail: dariaioana8@yahoo.com*

***Keywords:*** *UAV photogrammetry, GIS, RGB imagery, orchard monitoring, canopy height model, vegetation indices*

**ABSTRACT**
*Precision agriculture increasingly relies on unmanned aerial vehicles (UAVs) and GIS techniques for the high-resolution spatial characterization of vegetation. This study evaluates the use of UAV RGB imagery, combined with GIS techniques, for the individual and spatial characterization of trees in an orchard. A DJI Mini 2 SE drone was used to acquire aerial images over an area of approximately 600 m², containing 15 fruit trees, the images being processed photogrammetrically in WebODM to generate the orthophoto, DSM and DTM. Three methods of canopy height estimation were compared: CHM obtained as the difference between DSM and DTM, the buffer-DSM approach, and a CHM derived from point cloud classification using the Cloth Simulation Filter (CSF) algorithm in CloudCompare. To characterize vegetation variation, the RGB indices GLI and VARI were calculated at crown level and spatially interpolated using the IDW method. Field validation indicated, for the CSF-based method, a detection rate of 87% and an RMSE of 0.40 m. GLI and VARI values showed variations associated with differences in vegetation condition observed in the field. The results highlight the potential of integrating UAV RGB imagery, photogrammetry and GIS for the preliminary spatial characterization of individual orchard trees.*

**REZUMAT**
*Agricultura de precizie se bazează tot mai mult pe sisteme aeriene fără pilot (UAV) și tehnici GIS pentru caracterizarea spațială a vegetației la rezoluție ridicată. Studiul de față evaluează utilizarea imaginilor UAV RGB, combinate cu tehnici GIS, pentru caracterizarea individuală și spațială a pomilor dintr-o livadă. O dronă DJI Mini 2 SE a fost utilizată pentru achiziția de imagini aeriene asupra unei suprafețe de aproximativ 600 m², care conținea 15 pomi fructiferi, imaginile fiind procesate fotogrammetric în WebODM pentru generarea ortofotoplanului, DSM și DTM. Au fost comparate trei metode de estimare a înălțimii coronamentului: CHM obținut prin diferența DSM–DTM, abordarea buffer-DSM și un CHM derivat din clasificarea norului de puncte utilizând algoritmul Cloth Simulation Filter (CSF) în CloudCompare. Pentru caracterizarea variației vegetației au fost calculați indicii RGB GLI și VARI la nivelul fiecărui coronament și interpolați spațial prin metoda IDW. Validarea pe teren a indicat pentru metoda bazată pe CSF o rată de detecție de 87% și o eroare RMSE de 0,40 m. Valorile GLI și VARI au prezentat variații asociate cu diferențele de stare a vegetației observate în teren. Rezultatele evidențiază potențialul integrării UAV RGB, fotogrammetriei și GIS pentru caracterizarea spațială preliminară a pomilor individuali.*

## INTRODUCTION

Precision agriculture is a branch of sustainable agriculture that aims to make more efficient use of agricultural resources and reduce environmental impact. Advances in technology and data analysis capabilities have enabled precision agriculture to support decision-making in farming practices (*Sishodia et al., 2020*). Traditional vegetation monitoring methods generally rely on physical fieldwork, making them time-consuming and costly.

In this context, the increasingly widespread use of UAVs has reshaped agricultural practices, as unmanned aerial vehicles have advanced considerably in recent years and are now equipped with advanced imaging sensors capable of capturing aerial imagery at low cost over large areas (*Anzar et al., 2025*).

Individual tree detection in orchard monitoring allows for improved management practices. In addition, analysing each tree separately provides structural, geometric and positional information specific to each individual case (*Dong et al., 2020*). When crown boundaries are delineated with greater precision, the resulting geometric data — crown area and diameter — become more reliable, as the risk of confusion with neighbouring vegetation is reduced, supporting more accurate decisions on irrigation, fertilization and other management practices (*Ball et al., 2023*). Compared with satellite imagery, UAVs offer a clear advantage in terms of spatial detail and the frequency with which the same area can be surveyed, making them a more flexible solution for farmers (*Ponce et al., 2022*). However, limitations remain regarding battery life and the maximum area that can be covered within a single orchard (*Zhang et al., 2021*). Photogrammetric processing of UAV images, using techniques such as Structure from Motion (SfM) and Multi-View Stereo (MVS), makes it possible to derive several key products, including three-dimensional point clouds, digital orthophoto maps (DOM), digital surface models (DSM) and digital terrain models (DTM) (*Dong et al., 2020*).

These products can subsequently be used to obtain useful information about individual trees, such as height, 3D coordinates, crown diameter and crown area. Among the available approaches, the Canopy Height Model (CHM) is commonly used to estimate tree height, typically calculated as the difference between the digital surface model and the digital terrain model *(Vacca and Vecchi, 2024).*

However, comparing UAV-based height extraction methods on a university campus, Hao et al. (2022) reported that heights derived from CHM tend to be lower than field-measured values, while height extraction directly from the point cloud achieved a mean absolute error of 10.28 cm, outperforming the CHM-based approach.

UAV RGB image acquisition makes it possible to obtain spectral information from the visible domain. The spatial evaluation and monitoring of vegetation frequently relies on the calculation of spectral indices, which can provide useful information on vegetation status (*Gitelson et al., 2002*). Although many studies have focused on multispectral and hyperspectral data for vegetation assessment, RGB imagery also provides valuable information that can be used to characterize vegetation variability.

Vegetation indices derived from RGB bands, such as the Green Leaf Index (GLI) and the Visible Atmospherically Resistant Index (VARI), have shown potential for detecting variations in plant vigour and early signs of stress (*Banaszek and Szota, 2025*). For instance, Nur Anisa et al. (2020) demonstrated that the health of oil palm trees could be assessed using the VARI index derived from UAV imagery, highlighting the considerable potential of RGB-based data for vegetation health monitoring.

The present study aims to evaluate the feasibility of a low-cost UAV RGB workflow, combined with open-source GIS software, for the spatial and structural characterization of a small backyard orchard. Specific objectives were to: compare three methods of tree height estimation in terms of detection rate and accuracy against field measurements; calculate and interpret the GLI and VARI vegetation indices at individual tree level; and generate an interpolated spatial representation of index variability across the orchard using IDW.

## MATERIALS AND METHODS

The study was conducted in a private garden located in Blejoi, Prahova County, Romania (Figure 1), covering an area of approximately 600 m², which was used as an experimental area for tree analysis using photogrammetric and GIS-based methods. The study area included 15 fruit trees, for which spatial and structural characteristics were subsequently determined and RGB vegetation indices were calculated.



**Fig. 1 - Location of the study area in Blejoi, Prahova County, Romania.**
*(source: WebODM)*

Aerial image acquisition was carried out on 11 July 2026, starting at 11:30. Weather conditions at the time of the flight were favourable, with clear skies, an air temperature of approximately 24 °C and a wind speed of approximately 7 km/h; no significant shading of the study area was present during acquisition.

Data were acquired using a DJI Mini 2 SE drone equipped with an RGB camera. The flight was conducted at an altitude of 30 m, with the camera oriented at nadir (90°) and an image overlap of approximately 70–72%, resulting in a theoretical ground sampling distance (GSD) of approximately 1 cm at the flight altitude used. A total of 40 aerial images were acquired for the study area and subsequently used for photogrammetric reconstruction; the final orthophoto exported from WebODM was generated at a resolution of 5 cm/pixel, corresponding to the software's default orthophoto-resolution setting.

To validate the results obtained through photogrammetric methods, direct field measurements of tree height were subsequently carried out approximately one month after the flight date. Measurements were taken using a tape measure, an instrument associated with an estimated error of approximately ±10 cm. The one-month interval between UAV acquisition and field measurements was considered negligible for result comparison, as the expected growth of mature trees over this period is on the order of 1–3 cm.

Aerial images were processed in WebODM, producing an RGB orthophoto (used for colour analysis and tree digitization), a DSM, a DTM, and a raw photogrammetric point cloud (used independently for ground/surface classification, described below). Based on the orthophoto, 15 trees were identified and manually digitized, each assigned a unique identifier together with species, crown geometry and derived attribute values. Three methods of tree height estimation were compared. The first used the classical canopy height model, obtained as the difference between the digital surface model and the digital terrain model (*Vacca and Vecchi, 2024*):

$$CHM = DSM - DTM \tag{1}$$

For each tree crown, the corresponding CHM values were extracted to obtain an estimate of tree height. The second method relied solely on the DSM: the maximum DSM value inside each crown was compared with the mean DSM value in an external buffer ring, used as a local estimate of terrain elevation, with height calculated as the difference between the two.

The third method was applied directly to the raw point cloud, independently of WebODM's rasterized outputs: ground and vegetation points were separated using the Cloth Simulation Filter (CSF) algorithm in CloudCompare *(Zhang et al., 2016).* Ground points were rasterized at 0.1 m resolution using Delaunay triangulation to fill small data gaps, with cells lacking nearby ground points explicitly flagged as NoData. A surface model was generated in the same manner from the full point cloud, and the difference between the two produced a third, independently classified CHM dataset.

Two RGB-derived vegetation indices were calculated at crown level and averaged per tree: the Green Leaf Index (Louhaichi et al., 2001):

$$GLI = \frac{2G - R - B}{2G + R + B} \tag{2}$$

and the Visible Atmospherically Resistant Index *(Gitelson et al., 2002):*

$$VARI = \frac{G - R}{G + R - B} \quad (3)$$

where R, G and B are the reflectance values of the red, green and blue bands, respectively.

Both indices are sensitive to the proportion of green canopy cover and to biochemical changes in leaf pigmentation associated with vegetative stress. Relationships between the two indices and the structural parameters of the trees (height, crown area) were further examined using the Pearson correlation coefficient.

Finally, thematic maps of tree height, species, GLI and VARI were produced in QGIS.

The spatial distribution of GLI and VARI was interpolated using Inverse Distance Weighting (IDW) *(Shepard, 1968; Sobjak et al., 2023),* based on the 15 point values, with results clipped to the boundary of the study area.

## RESULTS

To characterize the spatial distribution of the orchard trees, four thematic maps were produced in QGIS: tree height, species, GLI, and VARI (Figure 2). Together, these maps provide an overview of the structural and RGB-derived vegetation characteristics of the analysed trees and allow the spatial variability among individual trees to be visually assessed.

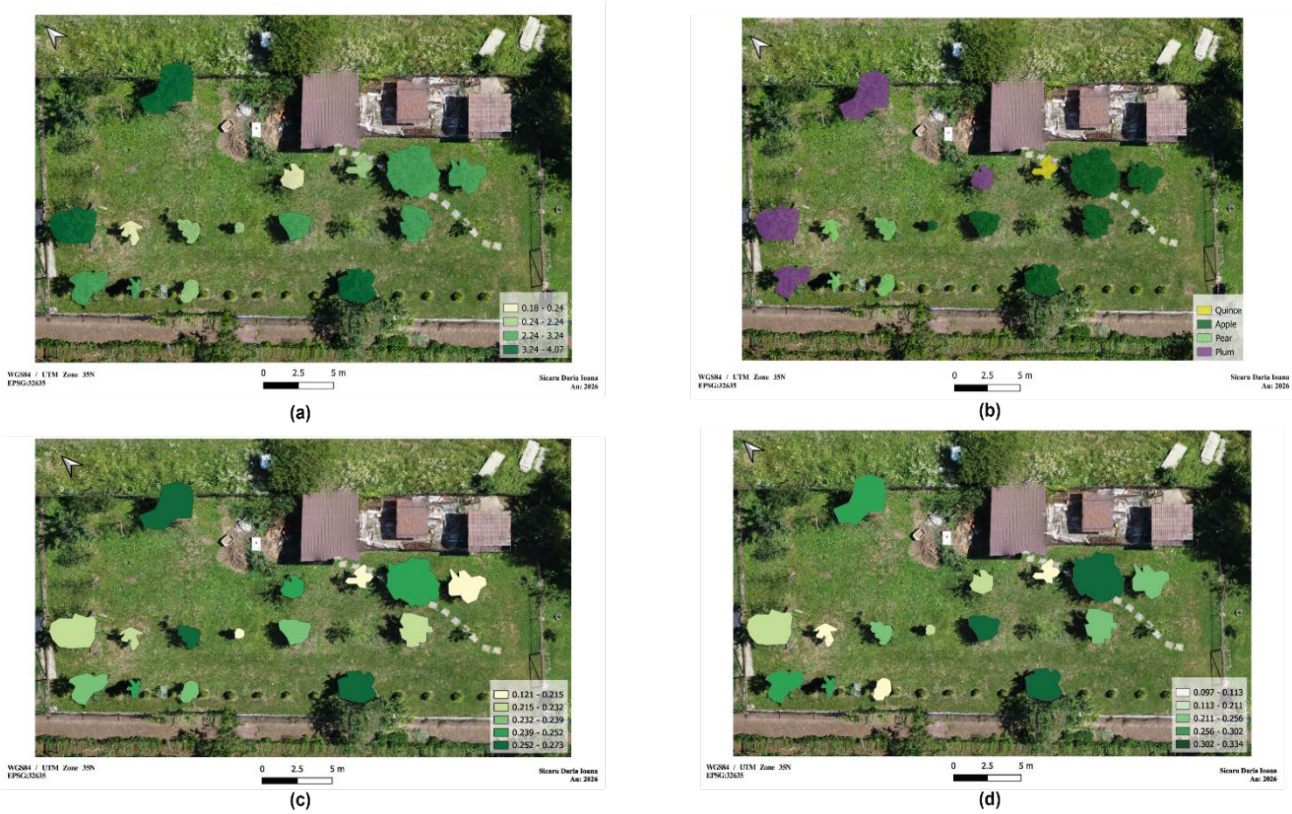



**Fig. 2 - Thematic maps of (a) tree height, (b) species distribution, (c) GLI, (d) VARI**

Three methods of tree height estimation were compared, as described in the previous section. Mean heights across the 15 trees were 1.16 m for the CHM method, 2.26 m for the buffer-DSM method, and 2.53 m for the point-cloud-based CHM (CloudCompare/CSF). Detection rate — the proportion of trees for which a method returned a height above a 0.3 m crown-detection threshold — and accuracy indicators (RMSE, MAE, mean bias), computed on the subset of 11 trees detected simultaneously by all three methods, are summarized in Tables 1 and 2.

The CSF-based method achieved both the highest detection rate (87%) and the lowest estimation error (RMSE = 0.40 m, MAE = 0.33 m), likely due to direct control over ground/vegetation point classification and the fine interpolation resolution used (0.1 m), compared with the automatic classification in the WebODM pipeline.

All three methods showed a negative bias, indicating systematic underestimation of tree height, most pronounced for the classical CHM approach; the close match between bias and MAE for each method

suggests the error is predominantly systematic rather than random, opening the possibility of a future calibration correction. Detection failures were concentrated at trees ID 5, 7, 8 and 12, with a progressive improvement across methods: the classical CHM missed 4 of 15 trees, buffer-DSM missed 3, and the point-cloud-based CHM missed only 2 (ID 7 and 8), likely reflecting small crown size, sparse foliage, shading, and the inherent limitations of RGB-only photogrammetric reconstruction. Overall, the CSF-based method was considered the most suitable for height estimation in this dataset.

**Table 1**

**Detection rate per method**

| Method | Trees detected | Total trees | Detection rate |
|---|---|---|---|
| CHM (DSM − DTM) | 11 | 15 | 73% |
| Buffer-DSM | 12 | 15 | 80% |
| CSF (CloudCompare) | 13 | 15 | 87% |

**Table 2**

**RMSE, MAE, mean bias per method**

| Method | RMSE (m) | MAE (m) | Mean bias (m) |
|---|---|---|---|
| CHM | 1.85 | 1.75 | −1.75 |
| Buffer-DSM | 0.55 | 0.47 | −0.42 |
| CSF (CloudCompare) | 0.40 | 0.33 | −0.25 |

GLI and VARI values were calculated for each of the 15 trees analysed (Table 3), ranging from approximately 0.12 to 0.27 for GLI and from approximately 0.10 to 0.33 for VARI.

**Table 3**

**Mean GLI and VARI values per tree**

| ID | Species | GLI Mean | VARI Mean |
|---|---|---|---|
| 1 | Apple | 0.21 | 0.24 |
| 2 | Apple | 0.22 | 0.26 |
| 3 | Apple | 0.26 | 0.33 |
| 4 | Apple | 0.24 | 0.30 |
| 5 | Quince | 0.12 | 0.11 |
| 6 | Apple | 0.23 | 0.29 |
| 7 | Plum | 0.24 | 0.21 |
| 8 | Apple | 0.19 | 0.20 |
| 9 | Pear | 0.26 | 0.26 |
| 10 | Pear | 0.24 | 0.18 |
| 11 | Pear | 0.25 | 0.27 |
| 12 | Pear | 0.22 | 0.10 |
| 13 | Plum | 0.24 | 0.29 |
| 14 | Plum | 0.23 | 0.23 |
| 15 | Plum | 0.27 | 0.27 |

Relationships between the two indices and tree structural parameters were examined using the Pearson correlation coefficient. A moderate positive correlation was found between GLI and tree height ($r = 0.402$), and a stronger positive correlation between VARI and height ($r = 0.672$) (Figure 3).

A positive association was also found between GLI and VARI themselves (r = 0.664). Given the limited sample size (N = 15), these correlation coefficients should be interpreted as indicative trends rather than robust statistical relationships.

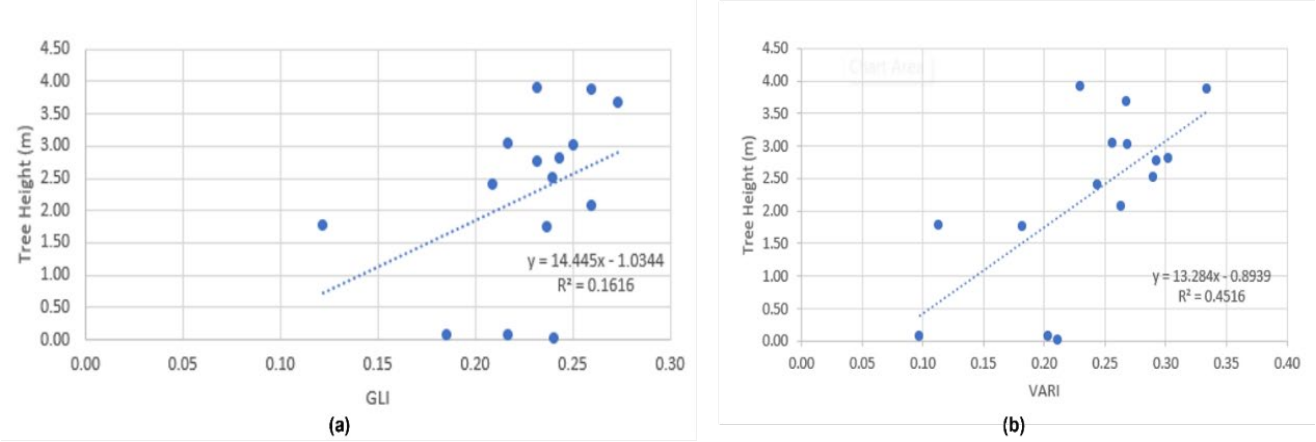



**Fig. 3 - Relationship between (a) GLI and tree height, and (b) VARI and tree height**

Field validation, carried out for the trees showing the lowest index values, confirmed the sensitivity of both indices to canopy health and foliage structure.

Tree ID 5 (quince), which had the lowest values of both indices (GLI = 0.12, VARI = 0.11), showed severe drying, curling and complete browning of the foliage in the field together with very low leaf density (Figure 4a, b). The low GLI reflects the geometric deficit of green canopy mass caused by visible soil between branches, while the low VARI reflects the biochemical degradation of green pigments and increased reflectance in the red band.

Tree ID 12 (pear) showed a contrasting pattern: a normal GLI (0.22), maintained by a well-developed, dense crown that covered the soil, but a markedly reduced VARI (0.10), explained by strong foliar chlorosis, most likely due to nutrient deficiency (Figure 4c, d). Direct comparison with a healthy pear leaf confirmed that VARI responded immediately to this change in leaf hue, illustrating its value as an early indicator of canopy stress not always captured by GLI alone.

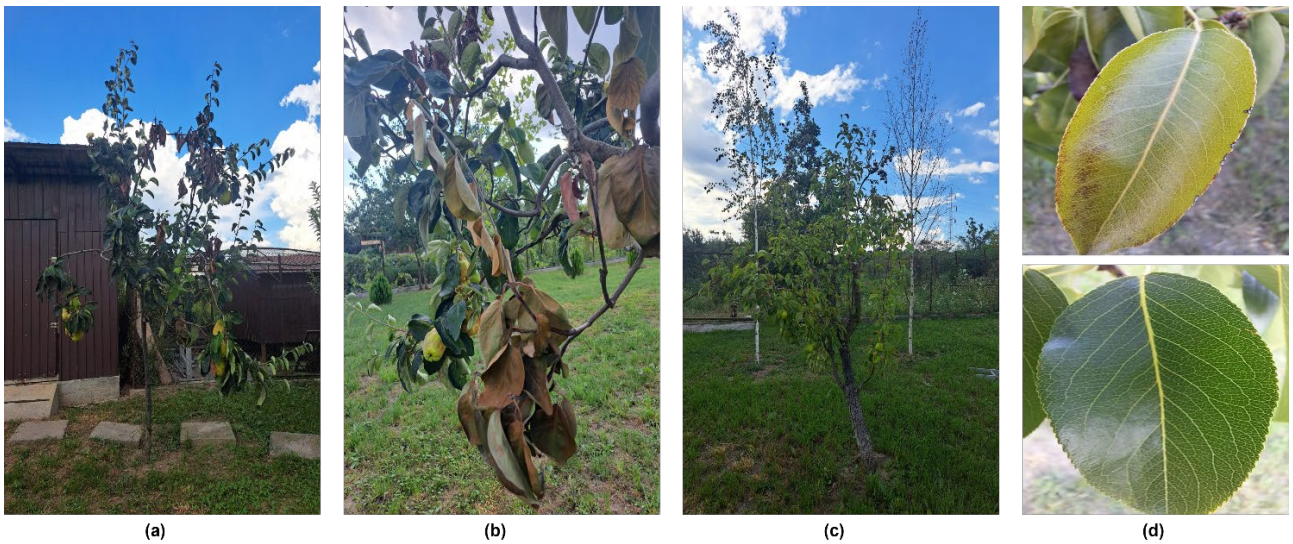



**Fig. 4 - Field validation of spectral anomalies:**
*(a) overall crown view of tree ID 5 (quince); (b) close-up of the foliage of tree ID 5; (c) overall crown view of tree ID 12 (pear); (d) direct comparison between a chlorotic leaf from tree ID 12 (top) and a healthy pear leaf (bottom).*

The spatial distribution of GLI and VARI was interpolated using the IDW method described in the previous section, producing continuous surfaces from the 15 point values, clipped to the boundary of the study area (Figure 5).

The resulting maps highlight zones where estimated index values are higher or lower depending on the values measured at neighbouring trees, allowing the transition from a point-based to a continuous representation of spatial variability within the orchard.




**Fig. 5 - IDW-interpolated spatial distribution of (a) GLI and (b) VARI**

It should be noted that these maps represent a spatial estimate based on the values available at the analysed points, rather than a direct measurement of the indices at every location within the orchard.

## CONCLUSIONS

This study evaluated the potential of a low-cost UAV RGB workflow, combined with open-source GIS tools, for the preliminary structural and spectral characterization of orchard trees. Among the three height-estimation methods tested, the point-cloud-based CHM (CSF algorithm) performed best, achieving the highest detection rate (87%) and the lowest estimation error (RMSE = 0.40 m), while all three methods showed a systematic tendency to underestimate tree height, most pronounced for the classical CHM approach.

The GLI and VARI indices proved sensitive to visible canopy stress observed in the field, with VARI showing a stronger relationship to tree height and reacting more clearly to early chlorosis symptoms, while GLI more directly reflected canopy density and coverage. The spatial interpolation of both indices further illustrated how index variation is distributed across the orchard, beyond the individual tree level.

The main limitations of the study are the small number of trees analysed, the use of a single flight, and the exclusive reliance on RGB imagery rather than multispectral data. Future work should extend this workflow to a larger and more diverse orchard, incorporate multispectral sensors, and automate data processing using Python.

## ACKNOWLEDGEMENT

The author would like to thank her family for their support in the acquisition of aerial data, including the use of the drone and the study site. This work was carried out as a preparatory study for the author's bachelor's thesis at the National University of Science and Technology POLITEHNICA Bucharest, Faculty of Biotechnical Systems Engineering.

## REFERENCES

[1] Anisa, Medina & Rokhmatuloh, Rokhmatuloh & Hernina, Revi. (2020). UAV application to estimate oil palm trees health using Visible Atmospherically Resistant Index (VARI) (Case study of Cikabayan Research Farm, Bogor City). E3S Web of Conferences. 211. 05001. 10.1051/e3sconf/202021105001.

[2] Anzar, S. M., Sherin, K., Panthakkan, A., Al Mansoori, S., and Al-Ahmad, H. (2025). Evaluation of UAV-Based RGB and Multispectral Vegetation Indices for Precision Agriculture in Palm Tree Cultivation, Int. Arch. Photogramm. Remote Sens. Spatial Inf. Sci., XLVIII-G-2025, 163–170, https://doi.org/10.5194/isprs-archives-XLVIII-G-2025-163-2025.

[3] Ball, James & Hickman, Sebastian & Jackson, Toby & Koay, Xian & Hirst, James & Jay, William & Archer, Matthew & Aubry-Kientz, Mélaine & Vincent, Gregoire & Coomes, David. (2023). Accurate

delineation of individual tree crowns in tropical forests from aerial RGB imagery using Mask R-CNN. Remote Sensing in Ecology and Conservation. 9. 10.1002/rse2.332.

[4] Banaszek, S.; Szota, M. (2025). A Semi-Automated RGB-Based Method for Wildlife Crop Damage Detection Using QGIS-Integrated UAV Workflow. https://doi.org/10.3390/s25154734

[5] Dong, X.; Zhang, Z.; Yu, R.; Tian, Q.; Zhu, X. (2020). Extraction of Information about Individual Trees from High-Spatial-Resolution UAV-Acquired Images of an Orchard. Remote Sens. 12, 133. https://doi.org/10.3390/rs12010133

[6] Gitelson, Anatoly & Kaufman, Yoram & Stark, Robert & Rundquist, Donald. (2002). Novel Algorithms for Remote Estimation of Vegetation Fraction. Remote Sensing of Environment. 80. 76-87. 10.1016/S0034-4257(01)00289-9.

[7] Hao, J. & Fang, Z. & Wu, B. & Liu, S. & Ma, Y. & Pan, Y. (2022). TREE CANOPY HEIGHT ESTIMATION AND ACCURACY ANALYSIS BASED ON UAV REMOTE SENSING IMAGES. The International Archives of the Photogrammetry, Remote Sensing and Spatial Information Sciences. XLIII-B2-2022. 129-134. 10.5194/isprs-archives-XLIII-B2-2022-129-2022.

[8] Louhaichi, Mounir & Borman, Michael & Johnson, Douglas. (2001). Spatially Located Platform and Aerial Photography for Documentation of Grazing Impacts on Wheat. Geocarto International. 16. 10.1080/10106040108542184.

[9] Ponce, J.M.; Aquino, A.; Tejada, D.; Al-Hadithi, B.M.; Andújar, J.M. (2022). A Methodology for the Automated Delineation of Crop Tree Crowns from UAV-Based Aerial Imagery by Means of Morphological Image Analysis. Agronomy, 12, 43. https://doi.org/10.3390/agronomy12010043

[10] Shepard, D. (1968). A two-dimensional interpolation function for irregularly-spaced data. *Proceedings of the 1968 23rd ACM National Conference*, 517–524. https://doi.org/10.1145/800186.810616

[11] Sishodia, R.P.; Ray, R.L.; Singh, S.K. (2020). Applications of Remote Sensing in Precision Agriculture: A Review. Remote Sens. 12, 3136. https://doi.org/10.3390/rs12193136

[12] Sobjak, R., de Souza, E.G., Bazzi, C.L. et al. (2023). Process improvement of selecting the best interpolator and its parameters to create thematic maps. *Precision Agric* 24, 1461–1496. https://doi.org/10.1007/s11119-023-09998-4

[13] Vacca, G.; Vecchi, E. (2024). UAV Photogrammetric Surveys for Tree Height Estimation. Drones, 8, 106. https://doi.org/10.3390/drones8030106

[14] Zhang, C., Valente, J., Kooistra, L. *et al. (2021).* Orchard management with small unmanned aerial vehicles: a survey of sensing and analysis approaches. *Precision Agric* 22, 2007–2052. https://doi.org/10.1007/s11119-021-09813-y

[15] Zhang, W.; Qi, J.; Wan, P.; Wang, H.; Xie, D.; Wang, X.; Yan, G. (2016). An Easy-to-Use Airborne LiDAR Data Filtering Method Based on Cloth Simulation. Remote Sens. 8, 501. https://doi.org/10.3390/rs8060501

# ASPECTS REGARDING THE COMPRESSION AND FAILURE BEHAVIOR OF CONCRETE CUBIC MINI-BLOCKS WITH RED MUD ADDITION

/

# *APECTE PRIVIND COMPORTAREA LA COMPRESIUNE ȘI RUPERE A MINI-BLOCURILOR CUBICE DIN BETON CU ADAOS DE NĂMOL ROȘU*

**Augustin VOINEA[1)], George IPATE[1)], Gheorghe VOICU[1)], Paula TUDOR*[1)], George-Mirel MIU[1)], Dorel STOICA[1)], Dorin Andrei CIRSTEA[2)]**

[1)] National University of Science and technology POLITEHNICA Bucharest / Romania;

[2)] National Institute of Research - Development for Machines and Installations Designed for Agriculture and Food Industry - INMA Bucharest / Romania

**Tel: 0040 723 850 975; *E-mail: paule.voicu@upb.ro*

***Keywords:*** *red mud, accelerated carbonation, compressive strength, finite element method, fracture mechanics, sustainable concrete*

## ABSTRACT

*This study evaluates the structural performance of a concrete mixture incorporating neutralized red mud sourced from the Valea lui Flam deposit (Tulcea, Romania). To reduce alkalinity, the residue was treated via accelerated carbonation ($CO_2$ bubbling for 3 hours), lowering the pH value to 9. The conditioned waste replaced 11% of the composite Portland cement in a standard C16/20 concrete mix. Cubic specimens (15×15×15 cm), prepared at SC CLASS BETON AGREGATE SRL, were tested at a curing age of 7 days using a computerized MATEST press. Experimental results indicated a maximum failure load of 211.606 kN, corresponding to a compressive strength of 9.405 MPa, and revealed a brittle failure mode driven by the high $Fe_2O_3$ content (44.60%). A parallel 3D finite element simulation (FEM in Ansys) successfully modeled stress concentration around a crack front, validating the observed hourglass-shaped macroscopic failure. Although binder dilution slightly reduces early-age strength, the matrix exhibits adequate compaction, proving highly viable for the manufacture of non-structural precast elements such as pedestrian pavers and kerbstones.*

## REZUMAT

*Această lucrare evaluează performanța structurală a unui amestec de beton care încorporează nămol roșu neutralizat provenit de la depozitul Valea lui Flam (Tulcea, România). Pentru reducerea alcalinității, reziduul a fost tratat prin carbonatare accelerată (barbotare cu $CO_2$ timp de 3 ore), coborând valoarea pH-ului la 9. Deșeul astfel condiționat a înlocuit 11% din cimentul Portland compozit într-un amestec de beton standard de clasă C16/20. Epruvete cubice (15×15×15 cm), preparate la SC CLASS BETON AGREGATE SRL, au fost testate la o vârstă de maturare de 7 zile, utilizând o presă computerizată MATEST. Rezultatele experimentale au indicat o sarcină maximă de rupere de 211,606 kN, corespunzătoare unei rezistențe la compresiune de 9,405 MPa, evidențiind un mod de rupere casantă determinat de conținutul ridicat de $Fe_2O_3$ (44,60%). O simulare paralelă 3D cu elemente finite (FEM în Ansys) a modelat cu succes concentrarea tensiunilor în jurul frontului de fisură, validând ruperea macroscopică sub formă de clepsidră. Deși diluarea liantului reduce ușor rezistența inițială, matricea prezintă o compactare adecvată, dovedindu-se extrem de viabilă pentru fabricarea elementelor prefabricate nestructurale, precum pavelele pietonale și bordurile.*

## INTRODUCTION

The rapid development of road and urban infrastructure drives the consumption of Portland cement—an industry that is a major source of carbon dioxide emissions and environmental degradation. Within the context of the current circular economy, the utilization of industrial solid waste represents a necessary pathway for the decarbonization of construction materials. One of the most problematic global waste products is red mud a highly alkaline byproduct of the Bayer process used to extract alumina from bauxite (*Bandopadhyay, A. & Debabrata, G., 2020*).

Storing this material in large-scale disposal sites—such as the one in the Valea lui Flam area of Tulcea County—entails environmental risks related to soil, groundwater, and air pollution (*Rice J.R., 1968*). The raw waste exhibits significant chemical and mineralogical variability depending on the source of the bauxite ore used in the refining process (*Myers, R.H. et al., 2016; Cablik, V., 2007*).

Recent research indicates that red mud possesses properties enabling its partial integration into cementitious compositions, yielding both economic and environmental benefits (*Duckworth, A.L. et al., 2019*). At optimal replacement levels, ultrafine particles act as nucleation sites and micro-fillers, accelerating hydration kinetics and densifying the interfacial transition zone (ITZ). However, determining this optimum is complex and requires advanced statistical techniques. Response Surface Methodology (RSM) and the three-level Box-Behnken experimental design (BBD) (*Box, G.E.P. & Behnken D.W., 1960*) are employed to model rheological properties and optimize the costs of multivariable cementitious mixtures (*Budige K. et al., 2026; Montgomery D.C., 2017*). Complementary techniques, such as the Non-dominated Sorting Genetic Algorithm II (NSGA-II), are successfully implemented for the multi-objective cost-performance optimization of cement composites, defining a clear Pareto front among strength, cost, and carbon dioxide emissions (*Budige K. et al., 2026; Montgomery D.C., 2017; Wang, Q., et al., 2025*).

The high alkalinity of red mud (pH 11–12.5), driven by sodium oxides ($Na_2O$), necessitates preliminary neutralization treatments to produce stable matrices (*Rice, J.R., 1968; Rai, S. et al., 2012;* Han, Y.-S. et al., 2017). Stabilization via accelerated carbonation with carbon dioxide ($CO_2$) is a method that lowers pH, fixes sodium into stable carbonate phases, and shortens setting times (*Wu, G. et al., 2025*).

The resulting composites exhibit reduced capillary porosity and a denser structure due to the contribution of stable iron ($Fe_2O_3$) and aluminum ($Al_2O_3$) oxides (*Zhang, C. et al., 2025*). To predict compressive strength based on pore structure geometry and anisotropy, the literature employs exponential mathematical models—such as the Ryshkewitch-Duckworth model—although modern correlations reveal discrepancies at low porosity values (*Eshelby, J.D., 1957*).

Alternatively, hybrid binder systems, such as geopolymers based on red mud and fly ash, offer high mechanical strength and a stable microstructure under various thermal pre-treatment conditions (*Zhang, H. et al., 2024*). These materials demonstrate enhanced durability against chemical attack, compensating for the limited pozzolanicity of the untreated waste, although prolonged exposure to acidic aqueous environments can lead to a decline in strength due to increased apparent porosity.

The study of the compression and fracture behavior of these new additive-enhanced structures must be grounded in the principles of linear elastic fracture mechanics, moving beyond traditional approaches based strictly on the strength of materials (*Anderson, T.L., 1994; Li, F. & Xu, J., 2024*). Asymptotic models describe the stress and strain fields surrounding a crack tip under axial loading (*SR EN 1992-1-1, 2004*). The energy available for defect propagation is assessed using energy-based criteria established by Griffith and Irwin, evaluated computationally via path-independent integrals such as the J-integral (*Rice, J.R. & Rosengren, J.F., 1968*).

Furthermore, modeling the variations in elastic energy density caused by inclusions employs the energy-momentum tensor, providing insights into configurational forces within the matrix. Finally, crack trajectory stability and deviation from the initial plane under mixed-mode loading are directly influenced by the non-singular T-stress component, according to kinematic analyses found in the literature. Additionally, the role of social perception regarding the use of eco-friendly materials is sometimes examined in behavioral and educational impact studies *(Voinea, A. et al., 2026).*

Determining the optimal substitution level in modified cementitious matrices involves analyzing rheological behavior at the interface between ultrafine particles and polycarboxylate ether (PCE) superplasticizers. Although classical studies indicate a theoretical replacement threshold in the 10%–15% range, the mechanism of physical water adsorption onto the high specific surface area of hematite ($Fe_2O_3$) and goethite radically alters hydration kinetics during the initial 24–72 hours. The high specific surface area of bauxite waste (typically measured between 10 and 30 $m^2/g$ via the BET method) increases the mixture's free water demand. Without rigorous control of the water-to-binder ratio, this phenomenon causes water to become trapped within the intracrystalline pores of the C-S-H (calcium silicate hydrate) gel phase, creating a large volume of interconnected voids and reducing the composite's maximum dry density.

The specific choice of an 11% replacement level in this study was statistically justified to maximize the physical micro-filler effect of the inert metal oxides without triggering the under-hydration associated with the dilution of active clinker. This precisely tuned percentage prevents sub-micron particles from agglomerating into textural defects, ensuring a dense interfacial transition zone (ITZ) between the cement paste and aggregates—a crucial prerequisite for limiting crack opening under concentrated axial stresses.

This study aims to experimentally evaluate the compressive behavior at 7 days of C16/20 concrete mini-cubes containing an 11% addition of carbonated red mud, manufactured and tested at the SC CLASS BETON AGREGATE SRL laboratory in Moara Nouă, Prahova.

The results obtained from destructive testing are correlated with a three-dimensional finite element method (FEM) simulation performed in Ansys to validate the sustainable material's compliance with the technical requirements of the SR EN 1338:2004 standard for paving blocks, applied in conjunction with the general structural design provisions of Eurocode 2.

## MATERIALS AND METHODS

The reference mix was designed for standard C16/20 class concrete with S3 consistency and a maximum aggregate size of 16 mm. The cement used to prepare the specimens was a composite Portland cement—standardized as SR EN 197-1-CEM II/B-M (S-V) 42.5N and produced by ROMCIM SA in accordance with Declaration of Performance 27-CPR. The binder contains Portland clinker, a composition that ensures stable long-term strength development within the hybrid concrete matrix.



**Fig. 1 - Location of the secondary raw material source (Red Mud)**

The red mud used in the experiment was sampled from the Valea lui Flam sludge disposal site in Tulcea County (originating from bauxite processing at ALUM SA Tulcea). Figure 1 illustrates the transition to dense-phase storage (56% moisture content), implemented to comply with European environmental directives and reduce the risk of leaching. Chemical oxide composition, determined via instrumental analysis, reveals that iron oxide constitutes the major component, as shown in the data summarized in Table 1.

**Table 1**

**Oxidative chemical composition of the red mud used (% mass).**

| $Al_2O_3$ | CaO | MgO | $K_2O$ | $Na_2O$ | $SiO_2$ | $Fe_2O_3$ | MnO | $TiO_2$ | PC | Total |
|---|---|---|---|---|---|---|---|---|---|---|
| 18.16 | 3.66 | 0.16 | 0.15 | 6.87 | 7.50 | 44.60 | 0.03 | 3.16 | 15.20 | 99.80 |

Due to the significant $Na_2O$ content (6.87%)—which creates high alkalinity detrimental to the structural stability of the concrete—a preliminary neutralization step was carried out. The sludge was placed in a specialized laboratory vessel equipped with a continuous mechanical stirring system. Industrial carbon dioxide ($CO_2$) was bubbled through the mixture for three hours, triggering the mineral carbonation of the soluble alkaline phases.

This process resulted in a controlled reduction of the suspension's pH to a stable value of approximately 9. Following neutralization, the red mud underwent a partial drying cycle, bringing its moisture content to a final working level of 46% prior to being fed into the mixer.

All proportioning, mixing, and casting operations were carried out at the authorized construction analysis and testing laboratory of SC CLASS BETON AGREGATE SRL, located in Moara Nouă village, Berceni commune, Prahova County. The experimental mix design involved the partial replacement of cement with a fixed percentage (11%) of modified red mud.

Samples were taken from the homogenized mixture and cast into standard cubic metal molds measuring 150x150x150 mm (Fig. 2). Following mechanical compaction on a vibrating table, the specimens were demolded after 24 hours and stored in a controlled laboratory environment (water immersion tank at 20±2°C) until the time of destructive testing. At the testing age (7 days), the analyzed cube weighed exactly 7.705 kg, resulting in an apparent density of 2282 kg/m³ for the modified concrete. The nominal compressive surface area of the specimen was 225 cm².

The determination of early compressive strength at 7 days was performed using a high-precision computerized MATEST press, model C109N (New Cybertronic series). This instrument is equipped with a

graphic display and a three-channel digital data acquisition system, enabling real-time monitoring of the applied load and remote data management via PC.

The cubic specimen (15x15x15 cm), weighing 7.705 kg, was centered on the testing machine platens. The loading rate was programmed in accordance with the SR EN 1338 standard, with a progressive load applied until structural failure. The digital system automatically recorded the stress-strain curve and the maximum failure load.



**Fig. 2 - The production process at the SC Class Beton Agregate SRL laboratory**




**Fig. 3 - Experimental setup for the strength test using the MATEST computerized press.**

To understand the microscopic mechanism of crack propagation in the matrix modified with iron oxides (derived from the 44.6% $Fe_2O_3$ content of red mud), a three-dimensional simulation was run in parallel using Ansys 2022 R2.

A block of similar dimensions (Bounding Box: 240x20x180 mm) subjected to a uniform pressure of 7.5 MPa was modeled. Discretization was performed using a program-controlled algorithm (Hex-dominant to Tetrahedral), generating 33,226 nodes and 11,021 elements.

The model was configured with isotropic properties typical of porous ceramic/cementitious materials: Young's modulus E = 22,360 MPa, Poisson's ratio $\nu$ = 0.2145, and a density of $2.024 \cdot 10^{-6}$ kg/mm³. The tensile strength was set at 9.829 MPa.

A semi-elliptical analytical crack (*Major Radius = 4 mm, Minor Radius = 2 mm*) was introduced to analyze the Stress Intensity Factors ($K_1$, $K_2$, $K_3$) under linear elastic conditions.

**RESULTS**

During the destructive test on September 6, 2026, the cubic mini-block containing 11% red mud exhibited brittle failure under a maximum load of 211.606 kN. The data obtained were automatically compiled by the Cyber-Plus system and are presented in Table 2.

**Table 2**

**Experimental compression test report (7 days)**

| Physical-mechanical parameters | Value |
|---|---|
| Physical-mechanical parameters | 225 cm² |
| Compression area (A) | 7.705 kg |
| Weight of the concrete cube | 2282 kg/m³ |
| Maximum failure load ($F_{max}$) | 211.606 kN |
| Compressive strength ($\sigma_c$) | 9405 N/mm² (MPa) |

Graphical analysis of the digital curve displayed on the MATEST press screen indicates a steep upward slope during the first 15 seconds, reaching a peak stress of 9.405 MPa, followed by an instantaneous drop in load. This graph is further validated by the 255-point load-displacement diagram, which shows a peak at the coordinates 7.05 s and 211.606 kN, demonstrating that the addition of red mud alters matrix stiffness and creates a dense structure that is, however, markedly brittle under rapid loading.




**Fig. 4 - Monitorizarea digitală și curba de cedare structurală**

Although the Ansys model was run using a different geometry and theoretical control parameters (maximum von Mises equivalent stress of 69.959 MPa and maximum total deformation of $8.17 \cdot 10^{-2}$ mm), the correlation with laboratory data provides important insights into the crack propagation behavior in mini-blocks.

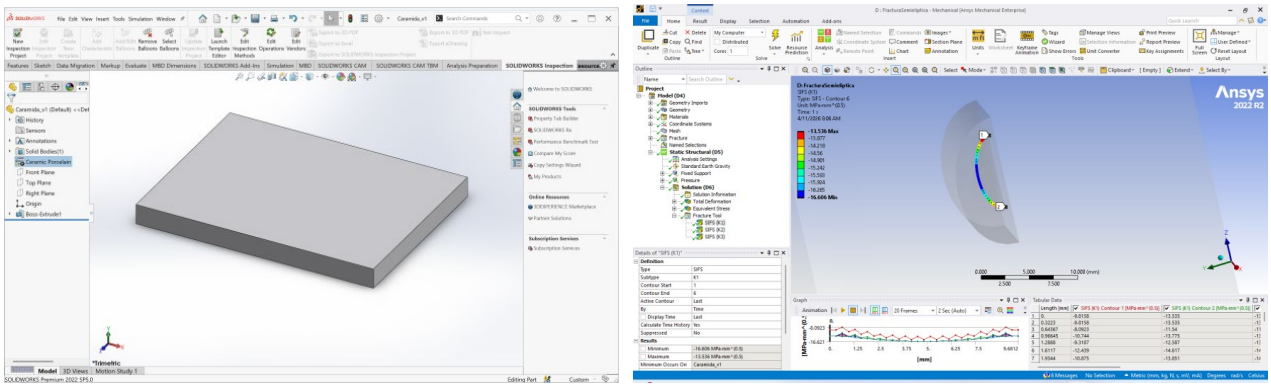



**Fig. 5 - Numerical simulation model and crack propagation analysis (Ansys)**

To provide a theoretical basis for the degradation process and the formation of fracture lines, data regarding stress evolution along the semi-elliptical defect front were extracted from the Ansys numerical simulation. The calculated values for Mode I (opening, $K_1$), Mode II (sliding shear, $K_2$), and Mode III (tearing/torsion, $K_3$) are essential for understanding the asymptotic behavior of the hybrid material.

Analysis of the data in Table 3 reveals that the $K_1$ factor exhibits exclusively negative values along the entire crack front, ranging from -8.09 to -16.60 MPa·mm$^{0.5}$. In fracture mechanics, a negative $K_1$ value indicates a local state of pure compression acting perpendicular to the defect faces, forcing them to remain closed. This explains why, during the initial phase of axial loading, micro-pores blocked by fine hematite particles offer significant resistance to crack propagation.

**Table 3**

**Distribution of Stress Intensity Factors (SIF) along the crack front in the specimen.**

| Contour length [mm] | $K_1$ Contour 1 [MPa·mm$^{0.5}$] | $K_1$ Contour 3 [MPa·mm$^{0.5}$] | $K_1$ Contour 6 [MPa·mm$^{0.5}$] | $K_2$ Contour 6 [MPa·mm$^{0.5}$] | $K_3$ Contour 9 [MPa·mm$^{0.5}$] |
|---|---|---|---|---|---|
| 0.00000 | -9.8158 | -13.530 | -13.536 | $5.223 \cdot 10^{-3}$ | $1.783 \cdot 10^{-3}$ |
| 0.64367 | -8.0923 | -11.990 | -13.784 | $4.922 \cdot 10^{-3}$ | $2.746 \cdot 10^{-3}$ |
| 0.96645 | -10.744 | -13.777 | -13.777 | $4.448 \cdot 10^{-3}$ | $3.158 \cdot 10^{-3}$ |
| 1.28880 | -9.3187 | -13.415 | -14.291 | $4.245 \cdot 10^{-3}$ | $3.441 \cdot 10^{-3}$ |
| 1.61170 | -12.439 | -14.622 | -14.623 | $3.680 \cdot 10^{-3}$ | $3.587 \cdot 10^{-3}$ |
| 3.54890 | -15.242 | -16.310 | -16.312 | $2.054 \cdot 10^{-3}$ | $1.983 \cdot 10^{-3}$ |
| 4.84060 | -15.567 | -16.605 | -16.606 | $1.714 \cdot 10^{-3}$ | $1.833 \cdot 10^{-3}$ |
| 5.16350 | -13.688 | -16.594 | -16.596 | $1.750 \cdot 10^{-3}$ | $-5.155 \cdot 10^{-3}$ |
| 7.74680 | -10.875 | -14.991 | -15.058 | $3.241 \cdot 10^{-3}$ | $-3.548 \cdot 10^{-3}$ |
| 9.35890 | -9.8161 | -13.530 | -13.537 | $5.349 \cdot 10^{-3}$ | $-1.904 \cdot 10^{-3}$ |

However, as the von Mises stress reaches the simulated peak value of 69.959 MPa, tangential components become active. Mode II (shear, $K_2$ ≈5.34·10$^{-3}$ MPa·mm$^{0.5}$) and Mode III (torsion, $K_3$ ≈3.58·10$^{-3}$ MPa·mm$^{0.5}$) induce sliding and twisting stresses at the cement-slurry interface. As the non-singular T-stress parameter becomes strongly positive, the crack trajectory is forced to deviate sharply from the initial propagation plane. This complex mixed-mode loading mechanism explains the appearance of inclined fracture lines and the hourglass-shaped macroscopic opening observed on the actual laboratory specimen.

To quantitatively evaluate the energy available for the propagation of the semi-elliptical defect induced in the paving block, the numerical simulation independently calculated the path-independent J-integral along six distinct integration contours. Mathematically, for the configured linear elastic model, the J-integral is equivalent to the elastic energy release rate G, based on the Griffith-Irwin energy criterion:

$$J = G = \frac{K_I^2}{E\prime} \tag{1}$$

where E'=E/(1-ν$^2$) for the plane strain state occurring within the hybrid concrete mini-block.

Substituting the experimental Young's modulus of the matrix (E = 22360 MPa) and Poisson's ratio ($\nu$ = 0.2145) yields a corrected modulus of $E'$ ≈ 23,438 MPa. At the point of maximum crack front length ($s$ = 4.8406 mm) – where the stress intensity factor $K_1$ reaches its maximum negative value of −16.606 MPa·mm$^{0.5}$ on contour 6 – the calculated value of the J-integral is 0.0117 N/mm (or J/m²).

From a mechanical standpoint, since $K_1$ is negative due to the 7.5 MPa compressive hydrostatic pressure exerted by the MATEST press platens, this calculated energy represents a closure energy barrier. The crack cannot initiate unstable Mode I (opening) propagation as long as the external loads do not exceed the crushing resistance of the hematite ($Fe_2O_3$) micro-filler, which structurally stabilizes the capillary pores of the composite Portland cement.

Unlike traditional physical forces in structural mechanics that act on geometric nodes, the material (or configurational) force represents the force exerted by the cementitious matrix on the defect or red mud inclusion. It characterizes the variation in the system's total energy associated with a change in the position or shape of the crack geometry:

$$F_m = \int_\Gamma \left( W\delta_{ij} - \frac{\sigma_{ij}(\partial u_{ij})}{\partial x_j} \right) n_j \, d\Gamma \tag{2}$$

where the Eshelby energy-momentum tensor (*Eshelby, J.D., 1957*) describes the strain energy density $W$ around the nodes discretized within the model's 11021 elements. The tangential component of the material force vector, determined along the faces of the defect, acts as a driving force for local degradation.

This force is closely correlated with the sign and magnitude of the non-singular T-stress term. In the Ansys simulation, the transition from the initial stable state to the sudden fracture of the cube is governed by the evolution of stresses associated with the Mode II ($K_2$, shear) and Mode III ($K_3$, torsion) stress intensity factors. As the T-stress exceeds the hybrid concrete's critical tensile limit (9.829 MPa) at the specimen's corners, the level of triaxiality increases exponentially. The mechanical energy input from the Matest press is no longer dissipated through global elastic deformations but becomes instantly available to accelerate local degradation. This energy surge explains the brittle structural failure and the evolution of microscopic crack orientations into a network of three-dimensional geometric macro-cracks (*Cotterell, B., & Rice, J. R., 1980*).

To gain deeper insight into the physical nature of the configurational force ($F_m$) calculated around the defect, it is necessary to analytically decompose the Eshelby stress tensor used in the finite element discretization. The energy-momentum tensor associated with the cementitious system containing inert red mud inclusions is defined based on the elastic strain energy density ($W$), in accordance with the relationship:

$$b_{lj} = W\delta_{ij} - \sigma_{ij}\frac{\partial u_i}{\partial x_j} \quad (3)$$

In this three-dimensional model comprising 11021 elements, the W component was evaluated by integrating the specific elastic strain field ($\varepsilon_{ij}$) and the stress tensor ($\sigma_{ij}$) at each Gauss point. The presence of fine $Fe_2O_3$ particles (44.60% of the waste mass) alters the local energy density by inducing geometric eigen - strains. Since the red mud phase – carbonated for 3 hours – possesses an internal textural porosity distinct from that of the surrounding C-S-H gel, the interface between the inclusion and the matrix becomes the site of a net configurational force.

Numerical integration along contour $\Gamma$ in Ansys Structural reveals that the material force vector tends to displace the inclusion or extend the edges of the semi-elliptical crack in order to minimize the body's free potential energy. The determined J-integral value of 0.0117 N/mm at 7 days indicates that, although the material exhibits early, stage mechanical brittleness due to the lack of long-term active silicate hydrates (the clinker dilution effect), the energy barrier opposing macro-crack propagation remains stable. This behavior confirms that the microstructural network achieved through the neutralization technology applied at SC Class Beton Agregate SRL is capable of stabilizing internal defects, thereby maintaining the block's integrity under moderate static loads.

The structural simulation indicates a massive stress concentration in the central area of the semi-elliptical defect introduced into the structural model (Fig. 6).

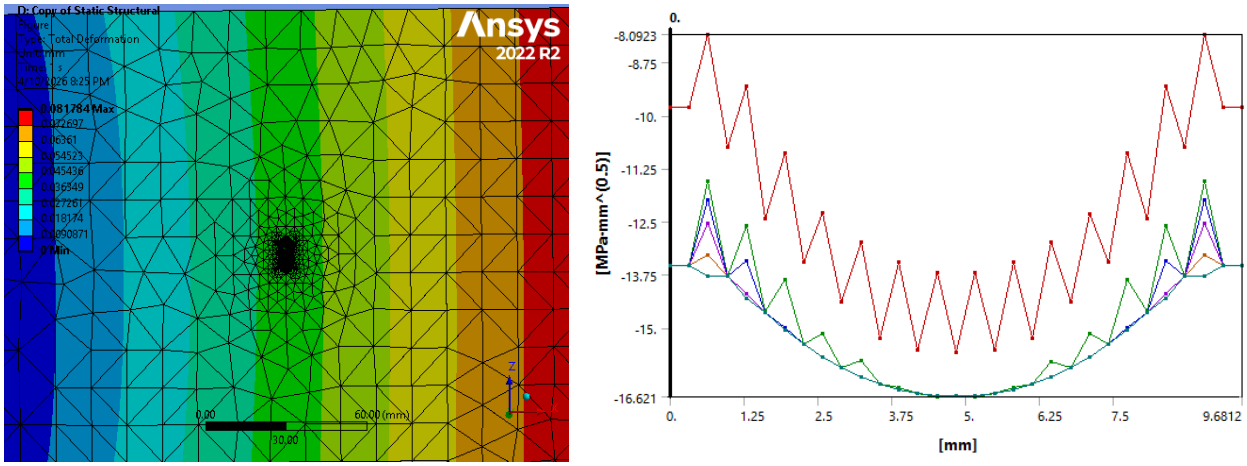



**Fig. 6 - Equivalent stresses in the structural model subjected to compression, and the evolution of the SIF ($K_1$)**

For the theoretical asymptotic study of defect propagation, a reference block discretized into 11021 elements and subjected to a pressure of 7.5 MPa was used. The von Mises stress concentration (maximum 69.959 MPa) around the central semi-elliptical crack and the negative $K_1$ factor values simulate the state of microscopic compression that red mud induces within the structural pores of the actual laboratory specimen (Fig. 6).

The laboratory-determined strength at 7 days (9.405 N/mm²) is lower than the theoretical value for standard C16/20 concrete. This behavior is attributed to the slower pozzolanic activity of the inert hematite ($Fe_2O_3$) phases in the red mud from Tulcea, which initially act merely as inert filler. However, extrapolation of

the hardening curve indicates that at the standard 28-day mark, the concrete will reach an estimated strength of 14–16 MPa, placing it within the range of sustainable non-structural materials.

To fully understand why the early 7-day strength recorded in the laboratory (9.405 MPa) is lower than that of a control concrete, it is necessary to analyze the kinetics of the chemical reactions between the mineralogical phases of the composite Portland cement (SR EN 197-1-CEM II/B-M) and the reactive components of the bauxite waste (*Hutchinson, J.W., 1968*). In the first phase of the process (the initial 24–72 hours), the hydration of tricalcium silicates ($C_3S$) from the clinker generates the primary calcium silicate hydrate (C-S-H) gel and releases a significant amount of portlandite, or calcium hydroxide (Ca(OH)2), in accordance with the classic equation (*Rice, J.R. & Rosengren, G.F.,* 1968):

$$2C_3S + 6H_2O \rightarrow \text{C-S-H (gel)} + 3Ca(OH)_2 \quad (4)$$

The calcium hydroxide formed is a friable, soluble phase vulnerable to chemical attack, contributing minimally to the structural strength of the material matrix. In concretes containing admixtures, the secondary pozzolanic reaction, triggered by the presence of red mud, comes into play only during the second phase (which intensifies after 7 days and continues up to 28–90 days) (*Kumar, A. & Singh, S., 2025*). The active silica ($SiO_2$) and amorphous aluminosilicates present in the residue consume the deleterious portlandite, converting it into additional C-S-H gels that block capillary porosity:

This delayed reaction explains why the hybrid mixture exhibits a strength penalty during the first week of curing, when the waste acts solely as an inert physical filler (*Bandopadhyay, A. & Debabrata, G., 2020*). However, the presence of residual sodium ions (Na+) from the sludge structure—even after neutralization via carbonation to pH 9—acts as a local alkaline catalyst that accelerates the formation of primary ettringite within the pores. Extrapolation of thermodynamic curves indicates that, as secondary pozzolanic hydration progresses, the structure will achieve a significant strength gain by the standard 28-day mark, ensuring superior microstructural densification and enhanced long-term durability (*Voinea, A. et al., 2026*).

To understand exactly where this hybrid mixture stands in relation to the rigorous requirements for road and pedestrian infrastructure, a direct comparative analysis was conducted (Table 4), using data from European standards and advanced research from the specialized literature as a baseline.

**Table 4**

**Comparative analysis of the performance and applicability of red mud concrete**

| Mix Type / Standard | Compressive Strength (28 days) | Water Absorption / Porosity | Validity and Scope of Application According to Standards |
|---|---|---|---|
| Experimental Concrete (11% RM) | 14.0 - 16.0 MPa (estimated) | Controlled porosity *(due to 3-hour carbonation)* | Recommended exclusively for light-traffic pedestrian pavers, secondary street curbs, and cast blocks for embankment stabilization. |
| Standard SR EN 1338 | Specified design class (typically > 30 MPa) | ≤ 6.0% *(Class 2, Marking B)* Splitting strength ≥ 3.6 MPa. | The experimental mix requires optimization with superplasticizers for heavy-traffic applications. |
| Optimal mix 10% RM *(Kumar & Singh, 2025)* | Increase resistance with +28.96% in the long term (180 days) | Minim (3,15%) la 10% RM Critical porosity threshold: 12.87%. | Fine particles act as nucleation sites and block open capillary channels. |
| Over-contaminated Mix (>20% RM) *(Dhapte & Sawant, 2021)* | Drastic drop in strength (26% collapse at 25% RM). | Escalate to > 4,06% *(macropore accumulation)*. | Severe dilution of the active silicate phases ($C_3S$ and $C_2S$) occurs, rendering the material unsuitable for structural or road applications. |

The experimental and numerical results obtained in this research highlight the complexity of using red mud as a partial cement replacement in sustainable concrete. A critical aspect deserving special attention is the contrast between short-term physical behavior and projected long-term structural dynamics. At 7 days, the recorded compressive strength (9.405 MPa) indicates a reduction in early-age mechanical performance compared to a C16/20 control concrete. This phenomenon, which is also confirmed by the literature, is directly attributed to the binder dilution effect. By substituting 11% of the composite Portland

cement with bauxite waste, the content of tricalcium silicates ($C_3S$) - which are responsible for early strength development - decreases proportionally.

However, an analysis based on linear elastic fracture mechanics, performed in Ansys, demonstrates that the hybrid material compensates for this loss through the microstructural optimization of the pore network. The strongly negative values of the Stress Intensity Factor ($K_1$) simulated along the semi-elliptical crack front indicate the existence of a stable internal micro-compression state. Although chemically inert during the initial stages of hydration, the ultrafine hematite ($Fe_2O_3$) particles act as a high-density physical filler. They block open capillary channels within the cement paste, thereby reducing the matrix's total porosity. This geometric compaction explains why the actual specimen exhibits adequate structural stability under concentrated static loads, despite the chemical dilution of the clinker.

Another key factor for the industrial viability of the paving stones is the accelerated carbonation treatment applied for three hours in the laboratory. Neutralizing the harmful $Na_2O$ component by bubbling carbon dioxide through the material not only lowers the residue's pH to a safe level of 9 but also converts free sodium into stable carbonate phases. This process mitigates one of the major drawbacks of untreated red mud: its tendency to trigger destructive delayed expansion via the alkali-silica reaction (ASR). Thus, through the early fixation of sodium and the geometric optimization of pore shapes, the experimental mixture avoids the critical threshold of structural degradation typically associated with composites heavily contaminated by raw waste.

From a macroscopic perspective, the appearance of hourglass-shaped fracture lines highlights the brittle nature of the failure, a characteristic influenced by the high iron content in the red mud. Numerical modeling provides the theoretical explanation here: when external pressure exceeds the cohesion limit, the interaction between secondary shear ($K_2$) and torsion ($K_3$) modes, driven by a positive T-stress parameter, forces cracks to deviate and propagate along oblique planes. This close correlation between laboratory physical phenomena and virtual simulation validates the reliability of the numerical model as a predictive tool.

The analysis clearly demonstrates that, by maintaining the percentage at 11%, the mixture falls within the structural safety range, avoiding the critical threshold for textural degradation (>20%) and offering a genuine decarbonization solution through the recycling of waste from Alum Tulcea.

## CONCLUSIONS

Based on experimental investigations conducted at the SC Class Beton Agregate SRL laboratory and correlations with the three-dimensional numerical simulation model, the following fundamental conclusions were formulated:

1. Neutralizing red mud sampled from the Valea lui Flam tailings pile (Tulcea) using the accelerated carbonation method ($CO_2$ sparging for 3 hours) enabled a controlled reduction of the pH to a value of 9. This step is important for reducing the risk of leaching sodium oxides ($Na_2O$, initially 6.87%) into the environment and for ensuring the textural stability of the cementitious matrix.
2. At 7 days of age, the cubic mini-block containing 11% red mud and 46% moisture exhibited a maximum failure load of 211.606 kN, yielding a stable compressive strength of 9.405 MPa. Although this value is lower than that of a reference C16/20 concrete due to inert iron hydrates ($Fe_2O_3$, 44.60%), the mixture demonstrates adequate structural compactness.
3. Numerical simulation in Ansys Structural demonstrated that, under the applied load, the tip of the semi-elliptical defect exhibits a strongly negative Mode I Stress Intensity Factor ($K_1$) (ranging from -13.53 to -16.60 $MPa \cdot mm^{0.5}$). This confirms that the material is in an initial state of pure compression that keeps the cracks closed, with final failure subsequently driven by shear ($K_2$) and torsion ($K_3$) components that cause the hourglass-shaped fracture lines to open.

The results validate the use of this hybrid mix (11% cement replacement) exclusively for the production of non-structural precast elements (light-traffic pavers, secondary kerbs, or cast elements for road embankment stabilization), offering a viable eco-friendly solution for industry decarbonization through the recycling of bauxite waste.

## REFERENCES

[1] Anderson, T. L. (1994). Fracture Mechanics -- Fundamentals and Applications (2nd ed.). CRC Press, Boca Raton.

[2] Bandopadhyay, A., & Debabrata, G. (2020). Use of bauxite residue for construction material—A review. In *Advances in Sustainable Construction Materials—Select Proceedings of ASCM* (pp. 561–571). Springer, Berlin/Heidelberg.
[3] Box, G.E.P., & Behnken, D.W. (1960). Some new three level designs for the study of quantitative variables. *Technometrics*, 2(4), 455–475.
[4] Budige, K., Katare, V.D., Barbuiya, S. (2026). Eco-efficient masonry units using fly ash and red mud: A comparative study of sandwich and hollow blocks. *Energy and Buildings*, 352, Article 116855.
[5] Cablik, V. (2007). Characterization and applications of red mud from bauxite processing. *Gospodarka Surowcami Mineralnymi - Mineral Resources Management*, 23(3), 27–38.
[6] Cotterell, B., & Rice, J. R. (1980). Slightly curved or kinked cracks. *International Journal of Fracture*, 16(2), 155–169.
[7] Dhapte, S. K., & Sawant, R. S. (2021). Potential Use of Bauxite Ore (Red Mud) in Paver Blocks. *International Research Journal of Engineering and Technology* (IRJET), 8(5), 472–476.
[8] Duckworth, A.L., Quirk, A., Gallop, R., Hoyle, R.H., Kelly, D.R., Matthews, M.D. (2019). Cognitive and noncognitive predictors of success. *Proceedings of the National Academy of Sciences*, USA, 116(47), 23499–23504.
[9] Eshelby, J.D. (1957). The determination of the elastic field of an ellipsoidal inclusion and related problems. Proceedings of the Royal Society of London. Series A. *Mathematical and Physical Sciences*, 241(1226), 376–396.
[10] Han, Y.-S., Ji, S., Lee, P.-K., & Oh, C. (2017). Bauxite residue neutralization with simultaneous mineral carbonation using atmospheric $CO_2$. *Journal of Hazardous Materials*, 326, 87–93.
[11] Hutchinson, J.W. (1968). Singular behavior at the end of a tensile crack in a hardening material. Journal of the Mechanics and Physics of Solids, 16(1), 13–31.
[12] Kumar, A., & Singh, S. (2025). Microstructural evolution and mechanical property enhancement of red-mud-blended cement concrete. *Scientific Reports*, 15, Article 4210.
[13] Li, F., & Xu, J. (2024). RSM-*based modelling for predicting and optimizing the rheological properties of red mud concrete. Scientific* Reports, 14, Article 3120.
[14] Montgomery, D.C. (2017). *Design and Analysis of Experiments* (9th ed.). John Wiley & Sons, New York.
[15] Myers, R.H., Montgomery, D.C., Anderson-Cook, C. M. (2016). *Response Surface Methodology: Process and Product Optimization Using Designed Experiments* (4th ed.). John Wiley & Sons, New York.
[16] Rai, S., Wasewar, K. L., Mukhopadhyay, J., Yoo, C. K., & Uslu, H. (2012). Neutralization and utilization of red mud for its better waste management. *Archives of Environmental Science*, 6, 13–33.
[17] Rice, J.R. (1968). A path independent integral and the approximate analysis of strain concentration by notches and cracks. *Journal of Applied Mechanics*, 35(2), 379–386.
[18] Rice, J.R., & Rosengren, G.F. (1968). Plane strain deformation near a crack tip in a power-law hardening material. *Journal of the Mechanics and Physics of Solids*, 16(1), 1–12.
[19] SR EN 1338:2004; Concrete Paving Blocks. Requirements and Test Methods. Romanian Standards Association (ASRO): Bucharest, Romania, 2004.
[20] SR EN 1992-1-1:2004; Eurocode 2: Design of concrete structures. Part 1-1: General rules and rules for buildings. Romanian Standards Association (ASRO): Bucharest, Romania, 2004.
[21] Voinea, A., Voicu, G., Savaniu, M., Lazarescu, A., & Tudor, P. (2026). Research on the utilization of carbonated red mud in sustainable construction materials (Paving Stones). *Materials*, 19(9), Article 1883.
[22] Wang, Q., et al. (2025). Cost–performance multi-objective optimization of quaternary cementitious composites using NSGA-II. *Buildings*, 15(22), Article 4074.
[23] Wu, G., Bai, J., Yilmaz, E., Feng, G., Han, Y., Li, J. (2025). Strength evolution and carbonation behavior of red mud–fly ash geopolymers under varying pre-curing conditions. *Construction and Building Materials*, 504, Article 144575.
[24] Zhang, C., Zhang, X., Wu, C., Yang, S., Yu, T., Wang, W., & Hu, Z. (2025). Development of high performance and low-carbon red mud based lightweight concrete: A novel strategy for transforming red mud into sustainable concrete. *Construction and Building Materials*, 491, Article 142714.
[25] Zhang, H., et al. (2024). Performance and microstructure of red mud–blended concrete under acidic conditions. *Construction and Building Materials*, 420, Article 131301.

# DISCRETE ELEMENT MODELLING OF SEED GRAVITATIONAL FLOW THROUGH DISCHARGE ORIFICES: RELEVANT PARAMETERS AND A PRELIMINARY METHODOLOGICAL FRAMEWORK

/

# *MODELAREA PRIN METODA ELEMENTELOR DISCRETE A CURGERII GRAVITAȚIONALE A SEMINȚELOR PRIN ORIFICII DE EVACUARE: PARAMETRI RELEVANȚI ȘI CADRU METODOLOGIC PRELIMINAR*

**Daniela-Andreea ZAMFIR*[1)], Sorin-Ștefan BIRIȘ[1)], Atanas ATANASOV[2)], Maria TĂNASE[3)], Mariana EPURE[4)]**

[1)] National University of Science and Technology POLITEHNICA Bucharest / Romania;
[2)] "Angel Kanchev" University of Ruse / Bulgaria;
[3)] Petroleum-Gas University of Ploiești, Prahova County / Romania;
[4)] INMA Bucharest / Romania
**Tel: (+40) 752.218.204; *E-mail: andreea.epure21@upb.ro*

***Keywords:*** *discrete element method, agricultural seeds, gravitational flow, discharge orifice, orifice geometry, parameter calibration*

## ABSTRACT

*In agriculture and the food industry, seeds often flow by gravity through discharge orifices, for example in hoppers and silos. Earlier studies described this flow with empirical equations and showed that the flow rate depends on the size, the shape of the orifice and on seed properties such as size, bulk density and moisture content. These equations estimate the average flow rate, but not the motion of individual seeds. The aim of this paper was to identify the main parameters that influence the flow of seeds through discharge orifices and to propose a preliminary methodology for studying them with the Discrete Element Method, a numerical method that simulates the motion of each particle. Classical studies and recent discrete element studies on agricultural materials were analysed. Published data showed that, for circular and square orifices with the same hydraulic diameter, the ratio of the flow rates (0.72–0.75) was lower than the ratio of their areas (0.785), so the effect of orifice shape could not be explained only by the orifice area. The parameters needed for a future model were grouped into measurable parameters, parameters that require calibration, geometrical parameters and validation indicators, and the next steps of the research were defined.*

## REZUMAT

*În agricultură și în industria alimentară, semințele curg adesea gravitațional prin orificii de evacuare, de exemplu în buncăre și silozuri. Studiile anterioare au descris această curgere prin ecuații empirice și au arătat că debitul depinde de dimensiunea, forma orificiului și de proprietățile semințelor, precum dimensiunea, masa volumică în vrac și umiditatea. Aceste ecuații estimează debitul mediu, dar nu și mișcarea fiecărei semințe. Scopul lucrării a fost identificarea principalilor parametri care influențează curgerea semințelor prin orificii de evacuare și propunerea unei metodologii preliminare pentru studierea lor cu Metoda Elementelor Discrete, o metodă numerică ce simulează mișcarea fiecărei particule. Au fost analizate studii clasice și studii recente de modelare prin elemente discrete a materialelor agricole. Datele publicate au arătat că, pentru orificii circulare și pătrate cu același diametru hidraulic, raportul debitelor (0,72–0,75) a fost mai mic decât raportul ariilor (0,785), deci efectul formei orificiului nu poate fi explicat numai prin arie. Parametrii necesari unui model viitor au fost grupați în parametri măsurabili, parametri care necesită calibrare, parametri geometrici și indicatori de validare, iar etapele următoare ale cercetării au fost definite.*

## INTRODUCTION

Many materials used in agriculture and the food industry are granular materials, made of many separate particles, such as seeds, grains, granular fertilisers and pelleted feed. During dosing, transport, storage and discharge, these particles move, collide and rub against each other and against the walls of the equipment. For this reason, their behaviour is difficult to describe with models that treat the material as a continuous medium *(Horabik and Molenda, 2016; Zhao et al., 2021).*

Experiments are necessary, but they cannot easily show what happens inside the material, for example the velocity of each particle or the forces between particles. Numerical simulation can help in this respect. The Discrete Element Method (DEM), proposed by Cundall and Strack (1979), represents the material as a set of individual particles and calculates the motion of each particle from the forces that act at its contacts with other particles and with the walls.

DEM has been used in agricultural engineering for soil, seeds, straw and fertilisers, and for processes such as tillage, sowing, harvesting, cleaning, transport and storage *(Maraveas et al., 2025; Tian et al., 2024; Walunj et al., 2023; Zhao et al., 2021).* These reviews also show that good results depend on how the particle shape is represented, on the chosen contact model and on the correct determination (calibration) of the model parameters, while the calculation time remains an important limitation *(Coetzee, 2017; Horabik and Molenda, 2016; Zhao et al., 2024).*

A simple example of such a process is the gravitational flow of seeds through a discharge orifice, which occurs in hoppers, silos and seed-metering devices. The flow rate through the orifice influences the dosing accuracy and the capacity of the equipment.

Classical studies described this flow with empirical equations. Beverloo et al. (1961) related the flow rate to the orifice diameter and the particle size, while Chang et al. (1990, 1991) measured the flow of wheat, corn, sorghum and soybeans through orifices of different shapes and related it to the hydraulic diameter of the orifice.

Using the data of Chang et al. (1990), Mieilă and Căsăndroiu (2009) studied how the shape of vertical orifices influences the flow rate of seeds. They found that, for the same hydraulic diameter, the flow rate through a circular orifice was only 72–75% of the flow rate through a square orifice.

They also suggested that there is a minimum orifice size below which the seeds can no longer flow, and that the properties of the seeds should be included more clearly in the equations. However, measurements of the total flow rate cannot show how the seeds move near the orifice.

Some recent studies have used DEM for this purpose. Zaki and Siraj (2019) simulated the discharge of spherical particles from a silo through circular, square and triangular orifices, and Wang et al. (2025) showed, for rice grains, that the discharge rate depends on how densely the particles are packed and how fast they move near the orifice. Such studies are, however, still few for agricultural seeds.

This paper represents the first stage of a doctoral research on the use of DEM for modelling granular materials in agriculture and the food industry. Its aim was to identify the main parameters that influence the gravitational flow of seeds through discharge orifices and to propose a preliminary methodology for studying them with DEM.

The specific objectives were: **(i)** to summarise the classical studies on seed flow through orifices; **(ii)** to describe how seeds are represented in DEM; **(iii)** to classify the parameters needed for a future DEM model; and **(iv)** to define the next steps of the research. The paper does not present DEM simulations; these will be carried out in the next stages.

## MATERIALS AND METHODS

### *Research approach*

This study is based on the analysis of published literature because no new experiments or simulations were performed. Articles were searched in ScienceDirect, MDPI and INMATEH – Agricultural Engineering using keywords such as “discrete element method”, “seeds”, “orifice”, “silo discharge”, “flow rate” and “calibration”. Classical studies on granular flow through orifices, review papers on DEM in agriculture and recent DEM studies on seed discharge and calibration were selected, with priority given to papers from the last ten years.

The analysed system is shown in Fig. 1. Seeds flow by gravity from a container through a vertical or a horizontal orifice (Fig. 1a). In DEM, each seed is represented as a particle that interacts with the other particles and with the walls (Fig. 1b).

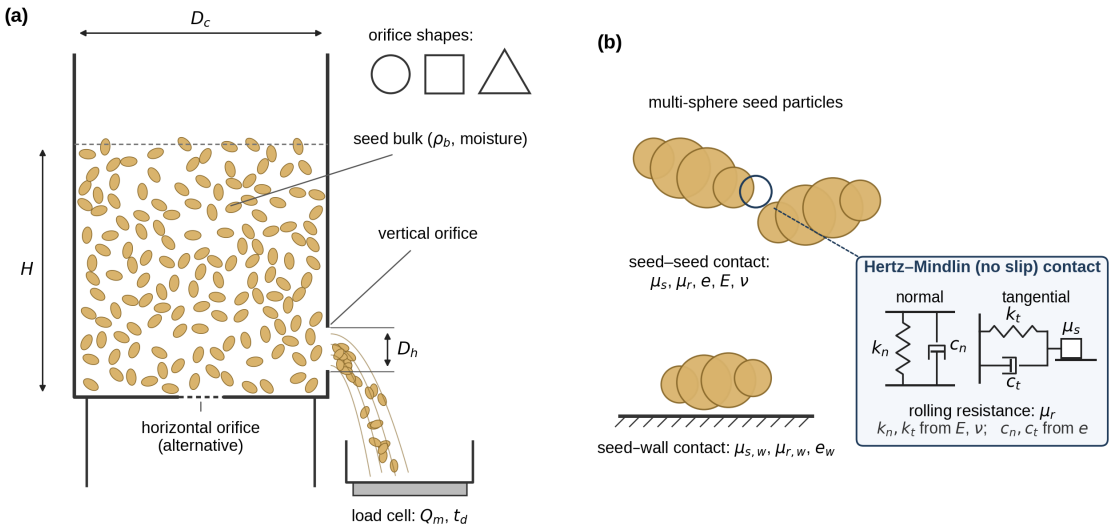



**Fig. 1 - Schematic representation of the analysed system: (a) gravitational discharge of seeds through a vertical or horizontal orifice; (b) representation of seeds and contacts in DEM**

*$D_c$ – container diameter; $H$ – filling height; $D_h$ – hydraulic diameter of the orifice; $Q_m$ – mass flow rate; $t_d$ – discharge time; $k_n$, $k_t$ – contact stiffness; $c_n$, $c_t$ – damping; $\mu_s$, $\mu_r$ – static and rolling friction coefficients; $e$ – coefficient of restitution; $E$, $\nu$ – elastic modulus and Poisson's ratio; $w$ – seed–wall contact*

***Equations used in the analysis***

To compare orifices of different shapes, the hydraulic diameter was used:

$$D_h = \frac{4A}{P} \tag{1}$$

where: $D_h$ is the hydraulic diameter, [m]; $A$ – orifice area, [m$^2$]; $P$ – orifice perimeter, [m]. For a circle, $D_h$ is equal to the diameter, and for a square, to the side length.

The classical equation of Beverloo et al. (1961), as given by Mieilă and Căsăndroiu (2009), is:

$$Q_m = C \cdot \rho_b \cdot g^{1/2} \cdot (D - k \cdot d)^{5/2} \tag{2}$$

where: $Q_m$ is the mass flow rate, [kg/s]; $\rho_b$ – bulk density, [kg/m$^3$]; $g$ – gravitational acceleration, [m/s$^2$]; $D$ – orifice diameter, [m]; $d$ – mean particle diameter, [m]; $C$ and $k$ – empirical constants (about 0.58 and 1.4).

Mieilă and Căsăndroiu (2009) used a simpler relation between the flow rate and the hydraulic diameter:

$$Q = K \cdot D_h^n \tag{3}$$

where: $Q$ is the volume flow rate, [m$^3$/h] (with $D_h$ in cm); $K$ and $n$ – experimental coefficients that depend on the seed type, moisture content and orifice shape.

The effect of orifice shape was expressed by the ratio between the flow rates through a circular and a square orifice with the same hydraulic diameter *(Mieilă and Căsăndroiu, 2009):*

$$C_f = \frac{Q_c}{Q_s} \tag{4}$$

where: $Q_c$ and $Q_s$ are the flow rates through the circular and the square orifice, respectively.

The flow rates published by Mieilă and Căsăndroiu (2009) for four seed types were plotted again, and the ratio $Q_c/Q_s$ was calculated for each orifice size and compared with the ratio of the orifice areas.

***Classification of parameters***

Each parameter needed for a future DEM model was placed in one of four groups: (M) parameters that can be measured directly in the laboratory; (C) parameters that are difficult to measure and must be calibrated, i.e. adjusted until the simulation reproduces a simple laboratory test; (G) geometrical parameters

of the equipment; and (V) validation indicators, i.e. results that can be measured and compared with the simulation.

## RESULTS AND DISCUSSION

### *Classical and DEM studies of seed flow through orifices*

The main studies are summarised in Table 1. The classical studies identified the same main parameters: orifice size, orifice shape and position, particle size, bulk density and moisture content. In all cases the flow rate increased strongly with the orifice size; for the seeds analysed by Mieilă and Căsăndroiu (2009), the exponent *n* in Equation (3) was between 2.52 and 2.79.

The flow rate of corn and wheat decreased when the moisture content increased, and vertical orifices discharged only 37–50% of the flow rate of similar horizontal orifices *(Chang et al., 1991).*

**Table 1**

**Classical and DEM studies on the flow of granular materials through discharge orifices**

| Study | Material and set-up | Studied parameters | Main findings | What DEM could add |
|---|---|---|---|---|
| ***Classical studies*** | | | | |
| Beverloo et al. (1961) | Granular materials; orifice in the container bottom | Orifice diameter, particle size, bulk density | $Q_m \propto \rho_b \cdot g^{1/2} \cdot (D - k \cdot d)^{5/2}$; a narrow zone near the orifice edge does not contribute to the flow | Explain the edge effect from the motion of particles |
| Chang et al. (1991) | Wheat, corn, sorghum, soybeans; six orifice shapes, vertical and horizontal | Orifice shape, size and position; seed type | Flow rate increases with $D_h$; vertical orifices give 37–50% of the horizontal flow | Compare the flow near vertical and horizontal orifices |
| Mieilă and Căsăndroiu (2009) | Data of Chang et al. (1990); circular and square vertical orifices, $D_h = 10{,}2 - 30{,}5$ cm | Orifice shape, $D_h$, moisture, seed type | $Q_c = C_f \cdot Q_s$, $C_f = 0{,}72 - 0{,}75$; $Q \propto D_h^{2.67}$; minimum $D_h \approx 2 - 2{,}5$ cm cm (not verified) | Explain $C_f$; include seed properties; minimum orifice size |
| ***DEM studies*** | | | | |
| Zaki and Siraj (2019) | Spherical glass beads; flat-bottomed silo | Circular, square and triangular orifices of equal area | Highest flow for the circular and lowest for the triangular orifice | Use real seed shapes |
| Wang et al. (2025) | Rice grains; flat-bottomed silo | Orifice position (eccentricity) | Flow rate depends on the packing and velocity of particles at the orifice | Apply the same approach to orifice shape |

The main limitation of these studies is that the effect of the seed properties is included in empirical coefficients (*C*, *k*, *K*, *n*), which must be determined again for each seed type and moisture content. Mieilă and Căsăndroiu (2009) noted larger errors for some seeds, especially wheat. The minimum orifice size was only estimated mathematically and was not verified by experiments. Moreover, the orifices studied were large (10.2–30.5 cm), while the orifices of seed-metering devices are only a few seed sizes wide.

DEM studies can add information about what happens inside the material. Zaki and Siraj (2019) showed that the constants of the Beverloo equation depend on the orifice shape, and Wang et al. (2025) explained the changes in discharge rate by the packing and velocity of the particles near the orifice. Parafiniuk et al. (2013) compared experiments and DEM simulations for the discharge of rapeseed from a model silo, Huang et al. (2024) used DEM to improve the prediction of discharge for pelleted feed, and Markauskas et al. (2015) showed that the way the shape of maize grains is represented changes the simulated discharge.

### *Effect of orifice shape*

The hydraulic diameter alone does not describe the orifice completely. For the same hydraulic diameter, a square orifice has a 27% larger area than a circular one, so the ratio of their areas is $\frac{\pi}{4} \approx 0{,}785$. Therefore, part of the higher flow rate through square orifices reported by Mieilă and Căsăndroiu (2009) is simply due to their larger area. Zaki and Siraj (2019), who compared orifices with the same area, found

instead the highest discharge rate for the circular orifice. The conclusion about which shape performs better therefore depends on how the orifices are compared.

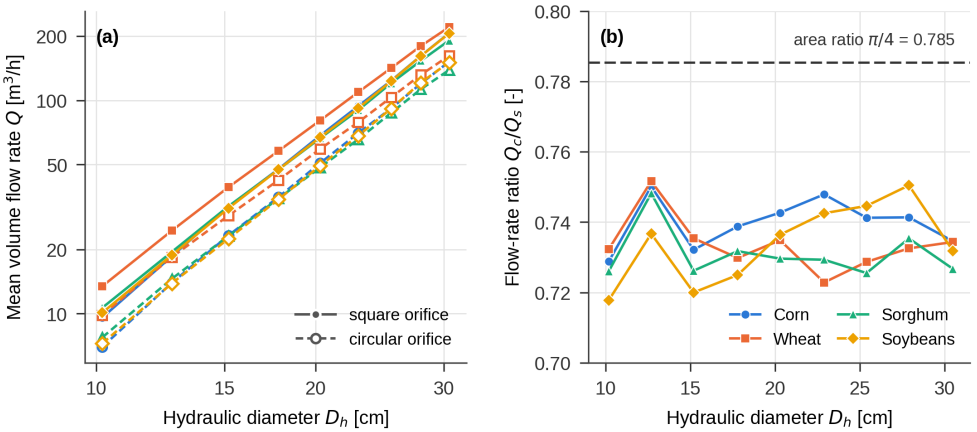



**Fig. 2 - Published flow rates of seeds through circular and square vertical orifices (a) and ratio of circular to square flow rates (b) as a function of hydraulic diameter**

*Data of Chang et al. (1990), as given by Mieilă and Căsăndroiu (2009); colours and markers indicate the seed type in both graphs; dashed line in (b) – ratio of the orifice areas*

Fig. 2b shows the ratio between the flow rates through circular and square orifices, calculated from the published data. All 36 values are between 0.718 and 0.752 (mean about 0.734), below the area ratio of 0.785, and they show no clear trend with orifice size or seed type. If only the area mattered, the two values would be equal. This means that the flow rate per unit area was about 5–8% lower for the circular orifice, so the orifice shape also has an effect of its own. The cause of this effect cannot be found from flow-rate measurements alone; it requires information about how the seeds move and pack near the orifice, which DEM can provide. This is a concrete question for the next stage of the research.

***Representation of seeds in DEM***

Seeds are usually not sticky (cohesive), so the Hertz–Mindlin (no slip) contact model is commonly used for them *(Zhao et al., 2021; Zhao et al., 2024).* In this model, the contact between two particles is described by springs and dampers in the normal and tangential directions, together with friction (Fig. 1b). The shape of a seed is often represented by several overlapping spheres; more spheres give a more realistic shape but increase the calculation time *(Markauskas et al., 2015).* Since the moisture content changes the properties of seeds *(Horabik and Molenda, 2016),* all parameters must be determined for the same moisture content.

Some parameters, such as seed dimensions and density, can be measured directly. Others, especially the friction coefficients, are usually calibrated: their values are changed until the simulated angle of repose (the slope of a pile of seeds) matches the measured one *(Dun et al., 2024; Wang et al., 2024).* Because different sets of parameters may give the same result in one test *(Coetzee, 2017),* the model must also be checked in a second, different test. For this reason, the orifices used for validation should be different from those used for calibration.

***Parameters for a future DEM model***

The parameters identified in this study are grouped in Table 2. The friction coefficients are the main parameters that need calibration, while the mass flow rate and the discharge time are the simplest results to compare with experiments. Future simulations should also include small orifices, only a few seed sizes wide, where blockage becomes more likely.

**Table 2**

**Parameters needed for the DEM modelling of seed flow through discharge orifices**

| Parameter | Influence on seed flow | Role in the DEM model | How it can be determined | Group |
|---|---|---|---|---|
| ***Seed properties*** | | | | |
| Seed size and shape | Influence packing, orientation and risk of blockage | Particle size and shape in the model | Calliper, image analysis | M |

| Parameter | Influence on seed flow | Role in the DEM model | How it can be determined | Group |
|---|---|---|---|---|
| Density and bulk density | Influence the mass flow rate | Particle mass | Pycnometer; weighing a known volume | M |
| Moisture content | Changes friction and flow rate | Parameters valid for one moisture level | Oven-drying method | M |
| Friction coefficients (static and rolling) | Higher friction reduces the flow and can cause blockage | Resistance to sliding and rolling | Inclined plane; calibration with the angle of repose | M / C |
| Coefficient of restitution, elastic modulus | Small effect in dense flow | Energy loss and stiffness at contact | Drop test; compression test | M / C |
| ***Geometrical parameters*** | | | | |
| Orifice shape and size | Change the orifice area and the flow rate | Model geometry (CAD) | Chosen in the design | G |
| Orifice position; container shape | Vertical orifices give lower flow rates | Model geometry (CAD) | Chosen in the design | G |
| ***Results used for validation*** | | | | |
| Mass flow rate, discharge time | Main results of the process | Calculated from the particles leaving the orifice | Weighing with a load cell | V |
| Particle velocity, blockage | Explain the effect of orifice shape | Obtained directly from the simulation | High-speed camera; repeated tests | V |

*M – measurable; C – requires calibration; G – geometrical; V – validation indicator*

***Proposed methodology***

The proposed methodology is shown in Fig. 3. This paper covers steps 1–4; the other steps will be carried out in the next stages of the doctoral research.

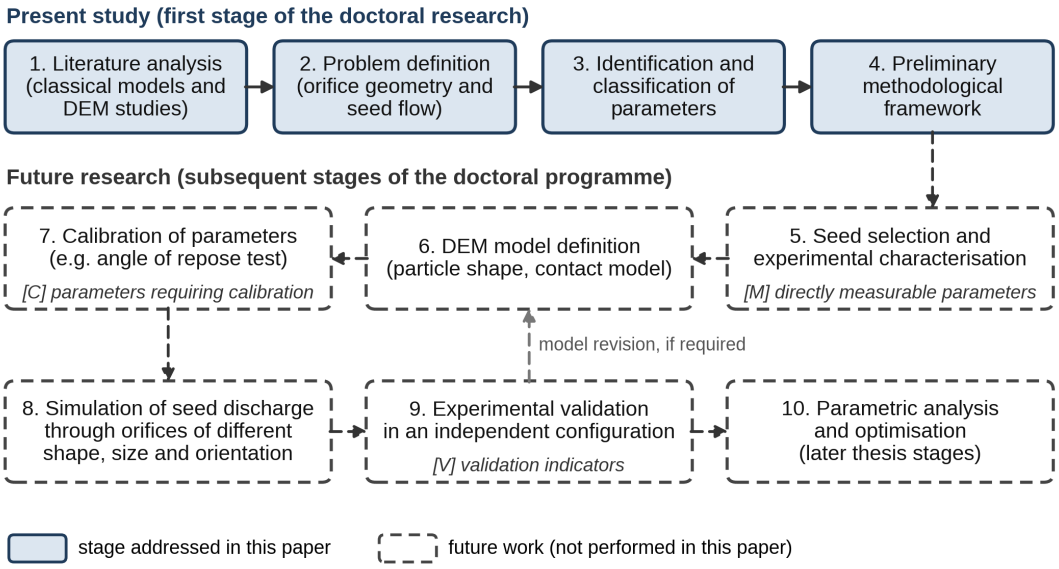



**Fig. 3 - Preliminary methodology for the DEM study of seed flow through discharge orifices**

*M – measurable parameters; C – parameters that require calibration; V – validation indicators*

In the next stage, a seed type will be selected and its basic properties will be measured in the laboratory at a known moisture content. A DEM model will then be built, and the parameters that cannot be measured will be calibrated using the angle of repose test. The model will be used to simulate the discharge of seeds through orifices of different shapes and sizes, compared both at the same hydraulic diameter and at the same area.

The results will be validated by experiments on orifices that were not used for calibration, by comparing the mass flow rate and the discharge time. Since this paper is based only on published data, the explanations proposed for the effect of orifice shape must still be checked by simulations and experiments.

## CONCLUSIONS

(1) DEM is a suitable method for studying the flow of seeds and other agricultural granular materials, because it shows the motion of each particle, which cannot be observed in experiments alone.

(2) The flow of seeds through discharge orifices depends on the properties of the seeds (size, shape, density, moisture content and friction) and on the geometry of the orifice and of the container.

(3) The effect of orifice shape depends on how the orifices are compared (same hydraulic diameter or same area). For the same hydraulic diameter, the published flow-rate ratio between circular and square orifices was lower than the ratio of their areas, so the shape has an effect that cannot be explained by the area alone.

(4) A reliable DEM model requires measured seed properties, calibration of the parameters that cannot be measured and validation against independent experiments. The next stage of the research will include selecting the seed material, measuring its properties, building and calibrating the DEM model and validating it for orifices of different shapes.

## REFERENCES


[1] Beverloo, W. A., Leniger, H. A., & van de Velde, J. (1961). The flow of granular solids through orifices. *Chemical Engineering Science, 15*(3–4), 260–269. https://doi.org/10.1016/0009-2509(61)85030-6

[2] Chang, C. S., Converse, H. H., & Steele, J. L. (1990). Flow rates of grain through vertical orifices. *Transactions of the ASAE, 33*(2), 601–606.

[3] Chang, C. S., Converse, H. H., & Steele, J. L. (1991). Flow rates of grain through various shapes of vertical and horizontal orifices. *Transactions of the ASAE, 34*(4), 1789–1796.

[4] Coetzee, C. J. (2017). Review: Calibration of the discrete element method. *Powder Technology, 310*, 104–142. https://doi.org/10.1016/j.powtec.2017.01.015

[5] Cundall, P. A., & Strack, O. D. L. (1979). A discrete numerical model for granular assemblies. *Géotechnique, 29*(1), 47–65. https://doi.org/10.1680/geot.1979.29.1.47

[6] Dun, G., Zhang, C., Ji, X., Meng, Q., Sheng, Q., & Wang, L. (2024). Simulation parameter calibration and test of pakchoi seeds based on discrete element method. *INMATEH – Agricultural Engineering, 73*(2), 391–405. https://doi.org/10.35633/inmateh-73-33

[7] Horabik, J., & Molenda, M. (2016). Parameters and contact models for DEM simulations of agricultural granular materials: A review. *Biosystems Engineering, 147*, 206–225. https://doi.org/10.1016/j.biosystemseng.2016.02.017

[8] Huang, T., Wu, B., Xie, F., Qian, H., Li, Z., Chen, P., & Xiang, Q. (2024). Characterisation of discharge and flow rate predictions for asymmetric wedge-shaped hoppers. *Biosystems Engineering, 245*, 96–105. https://doi.org/10.1016/j.biosystemseng.2024.07.007

[9] Maraveas, C., Tsigkas, N., & Bartzanas, T. (2025). Agricultural processes simulation using discrete element method: A review. *Computers and Electronics in Agriculture, 237*, 110733. https://doi.org/10.1016/j.compag.2025.110733

[10] Markauskas, D., Ramírez-Gómez, Á., Kačianauskas, R., & Zdancevičius, E. (2015). Maize grain shape approaches for DEM modelling. *Computers and Electronics in Agriculture, 118*, 247–258. https://doi.org/10.1016/j.compag.2015.09.004

[11] Mieilă, C., & Căsăndroiu, T. (2009). Aspects regarding influence of geometrical shape of orifices about seeds gravimetric flow rate. *Lucrări Științifice (INMATEH) [Scientific Papers (INMATEH)], 28*(2), 59–66.

[12] Parafiniuk, P., Molenda, M., & Horabik, J. (2013). Discharge of rapeseeds from a model silo: Physical testing and discrete element method simulations. *Computers and Electronics in Agriculture, 97*, 40–46. https://doi.org/10.1016/j.compag.2013.06.008

[13] Tian, Y., Zeng, Z., & Xing, Y. (2024). A review of discrete element method applications in soil–plant interactions: Challenges and opportunities. *Agriculture, 14*(9), 1486. https://doi.org/10.3390/agriculture14091486

[14] Walunj, A., Chen, Y., Tian, Y., & Zeng, Z. (2023). Modeling soil–plant–machine dynamics using discrete element method: A review. *Agronomy, 13*(5), 1260. https://doi.org/10.3390/agronomy13051260

[15] Wang, S., Xia, S., Chen, Y., Lou, C., Ren, D., & Li, Z. (2024). Particle motion of coated corn seed accumulation process based on discrete element method. *INMATEH – Agricultural Engineering, 72*(1), 375–390. https://doi.org/10.35633/inmateh-72-34

[16] Wang, Y., Han, Y., Li, A., Li, H., Gao, H., Sun, Z., Ji, S., Li, Z., & Jia, F. (2025). Numerical analysis of influence mechanism of orifice eccentricity on silo discharge rate. *Agriculture, 15*(5), 490. https://doi.org/10.3390/agriculture15050490

[17] Zaki, M., & Siraj, M. S. (2019). Study of a flat-bottomed cylindrical silo with different orifice shapes. *Powder Technology, 354*, 641–652. https://doi.org/10.1016/j.powtec.2019.06.041

[18] Zhao, H., Huang, Y., Liu, Z., Liu, W., & Zheng, Z. (2021). Applications of discrete element method in the research of agricultural machinery: A review. *Agriculture, 11*(5), 425. https://doi.org/10.3390/agriculture11050425

[19] Zhao, Z., Wu, M., & Jiang, X. (2024). A review of contact models' properties for discrete element simulation in agricultural engineering. *Agriculture, 14*(2), 238. https://doi.org/10.3390/agriculture14020238

# ADVANCED MONITORING OF AQUACULTURE SYSTEMS USING MULTISENSOR PREDICTIVE MODELS
# /
# *MONITORIZAREA AVANSATĂ A ACVACULTURII PRIN MODELE PREDICTIVE MULTISENZOR*

**Dan CUJBESCU[1)], Iulian VOICEA*[1)], Cătălin PERSU[1)]**
[1)] National Institute of Research - Development for Machines and Installations Designed to Agriculture and Food Industry - INMA Bucharest / Romania
**Tel: (+40) 752 161 780; *E-mail: voicea_iulian@yahoo.com*

***Keywords:*** *precision aquaculture, multisensor data, predictive models, real-time monitoring*

## ABSTRACT
*Modern aquaculture systems require continuous monitoring of environmental parameters and bioresource behavior to ensure high productivity and risk control. Traditional practices are based on visual observations and empirical decisions, which generates variability and reduces process reproducibility, and the lack of real-time data limits rapid intervention in critical situations, such as decreased dissolved oxygen or stress in fish. The development of digital technologies has led to precision aquaculture, based on the integration of sensors, acquisition systems and artificial intelligence algorithms, which continuously collect physical and chemical parameters of water and data on fish behavior through underwater imaging. The integration of these sources allows the transition from reactive monitoring to predictive control, through artificial intelligence models, especially machine learning and computer vision, identify patterns in data, estimate biomass, detect anomalies and anticipate the evolution of environmental parameters. Thus, decisions regarding feeding and environmental control are based on quantifiable predictions, and the integration of multisensor data increases the accuracy of models and reduces uncertainties. The paper proposes an integrated system for advanced monitoring, based on modular architecture, capable of ensuring real-time data acquisition and processing and decision support for optimizing technological processes.*

## REZUMAT
*Sistemele moderne de acvacultură necesită monitorizarea continuă a parametrilor de mediu și a comportamentului bioresurselor pentru a asigura productivitate ridicată și controlul riscurilor. Practicile tradiționale se bazează pe observații vizuale și decizii empirice, ceea ce generează variabilitate și reduce reproductibilitatea proceselor, iar lipsa datelor în timp real limitează intervenția rapidă în situații critice, precum scăderea oxigenului dizolvat sau apariția stresului la pești. Dezvoltarea tehnologiilor digitale a condus la acvacultura de precizie, bazată pe integrarea senzorilor, sistemelor de achiziție și algoritmilor de inteligență artificială, acestea colectând continuu parametri fizico-chimici ai apei și date privind comportamentul piscicol prin imagistică subacvatică. Integrarea acestor surse permite trecerea de la monitorizare reactivă la control predictiv, prin intermediul modelelor de inteligență artificială, în special învățarea automată și viziunea computerizată, identifică tipare în date, estimează biomasa, detectează anomalii și anticipează evoluția parametrilor de mediu. Astfel, deciziile privind hrănirea și controlul mediului se bazează pe predicții cuantificabile, iar integrarea datelor multisenzor crește acuratețea modelelor și reduce incertitudinile. Lucrarea propune un sistem integrat pentru monitorizare avansată, bazat pe arhitectură modulară, capabilă să asigure achiziția și procesarea datelor în timp real și suport decizional pentru optimizarea proceselor tehnologice.*

## INTRODUCTION
Aquaculture production has significantly increased in recent years due to the growing global demand for aquatic products (*FAO, 2024*). The expansion of the concept of precision aquaculture is based on the use of integrated systems capable of collecting and processing large volumes of data from heterogeneous sources. Recent studies highlight that the use of sensors, IoT networks and artificial intelligence algorithms allows the transformation of aquaculture operations into automated and reproducible processes, reducing the dependence on the human factor and subjective assessments (*D'Agaro, 2025; Føre et al., 2018*). In this context, each element of the aquatic system can become a source of data, contributing to the development

of robust predictive models for production management. Computer vision methods have experienced significant development in recent years, being used for biomass estimation, behavioral analysis and monitoring of fish health. These systems allow for pixel-level image analysis and feature extraction to identify behavioral patterns (*Rathi et al., 2017; Li et al., 2020*). In parallel, acoustic technologies and environmental sensors complement visual information, providing data on the spatial distribution of fish and physicochemical parameters of the water (*Føre et al., 2018, Hu et al., 2022*).

Artificial intelligence plays a central role in integrating and interpreting these data. Machine learning and deep learning models are used for growth prediction, optimization of feeding strategies and early detection of diseases (*Aung et al., 2025*). These approaches allow for the identification of complex relationships between environmental variables and the biological response of aquatic organisms, contributing to increasing the efficiency and sustainability of production systems (*Huang et al., 2021*).

However, the implementation of these technologies faces challenges related to data availability, implementation costs and the complexity of system integration. The lack of representative and standardized data sets can affect the performance of predictive models, and the integration of different types of sensors requires robust interoperability solutions (*Aung et al., 2025, Zheng et al., 2025*).

Despite these advances, several challenges remain. Data availability is limited in many aquaculture environments. Integration of heterogeneous systems is complex. Costs increase with system complexity. In this context, the development of an integrated system, based on predictive models and multisensor data fusion, is a necessary direction for increasing the performance and reliability of aquaculture processes. The paper proposes the study of integrated advanced monitoring systems, based on modular architectures, for real-time data acquisition and processing and decision support in aquaculture.

## MATERIALS AND METHODS

The paper uses a systems analysis approach applied to modern aquaculture monitoring systems. The analysis aims to identify functional architectures, technologies used and methods for integrating multisensor data within intelligent systems. Solutions based on sensors, underwater imaging and artificial intelligence algorithms are evaluated, with a focus on their ability to provide real-time monitoring and decision support.

The general structure of the analyzed system is presented in Fig. 1, where the three main modules are highlighted: acquisition, processing and decision support.

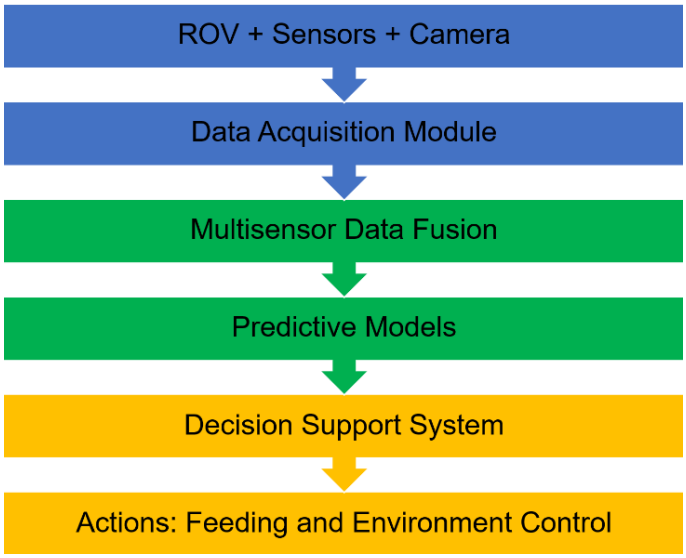



**Fig. 1 - Modular architecture of an intelligent aquaculture monitoring system**

Each module performs a distinct function within the system. The acquisition layer ensures the collection of raw data from the aquatic environment. The processing layer transforms raw data into structured information using artificial intelligence methods. The decision layer generates actionable outputs for system control.

The interaction between modules is defined by a unidirectional and feedback data flow, ensuring both monitoring and control capabilities.

The acquisition module integrates heterogeneous sensing technologies and must comply with safety and operational standards (ISO, 2018). The main categories of data sources are:

- environmental sensors for temperature [°C], dissolved oxygen [mg/L], and pH [-];
- underwater cameras for behavioral analysis;
- IoT networks for data transmission.

These technologies ensure continuous monitoring and data availability (*D'Agaro, 2025*). The sampling process is continuous and designed to capture dynamic variations in the aquatic environment. The multisensor configuration allows redundancy and improves data reliability.

Data integration is performed through multisensor fusion techniques.

The input vector is defined as:

$$X = \{X_1, X_2, \ldots, X_n\} \quad (1)$$

where each element represents a measured parameter from a specific sensor.

The integration process includes:

- synchronization of data streams;
- normalization of measurement units;
- elimination of noise and outliers;
- feature extraction.

This step is critical for ensuring consistency and usability of the data in predictive models.

The predictive model is expressed as:

$$\hat{y} = f(X) \quad (2)$$

where:

$\hat{y}$ represents the estimated variable, such as biomass [kg] or dissolved oxygen [mg/L];

$X$ represents the multisensor input vector, including temperature [°C], pH [-], and other parameters.

The function $f(\cdot)$ is implemented using machine learning or deep learning algorithms. These models are designed to capture nonlinear relationships between environmental variables and biological responses.

Typical outputs include:

- prediction of environmental parameter evolution;
- detection of abnormal system behavior;
- estimation of fish growth and biomass.

For comparative analysis, systems are evaluated based on technical and functional criteria.

**Table 1**

**Comparative analysis of aquaculture monitoring systems**

| Criterion | Sensor-based systems | Vision-based systems | AI-integrated systems |
|---|---|---|---|
| Data type | Physical parameters | Image/video data | Multisensor data |
| Real-time capability | Medium | High | Very high |
| Prediction capability | Low | Medium | High |
| System complexity | Low | Medium | High |
| Decision support | Limited | Partial | Advanced |

The table highlights that integrated systems with artificial intelligence offer the best performance in terms of prediction and decision support, due to the ability to integrate and analyze heterogeneous data (*D'Agaro, 2025; Aung et al., 2025*).

The comparative analysis highlights the trend of moving from isolated systems to integrated systems, capable of combining multisensor data and using predictive models (*Føre et al., 2018; Aung et al.,*

*2025*). This direction is essential for the development of precision aquaculture and for increasing operational efficiency, by reducing uncertainties and optimizing technological decisions.

The systems are evaluated using a set of performance indicators that reflect their operational capabilities. The main criteria include:

- accuracy of predictions;
- real-time processing capability;
- level of data integration;
- scalability of the architecture;
- robustness to noise and missing data.

The evaluation is performed comparatively, as shown in Table 1. Each system type is assessed based on its ability to meet the defined criteria.

## RESULTS

The results of the comparative analysis highlight the evolution of aquaculture monitoring systems from isolated data acquisition solutions to integrated intelligent systems based on multisensor data and predictive models.

The functional relationship between system modules is illustrated in Fig. 1 and directly influences system performance. Systems that ensure a continuous and structured data flow between acquisition, processing, and decision modules achieve higher efficiency and accuracy.

The predictive capability of the analyzed systems is strongly dependent on the structure of the input data vector X defined in relation (1).

The accuracy of the estimated output $\hat{y}$ increases with the number and diversity of input parameters. Systems based on a single data source generate limited results, while multisensor systems enable a more complete representation of the aquatic environment.

**Table 2**

**Performance comparison of aquaculture monitoring systems**

| Parameter | Sensor-based | Vision-based | AI-integrated |
|---|---|---|---|
| Data accuracy | Medium | High | Very high |
| Prediction capability | Low | Medium | High |
| Response time | High | Medium | Low |
| Integration level | Low | Medium | High |
| Decision support | Limited | Partial | Advanced |

The comparative evaluation presented in Table 2 is supported by recent studies in the field of precision aquaculture. The qualitative performance levels (low, medium, high) are derived from the comparative analysis of reported system capabilities in the cited literature.

Sensor-based systems provide reliable measurements of physicochemical parameters but have limited predictive capabilities (*Føre et al., 2018*).

Vision-based systems improve data accuracy and behavioral analysis through image processing techniques, enabling higher real-time capability (*Li et al., 2020*).

AI-integrated systems demonstrate superior performance due to the integration of multisensor data and the use of machine learning algorithms, which enhance prediction capability and decision support (*Aung et al., 2025, D'Agaro, 2025*).

The graphical representation in Fig. 2 illustrates the performance differences between monitoring systems, highlighting the superiority of AI-integrated solutions.

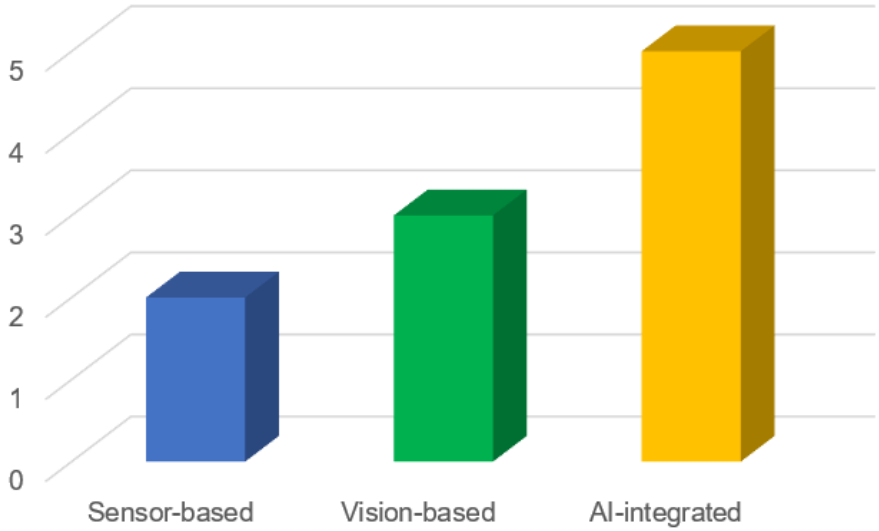



**Fig. 2 - Performance comparison of aquaculture monitoring systems**

The correlation between Fig. 2 and Table 2 confirms that performance improvements are directly linked to the level of data integration and processing capability. Systems with higher integration levels show better predictive accuracy and reduced response time.

The modular architecture presented in Fig. 1 enables this improvement by supporting efficient data flow and real-time processing. The acquisition module ensures continuous data input, while the processing module applies artificial intelligence algorithms for data fusion and prediction.

Multisensor integration plays a critical role in system robustness. It allows the detection of complex interactions between environmental parameters and biological responses. For example, simultaneous variation of temperature and dissolved oxygen can indicate stress conditions before visible symptoms appear.

Despite the advantages, AI-integrated systems require higher computational resources and more complex infrastructure. Data availability remains a limiting factor for model training.

However, the results demonstrate that the transition toward intelligent systems is necessary for improving efficiency, reducing uncertainty, and enabling real-time decision-making in aquaculture.

## CONCLUSIONS

This study examined advanced aquaculture monitoring systems through a systems-level lens. The analysis confirms a shift toward integrated, data-driven architectures.

Sensor-based solutions deliver stable measurements of environmental variables. Their role is well defined, yet narrow. They rarely provide predictive insight or actionable guidance on their own. Vision-based systems extend the scope to behavior and biomass. They perform well under controlled lighting and water clarity. Their robustness decreases in turbid environments, which limits general applicability. AI-integrated systems show the strongest potential. They combine heterogeneous inputs and enable prediction and early anomaly detection. However, performance depends on data quality, labeling consistency, and model validation protocols. Many studies report gains, but few provide standardized benchmarks. Transferability across farms and species is still uncertain. Multisensor fusion improves situational awareness. It also propagates noise if preprocessing is inadequate. The net benefit depends on filtering, alignment, and feature selection. Adoption barriers remain. Costs, data availability, and operational expertise constrain deployment.

Future work should prioritize rigorous validation, shared datasets, and reproducible metrics.

## ACKNOWLEDGEMENT

This research was supported by the Romanian Ministry of Research Innovation and Digitalization, through the project “Underwater Intelligent System (Robot) for the Protection of Life, Health and Growth Environment” – PN 23 04 01 03 – Ctr. 9N/01.01.2023 and by the Ministry of Agriculture and Rural Development – Romania - MADR through the Sectoral Project ADER 25.2.2 “Vertical Aquaponic Farm Adapted To Current Climate Changes”, Ctr. 18.07.2023.

## REFERENCES


[1] Aung, T., Razak, R. A., Nor, A. R. B. M. (2024). Artificial intelligence methods used in various aquaculture applications: A systematic literature review. *Journal of the World Aquaculture Society*, 56, e13107, DOI:10.1111/jwas.13107

[2] D'Agaro, E. (2025). Fish Farming 5.0: Advanced tools for a smart aquaculture management. *Applied Sciences*, 15(23), 12638, https://doi.org/10.3390/app152312638

[3] Føre, M., Frank, K., Norton, T., Svendsen, E., Alfredsen, J.A., Dempster, T., Eguiraun, H., Watson, W., Stahl, A., Sunde, L.M. and Schellewald, C., (2018). Precision fish farming: A new framework to improve production in aquaculture. *biosystems engineering*, *173*, pp.176-193,

[4] DOI:10.1016/j.biosystemseng.2017.10.014

[5] Huang, Y., Chen, Z., Yu, T., Huang, X., Gu, X. (2021). Agricultural remote sensing big data: Management and applications. *Journal of Integrative Agriculture*, 20(4), 868–878. DOI:10.1016/S2095-3119(17)61859-8

[6] Hu, W. C., Chen, L. B., Wang, B. H., Li, G. W., Huang, X. R. (2022). An AIoT-based water quality inspection system for intelligent aquaculture. In *2022 IEEE 11th Global Conference on Consumer Electronics (GCCE)* (pp. 551-552). IEEE, DOI:10.1109/GCCE56475.2022.10014181

[7] Li, D., Hao, Y., Duan, Y. (2019). Nonintrusive methods for biomass estimation in aquaculture with emphasis on fish: A review. *Reviews in Aquaculture*, 12(6), DOI:10.1111/raq.12388

[8] Rathi, D., Jain, S., Indu, S. (2017). Underwater fish detection using deep learning for water power applications. In *Proceedings of the IEEE International Conference on Computer Vision Workshops*.

[9] Zheng, Y., Chen, Y., Li, X., Peng, X. (2025). An IoT-based Aquaculture Environmental Monitoring System. In *Proceedings of the 2025 2nd International Conference on Big Data Analytics and Artificial Intelligence Application*, pp. 216-222, https://doi.org/10.1145/3788108.3788531

[10] *** FAO (2024). The State of World Fisheries and Aquaculture 2024. Food and Agriculture Organization of the United Nations, Rome.

[11] *** ISO (2018). Occupational health and safety management systems — Requirements with guidance for use (ISO 45001:2018). International Organization for Standardization.

# INFLUENCE OF SOIL MOISTURE ON MECHANICAL REQUIREMENTS DURING AUTOMATED SOIL SAMPLING

/

# *INFLUENȚA UMIDITĂȚII SOLULUI ASUPRA CERINȚELOR MECANICE ÎN TIMPUL PRELEVĂRII AUTOMATE A PROBELOR DE SOL*

**Alexandru IONESCU, Nicolae-Valentin VLĂDUȚ*, Florin NENCIU, Mario CRISTEA, Robert-Dorin CRISTEA, Dorin-Andrei CÎRSTEA, Alexandru-Cristian CIOACLĂ, Stefano-Andrea MANTOVANI, Dragos ANGHELACHE**
National Institute of Research - Development for Machines and Installations Designed to Agriculture and Food Industry - INMA Bucharest / Romania
**E-mail: vladut@inma.ro*

***Keywords:*** *soil moisture, penetration resistance, draft force, automated soil sampling, soil-tool interaction*

**ABSTRACT**

*This review examined how soil moisture content influenced the mechanical requirements of automated and robotic soil sampling systems. The mechanical behaviour of soil — including penetration resistance, shear strength, cohesion, internal friction angle, and soil-metal friction and adhesion — was shown to vary systematically with water content, with direct consequences for the forces, torques, and energy demanded by sampling probes, augers, and coring tools. Recent developments in autonomous ground and aerial soil sampling platforms were surveyed, with particular attention to actuator sizing, penetration-rate control, and moisture-adaptive strategies intended to reduce power consumption and mechanical wear. The relationships reported across cone penetrometry, tillage-tool draft force, and soil-tool adhesion studies were compared, and inconsistencies arising from differing soil textures, testing methods, and moisture ranges were discussed. The review concluded that moisture-responsive control, informed by real-time soil moisture or penetration-force feedback, represented a promising direction for improving the reliability, energy efficiency, and sample-core integrity of automated sampling equipment, while highlighting the need for standardized testing protocols and field-validated predictive models linking moisture content directly to probe-level force and torque requirements.*

**REZUMAT**

*Această lucrare de sinteză a analizat modul în care conținutul de umiditate al solului influențează cerințele mecanice ale sistemelor automate de prelevare a probelor de sol. S-a arătat că proprietățile mecanice ale solului — rezistența la penetrare, rezistența la forfecare, coeziunea, unghiul de frecare internă, precum și frecarea și aderența sol-metal — variază sistematic în funcție de conținutul de apă, cu consecințe directe asupra forțelor, cuplurilor și energiei necesare sondelor, burghielor și tuburilor de carotaj. Au fost trecute în revistă evoluțiile recente ale platformelor autonome terestre și aeriene de prelevare a probelor de sol, cu accent pe dimensionarea acționărilor, controlul vitezei de penetrare și strategiile adaptive la umiditate, destinate reducerii consumului de energie și a uzurii mecanice. Au fost comparate relațiile raportate în studiile de conometrie, forță de tracțiune și aderență sol-unealtă, fiind discutate neconcordanțele determinate de textura solului, metodele de testare și intervalele de umiditate. Lucrarea a concluzionat că un control adaptiv la umiditate, bazat pe umiditatea solului sau pe forța de penetrare măsurate în timp real, reprezintă o direcție promițătoare pentru îmbunătățirea fiabilității, eficienței energetice și integrității probelor, evidențiind și necesitatea unor protocoale de testare standardizate și a unor modele predictive validate în câmp.*

## INTRODUCTION

Soil sampling remains one of the most labour-intensive stages of precision agriculture, environmental site characterization, and agricultural research programmes, and it is increasingly being transferred from manual operators to automated and robotic systems capable of higher sampling density, better georeferencing, and reduced operator exposure to hazardous conditions *(Norby et al., 2024)*. Ground-based platforms equipped with hydraulic or electromechanical probes, augers, and coring tools, as well as emerging aerial sampling systems, must physically penetrate, cut, and extract soil under highly variable field conditions, and the soil itself behaves as a complex, moisture-dependent mechanical medium rather than a fixed material with constant properties *(Pang et al., 2023)*. Because the water content of soil governs

cohesion, internal friction, penetration resistance, and soil-tool adhesion, it directly determines the forces, torques, and power that a sampling mechanism must be capable of delivering, as well as the wear experienced by tools and the risk of core disturbance, jamming, or incomplete sample retrieval.

While the influence of moisture on tillage-tool draft force and on cone penetrometer readings has been studied for decades in the agricultural engineering and terramechanics literature, this body of knowledge has developed largely independently from the recent wave of research on autonomous soil sampling platforms, in which mechanical sizing decisions are often made empirically rather than through an explicit link to moisture-dependent soil behaviour *(Klopfenstein & Lussier Desbiens, 2024)*. At the same time, the growing availability of low-cost soil moisture sensors and force/torque feedback on robotic actuators has created a practical opportunity to size and control sampling mechanisms adaptively, adjusting penetration rate, applied force, or auger torque in response to real-time soil conditions rather than to fixed, worst-case design assumptions *(Eceoğlu & Ünal, 2024)*.

This review examined how variations in soil moisture content affect the mechanical requirements of automated soil sampling equipment. Rather than presenting new experimental data, it brought together and critically compared findings from soil mechanics, tillage-tool draft-force research, and the recent robotics literature on autonomous ground and aerial soil samplers.

The aim was threefold: first, to summarize the moisture dependence of the soil mechanical parameters most relevant to sampling — penetration resistance, shear strength, and soil-tool friction and adhesion; second, to examine how these parameters translate into force, torque, and power requirements for representative automated sampling mechanisms; and third, to identify aspects of this moisture–mechanics–automation relationship that remain insufficiently understood and require further research.

## MATERIALS AND METHODS

### Soil humidity conditions

Variations in water content directly affect soil cohesion, adhesion, plasticity, penetration resistance, and the interaction between the soil and the sampling tool. Consequently, the moisture condition of the soil can significantly influence the drilling torque, axial penetration force, extraction force, sampling time, collected sample mass, and the structural integrity of the obtained sample.

Under very dry conditions, soil particles exhibit limited cohesion and the sampled material may become highly friable and susceptible to fragmentation. During the penetration of the sampling tool, dry and compact soil can generate increased mechanical resistance, potentially resulting in higher drilling torque and axial force requirements. In addition, the collected sample may partially disintegrate during extraction, leading to material losses and reduced sample representativeness. Although adhesion to the sampling equipment is generally low under these conditions, excessive soil hardness may increase energy consumption and equipment wear.

As soil moisture increases, the cohesion between soil particles generally improves, facilitating the formation of a more stable and continuous soil sample. At an intermediate moisture range, the soil may provide favorable conditions for sampling, as it maintains sufficient cohesion to preserve the sample structure while avoiding excessive adhesion to the sampling tool. As illustrated in the generated figure, this range can be considered an optimum condition in which a well-formed soil core, increased sample mass, and improved sample quality may be obtained. From an operational perspective, the balance between soil cohesion and mechanical resistance can also contribute to improved sampling efficiency.

At higher moisture levels, however, the mechanical behavior of the soil changes significantly. The material may become increasingly plastic and deformable, resulting in greater adhesion to the surfaces of the sampling equipment. This phenomenon can cause smearing along the walls of the sampler and increase friction during penetration and extraction. Although wet soil may initially adhere effectively to the sampling tool, excessive moisture can negatively affect the recovery process by causing deformation, sticking, and partial loss of material.

Under very wet conditions, the soil may exhibit excessive plasticity and a pronounced adhesive behavior. The sample can adhere strongly to the sampling device, making its extraction and subsequent removal more difficult. Furthermore, the deformation of the soil during sampling may compromise the original structure of the collected material. Such conditions may therefore reduce sample quality and increase the time and mechanical effort required for the sampling operation.

The relationship between soil moisture and collected sample mass can consequently be expected to follow a non-linear trend. At low moisture levels, the mass of the recovered sample may be limited due to

fragmentation and material loss. With increasing moisture, improved cohesion can contribute to a greater quantity of retained soil, potentially reaching a maximum within an intermediate moisture range. Beyond this optimum point, excessive adhesion, plastic deformation, and material losses may again reduce the effective mass and quality of the collected sample.

Therefore, soil moisture should be considered a key parameter when evaluating and optimizing automated soil sampling systems. Monitoring the moisture content before sampling can provide valuable information regarding the expected mechanical requirements and may support the adjustment of operational parameters, such as penetration speed, rotational speed, applied axial force, and extraction conditions. The identification of favorable moisture conditions may ultimately contribute to reducing energy consumption, minimizing equipment wear, improving sample recovery, and ensuring a more representative soil sample for subsequent physical, chemical, or environmental analysis.

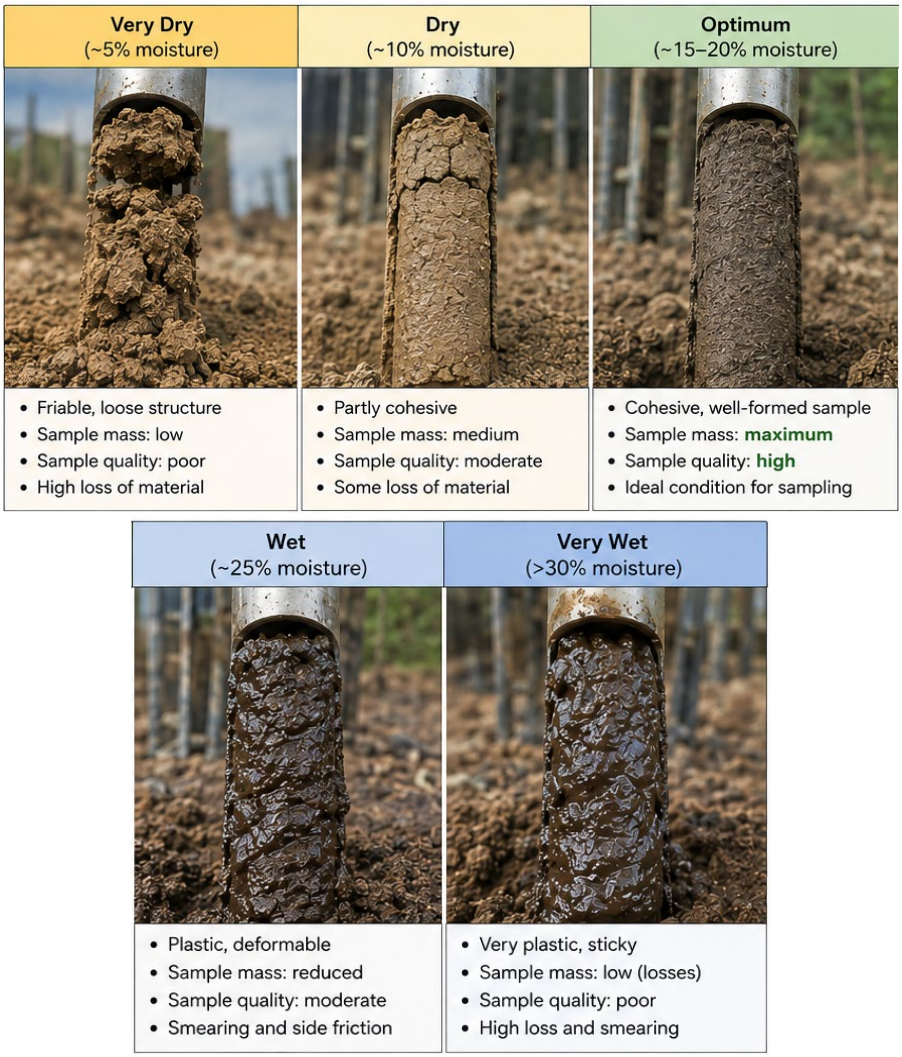



**Fig. 1 - Soil sampling based on humidity percentage**

**Soil mechanical behaviour as a function of moisture content**

Cone penetration resistance, commonly expressed through the cone index (CI) obtained with a standard cone penetrometer, has long served as an integrating indicator of soil strength for agricultural machinery design, and it responded strongly and consistently to changes in moisture content across the reviewed literature. At a given bulk density, penetration resistance decreased as moisture content increased, because water reduced inter-particle friction and altered the effective stress state within the soil matrix; conversely, drier soils close to their plastic limit exhibited markedly higher resistance to probe insertion. *(Pang et al., 2023)* modelled the penetration resistance of probes in cultivated soil using a spherical cavity-expansion approach and introduced density and moisture coefficients into the expansion-force formulation, obtaining a good fit between predicted and measured resistance across a range of densities (1.1–1.3 $Mg \cdot m^{-3}$) and moisture contents (10–20%). Their model illustrated that moisture content and bulk density

interacted rather than acted independently on penetration resistance, meaning that a sampling mechanism sized for a given force at one density–moisture combination could be substantially under- or over-designed at another.

This moisture sensitivity has direct implications for automated soil samplers: probes, coring tubes, and augers driven at constant velocity or under a constant force target encounter substantially different resistance profiles depending on antecedent soil moisture, which affects the peak insertion force, the achievable sampling depth, and the risk of probe deflection, buckling, or incomplete penetration in dry, compacted topsoil layers.

**Shear strength, cohesion and internal friction angle**

The classical Mohr–Coulomb failure criterion describes soil shear strength τ as the sum of a cohesive component c and a frictional component dependent on the normal stress σ and the internal friction angle φ:

$$\tau = c + \sigma \cdot \tan\varphi \quad (1)$$

where τ is the soil shear strength, [Pa]; c is the soil cohesion, [Pa]; σ is the normal stress on the failure plane, [Pa]; φ is the internal friction angle, [°].

Both cohesion and the internal friction angle were reported to vary systematically, but non-monotonically, with moisture content. Zhang et al. (2023), testing soil–rock mixtures in a large-scale direct shear apparatus, found that shear strength, cohesion, and internal friction angle all increased with moisture content up to an intermediate value (around 12% in their samples) and then decreased as moisture increased further, a pattern attributed to the transition from capillary-driven inter-particle cohesion at moderate saturation to a lubricating, strength-reducing effect once excess pore water began to separate soil particles. This non-monotonic behaviour is consistent with the general soil mechanics understanding that apparent cohesion in unsaturated soils arises primarily from capillary menisci between particles, an effect that is strongest at intermediate saturation and diminishes as the soil approaches either the dry or the fully saturated state.

For automated sampling systems, this means that the relationship between moisture content and the force required to shear or cut through soil during probe insertion is not simply monotonic, and a linear moisture–force correction applied across the full practical moisture range may be inaccurate near field capacity, where shear strength can locally peak rather than continuing to decline.

**Soil-metal friction and adhesion**

Beyond the internal mechanical behaviour of the soil itself, the interaction between soil and the metal or polymer surfaces of sampling tools was strongly moisture-dependent, and this interaction governed both the frictional drag along probe shafts and the sticking, or adhesion, of soil to tool surfaces. *Abbaspour-Gilandeh et al. (2018)* measured external soil friction and adhesion coefficients across several soil textures, moisture levels, and four contact materials (steel, cast iron, rubber, and Teflon), finding that the coefficient of friction increased with moisture content up to a maximum and then declined once the soil approached a fluid, near-saturated consistency; contact material had a statistically significant effect on both coefficients, with low-friction materials such as Teflon substantially reducing the sliding resistance compared with steel. A comparable moisture-dependent pattern was reported for soil–metal adhesion. *Li et al. (2024)* found that clay-loam soil showed weak adhesion below approximately 20% moisture content but strong adhesion once moisture exceeded 20% and approached the soil's liquid limit, and demonstrated that a non-smooth, convex subsoiler surface reduced tillage resistance by over 15% under high-adhesion conditions compared with a smooth surface — an approach directly transferable to the design of anti-stick coatings for coring tubes and auger flights operating in wet, cohesive soils. Earlier work on coated tillage tools reinforced this pattern: *Barzegar et al. (2016)* showed that an ultra-high-molecular-weight polyethylene (UHMW-PE) coating reduced draft force and soil-tool adhesion at both low (4%) and high (18%) moisture contents relative to an uncoated steel tine, with the largest relative improvement occurring in wetter, more adhesive soil.

Taken together, these friction and adhesion effects implied that the mechanical load on an automated sampling probe was not determined solely by the bulk soil resistance ahead of the tool tip, but also by the drag along the shaft or auger flight, which could increase substantially in moist, cohesive soils as

adhered soil built up on the tool surface — a phenomenon with direct consequences for actuator sizing, energy consumption, and the risk of sampler jamming.

**Table 1**

**Summary of literature-reported trends of soil mechanical parameters relevant to automated sampling with increasing moisture content**

| Mechanical parameter | Reported trend with increasing moisture content |
|---|---|
| Cone penetration resistance (CI) | Decreases at constant bulk density; moisture and density act interactively in probe-penetration models |
| Shear strength, cohesion, friction angle | Increases up to an intermediate moisture content, then decreases as saturation increases further |
| Soil–metal external friction coefficient | Increases with moisture up to a maximum, then declines near saturation; strongly material-dependent |
| Soil–metal adhesion | Weak below a texture-specific threshold (~20%); strong as moisture approaches the liquid limit |
| Draft force of soil-engaging tools | Generally decreases with increasing moisture in cohesive soils within the workable range |
| Tool wear rate | Governed jointly by tool/abrasive hardness ratio, texture and moisture; wear regime shifts accordingly |

**Mechanical requirements - Insertion force, torque and power demand**

The combined effect of moisture-dependent penetration resistance, shear strength, and soil-tool friction was reflected directly in the draft force, torque, and power requirements reported for both conventional soil-engaging tools and dedicated automated sampling mechanisms. Within the tillage-tool literature, *Cardei et al. (2019)*, reviewing the classical draft-force formulas used for soil-working machinery, showed that despite differing theoretical formulations, most established models converged on a structure in which draft force depended on a soil-resistance coefficient governed largely by moisture-sensitive cohesion and friction, tool geometry, and working depth — a generalization that offered a useful starting point for scaling the force requirements of automated probes and augers across different soil moisture conditions.

In dedicated soil-sampling robotics, the moisture–mechanics link became a first-order design constraint rather than a secondary consideration. *Klopfenstein and Lussier Desbiens (2024)*, developing the Terra-22 aerial drilling sampler for densely compacted agricultural soils, reported that an actively controlled drill penetration-rate strategy reduced torque requirements by 33% and axial force requirements by a factor of eight compared with a constant-penetration-speed controller, directly demonstrating that adapting the mechanical operating point of a sampler to instantaneous soil resistance — which is itself moisture-dependent — could yield an order-of-magnitude reduction in the peak forces that the on-board actuators and airframe needed to withstand. Similarly, *Eceoğlu and Ünal (2024)*, in a GIS-guided autonomous soil-drilling robot for orchard planting, used a gasoline-engine-driven auger sized to overcome the combined cutting, friction, and adhesion resistance of field soil, underscoring that even relatively simple auger-based automated tools required power trains sized with a margin for the moisture-driven variability of soil resistance rather than for a single nominal soil condition. On ground-based platforms intended for continuous, unattended operation, *Norby et al. (2024)* identified soil variability — including moisture-driven changes in strength and stickiness — as one of the principal design constraints shaping manipulator force capacity, sampling-tool selection, and platform mobility for autonomous site-characterization robots.

**Moisture-adaptive control and penetration-rate strategies**

A recurring theme across the recent automated-sampling literature was the shift from static, worst-case mechanical sizing toward moisture- or force-adaptive control. *Nguyen et al. (2025)*, describing a semi-autonomous robotic system for in-situ soil sampling, analysis, and mapping in precision agriculture, integrated real-time sensing and closed-loop control of the sampling mechanism to maintain reliable core acquisition across the variable soil conditions encountered during large-scale field trials, illustrating a practical implementation of moisture- and resistance-aware sampling logic operating alongside on-board soil-property analysis. This general approach — closing the loop between a resistance or moisture measurement

and the applied penetration force, rate, or torque — mirrored the strategy already validated for the Terra-22 drilling controller *(Klopfenstein & Lussier Desbiens, 2024)* and represented, across the reviewed studies, the most direct and effective way of reconciling the wide, moisture-driven variability of soil mechanical resistance with a mechanically compact, energy-efficient sampling actuator. A conceptual representation of such a control loop is given in Figure 2.

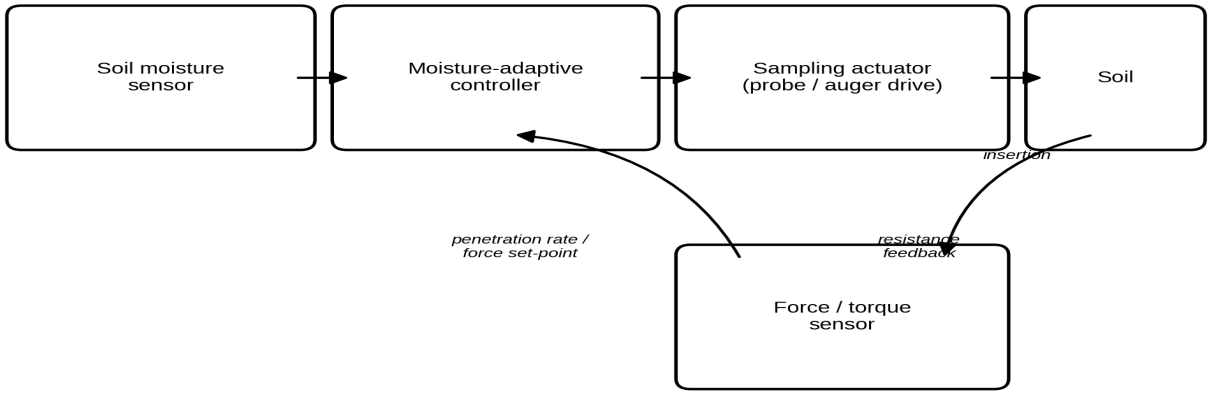



**Fig. 2 - Conceptual moisture-adaptive control loop for an automated soil sampling probe or auger**

**Wear, tool material and sample integrity considerations**

Moisture affected not only the instantaneous force and torque required for sampling, but also the longer-term wear behaviour of soil-engaging tools and, consequently, the maintenance burden and dimensional consistency of automated samplers over repeated use. *Malvajerdi (2023)*, reviewing wear and coating strategies for tillage tools, noted that wear mechanisms were governed jointly by tool hardness, soil abrasiveness, and moisture, with the ratio between tool and abrasive-particle hardness determining whether micro-cutting, micro-ploughing, or fragmentation-dominated wear regimes prevailed, and that coating strategies developed to reduce abrasive wear often also reduced adhesion-related drag in moist, cohesive soils. For automated probes and coring tools that must retrieve an intact, minimally disturbed soil core, moisture-driven adhesion additionally raised the risk of soil sticking inside the sampling tube, incomplete ejection, and cross-contamination between successive samples, an issue addressed through scraper mechanisms and low-friction coatings in automated sampling designs, and through anti-adhesion surface texturing in the tillage-tool literature *(Li et al., 2024)*.

## RESULTS

Comparing the studies reviewed above revealed both a consistent qualitative picture and a number of unresolved inconsistencies. Qualitatively, penetration resistance and draft force were widely reported to decrease as soil moisture increased over the low-to-moderate moisture range typical of workable agricultural soils, while soil-metal friction and adhesion increased with moisture up to a threshold and then declined as the soil approached a fluid consistency, and shear-strength parameters followed a broadly similar non-monotonic pattern. However, the exact moisture thresholds at which these trends reversed direction varied considerably between studies — for example, the moisture level marking the onset of strong adhesion differed between the soil textures and testing protocols used by Li et al. (2024) and Abbaspour-Gilandeh et al. (2018) — reflecting the strong dependence of these thresholds on soil texture, clay mineralogy, and the specific testing apparatus and normal loads applied, rather than the existence of a single, texture-independent moisture-response curve.

A further inconsistency concerned the transferability of tillage-derived force models to automated sampling geometries. Draft-force formulas reviewed by Cardei et al. (2019) were developed primarily for wide, shallow-working tillage tools such as plough bodies and cultivator shares, whose soil-failure mechanics differed substantially from the narrow, deep, largely axial penetration geometry of coring probes and augers used in automated sampling; while both families of tools were governed by the same underlying moisture-dependent soil parameters, direct application of classical tillage draft-force coefficients to probe insertion-force prediction required geometric adaptation that was not always made explicit in the automated-sampling literature. Finally, most of the reviewed automated sampling systems reported force, torque, or power outcomes for the specific soils and moisture conditions encountered during their field trials, without

systematically varying moisture as an independent test factor, which limited the extent to which their reported performance figures could be generalized to other soil types or seasonal moisture conditions.

Several aspects of the relationship between soil moisture and the mechanical requirements of automated soil sampling remained insufficiently characterized and merited further research. First, few studies to date had directly and systematically varied soil moisture content as an independent factor while measuring the insertion force, torque, and power demand of dedicated automated sampling probes or augers, as distinct from tillage tools; controlled, multi-texture experiments of this kind would allow the moisture-dependent soil mechanics reviewed here to be translated into predictive, geometry-specific force and torque models for sampler design. Second, the non-monotonic moisture response observed for shear strength, friction, and adhesion suggested that simple linear moisture-correction factors, of the kind sometimes used to adjust cone-index or draft-force readings, may be inadequate near field capacity, and more research was needed on moisture-response models capable of capturing this reversal across the full practical moisture range encountered in situ.

Third, while moisture-adaptive and force-adaptive control strategies had shown substantial benefits in reducing peak mechanical loads in early implementations such as the Terra-22 drilling controller, the sensing requirements, robustness, and generalizability of such closed-loop strategies across diverse soil types, textures, and structural conditions had not yet been systematically evaluated, and represented a promising avenue for combining low-cost soil moisture or force sensing with adaptive actuator control in next-generation automated samplers.

Finally, the long-term interaction between moisture-driven adhesion, tool wear, and sample integrity — including cross-contamination risk between successive samples — warranted dedicated study specifically for automated, repeated-use sampling tools, extending beyond the largely tillage-focused wear literature reviewed here.

## CONCLUSIONS

Soil moisture content was shown to exert a strong and largely predictable, though not always monotonic, influence on the mechanical parameters governing automated soil sampling, including penetration resistance, shear strength, cohesion, internal friction angle, and soil-metal friction and adhesion. These moisture-dependent soil properties translated directly into the insertion force, torque, and power that automated sampling probes, augers, and coring tools needed to deliver, and recent robotic sampling platforms that incorporated moisture- or resistance-adaptive control demonstrated substantial reductions in peak mechanical loads compared with fixed-parameter operation.

At the same time, considerable variability remained in the reported moisture thresholds governing the transition between low- and high-adhesion or low- and high-friction soil behaviour, and few studies had directly measured sampler-specific force and torque requirements across a controlled range of soil moisture conditions. Bridging the soil mechanics literature on moisture-dependent behaviour with geometry-specific, sampler-level force and torque models, and extending moisture- and force-adaptive control approaches to a broader range of platforms and soil types, were identified as priority directions for future research aimed at improving the reliability, energy efficiency, and sample integrity of automated soil sampling systems.

## ACKNOWLEDGEMENT

This work was supported by the National Research Authority, through the Project entitled: “An intelligent automated system designed for georeferenced soil sampling.” - **PN 23 04 01 02. Contract 9N/ 01.01.2023** and by the Program ADER 2023-2026, **ADER 25.1.2 / 14.07.2023**, “Tehnologie inovativă de prelucrare minimă a terenului agricol adaptată la schimbările climatice actuale”.

## REFERENCES

[1] Abbaspour-Gilandeh, Y., Hasankhani-Ghavam, F., Shahgoli, G., Shrabian, V. R., & Abbaspour-Gilandeh, M. (2018). Investigation of the effect of soil moisture content, contact surface material and soil texture on soil friction and soil adhesion coefficients. Acta Technologica Agriculturae, 21(2), 44–50. https://doi.org/10.2478/ata-2018-0009

[2] Barzegar, M., Hashemi, S. J., Nazokdast, H., & Karimi, R. (2016). Evaluating the draft force and soil-tool adhesion of a UHMW-PE coated furrower. Soil and Tillage Research, 163, 160–167. https://doi.org/10.1016/j.still.2016.05.016

[3] Cardei, P., Muraru, S. L., Sfîru, R., & Muraru, V. (2019). General structure of tillage draft force. Consequences in experimental and applicative researches. INMATEH – Agricultural Engineering, 59(3), 253–262. https://doi.org/10.35633/inmateh-59-28

[4] Eceoğlu, O., & Ünal, İ. (2024). Optimizing orchard planting efficiency with a GIS-integrated autonomous soil-drilling robot. AgriEngineering, 6(3), 2870–2890. https://doi.org/10.3390/agriengineering6030166

[5] Klopfenstein, H. B., & Lussier Desbiens, A. (2024). Terra-22: an aerial soil sampling in densely compacted agricultural fields. Drone Systems and Applications, 12, 1–14. https://doi.org/10.1139/dsa-2023-0010

[6] Li, J., Qi, H., Ma, Y., Gao, P., & Wu, B. (2024). Investigating soil adhesion and antiadhesion performance of nonsmooth subsoiler surfaces. Journal of Engineering, 2024, Article 7019756. https://doi.org/10.1155/2024/7019756

[7] Malvajerdi, A. S. (2023). Wear and coating of tillage tools: A review. Heliyon, 9(6), Article e16669. https://doi.org/10.1016/j.heliyon.2023.e16669

[8] Nguyen, T. H., Muller, E., Rubin, M., Wang, X., Sibona, F., McBratney, A., & Sukkarieh, S. (2025). A semi-autonomous robotic system for in situ soil sampling, analysis, and mapping in precision agriculture. IEEE Transactions on Field Robotics, 3, 22–39.

[9] Norby, J., Wang, S., Wang, H., Deng, S., Jones, N., Mishra, A., Pavlov, C., He, H., Subramanian, S., Thangavelu, V., Sihota, N., Hoelen, T., Johnson, A. M., & Lowry, G. V. (2024). Path to autonomous soil sampling and analysis by ground-based robots. Journal of Environmental Management, 360, Article 121130. https://doi.org/10.1016/j.jenvman.2024.121130

[10] Pang, J., Lin, X., Zhang, X., Ji, J., & Geng, L. (2023). Modelling and analysis of penetration resistance of probes in cultivated soils. PLOS ONE, 18(1), Article e0280525. https://doi.org/10.1371/journal.pone.0280525

[11] Zhang, Y., Lu, J., Han, W., Xiong, Y., & Qian, J. (2023). Effects of moisture and stone content on the shear strength characteristics of soil-rock mixture. Materials, 16(2), Article 567. https://doi.org/10.3390/ma16020567

# A DECADE OF AGRICULTURAL RESTRUCTURING IN SOUTH-WEST OLTENIA, ROMANIA: CULTIVATED AREA DYNAMICS AND COUNTY SPECIALIZATION

/

# *UN DECENIU DE RESTRUCTURARE AGRICOLĂ ÎN REGIUNEA SUD-VEST OLTENIA, ROMÂNIA: DINAMICA SUPRAFEȚELOR CULTIVATE ȘI SPECIALIZAREA JUDEȚEANĂ*

**Iulian Virgil GHIULEANU[1)], Daniel NIJLOVEANU*[2)], Corina CRUCERU[2)], Dragos-Nicolae DUMITRU[3)]**

[1)] University of Agronomic Sciences and Veterinary Medicine Bucharest (Doctoral student, Doctoral School: Plant and Animal Resources Engineering and Management), 59 Marasti Boulevard, District 1, 011464, Bucharest / Romania;

[2)] USAMV Bucharest, Faculty of Management and Rural Development, Slatina Branch, Olt County / Romania;

[3)] National Institute of Research - Development for Machines and Installations Designed to Agriculture and Food-Industry - INMA Bucharest / Romania

**E-mail: nijloveanu_daniel@yahoo.com*

***Keywords:*** *cultivated area, crop structure, territorial specialization, location quotient, South-West Oltenia.*

**ABSTRACT**

*This study analyzes the evolution of cultivated areas in the South-West Oltenia Region between 2016 and 2025, focusing on the changes in crop structure and territorial differences among Dolj, Gorj, Mehedinți, Olt and Vâlcea counties. The statistical data were obtained from the TEMPO-Online database of the National Institute of Statistics and processed in Microsoft Excel 365. The methodology combined chronological, structural and comparative analyses with the Location Quotient, the Herfindahl–Hirschman Index expressed on the 0–1 scale and a S.W.O.T. analysis. The regional cultivated area decreased by 6.56%, from 1,182,505 ha to 1,104,887 ha, while Mehedinți was the only county to record an increase. The crop structure underwent significant changes: rapeseed expanded by 74.77% and field peas by 289.12%, whereas grain maize, potatoes and vegetables declined by 36.32%, 81.02% and 41.57%, respectively. The Location Quotient revealed a strong specialization of Vâlcea in orchards, potatoes, green fodder and vegetables, while Dolj remained dominant in terms of absolute cultivated area. Territorial concentration was highest for grain legumes and lowest for vegetables. The results indicate that the reduction in cultivated area was accompanied by a broader restructuring of the regional agricultural profile and by the development of distinct, but potentially complementary, county specializations.*

**REZUMAT**

*Studiul analizează evoluția suprafețelor cultivate în Regiunea Sud-Vest Oltenia în perioada 2016–2025, urmărind schimbările produse în structura culturilor și diferențele teritoriale dintre județele Dolj, Gorj, Mehedinți, Olt și Vâlcea. Datele statistice au fost preluate din baza TEMPO-Online a Institutului Național de Statistică și prelucrate în Microsoft Excel 365. Metodologia a combinat analiza cronologică, structurală și comparativă cu utilizarea coeficientului de localizare, a indicelui Herfindahl–Hirschman exprimat pe scala 0–1 și a analizei S.W.O.T. Suprafața cultivată la nivel regional s-a redus cu 6.56%, de la 1,182,505 ha la 1,104,887 ha, Mehedinți fiind singurul județ care a înregistrat o creștere. Structura culturilor a cunoscut modificări importante: suprafața cultivată cu rapiță a crescut cu 74.77%, iar suprafața cultivată cu mazăre pentru boabe cu 289.12%, în timp ce porumbul boabe, cartofii și legumele s-au redus cu 36.32%, 81.02% și, respectiv, 41.57%. Coeficientul de localizare a evidențiat specializarea puternică a județului Vâlcea în livezi pe rod, cartofi, furaje verzi și legume, în timp ce Dolj și-a menținut dominația prin dimensiunea suprafețelor cultivate. Concentrarea teritorială a fost cea mai ridicată în cazul leguminoaselor pentru boabe și cea mai redusă în cazul legumelor. Rezultatele arată că reducerea suprafeței cultivate a fost însoțită de restructurarea profilului agricol regional și de conturarea unor specializări județene distincte, dar potențial complementare.*

## INTRODUCTION

Cultivated area is more than just a statistical indicator: it reflects how a region's agriculture uses its resources, adapts its crop structure, and responds to economic and environmental changes. Analyzing its evolution allows us to identify which crops are gaining ground, which are in decline, and the differences that

define the agricultural profile of each county. The South-West Oltenia region has a diverse agricultural profile, shaped by the natural and economic characteristics of its five constituent counties. Previous research has described the region as a relatively balanced agricultural area, but with a significant presence of cereals and oilseeds (*Ursu and Cofas, 2016*). In Olt County, wheat, sunflowers, grain maize, and rapeseed were identified as among the most prevalent crops in the structure of cultivated land (*Vânătoru et al., 2013b*). Changes in the agricultural structure are occurring in a context where land use is influenced by numerous factors. Vulnerability to drought and the variability of climatic conditions have been highlighted for the Caracal–Olt microregion, while studies on water erosion have shown the importance of crop selection and farming systems for land protection (*Nijloveanu et al., 2013; Vânătoru et al., 2013a*). At the national level, soil conservation, water management, and the sustainable use of land resources are considered essential for maintaining agricultural potential (*Buzatu et al., 2023*).

Crop structure is also an important component of agricultural risk management. Diversification, the adaptation of technologies, and efficient resource management can help reduce farms' vulnerability to climatic and economic fluctuations (*Ghiuleanu et al., 2023*). At the same time, trends are not uniform across all crops. Research on rapeseed has highlighted both its potential for expansion and the sector's sensitivity to climatic conditions and market changes (*Cruceru and Ghiuleanu, 2024a*). In the case of tomatoes, fluctuations in planted area and production indicate the need to modernize infrastructure and better adapt to risks specific to the vegetable sector (*Cruceru and Ghiuleanu, 2024b*). Previous studies provide important information on the regional agricultural structure, crop-related risks, soil conservation, and the evolution of distinct sectors. In this context, an updated comparative analysis of cultivated areas across all five counties can provide a more complete picture of agriculture in the South-West Oltenia region, highlighting not only the general trend but also changes in crop structure and territorial specialization.

The purpose of this study is to analyze trends in cultivated land area in the South-West Oltenia region from 2016 to 2025, based on statistical data provided by the National Institute of Statistics through the TEMPO-Online database, specifically the AGR108A matrix (*NIS, 2026*). The analysis aims to identify the main changes at the regional and county levels, compare the dynamics of crop groups, determine agricultural specializations using the location quotient, and assess territorial concentration using the Herfindahl–Hirschman Index. By integrating chronological, structural, and territorial analyses, the study aims to highlight how the profile of regional agriculture has changed over the past decade. The results are also summarized through a S.W.O.T. analysis, designed to transform statistical information into a clear picture of the strengths, weaknesses, opportunities, and threats facing agriculture in the South-West Oltenia region.

## MATERIALS AND METHODS

The research was based exclusively on official statistical data drawn from the National Institute of Statistics' TEMPO-Online database, specifically the AGR108A matrix—*"Area Cultivated with Major Crops, by Form of Ownership, Macroregions, Development Regions, and Counties"* (*NIS, 2026*). The data are expressed in hectares, cover the period 2016–2025, and refer to the South-West Oltenia region and its five constituent counties: Dolj, Gorj, Mehedinți, Olt, and Vâlcea. The statistical series were organized and processed in Microsoft Excel 365. The analysis tracked changes in the total cultivated area, the main crop groups, and individual crops, at both the regional and county levels. Absolute and percentage changes, fixed-base indices, average annual growth rates, shares of the total, and their changes in percentage points were calculated. The average annual growth rate (AAGR) was calculated based on the values from the first and last years of the period:

$$\boldsymbol{AAGR}(\%) = \left[\left(\frac{S_{2025}}{S_{2016}}\right)^{1/9} - 1\right] \times 100 \quad (1)$$

where *S2016* represents the cultivated area in the base year, *S2025* represents the cultivated area in the most recent year analyzed, and 9 represents the number of annual intervals between 2016 and 2025. To ensure a consistent interpretation of the results, the crops were classified into five categories. Variations between -5.00% and +5.00% were considered relatively stable. Increases greater than 5.00% but not exceeding 20.00% were classified as moderate expansion, and those exceeding 20.00% as strong expansion. Decreases greater than 5.00% but not exceeding 20.00% were considered moderate decline, while decreases exceeding 20.00% were classified as strong decline. Territorial specialization was analyzed using the Location Quotient (LQ). This compares the importance of a crop in a county's agricultural structure

with the importance of the same crop in the structure of the entire region. The Location Quotient compares the share of a crop group in a county's cultivated area with the share of the same group in the regional cultivated area (*U.S. Bureau of Labor Statistics, 2025*).

$$LQ_{ij} = \frac{S_{ij}/S_j}{S_{iR}/S_R} \quad (2)$$

where *Sij* represents the area of crop group *i* in county *j*, *Sj* represents the total cultivated area in that county, *SiR* represents the area of the same crop group in the South-West Oltenia region, and *SR* represents the total cultivated area at the regional level. An LQ value greater than 1 indicates that the crop's share exceeds the regional average. A value of 1 indicates a structure similar to the regional average, while a value less than 1 indicates a relatively low share. The coefficient does not express the absolute size of the area, but rather the relative importance of the crop in the county's agricultural profile. To determine territorial concentration, the Herfindahl–Hirschman Index (HHI) was used, calculated based on shares expressed as decimals on a scale of 0–1. The method involves squaring each county's share and summing the resulting values (*U.S. Department of Justice, 2024*).

$$HHI_i = \sum_{j=1}^{5} p_{ij}^2 \quad (3)$$

$$p_{ij} = \frac{S_{ij}}{S_{iR}} \quad (4)$$

where *pij* represents the share of county *j* in the regional area of crop group *i*, *Sij* represents the area of that group in the county, and *SiR* represents the total area of the same group in the South-West Oltenia region. The percentage shares were divided by 100 before being squared. Dividing the shares by 100 is necessary because the percentage values must be converted to decimal numbers before being squared. For example, a share of 42.37% is used in the calculation as 0.4237.

For the five counties, the theoretical minimum value of the index is 0.20, which occurs when the area is distributed equally, and the maximum value is 1.00, when the entire area is concentrated in a single county.

The higher the HHI value, the more geographically concentrated the crop area is. The values were compared across crop groups without using thresholds specific to economic competition analyses. In the final stage, the results were synthesized through a S.W.O.T. analysis. Strengths and weaknesses were identified based on the trends and specializations observed. Opportunities and threats represent potential directions and risks derived from the continuation of the observed statistical trends.

## RESULTS

This analysis tracks changes in cultivated land area in the South-West Oltenia region from 2016 to 2025, both at the regional level and within the five constituent counties. The results highlight changes in the territorial distribution, crop structure, and agricultural profile of each county. To provide as clear a picture as possible, the analysis examined variations in cultivated areas, rates of change, county shares, location quotient, and the degree of territorial concentration. The interpretation emphasizes the relevant changes and the differences that distinguish the agriculture of the region's counties.

### a) Trends in cultivated area at the regional and county levels

During the period under review, the cultivated area in the South-West Oltenia region fluctuated, but the overall trend was downward. The annual trends for the five counties are presented in Table 1.

**Table 1**

**Trends in cultivated land area in the Counties of the South-West Oltenia region**

| County/Region | 2016 | 2017 | 2018 | 2019 | 2020 | 2021 | 2022 | 2023 | 2024 | 2025 |
|---|---|---|---|---|---|---|---|---|---|---|
| | U.M.: Hectares | | | | | | | | | |
| Dolj | 493,159 | 478,872 | 482,226 | 513,832 | 481,868 | 484,101 | 476,745 | 477,664 | 470,112 | 481,618 |
| Gorj | 87,049 | 79,850 | 80,141 | 80,199 | 79,335 | 79,018 | 75,640 | 75,506 | 74,442 | 66,960 |
| Mehedinți | 150,733 | 143,595 | 144,333 | 146,373 | 145,837 | 152,512 | 149,274 | 157,823 | 149,354 | 154,906 |
| Olt | 381,038 | 364,933 | 368,491 | 376,632 | 379,262 | 351,314 | 319,910 | 346,450 | 404,996 | 347,559 |
| Vâlcea | 70,526 | 66,273 | 69,663 | 69,326 | 66,475 | 66,233 | 62,741 | 54,861 | 53,693 | 53,844 |
| **South-West Oltenia** | **1,182,505** | **1,133,523** | **1,144,854** | **1,186,362** | **1,152,777** | **1,133,178** | **1,084,310** | **1,112,304** | **1,152,597** | **1,104,887** |

(*NIS, own processing based on statistical data provided through TEMPO-Online, AGR108A*)

The region's cultivated area decreased from 1,182,505 ha in 2016 to 1,104,887 ha in 2025. The region thus lost 77,618 ha, equivalent to a 6.56% decline. However, this trend was not uniform, as periods of decline alternated with years in which the cultivated area partially recovered. The main differences among counties are summarized in Table 2, showing absolute and percentage changes, average annual rates of change, and shifts in their shares of the regional total.

**Table 2**

**Summary indicators of changes in cultivated land area in the Counties of the South-West Oltenia region**

| County/Region | Absolute change, 2016–2025 | Evolution 2016–2025 | Average annual rate | Share in the region, 2016 | Share in the region in 2025 | Index 2025, 2016=100 |
|---|---|---|---|---|---|---|
| | U.M.: Hectares | U.M.: Percentages | | | | |
| Dolj | -11,541 | -2.34% | -0.26% | 41.70% | 43.59% | 97.66 |
| Gorj | -20,089 | -23.08% | -2.87% | 7.36% | 6.06% | 76.92 |
| Mehedinți | 4173 | 2.77% | 0.30% | 12.75% | 14.02% | 102.77 |
| Olt | -33,479 | -8.79% | -1.02% | 32.22% | 31.46% | 91.21 |
| Vâlcea | -16,682 | -23.65% | -2.95% | 5.96% | 4.87% | 76.35 |
| **South-West Oltenia** | **-77,618** | **-6.56%** | **-0.75%** | **100.00%** | **100.00%** | **93.44** |

(*NIS, own processing based on statistical data provided through TEMPO-Online, AGR108A*)

Mehedinți was the only county that ended the period with a larger cultivated area than in 2016. The increase was 4173 ha, or 2.77%. Dolj, on the other hand, showed the most stable trend among the counties experiencing a decline, with a reduction of only 2.34%. he magnitude of the losses differed across counties. Olt recorded the largest reduction in absolute terms, at 33,479 ha, while Vâlcea and Gorj recorded the sharpest percentage declines, at 23.65% and 23.08%, respectively. These results show that the loss of cultivated land was much more pronounced in counties with a smaller contribution to the regional total. Despite the recorded decline, Dolj consolidated its position as the county with the largest cultivated area, increasing its regional share from 41.70% to 43.59%. Mehedinți also increased its share, from 12.75% to 14.02%. In 2025, Dolj and Olt together accounted for 75.05% of the region's cultivated area, confirming the dominant role of these two counties. Consequently, the regional trend masks distinct local situations: relative stability in Dolj, a slight expansion in Mehedinți, and more pronounced declines in Olt, Gorj, and Vâlcea. This differentiation represents one of the key characteristics of the period under analysis.

**b) Annual trends in cultivated area**

The annual analysis rounds out the overall picture and shows that the reduction in cultivated area did not occur continuously. The period was marked by alternating declines and recoveries, without the latter developing into a stable upward trend.

**Table 3**

**Annual trends in cultivated area in the South-West Oltenia region**

| Year | Cultivated area | Annual change | Annual change (%) | Difference from 2016 | Fixed-base index, 2016=100 |
|---|---|---|---|---|---|
| | U.M.: Hectares | | U.M.: Percentages | U.M.: Hectares | |
| 2016 | 1,182,505 | – | – | 0 | 100.00 |
| 2017 | 1,133,523 | -48,982 | -4.14% | -48,982 | 95.86 |
| 2018 | 1,144,854 | 11,331 | 1.00% | -37,651 | 96.82 |
| 2019 | 1,186,362 | 41,508 | 3.63% | 3857 | 100.33 |
| 2020 | 1,152,777 | -33,585 | -2.83% | -29,728 | 97.49 |
| 2021 | 1,133,178 | -19,599 | -1.70% | -49,327 | 95.83 |
| 2022 | 1,084,310 | -48,868 | -4.31% | -98,195 | 91.70 |
| 2023 | 1,112,304 | 27,994 | 2.58% | -70,201 | 94.06 |
| 2024 | 1,152,597 | 40,293 | 3.62% | -29,908 | 97.47 |
| 2025 | 1,104,887 | -47,710 | -4.14% | -77,618 | 93.44 |

(*NIS, own processing based on statistical data provided through TEMPO-Online, AGR108A*)

The first notable annual decline occurred in 2017, when the cultivated area decreased by 48,982 ha, or 4.14%. The recovery over the next two years peaked in 2019, when the region reached its highest value for the period, at 1,186,362 ha. The annual growth rate of 3.63% that year was the highest in the analyzed period. After

that point, the trend changed noticeably. Between 2020 and 2022, there were three consecutive declines, and in 2022, the cultivated area fell to 1,084,310 ha, the lowest figure for the period. That same year also saw the sharpest annual decline, of 48,868 ha, equivalent to a 4.31% decrease. The years 2023 and 2024 brought a partial recovery, supported by increases of 2.58% and 3.62%, respectively. However, this recovery did not continue in 2025, when the cultivated area decreased again by 47,710 ha, or 4.14%. The annual trend reflects a fluctuating regional agricultural landscape, in which years of recovery only temporarily offset the accumulated losses. The sequence of these variations explains why, despite some favorable periods, the cultivated area in 2025 remained below the level recorded at the beginning of the analysis. These fluctuations are also relevant in the context of the climate vulnerability previously identified for the Caracal–Olt microregion (*Vânătoru et al., 2013a*).

**c) Trends in the main crop groups**

Beyond the reduction in cultivated area at the regional level, the data also highlight a shift in how land has been used. Some crop groups have expanded their acreage, while others have lost a significant portion of their regional presence.

**Table 4**

**The main crop groups in the South-West Oltenia region**

| Crop group | 2016 | 2017 | 2018 | 2019 | 2020 | 2021 | 2022 | 2023 | 2024 | 2025 |
|---|---|---|---|---|---|---|---|---|---|---|
| | U.M.: Hectares | | | | | | | | | |
| Cereals for grain | 854,396 | 816,332 | 822,224 | 833,352 | 837,869 | 780,482 | 761,261 | 759,952 | 754,924 | 769,065 |
| Legumes for grain | 6999 | 20,100 | 23,249 | 19,788 | 24,773 | 19,705 | 19,315 | 23,568 | 21,617 | 19,077 |
| Oilseeds | 232,669 | 210,373 | 209,591 | 243,857 | 212,075 | 261,936 | 241,309 | 262,014 | 310,961 | 251,911 |
| Potatoes – total | 11,720 | 11,732 | 12,200 | 12,205 | 6960 | 3015 | 2966 | 1770 | 1655 | 2224 |
| Vegetables – total | 35,271 | 35,506 | 35,022 | 34,685 | 28,279 | 28,390 | 24,704 | 24,795 | 24,510 | 20,609 |
| Green forage from arable land | 51,125 | 49,088 | 51,982 | 51,741 | 53,332 | 48,905 | 44,086 | 49,528 | 48,025 | 51,715 |
| Strawberry fields in production | 443 | 420 | 421 | 421 | 425 | 412 | 415 | 426 | 419 | 416 |
| Orchards in production | 25,971 | 26,469 | 26,260 | 26,136 | 26,182 | 26,864 | 26,609 | 26,736 | 26,578 | 26,728 |

(*NIS, own processing based on statistical data provided through TEMPO-Online, AGR108A*)

Grain crops remained the region's primary crop group, even though the area planted with them decreased from 854,396 ha in 2016 to 769,065 ha in 2025. Oilseeds continued to play an important role, reaching 251,911 ha in the last year analyzed. For the other groups, trends were more varied, and the differences between the first and last years are summarized in Table 5.

**Table 5**

**Trends in the main crop groups in the South-West Oltenia region**

| Crop group | Absolute change | Change 2016–2025 | Average annual rate | Share in 2016 | Share in 2025 | Change in share (p.p.) | Index 2025, 2016=100 | Classification |
|---|---|---|---|---|---|---|---|---|
| | U.M.: Hectares | U.M.: Percentages | | | | | | |
| Cereals for grain | -85,331 | -9.99% | -1.16% | 72.25% | 69.61% | -2.65 | 90.01 | Moderate decline |
| Legumes for grain | 12,078 | 172.57% | 11.79% | 0.59% | 1.73% | 1.13 | 272.57 | Strong expansion |
| Oilseeds | 19,242 | 8.27% | 0.89% | 19.68% | 22.80% | 3.12 | 108.27 | Moderate expansion |
| Potatoes – total | -9496 | -81.02% | -16.86% | 0.99% | 0.20% | -0.79 | 18.98 | Strong decline |
| Vegetables – total | -14,662 | -41.57% | -5.80% | 2.98% | 1.87% | -1.12 | 58.43 | Strong decline |
| Green forage from arable land | 590 | 1.15% | 0.13% | 4.32% | 4.68% | 0.36 | 101.15 | Relatively stable |
| Strawberry fields in production | -27 | -6.09% | -0.70% | 0.04% | 0.04% | 0.00 | 93.91 | Moderate decline |
| Orchards in production | 757 | 2.91% | 0.32% | 2.20% | 2.42% | 0.22 | 102.91 | Relatively stable |

(*NIS, own processing based on statistical data provided through TEMPO-Online, AGR108A*)

The most notable increase was recorded for grain legumes. The area planted with these crops increased by 12,078 ha, or 172.57%. Although they started from a lower baseline, legumes represent the fastest-growing group. Oilseed crops also showed a favorable trend, gaining 19,242 ha, equivalent to an 8.27% increase. At the other end of the spectrum, potatoes recorded the sharpest decline, losing 81.02% of their cultivated area. The area planted with vegetables also decreased by 14,662 ha, or 41.57%. Cereals lost 85,331 ha, but the percentage decline of 9.99% was more moderate than that recorded for potatoes and vegetables.

The areas occupied by forage crops and fruit orchards remained relatively stable, recording increases of 1.15% and 2.91%, respectively. In contrast, the area planted with strawberries decreased by 6.09%.

The results suggest a reconfiguration of the regional agricultural profile: oilseeds and grain legumes have gained ground, while potatoes and vegetables have experienced considerable declines. Cereals remained dominant, but their downward trend indicates that even this category was not immune to the changes during the period analyzed. The high share of cereals and oilseeds confirms certain characteristics of the regional agricultural profile also identified in previous studies (*Ursu and Cofas, 2016*).

**d) Changes in the structure of cereal crops**

Grain cereals have retained their central role in agriculture in the South-West Oltenia region, but the structure of this group has changed noticeably. The reduction in total acreage has not affected all crops to the same extent; some have gained ground at the expense of others.

**Table 6**

**Areas planted with grains in the South-West Oltenia region**

| Category | Statistical level | 2016 | 2017 | 2018 | 2019 | 2020 | 2021 | 2022 | 2023 | 2024 | 2025 |
|---|---|---|---|---|---|---|---|---|---|---|---|
| | | U.M.: Hectares | | | | | | | | | |
| Cereals for grain | Main group | 854,396 | 816,332 | 822,224 | 833,352 | 837,869 | 780,482 | 761,261 | 759,952 | 754,924 | 769,065 |
| Wheat and rye | Subtotal/subgroup | 403,173 | 407,632 | 415,084 | 410,632 | 421,155 | 405,410 | 405,503 | 424,293 | 414,944 | 437,035 |
| Wheat – total | Subtotal/subgroup | 399,710 | 404,784 | 412,318 | 408,020 | 418,309 | 403,270 | 403,046 | 421,360 | 412,427 | 435,410 |
| Common wheat | Component crop | 399,471 | 404,633 | 411,840 | 407,825 | 417,845 | 402,082 | 402,998 | 421,228 | 411,930 | 434,519 |
| Barley and two-row barley | Subtotal/subgroup | 51,679 | 48,355 | 49,285 | 50,955 | 53,038 | 64,482 | 60,370 | 66,343 | 62,576 | 74,341 |
| Barley | Component crop | 41,771 | 38,705 | 38,546 | 40,988 | 43,090 | 51,861 | 50,144 | 55,861 | 51,202 | 61,808 |
| Oats | Component crop | 18,306 | 17,953 | 17,763 | 17,970 | 15,996 | 16,078 | 14,455 | 14,172 | 13,087 | 13,354 |
| Grain maize | Component crop | 362,148 | 323,975 | 321,221 | 337,175 | 331,339 | 280,227 | 268,223 | 242,332 | 251,924 | 230,618 |

(*NIS, own processing based on statistical data provided through TEMPO-Online, AGR108A*)

The total area planted with grains decreased by 85,331 ha, or 9.99%. This trend was primarily driven by a reduction in grain maize cultivation, while wheat and barley showed favorable growth. The main changes are summarized in Table 7.

**Table 7**

**Trends in the area planted with grains in the South-West Oltenia region**

| Category | Absolute change | Change 2016–2025 | Average annual rate | Share in 2016 | Share in 2025 | Change in share (p.p.) | Index 2025, 2016=100 | Classification |
|---|---|---|---|---|---|---|---|---|
| | U.M.: Hectares | U.M.: Percentages | | | | | | |
| Cereals for grain | -85,331 | -9.99% | -1.16% | 100.00% | 100.00% | 0.00 | 90.01 | Moderate decline |
| Wheat and rye | 33,862 | 8.40% | 0.90% | 47.19% | 56.83% | 9.64 | 108.40 | Moderate expansion |
| Wheat – total | 35,700 | 8.93% | 0.96% | 46.78% | 56.62% | 9.83 | 108.93 | Moderate expansion |
| Common wheat | 35,048 | 8.77% | 0.94% | 46.75% | 56.50% | 9.74 | 108.77 | Moderate expansion |
| Barley and two-row barley | 22,662 | 43.85% | 4.12% | 6.05% | 9.67% | 3.62 | 143.85 | Strong expansion |
| Barley | 20,037 | 47.97% | 4.45% | 4.89% | 8.04% | 3.15 | 147.97 | Strong expansion |

| | | | | | | | | |
|---|---|---|---|---|---|---|---|---|
| Oats | -4952 | -27.05% | -3.44% | 2.14% | 1.74% | -0.41 | 72.95 | Strong decline |
| Grain maize | -131,530 | -36.32% | -4.89% | 42.39% | 29.99% | -12.40 | 63.68 | Strong decline |

(*NIS, own processing based on statistical data provided through TEMPO-Online, AGR108A*)

Wheat strengthened its position in the region's cereal area. The area under cultivation increased by 35,700 ha, or 8.93%, and its share of the total area under cereals rose from 46.78% to 56.62%. By 2025, more than half of the region's cereal-growing area was thus occupied by this crop. A favorable trend was also recorded for barley and two-row barley, whose cultivated area increased by 22,662 ha, or 43.85%. As a result, their share in the cereal mix rose from 6.05% to 9.67%.

The most significant change, however, occurred with grain maize. The cultivated area decreased by 131,530 ha, equivalent to a 36.32% decline, and its share fell from 42.39% to 29.99%. Oat cultivation also lost 4952 ha, or 27.05%, but its impact on the regional total was smaller. The results reveal a clear shift in the region's cereal profile: wheat has become increasingly dominant, barley has expanded its presence, and grain maize has lost a significant portion of its cultivated area. Consequently, the overall decline in the area under cereals masks an internal restructuring that is far more interesting than the trend in the total figures suggests. The consolidation of wheat cultivation continues a pattern also observed in localities in Olt County, where this crop occupied the largest areas (*Vânătoru et al., 2013b*).

**e) Trends in oilseed crops and grain legumes**

Oilseed crops and grain legumes followed a different trend than the overall trend in cultivated areas. Both groups expanded between 2016 and 2025, but the growth was driven by a limited number of crops.

**Table 8**

**Areas cultivated with oilseeds and grain legumes in the South-West Oltenia region**

| Category | Statistical level | 2016 | 2017 | 2018 | 2019 | 2020 | 2021 | 2022 | 2023 | 2024 | 2025 |
|---|---|---|---|---|---|---|---|---|---|---|---|
| | | U.M.: Hectares | | | | | | | | | |
| Oilseeds | Main group | 232,669 | 210,373 | 209,591 | 243,857 | 212,075 | 261,936 | 241,309 | 262,014 | 310,961 | 251,911 |
| Sunflower | Component crop | 185,838 | 147,811 | 142,724 | 208,307 | 179,386 | 216,703 | 192,442 | 191,261 | 252,952 | 177,215 |
| Rapeseed | Component crop | 41,187 | 59,778 | 63,446 | 32,682 | 26,676 | 40,033 | 44,289 | 67,158 | 54,806 | 71,984 |
| Soybeans | Component crop | 4968 | 2714 | 2826 | 1912 | 5672 | 3917 | 4368 | 2603 | 2382 | 1493 |
| Grain legumes | Main group | 6999 | 20,100 | 23,249 | 19,788 | 24,773 | 19,705 | 19,315 | 23,568 | 21,617 | 19,077 |
| Field peas | Component crop | 4781 | 18,228 | 22,102 | 18,763 | 23,815 | 18,758 | 18,339 | 22,687 | 20,951 | 18,604 |
| Beans for grain | Component crop | 1888 | 1065 | 964 | 973 | 958 | 921 | 857 | 839 | 666 | 467 |

(*NIS, own processing based on statistical data provided through TEMPO-Online, AGR108A*)

The area planted with oilseeds increased by 19,242 ha, or 8.27%, reaching 251,911 ha in 2025. Grain legumes experienced a much sharper percentage increase, with their area growing from 6999 ha to 19,077 ha.

The changes within these two groups are presented in Table 9.

**Table 9**

**Trends in the area planted with oilseeds and grain legumes in the South-West Oltenia region**

| Category | Absolute change | Change 2016–2025 | Average annual rate | Share within its own group in 2016 | Share within its own group in 2025 | Change in share (p.p.) | Index 2025, 2016=100 | Classification |
|---|---|---|---|---|---|---|---|---|
| | U.M.: Hectares | U.M.: Percentages | | | | | | |
| Oilseeds | 19,242 | 8.27% | 0.89% | 100.00% | 100.00% | 0.00 | 108.27 | Moderate expansion |
| Sunflower | -8623 | -4.64% | -0.53% | 79.87% | 70.35% | -9.52 | 95.36 | Relatively stable |
| Rapeseed | 30,797 | 74.77% | 6.40% | 17.70% | 28.58% | 10.87 | 174.77 | Strong |

| | | | | | | | | |
|---|---|---|---|---|---|---|---|---|
| | | | | | | | | expansion |
| Soybeans | -3475 | -69.95% | -12.50% | 2.14% | 0.59% | -1.54 | 30.05 | Strong decline |
| Grain legumes | 12,078 | 172.57% | 11.79% | 100.00% | 100.00% | 0.00 | 272.57 | Strong expansion |
| Field peas | 13,823 | 289.12% | 16.30% | 68.31% | 97.52% | 29.21 | 389.12 | Strong expansion |
| Beans for grain | -1421 | -75.26% | -14.38% | 26.98% | 2.45% | -24.53 | 24.74 | Strong decline |

(*NIS, own processing based on statistical data provided through TEMPO-Online, AGR108A*)

Among oilseed crops, rapeseed showed the most favorable trend, gaining 30,797 ha, equivalent to a 74.77% increase. The expansion of the area under rapeseed is consistent with the potential of this crop highlighted in recent research, even though the sector remains sensitive to climatic and economic fluctuations (*Cruceru and Ghiuleanu, 2024a*).

The expansion of this crop offset the reduction in areas planted with sunflowers (by 8623 ha) and soybeans (by 3475 ha). In the case of soybeans, the 69.95% decline indicates a particularly strong decline. The increase in grain legumes was driven primarily by peas. The area planted with this crop increased by 13,823 ha, or 289.12%, representing the fastest expansion among the crops analyzed. In contrast, the area planted with beans for grain decreased by 1421 ha, corresponding to a 75.26% reduction.

Consequently, the favorable trend across these two groups was not uniform. Rapeseed and peas became the main drivers of growth, while soybeans and beans for grain saw a considerable reduction in their planted areas. The results highlight a clear reorientation of the crop structure, rather than a general expansion of all components.

**f) Trends in areas planted with potatoes, vegetables, and fruit crops**

The areas planted with potatoes and vegetables recorded some of the sharpest declines during the period analyzed. The declines particularly affected potatoes, field vegetables, and melons, while bearing orchards and vegetables grown in protected environments fared better.

**Table 10**

**Areas planted with potatoes, vegetables, strawberries, and fruit orchards in the South-West Oltenia region**

| Category | Statistical level | 2016 | 2017 | 2018 | 2019 | 2020 | 2021 | 2022 | 2023 | 2024 | 2025 |
|---|---|---|---|---|---|---|---|---|---|---|---|
| | | U.M.: Hectares | | | | | | | | | |
| Potatoes – total | Main group | 11,720 | 11,732 | 12,200 | 12,205 | 6960 | 3015 | 2966 | 1770 | 1655 | 2224 |
| Early, mid-season, and summer potatoes | Subtotal/sub group | 5079 | 5025 | 5375 | 5379 | 4134 | 705 | 1678 | 686 | 685 | 881 |
| Fall potatoes | Subtotal/sub group | 6641 | 6707 | 6824 | 6827 | 2826 | 2308 | 1288 | 1084 | 971 | 1344 |
| Vegetables – total | Main group | 35,271 | 35,506 | 35,022 | 34,685 | 28,279 | 28,390 | 24,704 | 24,795 | 24,510 | 20,609 |
| Field-grown vegetables | Subtotal/sub group | 23,482 | 23,770 | 23,213 | 23,198 | 16,190 | 17,164 | 14,424 | 14,475 | 14,296 | 10,196 |
| Vegetables grown in greenhouses and high tunnels | Subtotal/sub group | 599 | 555 | 664 | 662 | 683 | 680 | 664 | 767 | 733 | 989 |
| Fresh vegetables from home gardens | Subtotal/sub group | 10,839 | 10,831 | 10,791 | 10,505 | 11,096 | 10,235 | 9599 | 9537 | 9465 | 9419 |
| Tomatoes | Component crop | 6141 | 6116 | 6159 | 5981 | 4799 | 5206 | 4979 | 4993 | 4972 | 4876 |
| White cabbage | Component crop | 6607 | 6502 | 6495 | 6480 | 4928 | 5245 | 4621 | 4599 | 4561 | 4446 |
| Watermelons and melons | Component crop | 6819 | 6785 | 6742 | 6724 | 3505 | 3024 | 2592 | 2751 | 2743 | 2381 |
| Strawberry fields in production | Distinct indicator | 443 | 420 | 421 | 421 | 425 | 412 | 415 | 426 | 419 | 416 |
| Bearing orchards | Distinct indicator | 25,971 | 26,469 | 26,260 | 26,136 | 26,182 | 26,864 | 26,609 | 26,736 | 26,578 | 26,728 |

(*NIS, own processing based on statistical data provided through TEMPO-Online, AGR108A*)

The area planted with potatoes decreased from 11,720 ha in 2016 to only 2224 ha in 2025. During the same period, the area planted with vegetables fell from 35,271 ha to 20,609 ha. The extent and direction of these changes are summarized in Table 11.

**Table 11**

**Trends in the area planted with potatoes, vegetables, strawberries, and fruit orchards in the South-West Oltenia region**

| Category | Absolute change | Change 2016–2025 | Average annual rate | Index 2025, 2016=100 | Classification |
|---|---|---|---|---|---|
| | U.M.: Hectares | U.M.: Percentages | | | |
| Potatoes – total | -9496 | -81.02% | -16.86% | 18.98 | Strong decline |
| Early, mid-season, and summer potatoes | -4198 | -82.65% | -17.69% | 17.35 | Strong decline |
| Fall potatoes | -5297 | -79.76% | -16.26% | 20.24 | Strong decline |
| Vegetables – total | -14,662 | -41.57% | -5.80% | 58.43 | Strong decline |
| Field-grown vegetables | -13,286 | -56.58% | -8.85% | 43.42 | Strong decline |
| Vegetables grown in greenhouses and high tunnels | 390 | 65.11% | 5.73% | 165.11 | Strong expansion |
| Fresh vegetables from home gardens | -1420 | -13.10% | -1.55% | 86.90 | Moderate decline |
| Tomatoes | -1265 | -20.60% | -2.53% | 79.40 | Strong decline |
| White cabbage | -2161 | -32.71% | -4.31% | 67.29 | Strong decline |
| Watermelons and melons | -4438 | -65.08% | -11.03% | 34.92 | Strong decline |
| Strawberry fields in production | -27 | -6.09% | -0.70% | 93.91 | Moderate decline |
| Bearing orchards | 757 | 2.91% | 0.32% | 102.91 | Relatively stable |

(*NIS, own processing based on statistical data provided through TEMPO-Online, AGR108A*)

Potato cultivation decreased by 9496 ha, representing a decline of 81.02%. The decline was significant for both early and late potatoes, with their cultivated areas decreasing by 82.65% and 79.76%, respectively. The total area planted with vegetables decreased by 14,662 ha, or 41.57%. The largest contribution to this decline came from field-grown vegetables, which lost 13,286 ha. Among the crops analyzed, melons recorded the most severe contraction, at 65.08%, followed by cabbage, at 32.71%, and tomatoes, at 20.60%. The reduction in the area planted with tomatoes completes the picture of a sector characterized by fluctuations in both area and production (*Cruceru and Ghiuleanu, 2024b*).

However, not all components of the horticultural sector followed the same trend. Vegetables grown in greenhouses and high tunnels saw their area increase by 65.11%, even though they started from a low baseline. Orchards in production recorded an increase of 757 ha, or 2.91%, while the area of strawberry fields in production decreased moderately, by 6.09%.

These changes affected not only the size of the cultivated areas but also the internal structure of potato and vegetable crops.

**Table 12**

**Changes in the internal structure of areas planted with potatoes and vegetables**

| Category | Reference group | Share in 2016 | Share in 2025 | Change in share (p.p.) |
|---|---|---|---|---|
| | | U.M.: Percentages | | |
| Early, mid-season, and summer potatoes | Potatoes – total | 43.34% | 39.61% | -3.72 |
| Fall potatoes | Potatoes – total | 56.66% | 60.43% | 3.77 |
| Field-grown vegetables | Vegetables – total | 66.58% | 49.47% | -17.10 |
| Vegetables grown in greenhouses and high tunnels | Vegetables – total | 1.70% | 4.80% | 3.10 |
| Fresh vegetables from home gardens | Vegetables – total | 30.73% | 45.70% | 14.97 |

(*NIS, own processing based on statistical data provided through TEMPO-Online, AGR108A*)

The share of vegetables grown in open fields fell from 66.58% to 49.47%, a decrease of 17.10 percentage points. In contrast, home gardens now account for 45.70% of the vegetable-growing area, compared to 30.73% in 2016. The share of vegetables grown in greenhouses and high tunnels also increased, from 1.70% to 4.80%. In the case of potatoes, the change in structure was less pronounced. The share of fall potatoes increased from 56.66% to 60.43%, while early potatoes decreased from 43.34% to 39.61%.

The results show a strong decline in the areas planted with potatoes and vegetables, accompanied by an increase in the relative importance of home gardens and protected cultivation areas. Fruit orchards followed a different trend, remaining relatively stable and showing a slight expansion.

**g) Territorial Specialization of the Main Crop Groups**

The distribution of crops in 2025 highlights different agricultural profiles from one county to another. The areas used to determine these differences are presented in Table 13.

**Table 13**

**Areas used to calculate the location quotients in the counties of the South-West Oltenia region in 2025**

| County/Region | Total cultivated area | Cereals for grain | Oilseeds | Legumes for grain | Potatoes – total | Vegetables – total | Green forage from arable land | Bearing orchards |
|---|---|---|---|---|---|---|---|---|
| | U.M.: Hectares | | | | | | | |
| Dolj | 481,618 | 325,885 | 118,386 | 9551 | 888 | 6536 | 22,252 | 1977 |
| Gorj | 66,960 | 61,090 | 460 | 75 | 127 | 2729 | 3741 | 4398 |
| Mehedinți | 154,906 | 111,478 | 32,473 | 2472 | 559 | 2165 | 7302 | 6530 |
| Olt | 347,559 | 232,341 | 97,182 | 6862 | 61 | 5993 | 8486 | 2886 |
| Vâlcea | 53,844 | 38,271 | 3410 | 117 | 589 | 3186 | 9934 | 10,937 |
| **South-West Oltenia** | **1,104,887** | **769,065** | **251,911** | **19,077** | **2224** | **20,609** | **51,715** | **26,728** |

(*NIS, own processing based on statistical data provided through TEMPO-Online, AGR108A*)

Based on these areas, the location quotients were calculated according to the methodology described above. An LQ value greater than 1 indicates a presence above the regional average, while values less than 1 indicate a relatively low presence of the crop under analysis. The results are presented in Table 14.

**Table 14**

**Location quotients for the main crop groups in the counties of the South-West Oltenia region in 2025**

| County | Cereals for grain | Oilseeds | Legumes for grain | Potatoes – total | Vegetables – total | Green forage | Bearing orchards |
|---|---|---|---|---|---|---|---|
| | U.M.: Dimensionless | | | | | | |
| Dolj | 0.97 | 1.08 | 1.15 | 0.92 | 0.73 | 0.99 | 0.17 |
| Gorj | 1.31 | 0.03 | 0.06 | 0.94 | 2.18 | 1.19 | 2.72 |
| Mehedinți | 1.03 | 0.92 | 0.92 | 1.79 | 0.75 | 1.01 | 1.74 |
| Olt | 0.96 | 1.23 | 1.14 | 0.09 | 0.92 | 0.52 | 0.34 |
| Vâlcea | 1.02 | 0.28 | 0.13 | 5.43 | 3.17 | 3.94 | 8.40 |

(*NIS, own processing based on statistical data provided through TEMPO-Online, AGR108A*)

Dolj has the most balanced agricultural profile. Values close to 1 for grains, oilseeds, legumes, potatoes, and forage crops indicate that the county's structure is similar to that of the region. There is a slight orientation toward grain legumes, with an LQ of 1.15, and oilseeds, with 1.08, while bearing orchards are underrepresented. Gorj stands out for its vegetables and fruit orchards, for which the coefficients reach 2.18 and 2.72, respectively.

The county also exhibits moderate specialization in cereal cultivation, with an LQ of 1.31. In contrast, oilseeds and grain legumes have a very limited presence. Mehedinți has a profile oriented primarily toward potatoes and fruit orchards, with LQ values of 1.79 and 1.74.

For cereals and forage crops, the coefficients are close to 1, indicating a representation similar to the regional average. Olt stands out for its oilseeds and grain legumes, with values of 1.23 and 1.14. Potatoes are virtually absent from the county's profile, with an LQ of only 0.09, and green forage and bearing orchards are also underrepresented.

The most distinct profile belongs to Vâlcea County. The high values for fruit orchards (8.40), potatoes (5.43), forage crops (3.94), and vegetables (3.17) indicate a strong territorial specialization. These results do not necessarily mean that Vâlcea has the largest areas in absolute terms, but rather that these crops occupy a much more significant place in the county's structure than in the regional structure.

The location quotients thus outline three main profiles: diversified agriculture in Dolj, a focus on field crops in Olt, and specialization in potatoes, vegetables, forage crops, and orchards in Vâlcea. Gorj and Mehedinți round out this picture with a more pronounced presence of fruit crops.

**h) Territorial concentration of cultivated areas**

Location quotients indicate the relative importance of a crop within each county's profile, but they do not highlight how concentrated that area is at the regional level. To supplement the analysis, the Herfindahl–Hirschman Index was used, whose values increase as the area of a crop becomes concentrated in a smaller number of counties.

**Table 15**

**The geographic distribution and concentration of cultivated land in the South-West Oltenia region in 2025**

| Crop Group | Dolj | Gorj | Mehedinți | Olt | Vâlcea | HHI (0–1 scale) | Dominant County | Maximum percentage |
|---|---|---|---|---|---|---|---|---|
| | U.M.: Percentages | | | | | | | U.M.: Percentages |
| Cereals for grain | 42.37% | 7.94% | 14.50% | 30.21% | 4.98% | 0.301 | Dolj | 42.37% |
| Oilseeds | 47.00% | 0.18% | 12.89% | 38.58% | 1.35% | 0.386 | Dolj | 47.00% |
| Legumes for grain | 50.07% | 0.39% | 12.96% | 35.97% | 0.61% | 0.397 | Dolj | 50.07% |
| Potatoes – total | 39.93% | 5.71% | 25.13% | 2.74% | 26.48% | 0.297 | Dolj | 39.93% |
| Vegetables – total | 31.71% | 13.24% | 10.51% | 29.08% | 15.46% | 0.238 | Dolj | 31.71% |
| Green forage from arable land | 43.03% | 7.23% | 14.12% | 16.41% | 19.21% | 0.274 | Dolj | 43.03% |
| Bearing orchards | 7.40% | 16.45% | 24.43% | 10.80% | 40.92% | 0.271 | Vâlcea | 40.92% |

(*NIS, authors' calculations based on data from TEMPO-Online, AGR108A*)

Grain legumes had the most concentrated geographical distribution, with an HHI of 0.397. Dolj accounted for 50.07% of the regional area devoted to this group, and Olt for 35.97%. A similar situation was observed for oilseed crops, for which the HHI reached 0.386, with Dolj and Olt accounting for the majority of the cultivated area. Vegetables had the most balanced distribution among the groups analyzed, with an HHI of 0.238. Dolj accounted for 31.71% of the area, and Olt for 29.08%, with the remainder distributed among Gorj, Mehedinți, and Vâlcea. Thus, no county exceeded one-third of the region's total area under vegetable cultivation.

Grains and potatoes showed similar levels of concentration, with HHI values of 0.301 and 0.297, respectively. In the case of grains, Dolj accounted for 42.37% of the regional area. Potatoes had a more specific distribution, with areas concentrated mainly in Dolj, Vâlcea, and Mehedinți. Green forage and bearing orchards recorded HHI values of 0.274 and 0.271. Dolj dominated the distribution of forage, accounting for 43.03%, while Vâlcea was the leading fruit-growing county, accounting for 40.92% of the regional area of bearing orchards. Dolj had the largest areas for six of the seven groups analyzed, confirming its dominant role in regional agriculture. The exception was bearing orchards, which were concentrated primarily in Vâlcea. Taken together, the LQ and HHI values provide a clearer picture: Dolj dominates in terms of the size of its areas, while Vâlcea stands out for its relatively strong specialization in certain crops.

**i) Summary of the main changes in cultivated areas**

Taken together, the results show that agriculture in the South-West Oltenia region has faced not only a reduction in cultivated area but also a shift in crop structure. Some crops have actually expanded despite the regional decline, while others have lost a significant portion of their cultivated area.

**Table 16**

**Major changes in cultivated land area in the South-West Oltenia region**

| Crops | Area in 2016 | Area in 2025 | Absolute change | Trends 2016–2025 | Average annual rate | Index 2025, 2016=100 | Classification |
|---|---|---|---|---|---|---|---|
| | U.M.: Hectares | | | U.M.: Percentages | | | |
| **Crops with increasing cultivated areas** | | | | | | | |
| Field peas | 4781 | 18,604 | 13,823 | 289.12% | 16.30% | 389.12 | Strong expansion |
| Rapeseed | 41,187 | 71,984 | 30,797 | 74.77% | 6.40% | 174.77 | Strong expansion |
| Vegetables grown in greenhouses and high tunnels | 599 | 989 | 390 | 65.11% | 5.73% | 165.11 | Strong expansion |
| Barley | 41,771 | 61,808 | 20,037 | 47.97% | 4.45% | 147.97 | Strong expansion |
| Wheat – total | 399,710 | 435,410 | 35,700 | 8.93% | 0.96% | 108.93 | Moderate expansion |
| **Crops with declining cultivated areas** | | | | | | | |
| Potatoes – total | 11,720 | 2224 | -9496 | -81.02% | -16.86% | 18.98 | Strong decline |

| | | | | | | | |
|---|---|---|---|---|---|---|---|
| Beans for grain | 1888 | 467 | -1421 | -75.26% | -14.38% | 24.74 | Strong decline |
| Soybeans | 4968 | 1493 | -3475 | -69.95% | -12.50% | 30.05 | Strong decline |
| Watermelons and melons | 6819 | 2381 | -4438 | -65.08% | -11.03% | 34.92 | Strong decline |
| Field-grown vegetables | 23,482 | 10,196 | -13,286 | -56.58% | -8.85% | 43.42 | Strong decline |
| Grain maize | 362,148 | 230,618 | -131,530 | -36.32% | -4.89% | 63.68 | Strong decline |

(*NIS, own processing based on statistical data provided through TEMPO-Online, AGR108A*)

The largest increases were recorded for wheat, which gained 35,700 ha; rapeseed, with an increase of 30,797 ha; and barley and two-row barley, with an increase of 22,662 ha. Peas stood out with the fastest percentage growth, at 289.12%, becoming the main driver of the expansion in grain legumes. The largest reduction was in grain maize, which lost 131,530 ha. This decline had a decisive impact on the contraction of the total area planted with cereals. Significant reductions were also recorded for vegetables, by 14,662 ha; potatoes, by 9496 ha; and sunflowers, by 8623 ha.

The observed changes point to a more pronounced shift toward wheat, rapeseed, barley, and peas, alongside a reduction in grain maize, potatoes, and vegetable crops. At the same time, the territorial distribution remained highly differentiated: Dolj and Olt accounted for the largest share of field crops, while Vâlcea stood out for its specialization in fruit orchards, potatoes, vegetables, and green forage. The 2016–2025 period can be characterized by three main processes: a reduction in the area under cultivation at the regional level, a restructuring of the crop mix, and the accentuation of distinct county-level agricultural profiles. These results provide the basis for discussing the factors that influenced the observed transformations and their implications for agriculture in the South-West Oltenia region.

**j) Diagnostic synthesis of the results through a S.W.O.T. analysis.**

To synthesize the results, a S.W.O.T. analysis was conducted on the evolution of cultivated areas in the South-West Oltenia region. Since the analysis is based exclusively on the statistical data examined, the opportunities and threats represent potential directions and risks derived from the continuation of the observed trends.

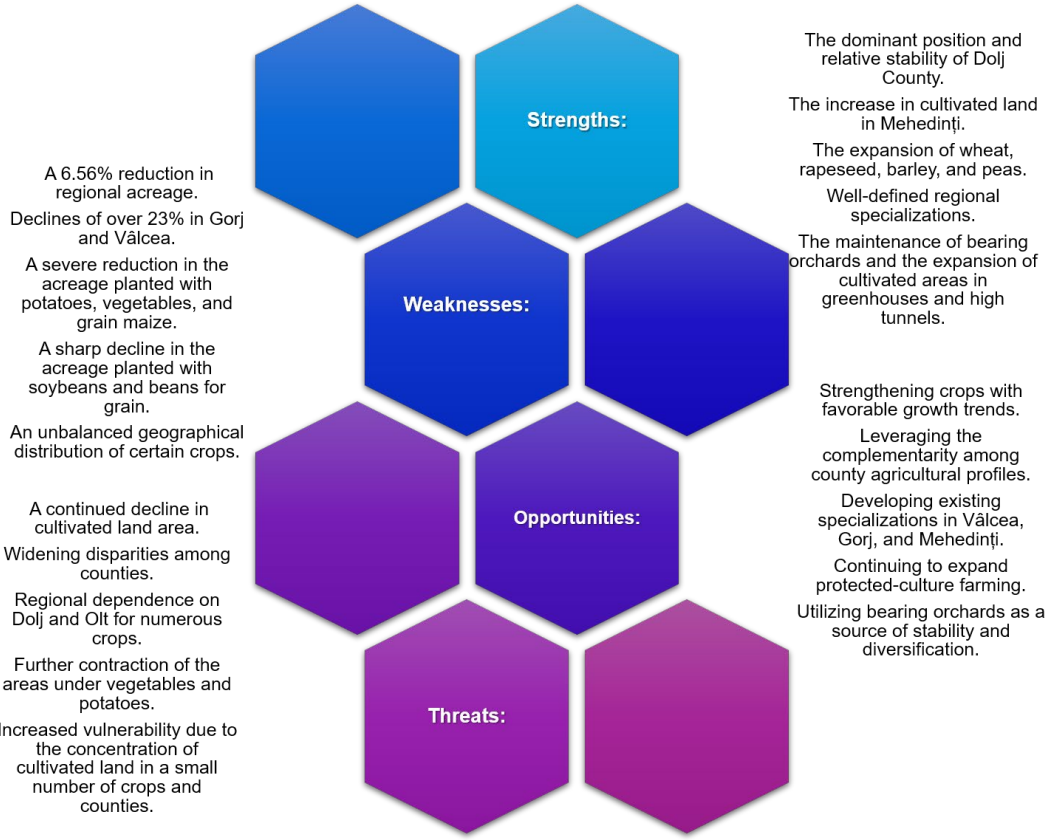



**Fig. 1 - Representative SmartArt diagram showing a S.W.O.T. analysis of trends in cultivated land area in the South-West Oltenia region**

*(Authors' own elaboration based on the study results)*

*Note: Opportunities and threats were identified based on statistical trends observed during the 2016–2025 period.*

The S.W.O.T. analysis highlights a significant contrast. The region has a solid grain-growing base, expanding crops, and clear county-level specializations, but these advantages are accompanied by a reduction in total acreage and a strong decline in certain crops. The most useful direction suggested by the results is to capitalize on territorial complementarity: Dolj and Olt through field crops, and Vâlcea, Gorj, and Mehedinți through their horticultural, fruit-growing, and forage crop profiles. The relevance of these directions is also supported by studies that emphasize the need for crop diversification, soil conservation, and agricultural risk management (*Buzatu et al., 2023; Ghiuleanu et al., 2023; Nijloveanu et al., 2013*).

The results highlight a regional agricultural sector undergoing restructuring, in which the general trend toward a reduction in cultivated area coexists with the expansion of certain crops and the emergence of distinct county-level agricultural profiles. Capitalizing on these differences can transform territorial diversity into a source of balance and complementarity for agriculture in the South-West Oltenia region.

## CONCLUSIONS

Agriculture in the South-West Oltenia region underwent a noticeable restructuring process between 2016 and 2025. The cultivated area decreased by 6.56%, but this overall trend masks significant differences between counties and among the main crops.

Mehedinți was the only county where the cultivated area increased, while Dolj maintained its stability and dominant position. At the other end of the spectrum, Gorj and Vâlcea recorded declines of over 23%. Dolj and Olt together accounted for 75.05% of the regional cultivated area in 2025, confirming the existence of a well-defined agricultural core.

The changes in crop structure are just as significant as the reduction in total cultivated area. Wheat, barley, rapeseed, and peas expanded, while grain maize, potatoes, and vegetables lost ground. The decline in the area planted with potatoes was particularly sharp, at 81.02%, indicating one of the most significant transformations in regional agriculture.

The territorial analysis highlights complementary county profiles. Dolj stands out for the size and diversity of its cultivated areas, Olt for its field crops, and Vâlcea for its specialization in fruit orchards, potatoes, vegetables, and forage crops. Gorj and Mehedinți complement this structure with a more pronounced presence of fruit crops.

The region is facing not only a decline in cultivated area but also a shift in its agricultural profile. Capitalizing on growing crops, preserving diversity, and leveraging the complementarities among counties can transform these changes into a foundation for more balanced regional development. However, the results reflect only the dynamics of cultivated areas, which is why a future analysis could incorporate crop production, yields, and economic value.

## REFERENCES

[1] Buzatu, C. S., Ghiuleanu, I. V., Tudor, V. C. (2023). *Dynamics of land fund and strategies on soil conservation and prevention of soil degradation in Romania*. *Scientific Papers Series Management, Economic Engineering in Agriculture and Rural Development*, 23(4), 149–156. https://managementjournal.usamv.ro/pdf/vol.23_4/Art14.pdf. Accessed January 7, 2026.

[2] Cruceru, C., Ghiuleanu, I. V. (2024a). *The area under oilseed rape in Romania: Evolution and trends*. In *Proceedings of the International Symposium ISB-INMA-TEH: Agricultural and Mechanical Engineering* (pp. 486–501). https://isbinmateh.inma.ro/wp-content/uploads/2025/11/Vol-ISB-INMA-TEH-2024.pdf. Accessed January 3, 2026.

[3] Cruceru, C., Ghiuleanu, I. V. (2024b). *Tomatoes in figures: Production, prices and outlook for the future*. In *Proceedings of the International Symposium ISB-INMA-TEH: Agricultural and Mechanical Engineering* (pp. 502–511). https://isbinmateh.inma.ro/wp-content/uploads/2025/11/Vol-ISB-INMA-TEH-2024.pdf. Accessed February 13, 2026.

[4] Ghiuleanu, I. V., Buzatu, C. S., Tudor, V. C., Panait, R., (Carbarău) Smedescu, C. A. (2023). *Risks analyses and challenges in crop management in Romania*. *Scientific Papers Series Management, Economic Engineering in Agriculture and Rural Development*, 23(4), 353–364. https://managementjournal.usamv.ro/pdf/vol.23_4/Art34.pdf. Accessed January 17, 2026.

[5] National Institute of Statistics [NIS]. (2026). TEMPO-Online database: *Area cultivated with main crops, by forms of ownership, macroregions, development regions and counties* (AGR108A; data for 2016–

2025). Accessed July 7, 2026, from http://statistici.insse.ro:8077/tempo-online/#/pages/tables/insse-table.

[6] Nijloveanu, D., Bozga, I., Tita, V., Vânătoru (Rădulescu), D. L. (2013). *Soil degradation in Olt County by the process of hydric erosion*. *Annals of the University of Craiova – Agriculture, Montanology, Cadastre Series, 43(1)*, 243–246. https://anale.agro-craiova.ro/index.php/aamc/article/view/46/46. Accessed March 11, 2026.

[7] U.S. Bureau of Labor Statistics. (2025, September 15). *QCEW location quotient details*. https://www.bls.gov/cew/about-data/location-quotients-explained.htm. Accessed March 8, 2026.

[8] U.S. Department of Justice, Antitrust Division. (2024, January 17). *Herfindahl–Hirschman Index*. https://www.justice.gov/atr/herfindahl-hirschman-index. Accessed January 18, 2026.

[9] Ursu, A., Cofas, E. (2016). *The territorial analysis of agricultural production structure. Case study: Region South-West Oltenia*. *Scientific Papers Series Management, Economic Engineering in Agriculture and Rural Development, 16(1)*, 535–542. https://managementjournal.usamv.ro/pdf/vol.16_1/Art84.pdf. Accessed February 13, 2026.

[10] Vânătoru (Rădulescu), D. L., Bozga, I., Nijloveanu, D., Tita, V. (2013a). *Climate change and its effects on culture in microregion Caracal–Olt*. *Annals of the University of Craiova – Agriculture, Montanology, Cadastre Series, 43(2)*, 237–240. https://anale.agro-craiova.ro/index.php/aamc/article/view/98/93. Accessed February 3, 2026.

[11] Vânătoru (Rădulescu), D. L., Bozga, I., Nijloveanu, D., Tita, V. (2013b). *Studies on the development of agriculture in Olt County*. *Annals of the University of Craiova – Agriculture, Montanology, Cadastre Series, 43(2)*, 231–236. https://anale.agro-craiova.ro/index.php/aamc/article/view/97/92. Accessed January 25, 2026.

# BETWEEN GROWTH AND DECLINE: STRUCTURAL AND TERRITORIAL SHIFTS IN CROP PRODUCTION IN SOUTH-WEST OLTENIA, ROMANIA (2016–2025)

/

# *ÎNTRE CREȘTERE ȘI DECLIN: SCHIMBĂRI STRUCTURALE ȘI TERITORIALE ALE PRODUCȚIEI VEGETALE DIN REGIUNEA SUD-VEST OLTENIA, ROMÂNIA (2016–2025)*

**Daniel NIJLOVEANU[1)], Iulian Virgil GHIULEANU[2)], Corina CRUCERU*[1)], Nicolae-Valentin VLĂDUȚ[3)], Stefano Andrea MANTOVANI[3)]**

[1)] USAMV Bucharest, Faculty of Management and Rural Development, Slatina Branch, Olt County / Romania;

[2)] University of Agronomic Sciences and Veterinary Medicine Bucharest (Doctoral student, Doctoral School: Plant and Animal Resources Engineering and Management), 59 Marasti Boulevard, District 1, 011464, Bucharest / Romania;

[3)] National Institute of Research - Development for Machines and Installations Designed for Agriculture and Food Industry - INMA Bucharest / Romania.

**E-mail: c.cruceru19@yahoo.com*

***Keywords:*** *crop production, agricultural restructuring, production dynamics, crop structure, territorial disparities, South-West Oltenia.*

**ABSTRACT**

*This study analyzes the dynamics and restructuring of crop production in the South-West Oltenia Region of Romania during 2016–2025. Statistical data were obtained from the National Institute of Statistics, TEMPO-Online database, AGR109A, and processed in Microsoft Excel. The analysis covered the regional level and its five constituent counties, using absolute and percentage changes, annual averages, year-on-year changes, territorial shares and changes in crop structure. The results indicate a selective restructuring rather than a uniform decline in agricultural production. Cereal production decreased by 8.66%, although wheat and barley output increased by 36.22% and 51.08%, respectively, while grain maize declined by 63.92%. Grain legumes recorded the strongest expansion among the main crop groups, increasing by 141.62%, mainly due to the growth of pea production. Oilseed production decreased by 10.74%, but the share of rapeseed rose from 26.28% to 47.40%, approaching that of sunflower. The most vulnerable sectors were potatoes, vegetables and green forage from arable land, whose production declined by 84.40%, 51.49% and 22.03%, respectively. Vegetable production under protected cultivation was a notable exception, increasing by 34.83%. From a territorial perspective, Dolj and Olt formed the main production core of the region. The findings highlight substantial year-to-year volatility, territorial concentration and dependence on a limited number of crops, emphasizing the importance of production diversification and greater agricultural resilience.*

**REZUMAT**

*Studiul analizează dinamica și restructurarea producției agricole vegetale din Regiunea Sud-Vest Oltenia în perioada 2016–2025. Datele statistice au fost preluate din baza TEMPO-Online a Institutului Național de Statistică, seria AGR109A, și prelucrate în Microsoft Excel. Analiza a fost realizată la nivel regional și pentru cele cinci județe componente, utilizând modificări absolute și procentuale, medii anuale, dinamici anuale, ponderi teritoriale și schimbări ale structurii culturilor. Rezultatele indică o restructurare selectivă, nu un declin uniform al producției agricole. Producția de cereale s-a redus cu 8.66%, deși grâul și orzul au crescut cu 36.22%, respectiv 51.08%, în timp ce porumbul boabe s-a diminuat cu 63.92%. Leguminoasele pentru boabe au înregistrat cea mai puternică expansiune dintre grupele principale, cu 141.62%, susținută în special de creșterea producției de mazăre. Producția plantelor uleioase s-a redus cu 10.74%, dar ponderea rapiței a avansat de la 26.28% la 47.40%, apropiindu-se de cea a florii-soarelui. Cele mai vulnerabile sectoare au fost cartofii, legumele și furajele verzi din teren arabil, ale căror producții au scăzut cu 84.40%, 51.49% și, respectiv, 22.03%. O excepție importantă a fost producția legumelor cultivate în solarii, care a crescut cu 34.83%. Din punct de vedere teritorial, Doljul și Oltul au format principalul nucleu productiv al regiunii. Rezultatele evidențiază creșterea volatilității și a concentrării teritoriale, subliniind necesitatea diversificării producției și consolidării rezilienței agriculturii regionale.*

## INTRODUCTION

Agriculture remains a vital sector for food security, the rural economy, and the sustainable use of land resources. Beyond production volume, the sector's stability depends on how crops adapt to climate change, soil degradation, market fluctuations, and risks that are increasingly difficult to anticipate. Sustainable land management and improved decision-making regarding crop structure are thus becoming key conditions for maintaining long-term productive capacity (*Buzatu et al., 2023; Ghiuleanu et al., 2023*).

In recent years, European crop production has been characterized by significant differences across crops, countries, and growing seasons (*Eurostat, 2025*). Drought and high temperatures have amplified the vulnerability of agricultural systems, and the risk can no longer be viewed as an isolated or strictly local phenomenon (*Rossi et al., 2023*). For Romania, climate change and shifts in soil temperatures may affect the stability of production and agriculture's ability to meet food demand (*Buzatu, Ghiuleanu, Mărcuță, et al., 2024*). In this context, the Common Agricultural Policy is placing increasing emphasis on farm resilience, efficient resource use, and the modernization of the agricultural sector (*European Commission, 2026*). Similarly, conservation and organic farming practices can help improve soil health and strengthen production resilience by reducing the intensity of tillage, maintaining plant residue cover, and implementing crop rotation (*Vlăduț et al., 2024*).

The South-West Oltenia region is an important agricultural area in Romania, but one characterized by natural conditions, production structures, and levels of specialization that vary from one county to another. Previous research has highlighted the existence of clear territorial differences in the structure of regional agricultural production (*Ursu and Cofas, 2016*). In Olt County, both the prospects for agricultural development and the effects of climate change and vulnerabilities associated with soil erosion have been analyzed (*Nijloveanu et al., 2013; Vânătoru (Rădulescu) et al., 2013a; Vânătoru (Rădulescu) et al., 2013b*). These findings indicate that regional performance cannot be assessed solely based on total output; rather, the distribution of production across counties and crops must also be considered.

At the same time, each crop group responds differently to production conditions. Grain maize performance can vary depending on the agricultural land and local soil characteristics, a finding also highlighted in research conducted in Dolj County (*Ștefan et al., 2022*). Within the oilseed crop sector, rapeseed has gained increasing importance at the national level (*Cruceru and Ghiuleanu, 2024a*), while the vegetable sector is influenced by differences between open-field production and protected cultivation, as well as by trends in prices and demand (*Cruceru and Ghiuleanu, 2024b*). The diversity of these trajectories warrants an analysis that goes beyond the evolution of total figures and examines the changes occurring within the main groups.

The 2016–2025 period is relevant because it includes both years with high production levels and episodes of widespread decline. Official data on crop production from 2024 indicate significant difficulties for several agricultural crops in Romania (*NIS, 2025*). However, a decline in total production does not mean that all crops followed the same trend. Some have strengthened their position, while others have become marginal, and these changes have altered the region's agricultural structure.

The aim of this study is to assess the dynamics and restructuring of crop production in the South-West Oltenia region during the period 2016–2025, based on data provided by the National Institute of Statistics (NIS) via TEMPO-Online, series AGR109A (*NIS, 2026*). The analysis examines the evolution of the main crop groups, annual variations, differences between counties, the territorial contribution to regional production, and structural changes within cereals, legumes, oilseeds, potatoes, vegetables, and forage crops. By identifying the most significant increases and decreases, the study aims to outline the strengths, vulnerabilities, and directions for the development of regional agriculture.

## MATERIALS AND METHODS

The statistical data were taken from the National Institute of Statistics' TEMPO-Online database, Table AGR109A—*"Crop Production for Major Crops, by Form of Ownership, Macroregions, Development Regions, and Counties."* The *"Total"* form of ownership was selected, and production was expressed in metric tons. According to the NIS methodology, the indicator represents the gross physical production obtained over a specific period, with data reported annually (*NIS, 2026*).

Data processing was performed in Microsoft Excel 365. Regional values were obtained by summing the production figures recorded in the five counties. For each crop group, the following were calculated: the absolute change between 2016 and 2025, the percentage change in production, the ten-year annual average, the minimum and maximum values, and the years in which these were recorded. Year-on-year

changes were calculated by comparing each year's production with that of the previous year. The percentage results were rounded to two decimal places.

To interpret the general trend, the changes from 2016 to 2025 were classified into five categories: strong decline for values below -20.00%, moderate decline for values between -20.00% and less than -5.00%, relatively stable trends for values between -5.00% and 5.00%, moderate expansion for values greater than 5.00% and up to 20.00%, and strong expansion for values greater than 20.00%. This classification was used to quickly distinguish between groups experiencing growth and those characterized by a decline in production.

The territorial analysis was conducted based on county-level production in 2025 and the changes recorded compared to 2016. Each county's contribution was determined as the share of its production in the regional total for the respective group. To analyze the internal structure of cereals, legumes, and oilseeds, the shares of component crops in the total production of each group were calculated for both 2016 and 2025. The differences between the two shares were expressed in percentage points to highlight whether a crop gained or lost importance within the group's structure.

The categories *"Rye and other cereals," "Other legumes,"* and *"Other oilseeds"* were determined by the difference between the group's total production and the sum of the individually listed crops. To avoid double counting, alfalfa and clover were treated as components of perennial forages, and forage maize as a component of annual forage crops. Forage roots were analyzed separately and were not added to the total forage crops on arable land.

In the final stage, the crops with the most significant percentage increases and decreases were selected. The residual categories *"Other legumes"* and *"Other oilseed crops,"* determined by difference, were excluded from this selection due to their small volumes and heterogeneous nature. Percentage changes were analyzed alongside absolute differences, as a high percentage change may stem from a very low initial level. The quantitative results and structural changes were subsequently synthesized through a S.W.O.T. analysis, based on the strengths, weaknesses, opportunities, and threats identified for regional agriculture. The research is descriptive in nature, and the results highlight trends and regional differences without attributing the observed changes to a single causal relationship. All calculations were performed using unrounded values; percentage results were rounded to two decimal places only for presentation.

## RESULTS

The results paint a picture of regional agriculture undergoing a visible process of change. The analysis begins with the evolution of the main crop groups, continues with the differences between counties, and then examines the changes that have occurred in the structure of cereals, oilseeds, legumes, vegetables, and forage crops. The 2016–2025 series shows that production did not follow a single trend: some crops expanded, others contracted sharply, and annual variations remained significant. The empirical basis of the analysis consists of statistical data from TEMPO-Online, series AGR109A, processed for the period 2016–2025 (*NIS, 2026*).

**Table 1**

**Production trends for the main crop groups in the South-West Oltenia region**

| Crop group | 2016 | 2017 | 2018 | 2019 | 2020 | 2021 | 2022 | 2023 | 2024 | 2025 |
|---|---|---|---|---|---|---|---|---|---|---|
| | U.M.: Metric tons | | | | | | | | | |
| Cereals for grain | 2,858,903 | 4,330,567 | 4,653,133 | 4,197,585 | 3,211,456 | 3,345,688 | 2,929,924 | 3,076,028 | 2,448,987 | 2,611,304 |
| Grain legumes | 12,299 | 50,856 | 29,570 | 42,131 | 35,102 | 48,010 | 36,234 | 43,571 | 24,188 | 29,717 |
| Oilseed crops | 420,806 | 634,417 | 581,620 | 705,900 | 440,798 | 666,268 | 518,376 | 577,527 | 315,500 | 375,600 |
| Potatoes – total | 144,216 | 192,441 | 185,297 | 156,190 | 82,619 | 47,536 | 40,104 | 15,526 | 12,610 | 22,504 |
| Vegetables – total | 528,649 | 614,268 | 645,029 | 587,681 | 515,250 | 564,963 | 343,009 | 323,681 | 283,959 | 256,444 |
| Green forage from arable land | 597,370 | 616,628 | 716,596 | 685,112 | 587,629 | 561,602 | 449,716 | 476,230 | 410,793 | 465,774 |

*(NIS, own calculations based on statistical data provided through TEMPO-Online, AGR109A)*

The data in Table 1 indicate a favorable period between 2017 and 2019, when several groups recorded high levels. Grain production reached 4,653,133 metric tons in 2018, compared to 2,858,903 metric tons in

2016, but subsequently declined to 2,611,304 metric tons in 2025. Oilseeds followed a similar trajectory, peaking at 705,900 metric tons in 2019 and reaching only 375,600 metric tons by the end of the period.

The most significant declines are seen in potatoes and vegetables. Potato production fell from 144,216 metric tons in 2016 to 22,504 metric tons in 2025, while vegetable production dropped from 528,649 to 256,444 metric tons. Conversely, grain legumes ended the period above their initial level, though with significant year-to-year fluctuations. The initial picture presented by the data is therefore not one of a uniform decline, but rather of an increasingly clear differentiation among crop groups.

**Table 2**

**Summary indicators of production trends for the main crop groups in the South-West Oltenia region**

| Crop Group | Production in 2016 | Production in 2025 | Absolute change | Change from 2016 to 2025 | Average annual production | Minimum production | Year of minimum | Maximum production | Year of maximum | Classification |
|---|---|---|---|---|---|---|---|---|---|---|
| | U.M.: Metric tons for production indicators and % for the 2016–2025 change; years and qualitative classification are indicated separately | | | | | | | | | |
| Cereals for grain | 2,858,903 | 2,611,304 | -247,599 | -8.66% | 3,366,358 | 2,448,987 | 2024 | 4,653,133 | 2018 | Moderate decline |
| Grain legumes | 12,299 | 29,717 | 17,418 | 141.62% | 35,168 | 12,299 | 2016 | 50,856 | 2017 | Strong expansion |
| Oilseeds | 420,806 | 375,600 | -45,206 | -10.74% | 523,681 | 315,500 | 2024 | 705,900 | 2019 | Moderate decline |
| Potatoes – total | 144,216 | 22,504 | -121,712 | -84.40% | 89,904 | 12,610 | 2024 | 192,441 | 2017 | Strong decline |
| Vegetables – total | 528,649 | 256,444 | -272,205 | -51.49% | 466,293 | 256,444 | 2025 | 645,029 | 2018 | Strong decline |
| Green forage from arable land | 597,370 | 465,774 | -131,596 | -22.03% | 556,745 | 410,793 | 2024 | 716,596 | 2018 | Strong decline |

*(NIS, own calculations based on statistical data provided through TEMPO-Online, AGR109A)*

The summary indicators in Table 2 provide a clearer picture of the trends. Grain legumes are the only group that recorded strong growth: production in 2025 was 141.62% higher than in 2016. However, this increase must be viewed in relation to the low initial level and the wide fluctuations in production over the period. Cereals and oilseeds recorded moderate declines of 8.66% and 10.74%, respectively.

The situation is much more difficult for potatoes, vegetables, and green forage. Potato production fell by 84.40%, and vegetable production by 51.49%. Green forage, in turn, recorded a decline of 22.03%. A key indicator is that, for all six groups, production in 2025 is below the annual average for the period. Furthermore, the highest values are concentrated primarily between 2017 and 2019, while most of the lowest values occur in 2024 or 2025, indicating a more pronounced decline toward the end of the analyzed period. This regional picture is consistent with official data on crop production in Romania in 2024, which highlights the difficulties faced by a significant portion of the major agricultural crops (*NIS, 2025*).

**Table 3**

**Year-on-year changes in production for the main crop groups in the South-West Oltenia region**

| Crop group | 2017 | 2018 | 2019 | 2020 | 2021 | 2022 | 2023 | 2024 | 2025 |
|---|---|---|---|---|---|---|---|---|---|
| | U.M.: % (year-on-year change) | | | | | | | | |
| Cereals for grain | 51.48% | 7.45% | -9.79% | -23.49% | 4.18% | -12.43% | 4.99% | -20.38% | 6.63% |
| Grain legumes | 313.50% | -41.86% | 42.48% | -16.68% | 36.77% | -24.53% | 20.25% | -44.49% | 22.86% |
| Oilseeds | 50.76% | -8.32% | 21.37% | -37.56% | 51.15% | -22.20% | 11.41% | -45.37% | 19.05% |
| Potatoes – total | 33.44% | -3.71% | -15.71% | -47.10% | -42.46% | -15.63% | -61.29% | -18.78% | 78.46% |
| Vegetables – total | 16.20% | 5.01% | -8.89% | -12.32% | 9.65% | -39.29% | -5.63% | -12.27% | -9.69% |
| Green forage from arable land | 3.22% | 16.21% | -4.39% | -14.23% | -4.43% | -19.92% | 5.90% | -13.74% | 13.38% |

*(NIS, own calculations based on statistical data provided through TEMPO-Online, AGR109A)*

The annual trends highlight the volatile nature of regional production. The year 2017 saw increases across all the groups analyzed, with the largest increases recorded for grain legumes (313.50%), cereals for grain (51.48%), and oilseeds (50.76%). However, this favorable trend was not sustained, as it was followed by frequent fluctuations between increases and decreases.

The years 2020, 2022, and 2024 are marked by simultaneous declines across all six groups, indicating periods of widespread decline. In 2025, a recovery is observed for five of these groups, but vegetables continued to decline by 9.69%. The 78.46% increase recorded by potatoes in the same year appears spectacular, but it stems from the very low level in 2024 and does not offset the losses accumulated previously. Consequently, the

annual variations confirm that isolated recoveries were not sufficient to reverse the negative trends of the entire period. The instability observed in the South-West Oltenia region is part of a broader European context characterized by significant variations in crop production across different crops and agricultural years (*Eurostat, 2025*). Climate risks, drought, and crop management challenges represent additional factors of vulnerability for agriculture in Romania and Europe (*Buzatu, Ghiuleanu, Mărcuță, et al., 2024; Ghiuleanu et al., 2023; Rossi et al., 2023*).

**Table 4**

**Production of major crop groups by county in the South-West Oltenia region in 2025**

| Crop group | Dolj | Gorj | Mehedinți | Olt | Vâlcea | Regional total |
|---|---|---|---|---|---|---|
| | U.M.: Metric tons | | | | | |
| Cereals for grain | 1,068,925 | 199,205 | 278,880 | 962,598 | 101,696 | 2,611,304 |
| Grain legumes | 13,893 | 128 | 3639 | 11,929 | 128 | 29,717 |
| Oilseeds | 159,255 | 438 | 38,714 | 169,578 | 7615 | 375,600 |
| Potatoes – total | 11,513 | 1132 | 5454 | 490 | 3915 | 22,504 |
| Vegetables – total | 98,256 | 23,263 | 24,845 | 81,899 | 28,181 | 256,444 |
| Green forage from arable land | 185,643 | 37,842 | 86,720 | 68,751 | 86,818 | 465,774 |

*(NIS, own calculations based on statistical data provided through TEMPO-Online, AGR109A)*

The regional distribution shown in Table 4 reveals a clear concentration of production in Dolj and Olt. Dolj ranks first in five of the six groups analyzed, with 1,068,925 metric tons of grains, 13,893 metric tons of legumes, and 185,643 metric tons of green forage. The county also leads in potato and vegetable production, even though the levels for these groups are much lower than in previous years.

Olt is close to Dolj in terms of grains and legumes and surpasses it in oilseeds, with a production of 169,578 metric tons. Mehedinți generally occupies an intermediate position, while Gorj and Vâlcea record lower volumes for most crops. However, these differences are not identical across all groups, suggesting the existence of distinct county-level agricultural profiles. Each county's actual contribution to the regional total is more clearly illustrated by the shares presented in the following table.

**Table 5**

**The counties' contribution to regional production of the main crop groups in 2025**

| Crop group | Dolj | Gorj | Mehedinți | Olt | Vâlcea | Regional total |
|---|---|---|---|---|---|---|
| | U.M.: % of regional production in 2025 | | | | | |
| Cereals for grain | **40.93%** | 7.63% | 10.68% | 36.86% | 3.89% | 100.00% |
| Grain legumes | **46.75%** | 0.43% | 12.25% | 40.14% | 0.43% | 100.00% |
| Oilseeds | 42.40% | 0.12% | 10.31% | **45.15%** | 2.03% | 100.00% |
| Potatoes – total | **51.16%** | 5.03% | 24.24% | 2.18% | 17.40% | 100.00% |
| Vegetables – total | **38.31%** | 9.07% | 9.69% | 31.94% | 10.99% | 100.00% |
| Green forage from arable land | **39.86%** | 8.12% | 18.62% | 14.76% | 18.64% | 100.00% |

*(NIS, own calculations based on statistical data provided through TEMPO-Online, AGR109A)*

The percentages in Table 5 confirm the central role of Dolj and Olt counties. Together, they account for 77.79% of the region's grain production, 86.89% of its legume production, 87.55% of its oilseed production, and 70.25% of its vegetable production. Dolj makes the largest contribution to five categories and accounts for more than half of the region's potato production, with a share of 51.16%. Olt ranks first in oilseeds, with 45.15%.

The distribution is more balanced for green forage, where Mehedinți and Vâlcea contribute nearly equal shares, at 18.62% and 18.64%, respectively. Mehedinți also plays an important role in potato production, accounting for 24.24% of the regional total. Therefore, although Dolj and Olt form the region's main productive core, the contributions of the other counties are significant for certain categories and complement Oltenia's agricultural profile. The concentration of productive functions in Dolj and Olt is consistent with the territorial

differences previously noted in the structure of agriculture in the South-West Oltenia region and with the important role of Olt County in regional agriculture (*Ursu and Cofas, 2016; Vânătoru (Rădulescu) et al., 2013b*).

**Table 6**

**Changes in the production of major crop groups by county in the South-West Oltenia region between 2016 and 2025**

| Crop group | Dolj | Gorj | Mehedinți | Olt | Vâlcea | South-West Oltenia region |
|---|---|---|---|---|---|---|
| | U.M.: % change between 2016 and 2025 | | | | | |
| Cereals for grain | -12.24% | -13.83% | -28.77% | **18.41%** | -50.46% | -8.66% |
| Grain legumes | 238.03% | -69.95% | -19.01% | **284.68%** | -24.26% | 141.62% |
| Oilseeds | -22.90% | **476.32%** | -47.70% | 22.38% | 382.88% | -10.74% |
| Potatoes – total | **-69.18%** | -97.05% | -69.84% | -97.21% | -88.08% | -84.40% |
| Vegetables – total | -56.39% | -58.69% | -59.98% | **-35.94%** | -50.67% | -51.49% |
| Green forage from arable land | -19.00% | -44.52% | **75.22%** | -58.75% | 3.61% | -22.03% |

*(NIS, own calculations based on statistical data provided through TEMPO-Online, AGR109A)*

Olt is the only county where grain production increased by 18.41%, while Vâlcea recorded the sharpest decline, at 50.46%. The regional expansion of legumes was driven almost exclusively by Olt and Dolj, where production rose by 284.68% and 238.03%, respectively. In the other three counties, this crop group declined.

The percentage increases in oilseed crops in Gorj and Vâlcea appear spectacular, but they start from very low initial levels and do not translate into dominant volumes at the regional level. The situation for potatoes and vegetables is much clearer: production declined in all five counties. For potatoes, the declines exceeded 97% in Gorj and Olt, while for vegetables, the smallest decline was also recorded in Olt, at 35.94%.

Green forage completes this contrasting picture. Mehedinți recorded a 75.22% increase, while Vâlcea remained relatively stable, with a 3.61% rise. In contrast, Olt lost 58.75% of its production. The results show that regional changes were not evenly distributed but altered the agricultural profile of each county differently.

The differences between counties should not be interpreted solely in terms of production volume, as research conducted in Olt County has also highlighted vulnerabilities associated with soil erosion and local climate change (*Nijloveanu et al., 2013; Vânătoru (Rădulescu) et al., 2013a*).

**Table 7**

**Trends in grain production and its main components in the South-West Oltenia region**

| Category | 2016 | 2017 | 2018 | 2019 | 2020 | 2021 | 2022 | 2023 | 2024 | 2025 |
|---|---|---|---|---|---|---|---|---|---|---|
| | U.M.: Metric tons | | | | | | | | | |
| Cereals for grain – total | 2,858,903 | 4,330,567 | 4,653,133 | 4,197,585 | 3,211,456 | 3,345,688 | 2,929,924 | 3,076,028 | 2,448,987 | 2,611,304 |
| Wheat – total | 1,325,051 | 1,916,770 | 1,944,697 | 1,937,152 | 1,462,325 | 1,868,870 | 1,597,982 | 1,712,787 | 1,618,126 | 1,804,921 |
| Barley, including two-row barley | 183,135 | 214,617 | 219,507 | 225,321 | 201,384 | 261,183 | 235,680 | 251,722 | 217,343 | 276,675 |
| Oats | 34,634 | 40,271 | 38,933 | 39,086 | 32,814 | 39,185 | 31,298 | 29,300 | 25,963 | 33,210 |
| Grain maize | 1,243,414 | 2,076,777 | 2,362,330 | 1,924,121 | 1,456,069 | 1,116,003 | 1,016,623 | 1,035,825 | 545,508 | 448,593 |
| Rye and other cereals* | 72,669 | 82,132 | 87,666 | 71,905 | 58,864 | 60,447 | 48,341 | 46,394 | 42,047 | 47,905 |

*(NIS, own calculations based on statistical data provided through TEMPO-Online, AGR109A)*

*Note: *The "Rye and other cereals" category was calculated as the difference between total grain production and the combined production of wheat, barley, including two-row barley, oats, and grain maize.*

The trends in the components presented in Table 7 show that the decline in total grain production masks a much more profound shift in its structure. In 2016, wheat and grain maize production were similar, at 1,325,051 and 1,243,414 metric tons, respectively. By 2025, wheat production had risen to 1,804,921 metric tons, while grain maize production had fallen to just 448,593 metric tons.

Thus, wheat production was approximately four times that of grain maize. Barley, including two-row barley, also showed a favorable trend, reaching its highest level for the period in 2025, at 276,675 metric tons. Oats remained a crop with a small and relatively stable contribution, while rye and other cereals saw a decline in production. Consequently, the transformation of the grain sector consists not only of a quantitative decline but, above all, of a clear shift in production from grain maize toward wheat and barley.

**Table 8**

**Changes in the structure of grain production in the South-West Oltenia region**

| Category | 2016 production | 2016 share | 2025 production | 2025 share | Production change | Change in share (p.p.) |
|---|---|---|---|---|---|---|
| | U.M.: Metric tons for production, % for shares and production change, and percentage points (p.p.) for changes in shares | | | | | |
| Wheat – total | 1,325,051 | 46.35% | 1,804,921 | 69.12% | 36.22% | 22.77 |
| Barley, including two-row barley | 183,135 | 6.41% | 276,675 | 10.60% | 51.08% | 4.19 |
| Oats | 34,634 | 1.21% | 33,210 | 1.27% | -4.11% | 0.06 |
| Grain maize | 1,243,414 | 43.49% | 448,593 | 17.18% | -63.92% | -26.31 |
| Rye and other cereals* | 72,669 | 2.54% | 47,905 | 1.83% | -34.08% | -0.71 |
| **Cereals for grain – total** | **2,858,903** | **100.00%** | **2,611,304** | **100.00%** | **-8.66%** | **0.00** |

*(NIS, own calculations based on statistical data provided through TEMPO-Online, AGR109A)*

*Note: *The category was determined by difference, according to the calculation presented in Table 7.*

The structural changes in Table 8 confirm the repositioning of the main cereal crops. The share of wheat increased from 46.35% in 2016 to 69.12% in 2025, representing a gain of 22.77 percentage points. Barley and two-row barley increased their combined share from 6.41% to 10.60%. Together, these two categories now account for 79.72% of regional cereal production, compared to 52.76% at the beginning of the period.

Conversely, grain maize lost 26.31 percentage points, and its share fell from 43.49% to 17.18%. Oats remained nearly unchanged in terms of share, while rye and other cereals fell to 1.83%. In just ten years, the grain structure thus shifted from a relative balance between wheat and grain maize to a clear dominance of wheat, supported by the expanding role of barley. Although the statistical data do not allow for the identification of a single cause for the decline in grain maize, research conducted in Dolj County highlights the influence of agricultural land and local conditions on the performance of this crop (*Ștefan et al., 2022*).

**Table 9**

**Trends in the production of grain legumes and oilseeds, as well as their main component crops, in the South-West Oltenia region**

| Category | 2016 | 2017 | 2018 | 2019 | 2020 | 2021 | 2022 | 2023 | 2024 | 2025 |
|---|---|---|---|---|---|---|---|---|---|---|
| | U.M.: Metric tons | | | | | | | | | |
| **Grain legumes – total** | **12,299** | **50,856** | **29,570** | **42,131** | **35,102** | **48,010** | **36,234** | **43,571** | **24,188** | **29,717** |
| Field peas | 8580 | 46,544 | 27,298 | 40,428 | 33,830 | 46,594 | 34,692 | 42,525 | 23,523 | 28,924 |
| Dry beans | 3323 | 2063 | 1899 | 1610 | 1272 | 1404 | 1126 | 1003 | 665 | 784 |
| **Oilseeds – total** | **420,806** | **634,417** | **581,620** | **705,900** | **440,798** | **666,268** | **518,376** | **577,527** | **315,500** | **375,600** |
| Sunflower | 300,572 | 466,272 | 434,747 | 629,879 | 366,882 | 536,720 | 393,375 | 379,491 | 198,931 | 192,328 |
| Rapeseed | 110,596 | 162,430 | 139,986 | 70,369 | 66,737 | 122,034 | 116,278 | 189,782 | 112,091 | 178,022 |
| Soybeans | 8610 | 5631 | 6800 | 4301 | 7074 | 5959 | 8379 | 6761 | 3400 | 2831 |

*(NIS, own calculations based on statistical data provided through TEMPO-Online, AGR109A)*

Within the legume crop group, field peas have become the mainstay of the group. Their production increased from 8580 metric tons in 2016 to 28,924 metric tons in 2025 and peaked at 46,594 metric tons in 2021. However, the trend has been volatile, alternating between years of growth and significant declines. Dry beans followed the opposite trajectory, declining almost continuously from 3323 to just 784 metric tons.

Oilseeds show an equally evident internal shift. Total production reached 705,900 metric tons in 2019, fell to 315,500 metric tons in 2024, and partially rebounded to 375,600 metric tons in 2025. Sunflower production ended the period at 192,328 metric tons, well below the 2016 level, while rapeseed production increased from 110,596 to 178,022 metric tons. Soybeans remained a crop with a small and declining contribution, reaching 2831 metric tons.

These two groups thus reflect similar patterns of internal substitution: field peas gained ground relative to dry beans, and rapeseed increasingly closed the gap with sunflowers. The extent of these changes becomes clearer when analyzing the shares in the following table.

**Table 10**

**Changes in the production structure of grain legumes and oilseeds in the South-West Oltenia region**

| Category | 2016 production | 2016 share | 2025 production | 2025 share | Production change | Change in share (p.p.) |
|---|---|---|---|---|---|---|
| | U.M.: Metric tons for production, % for shares and production change, and percentage points (p.p.) for changes in shares | | | | | |
| **Grain legumes – total** | **12,299** | **100.00%** | **29,717** | **100.00%** | **141.62%** | **0.00** |
| Field peas | 8580 | 69.76% | 28,924 | 97.33% | 237.11% | 27.57 |
| Dry beans | 3323 | 27.02% | 784 | 2.64% | -76.41% | -24.38 |
| **Oilseeds – total** | **420,806** | **100.00%** | **375,600** | **100.00%** | **-10.74%** | **0.00** |
| Sunflower | 300,572 | 71.43% | 192,328 | 51.21% | -36.01% | -20.22 |
| Rapeseed | 110,596 | 26.28% | 178,022 | 47.40% | 60.97% | 21.11 |
| Soybeans | 8610 | 2.05% | 2831 | 0.75% | -67.12% | -1.29 |

*(NIS, own calculations based on statistical data provided through TEMPO-Online, AGR109A)*

*Note: Any difference between the displayed component shares and 100.00% corresponds to the residual categories "Other legumes" and "Other oilseeds," which are not presented separately because of their low shares.*

Structural changes are particularly evident in the case of grain legumes. The share of field peas increased from 69.76% in 2016 to 97.33% in 2025, gaining 27.57 percentage points. At the same time, dry beans lost 24.38 percentage points and came to account for only 2.64% of the group's production. Other legumes have become nearly insignificant, accounting for only 0.03%. Consequently, the expansion of legumes has been accompanied by an almost complete concentration of production around field peas.

In the case of oilseeds, the shift led to a more balanced structure. Sunflowers reduced their share from 71.43% to 51.21%, losing 20.22 percentage points. Rapeseed followed the opposite trend, rising from 26.28% to 47.40% and gaining 21.11 percentage points. The gap between the two crops thus narrowed from 45.15 percentage points in 2016 to just 3.81 percentage points in 2025. Soybeans saw their share decline from 2.05% to 0.75%.

The results reveal two distinct shifts: legumes have become increasingly dependent on field peas, while oilseeds have transitioned from the clear dominance of sunflowers to a nearly balanced ratio between sunflowers and rapeseed. The growing role of rapeseed in the structure of oilseed crops is consistent with the trends identified for this crop at the national level, where cultivated area and production have undergone significant changes in recent years (*Cruceru and Ghiuleanu, 2024a*).

**Table 11**

**Trends in potato and vegetable production by major categories in the South-West Oltenia region**

| Category | 2016 | 2017 | 2018 | 2019 | 2020 | 2021 | 2022 | 2023 | 2024 | 2025 |
|---|---|---|---|---|---|---|---|---|---|---|
| | U.M.: Metric tons | | | | | | | | | |
| **Potatoes – total** | **144,216** | **192,441** | **185,297** | **156,190** | **82,619** | **47,536** | **40,104** | **15,526** | **12,610** | **22,504** |
| Early, mid-season, and summer potatoes | 67,444 | 75,606 | 78,822 | 72,862 | 45,169 | 9376 | 25,149 | 5428 | 5317 | 9561 |
| Fall potatoes | 76,772 | 116,835 | 106,475 | 83,328 | 37,450 | 38,160 | 14,955 | 10,098 | 7293 | 12,943 |
| **Vegetables – total** | **528,649** | **614,268** | **645,029** | **587,681** | **515,250** | **564,963** | **343,009** | **323,681** | **283,959** | **256,444** |
| Field-grown vegetables | 377,895 | 441,793 | 470,387 | 420,069 | 341,972 | 395,455 | 203,128 | 185,031 | 150,917 | 121,039 |
| Vegetables grown under | 20,424 | 24,270 | 27,691 | 23,583 | 25,193 | 25,120 | 21,734 | 25,205 | 23,307 | 27,537 |

| | | | | | | | | | | |
|---|---|---|---|---|---|---|---|---|---|---|
| protected cultivation | | | | | | | | | | |
| Fresh vegetables from home gardens | 130,330 | 148,205 | 146,951 | 144,029 | 148,085 | 144,388 | 118,147 | 113,445 | 109,735 | 107,868 |

*(NIS, own calculations based on statistical data provided through TEMPO-Online, AGR109A)*

Potato production has experienced one of the sharpest declines during the period under review. After peaking at 192,441 metric tons in 2017, total production fell rapidly, reaching just 12,610 metric tons in 2024. The rebound to 22,504 metric tons in 2025 represents an improvement over the previous year, but the level remains well below that at the beginning of the period. The decline affected early, mid-season, and summer potatoes as well as fall potatoes, indicating that the decline is not limited to a single category. An equally noticeable change is evident in vegetable production. The regional total fell from 528,649 metric tons in 2016 to 256,444 metric tons in 2025, the lowest level in the series. The main driver of this decline is open-field production, which fell from 377,895 to 121,039 metric tons. Vegetables grown in home gardens followed a less steep trajectory but still ended the period below the initial level. Vegetable production under protected cultivation represents a notable exception. It increased from 20,424 metric tons in 2016 to 27,537 metric tons in 2025 and remained relatively stable during the years when the other categories experienced significant volume losses.

Although it could not offset the decline in open-field production, its trend indicates a gradual shift in how regional vegetable production is achieved. This trend is also relevant in the context of analyses of production, prices, and prospects for Romania's tomato sector, for which protected cultivation may represent an important direction for development (*Cruceru and Ghiuleanu, 2024b*).

**Table 12**

**Trends in the production of green forage and major forage crops in the South-West Oltenia region**

| Category | 2016 | 2017 | 2018 | 2019 | 2020 | 2021 | 2022 | 2023 | 2024 | 2025 |
|---|---|---|---|---|---|---|---|---|---|---|
| | U.M.: Metric tons | | | | | | | | | |
| **Green forage from arable land – total** | **597,370** | **616,628** | **716,596** | **685,112** | **587,629** | **561,602** | **449,716** | **476,230** | **410,793** | **465,774** |
| Perennial forage | 521,611 | 530,612 | 599,019 | 587,885 | 488,229 | 504,715 | 396,043 | 408,101 | 350,416 | 398,410 |
| Alfalfa – green matter equivalent* | 402,607 | 401,403 | 453,582 | 470,416 | 372,210 | 376,876 | 297,652 | 316,941 | 259,664 | 302,412 |
| Clover – green matter equivalent* | 38,700 | 39,540 | 50,149 | 41,695 | 43,049 | 47,675 | 21,521 | 16,671 | 17,717 | 21,434 |
| Annual green forage | 75,759 | 86,016 | 117,577 | 97,227 | 99,400 | 56,887 | 53,673 | 68,129 | 60,377 | 67,364 |
| Forage maize** | 1068 | 1575 | 6241 | 9007 | 6836 | 12,784 | 8970 | 14,201 | 8227 | 9451 |
| Forage root crops*** | 6705 | 7011 | 13,168 | 17,004 | 11,524 | 11,309 | 56 | 60 | 60 | 741 |

*(NIS, own calculations based on statistical data provided through TEMPO-Online, AGR109A)*

*Note: *Alfalfa and clover are components of perennial forage crops. **Forage maize is included in the category of annual forage crops. ***Forage root crops are reported separately and are not included in the total forage crops on arable land.*

Green forage production on arable land peaked at 716,596 metric tons in 2018, after which it followed a predominantly downward trend. The lowest level, 410,793 metric tons, was recorded in 2024, and the rebound to 465,774 metric tons in 2025 recovered only a portion of the accumulated losses.

The group's performance was influenced in particular by perennial forages, which account for the largest share of total production and declined from 521,611 to 398,410 metric tons. Within the perennial forage category, alfalfa production fell from 402,607 to 302,412 metric tons, while clover production nearly halved, reaching 21,434 metric tons. Annual green forage crops experienced a less severe decline but ended the period at 67,364 metric tons, below the 2016 level.

Forage maize stands out with the highest percentage increase among the crops analyzed, with its production rising from 1068 to 9451 metric tons. However, its initially low production volume explains the magnitude of the percentage increase, and its share within the group remains modest. At the other end of the

spectrum, forage root crops declined from 6705 to just 741 metric tons, becoming a nearly marginal crop by the end of the period.

The decline in several forage components underscores the importance of sustainable land management and soil conservation measures for maintaining agriculture's productive capacity. In this regard, reducing the intensity of tillage, leaving crop residues on the surface, and practicing crop rotation are key strategies for protecting the soil and strengthening the resilience of agricultural systems (*Buzatu et al., 2023; Vlăduț et al., 2024*).

**Table 13**

**The most significant increases and decreases in crop production in the South-West Oltenia region**

| Type of change | Crop or category | 2016 production | 2025 production | Absolute change | 2016–2025 change |
|---|---|---|---|---|---|
| | U.M.: Metric tons for production and absolute change, and % for the 2016–2025 change | | | | |
| Increase | Forage maize | 1068 | 9451 | 8383 | 784.93% |
| | Field peas | 8580 | 28,924 | 20,344 | 237.11% |
| | Rapeseed | 110,596 | 178,022 | 67,426 | 60.97% |
| | Barley, including two-row barley | 183,135 | 276,675 | 93,540 | 51.08% |
| | Wheat – total | 1,325,051 | 1,804,921 | 479,870 | 36.22% |
| | Vegetables grown under protected cultivation | 20,424 | 27,537 | 7113 | 34.83% |
| Decrease | Forage root crops | 6705 | 741 | -5964 | -88.95% |
| | Potatoes – total | 144,216 | 22,504 | -121,712 | -84.40% |
| | Dry beans | 3323 | 784 | -2539 | -76.41% |
| | Field-grown vegetables | 377,895 | 121,039 | -256,856 | -67.97% |
| | Soybeans | 8610 | 2831 | -5779 | -67.12% |
| | Grain maize | 1,243,414 | 448,593 | -794,821 | -63.92% |

*(NIS, own calculations based on statistical data provided through TEMPO-Online, AGR109A)*

*Note: Residual categories calculated by difference were excluded from the ranking.*

The summary in Table 13 shows that the percentage change does not always reflect its impact on regional production. Forage maize recorded the largest percentage increase, at 784.93%, but the absolute gain was only 8383 metric tons, because the initial level was very low. In contrast, the 36.22% increase in wheat translated to an additional 479,870 metric tons, the largest increase in absolute terms. Field peas, rapeseed, barley, and vegetables grown under protected cultivation also recorded favorable trends. Among the crops that saw declines, forage roots recorded the sharpest percentage drop, at 88.95%, followed by potatoes, at 84.40%, and dry beans, at 76.41%.

However, the greatest quantitative impact was on grain maize, whose production fell by 794,821 metric tons. Significant losses were also recorded for field-grown vegetables, down by 256,856 metric tons, and potatoes, down by 121,712 metric tons.

Taken together, these trends reflect a selective restructuring rather than a simple across-the-board reduction in production. Wheat, barley, rapeseed, field peas, and vegetable production under protected cultivation gained ground, while grain maize, potatoes, field vegetables, and several low-volume crops declined sharply. This contrast defines the transformation of regional agriculture during the period under review.

**S.W.O.T. analysis**

The S.W.O.T. analysis highlights a region that retains a strong agricultural base, but whose structure is becoming more concentrated and uneven. Favorable trends in wheat, rapeseed, field peas, and vegetable production under protected cultivation offer real avenues for development, but these do not yet offset the losses incurred by grain maize, potatoes, and field-grown vegetables. The main challenge is not only to recover lost production volumes but also to maintain an agricultural structure that is sufficiently diversified and stable.

The identified directions are consistent with approaches that place sustainability, cooperation, and shared responsibility at the center of agricultural development, as well as with the strategic objectives of the Common Agricultural Policy regarding the modernization and increased resilience of the sector (*Buzatu, Ghiuleanu, Tudor, et al., 2024; European Commission, 2026*).

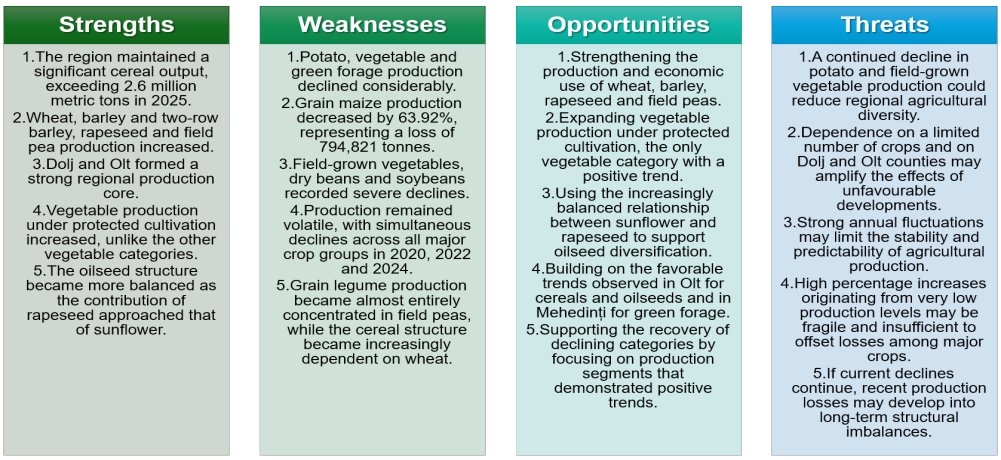



**Fig. 1 - Illustrative SmartArt diagram showing a S.W.O.T. analysis of trends in agricultural production in the South-West Oltenia region, based on results from 2016–2025**

*(Authors' own elaboration)*

Taken as a whole, the results do not merely reflect a decline in agricultural production, but rather a selective restructuring of it. The increase in the production of wheat, barley, rapeseed, field peas, and vegetables grown under protected cultivation contrasts with the strong decline in grain maize, potatoes, field vegetables, and certain forage crops. At the same time, Dolj and Olt have consolidated their position as the region's main productive hubs. The region continues to have a significant agricultural base, but its development is marked by volatility, territorial concentration, and dependence on a limited number of crops. Capitalizing on expanding sectors, maintaining productive diversity, and reducing identified imbalances are the main directions identified in the results for the 2016–2025 period.

## CONCLUSIONS

An analysis of the 2016–2025 period highlights a selective restructuring of agricultural production in the South-West Oltenia region. The 8.66% decline in cereal production masks a profound structural shift: wheat and barley production increased, while grain maize production fell by 63.92%. Grain legumes recorded the most favorable trend among the groups analyzed, driven mainly by increased pea production, and among oilseeds, the share of rapeseed has come considerably closer to that of sunflowers. The most vulnerable segments were potatoes, vegetable production (particularly open-field production), and certain forage crops. The 84.40% decline in potato production and the 51.49% reduction in total vegetable production indicate a significant loss of productive diversity. However, the positive trend in vegetables grown under protected cultivation is a favorable sign and may indicate gradual adaptation within the vegetable sector. From a geographical perspective, Dolj and Olt counties form the region's main agricultural hub, accounting for the bulk of production in the major crop groups.

This concentration shapes regional performance but also highlights dependence on a limited number of counties and crops. Consequently, the future development of regional agriculture should combine capitalizing on expanding segments with restoring productive diversity and reducing annual fluctuations. The competitiveness of the South-West Oltenia region will depend not only on the quantity produced but also on the ability of its agriculture to become more balanced and resilient.

## REFERENCES

[1] Buzatu, C. S., Ghiuleanu, I. V., Tudor, V. C. (2023). *Dynamics of land fund and strategies on soil conservation and prevention of soil degradation in Romania*. *Scientific Papers Series "Management, Economic Engineering in Agriculture and Rural Development"*, 23(4), 149–156. https://managementjournal.usamv.ro/pdf/vol.23_4/Art14.pdf. Accessed February 11, 2026.

[2] Buzatu, C. S., Ghiuleanu, I. V., Mărcuță, A. G., Popa, I. V. (2024). *Climate change and land temperatures and their impact on agriculture and society: A global investigation*. *Scientific Papers Series "Management, Economic Engineering in Agriculture and Rural Development"*, 24(4), 121–130. https://managementjournal.usamv.ro/pdf/vol.24_4/Art12.pdf. Accessed February 17, 2026.

[3] Buzatu, C. S., Ghiuleanu, I. V., Tudor, V. C., Oltenacu, N., Vlad, G. (2024). *Sustainability in agricultural work – our shared responsibility*. *Scientific Papers Series "Management, Economic*

*Engineering in Agriculture and Rural Development"*, 24(1), 147–156. https://managementjournal.usamv.ro/pdf/vol.24_1/Art14.pdf. Accessed September 5, 2026.

[4] Cruceru, C., Ghiuleanu, I. V. (2024a). *The area under oilseed rape in Romania: Evolution and trends*. In *Proceedings of the International Symposium ISB-INMA-TEH: Agricultural and Mechanical Engineering* (pp. 486–501). https://isbinmateh.inma.ro/wp-content/uploads/2025/11/Vol-ISB-INMA-TEH-2024.pdf. Accessed March 6, 2026.

[5] Cruceru, C., Ghiuleanu, I. V. (2024b). *Tomatoes in figures: Production, prices and outlook for the future*. In *Proceedings of the International Symposium ISB-INMA-TEH: Agricultural and Mechanical Engineering* (pp. 502–511). https://isbinmateh.inma.ro/wp-content/uploads/2025/11/Vol-ISB-INMA-TEH-2024.pdf. Accessed September 5, 2026.

[6] European Commission. (2026). Romania – *CAP Strategic Plan*. https://agriculture.ec.europa.eu/cap-my-country/cap-strategic-plans/romania_en. Accessed July 22, 2026.

[7] Eurostat. (2025). *Agricultural production – crops*. https://ec.europa.eu/eurostat/statistics-explained/index.php?title=Agricultural_production_-_crops. Accessed July 20, 2026.

[8] Ghiuleanu, I. V., Buzatu, C. S., Tudor, V. C., Panait, R., (Carbarău) Smedescu, C. A. (2023). *Risks analyses and challenges in crop management in Romania*. *Scientific Papers Series "Management, Economic Engineering in Agriculture and Rural Development"*, 23(4), 353–364. https://managementjournal.usamv.ro/pdf/vol.23_4/Art34.pdf. Accessed January 15, 2026.

[9] National Institute of Statistics [NIS]. (2025). *Producția vegetală la principalele culturi în anul 2024*. https://insse.ro/cms/ro/content/produc%C8%9Bia-vegetal%C4%83-la-principalele-culturi-%C3%AEn-anul-2024. Accessed March 9, 2026.

[10] National Institute of Statistics [NIS]. (2026). *TEMPO-Online database: Crop production for major crops, by type of ownership, macroregions, development regions and counties* (AGR109A; data for 2016–2025). http://statistici.insse.ro:8077/tempo-online/#/pages/tables/insse-table. Accessed August 17, 2026.

[11] Nijloveanu, D., Bozga, I., Tita, V., Vânătoru (Rădulescu), D. L. (2013). *Soil degradation in Olt County by the process of hydric erosion*. *Annals of the University of Craiova – Agriculture, Montanology, Cadastre Series, 43*(1), 243–246. https://anale.agro-craiova.ro/index.php/aamc/article/view/46/46. Accessed March 23, 2026.

[12] Rossi, L., Wens, M., De Moel, H., Cotti, D., Sabino Siemons, A.-S., Toreti, A., Maetens, W., Masante, D., Van Loon, A., Hagenlocher, M., Rudari, R., Meroni, M., Isabellon, M., Avanzi, F., Naumann, G., Barbosa, P. (2023). *European Drought Risk Atlas* (EUR 31682 EN, JRC135215). Publications Office of the European Union. https://doi.org/10.2760/608737. Accessed March 22, 2026.

[13] Ștefan, I.-O., Tița, V., Nijloveanu, D., Bold, N. (2022). *Research on the behavior of corn cultivated on a chernozem type soil from Boureni–Băilești area, Dolj County, Romania, depending on agrofund*. Scientific *Papers Series "Management, Economic Engineering in Agriculture and Rural Development"*, 22(2), 655–658. https://managementjournal.usamv.ro/pdf/vol.22_2/Art77.pdf. Accessed February 16, 2026.

[14] Ursu, A., Cofas, E. (2016). *The territorial analysis of agricultural production structure. Case study: Region South-West Oltenia*. *Scientific Papers Series "Management, Economic Engineering in Agriculture and Rural Development"*, 16(1), 535–542. https://managementjournal.usamv.ro/pdf/vol.16_1/Art84.pdf. Accessed January 6, 2026.

[15] Vânătoru (Rădulescu), D. L., Bozga, I., Nijloveanu, D., Tita, V. (2013a). *Climate change and its effects on culture in microregion Caracal–Olt*. *Annals of the University of Craiova – Agriculture, Montanology, Cadastre Series, 43(2)*, 237–240. https://anale.agro-craiova.ro/index.php/aamc/article/view/98/93. Accessed September 5, 2026.

[16] Vânătoru (Rădulescu), D. L., Bozga, I., Nijloveanu, D., Tita, V. (2013b). *Studies on the development of agriculture in Olt County*. *Annals of the University of Craiova – Agriculture, Montanology, Cadastre Series, 43(2)*, 231–236. https://anale.agro-craiova.ro/index.php/aamc/article/view/97/92. Accessed January 11, 2026.

[17] Vlăduț, N.-V., Atanasov, A., Ungureanu, N., Ivașcu, L.-V., Cioca, L.-I., Popa, L.-D., Matei, G., Boruz, S., Cerempei, V., Țîței, V., Nenciu, F., Milea, O.-E., Dumitru, Ș., Caba, I. (2024). *Trends in the development of conservation / ecological agriculture in the context of current climate change – A review. INMATEH – Agricultural Engineering*, 74(3), 980–1032. https://doi.org/10.35633/inmateh-74-86. Accessed September 15, 2026.

# LOCAL STRENGTHS, REGIONAL VULNERABILITIES: CROP YIELD DYNAMICS IN SOUTH-WEST OLTENIA, ROMANIA (2016–2025)

/

# *AVANTAJE LOCALE, VULNERABILITĂȚI REGIONALE: DINAMICA RANDAMENTELOR CULTURILOR ÎN REGIUNEA SUD-VEST OLTENIA, ROMÂNIA (2016–2025)*

**Corina CRUCERU[1)], Iulian Virgil GHIULEANU*[2)], Daniel NIJLOVEANU[1)], Oana-Elena MILEA[3)]**
[1)] USAMV Bucharest, Faculty of Management and Rural Development, Slatina Branch, Olt County / Romania;
[2)] University of Agronomic Sciences and Veterinary Medicine Bucharest (Doctoral student, Doctoral School: Plant and Animal Resources Engineering and Management), 59 Marasti Boulevard, District 1, 011464, Bucharest / Romania;
[3)] National University of Science and Technology POLITEHNICA Bucharest / Romania.
**E-mail: vghiuleanu@yahoo.com*

***Keywords:*** *crop yields, temporal dynamics, territorial disparities, regional agriculture, South-West Oltenia.*

## ABSTRACT

*This study examines the evolution of average crop yields per hectare in South-West Oltenia, Romania, during 2016–2025, using official data provided by the National Institute of Statistics through TEMPO-Online, AGR110A. The research combines temporal comparisons, multiyear averages, annual variation analysis and county-level comparisons for Dolj, Gorj, Mehedinți, Olt and Vâlcea, followed by a S.W.O.T. synthesis. The results reveal no uniform improvement in regional agricultural performance. The average yield of cereals for grain increased by only 1.46%, concealing a 25.04% rise in wheat and a 43.34% decline in grain maize. Sunflower and perennial forage yields also decreased considerably, by 32.90% and 29.63%, respectively. Across the nine representative categories, 45 annual declines were recorded compared with 36 increases, while six categories reached their minimum yield in 2024. Territorial differences were substantial: Olt displayed the most favourable comparative profile, although no county recorded a positive unweighted mean change across the analysed crops. The largest relative county gap, of 224.35%, was recorded for grain maize. The findings indicate selective and territorially fragmented agricultural performance, supporting the need for crop- and county-specific measures aimed at stabilising yields and adapting successful local practices.*

## REZUMAT

*Studiul analizează evoluția producției medii la hectar în Regiunea Sud-Vest Oltenia, în perioada 2016–2025, pe baza datelor oficiale furnizate de Institutul Național de Statistică prin TEMPO-Online, AGR110A. Cercetarea combină comparațiile temporale, mediile multianuale, analiza variațiilor anuale și comparațiile teritoriale pentru județele Dolj, Gorj, Mehedinți, Olt și Vâlcea, completate printr-o sinteză S.W.O.T. Rezultatele nu indică o îmbunătățire uniformă a performanței agricole regionale. Producția medie la hectar a cerealelor pentru boabe a crescut cu numai 1.46%, această evoluție ascunzând avansul grâului cu 25.04% și declinul porumbului boabe cu 43.34%. Scăderi importante au fost înregistrate și la floarea-soarelui, cu 32.90%, și la furajele perene, cu 29.63%. Pentru cele nouă categorii reprezentative au fost identificate 45 de scăderi anuale, față de 36 de creșteri, iar șase categorii au atins valoarea minimă în anul 2024. Diferențele teritoriale au fost considerabile: județul Olt a prezentat cel mai favorabil profil comparativ, deși niciun județ nu a obținut o evoluție medie neponderată pozitivă pentru toate culturile analizate. Cel mai mare decalaj relativ între județe, de 224.35%, a fost înregistrat la porumbul boabe. Rezultatele evidențiază o performanță agricolă selectivă și fragmentată teritorial, susținând necesitatea unor măsuri diferențiate pe culturi și județe, orientate spre stabilizarea randamentelor și adaptarea practicilor locale favorabile.*

## INTRODUCTION

Total production indicates the size of a harvest, but average yield per hectare provides a clearer picture of how efficiently agricultural land is used. The evolution of this indicator reflects the interaction among climatic conditions, soil quality, applied technologies, and management decisions. For this reason, yield analysis can reveal both the crops that are strengthening their performance and the sectors in which

favourable results occur only temporarily. Managing these differences is becoming increasingly important in a sector simultaneously exposed to climatic, technological, and economic risks (*Ghiuleanu et al., 2023*).

At the European level, variations in temperature and precipitation have increased the instability of crop production. The unusually warm and dry conditions recorded in Romania in the spring of 2024 illustrate the pressure exerted by climatic phenomena on agricultural crops (*Eurostat, 2025*). The European Drought Risk Atlas identifies Romania as one of the European countries facing a high risk of drought-related yield reductions, particularly for maize (*Rossi et al., 2023*). National analyses confirm the sensitivity of this crop and associate the severe droughts of 2020, 2022, and 2024 with lower yields and widening regional disparities (*Barna and Mănescu, 2025*). At the same time, changing temperatures require adaptation measures tailored to the specific characteristics of each agricultural area (*Buzatu et al., 2024a*).

The South-West Oltenia region provides a suitable setting for such an analysis because its five constituent counties differ in terms of natural conditions and agricultural profiles. Previous research has highlighted the importance of cereals and oilseed crops within the regional agricultural structure, as well as the territorial differentiation of resources and productive activities (*Ursu and Cofas, 2016*). In the Oltenia Plain, significant relationships have been identified between drought and the yields of wheat, maize, and sunflower, particularly in the period after 1990 (*Onțel and Vlăduț, 2015*). Climatic vulnerability has also been reported in the Caracal–Olt microregion, where the frequency and intensity of drought episodes affect agricultural stability (*Vânătoru (Rădulescu) et al., 2013a*).

Crop responses to these conditions are not uniform. Research on wheat in southern Romania has identified an association between water stress and yield levels, as well as the influence of phytosanitary factors that can limit performance even in years with better water availability (*Berca and Horoiaș, 2022*). For maize, trials conducted in the Boureni–Băilești area have shown that average yield per hectare can vary considerably depending on climatic conditions and fertilisation levels (*Ștefan et al., 2022*). These findings indicate that statistical fluctuations should not automatically be attributed to a single cause.

Important patterns also emerge in the case of oilseed and vegetable crops. Studies of rapeseed have highlighted fluctuations in cultivated area, production, and yields in Romania, the South-West Oltenia region, and Olt County, as well as the need to manage climatic and economic risks (*Cruceru and Ghiuleanu, 2024a*). In the case of tomatoes, variations in yields and production have been associated with the need to modernise infrastructure, improve irrigation systems, and adopt technologies capable of stabilising results (*Cruceru and Ghiuleanu, 2024b*). Therefore, a favourable regional value may conceal both differences among crops and important contrasts among counties.

In this context, agricultural policies are placing increasing emphasis on farm resilience, efficient resource use, and improved competitiveness. Romania's CAP Strategic Plan aims to develop a sustainable and economically viable agricultural sector while reducing disparities among farms and territories (*European Commission, 2026*). However, supporting these interventions requires up-to-date analyses capable of identifying not only the general direction of regional agriculture but also the crops and counties where the most important improvements or vulnerabilities occur.

The aim of this research is to assess the dynamics and territorial distribution of average yields per hectare in the South-West Oltenia region during the 2016–2025 period, based on data provided by the National Institute of Statistics through TEMPO-Online, series AGR110A (*NIS, 2026*). The analysis examines year-on-year changes, minimum and maximum values, the frequency of increases and decreases, differences among counties, and the gap between recent yields and the maximum performance recorded during the period. Through this approach, the research seeks to distinguish genuine stability from apparent equilibrium and to identify the county–crop combinations that can support the strengthening of regional agriculture.

## MATERIALS AND METHODS

The research was based on official statistical data obtained from the National Institute of Statistics' TEMPO-Online database, series AGR110A – *"Average production per hectare for the main crops, by form of ownership, macroregions, development regions and counties"* (*NIS, 2026*). The *"Total"* form of ownership was selected, and the data, expressed in kg/ha, cover the 2016–2025 period. The analysis focused on the South-West Oltenia region and its five constituent counties: Dolj, Gorj, Mehedinți, Olt, and Vâlcea.

The statistical series were organised and processed using Microsoft Excel 365. Nine representative crops and categories were selected for the general analysis: cereals for grain, wheat, grain maize, field peas, sunflower, rapeseed, potatoes, tomatoes, and perennial forage. The research was supplemented by a

detailed analysis of the main cereal, protein, oilseed, vegetable, and forage crops. The selection was based on the continuity of the statistical series, economic relevance, and the possibility of making territorial comparisons. The time-series analysis included the absolute and percentage changes between 2016 and 2025, the arithmetic mean of the ten annual values, the minimum and maximum values, and the years in which they were recorded. To capture instability, the number of years with increases and decreases, the largest annual increase, the sharpest annual decline, and the range between the minimum and maximum values were determined. The relative range was calculated by dividing this difference by the average value for the period.

To ensure a consistent interpretation of the changes, variations between −5.00% and +5.00% were considered relatively stable. Increases greater than 5.00% but not exceeding 20.00% were classified as *"Moderate increase"*, while those exceeding 20.00% were classified as *"Strong increase"*. Declines greater than 5.00% but not exceeding 20.00% were classified as *"Moderate decline"*, while those exceeding 20.00% were classified as *"Strong decline"*. The territorial analysis compared county-level yields with the regional level in 2025 and examined their changes relative to 2016. The counties with the maximum and minimum values, the absolute and relative gaps, the number of counties above the regional level, and the leading counties for each crop were identified. The relative gap was calculated by dividing the difference between the maximum and minimum values by the minimum value. Regional values were obtained directly from the NIS database and were not calculated as arithmetic means of county-level values.

For potatoes and vegetable crops, the gap between the 2025 yield and the maximum value recorded during the period was determined, while for forage crops, the averages for the 2016–2020 and 2021–2025 periods were compared. Each county's profile was summarized using the number of crops with positive or negative changes, the number of yields above the regional level, and the unweighted arithmetic mean of the changes recorded by the nine representative crops. Unavailable values were marked as "n.d." and were excluded only from calculations requiring the 2016 value, without being replaced by estimates. Percentages were rounded to two decimal places, while values expressed in kg/ha were presented without decimals. In the final stage, the time-series and territorial results were synthesized through a S.W.O.T. analysis based exclusively on the statistical findings. The method was descriptive and comparative and did not attribute the identified changes to a single causal factor. All calculations were performed using unrounded values; rounding was applied only to the results presented in the tables.

## RESULTS

The analysis of average yields per hectare during the 2016–2025 period reveals a regional agricultural sector characterised by a continuous alternation between growth and decline. The changes do not follow a common direction: some crops improved their yields, while others ended the period well below the maximum levels previously recorded. This time-series perspective makes it possible to identify both crops with stable performance and those exposed to substantial fluctuations.

The empirical basis of the analysis consists of the AGR110A series from TEMPO-Online, processed for the South-West Oltenia region and its five constituent counties (*NIS, 2026*).

**Table 1**

**Trends in average yield per hectare for representative crops in the South-West Oltenia region**

| Crop or category | 2016 | 2017 | 2018 | 2019 | 2020 | 2021 | 2022 | 2023 | 2024 | 2025 |
|---|---|---|---|---|---|---|---|---|---|---|
| | U.M.: kg/ha | | | | | | | | | |
| Cereals for grain | 3346 | 5305 | 5659 | 5037 | 3833 | 4287 | 3849 | 4047 | 3244 | 3395 |
| Wheat – total | 3315 | 4735 | 4717 | 4748 | 3496 | 4634 | 3965 | 4065 | 3923 | 4145 |
| Grain maize | 3433 | 6410 | 7354 | 5707 | 4395 | 3982 | 3790 | 4273 | 2164 | 1945 |
| Field peas | 1795 | 2553 | 1235 | 2155 | 1421 | 2484 | 1892 | 1874 | 1123 | 1555 |
| Sunflower | 1617 | 3155 | 3046 | 3024 | 2045 | 2477 | 2044 | 1984 | 786 | 1085 |
| Rapeseed | 2685 | 2717 | 2206 | 2153 | 2502 | 3048 | 2625 | 2826 | 2045 | 2473 |
| Potatoes – total | 12,263 | 16,363 | 15,150 | 12,758 | 11,803 | 15,770 | 13,518 | 8772 | 7616 | 10,085 |
| Tomatoes | 13,655 | 16,547 | 18,198 | 17,452 | 22,560 | 25,497 | 15,981 | 15,620 | 14,091 | 13,866 |
| Perennial forage | 12,644 | 13,490 | 14,759 | 14,146 | 11,412 | 11,517 | 10,217 | 9542 | 8459 | 8897 |

*(NIS, statistical data provided through TEMPO-Online, AGR110A)*

The data in Table 1 reveal strongly contrasting trends. The average yield of cereals for grain increased from 3346 kg/ha in 2016 to a maximum of 5659 kg/ha in 2018, but subsequently fell to only 3395 kg/ha in 2025.

Within this category, wheat ended the period at 4145 kg/ha, above its initial level, while grain maize declined sharply from a maximum of 7354 kg/ha in 2018 to 1945 kg/ha in 2025.

An unfavourable trend can also be observed for sunflower, whose yield decreased to 1085 kg/ha in 2025 after reaching 3155 kg/ha in 2017. Potatoes and tomatoes recorded the highest absolute values, but also considerable fluctuations. Tomato yield increased to 25,497 kg/ha in 2021 before falling to 13,866 kg/ha in 2025. In the case of potatoes, the minimum recorded in 2024 was followed by a recovery to 10,085 kg/ha.

The overall picture is completed by perennial forage, whose yield declined from 12,644 kg/ha in 2016 to 8897 kg/ha in 2025. Therefore, the similar values recorded by some crops at the beginning and end of the period should not be mistaken for stability, as substantial fluctuations occurred between these years.

**Table 2**

**Summary indicators of average yield trends for representative crops in the South-West Oltenia region**

| Crop or category | 2016 | 2025 | Absolute change | Change 2016–2025 | Period average | Minimum value | Year of minimum | Maximum value | Year of maximum | Classification |
|---|---|---|---|---|---|---|---|---|---|---|
| | U.M.: kg/ha, except for percentage change, years, and classification | | | | | | | | | |
| Cereals for grain | 3346 | 3395 | 49 | 1.46% | 4200 | 3244 | 2024 | 5659 | 2018 | Relatively stable |
| Wheat – total | 3315 | 4145 | 830 | 25.04% | 4174 | 3315 | 2016 | 4748 | 2019 | Strong increase |
| Grain maize | 3433 | 1945 | -1488 | -43.34% | 4345 | 1945 | 2025 | 7354 | 2018 | Strong decline |
| Field peas | 1795 | 1555 | -240 | -13.37% | 1809 | 1123 | 2024 | 2553 | 2017 | Moderate decline |
| Sunflower | 1617 | 1085 | -532 | -32.90% | 2126 | 786 | 2024 | 3155 | 2017 | Strong decline |
| Rapeseed | 2685 | 2473 | -212 | -7.90% | 2528 | 2045 | 2024 | 3048 | 2021 | Moderate decline |
| Potatoes – total | 12,263 | 10,085 | -2178 | -17.76% | 12,410 | 7616 | 2024 | 16,363 | 2017 | Moderate decline |
| Tomatoes | 13,655 | 13,866 | 211 | 1.55% | 17,347 | 13,655 | 2016 | 25,497 | 2021 | Relatively stable |
| Perennial forage | 12,644 | 8897 | -3747 | -29.63% | 11,508 | 8459 | 2024 | 14,759 | 2018 | Strong decline |

*(Authors' calculations based on NIS statistical data provided through TEMPO-Online, AGR110A)*

The summary indicators in Table 2 confirm that favourable developments were the exception rather than the rule. Wheat was the only crop classified as recording a *"Strong increase"*, with a 25.04% rise compared with 2016. Cereals for grain and tomatoes remained relatively stable, with changes of only 1.46% and 1.55%, respectively, between the first and last years of the period.

At the opposite end of the spectrum, grain maize recorded a decline of 43.34%, followed by sunflower, at 32.90%, and perennial forage, at 29.63%. The situation of grain maize is particularly relevant because its 2025 yield of 1945 kg/ha was also the minimum value for the entire period and remained far below the multiyear average of 4345 kg/ha.

The year 2024 represents a critical point for six of the nine categories analysed, as the minimum values for cereals, field peas, sunflower, rapeseed, potatoes, and perennial forage were recorded in that year. The recovery observed for some of these crops in 2025 was insufficient to offset the accumulated losses. Overall, the classification reveals a structure dominated by moderate or strong declines, while examples of sustained growth remain limited.

Without confusing yield with total production, the concentration of minimum values in 2024 occurred within a difficult agricultural context for Romania, also characterised by unusually warm and dry conditions during the spring (*Eurostat, 2025; NIS, 2025*).

The continued decline in grain maize in 2025 followed a period in which the severe droughts of 2020, 2022, and 2024 were associated nationally with lower yields for this crop (*Barna and Mănescu, 2025*).

**Table 3**

**Frequency and intensity of variations in average yield per hectare for representative crops in the South-West Oltenia region, 2016–2025**

| Crop or category | Years with increases | Years with decreases | Largest annual increase | Interval | Largest annual decline | Interval | Min–max range (kg/ha) | Range relative to the period average (%) |
|---|---|---|---|---|---|---|---|---|
| | U.M.: Number of years, kg/ha, and %, depending on the indicator | | | | | | | |
| Cereals for grain | 5 | 4 | 58.55% | 2016–2017 | -23.90% | 2019–2020 | 2415 | 57.50% |
| Wheat – total | 5 | 4 | 42.84% | 2016–2017 | -26.37% | 2019–2020 | 1433 | 34.33% |
| Grain maize | 3 | 6 | 86.72% | 2016–2017 | -49.36% | 2023–2024 | 5409 | 124.48% |
| Field peas | 4 | 5 | 74.81% | 2020–2021 | -51.63% | 2017–2018 | 1430 | 79.06% |
| Sunflower | 3 | 6 | 95.11% | 2016–2017 | -60.38% | 2023–2024 | 2369 | 111.41% |
| Rapeseed | 5 | 4 | 21.82% | 2020–2021 | -27.64% | 2023–2024 | 1003 | 39.68% |
| Potatoes – total | 3 | 6 | 33.61% | 2020–2021 | -35.11% | 2022–2023 | 8747 | 70.48% |
| Tomatoes | 4 | 5 | 29.27% | 2019–2020 | -37.32% | 2021–2022 | 11,842 | 68.27% |
| Perennial forage | 4 | 5 | 9.41% | 2017–2018 | -19.33% | 2019–2020 | 6300 | 54.74% |

*(Authors' calculations based on NIS statistical data provided through TEMPO-Online, AGR110A)*

*Note: The range relative to the period average represents the difference between the maximum and minimum values, expressed as a percentage of the period average.*

Table 3 shows that instability was reflected not only in the difference between 2016 and 2025 but also in pronounced year-to-year fluctuations. Of the 81 transitions analysed for the nine categories, 36 represented increases and 45 represented decreases, confirming the predominance of years with unfavourable developments.

Grain maize and sunflower stand out for their particularly high volatility. Both recorded only three years of increase and six years of decline, while the range relative to the period average reached 124.48% for grain maize and 111.41% for sunflower. Their largest annual increases, of 86.72% and 95.11%, respectively, were followed by sharp declines, indicating that isolated favourable results were unable to support a consistent trend.

Wheat and rapeseed displayed more balanced profiles, each recording five increases and four decreases. Wheat also recorded the lowest relative range, at 34.33%, followed by rapeseed, at 39.68%. In contrast, tomatoes recorded the largest absolute difference between the minimum and maximum values, at 11,842 kg/ha.

The results therefore highlight two distinct dimensions of risk: the frequency of declines and the intensity of variations, which are not always concentrated in the same crops. The volatility of grain maize and sunflower is consistent with research conducted in the Oltenia Plain, which identified significant relationships between drought years and the yields of the main crops (*Onțel and Vlăduț, 2015*). An increase in the frequency and intensity of droughts has also been reported for the Caracal–Olt microregion (*Vânătoru (Rădulescu) et al., 2013a*). Nevertheless, the more balanced profile of wheat should be interpreted cautiously, as water stress and phytosanitary factors can substantially affect yield from one year to another (*Berca and Horoiaș, 2022*).

**Table 4**

**Average yield per hectare for representative crops by county and in the South-West Oltenia region, 2025**

| Crop or category | Dolj | Gorj | Mehedinți | Olt | Vâlcea | South-West Oltenia region |
|---|---|---|---|---|---|---|
| | U.M.: kg/ha | | | | | |
| Cereals for grain | 3280 | 3261 | 2502 | **4143** | 2657 | 3395 |
| Wheat – total | 3805 | 3804 | 3284 | **4906** | 4681 | 4145 |
| Grain maize | 1898 | **3130** | 965 | 1579 | 2053 | 1945 |
| Field peas | 1455 | 1108 | 1454 | **1741** | 848 | 1555 |
| Sunflower | 1022 | 910 | 845 | 1254 | **1278** | 1085 |

| | | | | | | |
|---|---|---|---|---|---|---|
| Rapeseed | 2203 | 3405 | 2216 | 2750 | **3416** | 2473 |
| Potatoes – total | **12,966** | 8898 | 9760 | 7986 | 6527 | 10,085 |
| Tomatoes | 13,371 | 15,890 | 10,225 | **16,574** | 10,275 | 13,866 |
| Perennial forage | 8050 | 10,116 | **12,344** | 8237 | 8492 | 8897 |

*(NIS, statistical data provided through TEMPO-Online, AGR110A)*

The territorial distribution of yields in 2025 shows that regional agricultural performance is not concentrated in a single county. Olt nevertheless occupies the most favourable position, recording the highest values for cereals for grain → 4143 kg/ha, wheat → 4906 kg/ha, field peas → 1741 kg/ha, and tomatoes → 16,574 kg/ha.

The other counties stand out through specific advantages. Vâlcea leads in sunflower and rapeseed, with 1278 kg/ha and 3416 kg/ha, respectively; Gorj records the best result for grain maize, at 3130 kg/ha; while Dolj stands out for potatoes, with 12,966 kg/ha.

Mehedinți ranks first for perennial forage, with a yield of 12,344 kg/ha. Comparison with the regional level completes this picture: Olt exceeds the South-West Oltenia region value in six of the nine categories, while Gorj and Vâlcea exceed it in four categories each. Dolj and Mehedinți rank above the regional benchmark for only one crop each.

The results suggest the existence of distinct county-level agricultural profiles, with each territory achieving better performance in particular crop categories. This differentiation among county profiles continues a territorial pattern previously identified in the agriculture of the South-West Oltenia region (*Ursu and Cofas, 2016*).

At the local level, research conducted in Olt County has shown that neighbouring localities may obtain different results even under comparable natural conditions, with technology and input quality contributing to yield differentiation (*Vânătoru (Rădulescu) et al., 2013b*).

**Table 5**

**Territorial disparities in average yield per hectare for representative crops in the South-West Oltenia region, 2025**

| Crop or category | County with the maximum value | Maximum value | County with the minimum value | Minimum value | Absolute gap | Relative gap | Counties above the regional level |
|---|---|---|---|---|---|---|---|
| | U.M.: kg/ha, percentages, and number of counties, depending on the indicator | | | | | | |
| Cereals for grain | Olt | 4143 | Mehedinți | 2502 | 1641 | 65.59% | 1 |
| Wheat – total | Olt | 4906 | Mehedinți | 3284 | 1622 | 49.39% | 2 |
| Grain maize | Gorj | 3130 | Mehedinți | 965 | 2165 | 224.35% | 2 |
| Field peas | Olt | 1741 | Vâlcea | 848 | 893 | 105.31% | 1 |
| Sunflower | Vâlcea | 1278 | Mehedinți | 845 | 433 | 51.24% | 2 |
| Rapeseed | Vâlcea | 3416 | Dolj | 2203 | 1213 | 55.06% | 3 |
| Potatoes – total | Dolj | 12,966 | Vâlcea | 6527 | 6439 | 98.65% | 1 |
| Tomatoes | Olt | 16,574 | Mehedinți | 10,225 | 6349 | 62.09% | 2 |
| Perennial forage | Mehedinți | 12,344 | Dolj | 8050 | 4294 | 53.34% | 2 |

*(Authors' calculations based on NIS statistical data provided through TEMPO-Online, AGR110A)*

*Note: The relative gap was calculated by dividing the difference between the maximum and minimum values by the minimum value.*

The regional average does not always capture the disparities within the region. According to Table 5, the widest relative gap was recorded for grain maize: the maximum yield in Gorj, at 3130 kg/ha, was more than three times the minimum value recorded in Mehedinți, at 965 kg/ha.

The relative difference between the two counties therefore reached 224.35%. Substantial disparities were also observed for field peas, with a gap of 105.31%, and potatoes, with 98.65%. Potatoes recorded the largest absolute difference, at 6439 kg/ha, closely followed by tomatoes, with 6349 kg/ha.

These values should be considered in relation to the naturally higher yields of the two crops. Even the smallest relative gap, identified for wheat, reached 49.39%, indicating that none of the crops analysed had a genuinely uniform territorial distribution.

Rapeseed was the only crop for which three counties exceeded the regional level, whereas for cereals for grain, field peas, and potatoes, only one county exceeded this benchmark in each case. Regional performance therefore resulted from uneven territorial contributions rather than from similar yields across the five counties.

**Table 6**

**Changes in average yield per hectare for representative crops, by county and in the South-West Oltenia region, 2016–2025**

| Crop or category | Dolj | Gorj | Mehedinți | Olt | Vâlcea | South-West Oltenia region |
|---|---|---|---|---|---|---|
| | U.M.: Percentages | | | | | |
| Cereals for grain | -7.81% | 7.52% | -28.88% | **35.97%** | -25.28% | 1.46% |
| Wheat – total | 13.35% | 19.77% | -10.30% | **54.76%** | 50.32% | 25.04% |
| Grain maize | -52.84% | **2.25%** | -72.58% | -45.63% | -44.75% | -43.34% |
| Field peas | -12.45% | -37.82% | -30.00% | **0.81%** | n.d. | -13.37% |
| Sunflower | -39.78% | -23.40% | -64.89% | -2.34% | **42.00%** | -32.90% |
| Rapeseed | -15.43% | n.d. | -35.51% | 9.08% | **75.18%** | -7.90% |
| Potatoes – total | **-13.34%** | -25.53% | -24.26% | -25.11% | -40.30% | -17.76% |
| Tomatoes | 0.30% | **58.30%** | 4.42% | 3.28% | -34.17% | 1.55% |
| Perennial forage | -26.04% | -37.64% | **-1.70%** | -35.62% | -43.67% | -29.63% |

*(Authors' calculations based on NIS statistical data provided through TEMPO-Online, AGR110A)*

*Note: n.d. = change not determined because the value for 2016 is unavailable in the NIS database.*

The territorial analysis of changes between 2016 and 2025 reveals a region divided between several consistent improvements and numerous yield losses. Wheat recorded the most favourable trend, with increases in four of the five counties.

The most substantial results were observed in Olt, with 54.76%, and Vâlcea, with 50.32%, while Mehedinți was the only county to record a decline, of 10.30%.

The situation of grain maize was almost the opposite. With the exception of Gorj, where the yield increased slightly by 2.25%, all counties recorded considerable decreases.

The sharpest contraction occurred in Mehedinți, at 72.58%, followed by Dolj, at 52.84%. A widespread decline was also observed for potatoes and perennial forage, for which no county ended the period above its 2016 level.

Some crops nevertheless displayed strong territorial contrasts. For sunflower, the 42.00% increase recorded in Vâlcea coexisted with a 64.89% decline in Mehedinți. In the case of rapeseed, Vâlcea recorded the largest increase in the entire table, at 75.18%, while the value for Mehedinți decreased by 35.51%.

Tomatoes followed a favourable trend in four counties, whereas Vâlcea recorded a decline of 34.17%; at the regional level, the increase was only 1.55%.

These differences show that the same crop may follow entirely different trajectories within the region and that the regional result may conceal both substantial county-level improvements and severe declines. The unavailable values for field peas in Vâlcea and rapeseed in Gorj were retained as *"n.d."* and were excluded from the comparisons of changes over time.

**Table 7**

**Indicators of changes in average yield per hectare for the main cereal crops in the South-West Oltenia region**

| Crop or category | 2016 | 2025 | Absolute change | Change 2016–2025 | Period average | Deviation from the regional cereal yield in 2025 |
|---|---|---|---|---|---|---|
| | U.M.: kg/ha, except for percentage indicators | | | | | |
| Cereals for grain | 3346 | 3395 | 49 | 1.46% | 4200 | 0.00% |
| Wheat – total | 3315 | 4145 | 830 | 25.04% | 4174 | 22.09% |
| Barley and two-row barley | 3544 | 3722 | 178 | 5.02% | 3960 | 9.63% |
| Oats | 1892 | 2487 | 595 | **31.45%** | 2169 | -26.75% |

| | | | | | | |
|---|---|---|---|---|---|---|
| Grain maize | 3433 | 1945 | -1488 | **-43.34%** | 4345 | -42.71% |
| Sorghum | 2174 | 2349 | 175 | 8.05% | 2348 | -30.81% |

*(Authors' calculations based on NIS statistical data provided through TEMPO-Online, AGR110A)*

The apparent stability of the *"Cereals for grain"* category, which recorded an increase of only 1.46% between 2016 and 2025, conceals very different trends among its component crops. Wheat recorded the largest absolute gain, of 830 kg/ha, reaching 4145 kg/ha in 2025—22.09% above the overall yield for cereals for grain.

Oats recorded the largest percentage increase, at 31.45%, although their yield in 2025 remained 26.75% below the overall cereal yield. Barley and two-row barley increased by 5.02%, reaching 3722 kg/ha, while sorghum grew by 8.05% and ended the period at a value almost identical to its multiyear average. Grain maize represents the main negative exception. Its yield decreased by 43.34%, from 3433 kg/ha to 1945 kg/ha, and in 2025 it stood 42.71% below the level recorded for the cereals for grain category.

Therefore, the almost stationary trend of the overall category does not indicate uniform stability but results from the gains recorded for wheat, oats, barley, and sorghum offsetting the sharp decline in maize. However, the maize result should not be attributed to a single factor.

Experimental research conducted in the Boureni–Băilești area highlighted the influence of both climatic conditions and fertilisation levels on the yield of this crop (*Ștefan et al., 2022*).

**Table 8**

**Indicators of changes in average yield per hectare for protein and oilseed crops in the South-West Oltenia region**

| Crop | 2016 | 2025 | Absolute change | Change 2016–2025 | Period average | Deviation of the 2025 value from the period average |
|---|---|---|---|---|---|---|
| | U.M.: kg/ha, except for percentage indicators | | | | | |
| Field peas | 1795 | 1555 | -240 | -13.37% | 1809 | -14.03% |
| Dry beans | 1716 | 1583 | -133 | -7.75% | 1456 | 8.74% |
| Sunflower | 1617 | 1085 | -532 | **-32.90%** | 2126 | -48.97% |
| Rapeseed | 2685 | 2473 | -212 | -7.90% | 2528 | -2.18% |
| Soybeans | 1733 | 1897 | 164 | **9.46%** | 1907 | -0.55% |

*(Authors' calculations based on NIS statistical data provided through TEMPO-Online, AGR110A)*

Protein and oilseed crops did not follow a common trajectory. Soybean was the only crop to end the period with a higher yield than in 2016, recording an increase of 9.46%. Nevertheless, the 2025 value of 1897 kg/ha remained 0.55% below the multiyear average, indicating a recovery rather than the achievement of an exceptional level.

Among protein crops, the yield of field peas decreased by 13.37%, while the 2025 value stood 14.03% below the period average. Dry beans presented a different situation: although the final value was 7.75% lower than in 2016, it exceeded the multiyear average by 8.74%.

This example shows that the direction of a trend also depends on the benchmark selected for comparison. Among oilseed crops, rapeseed displayed the most balanced profile, with a decline of 7.90% between the beginning and end of the period and a 2025 yield only 2.18% below the multiyear average.

Sunflower, however, emerged as the group's main vulnerability: its average yield per hectare decreased by 32.90%, while the 2025 result was 48.97% below the period average.

The differences among crops are therefore sufficiently large to require a separate interpretation of each trajectory.

The relatively balanced profile of rapeseed does not exclude its exposure to risk, as previous research covering Romania, the South-West Oltenia region, and Olt County has highlighted yield fluctuations and the sector's sensitivity to climatic and economic conditions (*Cruceru and Ghiuleanu, 2024a*).

**Table 9**

**Changes in average yield per hectare and distance from the maximum for potatoes and the main vegetable crops in the South-West Oltenia region**

| Crop | 2016 | 2025 | Change 2016–2025 | Maximum value | Year of maximum | Difference from maximum | Distance of the 2025 value from the maximum (%) |
|---|---|---|---|---|---|---|---|
| | U.M.: kg/ha, except for years and percentage indicators | | | | | | |
| Potatoes – total | 12,263 | 10,085 | -17.76% | 16,363 | 2017 | 6278 | 38.37% |
| Tomatoes | 13,655 | 13,866 | 1.55% | 25,497 | 2021 | 11,631 | 45.62% |
| Dry onions | 9966 | 7195 | **-27.80%** | 12,671 | 2020 | 5476 | 43.22% |
| White cabbage | 18,867 | 13,796 | -26.88% | 26,416 | 2021 | 12,620 | **47.77%** |
| Peppers | 11,111 | 11,921 | **7.29%** | 15,187 | 2021 | 3266 | 21.51% |
| Watermelons and melons | 24,563 | 18,689 | -23.91% | 34,620 | 2021 | 15,931 | 46.02% |

*(Authors' calculations based on NIS statistical data provided through TEMPO-Online, AGR110A)*

The results presented in Table 9 show that the yields recorded in 2025 remained considerably below the maximum levels reached during the period. The only increases compared with 2016 were observed for peppers, at 7.29%, and tomatoes, at 1.55%.

Even in these cases, the values recorded in the final year were 21.51% and 45.62% below their previous maximum levels, respectively. The sharpest declines between 2016 and 2025 were recorded for dry onions, at 27.80%, and white cabbage, at 26.88%, followed by watermelons and melons, at 23.91%. White cabbage recorded the largest relative distance from its maximum, at 47.77%, while watermelons and melons registered the largest absolute difference, at 15,931 kg/ha. Most maximum values were concentrated in 2020–2021, except for potatoes, which reached their peak in 2017.

The widespread distance between the 2025 results and these maximum levels shows that the favourable performance achieved in previous years was not maintained.

From this perspective, the main challenge is not only to obtain high yields but also to sustain them over time. Fluctuations in tomato yields confirm the instability of the sector identified in previous research, which highlighted the need for investment in irrigation systems and modern technologies to stabilise production (*Cruceru and Ghiuleanu, 2024b*).

**Table 10**

**Changes in average yield per hectare for forage crops between the first and second halves of the 2016–2025 period**

| Crop or category | Average 2016–2020 | Average 2021–2025 | Absolute change in averages | Percentage change in averages | 2016 | 2025 | Change 2016–2025 |
|---|---|---|---|---|---|---|---|
| | U.M.: kg/ha, except for percentage indicators | | | | | | |
| Perennial forage | 13,290 | 9726 | -3564 | -26.82% | 12,644 | 8897 | -29.63% |
| Alfalfa, expressed as green-mass equivalent | 13,571 | 10,436 | -3135 | -23.10% | 12,943 | 9744 | -24.72% |
| Clover, expressed as green-mass equivalent | 17,276 | 10,418 | -6858 | **-39.70%** | 15,586 | 6698 | **-57.03%** |
| Annual green forage | 9157 | 10,039 | 882 | **9.63%** | 7674 | 9714 | 26.58% |
| Green maize for forage | 13,380 | 14,663 | 1283 | 9.59% | 7521 | 10,388 | **38.12%** |

*(Authors' calculations based on NIS statistical data provided through TEMPO-Online, AGR110A)*

*Note: "Perennial forage" and "Annual green forage" are aggregate categories, whereas alfalfa, clover, and green maize for forage are components of these categories. The values should not be summed.*

A comparison between the averages of the two halves of the period reveals a clear distinction between perennial and annual forage crops. The average yield of perennial forage decreased from 13,290

kg/ha in 2016–2020 to 9726 kg/ha in 2021–2025, corresponding to a decline of 26.82%. Clover recorded the most unfavourable trend: its average decreased by 39.70%, while the comparison between 2016 and 2025 indicates an even sharper decline, of 57.03%. Alfalfa followed the same direction, with a decrease of 23.10% between the two intervals and 24.72% between the first and final years.

By contrast, annual green forage and green maize for forage performed better during the second half of the period. Their average yields increased by 9.63% and 9.59%, respectively, while their 2025 yields exceeded the corresponding 2016 values by 26.58% and 38.12%.

The forage sector therefore did not follow a uniform trend: declining yields for perennial crops coexisted with improving yields for annual forage crops.

The categories included in the table were analysed as separate indicators and were not summed, because some represent aggregate groups while others are their components.

The importance of perennial crops extends beyond their productive role: they are among the crops with a strong capacity to limit erosion, whereas maize, sunflower, and potatoes provide less soil protection (*Nijloveanu et al., 2013*). In this context, conservation practices and continuous monitoring of soil conditions remain relevant (*Buzatu et al., 2023*).

**Table 11**

**Comparative profile of agricultural yields across the counties of the South-West Oltenia region**

| Indicator | Dolj | Gorj | Mehedinți | Olt | Vâlcea |
|---|---|---|---|---|---|
| | U.M.: number of crops and percentages, depending on the indicator | | | | |
| Crops with a positive trend | 2 | 4 | 1 | **5** | 3 |
| Crops with a negative trend | 7 | 4 | **8** | 4 | 5 |
| Crops with unavailable data | 0 | 1 | 0 | 0 | 1 |
| Crops above the regional level in 2025 | 1 | 4 | 1 | **6** | 4 |
| Leading positions among counties in 2025 | 1 | 1 | 1 | **4** | 2 |
| Unweighted average change, 2016–2025 | -17.12% | -4.57% | -29.30% | **-0.53%** | -2.58% |

*(Authors' calculations based on NIS statistical data provided through TEMPO-Online, AGR110A)*

*Note: The indicators were calculated for the nine representative crops analysed in Tables 4 and 6. The average change is an unweighted arithmetic mean, and n.d. values were excluded from its calculation.*

The summary of territorial indicators places Olt County at the forefront of the regional agricultural profile. It records five crops with a positive trend, six yields above the regional level in 2025, and four leading positions among the counties. Nevertheless, its unweighted average change remains slightly negative, at −0.53%, showing that the favourable results were almost sufficient to offset the declines recorded by the other crops. Vâlcea and Gorj occupy intermediate positions.

Vâlcea holds two leading positions and has four crops above the regional level, while its average change is −2.58%. Gorj displays the most balanced ratio between the two directions of change, with four increases and four decreases, resulting in an average of −4.57%. In both counties, one statistical series could not be assessed because the initial value was unavailable.

The most vulnerable profiles were observed in Dolj and Mehedinți. Dolj recorded seven declines and an average change of −17.12%, while Mehedinți accumulated eight declines across the nine crops and registered the most unfavourable average, at −29.30%. Nevertheless, each of these counties retained one leading position in 2025: Dolj for potatoes and Mehedinți for perennial forage.

The fact that none of the counties achieved a positive average confirms the predominantly unfavourable nature of the period, while also revealing local agricultural advantages that can be leveraged separately.

**Table 12**

**Extreme changes in average yield per hectare across county–crop combinations in the South-West Oltenia region**

| Type of change | Rank | County | Crop | 2016 | 2025 | Change 2016–2025 |
|---|---|---|---|---|---|---|
| | U.M.: kg/ha and percentages, depending on the indicator | | | | | |
| Increase | 1 | Vâlcea | Rapeseed | 1950 | 3416 | **75.18%** |
| | 2 | Gorj | Tomatoes | 10,038 | 15,890 | **58.30%** |
| | 3 | Olt | Wheat – total | 3170 | 4906 | **54.76%** |

| | | | | | | |
|---|---|---|---|---|---|---|
| | 4 | Vâlcea | Wheat – total | 3114 | 4681 | **50.32%** |
| | 5 | Vâlcea | Sunflower | 900 | 1278 | **42.00%** |
| Decline | 1 | Mehedinți | Grain maize | 3519 | 965 | **-72.58%** |
| | 2 | Mehedinți | Sunflower | 2407 | 845 | **-64.89%** |
| | 3 | Dolj | Grain maize | 4025 | 1898 | **-52.84%** |
| | 4 | Olt | Grain maize | 2904 | 1579 | **-45.63%** |
| | 5 | Vâlcea | Grain maize | 3716 | 2053 | **-44.75%** |

*(Authors' calculations based on NIS statistical data provided through TEMPO-Online, AGR110A)*

*Note: The ranking includes the nine representative crops and the five counties analysed in Table 6. County–crop combinations for which the 2016 value was unavailable were excluded.*

The ranking of extreme changes confirms that agricultural performance is linked to specific combinations of territory and crop. The largest increase was recorded for rapeseed grown in Vâlcea, whose yield rose by 75.18%, from 1950 to 3416 kg/ha. This was followed by tomatoes in Gorj, with an increase of 58.30%, and wheat in Olt, with 54.76%. Vâlcea occupies three of the top five positions for increases, owing to the results recorded for rapeseed, wheat, and sunflower. Nevertheless, the same county also appears among the sharpest declines in the case of grain maize.

This situation illustrates the selective nature of territorial advantages: a county may achieve very strong results for certain crops without these advantages extending across its entire agricultural profile. At the opposite end of the ranking, grain maize accounts for four of the five positions, with declines ranging from 44.75% to 72.58%. The sharpest contractions were recorded in Mehedinți, both for grain maize, at 72.58%, and sunflower, at 64.89%.

The concentration of declines around maize shows that the unfavourable trend of this crop is not an isolated county-level occurrence but a vulnerability affecting most of the region. At the same time, the distribution of increases across several crops indicates the existence of local pockets of strong performance that may provide a starting point for strengthening regional yields.

The spread of the maize decline across four of the five counties is particularly relevant given that Romania has been identified as one of the main European hotspots of drought-related maize yield losses (*Rossi et al., 2023*).




**Fig. 1 - SmartArt diagram illustrating the S.W.O.T. analysis of the dynamics and territorial distribution of average yield per hectare in the South-West Oltenia region, developed from the statistical results for 2016–2025**

*(Authors' own elaboration)*

The S.W.O.T. analysis shows that the region achieves strong agricultural performance, although this is concentrated in specific crops and counties. The main strategic direction emerging from the research is to

extend successful local practices while stabilising crops characterised by repeated declines and substantial fluctuations.

In this way, territorial differences may become sources of learning and adaptation rather than merely expressions of regional imbalances.

The results indicate selective agricultural performance rather than a widespread improvement in yields. Progress recorded for certain crops coexists with sharp declines and substantial territorial disparities, supporting the need for measures tailored to the profile of each county. These findings provide the empirical foundation for the conclusions of the research.

The directions formulated through the S.W.O.T. analysis (crop monitoring, technological adaptation, water management, and diversification) are consistent with the measures proposed to reduce risks in Romanian agriculture (*Ghiuleanu et al., 2023*).

The need for solutions adapted to local conditions is also supported by research concerning the effects of climate change on agriculture (*Buzatu et al., 2024a*).

However, transforming local advantages into regional resilience requires cooperation and long-term investment, in line with agricultural sustainability objectives and the priorities of Romania's CAP Strategic Plan (*Buzatu et al., 2024b; European Commission, 2026*).

## CONCLUSIONS

The analysis of average yield per hectare in the South-West Oltenia region shows that the 2016–2025 period was not characterised by uniform agricultural progress, but by a succession of increases and setbacks.

The apparent stability of certain regional indicators conceals substantial changes both among crops and across counties.

For cereals for grain, the regional increase of only 1.46% combines two opposing trends: a 25.04% increase in wheat yield and a 43.34% decline in grain maize. Substantial decreases were also identified for sunflower, perennial forage, and potatoes.

The predominance of 45 annual decreases over 36 increases, together with the concentration of minimum values for six categories in 2024, confirms the vulnerability of agricultural yields. The recovery observed in 2025 was genuine but insufficient to regain the previous maximum levels.

Territorial differences are equally significant. Olt displays the most favourable comparative profile, although none of the five counties recorded a positive unweighted average change across the crops analysed.

Moreover, the gap between county-level yields reached 224.35% for grain maize. The results confirm that no county performs uniformly well across all crops; instead, specific advantageous local combinations emerge, such as rapeseed in Vâlcea, tomatoes in Gorj, wheat in Olt, potatoes in Dolj, and perennial forage in Mehedinți.

The main conclusion of the research is that improving regional yields requires an approach differentiated by crop and county. Successful local practices can be assessed and adapted, while grain maize, sunflower, and perennial forage crops require greater attention in terms of yield stability.

Annual yield monitoring and comparison with multiyear averages would enable the early identification of deteriorating trends and provide a more precise basis for targeted interventions.

Future research could extend this analysis by correlating yields with cultivated areas, total production, and climatic, technological, and economic factors.

Such an extension would help explain the causes of the differences identified and provide a more comprehensive assessment of agricultural resilience in the South-West Oltenia region.

## REFERENCES

[1] Barna, F. M., Mănescu, A. C. (2025). *The impact of drought risk on maize crop in Romania. Sustainability*, 17(19), 8870. https://doi.org/10.3390/su17198870.

[2] Berca, M., Horoiaș, R. (2022). *NDMI use in recognition of water stress issues, related to winter wheat yields in Southern Romania. Scientific Papers Series "Management, Economic Engineering in Agriculture and Rural Development"*, 22(2), 105–112. https://managementjournal.usamv.ro/pdf/vol.22_2/Art12.pdf. Accessed September 15, 2026.

[3] Buzatu, C. S., Ghiuleanu, I. V., Tudor, V. C. (2023). *Dynamics of land fund and strategies on soil conservation and prevention of soil degradation in Romania. Scientific Papers Series "Management,*

*Economic Engineering in Agriculture and Rural Development*", 23(4), 149–156. https://managementjournal.usamv.ro/pdf/vol.23_4/Art14.pdf. Accessed February 11, 2026.

[4] Buzatu, C. S., Ghiuleanu, I. V., Mărcuță, A. G., Popa, I. V. (2024a). *Climate change and land temperatures and their impact on agriculture and society: A global investigation. Scientific Papers Series "Management, Economic Engineering in Agriculture and Rural Development"*, 24(4), 121–130. https://managementjournal.usamv.ro/pdf/vol.24_4/Art12.pdf. Accessed February 17, 2026.

[5] Buzatu, C. S., Ghiuleanu, I. V., Tudor, V. C., Oltenacu, N., Vlad, G. (2024b). *Sustainability in agricultural work – our shared responsibility. Scientific Papers Series "Management, Economic Engineering in Agriculture and Rural Development"*, 24(1), 147–156. https://managementjournal.usamv.ro/pdf/vol.24_1/Art14.pdf. Accessed September 5, 2026.

[6] Cruceru, C., Ghiuleanu, I. V. (2024a). *The area under oilseed rape in Romania: Evolution and trends. In Proceedings of the International Symposium ISB-INMA-TEH: Agricultural and Mechanical Engineering* (pp. 486–501). Accessed March 6, 2026. https://isbinmateh.inma.ro/wp-content/uploads/2025/11/Vol-ISB-INMA-TEH-2024.pdf

[7] Cruceru, C., Ghiuleanu, I. V. (2024b). *Tomatoes in figures: Production, prices and outlook for the future. In Proceedings of the International Symposium ISB-INMA-TEH: Agricultural and Mechanical Engineering* (pp. 502–511). Accessed September 5, 2026. https://isbinmateh.inma.ro/wp-content/uploads/2025/11/Vol-ISB-INMA-TEH-2024.pdf

[8] European Commission. (2026). *Romania – CAP Strategic Plan*. https://agriculture.ec.europa.eu/cap-my-country/cap-strategic-plans/romania_en. Accessed July 22, 2026.

[9] Eurostat. (2025). *Agricultural production – crops*. https://ec.europa.eu/eurostat/statistics-explained/index.php?title=Agricultural_production_-_crops. Accessed July 20, 2026.

[10] Ghiuleanu, I. V., Buzatu, C. S., Tudor, V. C., Panait, R., (Carbarău) Smedescu, C. A. (2023). *Risks analyses and challenges in crop management in Romania. Scientific Papers Series "Management, Economic Engineering in Agriculture and Rural Development"*, 23(4), 353–364. https://managementjournal.usamv.ro/pdf/vol.23_4/Art34.pdf. Accessed January 15, 2026.

[11] National Institute of Statistics [NIS]. (2025). *Producția vegetală la principalele culturi în anul 2024*. https://insse.ro/cms/ro/content/producția-vegetală-la-principalele-culturi-în-anul-2024. Accessed March 9, 2026.

[12] National Institute of Statistics [NIS]. (2026). TEMPO-Online database: Average production per hectare for the main crops, by forms of ownership, macroregions, development regions and counties (AGR110A; data for 2016–2025). Retrieved August 17, 2026, from TEMPO-Online.

[13] Nijloveanu, D., Bozga, I., Tița, V., Vânătoru (Rădulescu), D. L. (2013). *Soil degradation in Olt County by the process of hydric erosion. Annals of the University of Craiova – Agriculture, Montanology, Cadastre Series*, 43(1), 243–246. https://anale.agro-craiova.ro/index.php/aamc/article/view/46/46. Accessed March 23, 2026.

[14] Onțel, I., Vlăduț, A. (2015). *Impact of drought on the productivity of agricultural crops within the Oltenia Plain, Romania. Geographica Pannonica*, 19(1), 9–19. https://doi.org/10.5937/GeoPan1501009O.

[15] Rossi, L., Wens, M., De Moel, H., Cotti, D., Sabino Siemons, A.-S., Toreti, A., Maetens, W., Masante, D., Van Loon, A., Hagenlocher, M., Rudari, R., Naumann, G., Meroni, M., Avanzi, F., Isabellon, M., Barbosa, P. (2023). *European Drought Risk Atlas* (EUR 31682 EN, JRC135215). Publications Office of the European Union. https://doi.org/10.2760/608737.

[16] Ștefan, I.-O., Tița, V., Nijloveanu, D., Bold, N. (2022). *Research on the behavior of corn cultivated on a chernozem type soil from Boureni–Băilești area, Dolj County, Romania, depending on agrofund. Scientific Papers Series "Management, Economic Engineering in Agriculture and Rural Development"*, 22(2), 655–658. https://managementjournal.usamv.ro/pdf/vol.22_2/Art77.pdf. Accessed February 16, 2026.

[17] Ursu, A., Cofas, E. (2016). *The territorial analysis of agricultural production structure. Case study: Region South-West Oltenia. Scientific Papers Series "Management, Economic Engineering in Agriculture and Rural Development"*, 16(1), 535–542. https://managementjournal.usamv.ro/pdf/vol.16_1/Art84.pdf. Accessed January 6, 2026.

[18] Vânătoru (Rădulescu), D. L., Bozga, I., Nijloveanu, D., Tița, V. (2013a). *Climate change and its effects on culture in microregion Caracal–Olt. Annals of the University of Craiova – Agriculture, Montanology, Cadastre Series*, 43(2), 237–240. https://anale.agro-craiova.ro/index.php/aamc/article/view/98/93. Accessed September 5, 2026.

[19] Vânătoru (Rădulescu), D. L., Bozga, I., Nijloveanu, D., Tița, V. (2013b). *Studies on the development of agriculture in Olt County. Annals of the University of Craiova – Agriculture, Montanology, Cadastre Series*, 43(2), 231–236. https://anale.agro-craiova.ro/index.php/aamc/article/view/97/92. Accessed January 11, 2026.

# COMPARATIVE EVALUATION OF TWO INTELLIGENT ARCHITECTURES FOR HORTICULTURAL CROP PROTECTION

/

# *EVALUAREA COMPARATIVĂ A DOUĂ ARHITECTURI INTELIGENTE PENTRU PROTECŢIA CULTURILOR HORTICOLE*

**Augustina PRUTEANU*[1)], Iuliana GAGEANU[1)], Mihaela NIŢU[1)], Nicoleta Alexandra VANGHELE[1)], Andreea MATACHE[1)]**

[1)] National Institute of Research - Development for Machines and Installations Designed to Agriculture and Food Industry - INMA Bucharest / Romania.

*Tel: 0740 690 268; *E-mail: pruteanu_augustina@yahoo.com*

***Keywords:*** *intelligent crop protection; horticultural crops; bird deterrence; artificial intelligence; acoustic deterrence; laser deterrence; multimodal system*

## ABSTRACT

*Bird damage represents a persistent challenge in horticultural and fruit production, particularly where conventional deterrent methods may lose effectiveness because of bird habituation. Intelligent crop protection systems that combine automated detection with active deterrence may provide a flexible approach for reducing bird activity in cultivated areas. The present study aimed to comparatively evaluate two intelligent architectures developed for horticultural crop protection: an acoustic architecture and a multimodal acoustic-visual architecture. The experimental evaluation was conducted under real operating conditions over a 45-day monitoring period. The acoustic architecture relied primarily on acoustic deterrence with PIR-based motion detection, while the multimodal architecture combined acoustic and ultrasonic stimuli, laser-based visual stimulation and artificial-intelligence-assisted detection. System performance was evaluated using system efficiency, bird activity, reduction in bird activity and operational availability. Both architectures showed a progressive increase in the measured system-efficiency indicator during the monitoring period. The multimodal acoustic-visual architecture reached a mean efficiency of 81.4% and a maximum value of 97%, while the acoustic architecture recorded a mean efficiency of 76.8% and a maximum value of 91%. The total number of bird observations was 470 for the multimodal architecture and 621 for the acoustic architecture. Based on the initial and final daily counts, the calculated reduction in bird activity was 85.7% and 79.2%, respectively. Both systems maintained 100% operational availability during the experimental period. The results provide a comparative experimental basis for assessing intelligent and multimodal approaches to automated horticultural crop protection.*

## REZUMAT

*Pagubele provocate de păsări reprezintă o provocare persistentă pentru producția horticolă și pomicolă, în special în situațiile în care metodele convenționale de descurajare își pot pierde eficacitatea prin habituarea păsărilor. Sistemele inteligente de protecție a culturilor, care combină detectarea automatizată cu mecanisme active de descurajare, pot reprezenta o abordare flexibilă pentru reducerea activității păsărilor în zonele cultivate. Studiul de față a vizat evaluarea comparativă a două arhitecturi inteligente dezvoltate pentru protecția culturilor horticole: o arhitectură acustică și o arhitectură multimodală acustico-vizuală. Evaluarea experimentală a fost realizată în condiții reale de operare, pe parcursul unei perioade de monitorizare de 45 de zile. Arhitectura acustică s-a bazat în principal pe descurajare acustică și detectare prin senzori PIR, în timp ce arhitectura multimodală a combinat stimuli acustici și ultrasonici, stimulare vizuală bazată pe laser și detectare asistată de inteligență artificială. Performanța sistemelor a fost evaluată pe baza eficienței sistemului, a activității păsărilor, a reducerii activității acestora și a disponibilității operaționale. Ambele arhitecturi au prezentat o creștere progresivă a indicatorului de eficiență pe durata perioadei de monitorizare. Arhitectura multimodală acustico-vizuală a atins o eficiență medie de 81,4% și o valoare maximă de 97%, în timp ce arhitectura acustică a înregistrat o eficiență medie de 76,8% și o valoare maximă de 91%. Numărul total de observații privind păsările a fost de 470 pentru arhitectura multimodală și de 621 pentru arhitectura acustică. Pe baza numărului zilnic inițial și final, reducerea calculată a activității păsărilor a fost de 85,7%, respectiv 79,2%. Ambele sisteme și-au menținut disponibilitatea operațională la*

*nivelul de 100% pe parcursul perioadei experimentale. Rezultatele oferă o bază experimentală comparativă pentru evaluarea abordărilor inteligente și multimodale de protecție automatizată a culturilor horticole.*

## INTRODUCTION

Bird damage represents a persistent challenge for agricultural production, particularly in high-value crops and fruit-growing systems where birds can cause direct losses through feeding and indirect losses through contamination and crop disturbance. The management of avian pests is complex because bird populations, species composition and feeding behaviour vary among agricultural environments (*Nebel et al., 2019).* Moreover, the effectiveness of many conventional deterrent methods may decrease over time as birds become habituated to repeated and predictable stimuli *(Micaelo et al., 2023; Enos et al., 2021)*.

Bird deterrence methods include visual, acoustic, physical and chemical approaches, as well as technology-based solutions (*Micaelo et al., 2023; Egan et al., 2020; Mohamed et al., 2020*). Visual and acoustic deterrents are among the most investigated non-lethal approaches; however, their effectiveness depends on the target species, environmental conditions, spatial configuration and frequency of exposure. Studies of drones as non-lethal frightening devices indicate that standard commercial platforms may elicit weaker avoidance responses than natural predators, and that additional stimuli may be required to increase their deterrent effect (*Egan et al., 2020; Bhusal et al., 2022*). Reviews of bird-deterrence technologies have also emphasized habituation, variable effectiveness and the potential value of combining different deterrent mechanisms as continuing challenges for practical crop protection (*Micaelo et al., 2023; Enos et al., 2021*).

Recent developments in precision agriculture have created opportunities to integrate sensing, automated decision-making and targeted actuation into crop protection systems (Micaelo et al., 2023; Jalgoankar et al., 2026). Computer vision and deep-learning methods are increasingly used for real-time image interpretation, object detection and decision support, although field deployment remains challenging because of changing illumination, complex backgrounds, occlusion and variations in target size and position (*Ghazal et al., 2024*). These challenges are particularly relevant to bird detection, since birds may occupy only a small portion of an image and may be partially hidden by vegetation or other objects. Previous research in vineyard environments demonstrated improved bird-classification performance when image resolution was enhanced (*Bhusal et al., 2019*).

The integration of automatic detection with an active deterrence mechanism represents a further development toward targeted crop protection. Instead of continuously activating a deterrent over the entire protected area, sensor-based systems can trigger a response when a target is detected. Recent research has demonstrated the feasibility of combining deep-learning-based bird detection with automated laser actuation (*Chen et al., 2024; Elbers & Gonzales, 2021; Brown & Brown, 2021)*. *Chen et al. (2024),* for example, developed an automatic wild-bird repellent system integrating deep-learning-based detection, embedded computing and a rotating laser mechanism. Their field experiments demonstrated the feasibility of targeted, automated visual deterrence.

Laser-based deterrence has also been evaluated independently under experimental conditions. *Manz et al. (2024*) reported reductions in avian damage to sweet corn using laser scarecrows, with the observed treatment effects depending on distance and experimental conditions. These results support the potential of moving laser stimuli as a non-lethal visual deterrent, while also indicating that effectiveness depends on bird behaviour and the characteristics of the deployment environment. The combination of laser stimulation with other deterrent mechanisms is therefore of interest for the development of multimodal protection systems.

The transition from individual deterrent technologies toward integrated intelligent architectures is an important research direction. Recent reviews have identified sensing, automation, robotics and artificial intelligence as emerging components of technology-driven bird-deterrence systems (*Duttenhefner et al., 2025; Jalgoankar et al., 2026; Mohamed et al., 2020*). Sensor feedback and automated actuation may improve the targeting of deterrence actions, while long-term effectiveness, sensor robustness, scalability and economic feasibility remain important practical challenges *(Jalgoankar et al., 2026*). Recent work has also demonstrated the integration of artificial intelligence, acoustic sensing and automated deterrence in agricultural environments (*Jose & Mayan, 2025*).

Despite these developments, comparative experimental assessments of different intelligent deterrence architectures under field conditions remain limited. In particular, comparative studies are needed to characterize whether architectures combining several sensing and deterrence mechanisms produce different performance indicators from simpler systems under real operating conditions. Such comparisons

should also distinguish the overall performance of complete architectures from the individual contribution of specific deterrence mechanisms.

The objective of the present study was therefore to comparatively evaluate two intelligent architectures developed for the protection of horticultural crops against bird activity. The first architecture relied primarily on acoustic deterrence and PIR-based motion detection, while the second employed a multimodal strategy combining acoustic and ultrasonic stimuli, laser-based visual stimulation and artificial-intelligence-assisted detection. Both systems were evaluated under real operating conditions over a 45-day monitoring period using system efficiency, bird activity, reduction in bird activity, acoustic performance and operational availability as comparative indicators. The study provides an experimental basis for comparing complete intelligent crop-protection architectures under field conditions.

## MATERIALS AND METHODS

### *2.1. Experimental site and field conditions*

The field evaluation of the two intelligent architectures for horticultural crop protection was conducted in the Băneasa area of Bucharest, Romania, during June–July. Two production environments were considered. The multimodal acoustic-visual architecture was tested in a raspberry crop with an area of approximately 800 m², whereas the acoustic architecture was evaluated in an apple orchard with an area of approximately 1.5 ha. Images from the experimental investigations are presented in Figure 1.



**Fig. 1 - Aspects of the experimental research**

Both systems were evaluated under real operating conditions over a 45-day monitoring period. Bird activity was assessed from video recordings collected during the experimental period. The recorded video material was subsequently analyzed to determine the number of birds present in the monitored areas. The analysis refers to recorded bird observations and does not imply that individual birds were uniquely identified across observation periods.

The comparative evaluation considered system efficiency, bird activity, reduction in bird activity, operational availability, acoustic performance and energy autonomy.

### *2.2. Description of the intelligent architectures*

Both systems were developed using a modular configuration comprising three functional modules: power supply, detection and deterrence. The power-supply module consisted of photovoltaic panels, a solar charge controller, batteries and an inverter. The detection module included either an intelligent camera and central computing unit or PIR motion sensors. The deterrence module incorporated acoustic and visual deterrence devices.

#### 2.2.1. Multimodal acoustic-visual architecture

The multimodal acoustic-visual architecture combined intelligent visual detection with acoustic, ultrasonic and laser-based deterrence. Its main components included a solar power-supply system, an intelligent camera, an automatically controlled laser system, an ultrasonic generator with four loudspeakers and visual scare devices.

The intelligent camera was a colour camera with a resolution of 1920 × 1080 pixels (2 MP) and 360° rotation capability. Image processing was performed using an NVIDIA® Jetson™ Xavier NX module operating under Ubuntu Linux.

The laser deterrence system employed combined red and green laser beams with wavelengths of 650 nm and 532 nm, respectively. The declared beam power was 50–100 mW, with a divergence of 60° and a nominal unidirectional coverage of approximately 10,000 m². The ultrasonic subsystem comprised four loudspeakers, with a declared coverage of approximately 1,500 m², an acoustic pressure of 95–102 dB per loudspeaker and an operating frequency range of 15–25 kHz.

**2.2.2. Acoustic architecture**

The acoustic architecture was based primarily on acoustic deterrence combined with motion detection. The system included a solar power-supply system, nine PIR motion sensors, two sound generators, approximately 152 m of holographic reflective tape and four kites used as passive visual deterrence elements.

The PIR sensors had a detection range of up to approximately 7 m. The acoustic generator operated in random mode and produced predator and alarm sounds in the frequency range of 3–5 kHz, with a declared acoustic output of 105–110 dB at 1 m and a nominal coverage area of approximately 5,000 m².

Unlike the multimodal acoustic-visual architecture, the acoustic architecture did not employ AI-based visual detection, laser stimulation or ultrasonic stimulation. It nevertheless included passive visual deterrence elements in the form of holographic reflective tape and kites.

***2.3. Control algorithms and deterrence operation***

The control strategies of the two architectures were designed to reduce the predictability of the deterrence stimuli and to avoid repetitive activation patterns.

For the multimodal acoustic-visual architecture, bird detection by the intelligent camera initiated the deterrence sequence. The laser system operated using variable rotation patterns, with changes in beam direction and colour at irregular intervals of approximately 10–45 s. Acoustic and ultrasonic stimuli were also incorporated into the deterrence sequence.

For the acoustic architecture, the acoustic deterrence system operated either in random mode or in sensor-triggered mode. In random mode, activation intervals were generated within a programmable range of 5–30 min, with an activation duration of approximately 40 s. In sensor-based operation, activation was triggered by movement detected by the PIR sensors and maintained for approximately 40 s.

The acoustic system employed a variable sequence of predator sounds in order to reduce the predictability of the emitted stimuli.

***2.4. Acoustic measurements***

The acoustic performance of both architectures was characterized by measuring sound-pressure level at different distances from the loudspeakers. Measurements were performed at four volume settings: 25%, 50%, 75% and 100%.

For the multimodal acoustic-visual architecture, measurements were performed at distances of 1 m, 3.5 m and 28 m, as well as at approximately 29 m in the centre of the crop and 20 m outside the crop. For the acoustic architecture, measurements were conducted at 1, 3.5, 7, 14, 21 and 28 m.

Maximum and mean sound-pressure levels were recorded using a sound-level meter according to SR EN ISO 3744:2011, with a reported measurement accuracy of ±2%.

For multimodal acoustic-visual architecture, the maximum sound-pressure level at 100% volume was 97.6 dB at 1 m and 88.9 dB at 28 m. At the centre of the raspberry crop, the maximum recorded value was 99.2 dB.

For acoustic architecture, the maximum sound-pressure level at 100% volume decreased from 111.4 dB at 1 m to 82.6 dB at 28 m. These measurements were used to characterize the acoustic distribution of the deterrence signal under field conditions.

The two architectures were evaluated during the 45-day experimental period. Bird activity was quantified from video recordings, and the number of birds detected in the monitored areas was determined for the observation intervals.

### *2.5. Performance indicators and bird-activity assessment*

The temporal evolution of total system efficiency was monitored throughout the experimental period. The efficiency values represented the daily performance indicator assigned to each system during the field experiment. For the comparative analysis, minimum, mean and maximum efficiency values were determined.

The mean system efficiency over the 45-day period was calculated as equation (1):

$$E_{mean} = \frac{1}{n}\sum_{d=1}^{n} E_d \quad (1)$$

where $E_{mean}$ is the mean system efficiency (%), $E_d$ is the efficiency recorded on day d, and n is the number of monitoring days (n = 45).

For the multimodal acoustic-visual architecture, the recorded efficiency increased from 52% on day 1 to 97% on day 45, with intermediate values of 58%, 66%, 74%, 80%, 86%, 91%, 94% and 96% at the corresponding monitoring points. For the acoustic architecture, the efficiency increased from 46% on day 1 to 91% on day 45, with intermediate values of 50%, 56%, 62%, 69%, 74%, 78%, 83% and 87%.

The mean efficiencies calculated over the complete 45-day monitoring period were 81.4% for the multimodal acoustic-visual architecture and 76.8% for the acoustic architecture, while the maximum recorded efficiencies were 97% and 91%, respectively.

As a complementary indicator, the reduction in bird activity was calculated according to equation (2):

$$R_b = \frac{N_i - N_f}{N_i} x100 \quad (2)$$

where $R_b$ is the reduction in bird activity (%), $N_i$ is the initial number of birds recorded, and $N_f$ is the final number of birds recorded.

This indicator was treated separately from system efficiency. During the experimental period, 470 bird observations were recorded for the multimodal acoustic-visual architecture and 621 for the acoustic architecture, corresponding to mean daily values of 10.4 and 13.8 observations/day, respectively.

The minimum and maximum daily numbers were 3 and 21 observations for the multimodal architecture and 5 and 24 observations for the acoustic architecture. Based on the initial and final daily counts, the calculated reductions in bird activity were 85.7% and 79.2%, respectively.

The operational availability of both architectures was 100% during the 45-day experimental period.

### *2.6. Energy-autonomy assessment*

The energy autonomy of the two architectures was evaluated using the integrated photovoltaic power-supply systems. Additional photovoltaic capacity of 150 W for the multimodal acoustic-visual architecture and 120 W for the acoustic architecture was incorporated together with increased battery capacity.

The autonomy test was performed under predominantly cloudy conditions, with approximately four hours of sunlight per day. Battery state of charge was monitored during a prolonged period of limited solar availability.

After 96 h, the battery state of charge was 48% for the multimodal acoustic-visual architecture and 57% for the acoustic architecture. At 120 h, the corresponding values were 35% and 44%, respectively.

These measurements were used to characterize the ability of the photovoltaic-powered architectures to maintain operation under reduced solar availability.

## RESULTS

### *3.1. Evolution of total efficiency of the multimodal acoustic-visual architecture*

Evolution of total efficiency of the multimodal acoustic-visual architecture is presented in figure 2.

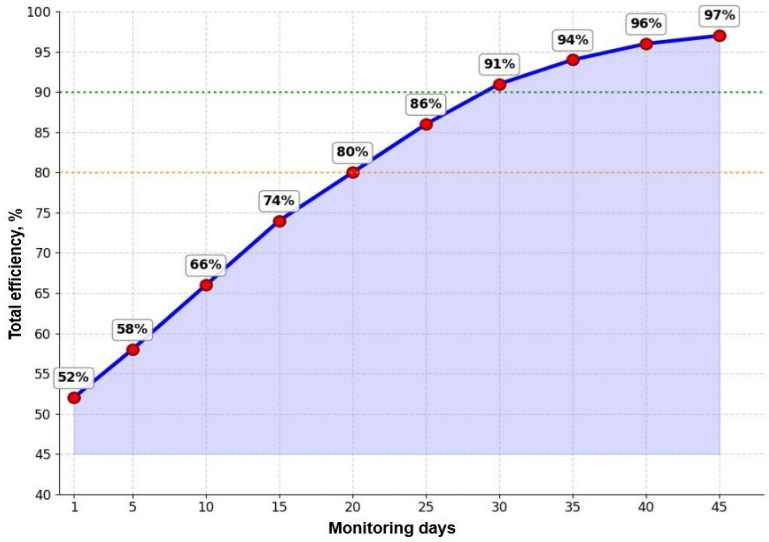



**Fig. 2 - Evolution of the total efficiency indicator of the multimodal acoustic-visual architecture**

Figure 2 shows the evolution of the total efficiency indicator for the multimodal acoustic-visual architecture during the 45-day field experiment. The efficiency increased progressively from 52% on the first monitoring day to 97% on day 45. Intermediate values of 58%, 66%, 74%, 80%, 86%, 91%, 94% and 96% were recorded during the monitoring period.

The mean efficiency calculated over the complete 45-day monitoring period was 81.4%, while the maximum recorded value was 97%. The observed increase describes the temporal evolution of the measured system-performance indicator; it should not be interpreted as evidence that a specific deterrence component was responsible for the change.

### *3.2. Performance of the multimodal acoustic-visual architecture*

The performance of the multimodal acoustic-visual architecture is presented in Table 1.

**Table 1**

**Maximum and mean sound-pressure levels of the multimodal acoustic-visual architecture**

| Distance from the speaker, m | Sound volume, % | | | | | | | |
|---|---|---|---|---|---|---|---|---|
| | 25 | | 50 | | 75 | | 100 | |
| | Sound pressure, dB | | | | | | | |
| | Maximum | Mean | Maximum | Mean | Maximum | Mean | Maximum | Mean |
| 1 m | 90.6 | 86.9 | 93.2 | 86.5 | 94.9 | 87.8 | 97.6 | 92.9 |
| 3.5 m | 87.2 | 80.6 | 90.2 | 83.9 | 93.8 | 86.0 | 93.5 | 89.3 |
| 28 m | 80.1 | 76.5 | 85.5 | 82.2 | 85.9 | 83.0 | 88.9 | 85.1 |
| Crop center, 29 m | 85.7 | 77.5 | 91.2 | 80.7 | 92.7 | 90.0 | 99.2 | 86.8 |
| Exterior crop, 20 m | 80.8 | 75.3 | 82.5 | 79.6 | 87.5 | 84.8 | 88.8 | 84.7 |

The acoustic measurements for the multimodal acoustic-visual architecture showed that sound-pressure levels varied with both the selected volume and the distance from the loudspeaker. At 100% volume, the maximum sound-pressure level was 97.6 dB at 1 m and 88.9 dB at 28 m. At the centre of the raspberry crop, located approximately 29 m from the loudspeaker, the maximum recorded value reached 99.2 dB, while the mean value was 86.8 dB. The measurements characterize the spatial distribution of the acoustic deterrence signal under the tested field conditions.

### *3.3. Evolution of total efficiency of the acoustic architecture*

The evolution of the acoustic architecture is presented in Figure 3.

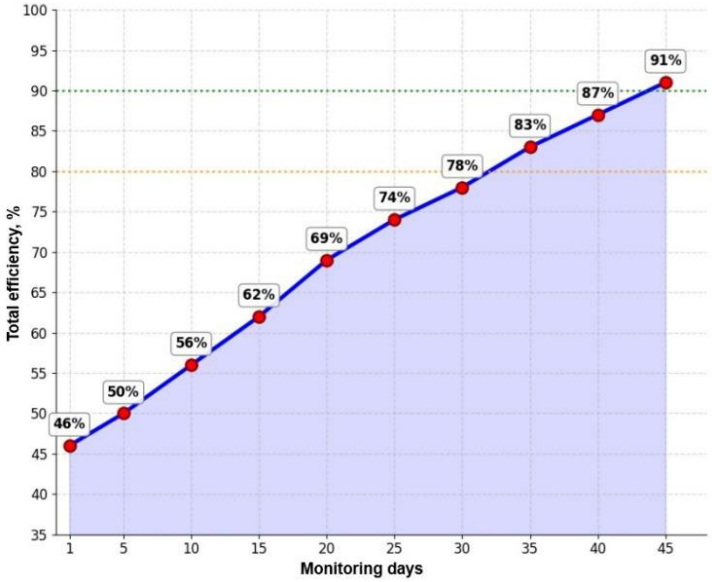



**Fig. 3 - Evolution of the total efficiency indicator of the acoustic architecture**

The acoustic architecture also showed a progressive increase in the total efficiency indicator during the 45-day period (Figure 3). The efficiency increased from 46% on day 1 to 91% on day 45, with intermediate values of 50%, 56%, 62%, 69%, 74%, 78%, 83% and 87%. The mean efficiency calculated over the complete period was 76.8%, while the maximum recorded value was 91%. The results describe an increasing temporal trend in the measured performance indicator under the tested field conditions.

### *3.4. Performance of the acoustic architecture*

The performance of the acoustic architecture is presented in Table 2.

**Table 2**

**Maximum and mean sound-pressure levels of the acoustic architecture**

| Distance from the speaker,m | Sound volume, % | | | | | | | |
|---|---|---|---|---|---|---|---|---|
| | 25 | | 50 | | 75 | | 100 | |
| | Sound pressure, dB | | | | | | | |
| | Maximum | Mean | Maximum | Mean | Maximum | Mean | Maximum | Mean |
| **1.0** | 95.8 | 90.2 | 99.9 | 97.9 | 106.2 | 102.5 | 111.4 | 104.3 |
| **3.5** | 83.8 | 82.7 | 97.0 | 91.5 | 98.3 | 95.7 | 103.4 | 95.8 |
| **7.0** | 82.3 | 79.4 | 88.1 | 86.3 | 94.1 | 85.1 | 98.2 | 89.8 |
| **14.0** | 78.9 | 76.6 | 84.2 | 83.0 | 89.7 | 83.5 | 91.3 | 87.5 |
| **21.0** | 77.4 | 74.7 | 80.4 | 79.6 | 85.0 | 81.7 | 89.0 | 79.6 |
| **28.0** | 77.0 | 73.8 | 80.2 | 77.8 | 81.1 | 78.7 | 82.6 | 82.0 |

The acoustic measurements for the acoustic architecture showed a clear decrease in sound-pressure level with increasing distance from the sound source. At 100% volume, the maximum sound-pressure level decreased from 111.4 dB at 1 m to 103.4 dB at 3.5 m, 98.2 dB at 7 m, 91.3 dB at 14 m, 89.0 dB at 21 m and 82.6 dB at 28 m. The results demonstrate the spatial attenuation of the acoustic signal and provide an experimental characterization of the sound distribution within the protected area. Compared with the multimodal acoustic-visual architecture, the acoustic architecture generated higher sound-pressure levels at short distances, while the two systems exhibited different spatial acoustic profiles.

The comparison also indicates that higher acoustic pressure alone did not correspond to higher overall system efficiency under the tested conditions.

The acoustic architecture produced higher maximum sound-pressure levels at short distances than the multimodal acoustic-visual architecture, but its mean system efficiency over the 45-day period was lower (76.8% compared with 81.4%). Because the two systems differed in detection strategy and deterrence configuration, this observation should be interpreted as a comparison of complete architectures rather than as an isolated test of acoustic intensity.

### *3.5. Comparative analysis of bird activity and system performance*

The comparative analysis of the two architectures, presented in Table 3, showed differences in the main field-performance indicators. The multimodal acoustic-visual architecture recorded a mean efficiency of 81.4%, compared with 76.8% for the acoustic architecture, while the maximum efficiencies were 97% and 91%, respectively. During the 45-day monitoring period, 470 bird observations were recorded for the multimodal architecture and 621 for the acoustic architecture. The corresponding mean daily values were 10.4 and 13.8 observations/day.

**Table 3**

**Comparative analysis of bird activity and system performance**

| Indicator | Multimodal acoustic-visual architecture | Acoustic architecture |
|---|---|---|
| **Minimum efficiency (%)** | 52 | 46 |
| **Mean efficiency (%)** | 81.4 | 76.8 |
| **Maximum efficiency (%)** | 97.0 | 91.0 |
| **Total bird observations** | 470 | 621 |
| **Mean daily bird observations** | 10.4 | 13.8 |
| **Minimum daily bird observations** | 3 | 5 |
| **Maximum daily bird observations** | 21 | 24 |
| **Reduction in bird activity (%)** | 85.7 | 79.2 |
| **Ultrasound** | Yes | No |
| **Laser system** | Yes | No |
| **AI detection** | Yes | No |
| **Operational availability (%)** | 100 | 100 |

The initial and final daily bird counts were also used to calculate the reduction in bird activity. For the multimodal acoustic-visual architecture, the number of birds recorded decreased from 21 to 3, corresponding to a reduction of 85.7%. For the acoustic architecture, the number decreased from 24 to 5, corresponding to a reduction of 79.2%.

These values describe the change between the initial and final daily observations and should be distinguished from the system-efficiency indicator.

Both architectures maintained 100% operational availability throughout the 45-day experiment. Therefore, the observed differences in the reported performance indicators occurred while both systems remained operational under the tested field conditions.

### *3.6. Discussion of the two architectures*

The comparative results indicate that both architectures were capable of reducing observed bird activity under real field conditions. The multimodal acoustic-visual architecture recorded higher values for the analyzed system-performance indicators, including mean efficiency, maximum efficiency and calculated reduction in bird activity. The difference in mean efficiency between the two architectures was 4.6 percentage points, while the difference in maximum efficiency was 6 percentage points. The total number of bird observations was also lower for the multimodal architecture (470 compared with 621).

The multimodal acoustic-visual architecture combined several deterrence mechanisms, including acoustic and ultrasonic stimuli, laser-based visual stimulation and AI-assisted detection, whereas the acoustic architecture relied primarily on acoustic stimulation and PIR-based motion detection, while also incorporating passive visual deterrents. The present comparison therefore concerns complete system architectures. Because the experimental design was not factorial or based on component removal (ablation), the individual contribution of laser stimulation, ultrasonic stimulation or AI-based detection cannot be isolated from the available data. An additional observation concerns the acoustic measurements. The acoustic architecture generated higher sound-pressure levels at short distances than the multimodal acoustic-visual architecture, but its mean system efficiency was lower.

This finding indicates that acoustic intensity alone does not describe the overall performance of an intelligent bird-deterrence system. Detection strategy, stimulus diversity and spatial distribution should also be considered when comparing complete system architectures.

Overall, the field experiment demonstrated that both architectures were capable of autonomous operation and were associated with reduced bird activity indicators over the 45-day monitoring period.

The multimodal acoustic-visual architecture recorded higher values for the analyzed performance indicators under the tested conditions, while the acoustic architecture also maintained sustained operation with PIR-based activation and 100% operational availability.

### *3.7. Energy autonomy*

The energy-autonomy test, presented in table 4, demonstrated that both architectures maintained substantial battery reserves during prolonged periods of limited solar availability.

**Table 4**

**Battery state of charge during the energy-autonomy test**

| Time | Multimodal acoustic-visual architecture (%) | Acoustic architecture (%) |
|---|---|---|
| **Start** | 100 | 100 |
| **24h** | 88 | 91 |
| **48h** | 74 | 80 |
| **72h** | 61 | 69 |
| **96h** | 48 | 57 |
| **120h** | 35 | 44 |

After 96 h, the battery state of charge was 48% for the multimodal acoustic-visual architecture and 57% for the acoustic architecture. After 120 h, the corresponding values were 35% and 44%. Because the photovoltaic capacities and battery configurations were different for the two architectures, the state-of-charge values should not be interpreted as a direct measure of comparative energy consumption. The results nevertheless characterize the ability of both photovoltaic-powered systems to remain operational during periods of reduced solar availability.

## CONCLUSIONS

The 45-day field experiment demonstrated the feasibility of two intelligent architectures for automated bird deterrence under horticultural and orchard field conditions. Both systems remained operational throughout the monitoring period, with an operational availability of 100%. The multimodal acoustic-visual architecture recorded a mean system efficiency of 81.4%, increasing from 52% at the beginning of the monitoring period to a maximum of 97%. The acoustic architecture recorded a mean efficiency of 76.8%, increasing from 46% to a maximum of 91%. Bird activity indicators decreased over the experimental period for both architectures. Based on the initial and final daily counts, the calculated reduction in bird activity was 85.7% for the multimodal acoustic-visual architecture and 79.2% for the acoustic architecture. The total number of bird observations was 470 and 621, respectively. The acoustic measurements showed different spatial sound-pressure profiles for the two architectures. The acoustic architecture generated higher sound-pressure levels at short distances, but this did not correspond to a higher mean system-efficiency value. The comparison therefore indicates that acoustic intensity alone is not sufficient to characterize the performance of a complete intelligent bird-deterrence architecture.The energy-autonomy tests showed that after 96 h the battery state of charge remained at 48% for the multimodal acoustic-visual architecture and 57% for the acoustic architecture, while after 120 h the corresponding values were 35% and 44%. These results characterize the operation of both photovoltaic-powered systems during a period of limited solar availability.

Under the experimental conditions investigated, the multimodal acoustic-visual architecture recorded higher values for the analyzed performance indicators than the acoustic architecture. However, the present experimental design does not allow the individual contribution of laser stimulation, ultrasonic stimulation or AI-based detection to be isolated.

Further studies using controlled comparative or factorial experiments, longer monitoring periods and species-specific observations are required to quantify the contribution of individual deterrence mechanisms and to assess long-term effectiveness.

## ACKNOWLEDGEMENT

This work was funded by the NUCLEU Programme 2023–2026, PN 23 04 01 06 "Intelligent mixed system for protection of agricultural crops against pests according to the Agriculture Concept 4.0", Contract no. 9N/01.01.2023.

## REFERENCES


[1] Bhusal, S., Bhattarai, U., & Karkee, M. (2019). Improving pest bird detection in a vineyard environment using super-resolution and deep learning. IFAC-PapersOnLine, 52(30), 18–23. https://doi.org/10.1016/j.ifacol.2019.12.483

[2] Bhusal, S., Bhattarai, U., Karkee, M., Majeed, Y., & Zhang, Q. (2022). Automated execution of a pest bird deterrence system using a programmable unmanned aerial vehicle (UAV). Computers and Electronics in Agriculture, 198, 106972. https://doi.org/10.1016/j.compag.2022.106972

[3] Brown, R. N., & Brown, D. H. (2021). Robotic laser scarecrows: A tool for controlling bird damage in sweet corn. Crop Protection, 146, 105652. https://doi.org/10.1016/j.cropro.2021.105652

[4] Chen, Y.-C., Chu, J.-F., Hsieh, K.-W., Lin, T.-H., Chang, P.-Z., & Tsai, Y.-C. (2024). Automatic wild bird repellent system that is based on deep-learning-based wild bird detection and integrated with a laser rotation mechanism. Scientific Reports, 14, 15924. https://doi.org/10.1038/s41598-024-66920-2

[5] Duttenhefner, J. L., ElSaid, A., & Klug, P. E. (2025). Machine learning to detect, classify, and count blackbirds damaging agriculture using drone-based imagery: Supporting AI-driven automation for deployment of damage management tools. Ecological Informatics, 92, 103495. https://doi.org/10.1016/j.ecoinf.2025.103495

[6] Egan, C. C., Blackwell, B. F., Fernández-Juricic, E., & Klug, P. E. (2020). Testing a key assumption of using drones as frightening devices: Do birds perceive drones as risky? The Condor, 122(3). https://doi.org/10.1093/condor/duaa014

[7] Elbers, A. R. W., & Gonzales, J. L. (2021). Efficacy of an automated laser for reducing wild bird visits to the free range area of a poultry farm. Scientific Reports, 11, 12779. https://doi.org/10.1038/s41598-021-92267-z

[8] Enos, J. K., Ward, M. P., & Hauber, M. E. (2021). A review of the scientific evidence on the impact of biologically salient frightening devices to protect crops from avian pests. Crop Protection, 148, 105734. https://doi.org/10.1016/j.cropro.2021.105734

[9] Ghazal, S., Munir, A., & Qureshi, W. S. (2024). Computer vision in smart agriculture and precision farming: Techniques and applications. Artificial Intelligence in Agriculture, 13, 64–83. https://doi.org/10.1016/j.aiia.2024.06.004

[10] Heath, S. K., & Long, R. F. (2019). Multiscale habitat mediates pest reduction by birds in an intensive agricultural region. Ecosphere, 10(10), e02884. https://doi.org/10.1002/ecs2.2884

[11] Jalgoankar, T. G., Badgujar, C. M., Kluever, B. M., & Klug, P. E. (2026). Emerging technology-driven bird deterrence methods for agricultural crop protection: A systematic literature review. Smart Agricultural Technology, 14, 102403. https://doi.org/10.1016/j.atech.2026.102403

[12] Jose, T., & Mayan, J. A. (2025). LoRaWAN and artificial intelligence integrated smart acoustic sensor network for bird species identification and deterrence system for farm protection. Measurement, 256(Part D), 118452. https://doi.org/10.1016/j.measurement.2025.118452

[13] Manz, S. T., Sieving, K. E., Brown, R. N., Klug, P. E., & Kluever, B. M. (2024). Experimental assessment of laser scarecrows for reducing avian damage to sweet corn. Pest Management Science, 80, 1547–1556. https://doi.org/10.1002/ps.7888

[14] Micaelo, E. B., Lourenço, L. G. P. S., Gaspar, P. D., Caldeira, J. M. L. P., & Soares, V. N. G. J. (2023). Bird deterrent solutions for crop protection: Approaches, challenges, and opportunities. Agriculture, 13(4), 774. https://doi.org/10.3390/agriculture13040774

[15] Mohamed, W. M. W., Naim, M. N. M., & Abdullah, A. (2020). The efficacy of visual and auditory bird scaring techniques using drone at paddy fields. IOP Conference Series: Materials Science and Engineering, 834(1), 012072.

[16] Nebel, C., Sumasgutner, P., Pajot, A., & Amar, A. (2019). Response time of an avian prey to a simulated hawk attack is slower in darker conditions, but is independent of hawk colour morph. Royal Society Open Science, 6, 190677. https://doi.org/10.1098/rsos.190677

[17] Pejchar, L., Clough, Y., Ekroos, J., Nicholas, K. A., Olsson, O., Ram, D., Tschumi, M., & Smith, H. G. (2018). Net effects of birds in agroecosystems. BioScience, 68, 896–904. https://doi.org/10.1093/biosci/biy104

# THE ROLE OF CANOPY ARCHITECTURE AND CANOPY MANAGEMENT IN OPTIMIZING GROWTH, FRUITING, AND FRUIT QUALITY IN FRUIT TREES

/

# *ROLUL ARHITECTURII ȘI MANAGEMENTULUI COROANEI ÎN OPTIMIZAREA CREȘTERII, FRUCTIFICĂRII ȘI CALITĂȚII PRODUCȚIEI LA POMII FRUCTIFERI*

**Oana-Elena MILEA[1)], Nicolae-Valentin VLĂDUȚ*[2)], Stefan DUMITRU[2)], Ana-Maria GROSU[1)], Corina CRUCERU[3)]**

[1)] National University of Science and Technology POLITEHNICA Bucharest / Romania;

[2)] National Institute of Research - Development for Machines and Installations Designed to Agriculture and Food Industry - INMA Bucharest / Romania;

[3)] USAMV Bucharest, Faculty of Management and Rural Development, Slatina Branch, Olt County / Romania.

**E-mail: vladut@inma.ro*

***Keywords:*** *canopy management, fruit trees, light interception, canopy architecture, fruit quality, productivity.*

**ABSTRACT**

*Canopy architecture and canopy management are essential components of modern fruit production systems, directly influencing light interception, photosynthetic efficiency, fruit quality and orchard productivity. The present study reviews and synthesizes recent scientific findings concerning the role of canopy structure, pruning practices and training systems in optimizing vegetative growth and fruiting in fruit tree species. The analysis highlights the importance of maintaining a balanced canopy structure that ensures efficient light distribution, adequate air circulation and a favorable balance between vegetative growth and reproductive development. The reviewed studies indicate that appropriate pruning and canopy management practices improve light penetration within the canopy, enhance fruit size, coloration and biochemical composition, and contribute to increased productivity. The response to pruning varies among species and depends on factors such as cultivar, rootstock, tree age, training system and environmental conditions. Furthermore, the integration of mechanized pruning technologies can improve labor efficiency and orchard management, although additional selective manual interventions may be required to maintain fruit quality. Overall, efficient canopy management represents a key strategy for improving orchard performance and ensuring sustainable fruit production.*

**REZUMAT**

*Arhitectura coroanei și managementul acesteia reprezintă elemente fundamentale ale tehnologiilor moderne de cultivare a pomilor fructiferi, influențând direct interceptarea luminii, eficiența fotosintezei, calitatea fructelor și productivitatea livezilor. Lucrarea prezintă o analiză și sinteză a rezultatelor raportate în literatura de specialitate privind rolul structurii coroanei, al sistemelor de conducere și al lucrărilor de tăiere asupra proceselor de creștere și fructificare la diferite specii pomicole. Rezultatele evidențiază faptul că optimizarea arhitecturii coroanei favorizează distribuția uniformă a luminii, îmbunătățește microclimatul intern al pomului și contribuie la creșterea producției și a calității fructelor. Efectele tăierilor diferă în funcție de specie, vârstă, portaltoi și condițiile de cultură, însă în toate cazurile acestea reprezintă instrumente importante pentru reglarea echilibrului dintre creșterea vegetativă și fructificare. De asemenea, utilizarea echipamentelor specializate și a tehnologiilor de mecanizare poate crește eficiența lucrărilor de întreținere a coroanei și poate contribui la dezvoltarea unor sisteme de producție durabile și performante.*

## INTRODUCTION

Arhitectura coroanei pomilor fructiferi reprezintă un factor esențial pentru creșterea productivității și îmbunătățirea calității fructelor, prin influența exercitată asupra interceptării și utilizării radiației solare în procesul de fotosinteză. Coroana este alcătuită din trunchi, ramuri, lăstari și frunze și îndeplinește un rol fundamental în interceptarea radiației solare și în desfășurarea proceselor fiziologice ale plantei *(Wani et al., 2021; Kumar & Sharma, 2020)*.

Densitatea coroanei, determinată de numărul, dimensiunea și distribuția frunzelor, influențează direct capacitatea pomului de a intercepta și valorifica radiația solară *(Hota & Chander, 2025)*. În acest context, o arhitectură corespunzătoare a coroanei trebuie să asigure un schelet solid, format din ramuri principale, secundare și terțiare bine distribuite și cu unghiuri de inserție favorabile, precum și o dispunere

eficientă a formațiunilor de rod și a aparatului foliar. Menținerea unui spațiu interior suficient pentru circulația aerului, concomitent cu asigurarea unui nivel adecvat de umbrire, contribuie atât la desfășurarea corespunzătoare a proceselor fiziologice, cât și la protejarea fructelor împotriva efectelor negative ale radiației solare excesive *(Kumar & Sharma, 2020)*.

Eficiența fotosintezei și, implicit, productivitatea pomilor sunt condiționate de disponibilitatea luminii și de interacțiunea acesteia cu temperatura, apa și fertilitatea solului *(Bhardwaj et al., 2025)*. O distribuție corespunzătoare a luminii în interiorul coroanei favorizează dezvoltarea florilor și fructelor prin stimularea producției de carbohidrați, în timp ce un frunziș viguros, cu o capacitate fotosintetică ridicată, contribuie la valorificarea eficientă a energiei solare.

Prin urmare, o coroană bine structurată trebuie să asigure un echilibru între interceptarea luminii, circulația aerului și protejarea fructelor împotriva radiației excesive. În același timp, menținerea formei fundamentale a pomului și a unor unghiuri largi de inserție ale ramurilor contribuie la formarea unui schelet robust, cu efecte favorabile asupra longevității pomului și a intrării acestuia pe rod *(Bhardwaj et al., 2025, Hota & Chander, 2025)*.

Managementul coroanei reprezintă o componentă fundamentală a tehnologiei moderne de cultivare a pomilor fructiferi, având ca obiectiv optimizarea arhitecturii vegetative prin controlul formei, dimensiunii și densității coroanei. Acesta include lucrările de formare, conducere și tăiere, prin care se urmăresc distribuția corespunzătoare a luminii și aerului în interiorul coroanei, menținerea echilibrului dintre creșterea vegetativă și fructificare și repartizarea eficientă a formațiunilor de rod *(Wani et al., 2021)*. Totodată, optimizarea arhitecturii coroanei permite maximizarea suprafeței foliare expuse la radiația solară și favorizează repartizarea substanței uscate către organele de reproducere, cu efecte asupra productivității și calității fructelor *(Khalil et al., 2023)*.

Un obiectiv esențial al managementului coroanei îl constituie optimizarea interceptării și penetrării luminii, deoarece nivelul și distribuția acesteia influențează fotosinteza, înflorirea, legarea și dezvoltarea fructelor, precum și producția, calitatea și colorarea acestora *(Hota & Chander, 2025)*.

În acest sens, formarea și întreținerea corespunzătoare a coroanei contribuie la îmbunătățirea randamentului și calității fructelor, la eficientizarea utilizării resurselor și la prelungirea duratei de viață a plantațiilor *(Bhardwaj et al., 2025)*. Dintre intervențiile tehnologice utilizate, tăierea are un rol deosebit în modelarea coroanei și reglarea proceselor de creștere și fructificare, prin îndepărtarea organelor vegetative neproductive sau afectate și îmbunătățirea condițiilor de iluminare în zona de rodire *(Wani et al., 2021)*.

În cadrul managementului coroanei, formarea și tăierea reprezintă intervenții distincte, dar complementare. Formarea pomului are ca obiectiv stabilirea și dirijarea arhitecturii coroanei, în special în primii ani de vegetație, prin alegerea și poziționarea ramurilor care vor constitui structura de bază a pomului.

Tăierea reprezintă una dintre principalele intervenții utilizate în acest proces, dar are un rol mai larg, fiind aplicată atât în perioada de formare, cât și ulterior, pentru menținerea și ajustarea structurii coroanei și pentru reglarea raportului dintre creșterea vegetativă și fructificare *(Wani et al., 2021)*

Prin îndepărtarea selectivă a unor organe vegetative, aceasta tăierea contribuie la stimularea regenerării, îmbunătățirea pătrunderii luminii în zona de rodire și crearea unor condiții favorabile pentru formarea mugurilor de rod și dezvoltarea fructelor *(Wani et al., 2021)*. Aplicarea intervențiilor încă din primii ani de vegetație este importantă pentru prevenirea formării unor coroane excesiv de viguroase, voluminoase și dense, care limitează distribuția luminii și pot afecta producția și calitatea fructelor *(Hota & Chander, 2025; Khalil et al., 2023)*.

Răspunsul pomilor la tăiere este influențat de momentul și intensitatea intervenției, precum și de soi, portaltoi, vârsta pomului, sistemul de conducere și condițiile pedoclimatice, determinând modificări atât ale creșterii vegetative, cât și ale fructificării *(Wani et al., 2021; Normand & Bally, 2026)*. În funcție de obiectivele tehnologice, se utilizează tăieri în uscat și în verde, ciupiri, tăieri de reducție și de rărire, precum și tăieri mecanizate de contur *(Wani et al., 2021)*.

În cazul tăierilor mecanizate, deși acestea pot contribui la standardizarea coroanei, reducerea necesarului de forță de muncă și creșterea producției, pot determina compactarea vegetației și diminuarea pătrunderii luminii în interiorul coroanei. Mika, Buler și Treder (2016) au constatat că, după trei ani de aplicare, pomii tăiați mecanizat au înregistrat producții superioare celor tăiați manual, dar și reduceri ale dimensiunii, greutății medii și intensității colorației roșii a fructelor. Prin urmare, alegerea și intensitatea tăierilor trebuie adaptate particularităților biologice ale pomului și condițiilor de cultură, iar în cazul tăierilor mecanizate, completarea acestora prin intervenții manuale selective și răritul corespunzător al fructelor poate

contribui la menținerea echilibrului dintre productivitate și calitatea producției *(Mika, Buler & Treder, 2016; Normand & Bally, 2026)*.

## MATERIALS AND METHODS

În vederea evidențierii rolului arhitecturii și managementului coroanei asupra creșterii, fructificării și calității producției la pomii fructiferi, au fost analizate și sintetizate informații provenite din literatura științifică de specialitate. Au fost luate în considerare studii care au investigat influența structurii coroanei asupra interceptării radiației solare, eficienței fotosintetice, distribuției luminii în interiorul coroanei și dezvoltării formațiunilor de rod, precum și cercetări referitoare la efectele diferitelor tipuri de tăieri și sisteme de conducere asupra creșterii vegetative, producției și calității fructelor. Informațiile identificate au fost analizate comparativ și interpretate în scopul evidențierii principalelor relații dintre caracteristicile arhitecturale ale coroanei, intervențiile de management aplicate și performanțele productive ale speciilor pomicole.

Arhitectura coroanei și sistemul de conducere influențează direct microclimatul intern al pomului și interacțiunile dintre organele vegetative și fructe. Cercetările au demonstrat că sistemele de conducere care favorizează divizarea și aerisirea coroanei permit o pătrundere mai eficientă a luminii solare, contribuind la creșterea producției și la îmbunătățirea calității fructelor (*Karunakaran et al., 2026*). Prin urmare, alegerea sistemului de conducere trebuie să urmărească optimizarea interceptării și distribuției luminii în interiorul coroanei, concomitent cu facilitarea operațiilor horticole, integrarea tehnologiilor de mecanizare, reducerea necesarului de forță de muncă și obținerea unor producții ridicate, caracterizate printr-o calitate superioară a fructelor (*Lang et al., 2022*; *Anthony & Minas, 2025*).

### Influența luminii

Interceptarea și distribuția radiației luminoase în interiorul coroanei reprezintă factori determinanți pentru desfășurarea proceselor fiziologice care susțin creșterea, dezvoltarea și fructificarea pomilor fructiferi. Maximizarea utilizării radiației solare este deosebit de importantă deoarece aceasta influențează intensitatea fotosintezei, diferențierea mugurilor, dimensiunea fructelor, acumularea zaharurilor, procesele de maturare și compoziția fructelor (*Karunakaran et al., 2026*).

Energia luminoasă absorbită de aparatul foliar este utilizată în procesul de fotosinteză pentru sinteza compușilor organici necesari formării, creșterii și maturării fructelor, motiv pentru care managementul coroanei trebuie orientat către asigurarea unei distribuții uniforme a luminii și a unei utilizări eficiente a acesteia de către suprafața fotosintetică (*Hota & Chander, 2025*).

Capacitatea coroanei de a intercepta și valorifica radiația solară este influențată de forma și orientarea pomului, densitatea de plantare, densitatea frunzișului, indicele suprafeței foliare (LAI), precum și de distribuția și suprafața foliară disponibilă pentru procesele fotosintetice (*Hota & Chander, 2025*; *Bhardwaj et al., 2025*).

Densitatea de plantare influențează, de asemenea, absorbția radiației solare la nivelul livezii. Deși creșterea numărului de pomi pe unitatea de suprafață poate determina o interceptare mai mare a luminii la nivelul plantației, densitățile excesive favorizează umbrirea reciprocă a coroanelor, cu efecte negative asupra producției, culorii și calității fructelor.

În consecință, eficiența utilizării luminii depinde de menținerea unui echilibru între dimensiunea pomilor, densitatea coroanei și distanțele de plantare (*Bhardwaj et al., 2025*).

Studiile realizate de Anthony și Minas (2025) au evidențiat faptul că lumina este distribuită mai uniform în coroanele plane, în timp ce sistemele de conducere caracterizate prin coroane complexe, cu mai multe șarpante verticale, prezintă o distribuție mai eficientă a vigorii vegetative, asociată cu creșterea greutății fructelor și a conținutului de substanță uscată.

În același timp, autorii subliniază că, deși obiectivul principal al sistemelor moderne de cultură este maximizarea interceptării luminii, distribuția acesteia în interiorul coroanei este la fel de importantă, deoarece în plantațiile tradiționale cu densitate redusă și coroane voluminoase zona de fructificare tinde să se deplaseze către partea superioară a pomului ca urmare a iluminării insuficiente a zonelor inferioare ale coroanei (*Anthony & Minas, 2025*).

Eficiența captării luminii este strâns legată de arhitectura coroanei. Coroanele înguste și dezvoltate predominant pe verticală favorizează o distribuție mai uniformă a radiației solare, în timp ce formele conice permit utilizarea eficientă a luminii, în special în regiunile apropiate de ecuator. Astfel, gradul de interceptare a luminii depinde atât de geometria coroanei, cât și de lungimea traseului parcurs de razele solare prin masa foliară (*Bhardwaj et al., 2025*).

Menținerea unui indice al suprafeței foliare optim și a unei structuri echilibrate a coroanei contribuie la distribuirea uniformă a luminii în interiorul acesteia și la reducerea efectelor negative generate de aglomerarea vegetației și umbrirea excesivă (*Bhardwaj et al., 2025*).

**Particularități ale răspunsului la tăiere în funcție de specie**

Efectele tăierilor asupra creșterii, fructificării și calității producției diferă în funcție de particularitățile biologice ale speciei, ceea ce impune adaptarea intensității și modului de intervenție la specificul fiecărei culturi. La citrice, principalul efect urmărit este îmbunătățirea pătrunderii luminii în interiorul coroanei, cu consecințe directe asupra caracteristicilor comerciale ale fructelor. Creșterea disponibilității luminii favorizează dezvoltarea fructelor, determinând sporirea dimensiunii acestora, a conținutului de suc și a concentrației de substanțe solide solubile *(Karunakaran et al., 2026)*. În cazul portocalului, intensitatea tăierii influențează în mod evident răspunsul vegetativ. Al-Saif et al. au evidențiat că intensificarea tăierii stimulează alungirea lăstarilor și dezvoltarea suprafeței foliare, deși volumul total al coroanei rămâne inferior celui înregistrat la pomii netăiați. Din punct de vedere productiv, cea mai ridicată recoltă a fost obținută în cazul tăierii severe, la 75%, urmată de tăierile de 50% și 25%. Aceste rezultate indică faptul că, la portocal, reducerea volumului coroanei prin tăiere poate fi însoțită de o intensificare a regenerării vegetative și de creșterea producției.

La mango, răspunsul la tăiere se evidențiază în special prin influența asupra înfloririi și a calității biochimice a fructelor. Spre deosebire de citrice, unde efectele sunt asociate în mod evident cu iluminarea coroanei și caracteristicile fizice ale fructului, la mango intervențiile asupra coroanei au fost asociate cu îmbunătățirea procesului de înflorire și a valorii calitative a producției *(Karunakaran et al., 2026)*. Rezultatele obținute de Asrey et al. (2013), pe parcursul a doi ani, la soiul de mango studiat în India, au arătat că pomii tăiați au produs fructe cu greutate mai mare și fermitate superioară a pulpei, precum și cu un conținut mai ridicat de carotenoizi, o capacitate antioxidantă mai mare și concentrații superioare de compuși fenolici comparativ cu pomii netăiați. Prin urmare, la mango, importanța tăierii nu se limitează la controlul arhitecturii coroanei, ci se reflectă și în modificarea compoziției biochimice și a proprietăților calitative ale fructelor.

La măslin, particularitatea răspunsului la tăiere este strâns legată de relația dintre creșterea vegetativă și încărcătura reproductivă. Rosati et al. (2018) au evidențiat că reducerea încărcăturii reproductive favorizează creșterea vegetativă, demonstrând existența unei competiții pentru resurse între dezvoltarea fructelor și formarea coroanei. În acest caz, tăierea trebuie privită nu doar ca o metodă de modelare a coroanei, ci ca un instrument de reglare a raportului dintre organele vegetative și cele reproductive. Modificarea acestui echilibru poate influența relațiile hidrice, activitatea fotosintetică și, implicit, productivitatea pomilor. Astfel, în cazul măslinului, eficiența tăierii este strâns legată de gestionarea încărcăturii de rod și de menținerea unui echilibru fiziologic între consumul de resurse pentru fructificare și dezvoltarea coroanei.

La măr, tăierea are un rol deosebit în controlul vigorii vegetative și în reglarea distribuției luminii în interiorul coroanei. Prin reducerea și redistribuirea masei vegetative se poate obține o arhitectură mai echilibrată, favorabilă pătrunderii luminii către zonele fructifere. O iluminare mai bună a coroanei este asociată cu îmbunătățirea mai multor caracteristici ale fructelor, inclusiv dimensiunea, fermitatea pulpei, intensitatea colorației și raportul dintre zaharuri și acizi. În cazul pomilor maturi, tăierea reduce suprafața foliară și activitatea fotosintetică la nivelul coroanei, dar poate favoriza pătrunderea luminii și eficiența utilizării apei. În acest context, o intensitate moderată a tăierii poate contribui la optimizarea arhitecturii coroanei și la menținerea unui echilibru fiziologic favorabil producției și calității fructelor *(Woldegebriel, 2025)*. În plus, la măr, producția este corelată cu interceptarea luminii, până la valori de aproximativ 50–60%, ceea ce evidențiază importanța gestionării arhitecturii coroanei pentru valorificarea eficientă a radiației solare *(Anthony & Minas, 2025)*.

La piersic, particularitățile managementului coroanei sunt strâns legate de sistemul de conducere și de densitatea de plantare, acestea influențând atât arhitectura pomilor, cât și productivitatea la nivel de pom și de suprafață. Sistemele de conducere urmăresc controlul vigorii și organizarea coroanei astfel încât să optimizeze interceptarea, distribuția și pătrunderea luminii, cu efecte asupra producției și calității fructelor. Spre deosebire de speciile la care efectele tăierii sunt analizate predominant prin răspunsul vegetativ sau prin modificarea caracteristicilor fructului, la piersic trebuie luată în considerare și relația dintre arhitectura individuală a pomului și configurația plantației. Densitatea redusă de plantare favorizează formarea unor coroane mai mari și un potențial mai ridicat de fructificare pe pom, dar poate întârzia intrarea pe rod, deoarece este necesară o perioadă mai lungă pentru formarea șarpantelor. În schimb, creșterea densității de

plantare determină sporirea producției raportate la unitatea de suprafață și permite atingerea mai rapidă a unor niveluri comerciale de producție *(Anthony & Minas, 2025)*.

Prin urmare, deși tăierea are la toate aceste specii funcția generală de reglare a arhitecturii coroanei și a raportului dintre creșterea vegetativă și fructificare, răspunsul pomilor este diferit.

## RESULTS

Analiza literaturii de specialitate a evidențiat faptul că arhitectura coroanei și intervențiile de management aplicate acesteia influențează în mod direct procesele fiziologice și productive ale pomilor fructiferi.

O distribuție uniformă a luminii în interiorul coroanei favorizează intensificarea fotosintezei, diferențierea mugurilor de rod și dezvoltarea fructelor, contribuind la creșterea producției și la îmbunătățirea caracteristicilor calitative ale acesteia.

Rezultatele analizate au arătat că sistemele de conducere care asigură o pătrundere mai eficientă a luminii și o aerisire corespunzătoare a coroanei conduc la sporirea greutății fructelor, îmbunătățirea colorației, a conținutului de zaharuri și a acumulării de substanță uscată. În același timp, densitatea excesivă a coroanei și a plantației poate reduce eficiența utilizării luminii și poate afecta negativ producția și calitatea fructelor.

Tăierea s-a dovedit a fi una dintre cele mai importante intervenții tehnologice pentru optimizarea arhitecturii coroanei. Prin eliminarea selectivă a organelor vegetative și redistribuirea masei foliare, aceasta contribuie la îmbunătățirea iluminării zonelor de rodire și la menținerea echilibrului dintre creșterea vegetativă și fructificare. Analiza comparativă a studiilor a arătat că răspunsul la tăiere diferă în funcție de specie. La citrice și măr sunt evidențiate efecte pozitive asupra producției și calității fructelor, la mango asupra caracteristicilor biochimice și comerciale ale fructelor, iar la măslin asupra raportului dintre dezvoltarea vegetativă și încărcătura reproductivă.

## CONCLUSIONS

Managementul coroanei reprezintă un factor determinant pentru obținerea unor producții ridicate și a unor fructe de calitate superioară în sistemele moderne de cultură a pomilor fructiferi. Arhitectura coroanei influențează direct interceptarea și distribuția luminii, eficiența fotosintezei și procesele de creștere și fructificare, motiv pentru care optimizarea acesteia trebuie să constituie un obiectiv principal al tehnologiilor de întreținere.

Tăierile și sistemele de conducere contribuie la menținerea unui echilibru între dezvoltarea vegetativă și cea reproductivă, favorizând pătrunderea luminii în interiorul coroanei și îmbunătățirea condițiilor microclimatice. Intensitatea și modul de aplicare a acestor intervenții trebuie adaptate particularităților biologice ale fiecărei specii, precum și condițiilor de cultură.

## REFERENCES

[1] Mika, A., Buler, Z., & Treder, W. (2016). Mechanical pruning of apple trees as an alternative to manual pruning. Acta Scientiarum Polonorum Hortorum Cultus, 15(1), 113-121.

[2] Wani, R. A., Din, S., Khan, M., Hakeem, S. A., Jahan, N., Lone, R. A., & Khan, J. (2021). Canopy management in fruit crops for maximizing productivity. Int J Chem Stud, 9(3), 160-165

[3] Hota, D., & Chander, S. (2025). Growth Manipulation through Canopy Architecture. *Advances in Growth Regulation of Fruit Crops*, 90-104, DOI: 10.1201/9781003354055-9.

[4] Kumar, K., & Sharma, S. (2020). Canopy management in fruit crops. Just Agric, 1(4). Khalil, A., Mir, M., Nabi, S., Mir, M. M., Iqbal, U., Nazir, N., ... & Wani, T. F. (2023). Canopy management. In Temperate nuts (pp. 209-245). Singapore: Springer Nature Singapore, https://doi.org/10.1007/978-981-19-9497-5_9.

[5] Bhardwaj, T., Kumar, V., Rana, V. S., & Sharma, S. (2025). Root and canopy regulation. Advances in growth regulation of fruit crops, 39-51.

[6] Normand, F., & SE Bally, I. (2026). Crop production: Canopy management. In The Mango: Botany, Production and Uses (pp. 466-494). GB: CABI, https://doi.org/10.1079/9781800622647.0020.

[7] Al-Saif, A. M., Abdel-Aziz, H. F., Khalifa, S. M., Elnaggar, I. A., Abd El-wahed, A. E. W. N., Farouk, M. H., & Hamdy, A. E. (2023). Pruning boosts growth, yield, and fruit quality of old Valencia orange trees: A field study. Agriculture, 13(9), 1720.

[8] Karunakaran, G., Kanupriya, C., Arivalagan, M., Laxman, R. H., Kumar, P., Manjunath, B. L., ... & Khadivi, A. (2026). Canopy management in two dragon fruit species through training systems for sustainable fruit production. Scientia Horticulturae, 355, 114545.

[9] Asrey, R., Patel, V. B., Barman, K., & Pal, R. K. (2013). Pruning affects fruit yield and postharvest quality in mango (Mangifera indica L.) cv. Amrapali. Fruits, 68(5), 367–380. https://doi.org/10.1051/fruits/2013070

[10] Rosati, A., Paoletti, A., Al Hariri, R., Morelli, A., & Famiani, F. (2018). Resource investments in reproductive growth proportionately limit investments in whole-tree vegetative growth in young olive trees with varying crop loads. Tree Physiology, 38(9), 1267–1277. https://doi.org/10.1093/treephys/tpy011

[11] Woldegebriel, A. M. (2025). Retracted: Canopy management improves better orchard light penetration, optimum tree growth, and fruit quality of apple (Malus domestica Borkh.) trees grown in mild winter tropical condition. European Journal of Horticultural Science, 90(1).

[12] Ma, H., Wang, K., Ma, J., Jiang, S., Liu, P., Yang, C., ... & Chang, H. (2025). Calculation method of canopy effective volume for fruit tree based on LiDAR point cloud data. Frontiers in Plant Science, 16, 1679027, https://doi.org/10.3389/fpls.2025.1679027.

[13] Anthony, B. M., & Minas, I. S. (2025). Canopy architecture impact on peach tree physiology, vigor diffusion, productivity and fruit quality. *Scientia Horticulturae*, *342*, 114025.

[14] Lang, R., Han, Y., Bai, X., & Bao, X. (2022). Influence of the metal flow in the keyhole molten pool on the molten pool stability in continuous variable polarity plasma arc keyhole vertical-up welding. *Journal of manufacturing processes*, *76*, 195-209, 10.1016/j.jmapro.2021.12.052.

# PHOSPHORUS TRANSFORMATION AND RECOVERY FROM POULTRY LITTER THROUGH PYROLYSIS: CHEMICAL FORMS, PROCESSES, AND PERSPECTIVES - A MINI-REVIEW

/

# *TRANSFORMAREA ȘI RECUPERAREA FOSFORULUI DIN AȘTERNUTUL AVICOL PRIN PIROLIZĂ: FORME CHIMICE, PROCESE ȘI PERSPECTIVE - MINIREVIEW*

**Mihaela Monica DINU[1)], Vasilica STEFAN[2)], Nicoleta RADU*[1)], Roxana Maria TUDOR[1)]**
[1)] Research and Development Institute for Plant Protection - ICDPP Bucharest / Romania;
[2)] National Institute of Research-Development for Machines and Installations Designed for Agriculture and Food Industry - INMA Bucharest / Romania.
**E-mail: nicolbiotec@yahoo.com*

**Keywords:** *phosphorus, poultry litter, phosphorus speciation, pyrolysis, phosphorus recovery, biochar, phosphorus circularity, phosphate fertilizers*

## ABSTRACT

*Phosphorus (P) is an essential macronutrient for agricultural production, but its inefficient use and accumulation in soils may cause environmental problems. Poultry litter represents an important secondary phosphorus source, containing inorganic phosphates, phytate, and other organic P compounds whose speciation influences fertilizer value and environmental mobility. This mini-review summarizes the main phosphorus sources and chemical forms in poultry manure and litter, the influence of poultry nutrition on P speciation, phosphorus transformations after soil application, and recovery strategies. Particular attention is given to pyrolysis and, to a lesser extent, hydrothermal treatment, which promote the transformation of organic P into predominantly inorganic calcium and magnesium associated phosphate phases while producing carbon-rich materials. Increasing pyrolysis temperature, at least up to approximately 450 °C, generally increases inorganic P and decreases water-soluble P, whereas Ca- and Mg-phosphate phases (e.g., hydroxyapatite and farringtonite) may become predominant at higher temperatures, potentially reducing immediate P availability and promoting slow release. Acid extraction, struvite precipitation, co-pyrolysis, and biochar–soil interactions are also discussed. Integrated recovery pathways can enhance phosphorus circularity by reducing nutrient losses, recovering a non-renewable resource, and valorizing poultry residues.*

## REZUMAT

*Fosforul (P) este un macronutrient esențial pentru producția agricolă, însă utilizarea ineficientă și acumularea sa în sol poate genera probleme de mediu. Așternutul avicol reprezintă o sursă secundară importantă de fosfor, conținând fosfați anorganici, fitați și alți compuși organici ai fosforului, a căror speciație influențează valoarea fertilizantă și mobilitatea în mediu. Prezenta minirecenzie sintetizează principalele surse și forme chimice ale fosforului din dejecțiile și așternutul avicol, influența nutriției păsărilor asupra speciației fosforului, transformările acestuia după aplicarea în sol și strategiile de recuperare. O atenție deosebită este acordată pirolizei și, într-o măsură mai mică, tratamentului hidrotermal, care favorizează transformarea fosforului organic în faze predominant anorganice de fosfați asociați cu calciu și magneziu, concomitent cu producerea unor materiale bogate în carbon. Creșterea temperaturii de piroliză, cel puțin până la aproximativ 450 °C, determină, în general, creșterea proporției de fosfor anorganic și reducerea fosforului solubil în apă. La temperaturi ridicate, fosfații de calciu și magneziu (de exemplu, hidroxiapatita și farringtonitul) pot deveni predominanți, reducând disponibilitatea imediată a fosforului și favorizând eliberarea lentă. Sunt discutate, de asemenea, extracția acidă, precipitarea struvitei, copiroliza și interacțiunile biocărbune–sol. Aceste abordări pot contribui la circularitatea fosforului și la valorificarea reziduurilor avicole.*

## INTRODUCTION

Phosphorus is an essential macronutrient required for plant growth and development. It participates in ATP-dependent energy transfer, nucleic-acid metabolism, membrane phospholipid synthesis and numerous phosphorylation reactions *(Raghothama, 1999; Vance et al., 2003)*. Despite its biological importance, phosphorus is often characterized by relatively low agronomic-use efficiency because a

considerable proportion of fertilizer P can become immobilized through adsorption, precipitation or incorporation into poorly soluble mineral and organic forms *(Shen et al., 2011)*.

Unlike nitrogen, phosphorus has no major atmospheric reservoir that can be directly exploited by conventional agriculture. Modern food production consequently depends strongly on geological phosphate resources and the fertilizers manufactured from them *(Cordell et al., 2009)*. Global phosphorus-use efficiency in cereal production has been estimated to be relatively low, with *Dhillon et al. (2017)* reporting an average value of approximately 16% using the difference method. This value should not be interpreted as a universal recovery coefficient because phosphorus-use efficiency varies with crop species, soil properties, fertilizer source, application rate and environmental conditions.

Phosphate rock is therefore both an agricultural resource and a strategic mineral resource. Most economically important phosphate deposits are sedimentary phosphorites, although igneous deposits also contribute to global phosphate production *(Pufahl & Groat, 2017)*. The conversion of phosphate rock into soluble fertilizers requires chemical processing, generally involving acidulation, which transforms relatively insoluble apatite minerals into more soluble phosphate compounds. At the same time, substantial amounts of phosphorus are continuously transferred from mineral fertilizer and feed ingredients into agricultural residues and animal manure. Poultry production is particularly important because phosphorus-containing feed ingredients, mineral supplements and endogenous phosphorus metabolism result in substantial P excretion. Poultry litter consequently represents a secondary phosphorus reservoir that can either be recycled directly to agricultural soils or processed to recover phosphorus in more controlled forms *(Bolan et al., 2010)*.

The environmental relevance of poultry litter is closely associated with phosphorus speciation. Total phosphorus concentration alone does not adequately describe its agronomic or environmental behavior. Poultry litter contains orthophosphate, calcium-associated phosphates, phytate and other organic phosphorus compounds. Their relative abundance depends on poultry diet, calcium supply, phytase supplementation, litter composition, storage and processing conditions *(Toor et al., 2005; He et al., 2007; Turner & Leytem, 2004)*. Thermochemical processing offers an alternative route for poultry-litter management. Pyrolysis converts the organic fraction into a carbon-rich solid while concentrating relatively non-volatile nutrients such as phosphorus, calcium and magnesium in the resulting biochar. Importantly, phosphorus does not simply remain chemically unchanged. Organic P is progressively transformed into inorganic phosphate species and subsequently into Ca- and Mg-associated mineral phases. Spectroscopic and diffraction studies have demonstrated that phosphorus transformations during pyrolysis and hydrothermal treatment are strongly temperature-dependent. Organic phosphate degradation and calcium-phosphate crystallization occur during thermochemical processing, with higher temperatures generally producing less soluble and more structurally stable phosphorus phases *(Uchimiya & Hiradate, 2014; Wang et al., 2015; Huang et al., 2018; Jiang et al., 2019)*.

The objective of this minireview is therefore to integrate phosphorus sources, phosphorus speciation in poultry residues, environmental behavior, recovery technologies and thermochemical transformation into a single chemical framework.

## MATERIALS AND METHODS

This mini-review was conducted as a structured narrative review. The objective was to identify, select, and critically evaluate studies published up to 2026 regarding phosphorus (P) dynamics in fertilizers, minerals, guano, and poultry-derived biochar.

### Search Strategy and Databases

Literature searches were executed across Web of Science, Scopus, PubMed, and Google Scholar using targeted word searches: ("phosphorus speciation" OR "phosphate forms") AND ("poultry manure" OR "chicken manure" OR "bat guano"); ("pyrolysis temperature") AND ("phosphate transformation" OR "pyrophosphate" OR "apatite") AND ("biochar"); ("phosphate rock genesis") AND ("SSP" OR "TSP" OR "DAP" OR "MAP") AND ("solubility"); ("phosphorus bioavailability") AND ("plant nutrition" OR "P-use efficiency"). Additional publications on phosphorus biogeochemistry, nutrient recovery from waste streams, fertilizer formulation, contaminant management and the EU regulatory framework were identified by backward citation searching of the selected articles and were included to provide context.

### Inclusion and Exclusion Criteria

Studies were selected based on the following inclusion criteria:

Peer-reviewed original research articles and reviews; Speciation analysis using advanced analytical techniques (NMR, XRD, XANES, FTIR); Investigation of the thermochemical treatment (pyrolysis or

hydrothermal carbonization) of poultry litter, other animal manures and guano across a temperature range of approximately 200–900 °C; Quantitative data regarding P solubility and bioavailability. Studies on other P-rich residues (e.g., sewage sludge, dairy residues and digestate) were included when they provided methodological or mechanistic comparisons. Studies on nutrient recovery from other waste streams, fertilizer formulation and contaminant removal were included when they informed the recovery options discussed for poultry residues. Exclusion criteria eliminated non-peer-reviewed publications (except legislative documents) and studies lacking an explicit focus on P forms, availability or recovery. Because this is a narrative review, no formal PRISMA screening procedure was applied.

## RESULTS AND DISCUSSION

### Major Sources of Phosphorus

#### *Phosphate rock*

Phosphate rock is the principal geological raw material for conventional phosphorus fertilizer production. Economically important deposits are dominated by sedimentary phosphorites, while igneous phosphate deposits constitute a smaller but technologically important resource *(Pufahl & Groat, 2017)*.

A major group of phosphate minerals is represented by apatites. Hydroxyapatite can be represented by **$Ca_5(PO_4)_3OH$.** Under acidic conditions, hydroxyapatite dissolution can be simplified as:

$$Ca_5(PO_4)_3OH + 4H^+ \rightarrow 5Ca^{2+} + 3HPO_4^{2-} + H_2O \quad (1)$$

This reaction illustrates the fundamental role of proton activity in phosphate-mineral dissolution. The resulting phosphate species participate in acid–base equilibria:

$$H_3PO_4 \rightleftharpoons H_2PO_4^- + H^+ \quad (2)$$

$$H_2PO_4^- \rightleftharpoons HPO_4^{2-} + H^+ \quad (3)$$

$$HPO_4^{2-} \rightleftharpoons PO_4^{3-} + H^+ \quad (4)$$

The relative proportions of $H_2PO_4^-$ and $HPO_4^{2-}$ are strongly dependent on pH. $H_2PO_4^-$ predominates below pH ≈ 7.2 ($pKa_2$ of phosphoric acid), whereas $HPO_4^{2-}$ predominates above this value; both ions are the main forms taken up by plant roots *(Schachtman et al., 1998)*. Consequently, phosphate solubility and mobility cannot be evaluated independently of soil or solution pH. In conventional agricultural systems, phosphorus is mined from phosphate rock, applied to land and partly lost to aquatic systems, mainly through erosion and surface runoff and, to a lesser extent, through leaching; this forms an open-loop flow with eventual sequestration in marine sediments *(Carpenter, 2008; Cordell et al., 2009)*.

**Calcium-phosphate precipitation.** Dissolved phosphate can react with calcium to form sparingly soluble mineral phases. A simplified reaction is:

$$Ca^{2+} + HPO_4^{2-} \rightarrow CaHPO_4(s) \quad (5)$$

Further precipitation can produce other calcium-phosphate phases:

$$3Ca^{2+} + 2PO_4^{3-} \rightarrow Ca_3(PO_4)_2(s) \quad (6)$$

and, under conditions favoring hydroxyl incorporation:

$$5Ca^{2+} + 3PO_4^{3-} + OH^- \rightarrow Ca_5(PO_4)_3OH(s) \quad (7)$$

These reactions are particularly relevant to animal manure because Ca and P are simultaneously abundant. During storage, soil application or thermal processing, their interaction can progressively shift phosphorus from soluble forms toward mineral-associated forms.

#### *Guano and Animal-Derived Phosphorus*

Guano represents an important historical example of nutrient recycling from animal-derived residues. Seabird guano contains phosphorus in forms that can contribute to plant nutrition, while prolonged environmental transformation can generate secondary phosphate minerals. Stable nitrogen-isotope ($\delta^{15}N$) studies have demonstrated that nutrients derived from seabird guano are incorporated into plant biomass *(Szpak et al., 2012)*. Because phosphorus has only one stable isotope ($^{31}P$), direct tracing of guano-derived P requires other approaches, such as radioisotope ($^{32}P/^{33}P$) labelling or the oxygen-isotope composition of phosphate ($\delta^{18}O$-P). Secondary phosphate minerals (e.g., hydroxylapatite and brushite) are also known to

form in long-term guano deposits, where acidic leachates from decomposing guano react with the surrounding minerals and rocks *(Audra et al., 2019)*, illustrating how organic animal-derived phosphorus can ultimately become incorporated into relatively stable mineral phases. The same general principle applies to poultry manure. Phosphorus initially originating from feed can undergo microbial mineralization, chemical precipitation and mineral transformation during manure storage and processing. Modern technological trends aim to divert poultry manure and avian guano away from environmental risks and into circular economic pathways, utilizing thermal, biological, and chemical transformation technologies.

**Phosphorus Speciation in Poultry Manure and Litter**

Poultry litter is chemically heterogeneous. Its phosphorus pool consists of both inorganic phosphorus (IP) and organic phosphorus (OP). *Toor et al. (2005)* demonstrated that phosphorus in broiler litter can include substantial quantities of dicalcium phosphate, aqueous phosphate and phytic acid. Importantly, the proportions depend on dietary composition. *He et al. (2007)*, using solution $^{31}P$ nuclear magnetic resonance spectroscopy and enzymatic hydrolysis, demonstrated that poultry manure contains multiple phosphorus forms, including orthophosphate, phytic-acid-derived P, other phosphomonoesters and phosphodiesters. *Turner and Leytem (2004)* similarly demonstrated that phosphorus in animal manures can be separated into chemically distinct fractions with substantially different environmental behavior. Sequential extraction should, however, be interpreted cautiously. *Hunger et al. (2005)* demonstrated that operational extraction procedures can overestimate particular phosphorus pools and therefore should not automatically be interpreted as direct measurements of mineralogical species.

***Inorganic phosphorus***

Inorganic phosphorus includes orthophosphate and mineral-associated phosphate. Calcium-associated phosphorus is particularly important in poultry litter because of the simultaneous presence of Ca and P. Their interaction can lead to the precipitation of dicalcium phosphate, as represented by Eq. (5).

The resulting mineral phase is generally less soluble than free orthophosphate. The importance of calcium-associated P is also supported by spectroscopic studies *(Hunger et al., 2004; Toor et al., 2005)*. The poultry-litter phosphorus pool can contain calcium-associated phosphate and calcium phytate, suggesting that Ca is an important structural component of both inorganic and organic P pools.

***Organic phosphorus***

Organic phosphorus in poultry litter includes phytate and other phosphomonoesters and phosphodiesters. Phytate is particularly important because plant-derived feed ingredients can contain substantial concentrations of phytic acid and its salts *(Turner, 2002)*. The enzymatic degradation of phytate can be represented schematically as:

**Phytate-P + $H_2O$ → lower inositol phosphates + inorganic phosphate(8)**

This should be regarded as a **schematic pathway**, not a single stoichiometric reaction, because phytase-mediated hydrolysis occurs through several sequential intermediates. A simplified representation is:

**Phytate → dephosphorylated inositol compounds + inorganic phosphate(9)**

Phytase supplementation can therefore influence both phosphorus utilization by poultry and the chemical composition of the phosphorus subsequently excreted in litter.

***Influence of Poultry Diet on Phosphorus Speciation***

The phosphorus concentration and speciation of poultry litter are strongly influenced by diet. Three factors are particularly important:

- dietary phosphorus concentration;
- phytase supplementation; and
- the calcium-to-available-phosphorus ratio.

*Leytem et al. (2007)* demonstrated that modifying dietary phosphorus and phytase affects the phosphorus concentration and solubility of broiler litter. Dietary modification can also change the amount of P lost in runoff from soils amended with poultry manure *(Vadas et al., 2004)*. Increasing phytase activity can improve the hydrolysis of phytate in the digestive tract, potentially reducing the amount of phytate-derived P excreted. Calcium is also critical because excessive Ca relative to available P can promote mineral phosphorus formation and alter phosphorus solubility. Consequently, poultry-litter P should not be regarded as a chemically uniform nutrient pool. Feed formulation determines, at least partly, whether excreted phosphorus occurs predominantly as soluble inorganic P, calcium-associated P or organic phosphorus.

**Phosphorus Transformations in Soil**

Following application to soil, poultry-litter phosphorus can undergo several competing processes:

- dissolution;
- adsorption;
- precipitation;
- mineralization;
- microbial immobilization;
- plant uptake; and
- transport with dissolved or particulate matter.

***Phosphate adsorption***

In acidic and highly weathered soils, Fe and Al oxides can strongly interact with phosphate.

A simplified surface-complexation representation is:

$$\equiv Fe\text{–}OH + H_2PO_4^- \rightleftharpoons \equiv Fe\text{–}H_2PO_4 + OH^- \quad (10)$$

This reaction is intentionally simplified because actual phosphate adsorption may involve inner-sphere complexes with different protonation states and surface configurations. Phosphate adsorption can reduce immediate solution concentrations while simultaneously creating a potentially reversible soil phosphorus reservoir.

***Calcium-phosphate precipitation in soils***

In neutral-to-alkaline or Ca-rich soils, precipitation of calcium phosphates can become increasingly important (Eqs. 5–7).

More stable phases can develop through subsequent reactions, including apatite-like minerals. Thus, phosphorus availability is controlled not only by total P input but also by soil pH, calcium concentration, Fe/Al mineralogy and organic matter.

***Environmental Mobility of Poultry-Litter Phosphorus***

The environmental risk associated with poultry litter depends strongly on the concentration of soluble and readily desorbable phosphorus. Water-soluble P, including dissolved organic P forms, can move with runoff *(Darch et al., 2014)* and contribute to eutrophication when losses reach aquatic systems *(Carpenter, 2008)*. Long-term repeated poultry-litter application can also produce phosphorus accumulation and stratification in agricultural soils *(Bolan et al., 2010)*. The transformation of a calcium-phosphate phase under acidic conditions can be represented as:

$$CaHPO_4(s) + H^+ \rightarrow Ca^{2+} + H_2PO_4^- \quad (11)$$

Similarly:

$$Ca_3(PO_4)_2(s) + 4H^+ \rightarrow 3Ca^{2+} + 2H_2PO_4^- \quad (12)$$

These reactions demonstrate why a decrease in water-soluble P does not necessarily mean that phosphorus has disappeared. It may instead have been transferred into a mineral reservoir that becomes soluble under different chemical conditions. This distinction is essential when evaluating biochar or other thermally processed manure products.

**Phosphorus Recovery from Poultry Litter**

Poultry litter can be managed through direct agricultural application or through technologies designed to concentrate and recover phosphorus. Direct application is the simplest recycling strategy. It returns phosphorus, nitrogen, potassium and organic matter to agricultural soils. However, repeated application based primarily on crop nitrogen requirements can result in phosphorus accumulation because the N:P ratio of poultry litter is considerably lower than that of crop uptake; rates calculated to meet crop N demand therefore supply P in excess of crop removal *(Bolan et al., 2010)*. Consequently, phosphorus-based nutrient management is important in regions with intensive poultry production.

***Chemical extraction***

Chemical extraction can transfer phosphorus from poorly soluble mineral phases into an aqueous phase. For tricalcium phosphate, dissolution proceeds as shown in Eq. (12), whereas for hydroxyapatite complete protonation to $H_2PO_4^-$ can be written as:

$$Ca_5(PO_4)_3OH(s) + 7H^+ \rightarrow 5Ca^{2+} + 3H_2PO_4^- + H_2O \quad (13)$$

These equations represent idealized mineral dissolution. Actual extraction systems contain multiple phosphate species, competing ions and potentially several mineral phases. The advantage of extraction is that phosphorus can be separated from the original solid matrix and subsequently recovered as a fertilizer product. Struvite precipitation: when phosphate is present in solution together with $Mg^{2+}$ and $NH_4^+$, phosphorus can be recovered as struvite:

$$Mg^{2+} + NH_4^+ + PO_4^{3-} + 6H_2O \rightarrow MgNH_4PO_4 \cdot 6H_2O(s) \quad (14)$$

At the pH range typically used for struvite crystallization (approximately 8–9), $HPO_4^{2-}$ is the dominant phosphate species, so the reaction is often written as $Mg^{2+} + NH_4^+ + HPO_4^{2-} + 6H_2O \rightarrow MgNH_4PO_4 \cdot 6H_2O(s) + H^+$. Struvite contains phosphorus, nitrogen and magnesium and can therefore function as a nutrient fertilizer. *Shashvatt et al. (2018)* demonstrated that $CO_2$-assisted phosphorus extraction from poultry litter can be coupled with selective recovery of struvite and potassium struvite. This approach illustrates the potential of combining extraction and precipitation rather than simply transferring phosphorus from one waste stream to another. Similarly, *Nishil et al. (2026)* combined acid leaching of poultry litter (pH ≈ 3.5) with precipitation at pH ≈ 9 in the presence of $Ca^{2+}$ and $Mg^{2+}$, recovering approximately 94% of the leached P as a mixture of struvite and hydroxyapatite; the spent litter was then converted into iron-loaded biochar, which removed approximately 82% of the residual P from the leachate and was proposed for use as a P-enriched soil amendment.

***Pyrolysis of Poultry Litter***

Pyrolysis is a thermochemical conversion process conducted under oxygen-limited or oxygen-free conditions. A generalized representation is:

$$Biomass \rightarrow biochar + CO_2 + CO + H_2O + CH_4 + H_2 + condensable\ organic\ compounds\ (bio\text{-}oil) \quad (15)$$

This is a process-level representation rather than a stoichiometrically balanced reaction because poultry litter contains proteins, carbohydrates, lipids, minerals and numerous other compounds. During pyrolysis, organic matter undergoes dehydration, decarboxylation, devolatilization and progressive aromatization. Phosphorus behaves differently from carbon and hydrogen because a substantial proportion of phosphorus remains associated with the solid mineral fraction. Consequently, removal of volatile organic matter produces an apparent concentration of phosphorus in the biochar. *Song and Guo (2012)* showed that pyrolysis temperature substantially changes the physicochemical properties of poultry-litter biochar, including pH, ash content, surface characteristics and nutrient composition.

**Transformation of Organic Phosphorus during Pyrolysis.** One of the most important changes during pyrolysis is the progressive conversion of organic phosphorus into inorganic phosphorus. The transformation can be represented schematically as:

$$Organic\text{-}P \rightarrow intermediate\ P\ compounds \rightarrow orthophosphate \quad (16)$$

**followed** by mineral association:

$$Orthophosphate \rightarrow Ca/Mg\text{-}phosphate\ minerals \quad (17)$$

These are not individual stoichiometric reactions but rather simplified representations of a series of thermal degradation and mineral-forming processes. *Li et al. (2018)* reported that raw poultry litter contained approximately 67.6% inorganic P and 32.4% organic P. With increasing pyrolysis temperature, the proportion of inorganic P increased substantially, reaching approximately 97% at 400 °C and approximately 99.8% at 450 °C in their experimental system. At higher temperatures (500–600 °C), a nominal organic P fraction of approximately 3–11% of total P reappeared; however, the authors attributed it to residual P that was not extractable by HCl rather than to genuine organic P, so it should not be interpreted as re-formation of organic phosphorus. In the same study, water-soluble P decreased from approximately 49.5% of total P in the raw litter to about 2.4% in biochars produced at 450 °C and above. *Jiang et al. (2019)* independently demonstrated the progressive transformation of poultry-litter phosphorus using X-ray diffraction, FTIR and solid-state NMR. Phytates decomposed at pyrolysis temperatures above approximately 300 °C, while poorly crystalline hydroxyapatite, already present in the raw litter (about 21% of P), increased to about 59% of P in biochars produced below 500 °C. Concurrently, water-extractable P decreased from 2.9 g $kg^{-1}$ in the raw litter to 0.3 g $kg^{-1}$ at 300 °C and to less than 0.2 g $kg^{-1}$ at 400 °C and above.

**Formation of Calcium- and Magnesium-Phosphate Phases.** After degradation of organic matter, phosphorus becomes increasingly associated with Ca and Mg.

Simplified mineral-forming reactions are:

$$Ca^{2+} + PO_4^{3-} \rightarrow Ca\text{–}P(s) \quad (18)$$

and:

$$Mg^{2+} + PO_4^{3-} \rightarrow Mg\text{–}P(s) \quad (19)$$

These equations represent families of mineral phases rather than unique compounds. Under suitable conditions, hydroxyapatite-like phases can form, as represented by Eq. (7).

At higher temperatures, more crystalline mineral phases can develop. *Jiang et al. (2019)* reported that, at 500 and 600 °C, labile $HPO_4^{2-}$ and phytates were almost completely converted into hydroxyapatite and newly formed farringtonite [$Mg_3(PO_4)_2$], the latter accounting for approximately 16–27% of P. More broadly, comparative thermochemical studies indicate that degradation of organic phosphorus and crystallization of calcium phosphate are strongly dependent on treatment temperature *(Huang et al., 2018)*.

**Condensed phosphates.** In addition to orthophosphate, thermal treatment can generate condensed phosphates such as pyrophosphate ($P_2O_7^{4-}$), formed by dehydration–condensation of adjacent orthophosphate groups, for example those of phytate ($2HPO_4^{2-} \rightarrow P_2O_7^{4-} + H_2O$). In poultry litter, a pyrophosphate signal was detected by solid-state $^{31}P$ NMR after heating at 100–200 °C but was no longer distinct at 300 °C and above, indicating that pyrophosphate formation is much less important than hydroxyapatite formation at higher temperatures *(Jiang et al., 2019)*. *Wang et al. (2015)* nevertheless identified pyrophosphate as a minor form of water-soluble P in poultry-litter biochar produced at 400 °C. Because pyrophosphate is hydrolysed to orthophosphate in soil through chemical and enzymatic (pyrophosphatase) processes, condensed phosphates can contribute to the gradual release of P from biochar.

**Temperature-Dependent Phosphorus Transformation.** The transformation of phosphorus during poultry-litter pyrolysis can be conceptually divided into several temperature ranges.

**Low-temperature region.** At approximately 200–300 °C, dehydration and initial thermal decomposition occur. Some organic P remains, while mineralization begins.

**Intermediate-temperature region.** At approximately 300–450 °C, degradation of organic phosphorus becomes pronounced and the inorganic P fraction increases rapidly. This range is particularly important because water-soluble phosphorus can decrease substantially while phosphorus remains potentially available through gradual mineral dissolution.

**High-temperature region.** Above approximately 450–500 °C, calcium-phosphate crystallization becomes increasingly important. The proportion of Ca-phosphate increases in this range, whereas Mg-phosphate phases such as farringtonite appear mainly above approximately 500 °C. Notably, hydroxyapatite in poultry-litter biochars can remain poorly crystalline even at 600 °C *(Jiang et al., 2019)*. The transformation can therefore be summarized as:

*Organic-P → orthophosphate → amorphous Ca/Mg-phosphate → crystalline Ca/Mg-phosphate* (20)

The exact sequence depends on feedstock composition, Ca:P and Mg:P ratios, moisture, heating rate, residence time and reactor configuration. Therefore, pyrolysis temperature should not be interpreted as an independent control variable.

**Phosphorus Release from Poultry-Litter Biochar.** *Wang et al. (2015)* demonstrated that pyrolysis of poultry litter can substantially increase total P concentration while simultaneously reducing water-soluble P. In their study, total P increased from approximately 13.7 g $kg^{-1}$ in raw litter to approximately 27.1 g $kg^{-1}$ after pyrolysis at 400 °C, while water-soluble P decreased from approximately 2.95 to 0.17 g $kg^{-1}$. This apparent contradiction—higher total P but lower soluble P—is chemically important. It indicates that pyrolysis concentrates phosphorus while simultaneously transforming it into less immediately soluble forms.

The subsequent release of phosphorus can be represented schematically as:

$$Ca\text{–}P(s) + H^+ \rightarrow Ca^{2+} + H_2PO_4^- \quad (21)$$

The rate of this process depends on mineral crystallinity, particle size, soil pH, proton supply and interactions with organic matter and root-derived compounds. Thus, poultry-litter biochar may function as a slow-release P source rather than an immediately soluble phosphate fertilizer.

**Biochar–Soil Interactions.** Biochar modifies the chemical environment of soil through changes in pH, cation exchange capacity, surface functional groups, dissolved organic carbon and mineral interactions. Meta-analyses have generally reported increases in soil P availability following biochar addition, although the magnitude depends strongly on feedstock, pyrolysis temperature, application rate and soil characteristics *(Gao et al., 2019; Glaser & Lehr, 2019; Tesfaye et al., 2021)*. In the meta-analysis of *Tesfaye et al. (2021)*, the largest effects were observed for manure-derived biochars, biochars produced below 300 °C, and acidic (pH < 5), fine-textured and P-poor soils. The effect is particularly relevant for manure-derived biochars because these materials contain substantial quantities of P, Ca and Mg. In acidic soil, proton-mediated dissolution of Ca–P phases (Eqs. 11 and 21) can facilitate P release.

In contrast, in alkaline Ca-rich conditions, phosphate may remain strongly associated with calcium-phosphate minerals. For example, pyrolysed dairy-processing sludge performed better than the raw material in an acidic soil but not in neutral soils *(McIntosh et al., 2022)*. Consequently, the agronomic performance of poultry-litter biochar cannot be predicted solely from total phosphorus concentration.

**Co-Pyrolysis for Engineered Phosphorus Fertilizers.** Co-pyrolysis provides an opportunity to manipulate phosphorus mineralogy during thermal treatment. The addition of magnesium, calcium or phosphate-containing materials can change the mineral phases formed during pyrolysis. A generalized representation is:

$$Ca^{2+}/Mg^{2+} + PO_4^{3-} \rightarrow Ca/Mg\text{-}phosphate(s) \quad (22)$$

*Lustosa Filho et al. (2017)* demonstrated that co-pyrolysis of poultry litter with phosphate and magnesium can generate slow-release fertilizer materials. The objective of this strategy is not necessarily to maximize water-soluble P. Instead, the aim is to engineer phosphorus-containing mineral phases that release P gradually after soil application. This distinction is fundamental for fertilizer design.

***Hydrothermal Carbonization***

Hydrothermal carbonization (HTC) represents an alternative thermochemical route for wet poultry residues. A simplified process representation is:

$$Wet\ poultry\ litter \rightarrow hydrochar + aqueous\ products \quad (23)$$

Unlike conventional dry pyrolysis, HTC can process wet feedstocks without extensive preliminary drying. Phosphorus transformation also occurs during HTC. *Heilmann et al. (2014)* reported that more than 90% of the total P of poultry, swine and cattle manures was retained in the hydrochars, largely as precipitated phosphate salts, from which P could subsequently be recovered by acid extraction. Comparative studies have shown that organic phosphate degradation and calcium-phosphate mineral formation occur during both pyrolysis and HTC, although the temperature ranges required for extensive mineral crystallization differ between the two processes *(Huang et al., 2018)*. *Santoro et al. (2024)* further demonstrated that solid-state $^{31}P$ NMR can provide detailed information about phosphorus environments in poultry-litter hydrochars. Research needs for scaling up HTC, including process-water management and nutrient recovery from the aqueous phase, have been reviewed by *Dang et al. (2024)*.

***Integrated Chemical Pathway for Phosphorus Recovery***

The complete phosphorus transformation pathway can be represented as:

**Poultry feed → poultry manure/litter → organic and inorganic P → thermochemical treatment → P-enriched biochar/hydrochar → extraction → soluble phosphate → recovered fertilizer**

This pathway combines the transformations described above: thermal mineralization of organic P (Eq. 16), association of the released orthophosphate with Ca and Mg (Eqs. 17–19), proton-driven dissolution of Ca–P phases during acid extraction (Eqs. 12, 13 and 21), and precipitation of the recovered phosphate as struvite (Eq. 14).

This integrated pathway connects waste management, thermochemical conversion and nutrient recovery.

***Phosphorus Mass Balance***

For a practical recovery system, phosphorus should be evaluated using a mass-balance approach:

$$P_{input} = P_{biochar} + P_{liquid} + P_{recovered} + P_{residual/lost} \quad (24)$$

where:

$\mathbf{P_{input}}$ is the phosphorus entering the treatment process;

$\mathbf{P_{biochar}}$ is phosphorus retained in the solid product;

$\mathbf{P_{liquid}}$ is phosphorus transferred to the liquid phase;

$\mathbf{P_{recovered}}$ is phosphorus recovered as a fertilizer product; and

$\mathbf{P_{residual/lost}}$ represents unrecovered phosphorus.

This framework is important because an increase in P concentration in biochar does not necessarily mean that phosphorus recovery efficiency has increased. Concentration and recovery efficiency are different parameters. For example, if organic matter is lost during pyrolysis while most phosphorus remains in the solid phase, the P concentration of the biochar increases even though the absolute quantity of phosphorus may remain approximately unchanged. Therefore, both concentration-based and mass-based indicators should be reported. At typical pyrolysis temperatures, most of the feedstock P is retained in the solid product; for example, P and K recoveries in biochar exceeded 75% during fast pyrolysis of poultry litter *(Pandey et al.,*

*2019)*, and approximately 98% of P was retained in biochar produced from dairy-processing sludge at 450 °C *(McIntosh et al., 2022)*.

**Environmental and Technical Limitations**

Despite its potential, poultry-litter pyrolysis presents several limitations.

First, phosphorus speciation depends strongly on feedstock composition and processing conditions. Results obtained at one pyrolysis temperature cannot necessarily be extrapolated to all poultry-litter feedstocks.

Second, high-temperature processing can decrease the immediate solubility of phosphorus. This may be beneficial from an environmental perspective but can reduce short-term fertilizer availability.

Third, poultry-litter biochar is strongly alkaline. Application to already alkaline soils can therefore create undesirable changes in soil pH. Conversely, in acidic soils this alkalinity can provide a liming effect that may itself increase P availability.

Fourth, phosphorus availability is controlled by mineralogy rather than total P concentration alone.

Fifth, pyrolysis modifies nitrogen differently from phosphorus. A substantial fraction of feedstock nitrogen can be lost to gaseous and condensable products during thermal treatment. Therefore, a P-rich biochar should not automatically be considered a complete NPK fertilizer.

Sixth, non-volatile trace elements present in poultry litter, particularly Cu and Zn from feed additives and, where arsenical additives have been used, As, are concentrated in the biochar together with P. *Wystalska et al. (2023)* found that most contaminants in poultry-manure biochars remained within permissible limits, although Cr exceeded the applicable threshold. For use as EU fertilising products, pyrolysis materials must meet the requirements of Component Material Category (CMC) 14, introduced into Regulation (EU) 2019/1009 by Delegated Regulation (EU) 2021/2088, including a molar H/Corg ratio below 0.7 and limits for PAH16 (6 mg $kg^{-1}$ dry matter), PCDD/F and ndl-PCB; limits for metals such as Cd, Cu, Zn and inorganic As apply to the final product through the product function category requirements of Regulation (EU) 2019/1009. Moreover, because poultry manure is an animal by-product under Regulation (EC) No 1069/2009 *(European Parliament & Council of the European Union, 2009)*, pyrolysis materials derived from it are admissible under CMC 14 only if an end point in the manufacturing chain has been determined under that Regulation *(European Parliament & Council of the European Union, 2019; European Commission, 2021)*.

Finally, the economic feasibility of phosphorus recovery depends on transport, drying requirements, reactor configuration, energy demand, extraction chemicals and the value of recovered phosphorus products.

**Research gaps**

Several key research priorities remain to elucidate phosphorus (P) dynamics during poultry litter pyrolysis and to optimize biochar utilization in sustainable agriculture.

***Standardized phosphorus speciation***

Different analytical approaches quantify distinct operational and chemical P pools. Sequential chemical extraction categorizes P based on operational solubility *(Hunger et al., 2005; Wang et al., 2022b)*, whereas solution $^{31}$P Nuclear Magnetic Resonance ($^{31}$P NMR) spectroscopy identifies organic P structures (e.g., monoesters, diesters, phytate) in liquid extracts *(Turner & Leytem, 2004; He et al., 2007; Laan et al., 2024)*. Conversely, solid-state $^{31}$P NMR, X-ray Diffraction (XRD), and Phosphorus K-edge X-ray Absorption Near-Edge Structure (XANES) spectroscopy characterize solid-phase crystalline and amorphous inorganic phosphate minerals directly within the biochar matrix without extraction artifacts *(Hunger et al., 2004; Jiang et al., 2019; Li et al., 2024; Liu et al., 2023; Santoro et al., 2024)*. Sequential extraction, solution $^{31}$P NMR, solid-state $^{31}$P NMR, XRD, and XANES should therefore be used in complementary rather than interchangeable ways to avoid misinterpreting P lability and transformation pathways.

***Linking mineralogy with plant availability***

More studies are needed to establish direct relationships between specific Ca/Mg-phosphate phases (e.g., hydroxyapatite, whitlockite, and amorphous Ca/Mg phosphates) and plant P uptake across diverse soil types *(Li et al., 2017; Novak et al., 2018)*. The dissolution of biochar mineral phases is strongly regulated by localized rhizosphere interactions, root exudate acidification, soil pH, and biochar particle size *(Pedersen et al., 2025)*. Quantifying how specific crystalline structures undergo weathering within the immediate "charosphere" is critical for predicting short- and long-term crop bio-accessibility *(Quilliam et al., 2013; Limwikran et al., 2019; Novak et al., 2018)*.

***Long-term field experiments***

Most studies remain laboratory- or greenhouse-based. Long-term field trials are required to determine how poultry-litter biochar behaves after repeated applications under realistic agricultural conditions *(Glaser & Lehr, 2019; Pan et al., 2021)*. Unresolved priorities include quantifying multi-year solubilization kinetics of recalcitrant Ca-P minerals in soil, evaluating cumulative impacts on soil pH and cation exchange capacity, and assessing shifts in soil microbial communities governing organic P mineralization *(Pan et al., 2021)*.

***Optimization of pyrolysis temperature***

There is no universal optimum temperature. Lower temperatures (300–400 °C) preserve more labile phosphorus fractions and organic matter and give higher biochar yields, but produce biochar with lower fixed carbon content and higher short-term leaching risks *(Song & Guo, 2012; Li et al., 2018; Aryal et al., 2024)*. Higher temperatures (500–700 °C) convert labile P into more stable Ca- and Mg-phosphate phases (e.g., hydroxyapatite and farringtonite) while producing condensed aromatic carbon structures resistant to microbial degradation *(Jiang et al., 2019; Pan et al., 2021)*. The optimal condition therefore depends on whether the desired product is:

- a directly applied slow-release fertilizer: moderate pyrolysis temperatures (approximately 300–450 °C) balancing P solubility with reduced runoff risk *(Li et al., 2018; Jiang et al., 2019)*;
- a phosphorus-rich intermediate for chemical extraction: higher-temperature biochars (above approximately 400 °C), in which mass loss increases P concentration and P is almost completely converted to inorganic forms *(Jiang et al., 2019)*;
- a carbon-sequestration material: high pyrolysis temperatures (>600 °C) maximizing carbon recalcitrance *(Pan et al., 2021)*; or
- a combined soil amendment: co-optimized process conditions or post-pyrolysis chemical modifications designed to optimize both carbon retention and nutrient availability *(Wang et al., 2022a)*.

***Integration with phosphorus recovery***

Future systems should evaluate pyrolysis and phosphorus extraction as integrated processes rather than independent technologies. Pre-treating poultry litter via chemical washing or mineral impregnation prior to pyrolysis can selectively mobilize organic P or direct mineral phase formation, yielding biochars with controlled release rates or high-purity secondary phosphate fertilizers *(Lustosa Filho et al., 2017; Barbosa et al., 2022; Padilla et al., 2023)*. A closed-loop example is the process described by *Nishil et al. (2026)*, in which acid leaching, struvite/hydroxyapatite precipitation and adsorption of residual P on biochar produced from the spent litter were combined, with recycling of the treated leachate towards zero liquid discharge. The integration of phosphorus recovery into poultry-waste management can contribute to the development of circular and resource-efficient fertilizer production systems. Nutrient recovery from wastewaters and residual biomass has been investigated as a viable strategy for obtaining fertilizer-related products *(Radu et al., 2007a; Radu & Meghea, 2007c)*. In particular, the reuse of spent microbial biomass in fertilizer manufacturing demonstrates the potential of waste-derived materials as secondary nutrient resources *(Radu et al., 2020)*. For poultry waste, phosphorus could similarly be recovered through suitable chemical or biological processes and subsequently incorporated into fertilizer formulations.

The interaction of recovered nutrients with calcium- and nitrogen-based compounds should also be considered when developing stable fertilizer products *(Radu et al., 2007b)*. Moreover, biosorption studies have shown that microbial biomass can remove heavy metals such as Cu and Co from dilute aqueous systems *(Dima et al., 2007; Radu et al., 2006)*; comparable approaches could help limit the transfer of feed-derived Cu and Zn from poultry-litter leachates into recovered P products. Thus, integrating phosphorus recovery with poultry-waste valorization could support the conversion of chicken-derived residues into useful fertilizer resources while reducing waste disposal requirements. Combining the energy recovered from pyrolysis with wet-chemical P extraction may provide a framework for more circular nutrient management, although its overall sustainability still needs to be demonstrated through mass-balance, techno-economic and life-cycle assessments.

## CONCLUSIONS

Poultry litter represents an important secondary phosphorus resource. Its phosphorus occurs in chemically diverse forms, including orthophosphate, calcium-associated phosphates, phytate and other organic phosphorus compounds.

The transformation of poultry-litter phosphorus is strongly influenced by poultry diet, calcium supply, phytase supplementation, soil chemistry and thermochemical treatment.

Pyrolysis produces particularly important changes in phosphorus speciation. Organic phosphorus is progressively degraded, inorganic phosphorus becomes dominant and Ca/Mg-phosphate minerals become increasingly important. Increasing temperature generally decreases water-soluble phosphorus while increasing the proportion of mineral-associated phosphorus.

The key transformation can be summarized as:

**Organic-P → orthophosphate → Ca/Mg-phosphate minerals**

These mineral phases can subsequently undergo acid-mediated dissolution:

**Ca/Mg-phosphate + $H^+$ → soluble phosphate**

The resulting phosphate can either be used directly as a slowly available nutrient or recovered through precipitation processes such as struvite formation:

$$Mg^{2+} + NH_4^+ + PO_4^{3-} + 6H_2O \rightarrow MgNH_4PO_4 \cdot 6H_2O(s)$$

Therefore, poultry-litter pyrolysis should not be viewed simply as a waste-to-biochar process. It can be considered a phosphorus-management and nutrient-recovery platform in which phosphorus speciation is deliberately modified to obtain a desired balance between stability, environmental safety and agronomic availability.

An integrated approach combining poultry nutrition, litter management, pyrolysis, phosphorus extraction and fertilizer recovery could contribute to a more circular phosphorus economy while simultaneously reducing the environmental risks associated with excessive poultry-litter application.

## REFERENCES


[1] Aryal, P., Vista, S. P., Dhakal, R., Basnet, B., Chand, P., Gyawali, S., & Pandit, N. R. (2024). Assessment of biochar quality and agronomic efficiency produced from rice-husk and saw-dust at different temperature regimes. Archives of Agriculture and Environmental Science, 9(4), 667-675. https://doi.org/10.26832/24566632.2024.090405

[2] Audra, P., De Waele, J., Bentaleb, I., Chroňáková, A., Krištůfek, V., D'Angeli, I. M., Carbone, C., Madonia, G., Vattano, M., Scopelliti, G., Cailhol, D., Vanara, N., Temovski, M., Bigot, J.-Y., Nobécourt, J.-C., Galli, E., Rull, F., & Sanz-Arranz, A. (2019). Guano-related phosphate-rich minerals in European caves. International Journal of Speleology, 48(1), 75-105. https://doi.org/10.5038/1827-806X.48.1.2252

[3] Barbosa, C. F., Correa, D. A., Carneiro, J. S. S., & Melo, L. C. A. (2022). Biochar phosphate fertilizer loaded with urea preserves available nitrogen longer than conventional urea. Sustainability, 14(2), 686. https://doi.org/10.3390/su14020686

[4] Bolan, N. S., Szogi, A. A., Chuasavathi, T., Seshadri, B., Rothrock, M. J., Jr., & Panneerselvam, P. (2010). Uses and management of poultry litter. World's Poultry Science Journal, 66(4), 673-698. https://doi.org/10.1017/S0043933910000656

[5] Carpenter, S. R. (2008). Phosphorus control is critical to mitigating eutrophication. Proceedings of the National Academy of Sciences, 105(32), 11039-11040. https://doi.org/10.1073/pnas.0806112105

[6] Cordell, D., Drangert, J.-O., & White, S. (2009). The story of phosphorus: Global food security and food for thought. Global Environmental Change, 19(2), 292-305. https://doi.org/10.1016/j.gloenvcha.2008.10.009

[7] Dang, C. H., Cappai, G., Chung, J.-W., Jeong, C., Kulli, B., Marchelli, F., Ro, K. S., & Román, S. (2024). Research needs and pathways to advance hydrothermal carbonization technology. Agronomy, 14(2), 247. https://doi.org/10.3390/agronomy14020247

[8] Darch, T., Blackwell, M. S. A., Hawkins, J. M. B., Haygarth, P. M., & Chadwick, D. R. (2014). A meta-analysis of organic and inorganic phosphorus in organic fertilizers, soils, and water: Implications for water quality. Critical Reviews in Environmental Science and Technology, 44(19), 2172-2202. https://doi.org/10.1080/10643389.2013.790752

[9] Dhillon, J., Torres, G., Driver, E., Figueiredo, B., & Raun, W. R. (2017). World phosphorus use efficiency in cereal crops. Agronomy Journal, 109(4), 1670-1677. https://doi.org/10.2134/agronj2016.08.0483

[10] Dima, G., Radu, N., Chirvase, A., & Pena, E. L. (2007). Studies regarding using biomass in bioremediation of wastewater with heavy metal. Revista de Chimie, 58(6), 561-565.

[11] European Commission. (2021). Commission Delegated Regulation (EU) 2021/2088 of 7 July 2021 amending Annexes II, III and IV to Regulation (EU) 2019/1009 of the European Parliament and of the Council for the purpose of adding pyrolysis and gasification materials as a component material category in EU fertilising products. Official Journal of the European Union, L 427, 140-148.

[12] European Parliament & Council of the European Union. (2009). Regulation (EC) No 1069/2009 of 21 October 2009 laying down health rules as regards animal by-products and derived products not intended for human consumption and repealing Regulation (EC) No 1774/2002 (Animal by-products Regulation). Official Journal of the European Union, L 300, 1-33.

[13] European Parliament & Council of the European Union. (2019). Regulation (EU) 2019/1009 of 5 June 2019 laying down rules on the making available on the market of EU fertilising products and amending Regulations (EC) No 1069/2009 and (EC) No 1107/2009 and repealing Regulation (EC) No 2003/2003. Official Journal of the European Union, L 170, 1-114.

[14] Gao, S., DeLuca, T. H., & Cleveland, C. C. (2019). Biochar additions alter phosphorus and nitrogen availability in agricultural ecosystems: A meta-analysis. Science of the Total Environment, 654, 463-472. https://doi.org/10.1016/j.scitotenv.2018.11.124

[15] Glaser, B., & Lehr, V.-I. (2019). Biochar effects on phosphorus availability in agricultural soils: A meta-analysis. Scientific Reports, 9, 9338. https://doi.org/10.1038/s41598-019-45693-z

[16] He, Z., Cade-Menun, B. J., Toor, G. S., Fortuna, A.-M., Honeycutt, C. W., & Sims, J. T. (2007). Comparison of phosphorus forms in wet and dried animal manures by solution phosphorus-31 nuclear magnetic resonance spectroscopy and enzymatic hydrolysis. Journal of Environmental Quality, 36(4), 1086-1095. https://doi.org/10.2134/jeq2006.0549

[17] Heilmann, S. M., Molde, J. S., Timler, J. G., Wood, B. M., Mikula, A. L., Vozhdayev, G. V., Spokas, K. A., Colosky, E. C., & Valentas, K. J. (2014). Phosphorus reclamation through hydrothermal carbonization of animal manures. Environmental Science & Technology, 48(17), 10323-10329. https://doi.org/10.1021/es501872k

[18] Huang, R., Fang, C., Zhang, B., & Tang, Y. (2018). Transformations of phosphorus speciation during (hydro)thermal treatments of animal manures. Environmental Science & Technology, 52(5), 3016-3026. https://doi.org/10.1021/acs.est.7b05203

[19] Hunger, S., Cho, H., Sims, J. T., & Sparks, D. L. (2004). Direct speciation of phosphorus in alum-amended poultry litter: Solid-state $^{31}$P NMR investigation. Environmental Science & Technology, 38(3), 674-681. https://doi.org/10.1021/es034755s

[20] Hunger, S., Sims, J. T., & Sparks, D. L. (2005). How accurate is the assessment of phosphorus pools in poultry litter by sequential extraction? Journal of Environmental Quality, 34(1), 382-389. https://doi.org/10.2134/jeq2005.0382

[21] Jiang, Y., Ren, C., Guo, H., Guo, M., & Li, W. (2019). Speciation transformation of phosphorus in poultry litter during pyrolysis: Insights from X-ray diffraction, Fourier transform infrared, and solid-state NMR spectroscopy. Environmental Science & Technology, 53(23), 13841-13849. https://doi.org/10.1021/acs.est.9b03261

[22] Laan, M., Strawn, D. G., Kayler, Z. E., Cade-Menun, B. J., & Möller, G. (2024). Phosphorus availability and speciation in soils amended with upcycled dairy-waste nutrients. Frontiers in Chemical Engineering, 5, 1303357. https://doi.org/10.3389/fceng.2023.1303357

[23] Leytem, A. B., Plumstead, P. W., Maguire, R. O., Kwanyuen, P., & Brake, J. (2007). What aspect of dietary modification in broilers controls phosphorus in litter: Dietary phosphorus, phytase, or calcium? Journal of Environmental Quality, 36(2), 453-463. https://doi.org/10.2134/jeq2006.0334

[24] Li, Q., Wu, Q., Zheng, X., Wang, P., Zou, D., Liu, F., & Xiao, Z. (2024). The conversion and migration behavior of phosphorus speciation during pyrolysis of different sludges. AIMS Environmental Science, 11(1), 1-20. https://doi.org/10.3934/environsci.2024001

[25] Li, W., Feng, X., Song, W., & Guo, M. (2018). Transformation of phosphorus in speciation and bioavailability during converting poultry litter to biochar. Frontiers in Sustainable Food Systems, 2, 20. https://doi.org/10.3389/fsufs.2018.00020

[26] Li, X., Rubæk, G. H., Müller-Stöver, D. S., Thomsen, T. P., Ahrenfeldt, J., & Sørensen, P. (2017). Plant availability of phosphorus in five gasification biochars. Frontiers in Sustainable Food Systems, 1, 2. https://doi.org/10.3389/fsufs.2017.00002

[27] Limwikran, T., Kheoruenromne, I., Suddhiprakarn, A., Prakongkep, N., & Gilkes, R. J. (2019). Most plant nutrient elements are retained by biochar in soil. Soil Systems, 3(4), 75. https://doi.org/10.3390/soilsystems3040075

[28] Liu, F., Xiao, Z., Fang, J., & Li, H. (2023). Effect of pyrolysis treatment on phosphorus migration and transformation of pig, cow and sheep manure. Sustainability, 15(12), 9215. https://doi.org/10.3390/su15129215

[29] Lustosa Filho, J. F., Penido, E. S., Castro, P. P., Silva, C. A., & Melo, L. C. A. (2017). Co-pyrolysis of poultry litter and phosphate and magnesium generates alternative slow-release fertilizer suitable for tropical soils. ACS Sustainable Chemistry & Engineering, 5(10), 9043-9052. https://doi.org/10.1021/acssuschemeng.7b01935

[30] McIntosh, S., Rose, T., Rose, A., Kearney, L., & Erler, D. (2022). Agronomic efficiency of phosphorus fertilisers recovered from milk processing waste. Agronomy, 12(10), 2341. https://doi.org/10.3390/agronomy12102341

[31] Nishil, B., Agrawal, K., Manna, P. R., Dixit, A., Shaikh, M. A. N., & Nawaz, T. (2026). Closed-loop process for phosphorus recovery from poultry litter. ACS Sustainable Resource Management, 3(3), 903-913. https://doi.org/10.1021/acssusresmgt.6c00066

[32] Novak, J. M., Johnson, M. G., & Spokas, K. A. (2018). Concentration and release of phosphorus and potassium from lignocellulosic- and manure-based biochars for fertilizer reuse. Frontiers in Sustainable Food Systems, 2, 54. https://doi.org/10.3389/fsufs.2018.00054

[33] Padilla, J. T., Watts, D. W., Novak, J. M., Cerven, V., Ippolito, J. A., Szogi, A. A., & Johnson, M. G. (2023). Magnesium activation affects the properties and phosphate sorption capacity of poultry litter biochar. Biochar, 5, 64. https://doi.org/10.1007/s42773-023-00263-5

[34] Pan, S.-Y., Dong, C.-D., Su, J.-F., Wang, P.-Y., Chen, C.-W., Chang, J.-S., Kim, H., Huang, C.-P., & Hung, C.-M. (2021). The role of biochar in regulating the carbon, phosphorus, and nitrogen cycles exemplified by soil systems. Sustainability, 13(10), 5612. https://doi.org/10.3390/su13105612

[35] Pandey, D. S., Katsaros, G., Lindfors, C., Leahy, J. J., & Tassou, S. A. (2019). Fast pyrolysis of poultry litter in a bubbling fluidised bed reactor: Energy and nutrient recovery. Sustainability, 11(9), 2533. https://doi.org/10.3390/su11092533

[36] Pedersen, I. F., Müller-Stöver, D. S., Lemming, C., & Gunnarsen, K. C. (2025). Particle size determines the short-term phosphorus availability in biochar produced from digestate solids. Waste Management, 191, 172-181. https://doi.org/10.1016/j.wasman.2024.11.006

[37] Pufahl, P. K., & Groat, L. A. (2017). Sedimentary and igneous phosphate deposits: Formation and exploration: An invited paper. Economic Geology, 112(3), 483-516. https://doi.org/10.2113/econgeo.112.3.483

[38] Quilliam, R. S., Glanville, H. C., Wade, S. C., & Jones, D. L. (2013). Life in the 'charosphere' – Does biochar in agricultural soil provide a significant habitat for microorganisms? Soil Biology and Biochemistry, 65, 287-293. https://doi.org/10.1016/j.soilbio.2013.06.004

[39] Radu, N., Bondar, E., Meghea, A., & Rau, I. (2006). Removal of copper and cobalt from diluted aqueous systems by biosorption processes. Revista de Chimie, 57(7), 711-717.

[40] Radu, N., Chirvase, A. A., Babeanu, N., Popa, O., Cornea, P., Pirvu, L., Bostan, M., Ciric, A., Mathe, E., Radu, E., Doni, M., Constantin, M., Raut, I., Gurban, A. M., & Begea, M. (2020). Study regarding the potential use of a spent microbial biomass in fertilizer manufacturing. Agronomy, 10(2), 299. https://doi.org/10.3390/agronomy10020299

[41] Radu, N., Lanyi, S., & Meghea, A. (2007a). Studies concerning the recovery of nutrients from industrial wastewaters as fertilisers. Journal of Environmental Protection and Ecology, 8(4), 866-874.

[42] Radu, N., Lanyi, S., Rau, I., & Chirvase, A. (2007b). Efecte generate de interacția ureei cu azotatul și dihidrogenofosfatul de calciu [Effects generated by the interaction of urea with calcium nitrate and calcium dihydrogen phosphate; in Romanian]. Revista de Chimie, 58(2), 158-162.

[43] Radu, N., & Meghea, A. (2007c). Studies concerning the use of microbial biomass by fertilisers manufacture. Journal of Environmental Protection and Ecology, 8(4), 824-834.

[44] Raghothama, K. G. (1999). Phosphate acquisition. Annual Review of Plant Physiology and Plant Molecular Biology, 50, 665-693. https://doi.org/10.1146/annurev.arplant.50.1.665

[45] Santoro, M. C., Ghanim, B. M., Kwapinski, W., Leahy, J. J., & Freitas, J. C. C. (2024). Solid-state NMR study of hydrochars produced from hydrothermal carbonization of poultry litter. ACS Omega, 9(46), 45759-45773. https://doi.org/10.1021/acsomega.4c02876

[46] Schachtman, D. P., Reid, R. J., & Ayling, S. M. (1998). Phosphorus uptake by plants: From soil to cell. Plant Physiology, 116(2), 447-453. https://doi.org/10.1104/pp.116.2.447

[47] Shashvatt, U., Benoit, J., Aris, H., & Blaney, L. (2018). $CO_2$-assisted phosphorus extraction from poultry litter and selective recovery of struvite and potassium struvite. Water Research, 143, 19-27. https://doi.org/10.1016/j.watres.2018.06.035

[48] Shen, J., Yuan, L., Zhang, J., Li, H., Bai, Z., Chen, X., Zhang, W., & Zhang, F. (2011). Phosphorus dynamics: From soil to plant. Plant Physiology, 156(3), 997-1005. https://doi.org/10.1104/pp.111.175232

[49] Song, W., & Guo, M. (2012). Quality variations of poultry litter biochar generated at different pyrolysis temperatures. Journal of Analytical and Applied Pyrolysis, 94, 138-145. https://doi.org/10.1016/j.jaap.2011.11.018

[50] Szpak, P., Longstaffe, F. J., Millaire, J.-F., & White, C. D. (2012). Stable isotope biogeochemistry of seabird guano fertilization: Results from growth chamber studies with maize (Zea mays). PLoS ONE, 7(3), e33741. https://doi.org/10.1371/journal.pone.0033741

[51] Tesfaye, F., Liu, X., Zheng, J., Cheng, K., Bian, R., Zhang, X., Li, L., Drosos, M., Joseph, S., & Pan, G. (2021). Could biochar amendment be a tool to improve soil availability and plant uptake of phosphorus? A meta-analysis of published experiments. Environmental Science and Pollution Research, 28, 34108-34120. https://doi.org/10.1007/s11356-021-14119-7

[52] Toor, G. S., Peak, J. D., & Sims, J. T. (2005). Phosphorus speciation in broiler litter and turkey manure produced from modified diets. Journal of Environmental Quality, 34(2), 687-697. https://doi.org/10.2134/jeq2005.0687

[53] Turner, B. L. (2002). Inositol phosphates in the environment. Philosophical Transactions of the Royal Society B: Biological Sciences, 357(1420), 449-469. https://doi.org/10.1098/rstb.2001.0837

[54] Turner, B. L., & Leytem, A. B. (2004). Phosphorus compounds in sequential extracts of animal manures: Chemical speciation and a novel fractionation procedure. Environmental Science & Technology, 38(22), 6101-6108. https://doi.org/10.1021/es0493042

[55] Uchimiya, M., & Hiradate, S. (2014). Pyrolysis temperature-dependent changes in dissolved phosphorus speciation of plant and manure biochars. Journal of Agricultural and Food Chemistry, 62(8), 1802-1809. https://doi.org/10.1021/jf4053385

[56] Vadas, P. A., Meisinger, J. J., Sikora, L. J., McMurtry, J. P., & Sefton, A. E. (2004). Effect of poultry diet on phosphorus in runoff from soils amended with poultry manure and compost. Journal of Environmental Quality, 33(5), 1845-1854. https://doi.org/10.2134/jeq2004.1845

[57] Vance, C. P., Uhde-Stone, C., & Allan, D. L. (2003). Phosphorus acquisition and use: Critical adaptations by plants for securing a nonrenewable resource. New Phytologist, 157(3), 423-447. https://doi.org/10.1046/j.1469-8137.2003.00695.x

[58] Wang, C., Luo, D., Zhang, X., Huang, R., Cao, Y., Liu, G., Zhang, Y., & Wang, H. (2022a). Biochar-based slow-release of fertilizers for sustainable agriculture: A mini review. Environmental Science and Ecotechnology, 10, 100167. https://doi.org/10.1016/j.ese.2022.100167

[59] Wang, Q., Zhang, N., Chen, Y., Qin, Z., Jin, Y., Zhu, P., Peng, C., Colinet, G., Zhang, S., & Liu, J. (2022b). The phosphorus availability in Mollisol is determined by inorganic phosphorus fraction under long-term different phosphorus fertilization regimes. Agronomy, 12(10), 2364. https://doi.org/10.3390/agronomy12102364

[60] Wang, Y., Lin, Y., Chiu, P. C., Imhoff, P. T., & Guo, M. (2015). Phosphorus release behaviors of poultry litter biochar as a soil amendment. Science of the Total Environment, 512-513, 454-463. https://doi.org/10.1016/j.scitotenv.2015.01.093

[61] Wystalska, K., Malińska, K., Sobik-Szołtysek, J., Dróżdż, D., & Meers, E. (2023). Properties of poultry-manure-derived biochar for peat substitution in growing media. Materials, 16(19), 6392. https://doi.org/10.3390/ma16196392

# STUDY OF MECHANICAL AND ELECTRICAL FAILURE POINTS OF AN AUTOMATED SOIL SAMPLING MACHINE

/

# *STUDIU AL PUNCTELOR DE DEFECȚIUNE MECANICĂ ȘI ELECTRICĂ ALE UNEI MAȘINI AUTOMATE DE PRELEVARE A PROBELOR DE SOL*

**Livia-Valentina BĂDESCU[1)], Marius-Adelin STUPARU[1)], Robert-Dorin CRISTEA*[2)]**

[1)] Volunteer at National Institute of Research - Development for Machines and Installations Designed to Agriculture and Food-Industry - INMA Bucharest / Romania;

[2)] National Institute of Research - Development for Machines and Installations Designed to Agriculture and Food Industry - INMA Bucharest / Romania.

**Tel: (+40) 771 717 451; *E-mail: robert.cristea@inma.ro*

***Keywords:*** *mechanical errors, soil sampling machine, electrical errors*

**ABSTRACT**

*This paper presents the optimisation of an automated soil sampling device controlled by an Arduino board and a Raspberry Pi board. The system addresses mechanical and electronic deficiencies in the sampling process. The alignment of the containers is achieved using electromagnetic chucks activated by a signal at maximum intensity. Voltage fluctuations in the brushed motor are eliminated using DC-DC (Direct Current-Direct Current) converters, ceramic capacitors, and optocouplers. The parameters are continuously logged in a CSV (Comma-Separated Values) file, and a safety feature stops data collection if GPS (Global Positioning System) coordinates are missing to ensure sample traceability. Evaluations confirm a significant increase in operational stability.*

**REZUMAT**

*Lucrarea prezintă optimizarea unui echipament automatizat pentru prelevarea probelor de sol controlat printr-o placă Arduino și o placă Raspberry Pi. Sistemul remediază deficiențe mecanice și electronice din procesul de eșantionare. Alinierea cuvelor se realizează prin cartele electromagnetice validate de un semnal la intensitate maximă. Fluctuațiile de tensiune ale motorului cu perii sunt eliminate prin convertoare DC-DC, condensatoare ceramice și optocuploare. Parametrii sunt arhivați continuu într-un document CSV, iar o funcție de siguranță oprește prelevarea în lipsa coordonatelor GPS pentru a garanta trasabilitatea eșantioanelor. Evaluările confirmă o creștere majoră a stabilității operaționale.*

## INTRODUCTION

The development of modern agriculture relies on automation and the accurate collection of data directly from the field, a process supported by mobile platforms for soil sampling and storage *(Łukowska et al., 2019)*. An important component of this process is the soil sample traceability system, which ensures that the samples are physically linked to the spatial data. However, the quality of the information and the physical samples obtained is often compromised by a variety of mechanical, electrical, and environmental errors.

A new sampling method must constantly address indexing and alignment issues *(Iváncsics, 1980)*. In hardware architectures where indexing relies on reading RFID (Radio-Frequency Identification) tags and the containers are placed close together, an error in locating the reference container or an accidental movement of the carousel—triggered by shocks—can result in the loss of the entire sample. The effect of these factors is exacerbated by harsh field conditions, which include the impact of dust and vibrations on moving components *(Nguyen et al., 2025)*. Furthermore, the composition of stony soil leads to mechanical deviations during sampling *(Hangen & Reck, 2024)*, while inconsistent sample processing causes significant distortions in the results *(Even et al., 2025)*.

Beyond the physical hardware, exact spatial coordinates are essential for reliable information. A poor or absent GPS signal introduces errors that directly degrades digital mapping, with positioning errors negatively impacting the quality of the final maps *(Blackford et al., 2022)*. This problem illustrates how signal degradation compromises the machine's navigation and the determination of the actual extraction point *(Yang et al., 2025; Zhou et al., 2025)*. Furthermore, the choice of location for collecting soil samples in the field affects the validity of the indicators obtained, and the evaluation of point-scale information leads to

significant estimation errors when the results are extrapolated to the total area of the agricultural plot *(Miralles et al., 2010; Gustavsson et al., 2005)*.

Electronic components can cause specific errors. Power supply fluctuations, radiation, interference, and voltage adjustments affect the sensors *(Effah et al., 2024; Schwamback et al., 2023).* Improper calibration of components results in invalid readings. In traceability system practice, even when data is saved to CSV files, display errors or data loss caused by incorrect wiring on the chassis may appear in the final document. In addition to these technological shortcomings, laboratory errors can also occur, which may completely distort the final assessment (*Tamminen, 2003*).

This article aims to detail precisely these categories of errors, providing an analysis of how they influence and limit the operation of an automated soil sampling and traceability system.

## MATERIALS AND METHODS

The project is based on a carousel with 12 trapezoidal-shaped containers, initially tested in the lab on a table. During laboratory testing, no electrical or magnetic interference issues have been encountered. To determine the exact position, inductive proximity sensors, powered by a 5V power supply, are mounted beneath the main board, and for indexing, a tag has been mounted on each container that will be read by an RFID reader. The location from which the soil sample was collected is determined using an Adafruit Ultimate GPS Breakout v3 module connected via the GPIO (General-Purpose Input/Output) pins to the Raspberry Pi 4, which includes an external antenna for better signal reception. The location data collected is directly linked to the index of each container to record the geographic location of the soil samples. The system is controlled by an Arduino board that communicates via the UART (Universal Asynchronous Receiver-Transmitter) protocol with a Raspberry Pi 4 for data processing. The information is exported as CSV files. The latitude and longitude for each sample are extracted from these files and used to create links to the OpenStreetMap platform so that the exact location can be viewed.

### Indexing error and reference cell detection

These specific types of operational errors typically occur due to an incorrect physical alignment between the electronic reader module and the identification label mounted directly on the well. Furthermore, the inherent mechanical play within the moving structure of the wells can easily cause a problematic situation where the label is successfully scanned by the system without the main discharge funnel being properly centered for the unloading phase. As illustrated in the image provided below, the reader module is mounted on a mechanically adjustable arm to help mitigate this spatial alignment issue. To ensure a highly reliable operation, the system microcontroller will validate the final position only after debouncing the incoming sensor signal to filter out any noise. This step guarantees a correct and safe alignment right before initiating the actual release of the collected soil sample into the container.

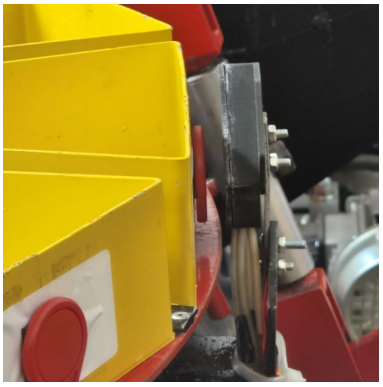


**Fig. 1 - RFID reader and tags setup for precise container identification**

### Vibrations

The continuous mechanical vibrations caused by the highly uneven agricultural terrain often throw the various moving components off-center and gradually loosen the physical connections between them. Consequently, the identification tags may unexpectedly shift from their original position or even become completely detached, making them entirely undetectable by the main software algorithm. To actively prevent any accidental movement of the central hopper, a dedicated inductive sensor mounted directly beneath the rotating carousel continuously detects a small metal plate securely attached to the bottom of each individual

container; the control program immediately halts the entire sampling process in the event of any unexpected movement. For additional protection against harsh field conditions, the metal plates can be safely embedded in custom recesses specially milled into the hopper wall and heavily coated with a durable layer of epoxy resin.

**Movement error**

A sudden motor jam frequently caused by small stones, extensive mud buildup on the main drive shaft, or unexpected physical interaction between the mechanical rocker arm and the collection container can significantly affect the carousel's smooth movement or even cause it to move completely accidentally.

The specific physical position of the container is continuously detected by a dedicated metal plate securely mounted directly beneath the rotating carousel, which is carefully monitored by an inductive proximity sensor, exactly as shown in the descriptive image provided below.

An unexpected loss of this sensor signal immediately indicates an accidental movement event, and the main control board will safely halt the entire sampling process to prevent further damage. Proactively protecting the vulnerable motor and the rotating shaft with a dedicated outer housing successfully prevents problematic mud buildup and subsequent mechanical jams during field operation.



**Fig. 2 - Close-up of the metal plates and sensors used for preventing movement errors of the carousel**

**Interference**

The strong magnetic noise generated by the active electric motors or the heavy presence of surrounding metal components can easily block or heavily distort the communication signal between the identification tag and the scanning reader. Furthermore, background electrical noise also significantly degrades the overall quality of the transmitted data during the sampling operation.

Whenever severe interference occurred in the field, reliable communication with the RFID tag reader became practically impossible, and the initial engineering solution was to use specialized shielded cables. Unfortunately, even following this hardware modification, problematic signal interference still occurred randomly. As a direct result of this persistent issue, the main reader module had to be completely reset every single time the automated system was initially started.

**Incorrect sensor calibration**

An inappropriate physical reading distance often causes significant identification errors during the automated process. A proximity sensor that is mounted too close mistakenly detects two separate containers simultaneously, while one that is positioned entirely too far away completely fails to read the necessary tags during the continuous rotation.

The implemented solution directly involves a dynamic software calibration routine integrated seamlessly within the main control program. Upon initial startup, the automated system carefully performs a complete full rotation to properly record the various incoming signal values and successfully establish the optimal detection threshold for reliable operation.

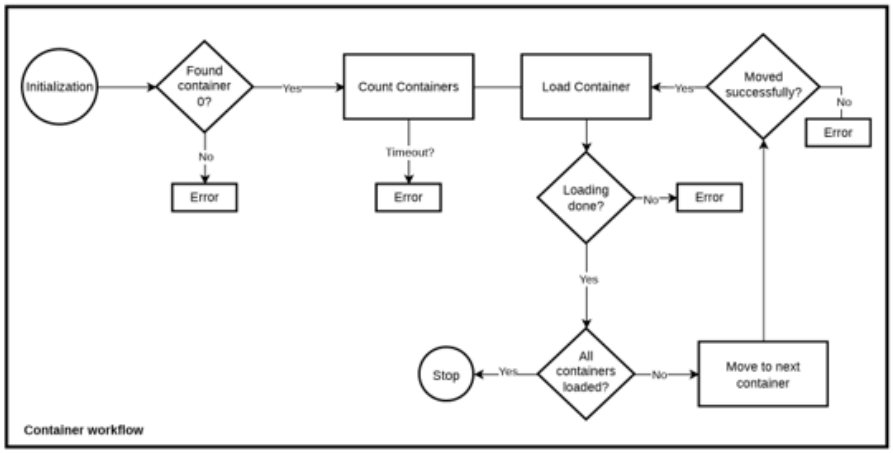



**Fig. 3 - Logical operation workflow diagram for validating and loading containers**

Figure 3 presents the steps of the control algorithm implemented for managing the bins during the sampling process. Immediately following the initialization stage, the program evaluates whether the reference container has been found and correctly positioned. If this condition is not met, an error state is triggered, which prevents soil release in the event of mechanical play or an incorrect alignment between the RFID reader and the tag.

When identification is successful, the equipment counts the containers and effectively begins the loading stage. A safety element clearly visible in the diagram is the continuous monitoring of the time allocated to each stage, because exceeding this duration indicates potential motor jams caused by mud or stones, prompting the system to automatically enter an error state. After a successful load, the microcontroller checks if all bins have been filled, and the process continues by either moving the carousel to the next container or entirely stopping the cycle.

**Power supply and voltage regulation**

Standard brush motors inherently generate exceptionally high power consumption spikes during initial startup sequences or immediately upon sudden physical impact with unexpected obstacles, directly causing severe voltage drops alongside significant electromagnetic interference in the surrounding environment.

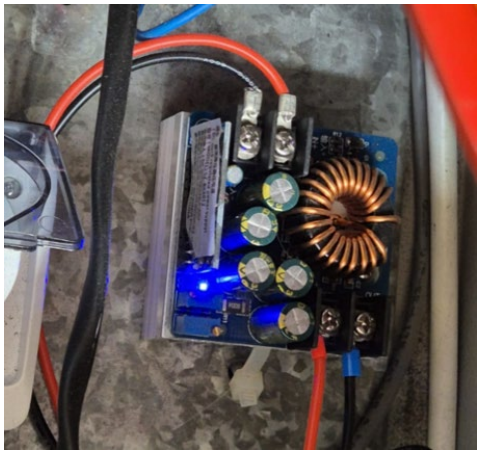


**Fig. 4 - DC-DC converter integrated into the power supply system**

To effectively counter this issue, completely separated DC-DC converters specifically designated for the main power and sensitive logic sections have been successfully integrated into the system's overall electrical circuit, exactly as illustrated in the following descriptive figure. Furthermore, the essential galvanic isolation required to safely protect the delicate control circuits is reliably provided by the specialized optocouplers seamlessly included in the mechanical relay modules, which are ultimately responsible for safely starting and stopping the active electric motors.

**Data storage errors**

If the standard CSV document opening function is currently set to a simple write mode, any new incoming data sets will completely overwrite the old existing information, unfortunately erasing the entire

recorded history. To effectively solve this specific software issue, the primary file access parameter must be permanently switched to a continuous append mode. By successfully utilizing this append feature, the main table header is initially written only one single time, and all subsequent data records are then automatically added directly to the bottom of the growing document.

**Errors caused by the GPS module**

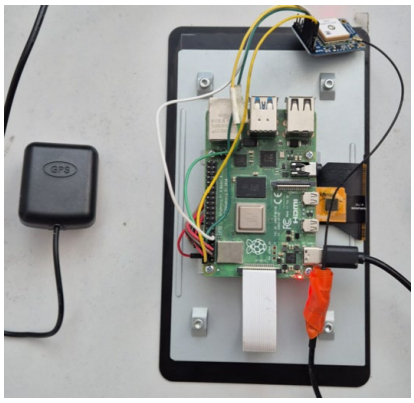


**Fig. 5 - Hardware configuration of the GPS module connected to the Raspberry Pi for soil sample traceability**

Various physical obstacles found in the typical agricultural environment frequently block the satellite GPS signal reception, ultimately resulting in completely null spatial coordinates, which negatively affects the correct association of the collected soil samples with their actual physical locations in the field. The main software algorithm must necessarily include a dedicated safety routine that continuously evaluates the overall connection quality; the total absence of valid spatial data should safely and temporarily halt the rotating carousel until the satellite signal is fully restored. For achieving far better geographic positioning, it is highly recommended to completely replace the standard tracking modules, such as the basic setup clearly shown in the image above, with advanced GNSS RTK (Global Navigation Satellite System Real-Time Kinematic) antennas, which are exceptionally capable of providing exact centimeter-level accuracy.

## RESULTS

The results from the functional evaluation demonstrate the viability of the proposed solutions for optimizing the automated soil sampling system. A summary of the remedied operational issues and their applied fixes is detailed in the Table 1. Each collection container is identified by reading the RFID tags mounted on them. To eliminate indexing errors caused by mechanical play, the microcontroller validates the unloading position only when the maximum signal intensity is detected, ensuring proper alignment.

**Table 1**

**Summary of mechanical and electrical failure points and implemented optimization solutions**

| Failure Category | Identified Issue | Implemented Solution |
|---|---|---|
| Mechanical errors | Incorrect container alignment and mechanical jams caused by shocks or mud buildup | The system reads RFID tags and validates the position at maximum signal intensity. Inductive sensors monitor metal plates to stop the equipment in case of accidental movement or jamming. |
| Electrical errors | Voltage fluctuations at brushed motor startup and magnetic noise | Integrating DC-DC converters and optocouplers ensures galvanic isolation of power circuits from logic ones. The system runs a dynamic sensor calibration upon startup. |
| Data storage and traceability | Overwriting historical data in the CSV document and GPS signal loss | The CSV file is opened in append mode to keep the history. A safety protocol temporarily stops the carousel upon GPS signal loss to guarantee the correct association of samples with their geographic location. |

Implementing dedicated DC-DC converters ensured separate power supplies for the power and logic sections, absorbing sudden voltage fluctuations. This solution protects the development board, and galvanic isolation is achieved through optocouplers included in the relay modules controlling the motors.

The program allowed for continuous updating of the main CSV file by writing new data lines at the bottom.

## CONCLUSIONS

In conclusion, the functional evaluation demonstrated the efficiency and reliability of the technical solutions integrated into this system. The method of identifying the containers by reading the cards, together with position validation at the maximum signal, resolved the indexing issues caused by the system's mechanics.

From an electrical standpoint, the separation of power circuits from logic circuits using DC-DC converters and optocouplers ensured stable operation and protected sensitive components from potential interference or voltage drops that occur when the motors are activated. At the same time, the programming logic implemented for continuous data saving in CSV format and the safety routine for monitoring the satellite signal guarantee process traceability. Thus, the system fulfills its intended purpose, establishing a correct and reliable association between each extracted soil sample and its actual geographic coordinates.

## ACKNOWLEDGEMENT

This work was supported by the National Research Authority, through the Project entitled: "An intelligent automated system designed for georeferenced soil sampling." -- PN 23 04 01 02. Contract no./date 9N/ 01.01.2023.

## REFERENCES

[1] Blackford, C., Heung, B., & Webster, K. (2022). Incorporating spatial uncertainty maps into soil sampling improves digital soil mapping classification accuracy in Ontario, Canada. *Geoderma Regional*. https://doi.org/10.1016/j.geodrs.2022.e00495

[2] Effah, E., Thiare , O., & Wyglinski , A. (2024). Hardware Evaluation of Cluster-Based Agricultural IoT Network. https://doi.org/10.1109/ACCESS.2024.3371900

[3] Even, R., Machmuller, M., Lavallee, J., Zelikova, T., & Cotrufo, M. (2025). Large errors in soil carbon measurements attributed to inconsistent sample processing. *SOIL*, 17-34. https://doi.org/10.5194/soil-11-17-2025

[4] Gustavsson, B., Luthbom, K., & Lagerkvist, A. (2005). Uncertainty in soil sampling - A case study. *Second World Conference on Sampling and Blending.*

[5] Hangen, E., & Reck, H. (2024). Minimizing sampling induced errors in Ks-measurements of stone bearing soils. *Soil & Tillage Research*. https://doi.org/10.1016/j.still.2023.105986

[6] Iváncsics, J. (1980). A new mechanical soil sampling method. *Communications in Soil Science and Plant Analysis*, 881-887. https://doi.org/10.1080/00103628009367088

[7] Łukowska, A., Tomaszuk, P., Dzierżek, K., & Magnuszewski, Ł. (2019). Soil sampling mobile platform for Agriculture 4.0. *2019 20th International Carpathian Control Conference.* IEEE. https://doi.org/10.1109/CarpathianCC.2019.8765937

[8] Miralles, D., Crow, W., & Cosh, M. (2010). Estimating Spatial Sampling Errors in Coarse-Scale Soil Moisture Estimates Derived from Point-Scale Observations. *Journal of Hydrometeorology*, 1423-1429. https://doi.org/10.1175/2010JHM1285.1

[9] Nguyen, T., Muller, E., Rubin, M., Wang, X., Sibona, F., & Sukkarieh, S. (2025). Towards Autonomous In-situ Soil Sampling and Mapping in Large-Scale Agricultural Environments. *2025 IEEE ICRA Workshop on Field Robotics.* https://doi.org/10.48550/arXiv.2506.05653

[10] Schwamback, D., Persson, M., Berndtsson, R., Bertotto, L., Kobayashi, A., & Wendland, E. (2023). Automated Low-Cost Soil Moisture Sensors Trade-Off between Cost and Accuracy. *Sensors*, 2451. https://doi.org/10.3390/s23052451

[11] Tamminen, P. (2003). Sampling and Laboratory Errors in Forest Soil Analysis. *Communications in Soil Science and Plant Analysis*, 1193-1209. https://doi.org/10.1081/CSS-120020437

[12] Yang, L., Tomioka, C., Hoshino, Y., Kamata, S., & Kikuchi, S. (2025). Research on EV Crawler-Type Soil Sample Robot Using GNSS Information. *Sensors*, 604. https://doi.org/10.3390/s25030604

[13] Zhou, H., Wang, J., Chen, Y., Hu, L., Li, Z., Xie, F., Wang, P. (2025). Neural Network-Based SLAM/GNSS Fusion Localization Algorithm for Agricultural Robots in Orchard GNSS-Degraded or Denied Environments. *Agriculture*, 1612. https://doi.org/10.3390/agriculture15151612

# SLUDGE TREATMENT AND MANAGEMENT IN WASTEWATER TREATMENT PLANTS USING MECHANICAL EQUIPMENT

/

# *TRATAREA ȘI GESTIONAREA NĂMOLURILOR ÎN STAȚIILE DE EPURARE A APELOR UZATE UTILIZÂND ECHIPAMENTE MECANICE*

**Cornelia Veronica DIMA[1)], Gheorghe VOICU*[1)], Gabriel-Alexandru CONSTANTIN[1)], Irina-Aura ISTRATE[1)], Alin-Nicolae HARABAGIU[2)]**

[1)] National University of Science and Technology POLITEHNICA Bucharest, Splaiul Independentei 313, Bucharest / Romania;
[2)] National Institute of Research - Development for Machines and Installations Designed to Agriculture and Food Industry - INMA Bucharest / Romania.
**Tel: (+40) 724 715 585; *E-mail: gheorghe.voicu@upb.ro*

***Keywords:*** *wastewater, sludge, treatment plant, coagulation, management, process*

**ABSTRACT**

*The water needed for daily consumption is taken from surface and underground sources, but it has a high level of contaminants and microorganisms, which are eliminated through the stages: primary, secondary and tertiary, which are carried out within the treatment plants, to protect urban settlements and the emissary against pollution. Most wastewater treatment plants use conventional treatment processes, which include coagulation, flocculation, sedimentation, filtration, aeration and disinfection, so that large quantities of sludge are produced by removing impurities from the water taken and from the various water treatment chemicals used in the treatment processes. It is particularly important to use an appropriate sludge treatment and disposal system, which is economical and technically feasible. Wastewater treatment plants use, in most cases, innovations and modern management strategies to improve the treatment, disposal and control of the release of sludge resulting from the treatment processes into the environment. Sludge management is of major importance in terms of quantities, handling costs, composition and environmental and regulatory requirements that any treatment plant must comply with.*

**REZUMAT**

*Apa necesară consumului zilnic, este preluată din sursele de suprafață și din cele subterane, însă deține un nivel ridicat de contaminanți și microorganisme, acestea fiind eliminate prin intermediul treptelor: primară, secundară și terțiară, ce se desfășoară în cadrul stațiilor de epurare, pentru protejarea așezările urbane și a emisarii împotriva poluării. Majoritatea stațiilor de epurare a apei uzate întrebuințează procese convenționale de tratare, dintre care fac parte, coagularea, floculareа, sedimentarea, filtrarea, aerarea și dezinfecția, astfel că , se produc cantități mari de nămol prin îndepărtarea impurităților din apa preluată și din diversele substanțe chimice de tratare a apei utilizate în procesele de tratare. Deosebit de importantă este utilizarea unui sistem adecvat de tratare și eliminare a nămolului, care să fie economic și fezabil din punct de vedere tehnic. Stațiile de epurare a apelor uzate folosesc , în cele mai multe cazuri, inovații și strategii moderne de management pentru a îmbunătăți tratarea, eliminarea și controlul eliberării nămolului rezultat în urma proceselor de tratare, în mediu. Gestionarea nămolului este de importanță majoră în ceea ce privește cantitățile, cheltuielile de manipulare, compoziția și cerințele de mediu și de reglementare pe care orice stație de epurare trebuie să le respecte.*

## INTRODUCTION

Water treatment plants typically employ modern innovations and management strategies to improve treatment and sludge disposal processes, as well as to prevent sludge discharge into the environment. Adopting such innovative, modern strategies can significantly contribute to compliance with permissible limits. The numerous advantages of these innovations and management strategies in water treatment include superior water quality, reduced operating costs, and lower energy consumption. (*USEPA, 2011*)

The coagulation-sedimentation process used in water treatment generates sludge based on aluminum or iron salts, containing sand particles and coagulants. Residues from industrial wastewater treatment plants are classified as industrial sludge; due to their high content of chemicals or heavy metals, they are categorized as hazardous waste regarding their handling.

Sludge consists of aggregates formed from various components, such as active microorganisms and extracellular polymeric substances, suspended in the wastewater. These aggregates, found in the activated sludge basin, are known as flocs. Flocs possess a highly complex internal structure in which water is strongly bound to the solid phase, making it difficult to separate from the solid surface by mechanical means. Consequently, in suspension, sludge exhibits fluid-like behavior, whereas as a dewatered cake, it displays characteristics of viscosity and elasticity. (*Zhang et al., 2017*)

Managing the sludge resulting from the water treatment process is a fundamental aspect, given the quantities generated, handling costs, sludge composition, and the environmental requirements and regulations that every wastewater treatment plant must meet.

Sludge volume, properties, and characteristics are influenced by the water source and type, the rate of treated water production, the level of contamination in the water source, the type of coagulant used, the dosage applied during treatment, and the plant's operating conditions.

The processing and management of sewage sludge from wastewater treatment plants are regulated by numerous legal acts issued by the European Union, such as the Waste Framework Directive. Given the current state of waste management technology, the formation of sewage sludge is unavoidable.

As for the stages of the wastewater treatment process, they remain quite conventional. The size of the wastewater treatment plant is the primary factor determining the technology used in the treatment process, (*Groseer et. al., 2016*). The subsequent stages of the sludge treatment process are: thickening, stabilization, conditioning, dewatering, sanitization, and, finally, drying. The number and type of sludge treatment processes depend not only on the nature and quantity of the sludge being processed but, above all, on the final disposal method for the sewage sludge.

## MATERIALS AND METHODS

Sludge, in the form of gelatinous particles, is formed during chemical coagulation and softening processes in water treatment plants. An important parameter influencing sludge characteristics is the configuration of the treatment plant system. There are numerous treatment system configurations, each generating sludge with its own specific characteristics. The expected characteristics of flocs for various water treatment configurations are presented in Table 1, (*Dharmappa et al., 1997*).

**Table 1**

**Expected floc characteristics for different configurations**

| | System configuration types | | |
|---|---|---|---|
| **Floc** | Conventional treatment | Direct filtration treatment | Contact filtration treatment |
| Floc volume | High | Medium | Law |
| Floc density | Law | Medium | High |
| Macro floc | High | Medium | Law |
| Micro floc | Law | Medium | High |

Sludge from wastewater treatment plants can contain a variety of microorganisms, depending on the source and quality of the raw water, the treatment method used, and the time of year the treatment takes place. Regarding the treatment and management of sludge from treatment plants, physical and chemical characteristics are paramount. Variations in the physical characteristics of sludges with different compositions are determined by variations in their physical structure. The sludge resulting from the coagulation process is composed of suspended matter present in the raw water, added coagulants, and a large amount of retained water.

During the coagulation-flocculation process, suspended solid particles and the coagulant interact to form flocs, which subsequently settle, generating sludge. Suspended solid particles include clay and sediment particles, color, causing colloids, algae, and other impurities. Clays and sediments are solids with a density of approximately 2600 kg/m$^3$; other components consist of coagulant agglomerations involving various ions and water molecules, all held together by weak electrostatic bonds.

The chemical characteristics of the sludge generally depend on the chemical composition of the raw water and the type of chemical coagulants used.

The quantities of sludge resulting from water treatment processes, whether in solid, semi-solid, or liquid form, account for between 3% and 5% of the volume of water entering the plant. The majority of this volume consists of wastewater resulting from filter backwashing; This typically contains less than 10% of the

solids removed during the plant's treatment process. Typical values reported for the quantities of sludge generated by various treatment methods are presented in Table 2, (*Anjithan, K., 2016*).

**Table 2**

**Typical production of sludge in WTP**

| Portion of plant flow | | |
|---|---|---|
| Sludge type | Range | Typical |
| Alum coagulation | 0.08 – 0.3% | 0.1% |
| Flotation (at reactor surface) | 0.01 – 0.1% | 0.06% |
| Flotation (at reactor bottom) | 0.001 – 0.04% | - |
| Iron coagulation | 0.08 – 0.3% | 0.1% |
| Lime-softening | 0.3 – 6% | 4% |

Sludge disposal from wastewater treatment plants is a crucial stage in the water treatment process, and the techniques used for this purpose face challenges and opportunities that necessitate change. Residues from treatment plants were often discharged into nearby watercourses, stored in lagoons for extended periods, or spread on land without adequate treatment (or indeed any treatment at all), leading to adverse environmental effects. Consequently, the direct discharge of sludge from treatment plants into water bodies negatively impacts downstream water quality and fails to comply with Environmental Protection Agency regulations. Under environmental regulations, sludge disposal will soon become an activity subject to permitting requirements. Large quantities of sludge are also disposed of in landfills. Sludge stored in open areas and washed by rainwater affects surface water quality. Groundwater quality can also be compromised due to the leaching of sludge components into the soil.

In the conventional treatment process involving coagulation and filtration, suspended particles and natural organic matter are removed from the water source through the addition of iron and aluminum salts and chemical coagulants, a process that generates sludge. In addition to the added chemical coagulant, the sludge contains mineral components and other elements derived from the raw water. Sludge is a mixture of liquid and solid phases and can be treated as waste. Although in certain cases it may be considered a natural resource, it often represents an unwanted economic and environmental burden. The quantities of sludge produced by wastewater treatment plants in modern society are enormous and continue to grow. The sources of this sludge and a brief description of it are presented in Table 3, (*Qrenawi et al., 2021*).

**Table 3**

**Sources of sludge from WT plants**

| Source of sludge | Description |
|---|---|
| Aluminum and iron precipitation | Sludge resulting from the precipitation of aluminum and iron from surface waters containing clay, silt, soil, colloids, and microorganisms, using chemical coagulants and polymers. |
| Coarse screening | Coarse screening prevents debris and fish from entering the intake structures. The coarse sludge accumulated on the screens includes rags, viscous matter, and large pieces of wood. |
| Flotation | Sometimes referred to as a sludge thickening technique, it results in the formation of a floating layer. This is collected uniformly in small plants and continuously in larger installations. |
| Pre-sedimentation | It takes place prior to conventional treatment and will result in the removal of large quantities of coarse sludge. |
| Scraping of slow sand filters | Scraping the surface of slow sand filters will sometimes result in the accumulation of semi-solid materials. |
| Worn-out shock absorbers | Solid materials used for the removal of constituents—including hardness, As, F, P, and certain organic substances—from water via sorption, and which have lost significant absorptive capacity or cannot be efficiently reactivated. |
| Off-site location | They are primarily used to prevent gravel, sand, and small stones from continuously moving toward the treatment plant. The materials retained typically include gravel, sand, and small stones. |
| Water softening | Removing $Ca^{2+}$ and $Mg^{2+}$ ions from raw water during precipitation results in water softening. This softening process produces calcareous sludge (lime sludge). |

The set of methods describing the infrastructure for the disposal and reuse of solids at wastewater treatment plants, as well as their operation, design, and planning, is generally referred to as sludge

management. The primary technical objective of sludge management is to reduce sludge quantities, particularly those destined for disposal. Sludge must be handled, transported, and ultimately disposed of in accordance with directives established by competent authorities. Reducing sludge water content and increasing solids content are key objectives of the sludge management process. Sludge management significantly influences the design of operations within wastewater treatment plants. Sludge removal and management must be controlled and executed according to the designed management system to ensure appropriate water quality. In the past, sludge from treatment plants was discharged into the nearest watercourses or sewer networks with minimal treatment. Currently, such sludge can no longer be discharged into sewer networks, as this practice would result in numerous negative effects. Furthermore, in compliance with effluent discharge standards, it cannot be released into natural water bodies. At present, sludge is discharged into a lagoon system located in the vicinity of the treatment plants, (*Dharmappa et al., 1997*).

In the research titled "Towards energy positive wastewater treatment plants", Gikas (*2017*) argues that the aeration process - considered a major energy consumer - can be improved by removing primary solids. Regarding energy consumption, this method can help enhance the efficiency of wastewater treatment plants. Unit operations can be combined; prime examples include simultaneous stabilization and sanitization, as well as dewatering with lime. Multifunctional processes should not be overlooked either; composting, for instance, provides stabilization while simultaneously achieving sanitization and drying at temperatures above 55°C. The number of possible unit processes is vast and continues to grow. In his research, the author notes that the resulting biosolids are thermally dried (to 80% solids) and transported to a gasifier, where the syngas produced is burned in a cogeneration engine. Wet oxidation has been promoted as an alternative to sewage sludge incineration; through this process, organic matter is converted into carbon dioxide, while water is released into the air and mineral residues remain.

The study titled "Environmental comparison of alternative sewage sludge treatments: an Italian case study", authored by *Lombardi et al. (2017*), suggests that replacing the direct spreading of sewage sludge with incineration helps reduce environmental toxicity for both humans and ecosystems. Thermal disposal of sewage sludge, specifically incineration, can yield a net energy gain only if the sludge's water content is below approximately 30%. Currently, the use of bioenergy appears to be the optimal solution to address the rising demand for energy and fossil fuels. Consequently, it is necessary to seek alternative solutions for the generation and management of municipal sewage sludge.

This paper examines the potential to utilize sewage sludge as a valuable organic product, specifically as biomass for renewable energy production, within small and medium-sized wastewater treatment plants. Implementing the described alternative wastewater and sludge treatment processes shifts the overall approach to wastewater treatment and enables sewage sludge management at the point of generation.

## RESULTS

The primary stage in sludge treatment consists of reducing its moisture content. Without this step, sludge treatment and management would be difficult and highly impractical. The techniques and costs associated with sludge treatment, transport, and final disposal are influenced by the quantity and properties of the sludge. Consequently, developing a comprehensive treatment system for a specific type of sludge requires a thorough understanding of the appropriate techniques available for processing that type of sludge. Reducing the quantity of sludge will inherently lead to lower facility operating costs.

To ensure cost-effective sludge management, it is important to reduce the sludge volume by increasing its solids concentration. An appropriate treatment method can achieve this. Sludge treatment and disposal processes can be classified as follows: thickening; chemical or physical conditioning; mechanical or non-mechanical dewatering; solids minimization; solids recovery; and final disposal. A general process flow diagram, illustrating the various methods and techniques used in sludge management, as well as the sequence in which they can be organized and grouped to form a complete treatment system, is presented in Figure 1. (*Qrenawi et al., 2021*). At the Pitești wastewater treatment plant, sludge retained in the settling tanks is directed partly to the activated sludge basin (as recirculated activated sludge) and partly to the thickening stage , as excess sludge, within the new mechanical sludge concentration units.

There are two primary sludge pumping stations, one of which serves two of the three primary settling tanks. Primary sludge is pumped to two radial gravity sludge thickeners for thickening. Polymer is added to improve thickener performance, enabling the concentrated primary sludge to reach a dry solids concentration of 5%. Progressive cavity pumps are provided for each thickener to transfer the concentrated sludge to the

concentrated sludge mixing chambers. Supernatant water is collected in the internal drainage network and flows by gravity to the supernatant storage tank.

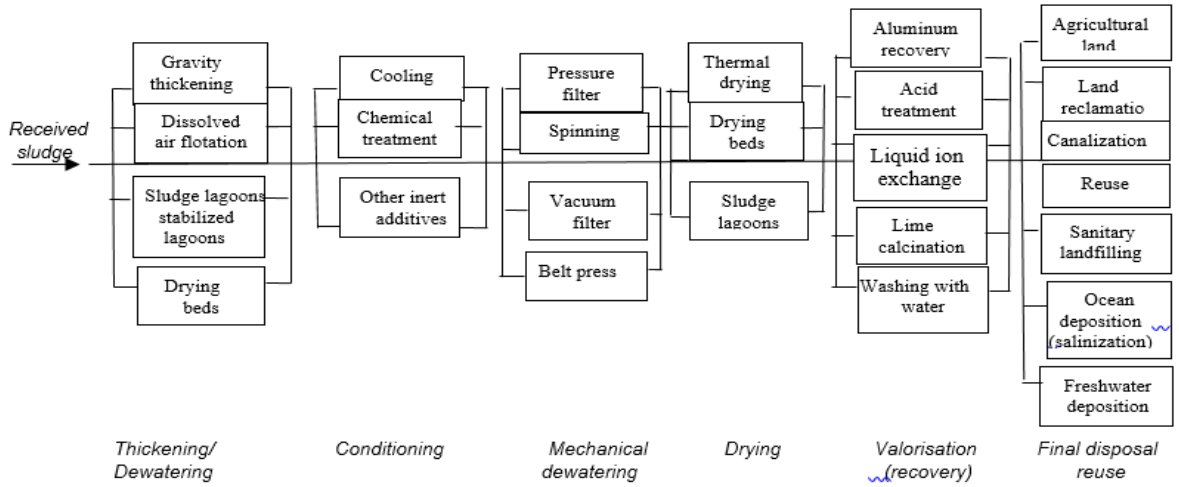



**Fig. 1 - Unit operations and processes for sludge management**

Each of the two recirculated activated sludge pumping stations is equipped with both duty pumps and standby units. Recirculated activated sludge is pumped into the anoxic zones of the two activated sludge basins.

The pumping equipment for the excess sludge pumping station is installed in the existing building located between the biological basins. Excess sludge is pumped to the mechanical sludge thickeners, where it undergoes thickening.



**Fig. 2 - Excess sludge pumping station**

To improve thickening performance, the sludge is chemically conditioned with a polyelectrolyte. Two mechanical thickening units are provided, located within the existing sludge processing building. The dry solids concentration following mechanical thickening is 6%. Progressive cavity pumps are provided for each thickener to transfer the thickened sludge to the thickened sludge mixing chambers. Supernatant is collected via the internal drainage network and flows by gravity to the supernatant storage tank.

Thickened sludges, derived from the gravity thickening of primary sludge and the mechanical thickening of excess sludge, are homogenized in two thickened sludge mixing chambers. The mixing tanks are equipped with agitators to homogenize the mixture and prevent sludge settling on the tank floor. Subsequently, the sludge is pumped to the three sludge digestion tanks (for the mineralization of organic matter within the thickened sludge). Duty and standby pumps are installed for the two mixing chambers to transfer the thickened sludge to the digesters.

As the anaerobic digestion process generates biogas, the gas is stored in three membrane, type biogas holders. Emergency equipment is also provided.

The sludge digestion process requires heating and the maintenance of the sludge at a temperature of 34–35°C. Consequently, two dual-fuel (natural gas/biogas) heating boilers were installed to provide the hot water required for the sludge heating process.

The actual heating takes place in heat exchangers located within the digested sludge recirculation/heating stations associated with the fermentation tanks. Biogas is collected from the top of

the fermenter and conveyed to three gas holders. A flow meter is installed at the inlet of the three gas holders to measure the quantity of biogas. Each gas holder is equipped with a dome-mounted ultrasonic sensor that measures the distance between the outer and inner layers, thereby determining the stored biogas volume. A flare burner has been installed to dispose of excess biogas whenever the cogeneration unit is not operational. The digested sludge is stored in two storage tanks. These tanks are equipped with agitators to ensure continuous sludge homogenization. From there, the sludge is sent for dewatering.

Sludge dewatering is carried out mechanically using centrifuges, with the incoming sludge being chemically conditioned using polyelectrolyte.



**Fig. 3 - Centrifuge pentru deshidratarea nămolului**

Three mechanical dewatering units are installed in the existing sludge processing plant (two operational and one standby), each equipped with a dedicated centrifugal feed pump, alongside a polyelectrolyte preparation station. The dry solids content after dewatering is 25%. The supernatant is collected in the internal sewerage network and conveyed by gravity to the supernatant storage tank. The dewatered sludge is stored in the designated dewatered sludge storage area.

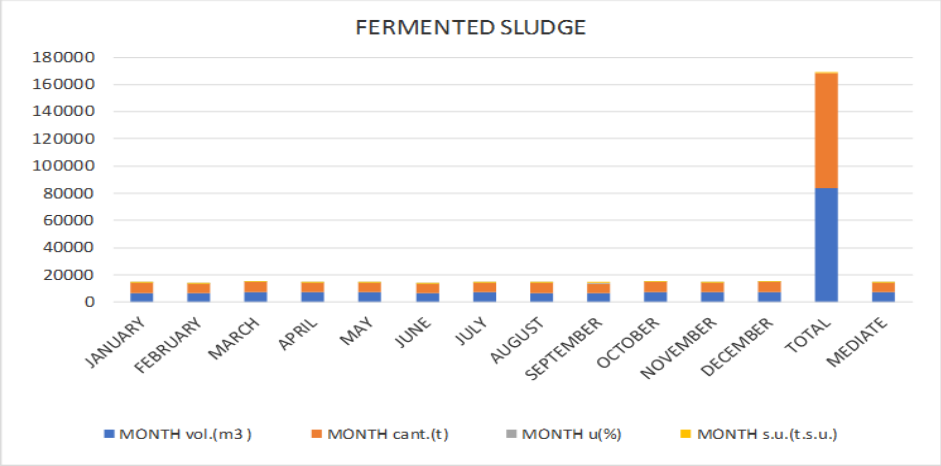



**Fig. 4 - Values for digested sludge – Pitesti Wastewater Treatment Plant**

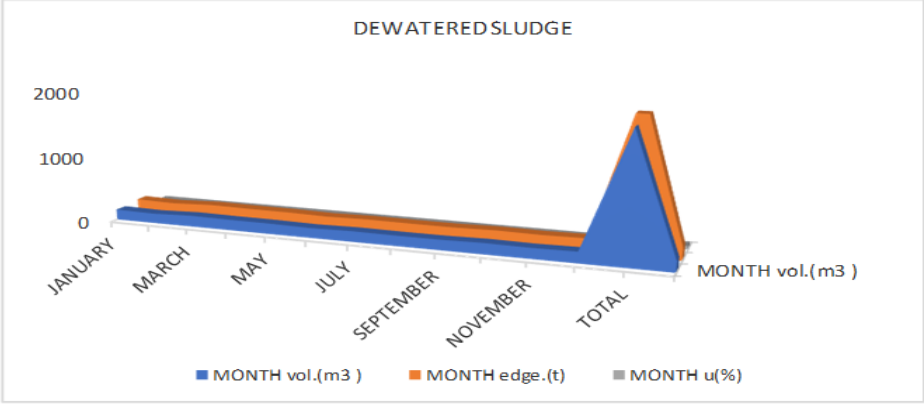



**Fig. 5 - Values for dewatered sludge – Pitesti Wastewater Treatment Plant**

The primary objective of sludge management is to reduce the quantity of sludge, particularly the portion destined for final disposal. Sludge handling, transfer, and final disposal must be carried out in accordance with directives established by competent authorities. Reducing the water content of the sludge and increasing the concentration of solids are also key objectives of the sludge management process, (*Anjithan, 2016*). Sludge management significantly influences the design and operation of water treatment plants. For existing plants, solid residue management systems can limit the facility's overall capacity if the design and operating conditions are inadequate. Sludge is sometimes stored temporarily before being sent for treatment, reuse, or transfer for disposal. Sludge removal and management must be controlled and executed according to the designed system to ensure appropriate water quality.

While a few years ago, sludge from water treatment plants was discharged into the nearest watercourses or sewer networks, either untreated or minimally treated, it can no longer be discharged into sewer networks today, as such a method would entail numerous negative effects. Strict standards regarding effluent discharge are a primary constraint, prohibiting discharge into natural water bodies. Consequently, the sludge is stored in lagoon systems located within the plant premises or in their immediate vicinity. (*USEPA, 2011*). Transport and final disposal costs account for the bulk of sludge management expenses; therefore, the most sustainable approach is to minimize the volume of sludge requiring final disposal. Particular emphasis is placed on reducing environmental impact and complying with disposal regulations established by the competent authorities.

## CONCLUSIONS

Sludge management issues must be taken into account when designing wastewater treatment plants. As the global population continues to grow, the volume of sludge generated by treatment plants follows the same upward trend; consequently, beneficial measures for sludge reuse must be adopted. Understanding sludge characteristics is essential for selecting and designing the most appropriate management, treatment, and disposal solutions. Using sludge in agriculture is an economical option; however, this approach is acceptable only if the sludge has a high content of valuable substances and minimal concentrations of pollutants. Sludge analysis and testing must be carried out throughout the entire management process to ensure that the negative impact associated with recovery and disposal options is minimized. During the design phase of water treatment plants, special attention must be paid to optimizing treatment operations and processes, as well as to aspects regarding sludge management and disposal. Sludge management requires long-term plans that comply with environmental regulations.

Reducing moisture content remains a critical priority for minimizing waste volume, thereby optimizing the facilities' operational and logistical costs. Modern technologies, such as centrifugation and polyelectrolyte conditioning, enable the achievement of high dry matter concentrations. Energy recovery via cogeneration using biogas generated during fermentation offers a sustainable solution for reducing the carbon footprint.

Integrating sludge management from the design phase is essential to prevent constraints on the facility's total capacity. Continuous monitoring of physicochemical composition ensures compliance with European standards and safe application in agriculture or disposal in landfills.

## REFERENCES

[1] Ahmad, T., Ahmad, K. and Alam, M., (2016). Characterization of sewage sludge and its safe disposal options, International Conference on Solid Waste Management, *Procedia Environmental Sciences*, Vol.35, pp.950–955, DOI:10.1504/IJEWM.2021.10033677.

[2] Anjithan, K., (2016. Management Practices of Water Treatment Sludge in Sri Lanka and Re-use Potential of Sludge Material, *International Journal of Environment and Waste Management* 27(1):93, DOI:10.1504/IJEWM.2021.10033677.

[3] Dharmappa, H., Hasia, A., Hagare, P., (1997). Management of residues from water treatment plants, Water Science and Technology, Water treatment plant residuals management, vol.35, no.8,pp.45–56, DOI:10.2166/wst.1997.0296.

[4] Generation, Treatment, and Disposal at Large Community Water Systems, Drinking Water

[5] Gikas, P., (2017). Towards energy positive wastewater treatment plants, *Journal of Environmental Management*, DOI:10.1016/j.jenvman.2016.05.061.

[6] Groseer, A., Neczaj, E., (2016). Enhancement of biogas production from sewage sludge by addition of grease trap sludge, *Energy Conversion and Management*, Vol. 125, 301-308, DOI:10.1016/j.enconman.2016.05.089.

[7] Hossain, K.M.I., (2024). Resilience of Wastewater Treatment Plants to Climate Change: Challenges and Adaptation Strategies, *International Journal of Business Social and Scientific Research*, 12(2):41-48, DOI: 10.55706/ijbssr12123.
[8] Ibrahim, K.S. Abdulkadir, M., Szegi, T., Makadi, M., (2025). Review of Sewage Sludge Composting Technologies**,** *Journal of Central European Green Innovation*, 13(2):45-62, DOI:10.33038/jcegi.7335
[9] Lombardi, L., Nocita, C., Bettazzi, E., Fibbi, D., Carnevale E., (2017). Environmental comparison of alternative treatments for sewage sludge: An Italian case study, *Waste Management*, vol. 69, p. 365-376, DOI:10.1016/j.wasman.2017.08.040.
[10] Industry Report.
[11] Isacu, M.D., (2014). Contributions on the efficiency of urban wastewater treatment plants / Contribuții cu privire la eficientizarea stațiilor de epurare orășenești, https: //dspace. upt.ro/jspui/ bitstream /123456789 /408/2 /BUPT_TD_Isacu%20Monica.pdf
[12] Lawrence, J., Giurea, R., Bettinetti, R., (2024). Preliminary correlations between climate change and wastewater treatment plant parameters, *WIT Transactions on Ecology and the Environment*, 262, articolul SDP240791. https://doi.org/10.2495/SDP240791
[13] Macoveanu, M., Teodosiu, C., Duca, G., (1997). Advanced treatment of wastewater containing non-biodegradable organic compounds, *Gh. Asachi Publishing House, Iași* / (in Romanian).
[14] Militaru, A.,C., Robescu, D., Panaitescu, V., (2011). Wastewater treatment plant for 100,000 inhabitants – case study – feasibility study on the modernization of the Pitești wastewater treatment plant, *11th National Conference with International Participation* (in Romanian), https://stiintasiinginerie.ro/wp-content/uploads/2014/01/74-STA%C5%A2IE-DE-EPURARE-PENTRU-100.000-LOCUITORI-%E2%80%93.pdf
[15] Qrenawi, L., Rabah, F., (2021). Sludge Management in Water Treatment Plants: A Literature Review, *International Journal of Environment and Waste Management*. 27(1):93, DOI: 10.1504/IJEWM.2021.111909.
[16] Ranieri, E., D'Onghia, G., Lopopolo, L., Gikas, P., Ranieri, F., Gika, E., Spagnolo, V., Herrera, J.A., Ranieri, A.C., (2024). Influence of climate change on wastewater treatment plants performances and energy costs in Apulia, south Italy. *Chemosphere*, 350, 141087, doi:10.1016/j.chemosphere.2023.141087
[17] Segneanu, E.,(2006) - Modernization of wastewater treatment plants, / Modernizarea stațiilor de epurare, https://dspace.upt.ro/jspui/bitstream/123456789/4342/1/BUPT_TD_Segneanu%20Emanoel.pdf
[18] USEPA (2011) Drinking Water Treatment Plant Residuals Management: Summary of Residuals
[19] Zhang, Q., Hu, J., Lee, D-J., Chang, Y.L, Y-J.,(2017). Sludge treatment: Current research trends, *Bioresource Technology*, 243(1159-1172), doi: 10.1016/j.biortech.2017.07.070.
[20] *** DIRECTIVE 2008/98/EC OF THE EUROPEAN PARLIAMENT AND OF THE COUNCIL of 19 November 2008, https://eur-lex.europa.eu/legal-content/EN/TXT/PDF/?uri=CELEX:02008L0098-20180705
[21] *** Pitești Wastewater Treatment Plant / Stația de epurare Pitești, https://www.apacanal2000.ro/
[22] *** USEPA (2011). Drinking Water Treatment Plant Residuals Management: Summary of Residuals Generation, Treatment, and Disposal at Large Community Water Systems, Drinking Water Industry Report.

# CAD-BASED DESIGN AND STRUCTURAL PERFORMANCE EVALUATION OF A SMALL-SCALE H-DARRIEUS VERTICAL AXIS WIND TURBINE FOR PRECISION AGRICULTURE APPLICATIONS

/

# *PROIECTAREA ASISTATĂ CAD ȘI EVALUAREA PERFORMANȚEI STRUCTURALE A UNEI TURBINE EOLIENE CU AX VERTICAL DE TIP H-DARRIEUS DE MICI DIMENSIUNI PENTRU APLICAȚII ÎN AGRICULTURA DE PRECIZIE*

**Bogdan Ovidiu DURAN[1)], Adrian PANDELE[1)], Dragos Mihail PREDA[1)], Gheorghe VOICU*[1)], Gabriel GHEORGHE[2)]**

[1)] National University of Science and Technology POLITEHNICA Bucharest, Biotechnical Systems Engineering Faculty, Bucharest / Romania;

[2)] National Institute of Research - Development for Machines and Installations Designed to Agriculture and Food Industry - INMA Bucharest / Romania;

**Tel: (+40) 724 715 585; *E-mail: gheorghe.voicu@upb.ro*

***Keywords:*** *precision agriculture; renewable energy; vertical axis wind turbine; H-Darrieus turbine; CAD modelling; finite element analysis; smart farming.*

## ABSTRACT

The use of small-scale vertical-axis wind turbines (VAWTs)—capable of powering remote monitoring and control devices in agriculture—offers distinct advantages due to their ability to operate under turbulent and multidirectional wind conditions. This paper describes the design of an experimental H-Darrieus vertical-axis wind turbine, developed as a renewable energy source for future precision agriculture technologies. The research encompassed the geometric design of the rotor, 3D CAD modelling of its structural components, and finite element analysis (FEM) of the proposed structure. Numerical studies were conducted across various loading conditions to analyse stress distribution, total deformation, and the system's mechanical behaviour. Furthermore, analysis of the rotor—featuring an improved blade design—indicates reduced structural deformation and acceptable stress levels in critical areas. The proposed design can serve as an experimental basis for subsequent aerodynamic studies and CFD analyses. The proposed methodology facilitates the design of more compact renewable energy systems capable of powering autonomous agricultural sensors and other smart technologies used on farms.

## REZUMAT

*Utilizarea turbinelor eoliene cu ax vertical (VAWT) de mici dimensiuni, capabile să alimenteze cu energie electrică dispozitivele de monitorizare și control de la distanță utilizate în agricultură, prezintă avantaje deosebite datorită capacității acestora de a funcționa în condiții de vânt turbulent și multidirecțional. Prezenta lucrare descrie proiectarea unei turbine eoliene experimentale cu ax vertical de tip H-Darrieus, concepută ca sursă de energie regenerabilă pentru viitoarele tehnologii din agricultura de precizie. Cercetarea a inclus proiectarea geometrică a rotorului, modelarea 3D CAD a elementelor sale structurale și analiza cu elemente finite (FEM) a structurii propuse. Au fost efectuate studii numerice pentru diverse regimuri de încărcare, în scopul analizei distribuției eforturilor, a deformării totale și a comportamentului mecanic al sistemului. În plus, analiza rotorului convențional cu design îmbunătățit al palelor indică o deformare structurală redusă și un nivel adecvat al eforturilor în zonele critice. Designul propus poate servi drept bază experimentală pentru studii aerodinamice și analize CFD ulterioare. Metodologia propusă facilitează proiectarea unor sisteme de energie regenerabilă mai compacte, capabile să alimenteze senzori agricoli autonomi și alte tehnologii inteligente utilizate în ferme.*

## INTRODUCTION

In the context of the accelerated development of modern society and the continuous increase in energy consumption, the use of renewable energy sources has become one of the main directions of research and development worldwide. Heavy reliance on fossil fuels has caused significant environmental pollution and greenhouse gas emissions, prompting the scientific community to shift its focus toward sustainable energy technologies with minimal environmental impact (*Kaygusuz, K..2009),* (*Jaber, S., 2013)*.

Wind energy stands out as a key form of renewable energy due to its abundant availability and the ability to convert wind's kinetic energy into electricity with relatively high efficiency (*Chaudhuri, A.et al., 2022)*. Advances in modern wind technology have enhanced the performance of energy conversion systems and lowered operating costs, establishing wind turbines as a vital component of contemporary energy systems (*Edwards, E. C.et al., 2023)*.

Most commercial applications employ Horizontal Axis Wind Turbines (HAWTs) due to their high aerodynamic efficiency and technological maturity (*Elkodama, A.et al., 2023)*. However, Vertical Axis Wind Turbines (VAWTs) have regained the interest of researchers thanks to their specific design and operational advantages, particularly for urban applications and small-scale power systems (*Cuevas-Carvajal, N. et al., 2022)*.




**Fig. 1 - Structural configurations of vertical-axis wind turbines used in experimental and urban applications** *(Manwell, J. F.et al., 2024).*

Vertical-axis wind turbines offer a number of significant advantages over conventional horizontal-axis turbines. Key among these are their independence from wind direction, low noise levels, the placement of the generator at the base of the structure, and the ability to operate in highly turbulent conditions (*Zhu, C.et al., 2026; Luo, W.et al.2023)*. These characteristics facilitate the integration of vertical-axis turbines into urban environments and experimental laboratory settings.

Among the various design configurations for vertical-axis turbines, the Darrieus and H-Darrieus types are considered the most aerodynamically efficient (*Jorge-Saúl, G. M.et al., 2025)*. The H-type rotor employs vertical blades connected to the central shaft via support arms, providing high structural rigidity and flexibility in the choice of air-foil profile (*Aboelezz, A., Ghali et al., 2022)*.

The aerodynamic behaviour of vertical-axis wind turbines is influenced by numerous geometric and operational parameters, such as rotor solidity, blade air-foil profile, tip-speed ratio (TSR), and the number of blades (*Tahzib, T. et al., 2022)*. The complex interaction between airflow and the rotor gives rise to transient aerodynamic phenomena—such as boundary layer separation and dynamic stall—that significantly impact turbine performance (*Zhu, C.et al., 2015)*.

In recent decades, modern numerical methods have become essential tools for the analysis and optimization of wind turbines. Computational Fluid Dynamics (CFD) enables the simulation of airflow around the rotor and the assessment of pressure and velocity distributions within the computational domain (*Radhakrishnan, J.et al., 2023)*. In parallel, structural analysis using the finite element method (FEM) is employed to evaluate the distribution of stresses and deformations in the turbine's structural components (*Luo, W.et al.2024)*.

In the case of vertical-axis turbines, rotor components are simultaneously subjected to bending, torsion, and vibration stresses generated by rotor rotation and aerodynamic forces (*Hameed, M. S.et al., 2015)*. Consequently, evaluating structural behaviour is a crucial step in the design and optimization process of the turbine assembly.

The finite element method enables the identification of critical zones characterized by high stress concentrations and allows for the optimization of the design configuration prior to the construction of an experimental prototype (*Wang, L.et al., 2016)*. Furthermore, modal analysis facilitates the determination of natural vibration frequencies and helps avoid resonance phenomena during rotor operation (*Roscher, B.2014)*.

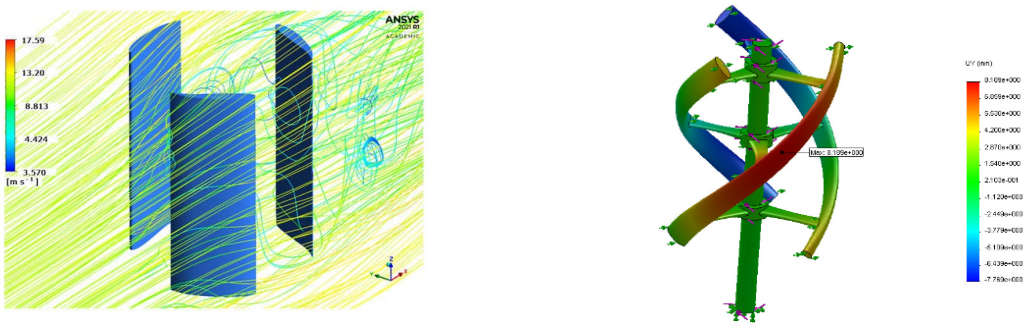



**Fig. 2 - Examples of numerical analyses: CFD** *(Gerrie, C.et al., 2023*) **and FEM** *(Aravind, S.et al., 2014)* **applied to vertical-axis wind turbines.**

The advancement of CAD technologies and modern additive manufacturing methods has significantly accelerated the prototyping and experimental development process for wind turbines (*Irwin, J. et al., 2013)*. Utilizing 3D printing for experimental components offers significant advantages regarding cost reduction and geometric flexibility (*Kao, R.H.et al., 2025)*.

Additive manufacturing via FDM (Fused Deposition Modelling) technology enables the rapid production of components with complex geometries and facilitates the implementation of design modifications derived from numerical and experimental analyses (*Olivera, A.F. et al., 2024)*. At the same time, integrating CAD models with CFD and FEM analyses allows for the development of modern engineering design and structural optimization workflows (*Turgut, A. et al.2019)*.

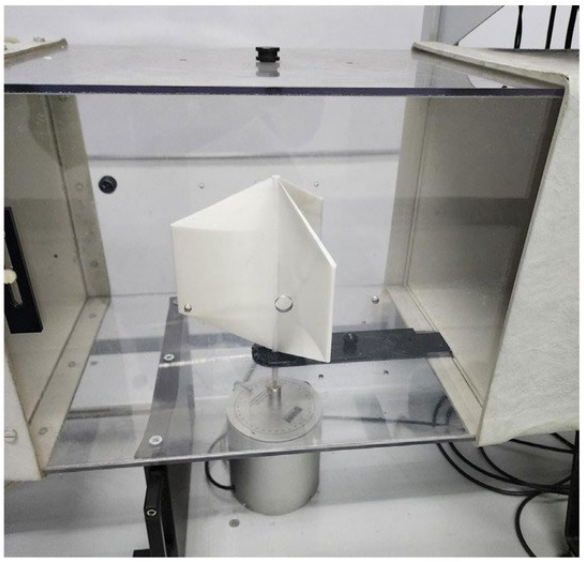


**Fig. 3 - Example of a wind turbine produced using additive manufacturing technologies for experimental wind applications.**
(*Ang, E.et al., 2025)*

This report analyses the development of an experimental H-Darrieus vertical-axis wind turbine model featuring three blades, intended for structural and experimental studies. The experimental model has a blade length of 500 mm and a rotor radius of 300 mm; it is designed for integration into a laboratory test rig and for conducting structural and numerical analyses.

The development process encompasses geometric sizing, CAD modelling, and FEM structural analysis. The approach employed aims to fully integrate the design stages into a unified engineering development workflow (*Rahman, M.et al., 2022)*.

The primary objective of the report is to develop and evaluate a functional experimental model of a vertical-axis wind turbine capable of enabling the investigation of the rotor's structural and mechanical behaviour under controlled laboratory conditions. To this end, the study focuses on optimizing the design configuration and evaluating the influence of geometric parameters on stress distribution and structural deformation.

The significance of this research stems from the need to develop efficient and accessible wind energy systems for urban applications and small-scale power generation. Vertical-axis wind turbines hold considerable potential in this field due to their high adaptability and ability to operate efficiently in conditions characterized by turbulence and frequent changes in wind direction (*Abdolahifar, A. et al., 2024)*.

## MATERIALS AND METHODS

Computer-aided modelling represents a fundamental stage in the development process of an experimental vertical-axis wind turbine, as it enables the precise definition of component geometry and their integration into a fully functional assembly. The use of CAD technologies facilitates both the optimization of the design configuration and the preparation of models required for numerical analyses and manufacturing processes.

In this report, the three-dimensional modelling of the wind turbine was carried out using parametric CAD software, which allows for the rapid modification of geometric dimensions and the automatic updating of associated components. This approach offers a significant advantage during the experimental phase, where design modifications frequently arise from structural or aerodynamic analyses.

The developed virtual model aimed to faithfully reproduce the actual configuration of the experimental turbine and ensure compatibility among all assembly components. At the same time, CAD modelling served as the basis for producing technical documentation, generating files required for 3D printing, and preparing Finite Element Method (FEM) analyses.

The wind turbine assembly was designed with an H-Darrieus configuration, featuring three blades arranged symmetrically around the central shaft. This configuration was selected due to its high structural stability and favourable aerodynamic performance under laboratory experimental conditions.

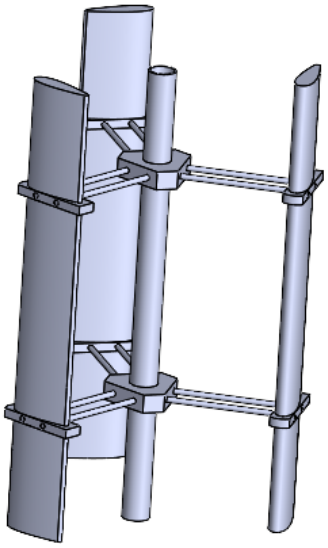


**Fig. 4 - CAD model of the H-Darrieus vertical-axis wind turbine assembly.**

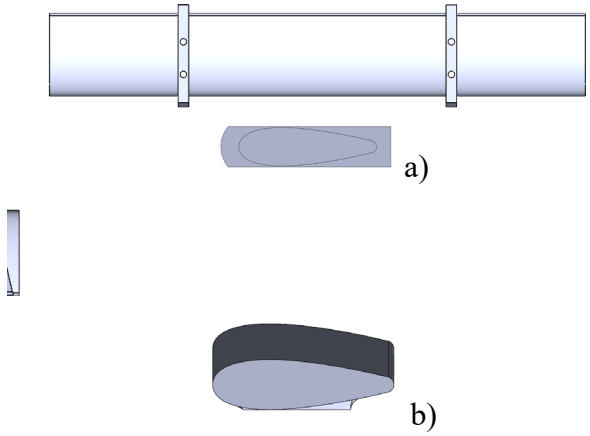



**Fig. 5 - Wind turbine blades for the two cases:** *a) the classical configuration; b) the new configuration.*

The general rotor geometry was established based on the main dimensions defined during the sizing phase: a blade length of 500 mm and a rotor radius of 300 mm. The symmetrical arrangement of the three blades helps reduce dynamic imbalances and ensures a uniform distribution of mechanical loads during operation.

The design process aimed to create a structure that is both compact and sufficiently rigid to withstand the stresses generated by rotor rotation and aerodynamic forces. The chosen configuration also allows for easy access to key components during assembly and experimental testing.

The turbine blade is the rotor's primary active component, responsible for converting the wind's kinetic energy into rotational mechanical energy. Consequently, its geometry directly influences the turbine's aerodynamic performance and operational stability.

A symmetrical air-foil profile, suitable for vertical-axis wind turbines, was used for the experimental model. Selecting a symmetrical profile enables efficient blade operation across various angular rotor positions and helps minimize torque fluctuations during rotation.

The CAD modelling process began by defining the air-foil coordinates in a two-dimensional plane, followed by the creation of a parametric sketch. Subsequently, the profile was extruded along the 500 mm length to generate the blade's complete three-dimensional geometry. Finally, the mounting sections required for connection to the rotor support arms were incorporated. The blade modelling aimed to strike a balance between structural rigidity and total mass reduction—a crucial factor for both the turbine's dynamic behaviour and its additive manufacturing process.

Once the individual components were modelled, they were integrated into a complete virtual assembly. The CAD assembly phase enabled the verification of geometric compatibility between components and the identification of potential structural interferences.

The virtual assembly facilitated an analysis of the blade's positioning relative to the shaft, the orientation of the support arms, and the overall layout of the rotor components. Furthermore, the CAD model allowed for a preliminary assessment of assembly access points and the space required to integrate experimental equipment.

Creating the 3D assembly enabled the simulation of assembly stages and served as the basis for exporting models to the software used for FEM and CFD analyses.

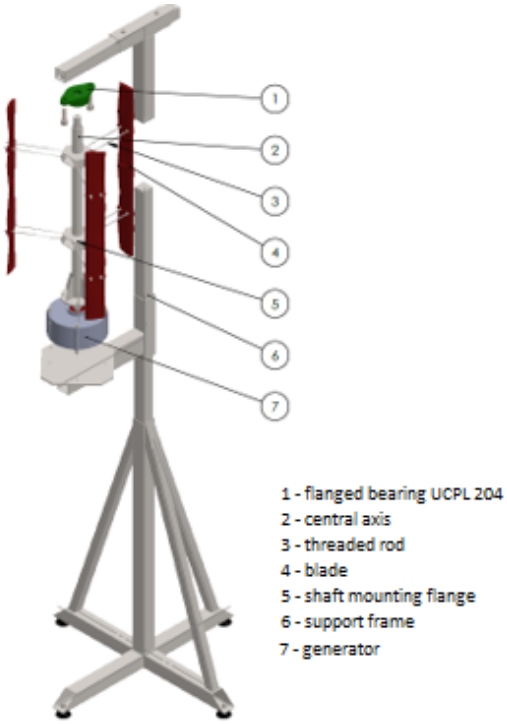



**Fig. 6 - Exploded view of the wind turbine assembly used to verify geometric compatibility between components.**

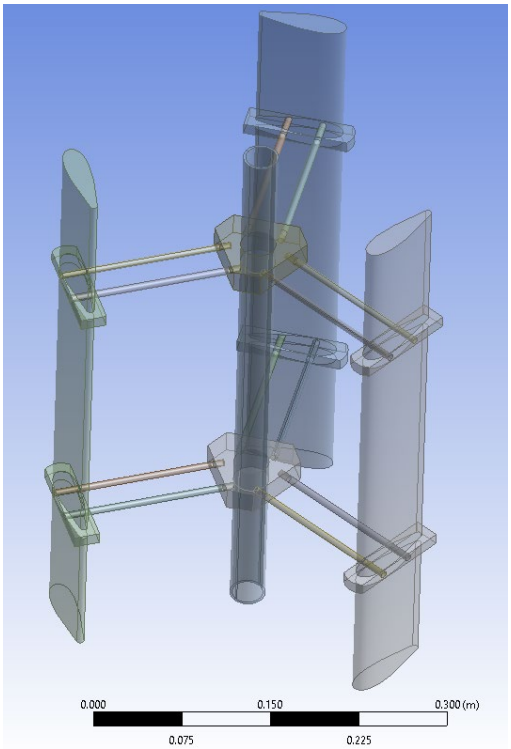



**Fig. 7 - The numerical model of the wind turbine used in the FEM analysis**

This chapter presents the CAD modelling process for the H-Darrieus vertical-axis wind turbine, highlighting the key development stages of the experimental assembly. The 3D models created enabled the precise definition of component geometry and their integration into a fully functional configuration.

The use of CAD technologies facilitated the optimization of the design configuration and the preparation of models required for subsequent manufacturing and numerical analysis stages. Furthermore, the resulting virtual model offers the flexibility needed to implement geometric modifications and develop alternative experimental configurations.

Finite Element Method (FEM) structural analysis is one of the most widely used numerical methods for evaluating the mechanical behaviour of structures subjected to various types of loads. In the case of vertical-axis wind turbines, FEM analysis allows for the estimation of stress distribution, deformation, and the dynamic behaviour of rotor components under conditions closely approximating actual operation.

In this study, structural analysis was performed on the H-Darrieus wind turbine experimental model to evaluate the structural integrity of key components and identify areas prone to high stress concentrations. The numerical study examined both the static behaviour of the assembly and the dynamic response of the rotor during operation.

The 3D model used in the FEM analysis was imported directly from the CAD environment, ensuring faithful preservation of component geometry and minimizing errors associated with the discretization process.

The numerical model used for the FEM analysis was developed based on the 3D turbine assembly created during the CAD modelling stage. To reduce computation time and simplify the discretization process, certain geometric details that were structurally insignificant were removed. The analysis focused on the rotor's main components—specifically the blades, support arms, and central shaft—as these are subjected to the highest loads during turbine operation. The final geometry was prepared to facilitate the generation of a uniform and numerically stable finite element mesh.

The numerical modelling process incorporated the mechanical properties of the materials used to manufacture the components, including the modulus of elasticity, Poisson's ratio, and material density.

The geometric model was discretized using three-dimensional finite elements capable of capturing the distribution of stresses and deformations within the rotor components. The quality of the discretization mesh directly influences the accuracy of the numerical results and the stability of the computational process.

A finer discretization was employed in areas characterized by significant geometric variations or high stress concentrations to enhance simulation accuracy. Conversely, larger elements were used in regions subject to lower structural loads, thereby helping to reduce total computation time.

The discretization process was validated through an analysis of finite element quality and an evaluation of the numerical results' convergence.

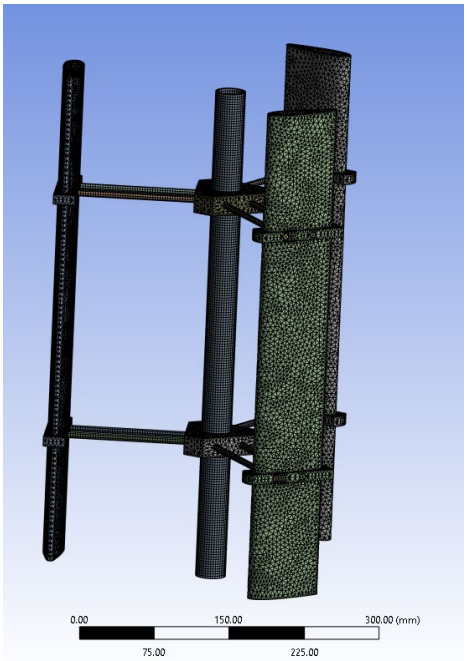



**Fig. 8 - The discretization mesh used in the structural analysis of the turbine.**

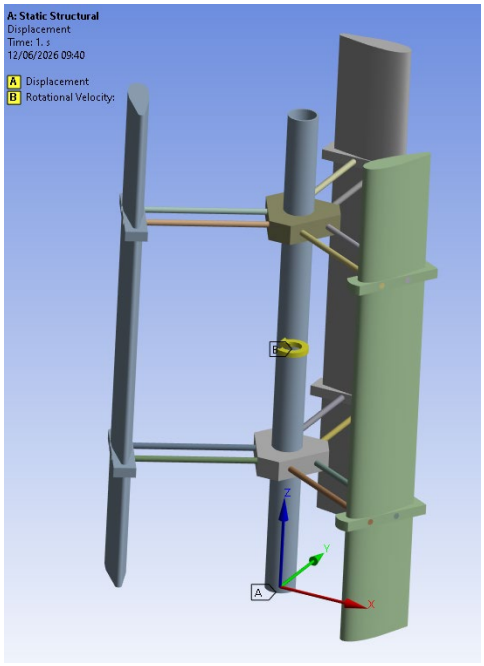



**Fig. 9 - Representation of boundary conditions and applied loads on the FEM model**

Defining boundary conditions and applied loads is a crucial step in obtaining meaningful numerical results. In this analysis, the central shaft was modelled as fixed to the supporting structure at the mounting point, simulating the actual installation conditions of the experimental turbine.

Equivalent forces—generated by airflow and rotor rotation—were applied to the blade and support arms. The loads considered in the model encompass both aerodynamic components and inertial effects resulting from the rotational motion.

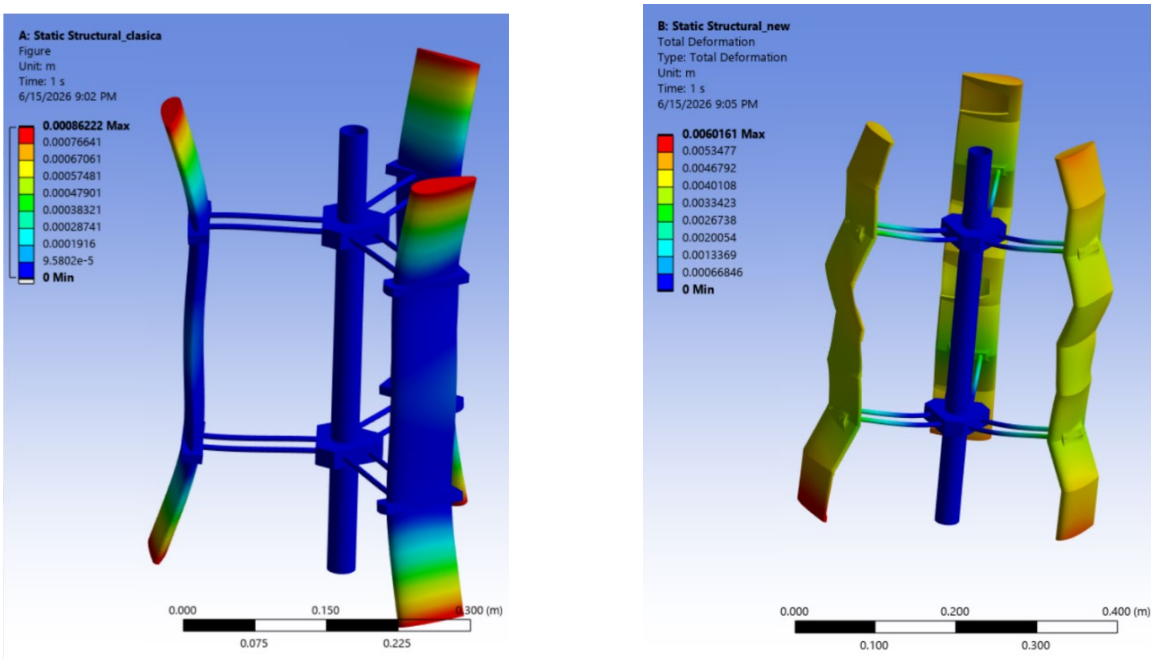
During turbine operation, the blades are subjected to simultaneous bending and torsional loads caused by the non-uniform pressure distribution across the airfoil surface. These effects lead to the emergence of critical zones characterized by high stress concentrations, particularly in the blade attachment regions.

## RESULTS AND DISCUSSION

Static structural analysis enabled the evaluation of the distribution of equivalent stresses and total deformations within the rotor components. The results indicate that peak stress values occur in the blade attachment zones and at the connection between the support arms and the central shaft.

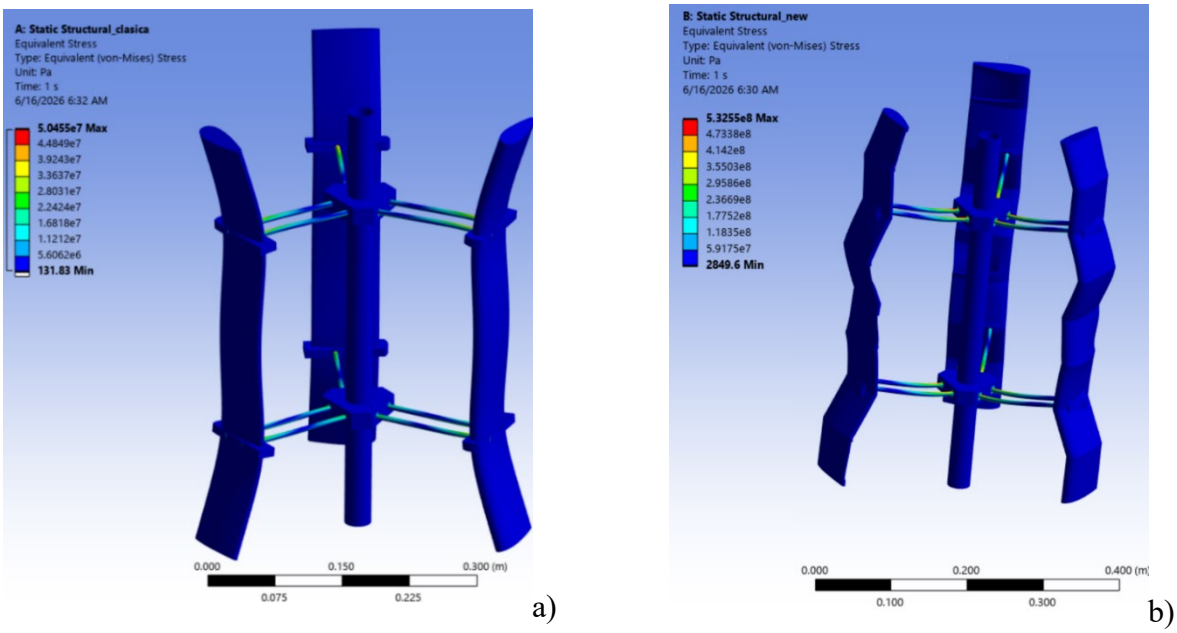
The stress distribution was influenced by both component geometry and the loading conditions applied during the simulation. Areas characterized by abrupt geometric variations or changes in cross-section exhibited higher local stress concentrations.

Maximum deformations were identified at the blade tips, resulting from bending effects caused by aerodynamic forces. However, the obtained values fall within acceptable limits for the experimental model's operation and do not lead to significant structural instabilities.




a) b)

**Fig. 10 - Distribution of deformations resulting from the structural analysis:**
*a) classic rotor; b) new rotor*




a) b)

**Fig. 11 - Equivalent stress distribution:**
*a) conventional turbine; b) new turbine*

As can be seen from Fig. 10, the deformation fields obtained directly illustrate how the classical rotor and the newly proposed rotor geometries differ. It can be clearly noted that in both geometries, the regions with maximal deformations occur near the free parts of the blades, whereas the central shaft and the regions that are constrained by the support arms are deformed much less. From the mechanical point of view, this is quite natural because of the cantilever behavior of the blade segments. The most important feature, however, lies in the fact that the new geometry introduces a new distribution of deformations along the blade segments.

Structurally speaking, the mentioned phenomenon is important since large deflections of the blade may change the intended geometry of the rotor. Although the material does not exceed the allowable stress, large deflections may affect the orientation of the blade relative to the flow, may increase cyclic loading at the joints, and decrease repeatability of the measurements in the lab. The relatively even distribution of deformations in the rotor under consideration is beneficial for the experimental setup, where stability of the geometry is crucial. This statement confirms the purpose of designing mentioned above: to develop a compact and sufficiently stiff rotor for experiments, but one that could be easily modified geometrically.

Equivalent-stress distributions presented in Fig. 11 are also a valuable complement to the deformations analysis. As can be seen from the simulations of both configurations, the numerical analysis reveals the most challenging areas to be those related to structural discontinuity points and interface areas for the load transfer, including the areas of blade connection and connection areas of the support arms and the shaft. This is quite obvious since the change in the cross-sectional properties causes stress concentration at certain areas. Similar observations were made in other finite-element analyses of VAWT blades (Hameed, M. S. et al., 2015; Wang, L. et al., 2016). In the current analysis, the stress distribution is local and not distributed over the major part of the rotor which proves that the overall structure is still rigid enough under the studied loading conditions.

The difference between global and local behavior of the structure is another key point demonstrated through the comparison of Figs. 10 and 11. The tips of the blades dominate the maximum deformations since they are far away from the zones where the load transfers take place, in contrast to the equivalent stresses that are generated in the vicinity of the joints. Therefore, the evaluation of deformations would not be enough for analyzing the rotor. Displacement together with the equivalent stress give a more holistic assessment of the components that must be observed during the tests. From the engineering point of view, blade geometry and stiffness determine the global displacements, while the joint geometry and local cross-sections determine the stresses.

This comparative analysis of the classical and novel designs indicates that the proposed geometry modification could help to enhance the structural performance without modifying the base H-Darrieus turbine structure. It is important for experimental studies since it is possible to use the same shaft and its support system together with other geometries of blades without altering the entire rotor. Thus, the parametric approach to CAD used in this study is directly related to the interpretation of the FEM results, which implies that the areas revealed by numerical simulations as those of high sensitivity could be modified in the CAD model and further studied without any redesigning of the entire rotor. This CAD-FEM analysis becomes especially important for small experimental turbines since there could be several designs to manufacture and test aerodynamically.

It is essential to keep in mind the limits of these results in relation to the adopted numerical model. While structural analyses have been done using equivalent loads due to aerodynamics and rotation, the real-life loading of a Darrieus turbine is transient and constantly changing depending on the position of the blades. Time-varying phenomena such as dynamic stall, velocity change, and load reversal may result in time-dependent behavior, which cannot be accounted for using a static structural analysis. Transient aerodynamics' crucial role in VAWT performance (Zhu, C. et al., 2023) and the need for combined structural-aerodynamic analysis to study loads (Luo, W. et al., 2024) have been discussed in previous research.

Another consequence relates to the envisioned use in precision agriculture. Small self-sufficient sensing and monitoring systems need energy sources that can be set up at the location where they operate and that work in varying wind directions as well as local turbulence. In this case, the H-Darrieus structure analyzed is appropriate for this purpose in that it does not have to align in yaw and it is compatible with distributed energy ideas. The structural analysis alone does not provide information about the electrical energy generation; yet, it shows that the experimental rotor suggested in this paper forms a consistent basis for future studies in aerodynamics, generator coupling, and energy yield. The difference here is essential

since the current paper proves the concept structurally but the energy contribution to agricultural devices should be proven experimentally and by means of CFD.

## CONCLUSIONS

In this study, a small-scale H-Darrieus vertical-axis wind turbine was designed and structurally analyzed as an experimental platform for possible renewable energy applications with a focus on the field of precision agriculture. The suggested process involved geometric sizing, parametric CAD modeling, and finite element analysis, which allowed assessing the rotor design before the prototype fabrication.

The chosen rotor design, involving three blades with the length of 500 mm and the rotor radius of 300 mm, led to a compact configuration appropriate for laboratory research. Parametric CAD modeling helped to define and assemble the turbine parts, check geometrical compatibility, and create the numerical model. Additionally, the use of a parametric approach allows making any future modifications without re-designing the whole assembly.

The FEA results revealed the blade connection area and the connection area between the support arms and the shaft as the regions of stress concentration. The maximum deformations occurred at the blade edges, which coincided with the bending deformation caused by the loads applied. According to the analyzed conditions, the numerical model showed the stable behavior of the structure without any deformation indicating a possible loss of the structural integrity.

The comparison between the traditional and innovative blade design reveals that the change of geometry affects deformation and equivalent stress distribution. The new blade geometry demonstrates a more controlled distribution of the deformation process with acceptable stresses in the connection areas. Therefore, we may conclude that small changes in the geometry of the blade can positively affect its performance without changing the fundamental structure of the H-Darrieus wind turbine. This is why CAD-FEM optimization technique is applicable for the design of prototypes.

At the same time, the results have to be considered from the perspective of the applied model. As mentioned above, the FEM analysis takes into account equivalent loads and, therefore, may be viewed as the structural screening process. In order to fully evaluate the dynamic and fatigue properties of the turbine, future research has to combine the transient CFD and FEM analysis with measurement of the rotational speed, torque, vibration and generated power. This will help us to correlate the structural analysis with aerodynamic and energy performance of the turbine and determine whether the new turbine is suitable for powering autonomous sensors in precision agriculture.

## REFERENCES

[1] Abdolahifar, A., & Zanj, A. (2024). Addressing VAWT aerodynamic challenges as the key to unlocking their potential in the wind energy sector. Energies, 17(20), 5052.

[2] Aboelezz, A., Ghali, H., Elbayomi, G., & Madboli, M. (2022). A novel VAWT passive flow control numerical and experimental investigations: Guided vane airfoil wind turbine. Ocean Engineering, 257, 111704.

[3] Ang, E., & Honra, J. (2025). Performance Analysis of a Novel 3D-Printed Three-Blade Savonius Wind Turbine Rotor with Pointed Deflectors. Fluids, 11(1), 9.

[4] Aravind, S., Sougathali, S., Ashokpandiyan, N., & Ganeshkarthikeyan, K. (2014). Trembling Analysis of Helical Blade Vertical Axis Wind Turbine (VAWT). Journal of Basic and Applied Engineering Research, 5, 71-77.

[5] Chaudhuri, A., Datta, R., Kumar, M. P., Davim, J. P., & Pramanik, S. (2022). Energy conversion strategies for wind energy system: Electrical, mechanical and material aspects. Materials, 15(3), 1232.

[6] Cuevas-Carvajal, N., Cortes-Ramirez, J. S., Norato, J. A., Hernandez, C., & Montoya-Vallejo, M. F. (2022). Effect of geometrical parameters on the performance of conventional Savonius VAWT: A review. Renewable and Sustainable Energy Reviews, 161, 112314.

[7] Edwards, E. C., Holcombe, A., Brown, S., Ransley, E., Hann, M., & Greaves, D. (2023). Evolution of floating offshore wind platforms: A review of at-sea devices. Renewable and Sustainable Energy Reviews, 183, 113416.

[8] Elkodama, A., Ismaiel, A., Abdellatif, A., Shaaban, S., Yoshida, S., & Rushdi, M. A. (2023). Control methods for horizontal axis wind turbines (HAWT): State-of-the-art review. Energies, 16(17), 6394.

[9] Gerrie, C., Islam, S. Z., Gerrie, S., Turner, N., & Asim, T. (2023). 3D CFD modelling of performance of a vertical-axis turbine. Energies, 16(3), 1144.
[10] Hameed, M. S., Afaq, S. K., & Shahid, F. (2015). Finite element analysis of a composite VAWT blade. Ocean Engineering, 109, 669-676.
[11] Irwin, J. (2013). Wind turbine blade CAD models used as scaffolding technique to teach design engineers. The Engineering Design Graphics Journal, 77(2).
[12] Jaber, S. (2013). Environmental impacts of wind energy. Journal of Clean Energy Technologies, 1(3), 251-254.
[13] Jorge-Saúl, G. M., & Ernesto, C. N. (2025). A Systematic Review of Technological Strategies to Improve Self-Starting in H-Type Darrieus VAWT. Sustainability, 17(17), 7878.
[14] Kao, R. H., Cheng, J. C., Tao, B., Chen, W. C., Hu, E. S., & Ma, C. (2025, July). Design and Performance of a 3D-Printed Vertical Axis Wind Turbine. In 2025 IEEE International Conference on Consumer Electronics-Taiwan (ICCE-Taiwan) (pp. 421-422). IEEE.
[15] Kaygusuz, K. A. M. I. L. (2009). Wind power for a clean and sustainable energy future. Energy Sources, Part B, 4(1), 122-133.
[16] Luo, W., Liu, W., Chen, S., Zou, Q., & Song, X. (2024). Development and Application of an FSI Model for Floating VAWT by Coupling CFD and FEA. Journal of Marine Science and Engineering, 12(4), 683.
[17] Luo, W., Liu, W., Yang, M., Chen, S., Song, X., & Wu, W. (2023). Load characteristics and extreme response of straight-bladed floating VAWT using a fully coupled model. Journal of Marine Science and Engineering, 11(1), 185.
[18] Manwell, J. F., Branlard, E., McGowan, J. G., & Ram, B. (2024). Wind energy explained: on land and offshore. John Wiley & Sons.
[19] Olivera, A. F., Chica, E., & Colorado, H. A. (2024). Design and manufacturing with 3D printing and life cycle analysis of a recyclable polymer-based H-Darrieus wind turbine. Engineered Science, 31, 1156.
[20] Radhakrishnan, J., Sridhar, S., Zuber, M., Ng, E. Y., & Shenoy, S. (2023). Design optimization of a Contra-Rotating VAWT: A comprehensive study using Taguchi method and CFD. Energy Conversion and Management, 298, 117766.
[21] Rahman, M., Whyte, O., Ilie, M., Soloiu, V., & Molina, G. (2022). Structural and Aerodynamic Characteristics Analysis of a Small V-shaped Vertical Axis Wind Turbine Rotor. International journal of green energy, 19(3), 279-299.
[22] Roscher, B. (2014). Structural optimization of a vertical axis wind turbine with aeroelastic analysis. M. Sc., Wind Energy and Aerospace Engineering, Technical University of Denmark and Delft University of Technology. Denmark.
[23] Tahzib, T., Hannan, M. A., Ahmed, Y. A., & Kamal, I. Z. M. (2022). Performance analysis of H-Darrieus wind turbine with NACA0018 and S1046 aerofoils: impact of blade angle and TSR. CFD Letters, 14(2), 10-23.
[24] Turgut, A., Kaya, Z., Özsoy, K., & Aksoy, B. (2019, November). Design and Manufacturing of Horizontal and Vertical Wind Turbine With 3D Printing Technology. In Proceedings on 2nd International Conference on Technology and Science.
[25] Wang, L., Kolios, A., Nishino, T., Delafin, P. L., & Bird, T. (2016). Structural optimisation of vertical-axis wind turbine composite blades based on finite element analysis and genetic algorithm. Composite Structures, 153, 123-138.
[26] Zhu, C., Yang, H., Qiu, Y., Zhou, G., Wang, L., Feng, Y., ... & Wang, T. (2023). Effects of the Reynolds number and reduced frequency on the aerodynamic performance and dynamic stall behaviors of a vertical axis wind turbine. Energy Conversion and Management, 293, 117513.
[27] Zhu, C., Zhu, Z., Qiu, Y., Na, W., Liu, N., & Wang, T. (2026). Contrasting Dynamic Stall Characteristics: Airfoil Behavior in VAWT Kinematics versus Equivalent Planar Motions. Energy, 140307.

# INTEGRATED WEED MANAGEMENT (IWM): SYNERGY BETWEEN CHEMICAL, BIOLOGICAL AND AGRONOMIC METHODS FOR SUSTAINABLE WEED CONTROL

/

# *MANAGEMENTUL INTEGRAT AL BURUIENILOR (IWM): INTEGRAREA METODELOR CHIMICE, BIOLOGICE ȘI AGROTEHNICE PENTRU COMBATEREA DURABILĂ A BURUIENILOR*

**Costin MIRCEA*[1)], Florin NENCIU[1)], Gheorghe STROESCU[1)], Andreea ENEA[2)], Raluca-Adriana ZOTA[3)], Floarea ȘERBANCEA[4)]**

[1)] INMA Bucharest / Romania; [2)] ARDS Secuieni, Neamt County / Romania; [3)] UNSTP Bucharest / Romania; [4)] IBA Bucharest / Romania

**E-mail: costinmircea@yahoo.com*

***Keywords:*** *Integrated weed management, sustainable agriculture, herbicide resistance, biological weed control, agronomic practices, weed ecology.*

## ABSTRACT

*Weed infestation is a major constraint to agricultural productivity, causing yield losses and increasing production costs. Intensive reliance on herbicides has contributed to herbicide resistance, environmental contamination, and potential health risks. Integrated Weed Management (IWM) offers a sustainable approach by combining chemical, biological, mechanical, and agronomic methods for long-term weed suppression. Evidence shows that crop rotation, cover crops, competitive cultivars, mechanical practices, biological agents, and rational herbicide use can reduce weed pressure, decrease herbicide dependence, and delay resistance development. IWM also strengthens agroecosystem resilience and biodiversity while supporting the sustainability of farming systems. Thus, IWM represents a shift from reactive weed control toward proactive and preventive management, contributing to sustainable agriculture and reduced environmental impact.*

## REZUMAT

*Infestarea cu buruieni reprezintă o constrângere majoră pentru productivitatea agricolă, provocând pierderi de producție și creșterea costurilor de producție. Utilizarea intensivă a erbicidelor a contribuit la apariția rezistenței buruienilor, contaminarea mediului și posibile riscuri pentru sănătate. Managementul integrat al buruienilor (IWM) oferă o abordare durabilă, prin combinarea metodelor chimice, biologice, mecanice și agrotehnice pentru combaterea buruienilor pe termen lung. Dovezile științifice arată că rotația culturilor, culturile de acoperire, soiurile competitive, practicile mecanice, agenții biologici și utilizarea rațională a erbicidelor pot reduce gradul de infestare, diminuând dependența de erbicide și întârziind dezvoltarea rezistenței. IWM contribuie, de asemenea, la creșterea rezilienței agroecosistemelor și a biodiversității, susținând durabilitatea sistemelor agricole. Prin urmare, IWM reprezintă o trecere de la combaterea reactivă la managementul preventiv al buruienilor, contribuind la dezvoltarea unei agriculturi durabile și la reducerea impactului asupra mediului.*

## INTRODUCTION

Weeds are among the most important biological constraints in agricultural production systems, competing with crops for light, water, nutrients, and space, and causing substantial yield and quality losses. It is estimated that weeds can reduce crop yields by 30–40% in the absence of effective control measures, making weed management a critical component of modern agriculture *(Oerke, 2006)*.

The impact of weed competition on crop development and the potential benefits of effective weed management are illustrated in Figure 1.




**Fig. 1 - Comparison of weed infestation in a maize crop: without weed control (left) and with integrated weed management (right)**

For decades, weed control has been dominated by chemical herbicides due to their high efficiency, ease of application, and relatively low cost. However, the excessive and repetitive use of herbicides with the same mode of action has resulted in the widespread evolution of herbicide-resistant weed species. Currently, more than 500 unique cases of herbicide resistance have been reported globally, affecting major cropping systems and threatening food security *(Heap, 2024)*. In addition, environmental pollution, residue accumulation in soil and water, and concerns regarding human and ecosystem health have intensified the demand for alternative weed management strategies.

The global increase in unique herbicide-resistance cases highlights the growing challenges associated with intensive reliance on chemical weed control *(Heap, 2026)*, as illustrated in Figure 2.

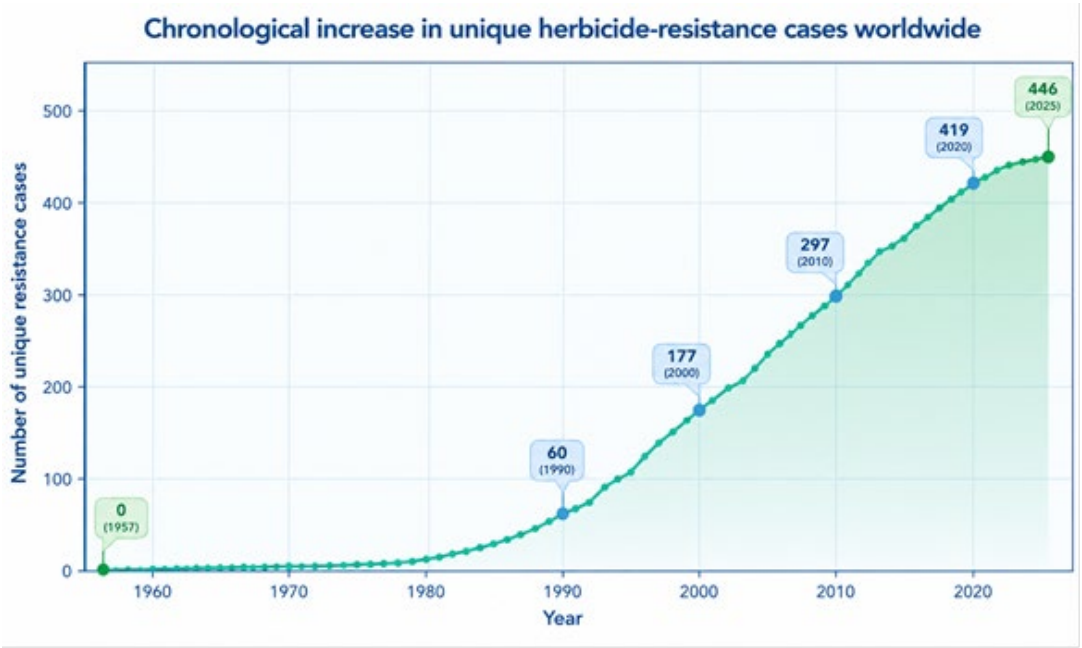



**Fig. 2 - Chronological increase in unique herbicide-resistance cases worldwide.**
*Source: Adapted from Heap, I. (2026), International Herbicide-Resistant Weed Database.*

In response to these challenges, Integrated Weed Management (IWM) has gained increasing attention as a holistic and sustainable approach. IWM is based on the coordinated use of multiple weed control methods, including agronomic, mechanical, biological, and chemical techniques, in order to maintain weed populations below economically damaging levels while minimizing negative environmental impacts *(Swanton & Weise, 1991; Harker & O'Donovan, 2013)*. Unlike conventional weed control, which often relies on a single method, IWM emphasizes system diversification and long-term ecological balance.

The main components of Integrated Weed Management and their complementary roles in sustainable weed suppression are illustrated in Figure 3.

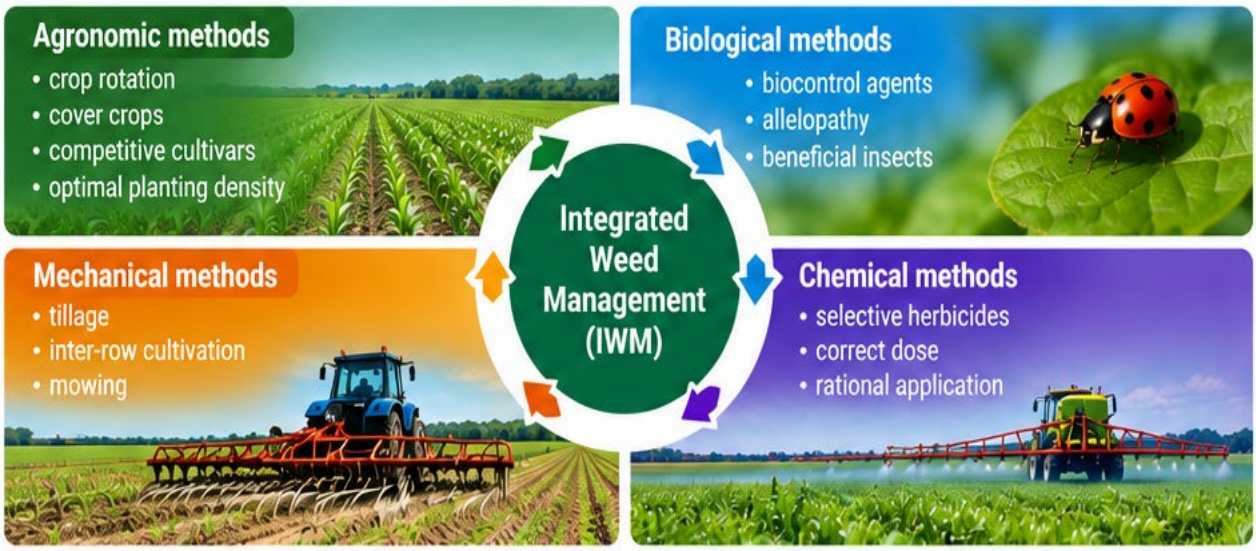



**Fig. 3 - Integrated Weed Management (IWM): combination of agronomic, biological, mechanical and chemical methods**

Previous studies have demonstrated the potential of individual alternative approaches, such as allelopathy, biological control agents, and optimized herbicide use, to suppress weed populations. Allelopathic interactions can inhibit weed germination and growth through the release of bioactive compounds, biological control exploits natural enemies of weeds, and rational herbicide management reduces selection pressure for resistant biotypes. However, when these methods are applied independently, their effectiveness is often limited by environmental variability and operational constraints.

The integration of these strategies within a unified framework offers a more robust and resilient weed management system. By combining preventive and curative measures, IWM not only improves weed control efficiency but also contributes to sustainable agricultural development by conserving natural resources and enhancing ecosystem services.

The aim of this paper is to analyze the concept of Integrated Weed Management and to evaluate the synergistic effects of combining chemical, biological, and agronomic methods for sustainable weed control.

This study provides a comprehensive synthesis of current scientific knowledge and highlights the role of IWM as a cornerstone of future weed management strategies.

## MATERIALS AND METHODS

This study is based on a comprehensive review of scientific literature concerning Integrated Weed Management (IWM) and its components. Relevant publications were collected from major scientific databases including Web of Science, Scopus, ScienceDirect, and Google Scholar. The search was conducted using keywords such as *integrated weed management*, *sustainable weed control*, *herbicide resistance*, *biological control of weeds*, *allelopathy*, *cover crops*, and *agronomic weed management*.

The literature selection focused on peer-reviewed articles, books, and international reports published mainly between 1990 and 2025. Preference was given to studies that evaluated combinations of weed control strategies or compared integrated approaches with single-method weed control systems. Both experimental and review papers were considered.

The collected information was analyzed and synthesized to:

- identify the main components of IWM,
- evaluate their individual and combined effectiveness,
- assess their impact on herbicide use reduction and resistance management,
- examine their contribution to sustainable agricultural systems.

This methodological approach allows a qualitative and comparative assessment of IWM as a holistic weed management strategy.

## RESULTS

The analysis of the reviewed literature highlights that Integrated Weed Management relies on the strategic combination of several complementary methods that act at different stages of the weed life cycle. The main components identified include agronomic, mechanical, biological, and chemical approaches. The functional roles and contributions of each IWM component are summarized in Table 1.

**Table 1**

**Main components of Integrated Weed Management (IWM) and their functional role**

| IWM Component | Methods Used | Main Role in Weed Control | Impact on Sustainability |
|---|---|---|---|
| **Agronomic** | Crop rotation, cover crops, optimal planting density, competitive cultivars | Prevention of weed establishment, reduction of the soil seed bank | Very high |
| **Mechanical** | Hoeing, harrowing, mowing, mulching | Direct destruction of young weeds | High |
| **Biological** | Pathogenic agents, phytophagous insects, allelopathy | Natural regulation of weed populations | Very high |
| **Chemical** | Selective herbicides, rotation of active substances | Rapid and effective control in critical situations | Moderate (when used rationally) |
| **Modern ecological** | Cover crops, bioherbicides, conservation agriculture | Reduction of weed pressure through natural processes | Very high |

### 3.1. Agronomic practices

Crop rotation, cover cropping, competitive crop cultivars, and optimized planting density were found to be among the most effective preventive measures. Crop rotation disrupts weed life cycles and reduces the dominance of species adapted to monoculture systems. Cover crops such as rye (*Secale cereale*), clover (*Trifolium spp.*), and mustard (*Sinapis alba*) significantly reduce weed emergence through competition and allelopathic effects. Several studies report weed biomass reductions of 40–70% when cover crops are integrated into cropping systems *(Teasdale, 1996; Liebman et al., 2001).*

Recent meta-analytical evidence confirms the role of cover crops in weed suppression. Dong and Zeng (2024), analyzing 250 site–year–management cases, reported average reductions of 62.6% in weed biomass and 45.4% in weed density after fall and winter cover crops. Mixtures were generally more effective than single species, although suppression declined after termination. These findings support the use of diverse, high-biomass cover crops within IWM systems *(Dong and Zeng, 2024).*

Summer legume cover crops can also contribute to IWM. *Zannopoulos et al. 2024* reviewed sunn hemp *(Crotalaria juncea L.)*, velvetbean *(Mucuna pruriens (L.) DC.)* and cowpea *(Vigna unguiculata (L.) Walp.).* During growth they suppress weeds through competition and allelopathy; after termination, their biomass can act as mulch. Sunn hemp and velvetbean reduced weed biomass by more than 50% under the reviewed conditions, while also providing potential soil, pest-regulation and carbon-sequestration benefits *(Zannopoulos et al., 2024).*

Cover crops suppress weeds through competition, soil coverage, and allelopathic effects. Their effectiveness varies with species, biomass production and cropping conditions. Examples of commonly used cover crops and their mechanisms of suppression are presented in Table 2.

**Table 2**

**Effect of different cover crops on weed biomass reduction**

| Cover Crop | Species | Main Control Mechanism | Reduction in Weed Biomass (%) |
|---|---|---|---|
| **Rye** | *Secale cereale* | Competition + allelopathy | 50–70 |
| **Mustard** | *Sinapis alba* | Allelopathy | 40–60 |
| **Clover** | *Trifolium pratense* | Competition + soil coverage | 30–50 |
| **Oat** | *Avena sativa* | Competition | 35–55 |

### 3.2. Mechanical methods

Mechanical weed control, including harrowing, hoeing, and mulching, provides immediate weed suppression and can reduce weed seed production. Its effectiveness is enhanced when mechanical operations are combined with agronomic practices that limit weed establishment.

### 3.3. Biological control

Biological control agents, including pathogenic fungi, insects, and allelopathic plants, can suppress specific weed species. Although biological methods are generally slower and more species-specific than herbicides, their integration into IWM can strengthen long-term population regulation and ecosystem stability.

### 3.4. Chemical control within IWM

Herbicides remain an important IWM component but are used rationally and in combination with non-chemical tactics. Rotating or combining active substances with different modes of action can reduce selection pressure for resistant biotypes. Integrated systems have been reported to reduce herbicide use by 30–60% without compromising crop yield *(Harker & O'Donovan, 2013).*

Farm-scale evidence also supports the integration of non-chemical practices in resistance management. Islam et al. (2026), analyzing 602 broadacre grain growers across 13 agroecological zones in Australia, found that herbicide resistance was associated with IWM adoption. Harvest weed seed control (HWSC) can reduce seed production of potentially resistant weeds without adding herbicide selection pressure. These findings support IWM as both a response to resistance and a proactive means of limiting its further development and spread *(Islam et al., 2026).*

### 3.5. Synergistic effects

The combined application of multiple strategies proved more effective than individual methods. Integrated systems consistently showed:

- lower weed density and biomass,
- reduced herbicide dependency,
- delayed evolution of herbicide resistance,
- improved soil quality and biodiversity.

A comparative evaluation between conventional weed control strategies and integrated systems demonstrates the advantages of IWM in terms of weed suppression efficiency, herbicide reduction, resistance management, and environmental impact. These differences are clearly illustrated in Table 3.

**Table 3**

**Indicative comparison of major weed control strategies**

| Control System | Reduction in Weed Density (%) | Reduction in Herbicide Use (%) | Resistance Risk | Ecological Impact |
|---|---|---|---|---|
| **Chemical only** | 80–90 | 0 | Very high | High |
| **Agronomic mechanical** | 40–60 | 70–100 | Low | Very low |
| **Biological** | 30–50 | 80–100 | Very low | Very low |
| **Integrated Weed Management (IWM)** | 75–90 | 30–60 | Low | Low |

*Note: Values represent indicative ranges synthesized from the reviewed literature and should not be interpreted as universal estimates.*

## DISCUSSION

Integrated Weed Management shifts weed control from a predominantly reactive approach toward proactive and preventive management. Its central principle is diversification: agronomic, mechanical, biological, and chemical measures act through different mechanisms and at different stages of weed establishment, growth, reproduction, and seed-bank replenishment. This diversification can improve the stability and durability of weed management while reducing dependence on any single tactic *(Harker & O'Donovan, 2013; Korres et al., 2019).*

### 4.1. Herbicide resistance management

Herbicide resistance represents one of the most important challenges to the long-term sustainability of chemical weed control. The repeated and intensive use of herbicides with the same mode of action

imposes strong selection pressure on weed populations, increasing the probability that resistant biotypes will survive and reproduce. Consequently, dependence on a limited number of herbicide mechanisms of action can progressively reduce the effectiveness of chemical weed control *(Harker & O'Donovan, 2013; Heap, 2026).*

Within an IWM framework, herbicides remain an important component of weed control, but they are integrated with agronomic, mechanical, biological, and preventive measures. The objective is not necessarily to eliminate herbicide use, but to reduce dependence on any single control tactic and to diversify selection pressures acting on weed populations. Crop rotation, competitive crops, cover crops, mechanical control, harvest weed seed control, and the rotation or combination of herbicide modes of action can therefore contribute to more durable resistance management *(Harker & O'Donovan, 2013; Korres et al., 2019).*

Recent evidence suggests that herbicide resistance and IWM are linked in a complex way. A 2026 farm-scale study of 602 Australian grain growers found that resistance was associated with IWM adoption, including harvest weed seed control. Practices adopted in response to resistance may also provide proactive benefits by reducing weed seed production and limiting further resistance development *(Islam et al., 2026).* This finding reinforces the importance of managing the weed seed bank and limiting the reproduction of resistant individuals. Preventing resistant weeds from producing viable seeds can complement chemical resistance management and reduce their frequency in subsequent generations. Because repeated use of any single tactic can impose selection pressure, diversification should include different herbicide modes of action and non-chemical tactics that affect weeds through different ecological mechanisms. The "many little hammers" approach can increase the durability of weed management by reducing the probability of adaptation to all measures simultaneously *(Liebman & Gallandt, 1997; Korres et al., 2019).*

The long-term effect of IWM on the development of herbicide-resistant weed populations compared with conventional herbicide-based systems highlights the importance of diversifying weed control tactics. Such diversification can reduce dependence on herbicides and potentially slow the development of herbicide resistance.

### 4.2. Environmental sustainability

Environmental sustainability is another major component of IWM. Intensive dependence on herbicides can contribute to environmental contamination, selection of resistant weed populations, and impacts on non-target organisms, although the magnitude of these effects depends on the herbicide, application rate, environmental conditions, soil characteristics, and management system. IWM addresses these concerns by combining chemical control with preventive and non-chemical approaches, thereby creating opportunities to reduce unnecessary chemical inputs and their associated environmental impacts *(Harker & O'Donovan, 2013; Deytieux et al., 2012).*

The environmental benefits of IWM are not necessarily derived from eliminating herbicides, but from reducing their dependence and integrating them more strategically within the cropping system. In a six-year field experiment, IWM-based cropping systems used fewer herbicides than a reference system while maintaining effective weed control, and the reduction in herbicide use was associated with lower environmental impact *(Bàrberi et al., 2009).*

Similarly, life-cycle assessment approaches have shown that the environmental performance of IWM depends on the complete cropping system rather than on an individual weed-control operation. Changes in crop sequence, soil tillage, mechanical weeding, and herbicide use can modify energy consumption, emissions, and pesticide-related impacts in different ways. Therefore, environmental assessment should consider the combined effects of all operations included in an IWM system *(Deytieux et al., 2012).*

Agronomic practices such as crop rotation and cover cropping can contribute to environmental sustainability by increasing crop diversity, improving soil cover, and modifying the ecological conditions that favor weed establishment. These practices may also contribute to long-term reductions in weed pressure by limiting weed recruitment and seed production. Mechanical and biological methods can further reduce dependence on chemical inputs, although their environmental benefits must be evaluated in relation to fuel consumption, soil disturbance, labor, and other operational requirements *(Harker & O'Donovan, 2013; Korres et al., 2019).*

The environmental performance of IWM should therefore be evaluated at the cropping-system level. A reduction in herbicide use does not automatically mean that the overall environmental footprint is reduced if it is replaced by intensive mechanical operations requiring additional fuel and field passes. Recent research illustrates this trade-off and emphasizes the importance of combining control methods according to

local conditions rather than assuming that one type of intervention is universally more sustainable than another.

Overall, IWM can contribute to environmental sustainability by reducing unnecessary pesticide inputs, diversifying weed control mechanisms, supporting crop and agroecosystem diversity, and reducing the ecological risks associated with excessive dependence on chemical control. Its environmental performance, however, remains strongly dependent on the specific cropping system, climate, soil conditions, weed community, and management practices employed.

### 4.3. Economic and practical considerations

The economic feasibility of IWM is an important factor influencing its adoption at farm level. Although diversified weed management can reduce dependence on herbicides and may lower chemical input requirements, IWM can also require additional field operations, machinery, labor, monitoring, and management time. Mechanical control measures such as inter-row cultivation, harrowing, or mowing may increase the number of field passes and consequently increase short-term operational costs. Therefore, the economic performance of IWM cannot be evaluated solely on the basis of herbicide expenditure.

The economic assessment of IWM should instead consider both short-term operational costs and longer-term benefits. Diversification of weed control tactics may reduce the risk of herbicide resistance and help maintain effective weed control when individual herbicides become less effective. Maintaining crop productivity and limiting the development of difficult-to-control weed populations may therefore provide economic benefits over longer time periods *(Harker & O'Donovan, 2013).*

Recent evidence demonstrates that the economic outcome of IWM is highly context dependent. A 2025 European case-study analysis found that IWM systems with reduced herbicide use could maintain crop yield without necessarily increasing workload, fuel use, or reducing profitability compared with local reference systems. However, the results also emphasized that the performance of IWM depended on the characteristics of the cropping systems and on the specific combination of practices adopted.

Similarly, the integration of chemical and mechanical practices can provide opportunities to reduce herbicide inputs without necessarily compromising weed control or crop yield. A meta-analysis of band herbicide application combined with inter-row cultivation found that integrated systems could reduce herbicide use while maintaining weed control and crop yield compared with broadcast herbicide application, although the results varied according to crop, herbicide timing and rate, spraying width, and cultivation frequency *(Ozaslan et al., 2024).*

Consequently, the economic viability of IWM depends on several interacting factors, including crop type, weed pressure, farm size, available machinery, labor availability, input prices, climate, and the level of technical knowledge required to implement diversified management strategies. Adoption may also be influenced by farmers' perceptions of risk and by the availability of advisory and technical support. IWM systems can be perceived as more complex than conventional herbicide-based programs because they require more detailed knowledge of weed biology, crop competition, timing of control measures, and field-specific conditions *(Harker & O'Donovan, 2013).*

For this reason, IWM should not be evaluated simply by comparing the cost of one weed-control operation with that of a herbicide application. A more appropriate economic assessment should consider the entire cropping cycle, including input costs, machinery and labor requirements, crop yield, resistance risk, and the long-term stability of weed control. The objective is therefore not necessarily to minimize the cost of individual interventions, but to achieve a sustainable balance between weed suppression, crop productivity, environmental performance, and long-term economic returns.

### 4.4. Emerging technologies in Integrated Weed Management

The development of precision agriculture and digital farming is creating new opportunities for improving IWM. Modern technologies can complement agronomic, mechanical, biological, and chemical practices by providing more accurate information on weed distribution, density, species composition, and spatial variability within agricultural fields. Rather than replacing established IWM practices, these technologies can improve the timing, precision, and efficiency of weed management interventions. *(Korres et al. 2019)* identified technological advancement, remote sensing, decision-support systems, robotics, and data-driven approaches as important components of the future development of IWM.

Precision agriculture allows weed management decisions to be adapted to spatial and temporal variability within a field. Global positioning systems, geographic information systems, variable-rate

technologies, and digital field mapping can be used to identify areas with different levels of weed infestation and to adjust management practices accordingly. This approach supports site-specific weed management, in which control measures are applied according to the actual distribution and characteristics of weeds rather than uniformly across the entire field *(Korres et al., 2019).*

Remote sensing provides additional opportunities for detecting and monitoring weed populations over large areas. Satellite imagery, multispectral and hyperspectral sensors, and high-resolution imaging systems can provide information that helps distinguish weeds from crops and identify areas with greater weed pressure. Remote sensing can therefore support weed mapping, monitoring of weed development, and evaluation of control effectiveness *(Maes & Steppe, 2019; Korres et al., 2019).*

Unmanned aerial vehicles (UAVs or drones) provide flexible, high-resolution field observations. Combined with machine learning and artificial intelligence, UAV imagery can support automated weed detection and classification, although environmental variability, data quality, algorithm performance, and field validation remain challenges *(Anam et al., 2024).*

Machine vision and AI can distinguish crops from weeds using morphological, spectral, and spatial characteristics, enabling automated decisions for mechanical removal or targeted herbicide application *(Vijayakumar et al., 2023; Anam et al., 2024).*

Site-specific herbicide application represents one of the most direct applications of these technologies within IWM. Smart sprayers can use cameras, sensors, GPS systems, and decision algorithms to activate individual nozzles when weeds are detected rather than treating the entire field uniformly. Such systems have the potential to reduce unnecessary herbicide applications while maintaining effective control of target weeds *(Vijayakumar et al., 2023).*

Robotic mechanical weeding provides another important pathway for reducing herbicide dependence. Autonomous or semi-autonomous robots equipped with machine vision can detect weeds and mechanically remove them using hoes, fingers, brushes, or other specialized implements. Recent developments include autonomous navigation, imaging sensors, sensor fusion, and deep-learning-based weed identification. However, high initial investment costs, operational complexity, variable field conditions, and the need for reliable real-time weed identification remain important limitations to widespread adoption *(Upadhyay et al., 2024).*

Decision-support systems (DSS) can integrate information from weed surveys, crop growth stages, weather conditions, soil characteristics, historical field records, remote sensing, and herbicide resistance information. Such systems can assist farmers in determining when, where, and how weed control should be implemented. The integration of DSS with remote sensing, machine learning, and field-level databases can improve the coordination of preventive, mechanical, biological, and chemical measures and strengthen the overall IWM strategy *(Korres et al., 2019).*

The integration of artificial intelligence, remote sensing, machine vision, robotics, and decision-support systems therefore represents an important transition toward data-driven IWM. These technologies have the potential to improve weed monitoring, increase the precision of interventions, reduce unnecessary herbicide use, and facilitate the integration of multiple control methods *(Korres et al., 2019; Vijayakumar et al., 2023; Anam et al., 2024)*. However, technological innovation should not be considered a substitute for ecological knowledge or established IWM principles. The effectiveness of digital weed management depends on data quality, detection accuracy, field conditions, equipment costs, operator skills, and compatibility with specific cropping systems *(Korres et al., 2019; Upadhyay et al., 2024).*

Emerging technologies should therefore be considered an additional layer of IWM that improves monitoring, decision-making, targeting, and automation. Their continued development may contribute to more precise, adaptive, and resource-efficient weed management systems, particularly when combined with preventive strategies aimed at reducing weed establishment, seed production, and herbicide resistance *(Korres et al., 2019; Islam et al., 2026)*.

## CONCLUSIONS

Integrated Weed Management (IWM) represents a sustainable approach to weed control based on the diversification and integration of complementary management strategies. The main conclusions of this review are:

1. **Biological and agronomic diversification.**

The integration of agronomic, mechanical and biological methods can reduce weed pressure by interfering with weed establishment, growth and reproduction at different stages of the weed life cycle. Crop

rotation, cover crops, competitive cultivars, mechanical control and biological agents can therefore complement each other and improve the consistency of weed suppression.

**2. Herbicide resistance management.**

Diversification of weed control tactics can reduce reliance on herbicides and decrease the selection pressure associated with repeated use of herbicides with similar modes of action. Within IWM systems, herbicides remain an important control tool, but their strategic use in combination with non-chemical methods can contribute to more sustainable resistance management and prolong the effectiveness of available herbicide options.

**3. Practical adaptation to local conditions.**

The effectiveness of IWM depends on the appropriate combination and timing of control methods according to the crop, weed spectrum and pressure, soil and climatic conditions, available machinery and labor, and economic constraints. Therefore, IWM should not be regarded as a universal fixed package of practices, but rather as an adaptive management framework that must be tailored to specific cropping systems and local conditions.

Overall, the evidence reviewed indicates that the long-term effectiveness and sustainability of weed management are enhanced when multiple complementary tactics are integrated rather than relying predominantly on a single control method. Future advances in precision agriculture, remote sensing, artificial intelligence and site-specific weed control may further improve the implementation and efficiency of IWM systems.

**ACKNOWLEDGEMENT**

This research was funded by The Ministry of Education and Research Project PN-IV-P6-840 6.1-CoEx-2024-0025 “Innovative strategies for ensuring nutritional security by stimulating the exploitation of sustainable protein resources PROfutureFOOD and Project PN 23 04 02 01, Contract no.: 9N/01.01.2023 SUSTAIN–DIGI-AGRI, Innovative biofertilizer production technology used to restore soil biodiversity and reduce the effects of drought on agricultural lands.

**REFERENCES**

[1] Anam, I., Arafat, N., Hafiz, M. S., Jim, J. R., Kabir, M. M., & Mridha, M. F. (2024). A systematic review of UAV and AI integration for targeted disease detection, weed management, and pest control in precision agriculture. *Smart Agricultural Technology, 9*, 100647. https://doi.org/10.1016/j.atech.2024.100647

[2] Bàrberi, P., Moonen, A. C., and N. M. Fontanelli. (2009). Integrated Weed Management systems allow reduced reliance on herbicides and long-term weed control. *Agriculture, Ecosystems & Environment, 132*(3–4), 237–242. https://doi.org/10.1016/j.agee.2009.04.009

[3] Chauhan, B. S., & Mahajan, G. (2014). *Recent Advances in Weed Management*. Springer.

[4] Deytieux, V., Nemecek, T., Freiermuth Knuchel, R., Gaillard, G., & Munier-Jolain, N. M. (2012). Is Integrated Weed Management efficient for reducing environmental impacts of cropping systems? A case study based on life cycle assessment. *European Journal of Agronomy, 36*(1), 55–65. https://doi.org/10.1016/j.eja.2011.08.004

[5] Dong, F., & Zeng, W. (2024). Effects of Fall and Winter Cover Crops on Weed Suppression in the United States: A Meta-Analysis. *Sustainability, 16*(8), 3192. https://doi.org/10.3390/su16083192

[6] Harker, K. N., & O’Donovan, J. T. (2013). Recent weed control, weed management, and integrated weed management. *Weed Technology*, 27(1), 1–11.

[7] Heap, I. (2024). The international survey of herbicide resistant weeds. Available online: www.weedscience.org

[8] Heap, I. (2026). The International Herbicide-Resistant Weed Database. Online. Available at: www.weedscience.org (accessed September 15, 2026).

[9] Islam, M. M., Llewellyn, R., & Monjardino, M. (2026). The relationship between herbicide resistance and the use of integrated weed management: Is it simply reactive? *Agricultural Systems, 233*, 104602. https://doi.org/10.1016/j.agsy.2025.104602

[10] Korres, N. E., Burgos, N. R., Travlos, I., Vurro, M., Gitsopoulos, T. K., Varanasi, V. K., Duke, S. O., Kudsk, P., Brabham, C., Rouse, C. E., & Salas-Perez, R. (2019). New directions for integrated weed

management: Modern technologies, tools and knowledge discovery. *Advances in Agronomy, 155*, 243–319. https://doi.org/10.1016/bs.agron.2019.01.006

[11] Liebman, M., Mohler, C. L., & Staver, C. P. (2001). *Ecological Management of Agricultural Weeds*. Cambridge University Press.

[12] Maes, W. H., & Steppe, K. (2019). Perspectives for remote sensing with unmanned aerial vehicles in precision agriculture. *Trends in Plant Science, 24*(2), 152–164. https://doi.org/10.1016/j.tplants.2018.11.007

[13] Oerke, E. C. (2006). Crop losses to pests. *Journal of Agricultural Science*, 144, 31–43.

[14] Ozaslan, C., Gürsoy, S., & DiTommaso, A. (2024). Band herbicide application combined with inter-row cultivation as a sustainable weed management strategy for reducing herbicide use: A meta-analysis. *Crop Protection, 175*, 106474. https://doi.org/10.1016/j.cropro.2023.106474

[15] Radosevich, S. R., Holt, J., & Ghersa, C. (2007). *Ecology of Weeds and Invasive Plants: Relationship to Agriculture and Natural Resource Management*. Wiley.

[16] Swanton, C. J., & Weise, S. F. (1991). Integrated weed management: The rationale and approach. *Weed Technology*, 5(3), 657–663.

[17] Teasdale, J. R. (1996). Contribution of cover crops to weed management in sustainable agricultural systems. *Journal of Production Agriculture*, 9(4), 475–479.

[18] Upadhyay, A., Zhang, Y., Koparan, C., Rai, N., Howatt, K., Bajwa, S., & Sun, X. (2024). Advances in ground robotic technologies for site-specific weed management in precision agriculture: A review. *Computers and Electronics in Agriculture, 225*, 109363. https://doi.org/10.1016/j.compag.2024.109363

[19] Vijayakumar, V., Ampatzidis, Y., Schueller, J. K., & Burks, T. (2023). Smart spraying technologies for precision weed management: A review. *Smart Agricultural Technology, 6*, 100337. https://doi.org/10.1016/j.atech.2023.100337

[20] Zannopoulos, S., Gazoulis, I., Kokkini, M., Antonopoulos, N., Kanatas, P., Kanetsi, M., & Travlos, I. (2024). The Potential of Three Summer Legume Cover Crops to Suppress Weeds and Provide Ecosystem Services—A Review. *Agronomy, 14*(6), 1192. https://doi.org/10.3390/agronomy14061192

# DATA STORAGE AND REMOTE TRANSMISSION USING AN EDGE COMPUTER IN A MOBILE SOIL SAMPLING PLATFORM

/

# *STOCAREA DATELOR ȘI TRANSMITEREA LA DISTANȚĂ UTILIZÂND UN COMPUTER EDGE ÎNTR-O PLATFORMĂ MOBILĂ DE EȘANTIONARE A SOLULUI*

**Dragoș-Valentin LUPU[1)], Robert-Dorin CRISTEA*[2)], Alexandru-Cristian CIOACLĂ[2)], Dorin-Andrei CÎRSTEA[2)], Daniel-Mirel DUMITRESCU[1)]**

[1)] National University of Science and Technology Politehnica Bucharest / Romania;

[2)] National Institute of Research - Development for Machines and Installations Designed to Agriculture and Food Industry - INMA Bucharest / Romania.

**Tel: 0771 717 451; *E-mail: robert.cristea@inma.ro*

***Keywords:*** *data, edge computing, edge storage, edge processing*

**ABSTRACT**

*In agriculture, beyond water, which is the most essential factor in yield success, one of the most crucial elements is soil quality. This was understood even by our ancient ancestors, who invented crop rotation so that the soil retained enough nutrients for all the plants grown in the field. As our understanding of biology and knowledge of agriculture grew, we developed new and more efficient ways to cultivate crops and increase harvest yields. One of these new ways is soil sampling, which provides a more in-depth analysis of the soil and helps with choosing the right fertilizer and crop that can be planted on a field. For a long time, soil sampling has relied heavily on manual labor. Technicians have had to physically travel into the field to collect soil samples, manually marking and recording their precise geographic locations. However, this highly manual process leaves a lot of room for human error, such as mislabeled coordinates, inaccurate mapping, or lost field notes. These inaccuracies make traditional methods unreliable and inefficient, especially when dealing with large-scale agricultural projects and expansive fields. With the rapid evolution of new technology, these labor-intensive tasks can be made much easier and far more accurate. By automating how location data is tracked and stored directly in the field, the risk of mistakes drops significantly. This paper aims to showcase one of the innovative ways soil sampling can be improved, demonstrating how modern systems can streamline the entire process.*

**REZUMAT**

*În agricultură, dincolo de apă, care este cel mai esențial factor în succesul recoltelor, unul dintre cele mai cruciale elemente este calitatea solului. Acest lucru a fost înțeles chiar și de strămoșii noștri din antichitate, care au inventat rotația culturilor pentru ca solul să rețină suficienți nutrienți pentru toate plantele cultivate pe câmp. Pe măsură ce înțelegerea noastră asupra biologiei și cunoștințele de agricultură au crescut, am dezvoltat metode noi și mai eficiente pentru a cultiva plante și a crește randamentul recoltelor. Una dintre aceste noi metode este prelevarea probelor de sol, care oferă o analiză mai aprofundată a solului și ajută la alegerea îngrășământului potrivit și a culturii care poate fi plantată pe un teren. Pentru o lungă perioadă de timp, prelevarea probelor de sol s-a bazat în mare măsură pe munca manuală. Tehnicienii au fost nevoiți să se deplaseze fizic pe teren pentru a colecta probe de sol, marcând și înregistrând manual coordonatele geografice precise ale acestora. Cu toate acestea, acest proces extrem de manual lasă mult loc pentru eroarea umană, cum ar fi coordonatele etichetate greșit, cartografierea inexactă sau notițele de teren pierdute. Aceste inexactități fac metodele tradiționale nesigure și ineficiente, în special atunci când se lucrează cu proiecte agricole la scară largă și terenuri extinse. Odată cu evoluția rapidă a noilor tehnologii, aceste sarcini care necesită multă muncă pot fi făcute mult mai ușoare și mult mai precise. Prin automatizarea modului în care datele de localizare sunt urmărite și stocate direct pe teren, riscul de greșeli scade semnificativ. Această lucrare își propune să prezinte una dintre modalitățile inovatoare prin care prelevarea probelor de sol poate fi îmbunătățită, demonstrând modul în care sistemele moderne pot eficientiza întregul proces.*

## INTRODUCTION

The evolution and integration of new technology, including sensors and edge computers, have led to widespread digitalization in our lives from our home appliances to sports and outdoor activities, this have made acquiring parts and developing new systems easier and cheaper than ever before *(Andriulo, F. C., et al., 2024)*. These new advances can be integrated into some of humanity's oldest fields, such as cooking and agriculture and are rapidly growing each day. This has led to the development of Agriculture 4.0 that aims to integrate technology in order to automate and better help large scale projects in productivity and sustainability *(Yang, D., et al., 2024)*. Agriculture 4.0 represents the incorporation of contemporary technologies such as artificial intelligence, Internet of Things (IoT), edge and cloud computing and many more into the agricultural industry. With the introduction of Agriculture 4.0 in the early 2010's, it keeps evolving each day, integrating and developing new technologies.

As a core part of Agriculture 4.0, Precision Agriculture (PA), has evolved at a rapid pace along with all technology, incorporating many of these new advances along the way, contemporary solutions rely heavily on data and Artificial Intelligence algorithms in order to make accurate decisions about fertilisation. Soil nutrients play a critical part in a plant health, sustainability and yield, mainly nitrogen (N), phosphorus (P), and potassium (K) as they are the most important nutrients *(Flores-Cortez, O., et al., 2026)*. As everting natural, these nutrients along with all the other factors, such as pH, that contribute to plant health are not constant in soil accurate sampling needs to be taken form the soil.

One of the most important technologies developed in the past decades are edge computers, that bring the data processing unit closer to the sensors that gather it and IoT (*Liang, S., et al.)*. Edge computing and IoT are used across all industries, but are especially useful in agricultural robots that need to cover large distances and at the same time collect, process and store data at the same time. In remote and large areas such as crop fields, where cloud-based systems are difficult and expensive to implement, this is where edge computers are most serviceable, as they are cheaper and make for great expansion of non-real-time systems. Using edge computing in agriculture, a machine can work fully autonomously without any need for human intervention. On large fields, where it is possible to lose connection due to the wide working area and remote location, the machine can gather and process data directly at its location. As it is working, the machine can update the work that it did as soon as a connection to the main network is established.

Agricultural robots are developed to reduce workloads, gather precise data, streamline and automate processes. They are equipped with sensors that collect and store data *(El-Ouati, M., et al., 2026)*. Precise data is the most important factor of an efficient system, so the data processing units need to have minimal latency for the collected data to be as exact as it needs to be. In the case of the Mobile Soil Sampling Platform (MSSP), the data that needs to be prepared is the location of the MSSP at the time the soil sample is taken.

This paper aims to explore an integrated data management structure developed for the MSSP, comprised of a Raspberry Pi 4 Model B serving as the main edge computer that is in charge of hosting a lightweight web server user interface, communicating with the main soil extraction mechanism through a synchronization handshake and executing data processing and storage. For the GPS data acquisition the Adafruit Ultimate GPS Breakout V3 was used, connected to the main edge computer via UART.

## MATERIALS AND METHODS

### System assembly and components

### The GPS Module

Sensors play a vital role in any IoT system: they bridge the gap between the real world and the digital world and collect the data the system needs in order to function *(Alahmad et al., 2023)*. Using the right sensors is one of the most important factors in building a machine. Which sensors are best depends on several factors, including but not limited to their core performance and the purpose the sensor serves in the machine.

The core performance traits required of our GPS module are:

- accuracy: to obtain the precise location of the MSSP at the exact time a soil sample is collected. Since each reading is permanent and cannot be changed, any variation or incorrect reading can, on large fields, lead to a misrepresentation of the field's fertility map;
- time to fix: for easier testing and faster soil collection. A long time to fix directly impacts the soil sampling time. Since the MSSP needs to send the handshake trigger after the GPS data

has been processed and stored each time it operates, this delay can accumulate into a meaningful loss of time over the course of a sampling cycle;

- sensitivity: which is useful if the MSSP is used in an orchard or on a field filled with shrubs. Dense tree and shrub foliage and trunks may obstruct satellite signals, making it harder for the GPS module to receive a strong signal. Choosing a GPS sensor with high sensitivity allows the MSSP to be used not only in open fields, but in orchards as well;
- number of channels: for better signal reliability. Tracking more satellites at the same time improves the ability to receive a reliable signal even when some satellites are obstructed or provide a weak signal, which translates into a lower margin of error;
- power consumption: since the MSSP runs on a battery, the GPS module needs to have low power consumption, as a full session of readings may take a considerable amount of time depending on the scale of the field. Low power consumption leaves more battery capacity available for the other systems attached to the MSSP.

Several low-cost GPS modules are commonly used in IoT applications, Table 1 compares the key specifications that are listed earlier of two of the most common used GPS sensors: Adafruit Ultimate GPS Breakout V3 and u-blox NEO-6M.

**Table 1**

**Comparison between Adafruit Ultimate GPS Breakout V3 and u-blox NEO-6M**

*(www.adafruit.com, 21 September 2026, www.u-blox.com, 25 September 2026)*

| GPS Module | Accuracy | Time to fix | Sensitivity | Number of channels | Power consumption |
|---|---|---|---|---|---|
| Adafruit Ultimate GPS Breakout V3 | 1.8 m | 34 s | -165 dBm | 66 | 20 mA – 25 mA |
| u-blox NEO-6M | 2.5 m | 27 s | -161 dBm | 50 | 39 mA |

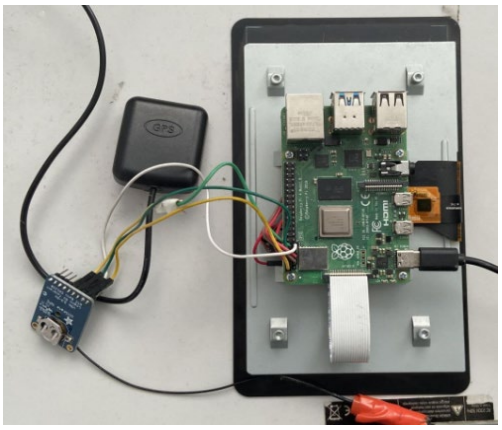


**Fig. 1 - Adafruit Ultimate GPS Breakout V3 and external antenna interfaced with the Raspberry Pi**

The GPS location of the MSSP is gathered with the Adafruit Ultimate GPS Breakout V3 (shown in the image above), which was chosen because it meets all the criteria above. It can track up to 22 satellites on 66 channels, with a position accuracy of 1.8 meters. The module was used with a ceramic patch antenna, which gives it a sensitivity of -165 dBm for more accurate data collection *(www.adafruit.com, 21 September 2026)*. It also has an internal battery that keeps track of time, so the time to fix is very low.

**The edge computer**

The integration of edge computing in agriculture for processing raw data and performing computationally intensive tasks will reduce latency and bandwidth usage *(Yang, D., et al., 2024)*. The promising features of edge computing are fast data processing and analysis that are done at the right where the data is collected, leading to quicker response time and speed of the whole machine *(Tahir, N., et al., 2025)*.

The main edge computer, a Raspberry Pi 4 Model B (RPi4B) (Fig. 2), was used to process and store the data. It was also used to host the web interface from which the data can be downloaded. The RPi4B has a quad-core 64-bit ARM Cortex-A72 processor running at 1.5 GHz, which is well suited to the amount of data that needs to be processed *(www.raspberrypi.com, 21 September 2026)*. Even though

the MSSP relies on battery power, energy consumption remains a minor concern, as the device only executes a single cycle before returning with the collected soil samples for recharging.

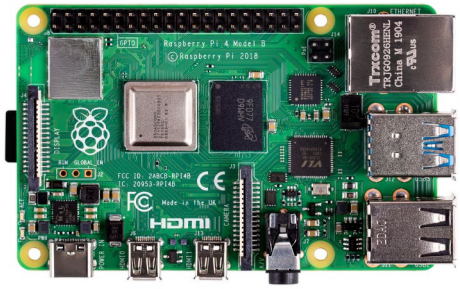


**Fig. 2 - Raspberry Pi 4 Model B**
*(https://www.optimusdigital.ro, 21 September 2026)*

**Software Implementation**

The RPi4B connects to the soil sampling mechanism, which transmits a trigger signal upon soil sample collection. It also communicates with the Ultimate GPS Breakout V3 via a UART interface at 9600 baud. During operation, the RPi4B waits for a numeric index provided by the trigger signal. Once triggered, the RPi4B retrieves the latest positioning data from the GPS module in NMEA 0183 format. The Python library pynmea2 is used to parse sentences starting with $GPGGA or $GNGGA to extract latitude and longitude coordinates. The GPS quality indicator is verified to ensure data accuracy. This method maximizes precision by sampling coordinates strictly at the moment of collection.

The moment a valid position is obtained, the sample index, current timestamp, latitude, and longitude are written to a CSV file, and a signal is sent back through the serial communication to indicate that the data was logged successfully. The handshake mechanism was used in order to prevent loss of synchronization between the sampling mechanism and the data logger. To keep the data organized, every time the MSSP begins a collection cycle of up to 10 soil samples, a new CSV file is created, named after the current time the process begins, with the corresponding headers for index, time of collection, latitude, and longitude. Using the CSV format for storing files is a great way of extending the system, as CSV files are universally compatible with a wide range of technologies while requiring little storage space. In the case of the MSSP, each file contains only a header row and ten rows of data, so the file size is exceptionally small, at under 1 KB per saved file. Since the data needs to be downloaded, the small file size is useful because it keeps download times extremely short.

**Web interface**

To allow for better data collection and monitoring, without requiring direct access to the RPi4B's file system, a simple web interface was implemented using Flask. Samourkasidis, A., et al. showed a proof of concept using a Raspberry Pi as a low-cost self-contained data repository where data can be downloaded. On each request, the application scans the local storage data folder in order to list all the CSV files generated by the system, including all past cycles, making them downloadable links on the web page. Since the RPi4B is connected to the local network, this interface allows the soil sampling data to be collected by all of the devices on the local network, without the need for any special software or physical access to the device. Having a simple, yet effective, data retrieval system, with all past data being preserved and easily accessible thanks to the timestamp-based file naming system, is an effective way of making the overall system more efficient.

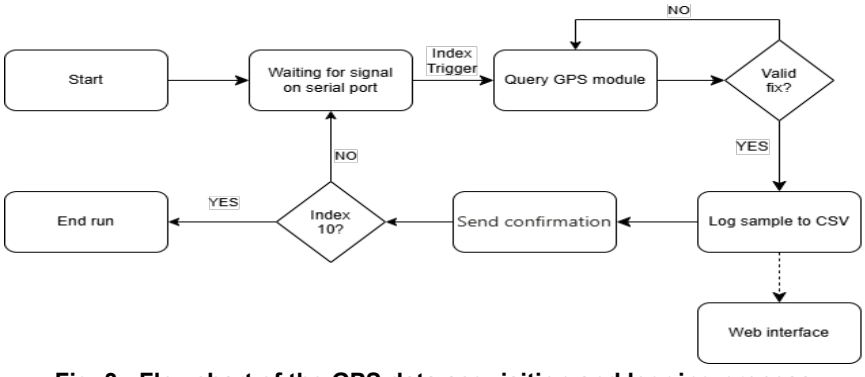



**Fig. 3 - Flowchart of the GPS data acquisition and logging process**

**Testing setup**

At the time of writing, the mechanical integration between the RPi4B and the MSSP's soil extraction mechanism was still in progress. In order to validate the data acquisition, processing, logging, and handshake logic, as well as the web interface, the trigger signal was simulated using an Arduino Uno, with a simple push button used to send the trigger signal. The Arduino reproduced the handshake procedure expected from the MSSP, transmitting the trigger pulse to the RPi4B and waiting for confirmation that the data had been logged to the CSV file. This approach allowed for testing the entire pipeline before full integration on the MSSP.

## RESULTS

Preliminary testing of the data acquisition, logging, handshake synchronization, and web interface pipeline was performed using the Arduino Uno simulated trigger described above, in the Testing setup section, in order to verify the correct operation of the system ahead of full implementation on the MSSP. The system was assembled and ran through a couple of cycles carried out under laboratory conditions.

During the testing trials, the RPi4B successfully received the trigger signal from the simulated Arduino circuit, retrieved a valid and correct position from the GPS module, created a CSV file correctly named after the current date and time, successfully logged the index, timestamp, latitude, and longitude to the correct CSV file (as in Fig. 2), and sent the handshake signal back to the Arduino to complete the logging pipeline. An ample testing on accuracy, time to process and log the data was not done at the moment of writing, however at the moment of testing the data seemed to be precise with no major variations between each data logged to the CSV files.

The web interface created to download and manage the CSV files was working as intended, correctly displaying and updating the list of every CSV file created, generating a download link for each file separately (as in Fig. 4) and generating a pin for every data logged on OpenStreetMap (As in Fig. 5). Every simulated cycle the new CSV file was automatically generated to the web page, after refreshing the page, verifying that the storage directory is scanned every request. The interface was tested using multiple devices connected to the local network and showed that the server was able to connect to multiple clients at the same time with no errors neither in loading the page or downloading the data.

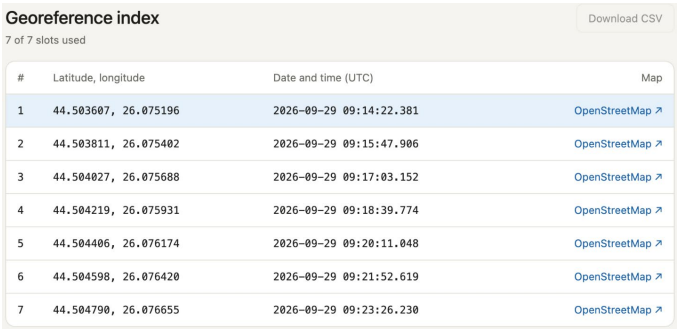



**Fig. 4 - Web interface displaying the georeference index and logged GPS coordinates**

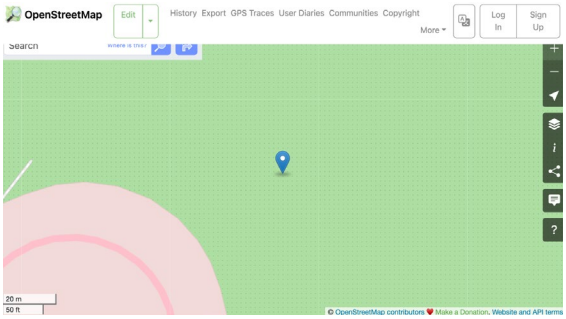



**Fig. 5 - Visualization of the logged GPS coordinates on OpenStreetMap**

Observing the testing of the data acquisition pipeline of the GPS module, an unusual behavior was observed in how the data was received by the RPI4B. On multiple testing rounds, when the trigger signal was pushed multiple times in a shot interval, the data was received by the RPi3B in batches of five, after that there was a short period of about 30 seconds where the system would not receive data. This behavior was observed

constantly enough on multiple testing rounds to be mentioned in the results. This abnormal behavior does not affect the logging system as, when implemented and ran on the MSSP, the soil sampling will be spread apart, even if the soil samples are close together, the time to dig is grater then the time interval needed to put the system in its unusual behavior.

## CONCLUSIONS

This paper presented the design and implementation of a data storage and remote transmission system for a Mobile Soil Sampling Platform, built around a Raspberry Pi 4 Model B edge computer and an Adafruit Ultimate GPS Breakout V3. The event-driven approach, in which GPS data was read only at the moment the soil sample was taken rather than continuously, proved more efficient in terms of storage time and data precision, while keeping the processor load of the Raspberry Pi 4 Model B to a minimum. The handshake mechanism between the sampling trigger and the data logger protected the system against desynchronization and false readings. The lightweight web interface and the simple organization of files by timestamp proved effective for data management across multiple devices connected to the network.

## ACKNOWLEDGEMENT

This work was supported by the National Research Authority, through the Project entitled: “An intelligent automated system designed for georeferenced soil sampling.” -- PN 23 04 01 02. Contract no./date 9N/ 01.01.2023.

## REFERENCES

[1] Alahmad, T., Neményi, M., & Nyéki, A. (2023). Applying IoT Sensors and Big Data to Improve Precision Crop Production: A Review. *Agronomy*, *13(10), 2603*. https://doi.org/10.3390/agronomy13102603

[2] Andriulo, F. C., Fiore, M., Mongiello, M., Traversa, E., & Zizzo, V. (2024). Edge Computing and Cloud Computing for Internet of Things: A Review. *Informatics*, *11(4), 71*. https://doi.org/10.3390/informatics11040071

[3] El-Ouati, M., Bimonte, S., & Tricot, N. (2026). Monitoring IoT and Robotics Data for Sustainable Agricultural Practices Using a New Edge–Fog–Cloud Architecture. *Computers*, *15*(1), *32*. https://doi.org/10.3390/computers15010032

[4] Flores-Cortez, O., Cordero, B., Arévalo, F., Pocasangre, C., & Melendez, W. (2026). A Portable IoT-Enabled System for Georeferenced Soil Nutrient Screening in Agricultural Fields. *Engineering Proceedings, 150(1), 117*. https://doi.org/10.3390/engproc2026150117 lady ada. (2026, August 20).

[5] Adafruit Ultimate GPS. Adafruit Industries. Retrieved September 21, 2026, from https://cdn.learn.adafruit.com/downloads/pdf/adafruit-ultimate-gps.pdf

[6] Liang, S., Jin, S., & Chen, Y. (2024). A Review of Edge Computing Technology and Its Applications in Power Systems. *Energies*, *17*(13), *3230*. https://doi.org/10.3390/en17133230

[7] Optimus Digital. (n.d.). Raspberry Pi 4 Model B 1GB [Photograph]. Retrieved September 21, 2026, from https://www.optimusdigital.ro/ro/placi-raspberry-pi/8615-raspberry-pi-4-model-b1gb-765756931168.html

[8] Raspberry Pi (Trading) Ltd. (2024). Raspberry Pi 4 Model B datasheet (Release 1.1). https://pip-assets.raspberrypi.com/categories/545-raspberry-pi-4-model-b/documents/RP-008341-DS-1-raspberry-pi-4-datasheet.pdf

[9] Samourkasidis, A., & Athanasiadis, I. N. (2017). A Miniature Data Repository on a Raspberry Pi. *Electronics, 6(1), 1*. https://doi.org/10.3390/electronics6010001

[10] Tahir, N., & Parasuraman, R. (2025). Edge Computing and Its Application in Robotics: A Survey. *Journal of Sensor and Actuator Networks*, *14(4), 65.* https://doi.org/10.3390/jsan14040065 u-blox. (2011). NEO-6: u-blox 6 GPS modules data sheet *(Document No. GPS.G6-HW-09005-E).* https://content.u-blox.com/sites/default/files/products/documents/NEO-6_DataSheet_%28GPS.G6-HW-09005%29.pdf

[11] Yang, D., Wu, J., & He, Y. (2024). Optimizing the Agricultural Internet of Things (IoT) with Edge Computing and Low-Altitude Platform Stations. *Sensors*, *24*(21), *7094*. https://doi.org/10.3390/s24217094

# THERMOFLUID MECHANISMS AND ADAPTIVE CONTROL IN ACTIVE ORCHARD FROST PROTECTION: A CRITICAL REVIEW OF AIR MIXING, HEATING, AND WATER-BASED SYSTEMS

/

# *MECANISME TERMOFLUIDICE ȘI CONTROL ADAPTIV ÎN PROTECȚIA ACTIVĂ A LIVEZILOR ÎMPOTRIVA ÎNGHEȚULUI: O ANALIZĂ CRITICĂ A SISTEMELOR DE AMESTECARE A AERULUI, ÎNCĂLZIRE ȘI UTILIZARE A APEI*

**Mihaela NIȚU*[1)], Iuliana GĂGEANU[1)], Augustina PRUTEANU[1)], Ana-Maria TĂBĂRAȘU[1)], Daria-Ioana SICARU[2)]**
[1)] National Institute of Research - Development for Machines and Installations Designed to Agriculture and Food Industry - INMA Bucharest / Romania;
[2)] National University of Science and Technology POLITEHNICA Bucharest / Romania.
**Tel: 0746 689 449; *E-mail: rosumihaelan@yahoo.com*

***Keywords:*** *orchard frost protection; thermofluid mechanisms; water mist; mobile heating; cyber-physical systems; adaptive control*

**ABSTRACT**
*This review examined how thermofluid mechanisms, actuator architecture, and adaptive control jointly determined the performance of active orchard frost-protection systems. Evidence published mainly during 2016–2026 was synthesized for air mixing, direct and mobile heating, sprinkler irrigation, mist/fog generation, and cyber-physical control. Wind machines redistributed sensible heat and were effective primarily under stable temperature inversions, whereas heating added energy but remained sensitive to plume transport, wind, fuel demand, and spatial non-uniformity. Water-based methods exploited latent heat, yet their safe operation depended on wet-bulb temperature, application rate, droplet transport, continuity, and ice load. Recent sensing, computational-fluid-dynamics, path-planning, and feedback-control studies improved spatial targeting and resource allocation, but many reported only simulated or microclimatic outputs rather than flower survival, fruit set, or yield. An integrated engineering framework was therefore proposed, linking frost state identification, multi-point sensing, state estimation, adaptive actuation, and four-level validation: process, microclimate, biological outcome, and resource/safety performance. The synthesis showed that future systems should combine complementary mechanisms conditionally, not simultaneously by default, and should be evaluated through standardized multi-season orchard trials.*

**REZUMAT**
*Lucrarea a analizat modul în care mecanismele termofluidice, arhitectura elementelor de acționare și controlul adaptiv au determinat împreună performanța sistemelor active de protecție a livezilor împotriva înghețului. Au fost sintetizate în principal rezultate publicate în perioada 2016–2026 privind amestecarea aerului, încălzirea fixă și mobilă, aspersiunea, generarea de ceață și controlul ciber-fizic. Mașinile de vânt au redistribuit căldura sensibilă și au fost eficiente mai ales în prezența inversiunilor termice stabile, în timp ce încălzirea a introdus energie, dar a rămas dependentă de transportul jetului, vânt, consum și neuniformitate spațială. Metodele cu apă au valorificat căldura latentă, însă funcționarea lor sigură a depins de temperatura bulbului umed, debit, transportul picăturilor, continuitate și încărcarea cu gheață. Senzorii, simularea CFD, planificarea traseului și reglarea în buclă închisă au îmbunătățit alocarea resurselor, dar multe studii au măsurat numai răspunsul tehnic sau microclimatic. A fost propus un cadru integrat care conectează identificarea stării de îngheț, estimarea, acționarea adaptivă și validarea procesului, microclimatului, răspunsului biologic și consumurilor.*

## INTRODUCTION

Spring frost remains a systems-engineering problem rather than a single-temperature problem. Flowering advances under warming climates, but the last damaging frost and the phenological window do not shift uniformly across regions, elevations, cultivars, and years. Belgian pear projections suggested fewer frost events during flowering on average, while preserving marked spatial differences and greater risk at higher elevations *(Drepper, Gobin, & Van Orshoven, 2022).* European tree species likewise displayed

contrasting changes in leaf-unfolding safety margins *(Bigler & Bugmann, 2018)*. Recent apple studies in China, Germany, and the Czech Republic further indicated that earlier phenology can maintain or locally increase exposure despite longer frost-free seasons (*Caspersen et al., 2025; Chen et al., 2024; Zahradníček et al., 2024)*. Consequently, equipment selection must begin with the event regime, canopy vulnerability, and local micrometeorology. Active frost protection acts through three main thermofluid pathways. Air-disturbance devices redistribute sensible heat from an inversion layer; heaters add sensible and radiative heat; and sprinklers or mist systems exchange latent and sensible heat while modifying humidity and radiation. These pathways are condition-dependent. Air mixing cannot create heat when the lower atmosphere is well mixed and uniformly cold. Water can protect tissue while freezing, but evaporation or interrupted delivery can intensify cooling. Heating can be displaced away from the crop by wind or buoyant plume rise. A useful review must therefore connect mechanism, boundary conditions, delivery architecture, and control rather than rank devices independently of the frost state.

Existing systematic and equipment reviews have compared broad protection categories and exposed a weak, heterogeneous evidence base *(Drepper, Bamps, Gobin, & Van Orshoven, 2022; Hu et al., 2018; Liu et al., 2025; Pan et al., 2024)*. A recent smart-frost-management review also synthesized sensing, modelling, artificial intelligence, and robotics *(Hua, Heinemann, & He, 2025)*. The distinct contribution of the present review is an integrated engineering framework that maps air mixing, heating, water application and adaptive control to measurable process, microclimatic, biological, and resource outcomes.

The objectives were to: (i) clarify the governing thermofluid mechanisms and their conditionality; (ii) critically compare stationary, mobile, and hybrid architectures; (iii) assess how sensing and control can allocate heat, airflow, and water spatially; and (iv) define a validation hierarchy for emerging orchard systems.

## MATERIALS AND METHODS

A structured critical review was conducted rather than a statistical meta-analysis because the available studies differed substantially in crop, frost regime, sensor placement, protected-area definition, intervention duration, and outcome reporting. Searches were completed through 3 September 2026 using ScienceDirect and ResearchGate for discovery, followed by verification against DOI records, journal pages, institutional repositories, or full texts. The principal keyword blocks combined “orchard” or “horticultural crop” with “frost protection”, “wind machine”, “air disturbance”, “heater”, “mobile heating”, “sprinkler”, “mist”, “fog”, “atomization”, “CFD”, “cyber-physical system”, “adaptive control”, or “path planning”.

Peer-reviewed English-language studies published from 2016 to 2026 were prioritized to meet the symposium recency requirement. Sources were retained when they described a physical mechanism, equipment architecture, control strategy, quantitative thermal response, biological response, or field-validation method relevant to active frost protection. Reviews were used to map the field and identify reporting gaps; experiments and models were used to extract quantitative outcomes. Studies on agricultural spraying or high-speed gas–liquid atomization were included only as transfer evidence for droplet generation and transport, not as proof of orchard frost-protection efficacy. Duplicate files and non-scientific project summaries were excluded. Evidence was classified by validation level: L1, component or process characterization; L2, simulation or controlled-environment microclimate; L3, orchard/field microclimate; and L4, biological or production outcome. Each source was evaluated for frost regime, scale, controls, spatial and temporal resolution, measured variables, resource reporting, and explicit limitations. Numerical comparisons were retained only when the source defined the comparison basis. This approach prevented large simulated percentage gains from being interpreted as equivalent to crop protection.

**Table 1**

**Mechanism-based applicability of active frost-protection systems**

| System | Primary mechanism | Favourable conditions | Failure modes | Main burdens | Evidence maturity |
|---|---|---|---|---|---|
| Air mixing | Redistribution of sensible heat from inversion layer | Radiative frost; low wind; positive inversion | Inversion absent; advective freeze; terrain-driven asymmetry | Electricity/fuel; noise; placement | L3 strong for microclimate; L4 limited |

| System | Primary mechanism | Favourable conditions | Failure modes | Main burdens | Evidence maturity |
|---|---|---|---|---|---|
| Direct heating | Sensible and radiative heat addition | Localized high-value crops; moderate transport losses | Wind advection; plume rise; non-uniformity | Fuel, emissions, labour, fire safety | L2–L3; biological evidence heterogeneous |
| Mobile heating | Heat addition plus forced convection and spatial targeting | Patchy canopy demand; navigable rows; real-time maps | Delayed revisit; navigation conflicts; short runtime | Fuel/battery, autonomy, safety | L2–L3 emerging |
| Overhead sprinkler | Latent heat released by continuous freezing | Adequate water; controlled wet-bulb conditions | Pump failure; evaporation; ice load; wind drift | High water/energy; infrastructure | L3–L4 comparatively mature |
| Mist/fog | Latent/sensible exchange; humidity and radiative modification | Low drift; tuned droplets; reliable atomization | Evaporative cooling; nozzle icing; insufficient deposition | Water, compressed air/pressure, maintenance | L1–L3; orchard L4 sparse |
| Hybrid system | Conditional combination of complementary pathways | State-aware supervisory control | Uncoordinated actuators can interfere | Highest integration and safety burden | Conceptual/emerging |

## RESULTS

### Frost state and energy balance as design constraints

The first control decision is whether the event is dominated by nocturnal radiative cooling or by advection of a cold air mass. Clear, calm nights commonly produce a stable inversion and cold-air pooling; under those conditions, canopy-scale mixing can recover heat stored aloft. In advective conditions, turbulent mixing is already strong and the entire air column may be cold, so heat addition, water-based protection, or combined strategies become more relevant. Terrain, row orientation, canopy porosity, soil heat storage, cloud cover, and background wind alter the local balance. The persistent spatial variability reported in frost-risk assessments argues against a single weather-station threshold for a heterogeneous orchard *(Caspersen et al., 2025; Drepper, Gobin, & Van Orshoven, 2022).*

For water-based systems, dry-bulb temperature alone is insufficient. Wet-bulb temperature represents the equilibrium reached under evaporation and therefore indicates how much early evaporative cooling may occur. Safe operation requires an application rate capable of offsetting radiative, convective, evaporative, and advective losses. Likewise, heater control should not target only outlet temperature: useful heat is the portion transported into vulnerable canopy volume and sustained during the critical exposure. These distinctions motivate spatial performance indicators such as protected canopy volume, duration above a phenology-specific threshold, and temperature uniformity.

### Air mixing: measurable warming but strong conditionality

Field evidence has moved from sparse point thermometry toward high-resolution three-dimensional observation. Heusinkveld et al. (2020) found rotation-averaged warming of up to about one-half of the inversion strength, approximately 3 K in their experiment, over a typical influence area of 3–5 ha at 1 m height. Even background wind below 1 m $s^{-1}$ produced pronounced upwind/downwind asymmetry. Slower rotations of 3–6 min enlarged the affected area without reducing mean enhancement, and modelling suggested a favourable horizontal tilt of approximately 8–16°. Engine heat and radiation were not negligible, meaning that a wind machine can combine redistribution with modest heat addition.

Dai et al. (2023) deployed approximately 9 km of fibre-optic sensing over 6.75 ha at 25 cm and 10 s resolution. One machine reduced a local 8 K inversion by 50% over 0.42 ha at 1 m and 0.46 ha at 2 m; a 30% reduction extended over about 2.81 and 2.52 ha, respectively. Mean canopy warming approached 3 K during a 40 min interval. These values demonstrate local thermofluid effectiveness, but they do not define a universal protected hectare figure. Only one machine configuration and weather episode were evaluated, while tissue temperature and flower survival were not the primary outcomes.

Oscillating frost fans in tea fields and broader air-disturbance reviews similarly show that jet trajectory, blade geometry, oscillation, canopy resistance, and inversion depth govern performance *(Hu et al., 2018; Kimura et al., 2017).* Accordingly, adaptive angle and rotational timing should be based on

measured inversion structure and wind direction. Using a fixed setting because it was optimal in one event risks warming non-target space or repeatedly missing the coldest rows.

**Heating and mobile high-velocity flow systems**

Heating increases the available energy but does not guarantee that energy reaches buds and flowers. Atam et al. (2020) developed a coupled thermofluid orchard model for estimating minimum energy demand, sizing equipment, and testing control strategies. The study reproduced field trends from the literature and showed the value of whole-orchard modelling, but a four-hour case required roughly five days of computation. Reduced-order modelling and model-predictive control were therefore proposed for operational use, together with optimized hot-air-source distribution and hybrid heat–water configurations. Romanian work has also described combined heat-and-smoke practices, but its descriptive design and limited controlled validation support contextual use rather than a quantitative efficacy claim *(Găgeanu et al., 2021).*

Recent apple-orchard CFD studies quantified the importance of heater orientation and mobility. Hua et al. (2024b) predicted that upwind-angled forced-air heaters protected a larger canopy volume than downwind arrangements. The maximum protected-canopy volume fraction among fixed layouts was 32.2%, whereas a mobile arrangement increased the metric by 1,180% relative to the first fixed layout and by 141.5% relative to two alternative fixed layouts. These are model-relative gains, not measured reductions in flower injury. They nevertheless show why route, revisit interval, and plume trajectory should be treated as coupled design variables. A subsequent multi-heater path-planning study used an improved A* algorithm and conflict-based search. In simulation, total path cost and computation time fell by 36.8% and 98.7%, respectively, while the estimated heater requirement decreased by 96.8% relative to fixed heating and 85.9% relative to traditional mobile heating *(Hua, He, Heinemann, & Zhu, 2025*). The magnitude of these improvements reflects the assumed demand map and optimization benchmark. Orchard trials must still verify localization, energy balance, navigation reliability, and tissue response under wind and terrain uncertainty.

A canopy-protection cyber-physical system supplied a more field-oriented demonstration. Temperature and wind direction were used to orient heating automatically, and a ground vehicle moved the source through apple rows. Compared with fixed-angle heating, protected time increased by 69.9% and 48.0% in two tests; comparison with a non-cyber-physical configuration yielded gains of 198.8% and 111.9%. Under wind, the temperature-increase ratio improved by 21.8% over fixed-angle operation and by 23.7% over the non-integrated system *(Hua et al., 2024a).* However, the vehicle remained manually controlled, gusts challenged orientation, runtime was about 1.5–2 h, and spatial/biological validation remained limited.

**Table 2**

**Representative quantitative evidence and the boundary of inference**

| Study | System/setting | Reported technical result | Inference limit | Level |
|---|---|---|---|---|
| *Heusinkveld et al. (2020)* | Wind machine; orchard field | Up to ~3 K; influence 3–5 ha at 1 m | Event- and inversion-specific; asymmetry under weak wind | L3 |
| *Dai et al. (2023)* | Wind machine; 3D field sensing | ~3 K mean canopy warming; 50% inversion reduction over ~0.42–0.46 ha | One machine/weather condition; no primary yield endpoint | L3 |
| *Hua et al. (2024a)* | Mobile cyber-physical heating | Protected time +48–69.9% vs fixed angle; +111.9–198.8% vs non-CPS | Manual vehicle; 1.5–2 h runtime; limited spatial/biological evidence | L3 |
| *Hua et al. (2024b)* | CFD fixed/mobile heaters | Mobile VPPC +141.5% to +1,180% vs fixed layouts | Model-relative metric; no flower or yield validation | L2 |
| *Hua, He, et al. (2025)* | Simulated multi-heater routing | Path cost −36.8%; computation −98.7%; estimated heaters −85.9 to −96.8% | Dependent on simulated demand and benchmarks | L2 |
| *Lu et al. (2018)* | Adaptive sprinkler; tea field | Canopy ~2.8 K warmer; remained above −1.2/0°C in reported events | Crop/region specific; continuity and micrometeorology critical | L3 |
| *Lu et al. (2025)* | Optimized smoke-machine layout | Up to 55.55% fewer units and 44.16% shorter wiring vs traditional layout | Single orchard; plume model/CFD; biological response not established | L2–L3 |

| Study | System/setting | Reported technical result | Inference limit | Level |
|---|---|---|---|---|
| *Zhang et al. (2026)* | LoRa + optimized fuzzy PID smoke/heating | Field canopy increase ~0.9–3.0 K; improved transient response | Control and microclimate evidence; multi-season biological validation needed | L3 |

**Water, sprinkling, mist and atomization**

Overhead sprinkling is the most mature water-based active method because freezing releases latent heat at the plant surface. A systematic review of 104 studies and 971 extracted data points found sprinklers among the most consistently effective interventions, but only nine studies reported variability sufficiently for robust quantitative synthesis *(Drepper, Bamps, Gobin, & Van Orshoven, 2022).* The finding supports the mechanism while also exposing low study validity and incomplete reporting. Pan et al. (2024) emphasized that application rate, cycling, meteorological conditions, water availability, and ice load must be co-designed rather than treated as independent operating choices.

Adaptive rate control offers a direct route to reduce water use and avoid insufficient application. In tea-field trials, a model using wind speed, air temperature, humidity, and water temperature regulated start/stop timing and variable application rate. The irrigated canopy remained above approximately −1.2°C during early-spring frost and 0°C during a heavier winter event, about 2.8 K above the non-irrigated area *(Lu et al., 2018).* Transfer to orchards requires re-estimation for canopy height, interception, nozzle spacing, fruit-tree critical temperature, and hydraulic response. Failsafe continuity remains essential because wet tissue can cool rapidly if freezing continues after water delivery stops. Fine mist and fog are attractive because they may reduce total water and distribute droplets within canopy air. Their effect is less straightforward than “smaller is better”. Finer droplets provide greater surface area and faster phase exchange, but they are more vulnerable to drift and complete evaporation, which extracts heat before water reaches the target. Coarser droplets have greater momentum and deposition but can increase runoff and ice load. Agricultural spray tests showed that fan operation, pressure, and target distance altered coverage markedly, while flat artificial targets did not reproduce irregular canopy interception *(Marin et al., 2017).* Such studies inform nozzle and transport design but cannot establish frost protection. Atomization research identifies Weber number, gas/liquid momentum ratio, viscosity, surface tension, and primary/secondary breakup as governing variables. Zhou et al. (2023) reviewed Kelvin–Helmholtz and Rayleigh–Taylor breakup mechanisms for liquid jets in supersonic crossflow. These relationships can guide injector development for high-velocity gas–liquid systems, yet combustion-flow evidence cannot be treated as orchard efficacy. A frost-protection design must revalidate droplet-size distribution, plume temperature, residence time, evaporation/freezing fraction, canopy deposition, drift, and safety under orchard-scale subsonic or exhaust-flow conditions.

**Adaptive monitoring and control**

The control objective should be defined as maintaining vulnerable tissue above a phenology-specific threshold with minimum water, energy, emissions, and risk. A single on/off thermostat cannot observe cold-air pooling or moving wind sectors. A practical sensing layer should combine distributed dry-bulb temperature at bud/canopy height, at least one vertical reference for inversion strength, relative humidity or wet-bulb temperature, wind speed/direction, and actuator telemetry. Leaf or bud temperature sensors can reduce uncertainty between air temperature and tissue exposure.

A state estimator can transform these measurements into a frost-regime label, spatial demand map, and confidence score. The supervisory controller then selects a mechanism: air mixing under a usable inversion; heat addition when the accessible air column is too cold; water application only when wet-bulb conditions, hydraulics, and continuity are safe; or a conditionally coordinated hybrid. Lower-level loops regulate fan angle/speed, heater output, pump pressure/flow, nozzle selection, and mobile route. Agricultural adaptive spraying has already shown that camera/PLC-based regulation can reduce applied volume, with a reported 13% saving in a field-sprayer prototype (Matache et al., 2017); however, frost protection requires stricter fail-safe logic because under-application can damage the crop.

Optimization should include constraints that are often omitted from thermal objectives: navigation clearance, combustion and fire safety, exhaust exposure, noise, pump reserve, water inventory, nozzle icing, battery/fuel state, communications loss, and safe shutdown. Low-carbon design studies and recent smoke-machine controllers illustrate how layout and closed-loop regulation can be optimized *(Lu et al., 2025; Wu & Wang, 2023; Zhang et al., 2026).* Their most transferable contribution is the control architecture, while smoke concentration, temperature increase, or algorithmic convergence remain intermediate outcomes.

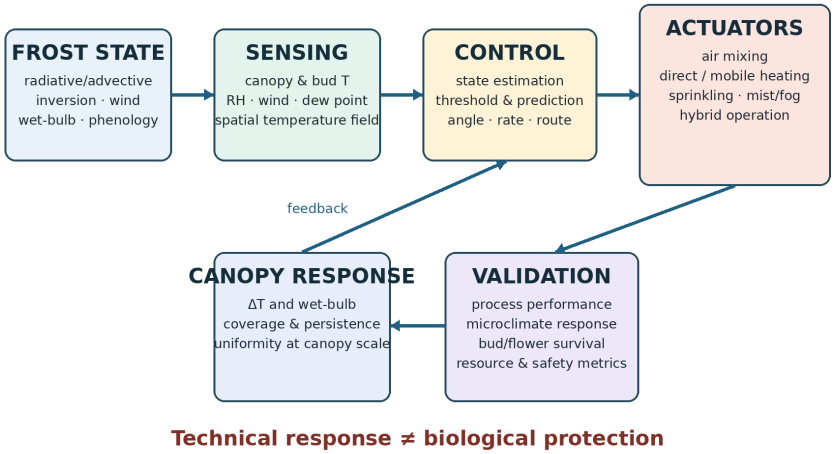



**Fig. 1 - Integrated engineering framework for conditional frost protection and closed-loop validation**
*The actuator set is selected from the estimated frost state; technical and biological outcomes are evaluated separately.*

### Integrated comparison and research priorities

No actuator dominates across all boundary conditions. Wind machines can cover relatively large areas with moderate operating inputs when an inversion exists, but their benefit collapses without accessible warm air. Heating is less dependent on inversion strength but more exposed to fuel cost, emissions, plume losses, and fire risk. Sprinklers can deliver strong biological protection when water supply and rate are adequate, yet require the greatest hydraulic continuity and can create ice-load and disease-management concerns. Mist/fog may reduce water demand, but the useful fraction is governed by coupled atomization, transport, evaporation, condensation, deposition, and freezing. A probabilistic decision-support study for German apple production further showed that strong technical or yield effects did not automatically improve net present value, reinforcing the need to evaluate local costs and avoided losses together *(Schmitz et al., 2025)*. Hybridization is justified only when mechanisms are complementary for the diagnosed event. Forced airflow can distribute added heat or carry droplets into cold zones, but excessive turbulence can also disperse fog. Warm combustion gases may accelerate atomization and transport, while also increasing plume buoyancy and evaporation. Sprinkling and heating can share the thermal burden, but poor coordination may waste energy or expose wet tissue during shutdown.

The engineering problem is therefore a constrained, state-dependent allocation problem, not a requirement to operate every actuator simultaneously. The evidence base remains dominated by short trials, simulations, and temperature-centric metrics. Drepper, Bamps, Gobin, and Van Orshoven (2022) found sparse reporting of randomization and variance; newer high-resolution studies improve spatial description but still rarely connect temperature fields to bud mortality, fruit set, yield, and quality. Standardized trials should report untreated and, where possible, active-comparator controls; sensor height and coordinates; minimum dry- and wet-bulb temperature; vertical inversion; wind; phenological stage; cultivar; soil and terrain; raw time series; uncertainty; resource use; and adverse effects. Multi-season replication is essential because a system optimized for one radiative event may fail in an advective or mixed event.

**Table 3**

**Minimum validation protocol for integrated orchard frost-protection systems**

| Validation tier | Core measurements | Minimum design/reporting | Decision supported |
|---|---|---|---|
| L1 Process | Outlet temperature/velocity; flow and pressure; droplet Dv10/Dv50/Dv90 or VMD; plume direction; actuator latency | Calibration, uncertainty, steady/transient conditions | Whether the device delivers the intended thermofluid state |
| L2 Microclimate | Canopy/tissue ΔT; wet-bulb temperature; inversion; protected volume/area; uniformity; duration above threshold | Distributed sensors, coordinates/heights, untreated control, full time series | Where and for how long protection is physically plausible |

| Validation tier | Core measurements | Minimum design/reporting | Decision supported |
|---|---|---|---|
| L3 Biological | Bud/flower mortality; fruit set; yield; quality; structural ice injury | Phenology/cultivar, randomized sampling, variance, repeated events/seasons | Whether thermal control becomes crop protection |
| L4 Resources & safety | Water, fuel/electricity, emissions, noise, labour, cost, fire/exhaust risk, failures | Per hectare and per protected hour; report downtime and interventions | Whether performance is operationally and environmentally viable |

## CONCLUSIONS

Active orchard frost protection should be designed as a condition-dependent thermofluid control system. Air mixing redistributes existing heat and therefore requires a usable inversion; heating adds energy but must control transport and spatial losses; water-based protection exploits latent heat but depends on wet-bulb temperature, delivery continuity, droplet behaviour, and ice load.

The strongest recent advance is the coupling of distributed sensing, spatial modelling, mobile actuation, and feedback control. These tools can target cold zones, adjust jet direction and water rate, and coordinate multiple devices. Nevertheless, large improvements in simulated path cost, protected canopy volume, temperature increase, or controller transients should not be presented as evidence of reduced crop loss without biological measurements.

A defensible integrated system should diagnose the frost state, choose complementary actuators conditionally, include fail-safe resource and safety constraints, and validate performance at four levels: process, microclimate, biological response, and resource/safety impact. Future progress depends on multi-season orchard experiments with transparent spatial data, comparator treatments, uncertainty reporting, and direct measurements of flower survival, fruit set, yield, and quality.

## REFERENCES

[1] Atam, E., Hong, S.-W., & Arteconi, A. (2020). Thermofluid modelling of large-scale orchards for optimal design and control of active frost prevention systems. Energies, 13(2), 378. https://doi.org/10.3390/en13020378

[2] Bigler, C., & Bugmann, H. (2018). Climate-induced shifts in leaf unfolding and frost risk of European trees and shrubs. Scientific Reports, 8, 9865. https://doi.org/10.1038/s41598-018-27893-1

[3] Caspersen, L., Schiffers, K., Milyaev, A., Neuwald, D. A., & Luedeling, E. (2025). Spring phenology projections for apples in southwestern Germany indicate persistent frost risk levels. Agricultural and Forest Meteorology, 374, 110824. https://doi.org/10.1016/j.agrformet.2025.110824

[4] Chen, R., Wang, J., Li, Y., Bai, R., Huang, M., Zhang, Z., Zhao, L., Qu, Z., & Liu, L. (2024). Higher risk of spring frost under future climate change across China's apple planting regions. European Journal of Agronomy, 159, 127288. https://doi.org/10.1016/j.eja.2024.127288

[5] Dai, Y., Boekee, J., Schilperoort, B., Veldhuis, M., & van de Wiel, B. J. H. (2023). Wind machines for frost damage mitigation: A quantitative 3D investigation based on observations. Agricultural and Forest Meteorology, 338, 109522. https://doi.org/10.1016/j.agrformet.2023.109522

[6] Drepper, B., Bamps, B., Gobin, A., & Van Orshoven, J. (2022). Strategies for managing spring frost risks in orchards: Effectiveness and conditionality—A systematic review. Environmental Evidence, 11, 29. https://doi.org/10.1186/s13750-022-00281-z

[7] Drepper, B., Gobin, A., & Van Orshoven, J. (2022). Spatio-temporal assessment of frost risks during the flowering of pear trees in Belgium for 1971–2068. Agricultural and Forest Meteorology, 315, 108822. https://doi.org/10.1016/j.agrformet.2022.108822

[8] Găgeanu, I., Tăbărașu, A., Cujbescu, D., Persu, C. I., & Gheorghe, G. (2021). Researches on the protection of vineyards and orchards against spring frosts using heat and smoke and using the resulting ash as soil amendment. Annals of the University of Craiova—Agriculture, Montanology, Cadastre Series, 51(2), 300–305.

[9] Heusinkveld, V. W. J., van Hooft, J. A., Schilperoort, B., Baas, P., ten Veldhuis, M.-C., & van de Wiel, B. J. H. (2020). Towards a physics-based understanding of fruit frost protection using wind machines. Agricultural and Forest Meteorology, 282–283, 107868. https://doi.org/10.1016/j.agrformet.2019.107868

[10] Hu, Y., Wu, W., De Melo-Abreu, J. P., & Shapland, T. M. (2018). Review of air disturbance technology for plant frost protection. International Journal of Agricultural and Biological Engineering, 11(3), 21–28. https://doi.org/10.25165/j.ijabe.20181103.3172

[11] Hua, W., He, L., Heinemann, P. H., & Zhu, M. (2025). Precision heating strategy based dynamic heater path planning for frost protection in apple orchards. Biosystems Engineering, 250, 117–132. https://doi.org/10.1016/j.biosystemseng.2024.12.002

[12] Hua, W., Heinemann, P. H., & He, L. (2024a). Canopy protection cyber-physical system (CPCPS) for smart agricultural management of frost damage in apple orchards. Computers and Electronics in Agriculture, 217, 108611. https://doi.org/10.1016/j.compag.2024.108611

[13] Hua, W., Heinemann, P. H., & He, L. (2024b). Heat transfer modeling with fixed and mobile heaters for frost protection in apple orchards. Computers and Electronics in Agriculture, 227, 109525. https://doi.org/10.1016/j.compag.2024.109525

[14] Hua, W., Heinemann, P. H., & He, L. (2025). Frost management in agriculture with advanced sensing, modeling, and artificial intelligent technologies: A review. Computers and Electronics in Agriculture, 231, 110027. https://doi.org/10.1016/j.compag.2025.110027

[15] Kimura, K., Yasutake, D., Nakazono, K., & Kitano, M. (2017). Dynamic distribution of thermal effects of an oscillating frost protective fan in a tea field. Biosystems Engineering, 164, 98–109. https://doi.org/10.1016/j.biosystemseng.2017.09.010

[16] Liu, T., Zhang, S., Sun, T., Ma, C., & Xue, X. (2025). Review of active plant frost protection equipment and technologies: Current status, challenges, and future prospects. Agronomy, 15(5), 1164. https://doi.org/10.3390/agronomy15051164

[17] Lu, Y., Hu, Y., Zhao, C., & Snyder, R. L. (2018). Modification of water application rates and intermittent control for sprinkler frost protection. Transactions of the ASABE, 61(4), 1277–1285. https://doi.org/10.13031/trans.12596

[18] Lu, Y., Zhang, W., Lin, Y., Cao, Z., Wu, H., Liu, L., Song, X., & Lu, Q. (2025). Design of anti-frost smoke machine system for mountain orchard based on multi-objective optimization. Scientific Reports, 15, 40681. https://doi.org/10.1038/s41598-025-21322-w

[19] Marin, E., Matache, M., Nițu, M., & Gheorghe, G. (2017). Experimental researches regarding assessment of coverage degree obtained by orchard spraying machine. Engineering for Rural Development, 16, 1239–1243. https://doi.org/10.22616/ERDev2017.16.N271

[20] Matache, M., Persu, C., Nițu, M., & Gheorghe, G. (2017). Vision system for spraying machine adaptive control. Engineering for Rural Development, 16, 358–363. https://doi.org/10.22616/ERDev2017.16.N071

[21] Pan, Q., Lu, Y., Hu, H., & Hu, Y. (2024). Review and research prospects on sprinkler irrigation frost protection for horticultural crops. Scientia Horticulturae, 326, 112775. https://doi.org/10.1016/j.scienta.2023.112775

[22] Schmitz, M., Zimmermann, A., Schiffers, K., Whitney, C., Balmer, M., & Luedeling, E. (2025). Model-based decision support for the choice of active spring frost protection measures in apple production. Agricultural Systems, 224, 104255. https://doi.org/10.1016/j.agsy.2024.104255

[23] Wu, H., & Wang, S. (2023). Design and optimization of intelligent orchard frost prevention machine under low-carbon emission reduction. Journal of Cleaner Production, 433, 139808. https://doi.org/10.1016/j.jclepro.2023.139808

[24] Zahradníček, P., Brázdil, R., Řehoř, J., Trnka, M., Bartošová, L., & Rožnovský, J. (2024). Past and present risk of spring frosts for fruit trees in the Czech Republic. Theoretical and Applied Climatology, 155, 965–984. https://doi.org/10.1007/s00704-023-04671-2

[25] Zhang, W., Lu, Y., Lin, Y., Cao, Z., Wu, H., Liu, L., Chen, Y., Hu, D., & Lu, Q. (2026). Design and experimental investigation of an anti-frost smoke machine using a fuzzy PID control strategy optimized by the Hippopotamus Optimization Algorithm. Agriculture, 16(10), 1113. https://doi.org/10.3390/agriculture16101113

[26] Zhou, Y., Han, Y., Zhao, J., Chen, X., & Yu, L. (2023). Review of atomization mechanism and spray characteristics of a liquid jet in supersonic crossflow. Chinese Journal of Aeronautics, 36(8), 1–23. https://doi.org/10.1016/j.cja.2023.03.010

# COMPARATIVE EVALUATION OF OIL EXTRACTION YIELD FROM DIFFERENT OILSEEDS USING A SMALL-SCALE SCREW PRESS

/

# *STUDIU COMPARATIV PRIVIND EXTRACȚIA MECANICĂ A ULEIULUI DIN DIFERITE SEMINȚE OLEAGINOASE UTILIZÂND O PRESĂ DE CAPACITATE MICĂ CU MELC*

**Mariana IONESCU*, Gabriel-Alexandru CONSTANTIN, Sorin-Ștefan BIRIȘ, Gheorghe VOICU, Neluș-Evelin GHEORGHIȚĂ, Mirela-Nicoleta DINCĂ, Nicoleta UNGUREANU, Bianca-Ștefania ZĂBAVĂ**
National University of Science and Technology POLITEHNICA Bucharest, Faculty of Biotechnical Systems Engineering, Bucharest / Romania
**E-mail: maneamaryana@gmail.com*

***Keywords:*** *oilseeds, vegetable oil, mechanical pressing, screw press, oil extraction, seedcake, oil yield*

**ABSTRACT**
*Mechanical pressing is a relatively simple method for extracting vegetable oils and is suitable for small-scale processing. The purpose of this study was to conduct a comparative evaluation of the oil recovery from various oilseeds using a screw press. Seven types of oilseeds were analyzed: white sesame, black sesame, flaxseed, dehulled pumpkin seeds, dehulled sunflower seeds, poppy seeds, and flaked almonds. For each type of raw material, a 200 g sample was subjected to mechanical pressing using a small stainless-steel screw press. The mass of extracted oil, the mass of the resulting seedcake, and material losses were determined, and the oil yield (OYD) was calculated. The results revealed considerable variations among analyzed oilseeds. The mass of extracted oil ranged from 50.88 to 81.84 g, corresponding to OYD values of 25.44 - 40.92%. Dehulled sunflower seeds yielded the highest amount of extracted oil and the highest yield (81.84 g and 40.92%, respectively), while poppy seeds exhibited the lowest values (50.88 g and 25.44%). The seedcake mass ranged from 111.25 to 145.38 g, while material losses varied between 3.65 and 6.95 g. The results provide comparative data on oil recovery and mass balance during small-scale mechanical pressing process of various oilseeds.*

**REZUMAT**
*Presarea mecanică reprezintă o metodă relativ simplă de extragere a uleiurilor vegetale, fiind potrivită în special pentru procesarea la scară mică. Scopul acestui studiu a fost evaluarea comparativă a cantității de ulei extrasă din diverse semințe oleaginoase, utilizând o presă cu melc. Au fost analizate șapte tipuri de semințe oleaginoase: susan alb, susan negru, semințe de in, semințe de dovleac decojite, semințe de floarea-soarelui decojite, semințe de mac și fulgi de migdale. Pentru fiecare tip de semințe, o probă de 200 g a fost supusă presării mecanice cu ajutorul unei prese de de capacitate mică, realizată din oțel inoxidabil. Au fost determinate masa uleiului extras, masa șrotului rezultat și pierderile de material, iar randamentul de ulei (OYD) a fost calculat. Rezultatele au evidențiat variații considerabile între tipurile de semințe analizate. Masa uleiului extras a variat între 50,88 și 81,84 g, corespunzând unor valori ale OYD cuprinse între 25,44 și 40,92%. Semințele de floarea-soarelui decorticate au înregistrat cea mai mare cantitate de ulei extras și cel mai ridicat randament (81,84 g și, respectiv, 40,92%), în timp ce semințele de mac au prezentat cele mai mici valori (50,88 g, respectiv 25,44%). Masa șrotului a variat între 111,25 și 145,38 g, în timp ce pierderile de material au fost cuprinse între 3,65 și 6,95 g. Rezultatele oferă date comparative privind recuperarea uleiului și bilanțul de materiale în procesul de presare mecanică la scară redusă a diferitelor materii prime oleaginoase.*

## INTRODUCTION

Lipids, like other nutrients, play a very important role in human nutrition. They are natural substances widely found in nature and include oils and fats of animal and plant origin. A vegetable oil is a fatty substance extracted from an oleaginous plant such as sunflower, flax, sesame, etc. Oleaginous plants are plants that have the particularity of accumulating oils mainly in seeds, nuts or fruits; their nutritional value is derived from their content of essential omega-3 and omega-6 fatty acids or vitamins *(Bouhadi, N., Chennit, B., Boudriche, L., 2018).*

The vegetable oil industry is a very important sub-sector of the food industry, processing a wide range of agricultural raw materials (oilseeds) to produce vegetable oil and meal as its main products *(Khobragade, U. H., Borkar, P., and Khobragade, A. D., 2021)*. Vegetable oils are a rich source of energy, providing approximately 9 kcal of energy per gram, whereas carbohydrates and proteins provide approximately 4 kcal per gram *(Rani, H., Sharma, S., Bala, M., 2021)*. Figure 1 shows global vegetable oil consumption from 2013 to 2026, broken down by oil type. The graph shows that palm oil has the highest consumption (78.3 million metric tons currently), followed by soybean oil, with a current consumption of 70.06 million metric tons *(***Statista, 2026).*

Vegetable oils are divided, based on their use, into two categories: edible and non-edible (or industrial) oils. Edible oils are used directly in food industry as cooking oil or as ingredients in margarine, mayonnaise, baked products, pastries, the canning industry, confectionery, etc. In addition to these edible products, vegetable oils are also used in the manufacture of non-edible products, such as varnishes, adhesives, synthetic resins, lubricants, soaps, paints, bactericides, cosmetics, greases, and waxes *(Boulard, C., Bardet, M., Chardot, T. et al, 2015).*

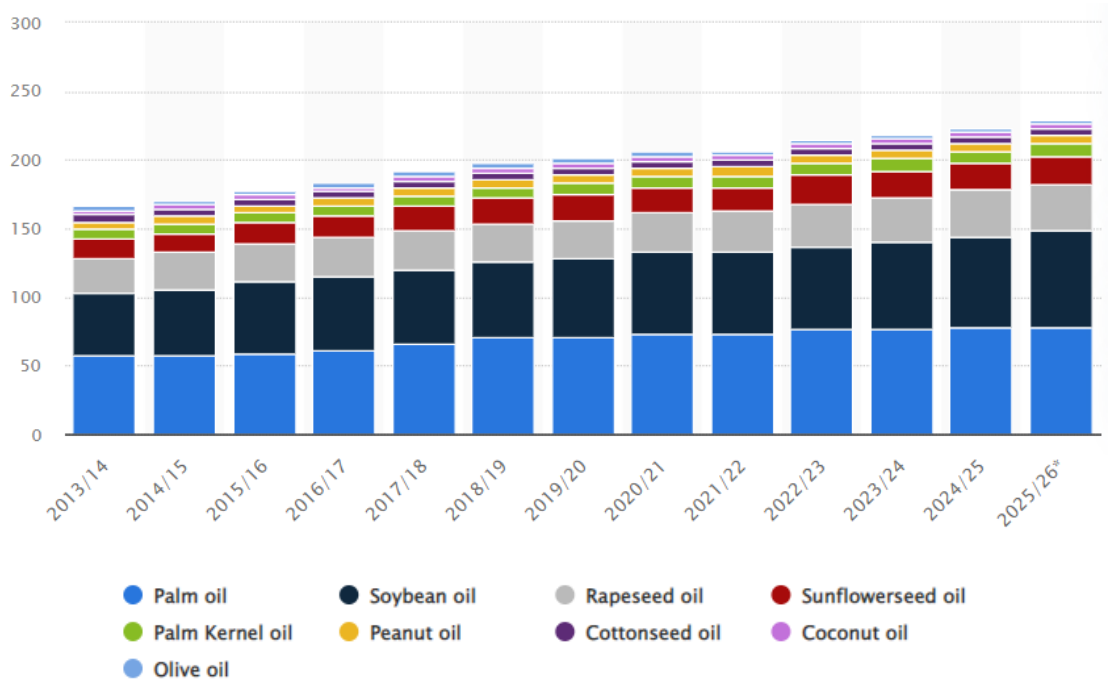



**Fig. 1- Global Vegetable oil consumption from 2013 to 2026, by oil type (in millions of metric tons)**
*(***Statista, 2026)*

To fulfill the growing demand for vegetable oils, for both industrial applications and human consumption, it is necessary to produce oil in large quantities and of high quality. Thus, numerous technologies have been developed for oil extraction, classified into traditional techniques (Ghanis), conventional methods (dry/wet separation, mechanical pressing, solvent or chemical extraction), and advanced techniques such as enzyme-assisted extraction (EAE), ultrasound-assisted extraction (UAE), microwave-assisted extraction (MAE), and supercritical fluid extraction (SFE). Currently, both conventional and advanced/modern techniques are used for vegetable oil extraction. However, conventional oil extraction techniques dominate the oil extraction industry *(Rani, H., Sharma, S., Bala, M., 2021).*

Mechanical pressing is recommended to be used for oil extraction only from oilseeds with an oil content exceeding 20%. The mechanical pressing of oilseeds involves separating the oil from the oilseed meal (a liquid-solid mixture) under the action of external compressive forces generated by machines called presses. The equipment employed for mechanical oil extraction are hydraulic presses and screw presses *(Sinha, L. K., Haldar, S., Majumdar, G. C., 2015; Cravotto, C., Claux, O., Bartier, M. et al, 2023)*. The hydraulic presses used to oilseeds compression is driven by fluid pressure. The high pressure applied in the hydraulic press yields a significantly higher oil yield than traditional oil processing methods. Further, the hydraulic press method has been improved upon by the screw press method, which offers slightly higher yields than the hydraulic press *(Rashid, M., Khalid, I., Sanghvi, G. et al, 2025).*

The advantages of mechanical pressing is the lower investment costs and the fact that it can be easily performed by moderately skilled personnel. The main disadvantage of this method is its low efficiency, as 8–14% of the oil remains in the cakeseeds *(Yusuf, A., 2018)*. Two types of mechanical pressing methods are defined, meaning the cold pressing and the hot pressing. As the name suggests, cold pressing method is performed at low temperature (below 50 °C) and pressure, while the hot pressing method requires high temperature and pressure. Due to the low temperature used, cold pressed oils are characterized by high quality, as the extraction process helps preserve their natural properties, flavor, and purity. The disadvantage of the cold pressing method is its lower oil extraction yield compared with hot pressing, which can recover up to 80% of the available oil in the raw material *(Kittiphoom, S., Sutasinee, S., 2015; Patel, V. R., Dumancas, G. G., Viswanath, L. C. K. et al, 2016)*.

The objectives of this study were to determine the mass of extracted oil, the mass of seedcake resulted from the process, the mass of material losses (oil and sediments), and the oil yield obtained at the pressing of different oilseed types.

## MATERIALS AND METHODS

In this study, the selected oilseeds were white sesame, flax, black sesame, pumpkin (dehulled), sunflower (dehulled), poppy, and almond (flaked). The oilseed samples were purchased from Bucharest, Romania. For the oil extraction process was used a small scale stainless steel oil press (Fig. 2 and Fig. 3).

The pressing machine is made of food grade 304 stainless steel and has a weight of 12 kg with the following dimensions: length 46 cm, width 18 cm, height 28 cm. Before starting the oil extraction, the press was pre-heated for about 5 minutes; the preheat switch did not need to be turned off afterwards, as the temperature adjusts automatically.




**Fig. 2 - Small scale stainless steel oil press**

*1 – feeding hopper; 2 – electric motor; 3 – oil collection tray; 4 – nozzle for cake outlet; 5 – press chamber (barrel)*

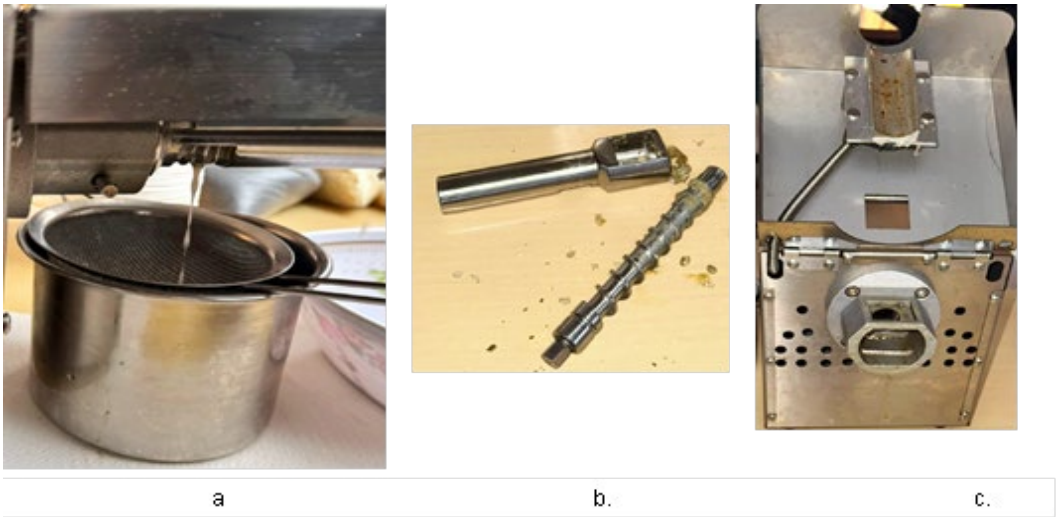



**Fig. 3 - Details of the small scale stainless steel oil press**

*a – oil evacuation and filtration; b – screw and press chamber (barrel); c – heating element of the press*

For the experiments, samples of 200 g from each of the selected oilseeds were prepared and fed through the press feeding hopper. The oilseeds are crushed by the rotating screw inside the press chamber. The crushing of the seeds is carried out by the rotating screw inside the barrel. The oil and the seedcake are simultaneously discharged through the oil output and the nozzle. The extracted crude oil and seedcake were weighed for further calculations.

**RESULTS**

Figure 4 shows different views of the oilseed samples prepared for the pressing process, along with the the process results, meaning the crude oil and the oilseed cakes.




**Fig. 4 - The results of the pressing process: samples, oils and seedcakes**

For the 200 g initial oilseed samples the following parameters were determined: the mass of seedcake, the mass of extracted oil, the mass of losses (oil and sediments), and the pressing oil yield. The material losses were calculated as the difference between the total mass of seedcake and oil and the initial sample mass. Table 1 presents the determined parameters after the pressing process of oilseed samples.

The abbreviations from the Table 1 represent: $M_T$ is the total mass of the sample, $M_S$ mean the mass of seedcake, $M_O$ is the mass of extracted oil and $M_P$ represent the mass of material losses (sediment and oil).

**Table 1**

**Determined parameters after pressing operation**

| Oilseed type | $M_T$ (g) | $M_S$ (g) | $M_O$ (g) | $M_{S+O}$ (g) | $M_P$ (g) | $O_{YD}$ (%) |
|---|---|---|---|---|---|---|
| **Pumpkin (dehulled)** | 200 | 118.82 | 74.23 | 193.05 | 6.95 | 37.115 |
| **Black sesame** | 200 | 130.14 | 63.41 | 193.55 | 6.45 | 31.705 |
| **Almond (flaked)** | 200 | 115.08 | 80.15 | 195.23 | 4.77 | 40.075 |
| **Flax** | 200 | 140.26 | 56.09 | 196.35 | 3.65 | 28.045 |
| **White sesame** | 200 | 132.71 | 60.77 | 193.48 | 6.52 | 30.385 |
| **Sunflower (dehulled)** | 200 | 111.25 | 81.84 | 193.09 | 6.91 | 40.92 |
| **Poppy** | 200 | 145.38 | 50.88 | 196.26 | 3.74 | 25.44 |

The oil yield of the pressing process from the Table 1 was calculated using Equation (1)*( Huang, S., Hu, Y. et al, 2019; Deli, S., Farah, M.M. et al, 2011; Chanioti, S., Tzia, C., 2017)* as follows:

$$O_{YD} = \frac{M_O}{M_T} \cdot 100 \quad [\%] \tag{1}$$

where:

$O_{YD}$ represent the oil yield (%), $M_O$ is the mass of extracted oil (g) and $M_T$ is the total mass of the sample (g).

According to the data presented in Table 1, it can be seen that the mass of the seedcake $M_S$ ranged from 111,25 to 145,38 g. The mass of extracted oil $M_O$ from the selected oilseeds varied between 50,88 and 81,84 g, while the material losses $M_P$, calculated as described previously, ranged from 3,65 to 6,95 g. It should be noted that the measured mass of extracted oil included the sediments from seedcake (which can be further separated by the decantation process) and the material losses included the oil loss (resulted from the collection and transfer of extracted oil into another container) and the sediments retained on the sieve during oil outlet.

The experiments results show that the poppy seeds obtained the highest seedcake mass of 145,38 g, with the lowest oil mass of 50,88 g, followed by flax seeds with seedcake mass of 140,26 g and oil mass of 56,09 g. The highest quantity of extracted oil was obtained in the case of dehulled sunflower seeds, with 81,84 g of extracted oil and 111,25 g of resulted seedcake, followed by the almond flakes with 80,15 g of extracted oil and 115,08 g of resulted seedcake. Thus the highest oil yield percentage was obtained in the case of dehulled sunflower seeds (40,92%), followed by the almond flakes oil yield (40,075%), while the lowest oil yield percentage was obtained for the poppy seeds (25,44%). The material losses, which were calculated as previously described, has the highest values in the case of pumpkin (6,95 g), while the lowest value was obtained for the flax seeds (3,65 g). In figures 5 to 8 are graphically illustrated the variation of: seedcake mass, material losses, extracted oil mass and pressing oil yield, which resulted from the mechanical pressing of selected oilseeds.

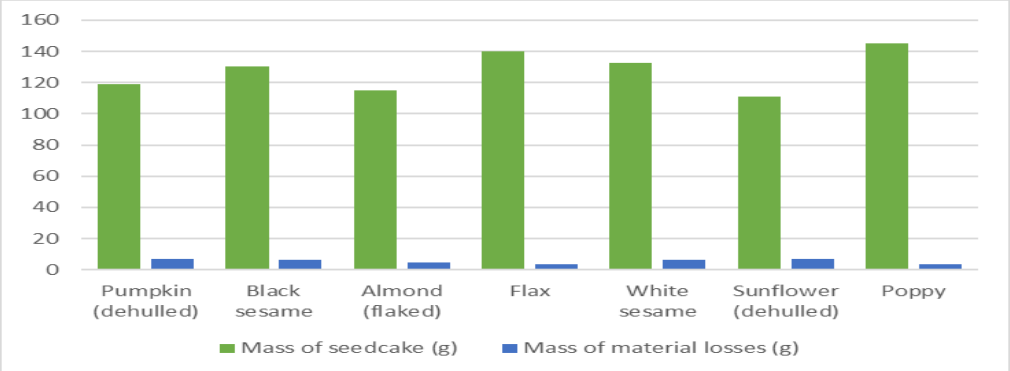



**Fig. 5 - Variation of seedcake mass and material losses after the mechanical pressing**

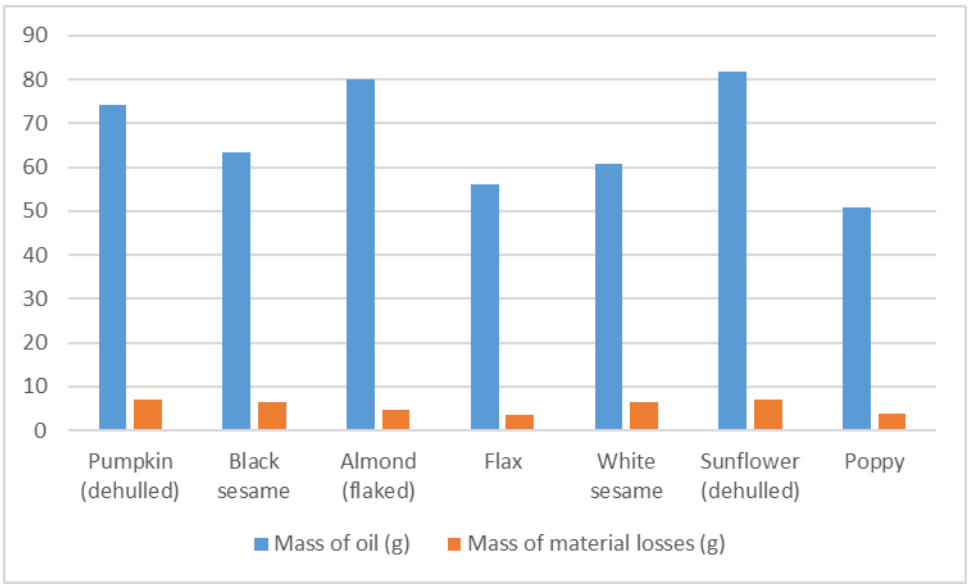



**Fig. 6 - Variation of extracted oil mass and material losses after the mechanical pressing**

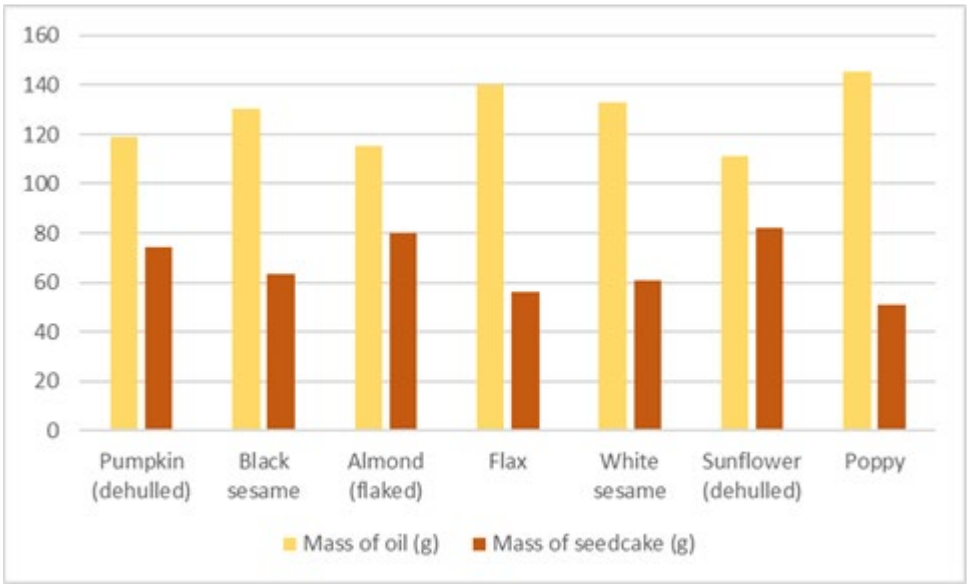



**Fig. 7 - Variation of extracted oil mass and seedcake mass after the mechanical pressing**

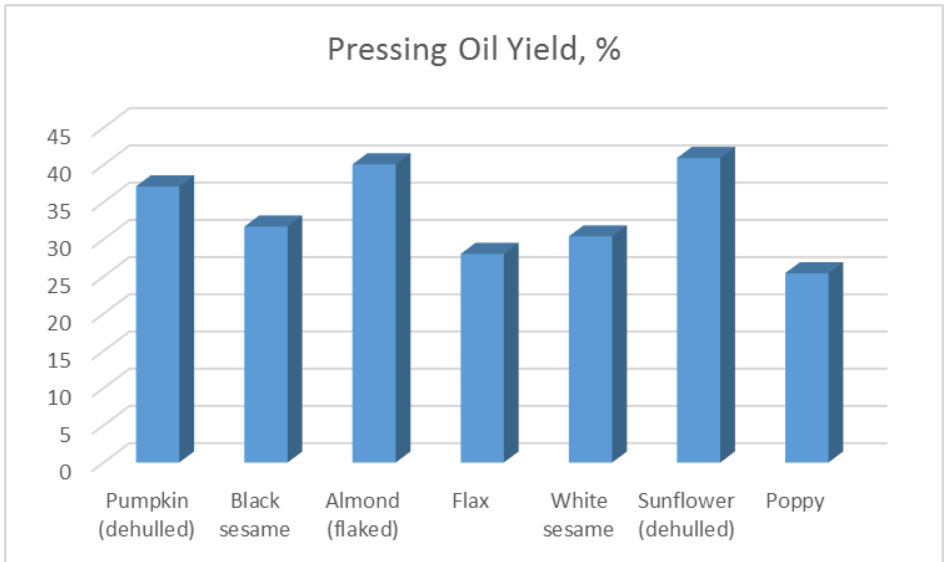



**Fig. 8 - Variation of pressing oil yield (%) for the selected oilseeds**

## CONCLUSIONS

White sesame, black sesame, flaxseed, dehulled pumpkin seeds, dehulled sunflower seeds, poppy seeds, and flaked almonds were pressed with a screw press, in order to determine the mass of extracted oil, the seedcake mass and the material losses (oil and sediments). The experimental results demonstrated that the type of oilseed had a significant influence on the amount of oil recovered by mechanical pressing. Dehulled sunflower seeds yielded the highest amount of extracted oil and the highest yield (81.84 g and 40.92%, respectively), while poppy seeds exhibited the lowest values (50.88 g and 25.44%). It was observed that the lower the amount of crude oil extracted, the higher the seedcake produced. The seedcake mass ranged from 111.25 to 145.38 g, while material losses varied between 3.65 and 6.95 g (approximately 1.83-3.48% of the initial sample mass), showing a high efficiency of the oil press.

The simultaneous determination of extracted oil, seedcake, and material losses provides useful information for assessing the mass balance of the pressing process. Further investigations should focus on the influence of operating parameters, such as pressing temperature, screw speed, and pressing conditions, on oil recovery. Also the influence of initial moisture content of the oilseeds and the treatments of the oilseed material (such as grinding, cooking) on the oil recovery and on the properties of both the extracted oil and the resulting seedcake, should be investigated.

## ACKNOWLEDGEMENT

This research was supported by the project CNFIS-FDI-2026-F-0049 “Asigurarea eficienței operaționale a bazei de aplicații practice pentru sisteme biotehnice în livezi, vii, solarii și grădini (EFIBIOTECH)”, from the Ministry of Education and Research through the Executive Agency for Financing Higher Education, Research, Development and Innovation.

## REFERENCES

[1] Bouhadi, N., Chennit, B., Boudriche, L. (2018). Sesame seeds and Flax Food oils: extraction and physicochemical characterizations, *Journal of Agroalimentary Processes and Technologies*, *24* (3), 136-142. https://journal-of-agroalimentary.ro/journal-of-agroalimentary-processes-and-technologies-2018-24-3/sesame-seeds-and-flax-food-oils-extraction-and-physicochemical-characterizations

[2] Boulard, C., Bardet, M., Chardot, T., Dubreucq, B., Gromova, M., Guillermo, Miquel, M., Nesi, N., Yen-Nicolaÿ, S., Jolivet, P. (2015). The structural organization of seed oil bodies could explain the contrasted oil extractability observed in two rapeseed genotypes. *Planta, 242*(1), 53–68. https://doi.org/10.1007/s00425-015-2286-4

[3] Chanioti, S., Tzia, C. (2017). Optimization of ultrasound-assisted extraction of oil from olive pomace using response surface technology: Oil recovery, unsaponifiable matter, total phenol content and antioxidant activity. *LWT - Food Science and Technology, 79,* 178–189. https://doi.org/10.1016/j.lwt.2017.01.029.

[4] Cravotto, C., Claux, O., Bartier, M., Fabiano-Tixier, A.S., Tabasso, S. (2023). Leading Edge Technologies and Perspectives in Industrial Oilseed Extraction. *Molecules. 9;*28(16), 5973. doi: 10.3390/molecules28165973.

[5] Deli, S., Farah, M.M., Tajul, A.Y., Wan, N.W.A. (2011). The effects of physical parameters of the screw press oil expeller on oil yield from Nigeria sativa L seeds*. International Food Research Journal, 18*(4), 1367-1373.https://www.researchgate.net/publication/279895772_The_effects_of_physical_parameters_of_the_screw_press_oil_expeller_on_oil_yield_from_Nigella_sativa_L_seeds.

[6] Huang, S., Hu, Y., Li, F., Jin, W., Godara, V., Wu, B. (2019). Optimization of mechanical oil extraction process from Camellia oleifera seeds regarding oil yield and energy. *Journal of Food Process Engineering*, *42*(6), e13157. https://doi.org/10.1111/jfpe.13157.

[7] Khobragade, U. H., Borkar, P., and Khobragade, A. D. (2021). Engineering Properties of Safflower Oilseeds. *International Journal of Engineering Science Invention (IJESI), 10*(4), 46-50. https://www.researchgate.net/publication/354751152_Engineering_Properties_of_Safflower_Oilseeds

[8] Kittiphoom, S., Sutasinee, S. (2015). Effect of microwaves pretreatments on extraction yield and quality of mango seed kernel oil. *International Food Research Journal, 22*(3), 960–964. https://www.researchgate.net/publication/282053642_Effect_of_microwaves_pretreatments_on_extraction_yield_and_quality_of_mango_seed_kernel_oil

[9] Patel, V. R., Dumancas, G. G., Viswanath, L. C. K., Maples, R., Subong, B. J. (2016). Castor oil: Properties, uses, and optimization of processing parameters in commercial production. *Lipid Insights, 9*, 1-12. https://doi.org/10.4137/LPI.S40233

[10] Rani, H., Sharma, S., Bala, M. (2021). Technologies for extraction of oil from oilseeds and other plant sources in retrospect and prospects: A review. *Journal of Food Process Engineering, 44*(11), e13851 https://doi.org/10.1111/jfpe.13851

[11] Rashid, M., Khalid, I., Sanghvi, G., Shankar, A., Saeed, F., Afzaal, M., Mehwish, Kundlas, M., Ndagire, C. T. (2025). Soybean Synergies: A Comprehensive Review on Novel Extraction Techniques and Their Role in Unlocking Health Potential. *Food Science & Nutrition, 13*(10), e70983. https://doi.org/10.1002/fsn3.70983.

[12] Sinha, L. K., Haldar, S., Majumdar, G. C. (2015). Effect of operating parameters on mechanical expression of solvent-soaked soybean-grits. *Journal of Food Science and Technology, 52*(5), 2942–2949. https://doi.org/10.1007/s13197-014-1340-8

[13] Yusuf, A. (2018). A Review of Methods Used for Seed Oil Extraction. *International Journal of Science and Research (IJSR). 7*(12), 1121804, 233-238. 10.21275/1121804.

[14] *** Statista. (2026). *Consumption of vegetable oils worldwide from 2013/14 to 2025/2026, by oil type (in million metric tons)*. https://www.statista.com/statistics/263937/vegetable-oils-global.

# COMPUTATIONAL ANALYSIS OF MILK FLOW DYNAMICS AND HEAT TRANSFER PERFORMANCE IN A PLATE HEAT EXCHANGERS - A REVIEW

/

# *ANALIZA COMPUTATIONALA A DINAMICII CURGERII LAPTELUI SI A PERFORMANTEI TRANSFERULUI TERMIC IN SCHIBATOARELE DE CALDURA CU PLACI - REVIEW*

**Florentina BRATOSIN[1)], Sorin-Ștefan BIRIȘ[1)], Mihaela BEGEA*[1)], Andreea-Ioana BADIU[1)], Alina-Daiana IONESCU[1)]**
National University of Science and Technology POLITEHNICA Bucharest / Romania
**E-mail: mihaela.begea@gmail.com*

***Keywords:*** *plate heat exchangers, milk flow, heat transfer, thermal efficiency.*

**ABSTRACT**

*Plate heat exchangers are widely utilized in the dairy industry for processes such as milk cooling and pasteurization because of their high heat transfer efficiency and compact design. The performance of these systems depends significantly on the milk flow patterns, velocity distribution within the narrow channels formed by the plates, and the effectiveness of heat exchange between the fluid and the heat transfer surfaces. This review provides a comprehensive analysis of how milk flow dynamics impact the overall heat transfer coefficient and the energy efficiency of the pasteurization process. Advanced numerical simulations and computational fluid dynamics (CFD) models are employed to examine temperature, velocity, and pressure distributions inside plate heat exchangers, facilitating the optimization of flow and heat transfer characteristics. Moreover, the review discusses the detrimental effects of fouling, caused by protein and mineral deposit formation on plate surfaces, which increase thermal resistance and energy consumption while reducing equipment lifespan and performance. Computational investigations of fouling mechanisms enable better understanding and prediction of deposit growth, leading to improved cleaning strategies and operational conditions. Integrating hydrodynamic, thermal, and fouling models is essential for designing efficient, and reliable dairy heat exchangers. The insights provided in this review support the advancement of plate heat exchanger technology in dairy processing, promoting enhanced safety, energy savings, and product quality.*

**REZUMAT**

*Schimbătoarele de căldură cu plăci sunt utilizate pe scară largă în industria lactatelor pentru procese precum răcirea și pasteurizarea laptelui, datorită eficienței ridicate a transferului de căldură și designului compact. Performanța acestor sisteme depinde semnificativ de modelele de curgere a laptelui, de distribuția vitezei în canalele înguste formate de plăci și de eficacitatea schimbului de căldură dintre fluid și suprafețele de transfer de căldură. Această analiză oferă o analiză cuprinzătoare a modului în care dinamica curgerii laptelui influențează coeficientul general de transfer de căldură și eficiența energetică a procesului de pasteurizare. Simulări numerice avansate și modele de dinamică computațională a fluidelor (CFD) sunt utilizate pentru a examina distribuțiile de temperatură, viteză și presiune în interiorul schimbătoarelor de căldură cu plăci, facilitând optimizarea caracteristicilor de curgere și transfer de căldură. Mai mult, analiza discută efectele negative ale murdăririi, cauzate de formarea depozitelor de proteine și minerale pe suprafețele plăcilor, care cresc rezistența termică și consumul de energie, reducând în același timp durata de viață și performanța echipamentelor. Investigațiile computaționale ale mecanismelor de murdărire permit o mai bună înțelegere și predicție a creșterii depozitelor, ducând la strategii de curățare și condiții de funcționare îmbunătățite. Integrarea în industria de procesare a laptelui a modelelor hidrodinamice, termice și celor de depuneri este esențială pentru proiectarea schimbătoarelor de căldură eficiente și fiabile. Informațiile furnizate în această analiză susțin avansul tehnologiei schimbătoarelor de căldură cu plăci în procesarea produselor lactate, promovând o siguranță sporită, economii de energie și o calitate sporită a produselor.*

## INTRODUCTION

Food safety and quality are crucial for food industry, including dairy industry, which relies significantly on thermal treatments like pasteurization to inactivate pathogens while preserving nutrients and sensory qualities. At present, High Temperature Short Time (HTST) pasteurization is the most widely used method in the dairy industry due to its optimal balance between ensuring microbiological food safety, energy consumption, and the preservation of the nutritional and sensory characteristics of milk (Indumathy et al., 2022). Plate heat exchangers dominate dairy processing due to high heat transfer rates, compactness, and energy recovery. They operate by transferring heat between two fluids separated by thin plates through conduction and convection. Counter-current flow is preferred for its superior heat transfer and energy recovery above 90%, reducing costs (*Shah & Sekulić, 2003; Kakaç et al., 2012*).

Compared to tubular exchangers, they offer higher heat transfer area per volume, flexibility in the number of plates, and lower costs but are sensitive to fouling and limited by viscosity, particle content, and pressure ratings (*Bansal & Chen, 2006; Sharma & Macchietto, 2021*). The corrugated configuration of the plates enhance turbulence, improving heat transfer and reducing process time (*Muley & Manglik, 1999; Tetra Pak, 2024*), while variations in milk's hydrodynamics and thermophysical properties with temperature and composition affect heat transfer efficiency (*Sharma & Macchietto, 2021*) and fouling from protein and mineral deposits raises heat transfer resistance and pressure drop, reducing performance (*Aboul Khail & Erişen, 2022*). Understanding the interplay of milk flow, heat transfer, and fouling via numerical simulations is vital for optimizing heat exchanger design, enhancing energy efficiency and product quality (*Indumathy et al., 2022*).

## REVIEW OF COMPUTATIONAL ANALYSIS OF MILK FLOW AND HEAT TRANSFER

Computational Fluid Dynamics (CFD) analysis is one of the most important methods used to investigate the hydrodynamic and thermal processes occurring in plate heat exchangers designed for the dairy industry. The complexity of the channel geometry, their small dimensions, and the inability to perform detailed experimental measurements inside the equipment have led researchers to focus on numerical methods capable of reproducing the distributions of velocity, pressure, and temperature under conditions close to actual operating conditions.

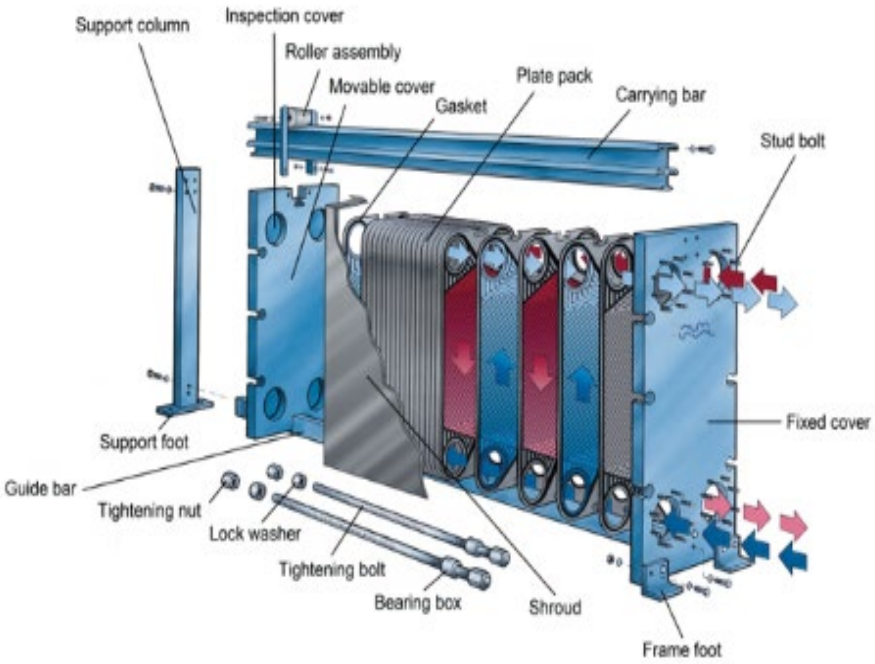



**Fig. 1 - Constructive configuration of a plate heat exchanger used in milk processing**
*(source Alfa Laval)*

Milk density affects flow distribution and hydrodynamic calculations, while viscosity controls flow resistance and regime in narrow heat exchanger channels. Thermal conductivity and specific heat capacity determine heat conduction and energy needed for temperature changes. These properties inform analytical and CFD models, influencing local temperature, pressure, velocity, and equipment efficiency (*Bergman et al.,*

*2020*). Milk is generally Newtonian in typical conditions, but products like cream and yogurt are non-Newtonian, requiring complex rheological models for accurate simulation (*Singh & Heldman, 2014*). Temperature mainly governs milk properties; as it rises, density and viscosity decrease, improving flow and convective heat transfer, while conductivity and heat capacity vary with composition and temperature, affecting key dimensionless numbers used to assess flow and heat transfer (*Kakaç et al., 2012*).

## PLATE TYPES AND DISTRIBUTION AREAS

Heat exchanger plates feature a corrugated herringbone design that directs flow and generates secondary turbulence, reducing thermal boundary layers and enhancing heat transfer. However, high velocities lead to pressure losses and higher pump energy, hence optimizing velocity is crucial in the design of modern heat exchangers (*Muley & Manglik, 1999*). Oppositely oriented corrugations create helical flow channels that increase turbulence, improve heat transfer, reduce deposits, and aid self-cleaning. Corrugation geometry can be adjusted to suit various processes, including those with fouling-prone fluids (*Alfa Laval*).

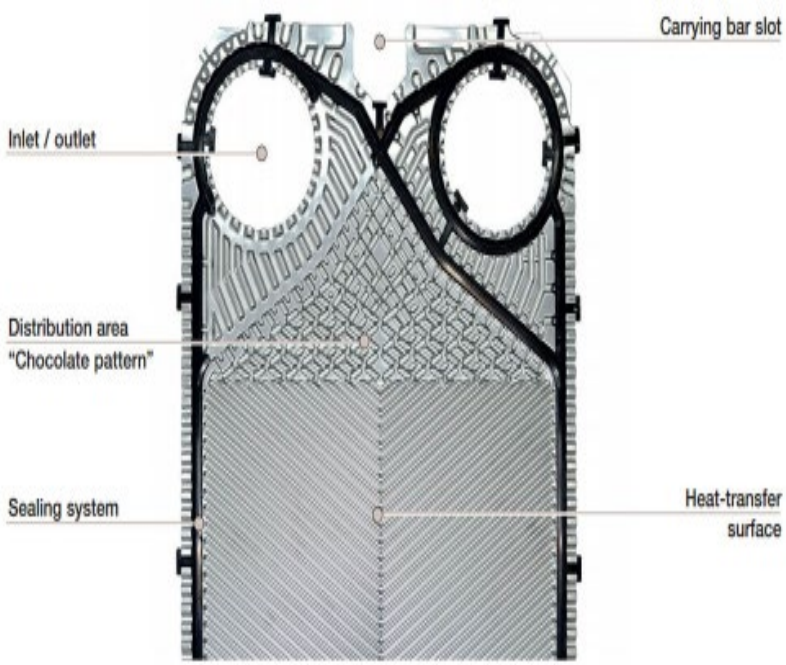



**Fig. 2 - Heat exchanger plate design**
*(source Alfa Laval)*

Heat exchanger plates can come in several design variants, as presented below.

Plates with large chevron angles create stronger turbulence and better heat transfer but cause higher pressure losses. Smaller angles reduce hydraulic resistance but lower heat transfer efficiency. Research aims to balance heat transfer and pumping energy (*Kakaç et al., 2012; Shah & Sekulić, 2003*). Double-wall plate heat exchangers, made of laser-welded plate pairs, prevent fluid mixing by containing leaks between the two plates, ensuring complete separation and avoiding contamination (*Alfa Laval*).

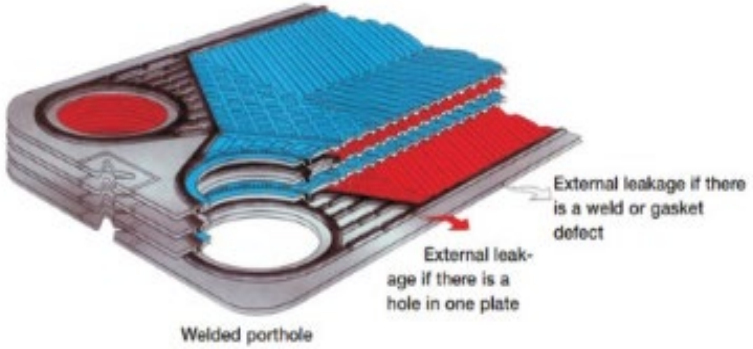



**Fig. 3 - Double-walled plates of a heat exchanger**
*(source Alfa Laval)*

Due to their wide channels, free of contact points**,** WideGap plates are suitable for processing fluids containing fibers or large particles. The channel geometry is designed to prevent the formation of solid bridges at the inlet area, facilitating fluid flow and reducing the risk of blockage or particle accumulation (*Alfa Laval*).

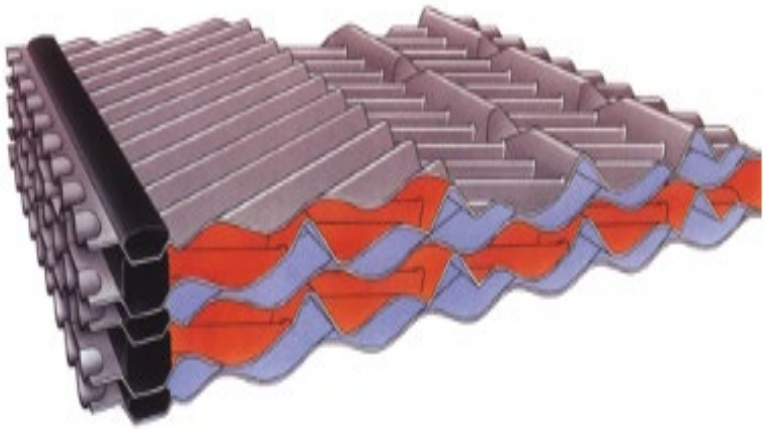


**Fig. 4 - WideGap plates for a heat exchanger**
*(source Alfa Laval)*

In case of semi-welded plates, the welded channels designed for process fluids enable the processing of aggressive or difficult-to-handle liquids in plate heat exchangers, while also extending the pressure range within which the equipment can operate. In addition, the welded configuration limits the exposure of the gaskets to the fluid, contributing to increased equipment durability and reliability (*Alfa Laval*).

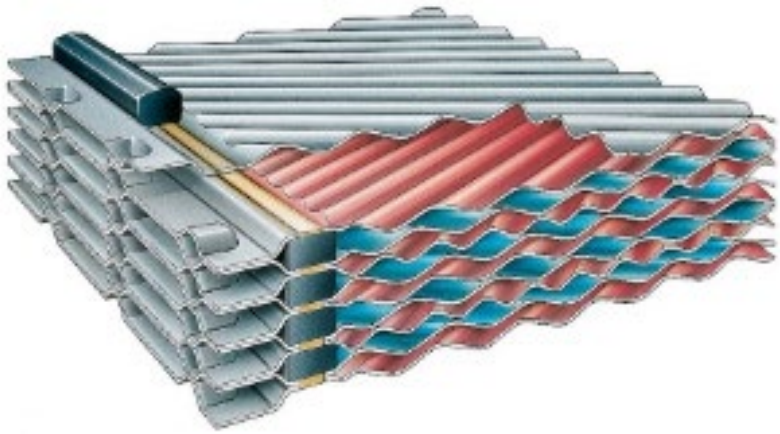


**Fig. 5 - Semi-welted plates for a heat exchanger**
*(source Alfa Laval)*

Diabon graphite non-metallic plates – the plates are manufactured from a graphite- and fluoroplastic-based composite, providing high resistance to hydrochloric acid and other corrosive substances. Unlike conventional graphite, Diabon F material has a non-porous and impermeable structure, which contributes to improved resistance under operating conditions.

These plates also exhibit increased resistance to cracking and breakage, both during handling and throughout their service life (*Alfa Laval*).

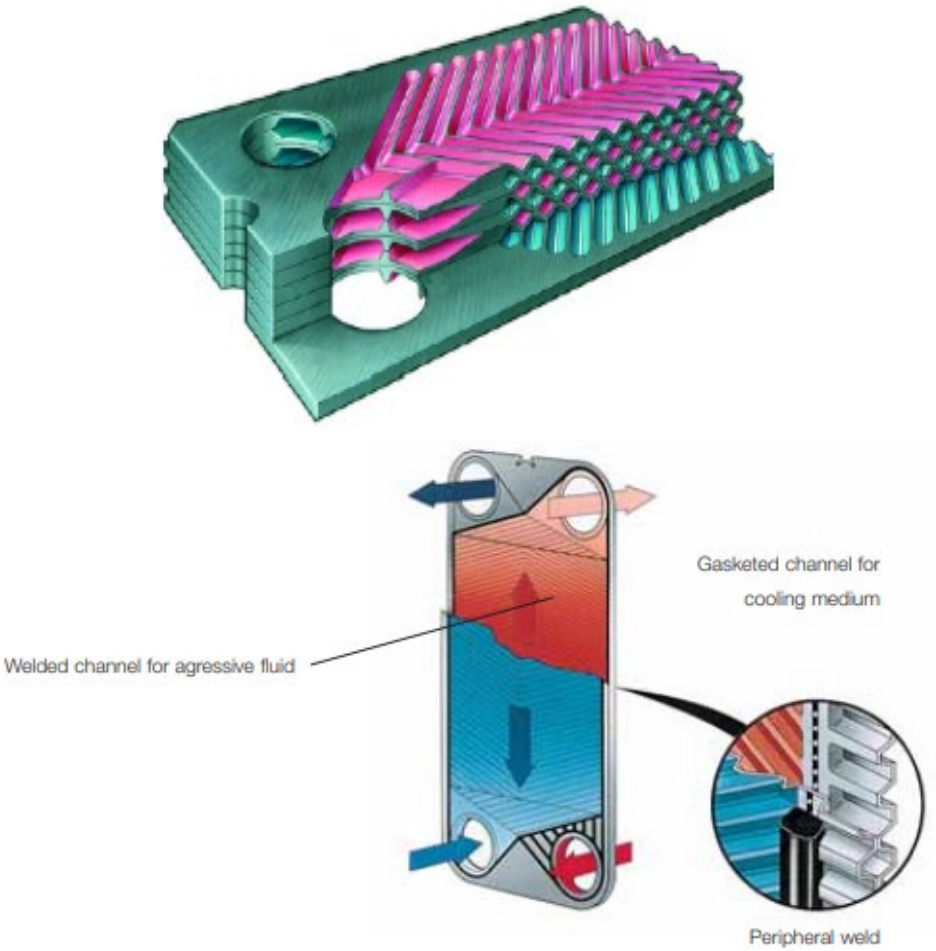



**Fig. 6 - Diabon Graphite non-metallic plates for a heat exchanger**
*(source Alfa Laval)*

The distribution area of the plates is manufactured by pressing them into a corrugated “chocolate” pattern, representing a specific feature of certain design configurations. This geometric configuration offers several important advantages:

- ensures uniform fluid distribution across the entire heat transfer surface, contributing to increased energy efficiency of the heat exchanger;
- reduces or eliminates stagnant zones (dead spots), thereby decreasing the risk of corrosion and deposit formation;
- contributes to reduced maintenance costs and increased equipment operating time by limiting deposit accumulation and maintaining stable process performance.

Numerical simulations reveal recirculation zones and vertical flows near plate corrugations, enhancing mixing and temperature uniformity but potentially causing stagnation and protein deposits at low velocities. These zones depend on plate geometry, flow rate, and fluid rheology. Reducing stagnation is key to improving heat transfer and reducing fouling, a major issue in milk processing (*Bansal & Chen, 2006*). Plates also differ by corrugation pattern into Low Theta and High Theta types, each with distinct features.




**Fig. 7 - Corrugated plates for a heat exchanger**
*(source Alfa Laval)*

The main characteristics of the "Low Theta" plate are represented by smaller chevron angle, lower pressure drop, lower heat transfer and lower flow resistance.

The main characteristics of the "High Theta" plate are represented by larger chevron angle, higher pressure drop, enhanced heat transfer, and higher flow resistance.

The two types of corrugation patterns, in turn, form three different types of channels, which are selected based on the required temperature program and the maximum allowable pressure drop.

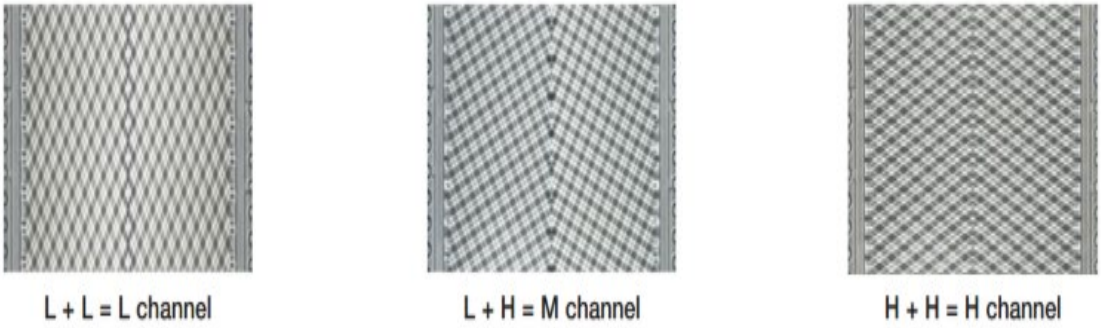



**Fig. 8 - The channels formed by the two types of corrugation**
*(source Alfa Laval)*

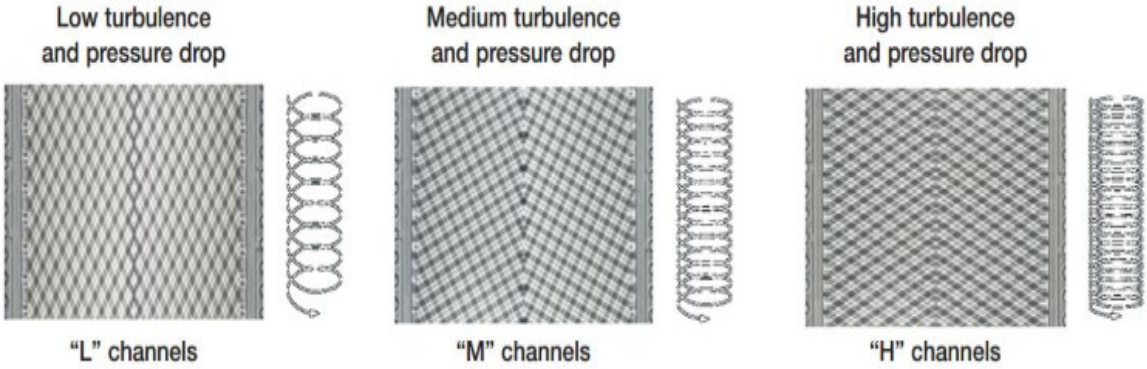



**Fig. 9 - Channel characteristics depending on flow**
*(source Alfa Laval)*

**Distribution Area - CurveFlow**

The CurveFlow design of the distribution area is intended to improve fluid distribution and ensure more efficient utilization of the pressure drop in the main heat transfer area. This configuration provides several advantages:

- **more compact heat exchanger dimensions** – improved heat transfer efficiency allows the use of a smaller number of plates;
- **increased energy efficiency** – uniform flow distribution limits deposit formation and contributes to reducing the energy required for pumping;
- **reduced maintenance costs** – the smaller number of plates facilitates cleaning operations and reduces costs associated with spare parts.

This new heat exchanger plate design improves fluid distribution and heat transfer, providing **up to 15% higher efficiency** compared with the traditional design. The non-circular ports also allow for a **higher flow capacity** at the same flow velocity. In addition, the increased velocity and shear stress in the heat transfer area can improve the **self-cleaning capability by up to 40%**, thereby reducing the risk of deposit formation.

The design also incorporates a **perpendicular corner guide**, which ensures proper plate alignment and contributes to maintaining reliable heat exchanger operation (*Alfa Laval*).

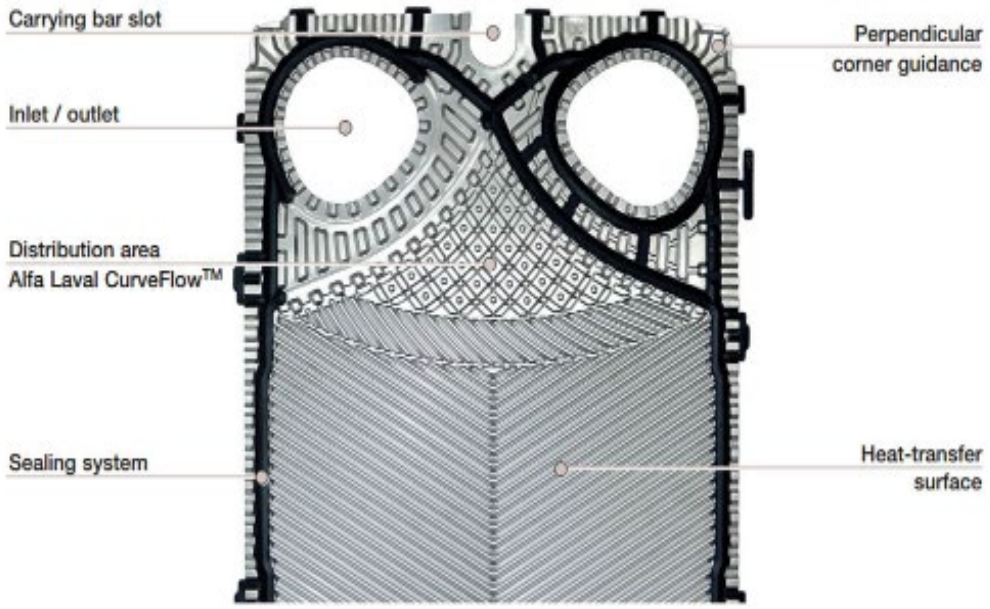



**Fig. 10 - Designing a new technology for heat exchanger plates**
*(source Alfa Laval)*

## NUMERICAL MODELLING OF MILK FLOW DYNAMICS AND HEAT TRANSFER

Milk's viscosity, density, and thermal conductivity vary with temperature and fat content, affecting heat exchange. Accurate modeling requires detailed thermophysical characterization since milk is a complex colloidal system with dispersed fat, proteins, lactose, and minerals, whose interactions define physical properties influenced by composition and processing (*Fox et al., 2015; Walstra et al., 2006*).

Density affects flow patterns, viscosity controls resistance and flow regime, while thermal conductivity and specific heat define heat conduction and energy needed for temperature changes.

Thermophysical properties are essential inputs for both analytical heat transfer models and CFD simulations, impacting local temperature, pressure, and velocity distributions, as well as energy efficiency evaluation (*Bergman et al., 2020*). Density, viscosity, thermal conductivity, and specific heat affect flow characteristics and heat transfer intensity. Using inaccurate or constant property values can cause significant errors in performance prediction (*Incropera et al., 2017*).

Temperature changes affect milk properties: as temperature rises, density and viscosity decrease, enhancing flow and convective heat transfer, while conductivity and heat capacity vary with composition, influencing dimensionless numbers important for heat transfer assessment (*Kakaç et al., 2012*). Fouling, caused by protein and mineral deposits during heat treatment, lowers heat transfer coefficient and increases pressure losses and energy use (*Indumathy et al., 2022; Versteeg & Malalasekera, 2007*). CFD solves mass, momentum, and energy equations to analyze transport phenomena and factors influencing efficiency.

Recent studies use 3D models with software like ANSYS Fluent, COMSOL, or OpenFOAM to evaluate geometry and operating effects. Numerical models incorporate milk's thermophysical properties and apply turbulence models like RNG k–ε and SST k–ω, which best fit chevron plate flows (*Aboul Khail & Erişen, 2022*).

Velocity distribution governs heat transfer and pressure loss, with pressure dropping from inlet to outlet based on flow rate and plate design. Raising flow rate increases turbulence and heat transfer but also pressure loss and energy use, requiring optimal flow regimes. Adjusting chevron angle, plate spacing, and corrugation depth enhances thermal efficiency without increasing size. Accurate CFD uses temperature-dependent milk properties validated by experiments and mesh analysis.

Advances in modeling improve flow and heat transfer understanding, enabling geometry optimization, energy savings, and fouling control—crucial for dairy heat exchangers (*Ferziger et al., 2020; Indumathy et al., 2022*). Uniform fluid distribution and sealing ensure safe, efficient operation (*Bansal & Chen, 2006; Sharma & Macchietto, 2021*). Milk's viscosity, density, and conductivity vary with temperature and fat, affecting heat exchange.

Fouling deposits reduce heat transfer and increase pressure loss and energy use (*Indumathy et al., 2022; Aboul Khail & Erişen, 2022*). Precise thermophysical data reflecting milk's complex colloidal makeup is vital to avoid CFD errors (*Walstra et al., 2006; Incropera et al., 2017*).

**Table 1**

**Principal equations and dimensionless numbers used in flow and heat transfer analysis**

| Mathematical Model/ Dimensionless Number | Equation | Parameters | SI Unit |
|---|---|---|---|
| **Continuity Equation** | $\Delta \cdot u = 0$ | $u, v, w$ **- velocity components** | $u, v, w: m \cdot s^{-1}$ |
| **Navier-Stokes Equations** | $\rho(\frac{\partial u}{\partial t} + u \cdot \nabla u) = -\Delta_p + \mu\nabla^2 u + \rho g$ | $\rho, p, \mu, u$ | $\rho: kg \cdot m^{-3}$ $\rho: Pa$ $\mu: Pa \cdot s$ $u: m \cdot s^{-1}$ |
| **Energy Equation** | $\rho c_p \left(\frac{\partial T}{\partial t} + u \cdot \nabla T\right) = k\nabla^2 T + \varphi$ | **T,** $c_p, k$ | **T: K** $c_p: J \cdot kg^{-1} \cdot K^{-1}$ $k: W \cdot m^{-1} \cdot K^{-1}$ |
| **Reynolds Number (Re)** | $Re = \frac{\rho u D_h}{\mu}$ | $D_h, \mu, \rho, u$ | **Dimensionless** |
| **Nusselt Number (Nu)** | $Nu = \frac{h D_h}{k}$ | $D_h, h, k$ | **Dimensionless** |
| **Prandtl Number (Pr)** | $Pr = \frac{\mu c_p}{k}$ | $\mu, c_p, k$ | **Dimensionless** |
| **Peclet Number (Pe)** | $Pe = Re \cdot Pr = \frac{u D_h}{\alpha}$ | $u, D_h, \alpha$ | **Dimensionless** |

Heat exchanger design must consider heat transfer, hydrodynamics, fouling prevention, and cleaning (*Bergman et al., 2020; Tetra Pak, 2024; Wang et al., 2021,2024*). Fouling decreases heat transfer, raises pressure losses, and complicates temperature control. HTST systems operate near 72 °C, typically with regeneration and pasteurization sections.

Process control uses empirical, nonlinear, neural network, and deep learning models for fault detection and fouling assessment. Combining dynamic modeling, CFD, and AI improves HTST pasteurization monitoring (*Fox et al., 2015*). Models based on fluid mechanics (continuity, Navier–Stokes, energy equations) yield velocity, pressure, and temperature fields (*Ferziger et al., 2020*).

Both steady-state and dynamic models analyze flow and heat transfer, with fouling impact being a major challenge. 1D models simplify geometry but may err for low aspect ratio plates; 2D models improve accuracy but omit factors like calcium and deposit re-entrainment (*Indumathy et al., 2022*).

Due to flow complexity, 3D CFD models provide realistic simulations of fouling but need extensive validation. Models range from single-phase to complex four-phase, describing protein denaturation and aggregation (*Indumathy et al., 2022; Singh & Heldman, 2014)*. Fouling models include Cleaning-in-Place cycles to reduce deposits and optimize cleaning, though reliable deposit mass prediction remains challenging.

Dimensional analysis aids in parameter reduction and fouling process optimization (*Indumathy et al., 2022*). Analytical solutions are difficult due to complex geometry; CFD uses finite volume methods with accurate boundary conditions reflecting milk's temperature-dependent properties (*Incropera et al., 2017*). Dimensionless numbers guide heat transfer estimations (*Kakaç et al., 2012*).

Advances in turbulence models and fouling simulations enable optimized designs. Mathematical modeling improves dairy heat exchanger efficiency and pasteurization, with minimal impact on most milk components except some vitamins (*Indumathy et al., 2022*).

Energy balance and integrated models simulate the pasteurization process, while Model Predictive Control maintains temperature accuracy (*Shah & Sekulić, 2003*).

**The future direction of research**

Future modelling research includes nonlinear optimization to find optimal inputs, development of linear parameter-varying (LPV) models for linearizing nonlinear HTST systems, and use of nonlinear identification methods like ARX and N4SID. Wavelet-fuzzy neural networks (FWNNs) and data-driven control

for SISO and MIMO systems are being explored. Modelling also focuses on integrating fouling dynamics into HTST system simulations for better control and accuracy.

Control research focuses on developing and applying Model Predictive Control (MPC) for pasteurization, using Economic MPC (EMPC) to optimize control accuracy and energy efficiency simultaneously. LPV control is applied to enhance system performance and robustness, while Genetic Algorithms (GA) help tune temperature controller parameters.

## CONCLUSION

Based on specialized literature, the main approaches used for the modelling, parametric identification, and control of HTST processes in the dairy industry have been presented. Researchers have shown that steady-state and dynamic models of plate heat exchangers, based on material and energy balances and fundamental operating principles, can describe the relationship between system inputs and outputs with relatively low complexity.

At the same time, these models can be integrated into control algorithms and used for performance analysis, system scale-up, and parametric sensitivity assessment. In addition, **"black-box" models** are used to describe nonlinear dynamics, as well as for process monitoring and control, although they do not provide information about the physical mechanisms governing system behavior.

An important aspect is the need to integrate the fouling phenomenon into the modelling of the pasteurization process, as deposit formation can alter the temperature profile and fluid flow, making process control more difficult. Models based on fundamental principles, together with model-based controllers, can ensure accurate tracking of reference values and effective disturbance rejection in HTST systems.

## REFERENCES


[1] Alfa Laval. (2024). *AlfaQ™ – Plate heat exchangers*. Alfa Laval;

[2] Aboul Khail, A., & Erişen, A. (2022). *A Review: CFD Approaches of Plate Heat Exchangers*. Archives of Computational Methods in Engineering, 29(6), 4197–4228. https://doi.org/10.1007/s11831-022-09839-z;

[3] Bansal, B., & Chen, X. D. (2006). *A critical review of milk fouling in heat exchangers*. Comprehensive Reviews in Food Science and Food Safety, 5(2), 27–33. https://doi.org/10.1111/j.1541-4337.2006.00004.x;

[4] Bylund, G. (1995). *Dairy Processing Handbook*. Tetra Pak Processing Systems, Lund, Sweden;

[5] Ferziger, J. H., Perić, M., & Street, R. L. (2020). *Computational Methods for Fluid Dynamics* (4th ed.). Springer;

[6] Fox, P. F., Uniacke-Lowe, T., McSweeney, P. L. H., & O'Mahony, J. A. (2015). *Dairy Chemistry and Biochemistry* (2nd ed.). Springer;

[7] Incropera, F. P., DeWitt, D. P., Bergman, T. L., & Lavine, A. S. (2017). *Fundamentals of Heat and Mass Transfer* (8th ed.). John Wiley & Sons;

[8] Indumathy, M., Sobana, S., Panda, B., & Panda, R. C. (2022). *Modelling and control of plate heat exchanger with continuous high-temperature short time milk pasteurization process – A review*. Chemical Engineering Journal Advances, 11, 100305. https://doi.org/10.1016/j.ceja.2022.100305;

[9] Kakaç, S., Liu, H., & Pramuanjaroenkij, A. (2012). *Heat Exchangers: Selection, Rating, and Thermal Design* (3rd ed.). CRC Press;

[10] Muley, A., & Manglik, R. M. (1999). *Experimental Study of Turbulent Flow Heat Transfer and Pressure Drop in a Plate Heat Exchanger With Chevron Plates*. Journal of Heat Transfer, 121(1), 110–117. https://doi.org/10.1115/1.2825923;

[11] Richalet, J., Darure, T., & Mallet, J. (2014). *Predictive Functional Control of counter current heat exchangers*. IFAC Proceedings Volumes, 47(3), 5345–5350. https://doi.org/10.3182/20140824-6-ZA-1003.02828;

[12] Shah, R. K., & Sekulić, D. P. (2003). *Fundamentals of Heat Exchanger Design*. John Wiley & Sons;

[13] Sharma, A., & Macchietto, S. (2021). *Fouling and cleaning of plate heat exchangers: Dairy application*. Food and Bioproducts Processing, 126, 32–41. https://doi.org/10.1016/j.fbp.2020.12.005;

[14] Singh, R. P., & Heldman, D. R. (2014). *Introduction to Food Engineering* (5th ed.). Academic Press;

[15] Tetra Pak. (2024). *Dairy Processing Handbook*. Tetra Pak Processing Systems;

[16] Versteeg, H. K., & Malalasekera, W. (2007). *An Introduction to Computational Fluid Dynamics: The Finite Volume Method* (2nd ed.). Pearson Education;

[17] Walstra, P., Wouters, J. T. M., & Geurts, T. J. (2006). *Dairy Science and Technology* (2nd ed.). CRC Press;
[18] Wang, H., Huang, F., Fazli, M., Kuang, S., & Yu, A. (2024). *CFD-DEM investigation of centrifugal slurry pump with polydisperse particle feeds*. Powder Technology, 447, 120204. https://doi.org/10.1016/j.powtec.2024.120204;
[19] Wang, L., Sundén, B., & Manglik, R. M. (2021). *Plate Heat Exchangers: Design, Applications and Performance*. WIT Press.

# REDUCING MECHANICAL DISTURBANCE AS A SOIL REGENERATION STRATEGY: IMPLICATIONS OF MINIMUM TILLAGE, NO-TILL, AND COMPACTION MANAGEMENT

/

# *REDUCEREA PERTURBĂRII MECANICE CA STRATEGIE DE REGENERARE A SOLULUI: IMPLICAȚII ALE MINIMUM TILLAGE, NO-TILL ȘI MANAGEMENTULUI COMPACTĂRII*

**Cristian RADU[1)], Gheorghe MATEI[1)], Sorin BORUZ*[1)], Stefan DUMITRU*[2, 3)], Valentin Nicolae VLADUȚ[3)], Lorena-Diana POPA[4)], Dragos ANGHELACHE[3)], Mihai NICOLESCU[5)], Oane-Elena MILEA[2)], Nicoleta UNGUREANU[2)]**

[1)] University of Craiova, Dolj County / Romania;
[2)] UNSTP Bucharest / Romania;
[3)] INMA Bucharest / Romania;
[4)] ARDS Secuieni, Neamt County / Romania,
[5)] ASAS Bucharest / Romania
**E-mail: stefan.dumitru2311@gmail.com, boruz.sorin@gmail.com*

***Keywords:*** *regenerative agriculture, conservation tillage, minimum tillage, strip-till, no-till, soil compaction, soil health*

**ABSTRACT**

*This review critically synthesizes current knowledge on soil tillage as a control point for soil regeneration, with emphasis on minimum tillage, strip-till, no-till and soil compaction management. Evidence from foundational studies, recent reviews and meta-analyses was compared to distinguish robust outcomes from context-dependent responses. Reduced disturbance generally lowers fuel use and erosion risk and can improve aggregate stability, residue protection and water infiltration, but the magnitude and direction of effects on bulk density, soil organic carbon, greenhouse-gas emissions and crop yield depend strongly on texture, climate, residue management, rotation, duration and traffic. Recent syntheses show that no-till is not universally superior to reduced or strip tillage: yield responses range from neutral to modestly negative or positive, while strip-till may narrow yield penalties where cold or dense seedbeds constrain direct seeding. Soil compaction remains a cross-cutting risk because heavy traffic can offset benefits of reduced tillage. Controlled traffic, moisture-aware field operations, optimized tyre pressure, targeted deep loosening and biologically driven pore formation are therefore integral to regenerative tillage strategies. Major knowledge gaps concern subsoil responses, long-term carbon accounting, N2O trade-offs, region-specific thresholds and sensor-based site-specific tillage. The review concludes that regenerative soil management should prioritize minimum necessary disturbance rather than adherence to a single tillage label.*

**REZUMAT**

*Articolul prezintă critic cunoștințele actuale privind lucrările solului ca factor major al regenerării, cu accent pe minimum tillage, strip-till, no-till și managementul compactării. Au fost comparate rezultate din lucrări fundamentale, articole de sinteză și meta-analize recente pentru delimitarea efectelor robuste de răspunsurile dependente de context. Reducerea perturbării mecanice diminuează, în general, consumul de combustibil și riscul de eroziune și poate îmbunătăți stabilitatea agregatelor, protecția prin resturi vegetale și infiltrarea apei, însă efectele asupra densității aparente, carbonului organic, emisiilor de gaze cu efect de seră și producției depind de textură, climă, managementul resturilor, rotație, durata aplicării și trafic. Sintezele recente arată că no-till nu este universal superior lucrărilor reduse sau strip-till. Compactarea rămâne un risc transversal, deoarece traficul greu poate anula beneficiile lucrărilor reduse. Traficul controlat, alegerea momentului în funcție de umiditate, presiunea corectă în pneuri, afânarea adâncă țintită și formarea biologică a porilor sunt componente esențiale ale strategiei regenerative. Sunt evidențiate lacune privind răspunsul subsolului, bilanțul carbonului, emisiile de N2O, pragurile regionale și lucrările diferențiate bazate pe senzori.*

## INTRODUCTION

Soil tillage remains one of the most consequential management decisions in arable systems because it simultaneously changes soil architecture, residue placement, aeration, water movement, root penetration, weed dynamics, fuel demand and the exposure of organic matter to decomposition. The historical dominance of mouldboard ploughing reflected its capacity to create a predictable seedbed and to control residues and weeds, but long-term intensive disturbance can accelerate aggregate turnover, organic-matter loss and erosion while increasing dependence on repeated traffic and energy *inputs (Six et al., 2000; Montgomery, 2007; Or et al., 2021).* Regenerative agriculture therefore treats tillage not as a fixed annual operation but as a disturbance to be justified against the ecological functions that must be preserved or restored.

The transition from conventional tillage to minimum tillage, strip-till or no-till is often presented as a simple continuum of declining mechanical disturbance. In practice, however, the agronomic consequences are determined by interactions among tillage intensity, permanent soil cover, crop diversification, traffic, soil moisture at operation, nutrient placement and local pedoclimatic constraints.

Reicosky (2015) emphasized that conservation tillage is not synonymous with conservation agriculture because reduced soil disturbance alone does not reproduce the system-level benefits expected when residue cover and crop diversification are absent. This distinction is particularly important in regenerative agriculture, where the objective is not the elimination of a specific implement but the recovery of soil functions such as aggregation, infiltration, rooting depth, biological activity and resilience to climatic stress.

Evidence accumulated during the last decade has also made clear that tillage responses are highly context dependent. The global meta-analysis of Pittelkow et al. (2015) showed that yield penalties under no-till varied with climate, crop and the simultaneous use of residue retention and rotation.

More recent syntheses continue to report substantial heterogeneity. Sun et al. (2024), using 5,191 comparisons from 551 studies, found a small average yield reduction under conservation tillage but no significant yield difference where the three core conservation-agriculture principles were implemented together.

Dou et al. (2024) found that strip-till maintained yields comparable with conventional tillage and exceeded no-till yields by 4.81% across the studies included in their meta-analysis. At the same time, recent European evidence indicates modest cereal-yield and yield-stability penalties under conservation agriculture, with minimum tillage reducing part of the gap relative to no-till *(Ceriani et al., 2026).*

Soil compaction complicates these comparisons. Reduced tillage decreases the number of traffic events, yet the absence of annual full-width loosening means that wheel-load management becomes more important.

Traffic-induced compaction increases mechanical resistance, decreases air and water transport and can reduce grain yield substantially *(Obour and Ugarte, 2021).* Conversely, deep loosening can temporarily improve root access but may have short-lived benefits if the causal traffic regime remains unchanged. The emerging regenerative perspective is therefore based on prevention first, targeted mechanical remediation when diagnosis confirms a limiting layer, and biological maintenance through roots, residues and pore-forming fauna.

The objective of this review is to critically assess the current evidence on minimum tillage, strip-till, no-till and compaction prevention as components of regenerative soil management.

The review focuses on: (i) physical and hydrological mechanisms; (ii) carbon and biological responses; (iii) yield, energy and greenhouse-gas trade-offs; (iv) machinery traffic and compaction prevention; (v) biological and site-specific strategies for structural recovery; and (vi) unresolved questions that require additional research before generalized recommendations can be made.

## REVIEW SCOPE AND METHODOLOGY

The paper was developed as a structured critical narrative review rather than as a formal PRISMA systematic review. The starting evidence base consisted of the technical literature underlying the original chapter on reduced tillage, direct seeding and compaction prevention, supplemented by a targeted update of peer-reviewed literature available through major publisher and scholarly indexing pages.

Priority was given to review articles, meta-analyses and long-term field syntheses because these sources provide stronger evidence for generalization across soils and climates than individual short-term experiments.

The core search concepts were combinations of the terms no-tillage, reduced tillage, minimum tillage, strip tillage, conservation agriculture, regenerative agriculture, soil compaction, controlled traffic, axle load, tyre pressure, soil organic carbon, aggregate stability, infiltration, cover crops, biopores, yield, greenhouse gases and meta-analysis.

Recent publications from 2015-2026 were prioritized, while older landmark studies were retained where they remain foundational for the interpretation of aggregate dynamics, compaction mechanisms or conservation-agriculture principles. Evidence was included when it reported soil physical, chemical, biological, agronomic, energetic or environmental responses directly relevant to tillage-system selection or compaction management.

Because tillage terminology is inconsistent across studies, the synthesis distinguishes between conventional inversion tillage, reduced/minimum full-width tillage, strip-till and no-till/direct seeding. Results reported as 'conservation tillage' were interpreted cautiously because that category may contain several practices with different disturbance intensities.

Numerical outcomes from meta-analyses are cited as evidence of average responses, not as universal expectations. Particular attention was given to moderators such as soil texture, precipitation, climate, study duration, residue retention, crop rotation and nitrogen management, since these factors frequently explain apparent contradictions among studies.

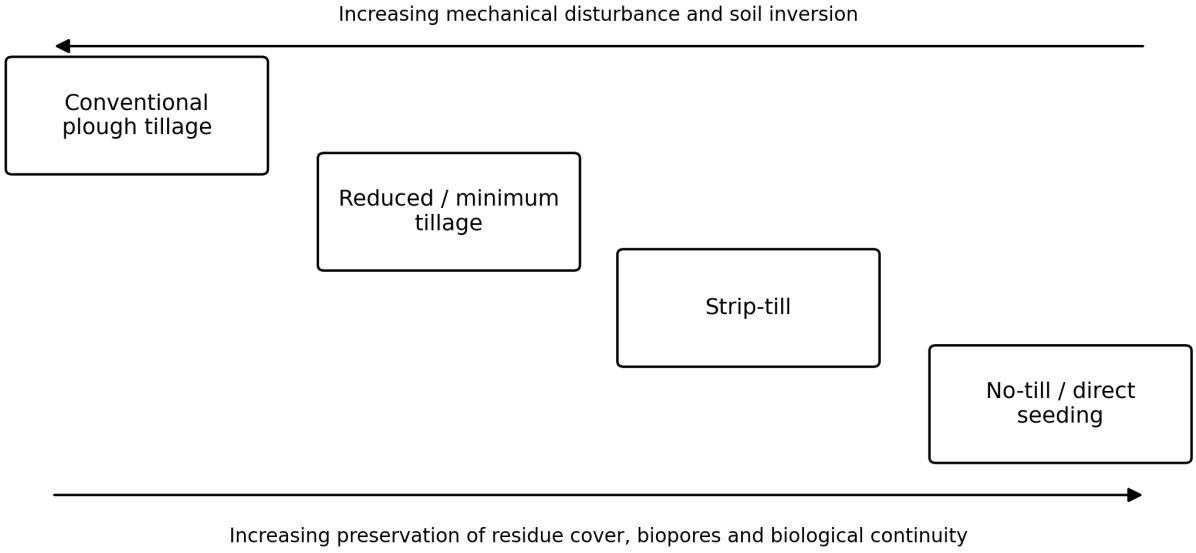



**Fig. 1 - Conceptual continuum from intensive inversion tillage to direct seeding in regenerative soil management**

## CONCEPTUAL DISTINCTIONS: DISTURBANCE INTENSITY IS NOT A SYSTEM BY ITSELF

The most important conceptual distinction is between a tillage operation and a farming system. Minimum tillage describes a reduction in the intensity, frequency or depth of soil disturbance relative to conventional practice. No-till describes crop establishment without prior full-width seedbed preparation, with disturbance largely confined to the seeding slot. Strip-till disturbs only narrow crop-row zones while leaving inter-row soil comparatively intact.

Conservation agriculture, by contrast, is a systems concept based on minimal disturbance, continuous organic cover and crop diversification *(Kassam et al., 2009; Reicosky, 2015)*. Regenerative agriculture is broader still and evaluates whether management actually restores soil functions over time.

This distinction explains why apparently similar 'reduced tillage' experiments can produce different outcomes. A shallow disc system that repeatedly pulverizes the same 10-15 cm layer may reduce fuel use compared with ploughing but still leave little surface residue, create a compacted layer beneath the worked zone and expose aggregates to rapid breakdown. A chisel-based system operating only when soil moisture is suitable may preserve substantially more residue and vertical pore continuity. Likewise, no-till with residue

removal and a narrow rotation can differ profoundly from no-till combined with high residue return, cover crops and diversified rotations.

Soil moisture at the time of traffic or tillage is a further source of variability. Mechanical resistance to penetration and draft changes strongly with water content and bulk density; dry soil often demands greater force, whereas wet cohesive soil is more susceptible to plastic deformation, smearing and compaction *(Cardei et al., 2019; Pang et al., 2023).*

Consequently, 'less tillage' cannot be evaluated without considering when the operation is performed and what mechanical state the soil is in. Regenerative management therefore replaces calendar-based tillage with condition-based tillage.

**Table 1**

| System | Typical disturbed area | Residue continuity | Main regenerative opportunity | Main risk / limitation |
|---|---|---|---|---|
| Conventional inversion tillage | Full width; commonly 20-30 cm or more | Low after tillage unless residue is rapidly restored | Rapid seedbed creation; mechanical weed and residue incorporation | Aggregate disruption, erosion exposure, repeated traffic, energy use |
| Minimum / reduced tillage | Full width, but fewer passes and/or shallower or non-inversion action | Moderate and implement-dependent | Lower fuel use; more residue retention; partial preservation of vertical continuity | Repeated shallow working may form dense layers; benefits depend on implement and timing |
| Strip-till | Narrow crop-row bands; inter-row undisturbed | High between rows | Warmer, loosened seed zone combined with protected inter-row soil | Specialized equipment and guidance; risk of repeated band compaction if poorly managed |
| No-till / direct seeding | Seeding slot only | High to very high | Maximum preservation of surface cover, biopores and biological continuity | Cold/wet seedbeds, weed shifts, nutrient stratification, traffic compaction if unmanaged |

## MINIMUM AND REDUCED TILLAGE: OPPORTUNITIES AND LIMITATIONS

Minimum tillage is often the most practicable first step away from intensive inversion tillage because it preserves operational flexibility while reducing disturbance and the number of passes. Chisel ploughs, paraplows, cultivators and vertical-tillage implements can loosen soil without complete inversion, thereby retaining more surface residue and reducing direct exposure to erosive forces.

The principal regenerative advantage is not merely the absence of the mouldboard plough but the possibility of maintaining a larger fraction of macroaggregates, root channels and residue cover while reducing energy requirements.

The physical response is nevertheless sensitive to implement design, depth and moisture. Deep chisel operations performed in sufficiently dry soil can create fissures and improve infiltration in dense layers, but the same implement used in wet clayey soil may smear the walls of the loosened zone and create only temporary apparent porosity.

Excessive depth also increases draft and fuel demand without necessarily improving crop performance. This is consistent with the broader mechanistic literature showing that tillage draft depends on soil strength, geometry, depth and operating conditions *(Cardei et al., 2019).* From a regenerative perspective, the appropriate depth is therefore the shallowest or most targeted depth that removes the diagnosed limitation.

Repeated disc tillage illustrates why a change of implement is not equivalent to a change of system. Although shallow discing can reduce the energy demand of primary tillage, repeated full-width operation may reduce residue cover and generate a dense zone immediately below working depth.

Such systems may perform adequately as transitional practices but can stall soil regeneration if the management objective remains repeated pulverization of the seedbed. Reicosky (2015) therefore argued that residue cover and biological continuity are essential dimensions that cannot be inferred from the term 'conservation tillage' alone.

Recent meta-analytical evidence supports a context-dependent interpretation. Sun et al. (2024) reported an average yield decrease of approximately 1.35% for conservation tillage relative to conventional tillage across a very large global database, but the difference became non-significant when no-till, straw mulching and crop rotation were implemented together.

This suggests that a reduced-tillage operation used in isolation is an incomplete proxy for the regenerative system. Similarly, the 2025 mega-analysis of 30 prior meta-analyses found no overall yield effect for no-tillage or reduced tillage, but strong variation with experimental setting, soil properties, residue management, irrigation and nitrogen rate *(Kasrija et al., 2025).*

The economic case for reduced tillage is usually stronger and less controversial than the yield case. Fewer high-draft operations reduce fuel, labour and machinery hours. However, net profitability also depends on machinery ownership structure, transition costs, weed-control strategy and whether reduced tillage enables timely sowing over a larger area.

The practical regenerative advantage is thus often a combination of lower operational cost and lower erosion risk rather than an immediate increase in yield.

## STRIP-TILL AS A FUNCTIONAL INTERMEDIATE

Strip-till is particularly relevant where full no-till creates seed-zone constraints but full-width tillage would sacrifice too much residue protection. By loosening only a narrow band, the system creates a warmer and often drier seedbed while preserving residue cover and pore continuity between rows. It can also support localized nutrient placement, which is advantageous where phosphorus or potassium stratification or early-season nutrient demand limits direct-seeded crops.

The 2024 meta-analysis by Dou et al. synthesized 53 articles and 290 paired comparisons and found that strip-till produced yields similar to conventional tillage and 4.81% higher than no-till on average. The effect was moderated by cropping system and mean annual temperature *(Dou et al., 2024).*

These results indicate that the agronomic value of strip-till is strongest where some mechanical improvement of the seed row is beneficial, rather than as a universal replacement for either no-till or conventional tillage.

A critical issue is spatial consistency. Repeatedly disturbing exactly the same band can create a highly differentiated soil profile, while traffic outside planned lanes can compact the inter-row zone. High-accuracy GNSS therefore adds value by aligning seed rows and tillage bands, but controlled traffic and crop-row repositioning strategies may be needed depending on system design. Strip-till should thus be regarded as a spatially selective tillage system whose success depends on precision of placement and traffic, not merely on reduced disturbed area.

## NO-TILL: SOIL PHYSICAL AND HYDROLOGICAL RESPONSES

No-till is the most restrictive form of mechanical disturbance considered in this review. By retaining the soil in a more continuous state between crops, the system preserves root channels, earthworm galleries and surface residue, but also removes the annual mechanical reset provided by seedbed cultivation. Consequently, its performance depends strongly on the initial condition of the soil and on the capacity of biological processes to maintain pore function.

Blanco-Canqui and Ruis (2018), in a review of approximately 200 studies, concluded that no-till generally improves wet aggregate stability, reduces soil compactibility and increases infiltration and plant-available water in many situations, but responses in bulk density, thermal properties and hydraulic behavior vary with soil type, climate and duration.

This helps explain a frequent apparent contradiction: the surface layer of no-till soil may be firmer or have higher bulk density than freshly tilled soil while still possessing more continuous macropores and greater structural stability. Bulk density alone is therefore an insufficient indicator of regenerative progress.

Hydrological benefits are closely tied to residue cover. Surface residues dissipate raindrop energy, reduce sealing and evaporation and slow overland flow. Continuous macropores then provide preferential infiltration pathways. These processes are particularly valuable in dryland systems where rainfall arrives in short, intense events.

Recent dryland evidence reinforces this interaction. Hashimi et al. (2026) found that no-till combined with straw retention increased surface SOC and wheat yield in their global dryland meta-analysis, while

climate and soil texture strongly moderated greenhouse-gas responses. Qin et al. (2024) likewise found that straw mulching could outperform no-till alone for yield and water-use efficiency in the Loess Plateau, illustrating that soil cover can be as important as disturbance reduction.

The main hydrological limitation occurs in poorly drained or already compacted soils. Direct seeding does not mechanically remove a pre-existing dense layer, and wet heavy-textured soils may warm and dry more slowly under residue. Under these conditions, strip-till or targeted loosening may provide a better transition pathway than immediate strict no-till.

The key principle is that no-till is most effective when it protects a functioning structure; it is less effective when expected to repair severe physical degradation without complementary measures.

## NO-TILL, SOIL ORGANIC CARBON AND BIOLOGICAL FUNCTION

Reduced disturbance can slow aggregate turnover and increase the physical protection of particulate organic matter within microaggregates, a mechanism described by Six et al. (2000). No-till also changes the vertical distribution of carbon by concentrating fresh residue inputs near the surface. For this reason, higher SOC concentrations in the upper centimetres are a common finding, whereas whole-profile sequestration is more variable.

Recent meta-analyses strengthen the need for depth-aware interpretation. Colunga et al. (2025) reported a mean SOC increase of 12.74% under conservation tillage in sandy soils of arid and semi-arid regions, with the strongest increase in the 0-20 cm layer and no significant gain at greater depths. He et al. (2023) found that no-till and residue retention increased SOC and influenced carbon mineralization, but responses varied with pH, depth, duration and nitrogen management.

Meng et al. (2024) likewise found that tillage effects on SOC and greenhouse-gas flux were modulated by soil and management conditions. Thus, a surface increase in SOC should not automatically be interpreted as equivalent whole-profile carbon sequestration.

Biological activity is similarly responsive to the interaction between disturbance and substrate supply. Li et al. (2020) reported increased bacterial diversity under no-till, with stubble retention and soil type acting as important moderators, while fungal diversity showed no significant overall response.

Li et al. (2024) found significant increases in several groups of extracellular enzyme activities under no-till, with crop diversity affecting the magnitude of the response. These findings support a systems interpretation: reduced disturbance creates a more stable habitat, but biological benefits depend on residue quality, crop diversity, nutrient inputs and climate.

The regenerative implication is that no-till should be paired with high biological carbon input. A low-biomass system with residue removal may preserve aggregates but provide insufficient substrate for long-term improvement. In contrast, crop rotations and cover crops maintain living roots for longer periods and supply chemically diverse inputs that support rhizosphere processes. The objective is therefore not simply to stop tillage but to replace mechanical disturbance with biological structuring.

## YIELD, YIELD STABILITY AND GREENHOUSE-GAS TRADE-OFFS

Yield remains the most important barrier to overgeneralization. The landmark global synthesis of Pittelkow et al. (2015) showed that no-till can reduce yields under some conditions, but penalties were much smaller when residue retention and crop rotation were combined with no-till and under dry climates where water conservation becomes a dominant benefit. The central lesson was not that no-till is yield-reducing, but that the response is conditional and management combinations matter.

The evidence has become more nuanced as larger syntheses have appeared. Sun et al. (2024) found a small overall yield penalty for conservation tillage but no significant penalty when the three conservation-agriculture principles were applied together.

Dou et al. (2024) showed that strip-till can outperform no-till in average yield while matching conventional tillage. Kasrija et al. (2025), synthesizing 30 meta-analyses, found no overall effect of no-till or reduced tillage on crop yield but identified strong variation by soil, residue, irrigation and nitrogen management. These results collectively argue against ranking tillage systems independently of site and complementary practices.

European evidence is especially relevant for temperate and continental production systems. Ceriani et al. (2026) reported an average cereal yield reduction of about 3% under conservation agriculture and a

9% decline in yield stability relative to conventional agriculture across the studies included in their analysis. Minimum tillage narrowed the yield gap compared with no-till, and clay content influenced both yield and N2O responses.

These findings are important because they challenge the assumption that reduced disturbance automatically increases resilience in every European environment. They instead support region-specific combinations and careful transition management.

Greenhouse-gas outcomes are equally complex. Reduced fuel use consistently lowers direct fossil-fuel emissions from field operations, but soil N2O can increase, decrease or remain unchanged depending on aeration, moisture, nitrogen rate and residue decomposition.

Kasrija et al. (2025) found a 10.5% increase in N2O under no-till across their second-order synthesis, whereas Meng et al. (2024) reported conditions under which reduced and no-tillage could suppress N2O. Hashimi et al. (2026) showed that dryland no-till effects depended strongly on texture, climate and residue retention. This inconsistency indicates that climate claims for no-till must include the entire greenhouse-gas balance and not rely solely on fuel savings or surface SOC.

The emerging consensus is therefore one of trade-offs. No single tillage system simultaneously maximizes yield, carbon storage, N2O mitigation, infiltration and operational simplicity in all contexts. Regenerative management is best interpreted as optimization across multiple functions, with the acceptable balance determined by local constraints and long-term system goals.

**Table 2**

| Synthesis | Evidence base | Key finding relevant to regenerative tillage | Critical interpretation |
|---|---|---|---|
| Pittelkow et al., 2015 | 5,463 paired observations / 610 studies | No-till yield response strongly depends on climate, crop and use of residue retention and rotation | System context matters more than the tillage label alone |
| Dou et al., 2024 | 53 studies / 290 paired comparisons | Strip-till yielded similarly to conventional tillage and 4.81% above no-till | Partial row-zone disturbance can reduce seedbed-related yield penalties |
| Sun et al., 2024 | 551 studies / 5,191 comparisons | Small mean conservation-tillage yield penalty; non-significant when three CA principles were combined | Integrated CA reduces risk of interpreting isolated no-till effects |
| Meng et al., 2024 | Meta-analysis of conservation tillage, SOC and GHG flux | SOC and N2O responses vary with soil and management; straw return is important | Climate benefits are conditional and should include residue and N management |
| Colunga et al., 2025 | 55 publications / 349 pairs in sandy arid-semiarid soils | SOC increased mainly in 0-20 cm under conservation tillage | Depth matters; surface enrichment is not whole-profile sequestration |
| Yan and Arthur, 2025 | 225 studies | Cover crops reduced bulk density and penetration resistance and increased aggregate stability and infiltration | Biological structuring is a major complement to reduced tillage |
| Kasrija et al., 2025 | 30 meta-analyses | No overall yield effect; no-till increased N2O on average; responses were context dependent | Second-order evidence confirms major trade-offs and moderator effects |
| Ceriani et al., 2026 | European meta-analysis | CA reduced cereal yield by ~3% and yield stability by ~9%; minimum tillage narrowed the gap | European adoption requires crop-, soil- and region-specific adaptation |
| Hashimi et al., 2026 | 87 peer-reviewed dryland studies | No-till with straw retention increased SOC and wheat yield; GHG effects depended on texture and management | Dryland benefits are strongest when water, residue and N management are integrated |

## SOIL COMPACTION AS A CROSS-CUTTING CONSTRAINT

Soil compaction is not simply the opposite of tillage. It is a structural degradation process in which pores are compressed and rearranged under mechanical stress, increasing resistance to penetration and

decreasing hydraulic and gaseous transport. Tillage can temporarily loosen compacted soil, but repeated traffic can recreate the problem rapidly. Conversely, no-till can preserve a stable pore network but cannot prevent compaction if high axle loads repeatedly cross wet soil.

Obour and Ugarte (2021) quantified the impact of traffic-induced compaction across 51 studies. Compaction strongly increased penetration resistance, decreased air permeability and saturated hydraulic conductivity down into the subsoil, and reduced grain yield of maize, wheat, barley and soybean by approximately 6-34% depending on crop and conditions.

Their analysis also suggested that hydraulic indicators may respond more sensitively than bulk density alone. This has an important diagnostic implication: a soil can suffer major pore-function losses before changes in bulk density appear dramatic.

Machinery weight is central to subsoil risk. Keller et al. (2019) demonstrated that historical increases in agricultural machinery mass have increased soil stress and the likelihood of adverse effects on soil functioning. Surface compaction is strongly affected by contact pressure, while deeper stress is increasingly controlled by total wheel or axle load. Larger tyres and tracks can reduce near-surface pressure, but they do not fully compensate for very high axle loads in wet soil.

Soil moisture determines vulnerability. When soil is near saturation, water occupies pore space and the soil skeleton has less capacity to support load without plastic deformation. Tillage or traffic under such conditions can smear pore walls and create persistent dense zones. In dry soil, penetration resistance and draft force may become very high, increasing energy requirements and tool wear. This dual response means that the mechanically safest operating window is neither extremely wet nor excessively dry, and reinforces the value of moisture-aware field scheduling *(Cardei et al., 2019; Pang et al., 2023).*

## COMPACTION PREVENTION: CONTROLLED TRAFFIC, TYRE MANAGEMENT AND TIMING

Prevention is usually more reliable than repeated remediation. Controlled Traffic Farming (CTF) concentrates wheel traffic on permanent lanes, protecting the majority of the cropped area from recurrent loading.

Yang et al. (2022), in a meta-analysis of compaction prevention, amelioration and alleviation measures, found a large positive mean crop-yield effect for controlled traffic and concluded that no single measure is sufficient across all situations. The significance of CTF is particularly high in no-till systems because the absence of annual loosening places greater value on preventing deformation in the first place.

Tyre inflation pressure should be adapted to the load and field operation. Lower field pressures within manufacturer limits increase the contact area and reduce topsoil stress. Dual wheels, wide low-pressure tyres and tracks can provide similar benefits.

These measures primarily protect the upper soil, while avoiding excessive axle load remains essential for subsoil protection. Regenerative machinery management therefore requires matching tractor and implement size to actual work requirements rather than maximizing power and ballast by default.

Traffic timing is equally important. Harvest operations often create the most severe loads because combines and grain transport equipment operate at high mass and may be forced into fields during wet periods. A tillage strategy cannot regenerate soil if the structural gains are repeatedly lost at harvest. Field logistics - including controlled unloading points, reduced in-field trailer traffic, temporary traffic lanes and delayed operations where feasible - should therefore be treated as soil-health practices rather than merely operational choices.

Precision guidance technologies are an enabling tool rather than a regenerative outcome by themselves. High-accuracy GNSS allows repeated traffic lanes, strip-till band alignment and targeted remediation. When combined with mapped penetration resistance, yield data, electrical conductivity and topography, guidance systems support a transition from uniform tillage to zone-specific intervention.

## TARGETED DEEP LOOSENING AND ITS LIMITS

Deep loosening or subsoiling remains justified where a compacted layer is clearly diagnosed and restricts root penetration or water movement. However, the regenerative criterion is corrective necessity rather than routine repetition. Working substantially deeper than the limiting layer increases energy demand and may disturb structurally functional subsoil. Working when soil is too wet can produce a narrow smeared slot rather than the intended network of fractures.

Evidence also shows that deep loosening effects can be temporary. Yang et al. (2022) found positive average yield responses to subsoiling and deep ploughing in compacted conditions, but their synthesis emphasized the value of a toolbox rather than a universal remedy. The durability of loosening depends on subsequent traffic, soil texture, biological activity and whether roots can occupy and stabilize the newly created fissures. Mechanical remediation without traffic reform often creates a cycle of compaction and repeated energy-intensive loosening.

The preferred sequence is therefore: diagnose the depth and spatial extent of the limiting layer; correct drainage problems if they are the underlying cause; loosen only where necessary and under moisture conditions that promote brittle fracture; immediately prevent re-compaction through traffic management; and introduce rooting systems that exploit and stabilize the loosened profile. This approach converts subsoiling from an annual operation into a targeted transition tool.

## BIOLOGICAL STRUCTURING: COVER CROPS, ROOTS AND BIOPORES

The long-term alternative to repeated mechanical loosening is biological structuring. Roots exert pressure, release exudates that support aggregation and leave pores after decomposition. Earthworms and other fauna further enlarge and connect pore networks. Cover crops extend the period during which living roots occupy the soil and can therefore complement reduced tillage by supplying both structural and carbon inputs.

A major 2025 global meta-analysis by Yan and Arthur, based on 225 studies, found that cover crops reduced bulk density by 3.2% and penetration resistance by 11.8%, while increasing water-stable aggregates by 15.9%, total porosity by 6.1% and infiltration by 37.2% on average.

The effects were moderated by climate, texture, cover-crop type and management. These results provide quantitative support for a key regenerative principle: the best replacement for mechanical soil loosening is not simply 'no operation', but active biological occupation of the profile.

The effectiveness of deep biopores is nevertheless conditional. Behrend et al. (2025) synthesized multiple long-term field experiments and found that tap-rooted precrops could improve subsoil root growth of subsequent spring crops, but yield benefits were most evident in dry years and long-term effects attributable to biopores were limited.

This result is important because it prevents overstatement of 'bio-drilling'. Roots can exploit and maintain pathways, but they do not always remove severe mechanical constraints quickly enough to replace corrective loosening.

The strongest strategy is therefore sequential: mechanical correction only where a severe barrier exists, followed by root systems that maintain the recovered pore space.

Mixtures combining fibrous-rooted grasses with tap-rooted broadleaves and legumes can provide complementary architectures and carbon qualities, but species selection must reflect water availability and crop sequence. In dry regions, an excessively competitive cover crop can deplete stored water and offset structural benefits.

**Table 3**

| Management option | Primary mechanism | Best use | Main limitation / evidence gap |
|---|---|---|---|
| Avoid wet-soil traffic | Limits plastic deformation and pore collapse | All systems; especially harvest and spring operations | Workable windows may be narrow; moisture thresholds are site-specific |
| Controlled Traffic Farming | Concentrates wheel loads on permanent lanes | No-till, strip-till and mechanized farms | Requires compatible widths, guidance and logistics |
| Low-pressure / wide tyres or tracks | Reduces topsoil contact stress | Routine field traffic | Does not remove deep stress from high axle loads |
| Targeted subsoiling | Fractures diagnosed compact layers | Severe compaction restricting roots or drainage | Benefits may be transient without traffic reform; energy intensive |
| Cover crops / deep-rooted precrops | Creates biopores and stabilizes aggregates | Maintenance and gradual structural recovery | Response varies with species, climate and soil; severe compaction may persist |
| Zone-specific tillage | Matches disturbance to measured limitation | Fields with mapped mechanical variability | Requires sensing, calibration and economic validation |

## PRECISION AND SITE-SPECIFIC TILLAGE FOR REGENERATIVE MANAGEMENT

One of the most promising research directions is the integration of regenerative principles with precision agriculture. Conventional tillage treats a field as mechanically uniform, yet compacted layers, texture, moisture and yield potential can vary sharply within a single field. If only a small fraction of the field is mechanically limiting, full-width deep tillage wastes energy and disrupts areas that do not require intervention.

Penetration-resistance sensing, apparent electrical conductivity, proximal soil sensors, yield maps and high-resolution elevation data can be combined to define management zones. The challenge is not data acquisition alone but the translation of sensor signals into biologically meaningful thresholds. Penetration resistance, for example, depends on moisture and bulk density; therefore, a single map produced under one moisture condition may misclassify compaction severity. Moisture-corrected or repeated measurements are needed before variable-depth tillage prescriptions can be considered robust.

Recent soil-tool interaction research provides an important parallel for precision tillage: mechanical requirements for penetration change systematically with soil moisture, density and resistance, so a fixed mechanical setting cannot be optimal across heterogeneous field conditions *(Cardei et al., 2019; Pang et al., 2023)*.

The same principle supports adaptive tillage. Future implements could adjust working depth, allowable draft load or disturbance intensity in response to measured resistance and moisture rather than follow a fixed depth. Such tools would operationalize the regenerative principle of minimum necessary disturbance at sub-field scale.

Economic validation is essential. Precision tillage adds sensors, control hardware and data-management costs. Its value will depend on how frequently mechanical limitations occur, the area avoided from unnecessary tillage, fuel prices and the longevity of corrected structure. Long-term field experiments comparing uniform deep tillage, sensor-guided variable-depth tillage and biologically maintained no-till are currently insufficient.

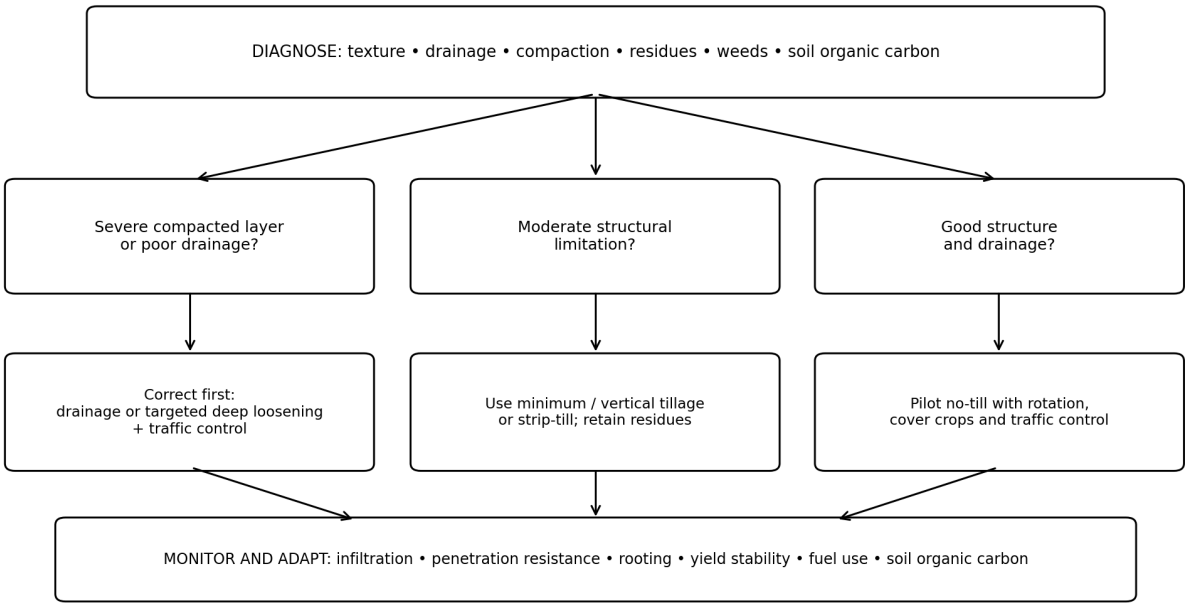



**Fig. 2 - Decision framework for selecting soil disturbance intensity within a regenerative management strategy**

## CRITICAL SYNTHESIS: WHAT THE EVIDENCE SUPPORTS

Several conclusions are sufficiently consistent across the literature to be treated as robust.

First, reducing disturbance and maintaining surface residues reduce the direct exposure of soil to erosion and lower field-operation energy demand.

Second, no-till and reduced tillage often improve aggregate stability and surface biological activity, but the response of bulk density and hydraulic properties is not uniform.

Third, crop yield is not determined by tillage intensity alone; climate, texture, residue management, rotation and transition quality are decisive moderators.

Fourth, compaction prevention through traffic management remains necessary in every system, including no-till.

Other commonly repeated claims are only partly supported. No-till does not universally increase whole-profile SOC. Surface stratification is common, and the depth distribution must be measured before carbon-sequestration claims are made *(Colunga et al., 2025).* No-till does not universally increase yield or yield stability; recent global and European meta-analyses show small average penalties or neutral effects, with substantial heterogeneity *(Sun et al., 2024; Kasrija et al., 2025; Ceriani et al., 2026).* Likewise, greenhouse-gas mitigation cannot be inferred from fewer tractor passes alone because soil N2O may respond in the opposite direction under wet, fine-textured or high-N conditions.

Strip-till deserves greater attention as a transitional and long-term system because it can preserve much of the inter-row soil while solving seed-zone limitations. Its average yield advantage over no-till in the analysis of Dou et al. (2024) indicates that selective disturbance may be a more rational endpoint than complete non-disturbance in some soils. The regenerative objective is therefore not ideological consistency but functional performance.

The strongest evidence also supports combining physical and biological approaches. Cover crops can improve porosity, aggregation and infiltration, but deep biopores do not always generate yield benefits and cannot be assumed to correct severe compaction rapidly *(Yan and Arthur, 2025; Behrend et al., 2025).*

Mechanical loosening remains useful when a real barrier exists, but its benefits must be preserved through controlled traffic and living roots. Regeneration is thus best viewed as a transition from repeated mechanical creation of porosity toward biological maintenance of porosity after initial constraints are corrected.

## KNOWLEDGE GAPS AND PRIORITIES FOR FUTURE RESEARCH

Despite extensive research, several uncertainties still limit evidence-based prescriptions. The first is the lack of standardized definitions. 'Minimum tillage', 'reduced tillage', 'conservation tillage' and even 'no-till' are applied to practices with different residue cover, disturbance width and auxiliary operations. Future experiments should quantify disturbed area, working depth, residue cover and traffic intensity rather than relying only on categorical labels.

Second, subsoil responses remain less studied than topsoil responses. Many carbon, microbial and physical assessments concentrate on 0-20 or 0-30 cm, yet compaction and root-access constraints often occur below these depths. Whole-profile SOC stocks, air permeability, saturated hydraulic conductivity and root architecture should be monitored together. The finding that conservation-tillage SOC gains may be concentrated near the surface *(Colunga et al., 2025)* makes depth-resolved sampling a priority.

Third, long-term greenhouse-gas accounting remains uncertain. Recent second-order syntheses report different N2O responses under no-till *(Meng et al., 2024; Kasrija et al., 2025),* and European evidence suggests interactions with clay content and crop type *(Ceriani et al., 2026*). Future work should measure CO2, N2O, CH4, fuel emissions and changes in SOC within the same experiments to avoid partial climate balances.

Fourth, the interaction between traffic and tillage needs better experimental separation. Many tillage comparisons change both soil disturbance and machinery passes, making it difficult to attribute effects. Factorial long-term designs that independently vary tillage intensity, axle load, tyre pressure and controlled traffic are needed to identify which component is responsible for structural change.

Fifth, biological alleviation requires more mechanistic and long-term evaluation. The 2025 cover-crop meta-analysis demonstrates substantial average improvements in physical properties, but species-specific rooting traits, water use, residue chemistry and persistence of biopores are still insufficiently connected to crop response. The conditional benefits observed by Behrend et al. (2025) show that 'bio-drilling' must be quantified rather than assumed.

Sixth, site-specific tillage is technically promising but lacks validated thresholds. Penetration resistance changes with moisture; bulk density is texture-dependent; yield maps integrate multiple stresses. Sensor-fusion approaches should therefore combine moisture, resistance, conductivity, topography and root observations. Machine-control algorithms then need agronomic thresholds that indicate when tillage is unnecessary, when shallow loosening is sufficient and when a deeper intervention is justified.

Finally, more evidence is needed from Eastern and South-Eastern Europe, including continental dryland environments and Chernozem-dominated systems. Regional calibration is essential because recent

syntheses repeatedly show that the direction of tillage response changes with precipitation, clay content, temperature, pH and management history. The scientific priority is no longer to ask whether no-till is 'better' than ploughing in general, but to predict which combination of disturbance, cover, rotation and traffic will optimize soil function at a specific site.

## CONCLUSIONS

The evidence reviewed here supports a shift from routine soil cultivation toward management based on minimum necessary disturbance. Minimum tillage can reduce energy demand and protect a larger fraction of the soil structure while maintaining operational flexibility. Strip-till offers an effective compromise where a prepared seed zone is needed but full-width disturbance is undesirable. No-till maximizes continuity of residue cover and biological pore networks, yet its success depends on the initial physical condition of the soil, diversified rotations, residue management and traffic control.

No system is universally optimal. Yield, carbon storage, greenhouse-gas emissions and water regulation respond differently across climates, textures and management histories.

Recent global and European syntheses show that the largest benefits occur when reduced disturbance is integrated with residue retention, crop diversification and careful nutrient and water management, whereas isolated adoption can generate trade-offs.

Compaction prevention is a central requirement of regenerative tillage. Controlled traffic, appropriate axle loads and tyre pressures, avoidance of wet-soil traffic and good harvest logistics should precede repeated mechanical remediation. Where a severe compacted layer is confirmed, targeted deep loosening can be justified, but its function should be transitional and followed by biological stabilization through living roots and residue inputs.

The most promising future direction is the integration of soil-health monitoring with precision control of disturbance. Regenerative tillage should evolve from uniform field-wide operations to site-specific interventions in which the soil is disturbed only where a measured limitation requires correction.

In this framework, the goal is not to defend a tillage label, but to maximize the long-term physical, biological and productive functions of the soil with the least necessary mechanical disruption.

## REFERENCES

[1] Behrend D., Athmann M., Han E., Küpper P.M., Perkons U., Bauke S.L., Köpke U., Kautz T., Gaiser T., Seidel S.J., (2025), Do biopores created by perennial fodder crops improve the growth of subsequent annual crops? A synthesis of multiple field experiments, Field Crops Research, vol.322, 109687, https://doi.org/10.1016/j.fcr.2024.109687.

[2] Blanco-Canqui H., Ruis S.J., (2018), No-tillage and soil physical environment, Geoderma, vol.326, pp.164-200, https://doi.org/10.1016/j.geoderma.2018.03.011.

[3] Cardei P., Muraru S.L., Sfîru R., Muraru V., (2019), General structure of tillage draft force. Consequences in experimental and applicative researches, INMATEH - Agricultural Engineering, vol.59, no.3, pp.253-262, https://doi.org/10.35633/inmateh-59-28.

[4] Ceriani R., Fohrafellner J., Maenhout P., Jarosch K.A., Weiss L., Di Bene C., Baratella V., Carboni G., Mereu V., Stefanova M., Fava F., Valkama E., (2026), Cereal yield, yield stability, and nitrous oxide release in European conservation agriculture: A meta-analysis, Field Crops Research, vol.341, 110386, https://doi.org/10.1016/j.fcr.2026.110386.

[5] Colunga S.L., Wahab L., Fierro Cabo A., Pereira E., (2025), Carbon sequestration through conservation tillage in sandy soils of arid and semi-arid climates: A meta-analysis, Soil and Tillage Research, vol.245, 106310, https://doi.org/10.1016/j.still.2024.106310.

[6] Dou S., Wang Z., Tong J., Shang Z., Deng A., Song Z., Zhang W., (2024), Strip tillage promotes crop yield in comparison with no tillage based on a meta-analysis, Soil and Tillage Research, vol.240, 106085, https://doi.org/10.1016/j.still.2024.106085.

[7] Fan X., Kong H., Zhao Y., Hu H., Jiang Z., Wang X., (2026), Global synthesis of agricultural practices on crop yield, soil organic carbon and greenhouse gas emissions, Journal of Cleaner Production, vol.540, 147529, https://doi.org/10.1016/j.jclepro.2026.147529.

[8] Hamza M.A., Anderson W.K., (2005), Soil compaction in cropping systems: A review of the nature, causes and possible solutions, Soil and Tillage Research, vol.82, no.2, pp.121-145, https://doi.org/10.1016/j.still.2004.08.009.

[9] Hashimi R., Ganjegunte G.K., Kumar S., Palmate S.S., Suthar J.D., (2026), Effects of no-tillage, mulching, drip irrigation, and nitrogen fertilization on greenhouse gas emissions, soil carbon sequestration, and crop yields in dryland agroecosystems: A meta-analysis, Agriculture, Ecosystems & Environment, vol.400, 110242, https://doi.org/10.1016/j.agee.2026.110242.
[10] He C., Chen Z., Qiu K.-Y., Chen J.-S., Bohoussou Y.N., Dang Y.P., Zhang H.-L., (2023), Effects of conservation agriculture on carbon mineralization: A global meta-analysis, Soil and Tillage Research, vol.229, 105685, https://doi.org/10.1016/j.still.2023.105685.
[11] Hobbs P.R., Sayre K., Gupta R., (2008), The role of conservation agriculture in sustainable agriculture, Philosophical Transactions of the Royal Society B: Biological Sciences, vol.363, pp.543-555, https://doi.org/10.1098/rstb.2007.2169.
[12] Kasrija L., Hui D., Ray A., Ren W., Wang L., Fay P.A., Smith D.R., Li J., Illukpitiya P., Tian H., (2025), Mega-analysis of no-tillage and reduced tillage impacts on crop yields and greenhouse gas emissions, Field Crops Research, vol.334, 110167, https://doi.org/10.1016/j.fcr.2025.110167.
[13] Kassam A., Friedrich T., Shaxson F., Pretty J., (2009), The spread of Conservation Agriculture: justification, sustainability and uptake, International Journal of Agricultural Sustainability, vol.7, no.4, pp.292-320, https://doi.org/10.3763/ijas.2009.0477.
[14] Keller T., Sandin M., Colombi T., Horn R., Or D., (2019), Historical increase in agricultural machinery weights enhanced soil stress levels and adversely affected soil functioning, Soil and Tillage Research, vol.194, 104293, https://doi.org/10.1016/j.still.2019.104293.
[15] Lal R., (2015), Restoring soil quality to mitigate soil degradation, Sustainability, vol.7, pp.5875-5895, https://doi.org/10.3390/su7055875.
[16] Li T., Li G., Lu Z., Zhao D., Li Y., Wang Z., Wen X., Liao Y., (2024), Crop diversification increases soil extracellular enzyme activities under no tillage: A global meta-analysis, Soil and Tillage Research, vol.235, 105870, https://doi.org/10.1016/j.still.2023.105870.
[17] Li Y., Song D., Liang S., Dang P., Qin X., Liao Y., Siddique K.H.M., (2020), Effect of no-tillage on soil bacterial and fungal community diversity: A meta-analysis, Soil and Tillage Research, vol.204, 104721, https://doi.org/10.1016/j.still.2020.104721.
[18] Meng X., Meng F., Chen P., Hou D., Zheng E., Xu T., (2024), A meta-analysis of conservation tillage management effects on soil organic carbon sequestration and soil greenhouse gas flux, Science of the Total Environment, vol.954, 176315, https://doi.org/10.1016/j.scitotenv.2024.176315.
[19] Montgomery D.R., (2007), Soil erosion and agricultural sustainability, Proceedings of the National Academy of Sciences, vol.104, pp.13268-13272, https://doi.org/10.1073/pnas.0611508104.
[20] Obour P.B., Ugarte C.M., (2021), A meta-analysis of the impact of traffic-induced compaction on soil physical properties and grain yield, Soil and Tillage Research, vol.211, 105019, https://doi.org/10.1016/j.still.2021.105019.
[21] Or D., Keller T., Schlesinger W.H., (2021), Natural and managed soil structure: On the fragile scaffolding for soil functioning, Soil and Tillage Research, vol.208, 104912, https://doi.org/10.1016/j.still.2020.104912.
[22] Pang J., Lin X., Zhang X., Ji J., Geng L., (2023), Modelling and analysis of penetration resistance of probes in cultivated soils, PLOS ONE, vol.18, no.1, e0280525, https://doi.org/10.1371/journal.pone.0280525.
[23] Pittelkow C.M., Liang X., Linquist B.A., van Groenigen K.J., Lee J., Lundy M.E., van Gestel N., Six J., Venterea R.T., van Kessel C., (2015), Productivity limits and potentials of the principles of conservation agriculture, Nature, vol.517, pp.365-368, https://doi.org/10.1038/nature13809.
[24] Qin W., Niu L., You Y., Cui S., Chen C., Li Z., (2024), Effects of conservation tillage and straw mulching on crop yield, water use efficiency, carbon sequestration and economic benefits in the Loess Plateau region of China: A meta-analysis, Soil and Tillage Research, vol.238, 106025, https://doi.org/10.1016/j.still.2024.106025.
[25] Reicosky D.C., (2015), Conservation tillage is not conservation agriculture, Journal of Soil and Water Conservation, vol.70, no.5, pp.103A-108A, https://doi.org/10.2489/jswc.70.5.103A.
[26] Sadiq F.K., Anyebe O., Tanko F., Abdulkadir A., Manono B.O., Matsika T.A., Abubakar F., Bello S.K., (2025), Conservation Agriculture for Sustainable Soil Health Management: A Review of Impacts, Benefits and Future Directions, Soil Systems, vol.9, no.3, 103, https://doi.org/10.3390/soilsystems9030103.

[27] Six J., Elliott E.T., Paustian K., (2000), Soil macroaggregate turnover and microaggregate formation: a mechanism for C sequestration under no-tillage agriculture, Soil Biology and Biochemistry, vol.32, no.14, pp.2099-2103, https://doi.org/10.1016/S0038-0717(00)00179-6.

[28] Sun J., Niu W., Du Y., Ma L., Huang S., Mu F., Zhang Q., Li G., Zhu J., Siddique K.H.M., (2024), Regionally adapted conservation tillage reduces the risk of crop yield losses: A global meta-analysis, Soil and Tillage Research, vol.244, 106265, https://doi.org/10.1016/j.still.2024.106265.

[29] Tebrügge F., Düring R.A., (1999), Reducing tillage intensity - a review of results from a long-term study in Germany, Soil and Tillage Research, vol.53, pp.15-28.

[30] Yang P., Dong W., Heinen M., Qin W., Oenema O., (2022), Soil Compaction Prevention, Amelioration and Alleviation Measures Are Effective in Mechanized and Smallholder Agriculture: A Meta-Analysis, Land, vol.11, 645, https://doi.org/10.3390/land11050645.

[31] Yan F., Arthur E., (2025), Cover crops alter soil physicochemical properties: A global meta-analysis, Geoderma, vol.460, 117436, https://doi.org/10.1016/j.geoderma.2025.117436.

# SPATIAL ANALYSIS OF FLOOD RISK USING GIS TECHNIQUES
# /
# *ANALIZA SPAȚIALĂ A RISCULUI DE INUNDAȚII UTILIZÂND TEHNICI GIS*

**Bianca-Ștefania ZĂBAVĂ[1)], Daria-Ioana SICARU*[1)], Gheorghe VOICU[1)], Mirela-Nicoleta DINCĂ[1)], Mariana IONESCU[1)], Georgiana MOICEANU[1)], Gigel PARASCHIV[1)]**
[1)] National University of Science and Technology Politehnica Bucharest / Romania.
**Tel: +40 770 783 029; *E-mail: dariaioana8@yahoo.com*

***Keywords:*** *environment, flood, GIS Techniques, spatial analysis*

**ABSTRACT**
*Flooding is a major natural hazard affecting urban environments, and the rapid pace of urbanization exacerbates the vulnerability of cities to such events. Like other densely developed areas, the Municipality of Bucharest—characterized by high land-use intensity and significant territorial transformations—requires an integrated analysis of the factors that contribute to flooding. This study aims to assess flood risk in Bucharest using GIS techniques. It integrates data on topography, the hydrographic network, and urban land use to identify high-risk zones. Geographic Information Systems (GIS) are employed to correlate and spatially represent these factors, providing a comprehensive overview of risk distribution across the municipality. The research findings can serve as a basis for identifying vulnerable areas and developing effective strategies for flood prevention and mitigation in the urban environment.*

**REZUMAT**
*Inundațiile constituie unul dintre riscurile naturale majore care afectează mediul urban, iar ritmul accelerat al urbanizării amplifică vulnerabilitatea orașelor în fața acestor fenomene. Asemenea altor zone intens dezvoltate, municipiul București — marcat de un grad ridicat de ocupare a terenului și de transformări teritoriale semnificative — necesită o analiză integrată a factorilor care favorizează producerea inundațiilor. Prezentul studiu urmărește evaluarea spațială a riscului de inundații în București, prin aplicarea tehnicilor GIS. Studiul vizează integrarea datelor privind relieful, rețeaua hidrografică și modul de utilizare a terenurilor urbane pentru a identifica zonele cu risc ridicat. Prin utilizarea Sistemelor Informaționale Geografice (GIS), se realizează o corelare și o reprezentare spațială a acestor factori, oferind o perspectivă de ansamblu asupra distribuției riscului la nivel municipal. Concluziile cercetării pot servi drept fundament pentru desemnarea ariilor vulnerabile și pentru elaborarea unor strategii eficiente de prevenire și atenuare a inundațiilor în mediul urban.*

## INTRODUCTION

Many nations face significant risks due to the increasing frequency and intensity of extreme weather events—such as typhoons, heatwaves, and floods—driven by global climate change. Both developing and developed countries face a serious threat from flooding *(Paprotny, D., Kreibich, H., Morales-Napoles, O. et al., 2020)*.

Flooding constitutes a particularly persistent and destructive global hydrometeorological hazard, causing significant loss of life, the degradation of critical infrastructure, and the destabilization of socio-economic systems. Driven by climate change, rapid urbanization, and improper land use, the frequency and intensity of these phenomena are steadily increasing. In areas characterized by poor infrastructure, inadequate urban planning, and uncontrolled development within floodplains, natural drainage capacity is diminished, turning episodes of heavy rainfall into events with severe consequences *(Arinabo, D., 2017).*

Flood risk is defined as the outcome of the interaction between hazard, exposure, and vulnerability, reflecting the likelihood of adverse effects on the built and natural environments. Accurate risk assessment requires reliable spatial and temporal data capable of capturing both current hydrological conditions and future scenarios.

Over the past two decades, Geographic Information Systems (GIS), remote sensing, and hydrological models have revolutionized flood risk analysis, enabling the efficient integration and processing of topographic, climatic, and urban data *(Arinabo, D., 2017).*

The expansion of urban areas and impervious surfaces reduces natural water infiltration and drainage capacity, thereby increasing the risk of flooding. Globally, the incidence and consequences of these phenomena have risen significantly, and the issue is becoming increasingly critical given projections that 68.4% of the world's population will be concentrated in urban areas by 2050 *(Bouchikhi, S., Chourak, M., Boushaba, F. et al., 2026).*

Numerous studies have shown that heavy rainfall in cities will intensify significantly in the future. Regarding water, global climate changes can lead to an increase in flood characteristics, such as peak flow, water volume, and duration. Climate change has resulted in an intensification of the intensity and frequency of extreme rainfall, a primary cause of frequent flooding *(Li, G., Liu, J., Shao, W., 2023; Xu, Z., Chen, H., Ren, M. et al., 2020).*

Rapid urban development, particularly in areas with inadequate infrastructure, increases vulnerability to flooding. Consequently, mapping flood susceptibility is crucial for identifying exposed areas, optimizing spatial planning, and implementing effective disaster risk reduction strategies *(Kaya, C. M., Derin, L., 2023).*

Flood susceptibility indicates the likelihood of a specific region being affected by floods, a factor influenced by various environmental, terrain, and climatic conditions. Creating maps for this purpose is an essential tool for identifying at-risk areas and for preventing and minimizing the impacts of flooding. Developing accurate maps requires combining topographic, hydrological, and meteorological information, as well as the appropriate selection of techniques, parameters, and data resolution *(Islam, T., Zeleke, E. B., Afroz, M. et al., 2025).*

Land-use changes and the expansion of areas that prevent water infiltration cause surface runoff to accelerate, thereby increasing flood risk ((2024) *(Dharmarathne, G., Waduge, A. O., Bogahawaththa, M. et al., 2024)*. This hazard is further exacerbated by climate change and the increasing frequency of extreme weather events *(Islam, M. B., Sultana, T., Rana, I. A. et al., 2024).*

In this context, identifying the most vulnerable areas and obtaining relevant flood data are crucial for developing prevention strategies and mitigating risks. Hydraulic modeling, statistical techniques, and machine learning are methods used to simulate, predict, and assess flood risk *(Kumar, V., Sharma, K. V., Caloiero, T. et al., 2023).*

Furthermore, remote sensing technologies and Geographic Information Systems (GIS) assist in monitoring and predicting floods, creating hazard and vulnerability maps, and supporting planning and intervention efforts *(Pakati, S. S., Shoko, C., Dube, T., 2025).*

In this context, GIS becomes an essential tool for analyzing flood susceptibility, offering the ability to visualize the potential extent of the phenomenon, integrate multiple factors, and support urban planning and risk management decisions.

This article analyzes the case of Bucharest, Romania's capital and the country's most representative example regarding the urban impact on river systems. The study integrates data on topography, the hydrographic network, and urban land use to identify high-risk areas.

Using Geographic Information Systems (GIS), these factors are correlated and spatially mapped, providing an overview of risk distribution at the municipal level. The results offer a better understanding of the effects of urbanization on watercourses and, more broadly, on the functioning of aquatic ecosystems influenced by human activity in the study area.

## MATERIALS AND METHODS

The Municipality of Bucharest is the capital of Romania and the country's most important political, economic, and cultural center. It is located in southeastern Romania, within the Romanian Plain—specifically, in the Vlăsia Plain, a subdivision thereof.

The municipality covers an area of approximately 240 km² and has a population exceeding 2.1 million inhabitants, according to data provided by the National Institute of Statistics for 2025. These characteristics highlight Bucharest's status as one of the largest urban agglomerations in Southeast Europe, featuring a high degree of urbanization *(Navarro, A., Baltariu, G.-C., Catalão, J., 2026)* .




**Fig. 1 - The location of Bucharest within Romania**
*(Meteoblue, n.d.)*

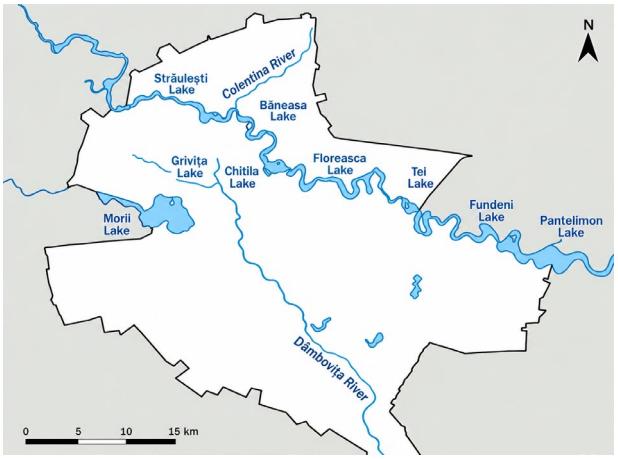



**Fig. 2 - The urban river network of Bucharest**
*(Meteoblue, n.d.)*

In the case of the municipality of Bucharest, the hydrographic network is structured around two main water courses: the Dâmbovița River and the Colentina River. They fulfill essential hydrological functions, being responsible for the drainage of meteoric waters and the transport of flows resulting from precipitation. Their positioning and orientation within the city determines the main runoff directions and influences the spatial distribution of areas susceptible to flooding *(Nkonu, R. S., Antwi, M., Amo-Boateng, M. et al., 2022).*

A spatial analysis of flood risk in the Municipality of Bucharest was conducted using QGIS software by integrating multiple spatial datasets. Three factors relevant to the occurrence and distribution of floods were considered: terrain slope, distance to watercourses, and land use/land cover (LULC).

The spatial information utilized in the evaluation comprised a Digital Elevation Model (DEM), datasets on land use and land cover, the waterway network, and the administrative limits of Bucharest Municipality. Each dataset was processed using QGIS and transformed to a unified coordinate reference system to maintain spatial compatibility. The DEM facilitated the extraction of terrain slope, whereas the waterway network helped in calculating the proximity to water bodies. Data regarding land use and land cover were employed to evaluate the impact of surface features and urban development on the likelihood of flooding.

## RESULTS

Analyzing flood risk in urban environments requires considering several determining factors that influence both the occurrence and the intensity of these phenomena. These factors include precipitation, surface runoff, terrain slope, the hydrographic network, urban drainage systems, and groundwater levels. In analyses conducted using GIS, these factors are modeled and integrated to identify vulnerable areas and assess flood risk.

Recent studies show a reduction in vegetated areas within the metropolitan zone due to rapid urbanization. This loss of vegetation, combined with an increase in impervious surfaces, leads to intensified surface runoff and an increased risk of flooding *(Revollo, N. V., Gil, V., Couto, F. T., 2025).*

The analysis of precipitation for the city of Bucharest was carried out based on the climate data provided by ERA5T, which provides information on average monthly and annual values. The average monthly amount varies between about 35–40 mm in the winter months and 70–80 mm in the spring and early summer months, when torrential rains occur frequently. In autumn, the values gradually decrease, and the total annual amount is about 550–600 mm.

Although precipitation is a significant factor in the occurrence of floods, it was not included in the spatial model developed for Bucharest. This is because spatial variations in precipitation across the city are minimal, and available data do not allow for the creation of a detailed climatic raster for reclassification purposes.

Regarding hydrography, information on Bucharest's rivers and lakes was required, as these directly influence flood risk. Data were extracted from OpenStreetMap (OSM) using the QuickOSM plugin for QGIS, which enables the rapid download of geographic features from a selected area. Hydrographic data are crucial for subsequently calculating distances to watercourses and identifying areas potentially more susceptible to water accumulation or overflow.

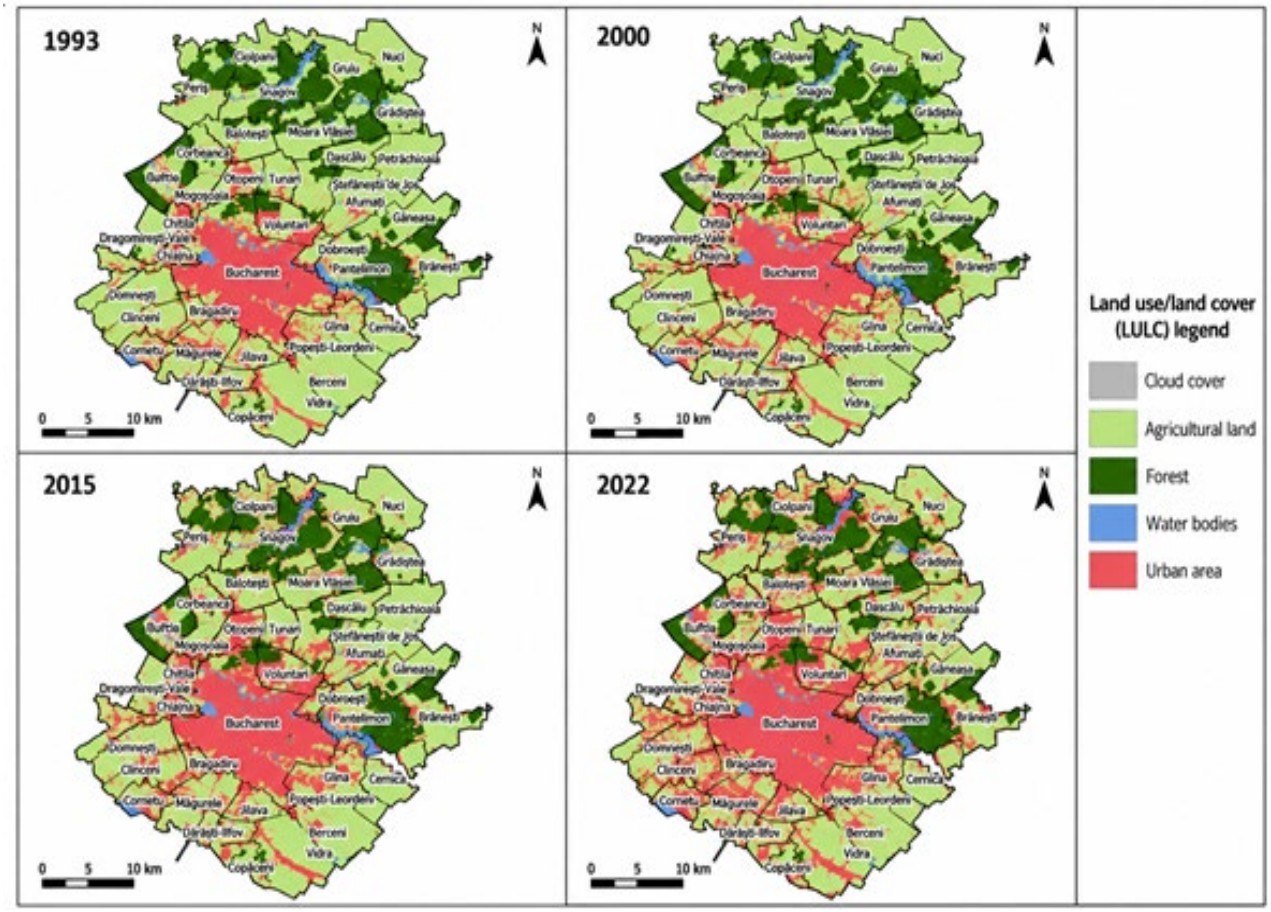



**Fig. 3 - Evolution of Land Use and Land Cover (LULC) in the Bucharest Metropolitan Area**

The land-use analysis for the Municipality of Bucharest was conducted using the CORINE Land Cover 2018 (CLC 2018) dataset, part of the Copernicus Land Monitoring Service program. This dataset is provided in vector format and features a standardized European land-use classification with a minimum mapping unit of 25 hectares. It provides essential information for assessing flood vulnerability based on surface types (built-up areas, green spaces, water bodies, infrastructure, etc.).

The spatial analysis aimed to integrate the three reclassified factors—slope, distance to watercourses, and land use (LULC)—into a final risk raster using a multi-criteria approach. The factors were combined with equal weights, as there are no published studies for the Municipality of Bucharest providing validated weights for them. The integration of the three factors was performed in QGIS using the Raster Calculator tool, based on the arithmetic mean of the reclassified rasters, according to the following formula:

$$FRI = \frac{S_r + D_r + LULC_r}{3} \quad (1)$$

where: FRI = Flood Risk Index, $S_r$ = Reclassified Slope, $D_r$ = Reclassified Distance to Watercourses, iar $LULC_r$ = Reclassified Land Use/Land Cover

The result is a raster with values ranging from 1 to 5, where 1 represents very low risk and 5 represents very high risk. The final raster was symbolized using a pseudocolor ramp with five equally distributed classes and an inverted ramp, so that high-risk areas are highlighted in red and low-risk areas in green.

The final flood risk map for the Municipality of Bucharest was generated by applying a spatial analysis method that combined the three selected factors. The spatial distribution of risk reveals a clear contrast between different areas of the city.

Risk levels are higher in the north and center of Bucharest, primarily due to high urban density and the presence of water bodies. Conversely, the western and southern peripheral areas exhibit low risk, as they feature steeper slopes, are located further from watercourses, and contain extensive vegetated areas. Situated between these two extremes are the medium-risk zones, which serve as transitions between dense

urban areas and natural landscapes, reflecting a moderate level of vulnerability resulting from the combination of the analyzed factors.

Although the proposed model provides an overview of the spatial distribution of potential flood risk in the Municipality of Bucharest, the results must be interpreted with certain methodological limitations in mind. The lack of data on the spatial variation of precipitation precluded the inclusion of the climatic factor, and in the absence of a locally calibrated AHP analysis, equal weights were assigned to the factors examined.

Furthermore, the availability of detailed historical flood data would allow for additional validation of the results, while the resolution of DEM and LULC data can influence the level of detail in the analysis, particularly in densely urbanized areas. Nevertheless, the applied methodology enables the coherent integration of the key spatial factors analyzed and provides a relevant basis for identifying areas potentially susceptible to flooding, as well as for the future development of more detailed analyses.

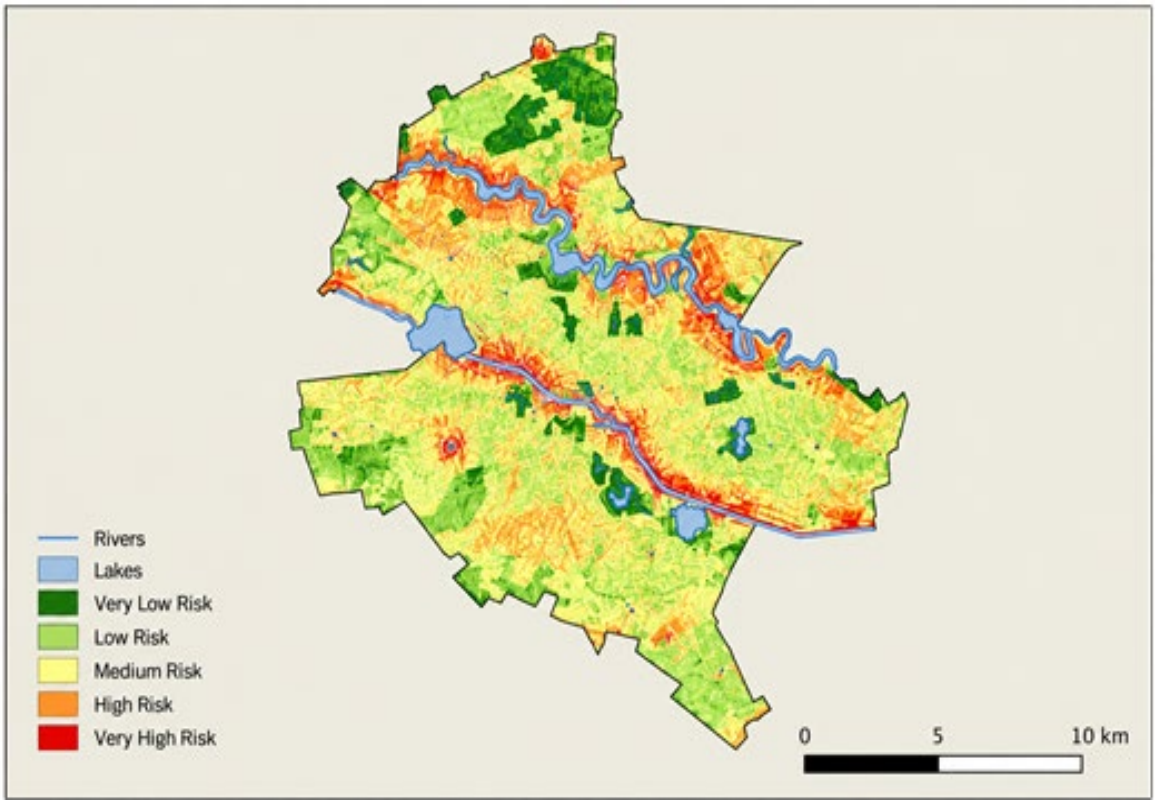



**Fig. 4 - Flood risk map for the Municipality of Bucharest**

## CONCLUSIONS

Spatial analysis conducted for the Municipality of Bucharest confirms that the risk of urban flooding can no longer be interpreted solely as a consequence of proximity to rivers, but rather as the result of an interplay between climatic hazards, inadequately adapted technical infrastructure, and the current model of urban development. Areas identified as high-risk coincide with densely built-up, low-permeability zones situated on low-lying terrain near major watercourses—specifically along the Dâmbovița River and in the vicinity of the lake system in the city's north.

Accelerated land impermeabilization emerges as the primary risk multiplier. The expansion of surfaces covered by asphalt, concrete, and built structures has reduced natural infiltration capacity and diverted increasingly large volumes of water directly into the sewerage network. Under these conditions, even moderate rainfall events can cause local system overloads, rapid water accumulation, and infrastructure blockages.

## REFERENCES

[1] Arinabo, D. (2017). The contribution of GIS in urban flood management.

[2] Bouchikhi, S., Chourak, M., Boushaba, F., & El Baida, M. (2026). Flood susceptibility mapping in urban areas based on analytical hierarchy process: A decade-long systematic literature review. *Journal of African Earth Sciences, 233*, 105903. https://doi.org/10.1016/j.jafrearsci.2025.105903

[3] Dharmarathne, G., Waduge, A. O., Bogahawaththa, M., Rathnayake, U., & Meddage, D. P. P. (2024). Adapting cities to the surge: A comprehensive review of climate-induced urban flooding. *Results in Engineering, 22,* 102123. https://doi.org/10.1016/j.rineng.2024.102123

[4] Islam, M. B., Sultana, T., Rana, I. A., Waseem, H. B., Murray-Tuite, P., Tingsanchali, T., & Mahfuz, M. (2024). Assessing the vulnerability of selected coastal informal settlements to floods in the Old Brahmaputra River floodplain, Bangladesh. *Urban Climate, 56*, 102078. https://doi.org/10.1016/j.uclim.2024.102078

[5] Islam, T., Zeleke, E. B., Afroz, M., & Melesse, A. M. (2025). A systematic review of urban flood susceptibility mapping: Remote sensing, machine learning, and other modeling approaches. *Remote Sensing, 17,* 524. https://doi.org/10.3390/rs17030524

[6] Kaya, C. M., & Derin, L. (2023). Parameters and methods used in flood susceptibility mapping: A review. *Journal of Water and Climate Change, 14*, 1935–1960. https://doi.org/10.2166/wcc.2023.035

[7] Kumar, V., Sharma, K. V., Caloiero, T., Mehta, D. J., & Singh, K. (2023). Comprehensive overview of flood modeling approaches: A review of recent advances. *Hydrology, 10,* 141. https://doi.org/10.3390/hydrology10070141

[8] Li, G., Liu, J., & Shao, W. (2023). Urban flood risk assessment under rapid urbanization in Zhengzhou City, China. *Regional Sustainability, 4*(3), 332–348. https://doi.org/10.1016/j.regsus.2023.08.004

[9] Navarro, A., Baltariu, G.-C., & Catalão, J. (2026). Three decades of land use and land cover changes in the Bucharest-Ilfov Development Region: From post-communist transition to EU accession. *Remote Sensing, 18*, 711. https://doi.org/10.3390/rs18050711

[10] Nkonu, R. S., Antwi, M., Amo-Boateng, M., et al. (2022). GIS-based multi-criteria analytical hierarchy process modelling for urban flood risk analysis and assessment, Accra Metropolis [Preprint]. *Research Square*. https://doi.org/10.21203/rs.3.rs-1712549/v1

[11] Pakati, S. S., Shoko, C., & Dube, T. (2025). Integrated flood modelling and risk assessment in urban areas: A review on applications, strengths, limitations and future research directions. *Journal of Hydrology: Regional Studies, 61,* 102583. https://doi.org/10.1016/j.ejrh.2025.102583

[12] Paprotny, D., Kreibich, H., Morales-Napoles, O., et al. (2020). Exposure and vulnerability estimation for modelling flood losses to commercial assets in Europe. *Science of the Total Environment, 737*, 140011. https://doi.org/10.1016/j.scitotenv.2020.140011

[13] Revollo, N. V., Gil, V., & Couto, F. T. (2025). Extreme precipitation and low-lying urban flooding in Bahía Blanca, Argentina. *Atmosphere, 16,* 511. https://doi.org/10.3390/atmos16050511

[14] Xu, Z., Chen, H., Ren, M., & Cheng, T. (2020). Progress on disaster mechanism and risk assessment of urban flood/waterlogging disasters in China. *Advances in Water Science*. https://doi.org/10.14042/j.cnki.32.1309.2020.05.008

[15] *** Meteoblue. (n.d.). Climate modelled data – Bucharest, Romania (ERA5T-based).

[16] https://www.meteoblue.com/ro/vreme/historyclimate/climatemodelled/bucure%C8%99ti_rom%C3%A2nia_683506

# INTEGRATED ASSESSMENT OF SOIL HEALTH AND REGENERATION: INDICATORS, DIGITAL TECHNOLOGIES AND ADAPTIVE MANAGEMENT

/

# *EVALUAREA INTEGRATĂ A SĂNĂTĂȚII ȘI REGENERĂRII SOLULUI: INDICATORI, TEHNOLOGII DIGITALE ȘI MANAGEMENT ADAPTIV*

**Cristian RADU[1)], Ștefan DUMITRU[*2, 3)], Nicolae-Valentin VLĂDUȚ[3)], Gabriel-Valentin GHEORGHE[3)], Alin HARABAGIU[3)], Sorin Dan IORDACHE[2)], Oana-Elena MILEA[2)], Sorin BORUZ[1)], Gheorghe MATEI[1)], Lorena-Diana POPA[4)], Mihai NICOLESCU[5)], Dragos-Nicolae ANGHELACHE[2,3)], Nicoleta UNGUREANU[2)]**

[1)] University of Craiova / Romania; [2)] UNSTPB Bucharest / Romania; [3)] INMA Bucharest / Romania; [4)] ASAS Bucharest / Romania

**E-mail: stefan.dumitru2311@gmail.com*

***Keywords:*** *soil health, soil regeneration, indicators, digital soil mapping, remote sensing, machine learning, adaptive management*

**ABSTRACT**

*Soil health is a functional property emerging from the interaction of physical, chemical and biological soil characteristics and from the capacity of soil to sustain ecosystem functions. This paper reviews current approaches to soil-health and regeneration assessment and develops an integrated methodological framework that combines field and laboratory indicators with digital soil mapping, remote and proximal sensing, geographic information systems and machine-learning methods. A set of 30 indicators is organized according to the main degradation processes considered in diagnosis: compaction, erosion, soil organic carbon depletion, nutrient imbalance, acidification, salinization, contamination and biodiversity loss. A conceptual Soil Health and Regeneration Index (SHRI/IRSS) is proposed to integrate normalized indicator scores while retaining the need for local calibration. Regeneration is treated as a measurable temporal trajectory rather than as a single favorable state. The proposed framework links measurement, diagnosis, intervention, monitoring and reassessment in an adaptive management cycle and provides a methodological basis for subsequent experimental calibration, spatial validation and long-term monitoring.*

**REZUMAT**

*Sănătatea solului reprezintă o proprietate funcțională rezultată din interacțiunea caracteristicilor fizice, chimice și biologice și din capacitatea solului de a susține funcțiile ecosistemice. Lucrarea analizează abordările actuale de evaluare a sănătății și regenerării solului și dezvoltă un cadru metodologic integrat care combină indicatorii determinați în teren și laborator cu cartarea digitală a solului, teledetecția, senzorii proximali, sistemele informaționale geografice și metodele de învățare automată. Un set de 30 de indicatori este organizat în raport cu principalele procese de degradare urmărite în diagnostic: compactare, eroziune, pierderea carbonului organic, dezechilibre nutritive, acidifiere, salinizare, contaminare și reducerea biodiversității. Este propus un Indice de Regenerare și Sănătate a Solului (IRSS/SHRI), destinat integrării scorurilor normalizate ale indicatorilor, cu menținerea necesității calibrării locale. Regenerarea este tratată ca o traiectorie temporală măsurabilă, nu ca o singură stare favorabilă. Cadrul conectează măsurarea, diagnosticul, intervenția, monitorizarea și reevaluarea într-un ciclu de management adaptiv și oferă baza metodologică pentru calibrare experimentală, validare spațială și monitorizare pe termen lung.*

## INTRODUCTION

Soil is the physical and biogeochemical foundation of agroecosystems, supporting biomass production, nutrient cycling, water infiltration and storage, carbon sequestration and biodiversity. Current soil-health concepts therefore extend beyond conventional fertility assessment and describe the continued capacity of soil as a living system to sustain multiple functions and ecosystem services (*Lehmann et al., 2020*). This broader perspective requires the simultaneous interpretation of structural, chemical and biological attributes rather than reliance on isolated analytical values.

A major difficulty is that soil properties are strongly context-dependent. Thresholds that are meaningful for one soil, climate or production system may be inappropriate for another because texture, parent material, topography, land use and management history modify both baseline values and functional

responses. Consequently, indicator interpretation should be linked to specific soil threats, functions and ecosystem services (*Bünemann et al., 2018; Rinot et al., 2019*).

Digital technologies have simultaneously expanded the spatial and temporal scale of soil observation. Digital soil mapping can transform point measurements into spatially continuous estimates, while topographic, climatic and spectral covariates, proximal sensing and machine-learning algorithms can support prediction in unsampled locations. These approaches increase information density, but they do not remove the need for field reference data, independent validation and pedological interpretation. Recent Soil Science-Informed Machine Learning approaches explicitly seek to combine predictive algorithms with process knowledge and observational constraints (*Minasny et al., 2024*).

The objective of this paper is to integrate these directions into a technical framework for assessing soil health and regeneration. Specifically, the study aims to: (i) organize an extended set of physical, chemical and biological indicators; (ii) connect indicators with degradation processes and candidate management interventions; (iii) formalize a conceptual Soil Health and Regeneration Index (SHRI/IRSS); and (iv) embed repeated assessment in an adaptive management cycle supported by spatial and temporal digital information.




**Fig. 1 - Conceptual cycle of integrated assessment and adaptive management. Original elaboration based on the synthesis framework and the principles discussed by Bünemann et al. (2018) and Rinot et al. (2019).**

## MATERIALS AND METHODS

The study was developed as a structured narrative synthesis combined with a methodological proposal. The analyzed literature covers soil quality and soil health concepts, indicator-based assessment, biological indicators, conservation and regenerative agriculture, digital soil mapping, remote and proximal sensing, and machine-learning applications. Priority was given to peer-reviewed studies and established methodological frameworks that provide explicit links among measurable soil properties, soil functions, degradation processes and management responses.

Indicators were selected according to seven operational criteria: functional relevance, sensitivity to management, availability of standardized or reproducible determination methods, repeatability, agronomic interpretability, analytical cost, and suitability for spatial and temporal monitoring. The resulting indicator architecture was subsequently grouped into physical, chemical and biological domains and linked to diagnostic questions, dominant threats and possible interventions. Because the present work is a methodological synthesis rather than a systematic review, the results are interpreted as a framework to be calibrated and validated

## RESULTS

The synthesis shows that individual measurements have limited diagnostic value when interpreted in isolation. High organic carbon does not exclude compaction, favorable pH does not demonstrate adequate biological activity, and sufficient nutrient reserves may coexist with restricted infiltration or poor aeration. A robust assessment therefore requires complementary indicators that describe soil structure and water relations, chemical status and biological functioning within the same diagnostic framework.

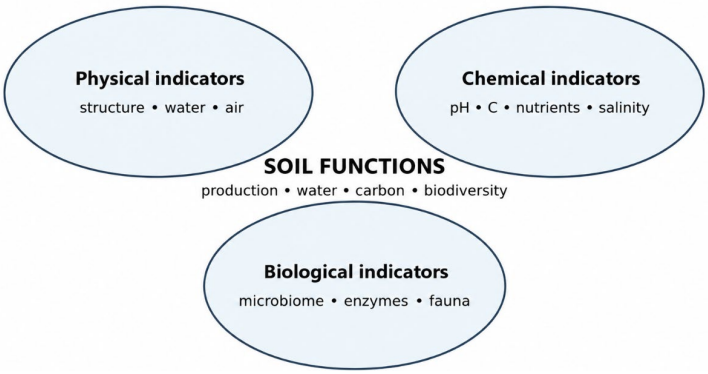



**Fig. 2 - The three complementary domains of soil health assessment. Original elaboration, conceptually** *adapted from Bünemann et al. (2018), Lehmann et al. (2020), and the (Moebius-Clune et al., 2016)*

**Table 1**

**Extended set of 30 indicators for integrated soil health assessment.**

| Domain | Indicator | Main method | Diagnostic relevance |
|---|---|---|---|
| Physical | Texture | hydrometer/pipette | hydraulic and mechanical behavior |
| Physical | Bulk density | core method | compaction |
| Physical | Total porosity | calculated from densities | pore space |
| Physical | Penetration resistance | penetrometry | root impedance |
| Physical | Aggregate stability | wet sieving | structural resistance |
| Physical | Infiltration | infiltrometry | water entry |
| Physical | Water-holding capacity | water-retention curve | plant-available water |
| Physical | Hydraulic conductivity | permeameter | water transport |
| Physical | Soil moisture | gravimetry/sensors | water regime |
| Physical | Effective depth | soil profile observations | rooting volume |
| Chemical | pH | potentiometry | soil reaction |
| Chemical | Organic carbon | dry combustion | organic matter and structure |
| Chemical | Organic matter | oxidation/calculation | fertility and aggregation |
| Chemical | Total nitrogen | Kjeldahl/combustion | N reserve |
| Chemical | Nitrate and ammonium | extraction + analysis | available N |
| Chemical | Available phosphorus | Olsen/Bray | available P |
| Chemical | Exchangeable potassium | extraction + AAS/ICP | available K |
| Chemical | CEC | standardized extraction | cation retention |
| Chemical | Base saturation | calculation | base status |
| Chemical | Electrical conductivity | conductometry | salinity |
| Chemical | Exchangeable Ca, Mg, Na | extracție + ICP/AAS | cation balance |
| Chemical | Potentially toxic metals | ICP/AAS | contamination |
| Biological | Soil respiration | incubation + $CO_2$ | biological activity |
| Biological | Microbial biomass | fumigation–extraction | community size |
| Biological | Dehydrogenase | enzyme assay | metabolic activity |
| Biological | β-glucosidase | enzyme assay | C cycling |
| Biological | Phosphatase | enzyme assay | P cycling |
| Biological | Earthworms | field counting | bioturbation and structure |
| Biological | Microbial diversity | DNA sequencing | taxonomic/functional diversity |
| Biological | Dissolved organic carbon | extraction + TOC | mobile C fraction |

Physical indicators describe pore architecture and the accessibility of water and air to roots *(Doran et al., 1996; Iheshiulo et al., 2023; Sheehy et al., 2015).* Bulk density and penetration resistance are useful for diagnosing compaction, while aggregate stability and infiltration characterize structural functioning. Chemical indicators capture soil reaction, nutrient reserves, salinity, and contamination. Organic carbon has a central role, but its interpretation must be contextualized according to texture, climate, and management history. Biological indicators can respond rapidly to management changes and complement physicochemical information. Earthworms, microbial biomass, respiration, and enzyme activities provide insight into biological processes that cannot be inferred solely from N, P, K, or pH.

- *From Indicators to Functions and Threats*

The relationships among indicators, soil threats and ecosystem functions are networked rather than one-to-one. Erosion, organic matter decline, contamination, compaction, biodiversity loss and salinization can simultaneously affect several soil functions, while a single indicator may respond to more than one degradation process *(Bünemann et al., 2018).* For this reason, the proposed architecture uses indicators as diagnostic evidence within a functional context rather than as independent pass/fail criteria.

For the present framework, the graphical synthesis was developed as original or conceptually adapted material so that the contribution of the proposed SHRI/IRSS architecture remains distinct from the source literature. This approach also facilitates direct linkage among indicators, degradation processes, spatial information and management decisions.

- *Digital Technologies and Spatio-Temporal Assessment*

A laboratory sample characterizes a limited soil volume, and uncritical extrapolation to an entire field may conceal within-field variability. The foundations of digital soil mapping and spatial validation are well established *(McBratney et al., 2003; Piikki & Wetterlind, 2021; Angon et al., 2023)*. Digital soil mapping uses relationships between observations and covariates to estimate the spatial distribution of properties. Covariates may include elevation, slope, aspect, climate, parent material, land use, vegetation indices, satellite imagery, and data from proximal sensors.

Recent digital soil mapping studies illustrate the value of combining environmental covariates with machine-learning algorithms for predicting soil properties, including total nitrogen *(Auzzas et al., 2024)*. At the same time, process-informed approaches emphasize that predictive accuracy alone is insufficient: model structure, calibration data, spatial dependence and the pedological plausibility of predictions must also be considered *(Minasny et al., 2024)*. Thus, digital models are most useful when they extend, rather than replace, direct soil measurements.

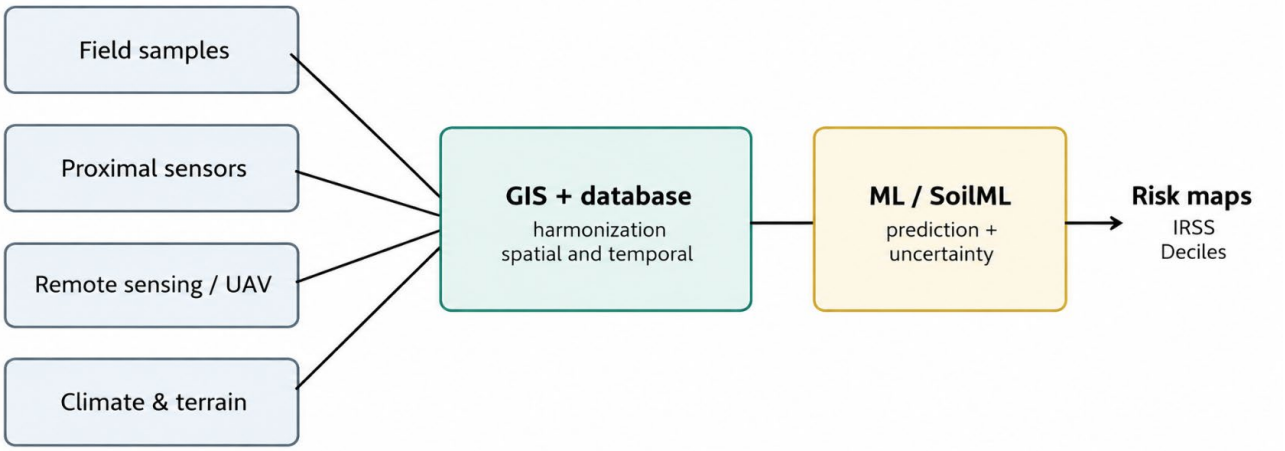



**Fig. 3 - Digital workflow for spatial soil health assessment. Original elaboration, conceptually adapted from the digital soil mapping and Soil Science-Informed Machine Learning literature**
*(Auzzas et al., 2024; Minasny et al., 2024).*

Remote sensing and proximal sensors can increase sampling efficiency and information density, but direct field and laboratory measurements remain necessary as reference observations for calibration and validation. For operational use, predictive performance should therefore be reported together with uncertainty, validation-set independence and the model domain of applicability. This requirement is especially important when spatial predictions are subsequently used to delineate management zones or prioritize interventions.

- *Proposal of the Soil Health and Regeneration Index (SHRI/IRSS)*

Integration of heterogeneous indicators requires conversion to comparable scores. Depending on indicator behavior, normalization may follow an increasing function for properties where higher values are favorable, a decreasing function where lower values are favorable, or an optimum-type function for variables such as pH. Because favorable ranges depend on soil type, climate, crop and management objective, normalization thresholds should be locally justified rather than transferred uncritically between systems.

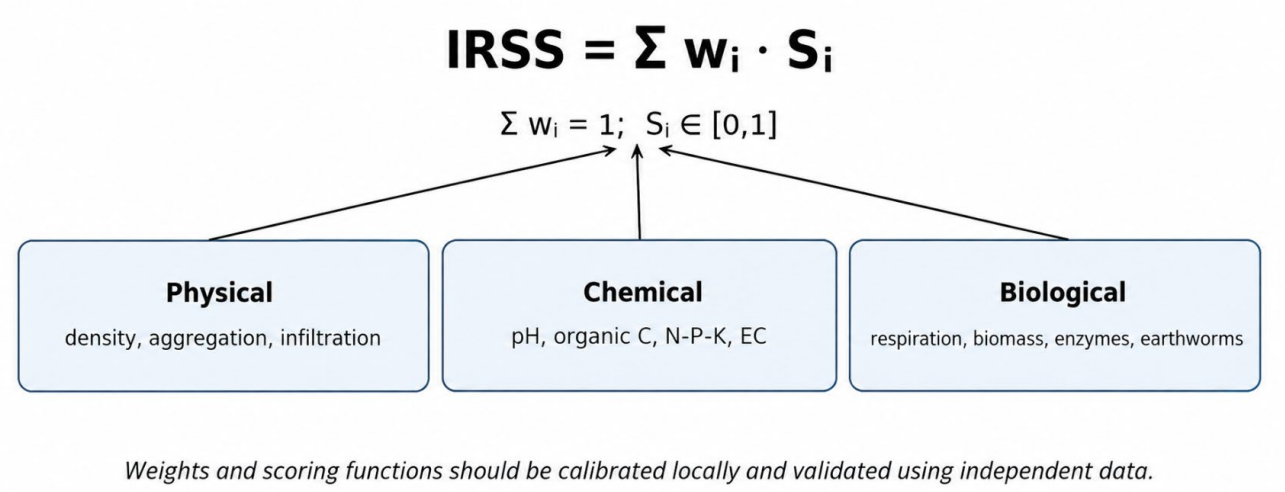



**Fig. 4 - Conceptual structure of SHRI/IRSS. Original elaboration. The formula is a methodological framework requiring experimental calibration and validation.**

For n indicators, the conceptual index can be written as IRSS = $\Sigma(w_i \cdot S_i)$, where $S_i$ is the normalized score of indicator i and $w_i$ is its weight, subject to $\Sigma w_i = 1$. Weights may be established from pedological expertise, multicriteria analysis, principal component analysis, statistical models or, preferably, empirical relationships between indicators and target soil functions. The index is therefore an integration structure, not a universal classification standard; its operational value depends on calibration for the soil, climate, crop and management context in which it is applied.

A simple weighted average may permit compensation between indicators, which can conceal severe limitations. Future calibration of SHRI/IRSS should therefore test penalty or constraint rules so that a high score for organic carbon, for example, cannot compensate for critical compaction or contamination above accepted limits. Such rules should be introduced only after validation with real datasets and sensitivity analysis of the resulting classifications.

- *Degradation, Regeneration and Interventions*

**Table 2**

**Diagnostic–indicator–intervention matrix. Interventions are options to be evaluated, not universal recommendations.**

| Process | Priority indicators | Interventions to evaluate |
|---|---|---|
| Compaction | bulk density; penetrometry; porosity | reduced traffic; deep-rooted crops; conservation tillage |
| Erosion | aggregation; infiltration; cover | cover crops; grass strips; contour farming |
| Organic C loss | organic C; organic matter; DOC | crop residues; compost; cover crops |
| Acidification | pH; base saturation | amendments; balanced fertilization |
| Salinization | EC; exchangeable Na | drainage; irrigation management |
| Nutrient imbalance | N; P; K; CEC | soil-test-based fertilization |
| Reduced biological activity | biomass; respiration; enzymes | organic inputs; diversification |
| Reduced biodiversity | microbial diversity; earthworms | reduced disturbance; diversification |
| Contamination | potentially toxic metals | source identification; remediation |

Regenerative agriculture is commonly associated with reduced soil disturbance, continuous soil cover, cover crops, diversified rotations, organic inputs and, where appropriate, livestock integration *(Khangura et al., 2023; Francaviglia et al., 2023; Somasundaram et al., 2020; Tadiello et al., 2023; Colombi et al., 2025)*. These practices should be interpreted as interventions whose effects must be tested against the diagnosed limitation. The designation 'regenerative' alone does not demonstrate improvement; effectiveness must be established through reproducible indicator changes and temporal comparison with a defined baseline.

- *Monitoring Soil Regeneration Over Time*

Regeneration is fundamentally a temporal property *(Bai et al., 2018; Six et al., 1999; Six et al., 2004)*. A single sampling campaign can characterize soil condition at a given moment, but it cannot demonstrate improvement attributable to an intervention. Monitoring should therefore begin with a baseline and maintain, as far as practicable, consistent sampling depth, positioning, analytical method and seasonal timing so that observed differences can be interpreted as temporal change rather than methodological variation.

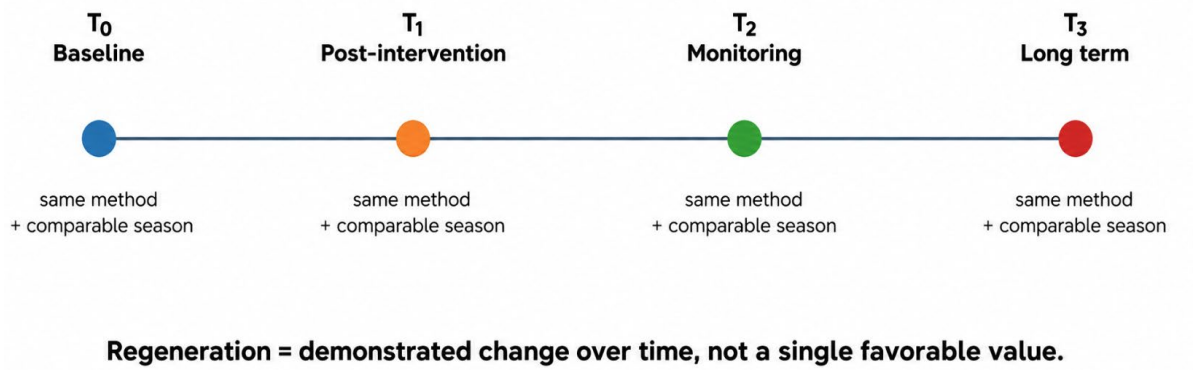



**Fig. 5 - Minimal temporal design for regeneration assessment. Original elaboration.**

For an indicator X, the absolute change may be expressed as $\Delta X = X_t - X_0$, while the mean rate of change is $(X_t - X_0)/\Delta t$. The same principle can be applied to SHRI/IRSS if scoring functions and weights remain comparable between monitoring dates. Experimental applications should additionally quantify uncertainty and use statistical models appropriate to the sampling design, particularly where repeated measurements, spatial dependence or heterogeneous management zones are present.

- *Adaptive Management*

Adaptive management converts monitoring results into an iterative decision process. After diagnosis, an intervention is selected according to the identified limitation, response indicators are defined, the practice is implemented, and the soil response is reassessed. If the expected response is not observed, the management hypothesis is revised and additional constraints are investigated. For example, limited improvement in infiltration after introducing cover crops may indicate persistent compaction, drainage limitations, unsuitable species, insufficient stand density or climatic constraints rather than a simple success/failure response.

This logic is consistent with assessment systems that connect physical, biological and chemical constraints with management planning. The proposed SHRI/IRSS framework extends that logic by explicitly incorporating repeated temporal assessment and spatial information from sensors, GIS and predictive models, thereby linking diagnosis with site-specific and adaptive management.

- *Integrated interpretation and methodological implications*

Three methodological implications emerge from the reviewed literature *(Bünemann et al., 2018; Lehmann et al., 2020; Rinot et al., 2019; van Es & Karlen, 2019).* First, no single indicator set is optimal for every soil and management objective; a minimum data set should be selected according to the target function and dominant threat, while the extended set supports detailed diagnosis. Second, biological indicators should be integrated more consistently because assessments based only on fertility chemistry can overlook early changes in soil functioning. Third, spatial extension through sensors and machine learning must be treated as an inference and validation problem rather than as a substitute for measurement.

A central validation requirement is the relationship between indicator scores and ecosystem services. Rinot et al. (2019) emphasize that holistic assessment should connect measured soil attributes with provisioning, regulating and supporting services, while Lehmann et al. (2020) place soil health within broader interactions involving water, climate, biodiversity and human well-being. Accordingly, validation of SHRI/IRSS should test associations not only among indicators but also with measurable functional outcomes such as infiltration, crop productivity, carbon storage and resilience to water stress.

The graphical elements used in the framework should remain traceable to their conceptual sources, while original synthesis diagrams are preferable when they integrate information from several studies. This preserves methodological transparency and avoids presenting literature-derived concepts as original experimental results.

- *Limitations and Future Directions*

The proposed framework remains conceptual. Optimal values and scoring thresholds are context-dependent; SHRI/IRSS weights have not yet been calibrated on an experimental dataset; biological indicators may vary seasonally; and digital models depend strongly on the representativeness of calibration data. Consequently, the index should not be used for normative soil classification until scoring functions, weights and decision rules have been validated against independent observations and relevant soil functions.

Priority research directions include the development of regional soil-health databases, multi-year calibration of SHRI/IRSS, integration of Sentinel and UAV observations with proximal sensing and soil spectroscopy, and evaluation of explainable and process-informed machine-learning models. Sensitivity analysis of indicator weights and normalization functions is also required to determine whether diagnostic conclusions remain stable under alternative parameterizations and to identify the indicators that most strongly influence the final assessment.

## CONCLUSIONS

- Integrated assessment of soil health and regeneration requires simultaneous consideration of physical, chemical and biological properties, interpreted in relation to soil functions, degradation threats and management responses. The proposed set of 30 indicators provides an extended diagnostic basis from which a purpose-specific minimum data set can be selected. Digital soil

mapping, remote and proximal sensing, GIS and machine-learning methods can increase spatial and temporal resolution, but their outputs require calibration and validation against field measurements and pedological knowledge.

- SHRI/IRSS is proposed as a conceptual structure for integrating normalized indicators rather than as a universal standard. Its scientific value depends on locally justified scoring functions, transparent weighting, sensitivity analysis and validation against measurable soil functions and ecosystem services. Regeneration should be demonstrated as reproducible change over time from a defined baseline. Within this framework, soil assessment becomes an adaptive cycle of measurement, diagnosis, intervention, monitoring and reassessment, providing a basis for future experimental validation and site-specific management.

**ACKNOWLEDGEMENT**

This work was supported by the MADR through Program ADER 2023-2026, project ADER 25.1.2 / 14.07.2023, “Innovative minimum tillage technology adapted to current climate change”

**REFERENCES**

[1] Bai, Z., Caspari, T., Ruiperez Gonzalez, M., et al. (2018). Effects of agricultural management practices on soil quality: A review of long-term experiments for Europe and China. Agriculture, Ecosystems & Environment, 265, 1–7. https://doi.org/10.1016/j.agee.2018.05.028

[2] Bünemann, E.K., Bongiorno, G., Bai, Z., et al. (2018). Soil quality – A critical review. Soil Biology and Biochemistry, 120, 105–125. https://doi.org/10.1016/j.soilbio.2018.01.030

[3] Doran, J.W., & Zeiss, M.R. (2000). Soil health and sustainability: Managing the biotic component of soil quality. Applied Soil Ecology, 15(1), 3–11. https://doi.org/10.1016/S0929-1393(00)00067-6

[4] Khangura, R., Ferris, D., Wagg, C., & Bowyer, J. (2023). Regenerative agriculture—A literature review on the practices and mechanisms used to improve soil health. Sustainability, 15(3), 2338. https://doi.org/10.3390/su15032338

[5] Lehmann, J., Bossio, D.A., Kögel-Knabner, I., & Rillig, M.C. (2020). The concept and future prospects of soil health. Nature Reviews Earth & Environment, 1, 544–553. https://doi.org/10.1038/s43017-020-0080-8

[6] Minasny, B., Bandai, T., Ghezzehei, T.A., et al. (2024). Soil Science-Informed Machine Learning. Geoderma, 452, 117094. https://doi.org/10.1016/j.geoderma.2024.117094

[7] Moebius-Clune, B.N., Moebius-Clune, D.J., Gugino, B.K., et al. (2016). Comprehensive Assessment of Soil Health – The Cornell Framework, Edition 3.2. Cornell University.

[8] Rinot, O., Levy, G.J., Steinberger, Y., Svoray, T., & Eshel, G. (2019). Soil health assessment: A critical review of current methodologies and a proposed new approach. Science of the Total Environment, 648, 1484–1491. https://doi.org/10.1016/j.scitotenv.2018.08.259

[9] Auzzas, A., Capra, G.F., Jani, A.D., et al. (2024). An improved digital soil mapping approach to predict total N by combining machine learning algorithms and open environmental data. Modeling Earth Systems and Environment, 10, 6519–6538.

[10] Schon, N.L., Fraser, P.M., & Mackay, A.D. (2023). Earthworms for inclusion as an indicator of soil biological health in New Zealand pastures. New Zealand Journal of Agricultural Research, 66(3), 208–223. https://doi.org/10.1080/00288233.2022.2041676

[11] Doran, J.W., Sarrantonio, M., & Liebig, M.A. (1996). Soil health and sustainability. Advances in Agronomy, 56, 1–54.

[12] Karlen, D.L., & Stott, D.E. (1994). A framework for evaluating physical and chemical indicators of soil quality. In J.W. Doran et al. (Eds.), Defining Soil Quality for a Sustainable Environment. SSSA Special Publication 35.

[13] Karlen, D.L., Doran, J.W., Andrews, S.S., & Wienhold, B.J. (2003). Soil quality: Humankind’s foundation for survival. Journal of Soil and Water Conservation, 58(4), 171–179.

[14] FAO. (2017). Voluntary Guidelines for Sustainable Soil Management. Global Soil Partnership, Food and Agriculture Organization of the United Nations, Rome.

[15] FAO/ITPS. (2015). Status of the World’s Soil Resources: Main Report. Food and Agriculture Organization of the United Nations, Rome.

[16] Chen, S., Arrouays, D., Mulder, V.L., Poggio, L., Minasny, B., Roudier, P., et al. (2022). Digital mapping of GlobalSoilMap soil properties at a broad scale: A review. Geoderma, 409, 115567. https://doi.org/10.1016/j.geoderma.2021.115567
[17] Wall, D.H., Nielsen, U.N., & Six, J. (2015). Soil biodiversity and human health. Nature, 528, 69–76. https://doi.org/10.1038/nature15744
[18] Li, Y., et al. (2020). Cropping systems in agriculture and their impact on soil health – A review. Global Ecology and Conservation, 23, e01118. https://doi.org/10.1016/j.gecco.2020.e01118
[19] Iheshiulo, E.M.-A., Larney, F.J., Hernandez-Ramirez, G., St. Luce, M., Liu, K., & Chau, H.W. (2023). Do diversified crop rotations influence soil physical health? A meta-analysis. Soil and Tillage Research, 233, 105781. https://doi.org/10.1016/j.still.2023.105781
[20] Sheehy, J., Regina, K., Alakukku, L., & Six, J. (2015). Impact of no-till and reduced tillage on aggregation and aggregate-associated carbon in Northern European agroecosystems. Soil and Tillage Research, 150, 107–113. https://doi.org/10.1016/j.still.2015.01.015
[21] Powlson, D.S., Whitmore, A.P., & Goulding, K.W.T. (2011). Soil carbon sequestration to mitigate climate change: A critical re-examination to identify the true and the false. European Journal of Soil Science, 62(1), 42–55. https://doi.org/10.1111/j.1365-2389.2010.01342.x
[22] Dick, R.P. (1994). Soil enzyme activities as indicators of soil quality. In J.W. Doran et al. (Eds.), Defining Soil Quality for a Sustainable Environment. SSSA Special Publication 35.
[23] Alkorta, I., Aizpurua, A., Riga, P., Albizu, I., Amézaga, I., & Garbisu, C. (2003). Soil enzyme activities as biological indicators of soil health. Reviews on Environmental Health, 18(1), 65–73. https://doi.org/10.1515/REVEH.2003.18.1.65
[24] Semenov, M.V., Zhelezova, A.D., Ksenofontova, N.A., Ivanova, E.A., Nikitin, D.A., & Semenov, V.M. (2025). Microbiological Indicators for Assessing the Effects of Agricultural Practices on Soil Health: A Review. Agronomy, 15(2), 335. https://doi.org/10.3390/agronomy15020335
[25] McBratney, A.B., Mendonça Santos, M.L., & Minasny, B. (2003). On digital soil mapping. Geoderma, 117(1–2), 3–52. https://doi.org/10.1016/S0016-7061(03)00223-4
[26] Piikki, K., & Wetterlind, J. (2021). Perspectives on validation in digital soil mapping of continuous attributes – A review. Soil Use and Management, 37(1), 7–21. https://doi.org/10.1111/sum.12694
[27] Angon, P.B., et al. (2023). An overview of the impact of tillage and cropping systems on soil health in agricultural practices. Advances in Agriculture, 2023, 8861216.
[28] Francaviglia, R., Almagro, M., & Vicente-Vicente, J.L. (2023). Conservation Agriculture and Soil Organic Carbon: Principles, Processes, Practices and Policy Options. Soil Systems, 7(1), 17. https://doi.org/10.3390/soilsystems7010017
[29] Somasundaram, J., et al. (2020). The ability of conservation agriculture to conserve soil organic carbon and the subsequent impact on soil physical, chemical, and biological properties and yield. Frontiers in Sustainable Food Systems, 4, 31. https://doi.org/10.3389/fsufs.2020.00031
[30] Tadiello, T., et al. (2023). Soil organic carbon under conservation agriculture in Mediterranean and humid subtropical climates: Global meta-analysis. European Journal of Soil Science. https://doi.org/10.1111/ejss.13338
[31] Colombi, G., Martani, E., & Fornara, D. (2025). Regenerative organic agriculture and soil ecosystem service delivery: A literature review. Ecosystem Services, 73, 101721. https://doi.org/10.1016/j.ecoser.2025.101721
[32] Six, J., Elliott, E.T., & Paustian, K. (1999). Aggregate and soil organic matter dynamics under conventional and no-tillage systems. Soil Science Society of America Journal, 63, 1350–1358.
[33] Six, J., Ogle, S.M., Breidt, F.J., Conant, R.T., Mosier, A.R., & Paustian, K. (2004). The potential to mitigate global warming with no-tillage management is only realized when practised in the long term. Global Change Biology, 10, 155–160. https://doi.org/10.1111/j.1529-8817.2003.00730.x
[34] van Es, H.M., & Karlen, D.L. (2019). Reanalysis validates soil health indicator sensitivity and correlation with long-term crop yields. Soil Science Society of America Journal, 83(3), 721–732. https://doi.org/10.2136/sssaj2018.09.0338

# MATHEMATICAL MODELS USED IN THE MECHANICAL-PNEUMATIC SOWING PROCESS

/

# *MODELE MATEMATICE UTILIZATE ÎN PROCESUL DE SEMĂNAT MECANO-PNEUMATIC*

**Dragoş-Nicolae ANGHELACHE[1, 2)], Ana-Maria TĂBĂRAŞU*[1)], Dragoş DUMITRU[1)], Eugen MARIN[1)], Nicoleta VANGHELE[1, 2)], Cristian RADU[2, 3)], Alexandru IONESCU[1, 2)], Melania CISMARU[1)], Nicolae-Valentin VLĂDUȚ*[1, 2)], Dragos Mihail PREDA[2)]**

[1)] INMA Bucharest / Romania; [2)] UNSTP Bucharest; [3)] University from Craiova / Romania.

**E-mail: anamariatabarasu22@yahoo.com; *valentin_vladut@yahoo.com*

***Keywords:*** *model, sowing, process, pneumatic, seeds*

**ABSTRACT**

*The sowing process is influenced by numerous parameters, the most important of which include the architecture of the distribution mechanism, travel speed, seed shape, chamber pressure, and the degree of soil levelling. This study aims to analyse mathematical models used globally for seed distribution within metering units, with the goal of optimizing the seeding process, reducing seed loss, and minimizing the impact on the soil.*

**REZUMAT**

*Procesul de semănat este influențat de foarte mulți parametri iar dintre aceștia cei mai importanți sunt: arhitectura aparatului de distribuție, viteza de deplasare, forma semințelor, presiunea din camera, gradul de nivelare al solului, etc. Lucrarea îşi propune să analizeze modele matematice utilizate pe plan mondial pentru distribuția semințelor în aparatele de dozare, în vederea optimizării procesului de înierbare, reducerii pierderilor de semințe și minimizarea impactului asupra solului.*

## INTRODUCTION

Grass establishment on agricultural land represents an essential step for obtaining high-quality crops and maintaining soil health. In modern orchards, maintaining a balance between productivity, soil resource protection, and reducing environmental impact is a major challenge. Controlled grass cover between rows of fruit trees or grapevines is an increasingly used agroecological technology, contributing to weed suppression, natural pest control, and reduced use of chemical fertilizers *(Hanna et al., 1995; Herea et al., 2019; Revenco and Ţîţei, 2021; Das et al., 2021).*

This technique involves establishing a herbaceous vegetation cover composed of perennial or temporary species that protects the soil, prevents erosion, improves water infiltration capacity, reduces soil compaction, and supports biodiversity. Through periodic mowing and proper vegetation management, soil fertility and biological activity are improved, while carbon sequestration contributes to maintaining natural soil fertility over the long term *(Webber et al., 2022; Baluszynska et al., 2022; Zanotelli et al., 2018).*

The effectiveness of grass establishment depends on the quality of the machinery used, which must ensure seedbed preparation, uniform seed distribution, seed incorporation, and rolling to achieve optimal seed–soil contact.

The present study focuses on an innovative machine for sowing grasses between rows of grapevines and fruit trees, which simultaneously performs soil tillage, transverse seed distribution, uniform seed dispersal close to the soil surface, seed incorporation, and rolling. The cutter rotor equipped with blades, driven by the tractor power take-off through a mechanical transmission, ensures seedbed preparation, while the electric metering device and pneumatic conveying system enable uniform seed dispersal.

The main technical characteristics include a 300 L hopper capacity, a sowing depth of 20–120 mm, a working width of 1.4 m, a required power of 45–50 hp, and a total mass of 453 kg. This machine provides the basis for developing an integrated mathematical model capable of simulating the behavior of similar machines under different working conditions, analyzing the interaction between design and operating parameters, and predicting seed distribution uniformity *(Dumitru et al., 2023; Manea, 2011).*

Through this model, the research aims to optimize the grass establishment process, reduce seed losses, and minimize the impact on the soil by integrating the principles of sustainable and agroecological agriculture. Thus, the study establishes a link between agronomic practice and advanced technological modeling, providing a predictive tool for the efficient management of grass-covered inter-row areas in orchards and vineyards..

## MATERIALS AND METHODS

The equipment is intended for sowing grasses between rows of grapevines and fruit trees and is designed to perform, in a single pass, a series of technological operations required for controlled grass establishment.

The sequence of operations performed by the equipment is schematically presented in Figure 1.

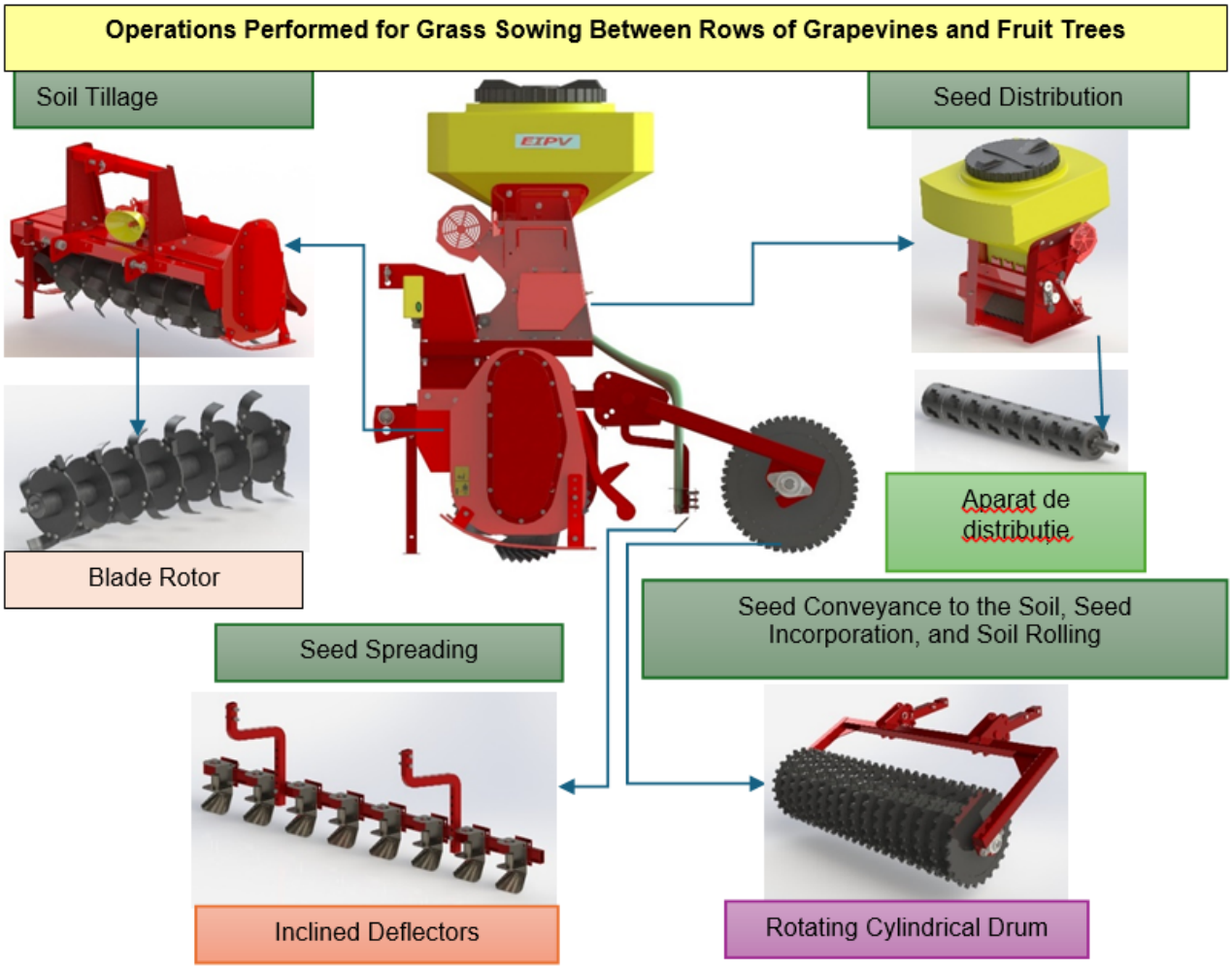



**Fig. 1 - Operations performed for grass sowing between rows of grapevines and fruit trees**

### Operating Principle

During field operation of the soil tillage and grass-sowing equipment, the tractor to which the machine is attached transmits rotational motion through the power take-off (PTO), which operates at a constant angular speed of 540 rpm. The motion is further transmitted to the horizontal blade rotor through a cardan shaft, a bevel gearbox, and a chain drive, resulting in a constant rotor angular speed of 96 rpm. The horizontal rotor, equipped with blades, cuts soil slices and carries them into a rotational motion, projecting them toward the metal housing of the machine.

This process results in soil crushing and loosening, with the soil remaining in a levelled layer located approximately 4–6 cm above the sowing depth, which is adjusted using the skids. Maintaining a constant rotor angular speed throughout operation ensures a uniform degree of soil fragmentation and prevents excessive pulverization, which could lead to a reduction in humus content.

Simultaneously with the soil tillage process, the sowing unit performs the transverse distribution of grass seeds. Seed metering is carried out using a cylindrical metering device driven electrically by a 12 V DC electric motor through a control device. The metered seeds are entrained by the airflow generated by a fan and pneumatically conveyed through flexible tubes to the spreading system. Seed spreading is performed close to the soil surface, across the entire working width, using inclined deflectors positioned forward in the direction of travel at an angle α. Uniform transverse distribution is ensured by channels formed by fan-shaped ribs, which define a dispersion angle β. This structural configuration enables controlled guidance of the seed flow and contributes to achieving uniform distribution over the working surface.

The seeds reaching the soil are subsequently taken up by the incorporation and rolling system, which introduces them into the soil surface layer and compacts it.

This system consists of a rotating cylindrical drum on which transverse plates are mounted at equal distances. The plates are provided with profiled ribs consisting of a recess with radius R, a beak, and a semicircular protrusion of the same radius. As the drum rotates, the seeds are incorporated to the required depth, while the soil above them is compacted and rolled, ensuring optimal seed–soil contact.

The synchronized operation of the equipment subassemblies enables all technological operations required for controlled grass establishment between rows to be performed in a single pass. This operating mode provides the physical and functional basis for developing an integrated mathematical model of the equipment's working process, capable of simulating its behavior under different operating conditions.

The functional diagram of the equipment is presented in Figure 2.

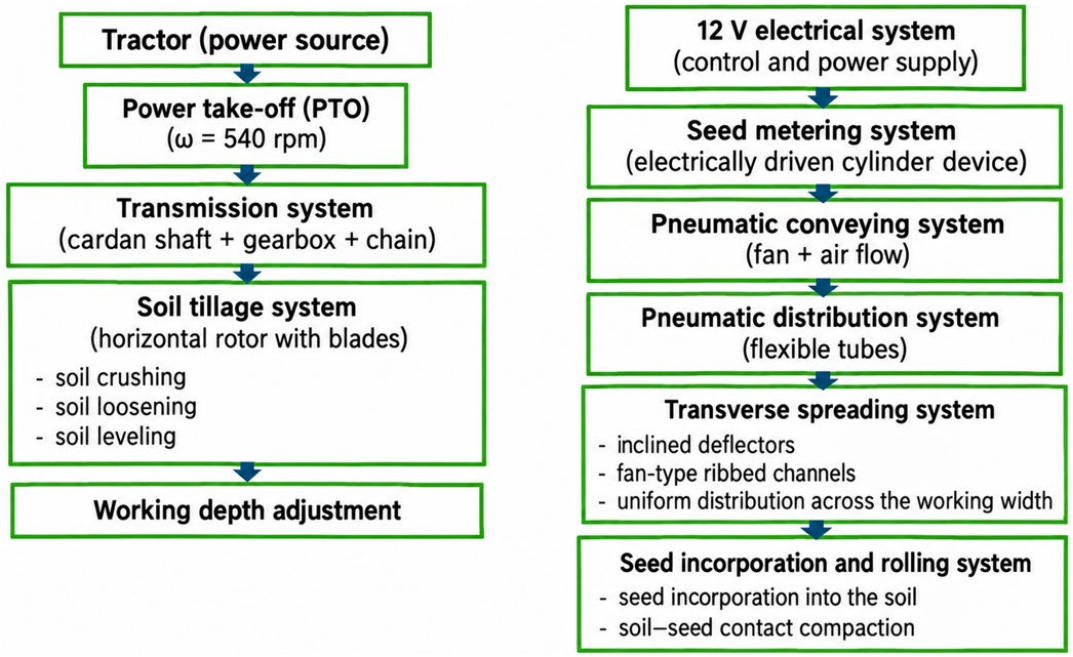



**Fig. 2 - Functional diagram of the equipment**

✓ ***Mathematical Model of Seed Distribution in Metering Devices***

Seed distribution represents one of the fundamental stages of the mechanized sowing process, directly influencing the seeding rate, distribution uniformity, and seed material use efficiency. For this reason, seed metering devices have been the subject of numerous theoretical and experimental studies, leading to the development of various mathematical models.

Classical distribution models are based on expressing the seed mass flow rate as a function of the active volume of the metering element and its rotational speed, with the general relationship expressed as:

$$Q_s = n \cdot V_u \cdot \rho_s \cdot \eta \quad (1)$$

where:

$Q_s$ – seed mass flow rate [kg/s];

n – rotational speed of the metering element [rev/s];

$V_u$ – effective volume of a groove [m³];

$\rho_s$ – bulk density of the seeds [kg/m³];

η – filling coefficient.

In recent studies, this model has been extended to account for the influence of the forward speed of the machine–tractor unit, vibrations, and the physical and mechanical properties of the seeds.

An important contribution was made by Manea (2011), who demonstrated that the actual seeding rate differs from the theoretical seeding rate when the operating speed varies, even when the seed flow rate is maintained constant. To describe this phenomenon, the author introduced nonlinear functional relationships for the filling coefficient, expressed as:

$$\eta(v) = a + b \cdot v + c \cdot v^2 \tag{2}$$

$$\eta(v) = \frac{1}{1+e^{k(v-v_0)}} \tag{3}$$

or

where:

$v$ is the forward speed of the seeder.

The coefficients a, b, and c were determined experimentally and depend on the geometry of the metering device, seed properties, and operating conditions.

Although these models are well suited to cereal seeders with centralized metering systems, they do not account for the specific characteristics of grass-seeding equipment, where:

- the seeds are very small and heterogeneous;
- seed metering is integrated with pneumatic conveying;
- seed distribution is performed over a wide working width rather than in rows.

✓ ***Model of Pneumatic Seed Conveying through Flexible Tubes***

Pneumatic seed conveying is a complex process characterized by the interaction between the gaseous phase (air) and the solid phase (seeds). The mathematical models used in this field are based on the principles of fluid mechanics and particle dynamics.

The motion of an individual seed in the airflow can be described by the fundamental equation of dynamics:

$$m\frac{dv}{dt} = F_d + F_g + F_f \tag{4}$$

where:

$F_d$ – aerodynamic drag force [N] [N];

$F_g$ – gravitational force [N];

$F_f$ – friction and impact forces with the tube walls [N].

The aerodynamic drag force is commonly expressed by the following relationship:

$$F_d = \frac{1}{2} C_d \cdot \rho_a \cdot A(v_a - v)^2 \tag{5}$$

where:

$C_d$ – aerodynamic drag coefficient;

$\rho_a$– air density [kg/m$^3$];

$A$ – seed cross-sectional area [m$^2$];

$v_a$– air velocity [m/s].

An essential parameter is the critical conveying velocity, which must be higher than the seed terminal velocity to prevent seed deposition and pipeline blockage. The literature indicates that, for small seeds, this velocity ranges from 5 to 15 m/s, depending on the species.

Current models separately consider:

- the acceleration regime;
- the steady-state regime;

- pressure losses along the tubes and through bends.
- However, these models are rarely integrated with the metering model, as the two processes are generally analyzed independently.

✓ ***Mathematical Model of Seed Spreading and Distribution Uniformity***

The uniformity of seed distribution at the outlet of the pneumatic system is analyzed using models that describe the behavior of the air–seed mixture within the distribution heads.

These systems include flow-guiding and flow-uniformizing elements designed to ensure the most uniform possible distribution of the seed flow among the conveying tubes.

Seed spreading at the outlet of the pneumatic system is described using ballistic and probabilistic models. The trajectory of a seed after leaving the deflector is described by the equations of seed motion:

$$x(t) = v_0 \cdot \cos \propto \cdot t \tag{6}$$

$$y(t) = v_0 \cdot \sin \propto \cdot t - \frac{1}{2}\ g \cdot t^2 \tag{7}$$

The transverse distribution is statistically evaluated using the coefficient of variation (CV):

$$CV = \frac{\sigma}{\mu} \cdot 100\% \tag{8}$$

where:

$\sigma$ – standard deviation

It measures the dispersion of individual values around the arithmetic mean.

In the context of sowing, it describes:

- variation in the amount of seeds across equal sections;
- differences between distribution points;
- temporal fluctuations in the seed flow rate.

$$\sigma = \sqrt{\frac{1}{n-1}\sum_{i=1}^{n}(x_i - \mu)^2} \tag{9}$$

where $x_i$ represents the measured values of the seed quantity.

$\mu$ – arithmetic mean

- Represents the mean value of the analyzed parameter.

In this case:

- the average quantity of seeds distributed;
- the average seeding rate..

$$\mu = \frac{1}{n}\sum_{i=1}^{n} x_i \tag{10}$$

Existing models highlight the role of flow-guiding cones, variations in cross-sectional area, and turbulence-dissipation elements in reducing distribution non-uniformity. However, most studies focus on row-crop sowing, without addressing the specific characteristics of the lateral seed distribution required for grass seeding in inter-row spaces..

✓ **Models of the Seed Incorporation and Rolling Process**

The process of seed incorporation into the soil and subsequent rolling is described using models that correlate soil–seed contact forces, working depth, and the degree of soil compaction. These models aim to ensure optimal seed–soil contact, which is essential for germination.

In the case of grass-seeding equipment, the incorporation process is additionally influenced by the soil structure between crop rows, the presence of existing vegetation, and the need to minimize soil

disturbance. The current literature provides partial models that are not integrated into a unified framework for the mechanical–pneumatic sowing process.

Seed incorporation and rolling are modeled using relationships that describe the pressure exerted on the soil and the seed penetration depth:

$$k_s = k \cdot \frac{F_t}{A_t \cdot \sigma_s} \tag{11}$$

where:

$F_t$ – force exerted by the roller [N];

$A_t$ – contact area [m$^2$];

$\sigma_s$ – soil resistance [N/m$^2$].

✓ ***Current Trends and Development Directions Identified in the International Literature***

The analysis of the specialized literature highlights a clear trend toward the development of integrated mathematical models capable of simultaneously describing seed metering, pneumatic conveying, distribution, and incorporation processes. Modern models are based on nonlinear functions, numerical approximation methods, and experimental validation.

Although the models developed by authors such as Manea (2011) represent an important reference in the optimization of the seed distribution process, they are primarily designed for conventional cereal seeders. In the case of equipment intended for grass seeding on agricultural land, there is a lack of integrated mathematical models that account for the specific characteristics of the operation, intermittent operating conditions, and specific agrotechnical requirements.

This gap justifies the need to develop, within the present doctoral thesis, an integrated mathematical model capable of simulating the behavior of grass-seeding equipment under different operating conditions and providing a scientific basis for optimizing its constructive and functional parameters.

## RESULTS

### Theoretical Foundations for Modeling the Working Process

- **General Considerations on Mechanized Grass Seeding**

Mechanized grass seeding is a complex technological process that integrates several operations: seedbed preparation, seed metering and distribution, pneumatic conveying, uniform spreading, and seed incorporation into the soil. The efficiency of the process is evaluated using indicators such as seed distribution uniformity, sowing depth, degree of soil loosening and compaction, as well as the energy efficiency of the equipment.

For the mathematical modeling of the process, a systemic approach is used, based on the functional relationships between input variables and output parameters. This approach enables the simulation of equipment behavior and the optimization of technological parameters under variable operating conditions.

- **Representation of the Working Process**

The working process of the grass-seeding equipment can be described using a block–parametric representation, which combines the logical structure of the functional subsystems with the mathematical relationships between the technological parameters.

This representation enables the visualization of energy and material flows, as well as the identification of critical parameters that influence equipment performance.

Figure 3 presents the block–parametric representation of the working process of the grass-seeding equipment, highlighting both the logical structure of the functional subsystems and the fundamental mathematical relationships between the input and output parameters.

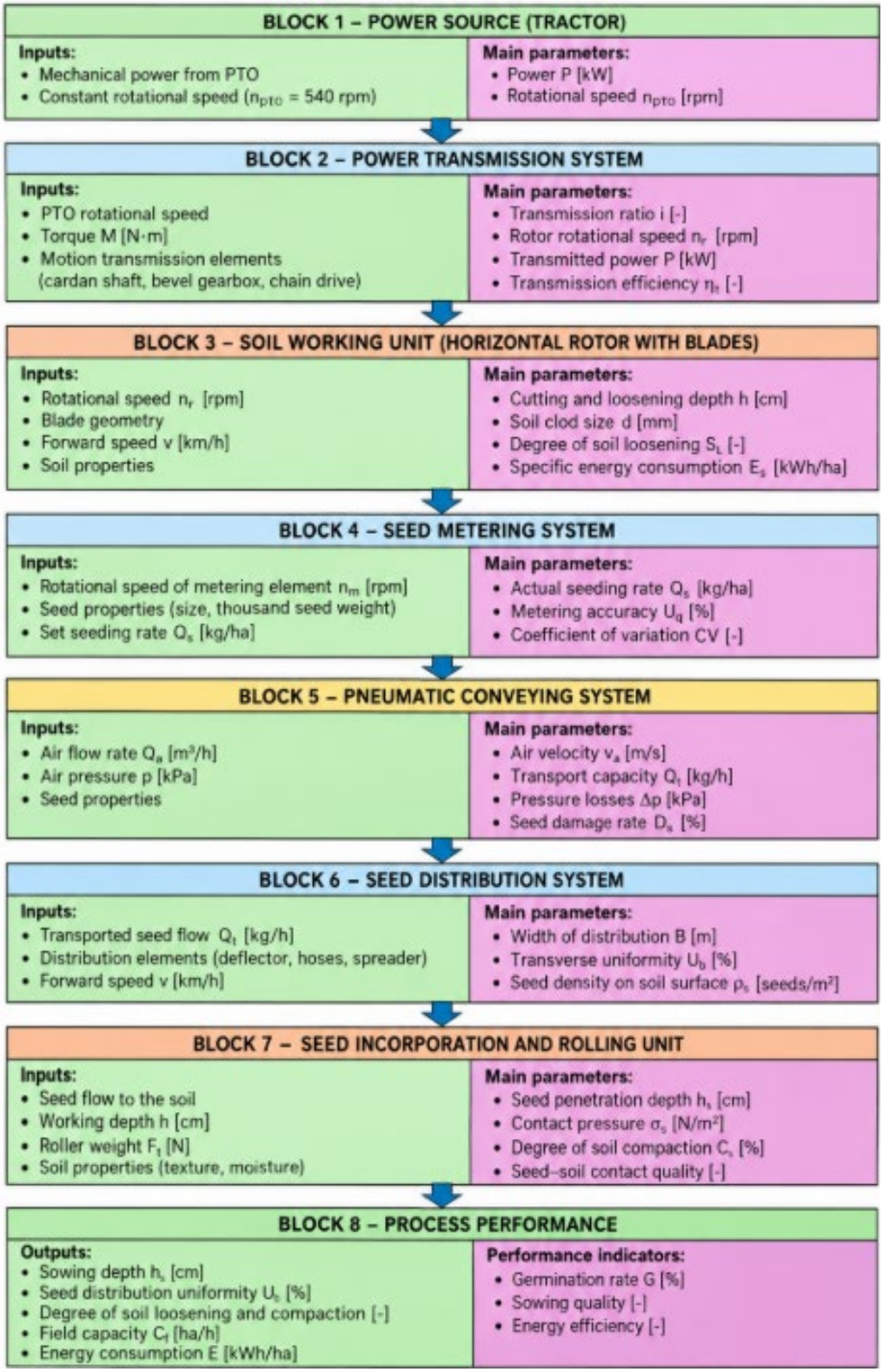



**Fig. 3 - Block–parametric representation of the working process of the grass-seeding equipment**

The fundamental vectors are defined as follows:

**- Input Variable Vector:**

$$X = (n_{PTO}, v, n_e, Q_a) \tag{12}$$

where:

- $n_{PTO}$ – tractor power take-off (PTO) rotational speed [rot/min];
- $v$ – forward speed [m/s];

- $n_e$ – rotational speed of the metering device electric motor [rot/min];
- $Q_a$ – air flow rate [m³/s].

**- Vector of Constructive and Technological Parameters:**

$$P = (i_T, \psi, \alpha, V_c, D_i, L_t) \quad (13)$$

where:
- $i_T$ – transmission ratio;
- $\psi$ – mechanical characteristics of the subassemblies;
- $\alpha$ – spreading angle [º];
- $V_c$ – hopper working volume [m³];
- $D_i$ – diameter of the distribution elements [m];
- $L_t$ – working width of the equipment [m].

**- Output Vector:**

$$P = (i_T, \psi, \alpha, V_c, D_i, L_t) \quad (14)$$

where:
- $Q_s$ – seed flow rate [kg/s];
- $U_l$ și $U_t$ – longitudinal and transverse distribution uniformity [%];
- $h_f$ – seed incorporation depth [m];
- $C_s$ – process efficiency coefficient.

These relationships allow the definition of a unified model of the following form**:**

$$Y = (Q_s, U_l, U_t, h_f, C_s) \quad (15)$$

which provides a comprehensive description of the equipment behavior as a function of the input parameters and the design characteristics of its subassemblies.

**Parametric Mathematical Representation**

The mathematical modeling of the system is carried out by defining the input parameters, state variables, and output parameters for each functional block. Examples of the fundamental relationships are:

**- Seed Flow Rate:**

$$Y = F(X, P) \quad (16)$$

where:
- $n_d$ – rotational speed of the metering cylinder [rot/min],
- $k_s$ – seed flow rate adjustment coefficient,
- $\rho_s$ – seed density [kg/m³].

Within the mathematical model, the seed density ρs\rho_sps represents the bulk density, expressed in kg/m³, and is used to correlate the volume delivered by the metering device with the seed mass flow rate.

***- Air flow rate:***

$$Q_a = f(n_v, D_v) \quad (17)$$

where:
- $n_v$ – fan rotational speed [rot/min];
- $D_v$ – air duct diameter [m].

***- Seed Distribution Uniformity:***

$$U = f(Q_s, Q_a, v, a) \quad (18)$$

***- Coefficient of Variation:***

$$CV = \frac{\sigma}{\mu} \times 100 \quad (19)$$

***- Process Efficiency:***

$$\eta(v) = a + b \cdot v + c \cdot v^2 \quad (20)$$

where:

- $v$ - forward speed [m/s];
- $a$, $b$, $c$ – experimentally determined coefficients.

This block–parametric representation provides the foundation for the development of the integrated mathematical model, enabling numerical simulation and optimization of the sowing process under different operating conditions.

- **Selection of Input and Output Variables**

Based on the block diagram, the input variables and output parameters were selected to directly reflect:

- the mechanical operation of the rotor and metering device;
- the pneumatic performance of seed conveying;
- seed distribution uniformity and sowing depth;
- the overall efficiency of the technological process.

This selection enables the experimental and simulation-based correlation of the results, facilitating the validation of the mathematical model and the adjustment of the optimal parameters..

- **Working Assumptions and Boundary Conditions**

To simplify the mathematical model and numerical simulation, the following assumptions are adopted:

- The soil is assumed to be uniform across the entire working width and free of major obstacles.
- Seeds are distributed independently, without complex interactions.
- The tractor forward speed and rotor rotational speed are constant.
- The pneumatic seed flow is uniform, with no significant losses.
- The geometric parameters of the deflectors and the distances between the discs are constant.
- External climatic factors (wind, rain) are not considered in the model.
- The model applies to seeds that are homogeneous in terms of mass and shape.
- These assumptions allow the development of a predictable and reproducible model, which can subsequently be validated experimentally.

- **Development of the Mathematical Model**

***the Operation of the Electrically Driven Cylindrical Metering Device***

The fluted-cylinder metering device is the main component responsible for controlling the seed flow rate. From a functional perspective, the mass flow rate of the distributed seeds depends on the rotational speed of the metering cylinder, its geometry, and the physical properties of the seeds.

The volumetric seed flow rate can be expressed by the following relationship:

$$Q_s = n_d \cdot V_c \cdot \eta_d \quad (21)$$

where:

- $n_d$ – rotational speed of the metering cylinder [rot/s];
- $V_c$ – volume conveyed per revolution of the cylinder [m³/rot];
- $\eta_d$ – groove filling coefficient.

The resulting seed mass flow rate is:

$$Q_s = Q_v \cdot \rho_s \quad (22)$$

where:

- $\rho_s$ bulk density of the seed [kg/m³].

The rotational speed of the metering cylinder is electrically controlled:

$$n_d = k_c \cdot U_c \quad (23)$$

where:

$k_e$ – electric motor conversion coefficient;
$U_e$ – supply voltage [V].

These relationships enable precise adjustment of the seeding rate through the electrical control of the metering device.

- **Modeling the Pneumatic Conveying Process through Flexible Tubes**

Pneumatic conveying of seeds is achieved by entraining them in an airflow generated by the fan. The essential condition for stable conveying is that the air velocity must be higher than the critical seed entrainment velocity.

The air flow rate is expressed as:

$$Q_a = A_t \cdot v_a \tag{24}$$

where:
$A_t$ – tube cross-sectional area [m²];
$v_a$ – air velocity [m/s].
The air velocity is correlated with the fan rotational speed:

$$v_a = k_v \cdot n_v \tag{25}$$

For efficient pneumatic conveying, the following condition must be satisfied:

$$v_a \geq v_{crit} \tag{26}$$

Pressure losses in the flexible tubes are modeled using:

$$\Delta p = \lambda \cdot \frac{L}{D} \cdot \frac{\rho_a \cdot {v_a}^2}{2} \tag{27}$$

where:
- $L$ – tube length;
- $D$ – tube diameter;
- $\lambda$ – pressure loss coefficient;
- $\rho a$ – *air density.*

- **Modeling the Seed Spreading System**

Seed spreading is influenced by the seed flow rate, air flow rate, forward speed, and deflector geometry. The transverse distribution can be modeled using a probability density function.

The effective spreading width is expressed as:

$$B = 2 \cdot h \cdot \tan(\frac{\beta}{2}) \tag{28}$$

The uniformity of transverse distribution is evaluated using the coefficient of variation:
where:
- $\sigma_t$ – standard deviation;
- $\mu_t$– mean value of the distribution.

The model allows the influence of the spreading angle β on distribution uniformity to be evaluated.

- **Modeling the Seed Incorporation and Rolling Process Using a Cylindrical Roller**

The seed incorporation process is determined by the geometry of the discs, the forward speed, and the rotational speed of the roller.

The seed incorporation depth can be expressed as:

$$h_f = f(R, n_t, v, p_s) \tag{29}$$

where:
- $R$ – disc radius;

- $n_t$ – roller rotational speed;
- $p_s$ – pressure exerted on the soil.

The degree of soil compaction is expressed by a compaction coefficient:

$$C_t = \frac{\rho_{sol,final}}{\rho_{sol,initial}} \quad (30)$$

This coefficient influences seed–soil contact and germination conditions.

- **Integration of the Subassemblies into a Unified Mathematical Model**

The overall mathematical model of the equipment is obtained by integrating the partial models corresponding to each subassembly. Thus, the sowing process can be described by a system of correlated functional relationships:

$$\begin{cases} Q_s=f(n_d,\rho_s,V_c) \\ Q_a=f(n_v,D_t) \\ U=f(Q_s, Q_a, v, \alpha, \beta) \\ h_{f=}f(n_t, v, R) \end{cases} \quad (31)$$

The unified mathematical model enables:

- numerical simulation of the sowing process;
- sensitivity analysis of the technological parameters;
- optimization of the seeding rate and distribution uniformity;
- establishment of the basis for the experimental validation presented in the following chapters.

## CONCLUSIONS

The study presents an integrated mathematical model of the seed metering and distribution process in pneumatic seeders, incorporating the geometric parameters of the metering cylinder and the functional parameters of the metering and pneumatic conveying systems.

Based on the analysis presented above, it can be concluded that the integrated mathematical model enables the estimation and optimization of seed flow rate and distribution uniformity, providing a basis for the design of precision pneumatic seeders. Experimental validation, complemented by 3D simulations using SolidWorks and EDEM, can confirm the accuracy of the model and the relevance of the proposed parameters.

The application of the recommended simulation and validation procedures will facilitate the optimization of the pneumatic sowing process for different seed types and forward speeds..

## ACKNOWLEDGEMENT

The results were obtained with the support of the Ministry of Research, Innovation and Digitalization through the Nucleu Program, contract no. 9 N / 01.01.2023, project PN 23 04 02 03 “Innovative technology for grassing the interval between rows of vines and fruit trees to avoid degradation of soil structure”.

## REFERENCES

[1] Hanna R, Zalom FG, Elmore CL (1995) Integrating cover crops into grapevine pest and nutrition management: The transition phase. *Sustain Tech Rev 7(3),* 11–14

[2] Herea, M., Talmaciu, M., Mocanu, I., & Talmaciu, N. (2019). Contributions to the knowledge of the structure of coleopters species collected from the apple tree fruit orchards. *International Multidisciplinary Scientific GeoConference: SGEM*, *19*(5.1), 125-132.

[3] Revenco, E., & Ţîţei, V. (2021). Înierbarea terenurilor agricole ca metodă de conservare a apei și protejare a solului: Ghid practic pentru producătorii agricoli. *Chişinău: S*, (60).

[4] Das, B., Kandpal, B. K., & Devi, H. L. (2021). Cover crops for orchard soil management. In *Cover Crops and Sustainable Agriculture* (pp. 147-168). CRC Press.

[5] Webber, S. M., Bailey, A. P., Huxley, T., Potts, S. G., & Lukac, M. (2022). Traditional and cover crop-derived mulches enhance soil ecosystem services in apple orchards. *Applied Soil Ecology*, *178*, 104569.

[6] Baluszynska, U. B., Rowinska, M., & Linczar-Malanczuk, M. (2022). Grass species as living mulches–Comparison of weed populations and their biodiversity in apple tree rows and tractor alleys. *Acta Agrobotanica*, *75*(1).

[7] Zanotelli, D., Vendrame, N., López-Bernal, Á., & Caruso, G. (2018). Carbon sequestration in orchards and vineyards. *Italus Hortus*, *2018*(3), 13-28.

[8] Dumitru, D., Bălțatu, C., Marin, E., Gheorghe, G. V., Manea, D., Mateescu, M., ... & Tăbăraşu, A. M. (2023). Study on the component elements of green cover equipment between the rows of vineyards and fruit trees, *Proceedings of ISB INMA TEH 2023, ISSN 2537 – 3773*, 656-665

[9] Dumitru, D. N., Marin, E., Gheorghe, G. V., Manea, D., Mateescu, M., Anghelache, D. N., ... & Harabagiu, A. (2024). Integration of edem by altair simulations for efficient distribution of large and small seeds in agricultural systems of vineyards and fruit trees. *INMATEH-Agricultural Engineering*, *74*(3).

[10] Manea, D. (2011). *Studii și cercetări privind optimizarea procesului de distribuţie al unei semănători de cereale păioase cu dozare centralizată [Studies and researches regarding optimization of the distribution process of a straw cereal sowing machine with centralized measuring]*. Teză de doctorat, Universitatea „Transilvania” din Brașov, Facultatea de Alimentație și Turism, Brașov.

# THERMO-MECHANICAL BEHAVIOUR OF BEESWAX-BASED OLEOGELS AND THEIR IMPACT ON THE NUTRI-SCORE PROFILE OF A REFORMULATED HAZELNUT SPREAD

/

# *COMPORTAMENTUL TERMO-MECANIC AL OLEOGELURILOR PE BAZĂ DE CEARĂ DE ALBINE ȘI IMPACTUL LOR ASUPRA PROFILULUI NUTRI-SCORE ÎNTR-O CREMĂ TARTINABILĂ DE ALUNE REFORMULATĂ*

**Anca-Ioana PUFLEA*, Sorin-Ștefan BIRIȘ, Mihaela BEGEA, Alexandru-Ionuț CIRIC**
Doctoral School of Biotechnical Systems Engineering - UNSP Bucharest / Romania.
**Tel: (+40) 723 015 908; *E-mail: anca.puflea@yahoo.com*

***Keywords:*** *oleogel; beeswax; inulin; Nutri-Score; hazelnut spread; thermo-mechanical behaviour; fat replacement.*

**ABSTRACT**

*Chocolate-hazelnut spreads typically combine a high added-sugar content with saturated-fat-rich lipid fractions, both of which penalise their Nutri-Score classification. This paper reports the nutritional reformulation of a commercial-type hazelnut spread through the substitution of sucrose with inulin and of the palm-oil-based lipid fraction with a sunflower-oil oleogel structured with beeswax. The control recipe and the reformulated product were characterised experimentally for dry matter, protein, fat, fatty-acid profile, sugars, fibre and sodium, and both were scored using the FSA/Nutri-Score algorithm. The oleogel was obtained by melting beeswax in sunflower oil under continuous stirring, followed by static cooling. Analytical results showed a reduction of over 60% in saturated fatty acids relative to the control, moving the reformulated product from Nutri-Score Class E to Class C. Replacing saturated fats with a beeswax-structured sunflower-oil oleogel, alongside the partial substitution of sugar with inulin, enables the reformulation of hazelnut spread by reducing saturated fatty acids by over 60% and improving its nutritional profile from Nutri-Score Class E to C, as demonstrated through analytical validation.*

**REZUMAT**

*Cremele tartinabile de ciocolată cu alune combină, de regulă, un conținut ridicat de zahăr adăugat cu o fracție lipidică bogată în acizi grași saturați, ambele reprezentând surse de penalizare pentru clasificarea Nutri-Score. Lucrarea prezintă reformularea nutrițională a unei creme tartinabile de tip comercial prin substituția zaharozei cu inulină și a fracției lipidice pe bază de ulei de palmier cu un oleogel pe bază de ulei de floarea-soarelui, stabilizat cu ceară de albine. Rețeta martor și produsul reformulat au fost analizate pentru determinarea substanței uscate, proteinelor, grăsimii, profilului de acizi grași, zaharurilor, fibrelor și sodiului, iar ambele au fost evaluate utilizând algoritmul FSA/Nutri-Score. Oleogelul a fost obținut prin topirea cerii de albine în ulei de floarea-soarelui sub agitare continuă, urmată de răcire statică. Rezultatele analitice au arătat o reducere de peste 60% a conținutului de acizi grași saturați față de martor, produsul reformulat trecând din clasa Nutri-Score E în clasa C. Înlocuirea grăsimilor saturate cu un oleogel pe bază de ulei de floarea-soarelui, stabilizat cu ceară de albine, alături de substituția parțială a zahărului cu inulină, permite reformularea cremei tartinabile de alune prin reducerea conținutului de acizi grași saturați cu peste 60% și îmbunătățirea profilului nutrițional de la clasa Nutri-Score E la C, așa cum a fost demonstrat prin validarea analitică.*

## INTRODUCTION

The Nutri-Score front-of-pack label classifies packaged foods from A to E using an algorithm adapted from the nutrient profiling model originally developed by the UK Food Standards Agency. The score is obtained by balancing negative points, allocated for energy, saturated fat, sugars and sodium, against positive points, allocated for fibre, protein and the proportion of fruit, vegetables, legumes and nuts. *(Hercberg et al., 2022)*

Spreadable hazelnut-cocoa products are structurally dependent on a solid fat fraction, usually palm oil, which provides spreadability and a stable crystalline network at room temperature, together with a high

sugar content that provides bulk and texture. Both components are heavily penalised by the Nutri-Score algorithm, so their simple reduction is not technologically viable without compromising product structure and sensory acceptance.

Oleogelation offers an alternative route: a liquid vegetable oil, rich in unsaturated fatty acids, is structured into a solid-like network by an organogelator such as beeswax, which crystallises on cooling into a three-dimensional wax-crystal matrix capable of immobilising the oil phase. The resulting oleogel can replace a saturated solid fat while retaining a markedly more favourable fatty-acid profile. Inulin, a soluble fibre extracted from chicory root, can similarly replace part of the sucrose fraction, acting as a bulking agent while contributing fibre points to the Nutri-Score calculation. *(Ropciuc et al., 2024, Żbikowska et al., 2022, De Los Santos-Trinidad et al., 2026, Karlović et al., 2026, Pușcaș et al., 2022, Perța-Crișan et al., 2023)*

This paper combines an experimental reformulation of a hazelnut spread using inulin and a beeswax-structured sunflower-oil oleogel with a literature-based synthesis of the thermo-mechanical behaviour of beeswax oleogels and of the laboratory-scale equipment used to obtain them, in order to contextualise the analytical results and to identify the process variables most likely to affect product texture in future optimisation work. *(Ropciuc et al., 2024, Żbikowska et al., 2022, De Los Santos-Trinidad et al., 2026, Karlović et al., 2026, Pușcaș et al., 2022, Perța-Crișan et al., 2023, Sivakanthan et al., 2024, Malvano et al., 2024, Hielscher Ultrasonics, n.d.)*

## MATERIALS AND METHODS

A commercial-type chocolate-hazelnut spread was used as control recipe. Its nutritional declaration per 100 g (2337 kJ / 559 kcal; 35 g fat, of which 16 g saturated; 55 g carbohydrate, of which 54 g sugars, and 0 g fibre; 4.6 g protein; 0.11 g salt; ~13% hazelnut content) was first scored with the FSA/Nutri-Score algorithm, confirming a Class E classification (score 26) and identifying saturated fat and sugars as the two components responsible for the maximum negative penalty (10 points each). This result justified the reformulation strategy described below. *(Hercberg et al., 2022)*

The oleogel was prepared by weighing 120 g of sunflower oil and 12 g of beeswax, heating the mixture on a water bath (bain-marie) at 62–65 °C until the wax was completely melted, avoiding thermal degradation of the oil.

The liquid phase was continuously stirred to ensure homogeneous dispersion of the molten wax, then cooled under static conditions at room temperature, allowing the wax to crystallise into the three-dimensional network that immobilises the oil and yields a solid oleogel (Fig. 1).




**Fig. 1 - Beeswax oleogel obtained by melting beeswax in sunflower oil, followed by static cooling.**

The reformulated spread was obtained by mechanically processing roasted, peeled hazelnuts in a high-speed blender until their own oils were released and a fluid hazelnut paste was formed. Dry ingredients

(inulin, raw cocoa powder and skimmed milk powder) were incorporated into the paste, followed by the solidified oleogel.

The mixture was homogenised until a smooth, glossy emulsion free of lumps was obtained; trace sucralose (<0.1%) was added at the end solely to adjust sweetness, followed by brief final mixing (Fig. 2).



**Fig. 2 - Reformulated hazelnut spread (inulin + beeswax oleogel).**

All physico-chemical analyses were performed on samples from a 600 g experimental batch, using standardised national (SR) and international (ISO) methods: dry matter/moisture by gravimetric drying (SR 2213-4:2007); total protein by Kjeldahl mineralisation, distillation and titration, N×6.25 (SR ISO 1871:2010); fatty-acid profile by gas chromatography of fatty-acid methyl esters after cold alkaline transesterification (SR EN ISO 12966-2:2017, SR EN ISO 12966-4:2015); reducing sugars by iodometric titration after Cu(II) reduction (SR 2213-13:2007); total fat by Soxhlet extraction with petroleum ether after acid hydrolysis (SR 2213-11:2007); and sodium by flame atomic absorption spectrometry after microwave acid digestion (SR EN 15505:2008). Salt content was calculated from the measured sodium content using the regulatory conversion factor (salt (g) = sodium (g) × 2.5). Fat isolation required solvent evaporation on a rotary evaporator (Fig. 3), one of several pieces of laboratory equipment relevant to oleogel-related sample processing.



**Fig. 3 - Rotary evaporator used for solvent removal during fat isolation.**

A literature-based synthesis complements the experimental work, comparing laboratory-scale equipment used for oleogel production and reporting published thermo-mechanical data on the effect of beeswax concentration, cooling rate and gelling-agent type on oleogel firmness.

Beyond the water-bath method used here, the literature describes three further categories of laboratory-scale equipment for oleogel structuring: magnetic hot-plate stirrers, ultrasonic probe homogenisers, high-shear rotor–stator mixers, and thermostatic cooling cabinets or baths. These alternatives are compared below, in relation to their expected effect on oleogel texture. *(Sivakanthan et al., 2024, Malvano et al., 2024, Hielscher Ultrasonics, n.d.)*

## COMPARISON OF LABORATORY-SCALE OLEOGEL-STRUCTURING EQUIPMENT

Four categories of laboratory-scale equipment are reported in the literature for the structuring step of oleogel production (Fig. 4): the magnetic hot-plate stirrer, equivalent in principle to the bain-marie method used in the present protocol but with mechanised, continuous agitation and more precise temperature control; the ultrasonic probe (sonotrode) homogeniser, which uses acoustic cavitation and intense micro-scale shear to disperse the gelling agent more finely; the high-shear rotor–stator mixer, a mechanical alternative to sonication, mainly used for pre-mixing at larger volumes; and the thermostatic cooling cabinet or bath, which imposes a controlled solidification temperature and cooling rate instead of static room-temperature cooling.

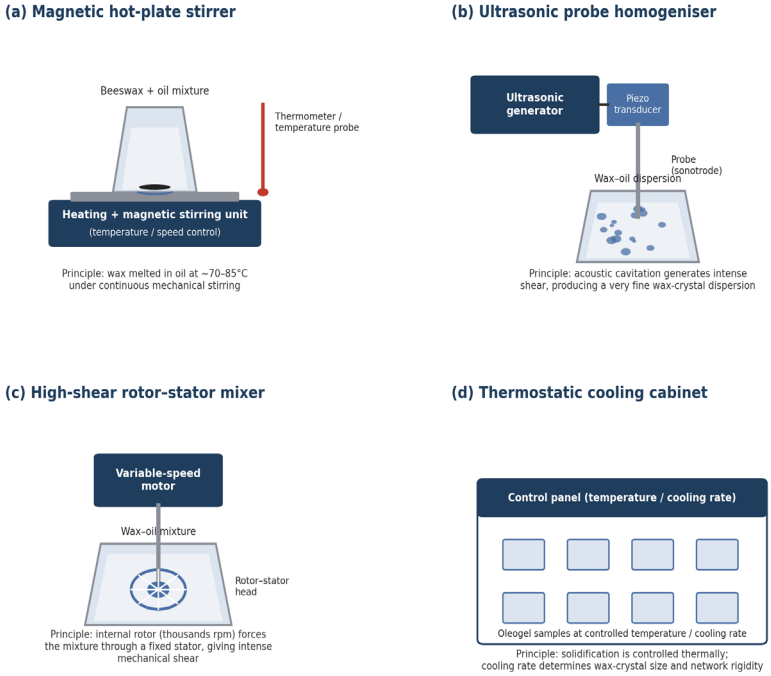



**Fig. 4 - Laboratory-scale equipment for oleogel structuring: (top-left) magnetic hot-plate stirrer; (top-right) ultrasonic probe homogeniser; (bottom-left) high-shear rotor–stator mixer; (bottom-right) thermostatic cooling cabinet.**

Table 1 **c**ompares the four categories on their operating principle, effect on the wax-crystal network, typical working volume, relative cost and recommended use, synthesised from the cited sources.

**Table 1**

**Comparison of laboratory-scale equipment used for beeswax-oleogel structuring.**

| Equipment | Principle | Effect on crystals | Typical volume | Cost | Recommended for |
|---|---|---|---|---|---|
| Magnetic hot-plate stirrer (present protocol) | Heating + mechanical stirring | Moderate homogenisation | 10 mL – few L | Low | Rapid screening; standard stability/ texture samples |
| Ultrasonic probe homogeniser | Acoustic cavitation; | Very fine dispersion; | 1 mL – 2 L | Medium–high | Fine structure, high homogeneity; |

| | | | | | |
|---|---|---|---|---|---|
| | micro-shear | smaller crystals | | | advanced research |
| High-shear rotor–stator mixer | Mechanical shear (rotor–stator) | Good dispersion; larger crystals than sonication | Hundreds mL – few L | Medium | Larger volumes; pre-mixing |
| Thermostatic cooling cabinet/bath | Precise control of cooling rate | Decisive for crystal size | Solidification step only | Low–medium | Reproducibility, regardless of homogenisation |

For a fine, reproducible oleogel structure, the ultrasonic probe homogeniser offers the best ratio between dispersion quality and process control, an advantage fully realised only when solidification subsequently takes place in a thermostatic cabinet with a controlled cooling rate; this combination is best suited to advanced structural optimisation.

For rapid recipe screening under limited resources — the situation of the present protocol (Fig. 1) — the bain-marie/hot-plate combined with static cooling remains adequate and is, in fact, the method most frequently reported for exploratory beeswax-oleogel work. *(Sivakanthan et al., 2024, Malvano et al., 2024, Hielscher Ultrasonics, n.d.)*

## RESULTS AND DISCUSSION

Table 2 compares four values per 100 g of product: the control (commercial) column reports the nutritional declaration of the unmodified commercial spread; the reformulated (theoretical) column gives the target values calculated from the reformulation recipe before laboratory analysis; the control (analytical) column reports the same control recipe as measured in-house using the analytical methods described above; and the reformulated (analytical) column reports the values actually measured for the reformulated spread, which are used for the final Nutri-Score classification.

**Table 2**

**Comparative nutritional profile of the control and reformulated hazelnut spreads (per 100 g).**

| Parameter | Unit | Control (commercial) | Reformulated (theoretical) | Control (analytical) | Reformulated (analytical) |
|---|---|---|---|---|---|
| Energy | kcal | 539 | 442 | 561 | 584 |
| Energy | kJ | 2252 | 1850 | 2338 | 2425 |
| Fat, total | g | 30.9 | 38 | 35.4 | 43.5 |
| of which saturates | g | 10.6 | 3 | 14.3 | 4.7 |
| Carbohydrate, total | g | 57.5 | 12.5 | 58.4 | 45.3 |
| of which sugars | g | 56.3 | < 3.0 | 53.0 | 31.2 |
| Fibre | g | 3.0 | 39.5 | 4.9 | 9.9 |
| Protein | g | 6.3 | 7.6 | 4.6 | 7.8 |
| Salt (Sodium) | g (mg) | 0.107 (44) | 0.110 (44) | 0.07 (27.2) | 0.07 (27.3) |

Nutri-Score calculation for the control spread yielded 7 points for energy, 10 for sugars (maximum penalty, above 45 g), 10 for saturated fat (maximum penalty, above 10 g) and 0 for sodium, for a total of 27 negative points; fibre contributed 5 positive points, and protein was disregarded because the negative score exceeded 11. The resulting score of 22 confirmed a Class E classification, consistent with the theoretical estimate from the commercial label.

For the reformulated spread, the same procedure yielded 7 points for energy, 6 for sugars, 4 for saturated fat and 0 for sodium (17 negative points), against 5 positive points for fibre, giving a raw score of 12 and a Class D classification. Saturated fat fell to only 4.7 g/100 g, close to the 3 g theoretical target and over 60% below the control, confirming the technological success of the oleogel substitution.

The largest deviation from the theoretical model concerned carbohydrates: although the recipe was designed without added sugar (<3 g sugars, 39.5 g fibre expected), the analytical report showed 31.2 g free sugars and only 9.9 g fibre.

This discrepancy is attributable to the purity of the inulin used: commercial food-grade inulin is not a chemically pure fructan and inherently contains a fraction of simple sugars, predominantly fructose, released during acid hydrolysis in the analytical procedure. Correcting the raw score by removing the 6 penalty points

attributable to this inulin-derived fructose fraction gives a corrected score of 6, placing the reformulated spread in Class C — an improvement of two Nutri-Score classes relative to the commercial control.

The magnitude of the change in saturated fat content is consistent with the thermo-mechanical behaviour reported for beeswax oleogels in the literature, which links oleogel firmness primarily to beeswax concentration and gelling-agent type rather than to the oil substrate itself. In peanut-oil oleogels, instrumentally measured firmness increased from 0.85 N at 2% beeswax to 14.01 N at 8% beeswax, a more than sixteen-fold, strongly non-linear increase concentrated between 4% and 6% wax content (Fig. 5).

This confirms that, below a threshold of roughly 4–6% structuring agent, a beeswax oleogel remains too soft to provide the solid-fat-like consistency required in a spreadable product. *(Żbikowska et al., 2022)*

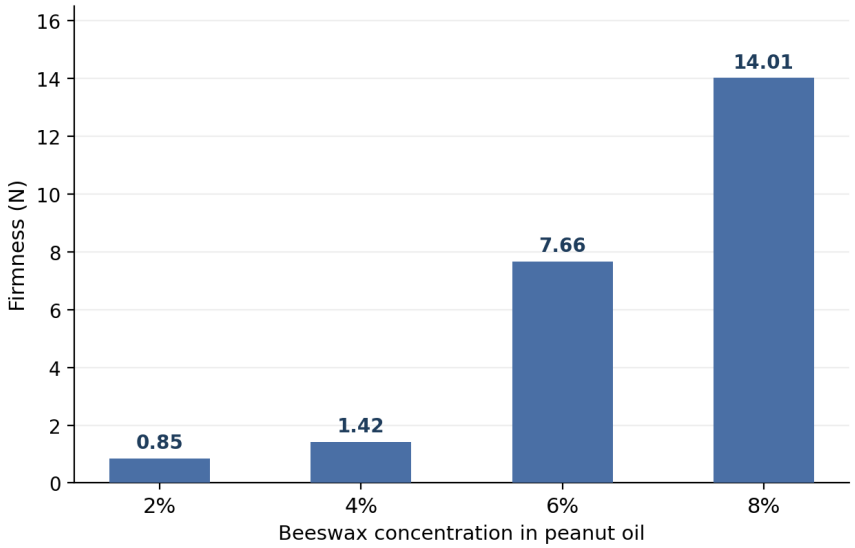



**Fig. 5 - Firmness of a peanut-oil oleogel as a function of beeswax concentration**
*(data from Żbikowska et al., 2022).*

Gelling-agent type has an even more significant effect than concentration alone: in a walnut-oil chocolate-butter formulation, a spread structured with 10% candelilla wax reached a hardness of 3521 g and an elastic modulus (G′) of 139 920 Pa, versus only 1136 g and 89 952 Pa for the equivalent monoglyceride-structured spread — a more than threefold difference in firmness at the same gelling-agent concentration (Fig. 6). *(Pușcaș et al., 2022)*

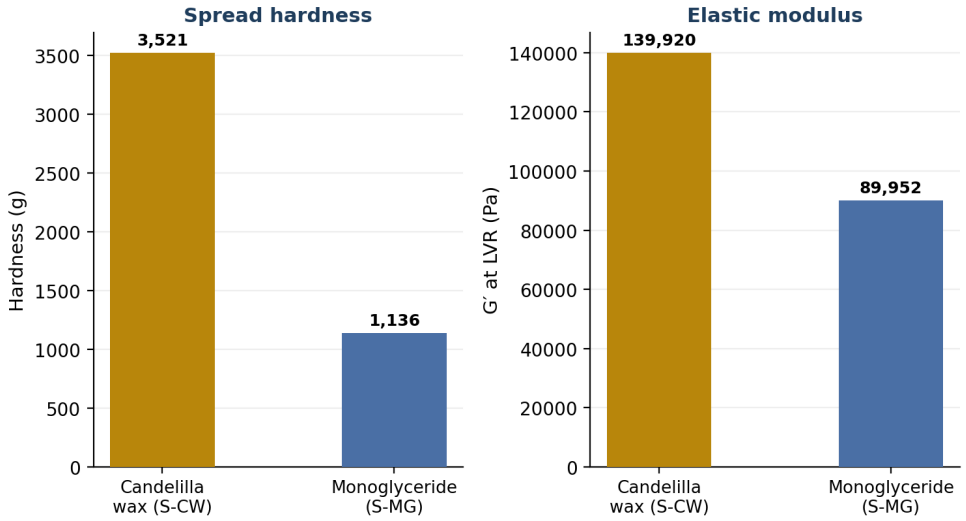



**Fig. 6 - Hardness and elastic modulus of walnut-oil spreads structured with candelilla wax versus monoglyceride, 10% w/w**
*(data from Pușcaș et al., 2022).*

Cooling rate also affects oleogel crystal size, but its effect on firmness is reported inconsistently across gelling-agent/oil systems: for a beeswax–stearic acid oleogel, slow cooling (0.5 °C/min) produced the most rigid network (G′ ≈ 107 400 Pa) and the largest, most uniformly distributed crystals, whereas other wax–oil systems in the literature become firmer under fast cooling.

The only consistent trend across studies is that faster cooling produces smaller crystals; its net effect on firmness must therefore be verified experimentally for each gelling-agent/oil combination rather than assumed from a single system. *(De Los Santos-Trinidad et al., 2026, Sivakanthan et al., 2024)*

Taken together, these results indicate that, of the process variables controllable at laboratory scale, gelling-agent concentration and type have a more significant and more predictable effect on oleogel texture than cooling rate. F

or the present work, the bain-marie/static-cooling method (Fig. 1) was adequate for a single-formulation proof of concept; a future optimisation of beeswax concentration would benefit from the ultrasonic-homogenisation and controlled-cooling equipment shown in Fig. 4, which the literature associates with finer, more reproducible wax-crystal networks. *(De Los Santos-Trinidad et al., 2026, Sivakanthan et al., 2024, Malvano et al., 2024, Hielscher Ultrasonics, n.d.)*

## CONCLUSIONS

Substituting the saturated-fat fraction of a commercial hazelnut spread with a beeswax-structured sunflower-oil oleogel, combined with partial replacement of sucrose by inulin, reduced saturated fatty acids by over 60% and moved the product from Nutri-Score Class E to Class C, an improvement confirmed analytically rather than only estimated theoretically.

The main deviation between the theoretical recipe and the analytical results originated in the intrinsic sugar fraction of commercial-grade inulin, which must be accounted for when interpreting Nutri-Score gains obtained through fibre-based sugar replacement.

The literature-based synthesis confirms that beeswax concentration and gelling-agent type are the process variables with the largest and most predictable influence on oleogel firmness, ahead of cooling rate, whose effect is system-dependent. Future work should therefore prioritise a systematic optimisation of beeswax concentration, supported where possible by ultrasonic homogenisation and controlled cooling, together with a lower-dosage, higher-purity inulin source to limit the analytical sugar deviation observed in this study.

This approach offers a promising strategy that can be extended to similar food matrices to enhance their nutritional profile while preserving their core organoleptic and structural properties.

## REFERENCES

[1] Hercberg, S., Touvier, M., Salas-Salvado, J., & Group of European scientists supporting the implementation of Nutri-Score in Europe. (2022). The Nutri-Score nutrition label: A public health tool based on rigorous scientific evidence aiming to improve the nutritional status of the population. International Journal for Vitamin and Nutrition Research, 92(3–4), 147–157. https://doi.org/10.1024/0300-9831/a000722

[2] Ropciuc, S., Dranca, F., Oroian, M. A., Leahu, A., Prisacaru, A. E., Spinei, M., & Codină, G. G. (2024). Characterization of Beeswax and Rice Bran Wax Oleogels Based on Different Types of Vegetable Oils and Their Impact on Wheat Flour Dough Technological Behavior during Bun Making. Gels, 10(3), 194. https://doi.org/10.3390/gels10030194

[3] Żbikowska, A. et al. (2022). Analysis of Stability, Rheological and Structural Properties of Oleogels Obtained from Peanut Oil Structured with Yellow Beeswax. Gels, 8(7), 448. https://doi.org/10.3390/gels8070448

[4] De Los Santos-Trinidad, J., Pintor-Jardines, A., Vernon-Carter, E. J., & Román-Guerrero, A. (2026). Modulation of physicochemical, textural, rheological, and thermal properties of beeswax oleogels based on the cooling rate and oil phase. Journal of the Science of Food and Agriculture. https://doi.org/10.1002/jsfa.70598

[5] Karlović, A., Banožić, M., Ačkar, Đ., Hasenay, S., & Šubarić, D. (2026). Aerogels and Oleogels as Functional Fat Replacers in Spreads — A Systematic Review. Applied Sciences, 16(3), 1654. https://doi.org/10.3390/app16031654

[6] Pușcaș, A., Tanislav, A. E., Mureșan, A. E., Fărcaș, A. C., & Mureșan, V. (2022). Walnut Oil Oleogels as Milk Fat Replacing System for Commercially Available Chocolate Butter. Gels, 8(10), 613. https://doi.org/10.3390/gels8100613

[7] Perța-Crișan, S., Ursachi, C.-Ș., Chereji, B.-D., & Munteanu, F.-D. (2023). Oleogels—Innovative Technological Solution for the Nutritional Improvement of Meat Products. Foods, 12(1), 131. https://doi.org/10.3390/foods12010131

[8] Sivakanthan, S., Fawzia, S., Mundree, S., Madhujith, T., & Karim, A. (2024). Effect of Cooling Rate on Properties of Beeswax and Stearic Acid Oleogel Based on Rice Bran Oil and Sesame Oil. Gels, 10(11), 697. https://doi.org/10.3390/gels10110697

[9] Malvano, F., Albanese, D., Cinquanta, L., Liparoti, S., & Marra, F. (2024). A Comparative Study between Beeswax and Glycerol Monostearate for Food-Grade Oleogels. Gels, 10(4), 214. https://doi.org/10.3390/gels10040214

[10] Hielscher Ultrasonics. Homogenizers – Working Principle, Use and Scale-Up. https://www.hielscher.com/homogenizers-working-principle-use-and-scale-up.htm

# STATIC STABILITY ANALYSIS OF THE NAIO OZ AUTONOMOUS AGRICULTURAL ROBOT OPERATING ON SLOPED TERRAIN

/

# *ANALIZA STABILITĂȚII STATICE A ROBOTULUI AGRICOL AUTONOM NAIO OZ ÎN CONDIȚII DE OPERARE PE TEREN ÎNCLINAT*

**Radu Nicolae SOARE*[1)], Andreea Alexandra FRUSINOIU[1)], Sorin Stefan BIRIȘ[1)], Edmond MAICAN[1)], Eugen MARIN[2)]**

[1)] UNSTP Bucharest, Faculty of Biotechnical Systems Engineering, Bucharest / Romania;
[2)] INMA Bucharest / Romania.
**E-mail: radunicolae11@yahoo.com*

***Keywords:*** *autonomous agricultural robot, Naio OZ, static stability, sloped terrain, agricultural robotics*

**ABSTRACT**

*The increasingly widespread use of autonomous agricultural robots has highlighted the importance of operational safety under different terrain conditions. This paper presents a technical assessment of the static stability of the Naio OZ autonomous agricultural robot operating on sloped terrain. The study focused on the influence of geometric characteristics, mass distribution, wheel configuration and center of gravity position on rollover resistance. The theoretical analysis was performed with a rigid-body model based on the technical specifications available in the manufacturer's documentation, the parameters not provided by the manufacturer being estimated and treated parametrically. The static behavior of the robot was evaluated under longitudinal and transverse inclinations for three working configurations, and the corresponding rollover and sliding limits were estimated. Transverse rollover was the critical mode in all cases, with static stability angles of 31.2°, 31.6° and 24.8°, corresponding to maximum recommended operating slopes of 40.4%, 40.9% and 30.8%. Particular attention was given to the relationship between the center of gravity height, track width and maximum permissible operating slope, and to the reduction of the stability reserve caused by uneven ground and emergency braking.*

**REZUMAT**

*Utilizarea pe scară tot mai largă a roboților agricoli autonomi a evidențiat importanța siguranței în exploatare în diferite condiții de teren. Lucrarea prezintă o evaluare tehnică a stabilității statice a robotului agricol autonom Naio OZ în condiții de deplasare pe terenuri înclinate. Studiul s-a concentrat asupra influenței caracteristicilor geometrice, distribuției maselor, configurației roților și poziției centrului de greutate asupra rezistenței la răsturnare. Analiza teoretică a fost realizată cu un model de corp rigid bazat pe specificațiile tehnice din documentația producătorului, parametrii nefurnizați de acesta fiind estimați și tratați parametric. Comportamentul static al robotului a fost evaluat pentru înclinări longitudinale și transversale, în trei configurații de lucru, fiind estimate limitele corespunzătoare de răsturnare și de alunecare. Răsturnarea transversală a fost modul critic în toate cazurile, cu unghiuri statice de stabilitate de 31,2°, 31,6° și 24,8°, corespunzătoare unor pante maxime de lucru recomandate de 40,4%, 40,9% și 30,8%. O atenție deosebită a fost acordată relației dintre înălțimea centrului de greutate, ecartament și panta maximă admisibilă de operare, precum și reducerii rezervei de stabilitate cauzate de denivelările terenului și de frânarea de urgență.*

## INTRODUCTION

The increasing development of agricultural robotics has created new possibilities for the automation of field operations, particularly in activities that require repetitive work, precise trajectory following and continuous operation in crop fields. Agricultural field robots integrate mechanical systems, sensing technologies, navigation, control and task-specific equipment, their operational performance depending on the coordinated operation of these subsystems *(Upadhyay et al., 2024)*. The development of autonomous platforms has therefore become an important research direction for improving the efficiency and flexibility of agricultural operations *(Rondelli, Franceschetti and Mengoli, 2022)*.

Unlike conventional agricultural machines operated by a human driver, autonomous agricultural robots must perform navigation and operational decisions while interacting directly with variable and partially

unpredictable field conditions. Agricultural environments may include irregular terrain, soil variability, obstacles and inclined surfaces, which can influence the mobility and stability of robotic platforms *(Quaglia et al., 2020; Rondelli, Capacci and Franceschetti, 2022)*. Consequently, the mechanical configuration of the mobile platform is an important factor in determining its ability to operate safely under field conditions.

Among the mechanical characteristics of an agricultural robotic platform, static stability is particularly relevant when the vehicle operates on inclined terrain. The inclination of the supporting surface modifies the relationship between the gravitational force acting through the center of gravity (CoG) and the contact area defined by the wheels or tracks. When the projection of the CoG approaches the boundary of the support polygon, the vehicle approaches a critical stability condition and the risk of rollover increases. For robotic platforms operating without a human operator, this assessment is particularly important, because the robot must maintain an adequate stability margin without direct intervention.

The stability of agricultural vehicles is influenced by geometry, wheel or track configuration, track width, wheelbase, mass distribution and CoG position. *Vidoni et al. (2015)* compared different vehicle configurations for robotic agricultural operations on side-slopes using a roll stability index and demonstrated the relevance of the mobile configuration for operation on inclined terrain. Research on tractors has clarified rollover mechanics and countermeasures *(Wang et al., 2024)*, showing that static lateral stability depends strongly on track width, CoG height, ballast and tire deformation *(Franceschetti et al., 2021; Majdan et al., 2021)*, and that attached implements can change the critical rollover angle significantly *(Jang et al., 2022; Kang et al., 2022)*. Similar analyses were performed on other self-propelled agricultural machines *(Chowdhury et al., 2023)*.

The static stability of self-propelled agricultural machines can be assessed using analytical models based on the geometry of the vehicle, the position of its CoG and the contact points with the terrain. *Petrović et al. (2021)* developed an analytical approach for determining the critical pitch and roll angles and the maximum permissible slope of self-propelled agricultural machines, considering the machine as a rigid body supported by three or four contact points and combining theoretical mechanics with three-dimensional analytical geometry. In addition, ISO 16231-2 defines a reference static stability angle (RSSA) and a machine operating slope (MOS) related by a safety factor of 1.5, values which were recently combined with terrain models to map rollover risk at field scale *(International Organization for Standardization, 2015; Puri et al., 2025)*.

For unmanned vehicles the problem is less documented. Standards for highly automated agricultural machines deal mainly with perception and protective zones and do not specify stability requirements *(International Organization for Standardization, 2018; Tiusanen et al., 2020)*, although tilting-platform tests on an orchard unmanned ground vehicle (UGV) showed that the implement configuration can change its longitudinal stability angle by more than 15° *(Rondelli, Capacci and Franceschetti, 2022)*.

The Naio OZ is a compact, electrically powered autonomous robot developed for market gardening and specialty crops. According to the manufacturer, the platform has four driven wheels and RTK-GNSS autonomous navigation *(Naïo Technologies, 2026)*. Published work on the OZ has focused mainly on its software, for example through the testing of weeding missions in virtual fields *(Robert et al., 2020)*, while its stability on sloped terrain has received little attention. Moreover, the available technical documentation does not provide all the parameters required for a direct determination of the CoG and of the rollover limits, so that a theoretical and parametric approach is appropriate.

The objective of this study was to perform a technical assessment of the static stability of the Naio OZ robot under longitudinal and transverse terrain inclinations, considering the influence of the geometric configuration, track width, CoG height and working equipment on the critical rollover and sliding conditions, and to derive recommended operating slopes that can be used as limits in mission planning.

## MATERIALS AND METHODS

The static stability analysis was performed for the Naio OZ autonomous agricultural robot (Fig. 1), developed by Naïo Technologies (France) for operations such as sowing, row marking, hoeing and weeding. The analysis was entirely theoretical: no experimental measurements were carried out, and the model was based on the technical specifications provided by the manufacturer and on a rigid-body representation of the robot on inclined terrain.



**Fig. 1 - Naio OZ autonomous agricultural robot**
*(source: Naïo Technologies)*
*front view of the robot during mechanical hoeing between crop rows, illustrating its narrow track width*

The main characteristics of the robot are given in Table 1. The declared data were taken from the manufacturer's documentation, which specifies a length of 1.30 m, a width of 0.47 m, a height of 0.83 m, a mass of 150 kg, four driven wheels, a maximum speed of 1.8 km/h and an autonomy of up to 8 hours. The wheelbase, the track width measured between the wheel contact centers and the CoG position are not published; they were therefore not assumed equal to the external dimensions, but estimated from the overall dimensions and from the layout of the robot, in which the battery pack and the four hub motors are placed low in the chassis. Because of this uncertainty, the CoG height and the track width were also varied parametrically.

**Table 1**

**Main characteristics of the Naio OZ robot used in the model**

| Characteristic | Value | Source |
|---|---|---|
| Overall length × width × height, [m] | 1.30 × 0.47 × 0.83 | declared |
| Robot mass, $m$, [kg] | 150 | declared |
| Wheel drive configuration | 4WD, 4 electric motors | declared |
| Maximum forward speed, [km/h] | 1.8 | declared |
| Wheelbase, $L_w$, [m] | 0.70 | estimated |
| Track width, $B$, [m] | 0.40 | estimated |
| CoG height (unladen), $h$, [m] | 0.33 | estimated |
| CoG longitudinal position (unladen) | mid-wheelbase | estimated |

Three working configurations were analyzed. Configuration C1 was the unladen robot. In configuration C2, a rear weeding toolbar with hoeing tools (25 kg) was attached, with its CoG 0.20 m behind the rear axle and 0.30 m above the ground. Configuration C3 added to C2 a transported load of 40 kg (e.g. harvest crates) placed on the upper deck, centered between the axles at a CoG height of 0.90 m. The masses and positions of the equipment were chosen as representative values. The resultant CoG of each configuration was obtained from the mass moments of its components:

$$x_G = \Sigma\, m_i\, x_i / \Sigma\, m\ ,\ h = \Sigma\, m_i\, z_i / \Sigma\, m_i \qquad (1)$$

where $m_i$ is the mass of component $i$, [kg]; $x_i$, $z_i$ – longitudinal and vertical coordinates of its CoG, [m]; $x_G$, $h$ – longitudinal position and height of the resultant CoG, [m]. The origin of the coordinate system

was placed on the ground, at the center of the support rectangle formed by the four wheel contact points, with the *x* axis pointing forward (Fig. 2).

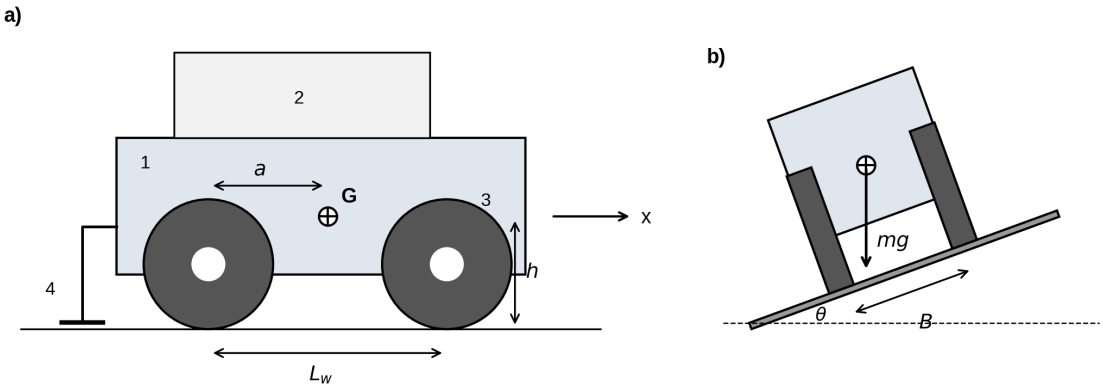



**Fig. 2 - Calculation scheme of the robot: a) side view; b) rear view on a transverse slope**
*1 - chassis with battery pack; 2 - transported load (configuration C3); 3 - drive wheel with hub motor; 4 - rear weeding toolbar; G - center of gravity*

The robot was treated as a rigid body resting on four point contacts, without suspension compliance or tire deformation, which is justified by its rigid chassis and low operating speed. Under static conditions, the robot was considered stable as long as the vertical projection of its CoG remained within the support polygon; the critical condition was reached when this projection coincided with the polygon boundary, i.e. when the normal reactions on the uphill wheels became zero. For a robot facing across the slope, the transverse static stability angle $\alpha_{lat}$ follows from:

$$\tan \alpha_{lat} = (B/2 - |y_G|) / h \tag{2}$$

and, for a robot facing up or down the slope, the uphill and downhill static stability angles are:

$$\tan \alpha_{up} = a / h , \quad \tan \alpha_{down} = (L_w - a) / h \tag{3}$$

where $B$ is the track width, [m]; $y_G$ – lateral offset of the CoG, [m]; $L_w$ – wheelbase, [m]; $a = x_G + L_w/2$ – horizontal distance between the rear axle and the CoG, [m]. For an arbitrary heading $\psi$ measured from the uphill direction and a slope angle $\theta$, the projection of the CoG along the vertical onto the support plane has the coordinates:

$$x_p = x_G - h \tan \theta \cos \psi, \quad y_p = y_G - h \tan \theta \sin \psi \tag{4}$$

and the robot is statically stable as long as $-L_w/2 \le x_p \le L_w/2$ and $|y_p| \le B/2$. The critical slope $\theta_{cr}(\psi)$ was found numerically for $\psi$ = 0...360° in steps of 5°, with a resolution of 0.001°. Sliding of the braked or driven robot was assumed to occur when the slope exceeded the friction limit:

$$\tan \theta_s = \mu \tag{5}$$

where $\mu$ is the wheel–soil friction coefficient, [-], taken between 0.4 (wet, loose soil) and 0.7 (dry, firm soil).

Following the approach of ISO 16231-2, each static stability angle was converted into a recommended machine operating slope, expressed in percent, by dividing the corresponding slope by the safety factor of 1.5:

$$MOS = 100 \cdot \tan \alpha_{min} / 1.5 \tag{6}$$

Finally, the reduction of the stability reserve produced by operational factors was estimated through equivalent tilt angles. A longitudinal deceleration $a_x$ [m/s$^2$] and a turn of radius $R$ [m] at speed $v$ [m/s] were converted into $\Delta\alpha = \arctan(a_x/g)$ and $\Delta\alpha = \arctan(v^2/(R\ g))$, respectively, and a level difference $\Delta z$ [m] between the left and right wheel tracks, typical when one track runs in a furrow and the other on the bed shoulder, into $\Delta\alpha = \arcsin(\Delta z/B)$. The effect of the tool draft force $F_d$ [N], applied at a height $h_d$ [m] above the

ground, on the uphill stability of configuration C2 was obtained from the moment equilibrium about the rear wheel contact line:

$$m\,g\,(a\cos\theta - h\sin\theta) - F_d\,h_d = 0 \tag{7}$$

where $g$ = 9.81 m/s$^2$ is the gravitational acceleration. All calculations were performed in Python using the NumPy library.

## RESULTS AND DISCUSSION

The mass, CoG position, static stability angles and recommended operating slopes obtained for the three configurations are summarized in Table 2. In all configurations the transverse static stability angle was the smallest, which confirmed that the narrow track width of the robot governed its stability. The weeding toolbar moved the CoG 0.079 m rearward and slightly downward, so that the transverse angle remained practically unchanged (31.6° instead of 31.2°), while the uphill angle decreased from 46.7° to 39.8° and the downhill angle increased to 52.8°. The transported load raised the CoG to 0.433 m and reduced the transverse angle to 24.8°, which represented a 20% loss of transverse stability compared with the unladen robot.

**Table 2**

**Mass properties, static stability angles and recommended operating slopes**

| Configuration | $m$ [kg] | $x_G$ [m] | $h$ [m] | $\alpha_{lat}$ [°] | $\alpha_{up}$ [°] | $\alpha_{down}$ [°] | MOS [%] transv. / long. |
|---|---|---|---|---|---|---|---|
| C1 – unladen | 150 | 0.000 | 0.330 | 31.2 | 46.7 | 46.7 | 40.4 / 70.7 |
| C2 – toolbar | 175 | −0.079 | 0.326 | 31.6 | 39.8 | 52.8 | 40.9 / 55.6 |
| C3 – toolbar + load | 215 | −0.064 | 0.433 | 24.8 | 33.5 | 43.7 | 30.8 / 44.1 |

The dependence of the critical slope on the heading of the robot is shown in Fig. 3. The stability domains had an approximately rectangular shape elongated along the direction of travel, and for headings deviating by more than about 30° from the fall line rollover took place about the downhill wheel line, the critical slope decreasing progressively to the transverse value at ψ = 90° and ψ = 270°. Comparing the domains with the sliding limits showed that, for the unladen robot and for the robot with the toolbar, sliding on wet soil (μ = 0.4, $\theta_s$ = 21.8°) preceded rollover in every direction, whereas on dry soil (μ = 0.6, $\theta_s$ = 31.0°) the two phenomena became almost simultaneous in the transverse direction. With the transported load, transverse rollover at 24.8° occurred before sliding whenever μ exceeded 0.46.

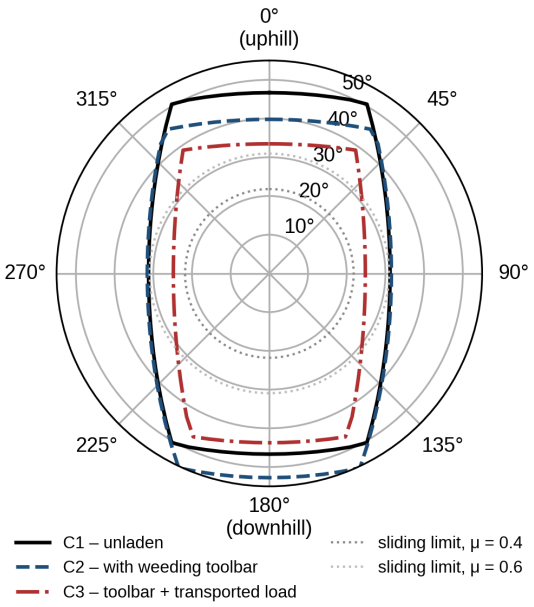



**Fig. 3 - Critical slope angle as a function of the heading of the robot**

*0° - robot facing uphill; 90° and 270° - robot travelling across the slope; dotted circles - sliding limits*

The sensitivity of the transverse stability angle to the CoG height and to the track width is presented in Fig. 4. For the estimated track width of 0.40 m, each 0.05 m increase of the CoG height between 0.33 m and 0.48 m reduced the transverse angle by 2.3–3.5°, and a variation of the track width by ±0.05 m shifted it by approximately ±3° at the unladen CoG height. The transverse angle fell below the wet-soil sliding limit only for CoG heights above 0.50 m, which corresponded to loads placed well above the upper deck. Since the CoG height and track width were estimated, Fig. 4 also indicates the range within which the actual stability angles are expected to lie.

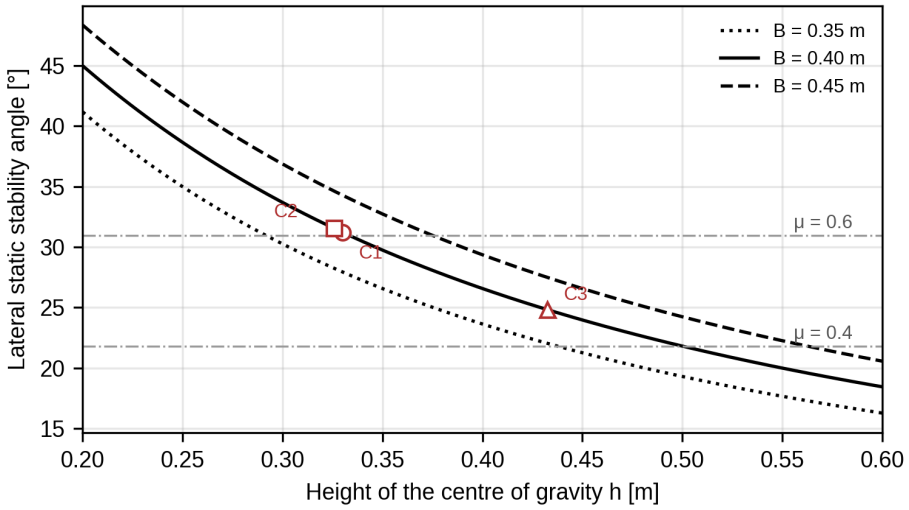



**Fig. 4 - Transverse static stability angle versus CoG height for three track widths**

*markers - configurations C1, C2 and C3 (B = 0.40 m); dash-dot lines - sliding limits for μ = 0.4 and μ = 0.6*

The equivalent reductions of the stability angle produced by the operational factors are given in Table 3. The centrifugal effect in a headland turn was below 1°, and the tool draft force reduced the uphill angle of configuration C2 by only 1.2–2.4°. In contrast, decelerations of 1.0–2.0 m/s$^2$ during an emergency stop generated equivalent tilts of 5.8–11.5°, and a level difference of 0.05–0.10 m between the wheel tracks consumed 7.2–14.5° of the transverse reserve. A lateral eccentricity of the transported load by 0.05 m further reduced the transverse angle of configuration C3 by 5.7°. When the most unfavorable transverse factors were combined for configuration C3 (0.05 m load eccentricity and 0.10 m level difference), the remaining transverse reserve on level ground was only 4.6°.

**Table 3**

**Reduction of the stability reserve caused by operational factors**

| Factor | Conditions | Direction affected | Δα [°] |
|---|---|---|---|
| Turning (centrifugal effect) | v = 0.5 m/s, R = 1.5 m | transverse | 1.0 |
| Tool draft force (C2) | $F_d$ = 150 / 300 N, $h_d$ = 0.10 m | uphill | 1.2 / 2.4 |
| Deceleration | $a_x$ = 0.5 / 1.0 / 2.0 m/s$^2$ | longitudinal | 2.9 / 5.8 / 11.5 |
| Level difference between tracks | Δz = 0.05 / 0.10 m | transverse | 7.2 / 14.5 |
| Lateral eccentricity of load (C3) | $y_G$ offset 0.02 / 0.05 m | transverse | 2.2 / 5.7 |

The transverse stability angles obtained for the OZ robot were lower than the 47–50° measured experimentally on a heavier tracked orchard UGV with a track width of 0.92 m *(Rondelli, Capacci and Franceschetti, 2022)*, which was consistent with the much narrower track of the OZ. Nevertheless, the recommended transverse operating slopes of 30.8–40.9% are likely to exceed the gradients of most market-gardening plots, so that under typical field conditions the practical limits will be set by sliding and by local terrain irregularities rather than by static rollover.

## CONCLUSIONS

- A rigid-body static model, based on the manufacturer's specifications and on estimated geometric parameters, allowed the rollover and sliding limits of the Naio OZ robot to be assessed without experimental measurements.

- Transverse rollover was the governing instability mode in all configurations, with static stability angles of 31.2° for the unladen robot, 31.6° with the rear weeding toolbar and 24.8° with an additional 40 kg load on the upper deck.
- Applying a safety factor of 1.5, the recommended transverse operating slopes were 40.4%, 40.9% and 30.8%, respectively, while the longitudinal limits were considerably higher.
- The rear toolbar mainly affected longitudinal stability, reducing the uphill stability angle by about 7°, whereas an elevated transported load reduced all stability angles and represented the most critical configuration.
- For the unladen robot and the robot with the toolbar, sliding on wet soil preceded rollover, so traction and braking limits, rather than overturning, will usually restrict operation on slopes.
- Level differences between the wheel tracks and emergency braking reduced the stability reserve far more than turning or tool draft; loads should be placed as low and as centered as possible, and traversing slopes with one track in a furrow should be avoided.
- The derived slope limits can be implemented in mission planning together with inclination monitoring by the on-board sensors; since the wheelbase, track width and CoG position were estimated, the results should be validated by weighing, CoG determination and tilting-platform tests.

**REFERENCES**

[1] Chowdhury, M., Ali, M., Habineza, E., Reza, M. N., Kabir, M. S. N., Lim, S.-J., Choi, I.-S., & Chung, S.-O. (2023). Analysis of rollover characteristics of a 12 kW automatic onion transplanter to reduce stability hazards. *Agriculture*, *13*(3), 652. https://doi.org/10.3390/agriculture13030652

[2] Franceschetti, B., Rondelli, V., & Capacci, E. (2021). Lateral stability performance of articulated narrow-track tractors. *Agronomy*, *11*(12), 2512. https://doi.org/10.3390/agronomy11122512

[3] International Organization for Standardization. (2015). *Self-propelled agricultural machinery — Assessment of stability — Part 2: Determination of static stability and test procedures* (ISO Standard No. 16231-2:2015).

[4] International Organization for Standardization. (2018). *Agricultural machinery and tractors — Safety of highly automated agricultural machines — Principles for design* (ISO Standard No. 18497:2018).

[5] Jang, M.-K., Hwang, S.-J., & Nam, J.-S. (2022). Simulation study for overturning and rollover characteristics of a tractor with an implement on a hard surface. *Agronomy*, *12*(12), 3093. https://doi.org/10.3390/agronomy12123093

[6] Kang, S., Kim, Y., Park, H., Kim, Y., Woo, S., Uyeh, D. D., & Ha, Y. (2022). Rollover safety and workable boundary suggestion of an agricultural platform with different attachments. *Agriculture*, *12*(8), 1148. https://doi.org/10.3390/agriculture12081148

[7] Majdan, R., Abrahám, R., Tkáč, Z., Drlička, R., Matejková, E., Kollárová, K., & Mareček, J. (2021). Static lateral stability of tractor with rear wheel ballast weights: Comparison of ISO 16231-2 (2015) with experimental data regarding tyre deformation. *Applied Sciences*, *11*(1), 381. https://doi.org/10.3390/app11010381

[8] Naïo Technologies. (2026). *OZ robot* [Product description]. https://www.naio-technologies.com/en/oz-robot/

[9] Petrović, D. V., Cerović, V. B., Radojević, R. L., & Mileusnić, Z. I. (2021). An approach to characterization of the agricultural self-propelled machines stability. *Journal of Terramechanics*, *93*, 51–63. https://doi.org/10.1016/j.jterra.2020.11.001

[10] Puri, D., Vita, L., Gattamelata, D., & Tulliani, V. (2025). Roll/tip-over risk analysis of agricultural self-propelled machines using airborne LiDAR data: GIS-based approach. *Machines*, *13*(5), 377. https://doi.org/10.3390/machines13050377

[11] Quaglia, G., Visconte, C., Scimmi, L. S., Melchiorre, M., Cavallone, P., & Pastorelli, S. (2020). Design of a UGV powered by solar energy for precision agriculture. *Robotics*, *9*(1), 13. https://doi.org/10.3390/robotics9010013

[12] Robert, C., Sotiropoulos, T., Waeselynck, H., Guiochet, J., & Vernhes, S. (2020). The virtual lands of Oz: Testing an agribot in simulation. *Empirical Software Engineering*, *25*(3), 2025–2054. https://doi.org/10.1007/s10664-020-09800-3

[13] Rondelli, V., Capacci, E., & Franceschetti, B. (2022). Evaluation of the stability behavior of an agricultural unmanned ground vehicle. *Sustainability*, *14*(23), 15561. https://doi.org/10.3390/su142315561

[14] Rondelli, V., Franceschetti, B., & Mengoli, D. (2022). A review of current and historical research contributions to the development of ground autonomous vehicles for agriculture. *Sustainability*, *14*(15), 9221. https://doi.org/10.3390/su14159221

[15] Tiusanen, R., Malm, T., & Ronkainen, A. (2020). An overview of current safety requirements for autonomous machines – Review of standards. *Open Engineering*, *10*(1), 665–673. https://doi.org/10.1515/eng-2020-0074

[16] Upadhyay, A., Zhang, Y., Koparan, C., Rai, N., Howatt, K., Bajwa, S., & Sun, X. (2024). Advances in ground robotic technologies for site-specific weed management in precision agriculture: A review. *Computers and Electronics in Agriculture*, *225*, 109363. https://doi.org/10.1016/j.compag.2024.109363

[17] Vidoni, R., Bietresato, M., Gasparetto, A., & Mazzetto, F. (2015). Evaluation and stability comparison of different vehicle configurations for robotic agricultural operations on side-slopes. *Biosystems Engineering*, *129*, 197–211. https://doi.org/10.1016/j.biosystemseng.2014.10.003

[18] Wang, L., Liu, F., Song, Z., Ni, Y., He, Z., Zhai, Z., Zhu, Z., Zhou, Z., Song, Z., & Li, Z. (2024). Advances in tractor rollover and stability control: Implications for off-road driving safety. *Computers and Electronics in Agriculture*, *226*, 109483. https://doi.org/10.1016/j.compag.2024.109483

# ANALYSIS OF RESEARCH TRENDS IN THE USE OF EVOLUTIONARY ALGORITHMS FOR THE MECHANICAL DESIGN OF AGRICULTURAL TECHNICAL SYSTEMS

/

# *ANALIZA TENDINȚELOR CERCETĂRII PRIVIND UTILIZAREA ALGORITMILOR EVOLUTIVI ÎN PROIECTAREA MECANICĂ A SISTEMELOR TEHNICE AGRICOLE*

**Andreea Alexandra FRUSINOIU*, Radu Nicolae SOARE, Sorin Stefan BIRIȘ, Adrian IOSIF**
UNSTP Bucharest, Faculty of Biotechnical Systems Engineering, Bucharest / Romania
**Tel: 0721 485 685; *E-mail: andreea.frusinoiu@stud.isb.upb.ro*

***Keywords:*** *evolutionary algorithms, genetic algorithms, multi-objective optimization, agricultural machinery design, surrogate-assisted optimization, metaheuristics*

***Abbreviations:*** *ANN – artificial neural network; CANFIS – coactive neuro-fuzzy inference system; DE – differential evolution; CMA-ES – covariance matrix adaptation evolution strategy; EA – evolutionary algorithm; ES – evolution strategies; FEM – finite element method; GA – genetic algorithm; HGA – hybrid genetic algorithm; MO – multi-objective; MOGA – multi-objective genetic algorithm; NSGA-II/III – non-dominated sorting genetic algorithm II/III; PSO – particle swarm optimization; SO – single-objective*

**ABSTRACT**

*The continuous development of agricultural technical systems and the increasing requirements for performance, energy efficiency, reliability, and sustainability have intensified research efforts focused on the application of advanced optimization methods in mechanical design. In this context, evolutionary algorithms represent an important class of optimization techniques inspired by natural processes of evolution and adaptation, being widely used to solve complex engineering problems characterized by multiple objectives and constraints. This paper presents an analysis of worldwide research trends regarding the application of evolutionary algorithms in mechanical design, with particular emphasis on agricultural technical systems. The study examines the main categories of algorithms reported in the scientific literature, including Genetic Algorithms, Evolution Strategies, Differential Evolution, and Particle Swarm Optimization, highlighting their application areas and advantages. The research aims to identify current trends, the most frequently addressed optimization objectives, and the main development directions in the field. The analysis reveals a significant increase in the interest for applying evolutionary algorithms to the design and optimization of agricultural machinery and equipment, contributing to improved functional performance, reduced resource consumption, and the development of innovative engineering solutions for modern agriculture. The findings emphasize the growing role of evolutionary optimization methods in supporting the design of efficient and sustainable agricultural technical systems.*

**REZUMAT**

*Dezvoltarea continuă a sistemelor tehnice agricole și creșterea cerințelor privind performanța, eficiența energetică, fiabilitatea și sustenabilitatea acestora au determinat intensificarea cercetărilor privind utilizarea metodelor avansate de optimizare în proiectarea mecanică. În acest context, algoritmii evolutivi reprezintă o categorie importantă de metode de optimizare inspirate din procesele naturale de evoluție și adaptare, fiind utilizați pentru rezolvarea unor probleme complexe caracterizate prin multiple obiective și constrângeri. Lucrarea prezintă o analiză a stadiului cercetărilor efectuate la nivel mondial privind aplicarea algoritmilor evolutivi în proiectarea mecanică, cu accent asupra sistemelor tehnice agricole. Sunt analizate principalele categorii de algoritmi utilizate în literatura de specialitate, precum algoritmii genetici, strategiile evolutive, evoluția diferențială și optimizarea prin roiuri de particule, evidențiindu-se domeniile de aplicare și avantajele acestora. Studiul urmărește identificarea tendințelor actuale de cercetare, a obiectivelor de optimizare abordate și a direcțiilor de dezvoltare din domeniu. Analiza evidențiază o creștere semnificativă a interesului pentru utilizarea algoritmilor evolutivi în proiectarea și optimizarea echipamentelor agricole, contribuind la îmbunătățirea performanțelor funcționale, reducerea consumului de resurse și dezvoltarea unor soluții inginerești inovatoare pentru agricultura modernă.*

## INTRODUCTION

The ongoing development of agricultural technical systems has led to increasing demand for their functional performance, energy efficiency, reliability, and sustainability. Because of the complexities of modern agricultural machinery operating under dynamic and varied conditions, it is necessary to consider the machines' operational efficiencies, energy use, environmental effects, and interactions with the soil, crop, or seed (*Filip et al., 2020; Maraveas et al., 2023*). When designing agricultural machinery, there is usually a non-linear relationship between the design variables and the performance metrics, a mixture of continuous and discrete variables, many potential local optima and expensive evaluations of performance (e.g., via finite element analysis, discrete element simulation or testing in the field).

Therefore, gradient-based methods may become trapped in a local optimum instead of the global one or may even be completely inapplicable. Evolutionary algorithms (EAs) have emerged as an alternative to gradient-based methods. The most well-known type of EA is the genetic algorithm (GA), developed by *Holland (1975)*. EAs operate by evolving a population of candidate solutions through selection, crossover and mutation processes. EAs require only the values of the objective function for each candidate solution, not its derivatives. Multi-objective versions of EAs, like NSGA-II (*Deb et al., 2002*) and NSGA-III (*Deb and Jain, 2014*), provide a collection of Pareto-optimal trade-off solutions in a single execution of the algorithm. This is particularly valuable when there are conflicting objectives, such as mass, strength, accuracy and energy consumption.

Existing reviews have covered bio- and nature-inspired algorithms in agricultural engineering in general (*Maraveas et al., 2023*), the optimization of machinery movement, including routing and fuel consumption (*Filip et al., 2020*), and, more recently, digital-twin and artificial-intelligence frameworks for machinery design (*Ding and Gao, 2026*). In these reviews, operational applications dominate, while the mechanical design of mechanisms, frames, working parts and transmissions receives comparatively little attention. In the strict sense, EAs include genetic algorithms, evolution strategies (ES), evolutionary programming, genetic programming and differential evolution (DE); particle swarm optimization (PSO) and ant colony optimization belong to swarm intelligence, although they are often analyzed together with EAs (*Filip et al., 2020*). In this paper, EAs form the central category.

The objective of the study was to analyze research trends in the application of EAs to the mechanical design and optimization of agricultural technical systems by answering four questions: (i) which algorithms and problem formulations are used; (ii) which design problems, variables and objectives are addressed; (iii) how the results are validated; and (iv) which research directions are emerging. Based on the answers, practical recommendations were formulated.

## MATERIALS AND METHODS

The study was carried out as a literature review of scientific publications on the use of evolutionary algorithms in agricultural engineering. The publications were selected from open-access journals and conference proceedings in the field, such as MDPI journals, IEEE Access, the International Journal of Agricultural and Biological Engineering and the CIGR Journal, focusing on studies in which an evolutionary algorithm was used to design or optimize an agricultural machine, one of its components or its operation.

Studies were included if (a) an EA was the main optimization method, (b) the application concerned an agricultural machine, one of its components or its operation, and (c) the design variables, objectives and results were reported in sufficient detail. Crop management applications without a machine component were excluded. One non-agricultural study, the structural optimization of an excavator boom (*Uzer, 2008*), was retained as a methodological reference because it describes a complete CAD–FEM–GA workflow directly transferable to agricultural machinery. The final set comprised fourteen primary studies published between 2008 and 2025; reviews, foundational algorithm papers and studies using non-evolutionary methods were cited only as context.

Each primary study was classified according to: the algorithm and its hybridization; the optimization level; the design or operating variables; the objectives; the single-objective (SO) or multi-objective (MO) formulation; and the type of validation (simulation, comparison with other algorithms, laboratory or field experiment). A study was classified as MO only if several objectives were optimized simultaneously, through a Pareto front or an explicit aggregation; an MO algorithm applied to a single objective was classified as SO, because the formulation of the problem, not the name of the algorithm, determines the nature of the optimization. Five optimization levels were distinguished: mechanism, structure or working part (dimensions, angles, cross-sections, operating settings); powertrain parameters (gear ratios); integrated mechanical–

control design; machinery operation (task sequence, machine allocation); and farm management (resources, timing). Operational studies were retained because their algorithmic developments can be transferred to design problems.

The general workflow common to the analyzed studies is shown in Fig. 1. The design variables are encoded as individuals of a population, and each individual is evaluated with a model of the machine, which may be analytical (kinematics), numerical (finite or discrete element method) or data-driven (regression, neural, neuro-fuzzy or Kriging surrogate). In a SO genetic algorithm, fitness is usually a decreasing function of the objective and constraints are handled by penalty terms. In NSGA-II, individuals are ranked by non-dominated sorting and, within a rank, by crowding distance, which preserves the diversity of the Pareto front (*Deb et al., 2002*); NSGA-III replaces the crowding distance with reference points and targets problems with more than three objectives (*Deb and Jain, 2014*). Two further elements are frequent: a hybrid step, in which a local or neighborhood search refines the best individuals, and a surrogate model that replaces an expensive simulation, making a population-based search affordable.

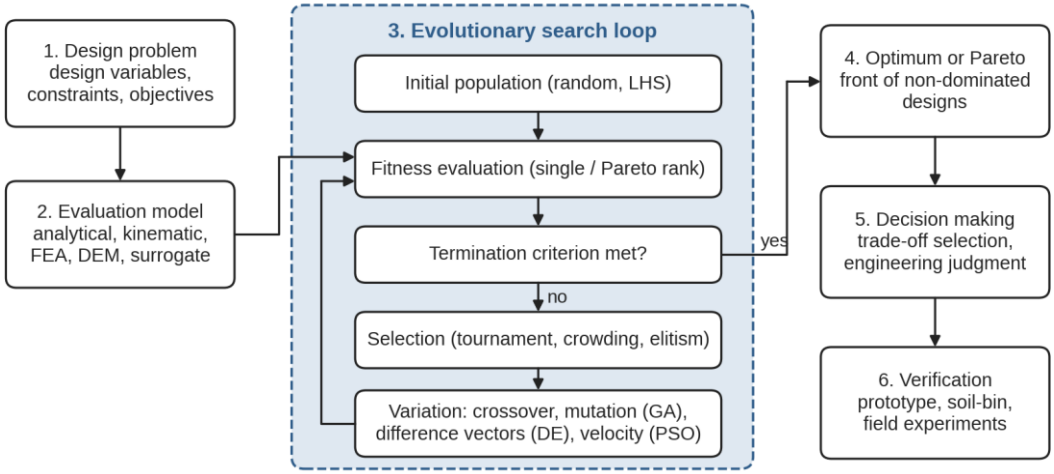



**Fig. 1 - General workflow of evolutionary optimization in the design of agricultural technical systems**

*LHS - Latin hypercube sampling; FEA - finite element analysis; DEM - discrete element method*

## RESULTS AND DISCUSSION

Table 1 summarizes the fourteen primary studies, and Fig. 2 shows their distribution by year, optimization level, formulation and validation.

**Table 1**

**Synthesis of the analyzed primary studies**

| Study | Application | Algorithm (hybridization) | Objective(s) | SO/ MO | Validation |
|---|---|---|---|---|---|
| Li et al. (2024) | Tractor steering trapezoid | GA + Powell local search | Relative steering-angle error | SO | Test on tractor |
| Uzer (2008) | Excavator boom (method reference) | GA + parametric CAD + FEM | Mass under stress constraint | SO | FEM |
| Hosseini et al. (2022) | Four-bar weeding mechanism | NSGA-II + goal attainment | Blade path error; transmission angle | MO | Prototype |
| Yu et al. (2025) | Peanut planter chassis | MOGA + FEM + Kriging surrogate | Chassis mass (lightweight design) | MO | FEM + field test |
| Oude and Adelkhani (2024) | Reversible plow stem | GA + FEM + ANN surrogate | Maximum von Mises stress | SO | FEM |
| Upadhyay et al. (2025) | Active–passive disc harrow | MO GA + regression models | Total power; tilled-soil cone index | MO | Soil bin + field |
| Yadav et al. (2025) | Mechatronic seed metering unit | MOGA + CANFIS surrogate | Miss, multiple and precision indices | MO | Laboratory test |
| Li et al. (2023) | Power-shift transmission | GA | Fuel consumption per unit distance | SO | Simulation |

| Study | Application | Algorithm (hybridization) | Objective(s) | SO/ MO | Validation |
|---|---|---|---|---|---|
| Chang et al. (2023) | Tractor driveline | NSGA-II + gradient crowding | Power loss rate; fuel consumption loss | MO | Simulation |
| Zhu and Eisaka (2009) | Sugar beet topper | GA; structure–control optimization | Contact-force tracking | SO | Simulation |
| Liu et al. (2024) | Scheduling, hilly areas | Improved NSGA-III + neighborhood search | Total scheduling time | SO | Case study; 3 algorithms |
| Liu et al. (2025) | Multi-cooperative scheduling | NSGA-II + simulated annealing | Scheduling cost; scheduling time | MO | Case study; 3 algorithms |
| Feng et al. (2025) | Multi-machine scheduling | GA + large neighborhood search | Total cost | SO | Case study; 6 algorithms |
| Erdoğdu et al. (2025) | Farm management | GA + fuzzy logic (alpha-cuts) | Cost, time, quality | MO | Numerical case study |

Seven studies address mechanisms, structures or working parts, two address powertrain parameters, one integrated mechanical–control design, three machinery scheduling and one farm management. All studies use a GA or a GA-based multi-objective variant, which confirms the dominant position of the GA family; no application of evolution strategies or differential evolution was found. Seven studies use a MO formulation and seven are SO, including one that uses NSGA-III for a single objective (*Liu et al., 2024*). Physical validation is reported in five studies, all published after 2021 (*Hosseini et al., 2022; Li et al., 2024; Upadhyay et al., 2025; Yadav et al., 2025; Yu et al., 2025*). Design studies published before 2010 are SO, whereas most studies published after 2020 include MO formulations and models built from simulation or experimental data; given the small sample, this indicates a direction rather than a quantified trend.

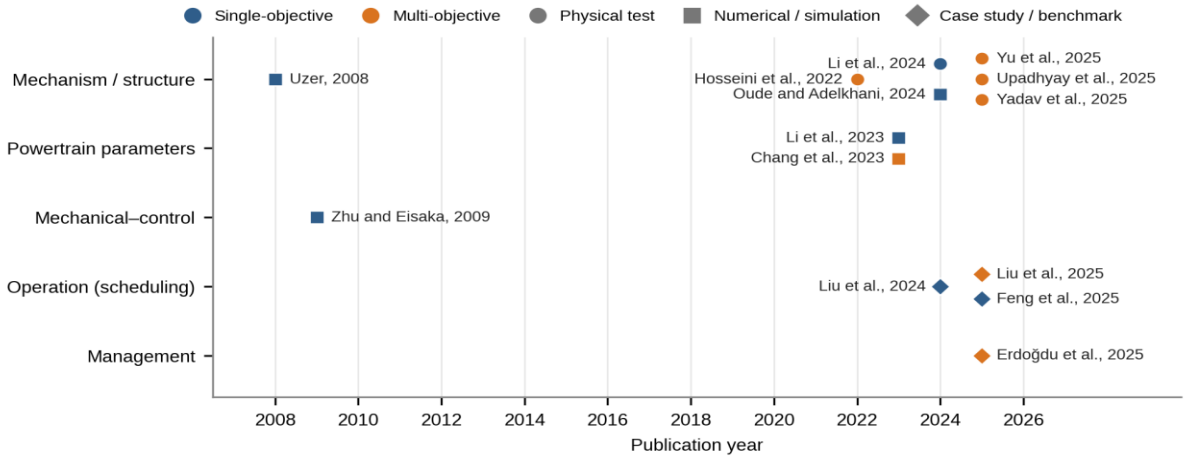



**Fig. 2 - Distribution of the analyzed primary studies by publication year, optimization level, formulation and validation**

**Single-objective design of mechanisms and structures.** The optimization of a tractor steering trapezoid by *Li et al. (2024)* is a representative example. The trapezoid should make the wheels turn around a common instantaneous center, which requires the outer and inner steering angles to satisfy the Ackermann condition (Fig. 3a); a real four-bar trapezoid can only approximate it (*Simionescu and Talpasanu, 2007*). For a 75 HP tractor with a track of 1.52 m and a wheelbase of 2.06 m, the initial bottom angle was the design variable and the relative error between actual and theoretical steering angles the objective. A hybrid GA combining global genetic search with Powell's local search changed the steering arm length from 240 to 210 mm and the bottom angle from 64° to 61°, reducing the objective from 19.5% to 17.8% (Fig. 3b). Compared with GA and the Powell method used separately, the hybrid reached the highest accuracy (98.07% vs. 94.02% and 93.03%) in the shortest time (18.06 vs. 21.06 and 19.54 min) (Fig. 3c).

The validation test reported a relative error of 1.49% between the measured and the optimized bottom angle, based on 20 repeated measurements (*Li et al., 2024*). This value confirms that the manufactured geometry corresponds to the optimized one, but it does not directly measure the reduction of

the steering-angle error, which shows that the validation metric must be chosen consistently with the optimization objective. *Zhu and Eisaka (2009)* compared, for a sugar beet topper, the GA optimization of the structural parameters of the existing machine with the simultaneous optimization of structural and control parameters after adding an actuator; the first approach was cheaper, while the second kept the contact force closer to the reference and was more robust. *Uzer (2008)* integrated a GA with automatic CAD generation and FEM analysis of an excavator boom; the optimized boom was 4.6% lighter than the initial design, which exceeded the design stress limit by about 10%, while satisfying the stress criterion. In all these studies, the algorithm does not replace mechanical modeling but operates on top of an analytical, numerical or simulation-based model.

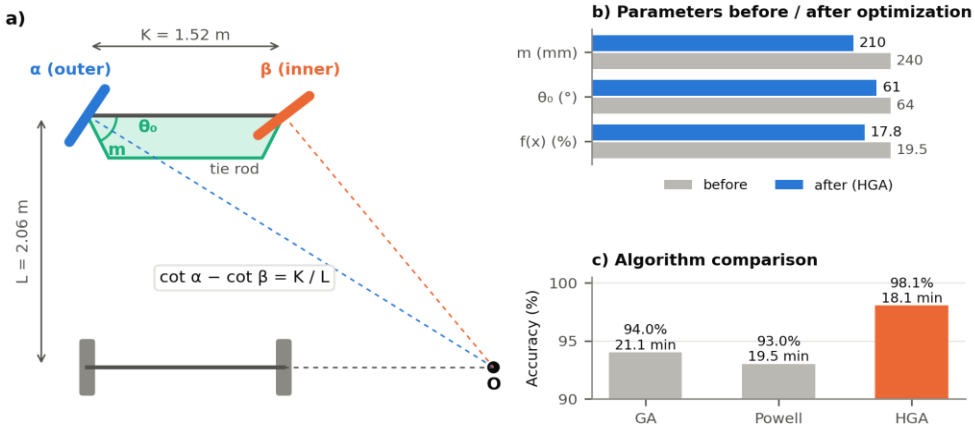



**Fig. 3 - Tractor steering trapezoid optimized with a hybrid genetic algorithm:**
*a) Ackermann steering geometry and design parameters; b) parameters before and after optimization; c) accuracy and computation time of GA, Powell and HGA*
*Data from Li et al. (2024); K - track; L - wheelbase; m - steering arm length; θ0 - initial bottom angle*

**Multi-objective and surrogate-assisted design.** *Hosseini et al. (2022)* synthesized a four-bar mechanism for an inter-row weeding tool by optimizing simultaneously the blade path and the transmission angle with a hybrid of NSGA-II and the goal attainment method and compared the prototype with tools designed by classical methods. *Yu et al. (2025)* sampled the finite element model of a peanut planter chassis with a Latin hypercube design, built a Kriging surrogate and applied a MOGA to it; the chassis mass was reduced by 28.9%, and field tests showed a plant-spacing qualification rate of at least 98%. *Oude and Adelkhani (2024)* analyzed 24 variants of a reversible plow stem by FEM, trained a neural network that predicted the maximum von Mises stress with about 99% accuracy and used it as the GA objective, reducing the maximum stress by 6%, to 295.2 MPa.

*Upadhyay et al. (2025)* built regression models from soil-bin tests on an active–passive disc harrow and used a MO GA to minimize the total power while maximizing soil pulverization; the optimal gang angle was 35.91–36.98° and the speed ratio 3.27–3.87, with maximum deviations between predicted and measured values of 18.50% and 13.11% in the soil bin and 19.79% and 19.47% in the field. *Yadav et al. (2025)* trained a coactive neuro-fuzzy inference system (CANFIS) on sticky-belt tests of a mechatronic seed metering unit ($R^2$ of 0.99 in testing) and used it as the fitness function of a MOGA that minimized the miss, multiple and precision indices. The optimum, obtained at 3.24 km/h, a 14 mm cell and a 50° plate inclination, gave indices of 5.04%, 6.60% and 11.06%, and the validation test showed relative errors of 1.30%, −3.12% and 0.80%. These studies share a common pattern: because each evaluation of a physical or FEM model is expensive, the EA is applied to a surrogate model, whether Kriging, a neural or neuro-fuzzy network or a regression model, built from simulation or experimental data. The approach makes population-based search affordable but transfers part of the uncertainty to the surrogate, which explains why validation deviations range from about 1% for laboratory tests to about 20% in the field.

**Powertrain parameters.** *Li et al. (2023)* optimized the speed ratios of a 16-gear power-shift transmission with a GA, minimizing fuel consumption per unit distance under a constraint on the ratio between adjacent gears; the ratio distribution was derived from the life-cycle use of the tractor, which spends most of its time between 4 and 20 km/h, and the optimized ratios improved fuel economy compared with the geometric series. *Chang et al. (2023)* formulated the problem as MO, minimizing both the loss rate of driving

power and that of specific fuel consumption with an NSGA-II modified by a gradient-crowding strategy, and reported reductions of 41.62% and 62.8%, respectively.

**Machinery operation.** *Liu et al. (2024)* proposed an improved NSGA-III for scheduling a machine performing several continuous tasks in hilly areas; although the algorithm is MO, the model has a single objective, the total scheduling time, which was reduced by 13.89%, 43.81% and 57.19% compared with NSGA-III, GA and the firefly algorithm. The same group later extended the problem to several cooperatives as a genuinely MO problem solved with a hybrid of NSGA-II and simulated annealing, reducing total cost by 3.1–9.8% and total time by 11.6–13.4% (*Liu et al., 2025*). *Feng et al. (2025)* combined a GA with an improved large neighborhood search and adaptive operators for scheduling under time windows, reducing the total cost by 171.40–460.39 CNY for 17 to 37 fields compared with six algorithms. Their encoding and neighborhood-search strategies can be transferred to design problems with discrete variables. At field level, the cost of a route depends strongly on the headland turning maneuvers (Ω-, U- and T-turns), which differ in the required headland width and turning time; as reviewed by *Filip et al. (2020)*, genetic, ant colony, simulated annealing and tabu search algorithms have been used for field coverage and routing, reducing the non-working routes of combine harvesters by 19.3–42.1%. Since a 5% gain in operating efficiency can reduce the cost of mechanized sugarcane harvesting by about 8%, the optimization of machine movement complements that of machine design.

**Hybridization and other bio-inspired methods.** Hybridization is present in almost all studies in two forms. Algorithmic hybridization modifies the search itself: GA with Powell's method (*Li et al., 2024*), NSGA-II with goal attainment (*Hosseini et al., 2022*) or simulated annealing (*Liu et al., 2025*), gradient crowding (*Chang et al., 2023*), neighborhood search operators (*Liu et al., 2024; Feng et al., 2025*) and fuzzy logic (*Erdoğdu et al., 2025*). Model hybridization connects the EA to a machine model through CAD and FEM (*Uzer, 2008*), Kriging (*Yu et al., 2025*), neural (*Oude and Adelkhani, 2024*), neuro-fuzzy (*Yadav et al., 2025*) or regression models (*Upadhyay et al., 2025*). For mechanical design, model hybridization appears to be the more important direction, because it decides whether realistic models can be optimized within an acceptable time, and it is the basis of the digital-twin approaches discussed by *Ding and Gao (2026)*. Swarm methods are applied to the same type of problems: a wheat seed feeding device was optimized with a MO PSO based on discrete element simulations (*Wang et al., 2020*), and no single algorithm suits all agricultural tasks (*Maraveas et al., 2023*).

**Comparison of algorithm families.** Table 2 compares the four main algorithm families with respect to mechanical design problems in agriculture. Genetic algorithms handle mixed variables and have mature multi-objective versions. Evolution strategies, including the covariance matrix adaptation variant (*Beyer and Schwefel, 2002; Hansen and Ostermeier, 2001*), and differential evolution (*Storn and Price, 1997*) are efficient on continuous problems with few control parameters, but were not identified in the analyzed agricultural studies. Particle swarm optimization (*Kennedy and Eberhart, 1995*) converges quickly but may converge prematurely.

**Table 2**

**Comparison of the main evolutionary algorithm families for agricultural machinery design**

| Family | Search principle | Main advantages | Main limitations | Typical agricultural uses |
|---|---|---|---|---|
| GA / NSGA-II / NSGA-III | Selection, crossover and mutation of encoded designs | Mixed variables; mature multi-objective versions; easy hybridization | Many parameters to tune; slow final convergence | Transmissions, linkages, frames, scheduling |
| Evolution Strategies (CMA-ES) | Gaussian mutation with self-adaptive step size | Efficient for continuous, correlated variables; few parameters | Less suited to discrete variables; rarely used in agriculture | Not identified in the corpus |
| Differential Evolution | Mutation by scaled difference vectors and greedy selection | Simple; few parameters; robust on continuous problems | Sensitive to F and crossover rate; limited use in machine design | Not identified in the corpus |
| Particle Swarm Optimization | Particle movement guided by personal and swarm best positions | Fast convergence; simple implementation | Premature convergence; handling of constraints | Seed metering devices, parameter tuning |

**Recommendations and limitations.** Based on the analyzed studies, the following recommendations can be formulated: (i) formulate the problem before choosing the algorithm, since for a

single objective a SO or hybrid GA is sufficient and a MO algorithm adds complexity without benefit; (ii) when objectives conflict, use a Pareto-based algorithm such as NSGA-II and report the whole front, not only the selected solution; (iii) when the machine model is expensive, build a surrogate from a planned set of simulations or tests and report its accuracy before optimizing on it; (iv) add a local search step when variables are continuous and the objective is smooth near the optimum; and (v) validate the optimized design experimentally with a metric that corresponds to the objective and report the predicted–measured deviation. The analysis is qualitative and based on a small, non-systematic sample, so the trends are indicative; a bibliometric analysis in Scopus or Web of Science with a documented protocol would be needed to quantify them.

## CONCLUSIONS

The analysis showed that genetic algorithms and their multi-objective variants were used in all analyzed studies, for the design of mechanisms, structures, working parts and transmissions and for the operation of agricultural machinery, while evolution strategies and differential evolution did not appear in the analyzed sample. The studies reflect a shift from single-objective toward Pareto-based multi-objective formulations, although the use of a multi-objective algorithm does not by itself make a problem multi-objective.

Hybridization was widespread: algorithmic hybrids improved convergence, while coupling evolutionary search with finite element, regression, neural, neuro-fuzzy or Kriging surrogate models made the optimization of realistic machine models feasible. Experimental validation was reported in only five studies, with deviations from about 1% to 20%, and should use a metric consistent with the optimization objective. Future research should move toward integrated frameworks in which structural, control and operating parameters of agricultural machines are optimized together.

## ACKNOWLEDGEMENT

The authors would like to acknowledge the support provided by the Faculty of Biotechnical Systems Engineering, National University of Science and Technology POLITEHNICA Bucharest, Romania, during the development of this research.

## REFERENCES

[1] Beyer, H.-G., & Schwefel, H.-P. (2002). Evolution strategies – A comprehensive introduction. *Natural Computing, 1*(1), 3–52. https://doi.org/10.1023/A:1015059928466

[2] Chang, F., Yuan, F., & Lu, Z. (2023). A multi-objective optimization method for a tractor driveline based on the diversity preservation strategy of gradient crowding. *Agriculture, 13*(7), 1324. https://doi.org/10.3390/agriculture13071324

[3] Deb, K., & Jain, H. (2014). An evolutionary many-objective optimization algorithm using reference-pointbased nondominated sorting approach, Part I: Solving problems with box constraints. *IEEE Transactions on Evolutionary Computation, 18*(4), 577–601. https://doi.org/10.1109/TEVC.2013.2281535

[4] Deb, K., Pratap, A., Agarwal, S., & Meyarivan, T. (2002). A fast and elitist multiobjective genetic algorithm: NSGA-II. *IEEE Transactions on Evolutionary Computation, 6*(2), 182–197. https://doi.org/10.1109/4235.996017

[5] Ding, P., & Gao, J. (2026). Digital twin- and AI-enabled intelligent optimisation design of agricultural machinery: A review. *Agronomy, 16*(11), 1038. https://doi.org/10.3390/agronomy16111038

[6] Erdoğdu, A., Dayi, F., Yildiz, F., Yanik, A., & Ganji, F. (2025). Combining fuzzy logic and genetic algorithms to optimize cost, time and quality in modern agriculture. *Sustainability, 17*(7), 2829. https://doi.org/10.3390/su17072829

[7] Feng, X., Chen, X., Huang, L., & Pu, P. (2025). A new multiple agricultural machinery scheduling via a genetic algorithm improved by large neighborhood search method. In *2025 IEEE 5th International Conference on Power, Electronics and Computer Applications (ICPECA)* (pp. 463–470). IEEE. https://doi.org/10.1109/ICPECA63937.2025.10928773

[8] Filip, M., Zoubek, T., Bumbalek, R., Cerny, P., Batista, C. E., Olsan, P., Bartos, P., Kriz, P., Xiao, M., Dolan, A., & Findura, P. (2020). Advanced computational methods for agriculture machinery

movement optimization with applications in sugarcane production. *Agriculture, 10*(10), 434. https://doi.org/10.3390/agriculture10100434

[9] Hansen, N., & Ostermeier, A. (2001). Completely derandomized self-adaptation in evolution strategies. *Evolutionary Computation, 9*(2), 159–195. https://doi.org/10.1162/106365601750190398

[10] Holland, J. H. (1975). *Adaptation in natural and artificial systems*. University of Michigan Press.

[11] Hosseini, H., Farzad, A., Majeed, F., Hensel, O., & Nasirahmadi, A. (2022). Multi-objective optimal design and development of a four-bar mechanism for weed control. *Machines, 10*(3), 198. https://doi.org/10.3390/machines10030198

[12] Kennedy, J., & Eberhart, R. (1995). Particle swarm optimization. In *Proceedings of ICNN'95 – International Conference on Neural Networks* (Vol. 4, pp. 1942–1948). IEEE. https://doi.org/10.1109/ICNN.1995.488968

[13] Li, B., Pan, J., Li, Y., Ni, K., Huang, W., Jiang, H., & Liu, F. (2023). Optimization method of speed ratio for power-shift transmission of agricultural tractor. *Machines, 11*(4), 438. https://doi.org/10.3390/machines11040438

[14] Li, B., Zhu, H., Fang, L., Zhu, Y., Fang, S., Li, F., & Xia, C. (2024). Optimum design of a tractor steering trapezoid based on a hybrid genetic algorithm. *IEEE Access, 12*, 87767–87775. https://doi.org/10.1109/ACCESS.2024.3400897

[15] Liu, H., Luo, J., Zhang, L., Wang, F., & Wang, S. (2025). Optimal scheduling of agricultural machines in hilly mountainous areas based on NSGA-II-SA hybrid algorithm with applications. *International Journal of Agricultural and Biological Engineering, 18*(5), 234–245. https://doi.org/10.25165/j.ijabe.20251805.9106

[16] Liu, H., Zhang, L., Zhao, B., Tang, J., Wang, F., & Wang, S. (2024). Research on agricultural machine scheduling in hilly areas based on improved non-dominated sorting genetic algorithm-III. *IEEE Access, 12*, 32584–32596. https://doi.org/10.1109/ACCESS.2024.3371176

[17] Maraveas, C., Asteris, P. G., Arvanitis, K. G., Bartzanas, T., & Loukatos, D. (2023). Application of bio and nature-inspired algorithms in agricultural engineering. *Archives of Computational Methods in Engineering, 30*(3), 1979–2012. https://doi.org/10.1007/s11831-022-09857-x

[18] Oude, K. K., & Adelkhani, A. (2024). Design and optimization of iron cow stem with flaps by finite element method and genetic algorithm. *Journal of Techniques, 6*(3), 52–65. https://doi.org/10.51173/jt.v6i3.1930

[19] Simionescu, P. A., & Talpasanu, I. (2007). Synthesis and analysis of the steering system of an adjustable tread-width four-wheel tractor. *Mechanism and Machine Theory, 42*(5), 526–540.

[20] Storn, R., & Price, K. (1997). Differential evolution – A simple and efficient heuristic for global optimization over continuous spaces. *Journal of Global Optimization, 11*(4), 341–359. https://doi.org/10.1023/A:1008202821328

[21] Upadhyay, G., Raheman, H., & Dubey, R. (2025). Regression models and multi-objective optimization using the genetic algorithm technique for an integrated tillage implement. *AgriEngineering, 7*(4), 121. https://doi.org/10.3390/agriengineering7040121

[22] Uzer, C. C. (2008). *Shape optimization of an excavator boom by using genetic algorithm* [Master's thesis, Middle East Technical University].

[23] Wang, Q., Li, Z., Wang, W., Zhang, C., Chen, L., & Wan, L. (2020). Multi-objective optimization design of wheat centralized seed feeding device based on particle swarm optimization (PSO) algorithm. *International Journal of Agricultural and Biological Engineering, 13*(6), 76–84. https://doi.org/10.25165/j.ijabe.20201306.5665

[24] Yadav, L. M., Sushilendra, A. R., Sunil, S., Vijayakumar, P., Nageshkumar, T., & Murali, M. (2025). Optimization of seeding performance of a mechatronic seed metering mechanism using integrated CANFIS-MOGA. *Agricultural Engineering International: CIGR Journal, 27*(4), 126–142.

[25] Yu, Y., Yi, D., Wang, J., Tan, X., Wang, X., Dong, W., & Song, Y. (2025). Lightweight design of the chassis framework for a self-propelled peanut planter in hilly areas based on finite element analysis. *International Journal of Agricultural and Biological Engineering, 18*(5), 117–126. https://doi.org/10.25165/j.ijabe.20251805.9447

[26] Zhu, Z., & Eisaka, T. (2009). Practical design method to improve an ordinary agricultural machine. In *Proceedings of the 11th WSEAS International Conference on Automatic Control, Modelling and Simulation* (pp. 407–412). WSEAS.

# OPTIMIZATION OF HEAT TRANSFER IN A HEAT EXCHANGER WITH TEMPERATURE RESTRICTIONS ON THE EXHAUST FLUE PIPE

/

# *OPTIMIZAREA TRANSFERULUI DE CĂLDURĂ ÎNTR-UN SCHIMBĂTOR DE CĂLDURĂ CU RESTRICȚII DE TEMPERATURĂ PE CONDUCTA DE EVACUARE A GAZELOR ARSE*

**Alexandru-Polifron CHIRIȚĂ*[1)], Florian-Andrei SCARLAT[1)], Ioan PAVEL[1)], Gheorghe ȘOVĂIALĂ[1)], Laurențiu VLĂDUȚOIU[2)]**

[1)] INOE 2000, Subsidiary Hydraulics and Pneumatics Research Institute / IHP, Cutitul de Argint 14, 040558 Bucharest / Romania;

[2)] INMA Bucharest / Romania

**E-mail: chirita.ihp@fluidas.ro*

***Keywords:*** *AMESim simulation, HX optimization, TLUD gasifier, sustainable heating, off-grid greenhouse*

**ABSTRACT**

*This paper presents a numerical simulation in AMESim of an embedded heat exchanger designed for year-round greenhouse vegetable cultivation using thermal energy from a Top-Lit Updraft (TLUD) biomass gasifier system. Rather than modeling the combustion process itself, the simulation evaluates heat transfer using a variable input thermal power from the TLUD ranging between 80% and 100%. To optimize heat transfer, the system incorporates a variable-speed fan controlled proportionally to the thermal output produced by the generator. The main objective is to maximize useful heat extraction for greenhouse heating while enforcing a strict exhaust flue gas temperature restriction between 180 °C and 200 °C to prevent deposit formation on the exhaust flue pipe. Using AMESim, the dynamic thermal behavior and fluid dynamics were analyzed across the entire operating range. The results demonstrate that proportional fan speed control effectively optimizes heat transfer efficiency while keeping flue gas temperatures securely within the safe 180–200 °C range. This approach enhances system longevity and provides an efficient, sustainable heating solution for off-grid agricultural applications.*

**REZUMAT**

*Această lucrare prezintă o simulare numerică, realizată în mediul AMESim, a unui schimbător de căldură integrat, destinat cultivării legumelor în sere pe tot parcursul anului prin utilizarea energiei termice furnizate de un sistem de gazeificare a biomasei de tip TLUD (Top-Lit Updraft). În loc să modeleze procesul de combustie propriu-zis, simularea evaluează transferul de căldură utilizând o putere termică de intrare variabilă, provenită de la sistemul TLUD, cuprinsă între 80% și 100%. Pentru optimizarea transferului de căldură, sistemul include un ventilator cu turație variabilă, controlat proporțional cu puterea termică generată. Obiectivul principal este maximizarea extracției de căldură utilă pentru încălzirea serei, respectând totodată o restricție strictă privind temperatura gazelor de evacuare (între 180 și 200 °C) pentru a preveni formarea depunerilor pe conducta de evacuare. Cu ajutorul software-ului AMESim, au fost analizate comportamentul termic dinamic și dinamica fluidelor pe întregul domeniu de funcționare. Rezultatele demonstrează că reglarea proporțională a turației ventilatorului optimizează eficient transferul de căldură, menținând în același timp temperatura gazelor de evacuare în intervalul sigur de 180–200 °C. Această abordare sporește durata de viață a sistemului și oferă o soluție de încălzire eficientă și sustenabilă pentru aplicații agricole independente de rețeaua energetică (off-grid).*

## INTRODUCTION

The demand for high-yield, high-quality agricultural produce in temperate and cold climate regions has driven a significant shift toward controlled-environment agriculture (CEA), particularly year-round greenhouse cultivation *(Ghiasi et al., 2024)*. Greenhouses offer a protected microclimate that shields crops from ambient thermal extremes, enabling extended growing and harvesting periods for high-value vegetable crops such as tomatoes, cucumbers, and peppers *(Cuce et al., 2016)*. However, operating greenhouses during severe winter months, when ambient outdoor temperatures drop well below freezing, presents a substantial technical and financial challenge *(Akpenpuun et al., 2023)*. Maintaining the indoor microclimate requiring optimal daytime temperatures about 18 °C *(Mahmood et al., 2025)* and nighttime temperatures

above 5 °C demands continuous, intensive thermal energy input. Historically, commercial greenhouse heating has relied heavily on fossil fuels, such as natural gas, heavy fuel oils, and liquefied petroleum gas (LPG). The heavy reliance on non-renewable fossil energy not only inflates operational costs, often exceeding 80% to 45% of total production expenses, but also contributes significantly to greenhouse gas (GHG) emissions, contradicting modern sustainability mandates in agriculture *(Cuce et al., 2016; Ghiasi et al., 2024)*.

To mitigate the environmental impact and reduce heating expenses, decentralized thermal systems fueled by renewable biomass have gained increasing traction in rural and off-grid agricultural operations *(Singh et al., 2023)*. Among the various agricultural residues available, pelletized agricultural waste, such as crop stalks, straw, pruning residues, and husks, represents an abundant, carbon-neutral energy source *(Papandrea et al., 2024)*. Thermal conversion of agricultural waste pellets via gasification offers a significantly higher thermodynamic efficiency and lower pollutant profile compared to direct combustion. Specifically, Top-Lit Updraft (TLUD) gasifiers have emerged as a highly promising technology for localized, off-grid heating applications *(Hailu, 2022)*. The TLUD gasifier operates on a stratified micro-gasification principle where pyrolytic combustion moves downward through a bed of biomass while primary air enters from the bottom, generating a rich producer gas (syngas) comprising carbon monoxide, hydrogen, and methane *(Mukunda et al., 2010)*. The syngas is subsequently combusted in a secondary burn chamber, producing high-temperature thermal energy suitable for greenhouse space heating.

Despite their potential, implementing TLUD gasifiers fueled by agricultural waste pellets for continuous greenhouse space heating poses distinct operational and thermofluidic challenges *(Singh et al., 2023)*. Agricultural waste pellets typically exhibit variable moisture content, higher ash fractions, and lower bulk density compared to premium wood pellets, leading to fluctuations in gasifier thermal output and fuel bed resistance *(Papandrea et al., 2024)*. Under real-world agricultural conditions, greenhouse heating loads fluctuate dynamically between day and night, requiring the thermal generator to modulate its input thermal power over a wide operating range, typically from partial load to full load *(Akpenpuun et al., 2023)*.

A critical technical bottleneck in biomass gasifier heating systems lies in the efficient extraction of thermal energy from flue gases while managing flue gas temperatures in the exhaust chimney *(Müller-Steinhagen et al., 2011; Chiriță et al., 2024)*. When hot flue gas flows through the gas-to-air heat exchanger, rapid heat transfer reduces the flue gas temperature prior to exhaust discharge. However, if the exhaust gas temperature drops below a critical threshold (in some cases around 180 °C) condensable hydrocarbons, organic tars, and moisture present in the flue gas begin to condense on the internal walls of the exhaust pipe *(Chiriță et al., 2024)*. This condensation mixes with fly ash particles to form sticky creosote deposits, causing rapid exchanger fouling, corrosion, reduced heat transfer efficiency, and severe chimney fire risks *(Müller-Steinhagen et al., 2011)*. Conversely, allowing exhaust flue gas temperatures to exceed 200 °C leads to unacceptable thermal losses, reduced system efficiency, and excessive thermal stress on flue pipe materials. Therefore, enforcing a strict exhaust flue gas temperature window between 180 °C and 200 °C is essential for long-term operational safety and heat transfer optimization *(Chiriță et al., 2024)*.

Achieving optimal heat extraction across a wide thermal power range while strictly confining exhaust flue pipe temperatures within the 180 °C to 200 °C safety margin requires active, responsive heat transfer control. Traditional fixed-speed air circulation fans fail to adapt to varying thermal generation rates, resulting in localized over-cooling during partial loads or insufficient heat recovery and elevated exhaust temperatures during full-load operations *(Kilkovsky et al., 2014)*. To overcome these limitations, modern thermal management employs variable-speed fans controlled proportionally to the generator's instant thermal output. By modulating the mass flow rate of the secondary coolant air through the heat exchanger, proportional fan control adjusts the convective heat transfer coefficient in real time, matching the variable heat flux from the gasifier exhaust *(Kilkovsky et al., 2014)*.

To design, evaluate, and optimize such complex, transient thermofluidic interactions without incurring high physical prototyping costs, system-level numerical simulation software is widely utilized *(Kilkovsky et al., 2014)*. Numerical simulation enables dynamic modeling of physical systems, accurately capturing fluid dynamics, transient convective and conductive heat transfer, and system control loops across diverse operational conditions *(Kilkovsky et al., 2014)*. While existing literature addresses general biomass gasification *(Mukunda et al., 2010)* and greenhouse energy efficiency *(Cuce et al., 2016; Mahmood et al., 2025)*, there remains a gap in evaluating heat exchanger control dynamics subject to narrow, strict flue gas exhaust temperature constraints under modulated thermal loads.

The main objective of this study is to perform a detailed numerical simulation in AMESim to optimize heat transfer in an embedded heat exchanger integrated with a TLUD biomass gasification system for off-grid greenhouse heating. Rather than modeling the complex chemical kinetics of combustion, this paper evaluates system dynamic heat transfer across a variable input thermal power spectrum ranging from 80% to 100%. The system integrates a proportional variable-speed fan control scheme designed to maximize useful heat extraction for the greenhouse microclimate while rigorously enforcing the exhaust flue gas temperature within the targeted 180 °C to 200 °C span, thereby preventing deposit formation and ensuring high operational efficiency throughout freezing winter cultivation periods.

## MATERIALS AND METHODS

The numerical simulation of the thermal energy recovery and greenhouse heating system was developed using Simcenter Amesim to evaluate dynamic heat transfer and thermofluidic interactions. Rather than modeling the complex chemical kinetics of the combustion process, the simulation focuses on the transient heat transfer mechanisms and the systemic response under a variable thermal load. The system architecture integrates a Top-Lit Updraft (TLUD) biomass gasifier (as a heat source), a counter-flow heat exchanger (HEX), a fan with variable-speed control, an exhaust flue pipe, and a medium-sized greenhouse.

Figure 1 details the block diagram, component parameterization, and simulation settings of the Amesim numerical model. The TLUD gasifier module generates a variable input thermal power ranging from 27 to 33 kW, representing operational loads between 80% and 100%. The output temperature from the gasifier is fixed at a constant 900 °C, generating an exhaust air mass flow rate that fluctuates between 0.0277 and 0.0333 kg/s. This high-temperature flue gas is directed into Side 1 of the counter-flow heat exchanger. The HEX block is geometrically defined by a characteristic length of 100,000 mm, a flow sectional area of 5,500 mm², and a total convective exchange area of 10,000,000 mm².

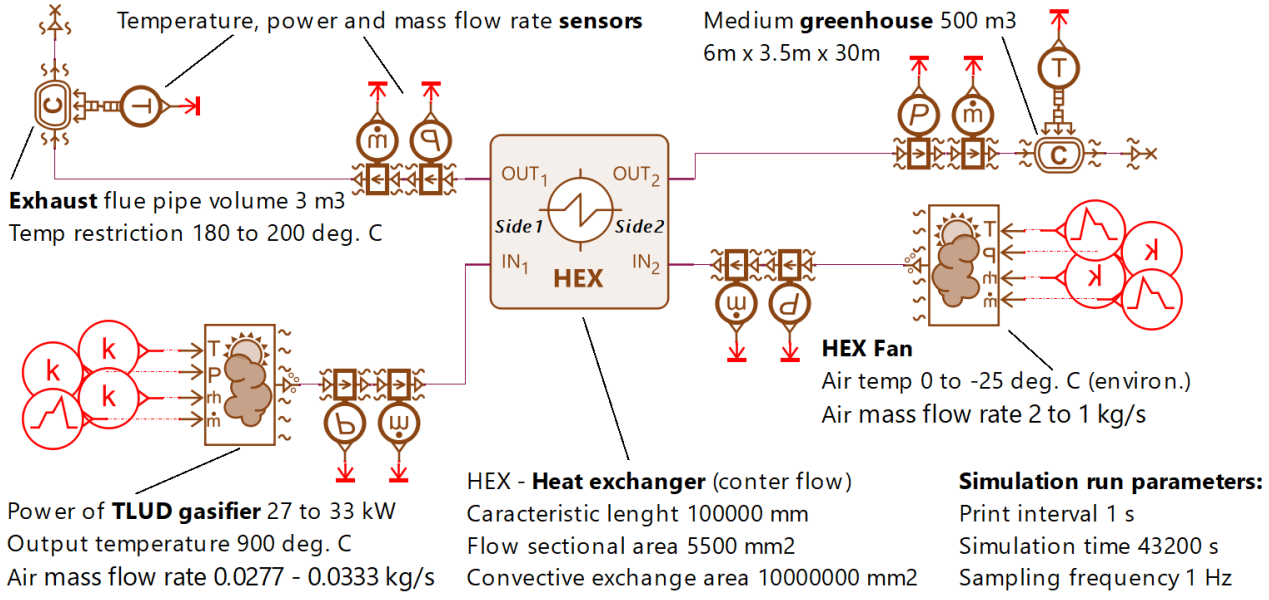



**Fig. 1 - Amesim numerical simulation model architecture of the greenhouse heating system**

On Side 2 of the HEX, a variable-speed fan introduces ambient environmental air to serve as the secondary coolant. The simulation imposes a severe winter climate scenario where the environmental intake air temperature steadily drops from 0 °C down to -25 °C. To optimize thermal recovery while strictly adhering to exhaust limitations, the fan is proportionally controlled, modulating the coolant air mass flow rate from 2.0 kg/s down to 1.0 kg/s based on the thermal output of the gasifier. The exhaust flue pipe is modeled with a discrete volume of 3 m³. A strict thermal restriction window of 180 to 200 °C is enforced on the exhaust flue pipe to prevent harmful condensation and rapid fouling.

The heated coolant air is continuously delivered to a medium-sized greenhouse with a total internal volume of 500 m³, modeled with physical dimensions of 6 m in width, 3.5 m in height, and 30 m in length. To accurately capture the transient system responses, the model is instrumented with temperature (T), power, and mass flow rate sensors at critical system nodes, including the exhaust pipe and the greenhouse interior.

The simulation solver was configured for a total run time of 43,200 s (equivalent to 12 hours), utilizing a sampling frequency of 1 Hz and a print interval of 1 s.

**RESULTS**

The dynamic simulation executed over the 43,200-second timeframe successfully captured the transient thermal and fluid dynamics of the gasifier-driven heating system operating under severe ambient temperature degradation. The integration of the proportional control loop allowed for continuous optimization of the convective heat transfer while enforcing systemic safety constraints.

Figure 2 illustrates the dynamic temperature profiles across the external environment, the greenhouse interior, and the exhaust flue pipe over the simulation duration. The environmental temperature acts as the primary thermal disturbance, declining linearly from an initial 0 °C to a severe -25 °C. In response to the TLUD heat input, the greenhouse interior temperature experiences a rapid initial spike, reaching approximately 11 °C. As the ambient temperature continues its severe drop, the greenhouse temperature gradually decreases but successfully avoids freezing, stabilizing near 1 °C before showing a slight upward recovery at the end of the thermal cycle. Crucially, the exhaust flue pipe temperature rapidly reaches the 180°C threshold and slowly climbs toward 190 °C. This confirms that the proportional fan control effectively maintains the flue gas strictly within the required 180 °C to 200 °C range, eliminating the risk of internal deposit formation and potential chimney fires.

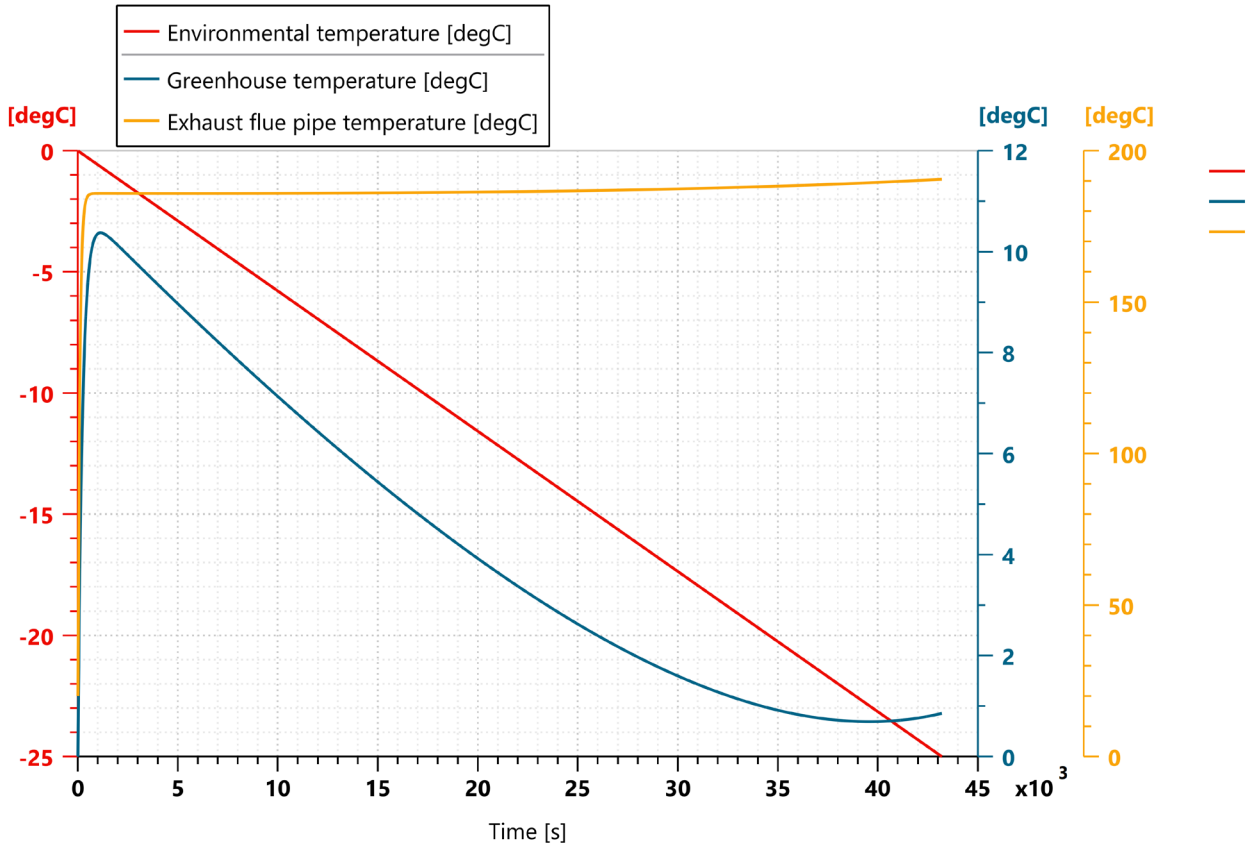



**Fig. 2 - Temperature dynamics over time (Environmental, Greenhouse, and Exhaust Flue Pipe temperature)**

The evolution of thermal power transferred and lost within the system is presented in Figure 3. The TLUD-generated thermal power increases linearly over the simulation period, scaling from approximately 27 kW up to about 33 kW. The heat flow successfully transferred through the heat exchanger into the greenhouse tracks this generation curve closely, rising from roughly 22 kW to 26 kW. Conversely, the thermal power lost through the exhaust flue pipe remains highly constrained, showing only a marginal increase from roughly 5 kW to 6.5 kW. This large differential between extracted useful heat and lost exhaust heat highlights the efficiency of the thermal recovery process.

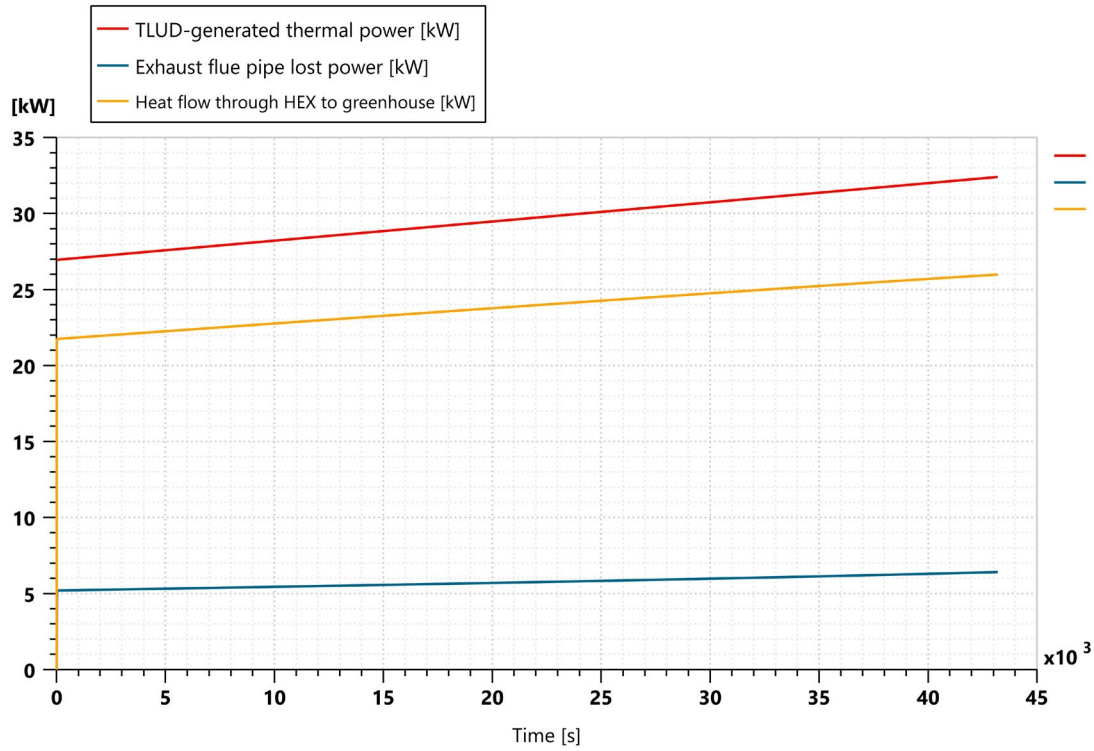



**Fig. 3 - Thermal power evolution over time (TLUD-generated power, heat flow to greenhouse, and flue pipe lost power)**

Figure 4 details the modulated mass flow rates across both sides of the heat exchanger. As the gasifier output scales up, the primary exhaust mass flow rate on Side 1 increases linearly from 0.0277 kg/s to 0.0333 kg/s. To counterbalance this increased thermal flux and prevent the exhaust temperature from exceeding the 200 °C upper limit, the variable-speed fan actively reduces the secondary coolant mass flow rate on Side 2. The Side 2 mass flow rate drops linearly from 2.0 kg/s to 1.0 kg/s. This dynamic, inverse adjustment of the coolant flow is the mechanism by which the convective heat transfer coefficient is modulated in real time to meet the thermal restriction on the flue pipe.

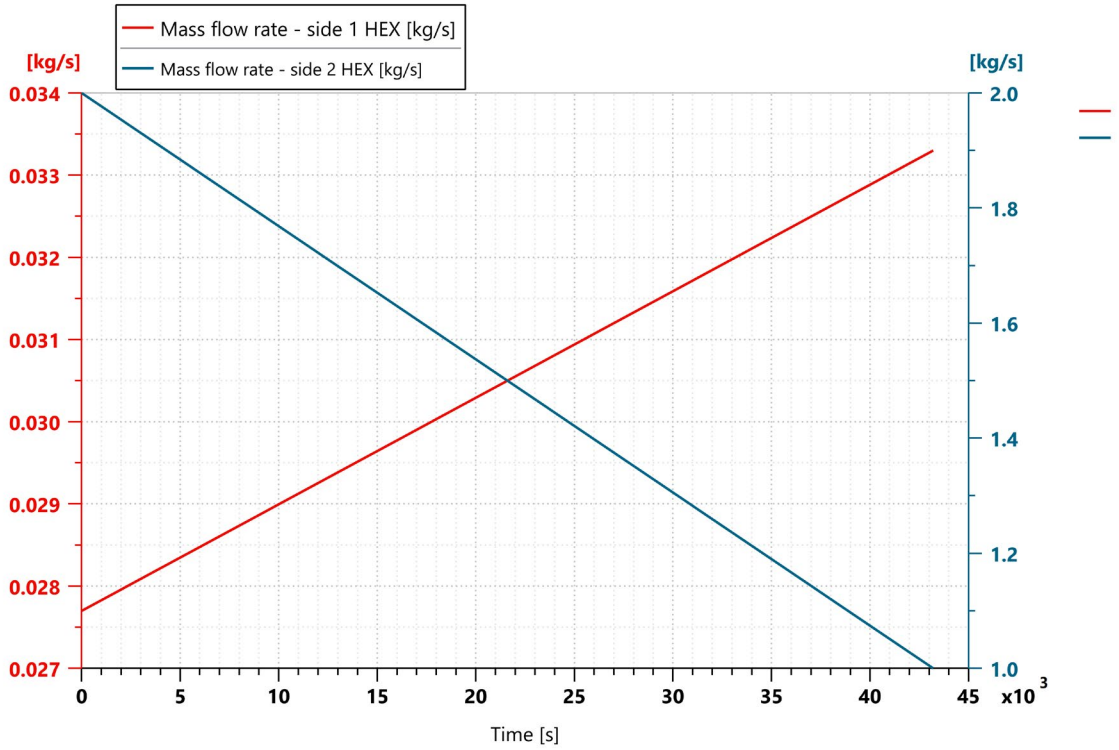



**Fig. 4 - Mass flow rates over time across Side 1 and Side 2 of the heat exchanger**

The sustained overall performance of the heat exchanger is verified by the metrics in Figure 5. The Number of Heat Transfer Units (NTU) remains highly stable, beginning at roughly 1.65 and gradually declining to approximately 1.55 by the end of the simulation. Similarly, the overall heat exchanger efficiency exhibits excellent stability, starting at 80% (0.8) and experiencing only a negligible drop to approximately 78% (0.78), despite the severe environmental cooling and actively modulated mass flow rates. This high efficiency confirms the proper design of the heat exchanger and thermofluidic viability of the dynamic thermal management approach.

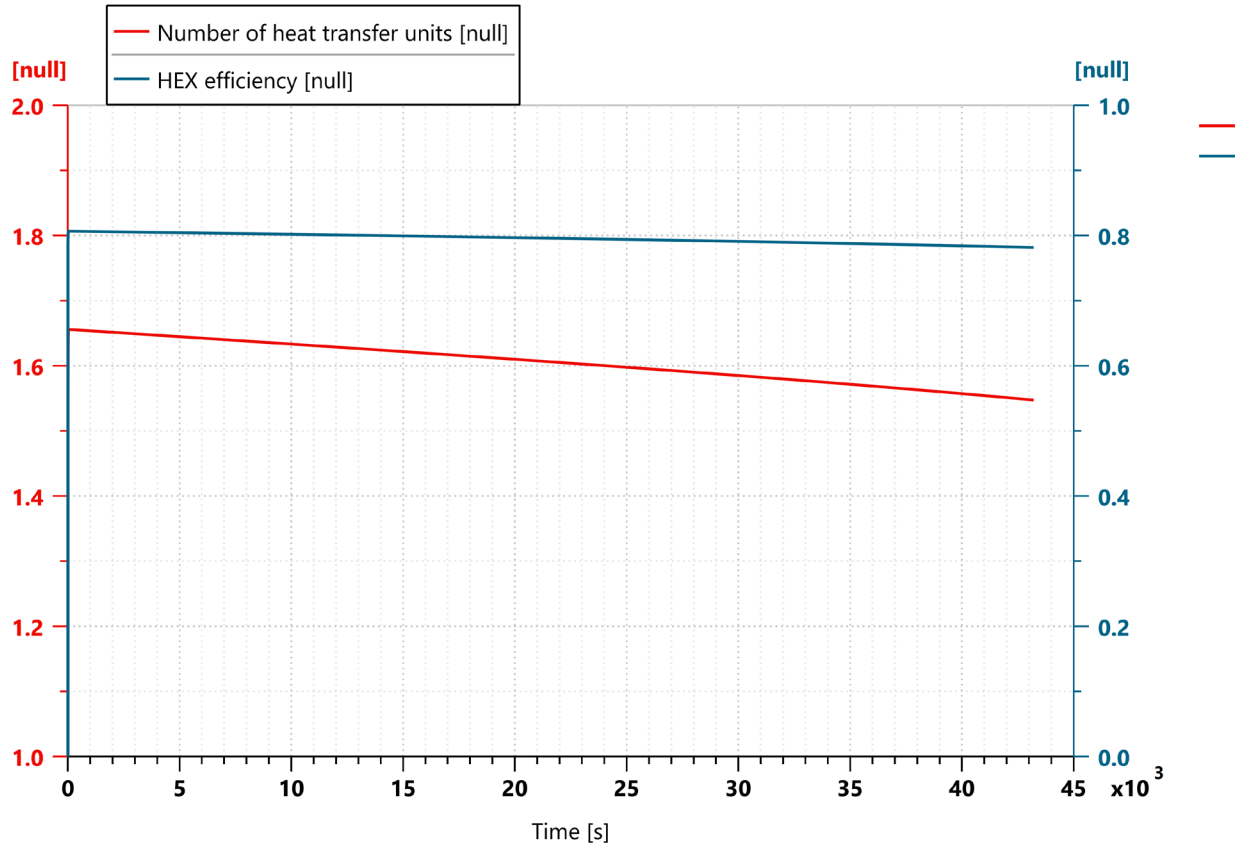



**Fig. 5 - Heat exchanger performance metrics over time (Number of heat Transfer Units - NTU, and HEX efficiency)**

## CONCLUSIONS

The numerical simulation conducted in Simcenter Amesim provides a comprehensive validation of the proposed dynamically controlled heat exchanger integrated with a Top-Lit Updraft (TLUD) biomass gasifier for off-grid greenhouse heating. The primary technical bottleneck in decentralized biomass heating systems, which is extracting maximum thermal energy while strictly managing exhaust flue gas temperatures, has been effectively resolved through the implementation of a proportional variable-speed fan control architecture. By modulating the secondary coolant air mass flow rate in direct response to the variable thermal output of the gasifier, the system successfully balanced the competing demands of optimal space heating and exhaust infrastructure safety.

The simulation results demonstrate that even under severe winter conditions, where the ambient environmental temperature dropped drastically from 0 °C to -25 °C, the thermal management system maintained the greenhouse microclimate safely above freezing temperatures. This capability is critical for controlled-environment agriculture in cold regions, ensuring crop survival and extending the cultivation season without relying on conventional fossil fuels. The utilization of pelletized agricultural waste (such as crop stalks, straw, and husks) within this highly efficient gasification framework provides an abundant, carbon-neutral alternative to expensive traditional fuels. Furthermore, the system exhibited robust heat transfer metrics, effectively converting a varying gasifier input of 27 to 33 kW into 21.5 to 26 kW of useful thermal energy directed into the greenhouse. This energy conversion sustained an overall heat exchanger efficiency of approximately 78% to 80% across the entire 12-hour operational thermal cycle.

Crucially, the dynamic modulation of the fan mass flow rate from 2.0 kg/s down to 1.0 kg/s successfully enforced the strict operational constraint on the exhaust flue pipe. The exhaust temperature was securely maintained within the narrow 180 °C to 200 °C safety window throughout the entire fluctuating load spectrum. Preventing the flue gas from dropping below the 180 °C threshold completely mitigates the risks of rapid exchanger fouling, corrosive condensation, and chimney fires, issues that frequently plague fixed-speed thermal recovery systems. Conversely, restricting the temperature from exceeding the 200 °C ceiling ensures that unnecessary thermal losses to the environment are minimized, maximizing the thermodynamic return on the biomass fuel.

The proposed TLUD gasifier and embedded heat exchanger system, coupled with proportional flow control, offers a highly efficient, safe, and sustainable heating solution for the agricultural sector. This decentralized approach significantly reduces operational heating expenses, which can otherwise account for up to 80% of production costs in controlled-environment agriculture, while simultaneously aligning with modern sustainability mandates to lower greenhouse gas emissions. The verified numerical findings provide a robust engineering foundation for future physical prototyping, experimental test bench development, and scaled field deployment in off-grid environments.

Beyond the immediate thermofluidic advantages, the integration of this TLUD gasifier system facilitates a fully decentralized, self-sustaining energy loop for off-grid agricultural operations. Agricultural residues generated directly on the farm can be systematically collected, dried, and pelletized to serve as an abundant, carbon-neutral fuel source. By repurposing this local biomass waste to generate the exact thermal energy required for greenhouse heating, farmers can establish a sustainable, closed-loop agro-energy system. This self-feeding architecture effectively insulates the farm from the volatility of external fossil fuel supply chains, drastically lowering both greenhouse gas emissions and long-term operational expenses. Ultimately, transforming organic farm waste into precisely controlled, life-sustaining heat for year-round crop cultivation represents a highly scalable and economically viable model for modern, eco-conscious agriculture.

## ACKNOWLEDGEMENT

This work was supported by a grant of the Ministry of Research, Innovation and Digitization, CCCDI - UEFISCDI, project number PN-IV-P7-7.1-PTE-2024-0035, within PNCDI IV.

## REFERENCES

[1] Akpenpuun, T. D., Ogunlowo, Q. O., Na, W. H., Rabiu, A., Adesanya, M. A., Dutta, P., ... & Lee, H. W. (2023). Review of temperature management strategies and techniques in the greenhouse microenvironment. *Adeleke Univ. J. Eng. Technol,* *6*(2), 126-147. https://research.knu.ac.kr/en/publications/review-of-temperature-management-strategies-and-techniques-in-the/

[2] Chiriță, A.-P., Pavel, I., Rădoi, R.-I., Matache, G., Șovăială, G., & Popescu, A.-M. C. (2024). Multi-Criteria Optimization of a Laboratory Top-Lit Updraft Gasifier in Order to Reduce Greenhouse Gases and Particulate Matter Emissions. *Processes, 12*(6), 1103. https://doi.org/10.3390/pr12061103

[3] Cuce, E., Harjunowibowo, D., & Cuce, P. M. (2016). Renewable and sustainable energy saving strategies for greenhouse heating: A comprehensive review. *Renewable and Sustainable Energy Reviews, 64*, 34–59. https://doi.org/10.1016/j.rser.2016.05.077

[4] Ghiasi, M., Wang, Z., Mehrandezh, M., & Paranjape, R. (2024). A Systematic Review of Optimal and Practical Methods in Design, Construction, Control, Energy Management and Operation of Smart Greenhouses. *IEEE Access, 12*, 2830-2853. https://doi.org/10.1109/access.2023.3346436

[5] Hailu, A. (2022). Development and performance analysis of top lit updraft: Natural draft gasifier stoves with various feed stocks. *Heliyon, 8*(8). https://doi.org/10.1016/j.heliyon.2022.e10163

[6] Kilkovsky, B., Stehlik, P., Jegla, Z., Tovazhnyansky, L. L., Arsenyeva, O., & Kapustenko, P. O. (2014). Heat exchangers for energy recovery in waste and biomass to energy technologies – I. Energy recovery from flue gas. *Applied Thermal Engineering,* *64*(1-2), 213-223. https://doi.org/10.1016/j.applthermaleng.2013.11.041

[7] Mahmood, F., Govindan, R., & Al-Ansari, T. (2025). Efficient energy management and temperature control of a high-tech greenhouse using an improved data-driven model predictive control. *Energy Conversion and Management: X, 26*, 100939. https://doi.org/10.1016/j.ecmx.2025.100939

[8] Mukunda, H. S., Dasappa, S., Paul, P. J., Rajan, N. K. S., Yagnaraman, M., Kumar, D. R., & Deogaonkar, M. (2010). Gasifier stoves – science, technology and field outreach. *Current Science, 98*(5), 627–638. http://www.jstor.org/stable/24111816

[9] Müller-Steinhagen, H., Malayeri, M. R., & Watkinson, A. P. (2011). Heat Exchanger Fouling: Mitigation and Cleaning Strategies. *Heat Transfer Engineering, 32*(3–4), 189–196. https://doi.org/10.1080/01457632.2010.503108

[10] Papandrea, S. F., Palma, A., Carnevale, M., Paris, E., Vincenti, B., Gallucci, F., & Proto, A. R. (2024). Characterization of Several Pellets from Agroforestry Residues: A Comparative Analysis of Physical and Energy Efficiency. *Fire, 7*(7), 239. https://doi.org/10.3390/fire7070239

[11] Singh, D. K., Raj, R., Tirkey, J. V., Jena, P., Parthasarathy, P., Mckay, G., & Al-Ansari, T. (2023). Progress and utilization of biomass gasification for decentralized energy generation: an outlook & critical review. *Environmental Technology Reviews*, *12*(1), 1–36. https://doi.org/10.1080/21622515.2023.2242014

# EVALUATION OF MECHANICAL PROPERTIES, WATER ACTIVITY, AND MOISTURE CONTENT OF GLUTEN-FREE PRETZELS

/

# *EVALUAREA PROPRIETĂȚILOR MECANICE, ACTIVITĂȚII APEI ȘI A UMIDITĂȚII LA COVRIGII AGLUTENICI*

**Mariana-Gabriela MUNTEANU[1)], Elena-Mădălina ȘTEFAN*[1)], Gheorghe VOICU[1)], Daiana-Alina IONESCU[1)], Gabriel-Alexandu CONSTANTIN[1)], Irina-Aura ISTRATE[1)], Loredana MORARI[1)], Zsofia-Krisztina LŐRINCZ[1)], Ana-Maria FETICU[1)], Gabriel-Valentin GHEORGHE[2)]**

[1)] UNSTP Bucharest / Romania;

[2)] INMA Bucharest / Romania.

**Tel: +40 726 043 472; *E-mail: stefanelenamadalina@gmail.com*

***Keywords:*** *gluten-free pretzels; cutting force; water activity; moisture content; texture; baking time*

## ABSTRACT

*Gluten-free bakery products present technological challenges related to the absence of gluten, particularly regarding structure and texture. The aim of this study was to characterize laboratory-produced gluten-free pretzels in terms of mechanical properties and water-related parameters. Two experimental variants were obtained by baking the products at 230 ºC for 13 and 15 min. Cutting force was determined using a HOUNSFIELD H1KS mechanical testing machine, while water activity and moisture content were measured using a Rotronic HygroLab system and KERN DBS moisture analyzer, respectively. Pretzels baked for 13 min showed a higher mean cutting force (72.89 N) than those baked for 15 min (51.51 N). Water activity decreased during 24 h of storage from 0.975 to 0.888 for samples baked for 13 min and from 0.953 to 0.865 for samples baked for 15 min. Moisture content showed a slight increase during storage. The results indicate that baking time was associated with differences in the mechanical resistance and water-related characteristics of gluten-free pretzels and may represent an important technological factor in further product optimization.*

## REZUMAT

*Produsele de panificație fără gluten ridică provocări tehnologice legate de absența glutenului, în special în ceea ce privește structura și textura. Scopul acestui studiu a fost caracterizarea unor covrigi fără gluten, produși în laborator, din perspectiva proprietăților mecanice și a parametrilor asociați conținutului de apă. Au fost obținute două variante experimentale prin coacerea produselor la 230 ºC, timp de 13, respectiv 15 minute. Forța de tăiere a fost determinată cu ajutorul unui aparat de testare mecanică HOUNSFIELD H1KS, în timp ce activitatea apei și conținutul de umiditate au fost măsurate utilizând sistemul Rotronic HygroLab, respectiv analizorul de umiditate KERN DBS. Covrigii copți timp de 13 minute au prezentat o forță medie de tăiere mai mare (72,89 N) comparativ cu cei copți timp de 15 minute (51,51 N). Activitatea apei a scăzut pe parcursul a 24 de ore de depozitare: de la 0,975 la 0,888 pentru probele coapte timp de 13 minute și de la 0,953 la 0,865 pentru cele coapte timp de 15 minute. Conținutul de umiditate a înregistrat o ușoară creștere în timpul depozitării. Rezultatele indică faptul că durata de coacere a influențat rezistența mecanică și caracteristicile legate de apă ale covrigilor fără gluten, constituind un factor tehnologic important pentru optimizarea ulterioară a produsului.*

## INTRODUCTION

Gluten-free products constitute an important category of food, intended mainly for people with gluten intolerance or diagnosed with celiac disease, but also for consumers who opt for a gluten-free diet (*Gallagher et al., 2004*). In recent years, the interest in the development and consumption of these products has increased, leading to increased research into identifying solutions for obtaining gluten-free products with appropriate technological, textural and sensory properties (*Gomez, 2022*).

Obtaining gluten-free bakery products represents a technological challenge, mainly due to the absence of gluten, which has an important role in the formation and stabilization of the structure of bakery products. The gluten network contributes to the structural and viscoelastic properties of the dough, and its elimination can affect the characteristics of the finished product, causing changes in its texture, elasticity and

resistance (*Gallagher et al., 2004; Gomez, 2022*). In this context, to obtain gluten-free products with properties close to those of conventional products, different types of gluten-free flours and starches are used, as well as ingredients with a role in improving the structure and technological properties of the finished product (*Gomez, 2022*).

The quality of gluten-free products is influenced both by the characteristics of the raw materials used and by the conditions of the technological process. Among the characteristics of the finished product, texture represents an important evaluation criterion, as it can influence the sensory perception and acceptability of the product by consumers. Therefore, research in this field aims to develop formulations and technologies that improve the technological, textural, and nutritional properties of gluten-free products (*Gallagher et al., 2004; Alibekova et al., 2026*).

In the present study, gluten-free pretzels were obtained under laboratory conditions, with the aim of evaluating their main physicochemical and textural characteristics. The characterization of the products involved determining the cutting force, water activity, and moisture content, parameters relevant for assessing the quality of the finished product.

Cutting force represents a relevant instrumental parameter for characterizing the textural properties of bakery products, providing information on their resistance to deformation and breakage. In the case of gluten-free products, textural properties are influenced by the composition and structure of the food matrix, and parameters such as firmness and elasticity are used to evaluate the mechanical behavior of the product (*Adazia et al., 2023*).

Water activity is an important parameter for evaluating the stability of bakery products, as it is associated with the possibility of microorganism development and, implicitly, with their microbiological stability and shelf life. At the same time, the mobility and redistribution of water during storage are associated with physical and sensory changes in bakery products, such as core drying, crust softening and increased firmness (*San et al., 2022*).

Moisture content, in turn, influences the sensory and textural characteristics of bakery products, as well as their changes during storage. In the case of crispy products, variations in water content and water activity can cause changes in the degree of crispiness, by affecting the mechanical properties of the product structure (*van Nieuwenhuijzen et al. 2008*).

The aim of the study was to evaluate the structural properties and water-related parameters of gluten-free pretzels obtained under laboratory conditions. In this regard, the cutting force, water activity and moisture content were determined, in order to assess the quality of the products and to compare the results obtained with the data available in the scientific literature.

## MATERIALS AND METHODS

The gluten-free pretzels were obtained under laboratory conditions, using a recipe based on rice flour. For the preparation of one batch, 1040 g of rice flour, 200 g of corn starch, 25 g of salt, 25 g of sugar, 20 g of baking powder, 36.3 g of sunflower oil, 900 ml of water, and 10 g of xanthan gum were used.

For the technological process and to ensure the reproducibility of the experimental determinations, the following equipment available in the food technology laboratory was used:

+ Dito Sama BE5 planetary mixer intended for the laboratory food industry, equipped with a 5 L capacity stainless steel bowl and transparent protective screen. The speed of the stainless steel spiral arm was adjusted by means of a 10-step electronic speed variator (operating range: 31–462 rpm), the installed motor power being 300 W.

+ commercial dough scalding unit, with a capacity of 6 L, with immersed electric heating elements, protective basket for samples, and electronic thermostat located on the main control panel for strict control of the solution temperature.

+ HOUNSFIELD H1KS mechanical testing machine equipped with a 1000 N load cell. The cutting device was a metal shear plate (guillotine-type blade) with an opening angle of 30°. Data acquisition, zero-point calibration, and generation of force-deformation curves were performed by computer using the dedicated QMat software

+ Rotronic HygroLab digital equipment specialized in water activity ($a_w$) analysis, equipped with a sealed capacitive HC2-AW measuring probe, for simultaneous monitoring of temperature and equilibrium relative humidity inside the chamber, with an accuracy of ±0.008.

+ KERN DBS gravimetric moisture analyzer equipped with an internal electronic balance with a weighing accuracy of d = 0.001 g and an upper heating unit with halogen lamps. The device has a digital display indicating in real time the temperature, process duration, and percentage evolution of the water removed.



**Fig. 1 - Gluten-free pretzels baked for 13 to 15 minutes**

Gluten-free pretzels were obtained according to the established recipe. The dry ingredients were introduced into the bowl of a Dito Sama BE5 planetary mixer, after which the liquid ingredients were gradually added. Mixing was carried out until a homogeneous dough was obtained. After mixing, the dough was left to rest for approximately 15 minutes, after which it was divided into pieces of approximately 35 g. Each piece of dough was manually shaped into a pretzel. The shaped pretzels were subsequently subjected to scalding by immersion for 1 minute in a solution prepared from 6 L of water and 400 g of sugar, maintained at a temperature of 95 ºC. After scalding, the products were baked at a temperature of 230 ºC using the FM electric pastry oven. Within the experimental research, two variants of experimental products were obtained, differentiated by baking time: 13 minutes and 15 minutes, respectively (Figure 1). After baking, the pretzels were cooled to an ambient temperature of 22 ºC and weighed, the mass of the finished product being approximately 27–28 g.

Prior to the determination of the mechanical properties, the samples were stored for 24 hours in polymeric material packaging, at ambient temperature.

The determination of the mechanical characteristics of the gluten-free pretzels was evaluated using the HOUNSFIELD H1KS mechanical testing machine, equipped with a cutting device (Figure 2). The testing system was equipped with metal shear plates with an opening angle of 30º, and the experimental data were recorded and represented in the form of force-deformation curves using the QMat software.

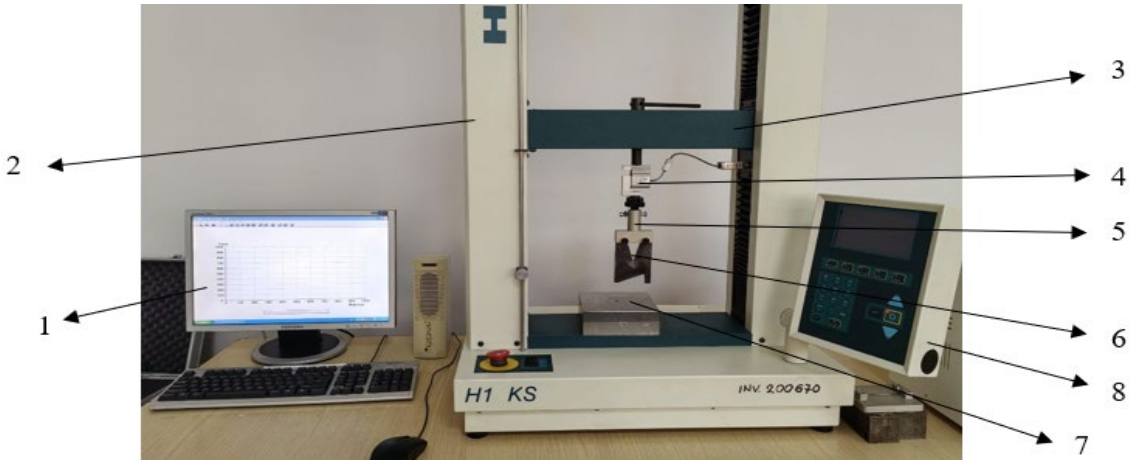



**Fig. 2 - HOUNSFIELD H1KS mechanical testing machine**

1 – computer; 2 – support columns; 3 – movable crosshead; 4 – 1000N load cell; 5 – cutting device mounting system; 6 – cutting device; 7 – pretzel holder; 8 – control panel

For each of the two batches, 6 individual pretzels were tested, with 3 determinations (cuts at different points) performed on each sample, resulting in a total of 18 tests per batch. The blade of the shear device

moved downward at a constant displacement speed set at 50 mm/min, covering a maximum vertical extension of 30 mm until complete sectioning of the pretzel cross-section. The parameter monitored was the maximum cutting force (expressed in N), automatically recorded at the point of structural failure.

Before each determination, zero-point calibration was performed. The samples were individually positioned on the apparatus support and subjected to the cutting process at a displacement speed of the cutting device of 50 mm/min, using a maximum vertical displacement range (extension) of 30 mm. Testing continued until complete sectioning of the sample (Figure 3). The maximum force value recorded during the cutting process was used as a parameter for characterizing the cutting resistance of the pretzels.



**Fig. 3 - Positioning and sectioning the pretzel sample in the shear device**

The water activity ($a_w$) was determined using the Rotronic HygroLab laboratory analyzer. Measurements were performed for both baking variants, both immediately after cooling the samples and after 24 hours of storage in packaging. The determinations were carried out at a temperature of 22 ºC, and the water activity values were recorded after stabilization of the instrument reading.

The moisture content of the samples was determined using the KERN DBS thermobalance, which operates on the thermogravimetric principle. The determinations were carried out for the samples baked for 13 and 15 minutes, both after cooling and after 24 hours of storage in packaging.

## RESULTS

For the evaluation of the mechanical properties of the gluten-free pretzels, two experimental variants were analyzed, corresponding to baking times of 13 and 15 minutes. For each variant, six individual samples were analyzed, and three cutting force determinations were performed for each pretzel. For the characterization of each pretzel, the mean of the three determinations was used, and the results obtained are presented in Table 1. In the case of the pretzels baked for 13 minutes, the mean values of the maximum cutting force for the six samples varied between 44.85 and 104.27 N, while the overall mean was approximately 72.89 N. For the samples baked for 15 minutes, the mean values of the maximum cutting force ranged between 39.73 N and 67.20 N, with an overall mean of approximately 51.51 N. Regarding the extension (vertical displacement of the knife during cutting) for the pretzels baked for 13 minutes, the mean values ranged between 12.59 and 27.47 mm, while the overall mean was approximately 20.08 mm. For the pretzels baked for 15 minutes, the mean extension values varied between 8.56 and 23.84 mm, with an overall mean of approximately 19.08 mm.

The data presented in Table 1 also highlight variability in the cutting force among the individual samples within each baking variant. The range of values was greater for the pretzels baked for 13 minutes compared with those baked for 15 minutes. The differences observed between samples belonging to the same type of sample may be associated with differences in shape and thickness resulting from manual shaping, as well as structural

non-uniformity. An original and relevant aspect introduced by the current mechanical study consists of the evaluation of the energy consumption during shearing (expressed in N·m), a parameter automatically recorded by integrating the area under the force-displacement curve up to the moment of complete sectioning of the sample. The data summarized in Table 1 reveal major discrepancies between the two technological variants. For the pretzels baked for 13 minutes, the total mechanical work consumed varied between 0.698 N·m and a maximum of 2.536 N·m. This increased energy confirms the presence of a structure with continuous internal resistance and high plasticity, generated by the strong interactions between the partially gelatinized starch and the elastic hydrocolloidal xanthan gum network, which retains a large amount of free water.

In contrast, the batch subjected to the prolonged thermal treatment of 15 minutes recorded a considerably lower overall energy consumption, with values ranging between 0.469 N·m and 1.469 N·m. From a physical point of view, although the outer crust of the 15-minute batch became more rigid, the extremely aerated, porous, and dehydrated crumb behaved as a brittle structure. Fracturing occurred almost instantaneously at low forces after penetration of the crust, substantially reducing the integral area under the curve and, consequently, the total energy required for mastication.

**Table 1**

**Results of cutting force determination for samples baked for 13 and 15 minutes**

| Time | Sample | Maximum force (N) | Mean maximum cutting force (N) | Extension (mm) | Mean extension (mm) | Energy consumption, (N·m) |
|---|---|---|---|---|---|---|
| Baked product 13 minutes | 1 | 191.80 | 99.64 | 27.80 | 16.45 | 1.639 |
| | | 36.24 | | 8.76 | | |
| | | 70.90 | | 12.80 | | |
| | 2 | 56.10 | 61.80 | 27.48 | 27.46 | 1.697 |
| | | 54.00 | | 27.40 | | |
| | | 75.30 | | 27.52 | | |
| | 3 | 78.00 | 71.26 | 27.92 | 17.36 | 1.237 |
| | | 60.70 | | 13.28 | | |
| | | 75.10 | | 10.88 | | |
| | 4 | 75.20 | 104.26 | 28.00 | 24.32 | 2.536 |
| | | 102.10 | | 17.28 | | |
| | | 135.50 | | 27.68 | | |
| | 5 | 45.70 | 44.84 | 28.00 | 22.30 | 1.000 |
| | | 36.44 | | 11.12 | | |
| | | 52.40 | | 27.80 | | |
| | 6 | 68.30 | 55.50 | 12.80 | 12.58 | 0.698 |
| | | 49.00 | | 15.60 | | |
| | | 49.20 | | 9.36 | | |
| Baked product 15 minutes | 1 | 68.80 | 54.80 | 7.48 | 8.56 | 0.469 |
| | | 43.20 | | 6.24 | | |
| | | 52.40 | | 11.96 | | |
| | 2 | 37.40 | 39.84 | 27.80 | 21.50 | 0.857 |
| | | 43.65 | | 28.00 | | |
| | | 38.48 | | 8.72 | | |
| | 3 | 36.32 | 39.73 | 13.92 | 16.64 | 0.661 |
| | | 38.52 | | 27.28 | | |
| | | 44.35 | | 8.72 | | |
| | 4 | 75.00 | 67.20 | 12.48 | 21.86 | 1.469 |
| | | 53.70 | | 25.20 | | |
| | | 72.90 | | 27.92 | | |
| | 5 | 64.20 | 64.60 | 28.00 | 22.06 | 1.425 |
| | | 67.30 | | 28.00 | | |
| | | 62.30 | | 10.20 | | |
| | 6 | 45.30 | 42.88 | 28.00 | 23.84 | 1.022 |
| | | 41.05 | | 15.52 | | |
| | | 42.30 | | 28.00 | | |

In addition to the maximum force values, the analysis of the force-displacement profiles corresponding to determinations *T1*, *T2*, and *T3*, corresponding to the three cuts performed for each sample, allows a more detailed characterization of how the pretzel structure responds to mechanical loading. For this purpose, the curves obtained for representative samples baked for 13 and 15 minutes were comparatively analyzed.

For the sample baked for 13 minutes, the curves corresponding to the three determinations generally show a relatively continuous evolution of force as a function of displacement. In the case of determination *T1*, a local maximum of approximately 85 N is reached at a displacement of approximately 10.5 mm, after which the force decreases with the progress of sectioning the pretzel. The increase in force observed toward the end of the displacement may be associated with the compaction of the material between the cutting device and the rigid support of the apparatus. The relatively smooth profile of the curves suggests a more progressive deformation of the pretzel structure before fracture. In the case of successive determinations, the shape of the curves is not identical, indicating the presence of local structural differences within the same product.

For the sample baked for 15 minutes, the force-displacement profiles exhibit large, frequent, and more pronounced oscillations of the force. In the case of determination *T1*, the initial maximum, of approximately 69 N, is reached at a displacement of approximately 7.5 mm, earlier than for the sample baked for 13 minutes.

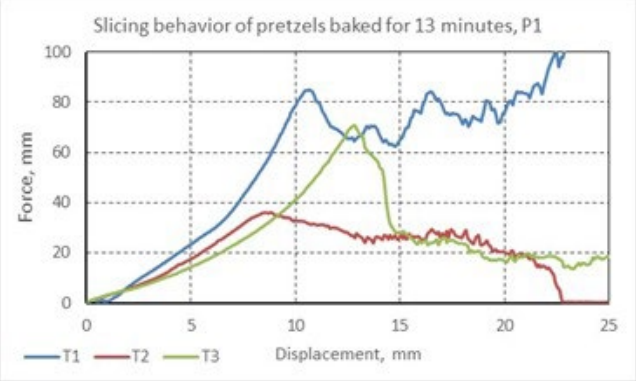



**Fig. 4 - Force–displacement profiles of gluten-free pretzels baked for 13 minutes**

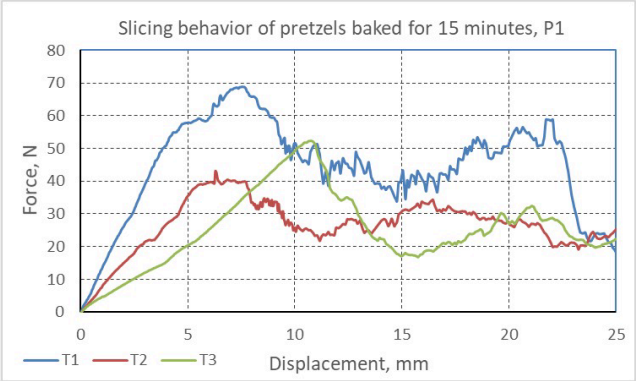



**Fig. 5 - Force–displacement profiles of gluten-free pretzels baked for 15 minutes**

The irregular appearance of the curves may be associated with the successive occurrence of local fracture events during the penetration of the cutting device into the product. This type of response is compatible with a more rigid structure and more susceptible to successive fracture compared with the more continuous profile observed for the sample baked for 13 minutes. A difference can also be observed in the region corresponding to larger displacements. For the sample baked for 13 minutes, some of the curves tend toward reduced force values after sectioning of the pretzel, whereas for the sample baked for 15 minutes, the *T2* and *T3* curves maintain residual force values of approximately 20–40 N over a larger portion of the displacement. This behavior suggests the maintenance of contact between the sectioned material and the cutting device.

The dynamics of the forces recorded during successive cuts at different points of the same product (Figure 3 and Figure 4) highlight another critical phenomenon specific to gluten-free bakery products: local structural anisotropy. In the case of the curves for the 13-minute batch (Figure 3), determination *T1* exhibits a clear peak in the central region (10.5 mm), whereas *T2* shows a much flatter evolution, plateauing at values below 40 N. This major discrepancy suggests a non-uniform distribution of gas bubbles and dough density caused by manual shaping. The area intersected by *T1* corresponds to a compact node, with low porosity, whereas the *T2* section indicates a large air cell or an area with reduced structural density, where the blade encountered minimal resistance. For the 15-minute batch (Figure 4), the superimposition of the *T1*, *T2*, and *T3* curves shows that, although there are variations in the amplitude of the peaks, the jagged profiles recur throughout the entire extension The presence of repeated force oscillations in the three determinations suggests a more heterogeneous fracture process in the 15-min samples. Such behavior could be associated with structural changes induced by prolonged baking, although porosity and microstructure were not directly measured. The comparison of the two sets of curves indicates that extending the baking time from 13 to 15 minutes was associated not only with changes in the maximum force values, but also with a change in the mechanical response of the product. For the sample baked for 13 minutes, the force evolution was more progressive, whereas the sample baked for 15 minutes exhibited a more irregular profile and a faster attainment of the initial maximum force. The differences between the *T1*, *T2*, and *T3* determinations performed on the same

product also highlight the local non-uniformity of the gluten-free matrix. This variability may be associated with local differences in porosity, thickness, and structural distribution resulting from manual shaping. However, the interpretation of these effects should be carried out with caution, as porosity and microstructure were not directly determined within the present study.

The values obtained were compared, for reference purposes, with those reported by Paykary et al. (2015) for gluten-free hard pretzels obtained using brewer's rice flour. In that study, the mechanical resistance of the products was evaluated using the cutting strength parameter, using a texture analyzer equipped with a guillotine-type blade, and the maximum force recorded during the test was considered the cutting force of the product. The values reported by the authors ranged approximately from 6.71 to 14.88 N, lower than those obtained in the present study, namely 72.89 N for the samples baked for 13 minutes and 51.51 N for the samples baked for 15 minutes. The differences between the two studies should be interpreted with caution, considering the differences in product formulation, raw materials used, sample geometry, and testing conditions.

The macrostructural differences observed between the two thermal treatment variants can be explained in terms of the kinetics of heat and mass transfer correlated with the rheology of hydrocolloids. During the baking process at 230°C, the removal of water from the outer layers of the dough directly dictates the phase transition of the macromolecular components. The higher overall mean cutting force obtained for the 13-minute batch (72.89 N), compared with the 15-minute batch (51.51 N), highlights a dense transitional structural state, characterized by a compact, partially gummy crumb. At this intermediate stage of baking (13 minutes), the network formed by xanthan gum and gelatinized corn starch still retains a high moisture content, exhibiting high shear resistance throughout the cross-section of the sample, without the occurrence of cleavage planes or macroscopic pores that would facilitate blade penetration. As the baking time is extended to 15 minutes, the phenomena of thermal expansion of gas microbubbles (leavening) and enhanced evaporation of free water induce the transformation of the compact matrix into a fixed cellular (alveolar) structure. The starch cell walls become much thinner and more rigid, while the overall density of the crumb decreases substantially. This phenomenon explains the decrease in the mean maximum force to 51.51 N; although the outer surface develops a harder crust, the internal mass of the pretzel becomes much more porous and easier to penetrate continuously by the blade of the HOUNSFIELD H1KS apparatus. The statistical analysis of the total shear energy values in Table 1 supports this kinetic hypothesis. The samples from the 13-minute batch require a considerably higher total mechanical work (reaching values of up to 2.536 N·m), as the blade must plastically deform a dense and cohesive material. In contrast, for the 15-minute batch, although the maximum point force required to break the crust remains significant, the rapid collapse of the internal alveolar walls drastically reduces the area under the force-displacement curve, stabilizing the energy consumption at considerably lower values (with a minimum of 0.469 N·m for Sample 1).

Therefore, optimization of the duration of the thermal treatment represents a technological tool for controlling not only the surface hardness but also the overall texture (gummy versus aerated/brittle) of bakery products based on rice flour. Water activity and moisture content were determined for both experimental sample variants, both after cooling the products and after 24 hours of storage in packaging. The values obtained are presented in Table 2.

**Table 2**

**Water activity and moisture content of the samples**

| Sample | Water activity, $a_w$ (22°) | Moisture content (%) |
|---|---|---|
| $Sample_{13\ min}$ after cooling | 0.975 | 20.68 |
| $Sample_{13\ min}$ after 24h | 0.888 | 25.64 |
| $Sample_{15\ min}$ after cooling | 0.953 | 21.64 |
| $Sample_{15\ min}$ after 24h | 0.865 | 23.00 |

For the samples baked for 13 minutes, water activity decreased from 0.975 after cooling to 0.888 after 24 h, while moisture content increased from 20.68% to 25.64%.

For the samples baked for 15 minutes, water activity decreased from 0.953 to 0.865, while moisture content increased from 21.64% to 23.00%.

In both experimental variants, a reduction in water activity was thus observed after 24 hours of storage. At both determination times, the samples baked for 15 minutes showed lower water activity values compared with those baked for 13 minutes. These results indicate differences in the water-related parameters between the two baking variants. However, based on the determinations performed, the shelf life or microbiological stability of the products cannot be directly established, as these would require monitoring over a longer

period and additional determinations. The opposite trends observed for moisture content and water activity may reflect differences between total water content and water availability within the product matrix.

**ACKNOWLEDGEMENT**

This research was supported by the project CNFIS-FDI-2026-F-0049 “Asigurarea eficienței operaționale a bazei de aplicații practice pentru sisteme biotehnice în livezi, vii, solarii și grădini (EFIBIOTECH)”, from the Ministry of Education and Research through the Executive Agency for Financing Higher Education, Research, Development and Innovation.

**CONCLUSIONS**

Within the study, gluten-free pretzels based on rice flour were obtained and characterized, with two experimental variants differentiated by baking time, 13 and 15 minutes, at a temperature of 230°C. For each variant, six individual products were analyzed, and the mechanical characterization revealed differences between the two batches. The pretzels baked for 13 minutes exhibited a higher mean cutting force, of approximately 72.89 N, compared with 51.51 N for the samples baked for 15 minutes.

The analysis of the force–displacement profiles also revealed differences in the mechanical response of the products. For the sample baked for 13 minutes, the curves generally showed a more continuous evolution of force, suggesting more progressive deformation before fracture. In contrast, the sample baked for 15 minutes exhibited a more irregular profile, characterized by successive force oscillations and faster attainment of the initial maximum, a behavior compatible with a more rigid structure and the occurrence of successive local fractures during cutting.

The differences observed between the *T1*, *T2*, and *T3* determinations performed on the same product highlighted the local non-uniformity of the pretzel structure, which may be associated with variations in shape, thickness, porosity, and structural distribution characteristic of manually shaped products. These aspects may contribute to the variability of the mechanical response within the same batch.

Water activity decreased after 24 hours of storage for both experimental variants, whereas moisture content showed a slight increase.

Overall, the results show that baking time is associated with both the level of mechanical resistance and the fracture behavior, as well as with water-related parameters of gluten-free pretzels. Determination of cutting force, analysis of force–displacement profiles, as well as evaluation of water activity and moisture content can provide useful information for the characterization and further optimization of the technological process.

**REFERENCES**

[1] Adzqia, F., Suwonsichon, S., & Thongngam, M. (2023). Effects of white sorghum flour levels on physicochemical and sensory characteristics of gluten-free bread. *Foods*, *12*(22), 4113. https://doi.org/10.3390/foods12224113

[2] Alibekova, Z., Bayisbayeva, M., Shamsudin, R., Bakhtybekova, A., Alibekov, R., & Aimenov, Z. (2026). Problems and approaches in the improvement of gluten-free bread texture: A comprehensive review. *International Journal of Food Science*, 2026, 5214023. https://doi.org/10.1155/ijfo/5214023

[3] Gallagher, E., Gormley, T. R., & Arendt, E. K. (2004). Recent advances in the formulation of gluten-free cereal-based products. *Trends in Food Science & Technology*, *15*(3–4), 143–152. https://doi.org/10.1016/j.tifs.2003.09.012

[4] Gómez, M. (2022). Gluten-free bakery products: Ingredients and processes. *Advances in Food and Nutrition Research*, *99*, 189–238. https://doi.org/10.1016/bs.afnr.2021.11.005

[5] San, H., Laorenza, Y., Behzadfar, E., Sonchaeng, U., Wadaugsorn, K., Sodsai, J., Kaewpetch, T., Promhuad, K., Srisa, A., Wongphan, P., & Harnkarnsujarit, N. (2022). Functional Polymer and Packaging Technology for Bakery Products. *Polymers*, *14*(18), 3793. https://doi.org/10.3390/polym14183793

[6] van Nieuwenhuijzen, N. H., Primo-Martín, C., Meinders, M. B. J., Tromp, R. H., Hamer, R. J., & van Vliet, T. (2008). Water content or water activity: What rules crispy behavior in bread crust? *Journal of Agricultural and Food Chemistry*, *56*(15), 6432–6438. https://doi.org/10.1021/jf800522c

# ECOTOXICITY ASSESSMENT OF PROCESS WATERS RESULTED DURING THE HYDROTHERMAL CARBONIZATION OF SPENT COFFEE GROUNDS

/

# *EVALUAREA ECOTOXICITĂȚII LICHIDELOR REZULTATE DIN CARBONIZAREA HIDROTERMALĂ A ZAȚULUI DE CAFEA*

**Ramona-Eugenia POPESCU[1)], Corina Violeta CHIRIȚĂ*[1)], Maria RÂPĂ[2)]**
[1)] UNSTP Bucharest, Biotechnical Systems Engineering Doctoral School, Bucharest / Romania;
*E-mail: ramona.popescu1008@stud.isb.upb.ro*
[2)] UNSTP Bucharest, Faculty of Materials Science and Engineering, Bucharest / Romania.
*E-mail: maria.rapa@upb.ro*
**Tel: (+40) 799 588 431; *E-mail: corina.chirita1806@stud.isb.upb.ro*

***Keywords:*** *spent coffee grounds (SCG), hydrothermal carbonization, circular economy, phytotoxicity, germination index*

***Abbreviations:*** *SCG – spent coffee grounds; HTC – hydrothermal carbonization; Gi – germination index; G – germination capacity; EC – electrical conductivity; TDS – total dissolved solids*

**ABSTRACT**

*Spent coffee grounds (SCG) are an abundant organic residue, most of which ends up in landfills. Although they are rich in organic matter and nutrients, their direct application to soil is limited by phenolic compounds and caffeine. Hydrothermal carbonization converts wet biomass in water, at moderate temperatures and autogenous pressure, into a solid hydrochar and a liquid phase rich in dissolved organic compounds and nutrients, whose phytotoxicity must be assessed before use. In this study, SCG were processed by hydrothermal carbonization under five operating conditions (samples HTC1–HTC5). The resulting liquids were diluted with distilled water at HTC liquid: water volume ratios of 1:25 and 1:50 and tested on mustard seeds for 6 days. Germination capacity, radicle length and the germination index (Gi) were determined relative to distilled water. The results showed that the following variants were non-phytotoxic (Gi > 80%): HTC1 at 1:25 (Gi = 152%) and 1:50 (Gi = 223%); HTC2 at 1:25 (Gi = 135%); HTC3 at 1:50 (Gi = 131%); HTC4 at 1:50 (Gi = 173%); and HTC5 at 1:50 (Gi = 133%). Gi values above 100% suggested a stimulating effect on radicle growth, which supports the use of diluted process water as a fertilizer.*

**REZUMAT**

*Zațul de cafea este un reziduu organic abundent, care ajunge în mare parte la depozitele de deșeuri. Deși bogat în materie organică și nutrienți, aplicarea sa directă pe sol este limitată de compușii fenolici și de cafeină. Carbonizarea hidrotermală transformă biomasa umedă, la temperaturi moderate și presiune autogenă, într-un produs solid, hidrocharul, și o fază lichidă bogată în compuși organici dizolvați și nutrienți, a cărei fitotoxicitate trebuie evaluată înainte de utilizare. În acest studiu, zațul de cafea a fost procesat prin carbonizare hidrotermală în cinci condiții de lucru (probele HTC1–HTC5). Lichidele obținute au fost diluate cu apă distilată la rapoarte volumice lichid HTC : apă de 1:25 și 1:50 și testate pe semințe de muștar timp de 6 zile, prin determinarea capacității de germinare, a lungimii radiculei și a indicelui de germinare (Gi). Au fost nefitotoxice (Gi > 80%) următoarele variante: HTC1 la 1:25 (Gi = 152%) și 1:50 (Gi = 223%); HTC2 la 1:25 (Gi = 135%); HTC3 la 1:50 (Gi = 131%); HTC4 la 1:50 (Gi = 173%) și HTC5 la 1:50 (Gi = 133%). Valorile Gi de peste 100% au sugerat un efect stimulator asupra creșterii radiculei, ceea ce susține utilizarea apei de proces diluate ca fertilizant.*

## INTRODUCTION

Coffee preparation generates over 6 million tonnes of spent coffee grounds (SCG) annually, originating from the soluble coffee industry, coffee shops and household consumption. One tonne of green coffee beans generates about 650 kg of spent coffee grounds, and approximately 2 kg of wet SCG are produced per kilogram of soluble coffee *(Mussatto et al., 2011).* Currently, this waste is mostly landfilled or incinerated, practices that emit greenhouse gases and generate significant environmental risks, particularly for aquatic environments *(Hu et al., 2025).*

Spent coffee grounds contain valuable organic compounds with a wide range of applications in the circular economy: cellulose (12%), hemicellulose (39%), lignin (24%), lipids (2%) and proteins (17%) *(Ballesteros et al., 2014),* along with caffeine, mineral nutrients (magnesium, calcium, potassium, iron and zinc) and other compounds with antioxidant activity. The valorization of this residue, in line with the circular economy principles and Directive (EU) 2018/851 on waste *(European Parliament and Council of the European Union, 2018)*, represents both a challenge and an opportunity for applied research *(Ungureanu and Vlăduț, 2026).* Polyphenols, mainly chlorogenic acids and their derivatives, are among the main bioactive compounds of SCG; they give SCG antioxidant and chelating properties, but together with caffeine they also inhibit plant growth, so SCG cannot be applied directly to soil even at low doses *(Hu et al., 2025; Pérez-Burillo et al., 2022).*

Hydrothermal carbonization (HTC) is emerging as one of the most promising technologies for the valorization of wet biomass, including spent coffee grounds. The process reproduces within a few hours, at laboratory and industrial scale, the geological transformations that led to the formation of coal over millions of years. It consists of the thermal treatment of wet biomass (agricultural waste, marine algae, agro-industrial residues, manure, sewage sludge, municipal solid waste etc.) in an aqueous medium at 150–250 °C and autogenous pressure, yielding a carbon-rich solid with high energy density (hydrochar) and a process liquid rich in soluble organic compounds *(Kambo et al., 2018; Wang et al., 2018).* Unlike pyrolysis, gasification and torrefaction, HTC does not require prior drying of the feedstock, which is a major techno-economic advantage for high-moisture residues, as it eliminates an energy-intensive and costly step. The relatively low operating temperature and the use of water as solvent also give HTC a favourable sustainability profile *(Wang et al., 2018).*

From a chemical perspective, HTC involves several simultaneous and sequential transformations: hydrolysis of the lignocellulosic fractions (cellulose, hemicellulose and lignin), followed by dehydration and decarboxylation of the intermediate products and by their condensation and polymerization into stable aromatic structures. Water has a dual role in this system, acting both as solvent and as reactant. At elevated temperatures, the increase in the ionization constant of water raises the concentration of $H^+$ ions, which promotes acid-catalysed reactions without any added acid *(Wang et al., 2018).*

Recent studies have addressed the valorization of SCG by HTC for a wide range of applications: high-quality solid fuels *(Afolabi et al., 2020; Sajadi et al., 2026; Wądrzyk et al., 2024),* adsorbents for the removal of hexavalent chromium from industrial effluents *(Freitas et al., 2026),* building materials *(Shao et al., 2025),* as well as the nutraceutical and agricultural *fields (Cervera-Mata et al., 2021; Valencia-Isaza et al., 2025).*

For the production of graphitic porous carbon for supercapacitors, HTC of SCG at 240 °C, followed by chemical activation with KOH at 600–700 °C, yielded a material with a specific surface area of 976 $m^2/g$ and a total pore volume of 0.535 $cm^3/g$ *(Nguyen et al., 2025).* Both by-products of SCG processing by HTC, the hydrochar and the process water, can therefore contribute to a circular and sustainable use of this residue.

The process water contains organic acids, furanic compounds, phenolic compounds and dissolved nutrients, and its acidity and content of reaction intermediates increase with reaction temperature *(Chu et al., 2026; Kambo et al., 2018).* Its nutrients make it a potential liquid fertilizer, but many of its organic constituents are phytotoxic, so it usually needs dilution before agricultural use *(Chu et al., 2026).* Concentrated process water from sugarcane by-products completely inhibited the germination of maize, lettuce and tomato seeds, whereas diluted process water stimulated seedling growth *(Fregolente et al., 2019).* The aqueous phase from cow manure digestate was too concentrated at a 1:30 dilution but allowed maize growth at 1:60 and 1:90 *(Celletti et al., 2021),* and the aqueous phase from brown seaweed improved the growth of bean plants *(Spagnuolo et al., 2023).* For SCG, the liquid phase obtained at 220 °C, with a 1:10 biomass-to-water ratio and residence times of 1 h and 12 h, showed potential as a fertilizer and as a source of bioactive compounds *(Popescu et al., 2026).*

The aim of this work was to establish the phytotoxic effect of the process waters resulting from the hydrothermal carbonization of spent coffee grounds under five sets of conditions, differing in temperature, residence time and solid-to-liquid ratio, on the germination and development of mustard seeds.

## MATERIALS AND METHODS

**Materials.** Spent coffee grounds resulting from daily coffee consumption were used. The SCG were washed with distilled water (about 10 L in total) until the electrical conductivity (EC) of the washing water

decreased from about 1.8 mS/cm to 14.27 µS/cm, and then dried in an oven for 2 days. This work focused on the process water, a by-product of HTC that is often ignored and considered waste, although it represents over 90% of the mass of the HTC products. It contains complex organic compounds (phenols, organic acids) and nutrients, and its characterization is needed for its subsequent valorization within the circular economy.

**Granulometric analysis.** The dried SCG were sieved with a Fritsch vibratory sieve shaker (Fig. 1), with a sieving time of 3 min and an amplitude setting of 0.5. The 90 µm fraction, selected on the basis of the granulometric analysis, was subjected to HTC.



**Fig. 1 - Fritsch vibratory sieve shaker used for the granulometric analysis of SCG**

**Hydrothermal carbonization.** The experimental variants are given in Table 1. For each variant, dried SCG (30 g, or 60 g for HTC5) were mixed with 300 mL of distilled water and processed in a laboratory autoclave reactor (Fig. 2a) under autogenous pressure. After the reaction, the hydrochar was separated from the liquid phase by vacuum filtration through a 1.2 µm filter (Fig. 2b), washed with water and ethanol and dried. The filtrate, referred to as process water, was kept for characterization and ecotoxicity testing.

**Table 1**

**Experimental variants of the hydrothermal carbonization of SCG**

| Sample code | Temperature [°C] | Time [min] | Solid : liquid ratio [g/mL] |
|---|---|---|---|
| HTC1 | 220 | 60 | 1:10 |
| HTC2 | 220 | 360 | 1:10 |
| HTC3 | 220 | 720 | 1:10 |
| HTC4 | 150 | 60 | 1:10 |
| HTC5 | 220 | 60 | 1:5 |

*Pressure was generated in situ (autogenous pressure)*



**Fig. 2 - Hydrothermal carbonization of SCG**

*a) laboratory autoclave reactor; b) separation of the process water by vacuum filtration*

**Characterization of the process waters.** The EC, total dissolved solids (TDS), salinity and pH of the process waters were measured with a multiparameter meter. The transmittance of the undiluted process waters was recorded with a UV-Vis spectrophotometer in the 200–800 nm range, and the value at 700 nm was used as an indicator of their colour intensity. The hydrochar yield was calculated with Equation (1):

$$\eta = \frac{m_{HC}}{m_{SCG}} x100 \quad [\%] \tag{1}$$

where:
$\eta$ – hydrochar yield, [%];
$m_{HC}$ – mass of dry hydrochar, [g];
$m_{SCG}$ – mass of dry SCG subjected to HTC, [g].

**Ecotoxicity test.** Filter paper discs were placed in Petri dishes, about 5 mL of process water diluted 1:25 and 1:50 (v/v) with distilled water (Fig. 3) were added to each dish, and 10 mustard seeds were distributed on the surface of the filter paper. After incubation at room temperature (24 °C) for 6 days, the germinated seeds were counted and the radicle length was measured with a graduated ruler (Mitelut and Popa, 2011); where a range of lengths was recorded for a dish, its midpoint was used. Distilled water (two dishes) was used as the reference, and an aqueous extract of untreated (non-autoclaved) SCG, diluted 1:25 and 1:50, was used for comparison. The germination index (Gi) was calculated with Equation (2):

$$Gi = \frac{G}{G_0} x \frac{L}{L_0} x100 \quad [\%] \tag{2}$$

where:
*Gi* – germination index, [%];
*G* – germination capacity of the seeds in the process water, [%];
$G_0$ – germination capacity in distilled water, [%];
*L* – mean radicle length of the seeds in the process water, [mm];
$L_0$ – mean radicle length in distilled water, [mm].

The mean of the two distilled water dishes was used as the reference ($G_0$ = 95%, $L_0$ = 12.5 mm). Gi is a very sensitive index, and values above 80% indicate the absence of phytotoxicity *(Tiquia et al., 1996).* Mustard seeds, which belong to the Brassicaceae family, were chosen for their remarkable capacity to accumulate heavy metals *(Arshed and Saleem, 2024; Lasat and Kochian, 2000).*

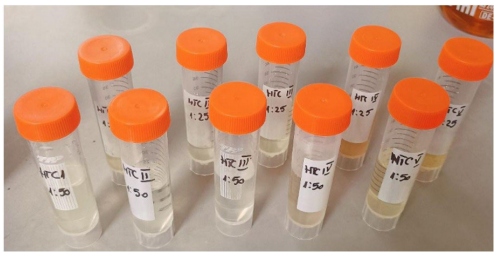


**Fig. 3 - Process waters diluted 1:25 and 1:50 with distilled water for the ecotoxicity test**

## RESULTS

### *Physicochemical characteristics of the process waters*

All process waters were acidic, with pH values between 4.33 and 4.87 (Table 2), which is consistent with the formation of organic acids during HTC (Kambo et al., 2018). HTC5, obtained with twice the amount of SCG, gave the most concentrated liquid, with an EC of 4.07 mS/cm and TDS of 3.19 g/L, about 1.8 and 2.6 times higher than HTC1. Extending the residence time at 220 °C from 60 to 360 and 720 min changed EC only slightly (2.31–2.53 mS/cm). HTC4, obtained at 150 °C, had the lowest EC (1.97 mS/cm) and was the least acidic (pH 4.87), but its transmittance at 700 nm was only 11.7%, compared with 91.2–94.5% for the other samples, which shows that it was much darker (Fig. 4).

The hydrochar yield ranged from 44.2% to 61.1%. At 220 °C and a residence time of 60 min, the yield was 46.5% (HTC1), and it was higher at the lower temperature of 150 °C (50.6%, HTC4), in agreement with the lower degree of conversion at milder conditions *(Wang et al., 2018).* The highest yield was obtained after 720 min (HTC3), which may be related to the deposition of secondary char formed by the polymerization of dissolved intermediates during long residence times.

**Table 2**

**Physicochemical characteristics of the process waters and hydrochar yield**

| Sample code | EC [mS/cm] | TDS [g/L] | pH [–] | Salinity [‰] | $T_{700}$ [%] | Yield [%] |
|---|---|---|---|---|---|---|
| HTC1 | 2.31 | 1.24 | 4.33 | 1.1 | 91.2 | 46.5 |
| HTC2 | 2.53 | 1.35 | 4.61 | 1.3 | 93.7 | 44.2 |
| HTC3 | 2.40 | 1.28 | 4.62 | 1.1 | 94.5 | 61.1 |
| HTC4 | 1.97 | 1.21 | 4.87 | 0.9 | 11.7 | 50.6 |
| HTC5 | 4.07 | 3.19 | 4.38 | 2.2 | 92.1 | 51.3 |

*$T_{700}$ – transmittance of the undiluted process water at 700 nm; yield calculated with Equation (1)*

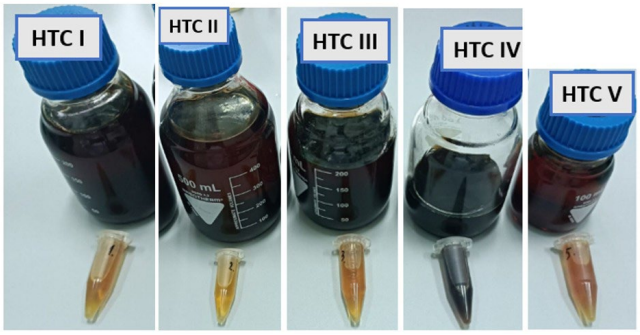



**Fig. 4 - Process waters obtained by HTC of SCG (samples HTC1–HTC5)**

***Germination and radicle growth***

At the 1:50 dilution, the process waters HTC1, HTC3 and HTC5 gave 90% germination and HTC4 gave 80%, close to distilled water (95%). At the 1:25 dilution, germination decreased to 50–60% for HTC1, HTC3, HTC4 and HTC5. HTC2 behaved in the opposite way, with 80% germination at 1:25 and only 30% at 1:50 (Table 3).

The longest radicles developed in the untreated SCG extract (34.0–39.6 mm) and in HTC1 (29.4–30.0 mm), more than twice as long as in distilled water (12.5 mm). At the 1:25 dilution, HTC3, HTC4 and HTC5 limited radicle growth to 5.0–7.5 mm, below the distilled water level, whereas at 1:50 the same process waters allowed radicles of 17.3–25.7 mm.

**Table 3**

**Germination capacity and radicle length of mustard seeds after 6 days**

| Sample | Dilution | *G* [%] | *L* [mm] |
|---|---|---|---|
| Distilled water, dish 1 | – | 100 | 7.5 |
| Distilled water, dish 2 | – | 90 | 17.5 |
| Distilled water, mean | – | 95 | 12.5 |
| Untreated SCG | 1:25 | 90 | 39.6 |
| Untreated SCG | 1:50 | 70 | 34.0 |
| HTC1 | 1:25 | 60 | 30.0 |
| HTC1 | 1:50 | 90 | 29.4 |
| HTC2 | 1:25 | 80 | 20.0 |
| HTC2 | 1:50 | 30 | 12.5 |
| HTC3 | 1:25 | 60 | 7.5 |
| HTC3 | 1:50 | 90 | 17.3 |
| HTC4 | 1:25 | 50 | 7.5 |
| HTC4 | 1:50 | 80 | 25.7 |
| HTC5 | 1:25 | 50 | 5.0 |
| HTC5 | 1:50 | 90 | 17.5 |

*G – germination capacity (10 seeds per dish); L – mean length of the measured radicles*

***Germination index***

Four variants had Gi values below the 80% threshold and were phytotoxic: HTC3 at 1:25 (38%), HTC4 at 1:25 (32%), HTC5 at 1:25 (21%) and HTC2 at 1:50 (32%) (Fig. 5). All other variants had Gi values

above 130%. HTC1 was the only process water that was non-phytotoxic at both dilutions (152% and 223%), and the untreated SCG extract was not phytotoxic at either dilution (300% and 200%). Examples of seedlings after 6 days are shown in Fig. 6.

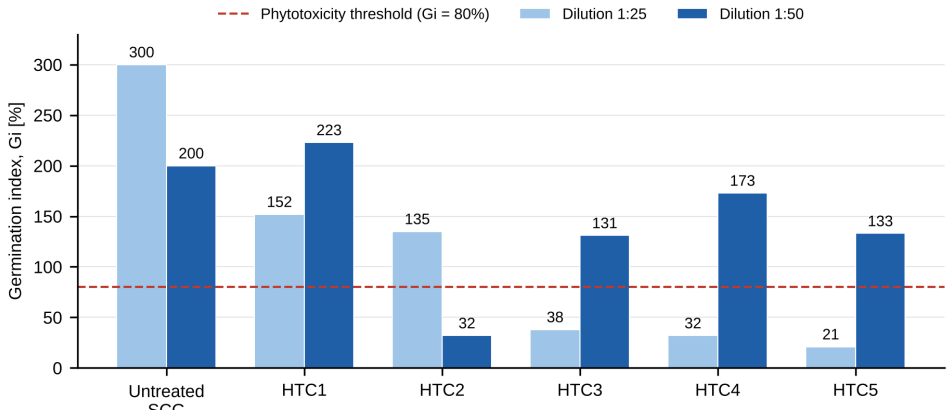



**Fig. 5 - Germination index of mustard seeds after 6 days**
*the dashed line marks the phytotoxicity threshold (Gi = 80%)*



**Fig. 6 - Mustard seedlings after 6 days**
*a) untreated SCG extract, 1:25; b) HTC1, 1:50*

***Influence of dilution and HTC conditions***

For HTC1, HTC3, HTC4 and HTC5, changing the dilution from 1:25 to 1:50 increased germination from 50–60% to 80–90%, and for HTC3, HTC4 and HTC5 radicle length increased 2.3 to 3.5 times. This dose–response relationship shows that the process water contains inhibitory compounds whose effect decreases with concentration, as also reported for process waters from other feedstocks (Celletti et al., 2021; Fregolente et al., 2019).

At the 1:25 dilution, *Gi* followed the order HTC1 (152%) > HTC2 (135%) > HTC3 (38%) > HTC4 (32%) > HTC5 (21%), which can be related to the HTC conditions (Table 1). The process water obtained at 220 °C for 60 min with a 1:10 ratio was the least phytotoxic, in agreement with Niu et al. (2021), who obtained the best lettuce growth with process water produced at 220 °C for 1 h. Extending the residence time to 720 min (HTC3) or lowering the temperature to 150 °C (HTC4) produced phytotoxic liquids at 1:25. The very low transmittance of HTC4 points to a higher load of dissolved coloured organic compounds, which may include intermediates that are not further converted at 150 °C.

The strongest effect was observed for HTC5 (*Gi* = 21%, radicles of 5 mm), whose process water also had the highest EC and TDS as a result of the doubled solid loading. Phenolic compounds, organic acids and furanic derivatives, which are typical of HTC process water and inhibit germination (Chu et al., 2026), are the likely cause of these effects.

HTC2 did not follow the trend of the other samples: only 3 of 10 seeds germinated at 1:50 (*Gi* = 32%), while at 1:25 *Gi* was 135%. This result may come from an error in labelling the dishes or from a local factor in the dish and has to be verified by repeating the test.

*Gi* values above 100% show that the radicles grew longer than in distilled water, which suggests that the diluted process waters and the untreated SCG extract supplied soluble nutrients that stimulated early seedling growth, as also reported for diluted process water on maize and tomato (Fregolente et al., 2019). Further studied should involve the repetition of the ecotoxicity test with at least three replicates.

## CONCLUSIONS

The process waters obtained by hydrothermal carbonization of spent coffee grounds were acidic (pH 4.33–4.87), and their dissolved solid content depended mainly on the solid-to-liquid ratio. The process water obtained at 150 °C was much darker than those obtained at 220 °C.

Dilution reduced the phytotoxicity of the process waters in a dose-dependent manner. At the 1:50 dilution, the process waters obtained at 220 °C for 60 and 720 min, at 150 °C for 60 min and at the 1:5 ratio were non-phytotoxic for mustard seeds (*Gi* of 131–223%), while at 1:25 the last three were phytotoxic (*Gi* of 21–38%). Longer residence time, lower temperature and higher solid loading therefore increased the phytotoxicity of the liquid phase.

The process water obtained at 220 °C for 60 min with a 1:10 ratio was the only one that was non-phytotoxic at both dilutions and is the most promising candidate for use as a liquid fertilizer. Diluted at least 1:50, the process water from spent coffee grounds can be considered for valorization as a liquid fertilizer, in line with the principles of the circular economy. Further work should repeat the test in triplicate, identify the inhibitory compounds and evaluate the effect of the process water on plant growth in soil.

## REFERENCES


[1] Afolabi, O. O. D., Sohail, M., & Cheng, Y.-L. (2020). Optimisation and characterisation of hydrochar production from spent coffee grounds by hydrothermal carbonisation. *Renewable Energy, 147*, 1380–1391. https://doi.org/10.1016/j.renene.2019.09.098

[2] Arshed, M. Z., & Saleem, A. (2024). Alleviation of chromium stress in *Brassica juncea* L. and soil remediation by plant growth promoting (PGP) bacteria. *Pakistan Journal of Scientific and Industrial Research Series B: Biological Sciences, 67*, 42–48. https://v2.pjsir.org/index.php/biological-sciences/article/view/3051

[3] Ballesteros, L. F., Teixeira, J. A., & Mussatto, S. I. (2014). Chemical, functional, and structural properties of spent coffee grounds and coffee silverskin. *Food and Bioprocess Technology, 7*(12), 3493–3503. https://doi.org/10.1007/s11947-014-1349-z

[4] Celletti, S., Lanz, M., Bergamo, A., Benedetti, V., Basso, D., Baratieri, M., Cesco, S., & Mimmo, T. (2021). Evaluating the aqueous phase from hydrothermal carbonization of cow manure digestate as possible fertilizer solution for plant growth. *Frontiers in Plant Science, 12*, 687434. https://doi.org/10.3389/fpls.2021.687434

[5] Cervera-Mata, A., Lara, L., Fernández-Arteaga, A., Rufián-Henares, J. Á., & Delgado, G. (2021). Washed hydrochar from spent coffee grounds: A second generation of coffee residues. Evaluation as organic amendment. *Waste Management, 120*, 322–329. https://doi.org/10.1016/j.wasman.2020.11.041

[6] Chu, Q., Liu, X., Feng, Y., Li, D., Yin, S., Chen, C., & Sha, Z. (2026). Process water from hydrothermal carbonization: From waste to liquid fertilizer and soil health amendment in circular bioeconomy. *Biochar, 8*(1), 96. https://doi.org/10.1007/s42773-026-00614-y

[7] European Parliament and Council of the European Union. (2018). Directive (EU) 2018/851 of 30 May 2018 amending Directive 2008/98/EC on waste. *Official Journal of the European Union, L 150*, 109–140. https://eur-lex.europa.eu/eli/dir/2018/851/oj

[8] Fregolente, L. G., Miguel, T. B. A. R., de Castro Miguel, E., de Almeida Melo, C., Moreira, A. B., Ferreira, O. P., & Bisinoti, M. C. (2019). Toxicity evaluation of process water from hydrothermal carbonization of sugarcane industry by-products. *Environmental Science and Pollution Research, 26*(27), 27579–27589. https://doi.org/10.1007/s11356-018-1771-2

[9] Freitas, C. P. M., Batista, G. D. F., Silva, M. D., Gomez, M. C., Arauzo, P. J., Cunha, F. F., & Kruse, A. (2026). From coffee waste to wastewater treatment: Optimization of hydrothermal carbonization and $H_3PO_4$ activation for Cr(VI) adsorption. *Journal of Hazardous Materials Advances, 21*, 100966. https://doi.org/10.1016/j.hazadv.2025.100966

[10] Hu, Y., Li, J., Wu, Y., Zhang, D., Qi, Z., & Yang, R. (2025). Spent coffee ground and its derivatives as soil amendments—Impact on soil health and plant production. *Agronomy, 15*(1), 26. https://doi.org/10.3390/agronomy15010026

[11] Kambo, H. S., Minaret, J., & Dutta, A. (2018). Process water from the hydrothermal carbonization of biomass: A waste or a valuable product? *Waste and Biomass Valorization, 9*(7), 1181–1189. https://doi.org/10.1007/s12649-017-9914-0

[12] Lasat, M. M., & Kochian, L. V. (2000). Physiology of Zn hyperaccumulation in *Thlaspi caerulescens*. In *Phytoremediation of contaminated soil and water*. CRC Press. https://doi.org/10.1201/9780367803148-8

[13] Mitelut, A. C., & Popa, M. E. (2011). Seed germination bioassay for toxicity evaluation of different composting biodegradable materials. *Romanian Biotechnological Letters, 16*(1), 121–129.

[14] Mussatto, S. I., Machado, E. M. S., Martins, S., & Teixeira, J. A. (2011). Production, composition, and application of coffee and its industrial residues. *Food and Bioprocess Technology, 4*(5), 661–672. https://doi.org/10.1007/s11947-011-0565-z

[15] Nguyen, T. P., Vu, T. N., Nguyen, D. H. M., Ho, T. T. A., Le, M. H., Ton, S. H. T., Tran, H. N., Luu, T. T. M., Nguyen, S. T., & Ho, V. T. T. (2025). Graphitic porous carbon fabricated from waste coffee grounds for supercapacitors. *Next Materials, 9*, 101021. https://doi.org/10.1016/j.nxmate.2025.101021

[16] Niu, Z., Wang, Z., Wang, J., Huang, H., Liu, W., Zhu, H., Wen, Y., & Liu, X. (2021). Phytotoxicity and nutrition behavior of process water obtained from the hydrothermal carbonization of poultry litter and its effect on lettuce germination and growth. *Environmental Science and Pollution Research, 28*, 58123–58134. https://doi.org/10.1007/s11356-021-14697-6

[17] Pérez-Burillo, S., Cervera-Mata, A., Fernández-Arteaga, A., Pastoriza, S., Rufián-Henares, J. Á., & Delgado, G. (2022). Why should we be concerned with the use of spent coffee grounds as an organic amendment of soils? A narrative review. *Agronomy, 12*(11), 2771. https://doi.org/10.3390/agronomy12112771

[18] Popescu, R.-E., Chiriță, C. V., Matei, E., Buse, T., Popa, M., Niță-Lazăr, M., Stănescu, M. M., & Râpă, M. (2026). Effect of hydrothermal treatment on some properties of spent coffee ground. *U.P.B. Scientific Bulletin, Series B, 88*(2), [299-308].

[19] Sajadi, A., Shekoohiyan, S., & Moussavi, G. (2026). Sustainable upcycling of face masks and spent coffee grounds into high-energy hydrochar via optimized co-hydrothermal carbonization. *Energy Reports, 15*, 109168. https://doi.org/10.1016/j.egyr.2026.109168

[20] Shao, J., Chen, Z., Wen, H., Su, L., & Li, Y. (2025). Evaluation on performance and carbon-sequestration of spent coffee grounds hydrothermal biochar concrete under multi-factor interaction. *Construction and Building Materials, 489*, 142394. https://doi.org/10.1016/j.conbuildmat.2025.142394

[21] Spagnuolo, D., Bressi, V., Chiofalo, M. T., Morabito, M., Espro, C., Genovese, G., Iannazzo, D., & Trifilò, P. (2023). Using the aqueous phase produced from hydrothermal carbonization process of brown seaweed to improve the growth of *Phaseolus vulgaris*. *Plants, 12*(14), 2745. https://doi.org/10.3390/plants12142745

[22] Tiquia, S. M., Tam, N. F. Y., & Hodgkiss, I. J. (1996). Effects of composting on phytotoxicity of spent pig-manure sawdust litter. *Environmental Pollution, 93*(3), 249–256.

[23] Ungureanu, N., & Vlăduț, N.-V. (2026). Sustainable valorization of spent coffee grounds within the circular economy: Innovative applications in food, agriculture, environmental, and industrial sectors. *Sustainability, 18*(8), 4127. https://doi.org/10.3390/su18084127

[24] Valencia-Isaza, A., Rufián-Henares, J. Á., Delgado-Osorio, A., & Fernández-Arteaga, A. (2025). New insights into the valorization of spent coffee grounds via hydrothermal carbonization: Emphasizing bioactive potential. *Bioresource Technology Reports, 31*, 102198. https://doi.org/10.1016/j.biteb.2025.102198

[25] Wądrzyk, M., Katerla, J., Janus, R., Lewandowski, M., Plata, M., & Korzeniowski, Ł. (2024). High-energy-density hydrochar and bio-oil from hydrothermal processing of spent coffee grounds—Experimental investigation. *Energies, 17*(24), 6446. https://doi.org/10.3390/en17246446

[26] Wang, T., Zhai, Y., Zhu, Y., Li, C., & Zeng, G. (2018). A review of the hydrothermal carbonization of biomass waste for hydrochar formation: Process conditions, fundamentals, and physicochemical properties. *Renewable and Sustainable Energy Reviews, 90*, 223–247. https://doi.org/10.1016/j.rser.2018.03.071

# NUMERICAL ANALYSIS OF ACOUSTIC PANELS USED FOR ROAD TRAFFIC NOISE REDUCTION

/

# *ANALIZA NUMERICĂ A PANOURILOR ACUSTICE UTILIZATE PENTRU REDUCEREA ZGOMOTULUI PROVENIT DIN TRAFICUL RUTIER*

**Ana-Maria GROSU[1)], Ovidiu VASILE[2)], Jazmina SCORȚEA[3)], Sorina Alexandra ZLATOIANU[3)]**

UNSTP Bucharest, Faculty of Biotechnical Systems Engineering, Bucharest / Romania;
*E-mail: ana_maria.grosu@upb.ro*

[2)] UNSTP Bucharest, Faculty of Biotechnical Systems Engineering, Department of Mechanics "Radu P. Voinea", Bucharest / Romania;
**Tel: 0722 172 700; *E-mail: ovidiu_vasile2002@yahoo.co.uk*

[3)] UNSTP Bucharest, Faculty of Biotechnical Systems Engineering, Bucharest / Romania

***Keywords:*** *acoustic barrier, perforated panel, sound absorption, transfer matrix method*

## ABSTRACT

*The paper proposes a numerical model, implemented in MATLAB, for evaluating the acoustic performance of a multilayer panel designed to reduce noise generated by road traffic. The analyzed structure consists of a perforated metal plate, a porous sound-absorbing layer, an air cavity, and a rigid backing. To characterize the acoustic behavior of the structure, the acoustic impedance of the perforated plate was determined using the Maa model, while the characteristic impedance and wave number of the porous material were calculated using the Miki model. The acoustic behavior of the multilayer assembly was evaluated by applying the Transfer Matrix Method (TMM), which enables the modeling of the interaction between the individual layers and the determination of the normal-incidence sound absorption coefficient and transmission loss (TL). The analysis was conducted over the frequency range of 100–4000 Hz.*

## REZUMAT

*Lucrarea propune un model numeric, implementat în mediul MATLAB, destinat evaluării performanței acustice a unui panou multistrat utilizat pentru reducerea zgomotului provenit din traficul rutier. Structura analizată este alcătuită dintr-o placă metalică perforată, un strat poros cu proprietăți fonoabsorbante, o cavitate de aer și un suport rigid. Pentru a caracteriza comportamentul acustic al structurii, impedanța acustică a plăcii perforate a fost determinată pe baza modelului Maa, iar impedanța caracteristică și numărul de undă corespunzător materialului poros au fost calculate utilizând modelul Miki. Comportamentul acustic al ansamblului multistrat a fost evaluat prin aplicarea Metodei Matricelor de Transfer (Transfer Matrix Method - TMM), care permite modelarea interacțiunii dintre straturile componente și determinarea coeficientului de absorbție acustică la incidență normală, precum și a pierderii prin transmisie (Transmission Loss - TL). Analiza a fost realizată în domeniul de frecvență 100-4000 Hz.*

## INTRODUCTION

Road traffic noise has become one of the most significant sources of environmental noise pollution in urban areas, with well documented effects on public health and quality of life. Acoustic barriers remain the most widely applied passive noise-control measure along highways, and their performance strongly depends on the material and structural configuration of the barrier panels *(Laxmi et al., 2022).* Conventional noise barriers are commonly built as multilayer panels combining a perforated metallic or polymeric plate with a porous absorbent material, since this configuration provides high sound absorption over a broad frequency range while remaining lightweight, durable, and cost effective *(Asdrubali and Pispola, 2007; Patil et al., 2024).*

The acoustic behaviour of perforated-plate absorbers has traditionally been described through the Maa model, which accounts for the viscous and inertial effects of air motion inside the perforations, while the acoustic properties of porous absorbent materials are commonly predicted with empirical models such as the Delany-Bazley model or it is improved version proposed by Miki *(Delany and Bazley, 1970; Miki, 1990).* Coupled with the Transfer Matrix Method, these models allow the acoustic response of multilayer panels to be predicted rapidly, without resorting to computationally expensive finite element simulations *(Lee and Kwon, 2004; Su et al., 2025).*

Numerous recent studies have focused on optimizing perforated-panel and porous-layer configurations for road-traffic noise mitigation, addressing either material level improvements, such as 3D-printed perforated geometries and hybrid aerogel absorbers *(Patil et al., 2024; Xue et al., 2024),* or structural-level solutions, such as active noise barriers and statistical-energy-analysis-based geometry optimization *(Wang et al., 2024; Wu et al., 2025).* However, numerical studies that combine the Maa and Miki models within a unified transfer-matrix implementation, specifically targeting the dominant frequency spectrum of road traffic noise, remain relatively scarce.

The aim of this paper was to develop a MATLAB based numerical model, using the Transfer Matrix Method combined with the Maa and Miki models, in order to predict the sound absorption coefficient and the transmission loss of a multilayer acoustic barrier panel, and to evaluate its acoustic performance in relation to the typical frequency spectrum of road traffic noise.

## MATERIALS AND METHODS

The acoustic barrier panel analysed in this study consisted of four layers, arranged from the sound source towards the rigid backing, as follows: a thin perforated plate, a porous absorbent layer, an air cavity, and a rigid wall (Fig. 1). This configuration is representative of noise barrier panels currently used along highways *(Patil et al., 2024; Wang et al., 2024).*

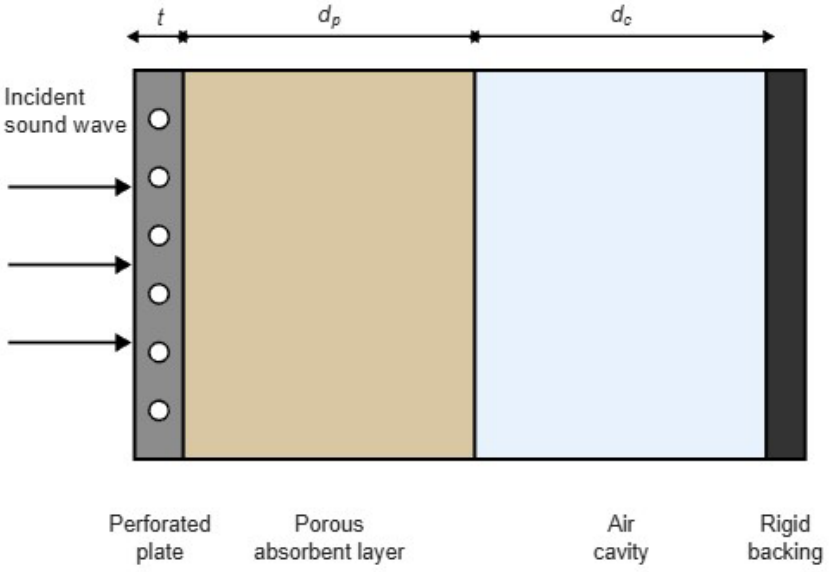



**Fig. 1 - Schematic of the multilayer acoustic barrier panel**

The normal incidence acoustic impedance of the perforated plate, $Z_{perf}$, was calculated using the Maa model, which accounts for the viscous resistance and the inertial reactance of the air oscillating inside the perforations, including the end correction:

$$Z_{perf} = R_{perf} + jX_{perf} \tag{1}$$

where $R_{perf}$ is the acoustic resistance and $X_{perf}$ is the acoustic reactance of the plate, both depending on the plate thickness $t$, the perforation diameter $d$, the perforation ratio $\sigma$, and the dynamic viscosity of air $\eta$.

The characteristic impedance $Zc$ and the complex wave number $k_c$ of the porous absorbent layer were obtained using the Miki model, an improved version of the classical Delany-Bazley formulation *(Miki, 1990):*

$$Z_c = \rho_0 c_0 \cdot (1 + 0.070 \cdot X^{-0.632} - j \cdot 0.107 \cdot X^{-0.632}) \tag{2}$$

$$k_c = k_0 \cdot (1 + 0.109 \cdot X^{-0.618} - j \cdot 0.160 \cdot X^{-0.618}) \tag{3}$$

where $X = \rho_0 f / \sigma f$ is a dimensionless parameter, $\sigma f$ is the flow resistivity of the porous material, $\rho_0$ and $c_0$ are the density and the speed of sound of air, and $k_0 = 2\pi f / c_0$ is the wave number in air.

The Transfer Matrix Method was used to combine the porous layer and the air cavity into a single two-port element:

$$[p_f;\ v_f] = [T] \cdot [p_b; v_b] \tag{4}$$

With a rigid backing ($v_b$=0), the input impedance of the porous-layer/air-cavity assembly, seen from the perforated plate, was obtained as $Z_{in}$ = *T11/T21*. The total surface impedance of the panel was then computed by adding the perforated-plate impedance in series:

$$Z_s = Z_{perf} + Z_{in} \tag{5}$$

Finally, the normal-incidence reflection coefficient *R* and the sound absorption coefficient *α* were calculated as:

$$R = \frac{\frac{Z_s}{Z_0} - 1}{\frac{Z_s}{Z_0} + 1}, \alpha = 1 - |R|^2 \tag{6}$$

where $Z_0 = \rho_0 c_0$ is the characteristic impedance of air. The transmission loss TL was computed in a similar manner, by considering air as a semi-infinite medium on both sides of the panel.

The complete model was implemented in MATLAB as a set of independent functions, corresponding to the Maa model, the Miki model, and the transfer-matrix assembly of the layers, which were combined in a main script performing the frequency sweep and the parametric analysis. Table 1 presents the parameters of the baseline configuration analysed in this study.

**Table 1**

**Baseline configuration parameters of the acoustic barrier panel**

| Parameter | Symbol | Value |
|---|---|---|
| Perforated plate thickness | t | 1 mm |
| Perforation diameter | d | 3 mm |
| Perforation ratio | σ | 10 % |
| Porous layer thickness | $d_p$ | 50 mm |
| Flow resistivity | $\sigma_f$ | 20 000 Ns/m⁴ |
| Air cavity depth | $d_c$ | 50 mm |

The frequency response of the panel was computed over the 100-4000 Hz range, corresponding to the dominant frequency content of road traffic noise *(Laxmi et al., 2022)*. In order to evaluate the influence of the main design parameters, three parametric studies were performed, in which the porous layer thickness (30, 50 and 80 mm), the perforation ratio (5%, 10% and 20%), and the air cavity depth (20, 50 and 100 mm) were varied independently, while the remaining parameters were kept equal to the baseline configuration.

## RESULTS

Figure 2 presents the sound absorption coefficient (a) and the transmission loss (b) of the baseline panel configuration. The absorption coefficient exceeded 0.9 within the 500-1800 Hz range, with a maximum value of 0.98 at approximately 600 Hz, corresponding to the quarter-wavelength resonance of the porous layer and air cavity assembly.

A secondary absorption peak was obtained near 1700 Hz, associated with the resonant behaviour of the perforated plate. The transmission loss increased monotonically with frequency, from approximately 5.7 dB at 100 Hz to 15.6 dB at 4000 Hz, following the general trend predicted by the mass law.

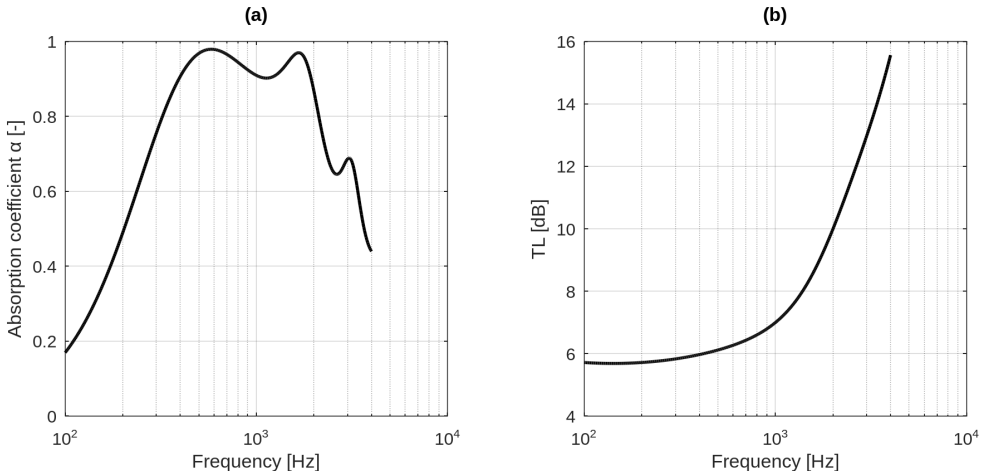



**Fig. 2 - Sound absorption coefficient (a) and transmission loss (b) of the baseline panel**

**Table 2**

**Absorption coefficient and transmission loss at octave-band frequencies (baseline configuration)**

| f [Hz] | 125 | 250 | 500 | 1000 | 2000 | 4000 |
|---|---|---|---|---|---|---|
| α | 0.245 | 0.637 | 0.968 | 0.909 | 0.867 | 0.440 |
| TL [dB] | 5.69 | 5.77 | 6.12 | 7.00 | 10.00 | 15.56 |

The influence of the porous layer thickness on the absorption coefficient is presented in figure 3. Increasing the thickness from 30 to 80 mm shifted the main absorption peak towards lower frequencies, from approximately 700 Hz to 550 Hz, and improved the low-frequency absorption below 400 Hz. However, above 2000 Hz, the absorption coefficient decreased regardless of the porous layer thickness, due to the increasing influence of the perforated-plate reactance.

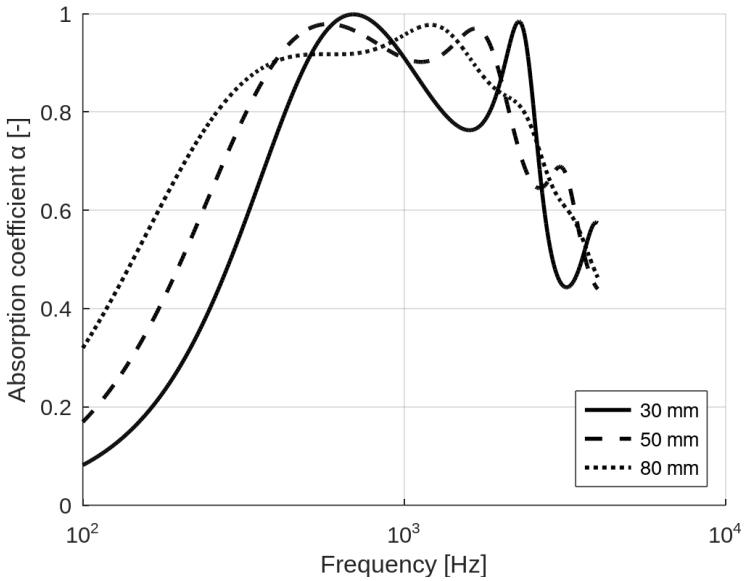



**Fig. 3 - Effect of the porous layer thickness on the absorption coefficient**

Figure 4 shows the effect of the perforation ratio on the absorption coefficient. A lower perforation ratio (5%) produced a narrower absorption band, with a pronounced drop above 1200 Hz, while a higher perforation ratio (20%) extended the high-frequency absorption up to 3500 Hz, at the expense of a slightly reduced peak absorption value. The 10% perforation ratio, used in the baseline configuration, provided a balanced trade-off between bandwidth and peak absorption.

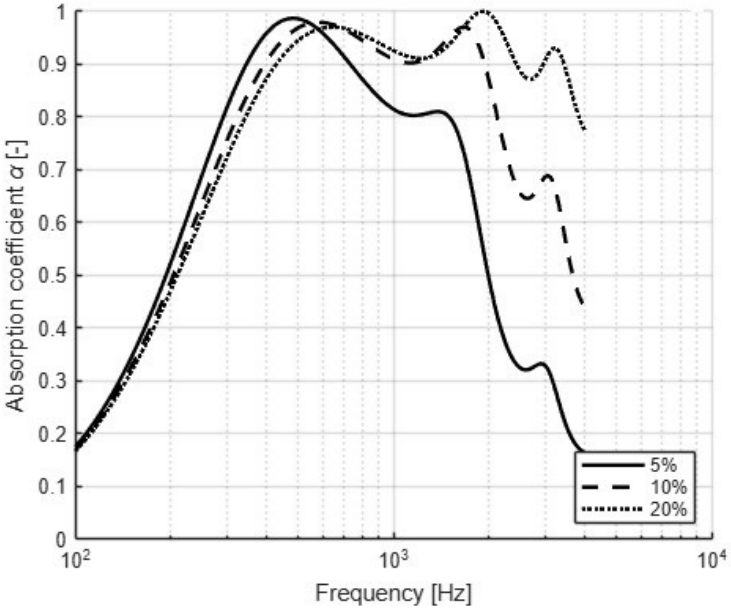



**Fig. 4 - Effect of the perforation ratio on the absorption coefficient**

Figure 5 superimposes the absorption coefficient of the baseline panel on the dominant frequency band of road traffic noise (500-2000 Hz), which mainly results from tyre-pavement interaction and engine noise.

The panel exhibited an absorption coefficient above 0.85 across almost the entire road traffic band, with values reaching 0.98 near 600 Hz. These results indicated that the baseline configuration was well suited for road-traffic noise mitigation, with the highest performance achieved in the frequency range that dominates the overall noise spectrum generated by vehicular traffic.

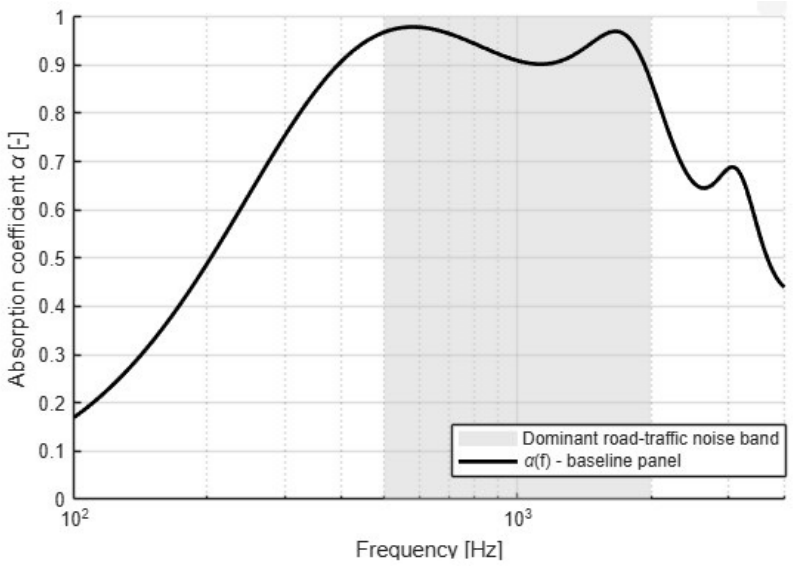



**Fig. 5 - Absorption coefficient of the baseline panel superimposed on the dominant road-traffic noise band**

## CONCLUSIONS

A numerical model based on the Transfer Matrix Method, combined with the Maa and Miki models, was developed in MATLAB to predict the acoustic performance of a multilayer barrier panel consisting of a perforated plate, a porous absorbent layer, an air cavity, and a rigid backing. The baseline configuration achieved a sound absorption coefficient above 0.85 within the 500-2000 Hz frequency range, matching the dominant spectrum of road traffic noise, while the transmission loss increased from 5.7 dB to 15.6 dB over the 100-4000 Hz range.

The parametric analysis showed that the porous layer thickness mainly controlled the position of the low-frequency absorption peak, while the perforation ratio of the plate governed the bandwidth of the high-

frequency absorption. The proposed numerical tool allowed a fast preliminary evaluation of alternative panel configurations, and could be further extended to include oblique sound incidence and different perforation geometries, in order to further optimize acoustic barrier panels for road traffic noise mitigation.

## REFERENCES

[1] Asdrubali, F., & Pispola, G. (2007). Properties of transparent sound-absorbing panels for use in noise barriers. The Journal of the Acoustical Society of America, 121(1), 214-221. https://doi.org/10.1121/1.2395916

[2] Delany, M. E., & Bazley, E. N. (1970). Acoustical properties of fibrous absorbent materials. Applied Acoustics, 3(2), 105-116. https://doi.org/10.1016/0003-682X(70)90031-9

[3] Laxmi, V., Thakre, C., & Vijay, R. (2022). Evaluation of noise barriers based on geometries and materials: A review. Environmental Science and Pollution Research, 29(2), 1729-1745. https://doi.org/10.1007/s11356-021-16944-2

[4] Lee, D. H., & Kwon, Y. P. (2004). Estimation of the absorption performance of multiple layer perforated panel systems by transfer matrix method. Journal of Sound and Vibration, 278(4-5), 847-860. https://doi.org/10.1016/j.jsv.2003.10.017

[5] Miki, Y. (1990). Acoustical properties of porous materials – Modifications of Delany-Bazley models. Journal of the Acoustical Society of Japan (E), 11(1), 19-24. https://doi.org/10.1250/ast.11.19

[6] Patil, C., Ghorpade, R., & Askhedkar, R. (2024). Analysing the impact of 3D-printed perforated panels and polyurethane foam on sound absorption coefficients. Modelling, 5(3), 969-989. https://doi.org/10.3390/modelling5030051

[7] Su, J., Liu, W., & Huang, N. (2025). Research on optimization of acoustic packaging performance of electric vehicle motor compartment based on transfer matrix theory. Medžiagotyra, 31. https://doi.org/10.5755/j02.ms.42507

[8] Wang, Y., Chang, Z., Chen, G., & Liu, J. (2024). Research on the arrangement of additional source for large space protection of an active noise barrier. Applied Sciences, 14(2), 885. https://doi.org/10.3390/app14020885

[9] Wu, H., He, L., Tao, Z., Zhang, D., & Luo, Y. (2025). An integrated SEA-deep learning approach for the optimal geometry performance of noise barrier. Machines, 13(8), 670. https://doi.org/10.3390/machines13080670

[10] Xue, Y., Nobles, L. P., Sharma, B., & Bolton, J. S. (2024). Designing hybrid aerogel-3D printed absorbers for simultaneous low-frequency and broadband noise control. Materials & Design, 242, 113026. https://doi.org/10.1016/j.matdes.2024.113026

# EXPERIMENTAL STUDY OF DUST COLLECTED FROM AN INDUSTRIAL CEREAL MILL DEDUSTING SYSTEM

/

# *STUDIU EXPERIMENTAL AL PULBERILOR COLECTATE DIN SISTEMUL DE DESPRĂFUIRE AL UNEI MORI INDUSTRIALE DE CEREALE*

**Liliana-Caliopi ISCRU, Daniel-Mirel DUMITRESCU, Gheorghe VOICU*, Paula TUDOR*, Gabriel-Alexandru CONSTANTIN**
UNSTP Bucharest / Romania
**Tel: 0723 850 975; *E-mail: paula.voicu@upb.ro*

***Keywords:*** *wheat milling, flour dust, dedusting, cyclone, particle size distribution, moisture content, drying kinetics*

## ABSTRACT

*This paper presents the physical characterization of the dust collected from four cyclones (C4, C6, C9 and C11) of the aspiration system of the milling section of an industrial wheat mill with a capacity of about 10 t/h, located in south-eastern Romania. The samples were subjected to sieve analysis, moisture content determination and monitoring of the drying process at 105 °C. The material retained in the cyclones consisted mainly of particles between 0.125 and 0.25 mm, the largest fraction being retained on the 0.20 mm sieve (26.12–42.23%), with median diameters $d_{50}$ of 0.181–0.224 mm. The proportion of particles finer than 0.06 mm did not exceed 6.89%. The moisture content ranged between 8.61 and 9.32% (wet basis); 68–80% of the water was removed in the first 3 minutes of drying, and the total drying time was 06:17–09:20 min. The results complement previous data on the material collected at the bag filters of the same mill.*

## REZUMAT

*Lucrarea prezintă caracterizarea fizică a prafului colectat din patru cicloane (C4, C6, C9 și C11) ale sistemului de aspirație al secției de măcinare a unei mori industriale de grâu cu o capacitate de circa 10 t/h, din sud-estul României. Probele au fost supuse analizei granulometrice, determinării umidității și monitorizării procesului de uscare la 105 °C. Materialul reținut în cicloane a fost format predominant din particule cu dimensiuni între 0,125 și 0,25 mm, fracția maximă fiind reținută pe sita de 0,20 mm (26,12–42,23%), cu diametre mediane $d_{50}$ de 0,181–0,224 mm. Ponderea particulelor sub 0,06 mm nu a depășit 6,89%. Umiditatea a variat între 8,61 și 9,32% (bază umedă); 68–80% din apă a fost eliminată în primele 3 minute de uscare, iar durata totală a uscării a fost de 06:17–09:20 min. Rezultatele completează datele anterioare privind materialul colectat la filtrele cu saci ale aceleiași mori.*

## INTRODUCTION

In the milling industry, grain reception, transport, cleaning, grinding, and sifting operations generate significant amounts of dust, consisting of fine flour particles, husk fragments, and mineral impurities. These particles are carried by airflow within the facility and, in the absence of an efficient capture system, settle in production areas or are released into the atmosphere (*Pranav and Biswas, 2016*). Prolonged exposure to flour dust is associated with respiratory and allergic conditions among workers; consequently, occupational exposure limits have been proposed for its inhalable fraction (*Stobnicka-Kupiec and Górny, 2017*). Measurements taken in grain milling facilities have revealed dust concentrations that vary depending on the specific technological operation and work area (*Sobczak et al., 2019*), and recent studies on flour mill workers confirm the health risks associated with this exposure (*Mishra et al., 2024*).

In the milling industry, the operations of reception, transport, cleaning, grinding, and sieving of cereals generate significant amounts of dust, formed from fine flour particles, fragments of outer layers, and mineral impurities. These particles are carried by the air currents from the installation and, in the absence of an efficient collection system, they settle in the production areas or are discharged into the atmosphere (*Pranav and Biswas, 2016*). Prolonged exposure to flour dust is associated with respiratory and allergic diseases of workers, which is why occupational exposure limit values have been proposed for its inhalable fraction (*Stobnicka-Kupiec and Górny, 2017*). Determinations carried out in cereal grinding units have highlighted dust concentrations that vary depending on the technological operation and the work area

(*Sobczak et al., 2019*), while recent studies on workers in flour mills confirm the health risks associated with this exposure (*Mishra et al., 2024*).

In addition to the effects on health, organic dust from mills is combustible and, at certain concentrations in air, can form explosive mixtures. The severity of the explosion depends directly on the fineness of the particles: for wheat flour dust with an average particle size of 84 μm, a maximum explosion pressure of 7.00 bar and an explosion constant of 16.9 bar·m/s were determined, while for particles with an average size of 50 μm, these values increased to 7.97 bar and 54.9 bar·m/s, respectively (*Kuracina et al., 2019*). The causes of such explosions in industrial grinding installations were analyzed by Freschi et al. (2017). Knowledge of the particle size distribution of the dust collected at different points of the installation is, therefore, important both for risk assessment and for the sizing of separation equipment.

For air purification, the aspiration systems of mills are equipped with cyclones and bag filters, the separation of the solid phase from the gaseous phase being influenced by the size and density of the particles. Bag filters cleaned by compressed-air pulses generally operate between two preset levels of pressure drop, and their selection influences the frequency of the cleaning cycles (*Krammer et al., 2003*).

The specific resistance of the dust layer deposited on the bags (filter cake) increases linearly with the filtration velocity (*Saleem et al., 2012*), while the cleaning efficiency depends on the pulse pressure and nozzle diameter, with a critical overpressure above which the performance no longer improves (*Lu and Tsai, 1998; Tsai et al., 2000*). Filter-aid solutions have also been proposed to reduce the pressure drop across the filter medium (*Hajar et al., 2015*).

The loading of bag filters can be reduced by the preliminary separation of part of the material in cyclones. These are simple pieces of equipment, without moving parts, whose efficiency depends on particle size and air-flow velocity, while the pressure drop can be estimated using experimentally validated calculation models (*Chen and Shi, 2007*). The combination of cyclonic separation with filtration led, in the case of a collector with a cyclone and filter cartridge, to a separation efficiency of approximately 99.86% at a flow rate of 50 m³/h, approximately 15% higher than that of a conventional cyclone (*Xie et al., 2018*).

In modern mills with pneumatic conveying, the intermediate products resulting from the grinding passages are conveyed in an air stream and separated from it in cyclones, the air then being directed to the central filter of the installation (*Voicu et al., 2013*). The dimensional characteristics of the intermediate products differ from one technological passage to another (*Constantin et al., 2021*), and their particle size distributions can be described by mathematical distribution functions, useful for estimating the material flows sorted into the compartments of the plansifter (*Voicu et al., 2014; Constantin et al., 2019*).

The literature regarding air filtration in cereal mills mainly addresses the modeling of flow through bag filters (*Solari et al., 2017; Solari et al., 2024*) and occupational exposure to dust. Within the same research direction, the authors previously presented the components of dust removal systems in cereal mills (*Iscru et al., 2024*) and characterized the material at the inlet and at the bottom of the bag filters of the cleaning and grinding sections of a wheat mill in southeastern Romania, obtaining average particle sizes of 0.563–1.191 mm for the cleaning section filter and 0.186–0.278 mm for the grinding section filter (*Iscru et al., 2025*). However, the material retained in the cyclones located upstream of the grinding section filter was not characterized.

The aim of the present paper is the physical characterization of the dust collected in cyclones C4, C6, C9, and C11 of the aspiration system of the grinding section of the S.C. Agro Chirnogi S.A. wheat mill, through particle size analysis, determination of moisture content and drying kinetics, as well as through the modeling of cumulative particle size distributions using the Chapman function and the ExpDec1 exponential function.

## MATERIALS AND METHODS

The experimental research was carried out at the wheat mill of S.C. Agro Chirnogi S.A. (Călărași County), a Bühler installation with pneumatic conveying, having a capacity of approximately 10 t/h (240 t/24 h) (*Iscru et al., 2024*). The air aspirated from the equipment of the grinding section is directed to the central filter of the section, with cyclones being installed along its path for the preliminary separation of particles (Fig. 1, Fig. 2).

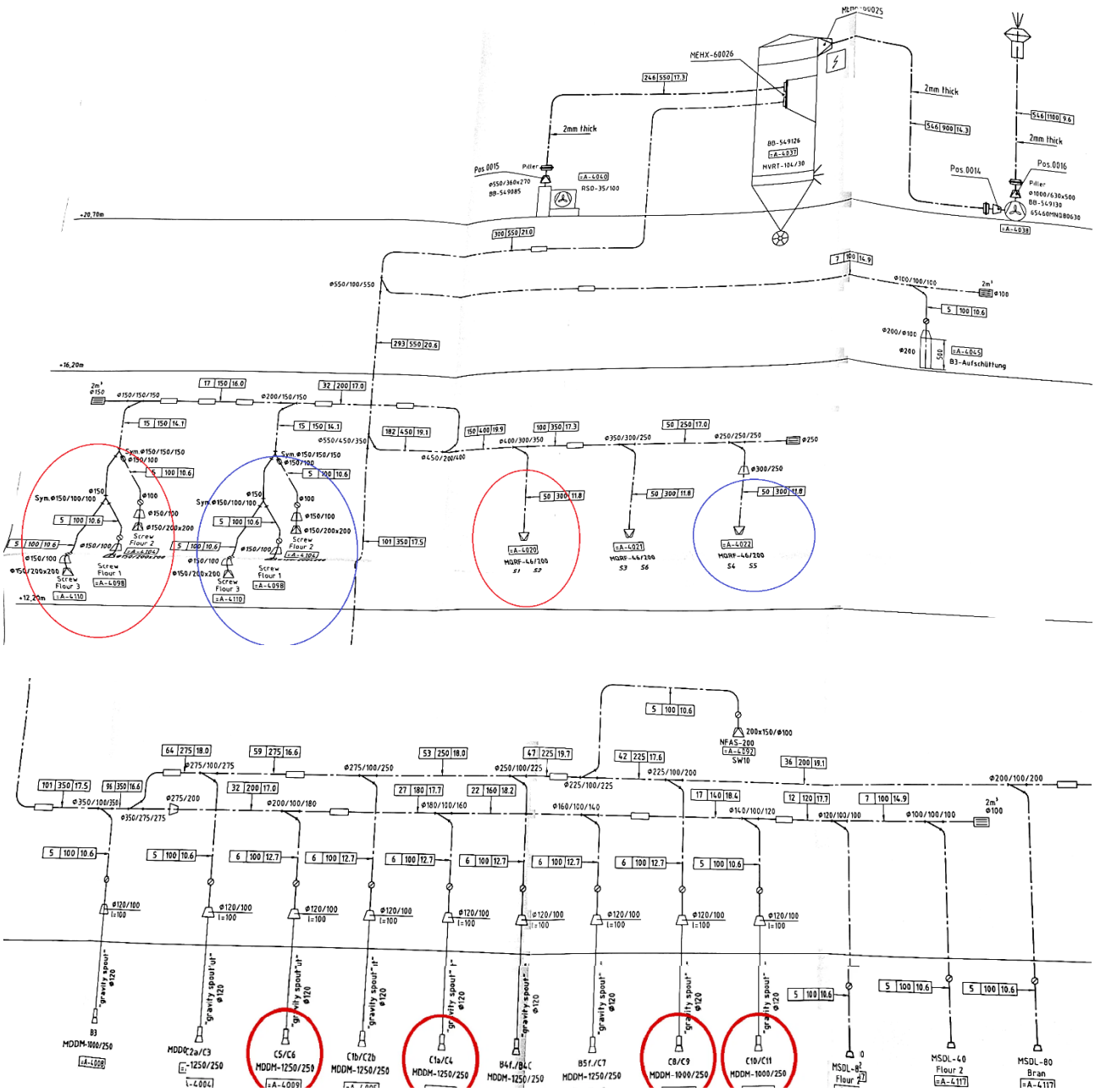



**Fig. 1 - Detail from the aspiration diagram of the wheat mill (Bühler MEHA-20308): connection of the roller mills to the aspiration collector of the central filter, including passages C1a/C4, C5/C6, C8/C9, and C10/C11**

The S1 technological passage consists of a group of machines that process the products resulting from the first passages of primary grinding of the wheat grain (break I and II), the extracted powders having an important proportion of suspended fine flour dust.

The filter is a Bühler MVRT-104/30 type, equipped with 104 filter bags with a diameter of 120 mm and a length of 3 m (*Iscru et al., 2025*). Air circulation is ensured by a low-pressure fan (3.0 kPa), while the cleaning of the bags is carried out by pulses of compressed air supplied by a high-pressure fan. The retained material is discharged through an MPSJ-28/30 rotary airlock, while the detachment of deposits from the hopper is assisted by a pneumatic hammer (Fig. 2).

Aspiration for the roller mills in the grinding section is achieved via individual branches with a 100 mm diameter, connected to the discharge outlet of each roller mill. These branches are equipped with adjustment dampers and connect to two horizontal manifolds that converge at the central filter (Fig. 1). In the system diagram, each section is characterized by its airflow rate, duct diameter, and air velocity (Table 1).

Passages C4, C6, and C11 connect to the lower manifold. The branch for roller mill C10/C11 (MDDM-1000/250) carries 5 m³/min at a velocity of 10.6 m/s; after this connection, the manifold has a diameter of 140 mm and carries 17 m³/min. Next, roller mill C1a/C4 (MDDM-1250/250) connects -

contributing 6 m³/min at 12.7 m/s - bringing the manifold to a diameter of 180 mm and a flow rate of 27 m³/min. Finally, roller mill C5/C6 (MDDM-1250/250) connects - also with 6 m³/min at 12.7 m/s - resulting in a lower manifold diameter of 200 mm and a flow rate of 32 m³/min.

**Table 1**

**Characteristics of the suction paths of the analyzed passages (based on diagram)**

| Pass | Roller mill | Branch: flow rate / ϕ / velocity | Collector | After flow rate / ϕ / velocity |
|---|---|---|---|---|
| C4 | C1a/C4, MDDM-1250/250 | 6 m³/min / 100 mm / 12,7 m/s | lower | 27 m³/min / 180 mm / 17,7 m/s |
| C6 | C5/C6, MDDM-1250/250 | 6 m³/min / 100 mm / 12,7 m/s | lower | 32 m³/min / 200 mm / 17,0 m/s |
| C9 | C8/C9, MDDM-1000/250 | 6 m³/min / 100 mm / 12,7 m/s | upper | 42 m³/min / 225 mm / 17,6 m/s |
| C11 | C10/C11, MDDM-1000/250 | 5 m³/min / 100 mm / 10,6 m/s | lower | 7 m³/min / 140 mm / 18.4 m/s |

Duct C9 connects to the upper manifold. The branch from roller mill C8/C9 (MDDM-1000/250) conveys 6 m³/min at 12.7 m/s; following this connection, the manifold measures 225 mm in diameter and conveys 42 m³/min. With the connection of the remaining roller mills, the upper manifold reaches a diameter of 275 mm and a flow rate of 64 m³/min.

The two manifolds merge into a 350 mm diameter duct which, after connecting to roller mill B3, conveys 101 m³/min at 17.5 m/s. This duct rises vertically to the +16.20 m level. There, it joins the suction manifold serving the MQRF-46/200 semolina purifiers and the flour conveyors, resulting in a 550 mm duct conveying 293 m³/min. Finally, a flow of 300 m³/min at a velocity of 21.0 m/s reaches the MVRT-104/30 filter, located at the +20.70 m level. The filter receives an additional 246 m³/min through a second inlet from the fan (Pos. 0015), and the cleaned air—totaling 546 m³/min—is exhausted via the main fan through a 900 mm duct.

Along the route, air velocity increases from 10.6–12.7 m/s in the roller mill branches to 16.6–19.7 m/s in the manifolds, and finally to 20.6–21.0 m/s in the main duct. Particles entrained from passages C4, C6, and C11 travel through the same collecting pipe, while those from passage C9 are transported along the upper collector to the point.

The dust samples were collected in October 2025 from cyclones C4, C6, C9, and C11, located on the aspiration circuit towards the central filter, corresponding to the grinding passages with the same designations.



**Fig. 2 - Images from inside the Chirnogi mill, showing the dust filter (left side) and the cyclone room (right side)**

The samples were sieved using an Analysette 3 Spartan vibrating sieve classifier (Fritsch, Idar-Oberstein, Germany) for 3 minutes. The set of sieves was selected according to the maximum and minimum particle sizes of each sample: for sample C4, sieves of 0.10, 0.14, 0.20, 0.355, 0.45, and 0.63 mm were used, while for samples C6, C9, and C11, sieves of 0.06, 0.08, 0.125, 0.20, 0.25, and 0.315 mm were used, together with the collecting pan.

The mass retained on each sieve was determined by weighing, and the results were expressed as percentages relative to the total sieved mass, calculating the partial percentages *p* (%), cumulative undersize *T(x)* (%), and cumulative oversize *R(x) = 100 − T(x)* (%).

*The moisture content analysis* was performed using a KERN DBS 60-3 moisture analyzer (*KERN & Sohn GmbH, Germany*), on samples of 2.027–2.120 g, at a temperature of 105 °C, in automatic mode. The residual mass (*D/W*, %) was recorded at 2 s intervals, and drying stopped automatically when the mass variation decreased below 0.05%. The final data were used to calculate the moisture content relative to the mass of the wet material ($w_{um}$%) and to the mass of the dry material ($w_{us}$%).

The moisture content relative to the wet mass, *wum*, and to the dry mass, *wus*, was calculated using the following equations:

$$w_{um} = \left(\frac{m_u - m_s}{m_u}\right) \cdot 100, (\%) \quad (1)$$

$$w_{us} = \left(\frac{m_u - m_s}{m_s}\right) \cdot 100, (\%) \quad (2)$$

where $m_u$ and $m_s$ are the masses of the wet and dry sample, respectively (g).

## RESULTS AND DISCUSSION

The particle size distributions of the samples collected from cyclones C4, C6, C9, and C11 are presented in Table 2, while the cumulative undersize curves *T(x)* are shown in Fig. 3.

**Table 2**

**Experimental particle size distribution of the powders collected from the cyclone hoppers**

| x (mm) | C4 *p* | C4 *T(x)* | C6 *p* | C6 *T(x)* | C9 *p* | C9 *T(x)* | C11 *p* | C11 *T(x)* |
|---|---|---|---|---|---|---|---|---|
| Sieve 0 mm | 6.20 | 0.00 | 6.89 | 0.00 | 4.32 | 0.00 | 0.00 | 0.00 |
| 0.06 | – | – | 0.83 | 6.89 | 0.53 | 4.32 | 0.12 | 0.00 |
| 0.08 | – | – | 21.80 | 7.72 | 7.69 | 4.85 | 5.52 | 0.12 |
| 0.10 | 21.00 | 6.20 | – | – | – | – | – | – |
| 0.125 | – | – | 27.40 | 29.52 | 24.87 | 12.54 | 23.82 | 5.64 |
| 0.14 | 28.60 | 27.20 | – | – | – | – | – | – |
| 0.20 | 38.40 | 55.80 | 26.12 | 56.92 | 37.41 | 37.41 | 42.23 | 29.46 |
| 0.25 | – | – | 4.01 | 83.04 | 16.23 | 74.82 | 14.96 | 71.69 |
| 0.315 | – | – | 12.95 | 87.05 | 8.95 | 91.05 | 13.35 | 86.65 |
| 0.355 | 1.40 | 94.20 | – | – | – | – | – | – |
| 0.45 | 1.20 | 95.60 | – | – | – | – | – | – |

The data in Table 2 demonstrate the high performance of the pre-separation stage, with the cyclones retaining most of the intermediate-sized particles ranging between 0.08 mm and 0.20 mm. This behavior is graphically illustrated in Fig. 3, where the cumulative curves highlight the region of maximum accumulation. In particular, in cyclone C11, the 0.20 mm fraction represents the largest proportion, accounting for 42.23% of the mass, with a similar pattern also being recorded for cyclones C4 (38.40% on the 0.20 mm sieve) and C9 (37.41%).

For the comparison of the samples, the characteristic dimensions $d_{10}$ and $d_{50}$ were determined from the T(x) curves by linear interpolation, i.e., the dimensions below which 10% and 50% of the sample mass are found, respectively (Table 3).

**Table 3**

**Characteristic parameters of particle size distributions**

| Sample | $d_{10}$ (mm) | $d_{50}$ (mm) | Material below value 0,06 mm* (%) | Material on the top screen (%) |
|---|---|---|---|---|
| **C4** | 0.107 | 0.188 | 6.20* | 3.20 (> 0.63 mm) |
| **C6** | 0.085 | 0.181 | 6.89 | 12.95 (> 0.315 mm) |
| **C9** | 0.110 | 0.217 | 4.32 | 8.95 (> 0.315 mm) |
| **C11** | 0.139 | 0.224 | 0.00 | 13.35 (> 0.315 mm) |

* For C4, the finest sieve was 0.10 mm; therefore, the value represents the material smaller than 0.10 mm.

For all samples, the largest part of the material was retained on the 0.125–0.20 mm sieves (0.14–0.20 mm for C4). The maximum fraction was recorded on the 0.20 mm sieve: 38.40% for C4, 26.12% for C6, 37.41% for C9, and 42.23% for C11. The median diameter $d_{50}$ varied between 0.181 and 0.224 mm. Samples C4 and C6 were the finest ($d_{50}$ = 0.188 and 0.181 mm, respectively, with 6–7% material in the collecting pan). Samples C9 and C11 were coarser ($d_{50}$ = 0.217 and 0.224 mm, respectively), and sample C11 practically did not contain particles below 0.06 mm.

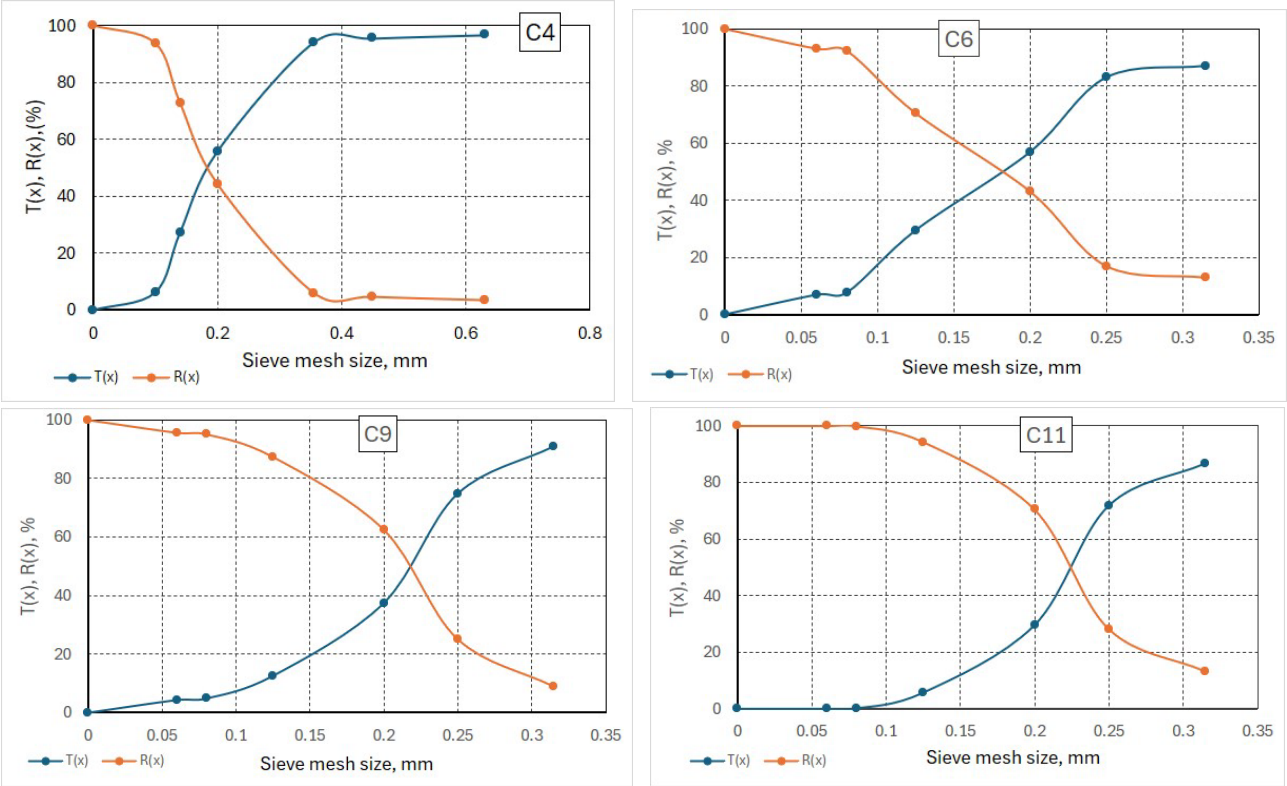



**Fig. 3 - Experimental cumulative undersize curves T(x) for the samples from cyclones C4, C6, C9, and C11**

The visual analysis of the fractions obtained from the sieving of the sample collected from Cyclone C6 (Fig. 4) showed that they are extremely fine, with a powdery appearance, light cream in color, with a tendency to agglomerate, specific to flour. The texture is relatively uniform, without the presence of coarse particles or visible impurities. The fraction above 0.315 mm has a granular appearance, yellowish-beige in color, and contains fragments of the grain outer layer.




**Fig. 4 - Visual analysis of the fractions obtained from the particle size analysis at cyclone C6**

The order of magnitude of the particles retained in the cyclones is close to that of the material previously collected at the filter of the grinding section, where the average size was 0.186–0.278 mm *(Iscru et al., 2025)*. The two values are not directly comparable, because there the weighted average size was calculated, while here the median diameter.

Under the conditions existing along the pneumatic routes for the transport and separation of fine particles, the moisture content of the material can influence the behavior of the particles during pneumatic transport, as well as their tendency to agglomerate or deposit on the surfaces of the equipment. Compared with the information provided by the particle size analysis, the determination of moisture content contributes to a more complete characterization of the powdery material collected in the dust removal system. Knowledge of this property is important because particles with different water contents may present distinct behaviors in the separation and filtration processes. Thus, the obtained result provides additional information regarding the operating conditions of the installation and the characteristics of the material collected at the analyzed sampling point.

The cumulative undersize curves were approximated by nonlinear regression in the Origin 8.0 program, using the Chapman function (3) and the ExpDec1 exponential function (4):

$$y = a \cdot (1 - e^{-b \cdot x})^c \tag{3}$$

$$y = y_0 + Ae^{-\frac{x}{t}} \tag{4}$$

where x is the size of the sieve openings (mm), and a, b, c, $y_0$, A and t are the regression coefficients. The quality of the approximation was evaluated by the coefficient of determination $R^2$. The same functions were previously used for the material collected at the mill filters (Iscru et al., 2025).

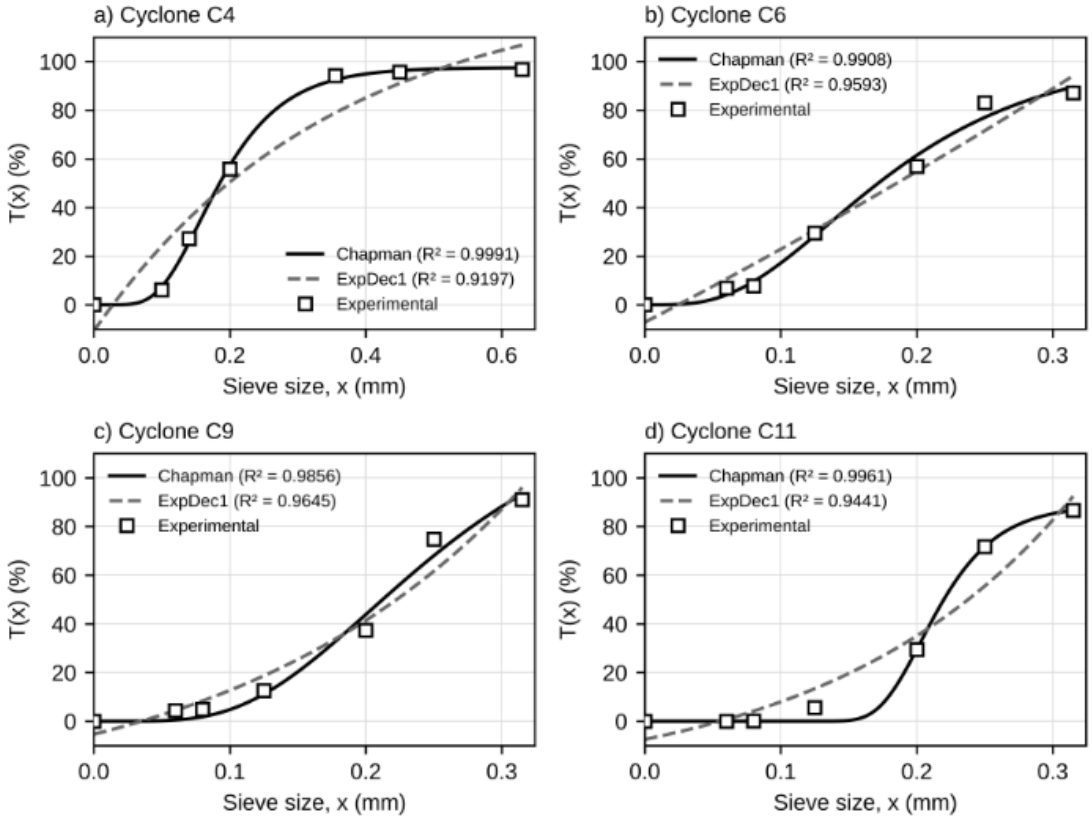



**Fig. 5 - Cumulative undersize curves *T(x)*: experimental points and the Chapman and ExpDec1 regression curves.**

The statistical indicators of the quality of the nonlinear regression with the models presented previously are presented in Table 4.

Both functions satisfactorily approximate the experimental data ($R^2 > 0.91$), however the Chapman function led to higher $R^2$ values for all samples (0.9856–0.9991), compared to 0.9197–0.9645 for the

exponential function (Table 4, Fig. 5). The difference is greater for samples C4 and C11, whose cumulative curves have a pronounced sigmoidal shape, which the exponential function cannot reproduce. For sample C11, the coefficient c of the Chapman function has a very high value (763.13), with a standard error greater than its value (±929.04), which shows that, for this sample, the individual coefficients are poorly determined, although the curve approximates the data well.

**Table 4**

**Analiza comparativă a indicatorilor de corelație statistică ($R^2$)**

| Equation | Indicator | Cyclone C4 | Cyclone C6 | Cyclone C9 | Cyclone C11 |
|---|---|---|---|---|---|
| Chapman Model | $R^2$ | 0.9991 | 0.9908 | 0.9856 | 0.9961 |
| | a | 97.4812 | 102.635 | 133.1038 | 88.9074 |
| | b | 14.7250 | 11.120 | 9.4302 | 32.6938 |
| | c | 9.8627 | 4.488 | 6.7557 | 763.1343 |
| Exponential Model | $R^2$ | 0.9197 | 0.9593 | 0.9645 | 0.9441 |
| | $y_0$ | 130.104 | -476.951 | -35.9114 | -27.9220 |
| | A | -140.911 | 469.737 | 30.5061 | 20.4206 |
| | t | 0.3510 | -1.613 | -0.2151 | -0.1776 |

The evolution of the residual mass during drying at 105 °C is presented in Table 5 and in Fig. 6. Based on these data, some indicators of the drying process were calculated (Table 5).

**Table 5**

**Moisture characteristics of the samples**

| Sampling point | Mass $m_u$ (g) | Mass $m_s$ (g) | Moisture content, $w_{um}$, (%) | Moisture content, $w_{us}$, (%) |
|---|---|---|---|---|
| **Cyclone C4** | 2.113 | 1.931 | 8.61 | 9.43 |
| **Cyclone C6** | 2.120 | 1.927 | 9.10 | 10.02 |
| **Cyclone C9** | 2.044 | 1.860 | 9.00 | 9.89 |
| **Cyclone C11** | 2.027 | 1.838 | 9.32 | 10.28 |

The moisture content on a wet basis was within a narrow range of 8.61–9.32%, the maximum difference between samples being 0.71 percentage points. The values are lower than those determined previously for the material from the filter of the grinding section (11.53% at the inlet and 12.63% at the discharge) (Iscru et al., 2025).

The continuous monitoring of the mass loss on the *KERN DBS 60-3* analyzer at a temperature of 105°C reflects the close relationship between the particle size of the material and the way in which the water is structurally fixed in the organic matrix of the powders (Table 6).

The evolution of the drying curves automatically traced by the device is shown in Fig. 6. It is found that the removal of the free surface water occurs rapidly in the first 60 seconds. Subsequently, the slope flattens, reflecting the slow removal of the capillary-bound water.

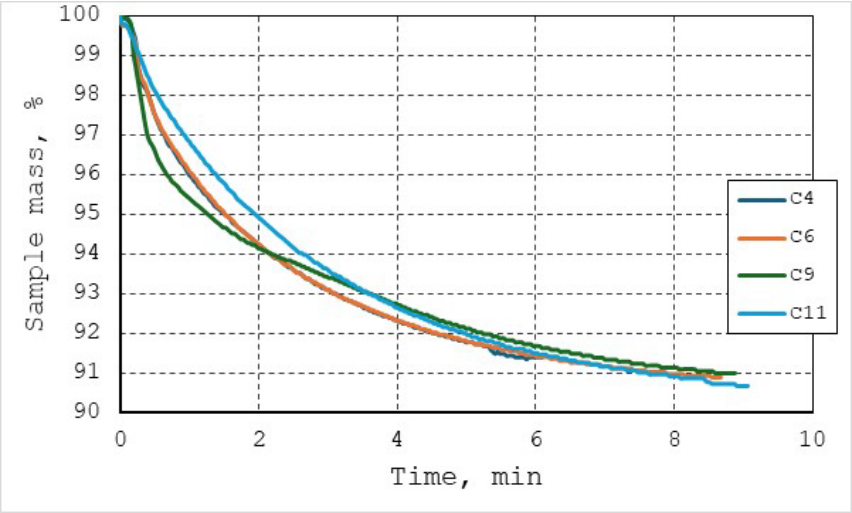



**Fig. 6 - Evolution of the residual mass of the samples over time, at 105°C on the KERN analyzer**

**Table 6**

**Indicatori ai procesului de uscare**

| Sample | Drying time, (min:s) | Average drying speed (%/min) | Water eliminated in the first minute (%) | Water eliminated in the first 3 min (%) |
|---|---|---|---|---|
| **C4** | 06:17 | 1.37 | 46 | 80 |
| **C6** | 08:56 | 1.02 | 42 | 75 |
| **C9** | 09:06 | 0.99 | 51 | 72 |
| **C11** | 09:20 | 1.00 | 33 | 68 |

From Fig. 6, it can be observed that the drying curves have the same shape in all the samples, presenting a rapid decrease in mass in the first minutes, followed by a gradual approach to constant mass. In the first 3 minutes, 68–80% of the water contained in the samples was eliminated. Sample C4 dried the fastest: 06:17 min, with an average drying rate of 1.37%/min. Samples C6, C9 and C11 had similar drying times (08:56–09:20 min) and average drying rates of approximately 1%/min. The drying time increased with the initial moisture content of the samples, with the exception of samples C6 and C9, whose moisture contents differ by only 0.10 percentage points. The drying time did not correlate with the fineness of the samples: sample C11, the coarsest, had the longest duration, and sample C6, the finest, an intermediate one.

## CONCLUSIONS

In the paper, the dust samples collected from cyclones C4, C6, C9 and C11 of the aspiration system of the grinding section of the S.C. Agro Chirnogi S.A. wheat mill, with a capacity of approximately 10 t/h, were physically characterized, through particle size analysis and through the determination of moisture and drying kinetics.

The material retained in the cyclones consists predominantly of particles with sizes between 0.125 and 0.25 mm, the maximum fraction being recorded on the 0.20 mm sieve for all samples (26.12–42.23%). The median diameter $d_{50}$ varied between 0.181 and 0.224 mm. Samples C4 and C6 were the finest, and samples C9 and C11 the coarsest. The proportion of particles below 0.06 mm was low (0–6.89%), which shows that the very fine fractions are entrained to a small extent in the material retained by the cyclones.

The cumulative particle size distributions were better approximated by the Chapman function ($R^2$ = 0.9856–0.9991) than by the ExpDec1 exponential function ($R^2$ = 0.9197–0.9645), the difference being more pronounced for the samples with curves of sigmoidal shape (C4 and C11).

The moisture content of the samples, on a wet basis, was within a narrow range of 8.61–9.32%, lower than that determined previously for the material from the filter of the grinding section.

During drying at 105 °C, 68–80% of the water contained in the samples was eliminated in the first 3 minutes. The total drying time was 06:17 min for sample C4 and 08:56–09:20 min for samples C6, C9 and C11. The drying time generally increased with the initial moisture content of the samples and did not correlate with their fineness.

The results complete the characterization of the material from the dust removal system of the mill, carried out previously at the bag filters, with data regarding the material retained in the cyclonic separation stage. The research will be continued through the simultaneous collection of samples from the cyclones and from the central filter, for the evaluation of the separation efficiency of the cyclones by size classes.

## REFERENCES

[1] Chen. J., Shi. M. (2007). A Universal Model to Calculate Cyclone Pressure Drop. *Powder Technology*. 171(3). 184-191. https://doi.org/10.1016/j.powtec.2006.09.014

[2] Constantin. G.A., Voicu. G., Ipate. G., Musuroi. G., Stefan. E.M., Munteanu. M.G., Stoica. D. (2019). Influence of motion type on granulometric distribution of grist obtained from some varieties of wheat and corn. 47th Symposium "*Actual Tasks on Agricultural Engineering*". Opatija. Croatia. 409-417

[3] Constantin, G.A., Voicu, G., Stefan, E.M., Munteanu, M.G., Musuroi, G., Voicea, I. (2021). Dimensional characteristics of grist intermediate products obtained in the first two technological passages in the reduction phase of an industrial milling plant. *E3S Web of Conferences*, 286, 04006, https://doi.org/10.1051/e3sconf/202128604006

[4] Freschi. F., Mitolo. M., Tommasini. R. (2017). Analysis of causation of a flour dust explosion in industrial plant. *IEEE Transactions on Industry Applications*. 53(6). 5182–5186. doi:10.1109/TIA.2017.2725947

[5] Hajar. S., Rashid. M., Nurnadia. A., Ammar. M.R. (2015). The characteristics of a formulated filter aids for fabric filters. *Powder Technology*. 283. 315–320.

[6] Iscru, L.C., Voicu, G., Dumitrescu, D., Toma, M.L. (2024). Collection and disposal of products with high dust content from grain mills. *Proceedings of the International Symposium ISB-INMATEH 2024*, Bucharest, Romania.

[7] Iscru. L.-C., Voicu. G., Stefan. E.-M., Constantin. G.-A., Ionescu. A.-D., Tudor. P. (2025). Aspects of the material characteristics of the filtration systems of a milling plant in the southeastern area of Romania. *Foods*. 14(7). 1202. https://doi.org/10.3390/foods14071202

[8] Krammer. G., Kavouras. A., Anzel. A. (2003). Optimization of pulse cleaning frequency during bag filter operation. *Chemical Engineering & Technology*. 26(9). 951–955. doi:10.1002/ceat.200303032

[9] Kuracina. R., Szabova. Z., Buranska. E. (2019). Study of explosion characteristics of the wheat flour dust clouds in dependence of the particle size distribution. *Research Papers Faculty of Materials Science and Technology Slovak University of Technology*. 27(44). 65–71. https://doi.org/10.2478/rput-2019-0007

[10] Lu. H.-C., Tsai. C.-J. (1998). A Pilot-Scale Study of the Design and Operation Parameters of a Pulse-Jet Baghouse. *Aerosol Science and Technology*. 29(6). 510-524. doi:10.1080/02786829808965587

[11] Mishra. J., Verma. K., Mohanty. S.K., Rath. I. (2024). Health risks and dust exposure among flour mill workers in Eastern India: A comprehensive study. *Current World Environment*. 19(2). 1022–1030. https://doi.org/10.12944/CWE.19.2.39

[12] Pranav. P.K., Biswas. M. (2016). Mechanical intervention for reducing dust concentration in traditional rice mills. *Industrial Health*. 54(4). 315–323. https://doi.org/10.2486/indhealth.2015-0180

[13] Saleem. M., Krammer. G., Tahir. M.S. (2012). The effect of operating conditions on resistance parameters of filter media and limestone dust cake for uniformly loaded needle felts in a pilot scale test facility at ambient conditions. *Powder Technology*. 228. 100–107. https://doi.org/10.1016/j.powtec.2012.05.003

[14] Sobczak. P., Mazur. J., Zawiślak. K., Panasiewicz. M., Żukiewicz-Sobczak. W., Królczyk. J.B., Lechowski. J. (2019). Evaluation of dust concentration during grinding grain in sustainable agriculture. *Sustainability*. 11(17). 4572. https://doi.org/10.3390/su11174572

[15] Solari. F., Tagliavini. G., Montanari. R., Bottani. E., Malagoli. N., Armenzoni. M. (2017). CFD model validation of a bag filter for air filtration in a milling plant. *Proceedings of the International Food Operations and Processing Simulation Workshop*. Barcelona. 73–81.

[16] Solari. F., Lysova. N., Montanari. R. (2024). Monitoring and control of air filtration systems: Digital twin based on 1D computational fluid dynamics simulation and experimental data. *Computers & Industrial Engineering*. 197. 110607. https://doi.org/10.1016/j.cie.2024.110607

[17] Stobnicka-Kupiec. A., Górny. R.L. (2017). Flour dust – aspiration fraction. Documentation of proposed values of occupational exposure limits (OELs). *Podstawy i Metody Oceny Środowiska Pracy*. 33(3). 91-120. https://doi.org/10.5604/01.3001.0010.4339

[18] Voicu. G., Biris. S.S., Stefan. E.M., Constantin. G.A., Ungureanu. N. (2013). Grinding characteristics of wheat in industrial mills. In: *Food Industry*. Chapter 15. InTech. Rijeka. 323–354.

[19] Voicu. G., Constantin. G.A., Ștefan. E.M., Casandroiu. T. (2014). Using of Granulometric Distribution Functions in estimating Flows of Grist sorted in a Plansifter Compartment. *Journal of EcoAgriTourism*. 10(1). 47-52

[20] Xie. B., Li. S., Jin. H., Hu. S., Wang. F., Zhou. F. (2018). Analysis of the performance of a novel dust collector combining cyclone separator and cartridge filter. *Powder Technology*. 339. 695–701. https://doi.org/10.1016/j.powtec.2018.07.103

[21] Tsai. C.-J., Tsai. M.-L., Lu. H.-C. (2000). Effect of filtration velocity and filtration pressure drop on the bag-cleaning performance of a pulse-jet baghouse. *Separation Science and Technology*. 35(2). 211-226. https://doi.org/10.1081/SS-100100152

# FUNCTIONAL PARAMETERS OF A MULTIPROCESS SYSTEM FOR HOMOGENEOUS STRAWBERRY NECTAR

/

# *PARAMETRII FUNCȚIONALI AI UNEI INSTALAȚII MULTIPROCES PENTRU NECTAR OMOGEN DE CĂPȘUNI*

**Andra-Valentina CIOBĂNESCU*, Sorin-Ștefan BIRIȘ, Mihaela BEGEA, Adrian IOSIF**
UNSP Bucharest, Doctoral School of Biotechnical Systems Engineering, Bucharest / Romania
**Tel.: (+40) 737 565 414; *E-mail: valentinaandra503@gmail.com*

***Keywords**: multiprocess installation; mixing; strawberry nectar; homogeneity; rheology; energy consumption.*

**ABSTRACT**

*This literature-based study developed an experimental framework for optimizing a multiprocess system for strawberry nectar mixing. Published research on nectar quality, strawberry pulp rheology and mixer energy efficiency was examined to identify relevant operating factors and responses. Agitator speed, mixing duration and vessel fill level were selected as proposed factors; spatial pulp distribution, viscosity, product stability and specific energy consumption were selected as responses. A sampling procedure at three vessel heights and comparisons at a predefined homogeneity threshold were specified. The reviewed studies showed that pulp structure and processing history influenced rheology and quality, and the proposed method identified the measurements required to determine reproducible operating conditions. However, the optimal settings could not be reported without trials on the actual equipment.*

**REZUMAT**

*Studiul, bazat pe literatura de specialitate, a elaborat un cadru experimental pentru optimizarea unei instalații multiproces de amestecare a nectarului de căpșuni. Au fost analizate cercetări privind calitatea nectarului, reologia pulpei și eficiența energetică a amestecării. Turația agitatorului, durata amestecării și gradul de umplere au fost selectate ca factori propuși, iar distribuția pulpei în vas, vâscozitatea, stabilitatea produsului și consumul specific de energie ca răspunsuri. A fost stabilită o procedură de prelevare la trei înălțimi și de comparare a condițiilor la un prag prestabilit de omogenitate. Studiile analizate au evidențiat influența structurii pulpei și a istoricului de procesare asupra reologiei și calității, iar metoda propusă a identificat măsurătorile necesare pentru a determina condiții de operare reproductibile. Cu toate acestea, parametrii optimi nu au putut fi determinați în absența încercărilor concrete pe echipament.*

## INTRODUCTION

Mixer selection in the food industry depends on material properties and the required operation. Niranjan et al. reviewed agricultural and food mixers and distinguished devices suited to low-viscosity liquids from those used for viscous materials. Thus, operating speed should be assessed together with impeller geometry and product rheology *(Niranjan et al., 1994).*

In accordance with the provisions of Order 510/2003, updated in 2024 (which transposes Directive 2001/112/EC, as amended in 2024), fruit nectar is the fermentable but unfermented product obtained by adding water and sugars and/or honey to fruit juice, fruit juice from concentrate, concentrated fruit juice, dehydrated fruit juice, fruit purée, or a mixture of these products, as well as sweeteners (for energy-reduced or with no added sugar nectars). The addition of sugars and/or honey is permitted only in quantities of up to 20% of the total mass of the finished product.

Strawberry nectar provides a practical case for assessing multiprocess mixing because fruit pulp must remain uniformly distributed in a liquid formulation. Lacey et al. prepared nectar from strawberry purée, water, sugar and citric acid and assessed properties including pH, colour and viscosity. Their formulation provides a published reference for selecting response variables, rather than a prescribed recipe for the proposed experiment (*Lacey et al., 2023).* Recent work linked raw-fruit ripeness with nectar colour acceptance, reinforcing the need to control fruit lots across trials (*Murray et al., 2024).*

Strawberry pulp can exhibit shear-thinning behaviour: Xing et al. reported decreasing apparent viscosity as shear rate increased. Maceiras et al. also found non-Newtonian behaviour in fruit purées,

including strawberry purée. Consequently, differences observed at different stirring speeds should be interpreted alongside viscosity and temperature measurements *(Xing et al., 2023; Maceiras et al., 2007).*

The aim of this paper is to define an experimental methodology for identifying a reproducible combination of agitator speed, mixing duration and fill level that reaches a target homogeneity with low specific energy use while retaining suitable nectar properties *(Lacey et al., 2023; Niranjan et al., 1994; Xing et al., 2023; Delaplace et al., 2023).*

## MATERIALS AND METHODS

A single strawberry nectar formulation should be used throughout each experimental series. Ingredient masses, initial temperature, pH and soluble solids should be recorded for each batch. The vessel working volume, impeller design and diameter, impeller clearance, recirculation arrangement and available speed range should be documented before testing. These controls allow operating regimes to be compared on the same product and equipment configuration *(Lacey et al., 2023; Niranjan et al., 1994; Xing et al., 2023).* The proposed independent factors are agitator rotational speed, mixing time and vessel fill level. Their numerical ranges must be selected after inspecting the actual installation and performing preliminary trials. Each operating condition should be replicated; ingredient composition and initial temperature should be kept as consistent as practical. No experimental trials are claimed in this paper *(Niranjan et al., 1994; Delaplace et al., 2023).*

At the end of each trial, samples should be taken from the upper, central and lower regions of the vessel. Soluble solids and a gravimetric pulp-content indicator should be determined in every sample. The coefficient of variation between sampling locations can quantify spatial differences; the acceptable limit must be declared before ranking the operating conditions. This proposed sampling method operationalizes the target of bulk uniformity *(Niranjan et al., 1994; Xing et al., 2023).*

Nectar quality should be characterized by pH, titratable acidity, apparent viscosity and suspension stability. Particle-size distribution and instrumental colour may be added when suitable instruments are available. These measurements reflect quality variables investigated in published studies of strawberry pulp, nectar and thermally treated purée. Product temperature should be recorded because processing can also influence rheological behaviour *(Lacey et al., 2023; Xing et al., 2023; Maceiras et al., 2007; Osorio et al., 2008).* Pilot-scale comparisons also documented colour and vitamin responses to strawberry-nectar processing *(Zia et al., 2025).*

Electrical energy used during each mixing trial should be divided by the processed nectar mass to obtain specific energy consumption in kWh/kg. Only operating conditions meeting the predefined homogeneity requirement should be compared for energy performance. This keeps the efficiency comparison tied to an equivalent processing task, consistent with the approach discussed by Delaplace et al. *(Delaplace et al., 2023).*

The sampling protocol should specify the mass or volume of each aliquot, the sampling port position and the delay between stopping the agitator and withdrawal. The same procedure should be used at every operating condition. Measurements from different vessel heights should first be reported separately, before a summary statistic is calculated; a single composite sample would conceal vertical differences in pulp distribution. The decision to accept a regime should use both the soluble-solids and pulp-content criteria *(Niranjan et al., 1994; Xing et al., 2023).*

For statistical analysis, replicate-level observations should be retained. A regression model can be fitted to the experimental factors and the measured responses only after inspecting the data and checking whether its residuals and experimental replication justify that model. Interactions are of particular interest because the effect of speed may depend on fill level or mixing duration. Any apparent optimum should subsequently be confirmed by independent trials at the selected setting rather than inferred solely from a fitted response surface.

These steps are proposed analytical procedures, not results reported by the cited studies *(Niranjan et al., 1994; Delaplace et al., 2023).*

## LITERATURE EVIDENCE AND PROPOSED EVALUATION

Published results identify factors to measure, but do not constitute experimental results for the multiprocess installation. Xing et al. reported a reduction in apparent viscosity with increasing shear rate for strawberry pulp.

Their original Figure 1 contains rheological curves for samples subjected to the treatments in their own study. Those curves justify measuring viscosity in the proposed work; they cannot be presented as trials conducted on the proposed mixer *(Xing et al., 2023).*

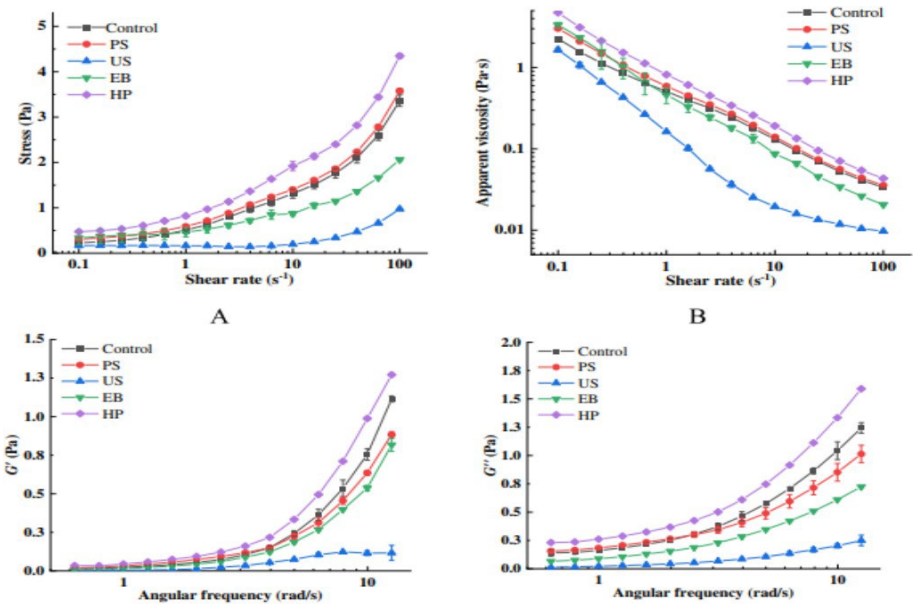



**Fig. 1 - Rheological properties of strawberry pulp**

*(reproduced from Xing et al., 2023).*

Thermal history should be recorded when interpreting rheological observations. Maceiras et al. found that temperature affected the apparent viscosity of fruit purées, while Osorio et al. observed changes in the viscosity of strawberry purée following the thermal treatments they investigated. Temperature effects must therefore be considered if the mixing process causes measurable heating *(Maceiras et al., 2007; Osorio et al., 2008).*

Xing et al. also found differences in particle size, suspension stability and microstructure between strawberry pulp samples subjected to different treatments. Their original microscopy images illustrate how structural observations can complement bulk quality measurements. Those treatments differ from the mechanical mixing proposed here, so their reported effects must not be transferred to this installation without testing *(Xing et al., 2023).* Further research on high-pressure homogenization reported changes in strawberry- pulp pectin fractions, indicating that any mechanical treatment should be assessed against compositional quality endpoints *(Xing et al., 2025).*

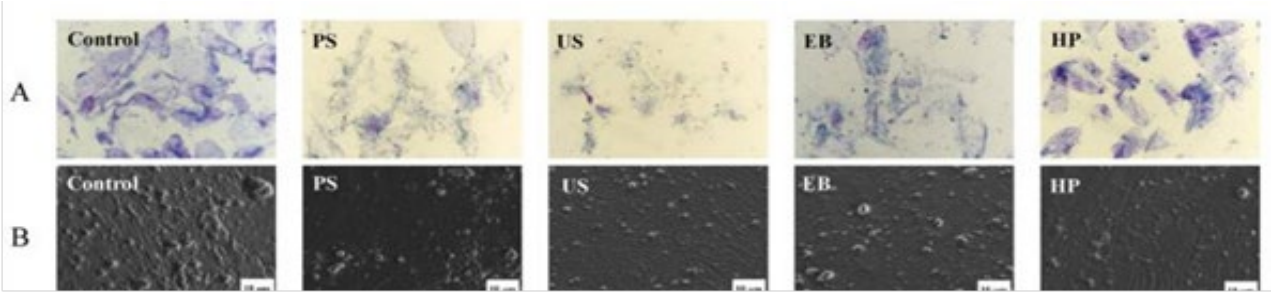



**Fig. 2 - Optical microscopy and cryo-SEM images of strawberry pulp**

*(reproduced from Xing et al., 2023).*

Energy performance must be evaluated at an equivalent homogeneity outcome. A lower instantaneous motor power may be offset by a longer required mixing time. The relevant comparison is therefore the energy required per kilogram to reach the same predefined spatial-uniformity threshold. Delaplace et al. proposed evaluating mixing equipment energy efficiency in relation to the task achieved, providing the rationale for this comparison *(Delaplace et al., 2023).*

The expected output of the proposed experiments is a measured relation between operating variables, spatial variability, nectar properties and specific energy use. The reviewed articles substantiate this study design, but none establishes the optimal speed, duration or fill level of the installation considered

here. These values will be reported only after tests on the real system *(Lacey et al., 2023; Niranjan et al., 1994; Xing et al., 2023; Delaplace et al., 2023; Maceiras et al., 2007; Osorio et al., 2008).*

Spatial consistency immediately after mixing is distinct from stability during storage; a nectar may be uniform when discharged yet separate later. Accordingly, a short storage observation at a fixed temperature should be reported as an additional product response, not substituted for measurements of in-vessel uniformity. The distinction is supported by research measuring both structural attributes and suspension stability of strawberry pulp *(Lacey et al., 2023; Xing et al., 2023).* Recent berry-purée research assessed the timing of ultrasound application and its sensory and rheological effects; those findings warrant consideration as comparative context, not as measured outcomes for this agitator *(Piecko et al., 2026).*

## CONCLUSIONS

Although no original equipment performance measurements or experimental optimization results were presented, the proposed methodology represents a promising strategy for evaluating a multiprocess mixing installation. Strawberry nectar is a suitable product for evaluating a multiprocess mixing installation because pulp distribution, rheology and energy demand can be measured.

The proposed protocol relates operating conditions to spatial homogeneity and nectar quality and compares specific energy use after a predefined homogeneity threshold has been reached. Optimal speed, mixing duration and vessel fill level must be determined in trials using the actual installation and a specified formulation.

## REFERENCES

[1] Delaplace, G., Xiao, J., Buendia, F., Jeantet, R., & Chen, X. D. (2023). Framework for choosing energy efficient mixing equipment whatever motions it induces: Example of application for planetary and helical ribbon mixers. Chemical Engineering Research and Design, 198, 173–183. https://doi.org/10.1016/j.cherd.2023.08.042

[2] Lacey, K. L., Moreno-Barreto, A., Pavón-Vargas, D., Cattani, L., Rinaldi, M., Rainieri, S., & Dhenge, R. (2023). A quality assessment of strawberry nectar stabilized by thermal and high-pressure processing conditions. Journal of Food Processing and Preservation. https://doi.org/10.1155/2023/5481142

[3] Maceiras, R., Álvarez, E., & Cancela, M. A. (2007). Rheological properties of fruit purees: Effect of cooking. Journal of Food Engineering, 80(3), 763–769. https://doi.org/10.1016/j.jfoodeng.2006.06.028

[4] Murray, H., Stipkovits, F., Lindner, M., Wühl, J., Halbwirth, H., & Gössinger, M. (2024). Conductivity at varying frequencies as a method for differentiating strawberry ripeness and association with colour acceptance of strawberry nectars. Journal of the Science of Food and Agriculture, 104(15), 9630–9639. https://doi.org/10.1002/jsfa.13787

[5] Niranjan, K., Smith, D. L. O., Rielly, C. D., et al. (1994). Mixing processes for agricultural and food materials: Part 5, review of mixer types. Journal of Agricultural Engineering Research. https://www.sciencedirect.com/science/article/pii/S0021863484710729

[6] Osorio, O., Martínez-Navarrete, N., Moraga, G., & Carbonell, J. V. (2008). Effect of thermal treatment on enzymatic activity and rheological and sensory properties of strawberry purees. Food Science and Technology International, 14(5_suppl). https://doi.org/10.1177/1082013208095328

[7] Piecko, J., Mieszczakowska-Frąc, M., Dickinson, N. J., Wrzodak, A., Celejewska, K., Frøst, M. B., Lange, B., Dandanell, C., Lewandowicz, J., & Jankowska, P. (2026). Ultrasound treatment in berry puree production: Effects on sensory, rheological, and chemical properties. Molecules, 31(2), 260. https://doi.org/10.3390/molecules31020260

[8] Xing, Y., Ma, Q., Wang, K., Dong, X., Wang, S., He, P., Wang, J., & Xu, H. (2023). Non-thermal treatments of strawberry pulp: The relationship between quality attributes and microstructure. Ultrasonics Sonochemistry, 98, 106508. https://doi.org/10.1016/j.ultsonch.2023.106508

[9] Xing, Y., Chen, G., Dong, X., Kou, L., Wang, J., & Xu, H. (2025). Impact of high-pressure homogenization on the homogalacturonan and rhamnogalacturonan-I regions of pectin in strawberry pulp and their interaction with anthocyanins. Food Chemistry, 494, 145989. https://doi.org/10.1016/j.foodchem.2025.145989

[10] Zia, H., Murray, H., Hofsommer, M., Moreno Barreto, A., Pavon-Vargas, D., Puzovic, A., Gędas, A.,

[11] Rincon, S., Gössinger, M., & Slatnar, A. (2025). Comparing the impact of conventional and non-conventional processing technologies on water-soluble vitamins and color in strawberry nectar: A pilot scale study. Food Chemistry, 463, 141078. https://doi.org/10.1016/j.foodchem.2024.141078

# ENHANCING HUMAN–MACHINE INTERACTION WITH SMART KNOBS AND HAPTIC FEEDBACK

/

# *ÎMBUNĂTĂȚIREA INTERACȚIUNII OM-MAȘINĂ CU BUTOANE INTELIGENTE ȘI FEEDBACK HAPTIC*

**Teodor Gabriel FODOREAN*[1)], Alin PLEȘA[2)], Emil-Octavian TEUȚAN[2)], Sergiu-Dan STAN[2)]**

[1)] INMA Bucharest / Romania;

[2)] Technical University of Cluj-Napoca, Faculty of Automotive, Mechatronics and Mechanical Engineering, Cluj-Napoca, Cluj County / Romania.

**Tel: (+40) 741 212 696; *E-mail: gabriel.fodorean@gmail.com*

***Keywords:*** *mechatronics, human–machine interaction, smart knob, interactive display, haptics, haptic feedback, external feedback, ergonomics, user experience, adaptive interfaces*

**ABSTRACT**

*This paper explores the integration of smart knobs, interactive displays, and haptic feedback in human–machine interaction (HMI). The proposed mechatronic approach enhances operator performance and ergonomics by combining tactile and visual cues. Smart knobs equipped with sensors and actuators provide precise control, while displays ensure adaptive information flow. The introduction of external haptic feedback sources, like actuators with force feedback, extends interaction beyond the control surface, enabling proactive alerts and improved situational awareness. Simulation evaluations demonstrate reduced error rates, faster task completion, and increased user confidence compared to conventional controls. The findings suggest that multimodal interfaces with haptics can significantly improve safety, efficiency, and user experience in industrial, agricultural, and assistive applications.*

**REZUMAT**

*Acest document explorează integrarea butoanelor rotative inteligente, a afișajelor interactive și a feedback-ului haptic în interacțiunea om-mașină (IOM). Abordarea mecatronică propusă îmbunătățește performanța și ergonomia operatorului prin combinarea indicilor tactili și vizuali. Butoanele rotative inteligente echipate cu senzori și actuatori oferă un control precis, în timp ce afișajele asigură un flux de informații adaptabil. Introducerea surselor externe de feedback haptic, cum ar fi actuatoarele cu feedback de forță, extinde interacțiunea dincolo de suprafața de control, permițând alerte proactive și o conștientizare situațională îmbunătățită. Evaluările prin simulare demonstrează o rată redusă de erori, finalizarea mai rapidă a sarcinilor și o încredere sporită a utilizatorului în comparație cu comenzile convenționale. Rezultatele sugerează că interfețele multimodale cu feedback haptic pot îmbunătăți semnificativ siguranța, eficiența și experiența utilizatorului în aplicații industriale, agricole și de asistență.*

## INTRODUCTION

Human–machine interaction (HMI) has evolved significantly, transitioning from mechanical levers and switches to touchscreens and voice control. While digital interfaces offer flexibility, they often lack tactile feedback, reducing operator confidence and precision.

The integration of **mechatronics** into HMI enables the design of **smart knobs** equipped with sensors, actuators, and programmable logic. When paired with interactive displays and **haptic concepts**, these knobs deliver both visual and tactile cues, reinforcing intuitive and reliable interaction.

This paper explores a mechatronic approach that combines **smart knobs, displays, and haptic feedback**—including feedback from **external sources**—to improve ergonomics, situational awareness, and adaptability across industrial and agricultural applications.

### Enhancing Situational Awareness

The mechatronic approach to HMI goes beyond simple button replacements; it creates a dynamic, multi-sensory feedback loop that significantly boosts situational awareness. In high-stakes environments, such as a factory floor or a combine harvester's cabin, a momentary lapse in attention can lead to errors or accidents. Traditional digital interfaces can exacerbate this by forcing the operator's gaze away from the task

to a screen. By contrast, a smart knob can provide a physical, haptic signal—a click, a resistance, or a vibration—that confirms an action has been taken without the operator needing to look. This allows the operator to keep their eyes on the process, whether they're monitoring a conveyor belt or navigating a field. Furthermore, haptic feedback can be used to communicate critical information, such as an impending system overload or an out-of-bounds parameter, through a distinct, easily recognizable tactile hint *(Hou, B., et al., 2019, Iafolla, L. et al., 2020, Kimura, F., 2009, Lee S. et al. 2021, Norman, D. 2013, Yavsan, E. et al. 2021).*

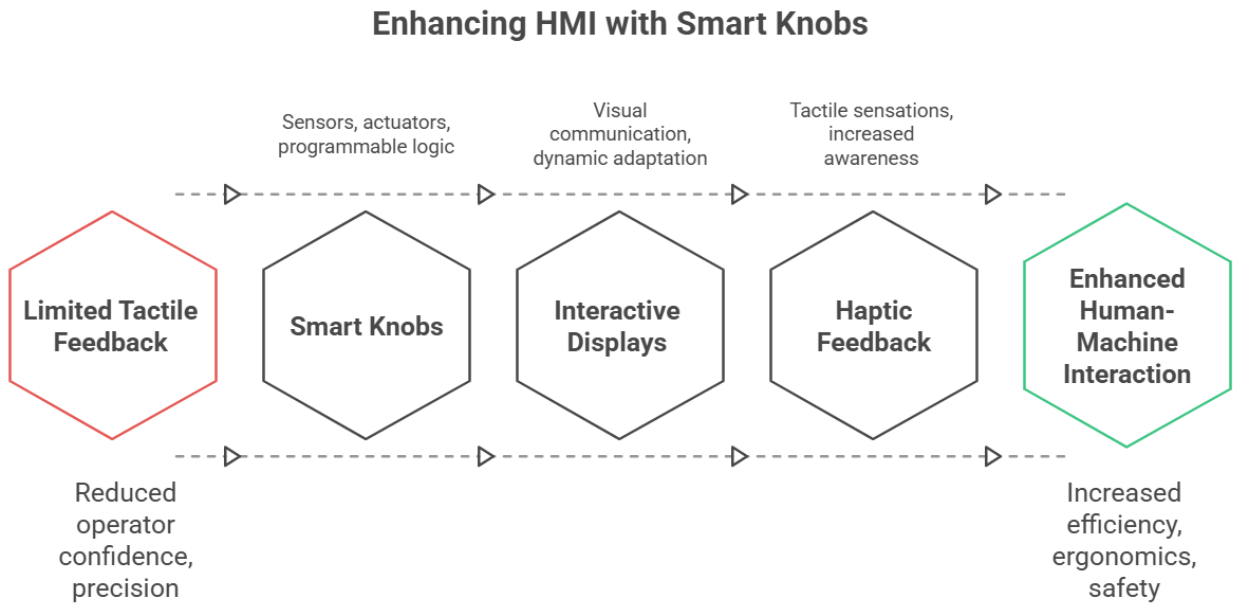



**Fig. 1 - Enhancing HMI with Smart Knobs**

**Improving Ergonomics and Adaptability**

A key advantage of this system is its inherent adaptability. Unlike fixed control panels, a mechatronic knob can be programmed to change its function, feel, and response based on the task at hand. For example, the same knob could adjust the temperature in one mode, and then, with a simple change on the display, control the speed of a motor in another. The tactile feedback can also be adjusted to match the context; a temperature adjustment might offer a smooth, continuous feel, while a critical safety setting could have a strong, ratcheting click. This dynamic reconfigurability reduces the number of physical controls needed, simplifying the cockpit or control room and improving ergonomics by minimizing repetitive hand movements. The system's ability to pull in feedback from external sources, such as sensor data from a machine, allows the knob to dynamically respond to the real-world state, providing a more intuitive and direct connection between the human and the machine.

**The Future of Industrial HMI**

This integration of smart knobs, interactive displays, and diverse haptic feedback represents a significant leap towards more intuitive and robust human–machine interaction. The system's ability to communicate complex information through both visual and tactile channels creates a more resilient interface that is less susceptible to environmental distractions or operator fatigue. By reinforcing the operator's actions with immediate and unmistakable physical feedback, the system not only improves precision and confidence but also reduces cognitive load. Looking forward, this approach could be extended to incorporate augmented reality overlays on the display, creating a seamless blend of virtual and physical controls. The ultimate goal is to create a truly symbiotic relationship where the machine doesn't just respond to commands, but actively collaborates with the human operator to achieve optimal performance and safety *(Lee S. et al. 2021, Norman, D. 2013, Yavsan, E. et al. 2021).*

**Real-World Applications in Agriculture and Industrial Machinery**

While the potential of these systems is clear, their adoption in agriculture and heavy industry has been cautious. However, the benefits are too significant to ignore. In a tractor, for instance, a single smart knob could be programmed to control different implements, from adjusting the depth of a plow to setting the seed rate on a planter. The knob could provide a ratcheting feel when adjusting seed rate, and a smooth,

continuous resistance when raising or lowering a heavy piece of equipment. This eliminates the need for a cluttered dashboard of dedicated buttons and levers.

For industrial machinery, such as a CNC mill or a robotic arm, a smart knob could be used for precise, millimeter-level adjustments. As the operator approaches a critical tolerance, the knob's haptic feedback could increase, providing a subtle but unmistakable warning that they're nearing a limit. This "feel" for the machine's state, without needing to constantly look at a display, is transformative for complex operations.

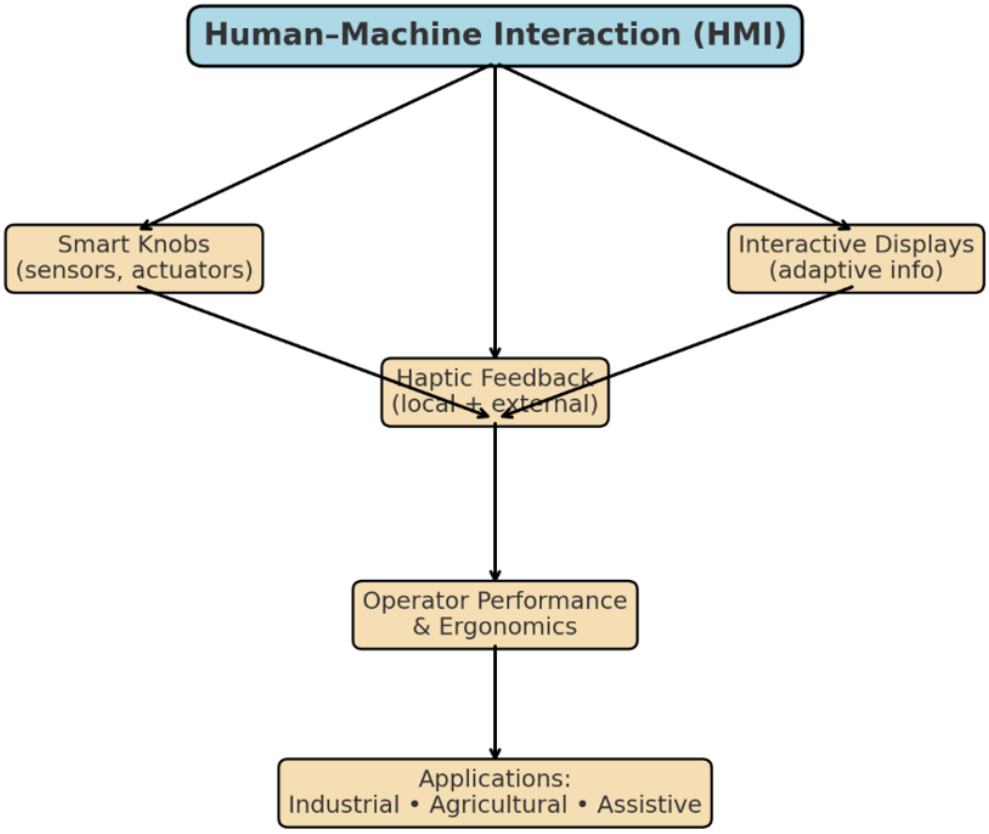



**Fig. 2 - HMI with Smart Knobs concept diagram**

**The Synergy of Multimodal Feedback**

The true power of this system lies in the synergy between its components. It's not just a knob, a display, or haptics; it's the seamless integration of all three. For example, a farming operator could use a smart knob to select a specific section of a field on a display. As they turn the knob, the display highlights the section, while the knob provides a physical "click" for each acre they pass over. Once they confirm the selection with a push on the knob, the haptic seat could give a brief vibration, confirming the command has been registered. This multimodal approach—visual, tactile, and physical—reduces cognitive load and minimizes the chance of error.

The integration of external feedback is especially crucial in these environments. A vibrating seat could alert a crane operator to an imbalance in their load, while a haptic wristband could warn a factory worker about an approaching piece of automated machinery. This ability to provide information through multiple senses makes the HMI more resilient and effective, especially in noisy, visually cluttered, or high-stress situations.

**The Path Forward: From HMI to Human-Machine Symbiosis**

Moving beyond simple control, the future of these mechatronic HMIs is about creating a symbiotic relationship between human and machine. This involves leveraging predictive algorithms and machine learning. A machine could learn an operator's preferred control settings, and the smart knob could automatically adjust its haptic feedback to match their style. Similarly, the system could provide proactive feedback; for instance, a knob could begin to vibrate subtly before an over-torque event occurs, giving the operator time to react before the machine even reports an error. This kind of predictive, collaborative

interaction holds the key to significant gains in both productivity and safety across a wide range of applications.

## MATERIALS AND METHODS

**Smart Knob Prototype**

- Equipped with a **rotary encoder** for position tracking
- **Capacitive sensing** for touch detection
- **Miniature vibration motor** for local haptic cues
- **Torque actuator** for resistance-based feedback

**Display Integration**

- **OLED/LCD interface** for real-time system visualization
- Contextual menus adapting to knob position and machine state
- Customizable dashboards for operator preferences

**Haptic Feedback System**

- **Local feedback**: vibration or resistance within the knob itself
- **External sources**: wireless modules driving haptic actuators on seats, gloves, or handheld devices to convey alerts such as overload, collision warnings, or environmental hazards
- **Control unit**: microcontroller (e.g., STM32, nRF52840) ensuring real-time synchronization of display, knob, and haptic signals

**Evaluation Approach**

- Usability tests with operators in simulated machinery environments
- Ergonomic assessment through NASA TLX workload measures
- Comparative analysis vs. traditional knobs and touchscreen-only controls

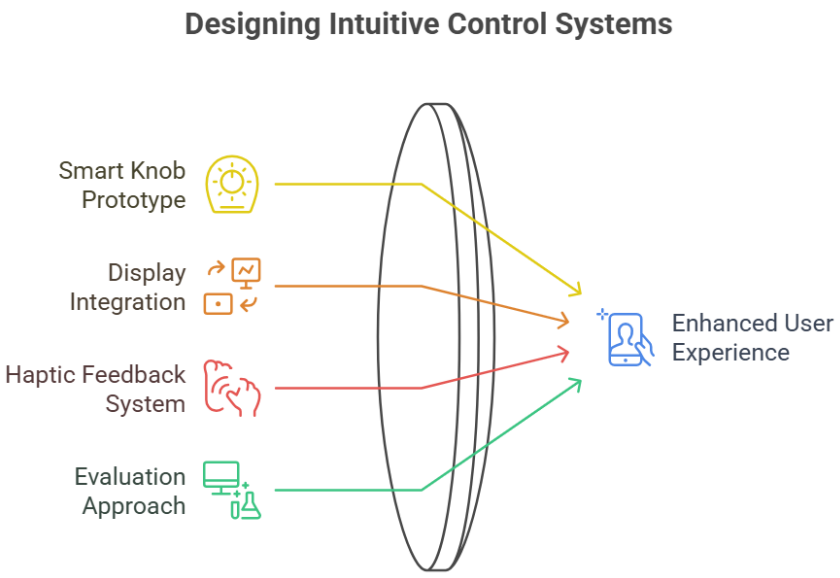



**Fig. 3 - Designing Intuitive Control Systems**

Operators reported higher confidence and faster task completion with smart knobs compared to touchscreen-only systems. Error reduction observed when external haptic alerts were introduced (e.g., vibration pulse indicating overload). Integration of visual + haptic channels improved situational awareness in complex tasks. Limitations identified:

- Increased power consumption for haptic actuators
- Need for robust synchronization between visual and tactile signals
- Added design complexity in embedding haptic actuators into machinery

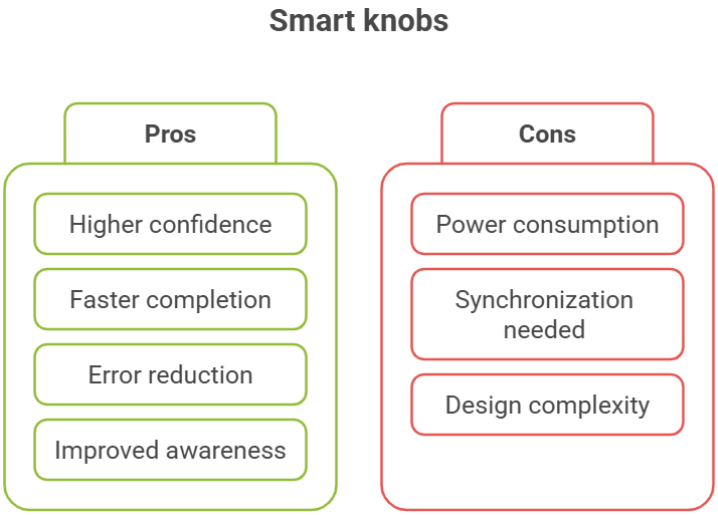



**Fig. 4 - Pros and cons for Smart Knobs**

## RESULTS

In industrial contexts, the system improved monitoring of multi-variable processes, especially when visual clutter was high. In agricultural machinery operation, external haptics allowed operators to maintain focus on the field while still receiving alerts about machine status. For assistive technologies, the prototype showed potential for accessible HMIs for visually impaired users, where haptics could replace or complement visual displays.

### Limitations and Challenges

Despite these advantages, the integration of haptic modules introduced challenges related to power consumption, synchronization of multimodal feedback, and user calibration preferences. Future work will focus on adaptive AI-based feedback that adjusts haptic intensity and frequency to user profiles and context.

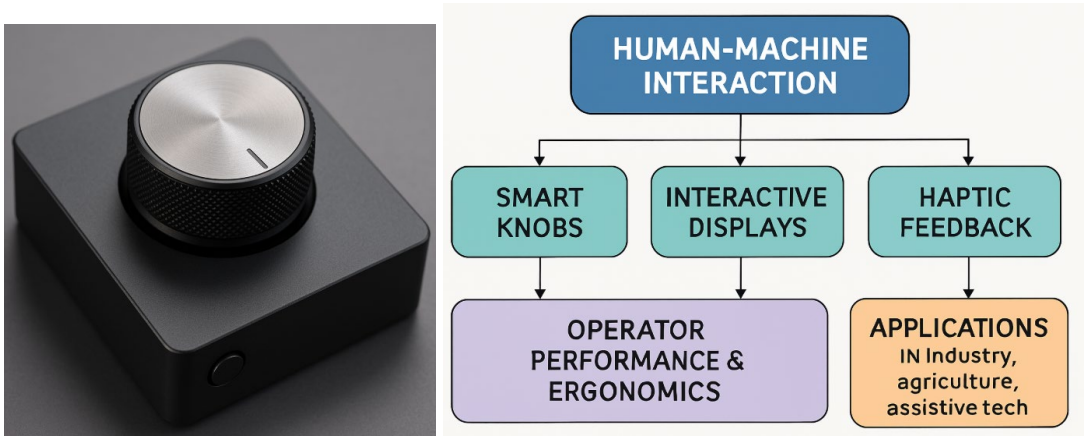



**Fig. 5 - Proposed Smart Knob and concept design**

## CONCLUSIONS

Smart knobs, when combined with displays and haptic feedback systems, provide a multimodal interface that enhances human–machine interaction. By delivering intuitive tactile and visual cues, such systems increase efficiency, ergonomics, and operator safety.

The inclusion of **external haptic sources** extends feedback beyond the control surface, enabling proactive alerts and adaptive responses. This approach has strong potential in **agricultural machinery, industrial systems, and assistive technologies**.

Future research will focus on **AI-driven adaptive feedback**, integration with IoT ecosystems, and advanced **multimodal ergonomics studies**.

**ACKNOWLEDGEMENT**

The authors would like to express their gratitude to the **Laboratory of Advanced Mechatronic Systems (LAMS), Technical University of Cluj-Napoca**, for their valuable support, resources, and collaborative environment that contributed to the development of this research.

**REFERENCES**

[1] Hou, B., Zhou, R., Gao, Z., Liu, X., Zhang, B., and Wang, Q. “An analog interface circuit for capacitive angle encoder,” Sensors, vol. 19, no. 14, 2019. doi: 10.3390/s19143116

[2] Iafolla, L., Filipozzi, M., Freund, S., Zam, A., Rauter, G., and Cattin, P. C., “Proof of concept of a novel absolute rotary encoder,” Sensors and Actuators A: Physical, vol. 313, 2020, Art. no. 111971. doi: 10.1016/j.sna.2020.111971

[3] Kimura, F., M. Gondo, A. Yamamoto, and T. Higuchi, “Resolver compatible capacitive rotary position sensor,” in Proc. 35th Annu. Conf. IEEE Industrial Electronics Society, 2009. doi: 10.1109/IECON.2009.5414883

[4] Lee, S. et al. (2021). “Smart rotary knobs with haptic feedback for industrial control.” *IEEE Transactions on Haptics*.

[5] Norman, D. (2013). *The Design of Everyday Things*. MIT Press.

[6] Yavsan, E., Kara, M. R., Karali, M., Gokce, B., and Erismis, M. A., “A novel high resolution miniaturized capacitive rotary encoder,” Sensors and Actuators A: Physical, vol. 332, 2021, Art. no. 113057. doi: 10.1016/j.sna.2021.113057

[7] *** BOEVX Technology, Knob-On Display: Physical Controls Design with Mechanical Haptics, Boevx Technical Documentation, 2021. https://www.boevx.com/knob-on-display/

[8] *** Goldenvision LCD Technology, How Can a Rotary Knob Screen Make the Center Console More Technological, Goldenvision Technical Report, 2025.https://www.goldenvisionlcd.com/News_1/96.html

[9] *** ISO 9241-210:2019. *Human-centred design for interactive systems*.

[10] *** Research in China, Automotive Smart Surface Industry Research Report, 2022, Beijing Research in China Information Technology Co., Ltd., 2023. http://www.researchinchina.com/Htmls/Report/2022/72828.html

[11] *** Synaptics Inc., Force-Sensing Touch Displays for Automotive Applications, Synaptics Corporation White Paper, 2025. https://www.synaptics.com/applications/automotive

[12] *** Panasonic Industry Europe GmbH, Magic Knob™: Capacitive Knob Technology for Automotive Applications, Panasonic Technical Specification, 2022. https://industry.panasonic.eu/products/components/rotary-input-devices/magic-knob

[13] *** STMicroelectronics, 1.3 Inch Round Smart Module Knob Display, ST Partner Products Technical Documentation, 2023. https://www.st.com/en/partner-products-and-services/1-3-inch-round-smart-module-knob-display.html

# CROP ROTATION AS AN ENVIRONMENTALLY FRIENDLY APPROACH TO IMPROVE FARM PRODUCTION

/

# *ROTAȚIA CULTURILOR CA O ABORDARE ECOLOGICĂ PENTRU ÎMBUNĂTĂȚIREA PRODUCȚIEI AGRICOLE*

**Mihaela NIȚU*[1)], Iuliana GĂGEANU[1)], Ana-Maria TĂBĂRAȘU[1)], Augustina PRUTEANU[1)], Mihai NICOLESCU[2)]**
[1)] National Institute of Research - Development for Machines and Installations Designed for Agriculture and Food Industry - INMA Bucharest / Romania;
[2)] ASAS Bucharest / Romania.
**E-mail: rosumihaelan@yahoo.com; *Tel.: 0746 689 449*

***Keywords:*** *crop rotation; soil health; crop diversification; agroecology; yield stability; decision support*

**ABSTRACT**

*Crop rotation is frequently presented as an intrinsically sustainable practice, although its performance depends on the functional contrast among crops, the length of the sequence, local soil and climate, and the accompanying management. This critical review evaluates how diversified rotations influence soil physical condition, carbon and nutrient cycling, biological communities, weed and disease regulation, yield, stability and farm-level feasibility. Peer-reviewed meta-analyses, long-term field experiments and methodological studies published up to 2025 were identified through focused searches in ScienceDirect and ResearchGate, followed by backward reference screening. The evidence consistently supports benefits relative to continuous monoculture, but effect sizes are heterogeneous. Stronger responses generally occur when rotations introduce legumes, contrasting rooting patterns, different sowing windows or cover crops, and when fertilizer and residue management are adjusted to the sequence. Conversely, merely increasing crop number does not ensure improved outcomes, and short-term yield, soil carbon and economic responses may diverge. A practical framework is proposed in which rotation design is treated as a constrained, multi-objective decision problem. The review concludes that crop rotation is best understood as an enabling ecological infrastructure whose value emerges from context-specific design, monitoring and adaptive management.*

**REZUMAT**

*Rotația culturilor este frecvent prezentată ca o practică implicit sustenabilă, deși performanța sa depinde de contrastul funcțional dintre culturi, durata secvenței, condițiile locale de sol și climă și managementul asociat. Acest review critic analizează influența rotațiilor diversificate asupra proprietăților fizice ale solului, ciclului carbonului și nutrienților, comunităților biologice, controlului buruienilor și bolilor, producției, stabilității și fezabilității la nivelul fermei. Meta-analize, experimente de lungă durată și studii metodologice, publicate până în 2025, au fost identificate prin căutări focalizate în ScienceDirect și ResearchGate, urmate de verificarea bibliografiilor. Dovezile susțin beneficii față de monocultură, însă mărimea efectelor este eterogenă. Răspunsurile sunt, în general, mai favorabile când rotația include leguminoase, sisteme radiculare contrastante, epoci diferite de semănat sau culturi de acoperire și când fertilizarea și gestionarea resturilor vegetale sunt adaptate secvenței. Simplificarea concluziilor la numărul de culturi este nejustificată, deoarece producția pe termen scurt, carbonul din sol și rezultatele economice pot evolua diferit. Este propus un cadru practic în care proiectarea rotației este tratată ca o decizie multiobiectiv, supusă constrângerilor locale.*

## INTRODUCTION

The simplification of crop sequences has supported specialization, mechanization and predictable logistics, but it has also repeatedly exposed soils and pest communities to the same crop traits and management disturbances. Continuous or narrowly alternating systems tend to concentrate nutrient demand, synchronize field operations, narrow residue quality and preserve ecological niches for specialized weeds and pathogens. Crop rotation counters this simplification by distributing contrasting crops through time. Its agronomic rationale is established, but the current relevance of rotation lies in its capacity to reorganize

several processes simultaneously rather than to deliver a single input substitution (*Bullock, 1992; Liebman and Dyck, 1993*).

Evidence accumulated during the last decade has strengthened the case for temporal diversification. Global syntheses associate crop diversification with higher production, associated biodiversity and multiple regulating services, while long-term experiments show that rotational diversity can increase resilience under adverse growing conditions (*Altieri et al., 2015; Bowles et al., 2020; Beillouin et al., 2021; Tamburini et al., 2020*). Recent meta-analyses also demonstrate that the identity of the preceding crop matters: legumes can provide an average yield advantage to the following crop, but the response declines as nitrogen fertilizer rates and baseline system diversity increase *(Zhao et al., 2022)*. Thus, crop rotation should not be described as universally beneficial without specifying the comparator, sequence, duration and management context.

This distinction is important for both scientific interpretation and farm implementation. A four-crop sequence can remain functionally narrow if all crops have similar rooting depth, phenology and management. Conversely, a shorter sequence may deliver a strong break effect when it alternates crop families, sowing seasons and resource-acquisition traits. Outcomes may also conflict: a cover crop can improve soil cover and water productivity without increasing the yield of every cash crop; a legume can reduce mineral nitrogen requirements yet provide limited residual nitrogen when most fixed nitrogen leaves the field in harvested seed; and a biologically desirable crop may be economically impractical where markets or machinery are absent (*Peoples et al., 2009; Attia et al., 2024*).

The objective of this review is to critically synthesize evidence on crop rotation as an environmentally friendly approach to farm production, with emphasis on (i) the mechanisms linking temporal crop diversity to soil and biotic processes; (ii) the strength and limits of reported effects on productivity and ecosystem services; and (iii) an operational framework for designing and monitoring rotations under commercial farm constraints. The intended contribution is not a universal rotation recipe, but a defensible set of design principles that can be adapted to temperate continental cropping systems, including those of Romania.

## MATERIALS AND METHODS

### *Review approach and search strategy*

A structured critical review was conducted rather than a de novo meta-analysis. Focused searches were performed in ScienceDirect and ResearchGate using combinations of the terms “crop rotation”, “crop diversification”, “soil health”, “soil organic carbon”, “microbial diversity”, “weed suppression”, “yield stability”, “legume pre-crop”, “economic performance” and “decision support”. The evidence base covered peer-reviewed publications available up to 2025. Backward reference screening was used to identify seminal studies and methodological papers. ResearchGate was used to locate bibliographic records or author-posted versions; evidence was attributed to the original peer-reviewed publication.

### *Eligibility and evidence hierarchy*

Priority was given to global or regional meta-analyses, syntheses of multiple experiments, and long-term field trials comparing diversified rotations with continuous monoculture or simpler sequences. Studies were retained when the rotation, comparator and reported response were sufficiently clear to support interpretation. Evidence on intercropping, agroforestry or variety mixtures was used only when a synthesis explicitly separated or contextualized temporal diversification. Non-peer-reviewed agronomic claims, untraceable numerical data and results without an identifiable comparator were excluded. This criterion led to the removal of the simulated experiment and unsupported numerical results included in the preliminary manuscript.

### *Synthesis framework*

Findings were organized into six linked domains: soil physical condition; carbon and nutrient cycling; soil biodiversity; weeds, pests and diseases; productivity and climate resilience; and operational feasibility. Quantitative effects are reported only when they originate from a clearly identified synthesis, and each value is interpreted within its original scope. No pooled effect was recalculated. The resulting framework therefore supports evidence-based comparison but does not claim the exhaustiveness or statistical independence of a new systematic review.

## RESULTS

### *Crop rotation as a process-based intervention*

The central mechanism of crop rotation is temporal functional diversity. Crops differ in root architecture, nutrient demand, residue chemistry, rhizosphere interactions, canopy development, sowing

date and harvest date. Alternating these traits changes the timing and location of resource capture and creates discontinuities in the life cycles of weeds and pathogens. The resulting benefits are indirect and cumulative: soil structure may improve through roots and residues; nutrient supply may become better synchronized with demand; microbial communities receive a wider range of substrates; and pest populations encounter an interrupted host sequence. These mechanisms interact, so attribution to a single cause is often inappropriate (*McDaniel et al., 2014a, 2014b; Tiemann et al., 2015*).

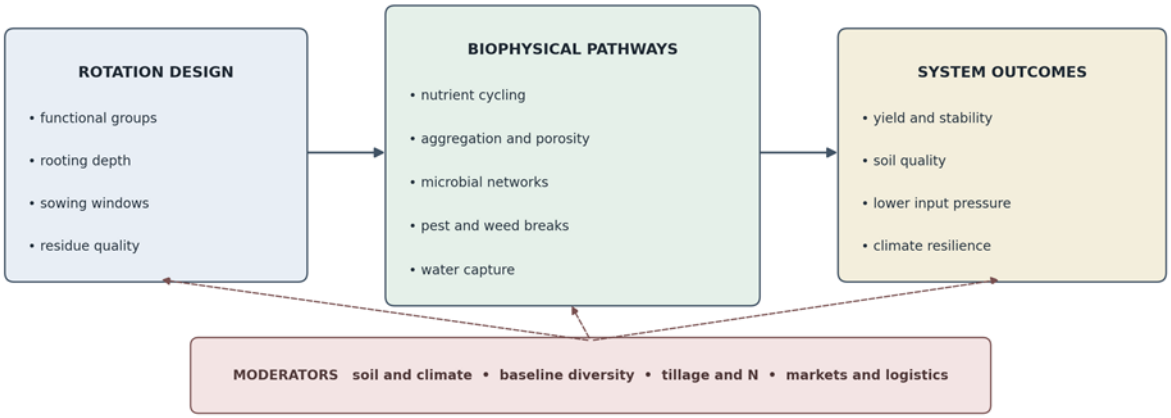



**Fig. 1 - Process-based framework linking crop-rotation design to system outcomes.**
*Source: authors' synthesis*

***Soil physical condition and water relations***

Rotations influence soil physical health through the amount, placement and decomposability of organic inputs and through differences in root diameter and depth. Fibrous-rooted cereals contribute dense root networks near the surface, while tap-rooted oilseeds, legumes or selected cover crops can explore deeper layers and create biopores. When residues are retained and traffic is well managed, these effects can support aggregation, porosity, infiltration and resistance to erosion. A meta-analysis of diversified rotations concluded that the strongest physical benefits occurred in sequences combining greater crop diversity with grain legumes and conservation tillage; nevertheless, responses differed among bulk density, aggregate stability, penetration resistance and hydraulic indicators (*Chahal et al., 2021; Iheshiulo et al., 2023*).

The evidence does not support the claim that rotation alone will correct compaction or water limitations. Heavy machinery operated on wet soil can override biological improvements, and deep-rooted crops cannot replace corrective action where a severe mechanical pan persists. Similarly, improved infiltration does not guarantee greater plant-available water if rainfall is insufficient or if an additional crop depletes water before the main crop. The practical implication is that rotation should be coordinated with controlled traffic, tillage intensity, residue cover and locally appropriate termination dates for cover crops.

***Soil organic carbon and nutrient cycling***

Diversified rotations alter carbon inputs by changing biomass quantity, root-to-shoot allocation and residue quality. Global syntheses report positive average effects on soil organic carbon, aggregation and aggregate-associated carbon, but the response is moderated by baseline carbon, climate, experiment duration and residue management (*Liu et al., 2022; Zheng et al., 2023; Li et al., 2024*). These findings justify cautious language: rotation can support carbon accumulation, especially when it increases total biomass returned to soil, but it is not an automatic or unlimited sequestration mechanism. Detectable changes may require several rotation cycles and can be concentrated in surface layers.

Nitrogen dynamics illustrate why crop identity matters. Symbiotic fixation can supply substantial nitrogen to legumes, yet the amount remaining for subsequent crops depends on biomass production, harvest index, residue removal and decomposition. Grain legumes may export much of the fixed nitrogen in seed; forage legumes or green manures generally return more nitrogen but carry opportunity costs. Across 11,768 paired observations, legume pre-crops increased the yield of subsequent crops by about 20% on average, with larger benefits in low-input and low-yield environments. The advantage declined as nitrogen fertilizer and baseline crop diversity increased, demonstrating that fertilizer savings must be determined locally rather than assumed (*Drinkwater et al., 1998; Peoples et al., 2009; Zhao et al., 2022*).

Residue diversity also affects microbial processing of carbon and nitrogen. Long-term rotation complexity changes microbial biomass, enzyme activity and decomposition of both high- and low-quality residues (*McDaniel et al., 2014a, 2014b; Tiemann et al., 2015*). A well-designed sequence therefore seeks a balance between residues that mineralize rapidly and provide near-term nutrients and residues that persist longer and contribute to soil cover and organic matter. This balance must be integrated with soil testing and nutrient budgets; otherwise, nitrogen immobilization after high-carbon residues or excess nitrogen after legumes can reduce efficiency and increase environmental loss.

***Soil biodiversity and biological functions***

Temporal plant diversity broadens the spectrum of root exudates and residues entering the soil and changes the duration of living-root cover. A meta-analysis found higher microbial richness and diversity under more diverse rotations, although the magnitude depended on the analytical method and experimental context (*Venter et al., 2016*). Long-term field evidence further links rotational diversity with changes in microbial community composition, aggregate formation and nutrient cycling (*Tiemann et al., 2015; Bender et al., 2016*). The relevant objective is not diversity as an isolated score, but the maintenance of functional communities that contribute to decomposition, nutrient retention and pathogen suppression.

Biological responses are slower and less predictable than simple fertilizer responses. Soil type, pH, moisture and pesticide history can dominate community composition, and a more diverse microbial profile does not automatically translate into higher yield. Accordingly, soil biology should be monitored alongside physical and chemical indicators. Potentially mineralizable carbon, soil respiration or microbial biomass can complement organic carbon, pH, available nutrients, aggregate stability and crop performance, provided that sampling depth, season and laboratory method remain consistent.

***Weed, pest and disease regulation***

Rotation suppresses weeds when it changes the timing of sowing, crop competition, disturbance and control measures. In a meta-analysis of 298 paired observations from 54 studies, diversified rotations reduced weed density by 49% on average, whereas the reduction in weed biomass was not statistically significant. Variation in planting dates explained more of the suppression than crop richness alone, reinforcing the importance of functional rather than numerical diversity (*Weisberger et al., 2019*). A sequence that alternates autumn- and spring-sown crops can expose weed cohorts to different mortality filters and reduce repeated selection for the same life-history strategy.

Disease control depends on host range, survival structures and the persistence of infected residue. Non-host intervals can reduce inoculum for specialized pathogens, but short breaks are ineffective for organisms that survive for many years or infect several crops. Volunteer plants and weeds can bridge the non-host period, while reduced tillage may preserve infected residues near the surface. Rotation must therefore be combined with resistant cultivars, clean seed, residue and volunteer management, and field surveillance (*Krupinsky et al., 2002*). Similar caution applies to arthropods: temporal crop diversity can interrupt resource continuity, yet mobile generalists may respond more strongly to landscape composition than to a single-field sequence (*Jaworski et al., 2023*).

***Productivity, stability and environmental performance***

Yield benefits arise through both nitrogen and non-nitrogen break-crop effects. A meta-analysis from China reported an average yield increase of about 20% relative to continuous monoculture, while a global synthesis of legume-based rotations found a comparable average advantage for the subsequent crop (*Zhao et al., 2020; Zhao et al., 2022*). More recent global evidence, based on 3,663 paired field-trial observations, reported that legume and non-legume pre-crops increased subsequent-crop yield by 23% and 16%, respectively, and that well-designed rotations can improve yield, nutritional output and revenue simultaneously (*Mudare et al., 2025*). These are average effects, not guaranteed farm-level outcomes.

Long-term North American experiments show that rotational diversification can protect maize yield under adverse growing conditions, indicating that the value of diversity becomes especially visible during climatic stress (*Bowles et al., 2020*). However, the effect is crop- and environment-specific. A water-demanding preceding crop may reduce yield in dry years, and a poorly timed cover crop may consume scarce spring water. Climate resilience therefore requires matching phenology and rooting depth to local rainfall patterns, not simply adding species.

Environmental benefits are also conditional. Rotation can reduce fertilizer and pesticide pressure by improving nitrogen supply and breaking pest cycles, and diversified systems frequently enhance several ecosystem services without compromising average yield (*Tamburini et al., 2020*). Yet soil carbon gains can be offset by other greenhouse-gas sources if nitrogen is poorly managed, and greater field diversity can

increase the number of operations. Evaluation should use a system boundary that includes fuel, fertilizer, pesticides, residue flows and all crops in the sequence rather than comparing one crop-year in isolation.

**Table 1**

**Selected quantitative evidence and its interpretation**

| Evidence domain | Scope | Reported effect | Critical interpretation |
|---|---|---|---|
| Crop diversification | 95 meta-analyses; >54,500 paired observations | Median crop production +14%; biodiversity +24% | Includes several diversification strategies; not a rotation-only estimate (Beillouin et al., 2021). |
| Legume pre-crop | 462 field experiments; 53 countries | Subsequent-crop yield +20% on average | Benefit decreases with higher N input and baseline diversity (Zhao et al., 2022). |
| Soil organic carbon | Global crop-rotation synthesis | SOC +6.6% relative to monoculture | Climate, duration, initial SOC and management moderate the response (Liu et al., 2022). |
| Aggregation and carbon | 1,924 observations across diversification strategies | Mean-weight diameter +7.5%; bulk SOC +3.3%; macroaggregate C +12.5% | Combined evidence for rotations, cover crops and intercropping; effects are not interchangeable (Li et al., 2024). |
| Soil microbial diversity | Meta-analysis of rotation studies | Microbial richness +15.11%; diversity +3.36% | Effect varies with analytical method; function should be assessed separately (Venter et al., 2016). |
| Weed regulation | 298 paired observations; 54 studies | Weed density -49%; biomass response not significant | Planting-date diversity was more influential than species count alone (Weisberger et al., 2019). |
| Recent global yield evidence | 3,663 paired observations; 738 experiments | Following-crop yield +23% after legumes and +16% after non-legumes | Average responses conceal sequence- and region-specific trade-offs (Mudare et al., 2025). |

***Economic feasibility and adoption constraints***

A rotation is economically viable only if its full sequence performs under the farm's resource and market constraints. Diverse systems can improve profitability by raising cash-crop yields, spreading risk and reducing selected inputs. Long-term Brazilian evidence found that diversified rotations under no-tillage increased grain yield and economic efficiency, with cover-crop costs compensated over the sequence rather than necessarily in the year of establishment (*Garbelini et al., 2022*). The recent global meta-analysis by Mudare et al. (2025) likewise indicates potential revenue gains, but the authors note the difficulty of estimating profit consistently across regions. Barriers include absent markets for legumes or minor crops, specialized harvesting and storage requirements, seed availability, contract restrictions, labor peaks and transition risk. These constraints explain why an agronomically sound crop can be unsuitable for a specific farm. Economic assessment should therefore include gross margin for every crop, machinery and storage compatibility, timing of cash flow, yield variability and the option value of maintaining alternative crops. A sequence with slightly lower expected margin but lower variance may be preferable where climatic and price risks are high.

***From generic prescriptions to measurable rotation design***

The evidence supports a shift from prescriptive lists to multi-objective design. Rotation planning must satisfy agronomic rules, legal and market requirements, machinery capacity and workload while pursuing soil, yield and environmental objectives. Formal representations of crop transitions make these constraints explicit and allow feasible sequences to be screened before field implementation (*Castellazzi et al., 2008*). Multi-criteria methods can then compare candidate rotations using indicators such as nitrogen balance, soil cover, pesticide pressure, gross margin and workability (*Liang et al., 2023*).

Digital tools are valuable when they structure reliable field histories and update decisions, not when they replace agronomic causality. A practical system should combine georeferenced crop records, soil analyses, yield maps, weather data and observations of weeds and diseases. Remote sensing can identify spatial anomalies, but it cannot by itself distinguish whether a yield response resulted from the preceding

crop, soil texture, input rate or weather. Data ownership, interoperability, farmer skills and transparent recommendations are therefore as important as algorithmic performance (*Klerkx et al., 2019*).

**Table 2**

**Operational criteria for designing and evaluating a crop rotation**

| Design criterion | Question | Minimum indicator | Main failure mode |
|---|---|---|---|
| Functional contrast | Do consecutive crops differ in family, rooting, phenology and residue quality? | Crop family; sowing window; rooting class; C:N class | More species but little ecological contrast |
| Nutrient logic | Does the sequence match nutrient supply to crop demand? | Whole-sequence N and P balance; soil test trend | Assumed legume credit or nutrient mining |
| Water and soil cover | Is water conserved without penalizing the following crop? | Days with cover; soil moisture at sowing; infiltration | Cover crop termination too late in dry conditions |
| Pest break | Is the non-host interval long enough for target organisms? | Host range; survival time; weed and disease records | Volunteers, shared hosts or persistent inoculum |
| Farm feasibility | Can crops be marketed, stored and harvested with available resources? | Gross margin; machinery fit; labor calendar; market access | Agronomically strong but operationally infeasible crop |
| Adaptive verification | Are outcomes compared over complete cycles? | Yield and variance; inputs; SOC; aggregate stability; pest pressure | Conclusions drawn from one crop-year or one indicator |

***Implications for temperate continental cropping systems***

For cereal-dominated systems in Romania and comparable temperate continental regions, the first priority is to avoid repeated winter cereals and to introduce functionally distinct break crops where soils, markets and water permit. Grain legumes can contribute nitrogen and a disease break; oilseeds change crop family and residue characteristics; spring crops diversify sowing and weed-control windows; and cover crops extend living-root cover between cash crops. The appropriate combination depends on rainfall distribution, soil water storage, erosion risk and access to buyers.

A defensible starting design should specify the target problem for each transition. For example, a legume should not be included merely to label the sequence “diverse”; its role may be nitrogen supply, an earlier harvest, reduced cereal disease pressure or an additional market. The following crop and fertilizer plan should be adjusted to that role. Likewise, a cover crop should have a defined service—soil cover, nitrogen capture, compaction alleviation or weed competition—and a termination rule linked to soil moisture and the next sowing date. This explicit logic makes the rotation testable and supports adaptive refinement.

***Limitations of the evidence base and research priorities***

The literature is strong in direction but uneven in transferability. Many experiments are concentrated in temperate regions and compare a few dominant crop systems. Definitions of “diverse” vary, and reported effects often combine crop identity, tillage, fertilization and residue management. Publication bias, non-independence among observations and short experimental duration can further inflate confidence. Meta-analyses resolve part of this problem but still aggregate systems with different baselines and management objectives *(Beillouin et al., 2021).* Future work should report complete sequences and management, not only the focal crop, and should evaluate at least one full rotation cycle. Priority indicators include yield and yield variance, input use, gross margin, soil carbon by depth, aggregate stability, nutrient balance, soil water and target pest pressure. Long-term experiments should be linked with commercial-farm data to test whether controlled results survive operational constraints. Decision-support research should publish agronomic rules, uncertainty and data provenance so that recommendations can be audited.

## CONCLUSIONS

1. Crop rotation is an ecological management infrastructure rather than a stand-alone input. Its benefits emerge when successive crops differ functionally in rooting, phenology, nutrient acquisition, residue quality and pest associations.
2. The strongest evidence supports improvements relative to continuous monoculture in subsequent-crop yield, soil carbon and aggregation, microbial diversity and weed regulation. Average effects are heterogeneous and must not be converted into guaranteed farm-level percentages.

3. Legumes are valuable but not automatically nitrogen-positive for the soil. Their contribution depends on biomass, nitrogen fixation, harvested nitrogen, residue handling and fertilizer adjustment in the following crop.
4. The number of crops is an inadequate design criterion. Rotation quality is better assessed through functional contrast, non-host intervals, soil cover, nutrient and water balances, and feasibility within machinery, labor and market constraints.
5. Evaluation should cover complete rotation cycles and integrate production, variability, inputs, soil indicators, pest pressure and economics. Digital tools can strengthen this process when they organize traceable data and transparent constraints.
6. For Romanian and other temperate continental systems, locally tested cereal-legume-oilseed-spring-crop combinations, supplemented by purpose-defined cover crops where water permits, offer a credible pathway to more resilient production without overstating universal benefits.

**ACKNOWLEDGEMENT**

This paper was supported by EIT FOOD Program, through project CROSAR 250725 “Crop Rotation Optimisation for Sustainable Agriculture in Romania” and by the Romanian Ministry of Research Innovation and Digitalization, through the project “Intelligent plant growth systems under controlled environmental conditions” – PN 23 04 01 04– Ctr. 9N/01.01.2023.

**REFERENCES**

[1] Altieri, M.A., Nicholls, C.I., Henao, A. and Lana, M.A., 2015. Agroecology and the design of climate change-resilient farming systems. Agronomy for Sustainable Development, 35, pp.869-890. https://doi.org/10.1007/s13593-015-0285-2

[2] Attia, A., Marohn, C., Shawon, A.R., de Kock, A., Strassemeyer, J. and Feike, T., 2024. Do rotations with cover crops increase yield and soil organic carbon? A modeling study in southwest Germany. Agriculture, Ecosystems & Environment, 375, 109167. https://doi.org/10.1016/j.agee.2024.109167

[3] Beillouin, D., Ben-Ari, T., Malézieux, E., Seufert, V. and Makowski, D., 2021. Positive but variable effects of crop diversification on biodiversity and ecosystem services. Global Change Biology, 27(19), pp.4697-4710. https://doi.org/10.1111/gcb.15747

[4] Bender, S.F., Wagg, C. and van der Heijden, M.G.A., 2016. An underground revolution: biodiversity and soil ecological engineering for agricultural sustainability. Trends in Ecology & Evolution, 31(6), pp.440-452. https://doi.org/10.1016/j.tree.2016.02.016

[5] Bowles, T.M., Mooshammer, M., Socolar, Y., Calderón, F., Cavigelli, M.A., Culman, S.W., Deen, W., Drury, C.F., Garcia y Garcia, A., Gaudin, A.C.M. et al., 2020. Long-term evidence shows that crop-rotation diversification increases agricultural resilience to adverse growing conditions in North America. One Earth, 2(3), pp.284-293. https://doi.org/10.1016/j.oneear.2020.02.007

[6] Bullock, D.G., 1992. Crop rotation. Critical Reviews in Plant Sciences, 11(4), pp.309-326. https://doi.org/10.1080/07352689209382349

[7] Castellazzi, M.S., Wood, G.A., Burgess, P.J., Morris, J., Conrad, K.F. and Perry, J.N., 2008. A systematic representation of crop rotations. Agricultural Systems, 97(1-2), pp.26-33. https://doi.org/10.1016/j.agsy.2007.10.006

[8] Chahal, I., Hooker, D.C., Deen, B., Janovicek, K. and Van Eerd, L.L., 2021. Long-term effects of crop rotation, tillage, and fertilizer nitrogen on soil health indicators and crop productivity in a temperate climate. Soil & Tillage Research, 213, 105121. https://doi.org/10.1016/j.still.2021.105121

[9] Drinkwater, L.E., Wagoner, P. and Sarrantonio, M., 1998. Legume-based cropping systems have reduced carbon and nitrogen losses. Nature, 396, pp.262-265. https://doi.org/10.1038/24376

[10] Garbelini, L.G., Debiasi, H., Balbinot Junior, A.A., Franchini, J.C., Coelho, A.E. and Telles, T.S., 2022. Diversified crop rotations increase the yield and economic efficiency of grain production systems. European Journal of Agronomy, 137, 126528. https://doi.org/10.1016/j.eja.2022.126528

[11] Iheshiulo, E.M.-A., Larney, F.J., Hernandez-Ramirez, G., St. Luce, M., Liu, K. and Chau, H.W., 2023. Do diversified crop rotations influence soil physical health? A meta-analysis. Soil & Tillage Research, 233, 105781. https://doi.org/10.1016/j.still.2023.105781

[12] Jaworski, C.C., Thomine, E., Rusch, A., Lavoir, A.-V., Wang, S. and Desneux, N., 2023. Crop diversification to promote arthropod pest management: A review. Agricultural Communications, 1, 100004. https://doi.org/10.1016/j.agrcom.2023.100004

[13] Klerkx, L., Jakku, E. and Labarthe, P., 2019. A review of social science on digital agriculture, smart farming and agriculture 4.0: New contributions and a future research agenda. NJAS - Wageningen Journal of Life Sciences, 90-91, 100315. https://doi.org/10.1016/j.njas.2019.100315

[14] Krupinsky, J.M., Bailey, K.L., McMullen, M.P., Gossen, B.D. and Turkington, T.K., 2002. Managing plant disease risk in diversified cropping systems. Agronomy Journal, 94, pp.198-209. https://doi.org/10.2134/agronj2002.1980

[15] Li, G., Yu, C., Shen, P., Hou, Y., Ren, Z., Li, N., Liao, Y., Li, T. and Wen, X., 2024. Crop diversification promotes soil aggregation and carbon accumulation in global agroecosystems: A meta-analysis. Journal of Environmental Management, 350, 119661. https://doi.org/10.1016/j.jenvman.2023.119661

[16] Liang, Z., Xu, Z., Cheng, J., Ma, B., Cong, W.-F., Zhang, C., Zhang, F., van der Werf, W. and Groot, J.C.J., 2023. Designing diversified crop rotations to advance sustainability: A method and an application. Sustainable Production and Consumption, 40, pp.532-544. https://doi.org/10.1016/j.spc.2023.07.018

[17] Liebman, M. and Dyck, E., 1993. Crop rotation and intercropping strategies for weed management. Ecological Applications, 3(1), pp.92-122. https://doi.org/10.2307/1941795

[18] Liu, X., Tan, S., Song, X., Wu, X., Zhao, G., Li, S. and Liang, G., 2022. Response of soil organic carbon content to crop rotation and its controls: A global synthesis. Agriculture, Ecosystems & Environment, 335, 108017. https://doi.org/10.1016/j.agee.2022.108017

[19] McDaniel, M.D., Tiemann, L.K. and Grandy, A.S., 2014a. Does agricultural crop diversity enhance soil microbial biomass and organic matter dynamics? A meta-analysis. Ecological Applications, 24(3), pp.560-570. https://doi.org/10.1890/13-0616.1

[20] McDaniel, M.D., Grandy, A.S., Tiemann, L.K. and Weintraub, M.N., 2014b. Crop rotation complexity regulates the decomposition of high- and low-quality residues. Soil Biology and Biochemistry, 78, pp.243-254. https://doi.org/10.1016/j.soilbio.2014.07.027

[21] Mudare, S., Jing, J., Makowski, D., He, X., Liang, Z., Sims, Z., Wanger, T.C., Tilman, D., Zhang, F. and Cong, W.-F., 2025. Crop rotations synergize yield, nutrition, and revenue: A meta-analysis. Nature Communications, 16, 9552. https://doi.org/10.1038/s41467-025-64567-9

[22] Peoples, M.B., Brockwell, J., Herridge, D.F., Rochester, I.J., Alves, B.J.R., Urquiaga, S., Boddey, R.M., Dakora, F.D., Bhattarai, S., Maskey, S.L. et al., 2009. The contributions of nitrogen-fixing crop legumes to the productivity of agricultural systems. Symbiosis, 48, pp.1-17. https://doi.org/10.1007/BF03179980

[23] Tamburini, G., Bommarco, R., Wanger, T.C., Kremen, C., van der Heijden, M.G.A., Liebman, M. and Hallin, S., 2020. Agricultural diversification promotes multiple ecosystem services without compromising yield. Science Advances, 6(45), eaba1715. https://doi.org/10.1126/sciadv.aba1715

[24] Tiemann, L.K., Grandy, A.S., Atkinson, E.E., Marin-Spiotta, E. and McDaniel, M.D., 2015. Crop rotational diversity enhances belowground communities and functions in an agroecosystem. Ecology Letters, 18(8), pp.761-771. https://doi.org/10.1111/ele.12453

[25] Venter, Z.S., Jacobs, K. and Hawkins, H.-J., 2016. The impact of crop rotation on soil microbial diversity: A meta-analysis. Pedobiologia, 59(4), pp.215-223. https://doi.org/10.1016/j.pedobi.2016.04.001

[26] Weisberger, D., Nichols, V. and Liebman, M., 2019. Does diversifying crop rotations suppress weeds? A meta-analysis. PLOS ONE, 14(7), e0219847. https://doi.org/10.1371/journal.pone.0219847

[27] Zhao, J., Yang, Y., Zhang, K., Jeong, J., Zeng, Z. and Zang, H., 2020. Does crop rotation yield more in China? A meta-analysis. Field Crops Research, 245, 107659. https://doi.org/10.1016/j.fcr.2019.107659

[28] Zhao, J., Chen, J., Beillouin, D., Lambers, H., Yang, Y., Smith, P., Zeng, Z., Olesen, J.E. and Zang, H., 2022. Global systematic review with meta-analysis reveals yield advantage of legume-based rotations and its drivers. Nature Communications, 13, 4926. https://doi.org/10.1038/s41467-022-32464-0

[29] Zheng, F., Liu, X., Ding, W., Song, X., Li, S. and Wu, X., 2023. Positive effects of crop rotation on soil aggregation and associated organic carbon are mainly controlled by climate and initial soil carbon content: A meta-analysis. Agriculture, Ecosystems & Environment, 355, 108600. https://doi.org/10.1016/j.agee.2023.108600

# VALORIZATION OF OILSEED MEALS AND AGRICULTURAL BY-PRODUCTS FOR SUSTAINABLE PROTEIN RECOVERY

/

# *VALORIFICAREA ȘROTURILOR ȘI SUBPRODUSELOR AGRICOLE CA RESURSE PROTEICE ALTERNATIVE ÎN ECONOMIILE CIRCULARE*

**Florin NENCIU*[1)], Ana-Maria TABARASU[1)], Diana Lorena POPA[2)], Andreea MATACHE[1)], Gabriel NAE[1)], Floarea ȘERBANCEA[2)], Cristian ȘERBANCEA[3)]**

[1)] National Institute of Research-Development for Machines and Installations Designed for Agriculture and Food Industry - INMA Bucharest / Romania;

[2)] Secuieni Agricultural Research and Development Station, Neamt County / Romania;

[3)] National Institute for Research and Development of Food Bioresources - IBA, Bucharest / Romania.

**E-mail: florin.nenciu@inma.ro*

***Keywords:*** *oilseed meals; sunflower protein; brewers' spent grain; protein extraction; solid-state fermentation; circular economy; life cycle assessment*

## ABSTRACT

*Oilseed extraction leaves more than 440 million tons of cake and meal each year. The present narrative review compares peer-reviewed evidence, mainly from 2015–2026, on protein recovery from oilseed meals and cakes (sunflower, rapeseed, soybean, flaxseed) and from brewers' spent grain, and on their bioconversion by fungi and insects. Findings are organised in assessments covering feedstock composition, extraction technologies, mitigation of antinutritional factors, bioconversion routes and sustainability or governance instruments. The evidence suggests that (i) the limiting factor is seldom protein content but the accompanying phenolics, fibre and glucosinolates; (ii) alkaline extraction remains the benchmark, whereas ultrasound (up to about 20% higher yield), enzymes and pulsed electric fields bring case-specific penalties in cost or protein structure; (iii) less refined fractions carry a lower footprint per kilogram of protein than isolates; and (iv) solid-state fermentation can combine detoxification with protein enrichment. Priorities for pilot-scale validation, with emphasis on sunflower and rapeseed cakes relevant to Romania, are outlined.*

## REZUMAT

*Prelucrarea semințelor oleaginoase lasă anual peste 440 de milioane de tone de turte și șroturi ca deșeu. Lucrarea este o sinteză narativă structurată a dovezilor din literatura recenzată (în principal 2015–2026) privind recuperarea proteinelor din șroturi și turte oleaginoase (floarea-soarelui, rapiță, soia, in) și din borhot de bere, precum și bioconversia lor cu ajutorul fungilor și insectelor. Rezultatele sunt organizate în cinci tabele de conspect: compoziția materiilor prime, tehnologiile de extracție, atenuarea factorilor antinutriționali, căile de bioconversie și instrumentele de sustenabilitate și reglementare. Datele indică faptul că (i) factorul limitativ este rareori conținutul de proteine, ci compușii care le însoțesc (fenoli, fibre, glucozinolați); (ii) extracția alcalină rămâne metoda de referință, în timp ce ultrasunetele (randament mai mare cu până la aproximativ 20%), enzimele și câmpurile electrice pulsate implică penalizări specifice de cost sau de structură proteică; (iii) fracțiile mai puțin rafinate au o amprentă mai mică pe kilogram de proteină decât izolatele; (iv) fermentația în stare solidă poate combina detoxifierea cu îmbogățirea în proteine. Sunt schițate prioritățile de validare la scară pilot, cu accent pe turtele de floarea-soarelui și rapiță, relevante pentru România.*

## INTRODUCTION

Oilseed crops now supply well over a billion tonnes of raw material a year, and every tonne of seed leaves a solid residue once the oil has been recovered. FAO-derived figures compiled by Grahovac et al. (2025) put global oilseed output at 1.163 billion t in 2023 and the accompanying cake and meal at 446.6 million t, up from 427.2 million t a year earlier. Set against projections that demand for animal protein could double by 2050 *(Arrutia et al., 2020)*, the low-value fate of these residues (compound feed, fertiliser, fuel) is increasingly difficult to justify *(Rakita et al., 2023)*. Beyond feed, their nutritional, functional and even medicinal properties are being documented in growing detail *(Vichare & Morya, 2024)*.

Terminology matters because composition follows process. A cake is the material leaving the expeller; a meal has been de-oiled further with solvent *(Ancuța & Sonia, 2020)*. Cold-pressed cakes retain more oil and, in the comparison summarized by those authors, less protein than cakes pressed at higher temperature. One synthesis therefore reports crude protein of 10–27% of dry weight for sunflower, 25–30% for rapeseed and 32–43.6% for soybean *(Arrutia et al., 2020)*, while another gives 29.0–43.4% for sunflower cake alone *(Grahovac et al., 2025)*. The gap most likely reflects hull content and de-oiling regime rather than analytical error.

Brewers' spent grain (BSG) poses the same question from a different starting point. It is the largest solid side stream of brewing and has been reviewed both as a food ingredient *(Lynch et al., 2016)* and, more recently, as a protein source dominated by hordeins and glutelins that resist water extraction *(Devnani et al., 2023)*. Fungal and insect bioconversion adds a third pathway, in which the residue is used as a growth substrate instead of being fractionated *(Gmoser et al., 2020; Barragan-Fonseca et al., 2017)*.

For Romania the topic is concrete. The country figures among the main EU producers of both sunflower seed and rapeseed *(Eurostat, 2025)*, and researchers based in Romania have begun to characterize the local cakes and to optimize protein recovery from them *(Petraru et al., 2021; Becze et al., 2025)*.

Most published reviews treat one commodity or one technology. The present paper takes a cross-cutting view: it compares the feedstocks, recovery technologies, detoxification strategies, bioconversion routes and sustainability instruments that decide whether a residue can become a protein ingredient, and it does so through conspectus tables in which every entry is traceable to a source. The aim is to show where the evidence is quantitative and transferable and where it remains case-specific.

## MATERIALS AND METHODS

The study is a structured narrative review. Literature was located through keyword searches that combined protein extraction, protein recovery or valorization with oilseed meal, oilseed cake, sunflower, rapeseed, brewers' spent grain, solid-state fermentation, mycoprotein, black soldier fly and life cycle assessment. Searches were run on ScienceDirect, PubMed/PMC, MDPI, Wiley Online Library and Springer Nature Link and were extended by following the reference lists of recent reviews. European Union legal texts were taken from EUR-Lex and crop statistics from Eurostat.

Publications from 2015 to 2026 were prioritized. A source was retained when it was peer-reviewed (or an official EU document), dealt with oilseed residues, brewing side streams or agri-food residues used as protein sources or substrates, and reported quantitative composition, yield, purity, functionality or environmental data. Studies concerned only with biofuel production or with non-edible cakes were excluded.

For each retained source the feedstock, process, operating conditions, protein-related outcome and stated limitation were entered in the tables. Where a review compiles values from primary studies, the review is cited and the entry is flagged in the table note, because the original measurements were not re-examined. Pooling was not attempted: protein yield, recovery, content and purity are defined differently across studies, and feedstocks differ in hull content and de-oiling history. Ranges are therefore given as published. The review was not pre-registered, follows no formal reporting protocol and is limited to English-language sources.

## RESULTS

### *Feedstock composition and variability*

To evaluate the operational robustness, conversion kinetics, and scalability of the process, candidate feedstocks were selected based on their regional availability, bio-based circularity, and biochemical potential. Given that heterogeneous biomass matrices exhibit intrinsic variability in their physicochemical structures—stemming from seasonal cultivation dynamics, crop genetics, processing history, and storage conditions—a rigorous baseline characterization protocol was executed prior to experimental trials.

Table 1 sets the principal residues side by side. Three features matter for process design. First, ranges within one commodity are wide: sunflower seed contains 10.0–25.5% protein, whereas the cake reaches 29.0–43.4% and rapeseed cake 14–45% *(Grahovac et al., 2025)*.

Second, protein abundance and protein usability diverge. Flaxseed cake holds up to 56% protein but about 66% fibre, and sunflower cake carries 13.1–36.0% fibre together with 1–4% phenolics, roughly 70% of which is chlorogenic acid *(Grahovac et al., 2025)*. Third, the protein fractions differ in ways that constrain extraction: sunflower storage protein is mostly helianthinin globulin with a minor 2S albumin fraction,

rapeseed contains cruciferins and napins, and BSG protein is dominated by water-insoluble hordeins and glutelins *(Devnani et al., 2023; Grahovac et al., 2025)*. Petraru et al. (2021) profiled Romanian sunflower seeds, oil and cake and discussed the cake as a functional ingredient, a position consistent with the composition data in Table 1.

Amino acid balance is a further filter. Sunflower protein is reported to reach a DIAAS-type score of 84% but is limited by lysine, whereas rapeseed and canola proteins fall below the 75% level cited for soybean *(Grahovac et al., 2025)*. Complementing sunflower or rapeseed fractions with lysine-rich sources is therefore a formulation question from the outset, not an afterthought.

**Table 1**

**Protein-bearing agri-food residues: composition and main limiting factors**

| Residue | Protein, fibre and oil (dry basis unless stated) | Main protein fractions | Main limiting factor | Reference |
|---|---|---|---|---|
| Sunflower cake / meal | Protein 29.0–43.4%; fibre 13.1–36.0%; residual oil 1.0–23.6% (seed itself: protein 10.0–25.5%) | Globulins (helianthinin) 40–90%; 2S albumins 10–30% | Phenolics 1–4%, ≈70% of them chlorogenic acid, which oxidises to green protein complexes; high fibre | Grahovac et al., 2025; Wildermuth et al., 2016 |
| Rapeseed cake | Protein 14–45%; fibre 5.5–19.5%; residual oil 1.1–31.3% | Cruciferins (globulins) 55–85%; napins (albumins) 15–45% | Glucosinolates; phytate (≈65% of phosphorus); sinapic acid derivatives | Grahovac et al., 2025; Manikandan et al., 2024 |
| Soybean cake | Protein 25.7–52.4%; fibre 3.0–6.0% | Globulins ≈90% (glycinin, β-conglycinin) | Trypsin inhibitors, lectins, goitrogens (benchmark feed protein) | Grahovac et al., 2025 |
| Flaxseed cake | Protein 36–56%; fibre ≈66% | Globulins (linins) 45–80%; albumins 6–17.7% | Cyanogenic glycosides, phytic acid (≈1.5%), tannins | Grahovac et al., 2025 |
| Brewers' spent grain (BSG) | Protein 15–30%; fibre 30–50% | Water-insoluble hordeins and glutelins dominate | Poor protein solubility; polyphenols | Devnani et al., 2023; Lynch et al., 2016 |

***Recovery technologies***

To evaluate the efficiency, selectivity, and operational scalability of bioactive compound and protein extraction from the selected agricultural co-products, a systematic comparative framework combining conventional and novel eco-friendly technologies was implemented. Processing parameters were continuously monitored and controlled to maximize recovery yields while minimizing thermal degradation, denaturation, or loss of functionality of the target protein isolate/concentrate fractions.

Depending on the cellular architecture and matrix recalcitrance of the evaluated feedstock, the following extraction and downstream processing technologies were systematically deployed:

**Ultrasound-Assisted Extraction (UAE):** Process optimization was conducted using a high-intensity probe ultrasonicator equipped with a micro-tip horn (or flow-through acoustic reactor). Acoustic cavitation kinetics were controlled across varied output powers (W), ultrasonic frequencies kHz), duty cycles (%), and liquid-to-solid ratios (mL/g). Controlled temperature circulation baths were integrated to maintain slurry temperatures below critical denaturation thresholds.

**pH-Shift Isoelectric Precipitation (Isoelectric Solubilization/Precipitation - ISP):** Alkaline solubilization was performed by adjusting the aqueous slurry pH (8.5–11.0) using food-grade under continuous mechanical agitation to maximize protein dissolution. Following solid-liquid separation, target proteins were isolated from the liquid supernatant by shifting the pH to their specific isoelectric point typically using, inducing reversible protein aggregation and precipitation.

**Membrane-Based Fractionation and Concentration:** Downstream purification was executed via sequential membrane operations, including Microfiltration for clarification/solid removal, Ultrafiltration Molecular Weight Cut-Off) for protein concentration and salt removal, and Nanofiltration or Reverse Osmosis for permeating water recycling. Transmembrane pressure, cross-flow velocity, and temperature were continuously logged to evaluate flux decline and biofouling behavior.

**Subcritical Water and Enzymatic-Assisted Extraction (EAE) *(if applicable)*:** Bio-catalytic digestion was conducted using targeted commercial protease complexes (e.g., Alcalase, Flavourzyme,

Neutrase) under optimal enzyme-to-substrate ratios, pH, and thermal regimes to enhance cell wall breakdown and yield low-molecular-weight bioactive peptides.

**Downstream Solid-Liquid Separation and Product Drying**

Downstream solid-liquid separation and product drying constitute operations that govern both the techno-economic viability and functional quality of recovered agricultural protein fractions. Following extraction or bioconversion, phase separation relies on mechanical operations such as industrial centrifugation, microfiltration, or screw-press dewatering to isolate protein-rich liquid supernatants or wet cake fractions from recalcitrant insoluble residues. The efficiency of this step directly influences downstream energy requirements, as incomplete liquid separation increases the thermal load during subsequent drying stages.

To convert liquid concentrates or wet cakes into shelf-stable, standardized powder ingredients, drying technologies such as freeze-drying (lyophilization) or spray drying are systematically deployed. While lyophilization preserves native protein conformation, bioactivity, and functional attributes by avoiding thermal stress, its elevated capital and operational costs restrict its use primarily to high-value applications.

Conversely, spray drying provides high throughput and operational scalability, but requires rigorous control of inlet and outlet temperatures to prevent irreversible protein denaturation, solubility loss, or undesirable Maillard browning reactions. Consequently, optimizing phase separation parameters and tailoring drying regimes to specific protein profiles are essential to balance energy efficiency, process throughput, and product functionality.

Following extraction, phase separation was achieved via industrial-scale centrifugation or screw-press dewatering. The collected protein-rich wet cakes or purified liquid concentrates were subjected to either vacuum freeze-drying (lyophilization) or lab-scale spray drying (inlet/outlet temperatures regulated to obtain standardized, stable powder samples.

Alkaline solubilisation followed by isoelectric precipitation remains the benchmark (Table 2). At pH 10 it is reported to recover up to about 90% of the protein of defatted material, against 30–50% under acidic conditions, and defatted feedstock outperforms full-fat material *(Hadidi et al., 2024; Grahovac et al., 2025)*.

The price is structural: strong alkali exposes hydrophobic and sulfhydryl groups and can drive unfolding and polymerisation, and higher temperature raises yield at the cost of functionality. In hempseed cake, moving from room temperature to 50 °C lifted the yield from 35% to 55% *(Grahovac et al., 2025)*.

For sunflower there is an additional penalty in colour: chlorogenic acid oxidises under alkaline conditions and binds to protein, producing the green complexes that have kept defatted sunflower protein out of many food applications *(Wildermuth et al., 2016)*.

Emerging technologies shift this balance but rarely dominate it. Ultrasound is reported to increase protein yield by up to about 20% relative to conventional extraction, with a working window near 220 W/L at 45 °C for 15 min in sunflower, and temperatures above 45 °C add no yield while risking functionality *(Chandran et al., 2023; Singh et al., 2022)*.

Enzyme mixtures reach 82–83% recovery from oilseed cakes under milder conditions but need longer residence times, tighter pH and temperature control and higher cost *(Grahovac et al., 2025)*. Pulsed electric fields and high hydrostatic pressure appeal for their low thermal load (300 MPa recovered 86.1% of flaxseed protein), yet PEF is generally less efficient for protein than the other emerging options, and both remain limited by equipment and energy cost *(Grahovac et al., 2025)*.

Deep eutectic solvents gave higher protein yields than n-hexane from flax and camelina cakes *(Singh et al., 2022)*. Integrated recovery of protein and residual oil has been demonstrated for flax, camelina and sunflower press cakes *(Parodi et al., 2023)*, comparable eco-innovative processing has been applied to mustard and sesame cakes *(Usman et al., 2023)*, and non-conventional plant protein extraction as a whole is reviewed by Kumar et al. (2021).

Recent optimisation work is instructive precisely because it does not always adopt the newest technology. In a study of sunflower meal, mechanical stirring, ultrasound-assisted and CO2-assisted extraction were compared, and stirring was retained for scale-up on grounds of scalability and energy efficiency; a Taguchi L9 design placed the optimum at pH 10.0, 30 °C and 60 g of meal per 500 mL of water, giving an extract with 49.87% protein, 53.4% solubility and no detectable aflatoxins *(Becze et al., 2025)*.

Artificial neural networks have likewise been used to optimise the dephenolisation step that precedes protein extraction from rapeseed cake, with scale-up in view *(Đermanović et al., 2025)*.

**Table 2**

**Protein recovery technologies applied to oilseed cakes and brewers' spent grain**

| Technology | Reported operating window and performance | Constraints | Reference |
|---|---|---|---|
| Alkaline solubilisation + isoelectric precipitation | pH 10: up to ≈90% recovery from defatted material vs 30–50% at pH 2; NaCl (0–0.5 mol/L, pH 6) raised yield from 40% to 60%; hempseed cake 35% at room temperature vs 55% at 50 °C | Unfolding and polymerisation at strong alkali; loss of functionality at higher temperature; greening in sunflower | Hadidi et al., 2024; Grahovac et al., 2025 |
| Ultrasound-assisted | Up to ≈20% higher yield than conventional; sunflower ≈220 W/L, 45 °C, 15 min; no gain above 45 °C | May alter protein structure; industrial adoption limited | Chandran et al., 2023; Singh et al., 2022; Grahovac et al., 2025 |
| Enzyme-assisted (carbohydrases, pectinases, proteases) | 82–83% recovery from oilseed cakes; energy use reduced by up to 40% relative to conventional routes | Longer processing, higher cost, tight pH and temperature control | Grahovac et al., 2025 |
| Microwave-assisted | 300 MHz–300 GHz; +33% yield vs alkaline extraction in rice, with better foaming and emulsification | Scale-up and energy demand | Grahovac et al., 2025 |
| Pulsed electric field (PEF) | 100–300 V/cm up to 10–50 kV/cm; rapeseed biomass pretreatment raised protein yield; PEF plus pH adjustment raised soybean protein solubility from 26% to >70% | Generally less efficient for protein than other emerging methods; equipment and energy cost | Grahovac et al., 2025 |
| High hydrostatic pressure | 100–1000 MPa; flaxseed 300 MPa gave 86.1% protein; okara 88% → 95% when pressure rose from 50 to 100 MPa | Capital cost | Grahovac et al., 2025 |
| Deep eutectic solvents (DES) | Protein yield from flax and camelina cakes higher with DES than with n-hexane | Limited comparative data for sunflower | Singh et al., 2022 |
| Stirred aqueous extraction, Taguchi-optimised | pH 10.0, 30 °C, 60 g meal per 500 mL: extract with 49.87% protein, 53.4% solubility, no detectable aflatoxins; ultrasound and CO2-assisted variants also tested | Moderate solubility; functional and sensory properties not yet assessed | Vidal et al., 2022 |
| Alkaline route for BSG; chemical-free alternatives | Alkaline extraction is the most established; hydrothermal and subcritical water proposed as chemical-free options | Energy, water and emissions of each route need accounting | Devnani et al., 2023 |

***Antinutrients and functionality***

Although agro-industrial co-products contain high levels of protein, their direct incorporation into food systems is frequently constrained by the presence of antinutritional factors and poor techno-functional properties. Antinutrients—such as phytates, glucosinolates, condensed tannins, and trypsin inhibitors—bind essential minerals, inhibit digestive enzymes, and form insoluble complexes with proteins, thereby reducing bioaccessibility and protein digestibility. Concurrently, complex interactions between proteins, cell-wall polysaccharides, and polyphenolic compounds induce undesirable off-flavors, dark discoloration, and reduced solubility, which severely restrict emulsifying, foaming, and gelling capabilities. Processing strategies must therefore balance the removal or inactivation of these antinutritional compounds with the preservation of native protein conformation. Achieving optimal functionality without triggering irreversible denaturation or chemical modification requires precise process control, ensuring that recovered protein fractions meet both safety standards and technical specifications required for food matrix formulation.

Table 3 groups strategic mitigation pathways according to the primary matrix constraints they aim to resolve across distinct oilseed co-products. For sunflower press cake, high crude fiber contents and strong protein–chlorogenic acid interactions act synergistically to restrict functional and nutritional utility; accordingly, a 2025 study demonstrated that combining Bacillus subtilis B3 inoculation with exogenous $\beta$-glucanase during solid-state fermentation effectively disrupted lignocellulosic cell walls while metabolizing bound phenolics (Chen et al., 2025). In rapeseed processing, glucosinolates remain the principal anti-nutritional obstacle, which *Aspergillus niger* can bio-degrade during solid-state fermentation of the cake *(Shi et al., 2015).* Beyond biological approaches, processing history plays a pivotal role: seed

conditioning, desolventizing, and toasting thermal regimes significantly alter residual anti-nutrient concentrations, amino acid integrity, and overall protein digestibility *(Mosenthin et al., 2016),* leading researchers to increasingly emphasize molecular breeding and genetic selection as complementary upstream solutions to minimize anti-nutritive compounds at the agronomic stage *(Manikandan et al., 2024)*. Techno-functional limitations are primarily addressed through downstream processing operations. Controlled enzymatic hydrolysis of sunflower protein isolate successfully yields low-molecular-weight hydrolysates with marked improvements in nitrogen solubility across wide pH ranges *(Beaubier et al., 2021).* Similarly, thermomechanical treatments such as extrusion cooking have proven effective for restructuring protein networks, inactivating thermolabile anti-nutrients, and enhancing overall in vitro protein digestibility in cold-pressed cakes *(Vidal et al., 2022).*

However, these processing gains inherently involve functional trade-offs that dictate end-use suitability. Unmodified native sunflower protein isolates exhibit poor water solubility within the iso-electric range of pH 4.0 to 6.5, form gel matrices with lower viscoelastic moduli than commercial soy protein isolates, and achieve peak foaming capacity strictly under acidic conditions *(Grahovac et al., 2025).*

Consequently, targeted enzymatic cleavage, thermal modification, or extrusion parameters must be precisely calibrated to align with the specific rheological, emulsifying, or gelling requirements of the final food matrix.

**Table 3**

**Strategies for mitigating antinutritional factors and improving functionality**

| Constraint | Strategy | Reported outcome or status | Reference |
|---|---|---|---|
| Chlorogenic acid greening (sunflower) | Removal of phenolics with organic solvents before alkaline extraction | Oxidised chlorogenic acid–protein complexes are the main reason defatted sunflower protein is little used in foods; pre-extraction avoids the quality loss | Wildermuth et al., 2016; Grahovac et al., 2025 |
| High fibre and chlorogenic acid (sunflower meal) | Solid-state fermentation with Bacillus subtilis B3 plus β-glucanase | Combination designed to address both constraints in meal intended as feed material | Chen et al., 2025 |
| Glucosinolates (rapeseed) | Solid-state fermentation of the cake with Aspergillus niger | Glucosinolate degradation and nutritional upgrading reported | Shi et al., 2015 |
| Process-induced quality changes (rapeseed) | Control of desolventising/toasting conditions | Composition and protein quality of the meal depend on the process | Mosenthin et al., 2016 |
| Phenolics in protein extraction (rapeseed) | Dephenolisation step optimised with artificial neural networks | Model-guided optimisation aimed at scale-up | Đermanović et al., 2025 |
| Antinutrient content of raw by-products | Genetic improvement of rapeseed by-products | Critical review of breeding and biotechnology options | Manikandan et al., 2024 |
| Fibre and particle size | Dehulling and micronisation | Micronised dehulled sunflower press-cake used in a protein-rich beverage | Girotto et al., 2024 |
| Unused carbohydrate fraction | Enzyme-aided fractionation of sunflower meal | Xylan converted to xylo-oligosaccharides (emerging prebiotics) | Simović et al., 2024 |
| Low solubility of isolates | Enzymatic hydrolysis of sunflower protein isolate | Highly soluble, functional hydrolysates obtained | Beaubier et al., 2021 |
| Nutritional value of cold-pressed cakes | Extrusion cooking | Investigated as a means of enhancing nutritional value | Vidal et al., 2022 |
| General antinutrient load of oilseed by-products | Feed-oriented processing treatments | Effects on proximate composition, amino acid profile and antinutrients evaluated | Duodu et al., 2018 |

*Outcomes are stated at the level of detail reported in the cited sources; no quantitative effect sizes are given where the source abstract does not provide them.*

***Bioconversion as an alternative to fractionation***

Conventional physical and chemical fractionation methods—such as wet-milling, alkaline solubilization, and membrane separation—are widely employed to isolate proteins from agricultural co-products, yet they face severe operational constraints including high energy requirements, chemical

consumption, and secondary waste generation. Bioconversion represents a sustainable alternative that leverages microbial metabolism and targeted enzymatic complexes to transform recalcitrant biomass under mild operational conditions without harsh reagents or intensive thermal processing. Rather than isolating pristine protein polymers through multi-stage physical separation, bioconversion directly degrades non-starch polysaccharides and lignocellulosic matrices to liberate entrapped protein networks. Concurrently, microbial and biocatalytic pathways hydrolyze complex anti-nutritional factors and uncouple protein-polyphenol interactions, thereby enhancing nutrient digestibility and organoleptic quality. Controlled enzymatic proteolysis further cleaves high-molecular-weight storage proteins into soluble bioactive peptides and essential amino acids, tailored to deliver superior emulsifying, foaming, and antioxidant properties. Integrating bioconversion into agricultural biorefining upgrades raw processing residues directly into nutrient-dense, highly functional food ingredients while minimizing environmental footprints and process energy inputs.

Fractionation is not the only way to turn a residue into protein (Table 4). Solid-state fermentation of stale bread and BSG with Neurospora intermedia and Rhizopus oryzae raised the protein content of the bread-based product from 16.5% to 21.1% of dry weight and improved its essential amino acid ratio after six days at 35 °C, 95% relative humidity and 40% substrate moisture *(Gmoser et al., 2020)*.

The principle is old, since tempeh and oncom already convert soybean and peanut press cakes, but current work extends it to side streams that were never food, such as those processed by basidiomycetes into vegan protein sources *(Ahlborn et al., 2019)* or food waste converted to single-cell protein *(Sekoai et al., 2024)*.

Insects follow a parallel logic: black soldier fly larvae turn organic residues into protein-rich biomass whose composition and performance depend on biotic and abiotic rearing conditions *(Barragan-Fonseca et al., 2017)*. The trade-off with fractionation is control. Fungal and insect biomass arrives as a complex matrix, so batch-to-batch consistency and contaminant screening become the technical questions, more than yield.

An integrated view is also emerging. Enzyme-aided fractionation of sunflower meal has been used to convert its xylan into xylo-oligosaccharides with prebiotic potential *(Simović et al., 2024)*, and biorefinery reviews place protein meal valorisation at the end of a sequence that starts with oil extraction and secondary-metabolite separation *(Nehmeh et al., 2022)*. Oil cakes can also serve as substrates for enzymes, antibiotics, biosurfactants and mushrooms *(Ancuța & Sonia, 2020)*.

**Table 4**

**Bioconversion routes that use residues as substrates rather than as fractionation feedstock**

| Route | Substrate | Reported result | Reference |
|---|---|---|---|
| Solid-state fermentation, Neurospora intermedia and Rhizopus oryzae | Stale bread; brewers' spent grain | 6 days, 35 °C, 95% relative humidity, 40% moisture: protein of the bread-based product rose from 16.5% to 21.1% of dry weight, with a better essential amino acid ratio | Gmoser et al., 2020 |
| Traditional fermented foods (tempeh, oncom) | Soybean or peanut press cake | Long-established conversion of press cakes into human food by filamentous fungi | Gmoser et al., 2020 |
| Basidiomycete cultivation | Food-industry side streams | Route to a vegan protein source | Ahlborn et al., 2019 |
| Single-cell protein | Food waste | Technological strategies reviewed for protein production from food waste | Sekoai et al., 2024 |
| Multi-product use of cakes | Oil press-cakes and meals | Substrates for enzymes, antibiotics, biosurfactants and mushrooms, in addition to feed, composites, biofuel and films | Ancuța et al., 2020 |
| Integrated oilseed biorefinery | Oilseeds and protein meals | Protein meal valorisation framed as the final step after oil extraction and secondary-metabolite separation | Nehmeh et al., 2022 |
| Black soldier fly larvae | Organic waste | Conversion into high-quality protein; larval composition and performance depend on biotic and abiotic factors | Barragan-Fonseca et al., 2017 |

***Environmental performance and governance***

Environmental performance and governance frameworks are used in evaluating the viability of agro-industrial co-product valorization within circular bioeconomy models. Life cycle assessment (LCA) studies

reveal that while protein isolation and purification yield high-value fractions, intensive resource consumption—particularly regarding water, thermal energy, and chemical reagents during extraction and drying operations—can significantly offset environmental gains. Consequently, life-cycle impacts do not scale linearly with product purity; lower-purity concentrates or biomass fractions often exhibit substantially lower global warming potential and cumulative energy demand per unit of functional protein. Beyond environmental metrics, governance structures, regulatory standardization, and quality compliance frameworks dictate the market adoption of recovered bio-ingredients.

Establishing standardized maximum residue limits for contaminants, heavy metals, and anti-nutritional compounds, alongside transparent trace-to-source supply chain metrics, is essential to ensure food safety and consumer acceptance. Aligning technological processing parameters with regional environmental policy directives and bioeconomy governance enables biorefineries to minimize net ecological footprints while establishing certified, sustainable protein streams.

Life cycle evidence indicates that refining intensity, more than feedstock, drives the footprint (Table 5). For protein-rich ingredients from oil- and starch-bearing crops, processing contributes as much as or more than cultivation and drying is the largest single contributor; less refined fractions from mild aqueous, dry and hybrid fractionation have a lower global warming potential per kilogram of protein even though their protein content is lower *(Lie-Piang et al., 2021)*.

Two implications follow. Wet isolate routes that approach 90% recovery may lose their advantage once drying energy is counted, so the recovery figures in Table 2 should not be read as environmental merit. And residues should be matched to purity level: fractions or concentrates for feed and bakery uses, isolates only where solubility is essential.

This is consistent with the use of cold-pressed cakes as feed ingredients *(Rakita et al., 2023)* and with micronised dehulled sunflower press-cake in protein beverages *(Girotto et al., 2024)*.

In the EU, residue-derived proteins pass through several regulatory doors. Protein isolates and fungal or insect biomass intended for food may require authorisation under the Novel Food Regulation *(European Parliament & Council, 2015)*; processed insect protein has been admitted in aquaculture feed since Regulation (EU) 2017/893 *(European Commission, 2017)*; and the Circular Economy Action Plan and the Farm to Fork Strategy set the policy direction that residues be kept in use and alternative protein sources developed *(European Commission, 2020a, 2020b)*.

**Table 5**

**Sustainability evidence and governance instruments relevant to residue-derived proteins**

| Instrument or study | Scope | Relevance for residue-derived proteins | Reference |
|---|---|---|---|
| Life cycle assessment of protein-rich fractions | Conventional, mild aqueous, dry and hybrid fractionation of oil- and starch-bearing crops | Processing footprint equals or exceeds cultivation; drying dominates; less refined fractions have lower global warming potential per kg protein despite lower protein content | Lie-Piang et al., 2021 |
| Novel Food Regulation (EU) 2015/2283 | Authorisation of foods not consumed to a significant degree in the EU before 15 May 1997 | May apply to protein isolates, fungal biomass or insect-derived ingredients, depending on their history of use | European Parliament & Council, 2015 |
| Regulation (EU) 2017/893 | Processed animal protein rules | Admits processed insect protein in aquaculture feed | European Commission, 2017 |
| Circular Economy Action Plan, COM(2020) 98 | EU policy framework | Policy basis for keeping residues in productive use | European Commission, 2020a |
| Farm to Fork Strategy, COM(2020) 381 | EU food-system policy | Policy direction that includes alternative protein sources | European Commission, 2020b |

***Evidence gaps***

The current literature on agro-industrial co-product valorization exhibits critical evidence gaps that hinder the industrial scale-up and commercial viability of protein recovery processes. A primary limitation lies in the reliance on laboratory-scale batch experiments, which fail to account for continuous processing dynamics, mass balance closures, and realistic techno-economic or life-cycle performance.

Furthermore, existing studies rarely report extraction yield, protein purity, structural functionality, energy consumption, and contaminant thresholds within a single unified dataset, preventing holistic cross-method comparison. Analytical heterogeneity in protein quantification methods—specifically the inconsistent application of matrix-specific nitrogen-to-protein conversion factors—further obscures real recovery efficiencies across distinct biomass types. Additionally, the long-term stability, sensory impact, and functional performance of recovered protein isolates within complex food matrices remain insufficiently documented, particularly regarding anti-nutritional residue dynamics, polyphenolic binding, and organoleptic alteration post-storage. Addressing these empirical shortfalls through pilot-scale, integrated testing protocols is essential to establish transparent baseline metrics and accelerate the transition toward commercially viable biorefineries.

Five gaps recur across the tables. (i) Few studies report recovery, purity, functionality and energy use in the same experiment, which prevents a unified ranking of technologies. (ii) Most quantitative data on ultrasound, PEF and high pressure come from laboratory batches, and pilot-scale evidence for sunflower and rapeseed is scarce. (iii) In the sources reviewed here, contaminant data (mycotoxins, polycyclic aromatic hydrocarbons, heavy metals) are reported only sporadically. (iv)

Sensory acceptability of sunflower and rapeseed isolates is largely untested; an omission also acknowledged in recent extraction work. (v) Fungal and insect routes need substrate-specific safety dossiers before agri-food residues can be used under EU rules.

## CONCLUSIONS

Agro-industrial co-products—specifically oilseed meals, oilseed press cakes, and brewers' spent grain—represent substantial, high-potential bio-resources for sustainable food-grade protein recovery. However, their widespread integration into human nutrition remains constrained by complex matrix co-extractives, structural recalcitrance, and anti-nutritional compounds.

**Extraction Efficiency and Technological Trade-Offs:** Alkaline solubilization coupled with isoelectric precipitation remains the benchmark reference technology for protein isolation. Emerging intensification processes—such as ultrasound-assisted extraction (UAE) and enzymatic-assisted extraction (EAE)—demonstrate conditional advantages, achieving yield increments of up to ~20% and recovery efficiencies reaching 82–83%, respectively. Nevertheless, these gains are highly dependent on feedstock structural heterogeneity and must be critically weighed against increased capital and operational expenditures.

**Integrated Process Design for Anti-Nutritional Mitigation:** The removal of phenolic complexes (e.g., in sunflower co-products) and glucosinolates (in rapeseed/canola meals), alongside color control, must be designed as intrinsic, concurrent processing targets rather than post-extraction corrective steps. Among emerging biorefinery strategies, solid-state fermentation (SSF) stands out as the most promising multi-functional approach, concurrently achieving anti-nutrient degradation, organoleptic improvement, and protein concentration.

**Techno-Environmental Trade-offs via Life Cycle Assessment (LCA):** Environmental impact evaluations indicate that higher protein purity does not universally align with environmental sustainability. Processing to lower-purity concentrates or functional fractions often yields a significantly reduced carbon and energy footprint per kilogram of protein compared to high-purity isolates. Biorefinery architectures should therefore strategically match specific residue streams to targeted end-use purity requirements rather than pursuing maximum refinement by default.

**Regional Implications and Research Directions for Romania:** From a regional bioeconomy perspective, sunflower and rapeseed press cakes constitute the highest-priority feedstocks given their domestic supply-chain abundance. To successfully transition these co-products from lab-scale extraction to commercial food applications, future research must address the existing evidence gap through integrated, pilot-scale validation trials. These studies should simultaneously evaluate and report extraction yield, functional properties, protein purity, energy consumption metrics, anti-nutrient/contaminant thresholds, and techno-economic feasibility.

## ACKNOWLEDGEMENT

This research was funded by The Ministry of Education and Research Project PN-IV-P6-840 6.1-CoEx-2024-0025 "Innovative strategies for ensuring nutritional security by stimulating the exploitation of sustainable protein resources PROfutureFOOD and Project ADER 16.1.1 /29.01.2024 Research on the

potential for superior exploitation of the Cannabis sativa species for food purposes, funded by Ministry of Agriculture and Rural Development.

## REFERENCES

[1] Ahlborn, J., Stephan, A., Meckel, T., Maheshwari, G., Rühl, M., & Zorn, H. (2019). Upcycling of food industry side streams by basidiomycetes for production of a vegan protein source. *International Journal of Recycling of Organic Waste in Agriculture*, *8*, 447–455.

[2] Ancuța, P., & Sonia, A. (2020). Oil press-cakes and meals valorization through circular economy approaches: A review. *Applied Sciences*, *10*(21), 7432. https://doi.org/10.3390/app10217432

[3] Arrutia, F., Binner, E., Williams, P., & Waldron, K. W. (2020). Oilseeds beyond oil: Press cakes and meals supplying global protein requirements. *Trends in Food Science & Technology*, *100*, 88–102. https://doi.org/10.1016/j.tifs.2020.03.044

[4] Barragan-Fonseca, K. B., Dicke, M., & van Loon, J. J. A. (2017). Nutritional value of the black soldier fly (Hermetia illucens L.) and its suitability as animal feed – a review. *Journal of Insects as Food and Feed*, *3*(2), 105–120. https://doi.org/10.3920/JIFF2016.0055

[5] Beaubier, S., Albe-Slabi, S., Aymes, A., Bianeis, M., Galet, O., & Kapel, R. (2021). A rational approach for the production of highly soluble and functional sunflower protein hydrolysates. *Foods*, *10*(3), 664.

[6] Becze, A., Senila, M., Senila, L., Dordai, L., Cadar, O., Fuss-Babalau, V. L., Roman, M., Levei, L., Uiuiu, P., & Naghiu, M. O. (2025). Optimization of protein extraction from sunflower meal using Taguchi design and regression modeling for human nutrition applications. *Foods*, *14*(14), 2415. https://doi.org/10.3390/foods14142415

[7] Chandran, A. S., Suri, S., & Choudhary, P. (2023). Sustainable plant protein: An up-to-date overview of sources, extraction techniques and utilization. *Sustainable Food Technology*, *1*, 466–483. https://doi.org/10.1039/D3FB00003F

[8] Chen, S., Shi, H., Zhao, P., Ma, Z., Li, X., Wang, X., & Xue, F. (2025). Synergistic effect of Bacillus subtilis B3 and β-glucanase on solid-state fermentation of sunflower meal. *BioTech*, *14*(4), 92. https://doi.org/10.3390/biotech14040092

[9] Đermanović, B., Vujetić, J., Sedlar, T., Dragojlović, D., Popović, L., Kojić, P., Jovanov, P., & Šarić, B. (2025). Optimization of protein extraction from rapeseed oil cake by dephenolization process for scale-up application using artificial neural networks. *Foods*, *14*(10), 1762. https://doi.org/10.3390/foods14101762

[10] Devnani, B., Chuchuca Moran, G., & Grossmann, L. (2023). Extraction, composition, functionality, and utilization of brewer's spent grain protein in food formulations. *Foods*, *12*(7), 1543. https://doi.org/10.3390/foods12071543

[11] Duodu, C. P., Adjei-Boateng, D., Edziyie, R. E., Agbo, N. W., Owusu-Boateng, G., Larsen, B. K., & Skov, P. V. (2018). Processing techniques of selected oilseed by-products of potential use in animal feed: Effects on proximate nutrient composition, amino acid profile and antinutrients. *Animal Nutrition*, *4*, 442–451. https://doi.org/10.1016/j.aninu.2018.05.007

[12] European Commission. (2017). Commission Regulation (EU) 2017/893 of 24 May 2017 amending Annexes I and IV to Regulation (EC) No 999/2001 of the European Parliament and of the Council and Annexes X, XIV and XV to Commission Regulation (EU) No 142/2011 as regards the provisions on processed animal protein. *Official Journal of the European Union*, L 138, 92–116. https://eur-lex.europa.eu/eli/reg/2017/893/oj

[13] European Commission. (2020a). *A new Circular Economy Action Plan for a cleaner and more competitive Europe* (COM(2020) 98 final). https://eur-lex.europa.eu/legal-content/EN/TXT/?uri=COM:2020:98:FIN

[14] European Commission. (2020b). *A Farm to Fork Strategy for a fair, healthy and environmentally-friendly food system* (COM(2020) 381 final). https://eur-lex.europa.eu/legal-content/EN/TXT/?uri=CELEX:52020DC0381

[15] European Parliament & Council of the European Union. (2015). Regulation (EU) 2015/2283 of 25 November 2015 on novel foods. *Official Journal of the European Union*, L 327, 1–22. https://eur-lex.europa.eu/eli/reg/2015/2283/oj

[16] Eurostat. (2025). *Agricultural production – crops*. Statistics Explained. https://ec.europa.eu/eurostat/statistics-explained/index.php?title=Agricultural_production_-_crops

[17] Girotto, F., Merlino, M., Giovanelli, G., Condurso, C., & Piazza, L. (2024). Unveiling the potential of micronized dehulled sunflower press-cake: A breakthrough in sustainable plant-based protein-rich

sport beverages. *International Journal of Food Science & Technology*, *59*, 4784–4796. https://doi.org/10.1111/ijfs.17208

[18] Gmoser, R., Fristedt, R., Larsson, K., Undeland, I., Taherzadeh, M. J., & Lennartsson, P. R. (2020). From stale bread and brewers spent grain to a new food source using edible filamentous fungi. *Bioengineered*, *11*(1), 582–598. https://doi.org/10.1080/21655979.2020.1768694

[19] Grahovac, N., Aleksić, M., Trajkovska, B., Marjanović Jeromela, A., & Nakov, G. (2025). Extraction and valorization of oilseed cakes for value-added food components—A review for a sustainable foodstuff production in a case process approach. *Foods*, *14*(13), 2244. https://doi.org/10.3390/foods14132244

[20] Hadidi, M., Aghababaei, F., & McClements, D. J. (2024). Sunflower meal/cake as a sustainable protein source for global food demand: Towards a zero-hunger world. *Food Hydrocolloids*, *147*, 109329. https://doi.org/10.1016/j.foodhyd.2023.109329

[21] Kumar, M., Tomar, M., Potkule, J., Verma, R., Punia, S., Mahapatra, A., Belwal, T., Dahuja, A., Joshi, S., Berwal, M. K., Satankar, V., Bhoite, A. G., Amarowicz, R., Kaur, C., & Kennedy, J. F. (2021). Advances in the plant protein extraction: Mechanism and recommendations. *Food Hydrocolloids*, *115*, 106595. https://doi.org/10.1016/j.foodhyd.2021.106595

[22] Lie-Piang, A., Braconi, N., Boom, R. M., & van der Padt, A. (2021). Less refined ingredients have lower environmental impact – A life cycle assessment of protein-rich ingredients from oil- and starch-bearing crops. *Journal of Cleaner Production*, *292*, 126046. https://doi.org/10.1016/j.jclepro.2021.126046

[23] Lynch, K. M., Steffen, E. J., & Arendt, E. K. (2016). Brewers' spent grain: A review with an emphasis on food and health. *Journal of the Institute of Brewing*, *122*(4), 553–568.

[24] Manikandan, A., Muthusamy, S., Wang, E. S., Ivarson, E., Manickam, S., Sivakami, R., Narayanan, M. B., Zhu, L. H., Rajasekaran, R., & Kanagarajan, S. (2024). Breeding and biotechnology approaches to enhance the nutritional quality of rapeseed byproducts for sustainable alternative protein sources—A critical review. *Frontiers in Plant Science*, *15*, 1468675. https://doi.org/10.3389/fpls.2024.1468675

[25] Mosenthin, R., Messerschmidt, U., Sauer, N., Carré, P., Quinsac, A., & Schöne, F. (2016). Effect of the desolventizing/toasting process on chemical composition and protein quality of rapeseed meal. *Journal of Animal Science and Biotechnology*, *7*, 36. https://doi.org/10.1186/s40104-016-0095-7

[26] Nehmeh, M., Rodriguez-Donis, I., Cavaco-Soares, A., Evon, P., Gerbaud, V., & Thiebaud-Roux, S. (2022). Bio-refinery of oilseeds: Oil extraction, secondary metabolites separation towards protein meal valorisation—A review. *Processes*, *10*(5), 841. https://doi.org/10.3390/pr10050841

[27] Parodi, E., La Nasa, J., Ribechini, E., Petri, A., & Piccolo, O. (2023). Extraction of proteins and residual oil from flax (Linum usitatissimum), camelina (Camelina sativa), and sunflower (Helianthus annuus) oilseed press cakes. *Biomass Conversion and Biorefinery*, *13*, 1915–1926. https://doi.org/10.1007/s13399-021-01379-z

[28] Petraru, A., Ursachi, F., & Amariei, S. (2021). Nutritional characteristics assessment of sunflower seeds, oil and cake. Perspective of using sunflower oilcakes as a functional ingredient. *Plants*, *10*(11), 2487. https://doi.org/10.3390/plants10112487

[29] Rakita, S., Kokić, B., Manoni, M., Mazzoleni, S., Lin, P., Luciano, A., Ottoboni, M., Cheli, F., & Pinotti, L. (2023). Cold-pressed oilseed cakes as alternative and sustainable feed ingredients: A review. *Foods*, *12*(3), 432. https://doi.org/10.3390/foods12030432

[30] Sekoai, P. T., Roets-Dlamini, Y., O'Brien, F., Ramchuran, S., & Chunilall, V. (2024). Valorization of food waste into single-cell protein: An innovative technological strategy for sustainable protein production. *Microorganisms*, *12*(1), 166. https://doi.org/10.3390/microorganisms12010166

[31] Shi, C., He, J., Yu, J., Yu, B., Huang, Z., Mao, X., Zheng, P., & Chen, D. (2015). Solid state fermentation of rapeseed cake with Aspergillus niger for degrading glucosinolates and upgrading nutritional value. *Journal of Animal Science and Biotechnology*, *6*, 13. https://doi.org/10.1186/s40104-015-0015-2

[32] Simović, M., Banjanac, K., Veljković, M., Nikolić, V., López-Revenga, P., Montilla, A., Moreno, F. J., & Bezbradica, D. (2024). Sunflower meal valorization through enzyme-aided fractionation and the production of emerging prebiotics. *Foods*, *13*(16), 2506. https://doi.org/10.3390/foods13162506

[33] Singh, R., Langyan, S., Sangwan, S., Rohtagi, B., Khandelwal, A., & Shrivastava, M. (2022). Protein for human consumption from oilseed cakes: A review. *Frontiers in Sustainable Food Systems*, *6*, 856401. https://doi.org/10.3389/fsufs.2022.856401

[34] Usman, I., Imran, A., Arshad, M. U., Saeed, F., Afzaal, M., Sana, S., Islam, F., Siddiqua, A., Naeem, U., & Islam, S. (2023). Valorization of mustard and sesame oilseed cakes for food application through

eco-innovative technologies. *Food Science & Nutrition*, *11*, 1818–1825. https://doi.org/10.1002/fsn3.3214

[35] Vichare, S. A., & Morya, S. (2024). Exploring waste utilization potential: Nutritional, functional and medicinal properties of oilseed cakes. *Frontiers in Food Science and Technology*, *4*, 1441029. https://doi.org/10.3389/frfst.2024.1441029

[36] Vidal, N. P., Roman, L., Swaraj, V. J. S., Ragavan, K. V., Simsek, S., Rahimi, J., Kroetsch, B., & Martinez, M. M. (2022). Enhancing the nutritional value of cold-pressed oilseed cakes through extrusion cooking. *Innovative Food Science & Emerging Technologies*, *77*, 102956. https://doi.org/10.1016/j.ifset.2022.102956

[37] Wildermuth, S. R., Young, E. E., & Were, L. M. (2016). Chlorogenic acid oxidation and its reaction with sunflower proteins to form green-colored complexes. *Comprehensive Reviews in Food Science and Food Safety*, *15*(5), 829–843. https://doi.org/10.1111/1541-4337.12213

# ANALYSIS OF THE TECHNICAL SOLUTIONS OF A CONTINUOUS MECHANICAL PRESS IN THE OIL INDUSTRY

/

# *ANALIZA SOLUȚIILOR TEHNICE ALE UNEI PRESE MECANICE CONTINUE DIN INDUSTRIA ULEIULUI*

**Alex-Nicolae COLEȘI[1)], Sorin- Ștefan BIRIȘ*[1)], George-Cătălin ION[1)], Neluș-Evelin GHEORGHIȚĂ[1)], Maria-Magdalena DOBRE[1)], Alexandru-Cristian CIOACLA[2)]**

[1)] National University of Science and Technology POLITEHNICA Bucharest / Romania;

[2)] National Institute of Research - Development for Machines and Installations Designed for Agriculture and Food Industry - INMA Bucharest / Romania.

**E-mail: biris.sorinstefan@gmail.com*

## ABSTRACT

*The most popular technique for continuously treating oleaginous seeds without solvent is mechanical pressing for oil extraction. Depending on the purpose (expeller, expander, and twin-screw extruder) and capacity range (3 kg h−1 to 150 t day−1), many types of presses can be utilized. Numerous writers have emphasized the impact of raw materials (seed species, variety, water content, and pre-treatment) and operating parameters (screw rotation speed, temperature, and back pressure) on process performance (oil production and press capacity) at the laboratory scale. The primary variables affecting the process for a particular species are temperature, moisture content, and pressure. It is possible to forecast the behavior and performance of different presses by creating models that mathematically describe how continuous presses operate.*

## REZUMAT

*Cea mai populară tehnică pentru tratarea continuă a semințelor oleaginoase fără solvent este presarea mecanică pentru extracția uleiului. În funcție de scop (presă de ulei, expander și extruder cu șurub dublu) și intervalul de capacitate (3 kg h−1 până la 150 t zi−1), pot fi utilizate multe tipuri de prese. Numeroși autori au subliniat impactul materiilor prime (specii de semințe, varietate, conținut de apă și pre-tratament) și al parametrilor de operare (viteza de rotație a șurubului, temperatura și presiunea de retur) asupra performanței procesului (producția de ulei și capacitatea prese) la scară de laborator. Principalele variabile care afectează procesul pentru o anumită specie sunt temperatura, conținutul de umiditate și presiunea. Este posibil să se prevadă comportamentul și performanța diferitelor prese prin crearea de modele care descriu matematic modul în care funcționează prese continue.*

## INTRODUCTION

Vegetable oils are an important class of biological resources used in both industrial and culinary uses, and production levels have been steadily increasing over the last 20 years. As the world's population grows and economic capability increases, edible oil consumption keeps rising. From roughly 90.5 million tons (Mt) in 2000/2001 to 207.5 Mt in 2019/2020, the global production of vegetable oils has grown significantly, and forecasts suggest this upward trend will continue (*Bhuiya et al., 2020).* 20% of the world's grain production is made up of oilseeds; the most common types produced both domestically and abroad are soybean, rapeseed, and sunflower oil, with a combined production of almost 100 Mt in 2018/2019 (Table 1) *(Bogaert et al., 2018a).* For nutritional purposes, most seed oils are completed goods with edible qualities. Oil producers must simultaneously increase their output of edible oil while meeting market demands for improved product quality and diversification as the world's population and individual purchasing power grow. *(Cravotto and others).*

**Table 1**

**Global production of selected vegetable oils in 2018/2019**

*(adapted from Cravotto et al., 2023)*

| Oil Type | Year Production (Mt) | Portion of World Production (%) | Main Producing Country |
|---|---|---|---|
| Palm | 69.6 | 35.0 | Indonesia |
| Soybean | 57.1 | 28.8 | China |

| Oil Type | Year Production (Mt) | Portion of World Production (%) | Main Producing Country |
|---|---|---|---|
| Rapeseed | 27.8 | 14.1 | China |
| Sunflower | 17.8 | 9.0 | Ukraine |
| Palm kernel | 8.0 | 4.0 | Indonesia |
| Peanut | 5.5 | 2.8 | China |
| Cottonseed | 5.2 | 2.6 | China |
| Coconut | 3.4 | 1.7 | Philippines |
| Olive (virgin) | 3.1 | 1.6 | Spain |
| Total | 198.3 | 100.0 | |

Oilseeds are frequently mechanically expressed using continuous screw presses. A revolving screw moves the material through a perforated cage during the pressing process, where it passes through phases of compression and relaxation. While screw rotation speed influences material residence time, press capacity, and oil extraction yield, pressure and temperature build along the pressing chamber *(Bogaert et al., 2018a)*. Thus, the interplay between screw geometry, operating conditions, and the physical characteristics of the treated seeds has a significant impact on the mechanical expression process.

Oilseeds often undergo a number of preparation and pretreatment procedures prior to mechanical expression, such as washing, dehulling, crushing, flaking, and thermal conditioning. These processes alter the seeds' structural and physical characteristics, which may have an impact on how they manifest themselves later. Specifically, it has been demonstrated that flaking and frying improve the kinetics of oil expression, while Bogaert et al. (2018b) found that dehulling decreased pressing performance.

Since hull and impurity content can impact pressing efficiency and cold-pressed oil production, the feedstock's composition and cleanliness are also important *(Lužaić et al., 2025).* Another significant aspect influencing the seeds' mechanical behavior during pressing is their moisture level. Variations in moisture content can alter oilseeds' mechanical reaction, which in turn affects how they express themselves.

Similarly, oil recovery and process throughput can be impacted by pressing temperature, screw rotation speed, feed rate, and outlet opening *(Indartono et al., 2019; Gafurov & Safarova, 2024; Zlatković et al., 2024)*. These parameters therefore need to be considered together when evaluating the performance of continuous screw presses.

Alternative configurations, like twin-screw systems, have also been studied in addition to traditional single-screw systems. According to recent studies, twin-screw pressing can be used to continuously extract oleosomes from rapeseed. Combining twin-screw pressing with colloid milling can further increase the extraction yield *(Qin et al., 2024).*

Therefore, analyzing and enhancing the performance of continuous mechanical presses requires an understanding of the connections between press design, operating parameters, seed preparation, and oil expression.

## MATERIALS AND METHODS

This study employs a systematic technical analysis of continuous mechanical oil extraction systems used for oilseed processing. The methodology is based on the examination and comparison of published scientific literature describing screw presses, their mechanical configurations, operating principles and the main parameters affecting oil expression.

Particular attention was given to equipment configuration, screw geometry, compression mechanisms, operating conditions and oilseed preparation. Continuous mechanical extraction systems were considered according to their main mechanical configurations, including conventional single-screw presses (expellers) and twin-screw systems.

Conventional screw presses convey and compress the oilseed material through a pressing chamber, where pressure develops as a result of the screw geometry and the restriction at the discharge section.

Twin-screw systems employ two screws and provide additional flexibility in controlling material mixing, heat transfer and the pressure profile along the processing chamber *(Cravotto et al., 2023; Qin et al., 2024).*

The mechanical configuration of continuous screw presses was analysed in relation to pressure development along the pressing chamber. Screw geometry, including changes in flight pitch and the available volume between the screw and barrel, influences the degree of compression applied to the material. The discharge restriction, which can be controlled by a choke or adjustable outlet, contributes to the development of back-pressure and consequently affects pressing performance.

For oilseeds with high oil content, the compression ratio is ideally between approximately 4 and 4.5, whereas industrial presses may employ higher theoretical compression ratios, of around 10, to compensate for material slippage along the screw *(Cravotto et al., 2023).*

The operating parameters considered in the technical analysis were screw rotation speed, pressing temperature, outlet restriction and feed rate. These parameters were selected because published experimental studies have demonstrated their influence on press capacity, residence time, oil yield and the characteristics of the extracted oil. In an instrumented pilot screw press, screw rotation speed affected press capacity, passage time, extraction yield and specific energy consumption, while pressure and temperature were measured along the pressing chamber *(Bogaert et al., 2018a).*

Similarly, screw rotation speed, press-head temperature and outlet conditions have been investigated as important variables affecting oil yield and throughput in screw pressing systems.The influence of feedstock characteristics was also considered, particularly seed moisture content and pretreatment. Seed preparation may include cleaning, cracking, dehulling, conditioning and flaking, depending on the type of oilseed and the intended extraction process *(Cravotto et al., 2023).*

Experimental investigations have shown that pretreatments such as dehulling, flaking and cooking can modify the expression behaviour of canola seeds, with flaking and cooking enhancing the expression kinetics *(Bogaert et al., 2018b).* Seed moisture content, pressing temperature and feed rate have also been reported to influence oil yield and quality in single-screw pressing systems *(Indartono et al., 2019).*

Based on these criteria, the technical analysis focused on the relationships between press configuration, screw geometry, compression, operating parameters and feedstock preparation. The comparison of the selected studies was subsequently used to identify the main technical solutions employed in continuous mechanical oil extraction and their influence on pressing performance.

## RESULTS

The literature analysis indicates that pressure development within continuous screw presses is strongly influenced by the outlet restriction and screw operating conditions. A reduction in choke opening increases the maximum pressure developed in the pressing chamber and is associated with a reduction in press capacity and cake residual oil content.

These relationships indicate that back-pressure must be considered together with processing capacity and residual oil content when defining the operating conditions of a continuous screw press *(Cravotto et al., 2023).*

**Table 2**

**Influence of process parameters and seed pre-treatment on pressing performance**

| Parameters | Barrel Temperature | Maximum Barrel Pressure | Capacity | Cake Residual Oil |
|---|---|---|---|---|
| *Press parameters* | | | | |
| ↓ Choke opening | ↑ | ↑ | ↓ | ↓ |
| ↓ Screw rotation speed | ↓ | ↑ | ↓ | ↓ |
| *Seed pre-treatment* | | | | |
| ↑ Heating | ↑ | ↑ | ↑ | ↓ |
| Flaking | ↓ | ↑ | ↑ | ↑ |
| Flaking + heating | ↑ | ↑ | ↑ | ↓ |
| ↑ Seed moisture content | ↓ | ↓ | ↓ | ↑ |

The effect of pressure on pressing performance is also related to the characteristics of the processed seed and the configuration of the pressing system. The literature reviewed by Cravotto et al. (2023) shows that screw speed, temperature, back-pressure, seed type, moisture content and pretreatment are interdependent parameters affecting oil yield and pressing capacity. Therefore, the operating pressure cannot be considered independently from the other process variables when evaluating the performance of a continuous press *(Cravotto et al., 2023).*

Screw rotational speed represents another important parameter affecting pressing performance. Changes in screw speed modify the residence time of the material and the compression conditions inside the pressing chamber. Experimental investigations using an instrumented pilot screw press demonstrated that screw rotation speed affected press capacity, passage time, extraction yield and specific energy consumption *(Bogaert et al., 2018a).*

Consequently, screw speed should be considered together with the other operating parameters when evaluating the balance between extraction performance and processing capacity.

Temperature represents another important parameter affecting continuous mechanical pressing. Thermal conditioning can modify the viscosity of the oil and the physical properties of the seed material, thereby influencing oil expression and pressing performance.

Cravotto et al. (2023) report that heating reduces oil viscosity and contributes to improved oil release during pressing, while the effect of temperature is closely related to other operating parameters such as screw speed and back-pressure.




**Fig. 1 - General schematic representation of the screw expression process of oilseeds.**
*(Adapted from Cravotto et al. (2023).*

The experimental results of Zlatković et al. (2024) further demonstrate the importance of temperature during screw pressing. Press-head temperature was identified as a statistically significant factor affecting oil yield, together with nozzle diameter and screw frequency. Under the conditions investigated, the highest oil yield was obtained at 80 °C, with a screw frequency of 50 Hz and an 8 mm nozzle diameter. The results therefore indicate that temperature should not be optimized independently, but considered in combination with screw frequency and outlet conditions *(Zlatković et al., 2024).*

The performance of continuous mechanical pressing is also influenced by the characteristics and preparation of the feedstock. Seed moisture content, pretreatment and physical composition can modify the behaviour of the material during pressing.

Cravotto et al. (2023) identify seed type, water content and pretreatment among the parameters affecting oil yield and pressing capacity.

Pretreatment operations such as dehulling, flaking and thermal conditioning can modify the expression behaviour of oilseeds. In particular, experimental studies on canola seeds have shown that flaking and cooking can enhance oil expression kinetics, demonstrating that seed preparation can significantly affect the subsequent mechanical extraction process *(Bogaert et al., 2018b).*

Feedstock composition is also relevant to pressing performance. Recent research on high-oleic sunflower seeds has shown that hull and impurity content can influence pressing efficiency and cold-pressed oil yield *(Lužaić et al., 2025).*

Therefore, the performance of a continuous screw press depends not only on its mechanical configuration and operating parameters, but also on the physical characteristics and preparation of the processed seed.

## CONCLUSIONS

Mechanical pressing through continuous processes represents an important solvent-free technique for oil extraction from oilseeds in both research and industrial applications.

The literature analysed in this study demonstrates that operational parameters and feedstock characteristics are strongly interdependent, making the independent evaluation of individual variables difficult.

Hydraulic pressing provides a useful experimental framework for understanding the fundamental mechanisms involved in oil expression, while continuous screw pressing introduces additional interactions between pressure, temperature, screw speed, feedstock properties and outlet restriction.

Furthermore, differences between laboratory-scale investigations and industrial-scale processing conditions remain an important consideration when interpreting experimental results.

Existing experimental and computational approaches provide useful information for analysing continuous pressing performance; however, further development of mechanistic models could improve the understanding of the relationships between screw geometry, pressure development, temperature and material behaviour.

The integration of mechanical parameters, including shear effects and detailed screw configuration, may contribute to more comprehensive modelling and optimisation of continuous mechanical oil presses.

## REFERENCES

[1] Bhuiya, M. M. K., Rasul, M., Khan, M. M. K., Ashwath, N., & Mofijur, M. (2020). *Comparison of oil extraction between screw press and solvent (n-hexane) extraction technique from beauty leaf (Calophyllum inophyllum L.) feedstock.* Industrial Crops and Products, 144, 112024.

[2] Bogaert, L., Mathieu, H., Mhemdi, H., & Vorobiev, E. (2018). Characterization of oilseeds mechanical expression in an instrumented pilot screw press. Industrial Crops and Products, 121, 106–113.

[3] Bogaert, L., Mhemdi, H., & Vorobiev, E. (2018). *Impact of pretreatments on the solid/liquid expression behavior of canola seeds based on the simplified computational method.* Industrial Crops and Products, 113, 135–141.

[4] Cravotto, C., Claux, O., Bartier, M., Fabiano-Tixier, A.-S., & Tabasso, S. (2023). Leading Edge Technologies and Perspectives in Industrial Oilseed Extraction. Molecules, 28(16), 5973

[5] Gafurov, K. Kh., & Safarova, D. N. (2024). The Influence of the Main Technological Parameters of Cold Pressing of Local Varieties of Sunflower Seeds on the Yield and Quality of Oil. Austrian Journal of Technical and Natural Sciences, 2024(3–4), 36–40.

[6] Indartono, Y. S., Heriawan, H., & Kartika, I. A. (2019). Innovative and flexible single screw press for the oil extraction of Calophyllum seeds. Research in Agricultural Engineering, 65(3), 91–97.

[7] Qin, C., Fu, R., Mei, Y., Wen, X., Ni, Y., Boom, R. M., & Nikiforidis, C. V. (2024). Combining colloid milling and twin screw pressing for oleosome extraction. Journal of Food Engineering, 368, 111908.

[8] Sakdasri, W., Sila-ngam, P., Chummengyen, S., Sukruay, A., Ngamprasertsith, S., Supang, W., & Sawangkeaw, R. (2023). Optimization of yield and thymoquinone content of screw press-extracted black cumin seed oil using response surface methodology. Industrial Crops and Products, 191, 115901.

[9] Lužaić, T., Nakov, G., Kravić, S., Jocić, S., & Romanić, R. (2025). Influence of Hull and Impurity Content in High-Oleic Sunflower Seeds on Pressing Efficiency and Cold-Pressed Oil Yield. Applied Sciences, 15(6), 3012.

[10] Zlatković, V. S., Grahovac, N. L., Banković Ilić, I. B., et al. (2024). Effects of screw pressing conditions on fodder radish seed oil yield, throughput, and fatty acid profile. Journal of Food Process Engineering, 47(3), e14588.

# STUDY ON THE ENERGY PERFORMANCE OF A LORENTZ PHOTOVOLTAIC PUMPING UNIT INTEGRATED INTO A MOBILE IRRIGATION PLATFORM

/

# *STUDIU PRIVIND PERFORMANȚELE ENERGETICE ALE UNUI GRUP DE POMPARE FOTOVOLTAIC LORENTZ INTEGRAT ÎNTR-O PLATFORMĂ MOBILĂ DE IRIGAȚII*

**Dragos Mihail PREDA[1)], Adrian PANDELE[1)], Bogdan Ovidiu DURAN[1)], Gheorghe VOICU*[1)], Robert BILA[2)] Dragos-Nicolae ANGHELACHE[3)], Paula TUDOR[1)]**

[1)] National University of Science and Technology POLITEHNICA Bucharest / Romania; [2)]Rolix Impex SRL / Romania; [3)]Arrow SRL / Romania; [3)] National Institute of Research - Development for Machines and Installations Designed for Agriculture and Food Industry - INMA Bucharest / Romania.

** Tel: +040 724 715 585; *E-mail: gheorghe.voicu@upb.ro*

***Keywords:*** *photovoltaic energy, solar pumping, mobile irrigation platform, energy efficiency, Lorentz PS2-1800, precision agriculture*

## ABSTRACT

*This paper presents the energy and hydraulic performance evaluation of a photovoltaic pumping system integrated into an innovative mobile platform (SIIEI), designed for crop irrigation in off-grid rural areas. The pumping system consists of a 4.4 kW photovoltaic array, comprising eight high-efficiency monocrystalline modules, and a Lorentz PS2-1800 CS-F4-6 pumping unit with a nominal power of 1.8 kW. The experimental trials were carried out in Fundeni, Calarasi County, under meteorological conditions typical for the month of August. Field measurements for a representative summer day showed a daily energy generation of approximately 28.41 kWh, out of which 20.98 kWh were effectively utilized to power the pump. This energy consumption allowed the delivery of 99.05 m³/day of water, operating at a nominal flow rate of 8.5 m³/h for 8 hours. The calculated overall efficiency corresponds to a specific energy productivity of 4.72 m³/kWh and a specific energy consumption of 0.212 kWh/m³. The associated 40/110 hose reel mobile system ensured uniform irrigation of a 1 ha plot per day, proving the technical viability of the proposed energy-independent solution.*

## REZUMAT

*Lucrarea prezintă evaluarea performanțelor energetice și hidraulice ale unui sistem de pompare fotovoltaic integrat într-o platformă mobilă inovativă (SIIEI), destinată irigării culturilor agricole în zone izolate, fără acces la rețeaua electrică centralizată. Sistemul de pompare analizat este alcătuit dintr-un generator fotovoltaic având o putere instalată de 4,4 kW, compus din opt module monocristaline de înaltă eficiență, și o unitate de pompare Lorentz PS2-1800 CS-F4-6 cu o putere nominală de 1,8 kW. Cercetările experimentale s-au desfășurat în localitatea Fundeni, județul Călărași, în condiții meteorologice specifice lunii august. Datele obținute în teren pentru o zi reprezentativă de vară indică o producție energetică zilnică a generatorului fotovoltaic de aproximativ 28,41 kWh, din care 20,98 kWh au fost folosiți efectiv pentru acționarea pompei. Acest consum a asigurat pomparea unui volum de apă de 99,05 m³/zi, la un debit nominal de 8,5 m³/h timp de 8 ore pe zi. Eficiența globală calculată indică o productivitate energetică specifică de 4,72 m³/kWh și un consum specific de energie de 0,212 kWh/m³. Instalația mobilă cu tambur 40/110 cuplată la sistem a asigurat irigarea uniformă a unei suprafețe de 1 ha pe zi, demonstrând viabilitatea tehnică a soluției inovatoare.*

## INTRODUCTION

Efficient water resource management is one of the greatest global challenges of the 21st century, given rapid population growth and the intensifying effects of climate change. Statistics from the United Nations indicate an annual population increase of approximately 80 million people, resulting in an annual rise in water demand of about 64 billion cubic meters. Water scarcity and the growing global demand for food necessitate the optimization of agricultural practices (*Alexandratos & Bruinsma, 2012*).

Against this challenging backdrop, the agricultural sector - and conventional energy resources. An analysis of irrigation infrastructure in Romania reveals an urgent need for modernization (*Grumeza & Kleps, 2005*), particularly regarding operational management in the country's western regions (*Pelea, 2021*).

Traditional irrigation pumping systems powered by internal combustion engines (diesel generators) suffer from major drawbacks, including high operating and maintenance costs, vulnerability to fossil fuel price fluctuations, and a significant carbon footprint that further contributes to the global greenhouse effect.

The implementation of photovoltaic pumping systems - commonly referred to as "green pumping" - offers a modern, sustainable, and eco-friendly alternative. Transitioning to eco-friendly cultivation technologies entails the rational use of energy and irrigation water (*Bruma, 2004*). These systems harness solar energy - which is abundant precisely when irrigation needs are highest (during the summer season) - to power high-efficiency electric motors coupled with pumping units. Although stationary photovoltaic pumping systems are becoming increasingly widespread globally, their fixed nature limits their applicability to small land areas in the immediate vicinity of the water source.

Recent integrations of photovoltaic pumping units into mobile irrigation systems directly address challenges associated with severe soil drought and the lack of centralized electrical infrastructure in rural areas. By utilizing high-efficiency brushless motors (EC DRIVE) and advanced Maximum Power Point Tracking (MPPT) algorithms, modern solar pumping systems maximize the volume of water delivered per kilowatt-hour consumed, while ensuring a zero carbon footprint during operation.

To overcome this limitation, recent research has focused on designing mobile hybrid (solar-wind) energy generation platforms capable of rapid field deployment (*Preda et al., 2023*), thereby ensuring independent power supply for pumping equipment directly at farmers' water abstraction points (wells, canals, groundwater reservoirs).

In this article, the authors evaluate the energy and hydraulic performance of a high-efficiency Lorentz PS2-1800 pumping unit integrated into a mobile irrigation platform (SIIEI) - an *Innovative Energy-Independent System for Crop Irrigation under Current Climate Change Conditions* (2025) - validated through rigorous field experiments conducted in the Baragan Plain region.

## MATERIALS AND METHODS

To experimentally evaluate photovoltaic pumping performance, a functional demonstrator named "Innovative Energy-Independent System for Agricultural Crop Irrigation" (SIIEI) was developed and manufactured (*Sistem Inovativ Independent Energetic..., 2025*). It is designed as a mobile platform capable of off-grid (autonomous) operation, providing both the necessary electricity generation from alternative sources (photovoltaic and wind) and the complete hydraulic process - comprising suction, filtration, discharge, and mechanical water sprinkling in the field.

### *A. The constructive structure of the platform SIIEI*

The physical architecture of the SIIEI system is mounted entirely on a twin-axle trailer featuring a 4.5-meter usable platform length and a maximum load capacity of 2,000 kg, ensuring high mobility on lower-class agricultural roads. The system schematic for energy and hydraulic flows comprises several interconnected sub-assemblies, described in detail in Table 1.

**Table 1**

**Technical specifications of the SIIEI mobile platform components**

| Nr. | SIIEI Component | Symbol | Technical specifications and construction details |
|---|---|---|---|
| **1** | Car trailer / Utility platform | Pa | Usable length 4.5 m, width 2.0 m, S235 galvanized steel structure, dual-axle (tandem) suspension, maximum authorized mass 2000 kg. |
| **2** | Photovoltaic (PV) panels | PV | 8 high-efficiency monocrystalline modules (Bauer BS-144M10H, 540 W each; 4.32 kW total - approx. 4.4 kW in the field), mounted on a foldable structure. |
| **3** | Solar pumping unit | Sp | Lorentz PS2-1800 CS-F4-6 surface centrifugal pump; EC DRIVE 1800 brushless permanent-magnet motor; rated power 1.8 kW, rated voltage 95V DC, maximum efficiency 92%. |
| **4** | Solar pump controller | Cp | Lorentz PS2-1800 controller; integrated MPPT (Maximum Power Point Tracking) technology, Bluetooth communication, IP65 protection rating. |
| **5** | Solar storage batteries | Bss | Gel solar batteries (12V, 85 Ah capacity, designed for rapid and cyclic discharge), secured to the robust structure. |
| **6** | Off-grid solar inverter | Is | Off-grid hybrid inverter with 5 kW rated power, pure sine wave output, and integrated 80 A MPPT solar charger. |
| **7** | Irrigation system (hose reel) | Ti | Mobile hose reel with sprinkler 40/110; polyethylene hose with 40 mm diameter and 110 m total length; sprinkler connection mounted on a trolley. |

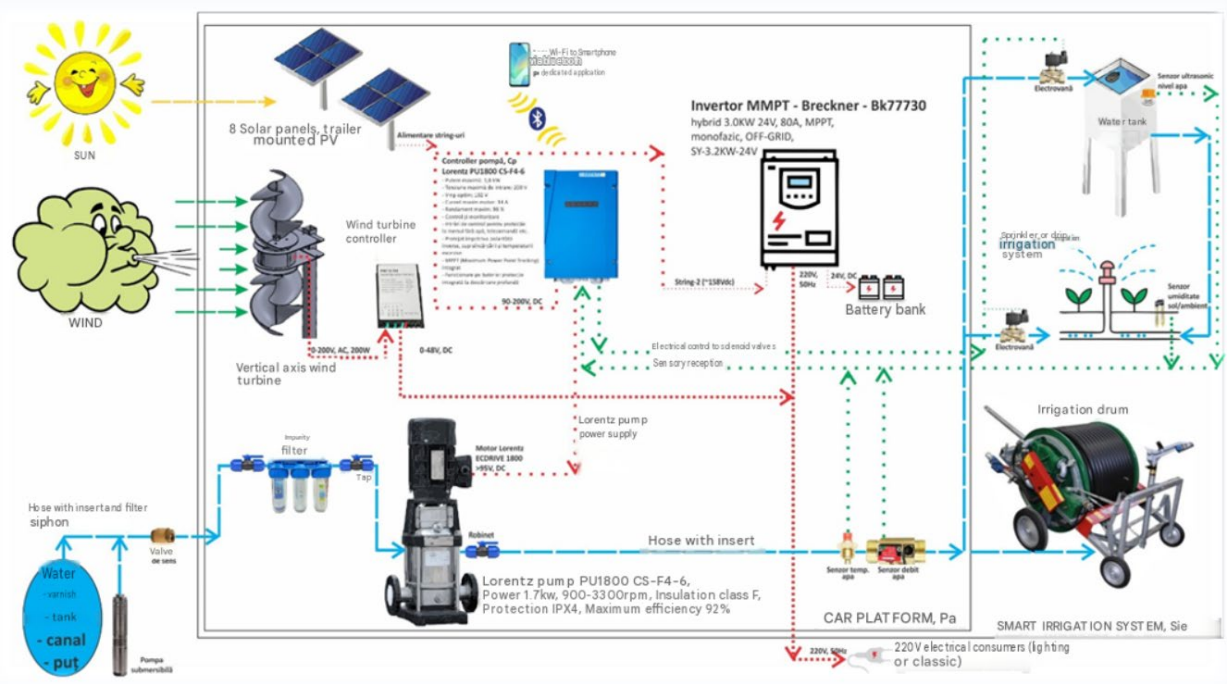



**Fig. 1 - Systemic diagram of the SIIEI smart irrigation system**



**Fig. 2 - Experimental setup of the mobile irrigation platform at Fundeni.**

*(a) Pumping and hydraulic connections; (b) 40/110 irrigation hose reel; (c) integration of the photovoltaic system and the PS2 controller.*

The experimental parameters and data acquisition methods are summarized in Table 2. Plane-of-array irradiance (G_POA) was measured using an SM206-Solar portable solar irradiance meter. According to the instrument specifications noted in the research log, the measurement range is 0.1 - 1999.9 W/m², with a resolution of 0.1 W/m² and a stated reading error of ±10%.

**Table 2**

**Experimental system and measurement instrumentation**

| Size / Subsystem | System | Range / Nominal value | Use in analysis |
|---|---|---|---|
| PV generator | 8 × 550 W modules | 4,4 kW | Solar source |
| Solar irradiance | SM206-Solar | 0,1–1999,9 W/m² | G_POA |
| PV surface temperature | InfiRay P2 Pro | from −20 to 550°C; ±2°C | Thermal response |
| PV electrical checks | UNI-T UT210E | DC current up to 100 A | Field verification |
| Pump / Controller | Lorentz PS2-1800 CS-F4-6 | 1.8 kW nominal | Pump power |
| Hydraulic output | LORENTZ CONNECTED / PS2 | Reported by the controller | Flow rate and volume |

The photovoltaic module surface temperature was measured using an InfiRay P2 Pro thermal imaging camera (256×192 detector, stated temperature accuracy of ±2°C). The measured surface temperature served as a practical proxy for the photovoltaic cell temperature during the field analysis.

Direct current (DC) and voltage measurements on the photovoltaic side were performed using a UNI-T UT210E DC clamp meter. Electrical power and pump flow rate were recorded via the Lorentz PS2-1800 controller and the LORENTZ CONNECTED/PumpScanner monitoring environment. Ambient temperature was recorded in the field measurement log.

The measurements were analyzed with hourly resolution for the time interval 06:00–19:00. For the one-hour intervals recorded in the field log, the hourly pumping energy was calculated as $E_i = P_i \cdot \Delta t$, with $\Delta t$ = 1 h. The daily pumping energy and the volume of pumped water were determined by summation:

$$E_p = \sum P_i \cdot \Delta t;\ V = \sum Q_i \cdot \Delta t \quad (1)$$

Subsequently, two complementary performance indicators were calculated: specific pumping energy, $e_s = E_p / V$ (kWh/m³), and water pumping energy productivity, $WP_E = V / E_p$ (m³/kWh). For a sample irrigated area of 1 ha, the equivalent gross irrigation rate, $d = 1000\ V / A$, was calculated, where $V$ is expressed in m³ and $A$ in m². This equivalent rate represents the pumped volume per unit area and does not include losses occurring during water application to the field.

The study represents a field performance assessment rather than a comprehensive test of overall system efficiency (from the electrical grid to the water output). Total dynamic head, instantaneous pressure, and flow rate (measured using an independent meter) were not recorded with the same hourly resolution; consequently, hydraulic power and overall pump efficiency were not calculated. The flow rate reported by the controller is treated as an operational variable, and the accuracy of the irradiance measuring device renders the G_POA value suitable for field correlations rather than for reference-level solar resource certification.

**Table 3**

**Hourly experimental data recorded on August 15, 2026**

| Time / Hour | G_POA (W/m²) | $T_{amb}$ (°C) | $T_{PV}$ (°C) | Pump power (kW) | Flow (m³/h) |
|---|---|---|---|---|---|
| 06:00 | 0 | 22.0 | 22.0 | 0.000 | 0.00 |
| 07:00 | 211 | 23.3 | 29.9 | 0.777 | 3.67 |
| 08:00 | 412 | 24.7 | 37.5 | 1.474 | 6.96 |
| 09:00 | 592 | 26.0 | 44.5 | 1.800 | 8.50 |
| 10:00 | 743 | 27.3 | 50.5 | 1.800 | 8.50 |
| 11:00 | 856 | 28.7 | 55.5 | 1.800 | 8.50 |
| 12:00 | 925 | 30.0 | 59.0 | 1.800 | 8.50 |
| 13:00 | 950 | 31.3 | 61.0 | 1.800 | 8.50 |
| 14:00 | 925 | 32.7 | 61.6 | 1.800 | 8.50 |
| 15:00 | 856 | 34.0 | 60.8 | 1.800 | 8.50 |
| 16:00 | 743 | 32.0 | 55.2 | 1.800 | 8.50 |
| 17:00 | 592 | 30.0 | 48.5 | 1.800 | 8.50 |
| 18:00 | 412 | 28.0 | 40.9 | 1.600 | 7.55 |
| 19:00 | 211 | 26.0 | 32.6 | 0.926 | 4.37 |

The solar and thermal profiles obtained during the test are shown in Fig. 3. Irradiance rose from 211 W/m² at 07:00 to a peak of 950 W/m² at 13:00, subsequently decreasing as evening approached. The smooth rise and fall of the G_POA value indicates a relatively stable summer day, free from major, short-term cloud-induced interruptions in the hourly dataset. The peak irradiance value was close to standard test conditions, providing suitable conditions for evaluating the upper limit of the pumping system's operating range.

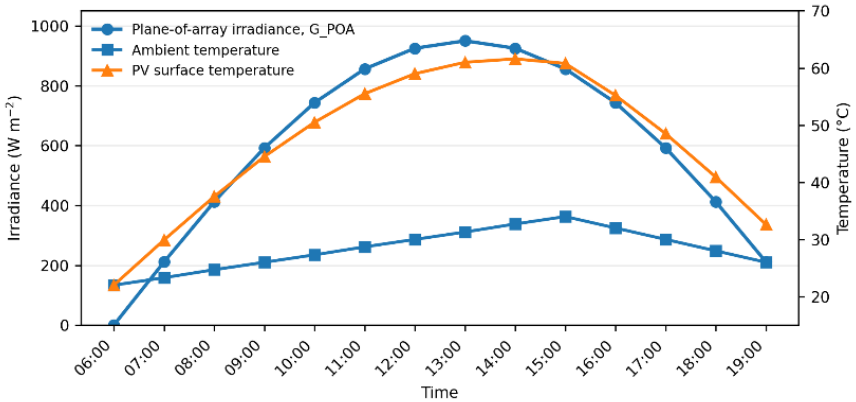



**Fig. 3 - Daily evolution of irradiance in the plane of the panels and of the temperature during the field test.**

The ambient temperature rose from 22.0°C at 06:00 to 34.0°C at 15:00. The photovoltaic panel surface temperature rose more rapidly, reaching 61.0°C at the time of peak irradiance and a daily maximum of 61.6°C at 14:00. The maximum difference between the panel surface temperature and the ambient temperature was 29.7°C at 13:00. The one-hour lag between peak irradiance and peak module surface temperature is consistent with the thermal inertia of the module structure. Such operating temperatures are significantly higher than the 25°C cell temperature used for the standard rating of photovoltaic systems and, consequently, entail a reduction in instantaneous photovoltaic conversion efficiency. However, in the current configuration, this thermal penalty did not result in a measurable reduction in pump flow rate during the period of high irradiance, as the photovoltaic system was oversized relative to the pump.

The pump's response is shown in Fig. 4. At 07:00, with an irradiance in the module plane (G_POA) of 211 W/m², the controller operated the pump at a power of 0.777 kW, and the recorded flow rate was 3.67 m³/h. At 08:00, the irradiance rose to 412 W/m², the pump power reached 1.474 kW, and the flow rate increased to 6.96 m³/h. By 09:00, at an irradiance of 592 W/m², the pump reached its rated limit of 1.8 kW, and the flow rate stabilized at 8.5 m³/h. The rated flow rate was maintained until 17:00, despite irradiance variations between 592 and 950 W/m² and panel surface temperatures ranging from 44.5 to 61.6°C. The period of operation at rated parameters was approximately eight hours.

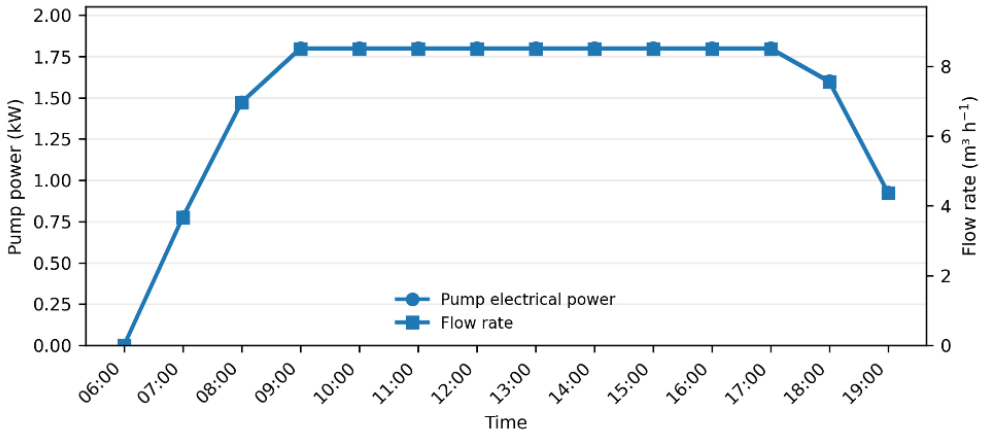



**Fig. 4 - The pump's electrical power and the flow rate reported by the controller throughout the test day.**

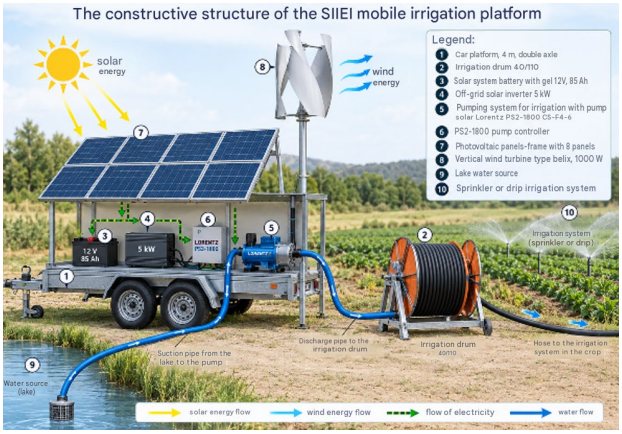





**Fig. 5 - Structural design SIIEI smart irrigation system, Fig. 6 - Image manufactured SIIEI smart irrigation system**

### *B. Lorentz PS2-1800 CS-F4-6 pumping unit*

The central component of the hydraulic subsystem is the high-efficiency pump unit manufactured by Lorentz. This centrifugal surface pump is specifically designed to operate directly on the direct current generated by photovoltaic panels (*Al-Ibrahim, 1997*). At the heart of the pump lies the EC DRIVE 1800 electric motor - a 1.7 kW EC (Electronically Commutated) motor (with a maximum hydraulic pumping power of 1.8 kW) powered by a nominal voltage of 95V DC. The motor operates without brushes, thereby reducing mechanical friction and eliminating the need for periodic maintenance, while simultaneously delivering exceptional overall efficiency of up to 92%. The unit features an IPX4 weather protection rating, making it ideal for operation under harsh agricultural field conditions.

The system is complemented by a Lorentz PS2-1800 electronic controller, which performs functions vital for stable, long-term operation: it implements a high-performance MPPT (Maximum Power Point Tracking) algorithm to ensure the electrical load constantly adapts to fluctuations in solar radiation intensity; it fine-tunes motor speed based on the voltage and current available at the photovoltaic panel terminals; and it provides integrated dry-run protection via a level sensor, as well as overvoltage and overcurrent protection.

### *C. Experimental research location and methodology*

The experimental research was conducted during August—a period characterized by a severe soil water deficit (*Canarache, 1990*)—in the area of Fundeni, Calarasi County (within the Bărăgan Plain geographical region in southeastern Romania). The specific pedoclimatic location provided a representative setting for testing the capabilities of the SIIEI system, as the area possesses high agricultural potential yet is frequently affected by prolonged soil drought.

The measurement and monitoring methodology involved the automated collection of electrical and hydraulic parameters using the PumpScanner (Lorentz App) smart application, installed on a smartphone connected via Bluetooth directly to the pump controller. The application enables the recording of the following parameters at 5-minute intervals: solar irradiance incident on the panels, voltage at the PV generator terminals, DC current drawn by the motor, instantaneous electrical power, pump speed, and estimated volumetric flow rate. Additionally, physical verification measurements were performed for sprinkler pressure (using a 10-bar glycerin-filled pressure gauge installed in the pipeline), and water distribution uniformity was evaluated using calibrated rain gauges (*Christiansen, 1942*).

Before measurements began, the photovoltaic panels were calibrated and oriented due south, set at an optimal tilt angle of 30° from the horizontal - suitable for the latitude of the Bărăgan Plain during summer. The Lorentz pumping unit was manually primed via the flexible suction line - equipped with an intake strainer and debris filter - while the 40/110 mobile reel unit was positioned at the edge of the experimental plot.

Local climatic conditions in Fundeni, Călărași County, directly determine the pumping system's energy productivity, given the direct relationship between solar irradiance and the pumped hydraulic flow rate. A summary of the average climatic conditions specific to the experimental period is presented in Table 3.

**Table 3**

**Average meteorological parameters for the Fundeni experimental site, Calarasi County**

| Determined meteorological parameter | Value determined in the field | Units |
|---|---|---|
| Global Horizontal Irradiance (GHI) | 3.58 | kWh / m² / zi |
| Direct Normal Irradiance (DNI) | 3.37 | kWh / m² / zi |
| Global Tilted Irradiance (GTI) | 4.19 | kWh / m² / zi |
| Average maximum air temperature in August 2026 | 31.0 | °C |
| Average minimum air temperature in August 2026 | 17.0 | °C |
| Average daily sunshine hours in August 2026 | 17.0 | zile |
| Estimated average total precipitation in August 2026 | 25..0 | mm |

Analysis of climate data indicates considerable solar radiation abundance during August, with an average daily Global Tilted Irradiance (GTI) of 4.19 kWh/m². High air temperatures (average highs of 31°C) combined with low precipitation (25 mm) create a soil-climate environment characterized by water scarcity, typical of the Bărăgan region. These weather conditions underscore the importance of implementing an independent system capable of ensuring optimal irrigation for the farm (*Popa, 20*21).

Testing also evaluated the dynamic response of the Lorentz PS2-1800 controller during the passage of cloud formations (episodic diffuse radiation below 300 W/m²).

Thanks to the rapid response of the integrated MPPT algorithm (reaction time under 1 second), the EC DRIVE motor speed was adjusted progressively, preventing sudden pump shutdown and water hammer effects in the discharge pipeline. The flow rate decreased proportionally to a safe minimum of 3.1 m³/h, resuming nominal operation as soon as the irradiance level exceeded the 650 W/m² threshold.

## RESULTS AND DISCUSSION

Field-based experimental research conducted at Fundeni monitored the performance of the Lorentz solar pumping unit over the course of a typical summer day (August 15). The objective was to highlight variations in key energy parameters - such as electricity generation, MPPT efficiency, and specific pumping

consumption - in close correlation with the hydraulic and quality indicators of water distribution provided by the mobile reel irrigation system.

***Energy and Hydraulic Performance Assessment***

On August 15, the mobile photovoltaic generator of the SIIEI platform - featuring a nominal installed capacity of 4.4 kW - delivered a total electricity output of approximately 28.41 kWh throughout the monitored daylight period (07:00–19:00).

Due to the physical power limitations of the EC DRIVE 1800 motor (maximum permissible input power of 1.8 kW) and the fact that the solar batteries reached full charge around midday, the electricity actually consumed by the pumping system amounted to 20.98 kWh.

This consumed energy enabled the continuous operation of the Lorentz pump at nominal speed for a duration of 8 hours (from 09:00 to 17:00), during which time the incident solar radiation remained consistently above the 700 W/m² threshold. The total volume of water pumped on this representative day was 99.05 m³ - drawn directly from the local water source - maintaining an average flow rate of approximately 8.5 m³/h.

Based on these measurements, two fundamental energy indicators were calculated to evaluate the overall efficiency of the solar pumping system:

$$E_p = \frac{Q_{total}}{E_{consummed}} = \frac{99{,}05\ m^3}{20{,}98\ kW} = 4{,}72\ m^3/kWh \quad (2)$$

$$E_s = \frac{E_{consummed}}{Q_{total}} = \frac{20{,}98\ kW}{99{,}05\ m^3} = 0{,}212\ kWh/m^3 \quad (3)$$

The specific water energy productivity of 4.72 m³/kWh and the extremely low specific consumption of 0.212 kWh/m³ confirm the outstanding performance of the Lorentz photovoltaic-hydraulic system, placing it above conventional AC pumping solutions using standard inverters, which typically incur substantial thermal and switching losses.

***Functional parameters of the mobile drum unit***

The irrigation process was carried out by hydraulically connecting the Lorentz pump to the mobile hose-reel irrigation unit (40/110 model). The end sprinkler mounted on the trolley was successively fitted with four different sizes of cylindrical nozzles (8, 9, 10, and 12 mm) to analyze flow rate and water jet radius behavior at a supply pressure maintained constant at the nominal value of 2.5 bar (*Nedelcu, 2010*). Detailed results of these tests are summarized in Table 4.

**Table 4**

**Functional parameters of the 40/110 mobile irrigation reel at a pressure of 2.5 bar**

| Nozzle diameter (mm) | Working pressure (bar) | System flow rate (m³/h) | Average jet radius (m) | Irrigated strip width (m) | Irrigation rate (m³/ha) |
|---|---|---|---|---|---|
| 8 | 2.5 | 2.2 | 26 | 36.4 | 54.95 |
| 9 | 2.5 | 2.4 | 28 | 39.2 | 55.66 |
| 10 | 2.5 | 2.6 | 29 | 40.6 | 58.22 |
| 12 | 2.5 | 3.0 | 29 | 40.6 | 67.17 |

Experimental results demonstrate that as the sprinkler nozzle diameter increases from 8 mm to 12 mm, the delivered volumetric flow rate rises in a controlled manner from 2.2 m³/h to 3.0 m³/h, while the average water jet radius extends from 26 m to a maximum of 29 m.

The width of the irrigated strip reaches a saturation point of 40.6 m at the maximum spray angle in the absence of strong crosswinds. The hose retraction speed was kept constant at 11 m/h, resulting in a total irrigation pass duration of approximately 7 hours.

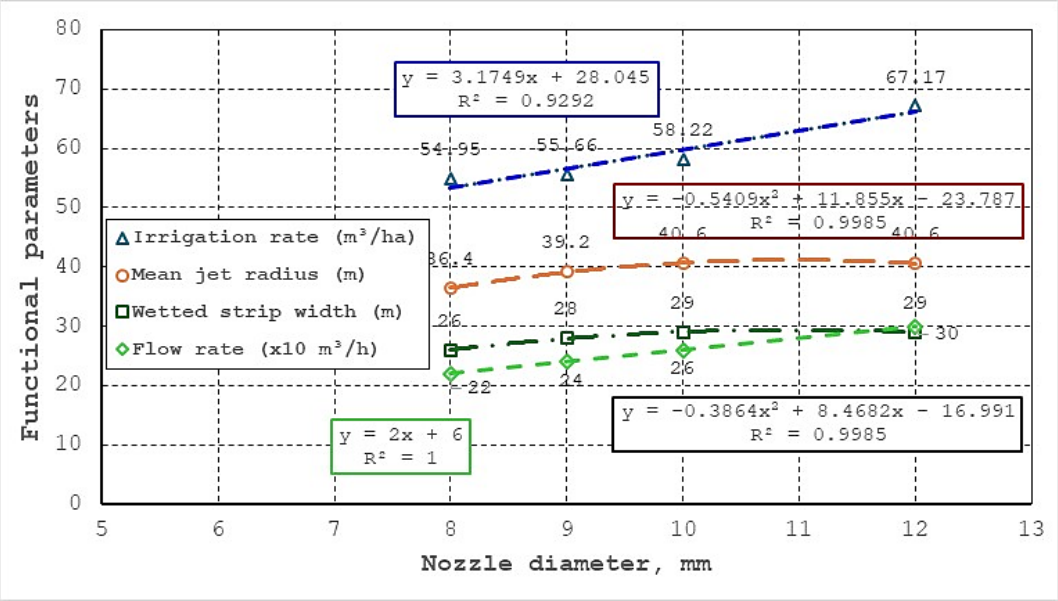



**Fig. 6 - Influence of nozzle diameter on the main operational parameters of the 40/110 mobile irrigation reel**

The applied irrigation rate varies in direct proportion to the hydraulic flow rate provided by the Lorentz pump and in inverse proportion to the width of the irrigated strip and the drum winding speed. Calculations indicate rate values ranging from 54.95 m³/ha to 67.17 m³/ha. This range falls perfectly within the limits recommended in agronomy for refreshing irrigation and maintaining the minimum level of active soil moisture, without exceeding the infiltration capacity of the medium-textured soils of the Bărăgan region (*Grumeza et al., 1989*).

***Hydraulic dynamics and the throttling effect (Throttling Effect)***

The relationship between the nozzle diameter (8 – 12 mm) and the flow rate (2.2 – 3.0 m³/h) at a constant pressure of 2.5 bar reflects the operating characteristic of the Lorentz PS2-1800 surface pump in relation to the system resistance curve:

- With the 8 mm nozzle, the small discharge cross-section creates additional hydraulic resistance (throttling effect). This forces the pump to operate at a higher discharge pressure to overcome head losses, reducing the delivered volumetric flow rate to just 2.2 m³/h.
- Switching to the 12 mm nozzle increases the discharge area by over 125%, lowering local resistance at the sprinkler and allowing the pump to operate in a range of higher hydraulic efficiency, thereby increasing the flow rate by ~36% (to 3.0 m³/h).

***Spray radius efficiency and kinematic saturation***

Extending the jet range from 26 m (8 mm nozzle) to 29 m (10 mm and 12 mm nozzles) demonstrates an aerodynamic saturation effect:

- Increasing the diameter to 10 mm provides sufficient momentum to the water mass to overcome air resistance and achieve the maximum coverage radius (29 m / 40.6 m wetted width).
- Increasing the diameter from 10 mm to 12 mm does not extend the spray radius (it remains 29 m); instead, it merely increases the flow rate and droplet size. This demonstrates that 10 mm is the optimal threshold for maximizing the coverage area at a pressure of 2.5 bar.

***Agronomic optimization of the irrigation rate and soil protection***

Varying the irrigation rate from 54.95 m³/ha (8 mm nozzle) to 67.17 m³/ha (12 mm nozzle) at the same reel retraction speed (11 m/h) offers flexible water management options:

- The 8–9 mm nozzle is ideal for the emergence stage or for heavier (clay) soils where water infiltration is slow; finer droplets prevent the breakdown of soil aggregate structure and the formation of a surface crust.

- The 12 mm nozzle provides a higher application rate (67.17 m³/ha)—necessary during peak crop water demand periods (e.g., flowering or grain filling in maize)—and is recommended for highly permeable soils (deep chernozems, sandy soils).

***Correlation with energy storage and operating time***

Since the Lorentz pump's flow rate is directly dependent on available solar energy, the choice of nozzle affects the time required to complete a pass:

- Using the 10 mm or 12 mm nozzle optimizes the daily irrigation window (8 hours of intense sunlight), allowing for the application of a larger volume of water (99 m³/day) without requiring additional battery storage for the evening hours.

## CONCLUSIONS

The theoretical and experimental research presented in this paper has technically and operationally validated the concept of an Innovative Energy-Independent System for Agricultural Crop Irrigation (SIIEI). The mobile demonstration platform successfully executed the complete hydraulic process under real-world daytime operating conditions in Fundeni, Călărași County.

The Lorentz PS2-1800 CS-F4-6 solar pumping unit proved to be a highly efficient component for the direct conversion of photovoltaic energy into hydraulic energy. The high efficiency of the EC DRIVE motor, combined with the precise operation of the controller's MPPT tracker, ensured a constant pumping flow rate of approximately 8.5 m³/h for 8 hours a day, even amidst inherent fluctuations in solar irradiance intensity.

Calculations of specific energy metrics—showing a specific water energy productivity of 4.72 m³/kWh and an energy consumption of only 0.212 kWh/m³—demonstrate the economic viability of this solution for small and medium-sized farmers in areas lacking access to the national electricity grid, offering virtually zero operating costs compared to conventional diesel generators.

The study opens up new research avenues regarding the full digitalization of water management by integrating data from the Lorentz PumpScanner application with wireless soil sensor networks (IoT) and weather forecasts to enable real-time automated irrigation decision-making.

## ACKNOWLEDGEMENT

This work was carried out as part of the doctoral study program at the Doctoral School of Biotechnical Systems Engineering, National University of Science and Technology POLITEHNICA Bucharest.

The authors wish to thank Prof. Gheorghe Voicu, PhD, Eng., for his scientific guidance throughout the doctoral research.

Acknowledgments are also extended to the company Rolix for the technical, material, and logistical support provided during the development, assembly, and field testing stages of the Innovative Energy-Independent System for Agricultural Crop Irrigation (SIIEI). Furthermore, the lead author thanks the co-authors for their collaboration on this article.

## REFERENCES

[1] Alexandratos, N. & Bruinsma, J. (2012). World agriculture towards 2030/2050: the 2012 revision.

[2] Al-Ibrahim, A. M. (1997). Optimum selection of direct-coupled photovoltaic pumping system in solar domestic hot water systems. The University of Wisconsin-Madison.

[3] Brumă, I.S. (2004). Ecological Vegetable Growing Technologies. *Horticulture Journal*, 2, (*in Romanian*).

[4] Canarache, A. (1990). Fizica solurilor agricole. *Ceres Publishing House*, Bucharest, (*in Romanian*).

[5] Christiansen, J.E. (1942). Irrigation by Sprinkling. *California Agricultural Experiment Station Bulletin,* No. 670, University of California, Berkeley, SUA.

[6] Grumeza, N., Merculiev, O., Klepș, C. (1989). Forecasting and scheduling of irrigation applications in irrigation systems. *Ceres Publishing House*, Bucharest (*in Romanian*).

[7] Grumeza, N., Kleps, C. (2005). Irrigation infrastructure in Romania. *Ceres Publishing House*, Bucharest (*in Romanian*).

[8] Nedelcu, M. (2010). Contributions on the optimization of the operating regime of irrigation installations by drum and hose sprinkling (Doctoral thesis, Transilvania University of Brașov), (*in Romanian*).

[9] Pelea, G.N. (2021). Current issues regarding the management of the exploitation and maintenance of irrigation systems located in western Romania (Doctoral thesis, Politehnica University of Timisoara), (*in Romanian*).
[10] Popa, A.S. (2021). Studies on updating the elements of the irrigation regime of corn and soybean crops in the locality of Martacesti, Braila County (Bachelor's thesis, Lower Danube University of Galati), (*in Romanian).*
[11] Preda D.M., Duran B.O., Pandele A., Ștefan V., Manoleli-Preda O.D., Ionescu A. (2023). Numerical Analysis of a Novel Vertical-Axis Wind Turbine Layout, INMATEH - Agricultural Engineering, Vol. 70, No. 2, 221-230.
[12] *** Innovative Energy-Independent System for Agricultural Crop Irrigation Under Current Climate Change Conditions, Financing Contract No. 431/390107/07.02.2023, SMIS 156177, ROLIX IMPEX SERIES SRL (2025).

# THE POTENTIAL FOR UTILIZING WOOL WASTE TO PRODUCE THERMAL AND ACOUSTIC INSULATION MATERIALS FOR CONSTRUCTION

/

# *POSIBILITĂȚILE VALORIFICĂRII DEȘEURILOR DE LÂNĂ PENTRU OBȚINEREA MATERIALELOR DE CONSTRUCȚIE TERMOIZOLANTE ȘI FONOABSORBANTE*

**Evelin-Anda LAZA[1)], Gabriela-Victoria MNERIE*[1, 2, 3)], Gabriel FODOREAN[1)], Elena-Mihaela NAGY[1)], Teodor VINTILĂ[4)], Ana-Cristina VASILE[5)], Aurelian GRUIN[5, 6)]**

[1)] National Institute of Research-Development for Machines and Installations Designed for Agriculture and Food Industry - INMA Bucharest / Romania;

[2)] Ioan Slavici University, Timișoara, Timis County / Romania;

[3)] National Research & Development Institute for Welding and Material Testing - ISIM Timișoara, Timis County / Romania;

[4)] University of Life Sciences "King Mihai I" from Timișoara, Timis County / Romania;

[5)] National Research & Development Institute URBAN-INCERC Timisoara Branch, 2 Traiana Lalescu Street, Timisoara, Timis County / Romania;

[6)] Faculty of Civil Engineering, Politehnica University of Timisoara, 2 Traiana Lalescu Street, Timisoara, Timis County / Romania.

**Tel: 0742 026 117; *E-mail: inmatm.mnerie@gmail.com*

***Keywords:*** *sheep wool waste, thermal insulation, acoustic insulation, circular economy, sustainable construction, natural fibres*

## ABSTRACT

*The recovery of low-value sheep wool waste as a secondary raw material is a promising route toward more sustainable construction products. This paper analyses the potential of sheep wool waste for thermal and acoustic insulation applications, considering fibre preparation, material density, binder selection and manufacturing route. Published studies report thermal conductivity values generally below 0.06 W/(m·K) for wool-based nonwovens and composites, while sound absorption coefficients above 0.7α have been measured for several configurations. The main technological limitations are moisture sensitivity, biological degradation, fire performance and reduced compressive strength when wool fibres are incorporated into structural matrices. A technological framework for sorting, cleaning, drying, fibrillation, binder mixing, forming and conditioning of wool-based insulation panels is proposed. The work also compiles literature-reported thermal and acoustic values to define a reference performance window for future experimental validation. The results support the use of wool waste as a renewable secondary resource for non-load-bearing thermal and acoustic insulation products.*

## REZUMAT

*Valorificarea deșeurilor de lână de oaie cu valoare scăzută ca materie primă secundară reprezintă o direcție promițătoare pentru obținerea unor produse de construcție mai sustenabile. Lucrarea analizează potențialul deșeurilor de lână de oaie pentru aplicații de izolare termică și fonică, luând în considerare pregătirea fibrelor, densitatea materialului, alegerea liantului și procesul de fabricație. Studiile publicate indică valori ale conductivității termice, în general, sub 0,06 W/(m·K) pentru materiale nețesute și compozite pe bază de lână, în timp ce pentru diverse configurații au fost înregistrați coeficienți de absorbție acustică de peste 0,7α. Principalele limitări tehnologice vizează sensibilitatea la umiditate, degradarea biologică, comportarea la foc și rezistența redusă la compresiune în cazul încorporării fibrelor de lână în matrice structurale. Se propune un cadru tehnologic pentru sortarea, curățarea, uscarea, fibrilarea, amestecarea cu liant, formarea și condiționarea panourilor termoizolante și fonoizolante pe bază de lână. De asemenea, lucrarea sintetizează valorile termice și acustice raportate în literatura de specialitate pentru a defini un interval de performanță de referință, necesar validării experimentale ulterioare. Rezultatele susțin utilizarea deșeurilor de lână ca resursă secundară regenerabilă pentru produse de izolare termică și fonică destinate elementelor nestructurale.*

## INTRODUCTION

The construction sector is under increasing pressure to reduce resource consumption, embodied emissions, and the volume of waste generated. In this context, agricultural and animal-derived residues can serve as secondary raw materials for bio-based construction products. Sheep's wool is of particular interest

because its keratin fibers form a porous network capable of trapping air while simultaneously providing hygroscopic and acoustic properties. Recent reviews identify thermal insulation and sound absorption as the most mature applications of sheep's wool in construction, while highlighting the need to control water consumption during processing and to improve durability and fire performance *(Midolo et al., 2024; Kicińska-Jakubowska et al., 2024).*

Low-quality wool obtained from sheep shearing is often unsuitable for textile processing and can consequently become a disposal issue. Transforming it into thermal insulation products creates a circular pathway from livestock waste to a value-added construction material.

Parlato et al. (2022) demonstrated the feasibility of a wool valorization chain for soft mats and semi-rigid thermal insulation panels, while Rubino et al. reported thermal conductivity values between 0.044 and 0.057 W/(m·K) for non-woven materials made from wool waste, as well as sound absorption coefficients ranging from 0.7 to nearly 1 at frequencies above 1 kHz *(Parlato et al., 2022 ; Rubino C. Et al., 2021).*

Dénes et al. obtained thermal conductivity values between 0.0324 and 0.0436 W/(m·K) for sheep wool composites prepared with acrylic-polyurethane resin and natural rubber latex. *(Dénes T.-O.et al., 2022).*

The aim of this paper is to synthesize the technological and performance-related information required for the development of thermal insulation panels made from sheep wool waste.

The specific objectives of this study are to identify the material's relevant properties, describe a recovery and manufacturing process, compare reported thermal and acoustic performance, and establish a baseline for subsequent experimental validation.

## MATERIALS AND METHODS

The material analyzed consists of low-quality sheep's wool obtained from shearing and sorting operations. For construction applications, the raw fiber must be separated from visible vegetable and mineral contaminants and subjected to a controlled cleaning process. The proposed process involves sorting, cleaning/washing, drying, mechanical fiber opening, mixing with a binder, forming, pressing, conditioning, and final characterization.



*a) Wool washing and degreasing* *b) Wool drying*

**Fig. 1 - Preparation of wool waste for experimental research**

The cleaning stage is particularly important because wool waste can contain grease, soil, plant debris, and biological contaminants. However, the water and energy requirements associated with washing can significantly impact environmental performance; therefore, future research should prioritize low-water or dry processing methods *(Midolo et al., 2024).*

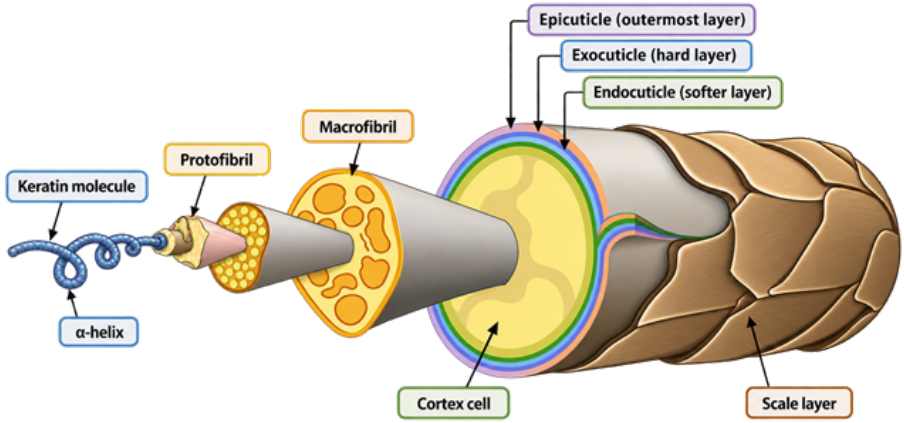



**Fig. 2 - Schematic representation of the wool fiber and its components**

Fiber morphology is relevant because the overlapping arrangement of cuticle scales and the wavy geometry of the fiber contribute to interlocking, elasticity, and the formation of air-filled pores. For a reproducible experimental program, fiber length distribution, moisture content, and bulk density must be determined prior to panel fabrication.




**Fig. 3 - Process flow for utilizing wool waste in thermal insulation panels**

Three material configurations were considered: unbound or lightly bonded fibrous mats; semi-rigid panels made of wool fibers and a binder; and composite materials in which wool acts as reinforcement or filler within a mineral or polymer matrix. For thermal insulation, semi-rigid fibrous panels offer a useful compromise between low density, dimensional stability and processability.

Key characterization parameters must include density, thermal conductivity, water absorption, water vapor permeability, sound absorption coefficient, compressive and flexural strength, dimensional stability, fire behavior, and biological resistance. Density, binder content, and panel thickness are particularly important, as they influence both pore structure and mechanical stability.

## RESULTS

The reviewed literature indicates consistent thermal insulation potential for sheep's wool. Dénes et al. (2022) reported values of 0.0324-0.0436 W/(m·K) for sheep's wool composites, while Rubino et al. (2021) reported 0.044-0.057 W/(m·K) for non-woven materials made from wool waste.

A 2026 study reported $\lambda$ = 0.031 W/(m·K) for sheep's wool-based biocomposites, alongside $\alpha$ = 0.85 at 1000 Hz and compressive strengths of up to 0.92 MP.

These values should be interpreted as measurements specific to each study rather than as a single standardized performance value *(Rubio et al. 2021, Dénes, et al. 2022; Saaidia et al., 2026)*

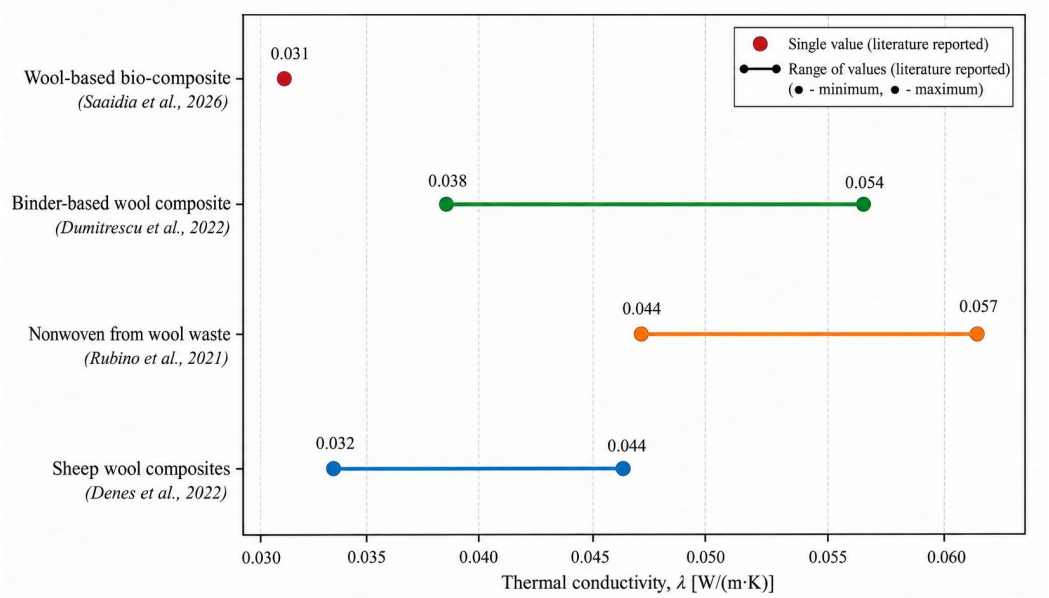



**Fig. 4 - Thermal conductivity ranges reported in the literature for selected wool-based materials**

The density range reported by Rubino et al. (2021) was 51-167 kg/m³. This result confirms that density is a key design variable. Excessive compression can reduce porosity, whereas insufficient consolidation may lead to dimensional instability and reduced handling strength. Consequently, optimization must aim at the combined response of density, thermal conductivity, and mechanical integrity, not just the minimization of λ *(Rubino et al., 2021).*

**Table 1**

**Selected thermal conductivity values reported in recent literature**

| Material / configuration | λ raportat [W/(m·K)] |
|---|---|
| Sheep's wool composites | 0,0324-0,0436 |
| Non-woven materials made from sheep wool waste | 0,044-0,057 |
| Sheep wool-based biocomposite | 0,031 |
| Wool-hemp/lime composite | 0,0738 |

The acoustic response of wool-based materials is also favorable. Rubino et al. (2021) measured absorption coefficients ranging from 0.7 to nearly 1 at frequencies above 1 kHz for nonwoven materials made from wool waste with a thickness of 50 mm. A 2025 study on a sheep wool biocomposite reported coefficients of up to 0.96, while Saaidia et al. (2026) reported α = 0.85 at 1000 Hz. Urdanpilleta et al. (2024) demonstrated that wool and soy protein biocomposites can achieve sound absorption coefficients close to 1 at medium and high frequencies *(Rubino et al., 2021; Urdanpilleta et al., 2024; Saaidia et al., 2026).*

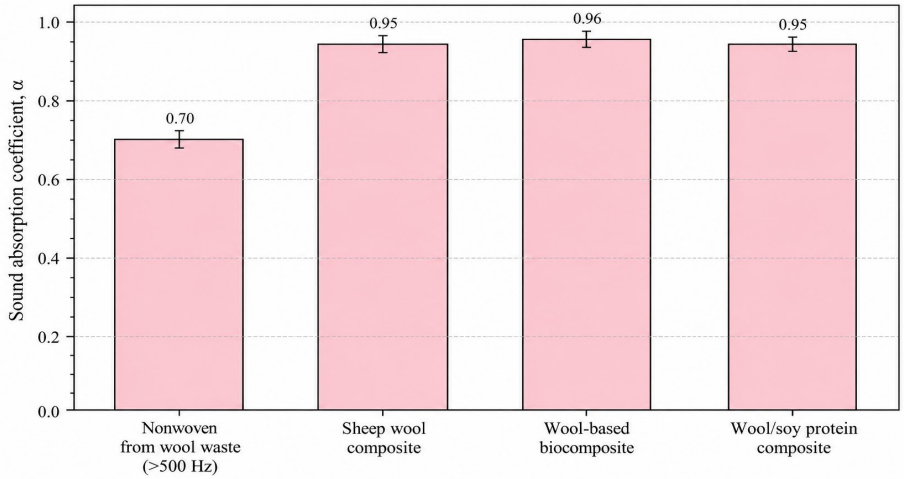



**Fig. 5 - Representative values of sound absorption reported in the literature**

**Table 2**

**Performance characteristics relevant to the development of wool-based construction materials**

| Property | Reference from the specialized literature | Technological implication |
|---|---|---|
| Thermal conductivity | 0.031-0.057 W/(m·K) in the selected studies | Suitable for non-load-bearing thermal insulation panels |
| Sound absorption | 0.70-0.96 in the selected configurations | Suitable for acoustic treatment and interior partitioning |
| Density | 51-167 kg/m³ in the tested non-woven materials | Key parameter for pore structure and stability |
| Humidity behavior | Hygroscopic characteristic performance changes with humidity | Requires vapor and water control |
| Compression | It can be susceptible to microorganisms and insects | Primarily used in non-structural applications |
| Biological resistance | It can be susceptible to microorganisms and insects | Requires humidity control and/or treatment |

The literature indicates that wool is better suited as a material for thermal insulation and acoustic treatment than as a primary load-bearing element. Research published between 2024 and 2026 also highlights the need to address issues regarding moisture, degradation in alkaline environments, fire behavior, and the impact of processing before transitioning to large-scale industrial use *(Midolo et al., 2024; Urdanpilleta et al., 2025; Saaidia et al., 2026).*

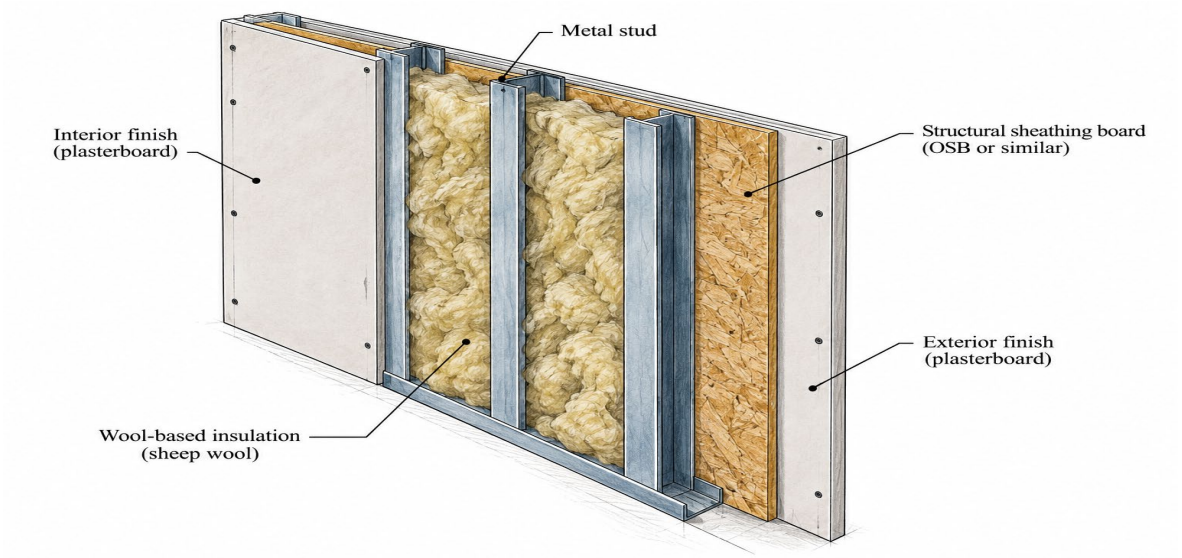



**Fig. 6 - Detail of a non-load-bearing wall with wool-based thermal and acoustic insulation**

The main advantage of wool waste lies in the combination of its renewable origin, low density, fibrous porosity, hygroscopicity, and sound absorption. The primary challenge is to retain these advantages while ensuring dimensional stability, a controlled response to moisture, adequate fire performance, and resistance to biological attack. Natural or low-impact binders can improve the environmental profile, but the choice of binder must be optimized with regard to mechanical and hygrothermal requirements.

A future research direction should include at least five density levels and three binder percentages, with a minimum of three replicates for each formulation. The dependent variables should be thermal conductivity, sound absorption, density, moisture absorption, and mechanical strength. Statistical analysis should be employed to quantify the effects of density and binder content and to identify an operating range that balances insulation performance with panel integrity.

From a circular economy perspective, the preferred pathway is a short regional supply chain: sheep farms, collection and sorting, low-water-consumption, pre-treatment, fiber opening, panel manufacturing, construction application, recovery or recycling. Parlato et al. (2022) demonstrated that the geographical concentration of raw wool availability can support the development of a regional value-added supply chain. Recent studies also show that wool waste can be combined with other bio-based or waste-derived materials

to produce functional thermal insulation products (*Parlato et al. 2022*; *Grzymisławska et al., 2024; Urdanpilleta et al., 2025; Saaidia et al.,2026)*.

## CONCLUSIONS

Sheep wool waste represents a technically promising secondary resource for the development of sustainable construction materials. The evidence analyzed supports the following conclusions: wool-based materials can achieve low thermal conductivity values; their fibrous and porous structure promotes high sound absorption; density, thickness, and binder content are critical technological variables; moisture behavior, biological resistance, and fire performance require dedicated testing; wool is better suited for non-load-bearing thermal insulation and acoustic treatment products than for primary structural elements; and low-water-consumption processing and the use of low-impact binders are important for maintaining the material's environmental advantage.

## ACKNOWLEDGEMENT

The presented results were obtained with the support of the UEFSCDI through the program PN 23 04 02 02, Objective 2 - Innovative technologies and equipment for the sustainable development of agroecological crops, in order to use them in conditions of energy efficiency, the protection of life, health and the environment, name of the work "Research on the use of wool waste to obtain organic fertilizers for agriculture in order to improve soil properties and reduce environmental pollution"

## REFERENCES

[1] Dénes, T.-O., Iştoan, R., Tămaş-Gavrea, D. R., Manea, D. L., Hegyi, A., Popa, F., & Vasile, O. (2022). Analysis of Sheep Wool-Based Composites for Building Insulation. Polymers, 14(10), 2109. https://doi.org/10.3390/polym14102109

[2] Grzymisławska, J., et al. (2024). Use of Waste Raw Materials in the Form of Hemp Shives and Waste Sheep Wool to Produce Composites Dedicated to Thermal Insulation. Journal of Natural Fibers. https://doi.org/10.1080/15440478.2024.2371902

[3] Kicińska-Jakubowska, A., et al. (2024). The Application of Sheep Wool in the Building Industry and in the Removal of Pollutants from the Environment. Processes, 12(5), 963. https://doi.org/10.3390/pr12050963

[4] Midolo, G., Del Zoppo, M., Porto, S. M. C., & Valenti, F. (2024). Recycling of wasted wool fibers from sheep shearing for green building components: A review. Case Studies in Construction Materials, 21, e03623. https://doi.org/10.1016/j.cscm.2024.e03623

[5] Parlato, M. C. M., Porto, S. M. C., & Valenti, F. (2022). Assessment of sheep wool waste as new resource for green building elements. Building and Environment, 225, 109596. https://doi.org/10.1016/j.buildenv.2022.109596

[6] Rubino, C., Bonet Aracil, M., Liuzzi, S., Stefanizzi, P., & Martellotta, F. (2021). Wool waste used as sustainable nonwoven for building applications. Journal of Cleaner Production, 278, 123905. https://doi.org/10.1016/j.jclepro.2020.123905

[7] Saaidia, R., Ben Othmane, A., Ayed, L., Boumediene, N., & Bouabidi, A. (2026). Thermal, Acoustic, and mechanical characterization of sheep Wool-Based Bio-Composites for sustainable construction. Energy and Buildings, 350, 116602. https://doi.org/10.1016/j.enbuild.2025.116602

[8] Savio, L., Pennacchio, R., Patrucco, A., Manni, V., Bosia, D., et al. (2022). Natural Fibre Insulation Materials: Use of Textile and Agri-food Waste in a Circular Economy Perspective. Materials Circular Economy, 4, 6. https://doi.org/10.1007/s42824-021-00043-1

[9] Urdanpilleta, M., del Rey, R., Leceta, I., Rodríguez, J. C., Alba, J., & Guerrero, P. (2024). Empirical modelling of the acoustic behavior of sheep wool/soy protein biocomposites. Journal of Building Engineering, 89, 109290. https://doi.org/10.1016/j.jobe.2024.109290

[10] Urdanpilleta, M., Leceta, I., Martín-Garín, A., Millán-García, J. A., Guerrero, P. M., & de la Caba, M. C. (2025). Valorized sheep wool biocomposites towards a more sustainable building sector: Thermal insulation, sound absorption, and resistance against insects. Developments in the Built Environment, 21, 100608. https://doi.org/10.1016/j.dibe.2025.100608

# INNOVATIVE TECHNOLOGIES FOR THE DEVELOPMENT OF FOOD PRODUCTS WITH ENHANCED FUNCTIONAL AND NUTRITIONAL VALUE

/

# *TEHNOLOGII INOVATIVE PENTRU DEZVOLTAREA PRODUSELOR ALIMENTARE CU VALOARE FUNCȚIONALĂ ȘI NUTRIȚIONALĂ ÎMBUNĂTĂȚITĂ*

**Cristian SORICĂ*[1)], Nicolae-Valentin VLĂDUȚ[1)], Laurențiu VLĂDUȚOIU[1)], Elena SORICĂ[1)] Florin NENCIU[1)], Alexandru IONESCU[1)]**

[1)] INMA Bucharest / Romania

*E-mail: cri_sor2002@yahoo.com*

***Keywords:*** *food fortification, nutrients, bioactive compounds, vacuum impregnation, encapsulation, extrusion*

## ABSTRACT

*The development of food products with enhanced nutritional and functional value was analysed in relation to technologies enabling the deliberate incorporation of nutrients and bioactive compounds into food matrices. Recent studies involving direct incorporation and reformulation, osmotic and vacuum-assisted mass transfer, encapsulation-assisted fortification, and extrusion and coating were reviewed. The analysed applications included proteins, vitamins, minerals, phenolic compounds, carotenoids and other bioactive constituents incorporated into bakery, dairy, fruit, vegetable and cereal-based products. Direct incorporation substantially improved food composition, although high addition levels sometimes affected technological and sensory properties. Osmotic and vacuum-assisted processes enabled the transfer of target compounds into porous food tissues, while encapsulation improved the protection and retention of sensitive fortificants. Extrusion and coating proved suitable for micronutrient incorporation into cereal-based foods, although nutrient retention varied during processing, storage and cooking. The results indicated that the selection of an appropriate technology should consider enrichment efficiency, nutrient stability, interactions with the food matrix and final product quality.*

## REZUMAT

*Dezvoltarea produselor alimentare cu valoare nutrițională și funcțională îmbunătățită a fost analizată în raport cu tehnologiile care permit introducerea controlată a nutrienților și compușilor bioactivi în matrici alimentare. Au fost analizate studii recente privind incorporarea directă și reformularea, transferul de masă prin procese osmotice și asistate de vid, fortificarea asistată de încapsulare, precum și extrudarea și acoperirea. Aplicațiile analizate au inclus proteine, vitamine, minerale, compuși fenolici, carotenoizi și alți constituenți bioactivi introduși în produse de panificație, lactate, fructe, legume și produse cerealiere. Incorporarea directă a îmbunătățit semnificativ compoziția produselor, dar nivelurile ridicate de adaos au putut afecta proprietățile tehnologice și senzoriale. Procesele osmotice și cele asistate de vid au permis transferul compușilor în țesuturi poroase, iar încapsularea a favorizat protecția și retenția compușilor sensibili. Extrudarea și acoperirea s-au dovedit adecvate pentru introducerea micronutrienților în produse cerealiere, însă retenția acestora a variat în timpul procesării, depozitării și preparării.*

## INTRODUCTION

Food fortification represents an important technological approach for increasing the nutritional value of commonly consumed foods through the deliberate incorporation of nutrients and other biologically relevant compounds. While traditional fortification has mainly focused on vitamins and minerals, current food-engineering strategies also address proteins and amino acids, polyunsaturated fatty acids, phenolic compounds, carotenoids and other bioactive constituents. Consequently, the development of nutritionally improved foods has evolved from the simple addition of micronutrients towards processing strategies adapted to both the fortifying compound and the characteristics of the food matrix (*Miano and Rojas, 2023).*

The technological route selected for enrichment strongly depends on food structure. In formulated products, nutrient-rich ingredients can be introduced directly during mixing or product reformulation. In contrast, intact porous matrices such as fruits and vegetables may be enriched through liquid-based mass-transfer operations. Osmotic processing is particularly suitable for this purpose because water removal from

the tissue can occur simultaneously with the inward migration of solutes from a concentrated external medium. Vacuum impregnation can further enhance this process by promoting the replacement of gases contained within the porous structure by an external solution containing the desired compounds.

These approaches have been increasingly investigated for the fortification of fruit and vegetable products with minerals, vitamins and bioactive compounds *(Asare et al., 2022; Haneef et al., 2024; Vinod et al., 2024).* Direct addition may nevertheless be unsuitable for nutrients that are unstable during processing or storage, poorly soluble, susceptible to oxidation or responsible for undesirable sensory changes.

Encapsulation provides an alternative approach in which the fortificant is first incorporated into a protective carrier and then introduced into the final food. Recent studies have identified liposomes, spray-dried microparticles and other food-grade delivery systems as suitable approaches for protecting vitamins and other bioactive ingredients used in fortified foods (*Espinoza-Espinoza et al., 2024; Rahim et al., 2025).*

Extrusion and coating represent additional technologies particularly suitable for staple cereal foods. In extrusion-based fortification, micronutrients are incorporated into a cereal flour mixture that is subsequently reconstituted into food particles, whereas coating deposits the fortifying material predominantly on the external surface of an already formed product. Both routes have been extensively investigated for fortified rice, where nutrient retention, sensory characteristics and stability depend on processing conditions and the chemical nature of the micronutrient *(Liu et al., 2025).* The effectiveness of a fortification process should not be evaluated solely on the basis of the quantity of fortificant initially added. Effective incorporation and retention, distribution within the food matrix, stability during subsequent processing and storage, effects on texture and sensory quality and, where available, bioaccessibility or bioavailability are also relevant technological criteria. From a process-engineering perspective, the technologies considered in this review also differ in the location and physical state of the fortificant within the final product. Direct reformulation disperses the added ingredient throughout the matrix, mass-transfer processes introduce soluble or dispersed compounds into pre-existing pores and intercellular spaces, encapsulation places the active compound within a protective carrier, while extrusion and coating either embed micronutrients within a reconstituted cereal structure or retain them mainly at the particle surface.

These differences influence exposure to oxygen, moisture, heat and washing or cooking media, as well as interactions with proteins, lipids and carbohydrates. Consequently, selection of a fortification route should consider the complete processing sequence and not only the chemical identity of the nutrient or bioactive compound *(Espinoza-Espinoza et al., 2024; Liu et al., 2025; Miano and Rojas, 2023).*

The aim of this paper was to analyze recent technological approaches used for the deliberate incorporation of nutrients and bioactive compounds into food products. Four main routes were considered: direct incorporation and food reformulation, osmotic and vacuum-assisted mass-transfer processes, encapsulation-assisted fortification, and extrusion and coating technologies. Particular attention was given to recent experimental studies reporting both processing conditions and quantitative results concerning nutrient incorporation, retention and final product quality.

The main technological routes considered in this review are summarized conceptually in Figure 1, which highlights the relationship between the mechanism of incorporation, the food matrix and representative nutrient or bioactive compound categories.

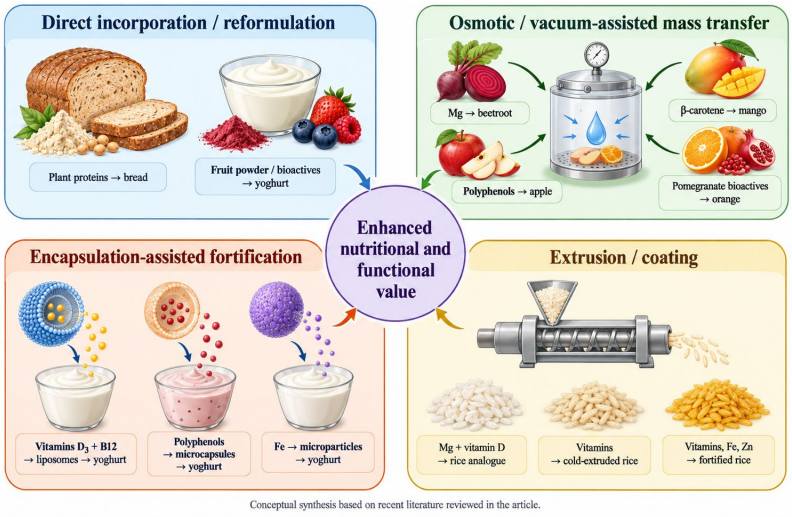



**Fig. 1 - Main technological routes for the incorporation of nutrients and bioactive compounds into food products**

## MATERIALS AND METHODS

The paper was prepared as a focused narrative review of recent peer-reviewed literature rather than as a systematic review or meta-analysis. Experimental studies were selected when they deliberately introduced an external nutrient or bioactive compound into a food matrix, described the relevant technological operation, and reported outcomes that allowed the effectiveness of incorporation to be assessed. Studies concerned only with preservation of naturally occurring nutrients, modification of endogenous compounds or improvement of bioaccessibility, without an intentional fortification step were not treated as core experimental evidence. Recent review papers were used to establish terminology, technological principles and the broader state of research. The experimental literature was organised according to the predominant mechanism of incorporation rather than according to nutrient class. The resulting groups comprised direct incorporation and reformulation, osmotic and vacuum-assisted mass transfer, encapsulation-assisted fortification, and extrusion or coating. For each study, attention was given to the food matrix, the incorporated compound, the carrier or treatment medium, the main processing sequence, subsequent preservation or preparation steps, and the reported effects on nutrient retention, stability, bioaccessibility and technological or sensory quality. This approach enabled comparison of both the advantages and the principal limitations associated with each technological route.

### Direct incorporation and food reformulation

Direct incorporation consists of adding a nutrient-rich or bioactive ingredient to the formulation of a food product before subsequent processing. The approach is particularly suitable for bakery, dairy and other formulated foods, where the added material can be dispersed throughout the matrix.

Álvarez-Quinteros et al. (2025) investigated bread enrichment using protein concentrates obtained from Plukenetia volubilis and Lupinus mutabilis. Wheat flour was partially substituted with different proportions of the two concentrates, and an optimisation procedure was used to identify a formulation combining improved protein quality with acceptable bread-making characteristics. The selected formulation contained 87% wheat flour, 4% lupin protein concentrate and 9% sacha inchi protein concentrate. Protein content, amino-acid composition, in vitro digestibility, PDCAAS and technological characteristics were subsequently determined. Lal et al. (2026) applied the same general technological principle to a dairy matrix by incorporating freeze-dried strawberry powder into set yoghurt at levels ranging from 2 to 12% (w/w). Physicochemical, textural, sensory and antioxidant characteristics were evaluated, while the selected formulation was further analysed by high-resolution mass spectrometry to characterise the bioactive compounds transferred from the fruit ingredient.

### Osmotic and vacuum-assisted mass-transfer technologies

Mass-transfer fortification uses an external liquid medium as a vehicle for transferring selected compounds into a solid food matrix. During osmotic treatment, water moves from the food into the hypertonic solution, while dissolved solutes can simultaneously penetrate the tissue. Vacuum treatment can intensify the process in porous foods by promoting the replacement of internal gases with the fortifying solution.

Kulczyński et al. (2025) investigated magnesium enrichment of beetroot using osmotic solutions containing magnesium oxide, citrate or chloride. Inulin, erythritol, xylitol and sucrose were evaluated as osmotic agents at different concentrations, together with variations in magnesium concentration, process time and temperature. Karlińska et al. (2025) used a 50% sucrose solution enriched with extracts from fragrant agrimony or rosehip during osmotic dehydration of Champion apples. Polyphenol levels of 2, 4 and 6 g/L were tested, while total and individual phenolic compounds incorporated into the apple tissue were determined by spectrophotometric and chromatographic methods. Fratta et al. (2025) used vacuum impregnation to introduce β-carotene into mango slices before solar drying. Emulsions containing β-carotene were prepared under different homogenisation conditions and used as impregnation media, enabling evaluation of both nutrient incorporation and retention after drying. Ismail et al. (2025) combined vacuum osmotic treatment with pomegranate juice concentrate for the enrichment of orange slices. The concentration of the osmotic medium, concentrate-to-fruit ratio and vacuum period were varied using a response-surface experimental design. The enriched samples were subsequently dried either by hot-air-assisted radiofrequency drying or conventional hot-air drying.

### Encapsulation-assisted fortification

Encapsulation-assisted fortification involves the preparation of a protective carrier containing the target compound followed by incorporation of the encapsulated material into the food matrix. Ferreira et al. (2026) developed food-grade liposomes coencapsulating vitamins D3 and B12. Different phospholipid systems and pectin-coated formulations were produced, lyophilised and subsequently incorporated into

yoghurt. Vitamin retention during storage, physicochemical stability, sensory properties and gastrointestinal behaviour were assessed. López-Astorga et al. (2025) microencapsulated a phenolic extract obtained from grape pomace by spray-drying using maltodextrin and gum arabic as wall materials. The resulting microparticles were incorporated into Greek-style yoghurt and compared with the non-encapsulated extract in terms of storage stability and gastrointestinal bioaccessibility.

Rebellato et al. (2025) developed ferrous sulfate microparticles using spray-drying followed by spray-chilling. The particles were incorporated into plant-based and dairy yoghurt formulations and compared with free ferrous sulfate. Iron content, stability, bioaccessibility and estimated bioavailability were subsequently evaluated.

**Extrusion and coating technologies**

Extrusion enables micronutrients to be embedded in a reconstituted cereal matrix, whereas coating applies the fortifying material mainly to the external surface of the product. Costa et al. (2026) developed rice-based analogues fortified with magnesium and vitamin D. Rice flour, cowpea flour and processed rice fractions were formulated with a vitamin-mineral premix containing magnesium sulfate and cholecalciferol, followed by shaping and drying. Ganachari et al. (2026) produced cold-extruded fortified rice analogues using rice flour, sodium alginate and a vitamin premix corresponding to 100, 125 or 150% of the target fortification level. Vitamin retention was assessed after extrusion and subsequent cooking.

Nader et al. (2026) compared coated and extruded fortified rice kernels containing vitamins A, B1, B3, B6, B9 and B12 together with iron and zinc. The products were stored for approximately two years under realistic supply-chain conditions in order to evaluate long-term micronutrient stability.

## RESULTS

**Effects of direct incorporation and food reformulation**

The bread formulation developed by Álvarez-Quinteros et al. (2025) showed that complementary plant protein concentrates could increase both the amount and nutritional quality of protein while preserving acceptable bread-making characteristics. The results also demonstrated the importance of assessing amino-acid balance and digestibility rather than considering total protein content alone.

For strawberry-fortified yoghurt, Lal et al. (2026) found that increasing the fruit powder level improved the concentration of phenolic compounds, flavonoids, vitamin C and carotenoids, but the most favourable formulation represented a compromise between compositional enhancement and sensory-technological quality. This illustrated a general limitation of direct fortification: the highest addition level is not necessarily the most appropriate product formulation.

**Effects of osmotic and vacuum-assisted mass transfer**

Kulczyński et al. (2025) showed that the chemical form of magnesium substantially influenced enrichment efficiency. Magnesium chloride produced greater enrichment than magnesium oxide or citrate, confirming the importance of mineral solubility, osmotic-medium composition and treatment time for mass transfer.

Karlińska et al. (2025) obtained a dose-dependent increase in apple polyphenols when plant extracts were added to the osmotic solution. Phenolic compounds that were absent from untreated apples were detected after processing, confirming actual transfer from the external medium rather than simple concentration of endogenous compounds. Fratta et al. (2025) demonstrated that vacuum impregnation with a suitable emulsion could introduce a lipophilic compound into mango tissue before drying. Although subsequent solar drying caused carotenoid losses, the impregnation step partially compensated for degradation during the preservation stage. Ismail et al. (2025) showed that pomegranate juice concentrate could function simultaneously as an osmotic medium and a source of bioactive compounds for orange slices. The study also illustrated the importance of integrating enrichment with the subsequent drying operation, because the final composition depended on both stages.

**Effects of encapsulation-assisted fortification**

Ferreira et al. (2026) showed that liposome composition strongly affected vitamin stability. Optimised phospholipid systems provided high retention of vitamin D3, while pectin-coated formulations were particularly effective in protecting vitamin B12. Incorporation into yoghurt did not produce relevant deterioration of product stability or sensory acceptance. The spray-dried grape-pomace system developed by López-Astorga et al. (2025) provided high encapsulation efficiency and improved the preservation of phenolic compounds during storage and simulated gastrointestinal digestion. The findings supported the use of carbohydrate-based wall materials as carriers for plant-derived bioactive compounds in dairy foods.

Rebellato et al. (2025) found that iron bioaccessibility after incorporation was strongly influenced by the surrounding food matrix. The study demonstrated that the performance of an encapsulated fortificant cannot be evaluated solely from particle characteristics, because the final food system can substantially modify nutrient availability.

**Effects of extrusion and coating technologies**

Costa et al. (2026) demonstrated that extruded rice analogues could simultaneously carry a vitamin and a mineral while maintaining technological characteristics compatible with a staple cereal product. Vitamin D remained comparatively stable during the first months of storage but declined during prolonged storage, indicating that successful incorporation does not automatically ensure long-term stability. Ganachari et al. (2026) reported considerable differences in vitamin stability after extrusion and cooking. The different retention profiles confirmed that the initial fortification level may need to include a controlled overage when predictable processing and cooking losses occur. The long-term comparison of Nader et al. (2026) showed relatively good stability for several B-group vitamins, iron and zinc in both coated and extruded fortified rice. Vitamin A was considerably less stable, and embedding it within an extruded matrix provided better protection in blended rice than surface coating under the investigated storage conditions. The results also highlighted the influence of blending uniformity and analytical sampling on the apparent stability of fortified staples.

**Comparative assessment of the investigated technologies**

The investigated approaches represented fundamentally different incorporation mechanisms: dispersion throughout a formulated matrix, solute transfer from a liquid phase into an existing food structure, introduction through a protective carrier, and embedding or deposition within cereal particles.

Their main technological characteristics and representative quantitative results are summarized in Table 1.

**Table 1**

**Comparative characteristics of recent nutrient-incorporation technologies**

| Technology | Food matrix | Introduced compound(s) | Representative result | Reference |
|---|---|---|---|---|
| Direct incorporation | Bread | Lupin + sacha inchi proteins | 20% protein; digestibility 0.86; PDCAAS 0.56 | *Álvarez-Quinteros et al., 2025* |
| Direct incorporation | Yoghurt | Strawberry bioactives | 8% freeze-dried powder selected as the optimum formulation | *Lal et al., 2026* |
| Osmotic dehydration | Beetroot | Mg | Maximum 683.96 mg Mg/100 g | *Kulczyński et al., 2025* |
| Osmotic dehydration | Apple | Polyphenols | Up to 827.1 mg GAE/100 g dry matter | *Karlińska et al., 2025* |
| Vacuum impregnation | Mango | Beta-carotene | 10.5 ppm increased to 20.4-24.0 ppm before drying | *Fratta et al., 2025* |
| Vacuum-osmotic treatment | Orange | Pomegranate bioactives | 21.57% solid gain under optimized treatment conditions | *Ismail et al., 2025* |
| Liposomal encapsulation | Yoghurt | Vitamins D3 + B12 | Approximately 100% D3 retention in optimized LS45 systems after 120 days | *Ferreira et al., 2026* |
| Spray-drying | Greek-style yoghurt | Grape polyphenols | 97.82% encapsulation efficiency | *López-Astorga et al., 2025* |
| Spray-drying/chilling | Yoghurt | Fe | 59.5% iron bioaccessibility in microparticles | *Rebellato et al., 2025* |
| Extrusion | Rice analogue | Mg + vitamin D | 278-287 mg Mg/100 g and 4.53-8.52 µg vitamin D/100 g | *Costa et al., 2026* |
| Cold extrusion | Rice analogue | Vitamins | Retention ranged from approximately 7% for thiamine to 75% for riboflavin | *Ganachari et al., 2026* |
| Extrusion/coating | Rice | Vitamins, Fe, Zn | Vitamin A half-life in blended rice: 6.8 months coated vs. 15.1 months extruded | *Nader et al., 2026* |

Overall, technology selection should be based on the complete food matrix-fortificant-process system rather than on the nutrient alone. Direct incorporation offers the simplest route for formulated products, mass-transfer processes are suited to porous tissues, encapsulation adds a protective delivery function, and extrusion or coating is particularly relevant to cereal staples. A cross-technology comparison further indicates that successful incorporation is only the first stage of an effective fortification strategy. Subsequent operations can modify the benefit obtained during enrichment: drying can degrade sensitive compounds introduced by impregnation, cooking can cause losses from fortified cereal products, and prolonged storage can reduce the concentration of unstable vitamins even when initial incorporation is

satisfactory. For formulated foods, the practical incorporation level may instead be limited by changes in structure, flavour or appearance. Encapsulation can reduce some stability problems, but introduces an additional carrier whose compatibility, release behaviour and processing cost must also be considered. Accordingly, the most informative evaluation is one that follows the fortificant across the complete processing, storage and preparation chain and relates nutritional improvement to the technological and sensory performance of the final food *(Ferreira et al., 2026; Fratta et al., 2025; Ganachari et al., 2026; Nader et al., 2026).*

The degree of structural modification required by each technology is another important distinction. Direct reformulation is appropriate when the product is manufactured from mixed ingredients and its composition can be adjusted before structure formation. By contrast, osmotic and vacuum-assisted processes preserve the recognisable geometry of fruits and vegetables and can therefore enrich an already formed product. Their effectiveness, however, depends on tissue porosity, permeability and the physicochemical compatibility between the fortifying medium and the target compound. This makes mass-transfer approaches attractive for minimally processed products, but also more sensitive to biological variability between raw materials than formulation-based methods *(Asare et al., 2022; Haneef et al., 2024; Vinod et al., 2024).* Encapsulation changes the objective from simply transferring a fortificant to controlling its protection and release. This is especially relevant when the active compound is poorly soluble, oxidation-sensitive or prone to interactions that could impair flavour, colour or nutritional availability.

The additional processing step can improve stability, but it also increases formulation complexity and requires the carrier to remain compatible with the food throughout manufacture, storage and digestion. Extrusion and coating address a different industrial problem: delivery of micronutrients through staple cereal foods in a form that can be blended, stored, transported and prepared using familiar household practices. In such systems, distribution uniformity, resistance to washing and cooking, and stability during long storage become as important as the initial fortification step *(Espinoza-Espinoza et al., 2024; Liu et al., 2025; Rahim et al., 2025).*

From an industrial perspective, the four technological routes should therefore be compared not only by enrichment efficiency but also by equipment requirements, ease of process control, compatibility with existing production lines, sensitivity to raw-material variability and the need for additional stabilization steps. A technologically successful fortified food is one in which the added nutritional value is maintained without creating unacceptable changes in processing behaviour or consumer-relevant quality. This broader criterion is particularly important when laboratory-scale results are translated into continuous or high-throughput production.

## FUTURE RESEARCH PERSPECTIVES

Although recent studies demonstrated the feasibility of incorporating diverse nutrients and bioactive compounds into food matrices, future investigations should extend beyond the amount of fortificant measured immediately after processing. Greater attention should be given to nutrient distribution, retention during realistic storage and domestic preparation, and bioaccessibility or bioavailability following digestion. The combined use of gastrointestinal digestion and cellular models may provide a more comprehensive assessment of the nutritional effectiveness of fortified foods *(López-Astorga et al., 2025; Rebellato et al., 2025).*

Comparison between published studies is currently limited by differences in food matrices, fortificant concentrations, process parameters and reporting methods. Greater standardisation of experimental protocols and reporting criteria would facilitate comparisons between technologies and support process optimisation. Sensory evaluation and long-term stability should also be assessed more systematically, particularly when increased fortification levels affect colour, texture or flavour.

A further priority is the transition from laboratory-scale studies to technically and economically viable industrial processes. Future work should address process scalability, energy and resource efficiency, management or reuse of fortifying solutions, carrier cost and stability, regulatory requirements, and integration with existing food-processing operations *(Asghari et al., 2024; Rahim et al., 2025).*

Particular potential exists for processes enabling the simultaneous incorporation of complementary nutrients and bioactive compounds and for the valorisation of nutrient-rich agricultural and food-processing resources.

## CONCLUSIONS

Recent studies demonstrated that foods with enhanced nutritional and functional value could be developed through direct incorporation, osmotic and vacuum-assisted mass transfer, encapsulation, extrusion and coating.

Direct incorporation represented the simplest enrichment route, whereas mass-transfer technologies were particularly suitable for porous food matrices. Encapsulation provided additional protection for sensitive compounds, while extrusion and coating enabled the fortification of cereal-based staple foods.

The effectiveness of these technologies depended on the characteristics of both the fortificant and the food matrix. Consequently, optimization should consider not only the amount of compound incorporated, but also its retention and stability during processing and storage, interactions with the food matrix, and the technological and sensory characteristics of the final product.

## ACKNOWLEDGEMENT

This work was supported by a grant from the Ministry of Research, Innovation and Digitalisation, under the PNCDI IV Programme, Programme 5.6, Subprogramme 5.6.1 - CoEx - Centres of Excellence, within the project "Nutritional security by innovative strategies for boosting sustainable protein resources exploitation" (PROfutureFOOD), project code PN-IV-P6-6.1-CoEx-2024-0025, Contract No. 11CoEx/02.03.2026.

## REFERENCES

[1] Álvarez-Quinteros, J. F., Lazo-Vélez, M. A., Cordero-Clavijo, L. M., Antunes-Ricardo, M., Avilés-González, J., Villacrés, E., & Serna-Saldívar, S. O. (2025). Protein concentrates from Andean plants (Plukenetia volubilis and Lupinus mutabilis): Impact on protein quality and in vitro biological activity in bread. *ACS Food Science & Technology*, 5(6), 2156-2166. https://doi.org/10.1021/acsfoodscitech.4c01079

[2] Asare, E. O., Bhujel, N. K., Čížková, H., & Rajchl, A. (2022). Fortification of fruit products - A review. *Czech Journal of Food Sciences*, 40(4), 259-272. https://doi.org/10.17221/28/2022-CJFS

[3] Asghari, A., Zongo, P. A., Osse, E. F., Aghajanzadeh, S., Raghavan, V., & Khalloufi, S. (2024). Review of osmotic dehydration: Promising technologies for enhancing products' attributes, opportunities, and challenges for the food industries. *Comprehensive Reviews in Food Science and Food Safety*, 23(3), e13346. https://doi.org/10.1111/1541-4337.13346

[4] Costa, E. S. L., Alves, T. T., Barreto, M. S., Oliveira, M. E. A. S., Carvalho, C. W. P., Antoniassi, R., Gomes, F. S., Torrezan, R., & Takeiti, C. Y. (2026). Designing fortified rice-based analogues for the elderly population. *ACS Food Science & Technology*, 6(3), 732-745. https://doi.org/10.1021/acsfoodscitech.5c01076

[5] Espinoza-Espinoza, L. A., Muñoz-More, H. D., Nole-Jaramillo, J. M., Ruiz-Flores, L. A., Arana-Torres, N. M., Moreno-Quispe, L. A., & Valdiviezo-Marcelo, J. (2024). Microencapsulation of vitamins: A review and meta-analysis of coating materials, release and food fortification. *Food Research International*, 187, 114420. https://doi.org/10.1016/j.foodres.2024.114420

[6] Ferreira, L. S., Luvizzotti, E. H., Ghiraldi, M., Chaves, M. A., & Pinho, S. C. (2026). Yogurt fortification with lyophilized liposomes coencapsulating vitamins D3 and B12: Physicochemical characterization, sensory evaluation and static in vitro digestion. *Journal of Food Science*, 91(2), e70870. https://doi.org/10.1111/1750-3841.70870

[7] Fratta, M., Salvador, P. V., Davidsson, H., & Gómez Galindo, F. (2025). Vacuum impregnation for β-carotene retention in mango prior to solar drying. *AIMS Agriculture and Food*, 10(3), 756-769. https://doi.org/10.3934/agrfood.2025039

[8] Ganachari, A., Nidoni, U., Hiregoudar, S., Ganachari, S., Ramappa, K. T., Naik, N., Vanishree, S., & Mathad, P. F. (2026). Development of vitamin-fortified rice analogs with a focus on extrusion and cooking stability and retention. *Journal of Food Science and Technology*, 63(9), 1682-1690. https://doi.org/10.1007/s13197-025-06337-5

[9] Haneef, N., Hanif, N., Hanif, T., Raghavan, V., Garièpy, Y., & Wang, J. (2024). Food fortification potential of osmotic dehydration and the impact of osmo-combined techniques on bioactive component saturation in fruits and vegetables. *Brazilian Journal of Food Technology*, 27, e2023028. https://doi.org/10.1590/1981-6723.02823

[10] Ismail, M., Özbek, H. N., & Göğüş, F. (2025). Combined vacuum osmotic dehydration by pomegranate juice concentrate and hot-air assisted radiofrequency drying to produce fortified orange slices. *Scientific Reports*, 15, 36001. https://doi.org/10.1038/s41598-025-19708-x

[11] Karlińska, E., Milala, J., Kosmala, M., & Klewicki, R. (2025). Osmotic dehydration of apples in a saccharose solution containing fragrant agrimony or rosehip extract. *Molecules*, 30(24), 4708. https://doi.org/10.3390/molecules30244708

[12] Kulczyński, B., Suliburska, J., Gramza-Michałowska, A., Sidor, A., Kowalczewski, P. Ł., & Brzozowska, A. (2025). The effect of osmotic dehydration conditions on the magnesium content in beetroot (Beta vulgaris L.). *Molecules*, 30(14), 3051. https://doi.org/10.3390/molecules30143051

[13] Lal, S., Singh, M. K., Rai, D. C., Dhyani, P., & Kumar, A. (2026). HR-MS metabolomics unveils the bioactive profile of set yoghurt fortified with freeze-dried strawberry powder. *Applied Food Research*, 6(1), 102007. https://doi.org/10.1016/j.afres.2026.102007

[14] Liu, J., Zheng, X., Khattak, S., Qv, Y., Wang, Y., Uyanga, V. A., Huo, Y., Liu, Z., Cui, Y., Chen, Y., & Liu, Y. (2025). A systematic review of post-harvest rice fortification: Technologies, sensory characteristics, consumer acceptance, and bioavailability. *Food Chemistry*, 485, 144491. https://doi.org/10.1016/j.foodchem.2025.144491

[15] López-Astorga, M., Leon-Bejarano, M., Gámez-Meza, N., Del Toro-Sánchez, C. L., Simsek, S., & Ovando-Martínez, M. (2025). Microencapsulated grape pomace extract as an antioxidant ingredient added to Greek-style yogurt: Storage stability an in vitro bioaccessibility. *Food Chemistry*, 477, 143550. https://doi.org/10.1016/j.foodchem.2025.143550

[16] Miano, A. C., & Rojas, M. L. (2023). Engineering strategies for food fortification. *Current Opinion in Food Science*, 51, 101033. https://doi.org/10.1016/j.cofs.2023.101033

[17] Nader, W., Sarkar, D., Adoko, M., de Pee, S., Ivarsen, E., Shkliar, V., Jensen, S. M., & Hein, J. (2026). Stability of vitamins and minerals in coated and extruded fortified rice kernels stored under real-life conditions over two years and implications for standards. *Rice Science*. Advance online publication. https://doi.org/10.1016/j.rsci.2026.03.007

[18] Rahim, M. A., Zahran, H. A., Jaffar, H. M., Ambreen, S., Ramadan, M. F., Al-Asmari, F., Castro-Muñoz, R., & Zongo, E. (2025). Liposomal encapsulation in food systems: A review of formulation, processing, and applications. *Food Science & Nutrition*, 13(8), e70587. https://doi.org/10.1002/fsn3.70587

[19] Rebellato, A. P., Teixeira, J. L. P., Milani, R. F., Alvim, I. D., Santana, T. M. S., Galland, F., & Morgano, M. A. (2025). Ferrous sulfate microparticles as a food fortification strategy: Application in plant-based yogurt and bioaccessibility assessment. *Food Research International*, 219, 116905. https://doi.org/10.1016/j.foodres.2025.116905

[20] Vinod, B. R., Asrey, R., Sethi, S., Menaka, M., Meena, N. K., & Shivaswamy, G. (2024). Recent advances in vacuum impregnation of fruits and vegetables processing: A concise review. *Heliyon*, 10(7), e28023. https://doi.org/10.1016/j.heliyon.2024.e28023

# EXTRUSION-GRANULATION OF SHEEP WOOL-BASED ORGANO-MINERAL FERTILISER AND CHARACTERISATION OF PROCESS AND PRODUCT

/

# *EXTRUDAREA-GRANULAREA ÎNGRĂȘĂMÂNTULUI ORGANO-MINERAL PE BAZĂ DE LÂNĂ DE OAIE ȘI CARACTERIZAREA PROCESULUI ȘI A PRODUSULUI*

**Gabriela-Victoria MNERIE[1, 2, 3], Evelin-Anda LAZA*[1], Elena-Mihaela NAGY[1]**

[1] National Institute of Research - Development of Machines and Installations Designed to Agriculture and Food Industry - INMA Bucharest / Romania;

[2] Ioan Slavici University, Timișoara, Timis County / Romania;

[2] National Research & Development Institute for Welding and Material Testing - ISIM Timisoara, Timis County / Romania.

*Tel: 0741 122 570; *E-mail: eveline_anda@yahoo.com*

***Keywords:*** *sheep wool, organo-mineral fertiliser, twin-screw extrusion, granulation, process conditions, product characterisation*

## ABSTRACT

*Sheep wool is a nitrogen-containing fibrous residue that can be incorporated into fertilising formulations, but its heterogeneous structure creates handling and processing constraints. This study assessed a continuous extrusion-granulation route for three organo-mineral formulations containing 10, 20 and 30% cut wool. The formulations were processed with a ZK25 co-rotating twin-screw extruder at a solids feed rate of 1.6 kg/h and an extrusion pressure of 15-20 bar, using zone temperatures of 40-40-50-85-85-65 °C and a single 5 mm die opening. The extrudate was dried at 60 °C for 6 h and subsequently granulated. More than 80% of the product was recovered in the 5-7 mm fraction, while moisture ranged from 3.2 to 7.3% and bulk density from 600 to 700 kg/m³. Complementary UHPLC-MS/MS and tomato-seed assays were used to characterise nitrogen release and preliminary biological response. The results showed marked differences among hydrolysis fractions and a concentration-dependent response in the seed assay. The study established a documented process window for further engineering optimisation.*

## REZUMAT

*Lâna de oaie este un reziduu fibros care conține azot și poate fi încorporat în formulări fertilizante, dar structura sa neomogenă generează constrângeri de manipulare și procesare. Studiul a evaluat o rută continuă de extrudare-granulare pentru trei formulări de îngrășământ organo-mineral cu 10, 20 și 30% lână tăiată. Formulările au fost procesate cu un extruder ZK25 cu doi melci corotativi, la un debit al componentelor solide de 1,6 kg/h și o presiune de 15-20 bar, utilizând temperaturile 40-40-50-85-85-65 °C și o matriță cu un singur orificiu de 5 mm. Materialul extrudat a fost uscat la 60 °C timp de 6 h și apoi granulat. Peste 80% din produs s-a încadrat în fracția 5-7 mm, umiditatea a variat între 3,2 și 7,3%, iar densitatea în vrac între 600 și 700 kg/m³. Analizele UHPLC-MS/MS și testele preliminare pe semințe de tomate au caracterizat eliberarea azotului și răspunsul biologic. Rezultatele au evidențiat diferențe între fracțiile de hidroliză și un răspuns dependent de concentrație.*

## INTRODUCTION

Sheep wool is increasingly considered a renewable agricultural feedstock because of its high protein and nitrogen content, but its fibrous structure and variable physical form impose specific requirements for handling and processing *(Broda et al., 2023; Gillespie et al., 2022; Giteru et al., 2023).* Recent studies have examined wool in powder and pellet forms as soil amendments and organic fertilising materials, indicating that material form affects practical behaviour and agricultural use *(Bradshaw and Hagen, 2022; Haque and Naebe, 2022)*.

A complementary research direction has focused on hydrolysis treatments intended to increase keratin accessibility and produce soluble nitrogen-containing fractions. Hydrolysed wool has been investigated as a potential agricultural input, while recent cultivation experiments have examined the effects of wool-derived hydrolysates and wool-based formulations on crop development and nutrient supply *(Gillespie et al., 2022; Sahin et al., 2025; Taskin, 2024).*

These approaches demonstrate the agricultural relevance of wool-derived fractions, but they address a different technological problem from the continuous conversion of fibrous material into a mechanically manageable granular product.

From an agricultural-engineering perspective, the chemical composition of wool represents only one part of the processing problem. The material must also be conditioned into a form that can be continuously introduced into equipment and subsequently stored, transported and distributed. Previous work on wool pellets and granular products has examined bulk density, moisture and water absorption, confirmed the relevance of physical descriptors when designed solid fertilising products *(Bradshaw and Hagen, 2022; Haque and Naebe, 2022; Nagy et al., 2024; Rom et al., 2025).*

Extrusion offers a continuous route in which conveying, mixing, mechanical shearing, thermal conditioning and shaping can be combined within the same processing sequence. Studies on biomass twin-screw extrusion show that screw configuration, liquid-to-solid ratio, pretreatment conditions and material characteristics can influence process response and product properties *(Cavailles et al., 2024; Jiao et al., 2024).* These findings are relevant to the present study because the investigated wool-containing formulations passed continuously through a twin-screw system before downstream cooling, drying and granulation.

The agricultural use of wool-based materials has also been examined in crop and soil experiments. Cut wool has been evaluated as a nitrogen source in winter wheat, while wool and alkaline hydrolysate have been investigated in sugar beet production and keratin hydrolysate has been assessed for effects on plant growth and mineral nutrition *(Broda et al., 2023; Karaca et al., 2023; Sahin et al., 2025; Taskin, 2024)*. These studies underline the need to consider both product composition and physical form when moving from agricultural potential toward an engineered fertiliser product.

The objective of the present study was to experimentally assess an extrusion-granulation route for sheep wool-based organo-mineral fertiliser and to relate formulation and operating conditions to the physical characteristics of the resulting product. The work focused on three formulations containing 10, 20 and 30% cut sheep wool, processed with a ZK25 co-rotating twin-screw extruder followed by cooling, drying and hammer-mill granulation. Physicochemical and preliminary biological analyses were treated as complementary assessments rather than as the principal engineering response variables.

Previous studies have demonstrated the agricultural potential of sheep wool and wool-derived hydrolysates, but fewer studies have addressed the continuous transformation of heterogeneous wool-containing mixtures into a granular fertiliser using an integrated extrusion-granulation route. From an agricultural-engineering perspective, the challenge is not limited to obtaining a chemically suitable formulation; the material must also be continuously conveyed, mixed, shaped, dried and reduced to a controlled particle-size fraction. The present study therefore focuses on the interaction between formulation composition and process conditions, with particular attention to the physical characteristics of the resulting granular product and to the limitations that remain relevant for subsequent scale-up and field application.

## MATERIALS AND METHODS

### Raw material and fertilising formulations

Experimental data were compiled from research activities carried out within project „Research on the use of wool waste to obtain organic fertilizers for agriculture in order to improve soil properties and reduce environmental pollution" during the documented project phases used for this study. Three target formulations were prepared with cut raw sheep wool as the main fibrous component and were identified according to their nominal wool content as R10, R20 and R30. R10, R20 and R30 contained 10, 20 and 30% cut wool by mass, respectively. The remaining components consisted of dry peat, urea, protein hydrolysate obtained with sodium or potassium hydroxide, bone meal and starch. All formulations were balanced to 100% by mass.

**Table 1**

**Composition of the investigated wool-based fertilising formulations**

| *Component* | *R10 [%]* | *R20 [%]* | *R30 [%]* |
|---|---|---|---|
| Cut raw wool | 10.0 | 20.0 | 30.0 |
| Dry peat, 20% moisture | 9.3 | 15.1 | 15.1 |
| Urea | 6.0 | 14.9 | 14.9 |
| NaOH wool-protein hydrolysate | 42.8 | - | - |

| | | | |
|---|---|---|---|
| KOH wool-protein hydrolysate | - | 29.0 | 20.0 |
| Bone meal | 2.1 | 6.0 | 6.0 |
| Starch | 29.8 | 15.0 | 14.0 |
| **Total** | **100.0** | **100.0** | **100.0** |

The formulation strategy was designed to investigate the effect of increasing the proportion of cut wool while maintaining a processable organo-mineral matrix. Wool acted as the fibrous and nitrogen-containing component, whereas peat contributed to the organic matrix and moisture-related behaviour. Urea provided an additional readily available nitrogen source, while the alkaline wool-protein hydrolysates represented processed nitrogen-containing fractions. Bone meal and starch were incorporated to adjust the formulation composition and improve the structural characteristics of the extruded material. Consequently, increasing the wool content simultaneously modified the fibre fraction, the proportion of hydrolysate and the balance between structural and readily available nitrogen sources.

**Extrusion-granulation equipment and operating conditions**

The technological route was implemented using components of an extrusion installation available at INMA. The processing line comprised a volumetric powder feeder with double screw, a ZK25 co-rotating twin-screw extruder, a forming die, a cooling chamber and a hammer mill for granulation. The peristaltic pump belonging to the complete installation was not used in the investigated process.

The feeding unit was a volumetric double-screw feeder designed for powdered materials with particle sizes between approximately 2 and 40 μm and a moisture content of up to 15%. The feed rate could be adjusted continuously within the range of 0.3-10 kg/h. Continuous feeding was used to limit variations in material throughput and in the properties of the processed product.

The extrusion unit was a ZK25 Collin twin-screw extruder equipped with two modular co-rotating screws. The screw diameter was 25 mm and the screw length was L = 30D; the maximum screw rotational speed was 400 rpm and the maximum declared throughput was 15 kg/h. The barrel was modular and equipped with independently heated and cooled processing zones with temperature sensors and ECS microprocessor control. The forming die had a single 5 mm opening and an independent heating system with an installed power of 5 kW. The cooling chamber reduced the material temperature before collection and subsequent granulation. The hammer mill had a 220 mm rotor operating at 1000 rpm and was driven by a 500 W single-phase motor. The extrusion installation used in the experimental campaign is shown in Fig. 1.




**Fig. 1 - ZK25 Collin co-rotating twin-screw extrusion installation used for producing the wool-based fertiliser**
*1 - peristaltic pump; 2 - powder feeder; 3 - extruder; 4 - die; 5 - cooling chamber*

The granulometric powder obtained after conditioning was incorporated into three organo-mineral formulations containing 10, 20 and 30% cut wool (R10, R20 and R30). The formulations were processed using a continuous extrusion-granulation route (Fig. 2), developed to convert the heterogeneous wool-

containing mixture into uniform granules. The process included continuous feeding, extrusion through a 5 mm die, cooling, drying and hammer-mill granulation, followed by the recovery of the final granular fertiliser. The sequence was designed to ensure stable processing and to produce a material with defined particle size, low moisture and suitable handling properties for subsequent storage and agricultural application.

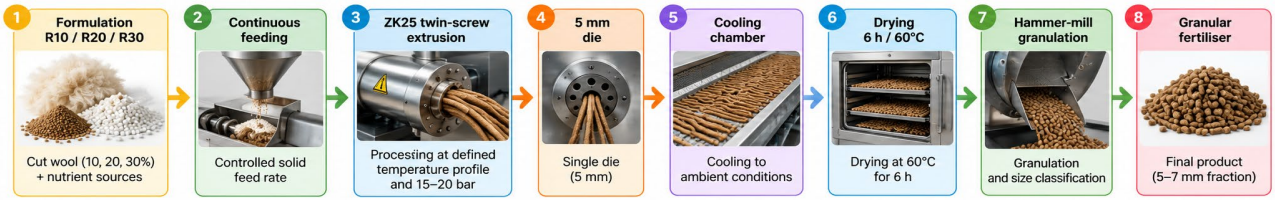



**Fig. 2 - Engineering sequence used for producing the wool-based granular fertiliser**

The formulated mixtures were introduced through the main feeding point in zone Z1. During processing, the co-rotating screws transported, mixed and subjected the material to mechanical shearing and thermal conditioning. The screw action generated pressure towards the forming die, while screw rotational speed was an adjustable machine variable. The documented trial window comprised a solids feed rate of 1.6 kg/h, an extrusion pressure of 15-20 bar, and zone temperatures of 40, 40, 50, 85, 85 and 65 °C for Z1-Z6. The extrudate was cooled and then dried at 60 °C for 6 h before hammer-mill granulation.

**Table 2**

**Main operating parameters of the extrusion-granulation process**

| Parameter | Unit | Experimental value |
|---|---|---|
| Solid feed rate | kg/h | 1.6 |
| Extrusion pressure | bar | 15-20 |
| Z1 temperature | °C | 40 |
| Z2 temperature | °C | 40 |
| Z3 temperature | °C | 50 |
| Z4 temperature | °C | 85 |
| Z5 temperature | °C | 85 |
| Z6 temperature | °C | 65 |
| Die opening | mm | 5 |
| Drying time | h | 6 |
| Drying temperature | °C | 60 |
| Hammer-mill rotor speed | rpm | 1000 |
| Hammer-mill motor power | W | 500 |
| Solid feed rate | kg/h | 1.6 |

The available documentation does not provide a separate experimental screw-speed value for each formulation, nor does it report torque, specific mechanical energy, residence-time measurements or formulation-specific throughput. These variables were therefore not reconstructed or inferred.

The selected thermal profile was intended to provide progressive conditioning of the formulation rather than abrupt heating. The relatively low temperatures in the first zones favour feeding and initial conveying, while the higher temperatures in zones Z4 and Z5 promote material softening and facilitate the passage of the formulation through the die. The reduction in temperature in the final zone supports the transition towards the forming section and reduces excessive thermal exposure. The 5 mm die opening was selected as a compromise between continuous extrudate formation and subsequent size reduction during hammer-mill granulation.

**Product characterisation and complementary analyses**

The obtained material was characterised using particle-size fraction, moisture content and bulk density as the principal physical descriptors. The documented product specifications were a 5-7 mm fraction

accounting for more than 80% of the material, final moisture of 3.2-7.3% and bulk density of 600-700 kg/m$^3$. These descriptors were selected because they directly described the transformation of the heterogeneous fibrous feedstock into a particulate product intended for subsequent handling and agricultural application. Representative products from R10, R20 and R30 are shown in Fig. 3.



*(a)* *(b)* *(c)*

**Fig. 3 - Granular wool-based fertiliser obtained from the three formulations**

*(a) R10 (10% wool), (b) R20 (20% wool) and (c) R30 (30% wool)*

A separate composite material, designated Pellet A, was analysed for nitrogen-bearing compounds after enzymatic and alkaline hydrolysis. Pellet A contained 39% wool hydrolysate, 11% cut wool, 12% fertiliser based on urea and NPK 20-20-0, 12% starch, 9% peat and 17% corn meal. Hydrolysed samples were dried, milled and homogenised. Free amino acids and nitrogen-bearing compounds were quantified by ultra-high-performance liquid chromatography-tandem mass spectrometry (UHPLC-MS/MS) using a hydrophilic interaction liquid chromatography (HILIC) column and isotope-labelled internal standards. Calibration covered 0.5-500 µg/L ($r^2 \geq 0.995$), spike recovery was 85-110%, analytical precision was below 10% RSD, and measurements were performed in triplicate. One-way ANOVA followed by Tukey HSD was used at $p < 0.05$. Preliminary biological validation used wool-derived extracts at concentrations of 0, 20, 40, 60 and 80%. Tomato seeds were evaluated at 120 and 192 h for germination percentage, root length, coleoptile length, root growth rate and coleoptile growth rate. Three observations were recorded for each condition. Two-way ANOVA assessed extract concentration, evaluation time and their interaction. Normality and homogeneity of variance were checked using the Shapiro-Wilk and Levene tests. Linear, exponential and four-parameter logistic dose-response models were compared using $R^2$, and EC50 values were estimated where supported by the fitted model.

## RESULTS

### Processing response of the three formulations

The three formulations were successfully processed through the investigated extrusion-granulation route. Increasing the wool fraction from 10 to 30% changed the balance between structural fibre, hydrolysate and other solid components, thereby defining three materially distinct feed formulations. Continuous feeding and formation of an extruded material were documented for all three variants.

The process operated at a solids feed rate of 1.6 kg/h and an extrusion pressure of 15-20 bar. The thermal profile increased from 40 °C in the first two zones to 85 °C in zones Z4 and Z5 and decreased to 65 °C in Z6. Together with the single 5 mm die opening, these conditions defined the documented processing window. The subsequent cooling and drying operations produced material suitable for hammer-mill processing. The hammer mill operated at 1000 rpm with a 500 W motor. The available dataset established process feasibility but did not permit calculation of throughput efficiency or energy demand for each formulation. The documented process window provided continuous extrusion and subsequent granulation for all three formulations. This finding is relevant because the introduction of wool fibres into an organo-mineral matrix may cause feeding irregularities, bridging or unstable conveying if the fibrous fraction is not adequately conditioned. The absence of documented interruption during the investigated trials indicates that the selected formulations and process conditions were compatible with the available equipment at laboratory scale. Nevertheless, process stability should be further quantified through measurements of torque fluctuations, specific mechanical energy, residence time and actual throughput.

### Physical characteristics of the granular product

More than 80% of the final material was recovered in the 5-7 mm particle fraction. Moisture ranged from 3.2 to 7.3%, while bulk density was approximately 600-700 kg/m$^3$. The product was therefore converted from an initially heterogeneous fibrous feedstock into a substantially more defined particulate form.

These measurements described the basic physical state of the product. They did not, however, establish flowability, mechanical durability, abrasion resistance or fertiliser-spreader metering performance.

The conversion of the initial fibrous material into a predominantly 5-7 mm granular fraction represents an important technological outcome of the investigated route. A relatively narrow dominant particle-size fraction is advantageous compared with untreated loose wool because it can facilitate storage, handling and subsequent dosing. At the same time, the reported fraction does not by itself demonstrate suitability for commercial fertilizer spreading, since flowability, abrasion resistance, mechanical durability and metering behaviour were not experimentally quantified.

The measured moisture interval of 3.2-7.3% indicates that the drying stage produced a comparatively dry final material. Moisture is particularly relevant for wool-containing granules because it can influence mechanical strength, storage stability, caking tendency and subsequent disintegration. The reported bulk density of approximately 600-700 kg/m³ also indicates a substantial increase in physical compactness compared with loose fibrous wool, although the study did not quantify the densification ratio relative to the untreated raw material.

**Physicochemical characterisation**

Free-nitrogen measurements differed markedly among the hydrolysis fractions (Table 3). Alkaline fractions generally showed higher values than the corresponding enzymatic fractions, while PAALU exhibited the highest value and the largest variability. Apparent nitrogen release spanned 0.16-38.06%. Because Pellet A contained hydrolysate, cut wool, urea and NPK 20-20-0, the PAALU value represented release from a composite matrix rather than a conversion yield from pure wool. The complementary amino-acid analysis also showed treatment-dependent profiles.

**Table 3**

**Free nitrogen measured after hydrolysis of wool-based materials**

| Treatment | Free N [mg/100 g] | Apparent N release [%] |
|---|---|---|
| Wool pellets | 30.02 ± 1.14 | 0.19 |
| WES | 63.47 ± 1.00 | 0.40 |
| WELU | 386.67 ± 5.73 | 2.42 |
| WAS | 188.63 ± 3.53 | 1.18 |
| WALU | 1108.00 ± 47.86 | 6.93 |
| PAES | 25.01 ± 0.16 | 0.16 |
| PAELU | 373.57 ± 3.53 | 2.33 |
| PAAS | 837.99 ± 12.11 | 5.24 |
| PAALU | 6090.39 ± 5174.67 | 38.06 |

**Preliminary biological response**

The preliminary seed assay demonstrated that the biological response was strongly dependent on extract concentration and exposure time. Germination declined markedly as extract concentration increased, indicating that the soluble fraction released from the tested wool-derived material can exert a measurable biological effect under the conditions of the assay. The fitted four-parameter logistic models provided high coefficients of determination for root-length response, with $R^2$ values of 0.989 at 120 h and 0.999 at 192 h.

The estimated EC50 values of 15.47% and 18.12% for the two assessment times indicate that root development responded sensitively to increasing extract concentration. This observation is relevant from a product-development perspective because biological response cannot be evaluated independently from nutrient concentration and soluble fractions. A material with high nitrogen release potential may require optimisation of formulation and application dose in order to avoid excessive local concentrations after soil application.

The seed test should nevertheless be regarded as preliminary biological screening rather than as evidence of field-level fertilizer performance. The experiment used three observations per condition and an extract-based exposure system, which differs from the physical and chemical environment of an agricultural

soil. Further validation should therefore use soil incubation, pot experiments and field trials at agronomically realistic application rates.

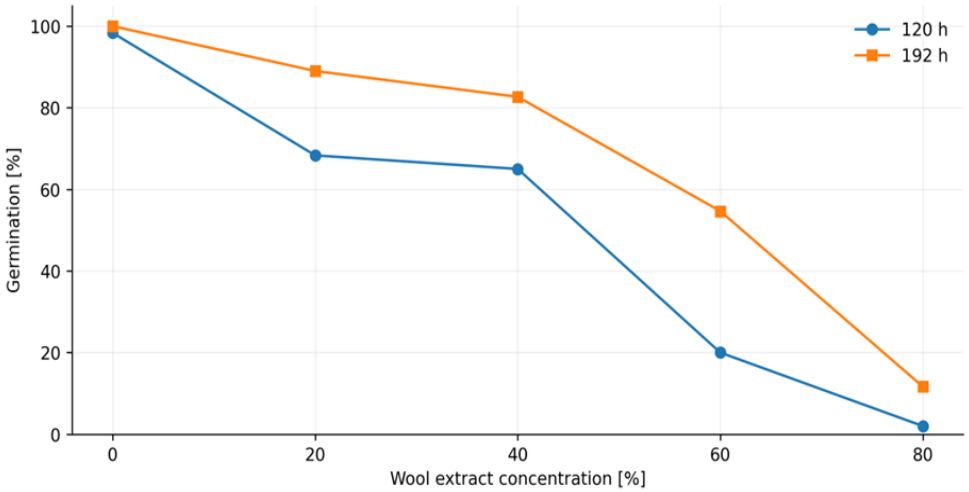



**Fig. 4 - Effect of wool-extract concentration on tomato seed germination at 120 and 192 h**

The germination assay showed a concentration-dependent response. Mean germination decreased from 98.33% at 0% extract to 2.00% at 80% extract after 120 h; at 192 h, it decreased from 100.00% to 11.67%. Root length was more sensitive than germination, with four-parameter logistic models yielding $R^2$ values of 0.989 at 120 h and 0.999 at 192 h and EC50 estimates of 15.47% and 18.12%, respectively. Concentration effects were significant at $p < 0.001$, while time was also significant and concentration × time interactions were detected for several biological endpoints. The values in Fig. 4 represent the means of three observations for each condition.

## CONCLUSIONS

The study demonstrated the feasibility of processing sheep wool-containing organo-mineral fertiliser formulations through a continuous extrusion-granulation route. Three formulations containing 10, 20 and 30% cut wool were processed using a ZK25 co-rotating twin-screw extruder followed by cooling, drying and hammer-mill granulation.

The documented processing window comprised a solids feed rate of 1.6 kg/h, an extrusion pressure of 15-20 bar and a $Z_1$-$Z_6$ temperature profile of 40-40-50-85-85-65 °C. The 5 mm die opening and subsequent conditioning produced a granular product in which more than 80% of the material occurred in the 5-7 mm fraction, with moisture of 3.2-7.3% and bulk density of approximately 600-700 kg/m$^3$.

Complementary physicochemical analysis showed marked differences among hydrolysis fractions, while the tomato-seed assay demonstrated a concentration-dependent biological response and greater sensitivity of root development than germination. These observations provided complementary information for future formulation and application studies.

The results should be regarded as process-development data rather than as a complete machine optimisation. Torque, electrical energy consumption, residence time, formulation-specific throughput, mechanical durability, flowability and fertiliser-spreader metering were not quantified. Future work should address these variables together with pilot-scale mass and energy balances and controlled agricultural validation.

## ACKNOWLEDGEMENT

The results were obtained with the support of MCID through the NUCLEU Program, contract no. 9N/01.01.2023 project PN 23 04 02 02 „Research on the use of wool waste to obtain organic fertilizers for agriculture in order to improve soil properties and reduce environmental pollution”.

## REFERENCES

[1] Bradshaw, T., & Hagen, K. (2022). Wool pellets are a viable alternative to commercial fertilizer for organic vegetable production. Agronomy, 12(5), 1210. https://doi.org/10.3390/agronomy12051210.

[2] Broda, J., Gawlowski, A., Rom, M., & Kobiela-Mendrek, K. (2023). Utilisation of waste wool from mountain sheep as fertiliser in winter wheat cultivation. Journal of Natural Fibers, 20(2), 2200047. https://doi.org/10.1080/15440478.2023.2200047.

[3] Cavailles, J., Vaca-Medina, G., Wu-Tiu-Yen, J., Labonne, L., Evon, P., Peydecastaing, J., & Pontalier, P.-Y. (2024). Aqueous pretreatment of lignocellulosic biomass for binderless material production: Influence of twin-screw extrusion configuration and liquid-to-solid ratio. Molecules, 29(13), 3020. https://doi.org/10.3390/molecules29133020.

[4] Gillespie, G. D., Dada, O., & McDonnell, K. P. (2022). The potential for hydrolysed sheep wool as a sustainable source of fertiliser for Irish agriculture. Sustainability, 14(1), 365. https://doi.org/10.3390/su14010365.

[5] Giteru, S. G., Ramsey, D. H., Hou, Y., Cong, L., Mohan, A., & Bekhit, A. E. D. A. (2023). Wool keratin as a novel alternative protein: A comprehensive review of extraction, purification, nutrition, safety, and food applications. Comprehensive Reviews in Food Science and Food Safety, 22(1), 643-687. https://doi.org/10.1111/1541-4337.13087.

[6] Haque, A. N. M. A., & Naebe, M. (2022). Waste wool powder for promoting plant growth by moisture retention. Sustainability, 14(19), 12267. https://doi.org/10.3390/su141912267.

[7] Jiao, T., Liang, F., Fang, G., Jiao, J., Huang, C., Tian, Q., Zhu, B., Deng, Y., Han, S., & Zhou, X. (2024). An integrated pretreatment strategy for enhancing enzymatic hydrolysis efficiency of poplar: Hydrothermal treatment followed by a twin-screw extrusion. Industrial Crops and Products, 211, 118169. https://doi.org/10.1016/j.indcrop.2024.118169.

[8] Karaca, U. Ç., Chalabee, O. A. H., & Saba, M. (2023). The effect of sheep wool fertilizer on some biochemical properties of a clay loam soil. Communications in Soil Science and Plant Analysis, 54(1), 48-61. https://doi.org/10.1080/00103624.2022.2109662.

[9] Nagy, E.M., Fodorean, T.G., Cioica, N., & Fechete-Tutunaru, L.V. (2024). Comparative research on wool pellets regarding some physico-chemical characteristics for their use in agriculture. Annals of Faculty Engineering Hunedoara - International Journal of Engineering, 22(1), 61-64.

[10] Nagy, E.M., Fodorean, T.G., Deac, T., & Fechete-Tutunaru, L.V. (2024). Research on wool waste processing technologies for use in agricultural crops. In Proceedings of ISB-INMA TEH 2024 Agricultural and Mechanical Engineering, ISSN 2537 – 3773, 722-727.

[11] Nagy, E.M., Fodorean, T.G., Laza, E.-A., & Fechete-Tutunaru, L.V. (2025). Research on the influence of the organic component on the characteristics of organo-mineral fertilizer pellets. Acta Technica Corviniensis - Bulletin of Engineering, 18(3), 37-41.

[12] Nagy, E.M., Fodorean, T.G., Laza, E.-A., & Gheres, M. (2025). Research on the influence of raw wool quality on the parameters for obtaining hydrolysate by the alkaline method. In Proceedings of ISB-INMA TEH 2025 Agricultural and Mechanical Engineering, p. 42-47.

[13] Nagy, E. M., Fodorean, T. G., Nica, D. V., Laza, E.-A., & Vintila, T. (2024). Researches for the physico-chemical characterization of some granular fertilizers obtained from native wool waste, in order to use them in agriculture. Scientific Papers. Series E. Land Reclamation, Earth Observation & Surveying, Environmental Engineering, 13, 320-325.

[14] Rom, M., Broda, J., Kukulski, T., Gawlowski, A., & Kobiela-Mendrek, K. (2025). The morphology of wool fibers biodegraded in natural conditions in soil. Journal of Natural Fibers, 22(1), 2446947. https://doi.org/10.1080/15440478.2024.2446947.

[15] Sahin, O., Yagcioglu, K. D., Kadioglu, Y. K., Ozturk, H. S., & Gunes, A. (2025). Valorization of sheep wool: Impact of keratin hydrolysate on the growth and mineral nutrition of lettuce, spinach, and radish plants. Journal of Soil Science and Plant Nutrition, 25, 2642-2652. https://doi.org/10.1007/s42729-025-02289-z.

[16] Taskin, M. B. (2024). Reducing mineral fertilizer usage: Utilizing sheep wool and alkaline hydrolysate for enhanced sugar beet cultivation. Sugar Tech, 26, 1653-1664. https://doi.org/10.1007/s12355-024-01426-9.

[17] PN 23 04 02 02, „Research on the use of wool waste to obtain organic fertilizers for agriculture in order to improve soil properties and reduce environmental pollution”, (2023-2026), Bucharest, NUCLEU programme contr. 9N/01.01.2023.

# SIMULATOR AND ACCELERATED TESTING OF SOME SINTERED COMPONENTS USED IN AGRICULTURAL MACHINERY

/

# *TESTARI IN REGIM SIMULATOR SI ACCELERAT PENTRU UNELE ELEMENTE SINTERIZATE DIN COMPONENTA UTILAJELOR AGRICOLE*

**Elena Mihaela NAGY*[1)], Teodor Gabriel FODOREAN[1)], Evelin-Anda LAZA[1)], Marius GHERES[2)]**

[1)] National Institute of Research-Development for Machines and Installations Designed for Agriculture and Food Industry-INMA Bucharest / Romania;

[2)] Technical University of Cluj-Napoca, Faculty of Automotive, Mechatronics and Mechanical Engineering, Cluj-Napoca, Cluj County / Romania.

**Tel: 0748 165 302; *E-mail:nagy_m2002@yahoo.co.uk*

***Keywords:*** *sintered components, bushing, pinion, agricultural machinery, accelerated testing*

## ABSTRACT

*Agricultural machinery contains many highly loaded components that must operate reliably under combined static, dynamic, thermal, and tribological loads. Powder metallurgy offers an attractive manufacturing method for such parts, as it allows for the production of complex geometries, low energy consumption, and favorable operational behavior in lubricated assemblies. This article presents a comparative experimental evaluation of two sintered components: a bushing from the B1 cardan shaft, manufactured by BINACCHI, and a driven pinion for the oil pump of a tractor engine. Dedicated test stands were used for testing under simulated and accelerated operating conditions, which reproduced the relevant operating loads. The results indicate stable operation, limited wear, and no significant loss of functional integrity for either component, supporting the applicability of sintered parts in agricultural transmissions and lubrication systems.*

## REZUMAT

*Mașinile agricole conțin numeroase componente supuse unor solicitări intense, care trebuie să funcționeze în mod fiabil în condiții de solicitări combinate statice, dinamice, termice și tribologice. Metalurgia pulberilor oferă o metodă de fabricație atractivă pentru astfel de piese, deoarece permite realizarea unor geometrii complexe, un consum redus de energie și un comportament favorabil în exploatare în ansamblurile lubrifiate. Acest articol prezintă o evaluare experimentală comparativă a două componente sinterizate: o bucșă de la transmisia cardanica B1, fabricatie BINACCHI și un pinion antrenat pentru pompa de ulei a unui motor de tractor. Pentru testare au utilizate standuri dedicate, în condiții de funcționare simulate și accelerate, care au reprodus sarcinile relevante de funcționare. Rezultatele indică o funcționare stabilă, o uzură limitată și nicio pierdere semnificativă a integrității funcționale pentru niciuna dintre componente, susținând aplicabilitatea pieselor sinterizate în transmisiile agricole și în sistemele de lubrifiere*.

## INTRODUCTION

Agricultural machines and equipment operate under particularly demanding conditions, characterized by variable loads, vibrations, friction, and wear, as well as exposure to dust, moisture, and soil particles. The failure of critical wear-resistant parts is responsible for over 50% of rural machinery breakdowns (*Wang, Y et al., 2023*).

In this context, the appropriate selection of materials and manufacturing processes represents an important factor in improving performance and reducing operating costs. One modern manufacturing process used for the production of specific mechanical components is powder metallurgy, through which sintered parts are manufactured.

Sintering is a manufacturing process in which metallic powders are compacted in dies to produce components with shapes and dimensions close to those of the final product. The compacted parts are subsequently heated to a temperature below the melting point of the main material.

During the heat treatment, particle bonding and consolidation take place, resulting in components with controlled mechanical and physical properties. An important advantage of this process is the possibility of producing components with complex geometries while requiring a reduced number of subsequent

machining operations. This can lead to lower material consumption and reduced manufacturing costs (*German, R. M., 2005*; *ASM International, 1998*).

In agricultural machinery manufacturing, sintered parts can be used for the production of components such as bushings, bearings, gears, pinions, cams, transmission components, and other parts subjected to friction and wear (*Gogaev, K. A., et al., 2016*; *Ilyushchanka, A. et al., 2017; ASM International, 1998*) Bushings and bearings manufactured using powder metallurgy are of particular interest due to the possibility of obtaining materials with controlled porosity. The pores can act as lubricant reservoirs, thereby contributing to friction reduction and improved operating performance (*Anselmo, L.M.,et al., 2022*).

This characteristic is particularly important for agricultural machinery mechanisms, where components are subjected to repetitive loads and must operate reliably under variable loading conditions (*Upadhyaya, G. S., 2002*).

Another significant advantage of sintered parts is the possibility of adjusting their chemical composition and material properties according to the intended application. By appropriately selecting the metallic powders, compaction pressure, and sintering parameters, components with properties tailored to specific loading conditions can be obtained *(Hu Q, et al., 2023*). Furthermore, modern powder metallurgy processes enable the manufacture of components with high dimensional accuracy and good reproducibility in mass production (*German, R. M., 2014*; *Davis, J. R., 1991).*

The use of sintered components can also provide significant economic and technological benefits. Reduced material waste, a lower number of machining operations, and the possibility of automating the manufacturing process contribute to increased production efficiency. In addition, the use of appropriate materials and manufacturing technologies can improve the operating characteristics of components and extend the service life of mechanical assemblies.

Before sintered components are used into machinery, their behaviour must be checked under conditions representative of the intended application. The two studies integrated here address distinct but complementary components.

The first evaluates sintered bushings intended to replace needle bearings in the universal joints of a BINACCHI B1 cardan transmission used on agricultural equipment. The second examines a sintered driven gear installed in the oil pump serving the engine fitted to wheeled agricultural tractors.

The common objective of this paper is to present and compare the reported simulated and accelerated test results for these components, focusing on thermal behaviour, dimensional change, visible damage and functional stability. Because the components were tested on different rigs and under different loading variables, the results are presented as two application-specific test programmes rather than as a direct quantitative comparison of wear resistance.

## MATERIALS AND METHODS

Each investigation used a test batch of eight sintered components manufactured by SC Sinterom SA Cluj-Napoca. The cardan-joint bushings (Figure 1) were produced from Ancorsteel 2000 steel powder (Höganäs) and the oil-pump driven gears (Figure 2), reference 110.08.012, were produced from Ancorsteel 4600 steel powder (Höganäs).



**Fig. 1 - Sintered Bushing**



**Fig. 2 - Sintered gear wheel**

The ***sintered bushings*** were intended to replace the sliding bearings of the B1 cardan joint and were tested on a dedicated test stand designed and built by INMA București, Cluj-Napoca Branch.

The stand for testing the bushings (Figure 3.) included a 15 kW electric motor and a speed of 1440 rot/min, while the belt transmission reduced the speed to 540 rot/min, which was the operating regime selected for the tests. The cardan shaft had a maximum torque of 210 N·m, and the hydraulic pump functioned as a brake capable of generating the resisting moment required for loading the joint.

The test program was designed around four inclination angles: 5°, 10°, 20°, and 30° and the duration of testing was derived from the nominal service conditions of the joint and adapted to an accelerated regime (Table 1). Temperature and dimensional variations were monitored with a digital multimeter, calipers, micrometers, and other precision instruments.

The cardan shaft is manufactured by Binacchi in Italy. Its main specifications include: maximum power: 12 kW; maximum torque: 210 N·m; minimum length: 600 mm; maximum length: 780 mm. This results in a variation of 180 mm in the distance between the two universal joints of the cardan shaft, which allowed for a maximum tilt angle of 30° during the experiments.

To determine the test method and the test program, the methods specified in the catalogs of BINACCHI (Italy), WALTERSCHEID GmbH (Germany), and INVOLINI (Italy) were used.

The durability of the cardan shaft is determined by the torque, the rotational speed, and the shaft's angle of inclination. The torque of the shaft was calculated based on the power and rotational speed at which the pump is operated on the test bench.

At a speed of 540 rpm, the power required to drive the pump is 11.2 kW, at this speed, the pump delivers a flow rate of 110 l/min at a pressure of 49 bar.

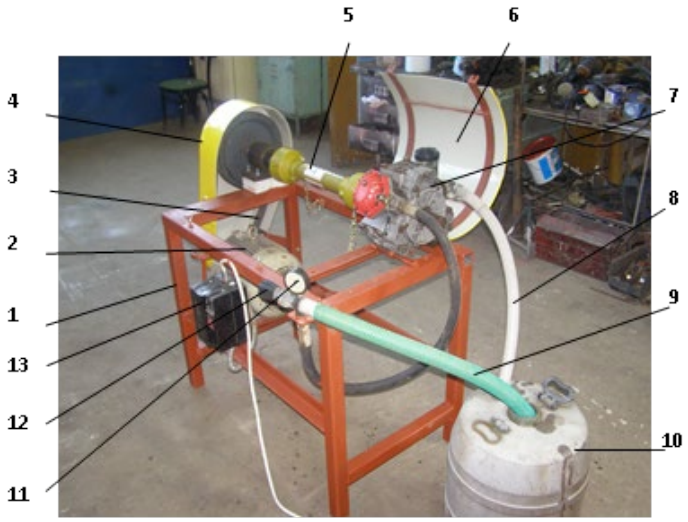



**Fig. 3 - Sintered bushing testing stand**

*1-Support frame, 2-Electric motor, 3-Belt drive, 4-Belt drive guards, 5-Cardan shaft, 6-Cardan shaft guards, 7-Pump, 8-Suction line, 9-Discharge line, 10-Tank, 11-Pressure gauge, 12-Pump pressure control valve, 13-Switch*

**Table 1**

**Test-time distribution**

| Inclination angle (°) | Nomogram time (h) | Weight | Accelerated test time (h) | Time per series (h) |
|---|---|---|---|---|
| 5 | 1200 | 1/12 | 8.30 | 25 |
| 10 | 550 | 1/6 | 16.70 | 23 |
| 20 | 136 | 1/4 | 25.00 | 8.5 |
| 30 | 28 | 1/2 | 50.00 | 3.5 |
| Total | — | 1/1 | 100.0 | 60 |

The ***driven-gear tests*** were performed on an INMA-designed stand (Figure 4) incorporating a 1.5 kW electric motor (1415 rot/min), a spur-gear transmission with helical teeth, the oil pump with a maximum discharge pressure of 3.5 bar at the test speed, an oil reservoir, a cooler, a pressure gauge and a flow-regulating valve. The oil pump is manufactured by SC Pulsor SA. Diesel engine oil M40 SUPER 2, API CC/CD, was used.

Through its design and operation, the test stand ensures both the load testing of the pump's driven pinion and the variation of the pump's resistance torque, as well as the cooling of the oil to maintain its temperature at levels similar to those encountered during operation.

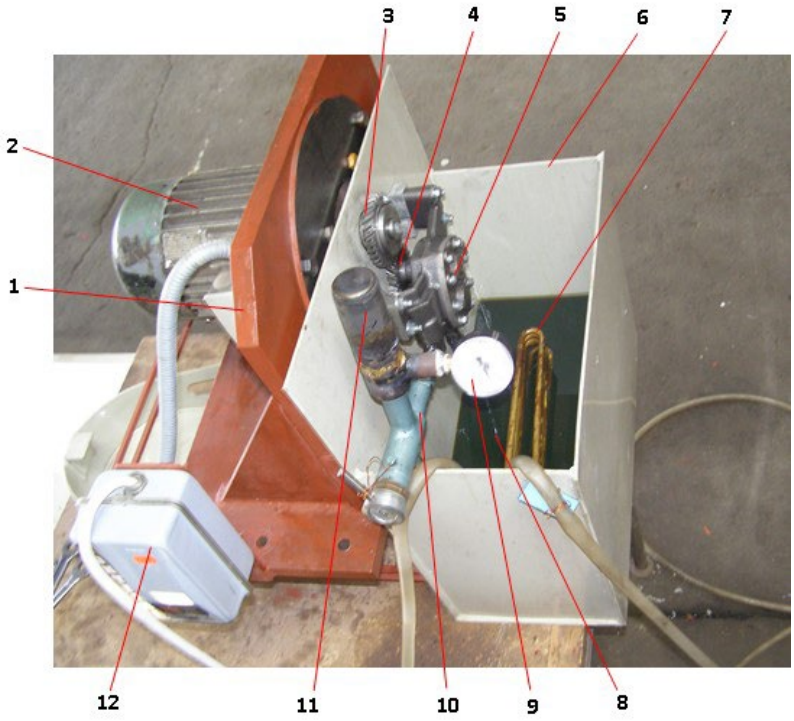



**Fig. 4 - Driven gears testing stand**

*1- Support frame, 2- Electric motor, 3 – Transmission drive pinion, 4- Transmission driven pinion,5 – Pump, 6 – Oil reservoir, 7 – Cooler, 8 – Pump suction line, 9 – Pressure gauge,10 – Pump discharge line, 11 – Flow control valve, 12 – Switch*

The test was based on an annual average pump operating time of 1500 h. A total of 300 h (20% of that reference duration) was assigned to testing at 2.5, 5 and 6 bar. The respective allocations are presented in Table 2.

Testing proceeded from the lowest to the highest pressure. Temperature was monitored during operation, and the pinions were measured before and after testing to assess wear.

**Table 2**

**Distribution of the driven-gear test time**

| Pressure (bar) | Share (%) | Test time (h) |
|---|---|---|
| 2.5 | 10 | 30 |
| 5 | 30 | 90 |
| 6 | 60 | 180 |
| Total | 100 | 300 |

## RESULTS

### Bushing behavior

The bushing tests showed a clear influence of cardan-joint inclination on the thermal regime. As the inclination angle increased, the operating temperature increased. For a 10° inclination, the measurements indicate an initial temperature of approximately 37 °C after one hour and a relatively stable thermal regime around 50–55 °C (Figure 3).

At a constant operating condition, temperature increased with accumulated operating time until a relatively stable thermal equilibrium was reached (Figure 4). The study also reports that the equilibrium temperature increased as the accelerated test period progressed, indicating the influence of wear on the thermal behavior.

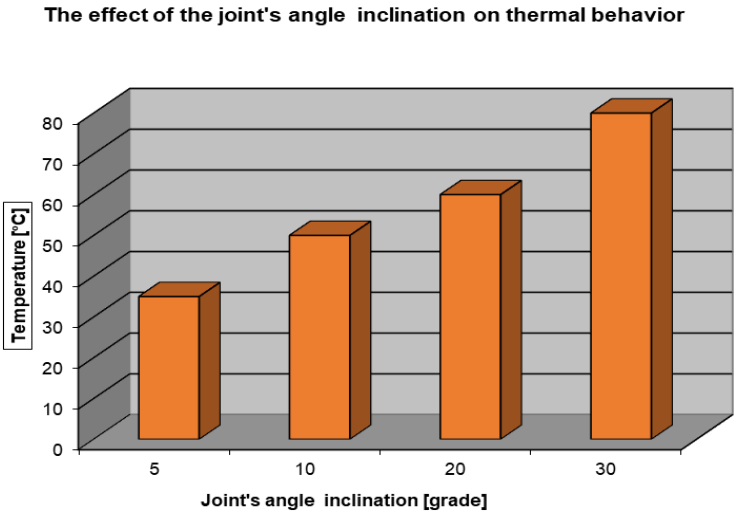



**Fig. 5 - The influence of joint`s angle on thermal behaviour**

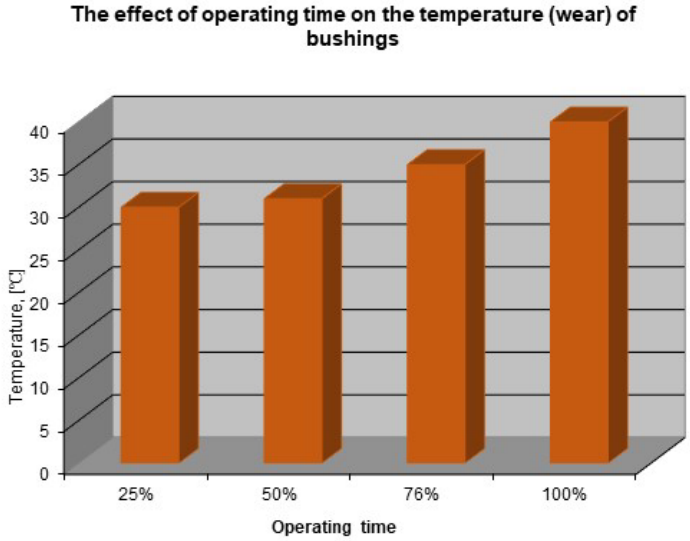



**Fig. 6 - The effect of operating time on temperature (wear)**

Dimensional inspection after testing showed that the outer diameter, which corresponds to the mounting surface in the cardan-joint fork, exhibited wear in the range 0.067–0.120 mm. This wear may be associated with the possibility of bushing rotation in the fork bore and with more pronounced heating at higher inclination angles. The inner diameter exhibited ovalization in the direction of the transmitted torque. By contrast, the width of the bushings remained largely unchanged, with a maximum wear of 0.06 mm.

**Driven-gear behavior**

The sintered driven gear operated throughout the programmed 300 h without phenomena requiring interruption of the tests. The pump pressure remained stable for each selected pressure setting, and the gear showed appropriate constructive-functional behavior and correct meshing with the driving gear.

After dismantling, visual inspection showed no significant pitting on the tooth flanks and the tooth surfaces retained an appropriate appearance. The wear at the tooth tip and root diameters was reported as 0.04 mm and 0.02 mm, respectively. The difference between the initial and final measurement over two teeth was 0.01–0.02 mm, while the difference in initial and final gear width was 0.04–0.06 mm.

The mass measurement did not provide a direct measure of material loss because the final mass was 1.7–2.8% higher than the initial mass. This increase is due to the oil being retained in the porous structure of the sintered gears during pressurized operation.

Although the two components belong to different subsystems, their behavior reflects the same broader advantages and limitations of sintered parts in agricultural machinery. In both cases, the test results show satisfactory functional performance, limited geometric change, and good compatibility with lubricated service conditions. The porous microstructure of the sintered material appears to have played a beneficial

role by retaining oil during operation, which helps explain the measured mass increase rather than mass loss.

## CONCLUSIONS

The combined results demonstrate that simulator and accelerated testing can provide useful experimental evidence for assessing the functional behavior and wear resistance of sintered components used in agricultural machinery.

The experimental evaluation of the two sintered components led to the following conclusions:

- Cardan-joint inclination has a direct influence on the thermal behavior of the sintered bushings; higher inclination angles resulted in higher operating temperatures.
- Wear of the bushings remained limited, and no significant degradation of functional behavior was observed.
- The sintered driven pinion tested in the oil pump operated safely at 2.5, 5, and 6 bar, with constant pressure throughout the test sequence.
- The pinion showed very small tooth wear and no meaningful loss of geometry or surface integrity/
- In both studies, the final mass increased because oil was retained in the porous sintered structure, confirming the tribological character of the material.
- Sintered components are suitable for agricultural transmission systems, especially when operating conditions are controlled and test-validated.
- The experimental evaluation of the two sintered components led to the following conclusions:

## REFERENCES

[1] Anselmo. L.M., Thiago de Souza Lamim, Matheus Hromatka, José Daniel Biasoli de Mello, Aloisio Nelmo Klein, Gisele Hammes, Cristiano Binder,(2022). Influence of post-sintering sizing process on the tribological behaviour of self-lubricating iron-based composite, Wear, Volumes 496–497,204287.

[2] Davis, J. R., (1991) ASM Handbook, Volume 4: Heat Treating. ASM International, Materials Park, Ohio.

[3] German, R. M., (2005), Powder Metallurgy & Particulate Materials Processing, Metal Powder Industries Federation, Princeton, New Jersey.

[4] German, R. M., (2014), Sintering: From Empirical Observations to Scientific Principles, Butterworth-Heinemann, Oxford, 2014.

[5] Gogaev, K. A., Voloshchenko, S. M., Podrezov, Yu. N., & Radchenko, A. K. (2016). Process approaches for producing complex composite inoculants by rolling of powder mixtures. I. Inoculant powder mixtures. Composition, structure, and properties. Powder Metallurgy and Metal Ceramics, 55, 5–6. DOI: 10.1007/s11106-016-9802-3.

[6] Hu Q, Wang M, Chen Y, Si Z and Zhang D (2023) Effects of sintering temperatures on the microstructure and mechanical properties of S390 powder metallurgy high-speed steel. Front. Mater. 10:1198776. doi: 10.3389/fmats.2023.1198776

[7] Ilyushchanka, A., Leshok, A. V., Rogovoy, A. N., & Rudakovsky, V. O. (2017). Application of sintered powder material FM-15 in the clutch coupling of “Belarus-3522” tractors. Agricultural Engineering, Research Papers**,** 49, 1–4.

[8] Upadhyaya, G. S., (2002), Powder Metallurgy Technology, Ed.Cambridge International Science Publishing, Cambridge, U.K.

[9] Wang, Y., Li, D., Nie, C., Gong, P., Yang, J., Hu, Z., Li, B., & Ma, M. (2023). Research Progress on the Wear Resistance of Key Components in Agricultural Machinery. Materials (Basel, Switzerland), 16(24), 7646. https://doi.org/10.3390/ma16247646

[10] *** ASM International (1998), ASM Handbook, Volume 7: Powder Metal Technologies and Applications, ASM International, Materials Park, Ohio.

[11] ***Binacchi srl, Alberi Cardanici, Catalogo generale, http://www.binacchi.it

[12] *** GKN Walterscheid GmbH., Gelenkwellen und Überlstkupplungen für Landmaschinen und Sonderbetriebe, Technisches Handbuch, http://www. Walterscheid.com

[13] *** Imovilli pompe S.r.l., Pompe, Catalogo generale, http://www.imovillipompe.it

# SIGNAL RECONSTRUCTION FROM FREQUENCY-DOMAIN THREE-DIMENSIONAL COMSOL SIMULATIONS OF WAVE PROPAGATION IN THIN CIRCULAR PLATE STRUCTURES

/

# *RECONSTRUCȚIA SEMNALELOR DIN SIMULĂRI TRIDIMENSIONALE COMSOL ÎN DOMENIUL FRECVENȚEI APLICATE PROPAGĂRII UNDELOR ÎN PLĂCI CIRCULARE SUBȚIRI*

**Andreea-Denisa GRIGUȚA, Mihai Valentin PREDOI***
Department of Mechanics, National University of Science and Technology POLITEHNICA Bucharest - Faculty of Biotechnical Systems Engineering, Bucharest / Romania
**Tel: 0214 029 250; *E-mail: mihai.predoi@upb.ro*

***Keywords:*** *non destructive characterization, pulse echo method, guided waves, signal reconstruction*

**ABSTRACT**

*Ultrasonic wave propagation in a circular plate is investigated under surface excitation produced by a centrally located piezoelectric transducer, with particular emphasis on the response measured by a receiving transducer positioned at a different location on the structure. Because the interpretation of experimentally acquired signals is strongly influenced by the testing configuration, numerical modeling is required to establish a reliable relationship between the measured response and the underlying wave propagation mechanisms. In this study, a three-dimensional finite element model is developed in COMSOL Multiphysics to simulate ultrasonic wave propagation within the circular plate. To reduce computational cost while preserving numerical accuracy, the analysis is performed in the frequency domain. A subsequent transformation procedure is then applied to reconstruct the corresponding transient response from the frequency-domain solution. The proposed methodology demonstrates that frequency-domain finite element simulations can reproduce ultrasonic wave responses with good fidelity while significantly reducing computational requirements compared with conventional time-domain analyses. This approach provides an efficient and robust framework for investigating guided wave behavior in plate structures and may be extended to other configurations involving ultrasonic sensing and structural health monitoring applications.*

**REZUMAT**

*Propagarea undelor ultrasonice într-o placă circulară este investigată în condițiile unei excitații de suprafață generate de un traductor piezoelectric amplasat central, cu accent particular pe răspunsul măsurat de un traductor receptor poziționat într-o altă locație pe structură. Deoarece interpretarea semnalelor achiziționate experimental este puternic influențată de configurația de testare, este necesară modelarea numerică pentru a stabili o relație fiabilă între răspunsul măsurat și mecanismele fundamentale de propagare a undelor. În acest studiu, este dezvoltat un model cu elemente finite tridimensional în COMSOL Multiphysics pentru a simula propagarea undelor ultrasonice în interiorul plăcii circulare. Pentru a reduce costul computațional, păstrând în același timp acuratețea numerică, analiza este realizată în domeniul frecvenței. Ulterior, se aplică o procedură de transformare pentru a reconstrui răspunsul tranzitoriu corespunzător din soluția obținută în domeniul frecvenței. Metodologia propusă demonstrează că simulările cu elemente finite în domeniul frecvenței pot reproduce cu fidelitate bună răspunsurile undelor ultrasonice, reducând în același timp semnificativ cerințele computaționale în comparație cu analizele convenționale în domeniul timpului. Această abordare oferă un cadru eficient și robust pentru investigarea comportamentului undelor ghidate în structuri de tip placă și poate fi extinsă la alte configurații care implică detecția ultrasonică și aplicații de monitorizare a integrității structurale.*

## INTRODUCTION

The progressive development of numerical simulation approaches has substantially contributed to the characterization of guided-wave propagation and its interaction with structural discontinuities, offering increasingly refined computational frameworks for the analysis of Lamb waves. Kazys et al. *(Kazys, et al.,*

*2006)* applied two- and three-dimensional finite element and finite difference techniques to investigate the interaction of Lamb waves with welded joints and defects in steel plates subjected to fluid loading.

Their results indicate that numerically generated leaky-wave fields can be exploited to estimate defect positions and to provide a detailed visualization of the scattering mechanisms induced by geometric and material discontinuities. In a related context, Alkassar et al. *(Alkassar, Agarwal, & Eman, 2017)* employed finite element models to examine wave propagation and mode conversion in thin plates containing notches, emphasizing the value of such simulations in elucidating dispersive characteristics and in clarifying the mechanisms through which incident waves interact with localized damage.

The investigation of nonlinear effects has also been addressed numerically: Chen et al. *(Chen , Deng, Gao, Hu, & Xiang, 2021)* simulated the generation of static components in layered plates and demonstrated, by means of finite element analysis, that nonlinear wave indicators exhibit pronounced sensitivity to interfacial deterioration, thereby offering a promising basis for the early identification of degradation.

Furthermore, Masurkar and Yelve *(Masurkar & Yelve, 2017)* integrated finite element simulations with experimental measurements to evaluate damage localization procedures based on Lamb waves and geodesic algorithms in both metallic and composite structures, showing that numerical modelling can effectively assist dispersion characterization, signal interpretation, and the refinement of localization accuracy. The theoretical foundations of ultrasonics have been developed and applied through complementary analytical, numerical, and signal-oriented methodologies, thereby strengthening both the fundamental understanding of guided-wave propagation and its practical implementation in the assessment of structural integrity.

Analytical formulations have played a particularly important role in establishing efficient predictive tools: Guo and Mal *(Guo & Mal, 1998)* proposed rapid analytical procedures for calculating Lamb waves generated by localized sources, providing a computationally efficient alternative to fully numerical treatments for certain classes of problems. In parallel, signal-processing research has addressed the practical interpretation of measured wavefields, as illustrated by Liu and Chen *(Liu & Chen, 2018)*, whose mode-selection and processing strategies enhance the physical interpretability of ultrasonic data in structural integrity evaluation.

More general theoretical treatments, such as that presented by Cheeke *(Cheeke, 2012)*, establish a broad connection between the underlying physics of elastic-wave propagation and the wide range of ultrasonic techniques employed in engineering practice, while Gravenkamp et al. *(Gravenkamp, Song, & Prager, 2012)* introduced advanced numerical methodologies for the accurate dispersion analysis of complex plate geometries. A further line of research has focused on the interaction between guided waves and structural defects: Chang and Mal *(Chang & Mal, 1998)* modelled the scattering of Lamb waves by discontinuities, whereas Martinez et al. *(Martinez, Pant, Yanishevsky, & Backman, 2017)* extended simulation frameworks to incorporate the residual stress fields associated with fatigue cracks, thereby improving the physical realism of damage-related wavefield predictions.

Electromechanical coupling has also been explicitly considered in computational studies; the piezoelectric wafer active sensor (PWAS)-based finite element investigation reported by Tashi, Abedian, and Khajehtourian *(Tashi, Abedian, & Khajehtourian, 2012)* demonstrates how coupled-field modelling can support crack detection strategies. In addition, Parrinello and Ghiringhelli *(Parrinello & Ghiringhelli, 2016)* formulated a transfer-matrix-based framework for analysing wave propagation in periodic media, providing an efficient means of characterizing wave behaviour in structured and repetitive configurations.

Further contributions have addressed more specialized geometries and loading conditions: Akbarov, Guliev, and Kepceler *(Akbarov, Guliev, & Kepceler, 2011)* investigated dispersion characteristics and wave-mode coupling in initially stressed and twisted cylindrical structures, while Rucka *(Rucka, 2010)* combined experimental measurements with numerical modelling to assess guided-wave-based damage detection in L-shaped joint configurations. Complementing these efforts, Tancredi *(Tancredi, 2011)* integrated experimental observations with finite element simulations of Lamb-wave propagation to support the identification of impact-induced damage in both metallic and composite plates, thereby illustrating the practical value of combined experimental–numerical methodologies in structural health monitoring applications.

The authors have previously reported results concerning conventional Lamb wave propagation *(Griguța & Predoi, 2021)*, *(Predoi, Griguta, & Petre, 2022)*, *(Griguța A. D., Predoi, Petre, & Rugină, 2025)*; however, these findings should be extended to account for the fact that cylindrical wave propagation can yield slightly different characteristics of the guided waves compared with those observed in semi-infinite plate

configurations. This distinction arises from the curvature-induced modification of the waveguide geometry, which influences the dispersion behaviour, modal structure, and propagation characteristics of the guided waves. Consequently, the results obtained for classical Lamb waves cannot be directly extrapolated to cylindrical structures without appropriate consideration of these geometrical effects.

This study presents a representative example of signal reconstruction performed in MATLAB, in which selected subsets of points from the frequency spectrum are considered. A finite number of spectral points is identified and subsequently imposed as input data for frequency-domain simulations conducted in COMSOL Multiphysics on a three-dimensional model of a circular thin plate. The numerical results obtained from the frequency-domain analysis are discussed and briefly compared with those derived from a time-dependent simulation of the same three-dimensional model.

## SIGNAL RECONSTRUCTION

To perform a frequency-domain analysis in the COMSOL Multiphysics environment, the amplitude spectrum associated with the chosen 200 kHz input excitation signal had to be established. For this purpose, an enveloped Gaussian waveform was employed as the reference excitation. The time-domain representation of this signal, showing its evolution as a function of time, is presented in Figure 1.

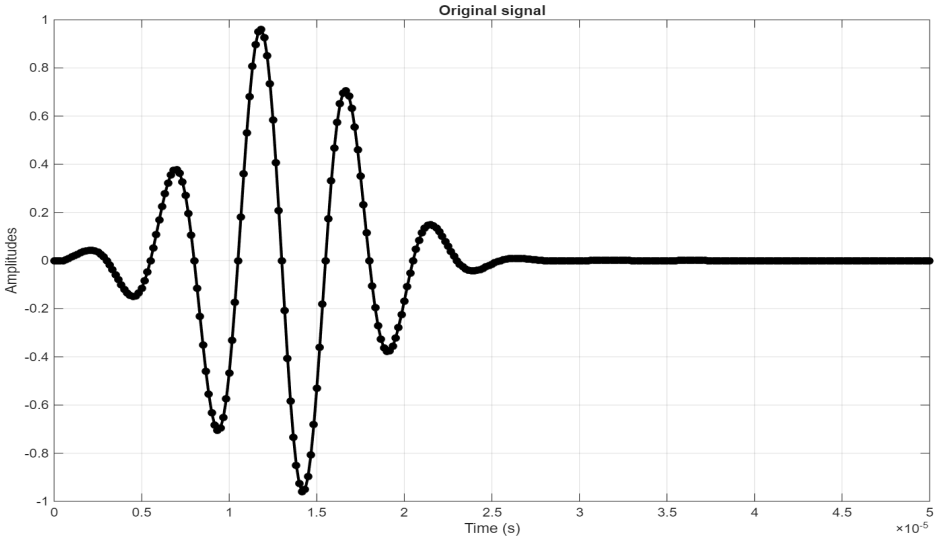



**Fig. 1 - Original signal input excitation**

Moreover, the amplitude spectrum was determined by means of a MATLAB implementation of the Fast Fourier Transform (FFT). In order to obtain an adequate representation of the spectral content, the overall temporal duration of the signal was increased.

This modification enabled the inclusion of a sufficiently extensive set of non-zero amplitude values in the neighbourhood of the signal's central frequency, thereby enhancing both the resolution and the interpretability of the resulting spectrum.

The calculated amplitude spectrum is depicted in the Figure 2.

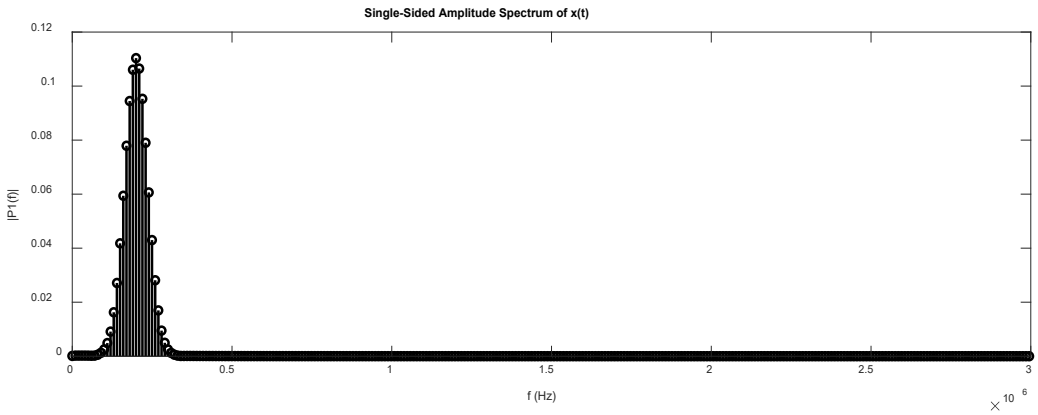
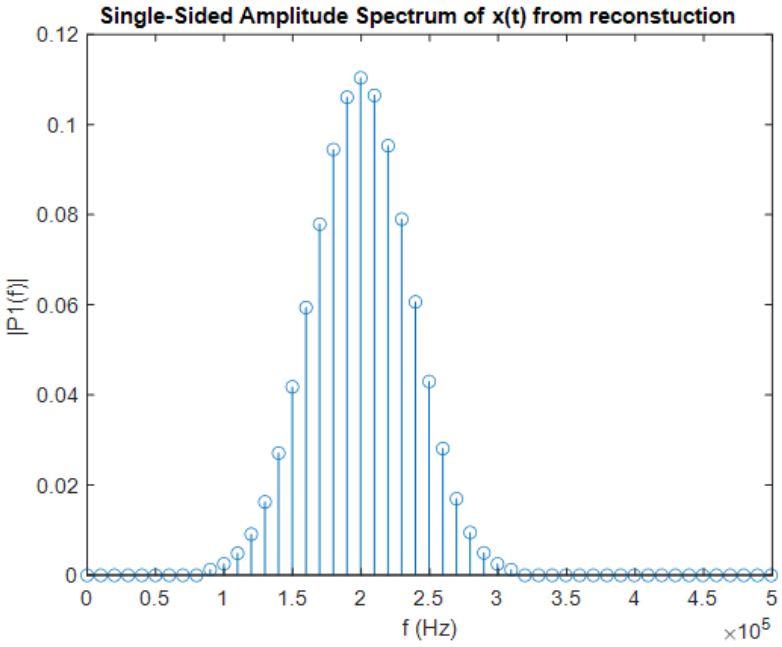



**Fig. 2 - Entire amplitude spectrum**

In order to preserve computational efficiency in the COMSOL simulations without compromising the physical representativeness of the model, a finite subset of frequency components was extracted from the signal envelope, and the reconstructed signal was subsequently compared with this reduced spectral representation. The selection criterion consisted of retaining exclusively those spectral components whose amplitudes were substantially different from zero. Consequently, the maximum number of discrete frequency points included in the amplitude spectrum was restricted to 23, corresponding to the frequencies exhibiting a meaningful contribution to the overall spectral content. This selection can be clearly observed in the magnified representation of the spectrum shown in Figure 3.




| | | |
|---|---|---|
| 9 | 5.6176e-04 | 7.9867e+04 |
| 10 | 0.0013 | 8.9850e+04 |
| 11 | 0.0025 | 9.9834e+04 |
| 12 | 0.0049 | 1.0982e+05 |
| 13 | 0.0091 | 1.1980e+05 |
| 14 | 0.0163 | 1.2978e+05 |
| 15 | 0.0271 | 1.3977e+05 |
| 16 | 0.0418 | 1.4975e+05 |
| 17 | 0.0594 | 1.5973e+05 |
| 18 | 0.0779 | 1.6972e+05 |
| 19 | 0.0945 | 1.7970e+05 |
| 20 | 0.1061 | 1.8968e+05 |
| 21 | 0.1104 | 1.9967e+05 |
| 22 | 0.1065 | 2.0965e+05 |
| 23 | 0.0953 | 2.1963e+05 |
| 24 | 0.0790 | 2.2962e+05 |
| 25 | 0.0606 | 2.3960e+05 |
| 26 | 0.0430 | 2.4958e+05 |
| 27 | 0.0281 | 2.5957e+05 |
| 28 | 0.0170 | 2.6955e+05 |
| 29 | 0.0095 | 2.7953e+05 |
| 30 | 0.0050 | 2.8952e+05 |
| 31 | 0.0025 | 2.9950e+05 |
| 32 | 0.0012 | 3.0948e+05 |
| 33 | 5.7625e-04 | 3.1947e+05 |

**Fig. 3 - Spectrum of the amplitudes considering 23 points**

The time-domain signal was reconstructed by applying the Inverse Fast Fourier Transform (IFFT) to the truncated spectrum, in which only a predefined subset of spectral amplitudes was retained as non-zero, see Figure 4.

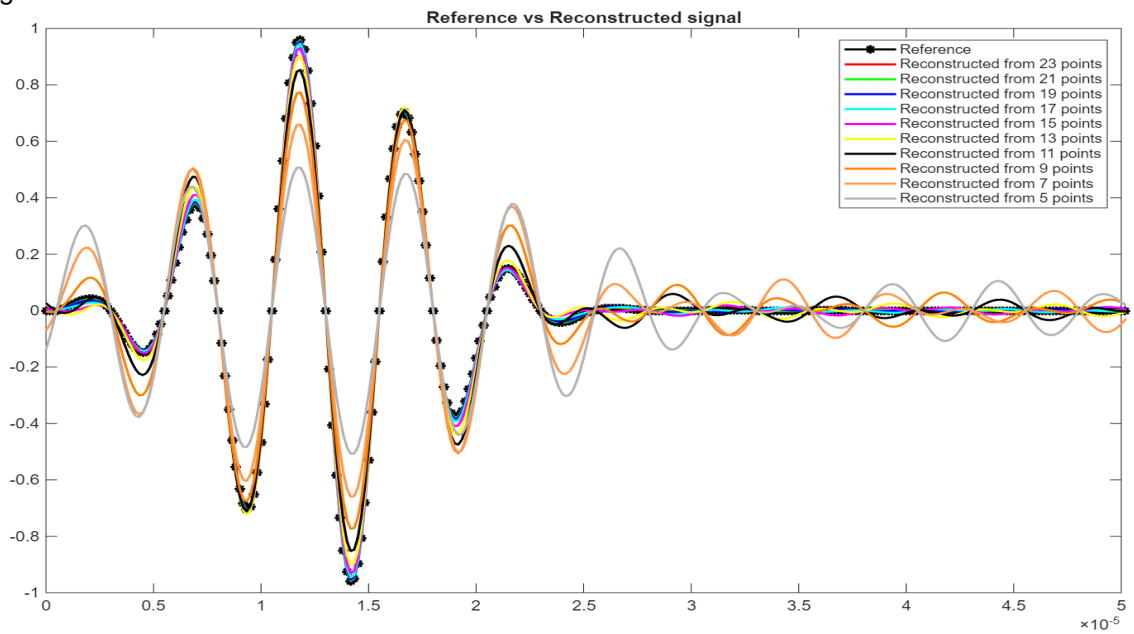



**Fig. 4 - Reference vs Reconstructed signals from subsets of spectra**

To further evaluate and optimize computational efficiency, the reconstruction procedure was carried out for several cases characterized by different numbers of retained spectral components.

The reference reconstruction was based on the complete set of 23 selected frequency components. Subsequent reconstructions were obtained by successively removing the frequency pairs situated at the greatest distance from the central frequency on both sides of the spectral envelope, thereby reducing the number of retained components from 23 to 5.

Furthermore, only odd numbers of frequency components were considered throughout this procedure, in order to maintain the symmetry of the spectrum with respect to the central frequency. This condition ensures a consistent and physically meaningful reconstruction of the corresponding time-domain signal. The reconstructed waveforms, superimposed on the original reference signal, are also presented in Figure 4, thus allowing a direct visual comparison between the initial signal and the approximations derived from the reduced spectral representations.

In order to enable a quantitative evaluation of the quality of the reconstructed signal with respect to the initial reference waveform, the convergence of the reconstruction process was assessed using the peak error. This metric quantifies the maximum deviation between the reconstructed and reference signals, thereby allowing a systematic analysis of the reconstruction accuracy. The corresponding evolution of the peak error is presented in Figure 5.

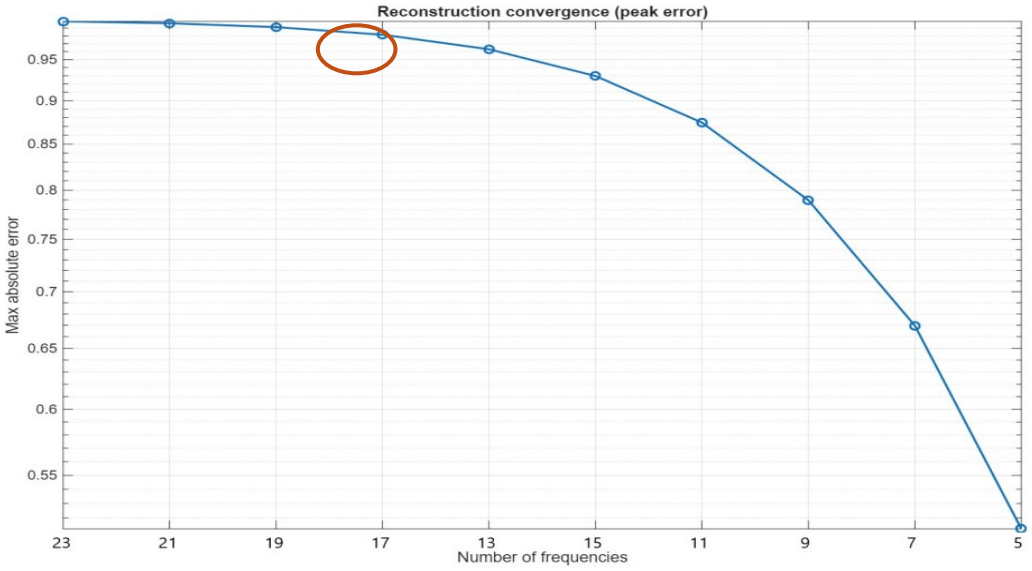



**Fig. 5 - Reconstructed convergence - peak error**

Based on the visual comparison of the superimposed waveforms, together with the quantitative assessment provided by the peak error metric, the reconstruction accuracy achieved with 17 frequency components is considered satisfactory.

This number of retained spectral components offers an appropriate compromise between computational efficiency and fidelity to the original reference signal, ensuring a reliable representation of the waveform while avoiding the inclusion of spectral components that do not contribute significantly to the reconstruction.

## FEM SIMULATION IN COMSOL FREQUENCY DOMAIN

The principal aim of the preceding chapter was to establish a clearly defined amplitude spectrum that could be directly implemented within the frequency-domain simulation framework of COMSOL Multiphysics.

Each discrete frequency component, together with its associated amplitude value, was considered as an independent input parameter for a separate simulation, from which the corresponding numerical solution was subsequently obtained. In addition, the geometric configuration of the model and the corresponding boundary conditions were established in accordance with the adopted three-dimensional modelling strategy, which is described in detail in the following section.

The thin plate was characterized by a thickness of 1 mm and a radius of 60 mm, and its geometry was created in COMSOL by means of a cylindrical representation. At the centre of the plate, an additional cylindrical domain with a radius of 2 mm was introduced in order to represent the region occupied by the piezoelectric transducer, as defined by the contact surface between the transducer and the plate.

See Figure 6 for details about the geometry and boundary conditions implementation.

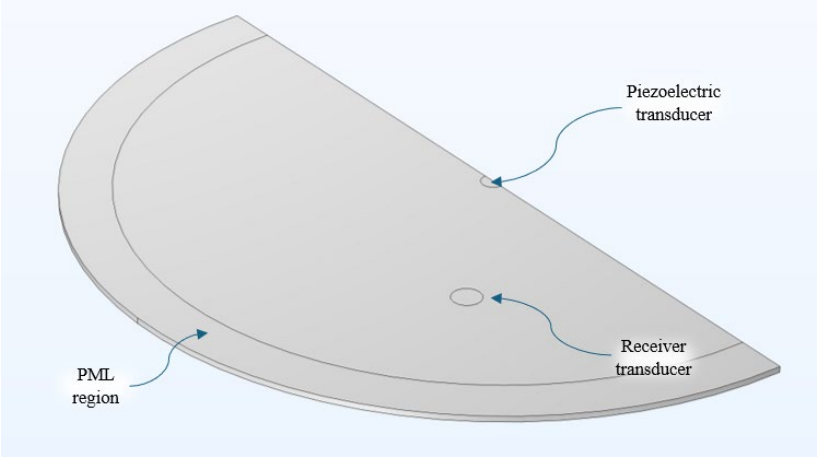



**Fig. 6 - Geometry and boundary conditions implementation**

With regard to the boundary conditions, a prescribed displacement was imposed on the surface region corresponding to the piezoelectric transducer. The magnitude of this applied displacement was defined according to the excitation amplitude associated with each individual frequency component of the reconstructed spectrum, Figure 7 b). In accordance with the number of frequency components selected in the preceding section, a total of 17 separate simulations were carried out. Each simulation was performed using the specific frequency value and its corresponding amplitude extracted from the previously defined amplitude spectrum.

The mesh was generated by taking into account the requirement that the maximum element length should not exceed one tenth of the wavelength, Figure 7 b). Consequently, a distinct mesh was employed for each simulation, corresponding to the specific frequency considered in that particular case.

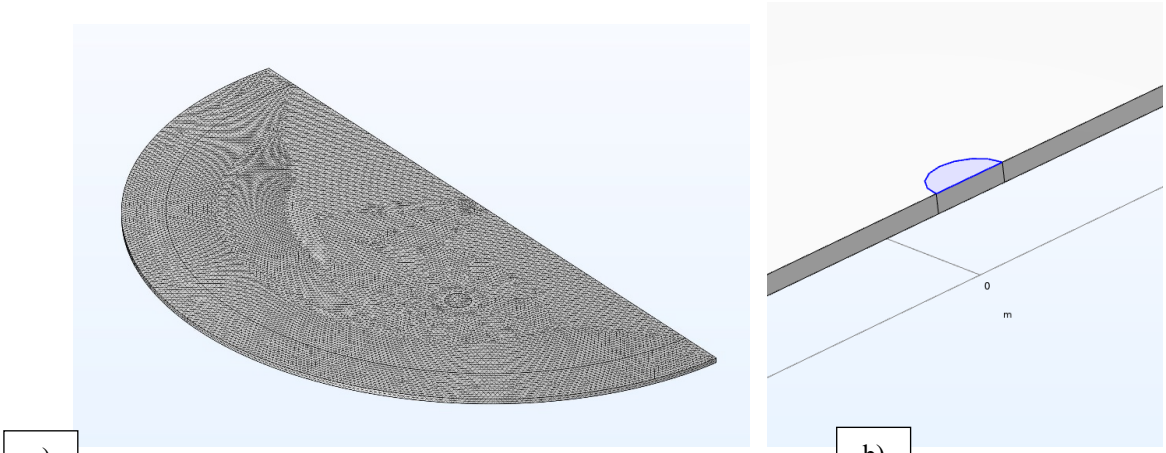



**Fig. 7**
**a) Mesh and b) Prescribed displacement implementation**

The visualizations of the total displacement field obtained from three simulations are presented in the figure, corresponding to the central frequency as well as to the first and last frequency components considered in the spectrum. These results provide a comparative representation of the displacement distribution within the plate for different positions across the selected frequency range.

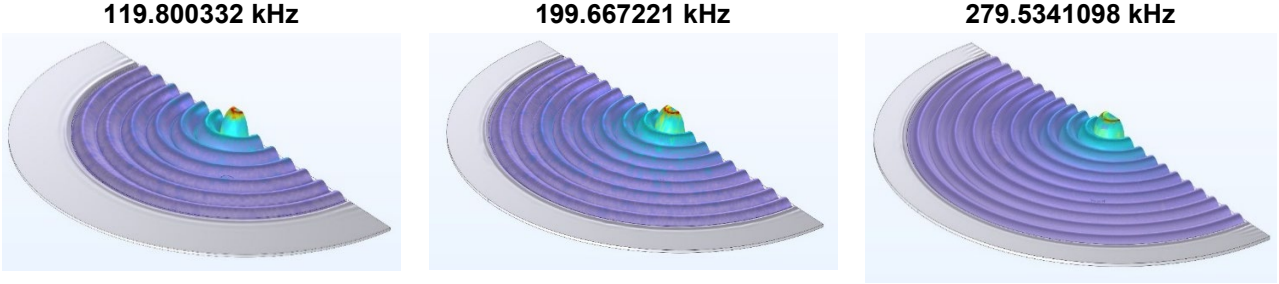



**Fig. 8 - Displacement field from central frequency, first and last frequency simulations**

Two distinct categories of results were obtained from the numerical simulations. The first category corresponds to the response evaluated over the surface representing the receiving transducer, thereby providing an averaged or spatially integrated measure of the signal that would be expected to be recorded in an experimental configuration.

The second category comprises discrete data points extracted along the radial direction of the plate, allowing the spatial variation of the response to be analysed as a function of the distance from the excitation region. Such pointwise measurements may be considered analogous to experimental data obtained by means of laser vibrometry, in which the surface motion is recorded at specific locations without requiring physical contact with the specimen.

### 1. Response evaluated on a average surface

In this case, the response was evaluated by computing the surface-averaged value of the transverse displacement field over the region corresponding to the receiving transducer. This approach provides a spatially integrated measure of the plate motion over the entire contact area of the receiver, rather than relying on the displacement at a single point.

Consequently, the obtained quantity can be regarded as representative of the overall signal that would be detected by a transducer covering the same surface area in an experimental configuration.By averaging the transverse displacement over this region, local variations in the wavefield are inherently accounted for, thereby yielding a more physically meaningful representation of the response measured by the receiving element.In this case the response was evaluated as the surface-averaged value of the transverse displacement field over the area corresponding to the receiving transducer.

By performing the 17 frequency-domain simulations and exporting the corresponding response values from COMSOL, the amplitude spectrum of the system response was reconstructed from the individual discrete simulation results. Each simulation provided the response associated with a specific frequency component and its corresponding excitation amplitude, thereby enabling the assembly of a complete spectral representation of the system behaviour. In this manner, the frequency-dependent response of the plate–transducer configuration could be characterized point by point, allowing the overall amplitude spectrum to be recovered from the set of individually computed solutions.

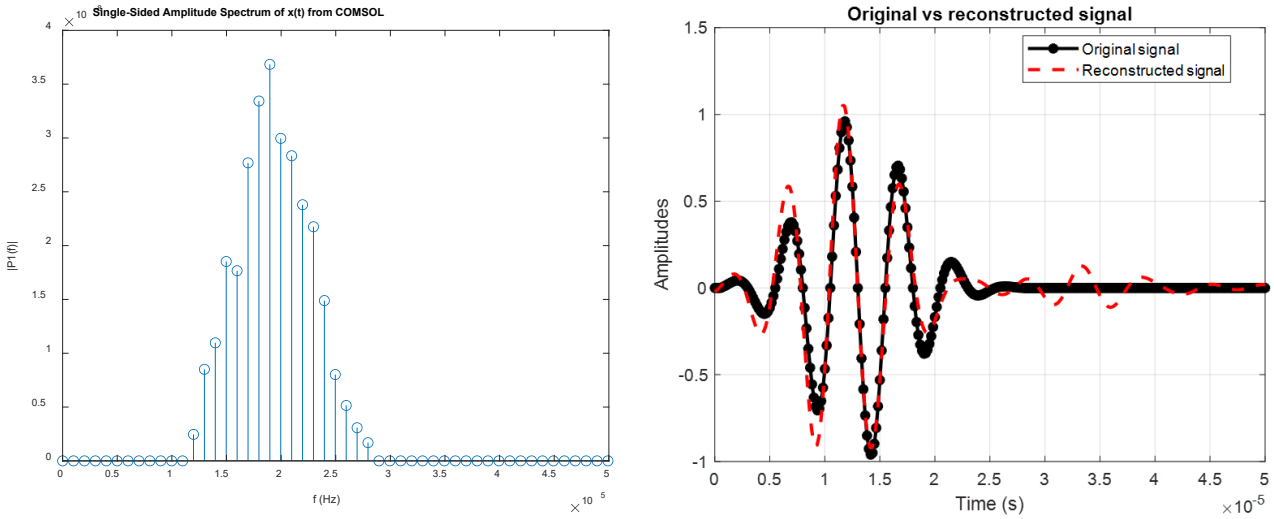



**Fig. 9 - Reconstructed spectrum and signal from the 17 COMSOL simulations**

The results shown in the Figure 7 indicate that the reconstructed signal, represented by the red line, closely resembles the original reference signal, depicted by the black dotted line. Although slight deviations can be observed between the two waveforms, the overall agreement is considered satisfactory, confirming that the reduced spectral representation provides an adequate approximation of the original signal.

### 2. Response evaluated from data set points

In this case, the transverse displacement field was extracted at a set of discrete points distributed along the radial direction of the plate, see Figure 9.

This approach allows the spatial variation of the displacement response to be analysed as a function of the radial position. As previously explained, this configuration is intended to reproduce the conditions of an

experimental laser vibrometry measurement performed along a line, in which the surface motion is recorded at individual locations without physical contact with the specimen.

By evaluating the displacement at successive radial positions, the propagation characteristics of the guided waves and their variation with distance from the excitation region can be more effectively examined.

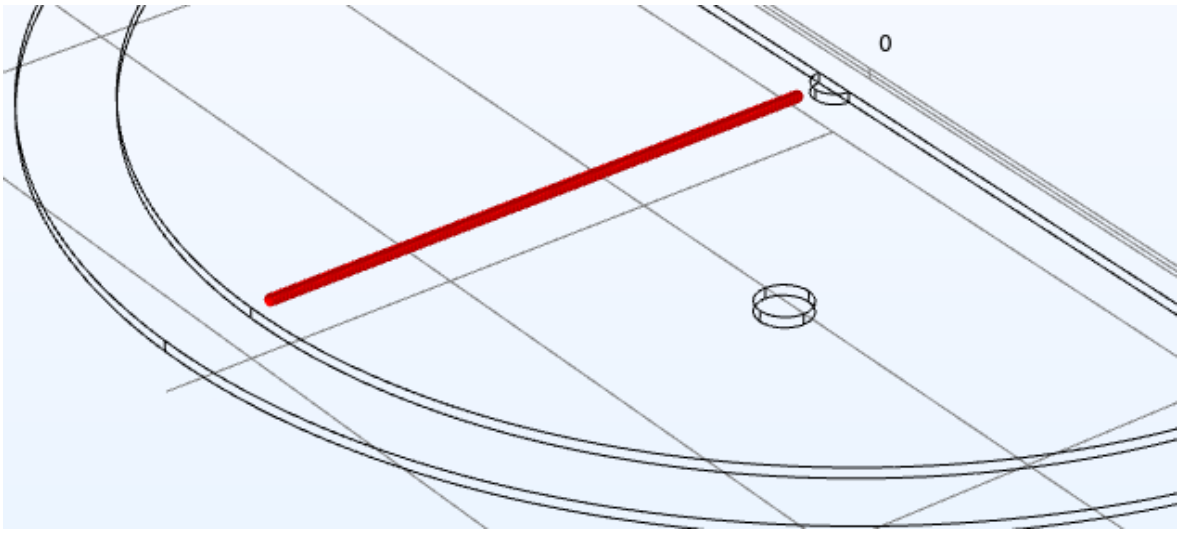



**Fig. 10 - The set of discrete points along the radial direction of the plate**

For this case, as an illustrative example, the recomposed amplitude spectrum corresponding to the 50th measurement point along the radial direction is presented in Figure 9 a). The corresponding reconstructed time-domain signal for this point is also shown in Figure 9 b).

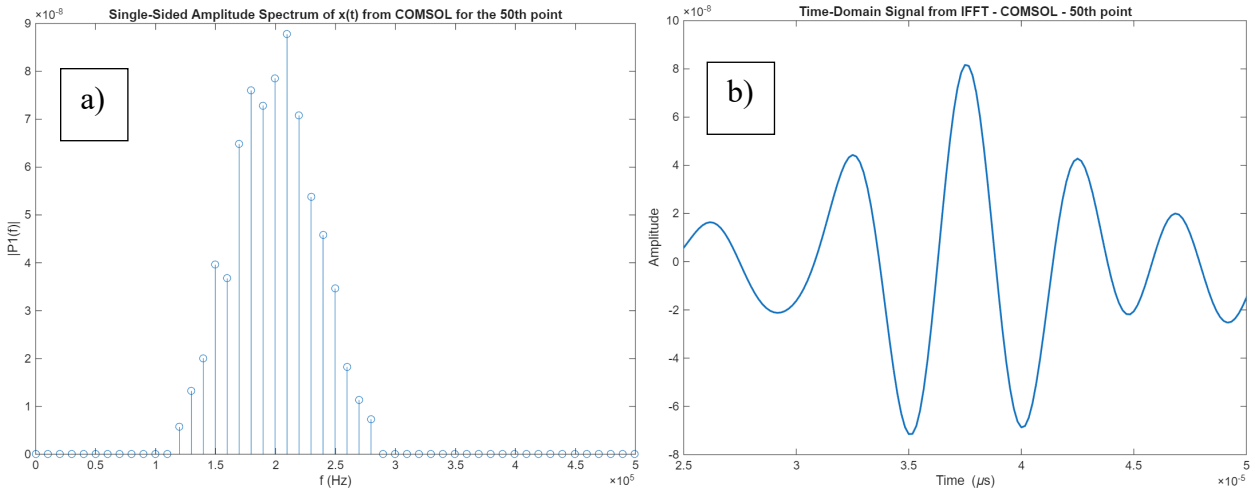



**Fig. 11 - Reconstrcuted a) spectrum and b) signal of a reading point**

The superimposed time-domain responses corresponding to the signals extracted from the evaluation points may be employed to construct displacement–time plots from which the group velocity can be determined.

During the graphical representation of the displacement–time plots obtained from the three-dimensional frequency-domain simulations, certain anomalies were identified as a consequence of phase errors introduced during the reconstruction of the signals.

Nevertheless, the group velocity was successfully computed and subsequently considered for comparison with the results obtained from the same three-dimensional model when analysed using a time-dependent formulation, in which the boundary condition was imposed by means of the Gaussian function associated with the original time-domain excitation signal.

Both computed group velocity results exhibit values of approximately 2500 m/s. However, in view of the anomalies identified during the signal reconstruction process, these results should be regarded as preliminary and require further investigation in order to confirm their accuracy and physical consistency.

## CONCLUSIONS

This work has investigated the modelling of guided waves through the combined use of signal-processing techniques and numerical simulation, with particular emphasis on extending the analysis towards fully three-dimensional computational frameworks. In contrast to numerous previous studies based on simplified or reduced-dimensional models, the present research demonstrates the feasibility and advantages of integrating advanced signal decomposition methods with three-dimensional numerical simulations in order to achieve a more realistic representation of wave propagation phenomena.

Furthermore, since the computational cost associated with frequency-domain simulations is considerably lower than that required for time-dependent analyses, this approach represents an efficient and effective means of characterizing the underlying physical phenomena.

The results presented in this paper demonstrate that a finite number of spectral components is sufficient for the accurate reconstruction of the corresponding time-domain signal. In particular, the response obtained through the surface-averaged evaluation exhibits an excellent level of agreement with the original reference waveform, thereby confirming the effectiveness of the proposed frequency-domain reconstruction strategy.

This outcome provides a promising basis for the further development of pulse–echo-based evaluation methods, for instance in applications involving the detection and characterization of defects within plate-like structures. Moreover, the results obtained from the set of discrete points distributed along the radial direction of the plate establish a solid foundation for the continuation of this research. This aspect is particularly relevant in view of the anomalies identified during the reconstruction process, which highlight the need for a more detailed analysis of the phase behaviour and spectral truncation effects.

Accordingly, further investigations are required in order to fully assess the accuracy, limitations, and practical applicability of the proposed approach.

The authors intend to address these aspects in future research, through complementary theoretical analyses and experimental investigations.

## ACKNOWLEDGEMENT

The authors gratefully acknowledge the Faculty of Biotechnical Systems Engineering at the National University of Science and Technology POLITEHNICA Bucharest for the financial support provided, which facilitated participation in the conference.

## REFERENCES

[1] Akbarov, S., Guliev, M., & Kepceler, T. (2011). Dispersion relations of axisymmetric wave propagation in initially twisted bi-material compounded cylinders. *Journal of Sound and Vibration, 330*, 1644-1664.

[2] Alkassar, Y., Agarwal, V., & Eman, A. (2017). Simulation of Lamb Wave Modes Conversions in a Thin Plate for Damage Detection. *11th International Symposium on Plasticity and Impact Mechanics, Implast 2016.*

[3] Chang, Z., & Mal, A. (1998). Wave propgation in a plate with defects. *Review of Progress in Quantitative Nondestructive Evaluation, 17*, 121-128.

[4] Cheeke, J. (2012). *Fundamentals and applications of ultrasonic waves.* CRC Press.

[5] Chen , H., Deng, M., Gao, G., Hu, N., & Xiang, Y. (2021). Modeling and simulation of static component generation of Lamb wave propagation in a layered plate. *Ultrasonics, 116*.

[6] Gravenkamp, H., Song, C., & Prager, J. (2012). A numerical approach for the computation of dispersion relations for plate structures using the Scaled Boundary Finite Element Method. *Journal of Sound and Vibration, 331*, 2543-2557.

[7] Griguța, A. D., Predoi, M. V., Petre, C. C., & Rugină, C. (2025). Methodologies for Dataset Analysis in Regard to Obtaining Material Characteristics Using Lamb Waves. *Special Issue MACROMOLECULAR SYMPOSIA - ICSAAM 2025*.

[8] Griguța, A., & Predoi, M. (2021). Generation of multi-modal Lamb waves for the inspection of thin aeronautical structures. *U.P.B. Scientific Bulletin, Series A, 83*(4).

[9] Guo, D., & Mal, A. (1998). Rapid calculation of lamb waves in plates due to localized sources. Los Angeles: Mechanical and Aerospace Engineering Department, University of California.

[10] Kazys, R., Mazeika, L., Barauskas, R., Raisutis, R., Cicenas, V., & Demcenko, A. (2006). 3D Analysis of interaction of Lamb waves with defects in loaded steel plates. *Ultrasonics, 44*, 1127–1130.

[11] Liu, Z., & Chen, H. (2018). Application and Challenges of Signal Processing Techniques for Lamb Waves Structural Integrity Evaluation: Part A-Lamb Waves Signals Emitting and Optimization Techniques. În *Structural Health Monitoring from Sensing to Processing* (pg. 61-86). IntechOpen.

[12] Martinez, M., Pant, S., Yanishevsky, M., & Backman, D. (2017). Residual stress effects of a fatigue crack on guided lamb waves. *Smart Materials and Structures, 26*(11).

[13] Masurkar, F., & Yelve, N. (2017). Lamb Wave Based Experimental and Finite Element Simulation Studies for Damage Detection in an Aluminium and a Composite Plate using Geodesic Algorithm. *International Journal of Acoustics and Vibration, 22*(4), 413-421.

[14] Parrinello, A., & Ghiringhelli, G. (2016). Transfer matrix representation for periodic planar media. *Journal of Sound and Vibration, 371*, 196-209.

[15] Predoi, M., Griguta, A., & Petre, C. (2022). Similarities between guided and longitudinal ultrasonic waves. *U.P.B. Scientific Bulletin, Series A, 84*(4).

[16] Rucka, M. (2010). Experimental and numerical study on damage detection in an L-joint using guided wave propagation. *Journal of Sound and Vibration, 329*, 1760-1779.

[17] Tancredi, S. (2011). Ph.D.: Experimental and numerical studies on low velocity impacts detection and damage identification in metal and composite structures using ultrasonic waves propagation (Lamb waves). Naples: University of Studies of Naples Federico II, Department of Aerospace Engineering.

[18] Tashi, S., Abedian, A., & Khajehtourian, R. (2012). The finite element simulation of lamb wave propagation in a cracked structure with coupled filed elements. *Advanced Materials Research, 463-464*, 618-623.

# EXPERIMENTAL VALIDATION AND NUMERICAL INVESTIGATION OF THE INFLUENCE OF EMBOSSMENTS ON THE FREE VIBRATION CHARACTERISTICS OF THIN PLATES

/

# *VALIDAREA EXPERIMENTALĂ ȘI INVESTIGAȚIA NUMERICĂ A INFLUENȚEI EMBOSĂRILOR ASUPRA CARACTERISTICILOR VIBRAȚIILOR LIBERE ALE PLĂCILOR SUBȚIRI*

**Laura-Mariana BARBU*[1)], Mihai Valentin PREDOI[2)]**

[1)] Ph.D. stud.eng., I.S.B. Doctoral School, Dept.of Mechanics, National University of Science and Technology POLITEHNICA Bucharest, Splaiul Independenței, 313, 060042, Bucharest / Romania;

[2)] Prof. Ph.D. Eng., Dept.of Mechanics, National University of Science and Technology POLITEHNICA Bucharest, Splaiul Independenței, 313, 060042, Bucharest / Romania.

**Tel: 0214 029 250; *E-mail: mihai.predoi@upb.ro*

***Keywords:*** thin plates, geometric embossments, modal analysis, free vibration, finite element analysis

## ABSTRACT

*Thin plate structures are widely used in automotive, aerospace, and mechanical engineering due to their favorable stiffness-to-weight ratio and manufacturing flexibility. Local geometric embossments can increase structural stiffness without a significant mass penalty, while also modifying the dynamic response of the component. This paper investigates the influence of a central rectangular embossment on the free vibration characteristics of a thin isotropic plate using COMSOL Multiphysics. A finite element model of the flat reference plate is first validated against experimental modal analysis results, showing good agreement between numerical and measured natural frequencies. The validated model is then used for a parametric study in which the embossment length and width are varied independently, while the depth and fillet radius are kept constant. For each configuration, the first ten structural natural frequencies are evaluated. The results show that increasing embossment length generally produces a monotonic increase in natural frequencies, whereas width variation leads to a more mode-dependent response, with some frequencies reaching a maximum at an intermediate configuration. The study confirms that embossment geometry can be effectively used to tailor the dynamic characteristics of thin plate structures.*

## REZUMAT

*Structurile de tip placă sunt utilizate pe scară largă în industria auto, aerospațială și în ingineria mecanică datorită raportului favorabil rigiditate–masă și flexibilității proceselor de fabricație. Modificările geometrice locale de tip embossment pot crește rigiditatea structurală fără o creștere semnificativă a masei, influențând în același timp comportamentul dinamic al componentei. Lucrarea investighează influența unui embossment dreptunghiular central asupra caracteristicilor vibrațiilor libere ale unei plăci subțiri izotrope utilizând COMSOL Multiphysics. Modelul cu elemente finite al plăcii plane de referință este validat prin compararea cu rezultatele analizei modale experimentale, evidențiind o bună concordanță a frecvențelor proprii. Modelul validat este ulterior utilizat într-un studiu parametric în care lungimea și lățimea embossment-ului sunt variate independent, în timp ce adâncimea și raza de racordare sunt menținute constante. Pentru fiecare configurație sunt analizate primele zece frecvențe proprii structurale. Rezultatele arată că majorarea lungimii produce, în general, o creștere monotonă a frecvențelor, în timp ce variația lățimii determină un răspuns mai dependent de modul de vibrație. Studiul confirmă că geometria embossment-ului poate fi utilizată pentru controlul caracteristicilor dinamice ale structurilor de tip placă subțire.*

## INTRODUCTION

Thin plate structures are widely used in mechanical, automotive, aerospace, marine, and civil engineering because of their favorable stiffness-to-mass ratio, relatively simple manufacturing processes, and capability to withstand different types of static and dynamic loads. *(R. Szilard, 1974) (Timoshenko, S. & Woinowsky-Krieger, S., 1959) (Leissa, 1969)* In many practical applications, these structures are exposed to mechanical excitation, impacts, aerodynamic loading, or other time-dependent disturbances, making the

evaluation of their vibration characteristics an important aspect of structural design. *(Predoi, 2011) (Leissa, 1969)*

The dynamic behavior of thin plates is mainly characterized by their natural frequencies and associated mode shapes *(Predoi, 2011) (Leissa, 1969)*. These quantities depend on the structural stiffness, mass distribution, material properties, geometry, and boundary conditions. *(Timoshenko, S. & Woinowsky-Krieger, S., 1959) (Gorman, 1982)* Consequently, even local modifications of the plate geometry may significantly influence the modal response of the structure.

A common approach for increasing the stiffness of thin structural components is the use of additional reinforcing elements, such as longitudinal or transverse stiffeners *(K. Zhang, J. Pan, & TR. Lin, 2021) (A. Hull & J. Maguire, 2014) (Zhongwei Zhao, et al., 2024)*. However, local geometric modifications can provide an alternative means of increasing out-of-plane rigidity without introducing separate structural components. In sheet-metal structures, embossments are frequently used for this purpose, allowing the local stiffness distribution to be modified while maintaining an integrated structural configuration *(Zhongwei Zhao, Bin Wang, & Ni Zhang, Optimization of local stiffener for controlling natural frequency of steel plates, 2025) (Lechao Tang, Zengming Feng, Jianjiao Deng, & Hangsheng Hou, 2025)*.

Although embossments are generally introduced to improve structural stiffness, their presence also modifies the vibration characteristics of the component. Changes in local geometry affect both stiffness and mass distribution and can therefore alter the natural frequencies and mode shapes of the plate. For this reason, understanding the relationship between embossment geometry and modal response is relevant during the early stages of structural design.

The present work investigates the influence of a central rectangular embossment on the free vibration characteristics of a thin rectangular plate. A finite element model of the reference flat plate is first assessed by comparison with experimental modal analysis results.

The validated numerical model is then used to investigate geometrically modified configurations in which the in-plane dimensions of the embossment are varied. Particular attention is given to the influence of embossment length and width on the natural frequencies of the plate and to the differences in sensitivity between the investigated vibration modes.

## REFERENCE PLATE AND NUMERICAL MODEL

The present investigation is based on a finite element model of a flat rectangular reference plate previously developed and experimentally assessed by the authors *(BARBU, TIRON, ALECU, & PREDOI, 2026)*. The reference plate has in-plane dimensions of 400 × 300 mm and was modeled under free-free boundary conditions.

The free vibration characteristics of rectangular plates under free-edge conditions have been extensively investigated in the literature and provide useful reference solutions for the assessment of numerical models *(Narita, Feb. 2022) (Y. Mochida, 2008)*. The finite element method is widely used for the numerical determination of natural frequencies and mode shapes of structures with complex geometries *(Petyt, 2010) (Bathe, 1996)*.

In the present study, the numerical model was developed in COMSOL Multiphysics using the measured geometric characteristics of the physical specimen. An eigenfrequency analysis was performed to determine the natural frequencies and corresponding mode shapes, while the rigid-body modes associated with the free-free configuration were excluded from the structural modal assessment.

The main geometric characteristics of the reference plate are summarized in Table 1.

**Table 1**

**Geometrical characteristics and mass of the reference plate**

| | |
|---|---|
| Length | 400 mm |
| Width | 300 mm |
| Height | 1.43 mm |
| Mass | 1404.28 g |

Further details regarding the development of the numerical model, the experimental procedure, and the numerical–experimental correlation are provided in *(BARBU, TIRON, ALECU, & PREDOI, 2026)*.

In the present work, the validated model is used as the baseline for the subsequent investigation of embossed configurations.

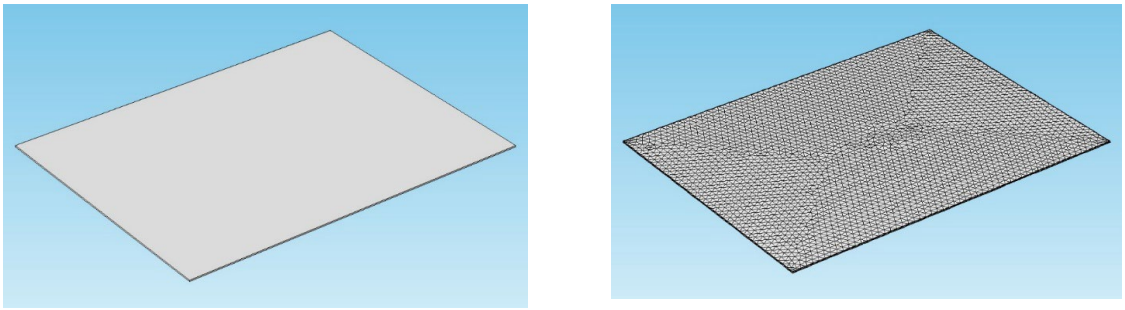


**Fig. 12 - Numerical model and finite element mesh of the reference plate**

## EXPERIMENTAL VALIDATION

Experimental validation of the reference configuration was previously performed by the authors and is described in detail in *(BARBU, TIRON, ALECU, & PREDOI, 2026)*. The plate was suspended using thin flexible elements in order to approximate free-free boundary conditions, mechanically excited at different locations, and its out-of-plane vibration response was measured using a laser vibrometer *(BARBU, TIRON, ALECU, & PREDOI, 2026)*. The recorded time-domain signals were processed in MATLAB to identify the structural natural frequencies. The comparison between numerical and experimental results showed good agreement. Relative differences remained below 2% for almost all identified modes, with a maximum deviation of 3.4% *(BARBU, TIRON, ALECU, & PREDOI, 2026)*. Based on this agreement, the finite element model was considered sufficiently reliable for the subsequent parametric investigation of the embossed configurations.

## PARAMETRIC INVESTIGATION OF THE EMBOSSED PLATE

### *Embossment Geometry and Investigated Configurations*

Following the validation of the reference plate model, the numerical investigation was extended to a geometrically modified configuration incorporating a centrally positioned rectangular embossment. The purpose of this stage was to evaluate the influence of the in-plane dimensions of the embossed region on the free vibration characteristics of the plate. The overall dimensions, thickness, and material properties of the plate were maintained identical to those of the reference configuration. The embossment geometry was defined by its length, width, fillet radius, and depth. The general geometry of the investigated model is presented in Figure 2, while the main geometric parameters are summarized in Table 2.

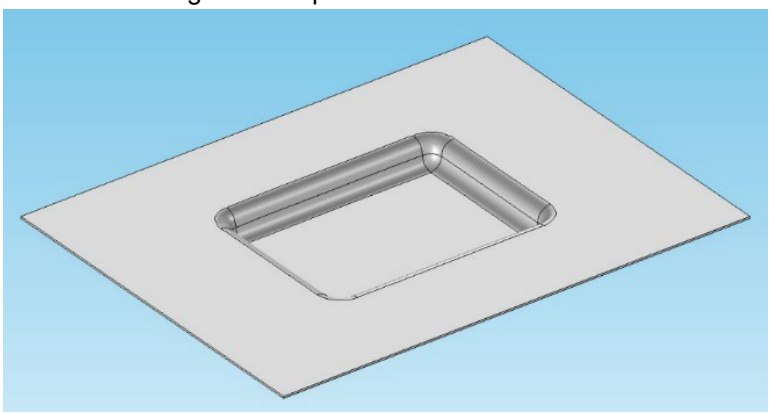


**Fig. 13 - Geometry of the rectangular plate with central embossment**

**Table 2**

**Main geometric parameters of the plate and reference embossed configuration**

| Parameter | Description | Value |
|---|---|---|
| $a$ | Plate length | 400 mm |
| $b$ | Plate width | 300 mm |
| $h_p$ | Initial plate thickness | 1.5 mm |
| $a_1$ | Reference embossment length | 200 mm |
| $b_1$ | Reference embossment width | 150 mm |
| $r$ | Fillet radius | 10 mm |
| $d$ | Embossment depth | 20 mm |

The configuration with an embossment size of 200 × 150 mm was selected as the common reference geometry for the parametric investigation. Starting from this configuration, the embossment length and width were varied independently in order to assess their individual influence on the modal response. The fillet radius was maintained constant at 10 mm for all configurations. Due to the adopted geometric construction, this value also corresponds to a constant embossment depth of 20 mm.

The first parametric series was obtained by varying the embossment length while maintaining its width at 150 mm. Four configurations were considered: L1 = 150 mm, L2 = 200 mm, L3 = 250 mm, and L4 = 300 mm. The corresponding geometries are shown in Figure 3.

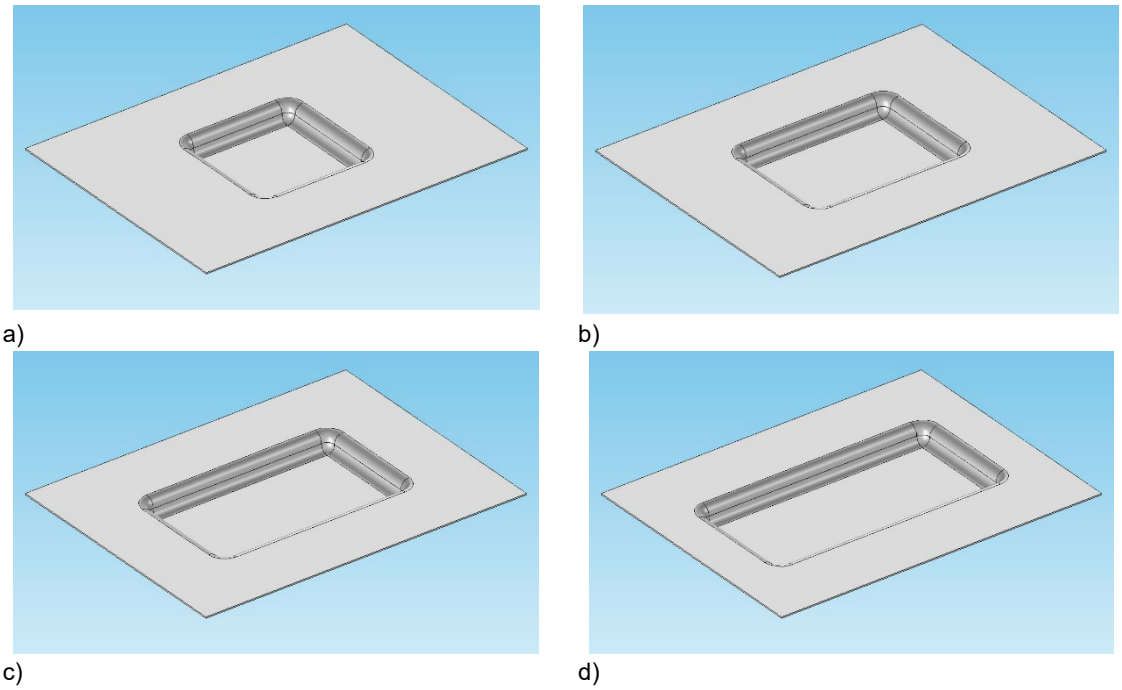



**Fig. 14 - Embossed plate configurations obtained by varying the embossment length:**
*(a) L1 = 150 mm; (b) L2 = 200 mm; (c) L3 = 250 mm; (d) L4 = 300 mm*

A second parametric series was generated by varying the embossment width while maintaining the length at 200 mm. The investigated configurations were W1 = 100 mm, W2 = 150 mm, W3 = 200 mm, and W4 = 250 mm. The corresponding geometries are presented in Figure 4.

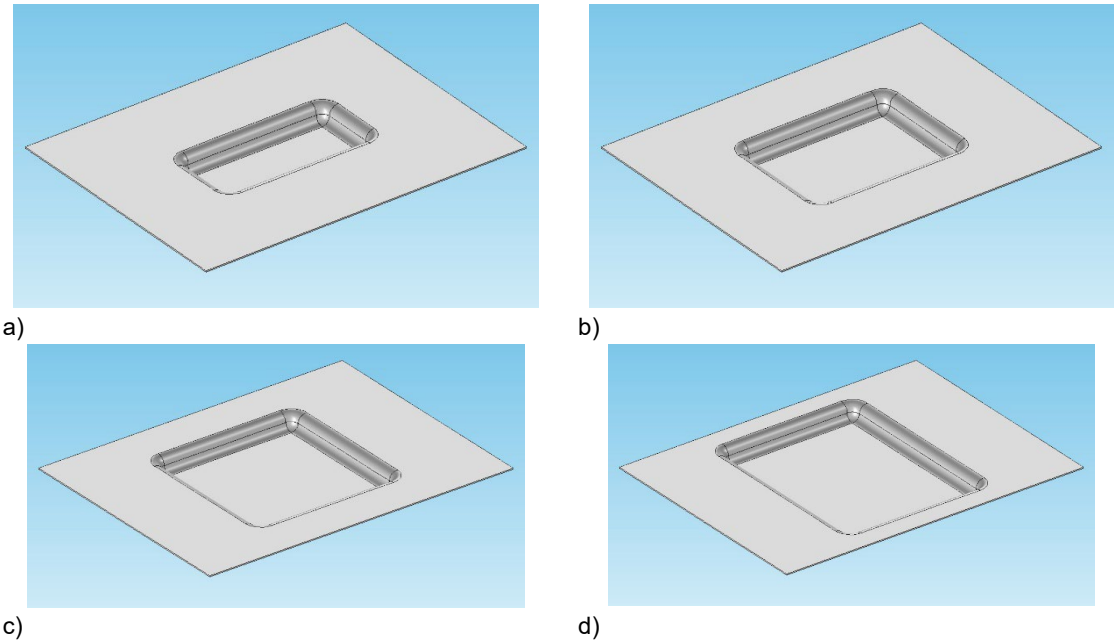


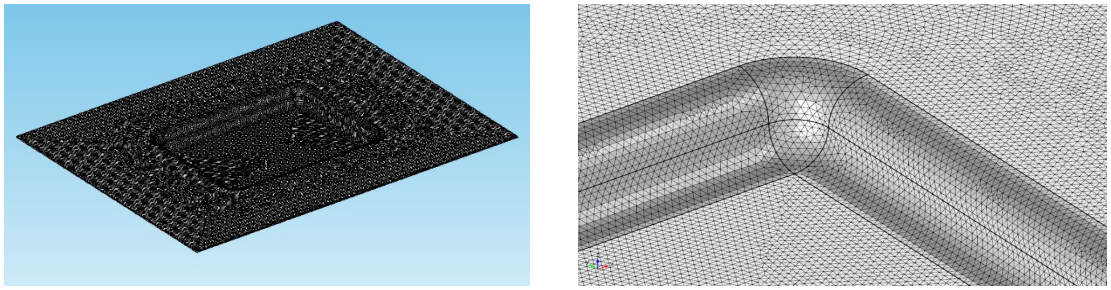

**Fig. 15 - Embossed plate configurations obtained by varying the embossment width:**
*(a) W1 = 100 mm; (b) W2 = 150 mm; (c) W3 = 200 mm; (d) W4 = 250 mm*

The 200 × 150 mm configuration is common to both parametric series and therefore corresponds simultaneously to configurations L2 and W2. It was used as the common reference configuration when comparing the influence of the longitudinal and transverse dimensions of the embossment. All remaining geometric parameters were maintained unchanged throughout the parametric analysis.

***Numerical Model and Mesh***

The numerical analyses were performed in COMSOL Multiphysics using the same general modeling methodology previously applied to the reference plate. Since the numerical model of the initial plate had already been validated experimentally, the same material properties, structural formulation, boundary conditions, and eigenfrequency analysis procedure were retained for all embossed configurations.

Consequently, the numerical investigation presented in this section focuses only on the influence of the geometric modifications introduced by the embossment. The finite element mesh was generated taking into account the additional geometric details associated with the embossed region. Particular attention was given to the transition between the flat plate surface and the embossed region, where the curved geometry requires an adequate spatial discretization. The same meshing strategy was maintained for all investigated configurations in order to ensure that the observed variations in the modal characteristics were primarily associated with changes in embossment geometry rather than with differences in numerical discretization. The finite element mesh used for the numerical analysis is illustrated in Figure 5. The general view shows the overall discretization of the plate, while the detailed view highlights the refined representation of the curved embossment region.



a) b)

**Fig. 16 - Finite element mesh of the embossed plate: (a) general view; (b) close-up of the embossment region**

For each investigated configuration, an eigenfrequency analysis was performed and the first ten structural natural frequencies were extracted for subsequent comparison. The very low-frequency solutions associated with rigid-body motion under free-free boundary conditions were excluded from the analysis, since they do not correspond to elastic deformation modes of the plate.

The resulting numerical data were then used to evaluate separately the influence of embossment length and embossment width on the modal response of the plate.

## RESULTS AND DISCUSSION

The numerical results obtained for the investigated embossed configurations were analyzed in order to evaluate separately the influence of embossment length and width on the modal response of the plate. For each configuration, the first ten structural natural frequencies were considered, while the rigid-body modes associated with the free-free boundary conditions were excluded from the comparison.

***Influence of Embossment Length***

The first parametric analysis investigated the influence of the embossment length while the remaining geometric parameters were maintained unchanged. The longitudinal dimension of the embossed region was progressively increased from configuration L1 to L4, corresponding to embossment lengths of 150, 200, 250, and 300 mm, respectively.

The first ten structural natural frequencies obtained for the four investigated configurations are presented in Table 3.

**Table 3**

**First ten natural frequencies obtained for the investigated embossment lengths**

| Mode | L1 [Hz] | L2 [Hz] | L3 [Hz] | L4 [Hz] |
|---|---|---|---|---|
| 1 | 77.020 | 96.296 | 121.280 | 139.340 |
| 2 | 79.243 | 106.780 | 148.290 | 185.610 |

| Mode | L1 [Hz] | L2 [Hz] | L3 [Hz] | L4 [Hz] |
|---|---|---|---|---|
| 3 | 112.960 | 131.340 | 161.280 | 198.470 |
| 4 | 136.310 | 151.560 | 172.580 | 201.020 |
| 5 | 140.140 | 157.310 | 178.840 | 204.950 |
| 6 | 152.170 | 174.300 | 219.840 | 276.980 |
| 7 | 236.930 | 243.180 | 251.950 | 278.470 |
| 8 | 259.280 | 261.050 | 276.820 | 298.690 |
| 9 | 272.760 | 281.140 | 291.280 | 358.070 |
| 10 | 351.840 | 360.850 | 363.370 | 390.980 |

The evolution of the first ten natural frequencies as a function of embossment length is illustrated in Figure 6.

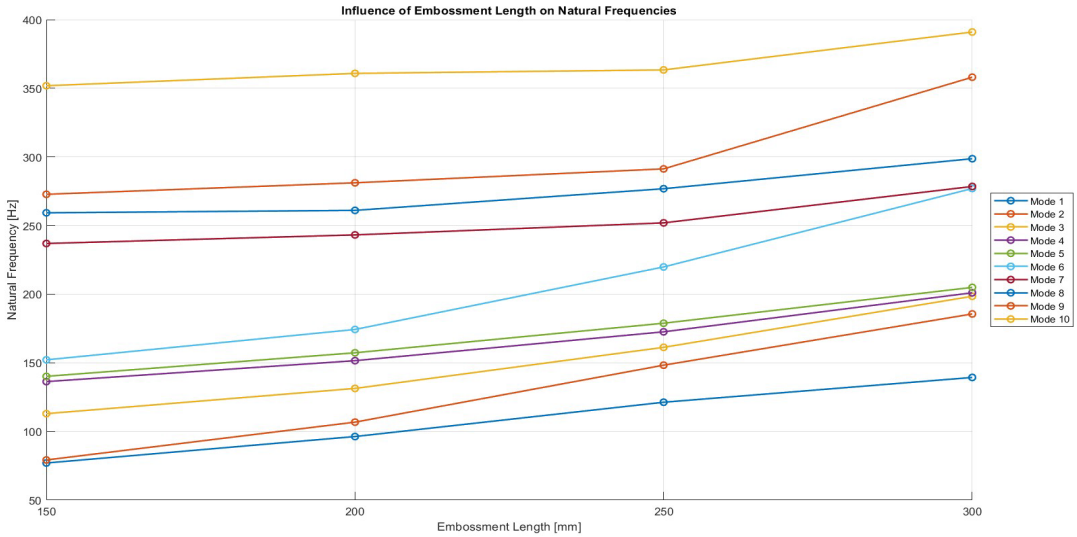



**Fig. 17 - Influence of embossment length on the first ten natural frequencies of the plate**

The results show a clear increase in the natural frequencies as the embossment length increases. This tendency is observed for all ten investigated modes, although the magnitude of the variation differs significantly from one mode to another. The strongest variations are observed for several lower and intermediate modes. For example, the second natural frequency increases from 79.243 Hz for configuration L1 to 185.610 Hz for L4, while the sixth frequency increases from 152.170 Hz to 276.980 Hz. In contrast, the tenth natural frequency increases from 351.840 Hz to 390.980 Hz, showing a considerably smaller relative variation. The graphical representation confirms that the influence of increasing embossment length is not identical for all modes. While some frequency curves exhibit a pronounced increase, others vary more gradually. This behavior indicates that extending the embossed region in the longitudinal direction modifies the dynamic stiffness of the plate in a mode-dependent manner.

Therefore, the effect of embossment length cannot be described as a uniform shift of the entire frequency spectrum, since each vibration mode responds differently to the change in local geometry.

***Influence of Embossment Width***

The second parametric analysis investigated the influence of embossment width while maintaining the remaining geometric parameters unchanged. The transverse dimension of the embossed region was progressively increased from 100 mm to 250 mm, corresponding to configurations W1–W4. Configuration W2 corresponds to the same 200 × 150 mm geometry as L2 and therefore represents the common reference configuration between the two parametric studies. The first ten structural natural frequencies obtained for the investigated configurations are summarized in Table 4.

**Table 4**

**First ten natural frequencies obtained for the investigated embossment widths**

| Mode | W1 [Hz] | W2 [Hz] | W3 [Hz] | W4 [Hz] |
|---|---|---|---|---|
| 1 | 76.335 | 96.296 | 112.660 | 106.300 |
| 2 | 95.153 | 106.780 | 116.040 | 120.390 |
| 3 | 115.840 | 131.340 | 148.620 | 160.850 |
| 4 | 116.060 | 151.560 | 181.200 | 184.950 |

| Mode | W1 [Hz] | W2 [Hz] | W3 [Hz] | W4 [Hz] |
|---|---|---|---|---|
| 5 | 134.420 | 157.310 | 185.780 | 210.130 |
| 6 | 166.670 | 174.300 | 187.150 | 211.480 |
| 7 | 211.870 | 243.180 | 298.370 | 278.480 |
| 8 | 226.460 | 261.050 | 322.120 | 341.020 |
| 9 | 249.330 | 281.140 | 367.600 | 353.810 |
| 10 | 329.280 | 360.850 | 388.080 | 356.990 |

The corresponding frequency evolution is presented in Figure 7.

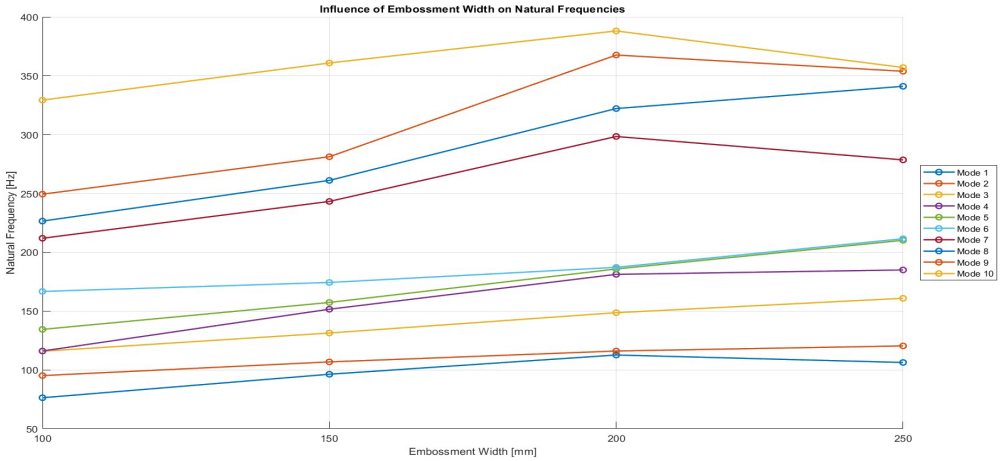



**Fig. 18 - Influence of embossment width on the first ten natural frequencies of the plate**

Increasing the embossment width also produces significant changes in the modal characteristics of the plate. However, unlike the length variation, the frequency evolution is not uniformly monotonic for all investigated modes.

Modes 2, 3, 4, 5, 6, and 8 exhibit a progressive increase in natural frequency from W1 to W4. In contrast, modes 1, 7, 9, and 10 reach their maximum value for configuration W3 and subsequently decrease for W4. For example, the seventh natural frequency increases from 211.870 Hz for W1 to 298.370 Hz for W3, before decreasing to 278.480 Hz for W4. Similarly, the tenth frequency increases from 329.280 Hz to 388.080 Hz and then decreases to 356.990 Hz. This non-monotonic behavior indicates that increasing the transverse dimension of the embossed region does not necessarily lead to a continuous increase in every natural frequency. The effect of the geometric modification depends on the interaction between the resulting stiffness redistribution and the deformation pattern associated with each individual vibration mode.

The observed trends also suggest that the eigenfrequency values should be interpreted together with the corresponding mode shapes, particularly in frequency ranges where neighboring modes may approach each other or change their relative order as the embossment geometry is modified.

***Comparative Influence of the Geometric Parameters***

The two parametric investigations highlight different effects of the longitudinal and transverse dimensions of the embossment on the dynamic response of the plate. Increasing the embossment length produces a clear and generally monotonic increase in all investigated natural frequencies. Although the magnitude of the variation differs from one mode to another, the overall evolution remains consistent throughout the analyzed configurations. The influence of embossment width is more complex. While several modes exhibit a continuous increase in frequency, others reach a maximum value for an intermediate configuration and subsequently decrease. This indicates a stronger dependence on the individual modal deformation pattern. The comparison therefore shows that the embossment length produces a more uniform evolution of the modal frequencies, whereas the embossment width generates a more mode-dependent response. Consequently, increasing the dimensions of the embossed region does not necessarily lead to the same dynamic effect for all vibration modes.

Overall, the results confirm that the in-plane dimensions of the embossment represent relevant design parameters for modifying the dynamic characteristics of thin plate structures. However, the geometric parameters should be evaluated in relation to the specific vibration modes of interest rather than considering only the overall size of the embossed region.

## CONCLUSIONS

The present study investigated the influence of a central rectangular embossment on the free vibration characteristics of a thin rectangular plate using a finite element model previously validated against experimental results.

The parametric analysis showed that the in-plane dimensions of the embossed region have a significant influence on the natural frequencies of the plate. Increasing the embossment length produced a clear and generally monotonic increase in all investigated frequencies, although the magnitude of the variation differed from one vibration mode to another.

The influence of embossment width was more complex. While several modes exhibited a progressive increase in natural frequency as the width increased, other modes reached a maximum value for an intermediate configuration and subsequently decreased. This behavior indicates that the effect of the geometric modification is strongly dependent on the individual mode shape and on the redistribution of structural stiffness within the plate.

The comparison between the two parametric studies therefore shows that the embossment length produces a more uniform evolution of the modal frequencies, whereas the embossment width generates a more mode-dependent response. Consequently, increasing the size of the embossed region does not necessarily produce the same effect on all vibration modes.

Overall, the results confirm that embossment geometry represents an effective design parameter for modifying the dynamic characteristics of thin plate structures. The obtained trends provide a basis for further investigations considering additional geometric parameters, such as embossment depth, fillet radius, position, and alternative embossment configurations.

## ACKNOWLEDGEMENT

The authors gratefully acknowledge the financial support provided by the Faculty of Biotechnical Systems Engineering, National University of Science and Technology POLITEHNICA Bucharest, which enabled their participation in this conference.

## REFERENCES

[1] Hull, & J. Maguire. (2014). Elastic response of an orthogonally reinforced plate. *Journal of Sound and Vibration, Vol. 333*.

[2] BARBU, L. -M., TIRON, A. C., ALECU, A., & PREDOI, M. V. (2026). FREE VIBRATION ANALYSIS OF RECTANGULAR PLATES REINFORCED WITH STRIPS. *U.P.B. Sci. Bull.*

[3] Bathe, K. (1996). Finite Element Procedures. *Prentice Hall,*.

[4] Gorman, D. (1982). Free Vibration Analysis of Rectangular Plates. *Elsevier*.

[5] K. Zhang, J. Pan, & TR. Lin. (2021). Vibration of rectangular plates stiffened by orthogonal beams. *Journal of Sound and Vibration, Vol. 513*.

[6] Lechao Tang, Zengming Feng, Jianjiao Deng, & Hangsheng Hou. (2025). The Factorial Fundamental Frequency Explicit Formulas for Homogenous Rectangular Thin Plates with Four Free Edges. *Journal of Vibration Engineering & Technologies, 13*. doi:https://doi.org/10.1007/s42417-024-01584-w

[7] Leissa, A. W. (1969). *Vibration of Plates.* NASA SP-160.

[8] Narita, Y. (Feb. 2022). Natural Frequencies of Isotropic Rectangular Plates in Improved Accuracy. *EPI International Journal of Engineering, Vol. 5*(Iss. 1).

[9] Petyt, M. (2010). Introduction to Finite Element Vibration Analysis. *Cambridge University Press*.

[10] Predoi, M. V. (2011). *Vibratii Mecanice - Modele si Aplicatii in Matlab.* Bucharest: Ed. Matrix Rom, p. 255.

[11] R. Szilard. (1974). Theory and Analysis of Plates: Classical and Numerical Methods. *Prentice Hall*.

[12] Timoshenko, S., & Woinowsky-Krieger, S. (1959). *Theory of Plates and Shells.* McGraw-Hill.

[13] Y. Mochida, S. I. (2008). Bounded Natural Frequencies of Completely Free Rectangular Plates. *Journal of Sound and Vibration, 311*, 1-8.

[14] Zhongwei Zhao, Bin Wang, & Ni Zhang. (2025). Optimization of local stiffener for controlling natural frequency of steel plates. *Construction and Building Materials, 468*.

[15] Zhongwei Zhao, Zeyuan Jin, Bin Wang, Ni Zhang, Ye Yuan, & Bingzhen Zhao. (2024). Design of stiffeners for steel plates with constraint on natural frequency. *Structures, 67*.

# ASPECTS REGARDING ANTI-FROST PROTECTION EQUIPMENT FOR FRUIT AND VINE CROPS

/

# *ASPECTE PRIVIND ECHIPAMENTELE PENTRU PROTECȚIA ANTI-ÎNGHEȚ A CULTURILOR POMICOLE ȘI VIȚEI DE VIE*

**Elena SORICĂ*, Carmen BRĂCĂCESCU, Cristian SORICĂ, Gabriel NAE**
INMA Bucharest / Romania
**E-mail: postelnicu.elena@yahoo.com*

***Keywords**: frost protection; orchards; vineyards; wind machines; micro-sprinklers; heaters; automation*

**ABSTRACT**

*Spring frost threatens fruit and vine crops when freezing temperatures coincide with flowering, fruit set or early shoot growth. To limit this risk, several anti-frost technologies can be implemented, including passive protection and monitoring, air mixing under thermal inversion, sprinkling and micro-sprinkling, fixed and mobile heating, and local electrical heating with automated control. Research findings illustrate the benefits of these mechanisms under specific frost and crop conditions. Air-mixing studies reported rotation-averaged air warming of about 50% of inversion strength (approximately 3 K) over 3–5 ha at 1 m height, and sprinkler studies reported favourable protection outcomes. In short apple-orchard heating tests, feedback control increased the mean protected-time fraction above −2 °C from 16.0% to 47.8%. Local heating with 15 W m$^{-1}$ cables reduced mean inflorescence injury from 41.3% in unheated controls to 13.1% in a single vineyard frost trial. The article also presents commercially available technical equipment implementing these technologies.*

**REZUMAT**

*Înghețurile de primăvară amenință culturile pomicole și vița de vie când temperaturile negative coincid cu înflorirea, legarea fructelor sau creșterea timpurie a lăstarilor. Pentru limitarea acestui risc pot fi implementate mai multe tehnologii anti-îngheț, printre care se numără protecția pasivă și monitorizarea, amestecarea aerului în condiții de inversiune termică, aspersiunea și microaspersiunea, încălzirea fixă și mobilă și încălzirea electrică locală asociată controlului automat. Rezultatele cercetărilor ilustrează beneficiile acestor mecanisme în condiții specifice de îngheț și de cultură. Studiile privind amestecarea aerului au raportat o creștere a temperaturii aerului, mediată pe rotație, de aproximativ 50% din intensitatea inversiunii (circa 3 K), pe 3–5 ha la înălțimea de 1 m, iar studiile privind aspersiunea au evidențiat rezultate favorabile. În teste scurte în livezi de meri, controlul prin feedback a crescut fracțiunea medie de timp protejat peste −2 °C de la 16,0% la 47,8%. Încălzirea locală prin cabluri de 15 W m$^{-1}$ a redus vătămarea medie a inflorescențelor de la 41,3% în martorii neîncălziți la 13,1% într-un test viticol cu un singur îngheț. Articolul prezintă, de asemenea, echipamente tehnice comerciale care aplică aceste tehnologii.*

## INTRODUCTION

Spring frost can damage flowers, recently formed fruit and young grapevine shoots during a short period that determines much of the seasonal crop potential. Protection is consequently a production requirement where vulnerable phenological stages overlap with freezing conditions. In orchards, the evidence reviewed by *Drepper et al. (2022)* showed that protection effectiveness was strongly conditional on crop and weather. For vineyards, the inflorescence damage measured by *Lamb (2009)* illustrated that visible frost injury can remain substantial even when a protective treatment is applied.

A warmer climate does not remove this exposure automatically. *Sgubin et al. (2018)* combined eight climate models, nine grapevine cultivars and three budburst models for French vineyards. Both the last frost date and budburst generally shifted earlier, but their relative movement determined the subsequent risk. Two phenological models projected increasing late-frost exposure in Alsace, Burgundy and Champagne, whereas a third gave an opposing response and performed less well against historical observations. These findings support local, cultivar-specific assessment and identify phenological uncertainty as a limitation of climate-based investment decisions. They do not establish that late-frost risk increases uniformly in every

winegrowing region. Frost type also determines the engineering problem. Radiation frost is associated with nocturnal radiative cooling and can develop an inversion containing warmer air above the crop. Advection frost involves the arrival of a cold air mass, often with stronger wind and little exploitable inversion. Equipment that redistributes existing atmospheric heat therefore has different operating limits from equipment that adds heat or maintains a water–ice layer on plant surfaces (*Snyder & de Melo-Abreu, 2005*). An equipment comparison needs to identify this difference before considering nominal capacity.

Recent research has improved the physical interpretation of wind-machine operation. *Heusinkveld et al. (2020)* examined mixing through field observations and modelling; *Boekee et al. (2023)* investigated the exchange of heat between air and plant organs; and *Dai et al. (2023)* resolved the spatial extent of the thermal response with distributed temperature sensing. These contributions progressively shift assessment from a temperature reading near the tower towards the entire canopy and the organs at risk.

Heating research has addressed distribution as well as installed power. *Hua et al. (2024a)* combined temperature sensing, adjustment of the heating direction and a mobile platform, while *Hua et al. (2024b)* modelled fixed and moving heaters. *Yum et al. (2025)* investigated airflow produced by electrically heated fans in an apple orchard, but explicitly left frost-prevention efficacy for subsequent field verification. Environmental evaluation adds another criterion: *Renaud-Gentié (2025)* reported that active vineyard protection methods differed substantially in their life-cycle impacts.

This narrative review synthesises those scientific contributions together with official documentation for equipment marketed for orchards and vineyards. Its objective is to compare operating principles, construction features, control functions and evidence of performance, and to identify where commercial specifications remain insufficient for agronomic evaluation. The technical presentation describes existing technologies, followed by research findings and an illustrated catalogue of commercial equipment. Particular attention is given to canopy geometry, energy or water delivery and the criterion used to define effective protection.

## MATERIALS AND METHODS

Frost protection technologies modify the heat balance of susceptible plant organs by reducing exposure, redistributing atmospheric heat, supplying heat from an external source or releasing latent heat as applied water freezes. Their working conditions depend on the frost mechanism, crop stage and layout, terrain, wind and humidity. A temperature measured in the open air is not necessarily the temperature of a flower or bud; the protected organ and the duration of its exposure therefore determine the required intervention (*Boekee et al., 2023; Snyder & de Melo-Abreu, 2005*).

### *Passive protection and monitoring*

Site selection, cold-air drainage, cultivar choice and management of vegetation or covers modify exposure before active equipment is started. The orchard review of *Drepper et al. (2022)* treated such measures together with active interventions and highlighted the dependence of reported effects on context. They provide the agronomic setting for machinery selection, while the present analysis concentrates on active equipment. Monitoring should characterise the protected organs and the vertical temperature profile. A lower sensor and an elevated sensor can help identify an inversion; humidity and wind observations help interpret water demand and the transport of heat.

### *Wind machines and air mixing*

A conventional wind machine comprises a tower, fan, transmission, drive unit and mechanism that changes the direction of the airflow. It draws warmer air towards the crop during an inversion and increases local convection. Canopy resistance and atmospheric motion affect the resulting plume (*Boekee et al., 2023; Heusinkveld et al., 2020*). The rotor speed determines fan operation, whereas the head-sweep period determines how frequently a sector receives the plume; these quantities must be distinguished from engine speed. Fixed towers provide a permanent installation; folding and portable structures facilitate maintenance and seasonal deployment. These arrangements are represented in the AgroFrost and Orchard-Rite commercial ranges (*AgroFrost; Orchard-Rite*).

### *Sprinkler and micro-sprinkler systems*

Over-plant sprinkling supplies liquid water whose freezing releases heat at the wetted surface. Adequate replenishment must offset cooling, including evaporation; early interruption or insufficient application can increase damage. Wet-bulb conditions are therefore relevant to operation. Under-tree sprinkling acts through heat exchange from the wetted ground and has a different protection mechanism *(Snyder & de Melo-Abreu, 2005).*

Conventional installations distribute water over a broad area. Targeted systems concentrate it on a vine row or tree crown. Netafim's Pulsar assemblies combine a pressure-compensating dripper, microtube, air-containing chamber, anti-drain valve and discharge head. StripNet uses a static head to produce a narrow rectangular pattern; GyroNet provides circular patterns through interchangeable swivels (*Netafim*). The emitter creates pulsation locally while the installation continues supplying water. Pump capacity, filtration, hydraulic uniformity, wind drift and the surface actually wetted determine whether the susceptible organs receive sufficient water. A low emitter flow alone does not establish a safe application rate for every frost event.

***Fixed and mobile heat generators***

Heaters add energy through combustion or electricity. Forced-air constructions use a fan to transport heated air, whereas distributed pots or candles release heat at many locations. Fixed units have a persistent spatial pattern; a mobile unit periodically revisits crop sectors. Heater direction and movement were explicit design variables in the field system and numerical model of *Hua et al. (2024a)* and *Hua et al. (2024b)*. Commercial examples include tractor-driven propane units, stationary rotating gas units and pellet burners that supplement wind machines (*AgroFrost*). A mobile arrangement must revisit each sector before its thermal benefit is lost. Generator output, transport losses and the temperature of the organs between passes therefore need to be considered together.

***Electrical heating and automated control***

Electric resistance cables transfer heat locally when installed around vine cordons. *Lamb (2009)* tested cable ratings of 5, 10 and 15 W $m^{-1}$, providing an early example of directly heating the crop structure. Infrared tubes represent a different electrical arrangement: Frolight describes tubes directed towards buds, control units, temperature sensors and management through the MyFrolight application (*Frolight*). Heat delivery depends on the position of the plant relative to the source, so a cable rating or installed electrical power alone cannot describe protection of the complete canopy.

Automation links sensing to starting, stopping, flow delivery or heater movement. The cyber-physical system of *Hua et al. (2024a)* combines canopy-temperature feedback, wind information and adjustment of a mobile heater. Commercial controls include temperature-triggered starting, machine telemetry and irrigation valve control (*Netafim*; *Orchard-Rite*). Sensor placement should represent the coldest susceptible crop sectors; high and low sensors can also identify the thermal reserve available to a wind machine. Electrical supply, communication, mechanical safety and continuity of water or fuel delivery remain practical requirements. Fig. 1 summarises the principal heat-transfer mechanisms.

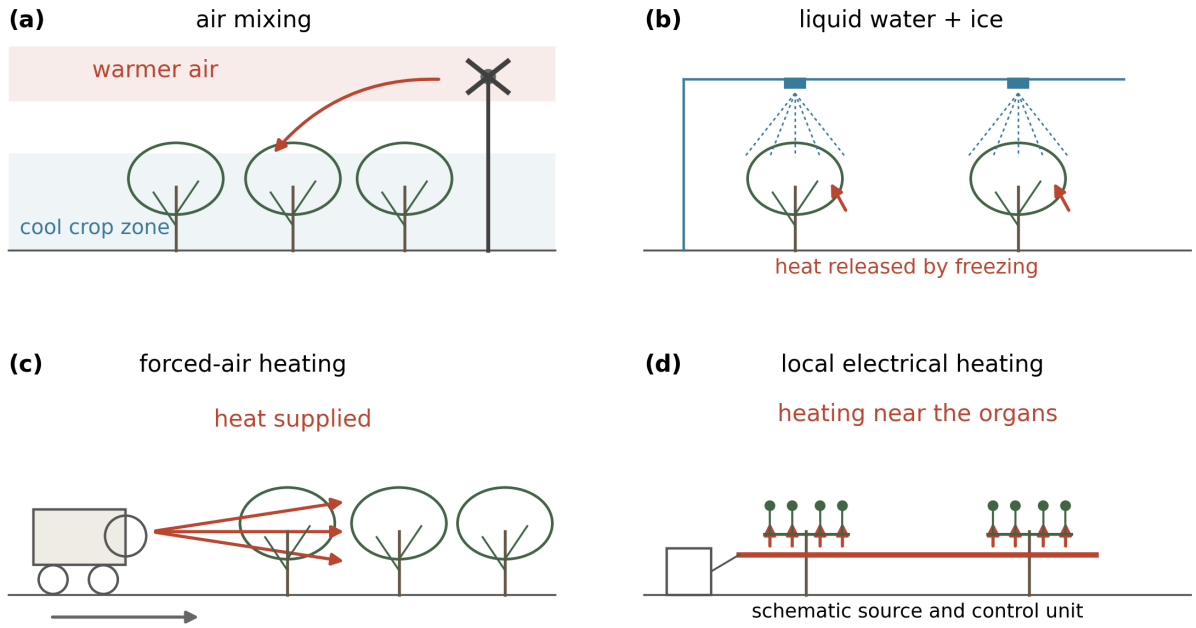



**Fig. 1. Principal mechanisms of anti-frost protection**

*(a) inversion mixing; (b) freezing of supplied water; (c) forced-air heating; (d) local electrical heating. Red arrows indicate heat transfer; the grey arrow indicates mobile-heater movement; blue dashed lines indicate water delivery.*

## RESULTS

### *Research findings and their conditions of validity*

Table 1 summarises scientific results from the studies introduced above. The values provide evidence about mechanisms and limitations rather than a common numerical ranking of equipment.

**Table 1**

**Scientific results for anti-frost protection equipment**

| Study | Crop and conditions | Reported result | Interpretation limit |
|---|---|---|---|
| *Heusinkveld et al. (2020)* | Fruit frost protection; field observations and modelling; 1 m assessment height | Rotation-averaged air warming reached about 50% of inversion strength (about 3 K) over 3–5 ha. | Conditional thermal response; the result does not define a universal protected area or crop-loss reduction. |
| *Boekee et al. (2023)* | Pear orchard, Netherlands; air profiles and tissue thermistors | Foliage limited plume penetration; at least 15 sweeps (about 75 min) were needed for optimal mixing in the observations. | Organ temperatures differed from air temperature. The reported time is specific to the observed canopy, not a universal start-up rule. |
| *Dai et al. (2023)* | 6.75 ha orchard; 9 km sensing fibre; local inversion about 8 K | Footprint for 50% inversion reduction: 0.42 ha at 1 m and 0.46 ha at 2 m. For 30%: 2.81 ha and 2.52 ha, respectively. | The instrumented orchard area was not the protected area. Footprints depend on the criterion and measurement height. |
| *Hua et al. (2024a)* | Apple orchard; paired 10 min heating tests; April 8 and 25, 2023 | On April 8, mean protected-time fraction was 47.8% with CPCPS versus 16.0% without CPCPS; threshold −2 °C. | Temperature-based proxy averaged over sensors; no whole-night or harvest validation. |
| *Hua et al. (2024b)* | Apple orchard; three-dimensional CFD; fixed and moving forced-air heaters | The tested fixed layouts reached at most 32.2% protected canopy volume; the simulated moving case improved that metric. | Numerical result for the modelled layouts; validation against crop injury and harvest outcomes remains necessary. |
| *Yum et al. (2025)* | Apple orchard, 896 m²; five two-stage fans; enclosing windbreak nets | Predicted airflow: about 0.5 m $s^{-1}$ to 18 m along rows and 0.9 m $s^{-1}$ to 21 m across rows. | Airflow prediction using measured outlet boundaries. The authors required subsequent frost-prevention field verification. |
| *Lamb (2009)* | Sauvignon Blanc within a 2 ha block; six replicates; one −3 °C event at about 30% capfall | Mean inflorescence damage: 41.3% in controls, 46.3% with unpowered cable, 28.2%, 16.5% and 13.1% at 5, 10 and 15 W $m^{-1}$. | Significant treatment effect ($P < 0.05$); single-event result. Later hail prevented assessment at harvest. |

*CFD: computational fluid dynamics. CPCPS: canopy protection cyber-physical system. Results are study-specific and are not directly comparable across rows.*

The wind-machine studies demonstrate why a single nominal area is inadequate. Thermal response varies across the field and changes with measurement height and the chosen threshold. The differing footprints reported by *Heusinkveld et al. (2020)* and *Dai et al. (2023)* cannot be read as directly contradictory capacity tests because their conditions and definitions differ. *Boekee et al. (2023)* further showed that foliage restricted plume penetration and that organ temperatures responded differently from air temperature. Thus a well-positioned air sensor can document mixing while still leaving uncertainty about colder organs elsewhere in the crop.

The heating studies support attention to heat placement and revisit time. The field improvement in protected time reported by *Hua et al. (2024a)* was a response of temperature measurements during short comparative tests. It did not quantify season-long yield preservation. The protected canopy volume in *Hua et al. (2024b)* was predicted numerically, and the airflow range in *Yum et al. (2025)* was also a model output. These results support prototype design and placement studies; their transfer to commercial machinery requires tests with comparable crop geometry and weather.

Electrical cables provide a different type of evidence. *Lamb (2009)* measured inflorescence injury, with a significant treatment effect, rather than relying only on warmer air. However, the trial experienced one frost event and a later hailstorm prevented a harvest comparison. The authors estimated approximately 43

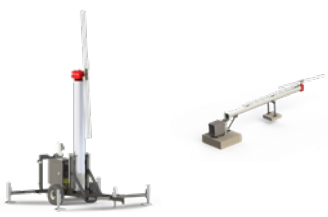
kW ha$^{-1}$ for the 10 W m$^{-1}$ cable layout at 3 m row spacing. This illustrates both the potential of local heating and the importance of electrical infrastructure. The value is specific to that layout and is not a specification for infrared-tube systems.

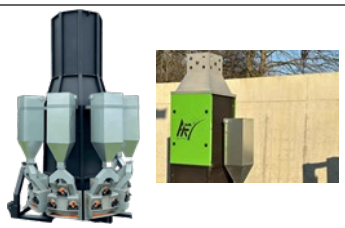
***Current commercial equipment and construction achievements***

Table 2 presents an illustrated catalogue of equipment listed by *AgroFrost*, *Orchard-Rite*, *Netafim* and *Frolight*. All specifications and nominal areas are manufacturer-declared; they are distinct from the research outcomes in Table 1. Figure captions identify the manufacturer website, while citations accompanying the specifications refer to the relevant technical sheet or product page.

**Table 2**

**Illustrated presentation of commercial anti-frost protection equipment**

| Equipment images | Equipment and construction | Principal manufacturer-declared characteristics |
|---|---|---|
| <br>**Fig. 2 - K10 (left) and K10F (right) wind machines**<br>*(source: https://www.agrofrost.eu)* | AgroFrost<br>K10 / K10F<br>Fixed tower and folding tower for air mixing. The folding arrangement uses a hydraulic cylinder. | Height: 10.60 m; rotor: 5.60 m, 560 min$^{-1}$; airflow: 109,000 m$^3$ min$^{-1}$; diesel drive: 129 kW. Nominal area: up to 6.5 ha; fuel: 18–20 L h$^{-1}$; tank: 400 L. Automatic start, high and low temperature probes, remote control. Drive power is not canopy heating power. (*AgroFrost*) |
| <br>**Fig. 3 - M7/M9 mobile wind-machine family**<br>*(source: https://www.agrofrost.eu)* | AgroFrost<br>M7 / M9<br>Mobile wind-machine family deployed on a stabilised trailer; representative field installation and product view. | Height: 7 m / 9 m; listed rotor speed: 540 min$^{-1}$; diesel drive: 105 kW; tank: 400 L. Nominal coverage: 5–6 ha. Temperature and wind sensors, automatic start and remote diagnostics. Coverage remains conditional on the inversion and site. (*AgroFrost*) |
| <br>**Fig. 4 - 2600 (left) and 2430 (right) wind machines**<br>*(source: https://orchard-rite.com)* | Orchard-Rite<br>2600 / 2430<br>Stationary wind machines with two-blade and three-blade rotors, respectively. | Fan-shaft height: 10.7 m; listed blade length: 6.05 m; blade pitch: 8°; concrete base: 5.35 m$^3$. Optional temperature-triggered starting and ORCell cellular monitoring. No common protected-area rating is assigned here; rotor and drive configurations require separate verification. (*Orchard-Rite*) |
| <br>**Fig. 5 - Portable (left) and laydown (right) wind machines**<br>*(source: https://orchard-rite.com)* | Orchard-Rite<br>Portable / laydown<br>Portable machine for seasonal deployment; tower-lowering option for reduced height when idle. | Portable unit: access through rows 2.28 m wide; propane or diesel packages. Laydown option: lowered height 2.38 m. Remote monitoring is available in selected markets. These are deployment characteristics, not evidence of equal thermal coverage. (*Orchard-Rite*) |

| Equipment images | Equipment and construction | Principal manufacturer-declared characteristics |
|---|---|---|
| <br>**Fig. 6 - FrostBuster F501 hot-air generator**<br>*(source: https://www.agrofrost.eu)* | AgroFrost<br>FrostBuster F501<br>Tractor-driven, trailed propane hot-air generator with two low lateral outlets. | Dimensions: 4.30 × 1.45 × 1.65 m; mass: 1,480 kg without cylinders; power-take-off: 540 min⁻¹; fuel: 30–35 kg h⁻¹. Fan flow: 23,500 m³ h⁻¹; maximum discharge temperature: 85 °C. Nominal area: up to 6.5 ha. Maximum lateral reach: 40 m per side in orchards, 30 m in vineyards. Crop response depends on the route and cooling between passes. (*AgroFrost*) |
| <br>**Fig. 7 - FrostGuard S20 (left) and V20 (right)**<br>*(source: https://www.agrofrost.eu)* | AgroFrost<br>FrostGuard S20 / V20<br>Propane burner with a stationary rotating fan; horizontal and upward discharge, respectively. | S20 sheet: 1.20 × 0.775 × 1.20 m; mass: 325 kg; fuel: 10.5 kg h⁻¹; nominal area: 0.5 ha; discharge: 80–90 °C; automatic start and smartphone control. (AgroFrost) V20 product page: 1.20 × 1.05 × 1.55 m; fuel: 10.5 kg h⁻¹; nominal area: 0.5 ha; temperature-triggered start. (*AgroFrost*) |
| <br>**Fig. 8 - Booster Pellet burner and field detail**<br>*(source: https://www.agrofrost.eu)* | AgroFrost<br>Booster Pellet<br>Pellet-fired supplemental burner positioned near a wind machine; family product view and field detail. | BR-P100: 100 kW; BR-P350: 300 kW; BR-P650: 600 kW. Listed hopper arrangements: 1, 4 and 7, respectively. Recommended input: 150 kW ha⁻¹. This is a commercial sizing recommendation; effective canopy heating and pellet consumption require site and fuel information. (*AgroFrost*) |
| <br>**Fig. 9 - Pulsar + StripNet assembly and vineyard installation**<br>*(source: https://www.netafim.com)* | Netafim<br>Pulsar + StripNet<br>Pressure-compensated pulsed emitter with a static head for narrow row-directed wetting. | Emitter flow: 12, 15 or 20 L h⁻¹; regulation range: 250–400 kPa. Strip width: 0.50 or 0.70 m according to nozzle; emitter spacing: up to 5 m; recommended mounting: 0.5 m above vines. Filtration: 130 µm. Values follow the 2026 sheet; adequate organ wetting requires hydraulic and crop-specific design. (*Netafim*) |
| <br>**Fig. 10 - Pulsar + GyroNet assembly and orchard installation**<br>*(source: https://www.netafim.com)* | Netafim<br>Pulsar + GyroNet<br>Pressure-compensated pulsed emitter with rotating head and interchangeable swivels for circular crown wetting. | Emitter flows: 8, 12, 15, 20 or 25 L h⁻¹; blue-pin anti-drain valve: 250–400 kPa; black-pin valve: 170–400 kPa. Circular 360° pattern; swivel selected for crown size. Filtration: 130 µm. Values follow the 2026 sheet; discharge per emitter is not the application rate per hectare. (*Netafim*) |
| <br>**Fig. 11 - Frolight infrared tube and vineyard installation**<br>*(source: https://www.frolight.com)* | Frolight<br>Infrared tubes and control units<br>Local electrical heating directed towards vine buds; manual, temperature-triggered or remote operation. | Master unit: three-phase 400 V supply with neutral; rated current 32 A; IP65; mass 10 kg; 12 tube connections. Maximum connected length: 1,200 m in total and 450 m per phase. MyFrolight supervision and expansion units support modular installation. Tube length and current do not establish protected area or verified heating power per hectare. (*Frolight*) |

*Images show the indicated model, configuration or family*

For air-mixing equipment, folding and portable structures address seasonal deployment and access between rows. Automatic starting, high and low temperature probes, and remote diagnostics provide information about both weather and machine status.

Stability and vibration sensing are documented for the AgroFrost M7/M9 family (*AgroFrost*). Orchard-Rite offers two- and three-blade stationary machines, portable units and a laydown option, with automatic starting and cellular supervision available as options (*Orchard-Rite*). These developments concern construction and control. Their contribution to safe organ temperatures still requires field measurements.

For forced-air heating, the contrast is between continuous treatment of a smaller sector and periodic treatment by a moving generator. The FrostGuard S20/V20 arrangements rotate at a fixed location, whereas the FrostBuster F501 depends on the tractor route and repeated passes (*AgroFrost*).

The declared treated areas therefore describe different operating patterns. A hot discharge temperature does not specify the temperature reached by buds at the most distant point or between passes. In combined systems, pellet boosters supply heat that can subsequently be redistributed by a wind machine (*AgroFrost*). Performance during an advective event remains dependent on heat loss and wind, even when extra thermal power is installed.

For water-based equipment, geometry is the main distinction between StripNet and GyroNet. Row-directed delivery is adapted to a narrow vine canopy, whereas a circular pattern can be selected for a tree crown. Pressure compensation and anti-drain components support delivery over variable terrain, but cannot compensate for an unsuitable nozzle pattern or inadequate water availability.

The consulted datasheets advertise water and energy savings of 70% for StripNet and 50% for GyroNet relative to standard full-coverage systems (*Netafim*). Those percentages are commercial comparisons whose baseline and frost-test conditions are not established by the research included here. They were therefore not entered in Table 1 as measured agronomic outcomes.

Frolight integrates infrared tubes with temperature-triggered power distribution and remote management (*Frolight*). The master-unit specifications make its connection architecture more explicit: a three-phase supply and multiple tube connections support a modular vineyard installation (Frolight).

However, connected tube length and electrical current are installation limits, not protected hectares or heat delivered to buds. The documentation does not provide a complete comparative dataset for bud-temperature uniformity, electricity use per effectively protected hectare or yield preservation.

***Technical characteristics and operating limits***

The K10 and K10F technical sheets specify a 5.60 m fibreglass rotor operating at 560 $min^{-1}$, an airflow of 109,000 $m^3$ $min^{-1}$ and a nominal area of up to 6.5 ha. The 129 kW diesel drive and declared fuel consumption of 18–20 L $h^{-1}$ describe the mechanical power supply (*AgroFrost*). These quantities do not express heat delivered to the canopy: the thermal effect of air mixing depends on the warmer layer available above the crop, plume distribution and interception by foliage.

The F501 technical sheet specifies a fan capacity of 23,500 $m^3$ $h^{-1}$, two lateral outlets and a maximum discharge temperature of 85 °C. Declared maximum lateral reach differs between orchards and vineyards: 40 m and 30 m on each side, respectively (*AgroFrost*). The S20 sheet describes a stationary 360° distribution pattern, an outlet 0.20 m above the ground and a discharge temperature of 80–90 °C (*AgroFrost*). Lateral reach, discharge temperature and nominal hectares describe different aspects of operation; none alone determines the temperature of the coldest flower or bud.

Model-specific characteristics establish mechanical, hydraulic and electrical operating limits. Rotor speed and fan flow describe air movement; burner temperature and fuel consumption describe the heat source; emitter discharge and pressure describe water delivery; connected tube length and rated current describe an electrical installation.

A protection criterion must additionally state the organ-temperature threshold, spatial extent and duration achieved under defined frost conditions.

This links machinery specifications to their agricultural function and permits comparison with the thermal and injury responses reported in Table 1. Resource demand and effective coverage must refer to the same crop area and operating period.

***Comparative engineering assessment***

A qualitative comparison of anti-frost protection technologies is presented within Table 3.

**Table 3**

**Qualitative comparison of anti-frost protection technologies**

| Technology | Main selection condition | Engineering advantage | Main verification need |
|---|---|---|---|
| Wind machine | Usable inversion; accessible warmer layer; suitable topography and canopy. | Redistributes existing atmospheric heat over a sector without wetting the crop. | Organ-temperature response and footprint under different inversions; noise and drive requirements. |
| Targeted sprinkling | Reliable water supply, hydraulic uniformity and wetting of susceptible organs. | Concentrates water on crop geometry; modular emitter selection. | Required application under wind and humidity; continuity, icing and ice-load effects. |
| Fixed / mobile forced-air heating | Heat input and distribution adequate for cooling; practical access or route. | Adds heat; directional or repeated delivery can treat selected sectors. | Temperature between passes, cold edges, fuel use and exposure to hot discharge. |
| Electrical cables / infrared tubes | Electrical capacity and a layout close to the organs requiring protection. | Local delivery and straightforward integration with temperature control. | Heating uniformity, peak demand, crop injury and interference with field operations. |
| Combined or automated system | Compatible equipment and control based on representative crop conditions. | Coordinates delivery and can respond to spatial or temporal variation. | Measured benefit over individual methods, sensor placement and reliability during the event. |

*These are selection and testing criteria, not numerical performance rankings.*

Coverage should be accompanied by a protection criterion. A manufacturer's maximum area, the area showing a specified inversion reduction, and the area in which a bud remains above a damage threshold are distinct quantities. A comparison should state which quantity was measured, its height, its duration and the initial weather conditions. The nominal hectares in Table 2 cannot consequently be substituted for the observed footprints in Table 1. A larger engine or hotter outlet may increase available capacity, but the useful result also depends on distribution and heat loss.

The same distinction applies to water delivery. Emitter flow in L $h^{-1}$ must be combined with emitter density and the wetted area before an application rate in mm $h^{-1}$ can be calculated. The unit identity 1 mm $h^{-1}$ = 10 $m^3$ $ha^{-1}$ $h^{-1}$ applies when the same hectare is used as the area denominator. For a targeted system, the application on wetted rows and the average abstraction per land hectare should both be reported. Pump power also depends on pressure and efficiency, so a percentage reduction in water flow does not by itself establish an identical energy saving.

Operational duration should be compared alongside instantaneous capacity. Fuel reserves, water storage or electricity supply must support the intended treatment over the event, including repeated passes where applicable. For mobile heaters, a practicable route should include turning and access time, because the coldest interval occurs between visits to a given sector. For fixed systems, accessible servicing points and representative sensors affect how faults are detected and corrected. These considerations are engineering implications of the respective layouts, not measured advantages assigned to a particular brand. They explain why maximum coverage and installed power are insufficient as sole selection criteria.

Resource use changes the practical comparison. A stationary installation requires investment and maintenance even in years with few frost hours; a mobile system adds route planning, tractor availability and labour during the event. *Renaud-Gentié (2025)* reported that candles had the highest impact in most environmental categories and wind machines the lowest in the vineyard scenarios assessed by her research team; rankings also changed with annual frost hours. This conference contribution supports using a life-cycle perspective, while its regional results cannot be transferred directly to another electricity mix, fuel supply or equipment lifetime. Environmental evaluation should be conditional on actually achieving the required protection.

***Evidence limitations and research priorities***

The strongest general limitation is the absence of a consistent link between equipment operation, organ temperature and crop outcome. *Drepper et al. (2022)* selected 104 studies from 8,970 records and found substantial weaknesses in study validity and reporting, including missing variability information. Sprinklers performed favourably across several outcomes, but heterogeneity limited broad comparisons.

That assessment explains why the present review does not designate one universally superior technology. Differences in frost type, crop stage and outcome remain central to interpretation.

A comparative testing programme should first describe inversion strength, wind, humidity, frost duration, cultivar and phenological stage. It should then monitor air and organ temperatures at several heights and distances, including field edges and points between heater passes. Unprotected reference sectors are needed to distinguish treatment effects from natural spatial variation. Damage to reproductive organs should be scored after the event, followed by crop yield where subsequent hazards permit. Replicated events would help establish how consistently each configuration works.

For wind machines, useful development questions concern tower height, airflow direction, sweep period and canopy resistance. For targeted sprinklers, priorities include catch-can uniformity, wetting of the organs at risk, emitter reliability during icing and the hydraulic capacity required during prolonged events. For mobile heaters, the relevant variables are route length, travel speed, outlet direction and cooling between passes. Electrical systems require assessment of heating uniformity, peak power demand and compatibility with pruning and harvesting. These are proposed engineering priorities derived from the synthesis, rather than results already demonstrated for every listed product.

Automation should be evaluated through its operational effect: earlier intervention when needed, response to a changing wind direction, adequate delivery at the coldest location and continued operation during power or communication faults. A common reporting framework could express water, fuel and electricity per hectare-hour meeting an explicitly defined organ-temperature criterion, together with damage and yield observations. Such testing would make research prototypes and commercial equipment more comparable and would support the development of systems adapted to local orchard and vineyard conditions.

## CONCLUSIONS

Anti-frost protection equipment must be matched to the frost mechanism and the sensitive crop organs. Wind machines are appropriate where a usable inversion supplies warmer air, whereas sprinklers and heaters introduce heat through different transfer processes. Their operating conditions and resource requirements prevent a universal ranking based on rated power or nominal hectares.

Current commercial achievements include portable and folding wind machines, automatic starting and telemetry, pressure-compensated pulsed emitters adapted to rows or crowns, rotating gas heaters, mobile forced-air generators and sensor-controlled infrared installations. These developments improve the options for deployment and control. Manufacturer specifications still require validation against a clear protection criterion under stated field conditions.

The reviewed research confirms that heat distribution, canopy resistance and the difference between air and organ temperature are central to performance. Mobile heating and feedback control showed promising thermal responses, while direct vine heating reduced inflorescence injury in a limited trial. Short field tests and numerical predictions do not establish long-term crop protection for commercially different equipment.

Further agricultural engineering work should combine spatial temperature monitoring with reproductive-organ damage, yield and measured resource consumption. Comparable trials over several frost events would clarify effective coverage and enable machinery selection and development on the basis of demonstrated protection, operational reliability and environmental performance.

## REFERENCES

[1] AgroFrost. https://www.agrofrost.eu/

[2] Boekee, J., Dai, Y., Schilperoort, B., van de Wiel, B. J. H., & ten Veldhuis, M.-C. (2023). Plant–atmosphere heat exchange during wind machine operation for frost protection. *Agricultural and Forest Meteorology, 330*, 109312. https://doi.org/10.1016/j.agrformet.2023.109312

[3] Dai, Y., Boekee, J., Schilperoort, B., ten Veldhuis, M.-C., & van de Wiel, B. J. H. (2023). Wind machines for frost damage mitigation: A quantitative 3D investigation based on observations. *Agricultural and Forest Meteorology, 338*, 109522. https://doi.org/10.1016/j.agrformet.2023.109522

[4] Drepper, B., Bamps, B., Gobin, A., & Van Orshoven, J. (2022). Strategies for managing spring frost risks in orchards: Effectiveness and conditionality—a systematic review. *Environmental Evidence, 11*, 29. https://doi.org/10.1186/s13750-022-00281-z

[5] Frolight. https://www.frolight.com/

[6] Heusinkveld, V. W. J., van Hooft, J. A., Schilperoort, B., Baas, P., ten Veldhuis, M.-C., & van de Wiel, B. J. H. (2020). Towards a physics-based understanding of fruit frost protection using wind machines. *Agricultural and Forest Meteorology, 282–283*, 107868. https://doi.org/10.1016/j.agrformet.2019.107868

[7] Hua, W., Heinemann, P. H., & He, L. (2024a). Canopy protection cyber-physical system (CPCPS) for smart agricultural management of frost damage in apple orchards. *Computers and Electronics in Agriculture, 217*, 108611. https://doi.org/10.1016/j.compag.2024.108611

[8] Hua, W., Heinemann, P. H., & He, L. (2024b). Heat transfer modeling with fixed and mobile heaters for frost protection in apple orchards. *Computers and Electronics in Agriculture, 227*, 109525. https://doi.org/10.1016/j.compag.2024.109525

[9] Lamb, D. W. (2009). Electrically heated cables protect vines from frost damage at early flowering. *Australian Journal of Grape and Wine Research, 15*(1), 79–84. https://doi.org/10.1111/j.1755-0238.2008.00034.x

[10] Netafim. https://www.netafim.com/

[11] Orchard-Rite. https://orchard-rite.com/

[12] Renaud-Gentié, C. (2025). *Life cycle assessment (LCA) to move towards more environmentally friendly winegrowing*. IVES Conference Series, GiESCO 2025, Geisenheim, Germany, July 27–31. https://ives-openscience.eu/giesco25-keynote7/

[13] Sgubin, G., Swingedouw, D., Dayon, G., García de Cortázar-Atauri, I., Ollat, N., Pagé, C., & van Leeuwen, C. (2018). The risk of tardive frost damage in French vineyards in a changing climate. *Agricultural and Forest Meteorology, 250–251*, 226–242. https://doi.org/10.1016/j.agrformet.2017.12.253

[14] Snyder, R. L., & de Melo-Abreu, J. P. (2005). *Frost protection: Fundamentals, practice and economics* (Vol. 1, Environment and Natural Resources Series No. 10). Food and Agriculture Organization of the United Nations. https://www.fao.org/4/y7223e/y7223e00.htm

[15] Yum, S.-H., Choi, S.-C., Kim, B.-G., Yoon, H.-K., & Kang, K.-J. (2025). A study on CFD analysis of airflow fan with electric heating wire in apple orchard. *Journal of Bio-Environment Control, 34*(3), 258–267. https://doi.org/10.12791/KSBEC.2025.34.3.258

# STATE OF THE ART IN RESEARCH ON THE INFLUENCE OF VIBRATIONS ON THE MOTION OF BODIES

/

# *STADIUL ACTUAL AL CERCETĂRILOR PRIVIND INFLUENȚA VIBRAȚIILOR ASUPRA MIȘCĂRII CORPURILOR*

**Andrei MĂGUREANU*[1)], Mihai Valentin PREDOI[2)], Andrei CRAIFALEANU[2)]**

[1)] Doctoral School of the Faculty of Biotechnical Systems Engineering, National University of Science and Technology POLITEHNICA Bucharest / Romania

[2)] Department of Mechanics, Faculty of Biotechnical Systems Engineering, National University of Science and Technology POLITEHNICA Bucharest / Romania;

**Tel: 07323 646 956; *E-mail: andreimagu2000@yahoo.com*

***Keywords:*** *vibration-motion coupling, contact mechanics, mobile robots, odometry, vibration control*

**ABSTRACT**

*The motion of a body in rolling or sliding contact with a surface is disturbed by vibrations that arise at the contact interface or are generated internally by the moving system, affecting motion accuracy, trajectory stability and overall dynamic performance. This paper reviews the current state of knowledge on vibration-motion coupling across railway, automotive, mobile robotics and conveyor applications. The contact interface is identified as the point at which vibration-induced force disturbances are generated, with classical contact mechanics theories providing the analytical basis for characterizing rolling and sliding forces, while more recent studies extend these theories to transient loading and omnidirectional wheel geometries. Vibrations are shown to degrade odometric position estimation through wheel slip and encoder corruption, motivating calibration-based, adaptive and sensor-fusion-based correction strategies. Control approaches for vibration rejection range from robust sliding-mode methods, offering strong stability guarantees at the cost of chattering, to data-driven predictive methods, more flexible but less theoretically mature. A critical comparison of existing modeling, experimental and control approaches shows that no current framework simultaneously achieves physical accuracy, computational efficiency and generality across system types. These gaps motivate a doctoral research program aimed at a unified theoretical framework, efficient computational models, dedicated experimental protocols and hybrid control strategies for vibration-motion coupling, illustrated by a first concrete contribution on the dynamics of a skew-mounted conveyor roller.*

**REZUMAT**

*Mișcarea unui corp aflat în contact de rulare sau alunecare cu o suprafață este perturbată de vibrații care apar la interfața de contact sau sunt generate intern de sistemul aflat în mișcare, afectând precizia mișcării, stabilitatea traiectoriei și performanța dinamică generală. Lucrarea prezintă stadiul actual al cunoștințelor privind cuplajul vibrație-mișcare în aplicații feroviare, auto, de robotică mobilă și de transport cu bandă. Interfața de contact este identificată drept punctul în care se generează perturbațiile de forță induse de vibrații, teoriile clasice ale mecanicii contactului oferind baza analitică pentru caracterizarea forțelor de rulare și alunecare, în timp ce studii mai recente extind aceste teorii la încărcări tranzitorii și la geometrii de roți omnidirecționale. Se arată că vibrațiile degradează estimarea odometrică a poziției prin alunecarea roților și perturbarea encoderelor, ceea ce motivează strategii de corecție bazate pe calibrare, adaptive și bazate pe fuziune senzorială. Strategiile de control pentru atenuarea vibrațiilor variază de la metode robuste de tip sliding-mode, cu garanții solide de stabilitate dar cu fenomenul de chattering, până la metode predictive bazate pe date, mai flexibile dar mai puțin fundamentate teoretic. O analiză critică a abordărilor actuale de modelare, experimentare și control arată că niciun cadru existent nu reușește simultan acuratețea fizică, eficiența computațională și generalitatea. Aceste lacune motivează un program de cercetare doctorală orientat spre un cadru teoretic unificat, modele computaționale eficiente, protocoale experimentale dedicate și strategii de control hibride, ilustrat printr-o primă contribuție privind dinamica unei role de transportor montate înclinat.*

## INTRODUCTION

Understanding how vibrations couple with the motion of bodies in contact with a surface has become increasingly important as engineering systems are pushed toward higher speeds, lighter structures and greater autonomy, conditions under which vibrational disturbances that were once negligible now measurably affect positioning accuracy, structural integrity and control performance. This paper surveys the current state of research on this coupling across railway, automotive, mobile robotics and conveyor applications, examining in turn the contact mechanics that generate vibration-induced forces, the degradation of odometric motion estimation, the control strategies developed to reject vibrational disturbance, and the modeling and experimental approaches used to study the problem. A critical comparison of these approaches is then used to identify the gaps that remain open in the field, which in turn define the objectives and methodology of the doctoral research program presented here, illustrated by a first concrete contribution on the dynamics of a skew-mounted conveyor roller.

The study of vibrations and their influence on the motion of bodies is an important area of research in mechanical engineering, with applications that extend across railway and automotive systems, mobile robotics and precision machinery. Vibrations can arise at the contact interface between a moving body and the surface it travels on, or they can be generated internally by rotating and reciprocating mechanical components. In both cases they introduce disturbances that affect the accuracy of motion, the stability of trajectories, and the overall dynamic performance of the system.

The motion of a body in contact with a surface is governed by well-established kinematic and dynamic principles which, under ideal conditions, lead to predictable and repeatable behavior. In practice, however, surface irregularities, mechanical flexibility, frictional non-idealities and structural resonances all give rise to vibrations that disturb the expected motion of the system, with consequences that are consistently significant from both a safety and a performance standpoint. In railway engineering, periodic irregularities in the track surface excite oscillatory motion in rolling stock that, beyond certain operating speeds, can develop into sustained lateral instabilities. In mobile robotics, vibrations transmitted through the wheels corrupt the encoder measurements used for position estimation, producing cumulative errors that cause the robot to deviate from its intended path over time. In road vehicles, the interaction between tire compliance and steering geometry can produce self-excited oscillations that reduce controllability and increase wear in steering components.

Den Hartog (1956) provided one of the earliest and most comprehensive treatments of such vibrational phenomena, establishing the theoretical foundations for analyzing free and forced vibrations in single and multi-degree-of-freedom systems and identifying the conditions under which resonance and instability arise. Despite the differences between these applications, the underlying physical mechanism is shared: a rolling or sliding contact interface through which vibrational energy is exchanged between the moving body and its environment, with measurable consequences for the gross motion of the system.

The primary motivation of this doctoral research is to develop a clearer and more rigorous understanding of this mechanism, with the aim of improving how vibration-induced motion disturbances are modeled, predicted and controlled in practical engineering systems.

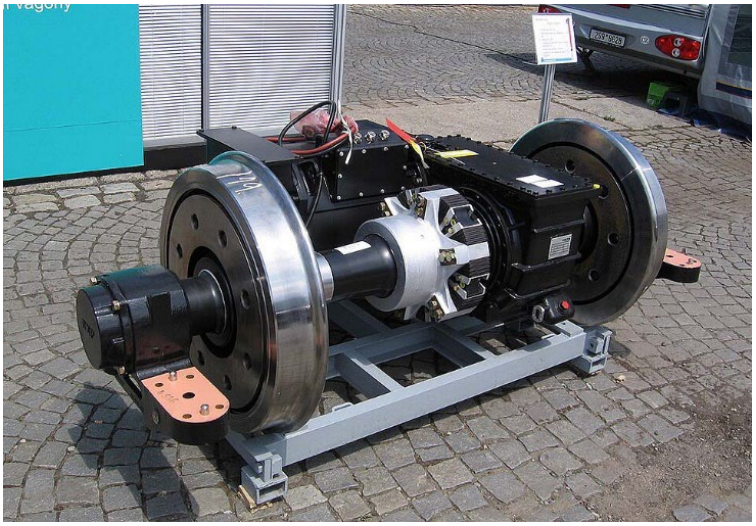


**Fig. 1 - Railway wheelset with traction motor**

The scientific study of vibrations in mechanical systems has a long history, rooted in the theoretical developments of the 18th and 19th centuries. The analysis of vibrating beams and plates, the formulation of contact mechanics, and the early treatment of friction and creep forces established the basic framework within which problems of vibration and motion are still studied today, a framework progressively extended over the 20th century by the demands of railway engineering, the automotive industry and, later, aerospace and robotics. Johnson (1985) consolidated the theoretical foundations of contact mechanics into a comprehensive treatment of the stress and deformation fields that arise when elastic bodies are brought into contact under normal and tangential loading, providing the analytical tools needed to characterize the forces generated at rolling and sliding interfaces. Building on this foundation, Kalker (1990) developed a rigorous three-dimensional treatment of the tangential contact problem for elastic bodies in rolling contact, establishing the mathematical relationships between relative slip, contact geometry and the resulting creep forces — relationships of direct relevance to vibration-motion coupling, since they describe how fluctuations in the contact state caused by vibrational loading translate into variations in the forces that drive and disturb motion.

The transient aspects of this problem were examined by Romano (2023), who compared classical, simplified and ODE-based rolling contact models and showed that the choice of theoretical framework has a significant effect on the predicted force-creepage response under transient excitation. Romano (2022) extended this to the case of spherical wheel rolling, demonstrating through analytical brush-theory modeling that steady rolling solutions exist under well-defined conditions, but that pure spinning requires the explicit incorporation of friction limits to be correctly described. In summary, the historical development of the field has been characterized by a progressive refinement of vibration and contact theories, moving from idealized steady-state descriptions toward models capable of capturing the transient and nonlinear behavior that governs real systems under operating conditions.

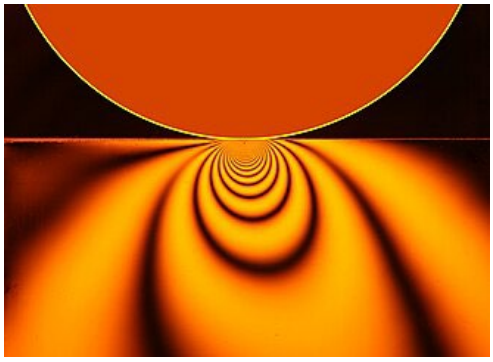


**Fig. 2 - Contact stress pattern at the wheel–surface interface**

The contact interface between a wheel and the surface it rolls on is the point at which all forces governing the motion of the body are generated. The geometry of the contact patch, the distribution of normal pressure within it, and the tangential forces it transmits are all determined by the mechanical properties of the contacting bodies, the applied normal load, and the kinematics of their relative motion. When vibrations are present, these quantities vary continuously in time, and the resulting fluctuations in contact force feed directly back into the dynamics of the system (Fig. 1).

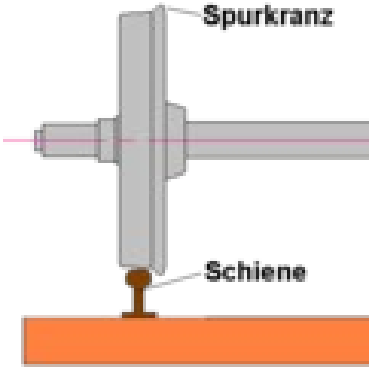



**Fig. 3 - Wheel–rail contact schematic**

Johnson (1985) established the theoretical basis for analyzing both the normal contact problem, which determines the contact patch size and pressure distribution, and the tangential problem, which governs the frictional forces responsible for driving and disturbing motion. Kalker (1990) developed this further in the specific context of rolling contact, providing the mathematical tools for computing creep forces under general three-dimensional contact conditions and validating them against experimental measurements.

For systems that use omnidirectional wheels, the contact problem is more complex because the geometry of the roller-based contact changes continuously as the individual rollers rotate. Manzl (2024) addressed this for Mecanum wheels by developing a friction model based on orthotropic contact properties, capturing the direction-dependent force generation behavior of the rollers in a form that is computationally efficient enough for real-time control applications, and validated experimentally across a range of operating conditions including cases where significant roller slip is induced by vibrational perturbations to the normal load. The influence of wheel construction on vibration-motion coupling was investigated by Zöller (2019) in the context of wheeled driving simulators, where solid and pneumatic tires were compared and solid tires were found to exhibit nonlinear dynamic behavior and greater lateral acceleration errors.

These studies collectively confirm that the contact interface must be treated as a dynamic element whose behavior under vibrational loading cannot be adequately described by static or quasi-static models.



**Fig. 4 - Mecanum wheels**

One of the most practically significant consequences of vibration-motion coupling in mobile systems is the degradation of odometric measurements. Odometry — the estimation of a vehicle's position and orientation from wheel rotation data — relies on the assumption that the relationship between wheel rotation and ground displacement is stable and well characterized during operation.

Vibrational disturbances disrupt this assumption through several mechanisms: impulsive disturbances cause momentary wheel slip, chassis oscillations introduce accelerations that cannot be separated from genuine translational motion at the wheel encoder level, and unequal excitation of the left and right drive wheels can produce apparent heading changes that are vibration artifacts rather than real maneuvers.

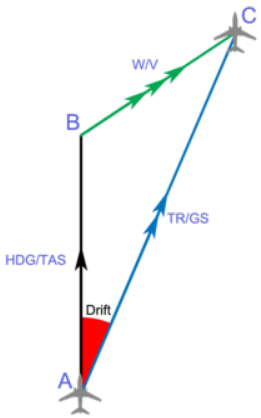



**Fig. 5 - Velocity vector diagram (heading, track, drift)**

Peng (2021) addressed the parameter calibration dimension of this problem, proposing a nonlinear optimization algorithm for omnidirectional robots that corrects systematic errors in the IMU and chassis geometry using only the sensors already present on the platform.

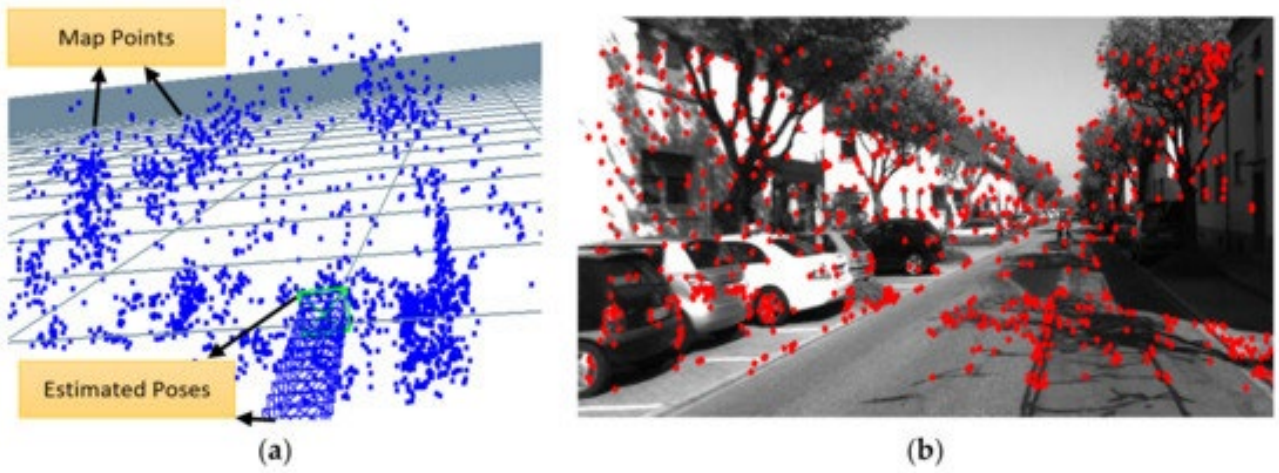



**Fig. 6 - Visual odometry: map points and estimated poses (a, b )**

While this approach is effective for fixed, geometry-related error sources, vibration-induced odometric errors are more difficult to handle because they depend on the terrain and operating conditions encountered during a mission and cannot be corrected by a single calibration.

Okawara (2025) tackled this more challenging problem by developing a LiDAR-IMU-wheel odometry system incorporating an online neural network that continuously adapts the kinematic model to the current terrain and motion conditions during operation, learning to compensate for the systematic components of vibration-induced encoder error even in previously unseen environments.

Franchini (2026) further demonstrated the importance of heterogeneous sensor fusion for maintaining accurate motion estimation in demanding environments, developing a state estimation framework for a lunar rover that integrates wheel, IMU and visual data to provide reliable odometry across all locomotion modes encountered on unstructured terrain.



**Fig. 7 - Non-pneumatic (airless) wheel**

Developing effective control strategies for systems subject to vibration-induced motion disturbances requires approaches that go beyond standard trajectory tracking controllers, since the disturbances affecting motion often share frequency content with the controlled dynamics of the system itself.

Preumont (2021) provided a thorough treatment of active vibration control strategies for mechanical structures, covering the design of feedback and feedforward controllers, actuator and sensor placement, and

the fundamental trade-offs involved in achieving effective vibration suppression without destabilizing the system.

At the trajectory tracking level, Moudoud (2024) proposed a fixed-time adaptive sliding mode controller for wheeled mobile robots operating under persistent external disturbances.

The sliding mode framework is well suited to vibration rejection because it drives the system state onto an invariant surface on which disturbances have no first-order effect on the tracking error (Fig. 2);

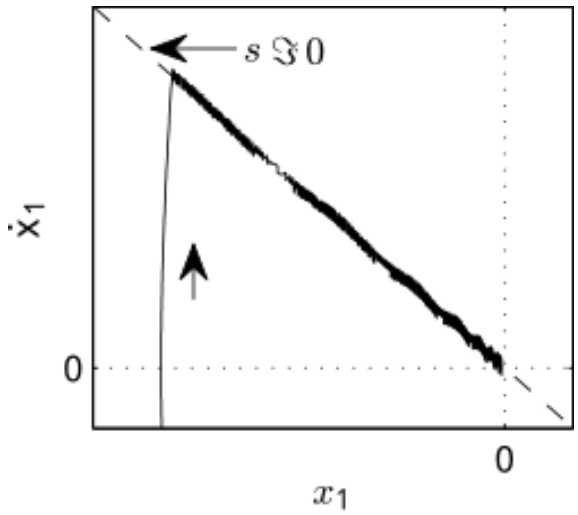



**Fig. 8 - Sliding-mode phase portrait converging to s = 0**

The adaptive component allows the controller to adjust to the observed disturbance level, and the fixed-time convergence property ensures that tracking errors are corrected within a bounded time regardless of their initial magnitude. In practice, however, the finite bandwidth of real actuators prevents exact sliding and introduces chattering — high-frequency oscillation of the control input around the sliding surface — which can itself excite vibrational modes and reintroduce the very disturbances the controller is intended to reject.

Rosenfelder (2025) explored a complementary approach, applying Extended Dynamic Mode Decomposition to design data-driven predictive controllers for nonholonomic mobile robots, representing the nonlinear system dynamics in a higher-dimensional linear space where standard predictive control methods can be applied.

A key finding was that purely data-based approaches encounter fundamental limitations when the geometric structure of the system dynamics is not explicitly accounted for, and that increasing the dimension of the lifted Koopman space does not monotonically improve control performance, since beyond a certain dimension additional lifting functions introduce numerical conditioning problems.

The systems in which vibration-motion coupling is studied vary considerably in mechanical configuration, operating environment and the nature of the motion performed. The most extensively studied category is that of bodies moving in rolling or sliding contact with a surface, encompassing railway wheelsets, road vehicle tires, industrial rollers and wheeled robotic platforms.

Goryacheva & Zobova (2021) provided a comprehensive review of dynamic problems in which the deformation of contacting bodies directly influences their motion, concluding that even in relatively simple configurations — a deformable cylinder rolling on a half-space — the influence of material compliance on deceleration dynamics is significant and cannot be captured by rigid-body models.

A second category consists of systems in which vibrations are deliberately used as the primary mechanism of locomotion: Takagi (2023) examined how periodic vibrational inputs can be converted into directed translational motion through asymmetric friction interactions, a mechanism exploited in pipe inspection robots, vibrating conveyor platforms and microrobotic systems. A third category consists of systems in which vibrations are an unwanted byproduct of operation.

Zhang (2024) showed that belt oscillations and drive-system non-uniformities in conveyor systems introduce positional errors in transported material that are difficult to compensate for at the control level alone, and Liu (2024) proposed active and passive damping strategies for suppressing belt oscillations, demonstrating measurable improvements in transport accuracy.



**Fig. 9 - Curved belt conveyor**

The theoretical treatment of vibration-motion coupling draws on two main bodies of knowledge: vibration theory, describing how mechanical systems respond to dynamic excitation, and contact mechanics, characterizing the forces generated at the interface between bodies in relative motion.

Rao (2011) provided a systematic framework for classifying and analyzing vibrational phenomena, distinguishing between free and forced vibrations and characterizing resonance conditions for single- and multi-degree-of-freedom systems. Popov (2010) presented a unified treatment of contact and friction phenomena, including frictionally induced vibrations — oscillations arising from the coupling between friction forces and structural compliance — representing one of the most direct mechanisms by which contact mechanics gives rise to vibration-motion coupling. The development of accurate computational models for vibration-motion coupling must capture the dynamics of the contact interface, the structural dynamics of the moving body, and the coupling between them, within a framework efficient enough for engineering design. Yu (2015) developed a detailed kinematic analysis of Mecanum wheel platforms, identifying sources of kinematic error from manufacturing tolerances, wheel deformation and contact geometry variations, errors that accumulate over time in a manner directly analogous to vibration-induced odometric drift.

D'Angelo (2024) presented a dynamic framework incorporating wheel-ground interaction forces, payload variations and structural flexibility, finding that structural flexibility introduces additional vibrational modes that couple with the translational and rotational degrees of freedom, producing motion disturbances that cannot be predicted without an adequate dynamic model. Siciliano et al. (2009) provided the broader robotics modeling context for such platform-specific models. For conveyor systems, Bhat (2025) identified the natural frequencies and mode shapes of belts as functions of tension, speed and load distribution, showing that certain operating speeds produce resonance conditions in which belt oscillations grow significantly in amplitude. Experimental investigation plays an essential role in validating theoretical and computational models and in characterizing phenomena difficult to capture analytically. Ewins (2000) established the foundations of experimental modal analysis for extracting natural frequencies, damping ratios and mode shapes, and Brandt (2011) complemented this with signal processing methods addressing noise, non-stationarity and limited frequency resolution in real measurement scenarios.



**Fig. 10 - Accelerometer / vibration sensor**

Raudmäe (2023) validated a Mecanum wheel modeling and simulation framework against experimental measurements, demonstrating good agreement including under significant vibrational excitation, while Muniandy (2012) developed a framework for detecting wheel slip from onboard sensor data and correcting its effect on odometric estimates in real time.

For conveyor systems, Zaher (2022) demonstrated that characteristic vibration signatures can be reliably distinguished from normal operating behavior using appropriate signal processing, and Uriarte (2018) characterized the vibrational phenomena arising in conveyor drive systems at various operating speeds and load levels.

The practical consequences of vibration-motion coupling for system performance have been documented across many domains. Emara (2022) demonstrated that standard kinematic controllers for wheeled mobile robots are inadequate when significant vibration-induced slip is present, and Bujňák (2025) showed that the omnidirectional kinematics of Mecanum-type platforms make them particularly sensitive to vibration-induced contact force variations.

Moosavi (2025) showed that the efficiency of snake-robot locomotion through body undulation depends critically on the dynamic interaction between the flexible body and the contact surface, and Jia (2025) found that vibrations from the drive system and surface irregularities can destabilize contact in climbing robots, causing loss of traction. Ushimi (2012) examined the sources and transmission paths of vibration in wheeled vehicles, finding that the structural transmission path plays a critical role in determining which vibrational modes most affect motion performance.



**Fig. 11 - Snake robot**

Slotine & Li (1991) provided a systematic treatment of nonlinear control techniques — Lyapunov stability analysis, sliding mode control and adaptive control — that underpins much of the applied research in vibration-aware control.

Achuthan (2018) developed a sensor fusion framework for mobile robot localization that maintains accurate estimates despite vibration-induced sensor noise, Safar (2012) addressed the localization challenges specific to omnidirectional platforms, and Jafarov (2016) and Abiyev (2017) explored robust and fuzzy-logic control respectively, illustrating the two main philosophical directions in vibration-aware control. Zaman (2023) showed that feedforward compensation based on a dynamic model of belt vibrations can significantly reduce positional errors in conveyed material.

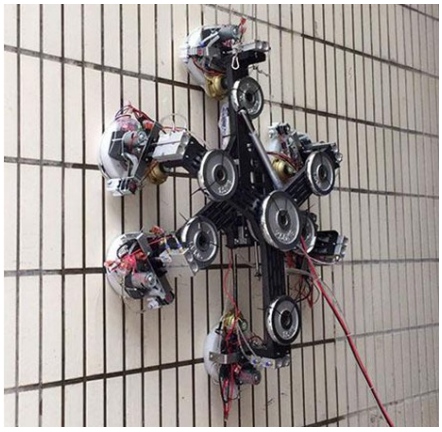


**Fig. 12 - Wall-climbing robot**

A number of important challenges remain open. Hellania (2025) noted that the computational resources available on a mobile platform impose strict limits on the model complexity usable for real-time motion planning.

Merino-Martínez (2021) showed, in the related context of acoustic emission analysis, that vibration signatures characteristic of one mechanical condition may not transfer directly to a system with a different structural configuration, pointing to the need for more general theoretical frameworks. Li (2025) demonstrated that online parameter adaptation can improve tracking performance under time-varying vibration-induced disturbance but also identified conditions under which purely adaptive approaches become unstable, and Guo (2026) showed that data-driven prediction models can be used effectively for vibration-aware motion planning provided appropriate physical consistency constraints are imposed.

A critical comparison of these approaches reveals a persistent trade-off between physical accuracy and computational efficiency. Analytical contact frameworks (Johnson, 1985; Kalker, 1990) are computationally efficient but rely on simplifying assumptions — elastic behavior, smooth geometry, quasi-static or linearized transient conditions — that limit their applicability under large vibrational disturbance; Johnson (1985) in particular noted that the tangential contact problem is fundamentally more complex than the normal problem because the frictional state depends on the entire history of relative motion, which is precisely what makes contact so sensitive to vibration.

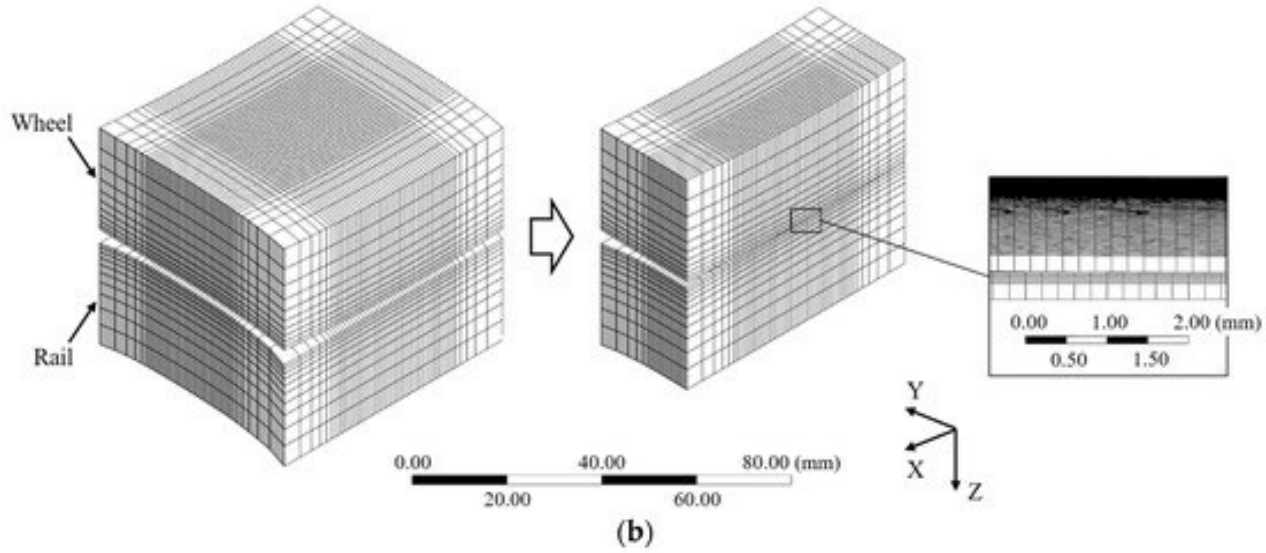



**Fig. 13 - Finite element mesh of the wheel–rail contact**

At the other extreme, finite element analysis (Bathe, 1996) can capture arbitrary geometry and nonlinearity but is computationally expensive and difficult to couple with real-time control, with accuracy depending critically on the relationship between the integration time step and the highest significant natural frequency — a constraint made more demanding when a system combines low-frequency rigid-body motion with high-frequency contact vibration. Intermediate approaches include the modal methods of Meirovitch

(2001), for whom modal truncation error — the neglect of higher modes in any finite modal model — is a genuine concern when excitation has significant broadband content, and the multibody framework of Shabana (2013), whose floating-frame-of-reference formulation separates rigid-body reference motion from small-amplitude elastic deformation but becomes problematic when vibrational amplitudes are not small relative to the contact patch, a limitation addressed by Bremer (2008) through a direct Ritz approach that accepts greater computational cost for improved accuracy under larger deformation.

For ground vehicles, Genta (1997) showed that road-induced vibration spans several decades of frequency, from long-wavelength undulations exciting rigid-body bounce and pitch to short-wavelength roughness exciting tire and suspension vibration, meaning no single model can adequately cover all relevant phenomena — a conclusion reinforced by Knothe & Grassie (1993) for the railway case and addressed, with mixed success, by the unified multibody framework of Popp & Schiehlen (2010).

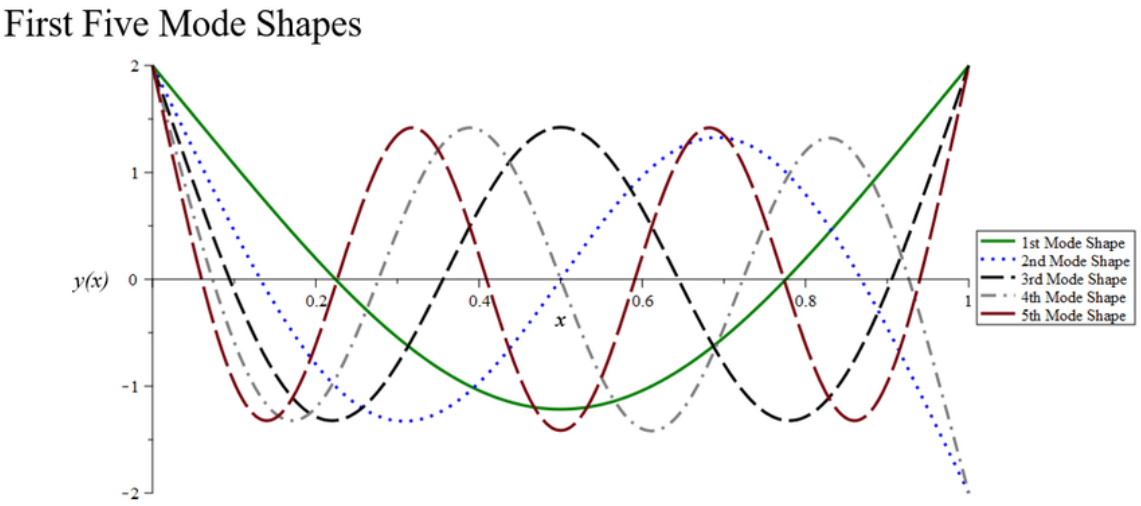



**Fig. 14 - First five mode shapes**

Experimental characterization presents its own challenges, since vibration and motion must be measured simultaneously at compatible spatial and temporal resolutions. Classical tools (Ewins, 2000; Maia & Silva, 1997; Brandt, 2011; McConnell & Varoto, 2008) were developed for stationary or quasi-stationary structures; Ewins (2000) noted that modal test quality depends as much on the excitation strategy as on the measurement hardware, a requirement difficult to satisfy when excitation is provided by contact with a moving surface rather than a controllable laboratory shaker.

McConnell & Varoto (2008) observed that the coherence function, a standard quality indicator, can give misleadingly high values for nonlinear systems, meaning standard laboratory quality checks cannot be applied uncritically to vibration-motion coupling measurements in operating systems.

Harris & Piersol (2002) showed that the peak amplitude of an impulsive contact force can be significantly higher than predicted by quasi-static analysis of the same surface irregularity, due to dynamic amplification from contact stiffness and rolling-body inertia — a key reason why vibration-induced disturbances in mobile systems are more severe than simple kinematic analysis would suggest. Maia & Silva (1997) further noted that identified modal parameters become increasingly sensitive to measurement noise when modes are closely spaced in frequency or significantly damped, a genuine challenge for the wide frequency and damping ranges relevant to vibration-motion coupling.

A further limitation is the difficulty of separating the contributions of different physical mechanisms — wheel slip, chassis vibration, steering-geometry error — to an observed motion deviation, a problem for which the sensor-fusion approaches described above offer practical but not fully explanatory solutions.

Control strategies fall broadly into model-based robust control, adaptive/learning-based control, and passive or semi-passive mitigation. Sliding mode control *(Moudoud, 2024; Slotine & Li, 1991)* offers the invariance property described above but is limited in practice by actuator-bandwidth-induced chattering. Adaptive and learning-based approaches *(Okawara, 2025; Li, 2025; Guo, 2026; Rosenfelder, 2025)* offer greater flexibility for time-varying and environment-dependent disturbances but weaker formal guarantees.

Passive and semi-passive mitigation *(Fuller, Elliott & Nelson, 1996; Isermann, 2005)* is fundamentally limited by a trade-off between low- and high-frequency isolation performance — directly

relevant to mobile robot suspension design, where the system must isolate the chassis from high-frequency surface roughness while retaining sufficient stiffness for precise low-frequency steering control.

The comparison suggests that the most promising direction lies in hybrid strategies combining the formal guarantees of model-based robust control with the adaptability of learning-based methods, anchored by physical models of the coupling mechanism.

This critical analysis identifies three key gaps that define the research space of this doctoral work. First, the absence of a general, unified theoretical framework for vibration-motion coupling across system types: Schiehlen (1997) identified this need in the multibody dynamics context nearly three decades ago, and while progress has been made in individual sub-domains, the general problem remains open.

Second, the modeling of contact dynamics under large vibrational loading, since classical theories *(Johnson, 1985; Kalker, 1990)* assume small relative motion and linear elastic behavior frequently violated in real systems; Pfeiffer & Glocker (1996) addressed the set-valued nature of unilateral contact forces under impulsive loading, directly relevant to the momentary loss-of-contact events that corrupt odometric measurements, but a comprehensive treatment of contact under large, broadband vibrational excitation remains an open challenge.

Third, the intersection of experimental measurement and physical modeling, since current experimental approaches *(McConnell & Varoto, 2008; Harris & Piersol, 2002)* are not well adapted to the simultaneous measurement of vibration and gross body motion in coupled dynamic systems.

Based on this analysis, the doctoral research pursues four objectives. The first is to develop a theoretical framework for vibration-motion coupling general enough to apply across wheeled platforms, conveyor systems and bodies in general rolling or sliding contact, building on the contact mechanics of Johnson (1985) and Kalker (1990) and the multibody formulations of Shabana (2013) and Schiehlen (1997), with particular emphasis on capturing the history-dependence of contact frictional state identified by Johnson (1985).

The second is to develop computational models implementing this framework with efficiency suitable for control design and real-time simulation, building on the modal methods of Meirovitch (2001) and the structural dynamics tools of Bathe (1996), targeting a level of efficiency comparable to that achieved by Manzl (2024) for Mecanum wheel contact.

The third is to design and implement experimental protocols for the simultaneous measurement of vibration and gross body motion, drawing on the signal processing methods of Brandt (2011) and McConnell & Varoto (2008) and the modal testing framework of Ewins (2000) and Maia & Silva (1997), using wheeled robotic platforms of the type studied by Raudmäe (2023) and Shafiq (2024) as test environments.

The fourth is to develop control strategies that explicitly account for vibration-motion coupling, building on the nonlinear control framework of Slotine & Li (1991) and the active vibration control methods of Preumont (2021) and Fuller, Elliott & Nelson (1996), incorporating the data-driven and adaptive elements demonstrated by Okawara (2025) and Li (2025), and validated on both wheeled platforms and conveyor systems of the type studied by Liu (2024) and Wang (2025).

The methodology follows a three-phase structure. The first phase addresses theoretical development, re-examining the conditions under which existing contact theories break down under large or rapidly varying vibrational loading and deriving extended formulations valid under these conditions, using a hierarchical modeling approach to address the multi-scale frequency character identified by Genta (1997) and Knothe & Grassie (1993).

The second phase addresses computational implementation, using multi-rate time integration schemes to handle the multi-scale temporal character identified by Bathe (1996), with tools validated first against analytical solutions and then against higher-fidelity finite element simulations.

The third phase addresses experimental validation and control design, instrumenting experimental platforms to measure vibrational response and gross body motion simultaneously, using the sensor fusion architectures of Okawara (2025) and Franchini (2026) as a starting point, with particular attention to the dynamic amplification of impulsive contact forces identified by Harris & Piersol (2002), and comparing control strategies against benchmarks drawn from Moudoud (2024) and Rosenfelder (2025).

A concrete first contribution to this research program has already been made through the study *Motion of a Skew Conveyor Module*, co-authored with Prof. Habil. Dr. Ing. Mihai Valentin Predoi, Andrei Craifaleanu and Ștefan Mihai Coadă, submitted to the Romanian Journal of Acoustics and Vibration.

That work investigates the motion of a platform equipped with a skew-mounted hinged roller, pulled in translation with constant velocity, through three progressively complex analytical models: a purely

kinematic model assuming pure rolling, a steady-state dynamic model incorporating sliding and rolling friction moments, and a vibratory dynamic model treating the axial oscillation of the roller as a stick-slip process driven by a velocity-dependent friction coefficient.

The study identifies the optimal roller shaft skew angle for maximum lateral displacement of a transported object and demonstrates that the kinematically optimal angle is significantly modified when friction effects are properly accounted for. In the vibratory model the axial motion of the roller is shown to be oscillatory, arising from the elastic compliance of the roller-shaft contact and sustained by the friction-velocity coupling, with the oscillation continuing until available mechanical clearance is consumed and a collision with the platform resets the motion — a direct, component-level instance of the broader vibration-motion coupling mechanism at the center of this doctoral research.

The dependence of the optimal skew angle on the sliding and rolling friction coefficients illustrates precisely the kind of vibration-parameter sensitivity that the general theoretical framework aims to capture across a wider class of systems, and the absence of direct comparisons with other authors in the technical literature, noted explicitly in that paper's own conclusions, reinforces the assessment made here that the field lacks a unified theoretical treatment — a gap the present doctoral work aims to address.

This review has shown that vibration-motion coupling is a physically fundamental feature of any body moving in rolling or sliding contact with a surface, not a phenomenon confined to a single application area. Classical contact mechanics provides the analytical basis for understanding how vibrational disturbance translates into fluctuating contact forces, but these theories were developed under assumptions of small relative motion that are frequently violated in practice.

Vibrations were shown to degrade odometric position estimation through wheel slip and encoder corruption, prompting correction strategies ranging from fixed calibration to adaptive, sensor-fusion-based methods. Control approaches for vibration rejection present a persistent trade-off between the stability guarantees of model-based methods, such as sliding mode control, and the flexibility of data-driven predictive methods, whose theoretical foundations remain comparatively immature.

The critical analysis carried out in this paper identified three open gaps that current research has not resolved simultaneously: the absence of a unified theoretical framework applicable across system types, the limited treatment of contact dynamics under large vibrational loading, and the lack of experimental methods adapted to the simultaneous measurement of vibration and gross body motion.

These gaps define a coherent doctoral research program — a unified theoretical framework, computationally efficient models, dedicated experimental protocols, and hybrid control strategies — of which a first concrete result has already been obtained through the study of a skew-mounted conveyor roller, where axial oscillation was shown to arise as a stick-slip process driven by a velocity-dependent friction coefficient. This result illustrates, at the component level, the broader coupling mechanism that the remainder of the doctoral research aims to characterize in a general and unified way.

## ACKNOWLEDGEMENT

The author acknowledges the Doctoral School of the Faculty of Biotechnical Systems Engineering at the National University of Science and Technology POLITEHNICA Bucharest for the financial support provided through the doctoral grant, which facilitated this research.

## REFERENCES

[1] Abiyev, R. (2017). Fuzzy Control of Omnidirectional Robot. *Procedia Computer Science, Vol. 120*.
[2] Achuthan, P. (2018). Omnidirectional ISI Device Design and Testing. *Procedia Computer Science, Vol. 133*.
[3] Bathe, K. (1996). *Finite Element Procedures*.
[4] Bhat, R. (2025). PLC Omni-Wheel Conveyor Sorting System. *Scientific Reports*.
[5] Brandt, A. (2011). *Noise and Vibration Analysis: Signal Processing and Experimental Methods*.
[6] Bremer, H. (2008). *Elastic Multibody Dynamics: A Direct Ritz Approach*.
[7] Bujňák, M. (2025). SpheriDrive Spherical Robot Platform. *Results in Engineering, Vol. 25*.
[8] D'Angelo, S. (2024). Control of Wheeled Mobile Manipulator on Pipe-Rack. *Robotics and Autonomous Systems, Vol. 171*.
[9] Den Hartog, J. D. (1956). *Mechanical Vibrations*.
[10] Emara, M. (2022). Digital Twin Control of Three-Wheel Omnidirectional Robot. *Procedia CIRP, Vol. 107*.

[11] Ewins, D. (2000). *Modal Testing: Theory, Practice and Application*.
[12] Franchini, G. (2026). State Estimation for Four-Wheeled Lunar Rover. *Acta Astronautica*.
[13] Fuller, C. R., Elliott, S., & Nelson, P. (1996). *Active Control of Vibration*.
[14] Genta, G. (1997). *Motor Vehicle Dynamics: Modeling and Simulation*.
[15] Goryacheva, I., & Zobova, A. (2021). Dynamics of Deformable Contacting Bodies with Sliding, Rolling, and Spinning. *International Journal of Mechanical Sciences*.
[16] Guo, T. (2026). Hierarchical Control of Wheel-Legged Robot. *Journal of Engineering Research*.
[17] Harris, C., & Piersol, A. (2002). *Harris Shock and Vibration Handbook*.
[18] Hellania, H. (2025). Mobile Robot Modeling with Battery Consumption. *Procedia Computer Science, Vol. 274*.
[19] Isermann, R. (2005). *Mechatronic Systems: Fundamentals*.
[20] Jafarov, S. (2016). Robust Control for Omnidirectional Robot. *Procedia Computer Science, Vol. 102*.
[21] Jia, P. (2025). Wall-Climbing Robot Design with Adaptive Mechanism. *Applied Ocean Research, Vol. 161*.
[22] Johnson, K. (1985). *Contact Mechanics*.
[23] Kalker, J. (1990). *Three-Dimensional Elastic Bodies in Rolling Contact*.
[24] Knothe, K., & Grassie, S. (1993). Modelling of Railway Track and Vehicle-Track Interaction at High Frequencies. *Vehicle System Dynamics, Vol. 22*.
[25] Li, C. (2025). Whale Optimization for Four-Steering AGV Control. *International Journal of Electrical Power and Energy Systems, Vol. 172*.
[26] Liu, K. (2024). Modeling and Control of Orthogonal Omni Conveyor. *Physica Scripta, Vol. 99*.
[27] Maia, N., & Silva, J. (1997). *Theoretical and Experimental Modal Analysis*.
[28] Manzl, P. (2024). Mecanum Wheel Orthotropic Friction Model. *Mechanism and Machine Theory, Vol. 193*.
[29] McConnell, K., & Varoto, P. (2008). *Vibration Testing: Theory and Practice*.
[30] Meirovitch, L. (2001). *Fundamentals of Vibrations*.
[31] Merino-Martínez, R. (2021). Low-Noise Nose Landing Gear Study. *Aerospace Science and Technology, Vol. 113*.
[32] Moosavi, S. (2025). Snake Robots: Design and Control Review. *Mechatronics, Vol. 112*.
[33] Moudoud, B. (2024). Sliding-Mode Trajectory Tracking for Wheeled Robot. *e-Prime – Advances in Electrical Engineering, Electronics and Energy, Vol. 10*.
[34] Muniandy, M. (2012). Reducing Odometry Error in Nonholonomic Robots. *Procedia Engineering, Vol. 41*.
[35] Okawara, T. (2025). LiDAR-IMU-Wheel Odometry with Neural Kinematics. *Robotics and Autonomous Systems, Vol. 187*.
[36] Peng, G. (2021). Chassis Parameter Calibration via Nonlinear Optimization. *Applied Mathematical Modelling, Vol. 95*.
[37] Pfeiffer, F., & Glocker, C. (1996). *Multibody Dynamics with Unilateral Contacts*.
[38] Popov, V. (2010). *Contact Mechanics and Friction: Physical Principles and Applications*.
[39] Popp, K., & Schiehlen, W. (2010). *Ground Vehicle Dynamics*.
[40] Preumont, A. (2021). *Vibration Control of Active Structures*.
[41] Rao, S. (2011). *Mechanical Vibrations*.
[42] Raudmäe, R. (2023). ROBOTONT Omnidirectional Robot Platform. *HardwareX, Vol. 14*.
[43] Romano, L. (2022). Spherical Wheels: Brush Theory Results. *Mechanism and Machine Theory, Vol. 173*.
[44] Romano, L. (2023). Transient Wheel–Rail Rolling Contact. *Tribology International, Vol. 186*.
[45] Rosenfelder, M. (2025). Koopman Predictive Control of Nonholonomic Robots. *Robotics and Autonomous Systems, Vol. 194*.
[46] Safar, M. (2012). Tip-Over Prediction for Omnidirectional Robot. *Procedia Engineering, Vol. 41*.
[47] Schiehlen, W. (1997). Multibody System Dynamics: Roots and Perspectives. *Multibody System Dynamics, Vol. 1*.
[48] Shabana, A. (2013). *Dynamics of Multibody Systems*.
[49] Shafiq, M. (2024). Navigation of Mecanum Wheel Robot. *Heliyon, Vol. 10*.
[50] Siciliano, B., Sciavicco, L., Villani, L., & Oriolo, G. (2009). *Robotics: Modelling, Planning and Control*.
[51] Slotine, J.-J., & Li, W. (1991). *Applied Nonlinear Control*.

[52] Takagi, Y. (2023). Kinematic Dual Snake Robot. *Mechatronics, Vol. 90*.
[53] Uriarte, C. (2018). Control of Small-Scale Conveyor Modules. *Procedia CIRP, Vol. 79*.
[54] Ushimi, N. (2012). Dual-Shaft Caster Odometer for Omnidirectional Robots. *Procedia Engineering, Vol. 41*.
[55] Wang, W. (2025). Piezoelectric Mecanum Wheel Robot. *Cell Reports Physical Science, Vol. 6*.
[56] Yu, S. (2015). Omnidirectional AGV with MY3 Wheels. *Perspectives in Science, Vol. 7*.
[57] Zaher, W. (2022). RL Path Planning for Omni-Wheel Conveyor. *IEEE Access, Vol. 10*.
[58] Zaman, M. (2023). Motion Control for Omnidirectional Conveyor. *IEEE Access, Vol. 11*.
[59] Zhang, Y. (2024). Kinematic Analysis and Trajectory Planning for Omnidirectional Conveyor Systems. *Actuators, Vol. 13, No. 11*.
[60] Zöller, C. (2019). Tire and Vertical Dynamics of Driving Simulators. *Transportation Research Part F, Vol. 61*.

# RESEARCH ON DEEP SOIL TILLAGE AND CONTROLLED APPLICATION OF LIQUID FERTILIZERS - A CASE STUDY IN THE SOUTH-EAST REGION OF ROMANIA

/

# *CERCETĂRI PRIVIND PRELUCRAREA PROFUNDĂ A SOLULUI ȘI INTRODUCEREA CONTROLATĂ A FERTILIZANȚILOR LICHIZI - STUDIU DE CAZ ÎN REGIUNEA SUD-EST DIN ROMÂNIA*

**Dragoș MANEA*[1)], Mihai GÎDEA[2)], Dragoș-Nicolae DUMITRU[1)], Alin HARABAGIU[1)], Larisa-Bianca IONICĂ[1)], Aura DUMITRESCU[1)]**

[1)] National Institute of Research - Development for Machines and Installations Designed for Agriculture and Food Industry - INMA Bucharest / Romania;

[2)] University of Agronomic Sciences and Veterinary Medicine of Bucharest / Romania.

**Tel: 0724350567; *E-mail: manea_dragos_05@yahoo.com*

***Keywords:*** *deep tillage, subsoiling, liquid biofertilizer, soil compaction, field performance, fuel consumption*

**ABSTRACT**

*A field case study was conducted in Jiliște, Vrancea County, South-East Romania, to evaluate a combined implement for deep soil loosening, clod fragmentation and controlled subsurface application of a liquid biofertilizer. The machine consisted of a five-tine subsoiler with tandem spiked rollers, a 500 L liquid tank, a 12 V pump and calibrated delivery nozzles. Tests were performed on chernozem developed on loess under wheat residues. Mean soil moisture at 10 cm was 22.87%. Because wet soil and residues caused roller clogging at greater settings, the operating depth was adjusted to 30 cm. The measured mean tillage depth was 25.53 cm (CV 2.71%), the mean working width was 224.67 cm (CV 2.72%), and the mean liquid injection depth was 14.8 cm (CV 2.95%). After tillage, bulk density decreased from 1.207 to 0.811 g cm−3, total porosity increased from 54.5 to 69.4%, and penetration resistance decreased from 1.10 to 0.82 MPa. In the energy trial, mean drawbar force ranged from 2300.3 to 2373.9 daN, while specific fuel consumption was 22.2 L ha−1. A subsequent operational trial achieved 1.71 ha h−1 effective field capacity and 22.8 L ha−1 fuel consumption. The results demonstrated stable depth control, uniform subsurface placement and acceptable energetic performance under field conditions.*

**REZUMAT**

*A fost realizat un studiu de caz în condiții de câmp, în comuna Jiliște, județul Vrancea, regiunea Sud-Est a României, pentru evaluarea unui echipament combinat destinat afânării profunde a solului, mărunțirii bulgărilor și aplicării controlate în substrat a unui biofertilizant lichid. Echipamentul a inclus un scarificator cu cinci ancore și tăvălugi cu colți, rezervor de 500 L, pompă de 12 V și duze calibrate. Solul a fost un cernoziom dezvoltat pe loess, cu resturi vegetale de grâu, iar umiditatea medie la 10 cm a fost 22,87%. Din cauza umidității și a resturilor vegetale, adâncimea reglată a fost stabilită la 30 cm. Adâncimea medie efectivă de lucru a fost 25,53 cm (CV 2,71%), lățimea medie 224,67 cm (CV 2,72%), iar adâncimea de injectare a biofertilizantului 14,8 cm (CV 2,95%). După lucrare, densitatea aparentă a scăzut de la 1,207 la 0,811 g/cm³, porozitatea totală a crescut de la 54,5 la 69,4%, iar rezistența la penetrare s-a redus de la 1,10 la 0,82 MPa. Consumul specific a fost 22,2–22,8 L/ha, iar capacitatea efectivă de lucru din testul final a fost 1,71 ha/h. Rezultatele confirmă uniformitatea lucrării și funcționarea integrată a sistemului în condiții reale de exploatare.*

## INTRODUCTION

Soil compaction and the formation of dense subsurface layers remain important constraints in mechanized agriculture because they restrict root penetration, reduce aeration and infiltration, and can increase the energy required for tillage. Mechanical loosening is therefore used when compacted layers cannot be adequately remediated by normal seedbed operations. A meta-analysis by Yang et al. (2022) showed that subsoiling and deep ploughing generally reduce penetration resistance, although the magnitude of the response depends strongly on soil, moisture and management conditions. Long-term field evidence likewise indicates that subsoiling may reduce bulk density and penetration resistance and improve soil water storage when the operation is appropriately matched to the field condition (*Zhao et al., 2022*).

The energetic cost of deep tillage is a major design and operational constraint. Tine geometry, spacing, depth and soil condition affect draft force, tractor slip and fuel use. Vanderhasselt et al. (2023) showed that subsoiler configuration has a clear impact on fuel consumption and the degree of soil disturbance, while Liu et al. (2023) reported significant relationships between tillage depth, traction requirement, slip and fuel consumption. Field tests of biomimetic subsoilers have also targeted the reduction of tillage resistance as a way to decrease the energy demand of deep loosening operations (*Wang et al., 2020*). These findings emphasize that the agronomic effect of loosening should be evaluated together with machinery performance rather than as an isolated soil treatment.

A second challenge is the efficient placement of fertilizers and microbial products. Surface application can expose liquid inputs to uneven distribution, runoff or rapid environmental losses, whereas subsurface placement can position the input directly within a mechanically loosened zone.

The concept is consistent with precision nutrient management, in which application rate, placement depth and spatial uniformity are key technological parameters.

Controlled subsurface liquid injection has been investigated as a way to combine loosening with nutrient placement, although adhesion and draft requirements may limit machine performance under difficult soil conditions. Recent work on liquid biofertilizers has additionally shown that biologically active liquid formulations can modify soil properties and microbial communities when they are properly prepared and applied (*Le et al., 2025; Shahzad et al., 2025*).

Deep tillage can also support crop rooting where dense layers limit access to water and nutrients. Field studies have reported improved deep root development under subsoiling compared with shallow rotary tillage (*Wang et al., 2021*), and recent research has shown that subsoil tillage can improve crop mechanical stability and yield-related traits under intensive production conditions (*Feng et al., 2024*). Nevertheless, the response is site-specific; deep tillage cannot be assumed to improve productivity in every soil and season, and excessive working depth may increase fuel use without proportional agronomic benefit (*Rubio et al., 2021; Vanderhasselt et al., 2023*).

The present study evaluated an integrated implement developed for deep soil tillage and controlled application of a liquid biofertilizer in a single pass. The objective was to quantify the main qualitative, energetic and operational indices under field conditions in the South-East region of Romania.

The assessment focused on working depth and width, changes in soil physical condition, uniformity of injection depth, tractor slip, draft and traction power, theoretical and effective field capacity, and fuel consumption.

The case study also documented practical limitations caused by moist soil and crop residues, because these factors directly influence whether a combined tillage-and-application technology can operate reliably in real farms.

## MATERIALS AND METHODS

The experiments were carried out near Jiliște, Vrancea County, Romania (field location identified in the experimental records as J62C+74C). The soil was a chernozem developed on loess, with a dark humus-rich surface horizon. Wheat stubble and fragmented straw remained on the soil surface after harvest. Soil moisture was measured at approximately 10 cm depth with an Extech MO750 meter. Three readings of 21.3, 22.7 and 24.6% gave a mean value of 22.87%. A rainfall event of approximately 7 l/m$^2$ had occurred one week before the measurements, and field observations showed locally wet soil adhering to the working parts.

The combined implement consisted of three functional modules: (i) a five-tine subsoiler equipped with tandem spiked rollers; (ii) a liquid biofertilizer application system with a 500 L tank, a Delavan 7812-201 12 V DC pump and calibrated nozzles; and (iii) an electrical command-and-control system enabling pump activation from the tractor cab and adjustment of pressure and flow.

The subsoiler frame was designed for deep loosening up to 55 cm under suitable conditions. During the reported test, however, the initial deeper setting caused residue and wet-soil accumulation on the spiked roller; the machine was therefore adjusted to a nominal depth of 30 cm to obtain stable operation. The liquid lines were positioned to inject the biofertilizer into the loosened soil zone, normally within the 10–20 cm layer.

The implement was operated with a New Holland T7060 tractor rated at 210 hp (156.6 kW), equipped with a 6.7 l six-cylinder turbocharged diesel engine. The tractor–implement unit was tested in two experimental stages. The partial field campaign quantified qualitative and energy indices at lower working speeds, while the final campaign determined operational time-use coefficients, effective field capacity and

fuel consumption under a later field operating regime. The two stages are reported separately because their speeds and calculated capacities were not identical.

Mean working depth and working width were determined from three replicated sets of measurements taken along the experimental plot. The field plot used for depth assessment was at least 100 m long and 50 m wide, with observations made at representative positions. A furrow-depth gauge and measuring tapes were used.

For each variable, the arithmetic mean, standard deviation and coefficient of variation were calculated. Uniformity was considered satisfactory when the coefficient of variation remained below 10%, in accordance with the criterion used in the experimental protocol.

Soil bulk density was determined with cylindrical cores of known volume (395.64 $cm^3$). Samples were weighed, oven-dried at 105°C to constant mass and reweighed. Total porosity was then calculated from the density data according to the experimental protocol. Penetration resistance was evaluated with a Wile penetrometer. Measurements taken before and after passage of the implement were used to quantify the immediate physical effect of loosening. The average profile height was also recorded at fixed reference points before and after tillage.

The liquid injection depth was evaluated by exposing transverse sections of the treated furrows at 25, 50 and 75 m along the test strip. The vertical distance from the soil surface to the visibly treated zone was measured with a graduated rule. The mean, standard deviation and coefficient of variation were calculated to characterize placement uniformity.

The biofertilizer used in the experiment was produced at INMA Bucharest from mature stabilized compost in an aerated bioreactor; the field study focused on placement and machinery performance rather than on a controlled crop-response comparison.

Working speed was determined by timing the tractor–implement unit over a known distance. Wheel slip was calculated from wheel travel measurements under no-load and working conditions. Draft force was measured tensometrically using 120 Ω strain gauges (KFG-6-120-C1-11 N15C2) mounted on the tractor linkage and a QuantumX 1615 data acquisition system.

Data were monitored and recorded with nSOFT/catman Easy software. Mean and maximum traction power were calculated from measured draft force and travel speed. Fuel consumption was determined by refilling the tractor fuel tank after a measured operating interval and relating the consumed volume to working time and treated area.

For the final operational trial, effective working time, auxiliary time, production time and total shift-related time were recorded with a stopwatch. The corresponding time-use coefficients were calculated from the experimental time balance.

Effective and performance field capacities were then derived from the treated area and recorded time. No inferential statistical test was applied because the reports describe an engineering field case study based primarily on replicated measurements, descriptive statistics and operational time accounting.

**Table 1**

| Parameter | Experimental condition / equipment |
|---|---|
| Location | Jiliște, Vrancea County, South-East Romania |
| Soil | Chernozem developed on loess; wheat residues on surface |
| Mean soil moisture at ~10 cm | 22.87% (21.3, 22.7, 24.6%) |
| Tractor | New Holland T7060, 210 hp (156.6 kW) |
| Tillage module | Five-tine subsoiler + tandem spiked rollers |
| Liquid application module | 500 l tank; Delavan 7812-201, 12 V DC pump; calibrated nozzles |
| Nominal depth during test | 30 cm after adjustment for wet soil/residue conditions |
| Liquid placement target | Loosened soil zone, approximately 10–20 cm |



**Fig. 1 - Tractor - implement unit during field testing in Jiliște, Vrancea County**

## RESULTS

The combined implement operated under conditions that were challenging for residue flow. At the initial deeper setting, moist soil and wheat residues accumulated on the spiked roller. Reducing the nominal setting to 30 cm eliminated repeated clogging sufficiently to continue the measurements and produced a visually homogeneous loosened strip. The measured mean depth was 25.53 cm. Across the three replicated sets, mean depth values ranged from 24.87 to 26.00 cm, and the overall coefficient of variation was 2.71%. The mean working width was 224.67 cm, with a coefficient of variation of 2.72%. These values indicate low spatial variability in both depth and width during the partial field campaign.

The immediate physical response of the soil was substantial. Mean bulk density decreased from 1.207 to 0.811 g/cm$^3$, a relative reduction of approximately 32.8%. Total porosity increased from 54.5 to 69.4%, corresponding to an increase of 14.9 percentage points. Mean penetration resistance decreased from 1.10 to 0.82 MPa, approximately 25.5% below the initial value. The reported mean profile height changed from 93.0 to 84.5 cm according to the fixed reference measurement used in the field protocol. Taken together, the measured variables showed that the passage of the implement produced an immediate loosening effect in the evaluated soil layer.

The subsurface placement of the liquid biofertilizer was also consistent along the test strip. Measured injection depths at 25, 50 and 75 m were 15.3, 14.5 and 14.6 cm, respectively. The resulting mean was 14.8 cm, with a standard deviation of 0.44 cm and a coefficient of variation of 2.95%. The variability therefore remained well below the 10% acceptance threshold used in the test protocol. The application system maintained liquid flow during the measurements, and the field inspection reported uniform delivery through the calibrated nozzles.

Two tractor speed regimes were evaluated in the energy campaign. In first slow gear, the measured speed was 3.97 km/h; the mean draft force was 2300.3 daN and the maximum was 2659.8 daN. In first fast gear, speed increased to 4.97 km/h; mean draft force was 2373.9 daN and the maximum was 2856.5 daN. Corresponding mean traction power increased from 33.83 to 43.72 hp, while the maximum traction power increased from 39.10 to 52.58 hp. Average wheel slip was 9.11% in the slower regime and 5.25% in the faster regime. The theoretical field capacity calculated from the 2.2467 m working width was 0.89 ha/h at 3.97 km/h and 1.12 ha/h at 4.97 km/h.

Fuel use during the partial energy trial was determined on a treated area of 0.18 ha. Effective working time was 0.202 h and hourly fuel consumption was 19.8 l/h. The resulting specific fuel consumption was 22.2 l/ha. These figures characterize the lower-speed energy test and should not be directly combined with the later operational-capacity measurements because the final trial was performed at a different working speed. In the final operational trial, the reported working speed was 6.9 km/h. Effective working time was 140.4 min, operating time was 152.4 min and production time was 170.4 min. The coefficient of operating-time use was 0.921, the production-time coefficient was 0.824, and the turning coefficient was 0.921. Effective field capacity reached 1.71 ha/h and performance field capacity was 1.41 ha/h. Specific fuel consumption was 22.8 l/ha, close to the 22.2 l/ha measured in the preceding energy trial despite the different operating regime.

Technical inspection after the campaigns found no major structural failure of the subsoiler frame, liquid tank, pump or electrical command system. The main limitations were minor and operational: the spiked roller tended to clog under wet conditions with abundant residues, and one nozzle on the central line detached during a clogging event. The reports consequently recommended regular roller cleaning under wet/residue-rich conditions, improved nozzle fastening, and redesign of the spiked roller geometry to increase clearance and reduce material accumulation.

**Table 2**

| Indicator | Before / setting | After / measured result | Change / variability |
|---|---|---|---|
| Working depth | Nominal setting: 30 cm | 25.53 cm mean | SD 0.69 cm; CV 2.71% |
| Working width | — | 224.67 cm mean | SD 6.11 cm; CV 2.72% |
| Bulk density | 1.207 g/cm$^3$ | 0.811 g/cm$^3$ | −32.8% |
| Total porosity | 54.5% | 69.4% | +14.9 % |
| Penetration resistance | 1.10 MPa | 0.82 MPa | −25.5% |
| Liquid injection depth | Target zone 10–20 cm | 14.8 cm mean | SD 0.44 cm; CV 2.95% |



**Fig. 2 - Field verification of the subsurface liquid injection depth**

**Table 3**

| Performance indicator | Partial energy trial | Final operational trial |
|---|---|---|
| Working speed | 3.97 / 4.97 km/h | 6.9 km/h |
| Mean draft force | 2300.3 / 2373.9 daN | - |
| Maximum draft force | 2659.8 / 2856.5 daN | - |
| Mean traction power | 33.83 / 43.72 hp | - |
| Wheel slip | 9.11 / 5.25% | - |
| Theoretical field capacity | 0.89 / 1.12 ha/h | - |
| Effective field capacity | — | 1.71 ha/h |
| Performance field capacity | — | 1.41 ha/h |
| Specific fuel consumption | 22.2 l/ha | 22.8 l/ha |
| Operating-time coefficient | — | 0.921 |
| Production-time coefficient | — | 0.824 |

## CONCLUSIONS

The field study confirmed that deep loosening and controlled subsurface application of a liquid biofertilizer can be integrated in a single tractor pass while maintaining stable working indices. Under the tested chernozem-on-loess conditions, the mean effective tillage depth was 25.53 cm and the mean working width was 224.67 cm, both with coefficients of variation below 3%. The liquid was placed at a mean depth of

14.8 cm with a 2.95% coefficient of variation, demonstrating uniform positioning within the loosened zone. The immediate soil response was characterized by a 32.8% reduction in bulk density, an increase in total porosity from 54.5 to 69.4%, and a reduction in penetration resistance from 1.10 to 0.82 MPa. Energy measurements showed mean draft forces of approximately 23–24 kN and specific fuel consumption of 22.2 l/ha in the partial trial. In the final operational test, effective field capacity reached 1.71 ha/h while fuel consumption remained similar at 22.8 l/ha. The main practical limitation was residue and wet-soil accumulation on the spiked roller, which required a reduction of the nominal depth and supports further optimization of roller clearance and nozzle fastening. Overall, the case study demonstrates that the combined technology is technically feasible for deep soil conditioning and controlled liquid input placement in South-East Romanian field conditions, provided that machine settings are adapted to soil moisture and residue load.

**ACKNOWLEDGEMENT**

This research was supported by project *Establishment and operationalization of a Competence Center for Soil Health and Food Safety* – CeSoH, Contract no. 760005/2022, specific project no.3, with the title: *Fertile and healthy soil through conservation and biological practices,* Code 2, financed through PNRR-III-C9-2022 – I5 (PNRR-National Recovery and Resilience Plan, C9 *Support for the private sector, research, development and innovation*, I5 Establishment and operationalization of Competence Centers).

**REFERENCES**

[1] Feng, X., Ma, D., Lei, T., Hu, S., Yu, X., & Gao, J. (2024). Subsoil tillage improved the maize stalk lodging resistance under high planting density. *Frontiers in Plant Science*, 15, 1396182. https://doi.org/10.3389/fpls.2024.1396182

[2] Le, T. Y. L., Lee, J., Shim, S.-Y., Jung, J., Kim, S.-R., Hong, S.-H., Lee, M.-G., & Hwang, S.-G. (2025). Effects of liquid bio-fertilizer on plant growth, antioxidant activity, and soil bacterial community during cultivation of Chinese cabbage (Brassica rapa L. ssp. pekinensis). *Microorganisms*, 13(5), 1036. https://doi.org/10.3390/microorganisms13051036

[3] Liu, K., Sozzi, M., Gasparini, F., Marinello, F., & Sartori, L. (2023). Combining simulations and field experiments: Effects of subsoiling angle and tillage depth on soil structure and energy requirements. *Computers and Electronics in Agriculture*, 214, 108323. https://doi.org/10.1016/j.compag.2023.108323

[4] Orzech, K., Wanic, M., & Załuski, D. (2021). The effects of soil compaction and different tillage systems on the bulk density and moisture content of soil and the yields of winter oilseed rape and cereals. *Agriculture*, 11(7), 666. https://doi.org/10.3390/agriculture11070666

[5] Rubio, V., Quincke, A., & Ernst, O. (2021). Deep tillage and nitrogen do not remediate cumulative soil deterioration effects of continuous cropping. *Agronomy Journal*, 113(6), 5584–5596. https://doi.org/10.1002/agj2.20927

[6] Shahzad, M., Hayat, R., Mujtaba, G., Rehman, W. U., et al. (2025). Biofertilizers in sustainable agriculture: Mechanisms, applications, and future prospects. *Discover Agriculture*, 3, 224. https://doi.org/10.1007/s44279-025-00318-0

[7] Vanderhasselt, A., Cool, S., D'Hose, T., & Cornelis, W. (2023). How tine characteristics of subsoilers affect fuel consumption, penetration resistance and potato yield of a sandy loam soil. *Soil and Tillage Research*, 228, 105631. https://doi.org/10.1016/j.still.2022.105631

[8] Wang, J., Wang, Z., Gu, F., Liu, H., Kang, G., Feng, W., Wang, Y., & Guo, T. (2021). Tillage and irrigation increase wheat root systems at deep soil layer and grain yields in lime concretion black soil. *Scientific Reports*, 11, 6394. https://doi.org/10.1038/s41598-021-85588-6

[9] Wang, Y., Li, N., Ma, Y., Tong, J., Pfleging, W., & Sun, J. (2020). Field experiments evaluating a biomimetic shark-inspired (BioS) subsoiler for tillage resistance reduction. *Soil and Tillage Research*, 196, 104432. https://doi.org/10.1016/j.still.2019.104432

[10] Yang, P., Dong, W., Heinen, M., Qin, W., & Oenema, O. (2022). Soil compaction prevention, amelioration and alleviation measures are effective in mechanized and smallholder agriculture: A meta-analysis. Land, 11(5), 645. https://doi.org/10.3390/land11050645

[11] Zhao, H., Qin, J., Gao, T., Zhang, M., Sun, H., Zhu, S., Xu, C., & Ning, T. (2022). Immediate and long-term effects of tillage practices with crop residue on soil water and organic carbon storage changes under a wheat–maize cropping system. *Soil and Tillage Research*, 218, 105309. https://doi.org/10.1016/j.still.2021.105309

# METHODS OF PRESERVING SOIL FERTILITY IN ARAD COUNTY, ROMANIA
# /
# *METODE DE CONSERVARE A FERTILITĂȚII SOLULUI ÎN JUDEȚUL ARAD, ROMÂNIA*

**Casiana MIHUȚ[1)], Sorin Tiberiu BUNGESCU*[1)], Nicolae-Valentin VLADUȚ[2)], Daniel POPA[1)], Anişoara DUMA-COPCEA[1)], Attila BLENEȘI-DIMA[1)], Aurelia MIHUȚ[1)], Veaceslav MAZĂRE[1)], Lavinia PETANEC[1)]**

[1)] University of Life Sciences "KING MIHAI I" from Timişoara, Timis County / Romania;

[2)] National Institute of Research - Development for Machines and Installations Designed for Agriculture and Food Industry - INMA Bucharest / Romania.

**Tel: 0723 699 380; *E-mail: sorin_bungescu@usvt.ro*

***Keywords:*** *soil fertility; alluvial; preluvosoil; conservative agricultural technologies; agricultural productions; PCA analysis; western Romania*

## ABSTRACT

*Soil fertility is essential for stable agricultural production under pedological and climatic variability. This study evaluated the effects of soil type and conservative management on crop productivity in Ususău, Western Romania, during 2022–2024. Alluvial soils and preluvosols were compared under conventional and conservative management based on organic fertilization and crop residues. Maize, wheat, and sunflower yields were evaluated in relation to soil type and management using Pearson correlation and principal component analysis (PCA). Conservative management increased yields for all crops, with maize increases exceeding 40% and a strong association with management (r ≈ 0.95). PCA confirmed soil–management differentiation.*

## REZUMAT

*Fertilitatea solului este esențială pentru stabilitatea producției agricole în condiții de variabilitate pedologică și climatică. Studiul a evaluat, în perioada 2022–2024, influența tipului de sol și a managementului conservativ asupra productivității culturilor din Ususău, vestul României. Solurile aluviale și preluvosolurile au fost analizate în sistem convențional și conservativ, cu fertilizare organică și menținerea resturilor vegetale. Producțiile de porumb, grâu și floarea-soarelui au fost corelate cu pH-ul, humusul și nutrienții disponibili prin corelație Pearson și PCA. Managementul conservativ a crescut producțiile, porumbul depășind 40% creștere (r ≈ 0,95). PCA a evidențiat rolul determinant al tipului de sol, modulat de management.*

## INTRODUCTION

Soil is the main support of agricultural production, and maintaining its fertility is an essential condition for the stability and efficiency of agricultural systems, especially in regions with intensive agriculture and high climatic variability. “Soil fertility is determined by the interaction of physical, chemical and biological soil properties and by their response to agricultural management practices applied over time (*FAO, 2017; FAO, 2026; Mihuț et al., 2024; Teng et al., 2024*).

At European and global level, the degradation of agricultural soils is manifested by the decrease in organic matter content, compaction, erosion and nutrient imbalances, processes accentuated by the intensification of agriculture and the effects of climate change. The reduction of humus has direct consequences on water retention capacity, nutrient availability and soil structure stability, negatively affecting agricultural production, especially under increasing climatic and water stress (*Chen et al., 2024; Teng et al., 2024; Vanghele et al., 2025*).

Conservative agriculture has emerged as an effective solution to limit these processes, by applying measures such as reducing the intensity of tillage work, keeping plant residues on the surface and using organic fertilization. Recent studies highlight that these practices improve soil health indicators and contribute to the stabilization of agricultural production, including under conditions of climate stress (*Mircov et al., 2025; Teng et al., 2024; van Wesemael et al., 2024; Gora et al., 2024; Vanghele et al., 2025*)

The application of organic fertilisers, in particular manure, is recognised for its positive effect on soil structure, cationic exchange capacity and availability of essential plant macroelements. Recent research confirms the role of organic fertilization and plant residue management in increasing the organic carbon

content and resilience of agricultural systems (*Diacono & Montemurro, 2010; Wang et al, 2024; Taghizadeh-Toosi et al., 2026; Burcea et al., 2024*).

In western Romania, agricultural soils have a high productive potential, but they are sensitive to degradation under the conditions of the application of intensive technologies. Recent studies emphasize the need to adapt agricultural technologies to regional soil particularities in order to maintain the fertility and stability of productions.

Ususău commune, located in the south-east of Arad County, in the area of influence of the Mureș River and the Lipova Hills, is a representative agricultural area for assessing the impact of conservation technologies on soil fertility. The pedological diversity of the territory, dominated by alluvial soils and preluvosols, allows the comparative analysis of the response of agricultural crops to conservation measures applied in pedoclimatic conditions specific to western Romania.

The purpose of this work is to evaluate the effect of the application of organic fertilization and the maintenance of plant residues on the level of agricultural productions and on their stability, in correlation with the pedological characteristics of the main soil types in Ususău, in the period 2022–2024. The results obtained provide a scientific basis for formulating recommendations on sustainable soil management on farms in the region.

## MATERIALS AND METHODS

### 2.1. Location and characterization of the study area

The research was carried out in the outskirts of Ususău, Arad County, on an agricultural area of 38 ha, used mainly for field crops. The area is located in the south-east of Arad County, near the Mureș River, benefiting from favorable conditions for agriculture, but also from hydrological and climatic influences specific to the meadow and adjacent hilly areas Figure 1.




**Fig. 1 - Location of the studied perimeter within Arad County, Romania**

Climatically, the region falls into the temperate-continental moderate type, with western influences. The average annual temperature is around 10.5–11.0°C, and the average annual rainfall is between 550 and 650 mm, with an uneven distribution throughout the year. The variability of the rainfall regime is an important factor that conditions the level and stability of agricultural productions (*Mihuț & Niță, 2018; Mircov et al., 2025*).

### 2.2. Soils analysed

From a pedological point of view, the studied territory is characterized by the presence of the following types of soil: alluvial, preluvosoil, gleyosol, luvosoil and eutricambisoil.

From an agricultural point of view, the detailed analysis focused on two dominant soil types, classified according to the Romanian Soil Taxonomy System (SRTS) and correlated with WRB (*Florea & Munteanu, 2012; IUSS Working Group WRB, 2022*):

*1. Alluvial soils, developed on recent fluvial deposits of the Mureș River, with variable texture and moderate to high fertility;*

*2. Preluvosols, clay-alluvial soils with Bt horizon, developed on loessoid deposits, characterized by weak acid reaction and medium to good natural fertility.*

The distribution of the analyzed areas is presented in Table 1.

**Table 1**

**Distribution of the studied area by soil type**

| Soil type | Area (ha) | Share (%) |
|---|---|---|
| Alluvial soil | 26 | 68.4 |
| Preluvosol | 12 | 31.6 |
| **Total** | **38** | **100** |

### 2.3. Soil fertility indicators

Based on specialized data for western Romania, the fertility characteristics of the analyzed soils fall into the following ranges:

1. pH: weakly acidic to neutral (6,0–7,0);
2. humus content: 2.2–3.5%, with higher values on alluvial soils;
3. car: 50–90 mg/kg;
4. mobile phosphorus: 30–65 mg/kg;
5. Potassium car: 150–240 mg/kg.

These values reflect a good to very good fertility level, which can be maintained and improved by applying appropriate agricultural technologies.

### 2.4. Crop structure and applied technologies

In the analyzed period (2022–2024), four agricultural crops representative of western Romania were cultivated on the studied area: corn (*Zea mays L.*), wheat (*Triticum aestivum L.*), sunflower (*Helianthus annuus L.*) and alfalfa (*Medicago sativa L.*).

The distribution of areas by crops and soil types is shown in **Table 2**.

**Table 2**

**Crop distribution by soil type**

| Crop | Alluvial soil (ha) | Preluvosol (ha) |
|---|---|---|
| Maize | 12 | 4 |
| Wheat | 5 | 6 |
| Sunflower | 5 | 1 |
| Alfalfa | 3 | 1 |

The structure of the crops was adapted to the soil conditions and biological requirements of the plants. Two technological variants were analyzed:

1. Intervention-free version, based on conventional tillage without the application of plant residues;
2. Variant with interventions, which included:

- application of manure at a dose of 25 t/ha, administered in the autumn of 2021;
- incorporation or maintenance of plant residues (straw, hobs, stems) on approximately 50% of the analyzed area, starting with 2022.

For each crop – soil type – technological variant combination, the yields obtained in 2022, 2023 and 2024 were analyzed, the multiannual averages being calculated, as well as the absolute and relative increases in yields, according to the statistical methodologies used in agronomy (Gomez & Gomez, 1984).

Alfalfa was analysed separately as it did not benefit from direct interventions during the study period, its productivity being influenced by residual soil fertility and biological capacity to fix atmospheric nitrogen.

The tillage of the soil was carried out according to its state of moisture and consistency, respecting the basic principles of conservative tillage of the soil. The mechanical interventions were carried out exclusively in the state of friable consistency, in order to avoid compaction and degradation of the soil structure, according to the recommendations formulated in the specialized literature (*Lal and Stewart, 2013*).

The assessment of the humidity status was carried out by organoleptic methods, currently used in practice, thus ensuring optimal conditions for maintaining the soil structure and reducing the number of secondary works.

### 2.5. Data analysis and processing methodology

The agricultural productions obtained in 2022, 2023 and 2024 were analyzed comparatively for each crop-soil type-technological variant combination. The multiannual averages, the absolute and relative production increases and the Pearson correlation coefficient (r) between the application of the interventions and the level of production were calculated.

In order to highlight the multivariate relationships between crops, soil types and applied technologies, the PCA (Principal Component Analysis) analysis was used, which allowed the identification of the main factors that explain the variation of agricultural productions.

## RESULTS

### 3.1. Soil characteristics and soil fertility level

The main soil types identified in Ususău commune have a good to very good fertility level, specific to western Romania. The characteristic values of soil reaction (pH 6.0–7.0), humus content (2.2–3.5%) and mobile nutrients (N, P, K) are summarized in Table 1 and reflect clear differences between alluvial and preluvosols.

**Table 1**

**Typical soil fertility parameters for the main soil types in Ususău commune (Western Romania)**

| Soil type | pH ($H_2O$) | Humus (%) | Available N (mg/kg) | Available P (mg/kg) | Available K (mg/kg) |
|---|---|---|---|---|---|
| Preluvosol | 6.0–6.5 | 2.2–3.0 | 55–75 | 35–55 | 160–210 |
| Alluvial soil | 6.5–7.0 | 2.5–3.5 | 65–90 | 40–65 | 180–240 |
| Gleysol | 5.8–6.5 | 2.0–2.8 | 45–65 | 25–40 | 140–190 |
| Luvisol | 5.8–6.4 | 1.8–2.4 | 40–60 | 20–35 | 130–180 |
| Eutric Cambisol | 6.0–6.5 | 2.0–2.6 | 50–70 | 30–45 | 150–200 |

According to Table 1, alluvial soils are distinguished by a higher humus content (2.5–3.5%) and better nitrogen and potassium reserves, explaining their higher productive potential. Preluvosoils show good values of chemical fertility, but are influenced by the presence of the Bt horizon, which can limit root development and water infiltration under compaction conditions.

### 3.2. Multiannual average yields by soil type and technology applied

The average multiannual yields (2022–2024) differ significantly depending on both the type of soil and the technology applied, as illustrated in Figure 2–4.

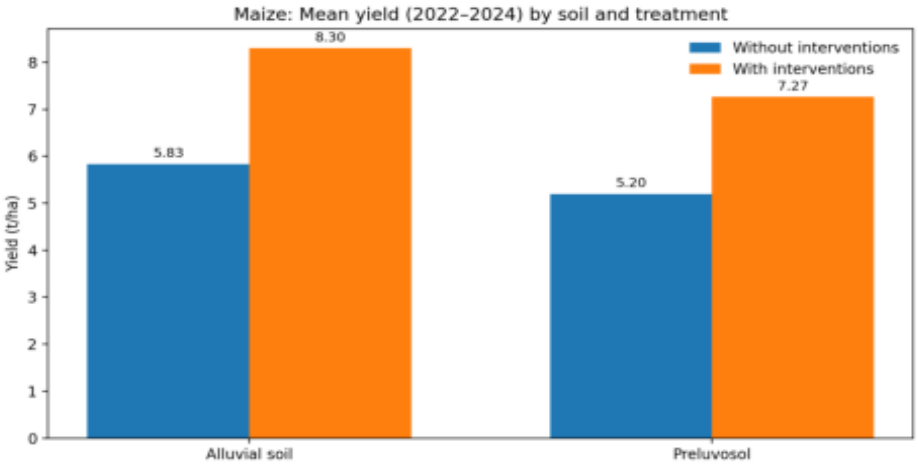



**Fig. 2 - Maize: Mean yield (2022–2024) by soil and treatment**

In maize crops, the average production increased from 5.8 t/ha to 8.3 t/ha on alluvial soil and from 5.2 t/ha to 7.3 t/ha on preluvosoil in the intervention variants (Figure 2). The differences are

consistent and confirm the ability of this crop to capitalize on the improvement of the nutrient and water regime of the soil.

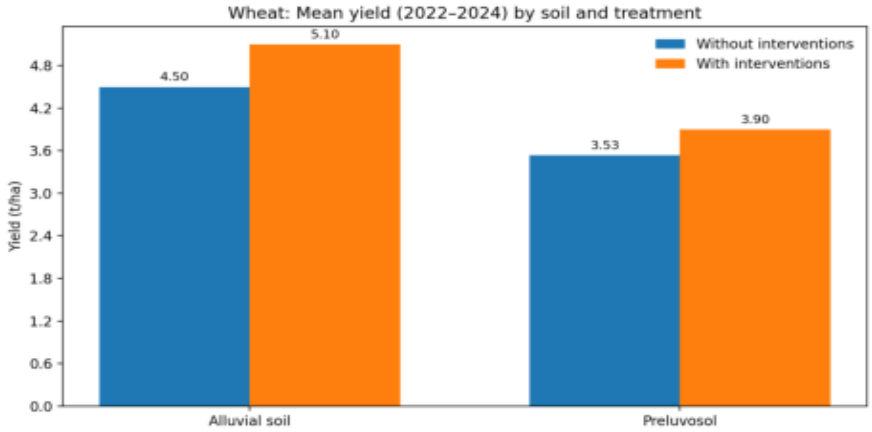



**Fig. 3 - Wheat: Mean yield (2022–2024) by soil and treatment**

In the case of wheat, average yields increased from 4.5 t/ha to 5.1 t/ha on alluvial soil and from 3.5 t/ha to 3.9 t/ha on prelusol soil (Figure 3). The increases are more moderate, reflecting the lower requirements of the crop compared to the rapid nutrient intake.

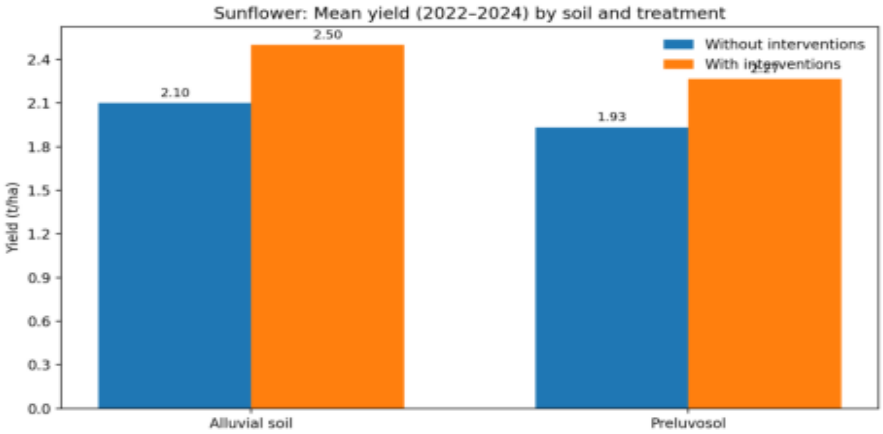



**Fig. 4 - Sunflower: Mean yield (2022–2024) by soil and treatment**

Sunflowers recorded average yields of 2.5 t/ha on alluvial soil and 2.3 t/ha on preluvosoil in the intervention variants, compared to 2.1 t/ha and 1.9 t/ha in the non-intervention variants (Figure 4), highlighting a positive response to conservation measures.

A consistent positive effect of the interventions (manure + plant residues) is observed on all the analyzed crops, with maximum amplitude in maize.

Agronomically, maize has high nutritional requirements and is very sensitive to nitrogen availability and water regime; organic matter-based interventions gradually increase N availability and improve water structure and retention, explaining the large increases in production (*Lal, 2004; Diacono & Montemurro, 2010*).

For wheat and sunflower, the response is positive, but more moderate, in accordance with the more stable behavior of the autumn crops (wheat) and the ability of the sunflower to efficiently capitalize on the water in the profile (*Florea & Munteanu, 2012; Lal and Stewart, 2013*).

### 3.3. Production dynamics (2022–2024)

The analysis of agricultural productions obtained in the period 2022–2024 highlights a clear effect of soil fertility conservation measures (application of manure and maintenance of plant residues), both on alluvial and preluvosoil.

For maize (Figure 5), intervention variants maintained a high and relatively stable level of production over all three years, compared to non-intervention variants, where fluctuations are more

pronounced. This indicates a buffering effect on climate stress by improving soil structure and water holding capacity.

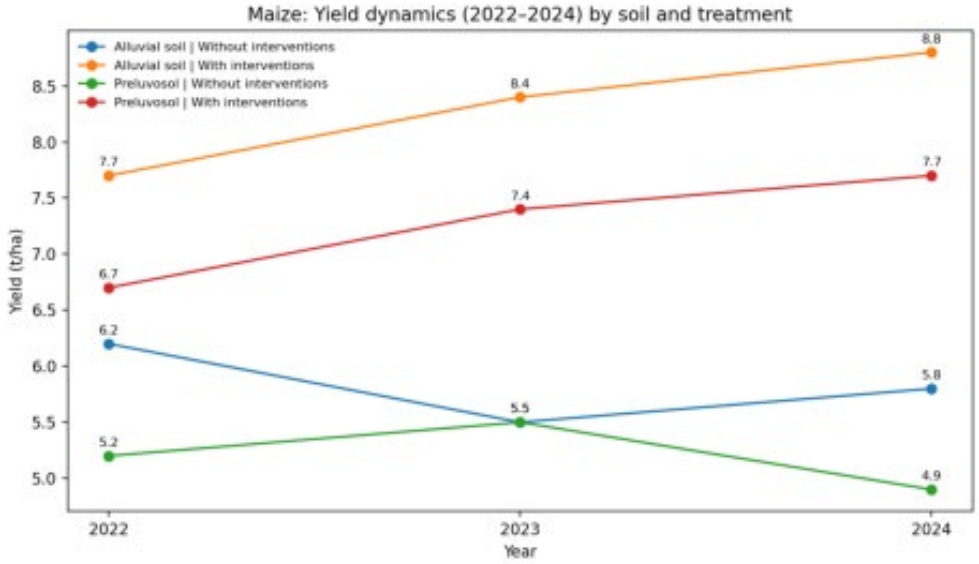



**Fig. 5 - Maize: Yield dynamics (2022–2024) by soil and treatment**

The average multiannual yields were 8.3 t/ha on alluvial soil and 7.3 t/ha on preluvosoil in the intervention variants, compared to 5.8 t/ha and 5.2 t/ha respectively in the non-intervention variants (Figure 5). The production increases (+43% on alluvial soil and +40% on preluvosoil) confirm the very good reaction of maize to the improvement of soil fertility and to the stabilization of the water regime.

For wheat (Figure 6) and sunflower (Figure 7), the annual dynamics show smaller variations, but the favorable trend for variants with interventions is constant, confirming the stabilization of productions over time.

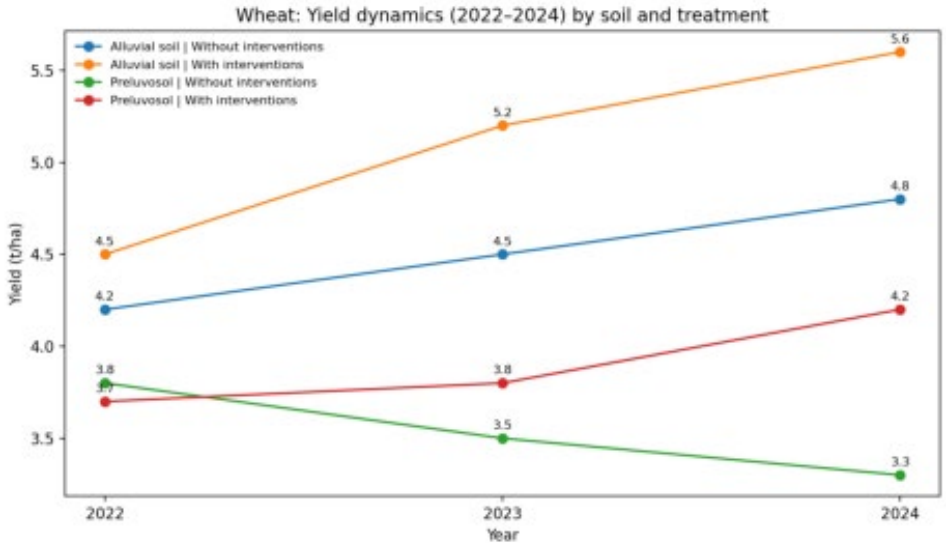



**Fig. 6 - Wheat: Yield dynamics (2022–2024) by soil and treatment**

In wheat, average yields increased from 4.5 to 5.6 t/ha on alluvial soil and from 3.5 to 3.9 t/ha on prelusosol (Figure 6). Increases are more moderate (11–13%), reflecting wheat's lower requirements for rapid nutrient intake and its ability to harness basic soil fertility.

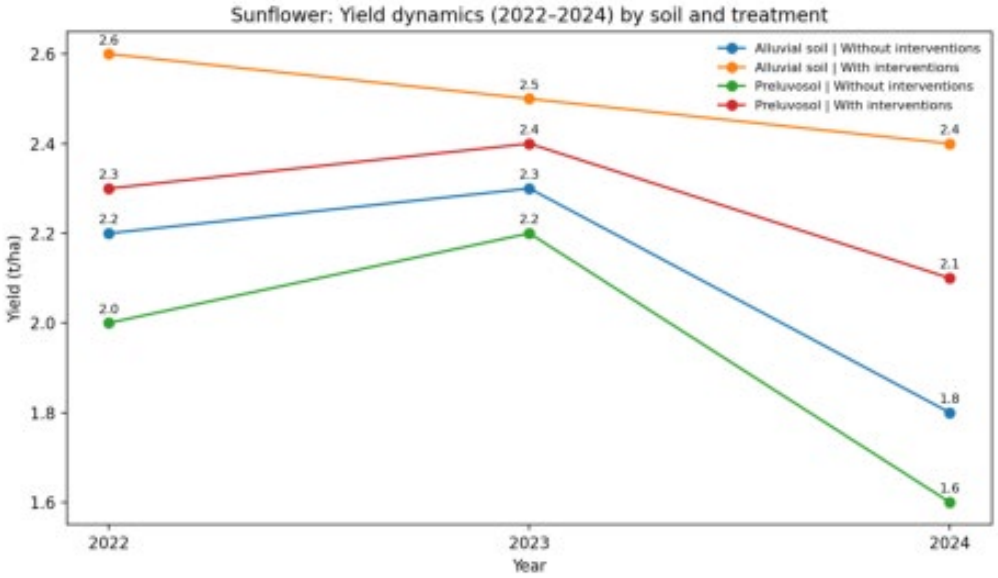



**Fig. 7 - Sunflower: Yield dynamics (2022–2024) by soil and treatment**

Sunflowers recorded significant percentage increases of 19–21% on both soil types (Figure 7). This crop effectively capitalizes on the structural improvements of the soil and the benefits brought by the maintenance of plant residues, especially in years of water deficit.

On all 3 crops, the "With interventions" curves are systematically above the "Without interventions" variants, indicating not only an increase in production, but also a stabilization of performance in different years.

This behavior is typical of organic matter input and vegetation cover/residue systems, which reduce evaporation, improve aggregation, and support biological activity, contributing to water and nutrient use efficiency (*Hobbs et al., 2008; Derpsch et al., 2010; Lal and Stewart, 2013; Teng et al., 2024; Gora et al., 2024*).

### 3.4. Correlation between interventions and production

The Pearson coefficient r, calculated between the application of the interventions (0/1) and the level of agricultural production, is graphically shown in Figure 8.

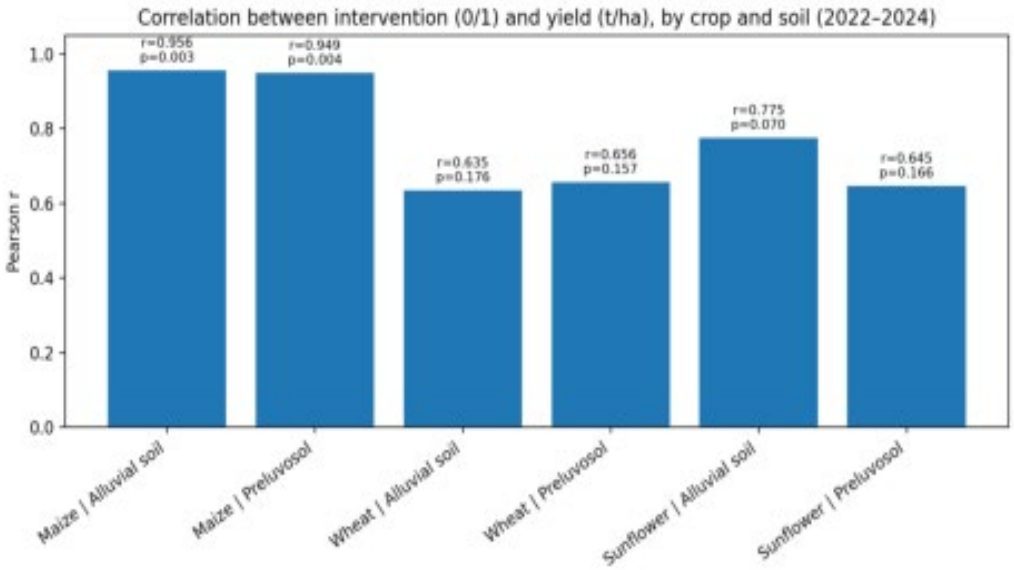



**Fig. 8 - Correlation between intervention (0/1) and yield (t/ha), by crop and soil (2022–2024)**

In maize, r is very high (≈0.95) on both soils, which indicates a very strong association between interventions and increased production. The very high values of the r-coefficient for corn indicate a very strong relationship between the applied technology and production.

For sunflower and wheat, the r-values are moderate (≈0.63–0.78), suggesting that, in addition to technology, other factors (climatic conditions, phenology) also influence the level of production.

These values confirm that the production increases are not random, but are closely linked to the application of fertility preservation measures, in particular to crops with high nutritional requirements.

### 3.5. PCA analysis and multivariate data structure

The results of the PCA analysis are presented in Figure 8, which highlights the distribution of observations in the main component space.

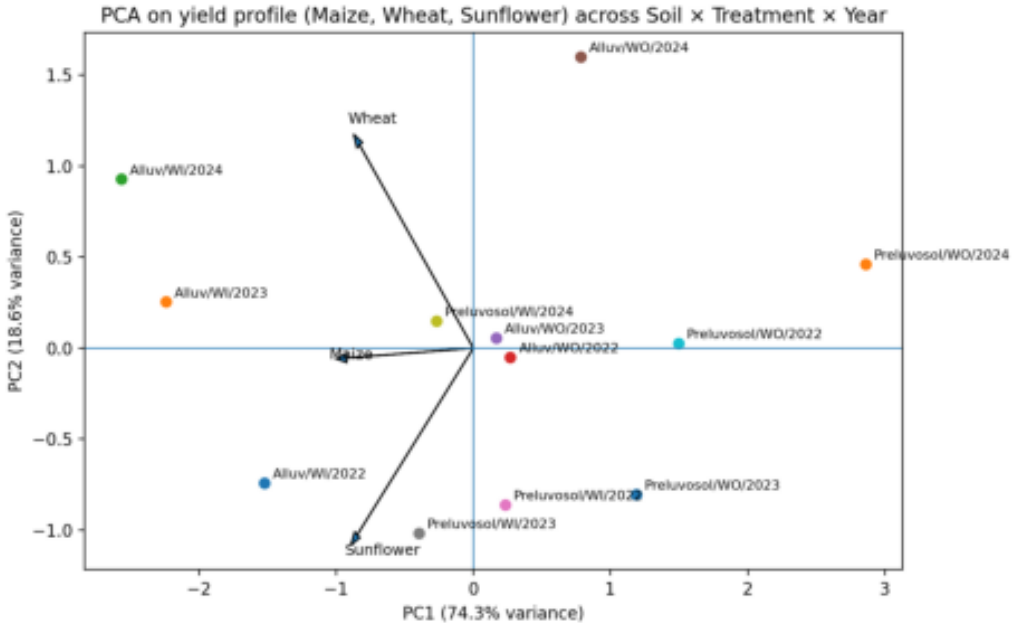



**Fig. 8 - PCA on yield profile (Maize, Wheat, Sunflower) across Soil × Treatment × Year**

FP1 explains 74.3% of the variation and is associated with an 'overall productivity' gradient (similar negative loads for all 3 crops), indicating that the intervention points tend to be shifted towards one end of the PC1 axis, corresponding to higher yields.

PC2 explains 18.6% and mainly separates the "wheat vs sunflower" component (opposite-sign loads), suggesting that certain years/soil-technology combinations favor one of these crops relatively more.

The distinct positioning of the observations corresponding to the alluvial soils from the preluvosoils confirms the role of soil type in modulating the response of crops to conservation measures.

The correlation of the results presented (tables 1 and figures 1–8), demonstrates that the level of soil fertility establishes the basic pedological framework of productivity, and the application of conservation technologies amplifies this potential by improving the water and nutrient regime.

The higher increases achieved in maize are explained by the high demands of this crop on nitrogen and water, while the more moderate response of wheat and sunflower reflects their better adaptability to variable fertility conditions.

The results obtained in Ususău commune show that the consistent application of soil fertility conservation measures leads to significant and stable production increases, especially on soils with high productive potential. Alluvial soils quickly capitalize on interventions due to their natural fertility, while preluvosoils benefit from progressive improvements in structure and water regime.

The differences between crops highlight the need to adapt agricultural technologies to the biological requirements of plants and the specific properties of the soil, in order to achieve high and sustainable yields in the long term.

## CONCLUSIONS

The results obtained in Ususău commune during 2022–2024 indicate that crop productivity was associated with both soil type and the applied agricultural management. Alluvial soils showed a higher productive potential than preluvosoils, consistent with their higher humus content and available nutrient levels.

The conservation variant, based on manure application and crop-residue management, produced higher multiannual mean yields than the conventional variant for all three analyzed crops. The strongest response was recorded in maize, for which mean yield increased from 5.8 to 8.3 t $ha^{-1}$ on alluvial soil and from 5.2 to 7.3 t $ha^{-1}$ on preluvosoil, corresponding to increases of approximately 43% and 40%, respectively. Wheat showed increases from 4.5 to 5.1 t $ha^{-1}$ and from 3.5 to 3.9 t $ha^{-1}$, while sunflower increased from 2.1 to 2.5 t $ha^{-1}$ and from 1.9 to 2.3 t $ha^{-1}$ on alluvial soil and preluvosoil, respectively.

Pearson correlation analysis showed a very strong association between the conservation variant and maize yield ($r \approx 0.95$), whereas moderate associations were obtained for wheat and sunflower ($r \approx 0.63–0.78$).

PCA explained 92.9% of the total variation through the first two components (PC1 = 74.3%; PC2 = 18.6%). PC1 represented the overall productivity gradient and differentiated the higher-yielding intervention variants, while PC2 mainly reflected differences in crop response. The distribution of observations also indicated that soil type modulated crop response to the applied management.

Overall, the results support the use of soil-specific conservation practices based on organic inputs, crop-residue management and tillage adapted to soil moisture conditions. Under the conditions investigated, these practices were associated with higher and more stable crop yields. Further multi-location and long-term studies are required before extending these findings to other soil and climatic conditions.

## ACKNOWLEDGEMENT

Pedological and agronomic study assessing the effects of conservative soil management practices on maize, wheat and sunflower yields during 2022–2024 on alluvial soils and preluvosoils in Ususău, Arad County, Romania. The analysis includes multiannual yields, Pearson correlations and PCA.

## REFERENCES

[1] Burcea, M., Oltenacu, V.C., Burcea, C.A., Oltenacu, N. (2024). Study on the influence of organic manure on soil fertility. Scientific Papers Series Management, Economic Engineering in Agriculture and Rural Development, 24(4), 115–120.

[2] Chen, S., Chen, Z., Zhang, X., Luo, Z., Schillaci, C., Arrouays, D., Richer-de-Forges, A.C., Shi, Z. (2024). European topsoil bulk density and organic carbon stock database (0–20 cm) using machine-learning-based pedotransfer functions. Earth System Science Data, 16, 2367–2383. https://doi.org/10.5194/essd-16-2367-2024

[3] Derpsch, R., Friedrich, T., Kassam, A., Li, H. (2010). Current status of adoption of no-till farming in the world and some of its main benefits. International Journal of Agricultural and Biological Engineering, 3(1), 1–25. https://doi.org/10.3965/j.issn.1934-6344.2010.01.0-0.

[4] Diacono, M., Montemurro, F. (2010). Long-term effects of organic amendments on soil fertility. A review. Agronomy for Sustainable Development, 30, 401–422. https://doi.org/10.1051/agro/2009040

[5] FAO (2017). Soil organic carbon: the hidden potential. Food and Agriculture Organization of the United Nations, Rome.

[6] FAO (2026). State of the World's Soil Resources – 2nd Edition. Food and Agriculture Organization of the United Nations, Rome.

[7] Florea, N., Munteanu, I. (2012). Sistemul Român de Taxonomie a Solurilor (SRTS). Editura Estfalia, București.

[8] Gomez, K.A., Gomez, A.A. (1984). Statistical Procedures for Agricultural Research. 2nd edition. John Wiley & Sons, New York, USA. ISBN: 978-0-471-87092-0

[9] Gora, M.K., Jat, H.S., Ladha, J.K., Choudhary, M., Sharma, P.C., Yadav, A.K., Singh, L.K., Sapkota, T.B., Singh, Y., Prajapat, K., Yadav, R.K., Jat, M.L., Krupnik, T.J., Gathala, M.K. (2024). Enhancing productivity, soil health, and reducing global warming potential through diverse conservation agriculture cropping systems in India's Western Indo-Gangetic Plains. Field Crops Research, 315, 109476. https://doi.org/10.1016/j.fcr.2024.109476.

[10] Hobbs, P.R., Sayre, K., Gupta, R. (2008). The role of conservation agriculture in sustainable agriculture. Philosophical Transactions of the Royal Society B: Biological Sciences, 363(1491), 543–555. https://doi.org/10.1098/rstb.2007.2169.

[11] IUSS Working Group WRB (2022). World Reference Base for Soil Resources: International Soil Classification System for Naming Soils and Creating Legends for Soil Maps. 4th edition. International Union of Soil Sciences, Vienna, Austria. ISBN: 979-8-9862451-1-9.

[12] Lal, R. (2004). Soil carbon sequestration to mitigate climate change. Geoderma, 123(1–2), 1–22. https://doi.org/10.1016/j.geoderma.2004.01.032.

[13] Lal, R., Stewart, B.A. (2013). Principles of Sustainable Soil Management in Agroecosystems. CRC Press, Boca Raton.

[14] Mihuț, C., Niță, L. Duma Copcea, A., Rinovetz, A. (2024). Assessment of the productive capacity of agricultural lands for their sustainable use. Scientific Papers Series Management, Economic Engineering in Agriculture and Rural Development Vol. 24, Issue 1.

[15] Mihuț, C., Niță, L. (2018). Atmospheric factors used to characterize soil resources. Research Journal of Agricultural Science, 50 (1), pg. 114-121.

[16] Mircov, V.D., Sărățeanu, V., Mihuț, C., Pușta, D.S., Durău, C.C. (2025). Impact of extreme weather conditions on the production of the main field crops in Western Romania over the 2018-2023 period–case study. Agriculture & Forestry/Poljoprivreda i šumarstv. Volume 71. Number 3. https://doi.org/10.17707/AgricultForest.71.3.06.

[17] Taghizadeh-Toosi, A., Nielsen, S.V., Elofsson, K. (2026). Potential of crop residues management for soil organic carbon sequestration in European countries until 2050: a simplified modelling approach. Soil Security, 22, 100221. https://doi.org/10.1016/j.soisec.2025.100221.

[18] Teng, J., Hou, R., Dungait, J.A.J. et al. (2024). Conservation agriculture improves soil health and sustains crop yields after long-term warming. Nat Commun 15, 8785. https://doi.org/10.1038/s41467-024-53169-6

[19] Vanghele, N.-A., Vlăduț, N.-V., Pruteanu, A., Matache, A., Vlăduțoiu, L.-C., Vrînceanu, N.-O. (2025). Novel solutions for mitigating drought impact and restoring soil functionality in agriculture. INMATEH – Agricultural Engineering, 76(2), 1352–1381. https://doi.org/10.35633/inmateh-76-112.

[20] van Wesemael, B., Abdelbaki, A., Ben-Dor, E., Chabrillat, S., d'Angelo, P., Demattê, J.A.M., Genova, G., Gholizadeh, A., Heiden, U., Karlshoefer, P., Milewski, R., Poggio, L., Sabetizade, M., Sanz, A., Schwind, P., Tsakiridis, N., Tziolas, N., Yagüe, J., Žížala, D. (2024). A European soil organic carbon monitoring system leveraging Sentinel 2 imagery and the LUCAS soil data base. Geoderma, 452, 117113. https://doi.org/10.1016/j.geoderma.2024.117113.

[21] Wang, Y., Zhang, Y., Liu, Y., Wang, L., Dong, Y. (2024). Effects of different tillage methods on soil properties and maize seedling growth in alternating wide and narrow rows rotation mode in the Songliao Plain of China. Geoderma, 452, 11FAO7120. https://doi.org/10.1016/j.geoderma.2024.117120.

# ANALYSIS OF TECHNICAL SOLUTIONS FOR INCREASING THE LATERAL STABILITY OF MOTOR-CULTIVATORS USED FOR MOWING SLOPED TERRAIN VIA ADAPTIVE MASS-BALANCING SYSTEMS

/

# *MOTOCULTOARE ANALIZA PRIVIND SOLUTIILE TEHNICE DE CREȘTEREA STABILITĂȚII LATERALE A MOTOCULTOARELOR UTILIZATE LA COSIREA TERENURILOR ÎNCLINATE PRIN SISTEME DE ECHILIBRARE ADAPTIVĂ A MASEI*

**Iulian DRENEA, Sorin-Stefan BIRIS*, Adrian IOSIF, Gabriel MUȘUROI, Raluca- Adriana ZOTA**
National University of Science and Technology POLITEHNICA Bucharest / Romania
**E-mail: biris.sorinstefan@gmail.com*

***Keywords:*** *garden tillers; traction; skidding; tires, sloping land*

**ABSTRACT**
*Garden tillers are designed and manufactured to ensure a wide range of agricultural work. One of the works is mowing, which can be done on both flat and sloping land. In Romania, sloping land represents around 20% of the total agricultural area of Romania. The accessibility of these areas by agricultural machinery raises some challenges due to the large angle of inclination of the land. Thus, for agricultural tractors and for some agricultural motor cultivators, access is limited by the risk of overturning and lateral skidding of the equipment. This article describes the theoretical part, the technical solutions and the validation method of these technical solutions, which reduce the risk of overturning and skidding, as well as increase the accessibility of sloping land by motor cultivators equipped for mowing, with the final result of increasing the agricultural area of Romania that can be worked mechanized and implicitly increasing productivity.*

**REZUMAT**
*Motocultoarele actuale sunt proiectate și realizate pentru asigurarea unei game cât mai mare de lucrarii din agricultura. Printre lucrările ce se pot executa se numără și lucrarea de cosirea ce se poate realiza atât pe terenuri plane cât si pe terenuri in panta. In România terenurile aflate in panta reprezinta in jur de 43% din totalul suprafetei agricole a României. Accesibilitatea acestor suprafete de catre utilajele agricole ridica unele provocari datorita marimi unghiului de inclinare a terenului. Astfel pentru tractoare agricole cat si pentru o parte din motocultoarele agricole accesul este limitat de existenta riscul de rasturnare cat si de derapare laterala a utilaje. Prin prezentul articol este descrisa partea teoretică, soluțiile tehnice cat si modul de validare a acestor solutii tehnice prin care se obtine diminuarea riscului de rasturnare si de deprapare cat si cresterea accesibilitati terenurilor in panta de catre motocultoare echipate pentru operatiunea de cosire avand ca rezultat final mărirea suprafatei agricole a Romaniei ce poate fi lucrata mecanizat si implicit cresterea productivitati*

## INTRODUCTION

According to official data, approximately 43% of Romania's agricultural area consists of sloping land (*Durability and Reliability of Mechanical Systems SYMECH, 2025).* This percentage represents 5,8 million hectares out of Romania's total agricultural area of 13,5 million hectares. Furthermore, official data indicate that 48% of Romania's total agricultural area consists of permanent grasslands *(https://iuls.ro/universitate/despre-universitate/)*. These figures highlight the importance of properly managing sloping land to prevent soil degradation and ensure sustainable agriculture *(Mocanu et al., 2012).* Of the total agricultural area situated on slopes, 1,53 million hectares are hay meadows, used primarily for hay production. It is worth noting that over 70% of permanent grasslands are located on sloping land, meaning that approximately 1,067 million hectares of hay meadows are situated on such terrain *(ro.wikipedia.org)* Consequently, grasslands on slopes of up to 15° present no operational difficulties, as they are accessible to tractors and walk-behind tractors. Grasslands on slopes exceeding 15° account for approximately 15–20% of the total sloping grassland area and are found primarily in high mountain regions. This slope threshold is critical for grassland management in Romania for several technical reasons, including the risk of walk-behind tractors tipping over or skidding. The area of grasslands in Romania situated on slopes ranging from 25° to

30° is estimated at approximately 150.000–200.000 hectares, representing about 3–4% of the total national grassland area.

The distribution of grasslands on these steep slopes is limited by natural factors and the difficulty of working the land. Many are located primarily in the Apuseni Mountains, the Eastern Carpathians (Harghita and Covasna counties), and the steep areas of the Banat Mountains. On these slopes, mechanization using standard machinery is practically impossible; maintenance is carried out almost exclusively by hand or through extensive sheep grazing, as sheep are better adapted to rugged terrain *(Dragoș et al., 2018).* This article presents a series of technical solutions designed to improve the ability of walk-behind tractors to perform mowing operations on terrain with slopes exceeding 15°.

## MATERIALS AND METHODS

The mechanization of agricultural work on sloping terrain poses a major challenge in hilly and mountainous areas. When mowing natural grasslands, the use of walk-behind tractors is often limited by the equipment's lateral stability. In operation, the safety limit for walk-behind tractors regarding transverse slope is between 20° and 25°. Exceeding this value leads to:

- an increase in the destabilizing moment,
- a reduction in the reaction force on the uphill wheel,
- a decrease in the contact patch area of the uphill wheel,
- a risk of the walk-behind tractor tipping over sideways.

Extending the operational limit to 30° would increase the area that can be mechanized and reduce the need for manual labor in difficult areas, thereby increasing mowing productivity. In light of this, the present study proposes an engineering approach based on controlling the position of the walk-behind tractor's lateral center of gravity by redistributing its mass according to the terrain slope.

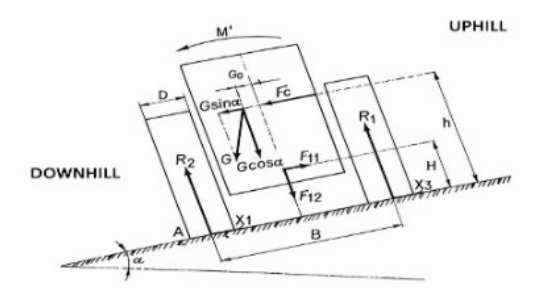



**Fig. 1- Forces and moments acting on an agricultural motor cultivator when working on sloping land** *(Tomescu et al., 1985)*

Theoretical model of the agricultural walk-behind tractor's lateral stability

To develop the mathematical model of the walk-behind tractor's lateral stability, the initial data shown in Fig. 1 were used. Thus, we have:

*Working assumptions based on Fig. 1*

It is assumed that:

- the walk-behind tractor is moving along contour lines,
- both wheels are in constant contact with the ground,
- maximum track width of the BCS 740 walk-behind tractor: B = 455 [mm],
- total mass of the walk-behind tractor equipped with a mower: m = 135 [kg],
- height of the walk-behind tractor's center of gravity: h [m],
- terrain inclination angle: α [degrees].

Based on the initial data, the expression for the destabilizing moment was determined as follows:

Regarding the destabilizing moment: for terrain with a transverse inclination angle α, the destabilizing moment relative to the downslope wheel is given by expression (2.1):

$$M_1' = mg\,h\sin\alpha \tag{2.1}$$

where: gravitational acceleration g = 9,81 [m/s²];

The destabilizing moment of the agricultural walk-behind tractor—which arises during operation and causes overturning or lateral skidding—can be counteracted by the stabilizing moment. The latter is expressed as follows:

The maximum stabilizing moment is given by formula (2.2)

$$M_S = mg\frac{B}{2}\cos\alpha \tag{2.2}$$

The parameter used to determine whether there is a risk of the agricultural walk-behind tractor tipping over or sliding is the lateral stability indicator, denoted as $K_s$. The expression for this stability coefficient is given by the ratio of the destabilizing moment to the stabilizing moment (2.3).

$$K_s = \frac{M_s}{M_1'} \tag{2.3}$$

Where, if $K_s > 1$ The walk-behind tractor is stable and not prone to tipping over.

This indicator is frequently used in the stability analysis of agricultural machinery.

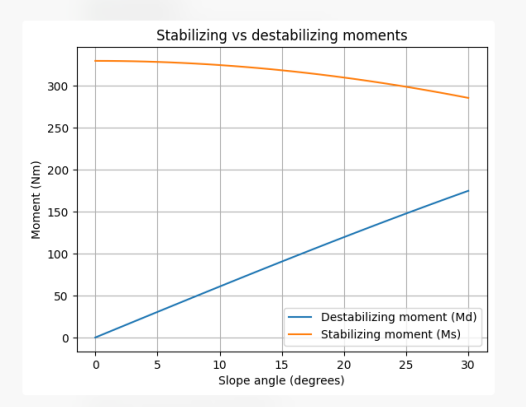



**Fig. 2 - Destabilizing moment and stabilizing moment as a function of the slope angle α**

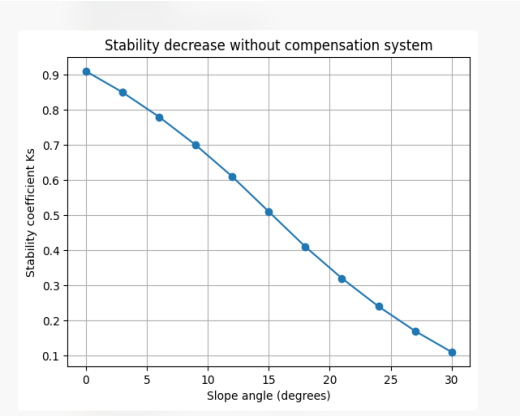



**Fig. 3 - Evolution of the lateral stability coefficient as a function of the slope angle α**

Figure 2 illustrates the variation of the stabilizing and destabilizing moments as a function of the terrain inclination angle (α); it shows that at an inclination angle exceeding 25°, the destabilizing moment becomes dominant, creating a risk of the walk-behind tractor overturning. Additionally, Figure 3 shows the variation of the stability coefficient for a walk-behind tractor lacking a system to compensate for the destabilizing moment.

Analysis of the stability coefficient formula yields the stability condition expressed by equation (2.4):

$$M_S > M_1' \tag{2.4}$$

Substituting the expressions for the destabilizing moment and the stabilizing moment yields the limiting condition:

$$mg\,h\sin\alpha < mg\frac{B}{2}\cos\alpha \tag{2.5}$$

$$h\sin\alpha < \frac{B}{2}\cos\alpha \tag{2.6}$$

$$h\,tag\,\alpha < 2B \tag{2.7}$$

From relationship (2.7), it follows that the lateral stability of the walk-behind tractor depends directly on:

- the track width of the walk-behind tractor,
- the height of the walk-behind tractor's center of gravity,
- the slope angle.

*Lateral displacement of the walk-behind tractor's center of gravity*

When operating on sloping terrain, the walk-behind tractor's center of gravity shifts away from its axis of symmetry toward the downhill wheel. Consequently, the projection of the center of gravity moves downslope by a distance $a_0$ (as shown in Fig. 1), according to the following formula:

$$a_0 = h\ tag\ \alpha \tag{2.8}$$

In this case, the overturning of the walk-behind tractor occurs when:

$$a_0 \geq \frac{B}{2} \tag{2.9}$$

By introducing an additional mass $m_a$ upstream—positioned laterally at a distance $d_r$—the two-wheel tractor's center of gravity shifts to a new position, and the center of gravity has the following new coordinates:

$$a_{CG} = \frac{mh\tan\alpha - m_a\ d_r}{m+m_a} \tag{2.10}$$

From relation (2.10), the condition for achieving the stability of the respective walk-behind tractor is derived:

$$a_{CG} < \frac{B}{2} \tag{2.11}$$

The information presented above forms the mathematical basis for the technical solutions proposed to balance the walk-behind tractor. The proposed technical solution involves using a movable or fixed counterweight on the upslope side of the machine to balance its center of gravity; this is illustrated in fig.4, which shows how the counterweight's position influences balance depending on the slope angle of the terrain.

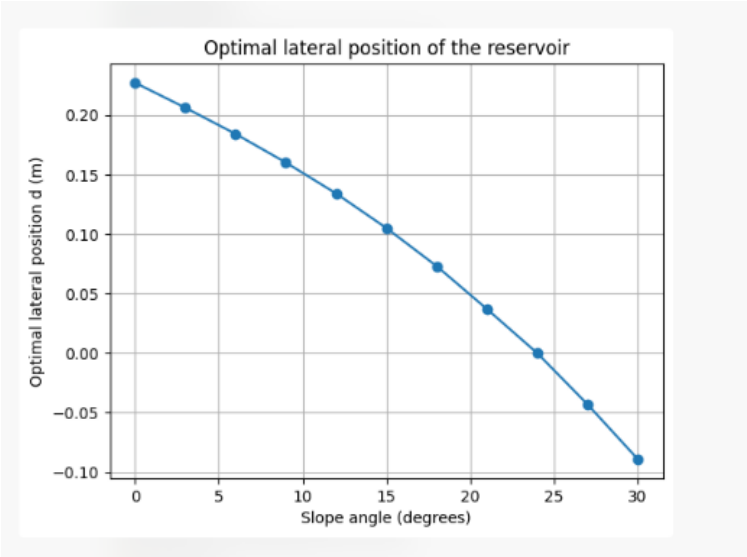



**Fig. 4 - Evolution of upstream counterweight positioning depending on the slope angle of the land**

Based on relations (2.7) and (2.10)—which establish the conditions required to balance the agricultural walk-behind tractor on slopes exceeding 15°—technical balancing solutions were determined, specifically involving the modification of the machine's center of gravity.

### 2.3 Proposed technical solutions for balancing the walk-behind tractor

#### *2.3.1 Current technical solutions for balancing the walk-behind tractor*

Currently, the technical solutions for balancing the walk-behind tractor include:

- Adjusting the tractor's track width
- Using dual tires
- Equipping the tractor with wheel counterweights
- Equipping the tractor with front-mounted counterweights
- Equipping the tractor with metal wheels
- Filling the tires with liquid
- Adjusting tire pressure

However, current technical solutions have certain technical and financial limitations. They require an additional financial outlay from the walk-behind tractor operator, as they are not included in the standard equipment. Furthermore, they demand time and additional technical resources on the part of the user. Another constraint is the limited applicability of these systems regarding terrain slope, which can vary during operation; existing systems cannot be quickly adjusted to compensate for slope changes. To address this, we propose a series of technical solutions that allow for the adjustment of the walk-behind tractor's center of gravity based on the terrain's inclination angle.

*New technical solutions for balancing the walk-behind tractor*

a) *Technical solution for balancing the walk-behind tractor using a system with two tanks and two pumps*

This system is illustrated in Fig. 5 and Fig.6.

The system's operating principle involves equipping the walk-behind tractor with two 15-liter side tanks. Only one tank—specifically the one on the upslope side—is filled during a given work pass. At the end of the row, water is transferred from the upslope tank to the downslope tank using two 12V mini-pumps powered by the tractor. This solution has the following technical specifications: water mass: ~15 kg; tank mass: 3–5 kg; mass of pumps and lines: 1–2 kg. The advantages of this solution include structural symmetry, balanced distribution of the machine's mass, no manual intervention required by the operator when changing direction, and the use of water as the fluid, which avoids environmental pollution. The disadvantages include electrical complexity, energy consumption, and permanent added mass.

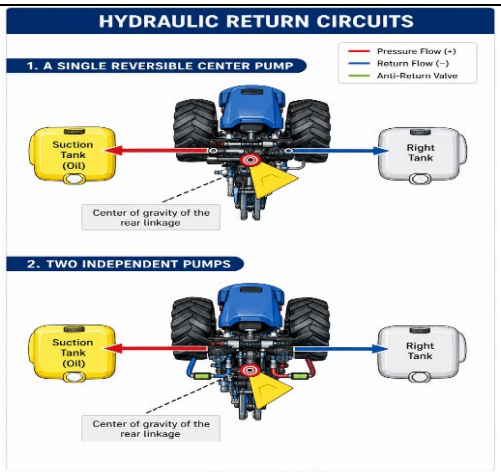



**Fig. 5 - Presentation of the position of the center of gravity of the motor cultivator depending on the location of the tanks**

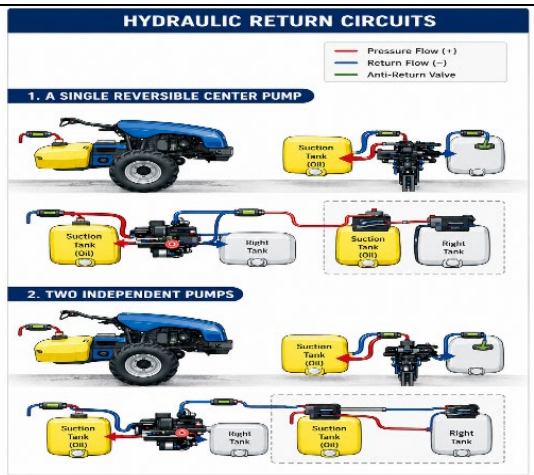



**Fig. 6 - Presentation of the technical solution with 2 tanks**

b) *Technical solution for balancing the walk-behind tractor using a single tank mounted on a movable arm*

The principle of the solution involves a single 15–20 liter tank mounted on a central articulated arm. This central arm allows for continuous lateral adjustment as well as progressive height adjustment of the

counterweight, depending on the slope. In this case, the stabilization equation for the agricultural walk-behind tractor regarding angle α is:

$$d_r = \frac{mh\ tag\ \alpha}{m_a} \quad (2.12)$$

Where:

$d_r$ – distance from the water tank to the walk-behind tractor's axis of symmetry [m]

m – mass of the walk-behind tractor [kg]

h – height of the counterweight above the ground [m]

$m_a$– additional mass (i.e., the water tank) [kg]

Advantages of the single-tank solution: continuous control of the tank's position relative to the walk-behind tractor's axis of symmetry; low total mass due to the use of water as the balancing fluid; high adaptability to terrain slope angles; no complex tools required for adjustments. Disadvantages of the single-tank solution: requires a rigid linkage; imposes additional structural loads on the walk-behind tractor.

c) *Technical solution using quick-mount counterweights attached to the walk-behind tractor's wheels*

The principle involves mounting a steel or cast-iron counterweight (with a fixed mass of 8–15 kg) onto the walk-behind tractor's wheels.

This counterweight is mounted only on the uphill wheel using a mechanical quick-attachment system. Advantages of the counterweight solution: simplicity (uses a single component), no electrical power required, and a robust system design. Disadvantages of the solution: lack of fine adjustment capability based on the terrain slope angle; requires operator intervention at the end of the row to remove the weight from the uphill wheel and mount it on the downhill wheel.

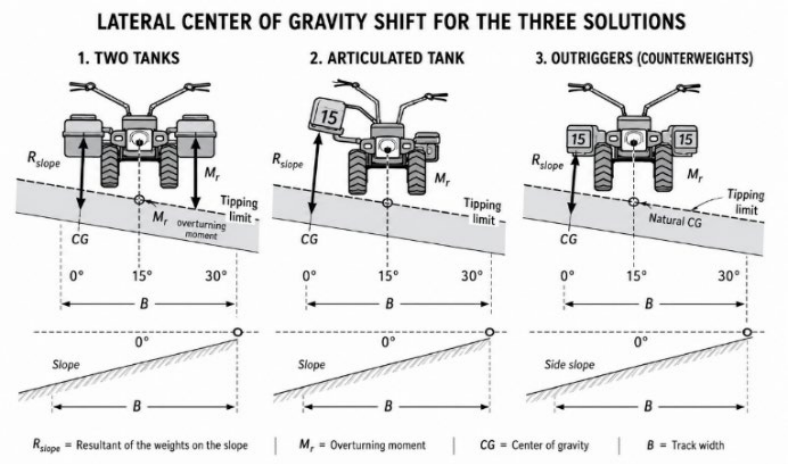



**Fig. 7 - Presentation of the 3 technical solutions for balancing the walk-behind tractor**

The three technical solutions presented for balancing the walk-behind tractor were analyzed based on a set of criteria to determine the optimal solution. The optimal solution—specifically, a single tank articulated on a movable arm—is the one that meets the majority of the selection criteria.

**Table 1**

**Analysis of technical solutions based on a series of criteria**

| Criterion | 2 Tanks | Articulated tank | Counterweights |
|---|---|---|---|
| Continuous adjustment | No | Yes | No |
| Energy consumption | Yes | No | No |
| Mass | Medium | Low | Low |
| Complexity | High | Medium | Low |
| Adaptation to variable angle | Good | Very good | Medium |

Furthermore, considering the three proposed technical solutions, we analyzed the variation of the stability coefficient in relation to these solutions; this is illustrated in Fig. 8, where the stability coefficient depends on the ground slope angle.

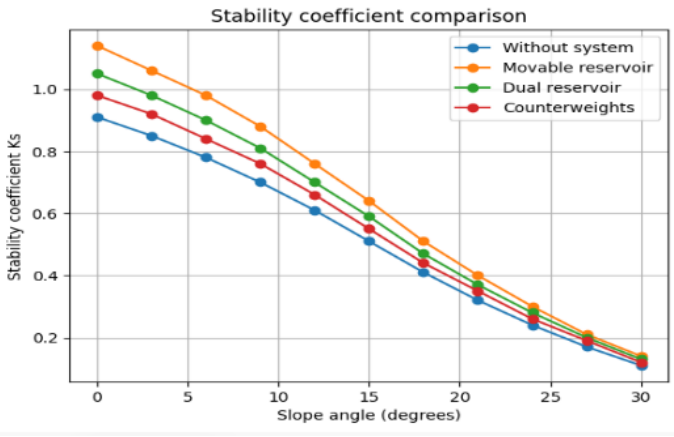



**Fig. 8 - Evolution of the stability coefficient depending on the proposed technical solution**

An analysis of the graph in Fig. 8 reveals that the technical solution involving the use of a movable reservoir ensures an adequate stability coefficient (Ks) value, thereby demonstrating the superiority of the articulated-arm solution featuring a single reservoir.

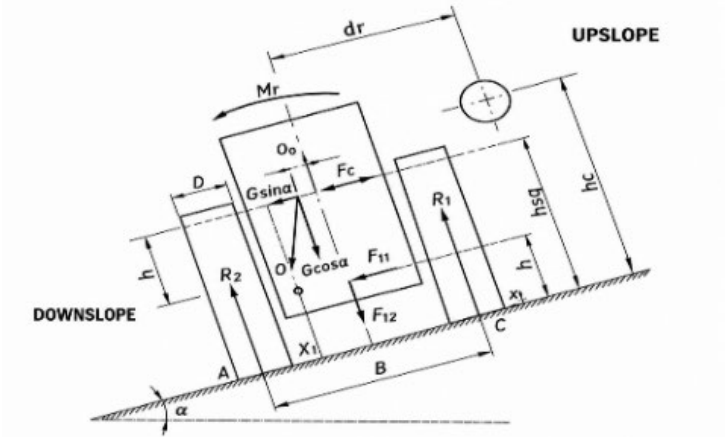



**Fig. 9 - The main forces and moments acting on the tiller when equipped with an upstream counterweight for balancing working on an inclined slope $\alpha$** *(Nițescu, 1973)*

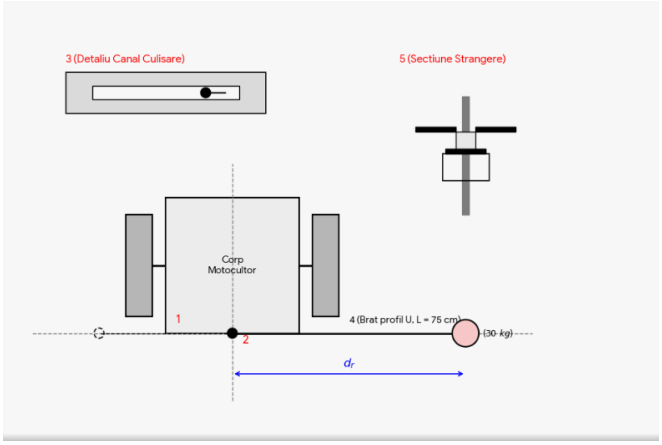



**Fig. 10 - Detailed presentation of the technical solution with articulated tank**

Detailed presentation of the technical solution featuring an articulated counterweight (Fig. 10)

On a side slope, the projection of the walk-behind tractor's center of gravity tends to shift outside the supporting base (the downslope wheel). Consequently, a counterweight $m_a$ (pos. 4, Fig. 10) is positioned on a bar at a distance $d_r$ (pos. 3, Fig. 10) on the upslope side; this effectively shifts the tractor's center of gravity back between the wheels, preventing a rollover. This load distribution reduces pressure on the bearings and half-shaft of the downslope wheel. The solution ensures maneuverability at the end of the row; when the tractor (pos. 1, Fig. 10) turns around to reverse direction, the "upslope" side becomes the

"downslope" side. If the weight were fixed, it would accelerate a rollover rather than prevent it. Therefore, a pivoting (pos. 2, Fig. 10) or sliding system is required to allow the weight to be shifted to the opposite side of the tractor. This addresses the issue where the downslope wheel—which already bears the majority of the load—might "dig" into the soil, while the upslope wheel could lift off, resulting in a loss of traction. By positioning the counterweight on the upslope side, the load on the downslope wheel is theoretically reduced, while the load on the upslope wheel is increased.

Practical Implementation (Tilting System)

For the system to operate efficiently at the end of a row, a central pivot is required, onto which an inverted U-shaped arm is mounted (Item 3, Fig. 10). When the walk-behind tractor reaches the end of the row and needs to turn, the system enables the weight to be unlocked, tilted, and re-locked within a maximum of 5–10 seconds. Additionally, the system limits swaying so the weight does not move freely; sudden swaying on a 25° slope could cause the machine to tip over due to inertia, which is why the counterweight is secured via a threaded rod (Item 5, Fig. 10).

Based on the mathematical model, calculations were performed to determine both the mass of the counterweight and its required coordinates relative to the terrain's inclination angle. However, these results must be verified through experimentation. The following section outlines the methodology and the test rig used to validate these calculations.

### 2.4 Experimental procedure

The experimental determination of the mass required for the front-mounted water tank (to balance the walk-behind tractor and prevent tipping) can be carried out using simple yet rigorously controlled practical methods. The aim is to verify whether the theoretically calculated value (derived from the mathematical model) is sufficient, too low, or too high under actual field conditions. The experiment to determine the optimal tank mass is conducted in two stages, as follows:

The first stage involves determining the contact patch areas between the walk-behind tractor's tires and a flat surface at various tire pressures and slope angles.

The second stage involves experimentally determining the required tank mass to ensure the walk-behind tractor remains stable without tipping over sideways.

#### *2.4.1 Laboratory test using a tilting platform to determine contact patch areas*

Required equipment: BCS 740 walk-behind tractor equipped with a mower attachment; a controlled slope (terrain or artificial ramp); an inclinometer (or digital angle gauge); a tape measure; and a bubble level.

Experimental steps for the first stage:

The BCS 740 walk-behind tractor, equipped with the mower, is placed on a test stand specifically constructed for the experiment. This stand allows for measurements to be taken at inclination angles ranging from 0 to 30 degrees.

Test Stand Description

Fig. 11a shows the test stand used to conduct the measurements. The stand consists of a metal structure made of welded profiles. Three hinge-type joints are welded to this structure, enabling the tilting of the experimental platform—which measures 1.5 x 0.8 m and is 15 mm thick, providing the rigidity needed to prevent deformation under the weight of the walk-behind tractor. Pressure-sensing plates are positioned on the upper surface to measure the contact area and contact load between the BCS 740 tractor's tires and the stand's flat surface. The stand allows the tractor to be secured to the platform; to tilt the platform to the desired angle, the stand is equipped with a manually operated M14 screw-and-nut mechanism (2 mm pitch). The stand enables the tilting of the support platform, allowing for an analysis of the difference in contact surface area between the downslope and upslope wheels of the tractor.




a)




b)

**Fig. 11 - a) Overview of the test stand; 1 metal frame, 2 experimental plate, 3 angle-measuring protractor, 4 level for checking stand flatness; b) 1 Tekscan pressure-sensing mat; 2 BCS 740 walk-behind tractor tire**

The contact patch areas for the two-wheel tractor's tires were determined at inflation pressures of 0.8, 1.0, 1.2, 1.5, 2.0, and 2.5 bar, across an angular range of 0° to 30° in 3° increments.

The Tekscan I-Scan system (running software v7.60) was used to determine the contact patch areas; this system comprises three components:

1. Sensors (Matrix Thin-Film): Ultra-thin sensor sheets (~0.1 mm) featuring thousands of pressure-sensitive cells (sensels). Tekscan offers over 200 shapes and sizes capable of measuring pressures ranging from very low (4 psi) to extremely high industrial levels (30,000 psi / 2,000 bar).
2. Data acquisition hardware (Evolution or VersaTek): The handle unit into which the sensor is inserted; it electronically scans all cells at extremely high speeds.
3. I-Scan software (v7.60): The system's "brain," running on a PC. It converts the sensors' electrical resistance into 2D and 3D color images, providing precise, real-time data on force, pressure, and location.

### *2.4.2 Laboratory tilt-platform test to determine the balancing system's arm length and the required counterweight mass.*

The same test rig and BCS 740 walk-behind tractor will be used. The experiment involves mounting a water tank—acting as a counterweight—on the upslope side of the tractor at the lateral distance $d_r$ used in the calculations. The tank is filled gradually (in increments of 5, 10, 15, and 20 liters), and the platform is tilted progressively to observe the maximum angle at which the tractor remains stable without tipping over sideways. The critical mass is confirmed if the tractor remains stable up to the reference slope angle (e.g., 25°–30°). Experimental confirmation is achieved through static testing under controlled slope conditions using incremental weights. The objective is to verify the calculated water mass threshold for: preventing rollover, balancing traction, and adapting to real-world ground conditions.

#### 2.4.2.1 Experimental steps:

Place the pressure sensor (load cell) on the device platform, then position the tractor on the platform so that its tires rest on the sensor.

Take initial measurements with the slope at 0°.

Gradually increase the transverse slope angle (in 3° increments up to 30°).

Record the angle at which the contact area of the upslope tire decreases (measurements indicate this begins at slope angles exceeding 12°) or when the upslope wheel loses contact with the platform. Begin loading the balancing device's arm—folded into the upstream position—with weights until the contact areas of the two walk-behind tractor tires are similar in size.

This allows for the verification of whether the actual weights closely match the calculated values, as well as the correct placement distance of the weights relative to the walk-behind tractor's axis of symmetry.

Using strain gauges is an excellent experimental method to validate: the calculated mass of the water tank, the pressure distribution between the wheels, and the tractor's balance on slopes. It allows for the precise determination of the slope angle at which the uphill wheel loses contact or begins to slip due to insufficient loading.

The contact area indicated by the strain gauge strip at a zero-degree slope angle serves as the reference baseline; as the slope angle is increased—say, to 30°—the contact area changes. A counterweight is then applied on the uphill side to restore the contact area as close as possible to the zero-degree baseline or to equalize the contact areas of the tractor's two wheels. By gradually adding weight on the uphill side until the contact area closely matches the initial one, the required weight can be determined experimentally and compared with the calculated value.

This is a practical calibration method for: determining the required weight of the uphill-mounted water tank, validating the mathematical model, and comparing theory with reality.

An experimental compensation principle is applied:

- Reference: the contact area $A_0$ is measured at a 0° slope (without counterweight).
- The reduction in contact area A is measured at a slope α (e.g., 30°), without water.
- Water/weight is gradually added upstream → the point is observed where:
- A_compensated ≈ $A_0$ ⇒ the upstream wheel is reloaded to the initial level
- The weight added at that point is the experimentally determined mass m_water.
- Relationship with the mathematical model

Theoretically, the water weight calculated mathematically is:

$$m_{theoretically\ water} = \frac{h_{cg}\, m \tan\alpha - \frac{B}{2} m}{d_r} \tag{2.13}$$

Using this method, one can obtain:

$$m_{experimental\ water} \rightarrow When\ A_{0\ compensate} \approx A_0$$

If the values are close, the mathematical model is valid, and the adopted technical solution satisfies the equilibrium condition for the walk-behind tractor on slopes with an inclination greater than 20°.

## RESULTS

The measurements yielded a series of contact patch areas for the walk-behind tractor's wheels at various tire pressures—specifically 0.8, 1.0, 1.2, 1.5, 2.0, and 2.5 bar—and at different platform tilt angles ranging from 0° to 30°. The minimum pressure of 0.8 bar and the maximum of 2.5 bar were used because these are the pressures specified by the tire manufacturer.

From the complete set of contact patch data, we selected the area values corresponding to a pressure of 1.2 bar, as this is the recommended tire pressure for mowing operations. These areas are presented in Table 2.

**Table 2**

**The correlation between tire pressure, terrain slope angle, and the contact patch.**

| Slope (Grade) | Upstream Pressure (bar) | Downstream Pressure (bar) | Upstream Patch (cm²) | Downstream Patch (cm²) |
|---|---|---|---|---|
| $0^0$ | 1.2 | 1.2 | 23,54 | 23,54 |
| 3° | 1.2 | 1.2 | 21.85 | 25.24 |
| 6° | 1.2 | 1.2 | 23.32 | 26.94 |
| 9° | 1.2 | 1.2 | 24.77 | 28.62 |
| 12° | 1.2 | 1.2 | 16.79 | 30.29 |
| 15° | 1.2 | 1.2 | 15.13 | 31.94 |
| 18° | 1.2 | 1.2 | 13.51 | 33.58 |
| 21° | 1.2 | 1.2 | 11.90 | 35.18 |
| 24° | 1.2 | 1.2 | 10.33 | 36.75 |
| 27° | 1.2 | 1.2 | 8.80 | 36.28 |
| 30° | 1.2 | 1.2 | 7.30 | 39.78 |

When mowing with the walk-behind tractor, the standard tire pressure (for 5.00-10 tires) should be lower than that used for transport or plowing. The ideal range is 1.0 to 1.2 bar (with a maximum of 1.4 bar if the ground is completely dry and smooth).

A pressure of 1.2 bar offers several advantages:

- vibration damping: The mowing attachment generates high-frequency vibrations. Lower pressure (1.0–1.2 bar) turns the tire into a natural shock absorber, protecting the tractor's transmission.
- traction and lateral stability: At 1.1 bar, the tire conforms better to ground irregularities, naturally increasing the contact patch (which you measured using Iscan). This prevents the tractor from sliding sideways (downhill) while mowing.
- terrain contouring: An over-inflated tire (above 1.6–2.0 bar) causes the machine to bounce over every mound or stone, disrupting the mowing blade's cutting height.

Analysis of the experimental data shows that on slopes exceeding 12°, the walk-behind tractor begins to exhibit a tendency to slide and roll over. Consequently, the experiments confirm that on slopes with an inclination of 15° or greater, the tractor encounters operational issues—specifically sliding and rolling. Based on the experimental data in Table No.2 We conducted an analysis to determine the mass of the counterweight and its placement relative to the walk-behind tractor's axis of symmetry.

The center of gravity of the walk-behind tractor shifts by a distance of Δx when on a slope.

$$\Delta_x = h_G \sin\alpha \quad [\text{m}] \tag{2.14}$$

Where $h_G$ is the height of the walk-behind tractor's center of gravity [m]

α is the ground inclination angle [degrees]

The height of the center of gravity can be approximated as equal to the wheel radius; therefore, the displacement of the center of gravity is expressed as follows:

$$\Delta_x = r\ tg\alpha \quad [\text{cm}] \tag{2.15}$$

The lever length required to restore the contact patch ratio to the ideal value involves calculating the exact distance (in meters) from the machine's axis of symmetry to the center of gravity on the U-profile, in order to achieve a perfect mass distribution (50%–50%) on the ground.

$$d_r = \frac{M\Delta_x}{m_b} \quad [\text{cm}] \tag{2.16}$$

Where M = mass of the walk-behind tractor [kg]

$m_b$ = = mass of the arm [kg]

Position of the U-profile outside the upstream wheel

$$L_{ext} = d_r - \frac{B}{2} \quad [\text{cm}] \tag{2.17}$$

The calculation results are presented in Table 3.

**Table 3**

**Analysis of the mobile tank solution for various terrain slope angles and tire pressures.**

| Slope (Grade) | Upstream Pressure (bar) | Downstream Pressure (bar) | Upstream Contact Patch (cm²) | Downstream Contact Patch (cm²) | Balancing Mass (kg) | Distance from Symmetry Axis $d_r$ (cm) | Position on U-profile - L_ext (Outside the wheel) | Technical notes and recommendations |
|---|---|---|---|---|---|---|---|---|
| 1 | 2 | 3 | 4 | 5 | 6 | 7 | 8 | 9 |
| 0° | 1.2 | 1.2 | 23.54 | 23.54 | 0 kg | Useless | Inside | The unit is inherently stable. No counterweight is installed. |
| 3° | 1.2 | 1.2 | 21.85 | 25.24 | 0 kg | Useless | Inside | The unit is inherently stable. No |

| | | | | | | | | |
|---|---|---|---|---|---|---|---|---|
| | | | | | | | | counterweight is installed. |
| 6° | 1.2 | 1.2 | 23.32 | 26.94 | 0 kg | Useless | Inside | Linear tire behavior. No arm required. |
| 9° | 1.2 | 1.2 | 24.77 | 28.62 | 0 kg | Useless | Inside | Upper limit of inherent stability at 1.2 bar. |
| 12° | 1.2 | 1.2 | 16.79 | 30.29 | 20 kg | 42.1 cm | 20.3 cm | First outward extension. The rod slides to the 42 cm mark. |
| 15° | 1.2 | 1.2 | 15.13 | 31.94 | 20 kg | 52.4 cm | 30.6 cm | Optimal balance. Compact and highly secure lever mechanism. |
| 18° | 1.2 | 1.2 | 13.51 | 33.58 | 20 kg | 62.6 cm | 40.8 cm | Design slope. Rod length reaches 62.6 cm. |
| 21° | 1.2 | 1.2 | 11.90 | 35.18 | 20 kg | 72.6 cm | 50.8 cm | Moderate dynamic load. Requires a rigid flat bar. |
| 24° | 1.2 | 1.2 | 10.33 | 36.75 | 20 kg | 82.4 cm | 60.6 cm | Maximum limit for a single arm and a weight of 20 kg. |
| 27° | 1.2 | 1.2 | 8.80 | 36.28 | 25 kg | 71.6 cm | 49.8 cm | Increased mass. For safety, 5 kg is added to the M14 rod. |
| 30° | 1.2 | 1.2 | 7.30 | 39.78 | 35 kg | 57.8 cm | 36.0 cm | Heavy-duty configuration for constant pressure (35 kg per rod) |

Thus, the data in Table No 3 indicate that at a slope of 12°, measures must be taken to reduce the risk of the walk-behind tractor sliding or rolling over. Table No 3 also highlights the position of the counterweight relative to the tractor's axis of symmetry. Based on the experimental data in Table 3, we determined the possible tire pressure combinations to optimize the counterweight's position, ensuring the entire assembly—tractor and counterweight—remains as compact as possible. When tire pressures differ, the wheels exhibit varying elastic stiffnesses: the downslope tire (at 1,5 bar) becomes stiffer and resists deformation, whereas the upslope tire (at 1,2 bar) is softer. This pressure differential creates a natural pneumatic correction that assists the mechanical arm by effectively shortening its lever arm.

To equalize the contact patches in this scenario, the distance $d_r$ from the tractor's axis of symmetry to the weight on the U-profile is calculated using the following formula:

$$d_r = \frac{(M\, r\, tg\alpha) - [W_{total}\ cos\alpha \left(\frac{K_{12}-K_{15}}{K_{12}+K_{15}}\right)\frac{B}{2}]}{m} \text{ [cm]} \quad (2.18)$$

Where $k_{12}$ is the tire stiffness at a pressure of 1,2 bar

$k_{1.5}$ is the tire stiffness at a pressure of 1.5 bar

$$\frac{K_{12}-K_{15}}{K_{12}+K_{15}} = -0{,}0828$$

**Table 4**

**Possible combinations and their effect on the position of the counterweight.**

| Slope (Grade) | Upstream / Downstream Pressure | Weight per arm | Distance from the axis of symmetry (cm) | Physical position on the U-profile | Machine behavior |
|---|---|---|---|---|---|
| 12° | 1.0 / 1.5 bar | 20 kg | 38,5 cm | ~16 cm outside the wheel | Much more stable; the machine no longer tends to require handlebar effort. |

| Slope (Grade) | Upstream / Downstream Pressure | Weight per arm | Distance from the axis of symmetry (cm) | Physical position on the U-profile | Machine behavior |
|---|---|---|---|---|---|
| 15° | 1.0 / 1.5 bar | 20 kg | 47,2 cm | ~25 cm outside the wheel | Safe zone. The arm is 5 cm shorter compared to the setup with equal pressures. |
| 18° | 1.0 / 1.5 bar | 20 kg | 56,8 cm | ~35 cm outside the wheel | Compact and rigid. Reduced risk of snagging obstacles upstream. |
| 21° | 1.0 / 1.5 bar | 20 kg | 66,2 cm | ~44 cm outside the wheel | Excellent steering control; the upper wheel no longer wanders. |
| 24° | 1.0 / 1.5 bar | 20 kg | 75,9 cm | ~54 cm outside the wheel | Ideal upper limit for the standard 20 kg weight. |
| 27° | 1.0 / 1.5 bar | 25 kg (recommended) | 69,1 cm | ~47 cm outside the wheel | The addition of 5 kg keeps the arm short and protects the U-profile. |
| 30° | 1.0 / 1.5 bar | 30 kg (recommended) | 65,5 cm | ~43 cm outside the wheel | The ultimate solution. An extremely compact and safe machine for extreme angles. |

Table No 4 shows that the chosen combination (1,0 bar upstream and 1.5 bar downstream) effectively resolves the issue requiring "heightened caution." Applying this asymmetric pressure (1,0 and 1,5 bar) as a general rule when entering steep areas radically improves the walk-behind tractor's behavior for two physical reasons:

1. The downstream tire (1,5 bar) becomes more rigid. It no longer "squashes" as much under the machine's 135 kg weight, preventing the unit from leaning further downslope.
2. The upstream tire (1,0 bar) remains flexible enough to "mold to the terrain," maintaining crucial traction to prevent the upstream wheel from slipping.

Building on this data, we took the concept a step further by adding a counterweight to the upstream tire. From an engineering perspective, this improves the operating method because the tire and counterweight work in tandem:

- Since the tires compensate for some of the imbalance through asymmetric pressure, the metal extension arm can be 5 to 7 centimeters shorter for each angle setting.
- A shorter arm results in a more compact footprint in the field (avoiding snagging on trees or mounds) and significantly reduces stress on the welds and the U55/U60 profile caused by vibrations.

This strategy transforms the walk-behind tractor into a vehicle with a simulated adaptive track width, making it perfect for safe mowing. With this data established, the next step is to conduct tests to verify the values derived from the calculations and analysis.

## CONCLUSIONS

1. Implementing a mobile tank articulated on the walk-behind tractor allows the center of gravity to be maintained close to the machine's longitudinal axis and significantly increases lateral stability on slopes of up to 30°.
2. Alternative solutions—such as dual tanks or quick-attach counterweights—offer fewer advantages and entail additional technical complexity, which may limit their applicability.
3. The mathematical model and quantitative analysis, correlated with graphs of moments and the stability coefficient, enable predictive estimation of the rollover risk and provide a guide for tank positioning based on the slope angle.
4. Increased lateral stability allows for the expansion of the area that can be mechanized, contributing to greater efficiency and safety in agricultural operations, particularly on steep terrain.

In conclusion, the articulated mobile tank solution represents the optimal choice regarding stability and adaptability, being directly applicable to the mechanization of previously inaccessible land.

**REFERENCES**

[1] Dumitru Tomescu, Gr. Raileanu, I.Vlădășel (1985) “"Tractor Maintenance and Repair – Manual for Agro-Industrial High Schools," Ceres Publishing House, Bucharest
[2] Gheorghe Nițescu (1973) “Tractor Mechanics” – Tehnică Publishing House, Bucharest
[3] Mocanu V (1997) Doctoral thesis “"Dynamic and energy optimization of units consisting of single-axle tractors and agricultural harvesting and transport machinery" – Brașov
[4] V. Mocanu, N. Dragomir, V. A. Blaj, T. A. Ene, Monica Alexandrina Tod (2012) The scientific paper “"Romania's Grasslands – Resources, Strategies for Improvement and Utilization" – Grassland Research and Development Institute, Brașov (part of the National Research and Development Institute for Soil Science, Agrochemistry and Environmental Protection – ICPA Bucharest)
[5] Marcela Dragoș, Neculai Dragomir, Marinel Horablaga, Dorin Rechițean (2018) The scientific paper Production dimension and potential of permanent grasslands of romania in relation to animals growth, "Ion Ionescu de la Brad" University of Life Sciences Iași
[6] Sorin-Stefan Biris, Iulian Drenea (2025) The scientific paper "Analysis of technical solutions for increasing the working capacity of motor mowers on sloping terrain" – OPROTEH 2025 Conference
[7] Sorin-Stefan Biris, Iulian DRENEA (2025) The scientific paper „ "Innovative solution for stabilizing a walk-behind tractor on sloping terrain using a water-tank counterweight" – conference 18th Symposium
[8] Durability and Reliability of Mechanical Systems SYMECH 2025
[9] *** site ro.wikipedia.org
[10] *** site https://iuls.ro/universitate/despre-universitate/
[11] *** site pajisti-grassland.ro

# EXPERIMENTAL EVALUATION OF A SMALL-SCALE ELECTRIC COMPOSTER UNDER DIFFERENT OPERATING CONDITIONS

/

# *EVALUAREA EXPERIMENTALĂ A UNUI COMPOSTOR ELECTRIC DE MICI DIMENSIUNI ÎN DIFERITE CONDIȚII DE FUNCȚIONARE*

**Elena-Melania CISMARU*[1)], Gigel PARASCHIV[1)], Gabriel-Alexandru CONSTANTIN[1)], Mirela-Nicoleta DINCĂ[1)], Elena-Mădălina ȘTEFAN[1)], Alina-Daiana IONESCU[1)], Nicolae-Valentin VLĂDUȚ[2)], Ana-Maria TĂBĂRAȘU[2)]**

[1)] National University of Science and Technology POLITEHNICA Bucharest - Faculty of Biotechnical Systems Engineering, Bucharest / Romania;

[2)] National Institute of Research - Development for Machines and Installations Designed for Agriculture and Food Industry - INMA Bucharest / Romania

**Tel: 0730 221 773; *E-mail: elena.cismaru@upb.ro*

***Keywords:*** *electric composter, vegetable waste, feeding regimes, operating conditions, temperature evolution, moisture content, composting performance*

## ABSTRACT

*The management of vegetable waste using small-scale electric composting systems represents an alternative for decentralized biodegradable waste treatment. This study aimed to evaluate the operational performance of a small-scale electric composter under different feeding regimes, focusing on temperature evolution, moisture conditions, material transformation, and mechanical operation. Experimental investigations were conducted using an Oklin GG-02 electric composter without the microbial starter recommended by the manufacturer. Three experimental conditions were investigated: batch feeding, progressive feeding (fed-batch), and the use of partially composted material from another composter of the same model as a biological inoculum. Material and ambient temperatures, moisture conditions, changes in material structure and volume, and mixing system operation were monitored. Under batch feeding, the material temperature reached 57°C after 24 hours, with a final mass reduction of 71.03%. The maximum temperature recorded under progressive feeding was 40°C, while the experiment using partially composted material reached 55°C after 24 hours. Progressive drying was observed under all experimental conditions, requiring moisture adjustments during extended operation. The mixing system operated without significant mechanical blockages, contributing to material fragmentation and homogenization. The findings highlight the importance of feeding strategy and moisture management in optimizing small-scale electric composter operation.*

## REZUMAT

*Gestionarea deșeurilor vegetale prin utilizarea sistemelor electrice de compostare de mici dimensiuni reprezintă o alternativă pentru tratarea descentralizată a biodeșeurilor. Prezenta cercetare a avut ca obiectiv evaluarea performanței operaționale a unui compostor electric în diferite regimuri de alimentare, cu accent pe evoluția temperaturii, umiditate, transformările materialului și funcționarea sistemului mecanic. Cercetările experimentale au fost realizate utilizând compostorul electric Oklin GG-02, fără adăugarea starterului microbiologic recomandat de producător. Au fost analizate trei variante experimentale: alimentarea în șarjă unică (batch), alimentarea progresivă (fed-batch) și utilizarea unui material parțial compostat, provenit dintr-un alt compostor de același model, ca inocul biologic. Au fost monitorizate temperatura materialului și a mediului ambiant, umiditatea, modificările structurii și volumului materialului, precum și funcționarea sistemului de amestecare. În regimul batch, temperatura materialului a atins 57°C după 24 de ore, înregistrându-se o reducere finală a masei de 71,03%. În regimul fed-batch, temperatura maximă a fost de 40°C, iar în varianta cu material parțial compostat s-au atins 55°C după 24 de ore. Uscarea progresivă a materialului a necesitat corectarea umidității. Sistemul de amestecare a funcționat fără blocaje semnificative, contribuind la fragmentarea și omogenizarea materialului. Rezultatele evidențiază importanța strategiei de alimentare și a gestionării umidității pentru optimizarea funcționării compostorului.*

## INTRODUCTION

The increasing generation of food and vegetable waste represents a significant challenge for sustainable waste management and resource recovery. According to the United Nations Environment Programme *(UNEP, 2024)*, approximately 1.05 billion tonnes of food waste were generated worldwide in 2022, with households accounting for 60% of the total amount. In the European Union, approximately 58.2 million tonnes of food waste were generated in 2023, highlighting the need for effective solutions for the management of biodegradable materials *(Eurostat, 2025)*. Composting represents an alternative for the biological treatment of organic waste, allowing the recovery of organic matter and its potential reuse in agricultural applications.

In recent years, increasing attention has been directed towards decentralized composting systems designed to process biodegradable waste close to its source of generation. Small-scale electric composters represent a technological solution for the treatment of organic waste in households, commercial facilities, and other locations generating relatively small quantities of biodegradable materials. These systems combine mechanical mixing, heating, and ventilation to facilitate material transformation under controlled operating conditions. However, their performance depends on the characteristics of the processed materials and the operating conditions of the equipment *(Jain et al., 2025; DeFelice and Stack Whitney, 2024)*.

Temperature, moisture content, aeration, and substrate composition are important parameters influencing the composting process. Temperature and moisture conditions are closely related to microbial activity *(Liang et al., 2003)*, while the aeration system contributes to oxygen supply, heat transfer, and water evaporation. Previous studies have demonstrated that airflow management can influence temperature evolution and moisture loss during small-scale composting *(Lai et al., 2024)*. Furthermore, the proportion of fresh vegetable waste and dry bulking materials affects the physical characteristics of the mixture, including its structure and porosity *(Guidoni et al., 2018)*. The feeding strategy represents another important operational parameter in composting systems. Batch operation involves introducing the entire quantity of material at the beginning of the process, whereas fed-batch operation consists of successive additions of fresh biodegradable material. Previous investigations have shown that feeding rate and substrate characteristics influence temperature evolution, moisture conditions, and the performance of fed-batch composting reactors *(Jolanun et al., 2005; Wang et al., 2017)*. In addition, the use of previously composted material as a starting substrate has been investigated as a strategy for influencing process development and maintaining favourable conditions for biological activity *(Sundberg and Jönsson, 2005; Yang and Zhang, 2022)*.

Although previous studies have investigated compost quality and the influence of individual process parameters, the operational behaviour of small-scale electric composters under different feeding conditions requires further experimental investigation. In particular, the interaction between feeding strategy, material moisture, temperature evolution, and mechanical mixing is relevant for evaluating equipment performance and identifying potential improvements in operating conditions. Independent evaluations of electric composting machines have also highlighted the need to distinguish waste mass reduction from the production of mature compost *(DeFelice and Stack Whitney, 2024; Azis et al., 2023; Schroeder et al., 2020)*.

Therefore, the present study aimed to evaluate the operational performance of an Oklin GG-02 small-scale electric composter under three experimental conditions: batch feeding, progressive feeding (fed-batch), and the use of partially composted material obtained from another composter of the same model as a biological inoculum. The experiments were conducted without the addition of the commercial microbial starter recommended by the manufacturer. Material and ambient temperatures, moisture conditions, changes in material structure and volume, and the operation of the mechanical mixing system were monitored to investigate the behaviour of the equipment under different operating conditions.

## MATERIALS AND METHODS

The experimental investigations were conducted using an Oklin GG-02 small-scale electric composter, manufactured by Oklin International Ltd. and designed for the decentralized processing of biodegradable organic waste. According to the manufacturer's specifications, the equipment has a processing capacity of 4-5.5 kg/day, overall dimensions of approximately 400×400×790 mm, and a maximum electrical power consumption of 240 W.

The composter comprises a stainless-steel processing chamber equipped with an electric heating system, a ventilation system, and a mechanical mixing mechanism consisting of a horizontal shaft fitted with rotating paddles. The mixing mechanism promotes the fragmentation and homogenization of the processed

material, while the heating and ventilation systems provide heat and facilitate moisture removal. The equipment also includes a deodorizing unit designed to reduce odours during operation.

The processing chamber is accessed through a top-mounted lid, which allows organic material to be introduced. A maximum filling level is marked inside the chamber, and a control unit manages the operation of the integrated systems. The general configuration and main structural components of the composter are presented in Fig. 1.

According to the technical documentation, the mixing mechanism is driven by a geared electric motor connected to the horizontal agitator shaft through a chain drive. The operating sequence described in the service documentation involves alternating clockwise and counterclockwise rotation, with short pauses between successive rotations. The ventilation system operates throughout the processing cycle, while the electric heating system is automatically controlled according to the equipment's temperature-control settings.

These systems operate together to provide mechanical agitation, air circulation, and heat input during material processing. All three experimental variants were conducted without the addition of Acidulo™, the commercial microbial starter recommended by the manufacturer, to evaluate the operational performance of the equipment under the investigated feeding and loading conditions.

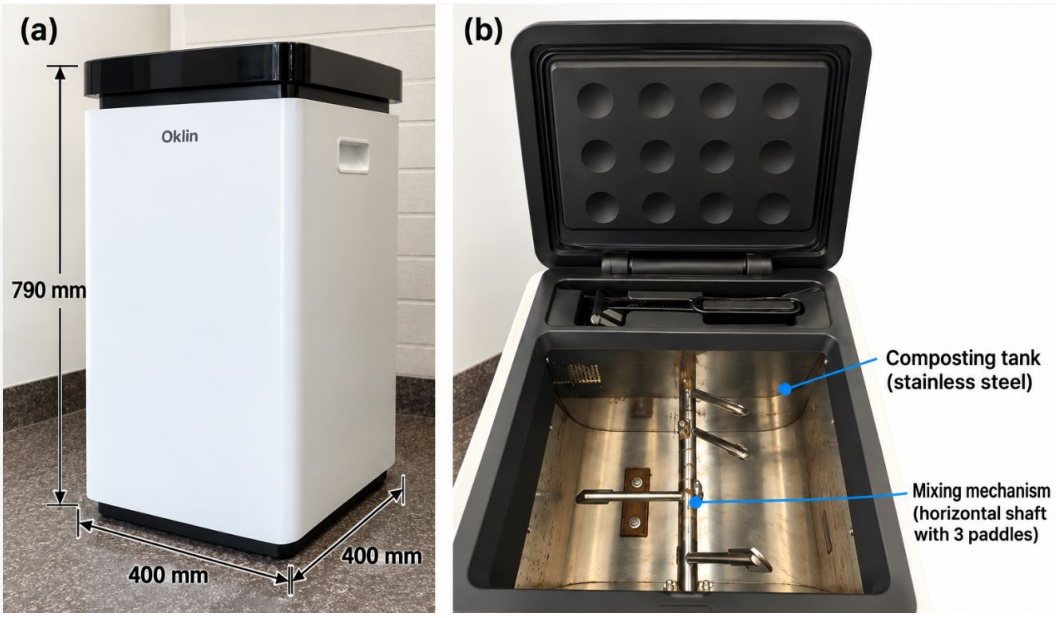



**Fig. 1 - Oklin GG-02 electric composter:**
*(a) external view and overall dimensions; (b) top view with open lid and main components*

**Raw materials and preparation**

The experimental material consisted of vegetables and vegetable residues obtained from local supermarkets, including lettuce, cabbage leaves, carrots, potatoes, cucumber peels, tomatoes and other biodegradable vegetable fractions. Fresh vegetable materials were combined with dry materials, mainly straw, hay and dried leaves, to improve the structure of the mixture and facilitate air circulation within the processing chamber.

Before loading, the vegetable materials were chopped into particles ranging approximately from 0.5 to 4.5 cm to facilitate mechanical mixing and increase the surface area available for biological degradation. The quantities of fresh and dry materials were weighed before introduction into the composter. The composition and initial loading conditions were established separately for each experimental variant.

**Experimental design**

Three experimental variants were investigated to characterize the operational behaviour of the Oklin GG-02 electric composter under different material-loading and feeding conditions: batch feeding, progressive feeding (fed-batch), and processing in the presence of partially composted material obtained from another composter of the same model.

The experimental programme was designed to examine the equipment's response to a single initial load, successive additions of fresh vegetable material, and the introduction of material that had undergone a previous processing stage. No commercial microbial starter was added in any of the experiments.

The experimental variants differed in their initial material composition, loading level, feeding schedule and monitoring duration.

Material and ambient temperatures were measured, while moisture conditions, changes in material appearance and apparent volume, and the operation of the mechanical mixing system were monitored. The results were compared descriptively to characterize the equipment under the investigated operating conditions.

The initial operating conditions of the three experimental variants are presented in Table 1.

**Table 1**

**Initial operating conditions of the experimental variants**

| Parameter | Experiment 1 (Batch) | Experiment 2 (Fed-batch) | Experiment 3 (Partially composted material) |
|---|---|---|---|
| **Fresh vegetable material (g)** | 5,999.6 | 1,000 | 500 |
| **Dry vegetable material (g)** | 212.8 | 330 | - |
| **Partially composted material (g)** | - | - | 2,180 |
| **Total initial mass (g)** | 6,212.4 | 1,330 | 2,680 |
| **Fresh-to-dry material mass ratio** | 28.2:1 | 3.03:1 | - |
| **Initial filling level** | Maximum recommended level | Approx. 25-30% | Approx. 30-35% |
| **Commercial microbial starter** | Not added | Not added | Not added |

*Note: the quantities presented in Table 1 refer exclusively to the initial loading of each experiment. Subsequent material additions are described in the corresponding experimental procedures.*

**Experimental variant 1 - Batch feeding**

The first experiment was conducted under batch feeding conditions, with the entire quantity of organic material introduced at the beginning of the process and no subsequent additions of vegetable material. The initial mixture consisted of 5,999.6 g of fresh vegetable material and 212.8 g of dry material, corresponding to a total initial mass of 6,212.4 g and a fresh-to-dry material mass ratio of 28.2:1. The processing chamber was filled up to the maximum level indicated by the manufacturer, without exceeding it.

No water or commercial microbial starter was added during the initial loading.

The equipment was operated for four days, during which material and ambient temperatures, moisture conditions, changes in material structure and apparent volume, and the operation of the mechanical mixing system were monitored. Following the measurements performed after 72 h, approximately 150 mL of water was sprayed onto the material to correct the observed drying. At the end of the experiment, the remaining material was collected and weighed to determine the reduction in mass.

**Experimental variant 2 - Progressive feeding (fed-batch)**

The second experiment was conducted under progressive feeding conditions to investigate the operational behaviour of the composter during successive additions of vegetable material.

The initial mixture consisted of 1,000 g of fresh vegetable material and 330 g of dry material, corresponding to a total initial mass of 1,330 g and a fresh-to-dry material mass ratio of 3.03:1. The initial filling level was approximately 25-30% of the useful chamber volume, leaving space for mechanical mixing and subsequent material additions.

Following the initial loading, fresh vegetable material was introduced progressively, generally in quantities of approximately 500 g per feeding. The additions were performed after the corresponding measurements, and their quantities were adjusted according to the observed condition of the processed material. Dry material was also added during certain feeding stages.

The experiment included 20 monitoring points (T1-T20). Material and ambient temperatures, moisture conditions, changes in appearance and apparent volume, and the operation of the mechanical mixing system were monitored. Water was added when excessive drying of the material was observed.

**Experimental variant 3 - Use of partially composted material as a biological inoculum**

The third experiment investigated the operational behavior of the electric composter in the presence of partially composted material obtained from another composter of the same model. This material consisted of biodegradable food waste that had undergone a previous processing stage.

The initial mixture consisted of 2,180 g of partially composted material and 500 g of fresh vegetable material, corresponding to a total initial mass of 2,680 g. The initial filling level was approximately 30-35% of the useful chamber volume. No water or commercial microbial starter was added during the initial loading.

After the first 24 h, the material and ambient temperatures were measured, and an additional quantity of fresh vegetable material and partially composted material was introduced. No further organic material was added during the subsequent monitoring stages. The experiment continued until monitoring point T8.

Material temperature, moisture conditions, changes in appearance and apparent volume, and the operation of the mechanical mixing system were monitored. Water was added when excessive drying of the processed material was observed. This variant was intended to characterize the behaviour of the equipment when the initial load included material that had already undergone a previous processing stage.

**Monitoring of operational parameters**

The operational behavior of the electric composter was evaluated by monitoring material and ambient temperatures, moisture conditions, changes in material appearance, structure and apparent volume, and the operation of the mechanical mixing, heating and ventilation systems.

Material temperature was measured periodically using a digital thermometer equipped with a temperature probe. The measurements were performed before feeding, water addition or other interventions to characterize the condition of the processed material at each monitoring point. Ambient temperature was recorded at the corresponding monitoring points.

The temperature difference between the processed material and the ambient environment was calculated using the following equation:

$$\Delta T = T_m - T_a \quad (1)$$

where:

$T_m$ is the material temperature (°C), $T_a$ is the ambient temperature (°C), and $\Delta T$ is the temperature difference (°C).

Moisture conditions were assessed qualitatively through visual inspection and tactile evaluation. Water was added when excessive drying of the material was observed, and these interventions were recorded during the experiments. No quantitative determination of material moisture content was performed. Changes in material color, texture, fragmentation and homogenization were monitored through direct observations and photographic documentation. Changes in apparent volume were assessed visually by observing the level occupied by the material in the processing chamber and comparing photographs taken at different monitoring points. The apparent volume was not measured using a standardized volumetric method.

Material odors were assessed qualitatively during the experiments. Observations concerning vapor release and condensation were also recorded. The operation of the mechanical mixing system was evaluated by observing the rotation of the horizontal shaft and mixing paddles, material homogenization and the occurrence of possible mechanical blockages. The operation of the heating and ventilation systems was assessed through direct observations of the equipment during processing.

For the batch experiment, the reduction in wet material mass was calculated using the following equation:

$$\eta_m = [(m_i - m_f)/m_i] x 100 \quad (2)$$

where:

$m_i$ is the initial mass of the material (g), $m_f$ is the final mass of the processed material (g), and $\eta_m$ is the reduction in wet material mass (%).

The recorded parameters and observations were compared descriptively to characterize the operational behaviour of the electric composter under the three investigated conditions. Because the equipment was equipped with an electric heating system, the measured material temperatures were not considered an exclusive indicator of biological activity.

## RESULTS

### Operational behaviour under batch feeding conditions

The first experimental variant was conducted under batch feeding conditions, with the processing chamber loaded up to the maximum filling level indicated by the manufacturer, without exceeding it.

After the first 24 h of operation, the material temperature reached 57°C, while the ambient temperature was 24°C, resulting in a temperature difference of 33°C. This initial stage was characterized by intensive vapour release, visible condensation and a pronounced reduction in the apparent volume of the processed material.

After 48 h, the material temperature decreased to 47°C, followed by a further reduction to 27°C after 72 h. At the final monitoring point, the material temperature reached 26°C, approaching the ambient temperature of 25°C. The evolution of material and ambient temperatures during batch operation is presented in Fig. 2.

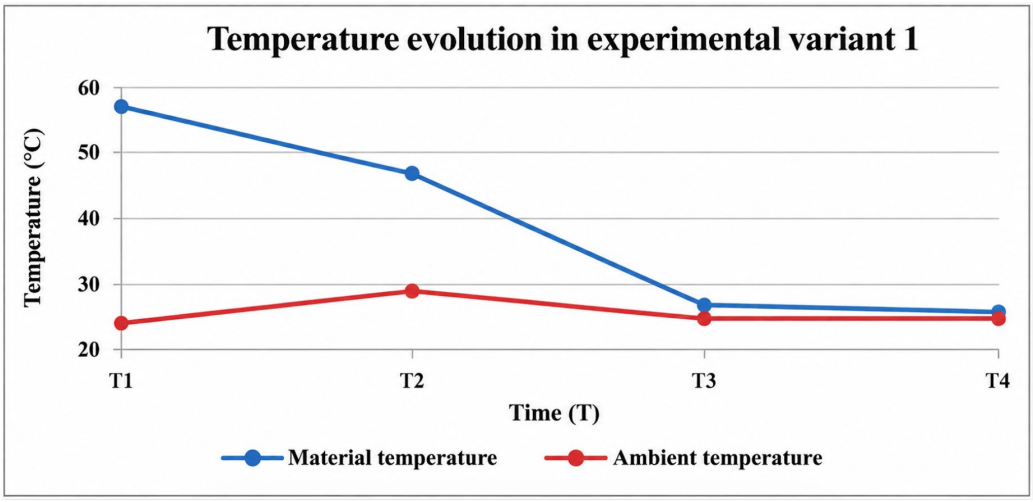



**Fig. 2 - Evolution of material and ambient temperatures during batch feeding**

The progressive decrease in temperature was accompanied by reduced vapour release and increased material dryness. After 72 hours, approximately 150 mL of water was added to correct the moisture conditions. However, the material exhibited a predominantly dry and fibrous structure at the final monitoring stage.

The initial mass of the material was 6,212.4 g, while the final mass was 1,800 g, corresponding to a mass reduction of 71,03%.

This reduction resulted from the combined effects of water evaporation, organic matter transformation, mechanical fragmentation, and possible material losses during handling. Therefore, mass reduction should not be interpreted exclusively as a measure of biological degradation.

The mechanical mixing system operated without observable blockages throughout the experiment, contributing to the fragmentation and homogenization of the processed material.

### *Operational behaviour under progressive feeding conditions*

The second experimental variant was conducted under progressive feeding conditions, with successive additions of fresh vegetable material and 20 monitoring points (T1-T20).

Material temperature fluctuated throughout the experiment. Temperatures of 37°C and 40°C were recorded at T6 and T10, respectively, with the highest recorded temperature occurring at T10. At this monitoring point, the temperature difference between the material and the ambient environment was 18°C.

At the other monitoring points between T1 and T15, material temperatures generally ranged from 27°C to 34°C. The evolution of material and ambient temperatures over the T1-T15 monitoring interval is presented in Fig. 3.

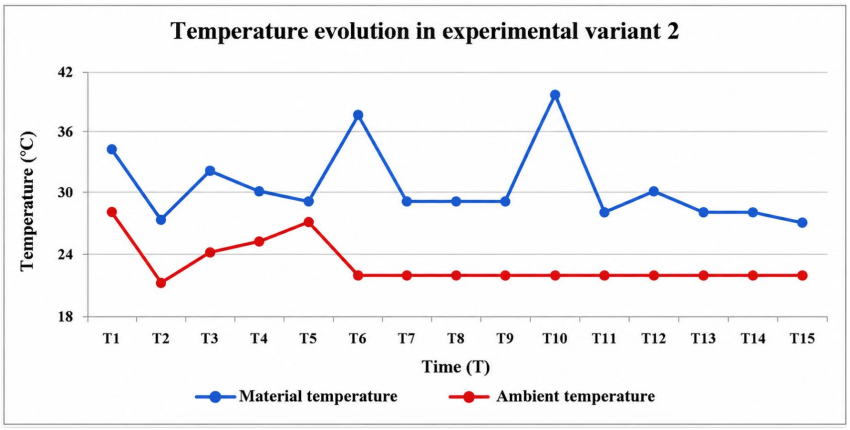



**Fig. 3 - Evolution of material and ambient temperatures during progressive feeding**

The successive addition of vegetable material allowed the operational behaviour of the composter to be observed under repeated feeding conditions. Previously introduced vegetable residues gradually became less distinguishable, while the processed material acquired a more homogeneous appearance. However, fibrous components remained visible for longer periods than the softer vegetable fractions. A recurring observation was the progressive drying of the processed material.

Despite the successive additions of fresh vegetable material, moisture corrections were required during the later monitoring stages. Following one of these interventions, the material temperature increased from 26°C at T18 to 30°C at T19. This temporal association suggests that moisture availability may have influenced the thermal behaviour of the system.

However, the observed increase cannot be attributed exclusively to water addition or biological activity, given the presence of the electric heating system and the other processes occurring within the material. Throughout the experiment, the mechanical mixing system operated without significant blockages and contributed to material fragmentation and homogenization.

***Operational behavior using partially composted material***

The third experimental variant investigated the behavior of the composter when partially composted material obtained from another composter of the same model was used as the initial substrate.

After the first 24 hours of operation, the material temperature reached 55°C, while the ambient temperature was 17°C, resulting in a temperature difference of 38°C. Following the measurements at T1, additional fresh vegetable material and partially composted material were introduced. The subsequent temperature evolution was therefore recorded after this intervention.

At the subsequent monitoring points, T2 and T3, the material temperature decreased to 22°C, approaching the ambience temperature. This decrease was accompanied by progressive material drying.

During the following stages, water was added to increase the moisture content. After these interventions, the material temperature increased progressively, reaching 36°C at T7. At the final monitoring point, T8, the temperature decreased to 26°C. The temperature evolution recorded during this experimental variant is presented in Fig. 4.

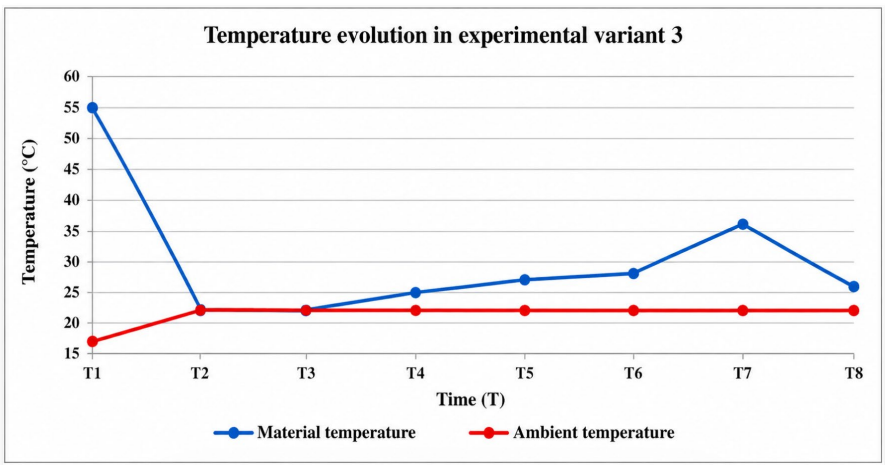



**Fig. 4 - Evolution of material and ambient temperatures during processing in the presence of partially composted material**

The initial thermal response was recorded in the presence of partially composted material. However, its contribution to temperature evolution could not be separated from the effects of electric heating, the composition of the initial load and the additional feeding performed after T1.

The temporary temperature increase observed following moisture corrections suggests a possible relationship between water availability and the thermal behavior of the system. Nevertheless, the relative contribution of moisture availability, biological activity and electric heating could not be quantified.

During the experiment, the processed material gradually became more homogeneous, while the previously introduced vegetable residues became less distinguishable. Fibrous components remained visible at the final monitoring point. The mechanical mixing system operated without significant blockages and contributed to material fragmentation and homogenization.

***Comparative analysis of the experimental variants***

The three experimental variants exhibited differences in temperature evolution, moisture conditions and changes in material appearance. The main experimental results are summarized in Table 2.

**Table 2**

**Comparative results of the experimental variants**

| Parameter | Experiment 1 (Batch) | Experiment 2 (Fed-batch) | Experiment 3 (Partially composted material) |
|---|---|---|---|
| **Maximum recorded material temperature (°C)** | 57 | 40 | 55 |
| **Ambient temperature at the maximum recorded material temperature (°C)** | 24 | Approx. 22 | 17 |
| **Temperature difference at the maximum recorded material temperature, ΔT (°C)** | 33 | 18 | 38 |
| **Material temperature at the final monitoring point (°C)** | 26 | Close to ambient temperature | 26 |
| **Progressive material drying** | Observed | Observed | Observed |
| **Moisture correction** | Performed | Performed | Performed |
| **Significant mechanical blockages** | Not observed | Not observed | Not observed |
| **Net wet mass reduction (%)** | 71.03 | Not determined | Not determined |

*Note: the reported temperature differences correspond to the monitoring points at which the maximum material temperature was recorded in each experimental variant. Net wet mass reduction was determined only for the batch experiment.*

The batch experiment exhibited a pronounced initial thermal response, with the material temperature reaching 57°C after 24 h, followed by a progressive decrease towards ambient temperature. A net wet mass reduction of 71.03% was recorded at the end of this experiment. Under progressive feeding conditions, the material temperature fluctuated during the monitoring period and reached a maximum of 40°C. In the experiment involving partially composted material, the temperature reached 55°C after 24 h, followed by a rapid decrease. Subsequent moisture corrections were associated with temporary increases in material temperature.

Progressive material drying was observed under all three experimental conditions, including the variant involving repeated additions of fresh vegetable material. Water addition was necessary at certain monitoring stages to correct the observed drying. These findings indicate that maintaining material moisture was an important operational challenge under the investigated conditions.

The recurring drying of the processed material should also be considered in relation to the operating configuration of the equipment. According to the technical documentation, the composter combines automatically controlled electric heating with mechanical agitation and ventilation. These systems can facilitate heat and moisture transfer from the processed material. However, because material moisture content, airflow rate and the energy supplied by the heating system were not measured quantitatively, their individual contributions to the observed drying could not be determined.

The processed material became progressively more fragmented and homogeneous in all three experiments, although fibrous components remained visible at the final monitoring stages. Changes in material structure and apparent volume may reflect the combined effects of mechanical fragmentation, mixing, water loss and biological transformation. The relative contribution of each process could not be quantified in the present study. The mechanical mixing system operated without significant blockages throughout the experiments, despite differences in initial loading level, material composition and feeding schedule. The observed fragmentation and homogenization indicate that the mixing mechanism remained operational under the investigated conditions.

The experimental variants differed in their initial material composition, loading level, subsequent feeding interventions and monitoring duration. Consequently, the observed differences cannot be attributed exclusively to the feeding strategy or to the presence of partially composted material. Furthermore, because the composter was equipped with an electric heating system, the measured material temperatures cannot be interpreted as an exclusive indicator of biological activity.

Overall, the results characterize the operational behavior of the Oklin GG-02 composter under the three investigated conditions and highlight the importance of considering feeding practices, moisture availability and the combined operation of the heating, ventilation and mixing systems when evaluating its performance.

## CONCLUSIONS

The experimental investigations conducted using the Oklin GG-02 electric composter highlighted differences in the operational behavior of the equipment under the three investigated feeding conditions.

Under batch feeding conditions, the material temperature reached 57°C after the first 24 hours, followed by a progressive decrease towards ambient temperature. At the end of the experiment, a mass reduction of 71.03% was recorded, resulting from the combined effects of water evaporation, organic matter transformation and mechanical processing. Under progressive feeding conditions, the material temperature exhibited fluctuations, reaching a maximum of 40°C. Successive additions of fresh vegetable material allowed the operational behavior of the equipment to be monitored over an extended period, while the processed material gradually became more homogeneous.

The use of partially composted material was associated with an initial temperature of 55°C after 24 hours. Subsequent moisture corrections were followed by temporary increases in material temperature, suggesting a possible relationship between water availability and the thermal behavior of the system. Progressive material drying was observed under all experimental conditions, highlighting the importance of moisture management during composter operation. The mechanical mixing system operated without significant blockages, contributing to material fragmentation and homogenization.

The results indicate that feeding conditions, moisture availability and the combined operation of the heating, ventilation and mixing systems are important factors influencing the operational behavior of small-scale electric composters. Further investigations should focus on quantitative moisture monitoring and the development of an integrated control strategy to reduce excessive material drying and improve operating conditions.

## ACKNOWLEDGEMENT

This research was supported by the project CNFIS-FDI-2026-F-0049 “Asigurarea eficienței operaționale a bazei de aplicații practice pentru sisteme biotehnice în livezi, vii, solarii și grădini (EFIBIOTECH)”, from the Ministry of Education and Research through the Executive Agency for Financing Higher Education, Research, Development and Innovation.

## REFERENCES

[1] Azis, F.A., Choo, M., Suhaimi, H. and Abas, P.E. (2023). The effect of initial carbon to nitrogen ratio on kitchen waste composting maturity. Sustainability, 15(7), 6191. doi:10.3390/su15076191.

[2] DeFelice, H. and Stack Whitney, K. (2024). Understanding electric composting machines as a potential household food waste management strategy. Food-Fueled, 1, e00004. doi:10.57912/25641639.

[3] Eurostat (2025). 130 kg of food wasted per person annually in the EU. Eurostat News, 16 October 2025.

[4] Guidoni, L.L.C., Marques, R.V., Moncks, R.B., Botelho, F.T., da Paz, M.F., Corrêa, L.B. and Corrêa, É.K. (2018). Home composting using different ratios of bulking agent to food waste. Journal of Environmental Management, 207, pp. 141-150. doi:10.1016/j.jenvman.2017.11.031.

[5] Jain, A., Singh, D.J. and Dikshit, A.K. (2025). Development and performance assessment of in-vessel home composters for food waste valorisation. Bioresource Technology Reports, 31, 102265. doi:10.1016/j.biteb.2025.102265.

[6] Jolanun, B., Tripetchkul, S., Chiemchaisri, C., Chaiprasert, P. and Towprayoon, S. (2005). The application of a fed batch reactor for composting of vegetable and fruit wastes. Thammasat International Journal of Science and Technology, 10(2), pp. 60-69.

[7] Lai, J.C., Then, Y.L., Hwang, S.S. and Lee, C.S. (2024). Optimal aeration management strategy for a small-scale food waste composting. Carbon Resources Conversion, 7(1), 100190. doi:10.1016/j.crcon.2023.06.002.

[8] Liang, C., Das, K.C. and McClendon, R.W. (2003). The influence of temperature and moisture contents regimes on the aerobic microbial activity of a biosolids composting blend. Bioresource Technology, 86(2), pp. 131-137. doi:10.1016/S0960-8524(02)00153-0.

[9] Oklin (n.d.). GG-02 Electric Composter: User Manual. Manufacturer's technical manual.

[10] Schroeder, J.T., Labuzetta, A.L. and Trabold, T.A. (2020). Assessment of dehydration as a commercial-scale food waste valorisation strategy. Sustainability, 12(15), 5959. doi:10.3390/su12155959.

[11] Sundberg, C. and Jönsson, H. (2005). Process inhibition due to organic acids in fed-batch composting of food waste - influence of starting culture. Biodegradation, 16, pp. 205-213. doi:10.1007/s10532-004-0628-1.

[12] United Nations Environment Programme (UNEP) (2024). Food Waste Index Report 2024: Think Eat Save - Tracking Progress to Halve Global Food Waste. Nairobi: UNEP.

[13] Wang, X., Pan, S., Zhang, Z., Lin, X., Zhang, Y. and Chen, S. (2017). Effects of the feeding ratio of food waste on fed-batch aerobic composting and its microbial community. Bioresource Technology, 224, pp. 397-404. doi:10.1016/j.biortech.2016.11.076.

[14] Yang, W. and Zhang, L. (2022). Addition of mature compost improves the composting of green waste. Bioresource Technology, 350, 126927. doi:10.1016/j.biortech.2022.126927.

# DEVELOPING AN OPERATIONAL MODEL FOR AGRICULTURAL KNOWLEDGE TRANSFER TO SUPPORT PUBLIC-PRIVATE PARTNERSHIPS IN ROMANIA

/

# *DEZVOLTAREA UNUI MODEL OPERAȚIONAL PENTRU TRANSFERUL CUNOAȘTERII AGRICOLE ÎN SPRIJINUL PARTENERIATELOR PUBLIC-PRIVATE DIN ROMÂNIA*

**Ioana Corina MOGA*[1)], Laurențiu CIORNEI[1)], Iulian VOICEA[2)]**

[1)] Centre for Studies and Research on Agroforestry Biodiversity "Acad. David Davidescu" (CSCBAS), Romanian Academy, Bucharest / Romania;

[2)] National Institute of Research-Development for Machines and Installations Designed for Agriculture and Food Industry - INMA Bucharest / Romania.

*Tel: +40.727.850.098; *E-mail: corinamoga@yahoo.com*

***Keywords:*** *public–private partnership, agricultural research, knowledge transfer, agricultural innovation, operational model*

**ABSTRACT**

*Public–private partnerships (PPPs) can facilitate the integration of agricultural research into farming practices by combining institutional capacities, financial resources and technological expertise. This paper investigates institutional and operational barriers to agricultural knowledge transfer in Romania and proposes a framework for strengthening cooperation between research institutions and the agricultural sector. The research draws on a workshop organised within Project ADER 21.1.1/2023, involving a questionnaire addressing research financing, knowledge-transfer mechanisms, education and institutional cooperation. The findings are complemented by field observations involving farms, cooperatives and agricultural associations in Iași County. Results indicate a prevailing orientation towards public funding, insufficient recognition of agricultural extension services and limited understanding of knowledge-transfer mechanisms. Field observations further reveal weak research–farmer interactions, administrative barriers and inadequate promotion of domestic research outcomes. Based on these findings, a seven-stage operational model is proposed, integrating needs assessment, research prioritisation, partnership formation, performance indicators, pilot demonstration, validation and feedback. The model provides a structured approach to connecting research capacities with agricultural needs, supporting technology adoption and creating the conditions for future PPP development.*

**REZUMAT**

*Cercetarea agricolă poate fi integrată mai eficient în practica fermierilor prin dezvoltarea parteneriatelor public-private (PPP), care valorifică complementaritatea capacităților instituționale, a resurselor financiare și a expertizei tehnologice. Lucrarea analizează barierele instituționale și operaționale care limitează transferul de cunoaștere în agricultura românească și propune un cadru pentru consolidarea cooperării dintre instituțiile de cercetare și sectorul agricol. Cercetarea se bazează pe un workshop organizat în cadrul proiectului ADER 21.1.1/2023, în care a fost aplicat un chestionar privind finanțarea cercetării, mecanismele transferului de cunoaștere, educația și cooperarea instituțională. Rezultatele sunt completate de observații din teren, realizate la ferme, cooperative și asociații agricole din județul Iași. Analiza evidențiază orientarea predominantă către finanțarea publică, insuficienta recunoaștere a rolului extensiei agricole și înțelegerea limitată a mecanismelor transferului de cunoaștere. Observațiile din teren indică relații reduse între cercetare și fermieri, bariere administrative și promovarea insuficientă a rezultatelor cercetării autohtone. Pe baza constatărilor, este propus un model operațional în șapte etape, care integrează identificarea nevoilor, prioritizarea cercetării, constituirea parteneriatelor, indicatorii de performanță, demonstrarea experimentală, validarea și feedbackul. Modelul urmărește conectarea capacităților de cercetare cu nevoile sectorului agricol, facilitarea adoptării tehnologiilor și crearea premiselor dezvoltării viitoarelor PPP.*

## INTRODUCTION

Public–private partnerships (PPPs) represent heterogeneous institutional and contractual arrangements through which public and private actors combine complementary resources, share

responsibilities and coordinate activities to achieve common objectives. Their configurations differ according to governance structures, contractual obligations, risk allocation and performance requirements (*Ke et al., 2024; Dhanshyam et al., 2024*). PPPs are therefore more than instruments for mobilising private financing; they constitute mechanisms of cooperation and public governance whose effectiveness depends on institutional design and measurable outcomes. Hodge and Greve (2007, 2010) emphasise the diversity of PPP models and the need to distinguish contractual partnerships from broader forms of public–private collaboration. Systematic reviews further identify governance, risk sharing, partnership formation and performance evaluation as central research dimensions (*Wang et al., 2018; Xiong et al., 2019*).

From an institutional economics perspective, PPPs can be explained through contractual incentives, transaction costs and the allocation of decision-making rights. Hart (2003) demonstrates that integrating investment and operational responsibilities may influence innovation incentives, costs and service quality. However, contractual arrangements alone cannot guarantee successful cooperation. Differences in organisational objectives, information asymmetries and conflicting interests require effective governance mechanisms, clearly assigned responsibilities and transparent evaluation procedures. Recent research confirms that PPP governance structures vary according to project characteristics and the distribution of risks and responsibilities (*Dhanshyam et al., 2024*).

An essential condition for effective PPP implementation is the appropriate allocation of risks and the establishment of performance-based contractual mechanisms. Risks associated with financing, technological development, market demand, operational activities and regulatory changes should be assigned to the partners best positioned to manage them. Moreover, performance indicators must reflect not only financial efficiency, but also service quality, technological reliability and long-term sustainability. The systematic analysis conducted by Wang et al. (2018) identifies risk allocation and performance evaluation as major dimensions of PPP research, while Xiong et al. (2019) emphasise the importance of governance arrangements in managing contractual complexity and institutional relationships.

In agriculture, PPPs are particularly relevant because technological development and production performance depend on the interaction of scientific knowledge, financing, infrastructure, managerial capabilities and market demand. Public research institutions contribute scientific expertise, experimental infrastructure and technological results, while private enterprises may provide capital, specialised equipment, commercial experience and access to agricultural markets. Agricultural partnerships may support research and innovation, irrigation, storage, processing, logistics, advisory services and technology dissemination. Nevertheless, their effectiveness depends on the compatibility of institutional objectives and the capacity to generate measurable benefits for participating actors. Maryono et al. (2024), in a systematic review covering 147 studies on multi-stakeholder partnerships in developing countries, identified substantial diversity in partnership arrangements and reported economic, social and technological benefits for farmers. However, the authors also highlighted conceptual inconsistencies between partnership types and the need for more systematic evaluation of their impacts.

Agricultural innovation partnerships must also be distinguished from conventional infrastructure-oriented PPPs. While formal PPPs generally involve long-term contractual obligations and risk-sharing mechanisms, agricultural innovation may additionally rely on research consortia, collaborative development agreements and intermediary organisations. Hall (2006) conceptualises agricultural PPPs within innovation systems, emphasising institutional interactions rather than exclusively contractual arrangements. Similarly, Hermans et al. (2019), analysing four agricultural PPPs in the Netherlands, demonstrate that partnership configurations influence knowledge development, network formation and technological diffusion, although complementary mechanisms may be required to facilitate market adoption.

The potential contribution of PPPs to agricultural development also depends on the distribution of benefits among participating stakeholders. Agricultural partnerships may generate economic advantages through improved productivity, reduced production costs and access to new markets, while contributing to environmental objectives through more efficient resource utilisation and sustainable production practices. However, these outcomes require clearly defined responsibilities, appropriate incentives and mechanisms for monitoring technological and economic performance. The findings of Hermans et al. (2019) and Maryono et al. (2024) indicate that partnership outcomes depend on institutional configurations, stakeholder participation and the capacity to translate collaborative activities into practical benefits for agricultural producers.

The agricultural innovation process extends beyond the linear transmission of technologies from research institutions to farmers. It involves interactions among researchers, agricultural producers, input suppliers, advisers, processors, professional associations and public authorities. Klerkx et al. (2010)

demonstrate that agricultural innovation networks evolve through continuous interactions with their institutional environments. Klerkx and Leeuwis (2009a, 2009b) further highlight the importance of innovation intermediaries and demand-driven research planning, identifying institutional barriers associated with information asymmetries, stakeholder coordination and the alignment of research priorities with agricultural needs.

The effectiveness of agricultural partnerships also depends on the institutional conditions enabling stakeholders to access and utilise innovations. Akullo et al. (2018), examining agricultural PPPs involving smallholder producers in Uganda, demonstrate how institutional practices influence technological opportunities and adoption. More recently, Tumwebaze et al. (2025), through a systematic literature review, examined knowledge-management practices in agriculture, emphasising the importance of knowledge creation, sharing and application, as well as the organisational and contextual conditions influencing these processes. These findings support the need to evaluate agricultural cooperation not only through formal institutional arrangements, but also through its capacity to generate practical technological and economic outcomes.

The persistent gap between agricultural research and its practical application remains a major challenge. Ben Farah and Amara (2025), through a systematic literature review, identify individual, organisational and external determinants influencing knowledge transfer from researchers to agricultural users. Digital technologies provide additional opportunities for improving information accessibility, stakeholder interactions and knowledge dissemination. However, their effectiveness depends on the interaction between technological infrastructure, institutional arrangements and users' capabilities, as discussed by Ahmadi et al. (2025) in their systematic review of digital knowledge transfer in the agri-food sector.

Agricultural extension services and intermediary organisations can play a decisive role in overcoming the institutional separation between research institutions and agricultural producers. Their functions may include identifying technological needs, facilitating access to research results, organising field demonstrations, supporting technology adaptation and collecting feedback from farmers. Such activities can reduce information asymmetries and improve the relevance of research programmes to agricultural demand. Klerkx and Leeuwis (2009a) demonstrate the importance of innovation brokers in connecting actors within agricultural innovation systems, while Ben Farah and Amara (2025) highlight the organisational and external factors influencing the effectiveness of knowledge-transfer channels.

Recent agricultural innovation research increasingly emphasises systemic approaches integrating institutional cooperation, demand-driven research and technological adoption. Ragasa et al. (2025) distinguish three successive policy frameworks: science and technology, agricultural innovation systems, and transformative innovation policy and scaling, emphasising the increasing importance of institutional coordination, demand articulation and systemic approaches to agricultural innovation. These perspectives indicate that research performance should be evaluated not only through scientific outputs, but also through the capacity to translate knowledge into practical economic, social and environmental benefits.

In Romania, strengthening the relationship between agricultural research institutions and the productive sector is particularly important for improving the valorisation of domestic research results. Effective knowledge transfer requires identifying farmers' technological needs, matching them with available research capacities, validating solutions under practical conditions and establishing functional communication and feedback mechanisms. Public–private cooperation may facilitate these processes by integrating scientific expertise, private-sector capabilities and intermediary organisations.

Within this context, the present study, conducted under Project ADER 21.1.1/2023, investigates institutional and operational barriers affecting agricultural knowledge transfer in Romania. Based on questionnaire findings and field observations, the research develops a demand-driven operational model integrating research–demand matching, comparative techno-economic validation and performance-based monitoring of institutional cooperation. The proposed framework aims to strengthen the practical utilisation of agricultural research results and establish conditions for future public–private partnerships.

## MATERIALS AND METHODS

The research was conducted within Project ADER 21.1.1/2023, focusing on the institutional capacity of public–private cooperation to improve agricultural performance and strengthen knowledge transfer between research institutions and agricultural producers. A mixed-methods approach was employed, combining a structured stakeholder questionnaire, qualitative analysis of open-ended responses and field-

based documentation. The methodology aimed to identify institutional, financial and operational barriers affecting the circulation of scientific and technological knowledge within the Romanian agricultural sector and to provide an empirical basis for developing an operational knowledge-transfer model.

The primary data collection activity consisted of a workshop organised by the Centre for Studies and Research on Agroforestry Biodiversity (CSCBAS “Acad. David Davidescu”), bringing together 38 participants representing universities, research institutions, farmers and farmers’ associations, public administration and relevant ministries, as well as doctoral researchers. A structured questionnaire comprising five items was administered to investigate agricultural research financing, knowledge-transfer mechanisms, education and institutional cooperation. As not all participants answered every question, the number of valid responses varied across questionnaire items. Consequently, the aggregated results were interpreted separately for each question, without assuming a uniform response rate across the entire questionnaire.

The first question examined perceptions concerning the financing of agricultural research. Respondents were requested to rank three potential funding sources on a scale from 0 to 10 points, according to their perceived contribution to strengthening the role of Romanian research in agricultural development. The analysis focused on the relative importance attributed to national public funding, non-reimbursable project financing and market-based financing.

The second question assessed the perceived importance of different channels for transferring value-generating information from knowledge producers to its users. Respondents evaluated the proposed knowledge-transfer mechanisms on a scale from 0 to 5 points. The assessment covered education, consultancy, agricultural extension, fairs and exhibitions, and other information-dissemination channels. Particular attention was given to the relative positioning of agricultural extension within the broader knowledge-transfer system.

The third question investigated the contribution of different educational levels to the dissemination of technological and scientific progress in agriculture. Using a scale from 0 to 5 points, respondents evaluated the role of vocational, secondary and university education, alongside other educational levels, in facilitating the circulation of knowledge and technological innovations towards agricultural users.

The fourth question employed an open-ended format, requesting participants to identify and rank the principal institutions and organisational structures potentially involved in public–private cooperation and agricultural knowledge transfer. Responses were examined qualitatively to distinguish between public–private partnership structures, research and educational institutions, intermediary organisations and other entities identified by participants. This analysis also assessed respondents' understanding of the institutional actors and their functions within the agricultural knowledge-transfer system.

The fifth question required respondents to develop a functional scheme illustrating the circulation of value-generating knowledge from its producers to its final users. The resulting schemes were subjected to qualitative content analysis, focusing on the identification of knowledge producers, intermediary actors, transfer mechanisms and end users. Based on the workshop documentation, the responses were classified into three categories: (i) schemes reflecting an incomplete or incorrect understanding of knowledge-transfer mechanisms; (ii) schemes identifying relevant actors and functional transfer channels, including agricultural extension and digital innovation platforms; and (iii) schemes omitting intermediary knowledge-transfer mechanisms.

The quantitative analysis was based on the aggregated results reported in the workshop documentation. The relative scores and percentages were interpreted as indicators of the importance assigned to different response categories, rather than as percentages of participants expressing a particular opinion. Qualitative responses were examined to identify recurring institutional barriers, misunderstandings concerning PPP structures and deficiencies in the representation of knowledge-transfer processes. As individual-level questionnaire data were not available for reanalysis, the assessment was restricted to descriptive interpretation, without inferential statistical testing.

The questionnaire-based investigation was complemented by field documentation undertaken in Iași County, Romania. The activities involved interactions with representatives of agricultural production farms, cooperatives, associations, Local Action Groups (LAGs), and production and processing organisations. The field investigation focused on the practical relationships between agricultural producers and Romanian research institutions, the accessibility and perceived relevance of domestic research results, the promotion of technological innovations and the institutional barriers affecting cooperation.

The qualitative information collected during field documentation was organised into thematic categories addressing: (i) farmers' professional training needs; (ii) research–farmer cooperation; (iii)

accessibility and promotion of domestic technologies; (iv) administrative and institutional constraints; (v) perceived technological quality and competitiveness; and (vi) the role of associative structures and intermediary organisations. The field observations were used to contextualise the questionnaire findings and identify convergent barriers affecting knowledge transfer.

Finally, the results of the questionnaire and field documentation were integrated through a qualitative synthesis to formulate an operational model for agricultural knowledge transfer. The model was structured around successive activities connecting the identification of agricultural needs with research prioritisation, institutional cooperation, technology demonstration, validation and feedback. The proposed framework was developed as a conceptual and operational output of the research; its implementation and effectiveness were not experimentally validated within the activities reported in this paper.

## RESULTS

The analysis of the questionnaire responses and field observations identified several institutional, financial and operational barriers affecting the transfer of agricultural research results to their potential users. The findings were organised into three interconnected dimensions: (i) perceptions regarding research financing and knowledge-transfer mechanisms; (ii) institutional understanding and practical functioning of the agricultural knowledge-transfer system; and (iii) barriers identified through interactions with agricultural stakeholders. These findings provided the empirical basis for developing a proposed operational model aimed at strengthening cooperation between research institutions, intermediary organisations and agricultural producers.

### *a. Research financing and market orientation*

The first questionnaire item examined the relative importance attributed to alternative sources of financing for agricultural research. The national budget received the highest reported share of the aggregated scores (19.77%), followed by non-reimbursable project funding (18.60%), while market-based financing was ranked last among the assessed alternatives. The difference between the two leading sources was 1.17 percentage points.

These findings indicate that respondents continued to associate the development of agricultural research primarily with public and grant-based financing mechanisms, rather than with direct demand from agricultural enterprises and other potential users of research results. Although public financing remains essential for research activities generating broad societal benefits, the limited importance assigned to market-based financing suggests insufficient integration of agricultural demand into research planning and funding mechanisms.

The results also highlight the need to distinguish between the financing of research activities and the commercial valorisation of research outputs. Public funding and competitive research grants may support scientific development, whereas cooperation with agricultural enterprises can contribute to defining research priorities, testing technologies under practical conditions and facilitating their subsequent adoption. Consequently, strengthening market orientation should not be interpreted as replacing public research financing, but as improving the interaction between public research capacities and agricultural demand.

### *b. Knowledge-transfer channels and agricultural extension*

The second questionnaire item investigated the perceived effectiveness of different mechanisms for transferring value-generating information from knowledge producers to agricultural users. Education received the highest reported share of the aggregated scores (16.03%), followed by consultancy (15.27%) and agricultural fairs and exhibitions (10.69%), while agricultural extension accounted for only 9.16%.

The results indicate that respondents assigned greater importance to education, consultancy, and fairs and exhibitions than to agricultural extension, despite the latter's essential role in connecting scientific knowledge with farmers' practical needs. The reported percentages represent shares of aggregated questionnaire scores and must not be interpreted as proportions of respondents selecting particular options.

The relatively low score attributed to agricultural extension suggests insufficient recognition of its role in facilitating the practical application of research results. This finding highlights the need to strengthen extension services as intermediary mechanisms supporting technology demonstration, adaptation, validation and feedback between research institutions and agricultural producers.

***c. Contribution of educational institutions***

The third questionnaire item examined the perceived contribution of different educational levels to the dissemination of technological and scientific progress in agriculture. University education and vocational education each accounted for 18.25% of the reported aggregated scores, while secondary education accounted for 10.32%. Lower-secondary education was identified in the workshop documentation as having the lowest perceived contribution. The identical scores attributed to university and vocational education indicate that respondents recognised the complementary importance of advanced scientific knowledge and practically oriented professional training. University institutions contribute to the generation and dissemination of specialised knowledge, while vocational education supports the development of competencies necessary for implementing technologies and improving agricultural practices.

The findings suggest that effective agricultural knowledge transfer requires coordinated educational pathways connecting scientific research, professional training and practical technological applications. Such coordination is particularly relevant to the adoption of new production technologies, which may require both an understanding of their technical principles and the acquisition of specific operational skills.

***d. Identification of institutional actors***

The fourth questionnaire item required participants to identify and rank the principal institutions and organisational structures potentially involved in PPP arrangements and agricultural knowledge transfer. The qualitative analysis revealed differences in respondents' understanding of the institutional actors and their potential roles. The responses included agricultural associations and cooperatives, business incubators, innovation centres, Local Action Groups (LAGs), clusters, research institutes, universities, public authorities, financial institutions and private enterprises. Although these entities may participate in public–private cooperation and agricultural knowledge-transfer networks, their institutional status does not automatically qualify them as PPP structures. Furthermore, some responses referred to governmental policies rather than institutions, indicating conceptual confusion between policy instruments and organisational actors. These findings suggest a need for clearer differentiation between formal PPP arrangements, potential partnership participants and intermediary organisations facilitating agricultural knowledge transfer.

The distinction is important because participation in agricultural innovation networks does not automatically confer PPP status on an institution or collaborative arrangement. A formal PPP requires an appropriate institutional and contractual framework, clearly defined responsibilities and an allocation of resources and risks.

The questionnaire documentation also recorded unanswered items, indicating difficulties among some participants in identifying relevant institutional structures. Taken together, these findings reveal conceptual ambiguities concerning the relationship between PPPs, agricultural innovation networks and knowledge-transfer organisations.

***e. Functional representation of knowledge-transfer mechanisms***

The fifth questionnaire item requested participants to develop a functional scheme describing how value-generating knowledge circulates from its producers to its final users.

The responses were classified into three qualitative categories. The first category comprised schemes reflecting an incomplete or incorrect understanding of knowledge-transfer mechanisms. These representations frequently confused knowledge producers, intermediary organisations and final users, or incorrectly assigned intermediary functions to actors primarily involved in agricultural production or processing. The second category included schemes identifying relevant actors and functional knowledge-transfer channels. Although described as less frequent than inadequate representations, these responses introduced mechanisms such as digital platforms, agricultural innovation hubs and extension services. Their inclusion indicates recognition among some participants of the need for intermediary structures connecting research institutions with agricultural users. The third category comprised schemes omitting knowledge-transfer intermediaries entirely, suggesting a predominantly linear interpretation of the relationship between research institutions and farmers.

The qualitative findings indicate that the circulation of agricultural knowledge was not consistently understood as a structured process involving distinct institutional roles, communication mechanisms and feedback relationships. This deficiency is particularly relevant because the

effectiveness of research valorisation depends not only on generating scientific results, but also on the institutional mechanisms through which those results reach potential users.

***Barriers identified through field documentation***

The field documentation undertaken in Iași County provided additional information concerning the practical relationship between agricultural research and production.

The observations indicated that cooperation between Romanian agricultural research institutions and farmers was perceived as sporadic and limited in scale. Stakeholders reported insufficient promotion of domestic research results, including certified seeds, improved animal breeds, production technologies and agricultural machinery, particularly when compared with the promotional activities of foreign agricultural input suppliers.

Administrative complexity was identified as a potential barrier to cooperation. Stakeholders also expressed concerns regarding the perceived competitiveness and quality of certain domestically developed technological products and the absence of sufficiently clear quality standards adapted to market requirements. These observations represent stakeholder perceptions documented during the field activities and should not be interpreted as independently verified assessments of the technological performance of Romanian research outputs.

Additional barriers concerned the limited integration of research institutions into agricultural value chains, from primary production to storage, processing and commercialisation. The insufficient visibility of domestic research results at agricultural fairs and exhibitions was also highlighted, alongside weak interactions between farmers and institutions providing pedological and agrochemical services.

The field observations further indicated a need for stronger professional competencies among farmers in financial management, marketing, business administration and agricultural policies. These requirements suggest that the transfer of technological knowledge should be accompanied by managerial and economic training to support the effective adoption and valorisation of innovations.

**Proposed operational model for demand-driven agricultural knowledge transfer**

Based on the questionnaire findings and field observations, a demand-driven operational model was developed to address the institutional and technological barriers limiting the valorisation of Romanian agricultural research. Unlike conventional linear knowledge-transfer approaches, the proposed framework integrates three interdependent mechanisms: (i) matching farmers' technological needs with domestic research capacities; (ii) comparative techno-economic validation of available solutions under practical farming conditions; and (iii) performance-based monitoring of institutional cooperation and technology adoption.

The model is structured around seven barriers identified in the ADER 21.1.1/2023 research, each associated with a specific corrective mechanism, responsible institutional actors and measurable performance indicators (Fig. 1). Its distinctive feature is the simultaneous assessment of technological suitability and institutional transfer efficiency, rather than considering knowledge dissemination as an end in itself.

The first mechanism establishes a structured connection between agricultural demand and research supply. Farmers, cooperatives and professional associations would submit technological needs using standardised descriptions of production constraints, expected improvements and implementation conditions. Research institutions would subsequently identify available technologies, research results or development capacities corresponding to these requirements. The proposed matching indicator is the proportion of documented agricultural needs for which a potentially applicable research solution is identified.

The second mechanism addresses concerns identified during field documentation regarding the competitiveness, accessibility and practical relevance of domestic research results. Technologies selected through the matching process would undergo comparative validation under relevant agricultural conditions, using reference practices or commercially available alternatives.

Evaluation criteria would include productivity, unit production costs, resource consumption, technological reliability and, where applicable, environmental performance. Transfer decisions would be based on documented results rather than exclusively on the availability or promotion of research outputs.

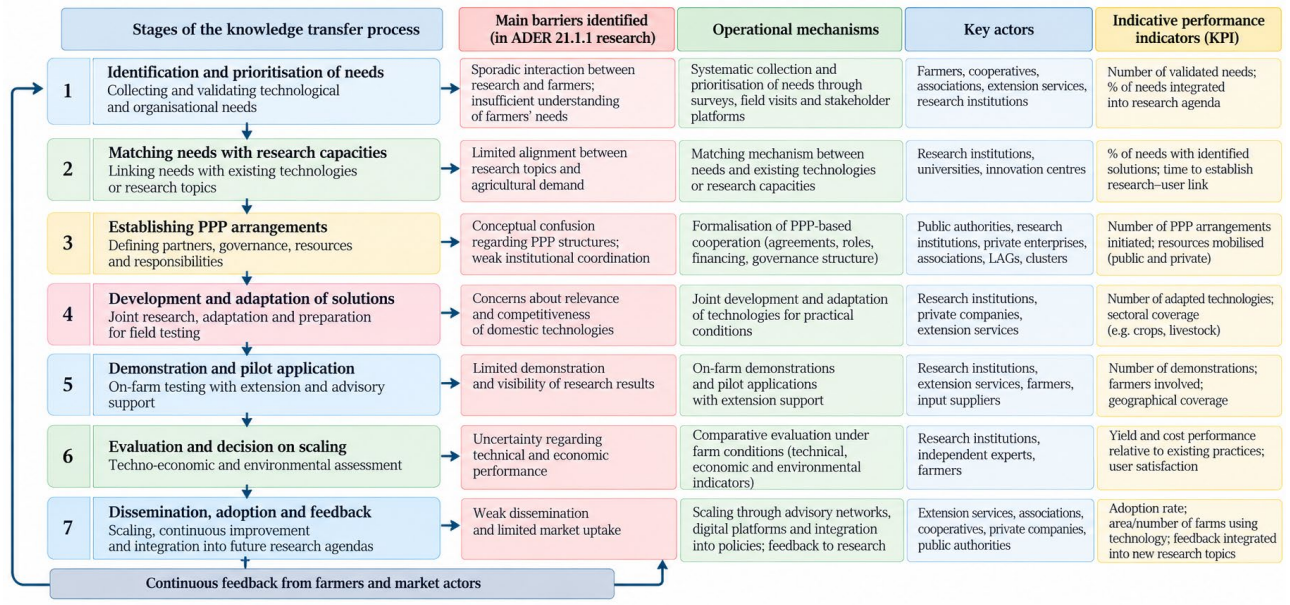



**Fig. 1 - Integrated operational model for agricultural knowledge transfer, linking identified barriers with intervention mechanisms, institutional actors and performance indicators.**

The third mechanism introduces institutional accountability into agricultural knowledge transfer. Research institutions would be responsible for technical documentation and scientific validation; agricultural extension and intermediary organisations would coordinate communication, demonstration activities and feedback collection; while farmers and private-sector partners would contribute practical requirements, testing conditions and operational information. Performance monitoring would cover both technological outcomes and the efficiency of institutional interactions.

To operationalise these mechanisms, the framework proposes a set of indicators covering demand–supply matching, response time, demonstration completion, comparative technological performance, adoption and feedback integration. The indicators are intended for subsequent implementation and validation; no measured performance values or adoption rates are attributed to the present study.

To enable quantitative assessment of the proposed model, six key performance indicators (KPIs) were defined, covering research–demand alignment, institutional responsiveness, technology validation, knowledge dissemination and practical adoption (Table 1). These indicators provide a standardised basis for evaluating the effectiveness of agricultural knowledge transfer during future pilot implementation.

**Table 1**

**Proposed key performance indicators for evaluating agricultural knowledge transfer**

| KPI | Definition and calculation | Unit |
|---|---|---|
| Research–demand matching rate | Agricultural needs matched with research solutions / Total validated needs × 100 | % |
| Institutional response time | Sum of days required to establish research–user connections / Number of connections established | days |
| Demonstration completion rate | Completed technology demonstrations / Planned demonstrations × 100 | % |
| Technology validation rate | Technologies meeting predefined technical and economic criteria / Total technologies tested × 100 | % |
| Technology adoption rate, within 12 months after demonstration | Farmers adopting validated technologies / Total farmers participating in demonstrations × 100 | % |
| Feedback integration rate | Documented feedback items incorporated into research activities / Total actionable feedback items × 100 | % |

The proposed model therefore transforms the institutional deficiencies identified through the questionnaire and field observations into a structured system of responsibilities, decision criteria and measurable outcomes. Its contribution lies in integrating demand-driven research prioritisation, comparative validation of domestic technologies and institutional performance monitoring within a single framework adapted to the barriers observed in Romanian agricultural knowledge transfer. The model

represents a methodological proposal requiring future pilot testing, rather than an experimentally validated PPP arrangement.

## CONCLUSIONS

The research identified significant institutional and operational barriers limiting the effective transfer of agricultural knowledge in Romania. The questionnaire results revealed a predominant orientation towards public and grant-based research financing, insufficient recognition of agricultural extension as a knowledge-transfer mechanism, and conceptual ambiguities regarding PPP structures and the roles of intermediary organisations. These findings indicate that the research-to-market gap is not exclusively a financial or technological problem but also reflects weaknesses in institutional coordination and knowledge-transfer mechanisms.

Field observations indicated the limited interaction between Romanian research institutions and agricultural producers, insufficient promotion of domestic research outputs, administrative barriers and concerns regarding their practical competitiveness. These findings underline the need to strengthen the connection between research priorities and farmers' technological requirements, supported by transparent validation procedures and effective intermediary services.

The main methodological contribution of the study is a demand-driven operational model integrating three complementary mechanisms: research–demand matching, comparative techno-economic validation of domestic technologies and performance-based monitoring of institutional cooperation. Six proposed KPIs provide measurable criteria for evaluating institutional responsiveness, technological validation, knowledge dissemination and adoption.

The model offers a structured basis for improving the valorisation of agricultural research and supporting future public–private cooperation. However, its effectiveness remains to be demonstrated through pilot implementation. Future research should validate the proposed indicators under practical agricultural conditions and quantify the economic, technological and institutional benefits generated by the model.

## ACKNOWLEDGEMENT

This research was carried out within the framework of Project ADER 21.1.1/2023, “Research on the Institutional Capacity of Public–Private Partnerships to Actively Contribute to Agricultural Performance in Terms of Productivity, Economic, Social and Environmental Outcomes”, funded by the Romanian Ministry of Agriculture and Rural Development (MADR) through the Sectoral Research and Development Plan for Agriculture and Rural Development 2023–2026 (ADER 2026).

## REFERENCES

[1] Akullo, D., Maat, H., & Wals, A. E. J. (2018). An institutional diagnostics of agricultural innovation; public-private partnerships and smallholder production in Uganda. *NJAS – Wageningen Journal of Life Sciences,* 84, 6–12. https://doi.org/10.1016/j.njas.2017.10.006

[2] Ahmadi, S., Amendolagine, V., & LaSala, P. (2025). Unpacking the impacts of digitalization of knowledge transfer in agri-food sector, through sociotechnical systems theory: A systematic literature review. *Agricultural and Food Economics*, 13, Article 51. https://doi.org/10.1186/s40100-025-00393-3

[3] Ben Farah, S., & Amara, N. (2025). Lab to farm: Mapping knowledge transfer channels and determinants from researchers’ perspective – A systematic literature review. *Journal of Innovation & Knowledge*, 10(1), 100650. https://doi.org/10.1016/j.jik.2025.100650

[4] Dhanshyam, M., Srivastava, S. K., & Biswas, I. (2024). Determinants of public-private partnership governance structures: Evidence from India. *Public Management Review*, 27(11), 2491–2513. *https://doi.org/10.1080/14719037.2024.2349125*

[5] Hall, A. (2006). Public-private sector partnerships in an agricultural system of innovation: Concepts and challenges. *International Journal of Technology Management & Sustainable Development*, 5(1), 3–20. https://doi.org/10.1386/ijtm.5.1.3/1

[6] Hart, O. (2003). Incomplete contracts and public ownership: Remarks, and an application to public-private partnerships. *The Economic Journal*, 113(486), C69–C76. https://doi.org/10.1111/1468-0297.00119

[7] Hermans, F., Geerling-Eiff, F., Potters, J., & Klerkx, L. (2019). Public-private partnerships as systemic agricultural innovation policy instruments – Assessing their contribution to innovation system function dynamics. NJAS – *Wageningen Journal of Life Sciences*, 88, 76–95.
[8] https://doi.org/10.1016/j.njas.2018.10.001
[9] Hodge, G. A., & Greve, C. (2007). Public–private partnerships: An international performance review. *Public Administration Review*, 67(3), 545–558. https://doi.org/10.1111/j.1540-6210.2007.00736.x
[10] Hodge, G. A., & Greve, C. (2010). Public-private partnerships: Governance scheme or language game? *Australian Journal of Public Administration*, 69(S1), S8–S22. https://doi.org/10.1111/j.1467-8500.2009.00659.x
[11] Ke, Y., Cheng, Z., Zhang, J., & Liu, Y. (2024). Making sense of the definition of public-private partnerships. *Built Environment Project and Asset Management*, 14(1), 4–21. https://doi.org/10.1108/BEPAM-01-2023-0009
[12] Klerkx, L., & Leeuwis, C. (2009a). Establishment and embedding of innovation brokers at different innovation system levels: Insights from the Dutch agricultural sector. *Technological Forecasting and Social Change*, 76(6), 849–860. https://doi.org/10.1016/j.techfore.2008.10.001
[13] Klerkx, L., & Leeuwis, C. (2009b). Operationalizing demand-driven agricultural research: Institutional influences in a public and private system of research planning in The Netherlands. *The Journal of Agricultural Education and Extension*, 15(2), 161–175. https://doi.org/10.1080/13892240902909080
[14] Klerkx, L., Aarts, N., & Leeuwis, C. (2010). Adaptive management in agricultural innovation systems: The interactions between innovation networks and their environment. *Agricultural Systems,* 103(6), 390–400. https://doi.org/10.1016/j.agsy.2010.03.012
[15] Maryono, M., KilLoes, A. M., Adhikari, R., & Aziz, A. A. (2024). Agriculture development through multi-stakeholder partnerships in developing countries: A systematic literature review. *Agricultural Systems,* 213, 103792. https://doi.org/10.1016/j.agsy.2023.103792
[16] Ragasa, C., Spielman, D. J., & Lynam, J. K. (2025). Agricultural innovation frames, policies, and instruments: Evolution, lessons, and future research. *Food Policy*, 137, 103008. https://doi.org/10.1016/j.foodpol.2025.103008
[17] Tumwebaze, R. P., Walsh, J. N., & Lannon, J. (2025). Knowledge management in the agriculture sector: A systematic literature review. *Knowledge Management Research & Practice*, 23(2), 131–148. https://doi.org/10.1080/14778238.2024.2359419
[18] Wang, H., Xiong, W., Wu, G., & Zhu, D. (2018). Public–private partnership in public administration discipline: A literature review. *Public Management Review*, 20(2), 293–316. https://doi.org/10.1080/14719037.2017.1313445
[19] Xiong, W., Chen, B., Wang, H., & Zhu, D. (2019). Governing public–private partnerships: A systematic review of case study literature. *Australian Journal of Public Administration*, 78(1), 95–112. https://doi.org/10.1111/1467-8500.12343

# ASSESSMENT OF THE ECONOMIC AND ENVIRONMENTAL IMPACT OF ALTERNATIVE PROTEINS DERIVED FROM LEGUMES, FUNGI, AND AQUATIC SOURCES

/

# *EVALUAREA IMPACTULUI ECONOMIC ȘI DE MEDIU AL PROTEINELOR ALTERNATIVE OBȚINUTE DIN LEGUMINOASE, CIUPERCI ȘI SURSE ACVATICE*

**Gabriel NAE*[1)], Florin NENCIU[1)], Andreea MATACHE[1)], Nicoleta VANGHELE[1)], Floarea ŞERBANCEA[2)], Margareta NAIE[3)], Simona-Florina ISTICIOAIA[3)]**

[1)] National Institute of Research - Development for Machines and Installations Designed to Agriculture and Food-Industry INMA Bucharest / Romania;

[2)] National Institute of Research and Development for Food Bioresources, Bucharest / Romania;

[3)] Agricultural Research - Development Station Secuieni / Romania.

**Tel: 0735 906 254; *Email: gabi.nae83@yahoo.com*

***Keywords:*** *alternative proteins, plant proteins, microbial proteins, insect proteins, cultured meat*

## ABSTRACT

*Given the projected growth of the global population, there is an inherent need for sustainable processes to secure essential food resources, such as proteins. Although conventional animal-based proteins are nutritious, they carry a high ecological cost due to greenhouse gas emissions, extensive land use, and substantial water consumption. Alternative proteins offer a new approach to meeting the increasingly significant global demand for food. Key examples of alternative proteins include single-cell proteins, plant-based meat, insects, and cultured meat. These proteins are derived from various sources, including plant materials (such as soy, lentils, and peas), microbial sources (such as fungi and algae), insects, and laboratory-grown meat. This paper evaluates the scientific literature regarding extraction and processing methods for alternative proteins and analyzes their economic and environmental impact. Although these alternative protein sources face various limitations that hinder their mass adoption in the short term, the implementation of appropriate policies and continued research will undoubtedly establish them as a viable option for global nutrition in the future.*

## REZUMAT

*Având în vedere creșterea preconizată a populației globale, există o nevoie inerentă de proceduri durabile pentru a asigura resurse alimentare indispensabile, cum ar fi proteinele. Consumul de proteine animale convenționale, deși nutritiv, este costisitor din punct de vedere ecologic din cauza emisiilor de gaze cu efect de seră, a utilizării extensive a terenurilor și a consumului substanțial de apă. Proteinele alternative reprezintă o nouă abordare care poate rezolva nevoile alimentare din ce în ce mai semnificative la scară globală. Printre cele mai importante proteine alternative se numără proteinele unicelulare, carnea pe bază de plante, insectele și carnea cultivată. Originea proteinelor alternative este diversă și poate proveni din materiale vegetale precum soia, linte și mazăre, proteine microbiene precum ciuperci și alge, proteine pe bază de insecte și carne cultivată în laborator. Lucrarea a evaluat lucrări științifice specializate privind metodele alternative de extracție și procesare a proteinelor și a analizat impactul lor economic și de mediu. Sursele alternative de proteine prezintă diverse limitări, ceea ce face dificilă implementarea în masă într-un timp relativ scurt, dar prin adoptarea unor politici adecvate și continuarea cercetărilor în domeniu, acestea vor reprezenta cu siguranță o alternativă viabilă pentru nutriția globală în viitor.*

## INTRODUCTION

Driven by rapid demographic growth, changing dietary patterns, and heightened environmental consciousness, there is an urgent need to explore sustainable food alternatives. Alternative proteins have emerged as a pivotal framework to meet these expanding global needs. As highlighted in recent literature, the most prominent categories include plant-based meat substitutes, microbial and single-cell proteins, edible insects, and cultured meat (*Munialo et al., 2022; Kouřimská & Adámková, 2016*).

In the processing of alternative proteins, various methods are used to transform these raw materials into products that can have food quality. Proteins obtained from plants are subjected to extrusion and fermentation to improve their texture and digestion. Microbial and insect proteins are dried, ground and

fermented to be more digestible, while cultured meat uses tissue engineering processes and cell culture methods to build muscle-like structures *(Kumar, S. et al, 2021).*

In the United States, Europe and parts of Asia, alternative proteins are becoming increasingly popular, partly due to environmental concerns and partly due to dietary preferences such as vegetarianism and veganism *(Sexton, AE et al, 2022).* However, it is known that there are several problems associated with alternative proteins such as regulatory obstacles, high manufacturing costs, customer acceptance problems and technological limitations in increasing production *(Alcorta, A. et al, 2021).*

A strategy is needed to address these issues in order to integrate alternative proteins into the global diet. *(Cedeno, FRP et al, 2025).*

Plant proteins come from a variety of sources, including plants, insects, and cell-based meat. Plant proteins, such as soy, peas, and chickpeas, have been around for a long time and are the most widely consumed alternative proteins (Fig. 1).

At the same time, insects, including crickets and mealworms, are becoming available as a sustainable source of protein due to their reduced water, land, and nutrient requirements compared to conventionally raised animals. On the other hand, cell-based meat, also known as lab-grown meat, is a more recent development in which meat is produced in a laboratory without animals *(Yadav, S. et al, 2025).*

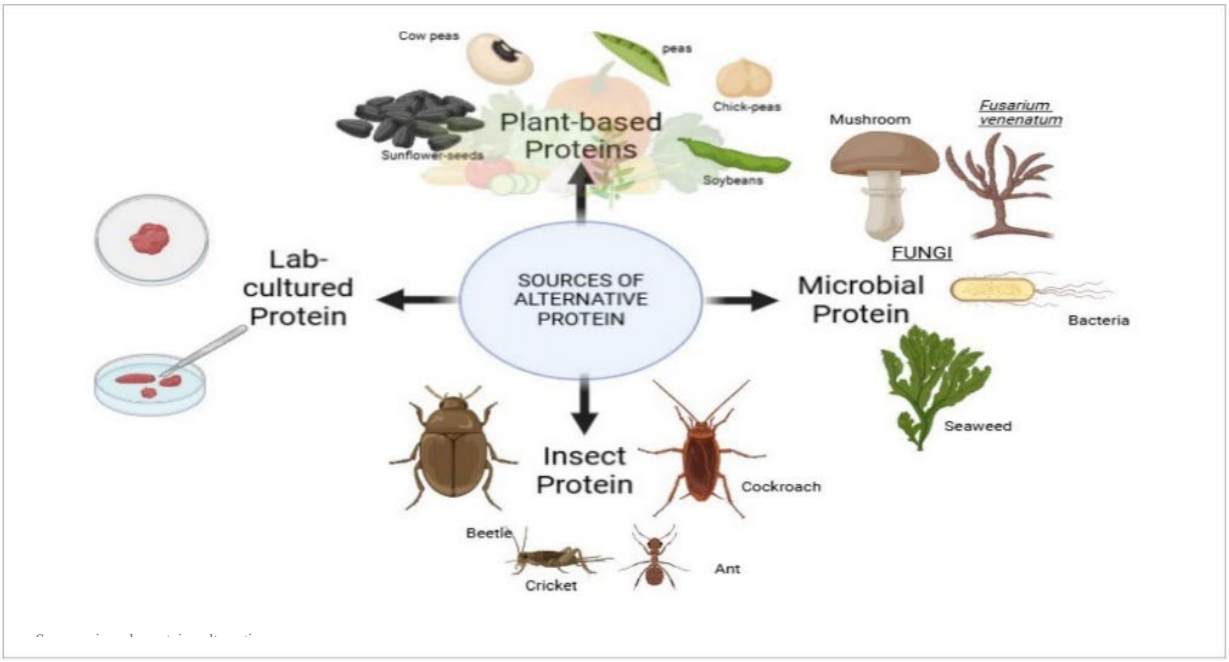



**Fig. 1 - The main alternative protein sources**
*(Kaur, S.P. et al, 2025)*

Traditional food production relies largely on animal protein sources, which have become increasingly unsustainable *(Jameel, S., 2023).* These production systems contribute substantially to environmental degradation, including deforestation, soil erosion and freshwater depletion *(Nguyen, TT et al, 2023)*.

At the same time, they have a significant contribution to greenhouse gas emissions, with cattle farming being responsible for approximately 14.5% of global anthropogenic emissions, mainly methane and nitrous oxide - gases with a significantly higher global warming potential compared to carbon dioxide *(Raihan, A., 2023)*.

The global population is projected to reach 8.5 billion by 2030, with the growth rate continuing to reach 9.7 billion by 2050 and possibly reach 10.4 billion by 2100. This unprecedented development comes with a significant constraint on natural resources, highlighting the critical need for sustainable development strategies to ensure equitable availability of essential goods such as land, fresh water and food *(Yang, Z. and Solangi, YA 2024)*.

This context generates an increasing demand for natural resources, which in turn impacts the global food supply, influences climate change and intensifies environmental degradation. Addressing these challenges requires modern solutions, such as alternative protein sources, to ensure sustainability (fig. 2), *(Nirmal, N. et al, 2025).*

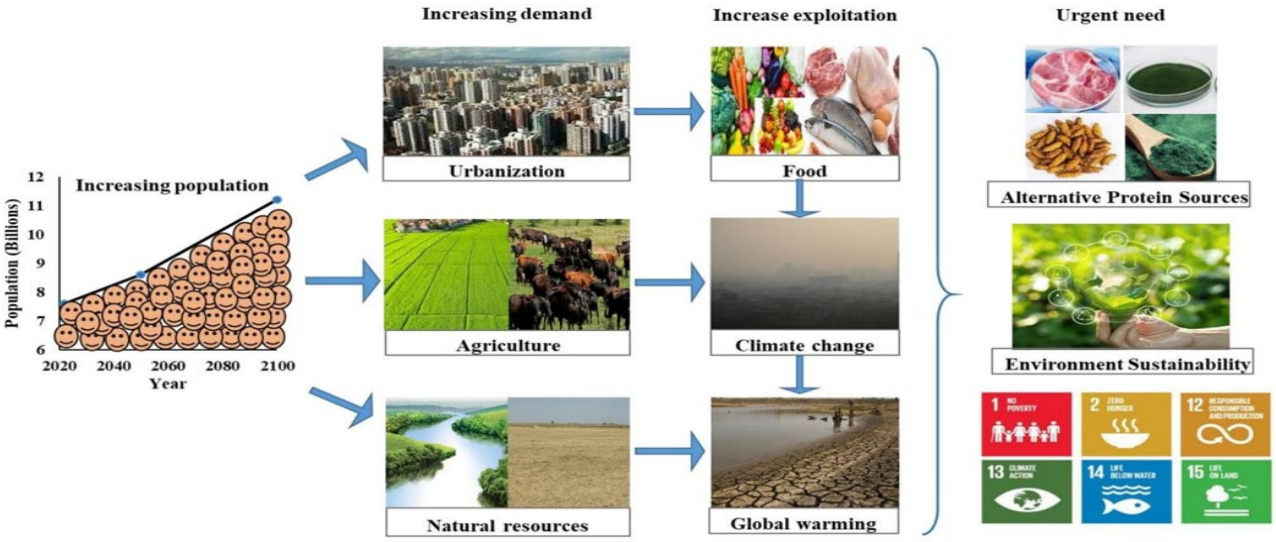



**Fig. 2 - Global population growth and the impact on natural resources, food supply and global warming**
*(Nirmal, N. et al, 2025)*

## 1.1 Alternative protein sources

### 1.1.1 Plant-based proteins

It is the most popular alternative to traditional proteins and includes legumes such as beans, lentils and peas, as well as whole grains, nuts and seeds. They are considered a more sustainable option, as vegetable proteins are rich in fiber, vitamins and minerals, making them a healthier choice *(Bryant, C. et al, 2021)*.

***Protein from legumes***

Legumes are identified as the edible seeds of leguminous plants such as beans and other legumes. They are an essential part of human nutrition as they are rich in protein, minerals, vitamins and caloric content. Due to their high protein content at affordable prices, legumes are commonly known as "poor man's meat". Legumes include, but are not limited to: beans, peas, pigeon peas, chickpeas, kidney beans, soybeans, lentils, cowpeas, black gram, etc. *(Chib, A. et al, 2024).*

***Soy protein***

Soybean is a legume plant grown primarily for its edible oil. It has a protein content of approximately 34-37%, including fiber. food and carbohydrates being comparatively higher than other cereals and legumes. Proteins lack some of the essential amino acids, such as cysteine and methionine, but possess all the remaining essential amino acids *(Yuliarti, O. et al, 2023).*

***Lentil protein***

Lentils are a member of the legume family and are described by their resemblance to a lentil; There are several varieties of lentils consumed such as green beans, red lentils, yellow pigeon peas, green and white peas, Bengal beans and black beans. Lentils contain essential amino acids such as leucine, phenylalanine, threonine and lysine and minerals such as iron, potassium, phosphorus, zinc and are rich in vitamin B *(Mistry et al., 2022).*

***Oilseed proteins***

Sunflower seeds, cottonseeds, rapeseeds, soybeans, and peanuts, which account for 68, 12, 7, 4, and 2% of global protein meal production, respectively, are the most abundant sources of protein. Some oilseed proteins lack sulfur-containing amino acids, as do animal proteins, but this can be corrected by adding a grain *(Surya Ulhas, R. et al, 2023).*

***Pea protein***

Peas are a well-known source of plant-based protein that has garnered significant attention in recent years. They are packed with protein, fiber, and antioxidants, and pea protein has a neutral flavor and is easily digestible *(Shanthakumar, P. et al, 2022).*

### 1.1.2 Microbial proteins (algae, bacteria, fungi)

***Mushrooms***

Mushrooms contain the sporocarps of edible mushrooms and the proteins of microfungal species such as yeast and molds *(Cardoso Alves, S. et al, 2023).*

Tempeh and Quora, a meat substitute, which have a protein content of approximately 45%, are made from the mycelium of *Fusarium venenatum.* Mycoproteins also have a high content of ribonucleic acid (RNA), which is characteristic of rapidly dividing cells. It should be noted that excessive consumption of RNA-rich foods can lead to health problems such as gout; therefore, it is essential to reduce the RNA content, usually through heat treatment *(Schweiggert-Weisz, U. et al, 2020).*

The diameter and length of the hyphae of *F.venenatum* allow them to give dishes a meat-like feel. The fungal protein contains 56% total protein content and 44% other nutrients. Edible mushrooms have a protein concentration of approximately 8.5–36.9%, much higher than that of many cereals and legumes *(Câmara, AKF et al, 2024).* The edible mushrooms with the highest protein content present in *Trichloma* are approximately 36.9%, and the lowest in *Tremella* is approximately 8.5% *(Yu, Q. et al, 2020).*

***Algae***

Given that seaweed is not widely consumed, there is less research on optimal digestion of seaweed. This makes it difficult to assess the quality of algae proteins *(Uma, G. et al., 2023).* In Compared to plant sources, microalgae and seaweed have a higher protein content. Microalgae can produce up to 70% of the proteins in cells, while soybeans produce only 30-40%. Some examples of algal protein sources are Spirulina (*Arthospira platensis)* and Chlorella *(Chlorella vulgaris, Chlorella protothecoides)* , *(Kurek, MA et al, 2022).*

**1.1.3 Insect proteins**

Edible insects contain a large amount of protein, lipids and other micronutrients, which contribute to improved dietary health in certain regions of the world. Some uncooked edible insects, such as *Sphenarium purpurascens,* have a protein content substantially higher than that of fish, pigs, poultry, cattle and many plant proteins. The insects most commonly consumed for protein are *Coleoptera beetles, Lepidoptera* and *Hymenoptera caterpillars,* wasps, bees and ants. Edible insects contain nutritionally valuable amino acids such as lysine, tryptophan, tyrosine, phenylalanine and threonine, as plant proteins do not contain these amino acids *(Rumpold, BA, and Schlüter, OK, 2013).*

**1.1.4 Lab-grown meat (clean meat)**

Lab-grown meat is also known as cultured or cell-based meat. This innovative method of producing animal proteins has the advantage that only the animals are fed and slaughtered *(Yuksel, S. and Mohr, JJ, 2023).* When growing meat in the laboratory, a very small number of animal cells, usually stem or satellite cells, are extracted at the beginning of the procedure and placed in a nutrient-rich culture medium *(Lima, M. et al, 2022).* Compared to traditional meat production, this method avoids the need to raise and slaughter animals, which has significant potential to address ethical concerns, reduce environmental impacts, and mitigate risks associated with zoonotic diseases *(Roy, B. et al, 2021).* It is also important to consider protein content, quality, and bioavailability, as well as the ecological footprint of additive proteins.

## MATERIALS AND METHODS

The paper evaluated specialized scientific papers on alternative protein extraction and processing methods. The next step was to determine the most eloquent scientific papers in the specialized literature on the proposed topic. The economic and environmental impact of various alternative protein extraction and processing methods was analyzed.

### 2.1 Alternative protein extraction methods

#### 2.1.1 Conventional extraction methods

***Solvent extraction*** - uses chemical solvents such as hexane, ethanol, or acetone to separate proteins from the source material. This extraction process is typically used for vegetable proteins, such as oilseeds (soybean, sunflower). The main benefit of solvent extraction is high protein yield and scalability. However, it also has limitations such as the use of volatile organic solvent residues in the final product and the risk of protein denaturation under harsh conditions *(Cui Q. et al, 2017)* .

***Aqueous extraction*** - proteins are extracted using water or a buffered solution (alkali and acids) at specific pH levels. It is widely used for the extraction of plant-based proteins, mainly rice and peas. Among the advantages of this method are that it is environmentally friendly, safe, simple and avoids the use of any harmful chemicals. Compared to the solvent extraction method, it has a lower efficiency *(Munialo, CD et al, 2023)*

***Mechanical extraction*** – the method does not involve the use of protein isolation chemicals or physical processes to separate proteins from raw materials, such as seeds, nuts or insects. This method

consists of grinding the raw material to break it down into smaller particles, followed by pressing or centrifugation to separate the protein-rich fractions from oils, water or solid residues. Mechanical extraction is used for oilseeds and insects. In combination with enzyme-assisted extraction, it improves the yield and quality of protein extracts *(Nadar, SS et al, 2018).*

***Isoelectric precipitation*** – consists of adjusting the pH of the solution to the isoelectric point, causing the precipitation of proteins. It exploits the principle of protein solubility at different pH levels. It is generally used for the extraction of proteins from plants and microbes. The benefits of this method lie in its ability to produce proteins with high purity and functionality. However, it requires precise pH control, and the acidic and alkaline conditions used can alter some proteins, affecting their nutritional and functional properties, *(Zhao, H. et al., 2020).*

***Thermal processing*** – involves heating raw materials to increase protein production, functionality or digestibility. The process consists of heating protein sources, such as insects, plant seeds or microbial biomass, at regulated temperatures, which are frequently combined with other extraction methods. Heat processing is used to deactivate antinutritional components, such as trypsin inhibitors from legumes, or to improve the sensory quality and texture of protein-based products. However, excessive heating can have negative consequences, such as protein degradation or loss of essential amino acids, thus reducing nutritional quality, *(Kaur, L. et al, 2022).*

**2.1.2. Innovative extraction methods**

***Enzyme-assisted extraction (EAE)*** - uses specific enzymes to improve protein recovery from biological sources. This method involves treating raw materials, such as plants, algae, or insects, with enzymes such as cellulases, proteases, or pectinases. This method is used in the food and pharmaceutical industries, having a high efficiency in producing high-quality proteins with minimal structural damage. EAE is valuable in industries, especially in the food and pharmaceutical industries. At the same time, it has limitations, such as the high cost of enzymes, longer processing times, and the need for precise control over reaction conditions to maintain efficiency *(Pojić, M. et al., 2018).*

***Ultrasound-assisted extraction (UAE):*** is a modern method that uses high-frequency sound waves to stimulate the extraction of proteins from various biological sources. In this method, the material is placed in a liquid medium and exposed to ultrasonic waves with a frequency of about 20 kHz. The method is flexible and can be used on a variety of protein sources, such as soy, legumes, microalgae and even insects *(Tiwari, BK, 2015).* The main advantage of the method is efficiency, as it requires a shorter processing time and operates at lower temperatures compared to conventional methods, which helps preserve the structure of sensitive proteins. However, there are some challenges, as high-intensity ultrasound can damage proteins, and scaling up the process for industrial use can be difficult *(Cravotto, G. and Binello, A., 2016).*

***Pulsed electric field (PEF)-assisted extraction*** - is an innovative extraction method that disrupts cell membranes with a short burst of high-voltage electrical pulses, enhancing the release of intracellular proteins and beneficial substances. In the process, raw materials such as microalgae, plant cells or microbial biomass are exposed to an electric field in a liquid medium *(Sweers, LJH et al., 2024).*

The main benefit is that the method is highly energy-efficient and environmentally friendly. However, it has limitations, including high initial equipment costs, the need for specialized systems to handle large-scale applications, and the variability of efficiency depending on the type and structure of the processed material *(Faizah N. et al., 2024).*

***Microwave-assisted extraction (MAE)*** - uses microwave energy to improve the extraction of proteins and other bioactive compounds from raw materials such as plants, algae or insects.

It has advantages such as shorter extraction times, lower solvent consumption, and increased energy efficiency. The method is particularly useful for materials with high water content or those that require gentle heating to maintain protein function and nutritional quality. The limitations are that it may be less effective for materials with low moisture content or for removing proteins firmly embedded in thick structures, *(Kumar S. et al, 2021).*

***High-pressure assisted extraction (HPAE)*** - is a novel method that uses hydrostatic pressure to increase protein recovery from a variety of biological materials, including plants, algae, and microbial biomass. This approach involves subjecting the raw materials to pressures ranging from 100 to 600 MPa (megapascals) in a liquid medium. High pressure damages cell walls and membranes, increases permeability, and encourages the release of intracellular proteins *(Kumar M. et al, 2021).*

### 2.2. Alternative protein processing methods

#### 2.2.1 Extrusion

Extrusion is the most commonly used processing technique. The method involves a high-temperature, high-pressure process in which a protein-based material is forced through a narrow opening using a screw mechanism inside an extruder. Extraction processing is of two types: high-moisture and low-moisture *(Ek, P. et al., 2020).* This method is extremely flexible and combines several unitary activities into a single system. Shearing, which is produced by the action of screws and material particles rubbing against each other, causes compaction, shearing, particle size reduction, phase transition, and molecular decomposition of the food material during the process, *(Sha, L., and Xiong, YL, 2020).*

#### *2.2.2. Cell shearing processes*

Cell shearing is a relatively new texturing method. In this technology, the upper cone remains stationary while the lower cone rotates at a predetermined speed. After the cell is sealed, the product is subjected to shear force and high temperatures (95–140 °C) in the space between the cones to reduce water evaporation. Compared to other high shear technologies, such as extrusion, shear flow is well defined due to its simple geometry and fewer shear cell parameters . This allows easy control over system and product properties, including fibril formation *(Dekkers, BL et al, 2018).*

#### *2.2.3. 3D printing processes*

Printing is described as a paste-like substance composed of protein powder, other chemicals, and water, applied layer by layer to create a structure. Inkjet printing and hot melt extrusion are two popular 3D printing techniques for food . However, this method works well with liquid materials because it is optimized for thermoplastic polymers with few constituents. When new components are added, the system must be re-optimized to identify important factors such as print viscosity, rheology, and cooking qualities *(McClements, DJ, and Grossmann, L., 2021).*

#### 2.2.4. Electrospinning

Electrospinning is described as a method that uses an electrical force to fabricate fibers at the micro and nanoscale. Although this method is mainly used in food delivery systems, it can also be useful in meat analog applications. Due to their complex secondary and tertiary structures, proteins, especially those derived from plants, are difficult to electrospinning. Even so, plant-based product compositions that resemble chicken strips can utilize electrospun zein fibers. The electrospinning process creates the well-formed fibrous structures needed in plant-based formulations, even though mechanical elongation is better at creating fibrous networks. However, for most plant proteins to spin well, a synthetic biopolymer may be required *(Ozturk, OK, and Hamaker, BR, 2023).*

## 3. RESULTS

The comparative findings obtained during the present paper are summarized in the table below, presenting a comprehensive overview of the composition, performance yields, and potential applications of each analyzed protein source.

**Table 1**

**Evaluation of various types of alternative proteins**

| No. Crt. | Plant-based proteins | Size | Microbial Protein/SCP | Insect proteins | Cultured meat | Reference |
|---|---|---|---|---|---|---|
| 1 | **Protein content (dry weight)** | - Moderate-high (20-40% depending on species)<br>- soy 30-40% | - Very high (40-80% depending on the body) | Typically 40–70%, depending on species | Similar to animal flesh (muscle cells), fat and texture varies | Joshi, VK, and Kumar, S., 2015 ; Rumpold, BA, and Schlüter, O. K. , 2013 |
| 2 | **Protein quality and amino acid profile** | - Medium to high protein content,<br>- Rich in lycopene, limited in methionine and cystine | - Very rich in protein (40–80%),<br>- essential amino acid profile balanced<br>- algae rich in leucine, lysine, isoleucine | - High protein content (40–70%)<br>- Good essential amino acid profile, rich in lysine, tryptophan, threonine, varies depending on species and diet. | - High protein content, matches conventional meats,<br>- Complete essential amino acid profile | Bleakley, S., and Hayes, M., 2017; Kurek, M.A. et al, 2022; Yuliarti, O. et al, 2023 |
| 3 | **Digestibility/bioavailability** | -PDCAAS 0.7-0.9; reduced by anti-nutritional factors | - High digestibility;<br>- Excess RNA in mushrooms can | - Good digestibility; chitin may reduce absorption | - High digestibility<br>- bioavailability, similar to | Kouřimská, L., and Adámková, A., 2016; Lima, |

| | | | | | | |
|---|---|---|---|---|---|---|
| | | (fats, tannins);<br>- Processing (fermentation, hydrolysis) improves bioavailability | cause health problems if left untreated;<br>- Fermentation improves use | - Processing (roasting, hydrolysis) improves bioavailability | beef or poultry | M. et al, 2022; Schweiggert-Weisz, U. et al, 2020 |
| 4 | **Environmental impact (land, water, greenhouse gases)** | - Smaller than conventional meat;<br>- unloaded requires agricultural land/water;<br>- variability depending on culture and region | - Reduced land use and greenhouse gas emissions compared to animals, but this depends of substrate and energy inputs. | - Lower than animals, efficient feed conversion, but challenges remain related to waste management and scaling | - Lowered to the ground, water and greenhouse gases, if renewable energy and resources are used effectively;<br>- energy consuming | Lynch, J., and Pierrehumbert, R., 2019; Poore, J., and Nemecek, T., 2018; |
| 5 | **Costs and scalability** | - Low to moderate cost.<br>- Competitive and supportive by those existing infrastructure. | - Moderately due to fermentation and downstream processing increases expenses<br>- Some processes are scalable, but purification of Food quality is expensive. | - Moderate scalability; moderate costs, because requires dechitinization in processing and security in controls | - High cost;<br>- Limited scalability, requires large investments | Joshi, VK, and Kumar, S., 2015; Kurek, M.A. et al, 2022; |
| 6 | **Consumer acceptance/culture** | - High in most regions,<br>- there is the perception of "processed" | - Mixture, algae/yeast somewhat accepted, but "there is stigma about microbes" | - High acceptance in certain areas of Asia, Africa, Latin America, America, but low in Western countries due to the perception of "disgusting" | - Mixed, intrigue, distrust, perception of "unnatural"/"lab-grown",<br>- Labeling and trust are essential. | Bryant, C., and Barnett, J., 2019; Hartmann, C., and Siegrist, M., 2017 |
| 7 | **Advantages** | - Widely available and affordable,<br>- Sustainable and with reduced impact on the environment<br>- Rich in fiber, vitamins and minerals | - High protein yield and complete amino acid profile | - High protein efficiency and rich in amino acid profile<br>- Rich in micronutrients. | - Biologically identical to animal meat, - Ethics (without animal slaughter)<br>- lower risk of zoonotic diseases. | Stephens, N. et al, 2018 |
| 8 | **limitation** | - Incomplete amino acid profile.<br>- Presence antinutritional factors, such as lectins, phytates, and oxalates.<br>- The allergenic potential of soybeans and peanuts | - Digestibility and taste problems (unwanted flavors of algae)<br>- Content high RNA (mycoproteins) requires processing<br>- Limited consumer acceptance | - Cultural and psychological barriers (the "disgusting factor").<br>- Reaction cross-allergic (with shellfish).<br>- Processing challenges for elimination of non-protein substances | - Very high production costs.<br>- Requires growth media with expensive components.<br>- The process is energy intensive.<br>- Limited scalability currently | Nirmal, N. et al, 2025 |

The comparative analysis shows clear trade-offs between protein density, amino acid profiles, and bioavailability across the evaluated alternatives. Microbial (SCP) and insect proteins offer the highest protein concentrations, matching or exceeding cultured meat and plant sources like soy. However, their raw nutritional value is often constrained by anti-nutritional factors, chitin, or high RNA levels in mycoproteins. Processing techniques such as fermentation, hydrolysis, and thermal treatment are essential to overcome these barriers, significantly improving digestibility (PDCAAS) and essential amino acid availability.

From an environmental and economic perspective, each protein category faces distinct scaling challenges. Plant-based proteins remain the most affordable and widely accepted option due to established agricultural infrastructure, despite higher land and water requirements. Conversely, cultured meat and microbial proteins dramatically reduce land use, but their industrial adoption is hindered by high production costs, energy demands, and technological bottlenecks. Furthermore, widespread market penetration for insect and lab-grown proteins relies heavily on overcoming psychological barriers (e.g., the "neophobia" or "disgust factor" in Western regions) and establishing clear regulatory frameworks.

## CONCLUSIONS

Protein content and quality vary depending on the protein source, with the lowest values being found in plant-based proteins, while microbial and insect proteins have medium-high content, and cultured meat has values similar to animal meat. Alternative protein sources offer important environmental, nutritional and ethical benefits, but widespread adoption requires overcome challenges such as cost, consumer acceptance and regulatory issues. Under certain conditions, regardless of alternative protein sources, the environmental impact is more or less reduced compared to conventional protein sources (animal origin). The lowest production costs are in the case of plant-based proteins, at the opposite end are protein sources from lab-grown meat, whose costs are high, and scalability is currently limited, requiring large investments. Alternative protein sources present various limitations, making mass implementation difficult in a relatively short time, but by adopting appropriate policies and continuing research in the field, they will certainly represent a viable alternative for global nutrition in the future.

## ACKNOWLEDGMENTS

This work was supported by a grant of the Ministry of Education and Research – National Authority for Research and UEFISCDI, project number PN-IV-P6-6.1-CoEx-2024-0025, contract no.11CoEX/2026, within PNCDI IV - Innovative strategies for ensuring nutritional security by stimulating the exploitation of sustainable protein resources PROfutureFOOD and Project ADER 16.1.1/29.01.2024 Research on the potential for superior exploitation of the Cannabis sativa species for food purposes, funded by the Ministry of Agriculture and Rural Development.

## REFERENCES

[1] Alcorta, A., Porta, A., Tárrega, A., Alvarez, MD, and Vaquero, MP (2021). Foods for plant-based diets: Challenges and innovations. *Foods 10* :293. https://doi.org/10.3390/foods10020293

[2] Bleakley, S., and Hayes, M. (2017). Algal proteins: Extraction, application, and challenges concerning production. Foods 6:33 https://doi.org/10.3390/foods6050033

[3] Bryant, C., and Barnett, J. (2019). Consumer acceptance of cultured meat: A systematic review. Front. Sustain. *Food Syst. 3:11* . doi: https://doi.org/10.3389/fsufs.2019.00011

[4] Bryant, C., van Nek, L., and Rolland, NC (2021). European markets for cultivated meat: A comparison of consumer attitudes and willingness to pay in the UK and the Netherlands. *Foods 9* :1297. https://doi.org/10.3390/foods9091152

[5] Câmara, AKF, Ozaki, MM, de Souza, PC, dos Santos, M., and Pollonio, MAR (2024). "Hybrid meat products: Using plant, fungi, and insect sources for flexitarian diets—technological, nutritional and sensory insights" in Food Analogues: Emerging Methods and Challenges. ed. A. P. Can, MG Saraç and DA Türkler (Switzerland: Springer Nature), 245–289.

[6] Cardoso Alves, S., Díaz-Ruiz, E., Lisboa, B., Sharma, M., Mussatto, SI, Thakur, VK, et al. (2023). Microbial meat: A sustainable vegan protein source produced from agri-waste to feed the world. *Food Res. International 166* :112596. https://doi.org/10.1016/j.foodres.2023.112596

[7] Cedeno, FRP, Olubiyo, OJ, and Ferreira, S. (2025). From microbial proteins to cultivated meat for alternative meat-like products: A review on sustainable fermentation approaches. *J. Biol. Eng.* 19:44. https://doi.org/10.1186/s13036-025-00509-9

[8] Chib, A., Gupta, N., Singh, J., Rishi, M., Verma, S., Langeh, A., et al. (2024). The plant advantage: Unlocking the secrets of plant-based proteins. *Plant. Arch. 24:75* . https://doi.org/10.51470/PLANTARCHIVES.2024.v24.no.1.075

[9] Cravotto, G., and Binello, A. (2016). "Low-frequency, high-power ultrasound-assisted food component extraction" in Innovative Food Processing Technologies (Amsterdam, Netherlands: Elsevier), 3–29.

[10] Cui, Q., Ni, X., Zeng, L., Tu, Z., Li, J., Sun, K., et al. (2017). Optimization of protein extraction and discoloration conditions for tea residues. Horticultural. Plant J. 3, 172–176. https://doi.org/101016/j.hpj.2017.06.003

[11] Dekkers, BL, Boom, RM, and van der Goot, AJ (2018). Structuring processes for meat analogues. *Trends Food Sci. Technol. 81* , 25–36. doi: https://doi.org/10.1016/j.tifs.2018.08.011

[12] Ek, P., Baner, JM, and Ganjyal, GM (2020). "Extrusion processing of cereal grains, tubers, and seeds" in Extrusion Cooking. ed. GM Ganjyal (Amsterdam, Netherlands: Elsevier), 225–263.

[13] Faizah, N., Widiyastuti, W., Setyawan, H., and Nurtono, T. (2024). Extraction of antioxidant and antibacterial agents from avocado (Persea americana) seed using pulsed electric field method. *Crop Ind. Prod. 222* :119803. https://doi.org/10.1016/j.indcrop.2024.119803

[14] Hartmann, C., and Siegrist, M. (2017). Consumer perception and behavior regarding sustainable protein consumption: A systematic review. *Appetite 112* , 227–234. https://doi.org/10.1016/j.appet.2017.02.004

[15] Jameel, S. (2023). "Climate Change, Food Systems and the Islamic Perspective on Alternative Proteins." *Trends in Food Science & Technology 138* : 480–490.

[16] Joshi, VK, and Kumar, S. (2015). Meat analogues: Plant-based alternatives to meat products—A review. Crit. rev. Food Sci. Nutrition 55, 1241–1245. https://doi.org/10.1080/10408398.2012.689381

[17] Kaur, L., Mao, B., Beniwal, AS, Abhilasha, KR, Chian, FM, and Singh, J. (2022). Alternative proteins vs animal proteins: The influence of structure and processing on their gastro-small intestinal digestion. *Trends Food Sci. Technol. 122* , 275–286. https://doi.org/10.1016/j.tifs.2022.02.021

[18] Kaur, SP, Sagar, NA and Rani, N. (2025). Alternative proteins: innovations in sources, processing, and consumption. *Front. Sustain. Food Syst. 9:* 1641712. https://doi.org/10.3389/fsufs.2025.1641712

[19] Kumar, M., Tomar, M., Potkule, J., Verma, R., Punia, S., Mahapatra, A., et al. (2021). Advances in the plant protein extraction: Mechanism and recommendations. *Food Hydrocoll. 115* :106595. https://doi.org/10.1016/j.foodhyd.2021.106595

[20] Kumar, S., Ghosh, P., and Agrawal, D. (2021). Single-cell protein: Production and process. Bioresour. *Technol. Rep. 15* :100728. https://doi.org/10.1016/j.biteb.2021.100728

[21] Kurek, MA, Onopiuk, A., Pogorzelska-Nowicka, E., Szpicer, A., Zalewska, M., and Półtorak, A. (2022). Novel protein sources for applications in meat-alternative products—Insight and challenges. Foods 11:957. https://doi.org/10.3390/foods11070957

[22] Kouřimská, L., and Adámková, A. (2016). Nutritional and sensory quality of edible insects. *NFS J. 4* , 22–26. https://doi.org/10.1016/j.nfs.2016.07.001

[23] Lima, M., Costa, R., Rodrigues, I., Lameiras, J., and Botelho, G. (2022). A narrative review of alternative protein sources: Highlights on meat, fish, egg and dairy analogues. *Foods 11* :2053. https://doi.org/10.3390/foods11142053

[24] Lynch, J., and Pierrehumbert, R. (2019). Climate impacts of cultured meat and beef cattle. Front. Sustain. *Food Syst. 3* :5. https://doi.org/.3389/fsufs.2019.00005

[25] McClements, DJ, and Grossmann, L. (2021). A brief review of the science behind the design of healthy and sustainable plant-based foods. NPJ Sci. *Food 5:17* . https://doi.org/10.1038/s41538-021-00099-y

[26] Mistry, K., Sardar, SD, Alim, H., Patel, N., Thakur, M., Jabbarova, D., et al. (2022). Plant-based proteins: Sustainable alternatives. *Plant Sci. Today* 2022:1652. two: 10.14719/pst.1652

[27] Munialo, CD, Stewart, D., Campbell, L., and Euston, SR (2022). Extraction, characterization and functional applications of sustainable alternative protein sources for future foods: A review. *Future Foods 6* :100152. https://doi.org/10.1016/j.fufo.2022.100152

[28] Munialo, CD (2023). A review of alternative plant protein sources, their extraction, functional characterization, application, nutritional value and pinch points to be the solution to sustainable food production. *International J. Food Sci. Technol. 59* , 462–472. https://doi.org/10.1111/ijfs.16467

[29] Nadar, SS, Rao, P., and Rathod, VK (2018). Enzyme assisted extraction of biomolecules as an approach to novel extraction technology: A review. Food Res. International 108, 309–330. https://doi.org/doi:10.1016/j.foodres.2018.03.006

[30] Nguyen, TT, U. Grote, F. Neubacher, MH Do, and GP Paudel. (2023). "Security Risks From Climate Change and Environmental Degradation: Implications for Sustainable Land Use Transformation in the Global South." *Current Opinion in Environmental Sustainability 63* : 101322.

[31] Nirmal, N., Anyimadu, CF, Khanashyam, AC, Bekhit, AE-dA, and Dhar, BK (2025). Alternative protein sources: Addressing global food security and environmental sustainability. *Sustainable Development, 33* : 3958-3969. https://doi.org/10.1002/sd.3338

[32] Ozturk, OK, and Hamaker, BR (2023). Texturization of plant protein-based meat alternatives: Processing, base proteins, and other constructional ingredients. *Future Foods 8* :100248. https://doi.org/10.1016/j.fufo.2023.100248

[33] Pojić, M., Mišan, A., and Tiwari, BK (2018). Eco-innovative technologies for extraction of proteins for human consumption from renewable protein sources of plant origin. *Trends Food Sci. Technol. 75* , 93–104. https://doi:10.1016/j.tifs.2018.03.010

[34] Poore, J., and Nemecek, T. (2018). Reducing food's environmental impacts through producers and consumers. *Science 360* , 987–992. https://doi:10.1126/science.aaq0216

[35] Raihan, A. (2023). "The Influence of Meat Consumption on Greenhouse Gas Emissions in Argentina." *Resources, Conservation & Recycling Advances 19* : 200183.

[36] Roy, B., Hagappa, A., Ramalingam, YD, Mahalingam, N., and Shaik, AB (2021). A review on lab-grown meat: Advantages and disadvantages. *Quest Int. J. Med. Health Sci. 4* , 19–24. https://doi:10.5281/zenodo.5201528

[37] Rumpold, BA, and Schlüter, OK (2013). Nutritional composition and safety aspects of edible insects. *Mol. Nutrition Food Res. 57* , 802–823. two: 10.1002/mnfr.201200735.

[38] Sexton, AE, Garnett, T., and Lorimer, J. (2022). Vegan food geographies and the rise of Big Veganism. *Prog. Hum. geogr. 46* , 605–628. https://doi.org/10.1177/03091325211051021 .

[39] Schweiggert-Weisz, U., Eisner, P., Bader-Mittermaier, S., and Osen, R. (2020). Food proteins from plants and fungi. *Curr. Opin. Food Sci. 32* , 156–162. https://doi.org/.1016/j.cofs.2020.08.003

[40] Sha, L., and Xiong, YL (2020). Plant protein-based alternatives of reconstructed meat: Science, technology, and challenges. *Trends Food Sci. Technol. 102* , 51–61 https://doi.org/10.1016/j.tifs.2020.05.022

[41] Shanthakumar, P., Klepacka, J., Bains, A., Chawla, P., Dhull, SB, and Najda, A. (2022). The current situation of pea protein and its application in the food industry. *Molecules 27* :5354. https://doi.org/10.10.3390/molecules27165354

[42] Stephens, N., Di Silvio, L., Dunsford, I., Ellis, M., Glencross, A., and Sexton, A. (2018). Bringing cultured meat to market: Technical, socio-political, and regulatory challenges in cellular agriculture. *Trends Food Sci. Technol. 78* , 155–166. https://doi.org/10.1016/j.tifs.2018.04.010

[43] Surya Ulhas, R., Ravindran, R., Malaviya, A., Priyadarshini, A., Tiwari, BK, and Rajauria, G. (2023). A review of alternative proteins for vegan diets: Sources, physico-chemical properties, nutritional equivalence, and consumer acceptance. *Food Res. International 173* :113479. doi: https://doi.org/10.1016/j.foodres.2023.113479

[44] Sweers, LJH, Mishyna, M., Ahrné, LM, Boom, RM, Fogliano, V., Patra, T., et al. (2024). Pulsed electric field processing of edible insect slurries induces thermally-assisted microbial inactivation. *Curr. Res. Food Sci. 10* :100940. https://doi.org/10.1016/j.crfs.2024.100940

[45] Tiwari, BK (2015). Ultrasound: A clean, green extraction technology. *TrAC Trends Anal. Chem. 71* , 100–109. two: https://doi.org/10.1016/j.trac.2015.04.013

[46] Uma, G., Jeraldine Nisha, S., Rameshbabu, D., Citarasu, T., and Immanuel, G. (2023). "Algal polymers, proteins, and pigments for industrial applications" in Haematococcus: Biochemistry. ed. R. Raja, S. Hemaiswarya, M. Narayanan, S. Kandasamy and KR Jayappriyan (Berlin, Springer Nature: Biotechnology and Biomedical Applications), 247–271

[47] Yadav, S., Kambhampati, V., and Mishra, S. (2025). "Future trends in food and dairy process engineering and business: A comprehensive exploration" in Engineering Solutions for Sustainable Food and Dairy Production: Innovations and Techniques in Food Processing and Dairy Engineering . *ed. SC Deka, C. Nickhil and AK Haghi (Berlin: Springer Nature Switzerland)* , 515–534

[48] Yang, Z., and Solangi, YA (2024). "Analyzing the Relationship Between Natural Resource Management, Environmental Protection, and Agricultural Economics for Sustainable Development in China." *Journal of Cleaner Production 450* : 141862

[49] Yu, Q., Guo, M., Zhang, B., Wu, H., Zhang, Y., and Zhang, L. (2020). Analysis of nutritional composition in 23 kinds of edible fungi., *J. Food Qual. 2020* :8821315.

[50] Yuksel, S., and Mohr, JJ (2023). Disrupting the plate: Cultured meat technology. Available online at: https://cmr.berkeley.edu/2023/07/disrupting-the-plate-cultured-meat-technology/ (Accessed Jul 31, 2023)

[51] Yuliarti, O., Muhd, B., Abdullah, F., Tan, MF, and Tay, JKK (2023). "Plant-based meat analogue" in Engineering Plant-Based Food Systems. ed. S. Prakash, BR Bhandari and C. Gaiani (Cambridge, MA: Academic Press), 169–183

[52] Zhao, H., Shen, C., Wu, Z., Zhang, Z., and Xu, C. (2020). Comparison of wheat, soybean, rice, and pea protein properties for effective applications in food products. *Journal of food biochemistry. 44* is 13157

# DEVELOPMENT AND EVALUATION OF INNOVATIVE FOOD PRODUCTS BASED ON HEMP SEEDS AND HEMP-DERIVED INGREDIENTS (*CANNABIS SATIVA* L.)

/

# *DEZVOLTAREA ȘI EVALUAREA UNOR PRODUSE ALIMENTARE INOVATOARE PE BAZĂ DE SEMINȚE DE CÂNEPĂ ȘI INGREDIENTE DERIVATE DIN CÂNEPĂ (CANNABIS SATIVA L.)*

**Alexandru Florin OLTEANU*[1, 2)], Gabriela Daniela CRIVEANU-STAMATIE[1)], Cristian FLOREA[1)], Serban CUCU[1)], Manuela RASCOL[1)], Tatiana ONISEI[1)]**

[1)] National Institute of Research and Development for Food Bioresources, INCDBA-IBA Bucharest, 6 Dinu Vintila Street, District 2, 021102, Bucharest / Romania;

[2)] University of Agronomic Sciences and Veterinary Medicine of Bucharest, USAMV Bucharest, 59 Marasti Blvd., District 1, 011464, Bucharest / Romania.

**Tel: 0771 520 310; *E-mail: alexandru-florin.olteanu@bioresurse.ro*

***Keywords:*** *hemp seeds, Cannabis sativa L., hemp protein powder, sensory analysis, hedonic test, gluten-free pasta, bakery products*

**ABSTRACT**

*Hemp seeds are rich in protein, fiber and minerals but remain underused in foods. This study developed four hemp-enriched products at pilot scale (muffins, cheese straws, bread rolls and gluten-free pasta) using hulled seeds, hemp flour or hemp protein powder at 5 to 100 g per 100 g of flour base. Consumer panels of 10 to 14 participants rated the products on a nine-point hedonic scale, and the products were analyzed for composition and microbiological quality; pasta cooking behavior was assessed. Muffins and cheese straws, containing 50 and 17 g of hemp seeds per 100 g of flour, obtained a mean hedonic score of 8. Bread rolls with 100 g of hemp flour per 100 g of wheat flour, plus brans and chia seeds, scored 4, whereas rolls with 5 g of hemp protein powder per 100 g of flour scored 8. Pasta made with hemp flour scored 6 and left dark particles and sediment in the cooking water, which the protein powder version did not. Cheese straws had the highest protein (19.85%) and fat (25.74%) contents. Yeasts, molds and Enterobacteriaceae were below 10 colony-forming units per gram in all products. Hemp ingredients can therefore enrich several cereal-based products.*

**REZUMAT**

*Semințele de cânepă sunt bogate în proteine, fibre și minerale, dar sunt insuficient utilizate. Studiul a dezvoltat la scară pilot patru produse cu cânepă (brioșe, sărățele cu brânză, chifle, paste fără gluten), cu semințe, făină sau pudră proteică de cânepă, în proporție de 5–100 g la 100 g de bază de făină. Produsele au fost evaluate de panouri de 10–14 consumatori (scară hedonică de nouă puncte) și analizate compozițional și microbiologic; s-a evaluat și comportamentul la fierbere al pastelor. Brioșele și sărățelele, cu 50 și 17 g de semințe la 100 g de făină, au obținut scorul mediu 8. Chiflele cu 100 g de făină de cânepă la 100 g de făină de grâu, plus tărâțe și chia, au obținut 4, iar cele cu 5 g de pudră proteică la 100 g de făină, 8. Pastele cu făină de cânepă au obținut 6 și au lăsat în apa de fierbere particule întunecate și sediment, nu și cele cu pudră proteică. Sărățelele au avut cele mai mari conținuturi de proteine (19,85%) și grăsimi (25,74%). Drojdiile, mucegaiurile și Enterobacteriaceae au fost sub 10 unități formatoare de colonii pe gram. Ingredientele din cânepă pot îmbogăți mai multe produse pe bază de cereale.*

**Abbreviations:** THC – $\Delta^9$-tetrahydrocannabinol; RH – relative humidity; SD – standard deviation; CFU – colony-forming units; n.d. – not determined; V1 – formulation with hemp flour; V2 – formulation with hemp protein powder; ANSVSA – National Sanitary Veterinary and Food Safety Authority.

## INTRODUCTION

Hemp (*Cannabis sativa* L.) is a multipurpose crop (*Crini et al., 2020; Visković et al., 2023*) whose seeds are increasingly regarded as a nutrient-dense food raw material. Hulled hempseed contains about one third protein and close to half fat, mostly unsaturated and with a favorable omega-6 to omega-3 ratio, together with dietary fiber, minerals and vitamins (*Farinon et al., 2020; Rizzo et al., 2023*). Hemp protein has

high digestibility (*Wang & Xiong, 2019*) and an amino acid score reported to be comparable to that of egg white (*Rizzo et al., 2023*). Besides whole and hulled seeds, hemp is processed into flour, oil and, from the press cake left after oil extraction, protein-rich meals, concentrates and isolates (*Leonard et al., 2020; Wang & Xiong, 2019*).

Despite this profile, hemp seeds remain underused in food (*Rizzo et al., 2023*). Legal restrictions introduced to curb the recreational use of cannabis rich in $\Delta^9$-tetrahydrocannabinol (THC) also limited the cultivation of low-THC industrial varieties, and the public confusion between industrial and drug hemp has discouraged research and investment in hemp foods (*Farinon et al., 2020; Rizzo et al., 2023*).

Many countries now distinguish between recreational and food use, and in the European Union maximum levels of THC have been set for hemp seeds and derived products (*European Commission, 2023*). Technological limitations also play a role, because some functional properties of hemp proteins restrict their use in food systems (*Leonard et al., 2020*).

Cereal-based products are a natural vehicle for hemp derivatives. In wheat bread, hemp seed cake flour at 5–40% raised the protein and phenolic contents but reduced porosity and increased hardness, while all samples remained acceptable to consumers (*Capcanari et al., 2023*). Hemp flour was also accepted by consumers in wheat bread, with a minor bitterness note (*Del Vecchio et al., 2025*), and hempseed protein isolate replacing 10–30% of the wheat flour in vegan muffins raised the protein content from 9.61% to 19.40% while maintaining overall sensory quality (*Du et al., 2025*). In durum wheat pasta, 5–40% hemp flour or 2.5–10% hemp cake increased the protein, fiber, ash and fat contents, hemp flour being the better raw material *(Teterycz et al., 2021)*.

Partial replacement of wheat flour with 5–20% hemp seed protein powder altered the cooking quality of pasta and improved its antioxidant capacity (*Axentii et al., 2023*), and a finer hemp flour at 7.5% substitution gave the best production performance and consumer acceptance among the levels tested (5–10%) (*Bonacci et al., 2023*).

Hemp is naturally gluten-free and has been used to improve gluten-free products (*Rizzo et al., 2023*). Up to 50% hemp flour in a gluten-free cake formulation increased the nutritional value, whereas higher levels impaired the physical and sensory properties (*Hayit et al., 2025*), and defatted hemp flour combined with rice flour was used to make gluten-free pasta (*Hastaoğlu et al., 2023*), and hemp press cake meal added at 5–30% to rice-based gluten-free sourdough bread was evaluated for its antioxidant, nutritional, technological and sensory effects (*Nakov et al., 2025*). This is relevant because gluten-free products are often nutritionally inferior to their gluten-containing counterparts, with low protein content among the main inadequacies (*Melini & Melini, 2019*).

The studies above, however, examined a single product category, and, to the best of our knowledge, the effect of the form of the hemp ingredient (seeds, flour or protein powder) and of its inclusion level has been little compared across different product types. In addition, no hemp-containing gluten-free pasta was found in the specialty stores consulted by the authors.

The aim of this study was therefore to develop four hemp-enriched products at pilot scale (muffins, cheese straws, bread rolls and gluten-free pasta), formulated with hulled seeds, hemp flour or hemp protein powder at different inclusion levels, and to evaluate their consumer acceptability, physico-chemical composition and microbiological quality.

## MATERIALS AND METHODS

### *Hemp-derived raw materials*

Hemp seeds (*Cannabis sativa* L., Secuieni-Jubileu variety) were supplied by the Secuieni Agricultural Research and Development Station (SCDA Secuieni) and processed by SC Canah International SRL (Salonta, Romania) into three ingredients.

Hulled seeds (hemp hearts) were obtained by mechanically breaking the whole seeds, grading them and separating the hulls by air aspiration at 15–20 °C. Hemp flour was produced by grinding the hulled seeds. Hemp protein powder was produced from the press cake (meal) remaining after oil extraction, which was ground in a stone mill and sieved at 45–48 °C.

The nutritional composition of the hulled seeds and of the protein powder, as stated in the supplier's technical specifications, is presented in Table 1.

**Table 1**

**Nutritional composition of the hemp-derived raw materials (supplier data, per 100 g)**

| Component | Hulled hemp seeds | Hemp protein powder |
|---|---|---|
| Protein [g] | 34 | 50 |
| Fat [g] | 48 | 11 |
| of which polyunsaturated fatty acids [g] | 37 | 7 |
| Carbohydrates [g] | 3.1 | 5.2 |
| of which sugars [g] | 2.6 | 4.1 |
| Dietary fiber [g] | 6 | 21 |
| Magnesium [mg] | 557 | 805 |
| Iron [mg] | 7.6 | 14 |
| Manganese [mg] | 5.7 | 12 |
| Zinc [mg] | 8.5 | 11 |

***Product formulations and manufacture***

Four products were developed and manufactured as pilot batches at the Pilot Experimental Station for Cereal and Flour Processing of INCDBA-IBA Bucharest: muffins with orange and hulled hemp seeds, cheese straws (savory biscuits) with hemp and sunflower seeds, bread rolls and gluten-free pasta. The formulations are given in Table 2, where the hemp inclusion level is expressed as grams of hemp ingredient per 100 g of non-hemp flour base. Bread rolls and pasta were each prepared in two variants: V1, containing hemp flour, and V2, in which hemp protein powder replaced hemp flour. This reformulation followed the sensory evaluation of V1; in the rolls, V2 also had a markedly lower hemp inclusion level and no added brans or chia seeds (Table 2).

**Table 2**

**Formulations of the experimental products (per batch)**

| Product | Hemp ingredient [g] | Flour base [g] | Hemp per 100 g flour base [g] | Other ingredients |
|---|---|---|---|---|
| Muffins | Hulled seeds, 50 | Wheat flour, 100 | 50.0 | 1 egg; orange juice, 150 mL; sour cream, 50 g; baking powder, coconut oil, raisins and orange zest, 5 g each |
| Cheese straws | Hemp seeds, 100 | White wheat flour, 600 | 16.7 | Cow's-milk telemea, 400 g; sheep's-milk telemea, 200 g; margarine, 150 g; sunflower seeds, 150 g; 1 egg (~50 g, for brushing); Himalayan salt, 50 g; caraway seeds, 50 g (total 1,750 g) |
| Bread rolls V1 | Hemp flour, 100 | Whole-wheat flour, 100 | 100.0 | Dry yeast, 7 g; salt, 5 g; psyllium bran, 50 g; oat bran, 60 g; wheat bran, 30 g; chia seeds, 15 g; olive oil, 30 g; water, 400–450 mL |
| Bread rolls V2 | Hemp protein powder, 50 | Whole-wheat flour, 1,000 | 5.0 | Dry yeast, 7 g; salt, 15 g; water, 600–650 mL |
| Pasta V1 | Hemp flour, 150 | Rice flour, 770 + cornmeal, 110 | 17.0 | Corn starch, 100 g; modified starch, 70 g; water, 350–400 mL |
| Pasta V2 | Hemp protein powder, 150 | Rice flour, 770 + cornmeal, 110 | 17.0 | Corn starch, 100 g; modified starch, 70 g; water, 350–400 mL |

Hulled hemp seeds (10–20 g) were optionally sprinkled on the rolls for decoration.

For the muffins, eggs were beaten until frothy and combined with melted coconut oil (35–40 °C), sour cream, orange juice and grated orange zest (wet phase). Sifted flour, baking powder, hemp seeds and a pinch of salt were homogenized separately (dry phase) and gradually incorporated into the wet phase under continuous mixing. Raisins, previously rehydrated in orange juice for 10–15 min and drained, were folded in at the end, and the batter was portioned into aluminum molds filled to about two thirds of their volume. For the cheese straws, the ingredients were tempered at room temperature for 20–30 min, the

cheeses were finely grated, and all ingredients were kneaded into a homogeneous, compact dough, which was rolled out, cut into strips, placed on parchment-lined trays, brushed with beaten egg and sprinkled with salt and caraway seeds. For the bread rolls, the dry ingredients were homogenized in a mixer and lukewarm water (35–40 °C) was added gradually until an elastic, non-sticky dough was obtained; after bulk fermentation in a covered, lightly oiled bowl, the dough was divided into pieces of approximately 120 g, shaped into rounds, proofed on parchment-lined trays and baked. For the pasta, rice flour, hemp ingredient, corn starch and modified starch were sifted and mixed, and water was added gradually until a homogeneous, slightly crumbly but compact dough was obtained; after resting, the dough was shaped in a pasta press (extrusion) into fusilli-type pasta, pre-dried and dried to a final moisture content below 13%. The main processing parameters are summarized in Table 3.

**Table 3**

**Main processing parameters of the experimental products**

| Stage | Muffins | Cheese straws | Bread rolls | Gluten-free pasta |
|---|---|---|---|---|
| Mixing / kneading | Wet phase 5–7 min and final mixing 5–7 min, 22–25 °C | 8–10 min, 20–22 °C | 8–10 min; dough 25–27 °C | 10–15 min, 20–25 °C |
| Fermentation / resting | – | – | Bulk: 30–40 min, 28–30 °C; final proofing: 20–30 min, 30–35 °C, RH 75–80% | Rest: 20–30 min |
| Forming | Molds filled to 2/3 | Dough rolled to 5–7 mm | ~120 g dough pieces (110–115 g after baking) | Extrusion, 6–10 MPa, 25–30 °C |
| Baking / drying | 180 °C, 20–25 min | 190 °C, 20–25 min | 220 °C, 18–20 min | Pre-drying 35–40 °C, 20 min; drying 40–60 °C, 3–6 h |
| Cooling | 20–30 min, rack | 30 min, rack | 30–40 min, rack | 1 h, 20–25 °C |
| Storage | 18–22 °C, RH 65–70%, max. 3 days | 18–22 °C, RH < 60% | 18–22 °C, RH 60–70%, 24–48 h | 18–22 °C, RH < 65% |

RH – relative humidity.

***Sensory evaluation***

Consumer acceptability was assessed in the sensory analysis laboratory of INCDBA-IBA Bucharest. The panels comprised 11 consumers for the muffins (7 women, 4 men; mean age 38 years), 14 for the cheese straws (11 women, 3 men; mean age 40 years), 14 for the bread rolls (10 women, 4 men; mean age 39 years) and 10 for the gluten-free pasta (7 women, 3 men; mean age 30 years). The panels for the bread rolls and the pasta evaluated the V1 formulations, and the reformulated V2 rolls were also scored in the hedonic test. Each product was evaluated individually, on a different day. Samples were coded and arranged for serving shortly before the analysis to prevent drying, hardening or cooling; pasta was evaluated after cooking. Room-temperature water was used to rinse the mouth between samples. Two tests were applied. In the descriptive test, attributes were scored on a 1–5 intensity scale (1 = imperceptible or weak; 2.5 = medium; 5 = very intense), covering appearance (e.g., exterior and interior color, crumb freshness, crumbliness, elasticity and pore uniformity for baked products; surface and shape retention for pasta), aroma, taste (e.g., hemp, sweet, salty, sour, bitter), texture (firmness at first bite, cohesiveness, adhesiveness, stickiness) and aftertaste. In the hedonic test, overall liking was scored on a 9-point scale (9 = like extremely; 5 = neither like nor dislike; 1 = dislike extremely).

***Physico-chemical analyses***

Analyses were performed on the finished products. Muffins and bread rolls were analyzed as dried crumb, as prescribed by the standards, and the results were recalculated to the initial product. Moisture was determined by oven drying 5 ± 1 g of sample at 130 °C for 120 ± 5 min. Crude protein was determined by the Kjeldahl method on a BUCHI KjelMaster K-375 system; the result was the mean of two determinations differing by no more than 0.5 g per 100 g of sample. Ash was determined by incinerating 2–3 g of sample in a muffle furnace at 750 °C (pre-ashing followed by 4 h of ashing), cooling in a desiccator and weighing to 0.1 mg; the result was the mean of two determinations, expressed to 0.01%. Fat was extracted from approximately 5 g of sample with petroleum ether (PA grade) on a FOSS Soxtec system (boiling 40 min,

rinsing 150 min, solvent recovery 15 min, solvent evaporation 10 min at 105 °C) and determined gravimetrically. Crude fiber was determined on approximately 1 g of sample by sequential digestion in boiling sulfuric acid and sodium hydroxide solutions in FiberBags, followed by drying at 105 ± 1 °C and ashing at 600 °C, with a blank run in parallel. Acidity was determined by titration with 0.1 mol/L NaOH in the presence of phenolphthalein, as follows: for baked products, 25 g of sample made up to 250 mL and a 50 mL aliquot; for pasta, 5 g of finely ground sample in 50 mL of water. The sugar content of the muffins was determined by iodometric titration (Fehling reagents, 0.1 mol/L sodium thiosulfate) after clarification with zinc sulfate and potassium ferrocyanide and acid inversion.

***Cooking behavior of pasta***

Cooking behavior was determined by volume displacement. Fifty grams of pasta were placed in a 500 $cm^3$ graduated cylinder containing approximately 300 $cm^3$ of room-temperature water, and the volume occupied by the pasta was calculated from the change in water level. The pasta was then cooked in 1 L of boiling water containing 7 g of salt until optimum cooking time, rinsed with 250 mL of cold water, and its volume was measured again; the volume increase was expressed as the ratio of cooked to raw volume. The odor during cooking, the shape retention of the pasta, and the odor and opalescence of the cooking water were recorded. A portion of the cooking water was poured into a 250 mL Berzelius beaker and left to stand, after which the sediment height was measured with a graduated ruler.

***Microbiological analyses***

Yeasts and molds were enumerated according to SR ISO 21527-1:2009 and Enterobacteriaceae according to SR ISO 21528-2:2017 (colony-count techniques). Results were expressed as CFU/g and assessed against the criteria of Order No. 27/2011 of the National Sanitary Veterinary and Food Safety Authority (ANSVSA) for the product category simple bakery products (ANSVSA, 2011).

***Data presentation***

Physico-chemical results are reported as mean ± standard deviation of replicate determinations. Sensory data were summarized descriptively, as mean scores and distributions of individual scores, and the descriptive attributes were represented as spider (radar) diagrams.

## RESULTS

***Physico-chemical composition***

The composition of the finished products is presented in Table 4. Cheese straws had the highest protein, fat and ash contents of the four products. Bread rolls had the highest moisture and crude fiber contents, with cheese straws second in crude fiber. Pasta had the lowest moisture, fat and ash contents, and its moisture content was below 10%. Sugars were determined only in the muffins. The composition of the dried crumb of muffins and rolls, on which the analyses of these two products were performed, is given in Table 5.

**Table 4**

**Physico-chemical composition of the finished products (g per 100 g of initial product, mean ± SD)**

| Parameter | Muffins | Cheese straws | Bread rolls | Gluten-free pasta |
|---|---|---|---|---|
| Moisture [%] | 38.69 ± 0.22 | 13.32 ± 0.21 | 45.78 ± 0.31 | 9.08 ± 0.08 |
| Protein [%] | 8.65 ± 0.26 | 19.85 ± 0.18 | 9.47 ± 0.63 | 7.04 ± 0.04 |
| Fat [%] | 13.05 ± 0.38 | 25.74 ± 0.11 | 5.50 ± 0.22 | 0.15 ± 0.03 |
| Ash [%] | 1.88 ± 0.03 | 2.94 ± 0.18 | 1.63 ± 0.07 | 0.85 ± 0.05 |
| Crude fiber [%] | 1.03 ± 0.01 | 6.63 ± 0.18 | 7.92 ± 0.47 | 1.46 ± 0.16 |
| Sugars [%] | 10.24 ± 0.32 | n.d. | n.d. | n.d. |
| Acidity [degrees] | 4.1 | 5.5 | 1.8 | 1.0 |

n.d. – not determined.

**Table 5**

**Composition of the dried crumb of muffins and bread rolls (g per 100 g, mean ± SD; moisture values without SD)**

| Parameter | Muffins | Bread rolls |
|---|---|---|
| Moisture [%] | 3.68 | 4.66 |
| Protein [%] | 13.84 ± 0.11 | 17.04 ± 0.47 |
| Fat [%] | 20.89 ± 0.13 | 9.90 ± 0.00 |

| Parameter | Muffins | Bread rolls |
|---|---|---|
| Sugars [%] | 16.47 ± 0.14 | n.d. |
| Ash [%] | 3.01 ± 0.01 | 2.93 ± 0.01 |
| Crude fiber [%] | 1.66 ± 0.02 | 14.25 ± 0.28 |

n.d. – not determined.

***Cooking behavior of pasta***

The V1 pasta reached optimum cooking in 6–7 min, retained its shape and increased its volume 2.8 times. Its cooking water was opalescent and, after standing, a substantial sediment containing small dark particles settled at the bottom of the beaker; dark particles were also visible on the surface of the dry and cooked pasta, and the bite was slightly grainy. The V2 pasta, in which hemp flour was replaced by hemp protein powder, was somewhat darker but uniform in color, without dark particles; its cooking water was opalescent, but no sediment rich in dark particles was formed.

***Sensory evaluation***

The descriptive sensory profiles are shown in Fig. 1 and the hedonic scores in Table 6. The muffins were light in color inside and outside, with a fresh crumb of high elasticity, a pleasant taste and smell, a weak hemp taste (1.2 on the 1–5 scale) and a low aftertaste (2.0). The cheese straws had a pleasant exterior and interior appearance, a predominantly cereal aroma and a salty taste; the hemp aroma (1.5) and the bitter taste were very low or imperceptible, and the firmness at first bite was high but not excessive. The V1 rolls had a pleasant exterior and interior appearance, good elasticity and medium pore uniformity; their crumb aroma was dominated by cereal and hemp notes, the bitter taste was above average (3.6), the consistency was dense and grainy, and the firmness of crust and crumb was medium (2.9 and 2.7), with low cohesiveness and adhesiveness (2.3 and 1.8). The V2 rolls were lighter in color and fluffier, with an improved taste. The V1 pasta had a pleasant surface appearance, kept its shape after cooking, a medium, neutral smell with a faint hemp note, medium firmness, a neutral to slightly bland taste and a medium degree of stickiness; the bitter and foreign tastes (1.3 and 1.4) were imperceptible or very weak, and the aftertaste persistence was low (2.1).

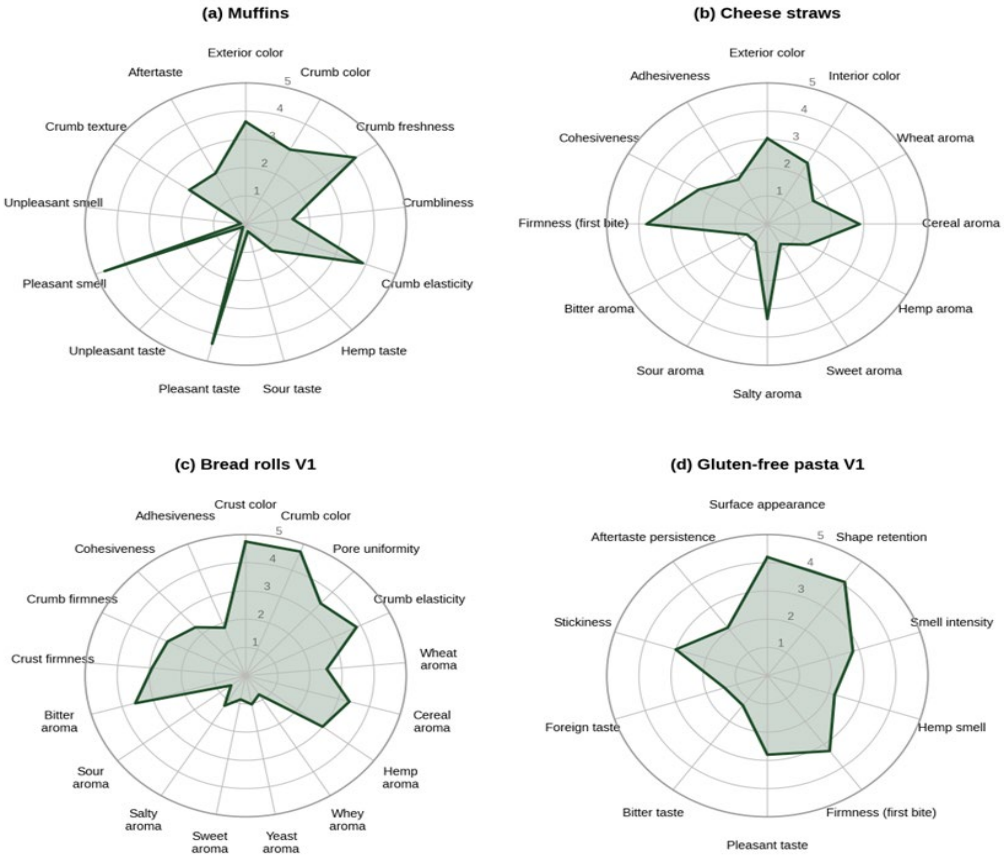



**Fig. 1 - Spider diagrams of the descriptive sensory profiles**

*(a) muffins; (b) cheese straws; (c) bread rolls V1; (d) gluten-free pasta V1. Mean scores on the 1–5 intensity scale.*

Muffins, cheese straws and the reformulated V2 rolls obtained a mean hedonic score of 8, whereas the V1 rolls obtained the lowest score, with 64% of the panelists scoring below 5 and 36% above 5.

**Table 6**

**Hedonic scores of the experimental products (9-point scale)**

| Product | Panel (n) | Mean score | Rating | Range of individual scores |
|---|---|---|---|---|
| Muffins | 11 | 8 | Like very much | 7–8 |
| Cheese straws | 14 | 8 | Like very much | 7–9 |
| Bread rolls V1 | 14 | 4 | Dislike slightly | – |
| Pasta V1 | 10 | 6 | Like slightly | 3–9 |

***Microbiological quality***

The counts of yeasts and molds and of *Enterobacteriaceae* were below 10 CFU/g in all four products, which therefore complied with ANSVSA Order No. 27/2011 (ANSVSA, 2011).

## CONCLUSIONS

Hemp seeds and their derivatives (hulled seeds, flour and protein powder) were successfully incorporated into four new products at pilot scale, with hemp inclusion levels ranging from 5 to 100 g per 100 g of non-hemp flour base. Muffins and cheese straws, containing hemp seeds at 50 and 17 g per 100 g of flour, respectively, were well accepted (mean hedonic score 8), and their hemp notes were weak or imperceptible. The cheese straws had the highest protein (19.85%) and fat (25.74%) contents, and the bread rolls the highest crude fiber content (7.92%).

Reformulation was decisive for the products made with hemp flour. The V1 rolls, with 100 g of hemp flour per 100 g of wheat flour plus brans and chia seeds, were dense, grainy and bitter and obtained a mean score of 4, whereas the V2 rolls, with 5 g of hemp protein powder per 100 g of flour, were lighter and fluffier and reached 8. Because several factors were changed simultaneously in V2 (the hemp ingredient, its inclusion level, and the brans and chia seeds), their individual effects could not be separated. In the pasta, replacing hemp flour with protein powder eliminated the dark particles and the sediment rich in dark particles in the cooking water, while the V1 pasta was moderately accepted (mean score 6). All products complied with the microbiological criteria applied.

Future work should separate the effects of the hemp ingredient and of its inclusion level, using larger consumer panels and including shelf-life studies, and should extend the use of hemp derivatives to other product categories, such as extruded snacks, breakfast cereals, plant-based beverages, protein bars and confectionery, as well as to the valorization of processing by-products such as hull fiber and press cake.

## ACKNOWLEDGEMENTS

This work was carried out within the framework of project ADER 16.1.1: “Research on the potential for high-value utilization of the *Cannabis sativa* species for food purposes,” funded by the Romanian Ministry of Agriculture and Rural Development (MADR) for the 2023–2026 period.

## REFERENCES

[1] ANSVSA. (2011). Order No. 27 of 6 June 2011 on the approval of the microbiological and hygiene criteria applicable to foodstuffs other than those covered by Commission Regulation (EC) No 2073/2005 of 15 November 2005 on microbiological criteria for foodstuffs. https://legislatie.just.ro/Public/DetaliiDocumentAfis/129504

[2] Axentii, M., Stroe, S.-G., & Codină, G. G. (2023). Development and Quality Evaluation of Rigatoni Pasta Enriched with Hemp Seed Meal. Foods, 12(9), 1774. https://doi.org/10.3390/foods12091774

[3] Bonacci, S., Di Stefano, V., Sciacca, F., Buzzanca, C., Virzì, N., Argento, S., & Melilli, M. G. (2023). Hemp Flour Particle Size Affects the Quality and Nutritional Profile of the Enriched Functional Pasta. Foods, 12(4), 774. https://doi.org/10.3390/foods12040774

[4] Capcanari, T., Covaliov, E., Negoița, C., Siminiuc, R., Chirsanova, A., Reșitca, V., & Țurcanu, D. (2023). Hemp Seed Cake Flour as a Source of Proteins, Minerals and Polyphenols and Its Impact on

the Nutritional, Sensorial and Technological Quality of Bread. Foods, 12(23), 4327. https://doi.org/10.3390/foods12234327

[5] Crini, G., Lichtfouse, E., Chanet, G., & Morin-Crini, N. (2020). Applications of hemp in textiles, paper industry, insulation and building materials, horticulture, animal nutrition, food and beverages, nutraceuticals, cosmetics and hygiene, medicine, agrochemistry, energy production and environment: A review. Environmental Chemistry Letters, 18(5), 1451–1476. https://doi.org/10.1007/s10311-020-01029-2

[6] Del Vecchio, L., Carini, E., Di Fazio, A., Chiodetti, M., Dall'Asta, C., Galaverna, G., & Cirlini, M. (2025). Enhancing wheat-bread with hemp flour: Impact on chemical, volatile, and sensory properties. Food Research International, 221, 117439. https://doi.org/10.1016/j.foodres.2025.117439

[7] Du, H., Baek, I., Jang, Y., Said, N. S., & Lee, W. Y. (2025). Effects on Physicochemical, Nutritional, and Quality Attributes of Fortified Vegan Muffins Incorporated with Hempseed as an Alternative Protein Source. Foods, 14(4), 601. https://doi.org/10.3390/foods14040601

[8] European Commission. (2023). Commission Regulation (EU) 2023/915 of 25 April 2023. http://data.europa.eu/eli/reg/2023/915/oj

[9] Farinon, B., Molinari, R., Costantini, L., & Merendino, N. (2020). The Seed of Industrial Hemp (Cannabis sativa L.): Nutritional Quality and Potential Functionality for Human Health and Nutrition. Nutrients, 12(7), 1935. https://doi.org/10.3390/nu12071935

[10] Hastaoğlu, E., Kelek, Z., & Çapar, D. (2023). Investigation of the Possibilities of Developing Gluten-Free Pasta Containing Hemp Pulp Flour and Rice Flour. Turkish Journal of Agriculture - Food Science and Technology, 11(11), 2080–2088. https://doi.org/10.24925/turjaf.v11i11.2080-2088.6240

[11] Hayit, F., Balıkcı, E., Yazıcı, L., & Bescanlar, S. (2025). Investigation of the Usability of Hemp Flour in the Production of Gluten-Free Cakes. Journal of Culinary Science & Technology, 23(4), 919–935. https://doi.org/10.1080/15428052.2024.2357282

[12] Leonard, W., Zhang, P., Ying, D., & Fang, Z. (2020). Hempseed in food industry: Nutritional value, health benefits, and industrial applications. Comprehensive Reviews in Food Science and Food Safety, 19(1), 282–308. https://doi.org/10.1111/1541-4337.12517

[13] Melini, V., & Melini, F. (2019). Gluten-Free Diet: Gaps and Needs for a Healthier Diet. Nutrients, 11(1), 170. https://doi.org/10.3390/nu11010170

[14] Nakov, G., Jukić, M., Soler, F., Syleimanova, S., Lukinac, J., Estivi, L., Brandolini, A., & Hidalgo, A. (2025). Enhancing the Antioxidant and Nutritional Profile of Gluten-Free Sourdough Bread Using Hemp Press Cake Meal. Foods, 14(20), 3571. https://doi.org/10.3390/foods14203571

[15] Rizzo, G., Storz, M. A., & Calapai, G. (2023). The Role of Hemp (Cannabis sativa L.) as a Functional Food in Vegetarian Nutrition. Foods, 12(18), 3505. https://doi.org/10.3390/foods12183505

[16] Teterycz, D., Sobota, A., Przygodzka, D., & Łysakowska, P. (2021). Hemp seed (Cannabis sativa L.) enriched pasta: Physicochemical properties and quality evaluation. PLOS ONE, 16(3), e0248790. https://doi.org/10.1371/journal.pone.0248790

[17] Visković, J., Zheljazkov, V. D., Sikora, V., Noller, J., Latković, D., Ocamb, C. M., & Koren, A. (2023). Industrial Hemp (Cannabis sativa L.) Agronomy and Utilization: A Review. Agronomy, 13(3), 931. https://doi.org/10.3390/agronomy13030931

[18] Wang, Q., & Xiong, Y. L. (2019). Processing, Nutrition, and Functionality of Hempseed Protein: A Review. Comprehensive Reviews in Food Science and Food Safety, 18(4), 936–952. https://doi.org/10.1111/1541-4337.12450

# STUDY ON THE MECHANICAL PROCESSING OF COMPOST
# /
# *STUDIU PRIVIND PRELUCRAREA MECANICĂ A COMPOSTULUI*

**Stefan DUMITRU*[1, 2)], Nicolae-Valentin VLĂDUȚ[1)], Gabriel-Valentin GHEORGHE[1)], Alin HARABAGIU[1)], Dragos-Nicolae DUMITRU[1)], Oana Elena MILEA[2)]**

[1)] INMA Bucharest / Romania;

[2)] UNSTPB Bucharest / Romania.

**E-mail: stefan.dumitru2311@gmail.com*

***Keywords:*** compost, mechanical processing, size reduction, mixing, turning, screening, equipment

**ABSTRACT**

*Composting is one of the main methods for recovering biodegradable organic waste, and process efficiency depends not only on biological and biochemical transformations but also on the mechanical operations applied to the material. This paper presents a review of compost mechanical processing, focusing on the relationship between material physical properties and the constructive and operating parameters of processing equipment. Size reduction, mixing, turning, conveying and screening operations are discussed together with the influence of moisture content, bulk density, porosity, particle-size distribution, feed rate and active-element speed. The literature indicates that particle-size reduction may intensify biodegradation by increasing specific surface area, while excessive comminution can reduce free air space and increase airflow resistance. Mechanical turning contributes to homogenization, disruption of compacted zones and redistribution of oxygen and moisture, but its frequency must be correlated with process stage and energy use. During finishing, screening separates particle-size fractions and improves product uniformity. The study highlights the need for an integrated engineering approach in which material characteristics and equipment parameters are analysed simultaneously to increase productivity, reduce specific energy consumption and obtain compost with uniform properties.*

**REZUMAT**

*Compostarea reprezintă una dintre principalele metode de valorificare a deșeurilor organice biodegradabile, iar eficiența procesului este condiționată nu numai de transformările biologice și biochimice, ci și de operațiile mecanice aplicate materialului. Lucrarea prezintă un studiu de sinteză privind prelucrarea mecanică a compostului, cu accent asupra relației dintre proprietățile fizice ale materialului și parametrii constructivi și funcționali ai echipamentelor. Sunt analizate operațiile de mărunțire, amestecare, întoarcere, transport și cernere, precum și influența umidității, densității aparente, porozității, granulometriei, debitului de alimentare și vitezei organelor active. Analiza literaturii evidențiază faptul că reducerea dimensiunii particulelor poate intensifica biodegradarea prin creșterea suprafeței specifice, dar o mărunțire excesivă poate diminua spațiul liber pentru aer și poate crește rezistența la curgerea aerului. Întoarcerea mecanică contribuie la omogenizare, destrămarea zonelor compactate și redistribuirea oxigenului și umidității, însă frecvența de lucru trebuie corelată cu stadiul procesului și cu consumul energetic. În etapa de finisare, cernerea asigură separarea fracțiilor granulometrice și îmbunătățirea uniformității produsului. Rezultatele studiului indică necesitatea unei abordări integrate, în care caracteristicile materialului și parametrii echipamentelor sunt analizați simultan pentru creșterea productivității, reducerea consumului energetic specific și obținerea unui compost cu proprietăți uniforme.*

## INTRODUCTION

Organic waste management represents a significant technological and environmental challenge, and composting offers the opportunity to transform a wide range of biodegradable residues into a stabilized product suitable for use as an organic soil amendment. Composting is a controlled bio-oxidative process in which organic matter undergoes mineralization and partial humification; the process's progression depends on the interaction between temperature, moisture, aeration, the C/N ratio, pH, and the physical structure of the material (*de Bertoldi et al., 1983; Haug, 1993; Insam, Bertoldi, et al. 2009*).

From a mechanical engineering perspective, composting involves a sequence of preparation and conditioning operations: raw material reception and sorting; size reduction (shredding); component

proportioning and mixing; windrow formation or reactor loading; turning and aeration; internal transport; maturation; and screening and recirculation of the coarse fraction. Mechanizing these operations aims to increase processing capacity, ensure material uniformity, and control the physical conditions under which biodegradation takes place (*Diaz and de Bertoldi, 2007; Haug, 1993; Rynk et al., 1992*). The physical properties of the material directly influence the operation of the equipment. Moisture content, bulk density, particle density, porosity, air-filled porosity, particle size distribution, and mechanical strength are correlated with both the aeration of the composting mass and the stresses encountered during transport, mixing, and turning (*Agnew and Leonard, 2003; Richard et al., 2004; Ahn et al., 2008*). Bulk density is also relevant for sizing transport capacities and estimating the power required for mechanical operations.

Shredding is one of the initial operations applied to plant materials and organic waste of non-uniform size. Reducing particle size increases the specific surface area accessible to microorganisms and can lead to a more homogeneous mixture. However, very fine particles can fill the voids between larger particles, thereby reducing air-filled porosity. Research on green waste has demonstrated that initial particle size significantly influences process kinetics and the characteristics of the final compost (*Zhang and Sun, 2014; Haynes et al., 2015*). Mechanically turning windrows or mixing material within reactors contributes to material redistribution, the homogenization of temperature and moisture, and the restoration of the porous structure. Turning frequency influences compost stability, temperature, and the dynamics of certain chemical compounds; however, increasing the frequency entails additional energy consumption (*Kalamdhad and Kazmi, 2009; Tiquia et al., 1997; Getahun et al., 2012*).

In the final stage, screening aims to separate mature compost based on particle size and to remove coarse fractions or impurities. Trommel screens are frequently used due to their continuous operation and ability to process heterogeneous materials. Their performance depends on drum diameter and length, perforation size, rotational speed, fill level, feed rate, particle size distribution, and the tendency of wet material to clog the screening surface (*Stessel, 1991; Wills and Finch, 2016; Kumar et al., 2024*).

The objective of this paper is to analyze the main mechanical processing methods for compost and to identify parameters that can be used to characterize the equipment's operational performance. The study is based on a review of the specialized literature and provides a foundation for future experimental research regarding productivity, energy consumption, particle size distribution, and separation quality.

## MATERIALS AND METHODS

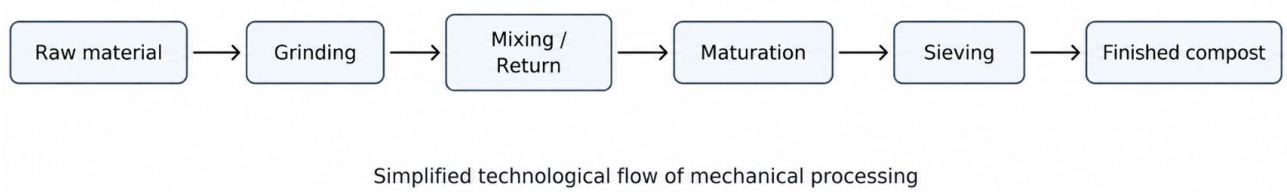



**Fig. 1 - Conceptual diagram of the main mechanical processing operations**
*(Zhang J. et al., 2019)*

This paper presents a comprehensive technical-scientific study. Publications regarding composting engineering, the physical properties of organic materials, shredding, mixing and turning, aeration, screening, and the assessment of compost maturity were analyzed. The structure of the analysis follows the technological processing flow, from raw material preparation to the production of the final compost fraction.

**Physical characteristics relevant to mechanical processing**

Moisture content influences material behavior during shredding, transport, and screening. Increased moisture can promote particle cohesion and adhesion, alter bulk density, and exacerbate the clogging of separation surfaces. At the same time, an inadequate water level limits microbiological activity. The relationship between moisture, density, air-filled porosity, and permeability is essential for the design and operation of composting systems (*Agnew and Leonard, 2003; Richard et al., 2004; Ahn et al., 2008; Ahn et al., 2009*).

Moisture content on a wet basis can be expressed by the relationship $W = (m_u - m_s) / m_u \times 100$ [%], where $m_u$ is the mass of the wet sample and $m_s$ is the mass of the sample after drying. Bulk density is determined by the ratio $\rho_b = m/V$ [kg·m$^{-3}$]. For particle size characterization, the proportion of a fraction i can be calculated as $p_i = m_i/m_t \times 100$ [%]. These parameters are simple yet useful for correlating material properties with equipment operating conditions. Air-filled porosity is a particularly important

characteristic for aerobic systems. Richard et al. (2004) demonstrated that air-filled porosity and permeability depend on moisture content and density, while the mechanical strength of the matrix contributes to structural changes caused by compaction. Consequently, a mechanical operation should be evaluated not only by the degree of fragmentation or mixing but also by its effect on the porous structure.

**Size reduction operation**

Shredding can be performed using knife-based shredders, hammer rotors, shafts with cutting elements, or combined systems. The choice of the active component depends on the material's nature: woody residues require different mechanisms compared to soft plant materials or partially stabilized compost. Key parameters include rotor speed, peripheral speed, feed rate, discharge opening, the geometry of the active components, and transmitted power.

The degree of size reduction can be characterized, in simplified terms, by the ratio $i_m = d_0/d_1$, where $d_0$ represents a characteristic dimension of the material before processing and $d_1$ the dimension after processing. From an energy perspective, specific energy $E_s = E/m$—or, for continuous operation, $e_s = P/Q$ (where P is the average power absorbed and Q is the mass flow rate)—is relevant. This indicator allows for the comparison of operating modes at different productivity levels.

Studies on green waste indicate that particle size influences both the decomposition rate and nutrient distribution. Zhang and Sun (2014) investigated initial sizes of 10, 15, and 25 mm and highlighted the importance of optimizing this parameter. Haynes et al. (2015) demonstrated that different particle size fractions of green waste exhibit varying chemical compositions and decomposition rates. Consequently, the technological objective is not to achieve the smallest possible size, but rather to produce a structure suitable for the process.

**Compost mixing and turning**

In windrow systems, turners may employ horizontal or vertical rotors equipped with paddles, blades, or flails. As the machine moves, the material is picked up, lifted, fragmented, and redeposited, resulting in homogenization and the restoration of porosity. In rotary reactors, mixing is achieved through the rotation of the drum and the movement of the material within it.

Key operating parameters include rotor speed, travel speed, penetration depth, working width, and material throughput. The turning frequency should be selected based on the evolution of temperature, moisture, and oxygen levels. Kalamdhad and Kazmi (2009) highlighted the effects of turning frequency on stability and chemical characteristics in rotary drum composting. In other systems, altering the turning frequency influenced material losses and the composting process (Tiquia et al., 1997; Getahun et al., 2012).

**Conveying and feeding**

Belt conveyors, scraper conveyors, screw conveyors, and loaders are used to move material between processing stages. Uniform feeding is important because significant fluctuations in flow rate are transmitted to the shredder, mixer, or screen, potentially altering mechanical load, power consumption, and processing quality. For a continuous flow, mass throughput can be expressed as $Q = m/t$ [$kg \cdot s^{-1}$ or $t \cdot h^{-1}$].

**Compost screening**

Screening is the process by which mature compost is separated into particle size fractions. Trommel screens perform both conveying and separation simultaneously, as the material is lifted and tumbled inside a perforated drum. The fine fraction passes through the perforations, while the oversize material is discharged at the end of the drum. The coarse fraction may be recirculated as bulking material, depending on its composition and the facility's technology.

Separation efficiency is influenced by drum rotation speed, residence time, fill level, perforation size, and material characteristics. Recent studies on trommels used in mechanical-biological treatment confirm the role of particle size distribution and operating conditions in separation performance (Kumar et al., 2024). For compost, moisture content is critical, as moist fine particles can form clumps and clog the perforations.

**Indicators for evaluating the working process**

Mechanical, technological, and energy-related indicators can be used to characterize compost processing equipment: mass throughput, degree of comminution, particle size distribution, separation efficiency, power consumption, specific energy, mixture uniformity, and the percentage of recirculated material. In experimental studies, these indicators can be correlated with the rotational speed of the working elements, travel speed, moisture content, and feed rate using regression models and experimental design methods.

## RESULTS AND DISCUSSION

A review of the literature indicates that mechanical processing should be viewed as a sequence of interdependent operations. Altering the particle size distribution through size reduction simultaneously changes the specific surface area, bulk density, and porous structure; these changes influence aeration and, consequently, the need for turning. Turning, in turn, can further fragment the material, and this evolution affects subsequent screening behavior.

**Table 1**

**Summary of the main mechanical processing operations for compost**

*(Adhikari B.K., et al., 2008)*

| Operation | Typical equipment | Active component | Key parameters | Evaluation indicators |
|---|---|---|---|---|
| grind | Chopper / mill | Knives, hammers, shafts | rotational speed, flow rate, humidity | particle size distribution, specific energy |
| shuffle | Mixer / drum | Paddles, drum | rotational speed, time, fill level | uniformity, productivity |
| Return | Mouldboard | Rotor with blades/hammers | rotational speed, speed, depth | flow rate, power, homogenization |
| Transport | Belt / screw conveyor | Strip, spiral | speed, inclination, flow rate | capacity, energy consumption |
| sifting | Trommel / screen | Perforated drum | rotational speed, flow rate, mesh size, humidity | efficiency, purity, refusal |

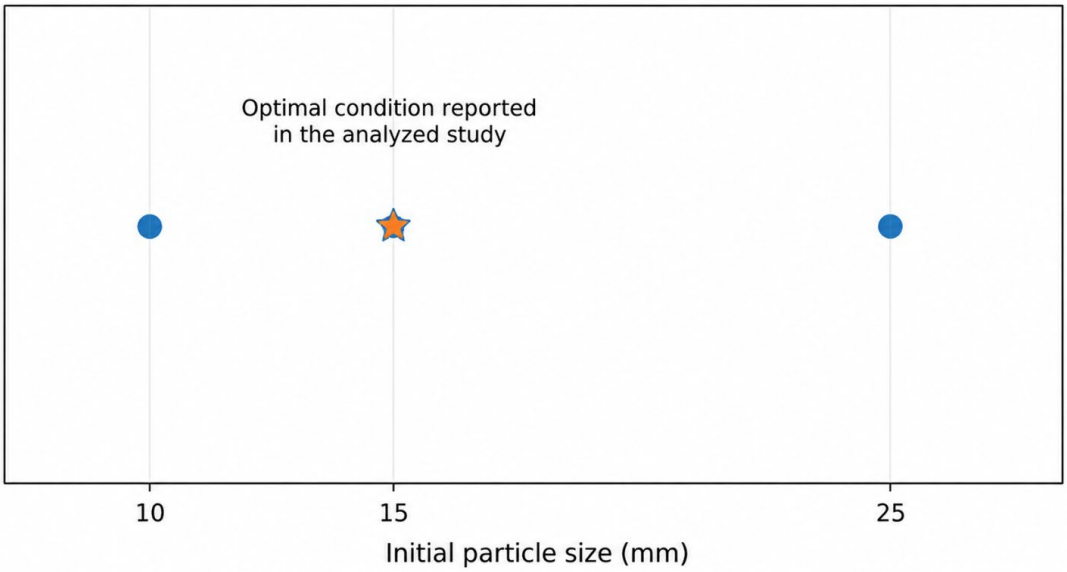



**Fig. 2 - Initial dimensions of the investigated particles and the reported optimal condition for the two-stage composting of green waste**

*adapted from (Zhang and Sun, 2014)*

Among the material properties, moisture content and particle size distribution have multiple effects. Moisture content alters density and cohesion, influences the load on active components, and can reduce screening efficiency. Particle size distribution determines the surface area available for biodegradation as well as the size of the voids within the matrix. Agnew and Leonard (2003),

Richard et al. (2004), and Ahn et al. (2008) demonstrate the need to correlate density, porosity, and permeability when analysing aeration processes.

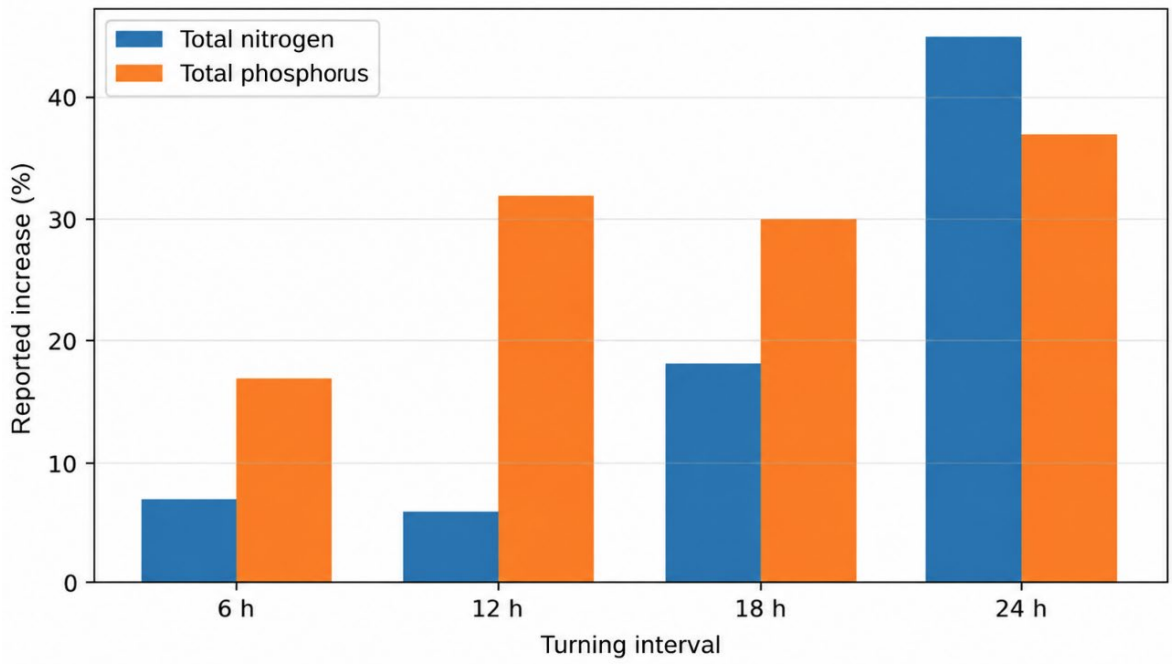



**Fig. 2 - Percentage increase in total nitrogen and total phosphorus at different turning intervals in a rotary drum composter**

*data reported by (Kalamdhad et al., 2009)*

Regarding size reduction, the literature does not support the concept of unlimited size reduction. Zhang and Sun (2014) obtained favorable results with an intermediate initial size under their experimental conditions, while Haynes et al. (2015) demonstrated that small and large green waste fractions differ in both composition and decomposition behavior. From a mechanical standpoint, further size reduction generally entails higher energy consumption and can generate an increased amount of fine particles.

Turning has a beneficial effect on homogenization and aeration, but it requires optimization. A frequency that is too low can promote compaction and non-uniformity, whereas an excessively high frequency increases the number of interventions and energy consumption, and may alter the thermal regime. Published results for rotary reactors and systems involving periodic turning confirm that frequency is a process parameter rather than a universal constant *(Kalamdhad and Kazmi, 2009; Getahun et al., 2012).*

**Table 2**

**Reference data extracted from studies used for the analysis of the mechanical process**

*(Insam H et al., 2007)*

| Parameter | Value / level | Reported result |
|---|---|---|
| Initial particle size | 10, 15, 25 mm | 15 mm under the study's optimal conditions |
| Return interval | 6, 12, 18, 24 h | 24 h: 45% increase in N; 37% increase in P |
| Trommel apertures | 80, 32, 16, 4 mm | organic recovery: 26.95% (80 mm), 95.82% (32 mm) |
| Specific consumption of the trommel | reported interval | 0.63–5.66 kWh/t |

In the screening stage, the objective is to obtain a final fraction with a particle size distribution suited to the intended application. Trommels are robust and suitable for heterogeneous materials, yet their efficiency is sensitive to feed rate and material condition.

The findings of Kumar et al. (2024) regarding trommels in a mechanical-biological treatment plant highlight the importance of the sequential selection of separation sizes.

For composting applications, this observation supports the use of separation stages or operating regimes tailored to the desired product.

**Table 3**

**Relationship between material properties and the mechanical process**

*(Gong X et al., 2013)*

| Factor | Possible mechanical effect | Possible technological effect | Optimization direction |
|---|---|---|---|
| High humidity | adhesion, agglomeration, increase in resistance | clogging, more difficult separation | conditioning of the material prior to screening |
| Particles that are too large | high shredding loads | slower degradation, non-uniformity | controlled fragmentation |
| Excessively fine particles | compaction, poor flow | reduction of the free air space | limiting the production of the fine fraction |
| Non-uniform flow rate | load and power variations | inconsistent processing quality | metered feeding |
| Excessive engine speed | higher wear and energy consumption | excessive fragmentation | establishing the optimal operating conditions |

The comparative analysis indicates that operating parameters must be established based on material properties and the objective of each specific operation. For the experimental study of compost processing equipment, a useful approach involves considering rotational speed (n), feed rate (Q), and moisture content (W) as input factors, while treating productivity, specific energy consumption, and particle size characteristics as response variables. Such an approach enables the identification of efficient operating ranges and the development of predictive models.

The quality of the final compost cannot be assessed solely by particle size distribution. Stability and maturity are distinct concepts evaluated through physicochemical, respirometric, and biological indicators (*Iannotti et al., 1993; Bernal et al., 1998; Bernal et al., 2009; Gómez et al., 2006; Tiquia, 2005*).

Consequently, mechanical optimization must be integrated with the biological requirements of the process to avoid situations where increased equipment productivity results in a structure unfavourable to composting.

## EXTENDED GRAPHICAL ANALYSIS BASED ON LITERATURE DATA

To deepen the analysis, graphs were generated based on numerical values published in the reference articles.

These graphs do not represent original experimental results; each legend explicitly indicates the data source. The open-access study by Zhang et al. (2019) compared turning intervals of 5, 7, 10, and 15 days, enabling an analysis of the effect of frequency on temperature, pH, total nitrogen, the germination index, and Solvita maturity.

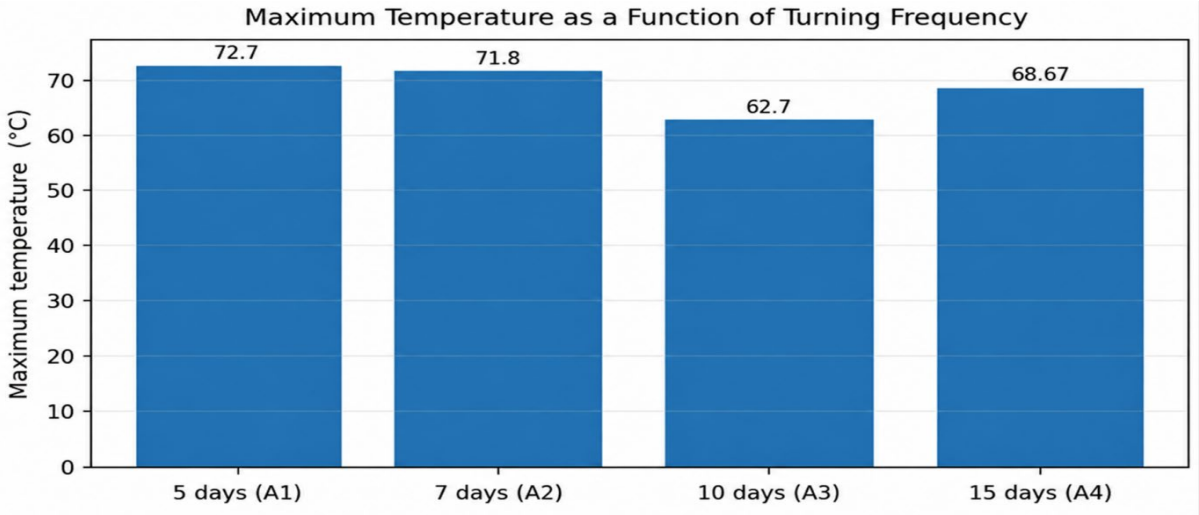



**Fig. 3 - Maximum temperatures reported for the four return frequencies.**

*Data reconstructed from (Zhang et al., 2019)*

The maximum temperatures were 72.7°C for A1, 71.8°C for A2, 62.7°C for A3, and 68.67°C for A4. Although A1 reached the highest maximum temperature, treatment A2—with turning every 7 days—exhibited the longest thermophilic phase, lasting approximately 41–42 days *(Zhang et al., 2019).*

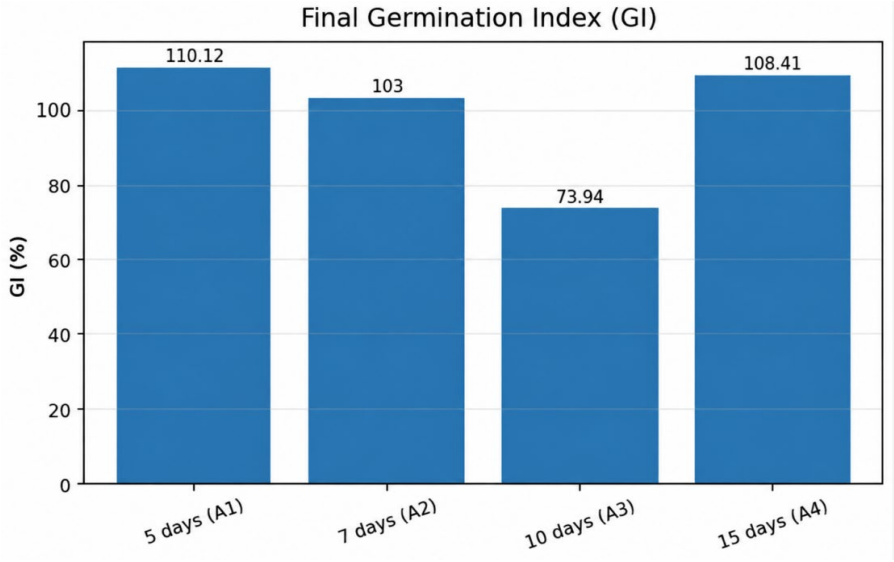



**Fig. 4 - Germination index at the end of the composting period.**
*Data redrawn from (Zhang et al., 2019)*

At the end, the germination index was 110.12% (A1), 103.00% (A2), 73.94% (A3), and 108.41% (A4). These values highlight that the turning frequency can alter the maturity and phytotoxicity of the product, although the effect depends on the compostable material and process conditions (*Zhang et al., 2019*).

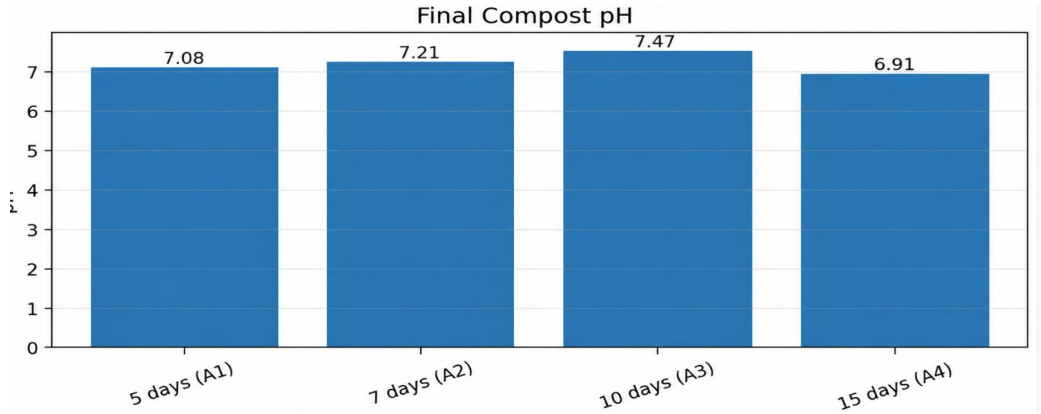



**Fig. 5 - Final pH as a function of turning frequency.**
Data redrawn from *(Zhang et al., 2019)*

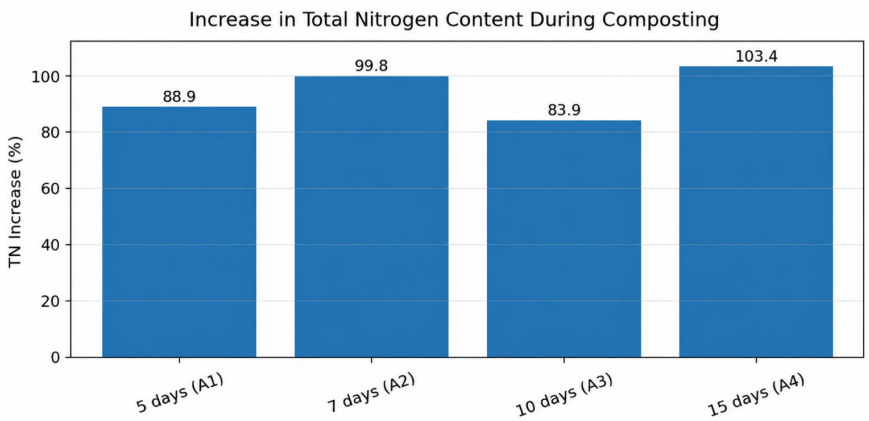



**Fig. 6 - Percentage increase in total nitrogen during composting.**
*Data redrawn from (Zhang et al., 2019)*

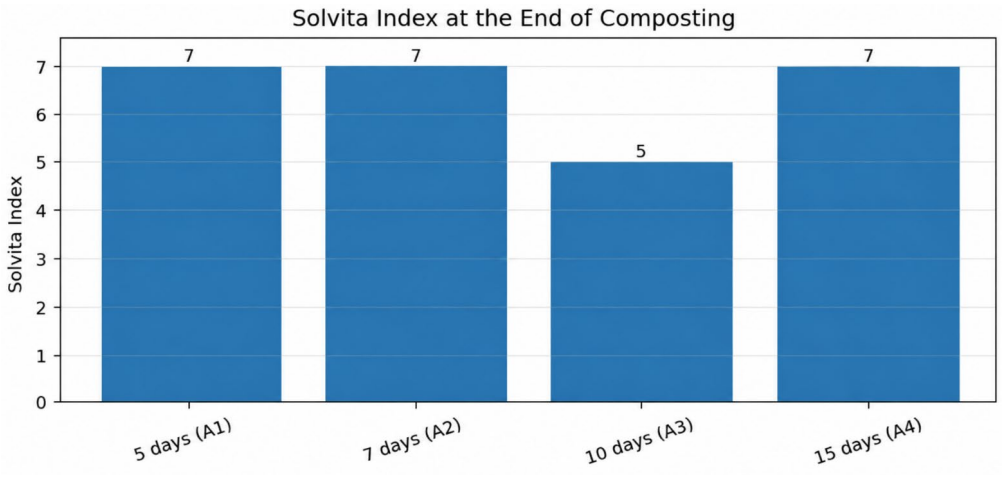



**Fig. 7 - Solvita index at the end of composting for the four turning regimes.**
*Data redrawn from (Zhang et al., 2019)*

**Table 4**

**Summary of final indicators reported for different return frequencies**
*(Zhang et al., 2019)*

| Treatment | Return interval | Tmax (°C) | Final pH | Final GI (%) | Final C/N | Final Solvita |
|---|---|---|---|---|---|---|
| A1 | 5 days | 72.7 | 7.08 | 110.12 | 16.12 | 7 |
| A2 | 7 days | 71.8 | 7.21 | 103.00 | 15.83 | 7 |
| A3 | 10 days | 62.7 | 7.47 | 73.94 | 16.56 | 5 |
| A4 | 15 days | 68.67 | 6.91 | 108.41 | 16.22 | 7 |

**Table 5**

**Evolution of total nitrogen and quality indicators reported in the study by** *(Zhang et al., 2019)*

| Treatment | NT increase (%) | Final total nutrients | Final organic matter | Observation |
|---|---|---|---|---|
| A1 | 88.9 | 5.41 ± 0.14% | 78,.44 ± 0.38% | return within 5 days |
| A2 | 99.8 | 5.75 ± 0.11% | 79.54 ± 0.98% | the longest thermophilic phase |
| A3 | 83.9 | — | — | Final GI below 80% |
| A4 | 103.4 | — | — | 15-day return |

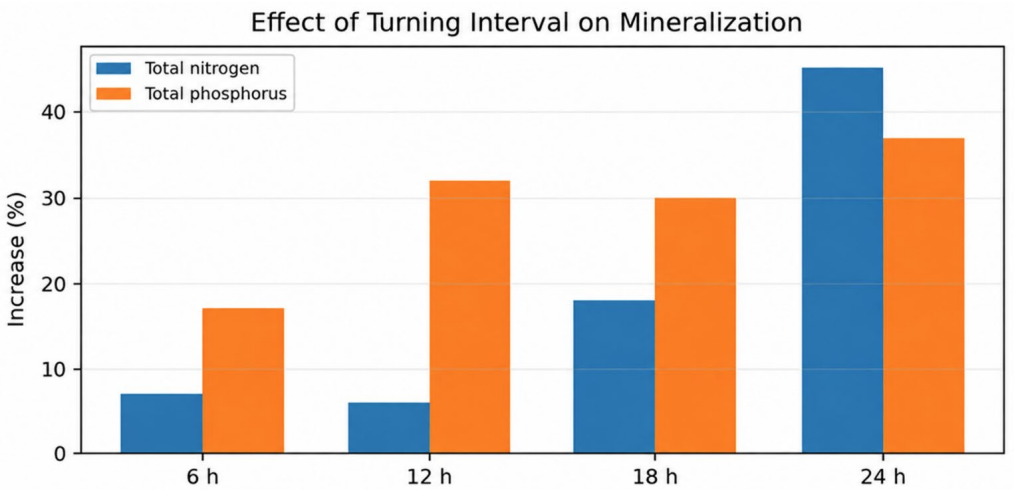



**Fig. 8 - Increase in total nitrogen and total phosphorus for different turning intervals in a rotary drum composter**.
*Data adapted from (Kalamdhad et al., 2009)*

In the rotary drum study, the increase in total nitrogen was 7%, 6%, 18%, and 45%, and the increase in total phosphorus was 17%, 32%, 30%, and 37% for the 6-, 12-, 18-, and 24-hour intervals, respectively. For the 24-hour regime, a maximum temperature of 58°C and a four-day thermophilic phase were also reported (*Kalamdhad and Kazmi, 2009*).

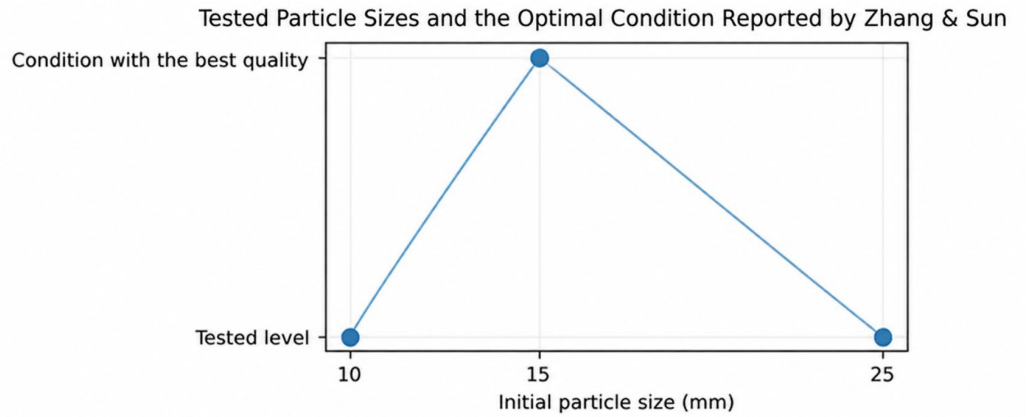



**Fig. 9 - Initial particle sizes investigated in green waste composting and the condition yielding the best compost quality**.
*Adapted from (Zhang et al., 2014)*

Zhang and Sun (2014) analyzed initial sizes of 10, 15, and 25 mm. Under their experimental conditions, the combination of 15 mm and 0.15% rhamnolipid yielded the highest-quality compost and resulted in a stable, mature product within 24 days. This conclusion should not be generalized as a universal optimum size, as the outcome is influenced by the raw material and the technology employed.

**Table 6**

**Particle size distribution and compositional trends of shredded green waste**
*summarized from (Haynes et al., 2015)*

| Particle size fraction | Reported observation |
|---|---|
| >20 mm | 25–32% of the sample mass; higher proportion of woody/lignified material |
| 10–20 mm | analyzed intermediate fraction |
| 5–10 mm | intermediate fraction; contributes to the <10 mm mass |
| 2–5 mm | relative increase in nutrients compared to the coarse fractions |
| 1–2 mm | higher content of macro- and micronutrients |
| 0,5–1,0 mm | faster N decomposition and mineralization |
| <0,5 mm | fine fraction, richer in nutrients and ash |

Haynes et al. (2015) separated five green waste samples into seven particle size classes. Overall, 39–54% of the mass was found in the <10 mm range, while the <20 mm fraction accounted for approximately 68–75% of the shredded mass. As particle size decreased, organic carbon content declined, whereas the content of macro- and micronutrients and ash increased (*Haynes et al., 2015*).

**Table 7**

**Physical relationships relevant to the mechanical process**,
*summarized from (Agnew et al., 2003; Ahn et al., 2008)*

| Parameter | Consequences of increasing the parameter | Implication for equipment |
|---|---|---|
| Moisture | filling of pores with water; modification of density | adhesion, agglomeration, screen blinding |
| Bulk density | reduction of air-filled porosity | higher mass load and mechanical strength |
| Compaction | decrease in permeability | increased need for loosening/turning over |
| Fine fraction | reduction of the voids between particles | risk of compaction and more difficult separation |

## CONCLUSIONS

Mechanical processing is an essential component of composting technologies, as preparation, mixing, turning, transport, and screening influence both the facility's capacity and the physical conditions under which the biological process takes place.

Moisture content, bulk density, porosity, and particle size distribution must be considered fundamental properties for material characterization. These factors influence the load on active components, aeration, the tendency for compaction, and separation efficiency.

Shredding should be optimized to achieve an appropriate particle size distribution rather than to minimize particle size absolutely. Excessive production of the fine fraction can reduce air void space and affect material behavior during subsequent operations.

Mechanical turning contributes to homogenization and aeration; however, frequency, rotor speed, and travel speed must be balanced against the composting stage and energy consumption.

Rotary drum screening is a suitable technical solution for compost finishing, with efficiency depending on the coordination of rotational speed, feed rate, perforation size, and material moisture content.

For further research, it is recommended to experimentally investigate the relationships between the speed of active components, feed rate, and moisture content on the one hand, and productivity, specific energy consumption, and particle size distribution on the other. These relationships can serve as the basis for optimizing the operational processes of compost processing equipment.

## REFERENCES

[1] Adhikari B.K., Barrington S., Martinez J., King S., (2008), Characterization of food waste and bulking agents for composting, Waste Management, 28(5), pp. 795–804.

[2] Agnew J.M., Leonard J.J., (2003), The physical properties of compost, Compost Science & Utilization, 11(3), pp. 238–264, DOI: 10.1080/1065657X.2003.10702132.

[3] Ahn H.K., Richard T.L., Glanville T.D., (2008), Laboratory determination of compost physical parameters for modeling of airflow characteristics, Waste Management, 28(3), pp. 660–670.

[4] Ahn H.K., Sauer T.J., Richard T.L., Glanville T.D., (2009), Determination of thermal properties of composting bulking materials, Bioresource Technology, 100(17), pp. 3974–3981.

[5] Bernal M.P., Alburquerque J.A., Moral R., (2009), Composting of animal manures and chemical criteria for compost maturity assessment. A review, Bioresource Technology, 100(22), pp. 5444–5453, DOI: 10.1016/j.biortech.2008.11.027.

[6] Bernal M.P., Paredes C., Sánchez-Monedero M.A., Cegarra J., (1998), Maturity and stability parameters of composts prepared with a wide range of organic wastes, Bioresource Technology, 63(1), pp. 91–99.

[7] Brewer L.J., Sullivan D.M., (2003), Maturity and stability evaluation of composted yard trimmings, Compost Science & Utilization, 11(2), pp. 96–112.

[8] Chang J.I., Hsu T.E., (2008), Effects of compositions on food waste composting, Bioresource Technology, 99(17), pp. 8068–8074, DOI: 10.1016/j.biortech.2008.03.043.

[9] de Bertoldi M., Vallini G., Pera A., (1983), The biology of composting: A review, Waste Management & Research, 1(2), pp. 157–176, DOI: 10.1016/0734-242X(83)90055-1.

[10] Diaz L.F., de Bertoldi M., (2007), History of composting, Waste Management Series, 8, pp. 7–24, DOI: 10.1016/S1478-7482(07)80005-4.

[11] Epstein E., (1997), The Science of Composting, Technomic Publishing Company, Lancaster, Pennsylvania.

[12] Getahun T., Nigusie A., Entele T., Van Gerven T., Van der Bruggen B., (2012), Effect of turning frequencies on composting biodegradable municipal solid waste quality, Resources, Conservation and Recycling, 65, pp. 79–84.

[13] Gómez R.B., Lima F.V., Ferrer A.S., (2006), The use of respiration indices in the composting process: a review, Waste Management & Research, 24(1), pp. 37–47.

[14] Haug R.T., (1993), The Practical Handbook of Compost Engineering, Lewis Publishers, Boca Raton, Florida.

[15] Haynes R.J., Belyaeva O.N., Zhou Y.F., (2015), Particle size fractionation as a method for characterizing the nutrient content of municipal green waste used for composting, Waste Management, 35, pp. 48–54, DOI: 10.1016/j.wasman.2014.10.002.

[16] Iannotti D.A., Pang T., Toth B.L., Elwell D.L., Keener H.M., Hoitink H.A.J., (1993), A quantitative respirometric method for monitoring compost stability, Compost Science & Utilization, 1(3), pp. 52–65.

[17] Iannotti D.A., Grebus M.E., Toth B.L., Madden L.V., Hoitink H.A.J., (1994), Oxygen respirometry to assess stability and maturity of composted municipal solid waste, Journal of Environmental Quality, 23(6), pp. 1177–1183.

[18] Insam H., de Bertoldi M., (2007), Microbiology of the composting process, Waste Management Series, 8, pp. 25–48, DOI: 10.1016/S1478-7482(07)80006-6.

[19] Kalamdhad A.S., Pasha M., Kazmi A.A., (2008), Stability evaluation of compost by respiration techniques in a rotary drum composter, Resources, Conservation and Recycling, 52(5), pp. 829–834.
[20] Kalamdhad A.S., Kazmi A.A., (2009), Effects of turning frequency on compost stability and some chemical characteristics in a rotary drum composter, Chemosphere, 74(10), pp. 1327–1334, DOI: 10.1016/j.chemosphere.2008.11.058.
[21] Keener H.M., Marugg C., Hansen R.C., Hoitink H.A.J., (1993), Optimizing the efficiency of the composting process, Science and Engineering of Composting: Design, Environmental, Microbiological and Utilization Aspects, Renaissance Publications, Worthington, Ohio.
[22] Kumar S., et al., (2024), Performance evaluation of trommel screens: A case study of a municipal solid waste treatment plant, Waste Management Bulletin, 2(2), pp. 83–94, DOI: 10.1016/j.wmb.2024.03.007.
[23] Rynk R., van de Kamp M., Willson G.B., Singley M.E., Richard T.L., Kolega J.J., Gouin F.R., Laliberty L. Jr., Kay D., Murphy D.W., Hoitink H.A.J., Brinton W.F., (1992), On-Farm Composting Handbook, NRAES-54, Northeast Regional Agricultural Engineering Service, Ithaca, New York.
[24] Lasaridi K.E., Stentiford E.I., (1998), A simple respirometric technique for assessing compost stability, Water Research, 32(12), pp. 3717–3723.
[25] Richard T.L., Veeken A.H.M., de Wilde V., Hamelers H.V.M., (2004), Air-filled porosity and permeability relationships during solid-state fermentation, Biotechnology Progress, 20(5), pp. 1372–1381, DOI: 10.1021/bp0499505.
[26] Liang C., Das K.C., McClendon R.W., (2003), The influence of temperature and moisture contents regimes on the aerobic microbial activity of a biosolids composting blend, Bioresource Technology, 86(2), pp. 131–137.
[27] Michel F.C. Jr., Reddy C.A., Forney L.J., (1996), Yard waste composting: studies using different mixes of leaves and grass in a laboratory scale system, Compost Science & Utilization, 4(1), pp. 85–96.
[28] Stessel R.I., (1991), A new trommel model, Resources, Conservation and Recycling, 5(2–3), pp. 183–197.
[29] Mohee R., Mudhoo A., (2005), Analysis of the physical properties of an in-vessel composting matrix, Powder Technology, 155(1), pp. 92–99.
[30] Tiquia S.M., Tam N.F.Y., Hodgkiss I.J., (1997), Effects of turning frequency on composting of spent pig-manure sawdust litter, Bioresource Technology, 62(1–2), pp. 37–42.
[31] Moral R., Paredes C., Bustamante M.A., Marhuenda-Egea F., Bernal M.P., (2009), Utilisation of manure composts by high-value crops: Safety and environmental challenges, Bioresource Technology, 100(22), pp. 5454–5460, DOI: 10.1016/j.biortech.2008.12.007.
[32] Rasapoor M., Nasrabadi T., Kamali M., Hoveidi H., (2009), The effects of aeration rate on generated compost quality, using aerated static pile method, Waste Management, 29(2), pp. 570–573.
[33] Sánchez-Monedero M.A., Roig A., Paredes C., Bernal M.P., (2001), Nitrogen transformation during organic waste composting by the Rutgers system and its effects on pH, EC and maturity of the composting mixtures, Bioresource Technology, 78(3), pp. 301–308.
[34] Stentiford E.I., (1996), Composting control: principles and practice, The Science of Composting, Springer, Dordrecht, pp. 49–59.
[35] Tiquia S.M., (2005), Microbiological parameters as indicators of compost maturity, Journal of Applied Microbiology, 99(4), pp. 816–828.
[36] Tiquia S.M., Tam N.F.Y., Hodgkiss I.J., (1996), Effects of composting on phytotoxicity of spent pig-manure sawdust litter, Environmental Pollution, 93(3), pp. 249–256.
[37] Tuomela M., Vikman M., Hatakka A., Itävaara M., (2000), Biodegradation of lignin in a compost environment: a review, Bioresource Technology, 72(2), pp. 169–183.
[38] Van der Gheynst J.S., Walker L.P., Parlange J.Y., (1997), Energy transport in a high-solids aerobic degradation process: mathematical modeling and analysis, Biotechnology Progress, 13(3), pp. 238–248.
[39] Wills B.A., Finch J.A., (2016), Wills' Mineral Processing Technology: An Introduction to the Practical Aspects of Ore Treatment and Mineral Recovery, 8th ed., Butterworth-Heinemann, Oxford.
[40] Wang P., Changa C.M., Watson M.E., Dick W.A., Chen Y., Hoitink H.A.J., (2004), Maturity indices for composted dairy and pig manures, Soil Biology and Biochemistry, 36(5), pp. 767–776.
[41] Wu L., Ma L.Q., Martinez G.A., (2000), Comparison of methods for evaluating stability and maturity of biosolids compost, Journal of Environmental Quality, 29(2), pp. 424–429.

[42] Zhang L., Sun X., Tian Y., Gong X., (2013), Effects of brown sugar and calcium superphosphate on the secondary fermentation of green waste, Bioresource Technology, 131, pp. 68–75.
[43] Zhang L., Sun X., (2014), Effects of rhamnolipid and initial compost particle size on the two-stage composting of green waste, Bioresource Technology, 163, pp. 112–122, DOI: 10.1016/j.biortech.2014.04.041.
[44] Zhang J., Ying Y., Yao X., (2019), Effects of turning frequency on the nutrients of Camellia oleifera shell co-compost with goat dung and evaluation of co-compost maturity, PLOS ONE, 14(9), e0222841, DOI: 10.1371/journal.pone.0222841.
[45] Zmora-Nahum S., Markovitch O., Tarchitzky J., Chen Y., (2005), Dissolved organic carbon (DOC) as a parameter of compost maturity, Soil Biology and Biochemistry, 37(11), pp. 2109–2116.

# PRECISION AGRICULTURE AND SUSTAINABLE PRACTICES IN ROMANIA: FARM PROFILES, DIGITAL GAPS AND EVIDENCE FROM SELECTED EU COUNTRIES

/

# *AGRICULTURA DE PRECIZIE ȘI PRACTICILE AGRICOLE DURABILE ÎN ROMÂNIA: PROFILUL EXPLOATAȚIILOR, DECALAJE DIGITALE ȘI COMPARAȚII CU STATE UE SELECTATE*

**Cristiana Silvia BUZATU[1)], Alina MĂRCUȚĂ[1)], Liviu MĂRCUȚĂ[1)], Iulian Virgil GHIULEANU*[2)], Răzvan Alexandru MATINCĂ[1)]**

[1)] University of Agronomic Sciences and Veterinary Medicine of Bucharest, 59 Marasti Boulevard, District 1, 011464, Bucharest / Romania;

[2)] University of Agronomic Sciences and Veterinary Medicine of Bucharest (Doctoral student, Doctoral School: Plant and Animal Resources Engineering and Management), 59 Marasti Boulevard, District 1, 011464, Bucharest / Romania.

**E-mail: vghiuleanu@yahoo.com*

***Keywords:*** *precision agriculture; farm digitalisation; sustainable agricultural practices; cover crops; crop rotation; Romania.*

**ABSTRACT**

*The study evaluates the adoption of precision agriculture and selected sustainable land-management practices in Romania compared with Czechia, Hungary, Croatia, France, Germany and Finland. The analysis used 2023 data from four Eurostat datasets, representing the latest information available when extracted on September 24, 2026. Indicators concerning agricultural holdings, utilised agricultural area, economic size, manager training and age, internet access, digital technologies, organic farming, soil cover and crop rotation were processed in Microsoft Excel 365. The methods included percentages, percentage-point differences, unweighted means, rankings, cartographic representations and Pearson correlation. Only 0.63% of Romanian agricultural holdings reported using precision agriculture, but they managed 1,444,130 ha, representing 11.51% of the utilised agricultural area included in the dataset. Adoption increased from 0.54% in holdings with a standard output of EUR 2000–7999 to 15.13% in those reaching at least EUR 100,000. Among holdings with a standard output of at least EUR 2000, internet access reached 24.45%, while farm management information systems were used by only 0.39%. Organic and in-conversion land accounted for 3.98% of the utilised agricultural area, and cover or intermediate crops represented 0.03% of arable land. The share of arable land associated with holdings in which crop rotation covered at least 75% of the arable area was 71.82%. Romania ranked last for five of the six comparative indicators and sixth for crop rotation. The association between precision agriculture and cover crops was positive but not statistically significant at the 5% level (r = 0.74; p = 0.058). The findings indicate limited and economically concentrated technological adoption, alongside substantial gaps between basic connectivity and the effective use of digital management tools.*

**REZUMAT**

*Cercetarea evaluează adoptarea agriculturii de precizie și a unor practici de gestionare durabilă a terenurilor în România, comparativ cu Cehia, Ungaria, Croația, Franța, Germania și Finlanda. Analiza utilizează date aferente anului 2023 din patru seturi Eurostat, acestea fiind cele mai recente informații disponibile la data extragerii, 24 septembrie 2026. Indicatorii privind exploatațiile agricole, suprafața agricolă utilizată, dimensiunea economică, pregătirea și vârsta managerului, accesul la internet, tehnologiile digitale, agricultura ecologică, acoperirea solului și rotația culturilor au fost prelucrați în Microsoft Excel 365. Au fost calculate ponderi, diferențe în puncte procentuale, medii neponderate, poziții comparative și coeficientul de corelație Pearson, iar distribuțiile teritoriale au fost reprezentate cartografic. Numai 0.63% dintre exploatațiile agricole din România au declarat utilizarea agriculturii de precizie, dar acestea au gestionat 1,444,130 ha, reprezentând 11.51% din suprafața agricolă utilizată inclusă în setul analizat. Ponderea adoptării a crescut de la 0.54% în exploatațiile cu o producție standard de 2000–7999 euro la 15.13% în cele de minimum 100,000 euro. În rândul exploatațiilor cu o producție standard de cel puțin 2000 euro, accesul la internet a ajuns la 24.45%, în timp ce sistemele informatice de management au fost utilizate de numai 0.39%. Suprafața ecologică și aflată în conversie a reprezentat 3.98% din SAU, iar culturile de acoperire sau*

*intermediare numai 0.03% din terenul arabil. Suprafața aferentă exploatațiilor în care rotația culturilor acoperă cel puțin 75% din terenul arabil a ajuns la 71.82%. România a ocupat ultima poziție pentru cinci dintre cei șase indicatori comparativi și locul al șaselea pentru rotația culturilor. Asocierea dintre agricultura de precizie și culturile de acoperire a fost pozitivă, dar nesemnificativă statistic la pragul de 5% (r = 0.74; p = 0.058). Rezultatele indică o adoptare tehnologică redusă și concentrată economic, precum și o diferență amplă între conectivitatea de bază și utilizarea efectivă a instrumentelor digitale de management.*

## INTRODUCTION

Precision agriculture uses information on soil, crops, machinery and operating conditions to adapt interventions to the variability within a farm. Guidance systems, sensors, variable-rate technologies and data-management applications can support more precise input use and the organisation of agricultural activities. Their effects are not identical across technologies or holdings. Cost reductions, productivity gains and lower environmental pressures depend on how the technology is applied, the characteristics of the farm and the user's ability to translate data into decisions (*Balafoutis et al., 2017; Finger et al., 2019*).

The adoption of these technologies varies considerably across holdings and territories. Farm size, production value, investment costs, manager training and access to technical support influence the capacity to introduce new equipment and applications. Studies conducted in European countries have found more frequent use among larger holdings and have shown that economies of scale can facilitate the recovery of investments (*Barnes et al., 2019; Paustian and Theuvsen, 2017*). In small farms, costs, technical complexity and the lack of suitable services may restrict adoption even when certain technologies are commercially available (*Mizik, 2023*). Manager characteristics provide an additional explanation, as age, training and experience may be associated with openness to digital tools without independently determining the decision to use them (*Tamirat et al., 2018*).

Internet access is a basic requirement for transmitting and using information, but it is not equivalent to the digitalisation of farm management. Farm management information systems organise data on operations, resources, costs and production, thereby supporting planning and control (*Fountas et al., 2015*). A considerable gap may remain between having a connection and using digital applications effectively. Differences in infrastructure, skills, costs and access to services contribute to the unequal distribution of data-driven farming (*Mehrabi et al., 2021*). Communication among farmers, technology providers, advisers and professional organisations can reduce some of these difficulties (*Kutter et al., 2011*).

Precision agriculture and sustainable agriculture are connected through the possibility of using resources more precisely, but they should not be treated as equivalent concepts. The use of a technology does not automatically demonstrate the implementation of soil-protection practices, while a holding may adopt crop rotation, cover crops or organic farming without using precision systems.

These practices describe different components of land management. Cover crops have been associated with the accumulation of soil organic carbon (*Poeplau and Don, 2015*), while diversified crop rotations have contributed to production stability in long-term agricultural experiments (*Bowles et al., 2020*). Their effects depend on climate, soil, crop sequence and the technology applied. Consequently, no single indicator can describe the overall sustainability of an agricultural system.

For Romania, examining these dimensions is relevant to both farm modernisation and agricultural resource management. Studies concerning the conservation of land resources and risks in crop management have shown the need to relate technologies to local land characteristics and climatic and economic pressures (*Buzatu et al., 2023; Ghiuleanu et al., 2023*).

Romania's CAP Strategic Plan includes objectives concerning farm viability, digitalisation, resilience and the sustainable management of resources (*European Commission, 2026*). Assessing the current situation nevertheless requires a distinction between the number of holdings using these technologies and the areas managed by them, as well as between internet access and the use of specific digital tools.

Eurostat data for 2023 allow several components to be examined simultaneously: the use of precision agriculture, the economic profile of holdings, manager training and age, internet access, farm management information systems, robotics and machinery for livestock management. Other statistical datasets provide information on organic and in-conversion areas, arable-land cover and crop rotation (*Eurostat, 2026a; Eurostat, 2026b; Eurostat, 2026c; Eurostat, 2026d*).

These indicators are derived from different statistical bases and must be compared using the definitions and denominators applicable to each share.

The literature reviewed explains factors that may influence technology adoption and the effects of specific agricultural practices. Romania's position is less clear when indicators of digitalisation, user profiles and land management are compared for the same year and against a constant group of countries. Such an analysis must avoid two erroneous interpretations: treating the total area managed by user holdings as the area on which a technology was actually applied, and interpreting a statistical association as a causal relationship.

The aim of this study is to assess the adoption of precision agriculture and selected practices associated with sustainable land management in Romania compared with six European Union Member States, using data for 2023. The analysis examines the shares of holdings and agricultural areas associated with precision agriculture, differences according to economic size, manager training and age, and access to the internet and digital technologies. The land-related component covers organic and in-conversion agricultural areas, forms of arable-land cover and crop rotation. The study also examines the association between the share of holdings using precision agriculture and the share of arable land under cover or intermediate crops. The results are interpreted descriptively and comparatively, and the main findings are synthesised through a S.W.O.T. analysis.

## MATERIALS AND METHODS

The study was based on statistical data for 2023 available in the Eurostat Data Browser. Four datasets were used: ef_mp_digi, covering internet access, farm management information systems, precision farming, robotics and machinery for livestock management; ef_mp_digicr, which differentiates the use of precision farming according to the economic size of the holding and the age and training of the manager; ef_lus_main, concerning agricultural land use; and ef_mp_soil, covering arable-land cover and crop rotation (Eurostat, 2026a; Eurostat, 2026b; Eurostat, 2026c; Eurostat, 2026d).

The ef_mp_digi, ef_mp_digicr and ef_lus_main datasets were updated by Eurostat on June 17, 2026, while ef_mp_soil was updated on August 14, 2026. The data were extracted on September 24, 2026. The year in which the datasets were updated does not alter the reference period of the indicators. All values analysed describe the situation in 2023, the latest year available at the time of extraction.

The tabular analysis covered Romania and six European Union Member States: Czechia, Hungary, Croatia, France, Germany and Finland. The same comparison group was maintained for the summary indicators so that Romania's position could be assessed against values calculated on comparable bases.

The selected group does not constitute a statistical sample of the European Union and was not used to estimate an EU average. The maps included all Member States for which the corresponding dataset provided numerical values. Countries without available data were left blank and were not treated as having a value of zero.

The data were organised and processed in Microsoft Excel 365. Depending on the analysis, the indicators were expressed as numbers of holdings, hectares, percentages, hectares per holding and percentage points. For the ef_mp_digicr dataset, the total number of holdings and total utilised agricultural area were obtained by summing the "precision farming" and "no precision farming" categories. The share of user holdings was calculated in relation to the total number of holdings within the same category, while the area share was determined against the corresponding utilised agricultural area (UAA). The average area per user holding was calculated by dividing the UAA associated with precision farming by the number of holdings reporting its use. The difference between the area share and the holding share was expressed in percentage points.

The profile of precision farming users was analysed according to the economic size of the holding and the training and age of its manager. Economic size was expressed through the holding's standard output and covered the following classes: EUR 2000–7999, EUR 8000–24,999, EUR 25,000–99,999 and at least EUR 100,000.

The difference between the two extreme classes was calculated by subtracting the share recorded for the first class from the share of holdings with a standard output of at least EUR 100,000. For manager training, practical experience only, basic agricultural training and full agricultural training were compared. The difference was calculated between the last and first categories. The group of managers under 35 years of age was obtained by summing the "less than 25 years" and "25–34 years" classes and was compared with the group of managers aged 65 years or over.

The indicators obtained from ef_mp_digi were aggregated across the four available standard-output classes starting from EUR 2000. Holdings with a standard output below EUR 2000 were not included in this

part of the analysis. The shares concerning internet access, farm management information systems, precision farming, robotics and machinery for livestock management were calculated against the total number of holdings included in the four classes. The technology categories are not mutually exclusive, as the same holding may use several types of technology. Their values were therefore not summed to construct an overall digitalisation indicator. This difference in statistical coverage also explains the distinction between the 0.63% share calculated for all holdings and the 1.05% value obtained for holdings with a standard output of at least EUR 2000.

Organic utilised agricultural area included fully converted land and land under conversion, excluding kitchen gardens. Its share was calculated against the total UAA of each country. The land-cover analysis included normal winter crops, cover or intermediate crops, plant residues and bare soil. Each category was related to the total arable-land area. The area excluded from the land-cover classification was presented separately. The *"multiannual plants"* category was not analysed because the exported data did not provide complete values.

Crop rotation was assessed using the arable area of holdings in which this practice covered at least 75% of the arable land. The share was calculated by dividing the area corresponding to this class by the total arable-land area. The indicator does not represent the exact number of hectares on which crop rotation was applied. It represents the entire arable area of the holdings included in the category defined by Eurostat.

Six indicators were selected for the comparative synthesis: the share of holdings using precision farming, internet access, the use of farm management information systems, the share of organic and in-conversion UAA, the share of arable land under cover or intermediate crops, and the share of land associated with holdings applying crop rotation to at least 75% of their arable area.

The reference mean was calculated as an unweighted arithmetic mean for the six countries compared with Romania. The difference was expressed in percentage points as Romania's value minus the group mean. Positions were established separately for each indicator in descending order. The indicators were not combined into a composite score because they refer to different statistical populations and reporting bases.

The association between precision farming and cover or intermediate crops was examined for the seven countries using the Pearson correlation coefficient. Precision farming was represented by the share calculated for holdings with a standard output of at least EUR 2000, while cover crops were represented by their share of arable land. The analysis also included the coefficient of determination for the linear trend and the two-tailed probability associated with the correlation coefficient. The statistical significance threshold was set at 5%. The correlation was interpreted descriptively, without implying a causal relationship.

The maps were produced in Excel using absolute values expressed in hectares. The relationship between precision farming and cover crops was represented by a scatter plot with a linear trendline. Percentages, percentage-point differences, average areas and statistical coefficients were presented to two decimal places, while the numbers of holdings and areas expressed in hectares were reported without decimals. The statistical results and the limitations of the indicators were synthesised through a S.W.O.T. analysis.

The method is descriptive and comparative. Data for a single year do not allow changes over time to be examined, while the limited number of countries restricts the interpretation of the correlation. Areas associated with user holdings represent the entire area managed by those holdings and not necessarily the hectares on which the technology or practice was applied.

The results describe the differences observed across indicators and countries without establishing causal effects of holding size, manager training, age or digitalisation.

## RESULTS

The comparison for 2023 reveals substantial differences among the seven countries analysed, both in the number of holdings using precision agriculture and in the utilised agricultural area managed by them. In Table 1, the total number of holdings and total UAA were obtained by summing the "precision farming" and "no precision farming" categories from the Eurostat ef_mp_digicr dataset.

The values refer to the statistical population covered by this dataset and should not be confused with totals reported in other Eurostat series (*Eurostat, 2026c*).

**Table 1**

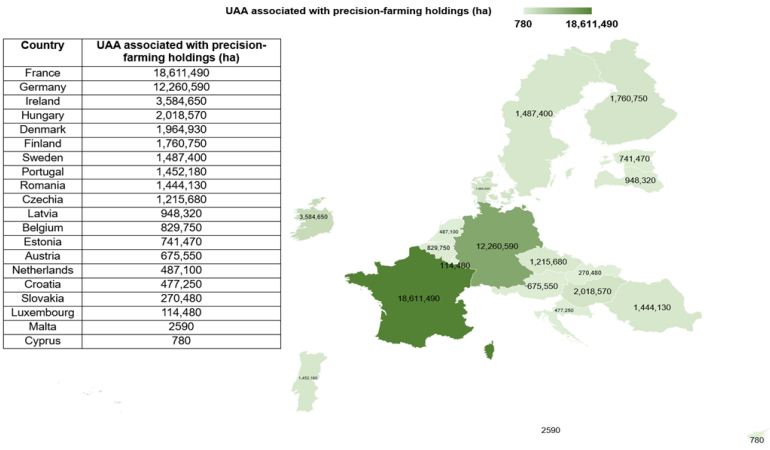
**Adoption of precision agriculture in Romania and selected EU Member States, in 2023**

| Country | Total holdings | Share of holdings (%) | Total UAA (ha) | Share of UAA (%) | Average UAA per precision-farming holding (ha/holding) | Difference (p.p.) |
|---|---|---|---|---|---|---|
| | U.M.: number of holdings, ha, percentages, ha/holding and percentage points, depending on the indicator | | | | | |
| Romania | 2,820,360 | 0.63% | 12,550,330 | 11.51% | 81.45 | 10.88 |
| Czechia | 32,720 | 4.92% | 3,521,210 | 34.52% | 755.08 | 29.60 |
| Hungary | 182,120 | 8.62% | 5,180,080 | 38.97% | 128.65 | 30.35 |
| Croatia | 143,740 | 12.83% | 1,251,710 | 38.13% | 25.88 | 25.30 |
| France | 356,340 | 47.12% | 27,201,240 | 68.42% | 110.84 | 21.30 |
| Germany | 251,130 | 47.42% | 16,585,540 | 73.92% | 102.95 | 26.50 |
| Finland | 42,100 | 64.87% | 2,264,330 | 77.76% | 64.47 | 12.89 |

*(Eurostat, data for 2023 from the ef_mp_digicr dataset, last updated June 17, 2026 and extracted September 24, 2026; own calculations)*
*Note: The area expressed in hectares represents the entire utilised agricultural area of the holdings that reported using precision agriculture, not the area on which the technologies were actually applied. The difference between the shares is expressed in percentage points.*

Romania has the largest number of holdings among the selected countries, at 2,820,360, but records the lowest share of precision agriculture users, at only 0.63%. These holdings manage 11.51% of the agricultural area included in the dataset, 10.88 percentage points above their numerical share. The average UAA per user holding reaches 81.45 ha, indicating that adoption is limited in frequency but concentrated among holdings managing larger areas. Finland ranks first for both adoption indicators: 64.87% of holdings and 77.76% of UAA are associated with precision agriculture. Germany and France record similar shares of holdings, at 47.42% and 47.12%, respectively, but the area share is higher in Germany, where it reaches 73.92%, compared with 68.42% in France. Czechia provides the clearest contrast between the frequency of adoption and the size of the areas managed. Only 4.92% of holdings use precision agriculture, but they account for 34.52% of the UAA analysed. The average area reaches 755.08 ha per user holding, the highest value in the table. Hungary records the largest difference between the area share and the holding share, at 30.35 percentage points, followed by Czechia, with 29.60 percentage points. In Croatia, precision agriculture is used by 12.83% of holdings, which manage 38.13% of UAA, although the average area of 25.88 ha is the lowest among the countries compared.

In all seven countries, the share of UAA exceeds the share of holdings using precision agriculture. This result indicates that these technologies are concentrated among holdings managing larger areas, although the size of the difference varies considerably between countries. The distribution of absolute values across European Union Member States with available data provides an additional perspective on this comparison. The tendency of precision agriculture to be adopted by holdings managing larger areas is consistent with the literature, which identifies farm size and economies of scale among the main factors influencing adoption (*Finger et al., 2019; Paustian and Theuvsen, 2017*).




| Country | UAA associated with precision-farming holdings (ha) |
|---|---|
| France | 18,611,490 |
| Germany | 12,260,590 |
| Ireland | 3,584,650 |
| Hungary | 2,018,570 |
| Denmark | 1,964,930 |
| Finland | 1,760,750 |
| Sweden | 1,487,400 |
| Portugal | 1,452,180 |
| Romania | 1,444,130 |
| Czechia | 1,215,680 |
| Latvia | 948,320 |
| Belgium | 829,750 |
| Estonia | 741,470 |
| Austria | 675,550 |
| Netherlands | 487,100 |
| Croatia | 477,250 |
| Slovakia | 270,480 |
| Luxembourg | 114,480 |
| Malta | 2590 |
| Cyprus | 780 |

**Fig. 1 - Utilised agricultural area associated with holdings using precision agriculture in European Union Member States with available data, in 2023 (U.M.: ha)**

*(Eurostat, data for 2023 from the ef_mp_digicr dataset, last updated on 17.06.2026 and extracted on 24.09.2026)*
*Note: The area shown represents the entire utilised agricultural area of holdings that reported using precision agriculture, not the area on which the technologies were actually applied. Values for Bulgaria, Greece, Spain, Italy, Lithuania, Poland and Slovenia are unavailable in the dataset analysed; the absence of data does not represent a value of zero.*

The territorial distribution of these areas shows a strong concentration in France and Germany. Holdings using precision agriculture manage 18,611,490 ha in France and 12,260,590 ha in Germany. The next values are considerably lower: Ireland records 3,584,650 ha, Hungary 2,018,570 ha and Finland 1,760,750 ha.

Romania accounts for 1,444,130 ha, placing it close to Portugal, with 1,452,180 ha, and Sweden, with 1,487,400 ha. Romania's value exceeds the 1,215,680 ha recorded in Czechia but represents only 7.76% of the corresponding area in France. Romania's comparatively favourable position in the ranking by absolute area contrasts with the low share of 11.51% reported in Table 1. The map must be interpreted in relation to the size of each country's agricultural area. A high absolute value does not automatically indicate a wider adoption of precision agriculture among holdings. Romania illustrates this distinction: the area associated with user holdings exceeds 1.4 million ha, although only 0.63% of the holdings included in the dataset reported using these technologies. In Finland, the absolute area is only approximately 317,000 ha larger than in Romania, but the share of user holdings reaches 64.87%. Absolute values and shares therefore describe different dimensions of adoption and should be examined together. The differences between countries raise the question of the characteristics of the holdings in which precision technologies are used. Economic size is the first criterion examined to define this profile.

**Table 2**

**Share of holdings using precision agriculture by economic size in Romania and selected EU Member States, in 2023**

| Country | EUR 2000–7999 | EUR 8000–24,999 | EUR 25,000–99,999 | ≥ EUR 100,000 | Difference (p.p.) |
|---|---|---|---|---|---|
| | U.M.: percentages and percentage points, depending on the indicator | | | | |
| Romania | 0.54% | 1.35% | 3.52% | 15.13% | 14.59 |
| Czechia | 0.36% | 1.18% | 3.23% | 20.45% | 20.10 |
| Hungary | 3.88% | 7.98% | 16.27% | 39.25% | 35.37 |
| Croatia | 9.37% | 18.56% | 34.56% | 54.55% | 45.18 |
| France | 5.55% | 14.74% | 33.32% | 70.26% | 64.71 |
| Germany | 13.26% | 30.08% | 48.92% | 68.76% | 55.51 |
| Finland | 42.68% | 63.38% | 73.16% | 79.88% | 37.20 |

*(Eurostat, data for 2023 from the ef_mp_digicr dataset, last updated on 17.06.2026 and extracted on 24.09.2026)*

*Note: Economic size is expressed through the standard output of the holding, in euros. The share was calculated by dividing the number of holdings using precision agriculture by the total number of holdings in the same economic-size class. The difference represents the share of the class with a standard output of at least EUR 100,000 minus the share of the EUR 2000–7999 class. The export analysed does not include holdings with a standard output below EUR 2000.*

The share of holdings using precision agriculture increases with economic size in all seven countries. Differences are already evident in the first class analysed, EUR 2000–7999, where the values range from 0.36% in Czechia to 42.68% in Finland. In the category with a standard output of at least EUR 100,000, the range shifts to values between 15.13% in Romania and 79.88% in Finland.

Romania records shares of 0.54% and 1.35% in the first two economic-size classes. The percentage rises to 3.52% in the EUR 25,000–99,999 category and to 15.13% among holdings with a standard output of at least EUR 100,000. The difference between the two extreme classes is 14.59 percentage points, the lowest value in the table. Nevertheless, the share recorded for Romania's highest class remains below the value reported in Finland even for holdings in the EUR 2000–7999 category.

France records the largest difference between the two extreme classes, at 64.71 percentage points. The share rises from 5.55% in the first category to 70.26% among holdings with a standard output of at least EUR 100,000. Germany follows the same pattern, increasing from 13.26% to 68.76%, with a difference of 55.51 percentage points. The gap reaches 45.18 percentage points in Croatia and 35.37 percentage points in Hungary.

Finland maintains the highest share in every economic-size class. Precision agriculture is used by 42.68% of holdings in the lowest category and by almost four fifths of those with a standard output of at least EUR 100,000. The results show an association between economic size and the adoption of precision technologies, but they also indicate that economic size alone does not explain the differences between countries. Wide gaps persist within the same economic-size class, supporting the examination of other characteristics of holdings and their managers.

The relationship between economic size and adoption is also explained in the literature through investment costs and expected profitability, while small farms frequently face constraints related to cost, technological complexity and access to professional support (*Barnes et al., 2019; Mizik, 2023*).

**Table 3**

**Share of holdings using precision agriculture by manager training in Romania and selected EU Member States, in 2023**

| Country | Practical experience only | Basic agricultural training | Full agricultural training | Difference (p.p.) |
|---|---|---|---|---|
| | U.M.: percentages and percentage points, depending on the indicator | | | |
| Romania | 0.53% | 1.75% | 5.02% | 4.49 |
| Czechia | 2.05% | 2.98% | 9.44% | 7.40 |
| Hungary | 3.96% | 11.29% | 23.06% | 19.09 |
| Croatia | 11.23% | 33.24% | 31.52% | 20.29 |
| France | 24.93% | 52.20% | 66.02% | 41.09 |
| Germany | 31.15% | 53.53% | 68.08% | 36.93 |
| Finland | 61.59% | 67.74% | 70.02% | 8.43 |

*(Eurostat, data for 2023 from the ef_mp_digicr dataset, last updated on 17.06.2026 and extracted on 24.09.2026)*

*Note: The share was calculated by dividing the number of holdings using precision agriculture by the total number of holdings in the same manager-training category. The difference represents the share associated with full agricultural training minus the share of managers with practical experience only. The indicators describe the association between manager training and the use of precision agriculture without demonstrating a causal relationship.*

Manager training clearly differentiates the level of precision agriculture use. In every country analysed, the share of holdings managed by individuals with full agricultural training exceeds the corresponding share for managers with practical experience only. The size of the difference nevertheless ranges from 4.49 percentage points in Romania to 41.09 percentage points in France.

Romania ranks last at all three training levels. Precision agriculture is used by 0.53% of holdings managed by individuals relying only on practical experience, by 1.75% in the basic agricultural training category and by 5.02% in the full agricultural training category. The increase between the first and last categories is clear, but the final value remains below the 9.44% recorded in Czechia and well below the levels reported by the other countries.

The largest differences occur in France and Germany. In France, the share rises from 24.93% for practical experience only to 66.02% for full agricultural training, resulting in a gap of 41.09 percentage points. Germany records a difference of 36.93 percentage points, with values of 31.15% and 68.08% at the two ends of the comparison. Hungary and Croatia occupy intermediate positions, with differences of 19.09 and 20.29 percentage points.

The pattern is not strictly ordered across all three training levels. In Croatia, the share associated with basic agricultural training, at 33.24%, exceeds the 31.52% recorded for full agricultural training. Finland presents another distinct situation: the share is already high among managers with practical experience only, at 61.59%, and reaches 70.02% for those with full agricultural training. The difference of 8.43 percentage points is small compared with France and Germany because adoption is widespread across all three categories.

The results indicate an association between the manager's agricultural training and the use of precision technologies, without allowing a causal relationship to be inferred. The managerial profile is examined further through a comparison of age groups.

The role of training should also be considered alongside access to demonstrations, workshops and professional networks, which are associated with adoption decisions. For smaller farms, cooperation and contractor services may reduce some of the existing constraints (*Kutter et al., 2011; Tamirat et al., 2018*).

**Table 4**

**Share of holdings using precision agriculture by manager age in Romania and selected EU Member States, in 2023**

| Country | Managers under 35 years of age | Managers aged 65 years or over | Difference (p.p.) |
|---|---|---|---|
| | U.M.: percentages and percentage points, depending on the indicator | | |
| Romania | 1.00% | 0.51% | 0.49 |
| Czechia | 4.42% | 3.24% | 1.18 |
| Hungary | 11.46% | 6.79% | 4.68 |
| Croatia | 20.93% | 7.80% | 13.13 |
| France | 54.46% | 24.11% | 30.35 |
| Germany | 52.47% | 37.77% | 14.69 |
| Finland | 75.84% | 54.04% | 21.80 |

*(Eurostat, data for 2023 from the ef_mp_digicr dataset, updated on 17.06.2026 and extracted on 24.09.2026)*

*Note: The category of managers under 35 years of age was obtained by adding the "under 25 years" and "25–34 years" classes. The share represents the ratio between holdings using precision agriculture and all holdings within the same manager-age group. The difference was calculated by subtracting the share for managers aged 65 years or over from the share for managers under 35 years of age.*

Managers under 35 years of age record a higher share of precision agriculture use than those aged 65 years or over in all the countries analysed. This difference is present both in countries with a high overall level of adoption and in those where these technologies are used by only a small proportion of holdings.

Romania once again ranks last. Precision agriculture is used by 1.00% of holdings managed by persons under 35 years of age and by 0.51% of those managed by persons aged 65 years or over. The difference of 0.49 percentage points is the smallest in the table, but it results from the low levels recorded by both age groups. A similar situation is observed in Czechia, where the shares are 4.42% and 3.24%, producing a gap of 1.18 percentage points.

France records the largest generational difference. The share reaches 54.46% among managers under 35 years of age, compared with 24.11% among those aged 65 years or over, resulting in a gap of 30.35 percentage points. Finland ranks first in both age groups, with 75.84% and 54.04%, although the difference remains substantial, at 21.80 percentage points. Germany records shares of 52.47% and 37.77%, with a gap of 14.69 percentage points.

In Croatia, the difference between the two age groups is 13.13 percentage points, exceeding the 4.68 percentage points observed in Hungary. These results indicate that manager age is associated with the use of precision agriculture, although the magnitude of the difference depends on the overall level of adoption in each country. A small gap does not automatically indicate a favourable situation, as demonstrated by the low values recorded in Romania and Czechia.

Economic size, training and age together outline the profile of holdings using precision agriculture. The analysis continues with internet access and the use of farm management information systems, two distinct components of agricultural digitalisation.

**Table 5**

**Internet access and use of farm management information systems among agricultural holdings in Romania and selected EU Member States, in 2023**

| Country | Total holdings analysed | Holdings with internet access | Share with internet access (%) | Holdings using farm management information systems | Share using farm management information systems (%) | Difference (p.p.) |
|---|---|---|---|---|---|---|
| | U.M.: number of holdings, percentages and percentage points, depending on the indicator | | | | | |
| Romania | 1,004,590 | 245,650 | 24.45% | 3960 | 0.39% | 24.06 |
| Czechia | 29,320 | 27,830 | 94.92% | 4080 | 13.92% | 81.00 |
| Hungary | 136,190 | 111,760 | 82.06% | 15,480 | 11.37% | 70.70 |
| Croatia | 107,620 | 73,870 | 68.64% | 12,080 | 11.22% | 57.41 |

| | | | | | | |
|---|---|---|---|---|---|---|
| France | 343,690 | 269,250 | 78.34% | 211,720 | 61.60% | 16.74 |
| Germany | 253,810 | 245,040 | 96.54% | 57,210 | 22.54% | 74.00 |
| Finland | 42,250 | 37,710 | 89.25% | 24,230 | 57.35% | 31.91 |

*(Eurostat, data for 2023 from the ef_mp_digi dataset, updated on 17.06.2026 and extracted on 24.09.2026)*

*Note: The absolute values were obtained by summing the four available standard-output classes: 2000–7999 euros, 8000–24,999 euros, 25,000–99,999 euros and at least 100,000 euros. Holdings with a standard output below 2000 euros are not included in the analysed export. The difference represents the share of holdings with internet access minus the share using farm management information systems. The two categories are not mutually exclusive and should not be added together.*

Internet access is considerably more widespread than the use of farm management information systems in all the countries analysed. The difference between the two indicators shows that connectivity is not accompanied to the same extent by the use of digital tools for managing agricultural holdings. Romania records the lowest shares for both indicators. Of the 1,004,590 holdings included in the economic classes analysed, 245,650 have internet access, representing 24.45% of the total. Only 3960 holdings use farm management information systems, corresponding to a share of 0.39%. The difference between the two indicators is 24.06 percentage points. The relatively small size of this gap does not indicate a favourable convergence between the indicators, but results from the low level of internet access.Germany has the highest share of holdings with internet access, at 96.54%, followed by Czechia with 94.92%, Finland with 89.25% and Hungary with 82.06%. The use of farm management information systems remains considerably lower in Germany and Czechia, where the corresponding shares are 22.54% and 13.92%. Consequently, the differences reach 74.00 percentage points in Germany and 81.00 percentage points in Czechia, the latter being the largest value in the table.

France and Finland show more extensive use of farm management information systems. France records 211,720 user holdings, representing 61.60% of the total, while Finland reaches 57.35%. Their differences relative to internet access are 16.74 and 31.91 percentage points, respectively, lower than those observed in Czechia, Germany, Hungary and Croatia.

The data distinguish between two stages of digitalisation: the availability of internet access and the use of information systems in farm management. The distance between them varies considerably among countries and shows that a high level of connectivity alone does not describe the extent to which farm management has been digitalised. The following analysis examines the use of specific agricultural technologies: precision agriculture, robotics and machinery for livestock management. The data used for this comparison come from the ef_mp_digi dataset (*Eurostat, 2026a*). The distinction between connectivity and the actual use of information systems is relevant because these systems transform data into support for farm-level decisions, while access to digital infrastructure remains unevenly distributed among holdings (*Fountas et al., 2015; Mehrabi et al., 2021*).

**Table 6**

**Share of holdings using precision agriculture, robotics and machinery for livestock management in Romania and selected EU Member States, in 2023**

| Country | Total holdings analysed | Holdings using precision agriculture | Share (%) | Holdings using robotics | Share (%) | Holdings using machinery for livestock management | Share (%) |
|---|---|---|---|---|---|---|---|
| | U.M.: number of holdings and percentages, depending on the indicator | | | | | | |
| Romania | 1,004,590 | 10,510 | 1.05% | 32,030 | 3.19% | 50,220 | 5.00% |
| Czechia | 29,320 | 1610 | 5.49% | 1130 | 3.85% | 2780 | 9.48% |
| Hungary | 136,190 | 15,020 | 11.03% | 3930 | 2.89% | 22,100 | 16.23% |
| Croatia | 107,620 | 17,030 | 15.82% | 2330 | 2.17% | 16,550 | 15.38% |
| France | 343,690 | 167,390 | 48.70% | 80,810 | 23.51% | 87,740 | 25.53% |
| Germany | 253,810 | 119,160 | 46.95% | 46,580 | 18.35% | 77,760 | 30.64% |
| Finland | 42,250 | 27,340 | 64.71% | 8090 | 19.15% | 6295 | 14.90% |

*(Eurostat, data for 2023 from the ef_mp_digi dataset, updated on 17.06.2026 and extracted on 24.09.2026)*

*Note: The absolute values were obtained by summing the four available standard-output classes, beginning at EUR 2000. Holdings with a standard output below EUR 2000 are not included. The technology categories are not mutually exclusive, as the same holding may use more*

*than one technology. The share of holdings using machinery for livestock management was calculated in relation to all the holdings analysed, not only livestock holdings. The comparison must therefore also be interpreted in relation to the agricultural profile of each country.*

The use of the three technology categories differs among the countries analysed. These categories are not mutually exclusive because the same holding may simultaneously use precision agriculture, robotics and machinery for livestock management. Their values should therefore not be added together to obtain a general measure of technological adoption.

In Romania, 10,510 holdings use precision agriculture, representing 1.05% of the total analysed. Robotics is used by 32,030 holdings, corresponding to a share of 3.19%, while machinery for livestock management is used by 50,220 holdings, or 5.00%. Romania exceeds Hungary and Croatia in the absolute number of holdings using robotics, but its low share reflects the influence of a much larger national base of more than one million holdings.

Precision agriculture records its highest shares in Finland, France and Germany, at 64.71%, 48.70% and 46.95%, respectively. Finland also ranks first in relative terms, although its absolute number of 27,340 holdings is considerably lower than the 167,390 recorded in France and the 119,160 in Germany. This contrast confirms the need to consider absolute values and shares together when comparing countries.

Robotics has a lower share than precision agriculture in six of the seven countries, with Romania being the exception. The highest values are recorded in France, at 23.51%, Finland, at 19.15%, and Germany, at 18.35%. At the opposite end are Croatia, with 2.17%, Hungary, with 2.89%, and Romania, with 3.19%.

Machinery for livestock management reaches its highest share in Germany, at 30.64%, followed by France, at 25.53%, and Hungary, at 16.23%. These percentages require cautious interpretation because the denominator includes all the holdings analysed, including those without livestock production. The indicator describes the prevalence of this machinery within the total population covered by the dataset, rather than the level of technological adoption among livestock holdings considered separately.

The results show that agricultural digitalisation does not follow a single pattern. Each country's position changes according to the technology examined, and a high absolute number of users can coexist with a low share. Following the assessment of the digital components, the analysis is extended to indicators associated with sustainable agricultural practices. The potential benefits of precision agriculture include more targeted input use, lower costs and environmental pressures, and the maintenance or improvement of productivity. The extent of these effects nevertheless depends on the technology applied and the context of the holding (*Balafoutis et al., 2017*).

**Table 7**

**Share of organic and in-conversion utilised agricultural area in Romania and selected EU Member States in 2023**

| Country | Total utilised agricultural area (ha) | Organic and in-conversion UAA (ha) | Share of organic UAA (%) | Difference from Romania (p.p.) |
|---|---|---|---|---|
| | U.M.: ha, percentages and percentage points, depending on the indicator | | | |
| Romania | 12,550,330 | 499,460 | 3.98% | 0.00 |
| Czechia | 3,521,210 | 537,230 | 15.26% | 11.28 |
| Hungary | 5,087,200 | 308,680 | 6.07% | 2.09 |
| Croatia | 1,506,220 | 121,790 | 8.09% | 4.11 |
| France | 27,201,240 | 2,599,660 | 9.56% | 5.58 |
| Germany | 16,585,540 | 1,852,660 | 11.17% | 7.19 |
| Finland | 2,264,330 | 312,370 | 13.80% | 9.82 |

*(Eurostat, data for 2023 from the ef_lus_main dataset, updated on 17.06.2026 and extracted on 24.09.2026; own calculations)*

*Note: Organic utilised agricultural area includes land fully converted to organic farming and land undergoing conversion, excluding kitchen gardens. The difference was calculated by subtracting the share recorded by Romania from the share of each country.*

The ranking of organic and in-conversion utilised agricultural area differs depending on whether the indicator is expressed in hectares or as a share of total UAA. France and Germany lead in absolute area, while Czechia and Finland occupy the first positions by share.

Romania records 499,460 ha of organic and in-conversion UAA, representing 3.98% of its total utilised agricultural area. The absolute value is close to that of Czechia, at 537,230 ha, but the structural difference is considerable. Czechia's share reaches 15.26%, standing 11.28 percentage points above Romania. This comparison shows that similar absolute areas can have different weights within the agricultural structure of each

country. France has the largest organic and in-conversion area among the selected countries, at 2,599,660 ha, followed by Germany with 1,852,660 ha. Their shares, however, are 9.56% and 11.17%, below those recorded by Czechia and Finland. In Finland, 312,370 ha account for 13.80% of total UAA, although the absolute area is smaller than that of Romania. Hungary and Croatia occupy intermediate positions by share, with 6.07% and 8.09%, respectively. Compared with Romania, the differences are 2.09 and 4.11 percentage points. Romania ranks last according to the share of organic UAA, although it does not have the smallest area expressed in hectares.

The results confirm that absolute values should be assessed in relation to the agricultural area of each country. The indicator describes the extent of organic farming and land undergoing conversion, but does not provide a general assessment of agricultural sustainability on its own. The territorial distribution across all EU Member States with available data is presented below.

| Country | Organic and in-conversion UAA (ha) |
|---|---|
| France | 2,599,660 |
| Germany | 1,852,660 |
| Austria | 691,940 |
| Portugal | 675,240 |
| Sweden | 556,700 |
| Czechia | 537,230 |
| Romania | 499,460 |
| Finland | 312,370 |
| Hungary | 308,680 |
| Denmark | 298,370 |
| Latvia | 297,410 |
| Slovakia | 258,200 |
| Ireland | 231,570 |
| Estonia | 224,350 |
| Croatia | 121,790 |
| Belgium | 95,690 |
| Netherlands | 87,890 |
| Luxembourg | 8740 |
| Cyprus | 7110 |

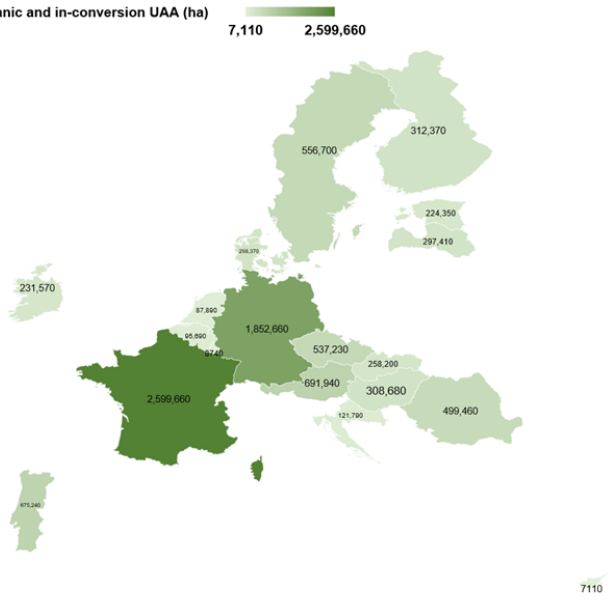



**Fig. 2 - Organic and in-conversion utilised agricultural area in EU Member States with available data, in 2023 (U.M.: ha)**

*(Eurostat, data for 2023 from the ef_lus_main dataset, updated on 17.06.2026 and extracted on 24.09.2026)*

*Note: The indicator includes certified organic utilised agricultural area and land undergoing conversion to organic farming, excluding kitchen gardens. Member States without available numerical values were not represented.*

The map confirms the leading positions of France and Germany in the distribution of organic and in-conversion agricultural area. France records 2,599,660 ha and Germany 1,852,660 ha. No other Member State represented exceeds one million hectares, clearly separating these two values from the remainder of the distribution.

A second group comprises Austria, with 691,940 ha, Portugal, with 675,240 ha, Sweden, with 556,700 ha, and Czechia, with 537,230 ha. Romania follows with 499,460 ha, standing 37,770 ha below Czechia. Romania's area exceeds the 312,370 ha recorded in Finland and the 308,680 ha in Hungary, although both countries have higher shares of organic area in their total UAA.

The distribution confirms the distinction between the physical extent of the area and its importance within the national agricultural structure. Romania occupies an intermediate position by number of hectares but ranks last among the selected countries according to its share of 3.98%. By contrast, Finland has a smaller absolute area but a share of 13.80%.

The map complements the comparison presented in Table 7 but does not permit a separate assessment of the general level of sustainability. Organic farming represents only one of the dimensions examined. The following analysis considers the structure of arable-land cover to identify differences among soil-protection practices.

The organic-farming data come from the ef_lus_main dataset (*Eurostat, 2026b*). In the literature, organic farming and conservation practices are examined within a broader framework that includes resource protection, adaptation to climate change and cooperation among actors in the agricultural sector (*Buzatu et al., 2024; Vlăduț et al., 2024*).

The type of arable-land cover complements the analysis of organically farmed areas by showing how land was classified under different forms of cover or management in 2023. The data reveal pronounced structural differences among the countries analysed.

**Table 8**

**Structure of arable-land cover in Romania and selected EU Member States, in 2023**

| Country | Total arable land | Excluded from the soil-cover classification | Normal winter crops | Cover or intermediate crops | Plant residues | Bare soil |
|---|---|---|---|---|---|---|
| | U.M.: ha and percentages, depending on the indicator | | | | | |
| Romania | 8,481,980 | 145,640 | 8,289,150 | 2260 | 3770 | 41,160 |
| Czechia | 2,518,810 | 369,520 | 1,333,320 | 193,950 | 186,720 | 435,290 |
| Hungary | 4,219,620 | 231,350 | 1,856,680 | 436,510 | 529,140 | 1,165,950 |
| Croatia | 877,820 | 65,720 | 289,750 | 30,530 | 137,900 | 353,920 |
| France | 16,963,990 | 86,750 | 11,188,550 | 3,697,490 | 1,048,790 | 942,410 |
| Germany | 11,644,580 | 614,570 | 6,236,760 | 1,734,740 | 2,393,080 | 665,420 |
| Finland | 2,246,610 | 1,001,530 | 110,370 | 271,520 | 495,660 | 367,530 |
| **Country** | **Total arable land (ha)** | **Excluded from the soil-cover classification (%)** | **Normal winter crops (%)** | **Cover or intermediate crops (%)** | **Plant residues (%)** | **Bare soil (%)** |
| Romania | 8,481,980 | 1.72% | 97.73% | 0.03% | 0.04% | 0.49% |
| Czechia | 2,518,810 | 14.67% | 52.93% | 7.70% | 7.41% | 17.28% |
| Hungary | 4,219,620 | 5.48% | 44.00% | 10.34% | 12.54% | 27.63% |
| Croatia | 877,820 | 7.49% | 33.01% | 3.48% | 15.71% | 40.32% |
| France | 16,963,990 | 0.51% | 65.95% | 21.80% | 6.18% | 5.56% |
| Germany | 11,644,580 | 5.28% | 53.56% | 14.90% | 20.55% | 5.71% |
| Finland | 2,246,610 | 44.58% | 4.91% | 12.09% | 22.06% | 16.36% |

*(Eurostat, data for 2023 from the ef_mp_soil dataset, updated on 14.08.2026 and extracted on 24.09.2026; own calculations)*

*Note: The percentages were calculated by dividing each category by the total arable-land area. The category "arable land excluded from the soil-cover classification" is distinct from bare soil and represents the area not included in the breakdown of soil-cover practices. Minor deviations from 100% may result from rounding. The "multiannual plants" category was not included because its values were unavailable in the analysed export. Considered separately, these indicators describe the type of arable-land cover and do not provide a direct assessment of sustainability or erosion risk.*

Romania has the highest concentration in a single cover category among the selected countries. Of its total arable-land area of 8,481,980 ha, 8,289,150 ha were classified under normal winter crops, representing 97.73%. Cover or intermediate crops accounted for only 2260 ha, or 0.03%, while plant residues were retained on 3770 ha, equivalent to 0.04%. Bare soil represented 0.49% of the total, and 1.72% of the arable land was excluded from the soil-cover classification.

France and Germany have a different structure. France recorded the largest area under cover or intermediate crops, at 3,697,490 ha, as well as the highest share, at 21.80%. Germany ranked second, with 1,734,740 ha and a share of 14.90%. Relatively high shares were also recorded in Finland, at 12.09%, and Hungary, at 10.34%, while Czechia and Croatia registered 7.70% and 3.48%, respectively.

Plant residues accounted for their largest relative shares in Finland, where the category represented 22.06% of arable land, and Germany, with 20.55%. Substantial shares were also recorded in Croatia, at 15.71%, and Hungary, at 12.54%. By contrast, bare soil accounted for 40.32% of Croatia's arable land and 27.63% of Hungary's. The corresponding shares were lower in France and Germany, at 5.56% and 5.71%, while Romania recorded the lowest value, at 0.49%.

The comparison of Finland with the other countries requires caution because 1,001,530 ha, representing 44.58% of its arable land, were excluded from the soil-cover classification. Czechia also recorded a relatively high excluded share, at 14.67%. In these cases, the detailed categories cover a smaller proportion of total arable land than in countries where the excluded share is limited.

The results reveal markedly different national patterns of arable-land cover, but they do not support a general sustainability ranking or a direct assessment of erosion risk. Each category must be interpreted together with the area excluded from the classification and the characteristics of the national agricultural structure. The analysis of crop rotation provides a complementary perspective on practices applied to arable land. The soil-cover structure was analysed using the ef_mp_soil dataset (*Eurostat, 2026d*). The relevance of cover crops extends beyond their statistical share because they are associated with soil protection, while a meta-analysis found higher stocks of soil organic carbon than in the agricultural reference systems (*Buzatu et al., 2023; Poeplau and Don, 2015*).

Crop rotation was analysed through the share of arable land belonging to holdings in which this practice covers at least 75% of the arable area. The indicator permits comparisons between countries independently of their total arable-land area, but it must be interpreted together with the absolute values.

**Table 9**

**Arable land of holdings in which crop rotation covers at least 75% of the arable area in Romania and selected EU Member States, in 2023**

| Country | Total arable land (ha) | Arable land associated with the ≥75% class (ha) | Share of total arable land (%) | Difference from Romania (p.p.) |
|---|---|---|---|---|
| | U.M.: ha, percentages and percentage points, depending on the indicator | | | |
| Romania | 8,481,980 | 6,091,850 | 71.82% | 0.00 |
| Czechia | 2,518,810 | 2,149,870 | 85.35% | 13.53 |
| Hungary | 4,219,620 | 3,071,310 | 72.79% | 0.97 |
| Croatia | 877,820 | 858,500 | 97.80% | 25.98 |
| France | 16,963,990 | 15,760,840 | 92.91% | 21.09 |
| Germany | 11,644,580 | 10,728,130 | 92.13% | 20.31 |
| Finland | 2,246,610 | 981,750 | 43.70% | -28.12 |

*(Eurostat, data for 2023 from the ef_mp_soil dataset, updated on 14.08.2026 and extracted on 24.09.2026; own calculations)*

*Note: The value for the ≥75% class represents the entire arable-land area of holdings included in this category, rather than the exact number of hectares on which crop rotation was applied. The share was calculated by dividing this area by total arable land. The difference represents the share of each country minus the share recorded by Romania.*

In Romania, holdings included in this category accounted for 6,091,850 ha out of a total arable-land area of 8,481,980 ha, corresponding to a share of 71.82%. In absolute terms, Romania ranks third among the seven countries analysed, after France and Germany. By share, however, it ranks sixth, ahead only of Finland.

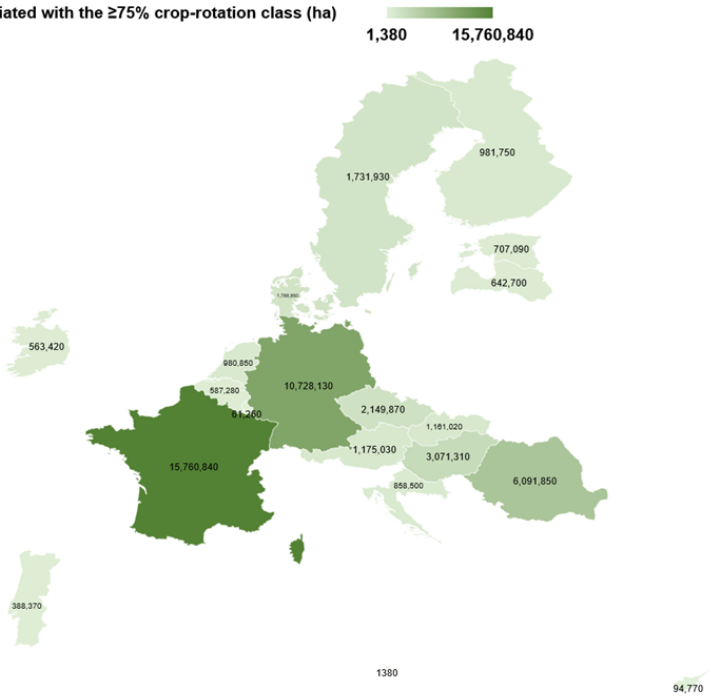
Croatia recorded the highest share, at 97.80%, standing 25.98 percentage points above Romania. Its associated area of 858,500 ha is nevertheless the smallest value in the table, owing to the country's smaller total arable-land area. France and Germany combine high shares, at 92.91% and 92.13%, with the largest absolute areas, at 15,760,840 ha and 10,728,130 ha, respectively.

Czechia also ranks above Romania, with a share of 85.35% and a difference of 13.53 percentage points. The closest value is recorded in Hungary, where the share reaches 72.79%, only 0.97 percentage points above Romania. Finland is the only selected country with a lower value than Romania, at 43.70%, or 28.12 percentage points less.

The values do not represent the exact area on which crop rotation was applied. They include the entire arable-land area of holdings where crop rotation covers at least 75% of the arable area. The results therefore describe the amount and share of arable land associated with holdings in this class and do not permit calculation of the exact number of hectares under crop rotation.

The relevance of crop rotation extends beyond the distribution of agricultural area. Long-term experiments conducted in North America associated diversified crop rotations with greater resilience of maize yields under adverse growing conditions (*Bowles et al., 2020*).

The difference between Romania's position by absolute area and its ranking by share confirms the influence of national arable-land size. The territorial distribution of absolute values for all EU Member States with available data is presented below in map form.




| Country | Arable land associated with the ≥75% crop-rotation class (ha) |
|---|---|
| France | 15,760,840 |
| Germany | 10,728,130 |
| Romania | 6,091,850 |
| Hungary | 3,071,310 |
| Czechia | 2,149,870 |
| Denmark | 1,788,850 |
| Sweden | 1,731,930 |
| Austria | 1,175,030 |
| Slovakia | 1,161,020 |
| Finland | 981,750 |
| Netherlands | 980,850 |
| Croatia | 858,500 |
| Estonia | 707,090 |
| Latvia | 642,700 |
| Belgium | 587,280 |
| Ireland | 563,420 |
| Portugal | 388,370 |
| Cyprus | 94,770 |
| Luxembourg | 61,260 |
| Malta | 1380 |

**Fig. 3 - Arable land of holdings in which crop rotation covers at least 75% of the arable area in EU Member States with available data, in 2023 (U.M.: ha)**

*(Eurostat, data for 2023 from the ef_mp_soil dataset, updated on 14.08.2026 and extracted on 24.09.2026)*

*Note: The values represent the entire arable-land area of holdings in which crop rotation covers at least 75% of the arable area. They do not represent the exact number of hectares on which crop rotation was applied. The map presents absolute values, which are also influenced by the size of each country's arable-land area; comparable shares are presented separately in Table 9.*

The map places France first, with 15,760,840 ha, followed by Germany, with 10,728,130 ha. Romania ranks third among the EU Member States for which numerical values are available. Its area of 6,091,850 ha is almost twice that recorded in Hungary, at 3,071,310 ha. Czechia accounts for 2,149,870 ha, while Denmark and Sweden record 1,788,850 ha and 1,731,930 ha, respectively.

Romania's position on the map is influenced by the large size of its arable-land area. Although its absolute value is the third highest among those available, the share of 71.82% presented in Table 9 places Romania second to last within the group of seven selected countries. Croatia presents the opposite situation: it records the highest share, at 97.80%, but the associated area amounts to only 858,500 ha.

The difference between rankings based on hectares and those based on shares shows that the map cannot be used alone to assess the prevalence of crop rotation. High absolute values may result from the size of the national arable-land area, even when the share of arable land associated with holdings in the analysed class is lower. Conversely, countries with smaller agricultural areas may record high shares without occupying leading positions by number of hectares.

Numerical values are unavailable in the analysed dataset for Bulgaria, Greece, Spain, Italy, Lithuania, Poland and Slovenia. Blank areas on the map should not be interpreted as zero values. The areas represented also refer to the entire arable land of holdings in which crop rotation covers at least 75% of the arable area, rather than the exact area on which the practice was applied.

Romania's position for crop rotation differs from those recorded for digitalisation, organic farming and cover crops. Comparing these indicators simultaneously identifies the areas in which its distance from the other countries is greater.

The comparison of the six indicators positions Romania against the same reference countries. The reference mean is arithmetic and unweighted and was calculated for Czechia, Hungary, Croatia, France, Germany and Finland. It does not represent the European Union average.

**Table 10**

**Romania's comparative position for the main indicators of agricultural digitalisation and sustainability, in 2023**

| Indicator | Romania | Czechia | Hungary | Croatia | France | Germany | Finland | Six-country mean | Romania's difference (p.p.) | Romania's rank |
|---|---|---|---|---|---|---|---|---|---|---|
| | U.M.: percentages and percentage points, depending on the indicator; rank: ordinal position | | | | | | | | | |
| Holdings using precision agriculture | 1.05% | 5.49% | 11.03% | 15.82% | 48.70% | 46.95% | 64.71% | 32.12% | -31.07 | 7 |
| Holdings with internet access | 24.45% | 94.92% | 82.06% | 68.64% | 78.34% | 96.54% | 89.25% | 84.96% | -60.51 | 7 |
| Holdings using farm management information systems | 0.39% | 13.92% | 11.37% | 11.22% | 61.60% | 22.54% | 57.35% | 29.67% | -29.27 | 7 |
| Organic and in-conversion UAA | 3.98% | 15.26% | 6.07% | 8.09% | 9.56% | 11.17% | 13.80% | 10.66% | -6.68 | 7 |
| Arable land under cover or intermediate crops | 0.03% | 7.70% | 10.34% | 3.48% | 21.80% | 14.90% | 12.09% | 11.72% | -11.69 | 7 |
| Arable land of holdings in which crop rotation covers at least 75% of the arable area | 71.82% | 85.35% | 72.79% | 97.80% | 92.91% | 92.13% | 43.70% | 80.78% | -8.96 | 6 |

*(Eurostat, data for 2023 from the ef_mp_digi, ef_lus_main and ef_mp_soil datasets; latest updates: 17.06.2026 for ef_mp_digi and ef_lus_main and 14.08.2026 for ef_mp_soil; data extracted on 24.09.2026; own calculations)*

*Note: The six-country mean is the unweighted arithmetic mean of the values recorded in Czechia, Hungary, Croatia, France, Germany and Finland and does not represent the European Union average. The difference was calculated as Romania's value minus the six-country mean. Negative values indicate a lower share in Romania. Rank 1 corresponds to the highest share among the seven countries. The first three indicators were calculated for holdings with an economic size of at least EUR 2000. For this reason, the precision-agriculture indicator is the value presented in Table 6, namely 1.05% for Romania, rather than the 0.63% reported in Table 1 for all holdings. Organic UAA was calculated in relation to utilised agricultural area, while the final two indicators were calculated in relation to arable land. For crop rotation, the area represents the entire arable land of holdings in which rotation covers at least 75% of the arable area, rather than the area actually under rotation. The indicators were not aggregated into a composite score.*

Romania records values below the six-country mean for all the indicators analysed. It ranks last for precision agriculture, internet access, farm management information systems, organic utilised agricultural area, and cover or intermediate crops. For crop rotation, Romania ranks sixth, ahead of Finland.

The largest difference concerns internet access. Romania's share of 24.45% is 60.51 percentage points below the reference-country mean of 84.96%. The difference for precision agriculture is -31.07 percentage points, while the use of farm management information systems records a gap of -29.27 percentage points. The precision-agriculture value of 1.05% differs from the 0.63% reported in Table 1 because the first three indicators in this comparison include only holdings with an economic size of at least EUR 2000.

Differences are also present in the indicators related to the agricultural practices analysed. Organic and in-conversion UAA represents 3.98% in Romania, compared with a mean of 10.66%, resulting in a difference of -6.68 percentage points. For cover or intermediate crops, Romania records 0.03%, which is 11.69 percentage points below the group mean. Crop rotation is the indicator for which Romania comes closest to the reference value: its share of 71.82% is 8.96 percentage points below the mean of 80.78%.

The rankings must be interpreted separately for each indicator. They are based on different statistical populations and denominators, namely holdings above a specified economic-size threshold, utilised agricultural area, or arable land. The values were therefore not aggregated into a single score, and Romania's seventh position for several indicators does not constitute a general ranking of Romanian agriculture.

The differences observed for precision agriculture and cover crops raise the question of a possible association between technology adoption and the application of this practice. The relationship between the two shares is examined separately for the seven countries analysed.

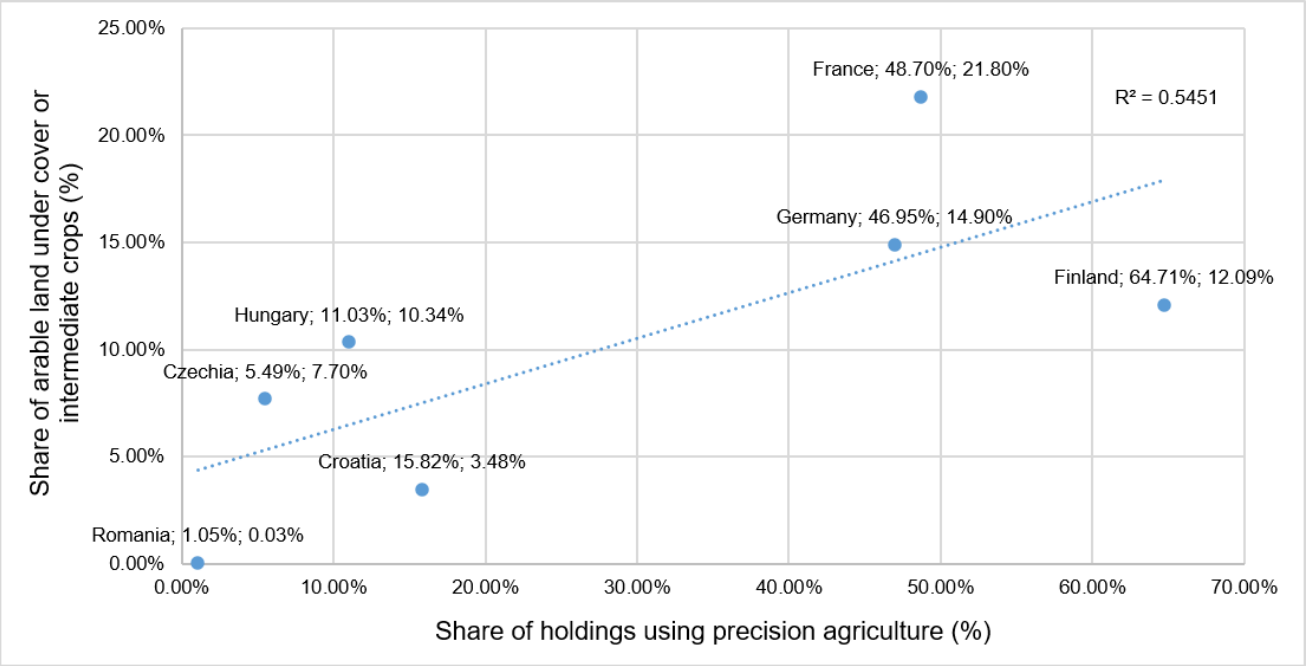



**Fig. 4 - Relationship between the share of holdings using precision agriculture and the share of arable land under cover or intermediate crops in Romania and selected EU Member States, in 2023 (U.M.: percentages)**

*(Eurostat, data for 2023 from the ef_mp_digi and ef_mp_soil datasets, updated on 17.06.2026 and 14.08.2026, respectively; data extracted on 24.09.2026; own calculations)*

*Note: For the seven countries analysed, the Pearson correlation coefficient is r = 0.74 ($R^2$ = 0.55; p = 0.058). The result indicates a positive descriptive association that does not reach the 5% statistical significance threshold and does not demonstrate a causal relationship.*

The distribution of the points indicates an upward trend: countries with higher shares of holdings using precision agriculture also tend to record higher shares of arable land under cover or intermediate crops. The Pearson correlation coefficient of r = 0.74 indicates a relatively strong positive linear association within the group analysed.

Romania is located near the lower end of both axes, with 1.05% of the analysed holdings using precision agriculture and only 0.03% of arable land classified under cover or intermediate crops. France combines a precision-agriculture share of 48.70% with the highest share of cover crops, at 21.80%. Germany records values of 46.95% and 14.90%, respectively, and is also positioned in the upper part of the distribution.

The relationship is not uniform across all countries. Finland records the highest share of precision agriculture, at 64.71%, but cover or intermediate crops account for 12.09%, below the values recorded in France and Germany. Croatia records 15.82% for precision agriculture but only 3.48% for cover crops. These differences explain why some points depart from the trend line.

The value of $R^2$ = 0.55 indicates that the linear model accounts for approximately 55% of the variation in the share of cover or intermediate crops observed across the seven countries. The remaining variation is not described by the linear relationship represented in the graph. The p-value of 0.058 is slightly above the 0.05 threshold; therefore, the association is not statistically significant at the 5% level.

The result should remain descriptive. The small number of countries, the use of data for a single year and the differences among national agricultural structures do not support a causal relationship between precision agriculture and cover crops. The association indicates a direction that could be examined using a larger number of countries and additional explanatory factors. A cautious interpretation is also required in relation to the literature: precision agriculture may support more efficient resource use and reduce certain environmental effects, but these potential benefits do not transform the statistical association identified here into a causal relationship (*Finger et al., 2019*).

The differences identified in digitalisation, organic farming, soil cover and crop rotation provide the statistical basis for the analysis of strengths, weaknesses, opportunities and threats.

**S.W.O.T. analysis**

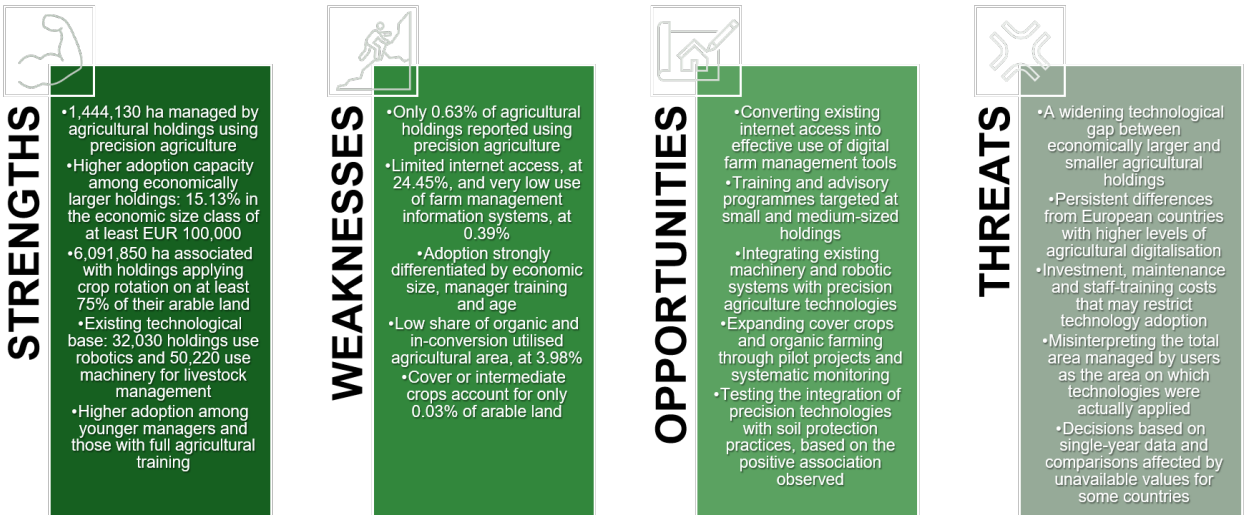



**Fig. 5 - Representative SmartArt illustrating the S.W.O.T. analysis of the adoption of precision agriculture and sustainable agricultural practices in Romania compared with selected EU Member States, in 2023**

(*Own determination based on the research results*)

The S.W.O.T. analysis reveals a contrast between the extent of the agricultural area associated with precision technologies and their limited adoption among holdings. Romania records 1,444,130 ha of utilised agricultural area managed by holdings that declared the use of precision agriculture, although these holdings represent only 0.63% of the total. The data indicate the existence of clusters of technology adoption, concentrated mainly among holdings in the higher economic-size classes, rather than widespread adoption throughout the agricultural sector.

The capacity of economically larger holdings to use these technologies represents the main strength. The share of precision-agriculture users reaches 15.13% in the class of at least EUR 100,000, compared with 0.54% in the EUR 2000–7999 class. Romania also has a base of holdings that use robotics or machinery for livestock management. Crop rotation complements this profile: holdings in which the practice covers at least 75% of the arable area account for 6,091,850 ha, the third-highest absolute value among the EU Member States with available data.

The main weaknesses concern the limited spread of digitalisation and some of the agricultural practices analysed. Internet access is reported by 24.45% of holdings with an economic size of at least EUR 2000, but only 0.39% use farm management information systems. The difference of 24.06 percentage points shows that connectivity does not automatically lead to the use of digital tools in farm management. Romania also ranks last in the comparison group for organic farming and cover or intermediate crops, with shares of 3.98% and 0.03%, respectively.

The opportunities arise from segments in which favourable conditions for adoption already exist. The 245,650 holdings with internet access form a much broader base than the 3960 holdings using farm management information systems. This difference could be reduced through training, advisory services and solutions adapted to holdings with limited resources. The results concerning manager training support this direction: the share of precision-agriculture users increases from 0.53% among managers relying exclusively on practical experience to 5.02% among those with full agricultural training. This direction is consistent with the objectives of Romania's CAP Strategic Plan, which seeks to improve the economic viability of holdings and develop a resilient and sustainable agricultural sector (*European Commission, 2026*).

The positive association between precision agriculture and cover crops, expressed by r = 0.74, provides a possible direction for pilot projects and further research. The result does not demonstrate that digitalisation causes the adoption of soil-protection practices, while the p-value of 0.058 does not confirm statistical significance at the 5% level. The relationship between the two indicators should be examined using multiannual series, a larger number of countries and indicators that capture actual implementation at plot level.

The main threat is the deepening of technological polarisation. If adoption remains dependent on economic size, economically larger holdings may consolidate their advantage while smaller farms remain outside the digitalisation process. Equipment costs, maintenance requirements and the need for specialised skills may widen this difference. The risk of technological polarisation is supported by studies identifying economic barriers to adoption and unequal access to data-driven agriculture (*Barnes et al., 2019; Mehrabi et al.,*

*2021*). In Romania, this risk adds to the difficulties already identified in crop management, including climatic pressures, resource-use problems and the need to adapt to new technologies (*Ghiuleanu et al., 2023*). A further risk arises from interpreting absolute values without examining their corresponding shares: the area managed by user holdings does not represent the area on which the technologies were actually applied.

The results describe an agricultural sector in which some holdings have the land, equipment and economic capacity to support technological adoption, while diffusion across the wider sector remains limited. The direction indicated by the S.W.O.T. analysis is to broaden access beyond economically larger holdings, convert connectivity into effective digital use and evaluate technologies together with the agricultural practices applied to the land. This section concludes the analysis of the results and provides the basis for the research conclusions.

## CONCLUSIONS

The research shows that the adoption of precision agriculture in Romania is limited and concentrated within specific categories of holdings. Although only 0.63% of holdings reported using these technologies, they manage 1,444,130 ha, representing 11.51% of the utilised agricultural area. The extent of the associated area therefore does not indicate a comparable level of adoption by number of holdings. Economic size most clearly differentiates users. The share of holdings using precision agriculture increases from 0.54% in the EUR 2000–7999 class to 15.13% among holdings with a standard output of at least EUR 100,000. Managers with full agricultural training and those under 35 years of age also record higher values than the corresponding comparison groups. These results identify segments with a greater capacity for adoption but do not demonstrate causal relationships.

Digitalisation remains incomplete. Internet access reaches 24.45% among holdings with an economic size of at least EUR 2000, while farm management information systems are used by only 0.39%. The difference of 24.06 percentage points shows that connectivity does not automatically lead to the integration of digital tools into farm management. The agricultural practices analysed produce mixed results. Organic and in-conversion UAA represents 3.98%, while cover or intermediate crops account for only 0.03% of arable land. By contrast, the arable land of holdings in which crop rotation covers at least 75% of the arable area reaches 6,091,850 ha, or 71.82%. Within the comparison group, Romania ranks last for five of the six indicators and sixth for crop rotation.

The association between precision agriculture and cover crops is positive, with $r = 0.74$, but is not statistically significant at the 5% level ($p = 0.058$). The result remains descriptive and does not demonstrate that technology use causes the adoption of soil-cover practices. Broader adoption would require narrowing the differences between economic-size classes, improving manager training and converting internet access into effective digital use.

The data cover only 2023, although the datasets were the most recent available at the time of extraction. The comparison is limited by unavailable values for some Member States and by the definitions of the indicators, as the areas managed by user holdings do not always represent the hectares on which a technology or practice was actually applied. Future analyses could use multiannual series and holding-level data to examine more precisely the relationships among farm structure, manager skills, digitalisation and land management.

## REFERENCES

[1] Balafoutis, A., Beck, B., Fountas, S., Vangeyte, J., van der Wal, T., Soto, I., Gómez-Barbero, M., Barnes, A., Eory, V. (2017). Precision agriculture technologies positively contributing to GHG emissions mitigation, farm productivity and economics. Sustainability, 9(8), 1339. https://doi.org/10.3390/su9081339. Accessed September 30, 2026.

[2] Barnes, A. P., Soto, I., Eory, V., Beck, B., Balafoutis, A., Sánchez, B., Vangeyte, J., Fountas, S., van der Wal, T., Gómez-Barbero, M. (2019). Exploring the adoption of precision agricultural technologies: A cross regional study of EU farmers. Land Use Policy, 80, 163–174. https://doi.org/10.1016/j.landusepol.2018.10.004. Accessed September 30, 2026.

[3] Bowles, T. M., Mooshammer, M., Socolar, Y., Calderón, F., Cavigelli, M. A., Culman, S. W., Deen, W., Drury, C. F., Garcia y Garcia, A., Gaudin, A. C. M., Harkcom, W. S., Lehman, R. M., Osborne, S. L., Robertson, G. P., Salerno, J., Schmer, M. R., Strock, J., Grandy, A. S. (2020). Long-term evidence shows that crop-rotation diversification increases agricultural resilience to adverse growing conditions in North America. One Earth, 2(3), 284–293. https://doi.org/10.1016/j.oneear.2020.02.007. Accessed September 30, 2026.

[4] Buzatu, C. S., Ghiuleanu, I. V., Tudor, V. C. (2023). Dynamics of land fund and strategies on soil conservation and prevention of soil degradation in Romania. Scientific Papers Series "Management, Economic Engineering in Agriculture and Rural Development", 23(4), 149–156. https://managementjournal.usamv.ro/pdf/vol.23_4/Art14.pdf. Accessed February 11, 2026.

[5] Buzatu, C. S., Ghiuleanu, I. V., Tudor, V. C., Oltenacu, N., Vlad, G. (2024). Sustainability in agricultural work – our shared responsibility. Scientific Papers Series "Management, Economic Engineering in Agriculture and Rural Development", 24(1), 147–156. https://managementjournal.usamv.ro/pdf/vol.24_1/Art14.pdf. Accessed September 5, 2026.

[6] European Commission. (2026). Romania – CAP Strategic Plan. https://agriculture.ec.europa.eu/cap-my-country/cap-strategic-plans/romania_en. Accessed July 22, 2026.

[7] Eurostat. (2026a). Internet facilities, robotics, precision farming and machinery for livestock management in farms by economic size of farm, farm type and NUTS 2 region (ef_mp_digi; data for 2023). Eurostat Data Browser. Last updated June 17, 2026. https://ec.europa.eu/eurostat/databrowser/view/ef_mp_digi/default/table?lang=en. Accessed September 24, 2026.

[8] Eurostat. (2026b). Main farm land use by NUTS 2 region (ef_lus_main; data for 2023). Eurostat Data Browser. Last updated June 17, 2026. https://ec.europa.eu/eurostat/databrowser/view/ef_lus_main/default/table?lang=en. Accessed September 24, 2026.

[9] Eurostat. (2026c). Precision farming by age and training of manager, size of farm and NUTS 2 region (ef_mp_digicr; data for 2023). Eurostat Data Browser. Last updated June 17, 2026. https://ec.europa.eu/eurostat/databrowser/view/ef_mp_digicr/default/table?lang=en. Accessed September 24, 2026.

[10] Eurostat. (2026d). Soil cover by arable land area, farm type, crop rotation and NUTS 2 region (ef_mp_soil; data for 2023). Eurostat Data Browser. Last updated August 14, 2026. https://ec.europa.eu/eurostat/databrowser/view/ef_mp_soil/default/table?lang=en. Accessed September 24, 2026.

[11] Finger, R., Swinton, S. M., El Benni, N., Walter, A. (2019). Precision farming at the nexus of agricultural production and the environment. Annual Review of Resource Economics, 11, 313–335. https://doi.org/10.1146/annurev-resource-100518-093929. Accessed September 30, 2026.

[12] Fountas, S., Carli, G., Sørensen, C. G., Tsiropoulos, Z., Cavalaris, C., Vatsanidou, A., Liakos, B., Canavari, M., Wiebensohn, J., Tisserye, B. (2015). Farm management information systems: Current situation and future perspectives. Computers and Electronics in Agriculture, 115, 40–50. https://doi.org/10.1016/j.compag.2015.05.011. Accessed September 30, 2026.

[13] Ghiuleanu, I. V., Buzatu, C. S., Tudor, V. C., Panait, R., (Carbarău) Smedescu, C. A. (2023). Risks analyses and challenges in crop management in Romania. Scientific Papers Series "Management, Economic Engineering in Agriculture and Rural Development", 23(4), 353–364. https://managementjournal.usamv.ro/pdf/vol.23_4/Art34.pdf. Accessed January 15, 2026.

[14] Kutter, T., Tiemann, S., Siebert, R., Fountas, S. (2011). The role of communication and co-operation in the adoption of precision farming. Precision Agriculture, 12(1), 2–17. https://doi.org/10.1007/s11119-009-9150-0. Accessed September 30, 2026.

[15] Mehrabi, Z., McDowell, M. J., Ricciardi, V., Levers, C., Martinez, J. D., Mehrabi, N., Wittman, H., Ramankutty, N., Jarvis, A. (2021). The global divide in data-driven farming. Nature Sustainability, 4(2), 154–160. https://doi.org/10.1038/s41893-020-00631-0. Accessed September 30, 2026.

[16] Mizik, T. (2023). How can precision farming work on a small scale? A systematic literature review. Precision Agriculture, 24(1), 384–406. https://doi.org/10.1007/s11119-022-09934-y. Accessed September 30, 2026.

[17] Paustian, M., Theuvsen, L. (2017). Adoption of precision agriculture technologies by German crop farmers. Precision Agriculture, 18(5), 701–716. https://doi.org/10.1007/s11119-016-9482-5. Accessed September 30, 2026.

[18] Poeplau, C., Don, A. (2015). Carbon sequestration in agricultural soils via cultivation of cover crops – A meta-analysis. Agriculture, Ecosystems & Environment, 200, 33–41. https://doi.org/10.1016/j.agee.2014.10.024. Accessed September 30, 2026.

[19] Tamirat, T. W., Pedersen, S. M., Lind, K. M. H. (2018). Farm and operator characteristics affecting adoption of precision agriculture in Denmark and Germany. Acta Agriculturae Scandinavica, Section B

– Soil & Plant Science, 68(4), 349–357. https://doi.org/10.1080/09064710.2017.1402949. Accessed September 30, 2026.

[20] Vlăduț, N.-V., Atanasov, A., Ungureanu, N., Ivașcu, L.-V., Cioca, L.-I., Popa, L.-D., Matei, G., Boruz, S., Cerempei, V., Țîței, V., Nenciu, F., Milea, O.-E., Dumitru, Ș., Caba, I. (2024). Trends in the development of conservation/ecological agriculture in the context of current climate change – A review. INMATEH – Agricultural Engineering, 74(3), 980–1032. https://doi.org/10.35633/inmateh-74-86. Accessed September 15, 2026.

# FROM LAND REGISTRATION TO TERRITORIAL PATTERNS: DYNAMICS AND CONCENTRATION OF REGISTERED LAND AREAS BY LAND-USE CATEGORY IN SOUTH-WEST OLTENIA, 2015–2024

/

# *DE LA CARTEA FUNCIARĂ LA PROFILUL TERITORIAL: DINAMICA ȘI CONCENTRAREA SUPRAFEȚELOR INTABULATE PE CATEGORII DE FOLOSINȚĂ ÎN REGIUNEA SUD-VEST OLTENIA, 2015–2024*

**Iulian Virgil GHIULEANU[1)], Cristiana Silvia BUZATU*[2)], Alina MĂRCUȚĂ[2)], Liviu MĂRCUȚĂ[2)], Răzvan Alexandru MATINCĂ[2)]**

[1)] University of Agronomic Sciences and Veterinary Medicine of Bucharest (Doctoral student, Doctoral School: Plant and Animal Resources Engineering and Management), 59 Marasti Boulevard, District 1, 011464, Bucharest / Romania;

[2)] University of Agronomic Sciences and Veterinary Medicine of Bucharest, 59 Marasti Boulevard, District 1, 011464, Bucharest / Romania.

**E-mail: buzatu.cristiana@managusamv.ro*

***Keywords:*** *land registration, cadastral records, land-use categories, agricultural land, territorial concentration, South-West Oltenia.*

**ABSTRACT**

*The study examines the dynamics, structure, and territorial concentration of land areas registered in the land book system in South-West Oltenia during the period 2015–2024. The analysis was based on official annual data provided by the National Institute of Statistics through the TEMPO-Online database, series TAZ0221, for the five counties of the region and six statistical series: total registered area and five land-use categories—arable land, pastures, hayfields, vineyards, and orchards. The data were processed using absolute and percentage changes, annual variations, structural shares, territorial gaps, contributions to regional growth, comparisons with the national level, and the two-county concentration ratio (CR2). The total registered area increased from 3,948,875 thousand m² in 2015 to 14,397,446 thousand m² in 2024, corresponding to a growth of 264.60%. Registered arable land recorded the largest increase, at 346.73%, and generated 59.91% of the overall regional increase, while its share in the total registered area rose from 45.72% to 56.02%. Dolj and Olt jointly accounted for 67.15% of regional growth, whereas Mehedinți contributed only 8.70%. At the national level, the region's share increased from 7.31% to 10.50% for the total registered area and from 7.08% to 12.25% for arable land. The CR2 ratio also rose, from 46.44% to 61.47% for the total area and from 71.24% to 81.96% for arable land. The findings indicate substantial progress in land registration, accompanied by increasing structural and territorial concentration. These results describe the evolution of registered areas and should not be interpreted as evidence of the physical expansion of land resources or as a measure of cadastral coverage.*

**REZUMAT**

*Studiul analizează dinamica, structura și concentrarea teritorială a suprafețelor intabulate în Regiunea Sud-Vest Oltenia, în perioada 2015–2024. Cercetarea s-a bazat pe datele statistice oficiale anuale furnizate de Institutul Național de Statistică prin baza TEMPO-Online, seria TAZ0221, pentru cele cinci județe ale regiunii și șase serii statistice: suprafața totală intabulată și cinci categorii de folosință – teren arabil, pășune, fâneață, vie și livadă. Datele au fost prelucrate prin calcularea modificărilor absolute și procentuale, a variațiilor anuale, ponderilor structurale, decalajelor teritoriale, contribuțiilor la creșterea regională, comparațiilor cu nivelul național și indicatorului de concentrare CR2. Suprafața totală intabulată a crescut de la 3,948,875 mii m² în 2015 la 14,397,446 mii m² în 2024, ceea ce corespunde unui avans de 264.60%. Terenurile arabile au înregistrat cea mai accentuată creștere, de 346.73%, și au generat 59.91% din sporul regional total, iar ponderea lor în suprafața intabulată a crescut de la 45.72% la 56.02%. Județele Dolj și Olt au contribuit împreună cu 67.15% la creșterea regională, în timp ce contribuția județului Mehedinți a fost de numai 8.70%. La nivel național, ponderea regiunii a avansat de la 7.31% la 10.50% pentru suprafața totală intabulată și de la 7.08% la 12.25% pentru terenurile arabile. Indicatorul CR2 a crescut de la 46.44% la 61.47% pentru suprafața totală și de la 71.24% la 81.96% pentru terenurile arabile. Rezultatele indică o creștere amplă a suprafețelor intabulate, însoțită de accentuarea concentrării structurale și teritoriale. Aceste*

*constatări descriu evoluția suprafețelor înregistrate și nu trebuie interpretate ca dovezi ale extinderii fizice a resurselor funciare sau ca măsură a gradului de acoperire cadastrală.*

## INTRODUCTION

Land administration depends on records that link the area and location of each property to its land-use category, rights holder, and legal status. In Romania, the cadastre and land registry form a unified and compulsory system of technical, economic, and legal records. This system enables the identification and representation of real properties, the registration of rights, the provision of information required by public institutions, and greater security in real estate transactions (*Romanian Parliament, 1996*). From this perspective, the registered area indicates the expansion of land records, not the physical growth of land resources.

The need for consistent land records is reinforced by the particular characteristics of land ownership in Romania. Developments after 1990 were accompanied by land fragmentation and a large number of owners using small plots (*Burcea et al., 2023*). Land-use categories also perform different agricultural and territorial functions. Arable land, pastures, hayfields, vineyards, and orchards cannot be examined solely in terms of the physical areas they occupy, because the way in which they are identified and registered affects the quality of the information available for land administration.

Systematic registration aims to incorporate properties into an integrated cadastre and land registry system. However, an evaluation of the National Programme for Cadastre and Land Registration showed that its initial objectives were difficult to achieve within the established timeframe. Rigid technical requirements, reliance on field surveys, and limited opportunities for incremental updating were identified among the factors that may slow the process (*Păunescu et al., 2022*). Recent analyses confirm the uneven implementation of the programme and identify problems related to ownership documents, institutional capacity, administrative procedures, and the integration of legal and technical components (*Gherheș et al., 2025*).

Geospatial technologies can support the collection, verification, and updating of cadastral data. Geographic information systems allow graphical and alphanumeric information to be linked and certain stages of cadastral documentation to be automated, thereby reducing processing time (*Tereșneu and Tereșneu, 2023*). However, these tools do not eliminate territorial differences or the problems generated by unclear legal situations. Registration progress must therefore be assessed both through the extent of the areas incorporated into the system and through their distribution among counties and land-use categories.

The connection between cadastre and agriculture becomes apparent when registered areas are differentiated by land use. Studies of Romania's land fund have examined changes in arable land, pastures, hayfields, vineyards, and orchards in relation to the use and conservation of soil resources (*Buzatu et al., 2023*).

Previous research on the South-West Oltenia Region identified territorial differences between the predominantly arable areas of Dolj and Olt and the profiles of counties where pastures, hayfields, or orchards are more prevalent, particularly Gorj and Vâlcea (*Ursu and Cofas, 2016*). These characteristics support a county-level analysis because an aggregated regional value may conceal different rates and structures.

The literature examined addresses either the operation and difficulties of systematic registration or the structure of the land fund and the agricultural use of land. The annual evolution of registered areas, disaggregated by both land-use category and county, remains less clearly documented. Such a distinction is necessary to avoid confusing progress in cadastral records with the expansion of agricultural land or a physical change in land use.

The aim of this research is to assess the dynamics, structure, and territorial distribution of registered land areas in the South-West Oltenia Region during the period 2015–2024, based on data provided by the National Institute of Statistics through the TEMPO-Online database, series TAZ0221 (*NIS, 2026*). The analysis examines the evolution of the total registered area and the main land-use categories, their contribution to regional growth, differences among Dolj, Gorj, Mehedinți, Olt, and Vâlcea counties, changes in territorial and structural shares, the region's position relative to the national level, and the concentration of registered areas in the two leading counties.

The research does not measure the actual degree of cadastral coverage and does not examine the physical conversion of land from one land-use category to another. The results describe the areas recorded in the land registry at the end of each year and identify the territories and categories in which the registration process advanced more rapidly or remained at a comparatively lower level.

## MATERIALS AND METHODS

The research was based on official statistical data obtained from the TEMPO-Online database of the National Institute of Statistics, series TAZ0221, *"Land areas registered in the land book by land-use categories"* (*NIS, 2026*). The indicator represents the total area of land for which the owner has been identified and a land book has been opened.

The data are reported annually, describe the situation at the end of each year, and are supplied to NIS by the National Agency for Cadastre and Land Registration. The values in the statistical series are expressed in thousands of square metres (thousand m²).

The analysis covered the period 2015–2024 and the five counties of the South-West Oltenia Region: Dolj, Gorj, Mehedinți, Olt, and Vâlcea. The total registered area and five land-use categories were examined: arable land, pasture, hayfield, vineyard, and orchard. Regional values were obtained by summing the data for the five counties. Comparisons with Romania were based on national values for the same years and categories, taken directly from series TAZ0221. The selected series were complete and contained no missing values; therefore, no estimates or interpolations were required.

The data were organised and processed using Microsoft Excel 365. The chronological analysis included the absolute and percentage changes between 2015 and 2024, the arithmetic mean of the ten annual values, and the average annual absolute increase. The latter was calculated by dividing the absolute change by the nine annual intervals between the ten observed years. Annual variations were calculated successively by dividing the difference between two consecutive years by the value recorded in the first year of each interval.

The contribution of each land-use category to the overall increase was calculated by dividing its absolute change by the change in the total registered area. In the territorial analysis, the county contribution represented each county's share of the absolute regional increase. Territorial shares were calculated by dividing county values by the regional total, while structural shares were obtained by dividing each land-use category by the total registered area within the same territory. Changes in shares were expressed in percentage points as the difference between the values recorded in 2024 and 2015.

To assess territorial disparities, the counties with the maximum and minimum values in 2024 were identified. The absolute gap was calculated as the difference between the two values, while the relative gap was obtained by dividing this difference by the minimum value. The maximum-to-minimum ratio shows how many times the area recorded by the leading county exceeds that of the lowest-ranked county. The analysis was supplemented by the leading county's share of the regional total for each category.

The position of the South-West Oltenia Region within the national context was assessed by comparing the regional and national percentage changes between 2015 and 2024. The difference between the two rates was expressed in percentage points. For each category, the region's share of the nationally registered area was also calculated for 2015 and 2024, together with the change in this share over the period.

Territorial concentration was analysed using the two-county concentration ratio (CR2), calculated as the combined share of the two leading counties in the regional registered area of each category. The indicator was determined for 2015 and 2024, and the difference between the two values was expressed in percentage points. Positive values indicate increased concentration in the two leading counties, while negative values indicate a less concentrated distribution. CR2 describes the distribution of registered areas among counties and is not an indicator of property ownership concentration or the number of agricultural holdings.

Percentages, ratios, and percentage-point changes were presented to two decimal places, while areas expressed in thousand m² were reported without decimals. In the final stage, the chronological, structural, and territorial results were synthesised through a S.W.O.T. analysis based on the statistical findings and the limitations of the indicator examined.

The method is descriptive and comparative. The increase in registered area was interpreted as an expansion of the land included in cadastral records, not as a physical increase in land resources. Series TAZ0221 does not allow the actual degree of cadastral coverage to be calculated because the values are not related to the total land area of each county.

The difference between the total registered area and the five categories examined also includes land uses that are not reported separately in this series and was not automatically classified as non-agricultural land. The data do not allow the causes of territorial differences to be identified or physical changes in land use to be confirmed.

## RESULTS

In the case of cadastral data, an increase in the registered area does not indicate a physical expansion of land resources. The indicator represents the area for which the owner has been identified and a land book has been opened by the end of each year. Its definition is consistent with the technical and legal functions of the cadastre and with the distinction between sporadic and systematic registration (*Romanian Parliament, 1996; Iordan et al., 2013; Begov-Ungur et al., 2025; NIS, 2026*). The results therefore describe the expansion of cadastral records in the South-West Oltenia Region, the rate of this process, and the differences among the main land-use categories.




**Fig. 1 - Panel of charts showing the evolution of registered areas by land-use category in the South-West Oltenia Region (U.M.: thousand m²)**

*(NIS, statistical data provided through TEMPO-Online, TAZ0221; own calculations based on aggregated data for Dolj, Gorj, Mehedinți, Olt, and Vâlcea counties)*

The charts indicate a continuous increase across all six series examined. The total registered area rose from 3,948,875 thousand m² in 2015 to 14,397,446 thousand m² in 2024, reaching 3.65 times its initial level. The rate of increase was not constant from one year to another. Larger increases occurred after 2018 and during the 2022–2023 interval, while other annual transitions recorded more moderate rates. Arable land remained the category with the largest registered area throughout the period. Its value increased from 1,805,404 thousand m² to 8,065,313 thousand m², representing the largest absolute increase among the land-use categories examined. The registered pasture area rose from 494,610 to 1,235,453 thousand m², while the registered hayfield area increased from 84,370 to 294,955 thousand m². The values recorded for vineyards and orchards were lower, but both categories followed an uninterrupted upward trajectory. The registered vineyard area increased from 44,599 to 146,874 thousand m², while the orchard area rose from 72,524 to 160,813 thousand m². The common direction of these series shows that the expansion of the area recorded in the land registry was not limited to arable land. However, differences between the initial values require absolute and percentage changes to be examined together, because a high relative increase may originate from a low initial value.

The comparison between the first and final years separates the size of the registered areas from the rate at which they were incorporated into the system. The summary indicators show how much each category contributed to regional growth and limit interpretations based solely on percentage values. The increase in registered areas forms part of the broader implementation of the National Programme for Cadastre and Land Registration. Evaluations of the programme indicate that progress in systematic registration must be considered together with the characteristics of the institutional framework and the difficulties encountered during implementation (*Păunescu et al., 2022; Gherheș et al., 2025*).

**Table 1**

**Summary indicators of the evolution of registered areas by land-use category in the South-West Oltenia Region**

| Land-use category | 2015 | 2024 | Absolute change | Change 2015–2024 | Period average | Average annual absolute increase | Contribution to total increase |
|---|---|---|---|---|---|---|---|
| | U.M.: thousand m², except for percentage indicators | | | | | | |
| Total registered area | 3,948,875 | 14,397,446 | 10,448,571 | 264.60% | 8,726,533 | 1,160,952 | 100.00% |
| Registered arable land | 1,805,404 | 8,065,313 | 6,259,909 | **346.73%** | 4,991,007 | 695,545 | **59.91%** |
| Registered pasture | 494,610 | 1,235,453 | 740,843 | 149.78% | 851,443 | 82,316 | 7.09% |
| Registered hayfield | 84,370 | 294,955 | 210,585 | 249.60% | 164,027 | 23,398 | 2.02% |
| Registered vineyard | 44,599 | 146,874 | 102,275 | 229.32% | 91,389 | 11,364 | 0.98% |
| Registered orchard | 72,524 | 160,813 | 88,289 | 121.74% | 112,102 | 9810 | 0.84% |

*(NIS, statistical data provided through TEMPO-Online, TAZ0221; own calculations)*

*Note: The average annual absolute increase represents the absolute change divided by the nine annual intervals. The contribution was calculated by dividing the increase in each category by the increase in the total registered area. The percentages of the categories do not add up to 100% because TAZ0221 does not provide separate data for all the other land uses included in the total.*

The total registered area increased by 10,448,571 thousand m² between 2015 and 2024, corresponding to a change of 264.60%. The average annual absolute increase was 1,160,952 thousand m². However, this indicator represents the mean across the nine annual intervals and does not imply that the same area was registered in each year.

Arable land recorded the strongest growth among the categories examined. Its registered area increased by 6,259,909 thousand m², or 346.73%, and contributed 59.91% to the increase in the region's total registered area. The average annual absolute increase of 695,545 thousand m² shows that a considerable part of the regional dynamics was associated with the registration of arable land. Hayfields and vineyards also recorded high percentage increases of 249.60% and 229.32%, respectively. However, their absolute areas remained considerably smaller: their contributions to the total increase were only 2.02% for hayfields and 0.98% for vineyards. The difference between the percentage growth rate and the effective contribution results from the low initial values of these categories. Orchards recorded the smallest relative increase, at 121.74%, although their registered area in 2024 was still more than twice its 2015 level.

Together, the five detailed land-use categories account for 70.84% of the increase in the total registered area. The remaining 29.16% corresponds to other land uses included in the total but not reported separately in series TAZ0221. This difference therefore cannot automatically be attributed to non-agricultural land. The dominant role of arable land is consistent with the structure of the agricultural land fund described at the national level. In the present research, however, the comparison concerns only registered areas and not the total physical extent of the land-use categories (*Burcea et al., 2023; Buzatu et al., 2023*).

Changes between the beginning and end of the period do not show how growth was distributed from one year to another. Annual variations identify the intervals during which the registered area increased more rapidly and the stages during which the process slowed.

**Table 2**

**Annual variations in registered areas by land-use category in the South-West Oltenia Region**

| Land-use category | 2015→2016 | 2016→2017 | 2017→2018 | 2018→2019 | 2019→2020 | 2020→2021 | 2021→2022 | 2022→2023 | 2023→2024 |
|---|---|---|---|---|---|---|---|---|---|
| | U.M.: percentages | | | | | | | | |
| Total registered area | 15.78% | 23.95% | 14.50% | **25.66%** | 11.05% | 16.70% | 6.64% | 16.64% | 9.53% |
| Registered arable land | 23.36% | 31.52% | 25.36% | **34.34%** | 12.68% | 15.95% | 4.93% | 11.15% | 7.32% |
| Registered | 10.89% | 14.16% | **15.69%** | 15.01% | 8.64% | 6.84% | 6.44% | 11.79% | 7.36% |

| | | | | | | | | | |
|---|---|---|---|---|---|---|---|---|---|
| pasture | | | | | | | | | |
| Registered hayfield | 13.16% | 12.62% | 13.35% | 16.30% | 12.68% | 13.07% | 9.81% | **28.94%** | 15.35% |
| Registered vineyard | 13.59% | 15.95% | 18.60% | **20.53%** | 14.11% | 15.36% | 7.02% | 13.84% | 9.05% |
| Registered orchard | 10.00% | 9.77% | 10.97% | 9.70% | 6.20% | 10.15% | 7.33% | 8.18% | **11.07%** |

*(NIS, statistical data provided through TEMPO-Online, TAZ0221; own calculations)*

*Note: Annual variations were calculated by dividing the difference between two consecutive years by the value recorded in the first year of the interval.*

None of the categories examined recorded a negative annual variation. For the total registered area, the largest increase occurred during the 2018–2019 interval, when the indicator rose by 25.66%. The lowest rate, 6.64%, was recorded between 2021 and 2022. The alternation between intervals of rapid growth and periods of more moderate change confirms that the expansion of the registered area did not proceed at a uniform rate.

Arable land recorded its largest variations during the first part of the period. The increases of 31.52% in 2016–2017 and 34.34% in 2018–2019 were followed by lower rates after 2020. The minimum annual variation for this category, at 4.93%, occurred during the 2021–2022 interval. The fact that arable land and the total registered area reached their maximum annual changes during the same interval indicates the influence of this category on regional dynamics.

Hayfields followed a different pattern. Their largest annual variation, at 28.94%, occurred in 2022–2023, after the rate had fallen to 9.81% in the previous interval. Vineyards recorded their highest increases during 2017–2018 and 2018–2019, at 18.60% and 20.53%, respectively, after which the annual values remained more moderate.

Orchards recorded the narrowest range of annual variation, with values between 6.20% and 11.07%. This pattern indicates a more consistent expansion than that of arable land or hayfields, although at a lower percentage rate. The variations presented in the table describe changes in the area recorded in the land registry, not changes in the physical area available for agriculture.

Annual variations do not reveal the administrative causes of faster or slower registration. However, the literature on the implementation of the National Programme for Cadastre and Land Registration (PNCCF) identifies the organisation of public procurement and the operational processes of service providers as relevant factors, although their separate effects cannot be determined from series TAZ0221 (*Păunescu et al., 2024a; Păunescu et al., 2025*).

Regional change results from the contributions of the five counties, whose series differed in both size and position throughout the period. Comparing the annual values makes it possible to identify changes in the leading county and the gaps that developed among the territories.

**Table 3**

**Evolution of the total registered area by county and at the level of the South-West Oltenia Region**

| County/Region | 2015 | 2016 | 2017 | 2018 | 2019 | 2020 | 2021 | 2022 | 2023 | 2024 |
|---|---|---|---|---|---|---|---|---|---|---|
| | U.M.: thousand m² | | | | | | | | | |
| Dolj | **952,440** | **1,223,149** | 1,475,564 | 1,670,534 | 2,278,924 | 2,688,182 | **3,343,559** | **3,543,014** | **4,276,355** | **4,928,926** |
| Gorj | 722,178 | 763,262 | 964,791 | 1,066,216 | 1,176,621 | 1,281,885 | 1,400,590 | 1,544,210 | 1,919,391 | 2,005,017 |
| Mehedinți | 645,963 | 722,004 | 787,301 | 833,360 | 905,834 | 969,662 | 1,106,290 | 1,165,446 | 1,379,024 | 1,554,601 |
| Olt | 881,280 | 1,054,690 | **1,482,539** | **1,872,000** | **2,633,107** | **2,885,878** | 3,309,511 | 3,458,929 | 3,712,351 | 3,921,051 |
| Vâlcea | 747,014 | 808,940 | 956,867 | 1,046,845 | 1,159,502 | 1,229,761 | 1,407,790 | 1,557,485 | 1,857,642 | 1,987,851 |
| **South-West Oltenia Region** | **3,948,875** | **4,572,045** | **5,667,062** | **6,488,955** | **8,153,988** | **9,055,368** | **10,567,740** | **11,269,084** | **13,144,763** | **14,397,446** |

*(NIS, statistical data provided through TEMPO-Online, TAZ0221; own calculations for the regional level)*

The total registered area increased every year in all five counties. Dolj started with the highest value, at 952,440 thousand m² in 2015, and reached 4,928,926 thousand m² in 2024. The county ranked first in 2015 and 2016, was temporarily overtaken by Olt, and regained the leading position in 2021.

Olt recorded the largest registered area during the 2017–2020 interval. The difference from Dolj was very small in 2017, at only 6975 thousand m², but widened in the following years. In 2021, the positions of the two counties were reversed again: Dolj reached 3,343,559 thousand m², while Olt recorded 3,309,511 thousand

m². By 2024, the gap between them had widened, with final values of 4,928,926 thousand m² in Dolj and 3,921,051 thousand m² in Olt.

Gorj and Vâlcea recorded similar values throughout most of the period and exchanged positions several times. In 2024, the total registered area amounted to 2,005,017 thousand m² in Gorj and 1,987,851 thousand m² in Vâlcea. Mehedinți remained the county with the lowest value in every year examined, although its registered area increased from 645,963 to 1,554,601 thousand m².

The change in the regional leader and the similar values recorded by certain counties show that the evolution cannot be described through a single ranking applicable to the entire period. At the same time, the absolute gap between Dolj and Mehedinți widened, making it necessary to compare both the growth rates and each county's contribution to regional change.

The increase in registered area across all five counties did not leave their contributions to the regional total unchanged. Different growth rates altered the territorial shares, even though none of the counties recorded a decrease in absolute terms.

**Table 4**

**Summary indicators of the territorial dynamics of the total registered area in the South-West Oltenia Region**

| County/Region | 2015 | 2024 | Absolute change | Change | Regional contribution | Share in 2015 | Share in 2024 | Change in share (p.p.) |
|---|---|---|---|---|---|---|---|---|
| | U.M.: thousand m², percentages, and percentage points, depending on the indicator | | | | | | | |
| Dolj | 952,440 | 4,928,926 | 3,976,486 | **417.51%** | **38.06%** | 24.12% | **34.23%** | **10.12** |
| Gorj | 722,178 | 2,005,017 | 1,282,839 | 177.63% | 12.28% | 18.29% | 13.93% | -4.36 |
| Mehedinți | 645,963 | 1,554,601 | 908,638 | 140.66% | 8.70% | 16.36% | 10.80% | -5.56 |
| Olt | 881,280 | 3,921,051 | 3,039,771 | 344.93% | 29.09% | 22.32% | 27.23% | 4.92 |
| Vâlcea | 747,014 | 1,987,851 | 1,240,837 | 166.11% | 11.88% | 18.92% | 13.81% | -5.11 |
| **South-West Oltenia Region** | **3,948,875** | **14,397,446** | **10,448,571** | **264.60%** | **100.00%** | **100.00%** | **100.00%** | **0.00** |

*(NIS, statistical data provided through TEMPO-Online, TAZ0221; own calculations)*

*Note: The regional contribution represents each county's share of the absolute increase recorded in the South-West Oltenia Region. The change in share represents the difference between the county's share in 2024 and its share in 2015.*

Dolj recorded the largest absolute increase, at 3,976,486 thousand m², and the highest growth rate among the counties examined, at 417.51%. The county generated 38.06% of the regional increase, while its share of the region's total registered area rose from 24.12% in 2015 to 34.23% in 2024, representing a gain of 10.12 percentage points.

Olt ranked second in both absolute increase, at 3,039,771 thousand m², and contribution to regional growth, at 29.09%. Its increase of 344.93% raised the county's share from 22.32% to 27.23%, a gain of 4.92 percentage points. Dolj and Olt were the only counties whose shares of the regional total increased.

Registered areas in Gorj and Vâlcea increased by 177.63% and 166.11%, respectively, but these rates remained below the regional increase of 264.60%. Consequently, Gorj's share decreased by 4.36 percentage points, while that of Vâlcea fell by 5.11 percentage points. These reductions in share do not indicate decreases in registered areas, but growth rates below that recorded for the region as a whole.

Mehedinți recorded the lowest percentage increase, at 140.66%, and contributed 8.70% to regional growth. Its share fell from 16.36% to 10.80%, with the loss of 5.56 percentage points being the largest among the five counties.

The dynamics of the period therefore strengthened the positions of Dolj and Olt, while the other three counties accounted for smaller shares of the regional total in 2024 than in 2015. The differentiation among the five counties is consistent with a territorial profile previously identified for agriculture in the South-West Oltenia Region (*Ursu and Cofas, 2016*). At the same time, a topographic and cadastral study conducted in Dolj indicates that modern information systems can improve the efficiency and accuracy of cadastral works, although this local finding does not, by itself, explain the county's statistical advance (*Călina et al., 2025*).

The situation in 2024 shows that a county's position depends on the land-use category examined. The total registered area alone is insufficient to describe its territorial profile because counties with lower values in one category may record high values in another.

**Table 5**

**Registered areas by land-use category, by county and at the level of the South-West Oltenia Region in 2024**

| Land-use category | Dolj | Gorj | Mehedinți | Olt | Vâlcea | South-West Oltenia Region |
|---|---|---|---|---|---|---|
| | U.M.: thousand m² | | | | | |
| Total registered area | **4,928,926** | 2,005,017 | 1,554,601 | 3,921,051 | 1,987,851 | 14,397,446 |
| Registered arable land | **3,566,859** | 366,499 | 802,086 | 3,043,381 | 286,488 | 8,065,313 |
| Registered pasture | 268,221 | **320,473** | 154,792 | 206,094 | 285,873 | 1,235,453 |
| Registered hayfield | 15,650 | **141,235** | 61,452 | 3182 | 73,436 | 294,955 |
| Registered vineyard | **61,174** | 20,565 | 20,808 | 32,141 | 12,186 | 146,874 |
| Registered orchard | 35,368 | 32,233 | 16,782 | **47,668** | 28,762 | 160,813 |

*(NIS, statistical data provided through TEMPO-Online, TAZ0221; own calculations for the regional level)*

Dolj recorded the largest total registered area, at 4,928,926 thousand m², and ranked first for arable land and vineyards. Its registered arable area reached 3,566,859 thousand m², while its vineyard area amounted to 61,174 thousand m². Olt ranked second for arable land, with 3,043,381 thousand m², but recorded the largest registered orchard area, at 47,668 thousand m².

Gorj had a different profile. The county ranked first for pastures, with 320,473 thousand m², and hayfields, with 141,235 thousand m². Vâlcea approached Gorj in terms of pasture area, recording 285,873 thousand m², and ranked second for hayfields, with 73,436 thousand m². At the same time, these two counties recorded the smallest registered arable areas, at 366,499 thousand m² in Gorj and 286,488 thousand m² in Vâlcea.

Mehedinți did not rank first in any of the categories examined. Arable land was its largest component, at 802,086 thousand m², while its total registered area amounted to 1,554,601 thousand m². At the regional level, registered arable land totalled 8,065,313 thousand m², far exceeding the areas registered as pastures, hayfields, vineyards, and orchards.

The distribution recorded in 2024 reveals two distinct situations within the registered areas: Dolj and Olt recorded high values for arable land, while Gorj and Vâlcea held stronger positions for pastures and hayfields. These results describe the structure of land already included in cadastral records and cannot automatically be extended to the entire land fund of each county. The intensity of territorial differences is examined separately through the maximum and minimum values and the gaps between counties.

The maximum and minimum values confirm that differences among counties do not have the same intensity across all land-use categories. The gaps must be interpreted together with the maximum-to-minimum ratio and the leading county's share because very high percentage values may result from a low minimum value.

**Table 6**

**Territorial gaps in registered areas by land-use category in the South-West Oltenia Region in 2024**

| Land-use category | County with maximum value | Maximum value | County with minimum value | Minimum value | Absolute gap | Relative gap | Max/min ratio | Leader's share |
|---|---|---|---|---|---|---|---|---|
| | U.M.: thousand m², percentages, and ratio, depending on the indicator | | | | | | | |
| Total registered area | Dolj | 4,928,926 | Mehedinți | 1,554,601 | **3,374,325** | 217.05% | 3.17 | 34.23% |
| Registered arable land | Dolj | 3,566,859 | Vâlcea | 286,488 | 3,280,371 | 1145.03% | 12.45 | 44.22% |
| Registered pasture | Gorj | 320,473 | Mehedinți | 154,792 | 165,681 | 107.03% | 2.07 | 25.94% |
| Registered hayfield | Gorj | 141,235 | Olt | 3182 | 138,053 | **4338.56%** | **44.39** | **47.88%** |
| Registered vineyard | Dolj | 61,174 | Vâlcea | 12,186 | 48,988 | 402.00% | 5.02 | 41.65% |
| Registered orchard | Olt | 47,668 | Mehedinți | 16,782 | 30,886 | 184.04% | 2.84 | 29.64% |

*(NIS, statistical data provided through TEMPO-Online, TAZ0221; own calculations)*

*Note: The relative gap was calculated by dividing the difference between the maximum and minimum values by the minimum value. The maximum-to-minimum ratio expresses the leading county's value as a multiple of the lowest value. The indicators describe the distribution of registered areas and do not represent degrees of cadastral coverage.*

The largest absolute difference occurs in the total registered area. The value recorded in Dolj exceeds that of Mehedinți by 3,374,325 thousand m² and is 3.17 times as high. The relative gap reaches 217.05%, while

Dolj accounts for 34.23% of the regional total. Therefore, even the leading county does not contain the majority of the region's registered area.

Arable land presents a stronger contrast. The maximum value recorded in Dolj, at 3,566,859 thousand m², is 12.45 times as high as the minimum value in Vâlcea, at 286,488 thousand m². The absolute gap amounts to 3,280,371 thousand m², while the relative gap reaches 1145.03%. Dolj accounts for 44.22% of the region's registered arable area.

The largest relative disparity is recorded for hayfields. The area in Gorj is 44.39 times as high as that in Olt, generating a relative gap of 4338.56%. This percentage must be interpreted in relation to the minimum value of only 3182 thousand m² recorded in Olt. Gorj accounts for 47.88% of the region's registered hayfield area, the highest leader's share among the categories examined.

The differences are smaller for pastures and orchards, although their distribution is still not uniform. The maximum pasture area, recorded in Gorj, is 2.07 times as high as the minimum in Mehedinți, while the orchard area in Olt is 2.84 times as high as that in Mehedinți. For vineyards, the value recorded in Dolj is 5.02 times that of Vâlcea and accounts for 41.65% of the region's registered area in this category.

These gaps describe the territorial distribution of the areas included in land records. They do not represent degrees of cadastral coverage because the calculation does not relate the registered area to the total physical area of each county. The observed differences may be associated with county size, land-use structure, or the rate of registration, but the separate contribution of these factors cannot be determined from series TAZ0221. Studies conducted at cadastral-sector level show that parcel identification and verification of land-use categories can be supported by GNSS and UAV technologies and geomatics applications (*Cioflan et al., 2025*). Establishing a physical change in land use, however, requires parcel-level examination and comparison of spatial information, not only the analysis of aggregated statistical values (*Cioflan, 2025*).

The gaps recorded in 2024 result from both the initial size of the registered areas and the different rates observed over the ten-year period. Comparing county-level changes indicates where the areas included in land records expanded most rapidly.

**Table 7**

**Changes in registered areas by land-use category, by county and at the level of the South-West Oltenia Region**

| Land-use category | Dolj | Gorj | Mehedinți | Olt | Vâlcea | South-West Oltenia Region |
|---|---|---|---|---|---|---|
| | U.M.: percentages | | | | | |
| Total registered area | **417.51%** | 177.63% | 140.66% | 344.93% | 166.11% | 264.60% |
| Registered arable land | **439.11%** | 203.97% | 146.70% | 387.24% | 289.89% | 346.73% |
| Registered pasture | **247.05%** | 159.21% | 67.11% | 238.73% | 103.87% | 149.78% |
| Registered hayfield | **652.04%** | 344.09% | 219.85% | 288.52% | 141.14% | 249.60% |
| Registered vineyard | **421.78%** | 204.13% | 81.82% | 223.22% | 157.90% | 229.32% |
| Registered orchard | **193.95%** | 177.34% | 79.81% | 72.55% | 141.47% | 121.74% |

*(NIS, statistical data provided through TEMPO-Online, TAZ0221; own calculations)*

*Note: Regional changes were calculated from the summed regional values and do not represent the average of the county percentages. High percentages for certain categories, particularly hayfields, must be interpreted together with the absolute values because they may result from low initial levels.*

Dolj recorded the largest increase in each of the six categories examined. The total registered area rose by 417.51%, while registered arable land increased by 439.11%. The highest value was recorded for hayfields, at 652.04%, followed by vineyards, at 421.78%. These percentages must also be interpreted in relation to their initial levels, which were lower for hayfields and vineyards than for arable land.

Olt recorded the second-largest increase in total registered area, at 344.93%. The county registered increases of 387.24% for arable land and 238.73% for pastures, but only 72.55% for orchards, the lowest county-level value for this category. This difference shows that the overall rate of land registration within a county was not reflected equally across all land-use categories.

The changes recorded in Gorj ranged from 159.21% for pastures to 344.09% for hayfields. In Vâlcea, the largest increase occurred in arable land, at 289.89%, while hayfields and orchards rose by 141.14% and 141.47%, respectively. Mehedinți recorded the smallest increase in total registered area, at 140.66%, as well as the lowest increases for pastures and vineyards, at 67.11% and 81.82%.

At the regional level, arable land recorded the largest increase among the categories examined, at 346.73%, followed by hayfields at 249.60% and vineyards at 229.32%. Orchards recorded the smallest regional increase, at 121.74%. Regional values were calculated from the summed areas of the five counties and do not represent the arithmetic mean of county percentages. Consequently, changes in counties with larger initial areas exert a greater influence on the regional result.

Growth rates do not show what proportion of the registered area is represented by each category. The structure in 2024 completes the analysis by relating arable land, pastures, hayfields, vineyards, and orchards to the total registered area of each territory.

**Table 8**

**Structure of registered areas by land-use category, by county and at the level of the South-West Oltenia Region in 2024**

| Land-use category | Dolj | Gorj | Mehedinți | Olt | Vâlcea | South-West Oltenia Region |
|---|---|---|---|---|---|---|
| | U.M.: percentages | | | | | |
| Registered arable land | 72.37% | 18.28% | 51.59% | 77.62% | 14.41% | 56.02% |
| Registered pasture | 5.44% | 15.98% | 9.96% | 5.26% | 14.38% | 8.58% |
| Registered hayfield | 0.32% | 7.04% | 3.95% | 0.08% | 3.69% | 2.05% |
| Registered vineyard | 1.24% | 1.03% | 1.34% | 0.82% | 0.61% | 1.02% |
| Registered orchard | 0.72% | 1.61% | 1.08% | 1.22% | 1.45% | 1.12% |
| **Subtotal of the five categories** | **80.08%** | **43.94%** | **67.92%** | **84.99%** | **34.55%** | **68.79%** |
| **Difference from the total** | **19.92%** | **56.06%** | **32.08%** | **15.01%** | **65.45%** | **31.21%** |

*(NIS, statistical data provided through TEMPO-Online, TAZ0221; own calculations)*

*Note: The percentages were calculated by dividing each category by the total registered area within the same territory. The difference from the total is a calculated value and includes land uses that are not reported separately in TAZ0221. It must not automatically be interpreted as non-agricultural land.*

At the regional level, arable land represents 56.02% of the total registered area. Pastures account for 8.58%, while hayfields, vineyards, and orchards have shares ranging from 1.02% to 2.05%. Together, the five categories account for 68.79% of the regional total, while the remaining 31.21% corresponds to land uses that are not reported separately in the series analysed.

Olt and Dolj have the highest shares of arable land within the structure of their registered areas. In Olt, arable land represents 77.62% of the total registered area, while the subtotal of the five categories reaches 84.99%. In Dolj, the share of arable land is 72.37%, and the five categories together account for 80.08%. These results explain the high absolute values recorded in the two counties and their major contribution to regional dynamics.

The structure is more diversified in Gorj and Vâlcea. In Gorj, arable land accounts for 18.28%, pastures for 15.98%, and hayfields for 7.04%. In Vâlcea, the shares of arable land and pastures are almost equal, at 14.41% and 14.38%, respectively. The subtotal of the five categories is 43.94% in Gorj and only 34.55% in Vâlcea, leaving differences from the total of 56.06% and 65.45%, respectively.

Mehedinți occupies an intermediate position. Arable land represents 51.59% of its total registered area, while the five categories analysed account for 67.92%. Vineyards and orchards have small shares in all counties, with the highest values being 1.34% for vineyards in Mehedinți and 1.61% for orchards in Gorj.

The difference from the total cannot automatically be considered non-agricultural land. It includes all land uses that form part of the total registered area but are not reported individually in TAZ0221. The percentages describe only the structure of the registered areas, not the complete structure of each county's land fund.

Comparing the structure in 2015 with that in 2024 shows how different registration rates altered the relative position of the land-use categories. Changes in shares do not imply that land was transferred from one category to another; they show that registered areas increased at different rates.

**Table 9**

**Changes in the structure of registered areas by land-use category in the South-West Oltenia Region**

| Land-use category | Share in 2015 | Share in 2024 | Change in share (p.p.) |
|---|---|---|---|
| | U.M.: percentages and percentage points | | |
| Registered arable land | 45.72% | 56.02% | **10.30** |
| Registered pasture | 12.53% | 8.58% | **-3.94** |
| Registered hayfield | 2.14% | 2.05% | -0.09 |
| Registered vineyard | 1.13% | 1.02% | -0.11 |
| Registered orchard | 1.84% | 1.12% | -0.72 |
| **Subtotal of the five categories** | **63.35%** | **68.79%** | **5.44** |
| **Difference from the total** | **36.65%** | **31.21%** | **-5.44** |

*(NIS, statistical data provided through TEMPO-Online, TAZ0221; own calculations)*

*Note: The shares were calculated in relation to the total registered area at the regional level. A decrease in share does not indicate a reduction in absolute area, but a slower rate of growth than that of the regional total.*

Arable land recorded the largest structural change. Its share of the total registered area increased from 45.72% in 2015 to 56.02% in 2024, a gain of 10.30 percentage points. This change resulted from the faster growth of the registered arable area compared with the regional total.

All the other categories lost share, although their registered areas increased in absolute terms. The largest decrease occurred for pastures, whose share fell from 12.53% to 8.58%, a reduction of 3.94 percentage points. The share of orchards decreased by 0.72 percentage points, while the changes recorded for hayfields and vineyards were smaller, at -0.09 and -0.11 percentage points.

The subtotal of the five categories increased from 63.35% to 68.79%, a gain of 5.44 percentage points. This increase was entirely attributable to arable land, whose structural gain offset the combined decreases in the shares of the other four categories. Conversely, the share of land uses not reported separately in TAZ0221 declined from 36.65% to 31.21%.

The results show a stronger orientation of the registered area towards arable land. They do not demonstrate the physical conversion of pastures, hayfields, vineyards, or orchards into arable land, because the statistical series records the cadastral registration status at the end of each year rather than changes in the use of individual parcels.

Placing the regional results in the national context shows whether the regional dynamics followed Romania's general pace or diverged from it. The comparison considers changes in registered areas and the share of the South-West Oltenia Region in the national value of each category.

**Table 10**

**Comparative changes and the share of the South-West Oltenia Region in registered areas at the national level, by land-use category**

| Land-use category | Regional change | National change | Difference (p.p.) | Region's share of the national total, 2015 | Region's share of the national total, 2024 | Change in share (p.p.) |
|---|---|---|---|---|---|---|
| | U.M.: percentages and percentage points | | | | | |
| Registered total area | 264.60% | 153.60% | 111.00 | 7.31% | 10.50% | 3.20 |
| Registered arable land | 346.73% | 158.03% | **188.70** | 7.08% | 12.25% | **5.17** |
| Registered pasture | 149.78% | 118.15% | 31.63 | 6.55% | 7.50% | 0.95 |
| Registered hayfield | 249.60% | 217.88% | 31.71 | 3.91% | 4.30% | 0.39 |
| Registered vineyard | 229.32% | 140.29% | 89.03 | 9.31% | 12.76% | 3.45 |
| Registered orchard | 121.74% | 114.29% | 7.45 | **14.97%** | **15.49%** | 0.52 |

*(NIS, statistical data provided through TEMPO-Online, TAZ0221; own calculations)*

*Note: The difference between the rates of change was calculated as the regional change minus the national change. The region's share was calculated by dividing the registered area in the South-West Oltenia Region by the national value for the same category and year.*

The South-West Oltenia Region recorded faster growth than the national level in all the categories analysed. The total registered area increased by 264.60% in the region, compared with 153.60% in Romania as

a whole, a difference of 111.00 percentage points. Consequently, the region's share of the national total increased from 7.31% in 2015 to 10.50% in 2024.

The largest regional advantage occurred for arable land. The increase of 346.73% in the South-West Oltenia Region exceeded the national increase of 158.03% by 188.70 percentage points. The region's share of the registered arable area at the national level rose from 7.08% to 12.25%. The gain of 5.17 percentage points was the largest among the categories analysed.

Vineyards also recorded much faster regional growth. The difference between the regional and national rates of change was 89.03 percentage points, while the region's share increased from 9.31% to 12.76%. For pastures and hayfields, the regional advantages were similar, at 31.63 and 31.71 percentage points, although the changes in their shares of the national totals were smaller.

Orchards followed a different pattern. In 2015, the region already accounted for 14.97% of the national registered area in this category, the largest initial share among the indicators analysed. Regional growth exceeded national growth by only 7.45 percentage points; consequently, the share increased moderately to 15.49% in 2024.

The increases in these shares show that registered areas grew faster in the South-West Oltenia Region than at the national level. This result cannot be interpreted directly as a higher degree of cadastral coverage, because the indicators do not relate the registered areas to the entire land fund available in the region and in Romania. The comparison describes only the region's position within the recorded national totals.

County-level changes and shifts in territorial shares indicate that registered areas may have become more concentrated in certain counties. The CR2 ratio measures the combined share held by the two leading counties and allows the degree of concentration in 2015 and 2024 to be compared.

**Table 11**

**Concentration of registered areas in the two leading counties of the South-West Oltenia Region, by land-use category**

| Land-use category | Top two counties, 2015 | Share in 2015 | Top two counties, 2024 | Share in 2024 | Change (p.p.) |
|---|---|---|---|---|---|
| | U.M.: percentages and percentage points | | | | |
| Registered total area | Dolj and Olt | 46.44% | Dolj and Olt | 61.47% | **15.03** |
| Registered arable land | Dolj and Olt | 71.24% | Dolj and Olt | 81.96% | 10.72 |
| Registered pasture | Vâlcea and Gorj | 53.35% | Gorj and Vâlcea | 49.08% | -4.27 |
| Registered hayfield | Gorj and Vâlcea | 73.79% | Gorj and Vâlcea | 72.78% | -1.01 |
| Registered vineyard | Dolj and Mehedinți | 51.95% | Dolj and Olt | 63.53% | 11.59 |
| Registered orchard | Olt and Dolj | 54.68% | Olt and Dolj | 51.64% | -3.05 |

*(NIS, statistical data provided through TEMPO-Online, TAZ0221; own calculations)*

*Note: The cumulative share, referred to as the CR2 concentration ratio, represents the share of the regional registered area in the respective category held by the two leading counties. Positive values indicate increased territorial concentration, whereas negative values indicate a less concentrated distribution.*

The concentration of the total registered area increased markedly. Dolj and Olt together held 46.44% of the regional total in 2015, while their combined share reached 61.47% in 2024, an increase of 15.03 percentage points. This result confirms the strengthening of their positions, also observed in their high contributions to regional growth.

Arable land had the highest level of concentration. The combined share of Dolj and Olt increased from 71.24% to 81.96%, meaning that more than four-fifths of the region's registered arable area was located in these two counties in 2024. The increase of 10.72 percentage points widened their difference from the other counties.

An important change also occurred in the case of vineyards. In 2015, the two leading positions were held by Dolj and Mehedinți, which together accounted for 51.95% of the regional area. In 2024, Olt replaced Mehedinți in this pair, and the combined share of Dolj and Olt reached 63.53%. The increase of 11.59 percentage points indicates both stronger concentration and a change in the territorial structure of this category.

Concentration decreased for pastures, hayfields, and orchards. Gorj and Vâlcea remained the two leading counties for pastures, but their combined share fell from 53.35% to 49.08%. The same pair continued to dominate the registered hayfield area, with a modest decrease from 73.79% to 72.78%. For orchards, Olt and Dolj retained the leading positions, but their combined share declined by 3.05 percentage points to 51.64%.

The results reveal two territorial patterns. The total registered area, arable land, and vineyards became more concentrated, while pastures, hayfields, and orchards became slightly more dispersed. The CR2 ratio

captures the contribution of the two leading counties but does not describe the differences among all five counties. Its interpretation therefore complements, rather than replaces, the analysis of territorial gaps and county shares.

Registered areas increased continuously, but at different rates across land-use categories, while territorial concentration became more pronounced in the case of arable land. To synthesise the advantages, limitations, and directions identified from these changes, the statistical findings were integrated into a S.W.O.T. analysis.

**S.W.O.T. analysis**

The S.W.O.T. analysis indicates a clear expansion of the areas entered in the land records, alongside an uneven territorial distribution. Registered areas in the South-West Oltenia Region grew faster than at the national level, and the region's share of the national total increased for all the categories analysed. This favourable result was supported largely by Dolj and Olt, which together generated 67.15% of the regional increase in the total registered area.

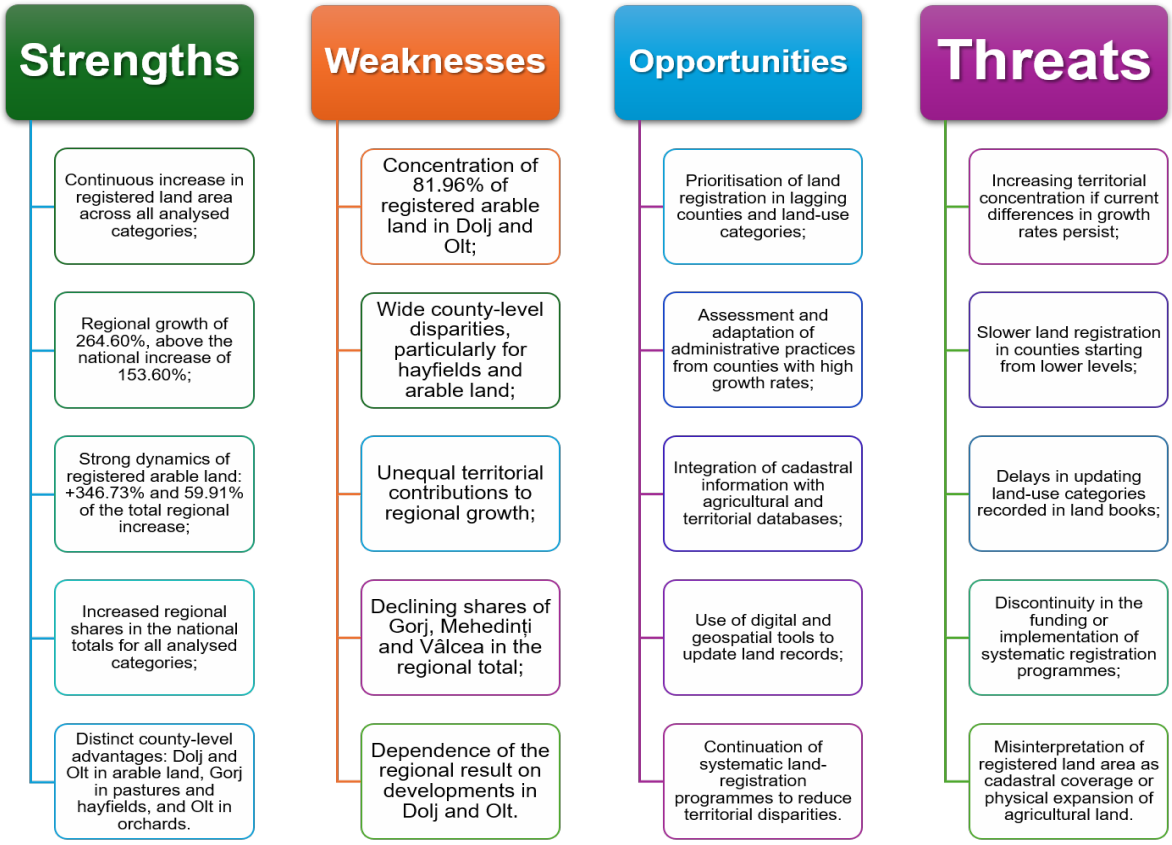



**Fig. 2 - Representative SmartArt diagram of the S.W.O.T. analysis of the dynamics and territorial distribution of registered areas by land-use category in the South-West Oltenia Region, based on the statistical results for 2015–2024**

*(Own determination based on the research results)*

The main limitation is the concentration of progress in a small number of counties and categories. The maximum-to-minimum ratio reaches 12.45 for arable land and 44.39 for hayfields. Regional progress may therefore coexist with considerably lower values in some counties. Mehedinți provides the clearest example, having recorded the smallest total registered area in every year and the lowest contribution to regional growth.

The opportunities concern extending the analysis by comparing registered areas with the corresponding land areas and integrating cadastral data with agricultural and territorial information. Such a comparison would allow counties and categories with slower registration rates to be assessed before intervention priorities are established.

The use of metadata and the integration of cadastral information with other territorial databases can support the comparison and updating of records (*Palamariu and Voina, 2015; Ispas Musceleanu, 2018*). Automating the preparation of documentation and using GIS tools can reduce data-processing time and facilitate the updating of cadastral information (*Terețneu and Terețneu, 2023; Coroian et al., 2025*).

The threats arise from the possible persistence of uneven territorial growth rates and the inappropriate use of the indicators. Persistent differences may also be associated with difficulties concerning the quality of the work, the resources involved, and the coordination of the systematic registration process, as identified in recent evaluations of the PNCCF (*Păunescu et al., 2024b; Gherheș et al., 2025*). An increase in registered area demonstrates neither an expansion of agricultural land nor the attainment of a particular degree of cadastral coverage. This distinction must be maintained if the statistical results are to be used correctly in agricultural and territorial decision-making.

## CONCLUSIONS

The analysis of registered areas in the South-West Oltenia Region shows a continuous increase in the area entered in the land records between 2015 and 2024. The total registered area increased from 3,948,875 to 14,397,446 thousand m², corresponding to a growth of 264.60%. Increases occurred in every year, in all five counties, and across all the land-use categories analysed. This result describes progress in land registration, not the physical expansion of the land fund.

Arable land was the main component of regional growth. Its registered area increased by 346.73% and generated 59.91% of the region's total increase. The share of this category in the total registered area rose from 45.72% to 56.02%. Pastures, hayfields, vineyards, and orchards increased in absolute terms but lost share because their growth rates were lower than that recorded for arable land.

Regional progress was unevenly distributed among counties. Dolj and Olt together contributed 67.15% of the increase in the total registered area and were the only counties whose shares of the regional total increased. Mehedinți remained in the last position throughout the period, and its contribution to regional growth was 8.70%. Differences were also pronounced among land-use categories. The maximum registered arable area was 12.45 times the county minimum, while the corresponding ratio for hayfields reached 44.39.

The position of the South-West Oltenia Region within the national total strengthened for all the categories analysed. Its share of Romania's total registered area increased from 7.31% to 10.50%, while its share of registered arable land rose from 7.08% to 12.25%. This development was accompanied by greater territorial concentration. The combined share of Dolj and Olt in the regional total increased from 46.44% to 61.47%, while their share of registered arable land rose from 71.24% to 81.96%.

The main conclusion is that registered areas increased substantially but unevenly. Growth in the South-West Oltenia Region exceeded the national rate, while the regional result became more dependent on the contributions of Dolj and Olt, particularly for arable land. Absolute values alone cannot establish registration priorities. They must be considered alongside the corresponding land areas, the stage of systematic registration, and agricultural and territorial data.

The limitations of the TAZ0221 series prevent the calculation of the actual degree of cadastral coverage because registered areas are not related to the entire land fund of each county. The data also do not allow the causes of territorial differences to be established or possible physical changes in land use to be identified.

Further analysis could compare registered areas with total land areas and with information on agricultural use, ownership, and systematic registration to distinguish more clearly between cadastral progress and the characteristics of the territorial structure.

## REFERENCES

[1] Begov-Ungur, A., Berindeie, I. A., Dimen, L. (2025). The effects of applying the law in cadastre activity – A comparative study of the resolutions that can be adopted for the registration of real estate properties in the land registry. Scientific Papers. Series E. Land Reclamation, Earth Observation & Surveying, Environmental Engineering, XIV, 788–793. https://landreclamationjournal.usamv.ro/pdf/2025/Art88.pdf. Accessed September 22, 2026.

[2] Burcea, M., Vlad, I. M., Oltenacu, N. (2023). Romania's agricultural land fund and the dynamics of the land ownership during the period 1990–2020. Scientific Papers Series "Management, Economic Engineering in Agriculture and Rural Development", 23(3), 77–84. https://managementjournal.usamv.ro/pdf/vol.23_3/Art9.pdf. Accessed February 22, 2026.

[3] Buzatu, C. S., Ghiuleanu, I. V., Tudor, V. C. (2023). Dynamics of land fund and strategies on soil conservation and prevention of soil degradation in Romania. Scientific Papers Series "Management,

Economic Engineering in Agriculture and Rural Development", 23(4), 149–156. https://managementjournal.usamv.ro/pdf/vol.23_4/Art14.pdf. Accessed February 11, 2026.

[4] Călina, J., Călina, A., Croitoru, A. (2025). Study on the impact of the application of information systems on the efficiency and precision of topo-cadastral works in the preparation of documentation for a road in Dolj County. Scientific Papers. Series E. Land Reclamation, Earth Observation & Surveying, Environmental Engineering, XIV, 816–826. https://landreclamationjournal.usamv.ro/pdf/2025/Art91.pdf. Accessed March 6, 2026.

[5] Cioflan, F. M. (2025). Assessment of land use changes in non-collectivized areas using geomatic applications: A case study in Vîrfurile, Romania. Scientific Papers. Series E. Land Reclamation, Earth Observation & Surveying, Environmental Engineering, XIV, 839–850. https://landreclamationjournal.usamv.ro/pdf/2025/Art93.pdf. Accessed January 16, 2026.

[6] Cioflan, F. M., Irimie, F., Sabău, N. C. (2025). Technical methodologies for cadastral plan development using GNSS and UAV technologies: A case study in Pietroasa, Romania. Scientific Papers. Series E. Land Reclamation, Earth Observation & Surveying, Environmental Engineering, XIV, 827–838. https://landreclamationjournal.usamv.ro/pdf/2025/Art92.pdf. Accessed September 10, 2026.

[7] Coroian, I., Chiorean, S., Sobolu, R., Ficior, D., Sestras, P., Rus, L.-P., Sabou, C.-S., Andronie, L. (2025). Advancing cadastral updates and GIS spatial analysis for forested areas. Scientific Papers. Series E. Land Reclamation, Earth Observation & Surveying, Environmental Engineering, XIV, 868–877. https://landreclamationjournal.usamv.ro/pdf/2025/Art96.pdf. Accessed September 8, 2026.

[8] Gherheș, V., Grecea, C., Vilceanu, C.-B., Herban, S., Coman, C. (2025). Challenges in systematic property registration in Romania: An analytical overview. Land, 14(5), 1118. https://doi.org/10.3390/land14051118. Accessed September 23, 2026.

[9] Iordan, D., Munteanu, B., Eni, I. (2013). Sporadic cadastre, systematic cadastre. Scientific Papers. Series E. Land Reclamation, Earth Observation & Surveying, Environmental Engineering, II, 133–136. https://landreclamationjournal.usamv.ro/pdf/vol.II/Art23.pdf. Accessed March 19, 2026.

[10] Ispas Musceleanu, A. (2018). Results of the study on integrating urbanism information into the cadastre and land book system. Scientific Papers. Series E. Land Reclamation, Earth Observation & Surveying, Environmental Engineering, VII, 152–155. https://landreclamationjournal.usamv.ro/pdf/2018/Art29.pdf. Accessed March 15, 2026.

[11] National Institute of Statistics [NIS]. (2026). TEMPO-Online database: Land areas registered in the land book by land-use categories (TAZ0221; data for 2015–2024). http://statistici.insse.ro:8077/tempo-online/#/pages/tables/insse-table. Accessed August 17, 2026.

[12] Palamariu, M., Voina, I. (2015). The use of metadata for completing the general cadastre in Romania. Scientific Papers. Series E. Land Reclamation, Earth Observation & Surveying, Environmental Engineering, IV, 135–140. https://landreclamationjournal.usamv.ro/pdf/2015/vol.IV/Art22.pdf. Accessed August 16, 2026.

[13] Păunescu, V., Kohli, D., Iliescu, A.-I., Nap, M.-E., Șuba, E.-E., Sălăgean, T. (2022). An evaluation of the National Program of Systematic Land Registration in Romania using the fit-for-purpose spatial framework principles. Land, 11(9), 1502. https://doi.org/10.3390/land11091502. Accessed August 16, 2026.

[14] Păunescu, V., Iliescu, A.-I., Sălăgean, T., Șuba, E.-E., Nap, M.-E. (2024a). An analysis of strategic goals and public procurement strategy regarding the implementation of the National Program for Land Registration in Romania. Land Use Policy, 146, 107334. https://doi.org/10.1016/j.landusepol.2024.107334. Accessed August 15, 2026.

[15] Păunescu, V., Iliescu, A.-I., Călin, M. C., Sălăgean, T., Kohli, D., Nap, M.-E., Șuba, E.-E. (2024b). A quality assessment of the Romanian National Program of Systematic Land Registration The point of view of local cadastral offices directors. Survey Review, 56(396), 284–299. https://doi.org/10.1080/00396265.2023.2233825. Accessed March 11, 2026.

[16] Păunescu, V., Kohli-Poll Jonker, D., Manea, R. M., Ciolacu (Călin), M., Iliescu, A. I. (2025). Operational issues in systematic land registration projects in Romania. A study case in a Romanian small and medium enterprise. Scientific Papers Series "Management, Economic Engineering in Agriculture and Rural Development", 25(1), 721–732. https://managementjournal.usamv.ro/pdf/vol.25_1/Art73.pdf. Accessed September 22, 2026.

[17] Romanian Parliament. (1996). Law No. 7/1996 on Cadastre and Real Estate Publicity, republished, with subsequent amendments and additions. https://legislatie.just.ro/Public/DetaliiDocumentAfis/69491. Accessed September 10, 2026.

[18] Tereșneu, C. C., Tereșneu, C. S. (2023). GIS facilities for the automation of cadastral documentations. Scientific Papers. Series E. Land Reclamation, Earth Observation & Surveying, Environmental Engineering, XII, 371–376. https://landreclamationjournal.usamv.ro/pdf/2023/Art48.pdf. Accessed September 22, 2026.

[19] Ursu, A., Cofas, E. (2016). The territorial analysis of agricultural production structure. Case study: Region South-West Oltenia. Scientific Papers Series "Management, Economic Engineering in Agriculture and Rural Development", 16(1), 535–542. https://managementjournal.usamv.ro/pdf/vol.16_1/Art84.pdf. Accessed January 6, 2026.

# EFFECT OF BUCKWHEAT FLOUR INCORPORATION ON PHYSICAL, STRUCTURAL AND SENSORY PROPERTIES OF WHEAT BREAD

/

# *INFLUENȚA ADAOSULUI DE FĂINĂ DE HRIȘCĂ ASUPRA PROPRIETĂȚILOR FIZICE, STRUCTURALE ȘI SENZORIALE ALE PÂINII DIN FĂINĂ DE GRÂU*

**Elena-Mădălina ȘTEFAN*, Gabriel-Alexandru CONSTANTIN, Mariana-Gabriela MUNTEANU, Gheorghe VOICU, Aura-Irina ISTRATE, Gabriel MUȘUROI, Mariana IONESCU, Alina-Daiana IONESCU, Elena-Melania CISMARU**
National University of Science and Technology POLITEHNICA Bucharest / Romania
**Tel: +40 726 043 472; *E-mail: madalina.stefan@upb.ro*

***Keywords:*** *buckwheat, wheat flour, bread, specific volume, porosity, elasticity, technological properties.*

**ABSTRACT**

*The incorporation of pseudocereals into bakery products is a strategy for raw-material diversification and nutritional improvement, but wheat flour replacement may affect dough development and final bread structure. This study evaluated partial replacement of wheat flour with 10, 20 and 30% buckwheat flour in terms of loaf mass, specific volume, height-to-diameter ratio (H/D), crumb porosity and elasticity, complemented by descriptive sensory assessment. Specific volume decreased from 346.90 cm³/100 g for the control to 297.03, 250.31 and 162.44 cm³/100 g, corresponding to reductions of 14.4, 27.8 and 53.2%. Porosity remained practically unchanged at 10% buckwheat (71.00% versus 71.20% for control) but decreased to 57.14 and 45.35% at 20 and 30%. Elasticity remained comparatively stable between 91.52 and 93.00%. Under the experimental conditions, 10% provided the most favorable technological compromise. The study highlights the need to optimize hydration, particle size and processing parameters when higher buckwheat incorporation is targeted.*

**REZUMAT**

*Încorporarea pseudocerealelor în produsele de panificație reprezintă o strategie de diversificare a materiilor prime și de îmbunătățire a profilului nutritional, dar substituirea făinii de grâu poate afecta dezvoltarea aluatului și structura produsului final. Studiul a urmărit să identifice influența substiturii parțiale a făinii de grâu cu 10, 20 și 30 % făină de hrișcă asupra masei, volumului specific, raportului H/D (înălțime/diametru), porozitîții și elasticității miezului, completate de o evaluare senzorială descriptivă. Volumul specific a scăzut de la 346,90 cm³/100 g la proba martor la 297,03; 250,31 și 162,44 cm³/100 g, corespunzător unor reduceri de 14,4%, 27,8 % și respective 53,2%. Porozitatea s-a menținut neschimbată la adaosul de 10% hrișcă (71,00% față de 71,20% la proba martor), dar a scazut la 57,14% și 45,35% la probele cu 20 și respective 305. Elasticitatea miezului a rămas relative stabilă, între 91,52 și 93,00%. În condițiile experimentale utilizate, nivelul de 10% a condus la cel mai favorabil rezultat, din punct de vedere tehnologic. Studiul evidențiază necesitatea optimizării hidratării, dimensiunii particulelor și parametrilor de process atunci când se urmărește creșterea proporției de făină de hrișcă.*

## INTRODUCTION

Bread is one of the most widely consumed cereal-based foods and therefore represents a suitable matrix for product reformulation. In recent years, bakery research has increasingly investigated pseudocereals, including buckwheat, amaranth, and quinoa, as ingredients that diversify sources of protein, dietery fibre, minerals, and bioactive compounds *(Atudorei et al., 2026)*. Among these materials, common buckwheat (*Fagopyrum esculentum Moench*) is of particular interest because its flour can be incorporated into wheat-based products while providing a markedly different chemical and functional composition.

Bucketwheat supplies starch, proteins, dietary fibre, minerals, and phenolic compounds. Particular attention has been paid to rutin and quercetin and to the contribution of outer grain fractions to mineral and fibre contents (*Atudorei et al., 2026, Brites L.T.G.F. et al., 2022, Nakov et al., 2022, Lukšič L. et al., 2016, Christa et al., 2008, Bonafaccia et al., 2003).* These characteristics justify its use in bakery products designed for improved nutritional profiles. However, compositional benefits cannot be considered independently of technological performance. Buckwheat flour does not contain proteins capable of

developing the characteristic wheat gluten network; consequently, wheat flour replacement simultaneously dilutes gluten and introduces components with different water-binding and structural properties.

In wheat dough, the gluten network contributes to viscoelastic behaviour and retention of carbon dioxide produced during fermentation. Partial replacement of wheat flour with buckwheat flour may therefore alter water distribution, dough development time, stability, extensibility and thermal behaviour (*Biduski B. et al., 2024, Coţovanu I. et al, 2021, Coţovanu I. et al, 2022, Coţovanu I. et al, 2023, Ştefan E-M et al., 2018, Inglett G.E. et al., 2009).* The extent of these changes depends not only on the substitution level, but also on flour extraction rate, particle size, the composition of the milling fractions, hydration and breadmaking technology (*Coţovanu I. et al, 2021, Coţovanu I. et al, 2022, Coţovanu I. et al, 2023)*

*Coţovanu I. et al, 2021* demonstrated that buckwheat milling fractions and addition levels produce different dough responses, showing that a nominal “buckwheat percentage” alone does not fully describe technological behaviour. Subsequent work by the same research group demonstrated that particle size can influence both rheology and final bread volume and texture (*Coţovanu I. et al, 2022, Coţovanu I. et al, 2023).* Thus, two formulations with the same buckwheat percentage may produce substantially different breads.

Published data concerning the substitution level tolerated by wheat bread are not fully uniform. Biduski et al. (*Biduski B. et al., 2024).* investigated 0, 10, 20 and 30% buckwheat flour and reported progressive deterioration of mixing properties, whereas bread quality was maintained up to 20%; at 30%, specific volume decreased and a denser, more crumbly structure developed. In contrast, Brites et al. *(Brites L.T.G.F. et al., 2022)* produced breads containing 30% refined or whole-grain buckwheat flour that were well accepted by consumers, although flour type strongly affected specific volume and colour. These differences emphasize the role of raw-material characteristics and processing conditions.

From a compositional perspective, increasing buckwheat content can increase dietary fibre, minerals and phenolic compounds *(Brites L.T.G.F. et al., 2022; Nakov G et al., 2022)*. Nevertheless, transformations during fermentation and baking must also be considered. *Lukšič L. et al., (2016)* demonstrated substantial transformations of rutin and quercetin during buckwheat sourdough bread preparation, while *(Brites L.T.G.F. et al., (2022)* monitored changes in these compounds during processing. Thus, the mere presence of buckwheat in a formulation is insufficient to predict the bioactive composition of the final bread.

The present work belongs to an experimental research direction previously initiated by the authors. In the study published by (*Ştefan E.-M. et al. 2018*), whole buckwheat flour addition to wheat flour caused clear changes in technological and farinographic properties. At 0, 10, 20 and 30% incorporation, water absorption increased from 58.6 to 61.2, 67.8 and 75.8%, whereas dough stability decreased from 7.9 to 6.2, 3.1 and 2.1 min. The results indicated greater water demand and reduced mixing stability as buckwheat content increased.

The current study does not repeat those rheological measurements and does not present previously published data as new results. Instead, it extends the research to the final baked product and investigates whether increasing buckwheat incorporation is reflected in measurable physical and structural bread characteristics. This distinction is important both methodologically and in terms of research integrity.

Accordingly, the objective was to evaluate the effect of partial wheat flour replacement with 10, 20 and 30% buckwheat flour on loaf mass, specific volume, H/D ratio, crumb porosity and elasticity, together with descriptive sensory appearance. The results are further discussed in relation to recent literature and the previously published rheological study, without assuming a statistical correlation between separate experiments.

## MATERIALS AND METHODS

White wheat flour roasted whole-grain buckwheat flour, dry baker's yeast, sugar, salt, potable water and sunflower oil were used. The buckwheat ingredient was the commercial product (Solaris, Romania), 500 g package; the label indicated Ukraine as the origin of the raw material. According to the manufacturer, the flour is produced from whole roasted buckwheat grains by slow milling in a traditional stone mill. Declared values per 100 g are 70.6 g carbohydrates, 12.6 g protein, 10.0 g dietary fibre and 3.1 g fat, with an energy value of 335 kcal.

Four formulations were produced: C – control containing 100% wheat flour; B10 – 10% buckwheat flour; B20 – 20% buckwheat flour; and B30 – 30% buckwheat flour. Percentages represent partial replacement of wheat flour. The basic recipe for approximately 500 g bread contained 325 g total flour, 210 mL water at approximately 35°C, sunflower oil, salt, sugar and dry yeast. The same processing scheme was applied to all formulations to enable direct comparison.

Samples were prepared using a Tefal Pain Plaisir bread maker. The programme included ingredient incorporation, mixing and kneading, fermentation/proofing and baking, with a total duration of approximately 85 min. Applying one programme to all formulations provides process consistency but also represents a limitation: hydration and processing time were not individually optimized for each buckwheat level. Literature indicates that water demand of wheat-buckwheat blends can increase with addition level *(Coţovanu I. et al, 2021; Ştefan E.-M. et al. 2018)*; therefore, constant water addition may affect formulations differently.

Loaf mass was measured approximately two hours after baking. The physical characteristics of bread were determined according to the Romanian standard SR 91:2207. Bread volume was determined by rapeseed displacement method and expressed as specific volume in cm³/100 g product. Specific volume was used as an integrative bread-quality indicator because it relates loaf expansion to product mass.

The H/D ratio was calculated from maximum loaf height (H) and mean diameter (D).

Crumb porosity was determined according to SR 91:2007, using a cylindrical specimen collected from the central crumb region. Porosity was calculated from the volume and mass of the crumb specimen and the density of compact crumb material and was expressed as percentage by volume.

Crumb elasticity was determined according to SR 91:2007. A cylindrical crumb specimen (30 mm in diameter and 60 mm in initial height) was compressed to half of its initial height for 1 minute and then allowed to recover for 1 minute, after which its height was measured. Elasticity was expressed as the percentage recovery relative to the initial specimen height.

Sensory evaluation was descriptive and considered external appearance, crust and crumb colour, pore structure, compactness, taste and aroma. Because no trained panel, hedonic scale or replicated sensory design was used, these observations are treated as descriptive support rather than statistical evidence of consumer acceptance.

Data processing included percentage differences relative to the control and analysis of trends.

## RESULTS

The experimental results are presented in Table 1.

**Table 1**

**Physical and structural characteristics of bread samples**

| Formulation | Mass (g) | Specific volume (cm³/100 g) | H/D | Porosity (%) | Elasticity (%) |
|---|---|---|---|---|---|
| Control – 100 % wheat flour | 472.6 | 346.90 | 0.587 | 71.20 | 91.60 |
| 10 % buckwheat – B10 | 481.3 | 297.03 | 0.524 | 71.00 | 92.72 |
| 20 % buckwheat – B20 | 480.9 | 250.31 | 0.462 | 57.14 | 93.00 |
| 30 % buckwheat – B30 | 469.2 | 162.44 | 0.492 | 45.35 | 91.52 |

The results show that the final loaf mass was 472.6 for the control, 481.3 g for B10, 480.9 g for B20 and 469.2 g for B30. The range was relatively narrow compared with changes in loaf volume. The samples B10 and B20 were approximately 1.8% heavier than the control, whereas B30 was approximately 0.7% lighter. These differences may reflect variation in baking losses and water retention, but the available dataset does not allow the mechanisms to be separated. Loaf mass should therefore not be interpreted independently as an indicator of improved or deteriorated quality.

Specific volume showed the clearest relationship with substitution level. The control had 346.90 cm³/100 g, whereas B10, B20 and B30 had 297.03, 250.31 and 162.44 cm³/100 g, respectively. Relative to the control, the reductions were 14.4%, 27.8% and 53.2%. The trend indicates progressively reduced loaf development, with a particularly strong effect at 30%.

Technologically, the reduction in volume may be interpreted through several interacting effects. First, wheat flour replacement reduces the proportion of gluten-forming proteins. Second, buckwheat fibre, protein and starch alter water distribution. Third, buckwheat particles may physically disrupt gluten-network continuity and modify interfaces surrounding gas cells *(Biduski B. et al., 2024; Coţovanu I. et al, 2021, Coţovanu I. et al, 2022, Coţovanu I. et al, 2023, Ştefan E-M et al., 2018).* These mechanisms were not directly measured in the current experiment, but they are supported by rheological literature.

The direction of the present findings agrees with *Biduski B. et al., 2024,* who studied exactly 0, 10, 20 and 30% buckwheat flour and observed progressive deterioration of dough mixing properties. In their system, major effects on specific volume and crumb structure became evident mainly at 30%, whereas bread

quality was maintained up to 20%. In the present experiment, volume reduction occurred earlier and was more pronounced. This difference should not be regarded as contradictory; rather, it illustrates the sensitivity of wheat-buckwheat systems to flour characteristics and process conditions.

*Brites L.T.G.F. et al., (2022)* reported specific volumes of 3.98 mL/g for control bread, 3.62 mL/g at 30% refined buckwheat flour and 3.05 mL/g at 30% whole-grain buckwheat flour. The present experiment used roasted whole-grain buckwheat flour, making the comparison with whole-grain flour particularly relevant while introducing an additional factor: thermal pretreatment before milling. Particle-size distribution was not experimentally determined, so its contribution cannot be separated.

Crumb porosity displayed a noteworthy response. The control had 71.20% porosity and B10 had 71.00%, a relative difference of only 0.28%. Therefore, although specific volume had already decreased by 14.4% at B10, the porous fraction of the crumb remained essentially unchanged. This suggests that the initial effect of buckwheat incorporation did not necessarily cause a proportional loss of internal aeration.

At B20, porosity decreased to 57.14%, approximately 19.7% below the control, while B30 reached 45.35%, approximately 36.3% below control. The simultaneous reduction in specific volume and porosity at the higher levels indicates formation of a more compact internal structure. Experimental photographs support this interpretation: sections of breads containing higher buckwheat percentages visually show a denser crumb and modified pore distribution.

The relationship between porosity and specific volume requires careful interpretation. Specific volume describes overall loaf expansion, whereas porosity describes the fraction of gas spaces within the crumb. They are associated but not equivalent. B10 demonstrates this distinction: the loaf was smaller, but the crumb-maintained porosity close to the control. From a technological perspective, this differentiation is useful when selecting formulations that preserve internal crumb structure despite moderate loss of overall volume.

Crumb elasticity was 91.60% for the control, 92.72% for B10, 93.00% for B20 and 91.52% for B30. The entire range was only 1.48 percentage points. Unlike volume and porosity, elasticity did not show progressive deterioration. B10 and B20 were slightly above the control, while B30 returned almost exactly to the control value.

This result demonstrates that a more compact loaf should not automatically be described as less elastic. The applied test measures recovery of crumb material after compression, whereas specific volume and porosity reflect formation and preservation of the gas-cell structure. Buckwheat components may alter cell density and geometry without proportionally reducing mechanical recovery of the solid matrix. Studies by (*Coţovanu I. et al, 2022, Coţovanu I. et al, 2023)* likewise show that volume, porosity and textural variables may respond differently depending on buckwheat fraction and particle size.

The calculated H/D ratios were 0.587 for the control, 0.524 for B10, 0.462 for B20 and 0.492 for B30. The decrease up to 20% indicates reduced vertical development. The slight increase at 30% should not be interpreted as quality recovery because B30 simultaneously exhibited the lowest specific volume and porosity. H/D is influenced by loaf geometry and must be evaluated together with volume and crumb structure.

Figure 1 presents the measured values and fitted regression trends for specific volume, crumb porosity, crumb elasticity, and the H/D ratio across increasing buckwheat flour substitution levels.

Regression analysis showed a decreasing trend in specific volume and crumb porosity with increasing substitution level. Linear models provided a good fit for these four treatment means ($R^2$ = 0.9751 and 0.9009, respectively). The H/D ratio also showed an overall decreasing trend, although the lower $R^2$ value (0.7003) and the increase at B30 indicate that the linear model did not fully capture the observed pattern. Crumb elasticity followed a non-linear trend, increasing up to B20 and decreasing at B30; therefore, a second-order polynomial model was used ($R^2$ = 0.9756). These regressions describe the four observed treatment means and should not be interpreted as validated predictive models.

An important part of the discussion concerns the conceptual relationship with the previously published rheological study (Ștefan E-M et al., 2018). At 0, 10, 20 and 30% buckwheat, water absorption increased from 58.6 to 75.8%, while dough stability decreased from 7.9 to 2.1 min. In the present bread experiment, at the same nominal levels, specific volume decreased from 346.90 to 162.44 cm³/100 g. The trends are technologically compatible: a system with increased water demand and reduced mixing stability may have lower capacity to preserve a stable gas-cell structure when hydration and processing are kept constant.

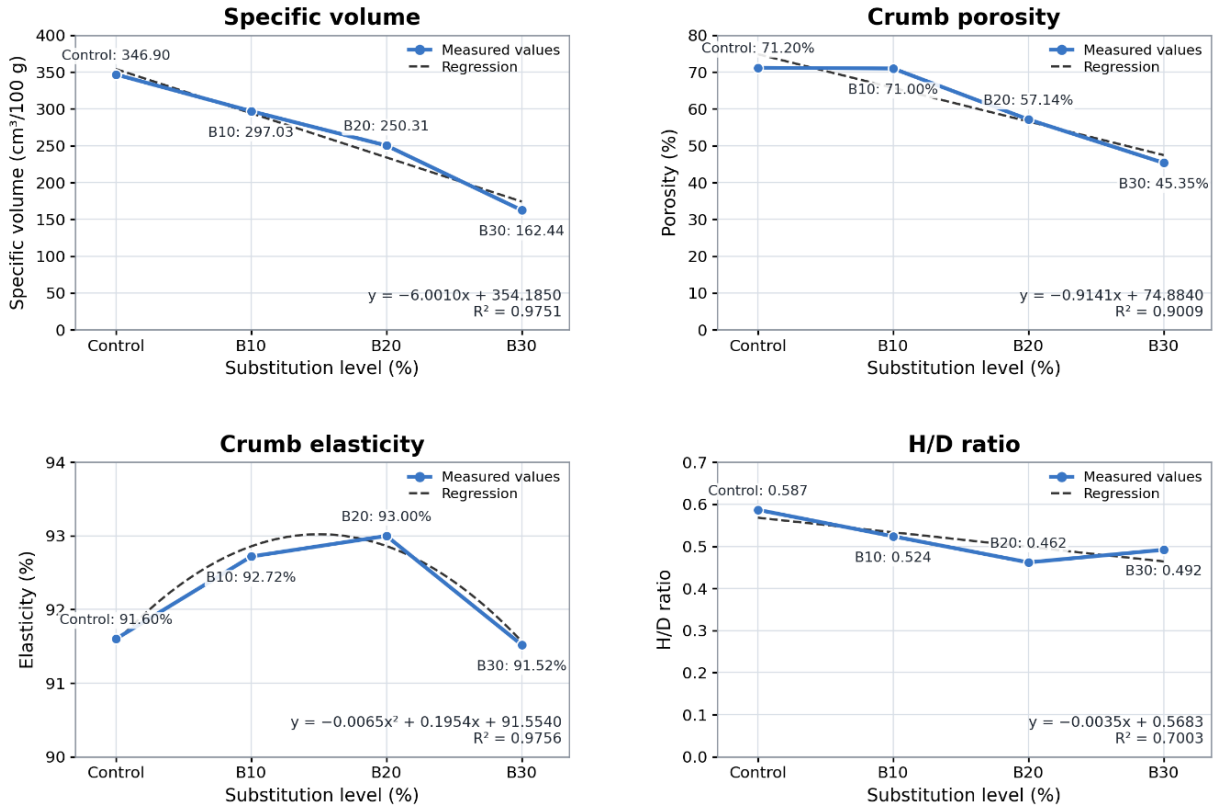



**Fig. 1 - Effect of buckwheat flour substitutional level on specific volume, crumb porosity, crumb elasticity and loaf H/D ratio**

Nevertheless, the two datasets originate from separate experiments. The previous study *(Ștefan E-M et al., 2018)* used whole buckwheat flour, whereas the current study more specifically used roasted whole-grain buckwheat flour. This difference in thermal pre-treatment prevents the two raw materials from being treated as identical. Therefore, no statistical correlation between farinographic and bread parameters is calculated, and a demonstrated causal relationship is not claimed.

Work by *Coţovanu and Mironeasa* (*Coţovanu I. et al, 2021; Coţovanu I. et al, 2022, Coţovanu I. et al, 2023)* provides additional explanation for variability among studies. Buckwheat fractions differ in composition, while large, medium and small particles can produce different rheological and baking responses. In optimized formulations, selected fractions may provide better performance than expected from total buckwheat concentration alone.

This observation has a direct implication for future experimental design: comparison of 10, 20 and 30% should be complemented by characterization of particle size, composition and hydration capacity.

Published nutritional studies explain why technological optimization is worthwhile. *Brites L.T.G.F. et al., (2022)* reported increased fibre and mineral content in breads containing whole-grain buckwheat flour, while *Nakov et al. (2022)* observed increasing levels of several nutritional and bioactive components with whole buckwheat incorporation.

However, the current study did not determine fibre, minerals, phenolics or antioxidant activity. Quantitative nutritional benefits must therefore not be directly attributed to B10-B30; literature is used to establish the relevance of the ingredient, not to replace missing measurements.

Similarly, claims concerning rutin and quercetin require caution. *Lukšič L. et al., (2016).* demonstrated major transformations of these flavonoids in sourdough systems, while Brites et al. monitored their evolution during processing. Final composition depends on species, milling fraction, fermentation and thermal treatment. These compounds were not measured in the current experiment and are therefore not used as criteria for selecting the optimum formulation.

Figure 2 and Figure 3 present images of all bread samples, showing their external appearance and crumb structure.




**Fig. 2 - External appearance of bread samples: Control (0% buckwheat flour), B10 (10% buckwheat flour), B20 (20% buckwheat flour), and B30 (30% buckwheat flour)**




**Fig. 3 - Crumb structure of bread samples with different levels of buckwheat flour substitution: Control (0% buckwheat flour), B10 (10% buckwheat flour), B20 (20%), and B30 (30% buckwheat flour)**

Visual assessment revealed progressive changes with increasing roasted whole-grain buckwheat flour incorporation. The control sample showed a regular, well-developed shape, a light-coloured crust and a homogeneous, well-aerated crumb. B10 remained visually close to the control, although the crust and crumb were slightly darker and a more pronounced surface crack was observed. Its crumb maintained a fine and relatively uniform pore distribution, consistent with the similar porosity values obtained for B10 and the control (71.00% and 71.20%, respectively).

At higher substitution levels, the differences became more pronounced. B20 exhibited reduced loaf development, a rougher and more irregular crust, darker colour and a more compact crumb with smaller and less distinct gas cells.

These changes were even more evident in B30, which showed the lowest loaf development, a markedly irregular and cracked surface and a dense, dark crumb with visibly reduced aeration. These observations were consistent with the decrease in specific volume from 346.90 cm³/100 g for the control to 250.31 and 162.44 cm³/100 g for B20 and B30, respectively, and with the corresponding decrease in porosity to 57.14 and 45.35%.

Overall, descriptive visual observations indicated a progressive darkening and a more compact crumb structure as buckwheat content increased. B10 was the formulation most similar to the wheat control, whereas structural changes became clearly evident at 20% and particularly at 30% incorporation. Nevertheless, crumb elasticity remained relatively stable (91.52–93.00%), indicating that the reduction in loaf volume and porosity was not accompanied by a proportional loss of crumb recovery after compression.

Literature confirms that buckwheat incorporation can modify bread colour, aroma and texture, although consumer acceptance is not determined by loaf volume alone. *Brites L.T.G.F. et al., (2022)* reported good acceptance of breads containing 30% refined or whole-grain buckwheat flour, whereas other studies have shown that sensory response depends on the product and formulation *(Nakov G., et al., 2022; Yıldız G et al., 2012).* Consequently, the more pronounced visual changes observed for B20 and B30 should not automatically be interpreted as sensory rejection.

Under the present experimental conditions, B10 represents the most favourable technological compromise. At this level, crumb porosity remained essentially identical to that of the control, elasticity was slightly higher, and the reduction in specific volume, although measurable, was considerably lower than at 20 and 30%. B20 may be considered an intermediate formulation; however, its approximately 28% reduction in specific volume and decrease in porosity to 57.14% indicate a need for process optimization.

Under the fixed processing conditions applied, B30 showed the greatest departure from the structural characteristics of the wheat control.

From an engineering perspective, these findings suggest several strategies for improving bread quality at higher buckwheat incorporation levels. Water addition could be adjusted for each flour blend based on farinograph or Mixolab measurements rather than kept constant, particularly considering the higher water absorption associated with increasing buckwheat flour addition *(Ștefan E-M et al., 2018)*. In addition, buckwheat particle-size distribution, mixing conditions, and fermentation time could be optimized. Sourdough, enzymes, or hydrocolloids may also be investigated as structure-modifying strategies, although their use would create different experimental systems and should therefore be evaluated separately *(Moroni A.V et al., 2011; Wronkowska M. et al., 2015).*

The contribution of the present study is therefore not the establishment of a universal optimum buckwheat percentage, but rather the identification of a system-dependent technological response. Under the formulation and processing conditions applied here, 10% roasted whole-grain buckwheat flour could be incorporated with relatively limited structural changes, whereas higher substitution levels increasingly affected loaf development and crumb structure and would require process adaptation. This interpretation is consistent with current literature, which indicates that buckwheat should not be regarded simply as a direct substitute for wheat flour, but as a raw material whose hydration requirements, particle characteristics, and functional behaviour need to be considered in bread formulation and process design.

## CONCLUSIONS

Partial replacement of wheat flour with buckwheat flour produced addition-level-dependent changes, most clearly reflected by specific volume and crumb porosity. Specific volume decreased by 14.4% at 10%, 27.8% at 20% and 53.2% at 30% relative to control. Porosity remained almost unchanged at 10% but decreased markedly at 20 and 30%. Crumb elasticity remained comparatively stable, demonstrating that structural quality indicators do not respond identically to substitution.

Under the fixed hydration and processing conditions used, the 10% formulation provided the most favourable technological compromise. The findings are compatible with the authors' previous rheological research, in which increasing buckwheat incorporation was associated with greater water absorption and lower dough stability; however, the experiments are separate and do not justify direct statistical correlation.

Comparison with published literature shows that the effect of buckwheat percentage depends on flour type, milling fraction, particle size, hydration and processing. Consequently, 20-30% incorporation should not be regarded as intrinsically unsuitable but as requiring technological optimization. Independent replication, complete flour characterization, water optimization and instrumental analysis of texture and crumb structure are required to validate and extend the present findings.

## ACKNOWLEDGEMENT

This research was supported by the project CNFIS-FDI-2026-F-0049 “Asigurarea eficienței operaționale a bazei de aplicații practice pentru sisteme biotehnice în livezi, vii, solarii și grădini (EFIBIOTECH)”, from the Ministry of Education and Research through the Executive Agency for Financing Higher Education, Research, Development and Innovation.

## REFERENCES

[1] Atudorei O., Atudorei D., Codină G.G., (2026). Pseudocereals in bakery products: a review of nutritional composition, health benefits and bakery applications. Foods, 15, 1283. DOI: 10.3390/foods15081283.

[2] Biduski B. et al., (2024). Dough rheology and internal structure of bread produced with wheat flour partially substituted by buckwheat flour: A step towards enhancing nutritional value. Food Structure, 39, 100364. DOI: 10.1016/j.foostr.2023.100364.

[3] Brites L.T.G.F. et al., (2022). Technological, sensory, nutritional and bioactive potential of pan breads produced with refined and whole grain buckwheat flours. Food Chemistry: X, 13, 100243. DOI: 10.1016/j.fochx.2022.100243.

[4] Brites L.T.G.F. et al., (2022). Antioxidant-enriched gluten-free bread made with buckwheat flour: evaluation of technological and nutritional quality. Cereal Chemistry. DOI: 10.1002/cche.10573.

[5] Bonafaccia G., Gambelli L., Fabjan N., Kreft I., (2003). Trace elements in flour and bran from common and tartary buckwheat. Food Chemistry, 83, 1-5. https://doi.org/10.1016/S0308-8146(03)00228-0

[6] Coţovanu I., Mironeasa S., (2021). Buckwheat seeds: impact of milling fractions and addition level on wheat bread dough rheology. Applied Sciences, 11, 1731. DOI: 10.3390/app11041731. https://doi.org/10.3390/app11041731

[7] Coţovanu I., Mironeasa S., (2022). Influence of buckwheat seed fractions on dough and baking performance of wheat bread. Agronomy, 12(1), 137. DOI: 10.3390/agronomy12010137. https://doi.org/10.3390/agronomy12010137

[8] Coţovanu I., Mironeasa C., Mironeasa S., (2023). Incorporation of buckwheat flour at different particle sizes and distinctive doses in wheat flour to manufacture an improved wheat bread. Foods, 12(8), 1730. DOI: 10.3390/foods12081730. https://doi.org/10.3390/foods12081730

[9] Nakov G., Temkov M., Damyanova S., Ivanova S., (2022). The effect of whole buckwheat flour addition on physico-chemical characteristics, biological active compounds and fatty acids profile of breads. Bulletin of the Transilvania University of Brasov, Series II, 15(64), 2. DOI: 10.31926/but.fwiafe.2022.15.64.2.12. https://doi.org/10.31926/but.fwiafe.2022.15.64.2.12

[10] Moroni A.V., Dal Bello F., Zannini E., Arendt E.K., (2011). Impact of sourdough on buckwheat flour, batter and bread: biochemical, rheological and textural insights. Journal of Cereal Science, 54(2), 195-202. DOI: 10.1016/j.jcs.2011.04.008. https://doi.org/10.1016/j.jcs.2011.04.008

[11] Lukšič L. et al., (2016). Rutin and quercetin transformation during preparation of buckwheat sourdough bread. Journal of Cereal Science, 69, 71-76. DOI: 10.1016/j.jcs.2016.02.011.

[12] Ştefan E.-M., Voicu G., Constantin G.-A., Ipate G., Munteanu M., (2018). Effect of whole buckwheat flour on technological properties of wheat flour and dough. Engineering for Rural Development. DOI: 10.22616/ERDev2018.17.N393.

[13] Wronkowska M. et al., (2015). Effect of adding fresh and freeze-dried buckwheat sourdough on gluten-free bread quality. International Journal of Food Science & Technology, 50(2), 313-322. DOI: 10.1111/ijfs.12622.

[14] Yıldız G., Bilgiçli N., (2012). Effects of whole buckwheat flour on physical, chemical, and sensory properties of flat bread, Lavaş. Czech Journal of Food Sciences, 30, 534-540. DOI: 10.17221/10/2012-CJFS

# FUNGAL BIOMASS IN CARRIER-BASED BIOREACTORS AS A BASIS FOR TREATING INDUSTRIAL EFFLUENTS WITH POTENTIAL AGRICULTURAL REUSE: REVIEW AND PRELIMINARY DATA

/

# *UTILIZAREA BIOMASEI FUNGICE IMOBILIZATE PE SUPORTURI ÎN BIOREACTOARE PENTRU EPURAREA APELOR UZATE INDUSTRIALE CU POTENȚIAL DE REUTILIZARE ÎN AGRICULTURĂ: ANALIZĂ BIBLIOGRAFICĂ ȘI REZULTATE PRELIMINARE*

**Ioana-Corina MOGA*[1, 2)], Ovidiu IORDACHE[3)], Bogdan CAZAN[3)], Gabriel PETRESCU[1)], Elena PERDUM[3)], Iulian VOICEA[4)], Răzvan RĂDULESCU[3)]**

[1)] DFR Systems SRL, Bucharest / Romania;

[2)] Centre for Studies and Research on Agroforestry Biodiversity "Acad. David Davidescu" (CSCBAS), Romanian Academy, Bucharest / Romania;

[3)] National Research and Development Institute for Textiles and Leather (INCDTP), Bucharest / Romania;

[4)] National Institute of Research-Development for Machines and Installations Designed for Agriculture and Food Industry - INMA Bucharest / Romania

**Tel: +40.727.850.098; *E-mail: corinamoga@yahoo.com*

***Keywords:*** *wastewater reuse, irrigation, industrial effluents, macromycetes, fungal biomass, MBBR*

**ABSTRACT**

*Industrial wastewater treatment and its potential reuse in agriculture require technological solutions capable of addressing complex pollutant mixtures while supporting sustainable water resource management. This paper examines the potential of fungal biomass immobilized on moving carriers for the biological treatment of industrial effluents, particularly those generated by the textile and leather industries. The research combines a critical review of biological treatment technologies and agricultural water reuse requirements with laboratory investigations conducted during the development of an integrated fungal-based treatment system. Experimental activities focused on the configuration of an aerated and mechanically mixed bioreactor, the cultivation and comparative assessment of seven macromycete strains in enriched liquid media, and the elemental characterization of selected fungal biomass using SEM-EDX analysis. The investigations identified fungal strains with favourable growth characteristics under the tested cultivation conditions and provided information relevant to inoculum selection and subsequent biofilm development. The study contributes to the experimental foundation of carrier-based fungal treatment systems and identifies technological considerations for their integration into wastewater treatment processes with potential applications in agricultural water reuse.*

**REZUMAT**

*Epurarea apelor uzate industriale și reutilizarea potențială a acestora în agricultură necesită soluții tehnologice capabile să trateze amestecuri complexe de poluanți și să contribuie la gestionarea durabilă a resurselor de apă. Lucrarea analizează potențialul biomasei fungice imobilizate pe suporturi mobile pentru epurarea biologică a efluenților industriali, în special a celor proveniți din industria textilă și industria pielăriei. Cercetarea îmbină analiza critică a tehnologiilor biologice de epurare și a cerințelor privind reutilizarea apei în agricultură cu investigații experimentale de laborator desfășurate în cadrul dezvoltării unui sistem integrat de tratare bazat pe biomasă fungică. Activitățile experimentale au vizat configurarea unui bioreactor aerat și prevăzut cu agitare mecanică, cultivarea și evaluarea comparativă a șapte tulpini de macromicete pe medii lichide îmbogățite, precum și caracterizarea elementală a biomasei fungice selectate prin analiza SEM-EDX. Investigațiile au permis identificarea unor tulpini cu caracteristici favorabile de creștere în condițiile de cultivare testate și au furnizat informații relevante pentru selecția inoculului și dezvoltarea ulterioară a biofilmului. Studiul contribuie la fundamentarea experimentală a sistemelor de epurare bazate pe biomasă fungică imobilizată și evidențiază aspecte tehnologice relevante pentru integrarea acestora în procese de tratare a apelor uzate cu potențial de reutilizare în agricultură.*

## INTRODUCTION

Irrigation is one of the largest uses of fresh water, and the reuse of treated wastewater is increasingly promoted as a way to reduce the pressure on freshwater sources (*Hashem and Qi, 2021*). In the European Union, Regulation (EU) 2020/741 sets minimum quality requirements and monitoring rules for reclaimed water used in agricultural irrigation (*Regulation (EU) 2020/741, 2020*). Reuse also brings risks, mainly from salinity, pathogens and heavy metals, which can affect soil properties and the safety of crops (*Hashem and Qi, 2021*).

From an agricultural perspective, wastewater reuse must be evaluated not only in terms of water availability, but also in relation to irrigation suitability, soil protection and crop safety. Reclaimed water may provide an alternative water resource and contribute to nutrient recycling; however, its long-term use requires consideration of salinity, nutrient balance, potentially toxic elements, organic micropollutants and microbiological hazards. These factors may influence soil properties, crop development and the accumulation of contaminants in agricultural systems. Consequently, the suitability of treated wastewater for irrigation depends on the combined assessment of treatment performance, intended crop use, irrigation practices and site-specific environmental risks (*Hashem and Qi, 2021; Regulation (EU) 2020/741, 2020*).

Recent research has highlighted the importance of considering contaminants of emerging concern when evaluating wastewater reuse in agriculture. These include pharmaceutical residues, pesticides, personal care product compounds and other persistent organic micropollutants that may remain in treated wastewater and enter agricultural soils through irrigation. Their environmental behaviour depends on physicochemical properties, soil characteristics, irrigation practices and plant uptake, with potential implications for crop safety and long-term soil quality. Christou et al. (2024), in a comprehensive review of sustainable wastewater reuse for agriculture, emphasise that conventional treatment processes may not completely eliminate these contaminants, supporting the need for advanced treatment technologies and integrated water quality monitoring. Furthermore, Okut et al. (2025) demonstrate the diversity of contaminants associated with agricultural wastewater and the relevance of combining biological, physical and chemical treatment methods according to wastewater characteristics and intended reuse applications.

Industrial effluents may present additional treatment challenges compared with municipal wastewater because of their variable composition and the presence of process-specific contaminants. Textile effluents contain dyes, salts, surfactants and process chemicals that conventional treatment removes only in part (*Holkar et al., 2016*), and tannery effluents add chromium and tannins. The consequences for crops are documented: in a pot experiment with a leafy vegetable irrigated with mixtures containing textile effluent, Pb and Cu were transferred from soil to plant with transfer factors above 1 (*Shammi et al., 2016*).

The moving bed biofilm reactor (MBBR) employs biofilm carriers maintained in motion within the reactor, providing a compact biological treatment configuration in which biomass can be retained without conventional sludge recirculation (*di Biase et al., 2019; Madan et al., 2022*). Combined with membrane bioreactor technology, MBBR has also been investigated for reducing treatment costs and environmental impacts in textile wastewater treatment (*Yang and López-Grimau, 2021*).

Fungi, particularly white-rot species, produce extracellular oxidative enzymes capable of transforming various organic pollutants, while fungal biomass may additionally contribute to contaminant removal through biosorption (*Pundir et al., 2024; Ghosh et al., 2023*). Fungal treatment systems include suspended or pelleted biomass in stirred and airlift reactors (*Espinosa-Ortiz et al., 2016; Cerrone and O'Connor, 2025*), immobilized fungal configurations and hybrid biological treatment processes (*Pundir et al., 2024; Baldessarelli et al., 2026*).

The use of fungal biomass immobilized on artificial carriers is particularly relevant for investigating the removal of selected organic micropollutants from complex wastewater matrices. Fungal treatment may involve extracellular enzymatic transformation and biosorption, while immobilization provides a means of retaining biomass within the reactor and supporting operation under continuous-flow conditions. A recent review by Baldessarelli et al. (2026), covering 71 studies on pellet-based and immobilized fungal bioreactors, identified pollutant-dependent removal performance and reported that carrier effects were particularly relevant for pesticides.

The review further identified wastewater sterility as an important operational factor in continuous immobilized systems, particularly through its effects on biomass stability, microbial competition and fungal activity. These findings support further investigation of carrier-based fungal technologies for wastewater containing agricultural and industrial organic contaminants, while emphasising the need to assess transformation products and their potential toxicity before considering treated water for agricultural reuse.

Several points are still open. Operation under non-sterile conditions, where fungi compete with bacteria, is a recurring concern (*Mir-Tutusaus et al., 2018*), although it has been tested on real textile wastewater in a rotating drum contactor (*Ardiati et al., 2024*). Biomass retention, foaming and shear in aerated and stirred reactors are practical issues, and design data for fungal systems appear to be scarce.

This paper has two parts. The first reviews technology options for treating industrial effluents with reuse in view and compares them with the quality classes of Regulation (EU) 2020/741. The second reports three preliminary results from the development of a combined fungal-MBBR treatment system: the configuration and operating window of a 5 L aerated and mechanically mixed bioreactor, the growth of seven macromycete strains on enriched media, and the elemental profile of two strains by SEM-EDX.

## MATERIALS AND METHODS

### *Bioreactor*

The laboratory bioreactor is a 5 L borosilicate glass vessel with four necks, used for the inoculation port (closed with a septum), the aeration line, a pH probe and a temperature probe. Oxygen was supplied by air sparging through a ceramic diffuser placed at the bottom of the vessel, and the content was mixed mechanically with an overhead paddle stirrer. The air line consisted of an air pump, an air filter, a flow control valve, a check valve and silicone tubing. The vessel was kept at temperature with a heating mantle (Biobase) and held on a laboratory stand. The design was prepared in AutoCAD. The moving carriers are made of high-density polyethylene (HDPE) with added cellulose (3 or 7%) and talc (5%), developed by one of the partners (DFR Systems) *(Moga et al., 2019).*

### *Strains and culture media*

Seven macromycete strains available as laboratory isolates were selected for preliminary growth screening, considering their potential relevance to fungal-based wastewater treatment: *Pholiota nameko* (PN1), *Hericium americanum* (HA2), *Pleurotus djamor* (PD3), *Ganoderma lingzhi* (GL4), *Lentinula edodes* (LE5), *Pleurotus citrinopileatus* (PC6) and *Flammulina velutipes* (FV7). Two liquid media were used: Sabouraud broth (Scharlau; glucose 40 g/L, peptone 10 g/L, final pH 5.6 ± 0.2) and YEG (yeast extract 10 g/L, glucose 20 g/L, final pH 6.5 ± 0.2).

A literature screening of the compounds available in the laboratory was used to select three mineral supplements, added to both media: $K_2HPO_4$ (1 g/L), $MgSO_4$ (0.5 g/L) and $FeSO_4 \cdot 7H_2O$ (0.05 g/L). The pH was readjusted after their addition with NaOH or HCl. Each strain was transferred from the stock inoculum (5 mL) into 80 mL of each medium and incubated for 28 days at 28°C. Growth was assessed visually at the end of incubation from the presence and size of the mycelial mass in the flask and classified as very good, good or none. No control without added mineral supplements was included.

### *SEM-EDX analysis*

*G. lingzhi* and *F. velutipes* were grown on Sabouraud agar and examined with a FEI Quanta 200 scanning electron microscope with a tungsten filament, in low vacuum mode with water vapour at 130 Pa to compensate for the charging of non-conductive samples, at an accelerating voltage of 10 kV. Elemental analysis was performed by energy-dispersive X-ray spectroscopy with an Ametek EDAX Element system (acquisition time 82 s, magnification 400x, maximum energy 10 keV).

## RESULTS

### *Technology options and reuse requirements*

Table 1 summarizes the biological treatment options reported in the literature for industrial effluents. Conventional activated sludge systems are widely applied, although the removal of recalcitrant dyes and dissolved salts remains limited (*Holkar et al., 2016*). MBBR technology provides a compact configuration with biomass retained on moving carriers, while hybrid MBBR–membrane systems have been investigated for treating complex wastewaters (*di Biase et al., 2019; Madan et al., 2022; Yang and López-Grimau, 2021*).

Fungal treatment systems offer additional enzymatic transformation and biosorption mechanisms, with biomass retention, oxygen transfer, shear stress and operation under non-sterile conditions representing important engineering considerations (*Pundir et al., 2024; Baldessarelli et al., 2026*).

**Table 1**

**Biological treatment options for industrial effluents considered in the literature**

| Option | Principle | Main advantages | Main limitations |
|---|---|---|---|
| Activated sludge | Suspended bacterial flocs, aeration, settling. | Mature, widely applied | Partial removal of recalcitrant dyes and salts (*Holkar et al., 2016*). |

| | | | |
|---|---|---|---|
| MBBR | Bacterial biofilm on free-moving carriers in an aerated tank. | Compact, no sludge recycling; combined with MBR for textile effluents *(di Biase et al., 2019; Yang and López-Grimau, 2021).* | Often combined with a further step such as MBR (*Yang and López-Grimau, 2021*). |
| Fungal pelleted reactors (stirred, airlift) | Free fungal pellets, enzymatic and sorptive action. | Low power and low shear in airlift; no carrier needed (*Espinosa-Ortiz et al., 2016; Cerrone and O'Connor, 2025*). | Pellet size control, foaming, weaker oxygen transfer; competition with bacteria in non-sterile operation (*Mir-Tutusaus et al., 2018*). |
| Fungal biofilm on rotating contactor | Fungal biomass immobilized on rotating support surfaces. | Biomass retained in the reactor *(Ardiati et al., 2024; Baldessarelli et al., 2026).* | Time needed to establish the biofilm; carbon source added in some systems (*Ardiati et al., 2024*). |

Reported treatment performance varies considerably according to reactor configuration, fungal species, wastewater composition and operating conditions. In a rotating drum biological contactor, immobilized Trametes hirsuta achieved 94% COD removal from non-sterile real textile wastewater under fed-batch conditions with 0.5% glucose supplementation (*Ardiati et al., 2024*). Recent reviews also identify the importance of fungal immobilization, biomass stability and operating conditions in determining pollutant removal performance (*Pundir et al., 2024; Baldessarelli et al., 2026*). The requirement for supplementary carbon sources must be considered when evaluating the operational feasibility of fungal treatment systems.

Table 2 gives the quality classes of Regulation (EU) 2020/741. The Regulation applies to treated urban wastewater, so for industrial effluents it serves only as a benchmark. Its indicators (*E. coli*, $BOD_5$, total suspended solids (TSS) and turbidity) are necessary, but salinity, metals and persistent organics also have to be controlled, as the transfer of Pb and Cu to a leafy vegetable show (*Shammi et al., 2016*). A biological stage acts mainly on organic load and colour. Turbidity, suspended solids and pathogens depend on separation and disinfection downstream, which in the system studied here are the settling and ultrasonic stages that follow the fungal-MBBR stage.

**Table 2**

**Minimum water quality classes for agricultural irrigation in Regulation (EU) 2020/741**

| Class | Crops | Irrigation method | *E. coli* [CFU/100 mL] | $BOD_5$ [mg/L] | TSS [mg/L] | Turbidity [NTU] |
|---|---|---|---|---|---|---|
| A | Food crops eaten raw, edible part in contact with water; raw-eaten root crops | All | ≤10 | ≤10 | ≤10 | ≤5 |
| B | Raw-eaten crops, edible part not in contact with water; processed food crops; non-food crops | All | ≤100 | ≤25 | ≤35 | - |
| C | As class B | Drip or other method avoiding contact with the edible part | ≤1000 | ≤25 | ≤35 | - |
| D | Industrial, energy and seeded crops | All | ≤10 000 | ≤25 | ≤35 | - |

*Note: For classes B, C and D, the $BOD_5$ and TSS values shown represent the concentration limits specified in Directive 91/271/EEC, to which Regulation (EU) 2020/741 refers; the Directive also provides alternative percentage-reduction requirements.*

***Implications for potential agricultural water reuse***

The potential agricultural application of treated industrial effluents requires a distinction between the removal of pollutants during wastewater treatment and the suitability of the resulting water for irrigation. Regulation (EU) 2020/741 establishes minimum quality classes for reclaimed urban wastewater according to crop categories and irrigation methods. Although these classes provide a useful reference for evaluating water quality, industrial effluents require additional consideration of source-specific contaminants, particularly dissolved salts, metals and persistent organic compounds. Therefore, compliance with conventional biological treatment indicators alone would not establish suitability for agricultural reuse (*Regulation (EU) 2020/741, 2020; Hashem and Qi, 2021*).

For the proposed fungal-MBBR system, this distinction provides a basis for defining subsequent experimental evaluation criteria. The biological stage is intended to address biodegradable organic matter and selected complex organic pollutants, while the integrated treatment configuration includes additional separation and downstream treatment processes. Assessment of the final treated water should combine

conventional parameters, including BOD5, suspended solids and microbiological indicators, with electrical conductivity, relevant metals and industrial contaminants selected according to wastewater composition. The interpretation of these measurements should also consider the intended crop category, irrigation method and potential effects on soil quality (*Regulation (EU) 2020/741, 2020*).

***Bioreactor configuration and operating window***

The bioreactor (Fig. 1) is built around three circuits: inoculation through a septum port, aeration, and monitoring of pH and temperature. Oxygen is supplied by sparging through the ceramic diffuser, and the content is mixed mechanically with an overhead paddle stirrer. Mechanical stirring is a known source of shear for mycelium (*Cerrone and O'Connor, 2025*), and moving carriers add collisions, so the stirring speed has to be set to keep the carriers suspended without detaching the biofilm. Foaming depends on both the air flow and the stirring speed, and a silicone antifoam at minimal dose is foreseen if needed. The outlet is an overflow protected against the loss of carriers.

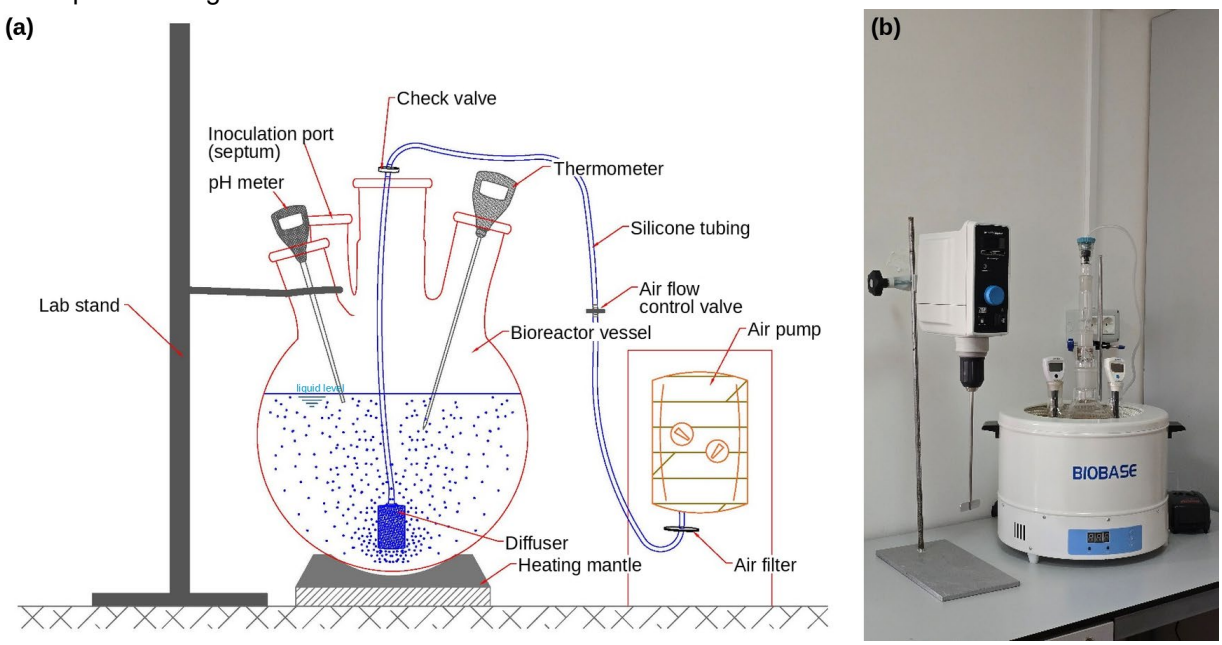



**Fig. 1 - Laboratory aerated and mechanically mixed bioreactor**

*(a) schematic of the assembly (stirrer not shown); (b) start configuration of the experimental setup*

Table 3 lists the starting operating values. The carrier filling ratio ranged from 20% to 40% (v/v) during the laboratory experiments. The air flow of 1-3 L/min is set to supply oxygen without excessive foaming and without projecting carriers out of the liquid, and the stirring speed is set separately, as explained above. The pH window of 5.5-7.0 is corrected through the septum port. The hydraulic retention time during the wastewater treatment stage ranged from 6 to 24 h, following the separate 28-day fungal inoculum cultivation stage (Table 4). Biofilm establishment on the carriers is required before continuous feeding, while subsequent performance will depend on biomass retention, fungal activity, oxygen transfer and operating conditions.

**Table 3**

**Starting operating parameters of the 5 L aerated and mechanically mixed bioreactor**

| Parameter | Starting value | Purpose |
|---|---|---|
| Vessel | 5 L borosilicate glass, four necks | Inoculation, aeration, pH and temperature ports |
| Aeration | Sparging, ceramic diffuser, 1-3 L/min | Oxygen supply |
| Mixing | Mechanical, overhead paddle stirrer | Keeps carriers suspended; speed set to avoid detaching the biofilm |
| Carrier fill | 20-40% v/v | Biofilm surface; validated hydrodynamically |
| pH | 5.5-7.0 | Corrected through the septum port |
| Temperature | 22-28 °C | Heating mantle; optional thermostatic bath |
| Retention time (continuous mode) | 6-24 h (12 h typical for dyes; 12-24 h or more for tannins) | Initial target |
| Foam control | Air flow and stirring speed; silicone antifoam at minimal dose if needed | Avoid loss of liquid and carriers |

***Fungal biomass: growth and elemental profile***

Four of the seven strains, *P. nameko*, *G. lingzhi*, *L. edodes* and *F. velutipes*, formed a large mycelial mass in both media (Table 4, Fig. 2). *P. citrinopileatus* grew only on YEG, *H. americanum* only on Sabouraud broth, and *P. djamor* did not grow on either medium within 28 days; the reason was not investigated. Based on the qualitative growth assessment, these four strains were selected as preliminary candidates for inoculum production and subsequent carrier colonisation experiments.

**Table 4**

**Growth of the strains after 28 days at 28°C (visual assessment)**

| Strain | Code | Sabouraud broth | YEG |
|---|---|---|---|
| *Pholiota nameko* | PN1 | Very good | Very good |
| *Hericium americanum* | HA2 | Good | None |
| *Pleurotus djamor* | PD3 | None | None |
| *Ganoderma lingzhi* | GL4 | Very good | Very good |
| *Lentinula edodes* | LE5 | Very good | Very good |
| *Pleurotus citrinopileatus* | PC6 | None | Good |
| *Flammulina velutipes* | FV7 | Very good | Very good |

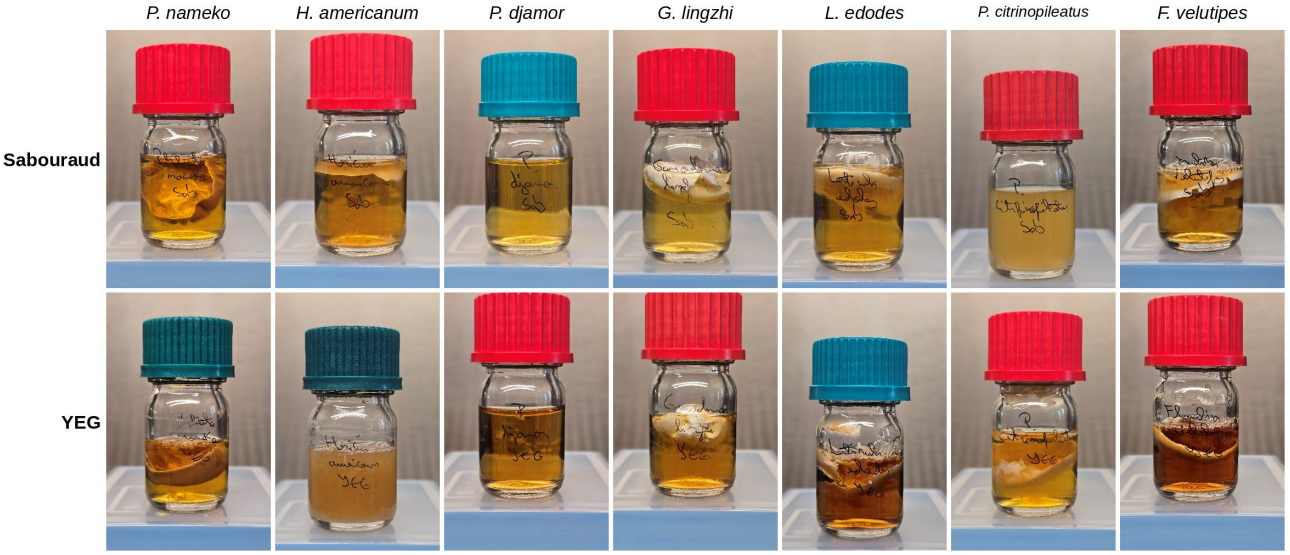



**Fig. 2 - Growth of the seven strains after 28 days at 28°C in Sabouraud broth and YEG medium, both with added $K_2HPO_4$, $MgSO_4$ and $FeSO_4 \cdot 7H_2O$**

The assessment is qualitative and no control without added mineral supplements was run, so the effect of the three salts cannot be separated from that of the base media. The positive effect of iron on mycelial growth reported for *L. edodes* (*Xiang et al., 2022*) therefore only motivates the supplements and was not tested here. The next measurement needed is the dry biomass per unit of medium, with and without supplements, and on carriers; the 28-day incubation is also long compared with the time scales of a continuous process.

The EDX spectra (Fig. 3) show carbon, nitrogen and oxygen as the main elements, as expected for organic biomass, with sodium and potassium as the only other elements in *G. lingzhi* and sulphur in addition in *F. velutipes*. Element maps (not shown) displayed these elements spread evenly, with no local accumulation at the scale of the maps. No distinct peaks attributable to heavy metals were identified in the recorded EDX spectra under the applied analytical conditions.

The data are qualitative. EDX is poorly suited to quantifying light elements such as C, N and O. At 10 kV the analysed volume can be as large as the diameter of a hypha, so the signal may include the agar medium underneath, and only one spectrum per strain is shown. The spectra therefore serve only as a baseline for comparison with biomass exposed to real effluent, for example to see whether chromium or other metals accumulate on the hyphae. Since filamentous fungi can bind heavy metals (*Ghosh et al., 2023*),

spent biomass from the treatment of metal-bearing effluents would need to be analysed before any use as a soil amendment.

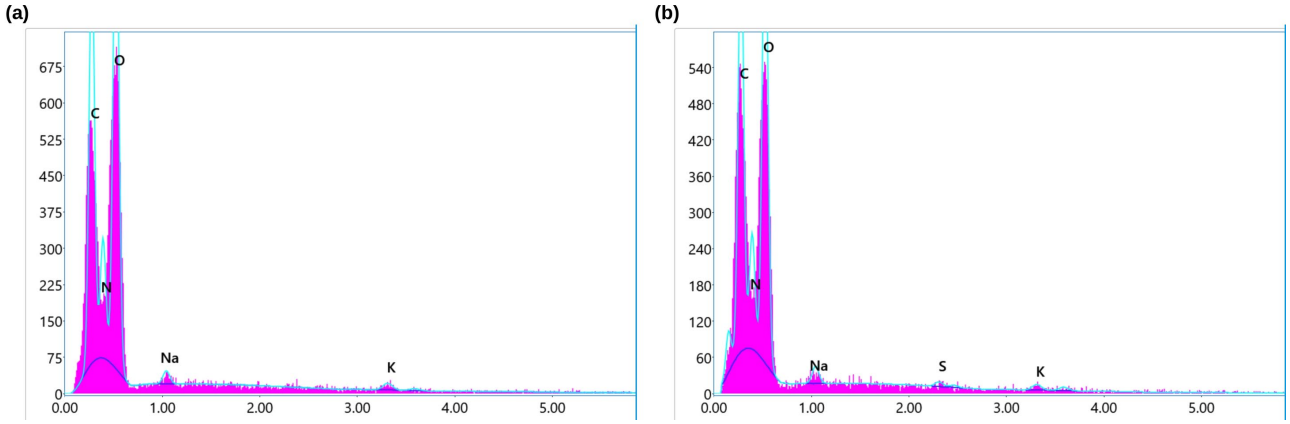



**Fig. 3 - EDX spectra of mycelium grown on Sabouraud agar: (a) G. lingzhi; (b) F. velutipes**
*Horizontal axis: energy [keV]; vertical axis: counts*

## CONCLUSIONS

The main conclusions are as follows:

1) Reuse in irrigation sets quality requirements (Table 2) that a biological stage cannot meet alone. For industrial effluents the fungal-MBBR stage must be followed by separation and disinfection, and salts and metals must be controlled in addition.
2) In the literature, the main engineering issues of fungal biofilm reactors are biomass retention, oxygen supply without shear, foaming and operation without sterile conditions.
3) A 5 L bioreactor aerated by sparging and mixed mechanically was configured with three circuits, and a starting operating window was defined (Table 3): air flow 1-3 L/min, carrier fill 20-40% v/v, pH 5.5-7.0 and 22-28 °C.
4) Four of seven strains (*P. nameko, G. lingzhi, L. edodes and F. velutipes*) grew very well on both enriched media and are inoculum candidates; P. djamor did not grow. EDX analysis identified C, N, O, Na and K in the examined samples, with S additionally observed in *F. velutipes*; no distinct heavy-metal peaks were identified in the recorded spectra.

Overall, the laboratory investigations provide a preliminary experimental basis for the development of a carrier-based fungal treatment system, particularly regarding bioreactor configuration, fungal strain selection and biomass characterisation. From an agricultural perspective, the relevance of this approach lies in its potential integration into multi-stage wastewater treatment systems designed to support water recovery and resource conservation. Subsequent experimental validation should address pollutant removal under representative operating conditions and assess the final effluent against microbiological, physicochemical and contaminant-specific criteria relevant to irrigation. Particular attention should be given to salinity, metal concentrations, organic pollutants and potential effects on agricultural soils and crops, consistent with the risk-based principles of Regulation (EU) 2020/741.

## ACKNOWLEDGEMENT

This work was supported by project 62PED/2025 (PN-IV-P7-7.1-PED-2024-1337) "Development and validation of a combined tri-component integrated system for wastewater treatment - 3treat", funded by UEFISCDI through the National Research, Development and Innovation Plan.

## REFERENCES

[1] Ardiati, F. C., Anita, S. H., Nurhayat, O. D., Chempaka, R. M., Yanto, D. H. Y., Watanabe, T., & Wilen, B.-M. (2024). Evaluation of batch and fed-batch rotating drum biological contactor using immobilized Trametes hirsuta EDN082 for non-sterile real textile wastewater treatment. J*ournal of Environmental Chemical Engineering, 12(4),* 113241. https://doi.org/10.1016/j.jece.2024.113241

[2] Baldessarelli, R., Bertrand, E., Seyssiecq, I., & Barca, C. (2026). Fungal bioreactors for treatment of emerging organic pollutants: Pellet-based and immobilized configurations. *Journal of Environmental Management, 414,* 130446. https://doi.org/10.1016/j.jenvman.2026.130446

[3] Cerrone, F., & O'Connor, K. E. (2025). Cultivation of filamentous fungi in airlift bioreactors: advantages and disadvantages. *Applied Microbiology and Biotechnology*, 109(1), 41. https://doi.org/10.1007/s00253-025-13422-4

[4] Christou, A., Beretsou, V. G., Iakovides, I. C., Karaolia, P., Michael, C., Benmarhnia, T., Chefetz, B., Donner, E., Gawlik, B. M., Lee, Y., Lim, T. T., Lundy, L., Maffettone, R., Rizzo, L., Topp, E., & Fatta-Kassinos, D. (2024). Sustainable wastewater reuse for agriculture. *Nature Reviews Earth & Environment, 5(7),* 504–521. https://doi.org/10.1038/s43017-024-00560-y

[5] di Biase, A., Kowalski, M. S., Devlin, T. R., & Oleszkiewicz, J. A. (2019). Moving bed biofilm reactor technology in municipal wastewater treatment: A review. *Journal of Environmental Management, 247*, 849–866. https://doi.org/10.1016/j.jenvman.2019.06.053

[6] Espinosa-Ortiz, E. J., Rene, E. R., Pakshirajan, K., van Hullebusch, E. D., & Lens, P. N. L. (2016). Fungal pelleted reactors in wastewater treatment: Applications and perspectives. *Chemical Engineering Journal, 283*, 553-571. https://doi.org/10.1016/j.cej.2015.07.068

[7] Ghosh, S., Rusyn, I., Dmytruk, O. V., Dmytruk, K. V., Onyeaka, H., Gryzenhout, M., & Gafforov, Y. (2023). Filamentous fungi for sustainable remediation of pharmaceutical compounds, heavy metal and oil hydrocarbons. *Frontiers in Bioengineering and Biotechnology, 11,* 1106973. https://doi.org/10.3389/fbioe.2023.1106973

[8] Hashem, M. S., & Qi, X.-B. (2021). Treated wastewater irrigation - a review. *Water, 13(11)*, 1527. https://doi.org/10.3390/w13111527

[9] Holkar, C. R., Jadhav, A. J., Pinjari, D. V., Mahamuni, N. M., & Pandit, A. B. (2016). A critical review on textile wastewater treatments: possible approaches. *Journal of Environmental Management, 182,* 351-366. https://doi.org/10.1016/j.jenvman.2016.07.090

[10] Madan, S., Madan, R., & Hussain, A. (2022). Advancement in biological wastewater treatment using hybrid moving bed biofilm reactor (MBBR): A review. *Applied Water Science, 12,* 141. https://doi.org/10.1007/s13201-022-01662-y

[11] Mir-Tutusaus, J. A., Baccar, R., Caminal, G., & Sarrà, M. (2018). Can white-rot fungi be a real wastewater treatment alternative for organic micropollutants removal? A review. *Water Research, 138,* 137-151. https://doi.org/10.1016/j.watres.2018.02.056

[12] Moga, I. C., Moisescu, C., Ardelean, I. I., Petrescu, G., Voicea, I., & Doroftei, B. I. (2019). New biofilm carriers for wastewater treatment. International *Journal of Conservation Science, 10(1),* 187-196. https://ijcs.ro/public/IJCS-19-17_Moga.pdf

[13] Okut, N., Hamzat, A. K., Rajakaruna, R. A. D. N. V., & Asmatulu, E. (2025). Agricultural wastewater treatment and reuse technologies: A comprehensive review. *Journal of Water Process Engineering, 69,* 106699. https://doi.org/10.1016/j.jwpe.2024.106699

[14] Pundir, A., Thakur, M. S., Prakash, S., Kumari, N., Sharma, N., Parameswari, E., He, Z., Nam, S., Thakur, M., Puri, S., Puranik, S., Kumar, S., Madhu, & Kumar, M. (2024). Fungi as versatile biocatalytic tool for treatment of textile wastewater effluents. *Environmental Sciences Europe, 36*, 185. https://doi.org/10.1186/s12302-024-01007-3

[15] Regulation (EU) 2020/741 of the European Parliament and of the Council of 25 May 2020 on minimum requirements for water reuse (2020). *Official Journal of the European Union, L 177,* 32-55.

[16] Shammi, M., Kashem, M. A., Rahman, M. M., Hossain, M. D., Rahman, R., & Uddin, M. K. (2016). Health risk assessment of textile effluent reuses as irrigation water in leafy vegetable Basella alba. *International Journal of Recycling of Organic Waste in Agriculture, 5(2),* 113-123. https://doi.org/10.1007/s40093-016-0122-x

[17] Xiang, Q., Zhang, H., Chen, X., Hou, S., Gu, Y., Yu, X., Zhao, K., Zhang, X., Ma, M., Chen, Q., Penttinen, P., & Chen, X. (2022). Enhanced effects of iron on mycelial growth, metabolism and in vitro antioxidant activity of polysaccharides from Lentinula edodes. *Bioengineering, 9(10),* 581. https://doi.org/10.3390/bioengineering9100581

[18] Yang, X., & López-Grimau, V. (2021). Reduction of cost and environmental impact in the treatment of textile wastewater using a combined MBBR-MBR system. *Membranes, 11(11),* 892. https://doi.org/10.3390/membranes11110892

# INTEGRATED DIGITAL SOLUTIONS IN AGRICULTURE
# /
# *SOLUȚII DIGITALE INTEGRATE ÎN AGRICULTURĂ*

**Iulian VOICEA*[1)], Florin NENCIU[1)], Cătălin PERSU[1)], Dan CUJBESCU[1)], Remus OPRESCU[1)], Iuliana GĂGEANU[1)], Roxana ZAHARIA[2)], Viorel FĂTU[2)], Corina MOGA[3)], Vlad-Nicolae ARSENOAIA[4)], Diana STEGARUS (POPESCU)[5)]**

[1)] INMA Bucharest / Romania;

[2)] ICDPP Bucharest / Romania;

[3)] DFR SYSTEMS Bucharest / Romania;

[4)] Faculty of Agriculture, Ion Ionescu de la Brad University of Agricultural Sciences and Veterinary Medicine, 700490 Iasi / Romania;

[5)] ICSI Valcea, Valcea County / Romania.

**Tel: 0752 161 780; *E-mail: voicea_iulian@yahoo.com*

***Keywords:*** *digital agriculture, precision agriculture, Internet of Things, artificial intelligence, UAV, farm management, interoperability*

**ABSTRACT**

*Agricultural digitalisation is one of the main development directions for increasing the precision of technological processes, optimizing resource use and enhancing the resilience of agricultural production systems. The paper presents, in an integrated manner, the main components of digital agriculture, namely sensor networks and the Internet of Things (IoT), remote sensing and unmanned aerial vehicles (UAVs), Big Data technologies, artificial intelligence (AI), farm management information systems (FMIS), variable-rate technologies and autonomous equipment. The methodology was based on documentary analysis and a comparative synthesis of recent scientific literature, with particular emphasis on the relationships between data collection and transmission, information processing and analysis, decision support and the automated execution of technological interventions. The results show that the efficiency of digital solutions increases considerably when they are interoperable and integrated into a coherent technological workflow based on the sequence measurement-transmission-analysis-decision-intervention-verification. The studies reviewed indicate the potential to reduce the consumption of water, fertilizers, plant protection products, fuel and labour, although the magnitude of these benefits is influenced by crop type, farm size, data quality and the degree of technological integration. At the same time, several barriers are identified, related to initial investment costs, communications infrastructure, the level of digital skills, data management and security, and compatibility among different platforms. In this context, a gradual approach to digitalisation is proposed, starting with monitoring and digital record-keeping and progressing toward automation and autonomy, so that investments can be adapted to the specific needs and technical capacity of each agricultural holding.*

**REZUMAT**

*Digitalizarea agriculturii constituie una dintre principalele direcții de dezvoltare pentru creșterea preciziei proceselor tehnologice, optimizarea utilizării resurselor și sporirea rezilienței sistemelor de producție agricolă. Lucrarea prezintă, într-o manieră integrată, principalele componente ale agriculturii digitale, respectiv rețelele de senzori și Internet of Things (IoT), teledetecția și vehiculele aeriene fără pilot (UAV), tehnologiile Big Data, inteligența artificială (AI), sistemele informatice pentru managementul fermei (FMIS), tehnologiile de aplicare variabilă și echipamentele autonome. Metodologia utilizată s-a bazat pe analiza documentară și pe sinteza comparativă a literaturii științifice recente, urmărind în special relațiile dintre colectarea datelor, transmiterea acestora, procesarea și analiza informațiilor, suportul decizional și realizarea automată a intervențiilor tehnologice. Rezultatele evidențiază faptul că eficiența soluțiilor digitale crește considerabil atunci când acestea sunt interoperabile și integrate într-un flux tehnologic coerent, bazat pe succesiunea măsurare–transmitere–analiză–decizie–intervenție–verificare. Studiile analizate indică posibilitatea reducerii consumurilor de apă, fertilizanți, produse de protecție a plantelor, combustibil și forță de muncă, nivelul beneficiilor fiind însă influențat de tipul culturii, dimensiunea exploatației, calitatea datelor și gradul de integrare tehnologică. Totodată, sunt identificate o serie de bariere asociate costurilor inițiale de investiție, infrastructurii de comunicații, nivelului competențelor digitale, gestionării și securității datelor, precum și compatibilității dintre diferitele platforme. În acest context, este propusă o abordare graduală a procesului de digitalizare, pornind de la monitorizare și evidență digitală și evoluând către automatizare și autonomie, astfel încât investițiile să fie adaptate nevoilor concrete și capacității tehnice a fiecărei exploatații agricole.*

## INTRODUCTION

Contemporary agriculture operates under increasing pressure on natural resources, higher climate variability, volatile production costs and reduced availability of skilled labour. Under these conditions, productivity can no longer be considered only in terms of machine capacity or the quantity of inputs applied. Information has become a production factor in its own right: the ability to measure the status of soil and crops, combine data from different sources and rapidly convert those data into technological decisions.

Digitalisation is therefore a new stage in the evolution of mechanisation, in which machines, sensors and operators are connected through communication systems and software platforms.

The concept is closely associated with Agriculture 4.0 and with the transition from uniform field management to spatially and temporally differentiated interventions based on data (*Rose and Chilvers, 2018; Fountas et al., 2020*).

In a broad sense, digital agriculture includes technologies for data acquisition, transmission, storage and analysis, together with systems able to convert analytical outputs into machine commands. The Internet of Things links sensors, weather stations, machinery, irrigation equipment and information platforms;

Big Data methods manage large and heterogeneous datasets; and artificial intelligence and machine learning support pattern recognition, image classification, yield prediction and anomaly detection.

The literature consistently shows that the value of these technologies does not arise from isolated use, but from integration into a coherent architecture in which observations are contextualised by field, crop, operation, growth stage and economic objective (*Wolfert et al., 2017; Alahmad et al., 2023; Soussi et al., 2024*).

Smart sensors constitute the layer in direct contact with the agricultural process. They may measure soil moisture and temperature, electrical conductivity, microclimatic parameters, water level and flow, machine position, fuel consumption or functional parameters of implements. Their value increases when measurements are georeferenced and repeated at a frequency sufficient to capture meaningful temporal and spatial variation. IoT networks can transmit data through Wi-Fi, cellular systems,

LoRaWAN and other protocols, while processing may take place locally at the edge or in the cloud. For agricultural applications, the communication solution must be selected according to distance, energy consumption, data volume, transmission frequency and available coverage. Consequently, the design of a digital agricultural system is simultaneously an agronomic, information-technology and engineering problem (*Alahmad et al., 2023; Sharma and Shivandu, 2024*).

Remote sensing adds the spatial dimension. Satellite imagery, machine-mounted cameras and UAVs allow field heterogeneity to be observed at parcel scale. Vegetation indices and multispectral images can reveal differences in vigour, water stress, nutrient deficiency or disease effects before they become easily visible to the human eye.

Progress in spatial, spectral and temporal resolution has transformed remote sensing into a core precision-agriculture tool (*Mulla, 2013*). UAVs complement satellites through flexible acquisition timing and very high spatial resolution; in certain configurations they can also perform localised application of crop-protection products, reducing operator exposure and enabling rapid intervention in areas that are difficult to access (*Guebsi et al., 2024; Nahiyoon et al., 2024*).

A further step is the transformation of observation into prediction. Machine-learning algorithms are used for disease and weed detection, image classification, biomass and yield estimation, and water and soil management.

The performance of these models depends directly on the quality and representativeness of training data. In agriculture, variability in cultivars, soils, illumination and weather can reduce the transferability of a model from one location to another. Local validation, model updating and explainability are therefore important for operational use. The integration of AI with IoT and remote-sensing data enables the transition from monitoring to early warning and predictive decision support (*Liakos et al., 2018; Delfani et al., 2024*).

Farm Management Information Systems represent the layer that connects technical observations to operational and economic records. A modern FMIS may integrate field boundaries, crops, operations, machinery, labour, inventories, documents and costs. Sensor and machinery data thereby acquire context and can be used for efficiency analysis.

FMIS have evolved from simple recordkeeping applications into platforms that support planning, traceability, compliance and data exchange with other systems (*Fountas et al., 2015; Basir et al., 2024*). For farms using several digital technologies, interoperability is critical: when each machine generates a

proprietary format, operators must repeatedly convert or re-enter information, reducing the benefits of automation (*Urdu et al., 2024*).

Digitalisation is also extending into autonomous execution. Driverless tractors, field robots and automatic guidance systems combine GNSS, perception sensors, path planning and motion control. Full autonomy requires high-accuracy positioning, reliable obstacle detection, safe response to unexpected events and robust control hardware.

Recent research demonstrates rapid progress but also emphasises the need for more robust sensors, multisource data integration and safety approaches specifically adapted to agricultural environments (*Qu et al., 2024; Liu et al., 2024*). From this perspective, Agriculture 5.0 is associated not only with automation but also with human-machine cooperation, sustainability and responsible use of data.

Adoption remains uneven. Initial investment, uncertainty concerning return on investment, internet infrastructure, lack of skills and difficulties integrating platforms are frequently reported barriers. Farm size influences the capacity to amortise investment, but modular and retrofit solutions can lower the entry threshold.

In parallel, questions of data ownership, privacy and cybersecurity are becoming increasingly important. Farmers need to know who stores their data, how data are used, whether they can be exported and under what conditions they can be transferred to another platform. Research on smart-farming data governance highlights the need for clear rules concerning access, sharing and protection of agricultural information (*Dibbern et al., 2024; Rouzky et al., 2026*).

The objective of this paper is to analyse the main digital solutions used in agriculture from the perspective of functional integration and value creation within the production process. Four questions are addressed: what role each technology category plays in the data flow; how monitoring is converted into decision and execution; which technical, economic and environmental benefits are reported in the scientific literature; and which conditions are required for gradual, scalable and secure implementation at farm level.

## MATERIAL AND METHOD

This paper is based on documentary analysis and technological synthesis. Scientific publications and review papers addressing digital agriculture, precision farming, IoT, sensors, Big Data, AI, UAVs, FMIS, interoperability, agricultural robots and data governance were considered.

To reflect the current state of the field, priority was given to literature published in 2023-2026, while earlier foundational studies defining major concepts such as Big Data in smart farming, FMIS and remote sensing in precision agriculture were retained. The selection focused on direct relevance to the integration of technologies at farm level and on the presence of conclusions concerning functionality, performance, benefits or adoption barriers.

The analysis was structured into four functional layers. The first layer, data acquisition, includes soil and microclimate sensors, machinery telemetry, GNSS, cameras, satellite imagery and UAVs. The second layer, communications and data management, includes IoT networks, local or cloud storage, databases and interoperability mechanisms.

The third layer, analytics and decision support, brings together agronomic indicators, GIS, predictive models, AI, machine learning and FMIS. The fourth layer is execution: auto-guidance, variable-rate application, automated irrigation, spraying UAVs, robots and autonomous tractors. This structure makes it possible to evaluate not only individual technologies but also the links between them.

For interpretation of benefits, results reported in review studies quantifying the effects of digital technologies on input use, productivity, labour requirements and fuel consumption were used. Maximum values reported in the literature are treated as indicative ranges rather than universally reproducible results.

Actual effects depend on crop, technology type, pedoclimatic conditions, baseline farm performance, spatial variability and implementation quality.

The paper therefore does not extrapolate percentages to a particular farm but uses them to compare the mechanisms through which digitalisation can create value.

Adoption barriers were grouped into four categories: economic, technical, organisational and data-governance related.

For each category, risk-reduction measures were formulated, including modular implementation, pilot testing, standardisation and interoperability, staff training, backup and cybersecurity policies, and definition of performance indicators before investment.

These elements were then used to formulate a four-stage implementation model: basic digitalisation and recordkeeping; connected monitoring; decision support and precision application; and advanced automation/autonomy.

**Table 1**

**Functional architecture of integrated digital solutions in agriculture**

| Layer | Representative technologies | Main role | Operational output |
|---|---|---|---|
| 1. Acquisition | Soil/microclimate sensors, GNSS, telemetry, satellite, UAV | Process sensing and georeferencing | Primary data on soil, crop, machinery and environment |
| 2. Communications & data | IoT, LoRaWAN, 4G/5G, edge/cloud, databases | Transmission, storage and synchronisation | Continuous accessible data flow |
| 3. Analytics & decision | GIS, FMIS, Big Data, AI/ML, agronomic models | Interpretation and prediction | Alerts, recommendations, prescription maps |
| 4. Execution | Auto-guidance, VRT, automated irrigation, UAV, robots | Implementation of decisions | Precise and documented intervention |

## RESULTS AND DISCUSSION

The analysis confirms that digital agriculture performs best as a cyber-physical system rather than as a collection of independent devices.

The technological flow begins with observation of the agricultural process and continues through data transmission, quality control, spatial and temporal contextualisation, analysis, recommendation and execution.

A new measurement after the intervention closes the control loop and allows the outcome to be evaluated. Without this loop, a sensor may generate data with no operational consequence, while a UAV may produce imagery that is never transformed into prescription maps or differentiated field operations. Integration is therefore the central criterion distinguishing a connected farm from a farm that merely owns several digital devices.

**Table 2**

**Main categories of digital solutions and suggested performance indicators**

| Category | Functions | Suggested indicators |
|---|---|---|
| Decision support | Satellite/UAV maps, forecasts, alerts, AI models | Response time, accuracy, reduction of unnecessary interventions |
| Farm Management | Fields, operations, machinery, inventory, costs, documents | Administrative time, cost/ha, inputs, traceability |
| Precision agriculture | Auto-guidance, VRT, mapping, on-the-go sensors | Overlap, input/ha, uniformity, energy efficiency |
| Automation/autonomy | Automated irrigation, robots, autonomous tractors | Labour hours, availability, safety, productivity |

At the acquisition layer, sensor density and sampling frequency must match the real variability of the field. Too few sensors may miss important zones, whereas excessive density may increase costs without generating proportional information. For soil moisture, sensor position should reflect texture, topography, irrigation layout and rooting depth.

For machine-mounted sensors, calibration and GNSS synchronisation are essential to prevent spatial displacement of data. Reviews of smart-sensor technology emphasise that accuracy, stability, energy consumption, maintenance requirements and protocol compatibility are as important as purchase price (*Soussi et al., 2024*).

IoT converts point measurements into continuous monitoring. In irrigation management, soil-moisture data can be combined with weather forecasts, evapotranspiration and crop growth stage. An algorithm may produce a recommendation or directly control valves and pumps.

The same principle can be used in greenhouses for temperature, humidity, CO2, lighting and fertigation. The key advantage is the reduction in time between the appearance of a deviation and the response. Nevertheless, automation without verification can amplify errors. Sensor failure or calibration drift

may produce incorrect commands. Robust systems therefore include safety limits, cross-checking between sensors, alerts for implausible values and the possibility of manual intervention.

Big Data becomes relevant when information is too large, fast and heterogeneous to be managed efficiently by conventional methods.

Agricultural sources include IoT sensors, machine telemetry, satellite imagery, UAV data, weather stations, soil analyses, operation records and economic data. Value is not created by volume alone but by the ability to connect observations to a decision. An agricultural dataset requires metadata, position, time, units, calibration information and links to the relevant field and crop.

Without these elements, combining datasets from different vendors becomes difficult. Wolfert et al. (2017) highlighted data quality and governance early in the development of smart farming; recent work increasingly focuses on semantic interoperability and controlled information exchange among platforms (*Urdu et al., 2024*).

Artificial intelligence adds the capacity to extract patterns from data. Crop applications include weed recognition, disease identification, maturity classification, biomass estimation and yield prediction. Resource-management models may estimate irrigation requirements or disease probability by combining microclimate, field history and crop status.

In practice, high performance in a laboratory does not guarantee identical performance in the field. A change in camera, illumination, cultivar or region can alter the data distribution. For critical applications, AI should therefore be combined with agronomic validation and with the ability to explain or verify recommendations. This approach increases user confidence and reduces the risk of automatically applying uncertain predictions (*Liakos et al., 2018; Delfani et al., 2024*).

UAVs perform two main roles: observation and intervention. In observation, a platform equipped with RGB or multispectral cameras can generate orthomosaics, surface models and vegetation indices. Repeated flights allow crop dynamics to be followed and zones with different development to be identified. Data are useful for stand establishment assessment, plant-density estimation, localisation of waterlogging, stress detection and definition of areas requiring ground inspection.

In intervention, spraying UAVs can treat well-defined zones with low carrier-water volume and high mobility. Constraints include battery endurance, payload, wind influence, regulatory requirements and the need for accurate calibration of flow rate and droplet spectrum. Recent literature shows that UAV effectiveness depends on the integration of imaging, algorithms and application systems, not only on the flight platform (*Guebsi et al., 2024; Nahiyoon et al., 2024*).

Variable-rate technologies provide a clear example of information being converted into action. Soil maps, vegetation imagery and on-the-go sensors can be transformed into prescription maps for fertilisation, seeding, spraying or irrigation. Benefits appear when spatial variability is sufficient to justify differentiated rates.

On relatively uniform fields, the advantage of VRT may be limited. On heterogeneous fields, however, site-specific application can reduce over-application and avoid under-dosing in productive zones. A prescription map should be generated from an agronomically valid model rather than from colour differences or a vegetation index alone; digital observation therefore has to be combined with biological and agronomic knowledge.

**Table 3**

**Examples of quantitative benefits reported for digital agricultural technologies**

| Technology/category | Benefit reported in review literature | Interpretation |
|---|---|---|
| Recording/mapping & guidance/CTF | Fertiliser reductions up to about 80% in selected applications | Upper values depend on context and within-field variability |
| Variable-rate technology (VRT) | Fertiliser reductions up to ~60% and pesticide reductions up to ~80% in selected cases | Requires agronomically validated prescriptions |
| Digital water management | Water savings of about 20-50% reported in some horticultural systems | Effect depends on irrigation system and climate |
| Robots / smart machines | Large labour reductions and, in some cases, lower diesel consumption | Benefit depends on autonomy level and annual utilisation |

| Technology/category | Benefit reported in review literature | Interpretation |
|---|---|---|
| FMIS | Yield improvements and reductions in labour/input use reported in selected studies | Higher value when FMIS is integrated with field data |

From an economic and environmental perspective, the evidence is promising but highly variable. Papadopoulos et al. (2024) synthesised 136 peer-reviewed papers together with empirical evidence from European projects and reported substantial reductions in fertiliser, pesticide, water, fuel and labour use for several categories of digital agricultural technologies. In selected cases included in that review, reductions of up to 80% were reported for certain inputs, water savings of 20-50% were observed, and major reductions in diesel use or labour requirements were achieved.

These values are upper outcomes from specific contexts and should not be interpreted as general promises. Their importance is mechanistic: better sensing and site-specific intervention can avoid unnecessary operations and replace conventional uniform management with differentiated management.

FMIS plays a transversal role by providing economic context and traceability for these operations. In a well-integrated system, tractor data can be automatically linked to the correct field and operation; fuel use can be compared against targets; input inventories can be updated after application; and yield maps can be analysed together with cost and fertilisation layers.

Digital recordkeeping reduces administrative effort and supports audits, but it can create another issue: platform dependence. If data cannot be exported in an open format or the farm history remains locked into one application, changing provider becomes difficult. Interoperability and data portability should therefore be included as procurement criteria alongside functionality and price (*Fountas et al., 2015; Basir et al., 2024; Urdu et al., 2024*).

Automation and autonomy move digitalisation into the execution layer. Auto-guidance systems are already mature for many operations and can reduce overlap, operator fatigue and path deviation.

Autonomous tractors and agricultural robots extend these functions through environmental perception and control without continuous human intervention. High-potential domains include repetitive operations, mechanical weed control, monitoring, selective harvesting and controlled-environment production. In open fields, the main challenges are robust obstacle detection, changing terrain, dust, vegetation, functional safety and interaction with people or other machines.

Recent reviews show that research is moving toward multisensor fusion, adaptive path planning and highly reliable control systems (*Qu et al., 2024; Liu et al., 2024*).

**Table 4**

**Adoption barriers and recommended mitigation measures**

| Barrier | Possible effect | Recommended measure |
|---|---|---|
| Initial investment / uncertain ROI | Delayed adoption | Limited-area pilot; baseline KPIs; modular implementation |
| Rural connectivity | Missing or delayed data | Edge computing; LPWAN; local storage with synchronisation |
| Limited digital skills | Partial use of the system | Training, simple procedures, technical support |
| Low interoperability | Duplicate entry and fragmented data | APIs, open standards, export testing before purchase |
| Security and data ownership | Commercial and operational risk | Role-based access, MFA, backup, contractual clauses and portability |

Adoption must be analysed as an organisational process rather than a purely technical choice. Dibbern et al. (2024) identify farmers' economic condition, infrastructure availability, technological knowledge, education, age, perceived technology reliability and concerns about security and privacy among major adoption factors and barriers.

These factors help explain why the same solution may succeed on one farm and be abandoned on another. Risk can be reduced by linking each investment to a measurable problem: excessive water use,

operational overlaps, insufficient traceability, high recordkeeping workload or strong crop variability. Baseline indicators should be measured before implementation and success evaluated over one or more seasons.

Data governance is becoming part of system performance. Agricultural datasets may include commercially sensitive information on productivity, costs, asset position and production practices. In a connected ecosystem, risks are not limited to loss of a file; they include unauthorised access, account lockout, data manipulation and service unavailability.

Recent work on smart-farming governance identifies a lack of sufficiently standardised governance frameworks and a need to improve farmer awareness of data security and privacy (Rouzky et al., 2026). Practical measures include role-based access, multifactor authentication, backups, regular updates, device inventories and clear contractual clauses concerning data ownership, reuse and export.

Interoperability is strategically important because farms frequently operate machinery and applications from several vendors. Technical interoperability requires exchange protocols and interfaces; semantic interoperability requires two systems to interpret concepts such as field, operation, rate, product, time and position in the same way.

European digital-agriculture initiatives compared by Urdu et al. (2024) show that interoperability should be addressed simultaneously at technical, semantic, organisational and security levels. Without it, the real cost of digitalisation increases through manual conversion, duplicate data entry and inability to automate the complete workflow.

For small and medium-sized farms, gradual implementation reduces investment risk. The first stage may consist of digital recordkeeping, field mapping and basic monitoring through GPS and a weather station. The second stage introduces IoT sensors and remote monitoring so that the farmer can receive alerts and compare trends. The third stage integrates satellite/UAV maps, decision-support models and variable-rate application.

The fourth stage includes advanced automation, robots and autonomy. Each stage should be justified by operational and economic indicators, and transition to the next stage should occur only after existing processes are stable. This strategy is consistent with sustainable digital transformation in which technology is selected to solve a concrete problem rather than merely to increase the amount of technology on the farm (*MacPherson et al., 2022; Arfasa and Tilahun, 2026*).

Overall, digitalisation generates the most consistent value when five conditions are met: high-quality data, adequate connectivity, interoperability, human competence and a clear economic model. Absence of one of these conditions can become the weak link of the entire system.

A high-performance AI application cannot compensate for incorrect input data; a precise sensor creates little value if there is no decision or actuator; and an advanced robot may remain underutilised if farm organisation is not adapted. Digital maturity should therefore be assessed at system level rather than by counting installed devices.

An emerging direction is the use of digital twins to represent a farm, crop or machine dynamically. Such a model is not simply a three-dimensional visualisation but a digital structure that is continuously updated with information from sensors, machines and management systems. In agriculture, a digital twin can combine soil, phenology, microclimate, input-use and machinery-status data to test scenarios before they are implemented in the field.

For example, the effect of a change in irrigation strategy or in the timing of field operations may be explored in terms of resource use and expected performance. Practical use requires reliable synchronisation between the real system and the model, sufficiently robust agronomic models and computational costs compatible with routine operation. Edge computing can complement the concept by processing data locally, reducing dependence on permanent cloud connectivity and shortening response time for critical operations.

The combination of digital models, local processing and connectivity may be particularly relevant on farms with uneven communication infrastructure or in processes that require rapid reaction.

Economic evaluation of digitalisation should extend beyond purchase price. Total cost of ownership includes hardware, software, licences, subscriptions, connectivity, calibration, maintenance, training, consumables, updates and possible integration costs with existing systems.

Benefits are also not always expressed directly as higher yield. Part of the value may arise from fewer overlaps, lower fuel consumption, reduced administrative workload, avoided losses, better traceability or more efficient allocation of labour.

Sound investment decisions therefore require comparison of the digital scenario with the baseline over several years while considering the actual utilisation rate of the system. A high-performance technology

used only a few days per year may have a longer payback period than a simpler tool used every day. Investment size should consequently be related to farm area, annual operating hours, technological intensity and the possibility of using the solution across several crops or operations.

The human factor remains decisive. Introducing a digital platform changes workflows, responsibilities and communication within the farm. Operators need to understand not only how to start a system but also what alerts mean, when a recommendation needs verification and how to proceed in the event of failure. Managers require skills for interpreting indicators and distinguishing normal variability from a genuine problem. Effective implementation includes written procedures, practical training, assignment of responsibilities and a transition period during which the digital system operates in parallel with the existing method.

This makes it possible to identify errors and adjust thresholds without disrupting production. Technology acceptance increases when users observe a concrete advantage and when the interface reduces rather than complicates daily tasks. This helps explain why software ergonomics, technical support and training quality may influence the final result as strongly as sensor accuracy or algorithm performance.

From a sustainability perspective, evaluation should include both reductions in agricultural inputs and the energy and material costs of the digital infrastructure itself. Sensors, servers, communications, batteries and robots consume energy and create material flows. Net benefit depends on equipment lifetime, repairability and reuse, energy source and the actual resource savings achieved in production.

In applications involving artificial lighting or intensive data processing, energy use may become significant. Conversely, fewer field passes, optimised fertiliser and crop-protection use and improved water management can reduce environmental impacts.

The appropriate perspective is therefore life-cycle and resource-balance based, in which digitalisation is justified by the total outcome rather than by the novelty of the technology. This approach is important for the transition from Agriculture 4.0, centred on connectivity and automation, toward systems in which technical performance is explicitly linked to resilience, resource efficiency and sustainability objectives.

## CONCLUSIONS

Digital agriculture should be understood as a transformation of sensing, decision-making and execution rather than as the simple introduction of electronic equipment. IoT sensors, remote sensing, UAVs, Big Data, AI, FMIS, variable-rate application and autonomous systems form a functional chain in which each component gains value through integration with the others. The most useful architecture is a closed loop: the process is measured, data are validated and analysed, a decision is formulated, the intervention is executed and the result is measured again.

The reviewed literature indicates substantial potential to reduce water, fertiliser, pesticide, fuel and labour use while improving productivity and traceability. Reported effects nevertheless vary widely across crops and production systems, and direct extrapolation should be avoided. Economic performance must be assessed locally using baseline indicators defined before investment and repeated measurements over successive seasons. The most reliable benefits are obtained when digitalisation is directed toward a real and measurable farm problem.

Interoperability and data governance are as important as sensor or algorithm performance. Data portability, standardisation, cybersecurity, access rights and the possibility of integrating different platforms should be included in technical specifications for future investments. Operator and manager training remains essential: automation does not eliminate the need for competence but shifts it from manual operation toward interpretation of information and supervision of complex systems.

For farms with limited resources, a modular transition is recommended, starting with digital recordkeeping and monitoring, progressing to decision support and precision application, and moving toward autonomy only where it is economically and technically justified. Under this approach, digital agriculture can contribute simultaneously to productivity, efficiency, sustainability and resilience.

The next stage of development will be deeper integration of sensors, AI and autonomous machines, supported by open standards and governance mechanisms that preserve farmers' control over their data and decisions.

## ACKNOWLEDGEMENTS

This paper was financed by MINISTRY OF AGRICULTURE AND RURAL DEVELOPMENT – ROMANIA - MADR – Sectorial Project ADER 25.2.2 /18.07.2023 Vertical Aquaponic Farm Adapted To

Current Climate Changes and Ministry of Research, Innovation and Digitalization through Program NUCLEU 9N/ 01.01.2023 - PROJECT PN 23 04 01 03.

## REFERENCES

[1] Alahmad T., Neményi M., Nyéki A. (2023). Applying IoT Sensors and Big Data to Improve Precision Crop Production: A Review. Agronomy, 13(10), 2603. doi:10.3390/agronomy13102603.

[2] Arfasa G.F., Tilahun Z.A. (2026). Advancing digital and climate-smart agriculture for sustainable and resilient food systems: A systematic review and future research directions. Information Processing in Agriculture, in press. doi:10.1016/j.inpa.2026.08.001.

[3] Basir M.S., Buckmaster D., Raturi A., et al. (2024). From pen and paper to digital precision: a comprehensive review of on-farm recordkeeping. Precision Agriculture, 25, 2643-2682. doi:10.1007/s11119-024-10172-7.

[4] Delfani P., Thuraga V., Banerjee B., et al. (2024). Integrative approaches in modern agriculture: IoT, ML and AI for disease forecasting amidst climate change. Precision Agriculture, 25, 2589-2613. doi:10.1007/s11119-024-10164-7.

[5] Dibbern T., Romani L.A.S., Massruhá S.M.F.S. (2024). Main drivers and barriers to the adoption of Digital Agriculture technologies. Smart Agricultural Technology, 8, 100459. doi:10.1016/j.atech.2024.100459.

[6] Fountas S., Carli G., Sørensen C.G., Tsiropoulos Z., Cavalaris C., Vatsanidou A., Liakos B., Canavari M., Wiebensohn J., Tisserye B. (2015). Farm management information systems: Current situation and future perspectives. Computers and Electronics in Agriculture, 115, 40-50. doi:10.1016/j.compag.2015.05.011.

[7] Fountas S., Espejo-García B., Kasimati A., Mylonas N., Darra N. (2020). The Future of Digital Agriculture: Technologies and Opportunities. IT Professional, 22(1), 24-28. doi:10.1109/MITP.2019.2963412.

[8] Guebsi R., Mami S., Chokmani K. (2024). Drones in Precision Agriculture: A Comprehensive Review of Applications, Technologies, and Challenges. Drones, 8(11), 686. doi:10.3390/drones8110686.

[9] Klerkx L., Jakku E., Labarthe P. (2019). A review of social science on digital agriculture, smart farming and agriculture 4.0: New contributions and a future research agenda. NJAS - Wageningen Journal of Life Sciences, 90-91, 100315. doi:10.1016/j.njas.2019.100315.

[10] Liakos K.G., Busato P., Moshou D., Pearson S., Bochtis D. (2018). Machine Learning in Agriculture: A Review. Sensors, 18(8), 2674. doi:10.3390/s18082674.

[11] Liu L., Yang F., Liu X., Du Y., Li X., Li G., Chen D., Zhu Z., Song Z. (2024). A review of the current status and common key technologies for agricultural field robots. Computers and Electronics in Agriculture, 227, 109630. doi:10.1016/j.compag.2024.109630.

[12] MacPherson J., Voglhuber-Slavinsky A., Olbrisch M., Schöbel P., Dönitz E., Mouratiadou I., Helming K. (2022). Future agricultural systems and the role of digitalization for achieving sustainability goals. A review. Agronomy for Sustainable Development, 42, 70. doi:10.1007/s13593-022-00792-6.

[13] Mulla D.J. (2013). Twenty five years of remote sensing in precision agriculture: Key advances and remaining knowledge gaps. Biosystems Engineering, 114(4), 358-371. doi:10.1016/j.biosystemseng.2012.08.009.

[14] Nahiyoon S.A., Ren Z., Wei P., et al. (2024). Recent Development Trends in Plant Protection UAVs: A Journey from Conventional Practices to Cutting-Edge Technologies-A Comprehensive Review. Drones, 8(9), 457. doi:10.3390/drones8090457.

[15] Papadopoulos G., Arduini S., Uyar H., Psiroukis V., Kasimati A., Fountas S. (2024). Economic and environmental benefits of digital agricultural technologies in crop production: A review. Smart Agricultural Technology, 8, 100441. doi:10.1016/j.atech.2024.100441.

[16] Qu J., Zhang Z., Qin Z., Guo K., Li D. (2024). Applications of Autonomous Navigation Technologies for Unmanned Agricultural Tractors: A Review. Machines, 12(4), 218. doi:10.3390/machines12040218.

[17] Rose D.C., Chilvers J. (2018). Agriculture 4.0: Broadening Responsible Innovation in an Era of Smart Farming. Frontiers in Sustainable Food Systems, 2, 87. doi:10.3389/fsufs.2018.00087.

[18] Rouzky R., Sarrafzadeh A., Sowells-Boone E., Pasandi H.B., Goins G. (2026). Data governance in smart farming: A systematic review of challenges and gaps. Information Processing in Agriculture, 13(2), 303-317. doi:10.1016/j.inpa.2025.11.006.

[19] Saini A.K., Yadav A.K., Dhiraj. (2025). A comprehensive review on technological breakthroughs in precision agriculture: IoT and emerging data analytics. European Journal of Agronomy, 163, 127440. doi:10.1016/j.eja.2024.127440.
[20] Sharma K., Shivandu S.K. (2024). Integrating artificial intelligence and Internet of Things (IoT) for enhanced crop monitoring and management in precision agriculture. Sensors International, 5, 100292. doi:10.1016/j.sintl.2024.100292.
[21] Soussi A., Zero E., Sacile R., Trinchero D., Fossa M. (2024). Smart Sensors and Smart Data for Precision Agriculture: A Review. Sensors, 24(8), 2647. doi:10.3390/s24082647.
[22] Urdu D., Berre A.J., Sundmaeker H., Rilling S., Roussaki I., Marguglio A., Doolin K., Zaborowski P., Atkinson R., Palma R., Faraldi M., Wolfert S. (2024). Aligning interoperability architectures for digital agri-food platforms. Computers and Electronics in Agriculture, 224, 109194. doi:10.1016/j.compag.2024.109194.
[23] Wolfert S., Ge L., Verdouw C., Bogaardt M.J. (2017). Big Data in Smart Farming - A review. Agricultural Systems, 153, 69-80. doi:10.1016/j.agsy.2017.01.023.

# THE EFFECTS OF CLIMATE CHANGE ON THE PRODUCTIVITY AND SUSTAINABILITY OF THE VEGETABLE SECTOR

/

# *EFECTELE SCHIMBĂRILOR CLIMATICE ASUPRA PRODUCTIVITĂȚII ȘI SUSTENABILITĂȚII SECTORULUI LEGUMICOL*

**Iulian VOICEA*[1)], Iuliana GAGEANU[1)], Florin NENCIU[1)], Cătălin PERSU[1)], Dan CUJBESCU[1)], Remus OPRESCU[1)], Roxana ZAHARIA[2)], Viorel FĂTU[2)], Corina MOGA[3)], Vlad-Nicolae ARSENOAIA[4)], Diana STEGARUS (POPESCU)[5)]**

[1)] INMA Bucharest / Romania;
[2)] ICDPP Bucharest / Romania;
[3)] DFR SYSTEMS Bucharest / Romania;
[4)] Faculty of Agriculture, "Ion Ionescu de la Brad" University of Life Sciences, Iași, Iasi County / Romania;
[5)] ICSI Râmnicu Vâlcea, Vâlcea County / Romania.
**E-mail: voicea_iulian@yahoo.com; *Tel.: +40 752 161 780*

***Keywords:*** *climate change; vegetable production; heat stress; drought; precision irrigation; adaptation; sustainability.*

## ABSTRACT

Climate change affects multiple economic sectors, but the agricultural sector is among the most exposed, as agricultural activities depend directly on climatic factors. The progression of climate change over the last two decades within Romania's agro-ecological zones indicates an intensification of negative impacts on agricultural production—including the vegetable-growing sector—driven by the occurrence of devastating meteorological events. These include extreme temperatures, frequent and catastrophic droughts, heavy downpours, floods, and winters characterized by minimal precipitation and above-freezing temperatures; such conditions promote the proliferation of diseases and pests, including the emergence of invasive harmful organisms. The agricultural sector will continue to be significantly affected, as the cultivation of high-yielding varieties and hybrids—selected for superior taste or specific processing and consumption traits—has narrowed the genetic resistance of vegetable crops to environmental stressors. Human activity has reduced the range of vegetable varieties that had evolved over time to adapt to environmental risks; through the directed process of evolution, humans have limited the use of these varieties as sources of germplasm. Adaptation strategies must be validated locally, taking into account water and energy consumption, as well as costs.

## *REZUMAT*

Schimbările climatice afectează multiple sectoare economice, dar sectorul agricol este unul din- tre cele mai expuse, deoarece activităţile agricole depind în mod direct de factorii climatici. Evoluţia schimbărilor climatice din ultimele două decenii în arealul agroecologic al Romaniei, denotă intensificarea efectelor negative asupra producţiei agricole, inclusiv al sectorului de legumicultură, prin influenţa și manifestarea de evenimente meteorologice devastatoare, ca: temperaturi extreme, secete frecvente și catastrofale, ploi cu averse, inundaţii, ierni cu minim de depuneri atmosferice și temperaturi pozitive, care intensifică proliferarea bolilor și dăunătorilor, inclusiv apariţia de organisme dăunătoare invazive. Sectorul agricol va fi și în continuare deosebit de afectat, deoarece introducerea în cultură a soiurilor și hibrizilor înalt productivi și cu caracteristici înalte gustative sau tehnologice de consum şi procesare a îngustat rezistenţa genetică a specimenelor legumicole la factorii de mediu. Sub acţiunea antropică s-a redus spectrul de specimene legumicole ce au evoluat în timp și care s-au acomodat la factorii de risc de mediu, omul singur în procesul dirijat al evoluţiei a mărginit utilizarea acestora ca surse de germoplasmă. Adaptarea trebuie validată local, ținând seama de consumul de apă, energie și costuri.

## INTRODUCTION

Vegetable crops are among the agricultural systems most sensitive to climatic conditions due to their relatively short production cycles, high commercial quality requirements, and vulnerability of their reproductive and edible organs. Their contribution to dietary diversity and nutritional security makes the stability of vegetable supply a strategic objective. Unlike certain field crops, vegetables are frequently marketed as fresh produce; therefore, even when biological yield is maintained, defects in colour, firmness,

shape, or appearance can substantially reduce marketable yield. Climate-related risks must be assessed through three interrelated dimensions: biological yield, marketable yield, and resource-use efficiency (*Bisbis et al., 2018; Dumitru et al., 2023; Zhou et al., 2024*).

Temperature is a major environmental factor influencing a wide range of vital physiological processes in vegetable crops, including seed germination, plant growth, flowering, fruit development, the duration of dormancy, as well as photosynthesis, respiration, transpiration, and other physiological processes that occur only within specific temperature ranges. The length of the growing season is also largely influenced by temperature. Thus, in regions characterised by higher temperatures, crop establishment can take place earlier, the growing period is generally shorter, and harvesting can begin sooner (*Hatfield and Prueger, 2015*).

However, excessively high or low temperatures negatively affect the growth, development, and fruiting of vegetable crops. High temperatures can cause excessive stem elongation, increased transpiration rates, reduced carbohydrate accumulation due to intensified respiration, and disturbances in pollination and fertilisation processes, particularly in fruit-bearing vegetable species. During the night, excessively high temperatures may interfere with carbohydrate mobilisation and translocation from leaves to growing and storage organs by affecting starch degradation and its conversion into soluble sugars.

In certain vegetable species, exposure to excessively high temperatures may inhibit the proper development of edible organs, as observed in lettuce, radishes, kohlrabi, early cabbage, and other temperature-sensitive crops. Conversely, low temperatures reduce respiration rates and consequently decrease the consumption of assimilates produced during the daytime. Prolonged exposure to low temperatures extends the growing season and delays crop maturity and harvesting.

As temperatures continue to rise beyond the physiological optimum, plants may experience metabolic and physiological disturbances, including increased respiration and catabolic activity, reduced photosynthetic assimilation, depletion of energy reserves, destabilisation of cellular colloidal systems, and ultimately cellular and tissue damage. Similarly, prolonged exposure to temperatures near the minimum threshold for growth results in weak and poorly developed plants, while temperatures below the species-specific tolerance limits may lead to irreversible injury and plant death *(Li et al., 2026).*

A more comprehensive understanding of the relationship between vegetable crops and temperature regimes can be achieved by examining specific physiological and developmental indicators. These include plant responses to air temperature, particularly the temperature requirements and thresholds associated with photosynthesis, vegetative growth, development, flowering, and fruit production.



**Fig. 1 - Response of eggplant / cucumber plants to daily temperature fluctuations**

Air temperature largely determines the intensity of photosynthetic activity and influences plant morphogenesis, growth rates, and development. Critical air temperatures represent positive or negative deviations from the optimal temperature ranges required for the normal physiological and vegetative processes of vegetable crops. These deviations constitute thermal risk factors that may lead to significant yield losses and, in extreme cases, complete crop failure, particularly when combined with water deficit.Air temperature directly influences leaf temperature and the temperature of other plant organs. Consequently, significant differences may occur between ambient air temperature and leaf temperature. These differences depend on the morphological and anatomical characteristics of the leaves, their orientation relative to solar radiation, canopy density, and other environmental and growing conditions (*Shah et al., 2024*).

Higher leaf temperatures are generally observed in vegetable crops and cultivars characterised by thick leaves. Under overheating conditions, relatively large temperature differences between leaves and the surrounding air, with leaf temperatures remaining lower than ambient temperatures, may occur in crops and

cultivars with deeply dissected or glossy leaves. Significantly higher temperatures are frequently recorded in crops cultivated under protected conditions, such as greenhouses and plastic tunnels (Fanourakis et al., 2025). Leaf temperature may increase considerably, particularly in early spring, when prolonged cloudy periods are suddenly followed by intense solar radiation. Such abrupt changes in environmental conditions can cause severe physiological stress and, in some cases, substantial damage to vegetable plants.

A sudden transition from low to high light intensity may induce physiological stress at the chloroplast level, commonly associated with photoinhibition or light-induced damage to the photosynthetic apparatus. The severity of this damage is generally greater under elevated temperature conditions. Plants require a certain acclimation period to adapt to changes in light intensity, whether increasing or decreasing. For example, tomato plants previously grown under light intensities of 3 or 6 kilolux (klx) may require approximately 8–10 days to acclimate to light intensities exceeding 15 klx.

Temperature also plays a crucial role in fruit and seed formation in vegetable crops. In many species, excessively low or high temperatures during pollination may cause pollen sterility, poor fruit set, reduced seed formation, and decreased fruit production. The reproductive stage is generally more sensitive to temperature stress than the vegetative stage (*Laxman et al., 2024*).

Increasing temperatures may damage reproductive organs before or during flowering, thereby reducing reproductive success and crop productivity. The effects of different temperature levels (20, 25, 30, 35, 40, and 45 °C) on pollen germination and pollen tube growth have been investigated in melon (Cucumis melo L.). The highest pollen germination percentage (64.33%) was recorded at 30 °C, whereas the lowest value (11.5%) was observed at 45 °C.

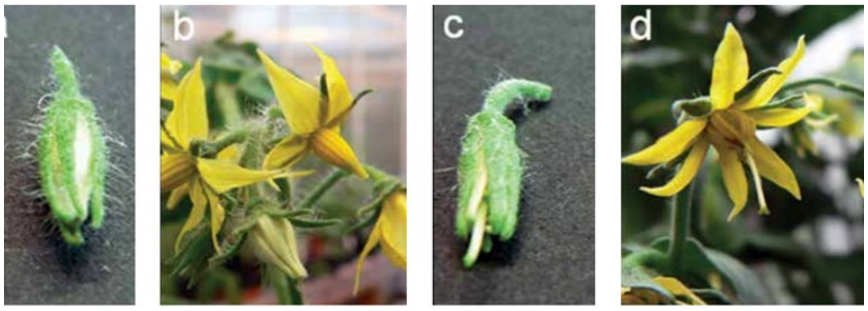



**Fig. 2 - Phenotypic Changes in Tomato Flowers Exposed to Prolonged Heat Stress Conditions**

Vegetable crops are frequently affected by late spring frosts and hoarfrost events. Cold-tolerant vegetable species may withstand temperatures of -5 to -8 °C, provided that the plants have been properly hardened and are well rooted. In contrast, cold-sensitive species, such as solanaceous crops, cucurbits, and beans, may die when temperatures drop to 0 °C, even under the mildest frost conditions (Novac et al., 2021).

Late spring frosts and hoarfrost, as well as early autumn frosts, occur under the influence of incoming cold polar air masses, which cause a sudden drop in air temperature, combined with continuous nocturnal cooling resulting from intense radiative heat loss. In most cases, this cooling is associated with rainfall or even sleet; however, the real frost hazard occurs only after skies clear, and it is usually more pronounced during the second or third night after the rains have ceased. The explanation for this phenomenon lies in the high specific heat capacity of water derived from precipitation, which acts as a protective factor against frost and hoarfrost.

Low temperatures, late spring frosts, and early autumn frosts may cause serious damage to vegetable crops. Frost injury to plants is difficult to predict, as it may range from leaf damage to the complete death of plant tissues. Of particular importance is the issue of chilling tolerance and frost resistance in vegetable plants. Chilling tolerance refers to the ability of vegetable crops to withstand low positive temperatures for a prolonged period of time (0–10 °C). Frost resistance refers to the ability of vegetable crops to survive temperatures below 0 °C, and in this case winter hardiness is also relevant (IPCC, 2022).

Early or late frost events are generally less harmful when they occur shortly after the resumption of plant growth and during developmental stages characterised by reduced intensity of vital physiological processes. Plant injury also depends on tissue water content, air humidity, light conditions, and other environmental factors. Thus, the plants or plant organs whose tissues contain higher amounts of water and lower concentrations of sugars are usually affected first.

The impact of extreme temperatures causes both reversible and irreversible changes in plants. Even when plant activity is fully restored, productivity declines and yield losses increase. In some cases, irreversible effects on vital physiological processes may also occur as a consequence of the secondary effects of stress conditions. Frost damage and plant death are associated with the coagulation (freezing) of water inside the cells. When ice forms in the intercellular spaces, cells die as a result of dehydration and mechanical injury caused by ice crystals (Fig. 3).



**Fig. 3 - Frost Damage in Pepper (a) and Tomato (b) Plants.**

## MATERIALS AND METHODS

All extreme meteorological phenomena occurring as a result of global warming are particularly harmful, both in their magnitude and, above all, through the disasters they may cause. Under the conditions of our country, drought is a specific climatic feature with major implications for agriculture. This phenomenon is caused by the absence of precipitation over prolonged periods. Drought is one of the most dangerous natural phenomena, representing a characteristic feature of the regional climate, conditioned by the uneven distribution of atmospheric precipitation in time and space against a background of high air temperatures. The annual decrease in precipitation, associated with rising temperatures, leads to a severe moisture deficit and a high frequency of droughts, strongly affecting the vegetable-growing sector. The negative effects of droughts depend not only on their duration but also on when they occur. Droughts occurring in April and May are dangerous because they delay soil preparation and the establishment of spring crops, whereas during the summer months they hinder plant growth and development (*IPCC, 2023; Novac et al., 2021*).

For perennial vegetable crops, soil moisture reserves in spring are important. When vegetation resumes, these crops already have a well-developed root system, allowing them to use soil water reserves much more efficiently. Therefore, the development of atmospheric drought during subsequent growth and development stages does not substantially influence the yields of these crops. The intensity of heat stress during June–August is highlighted by the sum of daily maximum air temperatures ≥ 32 °C. The limit of 32 °C represents the critical biological threshold for maximum air temperature beyond which the physiological optimum for the growth and development of agricultural crops is affected, the intensification of biological processes being directly correlated with the intensity of the “heatwave” phenomenon and the lack of water in the soil (soil drought). Thus, maximum air temperatures above the critical biological threshold of 32 °C, associated with moisture deficits in the air (atmospheric drought) and soil (soil drought), intensify thermal and water stress, with severe effects on plant growth and development (*Hatfield and Prueger, 2015; Novac et al., 2021*).

Given the high production costs of vegetables, very substantial economic losses may occur when production takes place under drought conditions. Normal growth and development processes can occur only in the presence of a certain amount of water. The importance of water derives from its role as a constituent element, a medium for biochemical and physiological reactions, and a means of transporting mineral substances and synthesised compounds. Water regulates plant temperature in hot weather through transpiration and evaporation (*Allen et al., 1998*). The edible parts of certain vegetable species (lettuce, spinach, orache, dill, cucumbers, etc.) readily lose their turgidity in the absence of water, acquire a wilted appearance, and lose freshness due to the development of mechanical tissues and the accumulation of alkaloids, thus reducing their commercial quality. In some crops (kohlrabi, carrots, radishes, cabbage), alternating dry periods and periods of excess moisture cause the edible parts to crack.

Large fluctuations in both atmospheric and soil moisture have an unfavourable impact on all vegetable species. Low air humidity intensifies plant respiration, resulting in wilting (Fig. 4), which primarily affects young plant organs. It affects pollination by causing the liquid on flower stigmas to disappear, making pollen grain germination difficult and incomplete. It favours the emergence and multiplication of certain

diseases and pests. Atmospheric humidity is very important for the growth and development of vegetable crops. Relative air humidity is managed according to the requirements of individual vegetable species (*Bisbis et al., 2018*).



**Fig. 4 - Wilting of cucumber plants under the effect of soil drought**

Soil moisture deficit also leads to a loss of plant turgidity and the appearance of wilting. Wilting may occur daily during the hours when outdoor temperatures are high, but in such situations it is temporary and does not cause harmful effects on plants. Prolonged wilting results from disturbances in water circulation caused by severe soil cooling, excess mineral salts in the soil, or a prolonged moisture deficit. The phenomenon is manifested by a gradual reduction in synthesis processes; ageing of hydrophilic colloids; progressive degradation of plastids; a two- to threefold increase in respiration; poor flower development and pollen formation; and disruption of fertilisation. When wilting becomes permanent and continues for several days, it becomes harmful to plants and may lead to crop failure. Similar effects may occur following sprinkler irrigation with cold water on hot days. Water deficit in plants may also result from applying excessive quantities of mineral substances. A high concentration of the soil solution is avoided through appropriate fertilisation and by maintaining soil water within normal limits. Under drought conditions, root system growth is inhibited, a process that may be caused by reduced assimilation, blockage of the transport of assimilates from leaves to roots and metabolites from roots to leaves, or increased rigidity of cell walls. The reduction of the assimilating surface and tissue dehydration have a significant negative impact on overall plant growth *(Shah et al., 2024).* In open-field vegetable cultivation, atmospheric drought poses a risk in addition to soil drought. Atmospheric drought results from excessive transpiration caused by extreme heat or hot, dry winds, when relative air humidity reaches 10–20%. Even if sufficient water is present in the soil, the rate of absorption becomes lower than the rate of transpiration, thereby creating a water deficit in the plant. Atmospheric drought is especially harmful to leafy vegetables, but it may also cause dehydration of the growing tips of young leaves in all other vegetable species. By applying short-duration irrigation in the morning, the soil surface is kept moist, enabling water evaporation and an increase in atmospheric humidity.

Moisture requirements and the harmful effects of insufficient moisture according to species: Tomatoes – depending on the development stage, water consumption is relatively high, ranging from 0.2 to 2.0 L/day per plant. Plants tolerate short periods of drought relatively easily, especially if they have previously been “hardened” or originate from direct sowing. Optimal atmospheric humidity is 56–65%, while a decrease below 45% accentuates the phenomenon of longistyly and makes pollination and fruit set more difficult; it also greatly increases transpiration losses (*Novac et al., 2021*).

Peppers – the optimal soil moisture level at the beginning of the growing season is 60–65% of the active moisture interval (IUA) and 70–75% of the IUA during fruiting. Soil drought causes poor growth, flower drop, small and deformed fruits, and reduced production. Peppers have higher atmospheric humidity requirements, the optimal level being 70–80%, especially during flowering and fruit setting. Potatoes have high moisture requirements, which is why plants must be supplied continuously with water to avoid drought even for short periods. Drought affects plant growth and development, negatively influencing the number and size of tubers. During this period, soil moisture should be maintained at 70–80% of field capacity.

Cucumbers. Moisture has a major influence on cucumber growth and development. Plants have a transpiration capacity of over 100 m³/ha/day, which implies a relative air humidity of 80–90%, as well as a high absorption capacity to reduce excessive water loss through transpiration. Optimal soil moisture is 70–80% of field capacity. If soil and atmospheric humidity are low, vegetative growth decreases and fruits become deformed because of pollination deficiencies (*Novac et al., 2021*).

Cabbage has high moisture requirements, with daily water consumption, depending on the growth stage, ranging from 0.2–0.4 L to 2.0–2.5 L per plant. Until heads form, soil moisture should be maintained at 70–75% of field capacity. Fluctuations in soil moisture after head formation cause head cracking in certain cultivars.

Carrots – moisture requirements are moderate. The crop has high water requirements during germination, when water consumption is equal to the mass of the seeds, and during the root-thickening stage, when optimal soil moisture should be 70–80% of field capacity. Both drought and excess moisture are harmful, causing lignification and an increase in the essential oil content of the roots, which gives them an unpleasant taste.

In sweet corn, the critical period for water extends from tassel emergence until after grain filling. Lack of water during this period, or keeping plants wilted for 3–4 consecutive days, reduces yield. For this reason, irrigation is required during the dry period of July–August.

Most vegetable plants have high water requirements and are major water consumers. The requirements of vegetable crops for soil and atmospheric moisture are determined by the degree of root system development and the morphological and anatomical characteristics of the leaves. Consequently, important differences occur among vegetable species according to their root systems. In certain species – onion, lettuce, spinach, pepper, eggplant, and tomatoes grown from transplants – the root system is distributed in the superficial soil layer, resulting in higher water requirements compared with directly sown crops, whose root systems are deeper. As a result, directly sown plants can obtain water more easily and tolerate fluctuations in moisture more effectively (*Allen et al., 1998*).

Considering the dimensions and structure of plant root systems, vegetable species are divided into four groups:

- Plants capable of extracting water efficiently from the soil and consuming it intensively through evaporation – beet. This crop responds well to irrigation.
- Plants capable of extracting water efficiently but consuming it sparingly – watermelon, melon, pumpkin, sweet corn, carrots, parsley, tomatoes, peppers, and beans. The most resistant to water shortage are watermelon, melon, sweet corn, and beans; pumpkin is less resistant because it consumes large amounts of moisture through evaporation.
- Plants with a low capacity to extract water but which consume it inefficiently – different varieties of cabbage, cucumber, eggplant, radish, turnip, lettuce, spinach, dill, and celery. These crops have high water requirements and respond well to irrigation.
- Plants with a low capacity to extract water from the soil but which consume it efficiently – onion and garlic. Despite their relatively low water consumption, they require high soil moisture during the first half of the growing season.

Water consumption varies according to the growth stage, increasing from germination to harvest. Initially, daily consumption per plant is low (10–30 g), but it increases after the development of the absorption and assimilation systems, reaching maximum values in summer: 340 g for beans, 240 g for carrots, 480 g for early cabbage, and 640 g for tomatoes *(Novac et al., 2021*).

## RESULTS

Hail, as a natural phenomenon, is a form of precipitation consisting of atmospheric water particles that fall to the soil surface in the form of ice. More specifically, hail forms when raindrops pass through layers of air with low temperatures (below 0 °C) (*EEA, 2024*).



**Fig. 5 - Hailstones of different shapes and sizes**

Essentially, the causes of hail formation are determined by the characteristics of atmospheric circulation interacting with those of the underlying surface. The cold air mass displaces the warm air mass through dynamic convection, forcing it to rise rapidly, a movement also involving thermal convection during the period preceding cold-air advection. Raised above 5,000–6,000 m altitude (sometimes even 10,000–12,000 m), the warm air cools rapidly, causing water vapour to condense and freeze into “pellets”. Under these conditions, the first electrical discharges occur, preceding or accompanying the fall of hail and the onset of the storm. In most cases, hailstorms begin suddenly. The duration of hailstorms is inversely proportional to the size of the hailstones. The shorter their duration, the larger the hailstones and the greater the mechanical impact they exert.

Hail is a climatic hazard which, although relatively rare, may cause large-scale natural disasters within a short time, locally or regionally, depending on the path of the cumulonimbus cloud that generated it. Field studies and the specialist literature indicate that almost all hail events have caused substantial losses to agriculture in general and particularly to unprotected open-field vegetable crops. The most severe damage caused by hail includes: (a) destruction of the plant leaf surface (ranging from minimal or partial damage to complete destruction); (b) loss of the harvest due to damage to the commercial appearance of fruits and edible organs of vegetable crops (which may be partial, allowing processing, or total); and (c) formation of a persistent ice layer, resulting in freezing of cell sap, cessation of sap circulation, destruction of foliage, and complete loss of the crop (*Babu et al., 2024*).

Because hail occurs most frequently during the warm season, it strikes agricultural crops at different developmental stages, disrupting the normal course of their biological cycle. A single hail event during a critical stage of plant development may be sufficient to destroy the entire harvest.

Hail can cause severe damage under the following conditions:

- when it occurs in the middle of the growing season, striking vegetable crops during flowering, crop formation, ripening, etc.;
- when it is accompanied by strong winds; when hailstone diameter exceeds 10 mm;
- when the phenomenon lasts for a long time;
- when the density of hailstones per 1 m² is very high;
- when a persistent ice layer forms (lasting from several hours to several days), causing freezing of cell sap, cessation of sap circulation, destruction of the foliage, and loss of the harvest;
- when it occurs after long periods of drought, with dry soil lacking cohesion, favouring intense erosion processes;

Cultivated agricultural plants and their plant residues, including spontaneous plants growing nearby, traditionally known as weeds, represent two inseparable components of agroecosystems: desired plants and undesired plants. The first group produces edible vegetables, while the second produces only biodegradable plant waste; however, if properly managed, this waste can be used to obtain fertile soil or a good humus layer to increase vegetable yields. Plant waste does not disappear by itself; its decomposition necessarily involves the intensive development of microorganisms, especially microscopic fungi, whose spores may become a virulent dust. Thus, crop residues and weeds carry a great diversity of pathogens, which cause diseases in the first group of plants, while facilitating fermentation and their conversion back into soil in the second group (*Pugliese et al., 2024*).

All the groups of living organisms mentioned – cultivated agricultural plants, weeds, and fungi – move from their location when two decisive factors are present above or below them: moisture and heat. Therefore, in vegetable crops with a strictly seasonal (not even annual) growing cycle, the phenomenon of drought or the impact of climate change on increasing the virulence of diseases and pests is debatable. This is because planned yields are not obtained during drought; consequently, growers do not rely on natural rainfall and sunshine but intervene in the crops through frequent and abundant irrigation, together with a thermal agent for producing heat (boilers with pipes or hoses), while conserving heat as much as possible (greenhouses).

In this context, we present only the most relevant examples of pathogens causing diseases in agricultural plants through activation of the deposited or stored biological reserve, since a contaminated substrate forms on or in both: (*Pugliese et al., 2024*)

- powdery mildew (Erysiphe sp.);
- cucumber powdery mildew (Sphaerotheca fuliginea);
- cucumber fusariosis (Fusarium oxysporum sp. cucumis);
- cucumber downy mildew (Pseudoperonospora cubensis);

- tomato late blight (Phytophtora infestans), where fruit falling or coming into contact with the soil during the growing season leads to abundant sporulation of the pathogen, followed by infection of leaves, stems, and fruits;
- black leaf spot (Alternaria brassicae);
- tomato fruit rot (Rhizoctonia solani) – at 18–20 °C and 90% humidity, affected fruit itself becomes a source of infection within 2–3 days;
- tomato root, stem, and fruit rot (Colletotrichum coccodes);
- soft rot (Erwinia carotovora);
- • white rot of bulbs (Sclerotium cepivorum) – the biological reserve in the soil can survive for more than 20 years;
- grey rot of bulbs (Botrytis allii);
- grey mould in tomatoes (Botrytis cinerea) – causes damage at 15–20 °C and humidity of [value missing in the source]; sclerotia survive in the soil for 7–8 years;
- soft rot of crucifers (Erwinia carotovora); • verticillium wilt (Verticillium dahliae);
- tobacco mosaic virus – TMV (Tobacco Mosaic Virus).

Most pathogens become active and affect vegetable crops in the presence of favourable humidity and temperature, but these conditions coincide with those needed for agricultural crops. Very few diseases develop in dry, warm weather at +25–27 °C, such as cucumber powdery mildew (Sphaerotheca fuliginea). Similarly, two types of rot develop in acidic, compacted soils with stagnant water: soft rot (Erwinia carotovora) and dry rot (Leptosphaeria maculans) (*Pugliese et al., 2024*).

Plant residues and growing plants provide favourable conditions for the development of another natural factor that carries, like raindrops or irrigation water, inoculum from certain pathogens: nematodes, mites, and some insects, particularly those with piercing-sucking mouthparts, including greenhouse whiteflies, aphids, thrips, true bugs, etc. This natural factor – microfauna – is just as dangerous to vegetable crops as plant residues carrying phytopathological inoculum. Therefore, several relevant examples of diseases of vegetable plants that occur after insects simply pierce them for their own physiological hydration are presented below: (*Ma et al., 2025*)

- tomato spotted wilt disease (Tomato spotted wilt virus) – associated with western flower thrips (Frankliniella occidentalis);
- melon and cucumber mosaic (Marmor cucumeris) – transmitted by 60 species of aphids;
- wilt or fusariosis (Fusarium oxysporium f.sp. lycopersici) – via root nematodes in the soil;
- brown leaf spot (Fulvia fulva syn. Cladosporium fulvum) – via aphids;
- soft rot of leek (Erwinia carotovora) – via aphids;
- tomato septoria leaf spot (Septoria lycopersici) – via aphids;
- verticillium wilt (Verticillium dahliae) – via root nematodes;
- tobacco mosaic virus – TMV (Tobacco Mosaic Virus) – via aphids;
- onion yellow dwarf virus (Onion yellow dwarf virus) – via aphids;
- tomato yellow leaf curl virus (Tomato yellow leaf curl virus) – via tobacco whitefly.

The choice of cultivars is an important mechanism through which farmers can adapt to the effects of climate change, combined with alternative strategies such as adapting fertilisation, irrigation, soil cultivation, and crop-rotation measures. The development of new cultivars tolerant to high temperatures, resistant to pests and diseases, with short growing seasons and high yields under stress conditions, together with the adoption of high-performance technologies and judicious management of natural resources, are the main strategies to be implemented to address the many challenges and shortcomings caused by climate change.

The experience and practice of many vegetable-growing units have shown that new cultivars commonly achieve important yield increases of 15–30% (Laxman et al., 2024; Schwarz et al., 2010).

The introduction of cultivars and hybrids into production must meet several requirements:

- they should exhibit genetic resistance to as many pathogens as possible;
- they should be well adapted to natural light conditions so that the adverse influence of low light intensity on plant growth is minimised;
- they should mature early, providing the highest possible early yield; they should tolerate lower temperatures in spring (advantage: earlier crop establishment);
- they should exhibit good tolerance to drought and extreme heat, etc.;
- the produce should withstand transport and handling.

## CONCLUSIONS

Climate change affects the vegetable sector through interacting thermal, water-related, and biological mechanisms. High temperatures and water deficits may reduce photosynthetic activity, disrupt pollination and fruit set, and accelerate quality deterioration. Late frosts, hail, intense rainfall, and episodic waterlogging add important risks that may be overlooked by strategies focusing exclusively on summer heat.

A robust adaptation strategy must combine locally tested tolerant cultivars, diversified crop management, soil conservation, monitored irrigation, drainage, appropriate crop protection, protected cultivation, and risk-based phytosanitary surveillance. Digital sensors and decision-support systems are useful when they close the loop between measurement, intervention, and verification; their implementation should be gradual and assessed using economically relevant indicators.

Future research should use multiannual, species-specific experiments in open-field and protected cultivation to quantify marketable yield, water and energy productivity, quality losses, and the combined effects of heat, drought, and phytosanitary pressure. These data would enable scientifically grounded comparisons between conventional and climate-adapted technologies, supporting practical recommendations for Romania and the wider region.

Potential yield is determined by the cultivated variety or hybrid, specifically by the genetic endowment of the cultivated plant, which may be expressed to a greater or lesser extent depending on the influence of other production factors. Thus, all early-maturing vegetable varieties require larger amounts of water than late-maturing ones because they are characterised by faster growth and development rates and a higher plant density per unit area.

## ACKNOWLEDGEMENTS

*This paper was financed by MINISTRY OF AGRICULTURE AND RURAL DEVELOPMENT – ROMANIA - MADR – Sectorial Project ADER 25.2.2 /18.07.2023 Vertical Aquaponic Farm Adapted To Current Climate Changes and Ministry of Research, Innovation and Digitalization through Program NUCLEU 9N/ 01.01.2023 - PROJECT PN 23 04 01 04 "Intelligent plant growth systems under controlled environmental conditions".*

## REFERENCES

[1] Alahmad T., Neményi M., Nyéki A. (2023). Applying IoT Sensors and Big Data to Improve Precision Crop Production: A Review. Agronomy, 13(10), 2603. https://doi.org/10.3390/agronomy13102603.

[2] Allen R.G., Pereira L.S., Raes D., Smith M. (1998). Crop Evapotranspiration: Guidelines for Computing Crop Water Requirements. FAO Irrigation and Drainage Paper 56, Rome: FAO.

[3] Babu R.R., Baishya L.K., Reddy A.G.K., et al. (2024). Climate Change Effects on Sustainable Vegetable Production in India: A Review. International Journal of Environment and Climate Change, 14(3), 804–814. https://doi.org/10.9734/IJECC/2024/v14i34089.

[4] Bisbis M.B., Gruda N., Blanke M. (2018). Potential impacts of climate change on vegetable production and product quality – A review. Journal of Cleaner Production, 170, 1602–1620. https://doi.org/10.1016/j.jclepro.2017.09.224.

[5] Dumitru E.A., Berevoianu R.L., Tudor V.C., et al. (2023). Climate Change Impacts on Vegetable Crops: A Systematic Review. Agriculture, 13(10), 1891. https://doi.org/10.3390/agriculture13101891.

[6] European Environment Agency (EEA) (2024). European Climate Risk Assessment. EEA Report 01/2024. Copenhagen: EEA. https://www.eea.europa.eu/en/analysis/publications/european-climate-risk-assessment.

[7] Fanourakis D., Tsaniklidis G., Makraki T., et al. (2025). Climate Change Impacts on Greenhouse Horticulture in the Mediterranean Basin: Challenges and Adaptation Strategies. Plants, 14(21), 3390. https://doi.org/10.3390/plants14213390.

[8] FAO (2021). The State of the World's Land and Water Resources for Food and Agriculture: Systems at Breaking Point. Rome: Food and Agriculture Organization of the United Nations.

[9] Fountas S., Espejo-García B., Kasimati A., Mylonas N., Darra N. (2020). The Future of Digital Agriculture: Technologies and Opportunities. IT Professional, 22(1), 24–28. https://doi.org/10.1109/MITP.2019.2963412.

[10] Guebsi R., Mami S., Chokmani K. (2024). Drones in Precision Agriculture: A Comprehensive Review of Applications, Technologies, and Challenges. Drones, 8(11), 686. https://doi.org/10.3390/drones8110686.

[11] Hatfield J.L., Prueger J.H. (2015). Temperature extremes: Effect on plant growth and development. Weather and Climate Extremes, 10, 4–10. https://doi.org/10.1016/j.wace.2015.08.001.

[12] IPCC (2022). Climate Change 2022: Impacts, Adaptation and Vulnerability. Working Group II Contribution to the Sixth Assessment Report, Chapter 5: Food, Fibre and Other Ecosystem Products. Cambridge University Press. https://www.ipcc.ch/report/ar6/wg2/chapter/chapter-5/.

[13] IPCC (2023). Climate Change 2023: Synthesis Report. Contribution of Working Groups I, II and III to the Sixth Assessment Report. Geneva: IPCC. https://www.ipcc.ch/report/sixth-assessment-report-cycle/.

[14] Laxman R.H., Kumar R., Ramesh K.V., Saini D.R., Sreekanth D., Verma R.K., Behera T.K. (2024). Impact of Climate Change on Vegetable Production and Management Strategies. Vegetable Science, 51(Special Issue), 11–21. https://doi.org/10.61180/vegsci.2024.v51.spl.02.

[15] Li Y., Zhang X., Xia C., et al. (2026). Molecular mechanisms and breeding strategies for heat tolerance in vegetable crops under global warming. Horticulture Research, 13(2), uhaf309. https://doi.org/10.1093/hr/uhaf309.

[16] Liakos K.G., Busato P., Moshou D., Pearson S., Bochtis D. (2018). Machine Learning in Agriculture: A Review. Sensors, 18(8), 2674. https://doi.org/10.3390/s18082674.

[17] Ma C.-S., Wang B.-X., Wang X.-J., Lin Q.-C., Zhang W., Yang X.-F., van Baaren J., et al. (2025). Crop pest responses to global changes in climate and land management. Nature Reviews Earth & Environment, 6, 264–283. https://doi.org/10.1038/s43017-025-00652-3.

[18] MacPherson J., Voglhuber-Slavinsky A., Olbrisch M., et al. (2022). Future agricultural systems and the role of digitalization for achieving sustainability goals. A review. Agronomy for Sustainable Development, 42, 70. https://doi.org/10.1007/s13593-022-00792-6.

[19] Millán S., Montesinos C., Campillo C. (2024). Evaluation of Different Commercial Sensors for the Development of Their Automatic Irrigation System. Sensors, 24(23), 7468. https://doi.org/10.3390/s24237468.

[20] Nair C.S., Manoharan R., Nishanth D., Subramanian R., Neumann E., Jaleel A. (2025). Recent advancements in aquaponics with special emphasis on its sustainability. Journal of the World Aquaculture Society, 56(1), e13116. https://doi.org/10.1111/jwas.13116.

[21] Novac T., Fala A., Timuș A., Conovali V., Țurcan E. (2021). Bunele practici în legumicultură în contextul schimbărilor climatice: Ghid practic pentru producătorii agricoli. Chișinău: UCIP IFAD/ACSA, 160 p. ISBN 978-9975-87-789-3. (Documentul consultat: paginile PDF 1–50.)

[22] Papadopoulos G., Arduini S., Uyar H., Psiroukis V., Kasimati A., Fountas S. (2024). Economic and environmental benefits of digital agricultural technologies in crop production: A review. Smart Agricultural Technology, 8, 100441. https://doi.org/10.1016/j.atech.2024.100441.

[23] Pugliese M., Gilardi G., Garibaldi A., Gullino M.L. (2024). The Impact of Climate Change on Vegetable Crop Diseases and Their Management: The Value of Phytotron Studies for the Agricultural Industry and Associated Stakeholders. Phytopathology, 114(5), 843–854. https://doi.org/10.1094/PHYTO-08-23-0284-KC.

[24] Schwarz D., Rouphael Y., Colla G., Venema J.H. (2010). Grafting as a tool to improve tolerance of vegetables to abiotic stresses: Thermal stress, water stress and organic pollutants. Scientia Horticulturae, 127(2), 162–171. https://doi.org/10.1016/j.scienta.2010.09.016.

[25] Shah I.H., Manzoor M.A., Wu J., Li X., Hameed M.K., Rehaman A., Li P., et al. (2024). Comprehensive review: Effects of climate change and greenhouse gases emission relevance to environmental stress on horticultural crops and management. Journal of Environmental Management, 351, 119978. https://doi.org/10.1016/j.jenvman.2023.119978.

[26] Zhang X., Feng G., Sun X. (2024). Advanced technologies of soil moisture monitoring in precision agriculture: A Review. Journal of Agriculture and Food Research, 18, 101473. https://doi.org/10.1016/j.jafr.2024.101473.

[27] Zhou R., Jiang F., Liu Y., Yu X., Song X., Wu Z., Cammarano D. (2024). Environmental changes impact on vegetables physiology and nutrition – Gaps between vegetable and cereal crops. Science of the Total Environment, 933, 173180. https://doi.org/10.1016/j.scitotenv.2024.173180.

# MODERN TECHNOLOGIES FOR SOIL REGENERATION
# /
# *TEHNOLOGII MODERNE DE REGENERARE A SOLULUI*

**Aura-Maria DUMITRESCU[1)], Vasilica STEFAN*[1)], Stefano-Andrea MANTOVANI[1)], Alex-Nicolae COLESI[2)], Maria-Magdalena DOBRE[2)]**

[1)] National Institute of Research-Development for Machines and Installations Designed for Agriculture and Food Industry-INMA Bucharest / Romania;

[2)] National University of Science and Technology Politehnica Bucharest / Romania.

**E-mail: auradumitrescu252@gmail.com*

***Keywords:*** *soil regeneration, minimum tillage, no-tillage, strip-tillage, soil compaction, precision agriculture.*

## ABSTRACT

*Soil degradation, manifested through erosion, compaction, and the decline in organic matter, represents a major challenge for sustainable agriculture. This paper analyzes modern soil regeneration technologies, focusing on the design and functional characteristics of machinery used in minimum tillage, no-tillage, and localized tillage systems such as strip-tillage. The methodology is based on a narrative review of published scientific studies, examining the relationships between the intensity of soil disturbance, crop residue management, machinery traffic, and the preservation of soil properties. The findings of the reviewed studies highlight the potential of reduced-disturbance systems to limit surface runoff and soil losses caused by erosion. However, the effectiveness of these technologies depends on soil and climatic conditions, machinery settings, axle load, tire pressure, and the number of field passes. Preserving soil organic matter requires the retention of crop residues and the integration of complementary practices, such as crop rotation and the use of cover crops. It is concluded that the appropriate selection and operation of agricultural machinery can contribute to soil regeneration within an integrated agricultural management system, whose effects should be assessed using specific indicators and long-term monitoring.*

## REZUMAT

*Degradarea solului, manifestată prin eroziune, compactare și diminuarea materiei organice, reprezintă o provocare majoră pentru agricultura durabilă. Lucrarea analizează tehnologii moderne de regenerare a solului, cu accent pe caracteristicile constructive și funcționale ale utilajelor utilizate în sistemele de lucrări minime, semănat direct și lucrări localizate de tip strip-tillage. Metodologia se bazează pe o sinteză narativă a studiilor științifice publicate, urmărind relația dintre intensitatea perturbării solului, gestionarea resturilor vegetale, traficul utilajelor și conservarea proprietăților solului. Rezultatele studiilor analizate evidențiază potențialul sistemelor cu perturbare redusă de a limita scurgerea de suprafață și pierderile de sol prin eroziune. Totodată, eficiența acestor tehnologii depinde de condițiile pedoclimatice, reglajele utilajelor, sarcina pe osie, presiunea pneurilor și numărul de treceri. Conservarea materiei organice necesită menținerea resturilor vegetale și integrarea unor practici complementare, precum rotația culturilor și utilizarea culturilor de acoperire. Se concluzionează că selectarea și exploatarea corespunzătoare a utilajelor agricole pot contribui la regenerarea solului, în cadrul unui sistem integrat de management agricol, ale cărui efecte trebuie evaluate prin indicatori specifici și monitorizare pe termen lung.*

## INTRODUCTION

As the foundation of agricultural output and a vital component of terrestrial ecosystems, soil is one of the most significant natural resources. Soil has a crucial role in ensuring food security, as evidenced by the fact that 98.8% of the food consumed globally is produced either directly or indirectly from it. At the same time, land and water resources are under more stress due to population growth and rising agricultural product demand (*Kopittke et al., 2019*).

Since soil offers a variety of ecosystem services, its significance goes beyond its role in production. Food, wood, fiber, and raw material production are examples of provisioning services; water filtering, pollutant and nutrient retention, flood mitigation, carbon storage, greenhouse gas regulation, and waste decomposition and nutrient recycling are examples of regulating services. Additionally, soil supports cultural services pertaining to heritage, recreation, and cultural identity *(Dominati et al., 2019)*.

The ability of soil health to adapt to agricultural interventions while maintaining crop productivity and ecosystem services is demonstrated. In addition to preserving vital processes including carbon transformations, nutrient cycling, soil structure maintenance, and pest and disease control, it depends on the interplay of physical, chemical, and biological characteristics. Soil condition cannot be evaluated with a single indicator since these processes are integrative. Rather, it is necessary to simultaneously monitor organic matter, pH, structure, moisture, nutrients, and biological activity *(Kibblewhite et al., 2008)*.

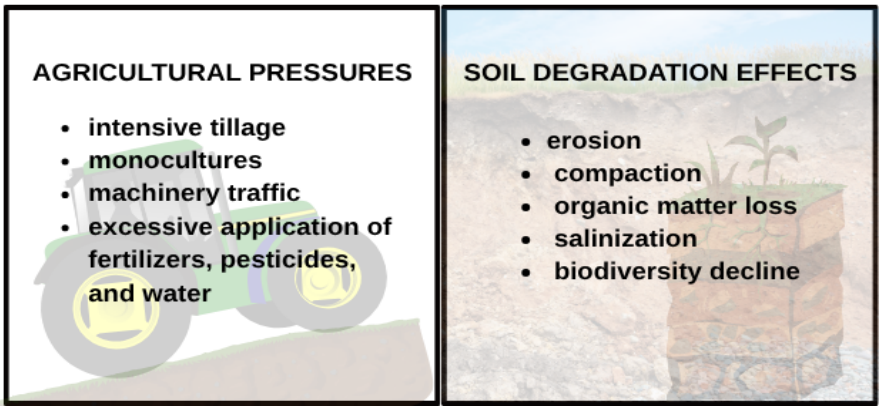



**Fig. 1 - Soil degradation: agricultural pressures and soil degradation effects**
*(Kibblewhite et al., 2008; Khangura et al., 2023; Musa et al. 2024; Obour and Ugarte, 2021)*

One of the primary causes of soil degradation is intensive agriculture. Organic matter loss, compaction, erosion, salinization, nutritional imbalances, and decreased biodiversity can result from repeated tillage, monoculture, uncontrolled mechanical traffic, improper irrigation, and excessive fertilizer application. Soil fertility, productivity, and its ability to deliver ecosystem services are all reduced by these processes. Over two billion hectares are impacted by various types of deterioration worldwide, and an estimated 75 billion tons of soil are lost each year due to erosion.

Technologies that can prevent degradation and restore soil functions are necessary under these circumstances. Soil structure, fertility, biological activity, and water-holding capacity can all be enhanced via conservation agriculture, crop rotation, cover crops, organic amendments, biochar, microbial biostimulants, and agroforestry systems. However, each area's characteristics and level of deterioration determine how effective these methods are.

| RA Principles | RA Practices | RA Benefits | Microbial Mechanisms |
|---|---|---|---|
| •Minimise soil disturbance<br>•Keep soils covered<br>•Keep living roots in soil year round<br>•Encourage diversity<br>•Integrate livestock | • No/minimum tillage<br>• Stubble retention<br>• Diverse crop rotations<br>• Multispecies cover crops<br>• Intercropping<br>• Composting and use biostimulants<br>• Rotational grazing<br>• Reduce synthetic inputs | • Improved soil health through<br>  • Increased soil carbon<br>  • Improved microbial functions and associated nutrient cycling<br>  • Improved soil moisture<br>  • Improved resilience to pests and diseases<br>• Nutrient rich food<br>• Reduced greenhouse gas emissions | •Liquid carbon pathway<br>•Improved uptake of water and minerals<br>•Enhanced soil aggregation, plant growth and photosynthesis |

**Fig. 2 - RA (Regenerative Agriculture) principles, practices, and purported benefits and mechanisms to improve soil health**
*Reproduced from (Khangura et al., 2023), Figure 1.*

Precision agriculture can support soil conservation by using spatial information to guide field operations and adapt interventions to local conditions. Within the tillage and seeding systems considered here, its relevance concerns the positioning of tilled strips and seed rows, the avoidance of unnecessary overlapping passes, and the organization of machinery traffic. Monitoring soil and crop variability provides a broader basis for site-specific management, while guidance and alignment translate this information into more consistent field operations *(Getahun et al., 2024)*.

The current evaluation concentrates on soil-working and seeding methods within this greater variety of regenerative approaches. Its purpose is to explore how reduced tillage, no-tillage, and strip-tillage, including precision guidance and residue management, may help limit erosion, compaction, and loss of organic matter. The design and operation of agricultural machinery, as well as the factors influencing its soil-protection performance, are presented.

## MATERIALS AND METHODS

This paper presents a narrative synthesis of published studies on minimum tillage, no-tillage, and strip-tillage. The analysis relates the technological characteristics of the equipment to three soil degradation processes: erosion, compaction, and organic matter decline. Quantitative findings are reported as results of the cited studies, with their comparative and contextual limitations, rather than as measurements obtained in the present work. Erosion, compaction, and the decrease of organic matter are degradation processes that impair soil health and productive potential. The literature on regenerative agriculture and tillage systems underlines the relationship between these processes, management methods, and the design characteristics of agricultural machinery. The application of agronomic principles and the mechanical tools used for field operations are both critical to soil conservation *(Kibblewhite et al., 2008; Musa et al., 2024; Khangura et al., 2023).*

The *minimum tillage*, *no-tillage*, and *strip-tillage* systems differ in terms of the soil surface area and depth affected, the proportion of crop residues retained on the soil surface, the number of operations, and the method used to prepare the seedbed. At the equipment level, these changes are associated with the type of active components, residue management, the construction of the seed slot or tilled strip, and control of seed placement depth. The degree of mechanical intervention in the soil is determined by the equipment's configuration and adjustment *(Dou et al., 2024).*

An example of the functional integration of strip-tillage operations is provided by the Mzuri Pro-Til system, which combines localized soil loosening, fertilizer application, and sowing in a single pass *(Jaskulska and Jaskulski, 2020).*

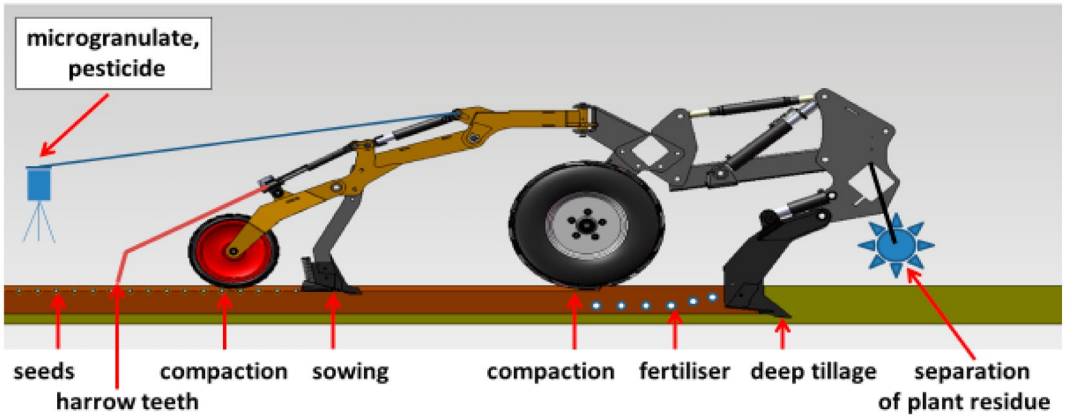



**Fig. 3 - Diagram of the agrotechnical practices performed with the use of Mzuri Pro-Til machine**
*(Jaskulska and Jaskulski, 2020)*

When evaluating erosion, crop residue cover, surface runoff, and sediment loss are pertinent indicators. Compaction can be characterized by bulk density and penetration resistance, in relation to machinery traffic. When it comes to organic matter, the carbon stock in the soil profile and the carbon concentration in the surface layer offer different kinds of information that must be interpreted by defining the bulk density and sampling depth *(Obour et al., 2021; Sun, Y. et al., 2015; Haddaway et al. 2017; Jacobs et al. 2010).*

The type of soil, crop, climate, length of practice implementation, and machinery setup all affect how tillage methods work. The direct comparison of results is limited by variations in measurement techniques and experimental settings. Rather than being regarded as generally applicable performance indicators for all fields, values provided in meta-analyses should be evaluated in reference to the systems being compared and the geographic area covered by the included research *(Obour et al., 2021; Sun et al., 2015; Haddaway et al., 2017; Jacobs et al., 2010).*

The synthesis is organized in three steps. First, soil disturbance and residue cover are considered in relation to runoff and sediment loss. Second, machinery traffic and operating conditions are examined in relation to compaction. Third, residue inputs and the duration of management practices are considered in

interpreting changes in organic matter. These findings are then brought together in a comparative table of equipment characteristics and operational requirements relevant to soil protection.

In order to help the interpretation of the operational trade-offs of systems, seedbed temperature, soil structural and biological indicators, energy requirements, and crop performance are also taken into account when reported by the selected studies.

## RESULTS

### 1. Erosion and the Area of Soil Disturbed

The main technological difference between the three systems is the spatial extent and location of soil disturbance. Depending on the implement and its settings, minimum tillage may disturb a large proportion of the surface while avoiding the intensity and inversion associated with conventional ploughing. In no-tillage, disturbance is concentrated in the seed slot, whereas strip-tillage prepares narrow zones corresponding to the future crop rows and leaves the inter-row areas largely undisturbed. The comparison must therefore consider the actual disturbed area and the residue cover remaining after the operation, rather than relying only on the name of the tillage system *(Lal, 1991; Jaskulska and Jaskulski, 2020).*

Cultivators with narrow shanks, chisels, or tools that integrate multiple actions can be used to carry out reduced tillage operations. The volume of soil displaced and the percentage of crop residues incorporated into the soil depend on the geometry of the tillage components and the working depth. When using direct seeders, the opener creates the seed slot while the cutting disk makes it easier to get through the crop residue layer *(Hoseinian et al., 2021).* Strip-tillage equipment adds extra components for residue control and localized preparation of the subsequent crop row. Soil protection therefore depends on the specific equipment configuration and the quality of its adjustment, rather than solely on the stated technological principle.

The degree of soil disturbance and seedbed conditions can both be affected by localized soil preparation. When compared to no-tillage, strip-tillage increases the temperature of the upper soil layer (0–5 cm) by about 1.2–1.4°C, bringing the temperature closer to what was observed during chisel plowing. An improved emergence rate index (ERI) reflects the improved germination and emergence circumstances brought about by this increase in soil temperature. However, there was no significant difference in soil moisture between the three regimes, and penetration resistance under strip-tillage was generally higher than under chisel plowing and comparable to that under no-tillage. These results show that reduced penetration resistance or notable variations in soil moisture are not always associated with better seedbed thermal conditions *(Licht and Al-Kaisi, 2005).*

According to a meta-analysis of published data from North American agricultural systems, minimum tillage decreased sediment loss by 64% and surface runoff by an average of 26% when compared to conventional tillage. In the comparison between conventional tillage and no-tillage, the reported reductions were 43% for runoff and 87% for sediment loss. It is not possible to immediately extend these values to different soil, slope, precipitation, or residue-management situations because they are aggregated data from the set of studies that the authors reviewed *(Fleming et al., 2025).*

Not all compounds carried by runoff will necessarily decrease if sediment loss decreases. Adoption of no-tillage decreased runoff and sediment loss, but it did not lower overall pesticide losses at the field edge in the same meta-analysis; pesticide concentrations in runoff water were greater. This result shows that a system's efficacy should be evaluated based on the particular indicator under consideration: limiting the transit of dissolved compounds and conserving soil particles are related but different goals *(Fleming et al., 2025).* The retention of crop residues on the soil surface is supported by the restriction of soil disturbance to narrow strips, which enhances soil protection and reduces erosion. Depending on the previous crop and row spacing, the strip-till one-pass method can retain between 62.7 and 82.0% of the residues from the previous crop. Additionally, in the conditions under investigation, this technique can reduce yearly soil loss by about 2.57–6.36 t $ha^{-1}$ when compared to traditional plough-based cultivation *(Jaskulska et al., 2020).*

### 2. Soil Compaction and Machinery Traffic

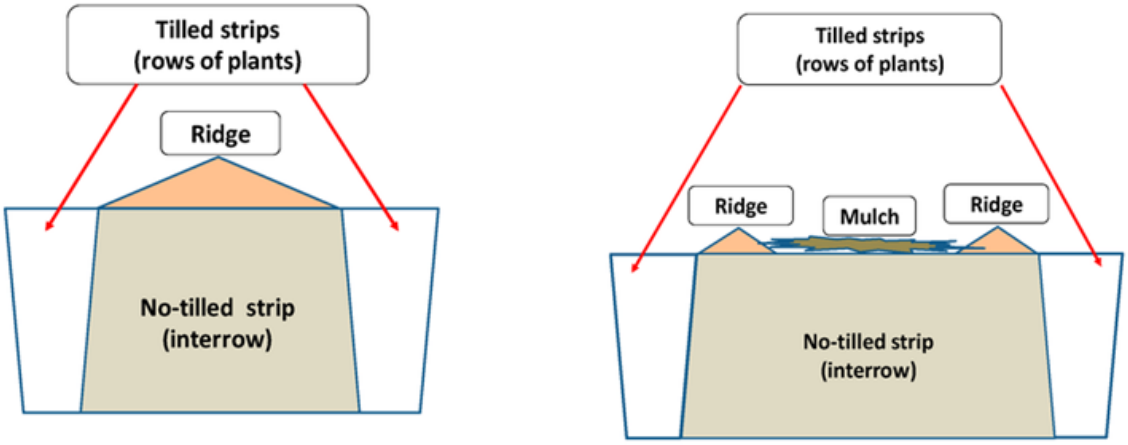
Reducing the number of field operations can lessen overall traffic, but none of the three tillage systems eliminates the pressures delivered to the soil by tractor and machinery wheels. Axle load, tire properties, number of passes, and soil moisture levels all affect soil compaction. Therefore, both the impact of active tillage components and the impact of machinery traffic over the field should be taken into account when evaluating machinery intended for soil preservation *(Yang et al., 2022; Vanderhasselt et al., 2024).*

Controlled traffic farming confines machinery passes to designated lanes, concentrating wheel-induced stresses in those areas and reducing traffic over the cropped soil between them. Its contribution to soil protection must be assessed together with axle load, tyre settings, soil moisture, and the number of passes. Prevention of repeated loading and measures intended to alleviate existing compaction address different stages of the problem. Their effectiveness varies with the depth and severity of compaction and with the agricultural system, so the expected benefits should be checked using appropriate soil physical indicators *(Yang et al., 2022; Antille et al., 2019).*

Combined implements can reduce the number of operations required for soil preparation. Soil quality and the placement of machinery traffic lanes in strip-tillage systems are both influenced by the precision of alignment between the seeder and the tool used to create the strips. In regions where compaction has been detected, localized soil loosening is a potential intervention; however, its application should be correlated with the depth of the affected layer and followed by soil property verification. These options arise from the design and operating principles of the machinery and do not, in the absence of measurements, constitute evidence of reduced compaction under all field conditions *(Yang et al., 2022).*

### 3. Organic Matter and Vegetative Cover

Retaining crop residues on the soil surface reduces soil exposure and retains a potential supply of organic matter. Direct seeders must get through the residue layer without sacrificing uniform seeding depth or forcing residues into the seed slot. Residues may be transferred from the prepared strip and persist in the spaces between rows in strip-tillage systems. When comparing the effects of tillage technologies on the soil, this distinct distribution needs to be explained *(Alvarez, 2024).*




a) b)

**Fig. 4 - Spatial arrangement of tilled strips and inter-row areas in strip-till one-pass technology: (A) 36 cm strip spacing; (B) 72 cm strip spacing.**

*(Jaskulska et al., 2020)*

Improvements in soil structure and biological activity are further advantages of less soil disturbance. When compared to traditional tillage, strip-till one-pass cultivation can boost the stability of 0.25–2.0 mm soil aggregates by about 12.7% and the glomalin content by 0.08 g $kg^{-1}$. Additionally, there may be a five-fold increase in earthworm biomass along with a rise in bacterial and fungal populations. When evaluating the sustainability and efficacy of machinery-based conservation tillage systems, these impacts emphasize the significance of taking into account not only crop residue retention and soil organic carbon content but also structural stability and biological markers *(Jaskulska et al., 2020).*

Changes in the area disturbed by tillage are apparent immediately after an operation, whereas changes in soil organic carbon require evaluation over a longer period. Their interpretation depends on the duration of the practice, residue inputs, soil conditions, and sampling depth. Higher organic carbon concentration near the surface does not, by itself, demonstrate an increase in carbon stocks throughout the soil profile. Comparisons should therefore distinguish surface concentration from profile stocks and account for sampling depth and bulk density. The direction and magnitude of the response must be interpreted for the particular tillage systems and soil layers being compared *(Haddaway et al., 2017; Bai et al., 2025).*

Soil depth and carbon stabilization mechanisms have a significant impact on the long-term consequences of reduced tillage on soil organic matter. When compared to traditional mouldboard plowing to

a depth of 25 cm, minimum tillage, which involves minimal soil disturbance at 5–8 cm, can result in higher organic carbon concentrations in the upper soil layer (0–5 cm). After several decades of less soil disturbance, values of 15.8 g $kg^{-1}$ under minimum tillage and 9.3 g $kg^{-1}$ under conventional tillage show a larger deposit of organic carbon at the soil surface. However, there is no statistically significant difference at a depth of 10–20 cm. Although the biochemically stabilized fraction cannot be entirely responsible for the increased organic matter accumulation, minimum tillage also encourages the production of surface macroaggregates. The significance of taking into account both sampling depth and sampling time when evaluating changes in soil carbon stocks is further highlighted by seasonal variations and the redistribution of organic matter during tillage activities *(Jacobs et al., 2010).*

Mechanical technologies can promote the conservation of organic matter when they are combined with sufficient plant residue inputs. Crop rotation, cover crops, and the retention of agricultural residues after harvest complement the reduction in soil disturbance induced by machines *(Fohrafellner et al., 2024).*

The combination of these results shows that choosing a seeder or tillage approach is only one aspect of a soil regeneration plan; changes in organic matter should be assessed over an extended period of time, taking into account the complete cropping system.

**Table 1**

**Technological Characteristics Relevant to Soil Protection**

| Criterion | *Minimum tillage* | *No-tillage* | *Strip-tillage* |
|---|---|---|---|
| Disturbed area | Variable; may cover a large proportion of the soil surface | Seed slot | Strips corresponding to the crop rows |
| Examples of components and implements | Cultivator, chisel, combination implement | Cutting disc, coulter, depth-control and closing elements | Residue-management discs, localized loosening component, strip-forming elements |
| Crop residues | The proportion retained depends on the components and their settings | Surface cover is intended to be maintained | Surface cover between the strips is intended to be maintained |
| Critical operational aspect | Actual intensity of soil disturbance | Residue cutting and uniform seed placement | Strip width and seeder alignment |
| Required verification | Disturbed area, soil cover, number of passes | Soil cover, sowing quality, machinery traffic | Soil cover between strips, alignment, machinery traffic |

*Authors' synthesis based on (Lal, 1991; Jaskulska and Jaskulski 2020; Jaskulska et al., 2020; Hoseinian et al., 2021; Alvarez 2024; Antille et al., 2019; Obour and Ugarte 2021; Yang et al., 2022; Vanderhasselt et al., 2024).*

The comparison highlights distinct technological trade-offs. No-tillage minimizes soil disturbance but requires effective residue cutting and consistent seed placement. Strip-tillage combines localized seedbed preparation with protected inter-row areas, making strip width and alignment with the seeder critical. Minimum tillage offers a wider range of implements and working depths, but its protective effect depends on the actual intensity of disturbance and the residue cover retained. Across all three systems, wheel traffic remains a separate source of soil stress. Consequently, machinery selection should combine disturbance control, residue management, sowing quality, and traffic organization, while changes in organic carbon require assessment over time *(Khangura et al., 2023; Haddaway et al., 2017).*

## 4. Energy Requirements and Crop Performance

An additional criterion for evaluating the performance of soil-conservation systems is energy consumption. When compared to conventional tillage, no-tillage can lower overall energy requirements to about 91% for maize, 93% for soybeans, and 92% for wheat. Depending on the farmed species and growth conditions, crop yield responses may differ. Soybean and wheat yields may be higher under no-tillage, although maize yields can be comparatively close to those produced under conventional tillage. These results emphasize how important it is to evaluate energy efficiency in light of crop output and the advantages of soil conservation. The entire agronomic effectiveness of conservation tillage systems depends on crop-specific responses and the environmental circumstances in which they are applied, even while reduced mechanical operations contribute to decreased energy use *(Rusu, 2014).*

The agronomic potential of strip-tillage is further illustrated by crop-specific results. When compared to conventional tillage, strip-tillage can boost sugar beet root yield and technological sugar production by approximately 6.6% and 8.2%, respectively, under the right growing circumstances. There was no apparent preference for either tillage method among the four sugar beet varieties. These findings indicate that, compared to traditional tillage, localized soil preparation can preserve or even increase crop output. However, in order to offer a thorough evaluation of the contribution of strip-tillage to soil regeneration and long-term agricultural sustainability, yield increases should be assessed in combination with direct measurements of soil physical, chemical, and biological parameters *(Górski et al., 2022).*

## CONCLUSIONS

Minimum tillage, no-tillage, and strip-tillage offer different ways of limiting soil disturbance and maintaining residue cover. Their contribution to erosion control depends on the actual disturbed area, the cover retained, and local soil and climatic conditions. Reductions reported in the literature should therefore be interpreted within the systems and contexts in which they were obtained.

Soil compaction cannot be assessed from tillage intensity alone. Wheel-induced stresses, soil moisture, axle load, tyre settings, and repeated passes remain relevant in all three systems. Traffic organization, combined operations, and appropriate machinery adjustment should be considered together when selecting soil-protection technologies.

Conservation of organic matter requires reduced disturbance to be combined with adequate plant residue inputs and complementary cropping practices. Surface carbon concentration and whole-profile carbon stocks provide different information, and changes should be evaluated over time. Machinery configuration and operation can support soil regeneration, but they form part of a broader management strategy rather than guaranteeing recovery independently of field conditions.

The reviewed studies additionally show that localized soil preparation can improve seedbed thermal conditions and that reduced-disturbance systems can lower energy requirements while maintaining or improving crop performance under specific conditions. These operational and agronomic benefits complement, but do not replace, direct evidence of changes in soil properties when assessing soil regeneration (*Górski et al., 2022; Licht and Al-Kaisi 2005; Rusu 2014).*

## REFERENCES

[1] Alvarez, R. (2024). A quantitative review of the effects of residue removing on soil organic carbon in croplands. Soil & Tillage Research, 240, 106098. https://doi.org/10.1016/j.still.2024.106098

[2] Antille, D. L., Peets, S., Galambošová, J., Botta, G. F., Rataj, V., Macak, M., Tullberg, J. N., Chamen, W. C. T., White, D. R., Misiewicz, P. A., Hargreaves, P. R., Bienvenido, J. F., & Godwin, R. J. (2019). Review: Soil compaction and controlled traffic farming in arable and grass cropping systems. Agronomy Research, 17(3), 653–682. https://doi.org/10.15159/AR.19.133

[3] Bai, X., et al. (2025). Can alternative tillage sequester carbon deeper? A global synthesis of deep-soil carbon stocks and fractions. European Journal of Soil Science, 76(6), e70251. https://doi.org/10.1111/ejss.70251

[4] Dominati, E. J., Maseyk, F. J. F., Mackay, A. D., & Rendel, J. M. (2019). Farming in a changing environment: Increasing biodiversity on farm for the supply of multiple ecosystem services. Science of the Total Environment, 662, 703–713. https://doi.org/10.1016/j.scitotenv.2019.01.268

[5] Dou, S., et al. (2024). Strip tillage promotes crop yield in comparison with no tillage based on a meta-analysis. Soil & Tillage Research, 240, 106085. https://doi.org/10.1016/j.still.2024.106085

[6] Fleming, D. E., Spencer, G. D., & Krutz, L. J. (2025). Pesticide runoff from conventional tillage, minimum tillage, and no-tillage cropping systems: Meta-analysis of published North American data. Journal of Environmental Quality, 54(5), 913–924. https://doi.org/10.1002/jeq2.70011

[7] Fohrafellner, J., Keiblinger, K. M., Zechmeister-Boltenstern, S., Murugan, R., Spiegel, H., & Valkama, E. (2024). Cover crops affect pool specific soil organic carbon in cropland – A meta-analysis. European Journal of Soil Science, 75(2), e13472. https://doi.org/10.1111/ejss.13472

[8] Getahun, S., Kefale, H., & Gelaye, Y. (2024). Application of precision agriculture technologies for sustainable crop production and environmental sustainability: A systematic review. The Scientific World Journal, 2024(1), Article 2126734. https://doi.org/10.1155/2024/2126734

[9] Górski, D., Gaj, R., Ulatowska, A., & Miziniak, W. (2022). Effect of strip-till and variety on yield and quality of sugar beet against conventional tillage. Agriculture, 12(2), 166. https://doi.org/10.3390/agriculture12020166

[10] Haddaway, N. R., Hedlund, K., Jackson, L. E., Kätterer, T., Lugato, E., Thomsen, I. K., Jørgensen, H. B., & Isberg, P.-E. (2017). How does tillage intensity affect soil organic carbon? A systematic review. Environmental Evidence, 6, 30. https://doi.org/10.1186/s13750-017-0108-9

[11] Hoseinian, S. H., Hemmat, A., Esehaghbeygi, A., Shahgoli, G., & Baghbanan, A. (2021). Development of a dual sideway-share subsurface tillage implement: Part 2. Effect of tool geometry on tillage forces and soil disturbance characteristics. Soil & Tillage Research, 215, 105200. https://doi.org/10.1016/j.still.2021.105200

[12] Jacobs, A., Helfrich, M., Hanisch, S., Quendt, U., Rauber, R., & Ludwig, B. (2010). Effect of conventional and minimum tillage on physical and biochemical stabilization of soil organic matter. Biology and Fertility of Soils, 46, 671–680. https://doi.org/10.1007/s00374-010-0472-x

[13] Jaskulska, I., & Jaskulski, D. (2020). Strip-till one-pass technology in Central and Eastern Europe: A MZURI Pro-Til hybrid machine case study. Agronomy, 10(7), 925. https://doi.org/10.3390/agronomy10070925

[14] Jaskulska, I., Romaneckas, K., Jaskulski, D., & Wojewódzki, P. (2020). A strip-till one-pass system as a component of conservation agriculture. Agronomy, 10(12), 2015. https://doi.org/10.3390/agronomy10122015

[15] Khangura, R., Ferris, D., Wagg, C., & Bowyer, J. (2023). Regenerative agriculture—A literature review on the practices and mechanisms used to improve soil health. Sustainability, 15(3), 2338. https://doi.org/10.3390/su15032338

[16] Kibblewhite, M. G., Ritz, K., & Swift, M. J. (2008). Soil health in agricultural systems. Philosophical Transactions of the Royal Society B: Biological Sciences, 363(1492), 685–701. https://doi.org/10.1098/rstb.2007.2178

[17] Kopittke, P. M., Menzies, N. W., Wang, P., McKenna, B. A., & Lombi, E. (2019). Soil and the intensification of agriculture for global food security. Environment International, 132, Article 105078. https://doi.org/10.1016/j.envint.2019.105078

[18] Lal, R. (1991). Tillage and agricultural sustainability. Soil & Tillage Research, 20(2–4), 133–146. https://doi.org/10.1016/0167-1987(91)90036-W

[19] Licht, M. A., & Al-Kaisi, M. (2005). Strip-tillage effect on seedbed soil temperature and other soil physical properties. Soil & Tillage Research, 80(1–2), 233–249. https://doi.org/10.1016/j.still.2004.03.017

[20] Musa, I. O., et al. (2024). Soil erosion, mineral depletion and regeneration. In S. A. Aransiola, B. R. Babaniyi, A. B. Aransiola, & N. R. Maddela (Eds.), Prospects for Soil Regeneration and Its Impact on Environmental Protection. Springer. https://doi.org/10.1007/978-3-031-53270-2_7

[21] Obour, P. B., & Ugarte, C. M. (2021). A meta-analysis of the impact of traffic-induced compaction on soil physical properties and grain yield. Soil & Tillage Research, 211, 105019. https://doi.org/10.1016/j.still.2021.105019

[22] Rusu, T. (2014). Energy efficiency and soil conservation in conventional, minimum tillage and no-tillage. International Soil and Water Conservation Research, 2(4), 42–49. https://doi.org/10.1016/S2095-6339(15)30057-5

[23] Sun, Y., Zeng, Y., Shi, Q., Pan, X., & Huang, S. (2015). No-tillage controls on runoff: A meta-analysis. Soil & Tillage Research, 153, 1–6. https://doi.org/10.1016/j.still.2015.04.007

[24] Vanderhasselt, A., D'Hose, T., Sneyders, M., & Cornelis, W. (2024). Effects of road- vs. field-recommended tyre inflation pressures and small variations in soil moisture content on traffic-induced soil compaction during seedbed preparation. Soil & Tillage Research, 241, 106109. https://doi.org/10.1016/j.still.2024.106109

[25] Yang, P., Dong, W., Heinen, M., Qin, W., & Oenema, O. (2022). Soil compaction prevention, amelioration and alleviation measures are effective in mechanized and smallholder agriculture: A meta-analysis. Land, 11(5), 645. https://doi.org/10.3390/land11050645